CMR2018
A JOINT EUROCMR/SCMR MEETING
5th EDITION
Improving Clinical Value by Technical Advances
Barcelona, Spain
31 January - 3 February 2018

Proceedings of CMR 2018 A Joint EuroCMR/SCMR Meeting

Barcelona, Spain. 31 January – 3 February 2018

Published: 31 January 2018

ID#: 363600

Effect of rare variants in Hypertrophic Cardiomyopathy genes on cardiac morphology in health and disease using machine-learning of CMR

Antonio de Marvao, MRCP, PhD[1] Carlo Biffi, MSc[2], Roddy Walsh[3], Georgia Doumou, MRes[4], Wenjia Bai, PhD[5], Timothy Dawes, FRCA, PhD.[2], Wenzhe Shi, PhD[2], Rachel Buchan, MSc[6], Iain Pierce, PhD[7], Paweł F. Tokarczuk, PhD[8], Thu-Thao Le, PhD[9], Siew Ching Kong, Bachelor of Science[9], Marina Quinlan, MSc[10], Anish N. Bhuva, MRCP MBBS[11], Hak Chiaw Tang, MBBS, MRCP (UK)[9], Calvin WL. Chin, Assistant Professor[12], Daniel Rueckert, PhD[3], James S. Ware, MRCP PhD[3], Sanjay Prasad, MD[13], Declan O'Regan, FRCR, PhD[14], Stuart Cook, PhD[9]

1. MRC London Institute of Medical Sciences, London, England, United Kingdom

2. Imperial College London, London, England, United Kingdom

3. Imperial College London, United Kingdom

4. MRC - Clinical Science Centre, United Kingdom

5. Imperial College London, London, United Kingdom

6. Royal Brompton Hospital, United Kingdom

7. Royal Brompton Hospital Trust, London, England, United Kingdom

8. Imperial College, London, England, United Kingdom

9. National Heart Centre Singapore, Singapore

10. Imperial College london, United Kingdom

11. Barts Heart Centre and Institute of Cardiovascular Science, UCL., London, England, United Kingdom

12. Duke-NUS Medical School, Singapore

13. Royal Brompton Hospital and Imperial College, London, England, United Kingdom

14. MRC London Institute of Medical Sciences, England, United Kingdom

Background: Hypertrophic cardiomyopathy (HCM) is an autosomal dominant Mendelian disease characterised by variable expressivity and penetrance. In the community, rare sarcomere variants are associated with increased risk of adverse cardiovascular events and linked to subtle structural changes in the absence of left ventricular (LV) hypertrophy. We aimed to define the effect of rare variants in HCM-associated genes on cardiac structure in both patients with HCM and healthy volunteers by using machine-learning analysis of cardiovascular magnetic resonance (CMR) imaging.

Methods: Patients with HCM diagnosed using standard clinical criteria were recruited at the Royal Brompton Hospital (n=622, 27% women, 77% Caucasian, 57±14 years) and the National Heart Centre Singapore (n=64, 22% women, 89% Chinese, 55±13 years). Healthy volunteers enrolled in the Digital Heart Project (n=1360, 55% women, 68% Caucasian,39±13 years). Patients underwent conventional CMR at 1.5T which was supplemented in healthy volunteers by high-resolution 3D b-SSFP cine imaging. Using cardiac atlas and machine learning techniques, CMRs were segmented and co-registered providing statistical models of phenotypic variation in the population adjusted for body surface area, sex, race, age and blood pressure. Subjects were sequenced with comprehensive gene panels and identified as genotype positive (G+) using stringent criteria (including frequency $<4.0 \times 10^{-5}$) in genes and variant classes previously associated with HCM. Individuals with variants not meeting these criteria were excluded (n=164). Those without any of these variants were considered genotype negative (G-).

Results: In healthy volunteers no subject met criteria for diagnosis of HCM. In this cohort, rare variants in thick filament genes (MYH7, MYBPC3; n=11) were associated with increased wall thickness (WT) at the base and

septum (Fig 1) compared to G- volunteers. No other variants were associated with phenotypic changes. In HCM, G+ (n=132) and G- patients had similar patterns of septal hypertrophy, but elsewhere WT was greater in G- patients. Thick filament G+ patients (n=104) had greater septal WT compared to both thin filament G+ and G- patients (Fig 2). G+ patients with thin filament variants (n=28) had significantly lower WT than other HCM subgroups (Fig 3).

Conclusion: Using 3D modelling we show that rare variants in thick filament genes are associated with a pattern of increased WT in healthy adults. In HCM we found that the previously reported association between G+ status and greater WT is driven by rare variants in thick filament genes. We demonstrate that integrating machine-learning-based analysis of CMR with genotypic data greatly increases the power to detect genotype-phenotype associations.

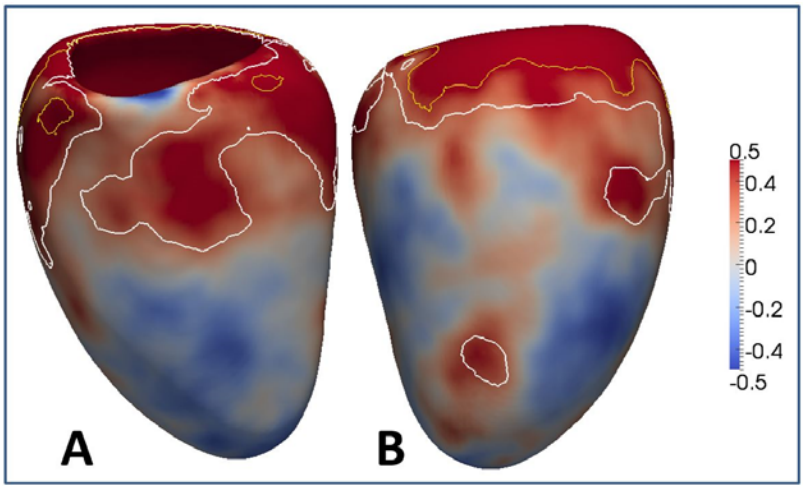

Figure 1 - Computational modelling of cardiac geometry in 1360 healthy volunteers using 3D CMR. Positive standardised beta coefficients indicate where rare variants in thick filament genes are associated with increased wall thickness when compared to genotype negative individuals. Contour lines indicate significant regions ($p<0.05$) before (white border) and after (yellow border) correction for multiple testing, respectively. LV projections are anterior (A) and lateral (B).

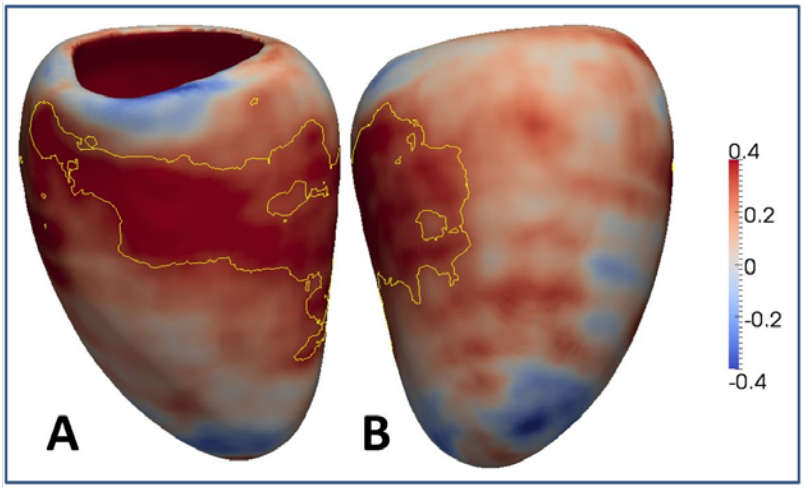

Figure 2 - Computational modelling of cardiac geometry in 686 patients with HCM using 2D CMR. Positive standardised beta coefficients indicate where rare variants in thick filament genes are associated with increased wall thickness when compared to rare variants in thin filament genotype positive individuals. Area enclosed by the yellow contour has a corrected $P<0.05$ (mass univariate linear regression). LV projections are anterior (A) and lateral (B).

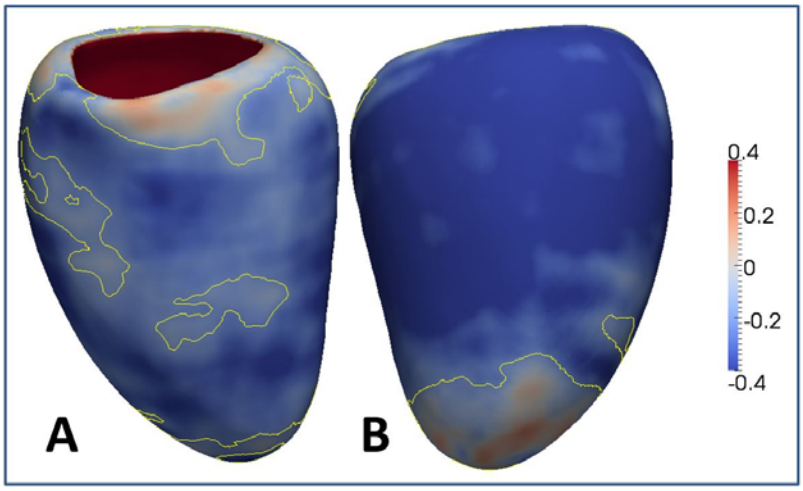

Figure 3 - Computational modelling of cardiac geometry in 686 patients with HCM using 2D CMR. Negative standardised beta coefficients indicate where rare variants in thin filament genes are associated with reduced wall thickness when compared to genotype negative HCM patients. Area enclosed by the yellow contour has a corrected P <0.05 (mass univariate linear regression). LV projections are anterior (A) and lateral (B).

ID#: 364558

Fractal analysis of right ventricular trabeculae in pulmonary hypertension

Timothy Dawes, FRCA, PhD.[1] Jiashen Cai, B.Eng (Hons), M.D.[2], Marina Quinlan[3], Antonio de Marvao, MRCP, PhD[4], Philip Ostrowski, MRCP PhD[5], Pawel Tokarczuk, PhD[5], Geoffrey Watson[6], John Wharton, PhD[5], Luke Howard[7], Simon Gibbs, PhD[8], Martin Wilkins, MD[5], Declan O'Regan, FRCR, PhD[3]

1. Imperial College London, London, England, United Kingdom

2. Duke-NUS Medical School, N/A, Singapore

3. MRC London Institute of Medical Sciences, England, United Kingdom

4. MRC London Institute of Medical Sciences, London, England, United Kingdom

5. Imperial College London, England, United Kingdom

6. Imperial College London, Brighton, United Kingdom

7. Imperial College Healthcare NHS Trust, England, United Kingdom

8. Imperial College Healthcare NHS Trust, London, UK, United Kingdom

Background: Survival in pulmonary hypertension (PH) depends on functional adaptation of the right heart. Conventional parameters of right ventricular (RV) function are often normal at diagnosis and may not detect early cardiac dysfunction. Trabeculae are known to adapt in PH and may provide a sensitive marker of disease. We assessed whether RV trabecular complexity, measured by fractal dimension (FD), predicts survival in patients with PH.

Methods: 256 patients (143 females, median age 67 years, inter-quartile range [IQR]: 52 to 74) with newly-diagnosed PH underwent cardiac magnetic resonance (CMR) imaging, right heart catheterization and six-minute walk distance testing with a median follow-up of 4.0 years. 256 healthy controls matched by age, gender, body surface area and race underwent CMR imaging. RV fractal dimension, volumes and function were assessed on short-axis cine images.

Results: Fractal dimension was highly reproducible in PH patients (median intraclass correlation coefficient 0.97, 95% confidence intervals [CI]: 0.96 to 0.98). Fractal dimension was higher in PH patients than healthy controls, with the greatest difference near the apex (maximum apical FD [MAFD]: median 1.39, IQR: 1.348 to 1.428 vs: 1.31, IQR 1.264 to 1.357, $p<0.001$. In PH patients, FD was associated with pulmonary vascular resistance ($r=0.30$, $p<0.001$). In univariate Cox regression analysis, MAFD was a significant predictor of death (hazards ratio [HR]: 1.256, CI: 1.011 to 1.560, $p=0.040$) and remained a significant independent predictor (HR: 1.305, CI: 1.022 to 1.666, $p=0.033$) in multivariate analysis controlling for non-invasive parameters (age, gender, race, PH subtype, World Health Organisation functional class, six-minute walk distance) and CMR volumetric parameters. Mean survival of PH patients in the first vs fourth MAFD quartile differed by 19.6 years (CI: 19.6 to 19.7).

Conclusion: Fractal analysis of RV trabecular complexity is a highly reproducible measure of remodeling in PH which is associated with outcome.

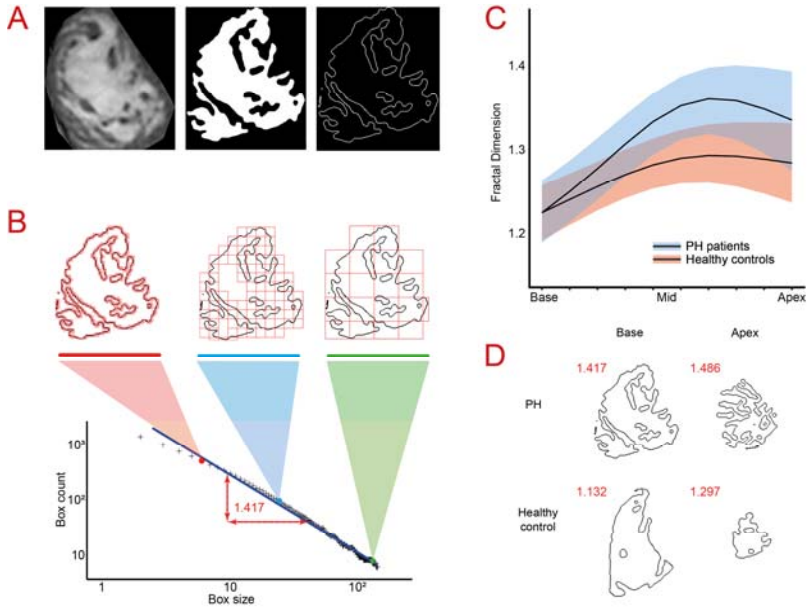

Figure 1. Fractal dimension analysis. A. Images show the process (left to right) of measuring fractal dimension (FD) from a single left ventricular short-axis (LVSA) slice. A region of interest is drawn around the right ventricle from which a binary mask of the blood pool is extracted followed by edge detection of the endocardium and trabeculae. B. Box-counting with a range of box sizes generates points on a log-log regression plot from which the gradient of a least squares linear regression fit (FD) is calculated. C. Line plot of FD in pulmonary hypertension (PH) patients (blue) and matched healthy controls (red) by right ventricular level. Ribbon denotes the inter-quartile range at each ventricular level. D. Trabecular and papillary muscle perimeter in one subject with PH (upper row) and one healthy control (lower row) in a single basal slice (left column) and apical slice (right column). FD for each slice is marked in red.

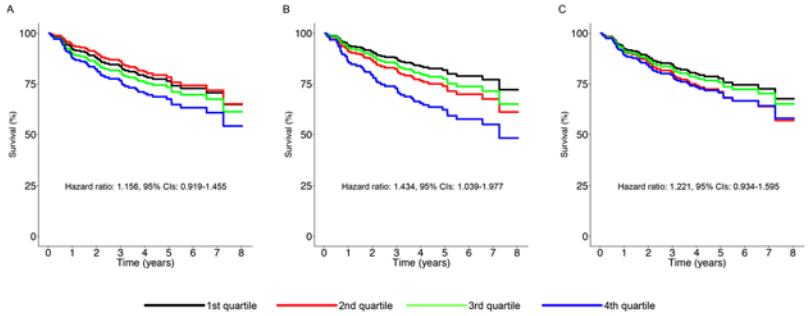

Figure 2. Cox regression analysis for the survival of pulmonary hypertension patients by quartile of global, maximum apical and maximum basal fractal dimension. Cox regression analysis models for the survival from diagnosis of 256 pulmonary hypertension (PH) patients by (A) global fractal dimension (FD), (B) maximum apical FD and (C) maximum basal FD. PH patients are divided into quartiles based on FD.

ID#: 366304

High resolution cardiac T1 mapping based on SUPER

Chenxi Hu, PhD[1]Dana C. Peters, PhD[2]

1. Yale University, CT

2. Yale University

Background: Cardiac T1 mapping (MOLLI)[1] is limited to a low image resolution because of the single-shot acquisition. Here we propose a new method to accelerate T1 mapping and therefore improve the resolution.

Methods: Figure 1 shows the rationale of SUPER[2], which represents “Shift Undersampling improves Parameter mapping Efficiency and Resolution”. Shift undersampling means that k-space in the phase-encoding (PE) direction is shifted and undersampled at every TI. The unsampled lines are zero-filled and the resultant k-space is Fourier transformed. The shift undersampling causes aliasing from equidistant voxels in the PE direction, but with a unique temporal modulation for signal at each voxel. The modulation separates the spectrum of the aliased relaxation signals in the measured signal. Dealiasing is performed by solving the least-squares cost function for each aliasing, using a customized Levenberg-Marquardt algorithm. T1 in the algorithm was bounded by 100ms and 5000ms to avoid local minima. With multi-channel coils, the coil sensitivity was derived from 24 low-frequency reference lines, and was employed in the reconstruction to allow for parallel imaging. Six healthy volunteers were studied with the standard and high-resolution SUPER MOLLI on a 3T scanner (Siemens Trio) after providing informed written consent. Parameters for the standard MOLLI: FOV: 360mmx270mm, matrix: 196x108, resolution: 1.9mmx2.5mm, slice thickness: 8mm, FA/BW/TR = 15/1395Hz/pixel/2.5ms, 11 TIs/17 heartbeats (i.e. 3(3)3(3)5 MOLLI), and GRAPPA factor of 2. SUPER MOLLI had the same parameters except the resolution was 1.4mmx1.4mm and matrix was 256x192. SUPER MOLLI used 4-fold acceleration, instead of 2-fold acceleration of MOLLI.

Results: Figure 2 shows the representative images from four subjects. SUPER MOLLI improved resolution, resulting in a better depiction of small structures and less Gibbs artifacts. The average myocardial T1 from the standard MOLLI and SUPER MOLLI was 1146ms ± 65ms and 1143ms ± 71ms ($p=0.26$), respectively, and the average blood T1 from the standard and SUPER MOLLI was 1669ms ± 49ms and 1644ms ± 55ms ($p=0.02$), respectively. The reconstruction time per pixel for SUPER MOLLI was 8.5ms ± 1.0ms.

Conclusion: We improved the resolution of MOLLI by using a new parameter mapping acceleration method. The method is applicable to many parameter mapping applications, and is clinically applicable due to its fast reconstruction. The improved resolution may benefit T1 mapping in small or thin structures, such as the papillary muscles, the RV, and small focal scars.

References 1. Messroghli DR, MRM 2004; 2. Hu C, ISMRM 2017

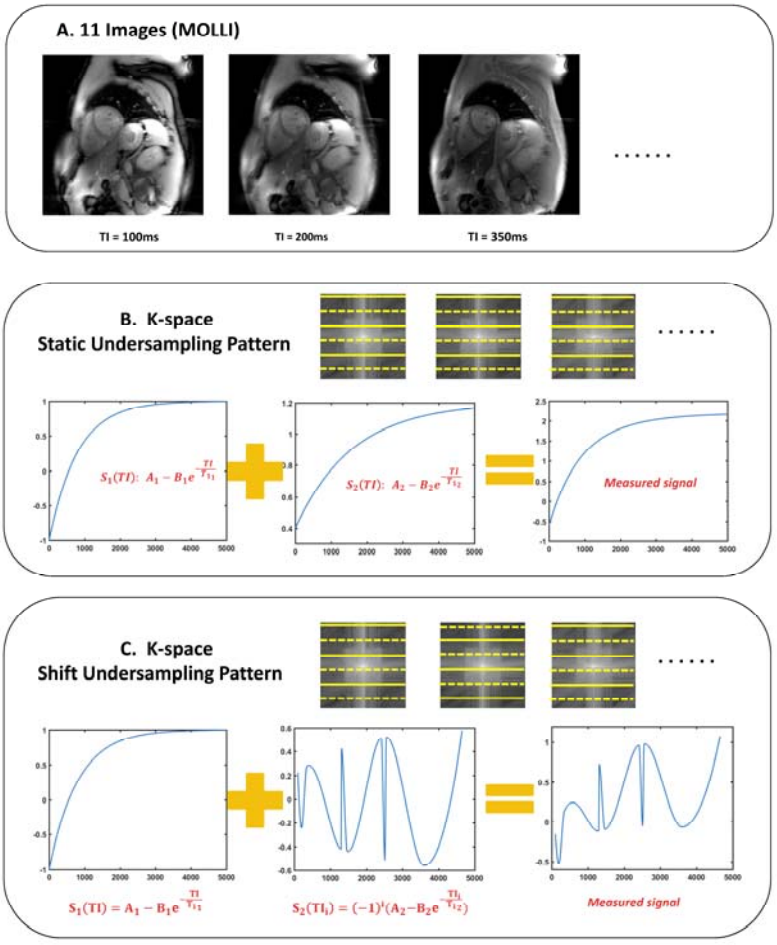

Figure 1. (Panel A) 11 images are to be acquired in MOLLI. (Panel B) K-space at each TI is undersampled in the same fashion, resulting in a pure aliasing of relaxation signals. The two signals are difficult to extract from the measured signal. (Panel C) K-space at each TI is undersampled but the sampling pattern is circularly shifted, resulting in a modulation of the relaxation signal before the aliasing. This modulation separates the two relaxation signals in the temporal frequency domain, facilitating extraction of the two relaxation signals.

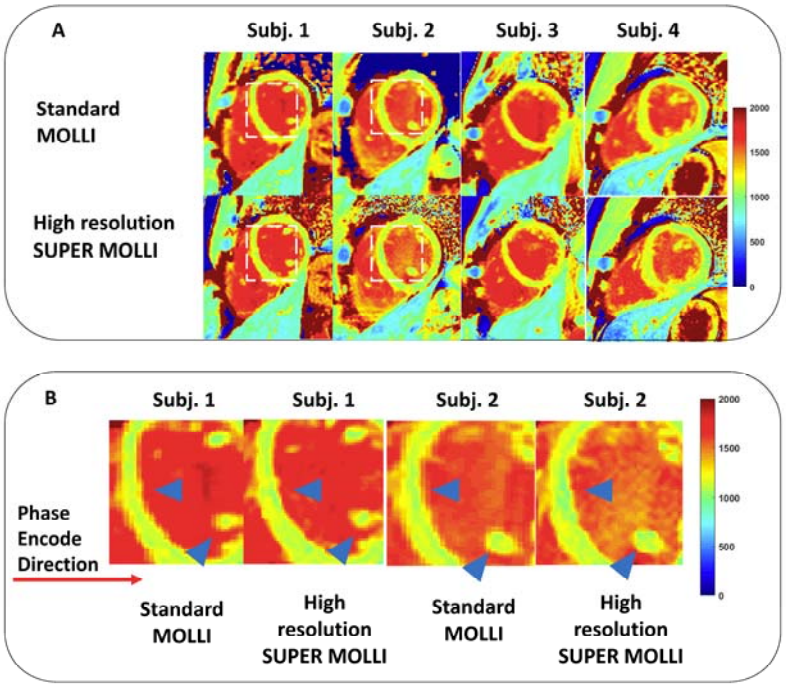

Figure 2. T1 maps reconstructed from the standard MOLLI (resolution: 1.9mmx2.5mm, image size: 196x108) and SUPER MOLLI (resolution: 1.4mmx1.4mm, image size: 256x192) in 4 healthy volunteers (Panel A) and the amplified images from subjects #1 and #2 demonstrating the resolution improvement in the left ventricle (Panel B). SUPER MOLLI led to clearer edges and less Gibbs ringing along the phase-encoding direction in the septal wall and papillary muscles (arrow heads).

ID#: 369021

3D High resolution imaging of ventricular scar: head-to-head comparison of three late gadolinium enhancement (LGE) sequences in a porcine infarct model at 1.5T

Rahul K. Mukherjee, MBBS[1] John Whitaker, BM BCh[2], Sébastien Roujol, PhD[1], Radhouene Neji, PhD[3], Giulia Ginami, PhD[4], Adriana D. M. Villa, MD[4], Henry Chubb, MRCP MRCPCH[5], Louisa O'Neill, MBChB[4], Steven Williams, MD PhD[6], John Silberbauer, MD[7], Matthew Wright, MBBS PhD[4], Mark O'Neill, MD DPhil[1], Rene Michael. Botnar, PhD[1], Claudia Prieto, PhD[8], Reza Razavi, MD, PhD[1]

1. King's College London, London, England, United Kingdom

2. King's College London/Beth Israel Deaconess Medical Centre, London, England, United Kingdom

3. Siemens Healthcare, MR Research Collaborations, Siemens Healthcare Limited, United Kingdom

4. King's College London, United Kingdom

5. Kings college London, England, United Kingdom

6. Kings College Londin, England, United Kingdom

7. Brighton and Sussex University Hospitals NHS Foundation Trust, United Kingdom

8. King's College London, England, United Kingdom

Background: Heterogeneous areas of scar identified with contrast-enhanced MRI (CE-CMR) have been related to the structural substrate of ventricular tachycardia in ischaemic cardiomyopathy. To create detailed 3D scar maps from CE-CMR and integrate into clinical mapping systems to facilitate substrate-guided ablation, a high spatial resolution is required to minimise partial volume effects and discriminate between regions of scar core and heterogeneous areas. This study was designed to systematically compare three 3D high resolution LGE techniques for assessment of scar and heterogeneous tissue in a porcine infarct model.

Methods: 6 pigs underwent a 180-minute occlusion of the left anterior descending artery followed by a 6-week recovery. All animals then underwent MR imaging at 1.5T (MAGNETOM, Aera, Siemens) using contrast steady-state to allow high resolution imaging of scar. A 3D inversion recovery (IR) balanced steady-state free precession (bSSFP) sequence was compared to IR gradient echo (GRE) and a recently proposed prototype Bright-blood and black-blOOd phase SensiTive T2-prep-IR (BOOST) sequences. All three sequences were 3D ECG-triggered with an isotropic spatial resolution (1.2mm x 1.2mm x 1.2mm) acquired in coronal orientation. Qualitative assessment of ventricular scar was performed by 2 independent observers using a 5-point Likert scale. Quantification of infarct size was made using the full width at half maximum (FWHM) technique whilst borderzone region was defined as areas between 20-50% of maximum pixel signal intensity.

Results: High resolution LGE images using each sequence are shown in Figure 1. Overall image quality was higher on the 3D-IR-bSSFP sequence (3.58, p= 0.021) compared to GRE and BOOST sequences. Lesion conspicuity relative to the LV cavity was significantly better on the BOOST sequence (3.50, p<0.001) whilst lesion conspicuity relative to normal myocardium was better on the bSSFP (4.0, p<0.001). There was a greater presence of artifacts on the GRE sequence (2.08, p<0.001) whilst there was no difference on assessment of transmural lesion extent (p=0.834, NS) – Figure 2. Moderate to good agreement was obtained between readers on image quality (k=0.667), lesion conspicuity relative to LV cavity (k=0.615) and transmural lesion extent (k=0.667). There was no difference between the sequences on assessment of LV scar volume (p=0.078) however, there was significant variability between the sequences on assessment of borderzone volume (Figure 3).

Conclusion: The 3D-IR-bSSFP technique demonstrated the best overall image quality and differentiation of infarct lesion from normal myocardium. However, there is significant variability between sequences on assessment of borderzone regions and comparison with a gold-standard is therefore warranted.

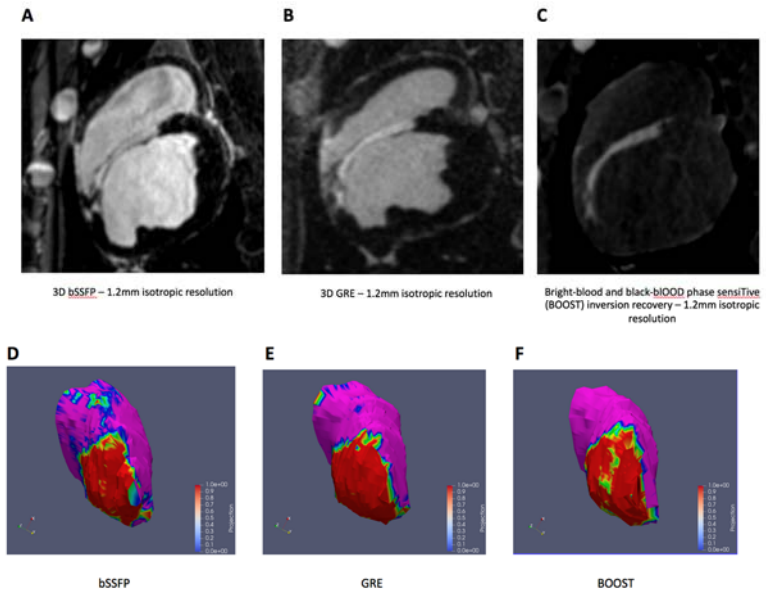

MR images of scar across three different LGE sequences (A-C) and corresponding 3D projection maps of scar from segmented images (D-F).

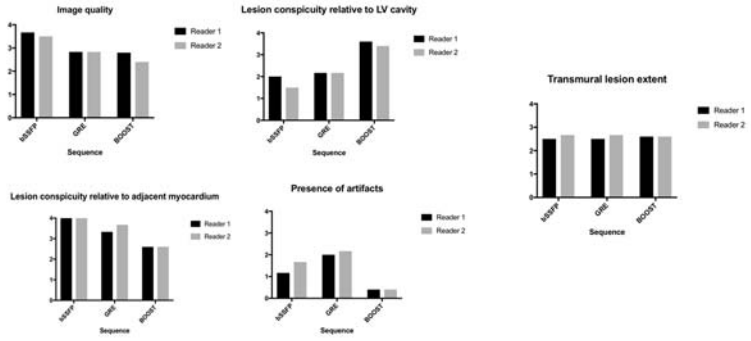

Qualitative assessment of different sequences for the degree of overall image quality, lesion conspicuity relative to LV cavity and normal myocardium, presence of artifacts and transmural lesion extent. All evaluations are means of scores assigned by two blinded readers of a 5-point scale. Overall image quality - 4 = excellent; 3 = good; 2 = moderate; 1 = poor; 0 = non-diagnostic; Lesion conspicuity relative to LV cavity/normal myocardium - 4 = excellent differentiation; 3 = good differentiation; 2 = moderate differentiation; 1 = poor differentiation; 0 = not able to differentiate; Presence of artifacts - 0 = none; 1 = minor; 2 = moderate; 3 = high artifact level; 4 = non-diagnostic; Transmural lesion extent - 0 = 0-24%; 1 = 25-49%; 2 = 50-74%; 3 = 75-100%.

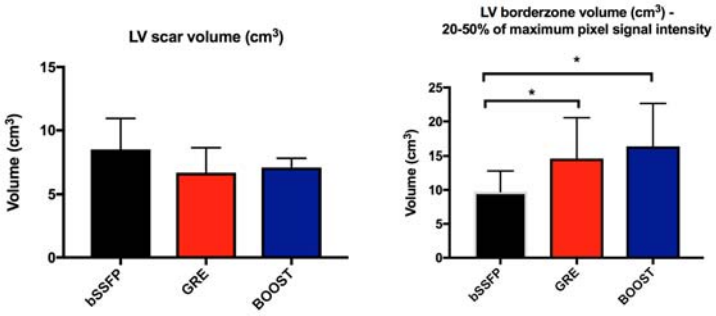

Quantification of LV scar volume (A) and LV borderzone volume (B) using FWHM and 20-50% of maximum pixel signal intensity. No difference in core LV scar volume was seen between the three 3D-IR sequences. Significant variability was seen in the LV borderzone volume between bSSFP (9.77cm3), GRE (14.61cm3) and BOOST (16.35cm3) sequences. Data shown as means SD; *p<0.05.

ID#: 370643

Free-breathing cine DENSE using phase-cycling with matchmaking and stimulated-echo image-based navigators

Xiaoying Cai, BS[1] Frederick H. Epstein, PhD[2]

1. University of Virginia, Charlottesville, VA

2. UVA Health System, Charlottesville, VA

Background: Cine DENSE is a well-established strain imaging technique that uses phase-cycling to suppress the artifact-generating echo due to T1-relaxation. During free-breathing (FB), respiration induces two types of artifacts: striping due to insufficient suppression of the T1-relaxation echo and blurring. We developed and evaluated a framework that addressed both types of artifacts for FB spiral cine DENSE.

Methods: For data acquisition, the framework utilized a 2D spiral cine DENSE sequence that supports golden angle rotation through time and localized generation of stimulated echoes. For reconstruction, the framework (Fig.1a) first selects phase-cycled interleafs acquired at matched respiratory phases using low residual T1-echo energy (rT1E) as the matching criterion, termed match-making. Then it reconstructs image-based navigators from post-subtraction interleafs (ps-interleaf) that are primarily comprised of the stimulated echo (termed ste-iNAVs). Lastly, the method estimates and compensates for motion between ps-interleafs using ste-iNAVs. The ste-iNAVs are focused to the heart with localized stimulated echo generation, which facilitates motion estimation.
Phantom datasets were acquired 6 times with the phantom moved between acquisitions to introduce motion between phase-cycled interleafs. Three different slice orientations were imaged and the motion seen by each slice was in-plane, through-plane and a combination of both, respectively. The rT1E of ps-interleafs was correlated to the amount of motion between phase-cycled interleafs.
FB DENSE datasets were acquired on 5 volunteers using a 3T system (Trio, Siemens) with field-of-view of 160 mm, 6 interleafs per image, TR of 15 ms, temporal resolution of 30 ms, spatial resolution of 3 mm^2, 3 averages, diaphragm navigator (dNAV) acquisition at end-diastole and 56 heartbeats in duration. Each dataset was reconstructed using both the match-making framework and the conventional dNAV-gated method. Reconstructions were evaluated by calculating overall rT1E for accepted data, magnitude signal-to-noise ratio (SNR), and phase quality (total variance of local derivative of phase) in the myocardium.

Results: An example ps-interleaf from phase-cycled interleafs acquired at matched positions demonstrated suppression of the T1-relaxation echo (Fig.2a, black curve), while an example ps-interleaf from phase-cycled interleafs acquired at mismatched positions had strong residual T1-echo signal (Fig.2a, red curve). The rT1E was highly correlated with the amount of motion between phase-cycled interleafs, and this relation stood for in-plane, through-plane, and combined motion (Fig.2c-e), which demonstrated that rT1E can be used to perform match-making. Striping artifacts (as in Fig.1f) can be removed with matched subtraction (Fig.1g). Motion compensation using ste-iNAVs further removed blurring artifacts (Fig.1h).
As shown in Fig. 3, reconstruction of volunteer images by the match-making framework had less artifacts and better phase quality than reconstruction by dNAV-gating (Fig.3a). Overall, the match-making framework reconstructed better images than dNAV-gating, with significantly lower rT1E, higher SNR and better phase quality (Fig.3b).

Conclusion: The proposed framework compensates for both striping and blurring artifacts in FB cine DENSE. Future work will develop an online version of the framework with adaptive acquisition to further improve image quality and efficiency.

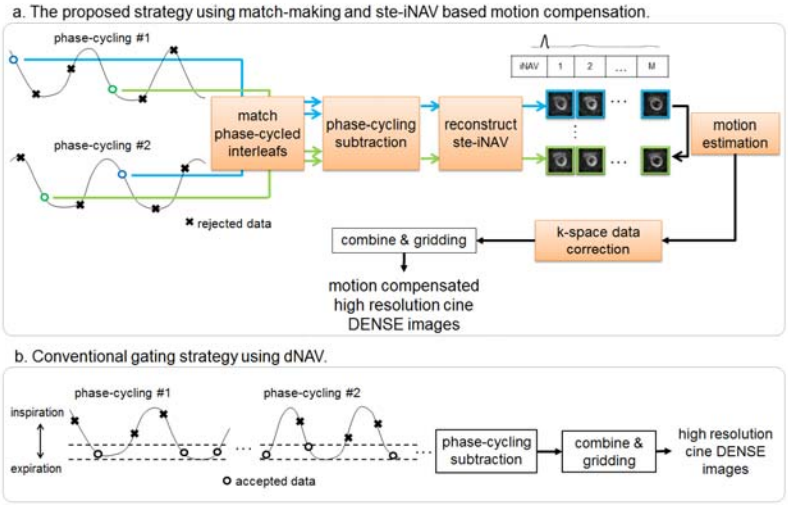

Fig.1. (a) Diagram of the proposed framework where (1) match-making is performed to identify phase-cycled interleafs at matched respiratory phases, (2) phase-cycling subtraction is performed with identified phase-cycling pairs, and (3) ste-iNAVs are reconstructed for motion estimation and compensation. (b) Conventional dNAV-gating strategy.

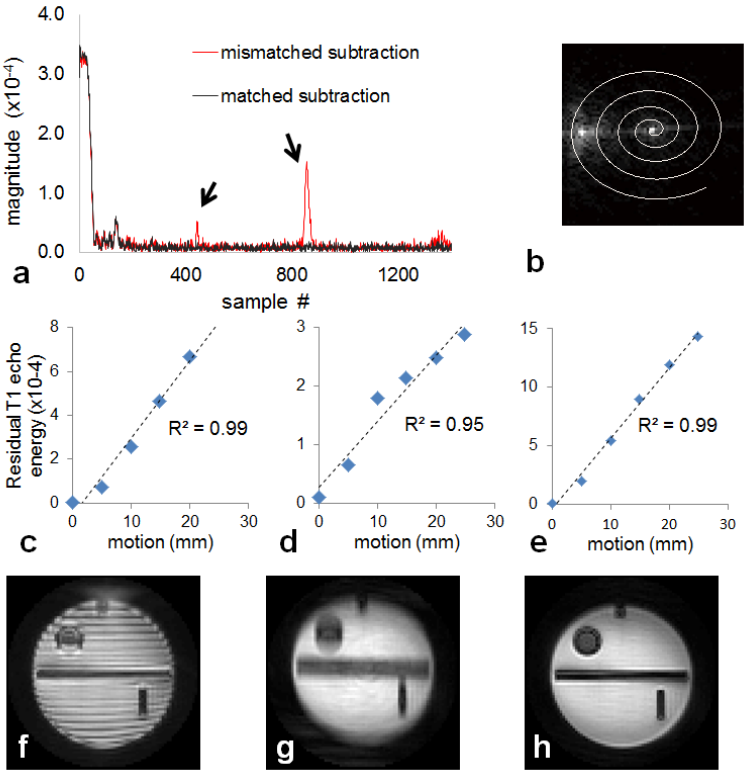

Fig.2. (a) Intensities of ps-interleafs along a spiral trajectory (as in (b)). Strong residual T1-echo signal (arrows) remains in the ps-interleaf from subtraction of mismatched phase-cycled interleafs, but the T1-echo signal is nulled by subtracting interleafs acquired at matched positions. (c-e) Residual T1-echo energy correlated well with motion between phase-cycled interleafs. The relation holds for in-plane motion (c), through-plane motion (d), and a combination of both types of motion (e). (f-h) Using the proposed framework, striping artifacts, as in (f), and blurring, as in (g), were removed and a high quality image was reconstructed (h).

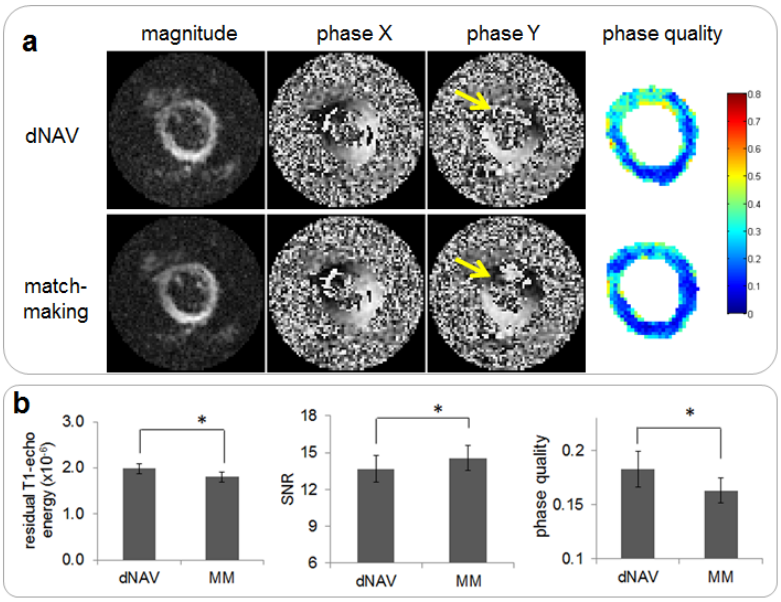

Fig.3. (a) Volunteer DENSE images at end-systole reconstructed from the same dataset using the match-making framework (bottom) and dNAV-gating (top). Images reconstructed by the match-making framework have higher SNR and better phase quality, as shown in the phase quality maps where low values indicate good phase quality. (b) Summary of image quality quantification. The match-making framework (MM) had significantly lower residual T1-echo energy, higher SNR and better phase quality than dNAV-gating. ($P<0.05$, paired t-test).

ID#: 370936

Feasibility and reproducibility of a free-breathing, multi-shot, navigated image acquisition for ventricular volume quantification during continuous exercise: A pilot study of healthy controls

Pei G. Chew, MBChB(Hons) [1]Peter P. Swoboda, PhD[2], Carrie Ferguson, PhD[3], Pankaj Garg, MD, PhD[4], Said Ibeggazene, BSc[3], Abigail Cook, MRes[3], Louise AE. Brown, MBChB, BMedSc[5], James R. Foley, MBChB BSc (Hons)[2], Graham J. Fent, MBChB, BSc[2], Sebastian C. Onciul[5], David M. Higgins, PhD[6], Sven Plein, MD PhD[5], Karen Birch, PhD[3], John P. Greenwood, PhD[5]

1. University of Leeds, Liverpool, England, United Kingdom

2. University of Leeds, Leeds, England, United Kingdom

3. University of Leeds, United Kingdom

4. University of Leeds, UK, Leeds, England, United Kingdom

5. University of Leeds, England, United Kingdom

6. Philips, Leeds, England, United Kingdom

Background: CMR image acquisition techniques during exercise typically require transient cessation of exercise or complex post-processing analysis, potentially compromising its clinical utility. We evaluated the feasibility and reproducibility of a novel image acquisition method for the assessment of biventricular physiological response during continuous physical exercise.

Methods: 10 healthy volunteers (80% men, age 25±2 years) underwent supine cycle ergometer (Lode) induced exercise CMR (Philips 1.5T Ingenia) on two separate occasions using a free-breathing, multi-shot, navigated, balanced steady-state free precession cine pulse sequence. Individual target heart rates (HR) for both moderate and high-intensity exercise were prescribed based on a prior supine cardiopulmonary exercise test (CPET). The scan protocol included a short axis ventricular volume stack and a 40 phase 4-chamber cine. Images were acquired at baseline, and during steady-state moderate and high-intensity exercise (55% and 75% maximal heart rate, respectively). Data were analysed by two independent observers and left and right ventricular (LV, RV) indices calculated.

Results: End-diastolic volume (EDV) of both LV and RV decreased during moderate and high-intensity exercise, although the reduction in indexed RVEDV (RVEDVi) was only observed during maximal exercise (Table 1). Similarly, a significant reduction in end-systolic volumes (ESV) was seen in both ventricles, whilst the reduction in indexed LVESV (LVESVi) was only evident during high-intensity exercise. Ejection fraction (EF) increased from rest to moderate and high intensity exercise in the LV (LVEF 58±5% vs 61±8% vs 68±3%, respectively; $p<0.001$), whereas RVEF was only significantly higher during high-intensity exercise (RVEF 58±7% vs 62±7% vs 66±4%; $p<0.01$). A biphasic change in global longitudinal strain (GLS) was observed; there was a significant increase in GLS during moderate-intensity exercise which appeared to plateau at maximal exercise. A similar biphasic change was observed for GLS rate (Table 1).

Intra-observer reproducibility of LV parameters was excellent at all three stages (Table 2), although measurements of RVESV were more variable. The reproducibility of both RVEF and RV cardiac indexes was however excellent. Similarly, inter-observer reproducibility of LV volumes, EF and cardiac indexes was excellent. Inter-scan LV and RV ejection fraction were highly reproducible at all 3 stages; RVESVi reproducibility was suboptimal.

Conclusion: This exercise CMR protocol using a novel free-breathing, multi-shot, navigated imaging method allows simultaneous assessment of the left and right ventricular response to continuous exercise. Intra and inter-observer reproducibility were excellent. Clinical feasibility and utility now needs to be established.

Table 1. Volumetric data for both left and right ventricle at baseline, and during steady-state moderate and high-intensity exercise.

Cardiovascular variables	Baseline	Moderate Intensity	High Intensity	P value (Baseline vs Moderate)	P value (Moderate vs High)	P value (Baseline vs High)
LVEDV (indexed) ml/m²	97±11	93±10	85±7	0.001	0.004	<0.001
LVESV (indexed) ml/m²	41±7	36±9	28±3	0.08	0.006	<0.001
LVSV (indexed) ml/m²	57±6	57±10	57±5	0.80	0.98	0.52
LVEF %	58±5	61±8	68±3	0.30	0.04	<0.001
LV cardiac index, L/min/m²	3805 ±721	5456 ±1448	7503 ±1055	0.001	0.001	<0.001
RVEDV (indexed) ml/m²	95±11	92±8	81±7	0.77	0.01	0.003
RVESV (indexed) ml/m²	40±10	35±8	28±5	0.04	0.04	0.004
RVSV (indexed) ml/m²	51±9	56±5	54±5	0.09	0.37	0.29
RVEF %	58±7	62±7	66±4	0.12	0.15	0.01
RV cardiac index, L/min/m²	3685± 907	5333± 1133	6991± 704	0.001	0.002	<0.001
GLS %	16.3 ±3.2	18.3 ±3.9	16.5 ±3.1	0.01	0.26	0.91
GLS rate %/s	135.9 ±59	218.3 ±101	285.8 ±106	0.07	0.11	0.004

Data as mean±SD. LVEDV, left ventricular end-diastolic volume; LVESV, left ventricular end-systolic volume; LVSV, left ventricular stroke volume; LVEF, left ventricular ejection fraction; LV, left ventricle; RVEDV, right ventricular end-diastolic volume; RVESV, right ventricular end-systolic volume; RVSV, right ventricular stroke volume; RVEF, right ventricular ejection fraction; RV, right ventricle; GLS, global longitudinal strain

Table 2. Coefficient of Variation (CoV) for the LV and RV cardiac indices

Stages	Cardiovascular variables	Coefficient variability for Reproducibility (%)		
		Intra-Observer	Inter-observer	Inter-scan
REST	LVEDVi LVESVi LVEF RVEDVi RVESVi RVSVi	<10	<10	<10
	LV CI RVEF RV CI	<10	<10	10-18
Moderate Intensity (55% max HR)	LVEDVi LVESVi LVSVi LV CI	≤10	≤10	6-16
	LVEF	<10	<10	<10
	RVEDVi RVSVi RVEF	<10	<10	<10
	RVESVi	12	12	16
	RV CI	<10	<10	12
High intensity (75% max HR)	LVEDVi LVESVi LVSVi	≤10	≤10	7-12
	LVEF LV CI	<10	≤10	<10
	RVEDVi RVSVi RVEF RV CI	≤10	≤10	≤10
	RVESVi	20	14	24

Data as %. LVEDV, left ventricular end-diastolic volume; LVESV, left ventricular end-systolic volume; LVSV, left ventricular stroke volume; LVEF, left ventricular ejection fraction; LV, left ventricle; RVEDV, right ventricular end-diastolic volume; RVESV, right ventricular end-systolic volume; RVSV, right ventricular stroke volume; RVEF, right ventricular ejection fraction; RV, right ventricle; GLS, global longitudinal strain; HR, heart rate

ID#: 371507

Simultaneous 3D Whole-Heart Bright-Blood Visualization of the Coronary Sinus and Heart Anatomy and Black-Blood PSIR Depiction of Atrial Walls for Non-Contrast Enhanced Interventional Planning

Giulia Ginami, PhD[1] Radhouene Neji, PhD[2], Karina Lopez, MRes[1], Sébastien Roujol, PhD[3], Peter Mountney, PhD[2], Reza Razavi, MD, PhD[3], Rene Michael. Botnar, PhD[3], Claudia Prieto, PhD[4]

1. King's College London, United Kingdom

2. Siemens Healthcare, MR Research Collaborations, Siemens Healthcare Limited, United Kingdom

3. King's College London, London, England, United Kingdom

4. King's College London, England, United Kingdom

Background: Quantification of atrial wall thickness plays a major role in the planning of electrophysiological (EP) procedures. Accurate and precise delivery of thermal energy during catheter ablation is important for the success of the procedure. Furthermore, pre-interventional knowledge of subject-specific variations in the anatomy of the coronary sinus (CS) facilitates catheterization. Here, we present a free-breathing 3D whole-heart phase-sensitive inversion recovery (PSIR) sequence suitable for non-contrast enhanced pre-interventional planning, offering simultaneous visualization of the atrial walls as well as of the heart and CS anatomy.

Methods: A 3D whole-heart bright-blood and black-blood PSIR (BOOST) bSSFP prototype sequence was implemented as in Fig.1. The proposed sequence partially resembles that described in (1), but exploits magnetization transfer contrast (MTC) instead of T2-preparation for improved visualization of the CS anatomy (2). Specifically, an MTC-IR module is applied for odd heartbeats (MTC-IR BOOST), while MTC preparation solely is performed for even heartbeats (MTC BOOST). The two bright-blood datasets are then combined in a PSIR-like reconstruction (3) to obtain a black-blood volume. The use of image-based navigation allows for estimation/compensation of translational respiratory motion with 100% scan efficiency and with predictable scan time (4). Data acquisition was performed in 6 healthy subjects on a 1.5T MR scanner (Siemens Magnetom Aera). Imaging parameters: isotropic spatial resolution 1.4mm^3, FOV=320x320x85-130mm, TE/TR=1.4/3.1ms, flip-angle=90deg, TI=140ms, MTC-preparation consisting of 8 off-resonance Gaussian pulses (BWTP=1.92, flip-angle=720deg, duration=20.48ms, off-resonance frequency offset=200Hz, pause between pulses=1.5ms). Signal to noise ratio of arterial (SNR_art) and venous (SNR_ven) blood was computed for the MTC-IR BOOST datasets, together with contrast to noise ratios (CNR_art and CNR_ven) with respect to myocardium.

Results: The proposed sequence depicts the CS with high contrast (Fig.2, Fig.3), similar to that of arterial blood (SNR_art=40.8±12.5, SNR_ven=38.7±10.5, CNR_art=27.0±1.4, CNR_ven=26.3±1.9, P=NS). Effective blood signal suppression is obtained for the black-blood PSIR BOOST dataset, thus highlighting vessel/atrial walls (Fig.2). The proposed sequence improves CS depiction when compared to approaches based on T2-preparation (Fig.3).

Conclusion: This novel 3D whole-heart free-breathing sequence shows potentials for non-contrast interventional planning of EP procedures by providing inherently co-registered high-contrast bright-blood visualization of the heart and CS anatomy together with black-blood depiction of atrial walls. Future work will include the use of acceleration techniques as well as strategies for non-rigid motion correction and, ultimately, validation in patients. 1) Ginami et al, MRM 2017, DOI:10.1002/mrm.26815; 2) Nezafat et al, MRM 2006, 58:1196-1206; 3) Kellman et al, MRM 2002, 47(2):372-383; 4) Henningsson et al, MRM 2012, 67(2):437-445.

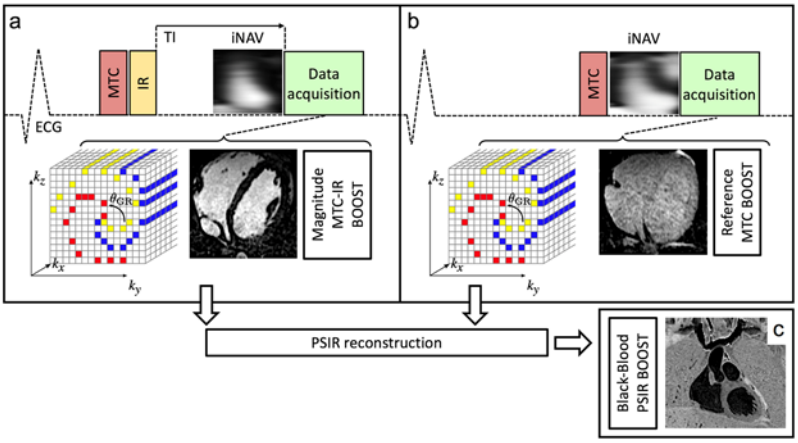

Figure 1: Proposed framework for bright-blood visualization of heart and coronary sinus (CS) anatomy and black-blood depiction of atrial walls. An MTC-IR module is applied in odd heartbeats (MTC-IR BOOST, a), thus allowing anatomy visualization while preserving signal from venous blood. MTC solely is exploited in even heartbeats, providing a second bright blood dataset (MTC BOOST, b). A 3D Cartesian trajectory with spiral profile order (Prieto et al., JMRI 2015, 41(3):738-746) is segmented over multiple heartbeats (yellow, red, blue) to account for cardiac motion. Translational respiratory motion is estimated with image-based navigation (iNAV) for each heartbeat independently. A complementary black-blood dataset (PSIR BOOST) for the depiction of atrial and vessel walls is obtained after PSIR computation involving the two motion-corrected and co-registered bright-blood datasets (c). Data acquisition is performed in free-breathing, at 100% scan efficiency, and with predictable scan time.

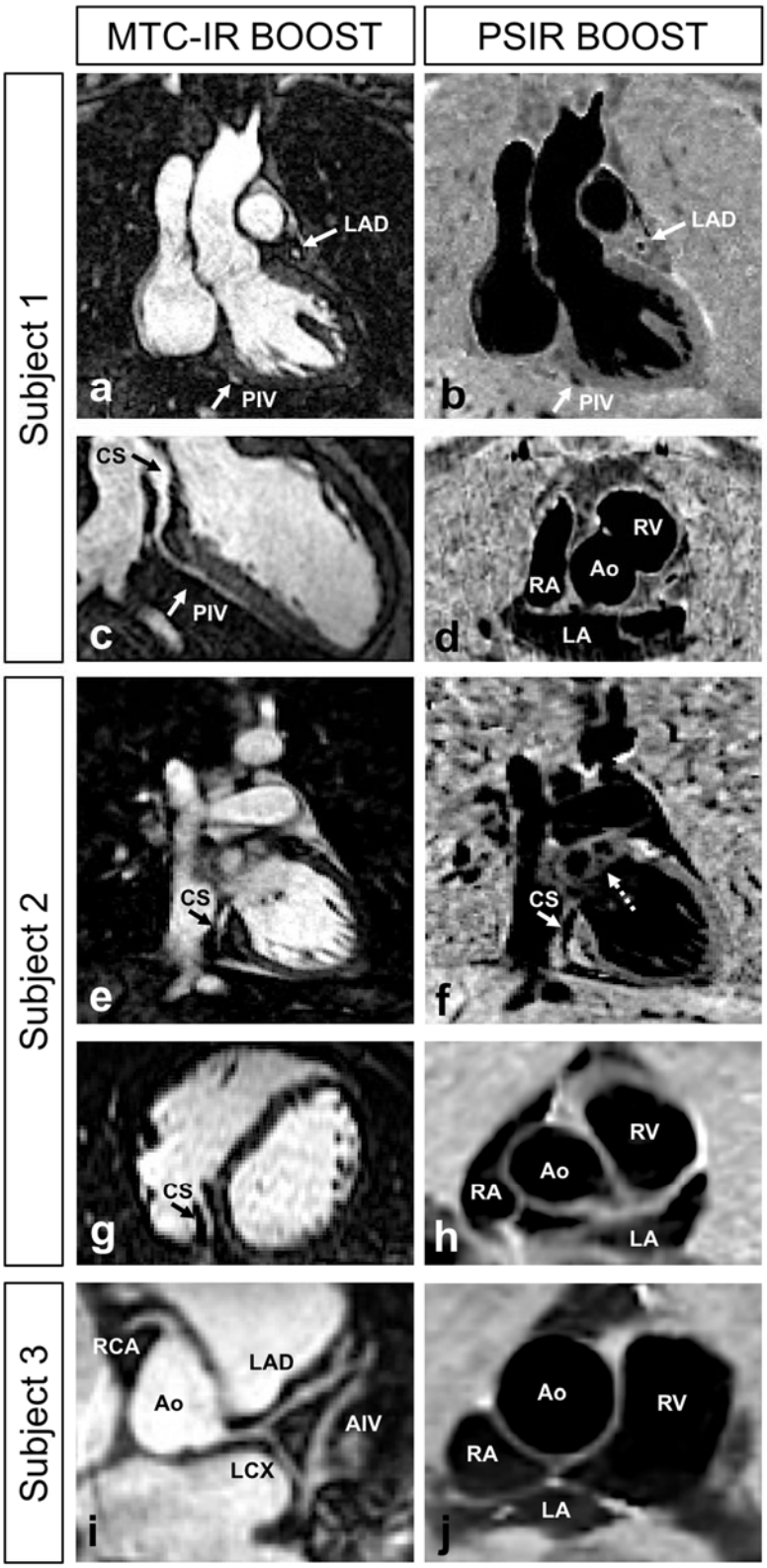

Figure 2: Images obtained with the proposed approach in 3 representative subjects. The first column (a,c,e,g,i) shows the bright-blood MTC-IR BOOST datasets, where venous structures are depicted with high contrast, similar to that of arterial blood. Black-blood PSIR BOOST datasets are displayed in the second column (b,d,f,h,j). Pronounced blood signal suppression leads to effective visualization of the atrial, ventricular, and aortic walls as

well as of the aortic valves (dotted arrow in f). Abbreviations: left coronary artery (LAD), posterior intraventricular vein (PIV), right ventricle (RV), aorta (Ao), right atrium (RA), left atrium (LA), coronary sinus (CS), right coronary artery (RCA), left circumflex coronary artery (LCX), anterior intraventricular vein (AIV).

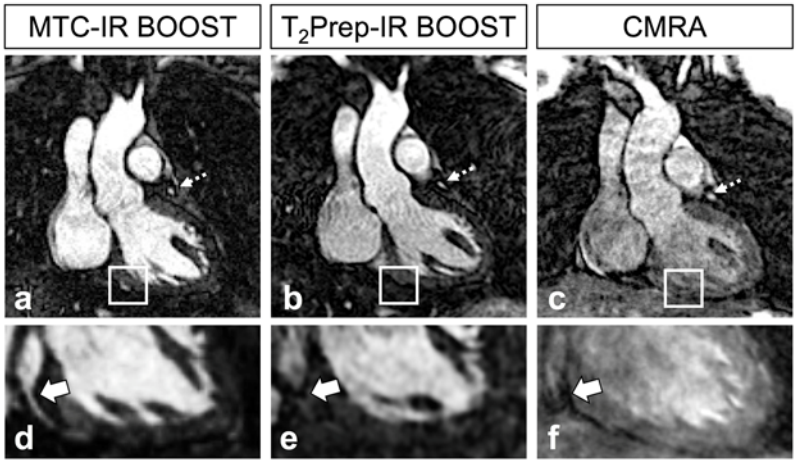

Figure 3: Bright-blood datasets obtained in one subject with the proposed approach for improved visualization of coronary sinus (CS) and veins (a) in comparison to T2-preparation based sequences. Dataset in (b) was obtained from the magnitude image (T2Prep-IR BOOST) of the recently published approach for simultaneous bright- and black-blood MRI described in Reference 1. The dataset in (c) was obtained with a conventional, T2-prepared, sequence for coronary MR angiography. Despite the effective visualization of arterial blood in (b,c), leading to sharp depiction of the coronary arteries (dotted arrows), the use of T2-preparation has a detrimental effect on the depiction of the CS and branching venous vessels (e,f and white rectangles in b,c). Conversely, with the proposed approach (a), both venous and arterial blood are depicted with high contrast. This offers high-contrast depiction of the CS and veins (d and white rectangle in a).

ID#: 371778

Biologic and Prognostic Validation of Delayed Enhancement (DE-) CMR for Cancer-Associated Cardiac Masses - Multimodality Comparison to Positron Emission Tomography (PET)

Angel T. Chan, MD, PhD[1] Josef Fox, MD[2], Rocio Perez Johnston, MD[2], Andrew Plodkowski, MD[3], Meridith P. Pollie, BS[4], Chaya Moskowitz, PhD[2], Jiwon Kim, MD[5], Richard Steingart, MD[3], Jonathan W. Weinsaft, MD[6]

1. Memorial Sloan Kettering Cancer Center, New York, NY

2. Memorial Sloan Kettering Cancer Center

3. Memorial Sloan Kettering Cancer Center, NY

4. Weill Cornell Medical College

5. Weill Cornell Medical College, New York, NY

6. Weill Cornell Medical Center, NY

Background: For patients with cardiac masses (C_{MASS}), CMR is widely used to differentiate cardiac neoplasm (C_{NEO}) from thrombus (C_{THR}) based on presence/absence of contrast enhancement, whereas PET assesses C_{MASS} biological activity. PET-derived biological validation of CMR contrast-enhancement as a criterion for differentiating C_{NEO} and C_{THR} as well as prognostic comparison of CMR and PET is lacking.

Methods: The population comprised C_{MASS+} patients and C_{MASS-} controls matched for cancer type/stage who underwent CMR (97% 1.5T) and PET within 3 (0.4±1.1) months: For CMR, C_{NEO} and C_{THR} were respectively defined via DE-CMR based on presence/absence of enhancement; lesions were quantified for size and tissue properties (SNR, CNR). PET was read blinded to CMR for diagnostic performance, and co-localized with CMR to assess C_{MASS} biological activity via FDG uptake. Clinical follow-up was performed to test prognosis in relation to C_{MASS} identified by CMR and PET.

Results: 74 patients with systemic cancer were studied, among whom 26 had C_{NEO} and 16 C_{THR} on CMR (32 controls). Leading cancer etiology differed between C_{NEO} (lung [19%], lymphoma [15%], sarcoma [15%]) and C_{THR} (lymphoma [50%], sarcoma [19%]) as did location ([C_{NEO}: RV 31%|RA 42%|LV 27%|LA 23%] [C_{THR}: RA 94%|LV 6%). LVEF (64±9% vs 64±9%; p=0.93), and clinical characteristics were similar (age, gender; p=NS). C_{NEO} and C_{THR} markedly differed with respect to quantitative CMR tissue properties (CNR: 17.5±17.6 vs 2.0±1.2; p<0.001) (Figure A): Magnitude of contrast enhancement (CNR) correlated with FDG uptake (r=0.45; p=0.009). Diagnostic performance of PET for CMR-evidenced C_{MASS} varied based on subtype: For CMR-evidenced C_{THR}, no cases were FDG avid (PET sensitivity=0%). For C_{NEO}, visual PET interpretation and quantitative cutoffs yielded reasonable sensitivity (65-73%) and high specificity (94%) (Figure B). C_{NEO} detected concordantly by CMR and PET were similar in size to those detected by CMR alone (18.5±26.6 vs 8.7±8.0cm^2; p=0.18). Location of C_{NEO} undetected by PET varied (RV 22%|RA 33%|LV 44%|LA 33%|pericardium 33%). During clinical follow-up of 1.7±1.6 years (p=0.9 between modalities), C_{NEO} on CMR conferred increased mortality to a greater magnitude (HR 2.73[CI=1.00-7.47]; p=0.04) than did C_{NEO} on PET (HR 2.11[CI 0.83-5.37]; p=0.13) (Figure C).

Conclusion: Contrast-enhancement provides a DE-CMR diagnostic criterion for C_{NEO} that parallels biologic activity on PET and predicts adverse prognosis among patients with systemic cancer.

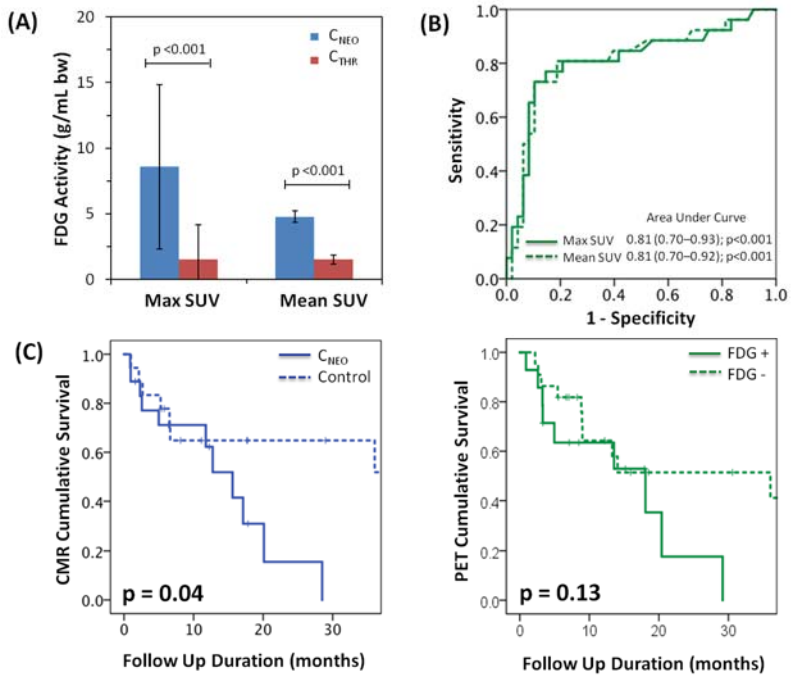

DE-CMR tissue characterization of cardiac masses in relation to PET biologic activity. (A) SUV uptake (mean±SD) among cardiac neoplasm (blue) and thrombus (red) as defined by PET. (B) Diagnostic performance of quantitative SUV cutoffs for assessment of CMR-defined cardiac neoplasm. (C) Kaplan-Meier curves for patient groups partitioned based on presence/absence of CMR-defined cardiac neoplasm (left) and PET FDG-avidity (right).

ID#: 372044

A quantitative comparison of navigator-gated Cartesian and self-navigated radial free-breathing 3D bSSFP whole-heart coronary MRA

John Heerfordt, MSc[1] Davide Piccini, PhD[2], Matthias Stuber, PhD[2]

1. Department of Radiology, University Hospital (CHUV) and University of Lausanne (UNIL) & Advanced Clinical Imaging Technology, Siemens Healthcare, Lausanne, Switzerland, Epallinges, Vaud, Switzerland

2. Center for Biomedical Imaging (CIBM), Lausanne, Switzerland, Vaud, Switzerland

Background: Navigator-gated acquisitions are the current state of the art for free-breathing 3D whole-heart coronary MRA. Due to long and unpredictable scan times, alternative approaches relying on self-navigation have been proposed. Our aim was to compare a Cartesian Navigator-Gated (CNG) imaging sequence, similar to protocols in large patient studies [1, 2], to a more recently published prototype Radial Self-Navigation (RSN) approach [3, 4, 5]. Such a comparison has not been performed to our knowledge. We hypothesize that RSN allows shorter and more predictable acquisition times compared to the CNG option while quantitative differences in image quality are investigated.

Methods: Examinations of healthy volunteers (N = 11, age 27.9 ± 5.4 years, 9 male) were performed with both sequences in alternating order on a 1.5T clinical scanner (MAGNETOM Aera, Siemens Healthcare) after obtaining informed consent. Both sequences were segmented and ECG-triggered implementing standard T_2-preparation and fat-saturation modules. Sequence parameters are found in Table 1. The acquisition times were recorded and quantitative measurements of visible vessel length and sharpness of the RCA and LM + LAD obtained [6]. Two-sided paired t-tests with $p < 0.05$ considered statistically significant were used for all comparisons. In addition, general image characteristics were compared visually.

Results: Image acquisition completed without user intervention in 10/11 subjects. In one subject respiratory drift occurred in the CNG acquisition and the volunteer was asked to move slightly to allow the acquisition to be completed. Quantitative results are reported in Table 2. The mean acquisition time for RSN was more than three times shorter than for CNG ($p < 0.05$) with a much reduced standard deviation of the scanning time. CNG provided significantly higher sharpness of the full vessels. No significant differences were found in vessel length and proximal vessel sharpness. Qualitatively, CNG resulted in a better visual delineation of the coronary arteries with a more homogeneous fat-saturation than RSN. In contrast, fewer respiratory motion artifacts originating from the chest wall and an improved homogeneity of the signal in the blood-pool can be reported for RSN (cf. Figure 1).

Conclusion: RSN enables highly predictable and significantly lower acquisition times when compared to CNG, which facilitates inclusion in clinical protocols. CNG yielded better vessel sharpness both quantitatively and visually. However, the larger acquired voxel size of the anisotropic CNG images provides a signal advantage. For examination of stenoses or congenital heart disease the robustness and simplicity of RSN has to be weighed against the superior vessel conspicuity of CNG. References:

[1] Sakuma H, Radiology 2005, 237(1):316-321
[2] Plein S, Lancet 2012, 379(9814):453–60
[3] Piccini D, MRM 2012, 68(2):571–579
[4] Monney P, JCMR 2015, 17:55
[5] Albrecht M, Eur Radiol 2017, Sep 8, Early view
[6] Etienne A, MRM 2002, 48(4):658-666

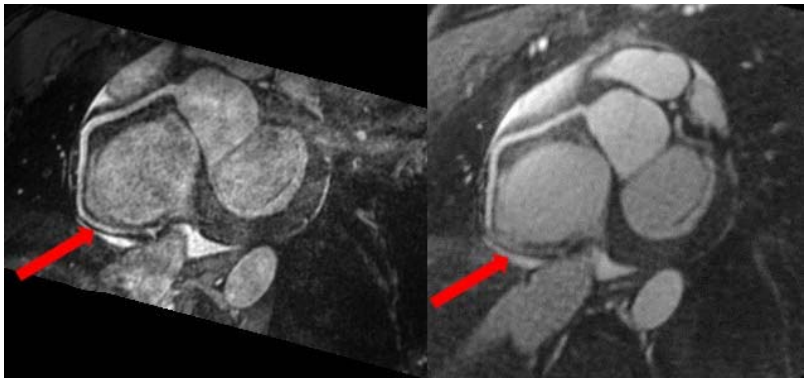

Figure 1. Reformats of the RCA from CNG (left) and RSN (right) Depicting a Sharpness Difference in the Distal Part of the Vessel

Table 1. Specification of Imaging Sequence Parameters

Parameter	Cartesian Navigator-Gated[a]	Radial Self-Navigation
Sampling Scheme	3D Cartesian centric-ordered	3D Radial Spiral Phyllotaxis
Respiratory Tracking	Navigator: tracking factor 0.6, window width 5 mm, fixed level	Self-navigation: 1D cross-correlation of blood pool along superior-inferior direction
Parallel Imaging	GRAPPA (factor 2)	n/a
FoV [mm^3]	280 x 280 x 120	210^3
Acquisition Matrix	256 x 256 x 80	192^3
Acquired Resolution [mm^3]	1.09 x1.09 x 1.50	192^3
RF Excitation	90º Slab-selective	90º Non-selective
TE/TR [ms]	1.91/3.82	1.57/3.14
Receiver Bandwidth [Hz/Pixel]	1030	1000

[a] The CNG parameters were similar to protocols in large studies [1, 2] but adapted to local conditions (GRAPPA instead of SENSE).

Table 2. Quantitative Results

Metric	Cartesian Navigator-Gated	Radial Self-Navigation	p-value
Acquisition time [minutes]	17:44 ± 5:16	5:31 ± 0:29*	$1.4 \cdot 10^{-5}$
Vessel length RCA [cm]	10.5 ± 1.9	9.9 ± 2.8	0.370
Proximal sharpness RCA [%]	50.3 ± 5.9	44.5 ± 8.8	0.079
Overall sharpness RCA [%]	46.9 ± 4.8*	39.0 ± 9.4	0.047
Vessel length LM + LAD [cm]	8.9 ± 1.9	7.4 ± 3.1	0.107
Proximal sharpness LM + LAD [%]	44.5 ± 8.8	39.7 ± 5.7	0.096
Overall sharpness LM + LAD [%]	48.2 ± 6.7*	37.8 ± 8.2	0.007

* indicates $p < 0.05$

ID#: 372007

Adenosine stress T1-mapping offers a novel gadolinium-free approach for perfusion assessment in hypertrophic cardiomyopathy

Betty Raman, MBBS, FRACP[1]Rina Ariga, MBBS, MRCP[2], Masliza Mahmod, MBChB, DPhil[2], Stefan K. Piechnik, PhD, MScEE[2], Alexander Liu, MBBS BSc[3], Alessandra Borlotti, PhD[3], Michael Jerosch-Herold, PhD[4], Jane M. Francis[5], Sanjay Sivalokanathan, MBBS, BSc[2], Erica Dall'Armellina, Sr., MD, DPhil[6], Matthew D. Robson, PhD[7], Hugh Watkins, FRS FMedSci[2], Vanessa M. Ferreira, MD, DPhil[2], Stefan Neubauer, MD, FRCP[2]

1. University of Oxford, Division of Cardiovascular Medicine, Oxfordshire, England, United Kingdom

2. University of Oxford, England, United Kingdom

3. University of Oxford, Oxford, England, United Kingdom

4. Harvard Medical School, Boston, MA

5. University of Oxford, OX39DU, England, United Kingdom

6. Leeds Institute of Cardiovascular and Metabolic Medicine, Division of Biomedical Imaging,University of Leeds, United Kingdom

7. OCMR, University of Oxford, England, United Kingdom

Background: Hypertrophic cardiomyopathy (HCM) is characterised by impaired myocardial perfusion reserve (MPR), a poor prognostic marker. HCM also displays blunted oxygenation (as seen on blood oxygen level dependent imaging; BOLD) due to impaired perfusion and increased metabolic demands. Adenosine stress T1 mapping has recently been shown to detect myocardium with impaired perfusion in patients with coronary artery disease. We sought to assess if adenosine stress T1-mapping can detect impaired MPR in HCM without contrast agents, and compared its diagnostic performance with non-contrast stress BOLD.

Methods: 62 subjects (31 HCM and 31 age- and gender- matched healthy controls) with no history of coronary disease underwent CMR (3T) including cine, rest and stress (adenosine 140 mcg/kg/min) BOLD, T1-mapping (Shortened Modified Look-Locker Inversion recovery – ShMOLLI) and first-pass perfusion, followed by late gadolinium enhanced (LGE) imaging. Stress BOLD and T1-maps were acquired for a mid-ventricular slice. Stress MPR was determined using Fermi function de-convolution method. Stress T1 reactivity and stress BOLD reactivity were estimated as a relative change in T1 (ΔT1) and heart-rate corrected BOLD SI during stress compared to rest, respectively. Region of interest (ROI) analyses of T1 maps were undertaken in hypoperfused, fibrotic (LGE) and remote (unaffected by LGE or hypoperfusion) regions. Clustered segmental analyses were undertaken for all measures.

Results: Compared with controls, subjects with HCM have significant impairment in stress MPR (2.3±1.2 vs 3.5±0.7), stress BOLD reactivity (5.8 ±6.0% vs 14.8±12.3%), and adenosine stress T1 reactivity (3.2±2.0% vs 6.0±1.9%) ($p<0.01$ for all). Hypo-perfused and fibrotic (LGE) myocardium on ROI analysis have significantly blunted T1 reactivity (ΔT1= 1.8±0.9% and 0.9±1.3%; p=ns) which are distinctly different from remote regions (5.2±2.4 %, $p<0.01$ for both) (Fig 1A). In LGE-absent segments, a stress T1 reactivity ΔT1 of 3.6 % has a good sensitivity of 84% and specificity of 84% for detecting impaired MPR (MPR<1.9) (AUC 0.88, 95% CI 0.81-0.93, $p<0.01$). In comparison, stress BOLD reactivity is significantly less predictive (AUC 0.62, 95% CI 0.54-0.71, $p<0.01$) in detecting impaired MPR, with a sensitivity of 57% and specificity 66% at an optimal BOLD threshold of 5.5% (Fig 1B).

Conclusion: Hypertrophic cardiomyopathy displays impaired stress T1 reactivity, stress BOLD reactivity and myocardial perfusion reserve. Hypo-perfused and fibrotic segments in HCM have significantly blunted T1 reactivity compared to remote LGE-negative myocardium and normal controls. Adenosine stress T1 reactivity provides a novel gadolinium-free method for the assessment of perfusion and is more accurate than stress BOLD in detecting impaired myocardial perfusion reserve in HCM.

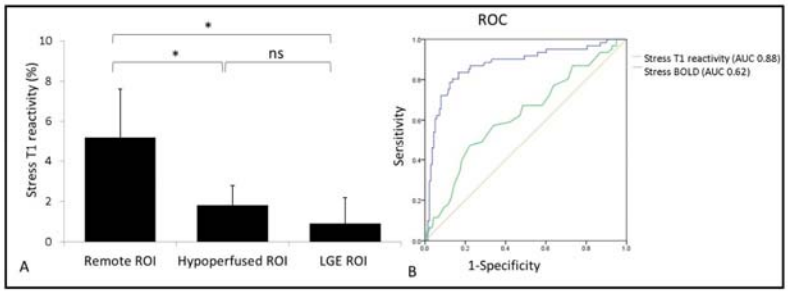

Figure1. (A) Stress T1 reactivity profiles of remote, hypoperfused, LGE+ regions of interest (*p<0.01; error bars represent standard deviation) (B) ROC curve depicts the diagnostic performance of stress T1 reactivity compared with stress BOLD reactivity for impaired myocardial perfusion reserve in HCM.

ID#: 372099

Microvascular Dysfunction is a Coronary Artery Specific Phenomenon, associated with Elevated Microvascular Resistance, Myocardial Hypo-Perfusion and Dysfunction - Time for a Paradigm Shift

Alexander Liu, MBBS BSc[1] Rohan S. Wijesurendra, MB BChir, MRCP[1], Joanna M. Liu, MBBS MRCP[2], Jeremy Langrish[3], Andrew Lucking[3], Robin Choudhury, MD[1], Adrian Banning[2], John C Forfar[3], Keith M. Channon, MD, FRCP[4], Stefan K. Piechnik, PhD, MScEE[4], Stefan Neubauer, MD, FRCP[4], Rajesh K. Kharbanda, MBChB, PhD[5], Vanessa M. Ferreira, MD, DPhil[4]

1. University of Oxford, Oxford, England, United Kingdom

2. University of Oxford, United Kingdom

3. John Radcliffe Hospital, United Kingdom

4. University of Oxford, England, United Kingdom

5. Oxford Heart Centre, England, United Kingdom

Background: In patients with angina but non-obstructed coronary artery disease (NOCAD), the pathological effects of coronary microvascular dysfunction (CMD) on the downstream myocardium remain poorly understood, hampering the development of effective therapies. Index of microcirculatory resistance (IMR) is a specific invasive marker of microvascular function. We characterized the effect of CMD in patients with angina by defining the relations between microvascular resistance (IMR) and downstream myocardial perfusion and contractile function, as assessed by cardiac magnetic resonance (CMR).

Methods: 80 subjects (60 outpatients with angina and 20 normal controls) underwent adenosine stress CMR to assess myocardial perfusion reserve index (MPRI), LV systolic and diastolic function (3D strain) and infarction (late gadolinium enhancement). During angiography, FFR and IMR were measured in consecutive vessels where possible (135/180) in patients. Infarcted segments were excluded.

Results: In a total of 96 non-obstructive vessels with FFR≥0.80, IMR was inversely correlated to MPRI (rho=-0.65), peak systolic circumferential strain (rho=0.57) and peak diastolic circumferential strain (rho=-0.50; all p<0.001). An IMR threshold of 25U accurately detected inducible hypo-perfusion (MPRI<1.40; 2SD below the mean MPRI of normal controls: 1.90±0.25) on ROC analysis (AUC 0.97±0.02, p<0.001, Figure 1). In the 20 patients with all 3 non-obstructive (FFR≥0.80) coronary arteries (NOCAD), CMD as defined by a high IMR≥25U occurred in a coronary artery specific fashion; as the number of vessels with high IMR (≥25U) increased, there were progressive reductions in global MPRI, with associated global impairments in LV systolic and diastolic strain (all p<0.01, Figure 2).

Conclusion: In patients with angina and NOCAD, we elucidated the novel concept of regional CMD localized to coronary artery territories, giving rise to the paradigm of single- or multi-vessel microvascular disease. This regional CMD is associated with increased microvascular resistance (IMR≥25U), impaired myocardial perfusion and contractile function. CMD can now be objectively demonstrated using CMR or IMR, offering patients with microvascular angina an objective diagnosis, and the treating clinician a firm indication for commencing therapy.

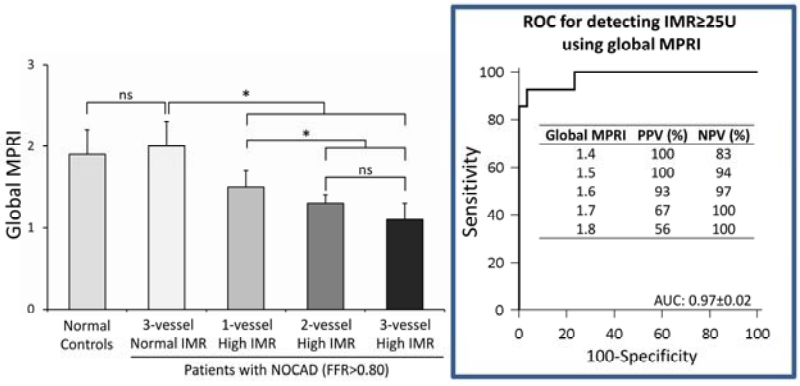

Figure 1. In patients with angina and non-obstructive coronary artery disease (NOCAD), as the number of coronary artery territories with elevated microvascular resistance (High IMR: ≥25U) increases, the global myocardial perfusion reserve index (MPRI) reduced in a step-wise fashion (Left bar-chart). Normal IMR (<25 U). On ROC

analysis (right panel), true positives were NOCAD patients with high IMR in ≥1 coronary artery; true negatives were normal controls and NOCAD patients with 3-vessel normal IMR. AUC: area under curve (<0.001); FFR: fractional flow reserve; PPV: positive predictive value; NPV: negative predictive value. Bars are mean and 1SD. *p<0.01; ns is p>0.10.

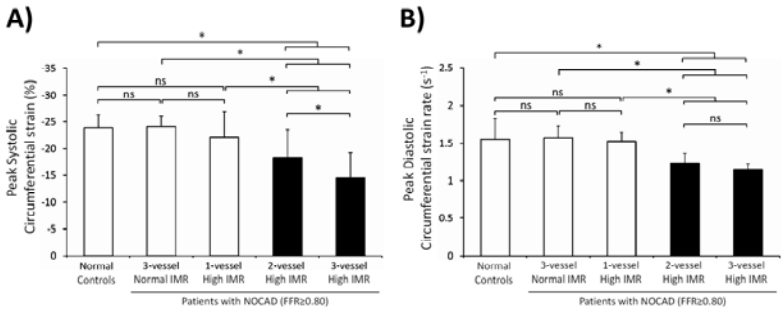

Figure 2. As the number of coronary artery territories with elevated microvascular resistance (High IMR: ≥25U) increases, there were gradual reductions in the A) global peak systolic circumferential strain and the (B) global peak diastolic circumferential strain rate. Abbreviations are as per Figure 1. Bars are mean and 1SD. *p<0.01; ns is p>0.10.

ID#: 372455

Four-minute whole-heart coronary MRA with sub-millimeter isotropic resolution and 100% respiratory scan efficiency

Aurelien Bustin, Biomedical Engineering[1]Radhouene Neji, PhD[2], Giulia Ginami, PhD[3], Tevfik F. Ismail, PhD MRCP[4], Imran Rashid, PhD FRACP[5], Rene Michael. Botnar, PhD[5], Claudia Prieto, PhD[6]

1. King's College of London, United Kingdom

2. Siemens Healthcare Limited, Frimley, England, United Kingdom

3. King's College London, United Kingdom

4. King's College London; Guy's and St Thomas' Hospitals NHS Foundation Trust, London, England, United Kingdom

5. King's College London, London, England, United Kingdom

6. King's College London, England, United Kingdom

Background: High-resolution isotropic coronary magnetic resonance angiography (CMRA) allows unrestricted reformatting in any desired imaging plane without loss of resolution, providing complete and detailed information on the coronary arteries and surrounding vessels. However, achieving sub-millimeter isotropic resolution with a conventional 1D diaphragmatic navigator (dNAV) gated CMRA is challenging due to long and unpredictable scan times. A 2D image-based navigator (iNAV) has been proposed as an alternative to dNAV resulting in 100% scan efficiency and reducing total scan time duration. In this study, we sought to achieve sub-millimeter Cartesian CMRA by combining 2D iNAV with an efficient variable density sampling scheme integrated into a compressed sensing (CS) framework to further accelerate the acquisition.

Methods: Undersampled variable-density (prototype VD-CASPR) sampling was implemented on a Siemens 1.5T Magnetom Aera scanner. VD-CASPR samples the phase-encoding plane following approximate spiral interleaves on the Cartesian grid with variable density along each spiral arm (Fig.1). A 2D iNAV precedes each spiral acquisition to enable beat-to-beat 2D translational respiratory motion correction without any data rejection. Five healthy subjects (4 females, 27±2 years) underwent free-breathing CMRA. Data were acquired with an ECG-gated bSSFP sequence, 18-channel body and 32-channel spine coils, fat-saturation and T2-prep pulses (FOV=320x320x160mm^3,TR/TE=3.7/1.63ms,FA=90°) with 0.9mm^3 isotropic resolution in mid-diastole with an undersampling factor of 5 and 9 (resulting in ~10x and 18x acceleration in comparison to fully sampled dNAV CMRA with 50% scan efficiency). Wavelet-based CS reconstruction with 2D translation motion correction was implemented offline. Two blinded readers scored the image quality. In addition, vessel sharpness and length of the RCA/LAD were measured using Soapbubble.

Results: The average scan time was 7min3s (x5) and 4min18s (x9) with 100% scan efficiency. The zero-filled reconstruction with VD-CASPR exhibits incoherent artefacts that behave like random noise and blurring (Fig.2). Sharpness is improved after motion correction. The proposed motion corrected CS reconstruction led to further improvements in terms of vessel sharpness and vessel length for both acceleration factors (Table 1). Visual and subjective image quality scores demonstrate that the proposed motion corrected CS reconstruction is robust even at high acceleration factors.

Conclusion: We demonstrate the feasibility of combining an efficient VD-CASPR sampling trajectory with 2D iNAV-based motion correction and CS reconstruction to obtain isotropic sub-millimeter CMRA under free-breathing. The proposed technique reduces scan time of sub-millimeter CMRA to clinically feasible durations. Ultimately, this technique might be useful for rapid screening of the major coronary vessels in patients with suspected coronary artery anomalies.

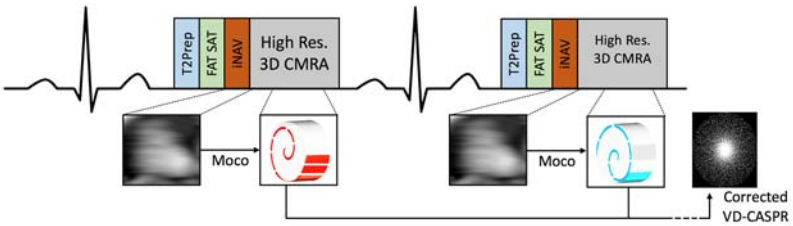

Figure 1 Proposed framework for sub-millimeter isotropic 3D whole-heart CMRA. VD-CASPR samples the phase-

encoding plane following approximate undersampled spiral interleaves on the Cartesian grid with variable density along each spiral arm. The undersampling scheme was developed such that high acceleration induces “noiselike” incoherent artefacts and avoid strong image disturbance from fold-over artefacts. A 2D iNAV navigator precedes each 3D whole-heart data acquisition to enable beat-to-beat 2D translational respiratory motion estimation and compensation with 100% scan efficiency. A template-matching algorithm was used to estimate superior-inferior and right-left translational motion, using end-expiration as respiratory reference position. Translational motion compensation was applied inline using linear phase modulation. Data were acquired without gating window during free-breathing with ECG-gated, fat-saturation prepulse, T2Prep (TE = 40ms) for contrast enhancement, with an acquisition window ~90-125ms, resulting in ~30 segments per cardiac cycle.

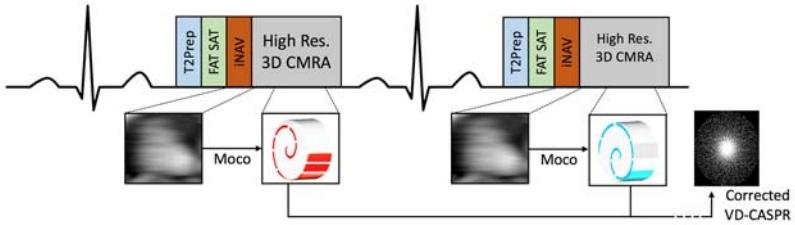

Figure 1 Proposed framework for sub-millimeter isotropic 3D whole-heart CMRA. VD-CASPR samples the phase-encoding plane following approximate undersampled spiral interleaves on the Cartesian grid with variable density along each spiral arm. The undersampling scheme was developed such that high acceleration induces “noiselike” incoherent artefacts and avoid strong image disturbance from fold-over artefacts. A 2D iNAV navigator precedes each spiral acquisition to enable beat-to-beat 2D translational respiratory motion estimation and compensation with 100% scan efficiency. A template-matching algorithm was used to estimate superior-inferior and right-left translational motion, using end-expiration as respiratory reference position. Translational motion compensation was applied inline using linear phase correction. Data were acquired without gating window during free-breathing with ECG-gated, fat-saturation prepulse, T2Prep (TE = 40ms) for improved blood-myocardium contrast, with an acquisition window ~90-125ms, resulting in ~30 lines per cardiac cycle.

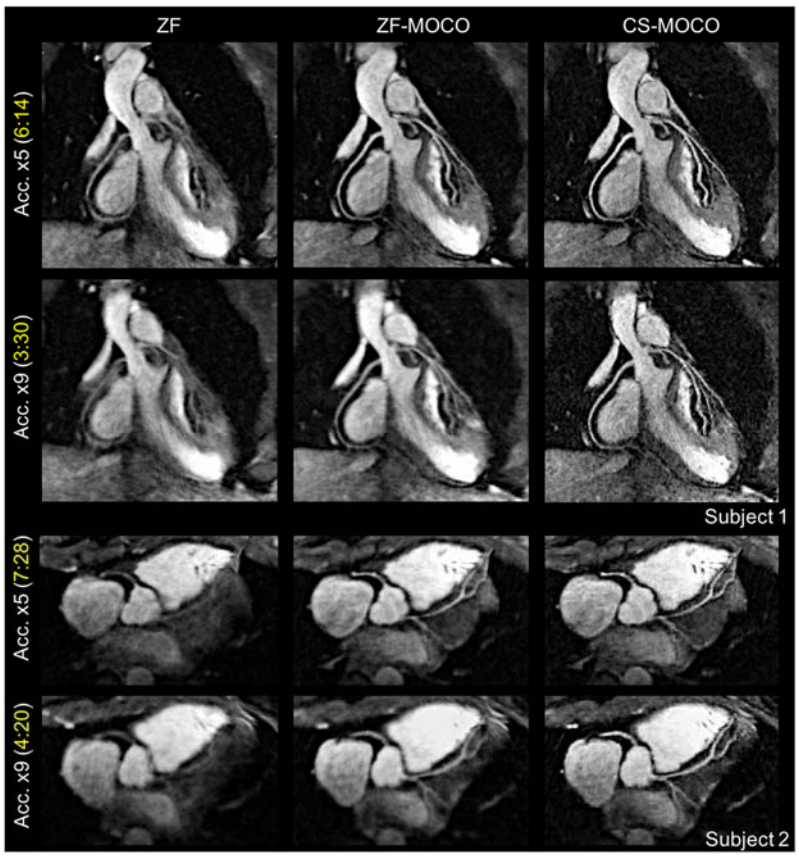

Figure 2 Visual comparison of CMRA images reformatted along the LAD and RCA arteries, acquired on two healthy subjects with isotropic resolution 0.9 mm3 and two different acceleration factors (x5 and x9), using the proposed VD-CASPR sampling. Standard zero filling reconstructions are shown (ZF, left column) along with the motion-corrected zero-filled (ZF-MOCO, middle column) and our motion-corrected compressed-sensing reconstructions (CS-MOCO, right column). The performance of the proposed VD-CASPR sampling is demonstrated on the ZF-MOCO reconstructions where high-resolution coronary arteries are shown without noticeable undersampling artifacts. Image quality and sharpness are further improved using wavelet-based CS, even for high acceleration factors (x9), resulting in a total scanning time of about 4 minutes.

ID#: 373641

The dependence of fatty remodeling of infarct territories on iron remnants from acute myocardial infarctions: a serial CMR study

Xingmin Guan, MS[1] Diego Hernando, PhD[2], Ivan Cokic, MD[3], Hsin-Jung Yang, PhD[4], Guan Wang, MD[1], Richard LQ. Tang, MD[5], Scott B. Reeder, MD, PhD[2], Rohan Dharmakumar, PhD[6]

1. Cedars-Sinai Medical Center

2. University of Wisconsin

3. Cedars-Sinai Medical Center, Los Angeles, CA

4. Cedars Sinai Medical Center, Los Angeles, CA

5. Cedars-Sinai Medical Center, CA

6. Cedars-Sinai Medical, CA

Background: Fatty remodeling of myocardial infarction (MI) is increasingly recognized to be associated with adverse outcomes. Evolving evidence supports the notion that iron deposition from hemorrhagic myocardial infarction is likely a key promoter of fatty remodeling of MI territories. However, whether the extent of fat deposition within the chronic MI zones depends on the extent of residual iron has not been studied, primarily because the previous investigations on the iron/fat axis were limited to histology (i.e. single time point). We investigated the temporal evolution of fat deposition and its relation to iron within MI territories using serial CMR in a validated animal model of hemorrhagic MI.

Methods: Hemorrhagic MIs were created in dogs(n=9) and surviving dogs (n=7) were followed for a period of 6 months. Contiguous, slice-and-resolution matched, short-axis, native mGRE and LGE images were acquired on a whole-body 3T MRI system on day 7, week 8 and month 6, post MI. Confounder-corrected R2*(or 1/T2*, an established measure of iron concentration) and proton density fat-fraction (PDFF) maps were constructed using a multi-echo water-fat separation algorithm. LGE images were used to identify MI and remote territories. These regions-of-interests were used to determine mean R2* and PDFF, as well relative R2* and relative PDFF estimates (compared to remote areas), of the MI territories. This was performed for all imaging slices at all time points. One-way ANOVA was used to determine the statistical differences.

Results: Representative findings from a dog with hemorrhagic MI followed over a 6-month period post MI are shown in Figure 1. Figure 2 shows the results of mean relative R2* and PDFF at 7 days, 8 weeks and 6 months post MI. R2* was not different between day 7 to month 6 ($p=0.12$) suggesting that iron concentration was constant between day 7 and month 6, post MI. However, relative PDFF increased from day 7 to 6 months post MI (~80% by week 8; and ~180% by month 6; $p<0.01$, at each time point). Regression analysis (adjusting for MI area), showed strong correlations between relative R2* and relative PDFF in chronic phases of MI (Figure 3), with the slope and r^2 increasing from 0.86±0.33 ($r^2=0.14$; day 7) to 2.52±0.55 ($r^2=0.52$; week 8) to 3.74±0.24 ($r^2=0.92$; month 6).

Conclusion: We conclude that the extent of fatty remodeling of chronic MI territories is strongly dependent on the extent of iron deposits from acute MI.

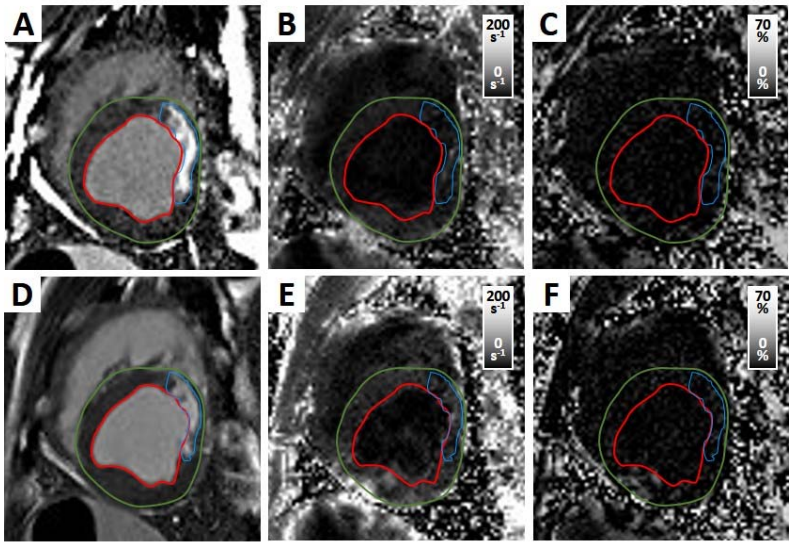

Figure 1. Representative LGE (A,D); R2* (B,E); and PDFF (C,F) from an animal after 8 weeks (A,B,C) and 6 months (D,E,F) post MI.

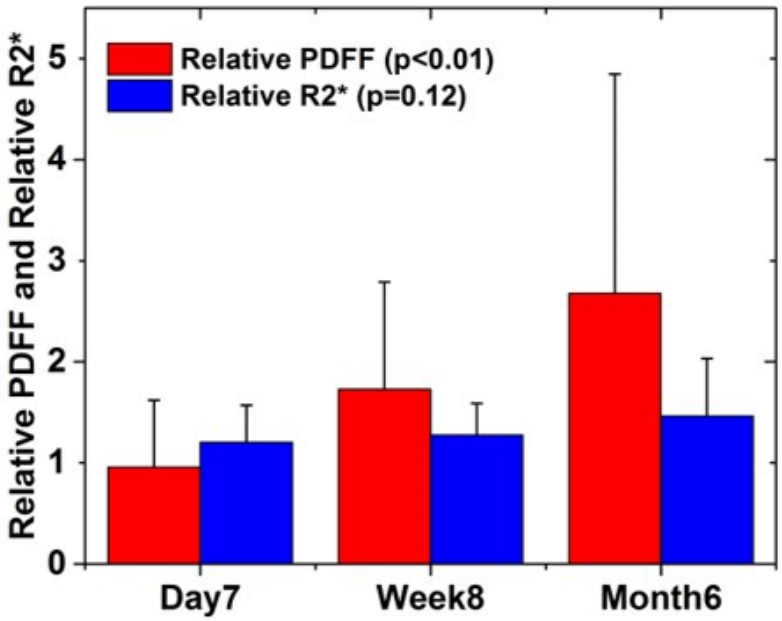

Figure 2. Mean relative PDFF and R2* value at day 7, week 8 and month 6 post MI. Relative PDFF increased over time (0.95 ± 0.66 (day 7), to 1.72 ± 1.06 (week 8), to 2.68 ± 2.17 (month 6)), but the relative iron concentration (R2*) remained approximately constant (1.20 ± 0.36 (day 7), to 1.28 ± 0.31 (week 8) and 1.46 ± 0.57 (month 6), p=0.12 (between day 7 and month 6)).

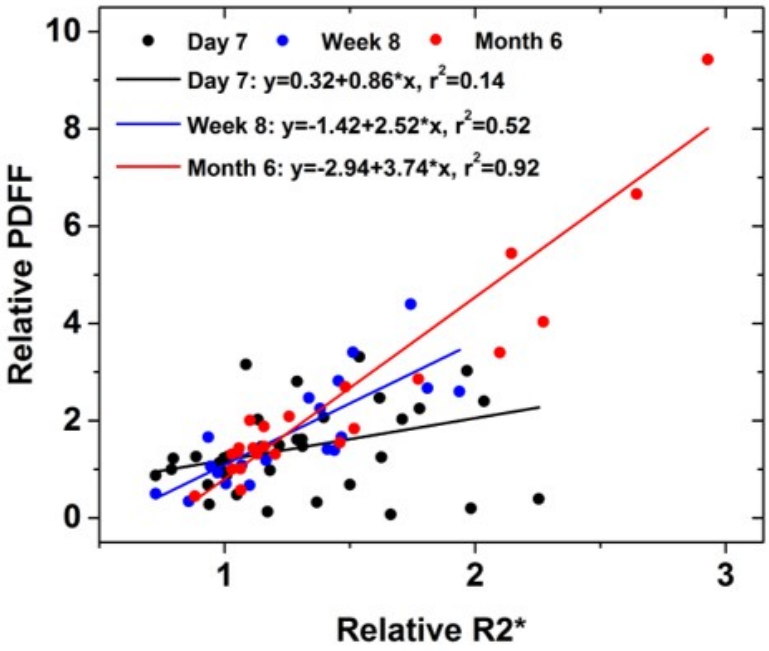

Figure 3. Scatter plot showing the relation between relative PDFF and relative R2* as determined from CMR on day 7, week 8 and month 6. Results from linear regression analysis are shown in the inset legend. Black line represents linear regression for Day 7, blue line represents linear regression for Week 8 and red line represents linear regression for Month 6.

ID#: 373833

Maldistribution of Pulmonary Blood Flow in Patients After the Fontan Operation Is Associated with Lower Exercise Capacity

Tarek Alsaied, MD, MSc[1] Lynn A. Sleeper, Sc.D.[2], Sunil J. Ghelani, M.D.[3], Nina Isabel. Azcue, BS Chemistry[4], Andrew J. Powell, M.D.[5], Rahul H. Rathod, MD[2]

1. Boston Children's Hospital, Cincinnati, OH

2. Boston Children's Hospital, Boston, MA

3. Boston Children's Hospital, MA

4. Boston Children's Hospital, Cambridge, MA

5. Harvard Medical School and Boston Children's Hospital, Boston, MA

Background: Maldistribution of pulmonary artery blood flow (MPBF) is a potential complication in patients who have undergone single ventricle palliation culminating in the Fontan procedure. Cardiac MRI (CMR) is the only modality that can evaluate MPBF in this population. The purpose of this study is to identify the prevalence and associations of MPBF and to determine the impact of MPBF on exercise capacity after the Fontan operation.

Methods: Patient inclusion criteria for this retrospective study were as follows: 1) status post Fontan, 2) CMR study and maximal cardiopulmonary exercise test (CPET) at Boston Children's Hospital with no intervening catheter or surgical interventions on the branch pulmonary arteries or veins, and 3) CMR blood flow measurements of the branch pulmonary arteries. MPBF was defined as >60% of pulmonary artery flow to one pulmonary artery. Exercise capacity was measured by percent of predicted oxygen consumption at maximum exercise (VO2 max %). Linear and logistic regression models were used to determine univariate and multivariable predictors of exercise capacity and correlates of MPBF.

Results: A total of 147 patients, who had CMR between 1999 and 2017, were included. Their mean age at CMR was 23.3 ±10.3 years and the median time between CMR and CPET was 2.8 months (interquartile range 0 -13.8 months). Fifty-four patients (37%) had MPBF (95% CI 29%-45%). The mean VO2 max % was 63 ± 16%. Patients with MPBF had lower VO2 max % compared to patients without MPBF (60 ±14% versus 65 ± 16%; p=0.035). Additional univariate predictors of lower VO2 max % included older age at CMR, older age at the Fontan operation, atriopulmonary connection Fontan, heart failure symptoms, presence of a fenestration, and a higher ventricular mass-to-volume ratio. On multivariable analysis, only older age at CMR, higher ventricular mass-to-volume ratio, and MPBF were associated with a lower VO2 max %. The univariate correlates of MPBF are shown in Table 1. On multivariable analysis, single ventricle dilation (end-diastolic volume >125 ml/m2) was independently associated with having MPBF (OR =2.8, 95% CI 1.9-3.7; p=0.03).

Conclusion: MPBF is common in patients after Fontan operation and is associated with single ventricle dilation. MPBF is an independent risk factor for lower VO2 max %. Efforts to normalize the distribution of pulmonary blood flow may lead to improvement in exercise capacity in this fragile patient population.

Medical History and Cardiac MRI univariate correlates of MPBF. Results are reported as mean ± standard deviation or frequency (percentage).

	All patients (n=147)	With MPBF (n=54)	Without MPBF (n= 93)	P value
Ventricular end-diastolic volume (ml/m^2)	98 ± 29	104 ± 35	94 ± 25	0.05
Ventricular end-systolic volume (ml/m^2)	49 ± 25	54 ± 26	46 ± 19	0.04
Dilated single ventricle (end-diastolic volume >125 ml/m^2)	21 (14%)	13 (24%)	9 (10%)	0.04

Damus-Kaye-Stansel anastomosis	36 (24%)	18 (33%)	18 (19%)	0.04
Atriopulmonary Fontan	33 (22%)	8 (15%)	25 (26%)	0.42
Systemic right ventricle	29 (20%)	11 (20%)	18 (19%)	0.54
Atrial arrhythmia	30 (20%)	10 (19%)	20 (22%)	0.43
Fenestration at the time of the Fontan operation	88 (60%)	36 (67%)	52 (56%)	0.17
Genetic diagnosis	11 (7%)	5 (9%)	6 (6%)	0.45

ID#: 374026

Staging reperfused myocardial infarctions with T2 CMR: insights into the dependence on infarction type with ex-vivo validation

Guan Wang, MD[1]Hsin-Jung Yang, PhD[2], Avinash Kali, PhD[3], Ivan Cokic, MD[4], Xingmin Guan, MS[1], Eric Johnson[5], Richard LQ. Tang, MD[6], Rohan Dharmakumar[7]

1. Cedars-Sinai Medical Center

2. Cedars Sinai Medical Center, Los Angeles, CA

3. Cedars-Sinai Medical Center: BIRI, CA

4. Cedars-Sinai Medical Center, Los Angeles, CA

5. Cedars-Sinai Medical Center and UCLA, Beverly Hills, CA

6. Cedars-Sinai Medical Center, CA

7. Biomedical Imaging Research Institute Dept of Biomedical Sciences, Cedars-Sinai Medical Center, Los Angeles,

Background: CMR-based staging of myocardial infarction (MI) with or without contrast agents relies on the resolution of edema in the chronic phase, which is determined on the basis of T2-based imaging. However, whether T2 CMR is sufficient for staging all MI types has not been investigated. We hypothesized that prolonged inflammation associated with chronic iron deposits following hemorrhagic MIs promote incomplete resolution of edema in the chronic phase which limit the capability of T2 imaging to stage hemorrhagic MIs.

Methods: Hemorrhagic (n=15) and non-hemorrhagic (n=9) MIs were created in dogs. Multi-parametric non-contrast mapping (T1, T2 and T2*) and LGE were performed at 1.5T and 3.0T at 5 days (acute) and 8 weeks (chronic) post MI. Relaxation values and LGE intensities of hemorrhagic, peri-hemorrhagic, non-hemorrhagic and remote territories were measured. Histopathology was performed to elucidate CMR findings.

Results: T2 of non-hemorrhagic MIs was significantly elevated in the acute phase relative to remote territories (39.8±12.8%(1.5T) and 27.9±16.5%(3.0T), $p<0.0001$ for both) but resolved to remote values by week 8 (-0.0±3.2%(1.5T, $p=0.678$) and -0.5±5.9%(3.0T, $p=0.601$)). In hemorrhagic MI, T2 of hemorrhage core was significantly elevated in the acute phase (17.7±10.0%(1.5T) and 8.6±8.2%(3.0T), $p<0.0001$ for both) but decreased below remote values by week 8 (-8.2±3.9%(1.5T) and -5.6±6.0%(3.0T), $p<0.0001$ for both). In contrast, T2 of the periphery of hemorrhage within MI zone was significantly elevated in the acute phase relative to remote territories (35.0±16.1%(1.5T) and 24.2±10.4%(3.0T), $p<0.0001$ for both) and remained elevated at 8 weeks post MI (8.6±5.1%(1.5T) and 6.0±3.3%(3.0T), $p<0.0001$ for both). The observed elevation in T2 in the peri-hemorrhagic zone of MIs and absence of T2 elevation in the non-hemorrhagic MI were consistent with ongoing or absence of histological evidence of inflammation, respectively.

Conclusion: Non-hemorrhagic MIs can be staged based on T2 changes in the MI territory. However, the incomplete resolution of T2 elevations in the periphery of hemorrhage associated with ongoing inflammation, well after scar formation, requires additional consideration of the spatial localization of sustained T2 elevations for staging hemorrhagic infarctions.

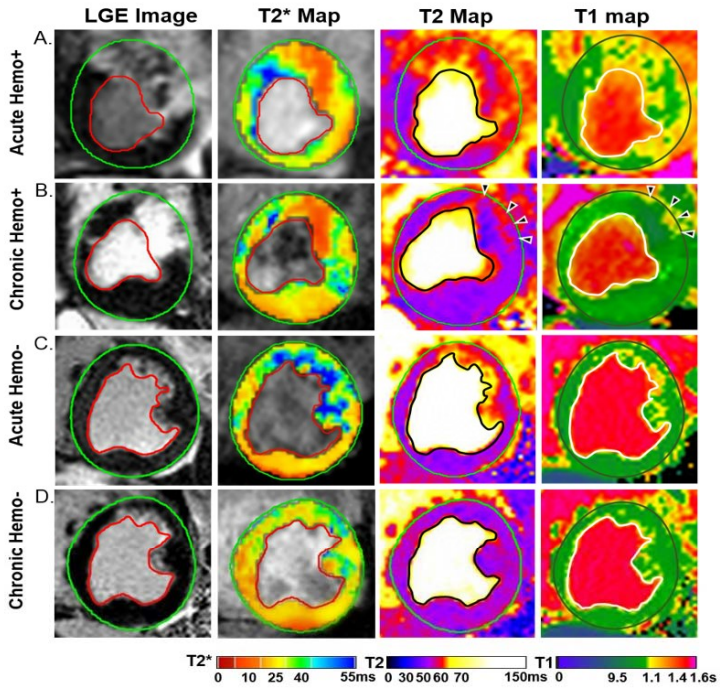

Figure 1 *Late-gadolinium-enhanced and Non-contrast-enhanced Relaxation Maps of Canine Hearts in the Acute and Chronic Phases of Reperfused Myocardial Infarction.* Panels A and B show representative LGE images, and native T2*, T2, and T1 maps acquired 5 days (acute) and 8 weeks (chronic) following reperfusion in a dog with hemorrhagic myocardial infarction. LGE images confirmed the presence of myocardial infarction. Marked T2* decreases were observed both in acute and chronic MI territories. Hyperintense edematous region were observed surrounding the relative hypointense core on T1 and T2 maps in acute hemorrhagic case, while persistent hyperintense surrounding the hemorrhagic area were also observed in the chronic stage (white arrowheads) on T2 maps. Panels C and D show representative LGE images, and native T2*, T2, and T1 maps acquired 5 days (acute) and 8 weeks (chronic) following reperfusion in another dog with non-hemorrhagic MI . Again, LGE images confirmed the presence of MI. Corresponding marked hyperintense and moderate hyperintense regions were observed on T2 map and T1 map in acute phase. Spotty hyperintense regions located within the MI zone were evident on T1 maps, while no hyperintense signal was observed within the MI territory on T2 maps in chronic phase.

Late-gadolinium-enhanced and Non-contrast-enhanced Relaxation Maps of Canine Hearts in the Acute and Chronic Phases of Referfused Myocardial Infarction.

ID#: 375691

Convolutional recurrent neural networks for dynamic cardiac MR image reconstruction

Chen Qin[1]Jo Schlemper[1], Jose Caballero, PhD[1], Anthony N. Price, PhD[2], Joseph V. Hajnal, PhD[2], Daniel Rueckert, PhD[1]

1. Imperial College London, United Kingdom

2. King's College London, London, England, United Kingdom

Background: The aim of this study is to accelerate cardiac cine magnetic resonance imaging (MRI) data acquisition by exploiting recurrent neural networks (RNN) for the reconstruction of images from undersampled data.

Methods: We propose a novel convolutional RNN (CRNN) architecture which learns representations in a recurrent fashion evolving over both time frames and iterations. In particular, the CRNN method models the recurrence of the iterative process by using recurrent hidden connections over iterations (CRNN-i unit), and spatio-temporal dependencies are simultaneously learnt exploiting bidirectional recurrent hidden connections across time sequences (BCRNN-t-i unit). Our architecture is illustrated in Fig. 1: we used N=10, and each block (Fig.1(a)) has 1 BCRNN-t-i layer, 3 CRNN-i layers and 1 CNN layer, interleaved by data consistency (DC) layers to incorporate the data fidelity.

The analysis was carried out using 10 fully sampled short-axis cardiac cine MR scans. The images were retrospectively undersampled using Cartesian undersampling masks and reconstructed assuming a single coil setup.

The method was compared to k-t FOCUSS, k-t SLR, 3D CNN-S and 3D CNN, in which 3D CNN-S and 3D CNN represent networks with 5 3D CNN layers in each block with and without shared weights respectively.

Results: The quantitative result is summarized in Table 1. The proposed method can outperform other baseline methods by a considerable margin at 6-fold and 9-fold undersampling rates in terms of mean squared error (MSE) and peak-to-noise-ratio (PSNR). A comparison of the visualization results of reconstructions and error maps from 9-fold undersampling data is shown in Fig.2 and their temporal profiles at x=120 is shown in Fig.3. As seen, our method can produce smaller residual error overall and more faithful reconstructions for those parts of the image around the myocardium where there are large temporal changes. In addition, the proposed method offers a very fast reconstruction and has less network capacity than 3D CNN, which is theoretically efficient and generalizes better.

Conclusion: We have presented a new RNN architecture for dynamic MRI reconstruction with the proposed variants of convolutional recurrent units which evolve over both time and iterations. The presented network is capable of producing faithful image reconstructions from highly undersampled data, and outperformed standard compressed sensing and low rank approaches as well as 3D CNN methods both in terms of reconstruction accuracy and speed, reflecting the effectiveness of the proposed method. The future extension is to exploit multi-coil information from parallel imaging to improve the reconstruction quality.

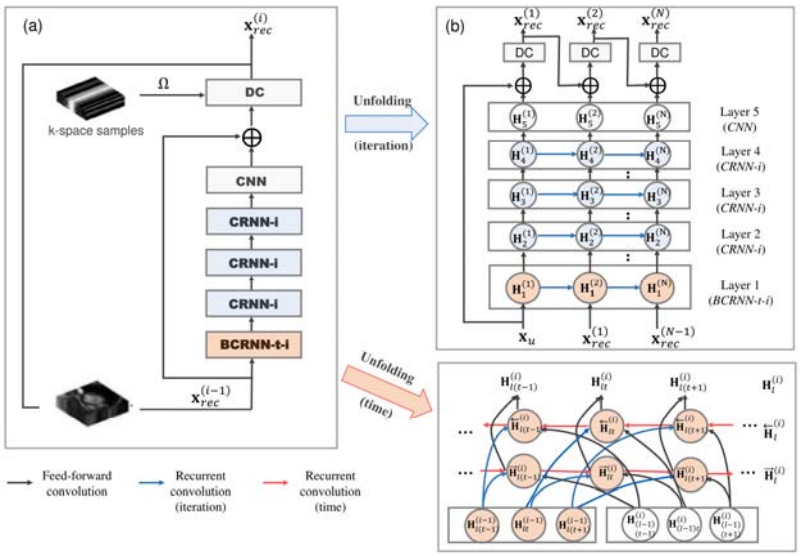

Figure 1: (a) The overall architecture of proposed CRNN network for MRI reconstruction. (b) The structure of the proposed network when unfolded over iterations. (c) The structure of BCRNN-t-i layer when unfolded over time sequence. The black arrows indicate feed-forward convolutions. The blue arrows and red arrows indicate recurrent convolutions over iterations and time sequence respectively.

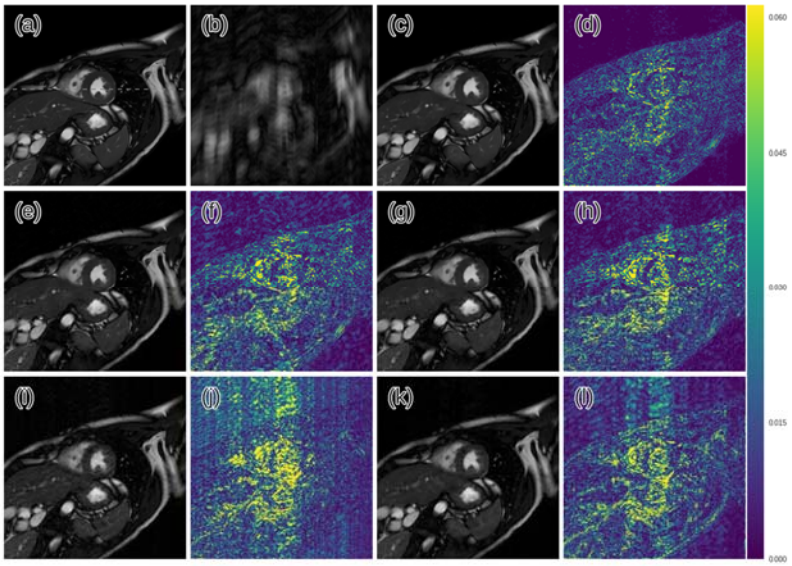

Figure 2: The comparisons of reconstructions on spatial dimension with their error maps. (a) Ground Truth (b) Undersampled image by acceleration factor 9 (c,d) the proposed CRNN (e,f) 3D CNN (g,h) 3D CNN-S(i,j) k-t FOCUSS (k,l) k-t SLR

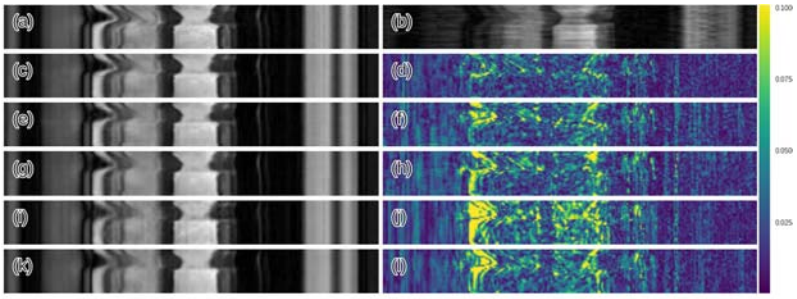

Figure 3: The comparison of reconstructions along temporal dimension with their error maps. (a) Ground Truth (b) Undersampled image by acceleration factor 9 (c,d) the proposed CRNN (e,f) 3D CNN (g,h) 3D CNN-S (i,j) k-t FOCUSS (k,l) k-t SLR

Table 1: Performance comparisons in terms of mean squared error (MSE) and peak-to-noise-ratio (PSNR) on dynamic cardiac data with different acceleration rates. MSE is scaled to 0.0001. Standard deviation is reported in the parenthesis. The best results are shown in bold.

Methods		k-t FOCUSS	k-t SLR	3D CNN-S	3D CNN	Proposed
Capacity		-	-	338,946	3,389,460	**262,020**
6-fold	MSE	6.00(2.29)	3.92(1.91)	3.76(1.28)	**2.90(1.02)**	2.93(1.31)
	PSNR (dB)	32.51(1.78)	34.51(2.15)	34.51(1.53)	35.64(1.46)	**35.67(1.84)**
9-fold	MSE	10.70(5.42)	7.68(4.28)	7.64(3.84)	7.03(2.71)	**6.05(3.33)**
	PSNR (dB)	30.11(2.00)	31.63(2.18)	31.61(1.84)	31.82(1.53)	**32.70(2.00)**
Reconstruction Time		15s	451s	8s	8s	**3s**

ID#: 375734

Combined high-resolution stress perfusion and scar assessment in patients with ischaemic cardiomyopathy

Adriana D. M. Villa, MD[1] Eva Sammut[2], Gabriella Di Giovine, MD[3], Jack Lee, DPhil[4], Matthew J. Ryan, MBChB MRCP[1], Khaled Alfakih, MD MRCP[5], Harry Pavlopoulos, MSc.MD.[6], Cian Scannell, BSc, MRes[7], Xenios Milidonis, MSc, PhD[7], Tevfik F. Ismail, PhD MRCP[8], Divaka Perera, MD[9], Reza Razavi, MD, PhD[10], Amedeo Chiribiri, MD PhD[10]

1. King's College London, United Kingdom

2. Bristol Heart Institute, Bristol, United Kingdom

3. King's College London, Novara, Piemonte, Italy

4. King's College London, England, United Kingdom

5. St. Thomas' Hospital, London; King's College London, England, United Kingdom

6. St Thomas Hospital, United Kingdom

7. King's College London, London, United Kingdom

8. King's College London; Guy's and St Thomas' Hospitals NHS Foundation Trust, London, England, United Kingdom

9. Guy's and St Thomas' NHS Foundation Trust, United Kingdom

10. King's College London, London, England, United Kingdom

Background: Myocardial scar and ischaemia frequently coexist in patients with ischaemic cardiomyopathy (ICM). It is recommended to assess stress-perfusion (SP) in combination with late gadolinium enhancement (LGE): while this is usually done with visual assessment, the feasibility of simultaneous LGE assessment and high-resolution quantitative perfusion has only been recently demonstrated (Villa ADM, JCMR 2016). In this study, we addressed the hypothesis that the accuracy of ischaemic burden can be improved by accounting for scar using combined high-resolution perfusion quantification and LGE assessment in patients with ischaemic cardiomyopathy.

Methods: Consecutive patients with ICM and LVEF<45% were included. All patients underwent high-resolution k-t adenosine SP at 1.5T (Philips Ingenia) or 3T (Philips Achieva) with a dual-bolus approach. Visual assessment was performed by two expert operators, blinded to clinical information. The analysis was repeated quantitatively with a semi-automated approach, using validated high-resolution deconvolution analysis and conventional semi-quantitative LGE threshold analysis (5SD). The combined assessment was performed as previously described, matching LGE and SP in terms of position and cardiac phase using a deformable template segmentation method. High-resolution myocardial perfusion reserve (MPR), LGE and fusion maps were then generated. Ischaemic burden was calculated with and without areas with LGE. All patients underwent invasive coronary angiography.

Results: 161 patients were included (LVEF 33.5±9.8). 93% had evidence of flow-limiting CAD on angiography, 42.6% demonstrated three-vessels disease (example case in Figure 1).
Visual assessment correctly identified the presence of CAD in 67.1% of patients (Table 1). Median ischaemic burden on visual assessment was 15.6%(0-31.3%) and scar burden 37.5%(31.3-43.8%).
Quantitative analysis agreed with coronary angiography in 84.5% of cases and similar results were observed on per-vessel analysis (Table 1).
When using an MPR cut-off of 1.5, the ischaemic burden was 21.2%(9.7-37.6%) on high-resolution analysis, dropping to 13.4%(5-23.3%) when LGE was taken into account (Figure 2). The average relative error in the estimation of the ischaemic burden caused by false-positive perfusion defects due to scar was 52.3±10.3%.

Conclusion: Our results demonstrate the accuracy of high-resolution quantitative SP and LGE assessment, demonstrating the need to account for areas of LGE when measuring ischaemic burden. When compared to visual assessment, combined analysis resulted particularly effective in the detection of peri-infarctual ischaemia, easily missed with visual assessment. These results support the use of combined quantitative assessment, and in particular in high-risk patients with ICM.

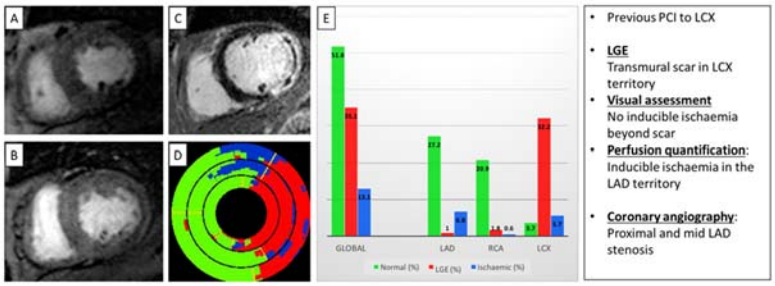

Figure 1: 51-year-old man with chest pain. Previous percutaneous coronary intervention (PCI) to left circumflex coronary artery (LCX). Late gadolinium enhancement (LGE) (panel C) shows a transmural scar in the LCX territory. Stress perfusion imaging (panel A) shows a perfusion defect, which is seen also on rest perfusion (panel B) and it is due to the presence of transmural scar, therefore on visual assessment there is no evidence of inducible ischaemia. Combined quantification (panel D) highlighted the presence of inducible ischaemia (blue) extending beyond the area of scar (red), which correlates with the angiographic finding of a proximal and mid LAD stenosis. Panel E shows the quantitative results with percentage of normal (green), scarred (red) and ischaemic (blue) myocardium. LAD: left anterior descending, RCA: right coronary artery.

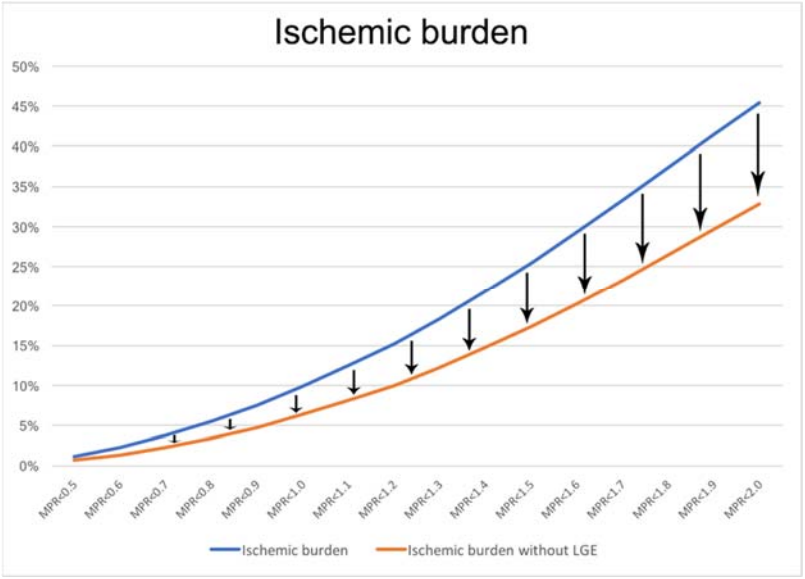

Figure 2: Percentage of ischaemic burden depending on the myocardial perfusion reserve (MPR) threshold chosen to identify ischaemic areas. There is an evident drop of ischaemic burden percentage after correction for LGE (arrows) ($p<0.0001$).

Percentage of diagnostic concordance between invasive coronary angiography and visual assessment of stress perfusion and between invasive coronary angiography and combined quantitative assessment ($p<0.0001$ quantitative vs visual assessment when using invasive coronary angiography as reference standard).

Concordance	Angio-Visual	Angio-Quantitative
CAD	67.1%	84.5%
RCA	67.7%	75.8%
LAD	59.0%	75.2%

LCX	65.2%	73.9%

CAD: coronary artery disease, RCA: right coronary artery, LAD: left anterior descending coronary artery, LCX: left circumflex coronary artery.

ID#: 378101

Validation of myocardial perfusion mapping: from invasive physiology to mapping

Tushar Kotecha, MRCP(UK) MBChB[1] Ana Martinez Naharro, MD[2], Daniel S. Knight[2], Rohin Francis, MBBS[3], Niket Patel, MBBS, MRCP[4], Deven Patel[5], Sundeep Kalra[5], John G. Coghlan, MD, MRCPI, FRCP[6], Philip N. Hawkins[7], Roby Rakhit, MD, FRCP[8], Timothy Lockie, MBChB, PhD[9], James Moon, MD[10], Sven Plein, MD PhD[11], Hui Xue, PhD[12], Peter Kellman, PhD[13], Marianna Fontana, MD, PhD[3]

1. Royal Free London NHS Foundation Trust, London, England, United Kingdom

2. UCL Department of CMR, Royal Free Hospital, London, England, United Kingdom

3. UCL Department of CMR, Royal Free Hospital, England, United Kingdom

4. The Royal Free Hospital, United Kingdom

5. Royal Free London NHS Foundation Trust, United Kingdom

6. Royal Free Hospital, London, England, United Kingdom

7. National Amyloidosis Centre, University College London, England, United Kingdom

8. Royal Free Hospital, England, United Kingdom

9. Royal Free Hospital, London, United Kingdom

10. UCL, England, United Kingdom

11. University of Leeds, England, United Kingdom

12. National Heart, Lung, and Blood Institute, Bethesda, MD

13. National Heart, Lung, and Blood Institute, National Institutes of Health, Bethesda, MD

Background: Myocardial perfusion CMR is routinely evaluated qualitatively. Quantitative analysis of myocardial perfusion CMR is feasible but has in the past been challenging and time consuming. Recently, a new motion corrected myocardial perfusion method with automated in-line perfusion mapping using the Gadgetron software framework has been proposed allowing free breathing acquisition and pixel-wise quantification of myocardial blood flow (MBF) and myocardial perfusion reserve (MPR). This novel method requires further clinical validation. Fractional flow reserve (FFR) is the current invasive reference standard for physiological assessment of coronary stenosis significance. The aim of this study was to compare myocardial perfusion mapping against invasively determined FFR.

Methods: Eighteen patients (9 male, age 62±10 years) with known or suspected coronary artery disease underwent CMR with adenosine stress and rest myocardial perfusion mapping in 3 short axis slices at 1.5T (Figure 1). Average MBF within myocardial segments supplied by each major epicardial coronary artery was measured on stress and rest myocardial perfusion maps. MPR was calculated as the ratio of stress and rest MBF. FFR was contemporaneously measured in all major epicardial arteries. FFR<0.80 was considered haemodynamically significant.

Results: FFR was determined in 46 vessels, with 10 vessels having FFR <0.80 (7 single vessel disease). Stress MBF and MPR were reduced in myocardial segments supplied by arteries with FFR <0.80 compared to arteries with FFR >0.80 (mean stress MBF: 1.87±0.52ml/g/min vs 2.83±0.54ml/g/min, mean MPR: 1.94±0.59 vs 3.15±0.99, both p<0.001, Figure 2). The optimum stress MBF to detect FFR<0.80 on a per-vessel basis was 2.22ml/g/min, with a sensitivity of 80%, specificity of 86% and receiver-operator characteristic area under curve (AUC) curve of 0.90 (p<0.001). The optimum MPR to detect FFR<0.80 was 2.65 with 90% sensitivity, 69% specificity and 0.85 AUC (p<0.001).

Conclusion: Automated stress perfusion mapping is able to accurately detect flow-limiting coronary disease as defined by invasive FFR. Stress MBF and MPR have similar diagnostic performance for the localization of perfusion defects to coronary territories. Myocardial perfusion mapping has the potential to transform CMR assessment of ischaemia by the addition of in-line automated quantitative analysis to routine perfusion imaging and merits further investigation with clinical endpoints.

Figure 1:
Examples of stress perfusion maps and coronary angiograms
Top row: normal stress perfusion and coronary angiogram
Middle row: stress perfusion defect in mid-distal septum and anterior wall corresponding to severe mid-LAD stenosis (blue arrow)
Bottom row: globally reduced stress perfusion corresponding to severe proximal three vessel disease (black arrows)

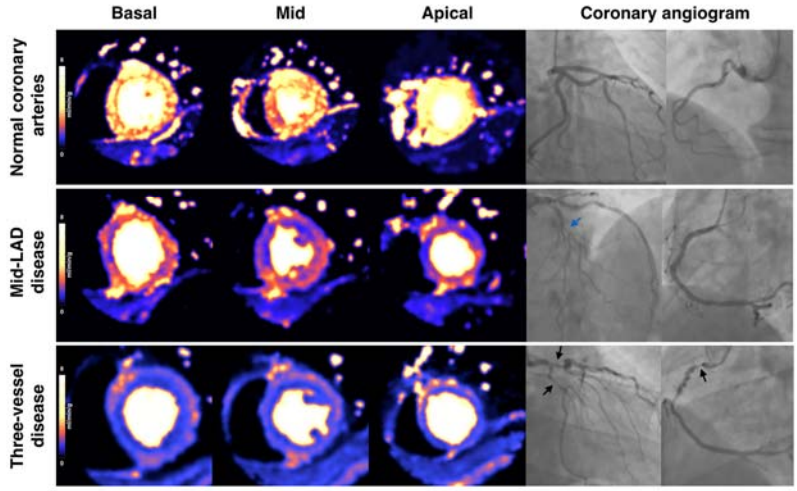

Figure 1

Figure 2:
Mean stress myocardial blood flow (MBF) and mean myocardial perfusion reserve (MPR) in myocardial territories supplied by vessels with normal (>0.80) and abnormal (<0.80) fractional flow reserve (FFR)

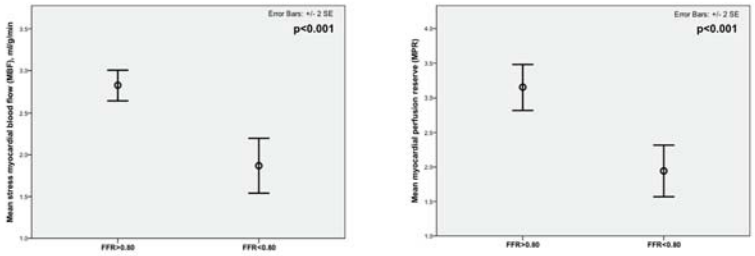

Figure 2

ID#: 378296

Coronary Hyper-Intensive Plaques Identified by Coronary Atherosclerosis T1-weighted Characterization Relates to Vulnerable Plaque Features and Clinical Severity in Patients with Acute Coronary Syndrome

Wei Yu, M.D, Ph.D[4]Wen Liu, M.D[1], Yibin Xie, PhD[2], Sijing Wu, M.D[3], Yanni Du, M.D[4], Zhenjia Wang, M.D[4], Zhaoyang Fan, Ph.D.[5], Li Dong, M.D, Ph.D[4], Yonghe Guo, Ph. D[3], Yi Liu, M.D[4], Xiaoming Bi, PhD[6], Jing An, M.D[7], Wei Liu, Ph. D[3], Debiao Li, PhD[2]

1. Department of Radiology, Anzhen Hospital, Capital Medical Universityl, Beijing, Beijing, China (People's Republic)

2. Cedars-Sinai Medical Center, Los Angeles, CA

3. Department of cardiology, Anzhen Hospital, Capital Medical University, Beijing, China (People's Republic)

4. Department of Radiology, Anzhen Hospital, Capital Medical University, Beijing, China (People's Republic)

5. Biomedical Imaging Research Institute, Cedars-Sinai Medical Center, CA

6. Siemens Healthcare, CA

7. MR Collaborations NE Asia, Siemens Healthcare,, Beijing, China (People's Republic)

Background: Recently, a novel CMR technique, coronary atherosclerosis T1-weighted characterization with integrated anatomical reference (CATCH), was developed for characterizing coronary atherosclerosis[1]. Using intracoronary optical coherence tomography (OCT) as reference, coronary hyper-intensive plaque (CHIP) detected on CATCH is associated with high-risk plaque morphology in patients with stable angina pectoris[1]. However, the association between CHIP and high-risk plaque features in patients with acute coronary syndrome (ACS) has not been reported. The purpose of this study is to investigate the relationship between CHIP and the clinical severity of ACS as well as high-risk plaque features on OCT.

Methods: Patients with clinically defined ACS (N=38) were prospectively included and underwent CATCH scanning to determine the plaque-to-myocardium signal intensity ratio (PMR). Patients were divided into 3 groups: unstable angina pectoris (UAP) (n=21), non-ST segment elevation myocardial infarction (NSTEMI) (n=6) and ST segment elevation myocardial infarction (STEMI) (n=11). Of the 38 patients, 23 lesions from 19 patients underwent invasive coronary angiography and pre-interventional OCT within 48 hours after CATCH examination.

Results: There was no significant difference in basic clinical characteristics between the 3 ACS groups (Table 1). Among all 38 patients, 26 (68.4%) patients had CHIPs with a PMR cutoff value of 1.0[2]. CHIPs were observed in 13 (61.9%) UAP patients, 5 (83.3%) NSTEMI patients, and 8 (72.7%) STEMI patients, respectively. The average PMR values was highest in patients with STEMI (1.5±0.7), followed by NSTEMI (1.4±0.5), and lowest in patients with UAP (1.2±0.3). Of the 23 lesions that underwent OCT, 16 (69.6%) were CHIPs. High-risk plaque features such as absence of calcification (P=0.047), plaque rupture (P=0.002), thrombus (P=0.007) and intimal vasculature (P=0.014) were associated with significantly higher PMR, except the presence of thin-cap fibroatheroma (P=0.65) and macrophage infiltrations (P=0.63) (Fig. 1). Table 2 shows plaque morphology assessed by OCT. Fig. 2 shows a representative patient case with a CHIP on CATCH.

Conclusion: This study shows that CHIPs detected on CATCH in patients with ACS are associated with different types of high-risk plaque features detected on OCT and the clinical severity of ACS.

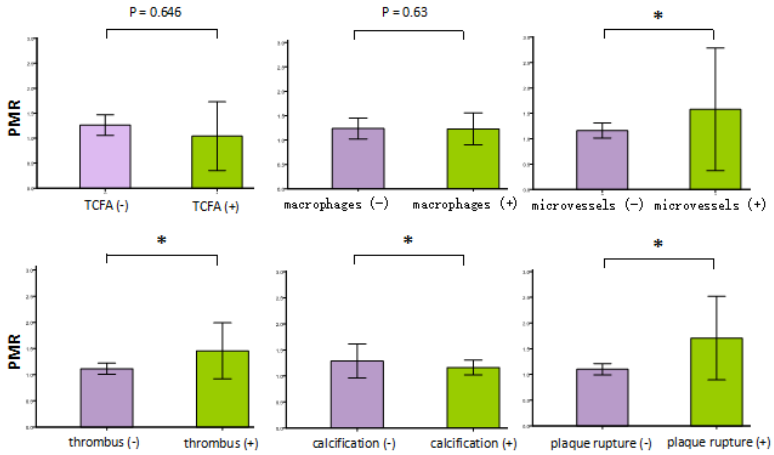

Figure 1 Relationship Between PMR and OCT Classifications Coronary plaques with vulnerable features as classified by OCT tended to be hyperintensive on CATCH. Star signs (*) denote statistical significance ($p < 0.05$). Positive sign (+) and negative sign (-) denote lesion groups with corresponding OCT grading. Plaque hyper-intensity is presented in terms of plaque to myocardium ratio (PMR) as described previously.

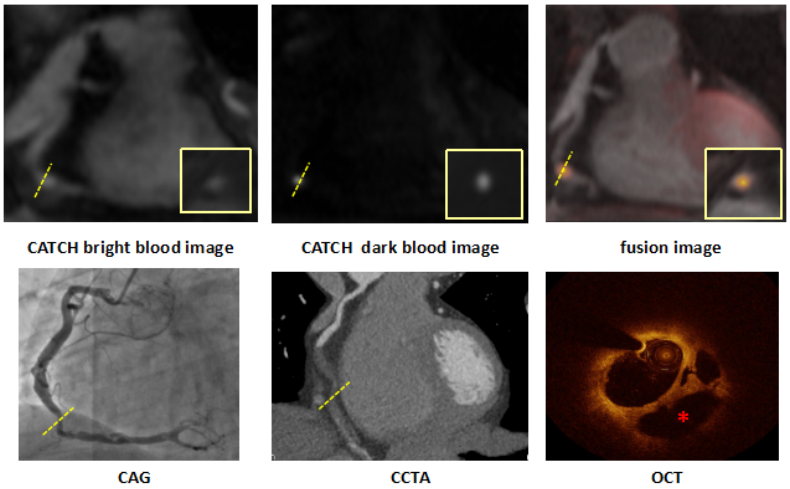

Figure 2 A representative patient case with a CHIP on CATCH A Patient with STEMI (38 y/o, male).CAG and CCTA shows significant stenosis in the middle segment of RCA, fusion image and CATCH dark blood shows high signal intensity in the area corresponding to the severe stenosis with PMR=1.6. The optical coherence tomography examination showed intrawall organized hemorrhage (*). STEMI = ST segment elevation myocardial infarction; CAG = coronary angiography; RCA = right coronary artery; PMR = plaque-to-myocardium signal intensity ratio.

Table 1 The Basic Clinical Characteristics in Each Group of Patients

Values are mean ±SD or n (%). PMR = the plaque-to-cardiac muscle signal intensity ratio. BP = blood pressure; NSTEMI = non-ST segment elevation myocardial infarction; STEMI = ST segment elevation myocardial infarction; CRP = C-reactive protein; HDL = high-density lipoprotein; LDL = low-density lipoprotein; T-chol = total cholesterol.

Table 1	**The Basic Clinical Characteristics and Angiographic Findings in Each Group of Patients**

	unstable angina (n=21)	NSTEMI (n=6)	STEMI (n=11)	P value
Age, yrs	56 ± 13	58 ± 12	51 ± 9	0.462
Male	18 (85.7)	5 (83.3)	10 (90.9)	0.736
BMI, kg/m^2	25.0 ± 4.2	23.5 ± 4.8	24.3 ± 3.5	0.805
Diabetes mellitus	10 (47.6)	4 (66.7)	3 (27.3)	0.105
Smoking	7 (33.3)	3 (50)	6 (54.5)	0.229
Dyslipidemia	2 (0.1)	0 (0)	1 (0.09)	0.833
Heart rate, beats/min	75 ± 10	67 ± 6	75 ± 8	0.207
Systolic BP, mmHg	128 ± 16	127 ± 18	115 ± 12	0.073
Diastolic BP, mmHg	74 ± 10	69 ± 7	76 ± 12	0.497
HDL, mmol/l	1.0 ± 0.2	1.2 ± 0.5	0.9 ± 0.3	0.202
LDL, mmol/l	2.3 ± 1.0	2.1 ± 0.8	2.2 ± 0.6	0.903
T-chol, mmol/l	3.9 ± 1.1	4.1 ± 1.1	3.6 ± 0.8	0.616
Triglycerides, mmol/l	1.4 ± 0.6	1.6 ± 0.4	1.5 ± 0.6	0.853
Homocysteine, µmmol/L	12.9 ± 9.2	11.8 ± 3.7	14.8 ± 9.4	0.771
CRP, mg/L	4.4 ± 7.5	11.5 ± 14.9	4.5 ± 7.1	0.224

ID#: 379015

Left atrial ejection fraction: a novel imaging biomarker for diagnosis and prognosis in heart failure with preserved ejection fraction

Prathap K. Kanagala, MBBS, MRCP[1] Anvesha Singh, MBChB, PhD[2], Jamal N. Khan, MBChB, PhD[3], Jayanth Arnold, BMBCh DPhil[3], Gerry p. McCann, MB ChB, MD[3], Adrian S. H. Cheng, NIHR Biomedical Research Centre, Glenfield Hospital, Leicester[4]

1. Aintree University Hospital, Liverpool, Department of Cardiovascular Sciences and NIHR Leicester Biomedical Research Centre, Glenfield Hospital, Leicester, Wirral, England, United Kingdom

2. Department of Cardiovascular Sciences and NIHR Leicester Biomedical Research Centre, Glenfield Hospital, Leicester, England, United Kingdom

3. Department of Cardiovascular Sciences and NIHR Biomedical Research Centre, Glenfield Hospital, Leicester, England, United Kingdom

4. Kettering General Hospital, Kettering, United Kingdom, United Kingdom

Background: Left atrial contractile function, as assessed by echocardiography is reportedly perturbed in heart failure (HF). We investigated the diagnostic and prognostic utility of left atrial ejection fraction (LAEF) quantified with cardiovascular magnetic resonance (CMR) in heart failure patients with preserved ejection fraction (HFpEF).

Methods: Subjects were recruited as part of Developing Imaging And plasMa biOmarkers iN Describing-HFpEF (DIAMOND-HFpEF): a single-centre prospective study. HFpEF inclusion criteria were: HF and left ventricular ejection fraction > 50%. Exclusion criteria were: myocardial infarction in the preceding 6 months, suspected or confirmed cardiomyopathy or constrictive pericarditis, non-cardiovascular life expectancy < 6 months, severe native valve/lung/kidney disease and standard CMR contraindications. For comparison, age- and sex-matched healthy controls were also recruited. The CMR protocol consisted of conventional cines, pre- and post-contrast modified-inversion-recovery-look-locker (MOLLI) and late gadolinium enhancement imaging at 3-Tesla. LAEF was calculated using the biplane method. Receiver operator characteristics (ROC) analysis, the net reclassification index (NRI) and Cox regression were used for diagnostic and prognostic assessments.

Results: One hundred and eighty eight subjects (HFpEF n=140, controls n=48) underwent CMR. Atrial fibrillation (AF) was present in 43 (31%) of HFpEF subjects. Overall, LAEF < 44% differentiated HFpEF from controls (area under curve [AUC] = 0.794; sinus rhythm 0.777). In comparison, AUCs for BNP, E/E';, maximum left atrial volume index and left ventricular mass were 0.861, 0.760, 0.723 and 0.664 respectively. Adding LAEF to a model comprising the above existing European Society of Cardiology (ESC) markers improved the overall NRI: in all subjects (56.8%, 95% confidence interval (CI) 22.400–91.100, p = 0.001); in sinus rhythm (53.8%, 95% CI 17.900–89.700, p = 0.003). During median follow-up of 616 days, there were 44 composite events (8 deaths, 36 HF hospitalisations) in HFpEF. Kaplan-Meier survival plots demonstrated association of lower LAEF with an increased risk of the composite endpoint across the HFpEF cohort (Log-Rank test: all patients p = 0.002; sinus rhythm p = 0.009). Using Cox regression, LAEF was an independent predictor of outcomes in all subjects (Hazard Ratio [HR] 0.673 per standard deviation increase, 95% CI 0.484–0.935, p = 0.018) and in sinus rhythm alone (HR 0.406; 95% CI 0.219–0.752; p = 0.004).

Conclusion: CMR-derived LAEF provides incremental diagnostic value beyond current ESC guidelines and is an important prognostic biomarker in HFpEF.

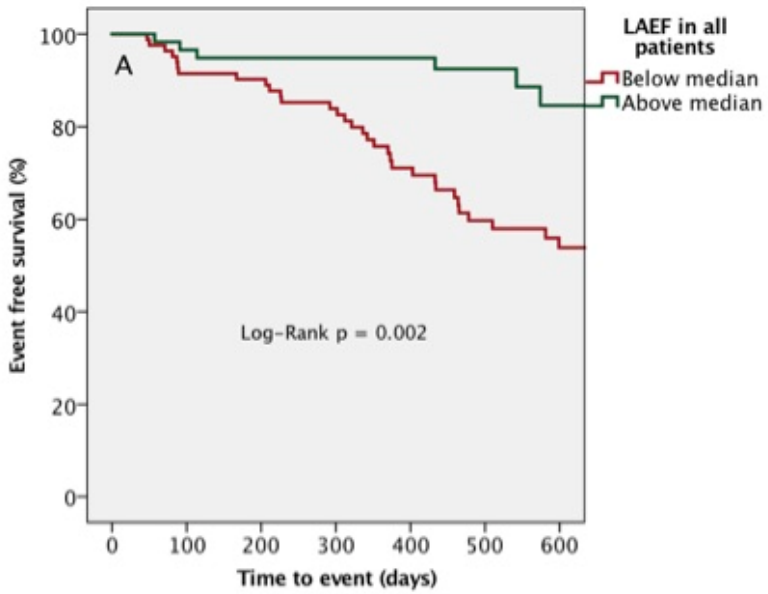

Kaplan-Meier survival plots stratified according to median LAEF in all patients

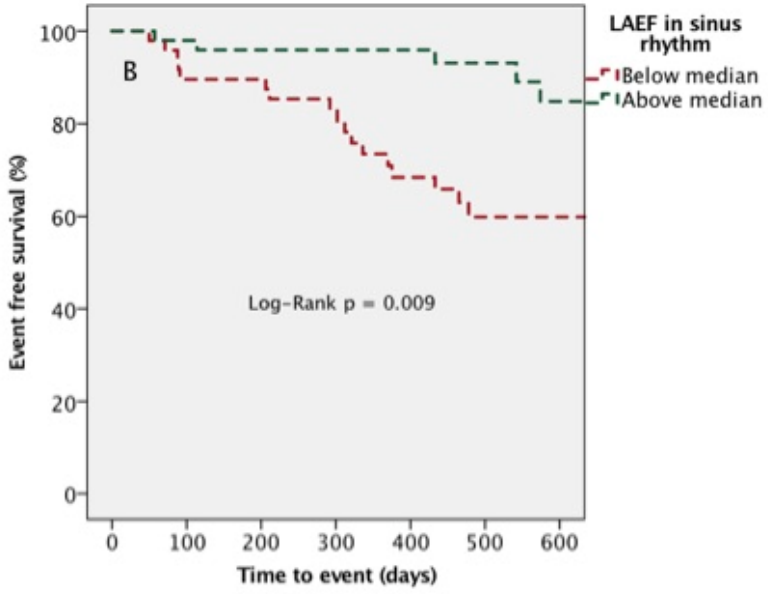

Kaplan-Meier survival plots stratified according to median LAEF in sinus rhythm

Receiver operator characteristics analysis for HFpEF diagnosis

		Sensitivity (%)	Specificity (%)	PPV (%)	NPV (%)	p value
Overall - all subjects including AF						

BNP	0.861	80	91	96	63	< 0.0001
E/E';	0.760	56	84	90	42	< 0.0001
LAVImax	0.723	58	76	86	41	< 0.0001
LV mass	0.664	51	78	86	38	0.001
LAEF	0.794	70	80	90	51	< 0.0001
ESC diagnostic markers combined	0.892	79	91	96	62	< 0.0001
ESC diagnostic markers combined **+ LAEF**	0.918	72	100	100	58	< 0.0001
Sinus rhythm subjects only						
BNP	0.821	75	91	94	65	< 0.0001
E/E';	0.749	84	56	79	64	< 0.0001
LAVImax	0.646	68	58	76	48	0.006
LV mass	0.660	50	76	80	44	0.003
LAEF	0.727	60	80	85	51	< 0.0001
ESC diagnostic markers combined	0.864	73	91	94	63	< 0.0001
ESC diagnostic markers combined **+ LAEF**	0.890	78	84	91	67	< 0.0001

Univariate and multivariate Cox regression models for the composite endpoint of death or hospitalization with heart failure

	All patients	**Sinus rhythm**

	Univariate		Multivariate		Univariate		Multivariate	
	Hazard ratio	**P value**	**Hazard ratio**	**P value**	**Hazard ratio**	**P value**	**Hazard ratio**	**P value**
Clinical								
Age	1.445 (1.045 – 1.998)	0.026			1.195 (0.808 – 1.766)	0.372		
Average DBP	0.673 (0.486 – 0.933)	0.017			0.580 (0.368 – 0.914)	0.109		
Prior HF hospitalization	3.547 (1.485 – 8.471)	0.004	3.954 (1.526– 10.244)	0.005	5.882 (1.749 – 19.789)	0.004	5.313 (1.567 – 18.017)	0.007
Asthma or COPD (%)	2.374 (1.211 – 4.656)	0.012	2.697 (1.238 – 5.874)	0.013	1.754 (0.736 – 4.180)	0.205		
Functional								
NYHA III/IV (%)	1.781 (0.964 – 3.293)	0.066			2.150 (0.985 – 4.691)	0.054		
Six minute walk test distance	0.678 (0.477 – 0.964)	0.030			0.536 (0.328 – 0.878)	0.103		
Minnesota Living With Heart Failure score	1.324 (0.949 – 1.847)	0.099			1.570 (1.010 – 2.440)	0.045		
Bloods								
Urea (mmol/L)	1.282 (1.002	0.048			1.479 (1.105	0.009	1.437 (1.050	0.023

	– 1.641)				– 1.981)		– 1.967)	
Log Creatinine (mmol/L)	1.317 (0.999 – 1.737)	0.051			1.509 (1.076 – 2.117)	0.017		
Haemoglobin (g/L)	0.741 (0.545 – 1.007)	0.055			0.711 (0.483 – 1.046)	0.083		
Log BNP (ng/L)	1.622 (1.136 – 2.315)	0.008			1.755 (1.158 – 2.661)	0.008		
Imaging								
E/E';	1.427 (1.073 – 1.896)	0.014			1.446 (1.019 – 2.052)	0.039		
LV mass	1.328 (0.999 – 1.765)	0.051			1.608 (1.047 – 2.471)	0.030		
RVEDVI	1.365 (0.995 – 1.871)	0.054	1.498 (1.076-2.084)	0.017	1.260 (0.827 – 1.917)	0.282		
RVEF	0.801 (0.623 – 1.030)	0.084			0.836 (0.614 – 1.140)	0.258		
LAVImax	1.330 (1.004 – 1.761)	0.047			1.398 (0.822 – 2.380)	0.217		
LAEF	**0.674 (0.495 – 0.918)**	**0.012**	**0.673 (0.484 – 0.935)**	**0.018**	**0.455 (0.267 – 0.777)**	**0.004**	**0.406 (0.219 – 0.752)**	**0.004**

ECV	1.474 (1.000 – 2.174)	0.050			1.363 (0.677 – 2.743)	0.386		
Presence of MI on CMR	1.891 (0.929 – 3.849)				2.061 (0.828 – 5.129)	0.120		

ID#: 373164

Native myocardial T1 for clinical diagnosis of cardiac amyloidosis: ready for prime time - a 715 patient prospective study

Andrea Baggiano[1]Michele Boldrini[2], Ana Martinez Naharro, MD[3], Tushar Kotecha, MRCP(UK) MBChB[4], Tamer Rezk, BSc[2], Rohin Francis, MBBS[2], Hossam Fayed, MBChB MSc MRCP(UK)[5], Richa Manwani, MRCP FRCPath[6], Daniel S. Knight[3], Helen J. Lachmann, MD[7], James Moon, MD[8], Peter Kellman, PhD[9], Julian D. Gillmore[10], Philip N. Hawkins[10], Marianna Fontana, MD, PhD[2], Ashutosh Wechalekar, MD[10]

1. Centro Cardiologico Monzino, Istituto di Ricovero e Cura a Carattere Scientifico, Italy

2. UCL Department of CMR, Royal Free Hospital, England, United Kingdom

3. UCL Department of CMR, Royal Free Hospital, London, England, United Kingdom

4. Royal Free London NHS Foundation Trust, London, England, United Kingdom

5. UCL Department of Cardiac MRI, Royal Free Pulmonary Hypertension Service, Pond Street, England, United Kingdom

6. UCL National Amyloidosis Center, Royal Free Hospital, United Kingdom

7. University College London, England, United Kingdom

8. UCL, England, United Kingdom

9. National Heart, Lung, and Blood Institute, National Institutes of Health, Bethesda, MD

10. National Amyloidosis Centre, University College London, England, United Kingdom

Background: Background: Cardiac amyloidosis is a challenging and underdiagnosed cause of heart failure. Native T1 is elevated in the two most common types of cardiac amyloidosis AL and ATTR (Figure 1). However, the diagnostic accuracy has only been tested on small retrospective studies leaving a knowledge gap, on the use of native T1 as a diagnostic test. Furthermore, renal failure is highly prevalent in systemic amyloidosis, but the impact of renal failure on the diagnostic accuracy of native T1 has never been investigated so far. **Aim:** The aim of this study is to assess the utility of native T1 to detect cardiac amyloidosis in a large prospective cohort of patients referred for suspected systemic amyloidosis.

Methods: Methods: A total of 715 patients with suspected systemic amyloidosis underwent, between 2015 and 2017, CMR with LGE and T1 mapping (with Modified Look-Locker Inversion recovery, MOLLI) and extensive clinical investigations including ECG, echo, blood biomarkers, SAP scintigraphy and cardiac or non cardiac biopsy. All ATTR patients also underwent cardiac 3,3-diphosphono-1,2-propanodicarboxylicacid (DPD) scintigraphy.

Results: Results: The final diagnosis was cardiac AL amyloidosis in 213, cardiac ATTR amyloidosis in 97 and no cardiac involvement in 405 (of which 197 had systemic amyloidosis and 208 did not have systemic amyloidosis). Chronic kidneys disease was highly prevalent in this population (31 CKD stage 1, 317 CKD stage 2, 235 CKD stage 3, 22 CKD stage 4; 145 had nephrotic range proteinuria). T1 was significantly elevated in both types of cardiac amyloidosis compared to patients with no cardiac involvement. This was associated with a high diagnostic accuracy in the overall population (AUC 0.933, 95%CI 0.913 to 0.949) (Figure 2). A native T1<1035ms was associated with 99% sensitivity to exclude cardiac amyloidosis whilst a native T1>1160ms was associated with 99% specificity to diagnose cardiac amyloidosis. There was no clinical significant correlation between native T1 and eGFR, the level of proteinuria or the serum albumin. The diagnostic accuracy was high and comparable in all CKD groups.

Conclusion: Conclusions: Native myocardial T1 enables the diagnosis of cardiac amyloidosis to be made reliably without the need of contrast agent in a large proportion of patients with suspected systemic amyloidosis. We propose a diagnostic algorithm for non contrast CMR applicable to the majority of patients (Figure 2).

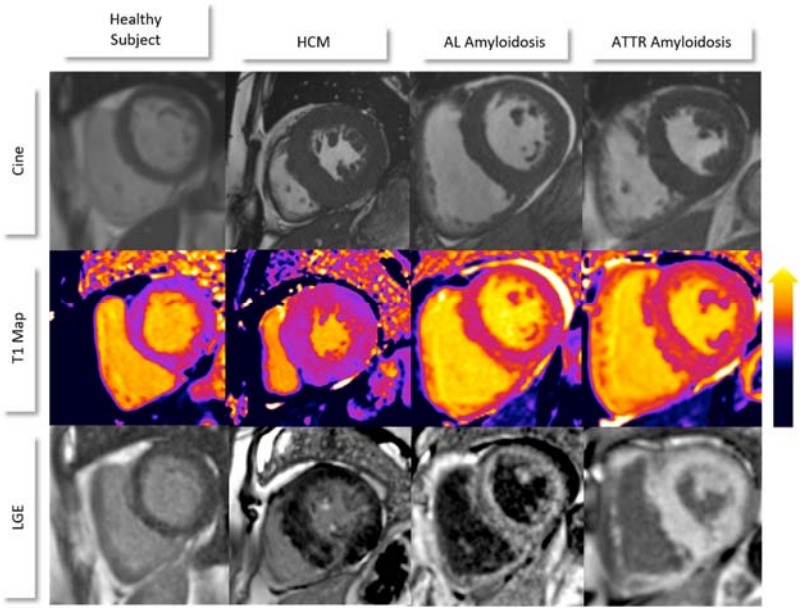

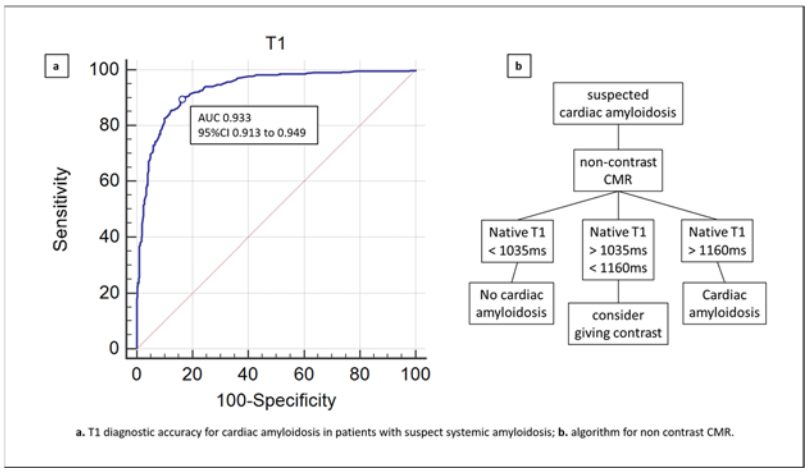

a. T1 diagnostic accuracy for cardiac amyloidosis in patients with suspect systemic amyloidosis; **b.** algorithm for non contrast CMR.

ID#: 373093

Progression of Myocardial Fibrosis in Aortic Stenosis: A Multicentre Cardiac Magnetic Resonance Study

Russell Everett, BSc MD[1] Lionel Tastet[2], Marie-Annick Clavel, DVM, PhD[3], Calvin Chin, MD PhD[4], Romain Capoulade, MD, PhD[5], Jacek Kwiecinski, MD[6], Miquel Gomez, MD, PhD[7], Christopher Tuck, BSc[1], Edwin J. van Beek, MD, PhD[8], Audrey Christina. White, BSE, CRCS (A)[9], Scott I. Semple, MSc PhD[10], David E. Newby, MD PhD[10], Philippe Pibarot, DVM, PhD[11], Marc R. Dweck, MD PhD[12]

1. University of Edinburgh, United Kingdom

2. Quebec Heart and Lung Institute, Department of Medicine, Quebec, Québec, PQ, Canada

3. Laval University, Canada

4. National Heart Center, N/A, Singapore

5. 2Quebec Heart and Lung Institute, Department of Medicine, Quebec, Canada

6. Centre for Cardiovascular Science, University of Edinburgh, UK, United Kingdom

7. Hospital del Mar Medical Research Institute. Universitat Autònoma de Barcelona. Barcelona, Spain

8. University of Edinburgh, Edinburgh, United Kingdom

9. Royal Infirmary, University of Edinburgh, UK, Scotland, United Kingdom

10. University of Edinburgh, Scotland, United Kingdom

11. Quebec Heart and Lung Institute, Department of Medicine, Quebec, Canada

12. University of Edinburgh, Edinburgh, Scotland, United Kingdom

Background: Aortic stenosis (AS) is accompanied by progressive left ventricular (LV) hypertrophy and myocardial fibrosis. Both are associated with an adverse long-term prognosis. We assessed the natural history of these processes and the impact of aortic valve replacement (AVR) using cardiac magnetic resonance (CMR) imaging.

Methods: Ninety-nine patients undergoing serial CMR imaging within two prospective observational AS studies were included (CMRAS, PROGRESSA). Sixty-one patients (age 61±12, 66% male, 43% mild, 34% moderate, 23% severe AS) did not undergo valve intervention (*natural history cohort)* with follow-up imaging at 2.1±0.7 years. Thirty-eight patients with symptomatic severe AS (age 66±8, 76% male) undergoing CMR prior to AVR (*AVR cohort)* had follow-up imaging at 1.5±0.5 years. Focal replacement fibrosis was assessed using late gadolinium enhancement (LGE). Extracellular expansion (a surrogate of diffuse fibrosis) was quantified using MOLLI T1 mapping and the indexed extracellular volume (iECV; LV end-diastolic volume * extracellular volume [ECV] fraction indexed to body surface area). Annualised change was analysed for all measures.

Results: In the natural history cohort, indexed left ventricular mass (LVMi) and iECV both increased over time (LVMi: 3 [1, 5] g/m2/yr, P<0.0001, iECV: 0.5 [0, 2.3] mL/m2/yr, P=0.006), with the fastest progression in those with most severe AS (r=0.41, P=0.001). There was no progression in ECV fraction suggesting that myocyte and extracellular expansion both occur at similar rates. Mid-wall LGE was present at baseline in 16 patients (26%), who demonstrated progression in LGE volume (1.6 [0.4, 4.1] g/m2/yr [1.5%/yr], P=0.001), including the development of new remote areas of LGE (n=4, Figure).

Following AVR, patients displayed a significant fall in both LVMi (-10 [-19, -5] g/m2/yr) and iECV (-2 [-3, -1] mL/m2/yr, both P<0.0001) accompanied by an improvement in diastolic function (E/e': -1.3 [-4.3, 1.1], P=0.012). By contrast, ECV fraction increased (1.2 [0.4, 2.2]%, P=0.002) suggesting that myocyte hypertrophy regresses faster than diffuse fibrosis. Mid-wall LGE was present in 10 patients (26%). There was no change in LGE mass following AVR, with no new LGE and no progression or resolution of existing LGE in any patient out to two years.

Conclusion: Myocardial hypertrophy and fibrosis increase in an exponential manner with fastest rates of progression in those with severe baseline disease. Post AVR, myocyte hypertrophy resolves more quickly than diffuse fibrosis. Whilst progression of focal replacement fibrosis is arrested by AVR, scarring already developed is irreversible. The EVOLVED trial will test whether operating promptly on patients with such scarring is beneficial.

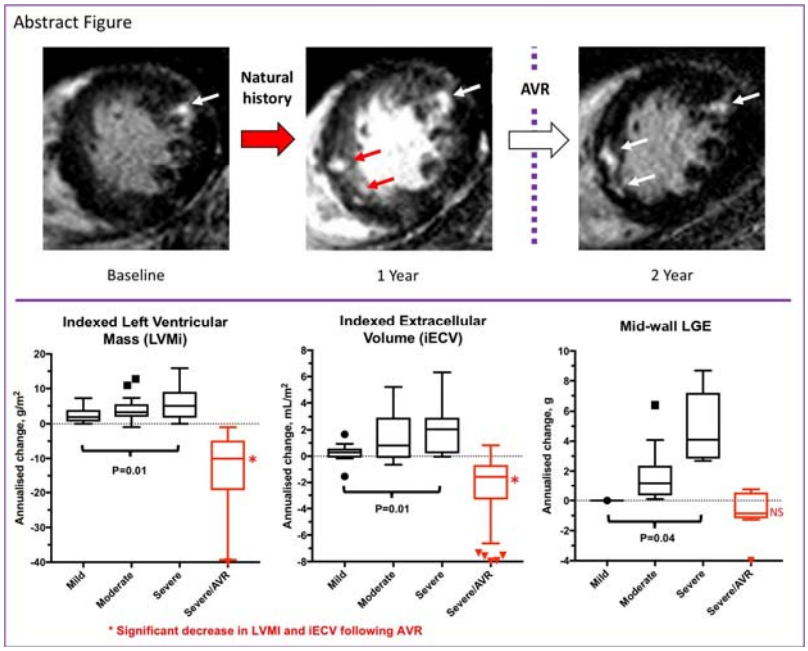
Abstract Figure
Natural history
AVR
Baseline
1 Year
2 Year
Indexed Left Ventricular Mass (LVMi)
Annualised change, g/m²
P=0.01
Indexed Extracellular Volume (iECV)
Annualised change, mL/m²
P=0.01
Mid-wall LGE
Annualised change, g
P=0.04
NS
Mild
Moderate
Severe
Severe/AVR
* Significant decrease in LVMI and iECV following AVR

Main figure

ID#: 373076

Creatine Kinase Kinetics are Increased in Obese Heart Failure: Is This The Answer to the Obesity Paradox?

Jennifer J. Rayner, BMBCh, MRCP(UK)[1] William T. Clarke, MChem, D.Phil[2], Mark A. Peterzan, BSc(Hons) MRCP(UK) MA[3], Christopher T. Rodgers, DPhil[3], Stefan Neubauer, MD, FRCP[4], Oliver J. Rider, MRCP, DPhil[5]

1. OCMR, University of Oxford, Oxford, England, United Kingdom

2. University Of Oxford Centre for Clinical Magnetic Resonance Research, England, United Kingdom

3. University of Oxford, Oxford, England, United Kingdom

4. University of Oxford, England, United Kingdom

5. University of Oxford, United Kingdom

Background: Obesity is associated with paradoxically improved prognosis in a wide range of diseases, including heart failure and coronary disease, despite being associated with diminished myocardial energetic stores. It has been shown that reduced activity of the creatine kinase shuttle, involved in transfer of ATP from the mitochondrion to the myofibril, is related to increased clinical events and mortality. We have previously demonstrated that the creatine kinase rate constant (k_f^{CK}) is elevated in obesity in the absence of cardiovascular disease (fig 1) – we therefore hypothesise that the rate constant of the creatine kinase shuttle will also be raised in obese heart failure.

Methods: 34 individuals with dilated cardiomyopathy (DCM) and ejection fraction (EF) 25-45% were recruited from a tertiary referral centre. 10 of these were normal weight (BMI 18.5-25 kg/m^2) and the remainder obese (BMI>30kg/m^2). Volunteers underwent comprehensive metabolic and anthropomorphic assessment, as well as MR imaging (3T Siemens) of visceral fat at the level of L5, hepatic fat and inflammation, and cardiac structure and function. They also underwent Triple Repetition time Saturation Transfer (TRiST) 1D-CSI ^{31}P magnetic resonance spectroscopy, which was used to measure apical myocardial k_f^{CK}.

Results: The 24 obese DCM participants had significantly greater BMI (37±5 kg/m^2 as opposed to 22±3 kg/m^2, p<0.001) but in addition larger fat mass (46±14kg as opposed to 17±10kg, p<0.001), greater visceral fat (214±111cm^2 as opposed to 76±35cm^2, p=0.002) and greater liver fat (5.0±3.9% as opposed to 1.1±0.9%, p=0.01). There were no significant differences in LV EDV (obese 230±57ml, normal weight 248±108ml, p=0.51), mass (obese 165±39g, normal weight 164±52g, p=0.97) or ejection fraction (obese 41±8%, normal weight 36±5%, p=0.09). However, k_f^{CK} was significantly higher in the obese group compared to normal weight (0.17±0.08s^{-1} as opposed to 0.08±0.07s^{-1}, p=0.02; fig 1). k_f^{CK} was significantly correlated with visceral fat volume (r=0.428, p=0.029; fig 2), but not with ejection fraction (r=0.015, p=0.942).

Conclusion: Here we demonstrate that myocardial k_f^{CK} is higher in obese DCM, than a normal weight group with the same cardiac structural and functional features. This supports the hypothesis that obesity is associated with a compensatory mechanism to maintain ATP delivery. It has previously been shown that low k_f^{CK} are associated with heart failure and mortality. Demonstrating the reverse in obesity, we suggest that this may provide a completely novel energetic basis underlying the obesity paradox.

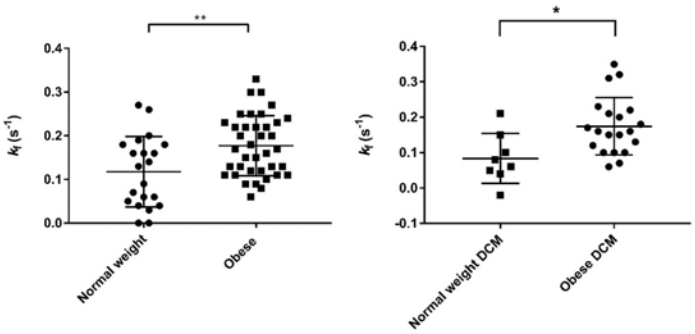

Figure 1 The obese DCM group has significantly higher creatine kinase forward rate constant (kf) than normal weight (R), in a similar pattern to that seen in normal heart (L). * p<0.05; ** p<0.01.

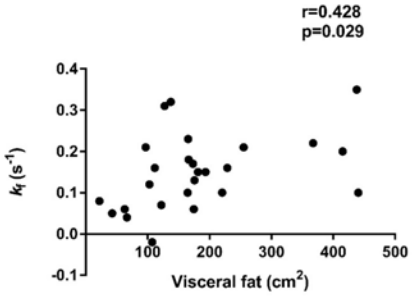

Figure 2 The forward rate constant of the creatine kinase reaction (kf) correlates with increasing visceral fat area.

ID#: 373034

CMR Longitudinal Strain Analysis in Aortic Stenosis

Nick B. Spath, BSc MD[1]Miquel Gomez, MD, PhD[2], Russell Everett, BSc MD[3], Scott I. Semple, MSc PhD[4], Calvin Chin, MD PhD[5], David E. Newby, MD PhD[4], Marc R. Dweck, MD PhD[1]

1. University of Edinburgh, Edinburgh, Scotland, United Kingdom

2. Hospital del Mar Medical Research Institute. Universitat Autònoma de Barcelona. Barcelona, Spain

3. University of Edinburgh, United Kingdom

4. University of Edinburgh, Scotland, United Kingdom

5. National Heart Center, N/A, Singapore

Background: There is interest in developing measures of myocardial health for patients with aortic stenosis in order to identify the early stages of left ventricular (LV) decompensation and optimise the timing of aortic valve replacement (AVR). We sought to investigate the relationship between longitudinal myocardial strain on cardiac magnetic resonance (CMR) and established markers of AS severity, LV remodelling and clinical outcomes.

Methods: CMR scans from 159 patients with aortic stenosis and 42 age and sex-matched controls were analysed using a commercially available strain analysis software package (CVI4.2®, Tissue Tracking Module, Circle Cardiovascular Imaging, Canada). LV endo-/epicardial diastolic contours were drawn in 2, 3 and 4-chamber long-axis, and all short-axis cine slices. After defining the RV insertion points, a fully automated strain analysis was performed to produce long-axis, short-axis and 3D strain calculations. Data for 2D and 3D LV global longitudinal strain (LVGLS) were used for analysis. Myocardial fibrosis was assessed using T1 mapping (indexed extracellular volume [iECV]) and late gadolinium enhancement (LGE). Mortality was assessed at a median of 1,466 days.

Results: Compared to control subjects, 2D LVGLS was unchanged in patients with mild or moderate AS but was lower in those with severe AS (P=0.015) and severe AS awaiting surgery (P=0.0024). Indeed substantial overlap in 2D LVGLS values was observed across the severity groups and only weak correlations were observed between2D LVGLS and echo parameters of stenosis severity (Vmax [P=0.005, r=0.244], mean gradient [Pr=0.248] and aortic valve area [P=0.020, r=-0.165]). Closer correlations were observed between 2D LVGLS and LV mass (r=0.428), iECV (r=0.420) and ejection fraction (r=-0.327 all P Kaplan-Meier plots did not demonstrate a difference in mortality between groups above and below the median 2D LVGLS. 3D LVGLS did not demonstrate significant association with any of the above measures.

Conclusion: 2D LVGLS measured on CMR is associated with disease severity and markers of LV decompensation in aortic stenosis. However substantial overlap in values between groups was observed and 2D LVGLS did not appear to predict clinical outcomes.

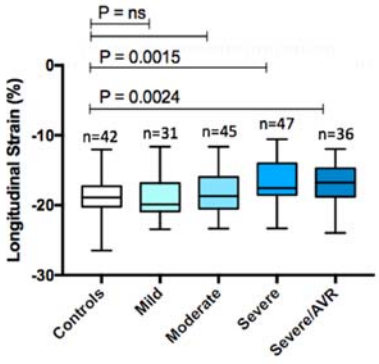

2D LVGLS vs AS Severity

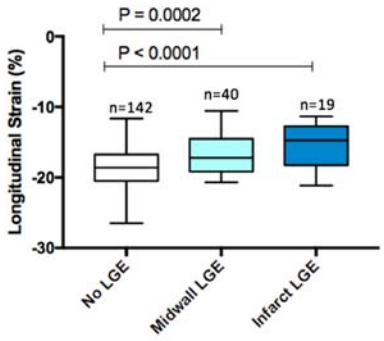

2D LVGLS vs LGE Distribution

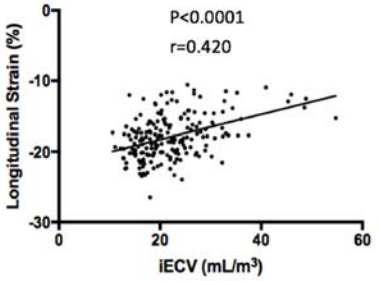

Correlation of 2D LVGLS vs iECV

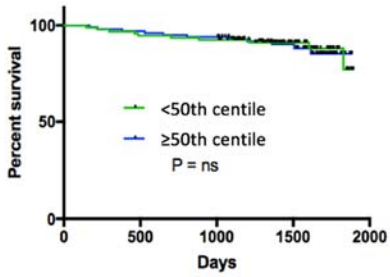

Survival by median 2D LVGLS

ID#: 372938

Prognosis and Cardiac function Outcome in Spontaneous Coronary Artery Dissection; SCAD UK study

Ahmed M.S.E.K. Abdelaty, University of Leicester[1] Abtehale Al-Hussaini[2], Jayanth Arnold, BMBCh DPhil[3], Gerry p. McCann, MB ChB, MD[3]

1. University of Leicester, UK, United Kingdom

2. University of Leicester, England, United Kingdom

3. Department of Cardiovascular Sciences and NIHR Biomedical Research Centre, Glenfield Hospital, Leicester, England, United Kingdom

Background: Spontaneous coronary artery dissection (SCAD) is an unusual though increasingly recognized cause of acute coronary syndrome mainly in young women, in the absence of conventional cardiac risk factors. The pathophysiology and prognosis remains poorly understood with controversy regarding the optimal management of SCAD. Aim

In this study, we report a large CMR series illustrating outcomes and prognosis including LV assessment in SCAD patients.

Methods: We recruited 174 SCAD patients and 52 age and gender matched control cases from the SCAD- UK research registry for the deep Phenotyping study. In this case series, the clinical and index case (SCAD) details were verified by examining clinical notes and angiographic data to confirm the diagnosis.
Patients and controls underwent a Cardiac MRI and peripheral arterial MR-angiography using our dedicated 3T cardiovascular scanner for a detailed assessment of LV function, LGE, and remote arteriopathies. Pulse wave velocity and aortic compliance were assessed using semiautomatic aortic tracking. Cardiac images include HASTE and localiser sequence, CINE images using TRUFISP, CINE SAX. Delayed contrast imaging was acquired following an MRA of the aorta.

Results: The mean age of SCAD 46.6 +/-6.4 vs Control 44.3 +/-7 years, with predominantly female cases (97%). The follow up median time for SCAD patients is 5.7 years. 30% presented with STEMI, 70%NSTEMI, 9.7 % of which were postpartum SCAD. Angiographic Characterisation of SCAD in this MRI series includes 4. 5% had Type I scad, 48.2% Type IIA, 28% Type IIB, 10.3% TYPE III, 9% with type V SCAD. 16.6% had multivessel SCAD and 13.7 % had recurrence. Mean EF (Ejection Fraction) in SCAD patients is 58.07%+/-7.85 vs 61.07%+/-6.783 in Controls (P 0.0136) The mean EF in conservative therapy 58.21%+/- 7.119, PCI, 55.42%+/- 6.578, CABG 51.44%+/- 9.44. One way Anova statistical comparison demonstrated no significance difference in EF amongst all therapy arms: conservative vs PCI (P 0.1187), Conservative VS CABG (0.0113), PCI VS CABG (P0.3044). There is no significant difference in mean EF between conservative and control group, though there was significance in mean EF between PCI and CABG group in comparison to control (PCI vs HV 0.0008), (CABG vs HV 0.0002).

Conclusion: SCAD remains to be under diagnosed with urgent need for guidelines for best management. This is the largest series of SCAD Cardiac MRI which demonstrates good functional outcome suggestive of good prognosis with preserved LV function in SCAD patients. This study also provides insight in to the difference in outcomes depending on the management of SCAD. Our study is suggestive of potential importance of minimal therapy where possible in Acute SCAD and provides consensus for conservative management of SCAD.

Table 1, CMR characterisation in SCAD

Characteristics	SCAD (N 174)	Control (N52)	P
Age (yrs)	46.6 +/-6.4	44.3 +/-7	0.3832 ns
Gender	97% Female	96%	

	3% Male	4%	
Ethnicity Caucasian Asian Afro-Caribbean	 97.14% (n165) 1.72% (3) 1.14% (2)	 94.2% (49) 3.84% (2) 1.92% (1)	
Cardiovascular Risk factors HTN Smoker Previous Smoker Current Smoker Diabetes	9% 10% 0% 2% 0%	1% 8% 0% 0% 0%	
LV EF % Conservative Therapy EF % PCI Therapy EF %	 58.07+/-7.485 58.21 +/-7.119	61.07+/-6.873	P 0.0136 Conservative vs PCI P 0.1187 Conservative vs.CABG P0.0113 Conservative vs. HV P0.1192 PCI vs. CABG P 0.3044 PCI vs. HV P0.0008 CABG vs. HV P 0.0002

CABG Therapy	55.42+/-6.578 51.44+/-9.44		
LVEDV(BSA)	85.24+/- 14.07	78+/-12.06	P 0.0009
LVESV(BSA)	37.3+/-11.1	32.1+/-7.4	P 0.0003
Myocardial Mass (BSA)	42+/-6.789	40.91+/-6.979	P 0.3485

ID#: 372145

Gadolinium-free Cardiac MRI Stress T1-mapping accurately diagnoses and differentiates between obstructive epicardial coronary artery disease and microvascular dysfunction

Alexander Liu, MBBS BSc[1] Rohan S. Wijesurendra, MB BChir, MRCP[1], Joanna M. Liu, MBBS MRCP[2], Andreas Greiser, Ph.D[3], Michael Jerosch-Herold, PhD[4], John C Forfar[5], Keith M. Channon, MD, FRCP[6], Stefan K. Piechnik, PhD, MScEE[6], Stefan Neubauer, MD, FRCP[6], Rajesh K. Kharbanda, MBChB, PhD[7], Vanessa M. Ferreira, MD, DPhil[6]

1. University of Oxford, Oxford, England, United Kingdom

2. University of Oxford, United Kingdom

3. Siemens Healthcare GmbH, Erlangen, Germany, Erlangen, Bayern, Germany

4. Harvard Medical School, Boston, MA

5. John Radcliffe Hospital, United Kingdom

6. University of Oxford, England, United Kingdom

7. Oxford Heart Centre, England, United Kingdom

Background: In patients with angina, accurate assessment of myocardial ischemia is important for clinical decision-making. No single non-invasive test exists that can accurately diagnose and distinguish between obstructive epicardial coronary artery disease (CAD) and coronary microvascular dysfunction (CMD). Cardiac magnetic resonance (CMR) adenosine stress T1-mapping can detect ischemia non-invasively without contrast agents. We performed the first prospective validation of stress T1-mapping against invasive coronary measurements for detecting obstructive epicardial CAD, defined by Fractional Flow Reserve (FFR<0.8), and CMD, defined by FFR≥0.8 and Index of Microcirculatory Resistance (IMR≥25U).

Methods: 90 subjects (60 patients with angina; 30 healthy controls) underwent CMR (1.5/3 Tesla; Siemens Healthcare, Erlangen, Germany) to assess LV function (cine), ischemia (adenosine stress/rest T1-mapping using a prototype and perfusion imaging) and infarction (late gadolinium enhancement). Patient FFR and IMR were assessed

Results: Normal myocardial stress T1 response (ΔT1) is 6.2±0.4% at 1.5-Tesla and 6.2±1.3% at 3-Tesla. Ischemic myocardium downstream of obstructive (FFR<0.8) epicardial CAD had almost no stress T1 response (ΔT1 0.7±0.7%). Myocardium downstream of non-obstructive (FFR≥0.8) coronary arteries with microvascular dysfunction (IMR≥25U) had a less-blunted stress T1 response (ΔT1 3.0±0.9%). On ROC analysis, a stress ΔT1 threshold of 1.5% accurately detected obstructive epicardial CAD (AUC: 0.97±0.02, p<0.001, sensitivity 93%, specificity 95%), while a less-blunted stress ΔT1 threshold of 4.0% accurately detected coronary microvascular dysfunction (AUC: 0.95±0.03, p<0.001, sensitivity 94%, specificity 94%, see Figure 1 for synopsis). Stress T1-mapping had superior diagnostic performance than gadolinium-based first-pass perfusion by visual analysis (AUC 0.85±0.04, p<0.001), semi-quantitative analysis (AUC 0.87±0.04, p<0.001) and absolute quantification of myocardial blood flow (AUC=0.91±0.03; p<0.001) for detecting obstructive epicardial CAD, all comparisons p<0.01.

Conclusion: This study is the first to show that CMR stress T1-mapping accurately detects and differentiates between obstructive epicardial CAD and CMD, without contrast agents - unparalleled by any existing non-invasive clinical tests. Stress T1-mapping can potentially become a new reference-standard non-invasive ischemia test.

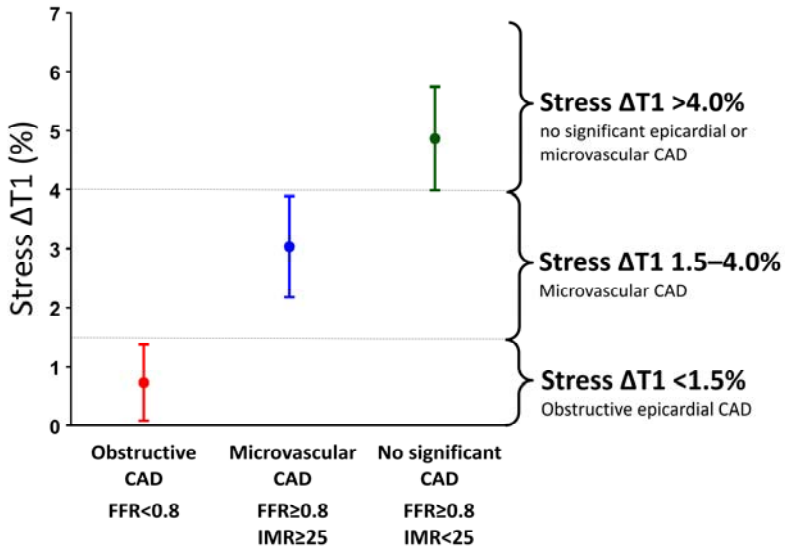

Figure 1: Detection and differentiation between epicardial and microvascular coronary artery disease (CAD) using gadolinium-free stress T1-mapping (ΔT1). Data are mean ± SD.

ID#: 371674

Hemodynamic flow changes in bicuspid aortic valve aortopathy are stable over time

Malenka Bissell, Md, DPhil[1] Aaron T. Hess, PhD[2], Margaret Loudon, DPhil[1], Victoria Stoll, DPhil, BMBCh[3], Stefan Neubauer, MD, FRCP[4], Saul Myerson, MD, FRCP[5]

1. Oxford University, United Kingdom

2. OCMR, University of Oxford, England, United Kingdom

3. University of Birmingham, Birmingham, England, United Kingdom

4. University of Oxford, England, United Kingdom

5. University of Oxford, Oxford, England, United Kingdom

Background: Hemodynamic flow changes likely contribute to aortic dilation in bicuspid aortic valve disease. To date follow-up data is limited. We therefore sought to examine flow changes in bicuspid aortic valve disease over time.

Methods: 100 bicuspid aortic valve participants underwent initial 4D flow CMR assessment. We performed a follow-up CMR scan 3 years after the initial visit in those without aortic valve intervention or other reasons to avoid CMR. The datasets were analysed using established 4D flow CMR analysis methods.

Results: 64 of the initial 100 patients were available for follow-up. The 36 who did not have a repeat scan were due to: aortic valve ± ascending aortic replacement/repair (19), endocarditis death (1), MRI contraindications at follow-up (2); declined follow-up (12) and lost to follow-up (2). Age range at initial study visit was 8-69 years. The 64 participants who returned for follow up showed a mean mid-ascending aortic growth rate of 0.31mm/year (range 0-1.7mm/year). There was no difference in growth rate between the pre-defined flow patterns of normal flow, right-handed helical flow and complex flow (p=0.78). There was also no significant progression of flow angle, flow displacement, or wall shear stress (p>0.05). 67% (4/6) patients with a left-handed flow pattern underwent AVR or aortic repair, compared to 19% (14/73) in the right-handed flow group. 15/64 (23%) participants had an aortic growth rate > 0.5mm/year. In this group progression of haemodynamic flow abnormalities was minimal: Peak velocity 2.4±0.6 m/s vs 2.4±0.6 m/s; flow angle 20±8 degree vs 20±11 degree; normalised flow displacement 0.139±0.063 vs 0.144±0.51; wall shear stress 0.88±0.28 vs 0.96±0.40 N/m2. Rotational flow values significantly increased in this population (29.8±11.7 vs 37.7±13.8 mm2/ms; p=0.017). Interestingly, these values also significantly increased in the significantly younger normal flow group (7.5±3.8 vs 18.4±7.6 mm2/ms; p=0.003).

Conclusion: This is the first large prospective longitudinal follow-up study using 4D flow CMR. The findings show overall slow progression of aortic size over 3 years, and hence, longer follow-up will be needed to fully assess the capability of 4D flow parameters for predicting outcomes (e.g. aortic dilation). A high proportion of participants with a left-handed flow profile underwent aortic valve and/or ascending aortic surgery, which raises the possibility that left handed helical flow may be a predictor of intervention, but numbers are very small in this study. While the degree of aortic valve stenosis and the majority of 4D flow CMR parameters remained largely stable, we observed an increase in rotational flow. Whether the rotational flow contributes to disease progression over time requires further study.

ID#: 371355

Selective heart rate inhibition optimizes exercise haemodynamics and energetic efficiency of the single ventricle in patients with Fontan circulation

Bram Ruijsink, MD[1]Phuoc Duong, MD[2], Mari Nieves Velasco Forte, MD[3], Esther Puyol Anton[4], Kuberan Pushparajah, MD[5], Alessandra Frigiola, MD, PhD[6], David Nordsletten, PhD[1], Reza Razavi, MD, PhD[1]

1. King's College London, London, England, United Kingdom

2. King's College London, United Kingdom

3. Kings College London, England, United Kingdom

4. King's College London, England, United Kingdom

5. Kings College London and Guy's & St Thomas' Hospital NHS Foundation Trust, Evelina London Children's Hospital, England, United Kingdom

6. Guys and St Thomas Hospital NHS Foundation Trust, England, United Kingdom

Background: The Fontan circulation is burdened with progressive decrease of cardiac performance leading to a high incidence of heart failure. This failure originates from inefficient haemodynamics rather than ischaemic burden. Previous physiological and computational modelling experiments suggest that in the biventricular heart, regulation of LV filling by the sub-pulmonary RV is a key factor in optimization of energy efficiency of cardiac output (CO) during exercise. In Fontan patients, this regulation of ventricular filling is severely impaired. Heart rate (HR) increases during stress result in a progressive fall in EDV and blunted CO response. We propose that the inability to regulate LV filling in Fontan patients during stress results in suboptimal CO augmentation and excessive energetic costs of contraction at increased HRs. Using Exercise CMR and a patient-specific biomechanical model of the heart, we explore this hypothesis and evaluate the potential role selective HR-inhibition in optimization of stress-haemodynamics in patients with a Fontan circulation.

Methods: 10 adult Fontan patients without a fenestration or significant collateral flow underwent two Exercise-CMR scans with identical workload and exercise time; one native test and one after administration of a selective HR inhibitor, ivabradine (HRi-test). Exercise data was obtained using real time imaging as previously described by La Gerche et al., Circulation CVI 2013. HR, cardiac volumes and function (EDV, ESV, SV, EF) were assessed at rest, moderate and high intensity exercise. Patient-specific exercise levels (cycle ergometer wattage) were determined based on a previous maximal cardiopulmonary exercise test results.

Results: Table 1, figures 1 and 2 describe the results the exercise tests. During exercise, ventricular filling falls with increasing HRs in patients with Fontan Circulation, resulting in a decrease in EDV (mean effect rest - high: -12±3% EDV, p<.01). This caused a drop in SV (mean effect rest - high: -9±4% SV, p<.01), leading to a blunted peak CO (peak-CO = 5.3±1 L/min). Selective HR-inhibition partly reverted the fall in EDV between the two tests (Mean effect +5±2% EDV, p<.01), resulting in increased SV (Mean effect -10±2%, p<.01). As a consequence, CO was mildly increased in the HRi test (Mean effect +5±2% CO, p<.01) despite the significantly lower HR (Mean effect -7±3%, p<.01). By investigating the observed changes using the biomechanical model, we can show that HRi reduces the cost of contraction (total active tension / beat) compared to the native situation, as the ventricle operates at more efficient EDV and ESV and better utilizes the Frank-Starling mechanism.

Conclusion: The absence of a sub-pulmonary ventricle in Fontan patients results in an inadequate haemodynamic response to stress in the Fontan circulation, leading to a sub-optimal CO response at high energetic costs. Selective HR-inhibition improves CO and energetic efficiency of the single ventricle during stress and therefore might be considered as a potential new treatment strategy in Fontan patients.

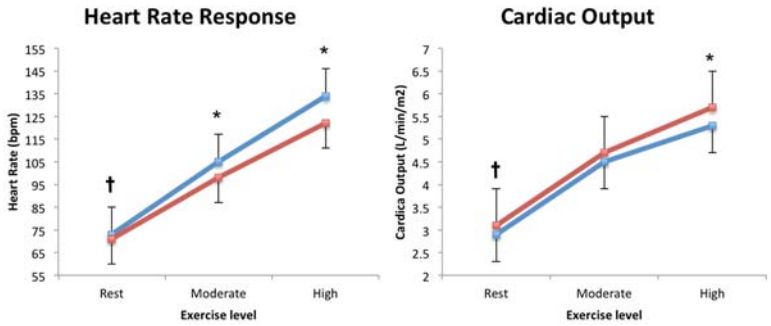

Effect of HR inhibition on exercise heart rate and cardiac output. Blue line represents native exercise MRI. Red line is the HR-inhibited test. All values are means±SD. An asterix means a significant difference at the corresponding exercise level between the native and HR-inhibited tests. A Dagger means a significant increase in baseline response from rest - high exercise. A) Heart rate response B) Cardiac Output response.

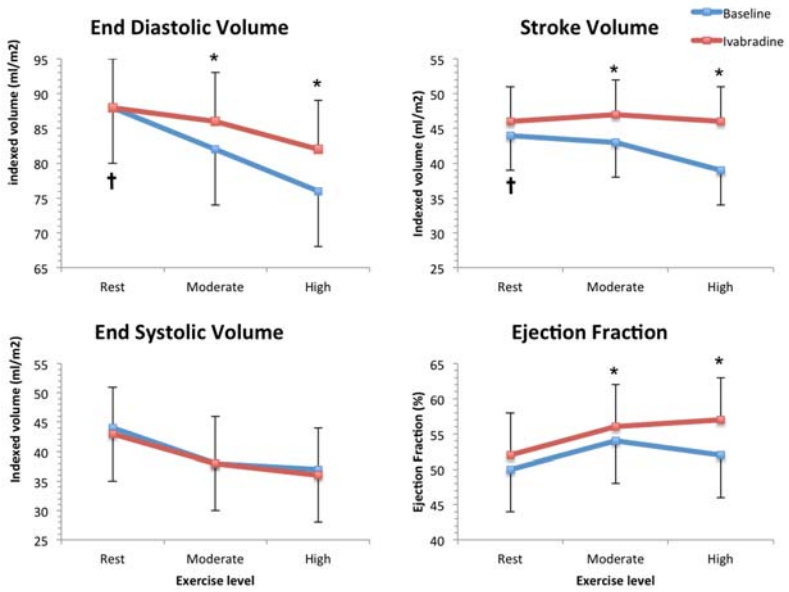

Effect of HR inhibition on cardiac function during exercise. Blue line represents native exercise MRI. Red line is after administration of ivabradine. All values are means±SD. An asterix means a significant difference before and after Ivabradine. A Dagger means a significant increase in baseline response from rest - high exercise. A) Indexed End Diastolic Volume, B) indexed End Systolic Volume, C) Stroke Volume, D) Ejection Fraction.

Heart Rate, Cardiac Output and Cardiac Volume response to exercise, before (native test) and after administration of ivabradine (HR-i test) in 10 patients with Fontan circulation. All values are means±SD. P-values express the significance of the mean effect of the native and Ivabradine exercise values (two-way repeated ANOVA). * Represents a significant difference (p<.05) at the corresponding exercise level from between the native and HRi-test.

	Native test			**HR-i test**			
	Rest	Moderate	High	Rest	Moderate	High	*p*-value
Heart Rate (beats per minute)	73±15	105±11	134±13	71±14	98±11*	122±12*	<.01
Cardiac Output (L/min/m^2)	2.9±0.4	4.5±0.7	5.3±0.9	3.1±0.5	4.7±0.8	5.7±0.9*	0.02

Single Ventricle (indexed)							
End Diastolic Volume (ml/m^2)	88±10	82±8	76±9	88±9	86±9*	82±9*	<.01
End Systolic Volume (ml/m^2)	44±9	38±9	37±9	43±9	38±9	36±10	0.17
Stroke Volume (ml/m^2)	44±6	43±5	39±4	46±5	47±5*	46±4*	<.01
Ejection Fraction (%)	50±5	54±6	52±7	52±5	56±7*	57±7*	<.01

ID#: 371395

Fully Quantitative Cardiac Magnetic Resonance Myocardial Perfusion Ready for Clinical Use: A comparison between Magnetic Resonance Imaging and Positron Emission Tomography

Henrik Engblom, MD, PhD[1] Hui Xue, PhD[2], Marcus Carlsson, MD, PhD[3], Cecilia Hindorf, PhD[4], Jenny Oddstig, PhD[4], Fredrik Hedeer, MD[5], Michael Hansen, PhD[6], Anthony H. Aletras, Ph.D.[7], Peter Kellman, PhD[8], Håkan Arheden, MD PhD[9]

1. Lund University, Skane University Hospital, Department of Clinical Sciences Lund, Clinical Physiology, Lund, Sweden, Lund, Sweden

2. National Heart, Lung, and Blood Institute, Bethesda, MD

3. Lund University, Skane University Hospital, Department of Clinical Sciences Lund, Clinical Physiology, Lund, Sweden, Skane Lan, Sweden

4. Skane University Hospital, Lund, Skane Lan, Sweden

5. Lund University, Skane Univeristy Hospital, Lund, Skane Lan, Sweden

6. National Heart, Lung, and Blood Institute, Bathesda, MD

7. Aristotle University of Thessaloniki/Lund University, Thessaloniki, Thessaloniki, Greece

8. National Heart, Lung, and Blood Institute, National Institutes of Health, Bethesda, MD

9. Lund University, Skåne University Hospital, Department of Clinical Sciences Lund, Clinical Physiology, Lund, Sweden, Lund, Sweden

Background: Recent studies have shown that quantification of myocardial perfusion (MP) at stress and myocardial perfusion reserve (MPR) offer additional diagnostic and prognostic information compared to qualitative and semi-quantitative assessment of myocardial perfusion distribution in patients with coronary artery disease (CAD). Technical advancements have enabled fully automatic quantification of MP using cardiac magnetic resonance (CMR) to be performed in-line in a clinical workflow. The aim of this study was to validate the use of the automated CMR perfusion mapping technique for quantification of MP using 13N-NH3 cardiac positron emission tomography (PET) as the reference method.

Methods: Twenty-one patients with stable CAD were included in the study. All patients underwent adenosine stress and rest perfusion imaging with 13N-NH3 PET and a dual sequence, single contrast bolus CMR on the same day. All patients had a coronary angiography performed within a month of the CMR exam. Global and regional MP were quantified both at stress and rest using PET and CMR.

Results: There was good agreement between global MP quantified by PET and CMR both at stress (-0.1±0.5 ml/min/g) and at rest (0±0.2 ml/min/g) with a strong correlation ($r=0.92$, $p<0.001$; $y=0.94x+0.14$, Figure 1). Furthermore, there was strong correlation between CMR and PET with regards to regional MP ($r=0.83$, $p<0.001$; $y=0.87x+0.26$) with a good agreement (-0.1±0.6 ml/min/g). There was also a significant correlation between CMR and PET with regard to global and regional MPR ($r=0.69$, $p=0.001$ and $r=0.57$, $p<0.001$, respectively).

Conclusion: There is good agreement between MP quantified by 13N-NH3 PET and dual sequence, single contrast bolus CMR in patients with stable CAD. Thus, CMR is viable in clinical practice for quantification of MP.

Figure 1

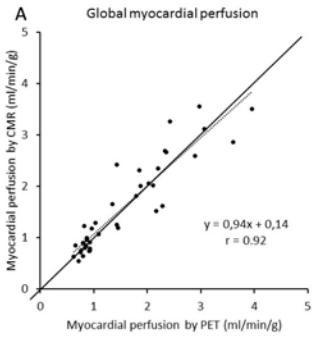
A
Global myocardial perfusion
Myocardial perfusion by CMR (ml/min/g)
Myocardial perfusion by PET (ml/min/g)
y = 0,94x + 0,14
r = 0.92
0
1
2
3
4
5

ID#: 367224

Gender Difference in Response to Adenosine Stress Perfusion CMR

Louise AE. Brown, MBChB, BMedSc[1] Sebastian C. Onciul[1], David A. Broadbent, MSc[2], Graham J. Fent, MBChB, BSc[3], James R. Foley, MBChB BSc (Hons)[3], Pankaj Garg, MD, PhD[4], Pei G. Chew, MBChB(Hons) [5], Kristopher D. Knott, MBBS MA[6], Peter P. Swoboda, PhD[3], Erica Dall'Armellina, Sr., MD, DPhil[7], Hui Xue, PhD[8], John P. Greenwood, PhD[1], James C. Moon, MD[9], Peter Kellman, Ph.D.[8], Sven Plein, MD PhD[1]

1. University of Leeds, England, United Kingdom

2. Leeds Teaching Hospitals NHS Trust, England, United Kingdom

3. University of Leeds, Leeds, England, United Kingdom

4. University of Leeds, UK, Leeds, England, United Kingdom

5. University of Leeds, Liverpool, England, United Kingdom

6. University College London, London, England, United Kingdom

7. Leeds Institute of Cardiovascular and Metabolic Medicine, Division of Biomedical Imaging,University of Leeds, United Kingdom

8. National Heart, Lung, and Blood Institute, Bethesda, MD

9. Barts Heart Centre, England, United Kingdom

Background: Gender differences in myocardial blood flow (MBF) have been reported in previous studies, predominantly using PET. Multiple studies have shown higher resting MBF in women, attributed to higher cardiac work at rest. However, these findings are not consistent over all studies, and changes in both rate-pressure product (RPP) -corrected rest and hyperaemic MBF have also been reported. Free-breathing motion corrected CMR methods with in-line MBF quantification have recently been reported and are expected to rapidly increase the use of quantitative perfusion CMR. Knowledge of CMR specific normal values is therefore important. Our aim was to examine the difference in resting and stress MBF between genders using quantitative perfusion CMR.

Methods: 50 healthy volunteers (21 male) attended for stress CMR with perfusion mapping. First pass myocardial perfusion CMR data were acquired, using adenosine pharmacological stress. Stress and rest perfusion images were acquired. MBF was calculated globally for the left ventricle from automatically generated quantitative maps. Myocardial perfusion reserve (MPR) was calculated as stress MBF/rest MBF. Correlations of MBF with RPP, blood pressure (BP) and heart rate (HR) were analysed, and flows corrected for these.

Results: There was no significant difference in age between the groups (Table 1). Resting MBF correlated with RPP (r=0.3, p=0.03), and resting heart rate (r=0.5, p= *Haemodynamics* There was no significant difference in resting HR between genders. Females had a lower systolic BP, however the change with stress was not significantly different between groups (3% increase). Both groups showed a significant increase in HR to adenosine infusion. The HR increase in females was significantly higher than in males (53% vs 37%). *Myocardial blood flow* Uncorrected MBF was significantly higher in females both at stress and rest. MPR was lower in females. (Figure 1a-c) Following correction for RPP, resting MBF remained significantly, higher in females (Fig 1d). After correction for heart rate, there was no longer a significant difference in hyperaemic flow (Fig 1e). The difference in MPR between genders was accentuated when calculated using HR corrected values (Fig 1f).

Conclusion:

- Women exhibit a greater haemodynamic response to pharmacological stress and this appears to be the main driver for difference in hyperaemic blood flow.
- The gender difference in MBF and MPR appears largely driven by the higher resting flows in females.
- Uncorrected MBF values are significantly different between genders both at stress and rest, with important implications in the interpretation of normal values.

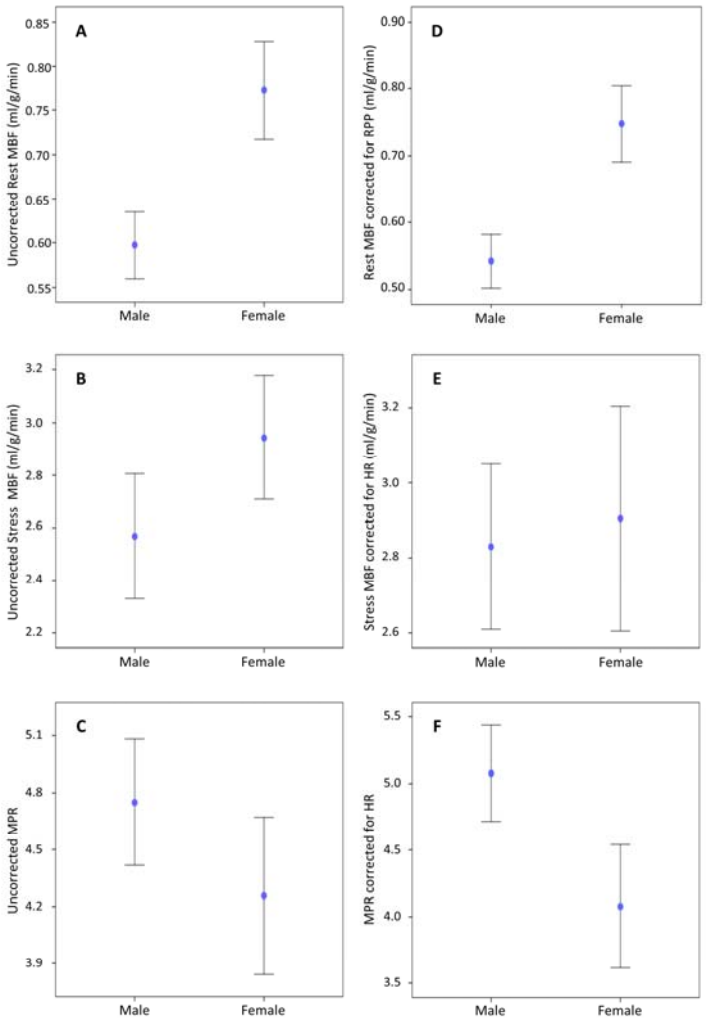

Figure 1 - Gender differences in whole heart mean: A) rest MBF, B) stress MBF, C) MPR, D) rest MBF corrected for RPP, E) stress MBF corrected for HR, F) MPR corrected for HR, Error bars – 95% CI of mean

Table 1 -

	Male		Female		
	Mean	SD	Mean	SD	p
Age	30.1	±15.6	27.6	±10.7	0.744
Resting HR	63.3	±9.0	64.2	±7.9	0.702
Stress HR	86.4	±14.3	98.0	±14.8	0.008**
% HR change	37	±18.7	53.4	±22.2	0.014*

Rest sBP	115.1	±11.9	108.5	±8.8	0.028*
Stress sBP	118.5	±13.3	111.6	±10.4	0.014*
% sBP change	2.9	±3.9	3.0	±7.2	0.94
Rest RPP	7324	±1526	6944	±1147	0.32
Stress RPP	10292	±2405	10959	±2076	0.30
% change in RPP	40.7	±20.8	59.1	±26.1	0.01*
Rest MBF	0.55	±0.08	0.72	±0.15	<0.001**
Stress MBF	2.57	±0.52	2.94	±0.62	0.028*
MPR	4.75	±0.73	4.26	±1.09	0.01*
Rest MBF (corrected for RPP)	0.54	±0.72	0.75	±0.15	<0.001**
Stress MBF (corrected for HR)	2.83	±0.52	2.90	±0.79	0.703
MPR (corrected for HR)	5.08	±0.73	4.08	±1.22	0.02*

sBP = systolic blood pressure. Significant at p=0.05, ** significant at p=0.01*

ID#: 364258

Factors limiting exercise in adults with transposition of the great arteries: an exercise cardiac magnetic resonance study

Frederik Helsen, MD[1] Piet Claus, MSc, PhD[2], Pieter De Meester, MD, PhD[3], Guido Claessen, MD, PhD[3], Alexander Van De Bruaene, MD, PhD[3], Charlien Gabriels, MD[4], Mathias Claeys, MD[5], Thibault Petit, MD[3], Els Troost, MD[4], Jens-Uwe Voigt, MD, PhD[4], Jan Bogaert, MD, PhD[5], Werner Budts, MD, PhD[4]

1. KU Leuven / University Hospitals Leuven, Vlaams-Brabant, Belgium

2. KU Leuven, Belgium

3. University Hospitals Leuven, Belgium

4. KU Leuven / University Hospitals Leuven, Belgium

5. KU Leuven / University Hospitals Leuven, Leuven, Vlaams-Brabant, Belgium

Background: Current understanding of exercise hemodynamics in patients with a systemic right ventricle (RV) is limited. Real-time cardiac magnetic resonance imaging during supine bicycle exercise (exCMR) could provide important physiological insights to guide future medical management. Our aims were to evaluate (1) differences between patients with complete transposition of the great arteries post atrial switch procedure (TGA-Mustard/Senning) and congenitally corrected TGA (ccTGA), and (2) differences between TGA-Mustard/Senning patients with a good vs. impaired peak oxygen consumption.

Methods: Thirty-three adults with a systemic RV (23 with TGA-Mustard/Senning and 10 with ccTGA) and recent cardiopulmonary exercise testing data underwent exCMR with simultaneous registration of radial arterial pressures. Heart rate reserve (HHR) was defined as the difference between peak exercise and resting HR. Right ventricular end-systolic pressure/volume relationship (RVESPVR), a surrogate of RV contractility, was calculated as 0.9 systolic blood pressure divided by RV end-systolic volume.

Results: Patients with TGA-Mustard/Senning were significantly younger than patients with ccTGA (34±7 years vs. 45±7 years, P<0.001) and had less severe tricuspid regurgitation on echocardiography (respectively mild/moderate/severe in 39 / 57 / 4 % vs. 10 / 50 / 40 %, P=0.020), whereas other baseline characteristics did not differ. The median percentage of predicted peak oxygen consumption (%ppVO2) was comparable between TGA-Mustard/Senning and ccTGA patients (70 [64 – 92] vs. 82 [61 – 88] %, P=0.875). During exercise, RV end-diastolic volume (EDVi) and stroke volume (SVi) of TGA-Mustard/Senning patients decreased linearly, whereas in ccTGA patients RVEDVi was stable and SVi increased. The HRR of ccTGA patients was lower (69±28 vs 90±18 bpm, P=0.014). The RVESPVR was comparable in both groups (Figure 1). The exercise response of the TGA-Mustard/Senning cohort with an impaired %ppVO2 (n=11, range 61 to 69%) differed from TGA-Mustard/Senning patients with a good %ppVO2 (n=12, range 70 to 105%) by a lower HRR (80±18 vs. 99±13 bpm, P=0.007) and a lower anaerobic threshold (42±9 vs. 60±12% of peak VO2, P<0.001). The decrease in RV EDVi and the increase in RVESPVR during exercise were comparable in both TGA-Mustard/Senning cohorts (Figure 2).

Conclusion: TGA-Mustard/Senning and ccTGA patients have different exercise hemodynamics. TGA-Mustard/Senning patients experience impaired ventricular filling during exercise, whereas ccTGA patients have a normal increase in stroke volume but a lower heart rate reserve. The difference between TGA-Mustard/Senning patients with a preserved versus an impaired peak oxygen consumption seems linked to diminished chronotropic competence and a lower physical fitness level.

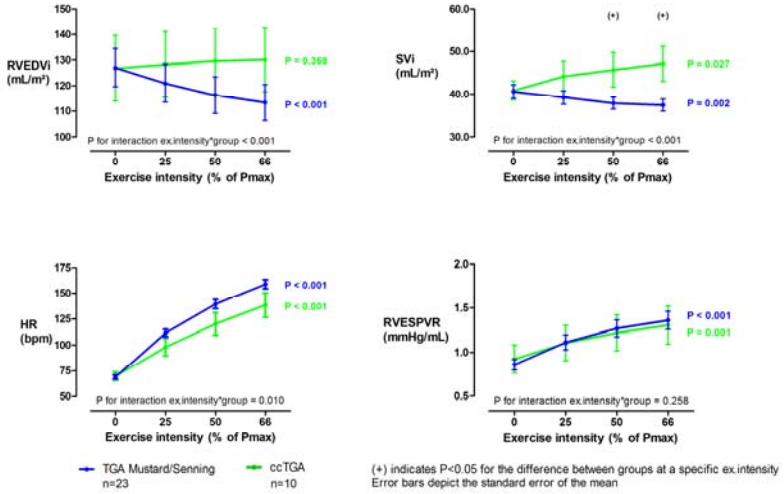

Figure 1: Changes during exercise in TGA-Mustard/Senning vs. ccTGA

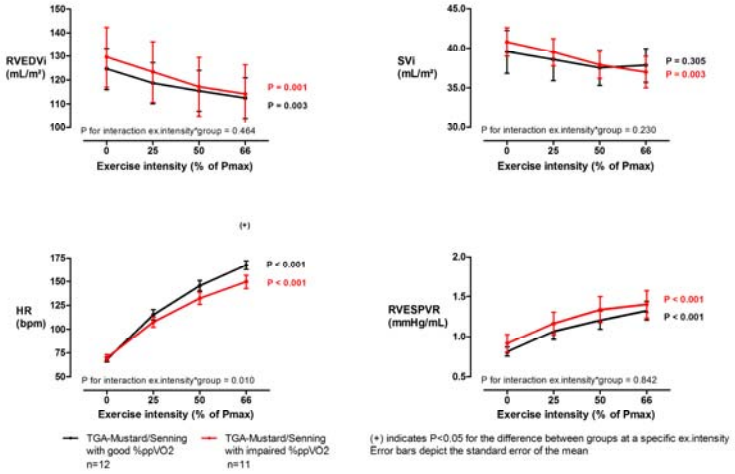

Figure 2: Changes during exercise in TGA-Mustard/Senning with good vs. impaired peak oxygen uptake

ID#: 364732

Ascending aortic wall shear stress in TGA patients after arterial switch operation in children and young adolescents

Roel LF. van der Palen, MD[1]Arno A.W. Roest, MD, PhD[2], Quirine S. Deurvorst[3], Pieter J. van den Boogaard, BSc[4], Lucia J.M. Kroft, MD[5], Nico A. Blom, MD, PhD[3], Hildo J. Lamb, MD, PhD[4], Jos J.M. Westenberg, PhD[5]

1. Division of Pediatric Cardiology, Department of Pediatrics, Leiden University Medical Center, Leiden, The Netherlands, Leiden, Zuid-Holland, Netherlands

2. Department of Pediatrics, Leiden University Medical Center, Leiden, The Netherlands, Zuid-Holland, Netherlands

3. Division of Pediatric Cardiology, Department of Pediatrics, Leiden University Medical Center, Leiden, The Netherlands, Zuid-Holland, Netherlands

4. Department of Radiology, Leiden University Medical Center, Leiden, The Netherlands, Zuid-Holland, Netherlands

5. Department of Radiology, Leiden University Medical Center, Leiden, The Netherlands, Leiden, Zuid-Holland, Netherlands

Background: Aortic root dilatation is an important complication seen in patients with transposition of the great arteries (TGA) after arterial switch operation (ASO). It is not well known how the altered geometry after ASO interact with aortic hemodynamics. During the ASO operation, the ascending aorta (AAo) is translocated to posterior and following the LeCompte procedure the main pulmonary artery runs in front of the AAo with the pulmonary bifurcation and pulmonary arteries embracing the AAo at the mid-AAo level. Wall shear stress (WSS), an hemodynamic parameter derived from 4D flow CMR, has been associated with vascular wall remodelling and may impact aortic dilatation [1]. The aim of this study was to evaluate ascending aortic WSS distribution in relation to post-ASO geometry using 4D flow CMR compared to a control cohort.

Methods: 28 pediatric patients (16.0±3.3 years) after ASO for simple TGA and 10 healthy volunteers (26.5±2.6 years) underwent an aortic 4D flow CMR and non-contrast enhanced 3D MR Angiography (NCE-MRA) on a 3.0 Tesla MRI scanner (Philips Healthcare). 4D flow CMR: retrospective ECG and respiratory navigator gating, spatial resolution=2.5x2.5x2.5mm3, temporal resolution=26.8-35.1ms, VENC=200cm/s, segmentation factor=2, SENSE=2.5 in anterior-posterior direction. NCE-MRA: Dixon sequence, respiratory navigator gating, resolution=2.5x2.5x2.5mm3, echo time/repetition time: 0.0-2.3/3.6-3.9ms). From 4D flow CMR, a peak systolic 3D aortic volume was automatically segmented using CAAS MR 4Dflow v1.1 software (Pie Medical Imaging BV) and was manually adapted where necessary. Three ascending neo-aortic segments of interest (proximal, mid and distal AAo) were determined from the 3D aortic segmentation by manually placing planes at anatomic landmarks along the AAo, indicating the segment borders (Fig 1.). Maximum 3D systolic WSS (WSSmax) and mean 3D systolic WSS (WSSmean) for three AAo segments were automatically determined (Fig 1.). 3D systolic WSS calculation was based on the algorithm previously described by Potters et al [2]. AAo diameters and Z-scores [3] were determined from NCE-MRA (Fig 1.).

Results: Baseline characteristics were comparable between TGA and healthy volunteers, except for age (Table 1). The proximal AAo diameter was significantly larger, whereas the mid-AAo diameter was significant smaller in TGA patients compared to healthy controls (Z-scores TGA vs healthy volunteers: aortic root: 4.98±2.04 vs 2.07±0.65, p<0.001; sino-tubular junction: 3.48±2.67 vs 1.38±1.30, p=0.010; mid-AAo: 0.31±3.06 vs 1.69±1.24, p=0.001). In TGA patients, segmental WSSmean and WSSmax was significantly lower in the dilated proximal AAo segment (WSSmean 1246±221 vs 1556±197 mPa, p<0.001; WSSmax 2776±509 vs 3607±491 mPa, p<0.001) compared to healthy volunteers; the distal AAo segment showed significant higher WSSmean and WSSmax values for TGA patients compared to healthy controls (WSSmean 1811±338 vs 1255±197 mPa, p<0.001; WSSmax 3664±962 vs 2631±631 mPa, p=0.003) (Table 2). The region of increased WSS visually corresponded with the location where the pulmonary bifurcation and branches embraces the AAo.

Conclusion: TGA-specific geometry related to the ASO, evidenced by neo-aortic root dilation and a sudden change in vessel diameter at mid-AAo level, leads to specific WSS distribution along the AAo in TGA patient which is different from that in healthy volunteers. Longitudinal follow-up studies are needed for correlation between changes in systolic WSS and progression of dilation and the consequence of the increased WSS at the distal AAo.
Acknowledgment: Grant supported by Netherlands Heart Foundation 2014T087. References 1. Guzzardi DG et al. Valve-Related Hemodynamics Mediate Human Bicuspid Aortopathy: Insights From Wall Shear Stress Mapping. J Am Coll Cardiol 2015; 66:892-900. 2. Potters, W.V., et al. Volumetric arterial wall shear stress calculation based on cine phase contrast MRI. J Magn Reson Imaging 2015; 41:505-16. 3. Kaiser T. et al. Normal values for aortic

diameters in children and adolescents--assessment in vivo by contrast-enhanced CMR-angiography. J Cardiovasc Magn Reson 2008; 10:56-63.

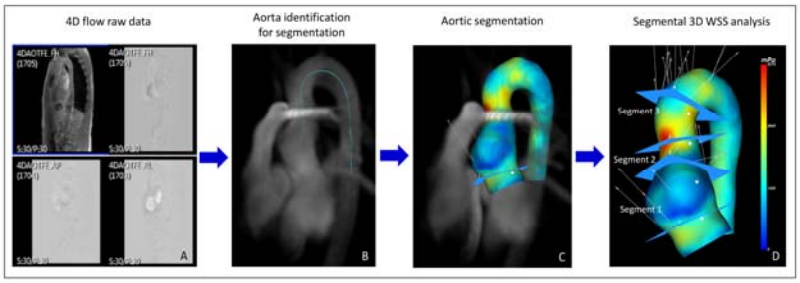

Figure 1. Aortic 4D flow CMR processing and analysis.

	TGA patients (n=28)	Healthy volunteers (n=10)	P-value
Patient and operative characteristics			
Male, n (%)	18 (63.4%)	5 (50.0%)	0.473
Age, years	16.0 ± 3.3	27.3 (24.9-28.4)	<0.001
Weight, kg	60.5 ± 14.0	68.3 ± 12.7	0.129
Height, cm	170.8 ±12.2	175.6 ± 6.6	0.250
Body Surface Area, m^2	1.7 ± 0.2	1.8 ± 0.2	0.137
LV ejection fraction, %	59.1 ± 5.7	62.0 ± 2.5	0.155
Transposition type, (%)			
TGA-IVS	21 (75.0%)		
TGA-VSD	7 (25.0%)		
Aortic diameters (mm)*			
Neo-aortic valve	23.0 [22.0-26.8]	19.5 [18.0-25.0]	0.010
Neo-aortic root, short axis, max	37.0 [33.3-41.0]	31.5 [29.0-33.3]	0.002
ST-junction	27.5 [24.0-32.0]	24.5 [23.8-27.3]	0.125
Mid ascending aorta	22.0 [21.0-24.0]	26.5 [25.0-29.3]	<0.001
Origin of BCT	22.0 [19.3-23.8]	23.5 [21.8-26.0]	0.056
Aortic Z-scores**			
Neo-aortic root, short axis, max	4.98 ± 2.04	2.07 ± 0.65	<0.001
ST-junction	3.48 ± 2.67	1.38 ± 1.30	0.010
Mid ascending aorta	0.32 ± 3.06	1.69 ± 1.24	0.001
Origin of BCT	-0.52 ± 1.21	0.20 ± 1.29	0.122

*Data are presented as median [Interquartile range]. **Data are presented as mean ±SD. Aortic Z-scores based on CMR derived normative data [2]. *Abbreviations:* ASO=arterial switch operation; BCT=brachiocephalic trunk; IVS=intact ventricular septum; LV=left ventricle; PA=pulmonary artery; TGA=transposition of the great arteries; VSD=ventricular septal defect

Table 2. Regional ascending aorta wall shear stress - per segment

	WSSmean (mPa)				WSSmax (mPa)		
	TGA patients	**Volunteers**	**P-value**		**TGA patients**	**Volunteers**	**P-value**
Proximal AAo	1246 ± 221	1556 ± 197	<0.001		2776 ± 509	3607 ± 491	<0.001
Mid AAo	1425 ± 271	1341 ± 325	0.427		3064 ± 638	2956 ± 545	0.636
Distal AAo	1811 ± 338	1255 ± 197	<0.001		3664 ± 962	2631 ± 631	0.003

Abbreviations: AAo=ascending aorta; TGA=transposition of the great arteries.

ID#: 366938

The relative contributions of myocardial perfusion, blood volume and extracellular volume to native T1 and native T2 at rest and during adenosine stress in normal physiology

Jannike Nickander, MD[1]Raquel Themudo, MD, PhD[2], Andreas Sigfridsson, PhD[3], Hui Xue, PhD[4], Peter Kellman, PhD[5], Martin Ugander, MD, PhD[6]

1. Karolinska Institutet, Stockholm, Stockholms Lan, Sweden

2. Karolinska Institutet, Stockholms Lan, Sweden

3. Karolinska Institute, Stockholm, Stockholms Lan, Sweden

4. National Heart, Lung, and Blood Institute, Bethesda, MD

5. National Heart, Lung, and Blood Institute, National Institutes of Health, Bethesda, MD

6. Karolinska Institutet, and Karolinska University Hospital, Stockholm, Sweden, Stockholms Lan, Sweden

Background: Both ischemic and non-ischemic heart disease can cause disturbances in the myocardial blood volume (MBV), myocardial perfusion and the myocardial extracellular volume fraction (ECV). Recent studies suggest that native myocardial T1 mapping can detect changes in MBV during adenosine stress, without the use of contrast agents. Furthermore, native T2 mapping could also potentially be used to quantify changes in perfusion and/or MBV. Therefore, the aim of this study was to explore the relative contributions of myocardial perfusion, MBV and ECV to native T1 and native T2 at rest and during adenosine stress in normal physiology.

Methods: Healthy volunteers (n=29, mean ± SD age 26 ± 5 years, 66% females) underwent 1.5T cardiovascular magnetic resonance imaging. Quantitative myocardial perfusion [ml/min/g] and MBV [%] maps were computed from first pass perfusion imaging at adenosine stress (140 microg/kg/min infusion) and rest following an intravenous contrast bolus (0.05 mmol/kg, gadobutrol). Native T1 and T2 maps were acquired before and during adenosine stress. T1 maps at rest and stress were also acquired following a 0.2 mmol/kg cumulative intravenous contrast dose, rendering rest and stress ECV maps [%]. T1, T2, perfusion, MBV and ECV values were measured by delineating a region of interest in the midmural third of the myocardium.

Results: During adenosine stress, there was an increase in myocardial native T1, native T2, perfusion, MBV, and ECV ($p \leq 0.001$ for all), Figure 1. Myocardial perfusion, MBV and ECV all correlated with both native T1 and native T2 at rest and stress, respectively (R^2 = 0.42 to 0.71, $p<0.001$ for all), Figure 2. Multivariate linear regression revealed that ECV and perfusion together best explained the change in native T2 (ECV beta 0.27, p=0.006; perfusion beta 0.69, $p<0.001$, model $R^2=0.75$, $p<0.01$), and native T1 (ECV beta 0.66, $p<0.001$; perfusion beta 0.38, $p<0.001$, model $R^2=0.84$, $p<0.001$).

Conclusion: Myocardial native T1, native T2, perfusion, MBV, and ECV all increase during adenosine stress. Changes in myocardial native T1 and T2 during adenosine stress in normal physiology can largely be explained by the combined changes in myocardial perfusion and ECV.

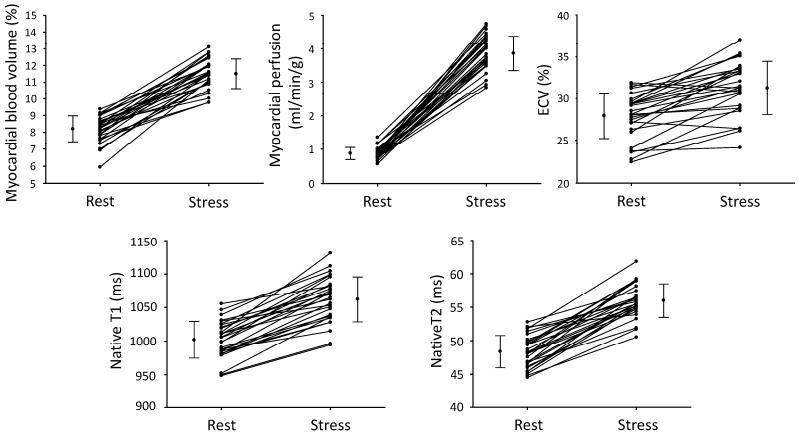

The change of myocardial blood volume, perfusion, ECV, native T1 and native T2 during adenosine stress

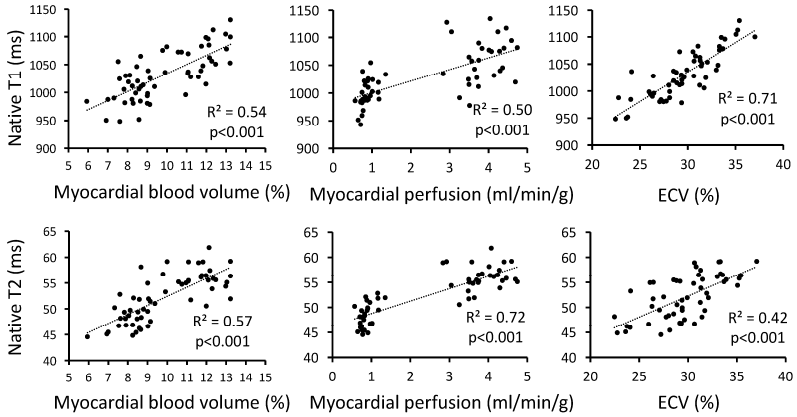

Correlations of myocardial blood volume, perfusion and ECV with native T1 and native T2, respectively.

ID#: 378206

Atlas based methods for understanding single ventricle pathologies

Kathleen Gilbert, BE(hons), PhD[1] Avan Suinesiaputra, PhD[2], Pau Medrano-Gracia, PhD[3], Nickolas Forsch, BS[4], James C. Perry, MD[5], Sanjeet R. Hegde, MD, PhD[5], Jeff Omens, PhD[6], Andrew D. McCulloch, PhD[6], Alistair Young, PhD[7]

1. University of Auckland, New Zealand, New Zealand

2. The University of Auckland, New Zealand, GRAFTON, Auckland, New Zealand

3. University of Auckland, Auckland, New Zealand

4. UC San Diego, San Diego, CA

5. UC San Diego/Rady Children's Hospital, San Diego, CA

6. UC San Diego, La Jolla, CA

7. University of Auckland, New Zealand, GRAFTON, Auckland, New Zealand

Background: Single ventricle pathologies account for 1-3% of all congenital heart defects in live-born children [1]. A recent study found the adult population with single ventricle pathologies is expected to grow by 60% in the next 10 years [2]. The Fontan registry has reported 42% of the recorded deaths were patients aged 20-30 [1]. We have modelled the ventricles of 76 cases from this cohort and created atlases to understand the variations in shape.

Methods: 76 cases were acquired from the cardiac atlas project which were listed as having undergone a Fontan procedure or having a condition which was a single ventricle physiology. 3D+time models were fitted of the dominant ventricle in each case using CIM (*Cardiac Image Modeller v8.1.6, Auckland, NZ)*. Expert cardiologists categorised each case as an anatomical LV or RV. The models underwent Procrustes alignment [3] and principal component analysis to evaluate the modes of variation in shape and function. Atlases were created for the ED shape, ES shape and the ES-ED shape differences, representing LV wall displacement. One-way ANOVA was used to assess the first 5 modes in each atlas and functional measures against the anatomic ventricle type. P-values<0.001 were considered to be significant.

Results: The ED atlas was able to explain 88% of the variation in the dataset in the first 10 modes, the ES 87% and the ES-ED difference 76%. The average shapes for the 42 systemic LV and 34 systemic RV were extracted from the atlases and are shown in Figure 1. The systemic RV';s were more spherical than the systemic LVs and had a different orientation of the inlet. Significant differences were found in shape between systemic LVs and systemic RVs between ES and ED (i.e. systolic differences added to the mean ED shape, Figure 2). The differences in the mode shows systemic LVs contracting more than systemic RVs in a regional fashion, with more motion along the lateral wall. This was also reflected in a significantly different EF, 49.9±6.8% for systemic LV and 38.2±8.6% for systemic RV.

Conclusion: Atlases of single ventricle patients add a powerful comparative tool to existing clinical information, and enable visualised regional differences in function between systemic RV and LV single ventricle pathologies.
References: 1. **Iyengar et al**.Intern Med J,44:148–155 2. **Coats et al**.Heart 2014;100:1348-1353. 3. **Medrano-Gracia et al**.JCMR,2014;16:56.

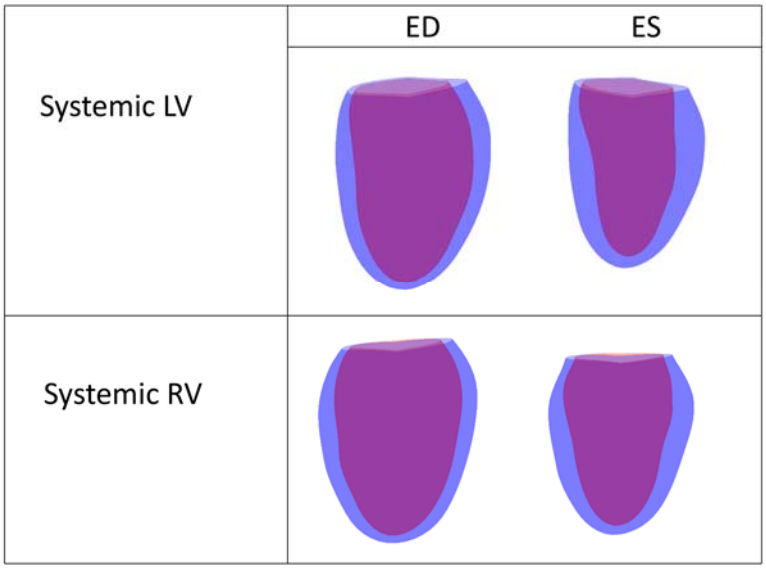

Average shapes of systemic LV and systemic RV at ED and ES

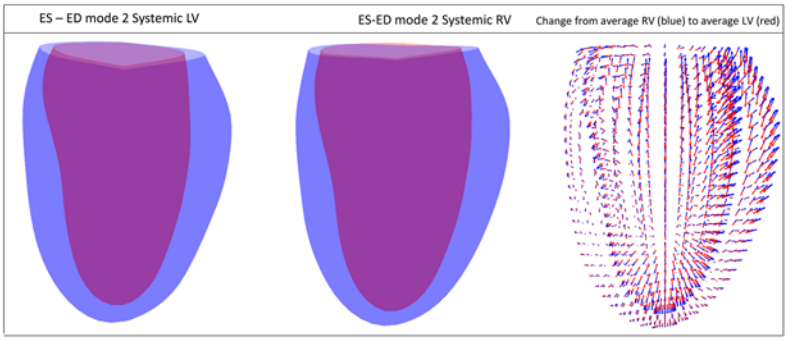

Average shape for systemic LVs, systemic RVs and the differences between them in EDES mode 2

ID#: 378394

MRI DENSE Strain Predicts Long-Term Survival and ICD Therapies with CRT Defibrillators

Kenneth C. Bilchick, MD, MS[1]Daniel A. Auger, PhD[1], Soham Shah, BS[2], Xiaoying Cai, BS[3], Rohit Malhotra, MD[2], Andrew Darby, MD[2], Michael Mangrum, MD[2], Pamela Mason, MD[1], John Ferguson, MD[2], Christopher M. Kramer, MD[1], Frederick H. Epstein, PhD[1]

1. University of Virginia Health System, Charlottesville, VA

2. University of Virginia Health System

3. University of Virginia, Charlottesville, VA

Background: Cardiac resynchronization therapy defibrillators (CRT-D) are routinely implanted in patients who meet guideline-based criteria; however, the benefit from CRT varies among patients, and better indicators of prognosis are needed. MRI strain and scar imaging has the potential to provide key data to inform long-term prognosis. The predictive value of cine displacement encoding with stimulated echoes (DENSE), which has been shown to provide highly accurate strain imaging in heart failure, has not been evaluated for long term prognostication after CRT-D with respect to overall survival and ICD therapies for ventricular tachycardia.

Methods: We performed complete MRI examinations for patients before CRT-D implantation. Late gadolinium enhancement (LGE) was used to evaluate myocardial scar, while cine DENSE was used to determine overall dyssynchrony based on the circumferential uniformity ratio estimate using singular value decomposition (CURE-SVD) and mechanical activation timing at the LV lead implant site. CURE-SVD ranges from 0-1, and values approaching 0 indicate more severe dyssynchrony. CRT-D implantation was performed as standard of care, and LV functional response was evaluated using echocardiography 6 months later. Cox proportional hazards regression was used to model associations among covariates of interest and survival outcomes.

Results: The 98 patients enrolled had a median age of 65.4 years (IQR 57.6-72.7 years), and 29/98 were female (Table 1). 51/98 had evidence of LGE, and among patients with LGE, the median percent scar volume was 10.4% (IQR 6.4% - 17.7 %). The median change in the left ventricular end-systolic volume (LVESV) 6 months after CRT was -18% (IQR -35% to +3%), and 55.1% met echocardiographic criteria for CRT response based on at least a 15% decrease in the LVESV. During a median follow-up of 3.3 years (IQR 1.4-4.4 years), 17 patients received appropriate ICD therapies for ventricular arrhythmias, and 27 patients experienced the outcome of death, left ventricular assist device (LVAD), or cardiac transplantation (DVADTX). The strongest MRI predictor of DVADTX during follow-up was the CURE-SVD (HR 7.7, 95% CI 1.4-41.4, P=0.01), and patients with CURE-SVD > 0.7 were 2.6 times more likely to have DVADTX (HR 2.56, 95% CI 1.17-5.64, P=0.019) (Figure 1). CURE-SVD was also associated with an increased likelihood of appropriate ICD therapies for ventricular tachycardia or DVADTX (HR 10.9, 95% CI 1.58-75.3, P=0.01) (Figure 2). The extent of LGE based on the percent scar volume was not significantly associated with either outcome after adjustment for CURE-SVD (P=0.42 for DVADTX and P=0.19 for the combined ICD therapies outcome). There was a trend for an association between late mechanical activation at the LV lead implant site and the survival outcomes (P=0.078). Greater degrees of echocardiographic CRT response at 6 months were associated with a decreased incidence of both clinical outcomes.

Conclusion: The pre-CRT use of CURE-SVD provides a reliable measure of long-term prognosis after CRT. Considering that CURE-SVD measures the extent of simultaneous stretch and contraction in opposing walls, patients with decreased CURE-SVD likely have a better survival after CRT and decreased arrhythmias because they have a therapeutic target that can be corrected with CRT. Greater use of cine DENSE to inform long-term survival after CRT, assess the risk of ICD therapies, and achieve optimal implementation of CRT promises to benefit many patients with heart failure who are CRT candidates.

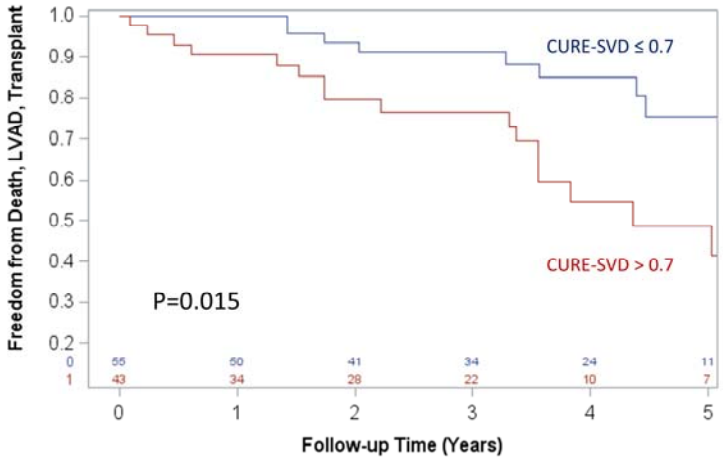

Freedom from DVADTX in CURE-SVD Subgroups

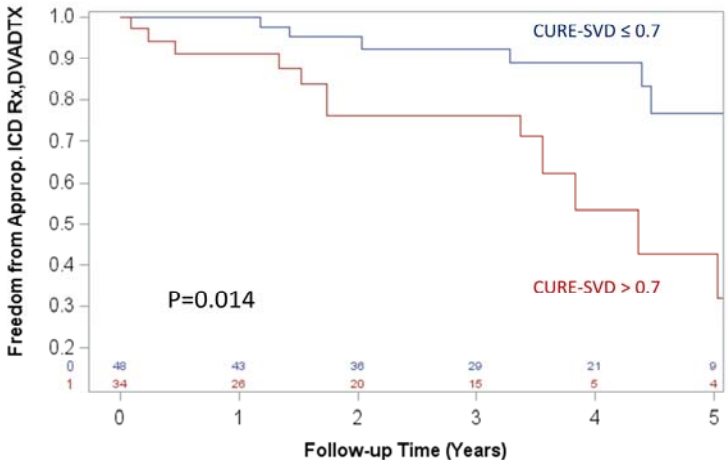

Freedom from Appropriate ICD Therapies and DVADTX in CURE-SVD Subgroups

Baseline Characteristics by CURE-SVD Group

Variable	All Patients (N=98)	CURE-SVD > 0.7 (Less Dyssynch.) (N=55)	CURE-SVD ≤ 0.7 (More Dyssynch.) (N=43)	P-Value

Age (years)	65.4 (57.6-72.7)	66.6 (61.0-75.7)	64.0 (54.7-71.0)	0.03
Gender (female)	29 (29.6)	10 (23.3)	19 (34.6%)	0.22
QRS (ms)	1545 (140-170)	150 (136-170)	160 (147-174)	0.08
QLV (ms)	105 (70.0-135.0)	90.0 (60.0-120.0)	120 (90.0-140.0)	0.0009
CURE-SVD	0.65 (0.41-0.81)	0.83 (0.77-0.90)	0.45 (0.33-0.54)	<0.0001
DVADTX	27 (27.6%)	17 (39.5%)	10 (18.2%)	0.02

ID#: 378447

Risk stratifying patients with suspected myocarditis with extracellular volume assessment by cardiovascular magnetic resonance imaging

Christoph Gräni, MD[1] Loïc Bière, MD, PhD[1], Christian Eichhorn, BSc[1], Kyoichi Kaneko, MD[1], Ayaz Aghayev, MD[1], Michael Steigner, MD[2], Michael Jerosch-Herold, PhD[3], Raymond Y. Kwong, MD, MPH[4]

1. Brigham and Women's Hospital, Harvard Medical School, Boston

2. Brigham and Women's Hospital, Harvard Medical School, Boston, Boston, MA

3. Harvard Medical School, Boston, MA

4. Brigham and Womens Hospital, Boston, MA

Background: Cardiovascular magnetic resonance imaging (CMR) has become a key investigative tool in patients with suspected myocarditis. Using T1 mapping, including extracellular volume (ECV) calculation, increased diagnostic accuracy in such presentations; however, its prognostic implications is unclear.

Methods: 179 patients with suspected myocarditis who underwent CMR evaluation, including T1 mapping, were identified. CMR findings including late gadolinium enhancement (LGE), left ventricular ejection fraction (LVEF), native T1 mapping, and ECV calculation were associated with time to first major adverse cardiac events (MACE) after CMR. MACE included a composite of all-cause death, heart failure hospitalization, heart transplantation, documented sustained ventricular arrhythmia, and recurrent myocarditis.

Results: At a median follow-up of 4.1 [interquartile-range (IQR) 2.2-6.1] years, 22 (12%) patients experienced a MACE. Mean age was 49±15 years and 79 individuals (44%) were female. Compared to mean native T1 (hazard ratio [HR] 1.00, 95% confidence interval [CI] 0.99-1.01, p=0.875), mean ECV (per 10%) was significantly associated with MACE (HR 2.09, 95%CI 1.07-4.08, p=0.031). Presence of ECV≥35% demonstrated significant univariable association with MACE (log-rank p=0.003) and when adjusted to LVEF (HR 3.42, 95%CI 1.42-7.94, p=0.006). In addition, ECV≥35% demonstrated more than 3-fold increased hazards to MACE adjusted to the effects of LGE presence (HR 3.14, 95%CI 1.29-7.36, p=0.012). In patients without LGE, ECV≥35% remained a prognostic discriminator (HR 6.6, p=0.010).

Conclusion: ECV calculation by CMR is a useful tool in the risk stratification of patients with clinically suspected myocarditis, incremental to LGE and LVEF.

ID#: 377470

Regional wall shear stress analysis in the aortic arch and its relation to dilation in bicuspid aortic valve disease

Aroa Ruiz-Muñoz, MSc[4]Lydia Dux-Santoy[1], Andrea Guala[2], Gisela Teixido-Tura, MD, PhD[1], GIULIANA MALDONADO, MD[3], Nicolas Villalva, MD[1], Filipa X. Valente, MD[3], Augusto Sao-Aviles, PhD[4], Laura Galian, MD[4], Laura Gutierrez, MD[4], Ruben Fernandez-Galera, MD[4], Teresa Gonzalez-Alujas, MD, PhD[4], David Garcia-Dorado, MD, PhD[4], Arturo Evangelista[4], José F. Rodríguez-Palomares, MD, PhD[2]

1. Hospital Universitari Vall d´Hebron. Vall d'Hebron Institut de Recerca. Universitat Autònoma de Barcelona, Catalonia, Spain

2. Hospital Universitari Vall d´Hebron. Vall d'Hebron Institut de Recerca. Universitat Autònoma de Barcelona, Barcelona, Catalonia, Spain

3. Hospital Universitari Vall d´Hebron. Vall d'Hebron Institut de Recerca. Universitat Autònoma de Barcelona, Barcelona, Spain

4. Hospital Universitari Vall d´Hebron. Vall d'Hebron Institut de Recerca. Universitat Autònoma de Barcelona, Spain

Background: Different bicuspid aortic valve (BAV) phenotypes are associated with different flow patterns and wall shear stress (WSS), which have been related to different expressions of BAV aortopathy. Despite some BAV dilate the proximal aortic arch, little is known about flow dynamics in this region. Thus, using 4D-flow MRI we aimed to analyse regional WSS in the arch in the different BAV phenotypes and its relation to dilation.

Methods: One hundred and eleven BAV patients underwent 4D-flow MRI with PC-VIPR sequence in a GE 1.5T scanner. Patients were classified according to the presence of arch dilation, which was considered based on previously published age-dependent reference value, and the fusion phenotype. The thoracic aorta was segmented from a 4D-flow derived angiography, without considering the supra-aortic vessels. Eight double-oblique analysis planes were distributed in the distal AscAo (planes 1-4, from the pulmonary level to the brachiocephalic trunk) and the aortic arch (planes 5-8, from the brachiocephalic trunk to the left subclavian artery).
Using in-house code, peak-systolic axial and circumferential WSS were calculated at 64 points distributed along the lumen contour for each plane, and contour-averaged axial ($WSS_{ax,avg}$) and circumferential ($WSS_{circ,avg}$) WSS were obtained. Also, the aortic wall was divided in 8 circumferential regions (anterior/left-anterior/left/left-posterior/posterior/right-posterior/right/right-anterior), and point-to-point averaged WSS and p-value were calculated for each plane and used to visualize regional maps.

Results: BAV phenotype was right-left (RL) in 74.8% patients, and RN in 25.2%. Arch was dilated in 56.7% BAV, affecting mainly the RN-phenotype (85.7% dilated RN vs 46.9% dilated RL).
Comparing BAV phenotypes, RN-BAV presented lower $WSS_{ax,avg}$ in the mid arch and higher $WSS_{circ,avg}$ along the distal AscAo and the arch (Table), coinciding with a higher rate of arch dilation. Also, dilated BAV compared to non-dilated had lower $WSS_{ax,avg}$ but higher $WSS_{circ,avg}$ in the distal AscAo and proximal-mid arch (Table), showing the relation between $WSS_{circ,avg}$ and arch dilation.
Regional WSS maps showed no differences in the axial WSS between BAV phenotypes (Figure 1A), but circumferential WSS was higher in the RN-BAV at all circumferential regions in the distal AscAo and proximal-mid aortic arch (Figure 1B). When comparing dilation, dilated BAV presented lower axial WSS (Figure 2A) but higher circumferential WSS in the right-to-posterior wall of the proximal arch (Figure 2B).

Conclusion: Proximal arch dilation is mostly associated with RN-phenotype. An increased circumferential WSS in the distal AscAo and aortic arch seems to be the most important flow determinant of the aortic morphotype seen in this population.

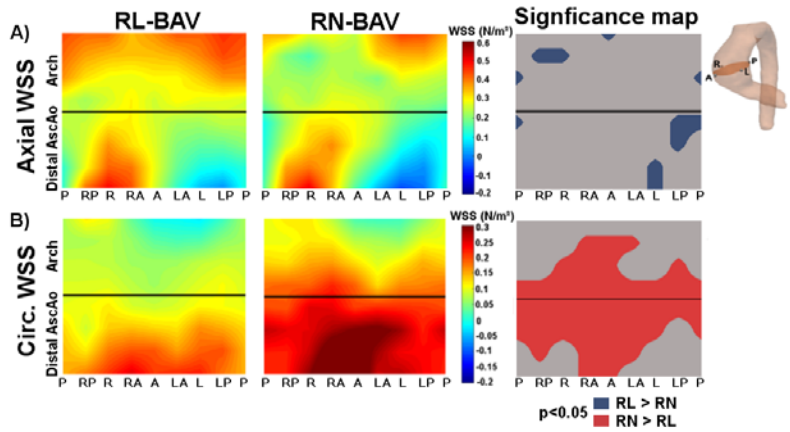

Figure 1. Axial and circumferential WSS and significance maps in BAV phenotypes.

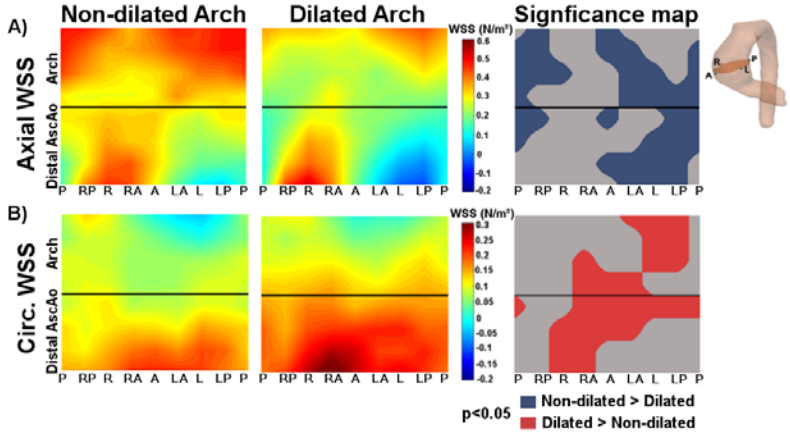

Figure 2. Axial and circumferential WSS and significance maps in BAV with and without arch dilation.

Table 1. Contour-averaged axial and circumferential WSS in BAV in the distal ascending aorta and the aortic arch. Mean±SD. * p<0.05 comparing RL vs RN-BAV or non dilated vs dilated arch BAV.

				BAV phenotype		BAV arch dilation	
	Region	Slice	BAV (n=111)	RL-BAV (n=83)	RN-BAV (n=28)	Non-dilated (n=48)	Dilated (n=63)
$WSS_{ax,avg}$ (N/m^2)	Distal AscAo	1	0.23±0.14	0.24±0.14	0.19±0.11	0.25±0.17	0.21±0.11
		2	0.23±0.14	0.24±0.15	0.20±0.10	0.27±0.17	0.19±0.11 *
		3	0.24±0.14	0.25±0.14	0.22±0.13	0.28±0.15	0.21±0.12 *
		4	0.25±0.16	0.26±0.17	0.23±0.11	0.31±0.18	0.21±0.12 *
	Aortic arch	5	0.26±0.15	0.27±0.16	0.24±0.12	0.31±0.16	0.23±0.14 *
		6	0.30±0.19	0.32±0.20	0.23±0.13 *	0.36±0.20	0.25±0.17 *
		7	0.35±0.25	0.32±0.20	0.23±0.13 *	0.42±0.27	0.29±0.22 *
		8	0.40±0.22	0.37±0.25	0.27±0.23	0.44±0.22	0.36±0.22
$WSS_{circ,avg}$ (N/m^2)	Distal AscAo	1	0.22±0.16	0.20±0.13	0.28±0.21 *	0.19±0.13	0.24±0.18
		2	0.19±0.15	0.17±0.13	0.27±0.19 *	0.16±0.12	0.22±0.17 *

		3	0.17±0.16	0.13±0.10	0.27±0.24 *	0.12±0.09	0.20±0.19 *
		4	0.13±0.12	0.10±0.08	0.22±0.19 *	0.09±0.07	0.16±0.15 *
	Aortic arch	5	0.11±0.10	0.09±0.07	0.18±0.15 *	0.08±0.06	0.13±0.12 *
		6	0.09±0.08	0.08±0.06	0.13±0.11 *	0.07±0.06	0.10±0.09
		7	0.06±0.07	0.05±0.05	0.09±0.10 *	0.05±0.05	0.07±0.08
		8	0.04±0.05	0.04±0.04	0.06±0.08 *	0.03±0.04	0.05±0.06

ID#: 377452

Differences in right ventricular-pulmonary vascular coupling between standard tetralogy of Fallot vs. Pulmonary atresia and association with other CMR and clinical indices

Sujatha Buddhe, MD MS[1] Samir Sarikouch, MD[2], Andreas Schuster, MD PhD MBA FESC[3], Philipp Beerbaum, MD[2], Mark Lewin, MD[4], Shelby Kutty, MD PhD MS-HCM[5]

1. Seattle Children's Hospital, Seattle, WA

2. Hannover Medical School, Germany

3. Department of Cardiology and Pneumology, University Medical Center Göttingen, Germany; Department of Cardiology, Royal North Shore Hospital, Sydney, Australia; The Kolling Institute, Northern Clinical School, University of Sydney, Sydney, Australia, Niedersachsen, Germany

4. Seattle Childrens' Hospital, WA

5. Children´s Hospital and Medical Center Joint Division of Pediatric Cardiology, University of Nebraska / Creighton University, Omaha, NE, USA, NE

Background: The right ventricle (RV) in repaired tetralogy of Fallot (rTOF) patients undergoes complex adaptation to chronic volume overload, not alone; but rather, coupled with the pulmonary arterial (PA) system. Traditional RV assessments provide limited appreciation into these mechanisms. We hypothesized that ventricular vascular coupling ratio (VVCR) assessed noninvasively by cardiac magnetic resonance (CMR) will provide unique insights into this relationship, because uncoupling is an important determinant of RV failure as reported in pulmonary hypertension. We sought to measure VVCR in standard TOF versus TOF with pulmonary atresia (PA) given the possible differences in vascular compliance.

Methods: Patients with rTOF>8 years age were recruited in a prospective trial for same day CMR, echocardiography and exercise stress testing. Traditional measures of biventricular size and systolic function were assessed. Sanz';s method was used to calculate VVCR as RV end-systolic volume/ pulmonary artery stroke volume, and indexed to body surface area to account for somatic growth. Subgroup analysis was performed for TOF vs. PA. Univariate and multivariate regressions were performed.

Results: A total of 260 subjects were included, 232 with TOF and 28 with PA. Mean age was 15.8±4.9 years and weight 55±18 kg. Mean non-indexed VVCR was 1.64±0.83, and was higher (abnormal) compared to published normal values (0.5-1.0). Mean indexed VVCR (VVCRi) in the cohort was 1.08±0.59; it was more abnormal in PA subgroup (1.35±0.71) compared to standard TOF (1.04±0.53; p<0.01; Figure) while traditional measures of RV size and function were not different. VVCRi had significant correlation with peak oxygen pulse on exercise testing (r=-0.33; p<0.001), RV ejection fraction (EF) (r=-0.44; p=<0.001), RV mass/volume ratio (r=-0.331; p<0.001), pulmonary regurgitation fraction (r=0.52; p<0.001) and LVEF(r=-0.31, p<0.001). VVCR was higher in subjects with NYHA class II (1.31±0.70; n=69) compared to NYHA class I (1.00±0.52; n=191; p<0.001; Figure). VVCRi also had independent association with peak oxygen pulse and NYHA class on multivariable analysis (R2=0.14); and this association improved with addition of RVEF and RV EDV to the model (R2=0.33).

Conclusion: It is feasible to noninvasively derive VVCR in children and adolescents with TOF using CMR. VVCRi is worse in subjects with PA compared to standard TOF. It has independent association with peak oxygen pulse and NYHA class, and this association improves when used in conjunction with RV volume and EF. Correlation with NYHA class and measures of exercise testing suggests its potential clinical value as an indicator of pulmonary arterial compliance and cardiovascular performance.

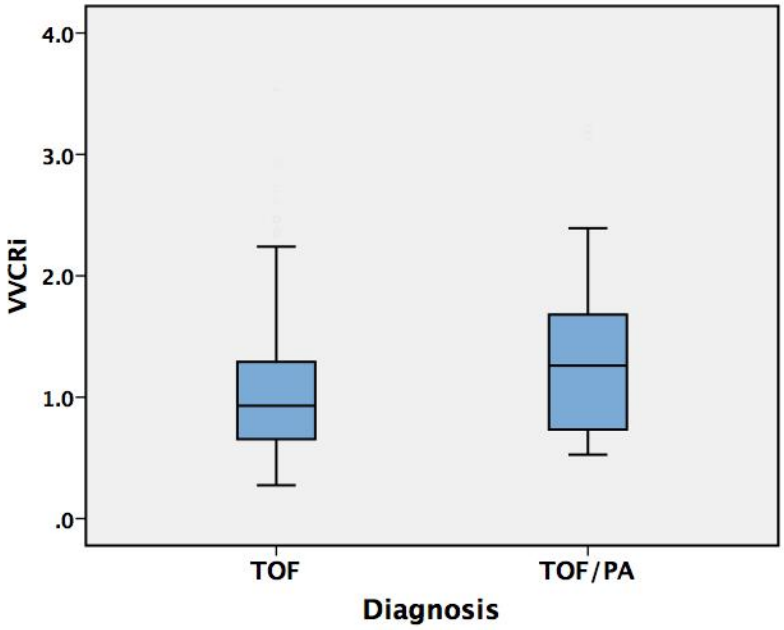

Boxplot showing distribution of VVCR in patients with TOF vs. PA

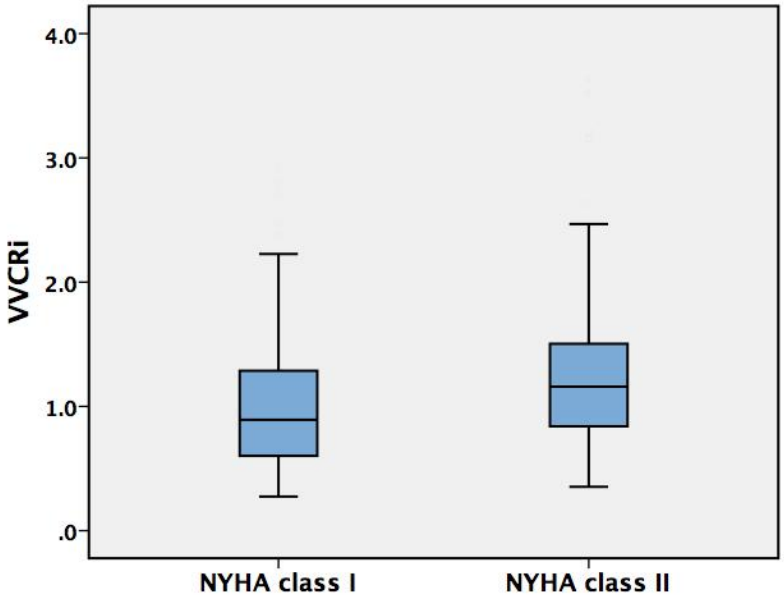

Boxplot showing distribution of VVCR in patients with NYHA class I vs. class II symptoms

ID#: 377627

In Vivo Quantification of Aortic Stiffness in Abdominal Aortic Aneurysm Patients: A Longitudinal Study

Huiming Dong, MS[1] Brian Raterman, BSRT[2], Prateek Kalra, MS[2], Richard White, MD[2], Arunark Kolipaka, PhD[2]

1. The Ohio State University Wexner Medical Center, Dublin, OH

2. Department of Radiology, The Ohio State University Wexner Medical Center, Columbus, OH

Background: Abdominal aortic aneurysm (AAA) is an abnormal vascular dilation of the abdominal aorta. Although the development of AAA is usually symptomless, AAA can eventually lead to life-threatening aortic rupture, making the disease a leading cause of death in the United States [1]. The diameter of an AAA is currently used as gold standard for evaluating the rupture risk in clinical practice. AAAs with diameter>=5.0 cm are considered high-risk, suggesting a larger chance of rupture when compared to those with diameter<5.0cm. However, studies have shown that large AAAs (>5.0 cm) may remain intact while small AAAs (<5.0 cm) can sometimes rupture, demonstrating that diameter is a poor indicator of rupture potential [2-4]. Aortic stiffness can be a better alternative as it can provide critical information about (1) the overall AAA mechanical integrity, (2) microstructure and (3) extracellular matrix (ECM) remodeling process of aortic wall, and thus potentially provides more accurate rupture risk evaluation [5-7]. Magnetic resonance elastography (MRE) is a novel phase-contrast MR technique by which the shear stiffness of soft tissues can be spatially estimated. Recent advancement in MRE has demonstrated that it is feasible to non-invasively evaluate aortic stiffness in vivo in healthy volunteers [8], AAA patients [5] and large animal models [9].The aim of this work is to serially follow AAA patients for every 6 months to obtain MRE-measured AAA stiffness for understanding the stiffness variation during the development of the disease.

Methods: In this study, 34 AAA patients were recruited. Each patient is serially scanned for every 6 months. Table I summarizes the number of patients and their visits. The patient recruitment criteria is (1) age≥20 years; (2) AAA diameter>3 cm; (3) no history of aortic vascular injury and vasculitis; (4) no history of surgical or endovascular repair of AAA; (5) no contradiction to receiving MR scans (e.g., no metal implants and not pregnant, no claustrophobia, etc.). All MR imaging was performed on a 3T MR scanner (Tim Trio, Siemens Healthcare, Erlangen, Germany) using a GRE MRE sequence [10]. All patients were scanned in a head first-supine position as demonstrated in Figure 1. The imaging parameters included: mechanical frequency=60 Hz; MEG frequency=60 Hz; three-directional motion encoding; FOV=400x400 mm2; slice thickness=6 mm; acquisition matrix size=128x64; No. of slices=3; No. of phase offsets=4; TE= 10.18 ms, TR = 14.29 ms. Magnitude images were masked to extract normal aorta and AAA region. Subsequently, effective aortic stiffness was obtained using local frequency estimation (LFE) algorithm via MRElab (Mayo Clinic, Rochester, MN).

Results: Figure 2 demonstrates the magnitude images, wave images and stiffness maps of one patient during his 3 serial visits. The mean AAA stiffness is 6.10 kPa, 8.34 kPa and 10.26 kPa. The mean AAA diameter is 55.59 mm, 57.12 mm and 57.64 mm for these 3 visits, respectively. The aortic stiffness has increased as the disease progresses. Figure 3 displays the mean AAA stiffness derived by pooling all patients. The mean AAA stiffness is 7.85±2.58 kPa, 8.00±1.22 kPa, 7.29±1.44 kPa, 10.28±0.32 kPa and 10.73 kPa for visit 1 to visit 5, respectively.

Conclusion: MRE demonstrated that aortic stiffness varied during the serial follow-ups, indicating changes in AAA wall integrity. The future work of this study includes studying AAA stiffness variation and its correlation to change in AAA diameter. The ultimate goal is to establish a standard of using MRE-derived aortic stiffness for more accurate AAA rupture risk evaluation. References [1] Kuivaniemi H, Platsoucas CD, Tilson 3rd MD. Aortic aneurysms: an immune disease with a strong genetic component. Circulation 2008;117(2):242-252. [2] Brewster DC, Cronenwett JL, Hallett JW Jr, Johnston KW, Krupski WC, Matsumura JS. Guidelines for the treatment of abdominal aortic aneurysms. Report of a subcommittee of the Joint Council of the American Association for Vascular Surgery and Society for Vascular Surgery. J Vasc Surg 2003;37:1106-17. [3] Nicholls SC, Gardner JB, Meissner MH, Johansen HK. Rupture in small abdominal aortic aneurysms. J Vasc Surg 1998;28:884-8. [4] Lederle FA, Wilson SE, Johnson GR, Reinke DB, Littooy FN, Acher CW, et al. Immediate repair compared with surveillance of small abdominal aortic aneurysms. N Engl J Med 2002;346:1437-44. [5] Kolipaka A, Illapani VS, Kenyhercz W, Dowell JD, Go MR, Starr JE, Vaccaro PS, White RD. Quantification of abdominal aortic aneurysm stiffness using magnetic resonance elastography and its comparison to aneurysm diameter. J Vasc Surg 2016;64(4):966-974. [6] Raghavan ML, Webster MW, Vorp DA. Ex vivo biomechanical behavior of abdominal aortic aneurysm: assessment using a new mathematical model. Ann Biomed Eng 1996;24:573-82. [7] Vorp DA, Vande Geest JP. Biomechanical determinants of abdominal aortic aneurysm rupture. Arterioscler Thromb Vasc Biol 2005;25:1558-66. [8] Damughatla AR, Raterman B, Sharkey-Toppen T, Jin N, Simonetti OP, White RD, Kolipaka A. Quantification of Aortic Stiffness Using MR Elastography and Its Comparison to MRI-Based Pulse Wave Velocity. J Magn Reson Imaging 2015;41(1):44-51. [9] Dong H, Mazumder R, Illapani VS, Mo X, Simonetti OP, White RD, Kolipaka A. In Vivo Quantification of Aortic Stiffness Using MR Elastography in Hypertensive Porcine Model. Magn Reson Med 2017,

DOI: 10.1002/mrm.26601. [10] Chamarthi S, Raterman B, Mazumder R, Michaels A, Oza V, Hanje J, Bolster B, Jin N, White RD, Kolipaka A. Rapid Acquisition Technique for MR Elastography of the Liver. Magn Reson Imaging 2014;32(6):679-683.

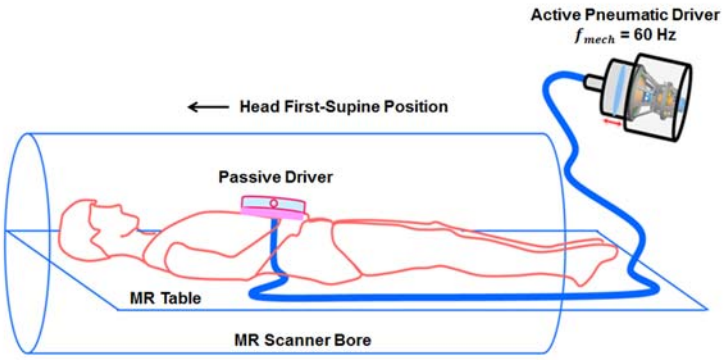

Figure 1. Patient Study Setup. Schematic of the experimental setup displays the placement of the passive driver on the patient abdomen and its connection to the pneumatic active driver located outside the scanner room via a plastic tube. A 60-Hz mechanical wave was induced in the abdominal aorta. All patients were positioned head first-supine position on the scanner table.

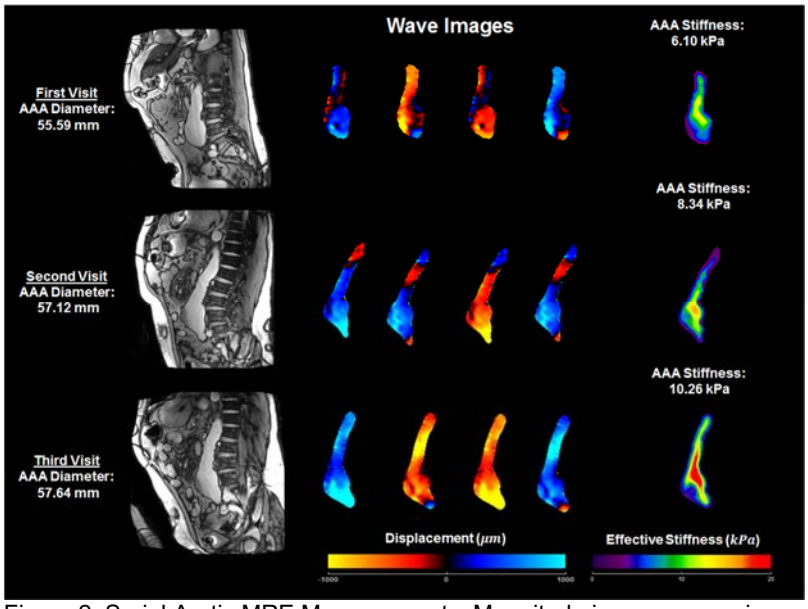

Figure 2. Serial Aortic MRE Measurements. Magnitude images, wave images and the corresponding aortic stiffness maps of one of the patients during his 3 serial visits are demonstrated. Reduction of aortic compliance can be clearly observed from the stiffness maps. The mean AAA diameter increased from 55.59 mm to 57.64 mm while the mean AAA stiffness increased from 6.10 kPa to 10.26 kPa.

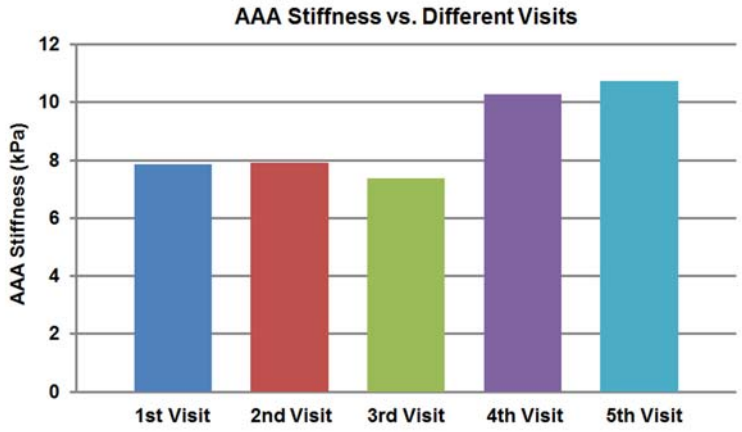

Figure 3. AAA Stiffness vs. Different Visits. The mean AAA stiffness by pooling all patients during each visit is 7.85±2.58 kPa, 8.00±1.22 kPa, 7.29±1.44 kPa, 10.28±0.32 kPa and 10.73 kPa for visit 1 to visit 5, respectively.

Table I. Summary of Patients and Visits

No. of Visits	No. of Patients	Mean AAA Stiffness (kPa)
1	34	7.85±2.58
2	13	8.00±1.22
3	7	7.29±1.44
4	4	10.28±0.32
5	1	10.73

ID#: 377725

CMR to assess treatment response in cardiac AL amyloidosis - findings from the ALchemy study

Ana Martinez Naharro, MD[1] Tushar Kotecha, MRCP(UK) MBChB[2], Andrea Baggiano[3], Michele Boldrini[4], Tamer Rezk, BSc[4], Rohin Francis, MBBS[4], Hossam Fayed, MBChB MSc MRCP(UK)[5], Daniel S. Knight[1], James Moon, MD[6], Peter Kellman, PhD[7], Julian D. Gillmore[8], Philip N. Hawkins[8], Marianna Fontana, MD, PhD[4]

1. UCL Department of CMR, Royal Free Hospital, London, England, United Kingdom

2. Royal Free London NHS Foundation Trust, London, England, United Kingdom

3. Centro Cardiologico Monzino, Istituto di Ricovero e Cura a Carattere Scientifico, Italy

4. UCL Department of CMR, Royal Free Hospital, England, United Kingdom

5. UCL Department of Cardiac MRI, Royal Free Pulmonary Hypertension Service, Pond Street, England, United Kingdom

6. UCL, England, United Kingdom

7. National Heart, Lung, and Blood Institute, National Institutes of Health, Bethesda, MD

8. National Amyloidosis Centre, University College London, England, United Kingdom

Background: Cardiac involvement in immunoglobulin light chain (AL) amyloidosis is the major determinant of survival. Cardiac response to chemotherapy is conventionally assessed by serum brain natriuretic peptide (NT-proBNP) and echocardiography, but neither quantify amyloid burden. The aim of this study was to evaluate cardiac AL amyloid serially using CMR withy T1 mapping at 3 months, 6 months and 1 year post chemotherapy.

Methods: 40 patients with cardiac AL amyloidosis were studied serially using CMR with T1 mapping extracellular volume measurement (a marker of the amyloid burden) at baseline and after 3 months, 6 months and 12 months of chemotherapy.

Results: At 6 months, 55% of patients achieved a complete or very good partial haematological response, and 45% patients a partial response or no response. Amyloid regression was not detectable at 3 months and was evident only in 7% patients at 6 months in the CR group. However, amyloid progression was detectable in 25% patients at 6 months, and 2% patients at 3 months. Although this occurred in the PR group, unexpectedly, it also occurred in the CR and VGPR groups (13% in PR, 5% in CR and 9% in VGPR). There was significant increase in native T1 ($p<0.01$) and LVEF reduction ($p<0.05$) in patients whose amyloid burden increased at 6 months. At one year, 70% patients achieved a CR or VGPR and 30% patients attained a PR or NR. Regression of amyloid was seen in 38% patients, all with CR or VGPR and 0 patients who achieved a PR or NR ($p<0.05$). 29% patients with changes in the ECV consistent with regression of amyloid had changes in late gadolinium enhancement. Amyloid regression was associated with reverse LV remodelling with significant reduction in LV mass and increase LVEDV ($p<0.05$ for both). The native T1 reduced only in patients with changes in the LGE pattern.

Conclusion: In newly diagnosed and treated AL amyloidosis, CMR demonstrates the dynamic biology of infiltration and deposition: increasing rapidly between 3 and 6 months, particularly if chemotherapy fails to switch off light chain production; regressing more slowly (by 1 year) if effective. Similar to cardiac iron by T2*, serial monitoring of myocardial end-organ infiltration has the potential for new AL amyloidosis therapeutic regimes based on myocardial organ response.

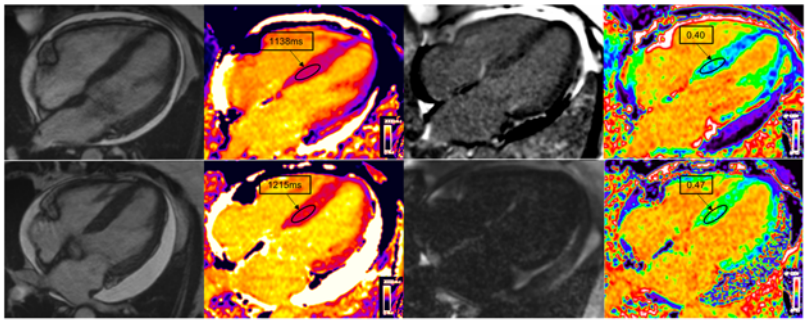

Baseline (top panel) and 6 months after chemotherapy (bottom panel) showing progression of AL amyloidosis by CMR. Top panel; 4 chamber view SSFP cine, corresponding 4Ch view native T1 map, late gadolinium enhancement (LGE) image and extracellular volumen fraction (ECV) map showing mildly elevated native T1 values,

no clear LGE and mildly elevated ECV values. Bottom panel; 4 chamber view SSFP cine, corresponding 4Ch view native T1 map, LGE and ECV map showing very high native T1 values, subendocardial LGE and moderately elevated ECV values

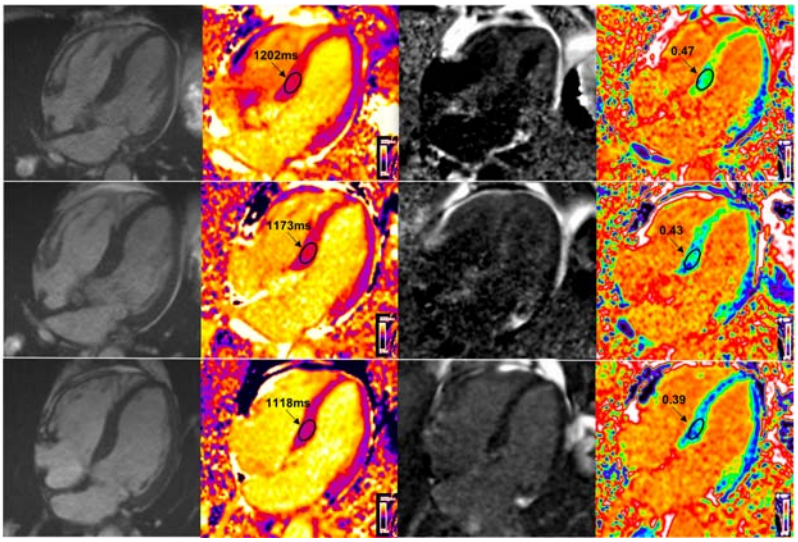

Baseline (top panel), 6 months after chemotherapy (mid panel) and 12 months after chemotherapy (bottom panel) showing regression of AL amyloidosis by CMR. Top panel; 4 chamber view SSFP cine, corresponding 4Ch view native T1 map, late gadolinium enhancement (LGE) image and extracellular volumen fraction (ECV) map showing elevated native T1 values, subendocardial LGE and moderately elevated ECV values. Mid panel; 4 chamber view SSFP cine, corresponding 4Ch view native T1 map, LGE and ECV map showing mildly elevated native T1 values, still subendocardial LGE and mildly elevated ECV values. Bottom panel; 4 chamber view SSFP cine, corresponding 4Ch view native T1 map, LGE and ECV map showing borderline native T1 values, no LGE and borderline ECV values

ID#: 377728

The prevalence of microvascular obstruction in cardiac sarcoidosis

Sabiha Gati, MRCP (UK), PhD[1] Vasilis Kouranos, PhD[2], Rakesh Sharma, MRCP PhD[3], Raj Khattar, PhD[2], Sanjay Prasad, MD[4], Dudley J. Pennell, MD[4], Kshama Wechalekar, MBBS DNB (Nuclear Medicine)[5], A John. Baksi, PhD MRCP[6]

1. Royal Brompton & Harefield NHS Trust, United Kingdom

2. Royal Brompton & Harefield NHS Trust, United Kingdom

3. MRCP PhD, London, United Kingdom

4. Royal Brompton Hospital and Imperial College, London, England, United Kingdom

5. Royal Brompton Hospital, London, England, United Kingdom

6. Royal Brompton Hospital and Imperial College London, London, London, England, United Kingdom

Background: Approximately 5% of patients with systemic sarcoidosis have clinically manifest cardiac involvement, yet the prevalence of sub-clinical cardiac involvement of sarcoidosis is reportedly between 20 and 70%. Despite the powerful utility of CMR and FDG-PET imaging now established in the diagnostic evaluation of such patients, this remains a challenging diagnosis. Microvascular obstruction (MVO) is a well-recognised feature following myocardial infarction. Following appreciation of hypovascular appearances akin to MVO on CMR in some patients with sarcoidosis, we hypothesised that these may be a manifestation of non-caseating granuloma and may be useful in facilitating the diagnosis of cardiac sarcoidosis. The aim of this study was to determine the prevalence of this MVO-like appearance on early gadolinium imaging in patients with cardiac sarcoidosis.

Methods: We performed a retrospective analysis of 181 consecutive patients seen in our tertiary centre combined cardio-respiratory sarcoidosis service between 2010 and 2017 with a diagnosis of cardiac sarcoidosis based on HRS criteria following MDT discussion. Evaluation included CMR, echocardiography, & FDG-PET imaging. Early gadolinium enhancement long axis sequences were assessed for the appearance of MVO and compared with CMR late Gadolinium and concurrent FDG-PET findings.

Results: Of the 181 patients, an MVO-like appearance was detected in 7% (n=13). None of the patients with MVO demonstrated an infarct pattern of late gadolinium enhancement. Of these 13 patients with MVO-like appearance, FDG-PET was performed in 12 individuals and demonstrated positive findings for active disease in 85% (n=11).

Conclusion: The appearance of MVO-like hypovascular regions on CMR is a not infrequent finding in patients with cardiac involvement of sarcoidosis. This may offer an additional diagnostic feature where present and may represent microvascular obstruction from non-caseating granuloma causing either direct or indirect macrovascular damage. This appearance does not appear to be limited to myocardial infarction and may be a feature of many non-ischaemic cardiomyopathies meriting further evaluation.

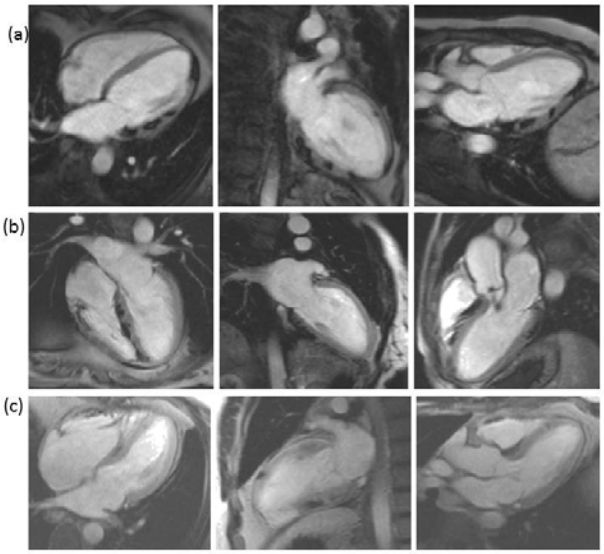

Examples from 3 patients with MVO-like appearance on early gadolinium enhancement imaging.

ID#: 377971

Role of myocardial strain assessed by CRM tissue-tracking to predict adverse cardiovascular events in cardiac amyloidosis.

Ilaria Dentamaro, MD[1] Alejandro Quijada-Fumero, MD[2], Lucia Rodríguez Eyras, MD[3], Nicolas Ezequiel. Villalva, MD[4], Filipa X. Valente, MD[5], Victor Pineda, MD[6], Gisela Teixidó-Turà, MD, PhD[7], Ruben Fernandez-Galera, MD[8], David Garcia-Dorado, MD, PhD[9], Arturo Evangelista[8], Hug Cuellar, MD, PhD[10], José F. Rodríguez-Palomares, MD, PhD[11]

1. Hospital Vall d'Hebron Barcelona, Bari, Puglia, Italy

2. (1) Hospital Vall d'Hebron, Department of Cardiology. VHIR, Universitat Autònoma de Barcelona, Barcelona, Spain., S/C de Tenerife, Canarias, Spain

3. (1) Hospital Vall d'Hebron, Department of Cardiology. VHIR, Universitat Autònoma de Barcelona, Barcelona, Spain., Mar del Plata, Buenos Aires, Argentina

4. (1) Hospital Vall d'Hebron, Department of Cardiology. VHIR, Universitat Autònoma de Barcelona, Barcelona, Spain, BARCELONA, Catalonia, Spain

5. Hospital Universitari Vall d´Hebron. Vall d'Hebron Institut de Recerca. Universitat Autònoma de Barcelona, Barcelona, Spain

6. (2) Hospital Vall d'Hebron, Department of Radiology. VHIR, Universitat Autònoma de Barcelona, Barcelona, Spain., Spain

7. Hospital Vall d'Hebron, Spain

8. Hospital Universitari Vall d´Hebron. Vall d'Hebron Institut de Recerca. Universitat Autònoma de Barcelona, Spain

9. (1) Hospital Vall d'Hebron, Department of Cardiology. VHIR, Universitat Autònoma de Barcelona, Barcelona, Spain., Spain

10. Hospital Universitari Vall d'Hebron, Spain

11. Hospital Universitari Vall d´Hebron. Vall d'Hebron Institut de Recerca. Universitat Autònoma de Barcelona, Barcelona, Catalonia, Spain

Background: Cardiovascular events are the major determinants of mortality in amyloidosis. CMR has been commonly used to diagnose cardiac involvement and the amount of LGE has been associated with a worse prognosis and death. However, the role of other CMR derived parameters of cardiac involvement such as myocardial deformation in this population are still unknown. Thus, the aim of our study was to analyze the prognostic value of the main variables derived from CMR in patients with cardiac amyloidosis.

Methods: Thirty-five patients with histologically proven amyloidosis underwent a CMR with LGE. Left ventricular volumes, ejection fraction, mass, and deformation parameters (radial, circumferential and longitudinal strain) were assessed using cine sequences. The number of segments with LGE was determined. Clinical parameters and cardiovascular events were collected at follow-up (hospitalization for heart failure, ventricular arrhythmias, stroke and cardiovascular mortality).

Results: All patients were followed for a mean period of 50 months. In this period, 46% presented a hospitalization for heart failure, 9% presented a ventricular arrhythmia, stroke 17% and cardiovascular death in 31%. The mean characteristics of the population with and without cardiovascular events are displayed on table 1. Among all different CMR derived variables, global circumferential strain and global longitudinal strain were significantly associated with cardiovascular events. In the multivariate analysis (including variables with a P-value > 0.1 in the univariate analysis), global circumferential strain was the main predictor of cardiovascular events beyond the presence of late gadolinium enhancement.

Conclusion: Patients with cardiac amyloidosis present a high rate of cardiovascular events. CMR constitutes an excellent imaging technique to risk stratify these population. However, circumferential strain (which is a surrogate of severe myocardial impairment) constitutes the main predictor of adverse cardiovascular events at follow-up.

	ALL	CARDIOVASCULAR EVENTS		
		without events	with events	P-value
Age (years)	77 ± 11	76 ± 12	78 ± 10	0,66
End-diastolic volume (mL)	134 ± 37	137 ± 35	133 ± 39	0,81
End-sistolic volume (mL)	65 ± 26	65 ± 25	66 ± 27	0,87
Ejection fraction (%)	52 ± 10	52 ± 9	51 ± 11	0,79
Left atrium area (cm2)	31 ± 8	31 ± 9	31 ± 6	1
Myocardial mass (gr)	151 ± 47	136 ± 42	166 ± 48	0,09
Segments with LGE (number)	6 ± 5	7 ± 5	7 ± 5	0,75
Global radial strain (%)	39 ± 15	42 ± 13	37 ± 16	0,38
Global circumferential strain (%)	-17 ± 5	-19 ± 3	-15 ± 5	0,023
Global longitudinal strain (%)	-12 ± 4	-14 ± 4	-11 ± 4	0,05

ID#: 375484

MR-Augmented Cardiopulmonary Exercise Testing in Young Adults with the Fontan Circulation

Nathaniel J. Barber, MBBS, MSc [1]Mun Hong Cheang, MBBS,BMedSci (Hons)[2], Bejal Pandya, MBBS[3], Steeden A. Jennifer, PhD [4], Vivek Muthurangu, MD[4]

1. UCL Institute of Cardiovascular Science & Great Ormond Street Hospital for Children, London, England, United Kingdom

2. Institute of Cardiovascular Science, University College London, United Kingdom

3. Barts Heart Centre, United Kingdom

4. Institute of Cardiovascular Science, University College London, England, United Kingdom

Background: The Fontan circulation is associated with significant exercise intolerance. It is generally believed that this is due to inadequate augmentation of cardiac output as a result of ventricular dysfunction and chronotropic incompetence. However, it is now well recognized that reduced skeletal muscle oxygen extraction is also an important determinant of poor exercise capacity. We have recently developed a MR augmented cardio-pulmonary exercise testing (MR-CPET), which allows simultaneous measurement of cardiac output (CO) and oxygen consumption (VO_2). Importantly, this enables calculation of arterio-venous oxygen content gradient (AVO) – a marker of tissue oxygen extraction. The aim of this study was to use MR-CPET to better understand the causes of exercise intolerance in young adults with the Fontan circulation.

Methods: Ten young adults with the Fontan circulation (8 male, 2 female) and ten age matched healthy controls (8 male, 2 female) underwent MR-CPET. Exercise was performed following a standardized ramp protocol on a supine MR compatible ergometer (Lode, Groningen, The Netherlands). All subjects were exercised to exhaustion. During exercise, oxygen consumption (VO_2), carbon dioxide production (VCO_2) and minute ventilation (VE) were measured using a commercial CPET system (Ultima, MedGraphics, St. Paul, USA) with a modified MR-compatible sampling tube. At the same time, aortic flow was continuously measured using a previously validated real-time UNFOLD-SENSE spiral PCMR sequence. Before and at peak exercise, ventricular volumes were assessed using a real-time radial SSFP k-t SENSE sequence.

Results: All participants were able to exercise with no adverse outcomes. The increase in VO_2 was significantly reduced in Fontan patients (Fig 1a). The HR response was also significantly (p-0.001) reduced in patients (Fig 1b). However, increase in CO was not significantly different (p=0.44) in patients and controls (Fig 1c). This was due to a trend towards higher SV response in patients. In addition, there was no significant difference in the increase in EF seen in patients and controls (p=0.25). Conversely, the increase in AVO during exercise was significantly (p=0.04) reduced in Fontan patients (Fig 1d).

Conclusion: In this study, we have shown that although Fontan patient have chronotropic incompetence during exercise, they do not have significantly reduced CO augmentation. However, we have shown that they have reduced AVO, suggesting a problem with tissue oxygen extraction that may better explain their reduced peak VO_2. This finding opens up the possibility of new intervention for exercise intolerance in Fontan patients – namely physical training.

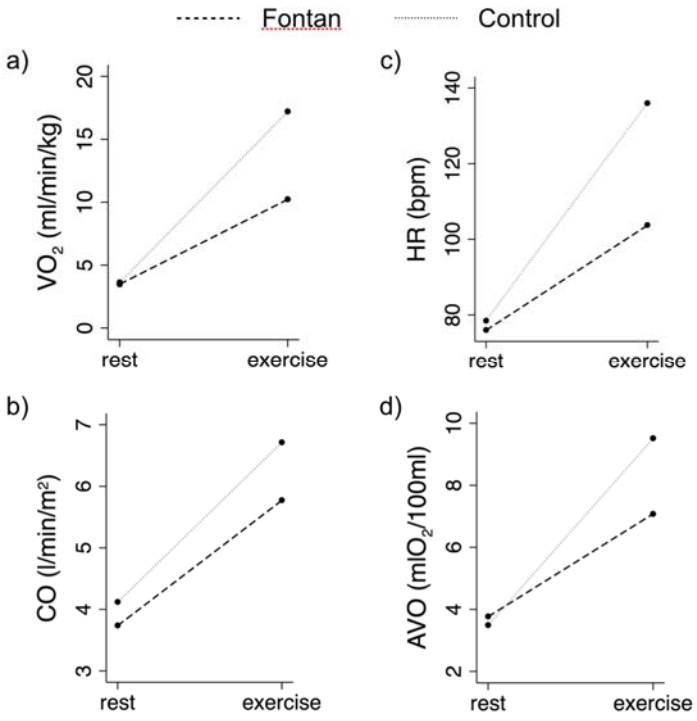
Fontan
Control
a)
VO_2 (ml/min/kg)
0
5
10
15
20
rest
exercise
c)
HR (bpm)
80
100
120
140
rest
exercise
b)
CO (l/min/m²)
3
4
5
6
7
rest
exercise
d)
AVO (mlO_2/100ml)
2
4
6
8
10
rest
exercise

ID#: 374495

Risk Stratification of Patients with Apparently Idiopathic Premature Ventricular Contractions: Data from a Multicenter International Cardiac Magnetic Resonance Study

Gaetano Nucifora, MD, PhD[10]Daniele Muser, MD[1], Pasquale Santangeli, MD, PhD[2], Jackson Liang, DO[2], Simon Castro, MD[2], Shingo Maeda, MD, PhD[3], Daniel Benhayon, MD[4], Mouhannad Sadek, MD[5], Ruben Casado Arroyo, MD, PhD[6], Elena Santarossa, MD[7], Benoit Desjardins, MD, PhD[1], Fermin C. Garcia, MD[1], David S. Frankel, MD[8], David J. Callans, MD[2], Francis E. Marchlinski, MD[2], Joseph Selvanayagam, FRACP, DPhil[9]

1. Hospital of the University of Pennsylvania, PA

2. Hospital of the University of Pennsylvania

3. Tokyo Medical and Dental University, Tokyo, Japan

4. Memorial Healthcare System, Hollywood, FL

5. University of Ottawa Heart Institute, ON, Canada

6. Université Libre de Bruxelles, Brussels Hoofdstedelijk Gewest, Belgium

7. Santa Maria della Misericordia University Hospital, Friuli-Venezia Giulia, Italy

8. Hospital of the University of Pennsylvania, Philadelphia, PA

9. Flinders University, Adelaide, SA, Australia, Bedford Park, South Australia, Australia

10. University Hospital of South Manchester, Sale, England, United Kingdom

Background: Few is known about the prognostic relevance of cardiac magnetic resonance (CMR) in patients with frequent premature ventricular contractions (PVCs) and negative routine diagnostic work-up. The aim of this study was to investigate the prevalence and prognostic significance of myocardial abnormalities absent on the basis of routine investigations but identified by CMR in this patient population.

Methods: This was a multicenter, international study that included 455 consecutive patients (43±16 years, 59% male) with frequent (>1000 /24h) PVCs (of multiple morphologies in 8% of cases) and negative routine diagnostic work-up who underwent a comprehensive CMR study, which included SSFP-cine imaging for wall motion abnormalities, FSE T1-weighted imaging for fatty infiltration and late gadolinium enhancement (LGE) imaging for necrosis/fibrosis. An abnormality of any CMR parameter was graded as a myocardial abnormality for correlation with long term major adverse cardiovascular events including sudden cardiac death (SCD) or nonfatal episodes of ventricular fibrillation or hemodynamically unstable sustained ventricular tachycardia requiring external cardioversion or appropriate implantable cardioverter defibrillator therapy.

Results: Myocardial abnormalities were found in 73 (16%) patients. Male gender (OR 4.02, 95% CI 1.71-9.48, p=0.001), family history of SCD and/or cardiomyopathy (OR 4.56, 95% CI 1.37-15.17, p=0.013), multiple morphologies of PVCs (OR 17.77, 95% CI 5.55-58.85, p=0.013), multiple morphologies of PVCs (OR 17.77, 95% CI 5.55-58.85, p<0.001) as well as left bundle branch block/superior axis morphology (OR 12.21, 95% CI 3.40-43.90, p<0.001), right bundle branch block/inferior axis morphology (OR 16.67, 95% CI 6.52-42.62, p<0.001) or right bundle branch block/superior axis morphology (OR 53.72, 95% CI 19.76-146.03, p<0.001) were all significantly related to the presence of myocardial structural abnormalities. After a median follow-up of 37 months, the composite endpoint occurred in 26 (6%) patients. Presence of myocardial abnormalities on CMR (HR 106.79, 95% CI 13.59-839.09, p<0.001) and multiple morphologies of PVCs (HR 4.28, 95% CI 1.89-9.68, p<0.001) were the only independent predictors of the composite endpoint. Survival free from the composite endpoint according to presence of myocardial abnormalities and multiple morphologies of PVCs is shown in Figure 1 A and B, respectively.

Conclusion: CMR can identify concealed myocardial abnormalities in 16% of patients with apparently idiopathic, frequent PVCs. Multiple morphologies of PVCs and presence of myocardial abnormalities independently predict worse clinical outcomes.

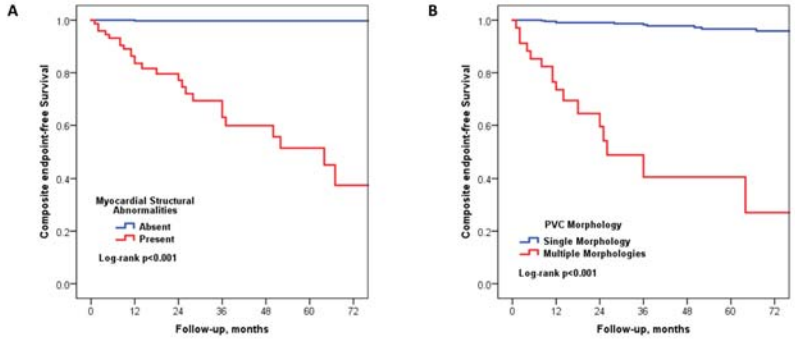

Survival free from the composite endpoint according to presence of myocardial abnormalities and multiple morphologies of PVCs

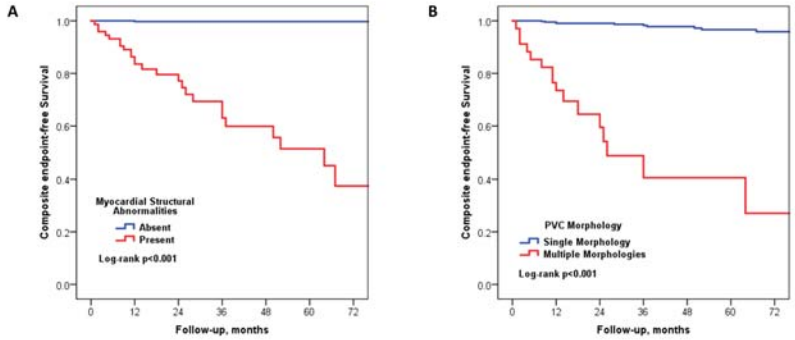

Figure 1

ID#: 374675

CMR-determined RV dysfunction but not dilatation correlates with prognostic reductions in Cardiopulmonary Exercise Performance in Repaired Tetralogy of Fallot

Imran Rashid, PhD FRACP[1] Adil Mahmood, B.Sc[1], Tevfik F. Ismail, PhD MRCP[2], Shelby Kutty, PhD, MD[3], David Celermajer, PhD DSc [4], Raj Puranik, PhD FRACP[5]

1. King's College London, London, England, United Kingdom

2. King's College London; Guy's and St Thomas' Hospitals NHS Foundation Trust, London, England, United Kingdom

3. University of Nebraska Medical Center, Omaha, Nebraska, USA, Omaha, NE

4. Royal Prince Alfred Hospital, University of Sydney, Camperdown, New South Wales, Australia

5. Royal Prince Alfred Hospital, University of Sydney, Camperdown, New South Wales, Australia

Background: The optimal timing for pulmonary valve replacement (PVR) in patients with repaired tetralogy of Fallot (rTOF) and severe pulmonary regurgitation remains contentious. Although a clear association between exercise capacity and outcome has been demonstrated, the prognostic impact of right ventricular (RV) dilatation remains unclear. We investigated whether CMR parameters, alone or in combination, correlate with prognostic reductions in exercise capacity in a large rTOF cohort.

Methods: Patients from the adult congenital heart service of two centres who had previously undergone CMR and standardised cardiopulmonary exercise (CPEX) protocols were included in the study. The indexed RV end-diastolic volume ($RVEDV_i$), indexed RV stroke volume ($RVSV_i$), RVEF, LVEF and pulmonary regurgitant fraction (PRF) were quantified by CMR. Univariable and multivariable regression analysis was performed to assess the association between CMR indices and CPEX-determined peak VO_2 or peak work (%Jones-predicted).

Results: A total of 163 patients were included (mean age 24.5±10.2 years, 59% males [Table 1]) and 33% had severe RV dilatation ($RVEDV_i$>150 ml/m^2). On univariable analysis, there was no significant correlation between $RVEDV_i$ and peak VO_2 (r=0.04, P=0.62) or peak work (r=0.136, P=0.08) (Fig 1A,B). Furthermore, neither PRF or LVEF had significant association with peak VO_2 or peak work (Fig1C-F), however, few subjects in this cohort (n=11) had moderate or severe LV dysfunction (LVEF≤45%). In contrast, RVEF and $RVSV_i$ had significant correlations with both peak VO_2 (RVEF r=0.33, P<0.0001; $RVSV_i$ r=0.263, P=0.0007) and peak work (RVEF r=0.340, P<0.0001; $RVSV_i$ r=0.361, P<0.0001) (Fig1G-J). Similarly, in the subset of patients with severe PR (PRF≥50%, n=17), RVEF and $RVSV_i$ but not $RVEDV_i$ correlated with CPEX performance (Fig 2). On multivariable analysis, RVEF remained a significant predictor of peak VO_2. For a previously established prognostic peak VO_2 threshold of <27ml/kg/min[1], ROC analysis demonstrated a Harrell';s c of 0.715 (95% CI 0.63 to 0.80) for RVEF.

Conclusion: CMR indices of RV systolic function (RVEF and $RVSV_i$) correlate better with CPEX performance than RV dilatation, highlighting the prognostic significance of RV dysfunction in this population. This finding was also observed in the context of severe PR and emphasises the importance of accurate assessment of RV function in rTOF patients to assess for interval changes that may be used to guide intervention.

References
1. Diller G-P, *Circulation* 112:828 (2005)

	All patients
Demographics	
Total patients	163
Age at CMR/CPEX (years)	24.5 ± 10.2
Male gender (%)	59
RVEF (%)	47.8 ± 9.9
LVEF (%)	57.3 ± 7.5
Previous palliation	
Blalock-Taussig shunt, n (%)	35 (21)
Central shunt, n (%)	2 (0.6)
Waterston shunt, n (%)	1 (0.6)
Brock procedure, n (%)	1 (0.6)
Ross procedure, n (%)	1 (0.6)
Age at previous palliation (years)	0.7 ± 1.1
Previous repair	
Transannular patch, n (%)	70 (43)
RVOT patch, n (%)	14 (9)
Homograft, n (%)	13 (8)
RV-PA conduit, n (%)	24 (15)
Valvectomy, n (%)	17 (11)
Valve-sparing repair, n (%)	11 (7)
Data unavailable, n (%)	14 (9)
Age at previous repair (years)	2.5 ± 2.9
Previous PVR, n (%)	70 (43)
Age at previous PVR (years)	24.1 ± 9.1

Table 1. Patient Demographic and Surgical Data. CPEX, cardiopulmonary exercise testing; RV-PA, right ventricle-to-pulmonary artery; RVOT, right ventricular outflow tract; PVR, pulmonary valve replacement. Data are mean ± SD.

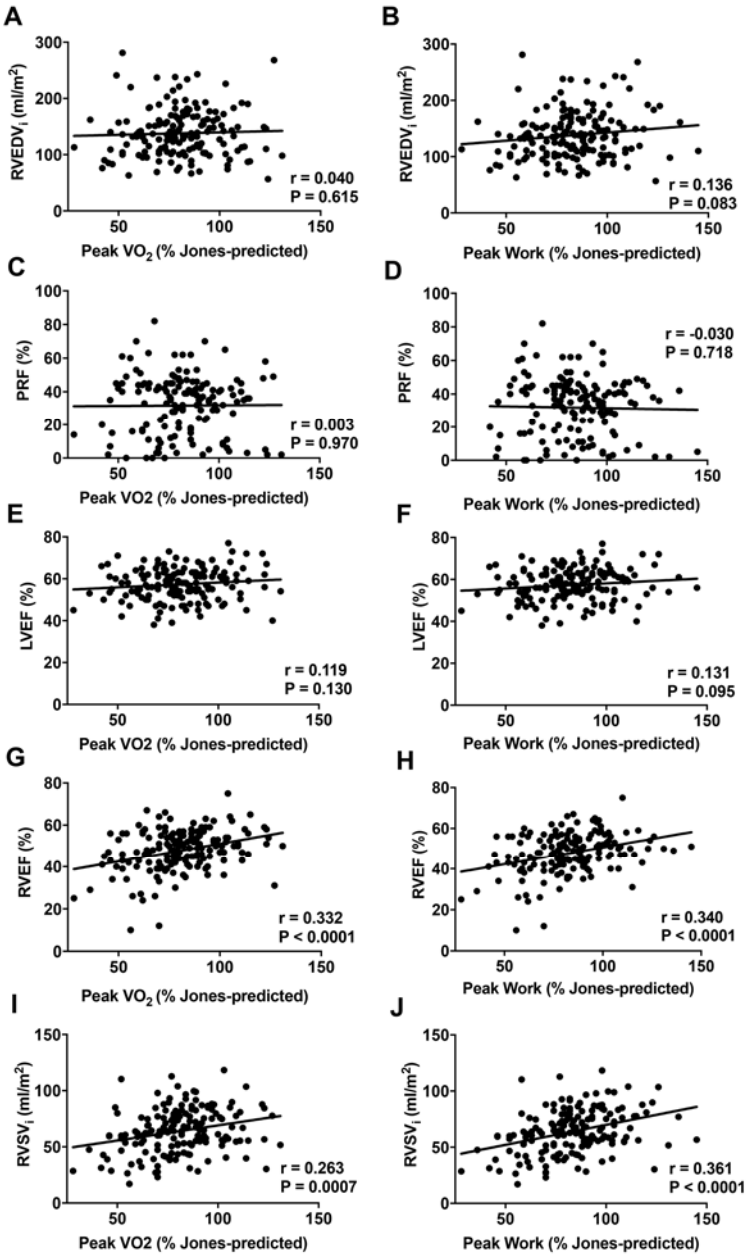

Figure 1. Univariable CMR determinants of CPEX performance in rTOF. There was no significant association between RVEDVi (A, B), PRF (C,D) or LVEF (E,F) with peak VO2 or peak work (% Jones-predicted). In contrast, indices of RV systolic function including RVEF (G,H) and RVSVi (I,J) had significant correlations with peak VO2 and peak work.

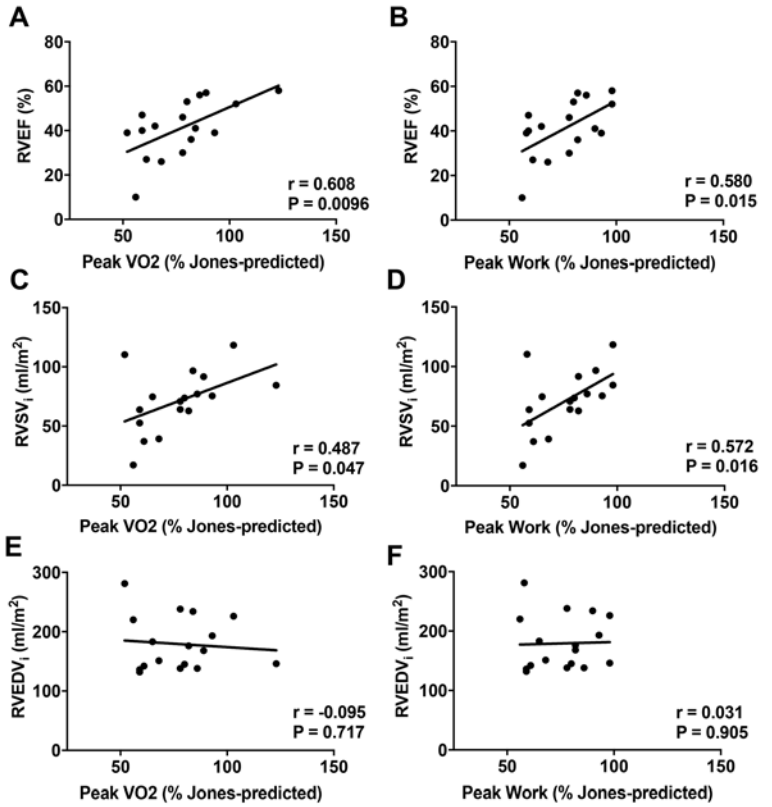

G

	rTOF + Severe PR			
	$RVEDV_i$<150ml/m²	$RVEDV_i$>150ml/m²	RVEF<40%	RVEF>40%
N	7	10	7	10
Peak VO_2 (% Jones-pred)	78 ± 8.6	77 ± 5.2	70.1 ± 5.7	83 ± 6.3

Figure 2. Univariable CMR determinants of CPEX performance in rTOF with severe PR. In the context of severe PR (PRF≥50%), RVEF (A,B) and RVSVi (C,D) but not RVEDVi (E,F) correlated with peak VO2 and peak work (% Jones-predicted) (Pearson correlation, n=17). G) RV systolic dysfunction (RVEF<40%) is a better discriminator of reductions in peak VO2 compared to severe RV dilatation (RVEDVi>150ml/m2), with subsequent ROC analysis demonstrating 90% sensitivity for RVEF<40% to detect a peak VO2 < 27ml/kg/min. Data are mean ± SEM.

ID#: 376732

Atrial Scar on CMR to Predict Pulmonary Vein Reconnection after Catheter Ablation for Paroxysmal Atrial Fibrillation

Hubert Cochet[4]Nora Al Jefairi[1], Claudia Camaioni, MD[2], Soumaya Sridi[1], Hubert Nivet[1], Francois Laurent[3], Michel Montaudon[3]

1. CHU Bordeaux, France

2. Barts Heart Center, London, England, United Kingdom

3. Unité d'imagerie cardio-thoracique, CHU Bordeaux, Pessac, Aquitaine, France

4. IHU LIRYC - CHU / Université de Bordeaux, France

Background: Pulmonary vein (PV) reconnection is frequent in patients showing atrial fibrillation (AF) recurrence after PV isolation (PVI). Its detection with cardiac magnetic resonance (CMR) may help predict outcome and guide redo procedures. We assessed the relationship between scar on CMR and PV reconnection after catheter ablation for paroxysmal AF.

Methods: Fifty-one patients with paroxysmal AF underwent CMR before PVI using either a conventional single-electrode catheter (N=28) or a circular multi-electrode catheter (N=23). At 3 months, a second CMR study was performed, followed by a systematic electrophysiological procedure to look for PV reconnection, regardless of AF recurrence. Pre-ablation fibrosis and post-ablation scar were quantified and mapped from late gadolinium-enhanced CMR. CMR results were compared to the distribution and extent of PV reconnection. CMR and electrophysiological findings were compared between catheter types.

Results: 3 months after successful PVI, scar gaps were found in 39(76%) patients, and 78(39%) veins. Electrical PV reconnection was detected in 45(88%) patients, and 99(50%) veins. The extent of PV reconnection related closely to the number of gaps ($R=0.55$, $P<0.001$), and to scar burden ($R=-0.63$, $P<0.001$). However, the agreement was only fair for the localization of PV reconnection ($k=0.37$, $P<0.001$), scar gaps particularly lacking sensitivity in areas of pre-existing fibrosis. The circular catheter was associated with shorter procedures ($P<0.001$), more scar ($P=0.01$), less gaps ($P=0.01$), and less reconnected veins ($P=0.03$).

Conclusion: PV reconnection is extremely frequent after PVI. CMR scar imaging accurately predicts its extent, but poorly predicts its location. Multi-electrode circular catheters induce more complete ablation.

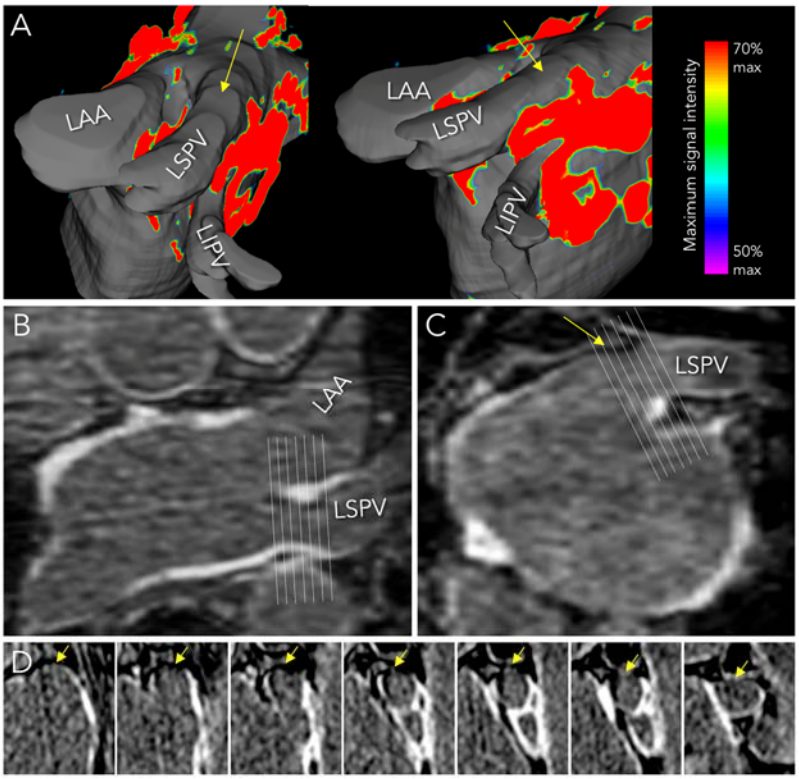

LGE-CMR showing a scar gap on left superior pulmonary vein 3 months after successful pulmonary vein isolation

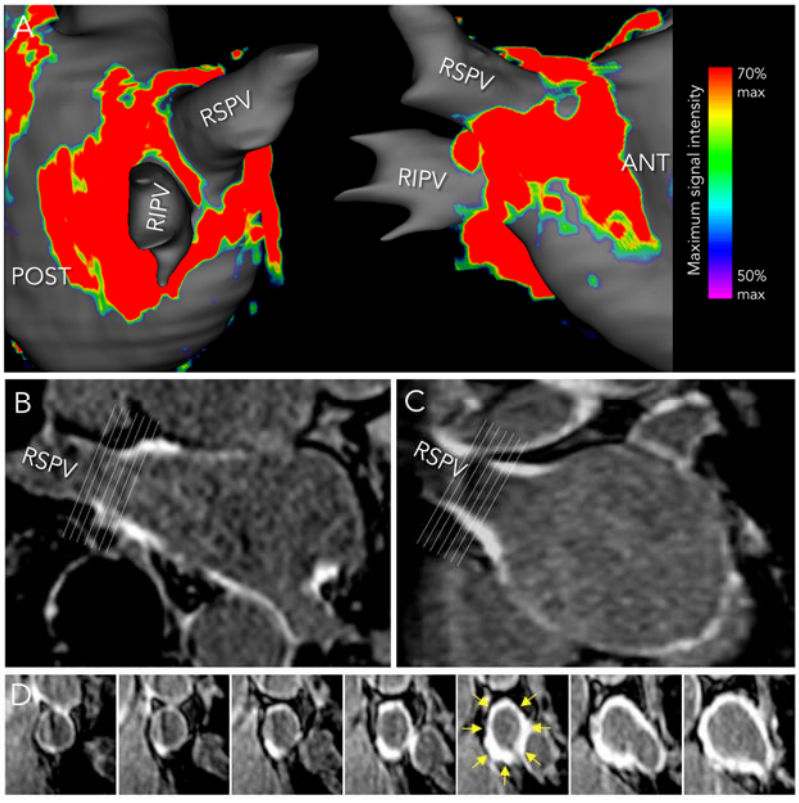

LGE-CMR showing circumferential scar on right pulmonary veins 3 months after successful pulmonary vein isolation

ID#: 376821

Recovery of left ventricular function with CRT. Is it enough to protect from arrhythmic events?

Adelina Doltra, MD, PhD[1] Juan Acosta, MD, PhD[2], Markus Linhart, MD, PhD[2], Mikel Martinez, MD[2], Jose T. Ortiz-Pérez, MD PhD[3], Ignasi Anguera, MD, PhD[4], Diego Penela, MD, PhD[2], Rosario J. Perea Palazón, MD PhD[5], Jose Maria Tolosana, MD, PhD[2], Lluis Mont, MD, PhD[2], Marta Sitges, MD, PhD[2], Antonio Berruezo, MD, PhD[2]

1. Hospital Clínic de Barcelona, Barcelona, Spain

2. Hospital Clínic de Barcelona, Spain

3. Hospital Clínic. Universitat de Barcelona, Catalonia, Spain

4. University Hospital of Bellvitge, Spain

5. Hospital Clínic. Universitat de Barcelona, Barcelona, Catalonia, Spain

Background: The improvement of left ventricle (LV) ejection fraction (EF) beyond >35% (current ICD indication) with cardiac resynchronization therapy (CRT) has been related to lower rate of malignant arrhythmic events at follow-up, opening the potential for even a downgrade from ICD-CRT to pacemaker-CRT if such an improvement occurs. Also, the presence of myocardial scar detected with late gadolinium enhancement (LGE) magnetic resonance (MR) is associated with malignant arrhythmia and sudden cardiac death. Whether scar assessment offers additional prognostic information over LVEF assessment in a CRT population is currently unknown. Therefore, our aim was to investigate if scar quantification with CMR predicts arrhythmic events in CRT patients despite the presence of LVEF improvement.

Methods: We prospectively included 187 patients that underwent CRT implantation (64.5±10.8 years, 53(28.3%) female, 70(37.4%) ischemic etiology, baseline QRS 161.5±29.9 ms, baseline LVEF 26.6±7.7 %). All patients underwent a LGE-MR before the implant, and the presence of scar was assessed. A conventional echocardiography was performed at baseline and at 12 month follow-up, and LVEF was quantified in both exams. Two cut-off values were pre-specified to define a significantly improved LVEF at 12-month echo: LVEF >35% (cutoff for ICD indications), and LVEF >40% (as stricter improvement criteria). Patients were followed-up for the occurrence of appropriate ICD discharge or sudden cardiac death (primary end-point).

Results: 27 patients (14.4%) reached the primary end-point at follow-up (mean follow-up 36.1±29.3). There were no significant differences in the event rate between patients with LVEF >35% and ≤35% (8(9.5%) vs. 19(18.4%), Log-rank p=0.129), although a trend was observed. Similarly, when using stricter criteria for LVEF improvement, no difference was found in the rate of events between the subgroups (8(11.9%) in LVEF>40% vs. 19(15.5%) in LVEF≤40%, Log-rank p=0.518). When the presence of scar was considered, all events occurred exclusively in patients with a scar (27(23.9%) vs 0(0%), p <0.0001), both in patients with and without LVEF improvement. The Figure attached shows the Kaplan Meier curves.

Conclusion: In CRT patients the presence of scar seems to determine the probability of malignant arrhythmia at follow-up. Although a non-significant trend is seen towards less events in patients with LV improvement, a significant risk for malignant arrhythmia exists particularly in the first years of follow-up, and even in patients with only mildly reduced EF. Our study supports the use of LGE-MR before CRT implant for arrhythmia risk assessment.

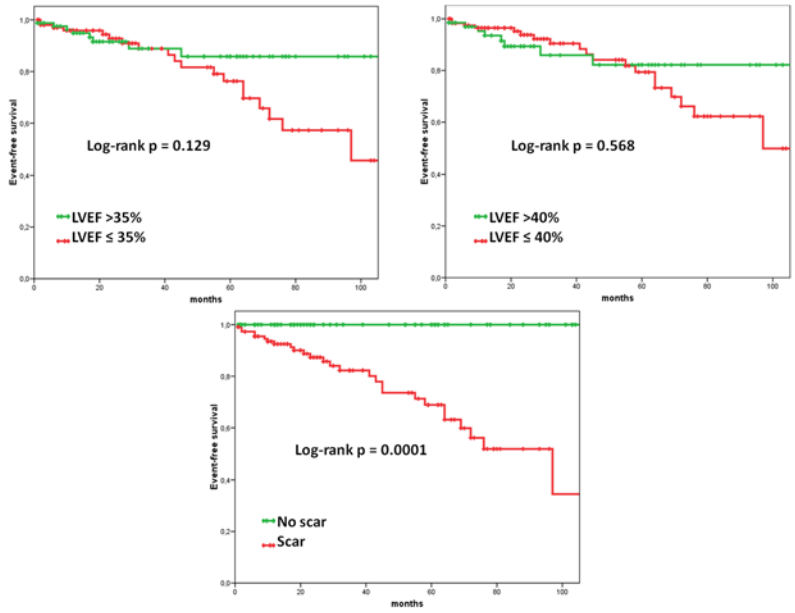

Kaplan Meier curves

ID#: 377022

Assessment of caval blood flow distribution in Fontan circulation using arterial spin labeled measurement of pulmonary perfusion

Joshua S. Greer, BS[1] Jerry Michael, MD[2], Barbara Burkhardt, M.D.[3], Animesh Tandon, MD, MS[3], Gerald F. Greil, MD, PhD[3], Tarique Hussain, MD, PhD[4], Ananth J. Madhuranthakam, PhD[5]

1. Dept. of Radiology, UT Southwestern Medical Center, Irving, TX

2. Dept. of Pediatrics, UT Southwestern Medical Center

3. Dept. of Pediatrics, UT Southwestern Medical Center, Dallas, TX

4. Dept. of Pediatrics, UT Southwestern Medical Center, TX

5. Dept. of Radiology, UT Southwestern Medical Center

Background: Uneven distribution of blood flow from the inferior vena cava (IVC) is suspected to play a role in the development of pulmonary arteriovenous malformations (PAVMs) in Fontan circulation due to the exclusion of hepatic blood flow from the affected lungs. Preferential flow can be observed using cardiac catheterization, and lung perfusion can be evaluated using scintigraphy, but non-invasive and non-ionizing techniques would be beneficial for repeated evaluation in children. The purpose of this study was to investigate the use of two arterial spin labeled (ASL) MR techniques, FAIR and pCASL, to quantify lung perfusion and assess the origin of pulmonary blood in Fontan patients, and validate these measurements with 4D-flow.

Methods: 20 patients with Fontan circulation (age 15.2 ± 2.4 years, 15 male) were scanned on a 1.5T Philips Ingenia between December 2016 and July 2017, with IRB approval and informed assent. ASL-MRI: FAIR perfusion signal is generated from the inflowing inverted blood from outside of the imaging plane, and does not discriminate based on the source of inflowing blood, thus measuring total lung perfusion. pCASL uses a labeling plane to invert blood in a vessel of interest, resulting in a perfusion image containing only blood originating from the labeled vessel. By labeling the IVC, lung perfusion images can be generated with only IVC blood, allowing for the contributions of each vena cava to be calculated from the differences between the ASL techniques. Both approaches used a coronal 2D-SShTSE, background suppression, and multiple averages over 2-3 minutes of guided breathing to improve SNR and reduce motion artifacts. A proton-density image was also acquired for quantification. 4D-Flow: 4D-flow images were acquired over 10-15 minutes, and analyzed using *FourFlow* to quantify differential IVC flow.

Results: Fig.1 shows ASL lung perfusion images showing good agreement with 4D-flow pathlines from the SVC and IVC from three representative subjects. The mean percentage of IVC flow to the right lung across all subjects using ASL was 52%, but varied from 28% to 71%. Mean total lung perfusion across all subjects was 469 ± 198 mL/100g/min, within the accepted normal range.

Conclusion: ASL can be used to simultaneously measure pulmonary perfusion and differential flow from the IVC in Fontan populations. This technique could be beneficial in follow-up patient examinations to evaluate the risk for PAVMs, and for non-invasively evaluating Fontan revisions. Future work includes confirming the level of agreement between ASL and 4D-flow.

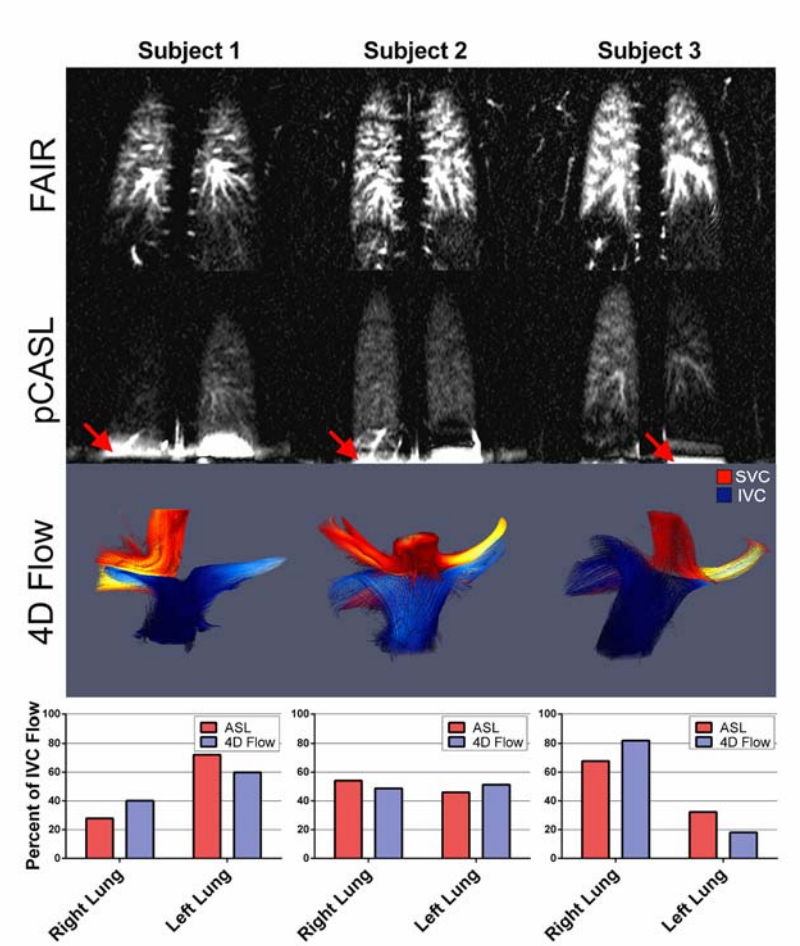

Figure 1: Coronal lung perfusion images from representative subjects acquired using FAIR (total perfusion) and pCASL (IVC contribution only), and 4D-flow pathlines from the SVC and IVC. The graphs show the calculated percentages of IVC flow to the left and right lungs, which are visually in agreement with the ASL and 4D-flow results for each subject. An artifact caused by pCASL labeling can be seen below the diaphragm (red arrows).

ID#: 374054

Ceroid-Induced Apoptosis of Siderophage-Derived Foam Cells Underlies the Perpetual Recruitment of Macrophages and Expansion of "Death Zone" in Hemorrhagic Myocardial Infarctions

Ivan Cokic, MD[1] Guan Wang, MD[2], Kolja Wawrowsky, PhD[2], Hsin-Jung Yang, PhD[2], Richard LQ. Tang, MD[3], Joseph Francis, B.V.Sc., Ph.D[4], Rohan Dharmakumar, PhD[5]

1. Cedars-Sinai Medical Center, Los Angeles, CA

2. Cedars-Sinai Medical Center

3. Cedars-Sinai Medical Center, CA

4. Louisian State University, LA

5. Cedars-Sinai Medical, CA

Background: Following erythrophagocytosis, iron-laden macrophages (siderophages) tend to oxidize surrounding LDL, accumulate cholesterol, produce ceroid-type lipopigment and transform into foam cells (FC). During the process of FC formation, part of the hemoglobin-derived iron forms a complex with developing ceroid. Ceroid is undegradable, cytotoxic and over time, can lead to lysosome destabilization, resulting in leakage of lysosomal contents and finally apoptosis of FC. Release of ceroid from apoptotic FC into the surrounding tissue constitutes a "death zone" containing toxic materials that may cause dysfunction and apoptosis of newly invading macrophages. This can further lead to a progressive accumulation of dead or dying phagocytic cells incapable of resolving the lesion but still capable of releasing cytokines, thereby promoting a self-perpetuating and amplifying loop of phagocyte ingress and apoptosis. Recent studies have shown that iron deposits within hemorrhagic MIs (h-MIs) facilitate perpetual recruitment of macrophages throughout the chronic phase of MI. The lack of efficient clearance of iron within h-MIs implies that macrophages cannot function properly within the environment of an abnormal iron deposition. We hypothesized that ceroid from apoptotic siderophage-derived FCs drives the perpetual increase in macrophage recruitment and expansion of "death zone" in h-MI.

Methods: Canines (n=10) were subjected to 3-hour occlusion of the LAD artery, followed by reperfusion. CMR studies were performed at 3T. Native T1 (MOLLI with bSSFP readout), T2 and T2*, and LGE were performed on day 5 and week 8 post-MI. Mean segmental T1, T2 and T2* values were measured using cvi^{42} (Circle Cardiovascular Imaging Inc.). After CMR on week 8, animals were sacrificed and explanted hearts underwent histopathological analysis. Sections stained with Prussian Blue were examined for autofluorescence of ceroid under confocal microscope. Apoptosis of siderophage-derived FCs was detected using cleaved caspase-3 antibody. Persisting phagocyte ingress was detected by MAC387 antibody (for newly recruited macrophages).

Results: All dogs exhibited intramyocardial hemorrhage on day 5 post-MI. Peri-infarct border zone of h-MIs exhibited significantly elevated T1 and T2 values relative to the infarct core and remote myocardium, suggestive of edema/inflammation and localized fat deposition (Figure 1). Histopathological evaluation demonstrated the enhanced regional colocalization of iron, ceroid, apoptotic FCs and newly recruited macrophages (Figure 2).

Conclusion: Our findings suggest that iron-ceroid complex from apoptotic siderophage-derived FCs promotes perpetual macrophage ingress, fluid extravasation and edema formation, and expansion of "death zone" in h-MIs. We conclude that iron-ceroid complex is a key driver of accelerated adverse LV remodeling in h-MIs.

Figure 1

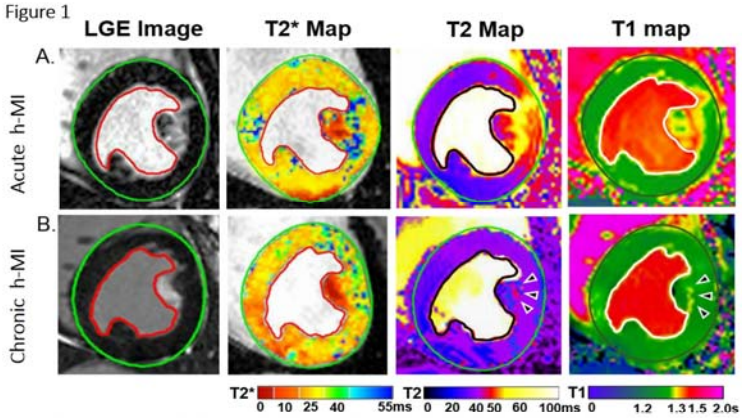

Figure 1. LGE and non-contrast-enhanced relaxation maps of canine hearts in the acute and chronic phases of reperfused myocardial infarction at 3.0T. Panels A and B show representative LGE images, and native T2*, T2, and T1 maps acquired 5 days (acute) and 8 weeks (chronic) following reperfusion in a dog with hemorrhagic myocardial infarction. Note that T1 and T2 values in the peri-infarct border zone remained substantially elevated (arrows) throughout the chronic phase of hemorrhagic MI (h-MI).

Figure 2

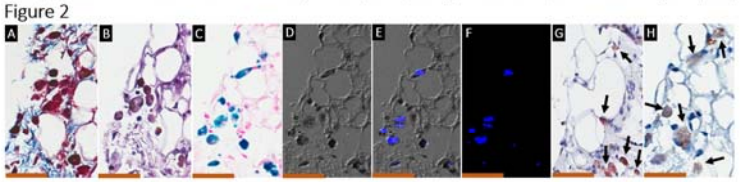

Figure 2. HISTOPATHOLOGY: Serial sections of the infarcted subendocardial myocardium 6 months post-MI stained with H&E **(A)**, elastin-modified Masson's trichrome stain **(B)** and Prussian Blue **(C)**. Note the extensive co-localization of fat (foam cells) with iron deposits. **Confocal Microscopy:** Autofluorescence of ceroid was examined in sections stained with Prussian Blue: **(D)** Differential Interference Contrast (DIC), **(E)** Excitation wavelength: 405 nm and Emission wavelength: 428-496 nm, **(F)** Overlay. Note the extensive co-localization of ceroid with iron and foam cells. **Foam Cell Apoptosis:** Positive immunohistochemical staining with Cleaved caspase-3 antibody confirmed the ongoing apoptosis of siderophage-derived foam cells (red stain; arrows) **(G)**. Ceroid deposition within the "death zone" appeared to be a highly potent chemoattractant for new monocytes/macrophages as evidenced by MAC387-positive immunohistochemical staining (brown stain; arrows) **(H)**. Scale bar equals 50 µm.

ID#: 374164

Prevalence of myocardial scar and myocardial inflammation in patients with sustained and non-sustained ventricular arrhythmias: A cardiac magnetic resonance and 18F-FDG cardiac PET study

Kalie Y. Kebed, MD[1] Erin Flatley, MSN, AGNP-BC[2], R. Parker Ward, MD[3], Joshua D. Moss, MD[4], Javid Ali, CNMT[5], Daniel Appelbaum, MD[6], Amita Singh, MD[5], Roderick Tung, MD[7], Amit R. Patel, MD[6]

1. University of Chicago, Chicago, IL

2. University of California San Francisco, San Francisco, CA

3. University of Chicago Medicine

4. University of California San Francisco

5. University of Chicago

6. University of Chicago, IL

7. University of Chicago Medical Center, IL

Background: Patients with ventricular tachycardia (VT) often have late gadolinium enhancement (LGE), representing myocardial scar, on cardiac magnetic resonance (CMR). Recently it has been shown that VT is also often associated with myocardial inflammation as determined by 18F-fluorodeoxyglucose (18F-FDG) uptake using cardiac positron emission tomography (PET). In this study, we sought to determine the relationship between myocardial 18F-FDG uptake and presence of LGE in patients with VT.

Methods: We retrospectively identified 40 patients without a known history of sarcoidosis referred for both CMR and PET for the evaluation of ventricular arrhythmias. Patients were divided into 2 groups based on burden of ventricular arrhythmias: non-sustained (NSVT) versus sustained VT. CMR was performed using a 1.5T scanner (Achieva, Philips). Standard cine- and LGE- CMR protocols were used. Prior to cardiac PET, patients were instructed to undergo a 24 hour carbohydrate fast and 12 hour strict fast to suppress physiologic myocardial glucose utilization. Cardiac PET images, along with low-dose CT images for attenuation correction, were acquired 60-90 minutes after the intravenous administration of 18F-FDG (10 mCi). Commercially available software was used to quantify CMR volumetric data. The presence of any myocardial LGE was defined as signal intensity >5 SDs above the mean signal intensity of normal myocardium. Cardiac PET images were considered positive if there was focal myocardial 18F-FDG uptake having greater activity than the left ventricular blood pool.

Results: The median time between CMR and PET was 14 days. There were 20 patients with NSVT and 20 with sustained VT. Age, gender, and LVEF were similar between groups. LGE was present in 12 (60%) patients with NSVT and 10 (50%) with VT. Myocardial 18F-FDG uptake was present in 7 (35%) patients with NSVT and 4 (20%) with VT. Both LGE and 18F-FDG uptake were present in 5 (25%) patients with NSVT and 3 (15%) with VT (Figure). LGE without 18F-FDG uptake was seen in 7 (35%) patients in both the NSVT and VT groups. 18F-FDG uptake in the absence of LGE was seen in only 2 (10%) patients with NSVT and 1 (5%) with VT.

Conclusion: LGE was present in the majority of patients with ventricular arrhythmias and was often associated with concomitant myocardial inflammation, whereas myocardial inflammation in the absence of LGE was uncommon.

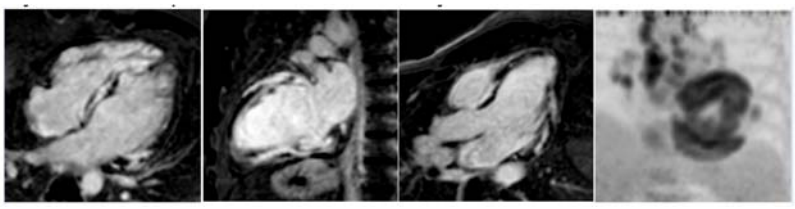

Late gadolinium enhancement and F18-FDG uptake (right image) of the myocardium in a patient with ventricular tachycardia.

ID#: 373522

Prognostic and incremental value of individual components of a cardiovascular magnetic resonance examination in patients with suspected ischaemic heart disease: long-term follow-up of CE-MARC

Peter P. Swoboda, PhD[1] James R. Foley, MBChB BSc (Hons)[1], Colin C Everett, MSc[2], Julia M Brown, MSc [2], Petra Bijsterveld, MA[2], Neil Maredia, MB ChB, MD [3], Manish Motwani, MB ChB, PhD [4], Sven Plein, MD PhD[5], John P. Greenwood, PhD[5]

1. University of Leeds, Leeds, England, United Kingdom

2. University of Leeds, United Kingdom

3. James Cook University Hospital, United Kingdom

4. Manchester Heart Centre, United Kingdom

5. University of Leeds, England, United Kingdom

Background: Cardiovascular magnetic resonance (CMR) is increasingly used for the investigation of suspected coronary heart disease (CHD). We aimed to investigate, in patients with suspected CHD which of inducible ischaemia, left ventricular ejection fraction (LVEF) and ischaemic scar assessed by CMR had the strongest association with long-term adverse outcomes and if any of these CMR components had incremental prognostic value over findings on invasive coronary angiography.

Methods: 752 patients from the CE-MARC (Clinical Evaluation of MAgnetic Resonance imaging in Coronary heart disease) study were followed up for a minimum of 5 years for major adverse cardiovascular events (MACEs) including cardiovascular death, acute coronary syndrome, unscheduled revascularization or hospital admission for cardiovascular cause. Prediction of time to first MACE was assessed by using log-rank test and Cox proportional hazards regression analysis.

Results: CMR and invasive coronary angiography were available in 676 patients in whom 114 (16.9%) had at least 1 MACE. Significant stenosis on coronary angiography (hazard ratio (HR) 2.7, 95% confidence interval (CI) 1.9-4.0, P<0.001), inducible ischaemia (HR 1.6, 95%CI 1.1-2.5, P=0.015) and ischaemic scar (HR 2.6, 95% CI 1.7-3.8, P<0.001) were independent predictors of time to first MACE. LVEF<55% (HR 1.4, 95%CI 0.9-2.0, P=0.11) did not predict time to first MACE in this population. After correction for baseline risk factors the presence of ischaemic scar was the only CMR parameter to significantly predict MACE (HR 2.2, 95%CI 1.48-3.48, P=0.0003). In stepwise multivariable Cox regression analysis, the addition of ischaemic scar to a model of age and stenosis on coronary angiography led to an improvement in prediction of MACE. All three components of age (HR 1.39, 95% CI 1.12-1.73, P=0.003), ischaemic scar (HR1.72, 95% CI 1.09-2.71, P=0.020) and significant stenosis on invasive coronary angiography (HR 1.81, 95% CI 1.16-2.83, P=0.010) had significant contributions to the model. The addition of inducible ischaemia and LVEF<55% did not lead to a statistically significant improvement in the model.

Conclusion: In patients with suspected CHD, inducible ischaemia and ischaemic scar by CMR are both associated with adverse outcomes on follow up. However only the presence of ischaemic scar has incremental prognostic value over conventional risk factors and significant stenosis identified on invasive angiography.

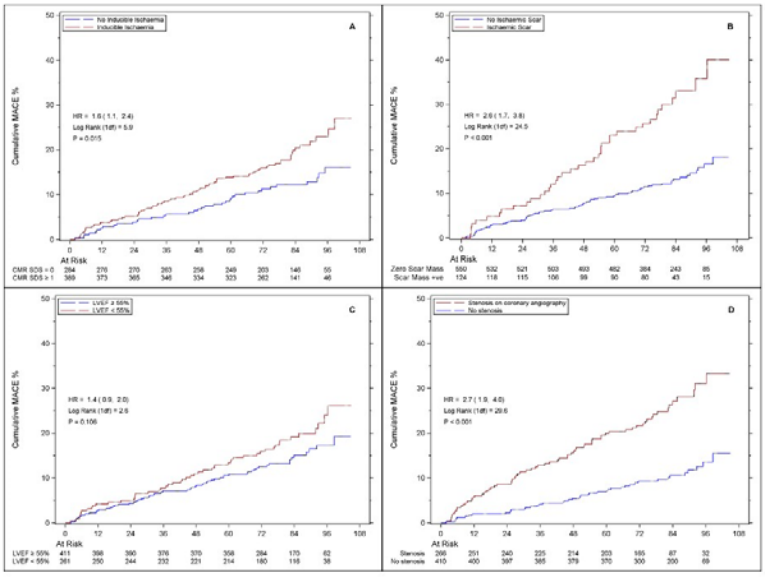

Cumulative incidence of MACE over time (months) according to the presence of A: inducible ischaemia, B: ischaemic scar, C: LVEF<55% or D: significant stenosis on invasive angiography

ID#: 374300

CMR-derived circumferential strain measures and the risk of ventricular arrhythmia in patients with prior myocardial infarction and implantable cardioverter defibrillator

Elisabeth H.M. Paiman, MD[1] Alexander F. Androulakis, MD[2], Rahil Shahzad, PhD[3], Qian Tao, PhD[4], Katja Zeppenfeld, MD, PhD[2], Hildo J. Lamb, MD, PhD[5], Rob J. van der Geest, PhD[4]

1. Department of Radiology, Leiden University Medical Center, Leiden, The Netherlands, Netherlands

2. Department of Cardiology, Leiden University Medical Center, The Netherlands, Netherlands

3. Department of Radiology, Leiden University Medical Center, Leiden, The Netherlands, Leiden`, Zuid-Holland, Netherlands

4. Department of Radiology, Leiden University Medical Center, The Netherlands, Leiden, Zuid-Holland, Netherlands

5. Department of Radiology, Leiden University Medical Center, Leiden, The Netherlands, Zuid-Holland, Netherlands

Background: Ventricular arrhythmia (VA) risk stratification in patients with ischemic cardiomyopathy remains challenging. Disturbed left ventricular (LV) contraction and relaxation, promoting adverse remodeling, may increase ventricular arrhythmogeneity. Aim of this study is to explore the association of CMR-derived global and regional systolic and diastolic circumferential strain measures, with the risk of VA in patients with myocardial infarction and implantable cardioverter defibrillator (ICD).

Methods: Patients with ischemic cardiomyopathy and ICD, who underwent CMR prior to ICD implantation, were retrospectively included. Segmental circumferential strain curves were extracted from bSSFP CMR using feature tracking. The subhazard ratio (SHR) for appropriate ICD therapy, with all-cause mortality as competing risk, was calculated for LV ejection fraction (LVEF), global strain, peak diastolic strain rate, mechanical dispersion and the extent of severely and moderately impaired strain (percentage of LV segments with peak systolic strain less than -5% and between -5% and 10%, respectively).

Results: In the primary (n=144) and secondary (n=37) prevention ICD group, respectively, 35 (24.3%) and 17 (45.9%) received appropriate ICD therapy and 17 (11.8%) and 1 (2.7%) died, during a median follow-up of 39.8 months (interquartile range 14.2-63.1). In patients with primary prevention ICD, the SHR was statistically significant for LVEF, global strain, peak diastolic strain rate, severely and moderately impaired strain, but not for mechanical dispersion. The risk associated with peak diastolic strain rate and moderately impaired strain was independent of LVEF (1.51 (1.01-2.25) per -0.25 s-1, p=0.04 and 1.52 (1.08-2.15) per +10%, p=0.02, respectively). The association with appropriate ICD therapy for moderately impaired strain was independent of severely impaired strain (SHR 1.69 (1.28-2.25) per +10%, p<0.001). In contrast, in patients with secondary prevention ICD, none of the CMR measures was associated with appropriate ICD therapy.

Conclusion: Circumferential peak diastolic strain rate and the extent of moderately impaired strain were associated with appropriate ICD therapy, independently of LVEF, in post-infarct patients with primary prevention ICD. Moderately, rather than severely impaired strain, was associated with the risk of VA. In patients with secondary prevention ICD, other mechanisms beyond disturbed LV contraction and relaxation, may be operative in ventricular arrhythmogenesis.

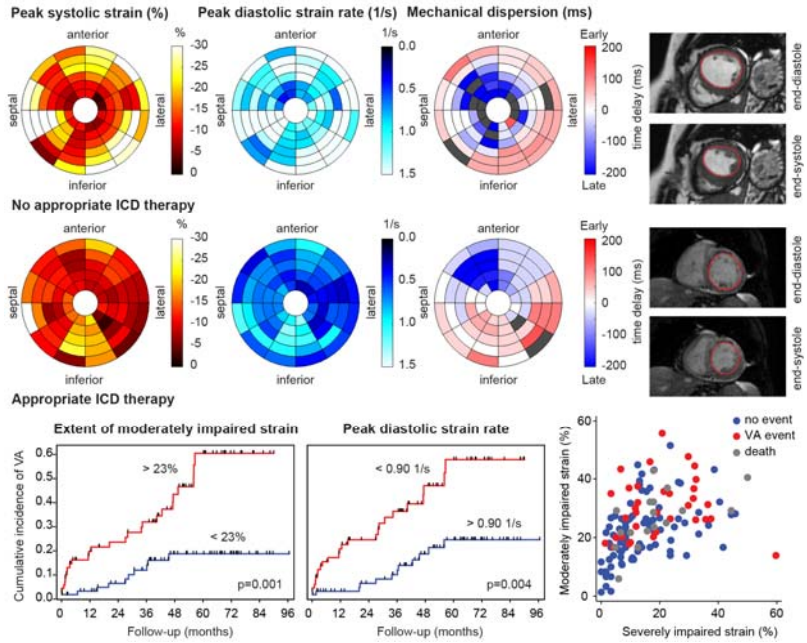

(upper panel) LV bullseye representation of circumferential peak systolic strain, peak diastolic strain rate and mechanical dispersion (extracted from short-axis bSSFP cine CMR). (upper panel, first row) 68-year-old man, without appropriate ICD therapy (LVEF 30%). (upper panel, second row) 50-year-old man, with appropriate ICD therapy at 40 months after ICD implantation (LVEF 26%). The extent of moderately impaired strain (strain between -5% and -10%) is relatively large and diastolic strain rate is low. The extent of severely impaired strain (strain less than -5%) and the mechanical dispersion are comparable in the presented cases. (lower panel, left) Kaplan-Meier curves of the cumulative incidence of appropriate ICD therapy in relation to moderately impaired strain and peak diastolic strain rate for the primary prevention ICD group, with the observed median as the cut-off. The association of moderately impaired strain and peak diastolic strain rate with appropriate ICD therapy was independent of LVEF. (lower panel, right) Scatter plot showing the relation between severely and moderately impaired strain.

ID#: 374461

Assessing myocardial fibre architecture in ex vivo specimens of congenital heart disease.

Cyril Tous, ME, MR, MB, BE, B.Sc[1] Alistair Young, PhD[2], Beau Pontre, PhD[3]

1. The University of Auckland, Auckland, Auckland, New Zealand

2. University of Auckland, New Zealand, GRAFTON, Auckland, New Zealand

3. The University of Auckland, New Zealand

Background: Thanks to improved surgical techniques, many children born with congenital heart defects are now surviving into adulthood, but these individuals have increased risk of cardiac dysfunction later in life. In the normal heart, the myocardial fibres are arranged in a continuous helical fashion. Disruptions to this pattern through structural remodelling of the tissue has been shown to adversely affect cardiac function. This study aims to evaluate how fibre architecture varies between specimens with two different types of congenital heart defects (CHD), namely tetralogy of Fallot (TOF), and transposition of the great arteries (TGA).

Methods: Diffusion tensor imaging (DTI) was performed on 12 *ex vivo* heart specimens with TOF(N=6) and with TGA(N=6). The age at the donation date ranges from 1 to 33 years (mean=13±9 years) with the time spent in 10% formaldehyde ranging from 28 to 57 years (mean=41±9 years). Specimens were scanned at room temperature (21°C) using a spin echo sequence with monopolar diffusion-encoding gradients. Imaging parameters used are: b=800 s/mm^2, 32 diffusion-encoding directions, averages=2, TR=1s, TE=57ms, slices=3, field of view= 200x200, acquisition voxel = 2x2x4. Mean fractional anisotropy (FA), mean diffusivity (MD) and mode were calculated across the myocardium. Diffusion metrics that characterise the myocardial fibre orientation, the helix angle (HA), transverse angle (TA) and sheet angle (SA) were also calculated. A polynomial fit of the measured angles across the myocardial wall was performed to characterise these metrics for each specimen. ANOVA test was used to assessed the mean differences in these metrics.

Results: In table 1, we observe no significant difference in FA, MD or mode between the two specimen groups. However, the slope of the polynomial fit of the helix angle is significantly different between the two groups ($p<0.002$). Figure 1 shows that the sheet angle is swapped (-35 degree in the septum, +35 degree elsewhere) compared to a healthy heart (+35 degree in the septum, -35 degree elsewhere).

Conclusion: Both TOF and TGA show reversed sheetlet (negative in the septum and positive elsewhere) compared to that seen in normal cardiac anatomy. A normal heart shows a slope in HA of -1.4 across the myocardial wall. We can conclude that the HA slope of a TGA is abnormal. The helix angle and the sheet angle are known to play a key role in the myocardial torsion required for normal cardiac function. Myocardial architecture remodelling between different types of CHD may cause additional stress in the myocardial muscle.

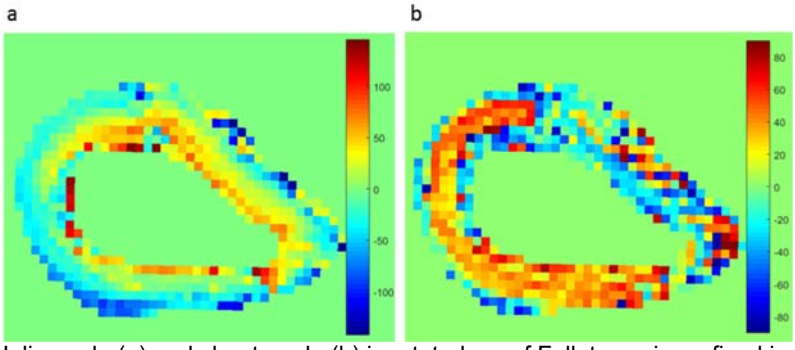

Helix angle (a) and sheet angle (b) in a tetralogy of Fallot specimen fixed in formalin.

DTI metrics according to the congenital heart disease

	TGA (N=6)	TOF (N=6)
FA	0.13±0.06	0.15±0.06

MD	$0.89x10^{-3}$±0.01	$0.87x10^{-3}$±0.01
mode	0.01±0.54	0.05±0.54
slope HA	-1.06±0.32	-1.32±0.38

ID#: 373183

Correlation of 4D flow MRI aortic wall shear stress to medial elastin fiber thinning in patients with a bicuspid aortic valve

Emilie Bollache, PhD[1]David Guzzardi, BSc[2], Chris Malaisrie, MD[3], Pim van Ooij, PhD[4], Jeremy D. Collins, MD[1], James Carr, MD[1], Patrick M. McCarthy, MD[1], Michael Markl, PhD[1], Paul W Fedak, MD, PhD[2], Alex J. Barker, PHD[1]

1. Northwestern University, Chicago, IL

2. University of Calgary, Canada

3. Northwestern University

4. Amsterdam Medical Center, Netherlands

Background: Bicuspid aortic valve (BAV) is associated with an increased risk of aortopathy, which is characterized by a degradation of the medial elastin fibers. In a previous study, a binary analysis of abnormally ‘elevated'; vs. ‘normal'; aortic wall shear stress (WSS) in BAV patients provided first evidence that regions with elevated WSS exhibited a higher degree of medial elastin fiber degeneration. The aim of the present study was to 1) quantitatively characterize regional aortic WSS in BAV patients compared to healthy controls, and 2) perform direct correlations of WSS to histological markers of elastin degradation.

Methods: Twenty BAV patients (Table 1) underwent prospective ECG- and respiratory navigator-gated aortic 4D flow MRI before surgery of the ascending aorta (1.5 or 3T, spatial / temporal resolution=2.2–3.8x1.7–2.7x2.2–3mm^3 / 36–43ms, venc=150-400cm/s). Aortic tissue samples were resected during surgery and their longitudinal and circumferential location was noted. Longitudinal zones 1 and 2 were defined, respectively, as the proximal and distal ascending aorta regions between the level of the inferior border of right pulmonary artery and the proximal takeoff of innominate artery (Figure 1). Each zone was subdivided into circumferential quadrants indicated by anterior, posterior, greater and lesser curvature. Histology was performed in each sample to assess mean elastin fiber thickness. Peak systolic 3D WSS was calculated throughout the aorta using 4D flow MRI data and a previously described method. Median WSS was extracted in regions of interest registered to each sample location using custom software (Figure 1). Twenty age- and gender-matched healthy volunteers (2 women; 48±14 years) were included as a control group representing physiologically normal WSS values.

Results: On average, 3 [1-8] aortic tissue samples were collected and analyzed in each patient, resulting in total n=73 samples (zone 1: n=61; zone 2: n=12). As expected, WSS was significantly increased in BAV patients when compared to controls in all regions except for the lesser curvature. In addition, WSS was significantly higher in the posterior and greater curvature regions than in the anterior location (Figure 2.a). Finally, a moderate but significant inverse correlation (r=-0.28, p=0.02) was found between increased WSS and reduced elastin fiber thickness (Figure 2.b).

Conclusion: The findings of this study demonstrate a significant correlation between 4D flow-derived aortic WSS and elastin fiber thickness at histopathology *in vivo*. Higher WSS was found to be associated with thinner elastin fibers which reflects elastin degradation, indicating the potential usefulness of non-invasive WSS to detect medial wall degeneration. Absolute WSS measurements could be more sensitive than binary maps and help refining risk stratification to improve decision making and provide patient-specific surgical strategies.

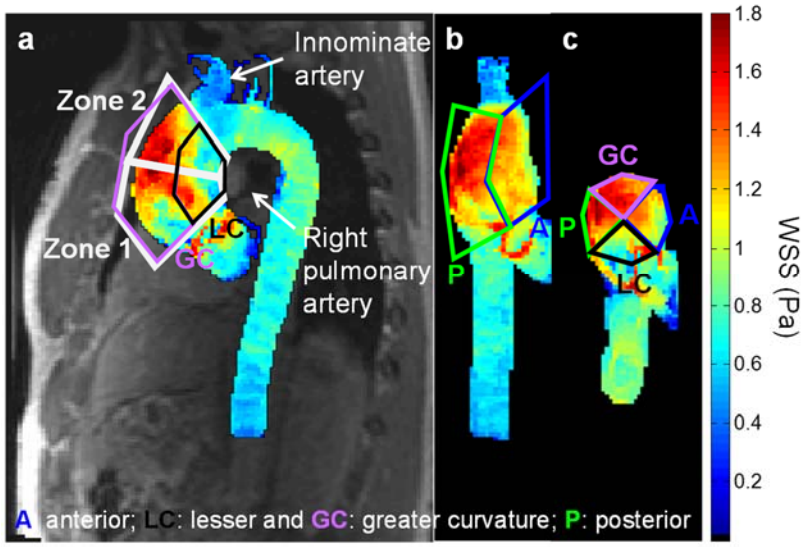

Extraction of local median aortic WSS from 4D flow MRI data according to resected tissue sample location. Longitudinal (zones 1 and 2) regions of interest (ROIs) were defined on sagittal orientation (a), while circumferential (A, P, GC and LC) ROIs were defined using sagittal (a), coronal (b) and axial (c) orientations.

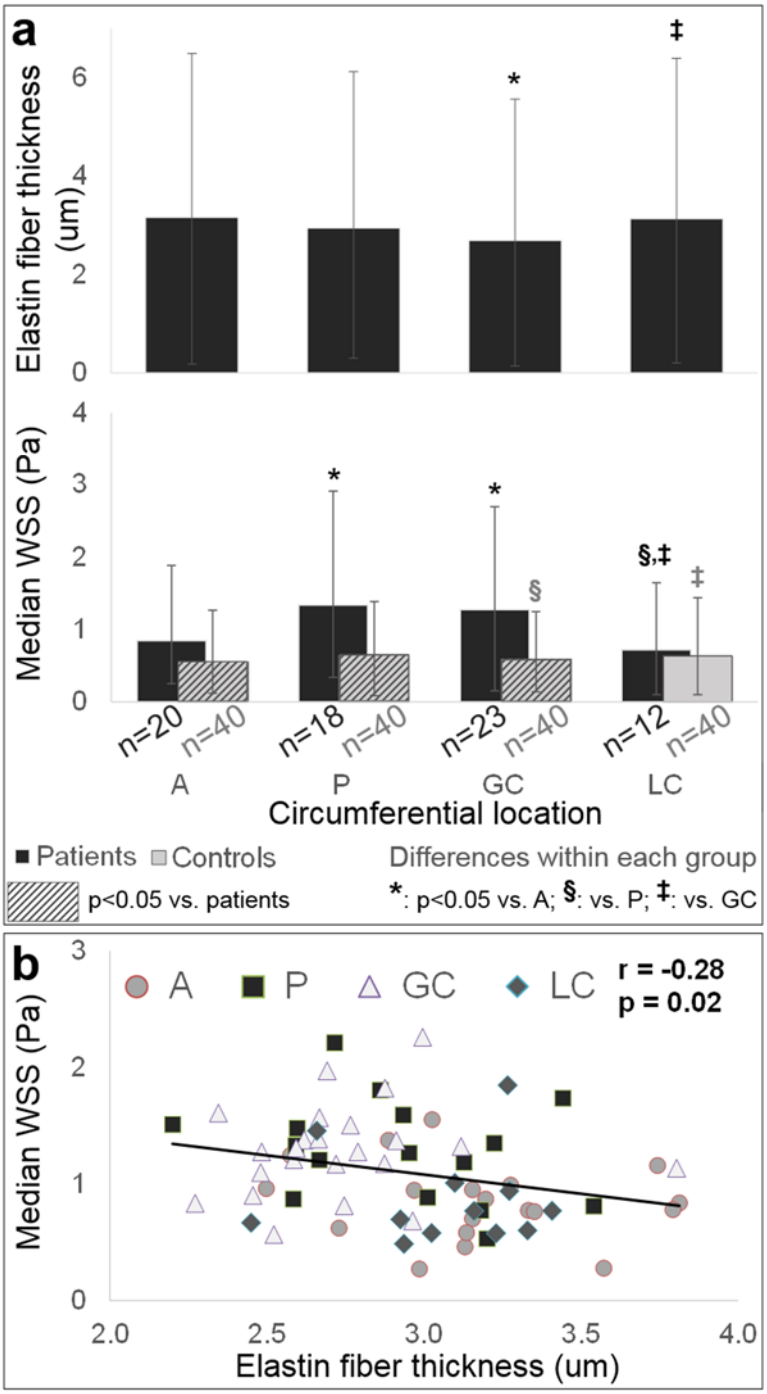

a. Elastin fiber thickness (top) and median aortic WSS (bottom) measurements in BAV patients (dark) and controls (light gray) according to the circumferential location, while pooling zones 1 and 2. n WSS measurements are reported, in regions where tissue was resected in patients and in all locations in controls. Data are represented as medians and interquartile ranges. b. Correlation between aortic medial elastin fiber thickness and WSS in BAV patients while pooling all locations. A: anterior; P: posterior; LC: lesser and GC: greater curvature.

BAV patients characteristics (n=20)

Women / men (n)	2 / 18

Age (years)	48±15
Sievers valve classification (n)	
type 0-lateral	2
type 1-RL	12
type 1-RN	1
type 2-RL/RN	5
Aortic stenosis (AS, n)	15
Aortic insufficiency (AI, n)	15
Mixed AS and AI (n)	10
Maximal aortic diameter (cm)	4.7±0.6

ID#: 373229

Surgical planning prediction of hepatic flow distribution for Fontan revisions using preoperative boundary conditions: a comparison with post-operative data

Phillip M. Trusty, MS[1] Zhenglun Wei, PhD[2], Timothy Slesnick[3], Mark A. Fogel, MD[4], Ajit Yoganathan, PhD[2]

1. Georgia Institute of Technology, Atlanta, GA

2. Georgia Institute of Technology

3. Emory University School of Medicine, Children's Healthcare of Atlanta

4. Children's Hospital of Philadelphia, Philadelphia, PA

Background: Fontan surgical planning has been used to provide insight for complex Fontan cases and while hypothesized to predict post-operative hemodynamics, no studies exist comparing surgical planning predictions with longer term post-operative results. The accuracy and effectiveness of surgical planning to predict hemodynamics, including hepatic flow distribution (HFD), is currently unknown. The purpose of this study is to compare surgical planning predictions with longer term post-operative data.

Methods: Five patients who underwent a Fontan revision operation due to the progression of PAVMs were included. Each patient was enrolled in a surgical planning protocol before the reoperation. Cardiac magnetic resonance (CMR) and phase-contrast CMR data was obtained for all patients both pre-operatively and post-operatively. Computational fluid dynamic simulations were performed to quantify HFD for the pre-operative, virtual proposed post-operative, and in vivo post-operative states using patient specific anatomies and blood flow waveforms reconstructed from CMR data. Surgical planning predictions were compared against post-operative data.

Results: Patient age was 12 [4.5-14] years at the time of reoperation, with post-operative follow up periods of 40 [2-96] months after Fontan revision. Four patients had an interrupted IVC with right-sided azygous continuation, three of which also had bilateral SVCs. Pre- to post-operative vessel flow rates changed on a patient and vessel specific basis, with no discernable trends based on patient age or follow up time. All pre-operative CFD simulations confirmed highly unbalanced HFD leading to PAVM progression. Despite the inconsistency in follow-up time, surgical planning accurately predicted HFD (within 10 points) for 3/5 cases (representative case shown in Figure 1). In the fourth case, pre-op flow rates were only available for outlet vessels, and estimations of the inlet flow rates were not sufficient for accurate surgical planning. The largest difference between the virtual proposed option and surgical implementation was seen in the final case, and this anatomical discrepancy clearly hindered the predictive power of surgical planning.

Conclusion: Even with the simplification of using pre-operative boundary conditions, surgical planning produced accurate estimations of post-op HFD for the majority of cases in this study. The effectiveness of surgical planning is highly dependent on the robustness of the proposed option, as variations in surgical implementation will exist. Improved predictions of vessel flow rates during the post-operative state are necessary to improve surgical planning predictions. Though this study focuses only on Fontan revisions, boundary condition prediction may have increased importance for stage 2-3 Fontan surgical planning.

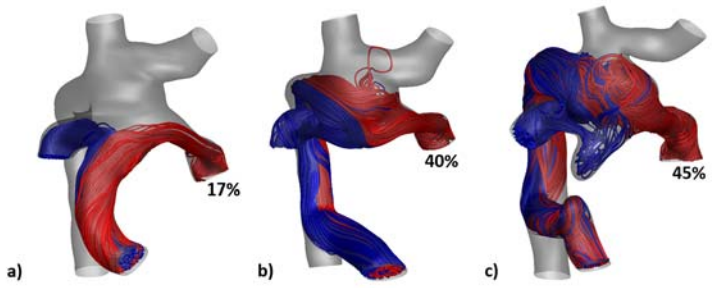

Figure 1: Flow field comparison between (a) pre-operative, (b) predicted, and (c) post-operative states. Post-operative state is an 8 year follow up. Streamlines colored by outlet vessel. Hepatic flow distribution is indicated by percentage to left pulmonary artery for each state.

ID#: 373282

Real-time flow using a golden-angle spiral acquisition

Rajiv Ramasawmy, PhD[1]Daniel Herzka, PhD[2], Robert J. Lederman, MD[3], Adrienne E. Campbell-Washburn, PhD[3]

1. National Institutes of Health, Bethesda, MD

2. National Institutes of Health

3. National Heart, Lung, and Blood Institute, National Institutes of Health, MD

Background: Real-time measurement of cardiac output has been shown to complement interventional cardiovascular MR procedures [1]. Beat-to-beat measurements of blood flow can monitor acute response to exercise provocation, where conventional segmented cardiac imaging, reliant on ECG triggering, is inadequate. We investigate the suitability of a golden-angle spiral acquisition to measure flow with two analyses: 1) real-time estimation of cardiac output and 2) retrospectively self-gated estimation of cardiac output, based on re-binning of beat-to-beat flow data.

Methods: Normal human subject studies were approved by the NHLBI institutional review board. Scans were performed on a 1.5T scanner (Aera, Siemens Healthcare, Germany). Real-time flow through the ascending aorta was acquired at rest for 18 seconds, and one subject was exercised on an MR-compatible ergometer (CardioStep, Ergospect, Austria).
An eight-shot spiral design [2] was modified to rotate by the golden angle (sequence parameters: TE/ TR = 1.6/ 9.2 ms, 2.7 x 2.7 mm^2 resolution). Flow data was analyzed three ways (fig 1): 1) as a real-time data stream using successive spiral arms (acceleration factor 4, temporal resolution 36.8 ms) to obtain beat-to-beat flow using an aortic ROI [3], 2) retrospective cardiac binning of spiral arms using the recorded ECG, and 3) retrospective cardiac binning of spiral arms using self-gating from the real-time flow data.
Images were reconstructed offline using iterative conjugate gradient SENSE [4] in Matlab (Mathworks, USA), and data was binned in to 30 cardiac frames to achieve a mean temporal resolution of 29.8 ms for retrospective reconstructions.
Reference ECG-gated Cartesian flow data was acquired with the following parameters: 1.4 x 1.4 mm^2 resolution, TE/TR = 2.8/5.0 ms, 3 averages, acceleration factor 3.

Results: There was no significant difference between cardiac output as estimated by the averaged real-time data, ECG-gated, self-gated and reference Cartesian GRE acquisition (Fig 2A&B) (Friedman test $p > 0.65$), though a slight over-estimation of cardiac output was measured by real-time (106 ± 8%), ECG-binned (102 ± 4%), self-gated (102 ± 4%) compared to reference Cartesian acquisitions. During exercise, the self-gated data preserved the expected flow profile, where the other techniques yielded erroneous or under-estimated data (fig 2C).

Conclusion: In this preliminary study, we have implemented a real-time flow sequence employing a golden angle sampling pattern to facilitate reconstruction of both a beat-to-beat and self-gated dataset. Self-gating is preferred over ECG-gating since ECG traces are unreliable under physiological provocations such as exercise. This may facilitate an improved workflow during cardiovascular intervention by enabling real-time monitoring of provocations and retrospective generation of averaged datasets Funding
This work was supported by the NHLBI DIR (Z01-HL006039, Z01-HL005062). References
[1] Barber N et al. *JCMR,* 2016; [2] Lee JH, et al. *MRM*. 2000. [3] Ramasawmy R, et al. *ISMRM* 2017; 2841. [4] Pruessman KP, et al. *MRM.*, 2001

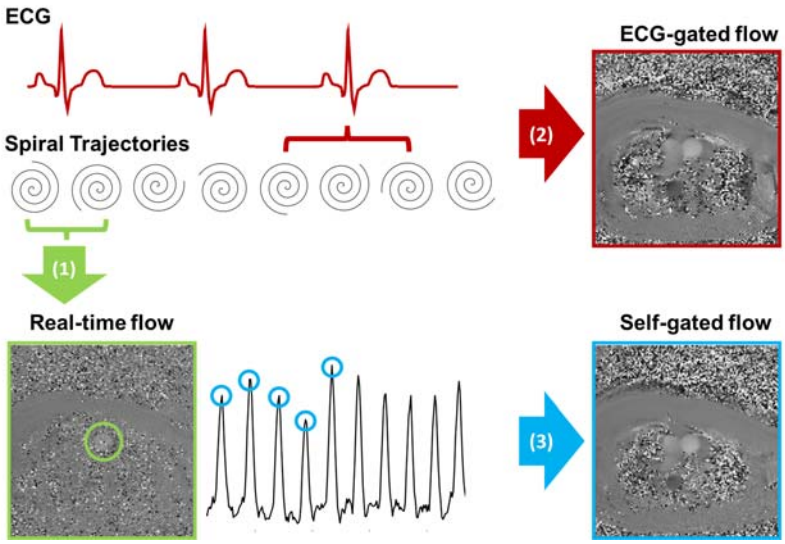

Fig 1: Schematic of golden-angle spiral data reconstruction 1) real-time data using two successive spiral trajectories (acceleration factor 4), 2) retrospective cardiac binning using the ECG as a reference, 3) retrospective self-gating using the peak detection from the real-time flow data from an approximate aortic ROI.

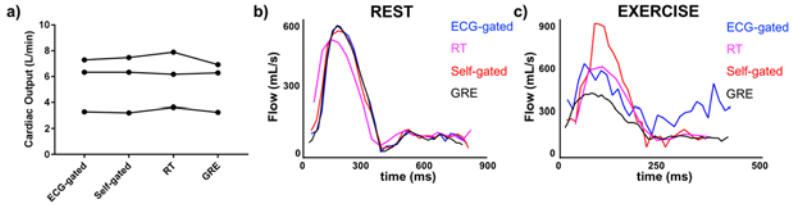

Fig 2: a) Comparison of cardiac output at rest across three healthy human subjects as estimated by the mean real-time (RT), ECG-gated golden-angle spiral, self-gated golden-angle spiral and reference ECG-gated Cartesian GRE analysis. No significant difference between the techniques was measured, indicating that the self-gating technique is robust. Example flow profiles have good agreement when acquired at rest b) but inadequate ECG gating yields erroneous data during exercise c), though the self-gated data maintained an expected flow profile.

ID#: 373460

Phenotype development in Cardiac Fabry disease proceeds through four stages: a prospective 182-patient study

Sabrina Nordin, MRCP [1] Rebecca Kozor, PhD[2], Katia Devorha. Menacho, MD[3], Amna Abdel-Gadir, MBBS.MRCP(UK)[4], Shanat Baig, MBBS[5], Ilaria Lobascio, MD[1], Elaine Murphy, FRCPath[6], Robin Lachmann, PhD[6], Atul Mehta, PhD[7], Peter Kellman, Ph.D.[8], Nicola Edwards, PhD[5], Uma Ramaswami, MD[9], Richard Steeds, MD[5], Derralynn Hughes, PhD[7], James C. Moon, MD[10]

1. Barts Heart Centre, United Kingdom

2. University of Sydney, Sydney, New South Wales, Australia

3. Barts Heart Centre, London, England, United Kingdom

4. University College London and Barts Heart Centre, London, England, United Kingdom

5. University Hospitals Birmingham, England, United Kingdom

6. National Hospital for Neurology and Neurosurgery, United Kingdom

7. Royal Free Hospital, England, United Kingdom

8. National Heart, Lung, and Blood Institute, Bethesda, MD

9. Royal Free Hospital, United Kingdom

10. Barts Heart Centre, England, United Kingdom

Background: Fabry disease (FD) is a rare, X-linked lysosomal storage disorder. Cardiovascular death is the leading cause of death in both sexes with men affected earlier than women. T1 is low in FD representing sphingolipid accumulation. We sought to refine further our understanding of myocardial disease development in FD using multiparametric CMR in a large FD cohort (adults and children, males and females).

Methods: A prospective, observational study of 182 FD (167 adults and 15 children; mean age 42±17 years, 37% male) with CMR (LV structure, function, native myocardial T1, LGE and ECV), 12-lead ECG and blood biomarkers (troponin and NT-proBNP).

Results: In children (n=15, age range 6-16 years), T1 was never below the normal range, but fell with age (r -0.78 in children/adolescents, r -0.41 in the whole cohort, both $p<0.001$). T1 fell faster with age in males compared to females pre LVH (r -0.54 males, $p=0.008$; r -0.276 females, $p=0.012$). LVH, LGE and ECG abnormalities occurred earlier in males. LGE always occurred in the presence of LVH in males, however, occurred without LVH in 18% of females. Once LVH was present, T1 demonstrated major sex dimorphism: with increasing indexed LVM in females, T1 and LVH became uncorrelated (r -0.239, $p>0.05$), but in male, the correlation reversed as T1 increased with indexed LVM (r +0.631, $p<0.001$; Figure 1).

Conclusion: These data propose four stages of Fabry myocardial phenotype development: Stage 1: silent myocyte storage starting in childhood. Stage 2: overt T1 lowering, progressing faster in men with ECG changes. Stage 3: gender independent scar/inflammation response with a sexually dimorphic myocyte hypertrophic response (worse in men) and stage 4: fibrosis, impairment and heart failure.

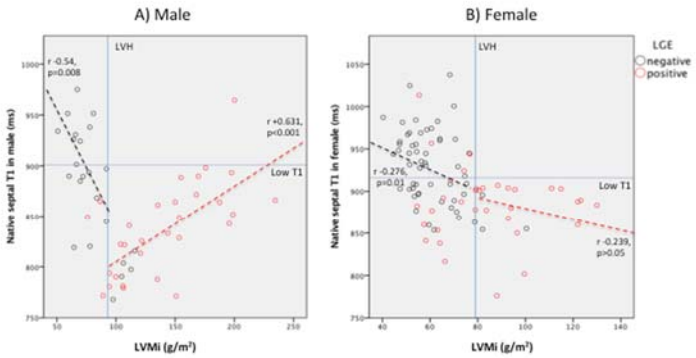

Figure 1: Relationship between native T1, LVMi and LGE in male and female Fabry disease showing a U shaped relationship of T1 to LVMi in males.

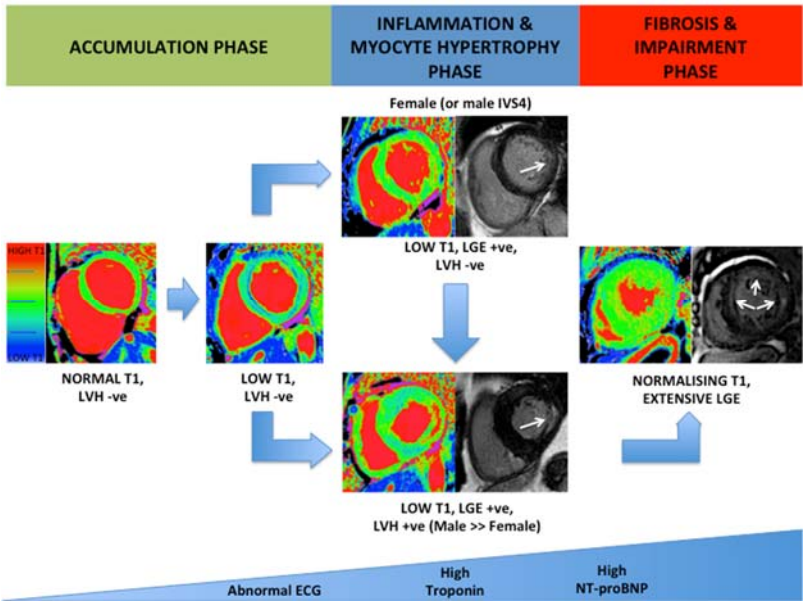

Figure 2: Disease developmental model of myocardial phenotype evolution in Fabry disease consisting of an accumulation phase (silent myocyte storage and overt T1 lowering), a myocyte hypertrophy and inflammation phase, and a fibrosis and impairment (late) phase.

ID#: 379503

Prognostic implications of apical hypertrophic cardiomyopathy

Mark Kennedy, BS[1] Clement F. Cholet, M.D.[2], Timothy C. Wong, MD MS[3]

1. University of Pittsburgh Medical Center, Wexford, PA

2. University of Pittsburgh Medical Center, Paris, France

3. University of Pittsburgh Medical Center, Pittsburgh, PA

Background: Apical hypertrophic cardiomyopathy (AHCM) has been reported to carry a benign prognosis, although some reports describe the occurrence of sudden death and other events. Current guidelines prescribe risk stratification algorithms irrespective of HCM phenotype category. We hypothesized that the combined endpoint of all-cause mortality, appropriate ICD shock, and heart failure would occur at similar rates in AHCM versus septal/diffuse HCM phenotypes.

Methods: We prospectively enrolled consecutive HCM patients referred for comprehensive evaluation, including stress echocardiography, ambulatory ECG, and cardiac MRI (CMR). CMR included extracellular volume fraction (ECV) measures of diffuse fibrosis. Clinical outcomes were ascertained by blinded medical record review. The t-test compared continuous variables; the log rank test and Cox proportional hazards regression analyzed time to event data. Our institutional review board approved the protocol.

Results: We followed 260 patients for a median of 2.7 years (IQR 1.0-4.2), of which 24 had AHCM. There were 6 events (2 deaths) in the AHCM group, and 30 events (15 deaths) in the nonapical HCM group; overall event rates were similar (Figure 1). In AHCM, family history, ventricular arrhythmia, wall thickness, and LGE extent did not associate with outcomes although higher ECV associated with the composite endpoint ($p = 0.047$). Overall, similar findings were observed in the non-apical HCM group.

Conclusion: A composite endpoint including mortality occurred similarly in AHCM versus the septal/diffuse HCM groups over short term follow up. AHCM prognosis may not be as benign as previously described. Although power was limited, several traditional risk markers did not associate with outcomes in the apical HCM group, with the exception of a CMR measure of diffuse fibrosis. Further work to characterize the role of additional prognostic variables, including ECV, is warranted.

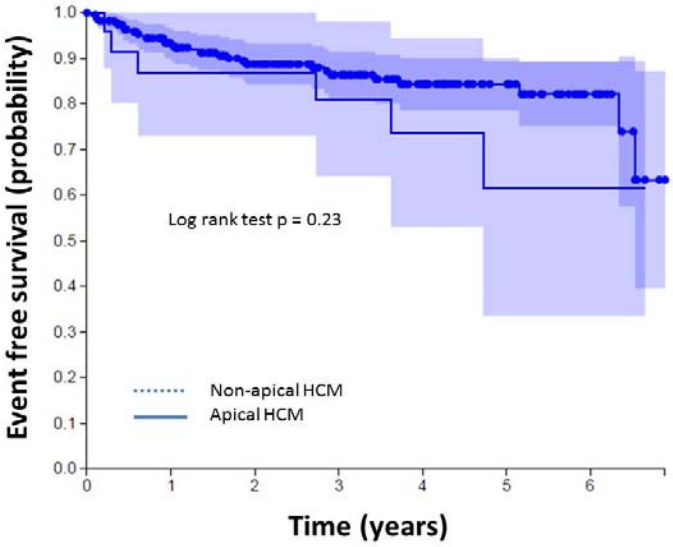
Event free survival (probability)
1.0
0.9
0.8
0.7
0.6
0.5
0.4
0.3
0.2
0.1
0.0
Log rank test p = 0.23
Non-apical HCM
Apical HCM
0
1
2
3
4
5
6
Time (years)

Figure 1

ID#: 379475

Incremental Value of Blood-oxygen-level-dependent in addition to stress-perfusion CMR at 3Tesla for Detecting Ischemia in Patients with Suspected Coronary Artery Disease

Ana G. Almeida, MD, PhD[1] Gustavo Lima Silva, MD[2], Rui Placido, MD[3], Claudio David, MD[2], Pedro Cardoso, MD[4], Luis Rosário, MD, PhD[4], Ana Francisco, MD[4], Pedro Canas, MD[4], Fausto Pinto, MD, PhD[2]

1. University Hospital Santa Maria, Lisbon, Portugal, Lisbon, Portugal

2. Cardiology - University Hospital Santa Maria, Lisbon, Lisboa, Portugal

3. Santa Maria University Hospital, Cardiology Department, Lisbon Academic Medical Center, CCUL, Lisbon, Portugal, Lisboa, Portugal

4. University Hospital Santa Maria, Lisbon, Portugal, Portugal

Background: Blood Oxygen Level Dependent (BOLD) CMR is an imaging sequence that reflects the myocardial oxygenation, through the effects on the relaxation time T2 by deoxyhemoglobin. During ischemia, perfusion and oxygenation may be dissociated. In this study we aimed to assess the incremental value of BOLD to detect myocardial ischemia in addition to stress-perfusion, for
detecting ischemia in patients with suspected coronary artery disease, using coronary angiography and FFR.as reference method for ischemia

Methods: Thirty-six consecutive patients (26 men; age 51±8.3 year-old,) with intermediate probability of CAD were included, after exclusion of patients with other significant heart disease Including ischemic heart disease, contra-indications to CMR and anemia. All underwent CMR at 3.0 Tesla followed by coronary angiography; an adenosine CMR stress BOLD and perfusion study was performed in short-axis orientation Quantitative coronary angiography plus FFR allowed the definition of normal or ischemic segments

Results: Coronary angiography detected 35 significant coronary lesions in 26 patients and the 16 LV segments were assigned to each of the coronaries. At rest, BOLD CMR, showed lower T2 values in segments with ischemia in comparison with the ones without ischemia (22.5±8.9 vs 31.4±11.6, p=0.001), based in coronary territories. After stress, ischemic segments showed no significant increase on the values of T2 (23.8±11.2, P=0.8) while non-ischemic showed significant increase in T2 (p=0.004). In comparison with perfusion, BOLD showed a lower sensitivity and specificity at rest and stress, for detecting patients with ischemia. However, the addition of BOLD to the perfusion assessment increased its sensitivity and specificity, with an AUC at ROC analysis of 0.85, 95%-CI [0.60-0.96],

Conclusion: BOLD CMR at 3T showed reduced values at ischemic myocardial segments as validated by coronary angio and FFR, both at rest and stress, leading to an incremental value to CMR stress-perfusion for the detection of ischemia. This new tool may prove to be useful for understanding ischemia mechanisms and impact the decision-making

ID#: 379076

The diagnostic value of Adenosine MR following a positive Coronary Calcium Score as a gatekeeper of invasive coronary angiography in 644 patients with stable chest pain.

Dorine Rijlaarsdam-Hermsen[1]Mallory Lo-Kioeng-Shioe[2], Dirkjan Kuijpers[3], Paul van Dijkman[3]

1. HMC Bronovo, Erasmus mc, Rotterdam, Zuid-Holland, Netherlands

2. Erasmus mc, Netherlands

3. HMC Bronovo, Netherlands

Background: The prevalence of significant coronary artery disease (CAD) in stable patients referred for evaluation of their chest pain is low and as a result the diagnostic accuracy of functional testing has declined. In current practice, about two-thirds of patients undergo non-invasive testing prior to elective cardiac catheterization, yet most patients have non-obstructive CAD. Our aim was to assess whether adenosine stress-only perfusion cardiac MR (CMR) following a positive coronary calcium score (CCS) is able to improve the diagnostic yield of coronary angiography (CCA).

Methods: From December 2004 to May 2011 consecutive patients with stable chest pain and CCS>0 referred CMR were enrolled. Pre-test likelihood was assessed according the ACC/ AHA guidelines on exercise testing.Images were visually analysed by an experienced radiologist and cardiologist in consensus. Patients with a perfusion defect were examined by CCA. Outcome was obstructive CAD defined as narrowing of ≥ 50% in the left main coronary or ≥ 70% stenosis in one or several of the major coronary arteries. Patients with normal perfusion entered follow up for major adverse coronary events (MACE).

Results: In total, 644 patients were included (mean age 63 year range 35-88, 50% men) of whom 13% had low, 72% intermediate and 15% high pre-test likelihood of CAD. Ischemia was present on adenosine MR in 13.4%. Of the patients with high pre-test likelihood 64.2% showed no ischemia, whereas of the patients with low pre-test likelihood 5.7% showed ischemia. Among the 86 (13.4%) patients with ischemia, 84 (98%) underwent CCA which showed obstructive CAD in 78 patients (93%) and no significant obstruction in 6 patients (7 %). 558 patients with a negative CMR entered follow up. Four (0.7%) patients had false negative CMR findings requiring revascularisation within 12 month after CMR. Sensitivity of CMR to detect relevant CAD was 0.95, specificity 0.99, negative predictive value 0.99, and positive predictive value 0.93.

Conclusion: In patients with stable chest symptoms CMR following a CCS>0 provides an excellent filter before CCA and increases the diagnostic yield of CCA to 93%.

ID#: 379376

Motion-corrected free-breathing LGE delivers superior imaging in half the time: a 400-patient study

Ilaria Lobascio, MD[1] Gabriella Captur, MD PhD MRCP MSc[2], Redha Boubertakh, PhD[3], Charlotte Manisty, MRCP PhD[4], Hui Xue, PhD[5], Peter Kellman, Ph.D.[5], James C. Moon, MD[6], Veronica Culotta, MD[7]

1. Barts Heart Centre, United Kingdom

2. Barts Heart Centre, London, England, United Kingdom

3. QMUL, England, United Kingdom

4. Barts Heart Centre and University College London, United Kingdom

5. National Heart, Lung, and Blood Institute, Bethesda, MD

6. Barts Heart Centre, England, United Kingdom

7. Barts Heart Centre, St Bartholomew's Hospital, England, United Kingdom

Background:

Novel free-breathing, motion-corrected (MOCO), averaged late gadolinium enhanced[1] (LGE) for the detection and quantification of scar introduces several advantages over breath held (bh) LGE[2], including minimal user input and no need for breath-holds. We hypothesised that MOCO-LGE would lead to superior image quality and reader confidence in the LGE rulings and faster acquisition times.

Methods:

400 consecutive clinical patients at one UK center underwent bh-LGE or MOCO-LGE at 1.5T. Clinical markers of patient vulnerability were recorded. LGE image quality was evaluated qualitatively and reader confidence and scan times were measured.

Results:

Qualitatively MOCO-LGE was better than bh-LGE (Fig.1) especially in clinically vulnerable patients (lower score better, 0.64 ± 1.25 *vs.* 2.37 ± 2.12, $P<0.0001$). Excellent image quality was more prevalent using MOCO-LGE compared to bh-LGE (78% vs 27%, $P<0.0001$). Blinded readers gave more concordant rulings on the presence/absence of LGE using MOCO-LGE compared to bh-LGE (kappa 0.82 [CI 0.74 - 0.91] *vs.* 0.76 [CI 0.66 - 0.86], respectively). There was greater inter-reader agreement of detected LGE patterns by MOCO-LGE compared to bh-LGE (kappa 0.79 [CI 0.72 - 0.86] *vs.* 0.77 [CI 0.69 - 0.85], $P= 0.008$) and reader confidence was also greater ($P<0.0001$). Total LGE scan time was 1.5 time faster with MOCO-LGE compared to bh-LGE (6:01 *vs*. 9:21 minutes, $P<0.0001$, Fig.2); acquisition of the SAX was also significantly faster with MOCO-LGE compared to bh-LGE in our centre (3:22 *vs.* 6:09 minutes, $P<0.0001$), with an annual cost saving for the UK NHS.

Conclusion:

MOCO-LGE is faster and superior to bh-LGE and cost-effective in a clinical service. At the Barts Heart Centre we now use MOCO-LGE on all our patients. The sequence is supported by the Gadgetron[4] framework and available as product for Siemens.

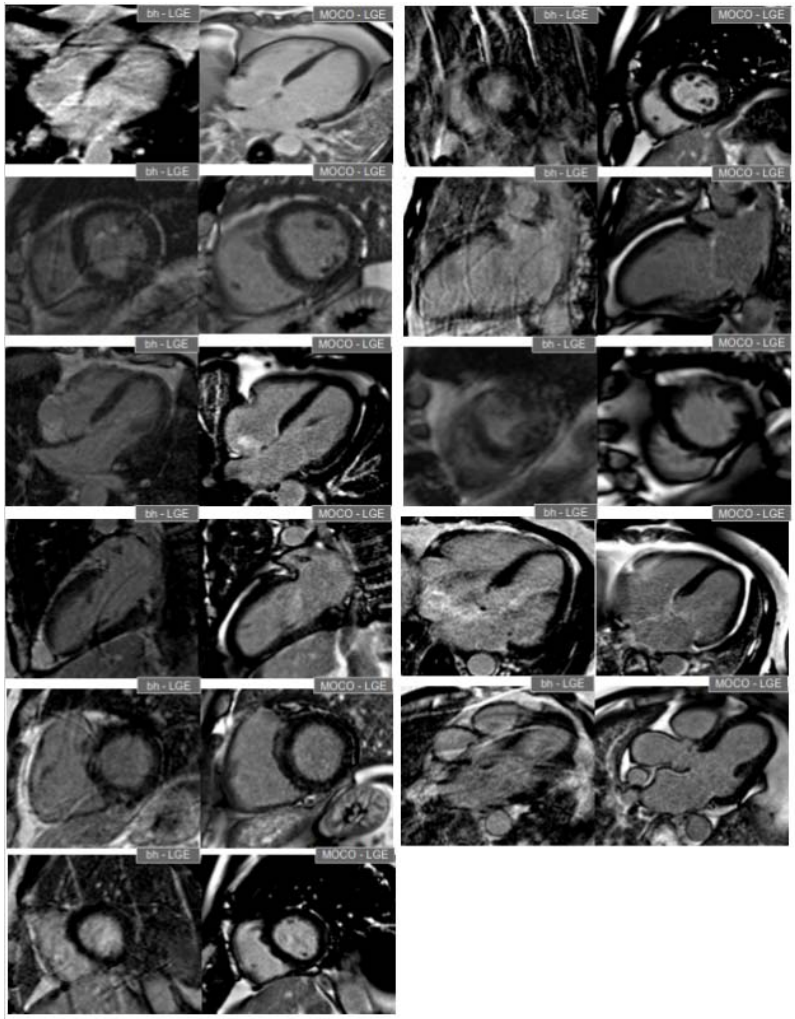

Figure 1. Same patient images comparing bh-LGE (left) and corresponding MOCO-LGE (right). In the setting of arrhythmia or inability to breath hold, MOCO-LGE clearly offers improved image quality compared with bh-LGE images.

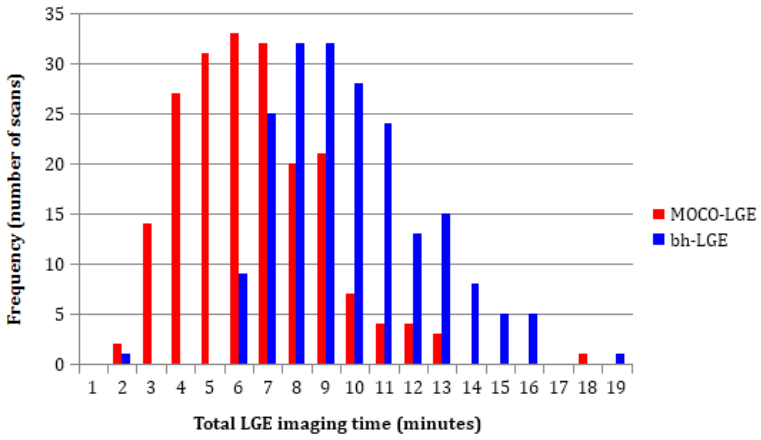

Figure 2. Total LGE imaging time is less when using MOCO-LGE vs. bh-LGE.

ID#: 378668

MRI DENSE Strain Imaging Provides a Superior Assessment for CRT Response Compared with 3D Echocardiography

Kenneth C. Bilchick, MD, MS[1] Daniel A. Auger, PhD[1], Xiaoying Cai, BS[2], Soham Shah, BS[3], Frederick H. Epstein, PhD[1]

1. University of Virginia Health System, Charlottesville, VA

2. University of Virginia, Charlottesville, VA

3. University of Virginia Health System

Background: MRI can effectively address the low cardiac resynchronization therapy (CRT) response rate by informing optimal patient selection and optimal left ventricular (LV) pacing sites. Cine displacement encoding with stimulated echoes (DENSE) has emerged as a very effective MRI strain imaging method that provides accurate strain measurements, excellent reproducibility, and rapid image analysis, particularly for patients with heart failure (HF) undergoing CRT. Although 3D echocardiography (3DE) is considered by many to be the echocardiographic method of choice for volumetric and strain analysis in HF, the comparative effectiveness of 3DE relative to MRI cine DENSE in predicting CRT response and identifying optimal LV pacing sites is unknown. As a result, we performed a head-to-head study of 3DE and MRI cine DENSE in CRT.

Methods: Prior to CRT, patients underwent MRI and echocardiographic imaging. Follow-up imaging was performed at 6 months. The MRI protocol included multislice 2D cine DENSE in short-axis and long-axis slices and late gadolinium enhancement (LGE). The LV pacing site based on fluoroscopic images was identified in 3D MRI coordinates. The circumferential uniformity ratio estimate with singular value decomposition (CURE-SVD) was used to determine the extent of simultaneous stretch and contraction in opposing walls with values approaching 0 indicating more severe dyssynchrony and values approaching 1 indicating greater synchrony. Mechanical timing of onset of contraction was also assessed with DENSE based on the circumferential strain curves (Figure 1). 3DE images were analyzed using commercial software, and the standard deviation in time to peak strain in 17 segments (3DE-SD17) and an adapted version of CURE-SVD for 3DE (3DE-CURE-SVD) were determined.

Results: The 60 patients with MRI and echocardiographic strain imaging prior to CRT had a median age of 65.4 years (IQR 59.0-71.0 years), and 22/60 were female (Table 1). In all patients, MRI CURE-SVD was associated with LV functional improvement based on the percent change in LVESV (LVESV-PERCHANGE) assessed 6 months after CRT (r=0.47, P=0.0002). In patients with 3DE, the standard deviation of time to circumferential strain in 17 segments (3DE-SD17) was not correlated with the LVESV-PERCHANGE (r=-0.08; P=0.63); however, a trend for an association with LV functional improvement was noted when 3DE strain was used to determine a modified CURE-SVD (r=0.27, P=0.09). The best echocardiographic linear regression model with the 3DE-CURE-SVD and the time to peak strain at the LV lead pacing site had an R^2 of 0.14 (P=0.11) for the outcome of LVESV-PERCHANGE (Table 2). In contrast, the multivariable linear regression model with MRI CURE-SVD and mechanical activation timing at the LV lead position had an R^2 of 0.36 (P<0.0001) for this outcome (Table 2), which further increased to an R^2 of 0.40 (P<0.0001) with the addition of scar by LGE at the LV pacing site.

Conclusion: MRI cine DENSE provides a more accurate determination of the extent of CRT response based on pre-CRT imaging than 3DE. Furthermore, activation times at the LV pacing site determined by cine DENSE MRI more strongly predict CRT response than echocardiographic strain measurements at the LV pacing site, and additional predictive capacity can be achieved by adding LGE imaging. These observations support MRI cine DENSE as the strain imaging of choice to identify likely CRT responders and guide selection of LV pacing sites.

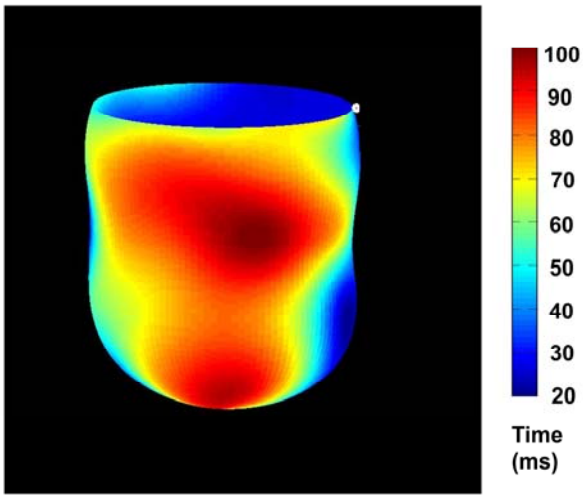

MRI DENSE 3D Mechanical Activation Map

Baseline Characteristics

Parameter	CRT Cohort (N=60)
Age (years)	65.4 (IQR 59.0-71.0)
Gender (female)	22 (36.7%)
QRS Duration	158 (IQR 146-180)
Q-LV (ms)	110 (IQR 75-140)
Ischemic Etiology of Cardiomyopathy	26 (43.3%)

Multivariable Linear Models

Linear Model for LVESV-PERCHANGE Based on Echocardiography (R^2=0.14, P=0.11)	Parameter	Standard Error	t-Value	P-Value	Standardized Coefficient
Intercept	-0.870	0.324	-2.68	0.012	0
Echo-CURE-SVD	0.751	0.383	1.96	0.059	0.341

Echo Time to Peak Strain at LV Pacing Site	0.00032	0.00027	1.18	0.25	0.205
Linear Model for LVESV-PERCHANGE **Based on MRI** **(R^2=0.36, P<0.0001)** **(Note: Addition of covariate of scar at LV pacing site in themodel increases R^2 to 0.40.)**	**Parameter**	**Standard Error**	**t-Value**	**P-Value**	**Standardized Coefficient**
Intercept	-0.222	0.117	-1.90	0.06	0
MRI-CURE-SVD	0.497	0.119	4.18	0.0001	0.471
Normalized MRI Mechanical Activation Time	-0.440	0.148	-2.97	0.005	-0.334

ID#: 378795

Association between cardiovascular magnetic resonance measures of extracellular volume and global longitudinal strain and comparison of their association with subsequent outcomes

Fredrika Fröjdh, MS[1] Eric Olausson[2], Louise Niklasson, MS[3], Maren Maanja, MD[4], Brian Feingold, MD, MS[5], Adam B. Christopher[6], Timothy C. Wong, MD MS[7], Christopher A. Miller, MBChB PhD[8], Javed Butler, MD, MPH[9], Yaron Fridman, MD[10], Peter Kellman, Ph.D.[11], Aatif Sayeed, BS[12], Martin Ugander, MD, PhD[13], Erik B. Schelbert, MD, MS[14]

1. Institute of Karolinska, Stockholm, Stockholms Lan, Sweden

2. Karolinska Institutet, and Karolinska University Hospital, Stockholm, Sweden, Stockholm, Sweden

3. Karolinska Institutet, Stockholms Lan, Sweden

4. Karolinska Institutet, Sweden

5. University of Pittsburgh School of Medicine

6. Children's Hospital of Pittsburgh of UPMC, Glenshaw, PA

7. University of Pittsburgh Medical Center, Pittsburgh, PA

8. University Hospital of Manchester, England, United Kingdom

9. Division of Cardiology, Deparment of Medicine, Stony Brook University, Stony Brook, NY

10. Asheville Cardiology Associates, Pittsburgh, PA

11. National Heart, Lung, and Blood Institute, Bethesda, MD

12. University of Pittsburgh School of Medicine, Pittsburgh, PA

13. Karolinska Institutet, and Karolinska University Hospital, Stockholm, Sweden, Stockholms Lan, Sweden

14. University of Pittsburgh; Heart and Vascular Institute of UPMC, PA

Background: We quantified 1) the extent to which left ventricular “structural” abnormalities (e.g., extracellular volume (ECV) measures of myocardial fibrosis) measures contribute to “functional” abnormalities (e.g., left ventricular global longitudinal strain (GLS), and 2) how these structural and functional metrics of disease compare in their relationship to subsequent outcomes. Both GLS and ECV represent key domains of cardiac disease promoting vulnerability to adverse outcomes. GLS reflects the culmination of any insult that promotes cardiomyocyte dysfunction, whereas ECV reflects a specific disease pathway, i.e., diffuse myocardial fibrosis.

Methods: In 1168 consecutive patients referred for CMR at 1.5T (Siemens), enrolled at time of CMR, we acquired standard cine imaging, late gadolinium enhancement (LGE), and modified Look-Locker inversion recovery (MOLLI) T1 mapping acquired before and after the administration of a gadolinium-based contrast agent (0.2 mmol/kg). ECV measures excluded myocardium with LGE of any origin. GLS analysis used commercial feature tracking software (cvi42) in three long axis planes. We excluded those with distinct diseases (hypertrophic cardiomyopathy, amyloidosis and congenital heart disease). The combined outcome endpoint was death or hospitalization for heart failure (HHF).

Results: Median ECV was 27% (range 18.2 to 46.4%), and median GLS was -15.9% (range -25.4 to -2.2%). ECV was modestly associated with GLS in univariable linear regression models (R2 0.05, $p<0.001$). This association persisted in a multivariable model with 20 clinical covariates ($p=0.007$), but ejection fraction and LV mass showed the strongest associations with GLS. Over a median follow-up time of 4 years, 180 events occurred (death/HHF). GLS associated most strongly with events based on chi square values in univariable Cox regression models. Univariable chi square was 111 for GLS and 63 for ECV. In fully adjusted Cox regression models (17 covariates), both ECV (HR 1.38 (95%CI 1.14-1.68) per 5% increment, $p=0.001$) and GLS (HR 1.51 (95%CI 1.20-1.90) per 5% increment, $p<0.001$) were among the principal variables associated with outcomes. Both variables exhibited “dose-response” relationships (Figure). Neither myocardial infarction nor focal, nonischemic LGE associated significantly with outcomes in multivariable models.

Conclusion: Metrics of left ventricular “structure” (myocardial fibrosis quantified by ECV) and “function” (global longitudinal strain measures) associate weakly to each other; GLS is not a proxy for ECV. Both metrics robustly associate with outcomes in a large cohort of consecutive patients. Combining both functional and structural metrics (i.e., GLS and ECV) may offer a more comprehensive assessment of cardiac disease and optimize risk stratification.

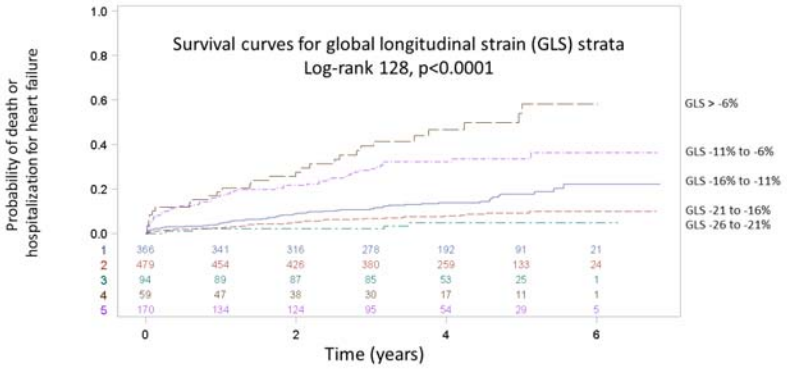
Survival curves for global longitudinal strain (GLS) strata
Log-rank 128, p<0.0001
Probability of death or hospitalization for heart failure
1.0
0.8
0.6
0.4
0.2
0.0
GLS > -6%
GLS -11% to -6%
GLS -16% to -11%
GLS -21 to -16%
GLS -26 to -21%
1 366 341 316 278 192 91 21
2 479 454 426 380 259 133 24
3 94 89 87 85 53 25 1
4 59 47 38 30 17 11 1
5 170 134 124 95 54 29 5
0
2
4
6
Time (years)

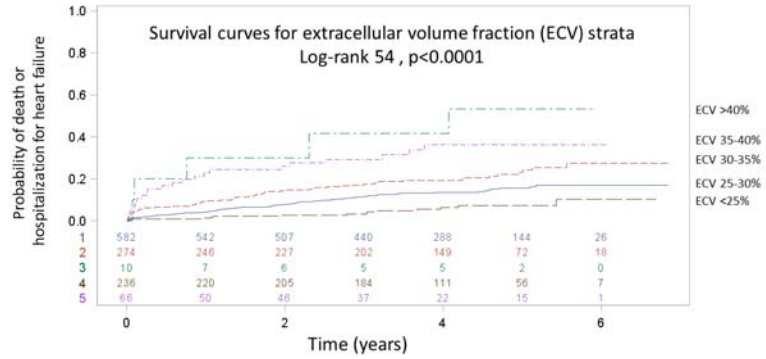
Survival curves for extracellular volume fraction (ECV) strata
Log-rank 54 , p<0.0001
Probability of death or hospitalization for heart failure
1.0
0.8
0.6
0.4
0.2
0.0
ECV >40%
ECV 35-40%
ECV 30-35%
ECV 25-30%
ECV <25%
1 582 542 507 440 288 144 26
2 274 246 227 202 149 72 18
3 10 7 6 5 5 2 0
4 236 220 205 184 111 56 7
5 66 50 46 37 22 15 1
0
2
4
6
Time (years)

ID#: 378944

Measuring myocardial performance across health and disease using contraction fraction

Rhodri Davies, MRCP, PHD[1] Heerajnarain Bulluck, MBBS PhD[2], Rebecca Kozor, PhD[3], Katia Devorha. Menacho, MD[4], Silvia Castelletti, MD[5], Sabrina Nordin, MRCP [6], Viviana Maestrini, PhD[7], Stefania Rosmini, MD, PhD[8], Marianna Fontana, MD, PhD[9], Thomas Treibel, PhD[8], James C. Moon, MD[8]

1. Barts Heart Centre, London, United Kingdom, CARDIFF, Wales, United Kingdom

2. Papworth Hospital NHS Trust, Cambridge, UK, England, United Kingdom

3. University of Sydney, Sydney, New South Wales, Australia

4. Barts Heart Centre, London, England, United Kingdom

5. UCL, N/A, Italy

6. Barts Heart Centre, United Kingdom

7. Sapienza University of Rome, Lazio, Italy

8. Barts Heart Centre, England, United Kingdom

9. UCL Department of CMR, Royal Free Hospital, England, United Kingdom

Background: The ejection fraction (EF) is so dominant as the leading cardiac imaging biomarker that it is often considered synonymous with systolic myocardial performance. An alternative, originally developed in echocardiography, is the myocardial contraction fraction (MCF), which is the ratio of LV stroke volume (SV) to LV myocardial volume (MV): MCF = SV/MV. It is dimensionless, easy to derive and has an intuitive interpretation, namely: the stroke volume produced per unit volume of myocardium.
Our aim is to see if MCF discriminates between different pathologies causing LV hypertrophy as well as healthy volunteers and veteran athletes (as an example of physiological hypertrophy), using cardiovascular MRI. We also investigate the relationship between MCF and NT-proBNP.

Methods: CMR was performed in five groups of subjects: 123 with severe aortic stenosis (AS), 68 with hypertrophic cardiomyopathy (HCM), 74 with cardiac amyloid (Am), 159 veteran athletes (VA) and 66 healthy volunteers (HV). Serum NT-proBNP concentration was measured at the time of scanning (only 29 of the HCM had NT-proBNP measurements and the VA BNP were measured on a different assay). End-diastolic, end-systolic and myocardial volumes were calculated using manual contouring on short axis images. EF, SV, LV mass and MCF were derived, with mass indexed to BSA (MCF and EF are dimensionless).

Results: Patient characteristics and quantitative results (mean ± standard deviation) are tabulated in figure 1. Figure 2 shows the 95% confidence intervals for MCF and EF for each group – there is a significant difference (all p <0.05) between pathological and physiological groups and between all pathologies except HCM *vs* AS. EF is unable to differentiate between physiological and pathological causes of LVH. The scatterplot in figure 3 shows a linear relationship between MCF and *log*(NTproBNP). The correlation coefficient is higher for MCF compared to other indices (MCF = 0.71, EF = 0.48, SV = 0.49, LVM=0.62), suggesting a tighter relationship (p<0.05).

Conclusion: In subjects with LVH, the myocardial contract fraction (MCF) discriminates health and disease better than ejection fraction and tracks BNP better.

	HV	VA	HCM	AS	AM
N	66	159	68	123	74
AGE	45 ± 13	55±9	54 ± 14	71 ± 9	71 ± 11
FEMALE	29 (47%)	115 (78%)	8 (28%)	53 (44%)	14 (19%)
NT-PROBNP	6 ± 3	-	212 ± 215	179 ± 259	368 ± 456
LV MASS (G/M2)	67 ± 14	80 ± 15	102 ± 42	99 ± 28	120 ± 34
LV EF (%)	67 ± 5	68 ± 6	73 ± 8	68 ± 14	55 ± 15
MCF	0.78 ± 0.16	0.77 ± 0.15	0.62 ± 0.22	0.54 ± 0.15	0.37 ± 0.2

Figure 1. Patient characteristics and quantitative results.

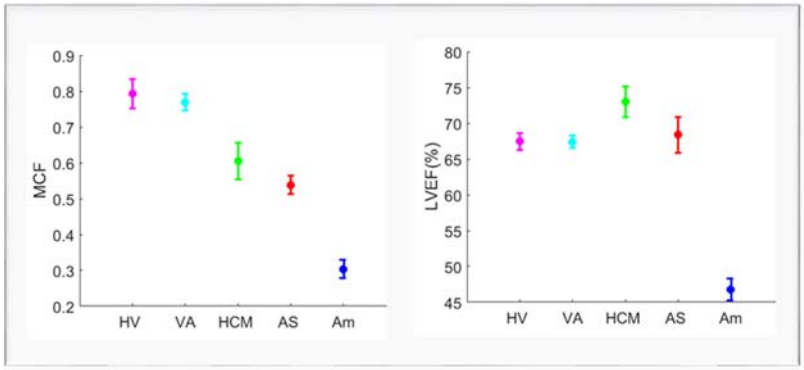

Figure 2. 95% confidence interval for each group

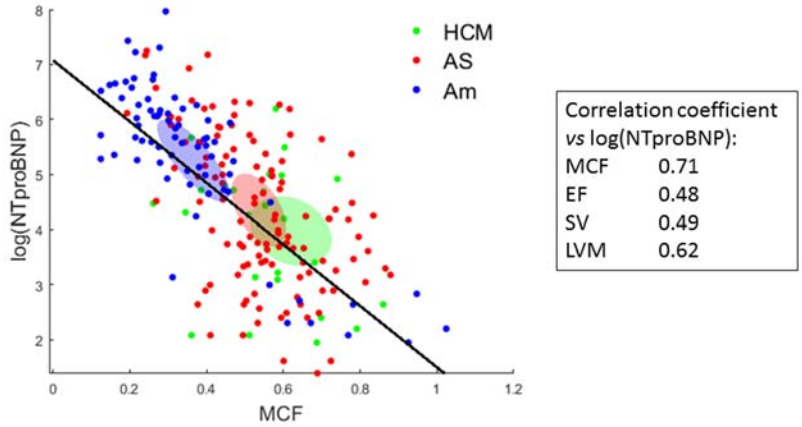

Figure 3. log(NTproBNP) as a function of MCF

ID#: 373292

Ventricular interaction at rest and during exercise in the pressure overloaded right heart: an exercise cardiac magnetic resonance study.

Mathias Claeys, MD[1] Jonathan Los[2], Guido Claessen, MD, PhD[3], Andre La Gerche, MD, PhD[4], Marion Delcroix, MD, PhD[3], Jan Bogaert, MD, PhD[1], Rik Willems, MD, PhD[5], Piet Claus, MSc, PhD[6]

1. KU Leuven / University Hospitals Leuven, Leuven, Vlaams-Brabant, Belgium

2. KU Leuven, Leuven, Belgium

3. University Hospitals Leuven, Belgium

4. Baker Heart And Diabetes Institute, Australia

5. University Hospitals Leuven, Leuven, Belgium

6. KU Leuven, Belgium

Background: The interventricular septum (IVS) plays an important role in mediating ventricular interactions. In pulmonary hypertension (PH) diastolic leftward septal shift through prolonged right ventricular (RV) contraction impedes left ventricular (LV) filling. As diastole shortens with increasing heart rate we hypothesize that this adverse ventricular interdependence worsens with exercise. Therefore we evaluated septal motion both at rest and during exercise in patients with PH and compared with healthy controls.

Methods: Twenty-five subjects (10 healthy controls and 15 PH patients) underwent exercise cardiac magnetic resonance imaging with simultaneous registration of invasive pulmonary and systemic arterial pressures using an ungated free-breathing steady-state free-precession cine imaging method. The LV and RV endocardial and epicardial borders of a mid-ventricular short-axis slice were traced during expiration at early-diastole (defined as mitral valve opening) and at end-diastole both at rest and during supine bicycle exercise at 25% of peak exercise capacity (peakVO2). Using custom software the septal curvature (SC), the LV eccentricity index (EI) and the RV to LV ratio (RVLV ratio) were calculated (Figure 1). A negative SC denotes a septum bowing the into the LV.

Results: The two groups were matched for age, sex and body composition. PH patients had significantly lower peakVO2 (14.3 ± 3.91 vs. 31.5 ± 10.6 ml.kg-1.min-1, $p<0.001$) and higher mean pulmonary artery pressures (43.8 ± 8.94 vs 18.3 ± 2.98 mmHg, $p<0.001$). At rest the IVS in PH patients was more displaced towards the LV as evident from a smaller SC and a higher EI ($p<0.01$ at early diastole and $p<0.05$ at end-diastole). Likewise RVLV ratio was significantly higher in PH patients ($p<0.01$ for both early- and end-diastole). Exercise did not influence septal motion in controls whereas it significantly increased leftward septal shift in PH patients both at early diastole ($p<0.01$ rest-to-exercise for SC, $p<0.001$ rest-to-exercise for EI and RVLV ratio; $p<0.01$ for interaction group*exercise; Figure 2) and end-diastole ($p<0.001$ rest-to-exercise for EI and RVLV ratio; $p<0.01$ for interaction group*exercise, Figure 3). In PH patients end-diastolic SC, EI and RVLV ratio correlated with RV ejection fraction both at rest ($r= 0.696$, $r=-0.676$ and $r=-0.75$ respectively, all $p<0.01$) and during exercise ($r=0.55$, $r=-0.628$ and $r=-0.642$ respectively, all $p<0.05$).

Conclusion: Adverse ventricular interaction in PH patients increases during exercise and is related to RV function. Therapeutic strategies aimed at reducing ventricular interdependence might have a significant impact on cardiac function especially during exercise.

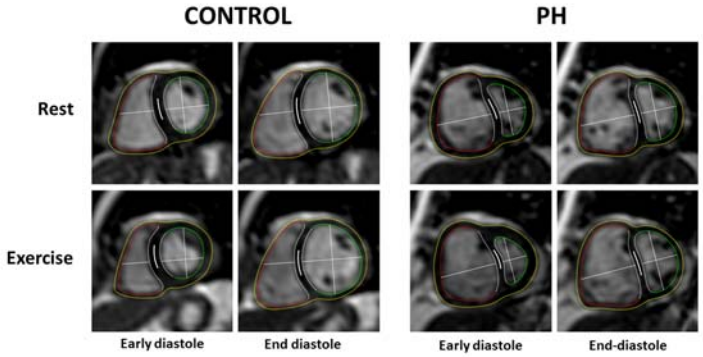

Figure 1. Early-diastolic and end-diastolic geometry at rest and during exercise.

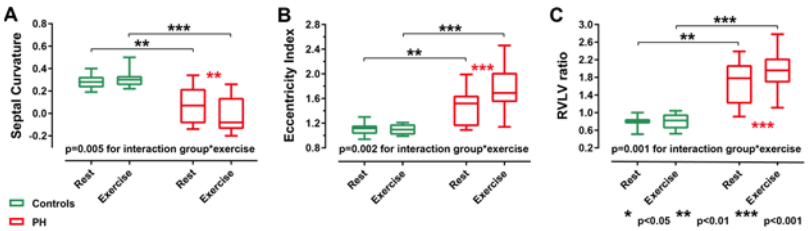

Figure 2. Early-diastolic ventricular interaction at rest and during exercise.

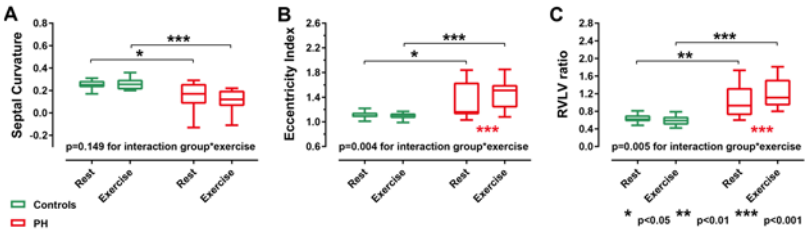

Figure 3. End-diastolic ventricular interaction at rest and during exercise.

ID#: 373293

Cardiovascular Magnetic Resonance Imaging to guide Transcatheter Aortic Valve Replacement: A Comparison with Computed Tomography

Agnes Mayr, MD[1] Gert Klug[2], Sebastian Reinstadler, MD[2], Martin Reindl, MD[2], Christof Kranewitter[1], Bernhard Metzler, MD[2]

1. University Clinic of Radiology, Medical University of Innsbruck, Austria

2. University Clinic of Internal Medicine III, Cardiology and Angiology, Medical University of Innsbruck, Austria

Background: To compare a comprehensive cardiovascular magnetic resonance (CMR) imaging protocol with contrast-enhanced computed tomography angiography (CTA) for guidance in TAVR evaluation.

Methods: Non-contrast three-dimensional (3D) “whole heart” CMR imaging for aortic annulus sizing and measurements of coronary ostia heights, contrast-enhanced CMR angiography (MRA) for evaluation of transfemoral routes as well as aortoiliofemoral-CTA were performed in 16 patients referred for evaluation of TAVR.

Results: Aortic annulus measurements by CMR and CTA showed a very strong correlation (r=0.956, p<0.0001; effective annulus area for CMR 430±74 vs. 428±78 mm² for CTA, p=0.629). Regarding decision for valve size there was an excellent agreement between CMR and CTA. Moreover, vessel luminal diameters and angulations of aortoiliofemoral access as measured by MRA and CTA showed overall very strong correlations (r= 0.819 to 0.996, all p<0.001), the agreement of minimal vessel diameter between the two modalities revealed a bias of 0.02 mm (upper and lower limit of agreement: 1.02 mm and -0.98 mm).

Conclusion: In patients referred for TAVR, CMR measurements of aortic annulus and minimal aortoiliofemoral diameters showed good to excellent agreement. Decisions based on CMR measurements regrading prosthesis sizing and transfemoral access would not have modified TAVR-strategy as compared to a CTA-based choice.

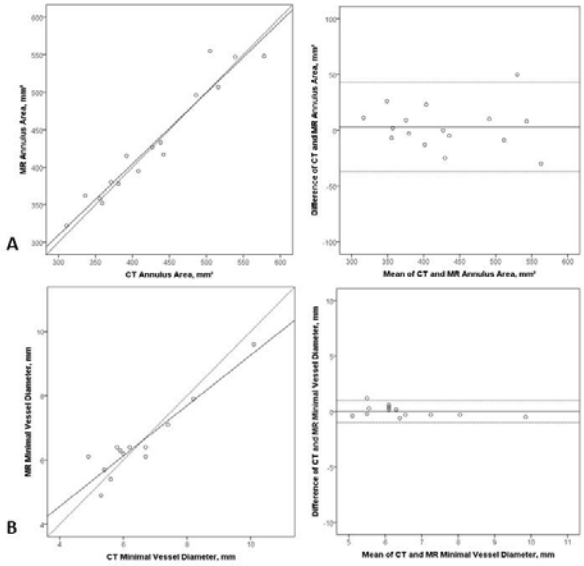

Correlation of the two methods

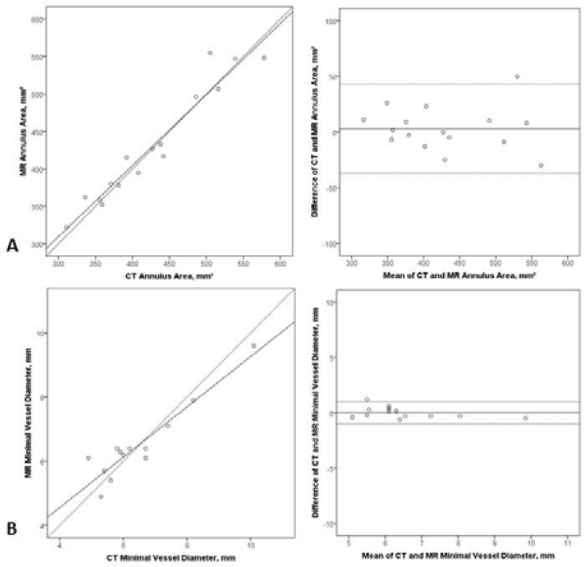

Linear correlations and corresponding Bland-Altman plots for agreement between methods of A) aortic annulus area and B) minimal aortoiliofemoral vessel diameter measured by CMR and CTA.

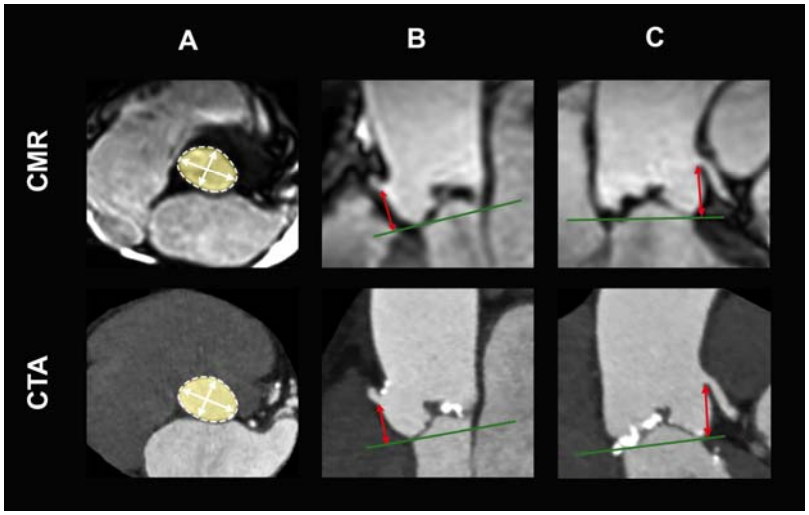

Imaging example of non-contrast 3D “whole heart” CMR or CTA measurements for (A) aortic annular measurements at hinge-point plane, (B) right coronary artery and (C) left main artery ostial height measurement in the longitudinal axis at a right angle to the hinge point plane.

ID#: 374464

Association of regional and systemic adipose tissue with coronary endothelial dysfunction in patients with HIV

Sahar Soleimanifard, PhD[1] Micaela Iantorno, MD[2], Michael Schär, PhD[3], Gabriele Bonanno, PhD[4], Gary Gerstenblith, MD[2], Robert G. Weiss, MD[5], Allison G. Hays, MD[6]

1. The Johns Hopkins Univeristy School of Medicine, Baltimore, MD

2. The Johns Hopkins Univeristy School of Medicine, MD

3. Russell H. Morgan Department of Radiology and Radiological Science, Johns Hopkins University School of Medicine, Baltimore, MD

4. Division of Cardiology and Division of MR Research, The Johns Hopkins University School of Medicine, Baltimore, MD, United States, MD

5. Russell H. Morgan Department of Radiology and Radiological Science, The Johns Hopkins University School of Medicine, Baltimore, MD, United States, MD

6. Division of Cardiology, The Johns Hopkins University School of Medicine, Baltimore, MD, United States, MD

Background: HIV infection is associated with increased coronary artery disease (CAD) and related events, but the underlying mechanisms are not well understood. Prior studies have shown that visceral adipose tissue is associated with cardiovascular events, independent of traditional risk factors[1]. This contribution to atherosclerotic development is thought to be from paracrine secretion of pro-inflammatory cytokines. We previously showed that impaired coronary endothelial function (CEF), an early marker of CAD, occurs in HIV[2]. In this work, we aim to investigate the relationship of body fat compartments (epicardial, subcutaneous, visceral, and hepatic fat) with CEF.

Methods: We studied 55 volunteers with HIV on stable anti-retroviral therapy (average age 55yo, range 34-72yo, 12 women, 16 with CAD based on prior imaging). Regional epicardial adipose tissue (EAT) and CEF, described as change in coronary cross-sectional area (%CSA) in response to isometric handgrip exercise, were measured in the mid right coronary artery on a 3T scanner as described before[2-3]. In a subset of 18 volunteers without CAD, abdominal subcutaneous and visceral adipose tissue were measured at the 4th lumbar vertebrae as a surrogate for systemic adipose tissue using a semi-automated tool developed in-house. Hepatic adipose tissue was characterized by fat fraction using a 6-echo Dixon sequence[4]. Figure 1 summarizes the acquisitions.

Results: The degree of exercise-induced %CSA change was inversely correlated with EAT thickness (r=-.47, p=0.0002) and area (r=-0.46, p=0.0004) in all volunteers (Figure 2). In the subgroup of patients with abdominal fat images, no association was found between %CSA change and systemic fat stores (subcutaneous: r=-0.02, visceral: r=-0.16, and hepatic fat fraction: r=-0.10, p=NS, Figure 3). In this group, a modest inverse relationship, between %CSA change and the ratio of visceral to subcutaneous fat was observed (r=-0.35, p=0.16). Hepatic fat fraction demonstrated a positive relationship, although not significant, with the ratio of visceral to subcutaneous adipose tissue (r=0.35, p=0.15).

Conclusion: In patients with HIV, regional epicardial adipose tissue is closely related to impaired CEF, an early marker and contributor of atherosclerosis. This association appears to be stronger than that of the systemic adipose tissue, as measured by abdominal subcutaneous, visceral, and hepatic fat. Although a larger study is warranted to evaluate for weaker relationships, these initial findings that regional fat is more closely related to impaired CEF than systemic fat are consistent with the hypothesis that local, possibly paracrine, factors contribute to accelerated atherosclerosis in HIV.

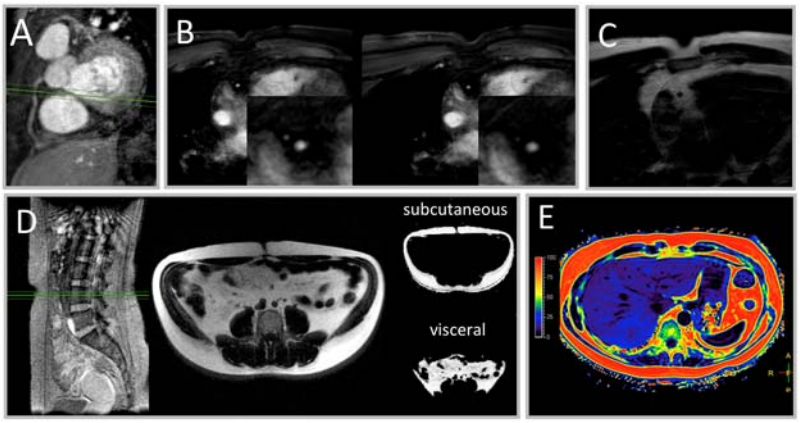

A) Three-dimensional targeted MRA image of the right coronary artery used for planning of subsequent two-dimensional images. B) Cross-sectional image of the mid right coronary artery at rest (left) and during handgrip-induced stress (right). C) Corresponding cross-sectional fat image demonstrating peri-coronary adipose tissue. D) Abdominal subcutaneous (top) and visceral (bottom) adipose tissue at the L4 level. E) Select slice from three-dimensional hepatic fat fraction images.

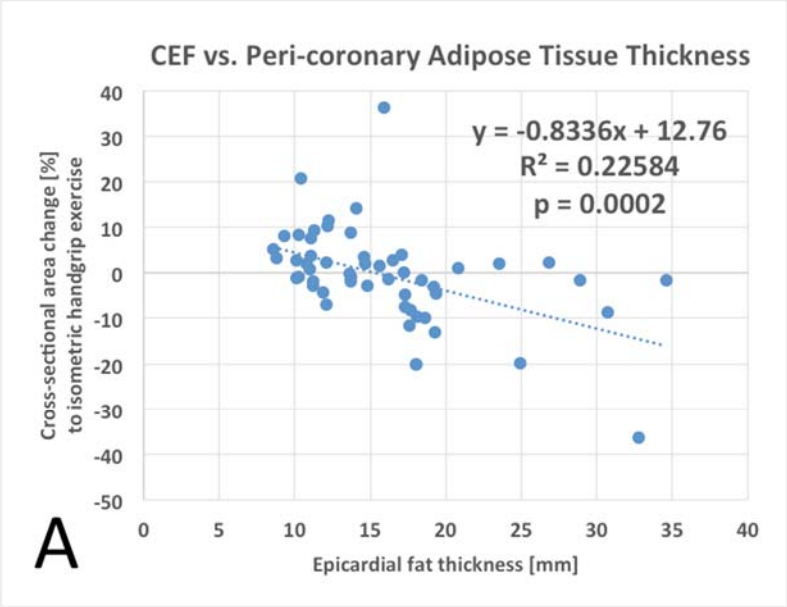

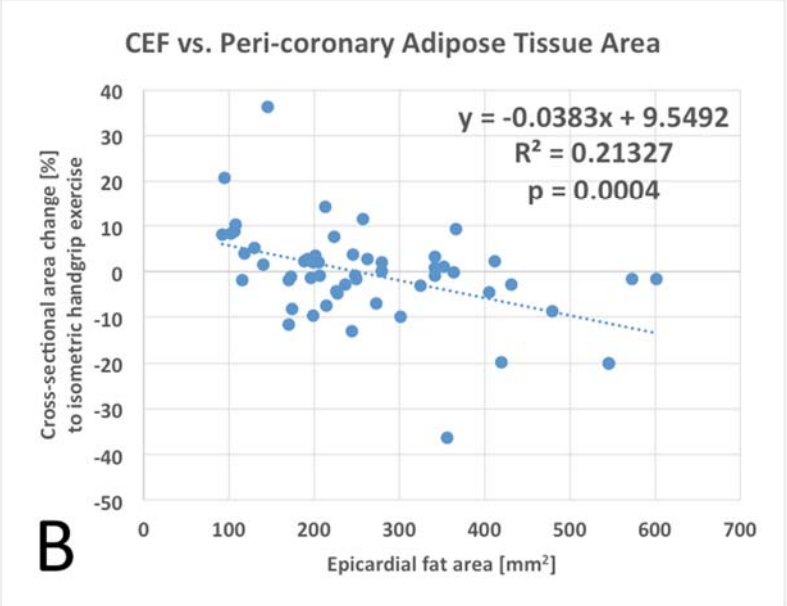

Coronary endothelial function (CEF) versus regional peri-coronary adipose tissue area [mm2] (A) and thickness [mm] (B) calculated using two-dimensional coronary artery images demonstrated in Figures 1B and 1C.

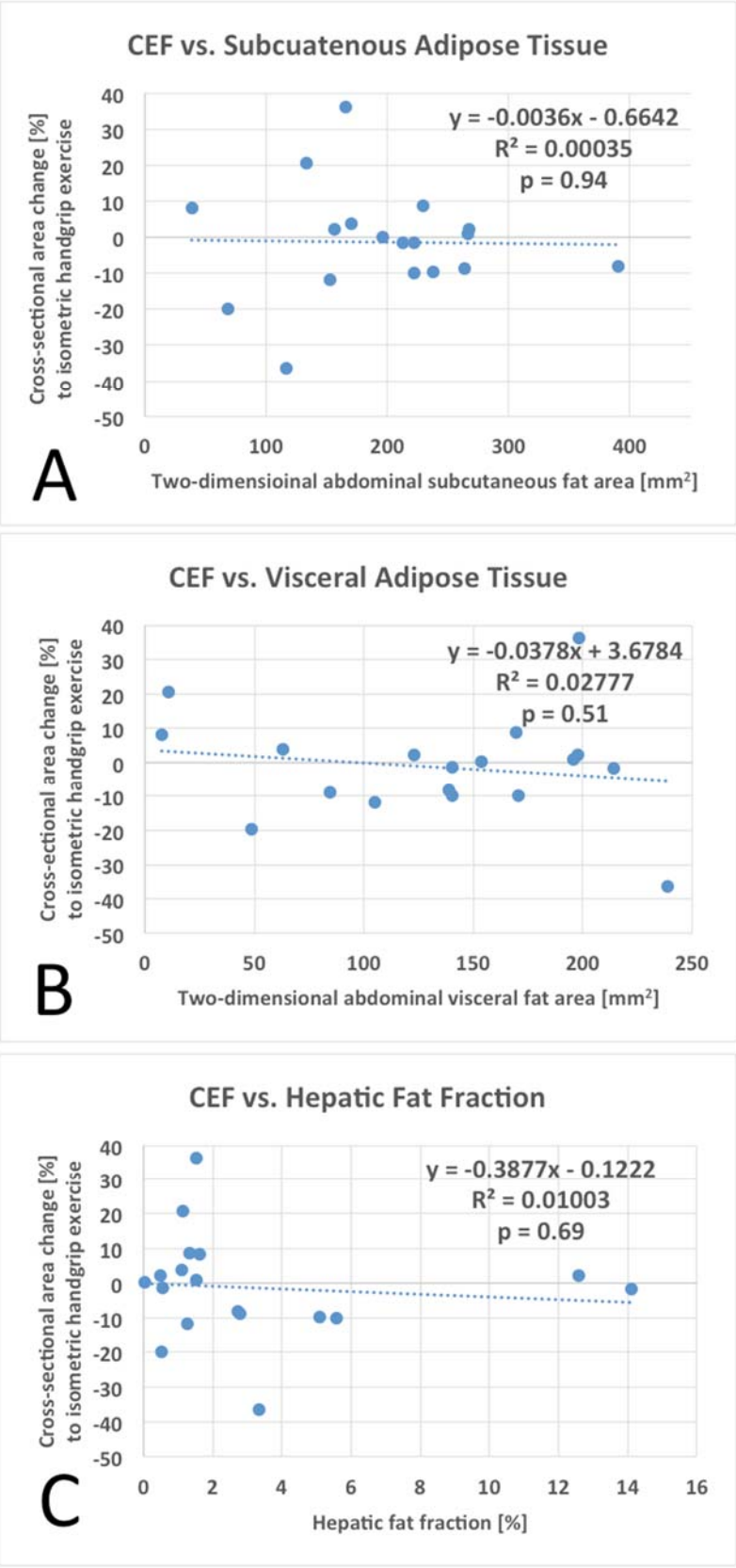

Coronary endothelial function (CEF) versus abdominal subcutaneous (A), visceral (B), and hepatic fat fraction (C)

using images demonstrated in Figures 1D and 1E.

References:

1. Mahabadi, Amir A., et al. "Association of epicardial fat with cardiovascular risk factors and incident myocardial infarction in the general population: the Heinz Nixdorf Recall Study." *Journal of the American College of Cardiology* 61.13 (2013): 1388-1395
2. Iantorno, Micaela, et al. "Coronary artery endothelial dysfunction is present in HIV-positive individuals without significant coronary artery disease." *AIDS*31.9 (2017): 1281-1289.
3. Hays, Allison G., et al. "Noninvasive visualization of coronary artery endothelial function in healthy subjects and in patients with coronary artery disease." *Journal of the American College of Cardiology* 56.20 (2010): 1657-1665
4. Yokoo, Takeshi, et al. "Nonalcoholic fatty liver disease: diagnostic and fat-grading accuracy of low-flip-angle multiecho gradient-recalled-echo MR imaging at 1.5 T." *Radiology* 251.1 (2009): 67-76.

ID#: 373640

Lipomatous Metaplasia of Hemorrhagic Myocardial Infarction is a Self-Perpetuating Process Driven by Foam Cell Formation and Iron Recycling

Ivan Cokic, MD[1] Guan Wang, MD[2], Xingmin Guan, MS[2], Hsin-Jung Yang, PhD[2], Richard LQ. Tang, MD[3], Diego Hernando, PhD[4], Scott B. Reeder, MD, PhD[4], Rohan Dharmakumar, PhD[5]

1. Cedars-Sinai Medical Center, Los Angeles, CA

2. Cedars-Sinai Medical Center

3. Cedars-Sinai Medical Center, CA

4. University of Wisconsin

5. Cedars-Sinai Medical, CA

Background: Fat deposition in old myocardial infarctions (MI) is a common finding. Based on autopsy reports and imaging studies over the last 30 years, it is estimated that fatty infiltration of post-MI scar shows an incidence of 50-80%. Fat depots are typically observed in the peri-infarct and border zones of old scars and have been linked to adverse clinical outcomes in the chronic post-MI setting. The mechanism of this fatty degeneration has conventionally been attributed to the process of “lipomatous metaplasia” (LM). A common feature of many disease processes associated with pathological fat accumulation is the iron-induced foam cell (FC) formation. The process of FC formation following erythrophagocytosis is accompanied by exocytosis of iron. Phagocytosis of this exocytosed iron by new macrophages can lead to a self-perpetuating and amplifying loop of FC formation. We investigated the spatial distribution and temporal accumulation of fatty infiltration in hemorrhagic MIs and their contribution to adverse LV remodeling.

Methods: Hemorrhagic MI in the LAD territory was created in 20 dogs. Animals were followed to 8-week (n=10) or 6-months (n=10) post MI. All dogs underwent cine, T2* and LGE CMR at 3T on day 7, week 8, and/or month 6 post-MI. LVEF and end-diastolic sphericity index (EDSI) were determined from cine images. All image analyses were performed using a commercial software. Animals were euthanized following week 8 or month 6 CMR scan and the hearts were explanted for histological evaluation.

Results: Reperfusion hemorrhage (Figure 1), chronic iron deposits (Figures 2&3), and LM (Figures 2&3) were detected in all dogs.There was no change in iron concentration (1/T2*) within MIs (day 7 to month 6 post-MI (P=0.12)).At week 8 and month 6 post-MI, individual FCs and mini-clusters of FCs were typically observed in the peripheral and border zones of hemorrhagic MIs where FCs exclusively colocalized with iron deposits (Figure 2). At month 6, larger fat depots which penetrated scar tissue at its internal core (Figure 3) were observed. Notably, these large FC clusters typically colocalized with iron deposits along the fat depot periphery, while the core of the growing adipose tissue was almost iron-negative. Propagation of LM throughout the scar core was significantly correlated with adverse LV remodeling (Figure 4).

Conclusion: Our findings reported herein support the notion that fatty degeneration of hemorrhagic MI is a self-perpetuating process driven by FC formation and iron recycling.

Figure 1

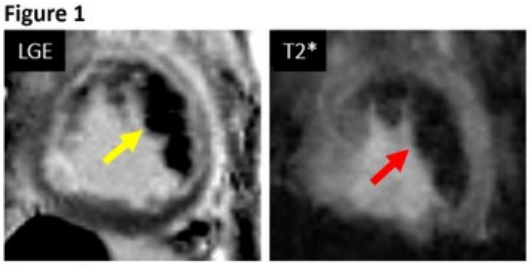

Figure 1. CMR: Representative LGE (**A**) and T2* (**B**) images acquired in a dog 7 days after acute MI confirming the presence of microvascular obstruction (MVO; yellow arrow) and hemorrhage (red arrow).

Figure 2

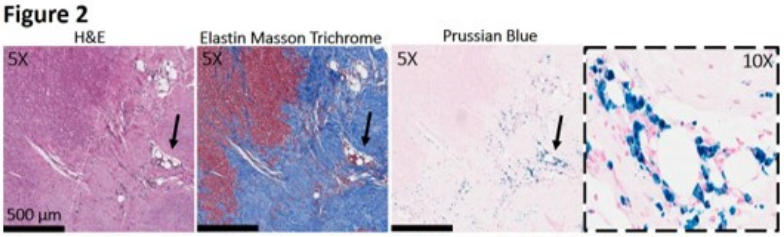

Figure 2. Serial paraffin sections from an **8-week-old hemorrhagic MI**. Individual foam cells in the peri-infarct border zone exclusively co-localized with chronic iron deposits.

Figure 3

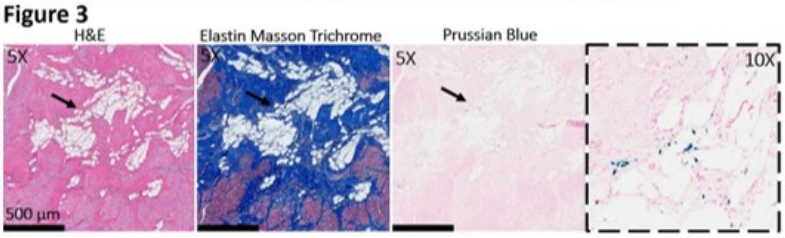

Figure 3. Serial paraffin sections from an **6-month-old hemorrhagic MI**. Larger foam cell clusters penetrated scar at its internal core and typically co-localized with iron deposits along the fat depot periphery. The core of the growing adipose tissue typically contained only traces of chronic iron deposits.

Figure 4

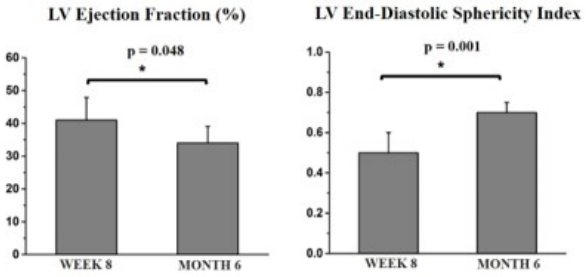

ID#: 373773

Automated aorta localization and quality control for cine CMR in the UK Biobank population cohort

Luca Biasiolli, DPhil[1] Evan Hann[2], Elena Lukaschuk, MSc[2], Valentina Carapella, DPhil[3], Nay Aung, MD, MRCP[4], Kenneth Fung, MBBS MRCP[5], Niall Moon, MChem[6], Jose Miguel Paiva, MSc[4], Henrike N. Puchta, MSc[6], Jennifer J. Rayner, BMBCh, MRCP(UK)[7], Mihir M. Sanghvi, MB BS, BSc[4], Katharine E. Thomas[8], Konrad Werys, PhD[6], Vicente Grau, PhD[9], Matthew D. Robson, PhD[10], Steffen E. Petersen, MD DPhil MPH FRCP[11], Stefan Neubauer, MD, FRCP[8], Stefan K. Piechnik, PhD, MScEE[8]

1. University of Oxford, Oxford, United Kingdom

2. University of Oxford, Oxford, England, United Kingdom

3. University of Oxford, Oxford, United Kingdom, England, United Kingdom

4. William Harvey Research Institute, NIHR Cardiovascular Biomedical Research Unit at Barts, Queen Mary University of London, Charterhouse Square, London, EC1M 6BQ, UK, England, United Kingdom

5. Queen Mary University of London, United Kingdom

6. University of Oxford, United Kingdom

7. OCMR, University of Oxford, Oxford, England, United Kingdom

8. University of Oxford, England, United Kingdom

9. University of Oxford, Oxford, UK, Oxford, England, United Kingdom

10. OCMR, University of Oxford, England, United Kingdom

11. Queen Mary University of London, London, England, United Kingdom

Background: Arterial stiffness is an independent predictor of cardiovascular morbidity and mortality. Aortic Distensibility (AoD), which measures stiffness, can be calculated using semi-automated methods to segment the aortic lumen on cine CMR. However, these methods require visual quality control and manual localization of the region of interest (ROI) of ascending (AA) and proximal descending (PDA) aorta, which limit AoD analysis in large-scale population-based studies such as UK Biobank. This study sought to develop and validate a fully automated method to 1) detect and locate the ROIs of AA and PDA, and 2) provide a quality control mechanism.

Methods: The automated algorithm to localize AA and PDA followed these steps: 1) foreground (axial image of the body) was segmented; 2) candidate ROIs for AA and PDA were detected by the Circular Hough Transform (CHT); 3) 18 local features were extracted to describe different characteristics of each candidate ROI (spatial, histogram- and shape-based features); 4) the Random Forest (RF) algorithm was trained on 1200 to learn how to identify the ROIs corresponding to AA and PDA based on the set of features; 5) In a separate test dataset (3900 scans), the RF algorithm assigned to each ROI the probability of corresponding to AA (or PDA). Location and radius of AA (or PDA) were given by the ROI that achieved maximum AA (or PDA) detection probability. To provide the ground truth, overall image quality (IQ=0-3 from poor to good) and aortic locations of 5100 cines (from UK Biobank) were assessed by 13 observers. Dice Similarity Coefficient (DSC) was used to calculate the agreement between ground truth and automatically detected ROIs. Finally, we investigated the association between AA·PDA detection probability and IQ scored by observers using Kruskal-Wallis rank test with multiple pairwise comparisons (Bonferroni).

Results: 51482 ROIs in 3900 scans (test data) were detected by CHT and classified with associated detection probability. Figure 1A shows ROC curves with AUC~100% and detection error of 0.6% for AA and 0.2% for PDA. Figure 1B shows excellent agreement with ground truth, with DSC≥0.9 in 94.8% of AA and 99.5% of PDA cases. AA·PDA detection probabilities of low-, mid- and high-IQ scans were significantly different (Figure 2A). ROC analysis indicated good ability to discriminate scans with IQ≥1 from those severely corrupted by artefacts (Figure 2B).

Conclusion: The proposed method for automated AA and PDA localization is very accurate, and AA·PDA probabilities provide a mechanism to detect low quality scans for further human review.

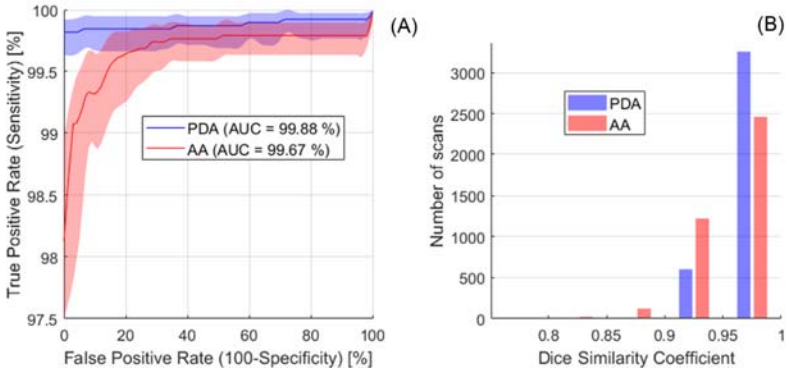

Figure 1. (A) Receiver Operating Characteristic (ROC) curves with 95% CIs for AA and PDA localization. Optimal threshold for AA probability at 0.18 (sensitivity = 99.6%, specificity = 83%) and for PDA at 0.09 (sensitivity = 99.8%, specificity = 100%). (B) Dice Similarity Coefficient (DSC) histogram showing excellent agreement with the ground truth (GT), where DSC(ROI,GT)=2·(|ROI∩GT|)/(|ROI|+|GT|)

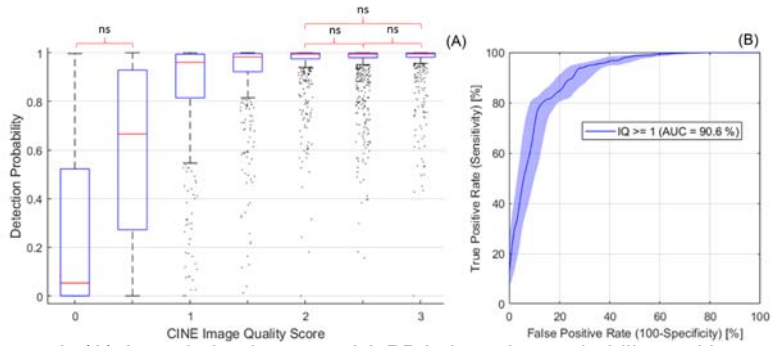

Figure 2. (A) Association between AA·PDA detection probability and image quality (IQ), where ns = not significant difference. (B) ROC curve with 95% CIs for detecting CINEs with IQ ≥ 1. Optimal thresholds for detection probability = 0.75 (sensitivity = 94%, specificity = 73%) and 0.95 (sensitivity = 81%, specificity = 86%).

ID#: 376835

Reproducibility of Regional and Global Longitudinal Strain Measurements Made Using Single Beat Strain-Encoded CMR

Neha Goyal, MD[1]Keigo Kawaji, PhD[2], Noreen T. Nazir, MD[1], Valentina Volpato, MD[1], Kohei Matsumoto, MA[2], John E. Blair, MD[1], Darius Dabir, MD[3], Lukas Stoiber, MD[4], Seyedeh Mahsa Zamani[5], Sebastian Kelle, MD[4], Victor Mor-Avi, PhD[1], Amit R. Patel, MD[1]

1. University of Chicago, IL

2. University of Chicago, Chicago, IL

3. University of Bonn, Bonn, Germany

4. German Heart Center Berlin, Berlin, Berlin, Germany

5. German Heart Institute Berlin, Berlin, Berlin, Germany

Background: Global longitudinal strain (GLS) determined by either echocardiography or cardiac magnetic resonance (CMR) has been shown to be a reproducible and independent predictor of prognosis. Although regional longitudinal strain (RLS) offers the promise of quantifying regional wall motion, which is important for the diagnosis of conditions that affect myocardial function regionally, its clinical use is not recommended by the current echocardiography guidelines. One reason for this is that the clinical utility of RLS is not yet well defined due to conflicting data regarding it reproducibility. The objective of our study was to assess test-retest, inter-, and intra-observer variability of RLS and GLS measured from single-beat strain-encoded (SENC) CMR images, during both resting conditions and dobutamine stress.

Methods: Fifteen subjects with known or suspected coronary artery disease were prospectively enrolled. CMR imaging was performed using a 1.5T scanner (Achieva, Philips; Best, The Netherlands) with a 5-channel array. SENC images (TR=13ms; TE=0.7ms; FA=30 degrees; 256x256mm^2; slice thickness=10mm; 24ms SENC magnetization prep prior to continuous 40ms [3 spiral interleaves] temporal phase over the R-R interval) were obtained during a single heart beat each at the basal, mid and apical short axis slice during resting conditions and after a 3-minute infusion of dobutamine (20 mcg/kg/min). For test-retest variability, images were acquired twice with slice position being separately re-planned. Epicardial and endocardial contours were drawn by two experienced observers independently during resting and stress conditions and twice by the same observer on resting images, stress images, and repeated images. RLS (16-segment model) and GLS were measured using MyoStrain software (Myocardial Solutions, Morrisville, NC). Test-retest, inter-, and intra- observer variability were assessed using intraclass correlation coefficient (ICC) as well as coefficient of variation (CoV).

Results: Of the 15 patients, 8 had a prior myocardial infarction. The average left ventricular ejection fraction was 52 ± 11%. Heart rate was 71 ± 12 bpm at rest and 94 ± 29 bpm under stress. GLS and RLS were successfully measured in all patients and all segments. The ICC and CoV values for GLS ranged between 0.91-0.99 and 2-8% and for RLS ranged between 0.80-0.92 and 11-17% (Table).

Conclusion: GLS and RLS can be measured using SENC images acquired using a single beat per slice acquisition. Test-retest, inter-, and intra- observer variability of measurements made during resting and stress conditions were excellent for GLS (r>0.9) and very good for RLS (r>0.8). Further studies are needed to determine the clinical utility of SENC-derived GLS and RLS.

Intraclass Correlation Coefficient and Coefficient of Variation for GLS and RLS.

	GLS		RLS	
Comparison	ICC	CoV	ICC	CoV
Test retest variability (Rest)	0.91	8%	0.80	17%
Test retest variability (Stress)	0.97	3%	0.84	16%
Inter-observer variability (Rest)	0.99	2%	0.92	11%

Inter-observer variability (Stress)	0.98	3%	0.90	12%
Intra-observer variability (Rest)	0.98	3%	0.87	11%
Intra-observer variability (Stress)	0.96	4%	0.86	13%

ID#: 375987

Z-score scaling for native T1 mapping: Application to normal data from different MR systems and to cardiac amyloidosis

Riccardo Kranzusch[1] Fabian Aus dem Siepen, MD[2], Stephanie Funk, MD[3], Leonora Zange, MD[4], Sarah Jeuthe, PhD[1], Tiago Ferreira da Silva, MSc[1], Titus Kühne, MD[1], Burkert Pieske, MD[5], Christoph Tillmanns, MD[6], Matthias G. Friedrich, MD[7], Jeanette Schulz-Menger, MD[8], Daniel R. Messroghli, MD[9]

1. Deutsches Herzzentrum Berlin and Charité University Medicine Berlin, Germany

2. University of Heidelberg, Germany

3. Working Group on Cardiovascular Magnetic Resonance, Experimental and Clinical Research Center, a joint cooperation between the Charité Medical Faculty and the Max-Delbrueck Center for Molecular Medicine and HELIOS Hospital Berlin Buch, Berlin, Berlin, Germany

4. Working Group on Cardiovascular Magnetic Resonance, Experimental and Clinical Research Center, a joint cooperation between the Charité Medical Faculty and the Max-Delbrueck Center for Molecular Medicine and HELIOS Hospital Berlin Buch, Berlin, Berlin, Berlin, Germany

5. German Heart Center Berlin, Berlin, Berlin, Germany

6. Diagnostikum Berlin, Germany

7. McGill University Health Centre, PQ, Canada

8. Working Group on Cardiovascular Magnetic Resonance, Experimental and Clinical Research Center a joint cooperation between the Charité Medical Faculty and the Max-Delbrueck Center for Molecular Medicine HELIOS Klinikum Berlin Buch, Germany, Berlin, Germany

9. Deutsches Herzzentrum Berlin and Charité University Medicine Berlin

Background: Cardiac T1 mapping using Modified Look-Locker inversion recovery (MOLLI) provides highly reproducible results for a given mapping protocol. However, comparability of the results from different sites is limited because normal ranges differ with field strength, system specifications, and MOLLI variants. Our aim was to study the comparability of Z-scores derived from MOLLI 5-3 data obtained from different MR systems, and to compare the diagnostic accuracy of Z-score mapping and conventional T1 mapping in patients with cardiac amyloidosis.

Methods: 15 healthy volunteers (mean age 25 ±4 years, 7 males) underwent cardiac T1 mapping at three sites on 4 different MR systems (1.5 T and 3 T from two different manufacturers) with the MOLLI 5(3)3 (beat) scheme. Normal values of septal mid-cavity myocardial T1 were derived for each MRI system. Z-scores are multiples of standard deviations (SD) from the normal mean. Based on the normal values, Z-score maps were generated from the volunteer data and compared to each other. In a second step, Z-score maps were generated from T1 maps acquired in patients with amyloidosis at 2 additional MR systems using normal data obtained with the same 5(3)3 MOLLI protocol: 1,5 T, 25 patients (mean age 65 ±10 years, 16 males) vs. 14 healthy volunteers (mean age 54 ±7, 7 males); and 3 T, 13 patients (mean age 68 ±12 years, all males) vs. 16 healthy volunteers (mean age 55 ±3 years, 11 males).

Results: Among healthy volunteers, there were significant differences between native myocardial T1 obtained with MOLLI 5-3 from different 3 T systems, but not between 1.5 T systems (Table 1). However, there was no significant difference between Z-scores of native T1 for 1.5 T, 3 T, or 1.5 T vs. 3 T (Table 1). In patients with cardiac amyloidosis, Z-score mapping yielded the same sensitivity and specificity for the detection of amyloid disease as native myocardial T1 mapping (Table 2, Figure 1).

Conclusion: Z-score mapping allows for standardizing results of native myocardial T1 mapping performed with different MR systems and field strengths, and yields the same diagnostic accuracy for the detection of cardiac amyloidosis as conventional native T1 mapping.

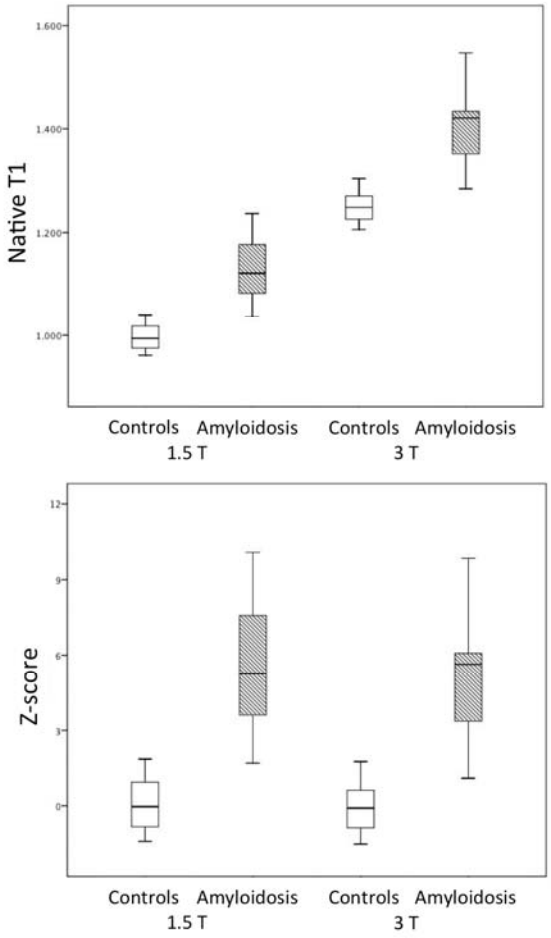

Distribution of native T1 and Z-scores in controls and patients with amyloidosis.

T1 Values and Z-Scores Derived from MOLLI 5-3

Manufacturer	Field strength	Native T1	Z-Score
Philips	1.5 T	1007 +/-29	-0.03 +/-0.99
Siemens	1.5 T	995 +/-20	-0.01 +/-0.98
Philips	3 T	1241 +/-47	-0.01 +/-1.00
Siemens	3 T	1214 +/-42	-0.01 +/-0.99

Sensitivity and Specificity of Native T1 and Z-Scores to Detect Amyloidosis

	Field Strength	Native T1	Z-Score

Sensitivity	**1.5 T**	0.92	0.92
	3 T	0.92	0.92
Specificity	**1.5 T**	1.0	1.0
	3 T	1.0	1.0

ID#: 376288

Is there a role for cardiac MRI stress imaging after an abnormal SPECT study?

Rohith Raghavendran, BS [1]Daniel R. Morgenstern, MS[2], Venkat Tondapu, BS[3], J. Ronald Mikolich, MD[4]

1. Sharon Regional Health System

2. University of Toledo College of Medicine, PA

3. Sharon Regional Health System/ NEOMED, Strongsville, OH

4. Northeast Ohio Medical University (NEOMED), Youngstown, OH

Background: For patients with known coronary atherosclerotic disease(CAD), stress testing may be appropriate every 5 years per ACC/AHA guidelines. Most commonly, a nuclear myocardial perfusion imaging (MPI) study is performed. If there is evidence of reversible ischemia, coronary arteriography (CATH) is often pursued. The CE-MARC trial demonstrated superiority of cardiac MRI stress imaging (CMR stress), especially with respect to a higher negative predictive value of 90.5% for CMR stress versus 79.1% for MPI. This study was designed to assess the potential role of CMR stress imaging, as an alternative to CATH, for stable CAD patients with an abnormal MPI.

Methods: The study cohort was composed of all stable CAD patients with an abnormal MPI during the first 6 months of 2015, derived from an institutional cardiac imaging database. Group A patients underwent CATH after the abnormal MPI, while Group B patients underwent CMR stress, at the discretion of the attending cardiologist. Patients from Group B who had an abnormal CMR stress went on to CATH. During a 2-year follow-up period, clinical outcomes, and cost of care for Groups A and B were computed and statistically compared. Clinical outcomes included cardiac death, fatal arrhythmia, myocardial infarction, and atrial fibrillation. Cost was computed from prevailing 2017 Medicare reimbursements, calculated as a mean cost per patient for Groups A and B. The 2017 Medicare reimbursements (cost) for MPI, MRI stress test and CATH were $1029.40, $1010.79, $2561. 92, respectively. The mean radiation dose for MPI is 12.5 mSv and 12.0 mSv for CATH. These published values were used for computation of the mean radiation dose per patient for both Groups A and B.

Results: Group A had 90 patients with an abnormal MPI who underwent CATH. Fifty-one had an abnormal CATH (57%), while 39 (43%) had no significant CAD on CATH. The average cost of care for the group A imaging strategy was $3,591 US/patient. Group B had 95 patients with an abnormal MPI and underwent CMR stress. Only 16 (17%) had an abnormal CMR stress and went on to CATH, while 79 (83%) had a normal CMR stress, requiring no further testing. The average cost of care for the Group B imaging strategy was $2,472 US/patient. The clinical outcome data is shown in Table 1. The mean radiation dose for Group A patients was 24.5 mSv, while the mean dose for Group B was 14.5 mSv. Group B patients had 40% reduction in radiation dose.

Conclusion: Cardiac MRI stress testing appears to be a reasonable option to coronary arteriography for stable CAD patients with an abnormal nuclear MPI, based on 2 year clinical outcome, cost and radiation exposure.

Table 1: Clinical Outcomes of Group A and B

Clinical Outcomes	Group A (N=90)	Group B (N=95)
Cardiac Death	3 (3.3%)	1(1%)
Fatal Arrhythmia	0	0
Myocardial Infarction	0	0
Atrial Fib	6(6.6%)	6(6.6%)

ID#: 376559

Clinical application of cardiac hyperpolarized magnetic resonance: initial experiences

Damian J. Tyler, Ph.D.[1] Oliver Rider, BMBCh, DPhil[2], Michael Dodd, DPhil[3], Angus Lau, Ph.D.[4], Andrew Lewis, MRCP[2], Jack Miller, DPhil[1], Mark A. Peterzan, BSc(Hons) MRCP(UK) MA[1], Claire Trumper[3], Stefan Neubauer, MD, FRCP[5]

1. University of Oxford, Oxford, England, United Kingdom

2. University of Oxford Centre for Clinical Magnetic Resonance, Oxford, England, United Kingdom

3. University of Oxford, United Kingdom

4. University of Toronto, Canada

5. University of Oxford, England, United Kingdom

Background: The recent introduction of hyperpolarized Magnetic Resonance (MR) spectroscopy has opened up a new window on *in vivo* metabolism and has been widely used to demonstrate physiological and pathological changes in pyruvate metabolism in the rodent heart. This work aims to demonstrate, for the first time, that hyperpolarized MR can detect physiological modulation of metabolism in the healthy human heart. In line with the Glucose Fatty-Acid cycle, proposed by Sir Philip Randle in 1963, we aimed to show changes in substrate selection in the healthy human heart during the transition from the fasted to the fed state.

Methods: All scanning was undertaken on a 3T Tim-Trio MR System (Siemens, Germany) and was approved as a physiological study by local and national research ethics committees. Five healthy male participants were initially scanned in the fasted state for assessment of pyruvate dehydrogenase (PDH) flux. They subsequently received a 70g oral glucose load and were rescanned one hour later. Hyperpolarized [1-^{13}C]pyruvate was generated in a SpinLab hyperpolarizer system (GE Healthcare, USA) and, following appropriate quality control measurements, was transferred to a Medrad syringe ready for patient injection. Hyperpolarized ^{13}C MR spectra were localised to the heart via slice selection and a surface coil placed directly over the heart. Data were reconstructed prior to thermal baseline subtraction and quantification.

Results: Hyperpolarized pyruvate was obtained with polarization levels of >40% and all injections were well tolerated with no adverse effects. Figure 1 shows example spectra acquired at 10s and 25s after the start of the injection into a fasted control participant, showing pyruvate arrival (10s) and metabolic conversion into lactate, alanine, bicarbonate and carbon dioxide (25s). As can be seen in Figure 2, the transition from the fasted to the fed state led to a 97% increase in the conversion of pyruvate into bicarbonate, indicative of an increase in flux through the key regulatory enzyme, PDH. No changes in the conversion of pyruvate to either lactate or alanine were observed.

Conclusion: This study has demonstrated the feasibility of undertaking metabolic studies with hyperpolarized pyruvate in the human heart. The transition from the fasted to the fed state led to an increase in the flux through PDH caused by a switch away from fatty acid oxidation towards glucose oxidation. Such studies will provide the basis for future clinical studies exploring the metabolic alterations that occur in the diseased heart.

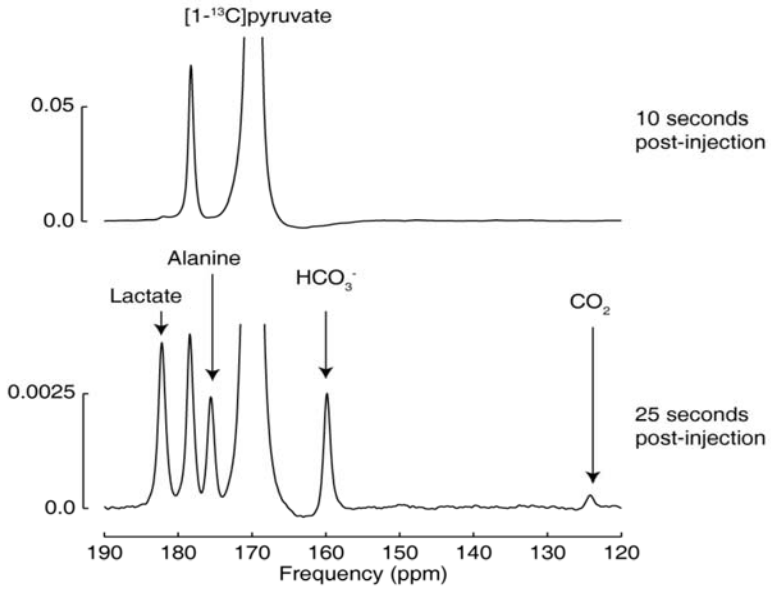

Figure 1: Example spectra acquired 10s and 25s following the injection of hyperpolarized [1-13C]pyruvate

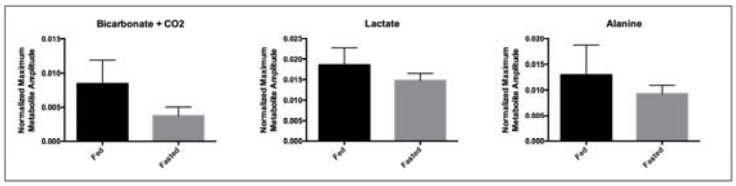

Figure 2: Quantifications showing increased flux through pyruvate dehydrogenase in the fed heart

ID#: 376672

Free-breathing Late Gadolinium-enhanced CMR to Identify the Cause of Myocardial Infarction with Non-obstructed Coronary Arteries

Pierre-Francois Lintingre[1] Claudia Camaioni, MD[2], Soumaya Sridi[3], Hubert Nivet[3], Francois Laurent[4], Michel Montaudon[4], Hubert Cochet[5]

1. CHU Bordeaux, Bordeaux, Aquitaine, France

2. Barts Heart Center, London, England, United Kingdom

3. CHU Bordeaux, France

4. Unité d'imagerie cardio-thoracique, CHU Bordeaux, Pessac, Aquitaine, France

5. IHU LIRYC - CHU / Université de Bordeaux, France

Background: Cardiac magnetic resonance (CMR) plays a pivotal role for the diagnosis of patients presenting with myocardial infarction and non-obstructed coronary arteries (MINOCA). However, the diagnosis remains uncertain in a significant number of patients, CMR being either negative or inconclusive. We assessed the diagnostic yield of CMR including high-resolution late gadolinium-enhanced imaging (HR-LGE) in patients with MINOCA.

Methods: Consecutive patients categorized as MINOCA after blood testing, ECG, coronary angiography, and echocardiography, underwent conventional CMR including cine, T2-weighted, first-pass perfusion and breath-held LGE imaging. HR-LGE using a free-breathing method was systematically added to the protocol when conventional CMR was negative or inconclusive, and was optional otherwise. Diagnoses retained after reviewing conventional CMR were compared to those retained after the adjunction of HR-LGE.

Results: From 2012 to 2016, 229 patients were included (age 56±17 years, 45% women). A definite diagnosis was retained after conventional CMR in 138(60%) patients: infarction in 56(24%), myocarditis in 57(25%), tako-tsubo cardiomyopathy in 22(10%), and other in 3(1%). In the remaining 91(40%) patients the diagnosis remained uncertain: negative CMR in 59(26%), consistent with multiple diagnoses in 32(14%). HR-LGE was performed in 172(75%) of the population, leading to a change in final diagnosis in 45(26%) of these patients, and to a lower rate of uncertain final diagnosis (29% vs. 50%, P<0.001). HR-LGE was particularly useful when TTE, ventriculography, and conventional CMR were negative.

Conclusion: HR-LGE imaging has high diagnostic value in patients with MINOCA. This has major diagnostic, prognostic and therapeutic implications.

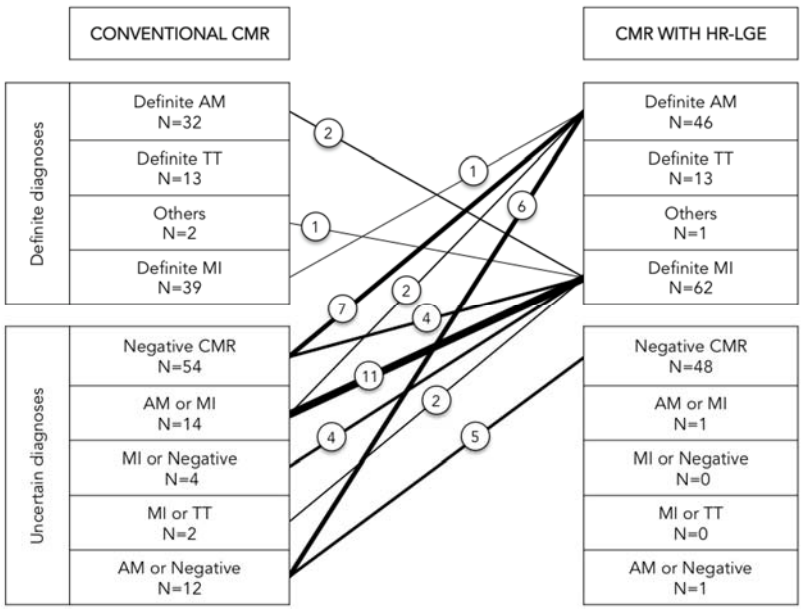

Diagnostic changes introduced by HR-LGE

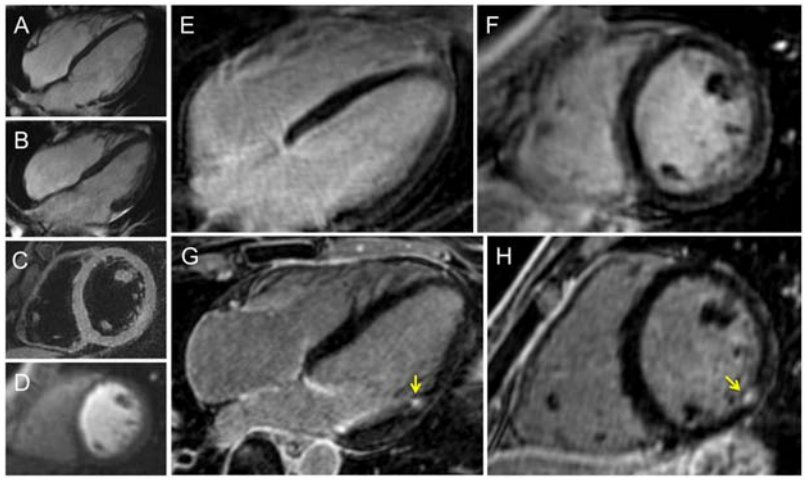

Focal micro-infarction revealed by HR-LGE in a 33yo women presenting with MINOCA

ID#: 376674

Prognostic Role of Cardiac Magnetic Resonance in Arrhythmogenic Right Ventricular Cardiomyopathy.

Giovanni D. Aquaro[1] Alessandro Pingitore[2], Andrea Barison, MD, PhD[3], Gianluca Di Bella[4], Giancarlo Todiere[5], Fausto Pizzino[6], Adriana Pantano[7], Pierluigi Festa[8]

1. Fondazione Toscana Gabriele Monasterio, Pisa (Italy), Toscana, Italy

2. Fondazione Toscana G.monasterio, CNR, Massa, Italy

3. Fondazione Toscana Gabriele Monasterio, Pisa (Italy), Pisa, Toscana, Italy

4. Università degli Studi di Messina, Dipartimento di Medicina Clinica e Sperimentale, Sicilia, Italy

5. Fondazione Toscana G.monasterio, CNR, Pisa, Italy

6. Fondazione Toscana Gabriele Monasterio and Scuola Superiore Sant'Anna di Pisa, Massa, Toscana, Italy

7. University of Trieste, Trieste, Italy, Trieste, Friuli-Venezia Giulia, Italy

8. Fondazione Toscana G.monasterio, CNR, Massa, Toscana, Italy

Background: We sought to evaluate the prognostic role of Cardiac Magnetic Resonance (CMR) in patients with definite, borderline and possible diagnosis of Arrhythmogenic Right Ventricular Cardiomyopathy (ARVC) and in patients with only 1 minor criterion as defined by the International Task Force (TF) in 2010.

Methods: We enrolled 745 patients with clinical suspect of ARVC and fulfilling at least 1 minor TF criterion (17 patients had a definite, 46 borderline, 62 possible diagnosis, while 620 patients with only 1 minor criterion were defined as “no-diagnosis”). Abnormal-CMR, was defined as the presence of ≥1 CMR abnormalities (including abnormalities of right ventricular and left ventricular wall motion, fat infiltration, late gadolinium enhancement, dilation and dysfunction of either ventricles).

Results: Abnormal-CMR, was found in 317(42.5%) patients. Median follow-up was of 1285 days (25th-75th 1205-3234). During this time 33 patients had cardiac events (sudden cardiac death, appropriate ICD shock and resuscitated cardiac arrest). Kaplan-Meier survival curve demonstrated that patients with definite ($p<0.0001$) and those with borderline ($p<0.0001$) diagnosi had worse prognosis than patients with possible and no-diagnosis (figure 1). Thirty-one events occurred in patients with abnormal-CMR. In patients with a definite diagnosis, 9/9 cardiac events occurred in patients with an abnormal CMR. Similarly, among patients with borderline diagnosis, 14/14 events occurred in patients with abnormal CMR. Instead, in patients with a diagnosis of possible, 1 event occurred in patients with abnormal CMR and 1 in those with negative CMR. Finally in subjects with no diagnosis, 7/8 events occurred in patients with an abnormal CMR (figure 2). Abnormal CMR had a prognostic role in patients presenting with NSVT at 24 h ECG Holter monitoring and in those with history of syncope (Figure 3). At multivariable Cox regression analysis a definite diagnosis (HR 14.7,95% CI 7.01-31.3,$p<0.0001$), abnormal-CMR (HR 11.9,95% CI 2.77-51.2,$p=0.0009$) and NSVT episode (HR 14.7,95% CI 2.23-12.1,$p=0.0001$) were independent predictors of the combined endpoint. Harrel-C statistic demonstrated that abnormal-CMR had an addictive prognostic role over a definite diagnosis to predict cardiac events (0.91, $p=0.0014$).

Conclusion: In patients with definite, and borderline diagnosis of ARVC/D, the presence of any CMR abnormalities including either RV and/or LV fat infiltration, not considered among TF criteria, is associated with worse prognosis. The abnormal CMR has a higher negative predictive value for cardiac events. Abnormal CMR is a strong independent predictor of cardiac events and has an additive prognostic role over definite diagnosis

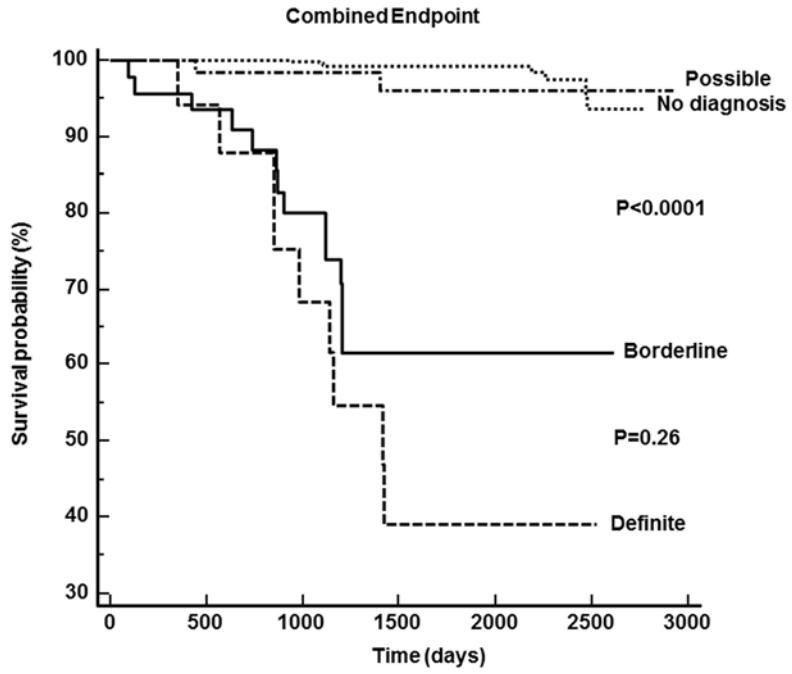

These Kaplan-Meier survival curves patients with definite and those with borderline diagnosis had worse prognosis than patients with possible and no diagnosis. No significant difference between definite and borderline diagnosis was found.

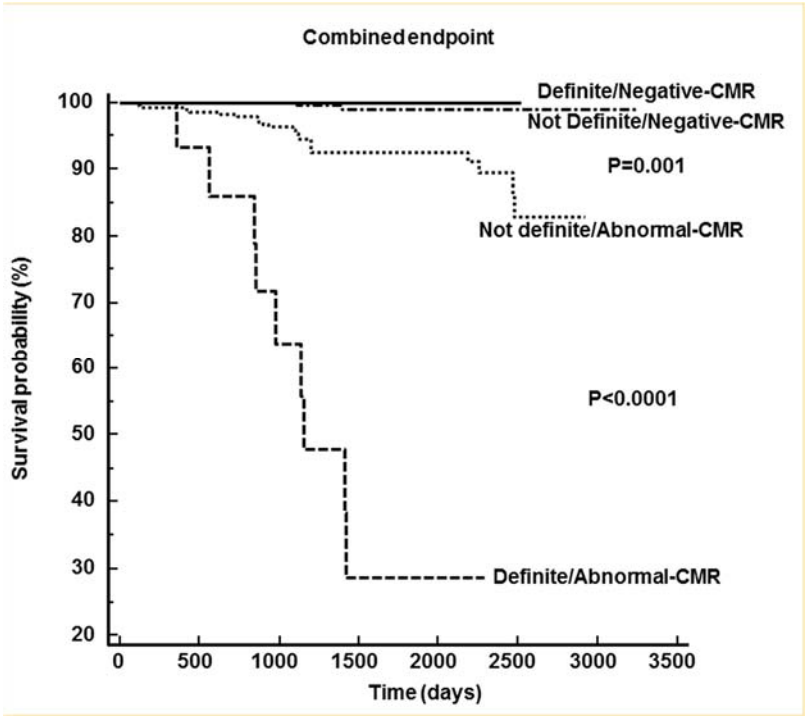

These curves demonstrated the prognosis role of an abnormal CMR: the worse prognosis was found in the group of patients with definite diagnosis and CMR, but no events occurred in subjects with definite diagnosis but negative CMR.

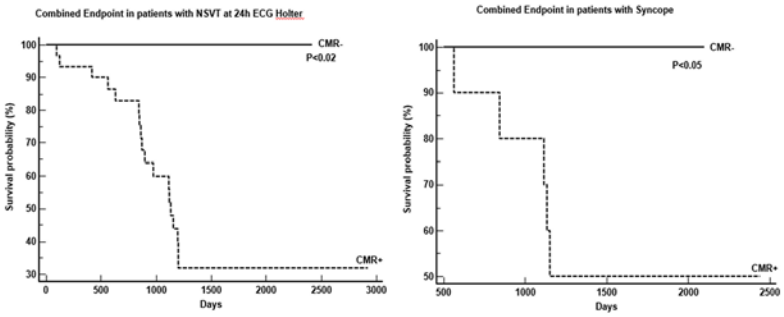

These graphs demonstrated that in patients with Syncope (left panel) and TVNS (right panel) the presence of abnormal CMR was associated to a worse prognosis.

ID#: 375556

Progression of aneurysm of the ascending aorta: A CMR perspective

Sebastian M. Boland, MBA[1] Daniel R. Morgenstern, MS[2], Rohith Raghavendran, BS [3], Venkat Tondapu, BS [3], J. Ronald Mikolich, MD[4]

1. Sharon Regional Health System, Rootstown, OH

2. University of Toledo College of Medicine, PA

3. Sharon Regional Health System

4. Northeast Ohio Medical University (NEOMED), Youngstown, OH

Background: The diagnosis of aneurysm of the ascending aorta (AAscAo) can be a clinical challenge, often remaining asymptomatic until a fatal or near-fatal event. A standard chest x-ray may not be adequate and the ascending aorta is often outside the 90-degree arc of 2D echo imaging, necessitating use of CT or MRI technology. The current recommendation by the ACCF/AHA and ESC regarding AAscAo imaging is for the diameter to be measured perpendicular to flow rather than in the axial plane . Published studies on progression of AAscAo have used CT axial dimensions (Park et al., 2017, European Journal of Cardio-Thoracic Surgery, 51, 959-964) . This study compiled and analyzed longitudinal data in patients with AAscAo (diameter >3.5cm perpendicular to flow) over a 5-year period using CMR.

Methods: fn institutional cardiac imaging database was queried for patients with AAscAo. 383 patients with an ascending aortic diameter exceeding 3.5 cm and at least one follow-up CMR constituted the study cohort. The mean diameter and rate of annual growth for five years after the initial diagnosis were computed. For purposes of measuring the cost saving effect of CMR versus CT serial imaging of AAscAo, the 2017 Medicare reimbursements rates were used. As of 2017, the cost of a CMR is $254.82 for patients with Medicare and $496.20 for patients with private insurance. The cost of CT is $486.10 for patients with Medicare and $720.50 for patients with private insurance.

Results: The mean diameter of the ascending aorta, measured perpendicular to flow, in patients diagnosed with AAscAo is 4.03 +/- 0.02 cm. The mean diameter is plotted on the line graph in Figure 1 below demonstrating the average change over the five-year period. The AAscAo diameter grew at an average rate of 0.59 mm/year, demonstrating a statistically significant increase in growth rate starting in the third year following diagnosis (p=0.03). After five years, the average diameter of the ascending aorta is 4.52 cm, representing an average total growth of 0.49 cm.

Conclusion: This study demonstrates a divergence from the current ACCF/AHA and ESC cardiac imaging interval recommendation for annual assessment of aneurysm of the ascending aorta size. Based upon the slow rate of growth for the first three years following diagnosis, this interval could be adjusted to every three years. Based on local reimbursement rates, adjustment to 3-year imaging intervals using CMR would decrease cost by $509.64/Medicare patient and $992.40/privately insured patient. Similarly, use of 3-year imaging intervals using CT would reduce cost by $972.20/Medicare patient and $1,441.00/privately insured patient.

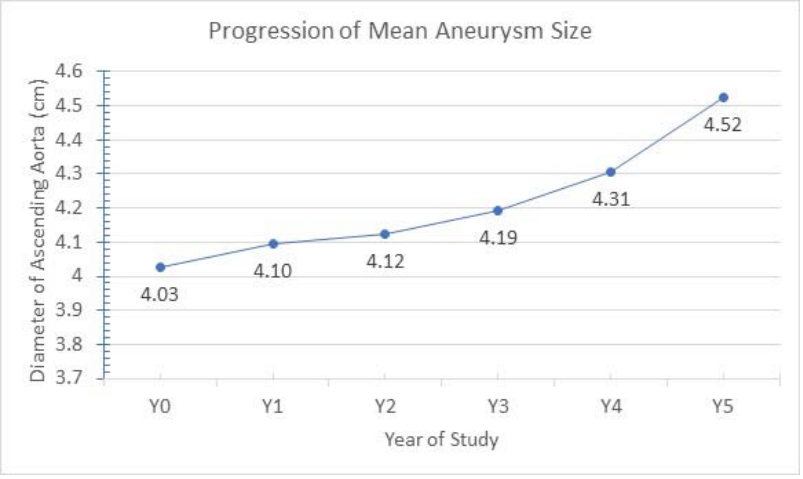

Figure 1 - Progression of Mean Aneurysm Size

ID#: 377548

Prognostic value of featuring-tracking cardiac magnetic strain parameters in ST-segment elevation myocardial infarction patients with a concurrent chronic total occlusion.

Joëlle Elias, MD[1]Ivo van Dongen, MD[1], Loes Hoebers, MD, PhD[1], Dagmar Ouweneel, PhD[1], Bimmer Claessen, MD, PhD[1], Peep Laanmets[2], Erlend Eriksen[3], Truls Ramunddal[4], Dan Ioanes[4], Rene van der Schaaf, MD, PhD[5], Robin Nijveldt, MD, PhD[6], Jan Tijssen, PhD[1], Jose Henriques, MD, PhD[1], Alexander Hirsch, MD, PhD[7]

1. Academic Medical Center Amsterdam, Netherlands

2. Nort-Estonia Medical Center, Estonia

3. Haukeland University hospital, Norway

4. Sahlgrenska, Sweden

5. Onze Lieve Vrouwe Gasthuis Amsterdam, Netherlands

6. VU University Medical Center, Netherlands

7. Erasmus Medical Center, Netherlands

Background: In the EXPLORE trial patients with ST-segment elevation myocardial infarct (STEMI) treated with primary percutaneous coronary intervention (PCI) and a concurrent chronic total occlusion (CTO), were randomized to PCI or conservative treatment of the CTO in the first week after STEMI. The main results did not show a significant benefit of CTO PCI on global left ventricular (LV) function. Although global LV function is routinely used to identify cardiac dysfunction, strain parameters are gaining more interest to identify more subtle LV dysfunction. The objective of this study was to determine the prognostic value of strain parameters by featuring-tracking cardiac magnetic resonance (FT-CMR) in STEMI patients with a CTO.

Methods: The EXPLORE trial included 302 STEMI patients with a CTO who were randomized to CTO PCI (148) or no-CTO PCI (154). In this EXPLORE strain substudy, we studied 200 of the 302 EXPLORE patients with a baseline CMR, of which 180 patients also had serial 4 month follow-up CMR. Endo-global longitudinal strain (GLS) was calculated from 3 long axis cine views. Global circumferential strain (GCS) and global radial strain (GRS) were calculated from 3 short axis (basal, mid and apical).

Results: Mean age was 60±10 years and 87% of patients was male. Baseline LV ejection fraction was 41.3(±11.8)% and end-diastolic volume 210.8(±53.4)ml. Baseline GLS, GCS and GRS by FT-CMR were significantly correlated with baseline global LV function ($p < 0.0001$ for all). Serial GLS measurements were available in 166 and GCS and GRS in 160 patients. GLS, GCS and GRS significantly improved at 4 months (mean difference: GLS: -1.8, 95%CI: -2.5 to -1.2; GCS: -1.2, 95%CI: -1.7 to -0.7; GRS: 7.1, 95%CI: 4.4-9.8, all $p<0.001$). However there was no treatment effect of CTO PCI on the recovery of global strain parameters. During a median follow-up of 3.9(±1.5) years 13 patients died. GLS, GCS and GRS were all univariate predictors for long-term mortality. In patients with impaired strain (GLS>-14.4 (median value)) compared to GLS <-14.4 survival was worse (87% versus 96%, Log-Rank p=0.04, figure).

Conclusion: GLS, GCS and GRS improved significantly over time in STEMI patients with a CTO. There was no difference between CTO PCI and no-CTO PCI on the recovery of strain. GLS, GCS and GRS were all associated with long-term mortality and patients with impaired strain had a worse survival.

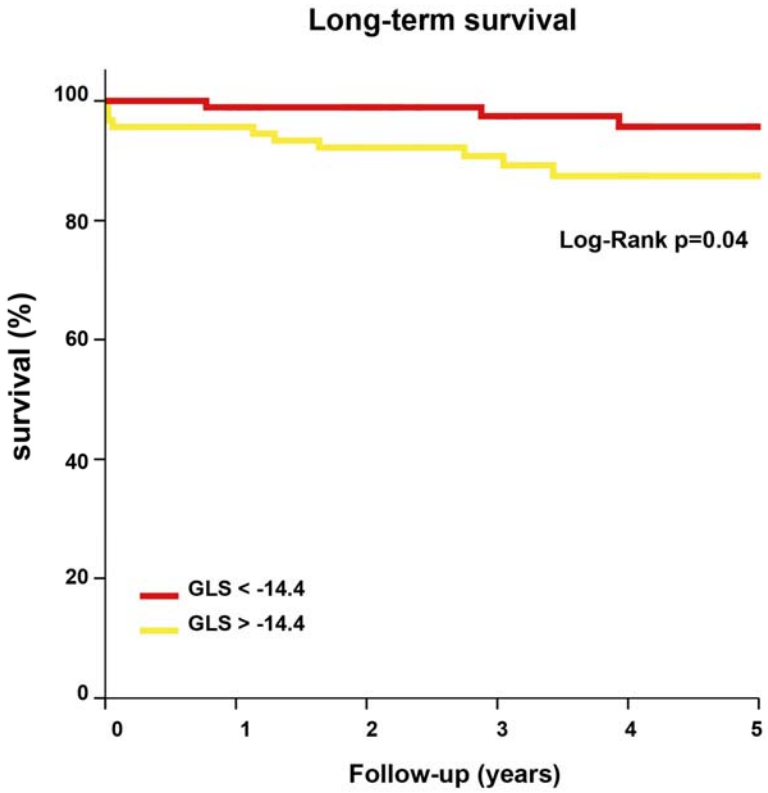

Survival curves

ID#: 377523

Subclinical Coronary Atherosclerosis in Young Women: Magnetic Resonance Coronary Vessel Wall Imaging as a Predictor of Coronary Plaque Burden

Khaled Z. Abd-Elmoniem, PhD, MHS[1] Ahmed H. Hamimi, MD/PhD - FRCR[2], Colleen Hadigan, MD, MPH[3], Jatin R. Matta, PA-C, DHSc[4], Ahmed Ghanem, PhD[5], Reham M. Elgarf, DDS[6], Ranganath Muniyappa, MD[7], Michael V. McConnell, MD, MSEE[8], Ahmed M. Gharib, MD[9]

1. National Institutes of Health, MD

2. National Institutes of Health, Bethesda, MD

3. NIAID, NIH

4. National Institutes of Health

5. National Institutes of Health, Rockville, MD

6. NIH, MD

7. NIH

8. Stanford University, Stanford, CA

9. National Institues of Health

Background: Risk stratification for Coronary Artery Disease (CAD) using traditional risk factors in women has not been as effective as in men. Consequently the mortality rate of young women (ages administration, and radiation exposure. Coronary wall thickness (VWT) determination using Magnetic Resonance Imaging (MRI) is potentially valuable for identifying early CAD in young women, possibly enabling early intervention. This study evaluates the value of this MRI method for the assessment of coronary plaque burden alone or in combination with traditional risk factors for CAD in a young low-risk population.

Methods: We prospectively evaluated 131 asymptomatic adults with at least one CAD risk factor. All subjects underwent coronary CTA for measurement of coronary calcification and coronary plaque burden scores, as well as 3 Tesla (3T) MRI for measurement of coronary VWT. Nonlinear multiple regression modeling with consideration for interactions with gender were performed to investigate the significance of association of traditional atherosclerotic risk factors and VWT with CTA-based plaque burden scores.

Results: The analysis included 62 women and 62 men with low/intermediate Framingham score (FrS) <20%.The age (mean age 45.0 ±14.5 years old) and BMI were not different between the groups. Age, gender, and VWT, individually, were significant predictors of all CTA-based coronary plaque burden scores. Additionally, gender was a significant effect modifier in associations with all plaque burden scores. In contrast to men where age remained the only significant independent predictor of coronary plaque, VWT was the only statistically significant independent predictor of coronary plaque burden scores in women.

Conclusion: In younger asymptomatic women, MRI VWT was the primary predictor of CTA-based coronary plaque burden, whereas age was most predictive of plaque in men. This study suggests that VWT may supplement traditional risk scores for CAD risk stratification in women without the additional risk of radiation from CTA. Further longitudinal studies are required to determine the potential implication and utility of this MRI technique on the preventative management of CAD in women.

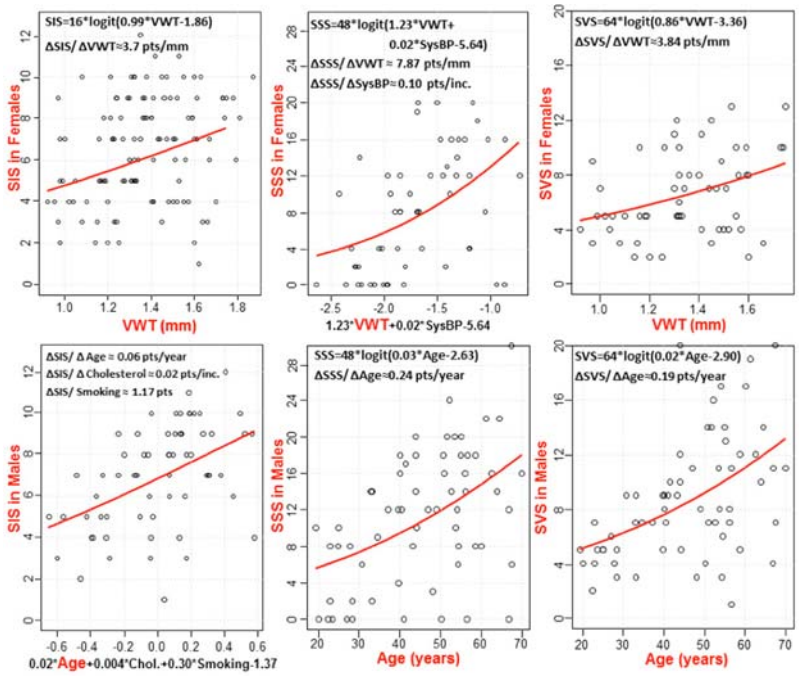

Figure 1: The binomial-logit regression models and the local marginal associations between the statistically significant predictors and normalized plaque burdens; SIS (left), SSS (middle), and SVS (right) in females (top) and males (bottom). Coronary wall thickness was the strongest predictor of plaque burden scores in females while age was the strongest predictor in males.

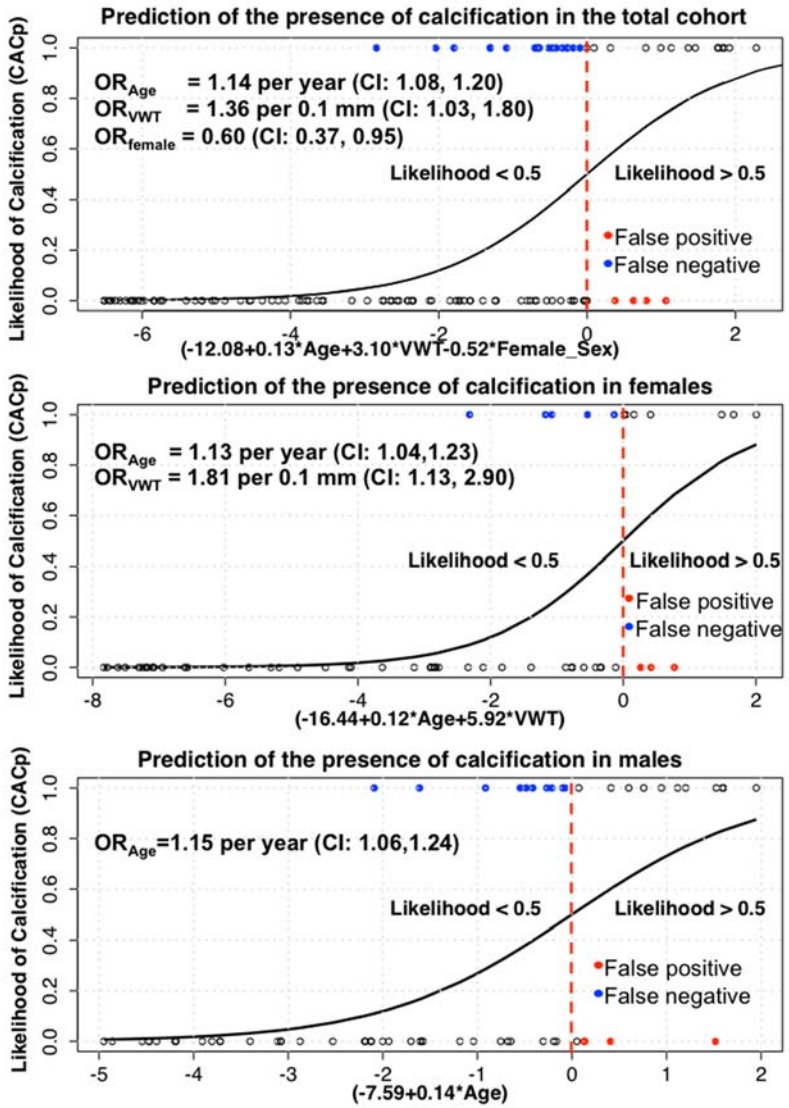

Figure 2: Predictive Probability curves showing: The likelihood of having calcified plaque in the total cohort (top), females (middle) and males (bottom) as a function of the statistically significant predictors; Age, VWT, and Sex in the total cohort in males, Age and VWT in females, and Age only in males.

ID#: 376998

Validation of right ventricular cardiac magnetic resonance feature tracking in patients with CTEPH (chronic thromboembolic pulmonary hypertension) after PEA (pulmonary endarterectomy)

Sabine Zitzmann, MD[1] Julia Vietheer, MD[2], Christoph Liebetrau, MD[2], Till Keller, MD[2], Jan Sebastian Wolter, MD[2], Steffen Kriechbaum, MD[2], Ulrich Fischer-Rasokat, MD[2], Stefan Guth, MD[3], Christoph Wiedenroth, MD[3], Christian W. Hamm, PhD[2], Andreas Rolf, MD[2]

1. Kerckhoff-Heart-Center, Department of Cardiology, Bad Nauheim, Germany, Frankfurt, Germany

2. Kerckhoff-Heart-Center, Department of Cardiology, Bad Nauheim, Germany, Germany

3. Kerckhoff-Heart-Center, Department of Thoracic surgery, Bad Nauheim, Germany, Germany

Background:

Introduction: In Patient with chronic thromboembolic hypertension (CTEPH) right ventricular (RV) function governs long term prognosis. Recently right ventricular strain analysis emerged as a quantitative measure with prognostic implication. Strain and strain rate are also considered to reflect myocardial contractility. Cardiac magnetic resonance (CMR) feature tracking (FT) has been shown to accurately and reproducibly quantify myocardial strain.

Aim: The goal of this study was to examine the correlation between CMR derived strain and strain rate parameters and hemodynamic measures of RV load and contractility (impedance (Ea), contractility (Emax) and RV-PA coupling (Ea/Emax)) and RV ejection fraction (EF) in patients with CTEPH 12 month after PEA (pulmonary endarterectomy).

Methods:

Methods: 85 patients with CTEPH underwent CMR and right heart catheterization (RHC) within 24 hours 12 month after PEA. Steady state free precession(SSFP) cine CMR sequences were analyzed retrospectively for end-systolic and -diastolic RV volumes and EF. RV strain and strain rate parameters were calculated using the feature tracking module from cvi42 (circle cardiovascular imaging, Calgary, Canada), yielding six strain parameters (GCS, GRS, GLS, GCSR, GRSR, GLSR). PAMP was obtained by RHC.

Results:

Results: Both RV strain and strain rate parameters correlated significantly but moderately with CMR derived RVEF, Ea and Ea/Emax (Table 1). We did not find any correlation between Emax and strain or strain rate parameters (Table 1).

Conclusion:

Conclusion: Strain and strain rate parameters correlated significantly with afterload measures (Ea), PA coupling (Ea/Emax) and RV-EF but not with contractility (Emax). RV strain and strain rate are therefore ideal measures for serial follow ups in CTEPH patients undergoing surgical, internventional or medical treatment.

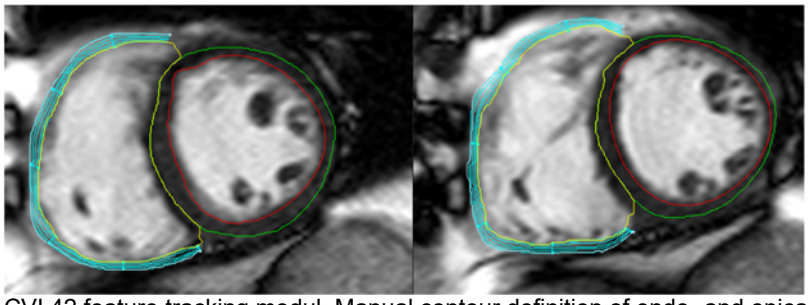

CVI 42 feature tracking modul. Manual contour definition of endo- and epicardial borders

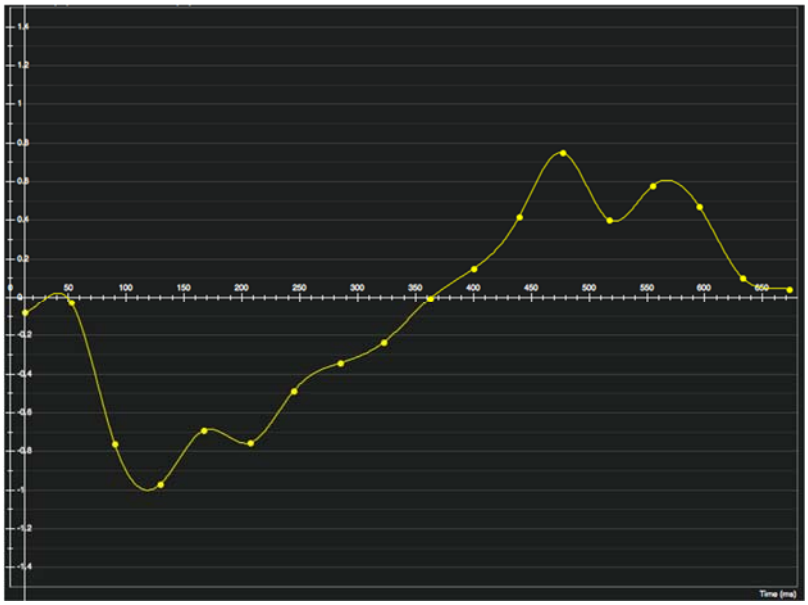

Computation of RV2D strain rate

Table 1. Strain correlations. EF - ejection fraction, RV - right ventricle, Ea - PA endsystolic pressure/volume ratio, Emax - RV endsystolic pressure/volume ratio, SAX - short axis, LAX - long axis, GRS(R) - global radial strain (rate), GCS(R) - global circumferential strain (rate), GLS(R) - global longitudinal strain (rate)

CMR measures of strain	EF r (P)	Ea r (P)	Emax r (P)	Ea/Emax r (P)
RV GRS SAX (%)	0.31(0.004)	-0.21(0.05)	0.009(0.9)	0.009(0.9)
RV GCS SAX (%)	-0.32(0.003)	0.23(0.03)	0.02(0.86)	0.02(0.86)
RV GLS LAX (%)	-0.32(0.003)	0.31(0.004)	0.08(0.47)	0.08(0.47)
RV GRSRsyst SAX (1/s)	0.30(0.004)	-0.1(0.36)	0.01(0.90)	0.01(0.90)
RV GCSRsyst SAX (1/s)	-0.35(0.001)	0.21(0.05)	0.05(0.66)	0.05(0.66)
RV GLSRsyst LAX (1/s)	-0.29(0.006)	0.16(0.14)	0.02(0.86)	0.02(0.86)

Table 2. Patients characteristics. SD - standard deviation, BNP - brain natriuretic peptid, NYHA - New York Heart Association, SixMWT - six minute walking test, PAMP - pulmonary artery mean pressure, TAPSE - tricuspid annular plane systolic excursion, EF - ejection fraction, EDV - end-diastolic volume, ESV - end-systolic volume, RV - right ventricle, SAX - short axis, LAX - long axis, Ea - PA endsystolic pressure/volume ratio, Emax - RV endsystolic pressure/volume ratio, GRS(R) - global radial strain (rate), GCS(R) - global circumferential strain (rate), GLS(R) - global longitudinal strain (rate)

	Observation number	Mean value (SD)
Patients characteristics		
Age (years)	85	55.9(16.6)
Gender (female,n,%)	85	34(40%)
Gender (male,n,%)	85	51(60%)
NT-Pro BNP (pg/ml)	71	334(646)
NYHA functional class	85	1.3(0.48)
SixMWT (m)	42	471(121)
Right heart catheterization measures		
PAMP (mmHg)	84	21.7(7.9)
Echocardiographic measures		
TAPSE (mm)	79	17.3(3.2)
CMR measures of function		
RVEDVindex (ml/m²)	85	76.8(22.7)
RVESVindex (ml/m²)	85	46.5(17.5)
RVSVindex (ml/m²)	85	30.4(12.8)
RVEF (%)	85	39.1(10.7)
Ea (PAMP/RVSVindex)	83	0.79(0.39)
Emax (PAMP/RVESVindex)	83	0.56(0.75)
Ea/Emax	83	1.69(0.69)
CMR measures of strain		
RV GRS SAX (%)	85	21.2(8.9)
RV GCS SAX (%)	85	-12.5(7.0)

RV GLS LAX (%)	85	-16.1(10.9)
RV GRSRsyst SAX (1/s)	85	1.12(0.54)
RV GCSRsyst SAX (1/s)	85	-0.69(0.46)
RV GLSRsyst LAX (1/s)	85	-1.08(0.76)

ID#: 378469

Left ventricular interstitial fibrosis and dysfunction in early chronic kidney disease: 2 year follow up study

Manvir K. Hayer, MBChB[1] Anna Price, MBChB[2], Charles Ferro, MD[3], Jonathan Townend, MD[3], Richard Steeds, MD[4], Nicola Edwards, PhD[4]

1. University Hospitals Birmingham, Birmingham, England, United Kingdom

2. University Hospitals Birmingham, United Kingdom

3. University Hospital Birmingham, United Kingdom

4. University Hospitals Birmingham, England, United Kingdom

Background: Patients with chronic kidney disease (CKD) have a disproportionately high risk of cardiovascular (CV) morbidity and mortality from the very early stages of CKD. This excess risk is believed to be the result of myocardial disease and myocardial fibrosis which are key mediators of CKD cardiomyopathy, commonly termed uremic cardiomyopathy (UC). This hypothesis is supported by recent observational data demonstrating increased native myocardial T1 values with advancing kidney disease and dialysis vintage. To date, there are no longitudinal data to confirm progression of fibrosis or define the natural history of these changes.

Methods: Patients with CKD stage 2 to 5 pre-dialysis, no history of CV disease or diabetes and healthy age matched volunteers were studied as part of an on-going British Heart Foundation funded study examining myocardial fibrosis in CKD. Cardiac magnetic resonance imaging (CMR) including T1 mapping (MOLLI) and late gadolinium enhancement (if eGFR >30ml/min/1,73m^2) was performed at baseline and at follow-up. Demographic, medical co-morbidities and blood and proteinuria data were collected prospectively. CV events were defined as death from CV disease, myocardial infarction, stroke, peripheral vascular disease, or hospital admission with heart failure.

Results: In total 30 patients (age 57 ± 10 years, male gender 60%) were studied. Over a mean follow up period of 2.7 ± 0.8 years, there was no change in left ventricular (LV) mass, volumes, ejection fraction, native T1 times and ECV with CKD or in healthy controls (Table 1 & Figure 1). Global longitudinal strain (GLS 20.6± 2.9 vs 19.8± 2.9 s^{-1}, p=0.03) and mitral annular planar systolic excursion (MASPE 13±2 vs 12±2 mm, p=0.009) decreased but were clinically insignificant. Mid-wall late gadolinium enhancement was present in 4 patients at baseline and was unchanged at follow up. There was no change in systolic blood pressure (129 ±12mmHg vs. 132 ± 17 mmHg). Renal function was stable in these patients over follow up (change in eGFR was minus 4ml/min/1.73m^2). No patients experienced a CV event.

Conclusion: In a cohort of patients with predominantly stable CKD, controlled blood pressure and without known CV disease or diabetes, there is no progression of myocardial fibrosis as assessed by T1 mapping and LGE over 2.7 years follow up. These findings are paralleled by stability of LV mass and systolic function. Further large scale longitudinal studies of patients at high risk of progression of renal disease are required.

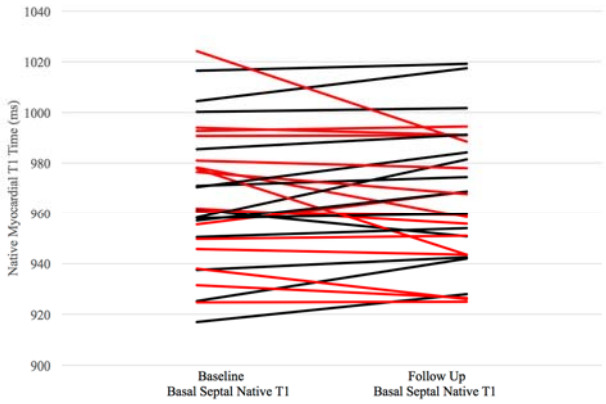

Figure1. The change in native myocardial septal T1 values between baseline and follow-up

Table 1. Demographic, biochemical and treatment data

	CKD Patients (n=30)		P Value
	Baseline	Follow Up	
Serum creatinine (mg/dL)	1.71 ± 1.02	1.96 ± 1.75	0.03
Glomerular Filtration Rate (ml/min/1.73m^2)	50 ± 21	46 ± 21	0.03
CKD stage			0.10
Stage 2 *n* (%)	13 (43%)	12 (40%)	
Stage 3 *n* (%)	11 (37%)	10 (33%)	
Stage 4 *n* (%)	6 (20%)	5 (17%)	
Stage 5 *n* (%)	0 (0%)	3 (10%)	
LVEF (%)	69 ± 9	71 ± 6	0.14
Left ventricular end diastolic volume index (ml/m^2)	67 ± 15	67 ± 11	0.92
Left ventricular end systolic volume index (ml/m^2)	20 ± 8	22 ± 13	0.52
Left ventricular mass indexed (g/m^2)	62 ± 14	62 ± 11	0.71
Native septal T1 time (ms)	967 ± 27	970 ± 26	0.19

Septal extracellular volume (%)	26.1 ± 2.2	26.6 ± 1.7	0.33
MAPSE (mm)	13 ± 2	12 ± 2	0.01
Global longitudinal strain (%)	20.6 ± 2.9	19.8 ± 2.9	0.03
Global longitudinal systolic strain rate (s^{-1})	1.12 ± 0.17	1.07 ± 0.22	0.26
Global longitudinal early diastolic strain rate (s^{-1})	0.92 ± 0.24	0.89 ± 0.26	0.57
Data are frequency (%), mean ± SD, or median and interquartile range.			

ID#: 378572

Mechanistic insight into TakoTsubo cardiomyopathy beyond apical ballooning by myocardial deformation and statistical shape modelling analysis

Giulia Pontecorboli, MD[1] Froso Sophocleous, MSc[2], Elena Giulia Milano, MD[3], Estefania De Garate, MD[4], Iwan Harries, MBBCh BSc[5], Tobias A. Fuchs, MD, FESC, FSCCT[6], Amardeep Dastidar, MBBS, MRCP[7], Anna Baritussio, MD[4], Giovanni Biglino, BEng, PhD[8], Chiara Bucciarelli-Ducci, MD, PhD[4], Benedetta Biffi[9]

1. University of Florence, Italy, Bristol Heart Institute, Bristol, UK, Firenze, Italy

2. Bristol Medical School, University of Bristol, United Kingdom

3. Bristol Heart Institute, Italy

4. Bristol Heart Institute, Bristol NIHR Biomedical Research Centre (Cardiovascular Section), University of Bristol, Bristol, England, United Kingdom

5. Bristol Heart Institute, Bristol, England, United Kingdom

6. Bristol Heart Institute, Bristol NIHR Biomedical Research Centre (Cardiovascular Section), University of Bristol, United Kingdom

7. BHI, United Kingdom

8. Bristol Heart Institute, School of Clinical Sciences, University of Bristol, Bristol, England, United Kingdom

9. University College London, London, United Kingdom

Background: Takotsubo cardiomyopathy (TCM) is a unique type of reversible cardiomyopathy mimicking an acute coronary syndrome. Although TCM was traditionally considered a benign reversible condition, it has been shown that it may be associated with inpatient morbidity and mortality. CMR imaging can provide unique insight into the anatomy and function of TCM patients.
This study aimed to describe ventricular deformations and morphology by means of 2D-Feature-tracking CMR (FT-CMR) and 3D-Statistical Shape Modelling analysis (SSM) in patients with TCM. We hypothesized that myocardial deformation patterns would identify patients at greatest risk for adverse in-hospital cardiovascular events.

Methods: Observational study performed at a tertiary centre in the South-West of England.Consecutive patients diagnosed with acute TCM based on clinical, angiographic and CMR findings were included. Clinical data (ECG, coronary angiogram, echocardiogram, peak troponin) were collected. The CMR protocol included long and short axis cines, T2-STIR, early and late gadolinium enhancement (LGE). Post-processing FT-CMR analysis of global peak radial (GRS), circumferential (GCS) and longitudinal (GLS) strain was performed from cine images.The latter were also used to reconstruct 3D LV peak systolic volumes as inputs for the SSM. A mean systolic LV configuration (‘template';) and deformations around this mean were computed, extracting shape vectors for further statistical analyses.

Results: We identified 37 acute TCM patients (66±11 years,35 females). Mean peak troponin T=785 ng/L (normal <14) and prolonged average QTc=486±52ms. No patient showed significant coronary stenosis on invasive coronary angiography. CMR was performed 4.8±3.0 days from admission. Mean left ventricular ejection fraction (LVEF) was 54±12%, all patients had CMR evidence of myocardial oedema, and 32% (n=12) presented in-hospital cardiovascular complications (Table 1). Risk of in-hospital cardiovascular events was associated with reduced GRS (OR=0.905, CI 0.830-0.985; p=0.02) and reduced GLS (OR=1.297, CI 1.041-1.616, p=0.02). Conversely, there was no association between the risk of cardiovascular events and GCS (p=0.43), peak troponin T (0.98),or QTc (0.45). SSM provided a mean systolic TCM ventricular configuration, with qualitative and quantitative additional insight into LV deformations. The dominant shape mode correlated significantly with EF, GLS and GRS (all p<0.001).

Conclusion: Ventricular deformation appears to carry prognostic information in patients with TCM, suggesting a potential role of shape biomarkers.

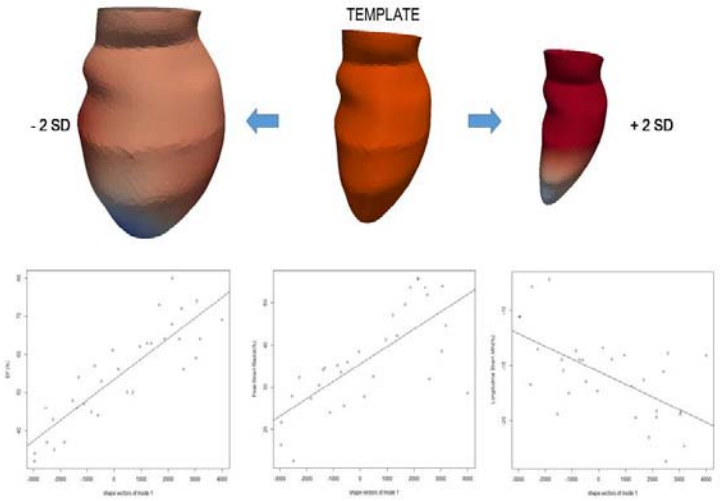

Top: Mean systolic configuration of the LV ('template') and extreme deformations around the mean in the studied population (+/- 2 standard deviations from the template). Bottom: The dominant shape mode (recapitulating 40% of shape variability) correlated with ejection fraction (EF%), global longitudinal strain (GLS) and global radial strain (GRS).

Table 1. In-hospital cardiovascular events in patients admitted with TCM

In-hospital cardiovascular events	12/37 (32.4%)
- Congestive heart Failure	5 (13.5%)
- Atrial Fibrillation	2 (5.4%)
- Ventricular Fibrillation	2 (5.4%)
- 2nd degree A-V block	1 (2.7%)
- Recurrence of chest pain with ST-elevation	1 (2.7%)
- TIA	1 (2.7%)

ID#: 378622

Comparing Myocardial Fibrosis Quantification Methods For Risk Stratification in Patients With Suspected Myocarditis Using Cardiac Magnetic Resonance Imaging

Christoph Gräni, MD[1]Christian Eichhorn, BSc[1], Loïc Bière, MD, PhD[1], Kyoichi Kaneko, MD, PhD[2], Ayaz Aghayev, MD[1], Michael Jerosch-Herold, PhD[3], Raymond Y. Kwong, MD, MPH[4]

1. Brigham and Women's Hospital, Harvard Medical School, Boston

2. Brigham and Women's Hospital and Showa University, Brookline, MA

3. Harvard Medical School, Boston, MA

4. Brigham and Womens Hospital, Boston, MA

Background: Although the presence of late gadolinium enhancement (LGE) using cardiac magnetic resonance imaging (CMR) is a significant discriminator of events in patients with suspected myocarditis, no data is available on the optimal LGE quantification method.

Methods: 670 consecutive patients (mean age 48 ± 16 years, 59% male) with suspected myocarditis were enrolled between 2002 and 2015. LGE thresholding by 2-7 standard deviations (SDs) above remote myocardium, and the full width at half maximum (FWHM) technique were analyzed. Further, a visual LGE presence score (LGE-VPS) (LGE present/absent in each segment) was assessed. Association with major adverse cardiac events (MACE) was analyzed in all methods. Inter-and intra-rater variability using intraclass-correlation (ICC) was performed.

Results: LGE extent varied significantly with the different quantification methods used. Ninety-eight (15%) patients experienced a MACE at a medium follow-up of 4.7 years. LGE quantification by FWHM, 2- and 3SD demonstrated univariable association with MACE (hazard ratio [HR] 1.05, 95% confidence interval [CI]: 1.02-1.08, p=0.001; HR 1.02, 95%CI: 1.00-1.04; p=0.001; HR 1.02, 95%CI: 1.00-1.05, p=0.035, respectively), whereas SD 4-7 showed no prognostic association. LGE-VPS was associated with MACE (HR 1.09, 95%CI: 1.04-1.15, p < 0.001). In the multivariable model FWHM, 2-SD quantification methods and LGE-VPS were independent outcome predictors (HR 1.04, 95%CI: 1.01-1.08, p=0.009; HR 1.02, 95%CI: 1.00-1.04, p=0.035; HR 1.07, 95%CI: 1.02-1.13, p=0.005, respectively). Best ICC was achieved in FWHM and LGE-VPS.

Conclusion: FWHM is the optimal semi-automated quantification method in risk stratifying patients with suspected myocarditis. Visual LGE scoring is a reliable alternative method and associated with outcome in these patients.

ID#: 378035

Radial Fast Interrupted Steady-State (FISS) Cine Imaging for the Evaluation of Heart Valves and Coronary Arteries

Ioannis Koktzoglou, PhD[1] Amit Pursnani, MD[1], Robert R. Edelman, MD[2]

1. NorthShore University HealthSystem, IL

2. NorthShore University HealthSystem, Evanston, IL

Background: Fast interrupted steady-state (FISS) is a newly-developed pulse sequence that enables cardiovascular imaging with high signal-to-noise ratio, inherent fat suppression, and reduced flow artifact compared to standard balanced steady-state free precession (bSSFP) [1]. Here we report our initial experience applying FISS for cine imaging of the heart, and in particular for evaluating coronary arteries and cardiac valves. Comparisons are made with cine bSSFP.

Methods: This study was approved by our institutional IRB and subjects provided written informed consent. Three volunteers were imaged at 1.5 Tesla (MAGNETOM Avanto, Siemens Healthineers, Germany). FISS consists of a highly-interrupted variant of bSSFP that uses radial k-space sampling and frequent spoiling of off-resonant and out-of-slice magnetization. Cine FISS was applied for generic imaging of the heart, en-face imaging of valves, and longitudinal imaging of the left main and anterior descending (LAD) coronary arteries. Comparisons were made with cine bSSFP acquired with identical sampling trajectory, slice thickness, receiver bandwidth, and in-plane spatial resolution.

Results: Compared to cine bSSFP, cine FISS greatly reduced signal from fat throughout the field of view, thereby suppressing chemical shift artifact and streak artifact from radial undersampling. For imaging of cardiac valves, cine FISS improved valve conspicuity during periods of rapid systolic flow when cine bSSFP images were degraded by flow artifact from out-of-slice magnetization. With cine FISS, the coronary arteries were well demonstrated throughout the cardiac cycle, but were poorly shown using cine bSSFP due to chemical shift artifact and partial volume averaging with surrounding epicardial fat.

Conclusion: We have demonstrated that FISS enables high-quality fat-suppressed cardiac cine imaging with reduced radial undersampling and flow artifacts, improved systolic display of valve anatomy, and enhanced depiction of the coronary arteries not feasible using standard cine bSSFP. [1] Koktzoglou I, Edelman RR. 2017 Aug 30. doi: 10.1002/mrm.26881
Acknowledgments: NIH R01 HL130093, R21 HL126015

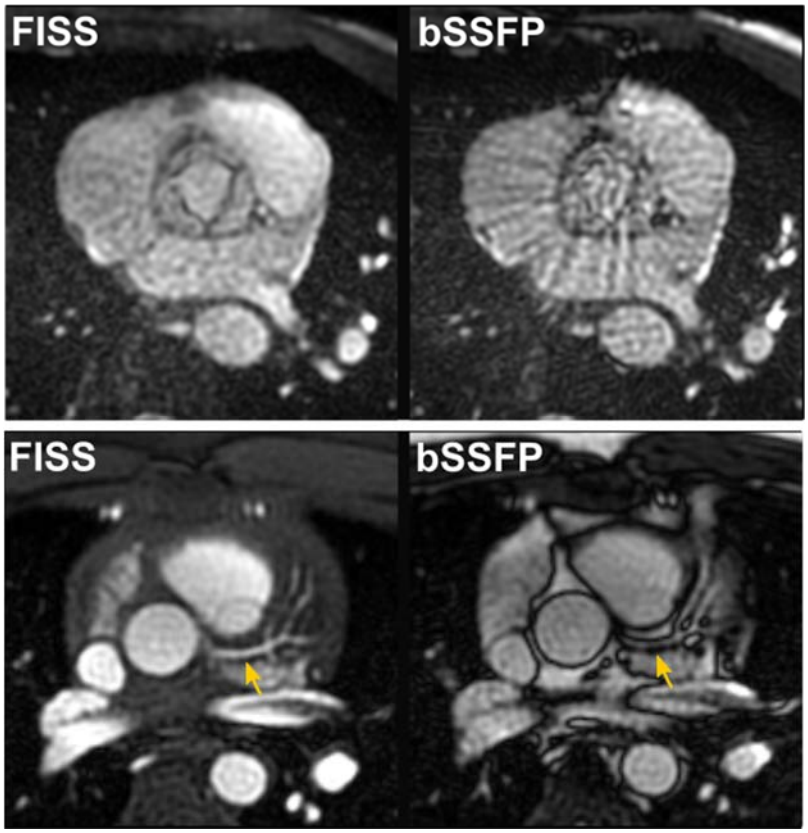

Comparisons of cine FISS and cine bSSFP. Top: Cine FISS shows improved systolic display of the aortic valve. Bottom: Cine FISS shows improved display of the left coronary artery (arrow).

ID#: 378377

The relationship between pulmonary artery-right ventricle coupling and right ventricle remodeling in untreated pulmonary artery hypertension patients

Yang Dong, BMsci[1] Weihao Li, BMSci[2], Ke Wan, MD[3], Yucheng Chen, MD[4]

1. Cardiology Department West China Hospital Sichuan University, Sichuan, China (People's Republic)

2. Cardiology Division, West China Hospital, Sichuan University, Chengdu, Sichuan, China (People's Republic)

3. Cardiology Division, West China Hospital, Sichuan University, Guoxue Xiang No. 37, Chengdu, Sichuan Province 610041, China, Sichuan, China (People's Republic)

4. Sichuan University West China Hospital, Sichuan, China (People's Republic)

Background: To find the relationship between pulmonary artery-right ventricle coupling (PA-RV coupling) and right ventricle remodeling derived from cardiac magnetic resonance (CMR) in untreated pulmonary artery hypertension patients.

Methods: Fifty untreated pulmonary artery hypertension patients were prospectively included from May 2016 to April 2017. All patients underwent CMR and right heart catheterization (RHC) within 72 hours. Ten healthy volunteers were enrolled as normal control and underwent CMR. PA-RV coupling was evaluated by pulmonary artery blood flow volume from phase contrast sequence and right ventricle end-sytolic volume from cine sequence. The relationship between parameters of right ventricle remodeling and PA-RV coupling was evaluated by Pearson';s correlation and multiple linear regression.

Results: PA-RV coupling of patients was significantly increased compared with normal control (2.74±2.13 vs 0.53±0.10,P<0.001). Right ventricle mass index (RVmassi) (r=0.640, P<0.001), right ventricle end-diastolic volume index (RVEDVI) (r=0.517, P<0.001) and ventricular mass index (VMI) (r=0.466, P=0.001) were significantly related to PA-RV coupling. As for myocardial fibrosis parameters, extracelluar volume (ECV) of posterior insertion point (PIP) was significantly related to PA-RV coupling (r=0.334, P=0.040). We also found that pulmonary vessel resistance index (PVRI) (r=0.507, P<0.001) and mean pulmonary artery pressure (mPAP) (r=0.392, P=0.009) were significantly related to PA-RV coupling. Multiple linear regression showed that PA-RV coupling was independently related with VMI (Beta=0.466, P<0.001), ECV of PIP (Beta=0.309, P=0.046)

Conclusion: PA-RV uncoupling lead to remodeling of right ventricle

ID#: 366612

Prognostic and Functional implications of Left Atrial Late Gadolinium Enhancement

Michael Quail, MBChB, PhD[1] Karl Grunseich, M.D.[2], Lauren A. Baldassarre, MD[2], Hamid R. Mojibian, MD[3], Mark Marieb, M.D.[2], Daniel Cornfeld, MD[4], Albert J. Sinusas, MD[5], Dana C. Peters, PhD[1]

1. Yale University

2. Yale University, CT

3. Yale School of Medicine, CT

4. Yale, CT

5. Yale University, New Haven, CT

Background: Left atrial (LA) late gadolinium enhancement (LGE) on cardiac magnetic resonance (CMR) imaging is indicative of fibrosis, and has been correlated with reduced LA function, increased LA volume, and poor procedural outcomes in cohorts with atrial fibrillation (AF). However, the role of LGE as a prognostic biomarker in cardiac disease more generally has not been examined. In this study, we aimed to assess the functional and prognostic significance of LA LGE.

Methods: We assessed LA fibrosis using a 3D LGE CMR sequence. Cine imaging was used to quantify LA and left ventricular (LV) size and function. Contemporaneous tissue Doppler echocardiographic data was available for 70% of patients to assess LV diastolic function (E, e';). New onset arrhythmia and mortality data were obtained from comprehensive notes review. The relationships between LA LGE and new onset atrial arrhythmia and mortality were assessed using multivariable logistic and Cox regression analysis. Simple linear relationships between LA LGE and LA and LV mechanical function were assessed using Spearman';s correlation.

Results: LA LGE images were acquired in 111 patients undergoing CMR imaging for diverse clinical indications (Table 1). Sixty-six patients had no prior history of atrial arrhythmia at baseline. During follow-up (2.7 years, [interquartile range 1.8-3.7years]) 15/66 patients developed new atrial arrhythmia(Figure 1). These patients had greater atrial fibrosis extent 6.8% (4.2-11.1%) compared to those without new arrhythmia 3.4% (2.4-4.8%), p=0.02. LA LGE was significantly associated with new-onset arrhythmia on multivariable logistic regression, with OR of 1.76 (1.03-3.01), p=0.04. Age was also associated with new arrhythmia in this model, while other measures of LA and LV volume and function were not (Figure 2). During follow-up, 5/111 died. Using Cox regression, LA LGE was found to be independently associated with time to all cause death, HR (hazard ratio) 1.82 (1.29-2.57, p<0.0005) and cardiac death, HR 1.83 (1.35-2.48, p<0.0005) including after adjustment for age and LVEF. There were significant relationships between LA LGE and both LA ejection fraction (r=-0.39, p<0.0005) and echocardiographic LV septal e'; (r=-0.24, p=0.04) and septal E/e'; (r=0.31, p=0.007).

Conclusion: LA LGE was associated with new onset atrial arrhythmia and mortality during follow-up, and increased LA LGE is associated with worse LA function and LV diastolic function. This study is the first to identify a prognostic role for LA LGE imaging in a cohort without prior atrial arrhythmia, and identifies LA LGE as a novel biomarker for atrial arrhythmia risk stratification.

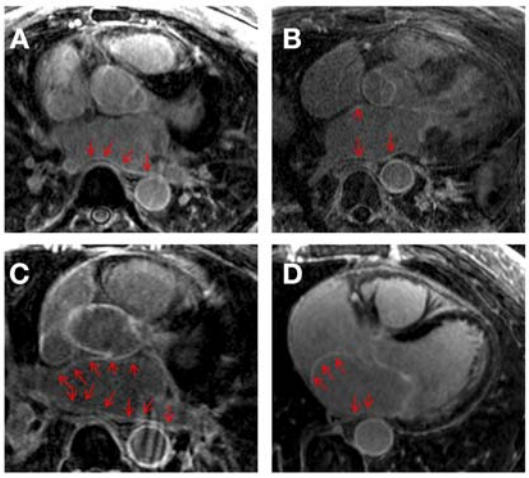

LA LGE images from four patients who developed either atrial fibrillation (A and B), or atrial tachycardia (C,D) during follow-up. Arrows point to LGE enhancement patterns.

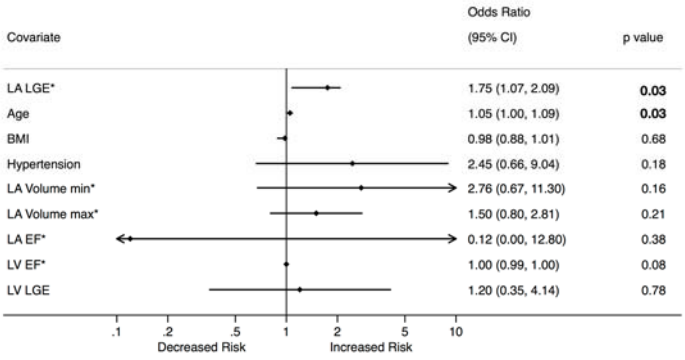

Forest Plot, showing Univariable Odds Ratios for risk of developing new atrial arrhythmia.

Table 1. Clinical Diagnoses of Study Participants.

Diagnosis	Total	Prior Atrial Arrhythmia	No prior Atrial Arrhythmia
DCM	36 (32.4%)	14 (31.1%)	22 (33.3%)
Pre-AF Ablation	25 (22.5%)	25 (55.6%)	-

Ventricular Arrhythmia	14 (12.6%)	2 (4.4%)	12 (18.2%)
HCM	8 (7.2%)	1 (2.2%)	7 (3.0%)
Sarcoid	8 (7.2%)	-	8 (12.1%)
ARVC	6 (5.4%)	-	6 (9.1%)
Normal/Family History	5 (4.5%)	-	5 (7.6%)
Coronary Disease	4 (3.6%)	-	4 (6.1%)
Valvular Disease	3 (2.7%)	1 (2.2%)	2 (3.0%)
Pericarditis	2 (1.8%)	2 (4.4%)	-

ID#: 366467

T2-Prepared Multidimensional Outer Volume Suppression for Coronary Imaging

David Y. Zeng, MS[1] Dwight Nishimura, PhD[2]

1. Stanford University, Stanford, CA

2. Stanford University

Background: We present a new sequence for combined T2-preparation and multidimensional outer volume suppression (OVS). For coronary imaging, OVS facilitates shorter scan times, higher resolution imaging, and reduced motion artifacts by suppressing signal outside a region of interest (ROI), while T2-preparation improves blood-muscle contrast [1]. Compared to other multidimensional OVS sequences based on 2D excitations [2,3], this new sequence offers lower SAR and sharper ROI definition.

Methods: The new sequence (Figure 1 left) consists of two consecutive blocks, each with a $90_{-60}180_{120}$ hard composite tip-down pulse [4], two 180_{90} hard refocusing pulses, and a selective tip-up pulse. The ROI (passband) is defined by the intersection of the spatial selectivity of the tip-up pulses used in the two blocks. For coronary imaging, a spectral-spatial sinc tip-up pulse with a fat stopband is used to leave fat saturated in the ROI. We compared our sequence against the sequence by Luo et al. that used a 2D tip-up pulse (Figure 1 right) [2] on a GE 1.5T scanner with an 8-channel cardiac coil. Phantom scans to examine OVS performance were acquired with a 2D gradient-echo sequence. Coronary scans (n=5) used an alternating-TR steady-state-free-precession 3D-cones sequence with 3D-iNAVs and translational motion correction [5]. Right coronary artery (RCA) and left anterior descending coronary artery (LAD) sharpness were evaluated with image edge profile acutance (IEPA) scores [6]. Image signal-to-noise ratio (SNR) was calculated by dividing the average signal in the left ventricle blood pool by image noise standard deviation in the background. Passband-to-stopband ratio (PSR) was used to evaluate OVS sequence suppression, calculated by dividing the mean passband signal by the mean stopband signal.

Results: Example phantom and coronary results are shown in Figure 2. Phantom cross section plots show a sharper transition band for the proposed sequence. IEPA scores of the RCA and LAD, SNR, and PSR are shown in Figure 3. The proposed OVS technique demonstrates significantly superior vessel sharpness, SNR, and PSR compared to the Luo sequence.

Conclusion: We have presented a sequence for T2-prepared, multidimensional OVS. Initial results indicate superior image quality compared to a previously reported 2D OVS sequence. Additionally, the proposed sequence has 45% less SAR which suggests potential viability for use at 3T. The phantom images demonstrate a sharper passband for the proposed sequence. Given also the superior PSR, the proposed sequence could be viable for scan acceleration with reduced FOV as demonstrated with previous sequences.

[1]Brittain,MRM,33:689,1995[2]Luo,MRM,74:1632;2014[3]Coristine,MRM,74:529,2014[4]Levitt,JMR,48:234,1969[5]Addy,MRM,74:614,2017[6]Delgado-Olabarriaga,SPIE,2712,1996

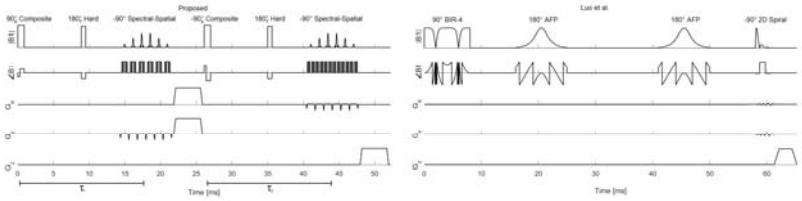

Figure 1: Pulse Sequence Diagrams. (Left) Proposed sequence. (Right) Luo's 2D OVS sequence to be compared against. Both sequences have total T2-preparation time of 50 ms.

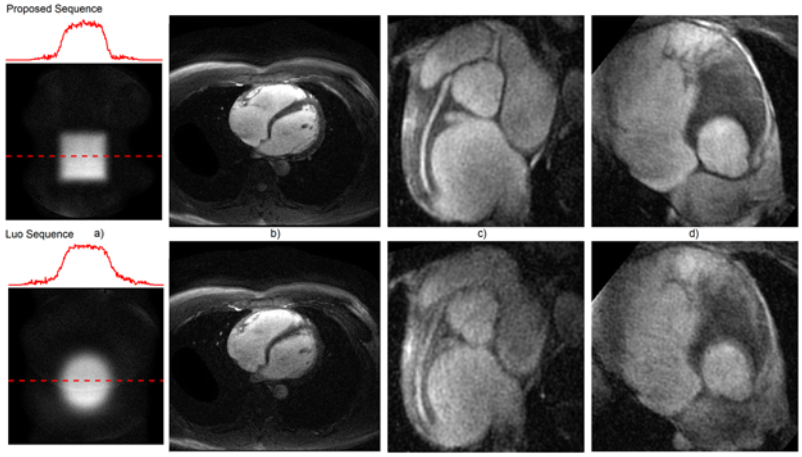

Figure 2: Phantom and In Vivo Results. (Top) Proposed sequence. (Bottom) Luo's 2D OVS sequence. (a) Phantom with OVS and line plot of cross section. (b) Axial view. (c) RCA. (d) LAD.

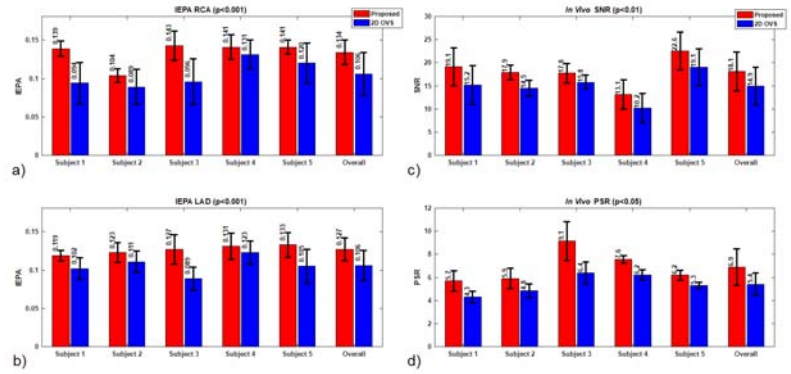

Figure 3: Quantitative Statistical Method Comparison. Paired two-tailed Student's t-tests are used to determine statistical significance. Higher is better for all values. For PSR, we select myocardium of the interventricular septum as passband and chest wall skeletal muscle as stopband. The passband and stopband are selected at the same superior-inferior position to normalize for receiver coil sensitivity.

ID#: 366543

Texture analysis applied on cardiac magnetic resonance T1 and T2 mapping in patients with biopsy-proven infarct-like acute myocarditis: initial results

Bettina Baeßler, M.D.[1]Christian Luecke, MD[2], Karin Klingel, MD[3], David Maintz, MD[1], Matthias Gutberlet, MD[4], Holger Thiele, MD[5], Philipp Lurz, MD, PHD[6]

1. University Hospital of Cologne, Department of Radiology, Nordrhein-Westfalen, Germany

2. University of Leipzig - Heart Centre, Department of Diagnostic and Interventional Radiology, Niedersachsen, Germany

3. Department of Molecular Pathology, Institute for Pathology and Neuropathology - University Hospital Tuebingen, Baden-Wurttemberg, Germany

4. University of Leipzig - Heart Centre, Department of Diagnostic and Interventional Radiology, Sachsen, Germany

5. Heart Center Leipzig University Hospital, Sachsen, Germany

6. University of Leipzig - Heart Centre, Department of Internal Medicine / Cardiology, Sachsen, Germany

Background: Texture analysis (TA) comprises a wide range of techniques modeling spatial distributions of pixel grey-levels for recognizing, classifying, and segmenting data based on their underlying texture. We hypothesize that applying TA on T1 and T2 maps derived from cardiac magnetic resonance (CMR) T1 and T2 mapping increases the diagnostic performance of CMR in patients with “infarct-like” acute myocarditis when compared to traditional Lake Louise criteria (LLC) and to quantification of native T1 and T2 alone, leading the way towards a novel way of tissue characterization based on CMR imaging.

Methods: In this prospective study, 33 patients with clinical suspicion of acute myocarditis defined by symptom duration ≤ 14 days and “infarct-like” clinical presentation were included. Patients underwent biventricular endomyocardial biopsy (EMB), cardiac catheterization and CMR imaging at 1.5T including native T1 and T2 mapping as well as standard LLC. 11 healthy subjects were included as controls. TA was applied on motion-corrected T1 and T2 maps using a freely available software package (MaZda version 4.6) by drawing a region of interest encompassing the entire myocardium. Step-wise dimension reduction and texture feature selection based on reproducibility, machine learning, correlation and logistic regression analyses was performed for selecting texture features enabling the diagnosis of acute infarct-like myocarditis, using EMB as the reference standard.

Results: EMB confirmed the diagnosis of acute myocarditis in 22 patients (EMB+), whereas 11 patients had no signs of acute inflammation on EMB (EMB-). Mean myocardial T2 showed a similar diagnostic performance when compared to LLC for differentiating EMB+ patients from healthy controls (area under the curve [AUC] in receiver operating curve [ROC] analysis: 0.86 for both, Fig. 1), whereas mean T1 demonstrated a slightly inferior diagnostic performance (AUC 0.78). Combining mean T2 with the run-length matrix texture feature T2 run-length non-uniformity (T2_RLNonUni), which is sought to represent the inhomogeneity of the underlying pixel-structure in a T2 map, showed a high diagnostic performance with an AUC of 1.00 as well as a sensitivity and specificity of 100% for differentiating EMB+ patients from healthy controls (Fig. 1). In a next step, we investigated the potential of texture features to differentiate between EMB+ and EMB- patients. In contrast to mean T1 and T2, which showed a similar and low diagnostic performance to LLC (AUC 0.61 for T1 and T2 and 0.64 for LLC, Fig. 2), combining T2_RLNonUni with another feature being thought to represent the inhomogeneity of the T2 map, grey-level non-uniformity (T2_GLevNonU), resulted in a high diagnostic performance with an AUC of 0.86 and a sensitivity and specificity of 91%, respectively (Fig. 2).

Conclusion: TA is feasible when being applied on native T1 and T2 maps and delivers interesting novel parameters for the diagnosis of acute infarct-like myocarditis. Especially the two parameters hypothesized to represent the inhomogeneity of the underlying pixel-structure in a T2 map showed a highly superior diagnostic performance when compared to LLC as well as to native T1 and T2 alone for differentiating EMB+ patients from healthy controls as well as from EMB- patients. Thus, TA may lead the way towards novel possibilities for tissue characterization in CMR imaging and allow for a more confident diagnosis of acute infarct-like myocarditis.

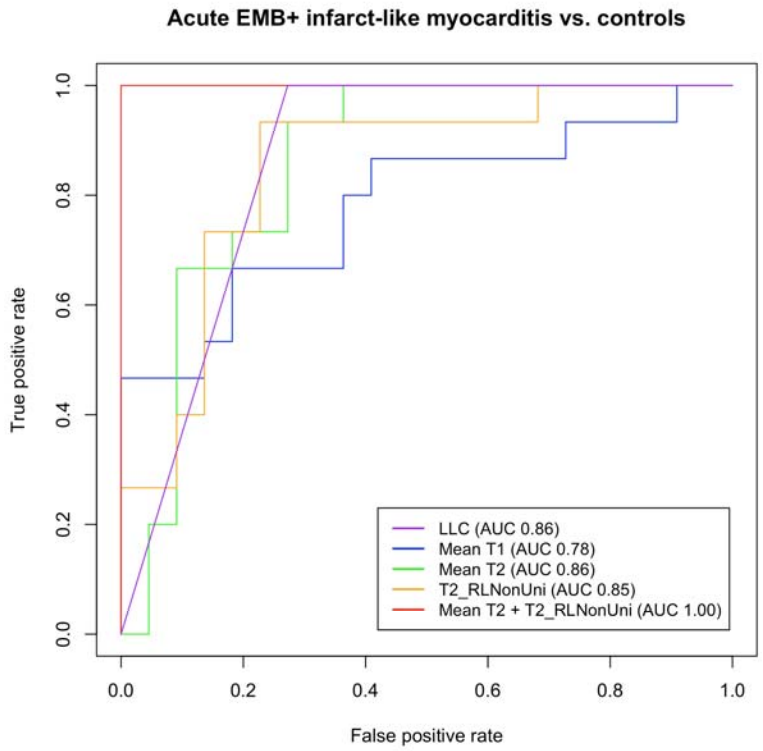

Fig. 1: ROC-Analysis for differentiating patients with EMB+ acute infarct-like myocarditis from healthy controls

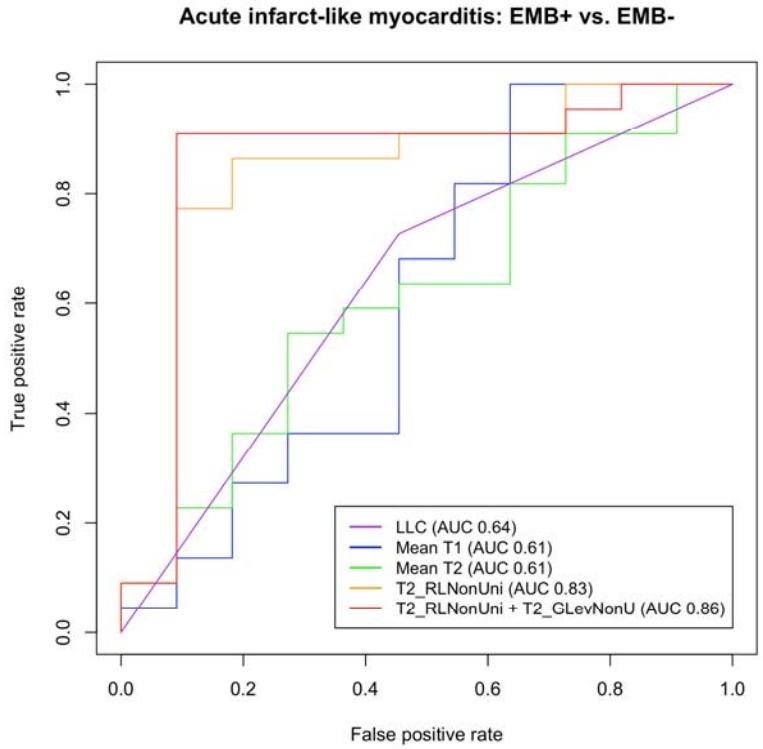

Fig. 2: ROC-Analysis for differentiating patients with EMB+ from those with EMB- acute infarct-like myocarditis

ID#: 363652

Exercise-induced cardiac remodelling in novice marathon runners

Andrew D'Silva, MBBS MRCP(UK)[1] Anish N. Bhuva, MRCP MBBS[2], Siana Jones, BSc MSc[3], Jet van Zalen, MSc [4], Rachel Bastiaenen, PhD[5], Katia Devorha. Menacho, MD[6], Amna Abdel-Gadir, MBBS MRCP[7], Thomas Treibel, PhD[8], Stefania Rosmini, MD, PhD[8], Manish Ramlal, MBChB MRCP[7], Paul R. Scully, MBBS MRes[6], Simiao Liu[9], Tee Joo Yeo, MBBS, MRCP (UK)[10], Bode Ensam, MBChB[11], Kyle Conley[12], Jacqueline Ah-Fong[13], Della Cole[11], Joao Augusto, MD[14], Yang Ye[15], Gabriella Captur, MD PhD MRCP MSc[6], Sabiha Gati, MRCP (UK), PhD[16], Camilla Torlasco, MD[17], Rajan Sharma, MD, MRCP[11], Riyaz Patel, MD FESC[7], Sanjeev Bhattacharyya[18], Alun Hughes, MBBS PhD[7], Guy Lloyd, MD FRCP[7], Charlotte Manisty, MRCP PhD[19], James Moon, MD[20], Sanjay Sharma, MD, FRCP[21]

1. St George's Univeristy of London, London, England, United Kingdom

2. Barts Heart Centre and Institute of Cardiovascular Science, UCL., London, England, United Kingdom

3. UCL, London, England, United Kingdom

4. eastbourne district general hospital, United Kingdom

5. Guy's and St Thomas NHS Foundation Trust, London, England, United Kingdom

6. Barts Heart Centre, London, England, United Kingdom

7. UCL, United Kingdom

8. Barts Heart Centre, England, United Kingdom

9. Bart's health, London, United Kingdom

10. National University Heart Centre Singapore, N/A, Singapore

11. St George's University of London, United Kingdom

12. University of Washington

13. St Georges' Hospital, Cheam, United Kingdom

14. Barts Heart Centre, Lisbon, Portugal

15. Department of Cardiology, Sir Run Run Shaw Hospital, College of Medicine, Zhejiang University, No. 3 Qingchun East Road, Hangzhou 310016, Zhejiang, People's Republic of China. Barts Heart Centre, St Bartholomew's Hospital, London, UK., United Kingdom

16. Royal Brompton & Harefield NHS Trust, United Kingdom

17. University of Milan-Bicocca. IRCCS Istituto Auxologico Italiano, Milan, Italy, Milan, Lombardia, Italy

18. Barts Heart Centre, St Bartholomew's Hospital, London, UK, United Kingdom

19. Barts Heart Centre and University College London, United Kingdom

20. UCL, England, United Kingdom

21. St George's University of London, England, United Kingdom

Background: Cardiac morphological adaptations are well documented across a variety of competitive athlete populations and sporting disciplines. Mass participation running events, such as marathons, are increasing in popularity and the precise extent of cardiac remodelling experienced by non-elite, novice runners remains unknown.

Methods: Novice marathon runners, aged 18-35 years, were evaluated in a longitudinal study, six months before the 2016 London Marathon (baseline) and within three weeks following the race (post marathon). Cardiac magnetic resonance (CMR) imaging at 1.5T with T1 mapping (MOLLI) and extracellular volume (ECV) quantification was performed. Left (LV) and right ventricular (RV) function, volumes and LV myocardial mass were assessed by cine SSFP sequences. Late Gadolinium enhancement (LGE) images were obtained after IV bolus injection of 0.1mmol/kg Gadolinium-based contrast to identify regional fibrosis.

Results: 67 subjects were included in the final analysis. The composition of this group was 54% male, with mean age 29 ±3.3 years and a median of 2 hours of regular exercise per week at baseline. LV end-diastolic volume (EDV) increased by 4.10%, RV EDV increased by 4.88%, LV mass increased by 5.47% and mean LV wall thickness increased by 1.73%, all reaching statistical significance. These proportional changes were similar

between men and women. At baseline, 2.99%, 5.97% and 11.94% subjects exceeded the upper limits of CMR reference values for LV hypertrophy, LV dilatation and RV dilatation, respectively. Post marathon, the proportion with LV hypertrophy was unchanged at 2.99%, the proportion with LV dilatation increased significantly to 20.90% and the proportion with RV dilatation also increased to 20.90%, though not reaching statistical significance. This supports a symmetrical biventricular eccentric remodelling response. Native T1 values were unchanged, however there was a significant absolute 1.12% fall in ECV. LGE was absent in all subjects.

Conclusion: Exercise-induced cardiac remodeling (EICR) was demonstrable in young runners following a first marathon. The final dimensions were modest in comparison to competitive endurance athletes, with the majority conserving normal geometry. The remodelling response was similar in men and women. The study demonstrated a fall in ECV post marathon training, which is consistent with cross-sectional studies comparing competitive athletes and sedentary control subjects. Though the native T1 values did not significantly change, the findings support athletic remodelling is a process driven by cellular hypertrophy with relative reduction in ECV. This work assists in defining the limits of physiological, athletic adaptation in non-elite marathon runners to better differentiate these common EICR changes from cardiomyopathies.

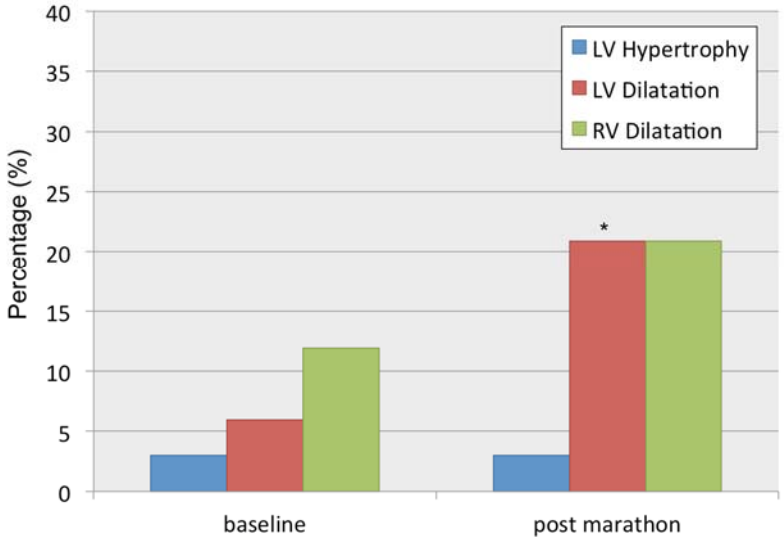

Figure 1. Bar chart showing percentage of subjects classed as having LV hypertrophy, LV dilatation, or RV dilatation grouped by study time point. Defined as an indexed LV mass, LV end-diastolc volume, or RV end-diastolic volume above the normal range for that individual according to published reference ranges stratified by decade of age and sex (Maceira AM JCMR 2006, Maceira AM EHJ 2006). The differences in proportions between study time points were assessed using McNemar's test with confidence intervals in parenthesis. For LV hypertrophy, 0% (0, 0); for LV dilatation, 15% (6, 24); for RV dilatation, 9% (-1, 19). LV indicates left ventricular; and RV, right ventricular.

Table 1. Changes in cardiac magnetic resonance findings between study visits.

	Baseline	**Post marathon**	**Absolute difference**	**Relative difference (%)**	**P value**
Indexed LV EDV (ml/m^2)	86.60 ±13.29	90.15 ±14.70	3.55	4.10	<0.01
Indexed RV EDV (ml/m^2)	93.99 ±15.02	98.58 ±16.18	4.59	4.88	<0.01
Indexed LV mass (g/m^2)	63.25 ±11.80	66.71 ±12.01	3.46	5.47	<0.01
Mean LV WT (mm)	6.95 ±0.94	7.10 ±0.85	0.12	1.73	0.02

Native T1 (ms)	1011 ±24.03	1009 ±36.28	--	--	0.66
ECV (%)	26.76 ±2.28	25.65 ±2.42	-1.12	-4.18	<0.01

Normally distributed measurements are presented as mean±SD and differences within group means were compared using paired t tests. Both absolute differences and differences relative to baseline are included for those values reaching statsitical significance, defined as a two-tailed value of $p<0.05$. ECV indicates extracellular volume; EDV, end-diastolic volume; LV, left ventricular; and RV, right ventricular; and WT, wall thickness.

ID#: 353267

The Right Ventricle in Aortic Stenosis: RV Hypercontractility assessed by CMR is an Early Marker of Clinical Decompensation and Cardiac Recovery in AS with Normal Left Ventricular Function

Marzia Rigolli, MBChB, MD[1] Sanjay Sivalokanathan, MBBS, BSc[2], Rohan S. Wijesurendra, MB BChir, MRCP[1], Rina Ariga, MBBS, MRCP[2], Margaret Loudon, MBChB, DPhil[2], Rafail A. Kotronias, MBChB MSc [3], Jane M. Francis[4], Theodoros Karamitsos, MD, PhD[5], Stefan Neubauer, MD, FRCP[2], Masliza Mahmod, MBChB, DPhil[2], Saul Myerson, MD, FRCP[1]

1. University of Oxford, Oxford, England, United Kingdom

2. University of Oxford, England, United Kingdom

3. University of Oxford, Oxford, United Kingdom

4. University of Oxford, OX39DU, England, United Kingdom

5. 1st Cardiology Department, Aristotle University of Thessaloniki, AHEPA Hospital, Thessaloniki, Greece

Background: In aortic stenosis (AS), right ventricular (RV) impairment is thought to occur late, associated with pulmonary hypertension (PH) and left ventricular (LV) dysfunction. However, increased pulmonary pressures may exist in the absence of detectable PH and the RV may also be directly affected by systemic afterload. Thus, RV changes may be present in AS without overt PH. If this was the case, the RV could be a useful early marker of decompensation. Cardiovascular magnetic resonance (CMR) is the most accurate modality for RV evaluation and may enable innovative RV deformation assessment in AS. We sought to examine the effect of increased LV afterload on RV function and RV strain in patients with AS and normal LV function pre and post aortic valve replacement (AVR).

Methods: 80 isolated AS (moderate, asymptomatic severe and symptomatic severe) and 28 matched-controls were prospectively enrolled. LV dysfunction, PH and other cardiomyopathies were excluded. CMR quantified biventricular parameters, including innovative RV strain by tissue-tracking, at baseline and 8 ± 2 months after AVR in the 21 symptomatic AS subjects who underwent AVR.

Results: RV ejection fraction (EF) significantly *increased* with AS severity (moderate AS: 62 ± 4%, asymptomatic severe AS: 68 ± 7%, symptomatic AS: 74 ± 4%, $p<0.001$). RV hypercontractility was confirmed by elevated RV strain (symptomatic AS: -17 ± 4% vs controls: -14 ± 4%, $p=0.02$). RVEF correlated strongly with AS degree (peak aortic velocity $r=0.62$, $p<0.001$), symptomatic status ($r=0.66$, $p<0.001$), and BNP ($r=0.51$, $p=0.01$). RVEF ≥71% had the best accuracy in detecting symptoms in moderate-severe AS (area under the curve 0.89, $p<0.001$), while RVEF <63% had 100% negative predictive value for presence of symptoms. RVEF also strongly correlated with LV recovery after AVR (mass regression $r=0.61$, $p=0.01$) and was the most powerful independent predictor of LV mass regression in all models. RV parameters were restored towards normal after AVR.

Conclusion: In patients with AS but normal LVEF, RV hypercontractility is associated with valve severity, symptomatic onset and signs of heart failure. RV function was the strongest independent predictor of LV mass regression after AVR. Thus, the RV may be a novel early marker of clinical decompensation and cardiac recovery after AVR, useful in risk stratification.

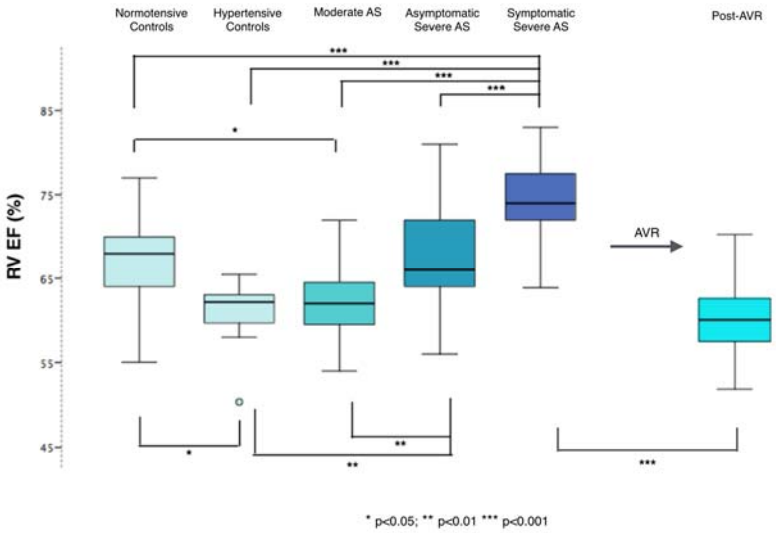

RV ejection fraction by CMR in AS and controls. *p<0.5 **p<0.01, ***p<0.001.

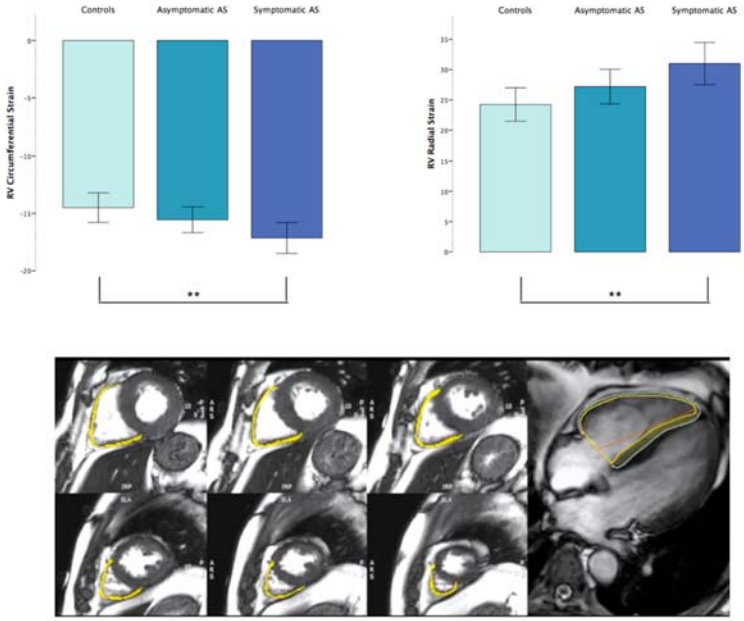

RV strain by CMR in AS and controls. **p<0.01.

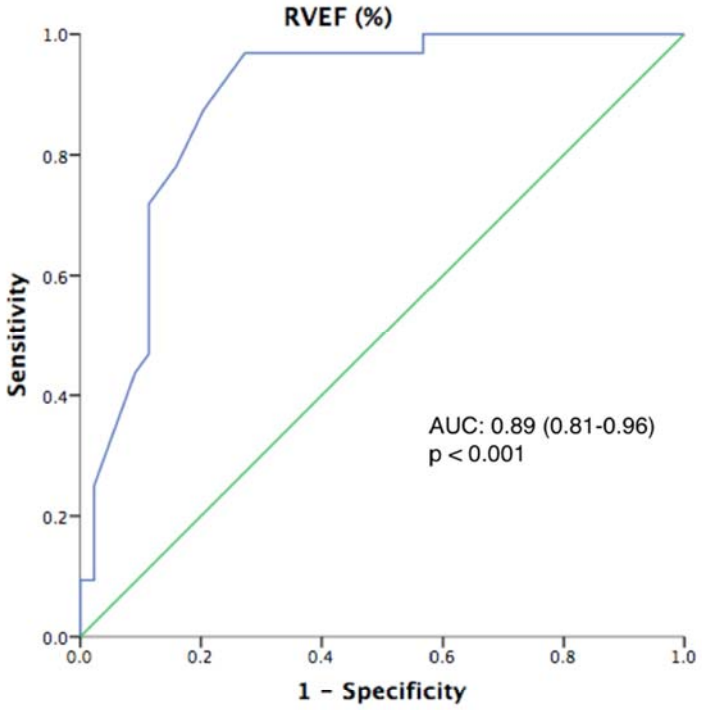

RVEF (%)	Sensitivity	Specificity	Positive Predictive Value	Negative Predictive Value	Accuracy
63%	100	39	54	100	65
65%	97	52	60	96	71
68%	97	73	72	97	83
71%	88	80	76	90	83

RV ejection fraction thresholds for symptoms detection in AS.

Baseline characteristics and CMR parameters in AS and Controls

	Symptomatic Severe AS	Asymptomatic Severe AS	Moderate AS	Controls	P-Value
Age, yrs	69 ± 8	69 ± 8	69 ± 7	66 ± 5	0.29
Male, n (%)	23 (66)	15 (68)	20 (87)	15 (54)	0.09
BSA, m^2	2.0 ± 0.2	1.9 ± 0.2	2.0 ± 0.2	1.9 ± 0.2	0.10
SBP, mmHg	135 ± 17	132 ± 13	140 ± 21	141 ± 19	0.34
DBP, mmHg	75 ± 10	75 ± 10	77 ± 8	81 ± 9	0.18

Peak Aortic Velocity - echo, m/s	4.6 ± 0.6	4.2 ± 0.5	3.3 ± 0.4	1.2 ± 0.1	**<0.001**
Aortic Valve Area - CMR, cm^2	0.81 ± 0.15	0.84 ± 0.15	1.31 ± 0.16	>2	**<0.001**
sPAP - echo, mmHg	26 ± 11	27 ± 7	29 ± 7	25 ± 5	0.72
Right-side CMR parameters					
RVEDV, ml	127 ± 36	131 ± 29	139 ± 35	151 ± 35	**0.04**
RVESV, ml	32 ± 10	42 ± 15	53 ± 14	54 ± 19	**<0.001**
RVSV, ml	95 ± 28	88 ± 19	87 ± 23	97 ± 20	0.32
RVEF, %	75 ± 4	68 ± 7	62 ± 4	65 ± 6	**<0.001**
RV Strain, circ %	- 17 ± 4	-16 ± 4	-15 ± 4	-14 ± 3	**0.04**
RA volume, ml	74 ± 22	72 ± 24	75 ± 23	67 ± 23	0.49

CMR parameters in follow-up AS pre- and post- AVR.

	Follow-up AS		**P-value**
	Pre-AVR	**Post-AVR**	
Right-side CMR parameters			
RVEDV, ml	123 ± 36	135 ± 30	0.06
RVESV, ml	32 ± 12	54 ±18	**<0.001**
RVSV, ml	92 ± 26	81 ± 16	0.07
RVEF, %	75 ± 4	61 ± 7	**<0.001**
RV Strain, circ %	-17 ± 4	-16 ± 4	**0.05**
RA volume, ml	75 ± 21	62 ± 13	**0.004**

ID#: 357052

The impact of heart rate and inotropy on LV flow patterns and energetics in the normal heart: a 4D flow dobutamine CMR study

Jonathan Sundin[1] Jan E. Engvall, MD, PhD[2], Eva Nylander, MD, PhD[3], Tino Ebbers, PhD[2], Ann F. Bolger, MD, PhD[4], Carl-Johan Carlhall, MD, PhD[5]

1. Linköping University, Linköping, Ostergotlands Lan, Sweden

2. Linkoping University, Linkoping, Ostergotlands Lan, Sweden

3. Linkoping University, Linköping, Ostergotlands Lan, Sweden

4. University of San Francisco, CA

5. Linköping university, Ostergotlands Lan, Sweden

Background: There is a growing interest in multidimensional intracardiac blood flow in health and disease as studied with 4D flow CMR. The effects of heart rate and inotropy on multidimensional flow patterns and energetics within the human heart remain undefined. Recently, reduced volume and end-diastolic kinetic energy (KE) of the portion of left ventricular (LV) inflow passing directly to outflow (Direct flow) have been shown to reflect inefficient LV pumping and to be a marker of LV dysfunction in heart failure patients.
In this study, we hypothesized that increasing heart rate and LV inotropy would result in an increased intraventricular blood flow efficiency. Therefore, we sought to investigate LV 4D blood flow patterns and energetics at increasing heart rate and LV inotropy with dobutamine infusion.

Methods: 4D flow and morphological CMR data were acquired on a 3T scanner in twelve healthy subjects: at rest and with dobutamine infusion to achieve a target heart rate approximately 60% higher than the resting heart rate. A previously validated method was used for flow analysis (Eriksson et al., JCMR 2010): pathlines were emitted from the end-diastolic (ED) LV blood volume and traced forward and backward in time to separate four functional LV flow components (Table). For each flow component, the KE at ED per milliliter blood volume was calculated.

Results: With dobutamine stress versus rest, heart rate, systolic blood pressure and stroke volume increased. Of the 4D flow parameters, the Direct flow';s proportion of EDV and its KE/mL at ED increased. Further, the Residual volume proportion of end-diastolic volume decreased. See Table and Figure for detailed results.

Conclusion: This study demonstrates that it is feasible to compare patterns of 4D flow within the normal human heart at rest and with stress. At higher heart rate and inotropy, by dobutamine infusion, the relative volume and pre-systolic KE of the most efficient, Direct flow component of the LV volume increased. The change in these markers may allow a novel assessment of LV dysfunction over a range of stress, and might assist in defining target heart rates in heart failure patients. Further, we found that increased heart rate and inotropy were associated with a decrease in the relative volume of the re-circulating residual volume: such a marker may improve risk assessment for LV thrombus formation in heart failure patients.

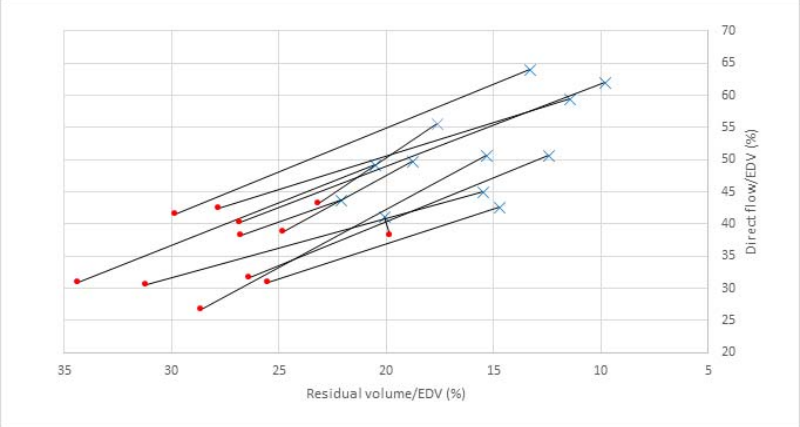

Volume proportion of EDV for Direct flow (Y-axis) and Residual volume (X-axis) at rest (red dots) and at dobutamine infusion (blue crosses) in healthy subjects.

Results at rest and with dobutamine infusion

	Rest	Dobutamine	P-value
Age	33±13		
Gender (f/m)	8/4		
HR (bpm)	66±9	108±13	<0.001
BP systolic (mmHg)	118±13	135±15	0.021
BP diastolic (mmHg)	68±9	63±8	0.251
LVEDV (mL)	153±28	139±35	0.004
LVESV (mL)	65±17	36±13	<0.001
LVEF (%)	58±5	74±5	<0.001
LVSV (mL)	88±13	102±25	0.010
CO (mL/min)	5770±1040	10960±2370	<0.001
DF/EDV (%)	36±6	51±8	<0.001
DF KE_{ED}/milliliter (µj/ml)	7.7±3	27.1±18.7	0.002
RV/EDV (%)	27±4	16±4	<0.001
RV KE_{ED}/milliliter (µj/ml)	1.5±0.5	3.3±1.6	0.002
DEF/EDV (%)	17±3	13±3	0.001
DEF KE_{ED}/milliliter (µj/ml)	5.8±2.5	20.5±20.4	0.002
RI/EDV (%)	20±4	20±3	0.615
RI KE_{ED}/milliliter (µj/ml)	3.7±1.4	9.2±3	<0.001

HR, heart rate; BP, blood pressure; LV, left ventricle; EDV, end-diastolic volume; ESV, end-systolic volume; EF, ejection fraction; SV, stroke volume; CO, cardiac output; DF, direct flow – blood that both enters and leaves the LV within one cardiac cycle ; KE_{ED}, kinetic energy at end-diastole; RI, retained inflow – blood that enters but does not leave the LV within one cardiac cycle; DEF, delayed ejection flow – blood that leaves but does not enter the LV within one cardiac cycle; RV, residual volume - blood that resides within the LV for at least two cardiac cycles. Level of significance was $P<0.05$

ID#: 369939

Evaluation of e-prime with Cardiac Magnetic Resonance Cine imaging—Preliminary Validation by Echocardiography

Dana C. Peters, PhD[7] Ricardo Gonzales[1], Chenxi Hu, PhD[2], Felicia Seemann, MS[3], Michael Quail, MD[4], Karl Grunseich, M.D.[2], Lauren A. Baldassarre, MD[2], Judith L. Meadows, MD[5], Albert J. Sinusas, MD[6], Hamid R. Mojibian, MD[5]

1. Universidad de Ingenieria y Tecnologia, Lima, Peru

2. Yale University, CT

3. Skane University Hospital, Department of Clinical Physiology, Lund University, and Department of Biomedical Engineering, Lund University, Sweden

4. King's College London, United Kingdom

5. Yale School of Medicine, CT

6. Yale University, New Haven, CT

7. Yale University

Background: Diastolic dysfunction, responsible for 40%-50% of all heart failure[1], is assessed by measurement of mitral annular early diastolic velocity, e';, by transthoracic echocardiography (TTE). e'; is a surrogate for left ventricular filling pressure[2];additionally, it has important implications for left atrial remodeling. Cardiovascular magnetic resonance (CMR) has limited application in measuring e';, but it is possible using tissue phase mapping[3]. Recently, a semi-automated feature tracking (FT) method was developed for tracking the mitral annular points on long-axis cine images[4]. In this work, we show the preliminary results of measuring e'; using 4-chamber cine, validated further against the results of TTE.

Methods: Twenty five patients (average age 50±14 years), imaged on a 1.5T clinical scanner (Siemens Healthcare, Erlangen) for diverse indications, were retrospectively enrolled in an IRB-approved study. The 4-chamber cine data (breath-held, segmented, bSSFP, 30 frames per cardiac cycle, 2x2x 8mm^3, TR/TE/Θ=3ms/1.5m/60°) were further analyzed to measure e';. All had TTE and 16 had a recent TTE within 3 months of the CMR study. The annular point displacement of the septal and lateral wall, relative to the mitral annular plane in begin-systole (Figure 1), was calculated using semi-automatic FT[4] in the software Segment[5]. Manual adjustment of points was performed when necessary, and the displacement was smoothed to eliminate discontinuities. The time derivative yielded the mitral annular septal and lateral velocity, and the peak of the velocity in the early diastolic frames was considered to be the CMR e';.

Results: The processing required less than five minutes per patient to track 30 frames and 3 long-axis views. There were excellent correlations between CMR and TTE e'; (R^2=0.80 and R^2=0.75, bias±2SD = -0.7±3.2 cm/s, and -1.1±3.6 cm/s, for the septal and lateral e';, respectively). The correlation was strengthened in patients who had recent TTE (R^2=0.92 and R^2=0.89 for septal and lateral e',Figure 2). Inter and intra-observer variability, analyzed in 10 patients, were 1.1 ± 0.8 cm/s and 0.2±1.2 cm/s for septal e';, and 1.5±0.8 cm/s and 0.8±1.2 cm/s for lateral e';, respectively.

Conclusion: We have validated a new methodology for measurement of e'; from CMR 4-chamber cine images, for diastolic function assessment.

References: 1. Caudron, Radiographics 2011; 2. Nagueh, European Journal of Echocardiography 2009; 3. Westenberg, Current cardiovascular imaging reports 2011. 4. Seemann F BMC Med Imaging 2017; 5. Heiberg, BMC medical imaging 2010.

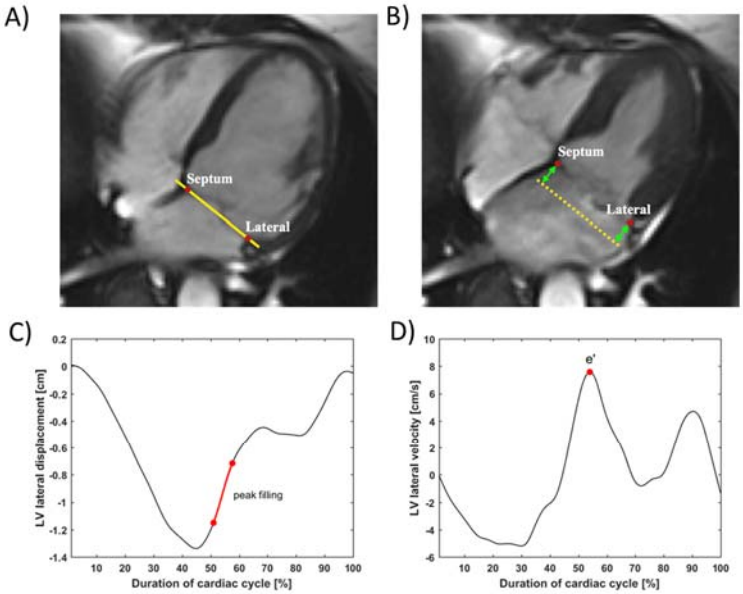

Figure 1. Illustration of the four steps in the calculation of e'. (a) In the end-diastolic (ED) frame, the septal and lateral mitral annular points (red) were manually labeled, which also defined the mitral annular plane (yellow). The software then automatically tracks the displacement of the two points relative to the ED annular plane, shown in (b) for the end-systolic (ES) frame. Manual adjustment of points is then performed if needed. (c) The resultant displacement curve for the lateral annular point, with the peak filling phase of the cardiac cycle highlighted. (d) The resultant velocity curve for the lateral annular point with the peak velocity (e') labeled.

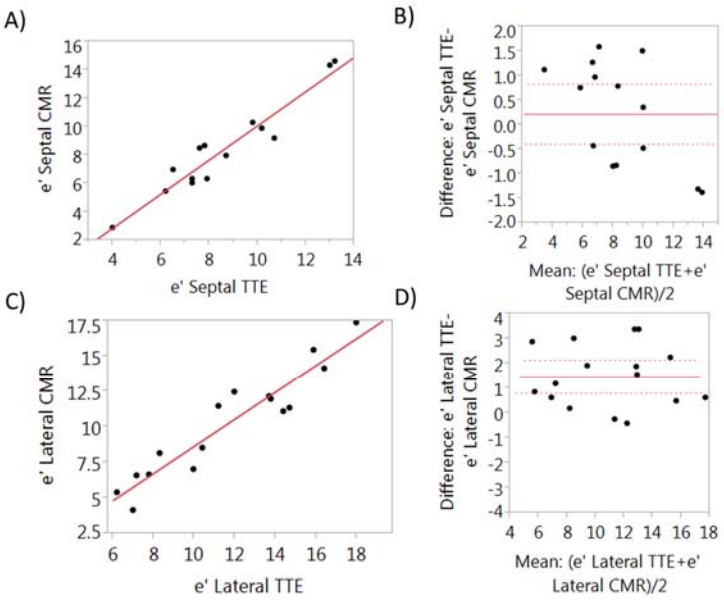

Figure 2. (a) Correlation (R^2=0.92) between e' septal from CMR with e' septal with recent TTE, and (b) its corresponding Bland-Altman plot with bias ± 2SD of -0.2 ± 2.1cm/s. (c) Correlation (R^2=0.89) between e' lateral from CMR with e' lateral with recent TTE, and (d) its corresponding Bland-Altman plot with bias ± 2SDs of -1.4 ± 2.4cm/s.

ID#: 367686

Relationship between CMR-derived parameters of ischemia / reperfusion damage and the timing of CMR after reperfused ST-segment elevation myocardial infarction

Anna Giulia Pavon, Cardio-Thoracic Vascular Department, San Raffaele Hospital, Milan, Italy[1] Pierre Monney, 1) Division of Cardiology and Center of Cardiac Magnetic Resonance, Cardiovascular Department, University Hospital of Lausanne, CHUV, Switzerland.[2], Gabriella Vincenti, Center of Cardiac Magnetic Resonance - University Hospital Lausanne-CHUV, Lausanne (Switzerland)[3], Tobias Rutz, 1) Division of Cardiology and Center of Cardiac Magnetic Resonance, Cardiovascular Department, University Hospital of Lausanne, CHUV, Switzerland.[2], Juerg Schwitter, 1) Division of Cardiology and Center of Cardiac Magnetic Resonance, Cardiovascular Department, University Hospital of Lausanne, CHUV, Switzerland.[2], Pier Giorgio Masci, 1) Division of Cardiology and Center of Cardiac Magnetic Resonance, Cardiovascular Department, University Hospital of Lausanne, CHUV, Switzerland.[2]

1. Cardiac MR Center-Cardiologiy Unit-University Hospital-CHUV-Lausanne, Switzerland, Lombardia, Italy

2. 1) Division of Cardiology and Center of Cardiac Magnetic Resonance, Cardiovascular Department, University Hospital of Lausanne, CHUV, Switzerland., Switzerland

3. Center of Cardiac Magnetic Resonance - University Hospital Lausanne-CHUV, Lausanne (Switzerland), Switzerland

Background: Objectives: To investigate the influence of cardiovascular magnetic resonance (CMR) timing after reperfusion on CMR-derived parameters of ischemia/reperfusion (I/R) in ST-segment elevation myocardial infarction (STEMI) patients. Background: In STEMI patients it is still questionable whether the timing of CMR after reperfusion impacts on CMR-derived I/R parameters.

Methods: Methods: The study originated from single-center registry prospectively including revascularized STEMI patients undergoing CMR during the index hospitalization. Between July 2014 and June 2017, 163 patients were included. Patients were divided according to the time between revascularization and CMR (Trevasc-CMR: Tertile-1≤43h n=54; Tertile-2: 44-93h, n=55; Tertile-3:>93h, n=54). T2-mapping derived area-at-risk (AAR; T2>mean+SD of remote) and intramyocardial hemorrhage (IMH; manual contouring), and late gadolinium enhancement (LGE)-derived infarct size (IS; signal >mean+5SD of remote) and microvascular obstruction (MVO; manual contouring) were quantified. T1-mapping was performed before and after (>15 minutes) Gd-based contrast-agent yielding extracellular volume (ECV) of infarct myocardium.

Results: Results: Main factors influencing I/R were homogenously balanced across Trevasc-CMR tertiles. CMR results are summarized in the Table. T2 of infarct and remote regions increased with the increase of Trevasc-CMR tertiles (figure, panel A). Differently from the entire study population and patients without IMH (figure, panel A and B), in patients with IMH the T2 of infarct did not increase with increasing Trevasc-CMR tertiles but rather showed a steady sustained augmentation (figure, panel C). In the whole study population and per-subgroup analysis, T2 of infarct broadly and significantly exceeded that of remote myocardium in each tertile, leading to comparable T2-mapping-derived AAR extent throughout Trevasc-CMR tertiles. Similarly, T2-mapping-based IMH detection and quantification was independent of Trevasc-CMR. Finally, IS and MVO were not influenced by Trevasc-CMR. In 68 patients without MVO, ECV of infarct region was comparable across Trevasc-CMR tertiles.

Conclusion: Conclusions: We acknowledge dynamic variation of T2 in infarct and remote myocardium in reperfused STEMI patients after reperfusion. However, these changes do not give rise to substantial variation of T2-mapping derived AAR estimation or other CMR-based parameters of I/R.

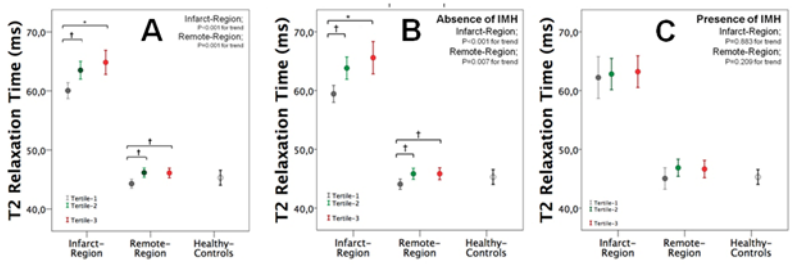

A) Overall study population (n=163) ; B) Patients without IMH (n=117); C) patients with IMH (n=46, 28%): *P<0.001; † P<0.05

Characteristics of the population

Characteristics	Overall (n=163)	Tertile-1 (n=54) $T_{revasc-CMR \leq 43h}$	Tertile-2 (n=55) $T_{revasc-CMR:44-93h}$	Tertile-3 (n=54) $T_{revasc-CMR>93h}$	P-Value For trend
Relaxation Times					
T2-mapping					
T2 infarct (ms)	62.8±6.4	60.0±4.9†·	63.5±5.6·	64.8±7.5†	<0.001
T2 remote (ms)	45.5±3.0	44.3±2.8·*	46.1±2.8·	46.1±3.0*	0.001
T1-mapping*					
T1 infarct (ms)*	1220±81	1172±63†·	1235±78·	1248±82†	<0.001
T1 remote (ms)*	1019±59	1004±37	1019±54	1034±76	**0.076**
ECV infarct (%)**	46.7 (41.5-52.0)	49.0 (41.6-53.1)	45.6 (41.7-52.9)	45.9 (40.1-49.5)	0.470
ECV remote (%)*	24.5 (22.1-27.1)	25.2 (22.0-27.0)	23.9 (22.3-25.7)	24.6 (22.0-28.3)	0.916
Infarct-related Measures					
AAR (g)	23±12	20±12	23±11	25±13	0.113
AAR (% LV)	18±8	17±9	19±9	18±8	0.385

IMH n, (%)	46 (28)	12 (22)	17 (31)	17 (31)	0.487
IMH extent (g)	2.8 (1.6-5.4)	2.8 (1.5-9.2)	3.0 (2.1-4.8)	2.4 (1.1-5.4)	0.794
IMH extent (% of LV)	2.0 (1.0-4.1)	2.7 (1.0-7.2)	2.4 (1.3-3.9)	1.9 (0.8-3.9)	0.681
IS (g)	16±13	15±12	16±12	19±14	0.271
IS (% of LV)	13±9	12±9	12±9	14±9	0.646

MVO n, (%)	73 (45)	23 (43)	25 (46)	25 (46)	0.921
MVO extent (g)	4.0 (2.3-7.9)	3.0 (2.0-4.2)	5.6 (3.0-7.8)	5.0 (2.3-11.4)	0.294
MVO extent (% of LV)	3.8 (1.8-6.9)	2.5 (1.5-4.5)	4.4 (2.0-6.9)	3.8 (1.9-8.0)	0.426
MSI	31 (7-55)	24(8-48)	36 (8-58)	26 (1-51)	0.258

Bonferroni';s post-hoc analysis, †P≤0.001; · P<0.05; *n=124 patients; ** ECV of infarct measured only in patients without MVO (n=68).

ID#: 371404

CMR Provides Superior Accuracy and Reduced Heterogeneity for Detecting Coronary Artery Disease: A Systematic Review and Meta-Analysis of Stress Imaging Methods using HSROC Methods in 23,051 Patients.

Lilia M. Sierra-Galan, MD, MCvT[1] Berrios-Barcenas Enrique, MD[2], Andrew E. Arai, MD[3], Victor A. Ferrari, MD[4], Micaela Ayala-Picazo, MLS[5], Jose S. Lainez-Zelaya, MD[6], Ingrid E. Flandes-Aguilar, MD[7], Begoña Parra-Laca, MD[5], Antonio J. Lugo-Dimas, MD[5], Julio C. Sauza-Sosa, MD[8], Grecia A. Jarillo-Guerrero, MD[6], Eulo Lupi-Herrera, MD[5], Maria-Elena Soto, MD, PhD[9]

1. American British Cowdray Medical Center, CDMX, Distrito Federal, Mexico

2. Spanish Hospital of Mexico, Mexico City Mexico, Mexico City, Mexico

3. National Heart, Lung and Blood Institute, National Institutes of Health, Bethesda, MD

4. Hospital of the University of Pennsylvania and Penn Cardiovascular Institute, Cardiovascular Division, Perelman School of Medicine, University of Pennsylvania, Philadelphia, PA, USA, Phila., PA

5. American British Cowdray Medical Center, Mexico

6. Mexican Institute of Transplantation SC, Cuernavaca, Morelos, Mexico, Mexico

7. American British Cowdray Medical Center, Distrito Federal, Mexico

8. American British Cowdray Medical Center, Mexico, Distrito Federal, Mexico

9. American British Cowdray Medical Center, Mexico City, Distrito Federal, Mexico

Background: Detection of coronary artery disease (CAD) and ischemia is important due to its high worldwide prevalence, its negative health impact, and the major economic implications of CAD-related disability. We reviewed the diagnostic performance of non-invasive stress imaging modalities to evaluate CAD vs. anatomic (traditional) and functional (updated) reference standards.

Methods: MEDLINE, EMBASE and SCOPUS were searched in English and Spanish from 1970-2015. We included all studies (prospective, retrospective and even case series) that included patients of any age and gender with known or suspected CAD and evaluated the sensitivity and specificity of stress echocardiography (SE), single emission computed tomography (SPECT), cardiovascular magnetic resonance (CMR), computed tomography perfusion (CTP) and positron emission tomography (PET) compared with invasive coronary angiography (ICA) and/or fractional flow reserve (FFR), and to that met the Cochrane guidelines including a score of >60% with STARD methodology; excluding those studies that included patients with known previous myocardial infarction, previous PCI with or without stent implantation, previous cardiac bypass surgery, heart transplantation, and the absence of ICA as a gold standard. The study was registered with the local IRB and in ClinicalTrials.gov (ID NCT03180060).

Results: Ten investigators extracted data and examined patient and study characteristics, and four investigators resolved all disagreements. We found 151 studies (54 SPECT, 43 Echo, 38 CMR, 9 PET, 7 CTP encompassing 23,051 patients) that met the inclusion/exclusion criteria. Summary point estimates of sensitivity and specificity were 77% and 85% for Echo, 82% and 74% for SPECT, 87% and 85% for CMR, 81% and 90% for CTP, and 88% and 80% for PET, with narrow 95% confidence intervals. However, on HSROC plots, SPECT and Echo had widely scattered sensitivity and specificity between studies. CMR had higher sensitivity than SPECT and Echo ($p<0.001$). PET had higher sensitivity than Echo ($p<0.001$). Echo and CMR had higher specificity than SPECT ($p=0.004$ and 0.01 respectively). Other comparisons with PET and CTP were not significant due to comparable results or inadequate sample size.

Conclusion: Cardiac stress testing by CMR, PET and CTP exhibit significantly greater diagnostic performance and much less scatter than SPECT and Echo. SPECT remains the most used imaging stress test for CAD detection despite its higher costs and lower diagnostic accuracy. CMR provides the greatest value for detection of CAD and will reduce downstream utilization of invasive procedures (catheterization and percutaneous coronary intervention) based on its higher accuracy vs. the more widely used Echo and SPECT techniques.

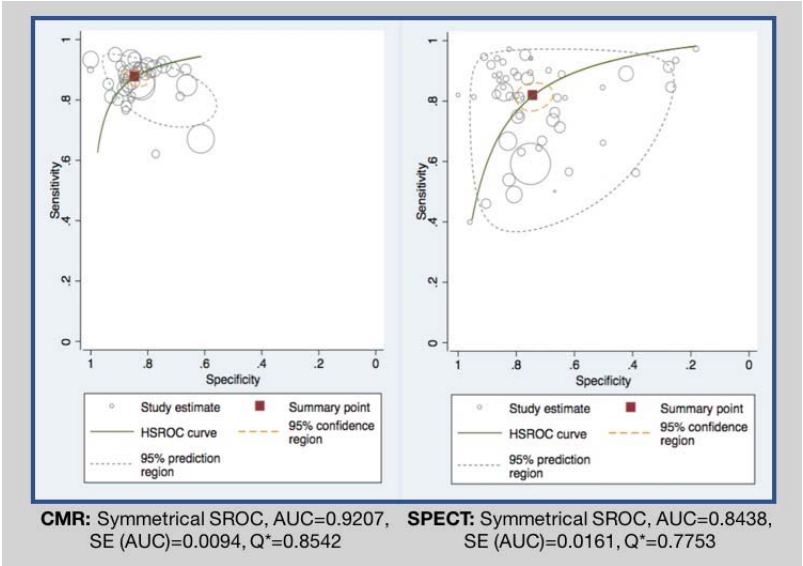

CMR: Symmetrical SROC, AUC=0.9207, SE (AUC)=0.0094, Q*=0.8542 **SPECT:** Symmetrical SROC, AUC=0.8438, SE (AUC)=0.0161, Q*=0.7753

These figures shown the summary receiver operating characteristic (HSROC) curves and Q* test of imaging modalities analyzed for CMR (left) and SPECT (left). The area within the orange dashed line indicates the 95% confidence region, the area within the light blue dashed line indicates the 95% predicted region, the bubbles indicates each included study in the analysis and its size indicates the sample size (n); the green line indicates the HSROC curve; and the red square corresponds to the summary point of the analysis for each imaging modality.

ID#: 371428

Cardiac Magnetic Resonance Imaging and Cardiac Computed Tomography versus Transesophageal Echocardiography for the Diagnosis of Left Atrial Appendage Thrombus: A Systematic Review and Meta-analysis

Tasnim Vira, MD[1] Petros Pechlivanoglou, PhD[2], Kim Connelly, MBBS, PhD[3], Harindra Wijeysundera, MD, PhD[4], Idan Roifman, MD[5]

1. Sunnybrook Health Sciences Centre, ON, Canada

2. Hospital for Sick Children, Toronto, ON, Canada

3. St. Michael's Hospital, ON, Canada

4. University of Toronto, ON, Canada

5. Sunnybrook Health Sciences Centre, University of Toronto, Toronto, ON, Canada

Background: Correct identification of left atrial appendage (LAA) thrombi is critical in atrial fibrillation and in those presenting with embolic phenomena as it may lead to initiation of anticoagulation. Transesophageal echocardiography (TEE) is the current gold standard for identification of LAA thrombi. However, TEE is semi-invasive and cannot be performed in certain patients. LAA thrombi can also be identified by cardiac computed tomography (CCT) and cardiac magnetic resonance imaging (CMR); however, the diagnostic performance of these techniques versus TEE is currently unclear. The objective of this study was to perform a systematic review and meta-analysis in order to address this knowledge gap.

Methods: We performed a systematic review and meta-analysis based on guidelines from the Preferred Reporting Items for Systematic Reviews and Meta-analysis Statement (PRISMA). EMBASE, MEDLINE and the Cochrane Database of Systematic Reviews were searched for articles between January 1, 1947 and July 31, 2017. 22 CCT and 4 CMR studies comparing the diagnostic performance of CMR and CCT to TEE for identification of LAA thrombi were ultimately included in the meta-analysis. Meta-regression was then performed to determine whether sensitivity and specificity differed between early and delayed image acquisition protocols for CCT vs. TEE. Meta-regression was also performed to compare the sensitivity and specificity between CCT and CMR.

Results: CCT demonstrated sensitivity and specificity of 0.99 (CI 0.93-1.00) and 0.94 (CI 0.90-0.97) respectively vs. TEE (see Figure 1). A subgroup analysis comparing early versus delayed protocol CT imaging was performed showing no significant differences in sensitivity (p-value = 0.17) however improved specificity of the delayed imaging protocols (p-value = 0.04). CMR demonstrated sensitivity and specificity of 0.80 (CI 0.63-0.91) and 0.98 (CI 0.97-0.99) respectively when compared to TEE (see Figure 2). The meta-regression analysis comparing the sensitivity and specificity of CCT vs. CMR in the identification of thrombi showed no significant difference between the two modalities (p-values 0.996 and 0.484, respectively).

Conclusion: In the first study to compare CCT and CMR for the diagnosis of LAA thrombi, our results indicate that both modalities had good to excellent sensitivity and specificity vs. TEE. Further, there was no significant difference in the sensitivity and specificity of CCT versus CMR. These results suggest that both CCT and CMR can be considered reasonable alternatives to TEE in the identification of LAA thrombi if TEE is unavailable or in those at high risk for undergoing the semi-invasive procedure.

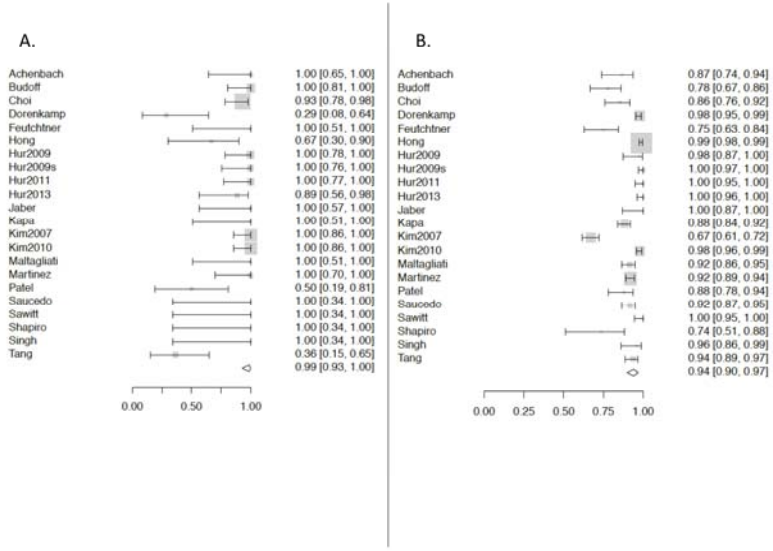

Figure 1. Forest plots of sensitivity (a) and specificity (b) of CCT vs. TEE.

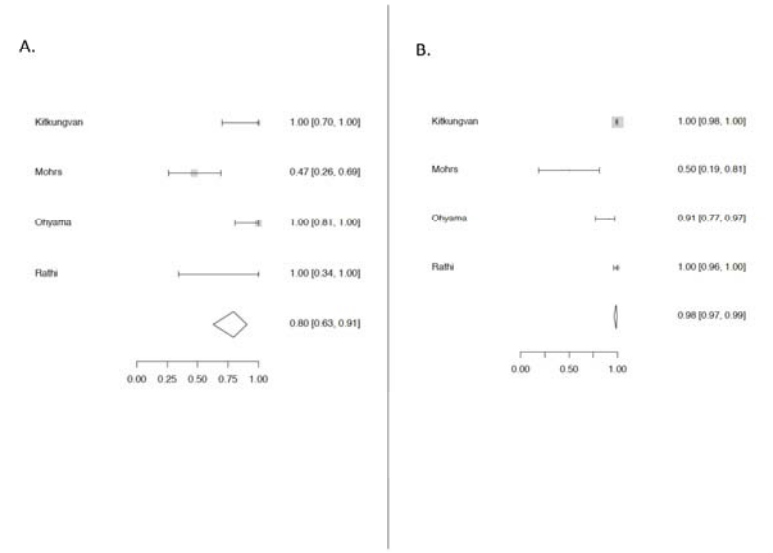

Figure 2. Forest plots of sensitivity (a) and specificity (b) of CMR vs. TEE.

ID#: 371358

Respiratory Self-Gated Stack-of-Stars 3D Cine MRI for the Proximal Coronary Arteries: Initial Steps towards Volumetric Endothelial Function Assessment

Gabriele Bonanno, PhD[1] Davide Piccini, PhD[2], Jerome Yerly, PhD[2], Li Pan, PhD[3], Xiaoming Bi, PhD[4], Allison G. Hays, MD[5], Matthias Stuber, PhD[2], Robert G. Weiss, MD[6], Michael Schär, PhD[7]

1. Division of Cardiology and Division of MR Research, The Johns Hopkins University School of Medicine, Baltimore, MD, United States, MD

2. Center for Biomedical Imaging (CIBM), Lausanne, Switzerland, Vaud, Switzerland

3. Siemens Healthineers, Baltimore, MD, United States

4. Siemens Healthineers, Los Angeles, CA, United States, CA

5. Division of Cardiology, The Johns Hopkins University School of Medicine, Baltimore, MD, United States, MD

6. Russell H. Morgan Department of Radiology and Radiological Science, The Johns Hopkins University School of Medicine, Baltimore, MD, United States, MD

7. Russell H. Morgan Department of Radiology and Radiological Science, Johns Hopkins University School of Medicine, Baltimore, MD

Background: Abnormal coronary endothelial function (CEF) represents a marker for sub-clinical atherosclerotic disease and an independent predictor of cardiovascular events[1,2]. Recently, a non-invasive method to quantify CEF was introduced that combined 2D spiral cine MRI with isometric handgrip exercise (IHE)[3] and those MRI-based responses were shown to be nitric oxide-dependent[4] and impaired in patients with coronary artery disease[3]. While atherosclerosis is a diffuse and patchy process; such 2D measures are local, give information about single coronary segments, and require a long and complex protocol[3]. The aim of this project was to develop a 3D coronary cine method to assess CEF in large portions of the coronary tree simultaneously investigating multiple segments. Here, we propose a stack-of-stars sequence that includes respiratory self-gating and 5D-GRASP[5] reconstruction to obtain a free-breathing targeted volumetric cine within 6 minutes (duration of IHE) and with <(1.5mm)^3 resolution.

Methods: For the prototype golden-angle-interleaved[6] stack-of-stars sequence, after CHESS fat-saturation, 20 radial spokes were acquired with the same azimuthal angle and center-out ordering in slice direction. Pulse oximetry was used for retrospective cardiac gating. For respiratory self-gating, a respiratory signal was automatically extracted using independent component analysis (ICA) of the k-space center signal[7,8] acquired every interleave and for all receiving coils (Figure 1).
A targeted stack-of-stars volume was prescribed using an interactive real-time sequence[9], in double oblique orientation to image the proximal right coronary arteries in 3 healthy volunteers in a 3T scanner (MAGNETOM Prisma, Siemens Healthcare).
The untriggered free-breathing golden-angle 3D stack-of-stars gradient-echo sequence was continuously acquired for 5';21” using a 30-channel coil array, 1.4mm isotropic resolution, 300x300x28mm^3 field-of-view, 3000 spokes/slice. Motion-unresolved gridded data[10] were displayed at the scanner. Offline, 5D-GRASP reconstruction was performed enforcing sparsity along the cardiac (15-phase) and respiratory (4-bin) dimensions (MATLAB, BART[11]).

Results: Gridded motion-unresolved data show blurring at the level of the heart (Figure 2A). After sorting and gridding, a diastolic cine image at end-expiration shows heavy streaking artifacts (Figure 2B). Reduced artifacts and improved depiction of the coronary artery are obtained with the 5D-GRASP reconstruction (Figure 2C). Multiplanar reformats[12] from diastolic and end-expiration 5D-GRASP data show good depiction of proximal RCAs in all 3 subjects (Figure 3).

Conclusion: The proposed respiratory self-gated 3D coronary cine MRI technique shows promising image quality and feasibility for imaging the proximal RCA in <6 minutes, while resolving cardiac and respiratory motion. Further work includes comparison with established 2D CEF measures, development of cardiac self-gating, and protocol optimization for higher spatial resolution.

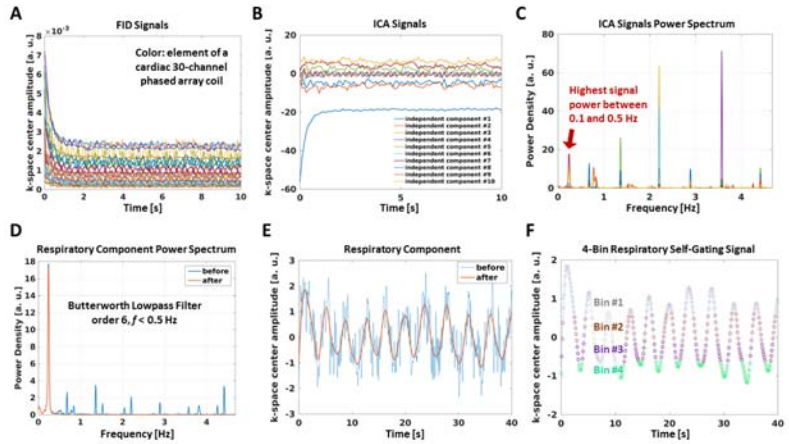

Figure 1. Respiratory self-gating method. The k-space center amplitude is recorded for every shot during the scan from the radial spoke at the center (in slice direction) of k-space and for all receiving coils (A). Independent component analysis is applied to reduce 30 coil signals to 10 components related to respiratory and cardiac activity, and magnetization variation due to steady state, etc. (B). The component with highest spectral power in the respiratory frequency range is selected (C). A respiratory self-gating signal is obtained after filtering out frequencies above 0.5 Hz (orange signal, D & E). Circles represent the respiratory position of each shot (F). Data are sorted in 4 respiratory bins for 5D-GRASP reconstruction.

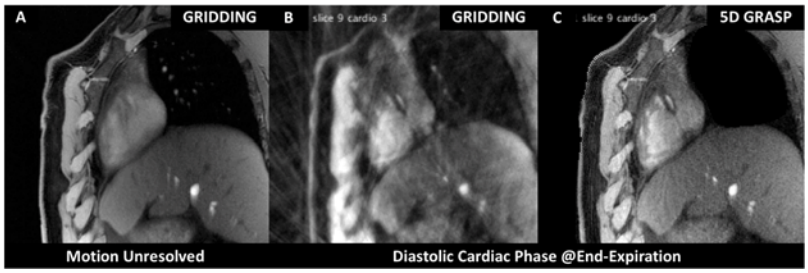

Figure 2. Selected slice of an example dataset. Gridding reconstruction of unsorted (and motion unresolved) volume as obtained at the scanner (A). After data sorting in 15 cardiac phases and 4 respiratory bins, a gridding reconstruction of a diastolic phase at end-expiration shows substantial streaking artifacts (B). The same slice shows improved image quality and coronary depiction after 5D-GRASP reconstruction along cardiac and respiratory motion states (C).

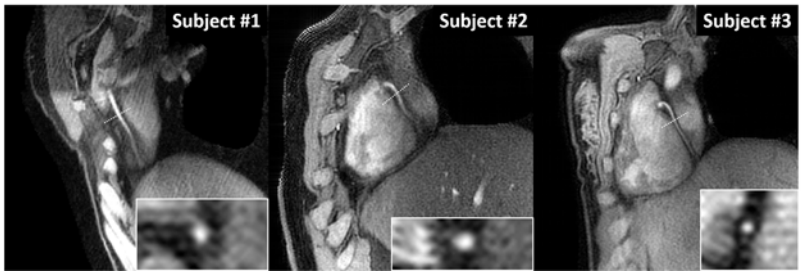

Figure 3. From the 5D-GRASP reconstruction, diastolic data at end-expiration are selected for best depiction of the coronary arteries and for future volumetric CEF assessment. Multiplanar reformats show good quality of proximal RCAs in all volunteers. Insets show reslicing of 2-fold zero-filled original data at the locations indicated by the dotted lines.

References

1. Ludmer PL, Selwyn AP, Shook TL, et al. Paradoxical Vasoconstriction Induced by Acetylcholine in Atherosclerotic Coronary Arteries. N Engl J Med. 1986;315(17):1046-1051. doi:10.1056/NEJM198610233151702.
2. Schächinger V, Britten MB, Zeiher AM. Prognostic impact of coronary vasodilator dysfunction on adverse long-

term outcome of coronary heart disease. Circulation. 2000;101(16):1899-1906.
3. Hays AG, Hirsch GA, Kelle S, Gerstenblith G, Weiss RG, Stuber M. Noninvasive visualization of coronary artery endothelial function in healthy subjects and in patients with coronary artery disease. J Am Coll Cardiol. 2010;56(20):1657-1665.
4. Hays AG, Iantorno M, Soleimanifard S, et al. Coronary vasomotor responses to isometric handgrip exercise are primarily mediated by nitric oxide: a noninvasive MRI test of coronary endothelial function. Am J Physiol Heart Circ Physiol. 2015;308(11):H1343-H1350.
5. Feng L, Grimm R, Block TK, et al. Golden□angle radial sparse parallel MRI: Combination of compressed sensing, parallel imaging, and golden□angle radial sampling for fast and flexible dynamic volumetric MRI. Magn Reson Med. 2016 Feb;75(2):775-88
6. Winkelmann S, Schaeffter T, Koehler T, Eggers H, Doessel O. An optimal radial profile order based on the Golden Ratio for time-resolved MRI. IEEE Trans Med Imaging. 2007;26(1):68-76. doi:10.1109/TMI.2006.885337.
7. Bonanno G, Piccini D, Maréchal B, Zenge MO, Stuber M. A New Binning Approach for 3D Motion Corrected Self-Navigated Whole-Heart Coronary MRA Using Independent Component Analysis of Individual Coils. Proc Intl Soc Magn Reson Med Volume 23. Milan, Italy; 2014. p 936.
8. Bonanno G, Hays AG, Weiss RG, Schär M. Self-Gated Golden Angle Spiral CINE MRI for Coronary Endothelial Function Assessment. Journal of Cardiovascular Magnetic Resonance (Suppl 1), F046, 2017.
9. Uecker M, Zhang S, Voit D, Karaus A, Merboldt KD, Frahm J. (2010), Real-time MRI at a resolution of 20 ms. NMR Biomed., 23: 986–994. doi:10.1002/nbm.1585
10. Jackson JI, Meyer CH, Nishimura DG, Macovski A. Selection of a convolution function for Fourier inversion using gridding [computerised tomography application]. IEEE Trans Med Imaging. 1991;10:473-478.
11. BART Toolbox for Computational Magnetic Resonance Imaging, DOI: 10.5281/zenodo.592960
12. Etienne A, Botnar RM, Van Muiswinkel AM, Boesiger P, Manning WJ, et al. (2002) "Soap-Bubble" visualization and quantitative analysis of 3D coronary magnetic resonance angiograms. Magn Reson Med 48: 658-666.

ID#: 371493

3D whole-heart free-breathing coronary lumen and vessel wall imaging with interleaved T2prep-IR

Giorgia Milotta, MSc[1] Giulia Ginami, PhD[2], Radhouene Neji, PhD[3], Claudia Prieto, PhD[1], Rene Michael. Botnar, PhD[4]

1. King's College London, England, United Kingdom

2. King's College London, United Kingdom

3. Siemens Healthcare, MR Research Collaborations, Siemens Healthcare Limited, United Kingdom

4. King's College London, London, England, United Kingdom

Background: Coronary lumen and vessel wall imaging is a powerful tool for the assessment of coronary artery disease (CAD). A 3D flow-independent approach for simultaneous lumen and vessel wall visualization (iT2prep) was proposed recently[1], based on an interleaved acquisition and subtraction of data with and without T2-preparation. However, this approach requires subject-dependent weighted subtraction to completely null arterial blood signal. We propose an interleaved T2prep-IR approach (iT2prep-IR) that: a) improves vessel wall to blood contrast, b) removes the need of weighted subtraction and c) incorporates 2D image-based navigators (iNAV) for 100% scan efficiency[2,3].

Methods: With the proposed prototype approach, a T2Prep-IR module is applied prior to data acquisition in odd heartbeats, whereas datasets in even heartbeats are obtained without preparatory pulses (Fig.1a). iNAVs are acquired in each heartbeat to estimate/compensate for translational respiratory motion without any data rejection. The two datasets are then non-rigidly co-registered before image subtraction. Sequence simulations were performed for the proposed and the iT2prep techniques. Furthermore, three healthy subjects were scanned under free-breathing on a 1.5T scanner (Siemens Magnetom Aera).

Results: *Simulations:* Sequence simulations of the proposed iT2Prep-IR approach (Fig.1b) show identical absolute blood magnetization in odd and even heartbeats (0.27 and 0.30), leading to complete blood nulling after subtraction and better myocardium-blood contrast compared to iT2prep (myocardium/blood ratio of 8.20 and 2.95 respectively). *Healthy subjects:* iT2prep-IR sequence generated higher signal-to-noise ratio (SNR) and contrast-to-noise ratio (CNR) between myocardium and blood in both odd and subtracted datasets (Table1). Results for three healthy subjects are shown in Fig.2. Aortic vessel wall thickness was quantified as proof of concept, showing a good agreement between iT2prep and iT2prep-IR sequences ($y = 0.7939x + 0.2842$, $R^2=0.93$). Improved nulling of the blood signal with iT2Prep-IR in comparison to both direct and weighted iT2prep subtraction was obtained with no need for weighted subtraction.

Conclusion: The proposed iT2prep-IR interleaved sequence showed promising results for blood signal nulling, SNR and CNR of the vessel wall and blood without the need of weighted subtraction. Future work will include the optimization of the motion correction pipeline and validation of the sequence performance for coronary vessel lumen and wall depiction in both healthy subjects and patients with CAD. **Bibliography** [1] M.E. Andia et al. *Magn. Reson. Med.*, vol.69(1): 150–7, 2013.
[2] M. Henningsson et al. *Magn. Reson. Med.*, vol.67(2), 2012.
[3] G. Cruz et al. *Magn. Reson. Med.*, vol.77(5): 1894-1908, 2016.

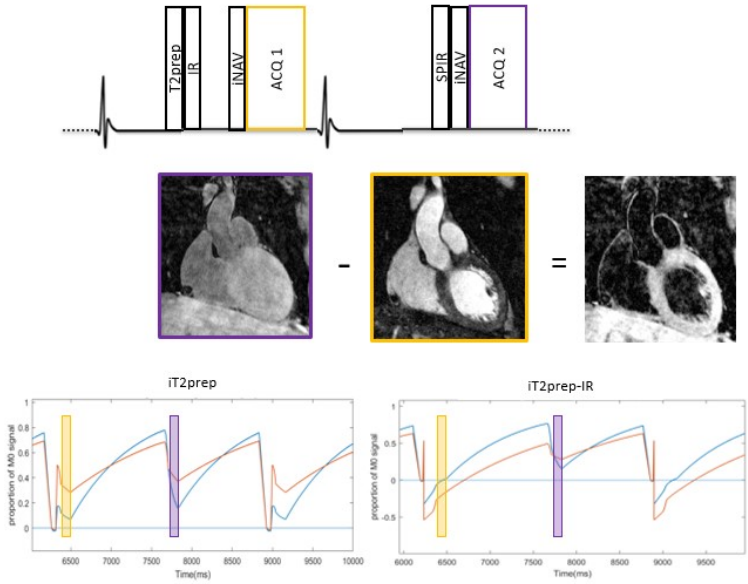

Fig.1: a) Proposed 3D whole-heart interleaved T2prep-IR sequence for simultaneous vessel wall and lumen imaging. Vessel wall images are obtained by subtracting two datasets, acquired with T2prep-IR preparation (lumen image) and without preparatory pulses. Even heartbeat acquisitions included a SPIR pulse for fat saturation, while a STIR like fat suppression (TI=110 ms) was used in odd heartbeats. T2prep=T2 preparation pulse, IR=inversion recovery pulse, iNAV= image navigator, SPIR= spectral pre saturation inversion recovery pulse, ACQ=acquisition. b) Magnetization evolution of blood (red line) and myocardium (blue line) obtained from extended phase graph simulations of iT2prep (left) and the proposed iT2prep-IR approach (right). Yellow rectangle: acquisition of first dataset (odd heartbeat). Purple rectangle: acquisition of second dataset (even heartbeat).

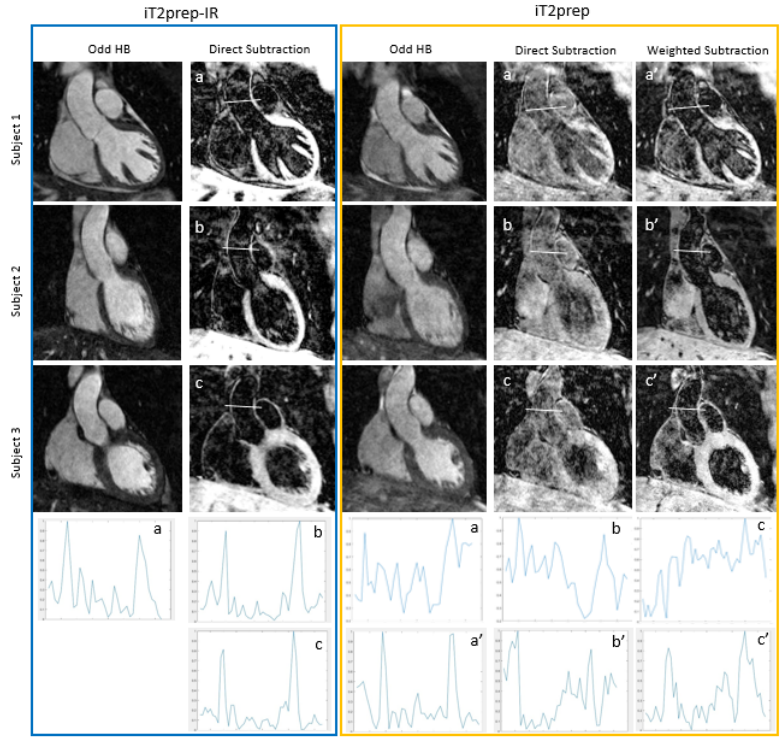

Fig.2: Images acquired for three healthy subjects with proposed iT2prep-IR (blue rectangle) and iT2prep (yellow rectangle) sequences for odd heartbeats (lumen visualization), after direct subtraction and after weighted subtraction (vessel wall images). Normalized pixel intensity profiles across the aorta are shown for the three

subjects (a, b and c) for both iT2prep-IR and iT2prep (after direct subtraction and weighted subtraction). A better nulling of the blood signal is observed with the proposed approach in comparison to both direct and weighted iT2prep subtraction. Both iT2prep-IR datasets were acquired with an ECG-triggered 3D Cartesian b-SSFP (1x1 mm in-plane resolution, 2 mm slice thickness, 320x320x144mm FOV, TR/TE = 3.6/1.6 ms, flip angle = 90°, TI=110ms, T2Prep duration=40ms, 14 startup echoes for iNAV). iT2prep acquisitions were performed with identical parameters for comparison purposes.

Table 1: Average SNR and CNR quantified in odd (lumen visualization) and subtracted (vessel wall) dataset for iT2prep-IR and iT2prep sequences on three healthy subjects.

	iT2prep-IR		iT2prep	
	odd	subtraction	odd	subtraction
SNR_{blood}	70.7±14	5.51±2.31	65.5±11	14.98±1.92
SNR_{myoc}	17.0±4.97	69±8.4	20.4±5.0	52.8±23
$CNR_{blood-myoc}$	18.6±7.4	24.1±5.6	12.8±5.5	10.9±8.5

ID#: 371547

Presence and Severity of Left Ventricular Diastolic Dysfunction Reflects Myocardial Interstitial Expansion

Andrea Cardona, MD[1] Karolina Zareba, MD[2], Akira Wada, MD[2], Abigail Shoben, Prof.[2], Giuseppe Ambrosio, MD, PhD[3], Subha Raman, MD, MSEE[4]

1. The Ohio State University Wexner Medical Center, Columbus, OH

2. The Ohio State University Wexner Medical Center, OH

3. Division of Cardiology - University of Perugia, Umbria, Italy

4. The Ohio State University, Columbus, OH

Background: Left ventricular diastolic dysfunction (LVDD) is highly prevalent and is associated with adverse cardiac outcomes. Myocardial fibrosis, as evaluated by late gadolinium enhancement cardiac magnetic resonance (LGE-CMR), contributes to diastolic dysfunction and is itself a strong predictor of cardiovascular events. The precise relationship between LVDD and extent of interstitial expansion by CMR T1 mapping-based myocardial extracellular volume fraction (ECV) computation has yet to be established. We investigated the association between LVDD and myocardial interstitial expansion indicated by ECV elevation.

Methods: We retrospectively identified a cohort of patients who had undergone clinical CMR with pre- and post-contrast T1 mapping as well as transthoracic echocardiography (TTE) with Doppler assessment of LVDD. T1 maps were acquired using a steady state free precession-based modified Lock-Locker inversion recovery (MOLLI) sequence. Diastolic function was classified as i) a dichotomous variable (i.e., normal vs. abnormal), ii) a nominal variable according to the individual patterns of presentation (grade 0-3), or iii) according to individual TTE parameters used for assessing LV diastolic function.

Results: Of 303 patients included in the final analysis (46% female, age 54±15 years), median LV ejection fraction by CMR was 52% (IQR=35-61%). The prevalence of LVDD was 60.1%. ECV was higher in patients with any degree of LVDD compared to those with normal diastolic function (35.9% vs. 24.2%, p<0.001). ECV was progressively higher with increasing severity of LVDD: normal diastolic function ECV = 27.2±5.6%, grade I LVDD ECV = 30.8±7.1%, grade II LVDD ECV = 34.7±7.7%, and grade III LVDD ECV = 40.1±14.7% (p for trend <0.001). By multivariate logistic regression, the presence of abnormal LV diastolic function independently predicted elevated ECV (odds ratio 2.64, 95%CI 1.40-5.01, p=0.003). The predictive value to detect an elevated ECV increased with the severity of LVDD. TTE-derived left atrial volume index and E/E'; ratio also independently predicted ECV elevation.

Conclusion:

LV diastolic dysfunction is significantly associated with the presence and severity of myocardial interstitial expansion as captured by CMR-based ECV elevation. Furthermore, increasing severity of LVDD strongly predicts progressively elevated ECV. This work supports ECV';s potential utility as a biomarker in LVDD clinical trials, and further studies are warranted exploring ECV elevation as targetable substrate for LVDD.

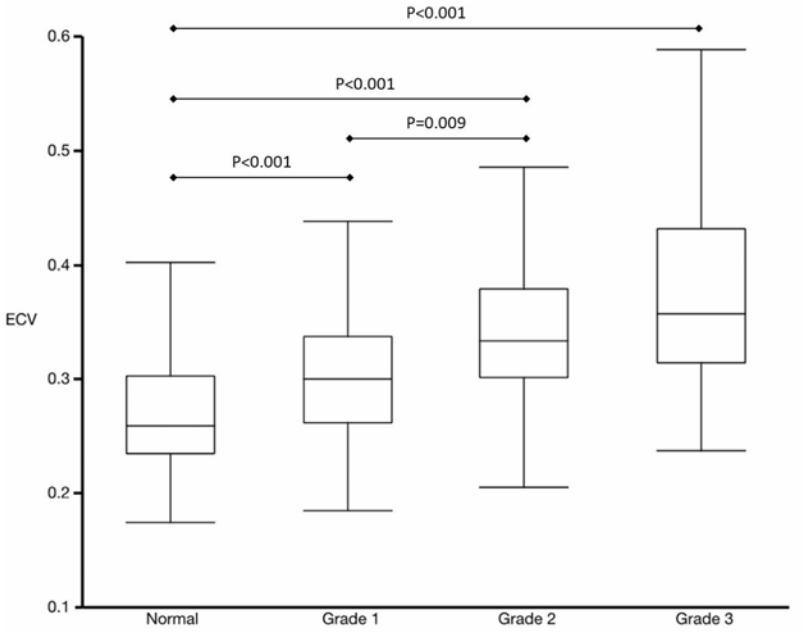

Relationship between ECV and successive grades of diastolic dysfunction. Box plot indicates medians and IQRs. P for trend=0.001. Horizontal lines show sub-group.

ID#: 371604

Long-term outcomes of unrecognized myocardial infarction in the elderly - Findings from the ICELAND MI study

Tushar Acharya[1] Thor Aspelund[2], Erik B. Schelbert, MD, MS[3], Jie Jane. Cao, MD, MPH[4], Christopher K. Dyke, MD[5], Anthony H. Aletras, Ph.D.[6], Sigurdur Sigurdsson[7], Gudmundur Thorgeirsson[8], Gudny Eiriksdottir[7], Tamara Harris, M.D., M.S.[9], Lenore Launer[9], Vilmundur Gudnason, MD, PhD[10], Andrew E. Arai, MD[11]

1. National Heart, Lung, and Blood Institute, NIH, Bethesda, MD

2. University of Iceland, Iceland

3. University of Pittsburgh; Heart and Vascular Institute of UPMC, PA

4. St Francis Hospital, NY

5. Alaska Heart and Vascular Institute, Anchorage, AK

6. Aristotle University of Thessaloniki/Lund University, Thessaloniki, Thessaloniki, Greece

7. Iceland Heart Association, Iceland

8. University of Iceland, Reykjavik, Hofuoborgarsvaoio, Iceland

9. National Institute on Aging

10. Iceland Heart Association, Kopavogur, Hofuoborgarsvaoio, Iceland

11. National Heart, Lung and Blood Institute, National Institutes of Health, Bethesda, MD

Background: CMR can identify unrecognized myocardial infarction (UMI) in the general population. UMI portends poor prognosis in the short-term but long-term outcomes are not known.

Methods: Community-dwelling participants of the ICELAND MI study (aged 67-93 years) were characterized with CMR at baseline (from 2004 to 2007) and followed over time to evaluate for all-cause death, incident MI, and heart failure (median follow-up of 10.9, 10.8, and 10.5 years respectively). Cox regression and Kaplan Meier time-to-event analyses was used to assess the relationship of UMI at baseline with future cardiovascular events and death.

Results: Of the 935 participants (mean age 76 years, 52% females), 91 (10%) had recognized MI (RMI) and 156 (17%) had UMI at baseline. After adjusting for age, sex, and diabetes, UMI by CMR was independently associated with increased risk of death (HR 1.60 [95% CI 1.26-2.02]), recurrent MI (HR 2.05 [95% CI 1.42-2.96]), and heart failure (HR 1.51 [95% CI 1.07-2.11]). At 3 years, UMI mortality rate (3%) was the same as no MI (3%) and lower than RMI (9%). At 5 years, UMI mortality rate (13%) increased and was higher than no MI (8%) but still lower than RMI (19%). By 10 years, UMI and RMI had similar mortality rates (49% and 51% respectively) that were significantly higher than no MI (30%) (P<0.001). Ten-year recurrent MI and heart failure rates of UMI (30%, 33%) were higher than no MI (13%, 19%) but lower than RMI (45%, 48%) (P<0.001).

Conclusion: With time, the mortality rate of UMI increases and is equivalent to that of RMI at 10 years follow-up. UMI has higher rates of recurrent MI and heart failure than no MI. Early detection and institution of appropriate therapy may potentially improve outcomes of UMI.

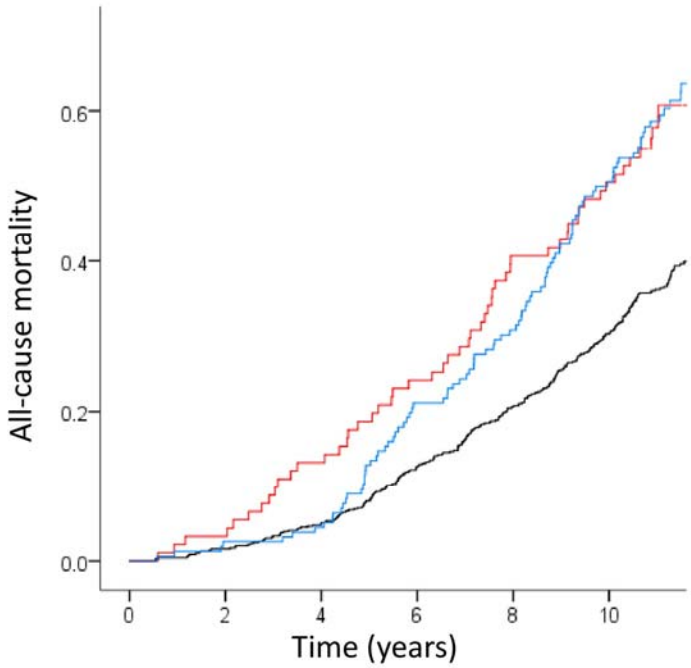

No MI	688	677	653	601	546	480
RMI	91	88	79	69	54	45
UMI	156	152	149	123	108	77

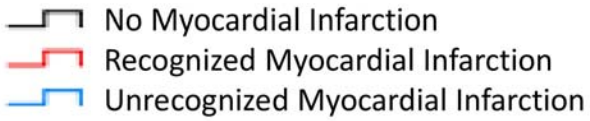

Figure. Kaplan-Meier survival analysis showing all-cause mortality in participants with no myocardial infarction, recognized myocardial infarction, and unrecognized myocardial infarction at baseline.

ID#: 371540

A bi-ventricular atlas for machine learning analysis of Hypertrophic Cardiomyopathy CMRs

Georgia Doumou, MRes[1] Antonio de Marvao, MRCP, PhD[2], Carlo Biffi, MSc[3], Roddy Walsh[4], Wenzhe Shi, PhD[3], Timothy Dawes, FRCA, PhD.[3], Wenjia Bai, PhD[5], Iain Pierce, PhD[6], Pawel F. Tokarczuk, PhD[3], Thu-Thao Le, PhD[7], Anish Bhuva, MRCP, MBBS[8], Hak Chiaw Tang, MBBS[7], Calvin WL. Chin, Assistant Professor[9], Daniel Rueckert, PhD[4], James S. Ware, MRCP PhD[4], Sanjay Prasad, MD[10], Declan O'Regan, FRCR, PhD[11], Stuart Cook, MRCP PhD[12]

1. MRC - Clinical Sciences Centre, London, England, United Kingdom

2. MRC London Institute of Medical Sciences, London, England, United Kingdom

3. Imperial College London, London, England, United Kingdom

4. Imperial College London, United Kingdom

5. Imperial College London, London, United Kingdom

6. Royal Brompton Hospital Trust, London, England, United Kingdom

7. National Heart Centre Singapore, Singapore

8. University College London, and Barts Heart Centre, United Kingdom

9. Duke-NUS Medical School, Singapore

10. Royal Brompton Hospital and Imperial College, London, United Kingdom

11. MRC London Institute of Medical Sciences, United Kingdom

12. National Heart and Lung Institute, Imperial College London, United Kingdom

Background: Integration of atlas-based machine learning analysis of cardiac magnetic resonance (CMR) with three-dimensional (3D) statistical modelling has been shown to be a powerful technique in imaging-genetics studies in the general population and in accurate prediction of patient outcomes in pulmonary hypertension. The use of machine learning segmentation methods in Hypertrophic Cardiomyopathy (HCM) has so far been limited by the lack of a large training set that encodes the wide spectrum of phenotypes that characterises this condition. We aimed to develop a HCM-specific bi-ventricular cardiac atlas and to assess whether it provides methodological advantage in the study of HCM.

Methods: In this study, 686 patients diagnosed with HCM using standard clinical criteria were recruited at the Royal Brompton Hospital (n=622, 27% women, 57±14 years) and the National Heart Centre Singapore (n=64, 22% women, 55±13 years). A previously published cardiac atlas derived from the Digital Heart Project healthy volunteer (HVOL) cohort (n=1,258 volunteers, 54% women, 40.6±12.8 years) was used for comparison. All participants underwent standard clinical CMR at 1.5T. The left ventricular (LV) short axis images from 200 randomly selected HCM subjects were manually labelled as LV myocardium, LV cavity or right ventricular (RV) cavity in end-diastole and end-systole (Fig. 1). This training set was used to create a probabilistic map and a common 3D template on which to co-register all segmentations. Using a previously published algorithm this atlas was used to guide the segmentation of the full HCM cohort (Fig. 2). 60 HCM datasets were segmented using the HCM or HVOL atlases and the results compared to manual labelling by the proportion of concordant voxels (Dice coefficient; 0 indicates no overlap and 1 indicates perfect agreement) and the mean surface distance (MSD; in mm).

Results: The HCM atlas-based segmentations were more accurate than the HVOL-guided segmentation for defining the LV endocardium (Dice: 0.86vs0.82; MSD: 0.98vs1.87), LV epicardium (Dice: 0.71vs0.59; MSD: 1.05vs1.88) and RV endocardium (Dice: 0.77vs0.67; MSD: 0.98vs4.06; Table 1) in HCM patients. The HCM and HVOL mean 3D shapes were computed and mean wall thickness plotted at each of the 46,000 vertexes in the model to show the morphological data encoded in the atlases (Fig. 3).

Conclusion: In this work, we created the first HCM-specific bi-ventricular cardiac atlas and demonstrate that a disease specific training set provides improved machine learning analysis of a phenotypically heterogenous population. The creation of this atlas presents the opportunity for statistically powerful, high-fidelity mapping of genotype-phenotype associations in HCM.

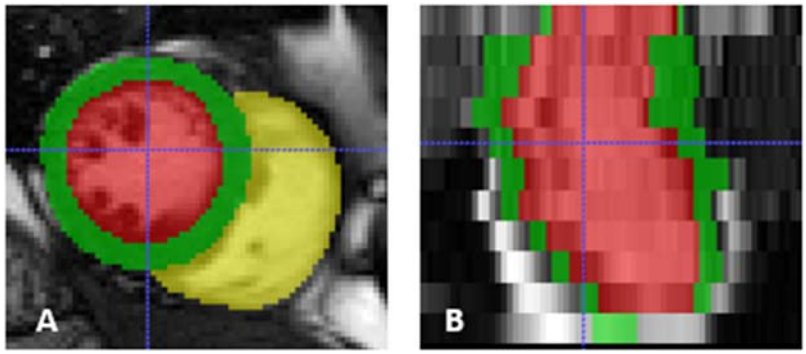

Figure 1. Short (A) and reformatted long axis (B) views demonstrating manual labelling of the LV cavity (red), LV myocardium (green) and RV cavity (yellow).

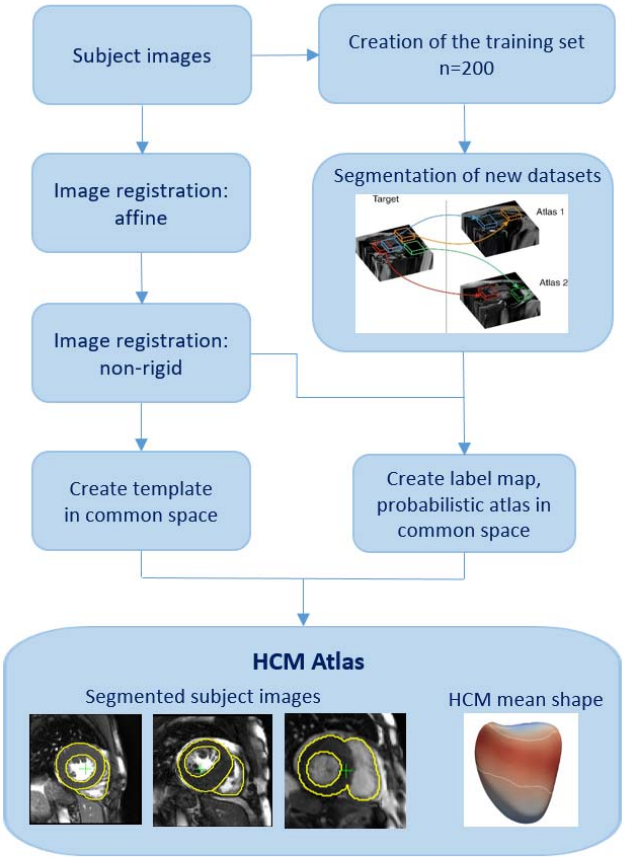

Figure 2. Atlas creation workflow.

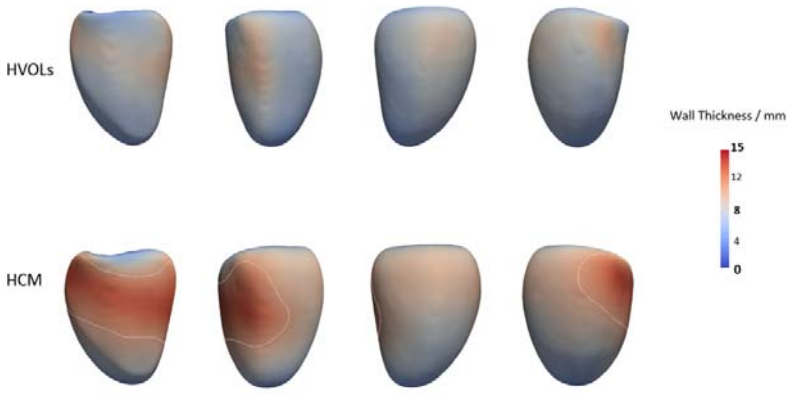

Figure 3. HVOLs population mean Wall Thickness (WT) plotted on the average 3D HVOLs atlas shape and HCM population mean WT plotted on the average HCM atlas shape. Septal, anterior, lateral and inferior en face projections are shown. The area enclosed by the yellow contour shows WT > 10mm.

Comparison of HCM and HVOL Atlas-Based Segmentation Results

	Dice metric HCM atlas	Dice metric HVOL atlas	Mean surface distance HCM atlas (mm)	Mean surface distance HVOL atlas (mm)
LV endocardium	0.857 ± 0.056	0.816 ± 0.075	0.976 ± 0.357	1.871 ± 1.274
LV epicardium	0.713 ± 0.084	0.593 ± 0.109	1.048 ± 0.501	1.882 ± 1.393
RV endocardium	0.767 ± 0.113	0.671 ± 0.141	0.980 ± 0.615	4.060 ± 2.660

ID#: 371673

Hemodynamic forces in the left and right ventricles of the human heart using 4D flow magnetic resonance imaging: phantom validation and reproducibility

Johannes Töger, PhD[1]Per M. Arvidsson, MD, PhD[2], Jelena Bock, PhD[3], Mikael Kanski, MD, PhD[2], Gianni Pedrizzetti, PhD[4], Marcus Carlsson, MD, PhD[3], Håkan Arheden, MD PhD[5], Einar Heiberg, PhD[6]

1. Lund University, Skåne University Hospital, Malmö, Sweden

2. Lund University, Skane University Hospital, Department of Clinical Sciences Lund, Clinical Physiology, Lund, Sweden, Lund, Skane Lan, Sweden

3. Lund University, Skane University Hospital, Department of Clinical Sciences Lund, Clinical Physiology, Lund, Sweden, Skane Lan, Sweden

4. University of Trieste, Trieste, Toscana, Italy

5. Lund University, Skåne University Hospital, Department of Clinical Sciences Lund, Clinical Physiology, Lund, Sweden, Lund, Sweden

6. Lund University, Skåne University Hospital, Department of Clinical Sciences Lund, Clinical Physiology, Lund, Sweden, Skane Lan, Sweden

Background: Hemodynamic force quantification (Figure 1) is a new method for quantification of biventricular function [1,2] which may be used to improve cardiac resynchronization therapy response [3,4]. The sensitivity of LV hemodynamic forces to field strength, respiratory gating and ventricle segmentation method have previously been evaluated [5]. However, phantom validation and in vivo reproducibility (same day, different scanner) and repeatability (different days, same scanner) have not been investigated.

Therefore, this study aims to validate hemodynamic force measurements in a phantom setup, and investigate in vivo reproduciblity and repeatability in controls.

Methods: A pulsatile flow phantom [6] (Figure 2) was imaged using 4D flow MRI and laser-based particle imaging velocimetry (PIV). Cardiac 4D flow MRI was performed in controls at 1.5T (n=23). Reproducibility was investigated using two 1.5T scanners (Achieva, Philips Healthcare, Best, The Netherlands and Magnetom Aera, Siemens Healthcare, Erlangen, Germany) on the same day (n=8). Subsets of controls were also imaged without respiratory gating (n=17), at 3T (same day, n=6), and 1-12 days later on the same scanner (n=9, median 6 days). Agreement was measured using intraclass correlation coefficient (ICC).

Results: Phantom validation showed good accuracy (Figure 2, Scanner 1: bias -14±9%, y=0.82x+0.08, R2=0.96, Scanner 2: bias -12±8%, y=0.99x-0.08, R2=1.00). Figure 1 c) shows mean LV forces for all subjects. Repeatability (Figure 3) was strong in the LV (0.09±0.07 vs 0.09±0.07 N, bias 0.00±0.04 N, ICC=0.87) and RV (0.09±0.06 vs 0.09±0.05 N, bias 0.00±0.03, ICC=0.83).

Furthermore, strong to very strong agreement was found for scans with and without respiratory gating (LV/RV: ICC=0.94/0.95), scans on different days (ICC=0.92/0.87), and 1.5T and 3T scans (ICC=0.93/0.94).

Conclusion: Results show high accuracy and reproducibility for both the LV and RV, supporting the use of hemodynamic forces for research and clinical investigations.

Acknowledgments
We thank Andreas Greiser at Siemens Healthcare, Erlangen, Germany, for providing the Siemens 4D flow sequence as the prototype work-in-progress package WIP785K.

References
1. Eriksson J et al. Physiol. Rep. 4(3):e12685, 2016.
2. Arvidsson PM et al. Am. J. Physiol. - Hear. Circ. Physiol. 312(2):H314–28, 2017.
3. Eriksson J et al. Sci. Rep. 7(1):2971, 2017.
4. Pedrizzetti G et al. Eur. Heart J. Cardiovasc. Imaging. 17(2):203–9, 2016.
5. Töger J et al. J. Cardiovasc. Magn. Reson. 18(Suppl 1):1–3, 2016.
6. Töger J et al. Magn. Reson. Med. 75(3):1064–75, 2016.

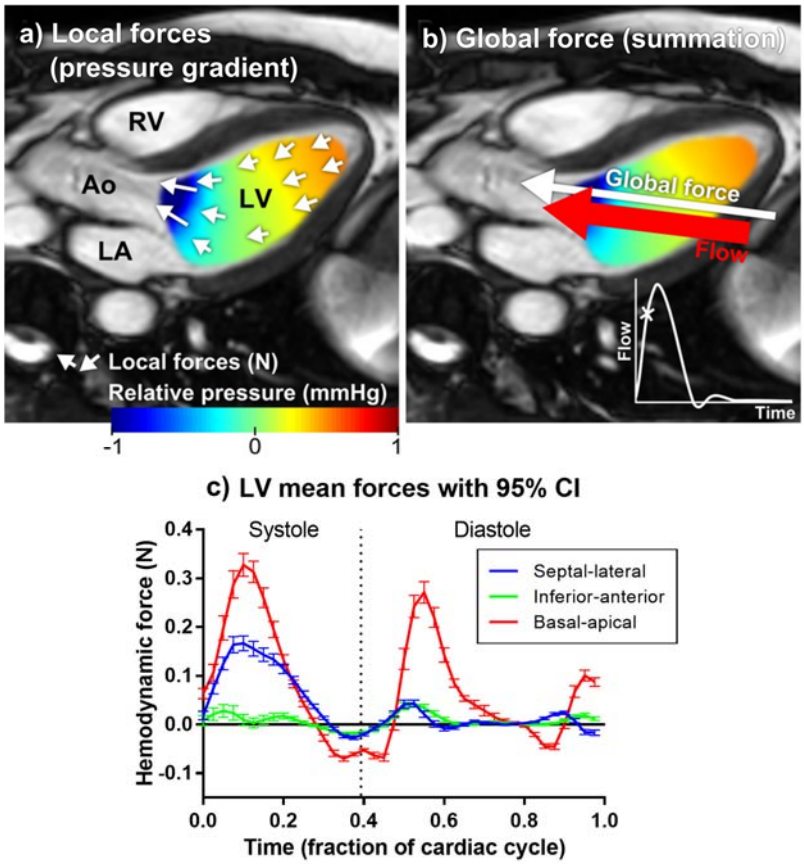

Figure 1: Visualization of hemodynamic forces. Panel a) shows how intraventricular pressure gradients give rise to local forces. Summation of the local forces produces the global hemodynamic force, as seen in panel b). Panel c) shows the mean LV forces in all subjects (n=23). Panels a) and b) reused with permission [2].

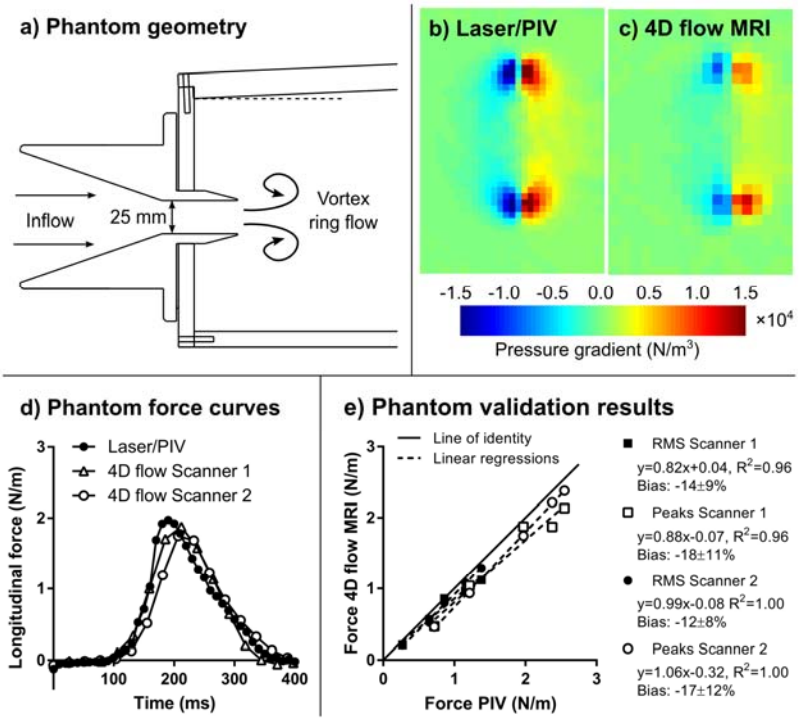

Figure 2: Phantom validation. A pulsatile flow phantom (Panel a) was imaged with a laser-based technique (PIV, particle image velocimetry) and 4D flow MRI. Panels b) and c) show the pressure gradient at one time instant computed from PIV and 4D flow velocities, respectively. Panel d) shows hemodynamic force curves for one pump setting (out of five). Panel e) shows a summary of results for RMS and peak forces on the both scanners, with a slight underestimation for both scanners.

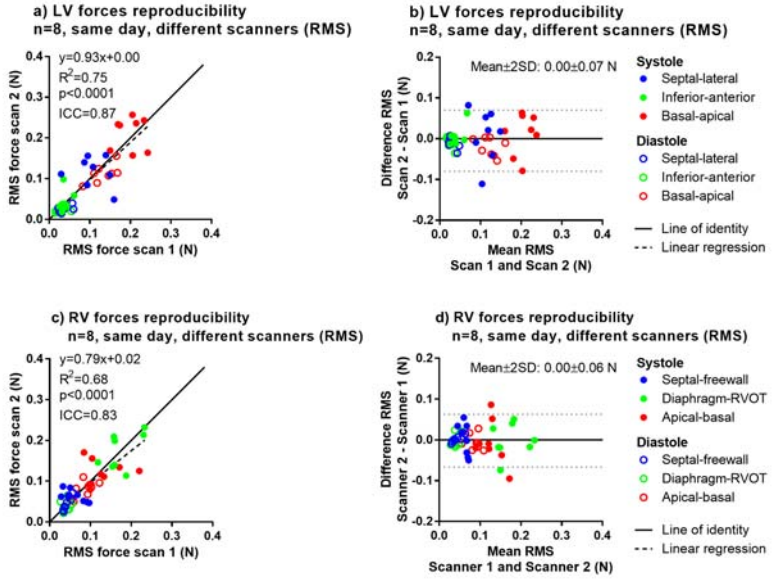

Figure 3: Reproducibility results. Panels a) and b) show LV results, and panels b) and c) show RV results. Strong agreement was found for both LV (ICC=0.87) and RV (ICC=0.83).

ID#: 371682

Automated versus manual valve tracking for assessment of valvular flow and regurgitation with 4D Flow MRI

Jos J.M. Westenberg, PhD[1] Arno A.W. Roest, MD, PhD[2], Pieter J. van den Boogaard, BSc[3], Jean-Paul Aben[4], Albert de Roos, MD, PhD[3]

1. Department of Radiology, Leiden University Medical Center, Leiden, The Netherlands, Leiden, Zuid-Holland, Netherlands

2. Department of Pediatrics, Leiden University Medical Center, Leiden, The Netherlands, Zuid-Holland, Netherlands

3. Department of Radiology, Leiden University Medical Center, Leiden, The Netherlands, Zuid-Holland, Netherlands

4. Pie Medical Imaging BV, Netherlands

Background: Valvular flow assessment is the main application of cardiac 4D flow MRI. However, manual tracking of multi-planar reformatting planes of each valve remains time-consuming and introduces observer-dependent variation that may hinder clinical use. Automated valve tracking may reduce analysis time and improve accuracy. The purpose of this study was to compare automated versus manual valve tracking in clinical 4D flow MRI data.

Methods: Data of 90 patients without shunt flow were retrieved from hospital database who underwent 4D flow MRI for valvular flow evaluation at 1.5T (Intera) or 3T MRI (Ingenia, Philips Healthcare). 4D flow MRI was performed with free breathing, VENC=150 cm/s in three directions, retrospective ECG-gating and Echo Planar Imaging factor 5 for acceleration. For valve tracking, two orthogonal cine steady-state free-precession (SSFP) views were used to identify aortic (AV) and pulmonary valve (PV) excursion. Also, 2- and 4-chamber cine SSFP views were used to identify mitral (MV) and tricuspid valve (TV) excursion. Manual valve tracking was previously performed for clinical evaluation using in-house developed software (Roes et al. Invest Radiol 2009). Automated valve tracking was performed with CAAS MR 4D flow v2.0 (Pie Medical Imaging) (Figure 1) with automatic aliasing and phase offset correction. The tracked valve excursion was used for through-plane motion correction. Automated versus manual tracking results were compared by paired samples t-tests for analysis time, coefficients of variation (COV) and differences between net forward flow (NFF) at each valve versus mean NFF among four valves and valve regurgitation fractions.

Results: Patient characteristics are presented in Table 1. Patients are divided into three groups: young (age<18 years) patients with repaired aorta coarctation (Coarc) (n=28), young and adult (age>18 years) patients with corrected atrioventricular septum defect (cAVSD) and adult patients with ischemic cardiomyopathy (IschCMP). Bland-Altman plots for NFF from manual and automated valve tracking are presented in Figure 2. Analysis times, regurgitation fractions and confidence intervals (CI) for differences in NFF and COVs are presented in Table 2. Analysis time was significantly shorter for automated versus manual tracking (13±3 minutes versus 23±3 minutes). Overall, CI in NFF were smaller for automated tracking and variation in NFF among the four valves improved to 5.2±3.0%, compared to 10.1±6.2% for manual tracking. Automated tracking resulted in statistically significant different regurgitation fractions for various valves among the three patient groups, although differences were marginally clinically significant.

Conclusion: Automated valve tracking reduces analysis time and positively impacts assessment of valvular flow in patients with repaired coarctation, corrected AVSD and ischemic cardiomyopathy.

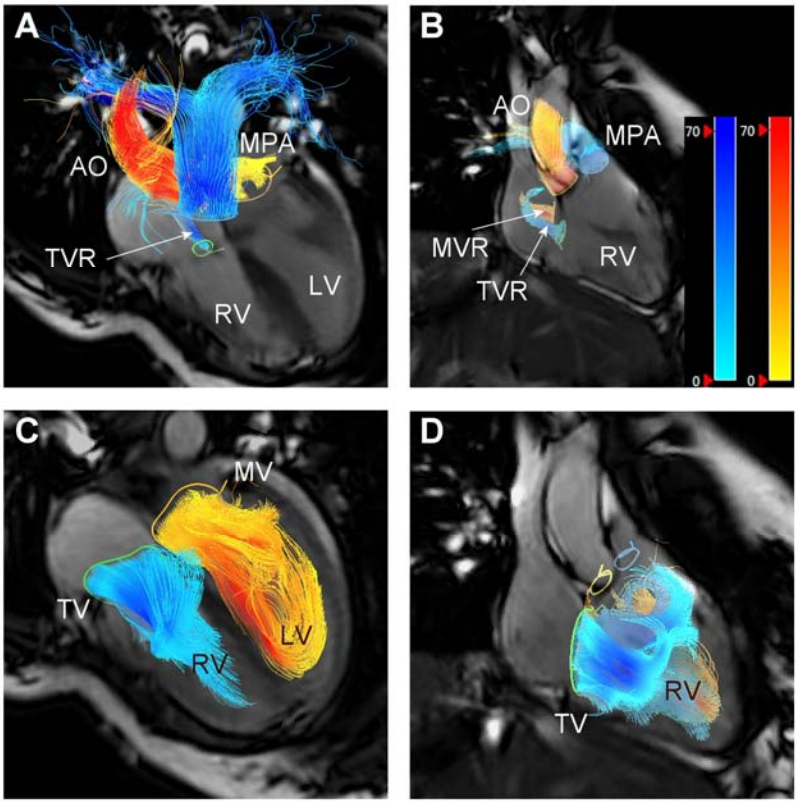

Figure 1. Valve tracking with 4D flow MRI. Four- (A) and two-chamber (B) view of the heart of a patient (16 year old girl) with corrected atrioventricular septum defect during systole and C and D are identical views during diastole. Ventricular in- and outflow is shown by streamline representation.

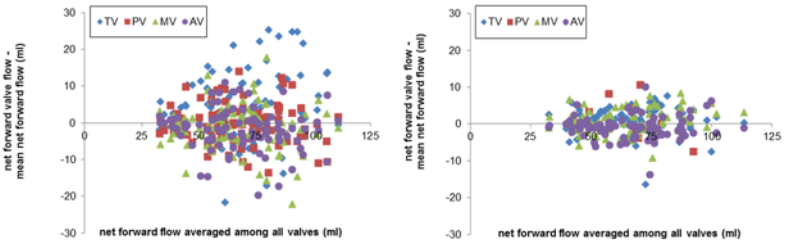

Figure 2. Bland-Altman plots for manual (left) and automated (right) valve tracking. The difference between net forward valve flow volume of each valve - mean net forward flow volume is plotted against the mean net forward flow averaged among the four valves.

Table 1. Patient characteristics

	Coarc	cAVSD	IschCMP	All
N	28	29	33	90
Mean age ± standard deviation (years)	13.4 ± 2.9	25.5 ± 11.7	60.8 ± 13.1	34.7 ± 23.0
<18 years | >18 years	28 | 0	9 | 20	0 | 33	37 | 53
Male | Female	18 | 10	8 | 21	22 | 11	48 | 42

Coarc: patients with repaired coarctation of the aorta; cAVSD: patients with corrected atrioventricular septum defect; IschCMP: patients with ischemic cardiomyopathy.

Table 2: Automated versus manual valve tracking for valvular flow assessment

		Coarc	cAVSD	IschCMP	All
Analysis time	**Automatic**	14 ± 3 minutes	13 ± 3 minutes	13 ± 2 minutes	13 ± 3 minutes
	Manual	23 ± 3 minutes	24 ± 3 minutes	23 ± 3 minutes	23 ± 3 minutes
	P-value	<0.001*	<0.001*	<0.001*	<0.001*
CI NFF tricuspid valve	**Automatic**	(-5 – 8ml)	(-8 – 9ml)	(-5 – 6ml)	(-6 – 8ml)
	Manual	(-6 – 29ml)	(-5 – 8ml)	(-18 – 18ml)	(-14 – 22ml)
	P-value	<0.001*	0.26	0.55	0.002*
CI NFF pulmonary valve	**Automatic**	(-5 – 4ml)	(-8 – 6ml)	(-8 – 9ml)	(-7 – 7ml)
	Manual	(-12 – 10ml)	(-4 – 4ml)	(-14 – 14ml)	(-11 – 10ml)
	P-value	0.44	0.06	0.33	0.63
CI NFF aortic valve	**Automatic**	(-6 – 6ml)	(-4 – 8ml)	(-7 – 6ml)	(-6 – 7ml)
	Manual	(-19 – 7ml)	(-6 – 5ml)	(-10 – 13ml)	(-14 – 11ml)
	P-value	<0.001*	0.005*	0.08	0.006*
CI NFF mitral valve	**Automatic**	(-8 – 5ml)	(-7 – 5ml)	(-7 – 4ml)	(-7 – 5ml)
	Manual	(-17 – 8ml)	(-6 – 5ml)	(-14 – 12ml)	(-13 – 9ml)
	P-value	0.002*	0.66	0.82	0.17
Tricuspid valve regurgitation fraction	**Automatic**	9.7 ± 6.9% (2% - 37%)	5.3 ± 3.2% (0% - 15%)	11.4 ± 6.9% (4% - 40%)	8.9 ± 6.4% (0% - 40%)
	Manual	5.5 ± 4.9% (0% - 24%)	5.1 ± 4.5% (0% - 21%)	11.2 ± 6.2% (0% - 26%)	7.5 ± 6.0% (0% - 26%)
	P-value	<0.001*	0.59	0.87	0.01*

Pulmonary valve regurgitation fraction	**Automatic**	1.2 ± 1.2% (0% - 5%)	2.0 ± 2.6% (0% - 12%)	2.4 ± 2.6% (0% - 12%)	1.9 ± 2.3% (0% - 12%)
	Manual	1.7 ± 1.8% (0% - 8%)	1.2 ± 2.3% (0% - 11%)	4.0 ± 4.6% (0% - 22%)	2.4 ± 3.5% (0% - 22%)
	P-value	0.10	0.01*	0.09	0.18
Mitral valve regurgitation fraction	**Automatic**	2.7 ± 1.7% (1% - 7%)	7.2 ± 4.2% (1% - 17%)	13.8 ± 9.7% (2% - 39%)	8.2 ± 7.8% (1% - 39%)
	Manual	2.7 ± 1.7% (1% - 9%)	13.8 ± 8.9% (2% - 36%)	11.7 ± 8.9% (1% - 32%)	9.6 ± 8.8% (2% - 36%)
	P-value	0.98	<0.001*	0.12	0.07
Aortic valve regurgitation fraction	**Automatic**	1.7 ± 3.7% (0% - 20%)	0.8 ± 0.8% (0% - 3%)	3.4 ± 3.4% (0% - 15%)	2.1 ± 3.1% (0% - 20%)
	Manual	2.8 ± 2.4% (0% - 8%)	0.5 ± 0.7% (0% - 2%)	3.3 ± 2.9% (0% - 11%)	2.2 ± 2.5% (0% - 11%)
	P-value	0.13	0.02*	0.87	0.62
COV NFF among four valves	**Automatic**	4.4 ± 2.7% (1% - 13%)	4.9 ± 3.5% (1% - 16%)	6.2 ± 2.5% (3% - 13%)	5.2 ± 3.0% (1% - 16%)
	Manual	13.6 ± 5.9% (2% - 24%)	4.3 ± 2.2% (1% - 10%)	12.3 ± 5.3% (4% - 26%)	10.1 ± 6.2% (1% - 26%)
	P-value	<0.001*	0.33	<0.001*	<0.001*

Mean values ± standard deviations. Ranges between parentheses. Coarc: patients with repaired coarctation of the aorta; cAVSD: patients with corrected atrioventricular septum defect; IschCMP: patients with ischemic cardiomyopathy; CI: confidence interval; NFF: net forward flow; COV: coefficient of variation. * implies statistically significant ($p<0.05$).

ID#: 371756

Tissue-Based Determinants of Right Ventricular Dysfunction in Ischemic Mitral Regurgitation - Incremental Utility of Non-ischemic Fibrosis Beyond CMR Evidenced Ischemia and Infarction Burden

Jiwon Kim, MD[6]Christiane Abouzeid, MD[1], Omar Khalique, MD[2], Javid Alakbarli, MD[1], Farhan Raza, MD[1], Meridith P. Pollie, BS[1], Ansh Johri, BS, MSE[1], Michael Villanueva[1], Robert A. Levine, MD[3], Mark B. Ratcliffe, MD[4], Richard B. Devereux, MD[5], Jonathan W. Weinsaft, MD[5], Martin A. Janich, PhD[7]

1. Weill Cornell Medical College

2. Columbia University Medical Center

3. Massachusetts General Hospital, MA

4. University of California San Francisco, San Francisco, CA

5. Weill Cornell Medical Center, NY

6. Weill Cornell Medical College, New York, NY

7. GE Healthcare, Germany

Background: Among patients with ischemic mitral regurgitation (iMR), right ventricular dysfunction (RV-dys) predicts adverse prognosis. LV ischemia, infarction, and non-ischemic septal midwall fibrosis (MWF) each have been associated with increased RV wall stress, providing a nidus for RV-dys. CMR enables integrated functional and tissue characterization; links between altered myocardial tissue properties and RV-dys are poorly understood.

Methods: Population comprised patients with iMR (≥mild) who prospectively underwent 3T CMR and echocardiography (echo) within 3 days (96% within 24 hours). CMR consisted of 3 components: (1) Stress (regadenoson) perfusion-CMR for LV ischemia; (2) DE-CMR for CAD pattern LV infarct (MI) size and non-ischemic pattern MWF (LGE confined to mid-myocardial or epicardial septum); (3) Cine-CMR for LV and RV volumes and function (RV-dys=EF<50%). Pulmonary systolic pressure (PASP) was quantified on echo; iMR was independently measured on both modalities.

Results: 84 iMR patients (68±10yo, 82% M) were studied; 32% had RV-dys. RV-dys patients had greater LV dilation (229±57 vs. 185±58 ml; p=0.002) and lower LVEF (39±8 vs. 59±6%; p<0.001), paralleling increased prevalence of advanced (≥moderate) MR by both echo (74 vs. 26%; p<0.001) and CMR (56% vs. 19%; p=0.001). Despite minimal increments in CMR-evidenced MI size (12±9 vs. 10±10%; p=0.05) and global LV ischemia (15±11 vs. 13±9%; p=0.06), RV-dys was strongly associated with non-ischemic tissue alterations as evidenced by a 10-fold increment in MWF among patients with RV-dys (52 vs. 6%; p<0.001): MWF was associated with RV-dys (regression coefficient [RC] 21.5, CI [.32-144]; p=0.002) independent of LV dysfunction (0.3 per 10-point LVEF decrement, [0.2-0.6]; p<0.001). Regarding RV remodeling, MWF was associated with geometric and functional maladaptation as evidenced by larger RV size (177±62 vs. 144±46 ml; p=0.02), increased mass (35±15 vs. 27±7 gm; p=0.04) and elevated PASP (52±22 vs. 34±11 mmHg; p=0.01), yielding higher aggregate wall stress (23±12 vs. 12±7 kPa; p<0.001). MWF prevalence increased in relation to RV wall stress, as evidenced by five-fold higher prevalence among patients in the top population-based RV wall stress tertile (Figure). Multivariate testing of RV wall stress components indicated MWF to be associated with PASP (OR=2.0 per 10 mmHg, [1.1-3.4]; p=0.02) independent of RV mass (OR=1.7 per 10 gm, [0.6-4.4]; p=0.3) and chamber volume (OR=1.0 per 10 ml, [0.8-1.1]; p=0.6) [model χ^2=14.5; p=0.002].

Conclusion: Among iMR patients, MWF is more strongly related to RV-dys than is LV MI or ischemia: MWF prevalence increases in parallel with increases in RV wall stress, secondary to MR associated increments in RV afterload.

Figure

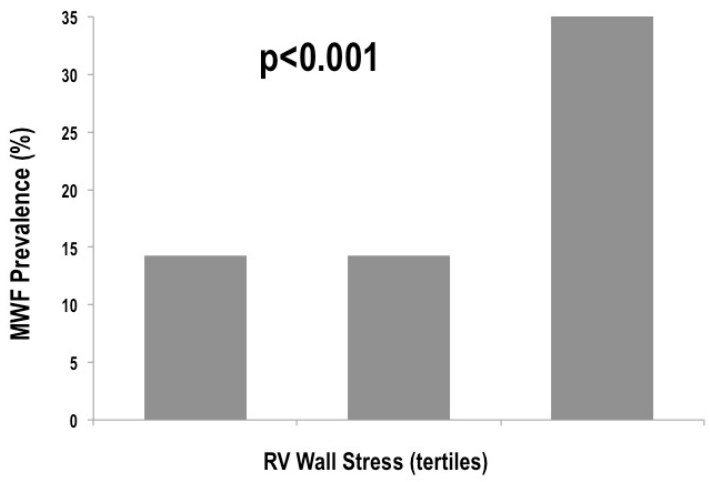

Prevalence of mid-wall fibrosis among population-based tertiles partitioned based on CMR-quantified RV wall stress. Note the increase in prevalence among patients with elevated RV wall stress ($p<0.001$).

ID#: 371899

Myocardial extracellular volume fraction derived from synthetic hematocrit can lead to significant clinical misclassification

Andrea Cardona, MD[1] Juliet Varghese, PhD[2], Giuseppe Ambrosio, MD, PhD[3], Orlando Simonetti, PhD[4], Subha Raman, MD, MSEE[5], Karolina Zareba, MD[6]

1. The Ohio State University Wexner Medical Center, Columbus, OH

2. The Ohio State University

3. Division of Cardiology - University of Perugia, Umbria, Italy

4. The Ohio State University, OH

5. The Ohio State University, Columbus, OH

6. The Ohio State University Wexner Medical Center, OH

Background: Cardiac magnetic resonance (CMR) using pre- and post-contrast T1 mapping allows precise quantification of the myocardial extracellular volume fraction (ECV) - a noninvasive biomarker of interstitial expansion. Recently, a method was proposed using the longitudinal relaxation of blood to generate a synthetic hematocrit (Hct), which can be used to calculate a synthetic ECV (Reference). We investigated the clinical accuracy and reliability of synthetic ECV estimation in discriminating subjects with normal vs. true abnormal ECV.

Methods: Subjects referred to our center for a clinical CMR over a period of 24 months were included. T1 maps were acquired using a steady state free precession-based modified Lock-Locker inversion recovery (MOLLI) sequence. Native and post-contrast T1 were determined in the mid myocardial septum and in the blood pool. Actual measured Hct was obtained on the same day of the exam in most patients. A total of 530 subjects with a wide range of health and disease were divided into derivation (265) and clinical (265) cohorts. The derivation cohort was used to estimate the parameters of the regression equation, based on the published model, in order to develop a local model which then was applied to the clinical cohort for the estimation of synthetic Hct and ECV.

Results: A total of 265 subjects (48.2±16.6 years, 50% female) were included in the clinical cohort. The mean measured Hct was 38.4±6.3% compared to a mean synthetic Hct of 38.4±5.9% with the locally-derived model, showing only modest intraclass coefficient agreement (ICC 0.58, 95%CI 0.47-0.67, p<0.001). The mean measured ECV was 27.6±6.5%, the mean synthetic ECV with the locally-derived model was 27.6±6.6% (ICC=0.95, 95%CI 0.94-0.96, p<0.001). While ICC was strong, differences between measured and synthetic ECV ranged from -5.4% to +5.5%. Using an established cut-off value of 29% for an abnormal ECV, we found that 24/110 (22%) were misclassified as normal vs. abnormal with the synthetic ECV estimation. Overall the locally-derived model showed moderate inter-rater agreement (Cohen's kappa coefficient=0.77, 95%CI 0.69-0.85, p<0.001). Applying the above mentioned published model revealed similar results.

Conclusion: In a large cohort of subjects referred for CMR, we demonstrated that synthetic ECV can potentially misclassify a large proportion of subjects even when adopting a locally-derived model. Such high misclassification coupled with the ease of direct Hct measurement in the vast majority of patients suggest that clinical use of synthetic ECV continues to be in question. Reference: Treibel et al. JACC Cardiovasc Imaging. 2016;9:54-63.

ID#: 372429

Optimized Prognosis Assessment in ST-Segment Elevation Myocardial Infarction Using a Cardiac Magnetic Resonance Imaging Risk Score

Thomas Stiermaier, MD[1] Alexander Jobs, MD[2], Suzanne de Waha, MD[2], Georg Fuernau, MD[2], Janine Pöss, MD[2], Steffen Desch, MD[3], Holger Thiele, MD[4], Ingo Eitel, MD[1]

1. University Heart Center Lübeck, Lübeck, Schleswig-Holstein, Germany

2. University Heart Center Lübeck, Germany

3. University Leipzig - Heart Center, Germany

4. Heart Center Leipzig - University Hospital, Sachsen, Germany

Background: Cardiac magnetic resonance (CMR) demonstrated great potential for the prediction of major adverse cardiac events (MACE) in ST-segment elevation myocardial infarction (STEMI). The aim of this study was to develop and validate a CMR based risk score for STEMI patients.

Methods: The scoring-model was developed and validated on STEMI cohorts from 2 independent randomized controlled trials (n=738 and n=458 patients, respectively) and included left ventricular ejection fraction (LVEF), infarct size (IS), and microvascular obstruction (MO). Primary endpoint was the 12-month MACE rate consisting of death, re-infarction, and new congestive heart failure.

Results: In the derivation cohort, LVEF ≤47%, IS ≥19%LV, and MO ≥1.4%LV were identified as the best cutoff values for MACE prediction. According to the hazard ratios in multivariable regression analysis, the CMR risk score was created by attributing 1 point for LVEF ≤47%, 1 point for IS ≥19%LV, and 2 points for MO ≥1.4%LV. In the validation cohort, the score showed a good prediction of MACE (area under the curve: 0.76). Stratification into a low (0/1 point) and high-risk group (≥2 points) resulted in significantly higher MACE rates in high-risk patients (9.0% versus 2.2%; p=0.001). Inclusion of the CMR score in addition to a model of clinical risk factors led to a significant increase of c-statistics from 0.74 to 0.83 (p=0.037), a net reclassification improvement of 0.18 (p=0.009) and an integrated discriminative improvement of 0.04 (p=0.010).

Conclusion: Our approach integrates the prognostic information of CMR imaging into a simple risk score that showed incremental prognostic value over clinical risk factors in STEMI patients.

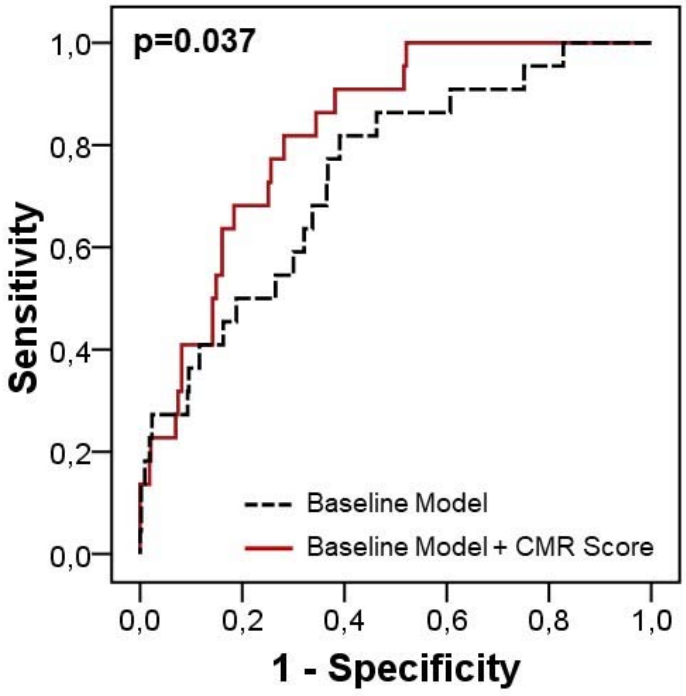

Incremental prognostic value of the CMR Score

ID#: 372894

Prognostic Value Of Global Circumferential Strain As Assessed By Feature-Tracking Cardiac Magnetic Resonance In Patients With A First St-Elevation Myocardial Infarction

Gaetano Nucifora, MD, PhD[1] Daniele Muser, MD[2], Chiara Tioni, MD[3], Ranjit Shah, MBBS, FRACP[4], Joseph Selvanayagam, FRACP, DPhil[5]

1. University Hospital of South Manchester, Sale, England, United Kingdom

2. Hospital of the University of Pennsylvania, PA

3. University Hospital "Santa Maria della Misericordia", Udine, Italy

4. South Australian Health and Medical Research Institute, Adelaide, SA, Australia, Prospect, South Australia, Australia

5. Flinders University, Adelaide, SA, Australia, Bedford Park, South Australia, Australia

Background: In recent year, several CMR techniques have emerged that permit us to directly assess myocardial deformation, which has been demonstrated to be more closely related to myocyte metabolism and contractility than left ventricular (LV) ejection fraction (EF). Among these techniques, CMR feature-tracking has gained prominence as a fast and accurate modality for the assessment of LV strain using the basic cine CMR sequences. It is still unknown whether CMR assessment of myocardial strain provides independent and incremental prognostic information in STEMI patients. The aim of the present study was therefore to investigate the prognostic utility of feature-tracking derived global circumferential strain (CS) in patients admitted with a first STEMI.

Methods: Consecutive patients (n = 180) admitted because of a first STEMI and referred to CMR with late gadolinium enhancement (LGE) imaging were included. All patients underwent immediate coronary angiography and primary PCI. CMR studies were performed using a 1.5 Tesla scanner after a median of 8 days. Cine-CMR and LGE images were analyzed offline to assess LV end-diastolic and end-systolic volume (EDV and ESV), LVEF, infarct size (IS) and the presence of microvascular obstruction (MVO). Furthermore, Cine-CMR basal, mid and apical short-axis images were analyzed offline to derive global CS using 2D Cardiac Performance Analysis Software (TomTec, Munich, Germany). Patients were followed-up (after CMR date) for a median duration of 95 months. The outcome event was a composite endpoint, which included *1)* cardiovascular death; *2)* aborted sudden cardiac death, defined as a nonfatal episode of ventricular fibrillation or sustained ventricular tachycardia requiring external cardioversion or appropriate implantable cardioverter defibrillator (ICD) therapy; and *3)* hospitalization for heart failure.

Results: The mean age of the study population was 60±12 years and 72% were male. Mean LVEDV index was 83±20 ml/m2 and mean LVEF was 50±13%; median infarct size was 13% (interquartile range, 5 to 30%) and 31% had MVO. Mean GCS was -16±5%. During follow-up, 40 (22%) patients experienced at least 1 event. At Kaplan-Meier analysis, the risk of outcome event increased significantly with worsening tertiles of global CS (log-rank $p<0.001$), increasing tertiles of IS (log-rank $p<0.001$) and with the presence of MVO (log-rank $p<0.001$). After adjustment for clinical and CMR imaging characteristics having univariate association with the outcome event at $p \leq 0.05$, global CS remained significantly and independently associated with the outcome event (HR 1.17 per %; 95% CI 1.03-1.33; $p = 0.013$). Of note, a significant increase of global χ^2 was observed when adding global CS to a model including clinical and non-contrast CMR variables (χ^2 change = 15.3; $p <0.001$) and to a model including clinical, non-contrast and LGE variables (χ^2 change = 5.7; $p=0.017$)

Conclusion: LV global CS assessed by CMR feature-tracking can predict a worse long-term prognosis in patients admitted with a first STEMI and treated with PCI. More importantly, the predictive ability of global CS was incremental to other clinical and especially CMR variables, including IS and MVO.

ID#: 372845

Motion-resolved free-breathing coronary MRA in heart transplant recipients at 3T

Jessica A.M. Bastiaansen, PhD[1] Lorenzo Di Sopra, MSc[2], Giulia Ginami, PhD[3], Hugues Vinzant, Jr., BSc[4], Juan F. Iglesias, MD[5], Sophie Degrauwe, MD[5], Samuel Rotman, MD[5], Davide Piccini, PhD[6], Jerome Yerly, PhD[6], Ruud B. van Heeswijk, PhD[5], Roger Hullin, MD[7], Matthias Stuber, PhD[6]

1. Department of Radiology, University Hospital (CHUV) and University of Lausanne (UNIL), Lausanne, Vaud, Switzerland

2. CIBM / CHUV / UNIL, Lausanne, Vaud, Switzerland

3. King's College London, United Kingdom

4. University Hospital (CHUV) and University of Lausanne (UNIL), Switzerland

5. Lausanne University Hospital (CHUV), Switzerland

6. Center for Biomedical Imaging (CIBM), Lausanne, Switzerland, Vaud, Switzerland

7. Lausanne University Hospital (CHUV), Lausanne, Vaud, Switzerland

Background: In heart transplant patients, there is a high prevalence of cardiac allograft vasculopathy (CAV) as a major cause of graft failure. A concentric thickening of the inner layer of the coronary vessel wall is often a characteristic of CAV in these patients[1]. Usually, conventional X-ray coronary angiography is used for detection of CAV. In this study, 3D whole-heart coronary magnetic resonance angiography was investigated as a possible alternative to invasive X-ray coronary angiography for the detection of luminal narrowing associated to the presence of CAV. The utilized 3D whole-heart sequence was integrated with cutting-edge strategies for respiratory motion compensation, allowing for volumetric acquisitions in free-breathing.

Methods: All study participants provided written informed consent, and the study was approved by the local ethics committee. Cardiac allograft transplant patients (n=23) ≥6 months after transplantation were recruited and underwent their routine clinical exams and cardiac MR examination. CAV severity was determined on the X-ray coronary angiograms in accordance with ISHLT guidelines[1]. We performed MRA on a 3T system (MAGNETOM Prisma) during and after gadolinium contrast agent injection[2,3], in a study design where vessel wall imaging and parametric mapping was also included. A prototype ECG-triggered free-breathing 3D radial GRE imaging sequence[4] using a lipid-insensitive water excitation pulse (LIBRE) [5] was used for imaging. In order to compensate respiratory motion, both datasets were reconstructed using 1D self-navigation[4] on the scanner software directly, and also using a respiratory-motion-resolved reconstruction using compressed sensing (k-t sparse SENSE) with 4 respiratory phases[6]. We then quantified coronary vessel sharpness [7]. Two-way ANOVA with repeated measures was performed and followed by a two-tailed Student';s t-test for paired data as post-hoc test. p

Results: Due to time constraints the second MRA (post-contrast) could not be acquired in 9 of the patients. Coronary reformats from MRA match with irregularities visible from X-ray angiograms (Figure 1). The end-expiration phase provided the best image quality for the motion-resolved-reconstructions (Figure 2A). Vessel sharpness was significantly improved using compressed sensing, both during slow-infusion and post-contrast (From 32.5% to 49.1% and 33.0% till 43.8%, Figure 2B). Respiratory self-navigation performs a motion-correction along one dimension (superior-inferior direction), however, respiratory-motion-resolved reconstruction may compensate for motion in multiple dimensions resulting in improved vessel conspicuity. Interestingly, comparing slow-infusion with post-contrast images vessel sharpness was not significantly changed using self-navigation. However, the motion-resolved reconstruction showed the highest average vessel sharpness when this data was acquired during slow-infusion (49.1%, Figure 2B).

Conclusion: To the best of our knowledge, this is the first report of self-navigated whole heart imaging during and post slow Gd infusion in heart transplant recipients at 3T. Coronary artery visualization was significantly improved when compressed sensing was applied on data acquired during slow infusion.

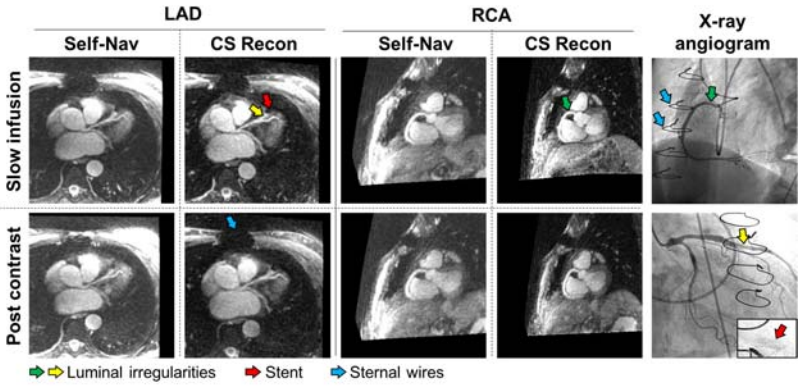

Figure 1. Coronary reformats of 3T MRA data obtained in a heart transplant recipient with corresponding X-ray angiograms. In each patient two free-breathing self-navigated whole-heart MRA acquisitions were performed, both during slow-infusion of Gd contrast agent and post-contrast injection. Each acquired self-navigated data set (Self-Nav) was also reconstructed using compressed sensing that provided respiratory-motion-resolved images (CS Recon). For the CS Recon, coronary reformats are shown at end-expiration.

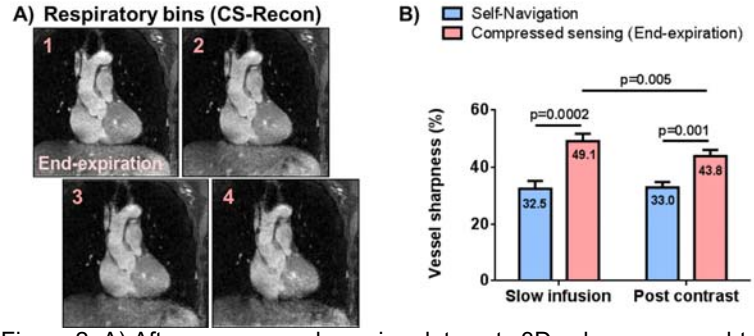

Figure 2. A) After compressed sensing data sets 3D volumes were obtained in different respiratory phases (respiratory bins). The phase corresponding to end-expiration typically provided the best image quality and was used for subsequent analysis. B) Vessel sharpness was generally improved in CAV patients when a respiratory-motion-resolved reconstruction with compressed sensing (both during slow Gd infusion and post contrast) was used. The best overall vessel conspicuity was obtained when data was acquired during slow infusion and reconstructed with compressed sensing.

References

[1] MR Mehra et al., J Heart Lung Transplant. 2010, 29(7):717-27

[2] Liu X, Bi X, Huang J, Jerecic R, Carr J, Li D. Contrast-Enhanced Whole-Heart Coronary Magnetic Resonance Angiography at 3.0 T: Comparison With Steady-State Free Precession Technique at 1.5 T. Investigative Radiology. 43(9):663-668

[3] Yang Q, Li K, Liu X, Bi X, Liu Z, An J, Zhang A, Jerecic R, Li D. Contrast-Enhanced Whole-Heart Coronary Magnetic Resonance Angiography at 3.0-T: A Comparative Study With X-Ray Angiography in a Single Center. JACC 2009 54(1): 69-76

[4] Piccini D, Littmann A, Nielles-Vallespin S, Zenge MO. Respiratory self-navigation for whole-heart bright-blood coronary MRI: methods for robust isolation and automatic segmentation of the blood pool. Magnetic resonance in medicine 2012;68(2):571-579.

[5] Bastiaansen JAM, Piccini D, van Heeswijk RB, Yerly J, Stuber M. Lipid insensitive free-breathing self-navigated coronary MR angiography at 3T using a novel water excitation method. SCMR (2017).

[6] Piccini D, Feng L, Bonanno G, Yerly J, Lim RP, Schwitter J, Sodickson D, Otazo R, Stuber M. Four-dimensional respiratory motion-resolved whole heart coronary MR angiography. MRM 2017; 77(4): 1473–1484

[7] Etienne A, Botnar RM, Van Muiswinkel AM, Boesiger P, Manning WJ, Stuber M. "Soap-Bubble" visualization and quantitative analysis of 3D coronary magnetic resonance angiograms. Magnetic resonance in medicine 2002;48(4):658-666.

References

ID#: 372948

Functional Late-Gadolinium Enhancement Imaging

Sebastian Weingärtner, PhD[1]Chetan Shenoy, M.D.[2], Marcel Prothmann, MD[3], Jeanette Schulz-Menger, MD[4], Mehmet Akçakaya, Ph.D.[5]

1. Electrical and Computer Engineering, University of Minnesota; Center for Magnetic Resonance Research, University of Minnesota; Computer Assisted Clinical Medicine, Heidelberg University, Minneapolis, MN

2. Cardiovascular Division, Department of Medicine, University of Minnesota, Minneapolis, MN

3. Working Group on Cardiovascular Magnetic Resonance, Experimental and Clinical Research Center, a joint cooperation between the Charité Medical Faculty and the Max-Delbrueck Center for Molecular Medicine and HELIOS Hospital Berlin Buch, Berlin, Berlin, Germany

4. Working Group on Cardiovascular Magnetic Resonance, Experimental and Clinical Research Center a joint cooperation between the Charité Medical Faculty and the Max-Delbrueck Center for Molecular Medicine HELIOS Klinikum Berlin Buch, Germany, Berlin, Germany

5. Electrical and Computer Engineering, University of Minnesota; Center for Magnetic Resonance Research, University of Minnesota, Minneapolis, MN

Background: Late Gadolinium Enhancement (LGE) based on inversion recovery imaging following contrast injection is the clinical gold-standard for depiction of scar in the heart [Kramer et al. JNuclMed 2015]. However, LGE is commonly restricted to a single cardiac phase, usually diastolic, to achieve the desired imaging contrast at a given time after the inversion pulse. Systolic LGE imaging has been shown to provide complementary information, with the potential of depicting scar that is concealed in diastolic imaging [Schuster et al. IntJCardvImag 2011]. Phase-resolved LGE imaging would allow the integrated assessment of multiple systolic and diastolic phases, potentially increasing diagnostic certainty. Furthermore, dynamic LGE imaging might allow tracking scar motility, potentially easing the assessment of residual viable tissue and facilitating the fusion of functional and viability information. In this study we sought to develop a method for phase-resolved LGE imaging using a steady-state Look-Locker approach and semi-quantitative data processing.

Methods: Sequence: Similar to [Weingärtner et al. MRM 2017] cardiac phase-resolved T1 weighted images are acquired using continuous FLASH pulses (Figure 1). After driving the magnetization to steady-state an inversion pulse is applied at a predetermined time after the R-wave. Images at multiple inversion times are acquired for each cardiac phase, while steady-state is re-reached over multiple heart-beats. Image acquisition is repeated multiple times by playing the inversion pulse at a different time within the heart-beat. Semi-quantitative T1 maps are then generated using a 2-parameter fit to the inversion-recovery curve ($S=A(1-2\exp(-t/T1))$). LGE contrast is finally synthesized with a virtual inversion time TI as $S_{LGE}=A(1-2\exp(-TI/T1))$, where TI is retrospectively chosen to null the signal of the healthy myocardium.
Imaging Experiments: The sequence was evaluated in 2 healthy subjects at 3T (23 y/o male, 28 y/o male) with the following imaging parameters: TR/TE/FA=5/2.6ms/3°, FOV=300x225mm2, resolution=1.9x1.9mm2, GRAPPA=2, slice=10mm, water-selective excitation, temp. resolution=60ms, breath-hold=17-19s. Additionally measurements were performed in 6 patients at 1.5T (48±21 y/o, 4 males) with the following imaging parameters: TR/TE/FA=6.7/3.2ms/6°, FOV=300x225mm2, resolution=2.1x2.1mm3, GRAPPA=2, slice=10mm, temp. resolution=80ms, breath-hold=15-18s.

Results: Diagnostic image quality was obtained in all subjects. Representative functional LGE images acquired in a healthy volunteer at 3T with a temporal resolution of 60ms show clear delineation of a thoroughly suppressed myocardium against the blood pool (Fig 2). Synthetic LGE images generated with the proposed method show image quality that is comparable to conventional 2D LGE. Despite an increased noise level, images acquire at 1.5T clearly depict transmural scar in the exemplary patient (Fig 3). The scar is visible against a thoroughly suppressed myocardium across all cardiac phases. Furthermore, dynamic LGE imaging reveals abnormal contractility of the scar tissue.

Conclusion: The proposed method allows, for the first time, generation of cardiac-phase resolved LGE images. Initial results indicate image quality comparable to reference LGE images at high fields, and clear scar depiction at low field strengths. Additionally, the proposed method allowed depiction of contractile abnormality of the scar tissue.

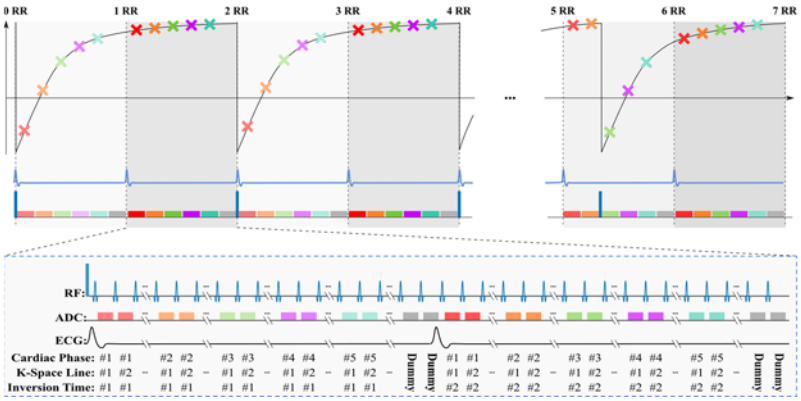

Sequence diagram of the proposed method for functional LGE imaging. Semi quantitative T1 maps are acquired using continuous FLASH pulses after inversion from the steady-state. Recovery to the steady-state spans multiple heart-beats, allowing to sample multiple time points of the inversion recovery curve for each cardiac phase. The steady-state look-locker experiment is repeated with varying position of the inversion pulse in the cardiac cycle to increase the sampling density of the inversion recovery curve.

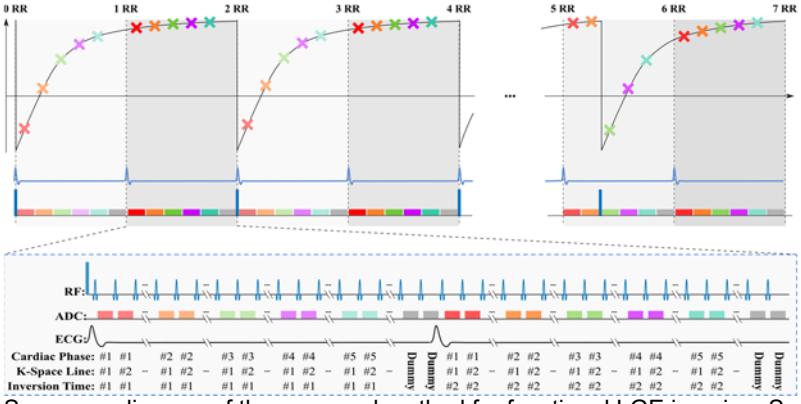

Sequence diagram of the proposed method for functional LGE imaging. Semi quantitative T1 maps are acquired using continuous FLASH pulses after inversion from the steady-state. Recovery to the steady-state spans multiple heart-beats, allowing to sample multiple time points of the inversion recovery curve for each cardiac phase. The steady-state look-locker experiment is repeated with varying position of the inversion pulse in the cardiac cycle to increase the sampling density of the inversion recovery curve.

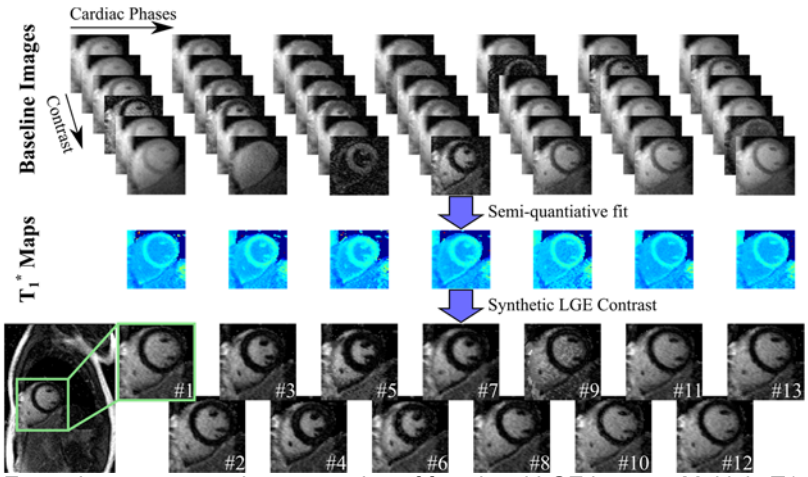

Example post-processing generation of functional LGE images. Multiple T1 weighted contrasts are acquired for each cardiac phase, based on a semi quantiative T1* fit, synthetic LGE contrast is generated. The resulting functional LGE images have a spatial resolution of 1.9x1.9mm2 and a temporal resolution of 60ms in a healthy

volunteer at 3T. Visually high image quality with thorough nulling of the healthy myocardium is observed throughout all cardiac phases, along with accurate temporal depiction of the cardiac function.

ID#: 373100

Aortic wall motion is critical to accurately simulate fluid dynamics at the aortic arch

Ramon Pons Cots, Grade in Chemical Engineering, Master in Chemical Engineering[1] Jordi Martorell, PhD[2], Arturo Evangelista, MD, PhD[3], José F. Rodríguez-Palomares, MD, PhD[4], Juan Carlos Cajas, PhD[5], Mariano Vazquez, PhD[5]

1. Institut Químic de Sarrià (IQS), Barcelona, Catalonia, Spain

2. Department of Chemical Engineering, IQS School of Engineering, Universitat Ramon Llull, Barcelona, Spain, Barcelona, Catalonia, Spain

3. Hospital Vall d'Hebron, Spain

4. Hospital Universitari Vall d´Hebron. Vall d'Hebron Institut de Recerca. Universitat Autònoma de Barcelona, Barcelona, Catalonia, Spain

5. Barcelona Supercomputing Center, Barcleona, Spain, Spain

Background: Differential fluid dynamics at the aortic wall may be at the origin of the diverse progression of aortic diseases such as aneurysms and dissections. The thoracic aorta is subject to pulsatile displacement that leads to a remarkable change of aortic geometry during the cardiac cycle. Highly complex techniques such as 4D-MRI or CT scan fail to completely characterize the state of the aortic wall. Fluid dynamics simulations, so far, have not been able to faithfully reproduce the aortic wall motion under complex fluidodynamic environments. Hypothesis: Wall motion must be incorporated in fluid dynamics simulations to accurately describe the biomechanical behavior of the aortic arch.

Methods: In patients with Marfan syndrome recruited at Hospital Vall d';Hebron, CT is used to precisely reproduce the thoracic aorta geometry. 4D-MRI flow data at the sinotubular junction are used to model blood flow profile entering the aortic arch. Both inputs are combined to perform fluid-solid interaction (FSI) simulations which couple aortic wall motion to blood flow. These simulations are compared to classic computational fluid dynamics (CFD), where wall is fixed. The calculations are performed using Alya, a software developed by the Barcelona Supercomputing Center. Shear stress gradients, vorticity and recirculation were calculated using the computer simulations and the differences between coupled and uncoupled simulations have been noted.

Results: Real blood flow is measured at the sinotubular junction and distal of the left subclavian artery using traditional flow MRI and compared with blood flow calculated using CFD or FSI. The delay observed in MRI between ascending aorta inlet and descending aorta outlet is due to flow accumulation after wall expansion and contraction. This delay can only be characterized using FSI simulations. Difference in velocity field alters most fluid dynamic parameters. Recirculation, shear stress gradients and vorticity are significantly different when simulations are performed including wall motion. Accurate mechanical properties of the vessel wall are critical for adequate results, those are calculated from pulse wave velocity of real data.

Conclusion: Fluid dynamic simulations of the aortic arch require fluid-solid interaction to properly map fluid behavior and wall motion of the vessel. These simulations improve the understanding of arterial biomechanics and could be a useful tool to predict aortic diseases progression. 4D-MRI combined with fluid-structure interaction can improve patient management in patients with aortic diseases.

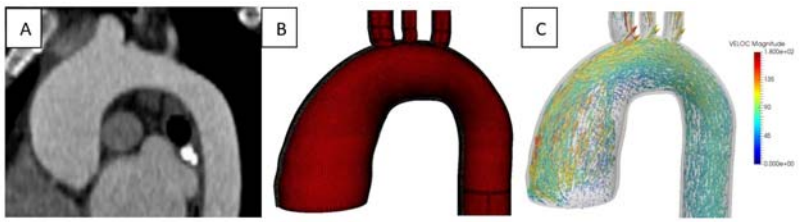

Aortic geometry and vessel wall reconstruction from CT (A) and meshing (B). Velocity profile along the aorta is then simulated, using 4D-MRI as input (C).

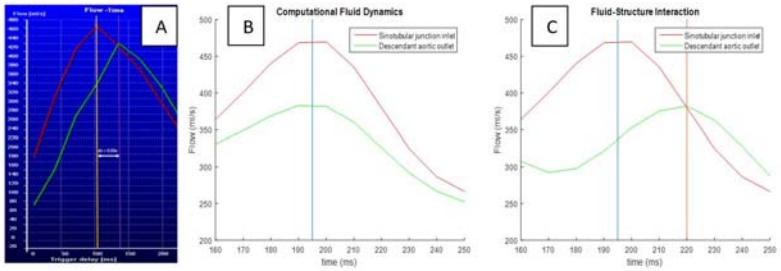

Flow at the sinotubular junction (red) and at the descending aorta (green) extracted from MRI data (A) is compared with flow obtained after CFD simulation (B) and FSI simulation (C).

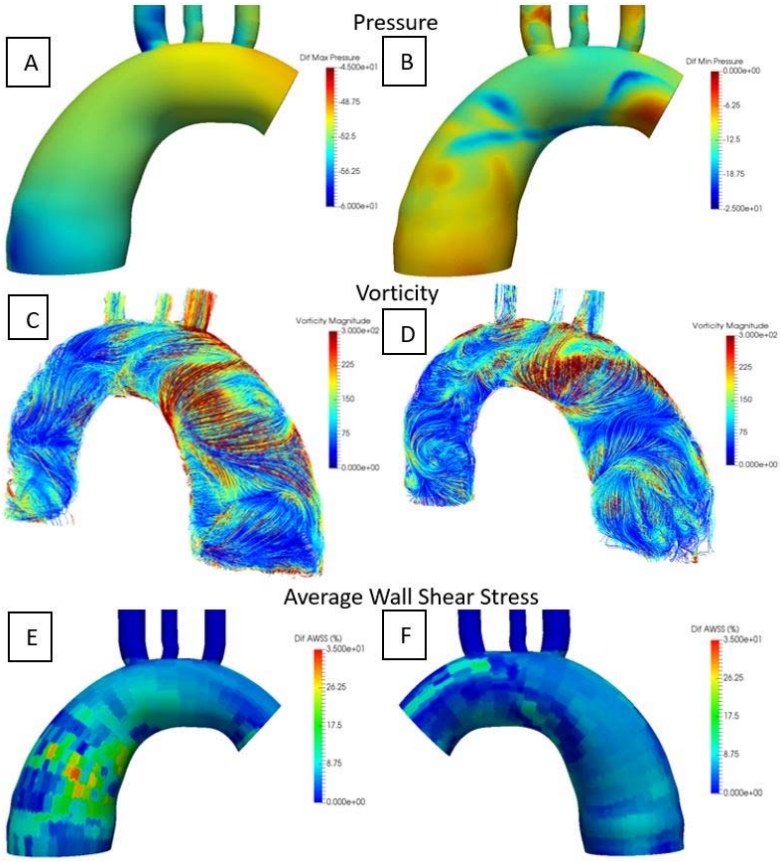

Maximum pressure during systole is significantly reduced when calculated using FSI (A) although minimum pressure during diastole is less affected (B). Vorticity peaks more distal to the aortic valve in FSI (D) than in CFD (C). Average wall shear stress (AWSS) decreases significantly during the systolic peak in the anterior face (E) of the ascending aorta, but not in the posterior face (F).

ID#: 372942

Gender Differences in Referral for Cardiovascular Magnetic Resonance (CMR) Imaging: Inaugural Findings from the Cardiovascular Imaging Registry of Calgary (CIROC)

Carmen P. Lydell, MD[1] Yoko Mikami, MD, Ph.D.[2], Michelle Seib, RN[1], Sarah G. Weeks, MD[3], Steven Dykstra, MSc[2], Sandra Rivest, RN[4], Rosa Sandonato, RN, BScN[2], Jacqueline A. Flewitt, MSc[1], Gary Dobko, Bsc[1], Bobby Heydari, MD, MPH[2], Andrew G. Howarth, MD, Ph.D[2], James White, MD, FRCP(C)[2]

1. Stephenson Cardiac Imaging Centre, Libin Cardiovascular Institute of Alberta, University of Calgary, Calgary, AB, Canada

2. Stephenson Cardiac Imaging Centre, Libin Cardiovascular Institute of Alberta, University of Calgary, AB, Canada

3. Libin Cardiovascular Institute of Alberta, University of Calgary, Calgary, AB, Canada

4. Stephenson Cardiac Imaging Centre, Libin Cardiovascular Institute of Alberta, University of Calgary, Canada, AB, Canada

Background: Gender-based differences in referral to diagnostic imaging remain an important but poorly studied aspect of cardiovascular care. To date, no published studies have evaluated the rate or indication distribution of clinical referrals for cardiovascular magnetic resonance (CMR) imaging between genders. The availability of such data may provide insight into the existence of relevant bias';s or emerging requirements relevant to the imaging community. Using data available from a large, prospective non-invasive cardiac imaging clinical registry we examined relative referral rates and referral indications for women versus men undergoing clinical CMR imaging over a 2.5-year period.

Methods: Between Feb 2015 and August 2017 a total of 4573 patients consented to and contributed 5795 CMR examinations to the Cardiovascular Imaging Registry of Calgary (CIROC). All cases were coded according to 18 referral indications and had standardized reporting performed using commercial software (Acuity®, Cohesic Inc, Calgary) and baseline questionnaires administered for demographics and quality of life (EQ5).

Results: CMR referrals were unevenly distributed between genders with 2788 males (58%) referred for 3383 studies (mean 1.2 per patient) versus 1784 females (42%) referred for 2412 studies (mean 1.4 per patient). No gender differences in age, EQ5 score or NYHA class were seen. The mean LVEF in women was 59.4 ± 11.3% with 111 (6%) having an LVEF of ≤ 40% versus a mean LVEF in men of 53.3 ± 14.1% with 499 (16%) having an LVEF of ≤ 40%. Gender-stratified referral indications are shown in Table 1 and shows differences in absolute referral numbers across most disease states. Percent distribution of referral indications were similar except for cardiotoxicity surveillance, coronary artery disease, congenital heart disease and ventricular arrhythmia / pre-ICD implantation. Interestingly, 30% of all CMR referrals in women were for cardiotoxicity surveillance (versus 5% in males). By comparison, only 9% of female CMR cases were referred for CAD (versus 17% in males).

Conclusion: At a large tertiary care CMR centre substantial differences were observed in referrals for women versus men. Recognizing site-bias, this study identified: i) reduced referral numbers for women across many indications that are not considered to have a gender bias, ii) growing clinical demand for cardiotoxicity surveillance using CMR, and iii) a lack of difference in NYHA class or Quality of Life between genders, suggesting similar disease severity at time of referral in women versus men.

Table 1: CMR referral characteristics in women versus men

	All N=4573	Women N=1784 (42%)	Men N=2788 (58%)
Demographics:			
Age (years)	52.7 ± 15.3	52.1 ± 15.1	53.3 ± 15.5
QOL score*	6.1 ± 1.7	6.3 ± 1.8	6.0 ± 1.5
NYHA (%)			
Class I-II	3855 (84%)	1477 (83%)	2378 (85%)
Class III-IV	717 (16%)	307 (17%)	410 (15%)
Diabetes (%)	492 (11%)	142 (8%)	350 (13%)
Hypertension (%)	1471 (32%)	503 (28%)	968 (35%)
Hyperlipidemia (%)	895 (20%)	250 (14%)	645 (23%)
CMR Features:			
LV EDV (ml)	175.2 ± 63.3	142.1 ± 42.9	196.1 ± 14.1
LV MASS (g)	116.6 ± 46.1	88.6 ± 30.6	134.7 ± 45.4
LV EF (%)	56.2 ± 14.0	59.4 ± 11.3	53.3 ± 14.1
RV EDV (ml)	168.6 ± 52.5	140.5 ± 39.1	186.7 ± 52.1
RV EF (%)	54.2 ± 9.6	56.6 ± 8.7	52.6 ± 9.7
LA vol (ml)	73.8 ± 32.9	64.1 ± 27.6	79.8 ± 34.3
Referral Indications:			
Cardiotoxicity Surveillance	672 (15%)	527 (30%)	145 (5%)
Coronary Artery Disease (viability / stress)	624 (14%)	156 (9%)	468 (17%)
Congenital Heart Disease	436 (10%)	218 (12%)	218 (8%)
Myocarditis	399 (9%)	135 (8%)	264 (9%)
Ventricular Arrhythmia (VT/VF/Pre-ICD)	367 (8%)	102 (6%)	265 (10%)
Non-Ischemic Dilated Cardiomyopathy	322 (7%)	86 (5%)	236 (9%)
ARVC (known / suspected)	304 (7%)	128 (7%)	176 (6%)
Hypertrophic Cardiomyopathy	288 (6%)	85 (5%)	203 (7%)
Pre/Post Pulmonary Vein Ablation	246 (5%)	54 (3%)	192 (7%)
Hypertrophic Cardiomyopathy	288 (6%)	85 (5%)	203 (7%)
Valvular heart disease	216 (5%)	94 (5%)	122 (4%)
Cardiac Amyloidosis	113 (3%)	34 (2%)	79 (3%)
Cardiac Sarcoidosis	111 (2%)	36 (2%)	75 (3%)
Cardiac mass	85 (2%)	28 (2%)	57 (2%)
Pulmonary hypertension	63 (1%)	35 (2%)	28 (1%)
Non-compaction cardiomyopathy	59 (1%)	18 (1%)	41 (2%)
Pericardial disease	45 (1%)	20 (1%)	25 (1%)
Other	223 (5%)	112 (6%)	111 (4%)

*EQ-5D standardized Quality of Life (QOL) questionnaire

Table 1: CMR referral characteristics in women versus men

ID#: 372883

Energetic and Vortex Size Alterations of Left Atrial Hemodynamics Using 4D Flow MRI: A Study in Patients with History of Paroxysmal Atrial Fibrillation

Julio Garcia, PhD[1] Mohammed S.M. Elbaz, PhD[2], Michael Bristow, MD[3], Carmen P. Lydell, MD[4], Andrew G. Howarth, MD, Ph.D[3], Bobby Heydari, MD, MPH[3], Frank S Prato, PhD[5], Maria Drangova, PhD[6], Rebecca E. Thornhill, PhD[7], Pablo Nery, MD[8], Stephen Wilton, MD[9], Allan Skanes, MD[10], Faramarz F. Samavati, PhD[2], James White, MD, FRCP(C)[3]

1. University of Calgary, Calgary, AB, Canada

2. University of Calgary, AB, Canada

3. Stephenson Cardiac Imaging Centre, Libin Cardiovascular Institute of Alberta, University of Calgary, AB, Canada

4. Stephenson Cardiac Imaging Centre, Libin Cardiovascular Institute of Alberta, University of Calgary, Calgary, AB, Canada

5. Lawson Health Research Institute, ON, Canada

6. Imaging Research Laboratories, Robarts Research Institute, ON, Canada

7. Medical Imaging, The Ottawa Hospital, ON, Canada

8. Electrophysiology, University of Ottawa, ON, Canada

9. Cardiac Sciences, Libin Cardiovascular Institute of Alberta, University of Calgary, AB, Canada

10. Department of Medicine, University of Western Ontario, ON, Canada

Background: Atrial fibrillation (AF) is a common arrhythmia associated with elevated morbidity and mortality from systemic thrombo-embolism. Left atrial (LA) energy dissipation may provide valuable insights for thrombogenic risk. However, such fluid dynamics are challenging to explore given 3-dimensional complexity. This study aimed to quantify viscous energy loss (EL), kinetic energy (KE) and vortex size to assess the complex hemodynamic of the LA in patients with paroxysmal AF and healthy controls.

Methods: 24 subjects (14 with paroxysmal AF, and 10 HC) were enrolled in an IRB-approved study protocol. Patients were required to be in sinus rhythm and not have mitral insufficiency. Imaging was performed using a 3T MRI scanner using a standardized protocol inclusive of ECG-gated 4D flow with adaptive respiratory navigator gating with whole heart coverage (Fig. 1A). 4D flow spatial resolution was 1.9-3.5x2.0-3.2x1.8-3.5 mm3, and temporal resolution was 39-47 ms. 4D flow dataset was pre-processed and a 3D phase contrast angiography (3D PC-MRA) was obtained. The 3D PC-MRA was used to segment the left sided chambers and proximal aorta, Fig. 1B. The LA was isolated, Fig. 1C, and used to calculate KE ($KE=1/2\times rho\times v^2$, where rho is the blood density = 1.06 g/mL and *v* the velocity field); and EL ($EL=\mu\sum(DV)$, where the dynamic viscosity was μ=0.004 Pa.s, D was the viscous dissipation on a voxel-by-voxel basis, and V was the voxel volume. The maximum vortex size as derived by lambda-2 detection was computed at the end systole. Volumetric median and total summation from KE and EL was obtained at peak systole and peak diastole (Fig. 2 and 3). All parameters were normalized to volume size.

Results: Age was 52±11 years in AF subjects and 42±15 years in HC (p=0.138). At peak systole, a significant decrease in EL was found in AF patients compared to HC for normalized median EL (HC: 3.8±3.3 mW/m3 vs. AF: 1.2±0. 7 mW/m3, p=0.001), total KE (HC: 24.50±7.12 J/m3 vs. AF: 16.85±9.70 J/m3, p=0.013), and total EL (HC: 18.51±8.53 W/m3 vs. AF: 5.70±2.34 W/m3, p<0.001). At peak diastole, significant decrease in KE was found in AF patients compared to HC for normalized median KE (HC: 12±11 mJ/m3 vs. AF: 5±4 mJ/m3, p=0.022), median EL (HC: 4.6±5.5 mW/m3 vs. AF: 1.2±0.6 mW/m3, p=0.001), total KE (HC: 51.98±22.063 J/m3 vs. AF: 22.21±10.86 J/m3, p<0.001), and total EL (HC: 17.90±12.96 W/m3 vs. AF: 4.90±1.75 W/m3, p<0.001). Vortical LA flow patterns were observed in all subjects and reliably followed a clockwise rotation pattern (viewed from ventricular side). Patients with AF demonstrated broader, more complex, and fractionated vortical flow patterns than HC. Maximum detected vortex size showed smaller vortices in HC as compared with AF patients (7.83±4.05 mm3 vs. 11.5±3.3 cm3, p=0.031).

Conclusion: This sentinel study demonstrated the quantification of viscous energy loss and vortex flow as derived from 4D flow MRI. The significant decrease in KE in AF patients may indicate the presence of a pressure overload in the LA. The reduced EL may indicate the presence of turbulent flow contributing to energy loss by turbulent dissipation. Such reduced LA energetics could potentially contribute to blood stagnation (flow stasis) and consequent LA thrombosis in AF patients. Reported results may support a potential prognostic role of LA vortex flow analysis in patients with atrial disease.

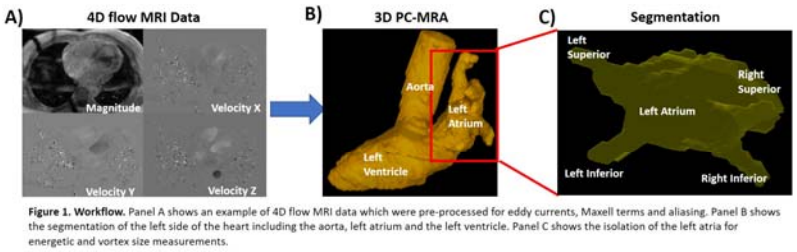

Figure 1. Workflow. Panel A shows an example of 4D flow MRI data which were pre-processed for eddy currents, Maxell terms and aliasing. Panel B shows the segmentation of the left side of the heart including the aorta, left atrium and the left ventricle. Panel C shows the isolation of the left atria for energetic and vortex size measurements.

Figure 1

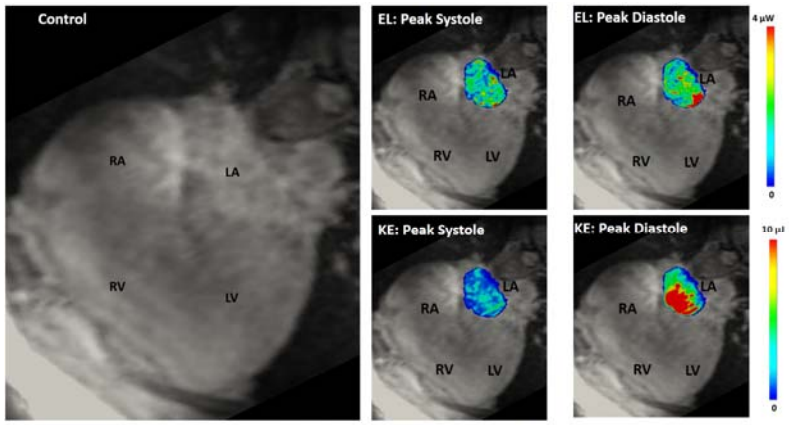

Figure 2. 4D flow energetics in a healthy control. RA: right atria; RV: right ventricle; LA: left atria; LV: left ventricle; EL: viscous energy loss; KE: kinetic energy.

Figure 2

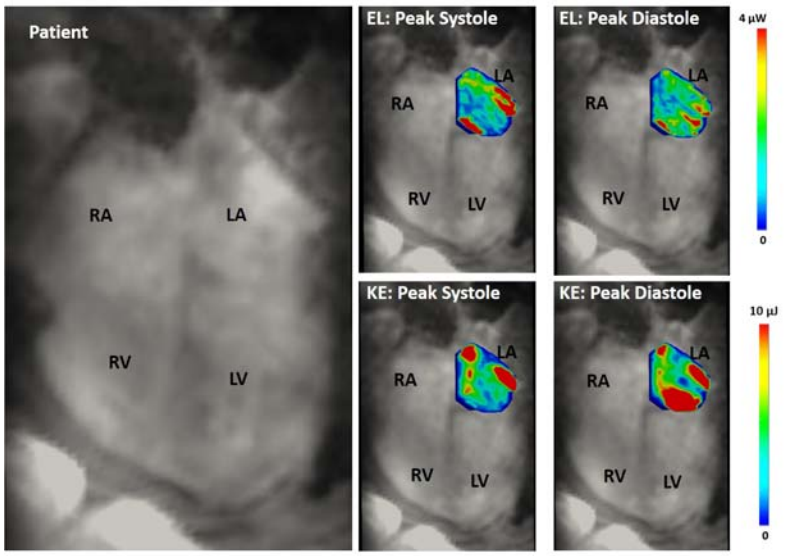

Figure 3. 4D flow energetics in a patient with atrial fibrillation. RA: right atria; RV: right ventricle; LA: left atria; LV: left ventricle; EL: viscous energy loss; KE: kinetic energy.

Figure 3

ID#: 372525

Effect of lipid storage and left ventricular hypertrophy on systolic strain in Fabry Disease

Antonia Camporeale, MD[1]Francesco Calvo, MD[2], Natalia Cobo Gomez, MD[3], Maurizio Pieroni, MD, PhD[4], Federico Pieruzzi, MD[5], Paola Lusardi, MD[6], Marco Spada, MD[7], Renzo Mignani, MD[8], Alessandro Burlina, MD[9], Silvia Pica, MD[10], Valentina Milani, PhD[10], Andreas Greiser, PhD[11], Massimo Lombardi, MD[12]

1. IRCCS Policlinico San DOnato, Milano, Italy

2. IRCCS Policlinico San Donato, Milano , Milan, Italy, Italy

3. QuironSalud Group Sagrado Corazón, Sevilla, Andalucia, Spain

4. ASL8 Arezzo San Donato Hospital Via Pietro Nenni, 20, Toscana, Italy

5. ASST Monza - San Gerardo Hospital, Lombardia, Italy

6. San Giovanni Bosco Hospital, Torino, Piemonte, Italy

7. Department of Pediatrics, University of Torino, Piemonte, Italy

8. Infermi Hospital, Rimini, Italy, Emilia-Romagna, Italy

9. S. Bassiano Hospital, Bassano del Grappa (VI), Italy, Italy

10. IRCCS Policlinico San Donato, Italy

11. Siemens Healthcare GmbH, Erlangen, Germany, Germany

12. IRCCS Policlinico San Donato, Milan, Italy, Lombardia, Italy

Background: Fabry disease (FD) is a rare lysosomal storage disorder. Sphingolipid accumulation in myocardial tissue and progressive left ventricular hypertrophy (LVH) lead to diastolic dysfunction and arrhythmias. Deterioration of systolic function, expressed as Global Longitudinal Strain by speckle tracking echocardiography, has also been described in patients with overt cardiac involvement. Cardiac Magnetic Resonance (CMR) allows both lipid storage detection by T1 mapping and functional evaluation by Feature Tracking. We aim to explore by CMR the link between progressive changes in myocardial structure and systolic strain parameters in a cohort of Fabry patients.

Methods: CMR (1.5T, Siemens Magnetom Aera) was performed in 54 patients with genetic diagnosis of FD (mean age 40±16, 22 M). LVH was defined as elevated indexed LV mass (LV mass ind) based on body surface area normalized cut-off values for age and gender. Native T1 value was measured using prototype ShMOLLI in the septum (average between short axis and horizontal long axis measurement). Low native T1 was defined as more than 2 SD below normal reference values (968±32 msec for males, 956±27 msec for females). Systolic strain parameters (peak global longitudinal, radial and circumferential; GLS, GRS, GCS) were obtained by contouring cine images, using dedicated post-processing software (Qstrain, Medis, Leiden). Results were compared with 9 healthy controls (mean age 45±15 years, 7 males).

Results: 27/54 patients (50%, mean age 46±16, 15 M) showed LVH (LVH+), all of them with low T1 value. Among patients without LVH (LVH-, mean age 35±16, 7M), 11 (41%) had low T1. GLS, GRS e GCS exhibited significant correlation with LM mass ind; correlation was positive for GLS (r 0,4; p 0,001) and GCS (r 0,4; p 0,008) and negative for GRS (r -0,35; p 0,01). T1 showed a negative correlation with GLS (r -0,4; p 0,006) and GCS (r -0,3; p 0,02) and a positive correlation with GRS (r 0,3 p 0,04). A progressive impairment of GSL, GRS and GCS was found comparing LVH+patients vs LVH-/lowT1 vs LVH-/normal T1, although without significant differences among groups (Figure 1). Strain values did not significantly differ among LVH-/normalT1 patients and controls while LVH-/lowT1 patients had a significantly higher value of GLS compared to controls (-18,1% vs -21,4%; p 0,02).

Conclusion: Sphingolipid storage in Fabry Disease leads to progressive impairment of systolic strain together with development of tissue and structural changes. GLS is significantly affected, compared to controls, in Fabry patients with lowT1 value even before manifestation of LVH.

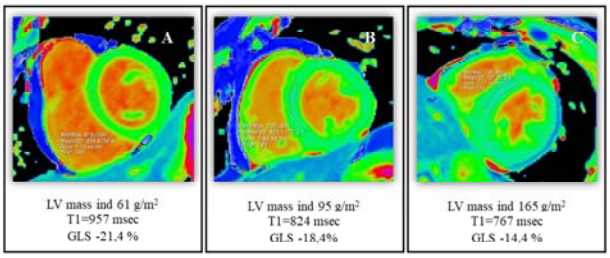

Figure 1. Progressive impairment of GLS according to increase in LV mass ind and decrease in T1 value in Fabry patients LVH-/normalT1 (A), LVH-/lowT1 (B) and LVH+/lowT1 (C).

Figure 1

ID#: 372573

Insulin resistance modifies the therapeutic effect of Omega-3 Acid Ethyl Esters on Left Ventricular Remodeling After Acute Myocardial Infarction: The OMEGA-REMODEL Randomized Clinical Trial.

Kana Fujikura, MD, PhD[1] Bobby Heydari, MD, MPH[2], Shuaib Abdullah, MD[3], Kyoichi Kaneko, MD, PhD[4], William Harris, PhD[5], Jiazuo H. H. Feng, MD[6], Michael Jerosch-Herold, PhD[7], Raymond Kwong, MD, MPH[8]

1. Brigham and Women's Hospital, Boston, MA

2. Stephenson Cardiac Imaging Centre, Libin Cardiovascular Institute of Alberta, University of Calgary, AB, Canada

3. University of Texas-Southwestern Medical Center

4. Brigham and Women's Hospital and Showa University, Brookline, MA

5. Sanford School of Medicine, University of South Dakota

6. Dartmouth-Hitchcock Medical Center

7. Harvard Medical School, Boston, MA

8. Brigham and Women's Hospital, MA

Background: Diabetes is associated with marked worsened outcomes after acute myocardial infarction (AMI). In the OMEGA-REMODEL trial, our group demonstrated that omega-3 fatty acid treatment (O-3FA) attenuated adverse left ventricular (LV) remodeling during the first 6 months after AMI via potential suppression of myocardial inflammation. This study hypothesizes that insulin resistance represents an underlying effect modifier to the response to O-3FA after AMI.

Methods: In this post-hoc sub-study, 203 AMI patients were categorized by presence of insulin resistance using median values of the following parameters: leptin to adiponectin ratio (LA), proinsulin to c-peptide ratio (ProC), linoleoylglycerophosphocholine level (LGP), and insulin resistance index (IRI). The effect modification of O-3FA treatment was also evaluated based on baseline serum insulin level. Within each parameter, degree of reduction in LV end-systolic volume index (LVESVI) and ejection fraction (LVEF) from baseline to post-treatment were compared between O-3FA and placebo group. Regression model was created to assess the correlation between the degree of change in serum O-3 index and LVESVI.

Results: As shown in images 1 and 2, insulin resistance as evident by high LA and ProC levels both attenuated the significant reduction of LVESVI and improvement of LVEF, from O-3FA treatment. Patients with insulin resistance based on a high LA also experienced an attenuated resolution of non-infarct myocardial extracellular volume expansion (-0.0018 vs. -0.0036, p = 0.87), compared to patients with a low LA (-0.023 vs. 0.016, p = 0.0054) (Image 3).

Conclusion: During the convalescence phase of acute infarct healing, insulin resistance appears to be an important modifying factor to the therapeutic response to O-3FA treatment towards improvement of LVESVI, LVEF, and non-infarct myocardial fibrosis.

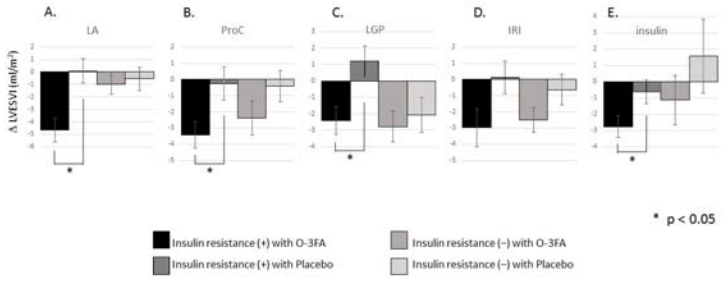

Change in LVESVI value from baseline to post-treatment of this study.

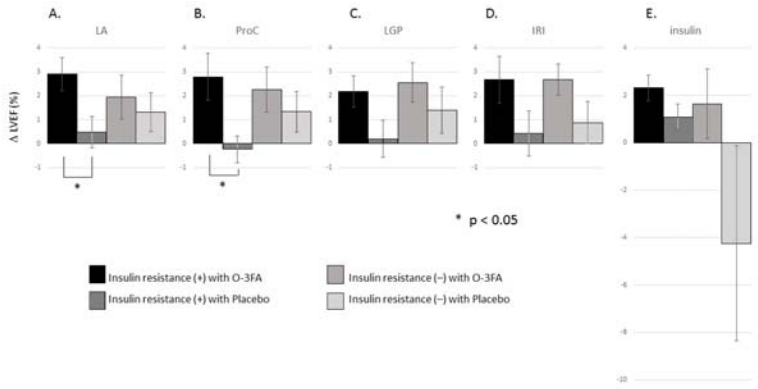

Change in LVEF value from baseline to post-treatment of this study.

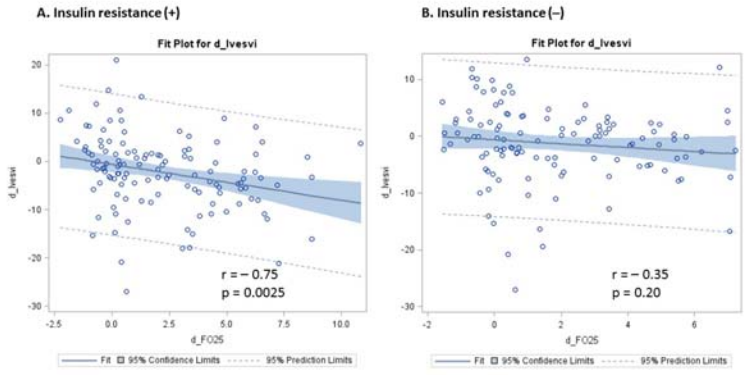

Scatter plot of difference in omega-3 index and LVESVI in patients with and without insulin resistance based on leptin to adiponectin ratio (LA).

ID#: 372604

Impact of Large Hiatus Hernia on Cardiac Function. An observational cohort study by Cardiac Magnetic Resonance.

Pamela Milito, Pamela.milito[1] Massimo Lombardi, MD[2], Emanuele Asti[3], Gianluca Bonitta[3], Francesco Bandera[3], Luigi Bonavina[3]

1. Università degli studi di Milano, Lombardia, Italy

2. IRCCS Policlinico San Donato, Milan, Italy, Lombardia, Italy

3. Università degli Studi di Milano, Lombardia, Italy

Background: Large hiatus hernia is defined as the presence of at least one third of the stomach in the chest and it is often associated with cardiorespiratory symptoms like post-prandial dyspnea, palpitations or chest discomfort. Our hypothesis was that large hiatus hernia interfers on mechanical heart performance, in particular after meal.

Methods: A prospective cohort study was conducted using cardiac magnetic resonance imaging to investigate how the herniated stomach in the chest affects cardiac chambers. Primary outcome was assessment of left atrial volumes variations before and after surgical repair. Between September 2014 to December 2016, 35 patients underwent cardiac magnetic resonance in the fasting state and after a standardized fatty meal, before and 3-months after laparoscopic repair.

Results: There were 31 females, mean age was 70.6 ± 9.1 years. None of the patients reported history of cardiac ischemia. Post-prandial dyspnea, chest discomfort and palpitations were reported by 74.3% of the patients.There was remarkable negative inversion of the delta-value of left atrial volumes before and after surgical repair (Δ Pre-operative 2.42 ± 12.65; Δ Post-operative -3.65 ± 8.05, p=0.018). A significant reduction was found only for right ventricle in end-diastolic volume (p=0.032), although an overall clinical trend in reduction of volume of the cardiac chambers (left and right atrium in end systole, and left ventricle in end diastole) was noted. In addition, both the left ventricle stroke volume (p=0.012) and the ejection fraction (p=0.010) were significantly reduced. Hiatal hernia size increased significantly after meal from 266.58 ± 316.12 ml to 325.64 ± 360.94 ml (p<0.010). There was a weak negative correlation between the ejection fraction of both ventricles and hernia size (p=0.051 for left ventricle, p=0.023 for right ventricle); in contrast, atrial volumes and stroke volumes were not related to hernia size (p=ns). After surgical repair, the standard fatty meal induced a statistically significant increase in left atrial volume (p=0.029), left ventricle volumes, both end-diastolic (p=0.010) and end-systolic (p=0.009) phases, and right ventricle end-systolic volume (p=0.046).

Conclusion: The global function of the heart was significantly impaired by a standardized meal in the presence of large hiatus hernia. Restoration of the cardiac physiological status and improvement of clinical symptoms were noted after surgical repair. Cardiac magnetic resonance with a challenge meal should be proposed to screen symptomatic patients with large hiatus hernia who may benefit from surgery.

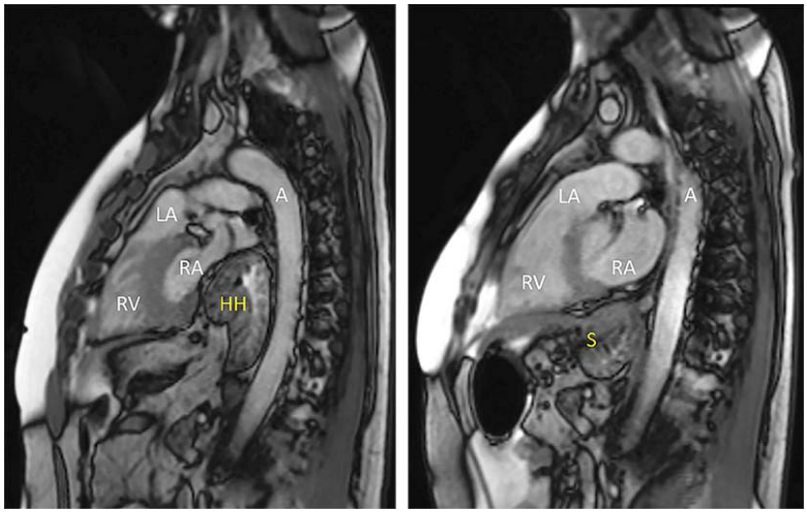

CMR images of hiatal hernia before and after surgical repair (A: Aorta, HH: Hiatal Hernia, LA: Left Atrium; RA: Right Atrium, RV: Right Ventricle, S:Stomach)

ID#: 372664

Magnetic Resonance Adenosine Perfusion Imaging as Gatekeeper of Invasive Coronary Intervention (MAGNET) - Results of the Randomized Controlled Trial

Dominik Buckert, M.D.[1] Simon Witzel[2], Wolfgang Rottbauer, M.D.[3], Peter Bernhardt, M.D.[4]

1. University Hospital Ulm, Neu-ulm, Bayern, Germany

2. University Hospital Ulm, Germany

3. Dept. Internal Medicine II, University Hospital Ulm, Baden-Wurttemberg, Germany

4. Heart Clinic Ulm, Ulm, Baden-Wurttemberg, Germany

Background: Cardiac magnetic resonance imaging (CMR) plays an increasing role in diagnosis and risk stratification of coronary artery disease (CAD) patients. With most studies focusing on diagnostic accuracy and prognostic value, evidence from trials prospectively evaluating its role in clinical pathways and decision processes is limited. Objective was the prospective and randomized evaluation of a CMR based management strategy for patients with stable CAD in comparison to a coronary angiography based approach.

Methods: Symptomatic stable CAD patients were randomized to diagnostic coronary angiography (group one) or to initial evaluation by adenosine stress CMR (group two). Subsequent revascularization was performed according to the results of the index procedure. Symptom burden and patient satisfaction were assessed by the Seattle Angina Questionnaire at baseline and during follow up.

Results: Two hundred patients were enrolled. Follow up of 3 years was completed in n=194 cases (97.0%). In group one, n=45 (45.9%) revascularizations were performed at initial examination. In group two, n=27 (28.1%) patients had myocardial ischemia on CMR and thus were referred to revascularization. Patients of both groups reported a moderate physical limitation and worse angina stability at initial assessment. At 12 months follow up, n=7 primary endpoints occurred (group 1: n=3, event-rate: 3.1%, group 2: n=4, event-rate: 4.2%, p=0.72). Patients of both arms showed improvement in angina stability, angina frequency and quality of life. There were significant differences in several SAQ scales in favor of group two. In the further course of the trial, a higher rate of cardiac endpoints occurred in group two resulting in failure to prove non-inferiority after 3 years.

Conclusion: A CMR based strategy for the management of patients with stable CAD was safe, reduced revascularization procedures and resulted in good symptom control at 12 months follow up. Optimal timing for re-assessment remains to be investigated.

ID#: 372430

We don't know how to measure wall thickness in HCM -Time for a guideline?

Gabriella Captur, MD PhD MRCP MSc[1] Charlotte Manisty, MRCP PhD[2], Rina Ariga, MBBS, MRCP[3], Ilaria Lobascio, MD[4], Claudia Camaioni, MD[5], Jenade Bonsu-Ofori, MSc[6], Shiro Nakamori, MD, PhD[7], Anish N. Bhuva, MRCP MBBS[8], Vlad Zaha, PhD[9], Timothy C. Wong, MD MS[10], Arthur Nasis, PhD[11], Mouaz H Al-Mallah, MD Ms[12], Sinitsyn Valentin, PhD[13], Diego Perez de Arenaza, MD[14], Iacopo Olivotto, MD[15], Raymond Y. Kwong, MD, MPH[16], Stefan Neubauer, MD, FRCP[3], Guy Lloyd, MD FCRP[2], Petros Nihoyannopoulos, MD[17], James Moon, MD[18]

1. Barts Heart Centre, London, England, United Kingdom

2. Barts Heart Centre and University College London, United Kingdom

3. University of Oxford, England, United Kingdom

4. Barts Heart Centre, United Kingdom

5. Barts Heart Center, London, England, United Kingdom

6. University College London, England, United Kingdom

7. Beth Israel Deaconess Medical Center, MA

8. Barts Heart Centre and Institute of Cardiovascular Science, UCL., London, England, United Kingdom

9. UT Southwestern, TX

10. University of Pittsburgh Medical Center, Pittsburgh, PA

11. Monash Heart, Australia

12. King Saud bin Abdulaziz University for Health Sciences, King Abdullah International Medical Research Center, King ABdulAziz Cardiac Center, Ministry of National Guard, Health Affairs, Saudia Arabia, Saudi Arabia

13. Federal Center of Medicine and Rehabilitation, Moscow, Moskva, Russia

14. Hospital Italiano de Buenos Aires, Buenos Aires, Argentina

15. Careggi University Hospital, Italy

16. Brigham and Womens Hospital, Boston, MA

17. Hammersmith Hospital, London, United Kingdom, England, United Kingdom

18. UCL, England, United Kingdom

Background: The left ventricular maximal wall thickness (MWT) is a daily part of our work. In hypertrophic cardiomyopathy (HCM), diagnostic thresholds, risk stratification and major treatment decisions depend upon it. However, measurement consistency has been questionable with a lack of established supporting guidelines. Differences may be down to modality (echocardiography[ECHO]/CMR), image quality, geography (US/European guidelines), and levels of interpretative experience.
We sought to define variability in HCM WT measurement. We did this in a standardized way–using excellent image quality, 2 modalities, and experienced readers from many countries.

Methods: *Datasets:* We assembled paired CMR and ECHO datasets from 20 centers worldwide. Only excellent images were kept. *Viewing platform:* Images were uploaded to a DICOM viewer with user interface for caliper measurement, and presented on a 15-inch laptop. We planned for a 15 minute analysis and for caliper data to export directly to Matlab for processing. *Grading:* Grading was conducted in 2015/2016 at 2 global single modality conferences (EuroECHO, SCMR) and one global cardiology congress (ESC). This used a face-to-face meeting and targeted the most senior imagers.

Results: *Graders:* 69 readers from 6 continents completed the analysis. 36%, 17% and 41% had respectively <5, 5-10 and >10yrs as full time imaging faculty. 33% were heads of department, service leads or international guideline committee members. *Measurements:* 63% and 78% of graders respectively, scored the CMR and ECHO image quality as excellent. For every HCM case, MWT measurements between modalities showed large inter-observer scatter and low intraclass correlation (ICCs from 0.23[95%CI, -0.33-0.58] to 0.73[0.62-0.81]). We presented 2 identical datasets twice (**Fig1**) to measure intra-observer scatter. These ICCs were better (CMR, 0.80 [0.70-0.88]; ECHO, 0.70 [0.53-0.83]). CMR measured thicker than ECHO (by ~4 mm, **Fig2,3**) and we observed greater inclusion of the septomarginal trabeculum by CMR compared to ECHO (127 vs 47, P<0.0001). Cross-modality agreement of MWT was better between US readers than Europeans (0.92 [0.81-0.99] vs 0.76 [0.69-0.82])

and better for senior readers than those with less experience (<5yrs, ICC, 0.92 vs 0.69). MWT discrepancies between CMR and ECHO, caused 2% of cases to be mis-stratified by the 30 mm risk threshold (47% due to CMR measuring higher).

Conclusion: Measurement of WT in HCM using best available image quality is currently a suboptimal test. Its repeatability is acceptable at best, poor at worst. Standardization of the MWT measurement method in guidelines, from current governing societies, is imperative and it may impact downstream patient decisions

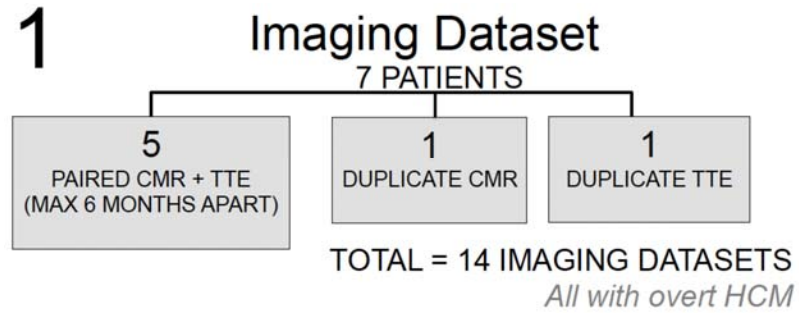

Organisation of the test dataset .

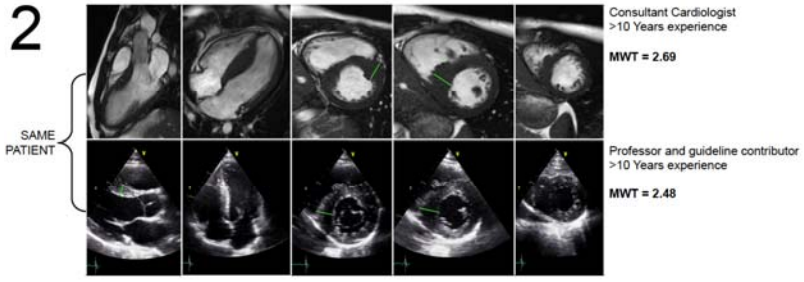

Snapshots of caliper measurements applied by readers.

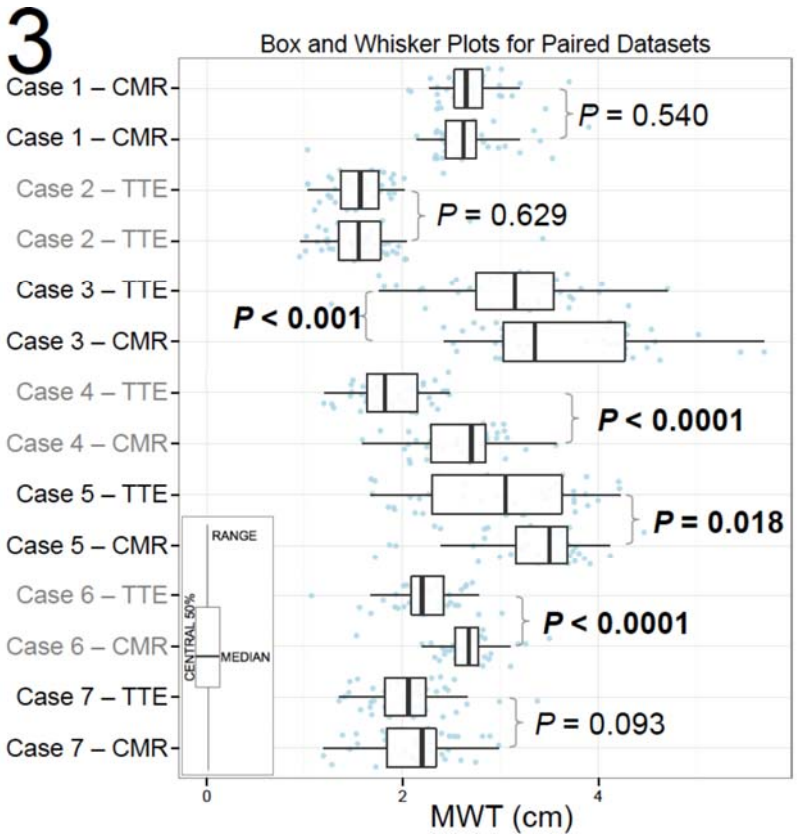

Box and whisker plots comparing maximal wall thickness (MWT) between pairs of HCM datasets (CMR and echo [TTE]). The first two datasets are identical duplicates of the same scan.

ID#: 372017

Fully Quantitative 3D Dynamic Contrast Enhanced (DCE) Imaging of Carotid Vessel Wall by Fast T1 Mapping

Nan Wang, M.S.[1] Anthony G. Christodoulou, PhD[2], Yibin Xie, PhD[2], Zixin Deng, M.S[2], Bill Zhou, B.S.[3], Wei Yu, M.D, Ph.D[4], Debiao Li, PhD[2]

1. Cedars-Sinai Medical Center/UCLA, Los Angeles, CA

2. Cedars-Sinai Medical Center, Los Angeles, CA

3. Cedars-Sinai Medical Center

4. Department of Radiology, Anzhen Hospital, Capital Medical University, Beijing, China (People's Republic)

Background: Dynamic contrast enhanced (DCE) CMR of the carotid vessel wall is a promising method for assessing the density and permeability of the vasa vasorum, which plays a significant role in the plaque inflammatory processes and disease progression[1]. However, carotid vessel wall DCE is yet widely utilized due to tough technical challenges: 1) it is difficult to simultaneously achieve submillimeter spatial resolution, adequate anatomical coverage, and temporal resolution at the same time, so current methods sacrifice one or more of these aspects[2,3]; 2) the nonlinearity between CMR signal intensity and contrast agent concentration can introduce errors in kinetic modeling. In this work, we developed a 3D DCE CMR method by dynamic T1 mapping with 0.7mm isotropic spatial resolution, 0.59s temporal resolution, and coverage of the entire carotid vasculature.

Methods: The proposed method employed the low-rank tensor (LRT) model[4]. Continuous scanning with non-selective SR prep followed by FLASH readout generated the T1 contrast dynamic change (Figure 1A). T1 mapping allowed direct contrast agent concentration quantification. A 3D Cartesian sampling pattern was implemented with randomized reordering in ky and kz directions (Figure 1B). The center k-space line was collected every 8 readout lines as LRT subspace training data[4]. Images were formulated as a 3-way tensor □ with voxel dimension **r** = (*x,y,z*), SR time □, and DCE time *t*. Correlation across the dynamic series allowed the tensor to be factorized as $\mathbf{A}_{(1)} = \mathbf{U\Phi}$. **Φ**, the weighted product of temporal basis functions describing T1 relaxation and contrast agent dynamics, is first determined from the subspace training data[4]. **U**, which contains spatial coefficients, is then recovered by fitting **Φ** to the remainder of the sparsely sampled data[4]. All data were acquired on a 3T Siemens Verio scanner from 12 healthy volunteers and 6 patients with known carotid atherosclerosis using: coronal orientation, FA=8º, echo spacing=11ms, temporal footprint=595ms, spatial resolution=0.7mm isotropic, FOV=150x150x26mm^3, scan time=9min. Gd contrast media was administered at the rate of 1.0ml/s (Gadovist, 0.1mmol/kg).

Results: Carotid DCE using the proposed method was successfully carried out in all subjects. Figure 2A shows a representative image set of high-resolution multi-phase DCE images from a healthy subject. Figure 2B shows the real-time signal evolution and quantification of contrast concentration. Figures 2C and 2D are examples of resultant kinetic parameter mapping in a healthy volunteer and a patient, respectively. Table 1 summarizes the statistical comparison of kinetic parameters between healthy volunteers and patients with known carotid atherosclerosis. Significant elevation was observed in patients for AUC, Ktrans, and Vp, suggesting increased vasa vasorum permeability and fractional plasma volume.

Conclusion: A novel high-resolution 3D DCE method based on dynamic T1 mapping was developed for imaging carotid vessel wall. Preliminary studies on healthy volunteers and patients with known carotid atherosclerosis demonstrated the feasibility to achieve high spatiotemporal resolution and large anatomical coverage at the same time. Further comparison with conventional DCE technique and validation with histology are warranted.

Reference:

1. Kerwin et al *Circulation* 2003
2. Dong et al *Radiology* 2011
3. Calcagno et al *NMR Biomed* 2015
4. Christodoulou et al ISMRM 2016

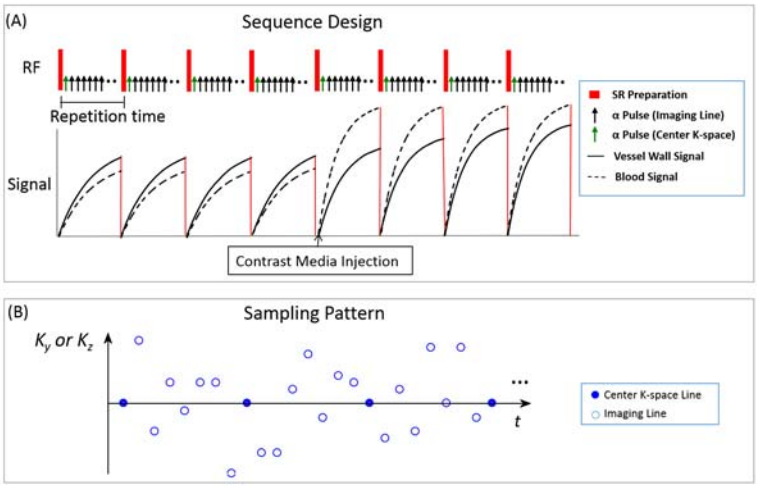

FIG. 1. (A): pulse sequence scheme for accelerated 3D DCE and corresponding simulated signal evolution for vessel wall and blood. Saturation recovery preparation is applied every TR followed by a 8º FLASH echo train. The entire k-space is traversed for 7 times with randomized sampling pattern. (B): simplified illustration of k-space sampling strategy. 3D Cartesian acquisition with randomized reordering in ky and kz directions is implemented according to a variable-density Gaussian distribution. A center k-space line is acquired every 8 readout lines as the LRT subspace training data.

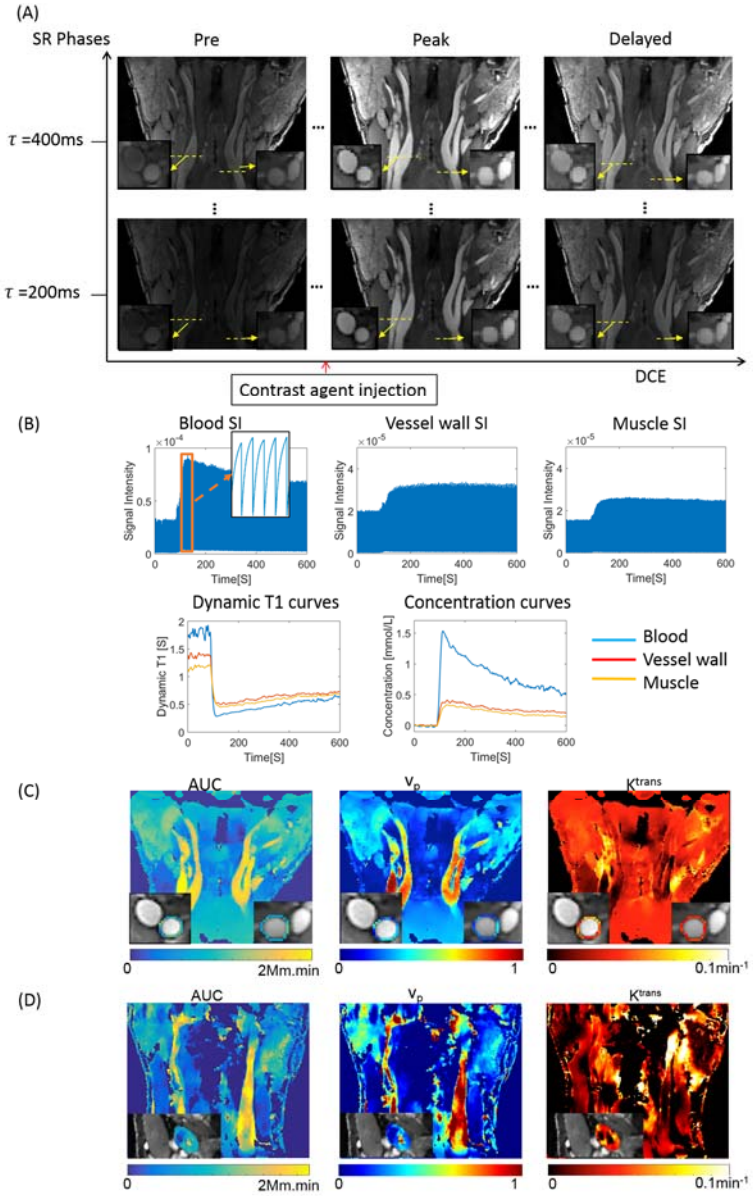

FIG. 2. (A): Representative image set of high-resolution 3D DCE of the carotid arteries. (B): Real-time signal evolution and conversion from CMR signal to contrast agent concentration in blood, vessel wall and muscle. (C): Typical kinetic parameter mapping in a healthy volunteer. (D): Typical kinetic parameter mapping in a patient.

Comparison of kinetic model parameters between healthy volunteers and patients with known carotid atherosclerosis

	Vp	Ktrans (min^{-1})	AUC (mM·min)
Control	0.1575±0.0377	0.0576±0.0108	0.6250±0.1099
Patient	0.2016±0.0546	0.0691±0.0145	0.9028±0.1340
P value	<0.01	0.011	<0.01

ID#: 372443

Whole-heart k-t PCA accelerated multi-venc 4D Flow CMR - a study in 45 healthy volunteers

Jan Robert Kroeger[1] Francesca Pavesio[2], Kilian Weiss, PhD[3], David Maintz, MD[4], Alexander Christian. Bunck, M.D.[4], Bettina Baeßler, M.D.[4], Daniel Giese, PhD[5]

1. University Hospital Cologne, Germany

2. University Hospital Cologne, Nordrhein-Westfalen, Germany

3. Philips Healthcare, Hamburg, Germany, Nordrhein-Westfalen, Germany

4. University Hospital of Cologne, Department of Radiology, Nordrhein-Westfalen, Germany

5. University Hospital Cologne

Background: Despite a recently published 4D Flow CMR consensus statement, the adoption of 4D Flow imaging into clinical routine is still hampered by its long scan times and limited accuracy for a wide range of velocities. The current study aims at demonstrating the feasibility of highly accelerated 4D Flow CMR in combination with a multi-venc acquisition technique tackling both of these issues.

Methods: 45 healthy volunteers were scanned on a 3 T Ingenia system (Philips, Best, the Netherlands) using a 32 channel surface coil. 4D flow measurements were obtained in a sagittal FOV covering the heart and its surrounding vessels leading to an average net acquisition time of 14 minutes. Mean scan parameters are presented in Table 1. Three vencs were acquired and reconstructed using a Bayesian unfolding algorithm to yield a single velocity/phase image per direction and a magnitude image. Additionally, a single-venc dataset (corresponding to the largest venc used) was reconstructed and quantitative flow parameters were compared.
3 regions of interest (ROI) were placed and analyzed (GTFlow Version..3.0, Gyrotools, Zurich, Switzerland): in the ascending aorta (AAo), in the main pulmonary artery (MPA), and in the left (LPA) and right (RPA) pulmonary artery. Differences in stroke volumes between AAo and MPA as well as between MPA and LPA+RPA were calculated. Moreover, particles were ejected in the MPA and their arrivals were counted in the LPA and RPA, approximately 1 cm downstream of the bifurcation. Loss of particles was calculated.

Results: The differences between stroke volumes in AAo and MPA were significantly lower in multi-VENC datasets compared to single-venc datasets (9,6 ± 7,8 ml vs. 25,4 ± 26,4 ml, $p<0.001$). A similar trend was found when comparing stroke volumes between MPA and LPA+RPA (7,2 ± 5,7 ml vs. 17,3 ± 10,5 ml, $p<0.001$). The loss of pathlines between MPA and LPA+RPA was significantly higher in the single-venc images compared to the multi-venc datasets (34,8 ± 18,4 % vs. 18,9 ± 7,5 %, $p<0,005$). On visual analysis, the multi-VENC datasets showed a more homogenous flow field and allowed for a better flow visualization with reduced pathline loss (Fig. 1).

Conclusion:

Multi-VENC 4D flow acquisition of the whole heart is feasible with an acceptable scan duration when using k-t acceleration. Mass conservation shows highly significant improvements in flow volumes and pathline statistics compared to a single-VENC acquisition. The presented acquisition may lead the pathway towards a translation of 4D flow CMR into clinical routine.

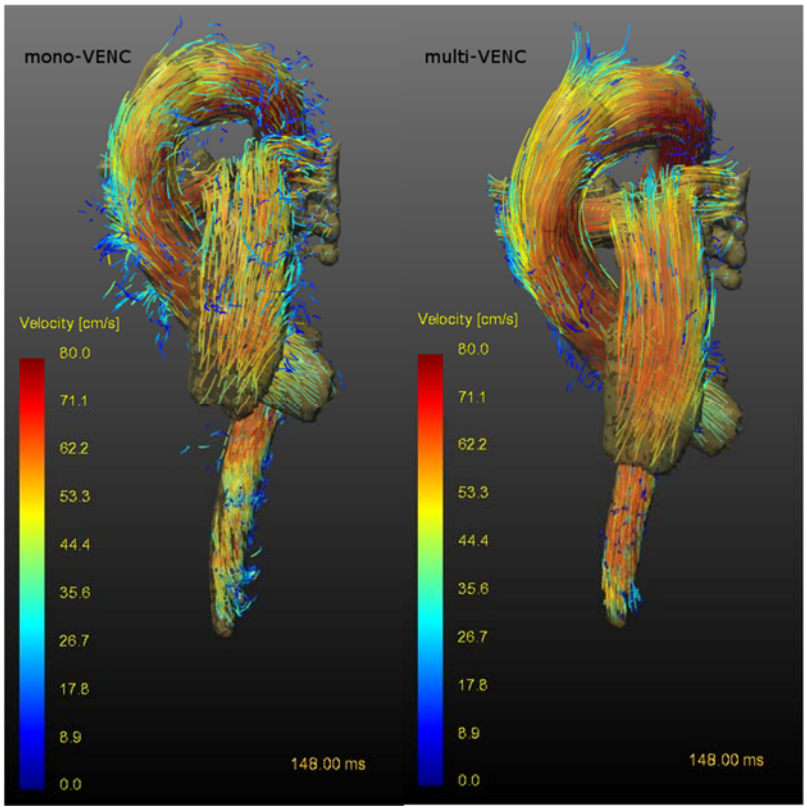

Figure 1: Example of particle traces ejected in the aorta and the pulmonary arteries of a single-venc (left) and multi-venc (right) reconstruction. Cleaner pathlines can be qualitatively observed in the multi-venc acquisition.

Table 1: Main scan parameters used. The net acceleration factor includes half-scan, a k-t space shutter and a nominal acceleration factor of 8. The net scan time includes the navigator efficiency (i.e., the nominal scan time was in the order of 7 minutes).

Venc [cm/s]	Net acceleration factor	Net scan time [min]	Breathing Navigator Efficiency [%]	Heart Phases	Resolution [mm^3]	Fiel of View [mm^3]
40, 100, 200	13.7 ± 1	13.8 ± 3.9	53.5 ± 11.1	24	2.5	247.8 ± 19.6 x 277.2 ± 22.1 x 71.2 ± 9.8

ID#: 372478

Segmental Longitudinal Myocardial Strains Can Distinguish The Healthy, Area-at-risk and Infarcted Myocardial Segments In Acute Ischaemic Reperfusion Injury

Salomon Narodden[1]Nicoleta Baxan[2], Sian Harding[2]

1. Imperial College London, London, England, United Kingdom

2. Imperial College London, United Kingdom

Background: An accurate assessment of myocardial disease phenotype is paramount in the fields of cardioprotection and regeneration. After ischemia-reperfusion MI (I/R-MI), myocardial segments could be permanently infarcted, or at risk for infarction (AAR; theoretically salvageable) or normal. The three segmental phenotypes could be respectively distinguished: (1) LGE positivity, (2) no LGE with abnormal T2 values and (3) no LGE with normal T2 values. It is hypothesized that the peak segmental longitudinal (LS) could distinguish the diseased phenotypes and the LS in (3) is different compared to segments from normal rats (4).

Methods: I/R-MI Lewis rats (96 segments, 5 rats) and normal rats (84 segments, 5 rats) were imaged using IntraGate Cine-high-frame rate at 60 frames per R-R interval of 150-170ms (Bruker-BioSpec 9.4T Ettlingen), conforming to AHA';s planes recommendations and 16-segments models. LGE was acquired using IR-FLASH (multi-slice inversion-recovery gradient-echo), area-at-risk(AAR) was assessed using T2-RARE mapping (multi-echo-spin-echo) and both series analysed in Segment (Medviso-AB, Lund). TomTec-2D CPA-MR (Unterschleissheim, Germany) was used to perform strain analysis of the three long axes views. The segments of I/R rats were assigned into either phenotype (1), (2) and (3); their LS were compared and (3) compared with (4).

Results: The three segmental phenotypes had LS characteristics: (1)mean=LS -3.07%, SE=2.75%, 32 segments, CI: -8.69 to 2.54%; (2)mean=-15.48%, SE=2.26%, CI: -20.13 to 10.83%, 27 segments and (3)mean=-26.02%, SE=1.40%, CI: -28.87 to 23.18%, 37 segments. The one-way ANOVA with Tukey';s multiple comparisons test showed: (2) versus (1): mean difference -12:41%, CI:-19.98 to -4.85%, p=0.0005; (3) versus (1): mean difference -22.95%, CI: -29.94 to -15.96%, $p < 0.0001$; and (3) versus (2) mean difference -10.54%, CI: -17.87 to -3.21%, p=0.0026. It was also observed that: (1) has paradoxical or severely reduced LS, (2) has a low LS strain or mildly low LS and (3) have a normal strain value or hyper-normal value. The post test for linear trend of the segments in I/R rats: slope -11.46, effect size R2=0.396, slope -11.46, p=0.02.

Conclusion: An abnormal segmental longitudinal strain was an indication that the segment was diseased, associated with either one or both: abnormal T2 value and LGE. A positive (paradoxical) longitudinal segmental strain was associated with transmural LGE whereas, in I/R MI, the segments with no LGE and normal T2 value could have hyper-normal strain values, an indication of compensation.

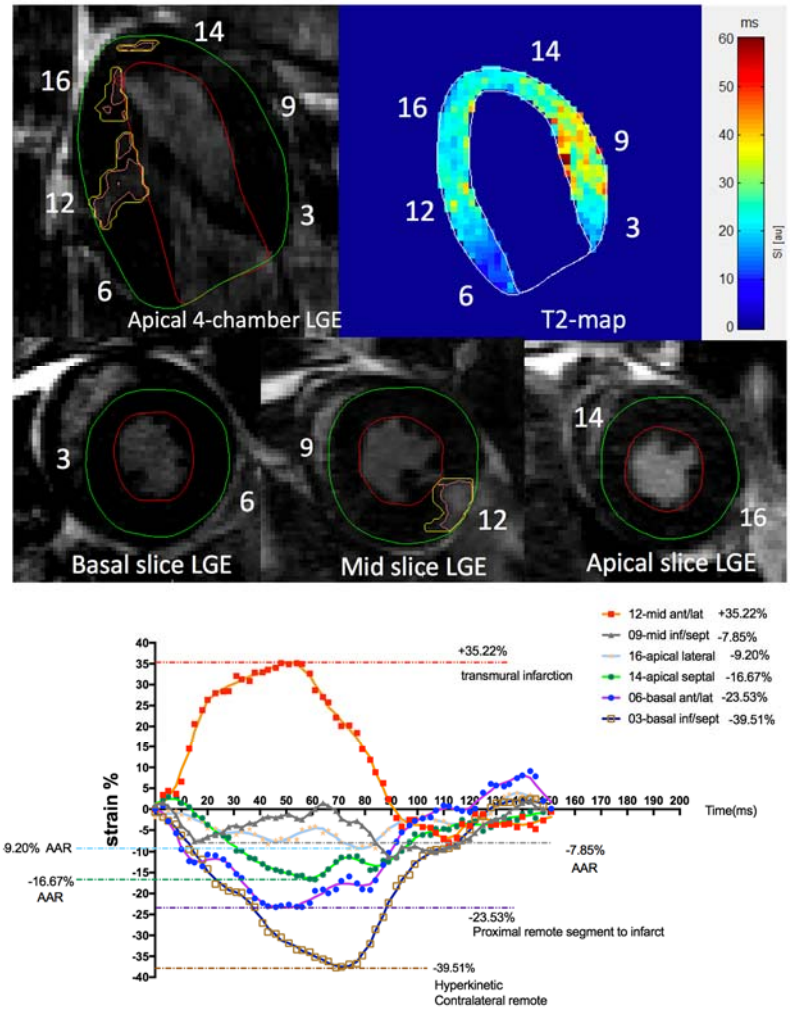

A representative example of MRI images from a rat with ischaemia-reperfusion myocardial infarction. LGE images and parametric T-2map are where indicated. Bottom picture is the segmental longitudinal strain curves of a 4-chamber view; where indicated are the peak strain values, the imaging phenotypes and the segments number according to AHA nomenclature.

Representative examples of MRI images and segmental strains

Segmental longitudinal strains according to imaging phenotypes in ischaemia-reperfusion myocardial infarction rats

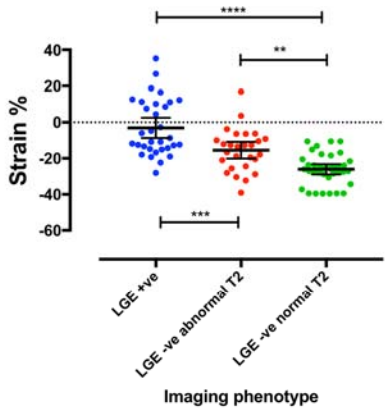

Each dot represents a myocardial segment and error bars indicate 95% confidence interval. One-way ANOVA with Tukey's multiple comparison test where ** P ≤ 0.01, *** P ≤ 0.001, and **** P≤ 0.0001

Segmental longitudinal strains in ischamia-reperfusion myocardial infarction rats versus segments of normal rats

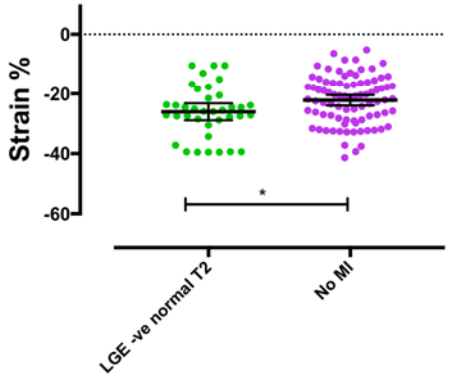

Each dot represents a myocardial segment and error bars indicate 95% confidence interval. Two-tailed t-test with Welch's correction where * P≤ 0.05

Comparative results of segmental strains according to their imaging phenotypes

Peak Segmental Longitudinal Strain according to Imaging Phenotypes

Imaging Phenotypes	LGE +ve	LGE -ve abnormal T2	LGE -ve normal T2
Number of segments	32	27	37
Minimum (%)	-28.04	-39.03	-39.51
25% Percentile	-14.69	-24.34	-29.68
Median (%)	-9.725	-13.43	-25.93
75% Percentile	10.91	-9.2	-21.01
Maximum (%)	35.22	16.92	-10.51
Mean LS strain (%)	-3.071	-15.48	-26.02
Std. Deviation	15.58	11.76	8.532
Std. Error of Mean	2.754	2.263	1.403
Lower 95% CI of mean	-8.687	-20.13	-28.87
Upper 95% CI of mean	2.545	-10.83	-23.18
D'Agostino & Pearson normality test			
K2	2.7	2.894	0.3443
P value	0.2592	0.2352	0.8418
Passed normality test (alpha=0.05)?	Yes	Yes	Yes
P value summary	ns	ns	ns

Table of peak segmental longitudinal strains according to imaging phenotypes

ID#: 372481

Differences in left ventricular volume and ejection fraction in patients with early and classic remodeling after acute myocardial infarction studied by cardiac MRI (CMR)

Martin Sinn, MD[1]Enver Guner. Tahir, MD[2], Ulf Radunski, MD[3], Maxim Avanesov, MD[4], Sebastian Bohnen, MD[5], Eric Freiwald[6], Patricia Uhlmann[7], Dennis Saering, PhD[8], Christian Stehning, PhD[9], Gerhard Adam, MD[10], Kai Muellerleile, MD[3], Gunnar Lund, MD[10]

1. Diagnostic and Interventional Radiology, University Hospital Eppendorf, Hamburg, Germany, Hamburg, Germany

2. University Medical Center Hamburg-Eppendorf, Hamburg, Hamburg, Germany

3. University Medical Center Hamburg-Eppendorg, Hamburg, Germany

4. UKE, Hamburg, Germany

5. University Heart Center Hamburg, Hamburg, Germany

6. Institute of Medical Biometry and Biostatistics, Germany

7. University Medical Center Hamburg-Eppendorf, Germany

8. FH Wedel Gemeinnützige Schulgesellschaft mbH, Hamburg, Germany

9. Philips Research Laboratories, Hamburg, Germany

10. University Medical Center Hamburg-Eppendorf, Hamburg, Germany

Background: Classic left ventricular (LV) remodeling after acute myocardial infarction (AMI) is defined as an increase of left ventricular end-diastolic volume index (LVEDVi) ≥20% within the first 3-6 months after AMI. However, some AMI patients have an initially dilated LV and show no further increase in LVEDVi during follow-up, which we defined as early remodeling. The purpose of this study was to analyze the exact course of LVEDVi with classic and early remodeling in relation to clinical characteristics.

Methods: We performed CMR in 90 consecutive patients (mean age 56 ±12 years) with reperfused first AMI to assess LV volumes, myocardial mass and function. Infarct size was obtained by late gadolinium enhancement (LGE) CMR. Patients underwent the baseline CMR 7 ±4 days after AMI. Follow-up scans were performed after 6 weeks, 3 months and 7 months. Early remodeling was defined as an increased LVEDVi >97 mL/m^2 in males and >90 mL/m^2 in females at baseline CMR.

Results: Two distinct different types of LV remodeling were observed. Eleven of 90 patients (12%) showed a classic remodeling with normal LVEDVi at baseline (75 ±14 mL/m^2), which significantly increased to 95 ±20 mL/m^2 at 7 week (*P* 2 at baseline and no further change of LVEDVi during follow-up. At baseline, patients with early remodeling had a significantly lower ejection fraction (EF) with 43 ±11 % compared to patients with classic remodeling (53 ±13%, *P* P P= ns). Time to reperfusion times showed significantly higher values for STEMI patients with early remodeling (median 26h, IQR: 6-57h) versus classic and also versus no remodeling patients (median 8h, IQR: 2-11, *P*= .037 and 3h, IQR: 2-11, *P*= .009). There were no significant differences between all three groups of NSTEMI patients.

Conclusion: Besides classic remodeling, 16% of our patientsshowed early remodeling, which is characterized by early LV dilatation after AMI and initially severely reduced EF with no recovery during follow-up. Early remodeling may result from prolonged time to reperfusion and represent a subgroup of patients at higher risk for heart failure and sudden cardiac death, requiring more intensive treatment to prevent these events.

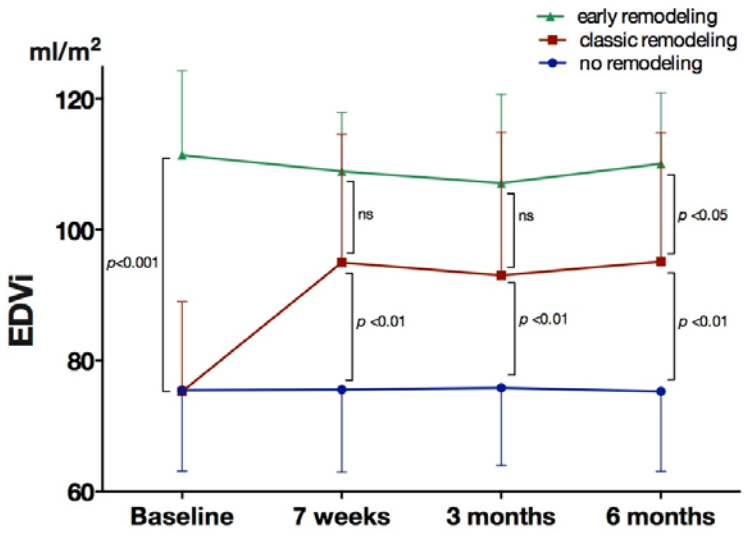

Serial development of EDVi of the different remodeling types

ID#: 371802

Physiological and clinical relevance of left atrial strain measured by feature-tracking magnetic resonance imaging in a large group of Chinese healthy volunteers and patients

Weihao Li, BMSci[1] Liuyu Yu, BMsci[2], Ke Wan, MD[3], Hong Liu[4], Jie Wang, BMSci[5], Yang Dong, BMsci[6], Jiayu Sun, MD[7], Yuchi Han, MD, MMSc[8], Yu-Cheng Chen, MD[9]

1. Cardiology Division, West China Hospital, Sichuan University, Chengdu, Sichuan, China (People's Republic)

2. Sichuan University West China Hospital, China (People's Republic)

3. Cardiology Division, West China Hospital, Sichuan University, Guoxue Xiang No. 37, Chengdu, Sichuan Province 610041, China, Sichuan, China (People's Republic)

4. Sichuan University West China Hospital, Chengdu, Sichuan, China (People's Republic)

5. Department of Cardiology, West China Hospital, Sichuan University, ChengDu, Sichuan, China (People's Republic)

6. Cardiology Department West China Hospital Sichuan University, Sichuan, China (People's Republic)

7. Sichuan University West China Hospital, Sichuan, China (People's Republic)

8. University of Pennsylvania, Philadelphia, PA

9. West China Hospital ,Sichuan University, Sichuan, China (People's Republic)

Background: Evaluation of LA is of great importance in understanding LA adaption to physiological and pathophysiological changes. The complex LA structure and function might be insufficiently described with diameters, volumes and EFs. Previous studies proposed feature tracking (FT) CMR as a promising approach to evaluate LA mechanics. We aimed to describe LA strains in a large group of Chinese healthy volunteers, HCM and HT patients, to explore the physiological factors impacting LA mechanics, and to evaluate their clinical discriminating value.

Methods: A total of 334 subjects (healthy volunteers, hypertension patients and HCM patients) were enrolled. CMR scan were performed at a 3.0-T scanner with retrospectively ECG-gated SSFP sequence during breath-holds. All CMR images were processed using Medis suit. Volume curves and longitudinal strain curves in 2ch and 4ch view and in 2ch-4ch biplane method were generated automatically after manual delineation, automatic tracking, visual inspection, manual adjustment until satisfactory. LA phasic volumes, EFs, and strains were obtained. 65(20%) subjects were randomly selected for reproducibility tests. Continuous variables were compared with ANOVA and Bonferroni's post-hoc analysis. Associations were measured by Pearson correlation. Multivariate regression was used to determine independent variables. ROC curves were used to assess discriminating values of volumes, EFs and strains.

Results: Reproducibility were good for FT-derived parameters. Biplane methods showed best reproducibility, and strains were less reproducible than EFs. Reservoir and conduit function showed significant gender differences, while booster pump function were similar. EFs and strains showed moderate correlation. Biplane EFs and strains were featured with smallest SD and highest correlation. Multivariate analysis in healthy volunteers confirmed male gender and older age independently associated with lower reservoir and conduit strain, and only older age was associated with higher booster pump strain. Considering all 3 groups, disease (HCM and hypertension), age, LVEF, and mass index were independent determinants of reservoir and conduit strains, and no single factor was significant in multivariate analysis for booster pump strains. Discriminative values of volumes, EFs, and strains were poor to fair. LA volumes had highest AUCs in most cases, while EFs had the best performance in discriminating HCM patients from HT patients.

Conclusion: We described LA strains in a Chinese population. Age and gender were independent determinants of LA mechanics in healthy volunteers. LA strain showed marked difference between healthy volunteers and patients and between patient groups. However, discriminating values of LA mechanics were less satisfactory.

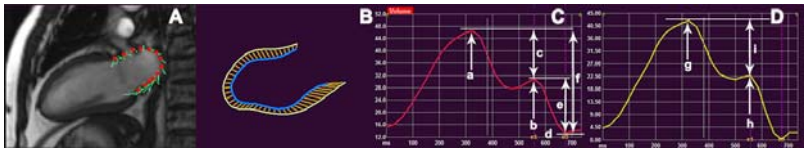

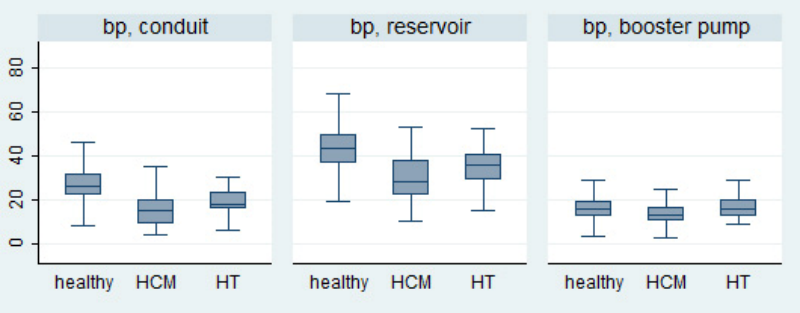

Reference values for volume phasic function& strains

	Phasic function			strain		
	2ch	4ch	biplane	2ch	4ch	biplane
Reservoir	64.2±9.1	64.5±8.3	63.7±7.7	48.1±14.5	39.6±12.3	29.3±5.5
Conduit	35.0±12.1	42.9±10.4	38.3±9.0	28.3±12.1	26.5±10.2	18.4±5.1
Booster pump	44.8±10.2	37.7±9.6	19.8±8.0	19.8±8.0	13.2±6.0	10.8±3.4

ID#: 371678

An advanced electrocardiographic prognosis score predicts heart failure hospitalization or death beyond CMR measures including global longitudinal strain and extracellular volume fraction

Maren Maanja, MD[1] Todd T. Schlegel, MD[2], Fredrika Fröjdh, MS[3], Louise Niklasson, MS[4], Björn Wieslander, MD PhD[5], Ljuba Bacharova, MD, DrS, MBA[6], Erik B. Schelbert, MD, MS[7], Martin Ugander, MD, PhD[8]

1. Karolinska Institutet, Sweden

2. Karolinska Institutet, Vaud, Switzerland

3. Institute of Karolinska, Stockholm, Stockholms Lan, Sweden

4. Karolinska Institutet, Stockholms Lan, Sweden

5. Department of Clinical Physiology, Karolinska Institutet and Karolinska University Hospital, Stockholm, Sweden, Stockholm, Stockholms Lan, Sweden

6. International Laser Center and Institute of Pathophysiology, Medical Faculty, Comenius University, Bratislava, Slovakia

7. University of Pittsburgh; Heart and Vascular Institute of UPMC, PA

8. Karolinska Institutet, and Karolinska University Hospital, Stockholm, Sweden, Stockholms Lan, Sweden

Background: Both advanced electrocardiography (A-ECG) and cardiovascular magnetic resonance (CMR) measures of function and tissue characterization are known to provide prognostic information. However, how these measures perform in relation to each other has not been studied head-to-head. Our aim was to create an A-ECG prognosis score, and compare to the prognostic value of CMR measures of function and tissue characterization.

Methods: Consecutive patients undergoing CMR at 1.5T and resting 12-lead ECG with a QRS duration <120 ms acquired within 30 days of CMR were included. CMR measures included feature tracking global longitudinal strain (GLS), infarct size by late gadolinium enhancement (LGE), non-ischemic scar size by LGE, extracellular volume fraction (ECV) in myocardium without any focal LGE, left ventricular (LV) end-diastolic volume index (EDVI), LV ejection fraction (LVEF), and LV mass index (LVMI). A-ECG analysis included conventional amplitudes and durations, derived vectorcardiographic (VCG) measures, and singular value decomposition measures of waveform complexity. An A-ECG prognosis score for 2 year survival was derived using multinomial logistic regression and bootstrapping, and compared to CMR measures with regards to survival free from hospitalization for heart failure or death using multivariate Cox regression and Kaplan-Meier analysis.

Results: Patients (n=759, median [interquartile range] age 55 [43-64] years, 43% female) had 102 events during 3.8 [2.6-4.8] years. The A-ECG prognosis score included (1) QTc, (2) VCG ST magnitude, (3) VCG ST spatial direction, (4) VCG QRS spatial direction, and (5) T-wave complexity, and had the highest univariate association with outcomes (chi^2 66, $p<0.001$) compared to all evaluated CMR measures (chi^2 10-60, $p<0.01$ for all). Multivariate analysis, where LVEF was excluded due to co-variance with GLS, showed an association with outcomes for GLS (chi^2 13.7), age (chi^2 12.1), A-ECG prognosis score (chi^2 10.6), and ECV (chi^2 6.0, $p\leq0.01$ for all; Kaplan-Meier log rank $p<0.0001$ for all, see Figures), and no significant relationship for the remaining CMR parameters. The A-ECG prognosis score was related to ECV, GLS, age and EDVI (global $R^2=0.37$, $p<0.001$).

Conclusion: In a consecutive clinical population with QRS<120 ms, a new A-ECG prognosis score provided prognostic information beyond CMR measures with known powerful prognostic performance. ECV, GLS, age and EDVI together only explained approximately one third of the A-ECG prognosis score, thus illustrating the unique and complementary prognostic information present in the ECG.

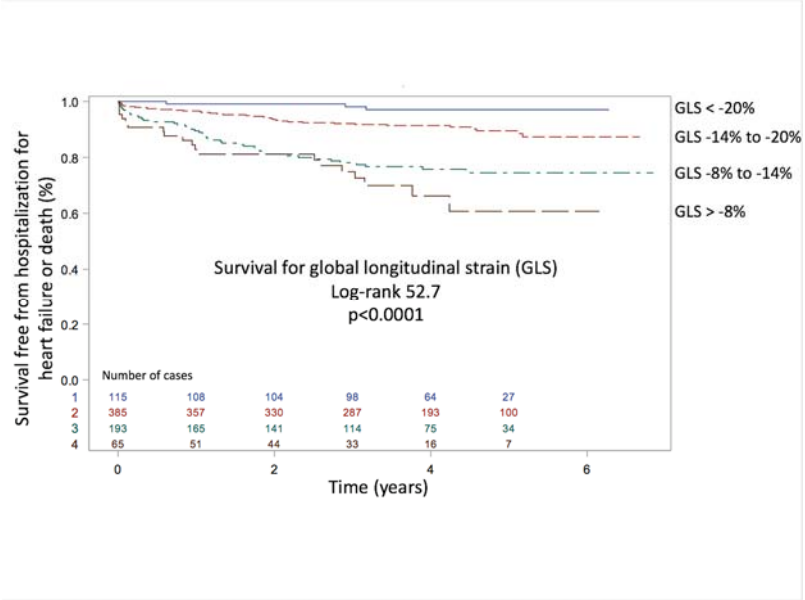
Survival free from hospitalization for heart failure or death (%)
1.0
0.8
0.6
0.4
0.2
0.0
GLS < -20%
GLS -14% to -20%
GLS -8% to -14%
GLS > -8%
Survival for global longitudinal strain (GLS)
Log-rank 52.7
p<0.0001
Number of cases
1 115 108 104 98 64 27
2 385 357 330 287 193 100
3 193 165 141 114 75 34
4 65 51 44 33 16 7
0
2
4
6
Time (years)

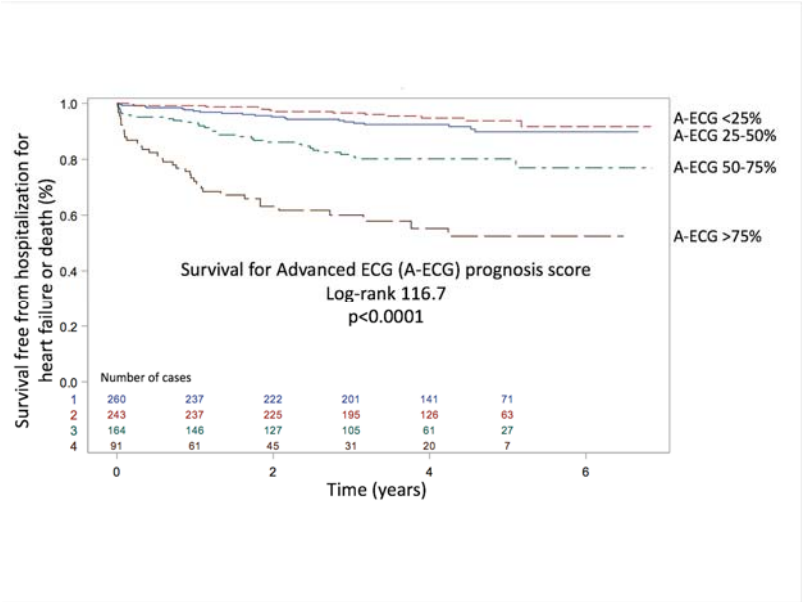
Survival free from hospitalization for heart failure or death (%)
1.0
0.8
0.6
0.4
0.2
0.0
A-ECG <25%
A-ECG 25-50%
A-ECG 50-75%
A-ECG >75%
Survival for Advanced ECG (A-ECG) prognosis score
Log-rank 116.7
p<0.0001
Number of cases
1 260 237 222 201 141 71
2 243 237 225 195 126 63
3 164 146 127 105 61 27
4 91 61 45 31 20 7
0
2
4
6
Time (years)

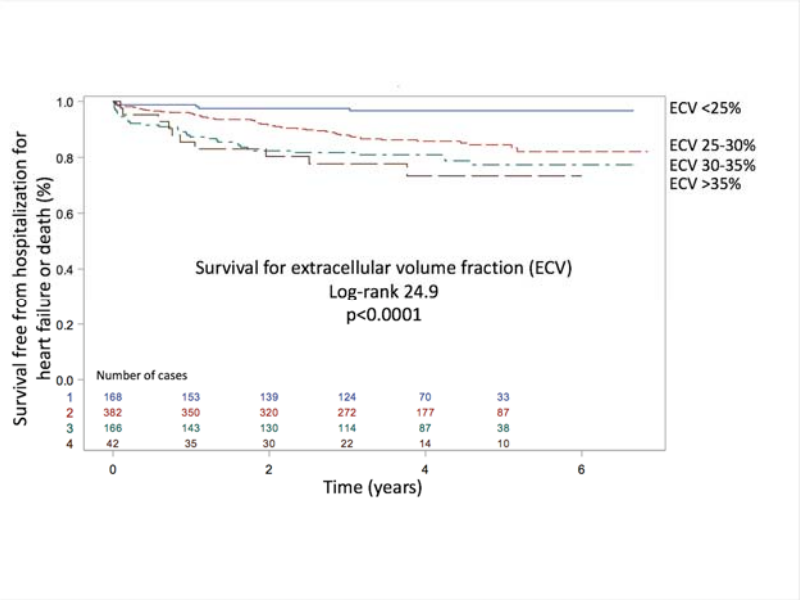
Survival free from hospitalization for heart failure or death (%)
1.0
0.8
0.6
0.4
0.2
0.0
ECV <25%
ECV 25-30%
ECV 30-35%
ECV >35%
Survival for extracellular volume fraction (ECV)
Log-rank 24.9
p<0.0001
Number of cases
1 168 153 139 124 70 33
2 382 350 320 272 177 87
3 166 143 130 114 87 38
4 42 35 30 22 14 10
0
2
4
6
Time (years)

ID#: 371793

Ticagrelor and left ventricular remodeling post-MI: assessment by cardiac magnetic resonance and molecular analysis.

Manuel Gutiérrez, MD[1] Guiomar Mendieta, MD[2], Gemma Vilahur, PhD, FESC[3], Laura Casani, PhD, DVM[3], Carmen Lambert[3], Soumaya Ben-Aicha[3], Antoni Capdevila, MD[4], Guillem Pons-Lladó, MD[5], Francesc Carreras, MD, PhD[5], Leif Carlsson, PhD[6], Alberto Hidalgo, MD, PhD[7], Lina Badimon, PhD, FESC[8]

1. Hospital de Viladecans, Institut Català de la Salut (ICS). Cardiovascular Research Center (CSIC-ICCC), IIB-HSCSP., Catalonia, Spain

2. Cardiology Department, Hospital Clinic de Barcelona. Cardiovascular Research Center (CSIC-ICCC), IIB-HSCSP., Catalonia, Spain

3. Cardiovascular Research Center (CSIC-ICCC), IIB-HSCSP. Barcelona, Catalonia, Spain

4. Radiology Unit. Hospital de la Santa Creu i Sant Pau (HSCSP), Barcelona, Catalonia, Spain

5. Cardiology Unit, Hospital de la Santa Creu i Sant Pau (HSCSP), Barcelona,, Catalonia, Spain

6. Cardiovascular and Metabolic Diseases, Innovative Medicines and Early Development Biotech Unit, AstraZeneca, Mölndal, Sweden, Mölndal, Sweden

7. Radiology Unit. Hospital de la Santa Creu i Sant Pau (HSCSP), Barcelona, Spain, Catalonia, Spain

8. Cardiovascular Research Center (CSIC-ICCC), IIB-HSCSP, Barcelona, Catalonia, Spain

Background: Antagonists of the ADP-receptor are the gold standard in antiaggregation therapy. However, their potential effects on functional myocardial recovery and cardiac healing after myocardial infarction (MI) are unknown. We have investigated, in an experimental preclinical pig model of MI whether ticagrelor and clopidogrel differently affect left ventricular remodeling post-MI.

Methods: Pigs (N=24) were randomized to: 1) clopidogrel (600mg; 75mg/qd); ticagrelor (180mg; 90mg/bid); and 3) control. MI was induced by closed-chest left anterior descending coronary artery balloon occlusion and treatment was given for 42days. Cardiac magnetic resonance imaging (CMR) was performed at day 3 and day 42. The following parameters of cardiac remodeling were assessed: global and regional function, wall edema and wall necrosis. Molecular analysis of AMP-activated protein kinase (AMPK) and Akt was performed in the ischemic and remote myocardium. All results were obtained blindly to treatment and experimental variables (time and sites).

Results: At day 3, CMR demonstrated that the extent of edema and of the infarct size were reduced and LVEF was improved by ticagrelor (all changes significant vs placebo and clopidogrel). At day 42, scar size was reduced and LVEF improved in ticagrelor-treated pigs (all changes significant vs placebo and clopidogrel). CMR-regional analysis revealed that while control and clopidogrel-treated pigs resulted to have severe and extensive wall motion abnormalities in the jeopardized myocardium and reduced myocardial viability, ticagrelor-treated pigs showed significant improvement ($\chi 2$ $p<0.05$). Only ticagrelor induced AMPK and Akt activation in the entire myocardium ($p<0.05$ vs. control and clopidogrel).

Conclusion: Ticagrelor significantly reduced myocardial structural and functional remodeling post-MI, improving cardiac healing compared to placebo and to clopidogrel.

This work has been partially funded by a competitive research grant from AstraZeneca.

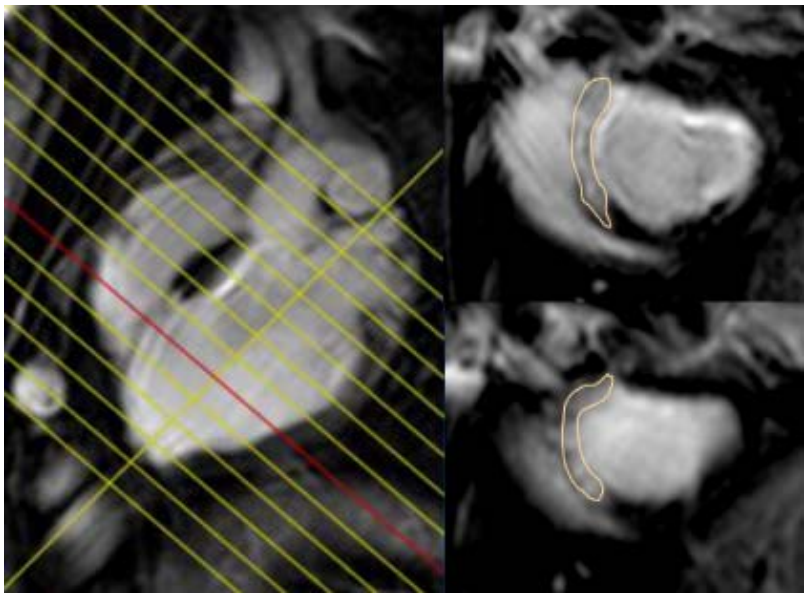

Left: Late Gadolinium Inversion Recovery image in long axis view. Right: two of the consecutive short axis LGE images of the short axis stack which was acquired to assess the whole myocardium.

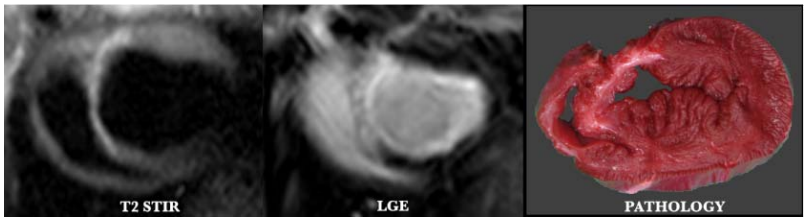

T2 STIR, Late Gadolinium Inversion recovery images and the corresponding pathologic specimen at mid ventricular level.

Magnetic resonance (CMR) imaging analysis. Edema assessed at day 3 post-MI (early remodeling phase).

	Group	**3 days post-MI**
	Control	23.5 ± 1.2
Edema (gr LV)	Clopidogrel	21.7 ± 0.9
	Ticagrelor	16.5 ± 1.0
	Control	36.5 ± 2.1
Edema (% of LV)	Clopidogrel	31.8 ± 1.5
	Ticagrelor	25.0 ± 1.6

ID#: 371794

Towards 4D flow High-resolution Imaging with a priori Knowledge Incorporating the Navier-Stokes equations and the discontinuous Galerkin method (4D flow HIKING)

Johannes Töger, PhD[1]Matthew J. Zahr, PhD[2], Karin Markenroth Bloch, PhD[3], Per-Olof Persson, PhD[2]

1. Lund University, Skåne University Hospital, Malmö, Sweden

2. Department of Mathematics, Lawrence Berkeley Laboratory and University of California, Berkeley, CA, USA

3. Lund University Bioimaging Center, Lund University, Lund, Sweden, Lund, Sweden

Background: Recent accelerated MRI methods exploit priori information, e.g. spatiotemporal correlations [1] or sparsity [2]. The Navier-Stokes equations describe blood flow physics accurately and can therefore give valuable a priori information for 4D flow, promising increased data quality and/or reduced scan times. However, previous Navier-Stokes 4D flow reconstruction methods are limited by simplified treatment of the Navier-Stokes equations [3] and not modelling MRI spatiotemporal smoothing [4].

We have recently developed a 4D flow reconstruction framework, called 4D flow high-resolution imaging with a priori knowledge incorporating the Navier-Stokes equations and the discontinuous Galerkin method (4D flow HIKING), including a high-order computational fluid dynamics (CFD) solver and a spatiotemporal smoothing model. Therefore, this study aims to investigate the performance of 4D flow HIKING in the presence of noise and low resolution in synthetic 2D data.

Methods: A reference CFD solution in a two-dimensional (2D) geometry was computed (Figure 1a). The reference solution was then downsampled (Figure 1b) with added noise to provide simulated MRI data corresponding to a) a consensus 4D flow sequence [5], b) low-resolution conditions, and c) high-noise conditions (Figure 2).

Downsampled data was used as input to the HIKING framework, which is based on three main components (Figure 3): 1) a *target function* measuring similarity between MR flow data and CFD solution, linked by the forward model **M**, 2) the *3DG CFD solver*, which computes the CFD solution from boundary conditions encoded in the parameter vector **μ**, and 3) *the adjoint equations* [6], used to compute the gradient of the target function. The target function is then minimized iteratively to reconstruct the high-resolution flow.

Results: The 4D flow HIKING method shows excellent reconstruction in all three 2D test cases (Figure 2). Convergence was attained after 220 minutes (55 iterations) on a 16-core computer (~60 CPU-hours).

Conclusion: The 4D flow HIKING framework shows excellent flow reconstruction performance in synthetic 2D tests. Future studies include 3D phantom validation and in vivo flow reconstruction.

References

1. Giese D et al. J. Cardiovasc. Magn. Reson. 16(1):42, 2014 [cited 2014 Jun 24].
2. Hsiao A et al. Am. J. Roentgenol. 198(3):250–9, 2012.
3. Rispoli VC et al. Biomed. Eng. Online. 14(1):110, 2015.
4. Funke SW et al. arXiv. :1607.03013v1, 2016.
5. Dyverfeldt P et al. J. Cardiovasc. Magn. Reson. 17:72, 2015.
6. Zahr MJ et al. Comput. Fluids. 139:130–47, 2016.
7. Wächter A et al. Math. Program. 106(1):25–57, 2006.

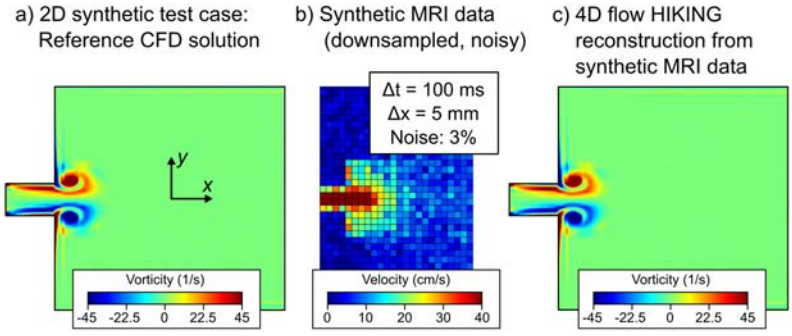

Figure 1: Setup of 2D synthetic numerical tests. Panel a) shows the reference CFD solution. Panel b) shows how

synthetic MRI data was constructed by downsampling the CFD data in space and time and adding noise. Panel c) shows the 4D flow HIKING reconstruction of the CFD data from the downsampled, noisy synthetic MRI data.

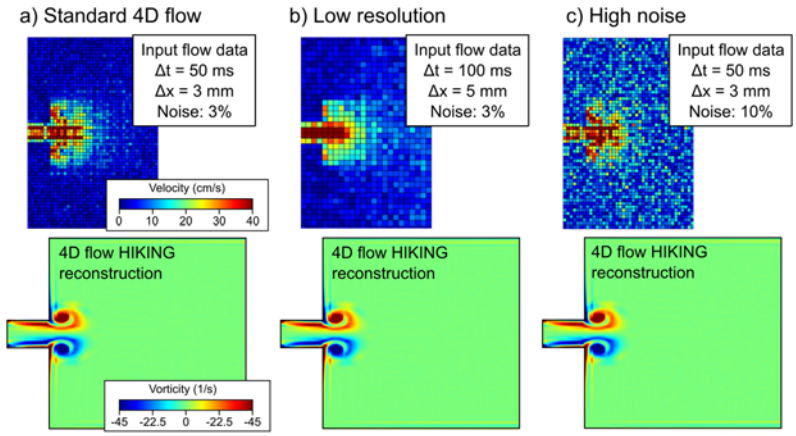

Figure 2: Results of 2D synthetic tests. Panels a, b and c show 4D flow HIKING reconstruction from downsampled, noisy data. In all three test cases, the reconstruction is very close to the reference CFD solution (Figure 1a).

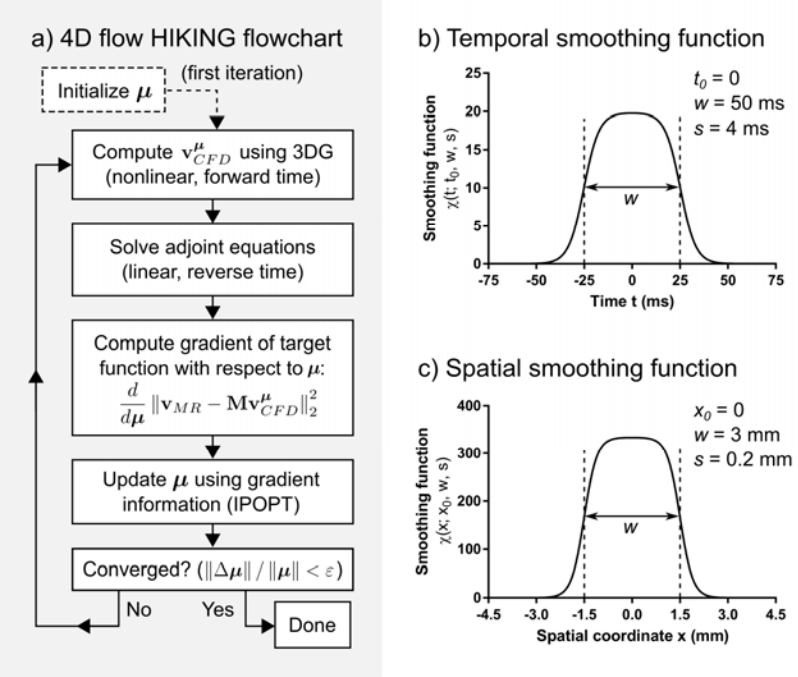

Figure 3: Technical overview of the 4D flow HIKING framework (a) and smoothing functions in the forward model M (b,c). Panel a) shows the 4D flow HIKING method. CFD simulation is performed using the 3DG solver. The spatial discretization is a 4th-order Discontinuous Galerkin (DG) method, and the temporal discretization is a 3rd-order implicit Runge-Kutta method. Gradients of the target function with respect to μ are computed using the adjoint equations, which enables efficient updates of the parameter vector μ using the IPOPT optimizer [7]. The optimization is stopped when the relative change in μ is below the threshold ε = 0.01. Panels b) and c) show the temporal and spatial smoothing functions χ used to approximate the 4D flow MRI velocity measurement process in the forward model M.

ID#: 371514

Blood pressure reduction with six months of exercise training is mediated by changes in proximal but not distal aortic stiffness as assessed by CMR

Anish N. Bhuva, MRCP MBBS[1] Andrew D'Silva, MBBS MRCP[2], Camilla Torlasco, MD[3], Niromila Nadarajan, MBBS MSc[4], Siana Jones, BSc MSc[5], Kristopher D. Knott, MBBS MA[6], Giulia Benedetti, MD[7], Paul R. Scully, MBBS MRes[7], Rachel Bastiaenen, PhD[8], Peter Kellman, Ph.D.[9], Guy Lloyd, MD FCRP[10], Nishi Chaturvedi, MD, MRCP[11], Sanjay Sharma, MD, FRCP[12], James C. Moon, MD[13], Alun Hughes, MBBS PhD[14], Charlotte Manisty, MBBS PhD[15]

1. Barts Heart Centre and Institute of Cardiovascular Science, UCL., London, England, United Kingdom

2. Cardiovascular Sciences Research Centre, St. George's, University of London, London, United Kingdom, London, England, United Kingdom

3. University of Milan-Bicocca. IRCCS Istituto Auxologico Italiano, Milan, Italy, Milan, Lombardia, Italy

4. University College London, London, United Kingdom

5. UCL, London, England, United Kingdom

6. University College London, London, England, United Kingdom

7. Barts Heart Centre, London, England, United Kingdom

8. Guy's and St Thomas' NHS Foundation Trust, United Kingdom

9. National Heart, Lung, and Blood Institute, Bethesda, MD

10. Barts Heart Centre and University College London, United Kingdom

11. University College London, United Kingdom

12. St George's University of London, England, United Kingdom

13. Barts Heart Centre, England, United Kingdom

14. UCL, United Kingdom

15. Barts Heart Centre and University College London, England, United Kingdom

Background: Exercise training is known to have beneficial effects on central (aortic) blood pressure (cBP), which is closely associated with cardiovascular risk. However the physiology remains poorly understood with effects on autonomic tone, body composition and aortic stiffness as proposed mechanisms. Regional aortic haemodynamics are of unknown importance. We studied the effects of first time marathon training on cBP and regional aortic stiffness using cardiovascular magnetic resonance (CMR).

Methods: Untrained healthy volunteers were recruited prior to starting an exercise training programme for the London Marathon. Assessment pre-training and two weeks post-marathon included cBP; anthropometry, maximum oxygen consumption (VO_{2max}) and phase contrast CMR (Siemens Aera 1.5T; 1.97 x 1.77mm^2, 9.24ms temporal resolution, Venc 150cm/s), in the ascending (AA) and proximal descending aorta at the level of the pulmonary artery (pDA) and at the level of the diaphragm (dDA). Transit times between AA and pDA, pDA and dDA, and AA and dDA were measured from flow velocity waveforms and regional and total pulse wave velocity (PWV) calculated. Aortic distensibility was measured at AA and pDA. Data are means (95% confidence intervals).

Results: 136 marathon completers (Median age 34 (range 21- 69), 49% male) underwent phase contrast CMR at baseline and follow up. At baseline, cBP was 109.8(102.0, 120.5)/ 76(71.5, 80.5) mmHg. PWV was lower in the ascending than descending aorta (4.39(3.72-5.35) vs 7.87(6.43-10.04) m/s) and AA and pDA distensibility were similar (8.63(5.34-11.32) and 8.49(5.53-12.32) 10^{-3}.$mmHg^{-1}$ respectively). After exercise training there was a reduction of 4.2(2.6, 5.9)/ 2.6(1.6, 3.5) mmHg in cBP and 2.4(0.3, 4.3) min^{-1} in heart rate. Exercise was associated with a -0.21(-0.01, -0.42) m/s reduction in total aortic PWV and a 0.83(0.2,1.46) 10^{-3}.$mmHg^{-1}$ increase in pDA distensibility. Older age and higher baseline systolic cBP (cSBP) was associated with greater reduction in cSBP. The reduction in cSBP was correlated with the reduction in PWV (or the increase in distensibility) in the proximal (AA to pDA) but not the distal (pDA to dDA) aorta (r = 0.18(0.02,0.32) and 0.03(-0.14,0.20) respectively). Change in weight or VO_{2max} were not associated with changes in cSBP.

Conclusion: Exercise training results in a reduction in central blood pressure; the reduction in cSBP can be explained, at least partially, by a reduction in aortic stiffness, particularly in the proximal aorta. MRI measurement of regional PWV offers new insights into the physiological mechanisms of exercise training.

ID#: 371466

3S SASHA myocardial T1 mapping with high accuracy and improved precision

Giovanna Nordio, Biomedical Engineering[1]Aurelien Bustin, Biomedical Engineering[2], Markus Henningsson, PhD[3], Freddy Odille, PhD[4], Claudia Prieto, PhD[3], Rene Michael. Botnar, PhD[1]

1. King's College London, London, England, United Kingdom

2. King's College of London, United Kingdom

3. King's College London, England, United Kingdom

4. Inserm, Vandoeuvre-lès-Nancy, Lorraine, France

Background: Free-breathing 3D quantitative myocardial T1-mapping allows for volumetric coverage of the heart providing higher signal-to-noise ratio (SNR) and spatial resolution than conventional 2D approaches. Recently a 3D saturation recovery based T1-mapping technique (3D SASHA[1]) was proposed. 3D SASHA achieves higher accuracy in the estimation of myocardial T1 but lower precision than the clinically used inversion recovery based 2D MOLLI[2] technique. We propose to further improve the precision of the 3D SASHA technique, while keeping its high accuracy, by employing a novel 3D denoising method which exploits spatio-temporal correlations in the T1-weighted images[3]. The proposed approach was tested in 10 healthy subjects and compared against 2D MOLLI acquisitions in terms of precision.

Methods: The 3D denoising technique imposes edge-preserving regularity and exploits the co-occurrence of spatial gradients in the acquired T1-weighted images by incorporating a multi-contrast Beltrami regularization. This technique corresponds to an extension of the 2D denoising approach proposed in[3].
3D SASHA and 2D MOLLI acquisitions were performed in 10 subjects on a 1.5T MR scanner (Ingenia, Philips, Best, The Netherlands). Acquisition parameters for 3D SASHA sequence included: FOV=300x300x90mm^3, TR/TE=3.2/1.6ms, resolution=1.4x1.4mm^2, slice thickness 8mm, FA=35°, parallel imaging SENSE factor 2, diaphragmatic navigator gating. Acquisition parameters for 2D MOLLI were: FOV=300x280mm^2, TR/TE=2.6/1.3ms, resolution=1.7x2.1mm^2, slice thickness 10mm, FA=35°.
The proposed 3D denoising technique was applied to the 3D SASHA datasets before pixel-wise T1 three-parameter fitting. A ROI was manually selected in the myocardial septum of 2D MOLLI and 3D SASHA T1-maps (apex, mid and base slices) to measure and compare the precision of the corresponding myocardial T1-values (WIlcoxon test).

Results: The proposed 3D denoising allows to obtain comparable precision (p=0.55) between 3D SASHA and 2D MOLLI iamging techniques (Figure 1), and it provides improved image quality, in terms of sharpness and suppression of noise, compared with the conventional T1-map (Figure 2).For all subjects the precision is improved after applying the 3D denoising technique on the 3D SASHA T1-maps (Figure 3).

Conclusion: The proposed 3D denoising technique enables 3D SASHA myocardial T1-mapping with high accuracy and high precision comparable to the conventional 2D MOLLI technique. The 3D denoising technique comes at no additional cost and could ultimately be beneficial to accurately detect and quantify interstitial fibrosis in the myocardium with high spatial resolution.

1Nordio G. et al,JMRI 2017;**2**Messroghli D et al.,MRM 2004;**3**Bustin A. et al,JMRI 2017.

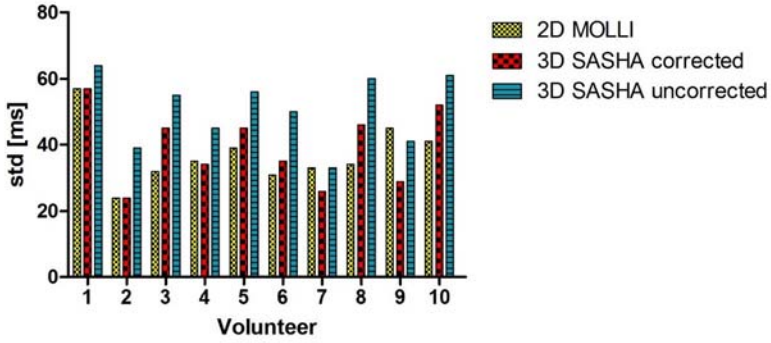

Graph comparing the precision of 2D MOLLI (yellow bar), 3D SASHA before (blue bar) and after (red bar) 3D denoising for all ten healthy subjects. The precision was measured in a ROI placed in the septum in a mid slice.

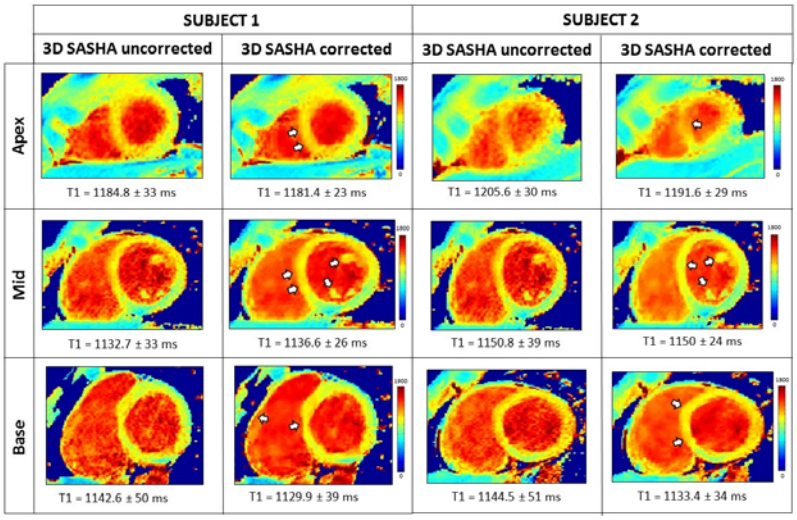

Myocardial T1 maps for two representative subjects. Representative T1 map of the apex, mid and base slice before (3D SASHA uncorrected) and after (3D SASHA corrected) 3D denoising are shown. Image quality was improved after 3D denoising, with a better delineation of the myocardial borders and the papillary muscles, as shown by the white arrows.

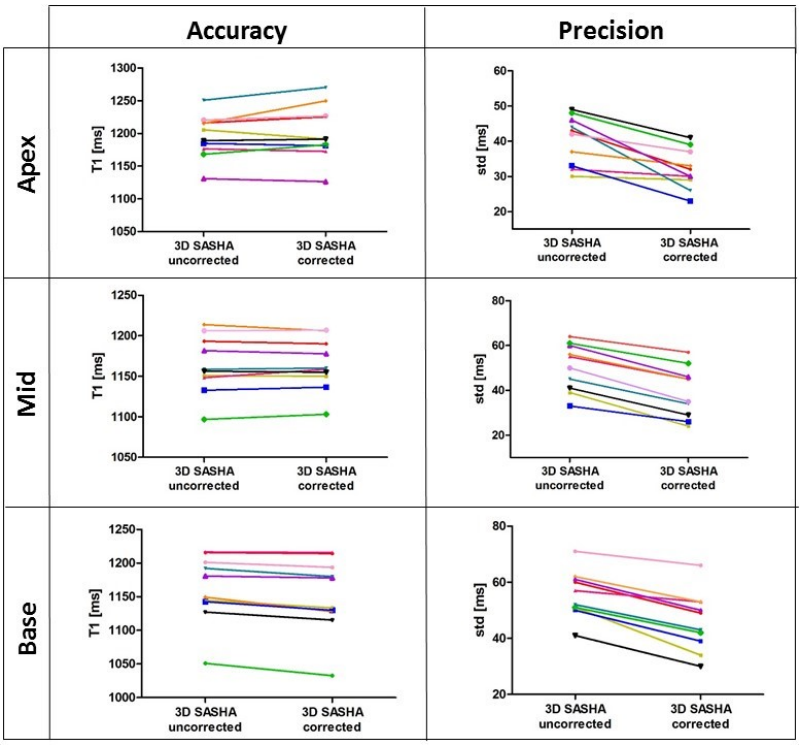

Comparison of the accuracy and precision of the 3D SASHA T1 map measured before and after applying the 3D denoising technique. The values have been measured in the septum of the myocardium for all the subjects in the apex, mid and base slices. Each color of the graph corresponds to a subject.

ID#: 371086

Precision and Accuracy of Coronary Cross-Sectional Area MRI Measurements Used to Measure Coronary Endothelial Function

Michael Schär, PhD[1] Sahar Soleimanifard, PhD[2], Gabriele Bonanno, PhD[2], Jerome Yerly, PhD[3], Allison G. Hays, MD[4], Robert G. Weiss, MD[5]

1. Russell H. Morgan Department of Radiology and Radiological Science, Johns Hopkins University School of Medicine, Baltimore, MD

2. Johns Hopkins University School of Medicine

3. Center for Biomedical Imaging (CIBM), Lausanne, Switzerland, Vaud, Switzerland

4. Division of Cardiology, The Johns Hopkins University School of Medicine, Baltimore, MD, United States, MD

5. Russell H. Morgan Department of Radiology and Radiological Science, The Johns Hopkins University School of Medicine, Baltimore, MD, United States, MD

Background: Coronary endothelial function (CEF) reflects vascular health and predicts cardiovascular events. MRI can now measure CEF noninvasively by quantifying changes in coronary artery cross-sectional area (CSA) in response to isometric handgrip exercise [1–4], an endothelial-dependent stressor [5]. But the CSA-change is only a few imaging pixels because of MRI';s limited spatial resolution. Despite this, phantom studies showed that radial MRI is capable of distinguishing a 3-4% area change for a 3-mm vessel, and the smallest detectable area change was independent of the voxel size [6]. We hypothesize that Fourier interpolation enables sub-pixel CSA-precision and test this with simulations and phantom measurements of CSA measurement precision and accuracy with spiral MRI used to measure CEF.

Methods: In-vivo Signal-to-noise Ratio (SNR): SNR of right or left coronary arteries imaged with the current CEF protocol [1] was measured in 10 subjects at 3T. SNR was determined by averaging and subtracting 2 cardiac phases [7]. **Simulations:** Area measurements of circular vessels were simulated varying partial volume (528 steps), vessel diameter (2.5-5mm), imaging voxel size Δx (0.4-1mm), SNR (10-150), and Fourier interpolation (factors 1, 2, 4, 8). Areas were measured with full-width at half-maximum and used to determine precision (standard deviation) and accuracy (mean of the difference from the true value). **Phantom:** A phantom with precision-drilled holes (diameters 3-3.42mm in steps of 0.02mm, each 5 times [6]) was placed in a container filled with gadolinium-doped water (T1~200ms). Spiral cine MRI was acquired 10 times orthogonal to the drilled holes with the current standard CEF protocol (Δx=0.89mm, 20 interleaves, 18s breath-hold) and a high-resolution protocol (Δx=0.6mm, 26 interleaves, 23s). Images were deblurred locally [8]. Precision, accuracy, and limit of area-change detection [6] were determined.

Results: In-vivo SNR: In-vivo coronary SNR with the standard CEF protocol was 53±19 (mean±standard deviation). **Simulations:** Fig. 1 shows that area measurements of a 3mm vessel without image interpolation vary up to 60%, and Fourier interpolation reduces this variation improving precision while slightly reducing accuracy. Precision and accuracy can be improved with increased spatial resolution as long as the SNR stays above 20 (Fig. 2). **Phantom:** Phantom measurements confirm the simulations (Fig. 3A-B). The limit of area-change detection is <4% for SNR>60, and <5% for SNR>30 with the current protocol, and <3.5% for SNR>40 with the high-resolution protocol (Fig. 3C).

Conclusion: Current CEF spiral MRI can detect CSA-changes of <5%, and can be improved to <3.5% with a voxel size of 0.6mm and sufficient SNR>40.

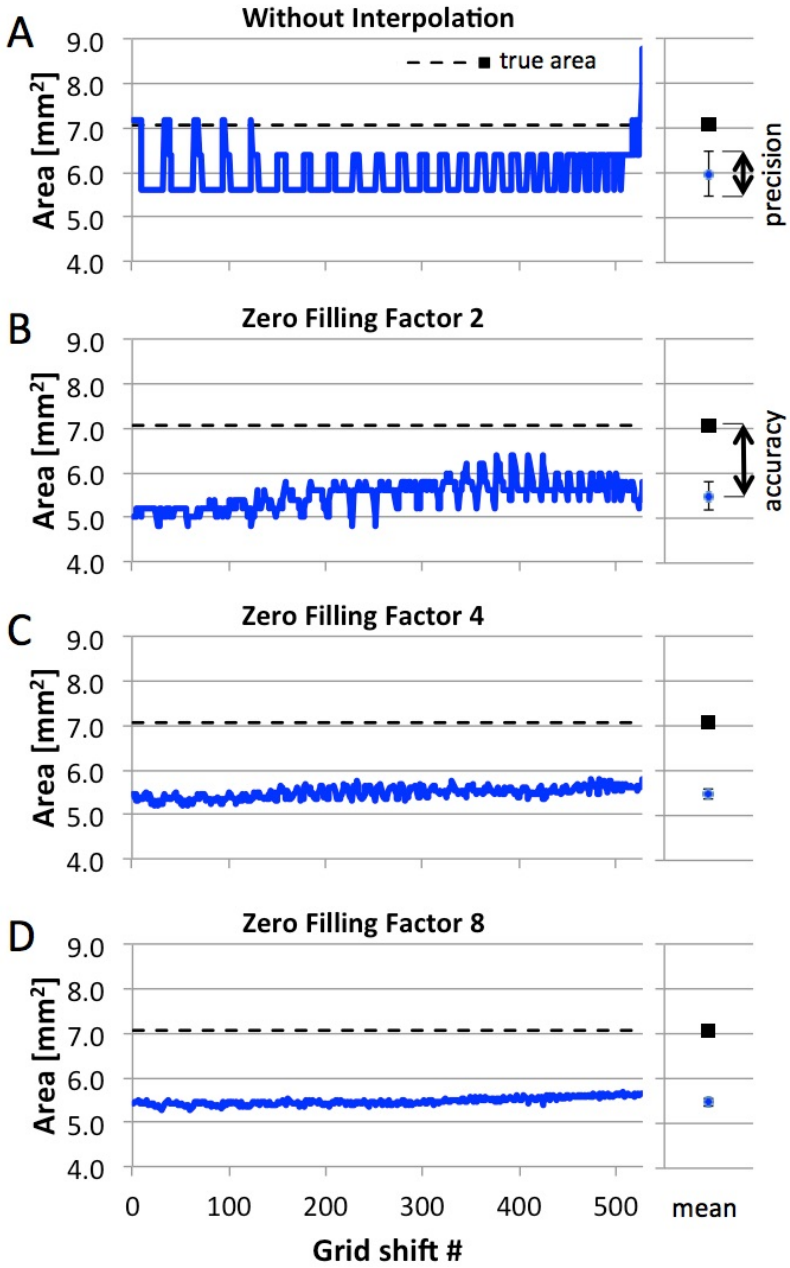

Figure 1: Simulated area measurements of a 3mm diameter vessel (SNR=150, Δx= 0.89mm) for 528 different imaging grid locations causing differences in partial volume effects. A) Measuring the area without interpolating the image leads to few discrete values and a rather large variation. B)-D) with Fourier interpolation applying zero-filling factors 2 (B), 4 (C), and 8 (D) the precision, as measured with the standard deviation of the area measures, is improved, while the accuracy, the difference of the mean of the measures to the true value, shows a larger underestimation. (error bars are standard deviations)

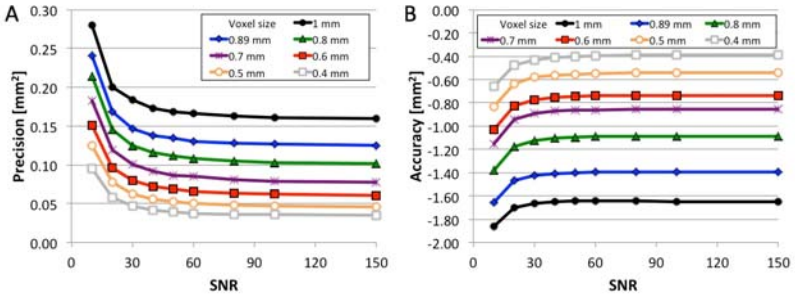

Figure 2: A) Precision and B) accuracy of simulated area measurements averaged over a range of vessel diameters from 2.5 to 5mm for a range of different SNR levels with a voxel size from 0.4 to 1mm.

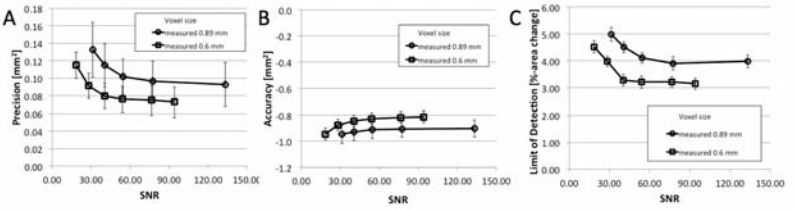

Figure 3: Measured A) precision and B) accuracy of area measurements, and C) limit of detection of area-change measurements averaged over a range of vessel diameters from 3 to 3.42mm for a range of different SNR levels with data acquired with voxel sizes of 0.89 and 0.6mm. The current standard protocol (Δx=0.89mm) can distinguish area changes of less than 5% even at a low SNR of 30. A potential protocol with improved resolution Δx=0.6mm and an SNR>40 would enable to measure a change of less than 3.5%.

References

1.	Hays AG, et al. J. Am. Coll. Cardiol. 2010;56:1657–65.
2.	Hays AG, et al. Circ. Cardiovasc. Imaging. 2012;5:341–8.
3.	Hays AG, et al. PLoS ONE. 2013;8:e58047.
4.	Iantorno M, et al. AIDS. 2017;31:1281–9.
5.	Hays AG, et al. Am. J. Physiol. Heart Circ. Physiol. 2015;308:H1343-1350.
6.	Yerly J, et al. Magn. Reson. Med. 2017 http://doi.wiley.com/10.1002/mrm.26646
7.	National Electrical Manufacturers Association. 2008.
8.	Noll DC, et al. Magn. Reson. Med. 1992;25:319–33.

ID#: 370875

Myocardial T1 mapping and Tissue-Tracking Strain Analysis with 1.5T Magnetic Resonance in Patients with Type 2 Diabetes Mellitus

Yukun Cao[1]Heshui Shi[2], Yue Cui[1], Xiangchuang Kong, doctor[3]

1. Department of Radiology, Union Hospital, Tongji Medical College, Huazhong University of Science and Technology, Wuhan, Hubei, China (People's Republic)

2. Department of Radiology, Union Hospital, Tongji Medical College, Huazhong University of Science and Technology, Hubei, China (People's Republic)

3. Deparment of Radiology,Union Hospital,Tongji Medical College,Huazhong University of Science and Technology, Hubei, China (People's Republic)

Background: Cardiac magnetic resonance (CMR) T1 mapping and tissue-tracking strain analysis are considered to be useful quantitative techniques that can evaluate myocardial tissue characterization and mechanic alterations, respectively, in early diabetic cardiomyopathy. The purpose of this study was to assess left ventricular myocardial T1 value, extracellular volume fraction (ECV), and systolic strains in asymptomatic patients with type 2 diabetes mellitus (T2DM) and its underlying relationship with clinical parameters.

Methods: We recruited 50 asymptomatic T2DM patients (mean age: 55±7 years; 28 males) and 32 healthy volunteers matched with sex, age, and BMI to undergo contrast-enhanced CMR examination. The myocardial native T1, post-contrast T1 and ECV values of left ventricle were measured in the T1 and ECV maps acquired by modified Look-Locker inversion recovery (MOLLI) technique. Left ventricular global systolic strain and strain rates were evaluated with routine cine images by tissue-tracking analysis software.The baseline clinical and biochemical indices were collected before CMR examination.

Results: The myocardial ECV and native T1 values were significantly higher in diabetic patients than that in controls. (ECV: 27.4 ± 2.5% vs. 24.6 ± 2.2%, $p < 0.001$; native T1: 1026.9 ± 30.0 ms vs. 1011.8 ± 26.0 ms, $p = 0.022$, respectively). However, the left ventricular global systolic strain, strain rate, volume, myocardial mass, ejection fraction, and left atrial volume were similar between diabetic patients and healthy controls. In diabetic patients, native T1 value was independently correlated to hemoglobin A1c level (standardized $\beta = 0.368$, $p = 0.008$). ECV was independently associated with hemoglobin A1c level (standardized $\beta = 0.365$, $p = 0.007$) and angiotensin-converting enzyme inhibitor (ACEI) treatment (standardized $\beta = -0.271$, $p = 0.042$).

Conclusion:

AsymptomaticT2DM patients have increased native T1 value and ECV indicative of myocardial extracellular interstitial expansion, which relates to poor glycemic control. AECI treatment can help ameliorate myocardial interstitial matrix remodeling.

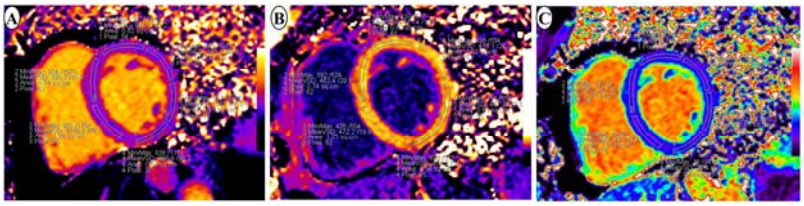

Representative maps of a healthy volunteer at the left ventricular middle short-axis segment with modified Look-Locker Inversion Recovery (MOLLI) sequence

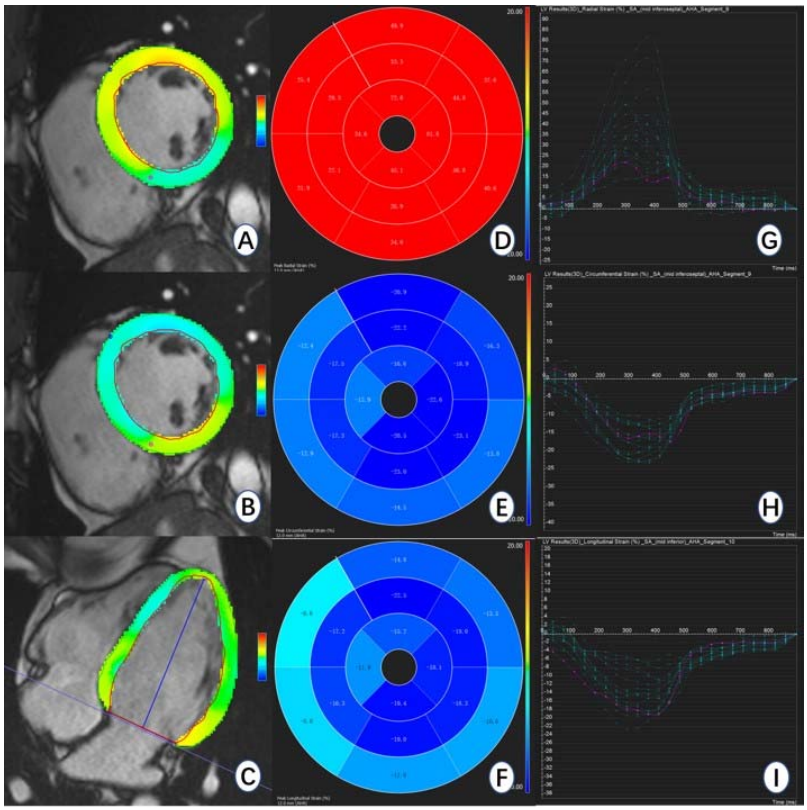

The diagram of the peak systolic strain analysis of the left ventricular myocardium in a healthy volunteer.

ID#: 370106

Automatic Quantification of Pulse Wave Velocity: Application for population-based CMR studies.

Rahil Shahzad, PhD[1] Arun Shankar, MSc[2], Raquel Amier, MD[3], Robin Nijveldt, MD, PhD[4], Jos J.M. Westenberg, PhD[5], Albert de Roos, MD, PhD[6], Boudewijn Lelieveldt, PhD[7], Rob J. van der Geest, PhD[8]

1. Department of Radiology, Leiden University Medical Center, Leiden, The Netherlands, Leiden`, Zuid-Holland, Netherlands

2. Leiden University Medical Center, Netherlands

3. VU University Medical Center, Amsterdam, Noord-Holland, Netherlands

4. Radboud University Medical Center, Nijmegen, Gelderland, Netherlands

5. Department of Radiology, Leiden University Medical Center, Leiden, The Netherlands, Leiden, Zuid-Holland, Netherlands

6. Department of Radiology, Leiden University Medical Center, Leiden, The Netherlands, Zuid-Holland, Netherlands

7. Department of Radiology, Leiden University Medical Center, Leiden, The Netherlands, Netherlands

8. Department of Radiology, Leiden University Medical Center, The Netherlands, Leiden, Zuid-Holland, Netherlands

Background: Pulse wave velocity (PWV) is a marker of arterial stiffness and is being used as a predictor of adverse cardiovascular events. PWV of the aortic arch can be derived from MRI, which has been well validated and widely used in clinical research[1]. Calculating PWV requires two components: (*i*) the length of the aortic arch, obtained using a stack of sagittal images (scout scan), and (*ii*) the transit time, obtained using a velocity encoded MR (VE-MR) scan (Figure 1). Current analysis methods are mostly manual or semi-automatic, being time consuming and operator dependent. We have developed a fully-automatic method which can estimate the PWV. [1] Bolster BD, et al. Accuracy of arterial pulse-wave velocity measurement using MR. JMRI 1998;8(4):878–888.

Methods: MRI data of 201 subjects was obtained as part of a large multi-center cohort[1] (Table 1). The proposed method has two main contributions: (*i*) multi-atlas-based segmentation[2] approach to segment the aorta and compute the length of the aortic arch in 3D, and (*ii*) detection and propagation of the 2D aorta contours on the VE-MR scan for computing of the time-velocity curves. Eight scout scans were used as atlases to segment the aortic arch and extract the centerline. The length was computed using the cutting plane of the VE-MR scan. The intersecting centerline points of the ascending and descending aorta were subsequently used to initialize and propagate the 2D aorta contours on the VE-MR scan. These contours were used to compute the velocity-time curves, from which the transit time was computed using the time-to-half-max method[3] (Figure 2). [1] van Buchem MA, et al. The heart-brain connection: A multidisciplinary approach targeting a missing link in the pathophysiology of vascular cognitive impairment. JAD 2014;42(s4). [2] Aljabar P, et al. Multi-atlas based segmentation of brain images: atlas selection and its effect on accuracy. Neuroimage 2009;46(3):726–738. [3] Groenink M, et al. Biophysical properties of the normal-sized aorta in patients with Marfan syndrome: evaluation with MR flow mapping. Radiology 2001;219:535–540.

Results: Automatic PWV assessment was successful in 193/201 (96%) of the subjects. In 8 subjects the method failed due to inferior image quality. The automatically obtained aorta length, the transit time and the computed PWV were compared to those obtained manually. The correlation between manual and fully automatic analysis of centerline length (R=0.98), transit time (R=0.90) and PWV (R=0.98) were excellent, with no significant absolute differences between the methods (Figure 3).

Conclusion: Fully-automatic method for computing the PWV was developed and evaluated. Results demonstrate that our method has good agreement with the manual approach. Our method is a valuable technique for large population-based studies.

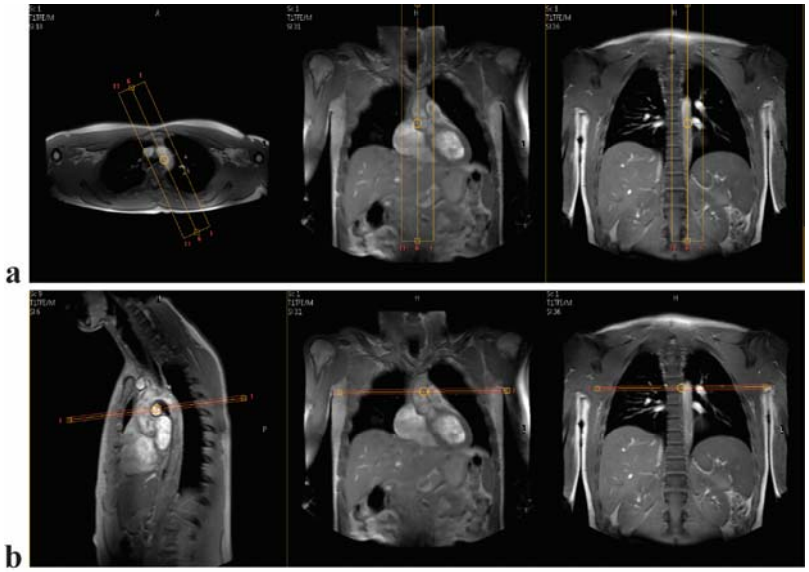

The MRI protocol included acquisition of a sagittal stack of images (11 slices, slice thickness 5 mm, reconstructed pixel size 1.8x1.8 mm) for imaging of the aortic arch (a) and a velocity-encoded (VE-MR) scan with high temporal resolution (TR/TE=4.7/2.8ms, true temporal resolution 9.8 ms) intersecting the proximal and descending aorta (b). All scans were acquired using a 3T MRI scanner from Philips Medical System (Best, The Netherlands).

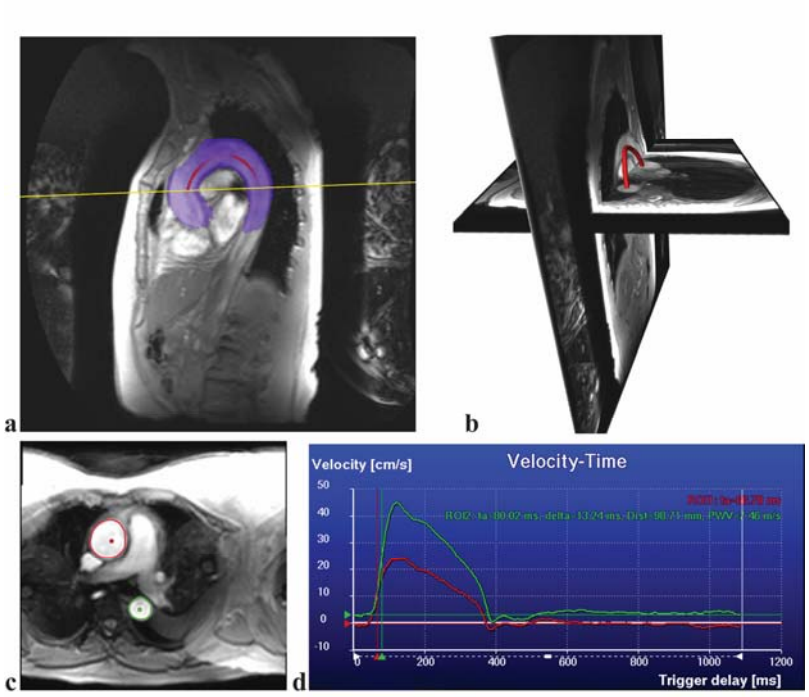

The resulting segmentation of the aorta after multi-atlas-based segmentation (in blue) and the calculated centerline (in red) on the sagittal images (a). The scout scan and the VE-MR scan with the extracted centerline represented in 3D (b). Automatically delineated ascending and descending aorta contours on the magnitude VE-MR scan, the two dots indicate the intersecting centerline point that were used as initiation (c). The computed velocity-time curves obtained from the phase VE-MR scan, used to compute the transit time (d).

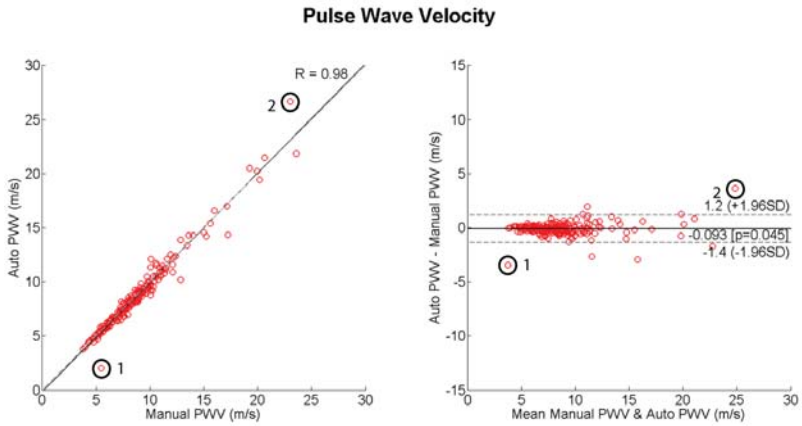

Pearson correlation and Bland-Altman plot for the PWV computation. The circled points show two extreme outliers. (1) The automatically delineated ascending aorta contours were inaccurate, resulting in erroneous transit-time and a low PWV. (2) The difference in the PWV caused due to the computed length of the proximal aorta, the automatic method overestimated the length.

Population characteristics. The included subjects fall in four categories: healthy controls, subjects with carotid occlusive disease (COD), subjects with vascular related cognitive impairment (VCI) and subjects with heart failure (HF).

Variable	Value
Sample Size	201
Men	129 (*64%*)
Age, *range*	68.5 (*59-91*)
Controls	37 (*18%*)
COD	40 (*20%*)
HF	62 (*31%*)
VCI	62 (*31%*)

Evaluation results of the proposed method. Where R is the Pearson correlation coefficient, B-A is the Bland-Altman bias, CI is the confidence interval and Abs diff is the average absolute difference.

Meaure	*R*	B-A (95% CI)	Abs diff
Centerline length (mm)	0.98	-1.0 (-9.3, 7.3)	3.3±2.8
Transit time (ms)	0.90	0.2 (-4.5, 5.0)	0.6±2.4
Pulse Wave Velocity (m/s)	0.98	0.0 (-1.4, 1.2)	0.4±0.5

ID#: 370393

Myocardial trabeculae improve left ventricular function: a combined UK Biobank and computational analysis

Timothy Dawes, FRCA, PhD.[1] Marta Serrani, PhD[2], Wenjia Bai, PhD[3], Jiashen Cai, BEng, MD[4], Pawel F. Tokarczuk, PhD[5], Philip Ostrowski, MRCP PhD[6], Hideaki Suzuki[7], Paul M. Matthews, MD, DPhil[3], Stuart Cook, PhD[8], Roberto Fumero[9], Maria Laura Costantino[9], Declan O'Regan, FRCR, PhD[10]

1. Imperial College London, London, England, United Kingdom

2. Department of Chemical Engineering and Biotechnology, University of Cambridge, United Kingdom

3. Imperial College London, London, United Kingdom

4. Duke-NUS Medical School, Singapore

5. Imperial College, London, England, United Kingdom

6. Imperial College London, England, United Kingdom

7. Imperial College London, United Kingdom

8. National Heart Centre Singapore, Singapore

9. Politecnico di Milano, Italy

10. MRC London Institute of Medical Sciences, England, United Kingdom

Background: Trabeculae form a complex mesh of myocardial strands that line the inner surface of the left and right ventricles. These are highly conserved structures in the mammalian heart, vital to cardiac embryonic development, but their importance in adults is unclear. Trabeculae have self-similar properties allowing their complexity to be measured by fractal analysis.

Methods: Left ventricular (LV) trabeculae were characterised using cardiac magnetic resonance imaging in 6791 participants from the first 10,000 persons imaged for the UK Biobank Imaging Enhancement (access agreement no. 18545). LV volumes, mass and fractal dimension, as a marker of trabecular complexity, were indexed to body surface area, analysed by machine learning and correlated with cardiovascular and anthropometric data by scaled linear regression.

To understand the effect of trabeculae on LV haemodynamics, a finite-element computational LV model was developed as a truncated ellipsoid with simulation of the cardiac cycle (Abaqus 6.10, SIMULIA, Dassault Systemes). Cardiac fibre orientation, tissue mechanical behaviour and contractile dynamics were based on physiological parameters. LV end-diastolic volume, mass, preload, afterload and heart rate were aligned to median values from the Biobank cohort. Heart rate and indexed systemic resistance were held constant. LV models with a smooth endocardial surface and with trabeculation equal to median Biobank fractal dimension were compared to identify the effects of trabeculae on ventricular haemodynamics under computational simulation.

Results: In Biobank participants, median fractal dimension was positively associated with indexed stroke volume (β=+0.25), cardiac output (β=+0.15), end-diastolic (β=+0.31) and end-systolic (β=+0.20) volumes and mean arterial pressure (β=+0.09) in vivo (n=6791, all $p<0.001$). Fractal dimension was negatively associated with heart rate (β=-0.11) and indexed systemic vascular resistance (β=-0.06, both $p<0.001$). Trabecular mass was weakly associated with stroke volume (β=-0.03, p=0.02) and end-diastolic volume (β=-0.03, p=0.03) and not significantly associated with cardiac output (β=-0.009, p=0.48), end-systolic volume (β=-0.02, p=0.26) and mean arterial pressure (β=+0.008, p=0.50).

In computational modelling, trabeculation were associated with increased indexed stroke volume (+32%), cardiac output (+32%), end-diastolic (+39%) and end-systolic (+46%) volumes and mean aortic pressure (+27%).

Conclusion: Myocardial trabeculae have significant clinical effects on LV function and cardiac output by increasing ventricular compliance. In vivo, this is associated with reductions in heart rate and systemic vascular resistance. These findings suggest that far from being a vestigial feature of cardiac development, LV trabeculae play an active and adaptive role in increasing ventricular function.

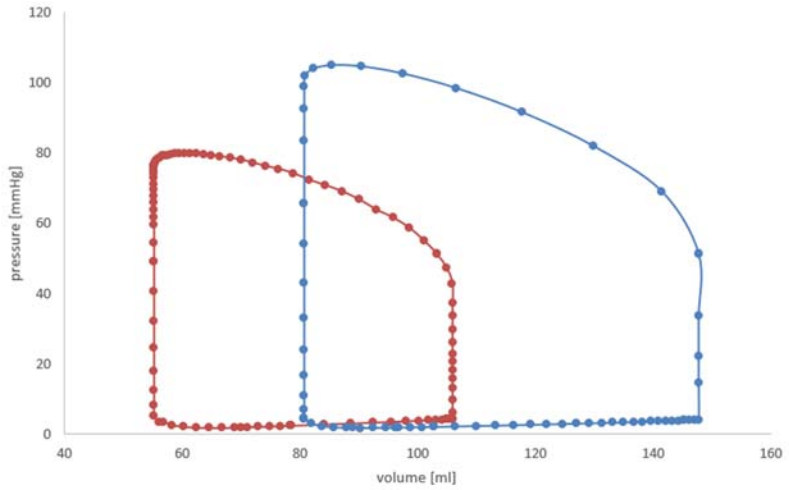

Figure 1. Computational modelling of ventricular haemodynamics over the cardiac cycle with smooth (red) and trabeculated (blue) endocardial surfaces.

UK Biobank Haemodynamic Data. All volumetric data refer to the left ventricle. Figures represent the median values and the inter-quartile range.

Parameter	Male (n=3175)	Female (n=3616)
Age (years)	63.8 (57.0 - 68.4)	62.2 (55.8 - 67.4)
Body surface area (m^2)	2.00 (1.90 - 2.12)	1.75 (1.65 - 1.86)
End-diastolic volume (mls)	172.2 (153.6 - 193.5)	138.6 (123.4 - 154.1)
End-systolic volume (mls)	79.0 (67.4 - 93.8)	62.5 (53.5 - 71.9)
Stroke volume (mls)	92.5 (79.1 - 107.7)	75.9 (64.4 - 87.2)
Ejection fraction (%)	53.9 (48.5 - 59.0)	54.8 (49.7 - 59.7)
Ventricular mass (g)	135.5 (120.5 - 152.8)	90.5 (79.5 - 102.6)
Mean global fractal dimension	1.187 (1.168-1.210)	1.177 (1.160 - 1.198)
Mean arterial pressure (mmHg)	99.9 (93.4 - 107.4)	94.9 (87.9 - 102.9)
Cardiac output ($L.min^{-1}$)	5.6 (4.8 - 6.6)	4.7 (4.0 - 5.5)

ID#: 367192

Long-term longitudinal prospective CMR study in patients with thalassemia major

Alessia Pepe, MD, PhD[1] Antonella Meloni, PhD[1], Laura Pistoia, MSc[1], Riccardo Righi, MD[2], Ada Riva, MD[3], Giuseppe Peritore, MD[4], Vincenzo Positano, MSc[1], Roberto Sarli, MD[5], Alessandra Quota, MD[6], Stefano Pulini, MD[7], Nicola Romano, MD[8], Andrea Olivi, MSc[9]

1. Fondazione G. Monasterio CNR Regione Toscana, Pisa, Toscana, Italy

2. Ospedale del Delta, Emilia-Romagna, Italy

3. Ospedale "SS. Annunziata" ASL Taranto, Taranto, Puglia, Italy

4. ARNAS Civico Di Cristina-Benfratelli, Palermo, Sicilia, Italy

5. Presidio Ospedaliero Orientale "M. Giannuzzi", Manduria (TA), Puglia, Italy

6. Ospedale, Gela (CL), Sicilia, Italy

7. Hematology, Ospedale Civile "Spirito Santo", Pescara, Italy, Pescara, Abruzzi, Italy

8. Azienda Ospedaliera Arcispedale, Reggio Emilia, Emilia-Romagna, Italy

9. Fondazione G. Monasterio CNR-Regione Toscana, Pisa, Toscana, Italy

Background: According to the International Guidelines, thalassemia major (TM) patients should perform a complete cardiac evaluation, including a CMR scan, every year. However, prospective CMR studies are limited beyond 3 years and longer-term studies are, therefore, important.
We aimed to determine longitudinal changes in cardiac iron and function assessed by CMR over 6 years in a large cohort of TM patients.

Methods: We considered 426 TM patients (205 males; 30.87±8.21 years) consecutively enrolled in the MIOT (Myocardial Iron Overload in Thalassemia) Network with a CMR follow-up (FU) study at 72 months (6 years). Myocardial iron overload (MIO) was quantified by the multislice multiecho T2* technique. Biventricular function was quantified by cine images.

Results: Four patterns of MIO were identified:no MIO (all segments with T2*≥20 ms), heterogeneous MIO and global heart T2*≥20 ms, heterogeneous MIO and global heart T2*<20 ms, and homogeneous MIO (all segments with T2*<20 ms). Figure 1 shows the frequency of the 4 patterns at both scans. An improvement in cardiac iron levels was detected in the 72% of patients showing MIO at the baseline (at least one pathologic segment) while, globally, a worsening was detected in 40 patients (Figure 2).
Biventricular end-diastolic volume indexes (EDVI) were significantly lower at the FU CMR. In patients with significant baseline MIO (global heart T2*<20 ms) a significant decrease in all biventricular volumes and a significant increase in left ventricular ejection fraction (EF) (mean difference: 3.83±8.48%, P<0.0001) as well as in right ventricular EF (mean difference: 1.79±9.04%, P=0.042) were detected with a concordant improvement of MIO status.
The 50.7% of the patients changed the type of chelator during the FU based on CMR results. The percentage of patients who changed the chelation therapy was significantly higher in patients with significant MIO than in patients without MIO (60.2% vs 46.2%; P=0.008).

Conclusion: Over a period of 6 years, the continuous monitoring of cardiac iron levels and a tailored chelation therapy allowed an improvement in more than 70% of patients with baseline MIO and a consequent improvement of biventricular function.

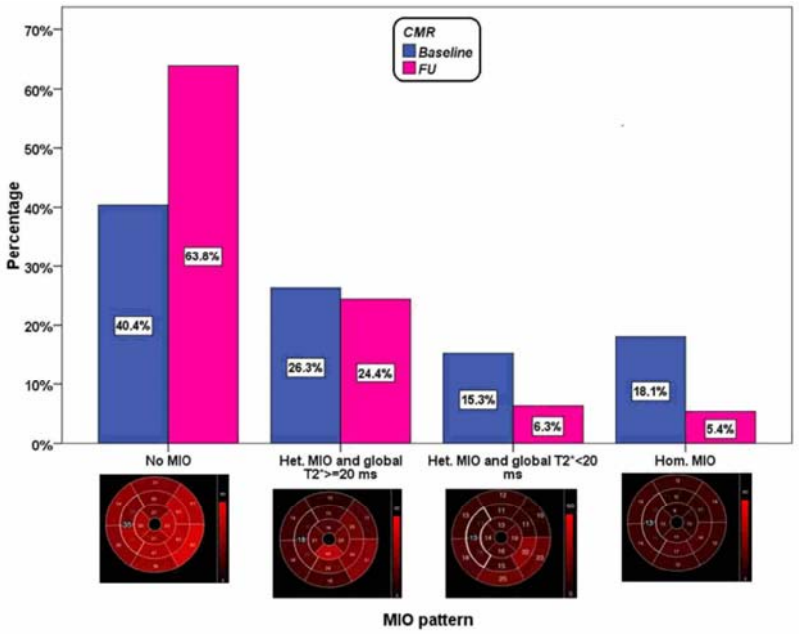

Figure 1

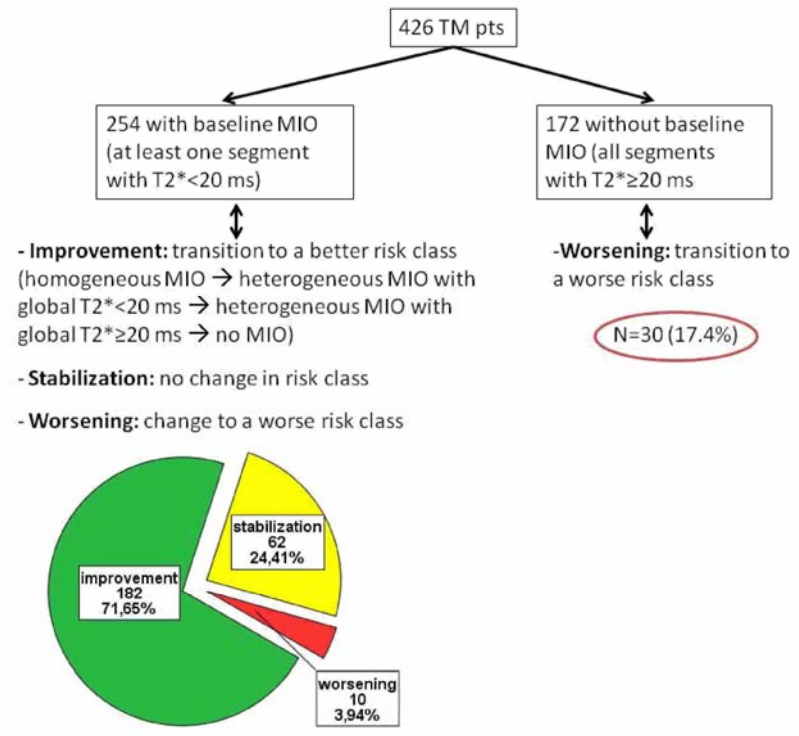

Figure 2

ID#: 367038

Myocardial Fibrosis in Myotonic Muscular Dystrophy: Highly Prevalent But Not Predictive of Pacemaker Implantation

Andrea Cardona, MD[1] William Arnold, MD[2], John Kissel, MD[2], Subha Raman, MD, MSEE[3], Karolina Zareba, MD[2]

1. The Ohio State University Wexner Medical Center, Columbus, OH

2. The Ohio State University Wexner Medical Center, OH

3. The Ohio State University, Columbus, OH

Background: Myotonic muscular dystrophy (MMD) is the most common muscular dystrophy in adults. Conduction system disease leads to cardiac arrhythmias and mortality in MMD, mitigated by timely permanent pacemaker implantation that has proven efficacy for prevention of sudden cardiac death (SCD). Cardiac magnetic resonance (CMR) studies have demonstrated high prevalence of myocardial fibrosis in MMD, though its association with surface conduction abnormalities remains uncertain. We explored the value of myocardial fibrosis by CMR in predicting pacemaker implantation in a cohort of consecutive patients with MMD.

Methods: Retrospective analysis of patients with genetically confirmed MMD was conducted. Standard 12-lead electrocardiography performed within 6 months of CMR exam was necessary for inclusion. Surface conduction abnormality was considered present if the PR interval was >200 msec and/or the QRS interval was ≥120 msec. Comprehensive CMR exams included cine imaging, myocardial T1 mapping, and late gadolinium enhancement (LGE). The presence and mass of LGE were assessed blinded to clinical data. Patients'; charts were reviewed up to 12 months post-CMR for occurrence of permanent pacemaker (PPM) implantation.

Results: A total of 61 patients, 38% male and age 43.1±14.4 years, were identified for inclusion. Overall, 37 (61%) showed a surface conduction abnormality and 25 (41%) demonstrated myocardial fibrosis by LGE-CMR. After a median time of 42 days from the CMR exam, 18 patients (29.5%) underwent PPM implantation. Demographic and clinical characteristics were not significantly different between the LGE-positive and LGE-negative groups. Importantly, no ECG parameters, including evidence of surface conduction abnormality, differed between LGE-positive and LGE-negative groups. By multivariate logistic regression analysis, the presence of a prolonged QTc interval (>450 msec) was the only predictor of PPM implant (OR 7.6, 2.0-25.3, p<0.002). Presence and amount of myocardial fibrosis by LGE did not predict PPM implantation.

Conclusion: Myocardial fibrosis in MMD is highly prevalent but not related to surface conduction abnormality and subsequent need for pacemaker. The complementary predictive value of myocardial fibrosis in the absence of surface conduction abnormalities warrants further evaluation in SCD risk stratification in this disease.

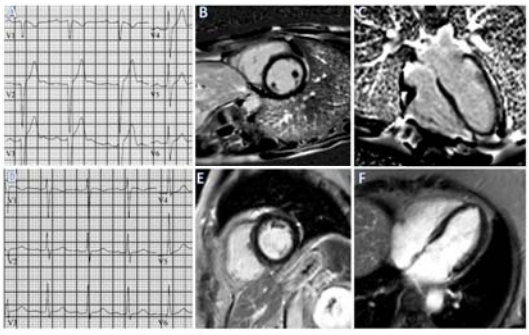

Figure. Upper panels (A-C) show an abnormal ECG with prolonged PR interval and borderline QRS interval (A) of a subject with no evidence of myocardial fibrosis by LGE-CMR (B,C) that received a PPM implant. Lower panels (D-F) show a normal ECG (D) of a subjects with evidence of extensive midwall fibrosis (E,F) who did not receive a PPM implant.

ECG and LGE findings in MMD

ID#: 368027

Comprehensive 3D Cine Steady-state Free Precession and 3D Cine Phase Contrast Cardiovascular Magnetic Resonance Examination

Mehdi H. Moghari, Ph.D.[1] Rob J. van der Geest, PhD[2], Andrew J. Powell, M.D.[3]

1. Harvard Medical School and Boston Children's Hospital

2. Department of Radiology, Leiden University Medical Center, The Netherlands, Leiden, Zuid-Holland, Netherlands

3. Harvard Medical School and Boston Children's Hospital, Boston, MA

Background: The typical CMR examination utilizes multiple 2D steady-state free precession (SSFP) and phase contrast (PC) sequences with repeated breath-holds. It requires careful planning of multiple imaging planes by a knowledgeable operator and yields blurred images in patients who are too young or ill to hold their breath. To address these deficiencies, we developed and tested a simply-planned, comprehensive, free-breathing 3D cine SSFP and 3D cine PC CMR examination.

Methods: The 3D cine SSFP and 3D cine PC sequences both utilized our “Heart-NAV” technique for prospective respiratory motion compensation [1]. Specifically, 4 excitations per cardiac cycle are re-purposed to generate a 1D signal that is routed into the scanner’s standard navigator processing system to track heart position. If all 4 signals are in end-expiration, cine data from the entire cardiac cycle is accepted. Both 3D cine sequences were acquired in the sagittal plane with an isotropic resolution of 2.0 mm and 30 phases per cardiac cycle. This facilitated off-line substitution of the SSFP images for the magnitude images of the PC dataset using a rigid-body registration algorithm. The result was a fused 3D cine dataset with the superior contrast-to-noise ratio of SSFP imaging and co-registered, superimposable flow data. To assess this approach, 15 patients (8 males, median age 18 yrs (range 11-58)) with informed consent underwent both a clinical 2D CMR study plus the 2 proposed 3D cine sequences on a 1.5T Philips Achieva scanner. First, the breath-hold 2D cine SSFP and free-breathing 2D cine PC sequence were acquired. Then, after receiving 0.15 mmol/kg gadobutrol contrast, the novel 3D cine SSFP (flip angle 60°, TE/TR 1.5/3.0 ms, SENSE x3), and 3D cine PC (flip angle 8°, TE/TR 2.1/3.8 ms, SENSE x4) sequences were performed. For comparison of ventricular parameters, the 3D cine SSFP data was reformatted into a short-axis plane.

Results: All 3D acquisitions were successfully completed. A 3D cine SSFP acquisition and its fusion with 3D cine flow data are shown in Fig. 1. The scan time was 6.3±1.8 min for 3D cine SSFP and 12.8±4.8 min for 3D cine PC. The mean 3D cine SSFP to 3D cine PC registration offset was 1.5±0.98 mm and 0.01±0.03°. The differences between 2D and 3D measurements of left ventricular parameters, ascending aorta and main pulmonary artery net blood flow, and Qp/Qs were all ≤9% (Table 1).

Conclusion: We developed and tested in patients a free-breathing 3D cine SSFP and 3D cine PC CMR examination with a scan time of ≈20 min, and found good agreement with 2D left ventricular and blood flow measurements. The single fused isotropic 3D cine dataset is well-suited for multiplanar reformatting, and provides a comprehensive anatomic and functional assessment. This strategy is a promising approach to simplify exam planning and eliminate breath-holding. References: [1] Moghari MH, MRM 2017. Funding: This work was supported by Higgins Family Noninvasive Imaging Research and Charles H. Hood Foundations.

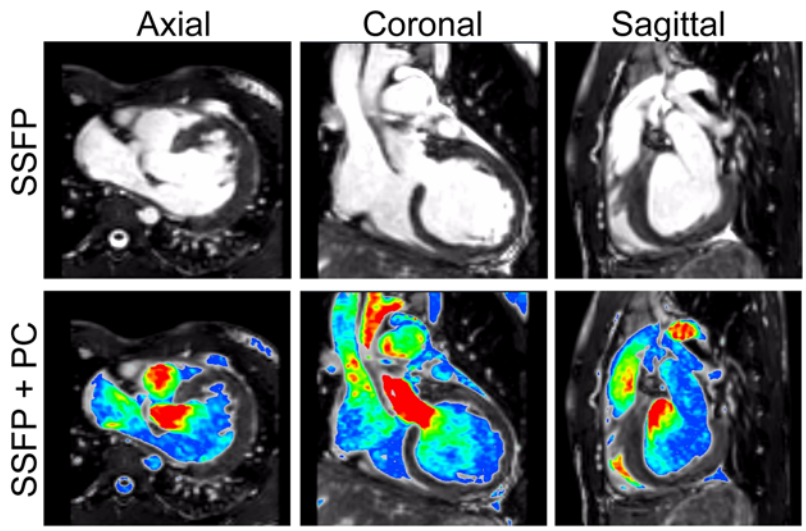

Figure 1: A representative example of a 3D cine steady-state free precession (SSFP) acquisition (top) and its fusion with a 3D cine phase contrast (PC) acquisition (i.e., velocity data) in axial, coronal, and sagittal orientations. The color represents the magnitude of the velocity vector.

Table 1: Comparison of 2D and 3D cine sequences for left ventricular and blood flow measurements (n=15). Values are mean ± standard deviation. AAo, ascending aorta; EDV, end-diastolic volume; EF, ejection fraction; ESV, end-systolic volume; MPA, main pulmonary artery, and SV, stroke volume.

	EDV (ml)	ESV (ml)	SV (ml)	EF (%)	Mass (g)	AAo Net flow (ml)	MPA Net flow (ml)	Q_p/Q_s
2D	169.9±59.3	71.1±28.3	98.7±34.9	58.6±7.4	97.0±32.9	82.7±33.6	84.6±31.8	1.0±0.1
3D	175.7±61.8	78.2±31.8	97.6±32.2	56.3±6.1	102.2±35.3	83.6±38.3	77.2±31.8	1.0±0.2
Mean difference (3D-2D)	5.9±8.6	7.0±7.3	-1.2±7.9	-2.3±3.3	5.3±9.9	0.9±16.1	-7.4±15.3	-0.1±0.2
Mean % difference (3D-2D)	3.4±5.5	9.3±9.5	-0.3±8.1	-3.7±5.6	5.8±11.8	-0.1±18.8	-8.9±21.4	-8.8±22.9
Correlation (3D vs. 2D)	0.99	0.98	0.98	0.90	0.96	0.91	0.88	-0.03
P-value (3D vs. 2D)	0.009	0.001	0.291	0.009	0.029	0.414	0.042	0.125

ID#: 368110

Diffusion tensor cardiovascular magnetic resonance assessment of recovered dilated cardiomyopathy

Zohya Khalique, MBBS[1] Pedro F. Ferreira, PhD[2], Andrew D. Scott, PhD[3], Sonia Nielles-Vallespin, PhD, MSc[4], Rick Wage, DCR (R)[5], David N. Firmin, PhD[6], Dudley J. Pennell, MD[7]

1. NIHR Cardiovascular Biomedical Research Unit, Royal Brompton Hospital, London, England, United Kingdom

2. Cardiovascular Magnetic Resonance Unit, Royal Brompton Hospital, Sydney Street, London, SW3 6NP, UK, England, United Kingdom

3. Royal Brompton Hospital, London, England, United Kingdom

4. NIH, MD

5. Royal Brompton Hospital NHS trust, England, United Kingdom

6. 1. Cardiovascular Magnetic Resonance Unit, Royal Brompton Hospital, Sydney Street, London, SW3 6NP, UK, England, United Kingdom

7. Royal Brompton Hospital and Imperial College, London, England, United Kingdom

Background: Diffusion tensor cardiovascular magnetic resonance (DT-CMR) can assess the microstructure of the myocardium in vivo, providing information on myocyte and sheetlet organisation. Impaired sheetlet mobility has been demonstrated in dilated cardiomyopathy (DCM) [1]. Approximately a third of DCM patients reverse remodel, exhibiting improved LV size and ejection fraction [2]. However, in these recovered DCM (R-DCM) patients there has been no study of microstructural recovery.

Methods: DT-CMR was performed in 11 DCM patients, 11 R-DCM patients and 11 healthy controls. R-DCM patients had normal LV size and ejection fraction (EF) within age and sex matched indexed reference ranges. All patients were New York Heart Association heart failure class I. Both R-DCM and DCM patients had a diagnosis of idiopathic DCM. A STEAM EPI sequence with b150 and b600 at 3T was used. LV myocyte orientation (helix angle, HA), sheetlet orientation (angle of the second eigenvector, E2A), EF and peak radial strain were calculated. R-DCM findings were compared to DCM and controls using the Mann-Whitney test.

Results: All groups were age and sex matched. In R-DCM, the median [IQR] EF at baseline was 28 [20]% and current EF was 63 [7]%. The EF was 32 [13]% in DCM, and 65 [4]% in controls.

The median systolic HA gradient (HAG) in R-DCM (0.85 [0.17]°/%) did not differ from DCM (0.68 [0.26]°/%, p=0.09) or control group (0.92 [0.19]°/%, p=0.15).

Diastolic E2A in the R-DCM group was 25 [8]°, similar to DCM 19 [13]° (p=0.09) and controls 19 [14]° (p=0.12). The systolic E2A in R-DCM was 59 [16]°; significantly greater than the DCM group (33 [18]° (p<0.001), but comparable to the control subjects (65 [5]°, p=0.04). E2A mobility was 35 [9]° in the R-DCM group; significantly greater than the DCM group (8 [15]°, p<0.001), but less than the control group (47 [13]° p=0.002). Peak radial strain was 0.39 [0.16] in R-DCM, greater than the DCM cohort, 0.17 [0.13] (p=0.01), but less than the control group, 0.55 [0.16] (p=0.02).

Conclusion: This is the first report of DT-CMR in R-DCM. Despite normal LV size and ejection fraction, R-DCM patients have persistent microstructural abnormalities, with sheetlet mobility impaired compared to controls. Sheetlet mobility may offer a role in disease monitoring and assessment of recovery.

References

1.Nielles-Vallespin S, J Am Coll Cardiol. 2017;69:661-76.
2.Merlo M, J Am Coll Cardiol. 2011;57:1468-76

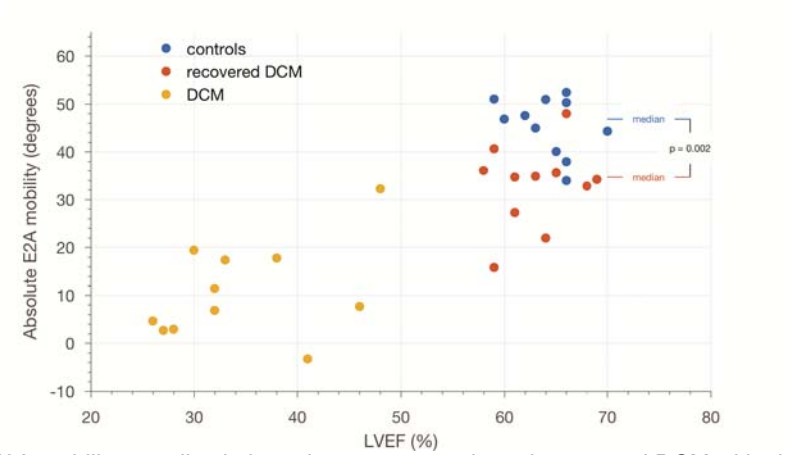

E2A mobility can discriminate between controls and recovered DCM with similar ejection fractions

ID#: 368195

3D Whole-Ventricle, Free-breathing, ECG-less, Myocardial T1 Mapping with CMR Multitasking

Jaime L. Shaw, MS[1] Anthony G. Christodoulou, PhD[2], Xiaoming Bi, PhD[3], Debiao Li, PhD[2]

1. Cedars-Sinai Medical Center/UCLA, CA

2. Cedars-Sinai Medical Center, Los Angeles, CA

3. Siemens Healthineers, Los Angeles, CA, United States, CA

Background: Myocardial T1 mapping is known to characterize both focal and diffuse myocardial fibrosis, important factors associated with adverse outcomes in cardiovascular disease.[1] Current 3D cardiac T1 mapping techniques are generally limited by the use of a respiratory navigator with long unpredictable scan times or multiple breath-holds with potential image misregistration. Additionally, the use of ECG gating is a source of error and reduced reproducibility in T1 mapping. We propose eliminating these limitations 3D T1 mapping with CMR Multitasking, a continuous acquisition technique using a low-rank tensor (LRT) imaging framework.[2,3]

Methods: The proposed sequence uses a prototype 3D stack-of-stars trajectory modified to collect auxiliary data interleaved with image data: odd readouts are image data incremented by the golden-angle, and even readouts are auxiliary data 0° trajectories at the center partition. The continuous acquisition sequence applies inversion recovery pulses at set intervals to achieve T1 recovery and collects small-angle FLASH readouts to sample the entire T1 recovery period. Sequence parameters were: fixed scan time of 9:52 min, 2.5 s between IRs, TE/TR = 2.8/6.1ms, flip angle = 5°, 20 slices, slice thickness = 4.0 mm, no slice gap, in-plane resolution = 1.7x1.7 mm^2.
First, real-time low-rank matrix images[4] were reconstructed from the image data and auxiliary data for cardiac and respiratory motion binning. Next, LRT reconstruction was performed using an explicit tensor subspace constraint estimated from the auxiliary data and a dictionary of Bloch equation T1 curves to produce 402 inversion time (TI) images (range: 3.6-2,476.0 ms, 12.2 ms temporal resolution) with 20 cardiac and 6 respiratory phases. Pixel-wise T1 maps were created by fitting to a FLASH-IR model at an end-expiration and a diastolic phase.
Six healthy subjects (3 female, age 35 ± 9) were scanned at 3T (Siemens Verio) with the proposed method as well as a 1.7x1.7x8.0 mm^3 breath-hold, ECG-gated, MOLLI 5(3)3.[5] For both methods, T1 was measured with an ROI in the septum

Results: The figure shows native T1 maps from the proposed 3D method from one healthy subject. T1 values in 3 out of 20 slices for all subjects from Multitasking 3D T1 mapping are shown in the table. The 3D Multitasking method underestimates T1 compared to MOLLI, although are within the published normal range at 3T. The bias between 3D Multitasking and MOLLI T1 values may potentially be due to the different steady-state behavior of blood flowing through the myocardium for different excitation schemes: a continuous-acquisition 3D volumetric FLASH excitation (Multitasking) versus less-frequent 2D slice-selective TrueFISP excitation (MOLLI).

Conclusion: We demonstrate the feasibility of a 3D free-breathing, ECG-less, T1 mapping technique to produce whole-ventricle T1 maps. The proposed method shows promise as a 3D T1 mapping technique in a fixed scan time with no dependence on heart rate or breath holds.
References:
1. Puntmann Circ Res 2016; 2. Shaw JL ISMRM 2017; 3. Christodoulou AG ISMRM 2017; 4. Christodoulou AG IEEE TBE 2013; 5. Xue H MRM 2013.

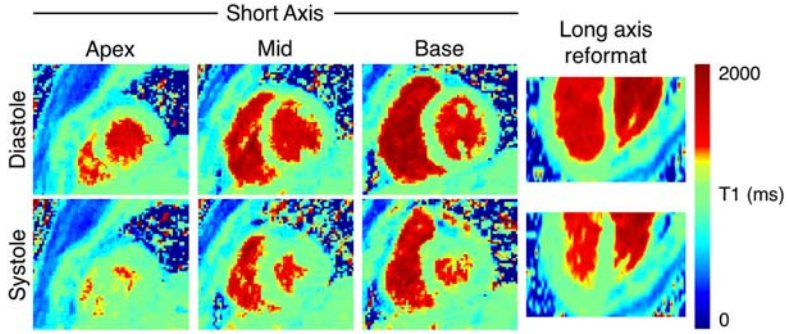

Native Myocardial T1 values from 3D Multitasking and 2D MOLLI T1 Mapping

T1(ms)	3D Multitasking	2D MOLLI
Base	1102 ± 70	
Mid	1147 ± 65	1276 ± 38
Apex	1156 ± 44	

ID#: 363910

Does raphe in bicuspid aortic valve have an impact on flow dynamics in the ascending aorta?

Aroa Ruiz-Muñoz, MSc[4]Lydia Dux-Santoy[1], Andrea Guala[2], Gisela Teixido-Tura, MD, PhD[1], GIULIANA MALDONADO, MD[3], Nicolas Villalva, MD[1], Filipa X. Valente, MD[3], Augusto Sao-Aviles, PhD[4], Laura Galian, MD[4], Laura Gutierrez, MD[4], Ruben Fernandez-Galera, MD[4], Teresa Gonzalez-Alujas, MD, PhD[4], David Garcia-Dorado, MD, PhD[4], Arturo Evangelista[4], José F. Rodríguez-Palomares, MD, PhD[2]

1. Hospital Universitari Vall d´Hebron. Vall d'Hebron Institut de Recerca. Universitat Autònoma de Barcelona, Catalonia, Spain

2. Hospital Universitari Vall d´Hebron. Vall d'Hebron Institut de Recerca. Universitat Autònoma de Barcelona, Barcelona, Catalonia, Spain

3. Hospital Universitari Vall d´Hebron. Vall d'Hebron Institut de Recerca. Universitat Autònoma de Barcelona, Barcelona, Spain

4. Hospital Universitari Vall d´Hebron. Vall d'Hebron Institut de Recerca. Universitat Autònoma de Barcelona, Spain

Background: The presence of raphe is a common finding in bicuspid aortic valve (BAV) and has been related to higher prevalence of significant aortic valvulopathy and increased rate of aortic surgery. However, its influence in flow dynamics and ascending aorta (AscAo) dilation has not been explored. Thus, using 4D-flow MRI we analysed if BAV patients with raphe present different alterations in AscAo flow dynamics and may benefit from a closer follow-up with advanced imaging.

Methods: One hundred and seventeen BAV patients (74.4% RL-BAV) with aortic diameters ≤55 mm and no severe valvulopathy assessed by echocardiography underwent 2D cine MRI and 4D-flow with PC-VIPR sequence in a GE 1.5T scanner. Valve morphology (fusion phenotype, raphe and calcification) was also determined by echo. Demographics and cardiovascular risk factors (hypertension, diabetes, dyslipidemia) were collected from clinical records. Aortic diameters by 2D cine MRI were used to obtain z-score for both sinuses (zsinus) and AscAo (zAscAo). AscAo morphotype was classified in non-dilated (zsinus<2 and zAscAo<2), root (zsinus>2 and zsinus>zAscAo) or ascending (zAscAo>2 and zAscAo>zsinus).
The thoracic aorta was semi-automatically segmented from an angiogram derived from the 4D-flow. Eight equidistant analysis planes orthogonal to the aortic centreline were distributed in the AscAo, from the sinotubular junction to the brachiocephalic trunk. Velocity data was exported to in-house code and peak-systolic velocity magnitude, jet angle, normalized flow displacement, and regional and contour-averaged axial and circumferential wall shear stress (WSS) were calculated for each plane. Also, systolic flow reversal ratio (SFRR), the ratio of backward to forward flow at systole, was obtained.

Results: Most BAV patients (69.2%) presented raphe, which mainly affected the RL-phenotype (73.6% RL-BAV vs 56.7% RN-BAV). No differences were found when comparing demographic and clinical variables between BAV with and without raphe, including aortic valvulopathy (p=0.39 for regurgitation, p=0.26 for stenosis). AscAo dilation morphotype was also similar in both groups (Table 1).
The analysis of AscAo flow dynamics showed no differences between groups, which presented similar velocity, flow eccentricity and contour-averaged WSS along the AscAo (Table 1 and Figure 1). Moreover, there were no regional differences in WSS distribution in the aortic wall (Figure 2).

Conclusion: The presence of raphe in BAV, in the absence of severe valvulopathy, has no impact on AscAo flow dynamics. Thus, the clinical impact of raphe is limited to the aortic valve itself, indicating that conventional follow-up with transthoracic echocardiography seems sufficient for these patients.

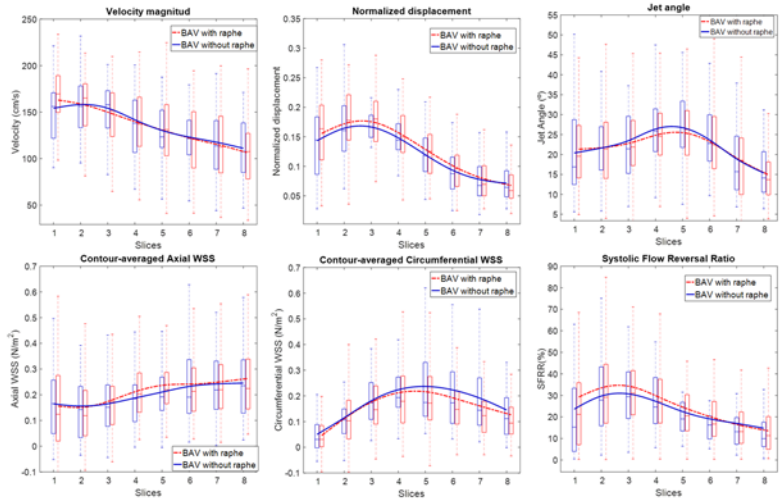

Figure 1. Flow variables distribution (mean value and boxplots) along the ascending aorta in BAV patients with and without raphe.

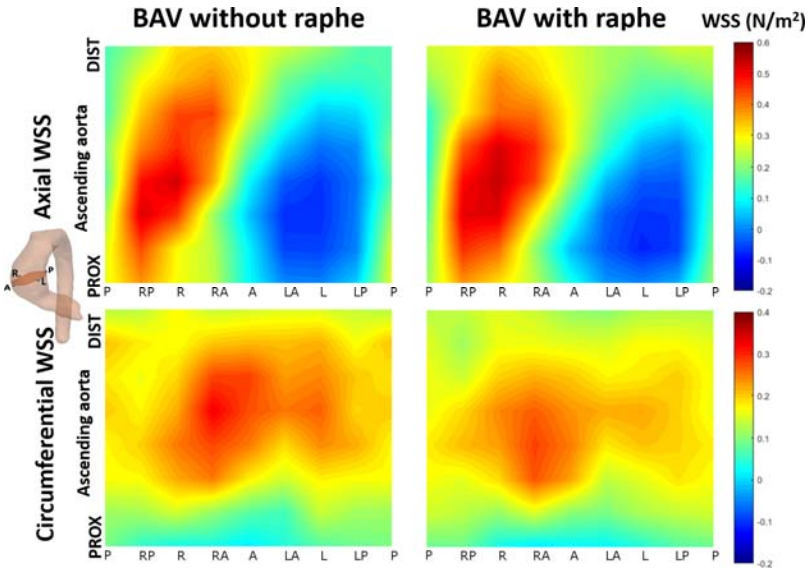

Figure 2. Mean regional axial and circumferential WSS for BAV patients without and with raphe.

Table 1. Dilation morphotype and flow dynamics in proximal, mid and distal ascending aorta in BAV.

		BAV without raphe (n=36)	BAV with raphe (n=81)	p-value
Ascending aorta dilation morphotype				0.81
Non-dilated		19.4	23.5	
Ascending		75	69.1	
Root		5.6	7.4	
Flow dynamics				
Velocity (cm/s)	Prox (slice 2)	158.8±36.7	158.34±37.0	0.95

	Mid (slice 5)	129.7±40.4	129.6±37.1	0.99
	Dist (slice 8)	110.9±41.1	106.0±32.9	0.49
Jet angle (°)	Prox (slice 2)	21.8±8.3	21.7±9.6	0.93
	Mid (slice 5)	26.9±8.7	25.4±9.2	0.40
	Dist (slice 8)	15.6±6.5	15.1±8.0	0.71
Norm. displ.	Prox (slice 2)	0.17±0.06	0.18±0.06	0.44
	Mid (slice 5)	0.12±0.04	0.12±0.04	0.65
	Dist (slice 8)	0.07±0.03	0.07±0.03	0.54
WSSax (N/m^2)	Prox (slice 2)	0.15±0.12	0.14±0.14	0.72
	Mid (slice 5)	0.21±0.12	0.25±0.14	0.15
	Dist (slice 8)	0.24±0.13	0.26±0.17	0.53
WSScirc (N/m^2)	Prox (slice 2)	0.11±0.09	0.12±0.12	0.52
	Mid (slice 5)	0.24±0.16	0.22±0.17	0.51
	Dist (slice 8)	0.14±0.13	0.13±0.14	0.55
SFRR (%)	Prox (slice 2)	30.6±20.2	34.4±28.9	0.48
	Mid (slice 5)	22.1±14.0	23.4±15.7	0.66
	Dist (slice 8)	14.7±14.5	13.6±11.4	0.66

ID#: 364234

Robust myocardial T1 measurement in PVC patients with arrhythmia-insensitive-SASHA (AI-SASHA)

Zachary B. Rodgers, MD, PhD[1] Srikant K. Iyer, PhD[2], Saharsh Dass, BS[3], Walter R. Witschey, PhD[4], Yuchi Han, MD, MMSc[4]

1. UNIVERSITY OF PENNSYLVANIA HEALTH SYSTEM, Philadelphia, PA

2. University of Pennsylvania

3. University of Pennsylvania, PA

4. University of Pennsylvania, Philadelphia, PA

Background: Current myocardial T1 mapping techniques perform poorly in the presence of premature ventricular contractions (PVCs), which are present in 40% of the general population[1] and ubiquitous in patients with heart disease. MOLLI,[2] the most common T1 mapping method, has several sources of error in PVCs: 1) intrinsic dependence on heart rate,[3] 2) PVC-induced motion artifacts, and 3) through-plane-motion-induced perturbation of the inversion recovery curve. This raises concern for confounding in studies demonstrating increased T1 in patients with ventricular arrhythmias.[4,5]

Saturation-recovery-based techniques (i.e., SASHA)[6] are robust against heart rate and through-plane motion, but still prone to motion artifacts. Furthermore, precision of SASHA T1 values is relatively poor,[7] thus, removing PVC-contaminated data prior to fitting is not feasible. This work proposes a free-breathing, arrhythmia-insensitive SASHA (AI-SASHA) pulse sequence to improve T1 mapping in patients with PVCs.

Methods: Ten subjects (age 42+/-17 years, 8 males), five with PVCs, were scanned (Siemens Avanto 1.5T) with 5(3)3 breath-hold MOLLI,[8] standard breath-hold SASHA with one non-saturated (NS) and ten saturation-recovered (SR) images,[6] and AI-SASHA, at a single mid-ventricular short-axis slice. To assess repeatability, one subject was scanned five times with each method. AI-SASHA consisted of a NS bSSFP acquisition followed by five 600 ms SR acquisitions and a four-second recovery period, repeated 10 times, producing 60 total images.[9] Scan time was 113+/-22 seconds. All processing was performed in Matlab (Figure 1). First, ECG data was used to eliminate PVC-corrupted images. Next, end-expiratory images were selected via respiratory self-navigating. This image subset then underwent non-rigid motion correction prior to T1 fitting. For standard MOLLI and SASHA sequences, motion correction was performed online.[10] For all methods, myocardial ROIs were manually segmented from T1 maps, and standard deviation (SD) of voxel-wise myocardial T1 values were calculated to assess precision.

Results: AI-SASHA achieved improved image quality compared to standard methods, especially in PVC patients (Figure 2). Myocardial mean T1 values (Figure 3a) were expectedly higher for all SASHA variants compared to MOLLI. Precision, represented by voxel-wise T1 SD (Figure 3b), was superior for AI-SASHA (67+/-15 ms) compared to SASHA (104+/-22 ms) and MOLLI (93+/-17 ms). SDs of mean myocardial T1 values in the single-subject repeatability assessment (Figure 3c) were considerably lower with AI-SASHA.

Conclusion: AI-SASHA is a promising approach for myocardial T1 quantification in PVC patients, achieving improved T1 precision and repeatability compared to standard SASHA and MOLLI. Reductions in scan time may be achieved by incorporating high-contrast image acquisition[9] to improve motion correction. **References:** [1] Paula-Barbosa MM, et al. *Exp Neurol.* 1989; [2] Messroghli DR, et al. *MRM* 2004; [3] Piechnik SK, et al. *JCMR* 2010; [4] Singh A, et al. *SCMR* 2016, p. 211; [5] Nakamori S, et al. *JMRI* 2017; [6] Chow K, et al. *MRM* 2014; [7] Kellman P, et al. *JCMR* 2014; [8] Kellman P, et al. *JCMR* 2012; [9] Chow K, et al. *JCMR* 2016; [10] Xue H, et al. *MRM* 2013; [11] Contijoch F, et al. *Circ. Arrhythm. Electrophysiol.* 2016; [12] Avants BB, et al. *Neuroimage* 2011.

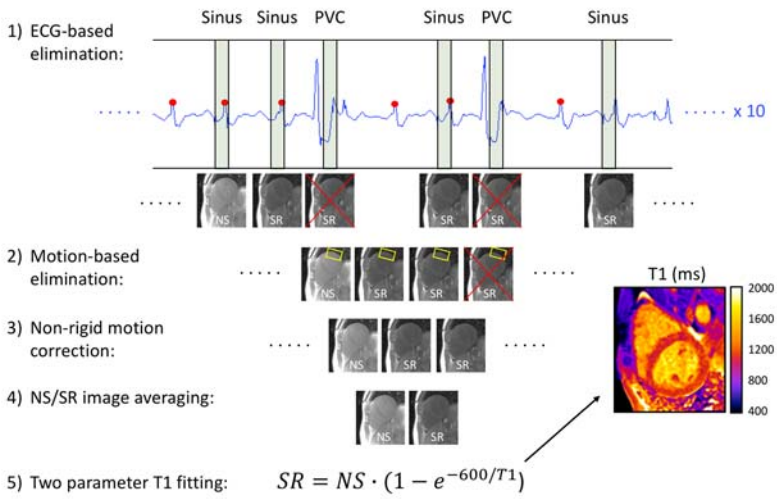

Figure 1: 60 initial AI-SASHA images (50 SR and 10 NS) are used to produce a final T1 map in the following steps: 1) Semi-automated elimination of PVC-corrupted images from acquisition-synced ECG data [11]. Red dots indicate ECG triggers for subsequent green acquisition windows. 2) Respiratory navigator based removal of images not acquired during end-expiration. Yellow box indicates the navigator window. 3) Non-rigid registration of images using ANTs [12]. 4) Averaging of the remaining images to produce a single NS and SR map. 5) Two-parameter T1 fitting. The total number of original images preserved for T1 fitting was 32+/-10 in PVC patients and 47+/-8 in controls.

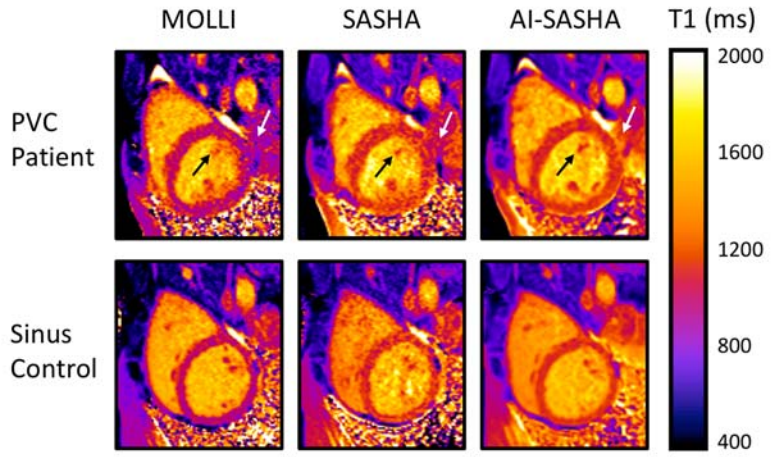

Figure 2: MOLLI, SASHA, AI-SASHA T1 maps from a representative PVC patient and control. In the PVC patient, AI-SASHA shows improved visualization of fine features such as papillary muscles (black arrows) and the posterior ventricular wall (white arrows) compared to standard MOLLI or SASHA.

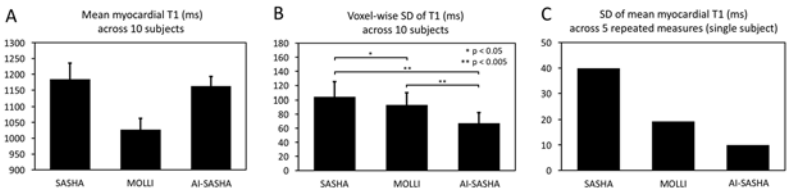

Figure 3: A) MOLLI mean myocardial T1 values were considerably lower than any of the SASHA variants. B) Precision of AI-SASHA is improved compared to MOLLI and SASHA. P-values were calculated from paired Student's T-tests. C) In a single subject, AI-SASHA had improved repeatability compared to MOLLI or SASHA.

ID#: 366324

A Quality Assurance Program for Standardizing T1-mapping for International Multicentre Studies - A Hypertrophic Cardiomyopathy (HCMR) Sub-Study

Qiang Zhang, Ph.D[1] Christopher M. Kramer, MD[2], Stefan Neubauer, MD, FRCP[3], Stefan K. Piechnik, PhD, MScEE[3]

1. University of Oxford Centre for Clinical Magnetic Resonance Research, Oxford, England, United Kingdom

2. University of Virginia Health System, Charlottesville, VA

3. University of Oxford, England, United Kingdom

Background: CMR T1-mapping has shown promise as a novel biomarker to support diagnostic, therapeutic and prognostic decision-making. It is clear that T1 measures depend on the acquisition method and other factors, as well as development of standardized quality assurance (QA) approaches. We report preliminary results of a T1-mapping QA program from the multinational HCMR study. We gratefully acknowledge all participating "HCMR study investigators" who will be named for the pending full publication.

Methods: 38 participating sites were distributed a dedicated HCMR T1 phantom, containing 9 compartments, arranged as a 3×3 array of plastic tubes filled with gels, to achieve T1/T2 combinations in the range of 50–3000 ms. The sites were also provided instructions and protocols to perform short-term repeated ShMOLLI T1-mapping acquisitions, and an inversion recovery spin-echo (IR-SE) as the reference T1-mapping method. We report early results on 46 scans acquired at 22 sites using MR systems from a single-vendor, evaluating the consistency of cardiac T1 measures in a combination of two field strengths 1.5T (33 scans), 3T (13 scans), and 3 software versions (21, 19, 6 scans). T1 values in the centre regions of each compartment were compared against the reference T1 to detect any patterns of departure from the norm.

Results: 286 T1-maps were analysed, with results shown in Fig. 1. 271 acquisitions converged completely with the expected pattern (Fig. 1, "Group 1"). Within the typical T1 range of tissues, including myocardium and blood (< 2000 ms), the ShMOLLI T1s showed high consistency with their characteristic relationship to the reference T1s in all the acquisitions. One clear outlier was caused by an artefact in a reference IR-SE acquisition (Fig.1, "Outlier 1"). 15 acquisitions showed departures in the long T1 range (Fig. 1, "Group 2"), attributed to the lack of adequate waiting time between acquisitions. All 46 datasets passed QA, by producing at least one ShMOLLI T1-map acquisition consistent with the expected pattern.

Conclusion: We demonstrate the successful deployment of a QA program for standardizing T1-mapping in a multicentre, single vendor setting, using 2 field-strengths and 3 software versions. Further analysis is required to assess the impacts of the identified minor departures from the protocol and to compare T1 measurements between vendors.

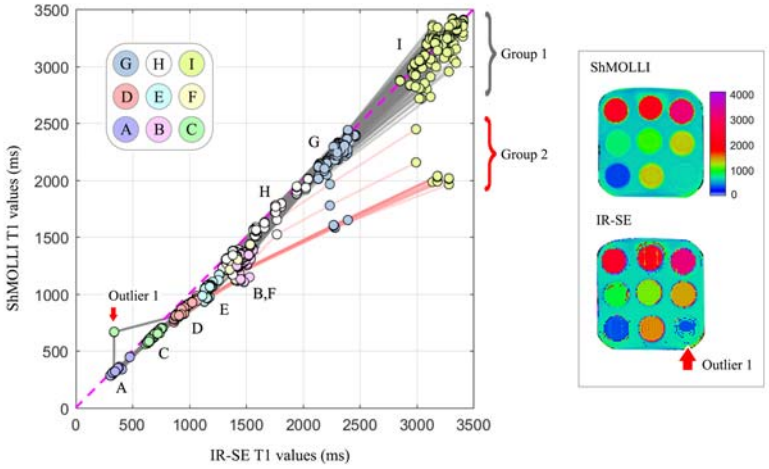

Figure 1. ShMOLLI T1 quality assessment measurements against IR-SE T1. 286 acquisitions from 46 scans. The 9 phantom tubes are shown as circles in the plot in 9 colours (A to I). "Outlier 1" demonstrates the source of one outlier (plot on the left, red arrow), caused by an artefact in the IR-SE T1-map (right panel, bottom, red arrow). Long-T1 tubes G, H, I allow extra sensitivity to detect small departures from measurement protocol. "Group 1" are

data points from acquisitions deemed to be within QA tolerance. “Group 2” show the capacity of the phantom design to detect discrepancy from the expected pattern at long-T1 range.

ID#: 378362

Role of gender in clinical presentation, morpho-functional and tissue characterization features of arrhythmogenic cardiomyopathy.

Anna Piccoli, MD[1]Manuel De Lazzari, MD, PhD[2], Alberto Cipriani, MD[2], Benedetta Giorgi, MD[3], Ilaria Rigato, MD, PhD[2], Sabino Iliceto, MD, PhD[2], Gaetano Thiene, MD[2], Martina Perazzolo Marra, MD, PhD[2], Domenico Corrado, MD, PhD[2], Cristina Basso, MD, PhD[2], Barbara Bauce, MD, PhD[4]

1. Division of Cardiology, Department of Medicine, University of Verona, Verona, Italy, Verona, Veneto, Italy

2. Department of Cardiac, Thoracic and Vascular Sciences, University of Padova, Italy, Italy

3. Department of Medicine, University of Padua Medical School, Italy, Padua, Veneto, Italy

4. Department of Cardiac, Thoracic and Vascular Sciences, University of Padova, Italy, Padova, Italy

Background: Arrhythmogenic cardiomyopathy (AC) is an uncommon disease characterized by diffuse or segmental loss of myocytes with replacement by fibro-fatty tissue. Even if this is an inherited disease, mostly transmitted with autosomal dominant trait, sex differences are commonly reported. We aimed to compare clinical features and cardiac magnetic resonance (CMR) findings at presentation in males and females with AC.

Methods: A total of 86 probands (37 females and 49 males) diagnosed as either “affected” or “borderline” according to 2010 Task Force Criteria were included. All patients underwent a CMR, performed following the complete AC protocol. Baseline clinical characteristics were compared by gender.

Results: Males showed a younger age at presentation (29 years vs 32; P = 0,026) and they were more frequently index cases (76% vs 40%, P=0,001) and competitive athletes (48% vs 14%, P=0,001). No gender difference was found considering the prevalence of definite and borderline diagnosis, whereas abnormal signal-averaged ECGs were more present in males than females (43% vs 19%, P=0,035). At CMR, males had higher prevalence of right ventricle (RV) dilatation (67% vs 30%, P=0,001) with lower RV ejection fraction (45% vs 56%, P=0,004). Consistently wall motion abnormalities of the RV were present more often in males than females (71% vs 46%, P=0,017) with a higher prevalence of scar in the RV anterolateral wall (63% vs 32%, P=0,005). Considering patients with a history of major cardiac events (MACE) at presentation, the presence of major imaging criteria at CMR resulted significantly higher in male gender (74% vs 42%, P=0,029).

Conclusion: In our study, we found similar frequency of “affected” and “borderline” subjects between males and females with no difference in cardiac events at presentation. Males showed right ventricles with bigger volumes, higher prevalence of wall motion abnormalities and lower ejection fraction. Among patients with MACE at presentation, the presence of major imaging criteria at CMR was significantly higher in male gender.

ID#: 378293

Characterize Ventricular Remodeling Features of Cardiac Sarcoidosis with Magnetic Resonance Imaging

Chenying Lu[1] David H. Feiglin[2], Ernest Scalzetti[3], Jiansong Ji[1], Tiemin Wei[1], Linchun Lv, medical practitioner[4], Kan Liu[3]

1. Lishui Hospital of Zhejiang University, China (People's Republic)

2. Upstate Medical University, Syracuse, NY

3. Upstate Medical University

4. Lishui Hospital of Zhejiang University, lishui, Zhejiang, China (People's Republic)

Background: The poor prognosis of cardiac sarcoidosis (CS) underscores the need for risk stratification. Cardiac magnetic resonance (CMR) can use late gadolinium enhancement (LGE) to identify chronic fibrosis/scar. Nevertheless, when LGE becomes detectable, it is often too late to reverse the pathological myocardial remodeling in CS patients. We investigate ventricular morphological features and characterize remodeling patterns, to improve the diagnostic/ prognostic values of the CMR for early-stage CS.

Methods: We studied 122 consecutive sarcoidosis patients who were referred for CMR evaluation for cardiac symptoms or abnormal electrocardiograms from August of 2008 to July of 2017. Using standard non-contrast CMR cine sequences, we determined left ventricular (LV) remodeling patterns based on both LV mass and ventricular geometric features. Relative wall thickness (RWT) was calculated as the sum of septal wall thickness and lateral wall thickness divided by LV end diastolic diameter. Four LV remodeling patterns were identified as type I: (concentric LV hypertrophy (LVH): increased LV mass with increased RWT (>0.42), type II: eccentric LVH: increased LV mass with normal RWT (≤0.42), type III: concentric remodeling: normal LV mass with increased RWT, and type IV: no remodeling: normal LV mass with normal RWT. Meanwhile, the presence and distribution of LGE and myocardial edema were assessed in the standard 17-segment LV model with either contrast T1-weighted 3-dimensional double inversion recovery images and non-contrast T2-weighted short-tau inversion recovery images. The LGE in each segment was categorized based on the locations of CS myocardial involvement (subepicardial, subendocardial, intramural, and transmural).

Results: CS was diagnosed in 38 of 122 (31.1%) patients based on updated Japanese Ministry of Health and Welfare, and Heart Rhythm Society. Systolic dysfunction (LVEF <50%) occurred in 18 of 38 (47.4%) CS patients. CS patients had overall higher LV wall thickness (0.48 vs. 0.37.) and LV mass index (58.99 vs. 48.94). Abnormal LV remodeling patterns (type I-III) were more common (65.7 % vs.10.7%) in CS patients. The concentric remodeling pattern (type III) was the most dominant (57.9%) phenotypes. Overall 26 CS patients were found to have myocardial LGE, and 10 of them had multiple patchy myocardial LGE. LGE was found in 58 of 476 (12.18%) LV segments. The most LGE appeared in intramural locations(61.07%), followed by subepicardial locations (32.76%). Only 2 patients had myocardial edema.

Conclusion: Integrating ventricular morphological features/ remodeling patterns into traditional clinical and imaging criteria significantly improves diagnostic sensitivity of early stage CS.

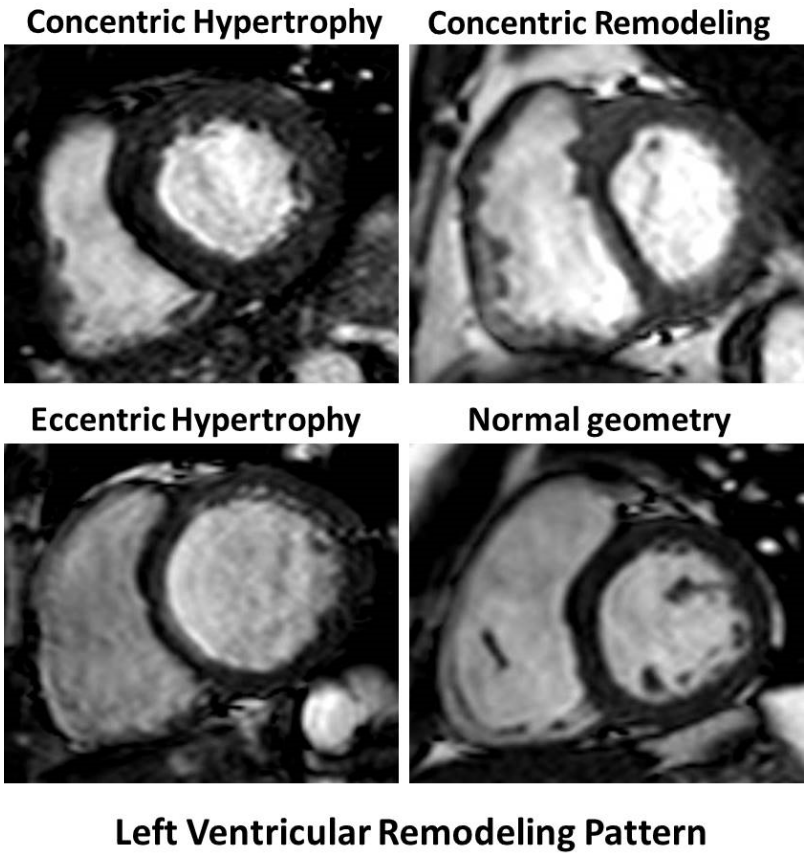

LV remodeling patterns. The example of a short-axis cine image.

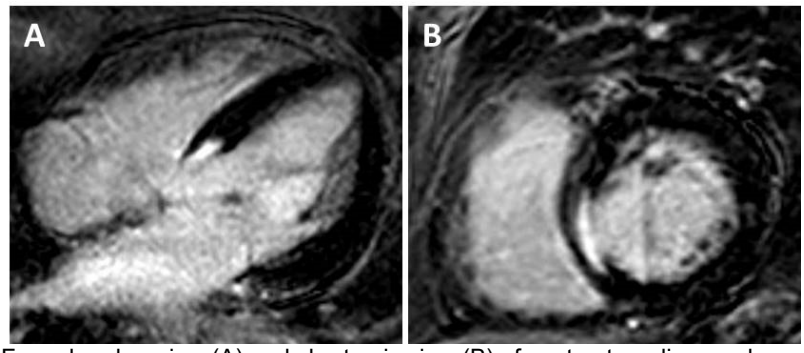

Four chamber view (A) and short-axis view (B) of contrast cardiovascular magnetic resonance. A 76-year-old man with a history of pulmonary sarcoidosis. Abnormal area of intramyocardial enhancement involving the basal anteroseptal segment, in a pattern and distribution which could be consistent with sarcoid. LVEF is 47.8%.

ID#: 378147

T1 mapping in myocardial regions without focal fibrosis in patients with Chagas heart disease

Rodrigo de Jesus Louzeiro. Melo, MD[1]Antonildes Nascimento. Assuncao, Jr., MD[2], Thamara Morais, MD[1], Fabio Fernandes, MD, PhD[1], Barbara Ianni, MD, PhD[1], Charles Mady, MD, PhD[1], Carlos E. Rochitte, MD, PhD[3]

1. Heart Institute (InCor), University of Sao Paulo, Brazil

2. Heart Institute (InCor), University of Sao Paulo, Sao Paulo, Sao Paulo, Brazil

3. Heart Institute - InCor - University of São Paulo Medical School and Hospital do Coração - Heart Hospital - HCOR, São Paulo, Brazil

Background: Chagas heart disease (CD) is characterized by extensive and progressive myocardial fibrosis identified by LGE-CMR, which usually is associated with irreversible adverse left ventricular remodeling and worse prognosis. T1 mapping, on the other hand, may identity subclinical diffuse changes potentially treatable. The goal of this study was to investigate T1 mapping indices in different clinical stages of CD assessed in myocardial regions without focal LGE.

Methods: Sixty-six patients with CD (clinical stages: 24 indeterminate, 12 abnormal ECG only, 13 with LV ejection fraction [LVEF] 40-50%, and 17 with LVEF <40%) and 18 healthy control subjects were enrolled to a 1.5T CMR exam (Philips Achieva, Best, The Netherlands). MOLLI short-axis images were acquired prior, and 15 minutes after an intravenous bolus of gadolinium-based contrast. Native T1 and extracellular volume (ECV) were calculated only for segments without focal LGE. T1 times were measured using CVI42 (Circle Cardiovascular Imaging, Calgary, Canada).

Results: No differences in ECV and native T1 were found when compared indeterminate and only abnormal ECG stages with control subjects. However, both groups LVEF 40-50% and <40% presented significantly expanded ECV when compared with other groups (p<0.01). Native T1 was also significantly higher in patients with LVEF 40-50% compared to controls (1054 ± 33ms versus 998 ± 43ms, p=0.02) (Figure 1 and 2).

Conclusion: Tissue characterization using T1 mapping in CD suggested a diffuse myocardial extracellular matrix expansion. Once T1 mapping changes may reflect disease activity and reversible damage, the finding of expanded ECV in myocardium without focal fibrosis warrants further investigation, particularly in patients with low-normal to mild left ventricular dysfunction.

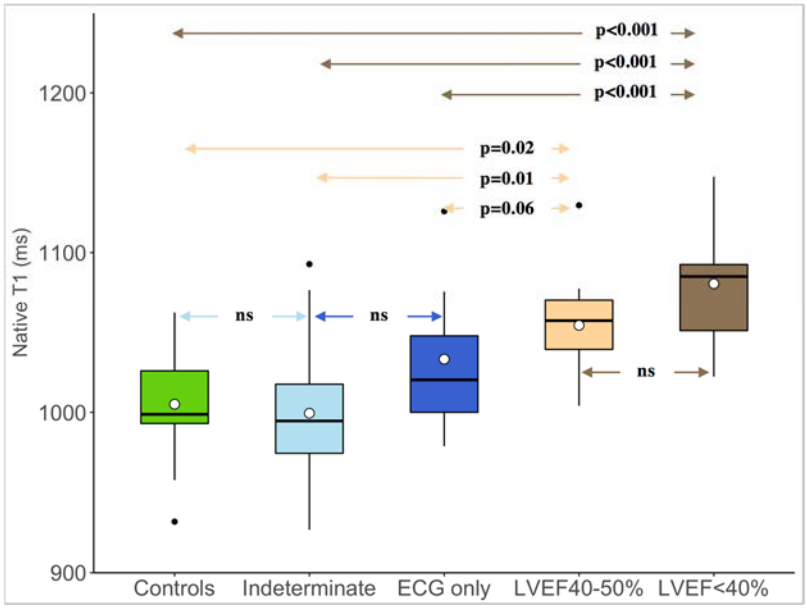

Figure 1. Native T1 by CMR in different clinical stages of Chagas Heart Disease.

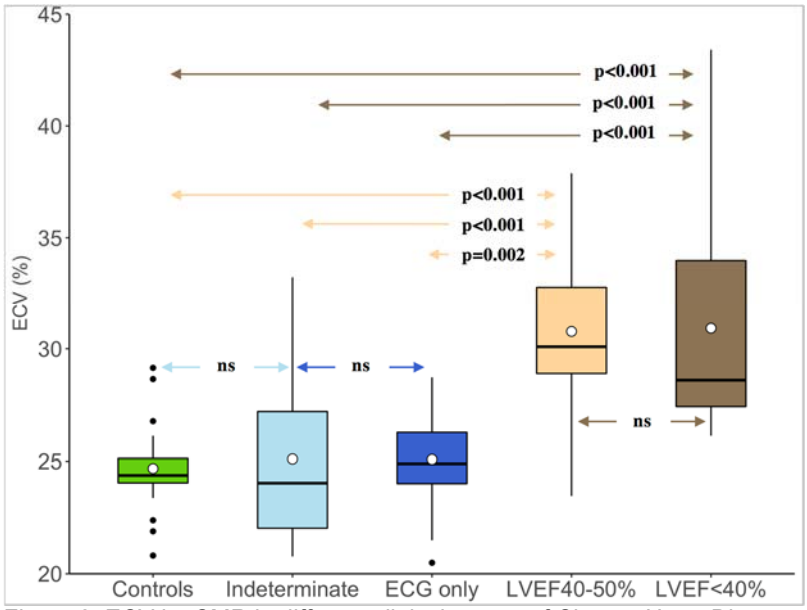

Figure 2. ECV by CMR in different clinical stages of Chagas Heart Disease.

ID#: 378115

Acute effects of haemodialysis on cardiac function and tissue characterisation

Tushar Kotecha, MRCP(UK) MBChB[1] Ana Martinez Naharro, MD[2], Suree Yoowannakul[3], Tamer Rezk, BSc[4], Michele Boldrini[4], Rohin Francis, MBBS[4], Daniel S. Knight[2], Philip N. Hawkins[5], James Moon, MD[6], Vivek Muthurangu, MD[7], Peter Kellman, PhD[8], Julian D. Gillmore[5], Andrew Davenport, MD[9], Marianna Fontana, MD, PhD[4]

1. Royal Free London NHS Foundation Trust, London, England, United Kingdom

2. UCL Department of CMR, Royal Free Hospital, London, England, United Kingdom

3. Royal Free London NHS Foundation Trust, United Kingdom

4. UCL Department of CMR, Royal Free Hospital, England, United Kingdom

5. National Amyloidosis Centre, University College London, England, United Kingdom

6. UCL, England, United Kingdom

7. Institute of Cardiovascular Science, University College London, England, United Kingdom

8. National Heart, Lung, and Blood Institute, National Institutes of Health, Bethesda, MD

9. UCL Centre for Nephrology, Univeristy College London, United Kingdom

Background: Renal failure with concomitant cardiac dysfunction is associated with poor prognosis. Studies have shown improvement in left ventricular (LV) dynamics after patients with LV impairment are established on dialysis. It has also been shown that native T1 is elevated in patients undergoing haemodialysis. However, the immediate effects of haemodialysis on these parameters are yet to be established. The aim of this study was to assess the acute effects of haemodialysis on biventricular haemodynamics, native T1 and myocardial T2.

Methods: Ten patients (8 male, age 65±17 years) with chronic renal failure and established on dialysis underwent non-contrast CMR scanning at 1.5T before and immediately after a haemodialysis session. Each study included either standard breath-held segmented or realtime SSFP cine sequences, and T1 and T2 mapping at base, mid and apical short axis levels. Average T1 and T2 were measured in each AHA segment and corresponding segments compared between scans.

Results: Following dialysis, mean reduction in body weight was 1.8±1.5kg and mean percentage reduction in extracellular to total body water ratio (ECW/TBW) was 0.0007±0.0067. Three patients had at least moderate LV dysfunction (LVEF<45%) at baseline. In these patients, there was significant improvement in LVEF following dialysis compared to those with pre-dialysis LVEF>45% (Mean change: LVEF<45% group +9.7±4.0% vs LVEF>45% group -1.3%±1.7%, $p<0.05$, Figure 1). In the cohort overall, there was significant reduction in LV mass index following dialysis (107±31g/m^2 vs 95±30g/m^2, $p<0.05$). There was correlation between change in LV mass and change in total body weight ($r = 0.82$, $p<0.05$, Figure 2). Native T1 was higher in those with LVEF<45% compared to those with LVEF>45% (pre-dialysis: 1090±43ms vs 1069±57ms, post-dialysis: 1070±34ms vs 1055±45ms, both $p<0.05$). Overall, native T1 and T2 were significantly lower post-dialysis (mean T1: pre-dialysis 1076±54ms vs post-dialysis 1060±43ms; mean T2: pre-dialysis 52.3±3.1ms vs post-dialysis 51.3±3.1ms, both $p<0.01$) with the reduction in both being greater in those with impaired LV function (Figure 3).

Conclusion: Haemodialysis results in immediate reduction in LV mass, native T1 and myocardial T2, consistent with reduction in myocardial oedema. Patients with impaired resting LV function also show acute improvement in LVEF likely due to a combination of improved loading conditions, myocardial mechanics and reduction in oedema. Furthermore, the difference in T1 and T2 pre- and post-dialysis is important to consider when planning the timing of serial CMR studies.

Figure 1: Change in left ventricular function following dialysis. Patients with baseline LVEF <45% (black lines) show significant improvement in function following dialysis compared to patients with baseline LVEF>45% (grey lines) (p<0.05).

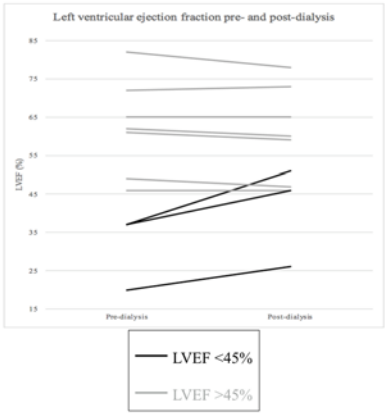

Figure 2: Correlation between change in LV mass index and change in total body weight pre- and post-dialysis

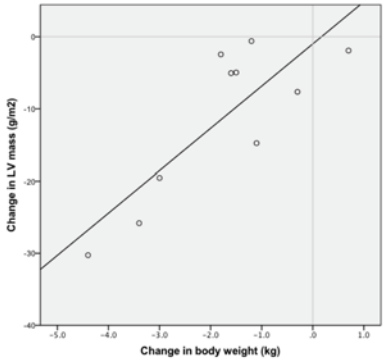

Figures 1 and 2

Figure 3: Change in native T1 and myocardial T2 following dialysis

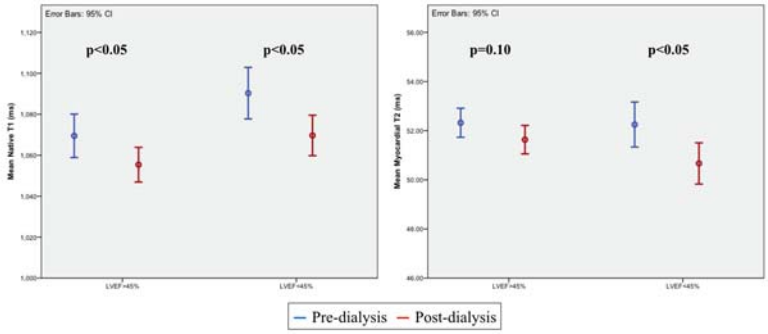

Figure 3

ID#: 378407

Cardiac involvement of asymptomatic carriers of Duchenne and Becker muscular dystrophy

Roman Panovsky, International Clinical Research Center, 1st Department of Internal Medicine/Cardioangiology[1]Tomas Holecek, International Clinical Research Center, Department of Medical Imaging[1], Vera Feitova, International Clinical Research Center, Department of Medical Imaging[1], Martin Pesl, International Clinical Research Center, 1st Department of Internal Medicine/Cardioangiology[2], Jan Machal, 1st Department of Internal Medicine/Cardioangiology, ICRC, St. Anne´s Faculty Hospital, Department of Pathophysiology[3], Lukas Opatril, International Clinical Research Center, 1st Department of Internal Medicine/Cardioangiology[1], Vladimir Kincl, International Clinical Research Center, 1st Department of Internal Medicine/Cardioangiology[1], Lenka Mrazova, Department of Pediatric Neurology[4], Veronika Stara, Department of Pediatrics[5]

1. St. Anne´s Faculty Hospital, Brno, Czech Republic, Czech Republic

2. St. Anne´s Faculty Hospital, Brno, Czech Republic, Brno, Jihomoravsky kraj, Czech Republic

3. Faculty of Medicine, Masaryk University, Brno, Czech Republic, Czech Republic

4. University Hospital Brno, Czech Republic, Czech Republic

5. University Hospital Motol, Second Faculty of Medicine Charles University, Prague, Czech Republic, Czech Republic

Background: Duchenne and Becker muscular dystrophy (DMD and BMD) is the X-linked recessive disorder caused by mutations in gene encoding muscle cell structural protein dystrophin. These abnormalities manifest in males by skeletal muscles impairment and in all surviving boys also by cardiac dysfunction in their twenties. Large number of female carriers will display cardiac involvement as well. The onset of cardiac disease appears long before their first cardiac symptoms. The aim of the study was to detect early cardiac abnormalities using cardiovascular magnetic resonance (CMR) including T1 mapping.

Methods: Thirty five asymptomatic DMD/BMD female carriers (37 ± 12 years) without any heart disease history underwent CMR examination at 1,5T MR scanner. Cine images for assessment of left ventricular (LV) volumetric and functional parameters, late-gadolinium-enhanced (LGE) images and pre- and post-contrast Modified Look-Locker Inversion recovery (MOLLI) images were acquired for assessment of extracellular volume (ECV).

Results: Carriers had not enlarged LV (end-diastolic volume 99 ± 17ml) and overall had normal global systolic LV function - LV ejection fraction (EF) 65 ± 6%. Concerning regional contractility, only 1 (3%) patient had slight regional hypokinesia. Six (17%) patients had LGE, all of them showed focal non-ischemic intramural LGE of the inferolateral LV wall. Mean ECV value of all cohort was 26,5 ± 2,0%; 6 (17%) patients had ECV ≥ 29,0% and only 10 (29%) patients had ECV ≤ 25,0%.

Conclusion: Despite no cardiac history and normal systolic function of undilated LV, almost one fifth of DMD carriers showed non-ischemic LGE. Important proportion of carriers had borderline or increased ECV as a sign of diffuse myocardial fibrosis.

ID#: 377431

High-Resolution Dynamic Topaz T1 Mapping Using Low Rank Tensor Regularization

Burhaneddin Yaman[1] Sebastian Weingärtner, Ph.D.[2], Nikolaos Kargas[3], Nicholas Sidiropoulos, Ph.D[4], Mehmet Akçakaya, Ph.D.[5]

1. Electrical and Computer Engineering, University of Minnesota; Center for Magnetic Resonance Research, University of Minnesota, Saint Paul, MN

2. Electrical and Computer Engineering, University of Minnesota; Center for Magnetic Resonance Research, University of Minnesota; Computer Assisted Clinical Medicine, Heidelberg University, Minneapolis, MN

3. Electrical and Computer Engineering, University of Minnesota

4. Electrical and Computer Engineering,University of Minnesota

5. Electrical and Computer Engineering, University of Minnesota; Center for Magnetic Resonance Research, University of Minnesota, Minneapolis, MN

Background: Myocardial T1 mapping is commonly performed using single-shot imaging with a temporal resolution of 150-200ms. However, for subjects with high heart rates such temporal resolution degrades the imaging quality and may hinder the quantification of mobile structures, such as papillary muscles. Recently a new sequence, called TOPAZ [Weingärtner et al, MRM2017], was proposed to acquire T1 maps in a cardiac phase-resolved manner at improved temporal resolutions. However, its spatial resolution was limited due to the breath-hold duration. Thus, it is desirable to improve the spatial resolution of TOPAZ, and regularization may be necessary to offset noise amplification. Low-rank matrix methods have been proposed for improving quantitative MRI [Zhang et al, MRM2015], but tensor regularization [Trzasko et al, ISMRM2011] may have more utility since TOPAZ datasets contain spatial, contrast and temporal dimensions. In this work, we use low-rank tensor regularization (LRTR) for high-resolution TOPAZ acquisitions, comparing global and local processing approaches.

Methods: In Vivo Imaging: Imaging was performed at 3T, using a 30-channel receiver coil array with resolution=1.3× 1.3mm^2, FOV=300×225 mm^2, temporal resolution=60ms, partial Fourier=6/8, in-plane acceleration=3 and ACS lines=24. This led to 11 cardiac phases and 5 different T1 weightings per phase for a total of 55 images in the dataset. **Reconstruction:** Images were reconstructed using GRAPPA. Subsequently, LRTR was applied to reduce noise amplification. PARAFAC decomposition, which uniquely factorizes a tensor into a sum of rank-one tensors, was used. Both global and local processing were implemented, as depicted in Fig. 1. Global processing of tensors consisted of all tissue types and contrasts, whereas the local approach processed smaller 2D patches across multiple contrast and cardiac phases, promoting locality. Global LRTR was performed by processing the whole dataset, while local LRTR was performed using overlapping 8×8×11×5 patches with a shift of 4. Processed patches in the local approach were combined via averaging to avoid blocking artifacts.

Results: Global LRTR was performed using a rank of 500, while local LRTR utilized a rank of 10. These ranks were chosen heuristically to maximize image quality. The spatial variability of myocardial T1 times was assessed as 219±54 ms for global and 153±23 ms for local LRTR, given as mean±std over cardiac phases. These provided improvements of 53.4% and 119.6% over the parallel imaging reconstruction, which had spatial variability 336±39ms. There were <1.5% absolute difference in the estimated mean T1 values using either LRTR approach compared to parallel imaging. Fig. 2 depicts the quantitative T1 maps of 6 representative cardiac phases. Noise inhomogeneity and residual noise artifacts are present in parallel imaging and global LRTR, respectively. These are considerably mitigated in local LRTR. Fig. 3 depicts the T1 values through the cardiac cycle for a cross-section of the heart. LRTR methods significantly eliminates noise artifacts, without apparent temporal blurring.

Conclusion: Locally low-rank tensor regularization has the potential to improve the spatial and temporal resolution of TOPAZ T1 mapping, allowing for joint characterization of cardiac function and viability information, at an in-plane spatial resolution of 1.3mm. **Funding:** NIH R00HL111410, NIH P41EB015894, NSF CCF-1651825 and NSF IIS-1704074

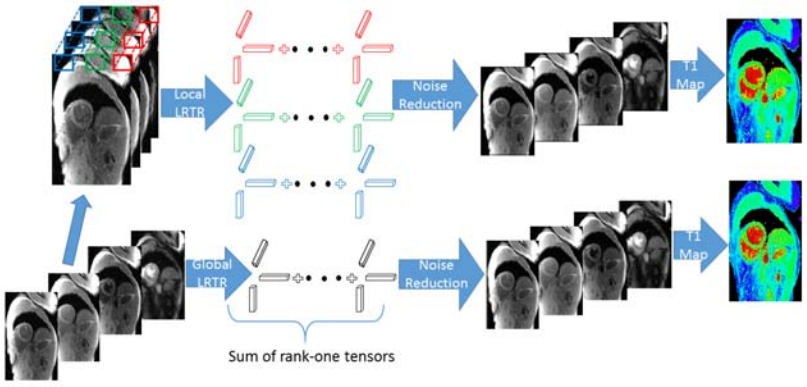

Figure 1: Flowchart of the low-rank tensor regularization (LRTR) approaches. Three-dimensional tensor decompositions are depicted, instead of the four-dimensional approach used in the study, in order to enable visualization. LRTR tries to represent all information in the dataset with a few rank-one tensors. Global LRTR process the whole dataset (i.e. all tissue types), whereas local LRTR is likely to process patches with similar features.

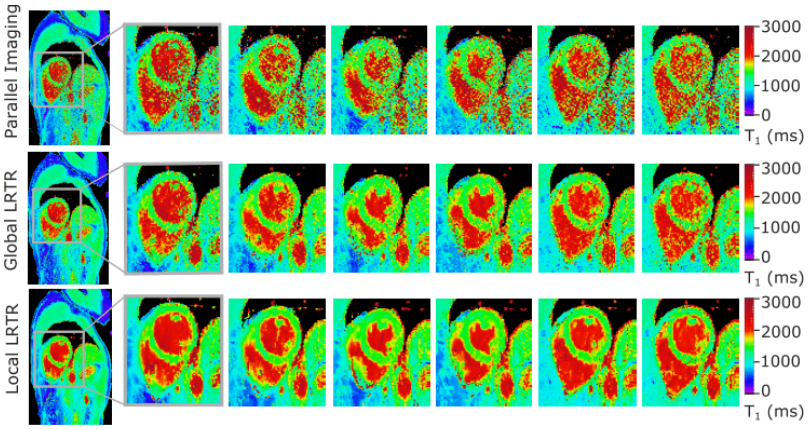

Figure 2: Dynamic quantitative T1 maps for representative cardiac phases generated by parallel imaging, global LRTR and local LRTR. Full field of view of images are shown on the left for first cardiac phases. Noise inhomogeneity and residual noise artifacts present in reference (top) and global LRTR, respectively, are considerably suppressed with local LRTR. Spatial variability of the T1 times with parallel imaging, global LRTR and local LRTR measured to 336±39 ms, 219±54 ms and 153±23 ms, respectively, quantitatively showing improvements with the local LRTR method.

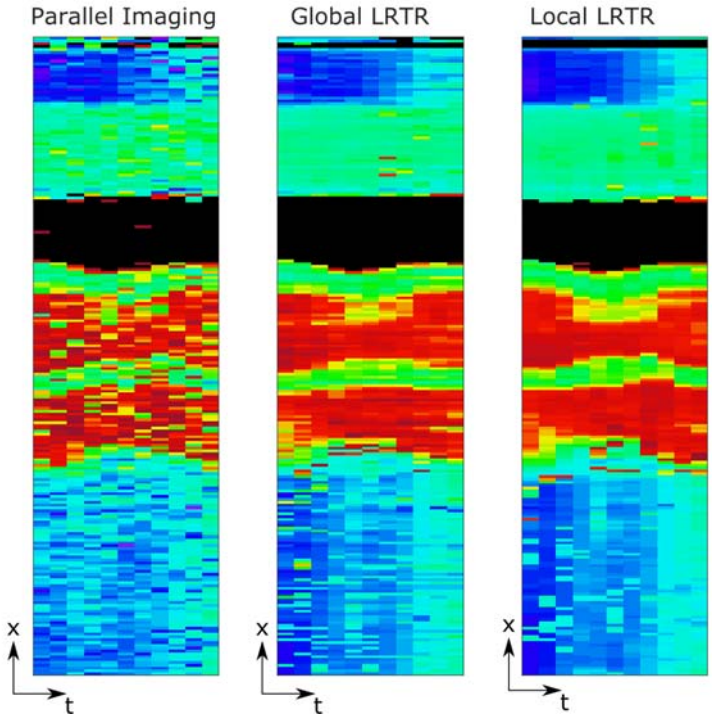

Figure 3: T1 times through cardiac phases for a cross-section of the heart is depicted for parallel imaging, local LRTR and global LRTR. Parallel imaging suffers from severe noise amplification that significantly degrades representing functionality of cardiac motion and hinders identifying tissue borders. Global and local LRTR methods enable well representation of functionality of cardiac motion by significantly eliminating noise artifacts while showing no temporal blurring.

ID#: 377219

Coronary 4D-Flow MRI using Stack-of-Stars Acquisition: towards noninvasive pressure gradient measurement in the coronary arteries

Zixin Deng, MS[1] Michael Loecher, PhD[2], Christopher Nguyen, PhD[3], Anthony G. Christodoulou, PhD[3], Zhengwei Zhou, MS,[3], Jaime L. Shaw, MS[4], Yibin Xie, PhD[3], Xiaoming Bi, PhD[5], Zhaoyang Fan, PhD[1], Daniel B. Ennis, PhD[6], Debiao Li, PhD[3]

1. Cedars-Sinai Medical Center, CA

2. University of California, Los Angeles, CA

3. Cedars-Sinai Medical Center, Los Angeles, CA

4. Cedars-Sinai Medical Center/UCLA, CA

5. Siemens Healthcare, CA

6. Department of Radiological Sciences, University of California, Los Angeles, CA, USA., CA

Background: In patients with suspected coronary artery disease selected for invasive catheterization procedures, ~50% were found with nonobstructive (<50% degree stenosis) or functionally nonsignificant (FFR>0.80) coronary lesions, resulting in unnecessary invasive procedures [1,2]. A recent noninvasive technique using 2D phase-contrast MRI and Navier-Stokes to estimate the pressure difference across a coronary stenosis has shown promise in identifying patients with functionally nonsignificant stenosis [3]. However, the method requires long scan times (30-40 min) and is prone to motion. This work aims to develop a 4D-Flow method using stack-of-stars (SOS) with golden-angle sampling in the coronary arteries and evaluate its feasibility in flow phantoms and healthy subjects, using Cartesian 4D-Flow as reference.

Methods: SOS 4D-Flow with ECG-triggering to diastole with navigator-gating was implemented for coronary imaging on a 3T system (Skyra, Siemens). *In vitro*: SOS and Cartesian were first compared in a flow phantom (constant volume velocity = 250 mL/min; reference diameter = 4.8 mm) with 0% and 50-60% diameter narrowing. Imaging parameters were: FA=15°; spatial resolution=0.6x0.6x3.2 mm^3; FOV=220 mm; VENC=45/110 cm/s, 1500/2000 projections per flow encoding direction, and 8/10 partitions were used for 0% and 50-60% narrowing, respectively, corresponding to ~12/16 min acquisition time with simulated 60 bpm ECG-triggering, matched to the same scan time as Cartesian (iPAT=2). Retrospective *k*-space undersampling of the SOS data was performed offline to evaluate the feasibility of scan time reduction. Cross-correlation in the maximum velocities across all imaging slices was performed for a range of SOS projections versus Cartesian, respectively. 5-6 contiguous slices were used for analysis. *In vivo:* scans were tested in one healthy subject (female, 61 yrs) with VENC= 40cm/s in the left coronary artery (7 slices) and similar imaging parameters.

Results: Good cross-correlation was preserved between SOS and Cartesian as SOS projection number decreased in the phantom studies (Table 1). Similar maximum velocities across each imaging slice were observed between Cartesian and SOS acquisitions over a range of total projections (Figure 1). Figure 2 shows the example images of Cartesian and SOS acquisition (920 projections, ~50% scan time reduction) in a healthy subject. Average maximum through-plane velocity was 11.5±0.8 cm/s and 11.6±2.4 cm/s for Cartesian and SOS, respectively.

Conclusion: Our preliminary results showed the feasibility of SOS 4D-Flow measurement in the coronary arteries. It has the potential to minimize motion sensitivity and reduce scan time as compared to conventional Cartesian imaging. In-vivo studies involving patients with coronary artery disease are underway to evaluate the performance of the method.

[1] Patel et al. AHJ, 2014;167; [2] Tonino et al. JACC, 2010;55; [3] Deng et al. MRM, 2017;77

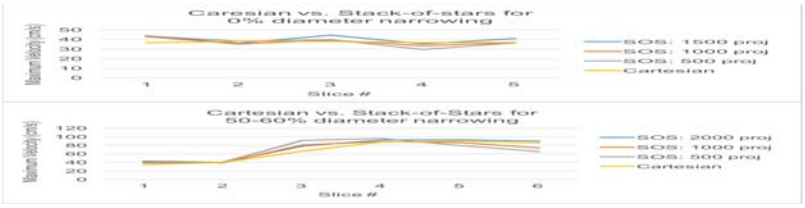

Figure 1. Cartesian versus stack-of-stars for 0% and 50-60% diameter narrowing

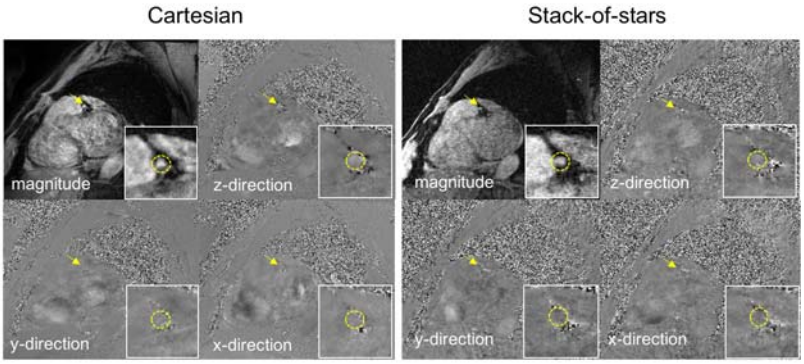

Figure 2. Example images from Cartesian versus stack-of-stars acquisition (920 projections, ~50% scan time reduction) in a healthy subject.

Table 1. Cross-correlation between the maximum velocities of SOS and Cartesian 4D-Flow methods for 0% and 50-60% diameter narrowing phantoms.

Cross-correlation (CC)	Projections		
0% narrowing:	**1500**	**1000**	**500**
	0.97	0.96	0.92
50-60% narrowing:	**2000**	**1000**	**500**
	0.94	0.91	0.89

ID#: 377989

Visualizing radiofrequency ablation lesions in scarred arrhythmia substrate using non-contrast T1-weighted cardiac magnetic resonance imaging

Susumu Tao, MD, PhD[1] Michael A. Guttman, MS[2], Sarah Fink, BA[3], Aravindan Kolandaivelu, MD[4], Ehud J. Schmidt, PhD[5], Daniel Herzka, PhD[3], Henry Halperin, MD, MA[6]

1. Johns Hopkins University, school of medicine, Baltimore, MD

2. The Johns Hopkins University, School of Medicine, MD

3. Johns Hopkins University, MD

4. Johns Hopkins University School of Medicine, MD

5. Johns Hopkins University, Towson, MD

6. Johns Hopkins University, Baltimore, MD

Background: One of the mechanisms for recurrence of arrhythmias after radiofrequency catheter ablation (RFCA) is incomplete ablation. Assessment of the completeness of ablation is especially difficult for scar-based arrhythmias. Non-contrast-enhanced T1-weighted (T1w) cardiac magnetic resonance (CMR) imaging with a long inversion time (TI) has demonstrated improved visualization of necrotic lesion cores. We hypothesize that this technique can be useful for quantifying the extent of acute RFCA lesions within and around scar, without the overestimation typically seen in delayed contrast-enhanced (DCE) CMR.

Methods: With IACUC approval, we performed electro-anatomical mapping and RFCA using a force-sensing catheter at 30W for 60sec in the left-ventricles of 8 chronically infarcted swine. Non-contrast-enhanced T1w and DCE post-RFCA were compared to gross pathology and histology. T1w parameters: TR/TE=5.4ms/2.7ms/25deg, TI=700 ms (2RR ECG-triggering), resolution=1.1X1.1X1.1 mm, BW=250 Hz/pixel, 80 slices/vol, respiratory-navigated, scan time=15-20 min. DCE was acquired 10 and 20 minutes post-injection, with similar parameters, but with TI=400 ms and 1RR ECG-triggering.

Results: In T1w CMR, all RFCA lesions were hyper-enhanced, while scar was hypo-intense, allowing discrimination between normal myocardium, scar, and RFCA lesions (Figure A, B). With DCE, lesion appearance varied with time after contrast-injection. RFCA lesions were iso-intense with chronic-scar, resulting in an inability to resolve them (Figure C-E). Of 59 lesions, 17 were in normal myocardium (NL, voltage > 1.5mV), 21 in border zone (BZ, 0.5-1.5mV), and 21 in scar (< 0.5mV). Lesion width and depth by T1w CMR correlated with pathology measures of necrosis (linear regression analysis: both r^2=0.94, p<0.001), without a systematic difference between them (p>0.05). CMR lesion volume was significantly different in NL, BZ, and scar (397 [interquartile range (IQR) 301-474] mm^3, 121 [IQR 87-201] mm^3, 66 [IQR 33-123] mm^3, respectively). RFCA force-time integral, impedance and voltage changes did not significantly correlate with BZ or scar volumes. Histology showed that ablation necrosis extended into fibrotic tissue in 26 lesions, and beyond in 14 lesions. In 7 lesions, necrosis expansion was blocked and redirected by fat.

Conclusion: T1w CMR can identify acute RFCA lesion necrosis inside and surrounding scar. Lesion formation in scar is affected by tissue characteristics, with fibrosis and fat acting as insulators. Use of T1W imaging may allow accurate monitoring of the completeness of ablation intra- and post-procedure.

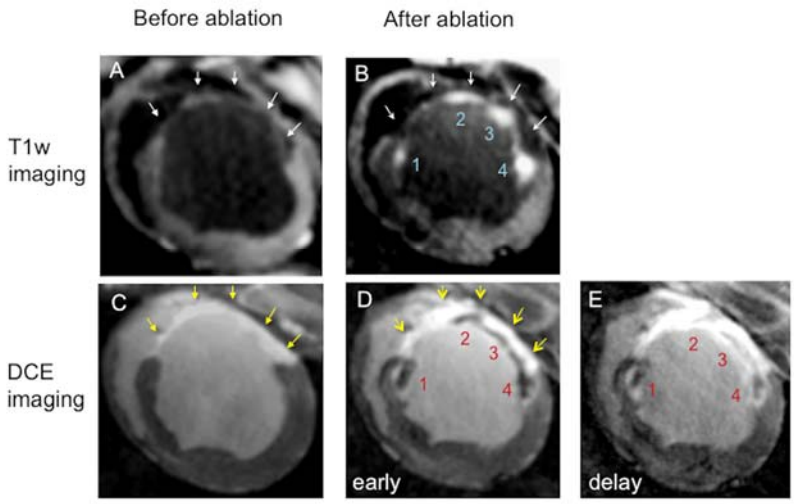

Figure: A, B: Comparison of T1w images obtained pre- and post- ablation. Ablation lesions in border zone (1,4) and scar (2,3) are enhanced, while scar (white arrows) is hypo-intense. Clear delineation of acute lesion borders was possible. Figures C-E: Comparison of DCE images before ablation (C), early (D: 10 minutes) and delayed (E: 20 minutes) post-ablation. Yellow arrows indicate scar. Since both acute lesion rims and scar are contrast enhanced, acute lesion size and borders were hard to resolve. Furthermore, lesion appearance in DCE varied with time post contrast injection (D,E) in a manner which may require better understanding of the pharmo-kinetics.

ID#: 377762

Predicting MACE recurrence in ventricular fibrillation cardiac arrest survivors: a cardiovascular magnetic resonance imaging study

Anna Baritussio, MD[1] Giovanni Biglino, BEng, PhD[2], Alessandra Scatteia, MD[3], Estefania De Garate, MD[1], Amardeep Ghosh Dastidar, MBBS(Hons), MRCP[1], Iwan Harries, MBBCh BSc[1], Ihab Diab, MD[4], Chiara Bucciarelli-Ducci, MD, PhD[1]

1. Bristol Heart Institute, Bristol NIHR Biomedical Research Centre (Cardiovascular Section), University of Bristol, Bristol, England, United Kingdom

2. Bristol Heart Institute, School of Clinical Sciences, University of Bristol, Bristol, England, United Kingdom

3. Division of Cardiology, Ospedale Medico-Chirurgico Accreditato Villa dei Fiori, Acerra, Naples, Italy, Naples, Campania, Italy

4. Bristol Heart Institute, United Kingdom

Background: Recurrence of Major Cardiovascular Adverse Events (MACE) in ventricular fibrillation (VF) cardiac arrest survivors is not rare. We sought to identify structural and functional myocardial predictors of MACE recurrence as provided by Cardiovascular Magnetic Resonance (CMR).

Methods: We retrospectively analysed the Bristol CMR registry to enrol VF cardiac arrest survivors. All patients underwent a 1.5 T CMR, comprehensive of long and short-axis cine and late gadolinium enhancement (LGE) sequences. LGE was quantified with a semi-automated software using the full width at half maximum method (cvi42, Circle Cardiovascular Imaging). Tissue tracking analysis software was used to assess myocardial deformation (cvi42, Circle Cardiovascular Imaging). Primary end-points were all-cause mortality, appropriate ICD discharge/anti-tachycardia pacing and hospitalisation for ventricular arrhythmias.

Results: We enrolled 121 patients [82% male, 62 (53-70) years]. CMR was performed within 13 (6-42) days from VF arrest. LV systolic function was mildly impaired [LVEF 54 (41-64)%], RV systolic function was preserved [RVEF 60 (53-65)%]. LGE was found in 71% of patients, median mass was 6.2 (0-15)% of the LV. Myocardial deformation was overall impaired [global longitudinal strain, -15.5 (-18.9- -12.3)%; global radial strain, 34.2 (25.2-45.2)%; global circumferential strain, -15.5 (-20.3- -11.9)%]. There was a significant correlation between LGE mass and myocardial deformation ($p<0.001$).On CMR, 75 patients (62%) were diagnosed with ischemic heart disease (IHD) and 20 (17%) with non-ischemic heart disease (NIHD); a structural normal heart was found in 26 (21%). Fifty-two per cent of patients were implanted with an ICD. After a median follow-up of 24 (6-41) months, 24 patients (18%) were lost to follow-up. Primary end-point was met in 24 patients (14 deaths, 10 appropriate ICD discharge). LVEF did not differ between patients with and without end-point ($p=0.128$), while RVEF was significantly lower in those meeting the end-point (58% vs 61%, $p=0.03$). LGE prevalence did not differ between patients with and without end-point ($p=0.075$) but its extent was significantly greater in patients meeting the end-point (LGE mass 8.6% of LV vs 4.1%, $p=0.02$).Myocardial deformation did not differ between patients with and without end-point. Patients with LGE mass >4.3% represented a subgroup at a higher risk of adverse events ($p=0.004$, log rank test).

Conclusion: The extent of LGE was the strongest predictor of recurrent adverse events in VF cardiac arrest survivors. Myocardial deformation did not show an additional role in patients'; risk stratification. The unique capability of CMR to provide accurate tissue characterisation may be useful in guiding the management of cardiac arrest survivors.

ID#: 377776

Parametric CMR and myocardial feature tracking identify early myocardial involvement in patients with systemic lupus erythematodes

Vera Lachmann, MD[1] Mareike Gastl, MD[2], Patrick Behm, MD[2], Philipp Sewerin, MD[3], Matthias Schneider, MD[3], Malte Kelm, MD[1], Florian Bönner, MD[4]

1. Division of Cardiology, Pulmonology and Vascular Medicine, Heinrich Heine University, Düsseldorf, Medical Faculty, Germany, Germany

2. Division of Cardiology, Pulmonology and Vascular Medicine, Heinrich Heine University, Düsseldorf, Medical Faculty, Germany, Düsseldorf, Nordrhein-Westfalen, Germany

3. Division of Rheumatology, Heinrich Heine University, Düsseldorf, Medical Faculty, Germany, Germany

4. Heinrich Heine University, Düsseldorf, Medical Faculty, Germany, Nordrhein-Westfalen, Germany

Background: Systemic lupus erythematodes (SLE) is an autoimmune, multisystemic connective tissue disorder, which predominantly affects young women. A variety of organs can be affected, contributing highly to morbidity and mortality in SLE. Cardiac involvement may manifest in coronary arteries, myocardium, endocardium and valves and pericardium. The prevalence for cardiac manifestations in patients with SLE is estimated to be more than 50 % and the risk for cardiovascular events such as myocardial infarction or stroke is 17 fold higher than in gender- and sex-matched healthy controls. Nevertheless, cardiac involvement remains asymptomatic in early stages of SLE and diagnostic tools such as electro- and echocardiography, cardiac enzymes and coronary angiography remain unsuspicious. Hence, parametric Cardiac magnetic resonance (CMR) and deformation imaging with myocardial feature tracking analysis (FTA) – well established for detection of myocardial inflammation in patients with myocarditis- may present a highly sensitive tool to detect cardiac involvement in early stages of SLE. We hypothesisze, that patients with SLE and persistent dyspnoea show early cardiac involvement by means of increased T2-times and impaired systolic and diastolic strain.

Methods: 15 women fulfilling the ACR criteria for SLE (37±14.81years, disease duration 13.75±8.47 years) with persistent dyspnoea (at least NYHA II) but absence of pathological findings in electro- or echocardiography were investigated with CMR at 1.5 Tesla (Achieva, Philips, Best, Netherlands). T2 mapping was performed using a respiration navigator gated Gradient-And Spin-Echo sequence (GRASE, 15 T2 echoes separated by 10ms, res: 1x1x10mm², 3 short axis slices). Images were post-processed using software based on the LabView environment for local T2 value generation (T2 mapping). Strain analysis was conducted entering cine-images into myocardial feature tracking (FTI) analysis software (TomTec Imaging Systems, Unterschleißheim, Germany). Parameters for analysis were T2-values, global longitudinal strain (GLS), peak early diastolic strain rate (SRe) and ejection fraction (EF). A cohort of age and gender matched volunteers served as controls.

Results: Patients with SLE showed- despite normal average ejection fraction (61.02±4.37%) - significantly impaired GLS and SRe (GLS: -22.92±3.48% vs. -26.92±3.14%; SRe: 1.53±0.25s^{-1} vs. 2.09±0.77s^{-1}; both $p<0.05$). Although there were no signs of late gadolinium enhancement, they revealed significantly increased T2-times compared to age matched healthy controls (67.09±3.12ms vs. 58.9±2.32ms, $p<0.01$).

Conclusion: In SLE patients presenting with persistent dyspnoea, but without pathological findings in electro- and routine echocardiography, CMR shows impaired systolic and diastolic deformation accompanied by a myocarditis-like T2 relaxation pattern. Thus, parametric CMR and myocardial feature tracking might early identify myocardial involvement in patients with SLE.

ID#: 375966

A history of pre-eclampsia is not associated with cardiomyopathy beyond the peripartum period

Lauren C. Coles, BSc[1] Eylem Levelt, MBBS, DPhil[2], Gerry p. McCann, MB ChB, MD[3], Philip Baker, BMBS, FRCOG[2], Tommy Mousa, MBBS, MRCOG[2]

1. Department of Cardiovascular Sciences, University of Leicester and NIHR Biomedical Research Unit, Glenfield Hospital, Leicester, England, United Kingdom

2. University of Leicester, England, United Kingdom

3. Department of Cardiovascular Sciences and NIHR Biomedical Research Centre, Glenfield Hospital, Leicester, England, United Kingdom

Background: Women with pre-eclampsia have an increased risk of cardiomyopathy in the peri-partum period (from the last month of pregnancy to five months after delivery). Pre-eclampsia is also associated with cardiovascular disease later in life, with a four-fold increased risk of hypertension and twice the risk of ischemic heart disease and cerebrovascular disease years after the affected pregnancy. Whether women with a history of pre-eclampsia also have an increased risk of cardiomyopathy outside the peripartum period, with persistent cardiac dysfunction and remodeling after pre-eclampsia, is unknown.

Objective - To determine whether a history of pre-eclampsia is associated with a cardiomyopathy beyond the peripartum period.

Methods: 19 primiparous women with a history of pre-eclampsia (mean age 27.8±4.1 years, BMI 29.2±6.2), and 12 healthy volunteers (mean age 28.1±2.4, BMI 28.2±6.3) with similar age, BMI and delivery date (12-24 months previously) underwent 3T CMR. Women with a history of chronic hypertension, cardiac, renal or hepatic disease or diabetes were excluded. CMR assessments included cine imaging and native T1 mapping. Ascending aortic cross-sectional area was measured at the level of the pulmonary artery bifurcation for calculation of aortic distensibility. Late gadolinium imaging was performed to rule out myocardial scarring and fibrosis.

Results: Women with a history of pre-eclampsia had a higher diastolic and mean arterial blood pressure, and heart rate than controls. There were no significant differences in left ventricular (LV) volumes or LV mass-to-volume ratio between the two groups. LV mass index was higher in controls. LV ejection fraction, peak circumferential systolic strain and longitudinal systolic strain were similar between women with a history of pre-eclampsia and controls. The numeric differences in native T1 time did not reach statistical significance. There was also no difference in ascending aortic distensibility between groups.

Conclusion: In women with pregnancies complicated by pre-eclampsia, whilst blood pressure abnormalities persist, there is no evidence that pre-eclampsia is associated with cardiomyopathy beyond the peripartum period. Further prospective, larger longitudinal studies are needed to confirm this.

Pre-eclampsia study results

	Characteristic	Control (n=12)	PET (n=19)	*P*-value
Anthropometric data	SBP, mmHg†	114.67±9.84	123.79±14.79	0.070
	DBP, mmHg†	73.50±7.39	83.16±10.87	0.011
	MAP, mmHg†	87.22±7.76	96.94±11.22	0.016
	HR, bpm†	70.58±8.88	79.11±12.26	0.036
CMR assessment of LV structure	LVEDVI, ml.m^{-2}*	80.50±14.00	77.00±12.00	0.260

	LVMVR, †	0.66±0.06	0.61±0.10	0.119
	LVMI, g. m^{-2}†	53.67±5.94	46.75±7.32	0.013
	Native T1, ms†	1247.04±35.56	1222.41±19.38	0.052
CMR assessment of LV function	LVEF, %†	59.17±5.87	56.8±5.65	0.281
	Global cPSS, %†	-19.84±2.43	-18.38±3.16	0.217
	Global lPSS, %†	-19.46±3.43	-20.62±2.36	0.330
CMR aortic stiffness assessment	AAD, $10^{-3}mmHg^{-1}$*	8.28±2.94	7.13±3.40	0.412

† Values expressed as mean ± standard deviations * Values expressed as median ± interquartile range. PET indicates pre-eclampsia; CMR, cardiac magnetic resonance; LV, left ventricular; SBP, systolic blood pressure; DBP, diastolic blood pressure; MAP, mean arterial pressure; HR, heart rate; LVEDVI, left ventricular end-diastolic volume index; LVMVR, left ventricular mass to volume ratio; LVMI, left ventricular mass index; LVEF, left ventricular ejection fraction; cPSS, circumferential peak systolic strain; lPSS, longitudinal peak systolic strain; AAD, ascending aortic distensibility.

ID#: 374659

Measuring myocardial tissue velocity with single breath hold Golden-Angle radial high temporal resolution phase contrast CMR: A comparison with pulsed wave tissue Doppler echocardiography

Alexander Fyrdahl, M. Sc.[1] Martin Ugander, MD, PhD[2], Andreas Sigfridsson, PhD[3]

1. Karolinska Institutet, Stockholms Lan, Sweden

2. Karolinska Institutet, and Karolinska University Hospital, Stockholm, Sweden, Stockholms Lan, Sweden

3. Karolinska Institute, Stockholm, Stockholms Lan, Sweden

Background: The standard method for assessing diastolic function is Doppler echocardiography of myocardial velocities. Obtaining high enough temporal resolution to measure this using MRI has been challenging, but highly undersampled radial imaging has potential to reach sufficient temporal resolution. The aim of this study was to determine the temporal resolution and temporal footprint needed to measure the myocardial tissue velocities directly with single breath hold phase contrast (PC) CMR using a Golden-Angle radial acquisition, and to compare to Doppler echocardiography.

Methods: Clinical patients (n=10, age 64±10 years, 60% female) referred for both CMR and echocardiography were scanned at 1.5T with a novel, variable temporal resolution PC pulse sequence. A segmented radial trajectory with through-plane shared velocity encoding was used to acquire short axis PC images at approximately 200 frames per second. Relevant imaging parameters were TE/TR 2.0/6.8ms, V_{ENC} 30 cm/s, voxel size 5x5x5mm^3 and a breath hold duration of 12 heartbeats. Images were reconstructed in a sliding window with fixed temporal resolution (frame increment) of 6.8ms and a variable temporal footprint ranging from 13.6ms to 86.4ms. Peak velocity within a region of interest was measured in the lateral wall using the commercially available software Segment (Medviso, Lund, Sweden). Echocardiographic velocities were obtained by pulsed wave tissue Doppler using conventional clinical methods. Mean velocities were compared with the paired t-test; $p<0.05$ was considered statistically significant.

Results: PC-CMR showed high correlation with Doppler across all temporal resolutions. The velocity did not differ between PC-CMR and Doppler for temporal footprints of 27.2–40.8ms. The strongest correlation and the lowest mean difference was found at a temporal footprint of 34ms (R^2=0.87, mean difference±2SD 0.2±2.0cm/s), see Figure 1. With temporal footprints <27.2ms the velocity was higher when measured by PC-CMR.

Conclusion: Lateral wall velocity measured with PC-CMR has excellent agreement with Doppler. While tests with more subjects and different imaging parameters are warranted, the data suggest that a temporal footprint ≤40.8ms is required for accurate measurement of myocardial tissue velocities when compared to Doppler. However, finding the peak velocity in the Doppler spectrum may be challenging due to intrinsic spectral broadening. Conservative Doppler measurements lead to underestimation, as does the temporal smoothing of a wide temporal footprint in PC-CMR, see Figure 2. Therefore, it cannot be excluded that the higher velocities in short temporal footprint PC-CMR are not an overestimation, but rather better estimates of the true velocity.

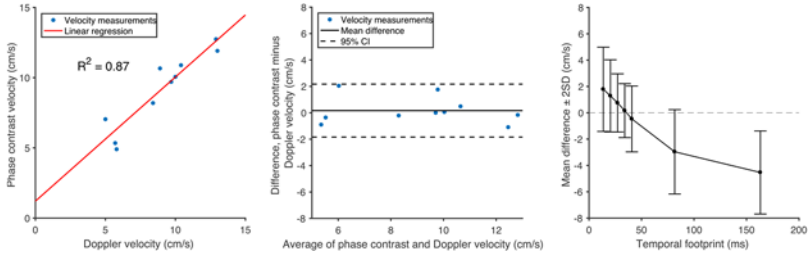

Figure 1: The correlation for a temporal footprint of 34 ms (left). Bland-Altman for the same temporal footprint shows low bias with a mean difference of 0.2 cm/s and narrow limits of agreement, 95% CI +/- 0.7 cm/s (middle). A temporal footprint between 27.2 and 40.8 does not differ from Doppler velocities. Bigger footprints tend to underestimates the Doppler velocity while smaller temporal footprints tend to measure higher velocities than Doppler (right).

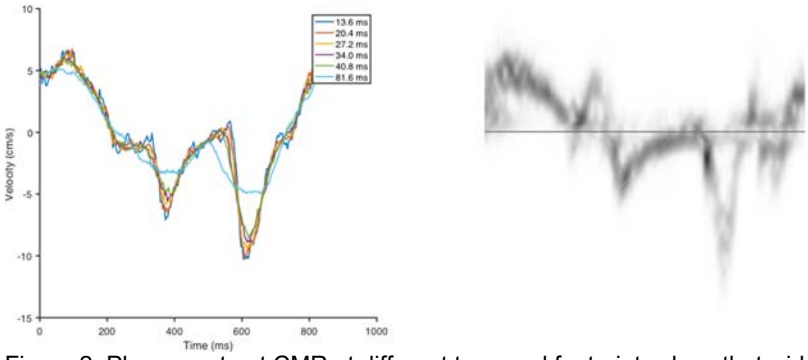

Figure 2: Phase contrast CMR at different temporal footprints show that wider temporal footprints tend to underestimate the velocity peaks (left). Corresponding Doppler spectrum in the same patient, for illustrative purposes (right). Note that heart rate differed between the two exams.

ID#: 374803

Determination of Conducting Channels from LGE CMR in patients with Myocardial Infarction- Comparison with Electroanatomic Mapping for Ventricular Tachycardia Ablation

Avanti Gulhane, M.D.[1] Saman Nazarian, MD, PhD[2], Harold Litt, MD-PhD[3]

1. Perelman School of Medicine, University of pennsylvania, Philadelphia, PA

2. University of Pennsylvania Perelman School of Medicine, PA

3. Perelman School of Medicine of the University of Pennsylvania, Philadelphia, PA

Background: LGE CMR is an excellent tool to evaluate scar in patients after myocardial infarction (MI). Electroanatomic mapping (EAM) is traditionally used to locate areas in scar tissue giving rise to ventricular tachycardia (VT) and guide ablation. However, new software using pixel signal intensity (PSI) algorithms has made it possible to locate conducting channels (CC) in scar tissue which form VT substrate using LGE CMR. We compared LGE derived CC with EAM findings in patients with VT post MI.

Methods: We evaluated retrospectively 31 patients with previous MI and VT who underwent CMR prior to EAM and VT ablation. 2D or 3D short axis LGE acquisitions were evaluated using ADAS-VT (Galgo Medical SL, Barcelona) to identify CC within myocardial layers from endocardium to epicardium. A PSI-based algorithm was applied to characterize the LGE area as scar core or border zone, using 60% and 40% of the maximum LGE intensity as thresholds. CC were identified topologically by finding border zone areas coursing through scar core, which are thought to represent corridors of viable tissue connecting through the core scar. CC detected by LGE CMR were compared with EAM findings and sites targeted for VT ablation on a per patient and per channel basis.

Results: Three patients had severe artifacts related to ICDs and could not be evaluated by the software. Of the remaining 28 patients, on a per patient basis, 12 CMR analyses were in total agreement with EAM sites, 15 had partial agreement and 1 had a total mismatch. A total of 106 channels were generated by the software, 56% subendocardial, 22% midmyocardial, and 23% transmural. 83 (79%) detected channels matched sites of VT ablation, 23 (22%) channels were detected only on CMR and not at EAM. The matching percentage was similar for subendocardial, midmyocardial and transmural channels.Channels were detected by LGE CMR analysis in 93/145 (64%) sites of EAM findings that led to VT ablation (table 1 – starred findings also showed voltage channels in the same locations)

Conclusion: LGE CMR PSI-based analysis showed good sensitivity (57%) and high (78%) positive predictive value in identifying sites of ablation and may be useful to help guide VT/PVC ablations. It also identified additional CC not detected at EAM; further follow-up would be required to determine if these areas may cause recurrent VT.

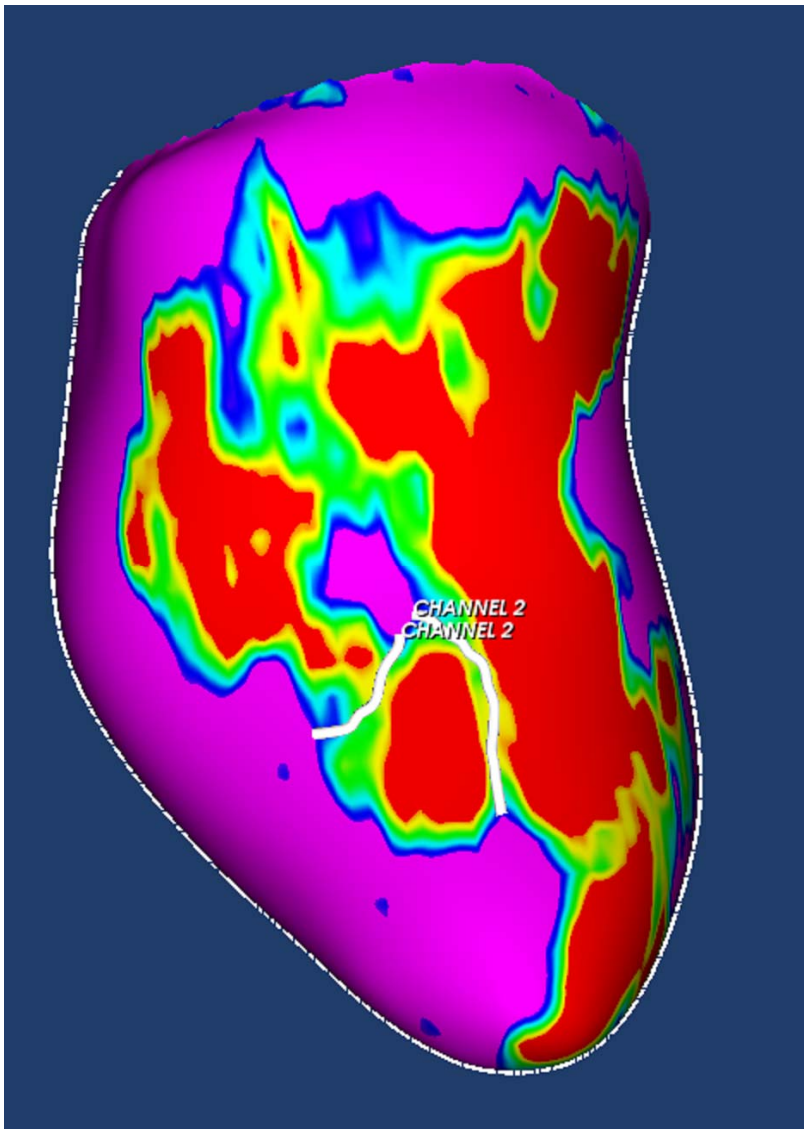

Conducting channel detected on LGE CMR

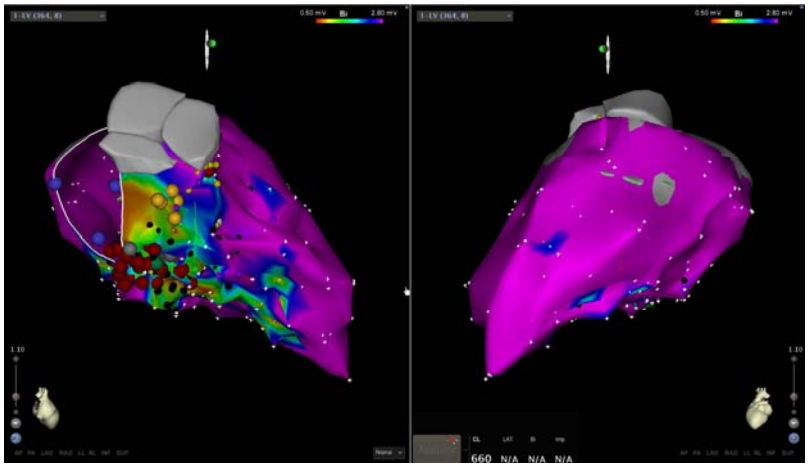

Electroanatomic map

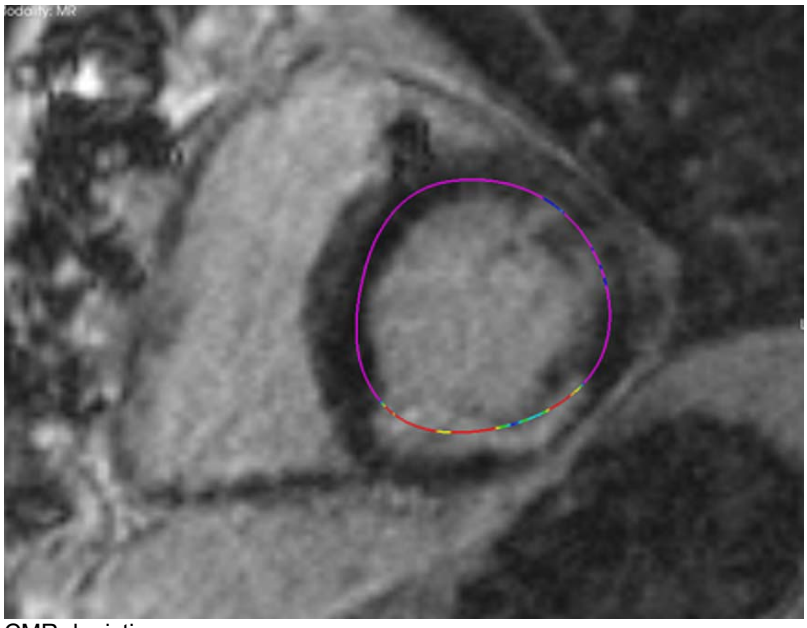

CMR depicting scar

Comparsion of EAM findings leading to VT ablation with LGE detected channels

EAM finding leading to VT ablation	LGE CMR matching
Voltage channels	35/56 (62.50%)
Late potentials	12/14 (85.70%)*
Fractionated potentials	12/15 (80%)*
Critical isthmus	5/9 (55.55%)
Induced VT	40/61 (65.60%)
PVC	10/16 (62.50%)

ID#: 374894

Increased Coronary Vessel Wall Thickness and Association with Myocardial Diastolic Function in Human Immune Deficiency Virus Infection.

Ahmed H. Hamimi, MD/PhD - FRCR[1] Khaled Abd-Elmoniem, PhD, MHS[2], Jatin R. Matta, PA-C, DHSc[3], Vandana Sachdev, MD[4], Hwaida Hannoush, MD[4], Colleen Hadigan, MD, MPH[5], Ahmed M. Gharib, MD[6], Julia Purdy, RN, MSN[4]

1. National Institutes of Health, Bethesda, MD

2. National Institutes of Health, MD

3. National Institutes of Health

4. NIH

5. NIAID, NIH

6. National Institues of Health

Background: Cardiovascular disease (CVD) is a rising cause of morbidly and mortality in human immune deficiency virus (HIV) infected patients. Coronary vessel wall (VW) thickening as measured by MRI in young HIV patients has demonstrated early coronary artery pathology. Further, early diastolic dysfunction and myocardial strain abnormalities were detected in HIV patients despite a preserved global myocardial function. The goal of this study is to assess both coronary vascular disease burden and its relation to myocardial function in adults with and controls.

Methods: In this prospective, cross-sectional study, a total of 100 HIV+ adults without known CVD and 30 matched healthy controls underwent time resolved phase-sensitive dual inversion recovery black-blood vessel wall magnetic resonance imaging (TRAPD) at 3T to measure proximal right coronary artery (RCA) wall thickness, and echocardiography to assess left ventricular function. Coronary Computer Tomography Angiography (CCTA) was also obtained to measure coronary calcification and overall coronary plaque burden. The presence of coronary calcification and Agatston score were recorded. Addition other non-calcified plaque was accounted for in segment involvement (SIS) and segment severity scores (SSS).

Results: There was no difference in age (HIV+48.6 ± 10.1 vs. controls = 46.3 ± 7.8 years), sex, body mass index and Framingham risk score between groups. VW measurements by MRI were successful obtained in 74 HIV-infected patients and 25 controls. HIV+ patients demonstrated a significantly thicker ($p<0.05$) coronary VW (1.5 ± 0.22mm) compared to controls (1.3 ± 0.18mm). Echocardiography measured ejection fraction (EF) and early (E) to late (A) ventricular filling velocities ratio (E/A) and all CCTA-based coronary plaque burden were not different between the two groups. However, in a regression analysis of HIV+ subjects, there was significant negative correlation between VW thickness and E/A ratio ($p<0.05$).

Conclusion: Subclinical coronary artery disease (CAD) is present in HIV-infected patients without a known history of CVD as shown by increased coronary VW thickness compared to controls. MRI detected the difference in subclinical CAD and not lumenography based CCTA method. This highlights the value of MRI for identifying positive arterial remodeling and/or diffuse coronary atherosclerosis or coronary vasculopathy associated with HIV. Furthermore, coronary VW thickness measured by MRI was associated with a detrimental effect on the myocardial function as demonstrated by the significant negative relationship between early mild diastolic dysfunction (impaired relaxation) depicted by decrease in E/A ratio on echocardiography.

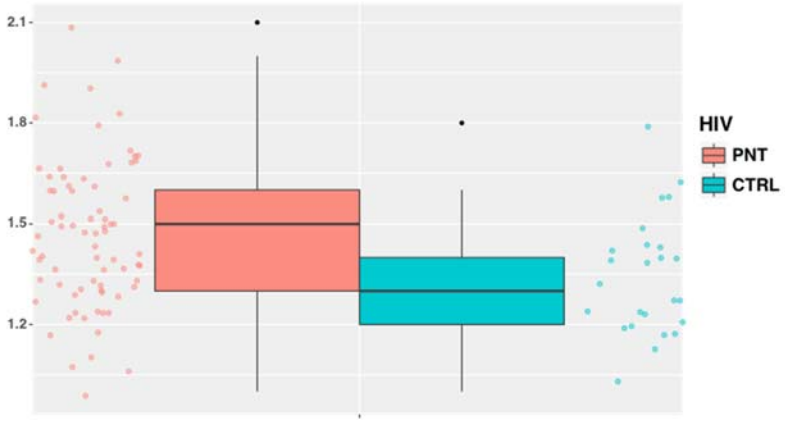

Figure1: Box plots of coronary vessel wall (VW) thickness measured by MRI in HIV-patients (red) and controls (green) showing statistically significant thicker VW in HIV-patients.

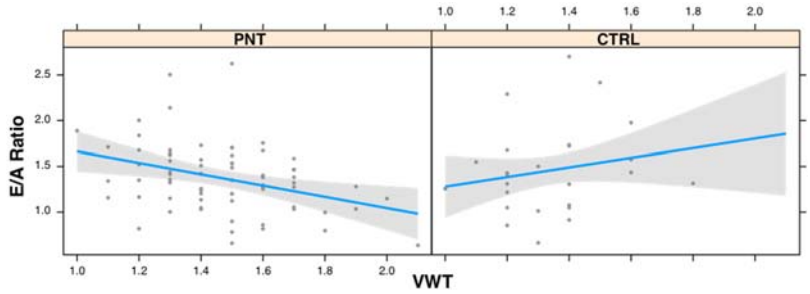

Figure 2: Regression analysis showing significant negative relation between increase coronary VW thickness and E/A in HIV-patients (PNT) but not in controls (CTRL).

ID#: 376550

Automated 3D CMR aortic morphometry demonstrates the enhanced value of volume indices as compared to diameters in hypertension and aneurysmal aortic diseases

Thomas Dietenbeck, PhD[1] Benjamin Dubourg, MD[2], David Rosenbaum, MD, PhD[3], Charles Roux, MD[2], Marine Bravetti, MD[2], Wafik Turki, MD[2], Samia Boussouar, MD[2], Nadjib Hammoudi, MD[4], Guillaume Lebreton, MD[5], Xavier Girerd, MD[6], Alain Giron, PhD[7], Philippe Cluzel, MD, PhD[8], Nadjia Kachenoura, PhD[9], Alban Redheuil, MD, PhD[3]

1. Sorbonne Universités, UPMC Univ Paris 06, INSERM UMRS 1146, CNRS UMR 7371, Laboratoire d'Imagerie Biomédicale, Ile-de-France, France

2. Département d'imagerie cardiovasculaire DICVRIT, Institut de Cardiologie, Groupe Hospitalier Pitié Salpêtrière APHP, Paris, France, France

3. Sorbonne Universités, UPMC Univ Paris 06, INSERM UMRS 1146, CNRS UMR 7371, Laboratoire d'Imagerie Biomédicale, Paris, Ile-de-France, France

4. Institut de Cardiologie, Groupe Hospitalier Pitié Salpêtrière APHP, Paris, France, France

5. Service de Chirurgie Thoracique et Cardiaque, Institut de Cardiologie, Groupe Hospitalier Pitié Salpêtrière APHP, Paris, France, Ile-de-France, France

6. Groupe hospitalier de la Pitié Salpétrière, APHP, Paris, France, Ile-de-France, France

7. Sorbonne Universités, UPMC Univ Paris 06, INSERM UMRS 1146, CNRS UMR 7371, Laboratoire d'Imagerie Biomédicale, F-75013, Paris, France, France

8. Sorbonne Universités, UPMC Univ Paris 06, INSERM, CNRS, UMR 7371, UMRS 1146, Laboratoire d'Imagerie Biomédicale, 75013, Paris, France, Ile-de-France, France

9. Sorbonne Universités, UPMC Univ Paris 06, INSERM UMRS 1146, CNRS UMR 7371, Laboratoire d'Imagerie Biomédicale, F-75013, Paris, France, Paris, Ile-de-France, France

Background: Currently, the aortic dilatation measure guiding the indication of prophylactic thoracic aorta surgery is based on local maximal aortic diameter. However, 50% of patients with aortic dissection following aneurysm have maximal aortic diameters below the recommended threshold for surgery. Aortic volumes integrate both aortic dilatation and elongation and may be more sensitive to changes in aortic geometry and less hampered by slice orientation and obliquity.

Methods: We studied 136 individuals (87 men, age: 54±15y): 25 healthy volunteers, 53 patients with hypertension (27 uncontrolled) and 58 patients with dilated ascending aorta (23 bicuspid) who underwent 3D SSFP ECG-gated and navigated CMR of the aorta.
Automated 3D aortic segmentation was performed and aortic length, maximal diameter and volume indices were measured from the sino-tubular junction to brachiocephalic artery for the ascending aorta (AAo) and from the left subclavian artery to the diaphragm for the descending aorta (DAo). Aortic measures were compared across groups using ANOVA and pairwise comparisons with Bonferroni correction.

Results: Compared to healthy individuals, AAo volume increased by 28% ($p<0.05$) in controlled hypertensives (HTc) and 44% ($p<0.05$) in uncontrolled hypertensives (HTu). This AAo volume increase resulted foremost from dilatation (HTc: +10%, $p<0.05$; HTu: +15%, $p<0.05$) but also from a modest elongation (HTc: +5%, $p=0.2$; HTu: +10%, $p<0.05$). When normalized to BSA, the volume increase remained significant in both hypertensive groups whereas the increase in diameter was only significant in HTu.
In patients with AAo aneurysm, the highly significant AAo volume augmentation found compared to healthy controls (tricuspid aneurysmal patients (APt): +170%, $p<0.001$; bicuspid aneurysmal patients (APb): +210%, $p<0.001$) contrasted with a smaller AAo diameter increase of only 45% (APt, $p<0.001$) and 50% (APb, $p<0.001$). The volume increase resulted from AAo dilatation but also from significant AAo elongation (APt: +30%, $p<0.001$; APb: +35%, $p<0.001$). These results remained significant when indexing to BSA.
The ratio between ascending and descending aortic volumes was unchanged in hypertensives when compared to healthy controls in favor of homogeneous dilatation of the thoracic aorta. However, this ratio significantly increased in aneurysmal patients (APt: +33%, $p<0.01$; APb: + 84%, $p<0.01$) and was significantly different between tricuspid and bicuspid patients ($p<0.01$).

Conclusion:

Aortic volume changes in hypertension and aortic diseases were more significant than diameter changes in MRI independent of BSA. Furthermore, the volume increase in hypertension reflects a homogeneous dilatation of AAo and DAo whereas aneurysmal patients had predominantly AAo dilatation and elongation. This pattern was further pronounced in bicuspid patients.

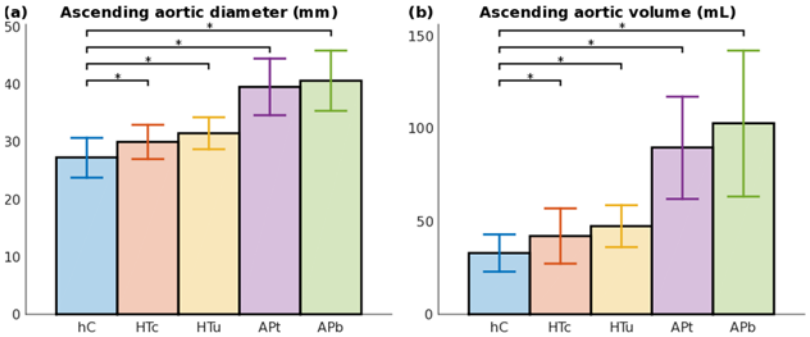

Changes in ascending aortic (a) diameter and (b) volume with hypertension and aneurysmal aortic diseases. Blue: healthy controls (hC); red: controlled hypertensives (HTc), yellow: uncontrolled hypertensives (HTu), purple: tricuspid aneurysmal patients (APt) and green: bicuspid aneurysmal patients (APb). * means $p < 0.05$ for comparisons against healthy controls.

Subjects characteristics for each group.

	Healthy controls	Controlled hypertensives	Uncontrolled hypertensives	Tricuspid aneurysmal patients	Bicuspid aneurysmal patients	p -value
N	25	26	27	35	23	
Gender (M/F)	14 / 11	11 / 15	17 / 10	26 / 9	19 / 4	
Age (y)	41 ± 14	52 ± 12	53 ± 12*	64 ± 9*	54 ± 18	< 0.001
cSBP (mmHg)	111 ± 13	122 ± 9*	134 ± 12*	121 ± 10	117 ± 18	< 0.001
AAo L (mm)	55 ± 8	58 ± 9	60 ± 7*	71 ± 10*	75 ± 13*	< 0.001
AAo D (mm)	27 ± 3	30 ± 3*	31 ± 3*	39.5 ± 5*	40.6 ± 5*	< 0.001
AAo V (mL)	33 ± 10	42 ± 15*	48 ± 11*	90 ± 27*	103 ± 40*	< 0.001
AAo D / DAo D	1.34 ± 0.12	1.32 ± 0.11	1.33 ± 0.11	1.50 ± 0.18*	1.66 ± 0.23*	< 0.001
AAo V / DAo V	0.71 ± 0.14	0.71 ± 0.17	0.72 ± 0.14	0.94 ± 0.26*	1.30 ± 0.56*	< 0.001

AAo: ascending aorta, DAo: descending aorta, cSBP: central systolic blood pressure, L: length, D: diameter, V: volume. p values for ANOVA across groups. * means $p < 0.05$ for comparisons against healthy controls.

ID#: 377065

Real-time assessment of myocardial deformation: the intra- and inter-observer agreement of LV strain using strain-encoded CMR imaging

Tomas Lapinskas, MD[1]Lukas Stoiber, MD[2], Sebastian Kelle, MD, PhD[3], Christian Stehning, PhD[4], Rolf Gebker, MD, PhD[2], Remigijus Zaliunas, MD, PhD[5], Burkert Pieske, MD[2], Sebastian Kelle, MD[2]

1. Medical Academy, Lithuanian University of Health Sciences, Kaunas, Kauno Apskritis, Lithuania

2. German Heart Center Berlin, Berlin, Berlin, Germany

3. German Heart Center Berlin, Berlin, Germany

4. Philips Research Laboratories, Hamburg, Germany

5. Lithuanian University of Health Sciences, Kaunas, Kauno Apskritis, Lithuania

Background: To date, cardiac wall motion analysis plays an important role for evaluation of myocardial contractile function. Recently developed strain-encoding (SENC) imaging technology provides fast real-time quantitative assessment of myocardial mechanics. The main aim of the study was to test intra- and inter-observer agreement of global left ventricular (LV) longitudinal and circumferential strain derived using cardiovascular magnetic resonance (CMR) SENC technology.

Methods: Twelve healthy volunteers underwent advanced CMR imaging using a 1.5 T MRI scanner (Achieva, Philips Healthcare, Best, The Netherlands). SENC images were acquired using newly developed real-time free-breathing technique (Myocardial Solutions, Inc., Morrisville, North Carolina, USA). Global LV longitudinal strain (Ell_{SAX}) was calculated from three short-axis (basal, mid-ventricular and apical) images, and global LV circumferential strain (Ecc_{LAX}) was derived from three long-axis (two-, three- and four-chamber) images by two experienced observers. To assess intra-observer agreement, strain analysis was repeated after 4 weeks.

Results: SENC imaging and analysis were fast with a 15 second scan time and a 90 second post-processing time for a complete quantitative assessment. Ell_{SAX} and Ecc_{LAX} demonstrated excellent intra-observer (ICC 0.95 (0.84 to 0.99) and 0.93 (0.77 to 0.98) for Ell_{SAX} and Ecc_{LAX} respectively) and inter-observer agreement (ICC 0.96 (0.88 to 0.99) and 0.94 (0.80 to 0.98) Ell_{SAX} and Ecc_{LAX} respectively). Bland-Altman plots demonstrate intra- and inter-observer reproducibility for left ventricular Ell_{SAX} and Ecc_{LAX} (Figure 1).

Conclusion: Myocardial deformation measurements derived using fast, real-time SENC imaging technique are highly reproducible. The newly developed SENC imaging technology may allow accurate and rapid assessment of myocardial deformation with a relevant decrease in imaging and analysis time.

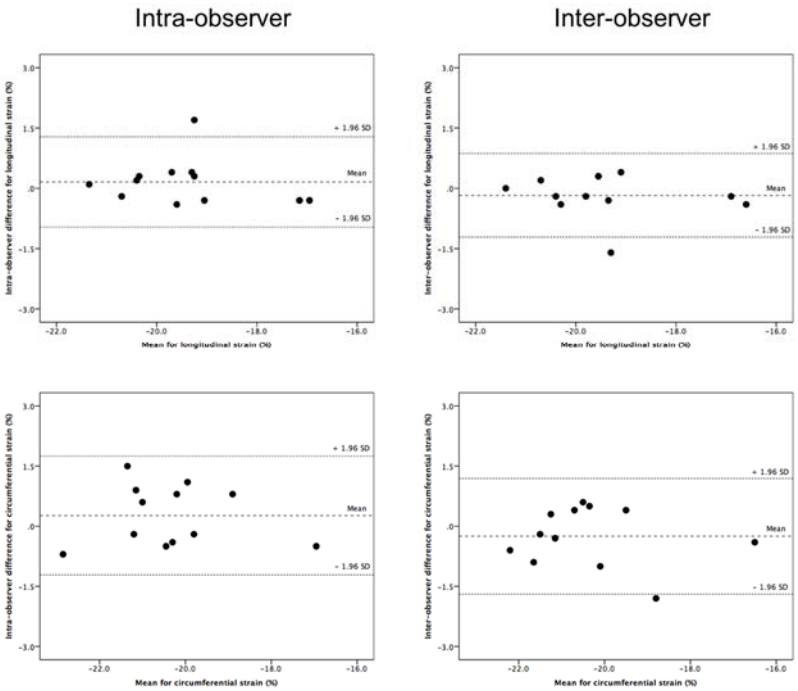

Bland-Altman plots with limits of agreement (1.96 standard deviation) demonstrate the intra-observer and inter-observer reproducibility of CMR strain-encoded imaging for LV strain parameters. The middle, dashed line is the mean of difference of measures. The upper and lower dotted lines are ± 1.96 standard deviation.

ID#: 376886

Added Value of MRI-based Vascular Calcification Visualization for the Assessment of Lower Extremity Arterial Stenosis in Patients with Peripheral Artery Disease Undergoing Quiescent Interval Single-Shot (QISS) MRA

Akos Varga-Szemes, MD, PhD[1] Taylor M. Duguay, BS[2], Thomas M. Todoran, MD[1], Megha Penmetsa, BS[1], Stephen R. Fuller, BS[1], Pal Suranyi, MD, PhD[1], Carlo N. De Cecco, MD, PhD[1], Domenico Mastrodicasa, MD[1], Robert R. Edelman, MD[3], Ioannis Koktzoglou, PhD[4], Shivraman Giri, PhD[5], U. Joseph Schoepf, MD[1]

1. Medical University of South Carolina, SC

2. Medical University of South Carolina, Charleston, SC

3. NorthShore University HealthSystem, Evanston, IL

4. NorthShore University HealthSystem, IL

5. Siemens Healthcare, IL

Background: The diagnostic accuracy of quiescent-interval single-shot (QISS) MRA to detect peripheral artery disease (PAD) has been shown to be similar to that of CTA. Unlike CTA, standard MR techniques are limited in the detection of vascular calcification. However, proton density-weighted, in-phase 3D stack-of-stars gradient-echo (PDIP-GRE) prototype pulse sequence has been shown to accurately depict calcifications in PAD. In this study we aimed to investigate the added value of calcification visualization on the diagnostic confidence and accuracy of detecting PAD and to compare the accuracy of calcium quantification between PDIP-GRE MRI and CTA.

Methods: Fourteen PAD patients (68±9 years) referred for lower extremity CTA (Siemens Force) prior to digital subtraction angiography (DSA) (Siemens Axiom Artis), were prospectively enrolled for a same-day 1.5T MRI (Siemens Avanto). Prototype QISS-MRA (FOV 400×260mm^2, TR/TE 3.5/1.4ms, flip angle 90°, in-plane resolution 1.0×1.0mm^2) was performed covering the abdominal aorta and lower extremity run-off. Prototype PDIP-GRE MRI (FOV 416mm, TR/TE 9.6/4.7ms, flip angle 4.5°, radial views 660) was acquired covering the iliofemoral region. Image evaluation was performed on a per-segment basis according to an 18-segment model. Two readers rated diagnostic confidence (3-point scale) and graded stenosis (< or >50%) on QISS-MRA without and with the visualization of calcification. Sensitivity and specificity were calculated using the McNemar-test with DSA as reference. Intra-arterial calcium was quantified using ImageJ (NIH) and compared between MRA and CTA using paired t-test and Bland-Altman analysis.

Results: A total of 252 vascular segments were evaluated with QISS-MRA and 84 segments were available for calcification assessment. Of those 84 segments, >50% stenosis was detected in 37 (44%), while calcium was present in 58 (69%). The diagnostic confidence (2.1 [1.9-2.3] vs. 2.3 [2.1-2.5]; P<0.0001) and the sensitivity and specificity of QISS-MRA in the detection of >50% stenosis (83.2% and 97.6% vs. 86.4% and 98.0%, respectively) were improved when calcification data were provided to the readers. Quantification of calcification showed no statistical difference between MRI and CTA (121±77mm^3 vs 127±84mm^3; P=0.0249), and Bland-Altman analysis revealed excellent agreement with a mean of differences at -5.8mm^3.

Conclusion: The visualization of lower extremity vascular calcification improved readers'; confidence and the diagnostic accuracy of QISS-MRA in detecting significant vascular stenoses. Quantification of vascular calcium with MRI showed good agreement with CTA. The PDIP-GRE MRI technique seems to be promising for the complex anatomical assessment in PAD, which could be beneficial in interventional procedure planning.

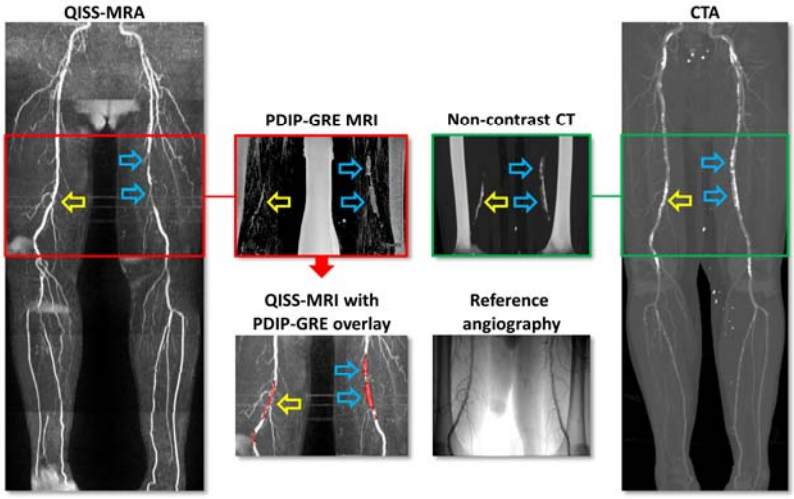

Corresponding QISS-MRA and CTA in a 72-year-old man with PAD. PDIP-GRE MRI (red frame) shows calcification of the right superficial femoral artery (yellow arrow) and two intra-vascular stents in the left superficial femoral artery (blue arrows). The composite image shows the calcification overlay on the QISS-MRA image. Corresponding non-contrast and contrast enhanced CT, as well as reference invasive angiography images are also displayed.

ID#: 373826

Donor and recipient characteristics are associated with CMR-derived cardiac structural and functional differences following heart transplantation

Ryan Dolan, MD[1] Amir Ali Rahsepar, MD[1], Julie Blaisdell[1], Kenichiro Suwa, MD[2], Kambiz Ghafourian, MD, MPH[3], Jane E. Wilcox, MD, MSc[4], Sadiya Khan, MD, MSc[3], Esther Vorovich, MD[3], Jonathan Rich, MD[3], Allen Anderson, MD[5], Jeremy D. Collins, MD[1], James Carr, MD[1], Michael Markl, PhD[1]

1. Northwestern University, Chicago, IL

2. Northwestern University Feinberg School of Medicine Department of Radiology, IL

3. Northwestern University

4. Northwestern University Feinberg School of Medicine, Chicago, IL

5. Northwestern Medicine, Chicago, IL

Background: Cardiac magnetic resonance (CMR) can be used for cardiac allograft surveillance following heart transplant (Tx) due to its ability to quantify regional myocardial tissue structure (edema using T2-mapping, fibrosis and interstitial expansion using T1-mapping and extracellular volume fraction (ECV)) and to measure global and regional left ventricular (LV) function [global LV function using 2D cine SSFP, myocardial velocities and dyssynchrony using tissue phase mapping (TPM)]. The goal of this study was to evaluate relationships between Tx donor and recipient characteristics and cardiac structure and function.

Methods: Ninety-one Tx recipients (51.0±17.0 years, 43% female, 5.6±5.6 years post-Tx) were prospectively recruited for CMR at 1.5T (Magnetom Aera or Avanto, Siemens, Erlangen, Germany), including 2D cine SSFP, T2-mapping, pre- and post- Gd contrast T1-mapping, and TPM. Global LV function parameters were calculated from a short-axis stack of 2D cine SSFP images. T2 and pre- and post-contrast T1 maps (to calculate ECV) were reconstructed on the MRI system and further analyzed using dedicated software (cvi42, version 5.3.6, Circle, Calgary, Canada). TPM data acquisition used a black-blood cine 2D phase-contrast sequence with tri-directional velocity encoding to quantify myocardial peak velocities and time to peak velocities (TTP) using an in-house tool (Matlab, Mathworks, Natick, MA). LV dyssynchrony was calculated using standard deviations of TTP. We evaluated baseline donor and recipient characteristics [demographics, clinical data, and immunologic status assessed by panel reactive antibody (PRA) and donor-specific antibody (DSA)] for correlation with CMR parameters (T2, T1, ECV, myocardial velocities, LV dyssynchrony, global function).

Results: Donor and recipient characteristics are summarized in Table 1. Increased donor age was positively correlated with elevated global T2 (r=0.30, P=0.02) and higher ECV (r=0.45, P<0.01, Figure 1) and correlated with declining peak diastolic longitudinal velocities (r=0.40, P<0.01, Figure 1). Female Tx recipients had significantly higher global T2 (52.4±4.4 ms vs. 50.0±4.4 ms, P=0.01) and T1 (1058±61 ms vs. 1023±60 ms, P=0.01) compared to male recipients. Recipient weight, BMI, and BSA were negatively associated with global T2 (r=-0.32, P<0.01; r=-0.27, P=0.03; r=-0.27, P=0.03). Donor BMI was positively associated with elevated global ECV (r=0.35, P=0.01). Donor-recipient BMI difference correlated positively with increased diastolic radial dyssynchrony (r=0.43, P<0.01, Figure 2). Recipients with positive DSA at time of Tx and at time of CMR had significantly higher global ECV (30.6±4.3% vs. 26.7±3.2%, P=0.03; 29.5±4.0% vs. 26.5±3.6%, P=0.02).

Conclusion: Donor and recipient characteristics are associated with altered global and regional allograft structure and function. Further investigation of the underlying pathophysiology and outcomes-based analysis of abnormal structural and functional CMR parameters is warranted.

Age at Scan	N=91	51.0 ± 17.0 yrs	**Height Rec**	N=70	172.7 ± 10.8 cm	**BSA**	N=70	1.94 ± 0.22 m²
Age at Tx	N=91	44.9 ± 17.9 yrs	**Height Donor**	N=64	174.7 ± 8.6 cm	**EF Don**	N=64	61.4 ± 6.1 %
Age Donor	N=64	28.0 ± 10.6 yrs	**Height Diff**	N=64	0.046 ± 0.035	**PRA Class I**	N=30	9.1 ± 22.2 %
Age Diff	N=64	1.05 ± 0.81	**WeightRec**	N=70	80.6 ± 16.2 kg	**PRA Class II**	N=30	5.9 ± 13.2 %
Sex Rec	N=91	38 (42%) female	**Weight Donor**	N=64	76.1 ± 14.9 kg	**Tx T Cross**	N=14	2 (14%) positive
Sex Donor	N=64	16 (25%) female	**Weight Diff**	N=64	0.199 ± 0.148	**Tx B Cross**	N=14	2 (14%) positive
Sex Diff	N=64	21 (33%) discordant	**BMI Rec**	N=70	26.6 ± 4.5 kg/m²	**Tx DSA**	N=48	35 (73%) positive
Race Rec	N=91	58%White, 25%Black,	**BMI Donor**	N=64	25.2 ± 4.8 kg/m²	**Scan DSA**	N=63	43 (68%) positive
		11%Hisp, 4%Asian	**BMI Diff**	N=64	0.200 ± 0.145	**CMV**	N=71	36 (51%) positive

Table 1: Donor and recipient characteristics. Number of patients for which information regarding a specific characteristic was available is listed next to each characteristic. Differences in age, height, weight, and BMI are relative: (X donor – X recipient)/X donor. Diff: difference, Tx: time of transplant, Rec: recipient, Cross: crossmatch.

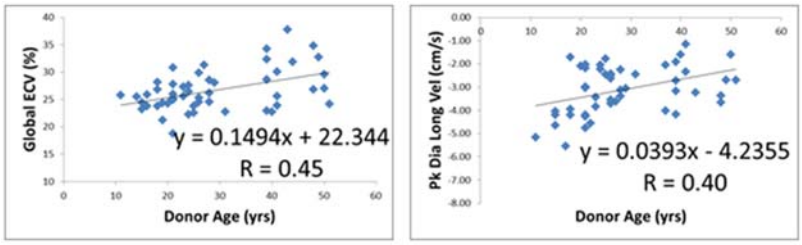

Figure 1: Correlation analyses of donor age and global ECV (on left) and donor age and peak diastolic longitudinal velocity (on right).

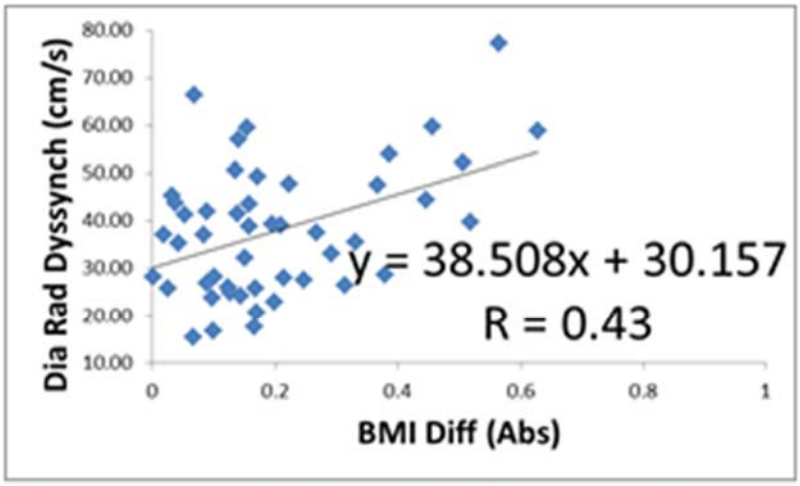

Figure 2: Correlation analysis between donor-recipient BMI difference and diastolic radial dyssynchrony.

ID#: 374425

T1 and T2 mapping at rest and stress for ischemic and scar detection in coronary artery disease: external validation in an independent cohort

Elen Elen, MD, FIHA[1] Tommaso D'Angelo, MD[2], Elif Peker, MD[3], Lea Winau, Bsc[4], Christophe Arendt, MD[5], Faraz Pathan, MBBS, FRACP[6], Thomas Vogl, MD[7], Andreas M. Zeiher, MD, PhD[8], Eike Nagel, MD, PhD[9], Valentina O. Puntmann, MD, PhD[10]

1. National Cardiovascular Center Harapan Kita, Jakarta-Indonesia; Institute for Experimental and Translational Cardiovascular Imaging, University Hospital Frankfurt-Germany, Tangerang, Banten, Indonesia

2. University of Messina, Messina, Sicilia, Italy

3. Goethe University Hospital Frankfurt, Frankfurt, Germany

4. Goethe University Hospital Frankfurt, Hessen, Germany

5. Goethe-University Frankfurt, Department of Diagnostic and Interventional Radiology, Frankfurt Am Main, Hessen, Germany

6. Goethe Institute for Experimental and Translational Cardiovascular Imaging, Sydney, New South Wales, Australia

7. Universitaetsklinikum Frankfurt, Germany

8. Goethe University Hospital Frankfurt, Frankfurt am Main, Hessen, Germany

9. University Hospital Frankfurt; Institute for Experimental and Translational Cardiovascular Imaging; DZHK Centre for Cardiovascular Imaging, Frankfurt, Germany

10. Universitaetsklinikum Frankfurt, Frankfurt Am Main, Germany

Background: Contrast-free myocardial perfusion CMR imaging would represent a considerable step change towards a fast and simple diagnostic method for detection of CAD. A previous study reported feasibility of T1 mapping in detection of ischemia and scar in a small number of patients. We undertook external validation of the T1 and T2 mapping at rest and stress for ischemia and scar detection in an independent cohort of patients with CAD.

Methods: We prospectively enrolled 46 CAD patients (71.7% male, age of 56.5(14) years). Contrast-enhanced adenosine stress myocardial perfusion CMR imaging and late gadolinium enhancement served as the diagnostic standard for the presence of ischemia and scar, respectively. T1 mapping MOLLI 3(2)3(2)5 FA50° and T2 mapping FLASH were performed in a single midventricular slice at rest and stress. 14 subjects with normal resting native T1 and no ischaemia/scar on contrast-enhancened imaging served as controls. A total of 69 segments were categorized in remote (n=24), ischemic (n=14), or scarred (n=21) segments by expert readers. Corresponding T1 and T2 values were measured at rest and stress by independent observer blind to the results of perfusion/LGE. Native T1 and T2 response (msec), reactivity (value between stress and rest, normalized for resting value, %) are reported.

Results: Native T1 values in controls have increased considerably in resonse to hyperaemia at stress compared to remote myocardium of patients (Tables 1 and 2, Figure 1A). In patients, scarred areas showed blunted response to hyperaemia, which was significantly differento to remote myocardium and areas of ischaemia, however, ischaemic segments could not be discerned from remote myocardium. Similarly, native T2 of controls has increased considerably compared to remote myocardium of patients. In patients, iscahemic and scarred areas both showed a blunted response compared to remote myocardium (Figure 1B)

Conclusion: We demonstrate that remote ischaemic myocardium shows reduced response/reactivity, detected by both tissue parametric measures. Whereas native t1 can identify scarred segments, differentiation between remote and ischaemic myocardium is not possible. On the contrary, native T2 show blunted response in ischaemic and scarred myocardium compared to remote myocardium. Differential responses of both measures may be complementary in identifying the signature of ischaemic and scarred tissue in CAD patients.

Segment	Response (msec)	P value	Reactivity (%)	P value
Native T1				
Normal	46.2 ± 20.2	0.01	4.2 ±2.0	0.001
Remote	25.1 ± 38.0		2.3 ± 3.5	
Ischemic	17.9 ± 40.7		1.6 ± 3.7	
Scarred	-12.4 ± 39.1		-0.95 ± 2.8	
Native T2				
Normal	5.5 ± 3.3	0.001	15.1 ± 9.2	0.001
Remote	3.5 ± 2.9		9.3 ± 7.7	
Ischemic	-0.64 ± 2.4		-1.4 ± 5.6	
Scarred	-1.4 ± 3.0		-2.8 ± 6.3	

Comparison	T1 response (msec)		T1 reactivity%		T2 response(msec)		T2 reactivity(%)	
	P value	Cohen's d	P value	Cohen's d	P value	Cohen's d	P value	Cohen's d
Normal-remote	0.062	0.69	0.271	0.64	0.059	0.68	0.068	0.68
Normal-ischemic	0.026	0.88	<0.001	2.15	<0.001	2.17	0.024	0.89
Remote-ischemic	0.551	0.18	<0.001	1.56	<0.001	1.58	0.570	0.19
Normal-scarred	<0.001	1.89	<0.001	2.18	<0.001	2.27	<0.001	2.17
Remote-scarred	0.011	0.97	<0.001	1.64	<0.001	1.71	0.015	1.03
Ischemic-scarred	0.037	0.97	1.000	0.26	0.461	0.24	0.489	0.79

Table 1 and 2

Figure 1

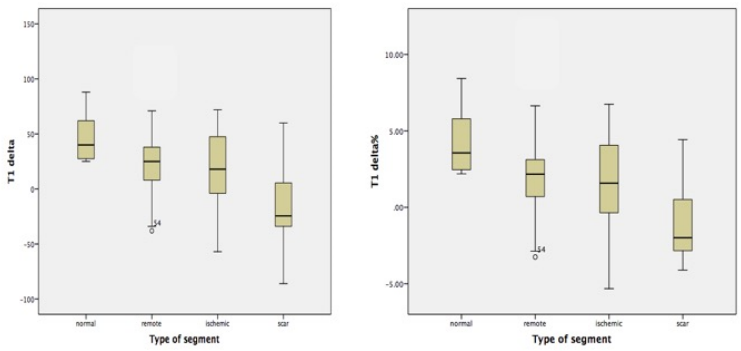

Figure 1

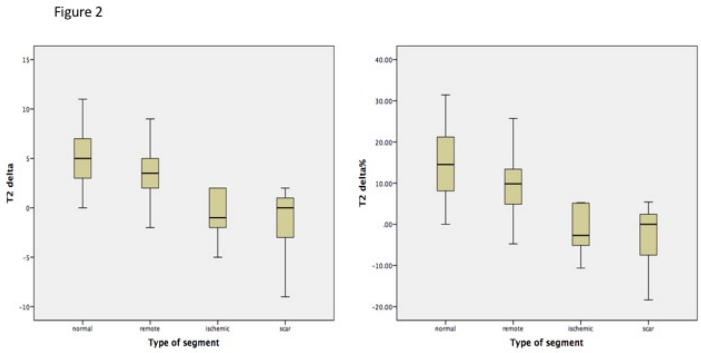
Figure 2
T2 delta
15
10
5
0
-5
-10
normal
remote
ischemic
scar
Type of segment
T2 delta%
40.00
30.00
20.00
10.00
.00
-10.00
-20.00
normal
remote
ischemic
scar
Type of segment

Figure 2

ID#: 373294

Value of cardiac MRI for assessment of aneurysm of the ascending aorta in patients with aortic valve Insufficiency

Ellianna J. Hoff[1] Sebastian M. Boland, MBA[2], Sreya Brahmandam[3], Daniel R. Morgenstern, MS[4], Selena J. Chandler[5], J. Ronald Mikolich, MD[6]

1. Sharon Regional Health System

2. Sharon Regional Health System, Rootstown, OH

3. Sharon Regional Health System, OH

4. University of Toledo College of Medicine, PA

5. Sharon Regional Health System, Willoughby, OH

6. Northeast Ohio Medical University (NEOMED), Youngstown, OH

Background: The current ACC/AHA and ESC guidelines recommend yearly monitoring of aneurysm size for patients with aneurysm of the ascending aorta > 3.5 cm diameter, measured perpendicular to flow. Recent data from Park et al (Eur J Cardiothorac Surg 51:959-964, 2017) suggest that co-existing aortic regurgitation (AR) may be an independent risk for progression of aneurysm size. However, Park et al used axial measurements, not perpendicular to flow dimensions, and included only moderate (2+) or worse AR, using CT as the imaging modality. Cardiac MRI (CMR) is ideal for assessing AAscAo size on a serial basis, without ionizing radiation. This study was designed to assess the long-term progression of AAscAo in patients with and without AR, using CMR.

Methods: An institutional cardiac imaging database was queried for all patients with AAscAo, defined as an ascending aorta diameter > 3.5 cm measured perpendicular to flow, who had 2 or more serial CMR studies. This patient cohort was divided into Group A (patients with AR) and Group B (patients with no AR). Serial ascending aortic diameter data were used to determine the mean diameter and rate of annual growth for four years after the initial diagnosis.

Results: The mean diameter of the ascending aorta, measured perpendicular to flow, for patients with and without AR is plotted on the line graph below demonstrating the average change over the four-year follow-up period. Patients with aortic valve insufficiency had a mean growth in the diameter of the ascending aorta of 0.06cm/year from years 1 to 3. From year 3 to 4, however, this value was 0.14cm/year. In contrast, those patients without aortic valve regurgitation had annual growth rates that remained static for both years 1 to 3 and year 3 to 4 (0.05cm/year for each). The mean radiation dose for a CT of the chest is 7 mSv with a cost of $486.10 (Medicare 2017 reimbursement). CMR has no radiation with a cost of $254.82 (Medicare reimbursement 2017). The 5-year cost savings of this approach is $115,640 per 100 patients with a radiation dose conservation of 35 mSv per patient.

Conclusion: Patients with aortic valve insufficiency in conjunction with an aortic aneurysm have an accelerated growth of the ascending aortic diameter as compared to those who do not have aortic regurgitation. The accelerated growth rate appears to begin 3 years after the initial diagnosis. Serial monitoring of these patients can be accomplished with CMR at a lower cost to the healthcare system, without the need for ionizing radiation.

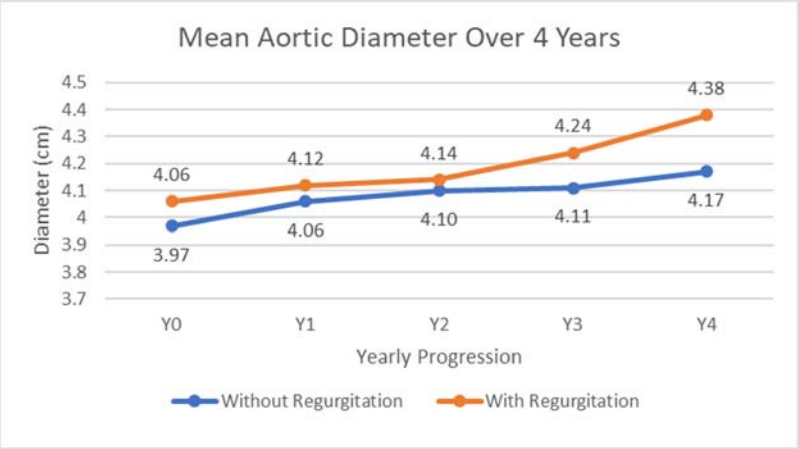

Graph 1

ID#: 373319

Subclinical Fabry Cardiomyopathy

Sabrina Nordin, MRCP [1]Rebecca Kozor, PhD[2], Shanat Baig, MBBS[3], Amna Abdel-Gadir, MBBS.MRCP(UK)[4], Katia Devorha. Menacho, MD[5], Stefania Rosmini, MD, PhD[6], Gabriella Captur, MD PhD MRCP MSc[5], Michel Tchan, PhD[7], Tarekegn Geberhiwot, PhD[8], Elaine Murphy, FRCPath[9], Robin Lachmann, PhD[9], Peter Kellman, Ph.D.[10], Uma Ramaswami, MD[11], Nicola Edwards, PhD[3], Derralynn Hughes, PhD[12], Richard Steeds, MD[3], James C. Moon, MD[6]

1. Barts Heart Centre, United Kingdom

2. University of Sydney, Sydney, New South Wales, Australia

3. University Hospitals Birmingham, England, United Kingdom

4. University College London and Barts Heart Centre, London, England, United Kingdom

5. Barts Heart Centre, London, England, United Kingdom

6. Barts Heart Centre, England, United Kingdom

7. University of Sydney, Australia

8. University Hospitals Birmingham, United Kingdom

9. National Hospital for Neurology and Neurosurgery, United Kingdom

10. National Heart, Lung, and Blood Institute, Bethesda, MD

11. Royal Free Hospital, United Kingdom

12. Royal Free Hospital, England, United Kingdom

Background: Fabry disease (FD) is a rare, X-linked lysosomal storage disorder. Cardiac involvement determines outcome therefore detecting early changes is important. A low T1 by CMR in FD reflects sphingolipid storage. In sarcomeric hypertrophic cardiomyopathy (HCM), a subclinical phenotype is present with, amongst other features, multiple myocardial crypts, anterior mitral valve leaflet (AMVL) elongation, abnormal trabeculae, and a higher ejection fraction. We hypothesized there would be a subclinical Fabry cardiomyopathy phenotype.

Methods: A prospective, international multicentre observational study of 100 left ventricular hypertrophy (LVH)-negative FD patients (mean age 39±15 years, 19% male) and 35 age- and gender-matched healthy volunteers (HV) (mean age 40±14 years, 25% male) underwent CMR including LV structure, function, native myocardial T1 and LGE, plus 12-lead ECG.

Results: In FD, 41% had a low T1 using a single septal region of interest, but this increased to 59% using a second slice, because T1 lowering was patchy. ECG abnormalities were present in 41% and twice as common with low T1 (53% vs 24%, p=0.005). When T1 was low, LV maximum wall thickness, indexed LV mass and LV ejection fraction were higher (MWT 9±1.5mm vs 8±1.4mm, p<0.005, LVMI 63±10g/m^2 vs 58±9g/m^2, p<0.05 and LVEF 73±8% vs 69±7%, p<0.01). LGE was more likely when T1 was low (27% vs 6%, p=0.01). FD had higher papillary muscle mass (LVPM) compared to HV (8±4g vs 6±2g, p<0.05), which also tracked low T1. FD had higher maximal apical fractal dimensions compared to HV (1.27±0.06 vs 1.24±0.04, p<0.005) and longer anterior mitral valve leaflets (AMVL, 23±2mm vs 21±3mm, p<0.005).

Conclusion: There is a detectable subclinical phenotype in FD consisting of sphingolipid storage (low T1), functional/architectural changes and ECG changes – a candidate group for enzyme replacement therapy (ERT).

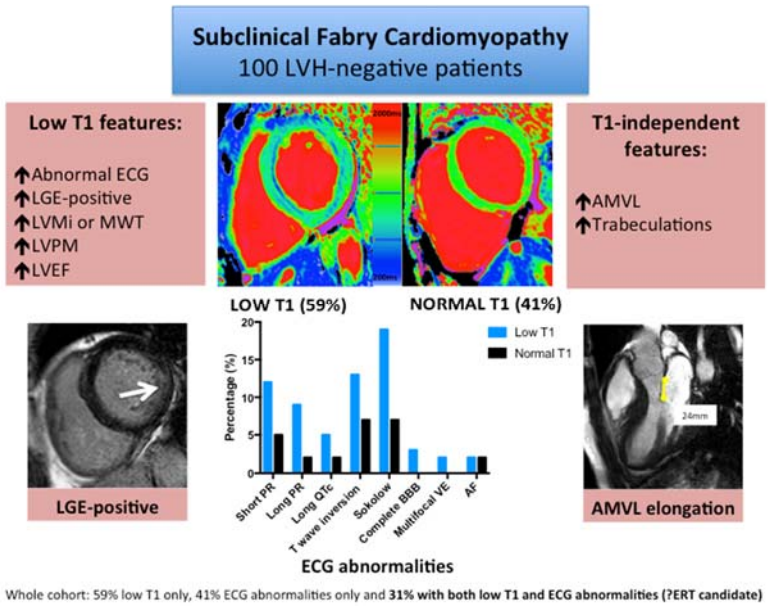

Central Illustration of Subclinical Phenotype of Fabry Cardiomyopathy

ID#: 378907

Myocardial Characterization and Strain as a Diagnostic Tool in Anthracycline-Induced Cardiotoxicity: A Preclinical Model

Cory V. Noel, M.D.[1] Nino Rainusso, MD[2], Jonathan Romero, B.S[3], Poonam Sarkar, PhD[3], Amol Pednekar, PhD[4], Robia Pautler, PhD[3]

1. Texas Children's Hospital - Baylor College of Medicine, Houston, TX

2. Texas Children's Hospital - Baylor College of Medicine, TX

3. Baylor College of Medicine, Houston, TX

4. Texas Children's Hospital, Houston, TX

Background: Anthracycline-based chemotherapy (AC) is at least partly responsible for improved survival of pediatric cancer patients. Cancer therapy-related cardiac dysfunction (CTRCD) is commonly observed in survivors of AC. The usual surveillance method for CTRCD is by transthoracic echocardiography. The purpose of our ongoing clinical study is to examine the effectiveness of MR-based myocardial tissue characterization by extracellular volume (ECV), and myocardial strain measurement for early detection of CTRCD in a pre-clinical model.

Methods: Forty mice aged 6-8 weeks were used in the CTRCD model. Ten mice served as controls with 30 mice receiving 3 mg/kg of intraperitoneal doxorubicin weekly for a total of 8 weeks to establish a chronic cardiotoxicity model. The mice underwent CMR at 4, 8 and 12 weeks. All mice were scanned on a Bruker 9.4 Tesla MRI. All mice were anesthetized by isofluorine for the study. Acquisition Protocol: The right and left ventricular volume and function was quantified from bSSFP cine sequence. T_1 mapping (modified Look Locker) sequence was performed prior and 15 minutes after intraperitoneal contrast injection. Strain information was acquired using Complementary Spatial Modulation of Magnetization techniques. Both T_1 and strain images are acquired at basal, mid-ventricular, and apical locations in short-axis. Data Analysis: The pre and post contrast T_1 was measured in the interventricular septum and the free wall and the blood (cvi[42], Calgary, CA). The ECV was calculated using T_1 and hematocrit values; the circumferential strain (ε_{cc}) was determined by using commercially available software (myocardial solutions, Morrisville, NC).

Results: Three control mice and one AC mouse died prior to the 4 week CMR. Box and Whisker plots for ECV, ε_{cc}, and ventricular ejection fractions are depicted in Figure 1. While ECV at 4 weeks were comparable ($p=0.24$), there was significant increase at 8 (6%,$p < 0.0006$) and 12 (8.5%,$p < 3*10^{-7}$) weeks post AC compared to controls at the same time points. There was corresponding significant decrease in LVEF and RVEF. Global ε_{cc} was significantly different between control and 4 and 12 week post AC. There was confined life style related slight increase of 0.8% (8 weeks) and 2.3% (12 weeks) of ECV in controls.

Conclusion: Myocardial tissue characterization with ECV, along with myocardial strain, may be useful diagnostic tools in patients in the earlier detection of CTRCD receiving AC. Larger clinical trials are needed to determine the value of these CMR techniques in this population.

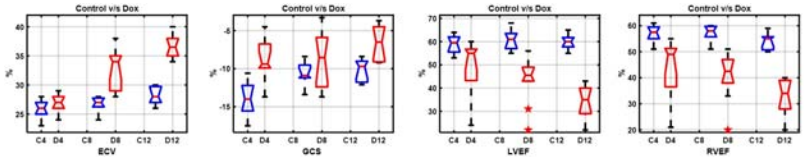

ECV, global circumferential strain (εcc), and ventricular ejection fractions in control and Dox mice. Dox = received intraperitoneal doxorubicin weekly; GCS = global circumferential strain; C = control; D = Dox; 4/8/12 = after 4/8/12 weeks, respectively

ID#: 378781

Different deformation behaviors assessed by Cardiac Magnetic Resonance-Feature Tracking analysis among patients with myocardial rupture due to myocardial infarction

Alice Niero, MD[1]Martina Previato, MD[2], Francesca Prevedello, MD[3], Alberto Cipriani, MD[4], Daniele Scarpa, Sr.[5], Benedetta Giorgi, MD[6], Carmelo Lacognata, MD[7], Luisa Cacciavillani, MD, PhD[8], Manuel De Lazzari, MD, PhD[4], Gino Gerosa, MD,PhD[9], Giuseppe Tarantini, MD, PhD[10], Sabino Iliceto, MD, PhD[4], Martina Perazzolo Marra, MD, PhD[4]

1. Depatment of Cardiac, Thoracic and Vascular Sciences. University of Padua. Italy, Italy

2. Depatment of Cardiac, Thoracic and Vascular Sciences. University of Padua. Italy., Italy

3. Depatment of Cardiac, Thoracic and Vascular Sciences. University of Padua, Padua, Veneto, Italy

4. Department of Cardiac, Thoracic and Vascular Sciences, University of Padova, Italy, Italy

5. Department of Cardiac, Thoracic and Vascular Science, University of Padua, Italy

6. Department of Radiology, Azienda Ospedaliera-University of Padua Medical School, Italy

7. Radiology, Azienda Ospedaliera Padova, Italy, Italy

8. Department of Cardiac, Thoracic and Vascular Sciences, Univerisity of Padua, Italy

9. Department of Cardiac, Thoracic and Vascular sciences, Univerisity of Padua, Italy

10. Department of Cardiac, Thoracic and Vascular sciences, University of Padua, Italy

Background: In the current era of urgent reperfusion therapy for ST-segment–Elevation Myocardial Infarction (STEMI), the incidence of post-infarction Myocardial Rupture (MR) is very low. Nevertheless, it carries with it a substantial mortality rate. We investigated whether strain imaging assessed by Cardiac Magnetic Resonance (CMR)-Feature Tracking (FT) could allow insights into the pathogenesis of the mechanism associated with this complication.

Methods: We enrolled a cohort of patients admitted for STEMI with suspected MR who underwent CMR between 2 and 10 days from admission. Patients with STEMI without MR who performed CMR on the same period served as controls. CMR-FT analysis was performed using a novel commercially available software (*Circle Cardiovascular Imaging Tissue Tracking, cvi42, Calgary, Alberta, Canada)* assessing radial, circumferential and longitudinal Peak Systolic Strain (PSS) both as global value, mean regional value in Infarct Area (IA), mean regional value in the Adjacent Zone (AZ) of the IA and finally in the residual segments. A sub-analysis was performed among left ventricle free wall MRs and the control group of STEMI patients (n=31) without MR. The difference on strain between IA and AZ has been considered as “wall stress index” (WSI). The IA has been identified on the basis of transmural late gadolinium enhancement (LGE) area.

Results: 15 patients (male 60%, mean age 69 ± 12 years) with STEMI complicated by MR were enrolled as case group. The population was composed by free wall MR (n=6), pseudoaneurysms (4) and ruptures in aneurysmatic infarcted areas (n=5). As control group, 52 patients with STEMI were analysed (male 64%, mean age 66 ± 15). On CMR-FT there was a significative difference between MR group and controls in term of global 2D radial, 2D circumferential and 3D longitudinal PSS (median values 3D global longitudinal PSS -6 vs -11, p= 0.03; 2dD global radial PSS 17 vs 28, p= 0.03; 2D global circumferential PSS -9 vs -16, p= 0.005; **table 1**). The comparison between free wall MRs (an example showed in **image 1)** and a subgroup of STEMI patients (n=31) showed a higher differential value in radial WSI (median values 20.2 vs 12.6; p= 0,014; **table 2).** Considering also the influence of global deformation on IA, the differential radial value indexed by global value of radial PSS was higher in MR patients than those without (1.62 vs 0.54, p=0.01).

Conclusion: In patients with myocardial infarction complicated by MR, strain values are worse than those without rupture, both considering global and regional values. Thus, global strain values seem to characterise those patients who, with similar EF and extension of myocardial infarction, are at risk of myocardial rupture. A higher WSI and its ratio with global radial PSS are associated with free wall MR in patients admitted for STEMI. These parameters take into account not only the IA, but also the complex interplay with non-infarcted myocardium and the WSI as possible pathogenic mechanism of MR in this group of patients.

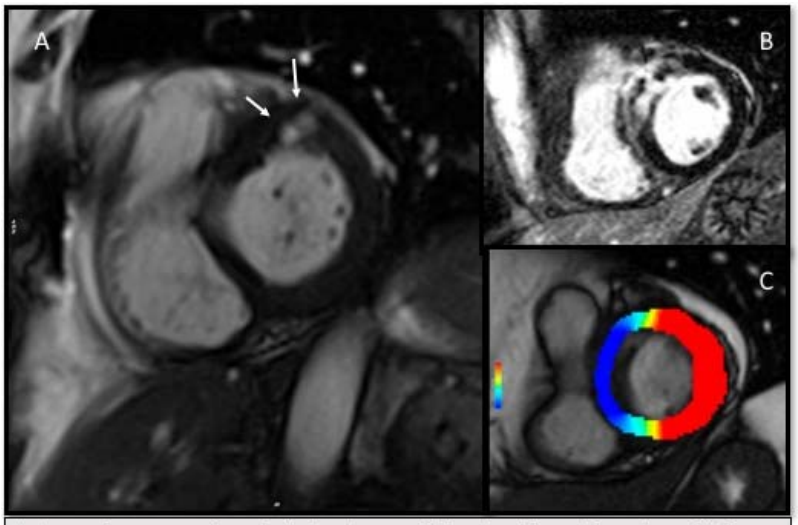

A: A magnetic resonance diagnosis of subacute myocardial rupture of the anterior wall complicating an acute STEMI. B: LGE demonstrating transmural scar on basal anterior segments. C: radial strain showing alterations on the corresponding segments.

Image 1

	STEMI patients (n=52)			***MRs patients (n=15)***			P
	Median	1st quartiles	3rd quartiles	Median	1st quartiles	3rd quartiles	
3D global radial PSS	30,76	20,74	37,12	21,02	15,71	29,57	0,216
3D global circumferential PSS	-12,24	-15,10	-7,44	-7,42	-11,27	-6,12	0,101
3D global longitudinal PSS	-11,01	-13,52	-7,05	-6,02	-10,01	-5,17	**0,027**
2D global radial PSS	28,30	20,16	34,65	17,07	15,95	27,42	**0,034**
2D global circumferential PSS	-15,74	-18,49	-10,89	-8,72	-12,80	-8,20	**0,005**
EF (%)	46,00	37,5	54,50	39	31	49,00	0,165

Table 1

	Free wall MRs (n=6)			***Control group (n=31)***			P
	Median	1st quartiles	3rd quartiles	Median	1st quartiles	3rd quartiles	
3D global radial PSS	27,43	19,02	31,16	34,28	28,33	41,27	0,200
3D global circumferential PSS	-9,78	-13,59	-6,05	-14,49	-15,83	-12,16	0,210
3D global longitudinal PSS	-10,01	-12,73	-6,38	-13,01	-14,41	-10,63	0,210
2D global radial PSS	23,58	15,96	30,68	32,31	27,11	38,72	0,162
2D global circumferential PSS	-12,17	-15,55	-8,20	-17,40	-19,66	-15,27	**0,035**
Radial WSI	20,05	18,54	26,29	12,64	6,87	16,26	**0,014**
Circumferential WSI	-7,21	-11,06	-2,97	-4,21	-7,36	-1,27	0,475
Longitudinal WSI	-5,63	-8,75	-2,32	-3,96	-10,88	,94	0,968
RATIO radial WSI/global PSS	1,62	1,12	4,17	,54	,32	,83	**0,014**
RATIO circumferential WSI/global PSS	-,02	-3,93	,74	,39	,08	1,03	0,221
RATIO longitudinal WSI/global PSS	-,07	-10,45	,27	,28	-,11	1,91	0,456
EF (%)	44,30	32,00	51,00	49	45,00	57,00	0,387

Table 2

ID#: 378610

Validation of fully automated quantitative myocardial perfusion by cardiovascular magnetic resonance compared to coronary sinus flow at 1.5T and 3T

Raquel Themudo, MD, PhD[1] Jannike Nickander, MD[2], Hampus Nyberg[3], Peter Kellman, Ph.D.[4], Hui Xue, PhD[4], Andreas Sigfridsson, PhD[5], Martin Ugander, MD, PhD[6]

1. Department of Clinical Physiology, Karolinska Institutet and Karolinska University Hospital, Stockholms Lan, Sweden

2. Karolinska Institutet, Stockholm, Stockholms Lan, Sweden

3. Department of Clinical Physiology, Karolinska Institutet, and Karolinska University Hospital, Stockholm, Sweden, Sweden

4. National Heart, Lung, and Blood Institute, Bethesda, MD

5. Karolinska Institute, Stockholm, Stockholms Lan, Sweden

6. Karolinska Institutet, and Karolinska University Hospital, Stockholm, Sweden, Stockholms Lan, Sweden

Background:

Quantitative CMR myocardial perfusion evaluation has been limited in part due to the moderate accuracy of the currently available qualitative and semiquantitative methods used to assess myocardial perfusion, and due to the lack of efficient absolute quantitative methods. We recently developed a Gadgetron software infrastructure for fully automated post-processing of first pass perfusion CMR images into quantitative color maps showing myocardial perfusion in the unit ml/min/g. The aim of this study was to validate quantification of MBF by quantitative perfusion color maps compared to an independent method of quantifying MBF by phase contrast coronary sinus (CS) flow imaging.

Methods:

Fifteen healthy subjects (mean age 26 years, 67% females) underwent CMR imaging at 1.5T and 22 healthy subjects (mean age 26 years, 50% females) underwent CMR imaging at 3T, including CS flow imaging and first-pass perfusion in 3 short-axis slices, prior to and during adenosine stress. First-pass perfusion images were analyzed by drawing regions of interest (ROIs) over the whole myocardium in the 3 short-axis slices in quantitative perfusion maps. Average myocardial perfusion weighted by slice area was obtained in mL/min/g. CS flow was determined by drawing an ROI in the coronary sinus in the velocity-encoded phase-contrast images. Coronary sinus flow in mL/min was divided by the left ventricle (LV) mass to obtain myocardial blood flow in mL/min/g. Linear regression analysis was performed to compare MBF from the quantitative perfusion maps with the MBF calculated from the CS phase-contrast images.

Results:

Quantitative myocardial perfusion at 1.5T from color maps at rest (mean±SD, n=15, 0.86±0.19 mL/min/g) and stress (n=15, 3.98±0.47 mL/min/g) correlated with MBF quantified as CS flow per gram LV mass (n=30, $y=1.07*x + 0.34$, $R^2=0.86$, $p<0.001$, mean±SD bias 0.48±0.61 ml/min/g). Quantitative myocardial perfusion at 3T from color maps at rest (mean±SD, n=21, 0.76 ± 0.20 mL/min/g) and stress (n=22, 3.47 ± 0.68 mL/min/g) correlated with MBF quantified as CS flow per gram LV mass (n=43, $y=0.85*x + 0.53$, $R^2= 0.81$, $p<0.001$, bias 0.23±0.68 ml/min/g).

Conclusion:

Automatic quantification of myocardial perfusion from first-pass perfusion CMR is feasible in clinical workflow at 1.5T and 3T, and shows a good correlation compared to the independent measure of CS flow per gram of LV mass.

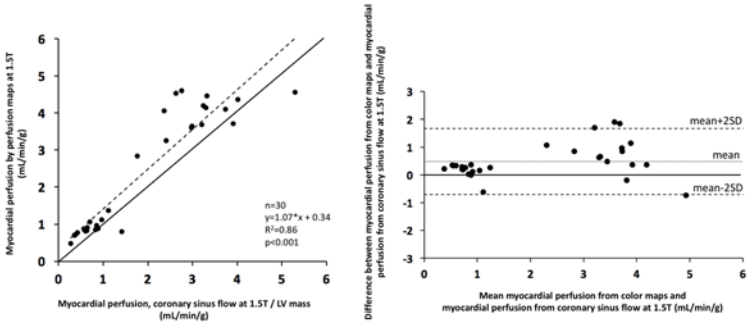

Correlation between quantitative perfusion by color maps and quantitative perfusion by coronary sinus flow at 1.5T

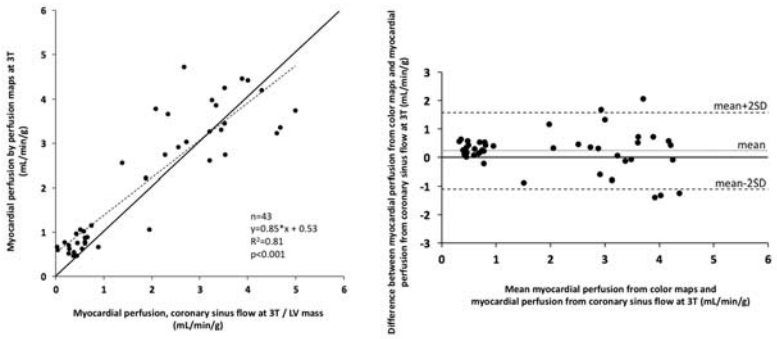

Correlation between quantitative perfusion by color maps and quantitative perfusion by coronary sinus flow at 3T

ID#: 378614

Reduced global longitudinal strain by feature tracking CMR is an independent predictor of all-cause mortality

Harsimar Singh[1] Lin Wang, MD[2], Rajasekhar Mulyala, M.D[3], James Nguyen, MD[4], Jie Jane. Cao, MD, MPH[5]

1. St. Francis Hospital, Greenvale, NY

2. St Francis Hospital The Heart Center, Roslyn, NY

3. St.Francis medical center, roslyn, NY

4. St. Francis: The Heart Center, NY

5. St Francis Hospital, NY

Background: Reduced longitudinal strain (LS) assessed by echocardiography is an important predictor of adverse clinical outcome. The prognostic value of LS assessed by feature tracking CMR is still under investigation. Furthermore, it remains unclear of the impact of tissue characterization using late gadolinium enhancement (LGE) on LS prognostication. In this study we assessed mortality risk associated with reduced global LS assessed using feature tracking in subjects who had comprehensive CMR evaluation.

Methods: We retrospectively analyzed 293 subjects who had CMR evaluation. Left ventricular function was assessed using balanced SSFP images. LGE imaging was acquired using phase sensitive inversion recovery sequence. Cine images of the 2, 3 and 4 chamber views were analyzed for global LS using commercial feature tracking software. All-cause mortality data was obtained from National Death Index. Logistic regression analysis was performed to determine the predictors of all-cause mortality.

Results: There were 235 patients and 57 normal controls. Mean age was 56±16 years and left ventricular ejection fraction (LVEF) 49±14%. LS was significantly reduced in patients than in control, -13.0±4.9 vs -17.7±2.2 ($p<0.001$). After mean follow up of 6.6 years30 subjects died. In the logistic regression analysis, reduced LS was significantly associated with all-cause mortality. In the multivariate regression analysis adjusting for age, LVEF, diabetes and hypertension reduced LS remained to be the most important predictor of mortality with Wald chi square 14.46 ($p<0.001$). When the model was further adjusted for the presence of LGE, reduced LS was the only predictor of mortality with Wald chi square 11.32 ($p<0.001$).

Conclusion: Reduced global longitudinal strain assessed by feature tracking CMR is an important risk for all-cause mortality. The risk remains significant even after altered myocardial tissue property defined by LGE was taken into consideration.

ID#: 378693

BART and Gadgetron Integration used for Real-Time Cardiac Cine Reconstruction

Mahamadou Diakite, PhD[1] Adrienne E. Campbell-Washburn, PhD[2], Hui Xue, PhD[3]

1. National Institutes of Health, Baltimore, MD

2. National Heart, Lung, and Blood Institute, National Institutes of Health, MD

3. National Heart, Lung, and Blood Institute, Bethesda, MD

Background: BART[1] is a powerful open-source software package that offers implementations of numerous MRI reconstruction algorithms. The algorithms are accessed through a set of command line tools using a custom intermediate file format. While the command line interface is suitable for exploring algorithms and reconstruction parameters, it does not, by itself, provide seamless integration with clinical MRI systems. We have leveraged the Gadgetron[2] streaming and reconstruction framework to provide tight, seamless scanner integration of BART on Siemens MRI systems and applied it for reconstruction of accelerated real-time cine imaging.

Methods: A new module (Gadget) was inserted into Gadgetron[2] reconstruction chain after individual readouts, in ISMRMRD[3] format, have been accumulated into data buffers. The data buffers are written to disk to allow BART command line processing. The BART commands are supplied in a shell script by the user. After the script execution, the resulting images are read back into the Gadgetron streaming pipeline and passed down the chain for any additional processing before being returned to the scanner host computer. Multi-slice real-time cardiac cine imaging was chosen as a test application for the proposed framework. A short axis stack of real-time SSFP images was acquired with the following parameters: TR/TE = 3.4/1.68ms, FA= 60^{o}, FOV=350x260mm^2, slice thickness = 8mm, GRAPPA rate 4, matrix size =160x120. The images were reconstructed using the following reconstruction configurations 1) Gadgetron-BART reconstruction, ESPIRIT with L1 regularization, 2) Gadgetron reconstruction, TGRAPPA. The main purpose was to demonstrate the seamless scanner integration of the BART toolbox for clinical imaging.

Results: Figure 1 shows a schematic diagram of the integration of BART gadget into Gadgetron reconstruction pipeline and inline display of images on the scanner host. Figure 2 shows three slices of the real-time cine cardiac images using the Gadgetron reconstruction and the Gadgetron-BART reconstruction. The average reconstruction time was: Gadgetron = 91.4ms/slice and Gadgetron-BART = 101.2ms/slice .

Conclusion: Our study demonstrates the integration of BART into the Gadgetron framework to perform reconstruction of accelerated real-time cine imaging in the clinical setting. The use of a configurable BART script allows deployment of many different BART reconstructions that can be integrated into Gadgetron reconstruction from the command line or deployed on the MRI scanner itself. Future work will include the cloud deployment of the framework to reduce the reconstruction time of multi-slice real-time cardiac cine.

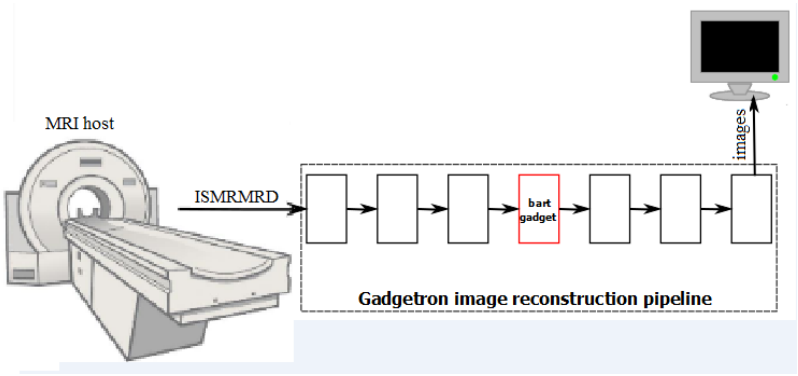

Figure 1: Integration of BART on Siemens MRI scanner. BART commands are loaded from a configurable shell script at runtime which enables flexible modification of the reconstruction steps without any recompilation of the source code.

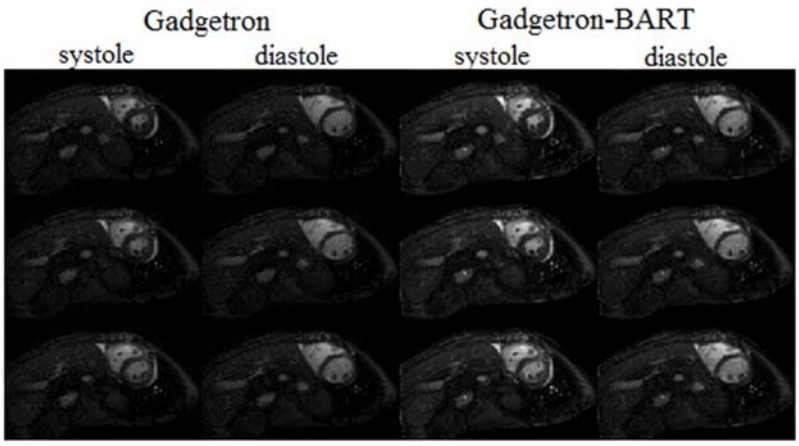

Figure 2: Three slices of the short axis stack of real-time cardiac cine images (systole/diastole) reconstructed on the Siemens MRI scanner with our standard Gadgetron reconstruction (first two columns) and Gadgetron-BART reconstruction (last two columns).

ID#: 379265

Myocardial inflammation and Edema Revealed by Cardiac Magnetic Resonance in Antiretroviral-Naïve and Antiretroviral- Exposed HIV Patients

Katia Devorha. Menacho, MD[1] Sara Elizabeth. Ramírez Flores[2], Jorge Luis. Alave[3], Flavio Santiago. Mosto[4], Daniela A. Salazar[5], Camilla Torlasco, MD[6], James C. Moon, MD[7]

1. Barts Heart Centre, London, England, United Kingdom

2. HOSPITAL FAP / CLÍNICA INTERNACIONAL, Lima, Lima, Peru

3. Asociación Civil Impacta Salud y Educación, Peru

4. Clínica Internacional, Lima, Lima, Peru

5. Universidad Peruana Cayetano Heredia, Lima, Lima, Peru

6. University of Milan-Bicocca. IRCCS Istituto Auxologico Italiano, Milan, Italy, Milan, Lombardia, Italy

7. Barts Heart Centre, England, United Kingdom

Background: Heart disease is a main contributor to morbidity and mortality in persons infected with human immunodeficiency virus (HIV). High risk is related to complex interactions between traditional risk factors, HIV infection itself and therapy effects. Both HIV and highly active antiretroviral therapy (HAART)HIV patients may be associated with cardiac abnormalities. This study aims to assess the extent of cardiac involvement in asymptomatic HIV patients by using advance Cardiac Magnetic Resonance (CMR) imaging.

Methods: A single, cross sectional centre study in Lima - Peru, 3T SIEMENS Prisma. *48 participants*: **18 patients** with **chronic HIV infection receiving ART**; **18 HIV patients naïve to ART** treatment and **12 healthy controls** selected by frequency matching age and sex. Patients with previous myocardial pathology were excluded from the study. Clinical information, physical exam and laboratory tests taken the same day of scanning. Myocardial structure, function and tissue characterization assessed by CMR: ventricular volumes, ejection fraction strain, native and post contrast T1 mapping, T2 mapping, extracellular volume ECV and late gadolinium enhancement (LGE).

Results: Compared with healthy controls, HIV-infected patients showed reduction in left ventricular function: lower ejection fraction (59.9% ± 3.9 vs 64% ± 2.1, *P= 0.002*), lower stroke volume (88.1 ± ± 18 vs 99.5 ± 12.3, P= 0.05) and lower global peak systolic circumferential strain (-21.5 ± 5.5 vs 27.7 ± 4.5, p<0.001). Signs of inflammation and diffuse fibrosis were higher in HIV patients than controls: native T1 mapping (1257.7 ± 25.1 vs 1222 ± 18.6, p =0.00) and edema assessed by T2 mapping (38.4 ± 1.9 vs 36.4 ± 1.7, p =0.003). Pericardial effusion and myocardial fibrosis assessed by LGE were three times higher when compared to controls. Myocardial fibrosis distribution was predominantly sub and mid-epicardium, in the inferolateral wall. See Table 1 and Figure 1. When comparing HIV patients receiving and not ART, patients who just started their ART showed reduction in LVEF (59.9 %± 3.9 vs 64% ± 2.1, P=0.05) and major incidence of pericardial effusion. There was not any significant difference in parameters to assess inflammation and edema.

Conclusion: CMR revealed that in asymptomatic HIV patients there is subclinical chronic myocardial inflammation: edema and pericardial effusion. Chronic inflammation may explain burden of fibrosis and alteration in cardiac function in patients and persists in patients regardless of whether receiving treatment for HIV.

	HIV patients N= 36	Health Control N= 12	P value
General characteristics			
Age, years	36 ± 11	39 ±13	0.180
Men %	31 (85%)	10 (81%)	0.56
Body mass index, mean (SD) kg/m²	23.9 ± 3.9	25.1 ± 2.3	0.457
Abdominal Circumference, mean (SD) cm	83.1 ± 12.7	83.7 ± 9.8	0.89
Systolic Blood Pressure, mean (SD) mmHg	107.4 ± 9.8	107.7 ± 15.3	0.32
Diastolic Blood Pressure, mean (SD) mmHg	69.3 ± 9.2	69.3 ±7.1	0.13
Laboratory exams			
Haemoglobin, mean (SD), mg/dl	13.1 ± 3.4	13.5 ± 1.7	0.54
Creatinine, mean (SD) mg/dl	0.8 ± 0.2	0.9 ±0.2	0.16
Cardiac Magnetic Resonance			
Left Ventricle End Diastolic Volume, mean (SD) ml	145.2 ± 28.1	156.8 ± 19.2	
Left Ventricle End Systolic Volume, mean (SD) ml	57.3 ± 12.7	55..3 ± 8.9	
Stroke Volume, mean (SD), mean (SD) ml	88.1 ± 18	99.5 ± 12.3	
Ejection Fraction mean (SD), %	59.9 ± 3.9	64 ± 2.1	
LV mass , mean (SD) g	106.1 ± 22.5	118.9 ± 23.6	
LV papillary muscle mean (SD), g	3.6 ± 1.1	3.6 ± 1.5	
Global Peak Systolic Circumferential Strain mean (SD) %	-21.5 ± 5.5	-27.7 ± 4.5	
T1 native mapping MOLLI mean (SD), ms	1257.7 ± 25.1	1222 ± 18.6	
T1 post contrast MOLLI, mean (SD), ms	652.1 ± 39.4	713.6 ± 38.1	
Extracellular Volume ECV 15min, mean (SD), %	26.7 ± 2.7	24.1 ± 1.1	
T2 mapping, mean (SD), %	38.4 ± 1.9	36.4 ± 1.7	
T2 ratio, mean (SD)	1.9 ± 0.8	1.4 ± 0.4	
Visible presence of Pericardial Effusion,	11 (31%)	1 (8%)	
Visible Presence of Late Gadolinium Enhancement,	12 (33%)	0 (0%)	

TABLE 1: Clinical, Laboratory and CMR parameters in HIV patients and Healthy controls

TABLE 1: Clinical, Laboratory and CMR parameters in HIV patients and Healthy controls

	HIV patients on ART N=18	HIV patients naïve to ART N=18	P value
General characteristics			
Age, years	34 ± 11	37 ± 12	0.49
Men %	16 (89%)	15 (83%)	0.86
CD4+ cell count	463.2 ± 276	721.8 ± 349	0.457
Cardiac Magnetic Resonance			
Left Ventricle End Diastolic Volume, mean (SD) ml	138.27± 31.3	154.7 ± 20.5	0.2
Left Ventricle End Systolic Volume, mean (SD) ml	56.7 ± 14.4	58..2 ± 10.3	0.7
Stroke Volume, mean (SD), mean (SD) ml	82.3 ± 19.6	96.5 ± 12.3	0.43
Ejection Fraction mean (SD), %	59.9 ± 3.9	64 ± 2.1	0.05
LV mass , mean (SD) g	58.8 ± 4.3	61.6 ± 2.5	0.96
LV papillary muscle mean (SD), g	3.6 ± 1.2	3.6 ± 0.7	0..92
Global Peak Systolic Circumferential Strain mean (SD) %	-22.5 ± 5.5	-26.5 ± 4.5	0.7
T1 native mapping MOLLI mean (SD), ms	1257.6 ± 31.7	1257 ± 11.4	0.95
T1 post contrast MOLLI, mean (SD), ms	654.8 ± 43.2	664.6 ± 31.6	0.51
Extracellular Volume ECV 15min, mean (SD), %	27.4 ± 2.8	25.6 ± 2.2	0.09
T2 mapping, mean (SD), %	38.2 ± 1.9	36.4 ± 1.7	0.54
T2 ratio, mean (SD)	2.0 ± 0.8	1.7 ± 0.4	0.12
Visible presence of Pericardial Effusion,	8 (44%)	3 (17%)	0.03
Visible Presence of Late Gadolinium Enhancement,	7 (38%)	5 (28%)	0.43

TABLE 2: CMR parameters in treated and non-treated HIV patients

TABLE 2: CMR parameters in treated an non-treated HIV patients

Figure 1: Pericardial effusion and late gadolinium enhancement in HIV patients

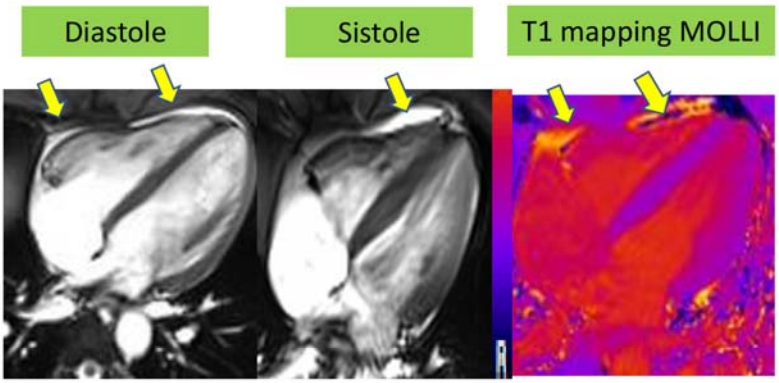

HIV patient with pericardial effusion on Cine SSFP (Diastole and systole). Yellow arrow shows effusion, confirmed by T1 mapping, higher pericardial

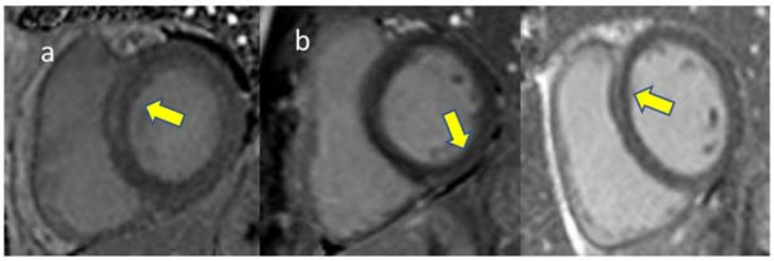

Three patients with HIV: Late Gadolinium enhancement in septum mid pattern wall (a, c) and inferolateral epicardium pattern

Pericardial effusion and gadolinium enhancement in HIV patients

ID#: 379314

Evaluation of LGE-CMR for predicting VT ablation sites in nonischemic cardiomyopathy - direct comparison with electroanatomic maps.

Avanti Gulhane, M.D.[1] Yahang Tan, M.D.[2], Saman Nazarian, MD, PhD[3], Harold Litt, MD-PhD[4]

1. Perelman School of Medicine, University of pennsylvania, Philadelphia, PA

2. Perelman School of Medicine, University of Pennsylvania, PA

3. University of Pennsylvania Perelman School of Medicine, PA

4. Perelman School of Medicine of the University of Pennsylvania, Philadelphia, PA

Background: LGE CMR enables characterization of fibrosis in patients of nonischemic cardiomyopathy. Electroanatomic mapping (EAM) is used to locate areas in fibrotic tissue giving rise to ventricular tachycardia (VT) and guide ablation. However, there are limitations with voltage mapping such as difficulties in identifying arrhythmogenic substrate, limited spatial resolution as well as long procedure times. A new software for LGE CMR analysis using pixel signal intensity (PSI) algorithms has made it possible to locate conducting channels (CC) in fibrotic tissue which form VT substrate. We compared LGE derived CC with EAM findings in patients with VT related to nonischemic disease.

Methods: We evaluated retrospectively 27 patients with nonischemic cardiomyopathy and VT who underwent CMR prior to EAM and VT ablation. 2D or 3D short axis LGE acquisitions were evaluated using ADAS-VT (Galgo Medical SL, Barcelona) to identify CC within LV myocardial layers from endocardium to epicardium. A PSI-based algorithm was applied to characterize the LGE area as scar core or border zone, using 60% and 40% of the maximum LGE intensity as thresholds. CC were identified topologically by finding border zone areas coursing through fibrous core, which are thought to represent corridors of viable tissue connecting through the fibrous scar. RV and papillary muscle scar cannot be evaluated by the software at present. CC detected by LGE CMR were compared with EAM findings and sites targeted for VT ablation on a per patient and per channel basis.

Results: A total of 42 channels were generated by the software. 32 (73%) detected channels matched sites of VT ablation. 10 (24%) channels were detected only on CMR and not at EAM. 8 patients did not show any CC on LGE CMR or abnormal EAM findings. LGE CMR PSI-based analysis showed high sensitivity (91%), good (76%) positive predictive value with 44% specificity and 73% negative predictive value for identifying sites of ablation.

Conclusion: LGE CMR PSI-based analysis shows promising results in detecting conducting channels to guide VT ablations in patients with nonischemic cardiomyopathies. Limitations of the current software include inability to identify RV or papillary muscle channels, which contribute to arrhythmia in nonischemic disease. Additional conducting channels detected that are not identified at the time of EAM procedure may lead to recurrent VT and need follow-up. Results should be validated in larger populations.

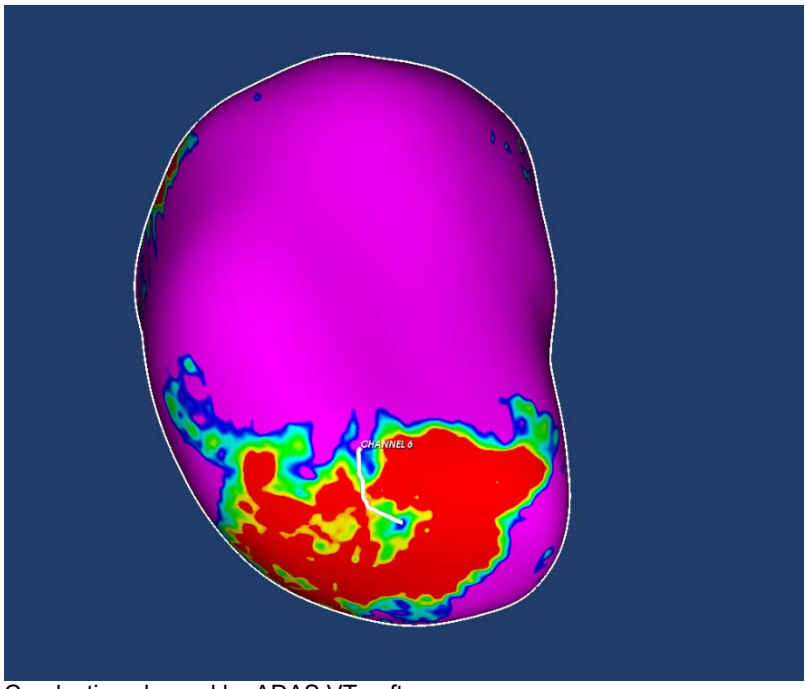

Condcuting channel by ADAS VT software

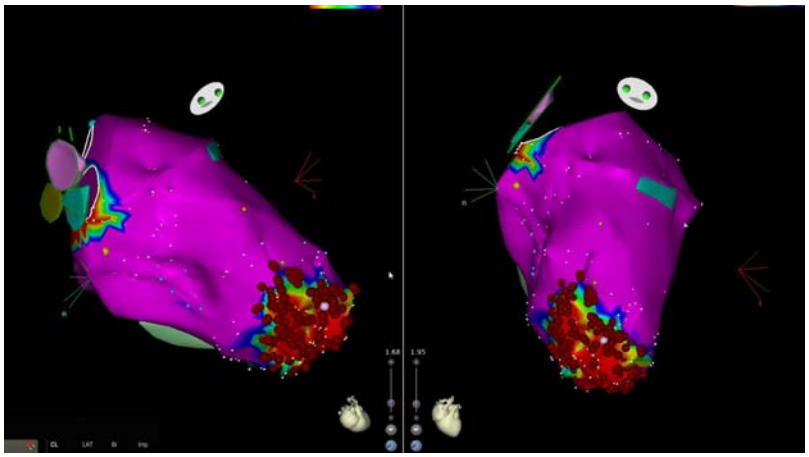
EAM

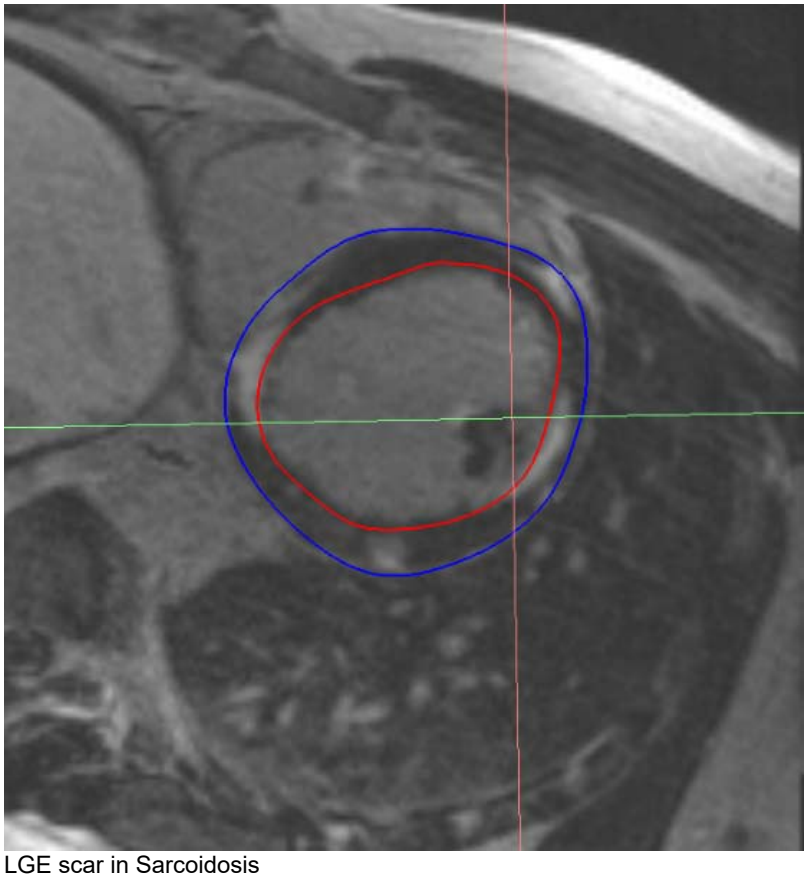

LGE scar in Sarcoidosis

Comparison of Conducting channels on LGE CMR with EAM findings in LV sites leading to VT ablation

		EAM findings in LV sites leading to VT ablation		
		Positive	Negative	Total
CC on CMR	Positive	32	10	42
	Negative	3	8	11
	Total	35	18	53

ID#: 379318

Cardiac outcome by CMR in SCAD

Abtehale Al-Hussaini[1] Ahmed M.S.E.K. Abdelaty, University of Leicester[2], Gerry p. McCann, MB ChB, MD[3], Jayanth Arnold, BMBCh DPhil[3]

1. University of Leicester, England, United Kingdom

2. University of Leicester, UK, United Kingdom

3. Department of Cardiovascular Sciences and NIHR Biomedical Research Centre, Glenfield Hospital, Leicester, England, United Kingdom

Background: Spontaneous coronary artery dissection (SCAD) is an unusual though increasingly recognized cause of acute coronary syndrome mainly in young women, in the absence of conventional cardiac risk factors. The pathophysiology and prognosis remains poorly understood with controversy regarding prognosis outcomes and the optimal management of SCAD. Aim
In this study, we report a large CMR series illustrating outcomes and prognosis including LV assessment and infarct size in SCAD patients.

Methods: 50 SCAD patients underwent a Cardiac MRI and peripheral arterial MR-angiography using our dedicated 3T cardiovascular scanner for a detailed assessment of LV function, LGE, and remote arteriopathies. Pulse wave velocity and aortic compliance were assessed using semiautomatic aortic tracking. Cardiac images include HASTE and localiser sequence, CINE images using TRUFISP, CINE SAX. Delayed contrast imaging was acquired following an MRA of the aorta. LGE was quantified using the full width half maximum technique using the CMR 42 software. Also, a 16-segment model was used to assess percentage of LGE in each segment. % LGE mass was compared across different therapy management (conservative, PCI, CABG) using a one way Anova statistical analysis

Results: The mean age of SCAD 42.1 +/-6.4 years, with predominantly female cases (97%). The follow up median time follow up time for SCAD patients is 5.7 years. 30% presented with STEMI, 70%NSTEMI, 9.7 % of which were postpartum SCAD. The mean LGE mass 3.887+/- 10.1. Mean LGE % in NSTEMI 2.746+/- 7.368 and in STEMI presentation 8.585+/- 16.19 (p 0.0518). LGE % in multivessel SCAD 3.476+/- 10.11, and 4.645 +/- 10.81 in non multivessel SCAD (P 0.6120). Mean LGE% in Recurrent SCAD 3.879+/- 8.337 and in single event SCAD 3.888+/- 10.38. LGE % in conservative therapy 3.546+/- 7.641, PCI 17.28+/. - 11.7, CABG 39.23+/- 26.75 with one way Anova test, P 0.0002 (Conservative vs PCI), P<0.0001 (conservative vs. CABG), P 0.0007 (PCI vs. CABG).

Conclusion: This study provides insight in to infarct size and potential outcomes following SCAD. We have demonstrated an overall minimal size infarct in SCAD patients, with no difference in myocardial injury in relation to presentation of Acute coronary syndrome, multivessel SCAD or recurrent SCAD. However, in conservative managed SCAD there was a significantly smaller infarct in comparison to those managed with PCI or surgical revascularisation. This study stipulates the potential consensus for clinical guidelines in support for conservative management of SCAD which appears to be associated with improved long-term prognosis

ID#: 379432

Detection of myocardial deformation changes assessed by CMR tissue-tracking in patients with acute myocarditis with preserved ejection fraction

Ana G. Almeida, MD, PhD[1] Miguel Menezes, MD[2], Claudio David, MD[3], Rui Placido, MD[4], Gustavo Lima-Silva, MD[2], Dulce Brito, MD, PhD[2], F austo Pinto, MD. PhD[2]

1. University Hospital Santa Maria, Lisbon, Portugal, Lisbon, Portugal

2. University Hospital Santa Maria, Lisbon, Portugal, Portugal

3. Cardiology - University Hospital Santa Maria, Lisbon, Lisboa, Portugal

4. Santa Maria University Hospital, Cardiology Department, Lisbon Academic Medical Center, CCUL, Lisbon, Portugal, Lisboa, Portugal

Background: Acute myocarditis presents in the majority of cases with benign manifestations and preserved ejection fraction However, the late evolution is still largely unknown, as it requires long follow-up times, and the possibility of adverse events at a distance can not be ruled out. This study aimed to assess myocardial deformation by CMR in the acute phase of myocarditis in patients with preserved ejection fraction (EF), and to estimate its relation to myocardial changes and to identify predictors of adverse clinical events and changes in ventricular function in a 3-year follow-up.

Methods: 44 consecutive patients (mean 40 year-old, 39 male) with acute myocarditis and normal EF were included and underwent CMR for LV volumes, ejection fraction, LGE and tissue-tracking (cvi42, Calgary) and followed for 3 years for MACE detection (heart failure, arrhythmia, death, ejection fraction or strain reduction>10%). LGE was quantified as percentages and longitudinal (GLS), radial (GRS) and circumferencial (GCS) strain was assessed in all patients. A control group of 18 normal individuals was assessed for comparison.

Results: In the acute phase LGE was 14.1 ± 7.2%. GLS and GCS were reduced in comparison to control group (p=0.001) and GCS was correlated with the LGE% (R=0.54, p=0.004). At 3-year follow-up, there were no deaths or heart failure; in 9 patients, EF and/or global strain reduced >10%. The LGE% (p=0,05) and the GCS at the acute phase were independent predictors of late reduction of EF or global strain, among age, gender, NT-proBNP, troponin I, LV volumes and EF and other deformational indices.

Conclusion: In patients with acute myocarditis and preserved EF, tissue-tracking CMR detected subclinical changes in myocardial deformation that were related to myocardial lesion mass. A higher mass of fibrosis and smaller values of circumferential strain in the acute phase were independent predictors of late LV dysfunction, suggesting being surrogate early markers of prognosis.

ID#: 378987

Myocardial Blood Flow falls during stress in Hypertrophic Cardiomyopathy. A Perfusion mapping study.

Claudia Camaioni, MD[1] Kristopher D. Knott, MBBS MA[2], Gabriella Captur, MD PhD MRCP MSc[3], Fabrizio Ricci[4], Redha Boubertakh, PhD[5], Hui Xue, PhD[6], Luis Lopes, MD, PhD [7], Saidi A. Mohiddin, FRCP, FESC[8], Steffen E. Petersen, MD DPhil MPH FRCP[9], Charlotte Manisty, MRCP PhD[10], Sven Plein, MD PhD[11], Peter Kellman, Ph.D.[6], James C. Moon, MD[8]

1. Barts Heart Center, London, England, United Kingdom

2. University College London, London, England, United Kingdom

3. Barts Heart Centre, London, England, United Kingdom

4. Department of Neuroscience, Imaging and Clinical Sciences, "G. D' Annunzio" University, Chieti, Italy, Pescara, Italy

5. QMUL, England, United Kingdom

6. National Heart, Lung, and Blood Institute, Bethesda, MD

7. Barts Heart Centre; UCL, United Kingdom

8. Barts Heart Centre, England, United Kingdom

9. Queen Mary University of London, London, England, United Kingdom

10. Barts Heart Centre and University College London, United Kingdom

11. University of Leeds, England, United Kingdom

Background: In hypertrophic cardiomyopathy (HCM), a myocardial perfusion reserve (MPR) < 1 is a possible finding. This has been described, but attributed to fitting errors in the model. Perfusion mapping may be able to inform. Therefore, we looked at myocardial blood flow in HCM i) hypothesising that MPR< 1 is a real finding and not just a model error; ii) assessing its prevalence and iii) finding any association with scar and hypertrophy.

Methods: HCM patients underwent adenosine stress perfusion CMR. We measured stress and rest myocardial blood flow (MBF, ml/g/min) for basal, mid and apical short axis views by using an automated in-line perfusion mapping. Transmural, endocardial, and epicardial MPR (tm-, endo- and epi-MPR) were calculated per segment and correlated with segmental wall thickness (WT) and late gadolinium enhancement (LGE), quantified by the 6 SD method. To prove the accuracy of the BTEX model, we re-scanned 1 HCM patient with endoMPR <1.

Results: 51 patients (30 ASH, 21 apical HCM, mean age 58 years, 81% male) were enrolled, for a total of 816 segments *(Tab. 1).* Reduced flow during stress was present, particularly in the endocardium (tm, endo, epi MPR < 1 prevalence: 6%, 13.9% and 4.3%). The repeated scan showed that even performing rest before stress, the endo MPR was still < 1 (Fig.1). An MPR < 1 was associated with LGE and increasing WT (LGE= p<0.001; WT p=0.002). More exactly, it was associated with both WT and LGE in apical HCM, but only with LGE in the ASH hypertrophy pattern (Fig.2).

Conclusion: Myocardial blood flow can fall in HCM during adenosine stress. This occurs in up to 14% of segments. It is a mainly endocardial phenomenon and associated with increased LGE and increased WT.

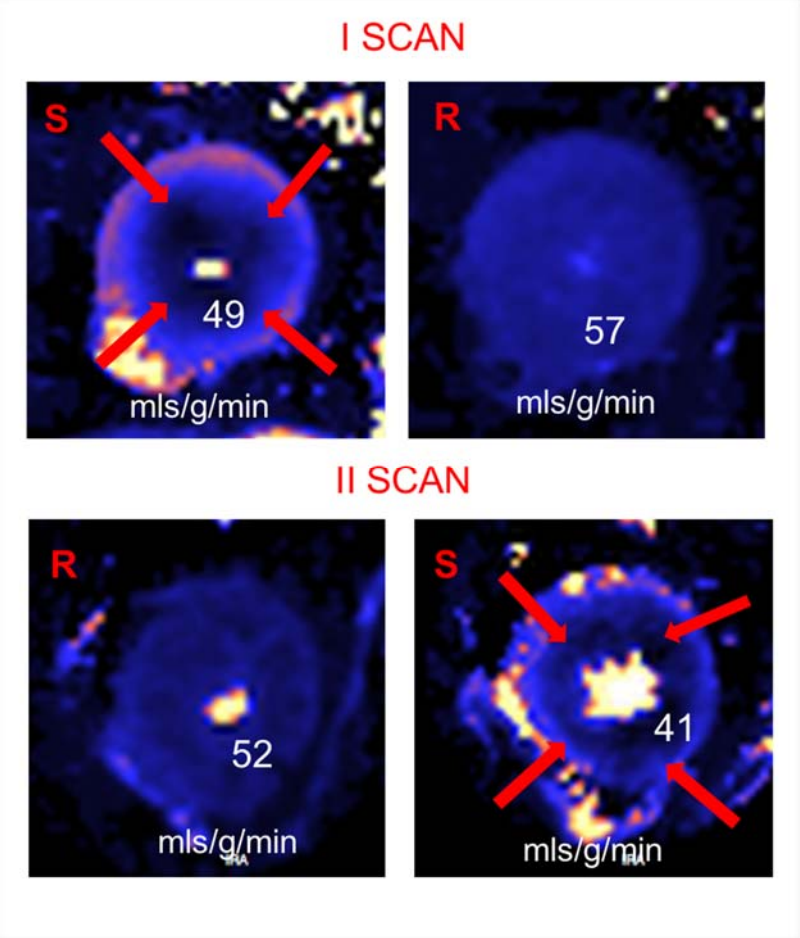

Fig. 1 The apical slice at stress showing an MPR less than 1 (top). We repeated (bottom) switching from stress-rest to rest-stress and the values remained consistent, supporting our hypothesis that reduced flow during adenosine in HCM is real.

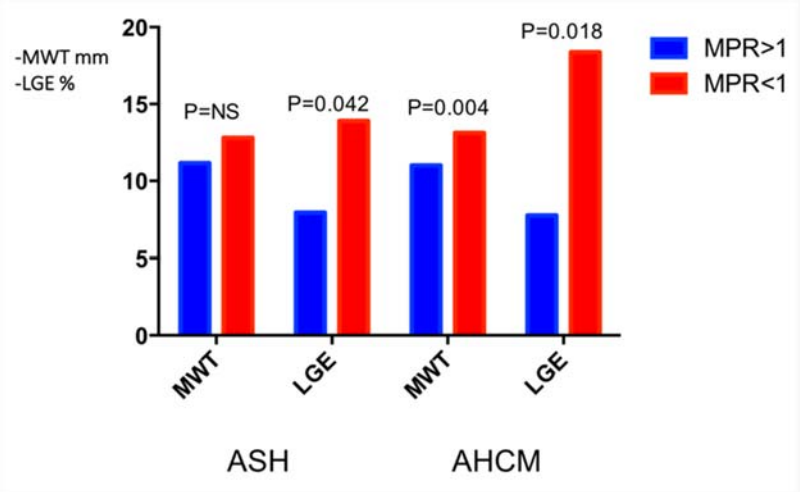

Fig. 2 An MPR <1 occurs with LGE and is associated with increased wall thickness in AHCM but not ASH patients.

HCM population baseline characteristics.

	OVERALL	ASH	aHCM	P-value
n	51	30	21	---
Age	57.8 ± 14	57 ± 15	58.8 ± 14.24	0.666
Female gender	10 (19)	6 (20)	4 (19)	0.933
BSA	2 ± 0.22	2 ± 0.24	1.9 ± 0.19	0.225
LV Mass_ind (g/m2)	166.8 ± 58.7	85.5 ± 27.4	83 ± 19.3	0.717
LVEDI (ml/m2)	74.4 ± 14.7	76.7 ± 15.5	71 ± 13.05	0.174
Average WT mm	11.2 ± 2.3	11.09 ± 2.6	11.4 ± 1.9	0.632
LGE %	8.35 ± 7.3	8.2 ± 7.9	8.6 ± 6.38	0.855
EF %	72.9 ± 7.6	71.8 ± 7.2	74.4 ± 8	0.233
Diabetes n (%)	9 (17%)	6 (20%)	3 (14)	0.598
Hypertension n (%)	22 (43%)	15 (50%)	7 (33)	0.237
tmMPR	2.3 ± 0.9	2.3 ± 1	2.3 ± 0.7	0.91
endoMPR	2 ± 0.8	1.9 ± 0.7	2 ± 0.7	0.828
epiMPR	2.5 ± 1	2.6 ± 1.1	2.5 ± 0.8	0.89

ID#: 378779

Diagnostic Performance of Fully Automated Pixel-wise Myocardial Blood Flow Maps of Stress and Rest CMR Perfusion in Patients

Li-Yueh Hsu, DSc[1] Matthew J. Jacobs, MSc[2], Mitchel Benovoy, PhD[3], Allison Ta, MD[4], Hannah Conn, BSc[5], Susanne Winkler, MD[6], Anders Greve, MD, PhD[7], Marcus Y. Chen, MD[1], Sujata M. Shanbhag, MD, MPH[4], W. Patricia Bandettini, MD[8], Andrew E. Arai, MD[1]

1. National Heart, Lung and Blood Institute, National Institutes of Health, Bethesda, MD

2. The Catholic University of America, Riverdale, MD

3. NIH/NHLBI, PQ, Canada

4. NIH/NHLBI, Bethesda, MD

5. National Heart Lung and Blood Institute, National Institutes of Health, Bethesda, MD

6. National Institutes of Health, Austria

7. National Institutes of Health, Denmark

8. National Heart, Lung and Blood Institute, National Institutes of Health, MD

Background: We previously developed a fully automated system to quantify myocardial blood flow (MBF) in units of ml/min/g at the pixel level for first-pass contrast-enhanced CMR perfusion. The diagnostic performance of the automatically generated MBF pixel maps was evaluated in patients with known or suspected coronary artery disease (CAD).

Methods: Eighty-one patients had regadenoson stress and rest CMR performed on a 1.5T scanner under an approved research protocol. Significant CAD was defined by quantitative coronary angiography (QCA) with 70% or more stenosis in at least one major vessel. Non-significant CAD was defined by 1) QCA with less than 70% stenoses in all major coronary arteries or by 2) CT coronary angiography with all coronary stenoses less than 30% and calcium score of 0. The automated MBF pixel maps were analyzed in six sectors per slice. MBF, myocardial perfusion reserve (MPR), relative MBF (rMBF) and relative MPR (rMPR) were analyzed by receiver operating characteristic curve for detecting significant CAD.

Results: The prevalence of significant CAD was 44%. Ischemic zone stress MBF was lower than remote sector MBF (1.33±0.55 vs. 2.50±0.77 ml/g/min, $p<0.01$). MPR was also lower in the ischemic sectors compared with the remote sectors (1.50±0.62 vs. 2.52±1.04, $p<0.01$). The diagnostic performance of MBF, MPR, rMBF, and rMPR is summarized in Figure-1. All quantitative metrics had very good to excellent sensitivity (from 83% to 92%) and area-under-curve (AUC, from 0.86 to 0.93). The major difference in the performance was related to the specificity which ranged between 73% and 91%. rMPR had the best overall accuracy of 91%.

Conclusion: Fully automated pixel-wise MBF quantification of stress and rest CMR perfusion had high diagnostic performance for detecting significant stenosis in patients with known or suspected CAD; however, incorporation of MPR and relative analysis of the quantitative metrics further improved the overall diagnostic accuracy.

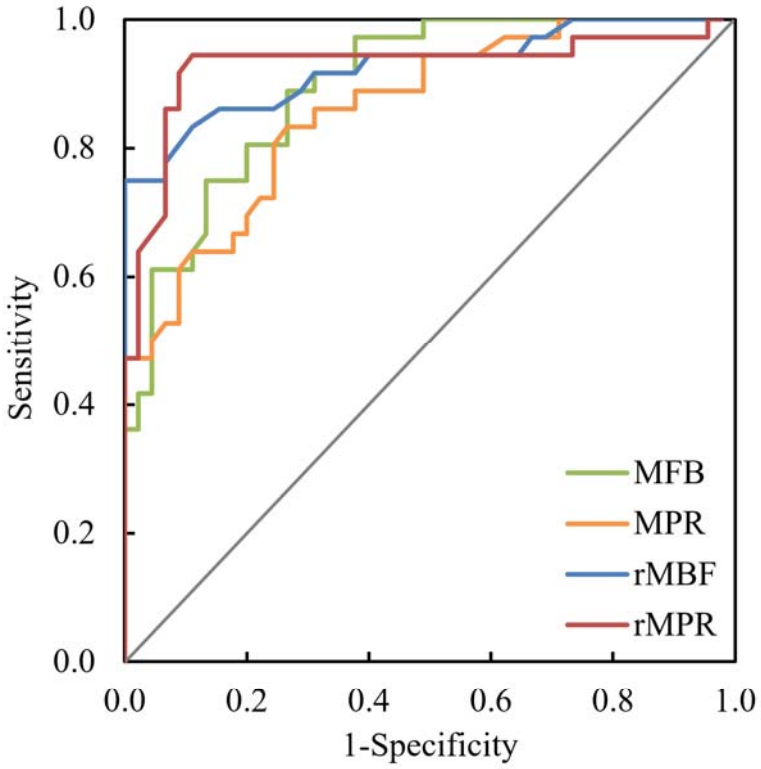

	Accuracy	Sensitivity	Specificity	AUC
MBF	80%	89%	73%	0.90
MPR	78%	83%	73%	0.86
rMBF	85%	86%	84%	0.93
rMPR	91%	92%	91%	0.93

Figure-1:

ID#: 378618

Histone Deacetylase Expression in the Human Heart and Brown Adipose Tissue Imaged In Vivo with Simultaneous PET-MR of 11C-Martinostat

Choukri Mekkaoui, Ph.D.[1]Hooker Hooker, Ph.D.[2], David Izquierdo-Garcia, Ph.D.[2], Frederick Schroeder, Ph.D.[2], Marcello Panagia, M.D. Ph.D.[2], Cheryl Cero, Ph.D.[3], Aaron Cypess, M.D. Ph.D.[3], Ciprian Catana, Ph.D.[2], David Sosnovik, M.D.[2]

1. Harvard Medical School - Massachusetts General Hospital - Athinoula A. Martinos Center for Biomedical Imaging - Boston, MA, Charlestown, MA

2. Harvard Medical School - Massachusetts General Hospital - Athinoula A. Martinos Center for Biomedical Imaging - Boston, MA

3. Translational Physiology Section - National Institute of Diabetes and Digestive and Kidney Diseases - Bethesda, MD

Background: Histone deacetylases (HDACs) modify chromatin packaging and gene transcription in mammalian cells. Preclinical studies have shown that the inhibition of class I HDACs can prevent, and even reverse, left ventricular hypertrophy and myocardial fibrosis. The role of HDAC in the adult human heart, however, remains poorly defined. In addition, there is limited data on the expression and role of HDAC in other metabolically active tissues such as brown adipose tissue (BAT). We aimed to assess the degree of HDAC expression in the human heart and other highly metabolically active tissues, *in vivo*, using PET-MR of a novel radiotracer (^{11}C-Martinostat)[1], targeting class I HDACs.

Methods: Six human volunteers were injected with ^{11}C-Martinostat and dynamic PET imaging was performed on an integrated 3T PET-MR scanner (Biograph, Siemens Medical) in 3D list-mode for 60 minutes. Static PET images were retrospectively reconstructed from the data acquired from 10 to 30 minutes after injection, using retrospective gating at end expiration. Mean SUVs were calculated from these images in the myocardium, skeletal muscle, bone marrow, subcutaneous white adipose tissue (WAT) and paravertebral BAT. Foci of paravertebral BAT were identified by calculating the water/fat ratio in each voxel (Dixon-based approach). In addition, quantitative PCR for Class I HDACs was performed in biopsies of WAT and BAT obtained in patients (n=7) undergoing abdominal surgery.

Results: The uptake of ^{11}C-Martinostat was highest in the heart (SUV = 4.4 ± 0.6, Figure 1) followed by bone marrow (1.6 ± 0.3) and BAT (1.0 ± 0.3). Uptake of the probe was far higher in BAT than WAT and skeletal muscle (Figure 2). The specificity of ^{11}C-Martinostat for class I HDACs was demonstrated with a suberoylanilide hydroxamic acid blocking study in a non-human primate. The increased density of Class I HDACs in human BAT (versus WAT) was demonstrated by PET-MR of ^{11}C-Martinostat and confirmed by PCR of the biopsy specimens (Figure 2).

Conclusion: Class I HDAC expression in the human heart and other metabolically active tissues can be imaged *in vivo* with PET-MR of ^{11}C-Martinostat. Moreover, PET-MR allows foci of BAT to be identified through a Dixon-based approach, a distinct advantage over PET-CT. The high levels of HDAC in the myocardium and BAT likely reflect their metabolic and morphological plasticity, and provides a potential therapeutic target. The ability to image HDAC expression *in vivo* could help facilitate the development of new agents to prevent and treat cardiometabolic disease.

References

1. Wey HY et al. Insights into neuroepigenetics through human histone deacetylase PET imaging. Sci Transl Med. 2016 10;8(351):106

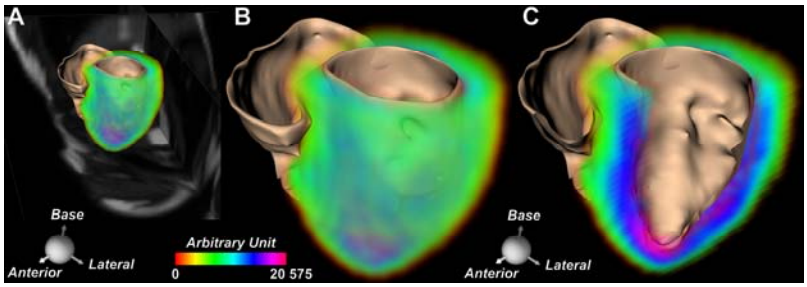

Figure 1. HDAC expression in the human heart imaged in vivo with PET-MR of 11C-Martinostat. The agent showed robust uptake in the heart and represents the density of Class I HDAC isoforms, HDAC 1, 2, and 3. The integrated PET-MR acquisition allows myocardial voxels in the PET dataset to be accurately identified and fused with a surface template of the heart, derived from the MR images.

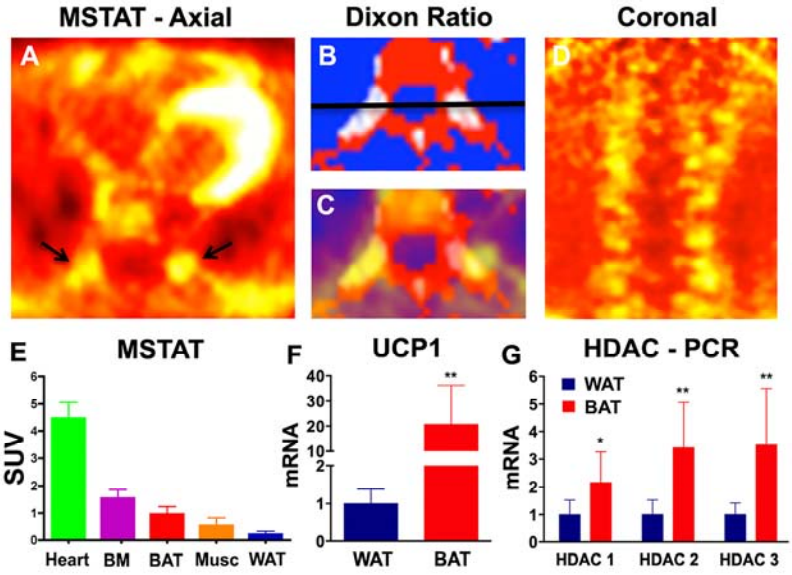

Figure 2. (A) Axial PET image in a human volunteer. Class I HDAC expression in foci of paravertebral brown adipose tissue (BAT, arrows) is high. (B) Ratio of water/fat in the Dixon fat image, acquired for attenuation correction of the PET data. BAT is identified by an intermediate ratio (white and light red/blue). (C) Fusion of the PET and Dixon ratio images and (D) Coronal PET image, in the plane of black line in panel (B), confirm high uptake of 11C-Martinostat (MSTAT) in BAT. (E) The uptake of the probe is highest in the myocardium, bone marrow (BM) and BAT. (F, G) Human biopsy specimens of BAT and WAT acquired during abdominal surgery. High levels of HDAC 1, HDAC 2 and HDAC 3 are seen in tissues with high UCP1 expression (BAT), confirming the imaging findings.

ID#: 378810

Toward Clinically-Practical Free-breathing Whole-Heart 3D Cine with Isotropic Resolution and High Contrast

Peng Lai, Ph.D.[1]Martin A. Janich, PhD[2], Anja Brau, PhD[1]

1. GE Healthcare, Menlo Park, CA

2. GE Healthcare, Germany

Background: Conventional 2D cine MRI is hindered by its lengthy series of breathheld scans at multiple cardiac views. Also, the inconsistent breathholding position in-between scans of different short-axis slices introduces slice misregistration and thus error to ventricular volume quantification. 3D cine, powered by recent fast imaging techniques (Tsao, MRM 2003), has enabled whole ventricle imaging in one breathhold. However, its resolution and coverage remains limited by the patient';s breathhold capability. Furthermore, 3D cine can suffer from low blood-myocardium contrast due to reduced in-flow blood enhancement. In this work, we aimed to develop a clinical solution to free-breathing whole-heart isotropic resolution 3D cine.

Methods: The proposed sequence collects 3D cine images at multiple slabs that covers the entire heart. Each slab images a thin volume to benefit from in-flow effects. Variable density k-t sampling was used for high acceleration. For robustness to respiratory motion, radial vieworder and golden angle increment was employed both in [ky, kz] and along time. Respiratory gating was performed prospectively on a per cardiac phase basis. In reconstruction, kat ARC (Lai, ISMRM 2009) was used to complete k-space non-iteratively utilizing spatiotemporal correlation. Respiratory motion was suppressed by motion-error-based regularization (Lai, ISMRM 2016) incorporated into katARC based on simultaneously recorded bellow signal. Specifically, such regularization balances between data synthesis accuracy and motion suppression, effectively relying more on data with less motion. 4 healthy volunteers were scanned on a GE 1.5T 450W scanner. Free-breathing 3D cine imaging was performed with 2.0x2.0 mm^2 in-plane resolution, 2.4mm slice thickness, 3 slabs covering the heart with 30 slices/slab and 6 overlapping slices, 16 views/segment, 6x acceleration, respiratory gating efficiency of 65%. The total scan time was ~3.5min.

Results: Figure 1 compares images obtained from the same volunteer. Free-breathing acquisition addresses the limited slice coverage and resolution with single-breathhold 3D cine (a & b). The proposed gating efficiently suppresses respiratory motion (e vs. d), providing sharpness similar to breathheld 3D cine, and enables 3D reformat of the whole-heart (f). Multi-slab acquisition (e) provides clearly higher blood-myocardium contrast than single-slab 3D cine (c). The reconstruction time was ~1.5min on a standard GE reconstruction system.

Conclusion: This work developed a free-breathing multi-slab technique for whole-heart isotropic-resolution 3D cine imaging. Based on our current results, the proposed multi-slab acquisition addresses the low contrast issue with single slab 3D cine and the proposed sampling scheme and non-iterative motion regularization can effective suppress respiratory motion with clinically practical processing time.

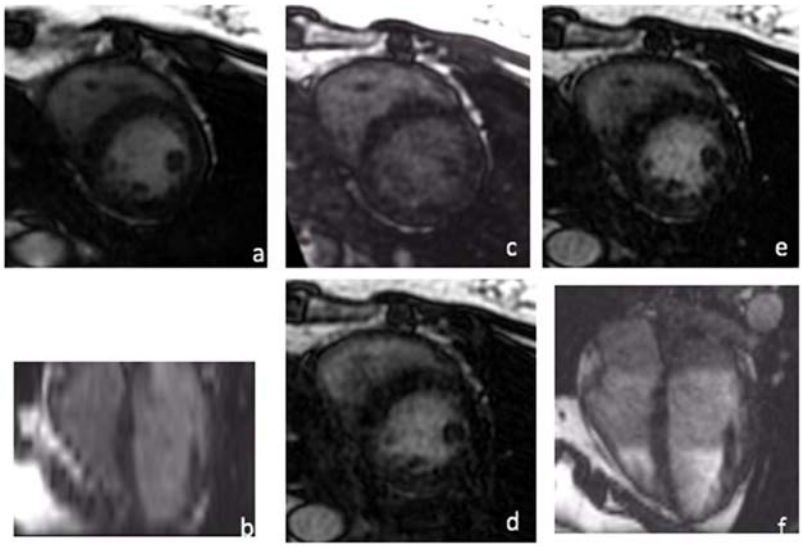

Figure 1. Breathheld short-axis 3DCine (a) and its 4-chamber reformat (b). Freebreathing whole-heart 3DCine (c). Multi-slab whole-heart 3D cine without gating (d) and proposed gating (e) and the 4-chamber reformat (f).

ID#: 378688

MR Augmented Right Heart Catheterization in children with pulmonary arterial hypertension: Prognostic Significance

Bejal Pandya, MBBS[1] Shahin Moledina, MD[2], Vivek Muthurangu, MD[3]

1. Barts Heart Centre, United Kingdom

2. UCL Centre for Translational Cardiovascular Imaging, Great Ormond Street Hospital, London, United Kingdom

3. Institute of Cardiovascular Science, University College London, England, United Kingdom

Background: Pediatric pulmonary hypertension (pPH) is characterized by increased pulmonary vascular resistance (PVR) and mean pulmonary artery pressure (mPAP). These hemodynamic markers only can be accurately measured at right heart catheterization (RHC). Recently, CMR assessment of right ventricular (RV) function has been shown to be prognostic in pPH. However, it is uncertain whether RHC or CMR provides superior prognostic information. MR augmented RHC provides a unique opportunity to simultaneously acquire conventional invasive measures, CMR metrics and markers that use both (i.e. pulmonary vascular resistance – PVR). The aim of this study was to investigate prognostic power of invasive versus CMR measures.

Methods: 87 children with PH patients (mean age = 7.6 y), 66% female, underwent invasive MR augmented catheterization. They were all classified as group 1 according to 2015 ESC/ERS guidelines. Simultaneous pressure measurements and MR flow data were collected, as well as biventricular volumes and function. PVR was calculated as trans-pulmonary pressure/pulmonary flow, pulmonary arterial compliance (PAC) was calculated pulmonary stroke volume/pulmonary pulse pressure. Cox proportional hazard analysis per z-score was performed using death/transplantation as the outcome.

Results: Median follow-up was 4.5 years (range 30 days – 2843 days). 10 patients died or underwent bilateral lung transplantation. Baseline mPAP was 45±18mmHg, mean systolic PAP was 65±24mmHg, PVRi 13±9.5 WUm^2, PAC 1.3±0.5ml/mmHg/ m^2, RVEF 52%±14%. On univariate analysis, mPAP (p<0.001, HR2.9), PVR (p<0.001, HR 2), PAC (p<0.001, HR 0.18), RV end systolic volume (p<0.001 HR 2.4), and RV ejection fraction (p<0.001, HR 0.3) were all significant independent prognostic indicators. Left ventricular CMR metrics and systemic arterial pressures were not prognostic. However, on multivariate analysis only RV ejection fraction was an independent predictor of outcome (p<0.03) – Fig 1.

Conclusion: Invasive assessment of children with PH provides valuable important diagnostic information. However, in our study we have shown that non-invasive CMR measures (specifically RVEF) are more powerful prognostic indictors. Importantly, this study is unique in that the CMR measures and invasive metrics were assessed contemporaneously during MR augmented RHC. Thus, we believe that non-invasive CMR is sufficient to evaluate prognosis in these children. This is important, as RHC is associated with morbidity and mortality in children and reducing the number performed is desirable.

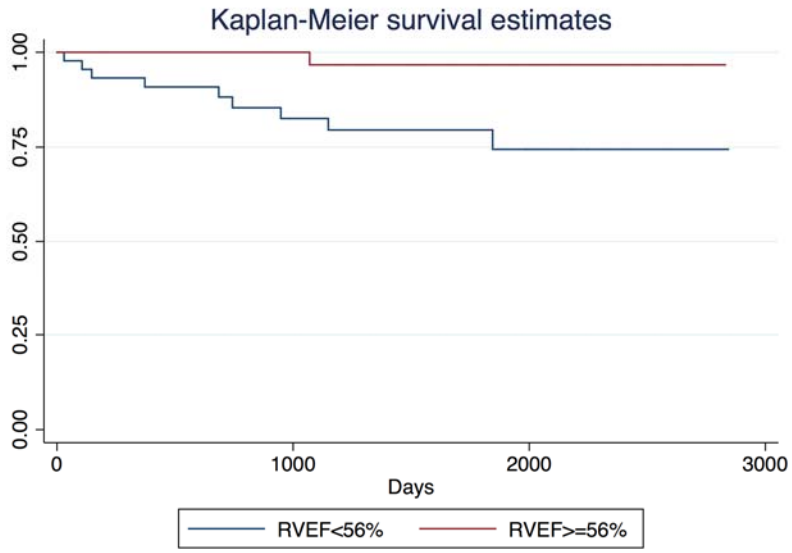

Kaplan-Meier Survival Estimated for RV Ejection Fraction

Results of Cox Proportional Hazard Analysis

Variable	Hazard Ratio	*p*-value
age	0.71	0.32
PVRi	2	<0.001
Pulmonary flow	0.55	0.13
Systolic PAP	3.1	<0.001
Diastolic PAP	2.7	<0.001
Mean PAP	2.9	<0.001
PULTAC	0.18	<0.001
RV end diastolic volume	1.7	<0.001
RV end systolic volume	2.4	<0.001
RV ejection fraction	0.3	<0.001
Arterial Elastance	2.3	<0.001

PVRi = indexed pulmonary vascular resistance, PULTAC = total pulmonary artery compliance, PAP = pulmonary artery pressure, RV = right ventricle.

ID#: 373304

Quantitative Coronary Flow Imaging using Breath-hold Cine FISS Arterial Spin-Labeled MR Angiography

Robert R. Edelman, MD[1] Ali Serhal, MD[2], Amit Pursnani, MD[2], Jianing Pang, PhD[3], Ioannis Koktzoglou, PhD[2]

1. NorthShore University HealthSystem, Evanston, IL

2. NorthShore University HealthSystem, IL

3. Siemens Healthcare, Chicago, IL

Background: CT angiography cannot always differentiate a hemodynamically significant lesion that requires intervention from one that does not. FFR CT is useful but provides only an indirect measure of flow . Phase contrast MRI can measure coronary flow but suffers from poor image quality and cannot image a coronary artery along its length. To overcome these limitations, we developed a cine fast interrupted steady-state (FISS) arterial spin-labeled (cFASL) technique that enables dynamic imaging and measurement of coronary flow .

Methods: The study was IRB-approved, and subjects provided written informed consent. Six volunteers were imaged at 1.5 Tesla (MAGNETOM Avanto, Siemens Healthcare, Erlangen, Germany). Flow tagging used an adiabatic inversion tag applied on alternate heartbeats at a user-selected cardiac phase, with complex subtraction of tagged and untagged images. Data were collected using the recently-described prototype FISS pulse sequence [1], which combines radial k-space trajectory with a modified balanced steady-state free-precession (bSSFP) readout where the steady-state magnetization is spoiled at frequent intervals. FISS differs from bSSFP in being less sensitive to artifacts from rapid systolic blood flow. FISS is intrinsically fat-suppressed, which decreases radial streak artifacts on the highly undersampled acquisitions needed for cine ASL. Typical imaging parameters: slice thickness ~ 2-3 mm, 3-8 bSSFP repetitions per FISS module, temporal resolution ~ 30-45 msec. A pulsatile flow phantom was used to validate cFASL flow measurements, cFASL flow velocity was quantified as the ratio of: (distance traveled by the leading edge of tagged blood)/(frame duration).

Results: Cine ASL imaging of the left main and left anterior descending coronary arteries was successfully obtained in all volunteers. Cine display of longitudinally-oriented cFASL images showed smooth progression of the tagged spins through the left main and LAD coronary arteries (Figure 1). Cine ASL obtained perpendicular to the coronary artery avoided out-of-slice motion of the tagged blood, thereby ensuring that arrival of the tagged bolus could be ascertained throughout the cardiac cycle.

Conclusion: We have demonstrated that coronary artery flow can be noninvasively observed and quantified using a breath-hold cine ASL technique. Potential misregistration of tagged and untagged images is minimized by interleaving the tagging RF pulse on alternate RR intervals. Flow within the left main coronary artery, along with the proximal and mid-portions of the LAD coronary artery could be observed and measured at multiple time points within the cardiac cycle.

[1] Koktzoglou I, Edelman RR. MRM 2017 Aug 30

Acknowledgments: NIH R01 HL130093, R21 HL126015

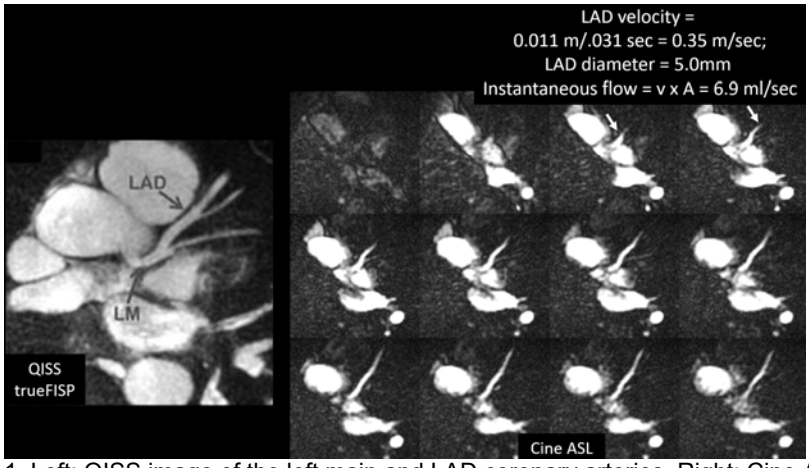

1. Left: QISS image of the left main and LAD coronary arteries. Right: Cine ASL. A single LAD velocity and flow measurement is shown, calculated from the displacement of the tagged bolus between frames 3 and 4.

ID#: 373720

Differential quantification of interstitial and dense myocardial fibrosis by high field MRI in a murine myocardial infarction model according to cardiac PW1 cell expression.

Khaoula Bouazizi, PhD[1] Marion Bouvet, PhD[2], Slawomir Kusmia, PhD[3], Philippe Cluzel, MD, PhD[4], David Sassoon, PhD[5], Nadjia Kachenoura, PhD[6], Jean-Sébastien Hulot, MD, PhD[5], Alban Redheuil, MD, PhD[7]

1. Institute of Cardiometabolism and Nutrition, France

2. INSERM UMRS 1166, Paris, Ile-de-France, France

3. Institute of Cardiometabolism and Nutrition, United Kingdom

4. Sorbonne Universités, UPMC Univ Paris 06, INSERM, CNRS, UMR 7371, UMRS 1146, Laboratoire d'Imagerie Biomédicale, 75013, Paris, France, Ile-de-France, France

5. INSERM UMRS 1166, France

6. Sorbonne Universités, UPMC Univ Paris 06, INSERM UMRS 1146, CNRS UMR 7371, Laboratoire d'Imagerie Biomédicale, F-75013, Paris, France, Paris, Ile-de-France, France

7. Sorbonne Universités, UPMC Univ Paris 06, INSERM UMRS 1146, CNRS UMR 7371, Laboratoire d'Imagerie Biomédicale, Paris, Ile-de-France, France

Background: Endogenous cardiac progenitor cells (CPC) hold great hope for future therapies in cardiac diseases. Despite the fact that different CPC have been identified[1], their specific roles remain ambiguous[2]. Cardiac PW1+ cells may contribute to cardiac fibrogenesis and remodeling[3]. We hypothesized that MRI could discriminate and quantify the dense and interstitial fibrosis in a murine myocardial infarction (MI) model.

Methods:

MRI was performed on a 4.0 T scanner (Bruker, Germany) in four groups: wild-type group (WT sham, n=2), PW1 knock-out (KO) group (KO sham, n=4), as well as in WT group (WT MI, n=6) and a PW1 KO group (KO MI, n=4) in whom MI was induced by ligation of the left anterior descending coronary artery. After 7 days, mice were euthanized and hearts explanted and fixed in formalin for MRI. A RARE sequence at different TRs was used to compute T1 maps (Fig.1A). Imaging parameters were: FOV=3.84x1.92cm, BW/pixel: 840Hz, three slices, TE=11.4ms, TR delays: 0.15-6.5ms, matrix=192x96. From T1 maps, fibrosis was quantified using a *k*-means clustering method on each slice (2D) and over the whole volume (3D) (Fig.1B,C). The fibrosis class was selected based on its mean T1 value (>normal myocardial T1). After MRI, hearts were cut into sections of 6µm and collagen was stained with Picrosirius Red for histological evaluation of fibrosis (Fig.1D).

Results: Good correlation (r=0.91, *P*=0.0002) was observed between MRI and histology for 3D dense fibrosis (Fig.2). MRI had a tendency to slightly overestimate dense fibrosis in mice hearts as revealed by the Bland-Altman analysis (mean difference: 2.7% and 95% limits of agreement:-0.6% to 6.1%). A good correlation was also observed between 2D and 3D MRI in terms of dense fibrosis (r=0.78, *P*=0.0006). In the KO sham and the WT sham groups, the amount of dense and interstitial fibrosis was approximately 5% and 25% respectively. In the MI groups, the amount of dense fibrosis in MRI was significantly lower in the KO group compared to the WT group (12.0% vs. 20.6%, *P*=0.009) and the amount of interstitial fibrosis in MRI increased in the KO group compared to the WT group (24.4% vs. 16.3%, *P*=0.06) (Fig.3).

Conclusion:

In this study, ex-vivo MRI was able to discriminate and quantify fibrosis subtypes (dense and interstitial) in normal and infarcted mice. Our results suggest that changes in cardiac PW1 expression may provide a novel therapeutic approach to influence fibrogenesis and improve cardiac regeneration.

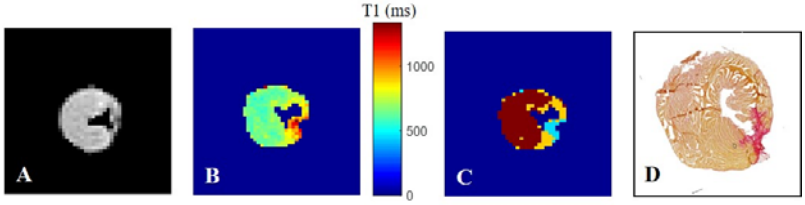

(A) A WT MI mouse heart section image acquired using the RARE sequence, (B) T1 map heart section and (C) the

corresponding k-means classification identifying myocardium (dark red), interstitial fibrosis (orange) and dense fibrosis (blue). (D) Representative photomicrograph of the same heart stained with Picrosirius red showing fibrotic remodeling (red) and myocardium (yellow).

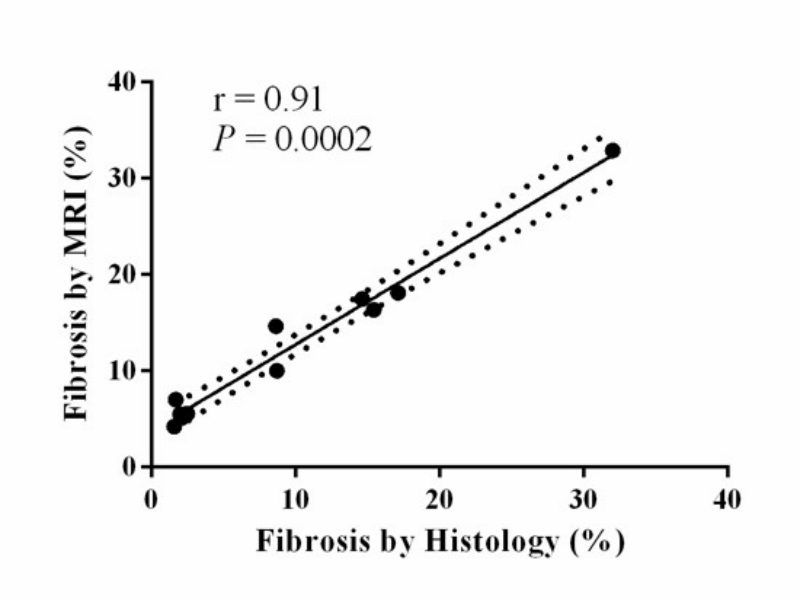

Linear regression plot for comparison between MRI and histology in terms of 3D dense fibrosis.

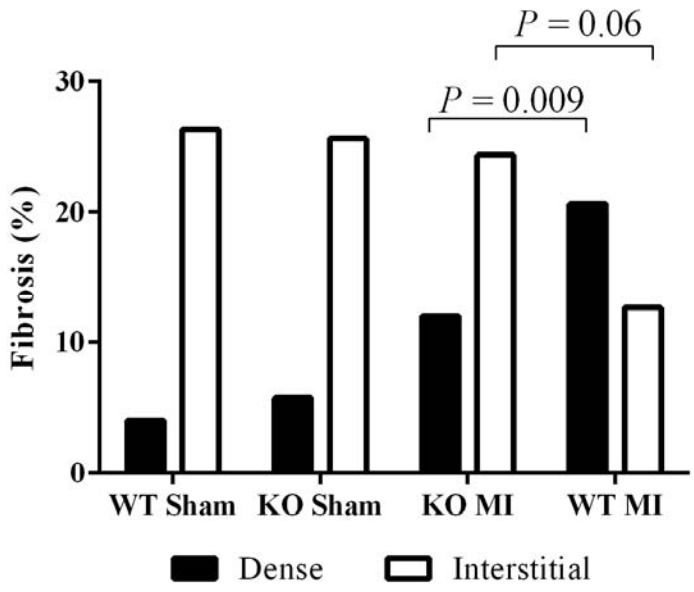

Quantitative analysis of the dense and interstitial components of fibrosis computed from 3D MRI.

ID#: 374298

Comprehensive Evaluation of Global and Regional Macroscopic and Microscopic Myocardial Fibrosis by Cardiac MR: Intra-individual Comparison of Gadobutrol Versus Gadoterate Meglumine

James Carr, MD[4]Amir Ali Rahsepar, MD[1], Ahmadreza Ghasemiesfe, M.D[2], Kenichiro Suwa, MD[3], Ryan Dolan, MD[4], Monda Shehata, MBBCH[5], Monica Korell, MPH[6], Julie Blaisdell[4], Nivedita Naresh, PhD[7], Michael Markl, PhD[4], Jeremy D. Collins, MD[4]

1. Northwestern University Feinberg School of Medicine, Chicago, IL

2. Yale New Haven Health, Bridgeport Hospital, Milford, CT

3. Northwestern University Feinberg School of Medicine Department of Radiology, IL

4. Northwestern University, Chicago, IL

5. SUNY Upstate Medical University, Manlius, NY

6. Northwestern University, IL

7. Northwestern University Feinberg School of Medicine, IL

Background: Late gadolinium enhancement cardiac MR (LGE-CMR) and extracellular volume fraction (ECV-CMR) are the reference standard for macroscopic and microscopic myocardial fibrosis. Due to the crucial role of myocardial scar detection using CMR and the increasing use of macrocyclic agents, we compared two macrocyclic contrast agents, gadoterate meglumine (Gd-DOTA; Dotarem, Guerbet, France) and gadobutrol (Gadavist, Bayer, Germany).

Methods: Forty subjects (61±11 years, 67.5% men) who underwent LGE-CMR using gadobutrol were recruited prospectively for a research CMR scan using Gd-DOTA at 1.5-T. Myocardial scar quantification was performed on short-axis PSIR Turbo-FLASH and True-FISP images using manual thresholding method as the reference standard. Moreover, we applied a threshold of 4SD above the mean signal intensity of the normal remote myocardium to quantify scar as a semi-automated method. Global and segmental LGE scar percentage (LGE%) were reported based on the AHA 16-segment model. T1-mapping was performed using a modified Look-Locker inversion recovery (MOLLI) technique. Data for three slices (base, mid, apex) were acquired during breath holding before and 12–25 minutes following the intravenous administration of extracellular Gd-contrast (0.2 mmol/kg). Pre- and post-Gd contrast T1-maps were analyzed on commercial software (CVI42 V5.3, Circle, Calgary, Canada) to generate segmental T1 and extracellular volume fraction (ECV) plots based on the AHA 16-segment model. Intraclass correlation coefficient (ICC) and the Wilcoxon signed rank test were used to check for reliability and differences in qualitative ratings between myocardial scar using the two GBCAs.

Results: Using manual thresholding, with PSIR Turbo-FLASH technique, LGE% was 9.9±9.77% and 9.4±9.79% for gadobutrol and Gd-DOTA, respectively (P>0.05) (ICC=0.99, 95% CI:0.97-0.99). Using manual thresholding, with PSIR SSFP technique, LGE% averaged 7.5±9.0% and 7.1±8.6% for gadobutrol and Gd-DOTA, respectively (P>0.05) (ICC=0.99, 95% CI:0.98-0.99). Using a 4SD threshold, with PSIR Turbo-FLASH technique, similar results were seen, with the LGE% of 9.5±9.7 and 9.2±9.3 for gadobutrol and Gd-DOTA (P=0.337) (ICC: 0.98, 95% CI: 0.95–0.99). Again, for 4SD threshold with PSIR SSFP technique, comparable values were observed, with the LGE% of 9.2±8.5 and 8.87±7.50 for gadobutrol and Gd-DOTA (P=0.736) (ICC: 0.98, 95% CI: 0.95–0.99). Averaged ECV for the CMR scan with Gadobutrol and Gd-DOTA were 28.40±4.88% and 28.46±4.73%, with perfect correlation (P>0.05) (ICC=0.98, 95% CI:0.94-0.99). Segmental analysis using manual/4SD thresholding with either PSIR Turbo-FLASH or True-FISP techniques revealed no difference in LGE% measured between two contrast agents (Figure 1). Moreover, for native T1 and ECV no difference in segmental analysis was observed between the two contrast agents for native T1 and ECV; however, contrast-enhanced T1 values were significantly different between the two contrast agents for all 16 segments (P<0.001) (Figure 2).

Conclusion: LGE- and ECV-CMR values derived from Gd-DOTA were comparable with values derived from gadobutrol. Gd-DOTA has equivalent diagnostic accuracy and performance compared to gadobutrol in identifying myocardial scar using LGE-CMR qualitatively and quantitatively.

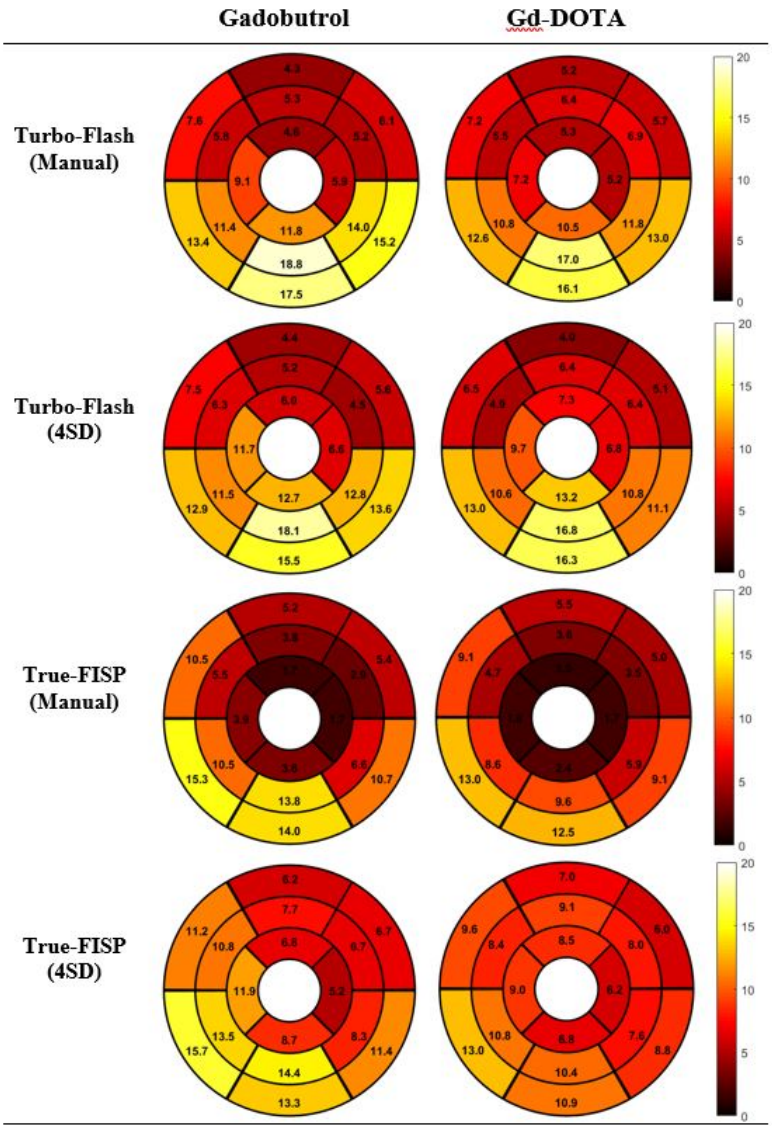

Figure 1. Segmental LGE% measurements between two contrast agents. No significant difference for any segments were observed for segmental analysis

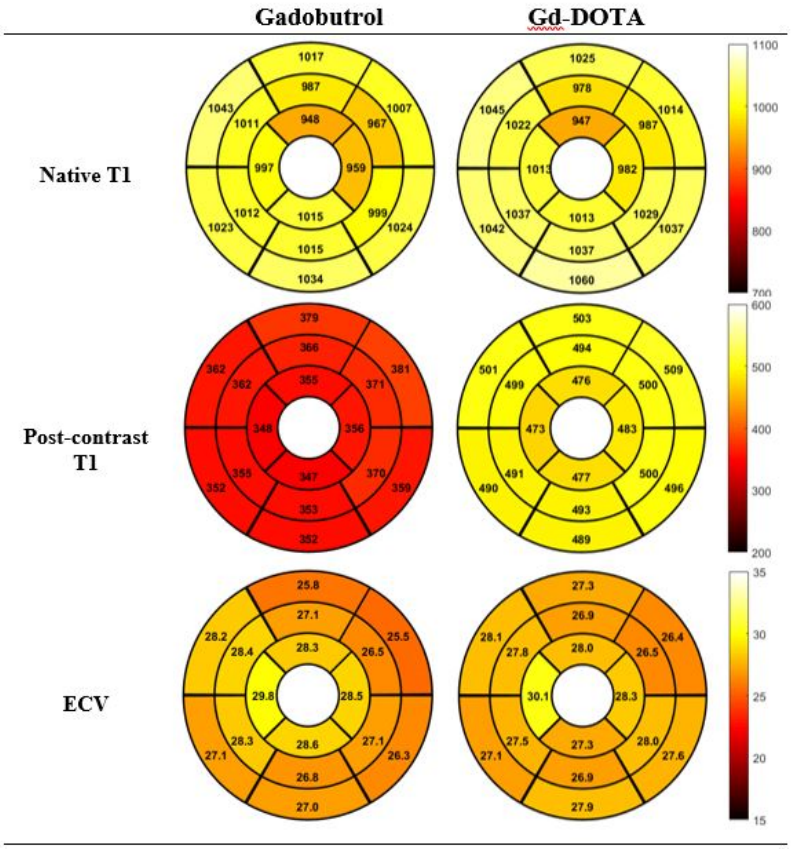

Figure 2. Segmental native-, post-contrast T1, and ECV for Gadobutrol and Gd-DOTA. ECV; extracellular volume fraction. No difference in segmental analysis were observed between two contrast agents for native T1 and ECV, however, contrast-enhanced T1 values were significantly different between the two contrast agents (P<0.001).

ID#: 374460

The Short-Term Prognosis Values of combined T1 Mapping and Feature Tracking by Cardiovascular Magnetic Resonance in Dilated Cardiomyopathy

Hui Liu, M.D.[1]Rui Chen, M.S.[2], Jingjing Wang, M.S.[2]

1. Guangdong General Hospital, Guangdong Academy of Medical Sciences, China (People's Republic)

2. School of Medicine, South China University of Technology, Guangzhou, China (People's Republic)

Background: The purpose of this study is to evaluate the prognosis value of combining T1 mapping with feature tracking in dilated cardiomyopathy (DCM) in short term follow-up.

Methods: Clinical baseline information, routine cardiovascular magnetic resonance (including late gadolinium enhancement(LGE)), feature tracking and T1 mapping analysis at 3.0T were also performed in 48 patients with DCM and 20 age- and sex-matched normal controls. Blood sample was taken just before CMR to measure hematocrit for ECV (extracellular volume fraction) calculation within 24 hours. All patients accepted optimal medication during the follow-up. Univariate and multivariate cox regression analysis were performed to detect the significant markers. To adjust the significant markers, a few variables recognized as risk factors clinically were manually added to the new multivariate cox model again. Furthermore, leave-one-out cross validation and time-dependent receiver of characteristics(ROC) were used to test the predictive performance of the new model in short term.

Results: Event-free survival was tracked at least 6 months and there were still 9 of DCM patients suffered from cardiovascular events within 12 months. No significant difference between patients with and without cardiovascular events in age (42.3±13.8vs 48.0±9.0, p=0.10) and gender (male:7(78%) vs 28(72%), p=1). Moreover, left ventricular ejection fraction(LVEF) in both groups is almost the same (21.8±9.0% vs 21.8±10.0%, p=1),much lower than that of normal controls (60.89±3.40%, p<0.001). Additionally, the parameters derived from feature tracking like global longitudinal strain(GLS) and global circumferential strain have no significant difference (p=0.90 and 0.77, respectively). Furthermore, the presence of LGE in CMR imaging interestingly have no significant difference (LGE present: 7(78%) vs 32(82%), p=1). Univariate cox regression analysis shows that ECV is the only marker with statistical significance(p<0.001). ECV in patients with and without events are 37.6%[quartile:37.1%,38.8%] and 29.9%[quartile:26.7%,32.8%] respectively. Only ECV still has statistical significance(p<0.001) in multivariate cox model. Using leave-one-out cross validation to test the performance of multivariate cox model, the time-dependent ROC shows that the area under curves(AUC) are 0.900, 0.871, 0.725 and 0.738(at 3 month, 6 month, 9 month and over 12 month respectively).

Conclusion: In DCM patients with severe systolic impairment, ECV is a strong independent marker prior to clinical information, routine CMR parameters and feature tracking parameters to predict adverse cardiovascular events in short term.

ID#: 374351

Non-Contrast Stress T1 Mapping CMR to Detect Mocardial Ischemia - Initial Experience

Sebastian Bohnen, MD[1] Ulf Radunski, MD[2], Jan Schneider, MD[3], Enver Guner. Tahir, MD[4], Maxim Avanesov, MD[5], Gunnar Lund, MD[6], Gerhard Adam, MD[6], Stefan Blankenberg, MD[7], Kai Muellerleile, MD[2]

1. University Heart Center Hamburg, Hamburg, Germany

2. University Medical Center Hamburg-Eppendorg, Hamburg, Germany

3. University Heart Center, Germany

4. University Medical Center Hamburg-Eppendorf, Hamburg, Hamburg, Germany

5. UKE, Hamburg, Germany

6. University Medical Center Hamburg-Eppendorf, Hamburg, Germany

7. University Heart Center Hamburg, Germany

Background: Stress perfusion Cardiovascular Magnetic Resonance (CMR) is an established noninvasive test to assess myocardial ischemia in coronary artery disease (CAD), but requires administration of gadolinium based contrast agents. The use of alterations in native myocardial T1 during vasodilation stress ("T1 reactivity") was recently proposed as a novel non-contrast approach to detect myocardial ischemia. We present our initial experience with stress T1 mapping at 1.5 and 3 Tesla.

Methods: Sixty-two patients with suspected or known CAD underwent CMR at 1.5 (n=30) or 3.0 Tesla (n=32). T1 mapping was performed on three short axis using the 5s(3s)3s-modified Look-Locker inversion-recovery (MOLLI) sequence at rest and under vasodilation stress 1 minute after administration of 400 µg regadenoson and was followed by a conventional stress perfusion CMR protocol. We defined T1 reactivity as the change in native T1 from rest to stress for 16 standard AHA segments. The presence of inducible ischemia was assessed by perfusion CMR on corresponding segments as reference. T1 reactivity was then compared between segments with and without stress-induced ischemia. Data are presented as mean (95% confidence interval).

Results: Remote myocardium showed a mean T1 increase from rest to stress ("T1 reactivity") of 22 (17-27) ms ($p<0.0001$). The mean T1 increase was 15 (8-23) ms at 1.5 Tesla ($p=0.0001$) and 28 (22-33) ms ($p<0.0001$) at 3 Tesla, respectively. We did not find a significant T1 reactivity in myocardial segments with inducible ischemia, the mean difference between rest and stress was -9 (-25-8) ms ($p=0.2997$). In addition, there mean T1 difference between rest and stress was -25 (-50-0) ms ($p=0.0504$) at 1.5 Tesla and 12 (-9-32) ms ($p=0.2592$) at 3 Tesla, respectively.

Conclusion: Native T1 of myocardium without inducible ischemia significantly increases under vasodilation stress ("T1 reactivity") at 1.5 and 3 Tesla. In contrast, we did not find a significant T1 reactivity in myocardium with inducible ischemia as defined by stress perfusion CMR. This phenomenon can be used to detect myocardial ischemia by non-contrast stress T1 mapping.

ID#: 376610

Prognostic Utility of Blood Oxygen Level Dependent (BOLD) Cardiovascular Magnetic Resonance (CMR) imaging in Asymptomatic Chronic Kidney Disease (CKD) Patients with and without Diabetes Mellitus.

Ranjit Shah, MBBS, FRACP[1] Susie Parnham, FRACP, PhD[2], Zach Liang, BSc[3], Gaetano Nucifora, MD, PhD[4], Karthigesh Sree Raman, MBChB, FRACP[5], Richard Woodman, PhD[6], Jonathan M. Gleadle, FRACP, DPhil[6], Joseph Selvanayagam, FRACP, DPhil[7]

1. South Australian Health and Medical Research Institute, Adelaide, SA, Australia, Prospect, South Australia, Australia

2. Flinders Medical Centre, Bedford Park, South Australia, Australia

3. Flinders University of South Australia, South Australia, Australia

4. University Hospital of South Manchester, Sale, England, United Kingdom

5. Flinders University of South Australia, Adelaide, South Australia, Australia

6. Flinders University, South Australia, Australia

7. Flinders University, Adelaide, SA, Australia, Bedford Park, South Australia, Australia

Background: Diabetes and CKD often co-exist and are both recognized risk factors for future cardiovascular events. We have previously shown that asymptomatic CKD patients have a blunted myocardial oxygenation response to stress, and that this is predictive of major adverse cardiac effects. However, whether this effect is independent of the presence of diabetes is unknown. In this study, we set out to compare the prognostic utility of BOLD in a CKD population with and without diabetes.

Methods: 65 CKD patients (27 with diabetes mellitus and 38 without diabetes mellitus) and no established or suspected coronary artery disease underwent BOLD CMR scanning at 3 Tesla. BOLD images were acquired at rest and after adenosine stress. BOLD SI Change was assessed semi-quantitatively. Patients were prospectively followed for adverse events (death, myocardial infarction, ventricular arrhythmia and heart failure (HF).

Results: The mean follow-up was 2.2 years. There were a total of 24 events in 15 (23%) participants: eight deaths, seven non-fatal myocardial infarctions, one ventricular arrhythmia and eight HF. Of these, 17 events were seen in 12 diabetic participants. Importantly, 30% (12/40) of participants with negative ΔSI had adverse events versus only 12% (3/25) of those with positive ΔSI.
On multivariate analysis (Table 1), the absolute BOLD CMR ΔSI was an independent predictor of adverse events in the 38 non-diabetic participants (HR 0.89, 95% CI 0.80-0.98, p=0.02), whereas it was not in diabetic participants. Participants with negative ΔSI had reduced event-free survival compared to those with positive ΔSI (Figure 1).

Conclusion: Blunted myocardial oxygenation response to stress is an independent predictor of adverse events in non-diabetic patients with CKD. Non-contrast BOLD CMR is a promising prognostic tool to assess silent myocardial ischaemia in CKD patients. Further studies in larger patient populations are in progress.

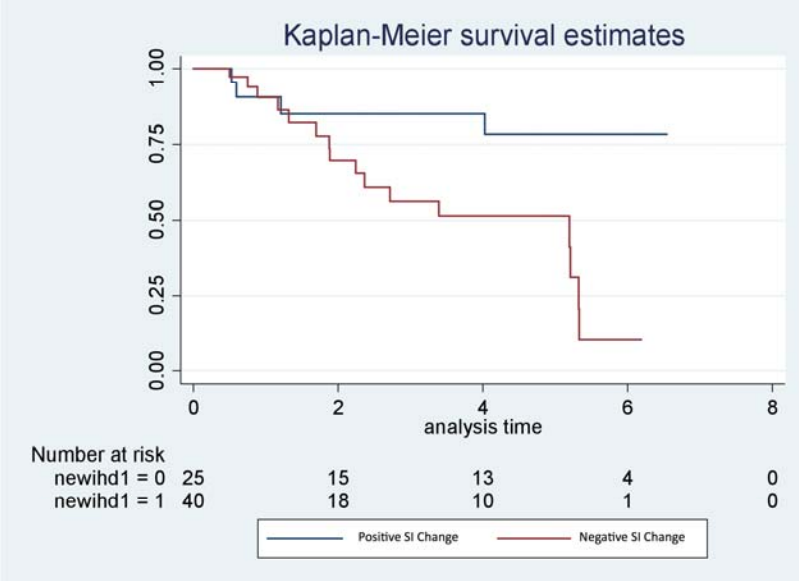

Figure 1: Kaplan-Meier survival graph showing CKD patients with negative BOLD SI change values had significantly higher major adverse cardiac events (MACE) rate compared to those with positive BOLD SI change values (p= 0.018).

Multivariate Analysis of Predictors of MACE in CKD Patients.

	Hazard Ratio	95% Confidence Interval	*p* value
Age	1.11	1.04-1.19	0.002
Diabetes mellitus	4.56	1.19-17.51	0.027
LVEF	0.94	0.89-1.00	0.055
RVEF	0.96	0.89-1.03	0.257
LV mass index	1.02	1.00-1.05	0.091
Absolute ΔSI (all participants)	0.98	0.92-1.04	0.45
Absolute ΔSI (non-diabetics)	0.89	0.80-0.98	0.019

ID#: 376365

Deep Learning for Fully Automatic Contouring of the Left Ventricle in Cardiac T1 Mapping

Evan Hann[1] Vanessa M. Ferreira, MD, DPhil[2], Stefan Neubauer, MD, FRCP[2], Stefan K. Piechnik, PhD, MScEE[2]

1. University of Oxford, Oxford, England, United Kingdom

2. University of Oxford, England, United Kingdom

Background:

Cardiac T1-mapping is an emerging technique for characterising the myocardial composition in a variety of cardiomyopathies. Like many other cardiac imaging techniques, image post-processing of T1-maps requires manual outlining of endocardial and epicardial borders. The manual process is laborious, and possibly prohibitive when it comes to large datasets in increasingly large-scale clinical trials, but this can be addressed by robust automatic methods and machine learning techniques.

Methods:

2000 short-axis ShMOLLI native T1-maps, covering the left ventricle with corresponding manual contours available from previous research studies conducted at our institution, were used. For development, data were randomly split into 75% training data and 25% validation data. We chose a convolutional neural network (U-net) of 19 convolutional layers, each layer with up to 512 3x3 trainable features, implemented with the TensorFlow software development library. The neural network was trained for 60 epochs. After training, the neural network was deployed to analyse all 2000 T1-maps to assess the overall speed and contour agreement, using a dice similarity coefficient, calculated as: (2 x intersection of automatic and manual contours) divided by (area of automatic contour + area of manual contour).

Results:

The entire processing of 2000 T1-maps took only 2 minutes and 11 seconds on a desktop computer equipped with an Nvidia Titan X GPU (graphical processing unit), i.e. ~7 milliseconds per slice. Median dice coefficients for both endocardial and epicardial contours were over 97%, and the interquartile range less than 2% (Table 1). Only one very apical short-axis slice could not be contoured automatically (Fig. 1A). 99% of the data (1979/2000 T1-maps) had automatic contours with dice coefficients better than 90%. Representative examples of cases with poor dice similarity are shown in Fig. 1B-D, and were all clearly attributable to poor T1-map quality due to artefacts, erroneous or ambiguous planning, and partial volume at apical slice positions. 99% of automatic contours had better dice similarity than the automatic contours shown in Fig. 1D.

Conclusion:

We achieved fully-automatic, unsupervised contouring of left ventricular short-axis T1-maps, with nearly-instantaneous and near-perfect agreement with human operators in 99% of 2000 T1-maps using Deep Learning.
We acknowledge NVIDIA for providing GPU used in this work.

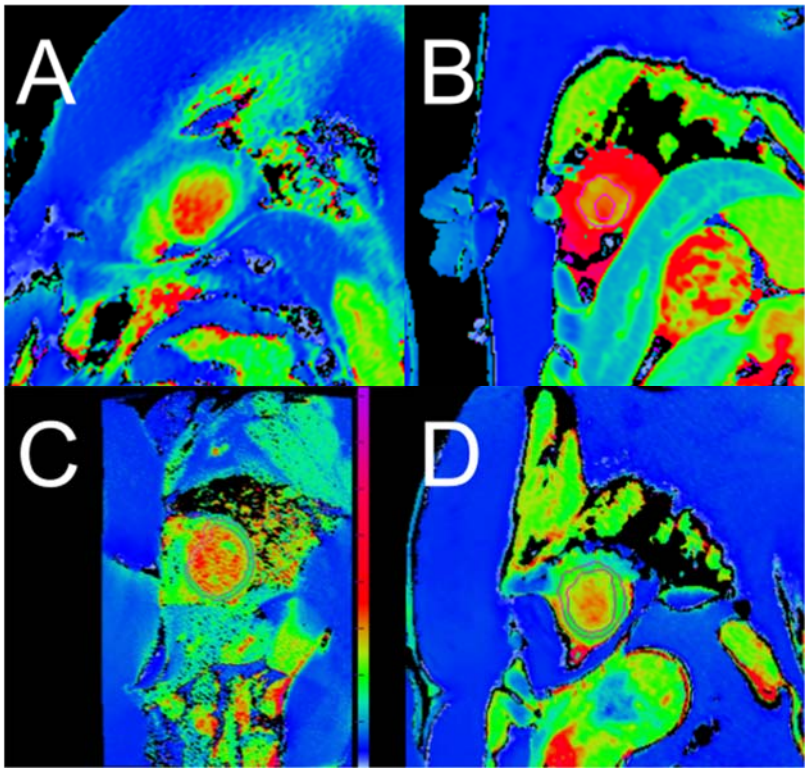

Representative examples of automatic contours with less than 90% dice coefficients: (A) contours not placed automatically due to extreme apical position with an oblique cut; (B) poor dice similarity due to very apical slice position; (C) poor dice similarity in poorly planned T1-map (severe wrap artifact and poor T1-reconstruction as seen by pixelated appearance); (D) despite having dice coefficients slightly less than 90%, the automatic contours in this case were acceptably placed. Cases with higher than 90% dice coefficients all had acceptable automatic contours.

Median and Quartiles of Dice Coefficients for Measuring Similarity between Automatic Contours and Manual Contours

Dice Coefficients (%): Median (Quartiles)		
Dataset	**Endocardial Contour**	**Epicardial Contour**
Training (N=1500)	97.20 (96.08 - 97.84)	97.41 (96.75 - 97.91)
Validation (N=500)	97.11 (95.92 - 97.85)	97.29 (96.58 - 97.84)
All (N=2000)	97.18 (96.07 - 97.88)	97.38 (96.70 - 97.90)

ID#: 375198

Clinical feasibility of 2-minute aortic 4D flow MRI: initial experience at two centers

Emilie Bollache, PhD[1] Kristopher D. Knott, MBBS MA[2], Redha Boubertakh, PhD[3], Ryan Dolan, MD[1], Claudia Camaioni, MD[4], Saadullah Ahmed-Villiers, MD[5], Thomas Treibel, PhD[6], James Carr, MD[1], Pim van Ooij, PhD[7], Jeremy D. Collins, MD[1], Julia Geiger, MD[8], James C. Moon, MD[6], Alex J. Barker, PHD[1], Steffen E. Petersen, MD DPhil MPH FRCP[9], Michael Markl, PhD[1]

1. Northwestern University, Chicago, IL

2. University College London, London, England, United Kingdom

3. QMUL, England, United Kingdom

4. Barts Heart Center, London, England, United Kingdom

5. Barts Heart Centre, United Kingdom

6. Barts Heart Centre, England, United Kingdom

7. Amsterdam Medical Center, Netherlands

8. University Children's Hospital Zurich, Switzerland

9. Queen Mary University of London, London, England, United Kingdom

Background: 4D flow MRI can be valuable in the comprehensive assessment of hemodynamic changes in congenital heart disease or aortic abnormalities. However, its use in clinical routine is still hampered by long scan times (5-15 min) and complex scan prescription including respiration control. Thus, we recently developed a highly k-t accelerated sequence with dedicated k_y-k_z-space sampling for the acquisition of aortic 4D flow MRI in 2 minutes during free breathing. A pilot study at a single center demonstrated its technical feasibility and good performance in quantifying flow indices compared to conventional respiratory-gated 4D flow MRI. The purpose of the present work was to further study the clinical feasibility of 2-minute aortic 4D flow MRI as an easy to use add-on to standard-of-care cardiothoracic MRI at two academic centers.

Methods: Healthy volunteers and patients were prospectively recruited at Northwestern University (NU) in Chicago, USA and Barts Heart Centre in London, UK. Prospective ECG-gated k-t accelerated (PEAK GRAPPA R=5) aortic 4D flow MRI was acquired during free breathing on Siemens scanners (Table 1). To minimize respiration artifacts, an initial filling of k-space corners followed by a centric reordering was used, to prioritize k-space center acquisition and thus favor contrast over as few respiratory cycles as possible once stable patient physiological and respiratory conditions are reached. Gd-contrast agent was injected (Barts: Dotarem, Guerbet; NU: Gadavist, Bayer) except in NU volunteers. Aortic wall edge sharpness, signal and noise inside the aorta were semi-quantitatively graded (from 1: low to 3: high quality), based on anatomic (magnitude) images and maximal intensity projection (MIP) of 4D flow-derived 3D phase-contrast MR angiogram (PCMRA).

Results: Highly accelerated aortic 4D flow data were successfully acquired in 37 consecutive subjects (Table 2): 12 healthy volunteers and 4 patients (3 with aortic valve stenosis and one with hypertension) at Barts, as well as 11 volunteers and 10 patients with various aortic disease (see representative examples in Figure 1) at NU. Total 4D flow scan time varied based on heart rate and averaged 2:02±0:28 minutes (see Table 2 for breakdown according to center and subject group). Examples of magnitude images as well as PCMRA and peak systolic velocity MIPs are shown in Figure 1, revealing overall good image quality as confirmed by the median image quality scores (Table 2). As expected, image quality was higher in post-Gd-contrast data. Finally, images reconstruction times reached 8:22±1:54 min at NU and were reported to average 11:50 min at Barts.

Conclusion: We confirmed in this bi-centric study that our 2-minute aortic 4D flow MRI sequence was easy to implement and use, providing short scan times and good image quality. Future work includes the development of faster reconstruction methods, to foster its use in a clinical setting and complement standard of care assessment of cardiovascular flow.

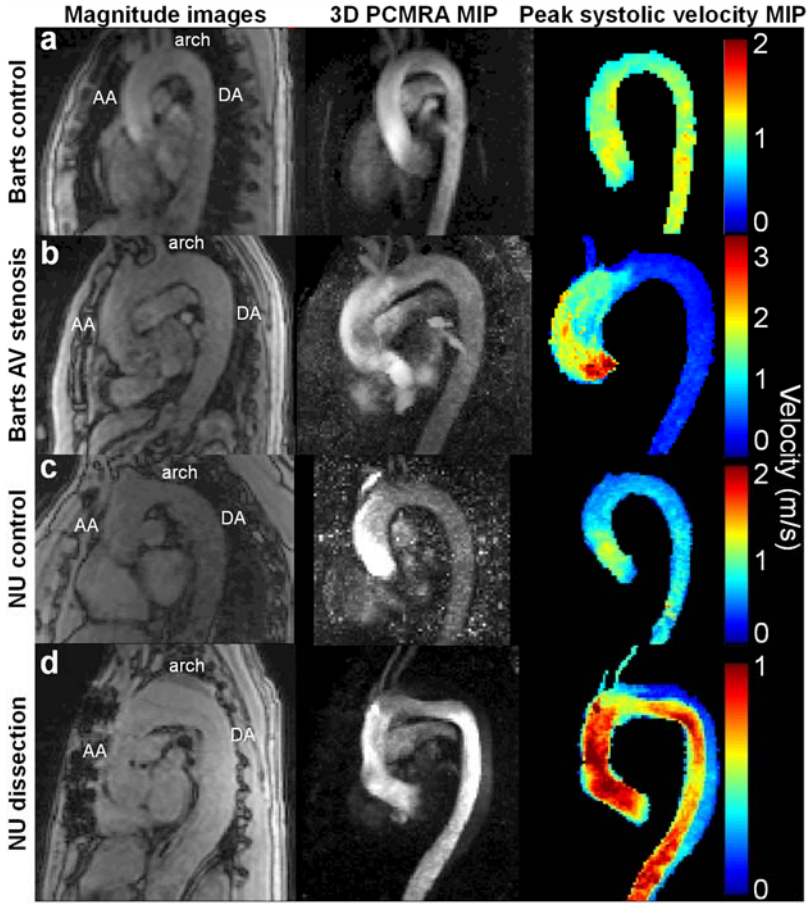

Examples of 2-min aortic 4D flow MRI data, from left to right: systolic magnitude images, PCMRA MIPs and peak systolic velocity MIPs obtained in a) Barts post-Gd-contrast 29-yo healthy woman, b) Barts post-contrast 81-yo patient with aortic valve (AV) stenosis, c) NU non-con 37-yo healthy man, and d) NU post-contrast 57-yo patient after repair of type A aortic dissection. Velocity MIPs were eroded by one pixel to suppress border noise.

Acquisition parameters used for the 2-minute aortic 4D flow MRI in Barts and NU centers.

	Barts	NU	
	all subjects	*volunteers*	*patients*
Scanner	1.5T Aera	1.5T Aera	1.5T Avanto
TR (ms)	4.2	4.2	4.1
TE (ms)	2.3	2.3	2.2
Flip angle (°)	15	7	15
Acq. matrix	160x80	160x80	160x80
FOV (mm^2)	360-400x270-300	360x270	360x270
SRes (mm^3)	3.4-3.8x2.3-2.5x2.8	3.4x2.3x2.6-3.3	3.4x2.3x2.8-3

N_{Seg}	4	4	4
TRes = N_{Seg}xTR (ms)	67.2	67.2	65.6
Slices (n)	24	24	24
Venc (cm/s)	150	150	150-250
Parallel imaging	PEAK GRAPPA (y-z-t) R=5		

TR: repetition time; TE: echo time; FOV: field of view; SRes: spatial resolution; N_{seg}: number of k-space segments per cardiac time frame; TRes: temporal resolution; Venc: encoding sensitivity; R: acceleration factor.

Subjects characteristics, scan time and image quality grading (provided as median [interquartile range]) obtained using k-t accelerated aortic 4D flow MRI according to center and population. AA: ascending aorta; DA: descending aorta.

	Barts		NU	
	volunteers (n=12)	*patients (n=4)*	*volunteers (n=11)*	*patients (n=10)*
Subjects characteristics				
Gender	9 women	3 women	4 women	3 women
Age	33±5 [25-45] years	73±13 [53-81] years	61±15 [31-77] years	60±10 [44-74] years
Weight	78±15 kg	68±11 kg	86±20 kg	88±13 kg
Heart rate	66±12 bpm	56±10 bpm	67±10 bpm	73±14 bpm
Scan time				
	1:58±0:18 min	2:24±0:28 min	1:55±0:14 min	2:05±0:44 min
Image quality grading: edge sharpness				
AA	3.0 (2.0-3.0)	3.0 (3.0-3.0)	3.0 (2.0-3.0)	3.0 (2.0-3.0)
arch	3.0 (2.8-3.0)	3.0 (2.5-3.0)	3.0 (2.0-3.0)	3.0 (2.0-3.0)
DA	2.5 (2.0-3.0)	2.5 (1.8-3.0)	2.0 (2.0-3.0)	2.0 (2.0-2.8)
Signal				
AA	3.0 (3.0-3.0)	3.0 (2.8-3.0)	3.0 (2.0-3.0)	3.0 (3.0-3.0)
arch	3.0 (2.0-3.0)	2.5 (1.8-3.0)	2.0 (2.0-3.0)	3.0 (3.0-3.0)

DA	2.5 (2.0-3.0)	2.5 (1.8-3.0)	2.0 (1.5-2.0)	3.0 (3.0-3.0)
Noise				
AA	3.0 (2.0-3.0)	2.0 (2.0-2.3)	2.0 (2.0-3.0)	3.0 (2.3-3.0)
arch	3.0 (2.8-3.0)	3.0 (3.0-3.0)	2.5 (2.0-3.0)	3.0 (3.0-3.0)
DA	2.5 (2.0-3.0)	2.0 (2.0-2.5)	2.0 (2.0-2.0)	3.0 (3.0-3.0)

ID#: 375834

Importance of operator training and rest perfusion on the diagnostic accuracy of stress perfusion CMR

Adriana D. M. Villa, MD[1] Laura Corsinovi, Locum Consultant Cardiologist and General Medicine Specialist, MD, PhD[2], Ioannis Ntalas, MD, PhD[3], Xenios Milidonis, MSc, PhD[4], Cian Scannell, BSc, MRes[4], Gabriella Di Giovine, MD[5], Nicholas Child[6], Catarina Ferreira[7], Muhummad Sohaib Nazir, MBBS MRCP[1], Julia Karady[8], Esmeralda Eshja[9], Viola De Francesco[10], Andreas Schuster, MD PhD MBA FESC[11], Tevfik F. Ismail, PhD MRCP[12], Reza Razavi, MD, PhD[13], Amedeo Chiribiri, MD PhD[13]

1. King's College London, United Kingdom

2. Cardiology Department, Basingstoke and North Hampshire Hospital, The UK, Basingstoke, England, United Kingdom

3. St. Thomas' Hospital, London; King's College London, United Kingdom

4. King's College London, London, United Kingdom

5. King's College London, Novara, Piemonte, Italy

6. Guys and St Thomas' Hospital, London, United Kingdom

7. Centro de Investigação Ciências da Saúde (CICS) - FCS UBI, Vila Real, Portugal

8. Department of Cardiology, Guy's and St Thomas' NHS Foundation Trust, London, United Kingdom, United Kingdom

9. ICS Maugeri Pavia, Pavia, Lombardia, Italy

10. King's College, London, United Kingdom

11. Department of Cardiology and Pneumology, University Medical Center Göttingen, Germany; Department of Cardiology, Royal North Shore Hospital, Sydney, Australia; The Kolling Institute, Northern Clinical School, University of Sydney, Sydney, Australia, Niedersachsen, Germany

12. King's College London; Guy's and St Thomas' Hospitals NHS Foundation Trust, London, England, United Kingdom

13. King's College London, London, England, United Kingdom

Background: Clinical evaluation of stress perfusion (SP) cardiac magnetic resonance (CMR) is based on visual assessment, which has shown high diagnostic accuracy in previous clinical trials. In these studies, however, visual assessment was performed by expert readers or by a core laboratory and the results may not be directly transferrable to clinical practice. Other factors, such as the level of training, the extent of ischaemia, and image quality could affect the diagnostic accuracy. Moreover, the role of rest images has not been clarified.
The aim of this study was to assess the diagnostic accuracy of visual assessment for operators with different levels of training and the additional value of rest perfusion imaging, and to compare visual assessment and automated quantitative analysis in the assessment of coronary artery disease (CAD).

Methods: We evaluated 53 SP-CMR requested for known or suspected CAD. All patients had invasive coronary angiography. Nine operators (equally divided in 3 levels of competency, according to SCMR guidelines) blindly reviewed each case twice with a 2-week interval, randomised with and without rest images. Late gadolinium enhancement was always available. Automated Fermi deconvolution was used for quantitative analysis and myocardial perfusion reserve calculated as stress/rest absolute perfusion estimates.

Results: Level-3 operators correctly identified CAD in 83.6% of the cases. This percentage dropped to 65.7% for level-2 operators and to 55.7% for level-1 operators. Quantitative analysis correctly identified CAD in 86.3% of the cases (p When rest images were available, a non-statistically significant trend towards more accurate CAD detection was observed in all competency groups (Figure 2) and in the overall analysis (69.6% vs 67.1%). However, when rest images were available, a significantly higher level of confidence was reported by the operators (p=0.022)(Figure 3) and subjective image quality was scored at a higher level (p=0.012).

Conclusion: Our study demonstrates that the level of training is the main determinant of the diagnostic accuracy in the identification of CAD. Level-3 operators performed at levels comparable with the results from clinical trials. Rest images did not significantly improve diagnostic accuracy, but contributed to higher confidence in the results. Automated quantitative analysis performed similarly to level-3 operators. This is of increasing relevance as recent technical advances in image reconstruction and analysis techniques are likely to permit the clinical translation of robust and fully automated quantitative analysis into routine clinical practice.

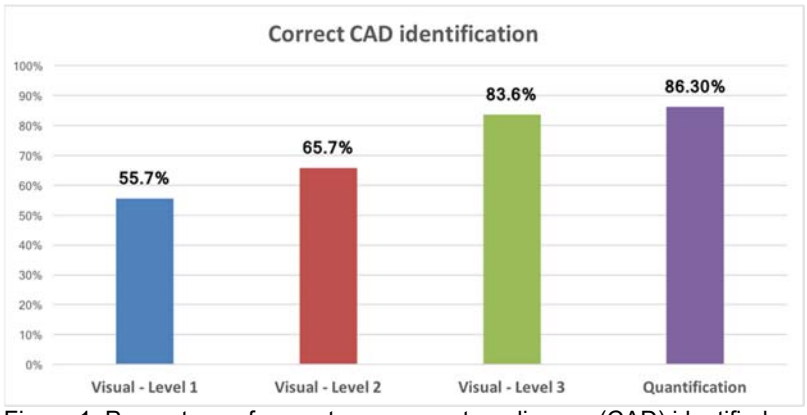

Figure 1: Percentage of correct coronary artery disease (CAD) identified on visual assessment based on the level of CMR training (p<0.001).

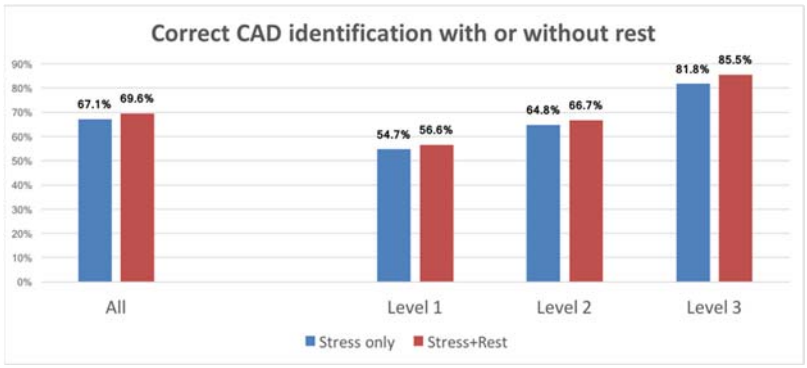

Figure 2: Percentage of correct coronary artery disease (CAD) identified on visual assessment at different operator skill level when using stress perfusion only and when using both stress and rest perfusion data.

Figure 3: Average operator confidence when using stress perfusion only and when using both stress and rest perfusion (p=0.022).

ID#: 375464

Obesity paradox and myocardial injury by cardiac magnetic resonance imaging in ST-elevation myocardial infarction

Georg Fuernau, MD[1] Thomas Stiermaier, MD[2], Mohammed Saad, MD[1], Janine Pöss, MD[1], Holger Thiele, MD[3], Ingo Eitel, MD[2]

1. University Heart Center Lübeck, Germany

2. University Heart Center Lübeck, Lübeck, Schleswig-Holstein, Germany

3. Heart Center Leipzig - University Hospital, Sachsen, Germany

Background: A so called obesity paradox with better outcome for overweight patients with acute ST-segment elevation myocardial infarction (STEMI) has been demonstrated in previous studies. The pathophysiological basis for this survival benefit in obese patients is unknown. A possible link of this observed phenomenon to myocardial injury measured by cardiac magnetic resonance imaging (CMR) has never been investigated before. Aim of this study was therefore to assess the correlation of the body mass index (BMI) with CMR detected markers of myocardial damage and clinical prognosis in acute reperfused STEMI patients.

Methods: The randomized multi-center AIDA-STEMI CMR substudy trial included in total 792 patients with acute STEMI and CMR was performed within 1-7 days after the index event. The left ventricular (LV) ejection fraction (EF), area at risk (AAR), myocardial salvage index (MSI), infarct size (IS), and microvascular obstruction (MO) were assessed with CMR. Patients were stratified by the median of body mass index (BMI). The primary clinical endpoint was long-term all-cause, secondary end-point major adverse cardiovascular (MACE) events rate consisting of death, re-infarction, and new congestive heart failure.

Results: Information on BMI was available in 778 (98%) of 792 patients. Median BMI was 27.3 (24.9-30.3) kg/m². Patient with a BMI below the median had a significant higher long-term mortality (4.1 vs. 1.5%, log-rank-test hazard ratio [HR] 2.66 [95% confidential interval {CI} 1.15-6.14], p=0.04). In contrast there was no difference in MACE rates over time (8.0 vs. 6.2%, log-rank-test HR 1.27 [95%CI 0.75-2.17], p=0.37). There was no association of BMI to any CMR finding reflecting myocardial damage and reperfusion injury (Table 1). In multivariable Cox-Regression-analysis in prediction of time to mortality including BMI and CMR parameters a BMI <median remained a significant prognosticator (HR 2.90 [95%CI 1.04-8.09], p=0.04).

Conclusion: The mortality benefit observed for overweight STEMI patients is not explained by differences in myocardial damage and reperfusion injury. Further studies are needed to ascertain the underlying cause of improved survival of obese infarction patients.

Table 1

Median and interquartile range	Overall	BMI <27.3	BMI ≥27.3	p-value
AAR (%LV)	34.9 (25.4-47.4)	34.9 (25.1-48.5)	34.9 (25.4-46.9)	0.56
IS (%LV)	16.7 (8.4-24.9)	16.8 (8.4-25.9)	16.3 (8.4-23.7)	0.41
MSI (%)	51.0 (32.9-69.1)	48.2 (31.3-68.8)	53.2 (34.8-70.5)	0.16
MO (%LV)	0.00 (0.00-1.76)	0.16 (0.00-1.88)	0.00 (0.00-0.15)	0.21
LV-EF	50.5 (43.3-57.6)	50.2 (42.0-56.8)	50.9 (44.0-58.3)	0.08

ID#: 377704

Prospective correction of patient-specific respiratory motion in T1 mapping

Michael A. Bush, M.S.[1] Orlando Simonetti, PhD[2], Rizwan Ahmad, PhD[2], Yingmin Liu, Ph.D.[1], Ning Jin, PhD[3], Juliet Varghese, PhD[4]

1. The Ohio State University, Columbus, OH

2. The Ohio State University, OH

3. Siemens Healthineers

4. The Ohio State University

Background: Myocardial T1 mapping is a popular CMR technique capable of assessing diffuse myocardial structural changes. T1-mapping techniques require multiple images acquired at varying inversion times to be registered with each other. Inversion-recovery source images are often acquired during free-breathing and non-rigidly registered to facilitate pixel-wise curve fit for T1 estimation. However, retrospective registration cannot correct for through-plane motion and performs poorly in deeper breathing subjects; this can lead to corruption of myocardial T1 by adjacent blood pool, artificially elevating T1 values and increasing variability. Breath-holding prevents through-plane motion and improves retrospective image registration but may not be possible in certain patient populations. Navigator gating can be used, but is impractical because in addition to the complex schemes used to trigger the IR source images, navigator gating would lead to prohibitively long scan times. To improve efficiency of free-breathing T1 mapping, we have developed a motion compensation method that prospectively adjusts the imaging slice by following a patient-specific model that describes the motion of the heart throughout the respiratory cycle. This method is expected to reduce through and in-plane motions, and thereby improve the accuracy of pixel-wise T1 measurements.

Methods: A training scan acquires two orthogonal image planes each heartbeat along with diaphragmatic navigator position. Heart motion is extracted by non-rigid registration and feature tracking, and modeled with respect to navigator position in 3D. A modified T1 mapping pulse sequence reads the coefficients of the models and updates the scan plane in real-time to follow the heart throughout the respiratory cycle. This prospective motion correction method (**PROCO**) was tested in 5 healthy volunteers and compared to maps generated under free-breathing plus retrospective image registration (**NOCO**). Means and standard deviations of myocardial T1 measured in a single short-axis slice in each subject were then compared between the two methods.

Results: The standard deviation in myocardial T1 was reduced in all **PROCO** acquisitions relative to **NOCO**. Reduced variability was most likely related to reduction of partial volume effects, avoiding corruption of myocardial signal with blood pool T1 values. T1 variability was similar across all volunteers using **PROCO**; with **NOCO**, variability was higher in subjects with deeper breathing motion. This illustrates the need for prospective correction especially in cases of deep-breathing. While the lower average myocardial T1 value observed with **PROCO** is consistent with reduced blood pool contamination, further work is required to validate this finding.

Conclusion: PROCO reduced variability in myocardial T1 measured in normal subjects compared to **NOCO**. **PROCO**';s reduction of through and in-plane motion prior to retrospective image registration may help to avoid corruption of myocardial T1 values by adjacent blood-pool.

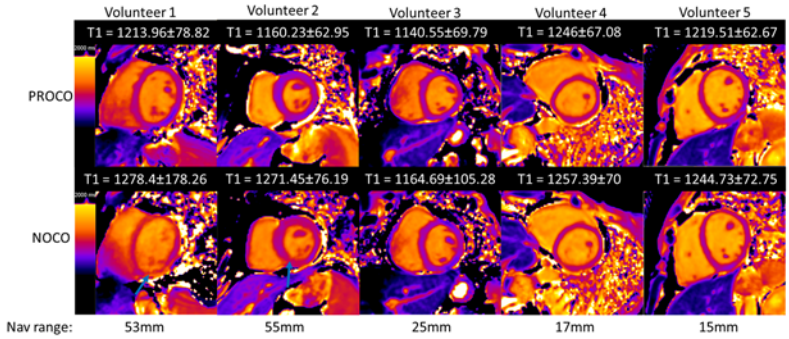

Figure 1. Application of PROCO and NOCO in T1 mapping of 5 volunteers. Respiratory motion leads to increased standard deviations in measurements of myocardial T1, which is significantly reduced in PROCO compared to NOCO. Blue arrows highlight significant areas of corruption of myocardial signal with blood pool T1 values.

T1 Mapping Results

ID#: 377861

When criteria for ICD implantation in the primary prevention of sudden death among patients with hypertrophic cardiomyopathy don't get along: an analysis of late gadolinium-enhancement and the European and American guidelines

Pedro Freitas[1] João Abecasis[2], Carla Saraiva[3], Daniel Jorge. Nascimento Matos[4], João Mesquita[5], Hugo Marques[6], António Ferreira[7]

1. Hospital de Santa Cruz, Carnaxide, Lisboa, Portugal

2. Hospital dos Lusíadas, Lisboa, Portugal

3. Hospital de Santa Cruz, Centro Hospitalar Lisboa Ocidental, Lisboa, Portugal

4. Hospital de Santa Cruz, Lisbon, Lisboa, Portugal

5. Hospital de Santa Cruz, Lisboa, Portugal

6. Hospital da Luz, Lisboa, Portugal

7. Hospital de Santa Cruz, Portugal

Background: The criteria for implantable cardioverter defibrillator (ICD) in patients with hypertrophic cardiomyopathy (HCM) differs between the European (ESC) and the American (ACC) guidelines. Recently, late gadolinium enhancement (LGE) in cardiac magnetic resonance (CMR) was proposed to improve patient selection. Our objective was to assess the prevalence and concordance between these criteria for primary prevention with ICD in a population of patients with HCM undergoing CMR.

Methods: A retrospective analysis was conducted in 3 centres where patients with HCM underwent CMR for diagnostic confirmation and/or risk stratification. Eligibility for ICD was determined according to the ESC criteria [HCM Risk-SCD at 5-years was categorized into 3 risk strata: low risk (< 4%; ICD not indicated); intermediate risk (≥4% to < 6%; ICD may be considered) and; high risk (≥6%; ICD should be considered)] and the ACC criteria (ICD not recommended, useful and reasonable). LGE was quantified semi-automatically using a signal intensity threshold of ≥6 standard-deviations above the average signal intensity of healthy myocardium. Patients were categorized according to the % of LGE as: ≤10%, 10-19.9%; ≥20%. Weighted κ (quadratic weights) was used to assess interrater agreement between classifications.

Results: From the 118 patients analysed (59% male; age 58 ± 15 years) 3.4% (n=4) had family history of sudden death, 12% (n=14) non-sustained ventricular tachycardia, 9.3% (n=11) had previous unexplained syncope, 4.2% (n=5) had LV maximum thickness ≥30 mm, and 21% (n=25) had LV outflow tract obstruction ≥ 50 mmHg.

According to the ACC guidelines, it would be reasonable to consider an ICD in 30 patients. Using ESC criteria, 12 patients would be eligible for ICD. The median HCM Risk-SCD score was 1.69% (IQR 1.3% - 2.2%). The median % of LGE was 1.3% (IQR 0.08% - 4%), with 2.5% (n=3) patients showing LGE ≥20% of total myocardial mass.

The concordance between these criteria is depicted in Figure 1 (green background representing concordance between scores). Weighted κ analysis revealed fair agreement between the ESC and ACC classifications [κ = 0.37 (95% CI = 0.19 – 0.55], p<0.001]. On the other hand, a poor agreement was found between ACC and LGE classifications [κ = 0.16 (95% CI = -0.02 to 0.35), p=0.024], while no agreement was present between ESC and LGE [κ = -0.02 (95% CI = -0.14 to 0.10), p=0.824].

Conclusion: In this population of patients with HCM undergoing CMR there was a large discrepancy between the 3 studied criteria for ICD implantation.

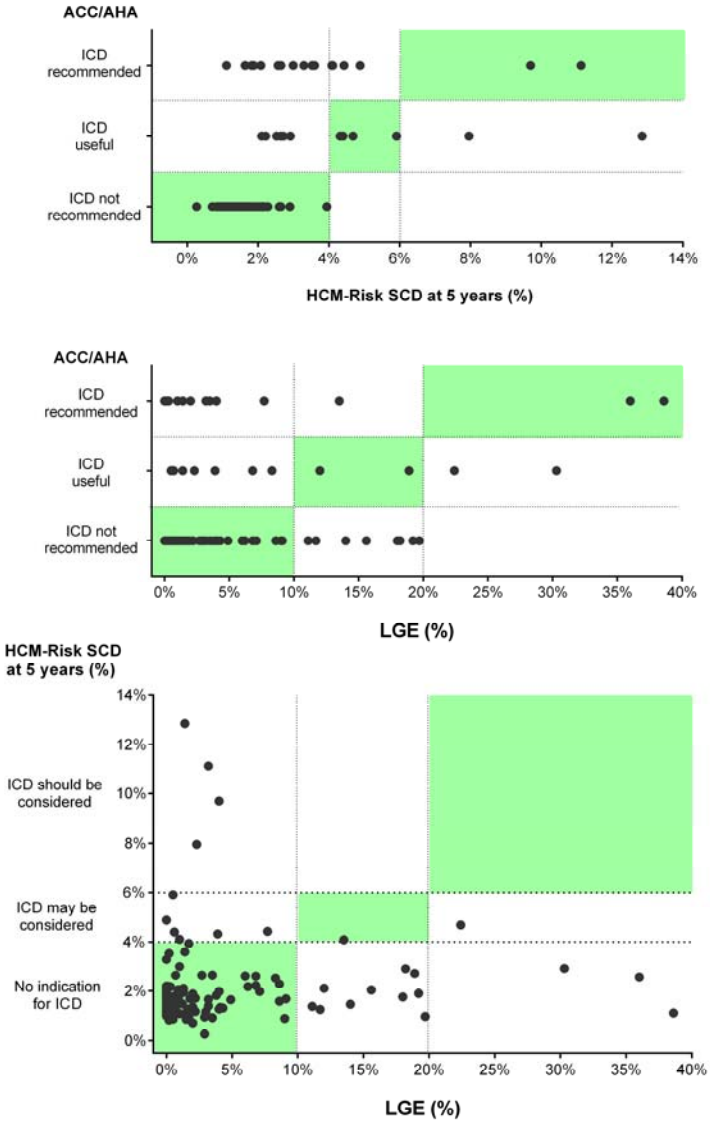

Figure 1. Concordance/discordance between the ESC, ACC and LGE classifications

ID#: 377872

T1 mapping for the prediction of treatment response in AL amyloidosis

Rosario J. Perea Palazón, MD PhD[1] Jose T. Ortiz-Pérez, MD PhD[2], Adelina Doltra, MD, PhD[2], Carlos Fernández de Larrea, MD PhD[2], Bladé Joan, MD PhD[2], Solé Manel, MD PhD[2], Susanna Prat-González, MD PhD[2], de Caralt Teresa M., MD PhD[2], Cibeira M. Teresa, MD PhD[2]

1. Hospital Clínic. Universitat de Barcelona, Barcelona, Catalonia, Spain

2. Hospital Clínic. Universitat de Barcelona, Catalonia, Spain

Background: Cardiac involvement in systemic AL amyloidosis is a leading cause of morbidity and mortality, and influences therapeutic options. Native myocardial T1 mapping and myocardial extracellular volume (ECV) derived from Cardiac Magnetic Resonance (CMR) have been shown to improve diagnostic accuracy, patient stratification and to monitor clinical changes in cardiac amyloidosis. The aim of this study was to characterize serial changes in native myocardial T1 and ECV in AL amyloidosis with cardiac involvement, and to investigate their relationship with the hematologic response.

Methods: We included 18 patients (11 men; 56±9y) with systemic AL amyloidosis. In 15 cases cardiac involvement was confirmed by endomyocardial biopsy and, in the remaining, presence of immunoglobulin light chains-derived amyloid deposits was demonstrated in another tissue. Subjects underwent serial CMR evaluation with T1 mapping and derived ECV before and 12 months after treatment. Native myocardial T1 values were compared with 18 healthy controls. The hematologic response to treatment was evaluated according to international consensus criteria and labelled as a dichotomous variable. CMR was performed with a 3T scanner. Standard cine and LGE sequences were performed. Before contrast administration, T1 mapping images using MOLLI sequence were acquired. To measure myocardial ECV contrast equilibrium was achieved by loading a bolus followed by a slow continuous infusion.

Results: At baseline, the prevalence of LGE was 89%. The pattern of LGE was subendocardial (56%), diffuse (33%) and 11% patients had no LGE. No significant differences were observed between responders and non-responders with regards to baseline and follow-up ejection fraction (56% vs 54%, p=NS and 54% vs 50%, p=NR respectively). Mean native myocardial T1 value was significantly higher in patients with amyloidosis at baseline than in healthy controls (1143.83±101.44 vs 1027.54±22.47 msec, p<0.0001).

The overall hematologic response rate was 61.1% and comprised complete response, very good partial response and partial response. Therapeutic failure rate was 38.9% and comprised early death, no response and progression disease. Native myocardial T1 prior treatment was higher in no-responders than in responders (1208.8±97.5 vs 1102.4±83.3 msec, p=0.027). In addition, responders showed lower ECV after treatment than non-responders (40.6±11.2 vs 75±17%, p=0.022). Finally, the absolute change in ECV from baseline to follow-up was higher in non-responder patients (17.0 vs 1.7%, p=0.04).

Conclusion: Changes in myocardial native T1 and ECV by CMR correlate with the haematological response to treatment. On top of an improved diagnostic yield for myocardial involvement in AL amyloidosis, characterization by T1 mapping correlates with response to treatment.

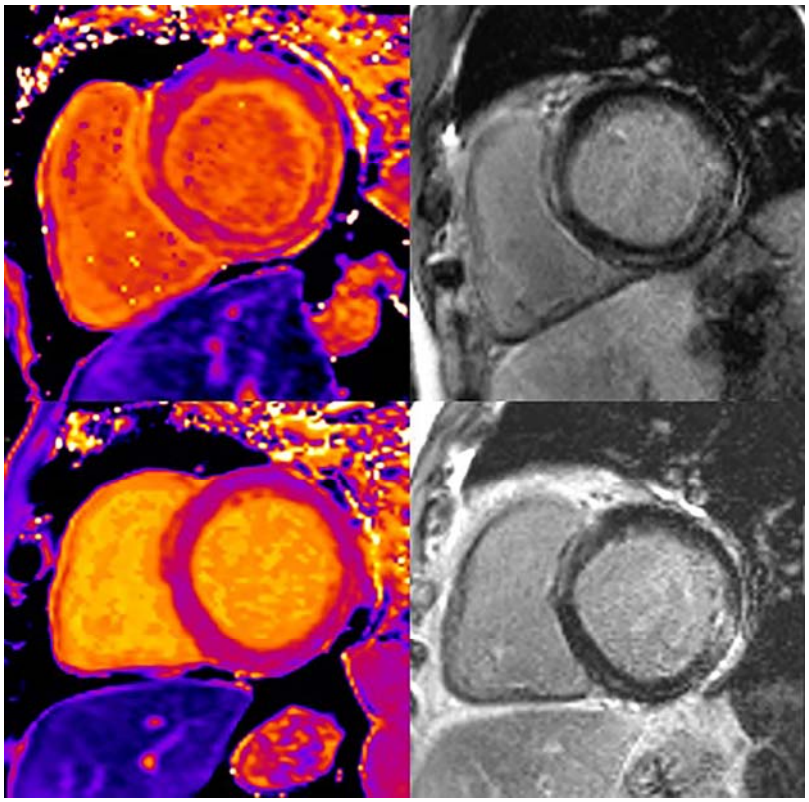

Short axis view of native T1 mapping (left), and LGE (right), before (top) and after (bottom) treatment in a responder patient.

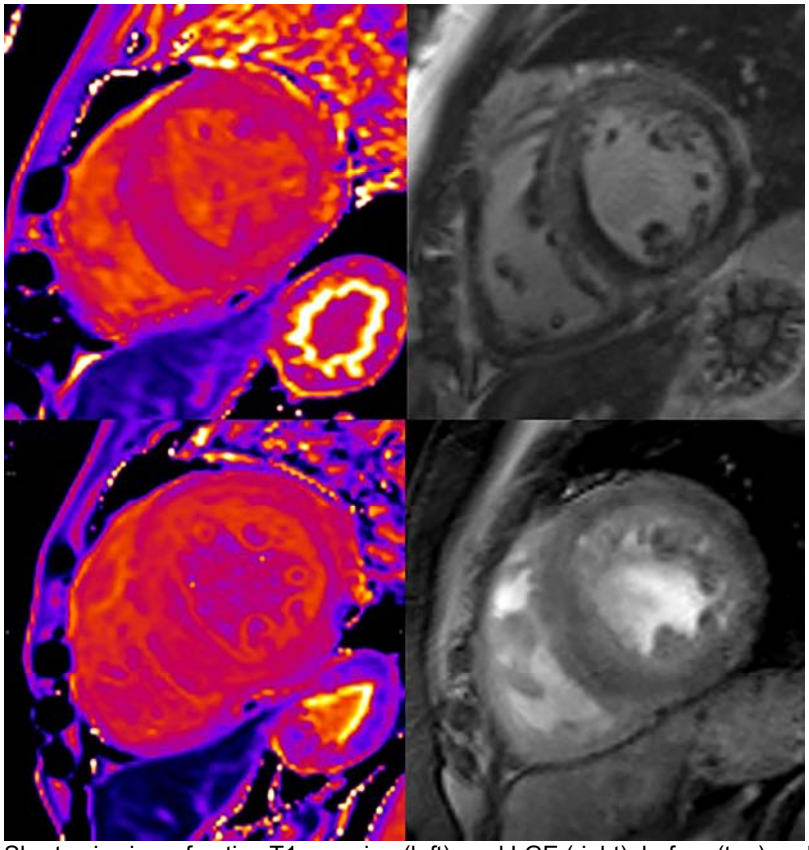

Short axis view of native T1 mapping (left), and LGE (right), before (top) and after (bottom) treatment in a non-responder patient.

ID#: 376910

RF Ablation of the Left Atrium and Pulmonary Vein Ostia is well Visualized by Non-contrast-enhanced MRI in a Swine Model

Michael A. Guttman, MS[1] Susumu Tao, MD, PhD[2], Daniel Herzka, PhD[3], Sarah Fink, BA[4], Ehud J. Schmidt, PhD[5], Henry Halperin, MD, MA[6], Aravindan Kolandaivelu, MD[7]

1. The Johns Hopkins University, School of Medicine, MD

2. Johns Hopkins University, school of medicine, Baltimore, MD

3. National Institutes of Health

4. Johns Hopkins University, MD

5. Johns Hopkins University, Towson, MD

6. Johns Hopkins University, Baltimore, MD

7. Johns Hopkins University School of Medicine, MD

Background: Atrial fibrillation recurrence after ablation is estimated at 30-50%. Many are due to incomplete ablation which resumes ectopic activity in 2-3 months. There is need for verification of permanent necrotic ablation. Inversion recovery (IR) MRI with long inversion time (TI) and no contrast agent demonstrated selective and stable enhancement of acute left ventricular RF ablation lesions in swine. Myocardium ablated to coagulation necrosis enhances due to T1 shortening. Enhancement is specific to necrotic lesion cores, allowing verification of permanently ablated tissue. We show that IR-MRI without contrast agent can also provide visualization of acute necrotic ablation lesions in the thin walled left atrium (LA) and pulmonary vein (PV) ostia.

Methods: Five swine underwent RF ablation (30W for 30-40 seconds) around the right superior PV ostia using conventional electroanatomic mapping. Animals were then transported to MR for 3D IR long-TI imaging using ECG-gating and respiratory navigator. Pixel size was 1.1x1.1x1.1 mm with 2x interpolation in slice direction, TI=700, acquisition time 15-18 mins. Animals were sacrificed and gross pathology of hearts examined.

Results: All ablation lesions were visualized on the LA wall and PV ostia. Lesions were readily distinguished from the blood pool. Electrical PV isolation was successfully performed in 2 cases. Results are shown in Figure 1 for both successful and unsuccessful PV isolation. Necrotic lesions are visibly enhanced and gaps are apparent, as corroborated by gross pathology.

Conclusion: IR-MRI with long-TI and no contrast agent can provide visualization of acute ablation lesions in the thin walled LA and PV ostia, as tested in a swine model. This imaging technique may allow verification of necrotic ablation to insure permanent conduction block and improve ablation outcome.

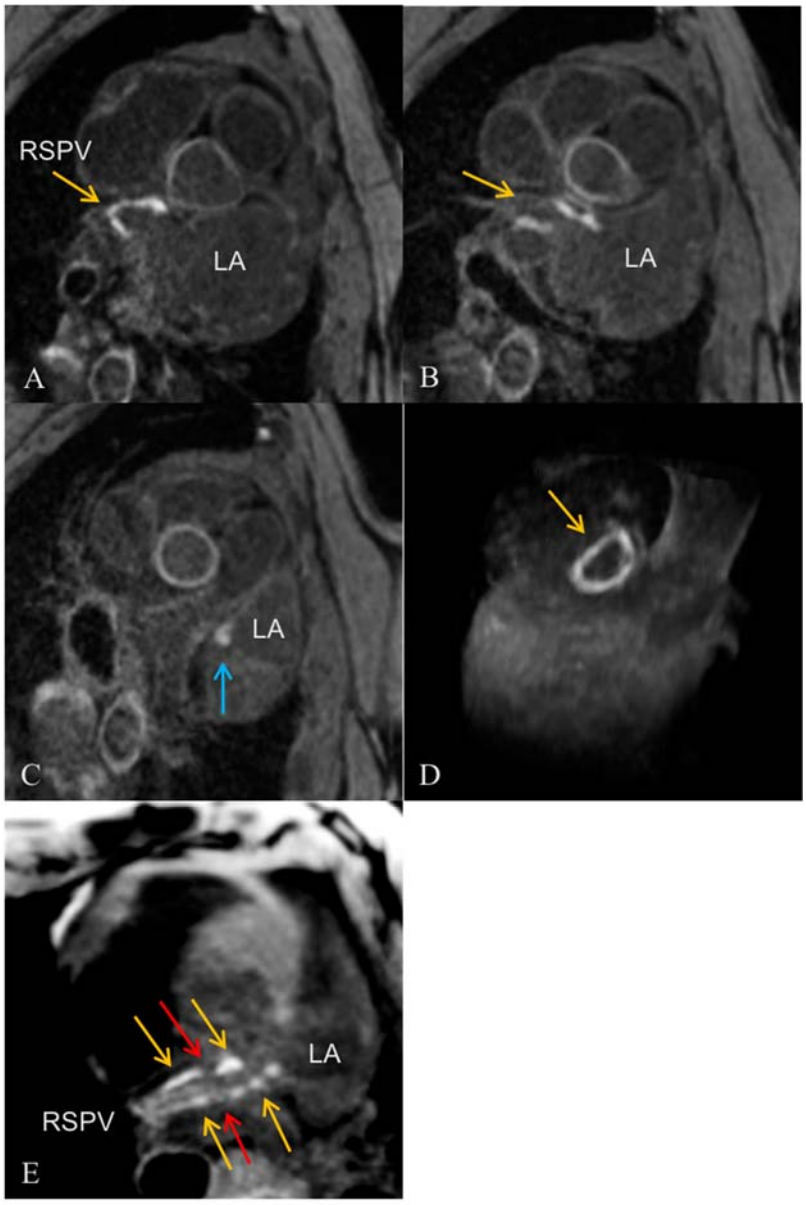

Figure 1. Inversion recovery MRI with long-TI after RF ablations in and near RSPV ostium. (A,B) After a successful PV isolation, continuous lines of enhanced ablation lesions are seen in these parallel slices (orange arrows). (C) A separate location in the LA was ablated (blue arrow). (D) When displayed as a 3D volume rendering, the ring formation of the ablations becomes apparent. (E) After an unsuccessful PV isolation, intermittent enhancement is seen (orange arrows) and gaps between ablations are apparent (red arrows).

ID#: 377115

Selective apheresis of C-reactive protein reduces myocardial reperfusion injury in patients with ST-segment elevation myocardial infarction

Tomas Lapinskas, MD[1] Lukas Stoiber, MD[2], Wolfgang Ries, MD[3], Christoph Garlichs, MD[3], Harald Darius, MD[4], Ahmed Sheriff, MD[5], Burkert Pieske, MD[2], Sebastian Kelle, MD[2]

1. Medical Academy, Lithuanian University of Health Sciences, Kaunas, Kauno Apskritis, Lithuania

2. German Heart Center Berlin, Berlin, Berlin, Germany

3. Diakonissenhospital, Flensburg, Germany

4. Department of Cardiology, Angiology, Nephrology and Conservative Intensive Care Medicine, Vivantes Klinikum Neukolln, Berlin, Germany

5. Department of Nephrology and Internal Intensive Care Medicine, Charité-Universitätsmedizin Berlin, Berlin, Germany

Background: Despite optimal myocardial reperfusion therapy using primary percutaneous coronary intervention (PPCI), the morbidity and mortality of ST-segment elevation myocardial infarction (STEMI) patients remain substantial. Cardiovascular magnetic resonance (CMR) is increasingly being used to quantify myocardial infarction (MI) size in studies investigating novel therapies targeting myocardial reperfusion injury. It has been demonstrated that circulating C-reactive protein (CRP) concentration during acute phase of STEMI is an important prognostic biomarker and may have impact on myocardial injury. This study aimed to determine whether the newly developed selective CRP apheresis initiated 24 ± 12 hours after the onset of symptoms could reduce myocardial injury size in patients presenting with acute STEMI.

Methods: Nineteen patients with acute STEMI were randomly assigned to receive CRP apheresis or control protocols after complete coronary revascularization. The primary study endpoint was myocardial injury size, measured by CMR T2-weighted imaging (myocardial edema) and late gadolinium enhancement (LGE) (MI size) in all subjects 5 ± 3 days after admission. The MRI-Core-lab was blinded.

Results: There were no severe apheresis-associated side effects. CRP apheresis reduced MI size (LGE percentage to LV mass) by 69%, when compared with the MI size of control subjects (12.0 ± 8.1 % (n = 12) vs. 38.8 ± 11.4 % (n = 7); p < 0,001). We observed two patients with zero infarct area in the CRP apheresis cohort. There was a trend toward lower extent of myocardial edema as measured by T2-weighted imaging in CRP apheresis group (39.6 ± 23.9 g vs. 61.0 ± 22.7 g; p = 0.100 for CRP apheresis and control group, respectively).

Conclusion: This blinded study demonstrated that in STEMI patients treated with PPCI, CRP apheresis initiated within 24 ± 12 hours after the onset of symptoms, may reduce acute myocardial injury.

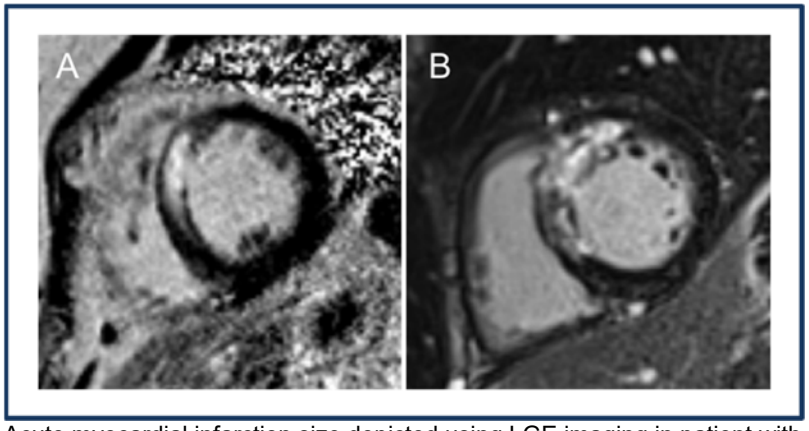

Acute myocardial infarction size depicted using LGE imaging in patient with CRP apheresis (A) and control (B)

ID#: 377191

T1-mapping as a biomarker for myocardial disease in Fabry disease

Alexander Hirsch, MD, PhD[1] Ali Zada, MSc[2], S. Matthijs. Boekholdt, MD, PhD[2], Marieke Biegstraaten, MD, PhD[2], R. Nils. Planken, MD, PhD[2], Maarten Groenink, MD, PhD[2], Mario Maas, MD, PhD[2], Carla E.M. Hollak, MD, PhD[2]

1. Erasmus Medical Center, Netherlands

2. Academic Medical Center, Netherlands

Background: In Fabry disease, better markers of disease progression are needed to refine guidelines on initiation and cessation of enzyme replacement therapy (ERT). Native T1 is decreased in Fabry patients and may be a good measure of cardiac involvement. In this study we assessed T1 in a relatively large Fabry population and investigated changes over time.

Methods: This study included 114 Fabry patients (245 scans). CMR included native T1 mapping with a Modified Look Locker Inversion recovery sequence and late gadolinium enhancement (LGE). T1 was measured on a basal short axis slice in the septum and in the inferolateral segment. Fabry patients were compared with hypertrophic cardiomyopathy (HCM) patients (n=20) and healthy controls (n=30). Linear mixed models were used to analyse the influence of baseline factors on the change of septal T1 over time.

Results: Mean septal T1 was 895±55ms in Fabry disease (age 40±15, 35% male) vs. 1015±42ms in HCM ($p<0.001$) and 984±30ms in controls ($p<0.001$). In Fabry disease, septal T1 was lower in men vs. women (870±56ms vs. 909±49ms, $p<0.001$) and lower in patients treated with ERT vs. untreated (881±55ms vs. 909±52ms, $p=0.01$). Of all patients, 39% were LGE+ and septal T1 was lower in these patients (LGE+ 863±49ms vs LGE- 916±49ms, $p<0.001$). However, inferolateral T1 was higher (968±69ms vs 912±48ms, $p<0.001$). In 71 Fabry patients ≥2 CMR studies were available with mean follow-up (FU) of 2.4±1.1 years and 2.9 scans/patient (range 2-5). There was a trend for an increase in inferolateral T1 over time (baseline 931±67ms, FU 941±70ms, $p=0.06$) but no change in septal T1 was observed (baseline 891±58ms, FU 894±57ms, $p=0.97$). Age, gender, and ERT were not associated with change of septal T1. However, in linear mixed model, including age, gender, ERT, and LGE, the change of septal T1 over time was different in LGE+ vs. LGE- patients (p-value for interaction=0.02). Septal T1 change was +2.9 ms/year in LGE+ patients vs. -2.2 ms/year in LGE-. This difference was even stronger in the inferolateral segment.

Conclusion: Native T1 was clearly decreased in this large cohort of Fabry patients, confirming it to be good biomarker for myocardial involvement. No overall change in septal T1 during 2.5 years was observed, but change in T1 in patients with or without LGE was different. LGE+ patients, with more advanced disease, had an increase in septal T1 compared to LGE- patients, suggesting partial pseudonormalization due to fibrosis even in the septum.

ID#: 377593

Impact of aortic geometrical characteristics on abnormal flow pattern in the proximal descending aorta in Marfan patients: a 4D flow MRI study

Andrea Guala[1]Lydia Dux-Santoy[2], José F. Rodríguez-Palomares, MD, PhD[1], Aroa Ruiz-Muñoz, MSc[3], GIULIANA MALDONADO, MD[4], Nicolas Villalva, MD[2], Ruben Fernandez-Galera, MD[3], Filipa X. Valente, MD[4], Laura Gutierrez, MD[3], Laura Galian, MD[3], David Garcia-Dorado, MD, PhD[3], Arturo Evangelista[3], Gisela Teixido-Tura, MD, PhD[2]

1. Hospital Universitari Vall d´Hebron. Vall d'Hebron Institut de Recerca. Universitat Autònoma de Barcelona, Barcelona, Catalonia, Spain

2. Hospital Universitari Vall d´Hebron. Vall d'Hebron Institut de Recerca. Universitat Autònoma de Barcelona, Catalonia, Spain

3. Hospital Universitari Vall d´Hebron. Vall d'Hebron Institut de Recerca. Universitat Autònoma de Barcelona, Spain

4. Hospital Universitari Vall d´Hebron. Vall d'Hebron Institut de Recerca. Universitat Autònoma de Barcelona, Barcelona, Spain

Background: Marfan syndrome (MFS) is a hereditary connective tissue disorder caused by mutation in the FBN1 gene. MFS typically presented diseases of the ascending aorta (AAo), (aortic dilation or type A dissection). Improvements in the management of the AAo in MFS has recently led to a marked increase in life expectancy. As a result, disease of the descending aorta (DAo) has emerged as a clinical issue in these patients. Recent studies in MFS have revealed the existence of abnormal vortex in the proximal DAo, with consequent lower wall shear stress (WSS) in the inner area, which were related to local dilation. However, any study has investigated the origin of these vortices. The aim of the present investigation was to investigate the relationship between aortic geometry and abnormal flow characteristics in the thoracic aorta of MFS.

Methods: Fifty-tree confirmed MFS patients were prospectively included from our Aortic unit. Inclusion criteria were: age > 18 years, absence of congenital heart diseases, aortic valve disease and contraindication for MRI. Also, 40 age-matched healthy volunteers (HV) were recruited. All participants underwent non-contrast-enhanced 4D flow-MRI, obtaining flow field and angiography. Geometric and flow parameters were determined at 20 planes through the thoracic aorta from sinotubular junction to proximal DAo. Geometric parameters (diameter, ellipticity and curvature) and flow characteristics (in-plane rotational flow IRF, systolic flow reversal ratio SFRR) were evaluated (see figure 1).

Results: Aortic diameters were significantly-larger in MFS in the proximal AAo ($p<0.001$) and in the proximal DAo ($p=0.028$) compared to HV, while no differences were found in the remaining region. Furthermore, ellipticity was increased and peak of aortic curvature was larger and more distal in MFS compared to controls (figure 2) Rotational flow (IRF, related to helicity) was reduced in MFS patients in the majority of the thoracic aorta, while systolic flow reversal ratio (SFRR, related to vortices) was increased in the proximal AAo and DAo. Bivariate correlation showed statistically-significant inverse relation between arch ellipticity ($R=-0.34$, $p=0.016$) as well as proximal DAo peak curvature ($R=-0.35$, $p=0.015$) and arch IRF. Maximum proximal DAo diameter was negatively correlated with local IRF ($R=-0.3$, $p=0.038$) and positively correlated with local SFRR ($R=0.605$, $p<0.001$)

Conclusion: Abnormal aortic ellipticity and curvature were evident in MFS patients and related to a reduction of flow helicity and increase of vorticity in the DAo. Longitudinal studies are needed to investigate the role of aortic geometry and flow distortion on the adverse clinical evolution of these patients

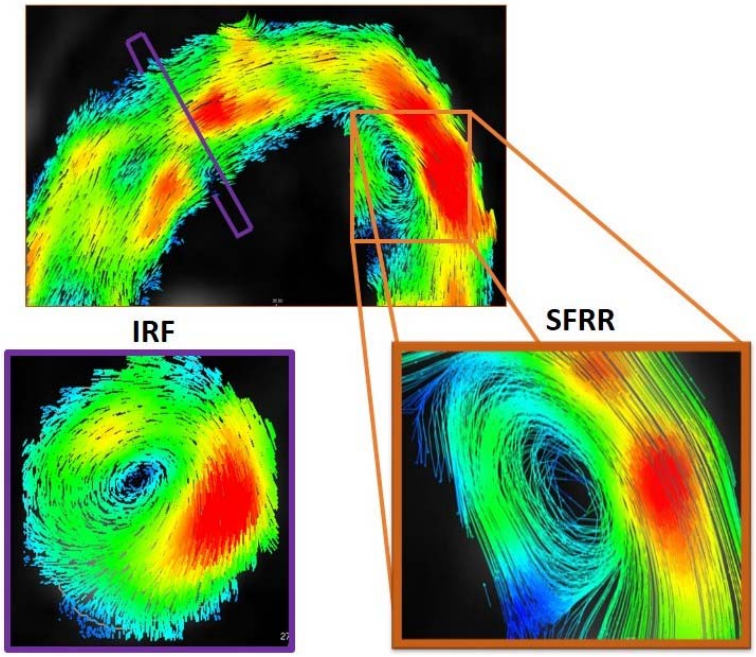

Figure 1: Visualization of in-plane rotational flow (IRF, bottom-left) and through-plane rotational flow (here measured with the systolic flow reversal ratio, bottom-right)

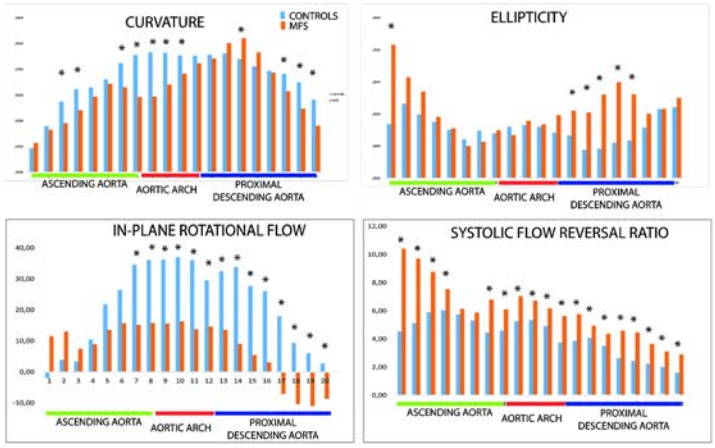

Figure 2: Curvature (top-left), ellipticity (top-right), IRF (bottom-left) and SFRR (bottom-right) at 20 planes in the thoracic aorta.

ID#: 377646

LA strain as an early imaging biomarker of Cardiotoxity: Cardiotox - CMR sub-study

Anna B. Reid, MBChB[1] Wendy Gamlin, BSE[2], Kim Linton, MBChB PhD[3], John Radford, MD FRCP[4], Matthias Schmitt, MD PhD[5], Laura Cove-Smith, MBChB PhD[6]

1. University Hospital of South Manchester, Liverpool, United Kingdom

2. University Hospital of South Manchester, Manchester, England, United Kingdom

3. University of Manchester, United Kingdom

4. The Christie NHS Foundation Trust, United Kingdom

5. University Hospital of South Manchester, United Kingdom

6. The Christie NHS Foundation Trust, Manchester, United Kingdom

Background: Anthracyclines remain an effective 1st line treatment for lymphoma and breast cancer but cardiotoxicity impacts on long term cardiovascular morbidity and mortality following treatment. There is pressing need to identify those at greatest risk of long term complications both in order to implement preventive strategies and tailor cost-effective surveillance. We previously established a rat model of progressive doxorubicin induced cardiomyopathy (Ref; Toxicol sciences 2014; 140(1)3-15) which demonstrated early atrial myopathy which correlated with changes in E/A ratio (phase contrast velocity CMR). We therefore decided to assess LA strain as an imaging biomarker in patients undergoing first line function as a marker of early cardiotoxicity.

Methods: 30 patients with no significant cardiac history receiving first line anthracycline-based chemotherapy underwent CMR at 1.5T (Phillips, the Netherlands) at baseline, half way through (mid-chemo), and at 4-6 weeks (post-chemo) (table 1). LV volumes were analysed from short axis SSFP cine-stack. Biplane LA volumes were obtained from 4- and 2-chamber SSFP cine images (cmr42, Circle Cardiovascular Imaging Inc., Calgary, Canada). Mean atrial strain and strain-rate parameters were also derived from these sequences using dedicated CMR feature tracking software (Diogenes® TomTec, Germany).

Results: There was a reduction in LV ejection fraction in all patients (mean reduction 10.5% ± 12.8%, $p<0.00001$). There was a trend towards increased LA volumes but this did not reach statistical significance (figure 1). There was a significant reduction in left atrial peak strain and other parameters of reservoir and conduit function (table 2). Whilst a trend towards reduced volumetric assessments of LA function, particularly reservoir function, was observed, this did not reach statistical significance. By contrast, booster pump function, which typically reflects reduced LV compliance, was not affected.

Conclusion: Anthracycline-based chemotherapy effects both ventricular and atrial function. Markers of reservoir and conduit function are particularly affected, reflecting deterioration in LA compliance. Strain imaging may be a more sensitive tool for the early identification of patients likely to develop longer-term cardiomyopathies.

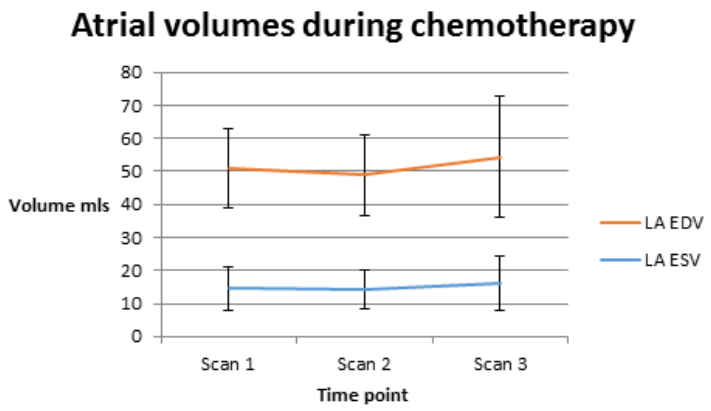

Changes in LA volumes during chemotherapy

Table 2: Changes in LA function with first line-anthracycline based chemotherapy

	Scan 1	Scan 2	Scan 3	p-value
LA Min (ml/m^2)	14.5 ± 6.5	14.1 ± 5.9	16.1 ± 8.2	0.06
LA Max (ml/m^2)	36.4 ± 12.0	34.7 ± 12.1	38.4 ± 18.5	0.25
LA Pre-A Contraction Volume (ml/m^2)	23.4 ± 9.1	22.5 ± 9.8	24.9 ± 11.7	0.16
Total Ejection Fraction (%)	60.8 ± 9.5	59.7 ± 7.5	58.6 ± 7.8	0.18
Reservoir				
LA expansion index (%)	1.68 ± 0.62	1.57 ± 0.51	1.51 ± 0.53	0.08
Total strain (%)	30.5 ± 8.8	26.8 ± 6.5	24.4 ± 5.6	0.002
Peak systolic strain rate (-1)	1.26 ± 0.39	1.15 ± 0.30	0.97 ± 0.32	0.001
Conduit				
Passive Ejection Fraction (%)	36.2 ± 11.7	36.2 ± 12.5	34.7 ± 11.1	0.28
Passive Strain (%)	16.2 ± 5.4	14.0 ± 5.3	12.1 ± 4.8	0.0002
Peak early negative strain rate (-1)	-1.0 ± 0.36	-0.84 ± 0.33	-0.75 ± 0.35	<0.0001
Booster Pump				
Active Ejection Fraction	38.2 ± 10.6	35.9 ± 10.0	36.1 ± 9.1	0.25
Active Strain (%)	14.3 ± 5.9	12.8 ± 4.2	12.2 ± 3.9	0.11

Peak late negative strain rate (-1)	-1.26 ± 0.42	-1.26 ± 0.42	-1.13 ± 0.38	0.23

Table 1: Patient Demographics

Baseline demographic		**Number (%)**
Gender	Male	14 (47)
	Female	16 (53)
Age	Range (years)	22-88
	Mean (years)	57
Ethnicity	White	28 (93)
	Afro-Carribbean	1 (3)
	Asian	1(3)
Diagnosis	NHL	19 (63)
	HL	6 (20)
	Breast Cancer	5 (17)
Performance Status	0	20 (67)
	1	10 (33)
Previous Chemotherapy	No	27 (90)
	Yes	3 (10)
Mediastinal XRT	Yes	1 (3)
	No	29 (97)
Chemotherapy Regimen	R-CHOP	19 (63)
	ABVD	6 (20)
	FEC-T	5 (17)
Cancer stage	No cancer (adjuvant)	5 (17)
	1	7 (23)
	2	6 (20)

	3	5 (17)
	4	7 (23)
Treatment Intent	Curative	23 (77)
	Adjuvant	5 (17)
	Palliative	2 (7)
Response (end of treatment)	Complete	20 (67)
	Partial	5 (17)
Disease Status end of study	Remission	26 (87)
	Relapse/progressed	4 (13)

ID#: 378151

Stop drawing circles! Deep learning for automating volumetric analysis

Rhodri Davies, MRCP, PHD[1] Thomas Treibel, PhD[2], Anish N. Bhuva, MRCP MBBS[3], Gabriella Captur, MD PhD MRCP MSc[4], Charlotte Manisty, MRCP PhD[5], Hui Xue, PhD[6], Peter Kellman, Ph.D.[6], James C. Moon, MD[2]

1. Barts Heart Centre, London, United Kingdom, CARDIFF, Wales, United Kingdom

2. Barts Heart Centre, England, United Kingdom

3. Barts Heart Centre and Institute of Cardiovascular Science, UCL., London, England, United Kingdom

4. Barts Heart Centre, London, England, United Kingdom

5. Barts Heart Centre and University College London, United Kingdom

6. National Heart, Lung, and Blood Institute, Bethesda, MD

Background: Delineating the myocardial borders is a key step in volumetric CMR analysis. This is typically done as a post-processing by drawing contours on short axis slices. Semi-automated tools help, but this remains a time-consuming, tedious, error-prone and subjective process with impaired reproducibility. Deep learning using convolutional neural networks has revolutionised automatic image analysis. In many domains, recent results on large datasets show their performance matches human efforts. Motivated by promising results from a recent Kaggle.com segmentation competition, we develop a novel deep neural network to automatically segment CMR short axis stacks.

Methods: A fully convolutional deep neural network was built based on an encoder-decoder architecture. We expose the cyclic nature of cardiac motion by regularising candidate segmentations to vary smoothly between frames across the cardiac phase. An ensemble of models, built using different network architectures, was used to avoid overfitting to the training data. Multiple sources of training data, including two datasets from the Cardiac Atlas Project was used to avoid overfitting to data from a particular MRI scanner. In total, 195 patient volumes studies, acquired at 1.5T and 3T were included, giving a total of 2432 images for training. Data augmentation was achieved using a statistical model of appearance. Quantitative evaluation was performed by k-fold leave-N-out cross-validation (with N=500, k=6), using two metrics (Dice, and mean perpendicular distance) to compare the automated segmentations to the “ground truth” manually-labelled contours.

Results: A mid-range GPU took 12 hours to train each model and 3 seconds to segment all short axis cines from a single patient. Figures 1 and 2 show the results of running the algorithm on an unseen (ie it was not in the training set) CMR study. Quantitative results are tabulated in figure 3.

Conclusion: We have applied a novel deep neural network to automate CMR volumetric analysis. The method produces near human-level performance. Our next step is to implement the method on the scanner using the Gadgetron framework to compute the contours *in line* so that they are presented to the user along with the raw images permitting post-hoc user editing, if necessary.

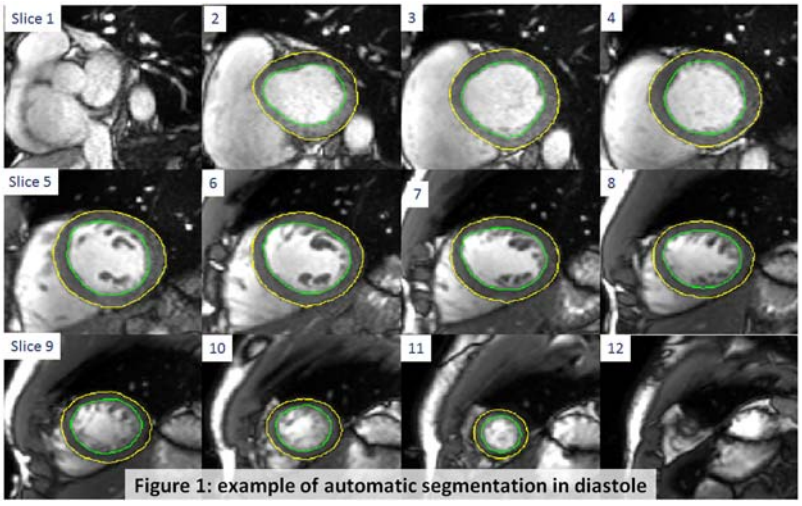

Figure 1: example of automatic segmentation in diastole

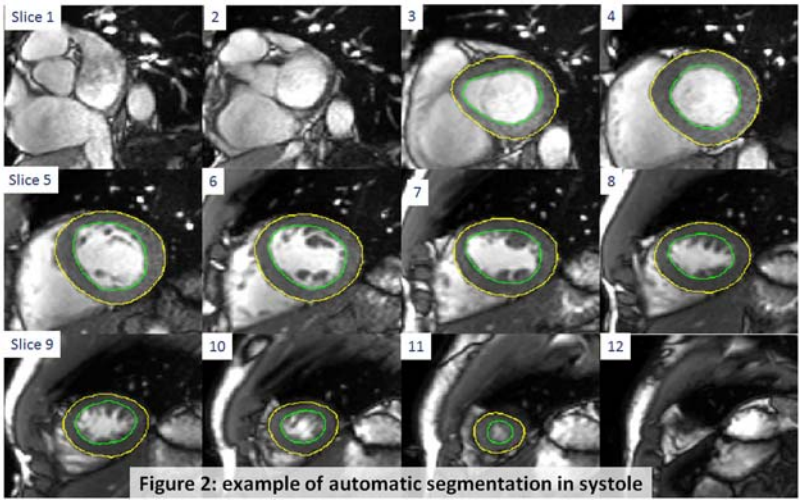

Figure 2: example of automatic segmentation in systole

	DICE (1=perfect agreement)	Mean perpendicular distance (0=perfect agreement)
Endocardial border	0.92	1.5 mm
Epicardial border	0.94	1.1 mm

Figure 3. Quantitative evaluation

ID#: 378322

Diffuse interstitial fibrosis is associated with reduced myocardial strain in heart failure with preserved and reduced ejection fraction

Xiaodan Zhao, PhD[1] Shuo Zhang, PhD[2], Yi Ying Han, BSc[3], David Sim, MBBS, MRCP[1], Fazlur Rehman Jaufeerally, MBChB[4], Arthur Mark Richards, MBChB, MD (Distinction), PhD, DSc, FRACP, FRCP,FAHA, FRSNZ[5], Seet Yoong Loh, MBBS, MRCP, M.Med [6], Dinna K.N. Soon, MBBS, MRCP, FAMS[7], Sheldon S. G. Lee, MBBS[8], Angela S Koh, MBBS, MPH, MMed, MRCP, FESC, FACC[1], Carolyn SP Lam, MBBS, PhD, MRCP, MS, FACC, FAMS, FESC[1], Liang Zhong, PhD[9], Ru San Tan, MBBS, MRCP[10]

1. National Heart Centre Singapore, Singapore

2. Philips Healthcare, Singapore, Singapore

3. Clinical Imaging Research Centre, Singapore

4. Singapore General Hospital; Duke-NUS Medical School, Singapore

5. National University Hospital, Singapore

6. Tan Tock Seng Hospital, Singapore

7. Khoo Teck Puat Hospital, Singapore

8. Changi General Hospital, Singapore

9. National Heart Centre Singapore; Duke-NUS Medical School, Singapore

10. National Heart Centre Singapore; Duke-NUS Medical School, Singapore, Singapore

Background: Myocardial fibrosis underlies cardiac mechanical dysfunction in heart failure (HF). Emerging cardiovascular magnetic resonance (CMR) techniques like mapping of left ventricular (LV) myocardial T1 and extracellular volume (ECV), and feature-tracking of LV-blood borders, can quantify LV diffuse fibrosis and myocardial strain, respectively. We aimed to study the relationships between LV native T1, ECV and strain in HF patients with preserved (HFpEF) and reduced ejection fraction (HFrEF).

Methods: HF patients from 6 centers in the country were prospectively enrolled to undergo CMR on a single 3.0T scanner (Philips, Ingenia) that was used throughout the study. In addition to late gadolinium enhancement (LGE) imaging for detection of focal macrofibrosis, native and post-contrast T1 mapping were performed using standard MOLLI imaging sequences with optimized with a second-based scheme at the mid and basal left ventricular (LV) short-axis (SAX) levels. Typical imaging parameters were: field of view 340 × 290 mm^2, acquired pixel size 1.8 × 1.8 mm^2 interpolated to 1.0 x 1.0 mm^2, slice thickness 8 mm; TR/TE 2.8ms/1.38 ms; flip angle 35°, minimal inversion time 87.7 ms; SENSE imaging factor 2. ECV maps were generated after applying off-line image motion correction and co-registration, as well as same-day hematocrit results. For comparison between HFpEF and HFrEF groups, pre-specified regions of interest for T1 and ECV analyses included (1) the entire myocardium within either the mid or basal SAX slice; remote myocardial tissue without LGE at the (2) LV septum; and (3) LV lateral wall. Global circumferential strain (GCS) was analysed from three SAX slices (basal, mid and apical) and three long axis (LAX) views (2-, 3- and 4-chamber) using a commercially-available post-processing workstation (Qstrain; Medis) (Figure 1). Within either HFpEF or HFrEF group, subjects were stratified into subgroups with and without focal lesions (i.e. LGE) for analysis. Analysis of variance (ANOVA) and linear regression analyses were performed; p-value smaller than 0.05 indicated statistically significant difference.

Results: 107 HF patients (27 HFpEF and 80 HFrEF) were enrolled (mean age 57±11 years; male-female ratio 85:22). GCS for both basal and mid SAX slices, and GLS from 3 LAX slices were significantly lower in HFrEF compared with HFpEF. No difference was found between HFpEF subgroups with and without focal LGE (**Table 1**). Among subjects without focal LGE (13 HFpEF; 28 HFrEF), there were moderate linear correlation between strains and respective native T1 measured at the entire SAX, septum and lateral wall (GCS: r=0.455, r=0.597, r=0.421; GLS: r=0.409, r=0.500, r=0.437, all p<0.05, Figure 2).

Conclusion: Diffuse fibrosis is associated with reduced strain. HFrEF exhibit more pronounced strain impairment than HFpEF for the same fibrosis extent. The correlation between strain and fibrosis appeared stronger when fibrosis was assessed with native T1 versus ECV, and when measured at the septum versus the lateral wall, implying that septal native T1 measurement may be suitable for noninvasive detection of diffuse fibrosis, monitoring of progression and response to treatment in HF patients.

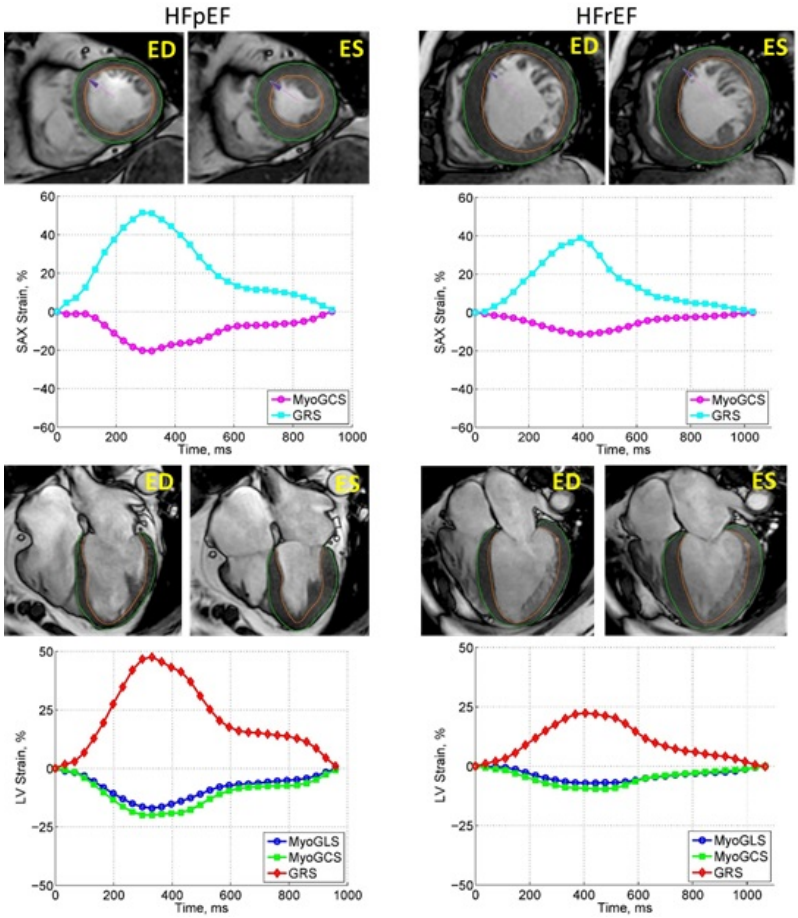

Figure 1. Short- (top) and long-axis (bottom) cine CMR images at end-diastole (ED and end-systole (ES) frames in HFpEF (left) and HFrEF subjects (right). Change in lengths of the endocardial contours (red) were tracked for calculation of global circumferential (GCS) and longitudinal strains (GLS) in the short- and long-axis slices, respectively. Corresponding strain-time plots are appended below the cine images. Global radial strain (GRS) plots are shown, but not analysed

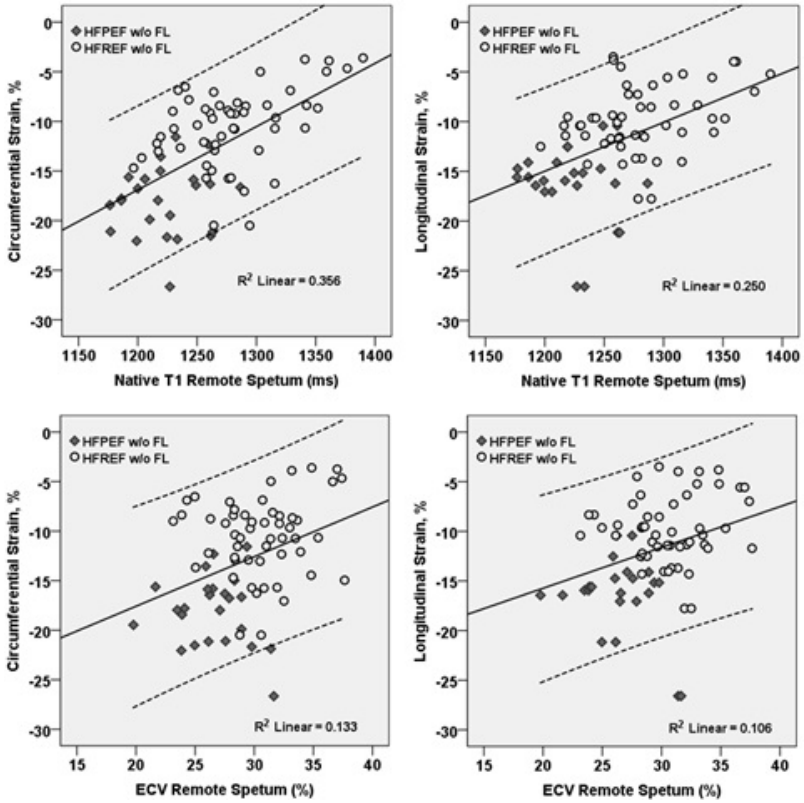

Figure 2. Correlation between global circumferential (left) and longitudinal strain values (right) and native T1 (top row) and extracellular volume (bottom row) measured at the septum in subjects without focal late gadolinium enhancement lesions (FL). Dotted lines denote 95% confidence intervals.

Table 1. Strain parameters among HFpEF and HFrEF subjects with (+) and without (-) focal late gadolinium enhancement lesions.

Strain	HFpEF Focal lesion + (n = 14)	HFpEF Focal lesion - (n = 13)	HFrEF Focal lesion + (n = 52)	HFrEF Focal lesion - (n = 28)	ANOVA P value
Basal GCS, %	-19.1 ± 4.4	-19.4 ± 3.5	-10.9 ± 3.5*#	-11.6 ± 4.2*#	<0.001
Mid GCS, %	-18.6 ± 2.7	-18.7 ± 3.4	-9.0 ± 3.6*#	-10.5 ± 3.5*#	<0.001
LV GLS, %	-16.2 ± 2.2	-16.3 ± 4.1	-8.2 ± 3.5*#	-9.9 ± 3.3*#	<0.001
GCS: global circumferential strain; GLS: global longitudinal strain; LV: left ventricle. * P < 0.05 between subgroup 1 and 2 or 3 or 4; # P < 0.05 between subgroup 2 and 3 or 4.					

ID#: 370485

The importance of Magnetization Transfer on simulation-based quantitative Magnetic Resonance Imaging techniques

Christos Xanthis, PhD[1] Sebastian Bidhult, MSc[2], Andreas Greiser, Ph.D[3], Kelvin Chow, PhD[4], Richard Thompson, PhD[5], Håkan Arheden, MD PhD[6], Anthony H. Aletras, Ph.D.[7]

1. Lund University, Skane University Hospital, Department of Clinical Physiology, Lund, Sweden, Skane Lan, Sweden

2. Lund University, Department of Clinical Sciences Lund, Clinical Physiology, Skane University Hospital, Lund, Sweden; Faculty of Engineering, Lund University, Department of Biomedical Engineering, Lund, Sweden, Skane Lan, Sweden

3. Siemens Healthcare GmbH, Erlangen, Germany, Erlangen, Bayern, Germany

4. Siemens Medical Solutions, Chicago, IL

5. Department of Biomedical Engineering, University of Alberta, AB, Canada

6. Lund University, Skåne University Hospital, Department of Clinical Sciences Lund, Clinical Physiology, Lund, Sweden, Lund, Sweden

7. Aristotle University of Thessaloniki/Lund University, Thessaloniki, Thessaloniki, Greece

Background: Recent studies in the field of simulation-based quantitative cardiovascular Magnetic Resonance Imaging (MRI) have shown simultaneous quantification of both T1 and T2 maps (Xanthis,2015 and Hamilton,2017). However, these studies do not investigate the effect of Magnetization Transfer (MT) on the T1/T2 estimates and are usually validated on phantoms where the MT effect is small. The main aim of this study was to investigate the effect of MT on simulation-based quantitative MR techniques.

Methods: A 5sec(3sec)3sec MOLLI prototype sequence (Kellman,2014) was modified to increase its T2 sensitivity. The duration of the sinc-shaped RF pulse of the bSSFP-readout was increased from 480μsec to 1050μsec to allow for excitation flip angles up to 180^{o} and a 5.12msec tangent/hyperbolic tangent adiabatic IR pulse was selected. The incorporation of advanced MR simulations was achieved through the SQUAREMR framework (Xanthis,2015). To investigate the performance of the SQUAREMR-MOLLI on the estimation of the T1 and T2 values in the absence of an MT effect, a set of three phantoms with no macromolecular content (aqueous solutions of 0.1mM, 0.2mM and 0.33mM MnCl2) was constructed. To investigate how the SQUAREMR-MOLLI performed with an increasing MT effect, a second set of three phantoms with an increasing macromolecular content (agar-gel phantoms of 2%, 4% and 8% agar) was constructed. T1 and T2 reference values were measured.

Results: In the manganese phantoms, the SQUAREMR-MOLLI demonstrated an increasing T2 accuracy with the increasing bSSFP excitation flip angle whereas the T1 accuracy remained the same across the entire range of the bSSFP excitation flip angles (mean T1 difference = 12±8msec). In the agar-gel phantoms, the phantom with the least agar gel concentration (agar 2%) presented a trend closer to the one appeared in the manganese phantoms whereas the phantoms with agar 4% and agar 8% presented larger T1 and T2 differences (figure1).

Conclusion: Changes on the flip angle of the bSSFP excitation pulse introduced different amounts of T2 modulation on the MR signal but also induced different MT effects on the phantoms with macromolecular content. The increased T2 modulation was confirmed on the phantoms with no MT effect where the SQUAREMR-MOLLI demonstrated an increasing T2 accuracy with the increasing bSSFP excitation flip angle. The increased MT effect was confirmed in the agar-gel phantoms. This study demonstrates for the first time that MT plays an important role in the simulation-based quantitative MR studies and points out the necessity of incorporating the study of MT in future techniques.

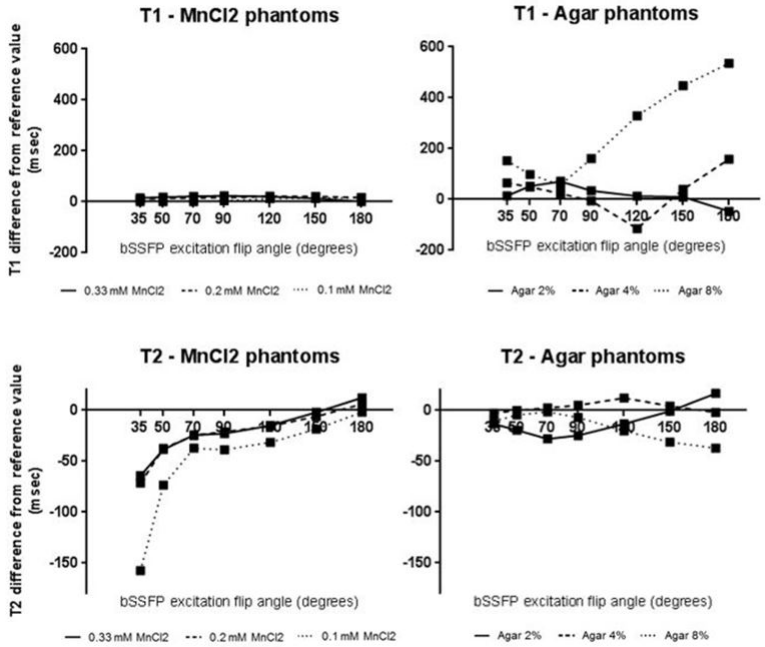

T1 and T2 differences of the SQUAREMR-estimated values from the reference values for each individual phantom, variant of the inversion pulse (2.56msec tangent/hyperbolic tangent adiabatic pulse, 5.12msec tangent/hyperbolic tangent adiabatic pulse and 10.24msec hyperbolic secant adiabatic pulse) and bSSFP excitation flip angle (35o, 50o, 70o, 90o, 120o, 150o and 180o) of the SQUAREMR-MOLLI. All experiments were performed on a Magnetom Aera 1.5T scanner (Siemens Healthcare, Erlangen, Germany). T1 and T2 reference values were measured with Inversion Recovery Spin Echo (Inversion Times = 21msec-8sec) and Spin Echo (TE:6-1000msec), respectively (TR>10msec). The reference T1/T2 values (in msec) of the phantoms were: MnCl2 0.1mM = 1387/220, MnCl2 0.2mM = 913/116, MnCl2 0.33mM = 639/72, Agar 2% = 2294/71, Agar 4% = 1892/39 and Agar 8% = 1218/19.

ID#: 371470

Myocardial scar imaging using contrast steady state in a chronic porcine infarct model

John Whitaker, BM BCh[1] Radhouene Neji, PhD[2], Rahul K. Mukherjee, MBBS[3], James Harrison, MRCP PhD[4], Steven Williams, MD PhD[5], Henry Chubb, MRCP MRCPCH[6], Louisa O'Neill, MBChB[7], Justo Julia[7], John Silberbauer, MD[8], Matthew Wright, MBBS PhD[7], Sébastien Roujol, PhD[3], Tevfik F. Ismail, PhD MRCP[9], Mark O'Neill, MD DPhil[3], Reza Razavi, MD, PhD[3]

1. King's College London/Beth Israel Deaconess Medical Centre, London, England, United Kingdom

2. Siemens Healthcare Limited, Frimley, England, United Kingdom

3. King's College London, London, England, United Kingdom

4. King's College London, England, United Kingdom

5. Kings College Londin, England, United Kingdom

6. Kings college London, England, United Kingdom

7. King's College London, United Kingdom

8. Brighton and Sussex University Hospitals NHS Foundation Trust, United Kingdom

9. King's College London; Guy's and St Thomas' Hospitals NHS Foundation Trust, London, England, United Kingdom

Background: We hypothesised that continuous contrast infusion could be used during late gadolinium enhancement (LGE) imaging to establish a stable myocardial T_1, thereby allowing extended acquisition for high-resolution 3D fibrosis imaging without significant change in inversion times (TI) for blood and myocardium.

Methods: All imaging was performed at 1.5T (MAGNETOM Aera, Siemens Healthcare, Germany). Eight pigs with chronic myocardial infarction were studied. Ten minutes after 0.1mmol/kg gadobutrol (Gd) bolus, TI scout was acquired in a single short axis slice. Clinical standard 2D-LGE scar sequences were acquired in 8 short axis slices using an inversion recovery (IR) sequence with phase-sensitive IR (PSIR) reconstruction (SSFP; linear k-space reordering; TE/TR/α: 1.21ms/3ms/45°; slice thickness: 6mm; in plane resolution: 1.4x1.4mm^2). Fifteen minutes following Gd bolus, 0.0011mmol/kg/min Gd infusion was commenced. TI-scout was repeated at regular intervals. 30 minutes following Gd bolus, isotropic navigator-gated ECG-triggered 3D IR sequence was acquired (SSFP; coronal orientation; linear k-space reordering; TE/TR/α: 1.58ms/3.6ms/90°; gating window = 7mm; resolution 1.2x1.2x1.2mm^3). Scar imaging was reviewed by 2 experienced observers who graded it on a 4 point scale according to image sharpness, image contrast, quality of myocardial nulling, complexity of scar pattern and overall scan quality. Signal-to-noise ratio (SNR) and contrast-to-noise ratio (CNR) were estimated using mean signal within blood, remote (healthy) myocardium and scar and standard deviation of signal within lung.

Results: Contrast steady state (CSS, <5% variation in blood/myocardium TI) was achieved in 7 pigs and maintained for up to 150 minutes (figure 1). Mean acquisition for CSS 3D-LGE imaging was 51 minutes. CSS 3D-LGE imaging was acquired using a total Gd dose of <0.2mmol/kg Gd. SNR_{Scar}, SNR_{Blood} and $CNR_{Scar\text{-}remote}$ was higher in CSS 3D-LGE imaging than the 2D-LGE imaging ($p<0.001$) (figure 3). SNR_{Remote} was lower in the CSS 3D-LGE than the 2D-LGE imaging ($p<0.05$), indicating more effective nulling of the myocardium. There was a significant median increase in sharpness (4.0vs2.5, p=0.026), contrast (4.0vs3.0, p=0.024), appreciation of scar complexity (4.0vs2.5, p=0.038) and overall scan quality (4.0vs2.5, p=0.041) in the CSS 3D-LGE imaging compared to the 2D-LGE imaging (figure 3).

Conclusion: CSS allows extended acquisition to facilitate high-resolution 3D-LGE imaging with improved SNR, CNR and overall image quality. CSS-LGE imaging may be valuable when detailed myocardial substrate assessment is required, for example when planning cardiac electrophysiology procedures. In addition, CSS-LGE imaging provides an experimental model in which post-contrast sequences may be compared with consistent contrast distributions.

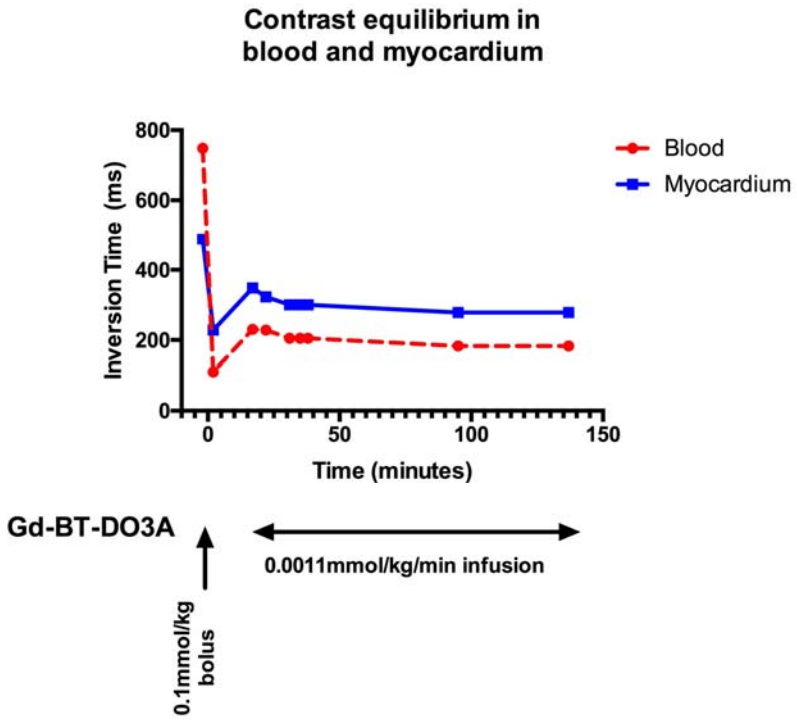

Example of time to inversion (TI) for myocardium and blood pool after gadobutrol (Gd-BT-D03A) bolus followed by infusion.

Multiplanar reconstructions of a 3D-LGE sequence acquired during contrast steady state (CSS).

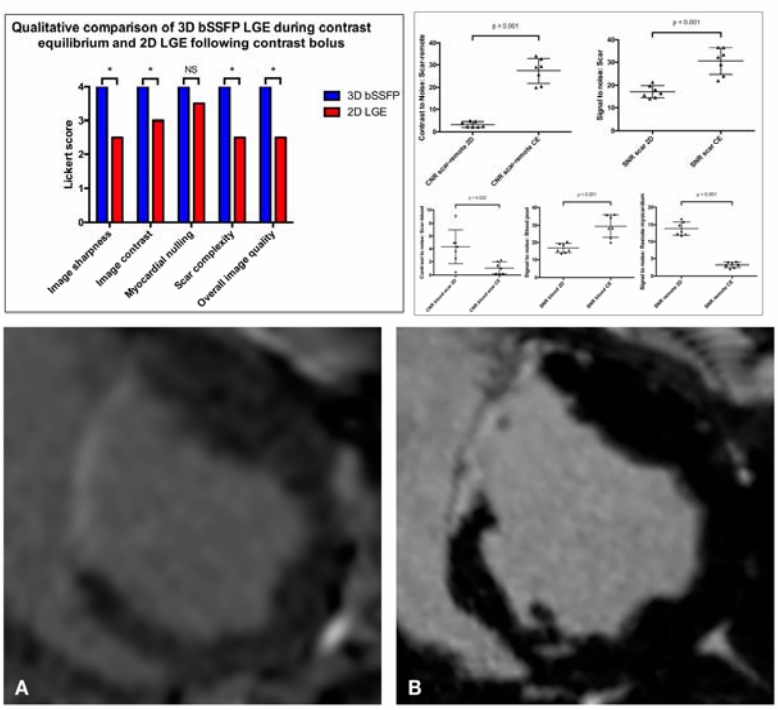

Top left: Qualitative comparison of gadobutrol (Gd) contrast steady state (CSS) 3D-LGE imaging and 2D-LGE imaging acquired following Gd bolus. Median scores from 2 observers are shown and have been compared using a Wilcoxon signed-rank test. Top right: Signal to noise (SNR) and contrast to noise (CNR) ratio compared between Gd CSS 3D-LGE imaging and 2D LGE imaging acquired following Gd bolus. Bottom pane:l: 2D-LGE (A) and CSS 3D-LGE mid ventricular short axis slice from the same pig demonstrating septal scar. Statistical significance is indicated by *($p<0.05$)

ID#: 371369

Clinical Impact of Magnetic Resonance Imaging in Non-Approved Cardiac Devices

Ibrahim M. Saeed, MD[2]Lina Ya'qoub, MD[1], Sanjaya Gupta, MD[2], Stanley Fisher, MD[3]

1. University of Missouri-Kansas City

2. Saint Luke's Mid-America Heart Institute, Kansas City, MO

3. Saint Luke's Marion Bloch Neuroscience Institute, Kansas City, MO

Background: For patients traditionally contraindicated for MRIs due to the presence of non-MR-conditional cardiac implantable electronic devices (CIED), we established the Patient Registry Of Magnetic resonance imaging in Non-Approved Devices (PROMeNADe). This involves significant resources including time for research nurses, electrophysiology staff, informed consent, and device interrogations. It is unknown if these MRIs have a clinical impact on patient care.

Methods: Patients with CIEDs undergoing clinical MRIs were enrolled. IRB-approved informed consent was obtained. Device interrogation was performed before and after each study. Pacemaker-dependent patients were paced asynchronously. Ventricular arrhythmia detections were disabled on ICDs. An ACLS-certified electrophysiologic nurse was present. A survey was sent to referring physicians to assess the clinical utility of MRI results.

Results: Since 09/2015 to 08/2017, 225 patients (74 F) were enrolled (51.8% pacemakers, 33.6% ICDs, 12.3% CRT-D, 2.7% abandoned leads), performing 274 MRIs, with no pt or device-related complications; 50% of surveys (112) were completed; 26% were for cardiac MRIs. Suspected diagnosis and prognosis changed in 25% and 29%, respectively for all studies; and 32% and 36%, respectively, for specifically CMRs. In over half, referring physicians stated the MRI changed planned medical or surgical treatment (see Figure).

Conclusion: Clinical MRIs, including cardiac studies, with non-conditional devices can be performed safely. Given the impact on patient care, our study justifies the extended resources needed in this process.

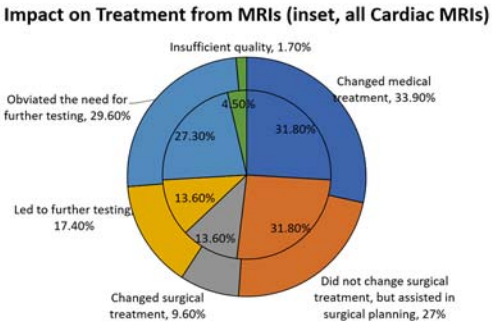

ID#: 371546

Automatic Optimal Frequency Adjustment for High Field Cardiac MR Imaging via Deep Learning

James W. Goldfarb, PhD[1] Joshua Cheng, RT[2], Jie Jane. Cao, MD, MPH[3]

1. St Francis Hospital

2. St Francis Hsopital

3. St Francis Hospital, NY

Background: Cardiac bSSFP CINE imaging at magnetic fields above 1.5T remains very sensitive to the setting of the synthesizer frequency. Suboptimal setting of this frequency causes severe banding, flow artifacts and artifactual signal loss and brightness. These artifacts often render images unsuitable for clinical decisions. The current solution is to obtain several images over a range of frequencies (a frequency scout) and select an optimal frequency by visually evaluating the images. Although this technique can be effective, there are several drawbacks. Firstly, it requires additional technologist training beyond the typical cardiac MR training. Also, the decision is time consuming because the optimal frequency varies significantly across imaging planes (HLA, VLA, LVOT and short-axis). Additionally, the decision can be quite subjective. The observer must pick a frequency optimal across the entire heart while excluding artifacts from implanted metal and flow. The purpose of this study was to develop and evaluate a deep learning approach for automatic cardiac MR frequency tuning at high fields.

Methods:

This study was performed at 3Tesla with a clinical Siemens Skyra imager. Frequency scouts from 100 patients referred for clinical evaluation were included in this IRB approved study; including 4 anatomical slice planes (mid short-axis, two-, three-, and four-chamber views). Thirteen images were obtained with frequencies ranging from -150 to 150 Hz with a 25 Hz increment. The 2D bSSFP frequency scout sequence had parameters matching CINE imaging: TR/TE= 2.5/1.25 ms, bandwidth 1095 Hz/pixel and slice thickness=8 mm.
A 3D linear convolutional neural network (CNN) (Figure 1) was used to determine the optimal frequency. The problem is three-dimensional in nature (two in-plane dimensions and one frequency dimension) Keras v2.0 and TensorFlow v1.3 (two open-source software libraries) were used for deep learning implementation. 200 image sets were used for 3D CNN training. The remaining 200 images sets were used for validation and visually inspected for optimal selection of frequency. The performance of the new method was evaluated with Pearson correlation when comparing manual and automated frequency determination.

Results: Training of the deep learning algorithm was performed in 50 epochs with excellent validation accuracy (Figure 2, R^2=0.99). Representative examples of the prospective application of the method are displayed in Figure 3. The frequency offset variance across subjects and imaging planes is well demonstrated. Additionally, the performance in subjects with artificial heart valves and sternal wires was excellent (Figure 3, top and bottom rows).

Conclusion: Deep learning using a 3D CNN is a viable solution for the determination of the center frequency at high fields for cardiac imaging. It can quickly provide similar results to an expert observer. In the future, the strategy may be applicable to improved frequency resolution and to frequency adjustments outside of the frequency scout range. This strategy should make 3T cardiac MR imaging accessible to a wider audience.

Layer (type)	Output Shape	Param #
input_1 (InputLayer)	(None, 1, 13, 208, 208)	0
block1_conv1 (Conv3D)	(None, 64, 13, 208, 208)	1792
block1_conv2 (Conv3D)	(None, 64, 13, 208, 208)	110656
block1_pool (MaxPooling3D)	(None, 64, 13, 52, 52)	0
dropout_1 (Dropout)	(None, 64, 13, 52, 52)	0
block2_conv1 (Conv3D)	(None, 128, 13, 52, 52)	221312
block2_conv2 (Conv3D)	(None, 128, 13, 52, 52)	442496
block2_pool (MaxPooling3D)	(None, 128, 13, 13, 13)	0
dropout_2 (Dropout)	(None, 128, 13, 13, 13)	0
block3_conv1 (Conv3D)	(None, 256, 13, 13, 13)	884992
block3_conv2 (Conv3D)	(None, 256, 13, 13, 13)	1769728
block3_pool (MaxPooling3D)	(None, 256, 6, 6, 6)	0
dropout_3 (Dropout)	(None, 256, 6, 6, 6)	0
flatten (Flatten)	(None, 55296)	0
fc1 (Dense)	(None, 256)	14156032
fc2 (Dense)	(None, 256)	65792
predictions (Dense)	(None, 1)	257

Total params: 17,653,057
Trainable params: 17,653,057
Non-trainable params: 0

Figure 1: 3D Convolutional Neural Network Used for Automatic Frequency Selection

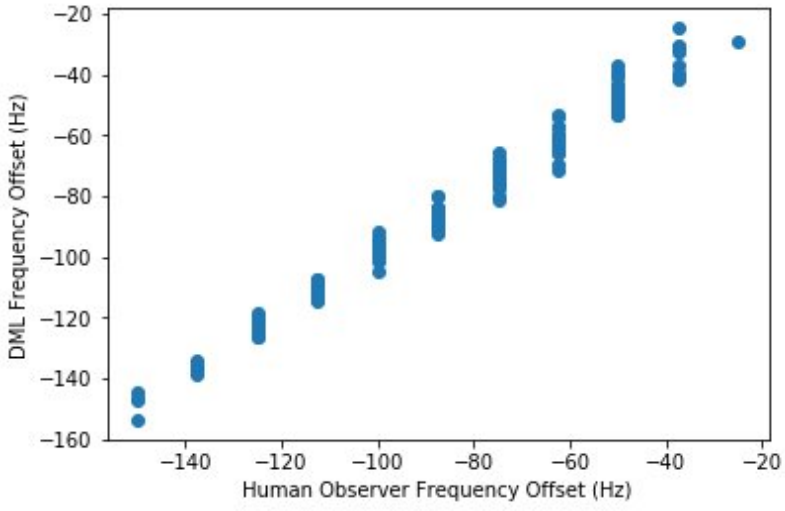

Figure 2: Plot of Automatic vs Manual Frequency Selection (R2=0.99)

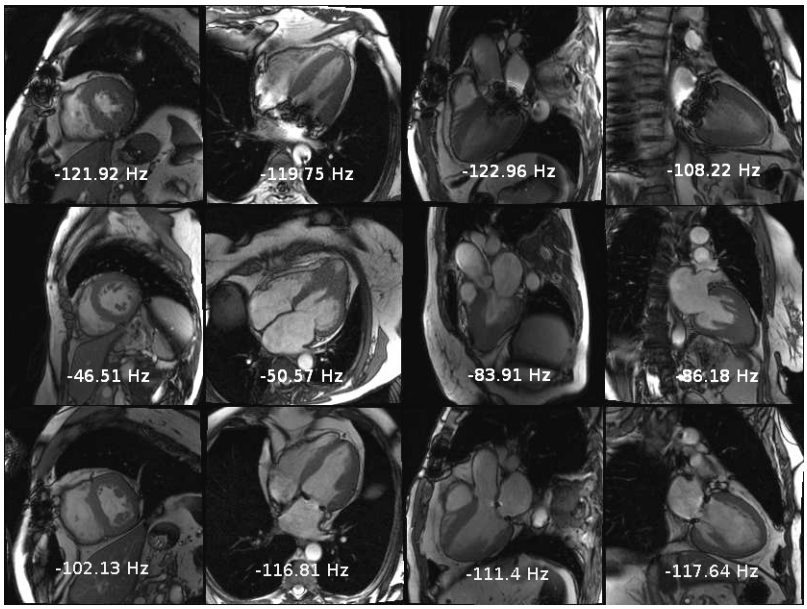

Figure 3: Examples of Automatic Frequency Selection (including two subjects with artificial mitral valves)

ID#: 371955

A novel acquisition strategy for Dark-Blood T1-TSE Imaging improves blood signal suppression, image sharpness, and overall clinical image quality

Wolfgang G. Rehwald, Ph.D.[1] Louis A. Klem[2], Stephen Darty, RT-N,MR; BSRS[3], Nestor Mena, B.A., A.S.[4], George Gamoneda, AS[5], Elizabeth Jenista, Ph.D.[6], David Wendell, PhD[3], Han Kim, MD[6], Gary McNeal, M.S.[7], Raymond J. Kim, MD[3]

1. Siemens Healthineers and Duke Cardiovascular MR Center, Chapel Hill, NC

2. Duke University, Chapel Hill, NC

3. Duke University Medical Center, NC

4. Duke University Hospital, Clayton, NC

5. Duke University Hospital, NC

6. Duke University, Durham, NC

7. Siemens Healthineers, Granbury, TX

Background: High spatial resolution dark-blood (DB) T1-turbo spin-echo (TSE) imaging is important for assessing cardiac morphology and characterizing masses. T1-mapping is helpful in examining diffuse processes, but suboptimal for detecting subendocardial abnormalities due to its limited spatial resolution (single shot technique). Unfortunately, conventional (CONV) TSE requires short TR of 1RR interval for sufficient tissue T1-weighting (T1W), but at most physiologic heart-rates (HR) such short TR prevents blood suppression, particularly at 3T. Long echo-spacing (ES) renders TSE readouts motion-sensitive causing myocardial signal-dropout. Both issues cause poor image quality (IQ) of most CONV T1-TSE images. We created a novel (NOV) T1-TSE acquisition-scheme combining longer blood-TR for complete blood suppression with shorter tissue-TR for optimal tissue T1W and designed readout pulses to shorten ES for reduced motion-sensitivity, while achieving a higher time-bandwidth product (BWTP) for sharper slice profiles.

Methods: Figure 1 shows CONV (1a) and NOV (1b) T1-TSE sequences with typical timing. NOV T1-TSE applies a DB preparation every other RR (blood-TR=2RR), but keeps tissue T1W commensurate with TR=RR by alternating true with dummy readouts. Blood-TR was determined by a devised algorithm (Figure 1). Hanning-filtered sinc pulses with a higher BWTP were truncated below 5% of peak-amplitude to reduce pulse-duration (excitation BWTP 1.6, 732µs, refocusing BWTP 2.3, 1300µs) while keeping their area essentially constant. 4 T1-TSE images of the same spatial and temporal resolution, 2 CONV and 2 NOV, were acquired at 2 locations per patient. Images were graded for IQ (4=excellent, 3=good, 2=poor, 1=non-diagnostic) by experienced readers. Myocardium signal-to-noise-ratio (SNR), blood-SNR and blood-to-myocardium-signal-ratio (BMR) were measured. All comparisons used paired t-tests.

Results: Patients (25F, 28M) had an RR of 916±151ms (MEAN±STDEV). CONV used blood-TR=RR. NOV used blood-TR=2RR by algorithm in all but 1 patient. CONV images required 8 echo trains (ET) in 8 RRs, NOV 6 ETs in 12 RRs. NOV acquisition time increased only 50% despite 100% longer blood-TR, due to faster readout of NOV (21 echoes at 3.94ms ES) vs CONV (16 at 5.27ms ES). NOV provided significantly better IQ (MEAN±SEM 3.58±0.07 vs 2.73±0.09, $p<0.001$) and darker blood by SNR (7.26±0.68 vs 14.65±1.09, $p<0.0001$) and BMR (0.175±0.09 vs 0.35±0.12, $p<0.0001$). CONV and NOV myocardium-SNR was identical (44.28±4.20 vs 44.83±4.44). NOV completely nulled blood magnetization, whereas CONV did not (Figure 1c). DB, sharpness, and overall IQ were drastically improved by NOV (Figure 2).

Conclusion: NOV T1-TSE allows image acquisition with excellent diagnostic quality and high spatial resolution, at any clinically-relevant HR, without affecting myocardium-SNR and T1W. T2-TSE imaging would equally benefit from the described shorter readout pulses.

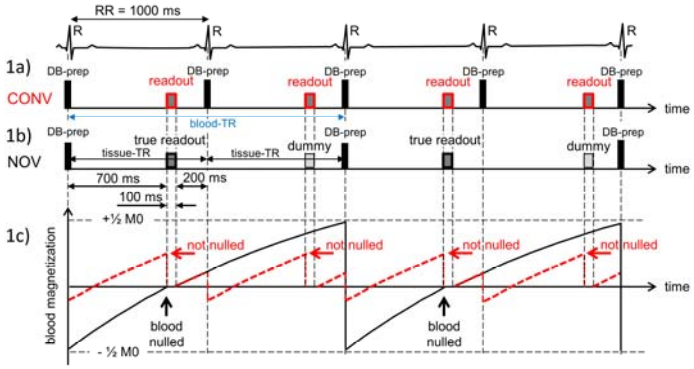

Figure 1a) conventional (CONV) T1-TSE sequence with DB preparation and readout occurring every RR interval, 1b) novel (NOV) T1-TSE sequence with DB preparation occurring every other heartbeat (blood-TR = two RR intervals) and true readouts alternating with dummy readouts (tissue-TR = one RR interval), but acquiring data only during true readouts. Blood-TR is set as a function of RR so that blood is nulled at any HR using the following devised algorithm: blood-TR=RR for RR>1250ms, 2RR for 600ms ≤RR≤1250ms, and 3RR for RR<600ms. 1c) blood magnetization T1-recovery (T1 =1900 ms at 3T) curve for CONV (dashed red) and NOV (solid black) showing failed blood nulling by CONV but excellent blood nulling by NOV.

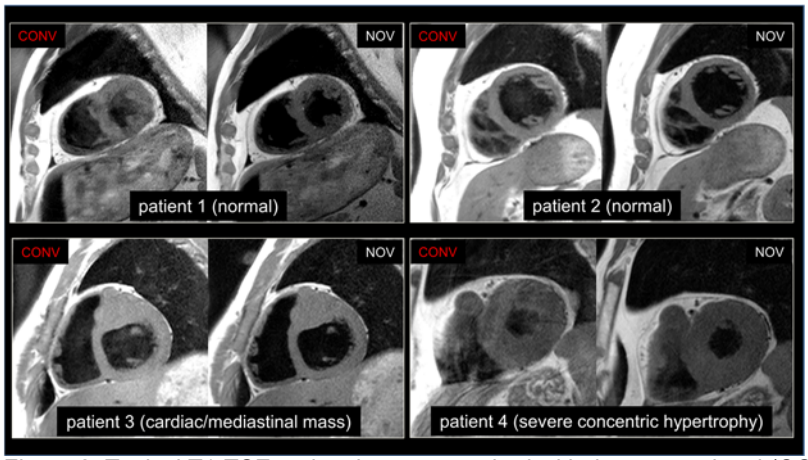

Figure 2: Typical T1-TSE patient images acquired with the conventional (CONV) and novel (NOV) T1-TSE sequence showing better blood suppression, image sharpness, and overall image quality of NOV compared to CONV. Typical parameters were FOV 340x255mm, resolution 1.4x1.4mm, slice thickness 5mm. CONV used TE 11ms and turbo factor (TF) 16, NOV TE 12ms and TF 21. Temporal solution was matched to ≈84ms. Acquisition took 8 (CONV) and 12 (NOV) heartbeats.

ID#: 372108

Novel insights into disease mechanism from in-vivo assessment of creatine kinase kinetics in hypertrophic cardiomyopathy.

Betty Raman, MBBS, FRACP[1] William T. Clarke, MChem, D.Phil[2], Rina Ariga, MBBS, MRCP[3], Masliza Mahmod, MBChB, DPhil[3], Sophia Godsland, MBBS[2], Moritz Jens. Hundertmark, MD[4], Jennie Han, BA [5], Hugh Watkins, FRS FMedSci[3], Christopher T. Rodgers, DPhil[6], Oliver J. Rider, MRCP, DPhil[7], Stefan Neubauer, MD, FRCP[3]

1. University of Oxford, Division of Cardiovascular Medicine, Oxfordshire, England, United Kingdom

2. University Of Oxford Centre for Clinical Magnetic Resonance Research, England, United Kingdom

3. University of Oxford, England, United Kingdom

4. University of Oxford, Department of Cardiovascular Medicine, Oxford, England, United Kingdom

5. University of Oxford, Division of Cardiovascular Medicine, England, United Kingdom

6. University of Oxford, Oxford, England, United Kingdom

7. University of Oxford, United Kingdom

Background:

Hypertrophic cardiomyopathy (HCM) is characterised by adverse remodelling and occasional progression to heart failure, a formidable sequela. The transition from hypertrophy to left ventricular dysfunction may be due to an impaired 'metabolic reserve' determined by creatine kinase (CK) reaction as described by Weiss *et al.* (PNAS, 2006). The CK reaction plays a critical role in maintaining cellular homeostasis, by buffering the production of adenosine triphosphate (ATP) at the myofibril, rapidly converting adenosine diphosphate (ADP) and phosphocreatine (PCr) to ATP when it is required. We therefore sought to characterise CK kinetics in HCM and assess its association with left ventricular hypertrophy and impairment in myocardial contractility.

Methods:

31 non-obstructive HCM patients (47±16 years, 71% male) and 16 (age-, BMI- and gender-matched) healthy controls underwent CMR at 3T including cine, late gadolinium enhanced (LGE) imaging. The pseudo-first-order forward CK rate constant (k_f) was measured with triple repetition time saturation transfer (TRiST) ^{31}P spectroscopy. Myocardial energetics (PCr/ATP) was also assessed by ^{31}P-MRS at rest. Using literature values for ATP concentration, CK flux was computed as $((PCr/ATP)\times k_f\times[ATP]_{literature})$. Global longitudinal (GLS), circumferential (GCS) and radial strain (GRS) were assessed from cine using feature tracking (FT-CMR) in all subjects.

Results:

Patients with HCM had higher left ventricular mass, maximum wall thickness and LGE compared to healthy controls. No significant difference was seen in resting rate pressure products between the two groups. Both resting myocardial energetics and CK k_f were significantly reduced in HCM: Rest PCr/ATP (HCM 1.96 ± 0.36, control 2.20 ± 0.40; P=0.03); k_f (HCM 0.15 ± 0.07 s^{-1}, control 0.22 ± 0.23 s^{-1}; P<0.01) (Fig 1A). A 34% reduction of CK ATP flux was seen in HCM compared with healthy controls (P<0.01) (Fig 1B). k_f and CK flux decreased in proportion to the degree of maximum left ventricular wall thickness (k_f r=-0.38; P<0.01); (CK flux r=- 0.528; P<0.01). Compared with healthy controls, HCM subjects had impaired myocardial contractility as assessed by GLS (mean difference ±SE +5.0±1.7%; P=0.04). GRS was significantly impaired (mean difference ±SE -10.0±3.0%; P=0.02) in HCM subjects with reduced CK flux (<1.3μmol $(g\ s)^{-1}$) compared to those with preserved CK flux. There was no correlation between GLS and k_f.

Conclusion: We have demonstrated that HCM is characterised by impaired CK-ATP flux, a substrate for left ventricular dysfunction, due to reduced k_f and resting energetics. CK kinetics correlated moderately with the degree of left ventricular hypertrophy. Impaired CK flux was associated with impaired myocardial contractility (GRS) in HCM.

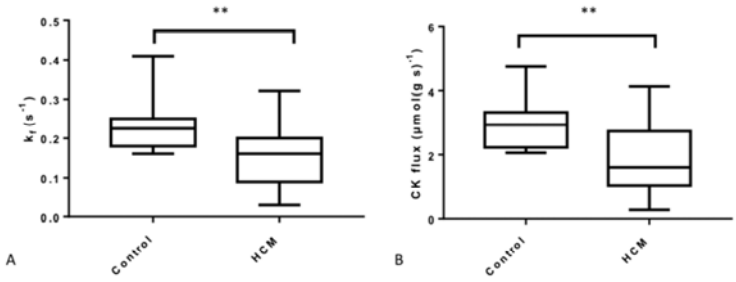

Fig1. Kf (A) and CK flux(B) were reduced in HCM compared with healthy controls. (**P<0.01; Error bars represent standard deviation)

ID#: 372261

Quantitative cardiac gene transfer imaging with CEST-MRI and a genetically encoded reporter gene

Moriel Vandsburger, PhD[2] Assaf Gilad[1]

1. Michigan State University

2. University of California, Berkeley, Berkeley, CA

Background: Gene therapy for heart failure has gained renewed interest with the availability of adeno-associated viral vectors (AAV), however quantitation of gene transfer/expression relies upon tissue biopsy or nuclear imaging. Magnetic resonance imaging (MRI) is standard for functional assessment of gene therapy outcomes. We tested whether the genetically encoded chemical exchange saturation transfer (CEST) – MRI reporter gene, Lysine Rich Protein (LRP), could be used to quantify gene expression following AAV9 mediated delivery to the heart.

Methods: The CEST-MRI reporter gene was cloned into an AAV9 vector and either administered systemically via tail vein injection or directly injected into the left ventricular free wall of mice (n = 45 total). Longitudinal in vivo CEST-MRI was performed at days 15 and 45 after direct injection or at 1, 60 and 90 days after systemic injection. Immunostaining was used to validate MR findings.

Results: Expression of LRP generated significantly greater peak CEST contrast following both direct (11.6 ± 4.4% LRP, 0.6 ± 2.0% AAV9-Empty, P = 0.01) and systemic (4.9 ± 4.3% LRP, -1.9 ± 2.1% AAV9-Empty, P = 0.01) AAV9 administration. CEST contrast following direct injection was focally elevated about the areas of reporter gene expression as confirmed by immunostaining (Figure 1). Although CEST contrast was consistently elevated in LRP expressing tissues, the magnitude of elevation varied between mice (Figure 2). Following intravenous administration of AAV9-LRP, spatially heterogeneous enhancement of CEST contrast was observed at 60 days post-administration (Figure 3). Mean myocardial CEST-contrast in the hearts of mice receiving AAV9-LRP was significantly greater than in mice receiving empty AAV9 or saline injections. Quantitative co-immunoprecipitation confirmed expression of LRP in the hearts of mice recieving AAV9-LRP. Terminal setpal thickness (0.90 ± 0.05mm LRP vs 0.94 ± 0.07mm AAV9-Empty, P=0.77 Direct; 0.99 ± 0.06mm LRP vs 0.95 ± 0.06mm AAV9-Empty, P=0.23 Systemic) was unchanged by LRP expression.

Conclusion: This study demonstrates the ability to serially quantify longitudinal changes in CEST contrast generated by expression of a genetically encoded CEST-MRI reporter gene in the mouse heart following AAV9 mediated delivery. Since CEST contrast is selectively 'turned on';, measurement of functional outcomes of gene therapy including tissue thickness, contractile function, fibrosis, and perfusion can be assessed in series in the same imaging session and correlated on an individualized basis. When desired functional outcomes are not achieved, whether failure is due to limited delivery, abrogated expression, or a lack of therapeutic effect despite adequate expression can be interrogated.

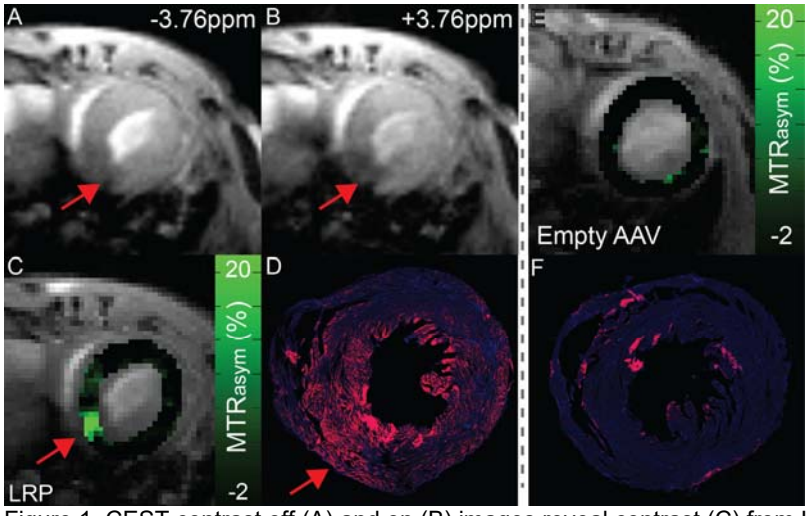

Figure 1. CEST contrast off (A) and on (B) images reveal contrast (C) from LRP as confirmed by immunostaining (D) that is not present when empty AAV9 is injected (E/F)

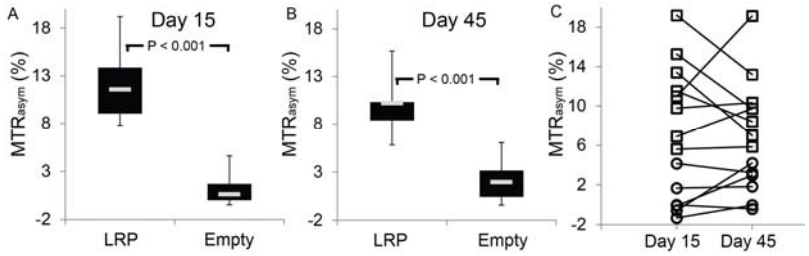

Figure 2. CEST contrast was significantly elevated in tissue expressing LRP at both time points

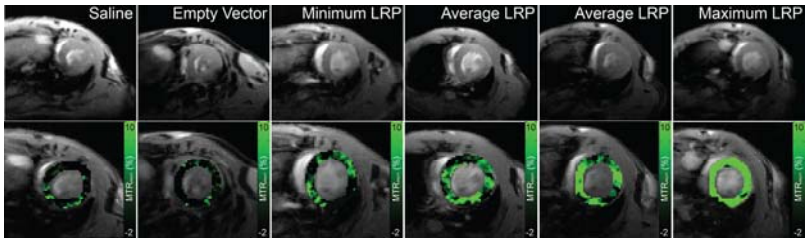

Figure 3. Representative CEST contrast maps at 60 days after systemic injection of either saline, empty AAV9, or AAV9 encoding for LRP

ID#: 372268

Machine Learning Based Modelling of Segmental Native T1 Distribution to Classify Cardiomyopathy State in Patients with Unexplained Left Ventricular Hypertrophy

Yoko Mikami, MD, Ph.D.[1]Mariam Narous, M.Sc.[1], Alessandro Satriano, Ph.D.[2], Rashed Alfagih, MBBS, MHSc[3], Reis Hansen[2], Steven Dykstra, MSc[1], Nowell M. Fine, MD, M.Sc.[4], Aneal Khan, MD, MSc[5], Rosa Sandonato, RN, BScN[1], Sandra Rivest, RN[6], Jacqueline A. Flewitt, MSc[2], Carmen P. Lydell, MD[2], Andrew G. Howarth, MD, Ph.D[1], Bobby Heydari, MD, MPH[1], James White, MD, FRCP(C)[1]

1. Stephenson Cardiac Imaging Centre, Libin Cardiovascular Institute of Alberta, University of Calgary, AB, Canada

2. Stephenson Cardiac Imaging Centre, Libin Cardiovascular Institute of Alberta, University of Calgary, Calgary, AB, Canada

3. King Fahad Cardiac Center, College of Medicine, King Saud University, Ar Riyad, Saudi Arabia

4. Libin Cardiovascular Institute of Alberta, AB, Canada

5. Alberta Children's Hospital Research Institute, Cumming School of Medicine, University of Calgary, AB, Canada

6. Stephenson Cardiac Imaging Centre, Libin Cardiovascular Institute of Alberta, University of Calgary, Canada, AB, Canada

Background: Unexplained left ventricular hypertrophy (LVH) can be due to hypertrophic cardiomyopathy (HCM), Anderson-Fabry disease (AFD), or cardiac amyloidosis (CA). We aimed to see if a machine-learning (ML) based algorithm could learn segmental native T1 distributions in these states and provide meaningful assistance for their future classification. The diagnostic performance of this model was compared to discrimination by global native T1 and post-contrast T1 (and partition coefficient (λ)) in their ability to differentiate cardiomyopathy state.

Methods: Eighty-eight patients (60% male; mean age=51.3±14.1years) with confirmed HCM (n=31), AFD (n=37) or CA (n=20) were studied. Patients were imaged at 3-Tesla using a protocol inclusive of short-axis T1 mapping (ShMOLLI) prior to and following gadolinium administration. Global native T1 and post contrast partition coefficient (λ) were calculated in addition to segmental native T1 values (12 basal and mid-ventricular segments). An ML ensemble classification model was constructed using segmental native T1 to discriminate each cardiomyopathy. The model was optimized and assessed by 5-fold cross-validation. Area under the curve (AUC) values of global T1 mapping (native), partition coefficient, and segmental ML-based modelling for the identification of each cardiomyopathy were compared.

Results: Mean global native T1 values were significantly different between each cardiomyopathy state, being lowest in AFD (1075±64ms), intermediate in HCM (1182±59ms), and elevated in CA (1307±100ms, P<0.0001). No overlap was observed between CA and AFD, with strong respective AUCs of 0.95 and 0.94. However, overlap was present for HCM versus both alternate cardiomyopathies with a modest AUC of 0.78. Partition coefficient showed significant elevation in CA versus both AFD and HCM (λ = 0.83±0.24 vs. 0.48±0.04 and 0.49±0.08; P<0.0001), however was not significantly different between HCM and AFD. Disease-specific maps of mean segmental native T1 (N=1034 segments) are shown in Figure 1. An ML model of segmental T1 provided strong discriminatory performance to identify each cardiomyopathy state, this tested by randomly selected cases: HCM with an AUC=0.89, AFD with an AUC=0.96, and CA with an AUC=0.98.

Conclusion: This study shows pilot feasibility for ML-based modelling of segmental native T1 values to discriminate HCM, AFD and CA. The overall diagnostic performance of this approach was superior to that achieved by either global T1 or post-contrast T1 (λ), the former failing to differentiate HCM from AFD or CA, and the latter failing to differentiate HCM from AFD. Expanded work is required to refine ML-based modelling for this purpose and requires external validation in a unique patient population.

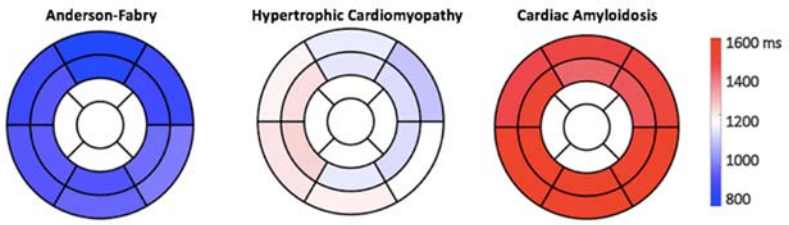

Figure 1. Segmental distribution of native T1 values in Anderson-Fabry disease, hypertrophic cardiomyopathy, and cardiac amyloidosis.

ID#: 372545

Comparison of Cardiac Magnetic Resonance-Derived Blood Oximetry to Invasive Catheterization in Heart Transplant Recipients

Juliet Varghese, PhD[1] Andrea Cardona, MD[2], Subha Raman, MD, MSEE[3], Rizwan Ahmad, PhD[4], Orlando Simonetti, PhD[1]

1. The Ohio State University, OH

2. The Ohio State University Wexner Medical Center, Columbus, OH

3. The Ohio State University, Columbus, OH

4. The Ohio State University

Background: Measurement of blood oxygen saturation (O2 sat) levels in the right heart provides an index of systemic oxygen consumption, valuable in the diagnosis and monitoring of patients with heart failure. Right heart catheterization (RHC) including O2 sat measurement and endomyocardial biopsy is also routinely performed for monitoring of post heart transplant status. A T2 mapping based, non-linear, multi-parameter estimation method was previously demonstrated to non-invasively determine blood O2 sat in the heart [1,2]. In this study, the accuracy of the technique is evaluated against RHC in a preliminary cohort of heart transplant recipients.

Methods: Six patients (age 48.3 ± 12.1 years, one female) undergoing clinically indicated RHC and endomyocardial biopsy were recruited for research cardiac MRI examination on a 1.5T scanner (Avanto, Siemens Healthineers). Six T2 prepared single-shot steady-state free precession (SSFP) images were acquired under free-breathing, across T2 preparation times ranging from 0 to 200 ms with corresponding inter-echo spacing (τ_{180}) of 0 to 25 ms (Figure 1). A short axis view of the right and left ventricles (RV and LV), and cross-sectional views of the pulmonary artery (PA) and aorta were acquired in each patient; the total acquisition time for each location was 30 seconds. The signal was measured in each image in ROIs placed in arterial and venous blood; arterial O2 sat was obtained with a pulse oximeter (SpO2), and hematocrit was measured from a blood sample. These data were jointly processed to estimate the unknown venous O2 sat and other remaining nuisance parameters of the Luz-Meiboom model (S_0, T_{2O}, τ_{ex} and α) [3,4]. O2 sat of the RV and MPA were then compared to catheterization results.

Results: MRI and RHC were performed on the same day. The comparison of O2 sat estimated from MRI in the RV and PA against catheter measurement in the PA is shown for each patient in Figure 2. Other physiological measurements obtained are shown in Table 1. The average absolute mean difference between O2 sat estimated in RV and RHC was 5.3 ± 4.4 % (range, 1% to 13%, ICC - 0.59). O2 sat estimated by MRI in the PA showed a similar, even smaller difference with RHC (4.8 ± 3.9%, range, 1% to 11%, ICC- 0.62).

Conclusion: The present study demonstrated good agreement between MR estimates of O2 sat in the right heart with invasive catheterization in a post heart transplant population. Patients typically undergo >10 RHCs and endomyocardial biopsies in the first year following heart transplant. The use of non-invasive measurement of oxygen saturation in combination with MR measurements of cardiac output, hemodynamics and myocardial tissue characteristics, warrants further prospective evaluation to comprehensively and non-invasively evaluate such patients towards fewer invasive procedures. **References: 1.** Varghese et al. JCMR 2016, 18(Suppl 1):W29. **2.** Varghese et al. 2017, 20th SCMR Abstract Suppl: F035. **3.** Wright et al. JMRI 1991, 1(3):275-283. **4.** Luz and Meiboom, J. Chem. Phys. 39(2): 366-370 (1963).

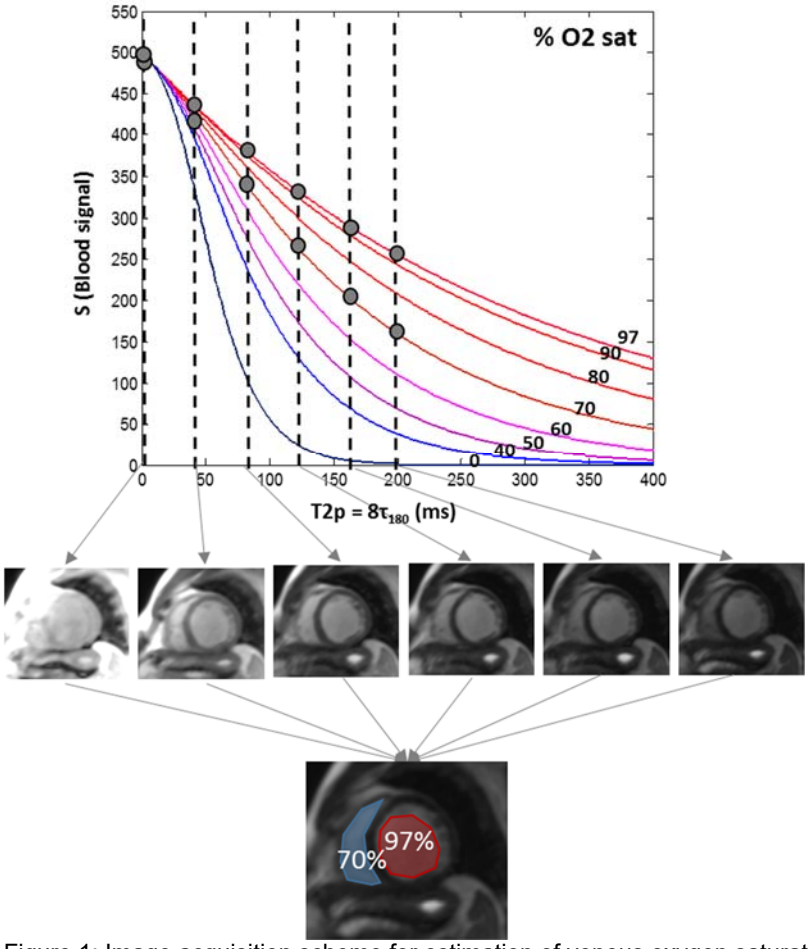

Figure 1: Image acquisition scheme for estimation of venous oxygen saturation in the right heart. T2 prepared blood signal is sampled across a range of interecho spacing and T2 preparation times to fit the Luz-Meiboom model. Arterial blood signal (from LV for RV O2 sat estimation, and from aorta for PA O2 sat estimation in this study) and O2 sat determined by pulse oximetry serves as a patient specific reference.

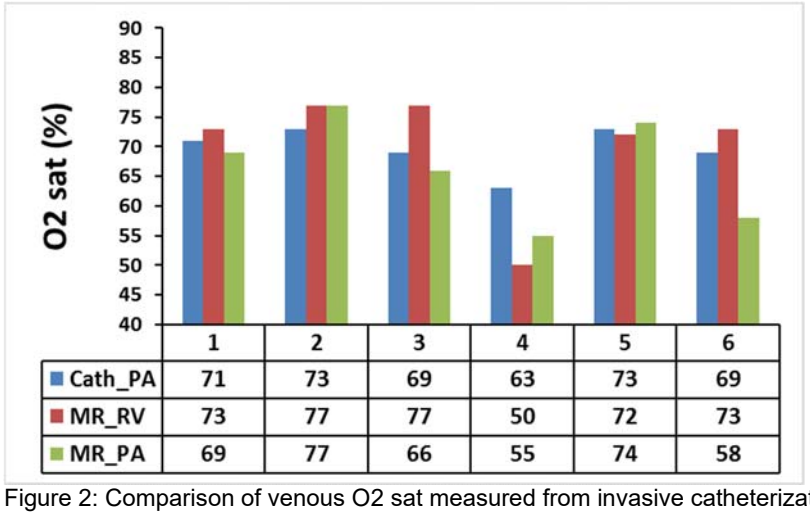

	1	2	3	4	5	6
Cath_PA	71	73	69	63	73	69
MR_RV	73	77	77	50	72	73
MR_PA	69	77	66	55	74	58

Figure 2: Comparison of venous O2 sat measured from invasive catheterization in the pulmonary artery (blue) and MRI (right ventricle-red, main pulmonary artery-green) in six heart transplant recipients.

Table 1: Mean ± standard deviation and range of physiological measurements made during RHC and MRI exams in the patient cohort.

Physiological Measurements	Mean ± SD	Range
SBP, mmHg	128.2 ± 25.1	105 – 166
DBP, mmHg	77.5 ± 13.9	59 – 98
BMI, kg/m^2	27.6 ± 6.2	17.6 – 34.7
Hct (%)	35.3 ± 6.7	23.5 – 40.8
Wedge pressure, mmHg	9.5 ± 2.9	5 - 13
Fick CO, L/min	5.8 ± 2.0	4.0 – 8.6
Biopsy grade		
0 (n = 3)		
1A (n = 3)		
SpO2 during MRI, %	97 ± 2	93 – 99
HR during MRI, bpm	85 ± 9	75 - 98
MRI CO, L/min	7.8 ± 2.6	4.8 – 10.9
Myocardial T1, ms	1058.9 ± 36.7	1003.8 – 1098.9
Myocardial T2, ms	60.35 ± 4.4	55.2 - 68

ID#: 373067

Intramyocardial injections guided by active MR-tracking for regenerative therapy

Steven Wenker, MD[1] Frebus van Slochteren, PhD[2], Peter Seevinck, PhD[3], Adriaan Kraaijeveld, MD, PhD[3], Thomas Lloyd[4], Scott Kimmel, MS[4], Maarten Bakker, TU/e[5], Patricia Dankers, PhD[5], Jouke Smink, MSc[6], Sascha Krueger, PhD[7], Cheyenne Tseng[8], Steven A.J. Chamuleau, MD, PhD[3]

1. Utrecht University Medical Center, Utrecht, Netherlands

2. University Medical Center Utrecht, Utrecht, Utrecht, Netherlands

3. Utrecht University Medical Center, Netherlands

4. Imricor

5. Eindhoven University of Technology, Netherlands

6. Philips Healthcare, Noord-Brabant, Netherlands

7. Innovative Technologies, Philips, Technology GmbH, Hamburg, Germany, Hamburg, Germany

8. University Medical Center Utrecht, Amsterdam, Noord-Holland, Netherlands

Background: Regeneration or protection of the failing heart using biologic therapies remains a promising but challenging application. Novel approaches aim at cardiac protection via local matrix support and sustained paracrine signaling. Although MRI is considered the gold standard for infarct assessment, it is rarely used to guide intramyocardial injections. MRI has important advantages over the currently used delivery methods in terms of accuracy, reproducibility, independency of patent coronary arteries, and exposure to ionizing radiation. In the MIGRATE project we have developed an actively tracked steerable MRI compatible injection catheter for the delivery of an MRI visible biomaterial for therapeutic treatment of the heart. In this study we have demonstrated the feasibility of this technique in four healthy pigs.

Methods: A steerable injection catheter with integrated receive coils for active tracking was adapted from an ablation catheter by Imricor. The catheter was connected to the iSuite iMRI platform installed on a 1.5T MRI (Philips Ingenia). For injections we used a supramolecular hydrogel crosslinked with dotarem which can directly be visualized on MRI (TU/e). Prior to the intervention a 3D-roadmap was acquired (free breathing, respiratory-gated and cardiac-triggered fat-suppressed T1-weighted 3D whole heart balance TFE-sequence) and a 3D shell of the endocardium with a fictive infarction border (ITK-SNAP) was created. During active tracking the location of the catheter-tip was tracked and rendered on the corresponding slices of the roadmap and inside the 3D shell (figure 1). Real time scanning was done by means of 2D balanced TFE sequences with a framerate of 2-5Hz.

Results: The catheter was introduced via the left femoral artery. Using active tracking the catheter was passed through the aortic valve and guided towards the desired location. Contact with the myocardium was confirmed by triggering a PVC on the surface ECG. Real time images were acquired during the injections (figure 2). Ex-vivo analysis showed several injections at the expected locations (figure 3), but not all injections could be identified. This could be due to leakage of the injections or unsuccessful injections caused by limited catheter stability due to lack of supportive devices, and the prototype nature of the injection catheter.

Conclusion: We showed the feasibility of guiding transendocardial injections with active catheter tracking and real time imaging to utilize the full potential of MRI for applications in cardiac regenerative therapy. The research was conducted by the MIGRATE consortium within the TKI-LSH framework and with financial support of the Hartstichting and Netherlands Heart Foundation.

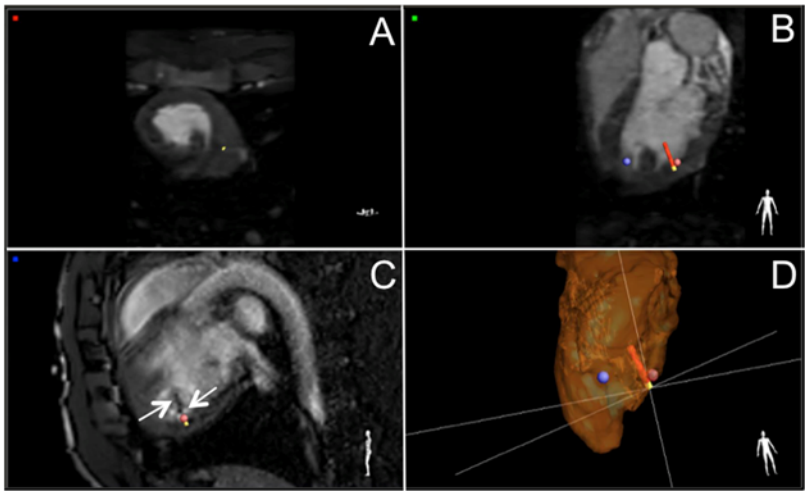

Figure 1. The catheter-tip is renderded in 3 orthogonal slices of the roadmap (A,B,C) and inside the 3D-shell (D).

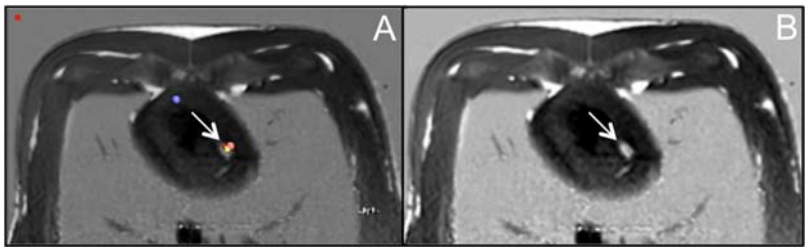

Figure 2. A. Passive tracking during injection B. Direct post-injection MR LGE PSIR imaging

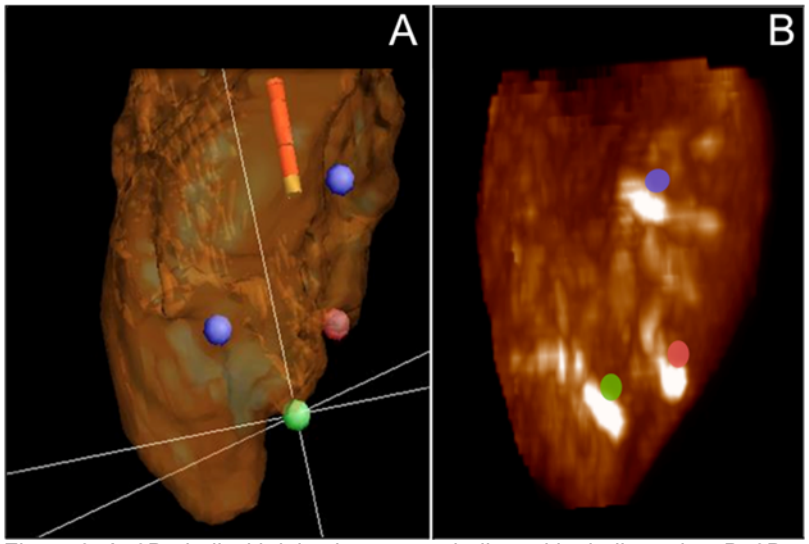

Figure 3. A. 3D-shell with injection targets indicated by bullet-points B. 3D-rendering of LGE-MR of ex-vivo heart

ID#: 372961

Automatic Ejection Fraction in Three Minutes

Okai Addy, Ph.D.[1]Bob Hu, MD[2], William Overall, Ph.D.[2], Juan Santos, Ph.D.[2]

1. HeartVista, Inc, Los Altos, CA

2. HeartVista, CA

Background:

One of the difficulties of providing consistent cardiac MRI across numerous clinical sites is the lack of highly trained technicians. To address this, we have trained a machine learning (ML) model to completely automate the examination of LV function, including determination of standard cardiac imaging planes, prescribing and scanning an appropriate free-breathing short-axis CINE stack, automatically drawing contours, and determining functional parameters such as ejection fraction (EF) and cardiac output. With our real-time based approach, we can go from initial image to completed EF assessment in less than 3 minutes.

Methods:

A typical cardiac LV function exam begins by localizing the patient';s standard cardiac planes. Then, a short-axis stack of CINE images is acquired, LV endocardial contours are segmented, and functional measures like EF are calculated.

To automate this process, we trained a convolutional neural network (CNN) in TensorFlow [1] using data from 58 patient studies acquired with the HeartVista Cardiac Package (HeartVista, Inc.; Los Altos, CA). From a total of 59,456 images, different networks were trained to perform the following prescription state transitions (Fig.1): moving from an arbitrary axial slice to a central cardiac axial slice; from there to a two-chamber view; from there to a short-axis view; and from there to either four-chamber or three chamber views. These trained networks could then be used sequentially to locate the complete set of standard views, in real time. After this localization, a stack of short-axis slices covering the entire left ventricle was automatically prescribed and HeartVista';s real-time, free-breathing CINE “HART” scan [2] was acquired and automatically analyzed.

During inference, the network continuously analyzed a series of real-time frames until a stable average prescription was determined. This minimized the effects of cardiac and respiratory motion. Using a single GeForce GTX Titan X GPU, total inference time was less than 60 ms.

To integrate this model into the scan, TensorFlow capabilities were added to HeartVista';s pipeline-based reconstruction engine to allow seamless bidirectional data transfer between MRI reconstruction nodes and TensorFlow graphs. Outputs of this hybrid MR/ML reconstruction were applied to update scan parameters. A separate TensorFlow graph was trained to automatically draw endocardial and epicardial contours.

In-vivo imaging was performed on a 1.5 T GE Signa scanner with the HeartVista Cardiac Package. Real-time spiral imaging was performed at 114 ms true temporal resolution, reconstructed at 30 frames per second and 15 inferences per second.

Results:

Figure 1 shows resulting image planes determined by the automatic procedure with a scan begun with an axial orientation inferior to the heart. Green lines on the images indicate the automatically generated prescription of the next orientation. In a feasibility test of 4 patients, the network successfully found all standard views and segmented both ventricles without operator intervention. All scans and reconstructions completed in under 3 minutes.

Conclusion: We have demonstrated the feasibility of using a neural network with scan feedback to automatically prescribe standard cardiac views and assess cardiac function. This was implemented within an extensible platform that can reduce the dependence of imaging quality on operator experience.

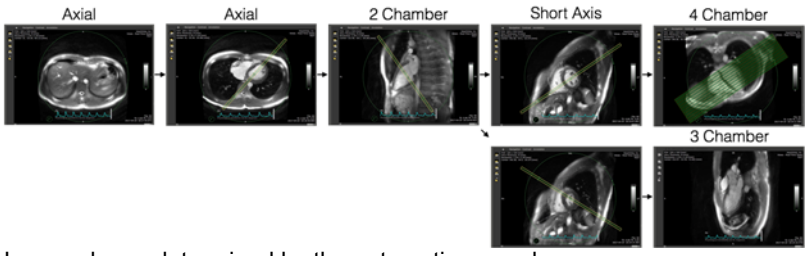

Image planes determined by the automatic procedure

ID#: 372975

Diagnostic yield, safety, and impact of cardiac MRI on treatment strategy in patients with cardiac devices

Eileen Gajo, BS, MD[1] Iva Golemi, MD[2], Amit Pursnani, MD[3], Robert Edelman, MD[4]

1. University of Chicago (NorthShore), Evanston Hospital

2. University of Chicago (Northshore), Evansotn, IL

3. NorthShore University HealthSystem, IL

4. NorthShore University HealthSystem

Background: Little evidence is available on the safety and diagnostic yield of cardiac MRI (CMRI) for the diagnosis of infiltrative cardiomyopathy (CMP) in patients with pre-existing pacemakers (PM) or intra-cardiac defibrillators (ICD). Potential hazards are thought to include lead heating that can cause tissue damage, inhibition of PM output, unintended cardiac stimulation leading to sustained tachycardia, or dislodgement of the device. Therefore, we sought to evaluate the diagnostic yield, safety, and impact of CMR on treatment strategy in patients with intra-cardiac devices suspected of having infiltrative CMP.

Methods: Utilizing radiology database keyword search software (Montage Healthcare Solution, Philadelphia PA), we found 18 CMR's were performed on patients with PM';s or ICD';s of which 13 were specifically for the evaluation of infiltrative CMP. One patient had an ICD; 12 had MRI-conditional PM';s. All patients were subjected to an institutional protocol for scanning including interrogation of their device both pre and post CMR. Variables monitored included pacing mode, ventricular and atrial capture threshold, sensing, lead impedance, and battery. Additionally, the protocol included monitoring of vitals and patient reported symptoms during the CMR. Charts were retrospectively reviewed for changes in these parameters. Second, the final biopsy diagnoses were gathered and compared to the CMR impression for accuracy.

Results: Seven (54%) of the patients reviewed had a PM placed for 3rd degree heart block; only 1 patient had an ICD. There were no clinically significant parameter changes detected on interrogation of the devices immediately post-CMR and at 3 month follow-up compared to pre-CMR settings for atrial and ventricular capture threshold, sensing, leading impedance, and battery life. Mean differences for atrial capture threshold, sensing, and lead impedance were 0.13V at 0.4mS, 0.07mV at 0.4mS, and 17.9 ohms, respectively. Mean differences for ventricular capture threshold, sensing, and lead impedance were 0.12V at 0.4mS, 1.1mv at 0.4mS, and 8.5 ohms, respectively. No patients had unstable vitals or symptoms during their CMR. Six of the 13 patients had CMR findings consistent with infiltrative CMP. Of these 6 patients, 5 had biopsies that confirmed the CMR diagnosis, with 4 patients having cardiac sarcoid and one with cardiac amyloid. Four patients had upgrades of their PM';s to ICD';s for secondary prevention. The patient with cardiac amyloidosis started appropriately medical therapy.

Conclusion: In this single-center study, CMR aids in the diagnosis of infiltrative CMP in patients with pre-existing pacemakers or defibrillators without adverse effects. Further studies are needed to validate these findings in larger cohorts.

ID#: 372950

Right Ventricular Remodelling following Pulmonary Valve Replacement in Patients with Tetralogy of Fallot

Victoria Stoll, DPhil, BMBCh[1] Lois Y. Kim[2], Mehreen Farooqi[3], Lucy Hudsmith, MD[4], Nigel Drury, PhD[3], Paul Clift, MD[5]

1. University of Birmingham, Birmingham, England, United Kingdom

2. University of Birmingham, Cheshire, United Kingdom

3. University of Birmingham, United Kingdom

4. Queen Elizabeth Hospital, Birmingham, England, United Kingdom

5. Queen Elizabeth Hospital, Birmingham, United Kingdom

Background: Advances in surgery have resulted in increased survival of children born with Tetralogy of Fallot. However, as these patients age they develop pulmonary regurgitation that over time causes right ventricular dilatation and dysfunction. Pulmonary valve replacement (PVR) is undertaken to prevent irreversible remodelling of the right ventricle (RV). The timing of this intervention remains controversial to ensure recovery of RV volumes and function. Previous studies have suggested that an RVEDV of <160ml/m^2, and less so an RVESV of <90ml/m^2 and RVEF >45%, will ensure normalisation of ventricular volumes post PVR. We sought to assess the recovery of RV volumes in patients who had undergone PVR.

Methods: 169 patients were identified who had undergone PVR between 2007 and 2017. Of these 59 patients (mean age at surgery 24.5±7.6yrs, 51% male) had an MRI scan before and after PVR.

Results: 36 (61%) patients had an EDV <160ml/m^2 (mean age 25.3±8.3yrs, 44% male) whilst 23 (39%) patients had an RVEDV ≥160ml/m^2 (mean age 23.1±5.9yrs, 61% male) prior to surgery. Of the 36 patients with an EDV <160ml/m^2 28 had normalisation of their RVEDV following PVR, whilst 8 had persistently elevated RVEDVs. Table 1 shows there was no difference in age at surgery, BMI, BSA or RVEF between those whose volumes normalised and those whose did not. The RVESV trended towards being smaller pre surgery in those whose volumes normalised (67±14ml/m^2) compared to those who volumes did not (78±10ml/m^2), p 0.05. However none of the patients whose volumes did not normalise had an ESV >90ml/m^2. LVEDV was larger in the patients whose volumes did not normalise (75±14 vs 63±14ml/m^2, p 0.04). Of the 23 patients with an EDV ≥160ml/m^2 pre-op 10 had normalisation of their RVEDV whilst 13 had persistently elevated RVEDVs. As shown in table 1 there was no significant difference in age at surgery, BSA, BMI or RVEDV. Of those whose RVEDV did not normalise all had an ESV of >90ml/m^2, however this was not a helpful predictor of recovery of function as 7 of the 10 whose volumes normalised also had an ESV >90ml/m^2. The RVEF was <45%, in all patients who failed to normalise their RV volumes, but also in 5 of the patients whose volumes recovered. The left ventricular parameters were all significantly different in patients who failed to normalise post-op with an increased LVEDV (88±13 vs 70±14ml/m^2, p 0.005) and LVESV (40±9 vs 29±10 ml/m^2, p 0.01) and lower LVEF (53±5 vs 59±8%, p 0.04) compared to those whose RV volumes normalised.

Conclusion: PVR restored RV volumes to within the normal range in 64% of patients with Tetralogy of Fallot. Current cut-off values for RVEDV were not reliably predictive of normalisation of RV volumes. Abnormal LV volumes and function were more prevalent in patients whose RV did not normalise post PVR and may provide additional predictive value for recovery of RV volumes. Incorporation of LV assessment may help improve current guidelines for decision making upon timing of PVR.

	Pre-op RVEDV <160ml/m²			Pre-op RVEDV ≥ 160ml/m²		
	RV volume normal post op	RV volume abnormal post op	p value	RV volume normal post op	RV volume abnormal post op	p value
Age at surgery (years)	24 ± 8	29 ± 10	0.25	23 ± 7	23 ± 6	0.85
BMI at surgery (kg/m²)	24 ± 3	24 ± 5	0.89	23 ± 9	21 ± 2	0.17
BSA at surgery (m²)	1.8 ± 0.3	1.7 ± 0.3	0.65	1.9 ± 0.2	1.7 ± 0.1	0.11
MRI timing post surgery (years)	3.6 ± 2.3	4.8 ± 1.7	0.18	2.3 ± 2.5	3.2 ± 2.1	0.19
RVEDV pre-op (ml/m²)	131 ± 20	136 ± 17	0.53	183.4 ± 10.4	219 ± 75	0.1
RVESV pre-op (ml/m²)	67 ± 14	78 ± 10	0.05	97 ± 20	131 ± 50	0.04
RVEF pre-op (%)	49 ± 9	43 ± 6	0.1	48 ± 10	41 ± 4	0.02
LVEDV pre-op (ml/m²)	63 ± 14	75 ± 14	0.04	70 ± 14	88 ± 13	0.005
LVESV pre-op (ml/m²)	24 ± 7	28 ± 7	0.2	29 ± 10	40 ± 9	0.01
LVEF pre-op (%)	62 ± 7	63 ± 4	0.6	59 ± 8	53 ± 5	0.04

ID#: 372955

Comprehensive flow, function, and viability MRI - Initial experience with a novel 30-minute protocol for structural heart disease

Michael Horowitz, MD, PhD[1] Tara A. Retson, MD, PhD[2], Darrin Wong, MD[3], Justin Sun[4], Peng Lai, Ph.D.[5], Albert Hsiao, MD, PhD[6]

1. UC-San Diego, San Diego, CA

2. University of California San Diego, San Diego, CA

3. University of California, San Diego, San Diego, CA

4. Temple University Lewis Katz School of Medicine

5. GE Healthcare, Menlo Park, CA

6. University of California, San Diego, CA

Background: Evaluation of structural heart disease with MRI can be technically challenging and time-consuming to perform using traditional planar imaging techniques. 4D Flow MR imaging has been proposed to help simplify structural cardiac MRI, but delineation of cardiac anatomy may not be optimal during the equilibrium phase of contrast-enhancement. We hypothesized that incorporation of first-pass contrast-enhanced breath-held 3D Cine and free-breathing 4D Flow into a single protocol could be used in place of traditional multiplanar SSFP to evaluate for structural defects, while minimizing scan time and improving resource utilization.

Methods:

With HIPAA-compliance and IRB approval, we retrospectively reviewed our initial experience with a 30-minute protocol in 51 consecutive patients referred for cardiac MRI between December 2016 and August 2017. Acquired images included volumetric SPGR-weighted 3D Cine, 4D Flow, and myocardial delayed enhancement imaging after routine administration of intravenous contrast. Post-contrast, traditional short-axis SSFP imaging was also performed to provide confirmatory data on cardiac volumetry and function.

Results:

First-pass contrast timing for 3D Cine was adequately performed in all patients, resulting in biventricular contrast-enhancement suitable for quantification of cardiac volumetry and function. For 37 patients, single breath-hold 3D Cine was typically performed in 24 seconds. For 14 patients, dual breath-hold 3D Cine was performed in 20 seconds per breath hold. Free-breathing 4D Flow MRI acquisitions were performed in all patients, taking an average of 10:28 minutes (range 8:09 - 12:57: minutes). We additionally present a few prototypical cases where the combination of sequences were contributory to diagnosis, including a patient with Noonan syndrome and a patient with pectus deformity and mitral regurgitation.

Conclusion:

Comprehensive evaluation of structural heart disease may be performed more efficiently by incorporating volumetric techniques for flow and function, as well as myocardial delayed enhancement. In addition to increasing patient comfort and compliance through an abbreviated scan time with reduced breath holds, the efficiency of this combined protocol can streamline MRI utilization and may enable further study and application of other novel pulse sequences.

ID#: 373035

Assessment of congenital vascular anomalies in people affected by Thalidomide

Julius Matthias. Weinrich, M.D[1] Lennart Well, M.D[1], Enver Guner. Tahir, MD[1], Beyer Rudolf, M.D[2], Maria Lindemann, M.D[3], Gerhard Adam, MD[4], Gunnar Lund, MD[4]

1. University Medical Center Hamburg-Eppendorf, Hamburg, Hamburg, Germany

2. Schön Klinik Hamburg Eilbek, Hamburg, Germany

3. Schön Klinik Hamburg Eilbek, Germany

4. University Medical Center Hamburg-Eppendorf, Hamburg, Germany

Background: Thalidomide embryopathy (TE) is a congenital disease resulting in anomalies caused by maternal intake of thalidomide between 1958 and 1963 mainly in Europe. About 2.500 thalidomide receivers are currently still alive in Germany. Initial post-mortem studies showed various cardiovascular birth defects caused by thalidomide, however, there are no current studies examining vascular malformations in now adult thalidomide receivers. This prospective study analysed the presence of vascular and organ malformations in adult thalidomide receivers using non-contrast enhanced magnetic resonance angiography (MRA).

Methods: Non-contrast enhanced MRA was performed in 60 subjects with TE (55±1.1 years, 26 men) using a 3T scanner. ECG-triggered images of the thorax, abdomen and pelvis were obtained by balanced turbo field echo sequences in coronal and sagittal planes. Two observers analyzed the scans for vascular and organ malformations. The observed malformations were compared to results from literature.

Results: We found 67 vascular anomalies in 48/60 (68%) subjects, 46 of them in the arterial and 21 in the venous system. Most vascular anomalies included the renal system (n=44, 66%) and the supraaortic branches (n=18, 27%). Two patients had a duplication of inferior vena cava, two a coeliac-mesenterico trunk, one patient an occluded right common iliac vein and one patient had an abberant renal vein. 12/60 (20%) patients had 13 abdominal organ anomalies which were mainly restricted to the renal system (10/13, 77%).

Conclusion: We observed vascular anomalies in 68% of the studied thalidomide receivers. Most anomalies were within ranges reported in literature but some had higher frequencies. Knowledge about higher frequency of vascular anomalies may be important for future medical treatment such as elective operations or vascular interventions.

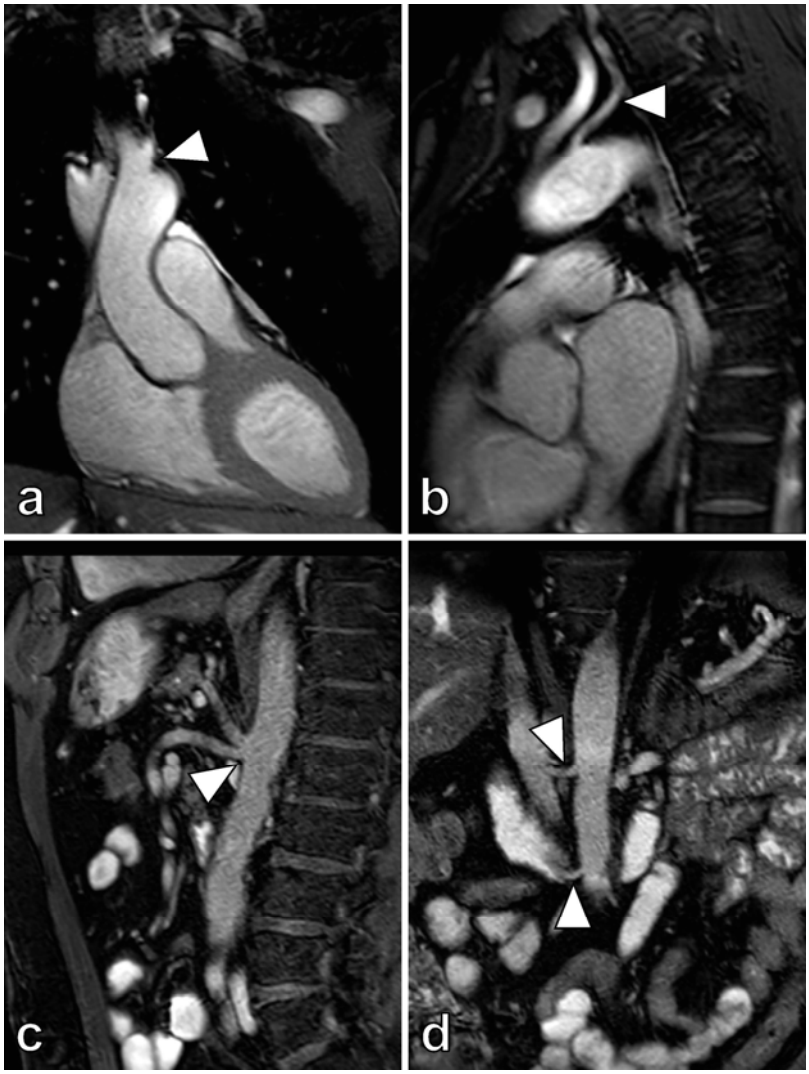

Typical arterial anomalies in Thalidomide receivers: bovine arch (a), left vertebral artery originated from the aortic arch (b); coeliac-mesenteric trunk (c) and two right sided renal arteries (d).

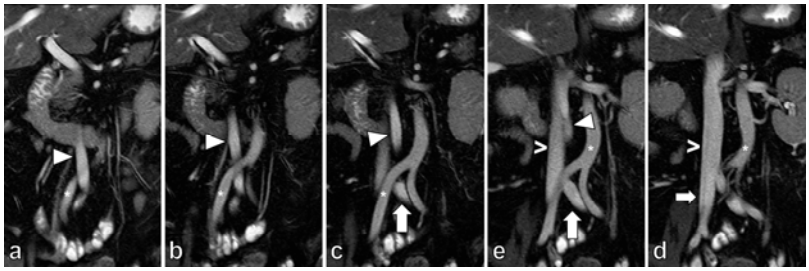

Doubled IVC in a 51-y/o female Thalidomide receiver, which is shown in coronal slices from anterior to posterior orientation (a to e). The doubled left sided IVC (arrowheads, a-d) arose from the common left iliac vein (arrow, c-e), then was located anterior of the right common iliac artery (white asterisks) and finally drained into the right IVC (open arrowhead, d and e) just below the left renal vein.

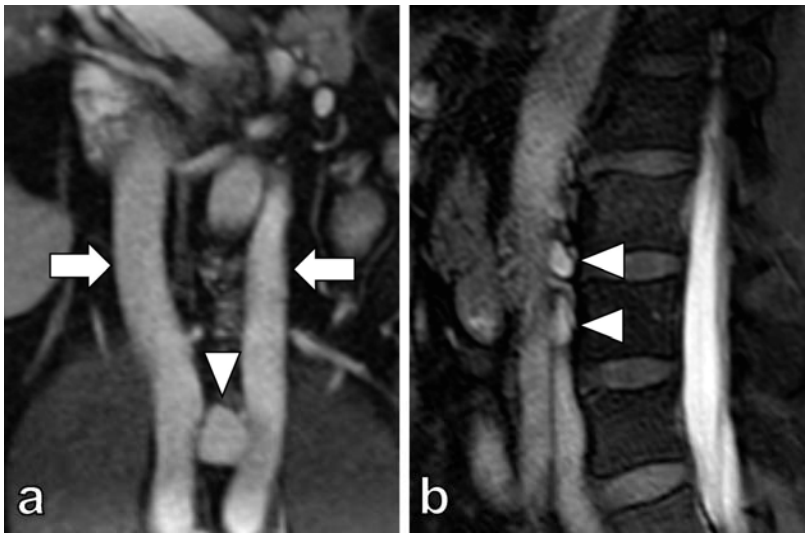

Venous anomalies in Thalidomide receivers. A doubled IVC was found in a 51 years old male subject (a; arrows). The left common iliac and left renal vein drained into the left IVC, which had no cranial run off, but was connected to the right IVC via a transverse interiliac vein at the lumbar level (a; arrowhead). Bifurcated retroaortic left renal veins (arrowheads) were found in a 51-years old female Thalidomide receiver (b).

ID#: 373037

The prognostic value of left ventricular strain assessed on cardiovascular magnetic resonance cine images in patients with light chain amyloidosis

Xiao Li[1] Yining Wang[2], Jian Li[1], Lu Lin[1], Jian Cao[2], Jing An, M.D[3], Zhengyu Jin[1]

1. Peking Union Medical College Hospital, China (People's Republic)

2. Peking Union Medical College Hospital, Beijing, China (People's Republic)

3. MR Collaborations NE Asia, Siemens Healthcare,, Beijing, China (People's Republic)

Background: To investigate the prognostic value of left ventricular strain assessed on cardiovascular magnetic resonance (CMR) cine images in patients with light chain (AL) amyloidosis.

Methods:

Seventy patients (age: 56±8 years; M/F: 46/24) and twenty healthy volunteers (age: 52±9 years; M/F: 10/10) were recruited prospectively. After informed consent, all subjects underwent standardized CMR scanning (3.0T, Magnetom Skyra Siemens, Germany) referring to Society for Cardiovascular Magnetic Resonance guidelines. Left ventricular strain were measured as the average total peak systolic strain in longitudinal, radial and circumferential direction on cine images using cvi42 software (version 5.3, Circle Cardiovascular Imaging, Canada). Follow-up on patients was done for all-cause mortality using Cox proportional hazards regression analysis.

Results: Patients demonstrated decreases in radial strain (31.5±14.3 % vs. 53.2±7.6 %, P<0.001), circumferential strain (-16.4±4.4 %, vs. -21.5±1.8 %, P<0.001) and longitudinal strain (-13.9±4.0 %, vs. -19.0±2.2 %, P<0.001), as compared to healthy controls. Patients also demonstrated decreases in left ventricular ejection fraction (LVEF) (64.0±14.5 % vs. 73.6±5.2 %, P=0.006) and indexed left ventricular end-diastolic volume (LVEDV) (57.4±13.9 ml/m^2 vs. 73.0±16.7 ml/m^2, P=0.001), and increases in left atrial area (LAA) (21.2±4.9 cm^2 vs. 18.8±2.9 cm^2, P=0.039) and indexed left ventricular mass (LVM) (89.7±27.1 g/m^2 vs. 60.9±13.2 g/m^2, P<0.001). During the follow-up for a median time of 12 months, 25 deaths occurred. Radial strain (hazard ratio [HR] 0.921, 95% confidence interval (CI) 0.860-0.987, P=0.019), circumferential strain (HR 0.778, 95% CI 0.637-0.952, P=0.015) and longitudinal strain (HR 0.764, 95% CI 0.609-0.960, P=0.021) were independently prognostic for mortality over LVEF, indexed LVEDV, LAA and indexed LVM.

Conclusion: We proved that radial strain, circumferential strain and longitudinal strain assessed on CMR cine images were independently prognostic for mortality in AL amyloidosis patients.

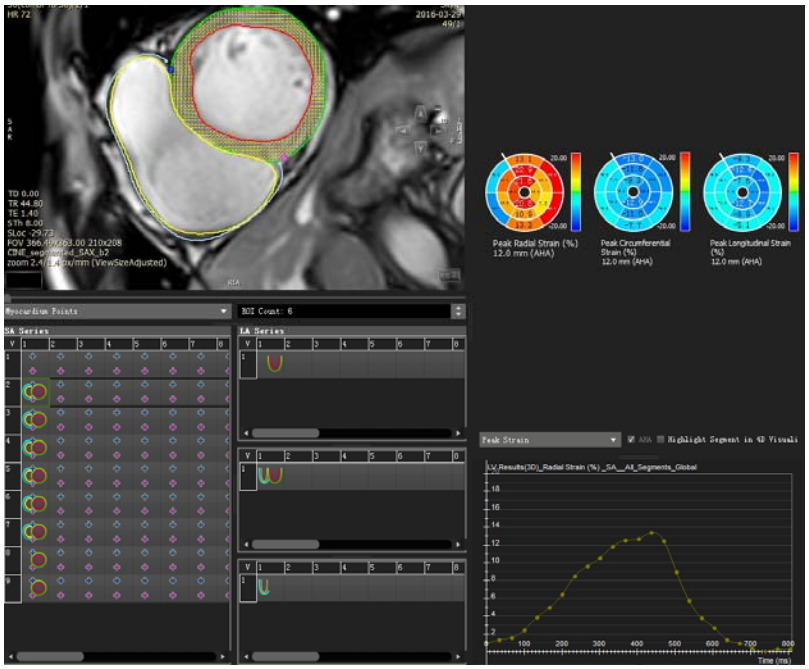

Figure 1. Left ventricular strain assessed semi-automatically by contouring the endocardium and epicardium on cine images

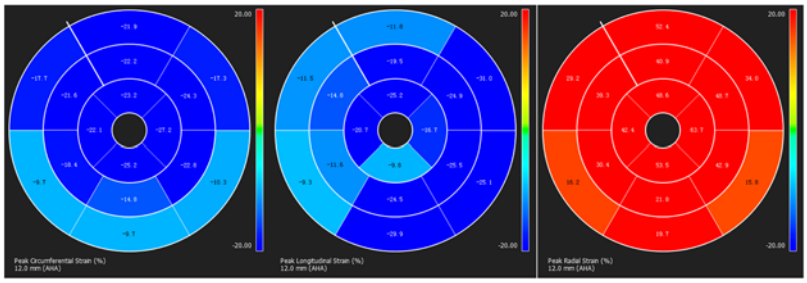

Figure 2. Bull's eye plot of left ventricular strain from a healthy volunteer.

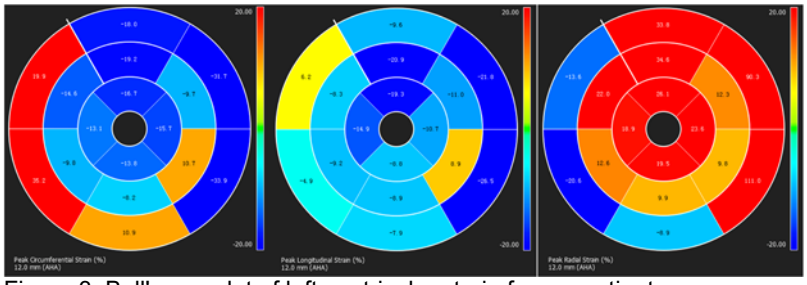

Figure 3. Bull's eye plot of left ventricular strain from a patient.

ID#: 373040

Cardiovascular magnetic resonance T2* for the assessment of myocardial ischemic reactions in hypertrophic cardiomyopathy

Mareike Gastl, MD[1] Jochen von Spizcak, MD[2], Alexander Gotschy, MD[3], Malte Kelm, MD[4], Hatem Alkadhi, MD[2], Florian Bönner, MD[4], Sebastian Kozerke, PhD[5], Robert Manka, MD[6]

1. ETH Zürich, University Hospital Zürich, Heinrich Heine University, Switzerland

2. University Hospital Zürich, Switzerland

3. ETH and University Hospital Zurich, Zurich, Switzerland

4. Heinrich Heine University, Düsseldorf, Medical Faculty, Germany, Nordrhein-Westfalen, Germany

5. ETH Zurich, Zurich, Zurich, Switzerland

6. University Hospital Zürich and ETH Zürich, Switzerland

Background: Hypertrophic cardiomyopathy (HCM) is characterized by a heterogeneity in clinical presentation, prognosis as well as structural abnormalities of the heart. Despite a macroscopic increase in left ventricular mass (LVM) and wall thickness, a mismatch between LVM and microcoronary circulation with corresponding ischemia has been implicated to cause myocyte degeneration and myocardial replacement fibrosis. In turn, this replacement fibrosis may deteriorate prognosis and outcome. Cardiovascular Magnetic Resonance (CMR) is able to characterize myocardial tissue by magnetic relaxation parameters (parametric mapping). In fact, T2* values have shown feasibility in identifying ischemic myocardial segments in patients with coronary artery disease (CAD). Therefore, we aimed to investigate structural alterations and myocardial ischemic reactions in a group of patients with hypertrophic non-obstructive/obstructive cardiomyopathy (HNCM/HOCM) using parametric CMR.

Methods: CMR was performed on a 1.5 Tesla MRI-System (Achieva, Philips, Best, Netherlands) using a 5-channel coil in patients with HNCM, HOCM and in healthy controls. T2* mapping was done using a single-breathhold multi-echo fast field-echo sequence (1 midventricular short axis slice, 6 echos) in addition to a 3D gradient-spoiled fast-field-echo sequence for late gadolinium enhancement (LGE). Images were post-processed off-line for T2* value generation by drawing a ROI within the IVS to avoid susceptibility artifacts. LGE was assessed by calculating the amount of fibrosis as % of LVM. Additional parameters were: 1) left ventricular mass per body surface area (LVMi) and 2) interventricular septum thickness (IVS).

Results: 107 patients with HCM (80 males, 51.0±16.4years) including 45 patients with HOCM (37 males, 51.0±15.2years) and 20 controls (12 males, 39.0±16.4years) received CMR. In comparison to the normal control group, patients with HCM showed significantly elevated IVS and LVMi alongside decreased T2* values (24.3±8.0 vs. 34.9±4.4ms, $p<0.01$). Comparing HCM patients with and without left-ventricular fibrosis, HCM patients with myocardial fibrosis exhibited significantly decreased T2* values (21.5±5.5 vs. 31.3±8.3, $p<0.01$). Showing the best area under the curve of 0.83, T2* values provided additional diagnostic accuracy of up to 85.2 % in differentiating HCM with and without left-ventricular fibrosis.

Conclusion: Except from morphological differences, parametric mapping identified a sub-group of HCM patients with decreased T2* values alongside myocardial replacement fibrosis. In this context, decreased T2* values may indicate ischemic alterations due to microvascular dysfunction consequently leading to myocardial replacement fibrosis. As left-ventricular fibrosis has been suggested influence on prognosis and cardiovascular events in patients with HCM, T2* mapping may potentially add information on identifying a higher risk sub-group of patients without the need for contrast agent.

ID#: 373041

Manganese-enhanced T1 mapping in myocardial infarction: validation with 18F-FDG PET/MR

Nick B. Spath, BSc MD[1] Adriana Tavares, MSc PhD[2], Gillian A. Gray, BSc PhD[3], Marc R. Dweck, MD PhD[1], David E. Newby, MD PhD[3], Phillip Yang, MD[4], Maurits A. Jansen, MSc PhD[3], Scott I. Semple, MSc PhD[3]

1. University of Edinburgh, Edinburgh, Scotland, United Kingdom

2. University of Edinburgh, United Kingdom

3. University of Edinburgh, Scotland, United Kingdom

4. Stanford University School of Medicine, CA

Background: Manganese-enhanced magnetic resonance imaging (MEMRI) is a promising tool in the assessment of myocardial viability and cardiac failure. We previously demonstrated that MEMRI with T1 mapping was effective in quantifying infarct size more accurately than with Gadolinium delayed-enhancement MRI (DEMRI). We have furthermore indicated potential to track and quantify altered calcium-handling in remodelling myocardium post-infarction. The present study aims to validate MEMRI viability against ^{18}F-FDG positron emission tomography/computed tomography (PET/CT).

Methods: Male Sprague-Dawley rats (180-300g) underwent permanent coronary artery ligation to induce anterior myocardial infarction (MI), or sham surgery. Animals (n=11 MI, n=2 sham) underwent dual assessment with MEMRI and 18F-FDG PET/CT, 10-12 weeks post-surgery. MRI was acquired using a 7T horizontal bore NMR spectrometer (Agilent Technologies, UK), maximum gradient strength 400mT/m. Pulse, respiration, and temperature were monitored. MEMRI was performed using intravenous manganese chloride (EVP1001-1, Eagle Vision Pharmaceuticals, Downingtown, USA; n=6 at 22 μmol/kg) and mangafodipir (Teslascan, IC Targets AS, Norway; n=7 at 44 μmol/kg).

Standard anatomical and functional imaging was acquired, followed by gradient-echo, cardiac-gated Modified Look-Locker Inversion recovery (MoLLI) sequences before and 20 min post-contrast at the maximal infarct short-axis slice. T1 colour maps were created using commercially available software (CVI4.2, Circle Cardiovascular Imaging, Canada) generating standardised T1 colour maps for ROI contouring.

Maintained under inhaled anaesthesia, animals were then transferred to a microPET/CT scanner (Nanoscan, Mediso Medical Imaging Systems, Hungary). Intravenous ^{18}F-FDG was administered and PET data were acquired continually for 60 min, followed by cardiac-gated PET/CT acquisition for 10 min. PET/MR images were co-registered in 1 short axis and 2 long axis views and fused, whereby contours were defined with PET uptake denoting viability.

Results: Infarct size assessed by MEMRI T1 mapping was smaller than by native T1 (mean 23.34 *vs* 18.68%, P=0.001) at 12 weeks. There was excellent agreement on infarct size between MEMRI T1 maps and ^{18}F-FDG PET (bias 1.294, 95%CI -24.98 to 25.57 P=0.688). In contrast, native T1 maps consistently overestimated infarct size (bias 25.76, 95% CI 7.51 to 44.01 P=0.031).

Conclusion: MEMRI T1 mapping identifies viable myocardium as well as ^{18}F-FDG PET and was superior to native T1 mapping. This validation, in conjunction with comparative data from MEMRI T1 mapping and ^{18}F-FDG uptake, informs the clinical translation of cardiac MEMRI where it has potential applications for the assessment of myocardial viability in various clinical contexts including myocardial infarction, cardiomyopathies and regenerative therapies.

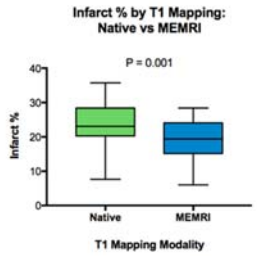
Infarct % by T1 Mapping:
Native vs MEMRI
P = 0.001
Infarct %
40
30
20
10
0
Native
MEMRI
T1 Mapping Modality

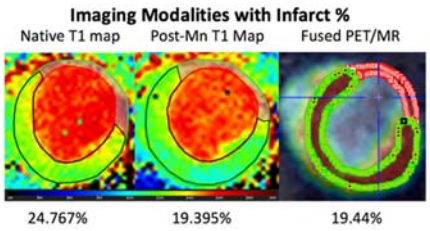
Imaging Modalities with Infarct %
Native T1 map
Post-Mn T1 Map
Fused PET/MR
24.767%
19.395%
19.44%

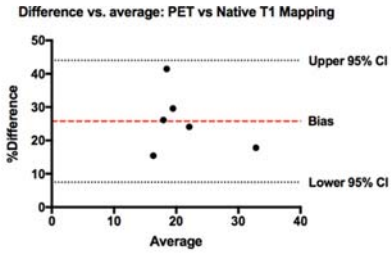
Difference vs. average: PET vs Native T1 Mapping
%Difference
50
40
30
20
10
0
Upper 95% CI
Bias
Lower 95% CI
0
10
20
30
40
Average

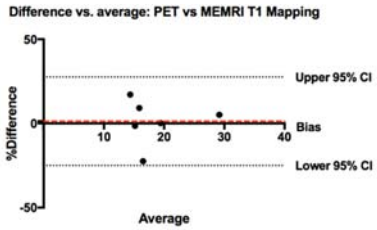
Difference vs. average: PET vs MEMRI T1 Mapping
%Difference
50
0
-50
Upper 95% CI
Bias
Lower 95% CI
10
20
30
40
Average

ID#: 373050

Myocardial Adaptation After Surgical Therapy Differs For Aortic Valve Stenosis And Hypertrophic Obstructive Cardiomyopathy

Rahana Parbhudayal, MD[1]Ahmet Güçlü, MD, PhD[2], Alwin Zweerink, MD[3], Paul S. Biesbroek, MD[4], Pierre Croisille, MD PhD[5], Patrick Clarysse, PhD[6], Michelle Michels, MD, PhD[7], Wim Stooker, MD, PhD[8], Alexander Vonk, MD, PhD[9], Albert C. van Rossum, MD, PhD[10], Jolanda Velden, van der, PhD[9], Robin Nijveldt, MD, PhD[11]

1. VU University Medical Center Amsterdam, The Netherlands, Noord-Holland, Netherlands

2. Isala Klinieken, Zwolle, The Netherlands, Haarlem, Noord-Holland, Netherlands

3. VU university medical center, Netherlands

4. VU University Medical Center, Amsterdam, Noord-Holland, Netherlands

5. Univ Lyon, UJM-Saint-Etienne, INSA, CNRS UMR 5520, INSERM U1206, CREATIS, Saint-etienne, Rhone-Alpes, France

6. 5Université Lyon, UJM-Saint-Etienne, INSA, CNRS UMR 5520, INSERM U1206, CREATIS, F-42023, Saint-Etienne, France, France

7. Erasmus Medical Center, Rotterdam, The Netherlands, Netherlands

8. Onze Lieve Vrouwe Gasthuis, Amsterdam, The Netherlands, Netherlands

9. VU University Medical Center Amsterdam, The Netherlands, Netherlands

10. VU University Medical Center, Noord-Holland, Netherlands

11. VU University Medical Center, Netherlands

Background: Surgical therapies in aortic valve stenosis (AVS) and hypertrophic obstructive cardiomyopathy (HOCM) aim to relief intraventricular pressure overload and improve clinical outcome. It is currently unknown to what extent myocardial adaptation concurs with restoration of intraventricular pressures, and whether this is similar in both patient groups. The aim of this study was to investigate changes in myocardial adaptation after surgical therapies for AVS and HOCM.

Methods: Ten AVS and ten HOCM patients were prospectively enrolled and underwent cardiac magnetic resonance (CMR) cine imaging and myocardial tagging with high temporal resolution (~14ms) prior to, and four months after aortic valve replacement (AVR) and septal myectomy, respectively. Two HOCM patients were unable to undergo follow-up CMR. Left ventricular (LV) volumes, mass, ejection fraction, wall thickness and wall thickening were derived from cine images. Circumferential strain was assessed at the septal and lateral wall at the mid ventricular level from the myocardial tagging images using the inTag software (CREATIS, Lyon, France) [and the SinMod motion estimation technique].

Results: Pressure gradients significantly reduced in both AVS and HOCM after surgery ($p<0.01$), with a concomitant decrease in left atrial volume ($p<0.05$) suggesting improved diastolic pressures. Also, LV mass and wall thickness reduced, but to a larger extent in AVS than in HOCM patients ($p<0.05$ for difference). Although surgery did not affect LV ejection fraction in both patient groups, a significant improvement in global wall thickening was observed in AVS patients (38 IQR [31,49] to 51 IQR [43,70] %, $p<0.05$). Not unexpectedly, there was a significantly worse septal systolic strain rate after septal myectomy compared with patients after valve replacement ($p=0.007$, see figure), with even a deterioration in systolic strain rate from pre to post myectomy (-28 IQR [-44,-17] to -13 IQR [-17,-6] %·s-1, $p=0.03$).

Conclusion: The present study demonstrates differences in myocardial adaptation in response to surgery for AVS and HOCM. Although both groups showed reductions in anatomical indices suggesting improved diastolic function, only AVS patients demonstrated a concomitant improved systolic myocardial function. The systolic functional deterioration after myectomy in HOCM seems to be inherent to an ongoing and irreversible disease.

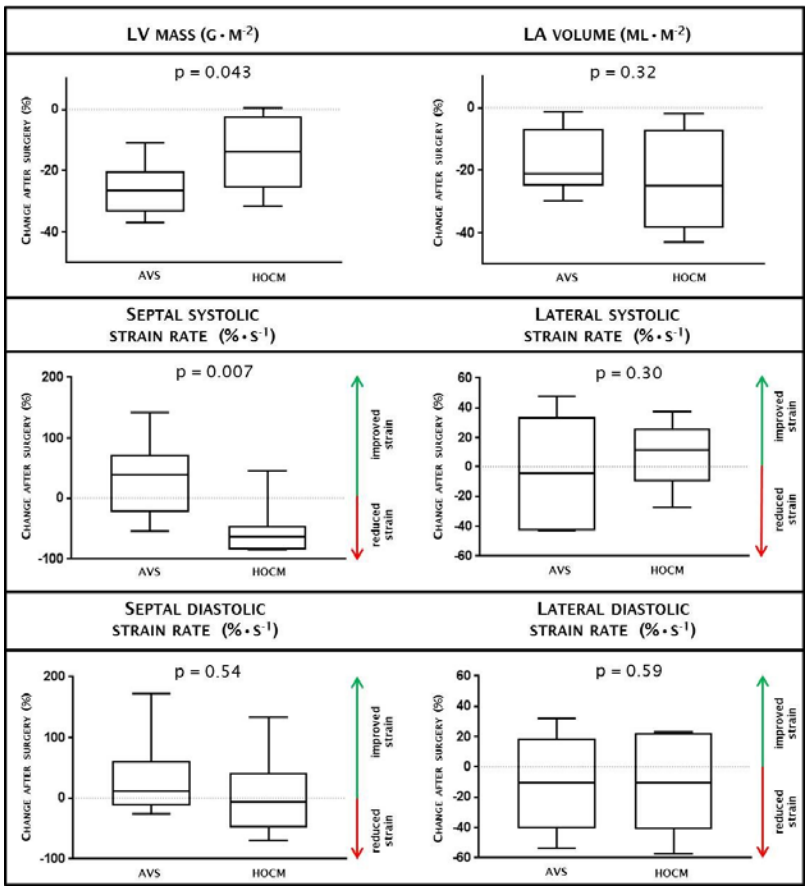
LV MASS (G • M-2)
p = 0.043
LA VOLUME (ML • M-2)
p = 0.32
CHANGE AFTER SURGERY (%)
AVS
HOCM
SEPTAL SYSTOLIC STRAIN RATE (%• S-1)
p = 0.007
LATERAL SYSTOLIC STRAIN RATE (%• S-1)
p = 0.30
improved strain
reduced strain
SEPTAL DIASTOLIC STRAIN RATE (%• S-1)
p = 0.54
LATERAL DIASTOLIC STRAIN RATE (%• S-1)
p = 0.59

ID#: 373051

Relationship between haemodynamic progression, left ventricular response and presence of myocardial fibrosis in aortic stenosis

Miquel Gomez[1]Russell Everett, BSc MD[2], Nick B. Spath, BSc MD[3], Calvin Chin, MD PhD[4], William Jenkins[5], Scott I. Semple, MSc PhD[6], Jacek Kwiecinski, MD[5], Marc R. Dweck, MD PhD[3], David E. Newby, MD PhD[6]

1. Parc de Salut Mar Barcelona, Barcelona, Catalonia, Spain

2. University of Edinburgh, United Kingdom

3. University of Edinburgh, Edinburgh, Scotland, United Kingdom

4. National Heart Center, N/A, Singapore

5. Centre for Cardiovascular Science, University of Edinburgh, UK, United Kingdom

6. University of Edinburgh, Scotland, United Kingdom

Background:

Myocardial fibrosis is an important driver of the transition from left ventricular hypertrophy to heart failure and adverse events in aortic stenosis (AS). Earlier diffuse fibrosis is associated with extracellular volume expansion that is detectable by T1 mapping, whereas late gadolinium enhancement (LGE) detects later replacement fibrosis.

Cardiac magnetic resonance (CMR) and biomarkers of myocardial damage were used to investigate if myocardial fibrosis is associated with disease progression both in terms of valvular stenosis and left ventricular (LV) hypertrophic response in AS patients.

Methods:

In a prospective observational cohort study, AS haemodynamic progression and changes in left ventricular mass were evaluated, at baseline and yearly by echocardiography. High sensitivity troponin I (hsTnI) levels were also determined. Patients with valve peak velocity progression >0,3 m/s/year were classified as fast valve progressors. Patients with increase of indexed LV mass >25 g/m2/year were classified as fast hypertrophic progressors. On CMR, we identified the total extracellular volume of the myocardium indexed to body surface area (iECV) as a marker of diffuse fibrosis.

Results:

163 patients diagnosed with AS (69 years; 69% male) were enrolled and followed up during a median period of 39 [19-43] months. Disease progression in terms of both the valve and LV hypertrophy was associated with baseline AS valve severity (r=0,49 and r=0,41, both p<0.001). 31% of patients were identified as fast valve progressors and 25% were fast hypertrophic progressors. Fast hypertrophic progressors had increased iECV values (iECV) (p=0,01) and increased hsTnI levels, fast valve progressors did not

Conclusion:

In AS patients, rapid progression of the hypertrophic response but not valve stenosis was related to increased markers of myocyte injury and diffuse myocardial fibrosis.

ID#: 373052

Translation of the Non-Invasive Measurement of Creatine Kinase Flux in Human Myocardium: from Bench to Magnet

Mark A. Peterzan, BSc(Hons) MRCP(UK) MA[1] Craig A Lygate, PhD[2], Hannah Lake, MNatSci(Hons)[3], Pete J. Cox, DPhil[4], Jennifer J. Rayner, BMBCh, MRCP(UK)[5], Moritz Jens. Hundertmark, MD[6], Andrew P. Apps, BMBCh MRCP(UK)[3], Rana A. Sayeed, PhD FRCS[7], Mario Petrou, PhD FRCS[8], George Krasopoulos, MD PhD[8], Stefan Neubauer, MD, FRCP[2], William T. Clarke, MChem, D.Phil[9], Christopher T. Rodgers, DPhil[10], Oliver J. Rider, MRCP, DPhil[3]

1. University of Oxford, Oxford, United Kingdom

2. University of Oxford, England, United Kingdom

3. University of Oxford, United Kingdom

4. John Radcliffe Hospital, Oxford, UK, United Kingdom

5. OCMR, University of Oxford, Oxford, England, United Kingdom

6. University of Oxford, Department of Cardiovascular Medicine, Oxford, England, United Kingdom

7. Oxford Heart Centre, Oxford, England, United Kingdom

8. Oxford Heart Centre, England, United Kingdom

9. University Of Oxford Centre for Clinical Magnetic Resonance Research, England, United Kingdom

10. University of Oxford, Oxford, England, United Kingdom

Background: ATP delivery from sites of production to sites of hydrolysis (phosphotransfer) is essential for normal contractile function. Reduced phosphotransfer reserve could serve as a final common pathway for diverse aetiologies to manifest as heart failure. As the prime temporal and spatial energy reserve, the creatine kinase (CK) system is an attractive candidate mediator of this pathway. CK mediates the equilibrium PCr^{2-}+ $MgADP^{-}$ + H^{+} □Cr + $MgATP^{2-}$.In vivo forward flux estimated by magnetisation saturation transfer is calculated as k_f *x* [PCr] where k_f is the pseudo-first order forward rate constant. Prior studies of k_f vs workload under non-ischaemic conditions have reported discordant results. In this study we aimed to 1) validate the measurement of CK k_f against biopsy-obtained CK activity and 2) in healthy hearts assess the response to catecholamine stress.

Methods: Validation of CK k_f 11 patients undergoing valve surgery (10 aortic, 1 mitral) underwent pre-operative CMR (3T Siemens) assessment of left ventricular (LV) function and ^{31}P magnetic resonance spectroscopy for (1) phosphocreatine (PCr)/ATP and (2) CK k_f by Triple Repetition time magnetisation Saturation Transfer (TRiST). In flash-frozen surgical LV biopsies, CK total activity (normalised to citrate synthase activity) and [total creatine] were assessed. Response to Catecholamine Stress 15 healthy volunteers (age 36 ± 10 yrs, BMI 23 ± 3 kg/m^2, SBP 114 ± 11, DBP 67 ± 8 mmHg) underwent the same MRI/MRS protocols and had repeated TRiST during moderate dobutamine stress (25 min infusion, target heart rate 65% of age-predicted maximum).

Results: Strong correlations were observed between non-invasive estimates of CK flux with ^{31}P-MRS and biopsy-obtained CK activity (CK k_f *x* [total creatine], r=0.65, p=0.03, Figure A; CK k_f *x* [PCr/ATP], r=0.74, p=0.014, Figure B). During sustained, moderate catecholamine stress (HR_{stress} 111 ± 10, rate-pressure product (RPP) 6,300 ± 1,700 to 16,600 ± 3,200 mmHg/s), RPP increased 2.5-3-fold, CK k_f increased 1.6-fold (from 0.14 ± 0.09 to 0.23 ± 0.12 s^{-1}) (Figure C, p=.004) and CK k_f as a proportion of workload (i.e. the percentage contribution of CK to ATP delivery) reduced (~1.5-fold).

Conclusion: We provide the first tissue validation of the non-invasive assessment of CK-mediated cardiac energy turnover rates with ^{31}P spectroscopy. Biopsy-assessed CK velocity and non-invasively estimated CK velocity were very well correlated. This is also the first human study showing that acutely increased cardiac workload is associated with increased CK forward velocity. This provides the basis for future translation of this technique for clinical studies.

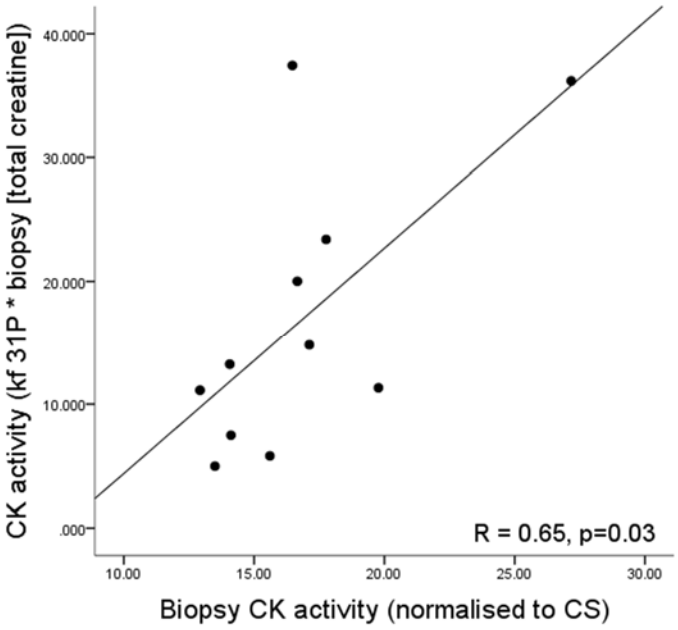

Figure A

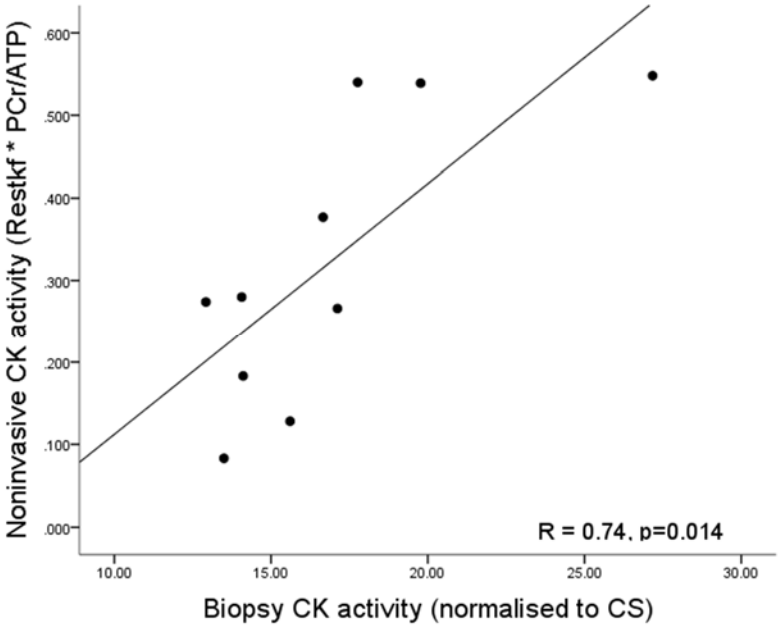

Figure B

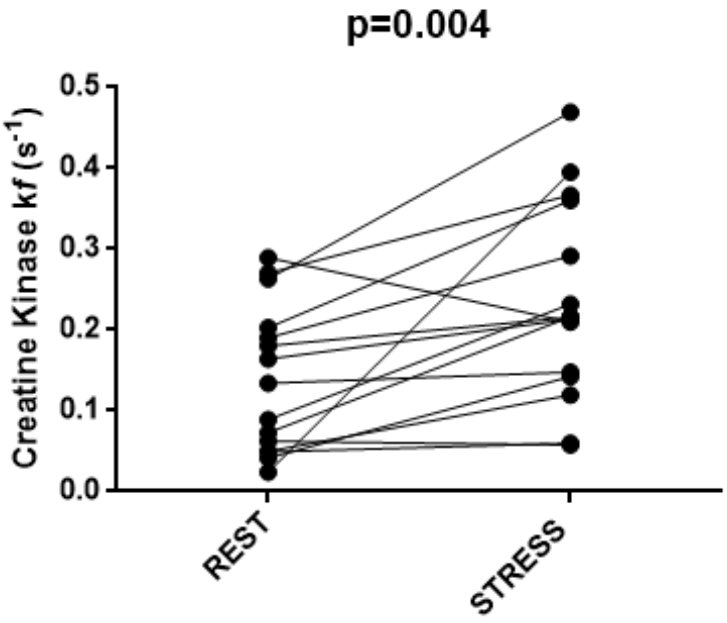

Figure C

ID#: 373053

Early detection of cardiac structural and functional abnormalities in adult Myotonic Dystrophy Type 1 patients using advanced cardiac magnetic resonance imaging

Kavitha Abdul Razak, Griffith University, Queensland, Austalia[1] Aaron Hawkins, Griffith University, Queensland[2], Tien Khoo, School of Medicine, Wollongong, University, NSW[3], Matthew Burrage, School of Medicine, University of Queensland, Queensland[4], Veera Challa, School of Medicine, Griffith University, Queensland[5], Richard Jackson, School of Medicine, Griffith University, Queensland[6], Arun Dahiya, Griffith University, Queensland[7], John Atherton, School of Medicine, University of Queensland, Queensland[8]

1. Logan Hospital, Meadowbrook, Australia, Meadowbrook, Australia

2. Logan Hospital, Meadowbrook, Queensland, Australia

3. Griffith University, Southport, Queensland, Australia

4. Logan Hosptial, Australia

5. Logan Hospital, Queensland, Australia

6. Logan Hospital, Queensland, Australia, Meadowbrook, Australia

7. Logan Hospital, Queensland, Australia, Queensland, Australia

8. School o, Queensland, Australia

Background: Myotonic Dystrophy type 1 (DM1), an autosomal dominant condition, is the most frequently inherited muscular dystrophy in adults and children. DM1 is characterised by progressive muscle weakness, wasting, myotonia and multi-system manifestations that include cardiac abnormalities, such as heart block, atrial or ventricular arrhythmias, cardiomyopathy and heart failure. Therefore, early diagnosis by a robust technique could result in important prognostic information. Although late gadolinium enhancement (LGE) imaging by cardiovascular magnetic resonance (CMR) has been shown to detect focal fibrotic changes, the use of CMR mapping techniques in detection of diffuse fibrosis/inflammation in DM1 patients has not been explored.

Methods: 38 DM1 patients were prospectively evaluated with clinical history, examination, genetic testing, transthoracic echocardiogram and CMR. 14 healthy control participants that were age and gender matched with the DM1 patients underwent CMR. Patients with symptomatic cardiac failure and any implantable cardiac device were excluded from the study.

Results: DM1 patients had higher CMR T2 values (58msec versus 52msec, p=<0.001), and CMR derived expanded extracellular volume (ECV) (31% versus 27%, p=<0.001) when compared to controls. There was a trend towards lower mean CMR left ventricle ejection fraction (LVEF) in DM1 patients compared to controls (57% versus 61%, p=0.06). Prevalence of LGE was low (5.7%). LVEF measured by echocardiogram and CMR was not significantly different.

Conclusion: DM1 patients showed higher ECV and T2 values compared to controls, which appear to be independent of the presence of LGE and LVEF. Our data suggest that CMR mapping techniques targeted towards evaluating myocardial oedema and interstitial fibrosis, by measuring myocardial T2 values and ECV respectively, can be used for early detection myocardial involvement in DM1 patients.

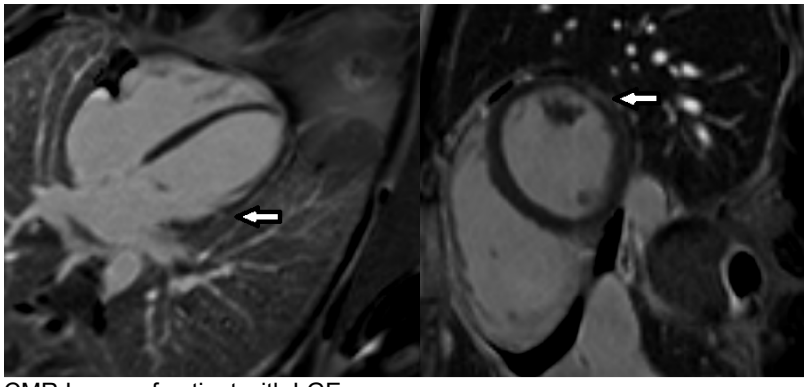

CMR Image of patient with LGE

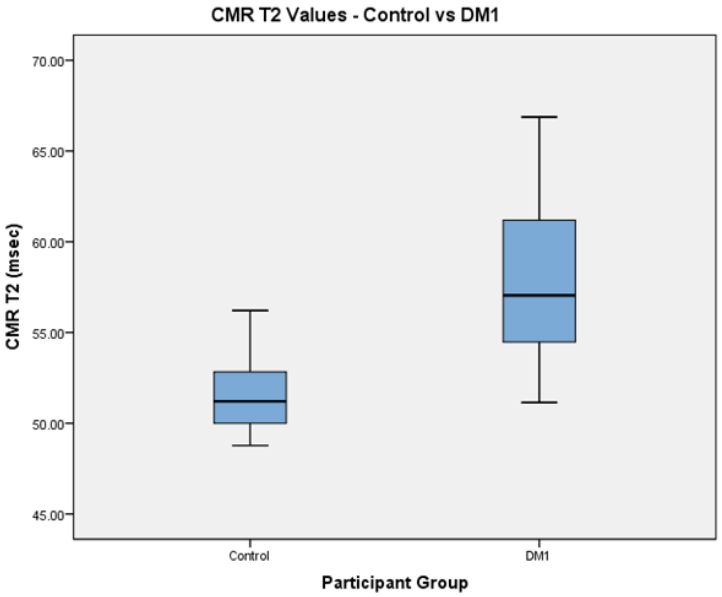

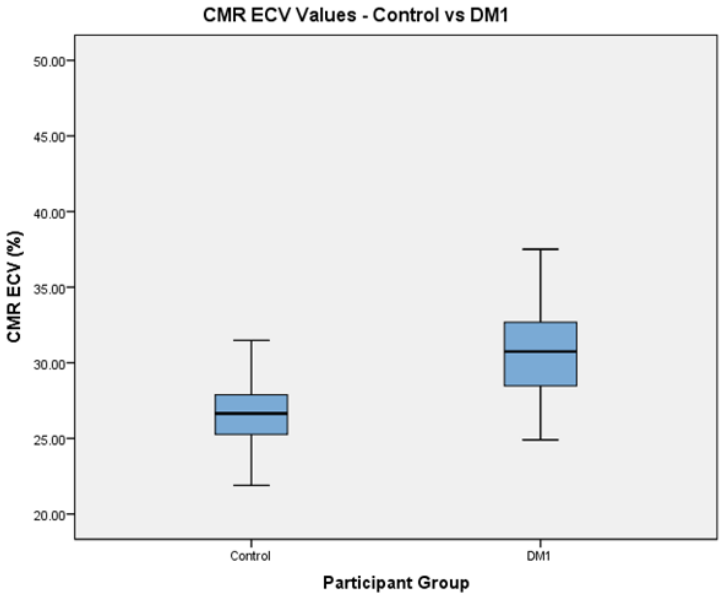

CMR ECV and T2 comparison graphs

Patient charecteristics

PATIENT CHARACTERISTICS	
Age, years (mean± SD, Min, Max)	43 ± 14.0 (20,69)

Gender		
Male, n (%)	22 (58)	
Female, n (%)	16 (42)	
BMI, kg/m^2 (mean ± SD)	24.5 ±5.70	
MIRS score (mean ± SD, n)	3.27 + 0.83	I=0, II=8, III=12, IV=16, V=1
CTG repeats lengths[1] (mean ± SD)	502.26 ± 319.31	
CTG repeat[1] **<200, n (%)** **>200, n (%)**	 3 (13) 20 (87)	
Systolic blood pressure (mean± SD), mm Hg	116.53 ± 11.27	
Diastolic blood pressure (mean± SD) mm Hg	73.94 ± 9.90	
Type 2 diabetes mellitus, n (%)	2 (5.4%)	
Smoker, n (%)	16 (43.2%)	
Dyslipidaemia, n (%)	11(29.7%)	

1. Missing data for CTG repeat 15 patients

ID#: 373061

Incremental value of cardiac deformation analysis in patients with troponin-positive chest pain and unobstructed coronary arteries: a cardiovascular magnetic resonance imaging study

Rocio Hinojar, MD[1] Jose Luis Zamorano, MD, PhD[2], Amparo Esteban, MD[3], Mª Angeles Fernández Mendez, MD[4], Ariana González-Gómez, MD[2], Jose Julio Jimenez-Nácher, MD, PhD[2], Covadonga Fernandez Golfin, MD[4]

1. RAMON Y CAJAL UNIVERSITY HOSPITAL, Madrid, Madrid, Spain

2. Ramon y Cajal University Hospital, Madrid, Madrid, Spain

3. Ramon y Cajal University Hospital, Spain

4. Ramon y Cajal University Hospital, Madrid, Spain

Background: Chest pain syndrome with raised troponin and unobstructed coronary arteries represents around 7-15% of all acute coronary syndromes (ACS). Cardiovascular magnetic resonance (CMR) has important diagnostic and therapeutic implications in this scenario. Impairment of left ventricular (LV) deformation is an independent predictor of cardiovascular (CV) outcomes in various CV conditions despite normal LV ejection fraction (LVEF). CMR feature tracking (CMR-FT) has recently emerged as a robust method that can provide quantitative measurements of myocardial mechanics with good reproducibility. The aim of our study was to evaluate LV strain parameters by CMR-FT in patients with troponin-positive chest pain and unobstructed coronary arteries

Methods: 64 patients admitted with chest pain, raised troponin and unobstructed coronary arteries and 65 healthy controls subjects underwent a conventional CMR study including assessment of oedema (T2-STIR) and late gadolinium enhancement (1.5 T). CMR-FT was applied to standard short and long-axis views of cine SSFP sequences (Circle CVI 42®, Calgary, Canada). Global peak longitudinal, circumferential and radial systolic strain values (GLS, GCS, GRS respectively) were measured in all subjects.

Results: 75% (n=48) of the patients had a definitive diagnosis of acute myocarditis (Amyo), 16% (n=10) acute myocardial infarction (AMI) and 9% (n=6) apical ballooning (AB). Patients showed impaired LV mechanics compared to controls (all patients vs. control, GLS: -15±3 vs. -19±3, GCS: -14 ± 7 vs. -19 ± 3, GRS: 26 ±6 vs. 37±9, p<0,001 for all). The subgroup of patients (n=45) with normal LVEF (FEVI>53%) and no evidence of myocardial LGE or edema (n=15) showed significantly impaired GLS, GCS and GRS (p<0,001 for both groups). The different final diagnosis (Amyo, AMI and AB) demonstrated different LV strain compared to controls (table). A subgroup of 16 patients had a serial scan in the convalescence stage (median of 5 months after symptoms), showing a trend to improvement in all strains in the subacute stage followed (1-3 months) followed by a slight deterioration after 6 months (figure).

Conclusion: LV deformation parameters are impaired in patients with chest pain, raised troponin and unobstructed coronary arteries, even in patients with normal LVEF or no evidence of myocardia LGE or edema, providing novel insight into the pathophysiology of the disease. A complete CMR study including CMR-FT appears promising in this particular scenario. Its potential to predict clinical outcomes needs further evaluation.

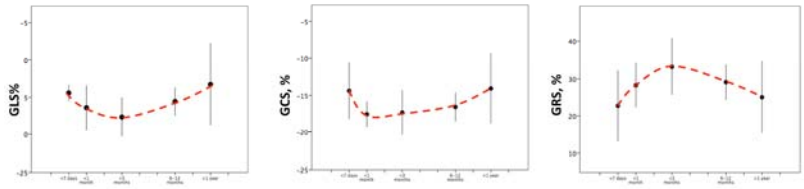

Time course of LV strain values as a function of time since onset of symptoms

	Controls (n=66)	Acute myocarditis n=48	Acute myocardial infarctions, n=10	Apical ballooning, n=6	p value
GLS, %	-19±3	-15 ±3	-14 ±4	12± 3	<0.001

GCS, %	-19 ± 3	- 14 ± 6	-16 ± 3	-8 ± 11	<0.001
GRS, %	37±9	26±5	29 ±7	19 ± 6	<0.001

ID#: 373062

Aliased flow planimetry by low-VENC phase-contrast CMR imaging for the assessment of effective orifice area in aortic valve stenosis: a proof-of-concept study

Fabrizio Ricci[1] Emilia D'Ugo[2], Domenico Rotondo, M.D.[3], Matteo Candeloro[4], Cesare Mantini[5], Antonio Raffaele Cotroneo[6], Sabina Gallina[2]

1. Department of Neuroscience, Imaging and Clinical Sciences, "G. D' Annunzio" University, Chieti, Italy, Pescara, Italy

2. Institute of Cardiology,, Italy

3. SS Annunziata Hospital, Chieti, Italy, Italy

4. "G.d'Annunzio" University, Chieti, Italy, Italy

5. Department of Neuroscience, Imaging and Clinical Sciences, "G. D' Annunzio" University, Chieti, Italy, Italy

6. Department of Neuroscience, Imaging and Clinical Sciences,, Italy

Background: Transthoracic echocardiography (TTE) is the preferred technique for assessing aortic stenosis (AS) severity, and effective orifice area (EOA) is the ideal way to quantify AS. Nevertheless, EOA is operator-dependent, influenced by a number of potential pitfalls and derived from the continuity equation, which requires three different measurements, yielding independent and random sources of error, increasing the propagation error probability eventually affecting the overall accuracy and precision of the measurement. In this study, we aimed to test the accuracy and precision of the aliased orifice area (AOA) planimetry by low-VENC phase-contrast CMR imaging, as a new, simple technique for the evaluation of AS severity.

Methods: Ten consecutive patients with moderate ($0.85cm^2/m^2 \geq EOA \geq 0.6cm^2/m^2$) or severe AS ($EOA < 0.6\ cm^2/m^2$) and 6 age- and sex-matched healthy volunteers underwent unenhanced CMR and TTE examinations. We performed a comprehensive analysis of the agreement and correlation among i) AOA planimetry by low-VENC phase-contrast CMR imaging, ii) geometrical orifice area (GOA) valve planimetry by CMR, iii) EOA by TTE (continuity equation method), and iv) multimodality hybrid EOA (EOA_{hybrid}), as obtained by substituting the LVOT area by CMR into the Doppler continuity equation (arbitrarily set as the gold-standard in reclassification analysis). Using a 3-chamber cine view for reference, a phase-contrast slice was prescribed through the tips of aortic valve leaflets, then by setting the VENC value down to 40-50 cm/s, with NEX of 5 and free-breathing acquisition, an aliased flow signal was detected. AOA planimetry was measured by contouring the aliasing artifact at its largest systolic appearance on phase-velocity maps. Correlations and agreement were assessed with the use of Pearson';s correlation and Bland-Altman method.

Results: AOA showed excellent inter-examination, intra-rater and inter-rater reliability (ICC: 0.953; 0.997; 0.998, respectively). We observed excellent pairwise correlation among AOA, EOA_{hybrid}, GOA and EOA ($P<0.001$), AOA yielding the highest grade of correlation with EOA_{hybrid} ($R^2=0.987$, $P<0.001$). Bland–Altman analysis demonstrated a good agreement between different methods, with the lowest bias for the comparison between EOA_{hybrid} and AOA. At exploratory reclassification analysis, 2 patients with severe AS by AOA and 3 patients with severe AS by EOA were reclassified downward to moderate AS by EOA_{hybrid}.

Conclusion:

Aliased orifice area planimetry by low-VENC phase-contrast imaging is a simple, reproducible, accurate and precise technique for the grading of aortic valve stenosis. Larger studies are warranted to confirm these promising preliminary results.

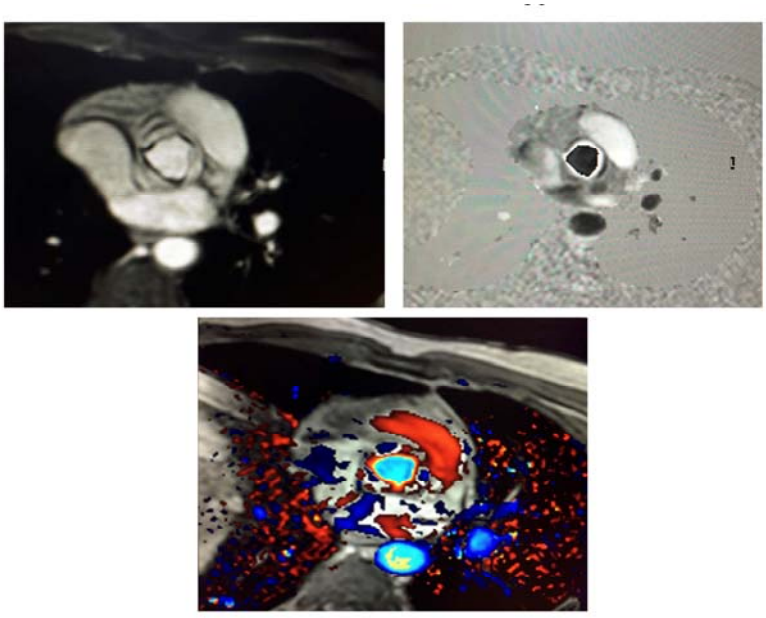

Aliased orifice area of the aortic valve in a healthy volunteer

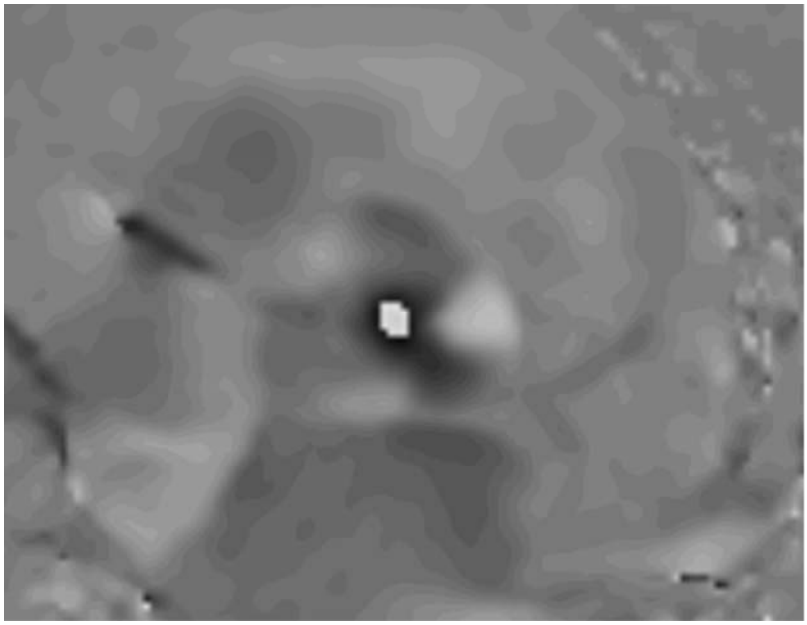

Aliased orifice area in a patient with severe aortic stenosis

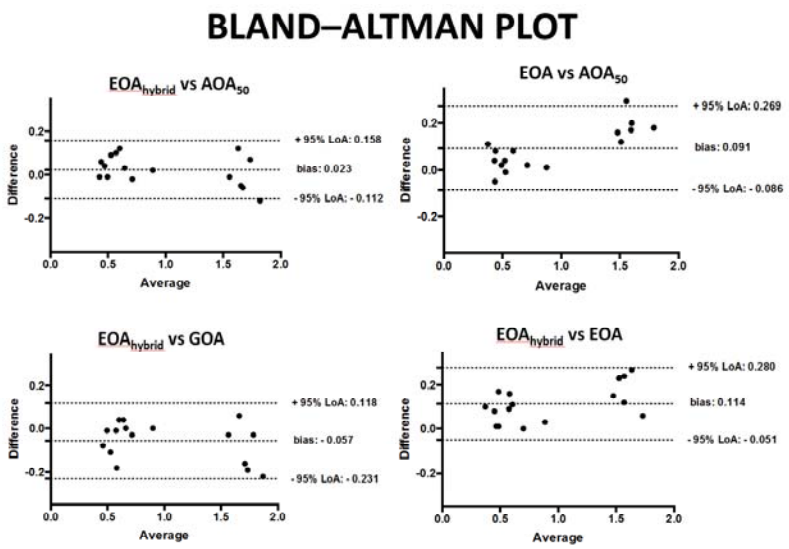

Bland Altman plots

ID#: 373064

Early Detection of Myocardial Involvement by T1 Mapping of Cardiac Magnetic Resonance in Idiopathic Inflammatory Myopathy

Liuyu Yu, BMsci[1] Jiayu Sun, MD[2], Yang Dong, BMsci[3], Qing Zhang, MD[1], Yucheng Chen, MD[2]

1. Sichuan University West China Hospital, China (People's Republic)

2. Sichuan University West China Hospital, Sichuan, China (People's Republic)

3. Cardiology Department West China Hospital Sichuan University, Sichuan, China (People's Republic)

Background: Polymyositis (PM) and dermatomyositis (DM) are common types of Idiopathic inflammatory myopathy (IIM), in which patients are at increased risk of suffering from adverse cardiovascular events. The aim of the study was to explore the value of cardiac magnetic resonance imaging in detecting myocardial involvement in PM/DM patients by T1 mapping technique.

Methods: Twenty-five PM/DM patients (13 male, mean age 50±12 years) with free of cardiovascular symptoms and preserved systolic function underwent CMR imaging, including biventricular function, late gadolinium enhancement (LGE) and T1 mapping sequences. Twenty-five healthy volunteers matched for age, sex served as controls. Myocardial native T1 and extracellular volume (ECV) were analyzed.

Results: Left ventricular volumes, mass, and ejection fraction were similar between PM/DM patients and control subjects. The LGE was only found in 19% of PM/DM patients but none of the control subjects. PM/DM patients showed significantly higher native T1 values (1263.7±84.0 vs. 1200.6±43.0, p=0.002) and expanded extracellular volume (ECV) (32.6±3.7 vs. 26.7±2.3, p<0.001) compare with control subjects. ECV in PM/DM patients showed the highest prevalence (60%) of abnormally increased values beyond the 95% percentile of controls. ROC analysis showed the ECV had the better performances to discriminate patients and controls than native T1 (P=0.03). There was a significant correlation between native T1 (r=0.710, p=0.0001) or ECV (r=0.508, p=0.01) and pro-NT-BNP.

Conclusion: T1 mapping of CMR is valuable to detect subclinical myocardial involvement in patients with PM/DM and both myocardial native T1 and ECV could serve as early imaging markers for myocardial impairment in PM/DM.

ID#: 373065

Improved segmental myocardial strain reproducibility using deformable registration algorithms in comparison with feature tracking CMR and speckle tracking echocardiography

Jie Wang, BMSci[1] Ke Wan, MD[2], Weihao Li, BMSci[3], Jiayu Sun, MD[4], Yucheng Chen, MD[4]

1. Department of Cardiology, West China Hospital, Sichuan University, ChengDu, Sichuan, China (People's Republic)

2. Cardiology Division, West China Hospital, Sichuan University, Guoxue Xiang No. 37, Chengdu, Sichuan Province 610041, China, Sichuan, China (People's Republic)

3. Cardiology Division, West China Hospital, Sichuan University, Chengdu, Sichuan, China (People's Republic)

4. Sichuan University West China Hospital, Sichuan, China (People's Republic)

Background: Left ventricular (LV) global myocardial strain measured by feature tracking (FT) cardiac magnetic resonance (CMR) has reasonable reproducibility, but segmental myocardial strain using this method is not acceptable due to poor reproducibility.There is a need for a better method to assess segmental wall motion using cine CMR. We aim to evaluate the reproducibility of LV segmental myocardial strain measured by deformable registration algorithms (DRA) on cine CMR in a group of healthy volunteers and patients with hypertrophic cardiomyopathy.

Methods: Sixteen healthy volunteers and 31 patients with hypertrophic cardiomyopathy（HCM） were recruited. All subjects had CMR and echocardiography exams within 12 hours of each other. LV global and segmental myocardial strains were analyzed by DRA, FT-CMR, and speckle tracking echocardiography (STE). The reproducibility of global and segmental strains of the three analysis methods were compared.

Results: The intra- and inter-observer agreements of global and segmental longitudinal strain (LS), circumferential strain (CS) and radial strain (RS) by DRA are better as compared to FT-CMR or STE. DRA showed the best observer agreement on segmental strain evaluated by ICC（LS：intra-observer variability range [0.98,1.00], inter-observer variability range [0.83,0.92], CS：intra-observer variability range [0.90,0.99], inter-observer variability range [0.80,0.97], RS: intra-observer variability range [0.84,0.99], inter-observer variability range [0.85,0.99]）. Segmental LS, CS and RS agreements evaluated by COV for FT-CMR and STE were poor. In addition, LV global myocardial strain of HCM were significantly lower than controls for all applied techniques but GCS by DRA had better accuracy compared to FT or STE for distinguishing HCM from healthy subjects（AUC 0.880 (DRA) vs. 0.577 (FT) or 0.736 (STE), $p < 0.05$, respectively）.

Conclusion: DRA is a reliable and robust analysis tool for segmental myocardial strain, which could be used for evaluation of regional myocardial dysfunction. In addition, global CS by DRA allows discrimination between HCM and normal controls with better accuracy compared to FT and STE.

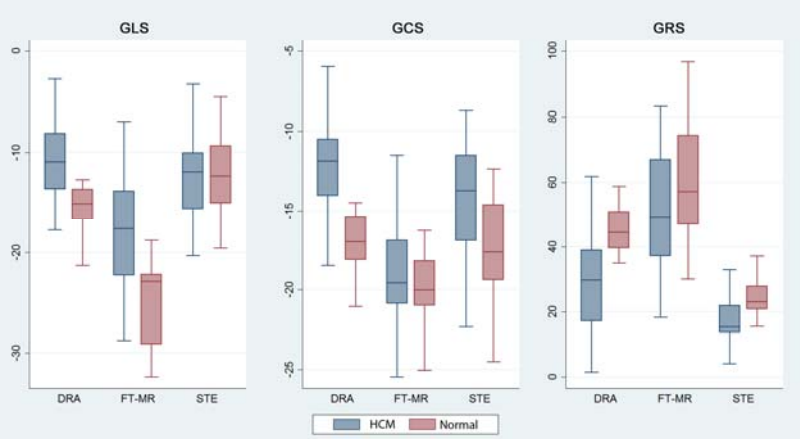

Global strain comparisons with different techniques between normal control and patients with HCM.All $p < 0.05$ vs. controls between different techniques or parameters.

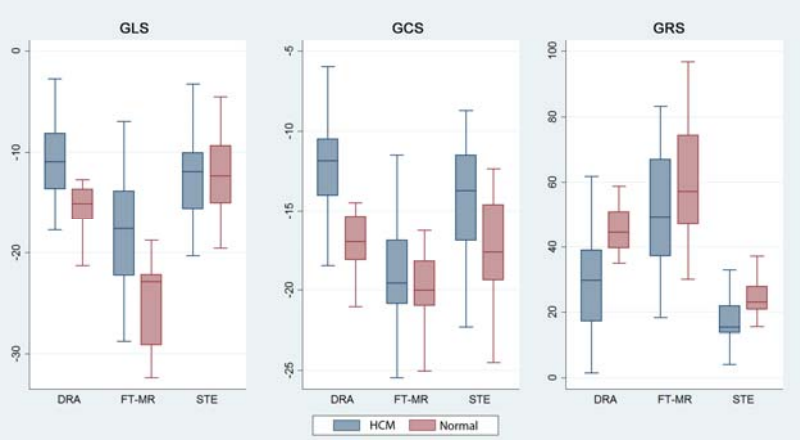

Global strain comparison with different techniques between normal control and patients with HCM.All p ＜0.05.

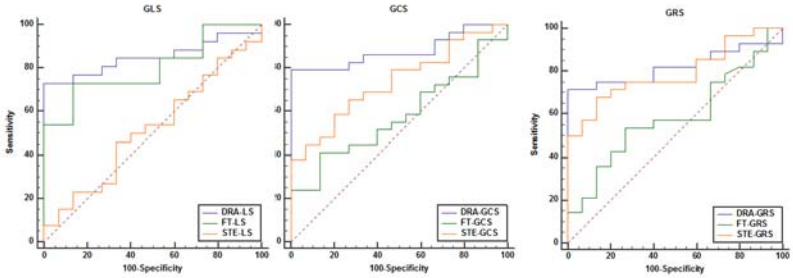

Receiver operating characteristic（ROC）curve of global strain for detection of HCM and normal controls.Pairwise comparison of ROC curves by GCS：p＜0.01(DRA-FT), p=0.04(DRA-STE), p=0.06(FT-STE), respectively.

ID#: 373070

Assessment of flow using phase contrast velocity mapping with radial acquisition ultrashort echo times for irregular heart rhythms

Michaela M. Hell[1] Jane M. Francis[2], Joanna d'Arcy[3], Stefan Neubauer, MD, FRCP[4], Stephan Achenbach[5], Saul Myerson, MD, FRCP[6]

1. Department of Cardiology, Faculty of Medicine, Friedrich-Alexander University Erlangen-Nürnberg, Germany, Germany

2. University of Oxford, OX39DU, England, United Kingdom

3. Division of Cardiovascular Medicine, Radcliffe Department of Medicine, University of Oxford, United Kingdom, United Kingdom

4. University of Oxford, England, United Kingdom

5. Department of Cardiology, Faculty of Medicine, University of Erlangen-Nürnberg, Germany, Germany

6. University of Oxford, Oxford, England, United Kingdom

Background: Phase contrast velocity mapping sequences utilising ultrashort echo time (UTE) radial k-space sequences have been used to reduce intravoxel dephasing at high velocities. Their ability to quantify flow has not been well assessed previously and we examined the accuracy of the UTE flow sequence in the quantification of mitral regurgitation, including patients with atrial fibrillation (who may benefit from radial sequences which acquire a proportion of central k-space with each line, as this may reduce flow quantification errors in very irregular rhythms).

Methods: Forty patients underwent cardiovascular magnetic resonance imaging for indirect mitral regurgitation quantification by assessment of aortic flow by a standard phase contrast sequence (TE 2.85 ms) and by a UTE phase contrast sequence (TE 0.65 ms), combined with LV stroke volume for calculation of mitral regurgitation. Retrospective acquisition was used in patients in sinus rhythm (30 patients), whereas patients in atrial fibrillation (10) were scanned prospectively. Mitral regurgitation was also quantified by comparing left and right ventricular stroke volumes. Bland-Altman analysis was used for comparison.

Results: UTE flow derived mitral regurgitation measurement showed modest agreement for patients in sinus rhythm (95% limits of agreement: ±38.2 ml; ±29.8%) and in atrial fibrillation (±33.7 ml; ±30.3%) compared to the standard flow method (see figure). The UTE flow method showed little systematic bias in patients with sinus rhythm (mean offset -4.4 ml / -3.5% compared to standard flow assessment), but there was a slight bias towards greater regurgitation with the UTE flow method in patients with atrial fibrillation (mean offset +15.2 ml; +14.0%). There were wider limits of agreement between the UTE flow method and the volumetric method in sinus rhythm (±48.4 ml; ±36.4%; mean offset: -12.2ml / -9%) and similar limits of agreement in patients with atrial fibrillation (±29.6 ml / 25.8%; mean offset: +12.0 ml / +10.3%).

Conclusion: UTE flow imaging for mitral regurgitation assessment compares reasonably well with standard flow imaging. With the relatively low number of patients with AF in this initial study, no superiority of UTE flow imaging was demonstrated for arrhythmic patients over standard flow imaging when comparing both to the volumetric method.

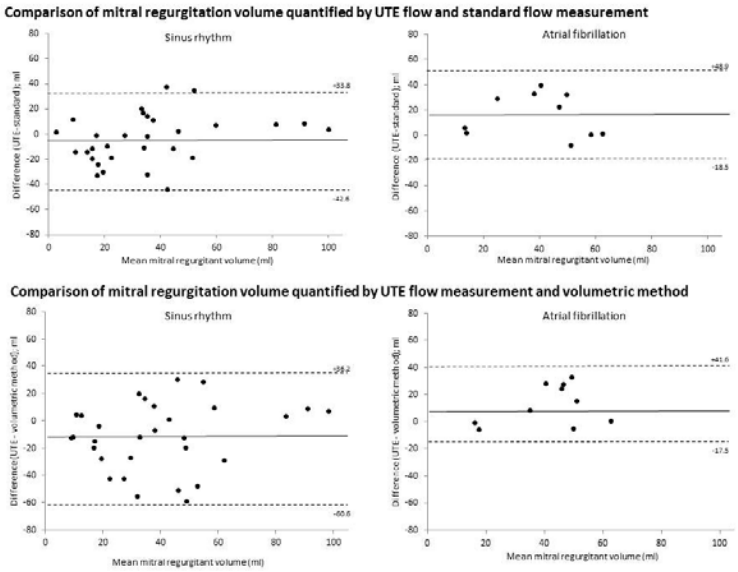

Comparison of mitral regurgitant volume quantified by UTE flow measurement with conventional methods

Comparison of mitral regurgitation volume quantified by UTE phase contrast imaging compared to conventional methods

Regurgitant volume (ml)		Total cohort (n=40)	Patients in sinus rhythm (n=30)	Patients in atrial fibrillation (n=10)
UTE flow versus standard flow methods	*95% limits of agreement*	±40.4	±38.2	±33.7
	Bias (offset)	+0.5	-4.4	+15.2
UTE flow method versus volumetric method	*95% limits of agreement*	±48.8	±48.4	±29.6
	Bias (offset)	-6.1	-12.2	+12.0

ID#: 373072

Cardiac ATP delivery rates in chronic severe mitral regurgitation

Mark A. Peterzan, BSc(Hons) MRCP(UK) MA[1] Jennifer J. Rayner, BMBCh, MRCP(UK)[2], Stefan Neubauer, MD, FRCP[3], William T. Clarke, MChem, D.Phil[4], Christopher T. Rodgers, DPhil[5], Oliver J. Rider, MRCP, DPhil[6]

1. University of Oxford, Oxford, United Kingdom

2. OCMR, University of Oxford, Oxford, England, United Kingdom

3. University of Oxford, England, United Kingdom

4. University Of Oxford Centre for Clinical Magnetic Resonance Research, England, United Kingdom

5. University of Oxford, Oxford, England, United Kingdom

6. University of Oxford, United Kingdom

Background: The creatine kinase (CK) system is the cardiomyocyte';s prime temporal and spatial energy reserve. CK mediates the equilibrium PCr^{2-}+ $MgADP^{-}$ + H^{+} □Cr + $MgATP^{2-}$.At a given pH, maximum forward flux is proportional to V_{max}[MgADP][PCr], where V_{max} is maximum forward velocity and depends on total enzyme activity. In vivo flux in the forward (ATP-generating) direction estimated by magnetisation saturation transfer is calculated as k_f *x* [PCr] where k_f is the pseudo-first order forward rate constant. There are few previous studies of left ventricular (LV) metabolic phenotype in human severe primary mitral regurgitation. We studied this as a model of metabolic adaptation to chronic volume overload.

Methods: 19 patients (age 67 ± 10, BMI 26 ± 8, 12 male) with severe primary mitral regurgitation awaiting surgical repair (NYHA class 2.0 ± 0.6) and 13 controls (age 48 ± 20, BMI 23 ± 3, 4 male) were recruited. All underwent cardiac magnetic resonance imaging (3T Siemens) for LV volumes (mL), function (LVEF %) and mass (g) and 31P magnetic resonance spectroscopy for (1) phosphocreatine (PCr)/ATP ratio by 3D ultra-short TE chemical shift imaging and (2) CK k_f by Triple Repetition time magnetisation Saturation Transfer (TRiST). All participants had normal LVEF (≥55%).

Results:

Patients had severe mitral regurgitant volume (LV stroke volume minus aortic forward flow 68 ± 35 vs 3 ± 5 mL, p<.001). Compared with controls, subjects had increased LVEDV (220 ± 64 vs 151 ± 47 mL, p=.001), LVEF (68 ± 7 vs 61 ± 4%, p=.002), and LV mass (135 ± 45 vs 90 ± 27 g, p=.001), with unaltered LV mass/LVEDV ratio (0.62 ± 0.10 vs 0.61 ± 0.12 g/mL). Severe mitral regurgitation was associated with reduced PCr/ATP ratios (1.57 vs 2.13, p=.001), unaltered CK k_f (0.15 ± 0.08 vs 0.17 ± 0.09 s^{-1}, p=.55) and unaltered estimated CK flux at rest i.e. k_f *x* PCr/ATP (0.24 ± 0.16 vs 0.36 ± 0.22, p=.12) (Figure).

Conclusion: This is the first study (to our knowledge) of CK k_f in the human LV adapted to chronic volume overload with preserved LV systolic function. In this setting, although PCr/ATP ratio is significantly reduced, we find no significant difference in CK k_f or resting CK forward flux estimated by the product (k_f *x* PCr/ATP). The degree of reduction in PCr/ATP (<1.60) is surprising given the supra-normal LVEF.

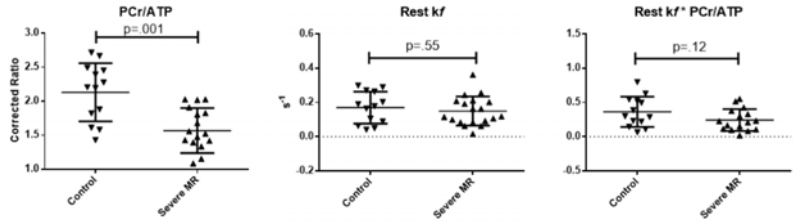

Blood- and saturation-corrected PCr/ATP ratio (left), CK kf (middle) and estimated CK flux (right).

ID#: 373073

Cardiac ATP delivery rates in chronic pressure overload

Mark A. Peterzan, BSc(Hons) MRCP(UK) MA[1] Jennifer J. Rayner, BMBCh, MRCP(UK)[2], Stefan Neubauer, MD, FRCP[3], William T. Clarke, MChem, D.Phil[4], Christopher T. Rodgers, DPhil[5], Oliver J. Rider, MRCP, DPhil[6]

1. University of Oxford, Oxford, United Kingdom

2. OCMR, University of Oxford, Oxford, England, United Kingdom

3. University of Oxford, England, United Kingdom

4. University Of Oxford Centre for Clinical Magnetic Resonance Research, England, United Kingdom

5. University of Oxford, Oxford, England, United Kingdom

6. University of Oxford, United Kingdom

Background: The creatine kinase (CK) system is the cardiomyocyte';s prime temporal and spatial energy reserve. CK mediates the equilibrium PCr^{2-}+ $MgADP^{-}$ + H^{+} □Cr + $MgATP^{2-}$.At a given pH, maximum forward flux is proportional to V_{max}[MgADP][PCr], where V_{max} is maximum forward velocity and depends on total enzyme activity. In vivo flux in the forward (ATP-generating) direction estimated by magnetisation saturation transfer is calculated as k_f *x* [PCr] where k_f is the pseudo-first order forward rate constant. There are no prior studies of CK $k_f$in the pressure-overloaded human heart. We studied isolated severe aortic stenosis as a model of metabolic adaptation to chronically increased left ventricular (LV) external work (pressure-stroke volume product).

Methods: 21 subjects with severe AS (age 71 ± 8, BMI 28 ± 5, 11 male, 3 in AFib) diagnosed by clinical echocardiography, preserved LV ejection fraction (LVEF), no coronary flow limitation or myocardial infarction and listed for aortic valve (AV) replacement, and 13 controls (age 48 ± 20, BMI 23 ± 3, 4 male, 3 in AFib) underwent 1H CMR imaging (3T Siemens) for LV volumes and mass, 31P magnetic resonance spectroscopy for (1) phosphocreatine (PCr)/ATP ratio by 3D ultra-short TE chemical shift imaging and (2) CK k_f by Triple Repetition time magnetisation Saturation Transfer (TRiST).

Results:

Subjects met criteria for severe AS (peak AV gradient 82 ± 20 mmHg, mean gradient 47 ± 13, dimensionless velocity index 0.22 ± 0.06). Compared with controls, subject LVs were hypertrophied (LV mass 138 ± 35 vs 90 ± 27 g, p<.001) and concentrically remodelled (LV mass/LVEDV ratio 1.06 ± 0.27 vs 0.61 ± 0.12, p<.001) with increased LVEF (71 ± 7 vs 61 ± 4%, p<.001).

Severe aortic stenosis was associated with reduced PCr/ATP ratios (1.71 ± 0.29 vs 2.13 ± 0.43, p=.006). No significant between-group differences were observed in rest k_f (0.17 ± 0.14 vs 0.17 ± 0.09) or CK flux estimated by rest k_f *x* PCr/ATP (0.26 ± 0.22 vs 0.36 ± 0.22, p=.23) (Figure).

Conclusion: In this first study (to our knowledge) of CK k_f in chronic human LV pressure overload, PCr/ATP ratio is significantly reduced with no signficant difference in CK k_f or resting CK forward flux estimated by the product (k_f *x* PCr/ATP).

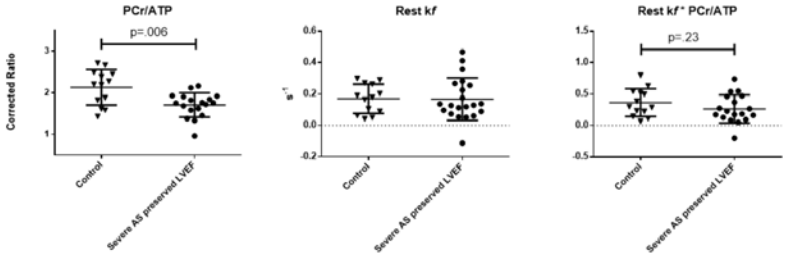

Blood- and saturation-corrected PCr/ATP ratio (left), CK kf (middle) and estimated CK flux (right).

ID#: 373081

'Crash diets' cause acute impairment of cardiac function with associated myocardial lipid accumulation

Jennifer J. Rayner, BMBCh, MRCP(UK)[1] Mark A. Peterzan, BSc(Hons) MRCP(UK) MA[2], Ines Abdesselam, PhD[3], Stefan Neubauer, MD, FRCP[4], Oliver J. Rider, MRCP, DPhil[5]

1. OCMR, University of Oxford, Oxford, England, United Kingdom

2. University of Oxford, Oxford, England, United Kingdom

3. Oxford University, Oxford, England, United Kingdom

4. University of Oxford, England, United Kingdom

5. University of Oxford, United Kingdom

Background: Very Low Calorie Diets (VLCD) are a highly effective and increasing utilised weight loss intervention that rapidly reduce liver fat, and reverse diabetes. Although these metabolic improvements would be expected to improve cardiac function, we hypothesised that the rapid mobilisation of hepatic fat, triggered by extreme caloric restriction, would be accompanied in the short term by an increase in myocardial triglyceride and functional decline.

Methods: 21 obese volunteers (6 male, 52 ± 13 years, BMI 37.1 ± 5.9 kg m^{-2}) underwent body composition analysis, MRI (3T Siemens) for abdominal visceral and liver fat quantification, LV structure and function, ^{1}H-MR spectroscopy to measure myocardial triglyceride content (MTGC), and echocardiography for diastolic function (e/e';), before and after one week, and eight weeks of VLCD (6-800kcal/day).

Results: After 7 days of VLCD, total body fat (by 6 ± 4% p<0.001), visceral fat (by 11 ± 15% p=0.005) and hepatic fat all fell significantly (by 42 ± 23% p<0.001, fig 1A). This was accompanied by a marked and rapid improvement in insulin resistance (HOMA-IR by 42 ± 31%, p=0.005), fasting total cholesterol, triglycerides and glucose (all p<0.01). Despite this, MTGC rose by 44% (p=0.038, fig 1B), and was associated with reductions in both systolic function (LVEF 66 ± 4% to 63 ± 5%, p=0.032, fig 2A; peak radial strain 53 ± 9% to 45 ± 9%, p=0.005, fig 2B) and diastolic function (e/e'; 8.5 ± 1.5 to 10.0 ± 3.1, p=0.024, fig 2C). This change in MTGC at one week correlated with both change in LVEF (r= -0.496, p=0.05, fig 3A) and diastolic function (peak diastolic strain rate; r=0.482, p=0.058, fig 3B). However at 8 weeks (n=10), although peripheral metabolic measurements continued to improve from baseline, MTGC as well as cardiac function had returned to normal (fig 1 and 2).

Conclusion: We have used multi-parametric MR to document the effects of lipid redistribution during VLCD, and its contrasting effects on peripheral markers of the metabolic syndrome and cardiac function. We demonstrate that although a 7 day period of severe caloric restriction results in marked improvement in hepatic fat and whole body insulin sensitivity, this comes at the cost of significant accumulation of myocardial fat and cardiac functional decline. This suggests that although these diet programmes are highly effective, they are likely to require careful monitoring in the early stages in individuals with cardiac disease.

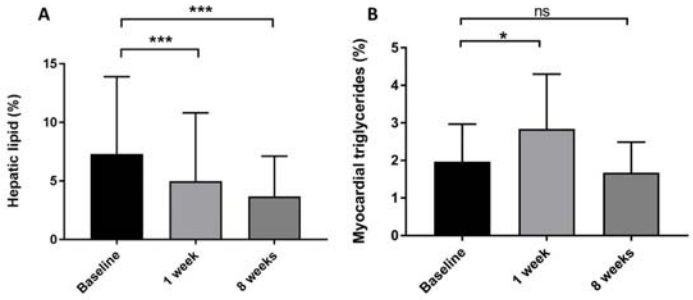

Figure 1: The acute and medium-term effects of VLCD on hepatic lipid (A) and myocardial triglyceride content (B). * indicates p<0.05; *** indicates p<0.001.

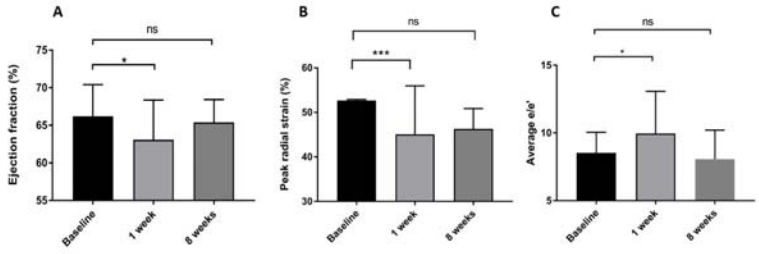

Figure 2: The acute and medium-term effects of VLCD on cardiac function - both systolic (ejection fraction, A; strain, B) and diastolic (e/e', C). * indicates p<0.05; *** indicates p<0.001.

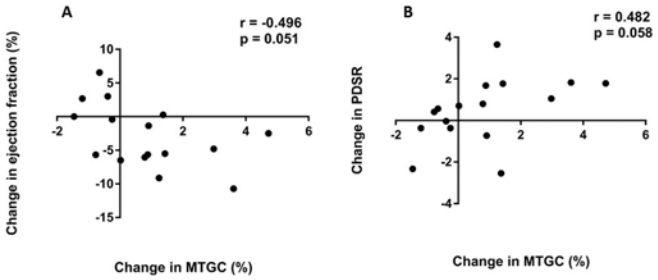

Figure 3: The change in myocardial triglyceride content at one week is associated with systolic (A) and diastolic (B) impairment

ID#: 373003

A novel Cardiac MRI-based 3D method to design personalized aortic valves: The sinus-mirror valve hypothesis

Michael Silberbach, MD[4]Xiao-Yue Han, BS, MS4[1], Craig S. Broberg, MD, MCR[2], Erik L. Frandsen, MD[3], Erin Madriago, MD[1], Sandra Rugonyi, PhD[1], Irving Shen, MD[4]

1. Oregon Health & Science University, OR

2. Oregon Health and Science University, Portland, OR

3. Seattle Children's Hospital, Seattle, WA

4. Oregon Health & Science University, Portland, OR

Background: Bicuspid aortic valve (BAV) is the most common congenital heart malformation and often leads to aortic insufficiency and stenosis requiring operative repair or replacement. We explored the use of the sinuses of Valsalva as templates to design personalized prostheses (sinus-mirror valves) in patients with tricuspid aortic valves (TAV) and BAV. We hypothesized that sinus-mirrored trileaflet valves predicted from patients with TAV or BAV will have the same valve coaptation areas, cusp height, and coaptation line orientation.

Methods: We studied patients with TAV and no stenosis/regurgitation (n=50*)* or BAV (n=50). All had cardiac MR angiography. Blinded DICOM data was exported to the Mimics Innovation Suite v17.0 (Materialise, Belgium) for segmentation and to 3-Matic for (1) wrapping and hollowing to isolate the 3D contour of the aortic sinuses, (2) identifying mirror planes of the three sinuses of Valsalva, and (3) mirroring the sinus shape across the mirror planes to produce sinus-matched aortic valve models. Closed valve coaptation areas, cusp height, and coaptation line orientation between TAV and BAV were compared.

Results: Regardless whether subjects had TAV or BAV there were three sinuses in all but 2 patients. Annulus-adjusted total valve coaptation areas of predicted valves from either BAV or TAV subjects were essentially identical (p=0.84), but adjusted right-left cusp coaptation area and cusp height were less in BAV than TAV (p=0.17)

Conclusion: Comparison of predicted sinus-mirror aortic valve morphology between TAV and BAV patients shows similar total valve coaptation areas suggesting that the sinus-mirror three-leafleted valves made from BAV patients will be competent. Personalized valves created by matching valve shape to sinus morphology in individual patients may decrease shear, improve hemodynamics, and increase coronary blood flow compared to off-the-shelf prosthetic aortic valves.

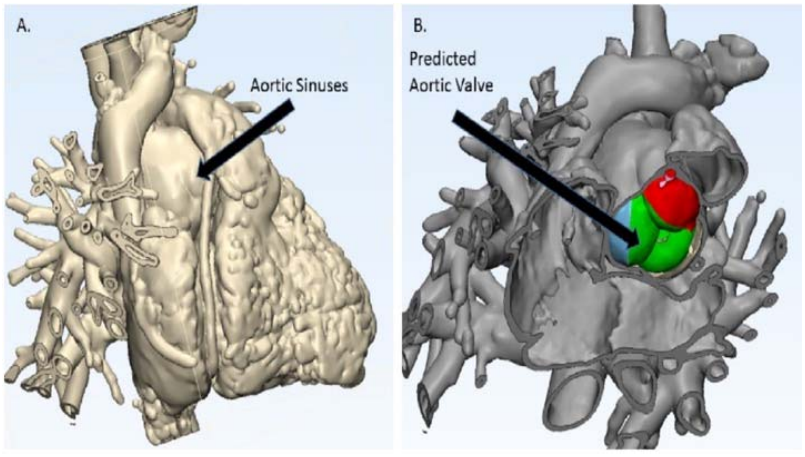

Sinus-mirrored trileaflet valves from subjects with bicuspid aortic valves

ID#: 373007

Towards improving applicability of respiratory self-gating (RSG): a multi-band approach

Chenxi Hu, PhD[1] Dana C. Peters, PhD[2]

1. Yale University, CT

2. Yale University

Background: Respiratory self-gating (RSG) has been developed for free-breathing cardiac cine imaging and has been mainly validated in the short-axis view[1-3]. However, there are recognized challenges in the other slice-planes, such as the long-axis and axial view, where the image has only subtle or zero diaphragmatic coverage[4]. Here the purpose is to develop a novel RSG approach that inserts multi-band excitation into the RF train of a cine sequence to enable the choice of a better RSG plane for monitoring the respiratory motion.

Methods: The proposed multi-band RSG radial cine sequence is illustrated in Figure 1. During each cardiac phase, a single projection is acquired twice, once using a multi-band excitation, which excites a navigator slice-plane while maintaining the steady-state of the imaging slice. While the slice position changes as multiple slices are to be imaged, the navigator plane remains stationary by adjustment of its excitation frequency. The subtraction of the multi-band projection and its single-band counterpart is used to monitor the "DC" signal for RSG. Healthy volunteers were imaged on a 3T scanner (Siemens) after providing written informed consent. Multiple imaging views, e.g. short-axis and axial, were imaged with the proposed technique. Sequence parameters were: image size 192x192, spatial resolution 1.6mmx1.6mm, slice thickness 3.5mm (axial) or 6mm (short-axis), 18-20 slices, 63 projections, 3 shots, 10-13 phases, 5 repetitions, GRE readout, TR/TE/q/ bandwidth =3.4ms/1.9ms/12°/1000 Hz/pixel, and total scan time=4-5 minutes. All of the imaging plane data was used to generate a conventional RSG signal.

Results: Figure 2 shows the smoothed RSG signals from multi-band RSG and conventional tracking. While the multi-band self-gating signal accurately depicts the respiratory motion, the conventional RSG signal is contaminated by the transient state in the beginning of each slice acquisition and the varying signal as the slice changes. In the axial view, due to the absence of diaphragm in some slices, respiratory motion cannot be continuously detected using conventional RSG. Figure 3 shows the end-systole and end-diastole images from the two views reconstructed with simple averaging and with the multi-band RSG. Several features are much improved in the multi-band approach.

Conclusion: The proposed method of multi-band self-gating improves applicability of RSG especially for certain slice-planes and during changes in slice location. This may greatly improve the appeal of self-gating in clinical practice.

References

1. Lai MRM 2008; 2. Larson MRM 2005; 3. Stehning MRM 2005; 4. Spincemaille Proc. ISMRM 2007

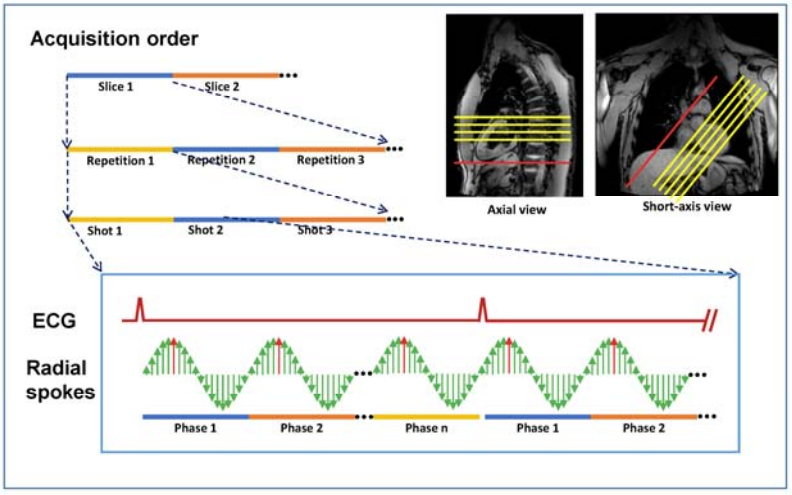

Figure 1. A schematic of the multi-band self-gating segmented radial cine sequence. For each slice, the sequence

samples through multiple shots with multiple repetitions. Each shot comprises acquisition of multiple cardiac phases with a series of sequentially applied radial spokes. After a fixed spoke in every phase, a multi-band excitation (red arrow) with the same angle as the previous spoke is applied to acquire signal from both the imaging plane and the navigator plane, which is placed in a respiratory motion sensitive slice (the red line shown in the images). A subtraction of the signal from the imaging plane only and the signal from the multi-band acquisition gives a tracking signal of the respiratory motion.

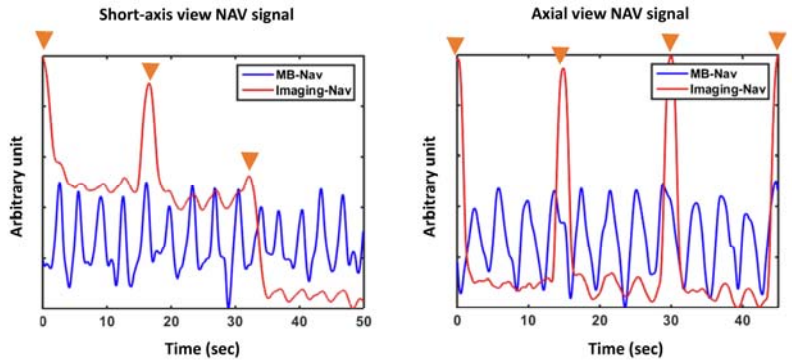

Figure 2. The self-gating signal from the multi-band approach and from the imaging plane itself (the conventional approach). The multi-band approach successfully detects the breathing motion in both short-axis and axial views. The imaging plane “DC” signal is successful in most time of the short-axis view except the period before entering steady state for each slice (arrow heads). In the axial view, the imaging plane “DC” signal contains incomplete breathing motion due to the absence of diaphragm in some slices. Signal is scaled for display.

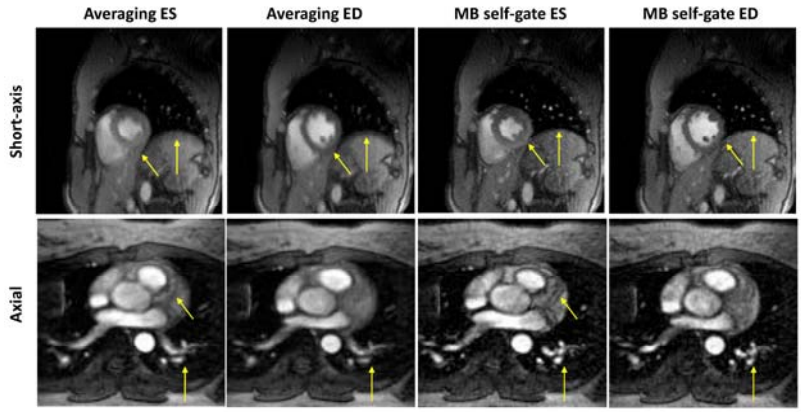

Figure 3. The retrospectively reconstructed end-systolic and end-diastolic images from the free-breathing multi-slice cine sequence by averaging the repetitions or using self-gating in both short-axis and axial view. Parallel imaging (radial SENSE) was used for both reconstruction. Considerable improvement is observed by using self-gating, including better sharpness of the papillary muscle and liver dome in the short-axis images and a better depiction of coronary vasculature and pulmonary veins in the axial view images.

ID#: 373095

Septal curvature during exercise in pulmonary hypertension- a pilot CMR study

Raj Puranik, PhD FRACP[1] Clare Arnott, MBBS FRACP[2], Danyi Zhu, phD[3], Jacqueline Stewart[4], David Celermajer, PhD DSc [5]

1. Royal Prince Alfred Hospital, University of Sydney, Camperdown, New South Wales, Australia

2. Royal Prince Alfred Hospital and University of Sydney, Camperdown, New South Wales, Australia

3. University of Sydney, Camperdown, New South Wales, Australia

4. Specialist MRI, Newtown, New South Wales, Australia

5. Royal Prince Alfred Hospital, University of Sydney, Camperdown, New South Wales, Australia

Background: Interventricular septal curvature (IVSC) during resting cardiac MRI (CMR) has been shown to be a valuable parameter in the non-invasive assessment of right ventricular (RV) afterload. Resting IVSC is predictive of both mean pulmonary artery pressure (MPAP) and pulmonary vascular resistance (PVR) in pulmonary arterial hypertension (PAH). No studies, however, have assessed the predictive value or utility of septal curvature ratio (septal to lateral curvature ratio) during exercise imaging.

Methods: Six patients with Type 1 PAH (age 47+/-16years, 67% female) and 13 healthy controls (age 50+/-16years, 46% female) underwent cardiopulmonary exercise testing, transthoracic echocardiogram and exercise CMR (1.5T Phillips) to >60% W max on a MRI safe cycle ergometer. Septal curvature was analysed at end-systole and end-diastole on short axis imaging using specially designed Matlab codes. Deviation towards the RV was defined as negative and towards the LV lateral wall as positive from the midline or ‘0'; point.

Results: The PAH patients had mean systolic PAP 53 +/- 24 mmHg, normal resting RV ejection fraction (57.0+/-5%) and a RV contractile reserve of 6% on submaximal exercise as compared to 14% in healthy controls ($p<0.001$). During submaximal exercise there was a significant difference in septal curvature at end-systole between groups. Those with PAH had a significantly ‘flatter'; IVSC, indicating marked leftward bowing of the septum into the LV cavity (Curvature ratio: Controls -1.082 versus PAH -0.520, $p=0.002$). At end-diastole during exercise the curvature ratio was also significantly different between groups, indicative of impaired LV filling (Controls -1.12 versus PAH -0.44, $p=0.029$). End-systolic curvature ratio on exertion correlated positively with invasive haemodynamics (PVR: Spearman rank 1.0, $p=0.001$; MPAP: Spearman 0.90, $p=0.04$; SPAP: Spearman 0.87, $p=0.005$) and negatively correlated with RV contractile reserve on exercise CMR (Spearman -0.76, $p=0.046$).

Conclusion: Interventricular septal curvature ratio at end-systole and end-diastole during submaximal exercise is abnormal in those with elevated RV afterload as compared to healthy controls. An abnormal end-systolic curvature ratio correlated with elevated PAP, PVR and reduced RV contractile reserve, in these subjects.

ID#: 373096

Thalassemia Intermedia: a truly cardiac iron-overload free disease?

Camilla Torlasco, MD[1] Elena Cassinerio, MD[2], Giovanna Graziadei, MD[3], Marco Capecchi, MD[4], Giuseppina Quattrocchi, MD[5], Angela Milazzo, MD[5], Amna Abdel-Gadir, MBBS MRCP[6], Cristina Giannattasio, MD[7], Gianfranco Parati, MD, PhD[8], James C. Moon, MD[9], Maria Domenica DOMENICA, MD[10], Patrizia Pedrotti, MD[11]

1. University of Milan-Bicocca. IRCCS Istituto Auxologico Italiano, Milan, Italy, Milan, Lombardia, Italy

2. "Ca' Granda" Foundation IRCCS, Milan, Italy, Lombardia, Italy

3. Fondazione IRCCS Ca' Granda Ospedale Maggiore Policlinico, Milan, Italy, Milan, Lombardia, Italy

4. "Ca' Granda" Foundation IRCCS, Milan, Italy, Italy

5. Department of Cardiology and Cardiac Surgery ASST Grande Ospedale Metropolitano Niguarda Milano, Italy, Lombardia, Italy

6. UCL, United Kingdom

7. Department of Cardiology and Cardiac Surgery ASST Grande Ospedale Metropolitano Niguarda Milano, Italy, Italy

8. IRCCS Istituto Auxologico Italiano, Milan, Italy, Italy

9. Barts Heart Centre, St Bartholomew's Hospital, London, UK, United Kingdom

10. "Ca' Granda" Foundation IRCCS-University of Milan, Milan, Italy, MILANO, Lombardia, Italy

11. ASST Grande Ospedale Metropolitano Niguarda, Lombardia, Italy

Background: Thalassemia Intermedia (TInt) patients accumulate iron, both from transfusion and from inappropriate increased intestinal absorption. Cardiac iron is cardiotoxic and can lead to heart failure and death. T2* is the gold standard for its assessment but T2* appears to miss mild iron overload in Thalassemia major due to susceptibility artefact, and a chosen cut point of (20msec). T1 mapping appears more sensitive. We assessed the cardiac iron burden by T2* and T1 mapping in TInt.

Methods: A single centre prospective study of 47 TInt patients and 32 healthy controls respectively. T1 mapping (modified look locker inversion recovery –MOLLI – Siemens Works in progress 448B - MOLLI) was compared to dark blood T2* at 1.5T (Avanto, Siemens Healthcare, Erlangen, Germany). Both were acquired on the same mid-ventricular short axis slice. Scans were analysed using "Thalassemia Tool".

Results: 1(2%) patient had low cardiac T2*, the other 48(98%) had normal T2*. By T1, 11(22%) had low T1 (including the low T2* patient), 38(78%) normal T1. T2* missed cardiac iron in 9 out of 10 subjects. The low T1, normal T2* group had mainly mild T1 lowering (T1 lowering by 2-5 standard deviations). Ferritin was significantly higher in this group, whilst age, Hb, liver T2* did not differ. See Table 1 for details about the patients'; cohort.

	All (n=47)	Normal T2* - Normal T1	Normal T2* - Low T1	p
Age (years)	44±11	44±11	43±10	p=0.36
Gender (M:F)	20:27	16:20	4:6	
Cardiac T2* (ms)	36±7	37±5	35±8	p=0.34
Cardiac T1 (ms)	935±60	960±23	872±44	p<0.001
Hb (g/dL)	9.3±1.4	9.2±1.2	9.6±1.6	p=0.45
Ferritin (µg/L)	1141±1355	780±588	2507±2359	p<0.01

Liver T2* (ms)	7.5±5.6	7.8±5.6	7.1±5.9	p=0.35

Conclusion: In TI, cardiac iron overload by T2* is uncommon, but T1 detects apparent missed cardiac iron in 20%. This group have higher ferritin supporting the hypothesis of increased iron burden and suggesting that whilst TI is considered more benign than Thalassemia Major, cardiac iron accumulation still occurs.

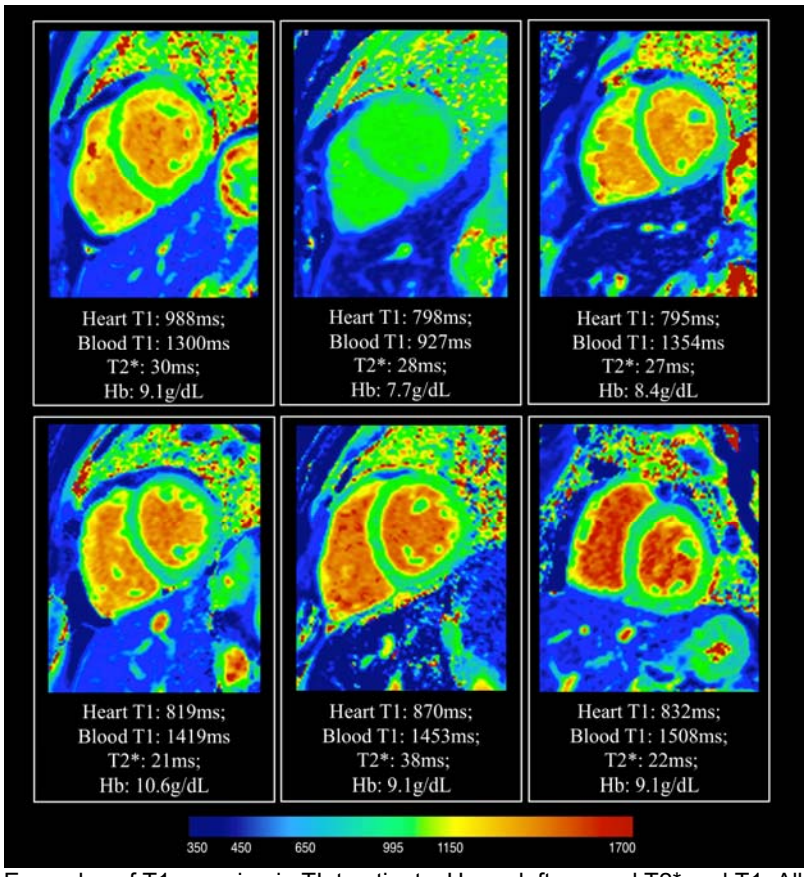

Examples of T1 mapping in TInt patients. Upper left: normal T2* and T1. All the other pictures: normal T2*, low T1.

Demographic Data, Blood and MRI Results in the Thalassemia Intermedia Patients

	All (n=47)	Normal T2* - Normal T1 (n=36)	Normal T2* - Low T1 (n=10)	p
Age (years)	44±11	44±11	43±10	0.36
Gender (M:F)	20:27	16:20	4:6	0.40
Cardiac T2* (ms)	36±7	37±5	35±8	0.34
Cardiac T1 (ms)	935±60	960±23	872±44	<0.01
Hb (g/dL)	9.3±1.4	9.2±1.2	9.6±1.6	0.45
Ferritin (µg/L)	1141±1355	780±588	2507±2359	<0.01

Liver T2* (ms)	7.5±5.6	7.8±5.6	7.1±5.9	0.35

ID#: 373166

2D/3D CMR-tissue tracking and tagging assessing early left ventricular dysfunction in isolated diastolic dysfunction (DD) spontaneous T2DM rhesus monkey

Zhu Tong[1] Yushu Chen, MD[2], Zhang Yu[3], Zeng Wen[4], Fabao Gao, MD,PHD[5]

1. Department of Radiology, WestChina Hospital, Sichuan University, Chengdu, Sichuan, China (People's Republic)

2. Molecular Imaging Center,Department of Radiology, West China Hospital. Sichuan University, Sichuan, China (People's Republic)

3. Molecular Imaging Center,Department of Radiology, West China Hospital. Sichuan University, China (People's Republic)

4. Sichuan Primed Biotech Group Co., LTD, Sichuan, China (People's Republic)

5. China West Hospital, Sichuan, China (People's Republic)

Background: To assess the feasibility of 2D/3D tissue tracking (TT) measured strain and compare strain values to those obtained with tagging in spontaneous T2DM rhesus monkeys diagnosed as isolated diastolic dysfunction (DD) in echocardiography previously.

Methods: 8 spontaneous T2DM rhesus monkeys with isolated diastolic dysfunction (DD) assessed by traditional echocardiography matched with 8 non-diabetic (ND) normal rhesus monkeys were recruited in this study. CMR tagging and CMR-TT were performed to quantify LV global circumferential and longitudinal peak strain (Ecc, Ell), time to peak strain (tEcc, tEll) and peak diastolic strain rate (SRc, SRl). Differences between groups, validity between 2D/3D TT with tagging and test-retest repeatability were evaluated respectively.

Results: The absolute value of tagging derived Ecc, Ell, SRc and SRl, CMR-TT 2D derived Ecc and SRc, and CMR-TT 3D derived Ecc significantly decreased in T2DM-DD monkeys compared with ND ($P<0.05$)(shown in table 1, fig 1 and fig 2). The absolute value of CMR-TT 2D derived Ecc, SRc and SRl were higher measured, but tEcc were lower measured compared with tagging ($p<0.05$). Besides, absolute value of CMR-TT 3D derived Ecc and SRc were higher measured, but tEcc were lower measured compared with tagging ($p<0.05$). Meanwhile, CMR-TT 2D derived Ecc (ICC=0.68, $p<0.05$) and tEll (ICC=0.65, $p<0.05$), and CMR-TT 3D derived Ecc (ICC=0.64, $p<0.05$) and Ell (ICC=0.67, $p<0.05$) agreed well with tagging (shown in table 2). Test-retest variability of CMR-2D derived Ecc (ICC=0.75, $p<0.05$), Ell (ICC=0.77, $p<0.05$), SRc (ICC=0.82, $p<0.05$) and SRl (ICC=0.76, $p<0.05$) were excellent, but test-retest variability of CMR-TT 3D derived parameters was lower.

Conclusion: CMR-TT derived strain and strain rate value were higher than tagging derived as a whole. However, CMR tagging and CMR-TT 2D are both able to reveal coexistence of systolic and diastolic dysfunction in a spontaneous T2DM rhesus monkeys which were diagnosed as early diastolic dysfunction by traditional echocardiography. CMR-TT 3D can find systolic dysfunction only. Compared with other CMR-TT derived parameters, CMR-TT 2D derived Ecc had highest sensitivity, validity and test-retest repeatability, so it may have the highest application value in this quantitative technique. Therefore, CMR-TT strain assessment is feasible in the early stage of diabetic cardiomyopathy and is likely to become the potential preferred quantification method.

Fig 1.

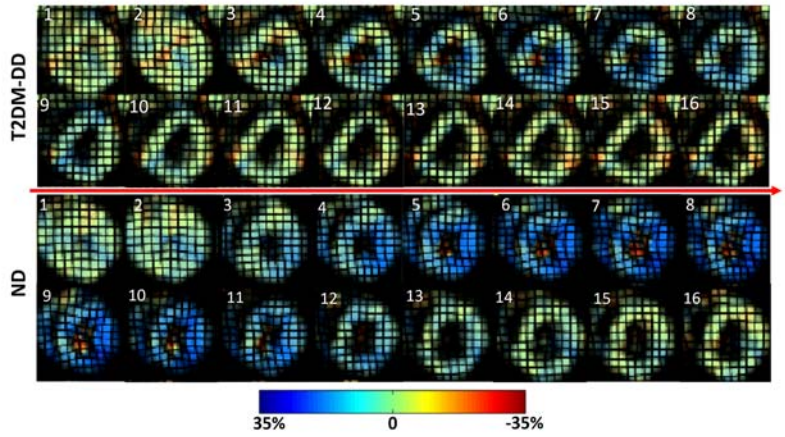

Time series of tagging circumferential strain color maps with grid tag overlay for a representative short-axis slice in a T2DM-DD (Row 1 and 2) and a ND (Row 3 and 4) monkeys respectively over one cardiac cycle. Color bar indicates circumferential strain in percentage.

Fig 2.

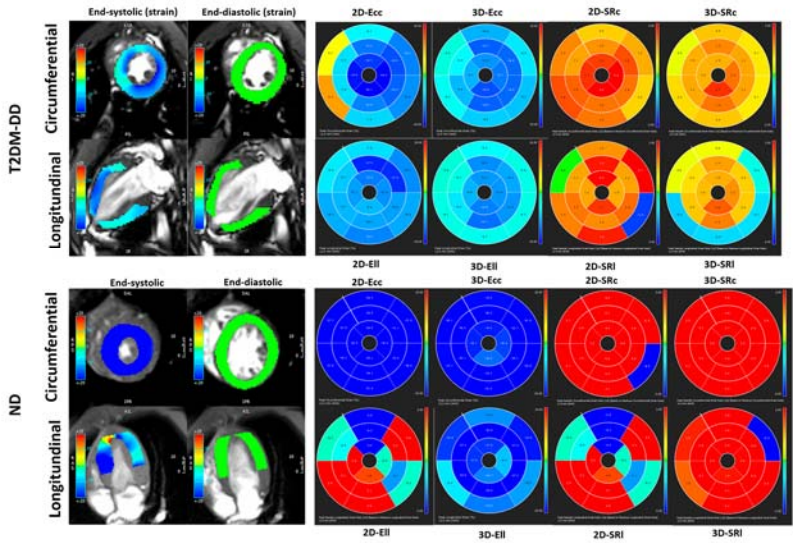

Color maps and 2D/3D polar maps of CMR-TT in end-systolic, end-diastolic phase and 16-segments depicting reduced systolic strain and diastolic strain rate in T2DM-DD monkey compared with ND in circumferential and longitundinal respectively.

Table 1. Tagging and CMR-TT Results in T2DM-DD Monkeys vs. ND Monkeys

Parameters	Tagging			CMR-TT 2D			CMR-TT 3D		
	T2DM-DD	ND	P	T2DM-DD	ND	P	T2DM-DD	ND	P
Ecc (%)	-9.97±3.29	-13.74±3.09	<0.05	-12.23±1.75	-18.89±3.92	<0.05	-13.40±1.60	-17.26±4.05	<0.05

tEcc (s)	0.28±0.04	0.25±0.05	0.13	0.24±0.34	0.23±0.02	0.86	0.23±0.023	0.22±0.03	0.46
CSR (%/s)	64.79±15.91	98.11±33.15	<0.05	141.63±29.36	196.75±52.84	<0.05	147.00±37.16	182.75±65.47	0.21
Ell (%)	-8.77±2.82	-13.94±1.64	<0.05	-8.77±2.82	-11.31±3.32	0.12	-9.65±1.86	-11.86±3.37	0.13
tEll (s)	0.27±0.02	0.24±0.05	0.16	0.25±0.03	0.22±0.06	0.12	0.25±0.03	0.24±0.16	0.58
LSR (%/s)	54.93±17.47	106.50±23.03	<0.05	148.75±31.29	144.75±44.26	0.84	72.13±76.93	123.88±49.00	0.13

Table 2. Agreement of all Parameters by CMR-TT and Tagging

Parameters	Paired samples t-test					Interclass correlation coefficient			
						Tagging/CMR TT 2D		Tagging /CMR TT 3D	
	Tagging	CMR-TT 2D	P	CMR-TT 3D	P	ICC Values (95%CI)	P	ICC Values (95%CI)	P
Ecc (%)	-11.85±3.65	-15.56±4.52	<0.05	-15.33±3.58	<0.05	98.00±67.80	<0.05	0.636 (-0.22/0.89)	<0.05
tEcc (s)	0.26±0.04	0.23±0.03	<0.05	0.23±0.03	<0.05	0.45 (-0.26/0.79)	0.07	0.336 (-0.36/0.73)	0.14
CSR (%/s)	81.45±30.44	169.19±50.16	<0.05	164.88±54.64	<0.05	0.29 (-0.16/0.70)	<0.05	0.296 (-0.20/0.70)	<0.05

Ell (%)	-11.36±3.48	-12.04±2.99	0.55	-10.75±2.87	<0.05	0.11 (-1.72/0.70)	0.42	0.671 (0.06/0.89)	<0.05
tEll (s)	0.26±0.04	0.24±0.05	0.09	0.24±0.02	0.33	0.65 (0.06/0.87)	<0.05	0.382 (-0.74/0.78)	0.18
LSR (%/s)	80.72±33.15	146.75±37.08	<0.05	98.00±67.80	0.26	0.04 (-0.27/0.44)	0.42	0.566 (-0.19/0.85)	0.06

ID#: 373111

Prevalence of inducible ischaemia across the strata of ejection fraction and according to the pattern of late gadolinium enhancement

Pamela Brown, MBBS[1] Sohail Iqbal, MBBS[2], Chris Miller, PhD[3], Gaetano Nucifora, MD, PhD[4], Matthias Schmitt, MD, PhD[3]

1. University Hospital South Manchester, Whitby, England, United Kingdom

2. University Hospital South Manchester, Manchester, United Kingdom

3. University Hospital South Manchester, United Kingdom

4. University Hospital of South Manchester, United Kingdom

Background: Recent studies have questioned the value of stress perfusion cardiac MRI (CMRI) in patients with severe left ventricular systolic dysfunction (LVSD) (Gulsin et al 2017). We sought to determine whether stress perfusion aids diagnosis above late gadolinium enhancement (LGE) and cine imaging across the strata of ejection fraction (EF).

Methods: Using the UHSM-redCAP database we analysed the reports of 1411 consecutive research consenting patients referred for stress CMRI between 02/2015-06/2017. We subsequently excluded all patients with a diagnosis of hypertrophic cardiomyopathy, Fabry';s and amyloidosis from analysis. All patients were scanned on a 1.5T or 3T Siemens scanner according to the SCMR standard protocol for adenosine stress perfusion (Kramer et al 2013) with adenosine infused at 140mcg/kg/min to 210mcg/kg/min. Scans were analysed and reported in an unblinded fashion; and EF, presence of inducible ischaemia and presence and pattern of LGE recorded.

Results: 1347 reports were analysed, 963 were male and 384 female, average age was 62 years old (19-88 years old). 780 (58%) had an ejection fraction >55%, 567 (42%) patients had an ejection fraction <55%. Overall presence of inducible ischaemia was 15% (Figure 1). The presence and pattern of LGE across the strata of ejection fraction is shown (Figure 2), LGE becomes more prevalent once EF falls below 55% with a preponderance for ischaemic LGE. Figure 3 demonstrates the presence of inducible ischaemia according to LGE pattern and ejection fraction. The presence of inducible ischaemia in those with no or non -ischaemic LGE is much lower than in those with ischaemic LGE. The prevalence of inducible ischaemia in those with non-ischaemic LGE is low (2-4%) across the ejection fraction strata

Conclusion: In a large UK cohort of patients presenting for clinically indicated chest pain assessment reversible ischaemia comprises 15%. This is similar to published trials (12.4%) (Greenwood et al 2016). The presence of reversible ischaemia in patients with non-ischaemic LGE i.e. those with dual pathology is 2-4% regardless of EF. Importantly, even in the absence of LGE reversible ischaemia was seen with a frequency ranging from 5% (severe LVSD) to 11% (normal EF). We conclude that stress perfusion imaging adds valuable information for the assessment of patients with chest pain across the EF strata.

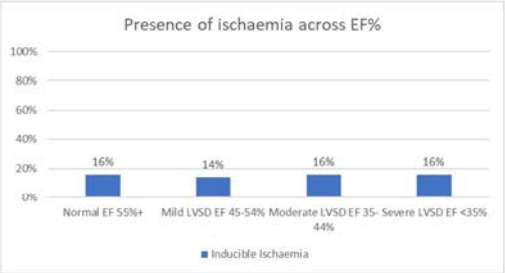
Presence of ischaemia across EF%
100%
80%
60%
40%
20%
0%
16%
14%
16%
16%
Normal EF 55%+
Mild LVSD EF 45-54%
Moderate LVSD EF 35-44%
Severe LVSD EF <35%
Inducible Ischaemia

Figure 1

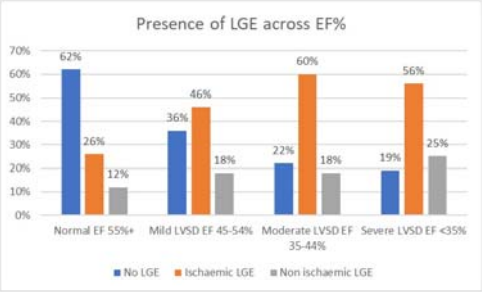
Presence of LGE across EF%
70%
60%
50%
40%
30%
20%
10%
0%
62%
26%
12%
36%
46%
18%
22%
60%
18%
19%
56%
25%
Normal EF 55%+
Mild LVSD EF 45-54%
Moderate LVSD EF 35-44%
Severe LVSD EF <35%
No LGE
Ischaemic LGE
Non ischaemic LGE

Figure 2

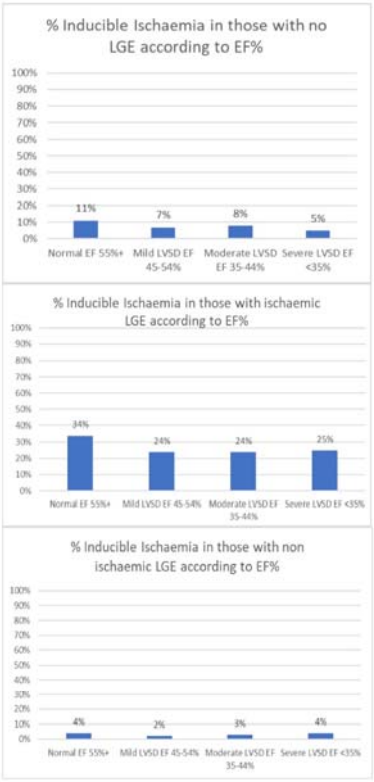
% Inducible Ischaemia in those with no LGE according to EF%
100%
90%
80%
70%
60%
50%
40%
30%
20%
10%
0%
11%
7%
8%
5%
Normal EF 55%+
Mild LVSD EF 45-54%
Moderate LVSD EF 35-44%
Severe LVSD EF <35%
% Inducible Ischaemia in those with ischaemic LGE according to EF%
34%
24%
24%
25%
Normal EF 55%+
Mild LVSD EF 45-54%
Moderate LVSD EF 35-44%
Severe LVSD EF <35%
% Inducible Ischaemia in those with non ischaemic LGE according to EF%
4%
2%
3%
4%
Normal EF 55%+
Mild LVSD EF 45-54%
Moderate LVSD EF 35-44%
Severe LVSD EF <35%

Figure 3

ID#: 373115

Left atrial deformation in patients with cryptogenic stroke: a cardiovascular magnetic resonance myocardial feature-tracking study

Johannes T. Kowallick, MD[1]Andreas Schuster, MD, PhD[2], Peter Witzenhausen, MD[1], Laura K. Wandelt[1], Mark Weber-Krüger, MD[1], Christina Unterberg-Buchwald, MD[3], Michael Steinmetz, MD[1], Gerd Hasenfuß, MD[1], Rolf Wachter, MD[1], Joachim Lotz, MD[4], Wieland Staab, MD[1]

1. University Medical Center Göttingen, Niedersachsen, Germany

2. University Medical Center Göttingen, Germany

3. University Medical Center Göttingen, Goettingen, Germany

4. University Medical Center Göttingen, Goettingen, Niedersachsen, Germany

Background: In ¼ of patients with ischemic stroke, no etiologic factor can be identified. Asymptomatic paroxysmal atrial fibrillation (AF) is often suspected to be the cause of these cryptogenic strokes (CS). AF is frequently associated with left atrial (LA) structural and functional alterations. Accordingly, the aim of this study was to examine LA deformation in patients with CS using cardiovascular magnetic resonance myocardial feature tracking (CMR-FT).

Methods: 29 patients with the diagnosis of CS underwent CMR imaging. Based on the initial cranial computed tomography (cCT), the patient group was divided into patients with previous ischemic lesions (recurrent CS) and patients without (first-time CS). LA deformation was analyzed based on CMR-FT of standard cine 4- and 2-chamber views including LA reservoir function (peak total strain [e_s], peak positive SR [SRs]), LA conduit function (passive strain [e_e], peak early negative SR [SRe]) and LA booster pump function (active strain [e_a], late peak negative SR [SRa]). Moreover, the “time to e_s”and “time to SRs” were calculated and expressed as a percentage of the entire cardiac cycle (**Figure 1**).

Results: Previous ischemic lesions were detected in5 of 29 patients (17%). LA conduit strain was lower in patients with recurrent CS as compared to first-time CS (6.4 ± 1.1 % vs. 10.3 ± 3.3 %, respectively, p=0.005). Furthermore, “time to e_s”and “time to SRs” were prolonged in patients with recurrent CS (47 ± 6 % vs. 57 ± 8%, p=0.007; and 19 ± 5% vs. 30 ± 7%, p=0.001, respectively). In multivariable regression models “time to e_s” and “time to SR” were independently associated with the presence of previous ischemic lesions (ß=0.41, p=0.006 and ß=0.51, p=0.015, respectively) after adjustment for traditional risk factors (age, gender, arterial hypertension, vascular disease and diabetes).

Conclusion: Prolonged time to peak LA reservoir strain and SR is associated with the presence of previous ischemic lesions in patients with CS. These findings propose advanced LA impairment as a distinct feature of CS which may be associated with unrecognized paroxysmal AF. Future research is warranted to confirm these findings alongside their prognostic implications in larger prospective clinical trials.

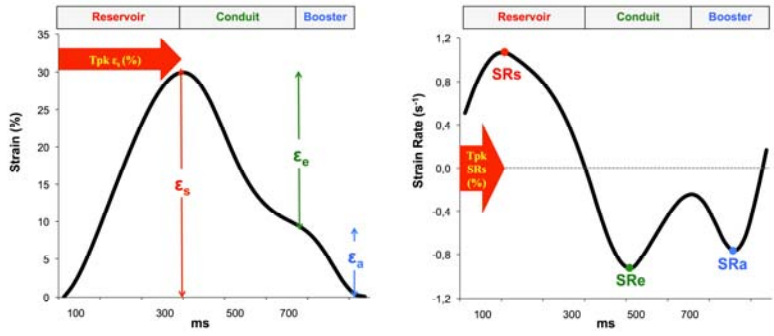

Figure 1: Left atrial strain and strain rate profiles as derived from cardiovascular magnetic resonance myocardial feature tracking (CMR-FT).

ID#: 373125

Blunted myocardial oxygenation response in Heart Failure with Preserved Ejection Fraction (HFpEF)

Kady Fischer, PhD[1] Dominik P. Guensch, MD, DESA[2], Melanie Artho, MD[2], Silvia Luescher[3], Bernd Jung, PhD[4], Christine Riggenbach[2], Hendrik von Tengg-Kobligk, MD[5], Balthasar Eberle, MD[6], Matthias G. Friedrich, MD[7]

1. McGill University Health Center, University Hospital Bern, Montreal, PQ, Canada

2. University Hospital Bern, Inselspital, Switzerland

3. University Hospital Bern, Inselspital, Bern, Bern, Switzerland

4. Inselspital Bern, Institute for Diagnostic, Interventional and Pediatric Radiology, Bern, Switzerland

5. Inselspital, Switzerland

6. Department of Anesthesiology, Inselspital / University Hospital Bern, Bern, Bern, Switzerland

7. McGill University Health Centre, PQ, Canada

Background: It has been suggested that approximately 50% of patients with heart failure have a preserved ejection fraction (HFpEF). While the underlying causes and pathophysiologic hallmarks are not well understood, newer insights target microvascular disease as a possible mechanism. Oxygenation-Sensitive (OS)-CMR is a technique that may be able to assess the microvascular function by calculating the oxygenation reserve during a vasoactive stimulus. OS-CMR can also detect global dysfunction in addition to regional oxygenation deficits. Thus with a breathing maneuver stimulus, we investigated the myocardial oxygenation reserve in an initial sample of HFpEF patients.

Methods: Twelve patients with heart failure and preserved LV ejection fraction (>50%) underwent a 3T-CMR exam. A vasoactive stimulus was induced with a breathing maneuver combining 60s of rapid-paced breathing (vasoconstrictive stimulus) immediately succeeded by a maximal breath-hold to induce vasodilation. The vasodilatory period was imaged using an SSFP-based OS cine in two short-axis slices (ECG-triggered, echo time 3.4ms, FA 35, uptake time 4 heart-beats). The OS response was calculated as a %-change between the start of the breath-hold, and the image obtained at 30s, and compared to previously obtained values from healthy control subjects (Figure A). Global dysfunction was defined as having at least 10 of the 12 AHA segments have an oxygenation drop (≤0%). A regional response was determined as having at least 2 segments ≤0%, with remote territory having a response at least 6.6% greater (1SD of controls).

Results: Patients were aged from 45-79 years (4 females / 8 males). All patients had an EF>50% (62±10%), a cardiac index of 2.9±1.3L/min/m^2, and a left atrial index of 44±18ml/m^2. The HFpEF patients showed a significantly attenuated OS response (0.6±4.5%, p<0.001) in comparison to the healthy controls (10.0±6.6%, n=44). Four of the patients demonstrated a global dysfunction (Figure C), three of which had no known history of macrovascular disease, while 6 patients had a regional response (Figure B).

Conclusion: In a preliminary sample, a majority of patients with HFpEF showed a blunted myocardial oxygenation response. One-third of this population presented with a global oxygenation dysfunction, and especially when macrovascular disease is absent this likely represents microvascular disease. Further research can highlight the association of the global and regional myocardial oxygenation dysfunction with other myocardial markers such as edema and fibrosis.

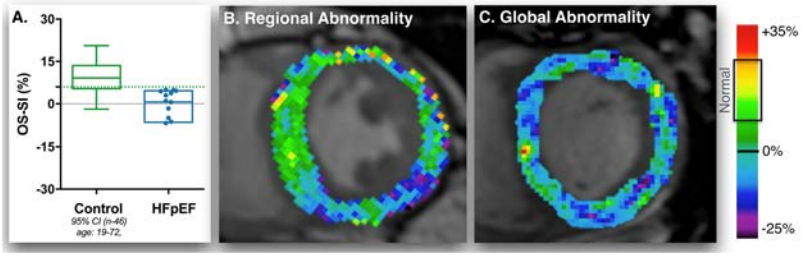

Myocardial oxygenation can be evaluated by measuring the %-change in oxygenation-sensitive signal intensity (OS-SI%). In the presence of a vasodilating breath-hold stimulus, healthy controls increase myocardial oxygenation, while in the first 12 HFpEF patients this response was blunted (A). This oxygenation abnormality can present as regional (B) with an oxygenation drop in a portion of the myocardium (blue), while normal in the other (green), or as a global drop in signal (C).

ID#: 372557

Diagnostic Utility of Vasodilator Cardiac Magnetic Resonance Imaging in Patients with Reduced Left Ventricular Ejection Fraction

Akhil Narang, MD[1]Keith Ameyaw, BA[2], Nimit Desai, MD[2], Keigo Kawaji, PhD[1], Victor Mor-Avi, PhD[3], Sandeep Nathan, MD[2], Luis Landeras, MD[2], Amit R. Patel, MD[3]

1. University of Chicago, Chicago, IL

2. University of Chicago

3. University of Chicago, IL

Background: While the diagnostic utility of vasodilator cardiac magnetic resonance (vCMR) in patients with suspected coronary artery disease (CAD) is reported to be high, its diagnostic performance in patients with reduced left ventricular ejection fraction (LVEF) is unclear. In patients with reduced LVEF, the presence of myocardial fibrosis coupled with reduced autoregulatory and vasodilator capacity of the microcirculation may reduce the diagnostic performance of vCMR. The purpose of this study was to determine the diagnostic utility of vCMR in patients with LVEF <50%

Methods: 113 consecutive patients with LVEF <50% who underwent a clinically indicated regadenoson vCMR for the detection of ischemia from 2010-2015 were included in the study. Imaging was performed using a 1.5 T scanner (Achieva, Philips) with standard clinical pulse sequences, which included cine-CMR, myocardial perfusion imaging during hyperemia and recovery, and late gadolinium enhancement. Three short-axis slices of the LV were obtained during first pass of contrast using a hybrid GRE-EPI pulse sequence. Perfusion defects were recorded if they persisted for ≥2 frames after peak enhancement of the LV cavity. The diagnostic performance of vCMR was determined using coronary revascularization within 3 months of vCMR as the reference standard in 2 groups of patients with LVEF <50%: (1) patients with ischemia (perfusion defect) who were referred for coronary angiography and (2) all patients who were referred for CA (with and without perfusion defect), including separate analysis in a subgroup of patients with LVEF <40%.

Results: Study patients were 61±14 years old, 65% male, and the LVEF was 40±10%. Perfusion defects were noted in 56 patients (50%) and 23/56 (41%) underwent coronary angiography (CA). Of these 23 patients, 20 (87%) were revascularized (**Figure**). Of the 57 patients with no ischemia noted on vCMR, 4 (7%) underwent CA and only 2 (3.5%) were revascularized. Among all patients referred for CA (with and without perfusion defect), the sensitivity for identifying coronary stenosis treated with revascularization was 91%. The diagnostic performance of both groups is listed in the **Table**.

Conclusion: In patients with reduced LVEF, ischemia detected by vCMR frequently results in revascularization; where as, the absence of ischemia rarely leads to revascularization. Among all patients referred for coronary angiography with reduced LVEF, vCMR has high sensitivity for detecting significant coronary artery stenosis.

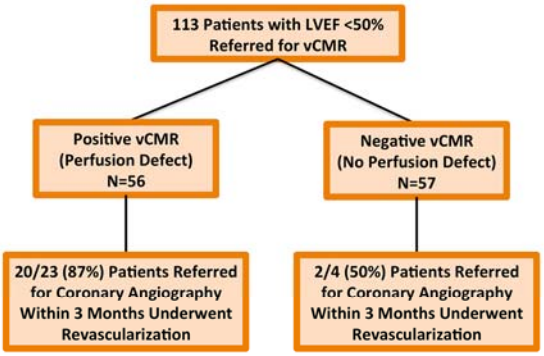

	All Patients Referred for Coronary Angiography (LVEF <50%), N=28	All Patients Referred for Coronary Angiography (LVEF <40%), N=14
Sensitivity	91%	91%
Specificity	40%	33%
Accuracy	79%	75%
Positive Predictive Value	88%	83%
Negative Predictive Value	50%	50%

ID#: 372571

Comparison of Intra-Cardiac Magnetic Resonance Blood Oximetry to Invasive Catheterization in Pediatric Patients with Congenital Heart Disease

Juliet Varghese, PhD[1] Yingmin Liu, Ph.D.[2], Ning Jin, PhD[3], Aimee Armstrong, MD[4], Kan Hor, MD[5], Rizwan Ahmad, PhD[6], Orlando Simonetti, PhD[1]

1. The Ohio State University, OH

2. The Ohio State University, Columbus, OH

3. Siemens Healthineers

4. Nationwide Children's Hospital

5. Nationwide Children's Hospital, Columbus, OH

6. The Ohio State University

Background: Blood oxygen saturation (O2 sat) measurement is important in shunt determination and interventional planning in pediatric patients with congenital heart disease (CHD). Currently, it requires invasive catheterization procedures involving radiation exposure. We previously demonstrated a non-invasive T2 mapping based method to determine O2 sat in the heart based on non-linear, multi-parameter estimation [1,2]. The present study evaluates the accuracy of the technique against invasive right heart catheterization (RHC) in a preliminary cohort of pediatric CHD patients.

Methods: Seven pediatric patients (age range, 22 mo – 16 yrs, two females) clinically indicated for cardiac MRI followed by RHC participated in the study. All subjects were scanned on a 3T MRI system (Skyra, Siemens Healthineers). Approximately 10 to 14 T2 prepared single-shot steady-state free precession (SSFP) images were acquired free-breathing, across different T2 preparation times (0 to 100 ms) and inter-echo spacing (0 to 25 ms) to fit the Luz-Meiboom model [3,4]. A short axis view of the right and left ventricles (RV and LV), and cross-sectional views of the superior vena cava (SVC), pulmonary artery (PA) and aorta were acquired in each patient; average acquisition time at each location was one minute. The signal measured in each image in ROIs placed in arterial and venous blood pools, arterial O2 sat from a pulse oximeter (SpO2), and hematocrit from a blood sample were jointly processed to estimate the unknown venous O2 sat and other remaining nuisance parameters of the model (S_0, T_{2O}, τ_{ex} and α). O2 sat of the RV, SVC and MPA were then compared to RHC results.

Results: All MRI and catheter measurements were obtained while patients were under general anesthesia and breathing room air. The average arterial SpO2 levels were 94 ± 8% (range, 76 % - 98 %) and average hematocrit levels were 37.7 ± 3.9% (range, 31 % – 41.4 %). Figure 1 compares O2 sat measured by catheterization and MRI for all patients. The average absolute mean difference between the MRI and invasive O2 sat measurements was 4.2 ± 2.6 % (range, 0% - 9%). A paired t-test between the two measurements showed no statistically significant difference ($p = 0.7$).

Conclusion: The present study examined the feasibility of non-invasive MR oximetry in pediatric CHD patients at 3T. MR estimates of O2 sat demonstrates good agreement with the clinical standard O2 sat RHC measurement. These results indicate that our multi-parametric approach to solve the L-M model may be more effective than previous attempts at deriving O2 sat from a single blood T2 measurement. Continuing studies aim at optimizing the image acquisition scheme as well as addressing issues such as the flow induced signal loss in the cardiac chambers and vessels that may occur, especially in the presence of congenital abnormalities. **References: 1.** Varghese et al. JCMR 2016, 18(Suppl 1):W29. **2.** Varghese et al. 2017, 20th SCMR Abstract Suppl: F035. **3.** Wright et al. JMRI 1991, 1(3):275-283. **4.** Luz and Meiboom, J. Chem. Phys. 39(2): 366-370 (1963).

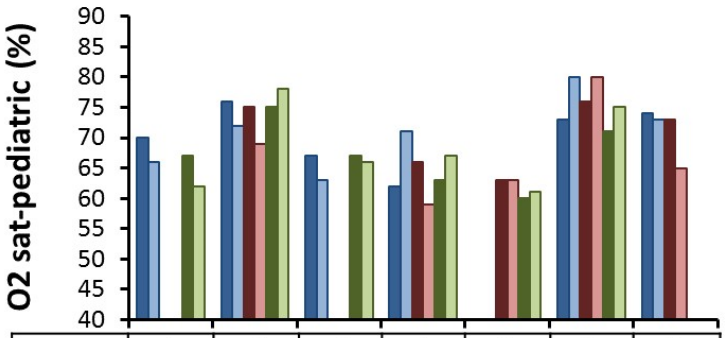

	1	2	3	4	5	6	7
Cath_RV	70	76	67	62		73	74
MRI_RV	66	72	63	71		80	73
Cath_SVC		75		66	63	76	73
MRI_SVC		69		59	63	80	65
Cath_PA	67	75	67	63	60	71	
MRI_PA	62	78	66	67	61	75	

Figure 1: Comparison of venous O2 sat measured from invasive catheterization and T2 prepared MR oximetry in seven patients with congenital heart disease. Measurements were made in the right ventricle (RV), superior vena cava (SVC) and pulmonary artery (PA). Empty cells indicate cases where a paired O2 sat measurement was not obtained.

ID#: 372529

Reduced Global Longitudinal Strain in Rheumatic Mitral Stenosis with Good Left Ventricular Ejection Fraction: A Cardiac Magnetic Resonance Feature Tracking Study

Elen Elen, MD, FIHA[1]Celly Anantaria. Atmadikoesoemah, MD, FIHA[2], Manoefris Kasim, MD, FIHA[2], Tommaso D'Angelo, MD[3], Faraz Pathan, MBBS, FRACP[4], Valentina O. Puntmann, MD, PhD[5], Eike Nagel, MD, PhD[6]

1. National Cardiovascular Center Harapan Kita, Jakarta-Indonesia; Institute for Experimental and Translational Cardiovascular Imaging, University Hospital Frankfurt-Germany, Tangerang, Banten, Indonesia

2. Department of Cardiology and Vascular Medicine, Faculty of Medicine Universitas Indonesia, National Cardiovascular Center Harapan Kita, Indonesia, Indonesia

3. University of Messina, Messina, Sicilia, Italy

4. Goethe Institute for Experimental and Translational Cardiovascular Imaging, Sydney, New South Wales, Australia

5. Universitaetsklinikum Frankfurt, Frankfurt Am Main, Germany

6. University Hospital Frankfurt; Institute for Experimental and Translational Cardiovascular Imaging; DZHK Centre for Cardiovascular Imaging, Frankfurt, Germany

Background: Chronic rheumatic heart disease has a persistent inflammatory process that can also affect the myocardium. Previous studies showed that echocardiography speckle tracking is realiable to detect subclinical left ventricular (LV) systolic dysfunction in patients with rheumatic mitral stenosis (MS). Cine-cardiac magnetic resonance (CMR) excellently depicts myocardial tissue to measure myocardial strain. We assessed LV myocardial strain by CMR feature-tracking (CMR-FT) in significant rheumatic MS.

Methods: We retrospectively analyzed LV feature-tracking in a total 42 subjects who underwent 1.5T-CMR examination: significant MS (n=25) without significant mitral regurgitation, aortic valve disease, and coronary artery disease (left ventricular ejection fraction (LVEF) ≥55%: n=10, LVEF <55%: n=15), and 17 healthy subjects. A 2D CMR-FT method was used to measure global longitudinal strain (GLS), global radial strain (GRS), and global circumferential strain (GCS). We analyzed these myocardial strain values in those three groups.

Results: Patients (40±11 years old, 63% female) had strong correlation between LVEF and GLS (r -0.78, p<0.001), GRS (r -0.78, p<0.001), and GCS (r -0.76, p<0.001). LVEF in healthy subjects, MS with good LVEF(≥55%), MS without good LVEF (<55%) were of 63.79±4.84, 62.81±7.32, and 40.38±10.56% (p<0.001). GLS, GRS, and GCS values for healthy subjects, MS with good LVEF, MS without good LVEF were respectively: -20.98±1.48, -15.71±3.57, and -10.27±2.77% (p<0.001); 46.62±8.26, 43.08±7.06, and 25.66±8.71% (p<0.001); -21.47±2.12, -20.46±2.45, and -14.39±3.32% (p<0.001). Compared with healthy subjects, GLS value in MS with good LVEF subjects was significantly reduced (p<0.001).While GRS and GCS values were not significantly different between healthy subjects and MS with good LVEF.

Conclusion: GLS was significantly reduced in rheumatic MS with good LVEF as assessed by CMR-FT, while GRS and GCS were significantly reduced only in rheumatic MS without good LVEF.

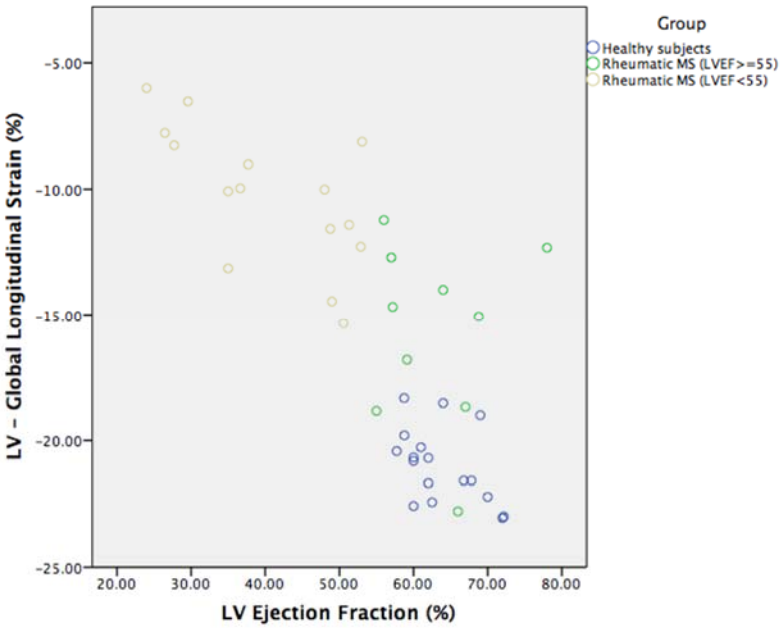

Global longitudinal strain in healthy subjects and patients with rheumatic mitral stenosis

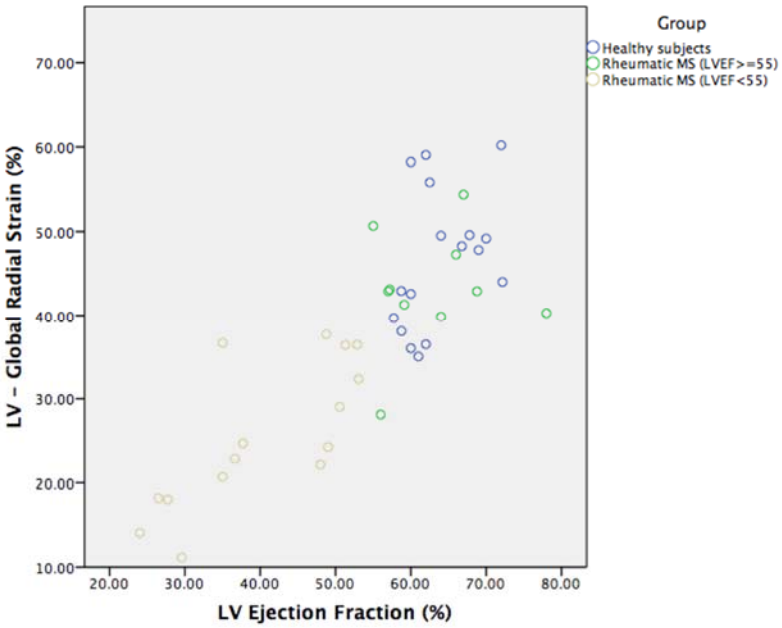

Global radial strain in healthy subjects and patients with rheumatic mitral stenosis

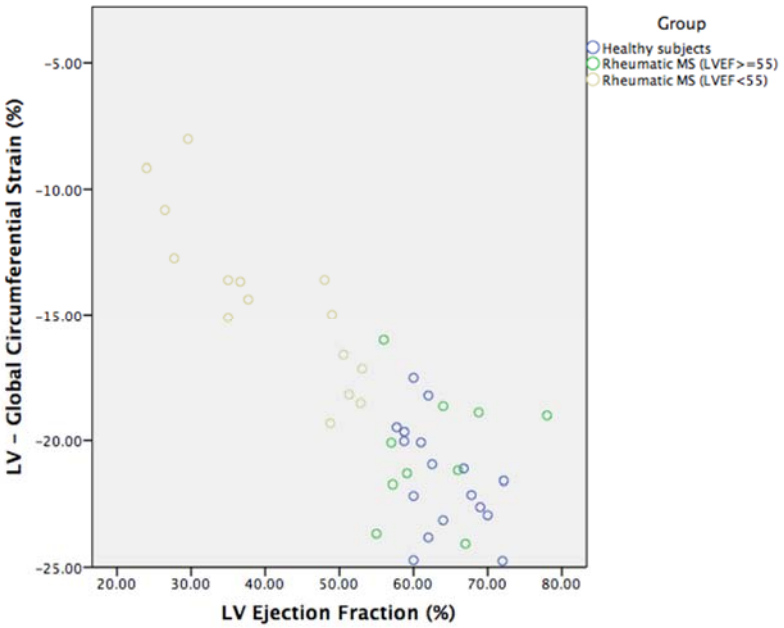

Global circumferential strain in healthy subjects and patients with rheumatic mitral stenosis

ID#: 372541

Metabolic Disease Impairs Response to Cardiac Rehabilitation - Insights from Skeletal Muscle Spectroscopy

Vidhya Kumar[1] Suzanne Smart[2], Beth McCarthy, BSRT[1], Subha Raman, MD, MSEE[3]

1. Ohio State University, Columbus, OH

2. Ohio State University

3. The Ohio State University, Columbus, OH

Background: Cardiac rehabilitation/secondary prevention (CRSP) programs reduce mortality, but less so in patients with metabolic abnormalities who have impaired mitochondrial function and ectopic lipid storage. With phosphorus magnetic resonance spectroscopy (PMRS), we assessed oxidative phosphorylation capacity (OXPHOS) and fat composition in response to CRSP in patients with differing severities of metabolic disease.

Methods: Patients referred for CRSP were prospectively enrolled and classified as having no/mild(N) or moderate/severe(S) metabolic abnormality based on the presence of < 2 or ≥ 2, respectively, metabolic syndrome features[1]. Patients in the 2 groups did not significantly differ in age, body size or left ventricular systolic function (**Table 1)**. Pre- and post-CRSP MRI/MRS included quadriceps muscle PMRS with resistive exercise[2] and fat quantification in muscle and liver using a three-point Dixon based sequence (TR = 11.1 s, TE = 2.39 s, BW = 1150 Hz, slice thickness = 4 mm). Phosphocreatine (PCr) concentrations were serially quantified and recovery time calculated with a best-fit mono-exponential function. Quantitative fat maps were generated from the Dixon sequence, with pixel intensity representing fat percentage.

Results: Twenty-one patients (10 in group N and 11 in group S) were enrolled. Across all patients, CRSP significantly improved exercise capacity from 6.8±3.4 to 8.9±4.0 METS (p = 0.001) with more modest improvement in OXPHOS (42.55±19.2 to 46.22±29.5 sec, p = 0.05). The presence of metabolic abnormalities impaired response to CRSP (**Fig. 1**). Patients with no/mild metabolic abnormality demonstrated significant improvements in exercise capacity and mitochondrial function that those with moderate/severe metabolic abnormality did not realize (Exercise capacity: 41.18±48.7% (N) vs. 7.33±24.08 (S), p = 0.05; PCr recovery time: 19.61±31.0% (N) vs. -21.81±43.8% (S), p= 0.03; **Fig.1**). Baseline levels of intramuscular and intrahepatic fat were higher in patients with severe metabolic abnormality but did not change significantly in response to CRSP in either group (baseline intramuscular = 7.4±3.1% (N) vs. 8.0±3.0%(S), p = 0.6, baseline intrahepatic = 4.9±5.3%(N) vs. 8.4±8.6%(S), p = 0.33).

Conclusion: A hybrid MRI/MRS protocol demonstrates impaired response to CRSP in patients with significant metabolic abnormalities. Larger-scale longitudinal studies are warranted to evaluate adequacy of current CRSP protocols that may warrant modification to improve outcomes for patients with more severe metabolic disease.

References:

1. Grundy SM, Cleeman JI, Daniels SR, et al. Diagnosis and management of the metabolic syndrome: an American Heart Association/National Heart, Lung, and Blood Institute Scientific Statement. *Circulation.* 2005;112:2735-2752.

2. Kumar V, Chang H, Reiter DA, et al. Phosphorus-31 Magnetic Resonance Spectroscopy: A Tool for Measuring In Vivo Mitochondrial Oxidative Phosphorylation Capacity in Human Skeletal Muscle. *Journal of visualized experiments : JoVE.* 2017.

Subject	Sex (% female)	Age (years)	BMI (kg/m²)	LVEF (%)	Smokers (% use)
No/Mild	26.7	61.1 ± 6.4	29.6 ± 6.5	54.1 ± 12.6	13.3
Moderate/Severe	31.6	55.9 ± 10.1	31.6 ± 4.9	49.2± 9.9	15.8
P-value	--	NS	NS	NS	--

Table 1. Baseline characteristics of enrolled subjects are shown. NS, not significant.

Table 1. Baseline characteristics of enrolled subjects are shown. NS, not significant.

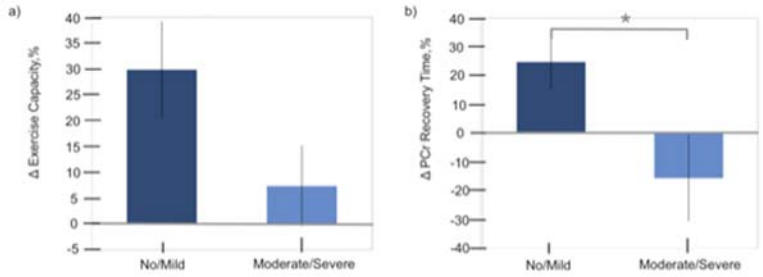

Figure 1. Comparison of changes in exercise capacity (a) and PCr recovery times (b, p < 0.05) in cohorts demonstrates impaired response of patients with severe metabolic abnormality following CRSP training.

Figure 1. Comparison of changes in exercise capacity (a) and PCr recovery times (b, $p < 0.05$) in cohorts demonstrates impaired response of patients with severe metabolic abnormality following CRSP training.

ID#: 372435

Cardiac Magnetic Resonance Myocardial Feature Tracking for Optimized Prediction of Cardiovascular Events Following Myocardial Infarction

Ingo Eitel, MD[1] Thomas Stiermaier, MD[1], Torben Lange, BSc[2], Karl-Philipp Rommel, MD[3], Alexander Koschalka, BSc[4], Johannes T. Kowallick, MD[5], Joachim Lotz, MD[6], Shelby Kutty, MD PhD MS-HCM[7], Matthias Gutberlet, MD[8], Gerd Hasenfuß, MD[5], Holger Thiele, MD[9], Andreas Schuster, MD PhD MBA FESC[10]

1. University Heart Center Lübeck, Lübeck, Schleswig-Holstein, Germany

2. DZHK (German Centre for Cardiovascular Research) partner site Göttingen, Niedersachsen, Germany

3. University Leipzig - Heart Center, Germany

4. University Medical Center Göttingen, Germany

5. University Medical Center Göttingen, Niedersachsen, Germany

6. University Medical Center Göttingen, Goettingen, Niedersachsen, Germany

7. Children´s Hospital and Medical Center Joint Division of Pediatric Cardiology, University of Nebraska / Creighton University, Omaha, NE, USA, NE

8. University of Leipzig - Heart Centre, Department of Diagnostic and Interventional Radiology, Sachsen, Germany

9. Heart Center Leipzig University Hospital, Sachsen, Germany

10. Department of Cardiology and Pneumology, University Medical Center Göttingen, Germany; Department of Cardiology, Royal North Shore Hospital, Sydney, Australia; The Kolling Institute, Northern Clinical School, University of Sydney, Sydney, Australia, Niedersachsen, Germany

Background: Cardiac magnetic resonance myocardial feature tracking (CMR-FT) is a new method that allows accurate assessment of global and regional circumferential, radial and longitudinal myocardial strain. The prognostic value of CMR-FT in patients with reperfused myocardial infarction (MI) is unknown. The aims of our study were to assess the prognostic significance of CMR-FT in a large multicenter study and to evaluate the most potent CMR-FT predictor of hard clinical events following MI.

Methods: We included 1235 MI patients (n=795 with ST-elevation MI and 440 with non ST-elevation MI) in this study at 15 centers. All patients were reperfused by primary percutaneous coronary intervention (PCI). Central core laboratory–masked analyses were performed to determine global left ventricular (LV) circumferential (GCS), radial (GRS) and longitudinal strain (GLS). The primary clinical endpoint of the study was the occurrence of major adverse cardiac events within 12 months after infarction.

Results: Patients with cardiovascular events had significantly impaired CMR-FT strain values ($p<0.001$ for all). GLS was identified as the strongest CMR-FT parameter of future cardiovascular events and emerged as an independent predictor of poor prognosis following MI even after adjustment for established prognostic markers. GLS provided an incremental prognostic value for all-cause mortality above LV ejection fraction (c-index increase from 0.65 to 0.73, $p=0.04$) and infarct size (c-index increase from 0.60 to 0.78, $p=0.002$).

Conclusion: CMR-FT is a superior measure of LV function and performance early after reperfused MI with incremental prognostic value for mortality over and above LV ejection fraction and infarct size.

ID#: 372600

Comparison of methods for quantitative assessment of left ventricular mechanical dyssynchrony by CMR feature tracking - a multicenter derivation/validation study

Daniel E. Loewenstein[1]Björn Wieslander, MD PhD[2], Einar Heiberg[3], Jimmy Axelsson[4], Igor Klem, MD[5], Robin Nijveldt, MD, PhD[6], Erik B. Schelbert, MD, MS[7], Peder Sörensson[8], Andreas Sigfridsson, PhD[9], David Strauss, MD, PhD[10], Brett D. Atwater, MD[11], Martin Ugander, MD, PhD[12]

1. Karolinska Institutet, Stockholm, Stockholms Lan, Sweden

2. Department of Clinical Physiology, Karolinska Institutet and Karolinska University Hospital, Stockholm, Sweden, Stockholm, Stockholms Lan, Sweden

3. Department of Clinical Physiology, Sweden

4. Department of Clinical Physiology, Karolinska Institutet, and Karolinska University Hospital, Stockholm, Sweden, Sweden

5. Duke University Medical Center, Durham, NC

6. Radboud University Medical Center, Nijmegen, Gelderland, Netherlands

7. University of Pittsburgh; Heart and Vascular Institute of UPMC, PA

8. Karolinska Institutet, Department of Molecular Medicine and Surgery, Stockholms Lan, Sweden

9. Karolinska Institute, Stockholm, Stockholms Lan, Sweden

10. FDA, Silver Spring, MD

11. Duke University School of Medicine, NC

12. Karolinska Institutet, and Karolinska University Hospital, Stockholm, Sweden, Stockholms Lan, Sweden

Background: Cardiac magnetic resonance (CMR) feature tracking (FT) has been validated against myocardial tissue tagging with good results. However, no consensus exists regarding which metric is optimal for quantitative assessment of left ventricular (LV) mechanical dyssynchrony by CMR-FT. We sought to derive and validate an optimal and automated index for identifying dyssynchrony in LBBB using CMR-FT.

Methods: We retrospectively identified patients from three centers (n=80), with LV ejection fraction (LVEF) ≤35%, no scar by CMR late gadolinium enhancement (LGE), and either normal electrocardiographic (ECG) QRS duration and normal frontal plane electrical axis (control, n=36), or left bundle branch block (LBBB, n=44) defined by Strauss' strict ECG criteria. Patients were randomized into a derivation cohort (n=40; LBBB n=22, control n=18) and a validation cohort (n=40; LBBB n=22, control n=18). CMR cine images in a midventricular short-axis plane or four chamber long-axis plane were assessed for presence of delay in time to first circumferential or longitudinal peak strain between the early and late activating segments, or using the uniformity ratio estimate for circumferential (CURE) or radial (RURE) strain using commercially available feature tracking module to the software (Segment, Medviso AB, Lund, Sweden). Delay times were measured either in ms or as percent of the cardiac cycle. Different automated dyssynchrony indices (n=28) were optimized in the derivation cohort, and applied to the validation cohort. The best dyssynchrony index was determined as the index with the highest lower limit of the 95% confidence interval (CI) of the area under the receiver operating characteristic curve (AUC) in the validation cohort.

Results: The best dyssynchrony index in the validation cohort was short-axis septal-to-lateral wall delay (SLD) with peak strain criteria expressed as an optimal percentage point of circumferential strain (SLD_{point}, AUC 0.93 (95% CI 0.84-0.99)). The optimal cutoff was 208 ms, yielding 94% sensitivity and 82% specificity in the validation cohort. For the purposes of comparison with prior published methods, SLD_{point} had diagnostic performance that did not differ from CURE (AUC 0.86 (95% CI 0.72-0.97), p=0.28) or earliest-to-latest segment delay (ELSD, AUC 0.84 (95% CI 0.69-0.96), p=0.23).

Conclusion: CMR-FT using the SLD_{point} index has excellent accuracy for detecting LV dyssynchrony in patients with LBBB, severely reduced LVEF and no myocardial scar. Both CURE and ELSD did not differ in diagnostic performance from SLD_{point}. ELSD has the added advantage that it can potentially be used to characterize LV contraction patterns in non-LBBB intraventricular conduction abnormalities.

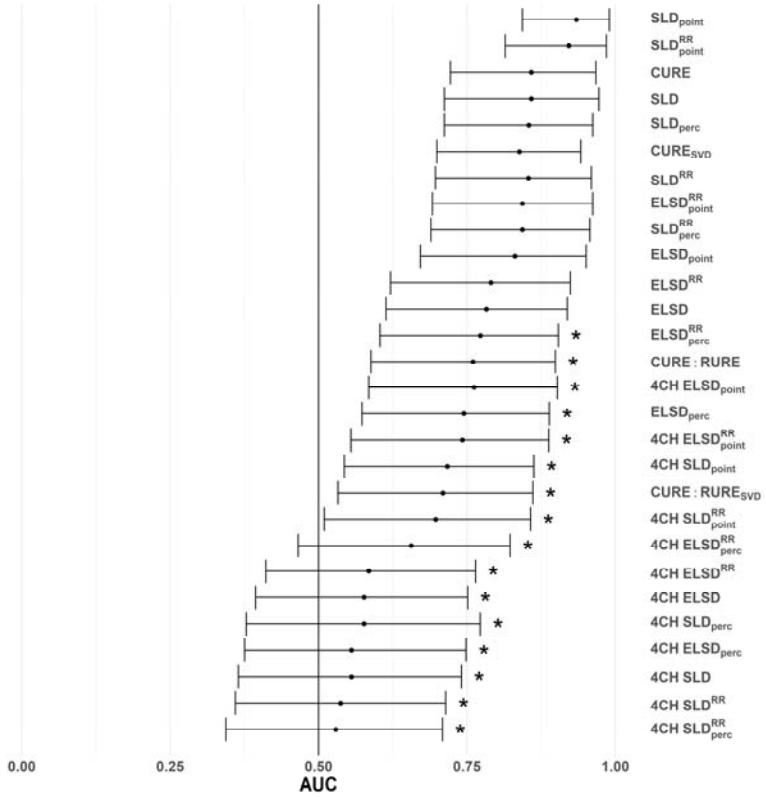

Figure 1. Area under the curve (AUC) for receiver operating characteristic (ROC) with 95% confidence interval for indices of dyssynchrony in the validation cohort. All indices are derived from a midventricular short-axis imaging plane unless denoted as 4CH, indicating the long-axis four chamber imaging plane. ELSD = earliest to latest segment delay, SLD = septal to lateral wall delay, CURE = circumferential uniformity ratio estimate, RURE = radial uniformity ratio estimate, SVD = Singular value decomposition. Notation for models using peak strain criteria expressed as an optimal percentage point (point) or an optimal percentage (perc) of circumferential strain. All time criteria were in ms unless denoted as RR, indicating that the time criteria were in percent of the cardiac cycle R-R interval. * denotes p <0.05 compared to SLDpoint.

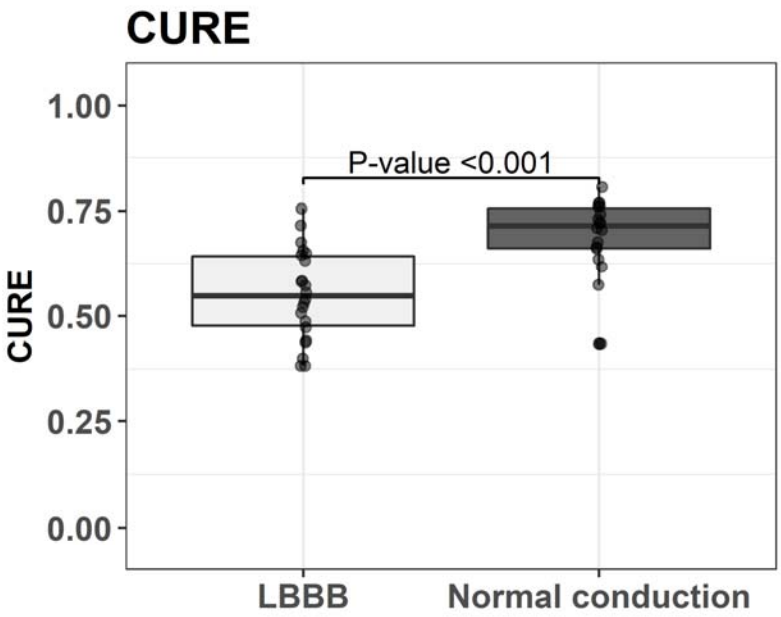
CURE
1.00
0.75
0.50
0.25
0.00
CURE
P-value <0.001
LBBB
Normal conduction

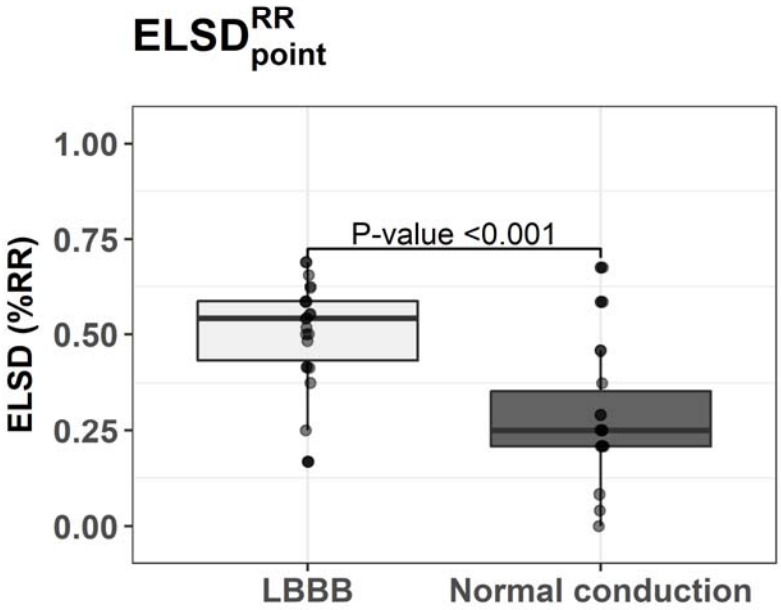
ELSD RR point
1.00
0.75
0.50
0.25
0.00
ELSD (%RR)
P-value <0.001
LBBB
Normal conduction

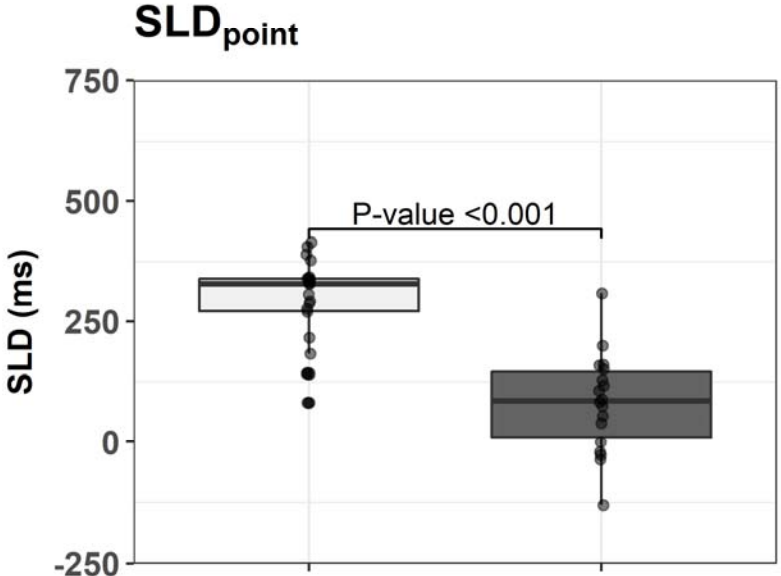
SLD point
750
500
250
0
-250
SLD (ms)
P-value <0.001

Figure 2. Boxplots showing distribution of dyssynchrony measurements from best performing model by dyssynchrony index in the validation cohort (LBBB n =22, Normal conduction n=18). All metrics are derived from a midventricular short-axis imaging plane. ELSD = earliest to latest segment delay, SLD = septal to lateral wall delay, CURE = circumferential uniformity ratio estimate. Test used: Wilcoxon test.

ID#: 372671

Associations Between Contractile Performance, Lipid Burden and Interstitial Fibrosis in Patients with Anderson Fabry Disease

Alessandro Satriano, Ph.D.[2]Cody Wu[1], Muhammad Afzal[3], Mariam Narous[4], Yoko Mikami, MD, Ph.D.[5], Aneal Khan, MD, MSc[6], Jacqueline A. Flewitt, MSc[2], Bobby Heydari, MD, MPH[5], Carmen P. Lydell, MD[2], Andrew G. Howarth, MD, Ph.D[5], Nowell M. Fine, MD, M.Sc.[7], James White, MD, FRCP(C)[5]

1. Stephenson Cardiac Imaging Centre, Canada

2. Stephenson Cardiac Imaging Centre, Libin Cardiovascular Institute of Alberta, University of Calgary, Calgary, AB, Canada

3. Stephenson Cardiac Imaging Centre, AB, Canada

4. University of Alberta, Canada

5. Stephenson Cardiac Imaging Centre, Libin Cardiovascular Institute of Alberta, University of Calgary, AB, Canada

6. Alberta Children's Hospital Research Institute, Cumming School of Medicine, University of Calgary, AB, Canada

7. Libin Cardiovascular Institute of Alberta, AB, Canada

Background: Anderson-Fabry Disease (AFD) is an X-linked genetic disorder associated with myocardial hypertrophy, lipid accumulation, and fibrosis. These respective abnormalities can be quantified through cine, T1 mapping and late gadolinium enhancement (LGE) CMR. Analyses of myocardial deformation are also permitted through 3D feature tracking strain analysis. In this study, we investigated the influence of lipid accumulation and hypertrophy on regional function in this population.

Methods: Thirty-five genetically confirmed AFD patients underwent a standardized CMR imaging protocol at 3 Tesla including multi-axial cine imaging, native T1 mapping, and LGE. Blinded analysis was performed using cvi42 to obtain global chamber volumes and T1. LGE distribution was coded using a 68 sub-segment model. 3D segmental strain amplitude and peak-systolic timing were computed using in-house validated software (GIUSEPPE). Statistical analyses were performed for segments without LGE to evaluate deformation characteristics related to lipid content and hypertrophy.

Results: The mean age was 43.5±15.6 years (69% female). The mean left ventricular (LV) mass index was 63.5±15.7g/m2 with an LV ejection fraction of 66.9±5.9%. 560 segments were evaluated with a mean wall thickness of 7.8±2.2 mm. 504 segments without LGE were available for analysis. The mean segmental native T1 was 1068±78ms and was lower in segments with increased (above median value) wall thickness (1036±71ms vs 1113+/-66ms, $p<0.0001$) (see Table 1). Segmental strain amplitude was significantly associated with wall thickness (e.g. circumferential: r=0.14; radial: -0.21; maximum principal: r=-0.11; $p<0.05$ for all), with lower strain values in segments above the median thickness (circumferential: -11.0±4.8% vs -12.1±4.5%, $p<0.05$; radial: 40.3±38.3% vs 58.6±47.6%, $p<0.0001$; maximum principal: 72.3±53.6% vs 89.9±60.2%, $p<0.0001$). Native T1 was not associated with strain amplitude, however did show correlation with time to peak strain (circumferential: r=0.28; radial: r=0.25; maximum principal: r=0.24; $p<0.0001$ for all).

Conclusion: This study shows that in patients with AFD reductions in strain amplitude are present in thickened myocardial segments despite no LGE , and are not related to native T1 (i.e. lipid burden). Such findings may be related to geometrical changes of the myocardial wall rather than a direct consequence of lipid deposition itself. An observed relationship was identified between native T1 and time to peak strain. Overall, it appears that amplitude and timing of contraction may be independently affected by geometry and lipid content, respectively. Further investigation of these findings is required.

Parameter	R (Global)	P-Value (Global)	R (Segmental)	P-Value (Segmental)
Circumferential				
Subendocardium	0.6100	**<0.005**	0.4043	**<0.0001**
Subepicardium	0.7634	**<0.0001**	0.3943	**<0.0001**
Transmural	0.6782	**0.001**	0.4250	**<0.0001**
Longitudinal				
Subendocardium	0.6024	**<0.005**	0.3164	**<0.0001**
Subepicardium	0.7166	**<0.0005**	0.3221	**<0.0001**
Transmural	0.6682	**0.001**	0.3487	**<0.0001**
Radial				
Transmural	-0.3514	0.13	-0.3335	**<0.0001**
Minimum				
Subendocardium	0.6120	**<0.005**	0.4000	**<0.0001**
Subepicardium	0.6886	**<0.001**	0.2931	**<0.0001**
Transmural	0.6823	**<0.001**	0.3964	**<0.0001**
Secondary	0.3148	<0.018	0.1863	**<0.005**
Subendocardium	0.6253	**<0.005**	0.2278	**0.0005**
Subepicardium	0.5582	**0.01**	0.2428	**<0.0005**
Transmural				
Maximum	-0.5117	**<0.05**	-0.4599	**<0.0001**
Transmural				
Thickness	0.4162	0.07	0.3807	**<0.0001**

Table 1: Segmental analysis of Native T1, Partition Coefficient and Left Ventricular myocardial deformation amplitude parameters in patients with genetically confirmed Anderson Fabry Disease, stratified for segments without LGE above and below the median wall thickness.

ID#: 372724

Quantitative Multi-Contrast CMR of Carotid Atherosclerosis: Pushing for Higher Clinical Value

Yibin Xie, PhD[1] Anthony G. Christodoulou, PhD[2], Nan Wang, M.S.[3], Zixin Deng, M.S[2], Bill Zhou, B.S.[1], Wei Yu, M.D, Ph.D[4], Debiao Li, PhD[2]

1. Cedars-Sinai Medical Center

2. Cedars-Sinai Medical Center, Los Angeles, CA

3. Cedars-Sinai Medical Center/UCLA, Los Angeles, CA

4. Department of Radiology, Anzhen Hospital, Capital Medical University, Beijing, China (People's Republic)

Background: Multi-contrast CMR has long been promised as a preferred noninvasive imaging solution for assessing carotid atherosclerosis. However, it has yet to become the standard of care procedure because of several longstanding challenges limiting its clinical value, including complex, motion-prone scans and difficulty in image interpretation due to its qualitative nature. By contrast, tissue relaxometry mapping offers high reproducibility and portability of its results[1,2]. In this study, we extend our previous single-scan concept of carotid artery CMR[3] to Quantitative Multi-contrast Atherosclerosis Characterization (qMATCH). The goal is to achieve multi-contrast CMR, including MRA, dark-blood vessel wall morphology, T1- and T2-weighted images, and quantitative relaxometry mapping, all in one 8-minute scan.

Methods: The proposed technique is formulated based on low-rank tensor (LRT) framework[4], exploiting the partial separability of spatial and contrast dimensions in the multi-contrast images to achieve vast acceleration. Variable-duration T2-IR preparations and a continuous spoiled gradient echo train were used to generate different T2 weightings and T1 weightings, respectively (Fig.1). Cartesian trajectory with Gaussian random variable-density sampling was designed for capturing the image contrast dynamics. All data were acquired on a 3T Siemens Verio scanner with the following parameters: coronal 3D slab, FOV=150x150x26mm^3, 0.7mm isotropic spatial resolution, FA=8°, TEs=20/30/40/50/60/70ms, scan time=8mins. Relaxometry mapping by qMATCH was tested in a custom phantom using standard spin echo sequence as the reference. In vivo imaging was performed in 7 healthy subjects and 9 patients with known carotid atherosclerosis. Carotid endarterectomy was performed in 3 patients and the plaque specimens were studied histologically and used as the reference.

Results: In the phantom study, T1 and T2 quantification by qMATCH showed high correlation with the spin echo reference (R=0.97). In the in vivo study, multi-contrast imaging with qMATCH showed satisfactory image quality in bright-blood MRA, dark-blood wall morphology, T1- and T2-weighted images and relaxometry mapping (Fig.2). Using sternocleidomastoid muscle as the region of interest, T1 quantification in the healthy subjects was 1041.4±21.2ms with qMATCH and 1142.2±20.7ms with MOLLI[5]. T2 quantification was 30.0±0.8 with qMATCH and 36.8±0.7ms with T2-SSFP[6]. Fig. 3 shows the qMATCH images acquired from a patient, compared with the conventional protocol and histological reference.

Conclusion: Preliminary results demonstrated the feasibility of qMATCH to provide a comprehensive assessment of carotid atherosclerosis in one scan. It can potentially evaluate multiple lesion characteristics including luminal stenosis (by bright-blood MRA), plaque burden (by dark-blood images), and plaque composition (by T1/T2 weighted images and relaxometry mapping). Additional advantages over conventional protocols include high-resolution 3D acquisition, large anatomical coverage, and inherently co-registered multi-contrast image set. Future work will focus on evaluating the diagnostic performance of qMATCH in a larger cohort with histological reference.

Reference: 1. Biasiolli, L. et al. JCMR (2013); 2. Coolen, B. et al. MRM (2016); 3. Fan, Z. et al. JCMR (2014); 4. Christodoulou, A. et al. ISMRM (2016); 5. Messroghli, D. et al. MRM (2004); 6. Giri, S. et al. MRM (2009).

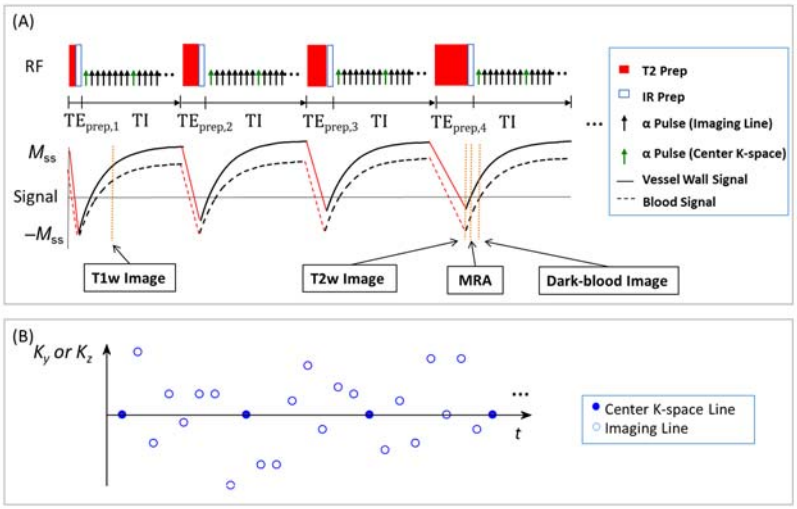

Figure 1. (A) Pulse sequence diagram for qMATCH and corresponding simulated signal evolution. The four sequence blocks shown in this diagram each has different duration of T2 preparation leading to different T2 weightings. Multi-contrast images, including MRA, dark-blood vessel wall, various T1-weighted and T2-weighted images are collected at the null point of vessel wall, null point of blood, half inversion period of the shortest T2IR prep and right after the longest T2IR prep, respectively. (B) Illustration of k-space sampling pattern for qMATCH. A 3D Cartesian trajectory was used with random reordering in the phase/partition encoding directions. A variable-density sampling scheme following the Gaussian distribution allowed higher sampling density in the central part of k-space for capturing the contrast change dynamics. A center k-space line was acquired every eight readout lines for LRT training data.

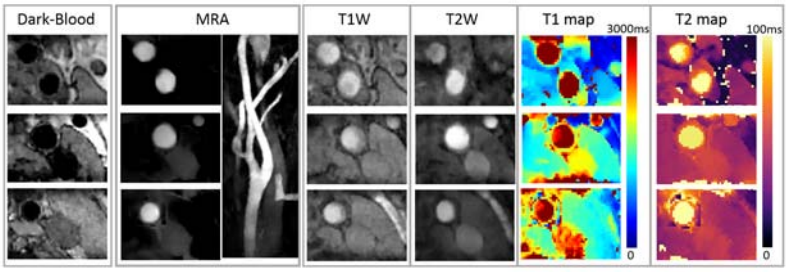

Figure 2. A representative qMATCH image set from a healthy subject. All images were acquired in coronal orientation with 0.7mm isotropic resolution. For presentation purpose, three reformatted transversal slice locations are shown here to represent the multi-contrast image set from qMATCH: Dark-Blood for visualizing vessel wall; MRA for visualizing lumen; T1-weighted and T2-weighted images for qualitative plaque characterization; and T1 and T2 mapping for quantitative plaque characterization.

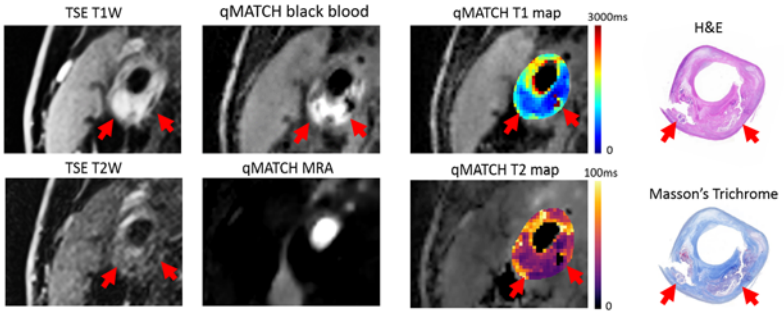

Figure 3. A representative case of a patient (80 y/o, male) with possible intra-plaque hemorrhage (IPH) in the carotid arterial wall. Conventional T1W TSE image showed a hyper-intense area in the plaque (arrows), suggesting possible methemoglobin deposit (T1 shortening). T2W TSE showed hypo-intense in the same area suggesting

subacute stage for the IPH (T2 shortening). Such trend was consistent with qMATCH findings as its relaxometry maps also showed decreased T1 and T2 values in the plaque area. Histological study of the ex vivo plaque specimen confirmed the presence of IPH.

ID#: 372727

Late Gadolinium Enhancement CMR Provides a Novel Tissue Marker of Adverse Left Ventricular Remodeling Independent of Conventional Genetic Risk Stratification in Friedreich's Ataxia

Jonathan W. Weinsaft, MD[1]Nadjia Kachenoura, PhD[2], Meridith P. Pollie, BS[3], Francoise Pousset, MD[4], Jiwon Kim, MD[5], Jonathan Y. Siden, BA, BSW[3], Virginie Bonnamain, PhD[6], Lise Legrand, MD[4], Stéphane Hatem, MD, PhD[7], Philippe Cluzel, MD, PhD[8], Odelya Pagovich, MD[3], Ronald Crystal, MD[3], Alexandra Durr, MD, PhD[9], Alban Redheuil, MD, PhD[10]

1. Weill Cornell Medical Center, NY

2. Sorbonne Universités, UPMC Univ Paris 06, INSERM UMRS 1146, CNRS UMR 7371, Laboratoire d'Imagerie Biomédicale, Ile-de-France, France

3. Weill Cornell Medical College

4. Hopital Pitie-Salpetriere, France

5. Weill Cornell Medical College, New York, NY

6. Adverum Biotechnologies, SAS, France

7. Hopital Pitie-Salpetriere, Ile-de-France, France

8. Sorbonne Universités, UPMC Univ Paris 06, INSERM, CNRS, UMR 7371, UMRS 1146, Laboratoire d'Imagerie Biomédicale, 75013, Paris, France, Ile-de-France, France

9. University Hospital Pitie-Salpetriere, France

10. Sorbonne Universités, UPMC Univ Paris 06, INSERM UMRS 1146, CNRS UMR 7371, Laboratoire d'Imagerie Biomédicale, Paris, Ile-de-France, France

Background: Cardiomyopathy is a leading cause of death among patients with Friedreich';s ataxia (FA). CMR has been used to identify altered left ventricular (LV) tissue properties in FA, but magnitude and impact of abnormal myocardial tissue substrate on LV remodeling is poorly understood.

Methods: The population comprised FA patients and age/gender matched controls undergoing contrast-enhanced CMR (1.5T) via a tailored protocol. CMR included (a) cine-CMR (SSFP) for LV structure/function, (b) DE-CMR (IR-GRE) for regional myocardial enhancement, and (c) T1 mapping (MOLLI) pre- and 10-minutes post-contrast (0.2mmol gadolinium) for global fibrosis via extracellular volume (ECV) calculation (derived from pre and post-contrast ROIs in LV septum and blood pool). CMR analysis was performed via an independent core lab blinded to clinical and genetic data.

Results: 39 subjects (20 FA [29±7 yo / disease duration = 14±6 years], 19 controls) prospectively underwent CMR. FA was associated with adverse LV remodeling, as evidenced by increased myocardial mass index and decreased chamber size (both $p<0.05$), with resultant increases in concentric LV remodeling quantified via volumetric and linear indices (both $p<0.001$) (Table). Despite absolute increases vs. controls, only 30% of FA patients met established cutoffs for LV hypertrophy based on established CMR normative cutoffs ($p=0.02$ vs. controls [0%]). Regarding LV function, LVEF ($p=0.21$) was similar between groups but FA patients had over 30% reduction in LV stroke volume (67±18 vs. 98±22ml, $p<0.001$) and decreased cardiac output ($p=0.01$) despite increased heart rate (78±13 vs. 66±13, $p=0.003$) and similar mean arterial pressure (102±9 vs. 104±10mmHg, p=49). DE-CMR tissue characterization identified LGE in 50% of FA patients (all controls LGE negative). Among FA patients with LGE, hyperenhancement was typically small (4±3% LV myocardium, 3±2 LV segments): All (9/10) FA patients with LGE had focal epicardial enhancement in the LV lateral wall (n=1 bilateral papillary LGE). LGE+ and – FA patients were similar with respect to conventional risk stratification based on maximum and minimum trinuclide repeat length (both p=NS): ECV values were similar in non-enhanced (LGE-) LV regions (p=NS). DE-CMR based partitioning demonstrated LGE+ FA patients to have more advanced LV remodeling, as evidenced by increased absolute ($p=0.07$) and indexed LV mass ($p=0.04$).

Conclusion: FA results in concentric LV remodeling, with decreased chamber size and reduced stroke volume despite compensatory increases in heart rate. Focal myocardial enhancement on DE-CMR is associated with increased LV hypertrophy among patients with Friedreich';s ataxia, providing a marker of adverse cardiac remodeling independent of conventional genetic risk stratification.

Friedreich's Ataxia-Associated LV Remodeling in Relation to Presence or Absence of CMR-Evidenced Late Gadolinium Enhancement

	Control	Friedreich's Ataxia	p	Friedreich's Ataxia		
				LGE -	LGE +	p
LV Structure and Function						
LV Mass	137 ± 29	161 ± 44	0.06	143 ± 23	179 ± 54	0.07
LV Mass Index	75 ± 13	93 ± 20	**0.002**	84 ± 10	102 ± 23	**0.04**
LV End-Diastolic Volume	151 ± 32	111 ± 34	**0.001**	104 ± 26	119 ± 40	0.3
LV EDV Index	83 ± 17	64 ± 14	**0.001**	60 ± 9	67 ± 18	0.3
LV End-Diastolic Diameter	5 ± 0.5	5 ± 0.6	**0.01**	5 ± 0.5	5 ± 0.7	0.3
LV End-Systolic Volume	53 ± 12	44 ± 21	0.1	38 ± 16	50 ± 24	0.2
LV ESV Index	29 ± 7	25 ± 10	0.2	22 ± 8	28 ± 12	0.2
Relative Mass (mass/EDV)	1 ± 0.2	1.5 ± 0.3	**<0.001**	1 ± 0.3	2 ± 0.4	0.3
Mean Wall Thickness	1 ± 0.2	1 ± 0.2	0.45	1 ± 0.2	1 ± 0.2	0.5
Relative Wall Thickness	0.3 ± 0.1	0.5 ± 0.1	**<0.001**	0.5 ± 0.1	0.5 ± 0.1	0.9
LV Ejection Fraction (%)	65 ± 5	62 ± 10	0.21	65 ± 10	59 ± 9	0.2
LV Stroke Volume	98 ± 22	67 ± 18	**<0.001**	66 ± 15	69 ± 21	0.7
LV Cardiac Output	6 ± 1	5 ± 1	**0.01**	5 ± 1	5 ± 2	0.5
Diffuse Fibrosis						
Pre-Contrast Myocardial T1	989 ± 36	962 ± 30	**0.01**	960 ± 29	964 ± 32	0.8
Post-Contrast Myocardial T1	410 ± 46	376 ± 53	**0.045**	371 ± 45	382 ± 62	0.7
Extracellular Volume	23 ± 3	24 ± 4	0.3	24 ± 4	24 ± 4	0.99
Genetic Repeats						
Maximum Number GAA Repeats	--	759 ± 240	--	725 ± 205	793 ± 280	0.6
Minimum Number GAA Repeats	--	544 ± 215	--	519 ± 189	570 ± 246	0.6

ID#: 372732

Identification and Sorting of End-Systolic and End-Diastolic images in Real-Time Cine Imaging Using Laplacian Eigenmaps and Image Registration

Anthony H. Aletras, Ph.D.[6]Kostas Haris, PhD, MSc[1], Sebastian Bidhult[2], Ellen Ostenfeld, M.D., Ph.D.[3], Katarina Steding-Ehrenborg[2], Pia Sjöberg, M.D.[4], Marcus Carlsson, MD, PhD[5]

1. Lund University, Skåne University Hospital, Department of Clinical Sciences Lund, Clinical Physiology, Lund, Sweden, Greece

2. Lund University, Skåne University Hospital, Department of Clinical Sciences Lund, Clinical Physiology, Lund, Sweden, Sweden

3. Lund University, Dept of Clinical Sciences, Clinical Physiology, Lund, and Skane University Hospital, Lund, Skane Lan, Sweden

4. Lund University, Skane University Hospital, Department of Clinical Sciences Lund, Clinical Physiology, Lund, Sweden, Sweden

5. Lund University, Skane University Hospital, Department of Clinical Sciences Lund, Clinical Physiology, Lund, Sweden, Skane Lan, Sweden

6. Aristotle University of Thessaloniki/Lund University, Thessaloniki, Thessaloniki, Greece

Background: Quantification of left-ventricular function in real-time free-breathing cine images requires the identification of end-diastolic (ED) and end-systolic (ES) images and their respiratory sorting (end-expiratory or end-inspiratory). Currently, the method of choice is their manual identification, a process laborious and time consuming [2]. The aim of this study was to develop a method for automatic identification of ES and ED images via manifold learning and image registration.

Methods: Eight healthy volunteers (4 females; age 24.9±4.4 years) were recruited and scanned with a 1.5T Siemens Aera MR-scanner (Siemens Healthineers, Erlangen, Germany). Short-axis real-time cine images covering the entire heart were acquired using an ECG-free free-breathing real-time bSSFP sequence (RT-SSFP): TE=0.94ms, temporal resolution 28.4ms, flip angle=56^{o}, 490 acquired timeframes and pixel size=2.7x2.7x8mm^3. A region of interest (ROI) enclosing the LV was manually selected. From each frame, a vector of all pixels in the ROI was extracted. This vector sequence was input to the Laplacian Eigenmaps (LE) dimensionality reduction method which creates a low-dimensional representation of its input so that the distances between each point and its k nearest-neighbors are minimized [1,3]. The low-dimension was selected to be 1 and, therefore, the low-dimensional points were scalar values. In this representation, the heart extreme deformations (ES-ED) were projected to opposite positions and therefore, their detection was reduced to local maxima and minima identification. Then, the detected ES-ED frames restricted to the initial ROI, were input to a rigid body registration algorithm. The vertical component of the estimated translation, dy, indicates the respiratory state of the frame. Frames with locally maximum dy are end-expiratory while frames with locally minimum dy are end-inspiratory.

Results: The detected end-expiratory and end-inspiratory ES and ED frames agreed with those identified by visual frame-by-frame inspection in 92.8%, 92.8%, 87.1% and 85.7% of cases, respectively. The result from LE analysis in one mid-ventricular slice of one volunteer is shown as an example in Figure 1. ES frames are projected to local maxima (black circles), while ED frames are projected as local minima. In Figure 2, the corresponding automatically detected end-expiratory ES and ED frames are shown. The computational time required for each dataset was less than 10s per slice.

Conclusion: In this study, we demonstrated that the identification of ES-ED frames in ECG-free free-breathing short-axis real-time cine MR images is possible using manifold learning techniques.

References:

[1] Usman et al., JMRI 2015
[2] Wu et al., JMRI 2015
[3] Belkin et al., Neural Comp 2003

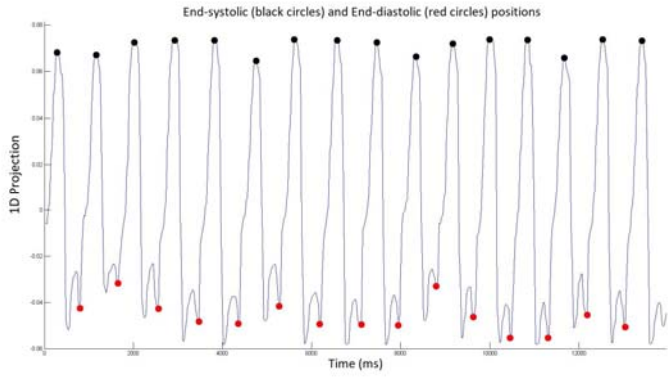

Mapping of the cine images into one dimension using Laplacian Eigenmaps. ES positions are local maxima and ED positions are local minima preceding ES positions. The appearance of more than one local minimum is due to the atrial contraction that precedes ventricular diastole. Therefore, the last local minimum is selected to represent the ED point.

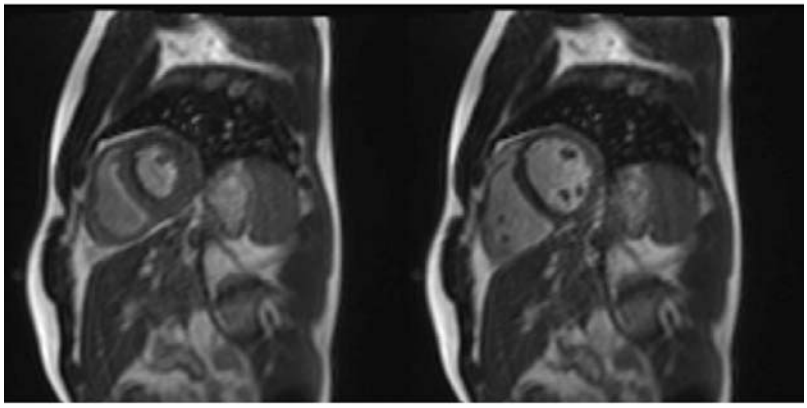

End-expiratory ES (Left) and ED (Right) frames detected by the proposed technique.

ID#: 372893

The use of novel non-contrast CMR techniques in the assessment of sub-clinical cardiovascular abnormalities in pediatric renovascular hypertension

Mun Hong Cheang, MBBS,BMedSci (Hons)[1] Nathaniel J. Barber, MBBS, MSc [2], Steeden A. Jennifer, PhD [3], Vivek Muthurangu, MD[3]

1. Institute of Cardiovascular Science, University College London, United Kingdom

2. UCL Institute of Cardiovascular Science & Great Ormond Street Hospital for Children, London, England, United Kingdom

3. Institute of Cardiovascular Science, University College London, England, United Kingdom

Background: The long-term effects of renovascular hypertension (RH) in children are not known. Pediatric RH is thought to have lower cardiovascular (CV) risk compared to adults because pediatric renal artery stenosis is seldom associated with CV disease and is frequently treatable. Resolution of hypertension may be achieved using renal artery angioplasty or surgical revascularization. However, it is not known if CV effects persist after successful treatment. Echocardiography is commonly used to assess these children. Nonetheless, it has well-known limitations with left ventricular (LV) assessment and is not used to assess vascular function. Cardiovascular magnetic resonance imaging (CMR) may be an ideal tool as it can perform myocardial and vascular assessment and may even detect sub-clinical myocardial changes using novel non-contrast techniques. This study aims to investigate the utility of CMR for the assessment of CV function in a cohort of optimally treated pediatric RH.

Methods: Forty-five children (15 RH, 15 essential hypertension (eHTN), 15 healthy controls (HC)) underwent CMR scan. All RAS and eHTN children received optimal treatment before recruitment. Aortic flow and LV assessment was performed with high-resolution breath-hold spiral phase contrast magnetic resonance (PCMR) and real-time radial SSFP sequence, respectively. Vascular function was assessed by calculating systemic vascular resistance (SVR) and total arterial compliance (TAC) from aortic flow and simultaneously acquired non-invasive blood pressure (BP) measurements. Cardiac timings were evaluated by measuring mitral inflow velocities using high temporal resolution real-time UNFOLD-SENSE spiral PCMR sequence. Systolic and diastolic LV mechanics (i.e. Radial (Rad) or Longitudinal (Long) systolic (S';), early diastolic (E';) or late (A';) myocardial velocity, E';/A'; ratio) were assessed by measuring myocardial velocities with self-navigated golden-angle spiral acquisition tissue phase mapping sequence. Image analysis was performed using in-house plug-ins for OsiriX software. Group comparisons (ANOVA) were used to identify abnormalities in RH and eHTN compared to HC.

Results: Although BP was similarly elevated in both groups, RH children had elevated SVR (p=0.01) while eHTN had lower TAC (p=0.003). Left ventricular remodelling (LV mass to volume ratio, MVR) was present in RH and eHTN (p≤0.04). While EF was normal, diastolic function (Long E';/A';) was significantly impaired in both hypertension groups (p<0.04).

Conclusion: Non-contrast CMR techniques can be used to detect sub-clinical changes in pediatric renovascular hypertension. Cardiovascular abnormalities remain present in RH children despite receiving optimal treatment. Although the CV effects of hypertension were similar in both cohorts, the vascular phenotype was different, with elevated SVR in RH and reduced TAC in eHTN.

Summary of cardiovascular profile of study population

	Healthy Controls n=15	Renovascular Hypertension n=15	Essential Hypertension n=15	P-value
SBP (mmhg)	103±11	122±8.4†	129±12‡	<0.001

DBP (mmhg)	52±6.6	63±12†	68±11‡	<0.001
MBP (mmhg)	74±5.9	88±8.6†	93±10‡	<0.001
SVR ($WU.m^2$)*	20±1.2	25±1.3†	23±1.2	0.018
TAC (ml/mmHg. $m^2.10^2$)	59±14	50±11	45±5.4‡	0.004||
$LVMht^{2.7}$ ($g/m^{2.7}$)	23±2.9	25±5.4	27±6.6	0.09
MVR(g/ml)	0.69±0.091	0.81±0.15†	0.83±0.14‡	0.008
EF (%)	69±3.4	73±9.1	69±4.4	0.46||
Long E'; (cm/s)	7.6±1.9	7.3±1.9	9.5±1.7‡§	0.004
Long A'; (cm/s)	2.2±0.49	2.7±0.87	3.6±0.76‡§	<0.001
Long E';/A'; ratio	3.5±0.7	2.8±0.67†	2.7±0.66‡	0.006

Abbreviations: HC=Healthy controls, RH=Renovascular hypertension group, eHTN=Essential hypertension group, SBP=Systolic blood pressure, DBP=Diastolic blood pressure, MBP=Mean blood pressure, SVR=Systemic vascular resistance, TAC=Total arterial compliance, LVMHT(2.7)=Left ventricular mass corrected by height to the power of 2.7. MVR=mass volume ratio, EF=Ejection fraction, Rad=Radial, Long=Longitudinal, E';=early diastolic myocardial velocity, A';=late diastolic velocity. Data presented as mean ± standard deviation. *- Logarithmic transformation was applied. †- P-value <0.05 when RH compared with HC. . ‡ - P-value <0.05 when eHTN compared with HC. §- P-value <0.05 when RH compared to eHTN. ||- ANOVA Welch (W) test was used.

ID#: 372896

Functional impact of CMR measures of diffuse myocardial fibrosis in patients with Duchenne muscular dystrophy

Joseph J. Pagano, MD[1]Regina De La Mora Cervantes, MD[1], Norman N. Musewe, MD, FRCP(C)[2], Aamir Jeewa, MD[1], Mike Seed, MBBS[3], Shi-Joon Yoo, MD[3], Lars Grosse-Wortmann, MD[1]

1. The Hospital for Sick Children, ON, Canada

2. The Hospital for Sick Children, Markham, ON, Canada

3. The Hospital for Sick Children, Toronto, ON, Canada

Background: Cardiomyopathy is the leading cause of death and morbidity in boys with Duchenne muscular dystrophy (DMD). Evidence of diffuse myocardial fibrosis, measured by cardiac magnetic resonance (CMR) relaxometry exists, however its functional impact requires evaluation. The study aimed to characterize measures of fibrosis in juvenile patients with DMD, using native T1 and extracellular volume (ECV), and examine their functional significance.

Methods: Subjects with DMD were retrospectively identified through our institutional CMR database. Studies included assessment of ventricular volumes, myocardial mass, late gadolinium enhancement (LGE), and T1 mapping using MOLLI, performed at 1.5T. The left ventricle (LV) was segmented into 6 segments, according to the American Heart Association model. Strain was derived using feature tracking of short axis and 4-chamber cine images. T1 and ECV values were compared to normative controls.

Results: Thirty-five boys with DMD and 28 male controls were included (age 13±3 vs. 14±3 years, p=0.06). Demographic information and CMR results are presented in Table 1. Nearly all CMR measures were different, including all measures of native T1 and ECV, except septal ECV. Nineteen boys with DMD (54%) had LGE, predominantly in the lateral wall. In boys with DMD, both T1 and ECV were increased in the free wall compared to the septum (p=0.02 and p<0.01, respectively), opposite to the finding in controls (p<0.01 and p<0.05, respectively). In boys with DMD, mean LV ejection fraction (LVEF) was lower in those with LGE (49±9 vs 54±4%, p=0.04), while T1 and ECV values were increased (Table 2), particularly in the LV free wall. Global LV native T1 and ECV did not correlate with LVEF, longitudinal, global radial, or global circumferential strain or strain rates. There were no correlations with septal or free wall T1 values, or ECV, and longitudinal strain or strain rate, except a weak correlation between free wall ECV and strain rate (Figure 1). On a segmental basis, native T1 only showed a weak correlation with circumferential strain rate (R2=0.02, p=0.04). There were weak correlations between segmental ECV and circumferential strain (R2=0.06, p <0.01), strain rate (R2=0.07, p<0.01), and radial strain rate (R2=0.03, p=0.03), however not with radial strain (p=0.16).

Conclusion: Boys with DMD demonstrate alterations in T1 and ECV, particularly in the lateral wall and with LGE. Absent or weak associations with myocardial mechanics suggest limited functional implications of diffuse myocardial fibrosis in juvenile patients. Whether this suggests independent pathophysiology and prognostic information from tissue characterization vs. strain requires further study.

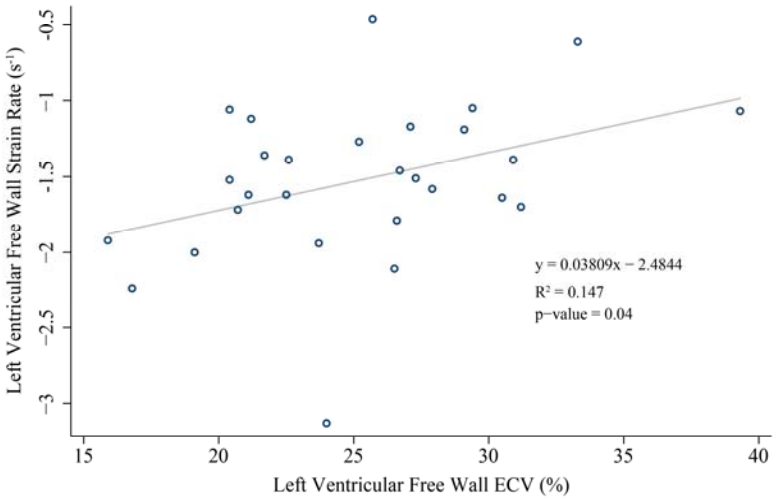

FIgure 1 - Left ventricular free wall ECV versus strain rate

Demographic and CMR values

	DMD	Controls	
	n=35	n=19	p-value
Age (years)	13±3	14±3	0.06
Height (cm)	133±12	165±18	<0.01
Weight (kg)	40±12	68±26	<0.01
HR (bpm)	93±16	72±15	<0.01
Hematocrit	0.46±0.03	0.45±0.03	0.42
LV mass (g/m2)	50±8	59±13	<0.01
LVEDVi (ml/m2)	84±16	95±13	0.01
LVESVi (ml/m2)	41±13	41±6	0.85
LVSVi (ml/m2)	43±9	55±9	<0.01
LVEF (%)	51±8	57±4	<0.01
RVEDVi (ml/m2)	79±14	103±19	<0.01
RVESVi (ml/m2)	37±7	50±10	<0.01

RVSVi (ml/m2)	42±10	53±11	<0.01
RVEF (%)	53±6	51±4	0.15
Native T1 (ms)			
Whole LV	1036±28	984±38	<0.01
IVS	1041±29	995±42	<0.01
Free wall	1060±45	967±39	<0.01
Blood T1 (ms)	1565±51	1532±72	0.03
ECV (%)	n=35	n=10	
Whole LV	22.1±3.0	20.0±2.6	0.05
IVS	21.3±3.2	20.9±2.9	0.73
Free wall	25.9±5.6	19.7±2.4	<0.01

DMD = Duchenne muscular dystrophy, LGE = late gadolinium enhancement, LV = left ventricle, LVEDVi = indexed left ventricular end-diastolic volume, LVESVi = indexed left ventricular end-systolic volume, LVSVi = indexed left ventricular stroke volume, LVEF = left ventricular ejection fraction, RVEDVi = indexed right ventricular end-diastolic volume, RVESVi = indexed right ventricular end-systolic volume, RVSVi = indexed right ventricular stroke volume, RVEF = right ventricular ejection fraction, IVS = interventricular septum, ECV = extracellular volume fraction

Comparisons between subjects with DMD based on LGE findings

	LGE+	LGE-	
	n=19	n=16	p-value
Age (years)	14±3	12±3	0.0682
LV LGE location	0	-	
Anterior	0	-	
Anteroseptal	2	-	
Inferoseptal	4	-	
Inferior	8	-	

Inferolateral	19	-	
Anterolateral	13	-	
Native T1 (ms)			
Whole LV	1045±25	1025±29	0.04
IVS	1049±31	1032±25	0.09
Free wall	1074±40	1042±45	0.03
Blood T1 (ms)	1560±56	1571±45	0.52
ECV (%)			
Whole LV	22.5±3.1	21.6±2.9	0.37
IVS	20.5±3.2	22.1±3.0	0.14
Free wall	28.6±5.6	22.7±3.6	<0.01

DMD = Duchenne muscular dystrophy, LV = left ventricle, LGE = late gadolinium enhancement, IVS = interventricular septum, ECV = extracellular volume fraction

ID#: 372921

MRI-guided catheterization in children and young adults with congenital heart disease using the pSAT sequence: Initial findings in diagnostic procedures.

Mari Nieves Velasco Forte, MBBS[1] Sébastien Roujol, PhD[2], Bram Ruijsink, MD[2], Israel Valverde, MD[3], Phuoc Duong, MD[4], Sascha Krueger, PhD[5], Tobias Schaeffter, PhD[6], Steffen Weiss, PhD[5], Tarique Hussain, MD, PhD[7], Kuberan Pushparajah, MD[8], Reza Razavi, MD, PhD[2]

1. Queen Elizabeth Hospital/King's College London, Glasgow, United Kingdom

2. King's College London, London, England, United Kingdom

3. King's College London, Andalucia, Spain

4. King's College London, United Kingdom

5. Innovative Technologies, Philips, Technology GmbH, Hamburg, Germany, Hamburg, Germany

6. Physikalisch-Technische Bundesanstalt (PTB), Braunschweig and Berlin, Germany, Berlin, Germany

7. Dept. of Pediatrics, UT Southwestern Medical Center, TX

8. Kings College London and Guy's & St Thomas' Hospital NHS Foundation Trust, Evelina London Children's Hospital, England, United Kingdom

Background: MRI is a promising alternative to fluoroscopy for the guidance of cardiac catheterization procedures. We have recently developed a partial saturation (pSAT) sequence which enables passive tracking with positive contrast of a gadolinium-filled balloon-wedge catheter. In this study, we sought to evaluate the performance of the pSAT sequence for MRI-guided catheterization in children and young adults with congenital heart disease (CHD).

Methods: 23 consecutive CHD patients were referred for MRI-guided catheterization for pulmonary vascular resistance (PVR) analysis; 4 patients could not be recruited, 16 were enrolled at our institutions and imaged using an XMR system (1.5T Philips Achieva combined BV Pulsera cardiac X-Ray unit); 3 patients were recruited at a different centre and scanned using a 1.5T Philips Ingenia MRI system. MRI-guidance was performed using the pSAT sequence and either the iSuite real-time visualization platform® (Philips) (12 patients) or an interactive imaging mode (5 patients). PVR analysis was recorded. Radiation dose and time, duration of catheterization performed under MRI-guidance and adverse events were reported. Fraction of time when the catheter tip was visible during real-time MRI imaging was also evaluated. Visualization of the heart anatomy and catheter balloon/blood contrast were each scored by 3 MRI-catheterisation experts (1-poor; 5-excellent).

Results: Patients'; characteristics and catheterization findings are summarised in Table 1. Median age was 5 years (range: 2 months-39 years). After initial evaluation, MRI guidance was not attempted in two patients, owing to the need of wire and patient instability, respectively. Of the remaining 17 patients, 37% underwent right heart catheterization, 42% underwent both left and right catheterization and 21% had single ventricle circulation. In 4 patients, the procedure was performed solely under MRI guidance, 3 Fontan patients had >50% performed under MRI (Figure 1). For the remaining part of the procedure in these cases and the rest of the patients (Figures 2) a stiffer catheter and/or a wire with the subsequent need for x-ray support was required. Median radiation time and dose were 11 min (IQ range:5.5-16.8) and 0.3 mGy.m^2 (IQ range:0.16-0.55), respectively. Mean catheterization time under MRI was 34±23 min. There was a significant trend towards needing x-ray support in smaller patients (p=0.03). Mean subjective image quality scores were 3.7±0.96 for heart visualisation and 4.6±0.6 for balloon/blood contrast. pSAT angle was 30-40° in all patients. During real-time MRI catheterization the balloon was visualized during 64±19% of the scanning time.

Conclusion: MRI-guided catheterization with simultaneous visualization of the catheter and cardiac anatomy using the pSAT sequence is feasible in patients with CHD. However, there remains a need for MRI-compatible guide-wires to enable cardiac catheterisation under MRI-guidance alone in patients with complex anatomy.

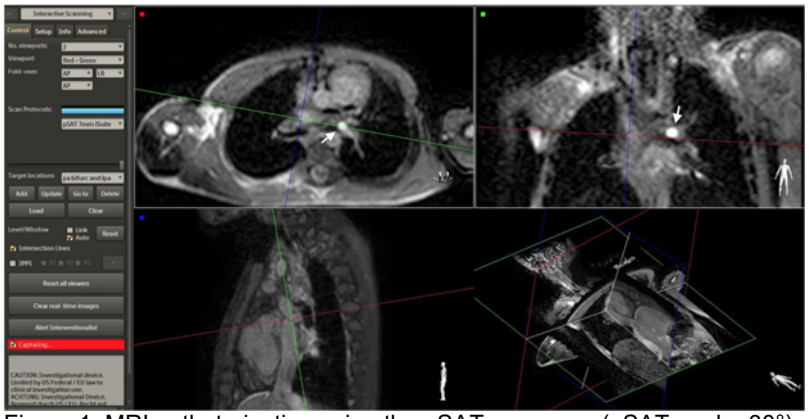

Figure 1. MRI-catheterization using the pSAT sequence (pSAT angle=30°) and the iSuite platform in a patient with Fontan circulation. The catheter is seen in the left pulmonary artery in both axial and coronal planes (top panels).

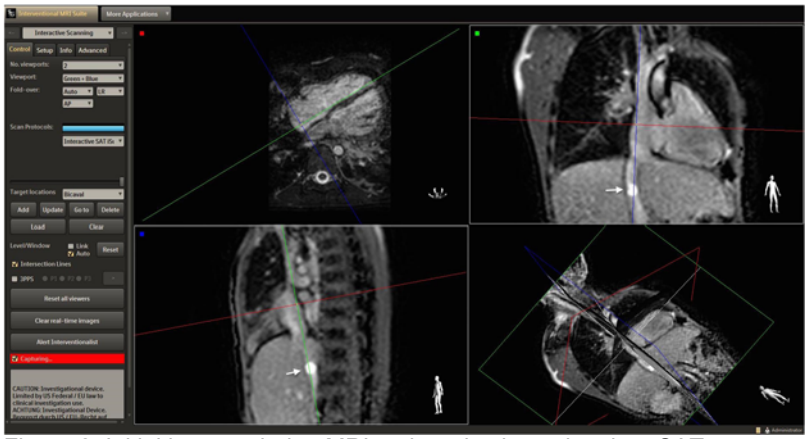

Figure 2. Initial images during MRI-catheterization using the pSAT sequence (pSAT angle=30°) and the iSuite platform in a patient with pulmonary stenosis (status post-correction of Total Anomalous Pulmonary Venous Drainage). The balloon at the tip of the catheter (white arrow) is seen in the inferior vena cava (IVC).

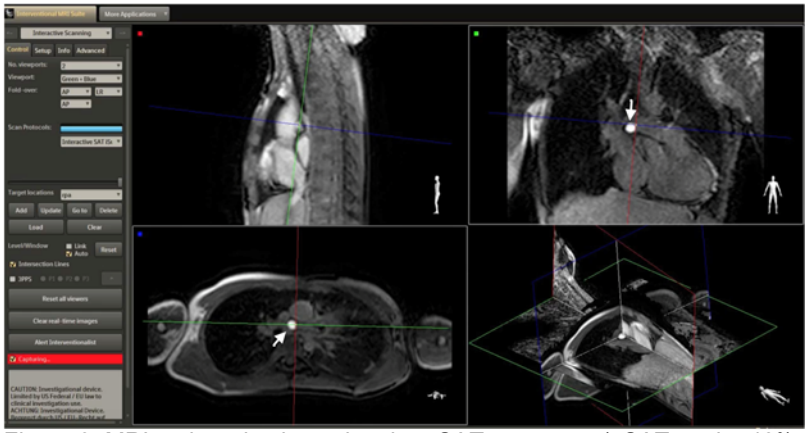

Figure 3. MRI-catheterization using the pSAT sequence (pSAT angle=40°) and the iSuite platform during right heart catheterization in a patient with Tetralogy of Fallot. Baloon-tip seen at the mid-portion of the right pulmonary artery.

Table 1. Catheterization findings in all patients. Measurements are shown as mean ± SD unless stated otherwise.

Age (median, range)	5.6 years (2 months – 39 years)
Body surface area (median, range)	0.51 m^2 (0.23 – 2)
Weight (median, range)	19 kg (5 – 98)
Height (median, range)	118 cm (58 – 175)
Previous cardiac procedure	50% of patients
Heart rate (bpm)	98±28
EtCO2 (kPa)	4.7±0.5
FiO_2 at baseline	0.3±0.1
IVC (mmHg)	9±4.3
RA (mmHg)	6.9±2.1
RV systolic (mmHg)	60±14.7
RV EDP (mmHg)	9.2±2.5
MPA mean (mmHg)	26.7±9.6
RPA mean (mmHg)	22.4±8.7
LPA mean (mmHg)	27.8±14
PA mean (under iNO, mmHg)	26.2±14.2
LA mean (mmHg)	8.6±2.9
Pulmonary capilary wedge (if LA not measured)	10.9±3
Transpulmonary gradient (rest)	15.4±12.6
Transpulmonary gradient (under iNO)	14.8±12.8
PVR (baseline; median, range; $WU.m^2$)	2.94 (0.28 – 32)
PVR under inhaled vasodilators when applied (iNO 20 ppm+FiO2 100%; median, range; $WU.m^2$)	2 (0.63 – 27.8)

ID#: 372849

Clinical Utility and Feasibility of Cardiac Magnetic Resonance Wideband Protocol in Patients with ICD and Ventricular Tachycardia

Amit R. Patel, MD[3]Amita Singh, MD[1], Keigo Kawaji, PhD[2], Noreen T. Nazir, MD[3], Andrew Beaser, MD[1], Virginia O'Keefe-Baker, APN[1], Diane Iovino, CCDS[1], Karima Addetia, MD[1], Victor Mor-Avi, PhD[3], Roderick Tung, MD[4]

1. University of Chicago

2. University of Chicago, Chicago, IL

3. University of Chicago, IL

4. University of Chicago Medical Center, IL

Background: The presence of implantable cardioverter defibrillators (ICD) has long been considered a contraindication to magnetic resonance imaging. Frequently, patients with ICD experience ventricular arrhythmias (VT) for which cardiac magnetic resonance (CMR) may provide valuable information regarding the presence and location of scar. Cine CMR and late gadolinium enhancement (LGE) imaging have characteristic artifacts (Figure 1 and 2) in the presence of ICDs which impair accurate assessment. We sought to: 1) quantify the frequency and severity of artifact on cine and LGE imaging quality; 2) assess how a modified wideband protocol could improve the diagnostic yield of LGE assessment in patients with ICDs who presented with clinical VT, and 3) determine whether wideband LGE findings correlated with invasive electroanatomic mapping.

Methods: CMR using a novel wideband protocol was performed at 1.5T (Achieva, Philips) in 21 patients with ICDs and VT. A general safety algorithm was followed for all patients before, during, and after CMR. Cine CMR, standard LGE, and wideband LGE imaging at a manually selected frequency shift were performed. Cine CMR images obtained in ICD patients and in 21 age-matched controls were used to determine and compare inter- and intra-observer variability of measurements. Standard and wideband LGE images were assessed for the presence of artifact using a global artifact score on a per-short axis slice basis and on a per-segment basis. The presence of LGE on wideband images was compared to findings from invasive electroanatomic mapping (Figure 2 and 3). Device interrogation was performed before and after CMR to assess for changes.

Results: Assessment of cardiac function on cine CMR images was limited, with greater inter-reader variability in left and right ventricular volumes and function, when compared to patients without an ICD (Table). There were no adverse patient or device related events. With standard LGE imaging, 74% of patients demonstrated some degree of hyperenhancement artifact (Figure 2), but this persisted in only 9% of patients after wideband LGE. The percentage of diagnostic quality short-axis LGE slices increased from 56% to 96% with WB imaging, with a significant reduction in global artifact score. Of the 14 patients who proceeded to invasive electroanatomic mapping for ventricular tachycardia ablation, wideband LGE assessment correlated in 10 cases (71%).

Conclusion: Assessment of cine CMR and standard LGE is markedly limited in patients with ICD. The use of wideband LGE significantly improves image quality and can accurately localize myocardial scar prior to an invasive ablation procedure for ventricular tachycardia.

	Percent Variability (%)	Intraclass Correlation (ICC)	Percent Variability (%)	Intraclass Correlation (ICC)
	ICD Subjects		EF-Matched Controls	
LVEDV (mL)	7.2 ± 6	0.91	4.2 ± 3.3	1
LVESV (mL)	13.1 ± 12.4	0.94	7.9 ± 9.9	1
LV EF (%)	12.2 ± 11.4	0.89	8 ± 7.7	0.96
LV Mass(g/m²)	31.7 ± 24	0.04	10.1 ± 7.2	0.91
RVEDV (mL)	28.5 ± 33.8	0.2	6.5 ± 6.4	0.96
RV ESV (mL)	34.8 ± 32.1	0.05	14 ± 16.1	0.95
RV EF (%)	44.1 ± 33.9	-0.22	10.5 ± 14.2	0.82

	Standard LGE	WB LGE
Diagnostic Slices on Short Axis (n,%)	118 (56%)	205 (96%) *
Global Artifact Score	3.8 ± 3	0.11 ± 0.3 *

Table of Reproducibility

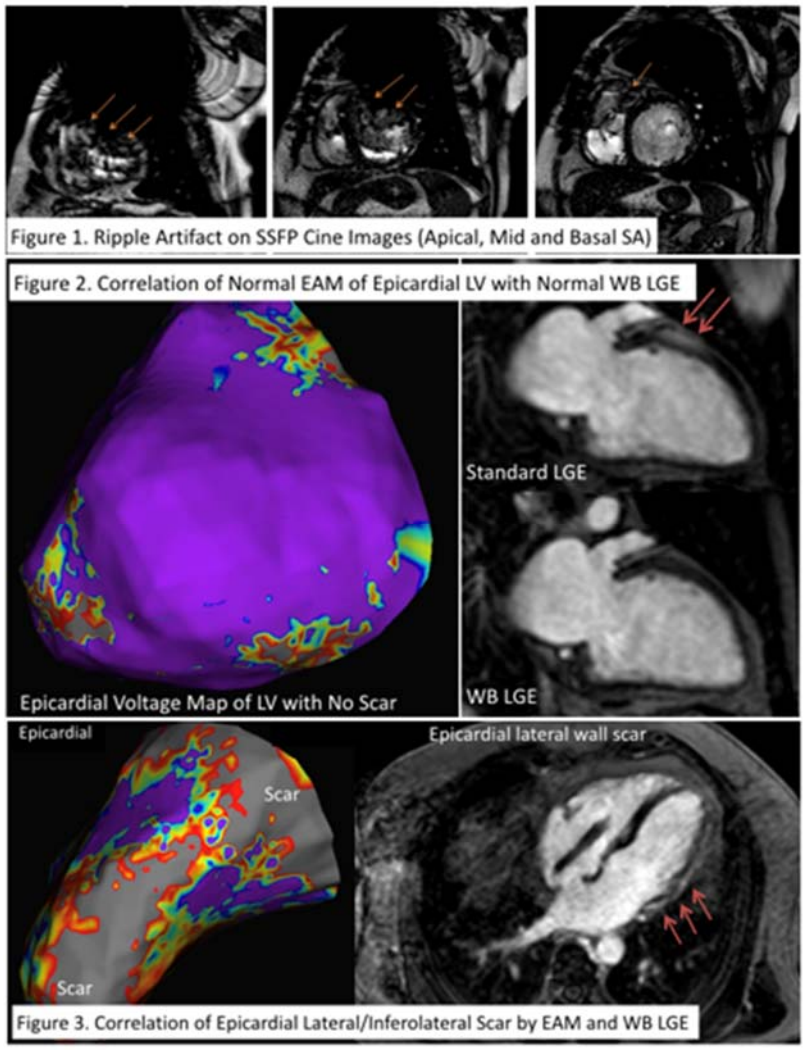

Figure of Examples

ID#: 372707

Influence of different post-processing tools on myocardial T1 and T2 relaxation times generated by cardiac T1 and T2 mapping

David Zopfs, M.D.[1] David Maintz, MD[2], Bettina Baeßler, M.D.[2]

1. University Hospital Cologne, Department of Diagnostic and Interventional Radiology, Cologne, Nordrhein-Westfalen, Germany

2. University Hospital of Cologne, Department of Radiology, Nordrhein-Westfalen, Germany

Background:
Previous studies have shown a high variability of myocardial T1 and T2 relaxation times between different sequences, field strengths and individuals, representing one of the main challenges of mapping techniques. Although an excellent technical reproducibility of T1 and T2 mapping has already been demonstrated, the potential influence of the post-processing software solution on generated T1 and T2 values still remains unclear. Thus, the purpose of the present study was to investigate the impact and reproducibility of different post-processing platforms on generated T2 and T1 relaxation times.

Methods: 11 healthy individuals were examined on a clinical 3T scanner including a gradient spin echo T2 mapping and a native Modified Look-Locker T1 mapping sequence (5(3)3 scheme). T1 and T2 maps were acquired at 3 slices in short axis view. Three different software solutions were used for post-processing of mapping data: a dedicated plugin for the open-source software OsiriX (software A), Intellispace Portal (version 9, Philips; software B), and cmr42 (Circle; software C). Maps generated i) on the scanner (scanner map) and ii) fitted separately using a mono-exponential fit (re-fitted map) were used for segmentation all three software solutions, respectively. Maps were segmented according to the 16-segments AHA-model. While averaging pixels within myocardial segments for segmental T1 and T2 calculation, the standard deviation (SD) within segments was recorded. Finally, myocardial T1 and T2 values as well as their corresponding SDs were averaged over all 16 segments in order to obtain global myocardial T1 / T2 / SD. Statistical analysis was performed using robust repeated-measures ANOVA with Tukey-type comparisons and intra-class correlation coefficients (ICCs).

Results: No systematic differences were found for global myocardial T1 and T2 between refitted and scanner maps within as well as between the three different software solutions (Table 1, Figure 1) with a good to excellent agreement (ICCs ranging from 0.611 to 0.980 for T1 and from 0.959 to 0.988 for T2). However, T1 values derived from scanner maps tended to be slightly lower when compared to re-fitted maps for all three software solutions. Similarly, no significant differences and an overall excellent agreement were observed for basal, midventricular and apical as well as for segmental T1 and T2 values, mean ICCs ranging from 0.618 to 0.960 for T1 and from 0.831 to 0.982 for T2. In contrast, SDs did not show a similar concordance across platforms, demonstrating significant differences between software C and the other two platforms (Table 2, Figure 2).

Conclusion: Myocardial T1 and T2 relaxation times appear to be independent of the used post-processing methods and thus can be used reliably used across different platforms. In contrast, SDs were not as reproducible across different platforms. This should be taken into account when aiming at elucidating the role of novel diagnostic parameters derived from T1 and T2 mapping such as madSD, which aim at quantifying the inhomogeneity of T2 values in the setting of myocardial inflammation.

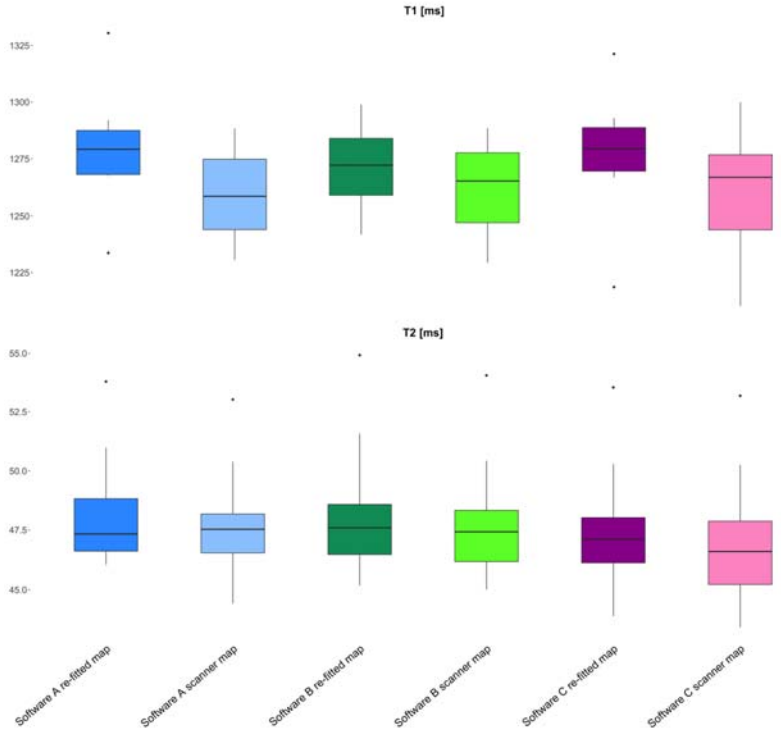

Figure 1. Box-Whisker plots for mean differences of myocardial T1 (top) and T2 relaxation times (bottom).

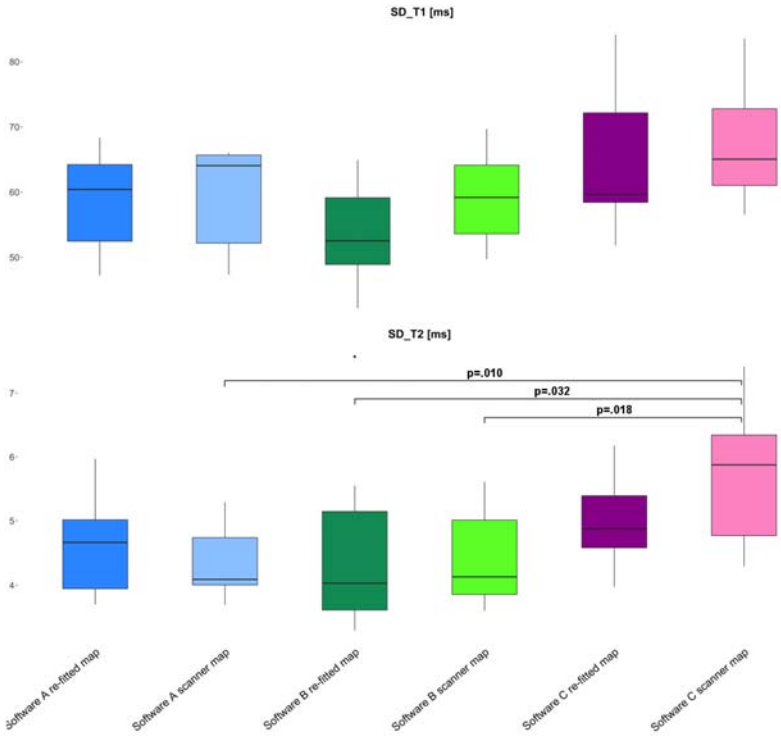

Figure 2. Box-Whisker plots for mean differences of corresponding SD of T1 (top) and T2 relaxation times (bottom).

Table 1: Comparison of mean values ± standard deviation (in ms) of myocardial T1 and T2 relaxation times.

	T1 [ms]	T2 [ms]
Software A refitted vs. scanner map	1279 ± 29 vs. 1259 ± 22, p=.576	48.2 ±2.4 vs. 47.7 ± 2.7, p=.977
Software B refitted vs. scanner map	1271 ± 28 vs. 1262 ± 21, p=.896	48.2 ± 3.0 vs. 47.8 ± 2.8, p=.989
Software C refitted vs. scanner map	1277 ± 31 vs. 1260 ± 30, p=.832	47.5 ± 2.6 vs. 47.0 ± 2.8, p=.998

Table 2: Comparison of mean values ± standard deviation (in ms) of SD (T1) and SD (T2).

	SD (T1) [ms]	**SD (T2) [ms]**
Software A refitted vs. scanner map	59 ± 8 vs. 59 ± 8, p=1.00	4.6 ±0.8 vs. 4.4 ± 0.5, p=.977
Software B refitted vs. scanner map	54 ± 8 vs. 59 ± 7, p=.875	4.5 ± 1.3 vs. 4.4 ± 0.8, p=.989
Software C refitted vs. scanner map	65 ± 13 vs. 68 ± 10, p=.997	5.0 ± 0.6 vs. 5.7 ± 1.1, p=.393

ID#: 372774

Initial Validation of Free-Breathing Navigator Cardiac Quantitative Susceptibility Mapping for Blood Pool Oxygenation as Verified Invasively via Right Heart Catheterization

Yan Wen, M.S.[1] Thanh D. Nguyen, PhD[2], Pascal Spincemaille, PhD[3], Zhe Liu[1], Javid Alakbarli, MD[4], Jiwon Kim, MD[5], Evelyn M. Horn, MD[4], Meridith P. Pollie, BS[4], Jonathan W. Weinsaft, MD[2], Yi Wang, PhD[6]

1. Cornell University

2. Weill Cornell Medical Center, NY

3. Weill Cornell Medicine, New York, NY

4. Weill Cornell Medical College

5. Weill Cornell Medical College, New York, NY

6. Weill Cornell Medical College, NY

Background: Quantitative susceptibility mapping (QSM) is an emerging technique for differential RV-to-LV oxygen saturation; an established indicator of cardiac performance. Pilot studies have applied QSM in volunteers or via non-contrast CMR – this technique has never before been tested using contrast-enhanced patient data.

Methods: QSM was acquired via an ECG-triggered free-breathing multi-echo 3D GRE sequence, which uses diaphragmatic navigators for motion tracking and real time data control (4mm window). QSM was performed on a clinical 3T scanner (GE 750W); images were acquired 20-30 minutes post gadolinium administration (0.2mmol/kg). QSM maps were reconstructed by first preparing the total field via graph cut phase analysis and chemical shift update methods, and then preforming field to source inversion with the total field inversion methods. QSM maps were scored for image quality using 3 point scale (3=excellent, 2=intermediate, 1=poor/uninterpretable), and compared to clinical right heart catheterization (RHC) data and ancillary CMR findings (DE-CMR late-gadolinium enhancement).

Results: 15 patients (age 69.6±7.22yr, 11 male, 11 HTN, 9 HLD, 12 CAD, 8 PCI, 6 CABG) underwent cardiac QSM (acquisition time 513±229s, typical resolution1.5x1.5x5 mm^3); 80% (12/15) of cases yielded interpretable results (image score≥2). The QSM maps showed RV blood susceptibility was higher than that of LV blood (234±60ppb vs. -81±68ppb; mean difference of 316±61ppb, $p<0.001$), which agreed with physiologic oxygenation differences between arterial/oxygenated blood (slightly diamagnetic) and venous/deoxygenated blood (highly paramagnetic) (**Figure 1A**). In 2 patients, whom underwent RHC (2.3±.6 weeks from CMR), QSM-derived differential RV-to-LV oxygen saturation, ΔSO_2, agreed with the RHC measurements in patient 1 (30.8% vs 29%, respectively), but the QSM based measurement was slightly lower than that of RHC in patient 2 (28.5% vs 35%, respectively) (**Figure 1B**). Among the remaining 10 patients, QSM-based calculations yielded differential RV-to-LV oxygen saturation (21.7±2.3%) that was consistent with physiologic norms. Ancillary analyses demonstrated altered myocardial tissue properties on QSM, including increased susceptibility corresponding to transmural late gadolinium enhancement on DE-CMR (**Figure 1C**).

Conclusion: In this initial validation study, cardiac QSM was successfully obtained in a substantial proportion of patients undergoing contrast-enhanced CMR. QSM yielded differential RV-to-LV blood pool oxygen saturation calculations that agree reasonably, with invasive measurements and physiologic norms. Further study is needed to improve QSM calculations by increasing higher spatial resolution, reducing motion artifacts, and optimzing regularization parameters for QSM reconstruction.

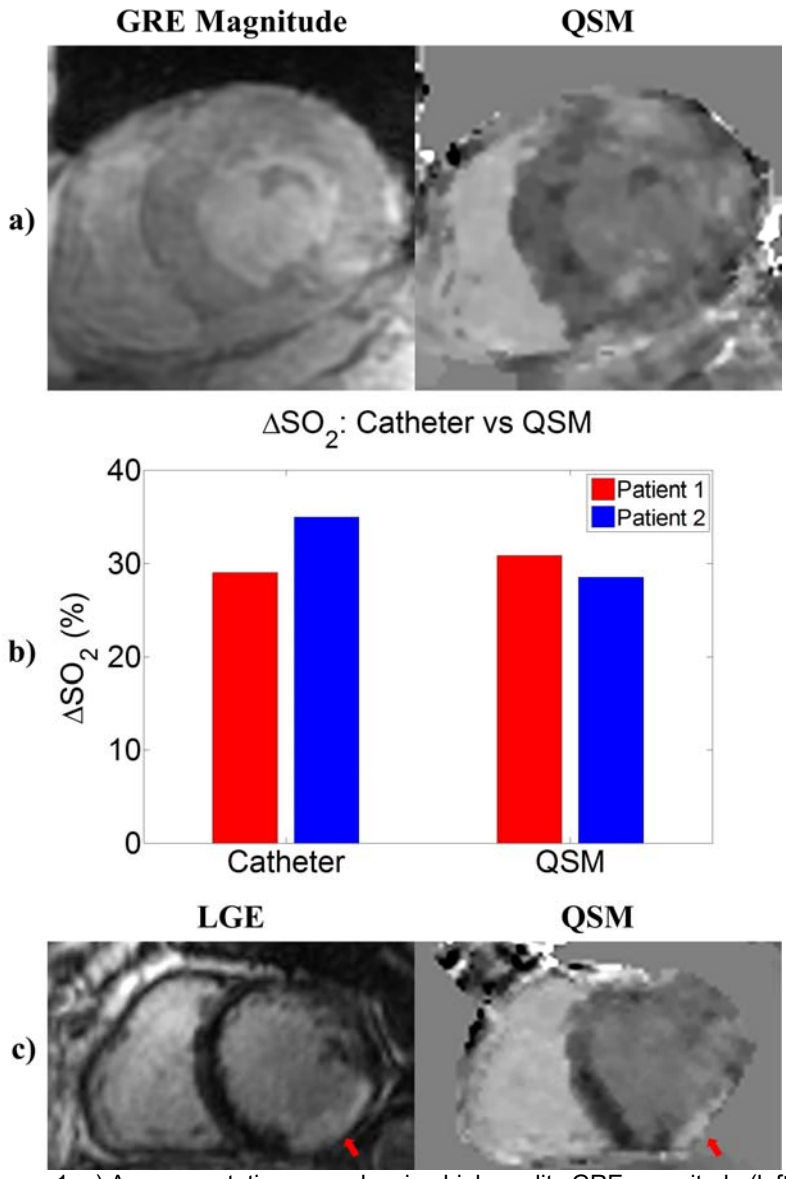

Figure 1: a) A representative case showing high quality GRE magnitude (left) and the corresponding QSM map (right) obtained with the free-breathing cardiac QSM sequence at 3T. b) Comparison of ΔSO2 measurements obtained with catheter and QSM. c) LGE image and QSM map of a transmural infarct (red arrows), showing good visual agreement.

ID#: 372775

Comparison of 4D Flow MRI to Doppler Echocardiography: Assessment of Mean Transvalvular Aortic Pressure Gradient

Alex J. Barker, PHD[3]Michael Rose, MS[1], Kelly Jarvis, PhD[2], Susanne Schnell, PhD[3], Kenichiro Suwa, MD[4], Joshua D. Robinson, MD, FACC[5], Cynthia K. Rigsby, MD, FACR[5], Michael Markl, PhD[3]

1. Northwestern University

2. Northwestern University, IL

3. Northwestern University, Chicago, IL

4. Northwestern University Feinberg School of Medicine Department of Radiology, IL

5. Ann & Robert H. Lurie Children's Hospital of Chicago, Chicago, IL

Background: Accurate estimation of aortic valve stenosis (AS) severity is necessary to guide medical therapy and intervention. Mean and peak transvalvular pressure gradients (PGs) are important indicators of AS severity. The non-invasive gold standard for PG determination is Doppler echocardiography (echo). 2D PCMRI and 4D flow have been shown to be moderately reliable alternatives to echo for measuring peak PGs; however, prior studies have not used optimized the temporal and spatial variance of the vena contracta to measure mean PG. Therefore, the aim of this study is to test a method to assess mean PG using 4D flow MRI. We hypothesize that 4D flow will produce PGs comparable to echo and that mean PGs from 4D flow will agree better with echo than peak PGs because of additional spatial and temporal velocity information available for mean PG.

Methods: 23 pediatric and young adult patients (age=14±5 (3-22) years, M:F=16:7) and 6 adult patients (age =56±10 (40-70) years, M:F=5:1) with diagnosed bicuspid aortic valve (BAV) underwent 4D flow MRI as part of this IRB-approved study. MRI scans were performed at 1.5T (Avanto or Aera, Siemens, Germany) with spatial resolution = 1.9-3.5x1.6-2.5x1.9-4.0 mm3, temporal resolution 36.8-39.2 ms, TE/TR/FA = 2.2-2.6ms/4.7-5.1ms/15° and velocity sensitivity = 150–400 cm/s. 4D flow data were corrected for velocity aliasing and phase offset errors (Maxwell terms, eddy currents). 3D PC-MR angiograms were computed from 4D flow data and a 3D segmentation of the aorta was obtained (Mimics, Materialise) to mask the velocity field. Velocity maximum intensity projections (MIP) were generated; peak velocity in the vena contracta was extracted (Fig 1A-B). A velocity-time curve similar to continuous wave Doppler (Fig 1C) was plotted at the location of peak velocity and its nearest neighbors (27 voxels, Fig 1D). Peak PGs were calculated using the simplified Bernoulli equation ($P=4v^2$). Mean PG was determined by tracing the velocity-time curve plots during systole and computing the mean of the trace (Fig 1D & F). Peak PGs and mean PGs for each patient were compared to a recent echocardiogram (<6 months).

Results: Doppler and 4D flow velocity-time curve plots are shown in Fig 1C-F. The slope of the regression for mean PG was lower than peak PG (Fig 2B, b=0.65 vs 0.80), indicating a systematic underestimation of both PG values; the quality of fit was higher for mean PG than peak PG (r^2=0.77 vs 0.70). Details are summarized in Fig 2. The mean time elapsed between 4D flow and echo was 60±58 days.

Conclusion: The bias and limits of agreement suggest moderate agreement between 4D flow and echo. While the quality of fit for 4D flow mean PG to echo was higher, MRI and echo must be assessed with minimum time elapsed between exams. Data collection using a same-day strategy is ongoing.

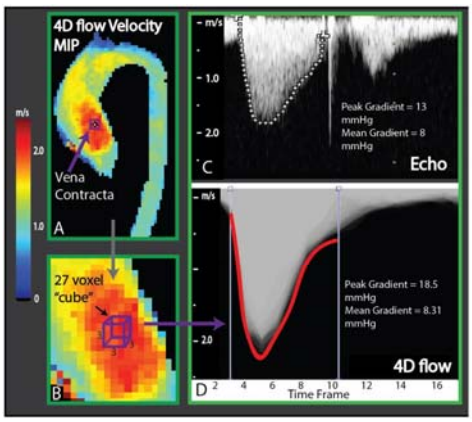

Fig 1: 4D flow velocity MIP of the aorta (A,B). Echo spectral Doppler (C) and 4D flow (D) velocity-time curves with mean pressure gradient traces (red lines/white dotted-lines). The peak velocity (white and black marker) is found in the vena contracta (A). Velocity-time curves (D) are plotted for the 27 voxels contained within the 3x3x3 voxel "cube" surrounding the peak velocity (purple box) (A, B).

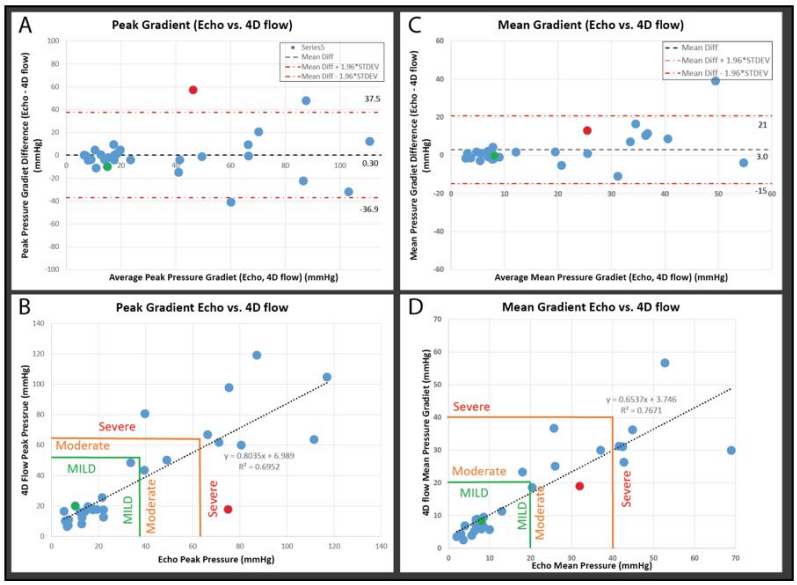

Fig 2: Bland-Altman plots comparing 4D flow and echo for peak (A) and mean (C) pressure gradients. Echo vs. 4D flow plots for peak (B) and mean (D) pressure gradients with trend lines and added mean and peak pressure gradient thresholds for mild, moderate and severe stenosis according to the ACC/AHA guidelines4. The green and red markers represent the patients highlighted in Figure 1 with good and poor agreement, respectively. 4D flow and echo showed no significant difference in either peak (36.8 ± 32.3 vs. 37.1 ± 33.58 mmHg, p=0.54) or mean pressure gradient (. 16.5 ± 13.5 vs 19.6 ± 18.1 mmHg, p=0.18). Bias between 4D flow and echo for both peak and mean pressure gradients (echo-4D flow: 0.3 and 3.0 mmHg) and limits of agreement (±37.2 and ±17.7 mmHg) can be seen in A and B. The slope and correlation between 4D flow and Doppler improved when comparing peak (b=0.80, r^2=0.70) to mean pressure gradient (b=0.65, r^2= 0.77).

ID#: 372818

Non-ECG, free-breathing myocardial T1-T2 mapping using CMR multitasking: Application to acute myocardial infarction

Anthony G. Christodoulou, PhD[1] Christopher Nguyen, PhD[1], Qi Yang, PhD[2], Yibin Xie, PhD[1], Nan Wang, M.S.[3], Jaime L. Shaw, MS[4], Debiao Li, PhD[1]

1. Cedars-Sinai Medical Center, Los Angeles, CA

2. Cedars-Sinai Medical Center, CA

3. Cedars-Sinai Medical Center/UCLA, Los Angeles, CA

4. Cedars-Sinai Medical Center/UCLA, CA

Background: Myocardial tissue characterization by quantitative mapping of T1 and T2 shows promise for diagnosing of myocardial infarction, ischemia, edema, and more [1]. A recent framework for joint T1-T2 myocardial mapping, CMR multitasking, removes the need for ECG triggering and breath-holding, and has shown good agreement with reference methods in healthy controls [2]. This abstract describes the first application of this method in patients, evaluating the ability of native T1-T2 multitasking to predict late gadolinium enhancement (LGE) in patients with suspected acute myocardial infarction (AMI).

Methods: Data were collected on a 3T Siemens Verio from *n*=5 patients with AMI. Each subject underwent: 1) native T1 mapping using MOLLI 5(3)3 [3]; 2) native T2 mapping using T2prep-SSFP mapping [4]; 3) native T1-T2 mapping using T2IR-FLASH multitasking; and 4) LGE imaging. MOLLI, T2prep-SSFP, and LGE images were collected at diastole during an end-inspiration breath-hold. CMR multitasking images were continuously acquired without ECG triggering or breath-holding over the course of 85 sec, resulting in cardiac- and respiratory-resolved images (16 cardiac bins and 5 respiratory bins); T1 and T2 values were fit at end-diastole and end-inspiration to match the reference method motion states. Segmentwise analysis was performed in six myocardial segments per subject.

Results: Comparison of multitasking T1 and T2 values (T1: 1177±147 ms; T2: 45.6±8.3 ms) to MOLLI (T1: 1206± 31 ms) and T2prep-SSFP mapping (T2: 44.3 ± 6.7 ms) were positively correlated (T1: r=0.90, T2: r=0.68) (**Figs. 1a, 2a**). Multitasking T1 showed a –29 ms bias (p=0.02) vs. MOLLI; multitasking T2 had no statistically significant bias (p=0.30) (**Figs. 1b, 2b**). Neither T1 mapping method on its own was predictive of LGE status, with the area under the curve (AUC) of the receiver operating characteristic (ROC) curve = 0.55 for MOLLI and 0.50 for multitasking (**Fig. 1c,d**); both T2 mapping methods were predictive of LGE status, with the ROC AUC = 0.71 for T2prep-SSFP mapping and 0.84 for multitasking (**Fig. 2c,d**). A 2D feature space of multitasking T1 and T2 values (**Fig. 3**) provided even greater diagnostic accuracy, with the pictured decision boundary yielding 100% sensitivity and 92% specificity.

Conclusion: Multitasking T1 and T2 maps showed similar diagnostic accuracy to the reference methods, with native T2 mapping being more predictive of LGE status than native T1, a potential result of the substantially larger fractional increase in T2 than T1 from edema associated with AMI [5,6]. The use of both T1 and T2 from the same multitasking scan further increased accuracy, demonstrating the value of obtaining multiple measurements. These initial results show great promise for non-ECG, free-breathing multiparameter mapping using CMR multitasking

1. Blume *JMRI* 2009
2. Christodoulou *SCMR* 2017
3. Xue *MRM* 2013
4. Giri *JCMR* 2009
5. Ferreira *J Thorac Imaging* 2014
6. Higgins *Am J Cardiol* 1983

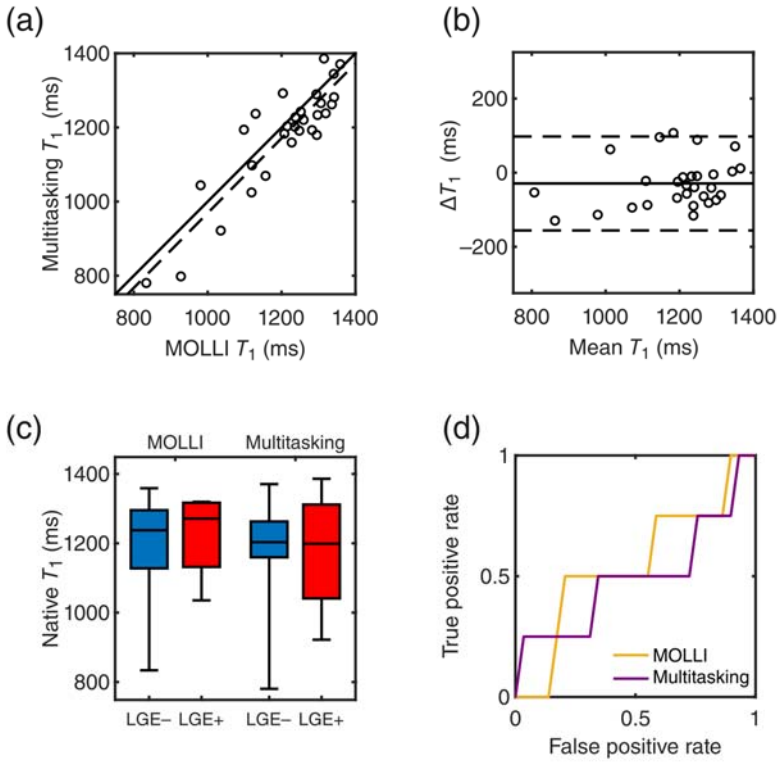

T1 mapping results. (a) Scatter plot comparing MOLLI and multitasking values. (b) Bland-Altman plot of the same data. (c) Box-whisker plots showing the median, interquartile range, and full range of results in each group. (d) ROC curves for native T1 as a predictor of LGE status.

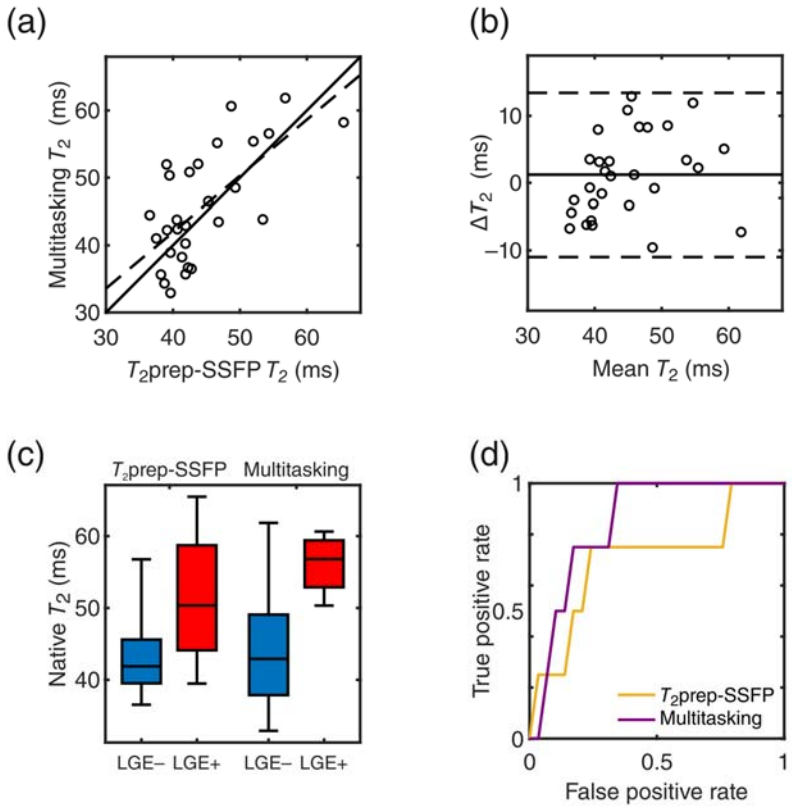

T2 mapping results. (a) Scatter plot comparing T2prep-SSFP and multitasking values. (b) Bland-Altman plot of the same data. (c) Box-whisker plots showing the median, interquartile range, and full range of results in each group. (d) ROC curves for native T1 as a predictor of LGE status.

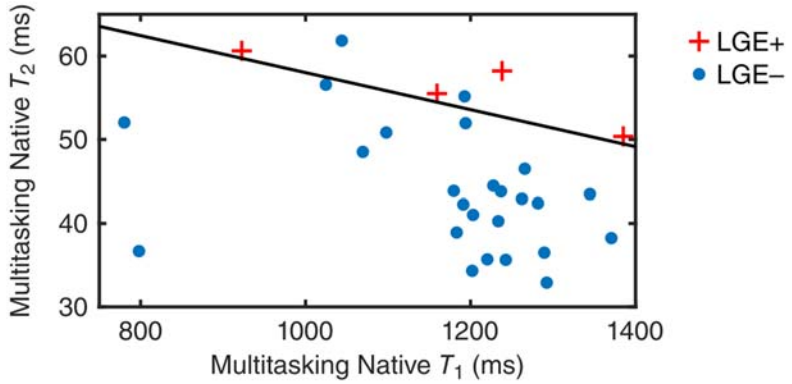

Multitasking T1-T2 mapping results in a 2D feature space. The picture decision boundary yields 100% sensitivity and 92% specificity.

ID#: 372821

Fetal Cardiac Cine MRI Using Doppler Ultrasound Gating

Fabian Kording[1]Jin Yamamura[2], Manuela Tavares de Sousa[2], Christian Ruprecht[1], Erik Hedström, MD, PhD[3], Anthony H. Aletras, Ph.D.[4], Andrew J. Powell, M.D.[5], P. Ellen Grant[6], Kai Fehrs[2], Hendrik Kooijman[7], Bjoern Schoennagel[2]

1. Department of Diagnostic and Interventional Radiology, University Medical Center Hamburg-Eppendorf, Hamburg, Germany, Germany, Germany

2. University Medical Center Hamburg-Eppendorf, Germany

3. Lund University, Skåne University Hospital, Department of Clinical Sciences Lund, Diagnostic Radiology, Lund, Sweden, Sweden

4. Aristotle University of Thessaloniki/Lund University, Thessaloniki, Thessaloniki, Greece

5. Harvard Medical School and Boston Children's Hospital, Boston, MA

6. Boston Children's Hospital, and Harvard Medical School

7. Philips GmbH, Germany

Background: Discordances of up to 29% between pre- and post-natal diagnoses of congenital heart disease (CHD) and a limited ability to measure blood flow using echocardiography encourages the development of new techniques to improve the accuracy of prenatal diagnoses of cardiovascular abnormalities [1]. Fetal cardiac magnetic resonance imaging (MRI) may provide a valuable adjunct [2]. However, fetal cardiac cine MRI requires an accurate trigger method in order to synchronize data acquisition with the cardiac cycle, unless time-consuming post-processing techniques are applied [3]. The aim of the study was to evaluate the image quality and clinical applicability of an external cardiac trigger device based on Doppler ultrasound (DUS) for fetal cardiac cine MRI.

Methods: To evaluate the DUS trigger device, 15 pregnant subjects (30-39 weeks gestation) were examined at 3 different imaging sites using 1.5T MRI scanners from Philips and Siemens. For fetal cardiac cine imaging, trigger signals were acquired with a newly developed MRI-compatible DUS device and transferred into the MRI scanner in real-time. Retrospectively triggered cine balanced steady-state free precession images were acquired in 2-chamber, 4-chamber, and short-axis views. Trigger signals were stored during data acquisition and were assessed for trigger sensitivity and variability. Cardiac cine endocardial blurring was quantified with a dedicated algorithm. Furthermore, two independent observers (B.S, J.Y) scored image quality ranging from 1 (poor image quality) to 4 (excellent image quality).

Results: The trigger signals of the fetal heart beat could be reliably detected without artifact at all imaging sites. The mean R-R interval was 433 ± 32 ms with a trigger variability of 26 ± 22 ms and a sensitivity for trigger detection of 96±4%. Cardiac chambers were clearly delineated, showing a good to excellent image quality (3.6 ± 0.6). The synchronous contraction of the ventricles was clearly visualized with a calculated endocardial blurring of 2.9 ± 0.6 pixels.

Conclusion: DUS triggering enables fetal cardiac cine MRI with good image quality and without motion artifacts. With the advantage of stable fetal cardiac trigger signals, the clinical benefit of fetal cardiac cine MRI for diagnosis of CHD can be further evaluated in future studies.

References: [1] Bensemlali M et al, J Am Coll Cardiol 2016;68:921–30.
[2] Wielandner A et al, Semin Fetal Neonatal Med 2013;18:286–97.
[3] Bidhult S et al, J Magn Reson Imaging 2017:1–11.
[4] Kording F et al, Magn Reson Med 2015;74:1257–65.

The study was supported by a grant of the German Research Foundation (DFG) (SCHO 1546/1-1), the Swedish Heart-Lung Foundation, Region of Skåne, and the Skåne University Hospital.

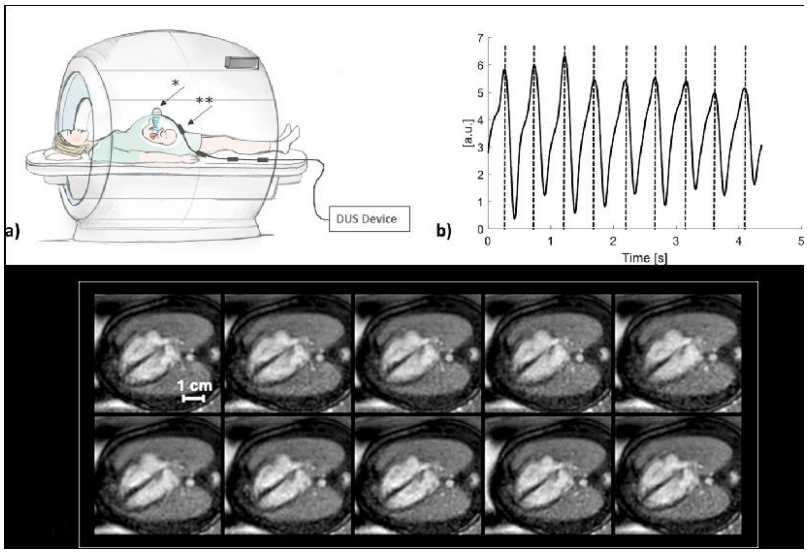

a) Schematic illustration of the experimental setup during fetal CMR showing placement of the Doppler ultrasound (DUS) transducer (*) on the maternal abdomen and the connecting cable (**) with cable traps to avoid electromagnetic interferences from radiofrequency pulses. Typical gating signals generated by the DUS device are shown in b). DUS-gated balanced SSFP cine images of the fetal heart in the 4-chamber view (gestational week 36) are shown in c).

ID#: 372269

LV patient specific models and shape analysis from 4500 UK Biobank studies

Kathleen Gilbert, BE(hons), PhD[1] Avan Suinesiaputra, PhD[2], Pau Medrano-Gracia, PhD[3], Stefan Neubauer, MD, FRCP[4], Stefan K. Piechnik, PhD, MScEE[4], Mihir M. Sanghvi, MB BS, BSc[5], Filip Zemrak, MD, MRCP[6], Kenneth Fung, MBBS MRCP[5], Jose Miguel Paiva, MSc[5], Elena Lukaschuk, MSc[7], Valentina Carapella, DPhil[8], Young Jin Kim, MD, PhD[9], Nay Aung, MD, MRCP[5], Aaron Lee, PhD, MBBS[5], Steffen E. Petersen, MD DPhil MPH FRCP[10], Alistair Young, PhD[11]

1. University of Auckland, New Zealand, New Zealand

2. The University of Auckland, New Zealand, GRAFTON, Auckland, New Zealand

3. University of Auckland, Auckland, New Zealand

4. University of Oxford, England, United Kingdom

5. William Harvey Research Institute, NIHR Cardiovascular Biomedical Research Unit at Barts, Queen Mary University of London, Charterhouse Square, London, EC1M 6BQ, UK, England, United Kingdom

6. William Harvey Research Institute, London, England, United Kingdom

7. University of Oxford, Oxford, England, United Kingdom

8. Simula Research Laboratory, Norway

9. Severance Hospital, Yonsei University College of Medicine, Seoul, Republic of Korea

10. Queen Mary University of London, London, England, United Kingdom

11. University of Auckland, New Zealand, GRAFTON, Auckland, New Zealand

Background: The UK Biobank is a prospective cohort study in which 100,000 participants will undergo CMR studies over the next five years. The pilot phase is now complete with 5065 participants analyzed [1]. We present a method for automatic generation of patient specific models (PSM) of the left ventricle (LV) and apply shape-based atlasing methods to quantify shape variations.

Methods: The steps required to make PSM and atlases of the LV at end-diastole (ED) and end-systole (ES) are shown in Figure 1. For each case, the manual contours and landmarks were drawn using CVI42 and converted to 3D points (step 1), the contours were then automatically fitted with a finite element model with a high stiffness (step 2) using the guide-point modelling minimisation method [2]. The contours underwent an automatic iterative in-plane adjustment in position, minimising their distance to the model, to correct for breath-hold mis-registration between slices. PSM for ED and ES frames were then created by fitting the models to the corrected contours with a lower stiffness (step 3). 1682 points were then sampled from each frame of the PSM (step 4). The points were aligned across all the models using Procrustes with scale factor adjustment to height as described in [3]. Principal component analysis (PCA) was used to assess the major modes of variation in the dataset.

Results: Atlases were successfully created for 4556 PSM (all those with sufficient contour, landmark and height information). The first 3 modes of the ED and ES atlases, with their shape classification and explained variation are shown in Figure 2.

The variations in shape were dominated by size (not attributable to height) and sphericity. These are consistent with the MESA study [3], providing direct comparison between cohorts. In future, these shapes can be assessed in conjunction with risk factors and other measures in the UK Biobank data.

Conclusion: We have created an atlas of ~4500 UK Biobank LV geometries. The modes show shape variations consistent with those seen in a separate large cohort [3]. **References** 1. Petersen SE et al. JCMR. 2017 **19**:18. 2. Young A et al. Radiology.2000; 216:597–602. 3. Medrano-Gracia P et al. JCMR.2014;16:56.

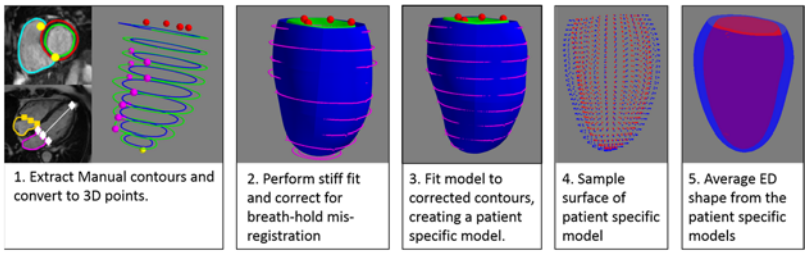

Figure 1: Steps required to make PSM and atlases

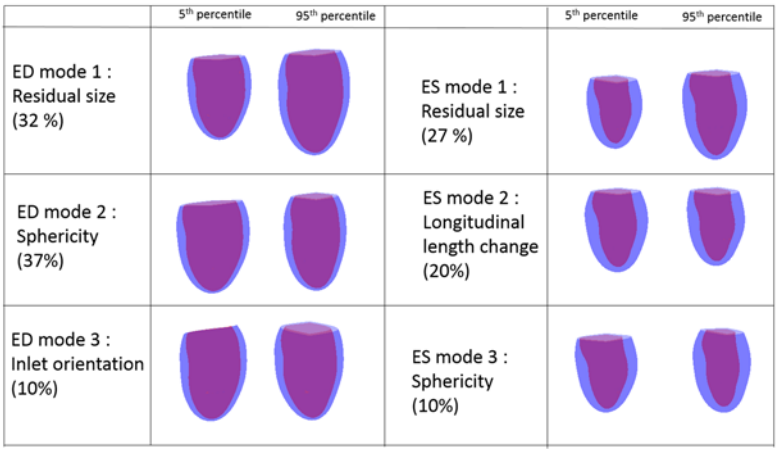

5th and 95th percentile of the first three modes from each of the ED and ES atlases (variance explained is shown in brackets). Viewpoint is from the anterior wall with the septum to the left.

ID#: 372281

Myocardial Contraction Fraction: Distribution, Determinants and Normal Reference Values in Adults

Michael L. Chuang, MD, ScM[7] Philimon N. Gona, PhD[1], Carol J. Salton, AB[2], Nathan J. Foster, MD[3], Connie W. Tsao, MD, MPH[4], Christopher J. O'Donnell, MD, MPH[5], Warren J. Manning, MD[6]

1. University of Massachusetts Boston, Framingham, MA

2. Beth Israel Deaconess Medical Center, MA

3. Consultants in Cardiology

4. Beth Israel Deaconess Medical Center, Boston, MA

5. Boston VAMC

6. Beth Israel Deaconess Medical Center, Harvard Medical School, Boston, MA

7. Beth Israel Deaconess Medical Center, Newton, MA

Background: Myocardial contraction fraction (MCF) is the ratio of left ventricular (LV) stroke volume to myocardial volume. MCF is a metric of appropriateness of LV mass, as well as an alternative measure of global LV systolic function complementary to LV ejection fraction (EF). Low MCF has been shown to be an independent predictor of adverse cardiovascular disease (CVD) events. We sought to determine whether CMR-derived MCF varies with sex and age in healthy community-dwelling adults, and to identify thresholds for low MCF.

Methods: Framingham Heart Study Offspring cohort members (N=1794) underwent CMR on a 1.5-T system (Philips Gyroscan NT). LV volumes, mass and EF were measured from a stack of bSSFP cine images obtained in the LV short-axis orientation (TR=3.2ms, TE=1.6ms, 60°FA, 1.9x1.6mm^2 in-plane resolution, THK=10mm, no gap). A healthy reference group (no myocardial infarction, heart failure, hypertension, wall-motion abnormality on CMR) was identified and stratified by sex and age group (<55, 55-64, ≥65y). We determined sex and age-group specific lower 10th percentile (P10) cutpoints in the reference group, then determined the prevalence of low (<P10) MCF in the overall cohort. Multivariable-adjusted logistic regression analysis was used to identify clinical factors associated with low MCF.

Results: The reference group comprised 852 Offspring (40% men), among whom MCF was significantly higher in women (0.94±0.13) than men (0.81±0.13), p<0.0001. The Table shows cutpoints for low MCF. MCF decreased significantly with greater age group in each sex (see Table). MCF was only modestly correlated (Pearson) with LV EF: r=0.14, p=0.008 men; r=0.19, p<0.0001 women. In the overall cohort (N=1730 after excluding 64 Offspring with prevalent myocardial infarction or heart failure), 14.7% of men and 14.8% of women had low MCF. On multivariable-adjusted logistic regression analysis accounting for age, sex and clinical factors, hypertension (hazard ratio, HR=1.54, 95% confidence intervals, CI=1.14–2.09); smoking (HR=2.15, CI=1.42–3.25); diabetes (HR=1.73, CI=1.12–2.66), and greater body mass index, BMI (HR=1.07 per kg/m^2, CI=1.04–1.10) were associated with greater hazards of low MCF. Age was not associated with lower MCF in this model which used age-specific thresholds.

Conclusion: Among healthy, community-dwelling adults, MCF, as determined using bSSFP CMR, is greater in women than men. MCF decreases with advancing age in each sex. In the overall population, lower MCF is associated with hypertension, smoking, diabetes and greater BMI. We presented sex and age-group means and lower 10th percentile limits for MCF which may be useful in both research and clinical settings.

	Men			Women		
	N	Mean±SD	P10	N	Mean±SD	P10
Age-Pooled	340	0.81±0.13	0.65	512	0.94±0.13	0.79
Age Group						

<55y	81	0.85±0.12	0.69	104	0.95±0.12	0.79
55 - 64 y	157	0.81±0.62	0.65	257	0.96±0.13	0.81
≥65y	102	0.80±0.13	0.65	151	0.91±0.12	0.77
P (for trend)		0.009			0.01	

MCF overall, and by age-group in the healthy reference group

ID#: 372306

Clinical value of dark blood late gadolinium enhancement without additional magnetisation preparation

Caroline M. Van De Heyning, MD PhD[1] Robert J. Holtackers, MSc[2], Muhummad Sohaib Nazir, MBBS MRCP[3], Imran Rashid, PhD FRACP[4], Ioannis Ntalas, MD, PhD[5], Haseeb Rahman, MD[5], Rene Michael. Botnar, PhD[4], Amedeo Chiribiri, MD PhD[4]

1. St. Thomas' Hospital, London; King's College London ; Antwerp University Hospital, Edegem, Belgium

2. Maastricht University Medical Centre, Maastricht, Netherlands

3. St. Thomas' Hospital, London; King's College London, England, United Kingdom

4. King's College London, London, England, United Kingdom

5. St. Thomas' Hospital, London; King's College London, United Kingdom

Background: Dark blood late gadolinium enhancement (LGE) is a promising cardiovascular magnetic resonance (CMR) technique, which may provide enhanced differentiation between subendocardial scar and the adjacent left ventricular blood pool compared with conventional bright blood LGE. A dark blood LGE method without the need for magnetisation preparation or software modification was recently proposed and evaluated in a small number of patients with ischaemic scar on a 1.5T scanner. This imaging strategy involves selection of a short TI-time to null the blood pool combined with phase-sensitive inversion-recovery (PSIR), resulting in a darker blood pool signal with preservation of a dark myocardium and bright scar. We sought to validate this novel dark blood LGE technique in a large cohort of patients at both 1.5 and 3T.

Methods: 250 consecutive patients referred for clinical CMR were enrolled and randomly allocated to 3 different scanners (Philips Ingenia 1.5T: n=86, Philips Achieva 3T: n=79 and Siemens Aera 1.5T: n=85). A routine CMR scan was performed with PSIR LGE imaging using both conventional nulling of the viable myocardium and nulling of the left ventricular blood pool. Presence and pattern of scar, global image quality and diagnostic confidence of both methods were separately assessed by 5 CMR readers, who were blinded to clinical data. Definite diagnosis of ischaemic or non-ischaemic scar was made by expert consensus.

Results: Complete bright and black blood LGE data sets were available in 243 patients. Ischaemic scar was detected in 57 patients by dark blood LGE and in 53 patients by bright blood LGE (23.5 vs 21.8%, p=0.125). All patients with a definite diagnosis of ischaemic scar were identified by dark blood LGE. A non-ischaemic scar pattern (excluding right ventricular insertion point fibrosis) was observed in 49 patients using dark blood LGE and in 56 patients using bright blood LGE (20.2% vs 23.1%, p=0.065). Similar trends were observed on all scanners. Global image quality was significantly higher for dark blood LGE than for bright blood LGE (all left ventricular segments correctly identified in 80.2 vs 70.4%, p=0.001)(see Table), resulting in a higher diagnostic confidence (81.1% vs 70.7%, p=0.001)(see Image).

Conclusion: Dark blood PSIR LGE imaging is a feasible, readily available CMR method to detect myocardial scar with improved image quality and operator confidence compared with conventional bright blood LGE imaging. There was a trend towards better identification of ischaemic scar by dark blood LGE, but less detection of non-ischaemic scar patterns compared with bright blood LGE.

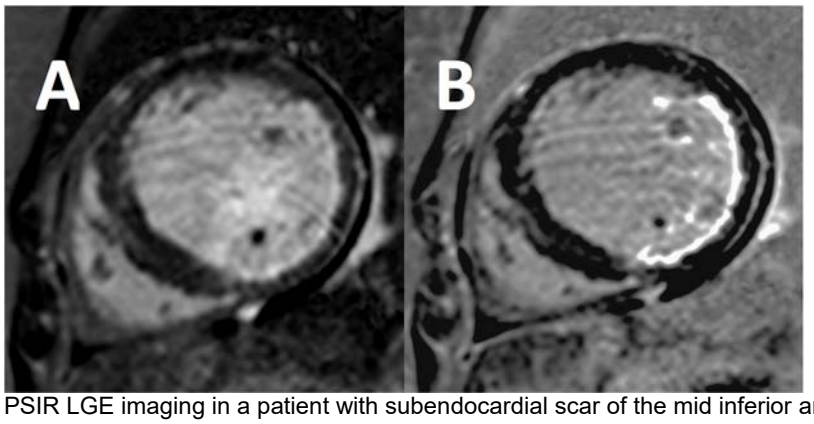

PSIR LGE imaging in a patient with subendocardial scar of the mid inferior and inferolateral wall by conventional

bright blood LGE (panel A) and by dark blood LGE (panel B). Scar could be differentiated from the blood pool with more operator confidence by dark blood LGE compared with bright blood LGE.

Global image quality as assessed by number of diagnostic left ventricular segments on LGE analysis

	Bright blood LGE	**Dark blood LGE**
All segments diagnostic	171 (70.4%)	195 (80.2%)
1 segment non-diagnostic	34 (14.0%)	24 (9.9%)
≥2 segments non-diagnostic	32 (13.2%)	21 (8.6%)
Non-diagnostic Scan	5 (2.1%)	2 (0.8%)

ID#: 372038

Evaluation of Pressure Drop using 4D Flow MRI: Clinical Feasibility in Patients with Bicuspid Aortic Valve

Julio Garcia, PhD[2]Fiona Burns[1], Xuexin Gao, PhD[3], Jacqueline A. Flewitt, MSc[4], Rosa Sandonato, RN, BScN[5], Michael Bristow, MD[5], Bobby Heydari, MD, MPH[5], Carmen P. Lydell, MD[4], Andrew G. Howarth, MD, Ph.D[5], Paul W Fedak, MD, PhD[6], James White, MD, FRCP(C)[5]

1. University of Calgary, AB, Canada

2. University of Calgary, Calgary, AB, Canada

3. Circle Cardiovascular Imaging Inc, Panarctic Plaza, Calgary, Canada, AB, Canada

4. Stephenson Cardiac Imaging Centre, Libin Cardiovascular Institute of Alberta, University of Calgary, Calgary, AB, Canada

5. Stephenson Cardiac Imaging Centre, Libin Cardiovascular Institute of Alberta, University of Calgary, AB, Canada

6. University of Calgary, Canada

Background: Bicuspid Aortic Valve (BAV) disease is associated with abnormal trans-valvular hemodynamics and varied progression to Aortic Stenosis (AS). This is typically identified through estimation of Peak Velocity (PV), Pressure Gradient (PG), and effective orifice area using Doppler echocardiography or 2D phase-contrast (2D PC) MRI. 4D flow MRI provides a more complete description of trans-valvular and downstream aortic flow. This allows for the quantification of Pressure Drop (PD), a novel marker to assess the physiologic impact of BAV disease. This study aimed to demonstrate the feasibility of 4D flow PD in patients with BAV and explore associations with conventional measures of flow obstruction.

Methods: Twenty-eight patients with BAV (47±15 years, 9 female) and eleven healthy volunteers with normal, tricuspid aortic valves (52±9 years, 2 female) were prospectively enrolled. MR imaging was performed at 3T inclusive of cine imaging, 2D PC, and 4D flow. Images were processed and analyzed using commercial software. 4D flow was analyzed at nine pre-defined locations extending from the left ventricular outflow tract (LVOT) to distal descending aorta (DDA) (Fig. 1). PD was calculated at each plane by quantifying the cumulative drop in pressure from the pre-valvular reference (LVOT). 2D PC-MR images were used to provide conventional measures of hemodynamic significance, including PV, peak PG, and mean PG.

Results: In BAV patients, the median peak PG was 12 mmHg (range 5 to 68 mmHg) as measured by 2D PC-MRI. Both BAV patients and healthy volunteers showed a progressive rise in PD from the sino-tubular junction to the DDA. However, BAV patients showed significantly higher PD than healthy volunteers ($p \leq 0.01$) for all planes (Fig. 2). At the mid-ascending aorta, the median PD was 3.31 mmHg in healthy volunteers versus 6.12 mmHg in those with BAV ($p=0.001$). Five BAV patients showed moderate-severe AS by 2D PC (peak PG >40mmHg) and demonstrated significantly higher PD than other BAV patients, particularly in the descending aortic segments ($p \leq 0.005$) (Fig. 2). A strong correlation ($R=0.88$, $p<0.05$) was observed between PD at the DDA and PV (Fig. 3).

Conclusion: 4D flow based PD is clinically feasible in patients with BAV and provides a physiologic description of valve-related hemodynamics through non-invasive pressure mapping. PD measurements show good correlation to conventional measures of valve-related flow obstruction. Further research is underway to explore how this novel marker may improve risk stratification in patients with BAV.

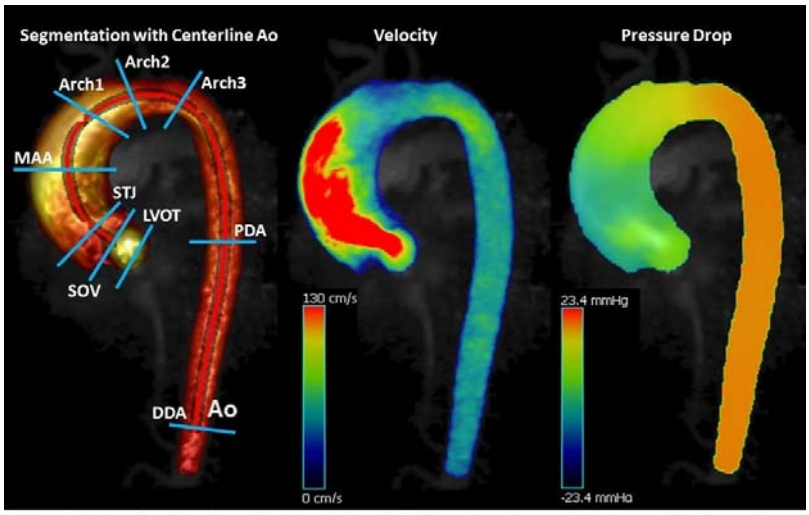

Figure 1: Example of patient with Type 0 Lateral BAV and moderate AS. Segmentation image shows location of 9 analysis planes. LVOT indicates left ventricular outflow tract, SOV indicates sinus of Valsalva, STJ indicates sinotubular junction, MAA indicates mid ascending aorta, PDA indicates proximal descending aorta, and DDA indicates distal descending aorta.

Figure 1

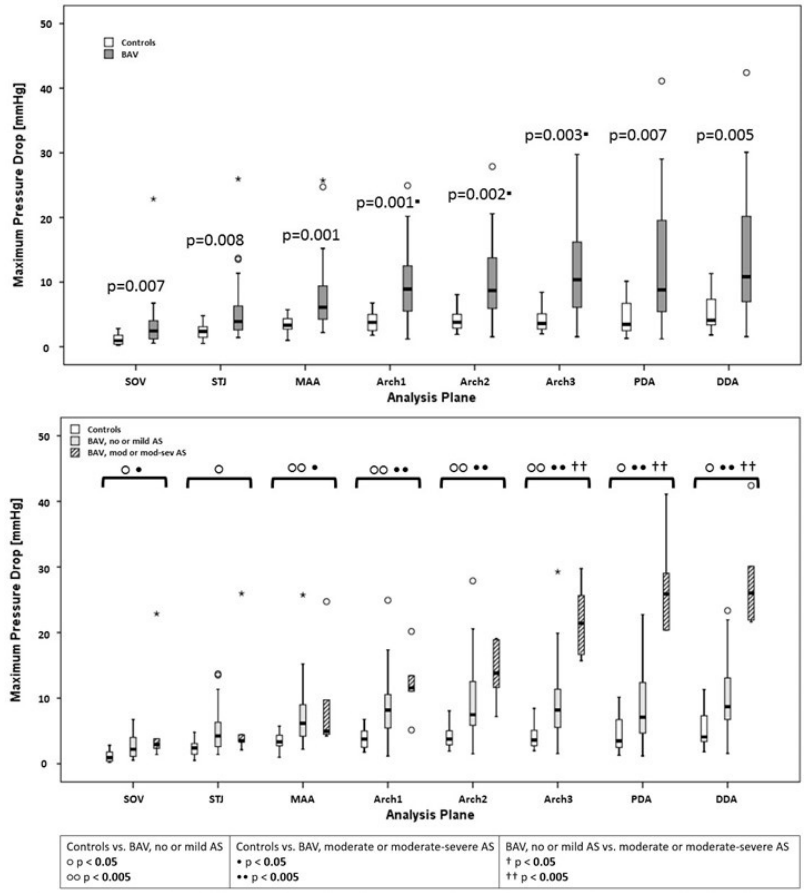

Figure 2: Boxplots illustrating distribution of PD data sets for 8 analysis planes relative to the LVOT reference. TOP: healthy volunteers (white) and all BAV patients (grey); ▪ indicates normally distributed data (student t-test used). BOTTOM: healthy volunteers (white), BAV patients with AS (striped), and BAV patients without AS (grey).

Figure 2

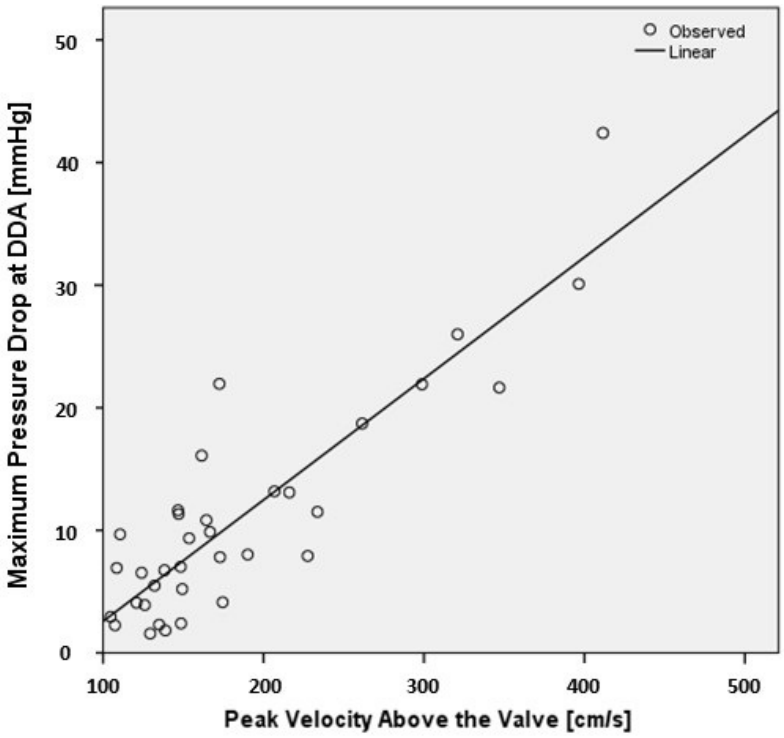

Figure 3: Linear regression results (R=0.88, p<0.05). PV and PD were measured by 2D PC-MRI and 4D flow respectively.

Figure 3

ID#: 372432

Non-Alcoholic Fatty Liver Disease is Associated with Increased Epicardial Adipose Tissue and Impaired Cardiovascular Remodelling and Function

Ines Abdesselam, PhD[1] Mohammad S. Siddiqui, MD[2], Rebecca Collen, BSN[3], Keri Hildick, PhD[4], Robert E. Cadrain, R.T. (MR), CNMT[5], Luca Biasiolli, DPhil[6], Joel L. Steinberg, MD[2], Michael Idowu, MD[2], Melissa J Contos, MD[2], Arun J. Sanyal, MD[3], Stefan Neubauer, MD, FRCP[7], Oliver Rider, BMBCh, DPhil[8]

1. Oxford University, Oxford, England, United Kingdom

2. Virginia Commonwealth University, VA

3. Virginia Commonwealth University, Richmond, VA

4. Perspectum Diagnostics Ltd, United Kingdom

5. Virginia Commonwealth University, Mechanicsville, VA

6. University of Oxford, Oxford, United Kingdom

7. University of Oxford, England, United Kingdom

8. University of Oxford Centre for Clinical Magnetic Resonance, Oxford, England, United Kingdom

Background: Nonalcoholic fatty liver disease (NAFLD) is associated with increased risk of cardiac mortality. NAFLD, especially NASH – non-alcoholic steatohepatitis, is thought to promote an increase in epicardial adipose tissue and therefore predicts myocardial dysfunction and aortic stiffness. The purpose of the study wasto investigate the relationship between liver steatosis, epicardial adipose tissue, and cardiovascular remodeling and function, but also to determine if the progression of the disease comes or not with an aggravation of these cardiovascular abnormalities

Methods: Asymptomatic subjects with biopsy-proven NAFLD were compared to normal BMI controls. Using MRI, systolic and diastolic functions, remodeling parameters, epicardial adipose tissue, but also aortic stiffening were measured.

Results: A total of 27 subjects with NAFLD and 19 controls were studied **Table**. Epicardial adipose tissue was significantly increased in NAFLD patients compare to controls (77.1 ±5.2 vs. 37.8 ±3.6mL; pFigure 1a. Interestingly, ascending aorta and proximal descending aorta distensibility were negatively correlated with epicardial adipose tissue (r=-0.40, p=0.06 and r=-0.41, p=0.03 respectively) while distal descending aorta was not. In addition, NAFLD was associated with decrease distensibility (4.4 ±0.4 vs. 7.2 ±0.4 10^{-3} $mm.Hg^{-1}$; pFigure 2a and increase pulse wave velocity (PWV= 10.3 ±1.4 vs. 5.4 ±0.5cm/s; p=0.006) **Figure 2b** compared to controls. NAFLD was also associated with lower EDV (60.8 ±3.8 vs. 71.3 ±3.2 ml, pFigure 3a, ESV (19.4 ±1.0 vs. 26.6 ±1.7 ml, p< 0.0001) **Figure 3b**, SV (38.3 ±1.7 vs. 44.7 ±2.2 ml, pFigure 3c, and increased LVMR (0.9 vs. 0.69, p< 0.0001). Subjects with NAFLD had higher peak systolic strain (1.5 vs 2.2 %, p< 0.0001), peak radial strain (38 vs. 33 %, p< 0.001) and time to peak longitudinal strain (375 vs. 314 ms, p< 0.04). One-way Anova analysis showed that epicardial adipose tissue increased with the severity of the disease (pFigure 1b, and is significantly correlated with liver fibrosis (r=0.43, p=0.02). The presence of NASH was also associated with further decrease of aortic distensibility (p=0.0004) **Figure 2c** and increase in PWV (p=0.02) **Figure 2d**. We also observed lower EDV (p< 0.0001) **Figure 3d**, ESV (p=0.004) **Figure 3e** and SV (p=0.001) **Figure 3f** in NASH group. One-way Anova analysis also showed that aortic distensibility was associated with liver steatosis (p=0.03) while PWV increased with fibrosis (p=0.009).

Conclusion: NAFLD is associated with subclinical evidence of diastolic dysfunction, myocardial remodeling, aortic stiffening, and increased epicardial adipose tissue. NASH, rather than simple steatosis, seems to be a higher risk of these complications.

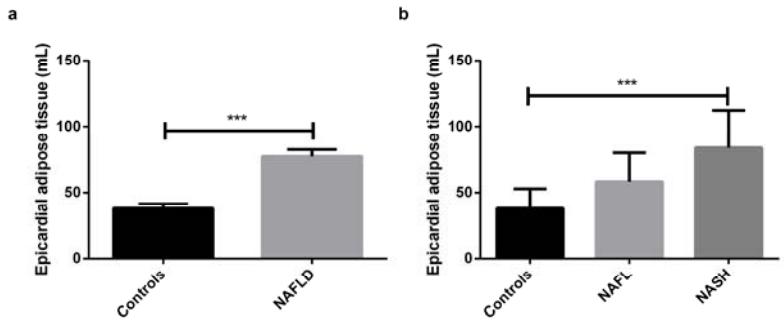

Figure 1: Comparison of epicardial adipose tissue accumulation between NAFLD patients and controls (a) and between controls, non-alcoholic fatty liver and non-alcoholic steatohepatitis groups (b). Data are presented as mean ± SEM

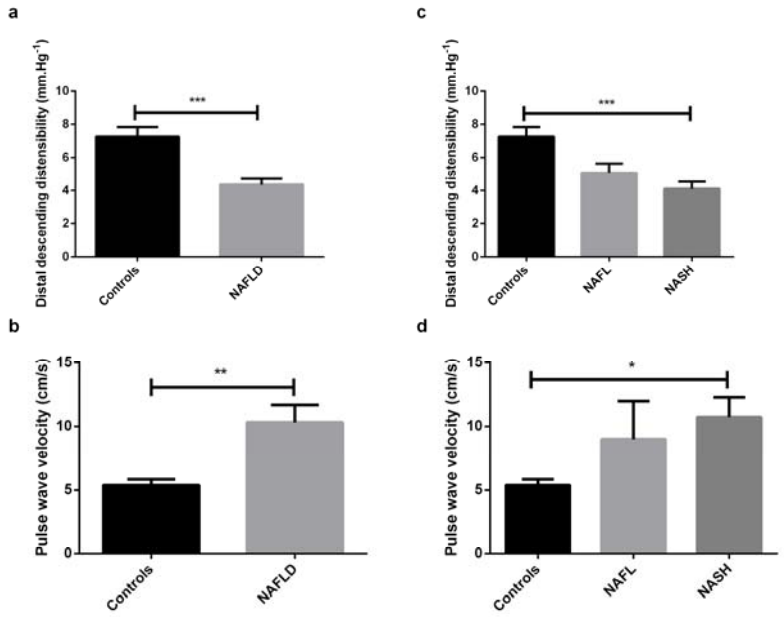

Figure 2: Comparison of aortic stiffness between NAFLD patients and controls (a,b) and between controls, non-alcoholic fatty liver and non-alcoholic steatohepatitis groups (c,d). Data are presented as mean ± SEM

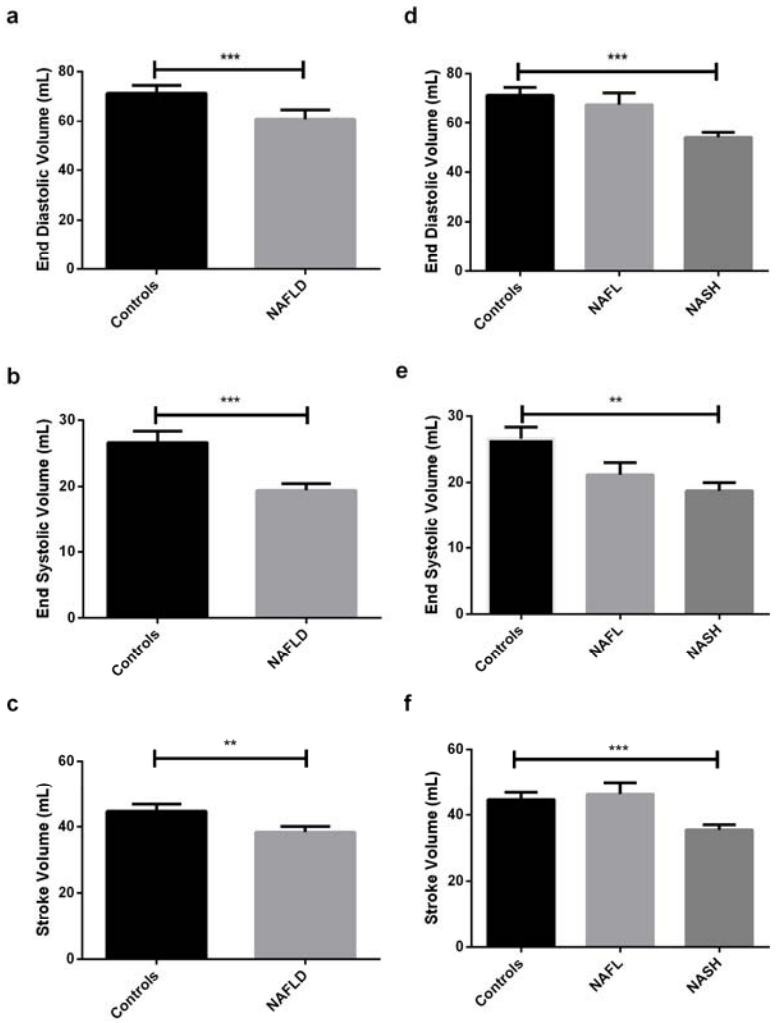

Figure 3: Comparison of cardiac volumes between NAFLD patients and controls (a,b,c) and between controls, non-alcoholic fatty liver and non-alcoholic steatohepatitis groups (d,e,f). Data are presented as mean ± SEM

Participants characteristics

	Lean	NAFL	NASH	p value
N	18	8	24	
Age, years	46 ± 2	53 ± 4	48 ± 3	ns
Gender, Men/Women	7/11	5/3	6/18	ns
BMI, $kg.m^{-2}$	21 ± 0	35 ± 2	38 ± 1	<0.0001
Type 2 diabetes, n	0	5	14	0.0002
Hyperlipidemia, n	0	7	15	<0.0001

Systolic blood pressure, $mm.Hg^{-1}$	115 ± 3	127 ± 7	124 ± 4	ns
Diastolic blood pressure, $mm.Hg^{-1}$	70	71	69	ns

Values as mean ±SEM

Abbreviations: NAFL, Non-alcoholic Fatty Liver; NASH, Non-alcoholic steatohepatitis; BMI, Body Mass Index

One-way Anova test was used to compare groups

ID#: 372433

Relative pressure gradients across the right ventricular outflow tract measured by 4D flow CMR

Piet Werner[1] Judith Zimmermann, MS[2], Nerejda Shehu, Dr.[3], Naira Mkrtchyan, Dr.[4], Heiner Latus, Dr.[5], Stefan Martinoff, MD[6], Anja Hennemuth, Prof. Dr.[7], Heiko Stern, Prof. Dr.[4], Peter Ewert, Prof. Dr.[4], Christian Meierhofer, Dr. Dr.[5]

1. Technical University Munich, Germany

2. Technical University Munich, Munich, Bayern, Germany

3. Pediatric Cardiology and Congenital Heart Disease, German Heart Center Munich, Muenchen, Bayern, Germany

4. Pediatric Cardiology and Congenital Heart Disease, German Heart Center Munich, Bayern, Germany

5. Pediatric Cardiology and Congenital Heart Disease, German Heart Center Munich, Munich, Bayern, Germany

6. German Heart Center Munich, Bayern, Germany

7. Charite - Universitätsmedizin Berlin, Berlin, Berlin, Germany

Background: Pressure gradients serve to grade severity of obstructive lesions in the cardiovascular system. The diagnostic ability to measure pressure gradients correctly and in a non-harmful way is crucial for the initial treatment and long-term follow-up of affected patients. Cardiac catheterization (CC) is the clinical gold standard for pressure gradient measurements. Recently, four-dimensional (4D) flow cardiovascular magnetic resonance (CMR) has been proposed as a non-invasive alternative to quantify relative pressure gradients across obstructive lesions in the aorta [1]. In this study CC was used to further quantify the precision and accuracy of relative pressure gradient measurements by 4D flow CMR. Therefore, patients were investigated with a primary or secondary impairment of the right ventricular outflow tract (RVOT) due to congenital heart disease (CHD).

Methods: 10 patients (mean age 27.3 years; age range 6 to 62 years) were included. 4D flow data was generated without sedation and administration of contrast agent. Patients'; relative pressure gradients were measured between the right ventricle and both pulmonary arteries by 4D flow CMR and CC consecutively (mean delay 1 day; delay range 0 to 1 day). Peak-instantaneous pressure gradients were computed based on acquired 4D flow vector fields by the Navier-Stokes and Pressure Poisson equations [2]. Precision and accuracy of 4D flow CMR measurements were quantified in comparison to peak-to-peak systolic pressure gradients estimated by CC.

Results: The range of peak-to-peak systolic pressure gradients was 6.5 to 45 mmHg. 4D flow CMR measurements show a moderate to good agreement compared to CC. The 95% limits of agreement are -14.2 to 14 mmHg. In 70% of measurements differences between methods have a deviation of ±5 mmHg or less that is supposed to be clinical irrelevant. 4D flow CMR gives accurate estimates of relative pressure gradients with a bias of -0.1 mmHg. Differences between methods are not significant ($p = 0.954$). The repeatability coefficient for intra-observer software analysis of 4D flow data is 4.9 mmHg.

Conclusion: Relative pressure gradient estimation by 4D flow CMR has proven its feasibility in context of impaired RVOTs due to CHD. The lack of precision is not explained by a lack of repeatability of 4D flow data analysis. However, the broad limits of agreement maybe attributable to single CC measurements. Further prospective studies should take measurements under more equal conditions in terms of sedation, measurements on the same day or at best taking 4D flow data during CC in the CMR environment.

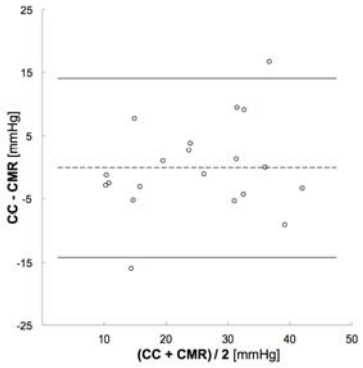

Bland-Altman plot for relative pressure gradients measured by CC and 4D flow CMR with 95% limits of agreement (solid lines) and bias (dashed line)

Limits	±5 mmHg or less	±10 mmHg or less	±15 mmHg or less
Proportion of differences	70%	90%	90%

Precision of 4D flow CMR relative pressure gradient estimation based on differences between measurements by CC and 4D flow CMR

[1] Riesenkampff, E., Fernandes, J. F., Meier, S., Goubergrits, L., Kropf, S., Schubert, S., . . . Kuehne, T. (2014). Pressure fields by flow-sensitive, 4D, velocity-encoded CMR in patients with aortic coarctation. *JACC Cardiovasc Imaging, 7*(9), 920- 926. doi:10.1016/j.jcmg.2014.03.017

[2] Meier, S., Hennemuth, A., Drexl, J., Bock, J., Jung, B., & Preusser, T. (2013). A Fast and Noise-Robust Method for Computation of Intravascular Pressure Difference Maps from 4D PC-MRI Data. *Statistical Atlases and Computational Models of the Heart. Imaging and Modelling Challenges, 7746*, 215-224. doi:10.1007/978-3-642-36961-2_25

References

ID#: 372358

Right Ventricular Function after Anthracycline Therapy

Thiago Ferreira. de Souza, MD, Msc[1] Ravi Shah, MD[2], Tomas G. Neilan, MD, MPH[3], Fabricio P. Brenelli, MD, PhD[4], Lício Velloso, MD, PhD[5], Wilson Nadruz, MD, PhD[4], Cesar Nomura, MD, PhD[6], José Roberto Mattos, MD, PhD[7], Michael Jerosch-Herold, PhD[8], OTAVIO R. COELHO-FILHO, MD, PhD, MPH[9], Thiago Quinaglia A. C. Silva, MD, PhD[5]

1. UNICAMP, Campinas, Sao Paulo, Brazil

2. Massachusetts General Hospital, Harvard Medical School, Boston, MA, USA, Newburyport

3. Massachusetts General Hospital, Harvard Medical School, Boston, MA, USA, MA

4. State University of Campinas, Sao Paulo, Brazil

5. State University of Campinas - UNICAMP, Sao Paulo, Brazil

6. Heart Institute - University of Sao Paulo, Sao Paulo, Brazil

7. State University of Campinas - UNICAMP - UNICAMP, Sao Paulo, Brazil

8. Harvard Medical School, Boston, MA

9. State University of Campinas - UNICAMP, Campinas, Sao Paulo, Brazil

Background: Anthracycline therapy is commonly associated with cardiovascular adverse effects including not only left ventricular (LV) but also right ventricular (RV) dysfunction. While recent data provide compelling evidence of the importance and prognostic significance of RV function in patients with heart failure (HF), few studies investigated the RV after anthracycline therapy. Given the thinner structure of the RV with fewer myofibrils, the RV may warrant more attention to the potential damage from cardiotoxic therapy. The goal of this study was to investigate the RV with cardiac magnetic resonance (CMR) imaging in breast cancer patients treated with anthracycline (240 mg/m^2).

Methods: Twenty-seven women with breast cancer (mean-age 51.8±8.9 years, BMI 26.9±3.6 kg/m^2), underwent CMR prior, and up to 3-times after anthracycline with matching measurements of serum cardiac biomarkers. The CMR protocol included assessment of LV and RV volumes and function.

Results: Before anthracycline, all subjects had normal LVEF (69.4±3.6%) and RVEF 55.1±9%) and LV and RV EF correlated significantly (ρ=0.42; P=0.031). At (351-700] days after anthracycline, LVEF and LV mas-index declined to 58±6% and 36±6 g/m^2 respectively (all, P<0.001). RVEF also decreased after anthracycline therapy, reaching a minimum averaging 46±8% at (231-368] days after anthracyclines (P<0.001 for comparison to baseline) (Figure 1). The RVEF showed a strong negative association with serum CK-MB measured during each CMR study (r=-0.5, P=0.013, Figure 2), independent of age, LV dysfunction, and follow-up time period. By contrast, LVEF showed a larger decline after anthracyclines (P<0.001 for all follow-up periods) compared to RVEF, but was not associated with CK-MB

Conclusion: Anthracycline therapy is associated with significant reduction in both LV and RV systolic function. The development of RV dysfunction after anthracyclines was independent of the degree of LV systolic dysfunction, and strongly associated with the serum cardiac biomarker CK-MB. The results of this study demonstrate that CK-MB is a marker specific to RV systolic dysfunction in patients receiving anthracycline therapy.

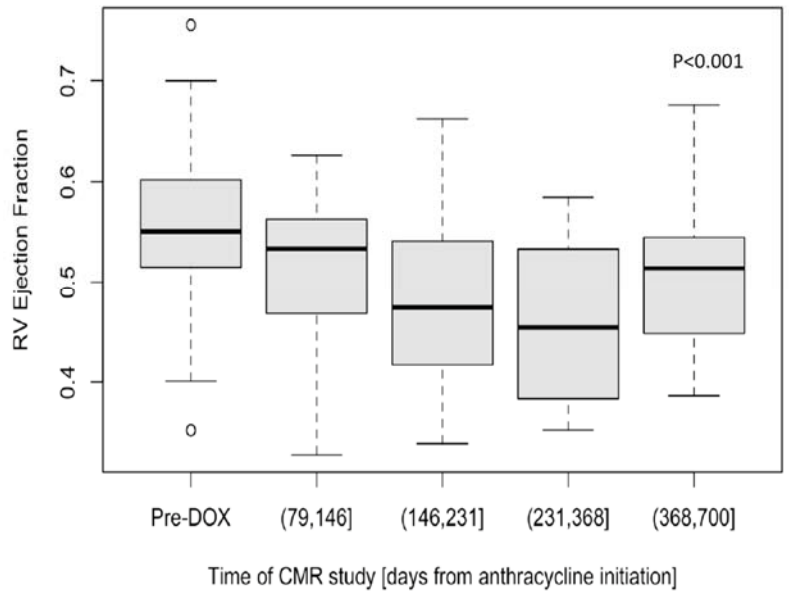

Figure 1

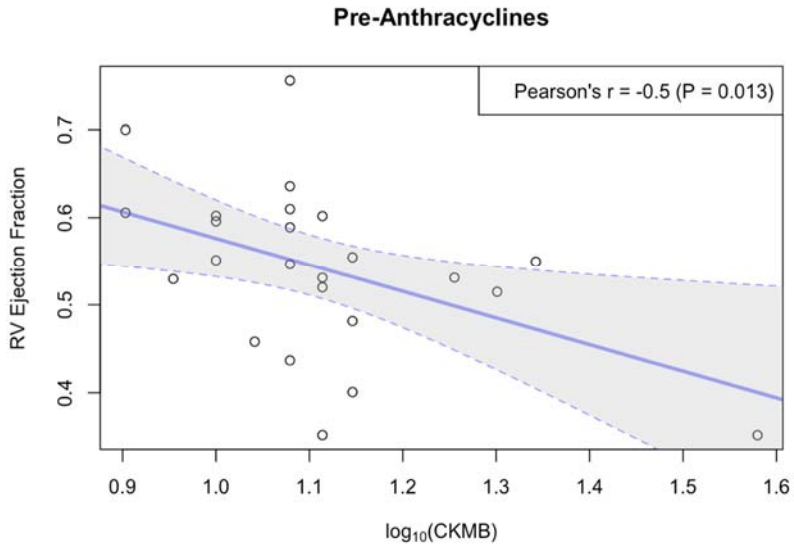

Figure 2

ID#: 372411

Age and Sex Dependent Effects of Trabeculae and Papillary Muscle Inclusion on Left Ventricular Volumetry by Cardiac Magnetic Resonance

Vincent Chen[1] Jeremy D. Collins, MD[2], Michael Markl, PhD[3], Alex J. Barker, PHD[3]

1. Northwestern University Feinberg School of Medicine

2. Northwestern University School of Medicine, Chicago, IL

3. Northwestern University, Chicago, IL

Background: Previous studies have reported age- and sex-specific normative values for global cardiac function (volumes, EF, mass) but the impact of including or excluding trabeculae and papillary muscle (TPM) from chamber volume has not been studied in detail. This study analyzed the impact of TPM handling on measures of global cardiac function in a large cohort of healthy subjects stratified by age and sex. We hypothesize that the effect of TPM handling on global cardiac function will be different between sexes but not among age groups.

Methods: 74 adult volunteers (n=74, m:f=36:38) free from known cardiac pathology underwent CMR at 1.5T (Aera, Siemens, Germany). Breath held short-axis 2D CINE SSFP images covered the left ventricle from apex to base, with TR/TE/FA = 3.0 ms/1.1 ms/60, slice thickness=6 mm, and interslice gap=4 mm. Age strata were 18-30 (n=14), 31-40 (n=19), 41-50 (n=12), 51-60 (n=11), and 61-80 (n=18). Analysis of global function (Circle cvi42 v5.3.0.) included automated detection of endocardial borders excluding TPM in end-diastole and end-systole, followed by manual correction. A thresholding algorithm detected papillary muscle based on contrast against blood pool; epicardial contours were manually drawn. Inclusion of TPM with LV volume was toggled by rounding of endocardial contours. Differences in end-diastolic volume (EDV), end-systolic volume (ESV), stroke volume (SV), ejection fraction (EF), and myocardial mass (LVM) were assessed between inclusion and exclusion of TPM with and from volume, and the magnitude of differences was compared between sexes and across age strata.

Results: TPM inclusion with volume significantly increased mean EDV (men: 13.6±1.0 mL; women: 9.2±1.2 mL) and ESV (men: 6.2±1.0 mL; women: 4.6±0.8 mL in women), and decreased mean EF (men: -0.8±0.3%; women: -1.2±0.5%). TPM inclusion with volume decreased mean LVM (men: -14.3±1.1 g; women: -9.7±1.2 g). Increase in volume after TPM inclusion was significantly greater in men than women for all volumes except indexed ESV. Decreases in EF were not significantly different between men and women. For men and women, no significant age-dependent effects of TPM handling on volumes, mass, or EF were found.

Conclusion: The decision to include TPM with LV chamber volume results in different age- and sex-specific normative values for global cardiac function depending on TPM handling during image analysis, with magnitude of difference dependent on sex. These findings highlight the importance of a systematic and transparent approach to TPM handling in CMR image analysis, especially for disease processes where there may be extensive cardiac remodeling.

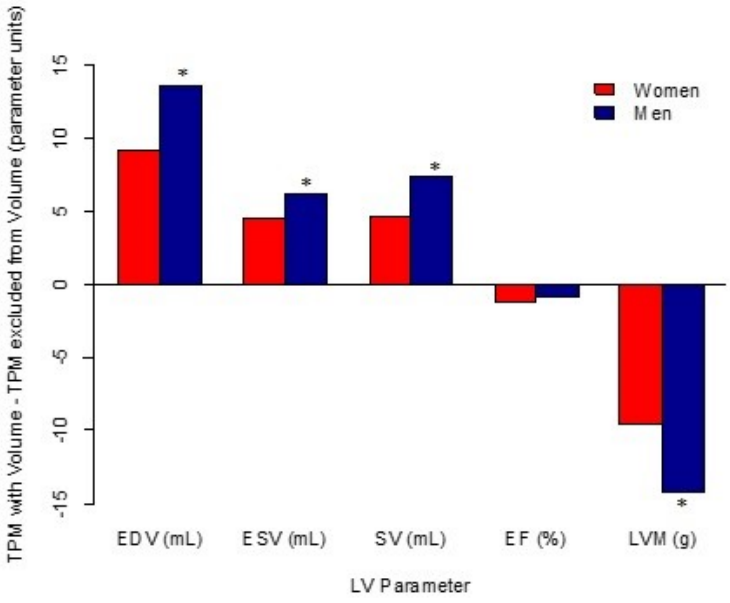

Impact of TPM Inclusion on LV Volumetry in Men and Women

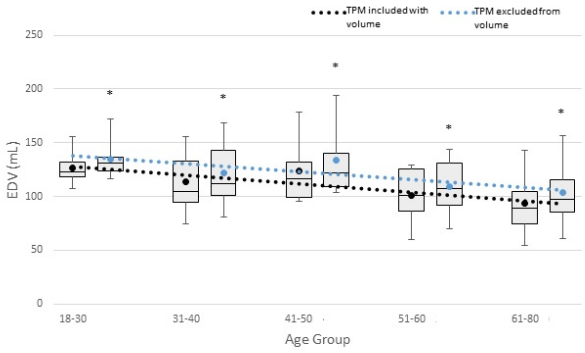

Effect of TPM on EDV in Adult Women over the Life Span

Global Cardiac Function in Men and Women by TPM Handling

	TPM Excluded from Volume			TPM Included with Volume		
	Men (n=36)	Women (n=38)	Men v. Women	Men (n=36)	Women (n=38)	Men v. Women
EDV, ml (sd)	130.0 (27.7)	111.0 (28.5)	$p < 0.05$	143.6 (29.2)	120.2 (30.0)	$p < 0.05$

EDV/BSA, ml/m^2 (sd)	63.1 (14.4)	60.5 (14.2)		69.6 (14.9)	65.5 (14.4)	
ESV, ml (sd)	46.8 (16.4)	35.4 (13.7)	p < 0.05	53.0 (18.8)	39.9 (15.9)	p < 0.05
ESV/BSA, ml/m^2 (sd)	22.8 (8.0)	19.2 (6.4)	p < 0.05	25.9 (2.2)	21.6 (7.3)	p < 0.05
SV, ml (sd)	83.2 (18.3)	75.6 (19.3)		90.4 (18.5)	80.2 (19.2)	p < 0.05
SV/BSA, ml/m^2 (sd)	40.3 (10.0)	41.4 (10.5)		43.7 (9.9)	43.9 (10.2)	
EF, % (sd)	64.5 (8.1)	68.6 (7.8)	p < 0.05	63.7 (8.4)	67.4 (8.1)	
LVM, g (sd)	149.1 (42.2)	103.1 (28.9)	p < 0.05	134.8 (39.8)	93.4 (26.4)	p < 0.05
LVM/BSA, g/m^2 (sd)	70.9 (16.6)	55.7 (12.6)	p < 0.05	64.0 (15.8)	50.5 (11.7)	p < 0.05

EDV = end diastolic volume; BSA = body surface area; ESV = end systolic volume; SV = stroke volume; EF = ejection fraction; LVM = left ventricular mass

ID#: 372446

Aortic stiffness is an independent predictor of concentric left ventricular hypertrophy in young adults with type 2 diabetes

Gaurav S. Gulsin, MBChB(Hons) MRCP(UK)[1] William Hunt, BSC (Hons)[2], Eylem Levelt, MBBS, DPhil[3], Daniel J. Swarbrick[4], Florence Lai[4], Thomas Yates[4], Melanie J. Davies, CBE[5], Gerald P. McCann, MBChB, MD[5]

1. The University of Leicester, Nottingham, England, United Kingdom

2. University of Leicester, Leicester, United Kingdom

3. University of Leicester, England, United Kingdom

4. University of Leicester, United Kingdom

5. University of Leicester, Leicester, England, United Kingdom

Background: The most deleterious consequence of developing type 2 diabetes (T2D) is a substantially elevated risk of cardiovascular disease, a feature that is magnified in younger adults. Patients with T2D have a two- to five-fold increased risk of developing heart failure (diabetic cardiomyopathy), which occurs independently of traditional risk factors such as hypertension, coronary artery disease and dyslipidemia. Despite being a widely recognised clinical entity, the etiology of diabetic cardiomyopathy is poorly understood and potential therapeutic strategies have not been adequately elucidated. Aortic stiffness (AoS) is frequently observed in patients with T2D and is independently associated with adverse cardiovascular events. AoS worsens across the glycemic spectrum and has been shown to contribute to subclinical cardiac dysfunction in T2D. However, the mechanisms linking AoS with adverse cardiovascular outcomes in T2D are unclear. Cardiovascular magnetic resonance (CMR) imaging can quantify AoS directly as aortic distensibility (AD). We hypothesised that AoS would be independently associated with cardiac remodeling in younger adults with T2D, which may predispose patients to heart failure.

Methods: Eighty patients with uncomplicated T2D (mean age 43.1±9.1yrs) and no prior cardiovascular disease underwent comprehensive CMR scanning, including LV volumes and function, pre- and post-contrast T1 mapping, aortic cine imaging and late gadolinium enhancement imaging. These were compared to 20 age-matched healthy controls. Blinded scans were analysed for ascending AD (AAD), descending AD (DAD), LV remodelling (LVmass/volume and LV mass index (LVMI)) and markers of focal and diffuse fibrosis. Multivariate linear regression assessed whether AoS independently predicted LV remodelling.

Results: Patients and controls were well-matched for age, gender and blood pressure (Table 1). There was no difference in LV ejection fraction (EF) or markers of diffuse fibrosis between groups (Table 1). T2D was associated with increased LV mass and concentric LV hypertrophy compared with controls (Table 1). Furthermore, AAD, DAD and mean AD were all lower in the T2D group (Table 1). When adjusted for age, systolic BP, BMI, heart rate, diabetes duration and HbA1c, AAD, DAD and mean AD were independent predictors LV mass index and LV mass/volume (Table 2).

Conclusion: This is the first study to demonstrate an independent association of aortic stiffening with cardiac remodelling in T2D. This suggests that ventricular/arterial interactions may play a significant role in cardiac risk in T2D. AoS may be a potential therapeutic target, independent of blood pressure control, to prevent heart failure in T2D.

Demographic details, LV volumes and function, markers of fibrosis and aortic characteristics in patients and controls

	T2D (n=80)	**Healthy controls (n=20)**	***P*-value**
Demographic details			
Age, years	43.1±9.1	38.8±10.9	0.087
Male gender, n (%)	40 (50)	11 (55)	0.613

Systolic BP, mmHg	131.4±18.0	126.1±13.7	0.269
Body mass index, kg/m^2	35.4±6.0	23.0±2.4	<0.001
HbA1c, %	7.6±1.6	5.4±0.3	<0.001
LV volumes and function, markers of fibrosis and aortic characteristics			
End-diastolic volume, mL	157.8±33.3	163.2±39.6	0.535
Ejection fraction, %	61.1±6.5	58.8±5.5	0.156
LV mass, g	99.5±24.8	89.1±36.9	0.017
LV mass index, g/m^2	40.9±8.2	35.8±12.0	0.028
LV mass/volume, g/mL	0.64±0.13	0.54±0.12	0.003
Mean native T1, ms	934.3±34.6	918.5±32.9	0.197
ECV, %	22.9±5.0	20.6±2.4	0.185
AAD, mmHg^{-1}x10^{-3}	4.85±2.21	6.12±1.78	0.010
DAD, mmHg^{-1}x10^{-3}	3.87±1.55	4.83±1.46	0.013

LV=left ventricle
ECV=extracellular volume fraction
AAD=ascending aortic distensibility
DAD=descending aortic distensibility

Pearson correlations and multivariate regressions

LV mass/volume	Univariate	Multivariate	LV mass index	Univariate	Multivariate
AAD (x10mmHg^{-3})	r=-0.417 *P*<0.001	β=-0.344 *P*=0.003	**AAD (x10mmHg^{-3})**	r=-0.424 *P*<0.001	β=-0.264 *P*<0.001
DAD (x10mmHg^{-3})	r=-0.425 *P*<0.001	β=-0.349 *P*=0.005	**DAD (x10mmHg^{-3})**	r=-0.437 *P*<0.001	β=-0.281 *P*<0.001

AAD=ascending aortic distensibility
DAD=descending aortic distensibility

ID#: 372447

Real-time cardiac cine using radial bSSFP sequence with trajectory auto-correction

Guoxi Xie, PhD[1] Xiaoyong Zhang[2], Wenlong Lv[3], Caiyun Shi[3], Shi Su[3], Bensheng Qiu, PhD[4], Xin Liu, M.D.[5]

1. School of Basic Science, Guangzhou Medical University, Guangzhou, China; Shenzhen Institutes of Advanced Technology, Chinese Academy of Sciences, China (People's Republic)

2. MR Collaborations NE Asia, Siemens Healthcare ,China, Guangdong, China (People's Republic)

3. Shenzhen Institutes of Advanced Technology, Chinese Academy of Sciences, China (People's Republic)

4. Centers for Biomedical Engineering, University of Science and Technology of China, Hefei, China, China (People's Republic)

5. Lauterbur Research Center for Biomedical Imaging, Shenzhen Institutes of Advanced Technology, Chinese Academy of Sciences, Shenzhen, China, Guangdong, China (People's Republic)

Background: Conventional cardiac cine is based on ECG-triggering, which is difficult to be used in arrhythmic patients. Real-time cardiac cine technique using radial sampling trajectories is an alternative method for imaging the arrhythmic patients. However, the technique is often hampered in trajectory error. To address this issue, a novel real-time technique with radial trajectory error auto-correction method was developed for cardiac cine and evaluated in patients with and without arrhythmia.

Methods: Sequence and Reconstruction: All acquisitions were based on a bSSFP sequence using radial trajectories and sliding window sampling scheme. Inspired by Ianni et al, a reconstruction method was developed for jointly estimating the radial trajectory errors, coil sensitivities, and dynamic images. The reconstruction was described as Eq. (1) (Figure 1A). **Experiment:** IRB-approved cardiac cine imaging was performed in 14 patients (8 with arrhythmia) on 3T (Siemens Verio, Germany) with a 32-element cardiac coil. 2D short-axis cine images were obtained in a stack of 7-12 contiguous slices spanning the entire left ventricle from the base to the apex. Imaging parameters included: TR/TE=3.0/1.52ms, FOV=220mm, bandwidth =1359Hz/pixel, spatial resolution=1.4×1.4×8.0mm^3, temporal resolution=36ms. Conventional CMR with ECG-triggering was conducted for comparison. **Image Analysis:** Left ventricular (LV) function parameters, including LV end-diastolic volume (LV-EDV), LV end-systolic volume (LV-ESV), and LV ejection fraction (LV-EF), were calculated and compared with those obtained by the conventional approach in patients without arrhythmia. To investigate whether the proposed method can improve the cardiac imaging in the presence of arrhythmia, contrast-to-noise ratio (CNR) between blood and myocardium were calculated for the arrhythmic patients. Statistical analysis was performed and significance was defined as $p < 0.05$.

Results: Using the proposed method to correct the radial sampling trajectories, signal intensity modulation and image blurry were improved (Figure 1B). Cardiac cine images obtained by the proposed method were comparable with those by conventional approach (Figure 2A). In addition, LV-EDV, LV-ESV and LV-EF between the proposed and conventional methods were well in agreement (Figure 2B). This demonstrated that the proposed method was feasibility for accurately evaluating patient';s LV function. For the study of the patients with arrhythmia, the images obtained by the proposed method showed significant improvement of image quality with better CNR between blood and myocardium and less motion artifacts (Figure 3).

Conclusion: A real-time cardiac cine technique was developed and evaluated on patients. Preliminary results demonstrated that the proposed technique has potential to be clinically useful for the patients with arrhythmia.

A

$$\arg\min \frac{1}{2}\left\|d - PF(\Delta k)\, S\rho\right\|_2^2 + \lambda\left\|G\,\rho\right\|_1 \qquad (1)$$

where P is sampling matrix, F is the NUFFT operator with trajectory correction Δk, ρ denotes the image. d is the acquired data, S is the coil sensitivity , λ is the regularization parameter, G is the sparsify transform operator. An alternative iterative algorithm was used for solving Eq. (1).

B

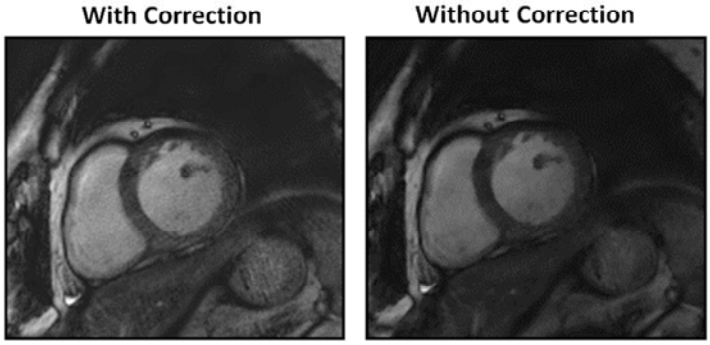

Figure.1. Image reconstruction model, and representative short axis images obtained from a patient with/without trajectory correction. Compared to the uncorrected reconstruction, the intensity modulations and blurring across the images were improved by the proposed method with trajectory correction (Figure 1B).

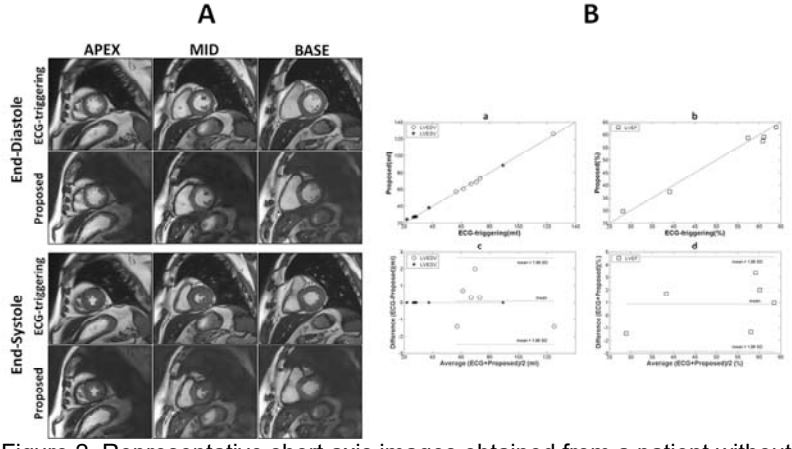

Figure.2. Representative short axis images obtained from a patient without arrhythmia and quantitative comparison results between the proposed method and conventional ECG-triggering approach. For the study of the patients without arrhythmia, the images obtained by the proposed method were comparable with those by conventional ECG-triggering approach (Figure 2A). Well agreements on measuring the LV-EDV, LV-ESV and LV-EF between the two techniques were realized according to the linear regression (Figure 2B, a&b) and Bland Altman analysis (Figure 2B, c&d).

A

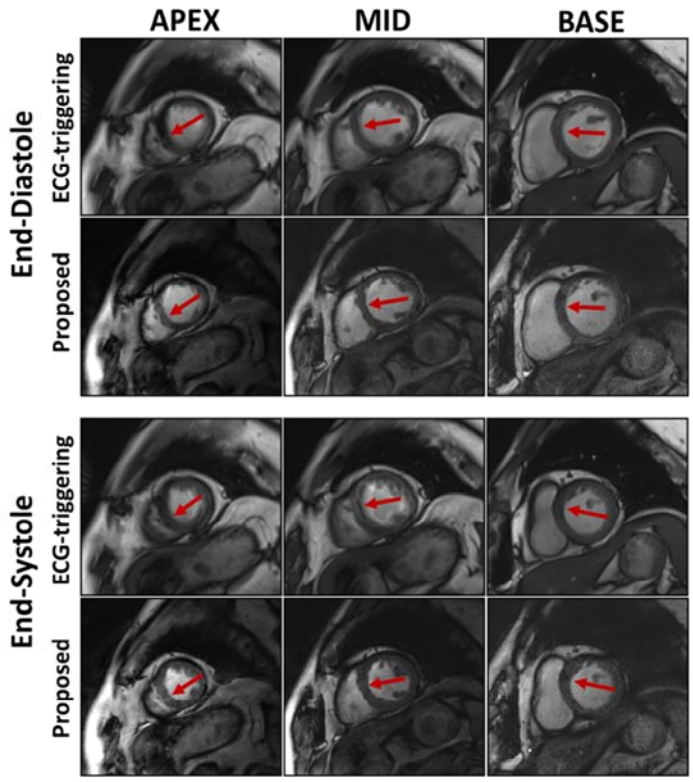

B

	Patient 1	Patient 2	Patient 3	Patient 4	Patient 5	Patient 6	Patient 7	Patient 8	Mean	P
ECG	12.5±3.1	6.5±2.7	7.8±3.3	10.2±2.1	8.3±2.1	9.6±2.1	11.2±3.0	6.9±3.1	9.1±3.9	0.004
Proposed	12.4±3.9	11.9±3.0	12.6±3.2	13.5±3.4	10.7±3.3	12.8±3.1	12.3±3.8	12.4±3.2	12.3±3.4	

Figure.3. Representative short axis images obtained from a patient with arrhythmia, and quantitative CNR analysis between the proposed method and conventional ECG-triggering approach. For the study of the patients with arrhythmia, obvious motion artifacts can be observed on the images obtained by the conventional ECG-triggering approach (red arrows on Figure 3A). The images obtained by the proposed method showed better CNR between blood and myocardium against those by the conventional ECG-triggering approach (Figure 3B).

ID#: 372457

Determination of the Optimal Method for 31P-Cardiac MR Spectral Analysis

Anna B. Reid, MBChB[1] Christopher A. Miller, MBChB PhD[2], Matthias Schmitt, MD PhD[3], Neal Sherratt[4]

1. University Hospital of South Manchester, Liverpool, United Kingdom

2. University Hospital of Manchester, England, United Kingdom

3. University Hospital of South Manchester, United Kingdom

4. NIHR / Wellcome Trust Manchester, United Kingdom

Background: 31P cardiac magnetic resonance spectroscopy (31P-CMRS) non-invasively measures the abundance of numerous metabolites in myocardium, giving insight into *in vivo* high energy phosphate metabolism. jMRUI software is commonly utilised for spectral analysis. Quantification can be performed manually, by fitting the acquired spectrum to 'prior knowledge'; of the particular spectral type. The aim of this of this study was to determine the feasibility and reproducibility of spectral analysis.

Methods: 15 patients with hypertrophic cardiomyopathy underwent 31P-CMRS at 3T (Achieva TX, Phillips, Best, Netherlands) using a dedicated, commercially available 31P- transmit and receive coil. Localisation was achieved using ISIS. A three dimensional voxel (same size in all patients) was positioned over the IVS. Three 31P-spectra were acquired using a standard, manufacturer-supplied sequence. Spectra were summed and analysed on jMRUI software allowing for pre-processing with 15Hz Lorenzian line broadening and phase correction. Firstly, fully automated peak identification and quantification was performed using the AMARES (Advanced Method for Accurate, Robust and Efficient Spectral fitting) fitting program (method A). Secondly, quantification was performed manually, with manual peak selection and calculation (method B). Thirdly, peaks were manually identified, with peak fitting and quantification performed using AMARES (method C). Line widths and amplitudes of peaks were determined. PCr/ATP ratio was calculated from the amplitudes of the PCr and γ-ATP peaks. Blinded quantification was performed twice, one month apart. Interclass-correlation coefficient (ICC) and Bland-Altman plots were used to assess reproducibility of PCr/ATP ratio.

Results: Mean PCR/ATP ratio determined by each method was 1.44 ± 0.63, 1.24 ± 0.38 and 1.33 ± 0.39, respectively, p=0.55. Of all potential spectra, 6 peaks could not be quantified by the software. In method A, three peaks could not be quantified (1 DPG, 2 PDE). One peak could not be quantified using method B (DPG). Two peaks could not be quantified using method C (both DPG). Method A displayed superior reproducibility with ICCs of 0.95, 0.15 and 0.71 for each method, respectively. Relative differences between mean PCR/ATP ratios were -0.05, -0.09, and -0.29 for each method, respectively.

Conclusion: Quantification of PCR/ATP derived from 31P-CMR spectra is reproducible when preformed using AMARES, despite failure of quantification of 3% of peaks.

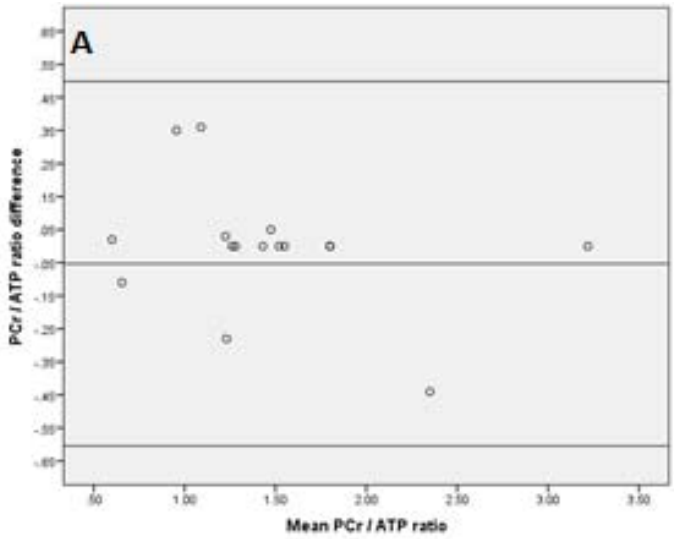
A
PCr / ATP ratio difference
Mean PCr / ATP ratio

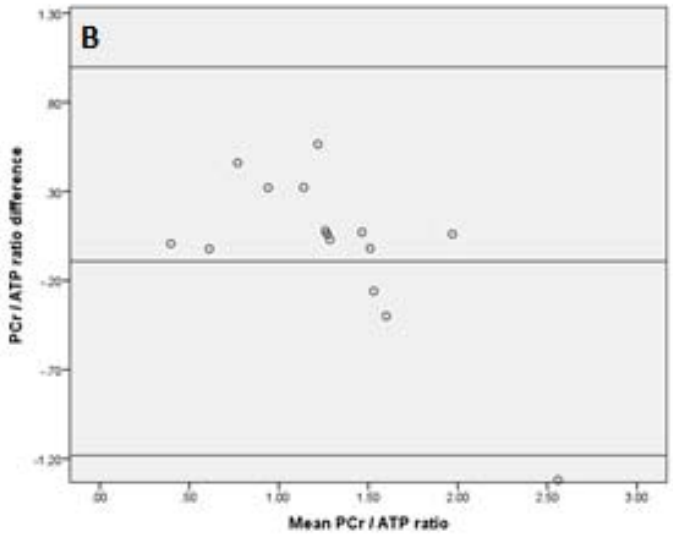
B
PCr / ATP ratio difference
Mean PCr / ATP ratio

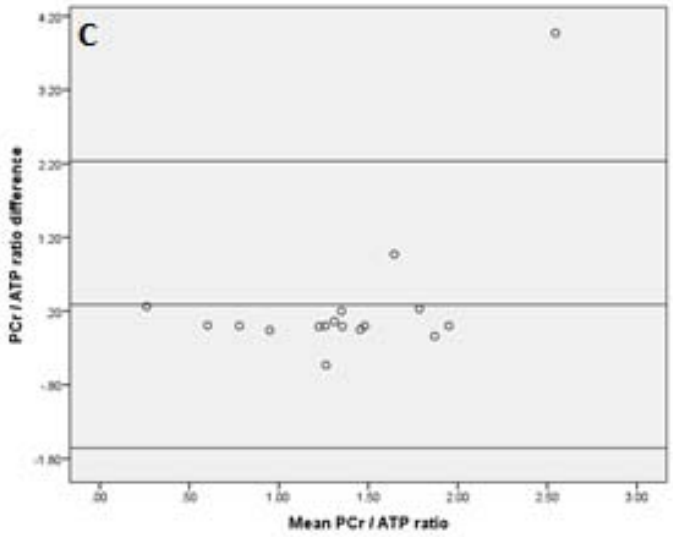
C
PCr / ATP ratio difference
Mean PCr / ATP ratio

Bland Altmann plots displaying the reproducibility of PCr/ATP quantification methods using A) method A, B) method B, and C) method C.

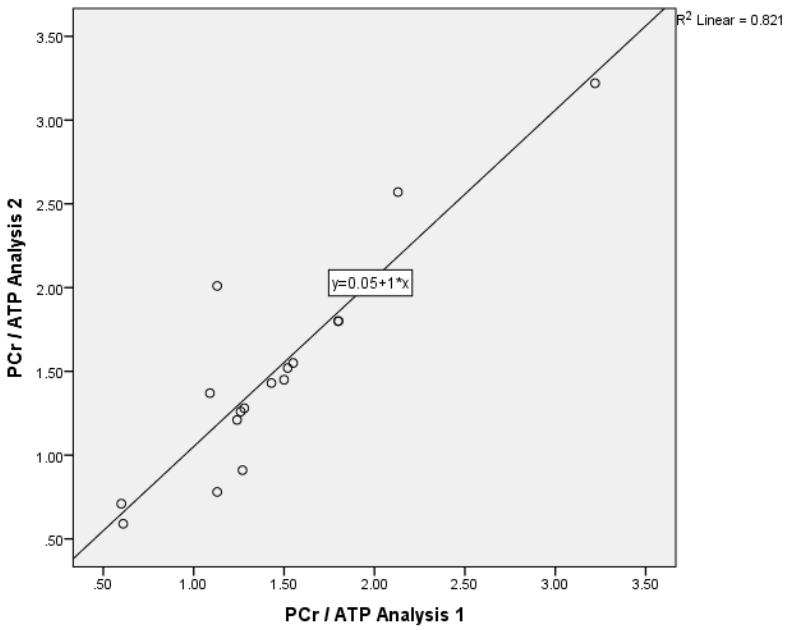

Interobserver correlation using AMARES for PCr/ATP quantification

ID#: 372467

Anisocytosis and its association with LV structure and function in the UK Biobank cohort

Marinos Koulouroudias, MBBS, BMedSci[1] Nay Aung, MD, MRCP[2], Kenneth Fung, MBBS BSc[1], Mihir M. Sanghvi, MB BS, BSc[2], Aaron Lee, PhD, MBBS[2], Jose Miguel Paiva, MSc[2], Jackie A. Cooper, CStat MSc[3], Stefan Neubauer, MD, FRCP[4], Steffen E. Petersen, MD DPhil MPH FRCP[5]

1. William Harvey Research Institute, NIHR Cardiovascular Biomedical Research Unit at Barts, Queen Mary University of London, Charterhouse Square, London, EC1M 6BQ, UK, London, United Kingdom

2. William Harvey Research Institute, NIHR Cardiovascular Biomedical Research Unit at Barts, Queen Mary University of London, Charterhouse Square, London, EC1M 6BQ, UK, England, United Kingdom

3. William Harvey Research Institute, NIHR Cardiovascular Biomedical Research Unit at Barts, Queen Mary University of London, Charterhouse Square, London, EC1M 6BQ, UK, United Kingdom

4. University of Oxford, England, United Kingdom

5. Queen Mary University of London, London, England, United Kingdom

Background: The red blood cell distribution width (RDW) is an inexpensive and widely available haematological index. It is the coefficient of variation of red blood cell volume, with higher values reflecting heterogeneity in red blood cell (RBC) sizes (anisocytosis). A number of studies have revealed an independent prognostic value for RDW in predicting mortality from heart failure and myocardial infarction (MI) as well as predicting the development of incident Heart Failure. No study to our knowledge has assessed the association of anisocytosis with LV structure and function in a cohort of individuals free from cardiovascular disease (CVD).

Methods: This was an observational cross-sectional study utilising data from the UK Biobank cohort study. Individuals underwent cardiac Magnetic Resonance Imaging (CMR) and had blood count indices measured. Left ventricular volumes, mass and ejection fraction were derived from the imaging studies. Interviews were performed at assessment centres to collect variables of interest. Individuals with self-reported CVD (defined as previous MI/Angina/Stroke) were excluded from the primary analysis. Multivariable regression models were built to assess the relation of CMR-derived parameters and RDW while controlling for various confounding variables (demographics, anthropometric measurements and CV risk factors). Haemoglobin levels were subsequently added to the final model to evaluate for the presence of any confounding.

Results: 3678 individuals free from self-reported CVD had both a CMR study and blood count data available (Figure 1). Univariate regression of CMR parameters versus RDW showed no significant relationship between the two. Multivariate analyses demonstrated statistically significant, but clinically likely irrelevant relationships between RDW and CMR parameters (Figure 2). A confounding effect was noted by the addition of Haemoglobin levels to the fully-adjusted model. All the above significant associations of RDW and CMR parameters were annulled, except for LV mass. At the same time, Haemoglobin was a relatively strong and statistically significant multivariate predictor for EDV, ESV and LV mass (Figure 3).

Conclusion: In this cohort of patients free of CVD, anisocytosis is associated with a very small albeit statistically significant increase in LV mass. Haemoglobin levels hold a stronger association with LV indices. The previously noted prognostic value of anisocytosis may be partly explained by its association with increasing LV mass.

Covariates	Mean ± SD or n (%)	Independent variables	Mean ± SD
Age, years	55 ± 8	LV EDV, ml	143 ± 34
Male	1660 (46)	LV ESV, ml	58 ± 20
Caucasian	3334 (93)	LV Mass, g	89 ± 24
Height, cm	170 ± 9	LV EF, %	59 ± 6
Weight, kg	75 ± 15		
Systolic BP, mmHg	139 ± 19	**Red Cell Indices**	**Mean ± SD**
Diastolic BP, mmHg	79 ± 10	RDW, %	13 ± 0.9 *
Diabetes Mellitus	194 (5.4)	Hb, g/dL	14 ± 1.2
Antihypertensive use	907 (25)	MCV, fL	91 ± 4
Statin use	433 (12)	MCH, pg	30 ± 1.8
Ever smoked	1923 (54)	MCHC, g/dL	34 ± 0.9
Family History of any CVD (parents)	1932 (54)		

Baseline characteristics for all covariates, independent variables and red cell indices used in the analysis *Median ± IQR

CMR Parameter	Effect Size (%) per SD increase in RDW	95 % CI	Adjusted p- value	Adjusted R^2
LV EDV	1.17	0.5 to 1.9	0.000727	0.49
LV ESV	1.13	0.1 to 2.2	0.029	0.38
LV Mass	1.09	0.4 to 1.8	0.0015	0.63
LV EF	0.02	-0.2 to 0.3	0.87	0.06

Effect size(%) per SD increase in RDW in individuals without CVD

CMR Parameter	Effect Size per SD increase in RDW (%)	95 % CI	Adjusted p-value	Effect Size per SD increase in Hb (%)	95 % CI	Adjusted p- value	Adjusted R^2
LV EDV	0.4	-0.2 to 1.1	0.2	-3.4	-4.1 to -2.8	0.000002	0.50
LV ESV	0.3	-0.7 to 1.4	0.5	-3.7	-4.7 to -2.7	0.00000002	0.39
LV Mass	0.8	0.1 to 1.5	0.02	-1.4	-2.1 to -0.7	0.000006	0.63
LV EF	0.03	-0.2 to 0.3	0.8	0.07	-0.2 to 0.3	0.6	0.06

Effect size (%) per SD increase in RDW or Haemoglobin in individuals without CVD

ID#: 372492

Added value of right ventricular 3-chamber view in patients with pulmonary hypertension using a comprehensive right ventricular myocardial systolic strain analysis with Feature-Tracking cardiac magnetic resonance.

Theresia Akhlaghi, B.Sc.[1]Göran Rådegran, M.D., Ph.D.[2], Roger Hesselstrand, M.D., Ph.D.[3], Einar Heiberg, PhD[4], Håkan Arheden, MD PhD[5], Ellen Ostenfeld, M.D., Ph.D.[6]

1. Lund University, Dept of Clinical Sciences, Clinical Physiology, Lund, and Skane University Hospital, Lund, Malmö, Skane Lan, Sweden

2. Lund University, Dept of Clinical Sciences, Cardiology, Lund, and Skane University Hospital, Lund, Skane Lan, Sweden

3. Lund University, Dept of Clinical Sciences, Rheumatology, Lund, and Skane University Hospital, Lund, Skane Lan, Sweden

4. Lund University, Skåne University Hospital, Department of Clinical Sciences Lund, Clinical Physiology, Lund, Sweden, Skane Lan, Sweden

5. Lund University, Skåne University Hospital, Department of Clinical Sciences Lund, Clinical Physiology, Lund, Sweden, Lund, Sweden

6. Lund University, Dept of Clinical Sciences, Clinical Physiology, Lund, and Skane University Hospital, Lund, Skane Lan, Sweden

Background: Pulmonary hypertension (PH) is a potentially devastating condition. Right ventricular (RV) dysfunction is a key determinant of prognosis, and better markers of early RV dysfunction are needed. Cardiac strain is a sensitive measure of myocardial dysfunction that appears to be affected before RV ejection fraction (RVEF) is reduced. At present, longitudinal RV strain is measured in the 4-chamber view (4CH) using cardiac magnetic resonance (CMR). Because RV dilatation also occurs in anterolateral direction in patients with PH, relying solely on 4CH might lead to an incomprehensive assessment of RV function and strain. In this study, RV strain was measured using CMR in a RV 3-chamber view (RV3CH) including the posterior and anterior free wall of RV. The aim was to evaluate if RV3CH has incremental diagnostic value to 4CH and midventricular short axis slice of the RV (RV-SA), in relation to assessment of RVEF, systolic pulmonary arterial pressure (sPAP) and pulmonary vascular resistance (PVR).

Methods: Fifty-one patients (60±16years, 76% female), 34 with PH and 17 with scleroderma being screened for but without PH, were prospectively included for RV evaluation using CMR. Longitudinal strain was analyzed in long axis images acquired in 4CH and the new RV3CH. Circumferential strain was analyzed in a short axis midventricular slice. Endocardial RV was manually delineated in 4CH, RV3CH and RV-SA (**Figure 1**), and strain was calculated with feature tracking in the software Segment (Medviso AB, Lund). Postsystolic contraction was defined as systolic contraction after pulmonary valve closure. Right heart catheterization was performed on clinical indications.

Results: Peak systolic strain was -17.6±1.6% in RV3CH, -17.4±1.7% in 4CH and -11.9±1.3% in RV-SA. Peak systolic strain from RV3CH correlated to RVEF (**Figure 2**), sPAP and PVR (r=-0.75, r=0.51, r=0.65, p<0.001 for all) (**Table 1**). Postsystolic contraction was detected in 17 patients in RV3CH, 12 in 4CH and 12 in RV-SA. Postsystolic contraction in RV3CH correlated to RVEF, sPAP and PVR (r=-0.71, r=0.69, r=0.58, p<0.001 for all) (**Table 1, Figure 2**). Positive predictive value of postsystolic contraction in RV3CH to detect RVEF<50%, mPAP≥25 and PVR>3WU, was 94%, 88% and 100%, respectively. Postsystolic contraction in 4CH or RV-SA did not correlate with RVEF, sPAP or PVR.

Conclusion:

Peak systolic strain from RV3CH using CMR correlates strongly to RVEF, sPAP and PVR. Presence of postsystolic contraction in RV3CH provides added predictive value of decreased RVEF, increased sPAP and PVR, while 4CH and RV-SA do not.

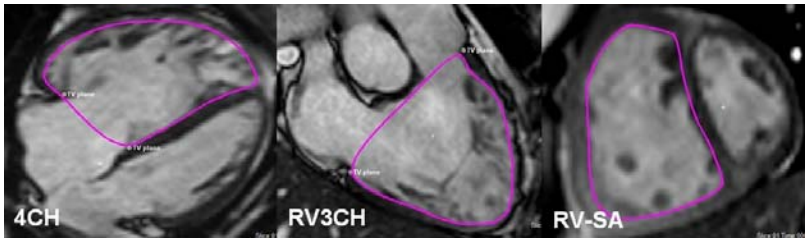

Figure 1: Manual Delineations of RV in Segment

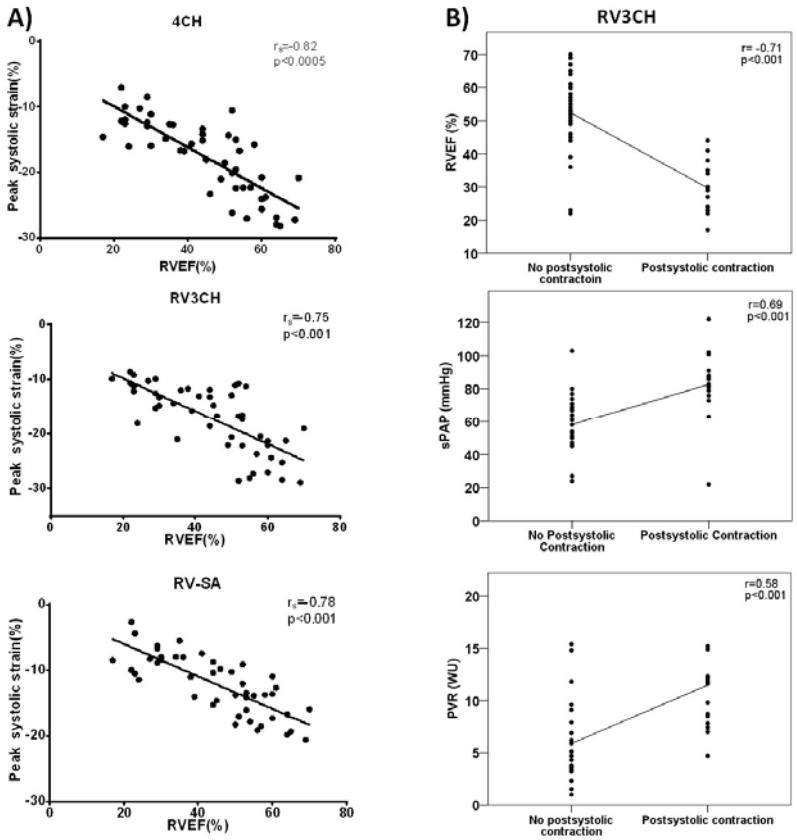

Figure 2: Scatterplots of A) peak systolic strain and RVEF in 4CH, RV3CH and RV-SA, and B) postsystolic contraction and RVEF, sPAP and PVR in RV3CH

Table 1: Association of peak systolic strain and postsystolic contraction to RVEF, sPAP and PVR

	RVEF		sPAP*		PVR*	
	R	P value	R	P value	R	P value
4CH Peak systolic strain	-0.816	<0.001	0.618	<0.001	0.835	<0.001
RV3CH Peak systolic strain	-0.752	<0.001	0.512	<0.001	0.650	<0.001
RV-SA Peak systolic strain	-0.780	<0.001	0.537	<0.001	0.522	<0.001

4CH Postsystolic contraction	-0.248	0.092	0.250	0.160	0.311	0.078
RV3CH Postsystolic contraction	-0.710	<0.001	0.685	<0.001	0.577	<0.001
RV-SA Postsystolic contraction	-0.266	0.070	0.147	0.405	0.115	0.516

4CH, 4 chamber view; RV3CH, right ventricular 3 chamber view; RV-SA, right ventricle short axis slice; RVEF, right ventricular stroke volume; sPAP, systolic pulmonary arterial pressure; PVR, pulmonary vascular resistance; RV, right ventricle; SA, short axis.
**Only patients with clinical indication underwent RHC (n=38) and was included in this test, excluding patient with scleroderma and no hypertension.*

ID#: 372504

High resolution in-vivo diffusion tensor cardiovascular magnetic resonance using a variable density interleaved spiral trajectory

Margarita Gorodezky, M. Sc.[1] Andrew D. Scott, PhD[2], Pedro F. Ferreira, PhD[3], Sonia Nielles-Vallespin, PhD, MSc[4], Peter D. Gatehouse, PhD[5], Dudley J. Pennell, MD[6], David N. Firmin, PhD[7]

1. Cardiovascular Magnetic Resonance Unit, Royal Brompton Hospital, England, United Kingdom

2. Royal Brompton Hospital, London, England, United Kingdom

3. Cardiovascular Magnetic Resonance Unit, Royal Brompton Hospital, Sydney Street, London, SW3 6NP, UK, England, United Kingdom

4. NIH, MD

5. NIHR Cardiovascular Biomedical Research Unit, Royal Brompton Hospital, London, England, United Kingdom

6. Royal Brompton Hospital and Imperial College, London, England, United Kingdom

7. 1. Cardiovascular Magnetic Resonance Unit, Royal Brompton Hospital, Sydney Street, London, SW3 6NP, UK, England, United Kingdom

Background: Diffusion tensor cardiovascular magnetic resonance (DT-CMR) provides novel microstructural information in several patient groups[1,2], however spatial resolution limits application in thinned myocardium. Single-shot spiral STEAM DT-CMR has demonstrated similar results to an established EPI sequence[3]. In this study interleaved spirals are used to increase spatial resolution, with a correction for motion-induced phase between interleaves.

Methods: A spiral STEAM sequence (figure 1a) with a reduced excitation field-of-view (FOV) in three directions[3] was modified to use interleaved variable-density spirals. Two variable density interleaves were acquired per image over 4 successive cardiac cycles (figure 1b). DT-CMR was performed (Siemens 3T-Skyra) in 7 healthy volunteers in a short-axis mid-ventricular slice in peak-systole during breath-holding. Data were acquired using the interleaved spiral sequence (2x2mm^2, TE=11ms, 17ms spiral, 22 breath-holds), a single-shot STEAM EPI sequence with matched resolution (figure 1c, 2x2mm^2, TE=34ms, 19ms echo-train, 11 breath-holds) and lower resolution single-shot spiral and EPI sequences as previously described[3] (2.8x2.8mm^2, 11 breath-holds, spiral: TE=11ms, 15ms spiral; EPI: TE=24ms, 13ms echo-train). Both EPI sequences used SENSE x2 and reduced phase FOV. All sequences used b_{main}=600s/mm^2 (10 averages) and b_{ref}=150s/mm^2 (1 average) in 6 diffusion-directions. The spiral data was reconstructed offline and data from the second interleave was corrected for motion-induced phase errors to match the first interleave[4]. The individual coil contribution to the images was weighted by coil sensitivity maps[5]. The diffusion tensor was calculated with in-house software (MATLAB). For interleaved spiral data the reconstruction was performed twice: with a matched number of averages (22 breath-holds, 10 averages) then with a matched acquisition time (11 breath-holds, 5 averages). Secondary eigenvector angulation (E2A), fractional anisotropy (FA), mean diffusivity (MD), the standard deviation of the transverse angle (stdTA) and percentage of negative eigenvalues (%nEV) were compared over the left ventricle (LV). The signal-to-noise-ratio (SNR) was compared in the septal wall.

Results: Figure 2 shows example DT-CMR parameter maps for a typical single volunteer. The average LV DT-CMR parameters; and SNR, %nEV and stdTA as quality measures are compared in figure 3. SNR is higher using spiral than the EPI at both resolutions, and at high resolution both the stdTA and %nEV lower for the spiral than EPI.

Conclusion: Variable density interleaved spiral trajectories with a correction for motion induced phase can increase the spatial resolution of in-vivo STEAM DT-CMR. These initial results suggest that interleaved spiral trajectories out-perform single-shot EPI at high spatial resolution. **References:** 1:Nielles-Vallespin S:JACC2017 2:Nguyen C: JCMR2014 3:Gorodezky M:ISMRM2016:Abstract3109 4:Scott A:NMRbiomedicine2016 5:Roemer P:MRM1990

Figure 1: STEAM sequences with a single interleave, constant density spiral readout (120x120mm2 FOV) (a), interleaved variable density spiral readout with an acquisition over 4 cardiac cycles (110x110-120x120mm2 FOV) (b) and an EPI readout (360x135mm2 FOV) (c). For the spiral acquisition asymmetric RF pulses were used. The images in the 6 diffusion-directions were acquired in a single breath-hold in both EPI and single interleave spiral sequences and in two breath-holds for the interleaved spiral sequence.

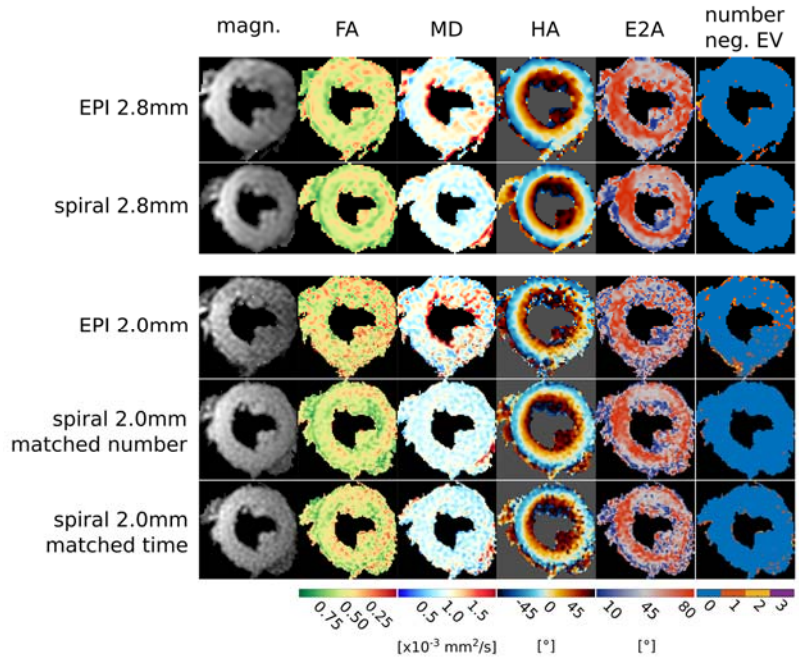

Figure 2: A calculated magnitude image at b=0s/mm2, DT-CMR parameter maps (fractional anisotropy (FA), mean diffusivity (MD), helical angle (HA), secondary angle angulation (E2A)) and negative eigenvalue maps from a typical volunteer are shown for both sequences and at both resolutions. For the interleaved spiral, two reconstructions, one with the matched number of averages and one with a matched acquisition time to the other sequences were performed.

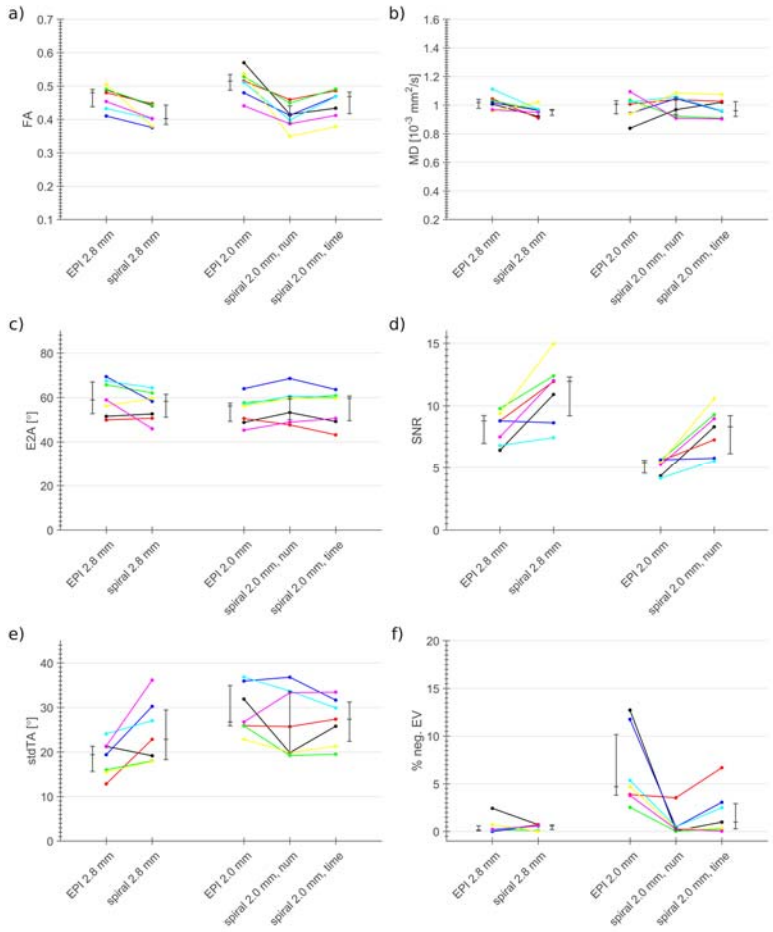

Figure 3: Comparison of the DT-CMR parameters and the data quality. The mean FA (a), MD (b) and median E2A (c) over the left ventricle are shown. (d) demonstrates an SNR comparison in the septal wall. Because of a low number of averages, no SNR calculation was performed for the time matched 2mm spiral. The data quality was compared using the standard deviation of the transverse angle (e) and the number of negative eigenvalues (f).

ID#: 372521

A deep learning approach for the segmental analysis of myocardial T1 mapping

Nicola Martini, PhD[1]Daniele Della Latta, BSc[1], Gianmarco Santini, MSc[1], Gabriele Valvano, MSc[1], Andrea Barison, MD, PhD[2], Carla Luisa Susini, MD[1], Francesco Avogliero, MD[1], Daniele De Marchi, RT[2], Luigi Landini, PhD[2], Dante Chiappino, MD[3]

1. Fondazione G. Monasterio CNR Regione Toscana, Massa, Italy

2. Fondazione G. Monasterio CNR Regione Toscana, Toscana, Italy

3. Fondazione G. Monasterio CNR Regione Toscana, Massa, Toscana, Italy

Background: T1 mapping is an emerging technique for the detection of acute and chronic myocardial injury. Regional analysis of T1 mapping is commonly performed according to the 17-segment model of the American Heart Association [1]. In this study, we propose a deep learning approach for the automatic segmentation of left-ventricle T1 maps.

Methods: We retrospectively studied native T1 maps acquired from 339 subjects using a modified Look-Locker inversion recovery (MOLLI) sequence [2] in mid-ventricular short-axis slices at 3.0 T. Six-segment reference analysis was performed by two expert operators by manually drawing endocardial and epicardial contours. Region-of-interests (ROIs) were also drawn in the LV and RV blood pools avoiding papillary muscles.
The proposed deep learning strategy is based on a fully convolutional neural network for multi-class semantic segmentation [3]. The deep network was trained to take the T1 map as input and to provide the segmented image with class labels, according to the ROIs previously defined. During training random rotations (max angle 45°) were used for data augmentation and weighted loss function to cope with class imbalance.
299 maps were used for training and 40 maps as ground truth for performance evaluation.
Jaccard and Dice similarity indexes were measured to evaluate the quality of the segmentation, while the agreement with operator results was assessed evaluating the mean T1 value in each compartment. In addition, the orientation of each myocardial segment was employed as an estimate of the angular error.

Results: Visual inspection of the automatic segmented maps showed a close agreement with manual segmentation in normal and pathological subjects (Fig. 1a and 1b). High Jaccard (0.961±0.028) and a Dice (0.980±0.015) values demonstrated good segmentation results. The angular error of 4.6±4.1 degrees reflected the high confidence in predicting the different heart orientation among subjects. The regional distribution of T1 values in myocardial segments and blood pools was well preserved by the proposed method as shown in Fig.2. No significant difference in the estimated T1 values between the operator and the deep learning approach (intraclass correlation coefficient, ICC=0.93) was found. The automatic segmental analysis took less than 1 second per T1 map.

Conclusion: The proposed method enables the automatic segmental analysis of myocardial T1 maps. No significant difference in the regional T1 values compared to manual measurements was found. This method can effectively facilitate the analysis of myocardial T1 mapping in clinical studies.

References

[1] Cerqueira MD et al. Circulation 2002;105:539-42. [2] Messroghli DR et al. MRM 2004;52(1):141-146. [3] Ronneberger O. et al., arXiv:1505.04597.

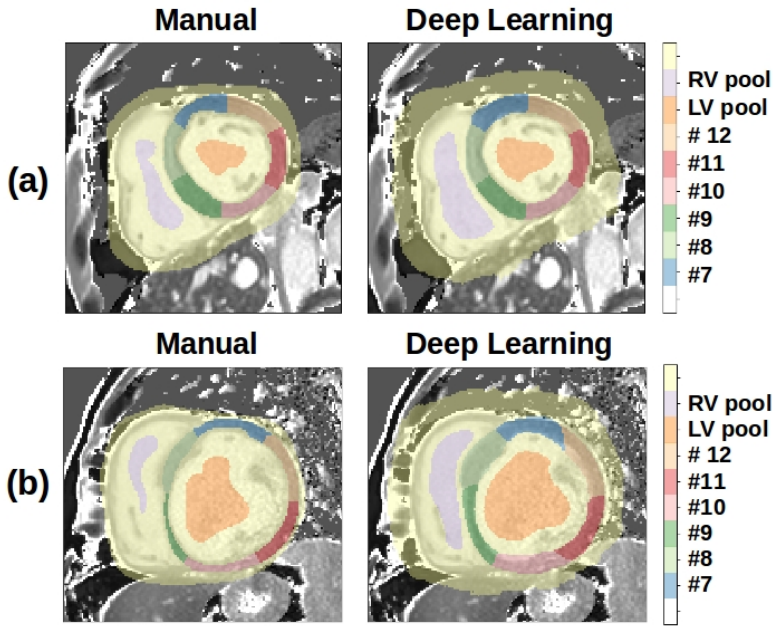

Fig.1. Segmentation results in (a) a normal subject and (b) a patient with dilated cardiomyopathy.

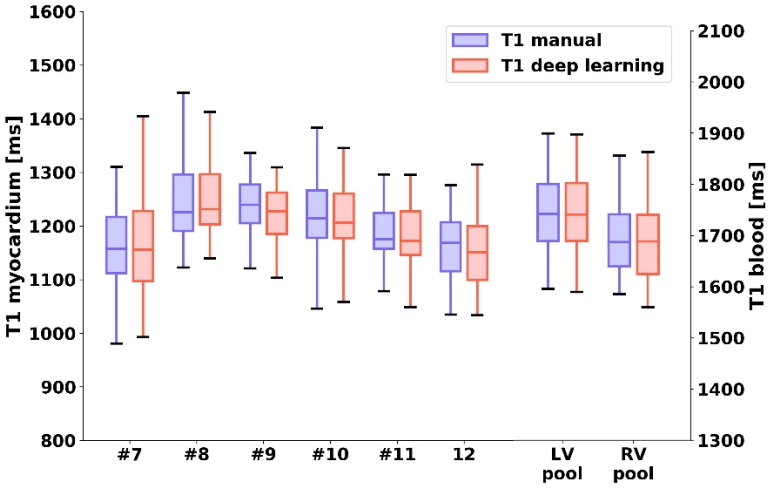

Fig.2. Boxplot of mean T1 values in myocardial segments and blood pools.

ID#: 372479

Assessment of Myocardial Fibrosis in Uremic Cardiomyopathy using Cardiac MR Native T1 Mapping: A Comparison with Coronary Artery Calcium Score

Shengjia Gu, M.D.[1] Qian Tao, PhD[2], Rob J. van der Geest, PhD[2], Wenjie Yang, Ph.D.[1], Fuhua Yan, Ph.D.[3]

1. Ruijin Hospital, Shanghai Jiao Tong University School of Medcine, China, Shanghai, China (People's Republic)

2. Department of Radiology, Leiden University Medical Center, The Netherlands, Leiden, Zuid-Holland, Netherlands

3. Ruijin Hospital, Shanghai Jiao Tong University School of Medcine, China, Shanghai, Shanghai, China (People's Republic)

Background:

End-stage renal disease (ESRD) patients treated with hemodialysis have high levels of interstitial myocardial fibrosis which causes structural abnormalities including left ventricular hypertrophy (LVH), termed uremic cardiomyopathy (UCM). Meanwhile, coronary artery calcium score (CACS) is an independent risk predictor of cardiac complications in chronic kidney disease as demonstrated in previous studies. As non-contrast native T1 value has been shown to have good correlation with cardiac fibrosis, the objective of this study is to investigate the value of native T1 mapping for the assessment of myocardial fibrosis in UCM for monitoring the cardiac status of ESRD patients.

Methods: 12 ERSD patients treated with hemodialysis who underwent both 3T CMR imaging (Philips Ingenia 3T) and Cardiac Calcium Scoring Scan (Siemens Somatom Definition Flash) were enrolled in this study. The CMR imaging protocol included cine SSFP and pre-contrast T1 mapping sequences. The full left ventricle was covered in around 10 short axis slices in both cine and T1 mapping, with the same in-plane resolution, slice thickness and gap. Left ventricular ejection fraction (EF) was measured from short axis cine. Global and segmental native T1 was measured from short axis slices using MASS software (research version 2017, Leiden University Medical Center). Segmental myocardial mass was measured from bull's eye view using Mass directly. Based on both short and long axis cine, the standardized segments (AHA) were identified by a radiologist with 6 year experience. Segmental native T1 were measured by the mean value of the same segments in consecutive slices. CACS AJ-130 and Volume-130 were quantified using the multimodality workplace (syngoMMWP VE50A, Siemens). Statistical analysis was performed using SPSS-23 software (IBM, Chicago, IL). Native T1 between low EF group and preserved LVEF group were compared by one-way ANOVA. Correlations between native T1, CACS and myocardial mass were assessed using Pearson';s analysis. K independent sample test was used to analyse the mean rank difference of native T1 values among 16 segments (segment 17 of apex is not included).

Results:

The mean global native T1 was 1285.9±36.5 ms. There was a significant difference of native T1 between low EF group and preserved LVEF group (1324.2±30.6 ms vs 1266.7±20.7 ms, p=0.003). Global native T1 was significantly correlated with the CACS AJ-130 and Volume-130 (r=0.789, p=0.002 and r=0.791, p=0.002, respectively). Bases on septal thickness ≥15mm, 66.7% (8/12) subjects showed myocardial hypertrophy. Segments 2, 14, 9 and 8 had the highest ranks of native T1 value (X^2=15.702, p=0.402), which indicated that septal segments appeared to be more prone to develop fibrosis.

Conclusion:

Native T1 value of ERSD patients is associated with structural abnormalities of the heart and highly correlated with structural and functional abnormalities of the left ventricle and CACS. Thus, native T1 is potentially clinically valuable for monitoring the cardiac status of ESRD patients treated with hemodialysis.

ID#: 372480

Quantification of the area-at-risk by post-contrast T1 mapping and detection of intramyocardial hemorrhage by post-contrast T2* mapping in reperfused STEMI patients

Nazia Chowdhury, BSc[1]Mei Xing Lim, BSc[2], Mervyn Chan, BSc[1], John Allen, PhD[3], Heerajnarain Bulluck, MBBS PhD[4], Derek J. Hausenloy, MBChB PhD[5]

1. Cardiovascular and Metabolic Disorders Program, Duke-National University Singapore Medical School: National Heart Research Institute Singapore, National Heart Centre, Singapore, Singapore

2. Cardiovascular and Metabolic Disorders Program, Duke-National University Singapore Medical School: National Heart Research Institute Singapore, National Heart Centre, Singapore, Singapore, Singapore

3. Centre for Quantitative Medicine, Office of Clinical Sciences, Duke-National University Singapore Medical School, Singapore

4. Papworth Hospital NHS Trust, Cambridge, UK, England, United Kingdom

5. Cardiovascular and Metabolic Disorders Program, Duke-National University Singapore Medical School; National Heart Research Institute Singapore, National Heart Centre, Singapore, Singapore, Singapore

Background: Pre-contrast T1 cardiovascular magnetic resonance (CMR) mapping, performed in the first week following ST-segment elevation myocardial infarction (STEMI), can quantify the edema-based area-at-risk (AAR). Pre-contrast T2* CMR mapping can detect intramyocardial hemorrhage (IMH) in STEMI patients. However, the inclusion of these pre-contrast CMR sequences substantially lengthens the scanning time. In this study, we investigate whether performing T1/T2*-mapping CMR after contrast can reliably quantify the edema-based AAR and detect IMH in reperfused STEMI patients. This has the potential to shorten the CMR scanning time, thereby making the procedure more tolerable for acutely unwell STEMI patients.

Methods: Eight STEMI patients reperfused by primary percutaneous coronary intervention (PPCI) at the National Heart Centre Singapore (NHCS) were prospectively recruited into the study following informed consent. Prior ethical approval of the study had been granted by the Singhealth Centralized Institutional Review Board. CMR was performed on a 1.5 Tesla scanner (Magnetom Avanto, Siemens Medical Solutions) at a median of 1.5 (1.0-3.8) days post-PPCI. Mid-left ventricular (LV) short-axis slices of pre-contrast T1-mapping (MOLLI) and post-contrast T1 mapping (performed within 8 minutes of post-contrast administration) were analysed for AAR, using a threshold of 2SD difference from remote myocardium. One mid-LV short-axis slice of pre-contrast and post-contrast T2* maps were analysed for the presence of IMH (defined as T2* value

Results: All STEMI patients were male, with wide range of ischemic times, median age of 57 (51-62) years old. There was an excellent correlation with the AAR quantified by post-contrast T1 when compared to pre-contrast images (R^2 0.958). There was minimal bias with acceptable limits of agreement (Bias -0.67±5.1%LV, P=0.52). 75% (6/8) of the patients had IMH present on pre- and post-contrast T2*-maps with similar T2* values within the hypointense cores (Post-T2*12.9±1.7msec vs. Pre-T2*13.1±2.6msec, P=0.834). The hypointense cores on the pre- and post-contrast T2*-maps were significantly lower as compared to remote myocardium (Pre-T2*: Core 13.1±2.6msec vs. Remote 32.6±3.8msec, P

Conclusion: T1 mapping CMR performed within 8 minutes of post-contrast administration can reliably quantify the AAR. Post-contrast T2* mapping CMR can detect IMH in reperfused STEMI patients. These approaches could potentially shorten CMR scanning time and make the procedure more tolerable for acute STEMI patients.

ID#: 372469

Feasibility of Fetal cine CMR based on Doppler Ultrasound Triggering and Compressed Sensing

Anthony H. Aletras, Ph.D.[8]Kostas Haris, PhD, MSc[1], Fabian Kording[2], Erik Hedström, MD, PhD[3], Sebastian Bidhult[4], Frederik Testud[5], Katarina Steding-Ehrenborg[4], Einar Heiberg, PhD[6], Christian Ruprecht[2], Håkan Arheden, MD PhD[7]

1. Lund University, Skåne University Hospital, Department of Clinical Sciences Lund, Clinical Physiology, Lund, Sweden, Greece

2. Department of Diagnostic and Interventional Radiology, University Medical Center Hamburg-Eppendorf, Hamburg, Germany, Germany, Germany

3. Lund University, Skåne University Hospital, Department of Clinical Sciences Lund, Diagnostic Radiology, Lund, Sweden, Sweden

4. Lund University, Skåne University Hospital, Department of Clinical Sciences Lund, Clinical Physiology, Lund, Sweden, Sweden

5. Siemens Healthcare AB, Skane Lan, Sweden

6. Lund University, Skåne University Hospital, Department of Clinical Sciences Lund, Clinical Physiology, Lund, Sweden, Skane Lan, Sweden

7. Lund University, Skåne University Hospital, Department of Clinical Sciences Lund, Clinical Physiology, Lund, Sweden, Lund, Sweden

8. Aristotle University of Thessaloniki/Lund University, Thessaloniki, Thessaloniki, Greece

Background: Fetal CMR is a growing research field where new imaging and reconstruction techniques allow for clinical evaluation of the fetal cardiac function. However, the extraction of reliable fetal ECG remains a difficult problem. Solutions based on retrospectively sorting the acquired MR data into the proper cardiac phases have been proposed [1]. The aim of this study is to demonstrate the feasibility of fetal CINE CMR within one breath-hold by retrospectively binning the Doppler Ultrasound (DUS) trigger signals within tyGRASP (tiny iterative Golden-angle RAdial Sparse Parallel) MRI [2,3].

Methods: The regional ethics board approved the study, and written informed consent was obtained from the study participants. Examinations were performed on a 1.5 T MAGNETOM Aera scanner (Siemens Healthcare, Erlangen, Germany). Short-axis fetal CMR images were acquired using a prototype radial bSSFP CINE sequence (TE/TR=1.9/3.9 ms, flip angle=60^{o}, pixel size 0.7x0.7x5 mm^3). 4,000 radial spokes with a tiny golden angle of order 7 (i.e. increment of 23.6^{o}) [3] were acquired within a breath-hold of 14s. An MR-compatible prototype DUS transducer [4], placed above the fetal heart, provided the cardiac synchronization signal for retrospective binning. Sixteen to 22 cardiac phases were obtained by tyGRASP compressed sensing reconstruction [3], implemented in MATLAB (Mathworks, MA, USA) [1]. The reconstruction time was approximately 5 min. Two blinded experts (S.E.H, H.A) visually evaluated the fetal images for both cardiovascular and extra-cardiovascular quality and potential diagnosis.

Results: Fetal images from a healthy volunteer (gestational week 38+4) are demonstrated. Figure 1 shows a short-axis view of the fetal heart at end diastole and end systole. In Figure 2, 20 reconstructed cardiac phases are shown. Both observers independently indicated high image quality.

Conclusion: The presented preliminary results demonstrate that DUS-gated fetal cine CMR with tyGRASP is feasible and provides high image quality. This method can be expanded and refined to incorporate free breathing, promoting the use of fetal CMR imaging in the clinical routine.

References

[1] Haris K et al JMRI 46:207 (2017)
[2] Feng L et al MRM 72:707 (2014)
[3] Wundrak S et al IEEE TMI 34:1262 (2015)
[4] Kording F et al MRM 74:1257 (2015)

Funding was provided by the Swedish Heart and Lung Foundation and by the Medical Faculty at Lund University. The authors thank Siemens Healthcare for providing support within the Master Research Agreement with Lund University and the Region of Skåne.

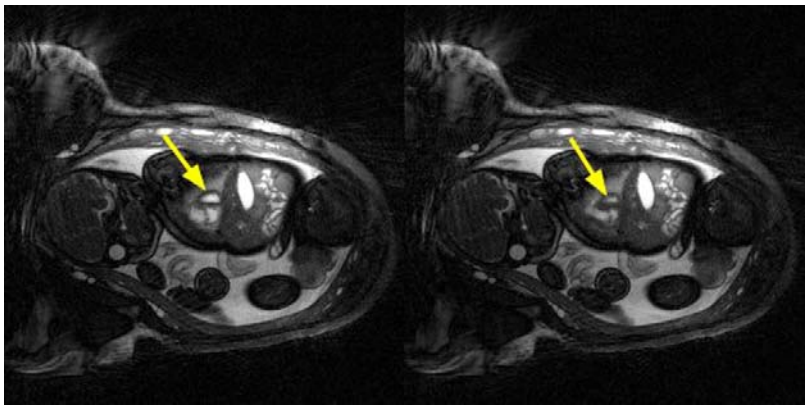

End-diastolic and end-systolic full-field-of-view slices of the fetus showing high image quality. The yellow arrow points to the left ventricle (short-axis view).

All twenty reconstructed cardiac phases from Figure 1, shown cropped and magnified.

ID#: 372471

4D flow MRI for the analysis of celiac trunk and mesenteric artery stenoses

Florian Siedek, MD[1]Daniel Giese, PhD[2], Kilian Weiss, PhD[3], Sebastian Brinkmann, MD[4], Wolfgang Schroeder, MD[4], Sandra Ekdawi, PhD[5], De-Hua Chang, MD[6], Christiane Bruns, MD[1], David Maintz, MD[7], Stefan Haneder, MD[5]

1. University Hospital Cologne, Nordrhein-Westfalen, Germany

2. University Hospital Cologne

3. Philips Healthcare, Hamburg, Germany, Nordrhein-Westfalen, Germany

4. University Hospital Cologne, Germany

5. Unversity Hospital Cologne, Nordrhein-Westfalen, Germany

6. University of Cologne, Nordrhein-Westfalen, Germany

7. University Hospital of Cologne, Department of Radiology, Nordrhein-Westfalen, Germany

Background: 4D flow MRI allows non-contrast-enhanced, time-resolved visualization of blood flow patterns and quantification of blood flow parameters in a 3D-volume. This facilitates the assessment and understanding of various blood flow characteristics including velocity (VelRP) and volume (VolRP) related parameter as well as stenosis assessment, blood flow distribution and wall shear stress (WSS).
This study aimed to show the feasibility of k-t accelerated 4D flow measurements in complex vascular territories, in this case for the celiac artery (CA) and superior mesenteric artery (SMA). Blood flow parameters were compared between healthy volunteers (HV) and patients (PAT) with stenosis of CA and/or SMA close to the vessel ramification known from contrast-enhanced computertomography (CE-CT) performed up to 3 months before 4D flow MRI. Comparison was undertaken based on the grade of CA- and/or SMA-stenosis.

Methods: In this prospective study 22 HV and 10 PAT were scanned at 3T (Tab.1). The 4D flow acquisition covered the CA, SMA and adjusting parts of the aorta (AO). Measurements of VelRP (peak velocity[PV], average velocity[AV]), VolRP (peak flow[PF], stroke volume[SV]), stenosis grade and WSS in the CA and SMA (5mm distal of the vessel ramification) and the AO (10mm proximal of CA) were conducted and analyzed. Two-sided t-test was used for statistical analysis regarding $p<0.05$ as significant.

Results: In PAT semiautomatic evaluation of prior CE-CT revealed 11 low- and 5 mid-grade stenoses of the CA and/or SMA. In HV no stenosis could be detected in the 4D dataset. VelRP (PV, AV) were significantly higher in PAT with low- and mid-grade stenoses than in HV [PV:$p<0.0001$; AV:$p=0.03$,$p<0.001$] without significant differences depending on the grade of stenosis (Fig.1, Fig.2). VolRP did not differ significantly between HV and PAT, however a trend towards lower PF and SV could be recognized in PAT with mid-grade stenosis. Comparison of CE-CT and 4D flow MRI revealed a high correlation regarding the estimated degree of stenosis (CA:$r=0.86$, SMA:$r=0.98$). PAT with middle-grade stenoses had a significantly higher average WSS magnitude (AWM) than healthy individuals ($p=0.02$). AWM was higher in PAT with low-grade stenosis (1.26vs.0.96N/m^2), however without statistical significance.

Conclusion: This study suggests that k-t accelerated 4D flow MRI is a technique for the thorough evaluation of complex flow characteristics also in smaller vessels such as the CA and SMA. 4D flow MRI is probably more suitable for functional evaluation than mere morphologic assessment using CE-CT. One of many prospective clinical applications could be preoperative evaluation before esophagectomy.

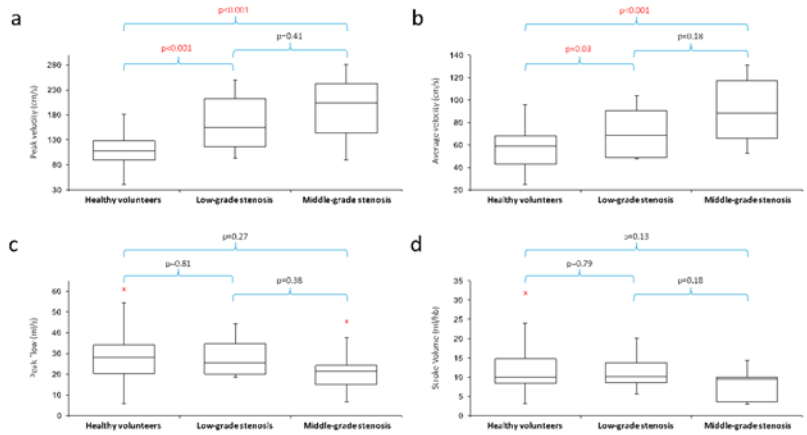

Figure 1: This panel shows four box and whisker plots of the values for A. peak velocity (PV), B. average velocity (AV), C. peak flow (PF) and D. stroke volume (SV) for healthy volunteers and patients with low- and middle-grade stenosis. Box and whisker plots present the five-number summary consisting of: the lowest mean R2* values, the lower quartile (25% percentile), median, upper quartile (75% percentile), and greatest mean R2* values. The colored asterisks indicate outliers.

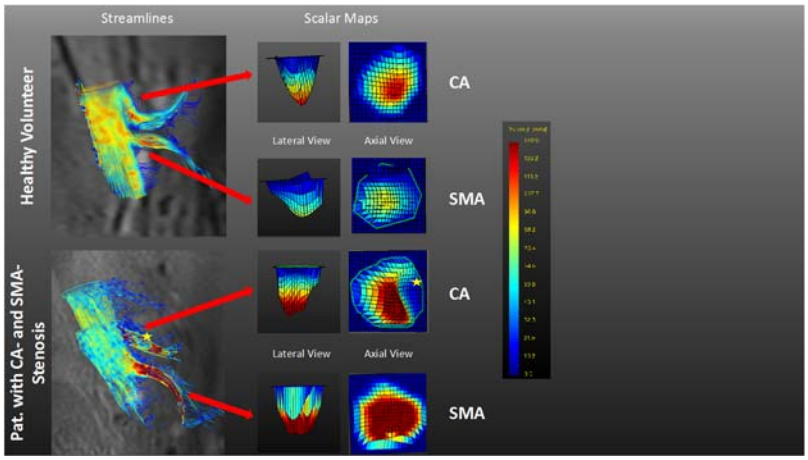

Figure 2: Illustration of flow pattern during systole using time-resolved 3D-streamlines which allow visualization of velocity changes and Scalar maps which show the distribution of blood flow velocity in the vessel lumen of the CA and SMA for a HV as well as a patient with known stenosis of the CA and SMA. Note - in the location of the yellow star 4D-flow shows a local turbulence with reduced blood flow velocity.

Table 1: Detailed information about the study population and the quantification and classification of the stenosis of the CA and SMA in patients according to the NASCET-criteria

		HV	Patients	
Gender	[m/f]	15 / 7	7 / 3	
Mean age ± SD	[y]	31.9 ± 12.6	74.7 ± 5.3	
Age range	[y]	23 - 77	66 - 82	
BMI	[kg/m^2]	23.3 ± 2.6	25.1 ± 2.8	
STenosis grading		N/A	low	middle

Numbers		N/A	11	5
Mean stenosis grade* ± SD	[%]	N/A	24.2 ± 6.1	61 ± 6.2
Range	[%]	N/A	15.4-33.9	50.1-68.2
*BMI = body mass index; m = male; f = female; y = years; HV = Healthy volunteers; SD = standard deviation; *according to NASCET = North American Symptomatic Carotid Endarterectomy Trial, N/A = not applicable*				

ID#: 372477

Weight Loss in Obesity is Associated with a Fall in the Creatine Kinase Rate Constant

Jennifer J. Rayner, BMBCh, MRCP(UK)[1] William T. Clarke, MChem, D.Phil[2], Mark A. Peterzan, BSc(Hons) MRCP(UK) MA[3], Stefan Neubauer, MD, FRCP[4], Christopher T. Rodgers, DPhil[3], Oliver Rider, BMBCh, DPhil[5]

1. OCMR, University of Oxford, Oxford, England, United Kingdom

2. University Of Oxford Centre for Clinical Magnetic Resonance Research, England, United Kingdom

3. University of Oxford, Oxford, England, United Kingdom

4. University of Oxford, England, United Kingdom

5. University of Oxford Centre for Clinical Magnetic Resonance, Oxford, England, United Kingdom

Background: Obesity is associated with diminished myocardial energetic stores, as determined by PCr/ATP, measured non-invasively with ^{31}P magnetic resonance spectroscopy. However, systolic function is typically maintained despite the diminished substrate reserve. Weight loss, either dietary or through bariatric surgery, is associated with restoration of the PCr/ATP ratio. We have previously demonstrated that creatine kinase rate constant (k_f^{CK}) is elevated in obese individuals with no cardiovascular disease, which may represent a compensatory mechanism to preserve ATP delivery. We hypothesised that intentional weight loss would reduce the requirement for increased enzyme activity, and hence k_f^{CK} would fall.

Methods: 23 obese individuals (53±13 years, 8 male, BMI 37±6 kg/m^{-2}) underwent comprehensive metabolic and anthropometric phenotyping with blood tests for cholesterol, glucose and insulin, body composition analysis, and MR (3T, Siemens) for abdominal visceral fat at the level of L5. They also had cardiac MR to determine cardiac structure and function. Triple Repetition time Saturation Transfer (TRiST) 1D-CSI ^{31}P magnetic resonance spectroscopy was used to measure k_f^{CK}. Participants then underwent repeat testing following a dietary weight loss intervention.

Results: Mean BMI in the cohort fell from 37 ± 6 kg/m^{-2} to 30 ± 10kg/m^{-2} (p=0.009, fig 2), with 14 volunteers losing more than 10% body fat (mean -20 ± 8%, p=0.004) and only 2 gaining weight. Visceral fat volume fell by 28 ± 26% (p<0.001, fig 1). Glucose (although within the normal range), cholesterol and triglyceride levels all fell (p<0.05). LV end-diastolic volume and mass fell (from 157± 8ml to 153±37ml (p=0.003) and 111±29g to 103±25g (p=0.042) respectively. k_f^{CK} fell from 0.20±0.10s^{-1} to 0.13±0.07s^{-1} (p=0.035), a value which was not statistically different from normal weight (fig 2). This change was correlated with change in both fat mass (r=0.623, p=0.006), and visceral fat volume (r=0.751, p=0.001, fig 3).

Conclusion: We demonstrate for the first time that a dietary weight loss intervention in an otherwise healthy obese population is associated with a fall in the creatine kinase forward rate constant. It has previously been shown that weight loss in this population is associated with an increase in the PCr/ATP ratio. Our findings may reflect a recalibration of the required k_f^{CK} in the context of replenished substrate pool (i.e. higher PCr levels). The impact of weight loss in diseases with more profound myocardial energetic deficit must be investigated to establish its safety.

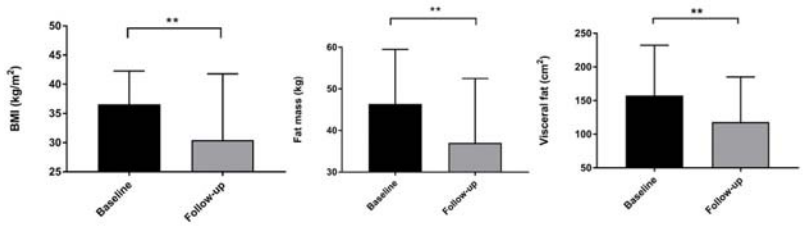

Figure 1: The impact of dietary weight loss on BMI (left), fat mass (centre) and visceral fat (right). ** indicates p<0.01.

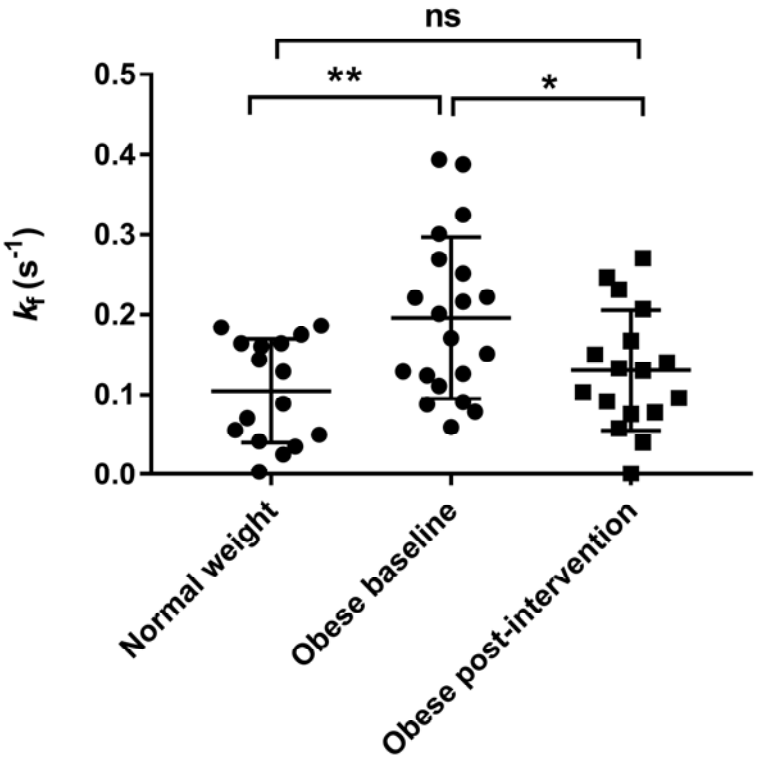

Figure 2: The forward rate constant (kf) of myocardial creatine kinase is higher in obesity than normal weight individuals, and returns to normal with weight loss. * p<0.05; ** p<0.01.

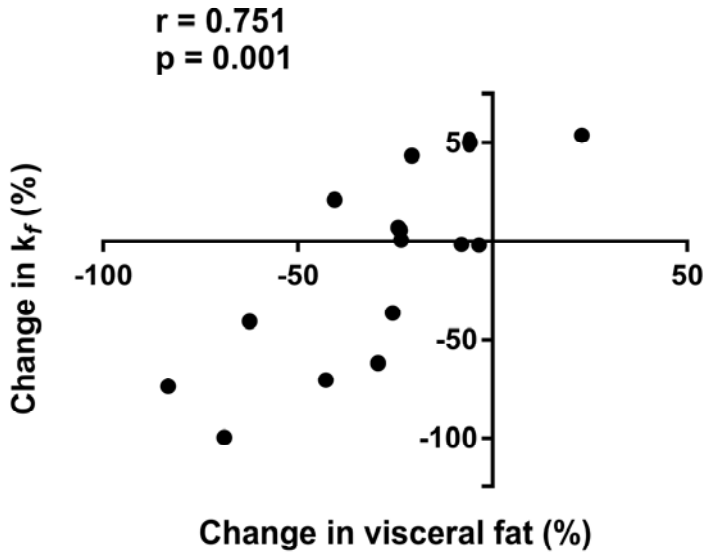

Figure 3: The change in visceral fat induced by weight loss, correlates with the change in creatine kinase kf

ID#: 371513

Aortic stenosis septal hypertrophy and its regression post AVR is more plastic in males than females: insights from a 3D cardiac atlas

Anish N. Bhuva, MRCP MBBS[1] Thomas Treibel, PhD[2], Antonio de Marvao, MB ChB, PhD[3], Carlo Biffi, MSc[4], Timothy Dawes, FRCA, PhD.[4], Georgia Doumou, MRes[5], Wenjia Bai, PhD[6], Ozan Oktay[7], Rhodri Davies, MRCP, PHD[8], Peter Kellman, Ph.D.[9], Nishi Chaturvedi, MD, MRCP[10], Daniel Rueckert, PhD[7], Declan O'Regan, FRCR, PhD[11], Alun Hughes, MBBS PhD[12], James Moon, MD[13], Charlotte Manisty, MBBS PhD[14]

1. Barts Heart Centre and Institute of Cardiovascular Science, UCL., London, England, United Kingdom

2. Barts Heart Centre, England, United Kingdom

3. MRC Clinical Sciences Centre, London, England, United Kingdom

4. Imperial College London, London, England, United Kingdom

5. MRC - Clinical Sciences Centre, London, England, United Kingdom

6. Imperial College London, London, United Kingdom

7. Imperial College London, United Kingdom

8. Barts Heart Centre, London, United Kingdom, CARDIFF, Wales, United Kingdom

9. National Heart, Lung, and Blood Institute, Bethesda, MD

10. University College London, United Kingdom

11. MRC London Institute of Medical Sciences, England, United Kingdom

12. UCL, United Kingdom

13. UCL, England, United Kingdom

14. Barts Heart Centre and University College London, England, United Kingdom

Background: Aortic stenosis (AS) is associated with asymmetric and variable LV remodeling before and after aortic valve replacement (AVR), with residual LVH associated with a worse prognosis in women. Global LV mass does not capture regional differences, so we explored early differences and the influence of gender on remodeling using a 3D computational approach.

Methods: 116 patients with symptomatic severe AS referred for AVR (54% male, 70±10years, AVAi 0.4±0.1cm^2) underwent clinical, echocardiography and CMR evaluation before and one year post AVR (RELIEFAS, NCT02174471). Segmentation and co-registration of 2D SSFP short axis cine acquisitions was used to produce 3D computational models of wall thickness and geometry. Computed global LV mass was indexed (LVMi) for body surface area (BSA). Perioperative changes were analysed by gender, and compared with age, gender and BSA matched healthy controls. Groups were compared by *t* tests and analysis of covariance, with p values corrected for false discovery rate.

Results: Patients with AS had increased LVMi than matched controls, mean difference 19.4g/m^2 (CI: 12.8-26.1 g/m^2), with greater wall thickness in 86% of the LV. AS was associated with septal concentric and lateral eccentric LV hypertrophy (Figure 1). Pre-operatively, AS subjects with normal global mass and geometry (n=17, 82% female, mass:volume < 1.15) had similar LVMi to matched controls, but greater infero-septal wall thickness pre-operatively (45% ventricular surface). The greatest reductions in LVMi post-operatively were localized to this region, but it remained relatively hypertrophied (29% ventricular surface) compared to matched controls. Male patients with AS had higher LVMi than females pre-operatively (93.8±22 g/m^2 vs 73.2±21.5 g/m^2, p<0.001), most marked in the inferoseptum. Post-operatively, septal relative wall thickness reduction was significantly greater in males than females (-15±11% vs -9±13%, p = 0.03) though the difference in LVMi was non significant (-17±16g/m^2 vs -10±20 g/m^2 p =0.059), Figure 2. Gender differences in % septal remodeling remained after accounting for age and change in valvuloarterial impedance (standardized ß= -0.24, p= 0.009).

Conclusion: 3D computational modeling reveals regionality and gender differences in LV hypertrophy and its regression following AVR, missed by conventional approaches. Patients with AS with normal conventional measures of geometry have a relatively hypertrophied inferoseptum, which regresses but does not normalize post AVR. Males have greater relative regression in septal wall thickness post AVR, and this may contribute to the disparity of outcomes post operatively.

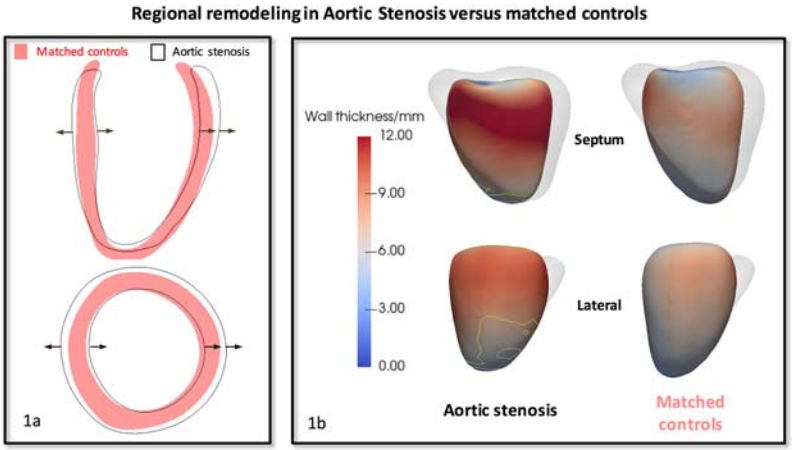

Figure 1a Ventricular four chamber and short axis cross-cuts showing a regional response of septal concentric and lateral eccentric hypertrophy (black contour = AS; red= matched controls). Figure 1b Mean shape and wall thickness in patients with aortic stenosis (left) and age, gender, BSA matched healthy volunteers (right). Red = thicker wall (mostly septal). Within yellow contour p values are < 0.05, 86% ventricular surface.

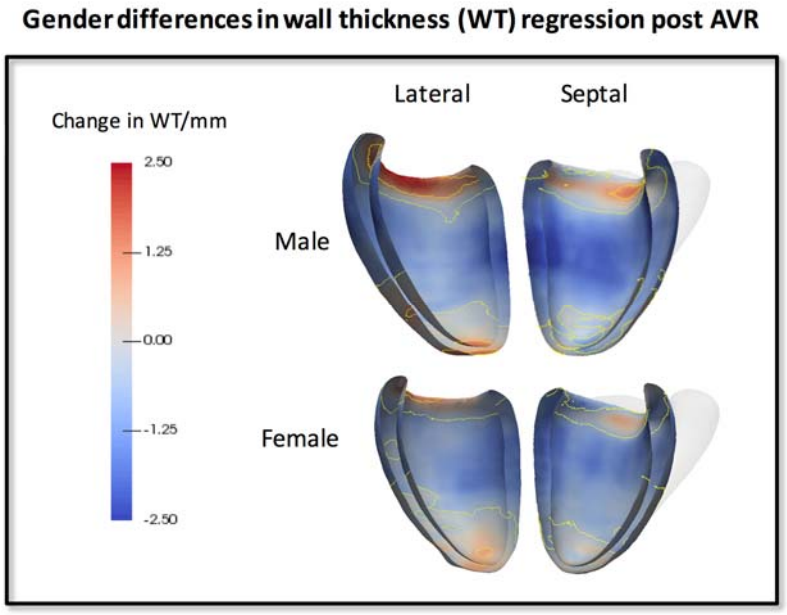

Figure 2 Average shape pre AVR for males (top) and females (bottom) for the lateral and septal walls (left and right). The colour represents the change in wall thickness (WT) after AVR, showing relatively more septal regression in males than females. Yellow contour represents p values < 0.05 for the change perioperatively for each gender (72% and 62% of the ventricle surface for males and females respectively, p< 0.05).

ID#: 371688

Treatment Effects of Chaperone Therapy with the Novel Oral Drug Migalastat on Cardiac Involvement in Fabry Disease

Jonas Müntze, MD[1] Tim Salinger, MD[2], Daniel Oder, MD[3], Kathrin Roblick, MD[3], Stefan Frantz, MD[3], Christoph Wanner, MD[3], Peter Nordbeck, MD[3]

1. Department of Internal Medicine I and Comprehensive Heart Failure Center, University Hospital Wuerzburg, Wuerzburg, Bayern, Germany

2. Department of Internal Medicine I and Comprehensive Heart Failure Center, University Hospital Wuerzburg, Bayern, Germany

3. Department of Internal Medicine I and Comprehensive Heart Failure Center, University Hospital Wuerzburg, Germany

Background: Fabry disease is an X-linked lysosomal storage disorder with versatile organ involvement. Cardiac symptoms manifest with myocardial hypertrophy and diffuse fibrosis, leading to progressive heart failure. Since 2001, enzyme replacement therapy has been available for specific treatment [1]. However, with regard to laborious intravenous delivery of enzyme replacement and highly varying genotypes as well as phenotypes [2], new drugs are warranted. Since June 2016, the chaperone Migalastat represents a novel oral form of specific therapy. This small molecule has been shown to stabilize the mutated α-galactosidase A (AGAL) in patients with Anderson-Fabry disease. Clinical impact on myocardial integrity is yet unknown.
This is a prospective monocentric study to evaluate cardiac integrity over time in patients with amenable AGAL mutations receiving Migalastat.

Methods: Until then, Migalastat therapy was initiated in a total 16 patients. All patients receive comprehensive characterization of cardiac morphology and function at baseline. First follow-up visit after begin of Migalastat therapy is scheduled after 3 months (FU 1), another after 12 months (FU 2). FU 1 include additional short-term diagnostics, FU 2 represents a regular annual examination with inpatient stay of 2 days. Patients receive cardiac MRI at baseline and FUP with early and late Gadolinium contrast if not contraindicated. Furthermore, several serum biomarkers such as AGAL activity and lyso-GB3 in leucocytes are monitored before therapy and with every follow-up.

Results: At FU 1, initial results from the first 10 patients suggest swift beneficial effects of Migalastat therapy on pain symptoms as well as cardiac morphology, reducing the myocardial mass index, measured by echocardiography, from 115.2±44 to 98.1±42 g/m² (p=0.001). MRI-measured myocardial mass index decreased from 156 to 115 g/m² in the first patient after 12 months of therapy. No significant change in myocardial fibrosis, as measured by late gadolinium enhancement, could be observed. Renal parameters remained stable with a GFR (MDRD) decrease from 91.1±30 to 82.1±23 ml/min/1.73 m² (p=0.017). Lyso-GB3 in leucocytes did not change significantly (11.0 vs. 12.40 ng/ml). Enzyme activity changed from median 0.06 (0.04 – 0.16) to 0.25 (0.06 – 0.37) nmol/min/mg proteine (p=0.33). None of the patients reported any side effects of the medication. With several additional patients anticipated to initiate Migalastat therapy, related follow-up visits over the next months at FAZiT will be included in further study analyses.

Conclusion: These first post-approval data suggest that oral chaperone therapy in Fabry disease can be a well-tolerated feasible alternative to enzyme replacement therapy in Fabry disease. Particularly positive effects include a swift decline in myocardial hypertrophy, detectable only several weeks after therapy initiation. Additional information on more subtle effects investigated by multiparametric imaging in amenable patients will be available after analysis of additional FU appointments in the near future.

References:

1. Oder D, Nordbeck P, Wanner C. Long Term Treatment with Enzyme Replacement Therapy in Patients with Fabry Disease. Nephron. 2016;134(1):30-36.

2. Oder D, Uceyler N, Liu D, Hu K, Petritsch B, Sommer C, Ertl G, Wanner C, Nordbeck P. Organ manifestations and long-term outcome of Fabry disease in patients with the GLA haplotype D313Y. BMJ Open. 2016;6(4):e010422.

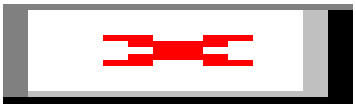

Reduction of the myocardial mass index (Echocardiography)

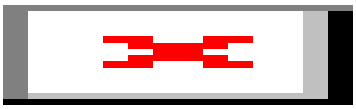

Cardiac MRI before start of therapy

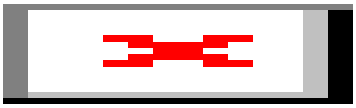

Cardiac MRI after 12 months of therapy

ID#: 371709

Diffuse myocardial fibrosis and coronary microvascular dysfunction are characteristic of HFpEF

Adrián I. Löffler, MD[1] Pelbreton C. Balfour, Jr., MD, MSc[2], Yang Yang, PhD[3], Daniel A. Auger, PhD[1], Moiz A. Nasir, BS[4], Christopher M. Kramer, MD[1], Li-Ming Gan, MD professor[5], Michael Salerno, MD, PhD[3]

1. University of Virginia Health System, Charlottesville, VA

2. University of Virginia Health System, Pensacola, FL

3. University of Virginia, VA

4. University of Virginia, Charlottesville, VA

5. Department of cardiology,Sahlgrenska University hospital, Hovås, Blekinge Lan, Sweden

Background: Heart failure with preserved ejection fraction (HFpEF) accounts for about 50% of HF cases with a mortality rate similar to HF with reduced EF. Despite this, evidence-based therapies for HFpEF are limited. The pathophysiology is poorly understood but may involve alterations of the extracellular matrix and systemic inflammation resulting in coronary microvascular dysfunction (CMD). CMR may enable better characterization of HFpEF and potentially help develop new therapies.

Methods: A single center pilot study, using a 1.5 T Siemens scanner, was performed to quantify diffuse myocardial fibrosis, MPR, and diastolic dysfunction in patients with HFpEF. SSFP cine was used to determine left ventricular (LV) function, LV mass, and LV volumes. LGE imaging and MOLLI T1 mapping was used to assess fibrosis and to calculate extracellular volume (ECV). Quantitative first-pass perfusion imaging, using a dual sequence approach, was used to calculate MPR (Figure 1). Spiral cine DENSE was used to calculate myocardial strain. Echocardiograms, cardiopulmonary exercise testing, and BNP were also obtained. Patients with LV EF < 45%, prior MI, pericardial disease, infiltrative cardiomyopathy, severe valvular disease, and known secondary cause of hypertension were excluded. T-tests and Fisher';s exact testing were used for comparing continuous and categorical variables respectively.

Results: 15 patients with HFpEF (age 64 ±11 years, 10 female) were compared to 10 normal (age 56 ±7 years, 4 female) controls as shown in Table 1. As expected, HFpEF patients had a higher incidence of hypertension ($p < 0.01$), higher PASP ($p < 0.01$), higher average E/e'; ($p < 0.01$), and lower VO2 max ($p = < 0.01$). Key CMR findings in HFpEF patients were a higher ECV ($p < 0.01$) and lower global MPR ($p < 0.01$). Of note, in this cohort there were no differences in LVEF ($p = 0.91$), LV mass index ($p = 0.64$), native T1 ($p = 0.70$), peak average circumferential strain ($p = 0.90$), or early diastolic circumferential strain rate ($p = 0.90$).

Conclusion: This cohort of HFpEF patients with mean EF>60%, absence of left ventricular hypertrophy, and normal strain parameters, had more diffuse fibrosis and impairment in global MPR suggestive of CMD. Reduction in global MPR is a known poor prognostic indicator. Future research is needed to develop specific therapies targeting fibrosis and perfusion in the HFpEF population.

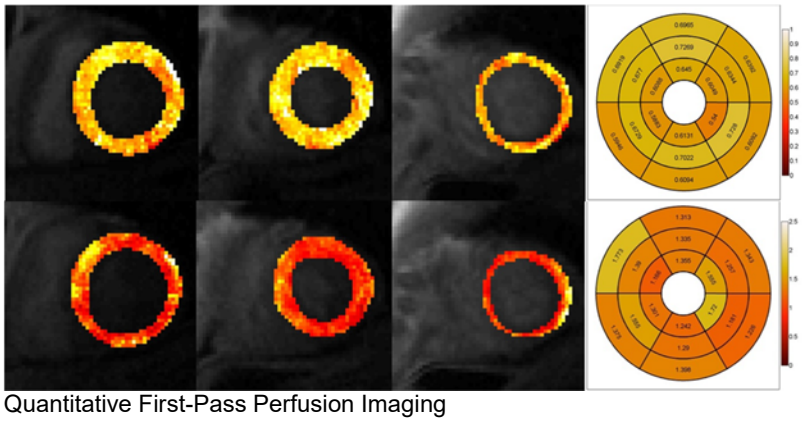

Quantitative First-Pass Perfusion Imaging

Table I. Clinical, CMR, Echocardiogram, and Stress test parameters comparing HFpEF subjects and Controls

	HFpEF (n=15)	Normal (n=10)	P value
Age (years)	64 ± 11	56 ± 7	0.04
Female sex	10 (67%)	4 (40%)	0.24
Caucasian	10 (67%)	10 (100%)	0.06
Hypertension	14 (93%)	2 (20%)	<0.01
BNP (pg/mL)	168 ± 161	21 ± 25	<0.01
Hematocrit (%)	37 ± 4	44 ± 5	<0.01
Left Ventricular Ejection Fraction (%)	62 ± 9	63 ± 7	0.91
Left Ventricular Mass index (g/m^2)	46.6 ± 15.5	44.0 ± 8.9	0.64
Peak average circumferential strain	-0.17 ± 0.04	-0.16 ± 0.03	0.90
Average e'_{SR} (s^{-1})	1.28 ± 0.79	1.59 ± 0.71	0.90
Native T1 (ms)	1038 ± 81	1027 ± 45	0.70
Extracellular volume	0.30 ± 0.04	0.25 ± 0.04	<0.01
Global myocardial perfusion reserve	1.94 ± 0.36	3.31 ± 0.41	<0.01
PASP on echocardiogram (mmHg)	38 ± 12	20 ± 3	<0.01
Average E/e';	14.1 ± 5.8	7.6 ± 2.9	<0.01
VO_2 max	14.6 ± 2.8	31.4 ± 7.0	<0.01

Continuous variables are reported as mean (SD).
Categorical variables are reported as frequency (%).
e'_{SR} = early diastolic circumferential strain rate.

ID#: 371718

Late enhancement and reverse left ventricular remodeling in percutaneous edge-to-edge mitral repair

Bernard P. PaelinckHiske Brouwer, Marc den Heijer, Dina De Bock, Tom Vandendriessche, Paul M. Parizel, Inez Rodrigus, Marc J. Claeys

Antwerp University Hospital, Belgium

Background: Percutaneous edge-to-edge repair with MitraClip is considered an alternative to surgical mitral valve repair in symptomatic severe mitral regurgitation at very high surgical risk. We aimed to evaluate the impact of myocardial late enhancement on reverse left ventricular remodeling following MitraClip.

Methods: Consecutive patients scheduled for MitraClip were prospectively studied. CMR (3.0 Tesla) and echocardiography were performed before MitraClip and at 6 months follow-up. Short-axis SSFP CMR images and late gadolinium enhancement short-axis CMR images covering the left ventricle were acquired. Mitral insufficiency was graded using color Doppler flow mapping (grade 1-4). ROC analysis was performed.

Results: Fifty-two patients underwent MitraClip procedure. Patients were excluded from the study due to contraindications for CMR (ICD, CRT, pacemaker) (n=19), due to renal insufficiency (glomerular filtration rate< 30 ml/min/1.73 m²) (n=5) and due to poor image quality (off-resonance artefacts MitraClip, insufficient respiratory cooperation, irregular heart rhythm) (n=14). Finally, 14 patients (75 years (range 66-83 years; M/F: 6/8); at high surgical risk (EuroSCORE II 4% (2-18,8 %)) with symptomatic severe (grade 3 or 4) mitral regurgitation (functional/degenerative/mixed n=12/1/1), left ventricular enddiastolic volume: 251 ml (102-448 ml); left ventricular EF 31% (16-60%)) were included in the study. In these patients MitraClip reduced the degree of mitral regurgitation (residual grade 1 (n=3), grade 2 (n=8) and grade 3 (n=3)). In 4 patients reverse left ventricular remodeling (left ventricular endsystolic volume reduction >10%) occurred. Late enhancement <16% predicted reverse left ventricular remodeling, while ≥16% predicted absence of reverse left ventricular remodeling. In 4 patients MACE occurred (mitral valve replacement n=1, death n=3), including one patient with reverse left ventricular remodeling.

Conclusion: CMR in patients requiring percutaneous edge-to-edge mitral repair is hampered by CMR contraindications (devices and renal insufficiency) and insufficient image quality (patient-related, MitraClip). In this pilot study, following MitraClip, no change of left ventricular volumes was measured at 6 months follow-up in patients with ≥16% myocardial late enhancement. Short-term reverse left ventricular remodeling at 6 months follow-up occurred in patients with <16% myocardial late enhancement.

ID#: 371675

CMR feature tracking for characterization of patients with heart failure with preserved ejection fraction.

Haruno Sakuma, MD[1]Masaki Ishida, MD, PhD[2], Yoshitaka Goto, MD[3], Wakana Makino, MD[1], Kakuya Kitagawa, MD, PhD[2], Yasutaka Ichikawa, MD, PhD[2], Taku Omori, MD[2], Kaoru Dohi, MD, PhD[2], Hajime Sakuma, MD, PhD[4]

1. Mie University Hospital, Tsu, Mie, Japan

2. Mie Universtiy Hospital, Japan

3. Department of Radiology, Mie University Hospital, Tsu, Mie, Japan

4. Department of Radiology, Mie University Hospital, Mie, Japan

Background: Heart failure with preserved ejection fraction (HFpEF) is a prevalent and growing public health problem. Although the pathophysiology of HFpEF is multifactorial, LV diastolic dysfunction, which is characterized by LV stiffness and relaxation, is the main cause of HFpEF. Previous studies demonstrated that LV extracellular volume fraction (ECV) is a noninvasive indicator of the LV stiffness. Another recent studies employing speckle-tracking echocardiography indicated that systolic function measures such as LV longitudinal strain (LS) are frequently abnormal in HFpEF patients. In addition, abnormal LS is of value to identify patients with HFpEF at high risk for cardiovascular events. However, the association between LS and indices of diastolic function by cardiac catheterization has not been fully investigated. CMR feature tracking technique allows for the reproducible assessment of LS from routine clinical cine MR images. However, the value of CMR feature tracking in identifying HFpEF patients with abnormal LS has not been investigated. Consequently, the purposes of the current study were to determine the prevalence and severity of GLS impairment in patients with HFpEF by using CMR feature tracking, and to evaluate the correlation between GLS measured by CMR feature tracking and invasive diastolic functional indices.

Methods: Eighteen patients with HFpEF and 18 age- and sex-matched control subjects were studied. Exclusion criteria included CAD, valvular disease, HOCM, sarcoidosis and amyloidosis. All subjects underwent cine CMR and pre- and post-contrast T1 mapping. In addition, invasive pressure-volume loops were obtained to evaluate LV diastolic properties in HFpEF patients. GLS and ECV were quantified from cine CMR and from pre- and post-contrast T1 mapping and hematocrit using cvi42, respectively.

Results: GLS was significantly impaired in HFpEF patients (-14.6±3.8%) than controls (-19.1±1.8%, p=0.0005) (Fig 1). Sixty-one percent (11/18) of HFpEF patients showed impaired GLS with the cut-off of -15.6%. HFpEF patients showed higher ECV (33.0±4.1%) compared with controls (29.7±3.9%, p=0.06). In HFpEF patients, GLS was strongly correlated with LV relaxation constant (tau) (r=0.72, p=0.0007) but not LV stiffness constant (beta) (r=0.002, p=0.99) (Fig 2).

Conclusion: CMR feature tracking is a noninvasive approach that can identify subgroup of HFpEF patients who had impaired GLS. Altered GLS measured by CMR feature tracking is significantly related with indices of impaired LV relaxation determined by invasive cardiac catheterization. These finding suggested that feature tracking analysis of routine cine MRI may permit identification of subgroup of HFpEF patients who had impaired GLS and severer diastolic dysfunction.

Figure 1. Comparisons for GLS and ECV between HFpEF patients and control subjects

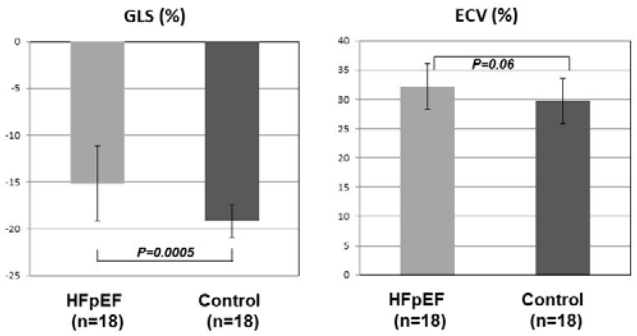

Figure 1. Comparisons for GLS and ECV between HFpEF patients and control subjects.

Figure 2. Correlations of CMR derived GLS with the LV relaxation constant (Tau) and LV stiffness constant (Beta) determined by cardiac catheterization in HFpEF patients.

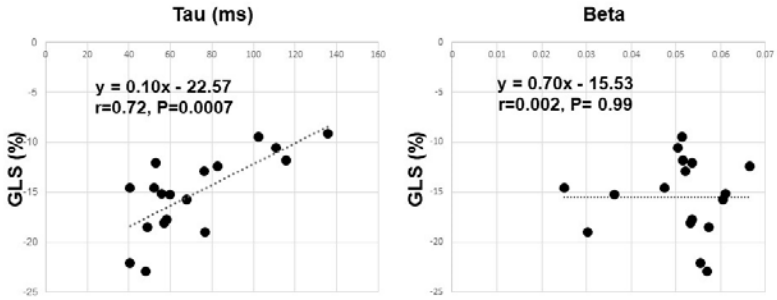

Figure 2. Correlations of CMR derived GLS with the LV relaxation constant (Tau) and LV stiffness constant (Beta) determined by cardiac catheterization in HFpEF patients.

ID#: 371799

Incremental Value of Extracellular Volume measured by cardiac magnetic resonance to Predict Reverse Remodeling in New Onset Non-ischemic Dilated Cardiomyopathy

Weihao Li, BMSci[1] Qing Zhang, MD[2], Yucheng Chen, MD[3]

1. Cardiology Division, West China Hospital, Sichuan University, Chengdu, Sichuan, China (People's Republic)

2. Sichuan University West China Hospital, China (People's Republic)

3. Sichuan University West China Hospital, Sichuan, China (People's Republic)

Background: Left ventricular reverse remodeling (LVRR) is regarded as an important surrogate marker in treated heart failure (HF) patients that implies a favorable outcome. Myocardial fibrosis detected by cardiac magnetic resonance (CMR) has becoming a new prognosticator in variety of heart diseases. Late gadolinium enhancement (LGE) and extracellular volume (ECV) for focal and diffuse fibrosis by CMR would predict LVRR in HF patients.

Methods: This study prospectively enrolled 116 patients (46 ± 15 years, 81% male) with newly diagnosed non-ischemic dilated cardiomyopathy (DCM) (HF symptoms ≤6 months, left ventricular ejection fraction (LVEF) ≤ 50% and left ventricular end-diastolic dimension (LVEDD) ≥ 55mm (male) or ≥ 50mm (female) by echocardiography at admission) and 45 age-matched normal subjects (46 ± 17 years, 60% male). Echocardiography and CMR were performed at baseline while echocardiography was repeated at 1-year follow up. LVRR was defined as a reduction in LVEDD of ≥10% and an increase in LVEF of ≥5%.

Results: LVRR occurred in 49 (42.2%) patients. The presence of LGE was found in 53 (45.7%) patients (LGE+, vs. LGE-). The ECV of ≥ 32.6% (derived from the normal subjects as mean+1.96SD) was observed in 48 (41.4%) patients (increased ECV, vs. normal ECV). The LVRR response rate was lower in the LGE+ than the LGE- group (17% vs. 63.5%), as well as in the increased ECV than the normal ECV group (20.8% vs. 57.4%) (Both $p<0.001$). When combined LGE and ECV measurement and divided the patients into 4 groups, the LVRR rate was the lowest in the patients with LGE+ and increased ECV while the highest in the patients with LGE- and normal ECV (10% vs. 73.3%, $p<0.001$). By multivariate logistic regression, the presence of LGE (OR: 0.075, 95% CI: 0.021-0.269, $p<0.001$), ECV (OR: 0.268, 95% CI: 0.081-0.881, $p=0.030$) and female gender (OR: 0.122, 95% CI: 0.023-0.633, $p=0.012$) were found to be independent risk factors of LVRR, adjusted for age, blood pressure and other clinical variables.

Conclusion: Both LGE and ECV for myocardial tissue characterization demonstrated their strength to predict LVRR in non-ischemic DCM patients over some conventional parameters.

ID#: 371951

CMR structural and fibrosis assessment predicts prognosis in chronic rheumatic valvular heart disease

Lilia M. Sierra-Galan, MD, MCvT[1] Angel L. Alberto-Delgado, MD[2], Julio C. Sauza-Sosa, MD[3], Fernanda Ortiz-Haro y Nassar, MD[4], Diego Reyes-Vazquez, MD[4], Alejandro Rey-Rodriguez, MD[3], Julio Lopez-Cuellar, MD[3], Ana-Camila Flores-Ventura, MD[5], Maria-Elena Soto, MD, PhD[6], Victor A. Ferrari, MD[7]

1. American British Cowdray Medical Center, CDMX, Distrito Federal, Mexico

2. Central Military Hospital, Mexico, City, Distrito Federal, Mexico

3. American British Cowdray Medical Center, Mexico, Distrito Federal, Mexico

4. American British Cowdray Medical Center, Mexico

5. Hospital de Diagnóstico. Clínica de Radiología BMP., San Salvador, San Salvador, El Salvador

6. American British Cowdray Medical Center, Mexico City, Distrito Federal, Mexico

7. Hospital of the University of Pennsylvania and Penn Cardiovascular Institute, Cardiovascular Division, Perelman School of Medicine, University of Pennsylvania, Philadelphia, PA, USA, Phila., PA

Background: Rheumatic heart disease (RHD) remains an important preventable cause of cardiovascular death and disability, with high disease rates in poor countries. Only rare data exist on myocardial involvement in chronic RHD, since echocardiography cannot assess the impact of myocardial fibrosis on outcomes. We performed a CMR evaluation of cardiac structural changes and fibrosis in patients with valvular heart disease (VHD) from RHD, vs. non-rheumatic VHD (NRHD).

Methods: A prospective IRB-approved CMR study of patients with VHD due to chronic RHD (G1), was designed to analyze cardiac structural changes and myocardial involvement with serial clinical follow-up compared to patients with NRHD (G2). Inclusion criteria were age >18 years, severe VHD, sinus rhythm and hemodynamically stability. If the patient went to surgery, a myocardial biopsy was retrieved. Exclusion criteria included the co-existence of known coronary artery disease (CAD). CMR-detected fibrosis was classified by presence and severity with a specifically designed score due to the diffuse and subtle presence of fibrosis in RHD, and confirmed by histology when possible. Statistical analysis; student T test and Pearson correlations.

Results: Twelve patients were included in each group with a mean follow-up of 26.9 $\pm$ 12.8 months, and mean age was 58 $\pm$ 15 for G1 and 54 $\pm$ 17 years for G2 (p=NS). VHD subtypes in G1 were: 5 mitral, 1 aortic, and 6 combined mitral and aortic; and G2: 2 mitral and 10 aortic. For chamber sizes, we found significant differences in left atrial size (LAS), G1: 58.3 $\pm$ 9.2 vs. 43.2 $\pm$ 6.0 mm, p=0.0001. Correlation of end-diastolic volume index with LV mass in G2 was (R=0.83) and in G1 (R=0.73) due to a weaker correlation in the mitral patients (R=0.18) and LV stroke volume index with LV mass in G1 in aortic patients (R=0.84) and in G2 (R=0.79). The stronger factors associated with surgical indication for mitral patients in G1 were NHYA functional class (R=0.80) and the presence of late gadolinium enhancement (LGE) (R=0.62), but not for aortic patients or G2. We eliminated 1 case from G1 for LGE analysis due to the development of renal failure (RF) after inclusion, and 3 from G2: one for development of RF and the other 2 due to previously unknown CAD. LGE was found in 100% of G1 and 82% of G2 (p=0.001), the maximum severity score for G1 was 25, and 15 points for G2 (p=0.006). In G1, 3 patients went to surgery and 2 in G2; histology confirmed myocardial fibrosis in the exact locations described by CMR in all 3 patients of G1. Mid-wall patchy LGE (MWPLGE) in G1 was 100% vs. 0% of G2 (p=0.0003). Mid-wall linear intramural LGE (MWLILGE) was similar in G1 (55%) and G2 (33%) (p=NS). MWLILGE was associated only in G2 with LAS (R=0.71), and with the indication for surgery only for G2 (R=0.56). MWLILGE was associated with aortics in G1 to LV mass (R=0.98) and to NYHA functional class. MWPLGE was associated only for mitrals in G1 to LV mass (R=0.98) and further to NHYA (R=0.62) and surgical indication (R=0.80). During the follow-up period 3 patients had MACE in both groups but only 1 patient died in G2.

Conclusion: This is the first study of the impact of structural and myocardial involvement in VHD due to RHD on patient outcomes. VHD from RHD causes distinctly different cardiac changes and myocardial involvement than degenerative VHD, with important prognostic impact. CMR has excellent correlation with histopathologic fibrosis, and may play a major role in diagnosis, prognosis and treatment of RHD-related VHD.

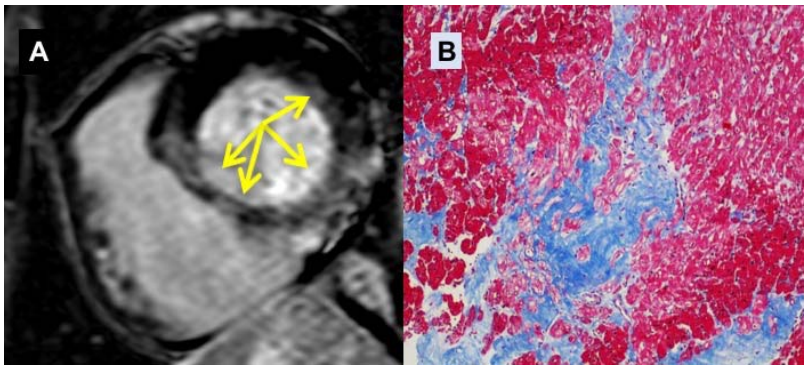

(A) LGE basal short-axis view showing diffuse, patchy LGE in a G1 patient confirmed by surgical biopsy shown in (B) stained with Masson's Trichrome. Fibrosis is shown in blue color.

ID#: 372050

Combining Native T1 Mapping and 3D Strain Analysis for Cardiac Amyloidosis Phenotyping

Alessandro Satriano, Ph.D.[2]Na'ama Avitzur, BscH[1], Muhammad Afzal[3], Mariam Narous[4], Yoko Mikami, MD, Ph.D.[5], Jacqueline A. Flewitt, MSc[2], Bobby Heydari, MD, MPH[5], Carmen P. Lydell, MD[2], Andrew G. Howarth, MD, Ph.D[5], Nowell M. Fine, MD, M.Sc.[6], James White, MD, FRCP(C)[5]

1. Cumming School of Medicine, University of Calgary, Canada

2. Stephenson Cardiac Imaging Centre, Libin Cardiovascular Institute of Alberta, University of Calgary, Calgary, AB, Canada

3. Stephenson Cardiac Imaging Centre, AB, Canada

4. University of Alberta, Canada

5. Stephenson Cardiac Imaging Centre, Libin Cardiovascular Institute of Alberta, University of Calgary, AB, Canada

6. Libin Cardiovascular Institute of Alberta, AB, Canada

Background: Native T1 mapping has been investigated as a non-contrast alternative for the identification of amyloid protein deposition in patients with suspected cardiac amyloidosis (CA). Strain based analyses have similarly been proposed for this purpose. As both may be achieved from a single, rapid MRI protocol we investigated relationships between these markers in patients with confirmed CA. Specifically, we studied the relationship between regional amyloid protein burden (measured by native T1) and changes in global and local tissue deformation (measured by 3D feature-tracking strain).

Methods: Twenty patients with confirmed CA were recruited and underwent a standardized CMR imaging protocol (3T), including multi-planar cine imaging, and basal and mid short axis native T1 maps using a Shortened Modified Look-Locker Inversion recovery (ShMOLLI) sequence. Left ventricular (LV) function, mass and native T1 (globally and segmentally) were measured using cvi^{42} (Circle Cardiovascular Imaging Inc.). 3D strain analysis was performed using in-house validated software (GIUSEPPE) in all directions of deformation at subendocardial, sub epicardial and transmural layers (globally and segmentally).

Results: The mean age was 70.4 ± 7.9 years (9 patients had light-chain, and 11 had transthyretin-related amyloidosis). The mean LVEF was 57.0 ± 13.1% with a mean LV mass index of 79.9 ± 29.7 g/m2. As per inclusion criteria, all patients showed diffuse myocardial enhancement by LGE. The mean native T1 (global) was 1311.55±108.6 ms while segmental native T1 values ranged from 886 to 1588 ms. Global longitudinal, circumferential, and maximum principal strain measures were -8.1±2.9%, -9.2±3.4%, and 41.7 ± 23.4% respectively. Segmental strain analysis demonstrated an apical sparing pattern for most deformation directions, the apical:basal strain ratio being significant at 1.5±0.5 (p=0.009) and 2.0±0.7 (p=0.002) for circumferential and maximal principal strain. Strong and significant relationships were found between 3D strain and native T1, both globally and segmentally (Table 1). At segmental level, the highest correlations were found for circumferential and maximum principal strain (p<0.0001).

Conclusion: Among patients with confirmed CA, regional amyloid protein burden (as measured by native T1 mapping) is associated with a progressive reduction in segmental deformation when measured by 3D feature tracking based strain analysis. This relationship was observed for multiple directions of deformation and was consistently demonstrated at both a global and segmental level. These findings provide cross-validation of these respective non-contrast imaging techniques in patients with CA. Whether their combined consideration may improve the accuracy of non-invasive screening for detection of CA remains to be studied within a larger cohort.

Parameter	R (Global)	P-Value (Global)	R (Segmental)	P-Value (Segmental)
Circumferential				
Subendocardium	0.6100	**<0.005**	0.4043	**<0.0001**
Subepicardium	0.7634	**<0.0001**	0.3943	**<0.0001**
Transmural	0.6782	**0.001**	0.4250	**<0.0001**
Longitudinal				
Subendocardium	0.6024	**<0.005**	0.3164	**<0.0001**
Subepicardium	0.7166	**<0.0005**	0.3221	**<0.0001**
Transmural	0.6682	**0.001**	0.3487	**<0.0001**
Radial				
Transmural	-0.3514	0.13	-0.3335	**<0.0001**
Minimum				
Subendocardium	0.6120	**<0.005**	0.4000	**<0.0001**
Subepicardium	0.6886	**<0.001**	0.2931	**<0.0001**
Transmural	0.6823	**<0.001**	0.3964	**<0.0001**
Secondary	0.3148	<0.018	0.1863	**<0.005**
Subendocardium	0.6253	**<0.005**	0.2278	**0.0005**
Subepicardium	0.5582	**0.01**	0.2428	**<0.0005**
Transmural				
Maximum	-0.5117	**<0.05**	-0.4599	**<0.0001**
Transmural				
Thickness	0.4162	0.07	0.3807	**<0.0001**

Table1: Linear Association between Native T1 and Strain Parameters (and Thickness).

ID#: 372062

Highly-Accelerated Simultaneous Multi-Slice CMR Using Outer Volume Suppression: Time-Efficient Characterization of Cardiac Function in A Single Breath-hold

Mehmet Akçakaya, Ph.D.[4]Sebastian Weingärtner, Ph.D.[1], Steen Moeller, Ph.D.[2], Sebastian Schmitter, Ph.D.[3]

1. Electrical and Computer Engineering, University of Minnesota; Center for Magnetic Resonance Research, University of Minnesota; Computer Assisted Clinical Medicine, Heidelberg University, Minneapolis, MN

2. University of Minnesota, Minneapolis, MN

3. Medical Physics and Metrological Information Technology, Physikalisch-Technische Bundesanstalt, Berlin, Germany, Berlin, Germany

4. Electrical and Computer Engineering, University of Minnesota; Center for Magnetic Resonance Research, University of Minnesota, Minneapolis, MN

Background: Cardiac magnetic resonance imaging is the clinical gold standard for assessment of cardiac function, routinely performed in most cardiac MRI protocols. However, covering the entire ventricle necessitates long scan-times with conventional methods, leading to increased patient discomfort and associated health-care costs [Hendel et al. JACC 2016]. Simultaneous multi-slice (SMS) imaging [Larkman et al. JMRI 2001] has been proposed for scan acceleration, by simultaneously exciting multiple slices and reconstructing these using coil information. The use of band shifts, as in CAIPIRINHA, has improved noise amplification in SMS imaging [Breuer et al. MRM 2005]. However, unfavorable coil geometries in cardiac applications limit the SMS acceleration compared to neuroimaging. In this study we sought to increase SMS imaging factors for cine imaging, by using CAIPIRINIHA band shifts in combination with a fast low-SAR outer-volume suppression (OVS) scheme to reduce inter-slice leakage.

Methods: Sequence: The proposed sequence uses retrospectively-gated FLASH imaging. SMS is enabled using an excitation pulse consisting of the sum of multiple sinc-shape pulses with different center frequencies, to simultaneously excite multiple slice locations. To increase dissimilarity between slices, spatial shifts are induced as proposed in CAIPIRINHA, using variational phase cycling of the RF pulses for each slice. OVS is achieved using interleaved regional saturation pulses to saturate chest and back signals on both sides of the heart (Fig. 1). To minimize the magnetization disruption induced by OVS pulses, both slabs are simultaneously saturated using a multi-band (MB) excitation.
Imaging Experiments: Imaging was performed in healthy subjects at 3T. For a time-efficient protocol, cine images were acquired after contrast injection. The following imaging parameters were employed: TR/TE/FA=4.3/2.1ms/12°, FOV=320x320mm2, resolution=1.7x1.7mm2, slice thickness=6mm, temp. resolution=41ms, breath-hold duration=15-17s, saturation slab=150 mm (each side, 2.4ms assymmetric sinc), RF peak shift = 15% [Auerbach et al. MRM 2013].

Results: Example images demonstrating the efficacy of MB-OVS in a single slice show thorough elimination of the chest and back signal, while maintaining high image quality in the selected slab around the heart (Fig. 2). Example images show excellent image quality with 5-fold SMS-accelerated cine images, when using the proposed OVS. Sharp delineation between the blood-pool and the myocardium in all slices facilitate functional assessment. On the other hand pronounced aliasing artifacts detriment the image quality of SMS cines without OVS due to high inter-slice leakage, precluding clinical evaluation.

Conclusion: The proposed technique enables multi-band acquisition of five slices. SMS acquisition of these slices ensure equal spacing and homogeneous coverage, minimizing sampling induced error in cardiac volumetry. This ultimately allows whole LV coverage with ten slices in a single breath-hold, without compromising temporal resolution, or image quality.

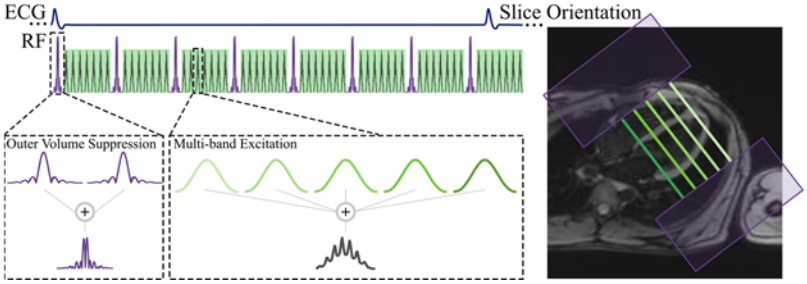

Sequence diagram depicting the proposed sequence for OVS multi-band cine imaging. Slice excitation is performed

with a pulsed obtained as the sum of five sinc-pulses at different center frequencies (green). These excitation pulses are interleaved with a multi-band rest-slab, simultaneously saturating two slabs one on each side of the heart (purple). Exemplar orientations of the slices and the rest slabs are indicated in the right panel.

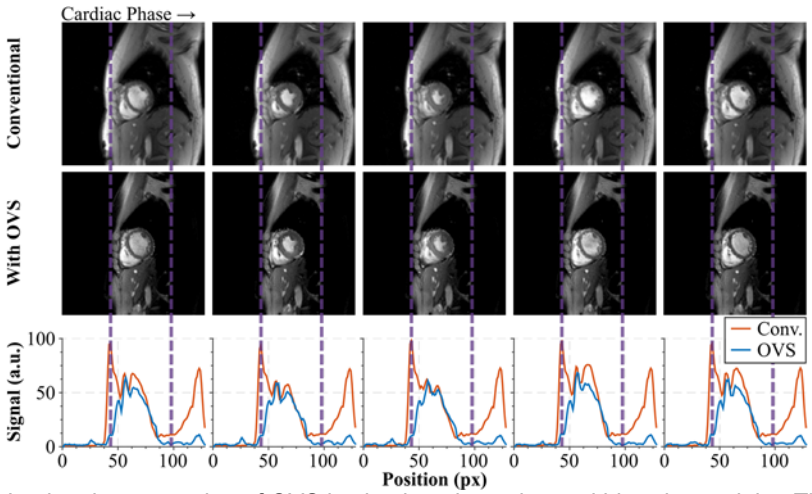

In-vivo demonstration of OVS in cine imaging using multi-band rest-slabs. The top row shows single slice FLASH cine imaging without and the middle row Cine images with interleaved multi-band rest slabs. The bottom row depicts signal intensity average across a box around the heart from anterior to posterior. Purple lines indicate the areas of saturation. Thorough suppression of signal outside the purple lines is achieved with the multi band rest slabs, leading to substantially lowered signal intensity, especially in the areas of chest and back. These images were acquired before contrast administration.

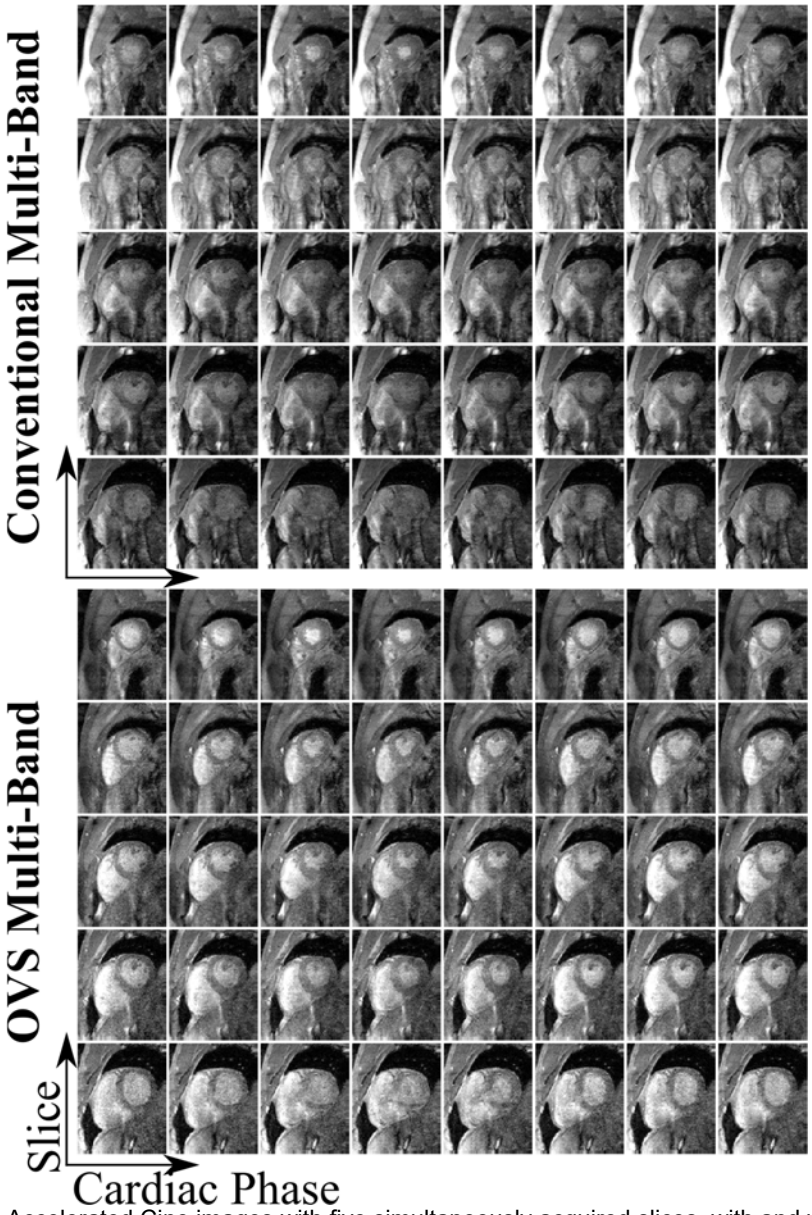

Accelerated Cine images with five simultaneously acquired slices, with and without interleaved OVS pulses. Substantial residual fold-over detriments the image quality when not using OVS pulses resulting in sub-clinical image quality. No residual fold-over is observed when using OVS pulses, providing clear myocardium blood interfaces suitable for cardiac volumetry.

ID#: 372089

4D Flow Evaluation of Altered Flow Patterns in Patients with Pulmonary Hypertension

Julio Garcia, PhD[2]Berkeley Scott[1], Jacqueline A. Flewitt, MSc[3], Jason Weatherald, MD[1], Israel Belenkie, MD[4], Carmen P. Lydell, MD[3], Andrew G. Howarth, MD, Ph.D[5], Bobby Heydari, MD, MPH[5], Michael Bristow, MD[5], John V. Tyberg, MD, PhD[2], James White, MD, FRCP(C)[5]

1. University of Calgary, AB, Canada

2. University of Calgary, Calgary, AB, Canada

3. Stephenson Cardiac Imaging Centre, Libin Cardiovascular Institute of Alberta, University of Calgary, Calgary, AB, Canada

4. University of Calgary, Canada

5. Stephenson Cardiac Imaging Centre, Libin Cardiovascular Institute of Alberta, University of Calgary, AB, Canada

Background: Pulmonary hypertension (PH) is a serious medical condition associated with significant morbidity and mortality. Recent advances in 4D flow MRI present new opportunities to explore novel markers in this population that may assist in evaluating therapeutic interventions or prognosis. In this pilot study we sought to evaluate the clinical feasibility of 4D flow MRI in patients with PH, describe patterns of flow, and describe their relationship to segmental flow quantification measures along the pulmonary arterial tree in addition to their influence on pulmonary arterial wall shear stress (WSS).

Methods: A total of 24 subjects, 11 with primary pulmonary hypertension (PHT) (age 24-85, mean 54, 9 female) and 13 healthy volunteers (age 24-77, mean 50, 2 female) underwent a standardized imaging protocol at 3 Tesla inclusive of cine and 4D flow imaging. A 3D phase contrast (PC) MRA was generated and used to visualize the pulmonary arterial tree and to label the following regions using pre-defined anatomic planes: right ventricle outflow tract (RVOT), ascending main PA, bifurcation of main PA, proximal LPA and proximal RPA (figure 1). 4D flow data was pre-processed and over-laid to allow analysis of each region for the presence of flow disturbances (vortical and helical) visually scored by streamline visualization, and 4D quantification of net flow, forward flow, peak velocity, retrograde flow and regurgitant fraction. Wall shear stress (WSS) was also calculated for the mPA, LPA and RPA regions, as shown in figure 3.

Results: Streamline visualization of all regions identified vortical flow in 64% of PH patients and 85% of healthy controls with a respective prevalence of helical flow in 18% and 31%. The appearance and location of vortices was different in PH patients with large, slowly precessing vortices in the main PA followed by small, faster preccessing vortices in the RPA. Normal subjects demonstrated small, fast precessing vortices in the main PA (figure 1D, top). Helical flow was rarely seen in the RPA of both normal and PH patients (figure 1D, bottom). Net forward flow was significantly reduced in PH versus controls (main PA: 25.2±0.01 vs 85.6±22.3 ml/beat, p=0.011). PH patients demonstrated greater asymmetry in net flow between the RPA and LPA with a ratio of 37.1±15.0 versus 30.3±14.3 in controls (p=0.25). Consistent with this we observed higher asymmetry in peak velocity (0.77±0.35 vs. 0.59±0.23, p= 0.007) and regurgitant flow (2.2±4.1 vs. 0.71±1.9, p= 0.034). WSS was 20% higher in the RPA versus LPA in PH patients while equally distributed in healthy controls.

Conclusion: 4D Flow was feasible in patients with PH and showed alterations in vortex location, size and rotational speed and resultant elevations in RPA flow and WSS. Whether such findings are contributory to, or a result of PA remodeling require further investigation.

Figure 1. 4D Flow visualization of the main pulmonary artery. A) x,y,z, vector component of 4D flow. B) magnitude component of 4D flow. C) Software designed computer segmentation of the mPA with 6 planes: RVOT, Bifurcation, LPA & RPA proximal, and LPA & RPA distal. D) Particle trace visualization of blood flow in the mPA, LPA and RPA using Ensight in a control (top) and PHT (bottom)

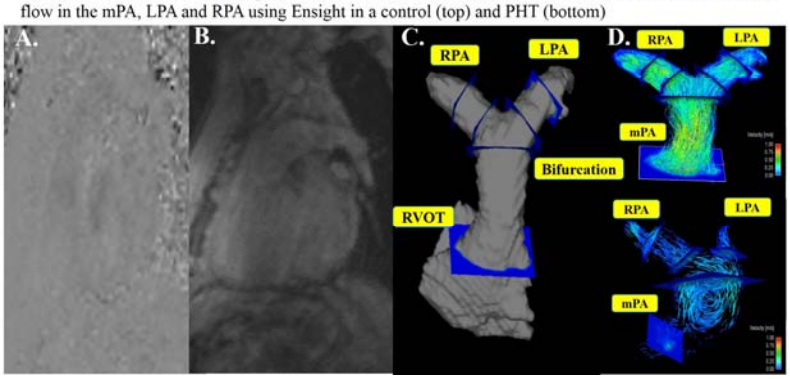

Figure 1

Figure 2. Evaluation of flow differences between the LPA & RPA using the total study population. Differences were evaluated in the left (white) and right (black) artery at the proximal planes (A,B) and distal planes (C,D). A) Net flow comparison between the LPAp and RPAp. B) Peak velocity comparison between LPAp and RPAp. C) Forward flow comparison at the LPAd and RPAd. D) Peak velocity comparison at the LPAd and RPAd. LPAp, proximal left pulmonary artery; RPAp, proximal right pulmonary artery; LPAd, distal left pulmonary artery; RPAd, distal right pulmonary artery.

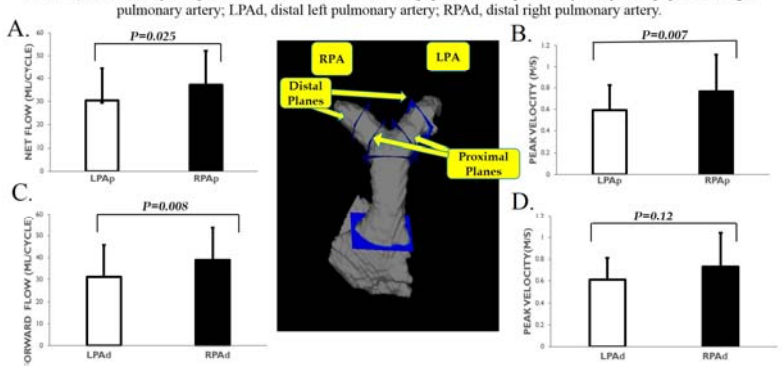

Figure 2

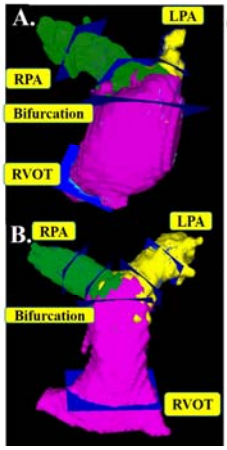

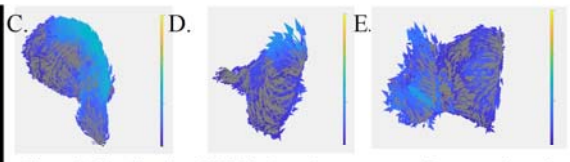

Figure 3. Visualization of WSS in the pulmonary artery. Segmentations of the main pulmonary artery in a PHT patient(A) and control (B) into three regions: mPA(purple), LPA(yellow) and RPA(green). Visualizations of WSS during systole (A-H) in the mPA (C and F), LPA (D and G), and RPA (E and H) were evaluated.

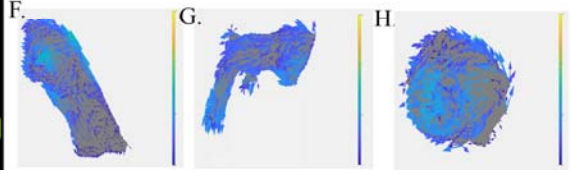

Figure 3

ID#: 371821

Normal Pediatric and Adult Regional Biventricular Myocardial Motion by Tissue Phase Mapping

Alexander Ruh, PhD[1] Kenny Sidoryk[2], Kai Lin, MD[1], Michael J. Rose, B.S.E[3], Joshua D. Robinson, MD, FACC[4], Cynthia K. Rigsby, MD, FACR[4], James Carr, MD[1], Michael Markl, PhD[1]

1. Northwestern University, Chicago, IL

2. Northwestern University

3. Ann & Robert H. Lurie Children's Hospital of Chicago, IL

4. Ann & Robert H. Lurie Children's Hospital of Chicago, Chicago, IL

Background: The assessment of both left (LV) and right ventricular (RV) motion is important for the understanding of the impact of heart disease on regional functional abnormalities of both cardiac chambers. CMR has emerged as a robust and reproducible imaging technique for the assessment of global and regional LV and RV function for analysis of changes in ventricular interactions in different cardiac pathologies. In this context, tissue phase mapping (TPM) allows for the quantification of regional myocardial velocities. However, previous studies have been limited to LV motion and data on pediatric and adult biventricular function is lacking. The goal of this study was thus 1) to develop TPM based analysis of myocardial velocities for both the LV and RV, 2) to assess the test-retest reproducibility of biventricular TPM, and 3) to establish normal regional biventricular velocity parameters in a cohort of pediatric and adult healthy volunteers.

Methods: Ten children (14±2y, 5m) and ten adults (44±16y, 7m) underwent standard CMR (1.5T Siemens Aera) including k-t accelerated (R=5) TPM using a black-blood prepared phase-contrast sequence with 3-directional velocity encoding in short-axis orientation (base, mid, apex; each in 1 breath-hold; in-plane res. = (1.6-2.4 mm)^2; temp. res. = 20-25 ms). To test reproducibility, all ten adults underwent a second TPM scan 15±5 days after the first. TPM data analysis included the delineation of RV and LV endo-/epicardial contours and calculation of time-resolved radial (v_r), circumferential (v_Φ), and long-axis (v_z) LV/RV velocities. For all components and slices the velocities were averaged over each ventricle to obtain global velocity time courses (Fig 3). For regional analysis, the velocities were also mapped onto an extended AHA model (16 segments for LV, 10 segments for RV, Fig 4). Systolic and diastolic peak velocities and times to peak (TTP) velocity were calculated for each segment and averaged over each ventricle to obtain global LV/RV peak values.

Results: Figure 1 depicts systolic and diastolic LV/RV velocities illustrating the feasibility of TPM for the assessment of biventricular motion in a 15-year-old pediatric subject. Bland-Altman plots show good agreement between segmental velocities of the two scans performed for the adults, Fig 2. Global velocity time courses (Fig 3) show similar cardiac motion dynamics for children and adults as well as for LV and RV. Quantitative differences were observed for diastolic peak values (Tab 1) with significantly reduced TTPs and increased peak velocities in children. Global peak velocities were significantly reduced and TTPs prolonged for the RV compared to the LV considering all subjects together (Tab 1). Figure 4 shows similar distributions of segmental peak velocities for LV and RV for both children and adults (decrease from base to apex, higher LV velocities). Notably, there was a significant inverse relationship between the increasing age and reduced diastolic LV v_r/v_z peak velocities ($r=0.69/0.78$, $p<0.001$) indicating generally reduced LV/RV velocities in adults compared to children (see also Tab 1). Moreover, diastolic v_r and v_z TTPs increase with age ($0.64<r<0.70$, $p<0.01$).

Conclusion: TPM enables a comprehensive analysis of global and regional biventricular myocardial motion with good reproducibility. Future studies are warranted to investigate the diagnostic value of TPM for the assessment of changes in biventricular motion in pediatric and adult patients with heart disease.

Fig. 1:
Myocardial in-plane velocity vector field mapped onto short-axis magnitude images (basal slice) of a representative pediatric subject (15y) during systole (left) and diastole (right).

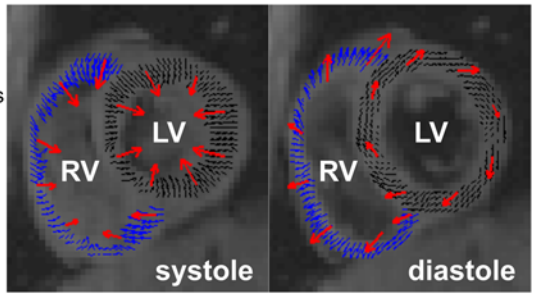

Fig. 2: Test-retest analysis for segmental peak velocities (LV and RV for systole and diastole = 520 data points) with Bland-Altman plots

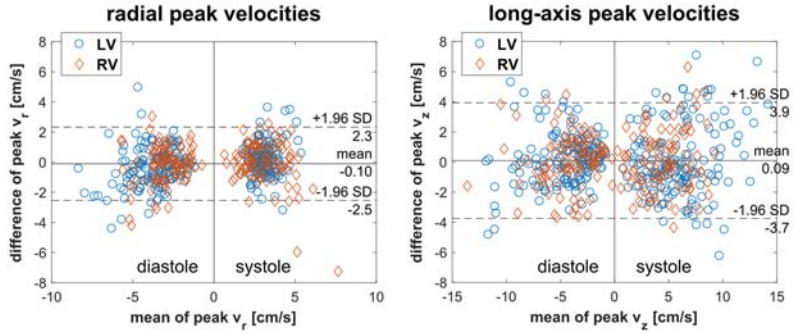

Fig. 3: Global radial (v_r), circumferential (v_Φ) and long-axis (v_z) velocity time courses (mean over all slices)

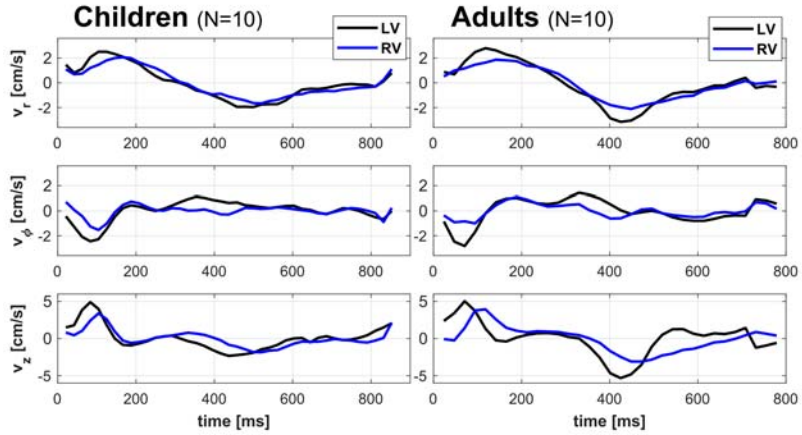

Fig. 4:

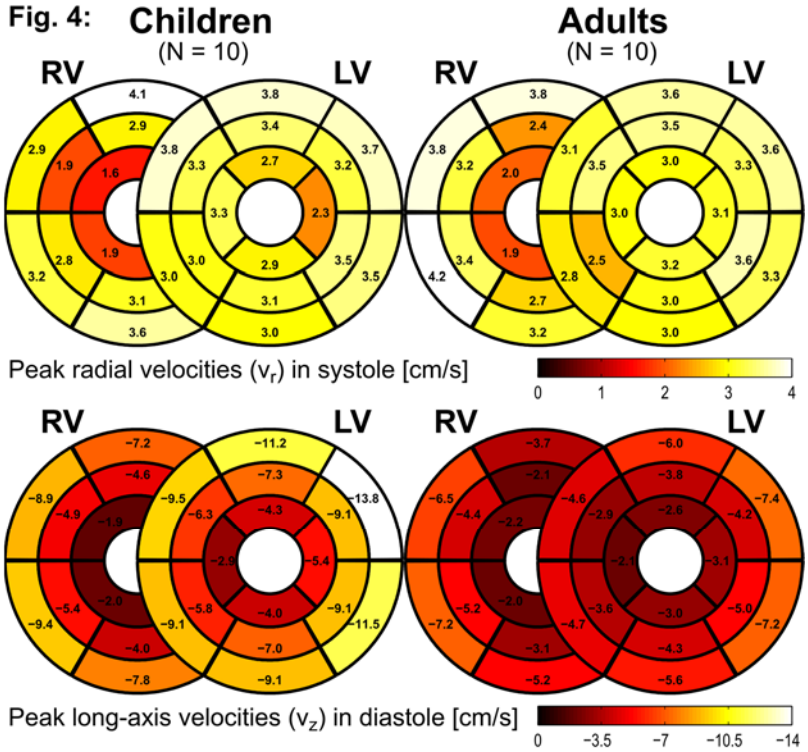

Tab. 1: Global values averaged over all segments

*p<0.05, **p<0.01		Left Ventricle		Right Ventricle		Children + Adults (N=20)	
		Children	Adults	Children	Adults	LV	RV
Peak v_r	Systole	3.2 ± 0.5	3.2 ± 0.4	2.8 ± 0.5	3.1 ± 0.5	**3.2 ± 0.5****	**2.9 ± 0.5****
[cm/s]	Diastole	**-5.0 ± 0.7***	**-3.8 ± 1.2***	-3.7 ± 0.9	-3.1 ± 0.7	**-4.4 ± 1.1****	**-3.4 ± 0.9****
Peak v_z	Systole	6 ± 2	6 ± 2	5 ± 2	5 ± 2	**6 ± 2****	**5 ± 2****
[cm/s]	Diastole	**-7.8 ± 1.5****	**-4 ± 2****	-6 ± 2	-4 ± 2	**-6 ± 2***	**-5 ± 2***
TTP v_r	Systole	121 ± 13	120 ± 30	140 ± 20	140 ± 20	**120 ± 20****	**140 ± 20****
[ms]	Diastole	**430 ± 30****	**490 ± 40****	**440 ± 40****	**510 ± 40****	460 ± 50	470 ± 50
TTP v_z	Systole	81 ± 7	90 ± 20	120 ± 30	110 ± 20	**86 ± 14****	**110 ± 20****
[ms]	Diastole	**420 ± 30***	**470 ± 40***	**450 ± 40***	**510 ± 60***	**450 ± 50****	**480 ± 60****

ID#: 371841

Effect of coffee consumption on cardiac structure and function from UK Biobank Imaging study

Kenneth Fung, MBBS MRCP[1] Nay Aung, MD, MRCP[1], Mihir M. Sanghvi, MB BS, BSc[1], Aaron Lee, PhD, MBBS[1], Jose Miguel Paiva, MSc[1], Elena Lukaschuk, MSc[2], Stefan Neubauer, MD, FRCP[3], Steffen E. Petersen, MD DPhil MPH FRCP[4]

1. William Harvey Research Institute, NIHR Cardiovascular Biomedical Research Unit at Barts, Queen Mary University of London, Charterhouse Square, London, EC1M 6BQ, UK, England, United Kingdom

2. University of Oxford, Oxford, England, United Kingdom

3. University of Oxford, England, United Kingdom

4. Queen Mary University of London, London, England, United Kingdom

Background: Coffee is widely reported to be the world';s most popular drink and the effect of its consumption on cardiovascular disease and outcomes has been of much interest and debate. But, there is currently no published data on its effects on cardiac structure and function.

This study aims to evaluate the association of coffee consumption and cardiac structure and function derived from cardiovascular magnetic resonance (CMR) imaging in the UK Biobank study.

Methods: This was a cross-sectional, observational cohort analysis of 5,065 UK Biobank participants who underwent CMR imaging that was previously analysed. Participants with known cardiovascular disease (angina, myocardial infarction and stroke), hypertension, arrhythmia, cardiomyopathy, hypercholesterolaemia and/or diabetes as well as those on medication for hypertension, high cholesterol and diabetes were excluded. Coffee consumption habits were recorded at the time of imaging and those recorded to drink >25 cups of coffee/day were excluded.

Association between coffee consumption and CMR-derived parameters of left ventricular (LV) structure and function were assessed using multivariate regression models adjusting for age, sex, ethnicity, Townsend deprivation index, current smoking, higher levels of education (university degree or professional qualification), height, weight, regular alcohol consumption (≥3 times/week), systolic blood pressure, resting heart rate and tea intake. Coffee consumption was analysed both as a continuous variable but also categorised into 5 groups (0, <1, 1-2, 3-4, ≥5 cups/day).

Results: Baseline characteristics of the 2,592 participants included in the final analyses are summarised in Table 1. Statistically significant increase in LV end-diastolic volume (LVEDV) and LV end-systolic volume (LVESV) are seen in those who consume ≥1 cup of coffee/day (Table 2). These effects are greatest in those who drink ≥5 cups/day. When coffee consumption is modelled as a continuous variable, each cup of coffee is associated with an increase of 0.57% (p <0.001) in LVEDV and 0.84% (p <0.001) in LVESV (Table 3).

Interestingly, the effect on LV mass is only significant in those with moderate coffee consumption (3-4 cups/day, effect estimate = 3.37%, p <0.001). Although the effect estimate on LVEF in those who drink 1-2 cups/day is statistically significant, the magnitude of the effect is small. There is no statistical significant effect seen on stroke volume.

Conclusion: No association is seen in low coffee consumption (<1 cup/day) with LV structure and function. Coffee consumption of at least 1 cup/day is associated with a very small increase in LVEDV and LVESV. However, its association with LVEF is not strong nor clinically significant.

	None (n = 526)	<1 cup/day (n = 191)	1-2 cups/day (n = 1035)	3-4 cups/day (n = 559)	≥5 cups/day (n = 281)	P value
Age (years)	58 (7.1)	60 (7.1)	60 (7.5)	60 (7.3)	59 (7.6)	<0.001
Sex (male)	190 (36.1%)	78 (40.8%)	427 (41.3%)	256 (45.8%)	140 (49.8%)	0.001
Ethnicity (Caucasian)	494 (93.9%)	180 (94.2%)	1014 (98.0%)	545 (97.5%)	279 (99.3%)	<0.001
Regular alcohol intake	163 (31.0%)	75 (39.3%)	491 (47.4%)	292 (52.2%)	127 (45.2%)	<0.001
Current smoker	14 (2.7%)	3 (1.6%)	17 (1.6%)	18 (3.2%)	14 (5.0%)	0.018
Higher level of education	259 (49.2%)	110 (57.6%)	578 (55.8%)	329 (58.9%)	145 (51.6%)	0.014
Systolic BP (mmHg)	133 (18.4)	136 (16.9)	134 (18.1)	135 (18.4)	135 (19.0)	0.617

Continuous variables displayed as mean (standard deviation) and categorical data are presented as numbers of participants (percentages) in each group of coffee consumption. *BP* = blood pressure.

Table 1 - Baseline characteristics

Table 2 - Effect estimate (percentage change compared with no coffee consumption) of daily coffee consumption on LV structure and function

	<1 cup/day		1-2 cups/day		3-4 cups/day		≥5 cups/day	
CMR Parameter	Effect estimate	P value	Effect estimate	P value	Effect estimate	P value	Effect estimate	P value
LV end-diastolic volume	0.27	0.828	1.81	0.027	2.91	<0.001	3.34	<0.001
LV end-systolic volume	1.31	0.483	3.47	<0.001	4.36	<0.001	5.35	<0.001
LV mass	0.56	0.670	1.33	0.122	3.37	<0.001	1.46	0.240
LV stroke volume	-0.48	0.732	0.75	0.406	1.96	0.068	2.02	0.126
LV ejection fraction	-0.43	0.366	-0.62	0.046	-0.54	0.138	-0.74	0.100

Effect estimate represent the percentage change of the CMR parameter compared with no coffee consumption in a multivariate regression adjusted for age, sex, ethnicity, Townsend deprivation index, current smoking, higher level of education (university degree or professional qualification), height, weight, regular alcohol consumption (≥3 times/week), systolic blood pressure, resting heart rate and tea intake. LV = left ventricular

Table 3 - Effect estimate (percentage change) of each daily cup of coffee consumed on LV structure and function

CMR Parameter	Effect estimate	P value
LV end-diastolic volume	0.57	<0.001
LV end-systolic volume	0.84	<0.001
LV mass	0.31	0.073
LV stroke volume	0.37	0.047
LV ejection fraction	-0.11	0.083

Effect estimate represent the percentage change of the CMR parameter in a multivariate regression with coffee consumption as a continuous variable. LV = left ventricular

ID#: 371850

'Anything but open-and-shut': Patient-specific, 3D printed heart valves within models of congenital heart disease

Nick Byrne[1]Mari Nieves Velasco Forte, MD[2], Alberto Gomez, PhD[3], Kuberan Pushparajah, MD[4], Israel Valverde, MD[5]

1. Guy's and St. Thomas' NHS Foundation Trust, King's College London School of Biomedical Engineering & Imaging Sciences, England, United Kingdom

2. Kings College London, England, United Kingdom

3. King's College London, United Kingdom

4. Kings College London and Guy's & St Thomas' Hospital NHS Foundation Trust, Evelina London Children's Hospital, England, United Kingdom

5. King's College London, Andalucia, Spain

Background: When derived from CMR data, a frequently observed limitation of patient-specific, 3D printed models of congenital heart disease anatomy is the incomplete representation or absence of valvular structures. These features can be critical to surgical decision-making and planning. The notion of a hybrid model of CMR and echocardiography data was demonstrated as one way to address this shortcoming. However, the fabrication of such a model remains manually laborious, dependent on research software and provides results that are difficult to verify. None of these qualities lend themselves to clinical translation. We present a clinical example of CMR-echocardiography registration and mutual segmentation to illustrate these deficiencies and motivate future work.

Methods: A diastolic, hybrid 3D model was constructed for a 6-year-old patient with transposition of the great arteries and straddling tricuspid valve. Structural representation of whole heart anatomy was segmented from 3D morphological CMR acquisition (1.5 T, Philips Achieva, bSSFP) using Mimics Medical v18.0 (Materialise NV, Belgium). Crude representations of valvular leaflets and attachments (including straddling chords) were segmented, using the same software, from 3D transthoracic echocardiogram (Philips, iE33), spatially registered to the CMR image. Landmark-based registration was performed using an eight-point picking protocol and rigid closed form algorithm within MITK Workbench v2016 (DKFZ, Germany). A 3D PDF demonstrated the hybrid model. A 3D printed representation of CMR data only was fabricated in rubber-like, TangoPlus acrylic, using an Objet500 Connex1 polyjet printer (Objet-Stratysys, USA-Israel).

Results: CMR segmentation required 3.5 hours; echocardiography segmentation required 2 hours; registration required 3.5 hours (Figure 1) Leaflet geometries were limited by the comparatively poor quality of the static echocardiogram. Registration was manually adjusted to give qualitatively good agreement in the vicinity of the valvular structures and papillary muscles at the expense of the remaining anatomy. Valvular anatomy was not incorporated into the printed model due to concerns that the polyjet support removal process would damage the delicate chord structures of the hybrid representation. The 3D PDF (Figure 3(a)-(c)) and 3D printed model (Figure 3(d)-(e)) were considered at multidisciplinary discussion and in pre-surgical planning.

Conclusion: The combination of CMR and echocardiography data can yield a hybrid model of congenital heart anatomy that includes structural representation of valvular structures. However, the approach presented is largely manual, time-consuming and highly operator dependent. It relies on research software and makes inefficient use of what is otherwise a time-resolved, echocardiogram. As a result, valvular depiction is crude and the accuracy of both its segmentation and then registration to CMR image space is difficult to understand. Parallel developments in image acquisition, segmentation and multi-modal registration will be necessary before 3D models that incorporate valvular anatomy are routinely used for surgical planning.

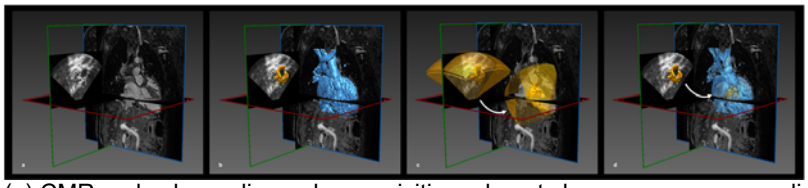

(a) CMR and echocardiography acquisitions do not share a common coordinate space and anatomical representation is misaligned; (b) 3D image segmentation is completed for CMR (blue) and echocardiography (orange) data sets individually; (c) Landmark based spatial registration is performed to align CMR and echocardiography acquisitions - the transformation of the 3D echocardiogram frustum (orange) is shown; (d) The

transformation is applied to the echocardiography segmentation geometry (orange) aligning it with the coordinate space of the CMR data (blue).

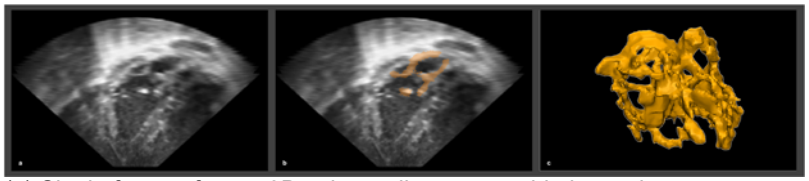

(a) Single frames from a 3D echocardiogram provide inconsistent representation of heart valves; (b) This limitation adversely affects image segmentation; (c) The resulting segmentation geometry provides a sub-optimal representation of leaflet and sub-valvular apparatus.

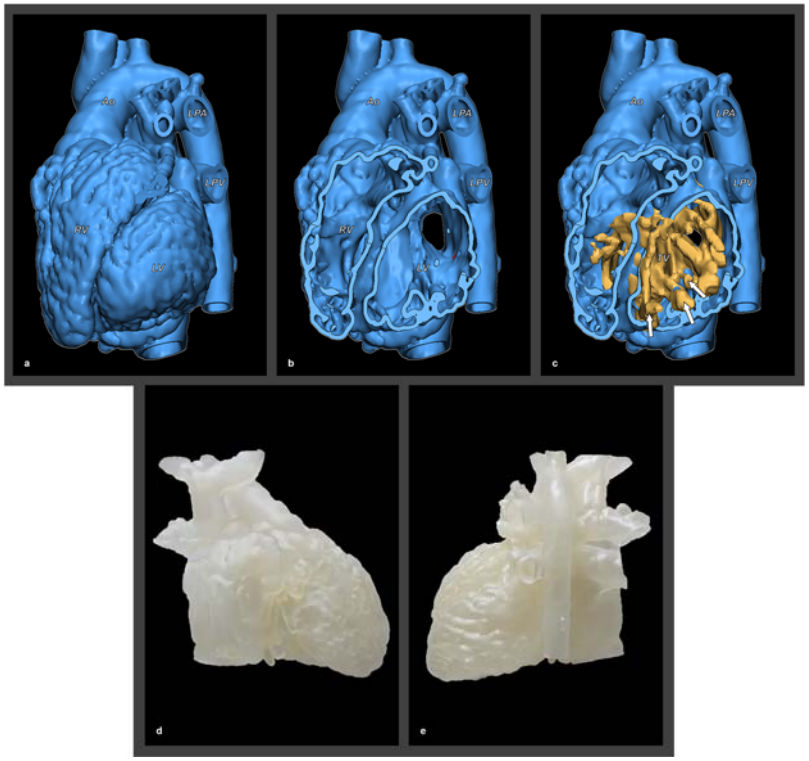

(a) An apical view of the CMR segmentation geometry; (b) The valvuar anatomy is absent from the CMR-derived model; (c) The addition of the echocardiography data demonstrates the tricuspid valve leaflet (TV) and the straddling chords (arrows); (d) Anterior and; (e) Posterior views of the 3D printed model.

ID#: 371863

Standardization of myocardial T2 mapping measurements: normal values and reproducibility in the presence of health and disease

Jasmin Haslbauer, MSc, cand.med.[1] Mengzhen Chen, Cand. med.[1], Yije Kim, Select state / province...[2], Hiwad Rashid, Bsc[2], Elen Elen, MD, FIHA[3], Faraz Pathan, MBBS, FRACP[4], Lea Winau, Bsc[5], Tommaso D'Angelo, MD[6], Andreas Greiser, Ph.D[7], Ralph Strecker, PhD[8], Eike Nagel, MD, PhD[9], Valentina O. Puntmann, MD, PhD[10]

1. Goethe University Hospital Frankfurt am Main, Frankfurt am Main, Germany

2. Universitaetsklinikum Frankfurt, Germany

3. National Cardiovascular Center Harapan Kita, Jakarta-Indonesia; Institute for Experimental and Translational Cardiovascular Imaging, University Hospital Frankfurt-Germany, Tangerang, Banten, Indonesia

4. Goethe Institute for Experimental and Translational Cardiovascular Imaging, Sydney, New South Wales, Australia

5. Goethe University Hospital Frankfurt, Hessen, Germany

6. University of Messina, Messina, Sicilia, Italy

7. Siemens Healthcare GmbH, Erlangen, Germany, Erlangen, Bayern, Germany

8. Siemens Healthineers, Frankfurt, Hessen, Germany

9. University Hospital Frankfurt; Institute for Experimental and Translational Cardiovascular Imaging; DZHK Centre for Cardiovascular Imaging, Frankfurt, Germany

10. Universitaetsklinikum Frankfurt, Frankfurt Am Main, Germany

Background: Quantifiable tissue characterisation using mapping techniques by CMR is becoming increasingly recognised as a valuable tool in the diagnosis and assessment of various cardiomyopathies. In previous analyses, pixel-wise quantification of longitudinal relaxation by T1 mapping has been shown as a reliable method to differentiate between healthy and pathological myocardial tissue in non-ischemic cardiomyopathies. T2 mapping has been used in a number of inflammatory cardiomyopathies, in querying the role of diffuse myocardial inflammation, as the predominant the pathological process. Standardization and reproducibility of T2 mapping measurements for clinical use has not been previously established.

Methods: A total of 51 subjects (controls, n=11; patients with LV hypertrophy n=1; and LV dilatation (n=32) underwent T2 mapping at 1.5 and 3T using T2 multi-echo SSFP (T2mapFLASH). Native T2 values were measured in a mid-ventricular short axis slice by drawing region of interest (ROI) conservatively within the septal myocardium (Figure 1). The reproducibility of measurements (the intra- and interobserver and interstudy reproducibility) of myocardial T2 mapping measurements has been assessed using Bland-Altman plots and Pearsons correlations.

Results:

Patients had significantly higher native T2 values compared to controls (native T2(msec): 1.5T: 49±4 vs 45±2; 3.0T: 42± 5 vs. 34±2, p<0.001). Intra- and inter-observer agreements for native T2 values across the whole cohort were very high (r=0.997; r=0.992, p<0.01 for both) . Similarly, the intra- and inter-observer coefficients of variation (CoV) for T2 (1.85%; 2.5%) values were low. There was an overall small bias in measurements for observer reproducibility; smaller bias and 95% confidence interval in an intra-observer setting (mean difference(95%CI): -0.04 [0.66, - 0.74]msec) compared to inter-observer measurements (0.18 [1.18, 0.81]msec). Comparison of reproducibility between controls and patients with LVH and DCM, respectively, as well as between 3 and 1.5T yielded no observable discrepancies in reproducibility (Figures 2 and 3).

Conclusion: Myocardial T2 mapping by CMR is a promising, reproducible method to characterize the contribution of myocardial inflammation in health and disease, at both clinically used field strenghts. Further work needs to be conducted to minimize the possibility of systematic bias by establishing standards in measurement, data acquisition and image analysis.

Figure 1

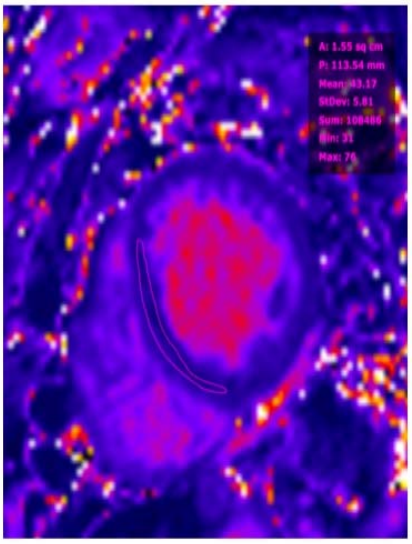

Figure 1

Figure 2

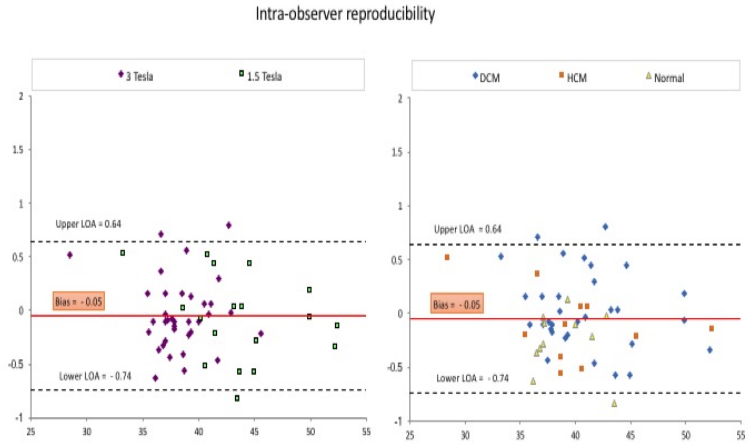

Figure 2

Figure 3

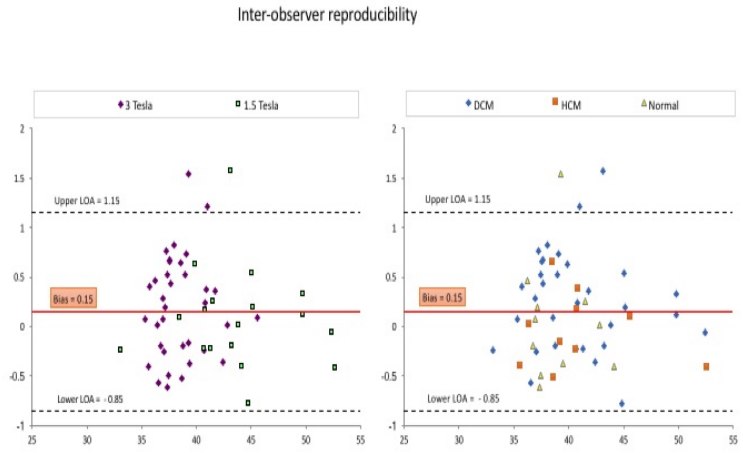

Figure 3

ID#: 371870

Dobutamine stress CMR out-performs LGE and adenosine in predicting CTO-PCI response (CARISMA_CTO preliminary results)

Silvia Pica, MD[1]Pietro Mazzarotto, MD[2], Gabriella Di Giovine, MD[3], Mario Bollati, MD[3], Francesco Calvo, MD[4], Antonia Camporeale, MD[5], Francesco Bedogni, MD[6], Gianluca Pontone, MD[7], Daniele Andreini, MD[7], Lorenzo Monti, MD[8], Alberto Maestroni, MD[9], Gioel Gabrio Secco, MD[10], Massimo Lombardi, MD[11]

1. IRCCS Policlinico San Donato, Multimodality Imaging Center, Milan, Italy

2. Ospedale Maggiore di Lodi, Milan, Lombardia, Italy

3. IRCCS Policlinico San Donato, Milano, Italy

4. IRCCS Policlinico San Donato, Milano , Milan, Italy, Italy

5. IRCCS Policlinico San DOnato, Milano, Italy

6. IRCCS Policlinico San Donato, Milano , Milan, Italy, san donato milanese, Lombardia, Italy

7. Centro Cardiologico Monzino, Italy

8. Humanitas Research Institute, Rozzano, Lombardia, Italy

9. ASST Valle Olona, Italy

10. A.O. Antonio e Biagio, Alessandria, Italy

11. IRCCS Policlinico San Donato, Milan, Italy, Lombardia, Italy

Background: It is debated whether percutaneous revascularization (PCI) of coronary chronic total occlusion (CTO) is superior to optimal medical therapy in improving symptoms, LV function and reducing MACE. Furthermore, PCI-CTO still presents complications with success procedural rate around 80%. Myocardial viability and ischemia assessment by cardiac magnetic resonance (CMR) imaging is suggested to identify pts who are more likely to benefit from PCI. However, which CMR protocol is the best for this purpose is not yet established. Aim of the study is to compare CMR protocols of myocardial viability/ischemia to predict clinical outcome in patients undergoing CTO-PCI

Methods: This is a multicentre, prospective, observational study, with estimated enrolment of 400 CTO pts eligible for PCI (Clinicaltrials.gov NCT03152825, CARISMA_CTO). All patients underwent stress CMR before PCI attempt and clinical follow-up in the following 12 months. In order to detect viability and/or regional myocardial ischemia, 3 different CMR protocols have been systematically applied: 1) adenosine-stress and LGE in pts with normal ejection fraction (EF) and no wall motion abnormalities (WMA), 2) high-dose-dobutamine and LGE in pts with WMA and EF ≥35%, 3) low-dose-dobutamine (LDD) in pts with EF <35%. Segmental contractility improvement at LDD and/or <75% LGE transmurality were considered a marker of viability, while the presence of induced WMA and/or perfusion defects by pharmacological stress a marker of myocardial ischemia. Short-term clinical responders to CTO-PCI were considered pts with at least one CCS/NYHA class improvement at 9±5 months FU

Results: Fifty-one pts have been enrolled so far. Twenty-three(47%) underwent adenosine, 13(25%) high dose and 10(19%) low-dose dobutamine. CTO-PCI was performed in 32(61%), successful in 24(75%).
Clinical responders were more likely found after successful CTO-PCI, 14(58%), as compared to 5(18%) if unsuccessful/not-attempted CTO-PCI (p=0.007). In clinical responders, myocardial viability based on LGE was found in 10(71%), as compared to 6(42%) based on LDD response. Inducible ischemia, assessed by adenosine or dobutamine, was found in 9(64%) of clinical responders. All pts with improved contractility after LDD, as compared to none without LDD response, were CTO-PCI responders (p=0.03). However, viability assessed by LGE alone, and/or the presence of inducible ischemia, were not predicting CTO-PCI response (p=0.6 and p=0.3, respectively).

FU data regarding LV global/segmental function changes will be provided in the next 4 months.

Conclusion: These preliminary results showed that low-dose-dobutamine stress CMR out-performs LGE and adenosine CMR in predicting CTO-PCI clinical improvement. Tailored CMR protocols may be required to improve accuracy in identifying CTO-PCI responders.

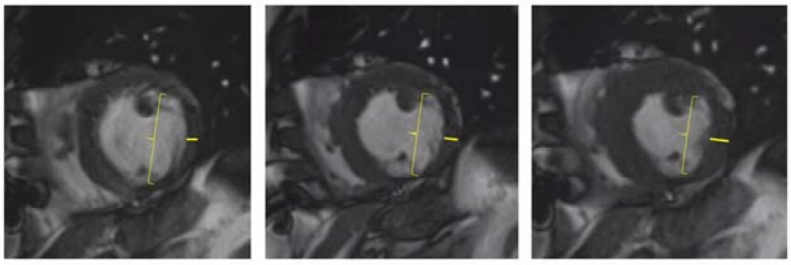

LV short axis cine SSFP in a pt with LCX CTO and clinical improvement at follow up. (left panel): baseline diastolic frame;(central panel): baseline systolic frame showing antero-lateral and infero-lateral wall thickening <50% vs baseline; (right panel): systolic frame during low dose dobutamine infusion showing contractility improvement of antero-lateral and infero-lateral wall, thickening >50% (likely viable)

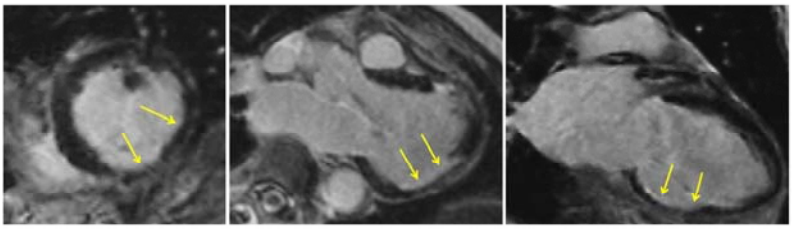

Same patient. LGE sequences showing inferior, infero-lateral and antero-lateral >75% LGE transmurality. Despite >75% LGE transmurality, dobutamine infusion induced a clear improvement of contractility at the same level

Baseline Characteristics of the study population

	Successful CTO-PCI pts (N=24)	**No-PCI pts* (N=27)**	**p-value**
Age, years	67±10	67±9	0.9
Male, n(%)	22(88)	24(88)	0.6
Hypertension, n(%)	16 (66)	17 (63)	0.6
Smoke, n(%)	15 (62)	21 (78)	0.2
Dyslipidaemia, n(%)	14 (58)	17 (63)	0.6

Diabetes, n(%)	13 (54)	6 (22)	0.04
Family History of CAD, n(%)	5 (21)	10 (37)	0.2
Prior STEMI, n(%)	8 (33)	14 (52)	0.2
Prior NSTEMI/UA, n(%)	13 (54)	7 (26)	0.02
Prior PCI other vessels, n(%)	20 (83)	20 (74)	0
Canadian Cardiovascular Society angina class (CCS), n(%) • **I** • **II** • **III** • **IV**	• 4(17) • 3(12) • 3(12) • 2(8)	• 0 • 3(11) • 3(11) • 4(15)	0.2
New York Heart Association functional class (NYHA), n(%) • **I** • **II** • **III** • **IV**	• 11(46) • 9(37) • 4(17) • 0	• 14(52) • 5(18) • 6(22) • 0	0.4
Cause of hospitalization, n(%) • **AMI/NSTEMI/UA** • **HF** • **Stable angina** • **Positive stress test** • **Incidental evidence of prior MI**	• 12(5) • 2(8) • 4(17) • 2(8) • 4(17)	• 5(18) • 4(15) • 5(18) • 8(30) • 4(15)	0.07
CTO vessel n(%) • **RCA** • **LAD** • **LCX**	• 18(75) • 2(8) • 5(21)	• 17(63) • 2(7)	0.7

		• 8(30)	
LVEDV index, ml	75±21	71±23	0.7
LV EF, %	53±15	54±16	0.8
Viability by LGE, n(%)	18(75)	6(22)	0.1
Viability by low-dose-dobutamine, n(%)	6(25)	0	0.09
Inducible ischemia by adenosine/dobutamine perfusion, n(%)	12(50)	4(15)	0.7

*No-PCI pts: unsuccessful/not-attempted CTO-PCI

ID#: 371903

Strain Encoding (SENC) Using EPI Readout

Yingmin Liu, Ph.D.[1] Rizwan Ahmad, PhD[2], Ning Jin, Ph.D.[3], Donel Tani, BS[4], Sid Fleischman, B.S.E.[5], Nael Osman, Ph.D.[4], Orlando Simonetti, PhD[2]

1. The Ohio State University, Columbus, OH

2. The Ohio State University, OH

3. Siemens Medical Solutions USA, Inc., OH

4. Myocardial Solutions, Inc., Morrisville, NC

5. Myocardial Solutions, Inc., NC

Background: Strain-encoded MRI (SENC) can directly measure through-plane strain in the left and right ventricles [1]. SENC has potential advantages over other techniques such as tagging and tissue tracking in that regional strain can be easily and automatically extracted from the image data. We demonstrate the feasibility of combining SENC encoding with an efficient echo planar imaging (EPI) based readout (EPI-SENC) to acquire high temporal resolution strain measurements in two heartbeats.

Methods: Selective SENC RF1 and tagging gradient SENC TAG create localized modulation of the magnetization in the transverse plane before it is tipped back by non-selective SENC RF2 pulse for imaging (Fig. 1). K-space ordering in EPI is linearly interleaved. To validate the sequence, a mechanical phantom (Fig. 2) was utilized; it consisted of a homogeneous silicone gel block and a non-ferromagnetic piston to compress the block periodically. Measurements with two different block dimensions, corresponding to compressions of -24% and -16%, were acquired with EPI-SENC and images were analyzed in SENC 4.1.2 (MyoCardial Solutions, NC, USA). Strain results were compared to those from HARP analysis of tagged images and the expected strain associated with the known phantom deformation. Three short-axis views and three long axis views from five healthy volunteers (IRB approved) were also scanned and quantified.

Results: Phantom and volunteers were scanned on a 1.5T scanner (Avanto, Siemens AG, Germany) with: spatial resolution 4.5mm x 4.5mm, TR 9.6ms, slice thickness 15mm, EPI factor 5, FA 12 degrees, BW 1920Hz/pixel, segment 20, acquisition matrix 40x96, and low and high tunings alternating every four echo trains. Representative phantom and volunteer images are shown in Fig. 3. Listed in Table 1 is the strain comparison for phantom, showing RMS of 1.6% at 24.0% compression, and 0.96% at 16.0% compression. Longitudinal strain from same five subjects scanned at different times yielded an average longitudinal strain difference of 0.4% and circumferential strain difference of 1.3%, showing good reproducibility.

Conclusion: Phantom validation shows the strain measured with EPI-SENC has a very high accuracy (<2%). Volunteer studies demonstrated that EPI-SENC strain results are comparable to tagging, but EPI-SENC offers high efficiency, acquiring each cardiac view in two heartbeats. EPI-SENC can potentially improve the acquisition efficiency of strain encoding without compromising the accuracy. References [1] Pan, L., et al, 2006. MRM, 55(2), pp.386-395.

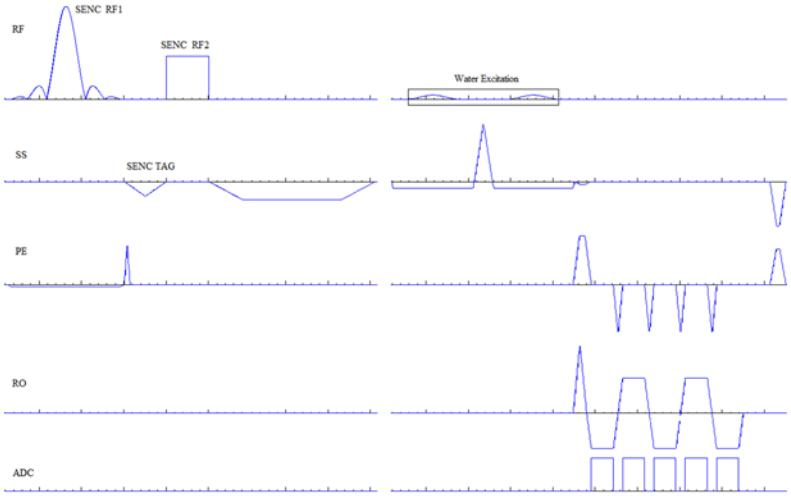

Fig. 1. Diagram of EPI-SENC pulse sequence with EPI factor of 5. Only one tuning is shown.

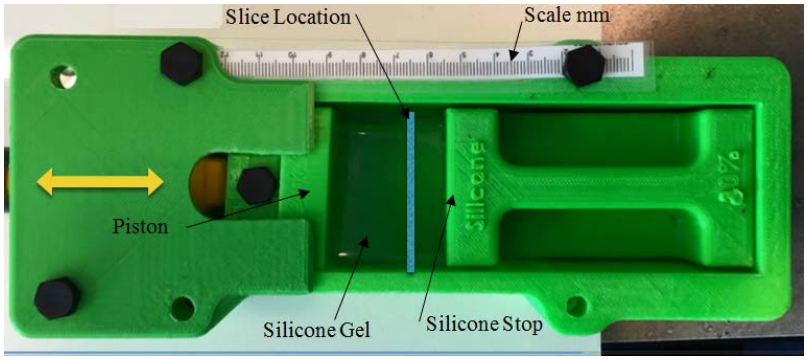

Fig. 2. The mechanical phantom to validate the accuracy of EPI-SENC sequence.

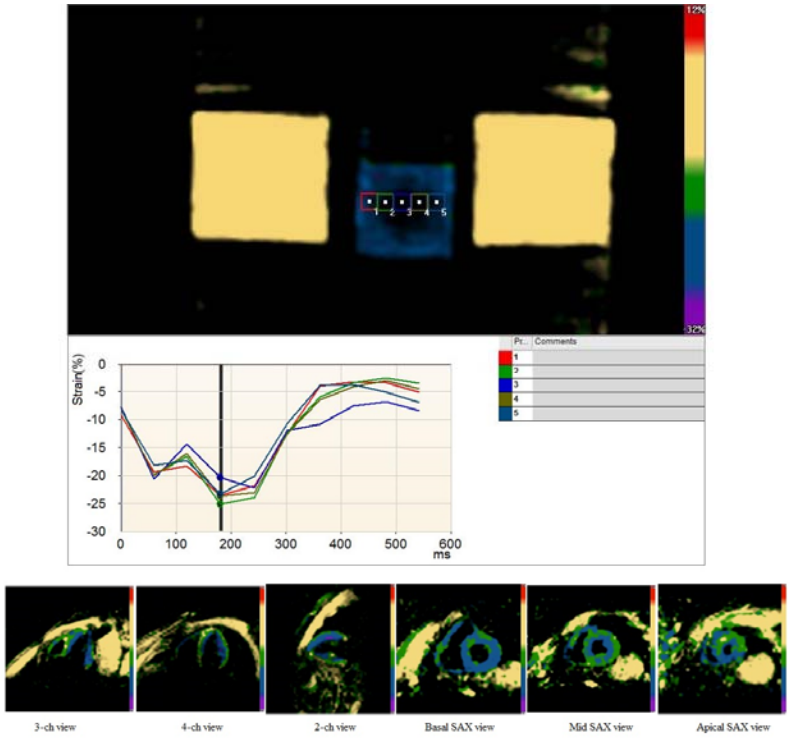

Fig. 3. EPI-SENC images from silicone gel phantom (top), only the middle gel block was compressed, and long and short axis cardiac views (bottom). Shown in the middle is the strain in a cardiac cycle for 5 probing points.

Table 1. Comparison between tagging (analyzed in HARP) and EPI-SENC images (analyzed in SENC 4.1.2) for two known strains from the gel phantom.

24.0% Compression				16.0% Compression			
Probe	HARP (%)	SENC EPI (%)	Error (%)	Probe	HARP (%)	SENC EPI (%)	Error (%)
1	-24.18	-23.52	-0.66	1	-17.41	-17.91	0.50
2	-25.35	-25.09	-0.27	2	-16.33	-17.09	0.76
3	-25.48	-22.23	-3.25	3	-15.67	-16.08	0.42
4	-24.32	-23.71	-0.60	4	-15.50	-17.26	1.76
5	-22.09	-23.24	1.15	5	-15.25	-14.55	-0.70
RMS			1.60	RMS			0.96

ID#: 371911

Standardisation of myocardial T1 mapping measurements for reproducible clinical use in the presence of health and disease

Mengzhen Chen, Cand. med.[1], Valentina O. Puntmann, MD, PhD[10]Jasmin Haslbauer, MSc, cand.med.[1], Hiwad Rashid, Bsc[2], Yije Kim, Select state / province...[2], Lea Winau, Bsc[3], Tommaso D'Angelo, MD[4], Faraz Pathan, MBBS, FRACP[5], Elen Elen, MD, FIHA[6], Ralph Strecker, PhD[7], Andreas Greiser, Ph.D[8], Eike Nagel, MD, PhD[9]

1. Goethe University Hospital Frankfurt am Main, Frankfurt am Main, Germany

2. Universitaetsklinikum Frankfurt, Germany

3. Goethe University Hospital Frankfurt, Hessen, Germany

4. University of Messina, Messina, Sicilia, Italy

5. Goethe Institute for Experimental and Translational Cardiovascular Imaging, Sydney, New South Wales, Australia

6. National Cardiovascular Center Harapan Kita, Jakarta-Indonesia; Institute for Experimental and Translational Cardiovascular Imaging, University Hospital Frankfurt-Germany, Tangerang, Banten, Indonesia

7. Siemens Healthineers, Frankfurt, Hessen, Germany

8. Siemens Healthcare GmbH, Erlangen, Germany, Erlangen, Bayern, Germany

9. University Hospital Frankfurt; Institute for Experimental and Translational Cardiovascular Imaging; DZHK Centre for Cardiovascular Imaging, Frankfurt, Germany

10. Universitaetsklinikum Frankfurt, Frankfurt Am Main, Germany

Background: The usage of tissue-mapping techniques in various cardiac conditions is increasingly popular, as it allows a robust tool in differentiating between normal and abnormal myocardial tissue. Several T1-mapping sequences have been proposed for pixel-wise quantification of longitudinal relaxation with variable reproducibility and precision of native T1 values. The ongoing optimisation of T1 mapping sequences by the vendors and others further compound a uniform solution for T1 mapping with established the normal values and pathological ranges, which are sequence-dependent. We undertook a head to head comparison of two MOLLI sequences for native T1 in reproducibility and discrimination between healthy and pathological myocardium.

Methods: A total of 51 subjects (controls, n=11; patients with LV hypertrophy n=1; and LV dilatation (n=32) underwent T1 mapping at 1.5 and 3T using FFM-MOLLI and VendorProduct MOLLI). Native T1 values were measured in a mid-ventricular short axis slice by drawing region of interest (ROI) conservatively within the septal myocardium (Figure 1). The reproducibility of measurements (the intra- and interobserver and interstudy reproducibility) of myocardial T1 mapping measurements has been assessed using Bland-Altman plots and Pearsons correlations. Discrimination between health and disease was performed using the ROC curve analysis.

Results: Patients had significantly higher native T1 values compared to controls for both sequences ($p<0.05$, Figure 2). Effect size by Cohen-D was 2.1 for FFM MOLLI and 1.7 for Vendor MOLLI, respectively. Intra- and inter-observer agreements for native T1 values across the whole cohort were very high (FFM MOLLI r=0.991; r=0.972; Vendor MOLLI: r=0.96 and r=0.89, for all). Similarly, the intra- and inter-observer coefficients of variation (CoV) for T1 (0.8%; 1.5% vs. 1.1% 2.7%) were low.There was an overall smaller bias in measurements for intra observer reproducibility compared to inter-observer measurements (Figure 3). Comparison of reproducibility between controls and patients with LVH and DCM, respectively, as well as between 3 and 1.5T yielded no observable discrepancies in reproducibility (Figures 2 and 3). AUCs across the cohort (controls vs. patients) were: 0.94 (0.86-0.99) vs. 0.79 (0.65 -0.95), respectively.

Conclusion: Different MOLLI sequences differ for normal values, effect sizes and in discrimination between health and disease. Myocardial T1 mapping with is a promising, reproducible method to characterize the contribution of myocardial disease, at both clinically used field strengths. Further work needs to be conducted to minimize the possibility of systematic bias by establishing standards in measurement, data acquisition and image analysis.

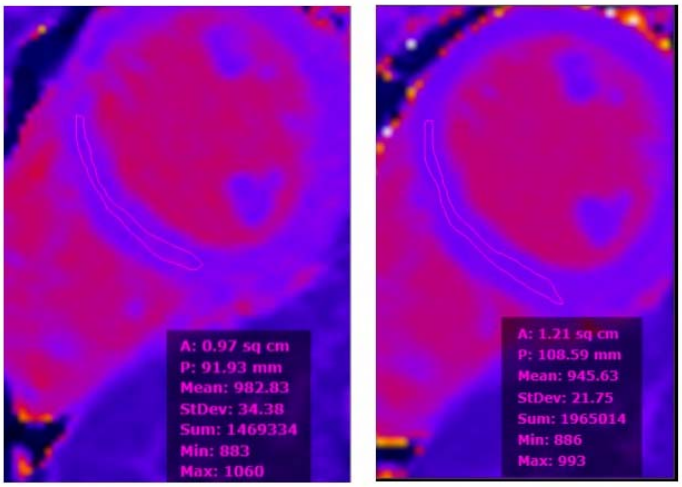

Figure 1

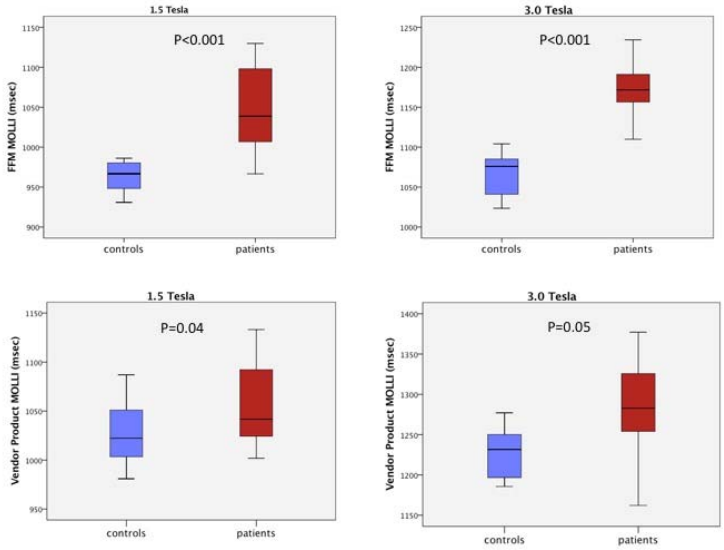

Figure 2

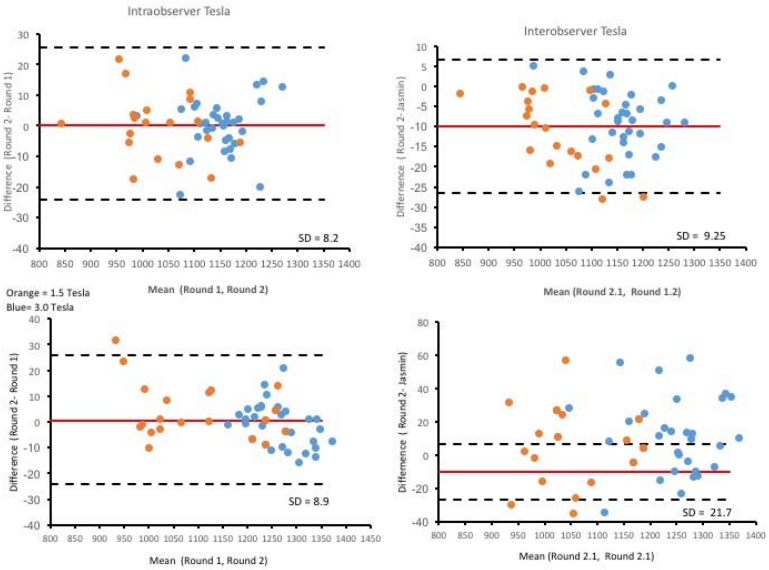
Intraobserver Tesla
Difference (Round 2- Round 1)
SD = 8.2
Mean (Round 1, Round 2)
Interobserver Tesla
Difference (Round 2- Jasmin)
SD = 9.25
Mean (Round 2.1, Round 1.2)
Orange = 1.5 Tesla
Blue= 3.0 Tesla
Difference (Round 2- Round 1)
SD = 8.9
Mean (Round 1, Round 2)
Difference (Round 2- Jasmin)
SD = 21.7
Mean (Round 2.1, Round 2.1)

Figure 3

ID#: 371912

Characterization of T2 and T2* relaxation and strain in disease progression post acute myocardial infarction

Nilesh R. Ghugre, PhD[7]Dipal Patel, BS Candidate[1], Idan Roifman, MD[2], Venkat Ramanan, MSc[3], Mohammad Zia, MD[4], Kim A. Connelly, MD, PhD[5], Graham Wright, PhD[6]

1. Sunnybrook Research Institute, Canada

2. Sunnybrook Health Sciences Centre, University of Toronto, Toronto, ON, Canada

3. Sunnybrook Research Institute, Toronto, ON, Canada

4. Sunnybrook Health Sciences Centre, Canada

5. St. Michaels Hospital and University of Toronto, Toronto, ON, Canada

6. Sunnybrook Research Institute, University of Toronto, ON, Canada

7. Sunnybrook Research Institute, University of Toronto, Toronto, ON, Canada

Background: Microvascular obstruction (MVO) is a common complication in acute myocardial infarction (AMI), which occurs in 50% of the ST-segment elevation of myocardial infarction (STEMI) patient population. Several studies have demonstrated that MVO is an independent predictor of adverse outcomes in AMI. In association with MVO, more recently, hemorrhage has been shown to be an active contributor to myocardial damage and inflammation, elevating the risk even further. The effects of these adverse consequences can be observed by serially assessing regional myocardial systolic function and inflammation in vivo using strain analysis and T2 mapping, respectively. The aim of our study was to longitudinally characterize T2 and strain in STEMI patients with and without MVO to observe the acute to chronic transition during disease progression.

Methods: The study involved patients (n=16) with reperfused STEMI with 3 visits at 48 hours, 4 weeks, and 6 months post-PCI. Imaging was serially performed on 1.5T clinical scanner. Cardiac function was assessed using a cine SSFP sequence. T2 was quantified for the detection of edema using a cardiac-gated free-breathing T2-prepared spiral imaging sequence: TE=2.9-184ms. T2* mapping was utilized for the identification of hemorrhage using a multi-echo gradient-echo acquisition with 8 echos, TE=1.4-12.7ms. Early and Late gadolinium enhancement (EGE, LGE) was employed to identify region of infarction and MVO. Patients were divided into two groups with and without MVO by identifying the hypo-enhanced core in EGE images. Two slices with infarct were chosen for analysis per patient per time point. T2, T2* and radial strain and circumferential strain were analyzed in infarct and remote segments using cvi42 software (Circle). Statistics were performed using 2-way ANOVA.

Results: MVO was identified on EGE images in 8 of the 16 patients (50%). At 48 hrs, the MVO+ group demonstrated low infarct T2* values or greater hemorrhage within the hypoenhanced region that was associated with reduced peak strain compared to the MVO- group. See Fig. 1 for representative images. T2* values were significantly lower in the MVO+ group at 48 hrs and 4 weeks relative to remote indicative of hemorrhage and remained low even at 6 months suggesting persistent hemorrhage. Edema characterized by T2 in infarct myocardium subsided within 4 weeks ($p<0.02$) in both groups, but at 6 months, resolved with significance only in the MVO- group where as remained elevated in the MVO+ group when compared to week 4. Radial and circumferential strain analysis in infarct regions showed significant recovery over time for only MVO- patients whereas recovery was blunted in MVO+ patients. See associated plots in Fig. 2. Strain in remote myocardium was not different between the groups and remained unchanged over time.

Conclusion: Edema, hemorrhage and strain progression in the infarct region for patients with microvascular obstruction fails to reach remote levels and has significantly less recovery rate compared to patients without microvascular obstruction. Remote myocardial alterations (T2) may further be an early indicator of adverse remodeling. Thus, our study shows that microvascular obstruction impacts disease progression by hindering the regional myocardial systolic function and edema recovery post-AMI.

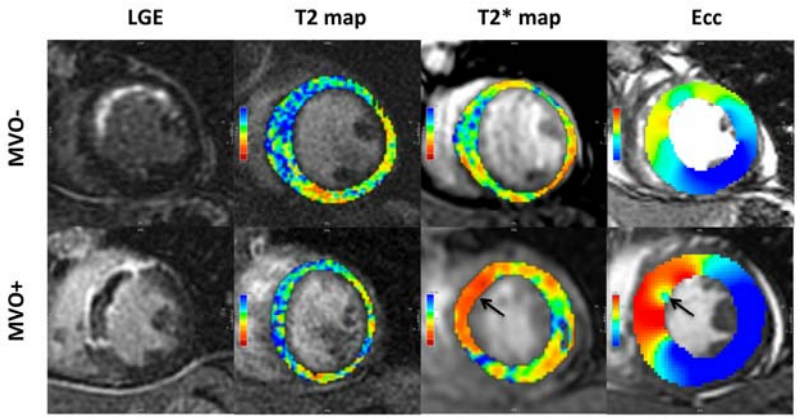

Figure 1: Representative short axis images from the two groups with MVO and no MVO at 48 hrs post-AMI. Arrows indicate hemorrhage on T2* map and compromised regional contraction on the peak circumferential strain map (Ecc) in the region of MVO.

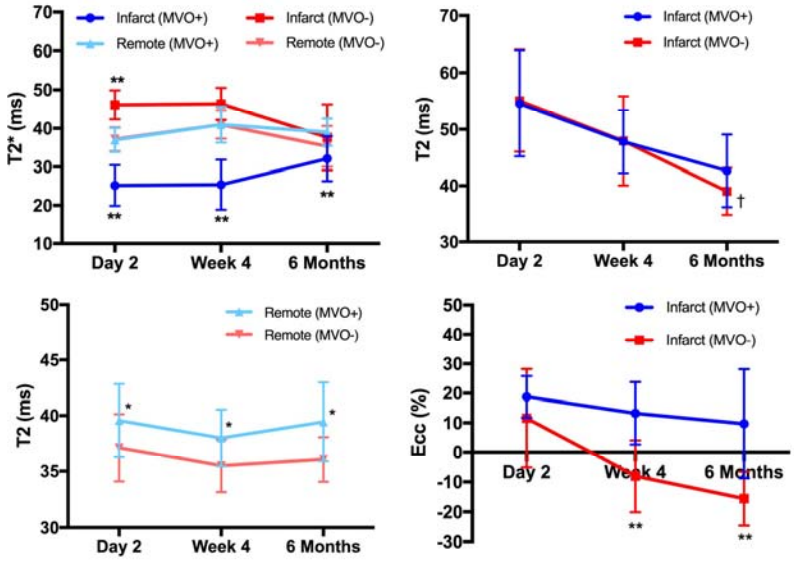

Figure 2: Evolution of T2*, T2 and peak circumferential strain (Ecc) in the infarcted and remote myocardium post-AMI.[**p<0.001 compared to remote (T2*) or other group (Ecc); *p<0.05 compared to other group; †p<0.05 compared to previous time point.]

ID#: 371371

Comparison of image quality with and without the use of an abdominal restrictive band in non-contrast enhanced, navigator 3D thoracic MRA

Richard Coulden, MB BS[1] Randeep Khosla, MB BS[1], Kent Greep, MD[2], James Pierce, MD[1], Raoul Pereira, MD[1], Kate Mracek, BSc[1], Emer Sonnex, MPhil[2]

1. University of Alberta Hospital, Canada

2. University of Alberta Hospital, Edmonton, AB, Canada

Background: The use of an elasticated abdominal band during 3D navigator, ECG triggered, non-contrast enhanced MRA (NCE-MRA) has been shown to reduce acquisition times. The superior image quality of NCE-MRA when compared to non-EKG triggered contrast-enhanced MRA in the thoracic aorta has also been shown. The purpose of our study was to compare measurement reproducibility and subjective image quality in NCE-MRA of the thoracic aorta with and without the use of a respiration restricting abdominal band.

Methods: Ethics committee approval and informed consent were obtained. Thirty volunteers (mean age 37.5, 16 males) underwent NCE-MRA twice. Both examinations were performed free-breathing, one using a restrictive abdominal band. Sixty data sets were anonymized and maximum intensity pixel (MIPs) reconstructions made in axial and sagittal oblique planes. Seven readers reviewed them for subjective quality and recorded 9 linear measurements (mms): Sinuses of Valsalva (SVS), sino-tubular junction (STJ), mid ascending aorta (MAA), proximal aortic arch (PAA), distal aortic arch (DAA) & mid descending aorta (MDA) and main pulmonary arteries (MPA), right proximal PA (RPA) and left proximal PA (LPA). One reader repeated measurements for intra-observer variability. Volunteer demographics (age, gender, height, weight, waist circumference) and acquisition times were also recorded.

Results: Scan times ranged from 4.4 - 9.9 minutes (mean 7.5; SD 1.5) in the 'no-band' group and 3.3 to 9.1 minutes (mean 6.0; SD 1.6) in the 'band' group. Mean reduction in acquisition time between the two groups was 1.5 mins or 19% of the standard technique. Although there was a significant decrease in acquisition times ($P < 0.0001$), there was no significant difference in subjective image quality assessment or linear measurements at any site in the 2 groups of data ($P = 0.67$). Interobserver agreement for diameter measurements was also excellent between both acquisition techniques (table 1).

Conclusion: Using a restrictive abdominal band reduces image acquisition times in NCE-MRA but does not result in reduced subjective or objective image quality. The use of a respiration suppression technique during NCE-MRA of the thoracic aorta should be considered when practicable to improve patient throughput in a busy cardiac MRI unit.

Table 1

	no band mean	no band stdev	band mean	band stdev
SVS mms	1.12	0.51	1.31	0.45
STJ mms	1.45	0.70	1.30	0.44
MAA mms	1.13	0.43	1.12	0.50
PAA mms	1.14	0.71	0.97	0.46
DAA mms	0.89	0.42	0.73	0.27
MDA mms	1.23	0.57	1.17	0.43
MPA mms	2.11	1.04	2.09	1.20
RPA mms	0.86	0.27	0.97	0.70

LPA mms	1.03	0.48	1.02	0.36

ID#: 371381

Automated detection of clinical and genetic effects on three-dimensional cardiac phenotypes using MR imaging and computational modelling.

Carlo Biffi, MSc[1] Antonio de Marvao, MRCP, PhD[2], Mark Ivan. Attard, MRCPCh[3], Timothy Dawes, FRCA, PhD.[1], Nicola Whiffin[4], Wenjia Bai, PhD[5], Wenzhe Shi, PhD[1], Katie Francis, MRCP, BM BCh (Oxon), MA (Cantab)[6], Hannah V. Meyer, MSc[7], Rachel Buchan, MSc[8], Stuart Cook, MRCP PhD[9], Daniel Rueckert, PhD[4], Declan O'Regan, FRCR, PhD[10]

1. Imperial College London, London, England, United Kingdom

2. MRC London Institute of Medical Sciences, London, England, United Kingdom

3. Imperial College, WOKING, England, United Kingdom

4. Imperial College London, United Kingdom

5. Imperial College London, London, United Kingdom

6. National Heart and Lung Institute, Imperial College London, Royal Brompton Hospital, United Kingdom

7. European Bioinformatics Institute (EMBL-EBI), United Kingdom

8. Royal Brompton Hospital, United Kingdom

9. National Heart and Lung Institute, Imperial College London, United Kingdom

10. MRC London Institute of Medical Sciences, England, United Kingdom

Background: The environmental and genetic determinants of cardiac physiology and function are still largely unexplained. Population-based studies have mainly relied on manually-derived global indices insensitive to regional remodelling. However, advanced cardiac image analysis offers an opportunity to uncover three-dimensional (3D) associations between high-dimensional cardiac traits and given explanatory variables.

Methods: A population mean ventricular shape storing 3D phenotypes at tens of thousands vertices is derived from automated image segmentation and co-registration algorithms of cardiac magnetic resonance (MR) images (Fig. 1). A 3D effect-size map for the association between a vertex-wise phenotype and a set of predictors is then derived through mass univariate regression. Threshold-free cluster enhancement is applied to increase sensitivity towards spatially extended signals before applying a false discovery rate correction.

Results: Our experiments on synthetic phenotypic signals showed that the proposed approach is powered to detect even low-intensity effects while providing robustness against false discoveries (Fig. 2). When applied on a healthy human dataset from the UK Digital Heart Project (N=1,124), the approach replicated the effect of a previously discovered genetic mutation (rs7183401 SNP) in a left ventricular mass (LVM) genome-wide association study (Fig. 3). The rs7183401 allele of the alpha kinase 3 (ALPK3) gene is implicated in early-onset cardiomyopathy in humans, but did not replicate when tested in a conventional linear regression setting against LVM.

Conclusion: We propose an automated and powerful approach that is able to detect the regional effects of a given explanatory variable throughout the heart and shows promise for population-based studies of cardiac structure and function.

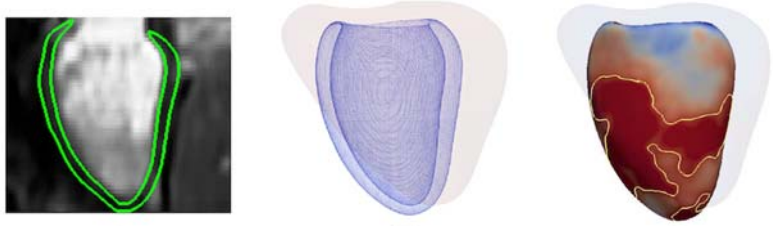

Cardiac MR images are automatically segmented (A) and co-registered to construct a mean ventricular shape storing at each vertex phenotypic parameters (B - left ventricle in blue, right ventricle in transparency). The proposed approach derives an effect-size map for the association between a given explanatory variable and a phenotype (C). Significant vertices are enclosed by yellow contours.

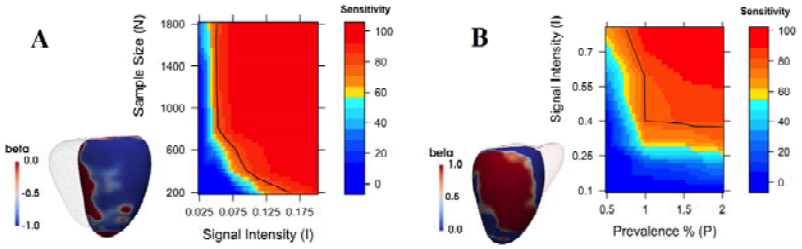

The sensitivity of the proposed approach as assessed on two synthetic signals and as a function of signal intensity and sample size (A) or prevalence of a given mutation when sample size is 1,800 (B). Signal A covers 60% of the left ventricle, while signal B the 30%. The black line indicates 80% sensitivity.

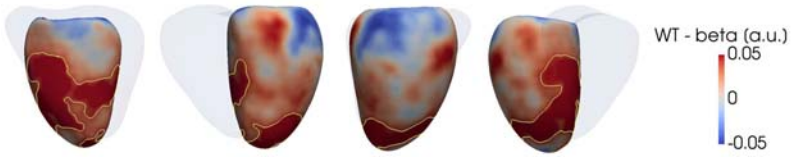

Standardized regression coefficients for the effect of rs7183401 allele on wall thickness (WT) adjusted for age, gender, body surface area and systolic blood pressure. Significant coefficients are enclosed by yellow contours.

ID#: 371382

Left ventricular feature tracking in real time CMR: Comparison with standard CINE bSSFP in sinus rhythm and atrial fibrillation

Kerstin Laubrock[1] Eckhart Thassilo von Loesch, MD[2], Johannes T. Kowallick, MD[3], Michael Steinmetz, MD[3], Martin Fasshauer, MD[2], Joachim Lotz, MD[4], Martin Uecker, Prof, PhD[5], Andreas Schuster, MD PhD MBA FESC[6], Christina Unterberg-Buchwald, MD[7]

1. UMG, Clinic of Cardiology, Institute of Diagnostic and Interventional Radiology, Germany

2. UMG, Institute of Diagnostic and Interventional Radiology, Germany

3. University Medical Center Göttingen, Niedersachsen, Germany

4. University Medical Center Göttingen, Goettingen, Niedersachsen, Germany

5. UMG, DZHK partner site, Institute of Diagnostic and Interventional Radiology, Germany

6. Department of Cardiology and Pneumology, University Medical Center Göttingen, Germany; Department of Cardiology, Royal North Shore Hospital, Sydney, Australia; The Kolling Institute, Northern Clinical School, University of Sydney, Sydney, Australia, Niedersachsen, Germany

7. University Medical Center Göttingen, Goettingen, Germany

Background: Evaluation of cardiac function including strain is crucial for the management of cardiac patients and can reliably be performed using cardiovascular magnetic resonance (CMR) imaging. However, impaired imaging quality using standard CINE bSSFP (CINE) sequences may occur in arrhythmias (e.g. atrial fibrillation) limiting this approach. In contrast real time bSSFP (RT) provides single beat images allowing functional analysis. Our objectives were to show feasibility and comparability of CMR feature tracking (CMR-FT) in RT images of volunteers in sinus rhythm (SR) and of patients in atrial fibrillation (AF).

Methods: For determination of strain parameters 29 patients in AF and 20 volunteers in SR were scanned on a 3 T scanner (Skyra, Siemens, Germany). Imaging included standard CINE and RT using radial acquisition and NLINV reconstruction (temporal resolution 33 ms; spatial resolution 1.6 mmx1.6 mm) in short-axis orientation (SA), two (2CV) and four chamber views (4CV). CMR-FT (3 repetitions per slice; QStrain Medis, Leiden, The Netherlands) was performed to quantify left ventricular global longitudinal strain (EII), global radial strain (Err) and global circumferential strain (Ecc). For RT three consecutive beats of each sectional plane were selected. Slices with insufficient tracking in more than 33% of the tracking points were excluded. Correlation of CINE and RT values were determined and intra- and interobserver (2 observers) variability were assessed applying Bland-Altman analysis, intraclass correlation coefficients and coefficient of variation.

Results: In RT software based sorting problems occurred in 7.1% of the images in SR and 6.3% of those in AF. Due to tracking failures caused by irregular contours in low image quality 14.7% of the RT and 19.6% of the CINE images were excluded in AF patients with no exclusions in volunteers. A significant correlation for CINE and RT was found for Ecc and EII in all sectional planes, with a trend of higher absolute values for EII in CINE vs RT. For Err only SR 2CV did not correlate significantly. (table 1, figure 1) In general, RT showed better image quality resulting in less tracking failures for patients with AF than CINE.

Conclusion: CMR-FT can be applied to images acquired using RT for Ecc, EII and Err in all planes. RT imaging improves yield of images and the whole performance of image analysis and interpretations in irregular heartbeats such as in atrial fibrillation. Functional analyses based on RT sequences carry high potential for optimized clinical assessments e.g. deformation imaging under ergometry stress in different clinical scenarios.

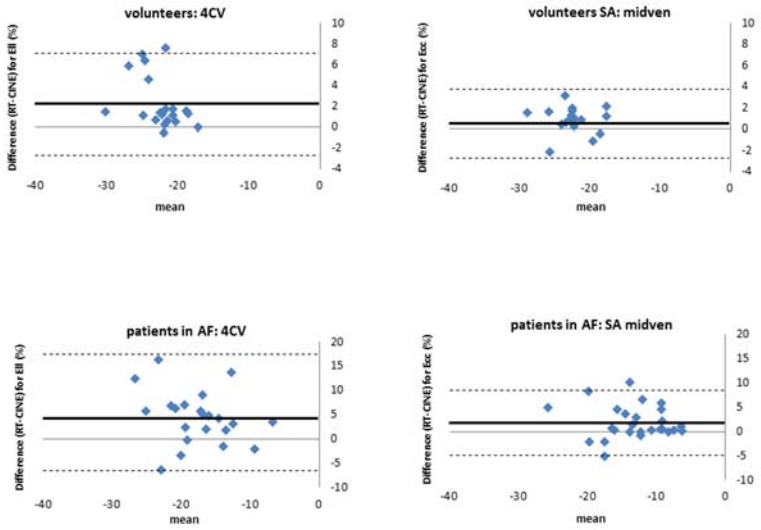

Fig 1: Bland-Altman plots with limits of agreement (95% confidence intervals) demonstrate the difference between global left ventricular ECC and global left ventricular Ell for RT and CINE in volunteers (sinus rhythm) and patients (atrial fibrillation)

Comparison of CMR-FT derived parameters for images in SSFP real time (RT) and Cine bSSFP during sinus rhythm and atrial fibrillation and Pearson correlation.

		normal volunteers in sinus rhythm (n=20; age 22-34; 8 male)				patients in atrial fibrillation (n=29; age 35-92; 21 male)			
		RT mean (SD)	CINE mean (SD)	r	p	RT mean (SD)	CINE mean (SD)	r	p
Ell [%]	**2 CV**	-22.37 (3,05)	-23.11 (3.01)	0.75	<0.001	-15.6 (6.1)	-18.5 (7)	0.004	0.005
	4 CV	-21.23 (2,74)	-23.4 (3.67)	0.73	<0.001	-14.9 (5.0)	-19.5 (6.3)	0.55	0.008
Ecc [%]	**SA apical**	-17.2 (2.12)	-19.46 (4.48)	0.91	<0.001	-15.4 (6.6)	-18.6 (7.2)	0.76	<0.001
	SA midven	-16.79 (2.88)	-17.29 (2.48)	0.82	<0.001	-12.0 (4.6)	-13.8 (5.1)	0.76	<0.001
	SA basal	-22.64 (2.95)	-23.93 (3.01)	0.78	<0.001	-13.8 (5.0)	-15.4 (4.1)	0.53	0.011
Err [%]	**2 CV**	54.34 (9.46)	58.85 (9.75)	0.39	0.091	35.6 (21.3)	45.6 (25.6)	0.86	<0.001
	4 CV	52.09 (9.24)	62.17 (15.16)	0.52	0.018	33.8 (12.0)	51.8 (23.1)	0.61	0.006
	SA apical	104.41 (96.1)	96.11 (49.12)	0.67	0.001	89.3 (46.7)	94.1 (45.3)	0.50	0.017
	SA midven	82.02 (28.69)	82.5 (24.18)	0.61	0.004	77.7 (33.6)	77.03 (30.8)	0.47	0.027
	SA basal	56.81 (16.65)	67.98 (23.51)	0.52	0.02	49.8 (28.9)	53,8 (26.2)	0.57	0.007

Results are reported as mean (SD). ECC, circumferential left ventricular (LV) strain; Ell, longitudinal LV strain, Err, radial LV strain, 2CV, two chamber view; 4CV, four chamber view; SA, short axis view. r, pearson correlation, values >4 indicating good correlation; p, < 0,05 level of significance

ID#: 371356

The heart in Wilson's disease. A 3-Tesla cardiac magnetic resonance imaging study.

Silvio Quick, MD[1]Nadine Katharina. Wässnig, MD[2], Felix M. Heidrich, MD[1], Marie Weidauer[3], Charlotte Hempel[3], Krunoslav Sveric, MD[3], Karim Ibrahim, MD[3], Uwe Speiser, MD[3]

1. Heart Center Dresden, Technische Universität Dresden, Dresden, Sachsen, Germany

2. Heart Center Dresden, Technische Universität Dresden, Sachsen, Germany

3. Heart Center Dresden, Technische Universität Dresden, Germany

Background: Wilson';s disease (WD) is an orphan disease, affecting 30 patients/ 1 million population. These patients show a reduced or absent function of a copper carrying protein, which leads to decreased copper elimination and copper accumulation in the liver and other organs. Pathological hepatic and neurological findings are typical characteristics. However, little is known about a copper overload on the heart. Aim of the present study was to evaluate cardiac manifestation of WD in one of the largest cohort of patients suffering from WD in Germany.

Methods: Patients with proven WD, based on clinical findings, laboratory examinations, copper content in liver biopsy and genetic examination, were referred to 3T cardiac magnetic resonance (CMR) including Cine-, T1-, T2-, T2*-, myocardial strain and late gadolinium enhancement sequences (LGE).

Results: 59 patients (age 45.3±17.4 years, 32 male) were compared to age and gender matched controls (45.5 ± 13.2, 32 male). At the time of presentation, cardiovascular abnormalities were not noted in any of the patients. In CMR mean left ventricular systolic function didn';t significantly differ between patients and controls (65.7 ± 4.4 % vs. 65.3 ± 2.8, p = 0.8). There was a small but nonpathological difference in the left ventricular volume (124.2 ± 38 vs. 139.4± 37, p = 0.34). WD patients showed a decreased RV systolic ejection fraction compared to controls (45.8 ± 3.2 % vs. 49.9 ± 7.9%, p = 0.001). However, none of the patients showed values below abnormality threshold. In contrast to that 6 of the 59 patients showed a reduced LV ejection fraction. Interestingly those patients were more severely affected by WD based on a special WD score. Furthermore, these Patients had elevated troponins and “myocarditis like pattern” in CMRI with evidence of edema and diffuse distribution LGE. In 20 patients (30%) and 5% (n=4) of the controls (p

Conclusion: Cardiac manifestation of WD seems possible, especially in the patients, who were severely affected by the disease. CMR is capable of revealing subclinical pathological findings. Cardiac involvement as fibrosis may affect prognosis in WD. Whether left ventricular clefts are related to genetic aberrations will be further investigated.

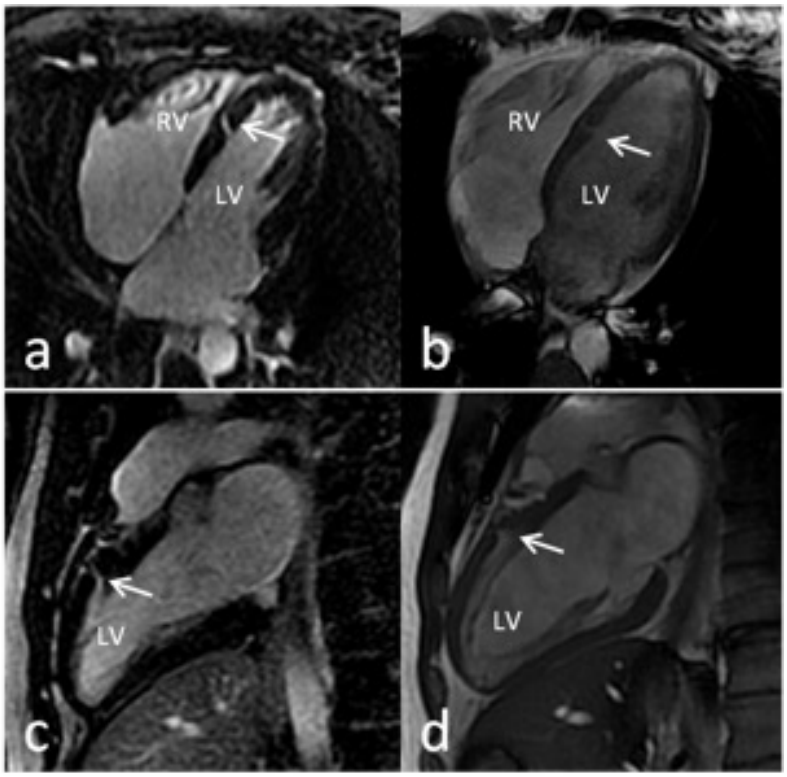

Left ventricular clefts in 2 different patients. A and C late gadolinium enhancement images, B and D cine sequences.

ID#: 371341

Cardiac magnetic resonance imaging to differentiate acute NSTEMI from acute ACS-like myocarditis

Enver Guner. Tahir, MD[1] Sebastian Bohnen, MD[2], Eric Freiwald[3], Martin Sinn, MD[4], Kai Muellerleile, MD[5], Maxim Avanesov, MD[6], Jitka Starekova, MD[5], Malte L. Warncke[7], Christian Stehning, PhD[8], Ulf Radunski, MD[5], Gerhard Adam, MD[9], Gunnar Lund, MD[9]

1. University Medical Center Hamburg-Eppendorf, Hamburg, Hamburg, Germany

2. University Heart Center Hamburg, Hamburg, Germany

3. Institute of Medical Biometry and Biostatistics, Germany

4. Diagnostic and Interventional Radiology, University Hospital Eppendorf, Hamburg, Germany, Hamburg, Germany

5. University Medical Center Hamburg-Eppendorg, Hamburg, Germany

6. UKE, Hamburg, Germany

7. Universitätsklinikum Hamburg Eppendorf, Germany, Hamburg, Germany

8. Philips Research Laboratories, Hamburg, Germany

9. University Medical Center Hamburg-Eppendorf, Hamburg, Germany

Background: Cardiac magnetic resonance (CMR) techniques including T2w and LGE imaging may have the potential to differentiate acute non-ST-segment elevation myocardial infarction (NSTEMI) from acute ACS-like myocarditis (ACSM). We investigated the clinical value of a separate and a combined use of different CMR techniques to discriminate NSTEMI from ACSM.

Methods: Cine, LGE and T2w CMR imaging were performed on a 1.5 T scanner (Philips, Achieva) in 20 patients with NSTEMI, 20 patients with ACSM and 20 controls. The CMR data were anonymized and visually evaluated in random manner by an independent observer blinded to all clinical information. The observer assigned the randomly presented CMRs to NSTEMI, ACSM or normal based on the observed pathological findings. At first, the available sequences were analyzed separately and then a combined evaluation of all three sequences was performed. The accuracy was calculated for each approach.

Results: Cine imaging alone had low accuracy for NSTEMI (AUC 0.50) and ACSM (AUC 0.50). T2w imaging alone had a good accuracy to detect NSTEMI (AUC 0.83) and ACSM (AUC 0.75). LGE also allowed a good identification of NSTEMI (AUC 0.75) and ACSM (AUC 0.83). A combination of all three techniques also resulted in the best accuracy for NSTEMI (AUC 0.83) and for ACSM (AUC 0.86). Compared to Cine imaging alone the other two approaches were significantly superior (T2w ($P<0.01$), LGE ($P<0.01$)) and combined approach ($P<0.0001$).

Conclusion: Differentiation between NSTEMI and ACSM is possible by using standard CMR techniques without the need for any clinical information. The best accuracy was achieved by a combined use of standard CMR sequences. CMR may have the potential to act as a gate keeper for further management of patients with NSTEMI and ACSM.

ID#: 371342

Differences of left and right heart involvement in patients with acute myocarditis.

Silvio Quick, MD[1] Nadine Katharina. Wässnig, MD[2], Matthias Lohr[3], Krunoslav Sveric, MD[3], Karim Ibrahim, MD[3], Uwe Speiser, MD[3]

1. Heart Center Dresden, Technische Universität Dresden, Dresden, Sachsen, Germany

2. Heart Center Dresden, Technische Universität Dresden, Sachsen, Germany

3. Heart Center Dresden, Technische Universität Dresden, Germany

Background: The purpose of the present study was to evaluate left and right heart involvement of patients with acute myocarditis.

Methods: CMR cine data of 37 patients with AM diagnosis by CMR according to the Lake Louise criteria as well as the data of 37 healthy were retrospectively analyzed. Analysis of global and segmental strain and strain rates of both ventricles were performed using a Feature Tracking Software. Follow up cMRI and data analysis was performed on an average of 5.1 months after the first presentation.

Results: Patients with AM showed no significant difference in right and left ventricular systolic function and dimensions compared to control group (table 1). In contrast to that global longitudinal strain (GLS) and global circular strain (GCS) were significantly reduced in patients compared to controls. Right ventricular strain parameters didn';t significantly differ between both groups (table 1).
In regard to LV and RV ejection fraction, we did not observe a significant difference between the parameters of patients at the initial presentation and during follow up. However GLS significantly improved in follow up examination (table 1).
There was a moderate to strong correlation between strain parameters GLS/GCS and extend of LGE (r= 0.51 and 0.53, $p < 0.05$). However, a negative correlation was also detected for LV-ejection fraction and LGE extent ($r = -0.55$, $p = 0.02$).
In the segmental myocardial strain analysis, we couldn';t detect any significant relationship between strain parameters and edema or capillary leakage. LGE extent was highest in basal and mid inferolateral segments. Patients with an impaired right ventricular function (< 40%) showed a reverse pattern of LGE, with highest amount in the septal segments (Figure 1). Furthermore regional septal strain was significantly reduced, while strain of the free lateral wall was preserved.

Conclusion: Myocardial strain imaging parameters, in particular GLS and GCS, are capable to detect subclinical changes in patients suffering from acute myocarditis, which were not detectable by LV-ejection fraction. LV-strain parameters are strongly correlated to the extent of LGE, however no superiority to LV-ejection fraction was evident. Reduced RV-ejection fraction is mainly due to reduced contractility of the interventricular septum and not to the lateral free wall.

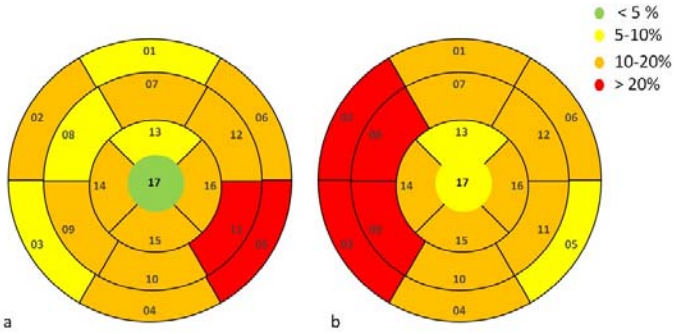

LGE distribution of patients with an preserved RV-ejection fraction (a) and reduced RV-ejection fraction (b)

Left and right ventricular function and volumes

	Myocarditis at presentation	Myocarditis at follow up	p-Value	Controls	p-Value
Left ventricle					
EF in %	61.5 ± 12.7	64.4 ± 8.6	0.2	64.7 ± 12.5	0.19
EDV in ml	145.8 ± 36.7	137.4 ± 30	0.06	150.7 ± 35.9	0.55
ESV in ml	57 ± 33.5	49.7 ± 21	0.1	53.5 ± 13.9	0.55
GLS in %	- 16.2	18	**0.023**	-18.1	**0.045**
GCS in %	-24.7	-25.2	0.2	-28.2	**0.012**
GRS in %	52	51.2	0.8	56.1	0.28
LGE in %	8.2	5.1	**0.001**		**0.001**
Right ventricle					
EF in %	47.6 ± 9.6	48.1 ± 9.1	0,9	49.5 ± 3	0.4
EDV in ml	151.4 ± 42	153 ± 35.5	0.67	140.6 ± 39.1	0.53
ESV in ml	77.4 ± 24.3	80.1 ± 24.9	0.4	74.8± 14.9	0.6
LS lat. free Wall	- 27.7 ± 9.2	- 28.3 ± 8.6	0.78	-29.1± 7.2	0.85
TS lat free Wall	20.3 ± 22.3	22.3 ± 21.8	0.89	-30.1± 47.2	0.27
EF, ejection fraction	EDV, end diastolic volume ESV, end systolic volume	GLS, global longituidinal strain GCS,global circular strain	TS, transversal Strain of the lateral free Wall LS, langitudinal Strain of the lateral free Wall		

		GRS, global radial strain			

ID#: 371426

Myocardial Scar Sub-Component Visualization using Multi-Parametric Cardiac Maps from a Single Scan

Zahra Hosseini[1] Nikolaos Tzemos[2], Raymond Yee[3], Maria Drangova, PhD[4]

1. Imaging Research Laboratories, Robarts Research Institute, London, ON, Canada

2. London Health Sciences, London, ON, Canada

3. London Health Sciences, Canada

4. Imaging Research Laboratories, Robarts Research Institute, ON, Canada

Background: Myocardial late gadolinium enhancement (LGE) has been demonstrated to predict patients'; response to interventional procedures such as cardiac resynchronization therapy in heart failure (HF). Assessment of myocardial scar and the identification of its sub-components have been of interest for those studying left ventricular (LV) remodelling and risks of sudden cardiac death. Non-invasive means of accomplishing these goals often include multiple imaging sequences (acquisition with and without fat-suppression, in addition to LGE), resulting in inevitably longer imaging sessions. In addition, appropriate selection of imaging parameters is crucial in the success of these imaging sessions. Recently, a new non-contrast based technique utilizing the information obtained from multi-echo GRE (ME-GRE) complex data has been developed. We demonstrate the robustness of this approach in healthy volunteers and present its application in HF patients.

Methods: Our institutional research ethics board approved this study and informed consent was obtained from all participants. Five healthy volunteers were scanned at 3T using a 4-echo 2D dark-blood imaging sequence. Short-axis, 2-chamber and 4-chamber long-axis images were acquired from the volunteers with the following imaging parameters: TR/TE/ESP: 940/2.23/1.27 ms, in-plane resolution: 1.5 × 1.5 mm^2, slice thickness: 6.0 mm, FA: 20°, BW: 1150 Hz/px, GRAPPA: 2. Four HF patients were also recruited and scanned with the same imaging protocol. In addition, the patients underwent LGE imaging 6-minutes after intravenous administration of contrast (0.1 mmol/kg - Gadovist). Complex channel ME-GRE data were saved. Quantitative R2*-, B0-, local frequency shift (LFS) and fat-fraction (FF) maps of the heart were generated for each channel using a channel-by-channel non-iterative phase error correction approach (Fig. 1) prior to combination.

Results: Example quantitative myocardial maps are shown from a healthy volunteer (Fig. 2) and an HF patient (Fig. 3). Notably, processing prior to channel combination renders visualization of coronary vessels (arrows, Fig. 2) and myocardium possible in all regions of the heart – even those adjacent to the lung interface. The FF map of the patient';s image (Fig. 3) demonstrates high signal within the myocardial wall and a decrease in LFS in the region of late gadolinium enhancement, suggesting that the quantitative maps can distinguish sub-components of myocardial scar, including fatty infiltration (FF) and collagen (LFS). An increase in R2* is also associated with the scar region.

Conclusion: Channel-by-channel processing of phase data results in robust quantitative myocardial maps of FF, LFS, R2*, despite proximity to lung, and is a promising tool for non-contrast LV scar characterization.

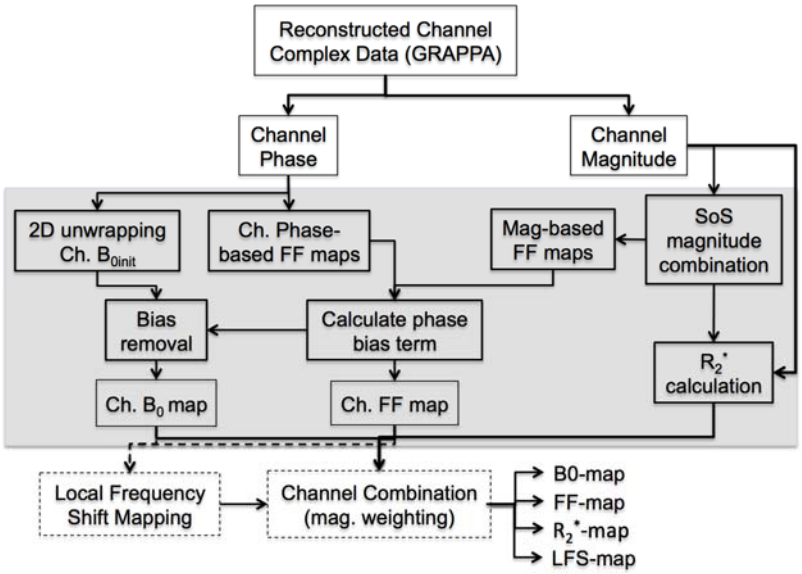

Figure 1: Flow diagram demonstrating the processing steps for generating single-channel quantitative maps prior to application of channel combination.

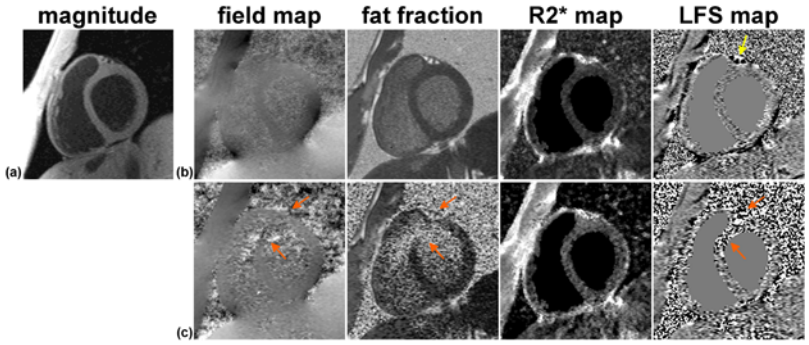

Figure 2: Short axis channel-combined magnitude image is shown as a reference in (a). Multi-parametric quantitative myocardial maps (healthy volunteer) generated via the steps of Fig. 1 are shown in (b). For comparison, the same maps generated using channel-combined complex data are also shown (c).

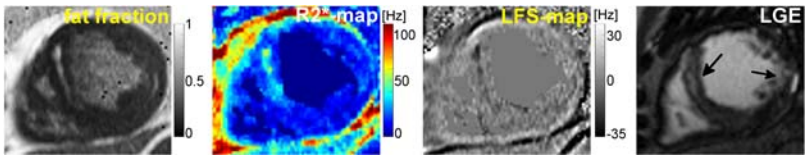

Figure 3: Sub-components of LV scar are clearly distinguishable on the multi-parametric quantitative maps. Clear delineation of fatty infiltration is seen on the fat-fraction map and scar tissue (corresponding to enhancement in LGE image) is clearly visible on the LFS-map. R2* is also elevated in the septal scar region.

ID#: 371453

Left atrial blood flow dynamics and hemostasis after electrical cardioversion of atrial fibrillation

Merih Cibis, PhD[1] Tomas L. Lindahl, MD, PhD[2], Tino Ebbers, PhD[3], Lars O. Karlsson, MD, PhD[4], Carl-Johan Carlhall, MD, PhD[5]

1. Linkoping University, Rotterdam, Netherlands

2. Linkoping University, Linköping, Sweden

3. Linkoping University, Linkoping, Ostergotlands Lan, Sweden

4. Linkoping University, Sweden

5. Linkoping university, Sweden

Background: Electrical cardioversion of atrial fibrillation is followed by a transient mechanical dysfunction of the atria, known as atrial stunning. During atrial stunning, the risk of post-cardioversion thromboembolism persists which may be associated with abnormal left atrial blood flow patterns. Our objective was to investigate left atrial 4D blood flow dynamics and hemostasis during left atrial stunning and at restored left atrial mechanical function.

Methods: Fourteen patients with atrial fibrillation were included. 4D Flow (figure 1) and morphological CMR data and blood samples were collected at two time-points: 2-3 hours (Time-1) and 4 weeks (Time-2) following cardioversion. We calculated left atrial mean velocity (V_{mean}), peak velocity (V_{peak}), mean vorticity (ω_{mean}) and near-wall vorticity (ω_{wall}) at early diastole and late diastole for both time-points. We investigated blood stasis by quantifying the volume of stasis ($Volume_{stasis}$) and the duration of stasis (T_{stasis}). Furthermore, hemostasis markers thrombin-antithrombin (TAT), sP-selectin, D-dimer and Willebrand Factor were analyzed. The relation between CMR-based stasis parameters and hemostasis markers were evaluated by linear regression analysis.

Results: The heart rate decreased (61 ± 7 vs. 56 ± 8 bpm, p=0.01) and the maximum change in the left atrial volume increased (8 ± 4 vs. 22 ± 15 %, p=0.009) over time. From time-1 to time-2: At early diastole, only V_{peak} decreased (56 ± 13 vs. 46 ± 9 cm/s, pmean (10 ± 2 vs. 15 ± 3 cm/s, ppeak (27 ± 8 vs. 52 ± 15 cm/s, pmean (24 ± 3 vs. 27 ± 3 1/s, pwall (26 ± 4 vs. 32 ± 4 1/s, pstasis (68 ± 11 vs. 57 ± 8 %, p=0.002) and $Volume_{stasis}$ (14 ± 9 vs. 9 ± 7 %, p=0.04) decreased. TAT also decreased over time (5.2 ± 3.3 vs. 3.3 ± 2.2 ug/L, p=0.008). We found a significant correlation between TAT and $Volume_{stasis}$ (r^2=0.69, pstasis (r^2=0.34, p=0.04) at Time-2 (figure 2).

Conclusion: In this longitudinal study, left atrial 4D Flow was altered and blood stasis was elevated at left atrial stunning compared to those at restored left atrial mechanical function. The blood coagulation marker TAT was also elevated at atrial stunning. The association between blood stasis and hypercoagulability suggests that assessment of left atrial 4D flow may add to the risk stratification of left atrial thrombus formation in patients with atrial fibrillation related atrial stunning.

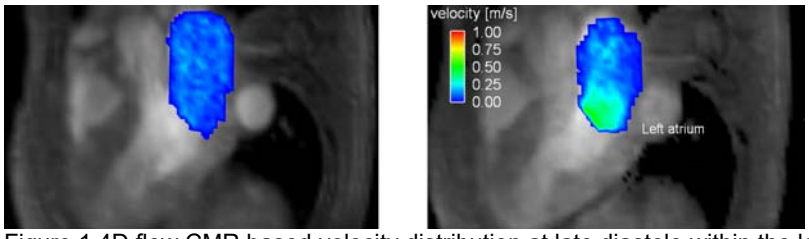

Figure 1 4D flow CMR based velocity distribution at late diastole within the left atrium in a patient with a history of persistent AF (Left panel) during left atrial stunning 2 hours after cardioversion and (Right panel) at restored left atrial mechanical function 4 weeks after cardioversion.

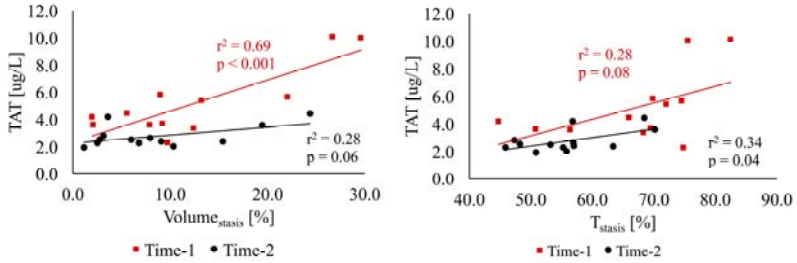

Figure 2 Linear regression analysis between: (Left panel) TAT vs. volume of stasis (Volumestasis) as a percentage of the LA volume at Time-1 (red) and Time-2 (black); (Right panel) TAT vs. duration of stasis (Tstasis) as a percentage of the cardiac cycle at Time-1 (red) and Time-2 (black).

ID#: 371455

High-resolution intracranial vessel wall MR imaging allows for black-blood angiographic visualization of the lenticulostriate artery at 3T: A validation against 7T TOF-MRA

Zihao Zhang, Ph.D.[1] Zhaoyang Fan, Ph.D.[2], Qingle Kong[1], Jing An, M.D.[3], Yan Zhuo, Prof.[1], Qi Yang, Ph.D.[4]

1. State Key Laboratory of Brain and Cognitive Science, Beijing MR Center for Brain Research, Institute of Biophysics, Chinese Academy of Sciences, China (People's Republic)

2. Biomedical Imaging Research Institute, Cedars-Sinai Medical Center, CA

3. Siemens Shenzhen Magnetic Resonance Ltd., China (People's Republic)

4. Xuanwu Hospital, China (People's Republic)

Background: The lenticulostriate artery (LSA) supplies the blood to the basal ganglia and its vicinity and impairment of the microvessel can lead to neurologic diseases such as strokes and vascular dementia. Noninvasive imaging of LSAs could be clinically useful to understand the mechanisms of microvascular pathologies or guide early therapeutic intervention. While 7T TOF-MRA has shown exquisite LSA visualization due to obtainable high spatial resolution, there are few MR methods available at clinical field strengths. In this study, we proposed to use a recently developed high-resolution intracranial vessel wall MR imaging technique to visualize the LSA in a black-blood (BB) fashion at 3T. The vessel-delineation quality of the BB-MRA approach was validated through a comparison with 7T TOF-MRA.

Methods: Twelve healthy volunteers were scanned with both BB-MRA at 3T (Siemens Prisma) and TOF-MRA at 7T (Siemens Magnetom). The BB-MRA was acquired using a recently developed inversion-prepared 3D variable-flip-angle turbo spin-echo (TSE) sequence with following imaging parameters: spatial resolution = $0.53x0.53x0.53mm^3$, TR/TE = 900/13 ms, echo train length = 52, acquisition time = 8min10sec. TOF-MRA was acquired with a spatial resolution of $0.23x0.23x0.34mm^3$ and a scan time of 7min23sec. Vascular tracing of middle cerebral arteries (MCAs) and LSAs was manually performed on the minimal and the maximal intensity projections (thickness 0.92mm) of BB-MRA and TOF-MRA, respectively. On the vascular skeletons, the number of stems and branches of LSAs were counted. The most prominent branch was chosen to measure the contrast-to-noise ratio (CNR), the length, and the distance between the origin and the visible extremity.

Results: In 9 out of 12 cases, the extracted vascular trees of TOF-MRA and BB-MRA are visually in good agreement (Fig. 1a). In remaining 3 cases, BB-MRA missed some tiny branches and distal segments of the LSAs, as Fig. 1b displays. The two acquisitions showed similar numbers of the LSA stems, but the number of branches in BB-MRA was smaller than in TOF-MRA in 3 cases (Table 1). The mean CNRs along the dominant branches are shown in Fig. 2. In both TOF-MRA and BB-MRA, CNR of LSA branches decreased with the distance to the parent MCA. Overall, 7T TOF-MRA yielded higher CNR than 3T BB-MRA. The Bland-Altman plots in Fig. 3 show similar distances measured in BB-MRA and TOF-MRA, but shorter length in BB-MRA.

Conclusion: Our study demonstrated the feasibility of using intracranial vessel wall MR to achieve BB-MRA of LSAs at a clinically available 3T system. Compared to 7T TOF-MRA, this approach is capable of depicting LSAs, particularly the stems and the proximal segments, with comparable image quality.

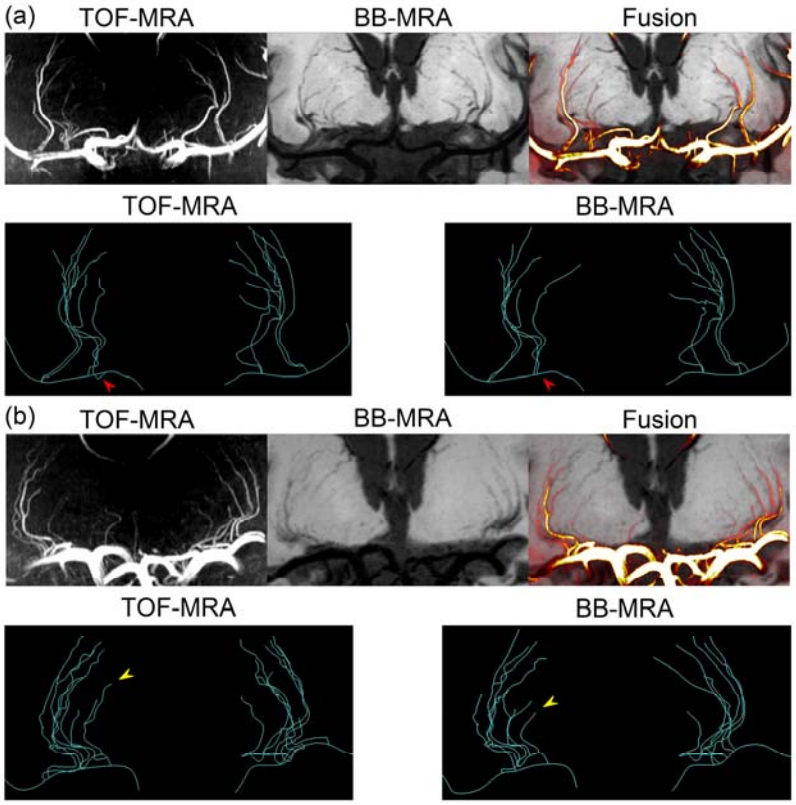

Figure 1 . (a) The coronal MIP of TOF-MRA and BB-MRA of one volunteer (slab thickness = 20mm), and their fusion view. The extracted vascular trees show high consistency between TOF-MRA and BB-MRA. The red arrowheads point to the mismatched proximal part of the LSAs. (b) The MIPs and the fusion view of another volunteer (slab thickness = 20mm). The vascular trees show more end branches of LSAs in TOF-MRA than BB-MRA, as pointed by the yellow arrowheads.

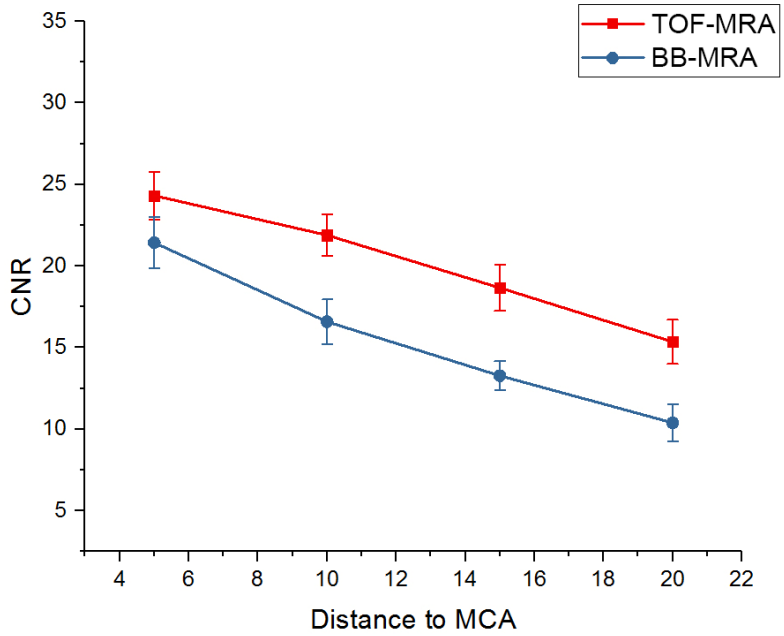

Figure. 2 The CNR of lumens to tissues measured in the images of 7T TOF-MRA and 3T BB-MRA. p = 0.204, 0.033, 0.001 and 0.003 for positions with 5, 10, 15, and 20mm distance to MCA, paired samples t test.

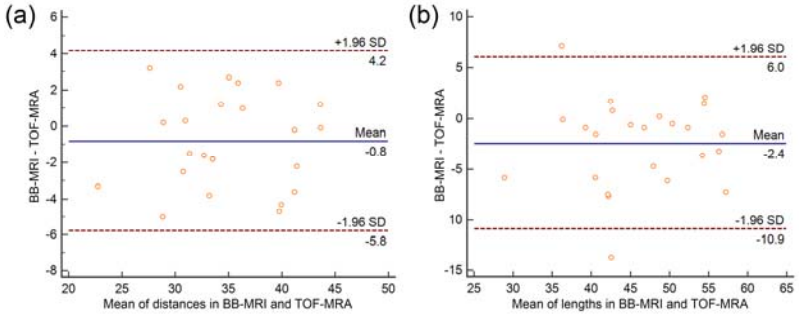

Figure 3. Bland-Altman plots represent the differences of (a) the distances and (b) the lengths measured in the predominant vascular trees of BB-MRA and TOF-MRA. p = 0.129 for distances, p = 0.011 for lengths, paired sample t test.

Table 1 . The number of stems and branches of perforating arteries visualized by 7T TOF-MRA and 3T BB-MRA, in left and right hemispheres respectively.

Subject	Left Hemisphere				Right Hemisphere			
	Stems		Branches		Stems		Branches	
	TOF-MRA	BB-MRA	TOF-MRA	BB-MRA	TOF-MRA	BB-MRA	TOF-MRA	BB-MRA
S01	2	2	5	4	3	3	6	5
S02	5	4	10	8	5	4	10	8
S03	3	3	7	4	5	5	12	10
S04	5	5	6	6	4	4	6	6
S05	5	5	11	7	5	5	10	10
S06	3	3	9	8	4	4	6	6
S07	4	4	7	6	2	2	6	5
S08	4	3	7	8	4	4	8	9
S09	4	5	10	10	5	5	9	8
S10	5	3	7	6	4	4	9	7
S11	4	4	6	6	4	4	6	5
S12	4	4	7	7	5	6	7	8

p = 0.486 for LH stems, *p* = 0.262 for LH branches, *p* = 0.877 for RH stems, *p* = 0.410 for RH branches, Mann-Whitney u test.

ID#: 371459

Respiratory motion correction for 4D Flow MRI using golden radial phase encoding

Daniel Giese, PhD[6] Christoph Kolbitsch, PhD[1], Claudia Prieto, PhD[2], Kilian Weiss, PhD[3], David Maintz, MD[4], Tobias Schaeffter, PhD[5]

1. Physikalisch-Technische Bundesanstalt (PTB), Braunschweig and Berlin, Germany, Berlin, Berlin, Germany

2. King's College London, England, United Kingdom

3. Philips Healthcare, Hamburg, Germany, Nordrhein-Westfalen, Germany

4. University Hospital of Cologne, Department of Radiology, Nordrhein-Westfalen, Germany

5. Physikalisch-Technische Bundesanstalt (PTB), Braunschweig and Berlin, Germany, Berlin, Germany

6. University Hospital Cologne

Background: 4D Flow CMR remains a time-consuming acquisition, also due to the subjects'; respiration. Respiratory gating can lead to low scan efficiency and long and unpredictable scan times, highly dependent on breathing patterns.
We present 4D Flow Golden Radial Phase Encoding (GRPE) which allows for respiratory motion-corrected 4D Flow CMR. Data can be binned into multiple respiratory phases in order to estimate respiratory motion and to assess respiratory dependent flows.

Methods: GRPE is a 3D Cartesian sampling scheme with phase encoding points located along radial lines in the ky-kz plane (Fig. 1). Data is acquired continuously over multiple cardiac and respiratory cycles using a golden angle increment. Data can be retrospectively binned based on both ECG and respiratory surrogate signals providing quantitative 4D Flow images at different breathing phases (Fig. 1).
GRPE was implemented in combination with 4D Flow on a 3T Ingenia (Philips, Best, the Netherlands) using a 32-channel cardiac coil. A square FOV of 250mm^3 with an isotropic resolution of 2.5mm^3 was chosen (TR/TE: 3.3/2ms, FA: 7°). The ECG signal was recorded as a surrogate signal. 800 GRPE lines per flow encoding direction were acquired leading to a total, predicted scan time of 16min. A self-calibrated iterative kt-SENSE reconstruction was used to obtain 4D Flow images re-binned into 20 cardiac phases in end-inspiration (INSP) and end-expiration (EXP) using 25% of the total data each (Fig. 1). Non-rigid respiratory motion was estimated between INSP and EXP yielding motion fields that were used to transform INSP to the same motion state as EXP. Averaged images were obtained by averaging EXP and INSP without motion correction (AVG) and by averaging EXP and INSP transformed to the same motion state as EXP (Moco-AVG).

Results: AVG images show blurring, impairing the visualization of small vessels (Fig. 2). Moco-AVG images show improved image quality and restored flow profiles.
Flow curves (Fig. 3) through the left and right pulmonary arteries indicate that the blood flow varies over the respiratory cycle, which is in agreement with previous studies. Flow in the aorta and main pulmonary artery however did not show a dependence on the breathing phase. Moco-AVG blood flow curves lie between INSP and EXP and describe an average of the blood flow over different respiratory phases.

Conclusion: We present a novel approach which yields respiratory-resolved 4D flow images in a single free-breathing acquisition allowing the reconstruction of time-resolved, respiratory motion-corrected 4D flow images in different respiratory states.

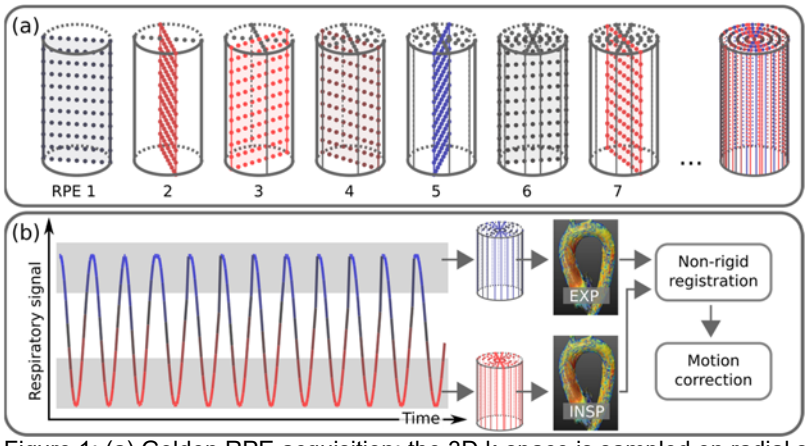

Figure 1: (a) Golden RPE acquisition: the 3D k-space is sampled on radial spokes in the ky-kz-plane which is rotated by the golden angle (111.24°) after each RPE step. (b) GRPE allows for retrospective binning of data into different respiratory motion states such as end-expiration (EXP) and end-inspiration (INSP). Non-rigid respiratory motion between EXP and INSP is determined and corrected for by transforming INSP to the same motion state as EXP.

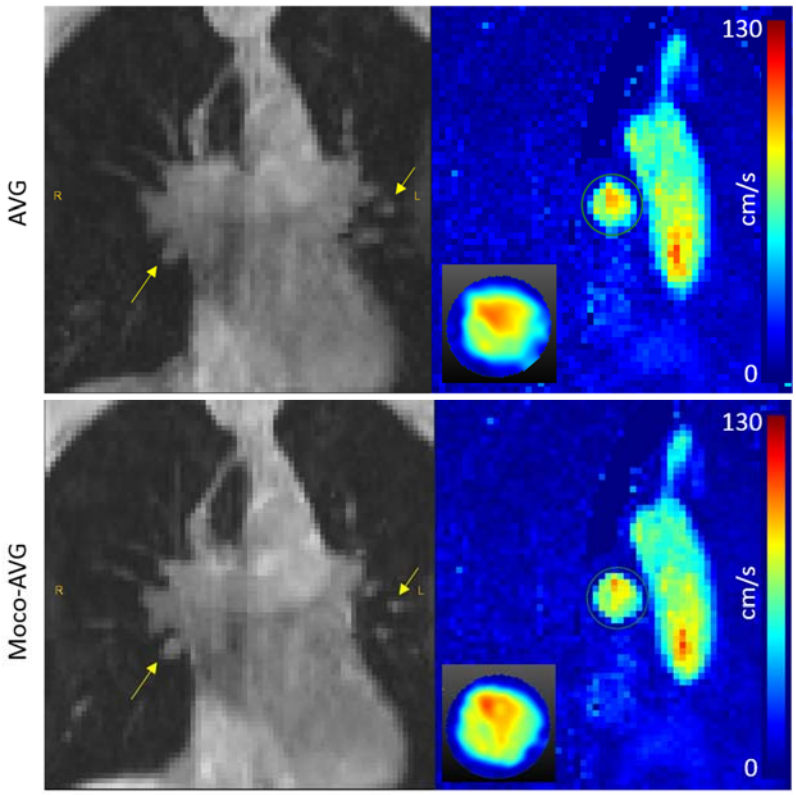

Figure 2: Respiratory motion leads to blurring of anatomical structures which can be clearly seen at small vessels in the lungs (yellow arrows) and also along the epicardium. This blurring also impairs the flow profiles of 4D flow images leading to distortions (elliptic rather than circular vessel cross sections) and blurred flow along vessel boundaries. Non-rigid respiratory motion correction improves visualization of anatomical features and ensures accurate flow profiles. AVG: average of EXP and INSP, Moco-AVG: average between EXP and INSP transformed to EXP motion state.

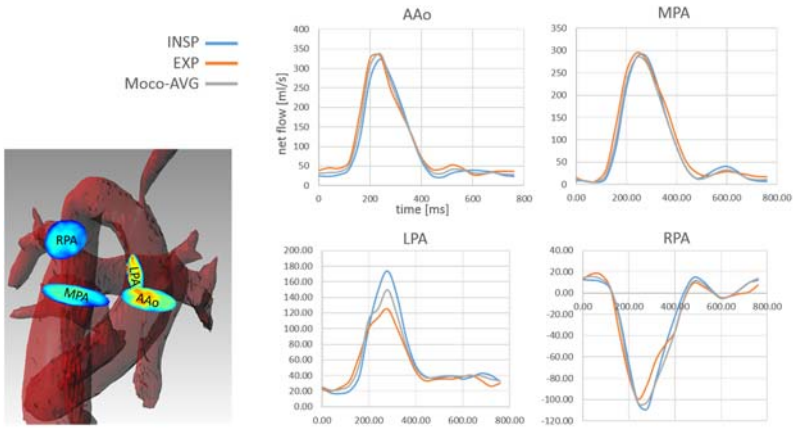

Figure 3: Resulting net flows in the four contours extracted from three different 4D Flow datasets: end-inspiration (INSP), end-expiration (EXP) and average between EXP and INSP motion-corrected to EXP (Moco-AVG). The ascending aorta (AAo) and main pulmonary artery (MPA) do not show a dependency on the respiratory cycle but the net-flow in the left and right pulmonary arteries (LPA and RPA) varies between end-inspiration and end-expiration. The Moco-AVG net flow curves lie between EXP and INSP. All ROIs were adapted to ensure the same location was selected in each motion state.

ID#: 371465

Myocardial remodeling and tissue characterization by CMR in endurance athletes

Soraya Merchan[1]Sandra Pujadas, Clínica Creu Blanca, Barcelona[2], Maite Doñate[3], Chi-Hion Li, Clínica Creu Blanca, Barcelona[3], Ana Cabanillas[4], Xavier Alomar[5], Guillem Pons-Lladó, MD, PhD[2], Francesc Carreras, MD, PhD[6], Ricard Serra-Grima[2]

1. Cardiac Imaging Unit, Cardiology Department, Salamanca University Hospital, Spain

2. Cardiac Imaging Unit, Cardiology Department, Hospital de la Santa Creu i Sant Pau, Universitat Autònoma de Barcelona, Spain

3. Cardiac Imaging Unit, Cardiology Department, Hospital de la Santa Creu i Sant Pau, Universitat Autònoma de Barcelona,, Spain

4. Clínica Creu Blanca, Barcelona, Spain

5. Clinica Creu Blanca. Barcelona, Spain

6. Cardiology Unit, Hospital de la Santa Creu i Sant Pau (HSCSP), Barcelona,, Catalonia, Spain

Background:

There is still some controversy about the benignity of structural changes observed in athlete';s heart, especially regarding the observation of increased biomarkers and the presence of myocardial fibrosis (MF). Our purpose was to evaluate by cardiovascular magnetic resonance (CMR) the presence of diffuse as well as focal MF in a series of high-performance veteran endurance athletes.

Methods: Thirty-four veteran healthy male endurance athletes, still being in regular training, with more than 10 years of training underwent a CMR. A cardiopulmonary exercise test was also performed to assess their maximal physical performance. The control group consisted in 12 non-trained normal individuals.

Results:

We found an increase in both, right and left ventricular volumes in the athlete';s group when compared with controls. There was no increase in indexed left ventricular myocardial mass despite of a significantly increased maximal myocardial wall thickness in comparison to controls. Native T1 values and extracellular volume (ECV) were normal in all cases. We did not find differences in native T1 values and ECV between both groups.In 3 athletes (9%) non-ischemic late gadolinium enhancement (LGE) was observed. We did not find a correlation between total training volume and presence of LGE nor with the ECV value.

Conclusion: Our results show that the majority of veteran endurance athletes present with myocardial remodeling without myocardial fibrosis as a physiological adaptive phenomenon. In the only 3 athletes with focal MF the LGE pattern observed suggests an intercurrent event not related with the remodeling phenomenon.

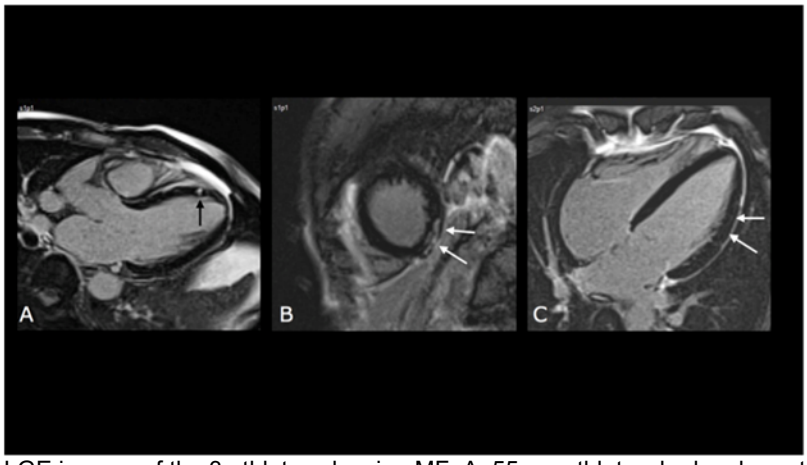

LGE images of the 3 athletes showing MF. A. 55 y.o athlete who has been training 10 hours/week in the last 28 years. Mesocardial LGE in the apical-septal wall is shown in a 3-chamber view image; B. 51 y.o athlete training 7 hours/week in the last 30 years. The short-axis view shows subepicardial LGE in the inferior apical wall; C. 55 y.o

athlete training 8 hours/week in the last 30 years. Mild intramyocardial LGE is the lateral wall is shown in the 4-chamber view.

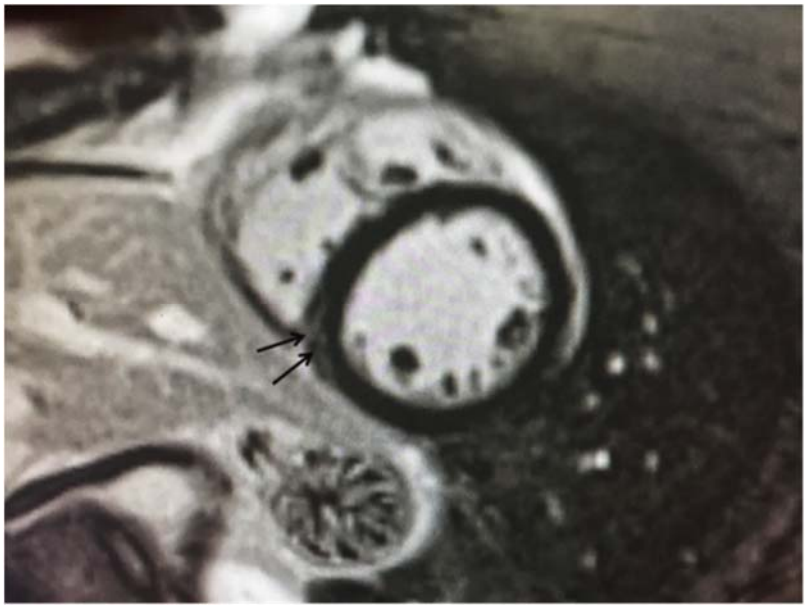

. 40 y.o male with a training history of 2 hours/week during 6 years (control group). A mid-ventricular short-axis view shows mild LGE in the inferior RV-LV junction.

Demographic and functional characteristics of endurance athletes and control subjects

	Athletes (n= 34)	Controls (n= 11)	P value
Age (y.o)	48.18±7.48	42.36±13.43	n.s
BSA (m2)	1.80±0.11	1.89±0.14	n.s
Training Volume (h/week)	9.38±3.52	3.08±1.52	<0.05
Training history (yrs)	28.06±10.84	9.38±3.02	<0.05
Rest heart rate (bpm)	56.03±8.87	70.33±15.42	<0.05
VO2 peak (ml/min/Kg)	60±6.53		

Peak heart rate (bpm)	176.27±10.32		
RER max	1.14±0.07		

Data are presented as mean value±SD
BSA, body surface area; VO2 peak, maximal oxigen uptake; RER max, maximal respiratory exchange ratio

CMR results

	Athletes (mean±SD)	Controls (mean±SD)	P value	
LVEDV (ml)	193.65±31.67	155.92±26.30	<0.001	
LVEDV index (ml/m2)	107.53±15.94	81.33±10.71	<0.001	
LVESV (ml)	72.47±15.98	57.75±13.96	<0.001	
LVESV index (ml/m2)	40.29±8.59	30.08±6.32	<0.001	
LVEF (%)	62.53±4.89	63±5.15	0.779	
RVEDV (ml)	204.44±37.50	165.58±31.90	0.003	
RVEDV index (ml/m2)	113.59±19.83	86.42±13.57	<0.001	
RVESV (ml)	76.12±20.69	64.67±17.15	0.086*	
RVESV index (ml/m2)	42.38±11.61	33.83±7.85	0.023*	
RVEF (%)	62.91±6.24	61.5±5.27	0.488	
Ratio RV-LV	0.96±0.10	0.96±0.14	0.968	
LVM (g)	124.59±22.13	124.54±32.23	0.996	
LVM index (g/m2)	69±11.05	65.25±15.73	0.372	
Max Wall Thickness (mm)	11±1.33	8.50±2.65	<0.001*	
LA area(cm2)	28.03±3.71	24.67±4.16	0.013	

T1 Mapping				
Native T1 septal (ms)	943.59±52.58	984.13±36.82	0.006*	NS
Native T1Lat (ms)	925.3±45.90	960.25±29.77	0.029*	NS
ECV Septal	0.25±0.02	0.22±0.02	<0.001	NS
ECV Lat	0.24±0.04	0.17±0.08	0.006	NS
Hematocrit (%)	0.42±0.02	0.46±0.04	0.001*	S
DE*	3 (12%)	0		

LVEDV, left ventricular end-diastolic volume; LVEF, left ventricular ejection fraction; RVEDV, right ventricular end-diastolic volume; RVEF, right ventricular ejection fraction; LVM, left ventricular mass; LA, left atrial; ECV, extracellular volume; DE, delayed-enhancement

ID#: 371539

Measurements of normal myocardial T1, partition coefficient and extracellular volume at 3 Tesla using MOLLI, ShMOLLI and SASHA

Tarik Hafyane, MSC[1]Nadia Iannino, MD[2], Nikola Stikov, PhD[3], Michel White, MD[4], François-Pierre Mongeon, MD[4]

1. Montreal Heart Institute, Laval, PQ, Canada

2. Montreal Heart Institute, Belgium

3. Montreal Heart Institute, PQ, Canada

4. Montreal Heart Institute, Canada

Background:

Sequences using inversion recovery (MOLLI and ShMOLLI) or saturation recovery (SASHA) techniques have been proposed to measure myocardial T1. Myocardial T1 measurements hold many promises for diagnosis of cardiomyopathies. However, different sequences produce different T1 measurement for normal myocardium in-vivo, therefore hampering their widespread clinical application. Our aim was to provide reference values for native myocardial T1, multiple post-contrast myocardial T1 and extracellular volume (ECV) using MOLLI, ShMOLLI and SASHA sequences at 3T in a group of healthy volunteers.

Methods:

Healthy volunteers (25, mean age 49 years, 36% male) underwent a CMR exam using a clinical 3T MRI system (Magnetom Skyra, Siemens Healthcare, Erlangen, Germany) with an 18-channel phased-array cardiac coil. T1 measurement images were acquired in a midventricular short-axis slice using MOLLI 5(3)3, ShMOLLI and SASHA sequences before and 2 times (5 and 20 minutes) after the injection of 0,1 mmol/kg of Gadobutrol (Gadovist, Bayer, Leverkusen, Germany). Native and post-contrast myocardial T1 were measured using a dedicated software (cvi42, Circle CVI, Calgary AB, Canada) after manually delineating the left ventricular endocardial and epicardial contours on the inline generated T1 map. The gadolinium contrast partition coefficient (PC) in myocardium was calculated using one native and 2 post-contrast T1 measurements. The myocardial ECV was calculated with the formula: ECV = PC x (1-Hematocrit).

Results:

Myocardial T1 values obtained with the SASHA sequence were substantially higher ($P<0.0001$ for all comparisons) than those obtained with MOLLI (Figure 1, 1493.41±51.67 vs.1215.04±34.40 for native T1, 639.38±47.40 vs. 519.77±37.92 ms for 5 minutes post contrast T1 and 788.80±41.90 vs. 675.06±36.20 ms for 20 minutes post contrast T1) and ShMOLLI (Figure 1, 1493.41±51.67 vs. 1195.01±51.67 for native T1, 639.38±47.40 vs. 501.49±33.51 ms for 5 minutes post contrast T1 and 788.80±41.90 vs. 635.38±30.16 ms for 20 minutes post contrast T1). PC and ECV measured with the ShMOLLI sequence were significantly higher than those measured with MOLLI and SASHA (Figure 2).

Conclusion:

MOLLI, ShMOLLI and SASHA sequences produce substantially different values for myocardial T1 and ECV measurements. We provide reference values for each commercially available T1 measurement sequence at 3T. The magnitude of the difference between sequences is less pronounced with ECV, where normal averages range between 21 and 26%.

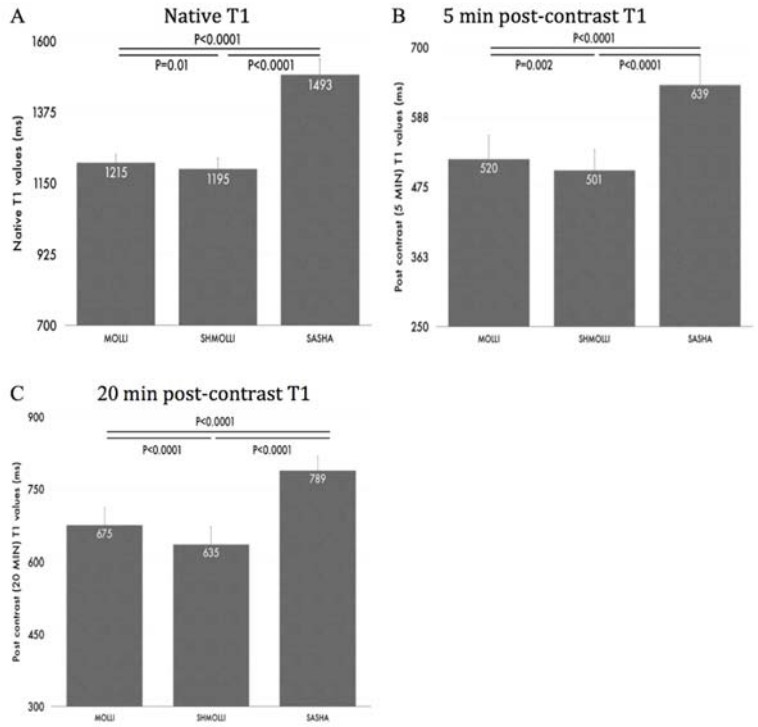

Figure 1: Myocardial native T1 (A), 5 minutes (B) and 20 minutes post-contrast injection (C) T1 measurements in a midventricular slice using MOLLI, ShMOLLI and SASHA sequences.

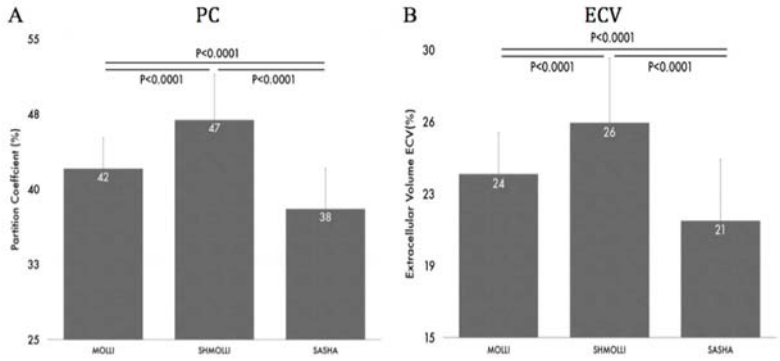

Figure 2: Myocardial partition coefficient (A) and extracellular volume (B) calculated in a midventricular slice using MOLLI, ShMOLLI and SASHA sequences derived T1 measurements.

ID#: 371500

Effects of food intake on Fontan hemodynamics assessed by a novel, dynamic CMR protocol

Jakob A. Hauser, MBBS[1] Alexander Jones, PhD[2], Bejal Pandya, MBBS[3], Vivek Muthurangu, MD[4]

1. University College London, Vienna, Wien, Austria

2. University of Oxford, United Kingdom

3. Barts Heart Centre, United Kingdom

4. Institute of Cardiovascular Science, University College London, England, United Kingdom

Background:

Food ingestion induces various short-term changes in cardiovascular physiology, including an increase in cardiac output (CO) and alterations in regional and global vascular resistances. In the univentricular (Fontan) circulation, abnormal fasting vascular resistance and low CO are thought to contribute to long-term complications such as protein losing enteropathy (PLE). We sought to describe the cardiovascular responses to a meal in Fontan patients.

Methods: Twenty-eight subjects (n=15 controls; median age 31 years [28-38]; n=2 with history of PLE) underwent fasting CMR flow measurement of the aorta (at sinus level and proximal to the iliac bifurcation) as well as the renal, carotid, celiac and superior mesenteric arteries (SMA). After drinking a high-energy liquid meal, this was repeated every ~7 minutes for ~50 minutes. Flow to the organs was quantified by RR-interval averaged spiral phase-contrast imaging within a single breath hold. Blood pressure was measured in 5-minute intervals to calculate vascular resistance through division by blood flow. Total arterial compliance was calculated as stroke volume / pulse pressure. Changes over time were assessed using multilevel linear regression and corrected for sex and age.

Results: In the fasting state, patients had significantly higher heart rates; total, mesenteric and lower limb vascular resistance; as well as lower stroke volume and a trend for lower total arterial compliance and lower CO. SMA resistance was significantly (~2-fold) higher in patients with PLE than in those without. Ingestion of the meal induced an overall drop in total, SMA and lower limb resistance. In the lower limb, this response was significantly more pronounced in patients as compared to controls. However, after 50 minutes postprandially, systemic and lower limb vascular resistance were still significantly higher in patients, whereas no difference was observed in the SMA. Moreover, postprandial SMA resistance was not different between patients with PLE and those without.

Conclusion: Patients with a univentricular circulation are able to produce a cardiovascular response to food ingestion similar to that of healthy subjects. This response appears to be largely independent of PLE status. By contrast, fasting hemodynamics, and particularly mesenteric vascular resistance, are abnormal in the Fontan physiology and, even more so, in patients with a history of PLE. This approach could aid identify patients at risk of poor outcome.

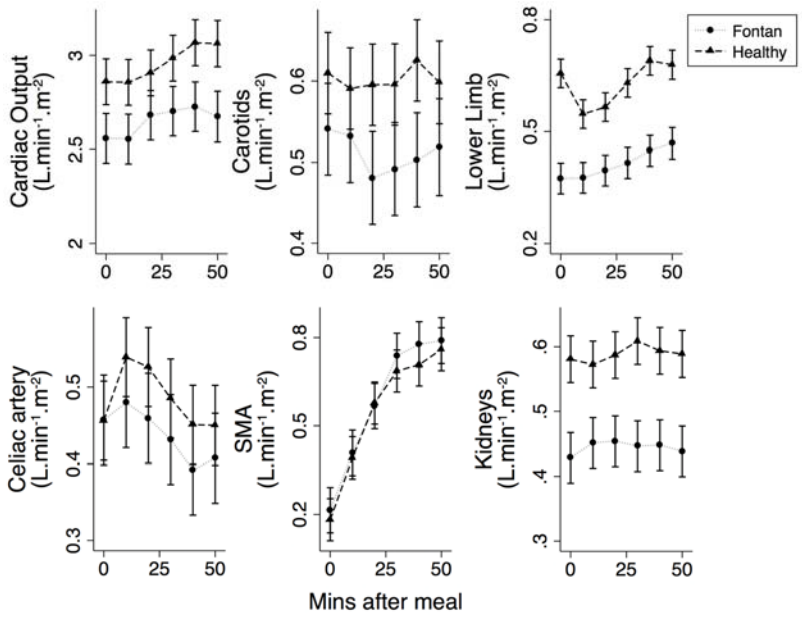

Global and regional flow response.

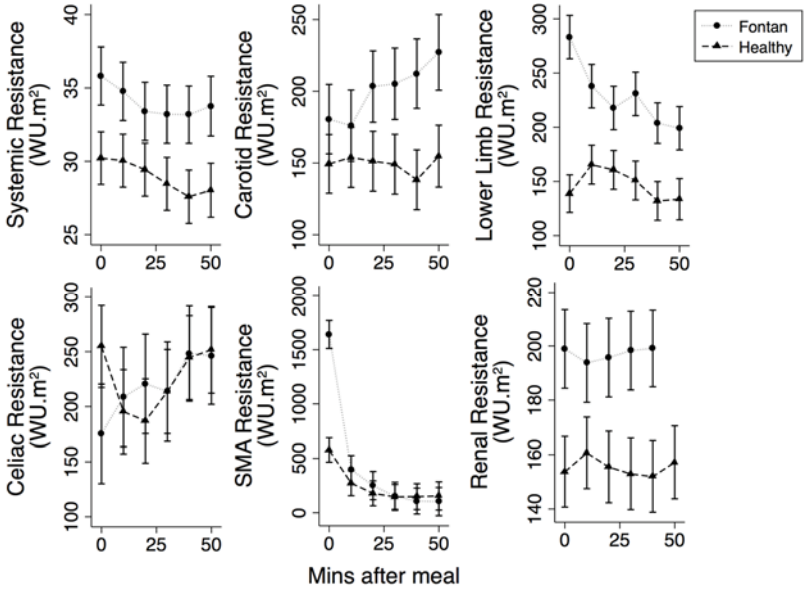

Global and regional resistance changes.

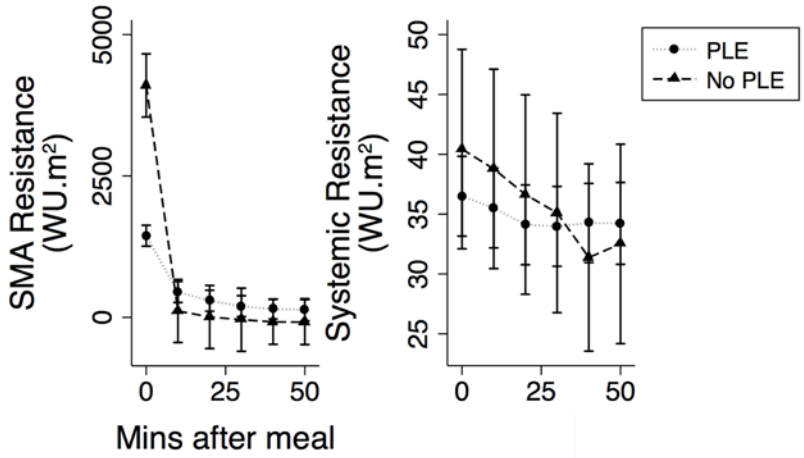

Effect of PLE-status on global and mesenteric resistances

ID#: 371054

Native myocardial T1 correlates with left ventricular volumes and function in patients treated with anthracycline

Iwan Harries, MBBCh BSc[1] Jonan Tan[2], Estefania De Garate, MD[3], Chris Lawton, PGC, BSC[1], Amardeep Ghosh Dastidar, MBBS(Hons), MRCP[3], Anna Baritussio, MD[3], Chiara Bucciarelli-Ducci, MD, PhD[3]

1. Bristol Heart Institute, Bristol, England, United Kingdom

2. University of Bristol, United Kingdom

3. Bristol Heart Institute, Bristol NIHR Biomedical Research Centre (Cardiovascular Section), University of Bristol, Bristol, England, United Kingdom

Background: The cardiotoxic effects of anthracycline chemotherapy have significant morbidity and mortality implications for cancer survivors. Native myocardial T1 mapping characteristics, determined by cardiovascular magnetic resonance (CMR) are known to be abnormal in patients treated with anthracycline. We sought to explore the relationship between native myocardial T1 mapping characteristics and cardiac structure and function.

Methods: An observational study of 126 consecutive adult cancer survivors referred for CMR (1.5T) was performed. Patients not treated with anthracycline (n = 32), those with concomitant confounding factors e.g. ischaemic heart disease (n = 23) and those in whom native T1 mapping sequences were not available (n=40), were excluded. The remaining 31 adult cancer survivors (24 [77%] female, mean age 57.2 ± 14.1 years) underwent CMR at median 8 years after anthracycline therapy (mean cumulative anthracycline dose 197.1 ± 116.8mg/m^2, 19 [61%] received radiotherapy). Native myocardial T1 maps were obtained in three short axis slices (base, mid and apex) using the optimized modified look-locker inversion recovery (MOLLI) sequence and mean global and mid septal myocardial T1 measured by two blinded readers in a total of 1054 myocardial segments.

Results: Mean global T1 (1034.6 and ± 31.9ms) and mid-septal T1 mapping characteristics (1044.2 ± 42.8ms) correlated significantly with all left ventricular volumetric (Indexed end-diastolic volume .485; P = 0.006, indexed end-systolic volume .501 ; P = 0.004) and functional (ejection fraction -.519, P = 0.003, mitral annular peak systolic excursion – 0.589; <0.001) parameters, except indexed left atrial volume (.252; P = 0.171). Anthracycline dose and radiotherapy did not correlate with measures of left ventricular volumes, function or native myocardial T1. Inter-observer variability, assessed by intra-class correlation coefficient showed good agreement, being 0.68 (P=0.001) and 0.71 (P<0.001), for mid septal and mean global T1, respectively.

Conclusion: In patients treated with anthracycline chemotherapy, novel imaging biomarkers of fibrosis (native myocardial T1 mapping) correlate significantly with multiple traditional measures of left ventricular volume and function and show good inter-observer agreement, with a single mid septal measure performing as well as mean global measures.

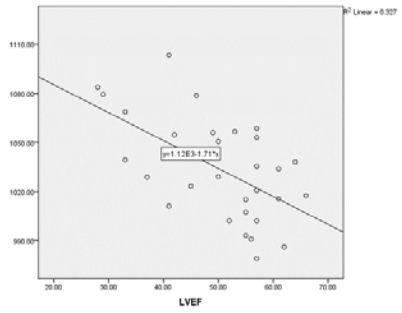
R² Linear = 0.327
1110.00
1080.00
1050.00
1020.00
990.00
y=1.12E3-1.71*x
20.00
30.00
40.00
50.00
60.00
70.00
LVEF

ID#: 371480

Flexible 3D printed acrylic insert to maintain in-vivo shape: Application to ex vivo imaging of chronic myocardial infarction in swine

John Whitaker, BM BCh[1] Radhouene Neji, PhD[2], Nick Byrne[3], Kawal Rhode, PhD[4], Rahul K. Mukherjee, MBBS[5], James Harrison, MRCP PhD[4], Steven Williams, MD PhD[6], Henry Chubb, MRCP MRCPCH[7], Louisa O'Neill, MBChB[8], Orod Razeghi, BSc, PhD[9], Steve Niederer[8], Mark O'Neill, MD DPhil[5], Reza Razavi, MD, PhD[5], Sébastien Roujol, PhD[5]

1. King's College London/Beth Israel Deaconess Medical Centre, London, England, United Kingdom

2. Siemens Healthcare Limited, Frimley, England, United Kingdom

3. Guy's and St. Thomas' NHS Foundation Trust, King's College London School of Biomedical Engineering & Imaging Sciences, England, United Kingdom

4. King's College London, England, United Kingdom

5. King's College London, London, England, United Kingdom

6. Kings College Londin, England, United Kingdom

7. Kings college London, England, United Kingdom

8. King's College London, United Kingdom

9. King's College London, London, United Kingdom

Background: High resolution ex-vivo CMR offers unparalleled detail when used for the experimental assessment of cardiac lesions. Comparison between in-vivo and ex-vivo imaging is often limited by conformational changes that occur when the heart is removed. We present a novel strategy to maintain in-vivo shape during ex-vivo imaging in which a deformable 3D printed scaffold created from in-vivo imaging data is inserted into the left ventricular (LV) cavity.

Methods: Eight pigs with chronic myocardial infarction were studied. All imaging was performed at 1.5T (MAGNETOM Aera, Siemens Healthcare, Germany). 3D whole heart was acquired following a 0.1mmol/kg bolus of Gadovist (gadobutrol, Gd) using an ECG-triggered navigator-gated inversion recovery spoiled gradient echo sequence (resolution: 1.4mm x 1.4 mm x 2mm). In-vivo 3D-LGE imaging used an ECG-triggered navigator-gated inversion recovery steady state free precession sequence (resolution 1.2mm x 1.2mm x 1.2mm). The left ventricular blood pool including aortic root was segmented from the 3D whole-heart in-vivo scan. The segmentation geometry was refined within 3-Matic Medical 10.0 (Materialise NV, Leuven, Belgium). The 3D scaffold was 3D printed in TangoPlus FullCure930 plastic using an Objet500 Connex1, polyjet 3D printer (Objet-Stratasys, Israel). A week after in-vivo CMR, further Gadovist was given 20 minutes before the heart was arrested in diastole using intravenous potassium chloride (KCl). The thorax was opened and the heart removed. Additional intracoronary KCl was administered. The 3D printed insert was passed across the mitral valve, correct orientation was ensured by the positioning of the aortic portion of the insert across aortic valve. Ex vivo imaging was performed using 0.4mm x 0.4mm x 0.4mm^3 isotropic 3D T_1-weighted spoiled gradient echo sequence commenced within an hour of removing the heart.

Results: 7 ex-vivo scans using 3D scaffold were acquired. Example 3D printed scaffold inserted into an excised heart is shown in Figure 1. In 6 cases the scaffold was successfully passed across the mitral valve. In a single case an incision at the basal infero-lateral wall was required. External examination demonstrated that the scaffold maintained the LV shape during ex-vivo CMR acquired over 4 hours. LV endocardial shape observed for the ex-vivo imaging corresponded with the in-vivo shape, as shown in Figure 2.

Conclusion: We have presented a novel approach to maintain the in-vivo shape of the heart during ex-vivo imaging which may facilitate accurate comparison and minimise registration errors introduced by deformation of the heart when it is removed from the thorax.

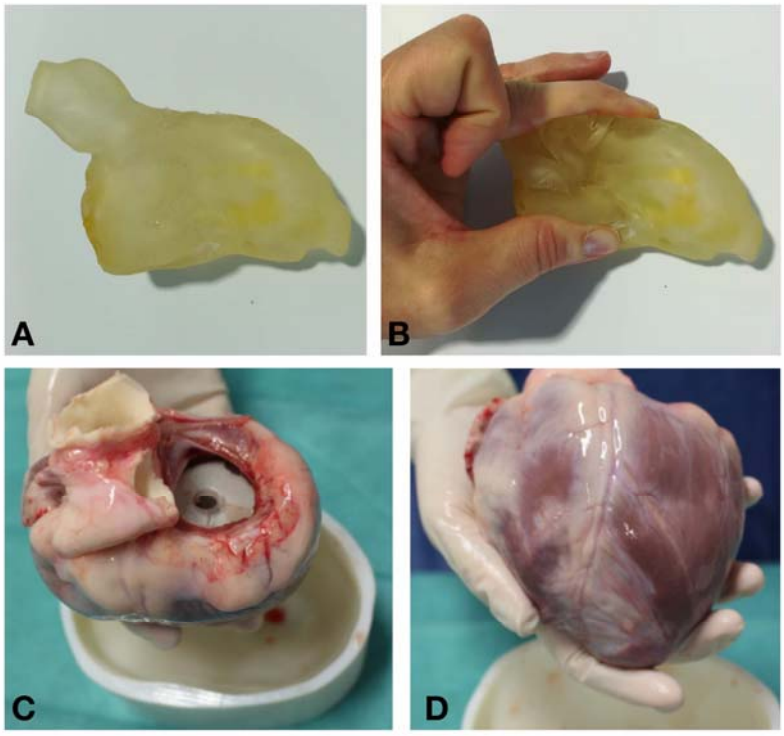

Figure 1: Deformable 3D printed scaffold demonstrating compressibility and external aspect of left ventricle with insert inside prior to ex-vivo CMR scanning. A: 3D printed insert. B: Demonstration of deformability of 3D printed insert to allow passage across the mitral valve. C: Basal aspect of heart in which 3D printed is seen through the mitral valve D: Anterior view of heart with left ventricular insert inside demonstrating maintenance of in-vivo shape

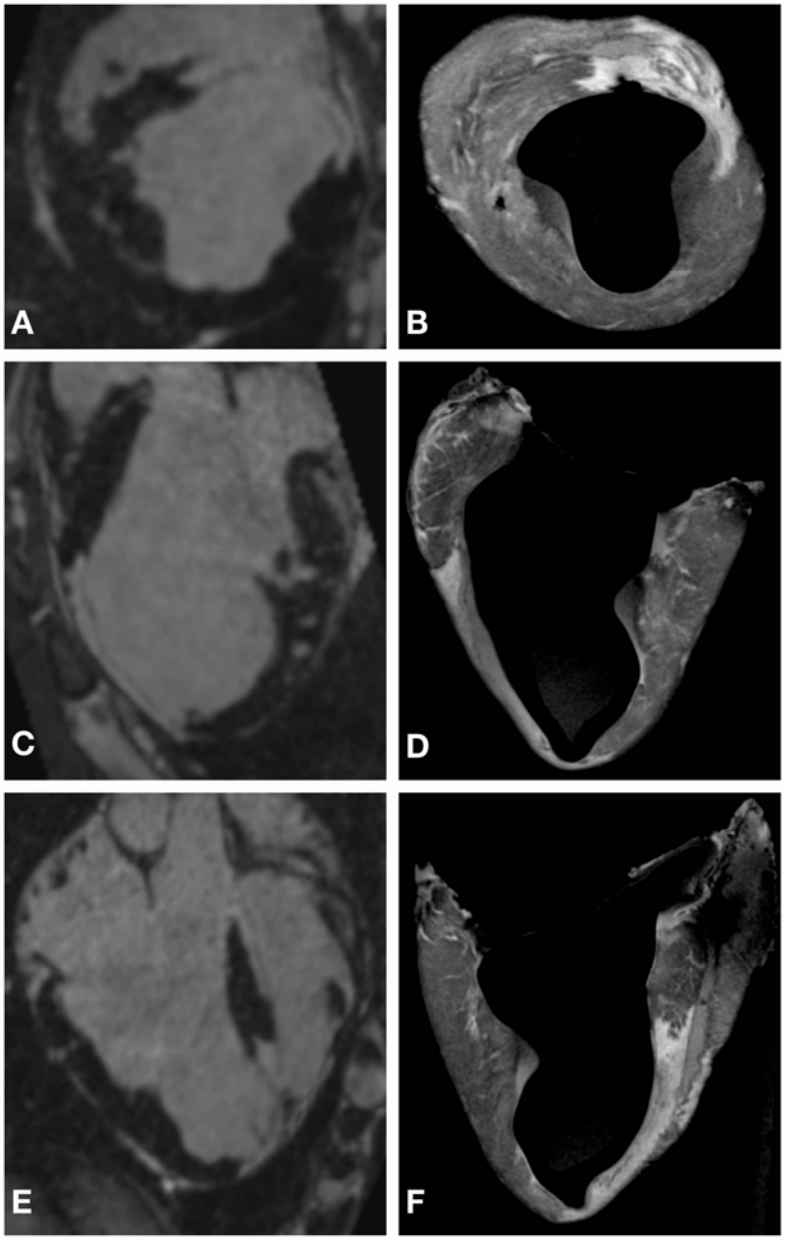

Figure 2: A and B: Multiplanar reconstruction (MPR) in short axis orientation from in-vivo (A) and ex vivo (B) scan. C and D: MPR in 2-chamber orientation from in-vivo (C) and ex-vivo (D) scan. E and F: MPR in 3-chamber view from in-vivo (E) and ex-vivo (F) scan demonstrating correspondence between shape of left ventricle in in-vivo and ex-vivo condition.

ID#: 371646

Late characterisation of cardiac effects following Anthracycline and Trastuzumab treatment in breast cancer patients

Joseph Selvanayagam, FRACP, DPhil[1] Rebecca Perry, BSc, PhD[2], Ashlee Kimball, BaMRS[3], Sanjana Patil[4], Suchi Grover[5], Karthigesh Sree Raman, MBChB, FRACP[6]

1. Flinders University, Adelaide, SA, Australia, Bedford Park, South Australia, Australia

2. Flinders University of South Australia, Bedford Park, South Australia, Australia

3. Flinders University, Australia

4. Flinders University, Adelaide, South Australia, Australia

5. Flinders Medical Centre, Flinders University, Australia

6. Flinders University of South Australia, Adelaide, South Australia, Australia

Background: Anthracycline (A) and trastuzumab (T) chemotherapy have well recognized cardiac toxicity, potentially leading to significant morbidity and mortality. Our previous work in 46 prospectively enrolled breast cancer patients showed early left ventricular (LV) and right ventricular (RV) function decline at 1 and 3 months, but only persistent RV dysfunction at 12 months which correlated with myocardial oedema observed early (1 and 3 months) after administration of chemotherapy regimes.

Methods: To investigate late cardiac effects, the same cohort were re-imaged with advanced Cardiovascular Magnetic Resonance (CMR) imaging including T1 mapping 5 +/- 1 year post chemotherapy.

Results: 26 out of 46 (56%) patients underwent follow up imaging. A statistical but non-clinically significant decrease was observed in LV ejection fraction (EF) from baseline to 5 years (72 to 65%, p=0.004). Subjects with initial drop of LVEF by >10% at 3 months (n=5) or at 12 months (n=3) did not demonstrate any difference in LV or RVEF at 5 years. No correlation was observed between myocardial oedema and LV or RVEF at 5 years. At 5 years, T1 values were within normal limits overall (935± 48ms). One patients had significantly elevated (>1000ms) T1 values with no correlation to LV or RVEF. No subjects demonstrated replacement myocardial fibrosis at 5 years.

Conclusion: Using advanced CMR, contemporary chemotherapy regimes demonstrate minimal long term cardiac toxicity. There is minimal late diffuse and no replacement fibrosis. This study suggests limiting serial imaging in these patients at 12 months.

ID#: 371647

Pre and post-contrast dark-blood SASHA T1 mapping - an initial feasibility study

Gabriella Captur, MD PhD MRCP MSc[1] Saima Azam[2], Dina Radenkovic, DR[2], Patricia Feuchter, Barts[3], Lizette Cash[4], Redha Boubertakh, PhD[5], Mark Westwood, MBBS MD FRCP FESC[4], Peter Kellman, PhD[6], James Moon, MD[2]

1. Barts Heart Centre, London, England, United Kingdom

2. UCL, England, United Kingdom

3. Barts Heart Center, England, United Kingdom

4. Barts, England, United Kingdom

5. QMUL, England, United Kingdom

6. National Heart, Lung, and Blood Institute, National Institutes of Health, Bethesda, MD

Background: T1 mapping in dilated cardiomyopathy (DCM) is challenging as currently available sequences have in-plane resolution issues and many DCMs are thin-walled, meaning neighbouring blood pool contamination and partial volume errors not only increase, but have a bias with wall thickness confounding the detection of disease-related changes [1]. We proposed a novel approach to overcome these and secured SCMR 2017 Seed Grant funding. We present initial results.

Methods: We propose a saturation recovery with single-shot acquisition T1 mapping sequence (SASHA) that uses a dark blood (DB) preparation, variable flip angle (VFA) and modified sampling strategy optimised for 2-parameter fitting, for better T1 mapping of thin-walled hearts.
The study consists of *implementation, phantom testing* and *clinical testing*.
Phantom testing using the T1MES phantom [2], compared the sequence at various heart rates (60, 95, 98, 105bpm) relative to conventional modified Look-Locker inversion recovery (MOLLI), bright blood SASHA, and gold standard slow inversion recovery spin echo (IRSE).
Clinical testing was pre and post contrast in 10 subjects (57 ± 16 years; 4 male) at 1.5T (Siemens, Aera). Blood:myocardial signal intensities were quantified in saturation images and T1 times in maps, using manually drawn regions of interest. Endo to epicardial profiles of cross-myocardial T1 times at the midseptum were compared on maps for the extent of blood pool contamination.

Results: *Implementation:* We used a motion-sensitized driven equilibrium (MSDE) magnetization preparation [3] (**Fig1a**) for enhanced B_1^+ insensitivity. MSDE parameters tested were TE_{MSDE} = 5, 10 ms and gradients: amplitude (GA) = 2, 3, 4, 5, 7, 10, 20 mT/m. *Phantom testing:* Bright blood and DB SASHA had less heart rate dependent biases compared to MOLLI and better agreement with IRSE (**Fig2**). *Clinical testing:* In vivo the TE5 GA10 MSDE preparation achieved the best combination of blood suppression and myocardial motion insensitivity (**Figs1b** and **3a**). Cross-myocardial profile analysis revealed aberrant T1 times towards the myocardial borders by conventional sequences (**Fig3b**) but more consistent T1 times using DB SASHA.

Conclusion: DB SASHA T1 mapping with adiabatic MSDE preparation developed thanks to the 2017 SCMR Seed Grant Program, has technical, phantom and initial clinical features that suggest it may be superior to conventional T1 mapping approaches for the thin-walled heart (e.g. DCM).

References 1.Kellman et al. JCMR2014
2.Captur et al. JCMR2016
3.Wang et al. MRM2007

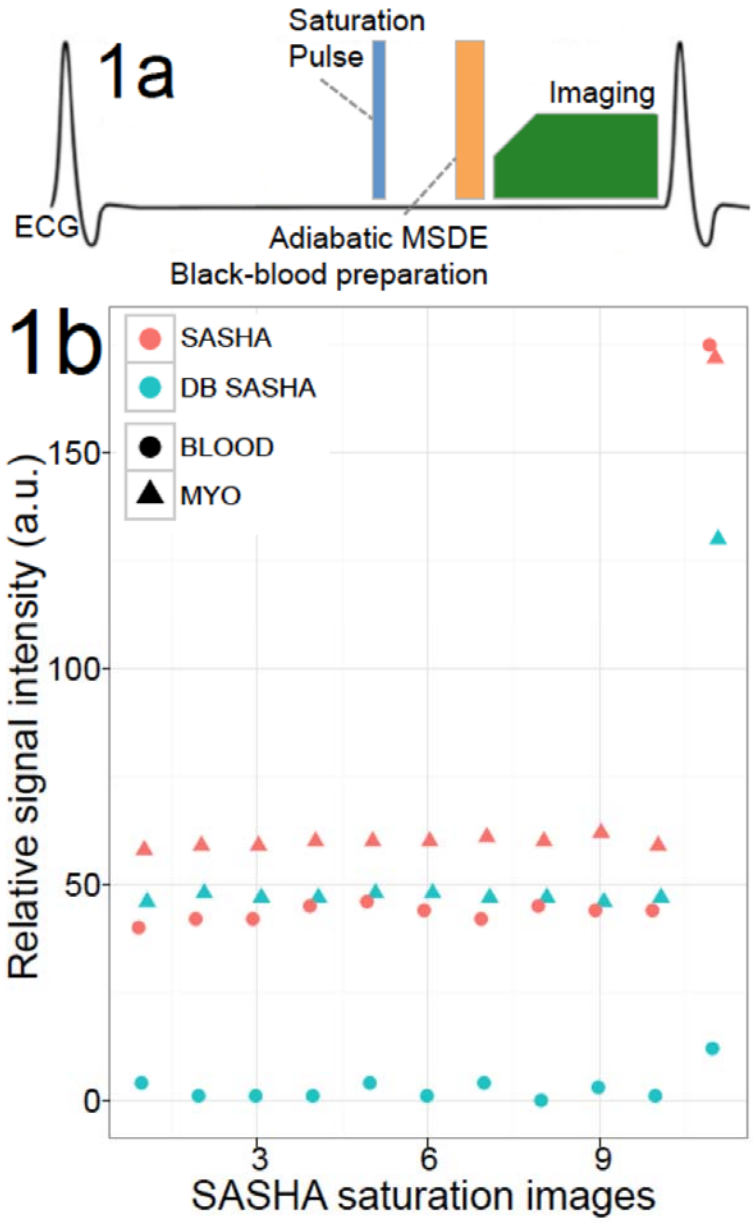

1a. An adiabatic MSDE preparation is inserted directly before the imaging pulses. In MSDE, blood-signal suppression is caused by symmetric dephasing gradients before and after a refocusing pulse, causing incomplete refocusing of moving tissue, increasing blood/myocardial contrast. 1b. Precontrast blood and myocardial signal intensities at the various inversion times of bright blood and DB SASHA. DB SASHA shows almost complete suppression of the blood signal.

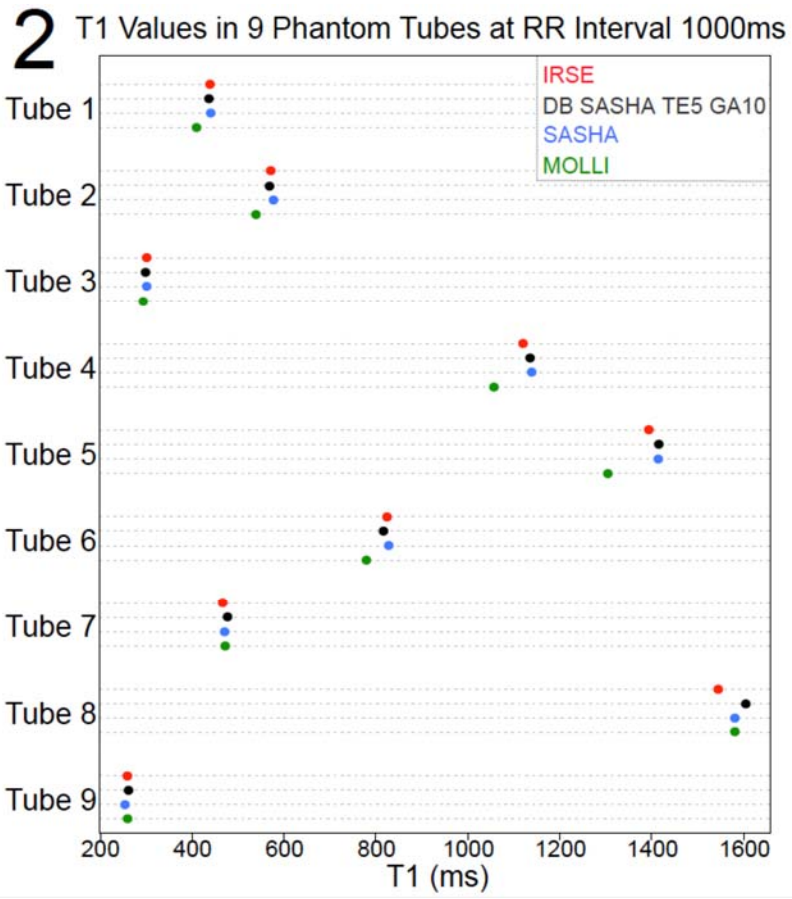

Comparison of T1MES tubes T1 values by slow inversion recovery spin echo and competing sequences here at simulated heart rate of 60 bpm.

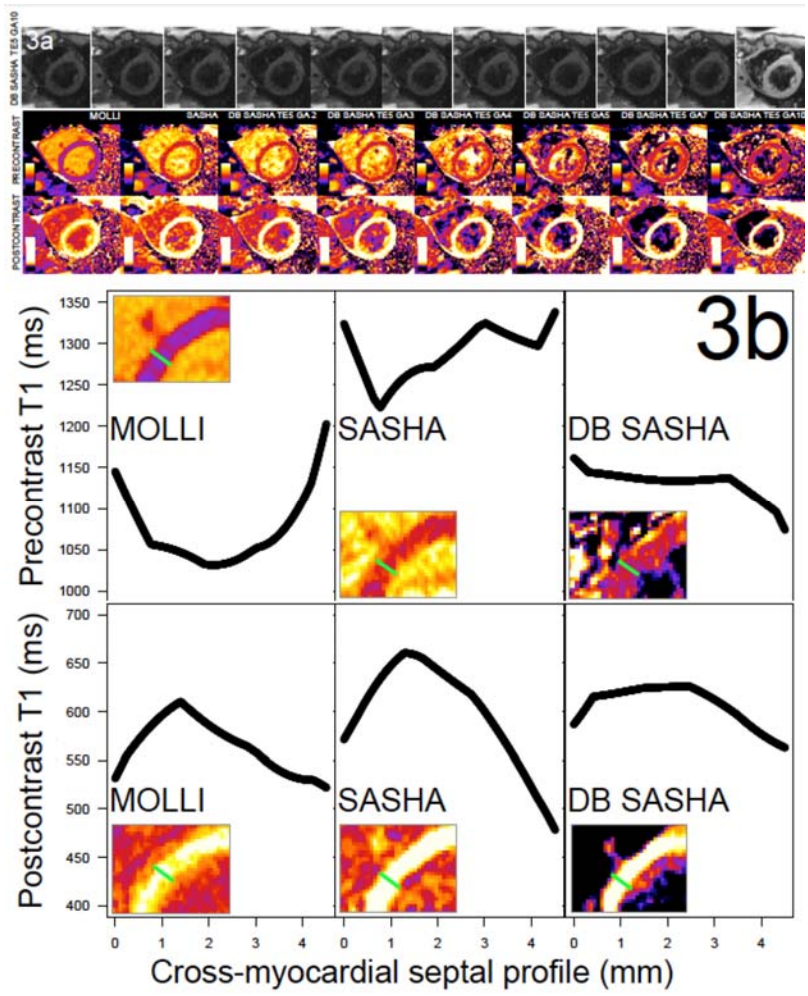

1a. In vivo results of DB SASHA T1 mapping. Top row: visually good suppression of the blood-signal in serial saturation images (and anchor) with precontrast DB SASHA TE5 GA10. Bottom rows: comparing precontrast and postcontrast T1 maps of MOLLI, bright blood SASHA and the various TE/GA DB SASHA combinations 1b. Conventional sequences show deranged T1 times at the endocardial borders due to blood pool contamination-less so with DB SASHA (5mm cross-myocardial septal profiles are shown in green).

ID#: 371663

Impairment of coronary flow reserve determined by the CMR coronary sinus flow measurement in patients with heart failure with preserved ejection fraction.

Yoshitaka Goto, MD[1]Masaki Ishida, MD, PhD[2], Haruno Sakuma, MD[3], Wakana Makino, MD[3], Motonori Nagata, MD[1], Yasutaka Ichikawa, MD[4], Kakuya Kitagawa, MD[5], Hajime Sakuma, MD, PhD[6]

1. Department of Radiology, Mie University Hospital, Tsu, Mie, Japan

2. Mie Universtiy Hospital, Japan

3. Mie University Hospital, Tsu, Mie, Japan

4. Radiology, Mie, Japan

5. Department of Radiology Mie university hospital, Mie, Japan

6. Department of Radiology, Mie University Hospital, Mie, Japan

Background:

Heart failure with preserved ejection fraction (HFpEF) is closely associated with LV diastolic dysfunction in the disease development and progression. Recent studies indicated that impaired global longitudinal strain (GLS) in LV is related to LV diastolic dysfunction in HFpEF. In addition, endothelial dysfunction is recognized as an additional mechanism leading to cardiac dysfunction in HFpEF. However, it has not been fully understood whether coronary flow reserve (CFR), which is an index of left ventricular microvascular function, is impaired in patients with HFpEF. The purposes of this study were to investigate the severity of CFR and LV GLS alterations in HFpEF patients as compared to patients with diastolic dysfunction without heart failure symptom, and to investigate the diagnostic value of CFR and GLS for identifying HFpEF in the subjects with preserved EF.

Methods:

Eleven patients with HFpEF, 11 patients with diastolic dysfunction without heart failure symptom (DD) and 11 age- and gender matched control subjects were retrospectively enrolled from patients who underwent CMR study including stress and rest coronary sinus flow measurements, cine CMR and LGE CMR. Exclusion criteria included CAD, valvular disease, HOCM, sarcoidosis and amyloidosis. CFR was calculated as the ratio of stress blood flow divided by rest blood flow in the coronary sinus. LV volumetric and functional parameters including LV GLS were measured in cine CMR.

Results:

CFR was significantly decreased in HFpEF patients (2.1±0.4) in comparison to DD patients (2.9±0.8, p=0.04) and control subjects (4.2±1.0, pFig 1a). LV GLS in HFpEF patients (-13.9±0.8) was significantly impaired than in DD patients (-17.9±0.8 p(Fig 1b). Of the 33 subjects, the area under the ROC curve (AUC) of CFR and LV GLS for identifying HFpEF was 0.888 and 0.872, respectively **(Fig 2)**. Linear regression analysis demonstrated that CFR had weak association with GLS (β = -0.1263, R2 = 0.136, p = 0.035) and moderate association with LV mass index (β = -0.0284, R2 = 0.2797, p = 0.002).

Conclusion:

BothCFR and LV GLS are significantly impaired in patients with HFpEF than in patients with diastolic dysfunction without heart failure symptom. In the subjects with preserved EF, CFR and LV GLS are weakly associated with each other. High AUC suggested that impairments of CFR and LV GLS measured by CMR may be of value to identify HFpEF patients in the subjects with preserved EF.

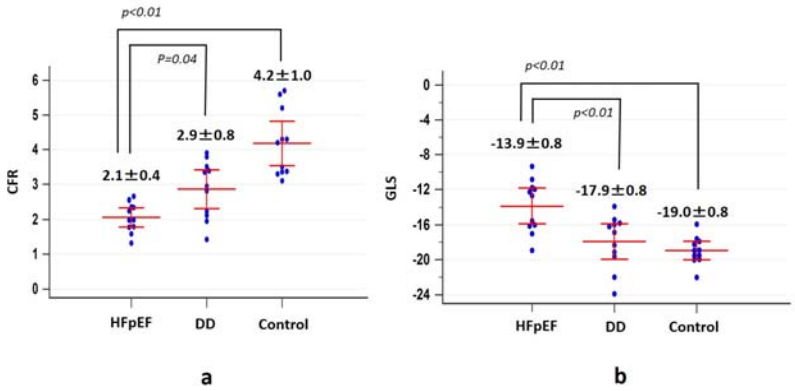

Figure 1.

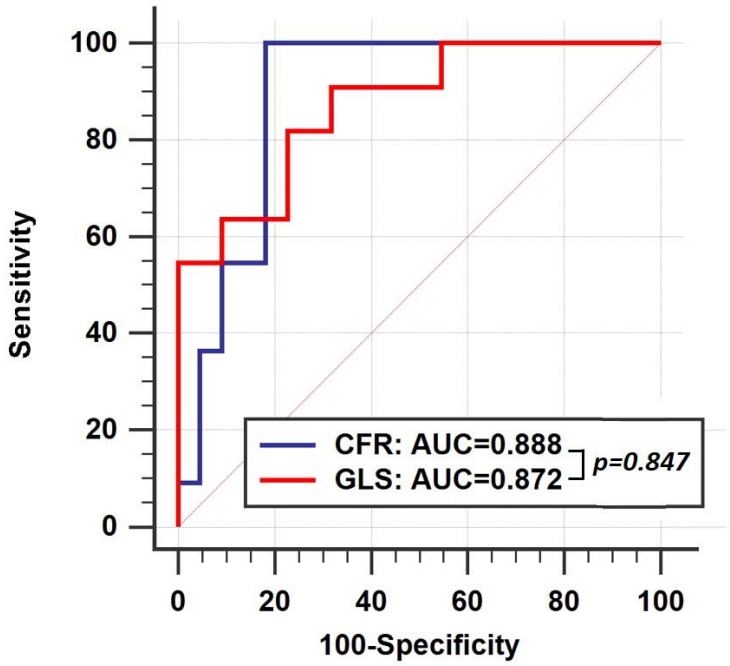

Figure 2.

ID#: 371556

Prevalence of Left Ventricular Noncompaction pattern among patients with Congenital Dyserythropoietic Anemia Type I - Cardiac Magnetic Resonance assessment

Aryeh Shalev[1] Hadar Abramovich-Yoffe[2], Orit Barrett[3], Hanna Shalev, Pediatric Division, Faculty of Health Sciences[3], Aviva Vivianne. Levitas[4]

1. Soroka University Medical Center, Ben-Gurion University of the Negev, Beer-Sheva, Israel., Omer, Israel

2. Ben Gurion University of the Negev, Beer-Sheva, Israel, Israel

3. Soroka University Medical Center, Ben Gurion University of the Negev, Beer-Sheva, Israel, Israel

4. Soroka University Medical Center, Ben-Gurion University of the Negev, Beer-Sheva, Israel., Israel

Background: Congenital dyserythropoietic anemia type I (CDA1) is a rare autosomal recessive disease characterized by macrocytic anemia, ineffective erythropoiesis and secondary hemochromatosis. Left ventricular noncompaction (LVNC) is a cardiomyopathy with potentially serious outcomes that is commonly attributed to intrauterine arrest of normal compaction during the endomyocardial morphogenesis. LVNC pattern, however, might exist in various hemoglobinopathies. We sought to determine whether the pattern of LVNC is more prevalent among patients with CDA1 as compared with subjects without CDA1.

Methods: We conducted a retrospective cohort study of all CDA1 patients that underwent cardiac magnetic resonance imaging (CMR) during a 6-year period (2010-2016) at our center as part of routine assessment of myocardial iron overload. The study population consisted of 32 CDA1 patients (median age 17.5, range 6-61years), all carrying the same CDAN1 founder mutation. The control group consisted of 64 subjects without CDA1, that were age (±5 years range)- and gender-matched. The distribution of non-compaction was assessed by qualitative analysis of 17 segments for the assessment of presence or absence of any degree of non-compaction. A segment was regarded as non-compacted if its visual appearance clearly suggested the presence of two myocardial layers with different degrees of tissue compaction. In each of the three end-diastolic long-axis views (basal, mid-cavity and apical), the segment with the most pronounced trabeculations was chosen for measurement of the thickness of the non-compacted and the compacted myocardium perpendicular to the compacted myocardium. The ratio of non-compacted to compacted myocardium (NC/C ratio) in end-diastole was calculated for each of the three long-axis views, and only the maximal ratio was then used for analysis. Left ventricular non-compaction was diagnosed when NC/C ratio > 2.3 in end diastole. Cardiac iron levels were measured in CDA1 patients using a breath-hold multiecho gradient T2* sequence sampled across regions of interest in the LV septum. The myocardial iron content (MIC) was quantified in milliseconds and than transformed to tissue iron content (mg/gr tissue) by conversion formulas.

Results: In multivariate analysis, the presence of CDA1 was an independent risk factor for NC/C ratio>2.3 (adjusted OR=11.46, 95%CI=2.6-50.68, P-value=0.001). CDA1 was strongly associated with increased number of myocardial segments exhibiting LVNC pattern. There was no evidence for myocardial iron overload among CDA1 patients.

Conclusion: Patients with CDA1 have a higher prevalence of LVNC pattern than normal individuals. Unfolding the natural course of LVNC pattern and its clinical implications among CDA1 patients may eventually improve patients'; care.

ID#: 370492

Defining the Association between the Extent and Location of Mid-wall Late Gadolinium Enhancement and Outcome in Dilated Cardiomyopathy

Brian Halliday, BSc MBChB[1] A John. Baksi, PhD MRCP[2], Cemil Izgi, MD[3], Monika Arzanauskaite, MD[4], Simon J. Newsome, MA MSc[5], Ankur Gulati, MD[6], Aamir Ali, MBBS[6], Amrit S. Lota, BMBCh BA[7], Upasana Tayal, BMBCh[6], Vass Vassiliou, MA, MD[8], Stuart Cook, MD PhD[9], Francisco Alpendurada, MD PhD[6], John Cleland, MD PhD[10], Dudley J. Pennell, MD[11], Sanjay Prasad, MD[11]

1. Royal Brompton Hospital and National Heart and Lung Institute, Imperial College London, London, England, United Kingdom

2. Royal Brompton Hospital and Imperial College London, London, London, England, United Kingdom

3. Cardiovascular Magnetic Resonance Unit, Royal Brompton Hospital, London, UK, England, United Kingdom

4. Royal Brompton Hospital and Liverpool Heart and Chest Hospital, United Kingdom

5. London School of Hygiene and Tropical Medicine, England, United Kingdom

6. Royal Brompton Hospital, England, United Kingdom

7. CMR Unit Royal Brompton Hospital and National Heart and Lung Institute, Imperial College London, London, England, United Kingdom

8. Royal Brompton, London, England, United Kingdom

9. Imperial College, London, United Kingdom

10. Imperial College, London, England, United Kingdom

11. Royal Brompton Hospital and Imperial College, London, England, United Kingdom

Background: Precise phenotypic characterisation of dilated cardiomyopathy (DCM) is required in order to personalise therapy and improve outcomes. Mid-wall late gadolinium enhancement (LGE) is known to predict adverse outcomes. However, there is a lack of data examining the relationship between the extent and location of LGE and outcome.

Methods: We recruited consecutive patients with DCM referred for CMR between 2000 and 2011. The presence of mid-wall LGE was determined by 2 independent specialists with a third adjudicating if necessary. LGE quantification was performed by 2 independent specialists using the full-width at half maximum technique. A blinded panel adjudicated outcome events. The association between the extent and location of LGE and all-cause mortality and an arrhythmic composite of sudden death and aborted sudden death, was examined using proportional hazard modelling. The Akaike information criterion (AIC) was used to compare the quality of each model in predicting the outcome, with smaller values indicating more optimal fit.

Results: Overall, 874 patients (588 male, median left ventricular ejection fraction [LVEF 39%], median age 52 years) were followed-up for a median of 4.9 years. Mid-wall LGE was present in 300 (34.3%) cases (median extent 3.8%, IQR 2.0:6.7%; septum only: 142, left ventricular free-wall only: 42, both septum and free-wall: 116). There was agreement on LGE presence in 828 cases (94.7%) and an absolute mean difference of 0.87% in LGE quantification between operators (intraclass correlation coefficient – 0.87). The presence of LGE was associated with greater all-cause mortality (HR 2.39; 95%CI 1.73:3.29; p<0.0001) and major arrhythmic events (HR 4.12; 95%CI 2.64:6.45; p<0.001). Estimated HRs for patients with LGE extent of 0-2.5%, 2.5-5% and >5%, compared to patients without LGE were 2.01 (95%CI 1.25-3.23), 2.38 (1.50-3.78) and 2.76 (1.81-4.21) for the primary end-point respectively and 2.92 (95%CI 1.51-5.65), 4.28 (2.38-7.68) and 5.14 (3.01-8.79) for major arrhythmic events respectively. Analyses yielded similar results after adjustment for LVEF. *Figure 1* demonstrates how modelling LGE as a linear measure or based on the square root of the HR underestimates risk in most patients. The extents of LGE with the largest c-statistic for the prediction of the primary and secondary end-points were 1.29% (c-statistic 0.70) and 0.71% (c-statistic 0.70) respectively. The presence of LGE only in the septum and in both the septum and the free-wall was associated with greater all-cause mortality (septum: HR 2.76; 95%CI 1.88:4.06, both: HR 2.67; 1.76:4.04) and major arrhythmic events (septum: HR 3.25; 95%CI 1.86:5.67; both: HR 6.09; 95%CI: 3.66:10.13). LGE occuring only in the free-wall was not associated with an increased incidence of death (HR 0.74; 95%CIs 0.27:2.04) or major arrhythmia (HR 2.08; 95%CIs 0.72:5.97). Models based on the location of LGE had the lowest AIC, compared to models based on increasing extent of LGE or the LGE extent cut-off with the largest c-statistic, and therefore appear to be the most effective in the prediction of risk (*Table 1*).

Conclusion: There is a non-linear relationship between LGE extent and outcome. The presence of septal LGE appears to be most important in determining risk.

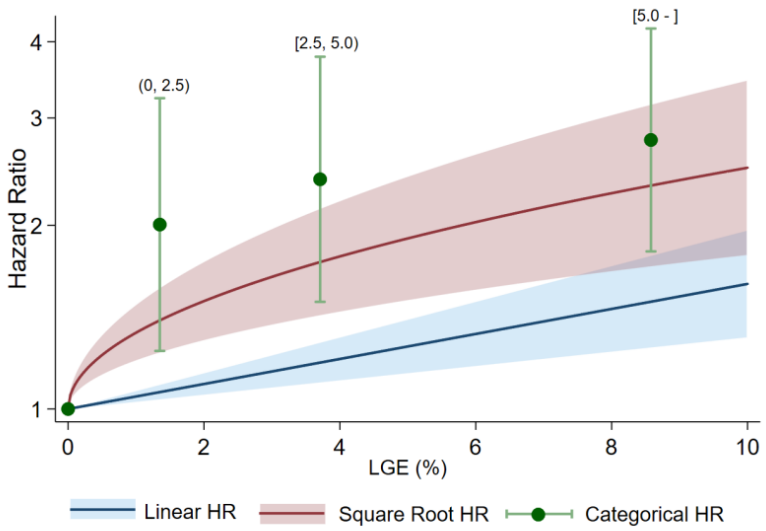

All-Cause Mortality (Unadjusted)

Estimated hazard ratios for the primary end-point based on increasing extent of LGE, together with statistical modelling of the data based on a continuous linear relationship or the square root of the hazard ratio, both of which underestimate risk in most patients.

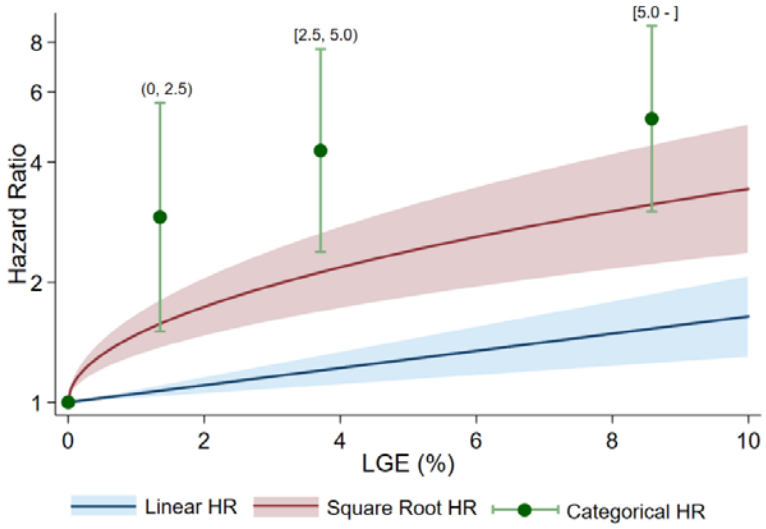

ASCD & SCD (Unadjusted)

Estimated hazard ratios for the secondary end-point based on increasing extent of LGE, together with statistical modelling of the data based on a continuous linear relationship or the square root of the hazard ratio, both of which underestimate risk in most patients.

A

			Mortality	Proportional Hazard Modelling		
			n (%)	HR (95% CI)	P	AIC
Presence & Extent	LGE (Binary) [Any]	0%	73 (12.7)	1.00	<0.0001	1844.1
		>0%	77 (25.7)	2.39 (1.73, 3.29)		
	LGE (Binary) [Cut-off]	<1.29%	81 (13.1)	1.00	<0.0001	1842.0
		≥1.29%	69 (26.8)	2.51 (1.82, 3.47)		
	LGE (4 Groups)	0%	73 (12.7)	1.00	<0.0001	1846.8
		>0% & <2.5%	22 (22.7)	2.01 (1.25, 3.23)		
		≥2.5% & <5%	24 (24.2)	2.38 (1.50, 3.78)		
		≥5%	31 (29.8)	2.76 (1.81, 4.21)		
Location	LGE (by Location)	Absent	73 (12.7)	1.00	<0.0001	1838.6
		Septal Only	41 (28.9)	2.76 (1.88, 4.06)		
		Non-Septal Only	4 (9.5)	0.74 (0.27, 2.04)		
		Both	32 (27.6)	2.67 (1.76, 4.04)		
	LGE (Septal)	**No**	**77 (12.5)**	**1.00**	**<0.0001**	**1835.0**
		Yes	**73 (28.3)**	**2.77 (2.01, 3.82)**		

B

			ASCD & SCD	Proportional Hazard Modelling		
			n (%)	HR (95% CI)	P	AIC
Presence & Extent	LGE (Binary) [Any]	0%	29 (5.1)	1.00	<0.0001	1026.6
		>0%	55 (18.3)	4.12 (2.64, 6.45)		
	LGE (Binary) [Best]	<0.71%	30 (5.2)	1.00	<0.0001	1027.0
		≥0.71%	54 (18.6)	4.08 (2.62, 6.36)		
	LGE (4 Groups)	0%	29 (5.1)	1.00	<0.0001	1027.7
		>0% & <2.5%	13 (13.4)	2.92 (1.51, 5.65)		
		≥2.5% & <5%	18 (18.2)	4.28 (2.38, 7.68)		
		≥5%	24 (23.1)	5.14 (3.01, 8.79)		
Location	**LGE (by Location)**	**Absent**	**29 (5.1)**	**1.00**	**<0.0001**	**1022.9**
		Septal Only	**21 (14.8)**	**3.25 (1.86, 5.67)**		
		Non-Septal Only	**4 (9.5)**	**2.08 (0.72, 5.97)**		
		Both	**30 (25.9)**	**6.09 (3.66, 10.13)**		
	LGE (Septal)	No	33 (5.4)	1.00	<0.0001	1025.4
		Yes	51 (19.8)	4.19 (2.71, 6.48)		

Proportional hazard modelling and Akaike Information Criterion analysis of the primary and secondary end-points

ID#: 369700

Diffuse Myocardial Fibrosis in Pediatric Patients with Marfan and Loeys-Dietz Syndromes

Gauri R. Karur, MD[1] Joseph J. Pagano, MD[2], Timothy Bradley, MBChB[3], Mike Seed, MBBS[4], Shi-Joon Yoo, MD[4], Lars Grosse-Wortmann, MD[2]

1. The Hospital for Sick Children, University of Toronto, Toronto, ON, Canada

2. The Hospital for Sick Children, ON, Canada

3. University of Saskatchewan, Saskatoon, SA, Canada

4. The Hospital for Sick Children, Toronto, ON, Canada

Background: Although most patients with Marfan (MFS) and Loeys-Dietz (LDS) syndromes have good ventricular function, intrinsic cardiomyopathies have been described. The aims of this study were (1) to assess the degree of fibrotic myocardial remodeling, as evidenced by myocardial T1 time and extracellular volume fraction (ECV), and (2) to test for any impact of fibrosis on function, in patients with MFS and LDS.

Methods: We retrospectively reviewed consecutive cardiac magnetic resonance (CMR) studies of 41 pediatric patients with either gene-positive MFS or LDS who underwent T1 mapping using a modified Look-Locker inversion recovery technique (MOLLi). Patients with significant aortic or mitral valve disease, history of complicated post-operative course or complete heart block were excluded (n=6). Patients were compared with healthy controls.

Results: CMR studies of 12 patients with MFS, 23 patients with LDS, and 49 controls were analyzed (see Table 1). Compared with controls, patients with MFS, LDS and the combined MFS/LDS cohort demonstrated longer mean LV native T1 time and ECV ($p=0.0058$ and $p=0.02$ for MFS, $p<0.0001$ and $p=0.04$ for LDS and $p<0.0001$ and $p=0.02$ for the combined MFS/LDS cohort respectively, see Figure 1). Mean left ventricular (LV) native T1 time was significantly longer in LDS compared with MFS ($p=0.03$). Compared with controls, the combined MFS/LDS cohort had higher Z-scores for LV end-diastolic volume (EDV, $p=0.01$) and lower Z-scores for LV ejection fraction (EF, $p<0.0001$), while LV mass Z-scores were similar ($p=0.92$). Between LDS and MFS, Z-scores for LV EDV ($p=0.37$), EF ($p=0.45$) or mass ($p=0.18$), were also similar. There was no correlation between LV native T1 time or ECV and Z-scores of LV EF or EDV. There was a trend towards shorter native T1 time in patients receiving Losartan (1033±54ms vs. 1057±24ms, $p=0.07$), despite the higher percentage of previous aortic root replacement and patients with LDS in this group. Previous surgery was not related to native T1 time or ECV.

Conclusion: CMR markers of diffuse myocardial fibrosis are elevated in pediatric patients with MFS, and especially in LDS, even in the presence of preserved LV function. The prognostic and pathogenic significance of this finding will need to be investigated in larger longitudinal studies and to determine whether angiotensin receptor blockers have an anti-fibrotic effect in LV myocardium, in patients with MFS and LDS.

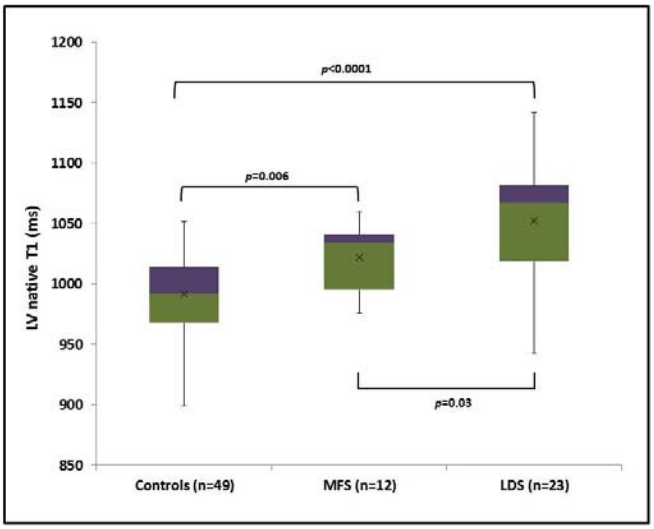

Figure 1: Box and whisker plot showing left ventricular (LV) native T1 time in Marfan Syndrome (MFS) and Loeys Dietz Syndrome (LDS).

Table 1: Characteristics of the combined cohort (MFS/LDS), MFS, LDS and controls depicted as mean ± SD. MFS - Marfan syndrome, LDS - Loeys Dietz syndrome, ECV - extracellular volume fraction, LV - left ventricle, EDVi - indexed end-diastolic volume, EF - ejection fraction, Mi - indexed mass , AoR - aortic root.

	MFS/LDS (n=35)	MFS (n=12)	LDS (n=23)	Controls (n=49)	MFS/LDS vs. controls p value	MFS vs. controls p value	LDS vs. controls p value	MFS vs. LDS p value
Males, n (%)	23(66)	8(67)	15(65)	28(57)	0.6	0.6	0.6	0.7
Age, years	11.9±4.9	15.4±2.2	10.1±5.0	13.8±2.8	0.05	**0.04**	**0.003**	**0.0001**
T1, ms	1042±46	1022±29	1052±50	991±37	**<0.0001**	**0.006**	**<0.0001**	**0.03**
ECV, %	25.3±5.0	23.5±0.7	25.8±5.6	20.8±2.4	**0.02**	**0.02**	**0.04**	0.3
LVEDVi, mL/m2	99.9±30.0	118.0±38.8	90.0±18.5	91.3±13.1	0.13	**0.04**	0.77	**0.03**
LVEDV Z-score	1.4±2.0	1.9±2.6	1.2±1.7	0.37±1.6	**0.01**	0.07	0.07	0.37

LVEF, %	53.8±3.9	53.3±3.9	54.0±4.0	58.2±4.6	**<0.0001**	**0.001**	0.0004	0.62
LVEF Z-score	-1.8±0.9	-2.0±0.9	-1.7±1.0	-0.75±1.1	**<0.0001**	**0.001**	0.001	0.45
LVMi, g/m2	53.5±13.4	62.1±14.6	48.8±10.3	54.8±12.3	0.67	0.13	**0.01**	**0.01**
LVM Z-score	-0.55±1.6	-0.04±1.6	-0.84±1.6	-0.59±1.9	0.92	0.32	0.58	0.18
LVM/EDV	0.55±0.1	0.54±0.1	0.55±0.1	0.60±0.1	**0.02**	0.07	0.08	0.84
AoR Z-score	2.17±1.8	5.7±3.0	2.6±1.5	not measured	N/A	N/A	N/A	**0.0047**

ID#: 370481

coreMRI: an online web platform for database generation in simulation-based quantitative MR methods

Christos Xanthis, PhD[1] Anthony H. Aletras, Ph.D.[2]

1. Lund University, Skane University Hospital, Department of Clinical Physiology, Lund, Sweden, Skane Lan, Sweden

2. Aristotle University of Thessaloniki/Lund University, Thessaloniki, Thessaloniki, Greece

Background: Recent studies (Ma, 2013 and Xanthis, 2015) have shown that the incorporation of Magnetic Resonance Imaging (MRI) simulations could significantly improve quantitative MRI through the generation of a database of simulated MR signals. However, several MR research groups do not have access to an MR simulation platform or the computational resources required to develop such an advanced MR simulation platform. In this study we present coreMRI, a MR simulation platform as a web service for database generation in simulation-based quantitative MR methods.

Methods: The simulation framework was developed on the cloud (AWS - aws.amazon.com) and GPU-based instances were utilized through the CUDA-C environment. Distribution and process of data was performed through the MATLAB single-program-multiple data (spmd) framework whereas a dynamic web-page was developed for bridging the user with the platform (figure1). The performance of coreMRI was evaluated on Amazon p2-type instances (1, 8 and 16 GPUs, NVIDIA K80). A MOLLI sequence (Messroghli, 2004) was simulated on 5901000 spins covering a large range of native myocardial T1 and T2 values (T1=700–1700msec, T2=20–300msec, T1 and T2step=1msec, 21 spins across slice-profile). The pulse sequence consisted of 157869 discrete time-steps and a database of 281000 entries, each with 8 points, was generated. On a second experiment, a Gradient-Echo (GE) sequence was simulated on 1486905 spins covering typical relaxation times of tissues in the brain (Ma, 2013) (T1= 100–5000 msec, T2= 20–3000msec, T1step= 20msec and T2step= 10msec). For each T1-T2 combination different off-resonance frequencies were simulated covering a BW of 200Hz with an increment of 10Hz. The pulse sequence consisted of 810497 discrete time-steps and a database of 1486905 entries, each with 1000 points, was generated. The second experiment was performed on a p2-type instance with 16 GPUs.

Results: Figure 2 demonstrates the speedup recorded for the spmd framework on the first experiment with 8 and 16 GPUs compared to a single-GPU configuration. The generation of the database of simulated MR signals took 106sec for the first experiment and 442sec for the second experiment on the 16 GPUs configuration.

Conclusion: The generation of extended databases of simulated MR signals to be used in simulation-based quantitative MR methods can now be publicly available and common to the entire MR research community through the online web-platform coreMRI (www.coremri.com). coreMRI does not require programming expertise for the development of an advanced MR simulation platform or upfront investment for purchasing advanced computer systems.

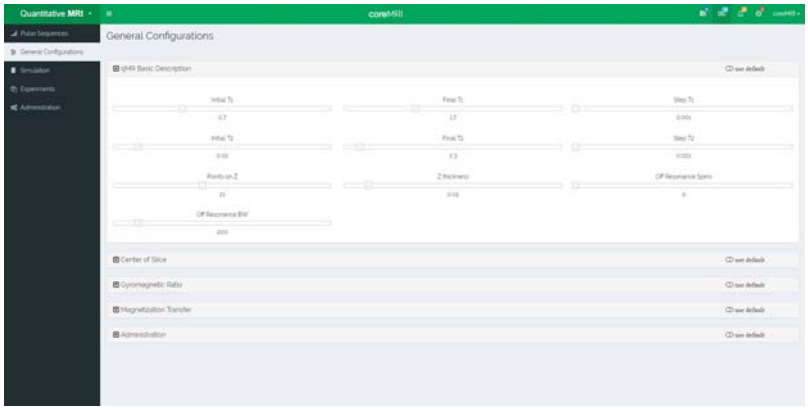

coreMRI web-interface (www.coremri.com) for configuring the characteristics of the database to be used in simulation-based quantitative MR methods.

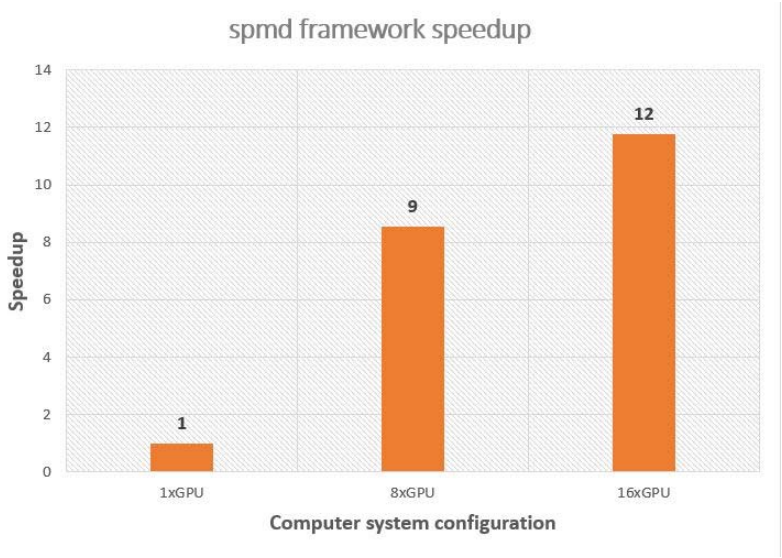

Speedup of spmd framework with 8 and 16 GPUs (NVIDIA K80) compared to a single-GPU configuration

ID#: 370651

Beyond the MagnaSafe Trial; Where Do We Go from Here? A Focus Beyond Simply CMR Safety

Robert W. Biederman, MD, FACC, FAHA[1] Loretta Gevenosky, R.N.[1], Huma Samar, M.D.[2], Ronald B. Williams, B.A.[3], Richard Lombardi, RT (mr)(r)[4], Moneal Shah, M.D.[5], Christopher Bonnet, M.D.[1], Mark Doyle, Ph.D.[1]

1. Allegheny General Hospital, Pittsburgh, PA

2. VA Loma Linda Medical Center, Pittsburgh, PA

3. Allegheny General Hospital, Washington, PA

4. Allegheny General Hospital

5. Allegheny General Hospital, pittsburgh, PA

Background: Today, MRI is infrequently performed in patients with conventional PM/ICD';s. While recent studies such as MagnaSafe published in *NEJM* for non-thoracic imaging have unequivocally documented MRI safety in those with implanted devices, the clinical value has not been considered. A myopic focus on safety continues potentially prohibitive for future dissemination of this concept.

Hypothesis MRI in patients with PM/ICD';s is crucial to existing diagnosis and may often substantially alter diagnosis and patient management.

Methods: An evaluation of consecutive patients with PM/ICD';s who underwent MRI (GE 1.5T,WI) over 10 yrs (95% and CRT';s (and 12 retained leads and 6 loop recorders). Specific criteria were followed to objectively determine if the diagnosis via MRI altered pt care. Accordingly, to attempt to objectify value, four questions were answered within 1 week of MRI by both MRI technologist and MRI physician(s): 1) Did primary diagnosis change? 2) Did MRI provide additional information to existing diagnosis? 3) Was the pre-MRI (tentative) diagnosis confirmed? 4) Did pt management change? If 'Yes'; was answered to any question, it was considered that MRI was of value to pt diagnosis and/or impending therapy.

Results: A total of 465 patients underwent CMR scanning with PM/ICD's over ~7 years. The average MRI times was 22±43min of which 326 (70%) were neurology/neurosurgery, 38 (12%) were musculoskeletal and 101 (22%) were cardiovascular cases. Upon review of the neuro/neurosurgery MRI';s, 289 (89%) provided additional information. The diagnosis changed in 175 (54%), while medical therapy changed for 175 (54%). In only 38 (12%) did MRI simply confirm original diagnosis. In 101 cardiac cases, CMRI provided additional data. In 82 pts (81%), CMRI changed the original diagnosis and in 49 (49%), patient care. CMRI did not contribute in 23 (23%) due to uninterpretable ICD artifact. In essence, 83% of cardiac cases benefited from MRI. Finally, in the 38 musculoskeletal cases, MRI provided additional information in 35 (92%) and in 29 (76%), MRI changed care. One patient (Dx: Glloblastoma mutliforme) was imaged without harm 9 times over >4 years. Importantly, with careful attention to device reprogramming and MRI sequences, no safety or device issues were encountered in any patient at any time.

Conclusion: MRI in patients with PM/ICD';s adds substantial clinical value to diagnosis and subsequent management greatly justifying any residual inherent risk. To our knowledge, this is the first study to focus solely on the diagnostic value of implantable devices under the notion that safety can be routinely accomplished.

ID#: 370666

Outcomes Prediction in PAH via the CardioMEMs Implantable Pulmonary Artery Device Integrated with CMR; Does CMR-Derived Emax have a Prognostic Role in Advanced PHTN?

Robert W. Biederman, MD, FACC, FAHA[1] Raymond Benza, M.D.[1], Priscilla I. Correa-Jaque, CCRC[2], Geetha Rayarao, M.S.[3], Mark Doyle, Ph.D.[1]

1. Allegheny General Hospital, Pittsburgh, PA

2. Allegheny General Hospital, PA

3. Allegheny General Hospital, PIttsburgh, PA

Background: Management of patients with pulmonary hypertension (PHTN) is difficult, time consuming and expensive due to the requirement, amongst many, for frequent rigth heart catheterizations (RHC). A non-invasive approach to limit RHC would have obvious advantage. We investigated the combined use of the CardioMEMs HF System (Abbott) and Cardiovascular MRI (CMR) to provide prognostic information. CMR can be used to measure RV volume/morphology while the CardioMEMs device used to simultaneously measure PA pressures within the MRI environment.

Hypothesis We hypothesize that the PV maximal myocardial elastance (Emax) derived from CardioMEMSTM pressure and CMR RV volumes provides prognostic value in PAH patients.

Methods: Seventeen PAH patients with NYHA Class III and a recent hospitalization for RHF underwent CMR/CardioMEMs evaluation for CMR-derived RV-Emax one month post implant and at 4 months post implant. Linear regression analysis of CMR metrics was performed to identify predictors of the number of SAE's as related to clinical metrics.

Results: Patients were followed for 22±10 months and cumulatively experienced 34 severe adverse events (SAE) including death remote from implant (4). The baseline PV Emax (pulse pressure /end-systolic RV volume) (method of Sanchez/Fuster) was identified as the strongest predictor (separately or in conjunction with other variables) in predicting number of SAEs (r=0.67, p Fig 1. The RV Emax assessed at 4 months post implant trended higher vs baseline (0.53±0.29 vs 0.63±0.3) but was not narrowly not predictive of SAEs (p=0.07).

Conclusion: Non-invasive assessment of PV elastance (RV-Emax) at baseline was predictive of the number of SAEs, particularly death, in patients with advanced PAH with a threshold >0.42 being 100% predictive of an SAE. Interestingly, treatment in these patient trended to increase Emax which suggests, counterintuitively, that Emax now moves in a deleterious direction. Finally, we note that the baseline CMR-derived RV Emax was strongly predictive of SAE events in this PHTN population which, potentially, may be a pharmacologically modifiable variable.

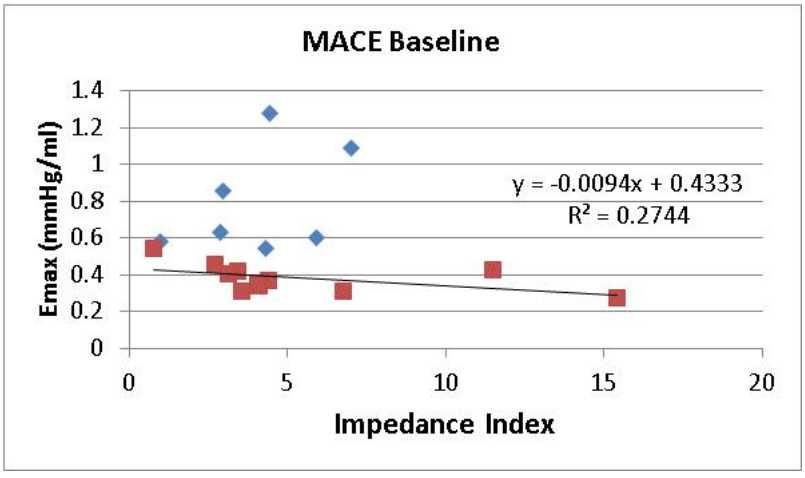

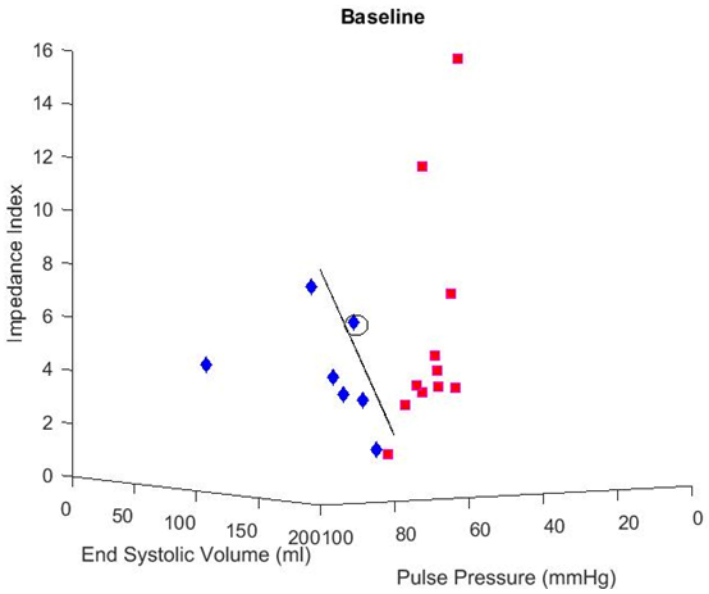
Baseline
Impedance Index
16
14
12
10
8
6
4
2
0
0
50
100
150
200
End Systolic Volume (ml)
100
80
60
40
20
0
Pulse Pressure (mmHg)

ID#: 370723

Long-term prognostic implications of previous silent myocardial infarction detected by cardiovascular magnetic resonance in patients presenting with first acute myocardial infarction

Raquel Amier, MD[1]Martijn Smulders, MD[2], Wiesje Van der Flier, PhD[3], Sebastiaan Bekkers, MD, PhD[2], Alwin Zweerink, MD[4], Cornelis Allaart, MD, PhD[5], Ahmet Demirkiran, MD[3], Sebastiaan Roos, MD[3], Paul Teunissen, MD, PhD[3], Yolande Appelman, MD, PhD[3], Niels van Royen, MD, PhD[3], Raymond J. Kim, MD[6], Albert C. van Rossum, MD, PhD[7], Robin Nijveldt, MD, PhD[3]

1. VU University Medical Center, Amsterdam, Noord-Holland, Netherlands

2. Maastricht University Medical Center, Netherlands

3. VU University Medical Center, Netherlands

4. VU university medical center, Netherlands

5. VU university medical center, Amsterdam, Netherlands

6. Duke University Medical Center, NC

7. VU University Medical Center, Noord-Holland, Netherlands

Background:

Up to 54% of myocardial infarction (MI) occurs without apparent symptoms. The prevalence and long-term prognostic implications of previous silent MI in patients presenting with seemingly first acute myocardial infarction (AMI) are unclear. This study aimed to investigate the prevalence of silent MI in patients presenting with first AMI, and its relation with mortality and major adverse cardiovascular events (MACE) at long-term follow-up.

Methods: A two-center observational longitudinal study was performed in 392 patients presenting with first AMI between 2003-2013, who underwent LGE-CMR exam within 14 days post-AMI. Silent MI was assessed on LGE-CMR images by identifying regions of hyperenhancement with an ischemic distribution pattern in other territories than the AMI. Mortality and MACE (all-cause death, reinfarction, coronary artery bypass surgery and ischemic stroke) were assessed at 6.8 ± 2.9 years follow-up.

Results: Thirty-two patients (8.2%) showed silent MI on LGE-CMR. Compared to patients without silent MI, mortality risk was higher in patients with silent MI (hazard ratio [HR] 3.33, 95% CI 1.34 – 8.27, p=0.009), as was risk of MACE (HR 3.55, 95% CI 1.66 – 7.55, p=0.001), both independent from clinical characteristics, CMR-derived left ventricular ejection fraction and (acute) infarct size.

Conclusion: Silent MI occurred in 8.2% of patients presenting with first AMI and was a strong, independent predictor of poorer long-term clinical outcome, with a more than three-fold risk of mortality and MACE. Silent MI holds prognostic value over important traditional prognosticators in the setting of AMI, indicating that these patients represent a high-risk subgroup warranting clinical awareness.

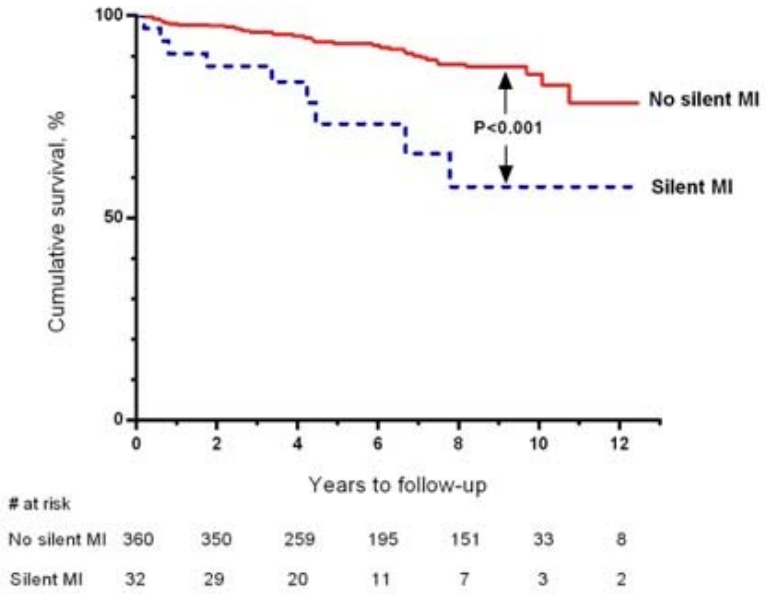

# at risk							
No silent MI	360	350	259	195	151	33	8
Silent MI	32	29	20	11	7	3	2

Kaplan-Meier curve showing increased mortality in patients with silent MI compared to those without silent MI

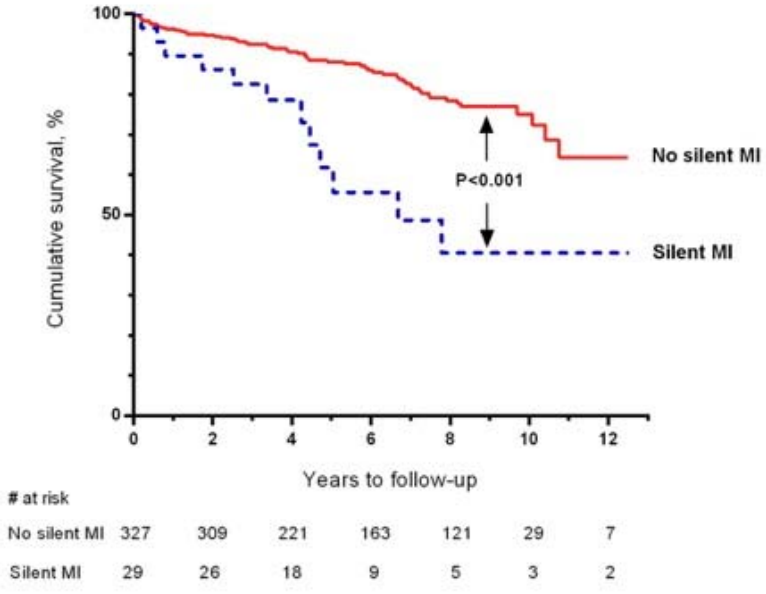

# at risk							
No silent MI	327	309	221	163	121	29	7
Silent MI	29	26	18	9	5	3	2

Kaplan-Meier curve showing increased MACE in patients with silent MI compared to those without silent MI

Uni- and multivariable Cox regression analyses of silent MI and clinical outcome

	Univariable	P-value	Multivariable*	P-value
	HR (95% CI)		HR (95% CI)	

Death	3.69 (1.77-7.67)	<0.001	3.33 (1.34 - 8.27)	0.009
MACE (death, reinfarction, ischemic stroke, coronary artery bypass grafting)	3.05 (1.64-5.70)	<0.001	3.55 (1.66 – 7.55)	0.001

HR indicates hazard ratio; CI, confidence interval, MACE, major adverse cardiovascular events

* Adjusted for age, sex, study site, pre-hospital medication, type of acute myocardial infarction (with or without ST-elevation), reperfusion strategy (direct, deferred or none), left ventricular ejection fraction, (acute) infarct size

ID#: 370884

CMR-derived Strain in Adult Cancer Survivors with a Normal Left Ventricular Ejection Fraction: an Age and Sex Matched Case Control Study

Iwan Harries, MBBCh BSc[1]Natasha ffrench-Constant, BSc[2], Estefania De Garate, MD[3], Amardeep Ghosh Dastidar, MBBS(Hons), MRCP[4], Chris Lawton, PGC, BSC[1], Anna Baritussio, MD[4], Chiara Bucciarelli-Ducci, MD, PhD[4]

1. Bristol Heart Institute, Bristol, England, United Kingdom

2. University of Bristol, United Kingdom

3. CMR Unit - Bristol Heart Institute, Bristol, England, United Kingdom

4. Bristol Heart Institute, Bristol NIHR Biomedical Research Centre (Cardiovascular Section), University of Bristol, Bristol, England, United Kingdom

Background: Adult cancer survivors are at increased risk of cancer therapeutics-related cardiac dysfunction (CTRCD). Echocardiography-derived left ventricular strain is reported to be abnormal in this population, even in the context of a normal left ventricular ejection fraction (LVEF). We sought to determine if cardiovascular magnetic resonance (CMR)-derived left ventricular strain is abnormal after cancer therapy in this age and sex matched case-control study.

Methods: 126 consecutive adult cancer survivors undergoing comprehensive 1.5T CMR were retrospectively identified. Those with abnormal LVEF (n = 65) or concomitant confounding factors e.g. ischaemic heart disease (n = 21) were excluded. The remaining 40 adult cancer survivors (27 [68%] female, mean age 55.0 ± 12.6 years) with normal LVEF (61.4 ± 5.8%) served as the study population. CMR was performed at mean 7 years after cancer therapy (mean cumulative anthracycline dose 244.8 ± 87.7mg/m2, 29 [50%] received radiotherapy) and were compared with 40 age and sex matched controls (27 [68%] female, mean age 54.9 ± 15.1 years) with normal CMR findings (normal volumes, function, absence of scar or significant cardiac pathology) and no history of cancer therapy. Left ventricular strain analysis was undertaken using short and long-axis SSFP cines by an experienced CMR reader blinded to clinical details using post-processing software (CVI 42, Circle Cardiovascular Imaging, Calgary, Canada).

Results: Albeit within the normal range, LVEF (61.4 ± 5.8 vs. 64.8 ± 5.4%, P = 0.009), was significantly lower in cancer survivors compared to controls, largely driven by increased indexed end systolic volume (27.5 ± 9.8 vs. 23.2 ± 4.7ml/m2, P = 0.015), though all values remained within normal limits. All other measures of left ventricular, right ventricular and left atrial volume and function were similar (P > 0.05 in all cases). However, peak global longitudinal (-18.1 ± 2.5 vs. -21.0 ± 2.4%; P < 0.0001), peak global radial (35.0 ± 6.4 vs. 41.5 ± 6.5%; P < 0.0001) and peak global circumferential strain (-18.8 ± 2.3 vs. -21.0 ± 2.0%; P < 0.0001) were on average 14%, 16% and 10% lower in cancer survivors compared to controls, respectively.

Conclusion: Patients treated with cancer therapy with a normal LVEF had significantly impaired CMR-derived measures of left ventricular strain compared to an age and sex matched control population. Strain imaging could provide complementary discriminatory information to traditional LVEF-focussed evaluation of cardiac function in adult cancer survivors.

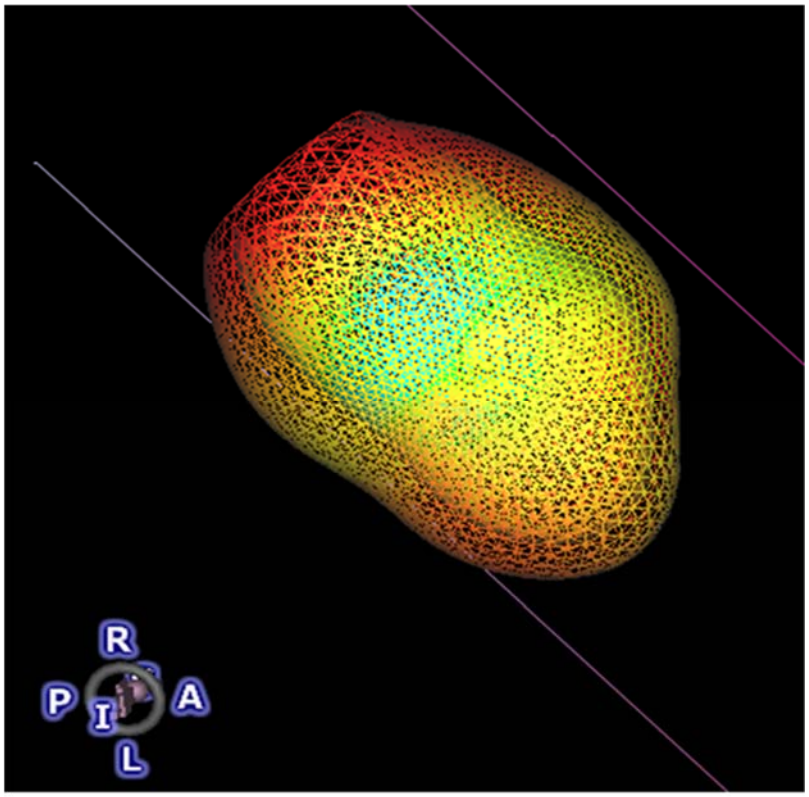
R
P
A
I
L

ID#: 370887

Novel Real-time Feedback Slice Tracking with a Predictive Algorithm and Spatially Resolved MR-compatible Ultrasound for Cardio-vascular MRI.

Lindsey A. Crowe[1] Francesco Santini[2], Laura Gui, PhD[3], Pauline Guillemin[4], Pamina Bernou[4], Myriam Roth[5], Gibran Manasseh, MD[6], Oliver Bieri[7], Rares Salomir, PhD[6], Jean-Paul Vallée[4]

1. Geneva University Hospitals, Geneva, Geneve, Switzerland

2. University Hospital Basel, University of Basel, Switzerland

3. University of Geneva, Switzerland

4. Geneva University Hospitals, Geneve, Switzerland

5. University of Geneva, Geneve, Switzerland

6. Geneva University Hospital, Geneve, Switzerland

7. University of Basel Hospital, Switzerland

Background: Cardiac MRI has the potential to depict the cardiac valves with high resolution, for functionality, morphology and flow. We propose a method of ultrasound guidance for motion compensation during MR acquisition, with a future-predicting algorithm illustrated in high-resolution cine of a ‘breathing'; phantom.

Methods: Ultrasound used a clinical Siemens ACUSON Antares. The P7-3-like linear-array probe (192-element) was built MR-compatible with advanced electromagnetic shielding on the transducer casing inner face. An 8m multi-channel cable (electromagnetically shielded with a non-magnetic dense mesh set to common ground with the Faraday cage) transferred signals between the US probe and control unit. Adjustment of impedance matching compensated increased capacity of the long cable. A phantom bottle of acoustic gel, in a water bath, was placed centrally above a 11cm loop coil. The bottle was attached to a robot simulating respiratory motion (amplitude 20mm, head-foot direction, figure 1). Probe orientation ensured no out-of-plane motion. The horizontal motion vector was imaged by second harmonic ultrasonography and tracked via the acoustic speckle shift. The US field depth was 14-16cm, frame rate 25-30 images/second, slice thickness 5mm, carrier frequency 3.3MHz, receive central frequency 6.6MHz. US images were sent in near real-time to an external PC, which extracted the average motion vector in a user-defined ROI, an communicated to the MR system on-the-fly. A second algorithm predicted the future position of the moving object (60ms) via parabolic fitting of the previous datapoints. A conventional cardiac-triggered segmented balanced-SSFP sequence was modified in order to adapt the slice positioning in quasi-realtime according to the information received from the ultrasound. Real-time bSSFP images were acquired on a Siemens 3T PRISMA to determine the optimum number of points for fitting. High-resolution cine bSSFP was acquired with acquisition longer than 30s. The cine images were assessed for visual sharpness and quantified with a Canny filter (hysteresis threshold, normalising gradient images to binary mask) counting sharp edge ‘pixels';.

Results: Figure 2 shows the time profile of 200 real-time images with no correction and the parabolic prediction. Quantitatively the standard deviation of motion was 8.86mm uncorrected, 0.68mm for the corrected, and 0.53mm with prediction. Cine images showed clear improvement with parabolic predictive correction compared to uncorrected images (figure 3A). The canny-filtered images showed ‘gaps'; where affected by motion artifacts. Quantification showed the predictive correction was closest to the static gold-standard image (figure 3C). Pixels were quantified as a measure of sharpness: Static 494, uncorrected 323, normal (on the fly) correction 404, parabolic prediction correction 467 pixels.

Conclusion: With this multimodality method, we corrected respiratory motion-blurring artifacts in long high-resolution cine acquisitions. The on-the-fly correction was further improved by the addition of a prediction algorithm using parabolic fitting of previous points.

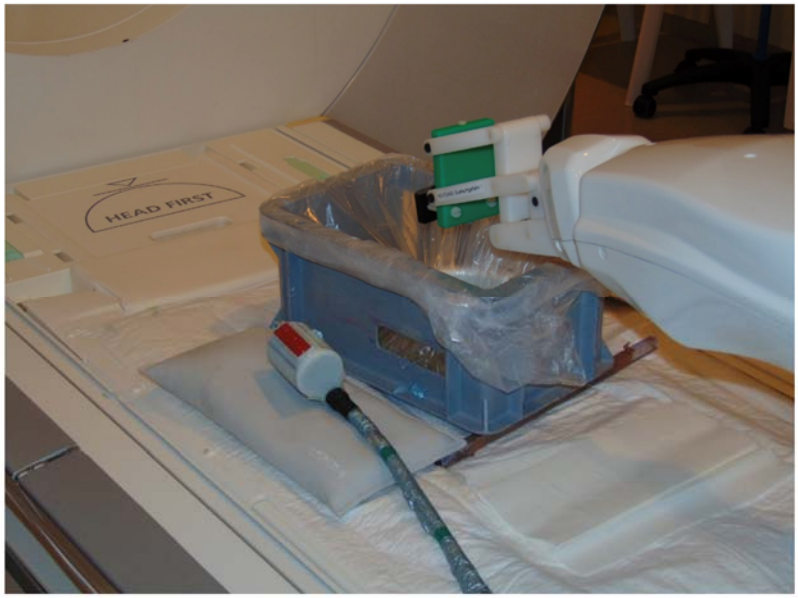

Figure 1. Set up of phantom and robot.

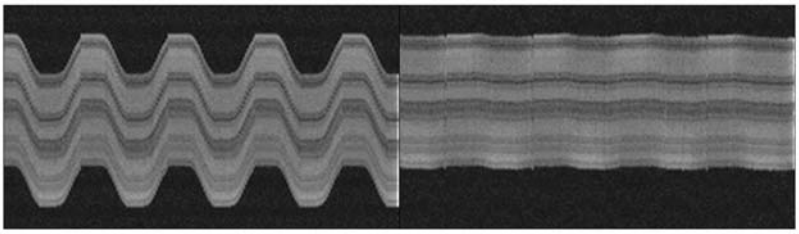

Figure 2. Profile of time dimension of 200 real-time images acquired with no correction and parabolic predictive correction. Images were bSSFP with TR/TE 17.13/2.56ms, 56ms, resolution 1mm, slice thickness 5mm.

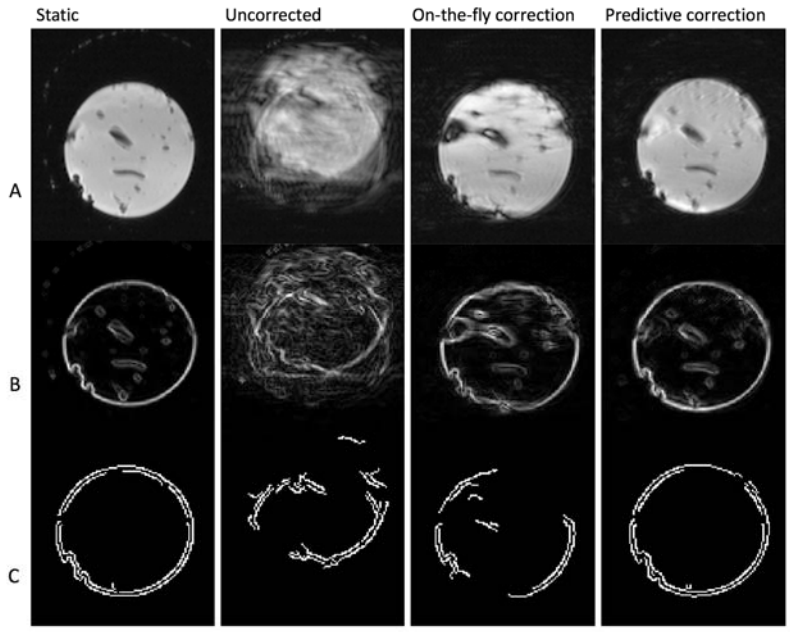

Figure 3. A: Cine images. Static, uncorrected, normal (on-the-fly) correction, parabolic prediction correction. Parameters were bSSFP with flip angle 57, TR/TE 18.2/1.54ms, simulated RR 1000ms, 0.88mm resolution and 51

cardiac phases, 30 second ‘breathold’; B: Gradient image; C: Quantification of sharpness by a Canny filter of the gradient edge image of the cine, normalised and with background noise removed by hysteresis threshold. Pixels in the bottom row indicate sharp edges and can be quantified as a measure of sharpness: Static 494, uncorrected 323, normal (on the fly) correction 404, parabolic prediction correction 467 pixels.

ID#: 370548

Flow asymmetry in the aortic root in TGA patients after arterial switch operation

Roel LF. van der Palen, MD[1] Jos J.M. Westenberg, PhD[2], Quirine S. Deurvorst[3], Pieter J. van den Boogaard, BSc[4], Lucia J.M. Kroft, MD[2], Nico A. Blom, MD, PhD[3], Hildo J. Lamb, MD, PhD[4], Arno A.W. Roest, MD, PhD[5]

1. Division of Pediatric Cardiology, Department of Pediatrics, Leiden University Medical Center, Leiden, The Netherlands, Leiden, Zuid-Holland, Netherlands

2. Department of Radiology, Leiden University Medical Center, Leiden, The Netherlands, Leiden, Zuid-Holland, Netherlands

3. Division of Pediatric Cardiology, Department of Pediatrics, Leiden University Medical Center, Leiden, The Netherlands, Zuid-Holland, Netherlands

4. Department of Radiology, Leiden University Medical Center, Leiden, The Netherlands, Zuid-Holland, Netherlands

5. Department of Pediatrics, Leiden University Medical Center, Leiden, The Netherlands, Zuid-Holland, Netherlands

Background: Aortic root dilatation is an important complication in patients with transposition of the great arteries (TGA) after arterial switch operation (ASO). It is not known whether aorta hemodynamics may impact aortic root dilatation in these patients. Systolic flow displacement (FD) is a hemodynamic parameter that has been correlated with ascending aortic (AAo) growth in patients with bicuspid aortic valve [1]. The aim of this study was to evaluate FD in relation to AAo geometry using 4D flow CMR in TGA patients after ASO.

Methods: 28 pediatric patients (16.0±3.3 years) after ASO for simple TGA and 10 healthy volunteers (26.5±2.6 years) underwent an aortic 4D flow CMR and non-contrast enhanced 3D MR Angiography (NCE-MRA) on a 3.0 Tesla MRI scanner (Philips Healthcare). **4D flow CMR**: retrospective ECG and respiratory navigator gating, spatial resolution=2.5x2.5x2.5mm^3, temporal resolution=26.8-35.1ms, VENC=200cm/s, segmentation factor=2, SENSE=2.5 in anterior-posterior direction. **NCE-MRA**: Dixon sequence, respiratory navigator gating, resolution=2.5x2.5x2.5mm^3, echo time/repetition time=0.0-2.3/3.6-3.9ms). AAo diameters and Z-scores [2] were determined from NCE-MRA (Fig 1). From 4D flow CMR, a peak systolic 3D aortic volume was automatically segmented using CAAS MR 4Dflow v1.1 software (Pie Medical Imaging BV) and was manually adapted where necessary. Eight cross-sectional planes were manually placed along the AAo. For each cross-sectional 2D plane, the border of the aorta was manually adapted where necessary and normalized FD was automatically determined using CAAS MR 4Dflow v2.0 software (Fig 1). FD was defined as the distance between the anatomical center of the vessel and the center peak velocity of the forward flow at peak systole, divided by vessel contour diameter [3]. The direction of FD within the aorta was assessed and classified in one of 8 directions (i.e. anterior, posterior, right, left, right-anterior, right-posterior, left-anterior, left-posterior).

Results: The proximal AAo was significantly dilated in TGA patients compared to controls at the level of the neo-aortic root (Z-score 4.98±2.04 vs 2.07±0.65, p<0.001) and sino-tubular junction (STJ) (3.48±2.67 vs 1.38±1.30, p=0.010) (Table 1). FD was significantly higher in TGA patients at level of the neo-aortic root (p=0.002) and STJ (p=0.011) (Fig 2). The FD direction in the AAo in TGA patients was different compared to controls (Fig 3). Furthermore, distinct FD differences between TGA patient subgroups based on pre-operative great artery position (data not shown) were detected: TGA patients with a right-anterior or right-sided position of the aorta (compared to the pulmonary artery) showed more FD to the right-side of the AAo (level aortic root and STJ), whereas a left-anterior or anterior position of the aorta resulted in more FD to the left-side of the aortic wall. There was a moderate association between the FD and neo-aortic Z-score at the level of the neo-aortic root and STJ (data not shown).

Conclusion: TGA patients after ASO have more flow asymmetry (i.e. higher magnitude and directionality of FD) in the proximal AAo, which was significantly dilated. Pre-operative great artery position is related to the direction of FD, which may have contributed to the progression of neo-aortic root dilation. **References:** [1.] Burris NS. et al. Invest Radiol. 2014;49:635-9 [2.] Kaiser T. et al. J Cardiovasc Magn Reson 2008; 10:56-63 [3.] Sigovan M. et al. J Magn Res Imaging. 2011;34:p1226-30

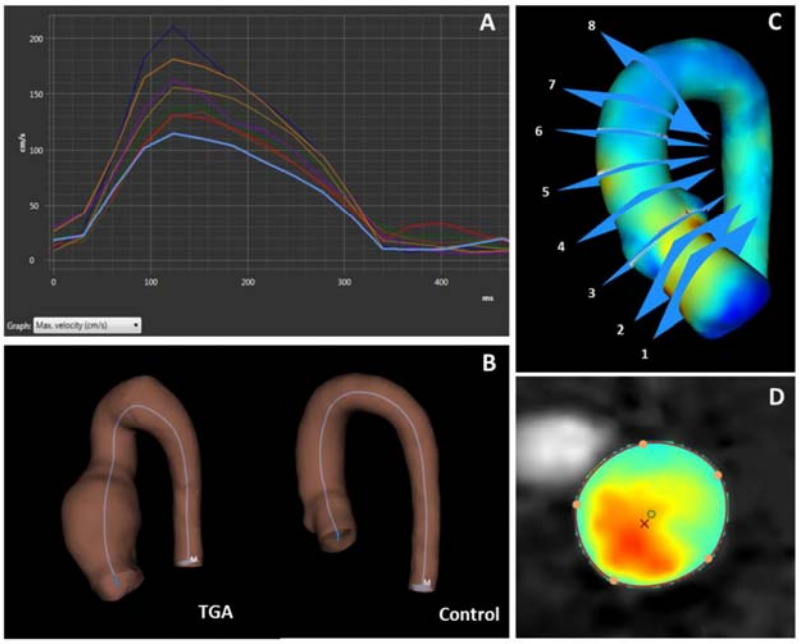

Figure 1. 3D segmentation and positioning of the eight cross-sectional planes for determining flow displacement.

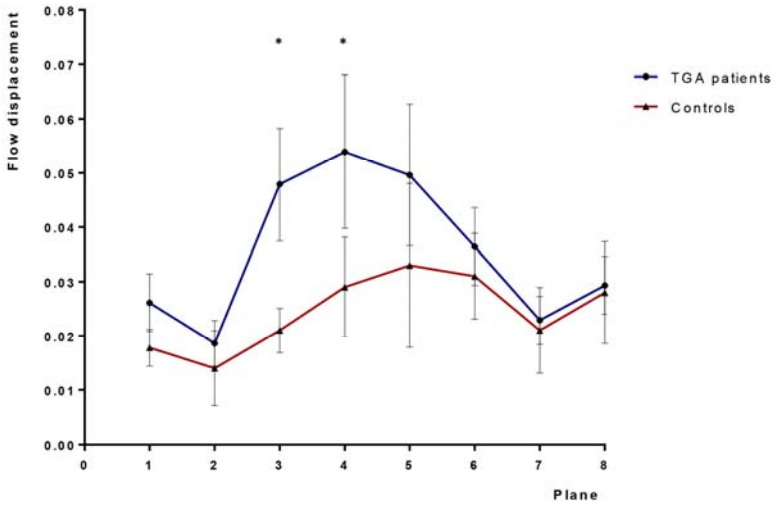

Figure 2: Flow displacement along the ascending aorta.

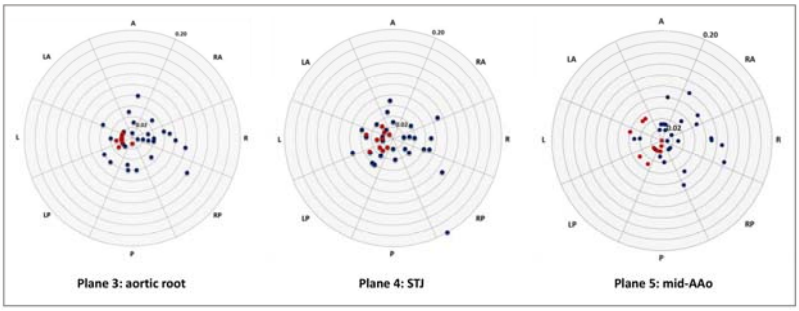

Figure 3: Magnitude and flow displacement direction profiles.

Table 1. Baseline characteristics and CMR measurements

	TGA patients (n=28)	Healthy volunteers (n=10)	P-value
Patient characteristics			
Male, n (%)	18 (64.3%)	5 (50.0%)	0.473
Age, years	16.0 ± 3.3	27.3 (24.9-28.4)	<0.001
Weight, kg	60.5 ± 14.0	68.3 ± 12.7	0.129
Height, cm	170.8 ±12.2	175.6 ± 6.6	0.250
Body Surface Area, m^2	1.7 ± 0.2	1.8 ± 0.2	0.137
LV ejection fraction, %	59.1 ± 5.7	62.0 ± 2.5	0.155
Transposition type, (%)			
TGA-IVS	21 (75.0%)		
TGA-VSD	7 (25.0%)		
Great artery position, (%)			
Aorta right anterior to PA	15 (53.6%)		
Aorta right side to PA	3 (10.7%)		
Aorta anterior to PA	7 (25.0%)		
Aorta left anterior to PA	3 (10.7%)		
Aortic diameters (mm)*			
Neo-aortic valve	23.0 [22.0-26.8]	19.5 [18.0-25.0]	0.010
Neo-aortic root, short axis, max	37.0 [33.3-41.0]	31.5 [29.0-33.3]	0.002
ST-junction	27.5 [24.0-32.0]	24.5 [23.8-27.3]	0.125
Mid ascending aorta	22.0 [21.0-24.0]	26.5 [25.0-29.3]	<0.001
Origin of BCT	22.0 [19.3-23.8]	23.5 [21.8-26.0]	0.056
Aortic Z-scores**			
Neo-aortic root, short axis, max	4.98 ± 2.04	2.07 ± 0.65	<0.001
ST-junction	3.48 ± 2.67	1.38 ± 1.30	0.010
Mid ascending aorta	0.32 ± 3.06	1.69 ± 1.24	0.001
Origin of BCT	-0.52 ± 1.21	0.20 ± 1.29	0.122

*Data are presented as median [Interquartile range]. **Data are presented as mean ± SD. Aortic Z-scores based on CMR derived normative data [2]. Abbreviations: ASO=arterial switch operation; BCT=brachiocephalic trunk; IVS=intact ventricular septum; LV=left ventricle; PA=pulmonary artery; TGA=transposition of great arteries; VSD=ventricular septal defect

ID#: 370576

Serum Uric Acid Level During Acute MI Modifies the Therapeutic Effects of High Dose Omega-3 Fatty Acids on Left Ventricular Remodeling

Kyoichi Kaneko, M.D., Ph.D[1]Bobby Heydari, MD, MPH[2], Shuaib Abdullah, MD[3], Kana Fujikura, MD, PhD[4], William Harris, PhD[5], Jiazuo Feng[6], Michael Jerosch-Herold, PhD[7], Raymond Y. Kwong, MD, MPH[8]

1. Brigham and Women's Hospital, Brookline, MA

2. Stephenson Cardiac Imaging Centre, Libin Cardiovascular Institute of Alberta, University of Calgary, AB, Canada

3. University of Texas-Southwestern Medical Center

4. Brigham and Women's Hospital, Boston, MA

5. Sanford School of Medicine, University of South Dakota

6. Dartmouth-Hitchcock Medical Center

7. Harvard Medical School, Boston, MA

8. Brigham and Womens Hospital, Boston, MA

Background: Serum uric acid (UA) is considered as a marker of cardiovascular inflammation and high UA levels are associated with adverse outcome in patients with acute MI. In the OMEGA-REMODEL trial, our group has reported that omega-3 fatty acid (O3-FA) therapy reduces systemic inflammation, non-infarct myocardial fibrosis and adverse remodeling of left ventricle during the first 6 months after an acute MI. We hypothesized whether serum UA level on admission can be an effect modifier after 6 months in patients with AMI.

Methods: 235 patients presented with AMI, double-blind randomized to O3-FA or placebo, were divided into 2 groups according to median of serum UA on admission. 3.0 tesla cardiac magnetic resonance (CMR) were performed and we analyzed left ventricular end systolic volume (LVESV) and non-infarct myocardial extracellular volume (ECV) at 2-4 weeks and 6 months after AMI. In high UA group and low UA group, we compared the change of LVESV, LVEF and ECV from baseline to post treatment between O-3 FA group and placebo group.

Results: As shown in images, in high UA group, O3-FA therapy significantly reduces LVESV (-5.23 ± 2.04 ml vs 0.39 ± 1.84 ml, p=0.043) whereas there is not significant reduction in low UA group (-2.11 ± 1.89 ml vs -6.07 ± 1.65ml, p=0.117). In addition, in high UA group, patient who received O3-FA demonstrated no progression of non-infarct myocardial fibrosis (-0.0066 ± 0.0085 vs 0.0047 ± 0.0079, p=0.166), whereas a significant progression was observed among patients in the low UA group (-0.016 ± 0.0087 vs 0.0089 ± 0.0092, p=0.027).

Conclusion: AMI patients with a high serum UA level were more likely to experience the benefits in post-MI cardiac remodeling, offered from anti-inflammatory effects of O3-FA.

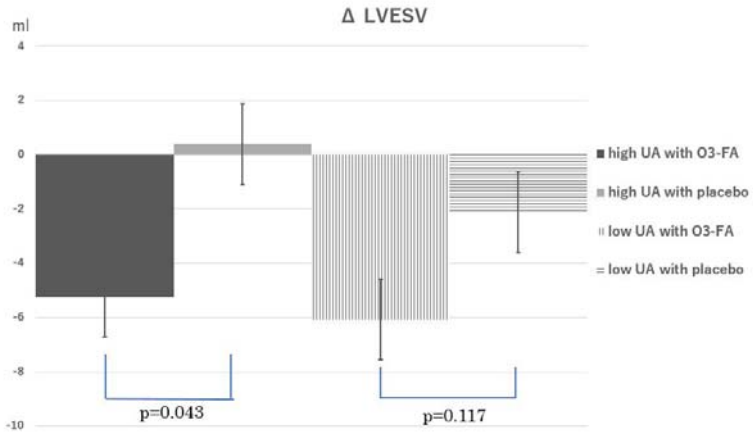

Change of LVESV in 4 groups from baseline to 6 months after therapy

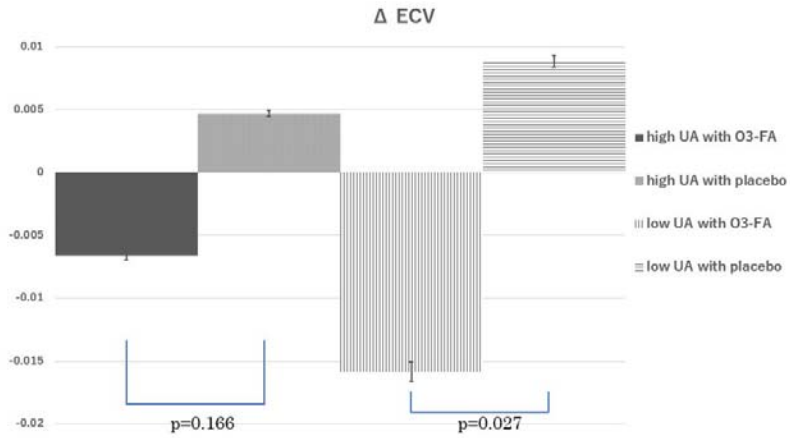

Change of ECV in 4 groups frombaseline to 6 months after therapy

ID#: 370637

Safety and Image Quality of the Combined use of Cardiac MRI and the CardioMEMS HF System in Progressive PAH; a Proof of Concept Study

Robert W. Biederman, MD, FACC, FAHA[1]Mark Doyle, Ph.D.[1], Priscilla I. Correa-Jaque, CCRC[2], Geetha Rayarao, M.S.[3], Raymond Benza, M.D.[1]

1. Allegheny General Hospital, Pittsburgh, PA

2. Allegheny General Hospital, PA

3. Allegheny General Hospital, PIttsburgh, PA

Background: Ongoing evaluation of right ventricular (RV) function and ventriculovascular coupling (VVC) are fundamental to predicting outcome in pulmonary hypertension (PHTN). The CardioMEMS HF System (Abbott) is a recently FDA device approved used for wireless monitoring of PA pressure in HF patients and is permanently implanted in the pulmonary artery during a RHC. We tested the safety and image impact of using this system combined with cardiac MRI (CMR) to obtain coincident pressure and right heart MRI volumetric data in patients with advanced PAH. Hypothesis Safety and image quality of CMR imaging will not be compromised with implantation of the CardioMEMS device in the distal pulmonary vasculature.

Methods: Methods PAH patients with NYHA class Ill and a recent hospitalization for RHF were enrolled. Sensor implants were performed in a Cath Lab and CMR lab. After 1 and 4 months, patients underwent PV/PA evaluation using a CMR non-contrast protocol to measure RV volumetrics, main pulmonary artery volumes, dimensions, VVC and flow. Interrogation of the CardioMEMS device was performed in the CMR room just outside the magnet bore (inside 5 Gauss line). SNR and CNR were temporally evaluated as well as graded subjectively via CMR cardiologist expert and CMR physicist. Image quality as assessed via CNR and SNR were performed. Patient monitoring to include BP, HR, 02 saturations, visual monitoring as well as direct CardioMEMS device interrogation throughout (before during and after) the CMR were performed. Reader evaluation was additionally assessed for image degradation, artifacts and paramagnetic interferences.

Results: No MRI safety, hemodynamic or CardioM EMS device issues were encountered in the first 17 patients in the MRI environment at either time point representing 31 individual CMR examinations. As well, there were no paramagnetic image degradation/artifacts affecting SNR or CNR. A full cohort of traditional cardiac metrics were performed without limitations or compromise.

Conclusion: Non-invasive assessment of CMR hemodynamics and physiology are possible when integrating a novel, implantable pulmonary hemodynamic monitor within the CMR. There were neither adverse safety signals nor paramagnetic effects. This initial work supports the safety and efficacy of the CardioMEMS device in the MRI environment further adding to its intrinsic value in advanced PHTN.

ID#: 370855

Tracking Electromechanical Activity in Ultra-thin Layers of Cardiac Tissue on 3T MRI Scanners

Vladimir Shusterman, MD, PhD[1] Xiaodong Zhu, PhD[2], Daniel Thedens, PhD[2], Stacy Hoffman, BA[3], Jin-Young Yoon, PhD[2], Gina Morgan, MS[4], Barry London, MD, PhD[5]

1. PinMed, Inc., Iowa City, IA

2. The University of Iowa

3. PinMed, Inc.

4. The University of Iowa, Iowa City, IA

5. The University of Iowa, Iowa city, IA

Background: Distinguishing contracting from non-contracting cardiac tissues is essential for the diagnosis and tracking of heart failure. We developed an MRI-compatible model for studying ultra-thin layers of cardiac tissue (ULCTs) and used it to test the feasibility of tracking contractile activity in ULCTs.

Methods: Contracting ULCTs (~50-100 microns) were obtained from cultured multicellular preparations of rat neonatal cardiomyocytes plated on rectangular plates (4.5 x 2.0 cm; Fig. 1a) or circular plates (diameter: 10 cm; Fig. 1b). A series of imaging experiments was performed on 3T scanners (Siemens Trio and GE Discovery) with the testing plate placed inside the 8-channel head coil (Fig.1c). The two-dimensional, gradient-echo CINE sequence was applied using the following parameters: FOV: 192 x 128 mm, FA: 65°, TR: 4.3 ms, TE: 1.2 ms, slice thickness: 4 mm, number of averages: 75. The CINE images were obtained at ~12.8-ms time intervals. An MRI-compatible,12-lead ECG system with thin (75 microns), non-metal electrodes (PELEX-MAX, PinMed, Inc.) was used to track and stimulate (pace) electrophysiological activity in the ULCTs, as well as to trigger the scanner, as shown in Fig. 1c.

Experiments were performed using: a) tissue-free culture (control), b) spontaneously beating ULCTs, and c) electrically activated (paced) tissues. Fig. 2 shows an example of a ULCT image (Fig. 2a), as well as the image with an approximately 2-cm^2 region of interest (ROI) (Fig. 2b). To track the patterns of tissue contraction and estimate the contraction-wave propagation velocity, the local maxima (LM) of the image intensity gradients were computed using the derivative of a Gaussian filter and depicted as level (contour) curves. The contraction velocity (CV) was estimated in the ROI as: $CV = PD/(MD_{LM} \times TI)$, where PD is the pixel-to-pixel distance (0.47 mm), MD_{LM} is the mean positive difference between LM in consecutive CINE images (Fig. 2c) for all rows in the ROI matrix, and TI is the time interval between consecutive CINE images.

Results: The ULCTs exhibited spontaneous mechanical contractions in the individual tissue strands (~1-4 mm long) at approximately 30-60 bpm (Fig. 3a). Pacing (0.5-2V) at 60-120 bpm produced synchronous contractions of all tissue strands on the plate (Fig. 3b). The ULCT images showed the contraction of different myocardial strands (Fig. 3c), which were delineated using level (contour) curves (Fig. 3d).To examine the impact of noise and scanner-vibration artifacts on the MR image pattern and quality, MR images were also obtained using cell-free chambers filled with the culture medium (Fig. 3e). Note the difference between heterogeneous patterns of contracting strands (Fig. 3c) compared with the homogeneous patterns of cell-free images (Fig. 3e). The dynamical changes associated with the contractions of myocardial strands were visually trackable in the sequences of CINE images (to be presented). The mean speed of the mechanical contraction was 5.1 ± 2.9 mm/s, which was in excellent agreement with previous studies. The electrical conduction velocity (estimated to be 0.24-0.29 m/s in our study) was also comparable to that in previous studies performed in confluent monolayers of neonatal rat ventricular myocytes.

Conclusion: Electromechanical activity can be tracked simultaneously in ULCTs using 3T scanners. Translating these results to in-vivo localization of non-contracting tissues in the failing heart requires further study.

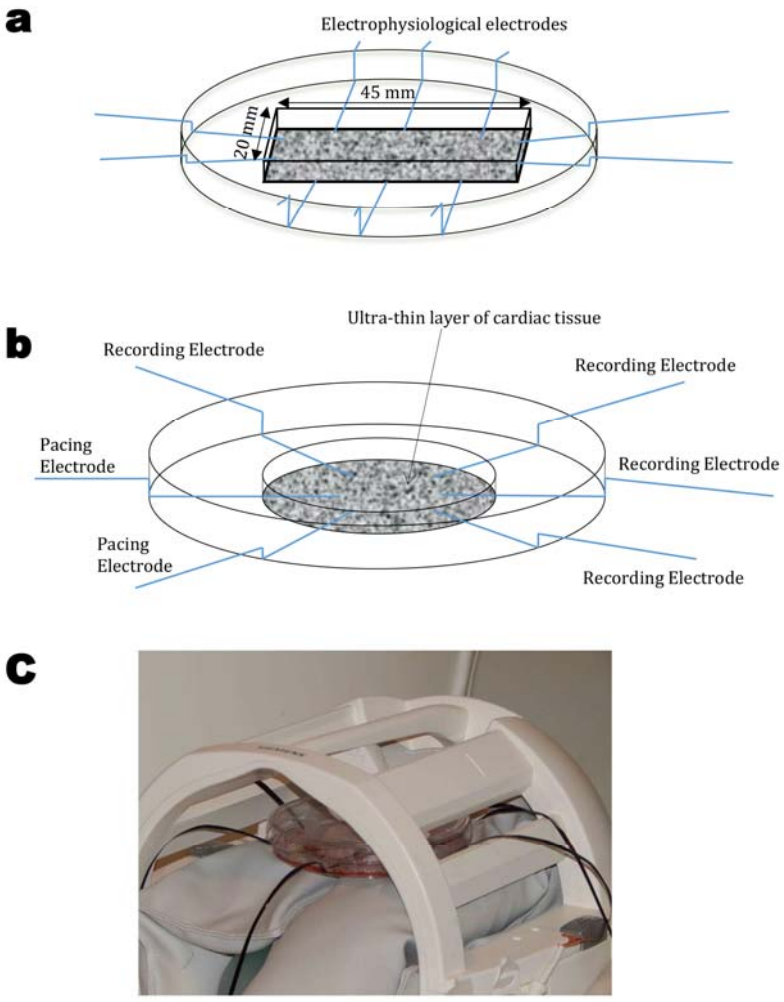

Fig. 1

Fig.1. An MR-compatible model for studying ultra-thin layers of cardiac tissue.

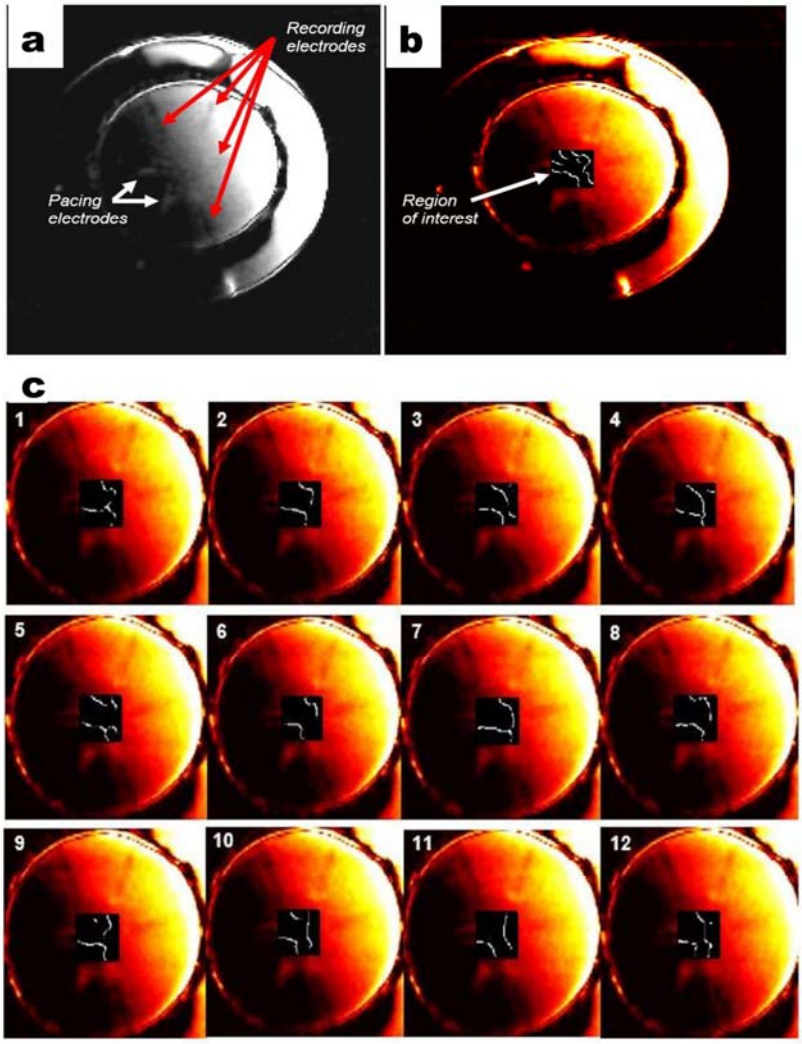

Fig. 2

Fig. 2. Example CINE images of the ultra-thin layers of cardiac tissue, with contraction patterns (depicted as contour plots) in the region of interest on circular plates (see text for details).

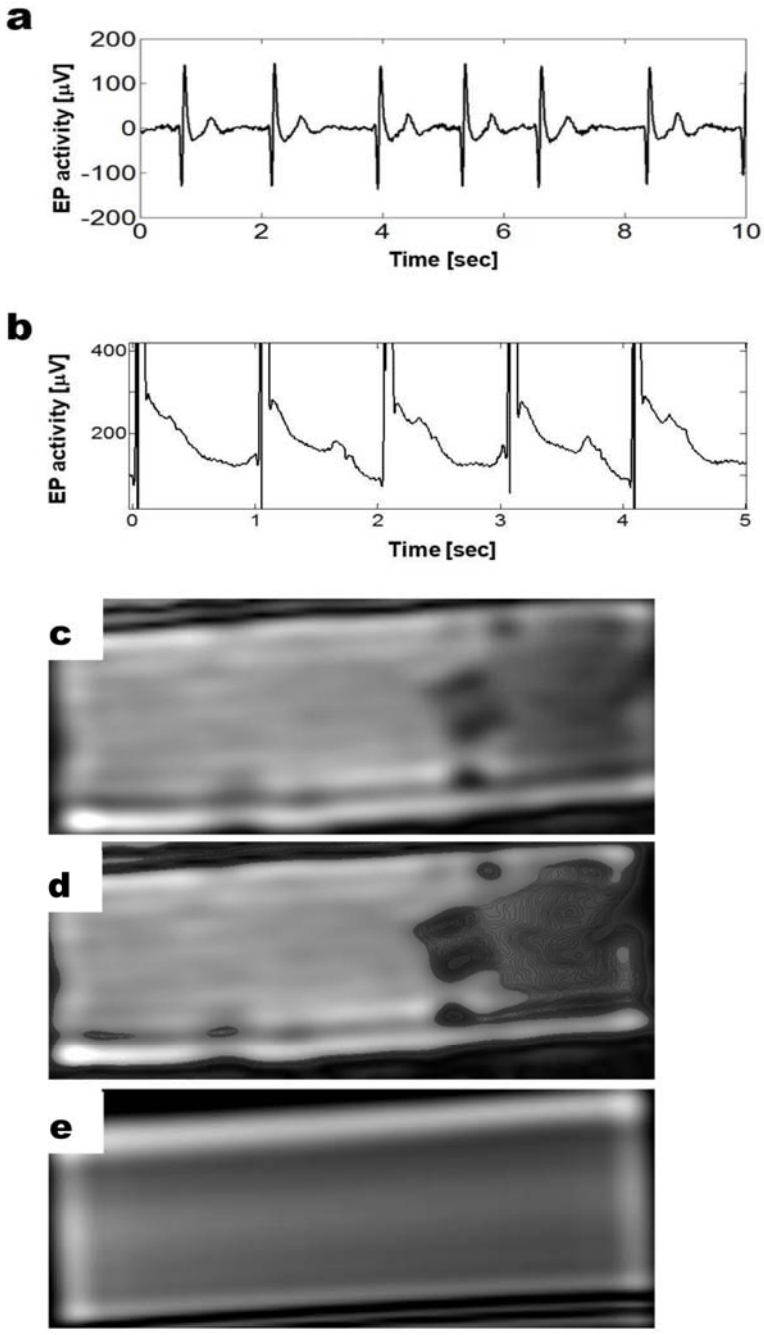

Fig. 3

Fig. 3. Examples of electrophysiological activity and CINE images of the ultra-thin layers of cardiac tissue and tissue-free (control) preparations on rectangular plates.

ID#: 370928

What have we Learned from Echo-TAVR; Can we apply it to CMR-TAVR?

Victor Farah, MD[1]Mark Doyle, Ph.D.[1], Sahadev Reddy, MD[1], Manik Veer, MD[2], Robert W. Biederman, MD, FACC, FAHA[1]

1. Allegheny General Hospital, Pittsburgh, PA

2. Allegheny General Hospital

Background: Transcatheter aortic valve replacement (TAVR) is increasingly performed in patients with severe aortic stenosis with high surgical risk and recently with moderate surgical risk all at acceptable mortality. The transcatheter valve is implanted in a suture-less fashion and therefore it has a high risk of developing perivalvular aortic leak (PVL). The presence of PVL and its severity carry an independent adverse prognostic sign for those patients post TAVR. Hypothesis
We hypothesize that PVL following TAVR will cause CHF decompensation in patients with concentrically adapted LVs to an isolated AS, while chronic AR pre-TAVR with an eccentrically adapted LVs will prevent decompensation.

Methods: 121 consecutive patients who underwent TAVR between January 2014 and September 2015 were reviewed. Demographic data and echocardiographic findings pre and one year post TAVR were retrospectively collected and analyzed and admissions to the hospital with congestive heart failure decompensation diagnosis were documented.

Results: PVL severity was estimated visually qualitatively without quantitative measurements in 100% of the patients. The patients were divided into 4 groups depending on the presence of AR pre and post TAVR. We had 4 groups, (Pre - AR, Post - PVL) (Pre - AR, Post + PVL) (Pre + AR, Post - PVL) (Pre + AR, Post + PVL). Hospitalization for CHF in each group was reviewed. In the (Pre - AR, Post + PVL) group, 7 (39%) episodes of CHF requiring hospitalization within one year post procedure occurred and represented the group with the highest rate of CHF hospitalization. Correlation between the degree of pre TAVR AR and post TAVR congestive heart failure episodes was weakly negative, r = - 0.2 ($p < 0.02$) (fig 1).

Conclusion: Accurate evaluation of PVL after TAVR is critical as it is highly prognostic for morbidity and mortality. While the presence of AR in the PARTNER Trials has been shown to be an adverse finding, we show that upon categorization of those patients, the presence of a mild to moderate degree of aortic regurgitation pre-TAVR is beneficial to patients who develop post-TAVR PVL, thus serving as an effective predictor of clinical outcomes in such patients. In that CMR is the 'gold-standard'; for AR quantitation, we propose that CMR may better provide insight into the likely physiologic method explanatory for this paradox. We believe it is time to incorporate cardiac MRI into the armamentarium for TAVR patients.

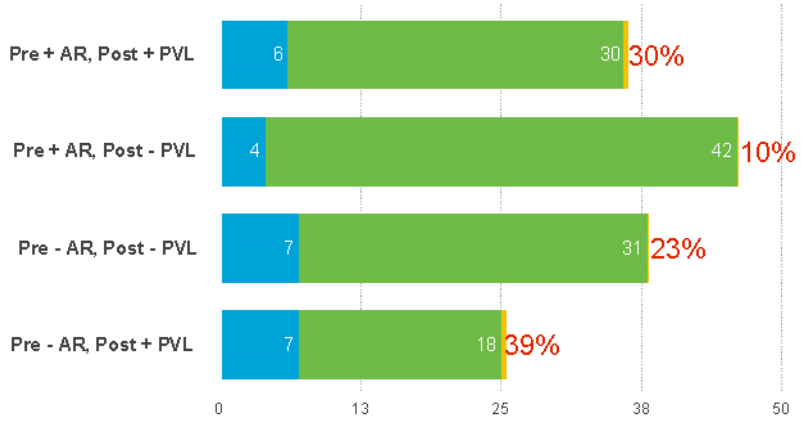

ID#: 371092

Assessment of automatic late gadolinium enhancement scar tissue analysis techniques in HIV-cardiomyopathy

Yoko Kato, MD, Ph.D[1] Bharath Ambale-Venkatesh, Ph.D[2], Michio Ozaki, BS,RT[2], Elzbieta Chamera, RDCS[1], Mohammad Ostovaneh, MD, Ph.D[2], Rob van Der Geest, Ph.D[2], Robert Kaplan, Ph.D[3], Jason Lazar, MD, MPH[4], Jorge R. Kizer, MD[3], Joao A.C. Lima, MD, MBA[1]

1. Johns Hopkins University, Baltimore, MD

2. Johns Hopkins University

3. Albert Einstein College of Medicine

4. SUNY Downstate Medical Center

Background: The quantification of scars in HIV cardiomyopathy is complicated by their diffuse nature and by the varied patterns found. The goal of this study was to understand scar distribution in women with, or at risk for HIV infection, and evaluate the performance of automatic late gadolinium enhancement (LGE) scar analysis methods.

Methods: This study included non-ischemic women with and without HIV infection, but similar behavioral risk factors, participating in the Women';s Interagency HIV Study (WIHS). 2D mulit-shot LGE with whole heart coverage was performed on Philips 3T scanner with high resolution of 0.63 x 0.63 mm and slice thickness of 10 mm. In the manual analysis, we assessed the distribution of myocardial scar tissues and segmentation was performed manually, which we treated as the gold standard of scar quantification. In the automatic scar analysis, the normal tissue and the scar tissue with highest signal intensity were selected automatically. Then the scar was detected using intensity thresholds of 2SD, 4SD, 6SD, 8SD above the normal myocardium, as well as the full width half maximum (FWHM) method. We compared the LGE volume as percentage of myocardium between manual and each automatic method. The comparisons were performed in whole myocardium and in each segment from AHA 16 segment model. Statistical assessments were performed using paired t-test to assess the difference, linear regression analysis to assess the correlation coefficient, and Bland-Altman plot to assess the concordance of methods compared to the manual method.

Results: 34 randomly chosen participants were included. Patient characteristics were - mean age: 53.3+-9.1 years old, ejection fraction (EF): 55.4+-6.1 %, myocardial mass: 81.9+-21.9 g, myocardial scar percentage: 8.6+-3.6% (mean+-SD). All the cases presented LGE positive, while scar percentage showed no correlation with LVEF (R-squared = 0.0027, p=0.77). Scar was mostly localized to basal inferoseptum to inferolateral segments and mid septum to inferior wall segments. The global scar percentage was most comparable to manual when using 8SD (Manual vs. 8SD = 8.5+-3.8 vs.9.4+-10.5, (mean+-SD (%)), p=0.603) with low correlation coefficient (R2 = 0.19, p manual). In segmental analysis, automatic 8SD analysis showed significantly larger scar percent than manual (8SD >= manual) in AHA segments 1-3 (basal anterior and septal walls). Significantly smaller percentages (8SD =< manual) were observed in segments 10-12 (basal lateral and inferior walls, and all mid-ventricular segments). In the apical segments (segments 13-16) the automatic 8SD analysis presented significantly larger scar percentage than manual (8SD > manual, p<0.01)).

Conclusion: Subclinical scar development was observed in these women with, or at risk for, HIV with preserved LVEF. Automatic scar analysis was susceptible to cardiac throughplane motion, which caused overestimation in the apical segments (segments 13-16) and the left ventricular outflow tract segments (segments 1 -3). The mid segments underestimated LGE when using 8SD. Care should be taken when interpreting scar analysis using completely automatic methods.

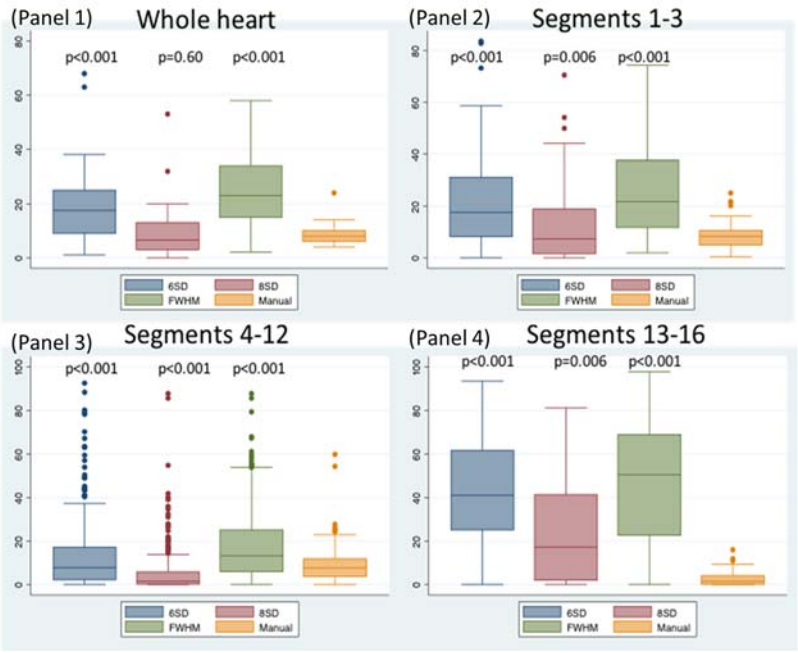

Figure. Scar percent on y-axis. Panel 1 is box plots for whole heart. Panel 2 is box plots for segments 1-3 combined. Panel 3 is box plots for segments 4-12 combined. Panel 4 is box plots for segments 13-16 combined.

ID#: 371128

Steady State MRA of the Thoracic Aorta Using IR SSFP and a High Relaxivity Contrast Agent

James Carr, MD[5]Olivia D. Reese[1], Pascale Aouad, MD[2], Matthew Barrett, MD[2], Monica Korell, MPH[3], Kaitlin Crawford[4], Julie Blaisdell[5], Louise Collins, M.Eng[2], Jeremy D. Collins, MD[6]

1. Northwestern Univeristy, Chicago, IL

2. Northwestern Memorial Hospital

3. Northwestern University, IL

4. Univeristy of Notre Dame

5. Northwestern University, Chicago, IL

6. Northwestern University School of Medicine, Chicago, IL

Background: Thoracic aortic disease is evaluated using MR imaging techniques. The high risk for dissection and rupture of TAA necessitates accurate imaging that can be used serially on patients without radiation exposure. First pass MRA (FP-MRA) (image 2) is commonly used, requiring patient breath-hold and careful timing of the contrast bolus. Steady state MRA (SS-MRA) (image 3) is a new technique that does not require patient breath-hold and yields a high signal to noise ratio. The objective of this study is to compare FP-MRA to SS-MRA for evaluation of patients with thoracic aortic aneurysms.

Methods: 72 adults who underwent cardiovascular MRA using FP-MRA and SS-MRA were retrospectively identified. A 1.5T scanner with a double dose of gadobutrol was used within the date range of July 1st 2015 to April 30th 2017. Following the AHA guidelines, aortic diameters were measured at six locations within the thoracic aorta for each sequence. Diameters were averaged at each anatomical position and compared using a paired t-test. Interobserver reliability was assessed by intraclass correlation coefficient. Two physicians independently assessed the thoracic aorta at four locations for: image quality [1-5], presence of artifact [1-4], signal-to-noise ratios [1-4], contrast-to-noise ratios [1-4], and wall conspicuity and sharpness [1-4]. Mean qualitative scores for FP-MRA and SS-MRA studies were compared for each reviewer using a paired t-test. ICC testing was done to compare Reviewer 1 and Reviewer 2 for FP-MRA and SS-MRA studies.

Results: There was no difference in aortic diameters between the two sequences. Means for the aortic diameters between the FP-MRA and the SS-MRA at all six locations showed minimal mean differences (0.0118 to 0.0457mm) (Image 1). The paired samples correlations at each location showed very good correlation ranging from 0.886 to 0.957. When comparing the mean aortic diameters measured by two reviewers ICC>0.88 for all anatomical locations. Qualitative analysis showed no significant differences between FP-MRA and SS-MRA images (Table 1). Image quality is comparable between FP-MRA and SS-MRA images. Comparing both reviewer';s qualitative scores, ICC=0.944 (FP-MRA) and ICC=0.841 (SS-MRA).

Conclusion: SS-MRA is feasible with a high relaxivity contrast agent and is comparable to FP-MRA for measuring aortic dimensions and image quality. SS-MRA could be used as a back up to regular FP-MRA in situations where there is poor contrast timing or motion artifact.

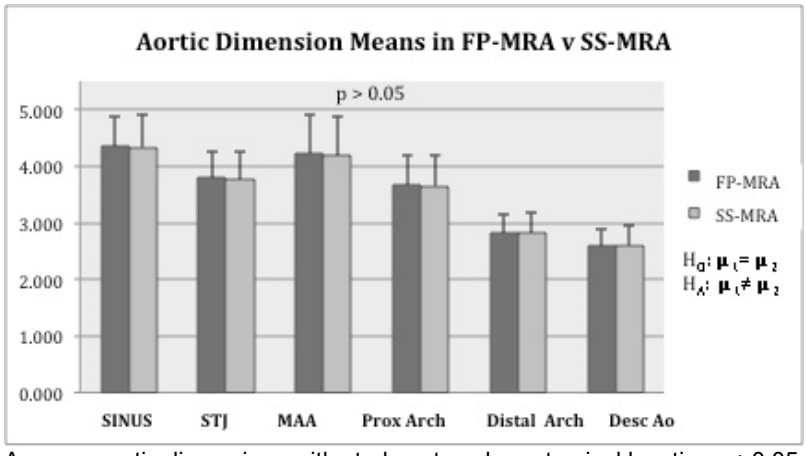

Average aortic dimensions with st. dev at each anatomical location. p>0.05.

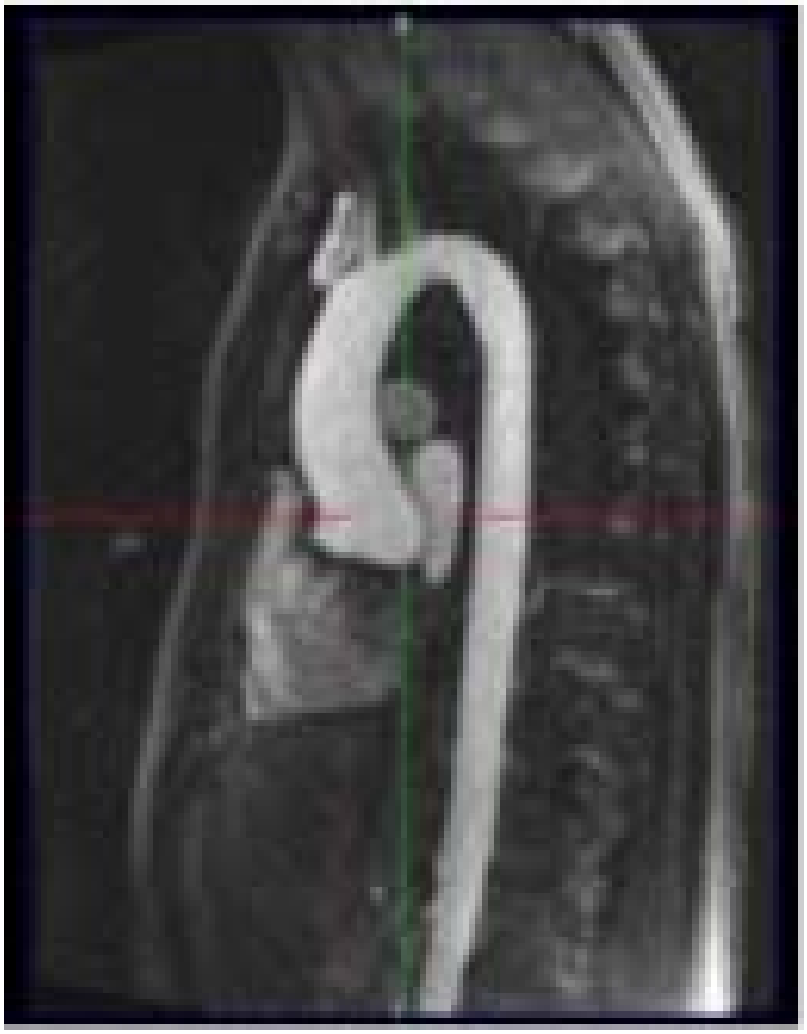

FP-MRA

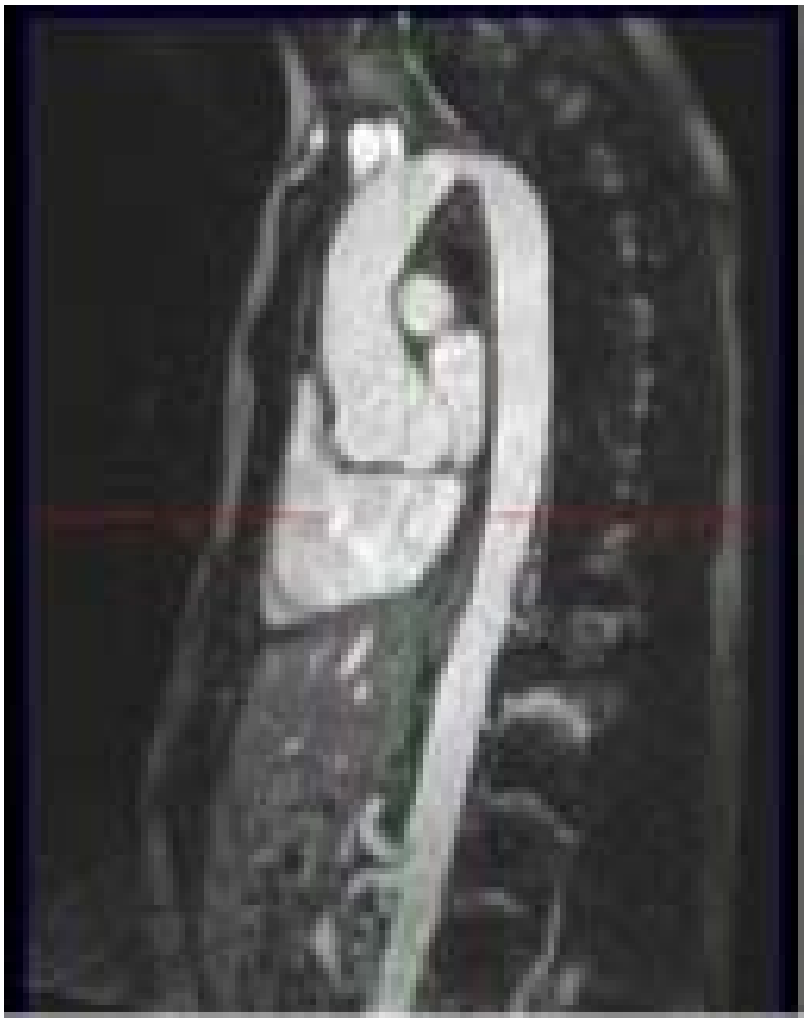

SS-MRA

Mean Qualitative Scores

	Reviewer 1 FP-MRA	Reviewer 1 SS-MRA	Reviewer 2 FP-MRA	Reviewer 2 SS-MRA
Image Quality [1-5]	3.49	3.61	4.07	3.70
Artifact [1-4]	2.88	2.89	3.43	3.05
Signal-to-Noise [1-4]	3.09	2.96	3.46	3.20
Contrast-to-Noise [1-4]	2.85	2.90	3.46	3.23
Wall Conspicuity [1-4]	2.97	3.19	3.51	3.52

Table 1. Average qualitative review scores. Image quality, wall conspicuity, SNR, and CNR rated with 5 or 4 being the best score and 1 being the lowest score. Amount of artifact was rated with 4 being the most artifact and 1 being the least artifact. P-value greater than 0.05 for all FP-MRA to SS-MRA comparisons.

ID#: 371153

Can atrial size and shape predict which patients experience a decline in left ventricular ejection fraction after surgery for mitral regurgitation?

Jessica Webb, BM BCh MRCP[1] Tom Jackson, MBBS[2], Muhummad Sohaib Nazir, MBBS MRCP[2], Lauren Fovargue, PhD[2], Gerald Carr-White, PhD[3], Vassilios Avlonitis, MBBS[4], Christopher Blauth[4], Reza Razavi, MD, PhD[1], Pablo Lamata, PhD, MSc[5]

1. King's College London, London, England, United Kingdom

2. King's College London, United Kingdom

3. Guy's and St Thomas' NHS Foundation Trust, United Kingdom

4. Guys and St Thomas' NHS Trust, United Kingdom

5. King's College of London, England, United Kingdom

Background: Mitral regurgitation (MR) surgery can cause *de novo* postoperative systolic impairment that persists long term, despite prior normal left ventricular ejection fraction (LVEF). Left atrial (LA) volume predicts LVEF outcome post surgery and correlates with pulmonary artery systolic pressure (PASP). Our goal was to test if atrial size and shape can predict patients who will experience a decline in LVEF following MR surgery.

Methods: 25 consecutive patients referred for MR surgery were prospectively recruited and underwent cardiac magnetic resonance (CMR) and echocardiography before and six months after surgery. A 3D statistical shape model of the LA was built after CMR manual segmentation and fully automatic 3D model construction. Linear discriminant analysis found the anatomical characteristics that predict the decline in LV function, and cross-validation was used to test the generality of prediction power. .

Results: 68% of the patients were male with a median age of 73.7 ± 12 years. The patients were categorised into groups (group 1: normal LVEF to normal LVEF n=5; group 2: normal LVEF to impaired LVEF, n=8; group 3: impaired LVEF to impaired LVEF, n=12). Atrial shape identified all patients that experienced LV function decline (group 2) with respect to those that maintained a normal function (group 1) with excellent performance (AUC 1). The adverse anatomy showed more spherical atria, Figure 1. Furthermore, the LA measurement taken from the 3-chamber view for both echocardiography and CMR, normalised by body surface area, was higher in patients in group 2 than in group 1; Echocardiography: 1.8 ± 0.2 v 1.5 ± 0.3 mm/m2 (p 0.02); CMR: 1.9 ± 0.3 v 1.5 ± 0.2 mm/m2 (p 0.02) respectively.

Conclusion: Dilated atria can predict LV functional decline following MR surgery. Atrial remodelling is thus a signature of disease progression and burden. Moreover, the most relevant anatomical features to predict LV function decline can be easily measured with conventional echocardiography. A comprehensive MRI and 3D computational study does increase the prediction power, and further research is needed to define the trade-off between anatomical detail and predictive power. Atrial anatomy can predict LVEF at 6 months following MR surgery, and the relevant shape features can be assessed on the parasternal echocardiographic view.

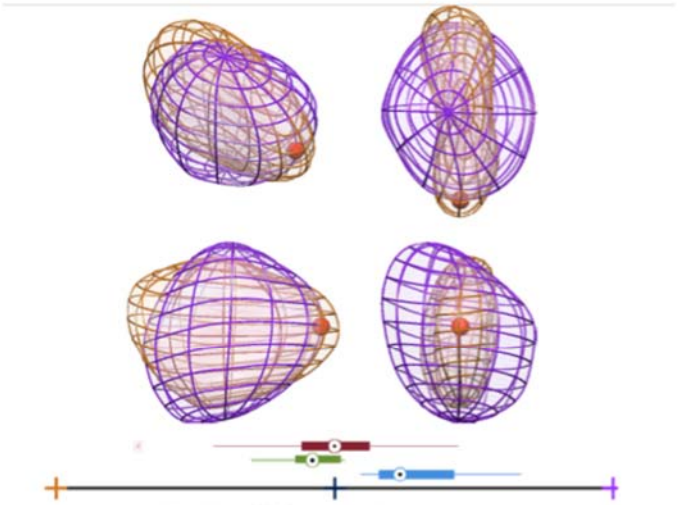

Figure 1: TOP: The anatomical change that predicts LV function decline, illustrated by the extreme shapes leading to a positive outcome (group 1 in purple) and the decline (group 2 in orange shape). Four alternative views are provided, where the red dot is located at the left end of the atria. BOTTOM: box plot of the shape coefficients of the three groups (blue, green and red respectively for groups 1, 2, 3), with the p-value and AUC of the comparison between groups 1 and 2.

Figure 1

ID#: 370958

The effect of cardiac allograft vasculopathy and fibrosis on the extracellular volume in heart transplant recipients: a preliminary study

Ruud B. van Heeswijk, PhD[1] Jessica A.M. Bastiaansen, PhD[2], Juan F. Iglesias, MD[1], Sophie Degrauwe, MD[1], Samuel Rotman, MD[1], Jerome Yerly, PhD[3], Giulia Ginami, PhD[4], Matthias Stuber, PhD[3], Roger Hullin, MD[5]

1. Lausanne University Hospital (CHUV), Switzerland

2. Department of Radiology, University Hospital (CHUV) and University of Lausanne (UNIL), Lausanne, Vaud, Switzerland

3. Center for Biomedical Imaging (CIBM), Lausanne, Switzerland, Vaud, Switzerland

4. King's College London, United Kingdom

5. Lausanne University Hospital (CHUV), Lausanne, Vaud, Switzerland

Background: Cardiac allograft vasculopathy (CAV) occurs with a high prevalence in cardiac allografts and is a major cause of mid-term to late graft failure. It is characterized by concentric thickening of the innermost layer (tunica intima) of the coronary vessel wall[1]. CAV is usually detected using X-ray coronary angiography and manifests as irregular luminal narrowing that often affects a large portion of the vessel. One of the sequelae of CAV is a reduced myocardial oxygenation, which results in an increase of interstitial fibrosis with subsequent rise in extracellular volume (ECV), and thus in T_1 relaxation time, which can both be mapped with MRI[2]. The goal of this study was therefore to investigate whether the extent of interstitial fibrosis assessed in endomyocardial biopsy and the presence of CAV are linked with the myocardial T_1 relaxation time and ECV as assessed by cardiac MRI.

Methods: The study was approved by the local ethics committee; all participants provided written informed consent. Cardiac allograft transplant patients (n=26) ≥6 months after transplantation were recruited and underwent their routine endomyocardial biopsy (EMB) exam and X-ray coronary angiogram. This was followed by T_1 mapping (MOLLI[3], 1 midventricular slice) at 3T (Siemens Prisma) before and after gadolinium contrast agent injection. Histopathological staining of the EMB (3 slides for myocardium and 3 slides for fibrotic tissue, Fig.1A-B) and automated image analysis were used for quantification of interstitial fibrosis. The severity of CAV was determined from the coronary angiogram in accordance with ISHLT guidelines[1]. T_1 maps pre- and post-gadolinium were calculated, and the average myocardial T_1 and ECV were computed (Fig.1C-D). A Pearson correlation was calculated to ascertain whether there is a link between T_1/ECV values and the EMB fibrosis. A Student';s t-test was used to test whether differences in T_1 and ECV exist between patients with and without CAV.

Results: The magnitude of interstitial fibrosis in EMB correlated significantly with the ECV (P=0.02), while it showed a trend with the T1 relaxation time (P=0.06, Fig.2A-B), in accordance with correlations reported in patient cohorts with other diseases[4,5]. CAV was present in 4/26 patients. Both ECV and T_1 differed significantly between the patients with and without CAV (P=0.03, Fig.2C-D), despite the low number of patients with CAV.

Conclusion: EMB-determined interstitial fibrosis is linked with both ECV and T_1 relaxation in heart transplant recipients. The presence of CAV appears to elevate both T_1 and ECV as well, although this remains to be confirmed in a larger cohort.

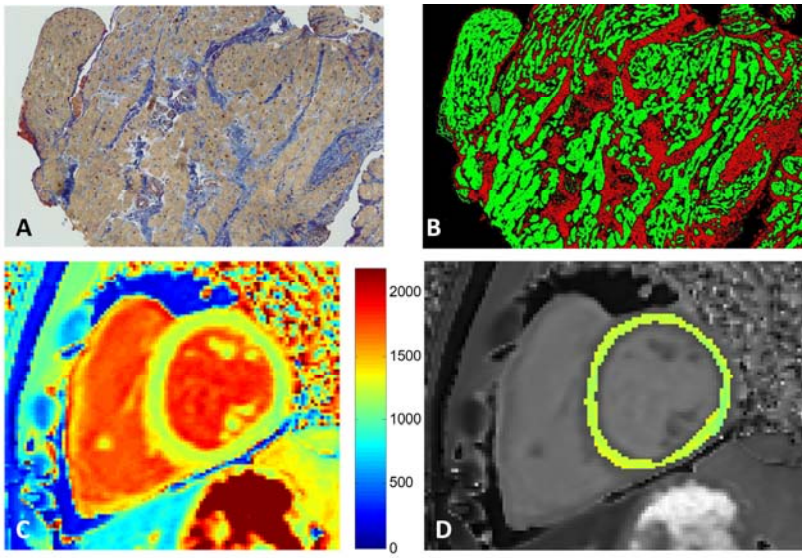

Figure 1. Examples of biopsy and T1 map analyses. A) An EMB is stained blue for collagen/fibrosis and brown for muscle. B) The same specimen underwent automated segmentation in Tissue IA Slidepath, which results in a clear delineation of myocytes (green), fibrosis (red), and other tissues (black). C. A midventricular T1 map demonstrates a homogeneous myocardium (with color bar in ms). D. The segmented T1 values of the myocardium in color overlaid on the rest of the map.

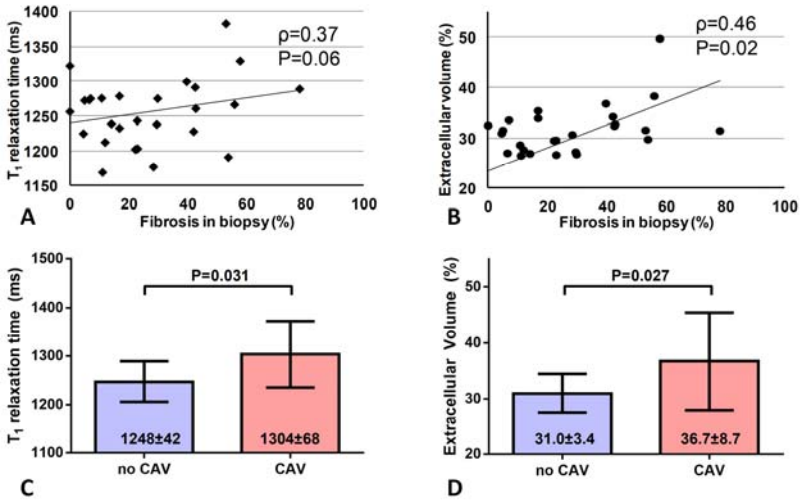

Figure 2. Fibrosis and vasculopathy versus parametric mapping. A-B) EMB fibrosis correlates weakly with the T1 relaxation time and strongly with the ECV in this small patient cohort. C-D) Patients with CAV demonstrated a significantly higher T1 relaxation time and ECV than their counterparts without CAV.

ID#: 370963

Left-Ventricular Strain Reference Values of Healthy Volunteers by Age and Gender as Measured with 3D Tissue Tracking

Volker Rasche, PhDYangyang Qu, MSc, Jan Paul, PhD, Dominik Buckert, MD, PhD

University Hospital of Ulm, Ulm, Baden-Wurttemberg, Germany

Background: CMR strain analysis by tissue tracking provides additional insight into left-ventricular (LV) mechanical function. Reference values from volunteers without history of cardiovascular disease are required as important step towards broad clinical application.
In this study, we investigate and compare strain values obtained from 3D tissue tracking, for different age and gender groups.

Methods: 150 healthy volunteers in three age groups ($G_{20\text{-}40\ years}$, $G_{41\text{-}60\ years}$, and $G_{61\text{-}80\ years}$) were investigated, subdivided into males/females with 25 volunteers each.
Global peak strain (radial, circumferential and longitudinal) was derived by CMR tissue tracking (cvi42 v5.3.8, Circle, Calgary, Canada) in standard steady-state free precession (SSFP) cine images acquired at 1.5T. Strain was calculated in the 17-segment AHA model using 3D (short axis stack, long axis 2-, 3-, and 4-chamber view) tracking.

Results: Radial peak strain for each group is presented in Figure 1, with 41.6%±12.2%, 43.7%±14.3%, and 48.0%±11.5%, for $G_{20\text{-}40}$, $G_{41\text{-}60}$, and $G_{61\text{-}80}$, respectively. Peak radial strain was significantly increased (more radial shortening) in $G_{61\text{-}80}$ compared to $G_{20\text{-}40}$, and in females compared to males, especially in $G_{61\text{-}80}$.
Circumferential strain (Figure 2) was -16.5%±2.3% ($G_{20\text{-}40}$), -16.5%±3.0% ($G_{41\text{-}60}$), and -18.0%±2.5% ($G_{61\text{-}80}$). Absolute strain was significantly increased (more circumferential shortening) in $G_{61\text{-}80}$ compared to the other groups, and significantly increased in females compared to males, especially in $G_{61\text{-}80}$.
For longitudinal strain (Figure 3), values were -15.3%±2.1% ($G_{20\text{-}40}$), -14.7%±2.5% ($G_{41\text{-}60}$), and -16.1%±2.3% ($G_{61\text{-}80}$). Absolute peak longitudinal strain was significantly increased (more longitudinal shortening) in $G_{61\text{-}80}$ compared to $G_{41\text{-}60}$, and in females compared to males, especially in $G_{61\text{-}80}$.

Conclusion: In summary, peak strains were increased in older volunteers and females. The increased strain values in older volunteers imply the increased contraction as a compensation mechanism for reduced heart rates and LV size. The increased strain values in females might be associated with the smaller LV size compared to males.
In conclusion, healthy reference values differ significantly by age and gender, and thus should be reported separately for each group.

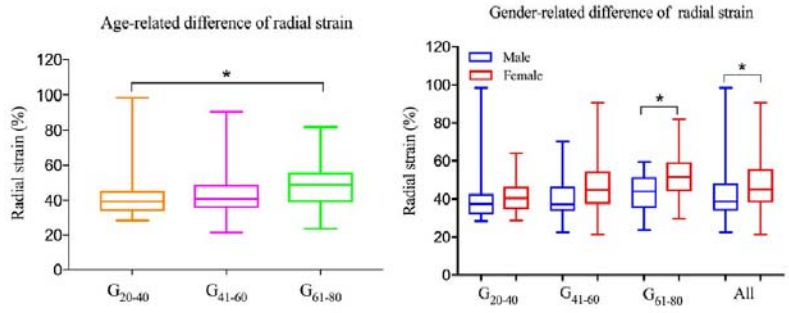

Figure 1: Global peak radial strain for each age and gender group.

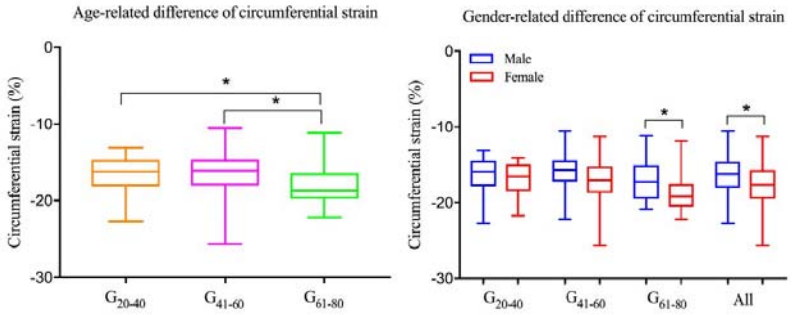

Figure 2: Global peak circumferential strain for each age and gender group.

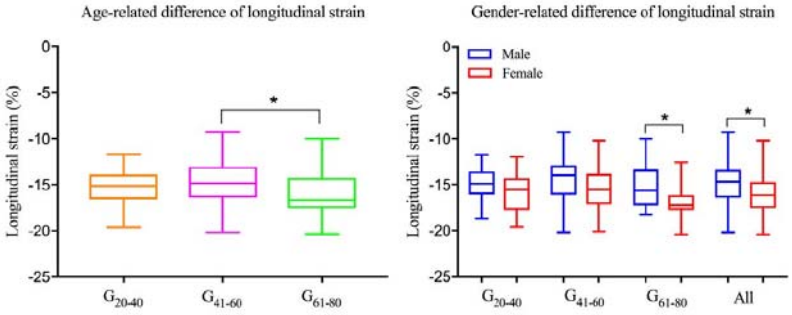

Figure 3: Global peak longitudinal strain for each age and gender group.

ID#: 370983

Cine-CMR Guided Predictive Model for Echocardiography-Based Assessment of Right Ventricular Remodeling - Validation of Novel Linear-Based Indices

Jiwon Kim, MD[4] Javid Alakbarli, MD[1], Farhan Raza, MD[1], Ansh Johri, BS, MSE[1], Michael Villanueva[1], Meridith P. Pollie, BS[1], Martin A. Janich, PhD[2], Evelyn M. Horn, MD[1], Richard B. Devereux, MD[3], Jonathan W. Weinsaft, MD[3]

1. Weill Cornell Medical College

2. GE Healthcare, Germany

3. Weill Cornell Medical Center, NY

4. Weill Cornell Medical College, New York, NY

Background: Right ventricular hypertrophy (RVH) is an adverse prognostic marker stemming from RV pressure and volume overload. Cine-CMR is well validated for 3D RV quantification, whereas echo is widely applied as an initial 2D screening test for the RV. Cine-CMR has yet to be used to inform application of optimal echo linear indices to identify RVH.

Methods: The population comprised pts at risk for RVH due to pulmonary hypertension (PH) or mitral regurgitation-associated RV pressure/volume overload. All pts underwent CMR and echo by standardized protocol. Cine-CMR (SSFP) quantified RV structure/function based on volumetric planimetry, as well as linear-derived RV chamber length/width and wall thickness. Echo-derived RV linear dimensions were acquired in co-localized spatial locations, blinded to CMR results.

Results: 113 subjects (66±12 yo, 71% male) prospectively underwent CMR and echo (Δ3±8 days); 35% had RVH via established cine-CMR volumetric criteria. Pts with RVH had increased RV chamber size (209±60 vs. 133±37 ml) and decreased RV function (45±11 vs. 55±10%; both p<0.001) on cine-CMR, corresponding to higher PA pressure on echo (65±27 vs. 35±12 mmHg) and increased aggregate RV wall stress (25±14 vs. 12±7 kPa; both p<0.001). Linear indices demonstrated cine-CMR-derived RV width (r=0.72) and length (r=0.68, both p<0.001) to correlate with RV volume, paralleling results obtained at co-localized echo landmarks (r=0.70 and r=0.49, both p<0.001 [**Figure A**]). Cine-CMR multiplanar assessment of RV wall thickness demonstrated volumetric RVH to manifest globally, as evidenced by similar increments in wall thickness in the RV outflow tract (4.0±1.2 vs. 3.1±0.9 mm; p<0.001), free wall (3.6±1.3 vs. 2.8±0.9 mm; p=0.001), and inferior wall (3.5±1.1 vs. 2.7±0.7 mm; p<0.001): Echo-derived RV thickness similarly differentiated pts with cine-CMR volumetric RVH (all p<0.001 [**Figure B**]). RV volumetric remodeling (mass/volume) paralleled linear data, as evidenced by increments in cine-CMR and echo-derived RV relative wall thickness among pts with volumetric concentric RVH (both p<0.001). In multivariate analysis, cine-CMR volumetric RV mass was independently associated with CMR RV thickness (partial r=0.46), chamber length (r=0.42) and width (r=0.46, all p<0.001) [model R=0.78, p<0.001]; substitution of echo-quantified RV wall thickness (r=0.54, p<0.001), chamber width (r=0.41, p<0.001), and chamber length (r=0.23, p=0.02) [model R=0.79, p<0.001] demonstrated similar magnitude of independent correlations with cine-CMR volumetric RV mass.

Conclusion: Volumetric RVH is independently associated with global increments in RV wall thickness and chamber dimensions. Cine-CMR informed analysis provides validation of multiplanar linear echo indices for identification of adverse RV remodeling.

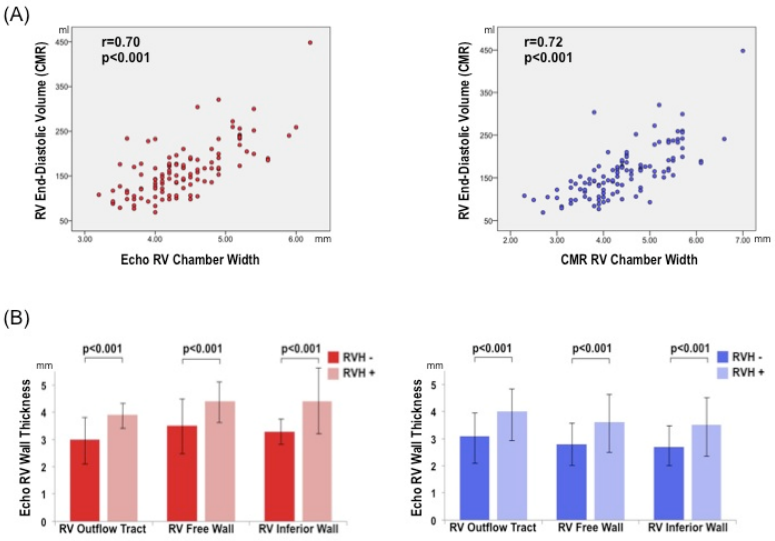

(A) Correlations between CMR-quantified RV end-diastolic volume and linear RV chamber width quantified by echo (r=0.70, p<0.001) and CMR (0.72, p<0.001) respectively. (B) Echo quantified multiplanar wall thickness stratified by CMR evidenced RVH (p<0.001 for all).

ID#: 370953

Creatine chemical exchange saturation transfer (CrCEST) voxel and ROI-wise decay maps at 3T for the study of peripheral artery disease

Helen L. Sporkin, BS[1]Roshin C. Mathew, MD[2], Christopher M. Kramer, MD[3], Steven P. Allen, PhD[4], Craig H. Meyer, PhD[1]

1. University of Virginia, Charlottesville, VA

2. University of Virginia Health System

3. University of Virginia Health System, Charlottesville, VA

4. University of Virginia

Background: Peripheral artery disease (PAD) is characterized by distal artery atherosclerosis, commonly leading to lower limb claudication and ischemia. PAD affects over 200 million people globally and increases major coronary event risk by >20%. The CrCEST signal decay can quantify metabolism spatially in the calf post-exercise. The current method, ^{31}P magnetic resonance spectroscopy (MRS), suffers from three orders of magnitude lower signal than CrCEST, is not specific to free creatine, only provides non-imaging data in large muscle regions, and requires ^{31}P coils [Kogan et al *MRM* 2014]. We proposed that CrCEST would provide whole-ROI and voxel-specific information on creatine metabolism to assess ischemia in PAD.

Methods: We applied CrCEST in 7 healthy and 2 PAD patients who performed plantarflexion ergometry to exhaustion or claudication. Creatine levels were measured over 10min in a Siemens 3T Trio scanner using a pulse sequence developed at University of Pennsylvania [Haris et al *Nature Medicine* 2014]. Water saturation with shift reference (WASSR) and B1 maps were collected for B0 and B1 correction. Six images were acquired over 30s intervals with saturation frequency offsets of ±1.3, ±1.8, and ±2.3ppm. The CEST effect reduces the signal at +1.8ppm compared to the reference at -1.8ppm, referred to as $CrCEST_{asym}$. A 500ms saturation pulse train was applied consisting of five 99.6ms Hanning-windowed pulses with 150Hz B1 amplitude and 0.4ms inter-pulse delay. Imaging parameters were single-shot spoiled gradient-echo readout with centric encoding, fat saturation, flip angle 10°, FOV 160x160mm, matrix 144x144, TR 6.0ms, TE 2.9ms, slice thickness 10mm.

Results: $CrCEST_{asym}$ maps for each time point were made for an ROI of the calf using a toolkit developed at UPenn. Creatine decay maps were created on both a voxel and ROI-wise basis by fitting the $CrCEST_{asym}$ time course to a monoexponential function to determine the decay time constant. Voxel-wise maps were not used in normal subject data due to insufficient temporal resolution to model fast decay. The 2 PAD voxel-wise fits had a mean R^2=0.9386. Mean whole-ROI was 71±20sec for the normal subjects and 193±90sec for PAD patients.

Conclusion: Voxel-wise maps and whole ROI estimates of the creatine decay constant were created from CrCEST data. Preliminary data suggests its ability to differentiate PAD from normal subjects, and further PAD studies are planned. Temporal resolution remains an issue in modeling fast decays. Planned work in pulse sequence design and image interpolation will address this.

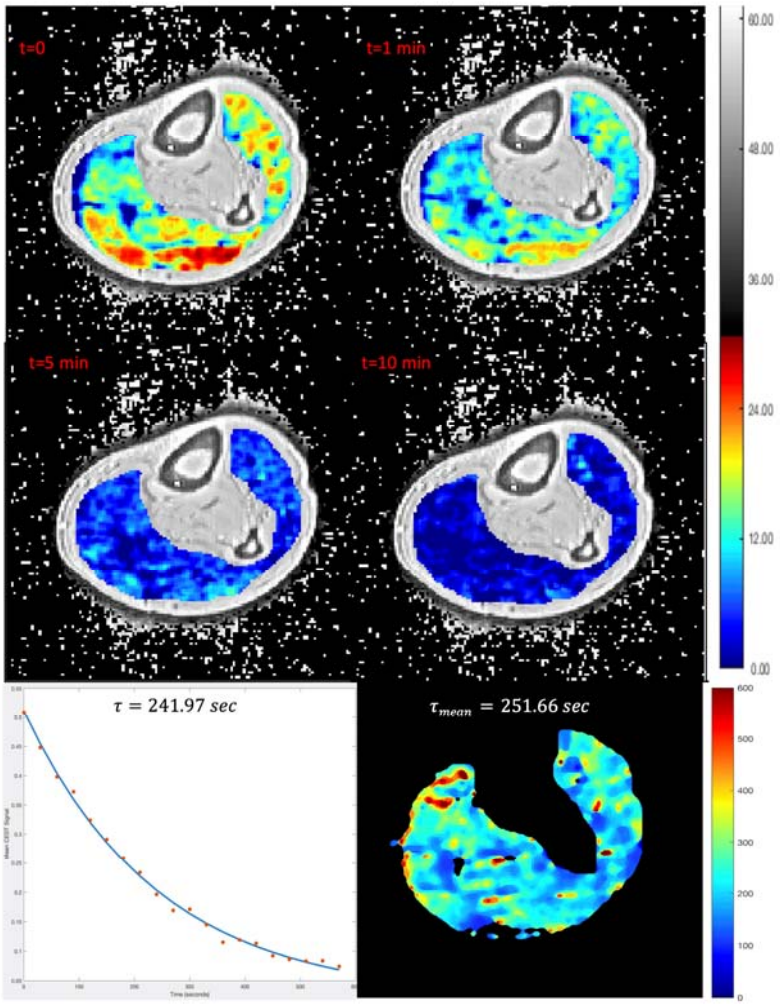

Top and Middle rows: $CrCEST_{asym}$ images at 0, 1, 5, and 10min in one PAD patient after exercise to exhaustion, with an ROI containing the gastrocnemius, tibialis anterior, and soleus muscles. Bottom left: A monoexponential fit of the entire ROI, with decay constant $\tau = 241.97sec$. Bottom right: CrCEST decay map showing τ from a monoexponential voxel-wise fit, with an average $\tau = 251.66sec$ and R^2 =0.9719.

CrCEST map and decay

ID#: 371326

Easy 2D measurements to predict left atrial sphericity in patients with paroxysmal atrial fibrillation

Albert Teis[1]Felipe Bisbal[2], Xavier Alomar[3], Alejandro Silveira[2], Francisco Gual-Capllonch[2], Roger Villuendas[2], Antoni Bayes-Genis, Department of Medicine, Universitat Autònoma de Barcelona, Barcelona[2]

1. Hospital Universitari Germans Trias. Badalona. Bacelona. Spain., Badalona, Spain

2. Hospital Universitari Germans Trias i Pujol, Spain

3. Clinica Creu Blanca. Barcelona, Spain

Background: The degree of left atrial sphericity (LAS) derived from 3D-left atrial angiographies (LAA), is a good predictor of post-ablation recurrences in patients with atrial fibrillation (AF), and also allows reclassification for the risk of embolism in these patients. However, its calculation can be laborious and limited to those centers who have the specific software.
Very limited data has been published regarding the use of two dimensional (2D) measurements in order to estimate the LAS. Moreover, they usualy come from echo-lab, and with no direct correlation to LAS derived from 3D-LAA. Our goal is the generation of a model that easily estimates the degree of LAS using 2D measurements from standard CMR SSFP long axis cine images.

Methods: We studied a cohort of 31 consecutive patients with AF sent for 3D-LAA prior to ablation, to whom the degree of LAS was calculated using a specific software. Standard longitudinal CMR SSFP cines images (2Ch, 3Ch and 4Ch projections) were also performed in all cases. We measured the left atrial longitudinal and transversal diameters and the left atrial área in each of those projections (fig 1). Then we mathematically generated a model of estimation of LAS derived from those 2D measures.

Results: We performed 3D-LAA and subsequently calculated LAS in 31 patients. 75% were men. Average age 60a (38-80a). Derived 3D left atrial volume was 104.4 ± 28ml. Average degree of LAS was 81.7 ± 2.9%. Mean left atrial diameters (mean ± SD; mm) were: Transveral (trans) 4Ch 53.2 ± 7.4; Longitudinal (long) 4Ch 65.8 ± 8.66; Trans-3Ch 44.8 ± 7.76; Long-3Ch 67.98 ± 6.42; Trans-2Ch 54.98 ± 5.97; Long-2Ch 66.33 ± 6.53. Left atrial areas (mean ± SD; mm2) were: 4Ch 31.14 ± 6.56; 3Ch 26.4 ± 5.58; 2Ch 30.17 ± 5.74.
The mathematical model that better correlate with the degree of LAS was:
LAS = 81.35+(0.114 * Trans4ch) + (0.132 * Long4ch) - (0.219 * Area4ch) - (0.13 * AP3ch) - (0.347 * Long3ch) + (0.504 * Area3ch) - (0.125 * AP2ch) + (0.233 * Long2ch) + (0.23 * Area2ch), with a correlation of r=0,71.
Compared to previously reported LAS estimation models (derived from 2D measurements from the echo-lab; atrial spherical index), the correlation with LAS was clearly superior in our model (r = 0.71 vs. 0.401).

Conclusion: Two dimensional measurements could we performed in all patients. The mathematical model generated from those measurements had a good correlation with the degree of LAS. In conclusion, we can easily get an approximation to LAS using simple 2D measures from standard CMR SSFP-cine longitudinal projections.

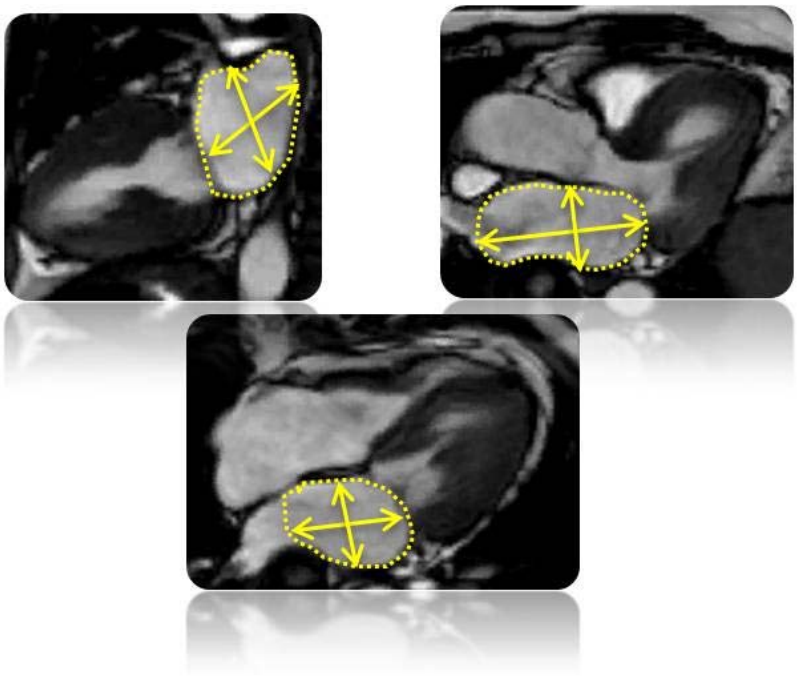

LA measurements

Left Atrial Sphericity (LAS) Calc.		
Variables	Values	Units
Trans-2ch		mm
Long-2ch		mm
Area-2ch		mm2
Tans-3ch		mm
Long-3ch		mm
Area-3ch		mm2
Trnas-4ch		mm
Long-4ch		mm
Area-4ch		mm2
LAS		%

Left Atrial Sphericity (LAS) Calc.		
Variables	Values	Units
Trans-2ch	54,8	mm
Long-2ch	63,8	mm
Area-2ch	30,2	mm2
Tans-3ch	44,3	mm
Long-3ch	68,3	mm
Area-3ch	26,2	mm2
Trnas-4ch	52,3	mm
Long-4ch	66,15	mm
Area-4ch	30,9	mm2
LAS	**79,95**	%

ID#: 371218

Prognostic value of midwall fibrosis in patients with preserved ejection fraction and structurally normal heart (pilot study)

Avirup Guha, MBBS, MD[1] Andrea Cardona, MD[2], Haikady Nagaraja, PhD[1], Subha Raman, MD, MSEE[3], Karolina Zareba, M.D.[2]

1. Ohio State University, Columbus, OH

2. The Ohio State University Wexner Medical Center, Columbus, OH

3. The Ohio State University, Columbus, OH

Background: Non-ischemic midwall fibrosis by cardiac magnetic resonance (CMR) imaging is associated with adverse cardiac outcomes in patients with depressed left ventricular ejection fraction. The prognostic value of midwall fibrosis in a structurally normal heart is unknown. We hypothesize that midwall fibrosis is associated with adverse cardiac outcomes in patients with no structural heart abnormalities.

Methods: Retrospective analysis of patients with preserved ejection fraction (EF) ≥ 50% who were referred for a clinical CMR scan in 2012 was conducted. Patients with the following findings were excluded: left ventricular hypertrophy, ventricular enlargement, hypertensive heart disease, myocardial infarction, any structural abnormalities, infiltrative disease, greater than mild valvular disease, atrial arrhythmias, cancer, and channelopathies predisposing to arrhythmias. Patients were divided into 2 groups, those with non-ischemic midwall fibrosis by late gadolinium enhancement (LGE) CMR and those without evidence of fibrosis (control group). Patients charts were reviewed for the following endpoints: new onset heart failure, arrhythmias (atrial or ventricular), initiation of antiarrhythmic therapy or ablation of ventricular arrhythmias, and death. Groups were compared using Fisher exact tests (for nominal variables) and 2 sample t-tests (for continuous variables). Multiple logistic regression was used to compare the odds of an endpoint event between groups.

Results: Eighty-nine patients were included in the study, 62.9 % female, mean age 47±14 years. Overall, 31 patients exhibited midwall fibrosis and 58 patients had no LGE on CMR. Baseline clinical characteristics and comorbidities did not differ between the groups (table 1). During a median follow up of 4.6±1.1 years, patients with midwall fibrosis tended to have more new onset heart failure, were initiated on antiarrhythmic therapy, and had more ventricular ablations, when compared to the control group. Eight patients (26%) met the combined endpoint in the midwall fibrosis group vs. 4 (7%) in the control group (table 2) (p=0.005, after controlling for the length of follow-up). For a given duration of follow-up, the OR for an event in the midwall fibrosis group was 6.53 when compared to the no-fibrosis group (95% CI 1.75-28.75).

Conclusion: We demonstrate that adverse cardiac outcomes are significantly more prevalent in patients with preserved EF and structurally normal heart who exhibit non-ischemic midwall fibrosis on LGE-CMR. This pilot study warrants a larger investigation to fully examine this association and its clinical impact.

Table 1

Variable (N, %)	Midwall Fibrosis (N= 31)	No fibrosis (N=58)	p-value
Length of follow-up (years)	4.2±1.4	4.8±0.9	0.03
Age (years)	48±15.5	47±13.5	0.76
Female	16 (52%)	40 (69%)	0.11
Hypertension	12 (38.7%)	21 (36.2%)	0.82
Diabetes Mellitus	3 (9.7%)	3 (5.2%)	0.42
Obstructive Sleep Apnea	7 (22.6%)	7 (12.1%)	0.23

Coronary artery disease	7 (22.6%)	11 (19%)	0.78
Stroke	2 (6.5%)	1 (1.7%)	0.28
Tobacco use	8 (25.8%)	15 (25.9 %)	0.99
Hyperlipidemia	10 (32.3%)	21 (36.2 %)	0.82
Chronic kidney disease	0	2 (3.4%)	0.54
Peripheral artery disease	2 (6.5%)	0	0.12
Rhythm monitoring	22 (71%)	44 (75.9%)	0.6
None	9 (29%)	14 (24.1%)	
Holter Monitor	16 (51.6%)	28 (48.3%)	
Event Monitor	4 (12.9%)	14 (24.1%)	
LINQ or pacemaker	2 (6.5%)	2 (3.5%)	
Mean PVC burden on 24 hour Holter monitoring	5042±8045	7088±12905	0.57

ID#: 371249

Impact of aortopulmonary collateral flow on single ventricle function and blood flow haemodynamics in patients after the Fontan procedure: a longitudinal CMR study

Heiner Latus[1]Pia Kruppa[2], Bettina Reich[2], Stefan Rupp[3], Christian Apitz[4], Inga Voges, MD[5], Christian Jux[3], Markus Khalil[3], Kerstin Gummel[3]

1. German Heart Centre Munich, Munich, Bayern, Germany

2. Pediatric Heart Centre Giessen, Germany, Germany

3. Pediatric Heart Centre Giessen, Germany

4. Department of Pediatric Cardiology, Ulm, Germany, Germany

5. Royal Brompton, London, United Kingdom

Background: Single ventricle (SV) patients are affected by various extent of aortopulmonary collateral (APC) flow. Although frequently closed by transcatheter procedures, the long-term clinical significance of APC remains unknown. The aim of our study was to assess the impact of APC flow on SV properties and blood flow haemodynamics in Fontan patients by using serial cardiac magnetic resonance (CMR) data.

Methods: Fontan patients who had two CMR examinations with a time interval of at least 4 years as part of their routine clinical assessment were included. The protocol consisted of standard short-axis cine volumetry and 2-dimensional blood flow measurements in the inferior vena cava (IVC), the superior vena cava (SVC) and the ascending aorta (Ao). Aortopulmonary collateral flow was calculated as Ao – (SVC + IVC).

Results: Forty-five Fontan patients (age at first CMR 12.5 ± 6.4 years, mean follow-up 5.2 ± 0.9 years) without APC closure between the two CMR studies and without patent tunnel fenestration were included. Functional classand transcutaneous oxygen saturations (94 ± 4 to 94 ± 5 %, p=0.32) remained stable. Heart rate decreased significantly from 80 ± 16 to 73 ± 19 bpm (p=0.01) while SV end diastolic volume (80 ± 25 to 88 ± 40 ml/m^2, p=0.14) and ejection fraction remained constant (EDVi 80 ± 25 to 88 ± 40 ml/m^2, p=0.14; EF 56 ± 12 to 55 ± 8 %, p=0.70). Aortic flow decreased significantly (3.3 ± 1.0 to 2.9 ± 0.8 l/min/m^2, p=0.01), IVC flow remained equal (1.6 ± 0.5 to 1.6 ± 0.4 l/min/m^2), while SVC flow (1.0 ± 0.3 to 0.8 ± 0.3 l/min/m^2, p=0.003) and APC flow (0.8 ± 0.7 to 0.5 ± 0.7 l/min/m^2, p=0.005) decreased significantly. Qp/Qs ratio showed significant decrement from 1.3 ± 0.3 to 1.2 ± 0.3 (p=0.02). Higher APC flow during first CMR exam was not associated with impairment of clinical status, changes in oxygen saturation nor SV dilatation or dysfunction.

Conclusion: APC flow gradually decreases over time in Fontan patients. Baseline APC flow at first CMR was not associated with clinical deterioration or adverse ventricular remodelling at follow-up. These findings might suggest a conservative strategy regarding APC embolization.

ID#: 364453

Regional Changes in Myocardial Strain During 6-month Exposure to Cardiotoxic Chemotherapy: Is there a Phenotype for Cardiotoxicity?

Reis Hansen[1]Alessandro Satriano, Ph.D.[1], Joelle Chartrain[2], Bobbi-Jo Blume[3], Yoko Mikami, MD, Ph.D.[2], Christina Sheppard, RN MN[4], Andrew G. Howarth, MD, Ph.D[2], Carmen P. Lydell, MD[1], Bobby Heydari, MD, MPH[2], James McMeekin, MD[5], Douglas A. Stewart, MD[6], Jan-Willem Henning, MBChB, FRCPC[6], Nowell M. Fine, MD, M.Sc.[7], Brian Clarke, MD FRCPC FACC[6], James White, MD, FRCP(C)[2]

1. Stephenson Cardiac Imaging Centre, Libin Cardiovascular Institute of Alberta, University of Calgary, Calgary, AB, Canada

2. Stephenson Cardiac Imaging Centre, Libin Cardiovascular Institute of Alberta, University of Calgary, AB, Canada

3. Stephenson Cardiac Imaging Centre at the Libin Cardiovascular Institute of Alberta, AB, Canada

4. Cardio-Oncology and Cardiac Function Clinics, South Health Campus, Libin Cardiovascular Institute of Alberta, AB, Canada

5. University of Calgary, AB, Canada

6. University of Calgary, Libin Cardiovascular Institute, AB, Canada

7. Libin Cardiovascular Institute of Alberta, AB, Canada

Background: Cancer therapeutics-related cardiac dysfunction (CTRCD) is of growing clinical concern. While measurements of global longitudinal strain (GLS) show benefit versus left ventricular ejection fraction (LVEF) for the surveillance of cardiotoxicity, spatial characterization of this disease may be of incremental benefit. Using cardiovascular magnetic resonance (CMR) based 3D strain analysis we aimed to characterize the spatial distribution of contractile dysfunction experienced by the LV over a 6-month exposure to cardiotoxic chemotherapy.

Methods: Fifty-five patients (50 breast cancer, 5 lymphoma) prescribed Anthracycline (Anth, N=10), Trastuzumab (Tr, N=15) or combination (Anth-Tr, N=30) chemotherapy underwent CMR imaging at 3T using a standardized protocol prior to chemotherapy exposure (baseline) and after 6 months of treatment (110 studies total). 3D strain analysis was performed from registered multi-axial 2D cine images to obtain both global and segmental strain amplitudes and rates. Six-month changes in segmental values were derived for all measures of strain and stratified according to chemotherapy regimen.

Results: Mean age was 50±9.9 years, 51 female. The mean LVEF at baseline and 6-months was 65.1±4.7% and 60.8±4.8%, respectively ($p<0.001$). Among all patients, global longitudinal strain and strain rate dropped from -12.7±2.0% and -4.7±2.1 1/s at baseline to -11.7±1.9% and -3.7±1.8 1/s at 6-months ($p=0.008$ and 0.005, respectively). Global minimum principal strain and strain rate dropped from -26.0±2.8% and -12.0±4.5 1/s at baseline to -24.9±2.7% and -10.4±3.4 1/s at 6-months ($p=0.03$ and 0.04, respectively). In the combination Anth-Tr group LVEF dropped from 64.8±5.1% to 60.1±4.4% ($p<0.001$) and global longitudinal strain from -12.6±1.7% to -11.2±1.7% ($p=0.002$). Segmental reductions in longitudinal and minimum principal strain ranged widely from 0% to an 8% absolute reduction at 6-months (Figure 1). A strong geographic predisposition of CTRCD for the apical and septal segments was observed with sparing of basal and anterolateral wall segments.

Conclusion: CTRCD shows predisposition for the apical and septal segments of the LV with sparing of the basal and anterolateral segments. Consideration of this phenotype may be important for optimal surveillance strategies, particularly among patients where apical visualization may be limited using echocardiographic techniques. Expanded investigation in larger cohorts is warranted.

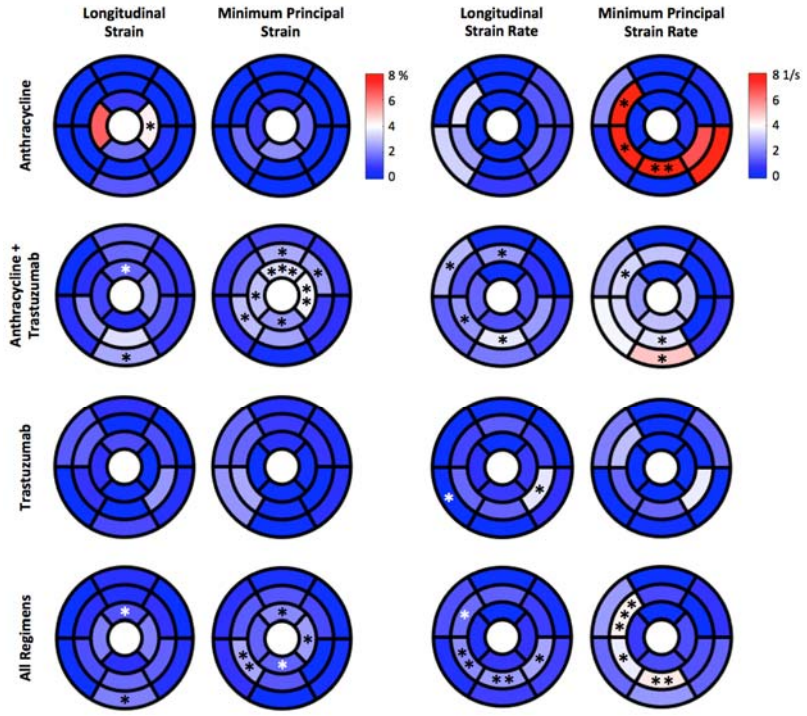

Figure 1. Six-month change in segmental Longitudinal and Minimum Principal Strain Amplitudes and corresponding Strain Rates in patients receiving regimens: Anthracycline alone, Anthracycline plus Trastuzumab, and Trastuzumab alone. P-values correspond to t-tests and Wilcoxon signed-rank tests of segmental values between baseline and 6 months (*p<0.05, **p<0.01, ***p<0.001).

ID#: 364819

Cross-Vendor Validation of Synthetic ECV Calculation at 1.5 Tesla

Graham J. Fent, MBChB, BSc[1] James R. Foley, MBChB BSc (Hons)[1], Pankaj Garg, MD, PhD[2], Louise AE. Brown, MBChB, BMedSc[3], Pei G. Chew, MBChB(Hons) [4], Sebastian C. Onciul[3], Peter P. Swoboda, PhD[1], John P. Greenwood, PhD[3], Sven Plein, MD PhD[3]

1. University of Leeds, Leeds, England, United Kingdom

2. University of Leeds, UK, Leeds, England, United Kingdom

3. University of Leeds, England, United Kingdom

4. University of Leeds, Liverpool, England, United Kingdom

Background: Previous studies have demonstrated a correlation between native blood pool T1 values and blood haematocrit (Hct). This allows estimation of Hct which can then be used to calculate *synthetic* myocardial extracellular volume fraction (ECV) which strongly correlates with conventionally calculated ECV, removing the time and cost associated with taking a blood Hct sample. Although *synthetic* ECV equations at 1.5T using a Modified Look-Locker Inversion Recovery acquisition (MOLLI) pulse sequence have been individually published for Philips and Siemens platforms, no study has shown whether they are interchangeable across these platforms. We hypothesised that previously published *synthetic* ECV equations would provide accurate estimation of ECV on an alternative vendor platform.

Methods: The study population included 101 patients with valvular heart disease, ST-elevation myocardial infarction or suspected cardiomyopathy. All patients were scanned at 1.5T on the same scanner (Philips, Ingenia, Best, The Netherlands). MOLLI schemes were used to acquire T1 maps produced prior to and 15 minutes after administration of either 0.2 mmol/kg Gadopentate Dimeglucide (Magnevist, Bayer Schering) or 0.15 mmol/kg Gadobutrol (Gadovist, Bayer Schering). T1 values were measured using post processing software (Circle CVI 42, Calgary, Canada). Conventional ECV was calculated using laboratory Hct and *synthetic* ECV was calculated by deriving Hct from published equations derived on a Siemens 1.5T platform and a second equation derived on the same 1.5T Philips scanner used in this study (see below):

Conventional ECV equation: (1-Hct) x (Δ myocardial T1)/(Δblood pool T1) Siemens 1.5T *synthetic* ECV equation: Synthetic Hct MOLLI = (866 x (T1blood)) -0.1232 Philips 1.5T *synthetic* ECV equation: Synthetic Hct MOLLI = (922.6 x (1/T1blood)) – 0.1668

Results: Results are summarised in figure 1 (Panel A: Bland Altman analysis of *synthetic* ECV calculated using Siemens and Philips 1.5T equations and panel B: *synthetic* ECV calculated using Siemens and Philips 1.5T equations plotted against conventionally calculated ECV). Bland-Altman analysis showed that *synthetic* ECV calculated using the 1.5T Siemens equation was associated with a minimal negative bias of -0.4%, 95% C.I. 0.06, 0.72% with respect to values calculated using the Philips 1.5T equation.

Conclusion: Although ideally *synthetic* ECV equations should be calibrated locally, we have demonstrated that previously published equations using MOLLI pulse sequences on Philips and Siemens 1.5T scanners are interchangeable with a clinically negligible bias between the two equations.

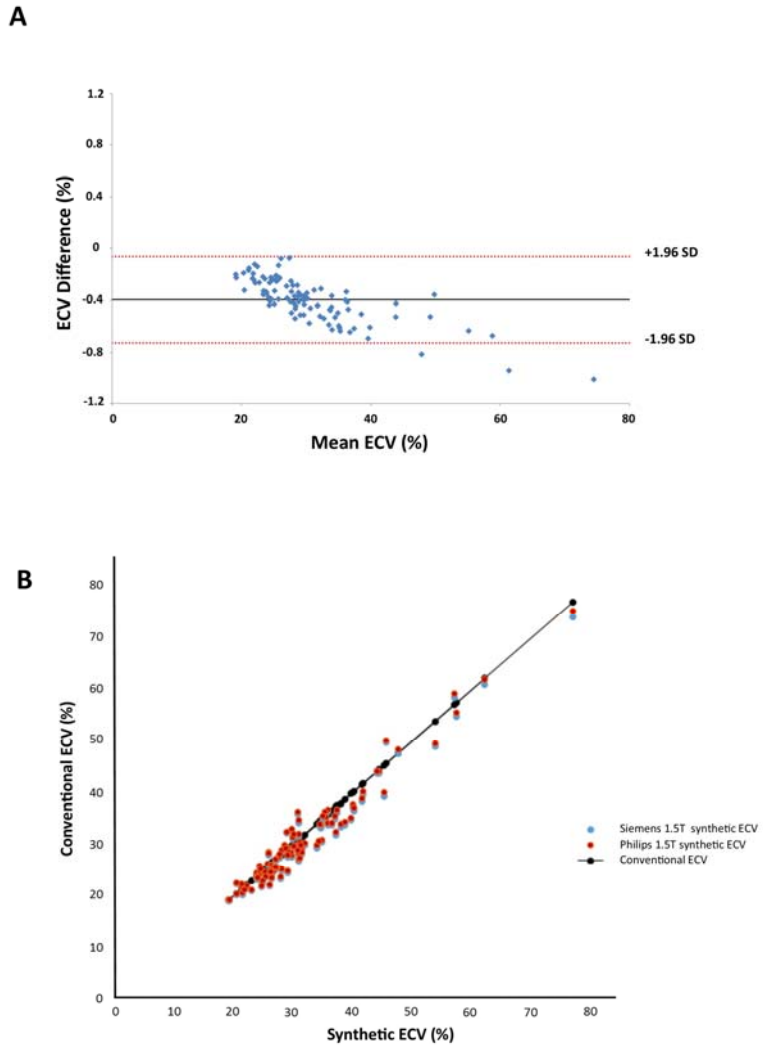
A
ECV Difference (%)
Mean ECV (%)
+1.96 SD
-1.96 SD
B
Conventional ECV (%)
Synthetic ECV (%)
Siemens 1.5T synthetic ECV
Philips 1.5T synthetic ECV
Conventional ECV

Figure 1

ID#: 365354

Inter-vendor reproducibility of left and right ventricular cardiovascular magnetic resonance myocardial feature-tracking

Roman J. Gertz, BSc[1] Torben Lange, BSc[2], Johannes T. Kowallick, MD[3], Sören Backhaus, MD[4], Michael Steinmetz, MD[3], Wieland Staab, MD[3], Shelby Kutty, MD PhD MS-HCM[5], Gerd Hasenfuß, MD[3], Joachim Lotz, MD[6], Andreas Schuster, MD PhD MBA FESC[7]

1. DZHK (German Centre for Cardiovascular Research) partner site Göttingen, Göttingen, Niedersachsen, Germany

2. DZHK (German Centre for Cardiovascular Research) partner site Göttingen, Niedersachsen, Germany

3. University Medical Center Göttingen, Niedersachsen, Germany

4. Georg-August-University Göttingen Universitätsmedizin, Nordrhein-Westfalen, Germany

5. Children´s Hospital and Medical Center Joint Division of Pediatric Cardiology, University of Nebraska / Creighton University, Omaha, NE, USA, NE

6. University Medical Center Göttingen, Goettingen, Niedersachsen, Germany

7. Department of Cardiology and Pneumology, University Medical Center Göttingen, Germany; Department of Cardiology, Royal North Shore Hospital, Sydney, Australia; The Kolling Institute, Northern Clinical School, University of Sydney, Sydney, Australia, Niedersachsen, Germany

Background: Since the diagnostic and prognostic potential of cardiovascular magnetic resonance feature-tracking (CMR-FT) has been demonstrated we investigated the interchangeability of global left and right ventricular strain parameters between different CMR-FT software solutions.

Methods: CMR-cine images of 10 patients with normal biventricular function (LVEF: 69.0% ± 3.3%; RVEF: 59.4% ± 7.1%) and 10 patients with significantly impaired left and right ventricular ejection fractions (LVEF 37.0% ± 9.8%; RVEF 40.0% ± 11.3%) were analyzed using two different types of FT-software. Global left and right ventricular longitudinal strain (LV GLS, RV GLS), global left ventricular circumferential (GCS) and radial strains (GRS) were assessed. Differences in intra- and inter-observer variability within and between software types based on single and up to three repeated and subsequently averaged measurements were evaluated. Global strain parameters were correlated with corresponding ejection fractions.

Results: Inter-vendor agreement was highest for GCS followed by LV GLS. GRS and RV GLS showed lower inter-vendor agreement (Table 1, Figure 1). Variability was consistently higher in normal subjects as compared to the patient group. Intra-vendor reproducibility was excellent for GCS, LV GLS and RV GLS, but lower for GRS (Table 1). The impact of repeated measurements on reproducibility was most pronounced for GRS and RV GLS on an intra-vendor level. Correlation between the LVEF and LV GLS and GCS was excellent with both types of software. RV GLS and GRS showed significant but weaker correlations with corresponding ejection fractions (Figure 2).

Conclusion: Reproducibility of CMR-FT is not negatively influenced by cardiac pathology with LV GLS and GCS qualifying as the most robust parameters within and between individual software types. Since both parameters can be interchangeably assessed with different software solutions they may enter the clinical arena for optimized prediction of cardiovascular mortality in various pathologies.

Inter-vendor agreement and intra- and inter-observer variablity for global longitudinal, global circumferential and global radial strain based on three averaged measurements (R3)

		TomTec versus QStrain			TomTec			QStrain		
		Mean Difference (SD of the Diff.)	ICC (95% CI)	CoV (%)	Mean Difference (SD of the Diff.)	ICC (95% CI)	CoV (%)	Mean Difference (SD of the Diff.)	ICC (95% CI)	CoV (%)
Intra-observer	LV GLS %	1.00 (2.23)	0.97 (0.92–0.99)	12.70	-0.15 (0.64)	1.00 (1.00–1.00)	3.79	0.24 (0.87)	1.00 (0.99–1.00)	4.78
	GCS %	0.66 (2.73)	0.98 (0.95–1.00)	11.50	-0.49 (0.56)	1.00 (0.99–1.00)	2.41	0.03 (0.74)	1.00 (1.00–1.00)	3.08
	GRS %	-12.16 (8.67)	0.62 (0.00–0.88)	34.28	-0.85 (3.00)	0.96 (0.90–0.99)	15.29	-2.45 (4.59)	0.97 (0.90–0.99)	14.07
	RV GLS %	2.78 (6.21)	0.80 (0.49–0.92)	32.47	-0.62 (1.14)	0.99 (0.98–1.00)	6.55	0.59 (1.38)	0.99 (0.98–1.00)	6.61
Inter-observer	LV GLS %	-0.72 (2.88)	0.96 (0.89–0.98)	16.03	0.52 (0.94)	1.00 (0.98–1.00)	5.41	0.18 (0.72)	1.00 (0.99–1.00)	3.96
	GCS %	-0.51 (2.40)	0.99 (0.96–0.99)	10.08	0.17 (1.09)	1.00 (0.99–1.00)	4.64	0.23 (0.91)	1.00 (1.00–1.00)	3.76
	GRS %	-14.78 (8.72)	0.53 (0.00–0.85)	32.98	0.17 (3.00)	0.96 (0.89–0.98)	15.67	4.51 (6.87)	0.89 (0.64–0.96)	23.59
	RV GLS %	0.63 (5.12)	0.86 (0.65–0.95)	28.75	0.40 (1.13)	0.99 (0.99–1.00)	6.30	0.19 (0.80)	1.00 (0.99–1.00)	3.89

SD, standard deviation; Diff., differences; ICC, intra-class correlation coefficient; CoV, coefficient of variation; CI, confidence interval; LV GLS, global left ventricular longitudinal strain; GCS, global left ventricular circumferential strain; GRS, global left ventricular radial strain; RV GLS, global right ventricular longitudinal strain

Table 1

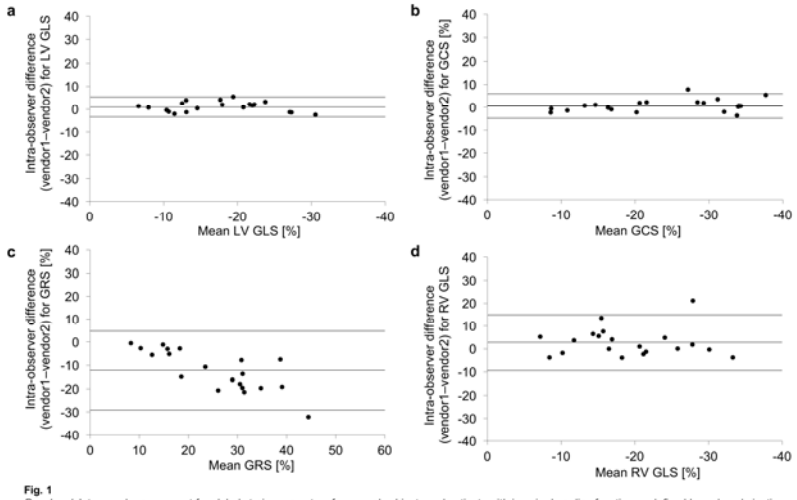

Fig. 1
Panel a–d. Inter-vendor agreement for global strain parameters for normal subjects and patients with impaired cardiac function as defined by reduced ejection fraction based on three averaged measurements (R3). Bland-Altman plots with limits of agreement (95% confidence intervals) demonstrating the CMR-FT derived reproducibility on an intra-observer level are being displayed

Fig. 1

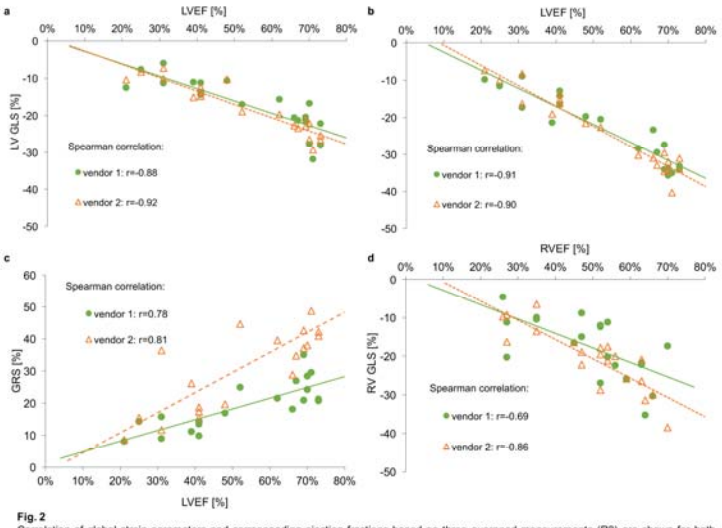

Fig. 2
Correlation of global strain parameters and corresponding ejection fractions based on three averaged measurements (R3) are shown for both types of software and each parameter respectively. *Panel a*: correlation between LV GLS and LVEF; *Panel b*: correlation between GCS and LVEF; *Panel c*: correlation between GRS and LVEF; *Panel d*: correlation between RV GLS and RVEF. LV GLS, global left ventricular longitudinal strain; GCS, global left ventricular circumferential strain; GRS, global left ventricular radial strain; RV GLS, global right ventricular longitudinal strain; r, Spearman´s correlation coefficient; LVEF, left ventricular ejection fraction; RVEF, right ventricular ejection fraction

Fig. 2

ID#: 365387

Atrial Mechanics and their Prognostic Impact in Takotsubo Syndrome: A Cardiovascular Magnetic Resonance Imaging Study

Sören Backhaus, MD[1] Thomas Stiermaier, MD[2], Torben Lange, BSc[3], Amedeo Chiribiri, MD PhD[4], Johannes Uhlig, MD MPH[5], Johannes T. Kowallick, MD[6], Roman J. Gertz, BSc[7], Boris Bigalke, MD[8], Adriana Villa, MD[9], Joachim Lotz, MD[10], Gerd Hasenfuß, MD[6], Holger Thiele, MD[11], Ingo Eitel, MD[2], Andreas Schuster, MD PhD MBA FESC[12]

1. Department of Cardiology and Pneumology, University Medical Center Göttingen, Germany, Niedersachsen, Germany

2. University Heart Center Lübeck, Lübeck, Schleswig-Holstein, Germany

3. DZHK (German Centre for Cardiovascular Research) partner site Göttingen, Niedersachsen, Germany

4. King's College London, London, England, United Kingdom

5. University Medical Center Göttingen, Institute for Diagnostic and Interventional Radiology, Niedersachsen, Germany

6. University Medical Center Göttingen, Niedersachsen, Germany

7. DZHK (German Centre for Cardiovascular Research) partner site Göttingen, Göttingen, Niedersachsen, Germany

8. University Medical Center Berlin, Department of Cardiology and Pneumology, Berlin, Germany

9. St. Thomas' Hospital, London; King's College London, London, England, United Kingdom

10. University Medical Center Göttingen, Goettingen, Niedersachsen, Germany

11. Heart Center Leipzig - University Hospital, Sachsen, Germany

12. Department of Cardiology and Pneumology, University Medical Center Göttingen, Germany; Department of Cardiology, Royal North Shore Hospital, Sydney, Australia; The Kolling Institute, Northern Clinical School, University of Sydney, Sydney, Australia, Niedersachsen, Germany

Background: The exact pathophysiology of Takotsubo Syndrome (TTS) remains not fully understood with most studies focussing predominantly on ventricular mechanics and associated ballooning patterns. This study aimed for further investigation of left (LA) and right atrial (RA) involvement employing atrial cardiovascular magnetic resonance feature tracking (CMR-FT).

Methods: This multicentre study recruited 152 TTS patients who underwent CMR on average within 3 days after hospitalisation. LA and RA reservoir (total strain ε_s and peak positive strain rate (SR) SRs), conduit (passive strain ε_e and peak early negative SRe) and booster pump function (active strain ε_a andpeak late negative SRa) were assessed in a core-laboratory. Results were compared to a control group of 20 patients with normal biventricular function. Twenty patients underwent follow-up CMR (median 3.5 months, IQR 3-5). All patients were approached for general follow-up.

Results: Left but not right atrial reservoir and conduit function were impaired during the acute phase as compared to the control group (ε_s p=0.003, SRs p=0.05, ε_e ps pe p=0.001, SRe p=0.04). Left and right atrial booster pump function were increased in the acute setting (LA-ε_a p=0.038, SRa p=0.003 and RA-ε_a p=0.005, SRa p=0.002) without changes at follow-up. LA booster pump (ε_a HR 0.32 95% CI 0.1–1.02 p=0.0495) and reservoir function (ε_s HR 0.31, 95 CI 0.01–0.98 p=0.046) predicted mortality irrespectively of patients'; age.

Conclusion: Acute phase TTS is characterized by transient impairments in left atrial reservoir and conduit functions and enhanced right and left atrial active booster pump functions. Both left atrial booster pump and reservoir functions identify patients at risk for adverse events. Our results propose atrial booster pump function as a distinct feature in TTS with compensatory action in the acute setting and implications for mortality prediction.

ID#: 366551

Diagnostic performance of cardiac magnetic resonance T1 and T2 mapping in patients with biopsy-proven DCM-like acute myocarditis

Bettina Baeßler, M.D.[1]Christian Luecke, MD[2], Karin Klingel, MD[3], David Maintz, MD[1], Matthias Gutberlet, MD[4], Holger Thiele, MD[5], Philipp Lurz, MD, PHD[6]

1. University Hospital of Cologne, Department of Radiology, Nordrhein-Westfalen, Germany

2. University of Leipzig - Heart Centre, Department of Diagnostic and Interventional Radiology, Niedersachsen, Germany

3. Department of Molecular Pathology, Institute for Pathology and Neuropathology - University Hospital Tuebingen, Baden-Wurttemberg, Germany

4. University of Leipzig - Heart Centre, Department of Diagnostic and Interventional Radiology, Sachsen, Germany

5. Heart Center Leipzig University Hospital, Sachsen, Germany

6. University of Leipzig - Heart Centre, Department of Internal Medicine / Cardiology, Sachsen, Germany

Background: In contrast to acute myocarditis presenting with “infarct-like” symptoms, where traditional Lake Louise criteria (LLC) as well as novel mapping techniques such as native T1 and T2 mapping have been demonstrated to achieve good diagnostic performance, the diagnosis of acute myocarditis in patients presenting with signs of dilated cardiomyopathy (DCM) still is extremely challenging. Thus, the aim of the present study was to test the usefulness of native T1 and T2 mapping for the diagnosis of endomyocardial biopsy (EMB) proven acute myocarditis with DCM-like presentation in comparison to LLC.

Methods: In this prospective study, 30 patients with clinical suspicion of acute myocarditis defined by symptom duration ≤ 14 days and “DCM-like” clinical presentation (ejection fraction < 50% and clinical signs of heart failure) were included. Patients underwent biventricular EMB, cardiac catheterization and CMR imaging at 1.5T including native T1 and T2 mapping as well as standard LLC. After segmentation of T1 and T2 maps using a dedicated Osirix plug-in, myocardial T1 and T2 values were averaged over the entire myocardium (mean myocardial T1 / T2). Statistical analysis was performed using Welch';s independent T-test and receiver operating curve (ROC) analyses in order to determine single or combined diagnostic parameters enabling the diagnosis of biopsy-proven acute DCM-like myocarditis, using EMB as the reference standard.

Results: EMB confirmed the diagnosis of acute myocarditis in 20 patients (EMB+), whereas 10 patients had no signs of acute inflammation on EMB (EMB-). Mean myocardial T1 and T2 showed significant differences between EMB+ and EMB- patients (T1: 1091 ± 78 vs. 1036 ± 92 ms, p = 0.05; T2: 64 ± 4 vs. 60 ± 5 ms, p = 0.01). In ROC analyses, T1 as well as T2 showed a superior diagnostic performance when compared to LLC (AUC: 0.72 for T1, 0.78 for T2, 0.55 for LLC, Fig. 2). Using a cut-off of ≥ 1061 ms for T1 and of ≥ 61 ms for T2 resulted in a diagnostic sensitivity of 75% and 90%, respectively and a specificity of 80% and 70%, respectively. Although the combination of T1 and T2 finally resulted in a further increased diagnostic performance with an AUC of 0.81 in ROC analysis (Fig. 2), the use of a combined cut-off of T1 ≥ 1061 ms and T2 ≥ 61 ms (i.e. both criteria met) did not further increase diagnostic certainty (sensitivity 70%, specificity 80%). Mean T1 and T2 demonstrated a moderate correlation with a Pearson';s correlation coefficient of 0.44.

Conclusion: In the patient cohort with DCM-like acute myocarditis, native T1 and T2 mapping might deliver potent novel diagnostic parameters, which are far superior to traditional LLC. Since our data showed a significant correlation between the two parameters, combining them in a model does not appear to be of additional diagnostic value. Thus, T1 and T2 might be used interchangeably for a future more sensitive and specific non-invasive diagnosis of acute myocarditis in this difficult-to diagnose patient group, offering the potential for the development of novel treatment options.

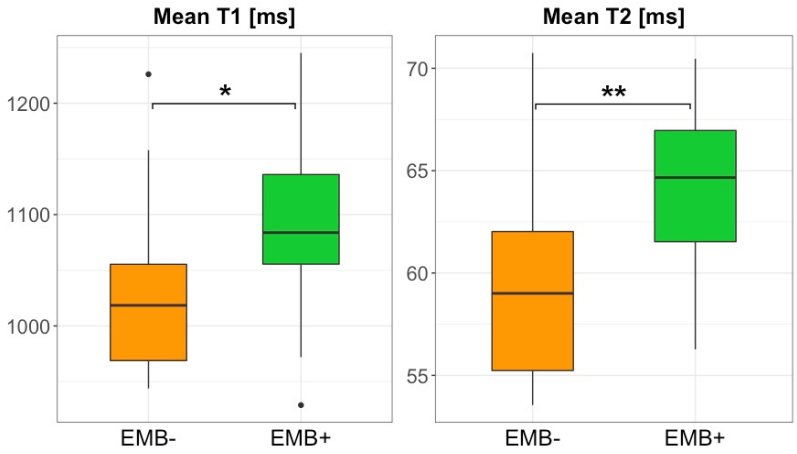

Fig. 1: Differences of mean myocardial T1 and T2 between EMB+ and EMB- patients with acute DCM-like symptoms

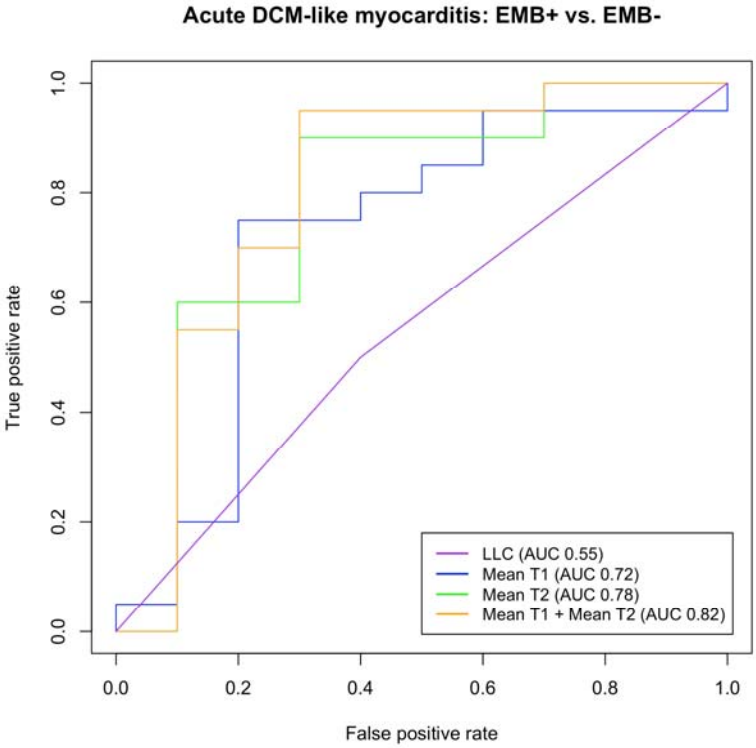

Fig. 2: ROC-Analysis for differentiating patients with EMB+ from EMB- acute DCM-like myocarditis. LLC - Lake Louise criteria

ID#: 366958

Stress cardiovascular magnetic resonance for evaluation of antineoplastic associated cardiotoxicity in a real-world cohort of breast cancer patients

Vinh Q. Nguyen, MD[1] Mariana L. Henry, BS[2], Albert J. Sinusas, MD[3], Dana C. Peters, PhD[4], Judith L. Meadows, MD[5], Imran Hafeez, MD[2], Steffen Huber, MD[5], Hamid R. Mojibian, MD[5], Isabel Oliva, MD[6], Anna Bader, MD[2], Jonathan Killam, MD[2], Syed Latif, MD[2], Sarah Hull, MD[2], Jessica Coviello, APRN[2], Michael Labrec, RTMR[2], Lauren A. Baldassarre, MD[7]

1. Yale School of Medicine, New Haven, CT

2. Yale School of Medicine

3. Yale University, New Haven, CT

4. Yale University

5. Yale School of Medicine, CT

6. Yale School of Medicine, MADISON, CT

7. Yale University, CT

Background: Breast cancer therapies, such as trastuzumab/pertuzumab (T/P), anthracyclines (AC) and radiation (R) may result in cardiotoxicity. Left ventricular (LV) dysfunction may manifest as decreased left ventricular ejection fraction (LVEF), abnormal global longitudinal strain (GLS), microvascular dysfunction as assessed by a decreased global sub-endocardial/sub-epicardial myocardial perfusion index ratio (SS-MPIR), or late gadolinium enhancement (LGE).

Methods: A retrospective search of the electronic medical record was performed for female patients with breast cancer and concern for cardiomyopathy who had a stress CMR between July 2013 and July 2017. CMR imaging (1.5T, Siemens, Erlangen, Germany) included cine imaging (SSFP), first-pass vasodilatory stress-only perfusion (ssGRE) with regadenoson 0.4mg and 0.05mmol/kg gadolinium at 3cc/s, and LGE sequences. Quantitative parameters were processed by an expert CMR reader (CVI42, v5.6.4, Calgary, Canada) for LV volume and function, feature tracking GLS, and SS-MPIR (Figures 1&2). Chart review was performed for cardiovascular risk factors, medications, and transthoracic echocardiogram (TTE). Correlations between breast cancer therapies, CMR parameters, and SS-MPIR were analyzed using SPSS v24.0.

Results: Thirteen patients were studied (Table 1). Six patients had follow-up TTEs demonstrating a new cardiomyopathy (average LVEF 42.8%), with an average interval decrease in LVEF of 17.6% from pre-treatment TTE (average LVEF 60.4%). On subsequent CMR, the entire cohort average LVEF was 59.7% and GLS was -15.12%. Five patients had follow up TTEs after CMR, all with normal LVEF (average 55.6%).

Three patients had perfusion defects and/or LGE consistent with ischemic heart disease (IHD), and 1 patient had a non-ischemic pattern of LGE. The average SS-MPIR at stress was 0.98. When all ischemic segments were excluded, it was 1.00, and when all patients with IHD were excluded, the SS-MPIR was 1.02. CMR LVEF correlated with SS-MPIR when all segments were analyzed ($r= 0.899$, $p < 0.01$), when ischemic segments were excluded ($r= 0.643$, $p=0.024$), and when patients with IHD were excluded ($r= 0.807$, $p=0.009$). No significant correlation was found between different breast cancer therapies and CMR SS-MPIR or GLS.

Conclusion: Stress CMR is a feasible clinical tool to evaluate antineoplastic cardiotoxicity. In our real world cohort, LVEF had recovered at the time of CMR, SS-MPIR was normal based on published references, and CMR LVEF positively correlated with SS-MPIR. GLS was abnormal and may be a marker of preclinical LV dysfunction. Prospective study of a larger cohort with stress CMR at the time of depressed LVEF is needed to define an association between microvascular dysfunction and antineoplastic cardio-toxicity.

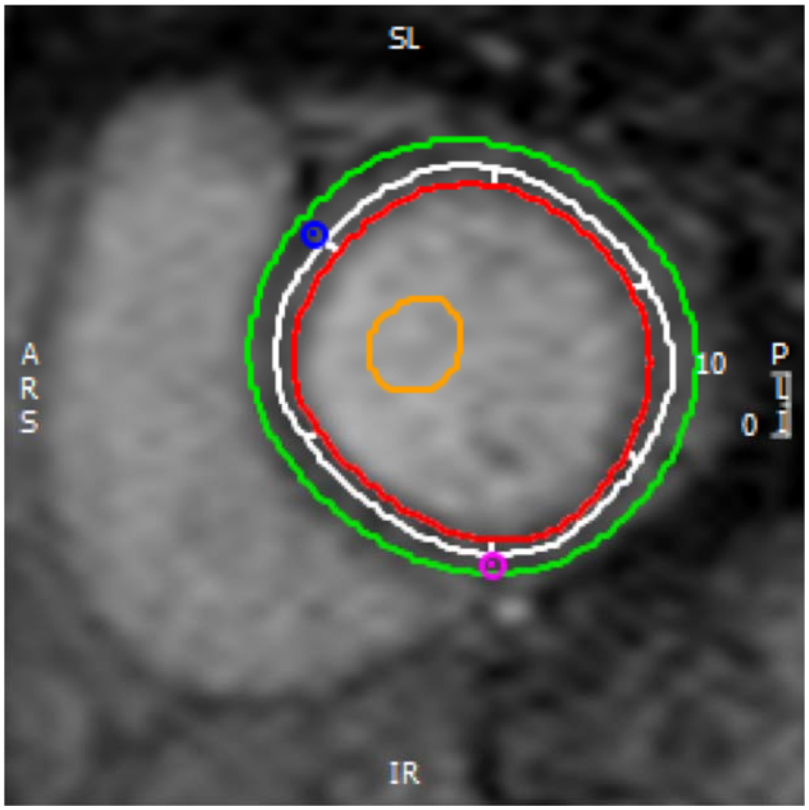

First-pass vasodilatory stress with regadenoson. Endocardium (red) and epicardium (green) contours were manually outlined for sub-endocardial/sub-epicardial myocardial perfusion index ratio analysis. To normalize to the arterial input function, a region of interest was drawn inside the LV blood pool (orange). The white contour circumscribes the sub-endocardial layer to be analyzed as shown.

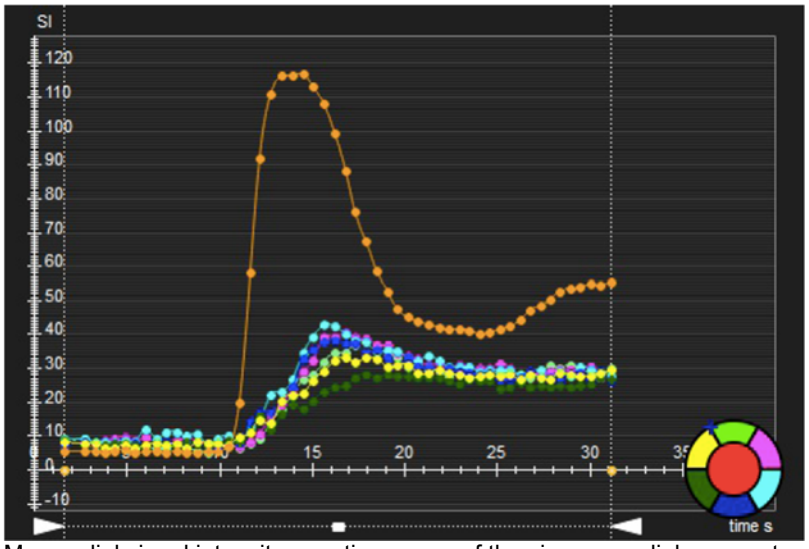

Myocardial signal intensity over time curve of the six myocardial segments and the LV blood pool, represented by the color palette to the bottom right. Myocardial perfusion index is the ratio between the maximum slope of one segment and the maximum slope of the blood pool (orange curve). All six segments were averaged to obtain a global sub-endocardial/sub-epicardial myocardial perfusion index ratio.

Patient Characteristics

PATIENT CHARACTERISTIC	MEAN/FREQUENCY
Average Age (years)	58.8
Coronary Artery Disease	23.1%
Diabetes Mellitus	7.7%
Family History	7.7%
Female	100%
Hyperlipidemia	46.2%
Hypertension	30.8%
Obesity	38.5%
Peripheral Arterial Disease	7.7%
Smoking	53.8%
Valvular Disease	23.1%
CARDIAC MEDICATIONS	
ACE Inhibitors/ARB	53.8%
Beta Blockers	15.4%
Statin	53.8%
ANTINEOPLASTIC THERAPY	
Anthracyclines	61.5%
Aromatase Inhibitors	38.5%
Trastuzumab/Pertuzumab	46.2%
Radiation Therapy	76.9%

ID#: 364069

Tissue tracking versus feature tracking for strain measurement on cardiac magnetic resonance

Jimmy C. Lu, MD[1] Sunkyung Yu, MS[2], Maryam Ghadimi-Mahani, MD[2], Prachi Agarwal, MD[2], Adam Dorfman, MD[2]

1. University of Michigan, Dexter, MI

2. University of Michigan, MI

Background: Left (LV) and right ventricular (RV) strain are important early indicators of ventricular dysfunction, but significant intervendor variability has been demonstrated on echocardiography. This study aimed to compare strain measurements and reproducibility by tissue tracking and feature tracking software on cardiovascular magnetic resonance (CMR) images.

Methods: In 25 patients with repaired tetralogy of Fallot (median 33 years old, interquartile range [IQR] 25-38 years) who had undergone CMR and exercise test within 6 months (median 0 days, IQR 0-19 days), LV and RV global circumferential (GCS) and longitudinal strain (GLS) were measured from CMR images. Tissue tracking (TT) was performed with cmr^{42} (Circle Cardiovascular Imaging, Calgary, Canada); feature tracking was performed with 2D CPA MR (Tomtec, Unterschleissheim, Germany). Using TT, diastolic endocardial and epicardial contours were drawn on all short axis and long axis images. Using FT, LV short axis contours were drawn at 3 levels, LV long axis contours were drawn on 2-chamber, 3-chamber, and 4-chamber slices, and RV contours were drawn on single short axis and 4-chamber slices (with septum excluded). All contours were evaluated visually for adequate tracking and revised as necessary. Time to process was measured from opening the study to acceptance of contours. Measurements were repeated ≥1 week later for intraobserver variability. Intraobserver reproducibility in each method was evaluated using Bland-Altman limits of agreement and coefficient of variation.

Results: Measurements were feasible in all but 1 patient (LV obscured due to embolization coil artifact). Mean time to process was similar (TT 10.2±3.1 min vs FT 9.0±1.7 min, p=0.10). Fewer patients required contour revision by TT than by FT. Both TT and FT measurements had similar correlations with LVEF and RVEF; RV GLS correlation with RVEF did not reach significance by either method. With the exception of LV GCS, strain was mildly underestimated by FT relative to TT, with mean difference ~3%. Intraobserver reproducibility had better agreement with TT (Figure). Coefficients of variation were lower with TT than FT for LV GLS (5.0 vs 12.9%), RV GCS (7.9 vs 17.5%), and RV GLS (7.3 vs 23.5%), but were similar for LV GCS (7.5 vs 7.6%). Neither TT nor FT measurements correlated with exercise capacity or maximal oxygen consumption in this small cohort.

Conclusion: LV and RV strain measurements are more reproducible by TT than FT, particularly for longitudinal strain. Systematic differences suggest that strain measurements by these two methods are not interchangeable. Further data are necessary in larger cohorts to evaluate correlation with clinical outcomes.

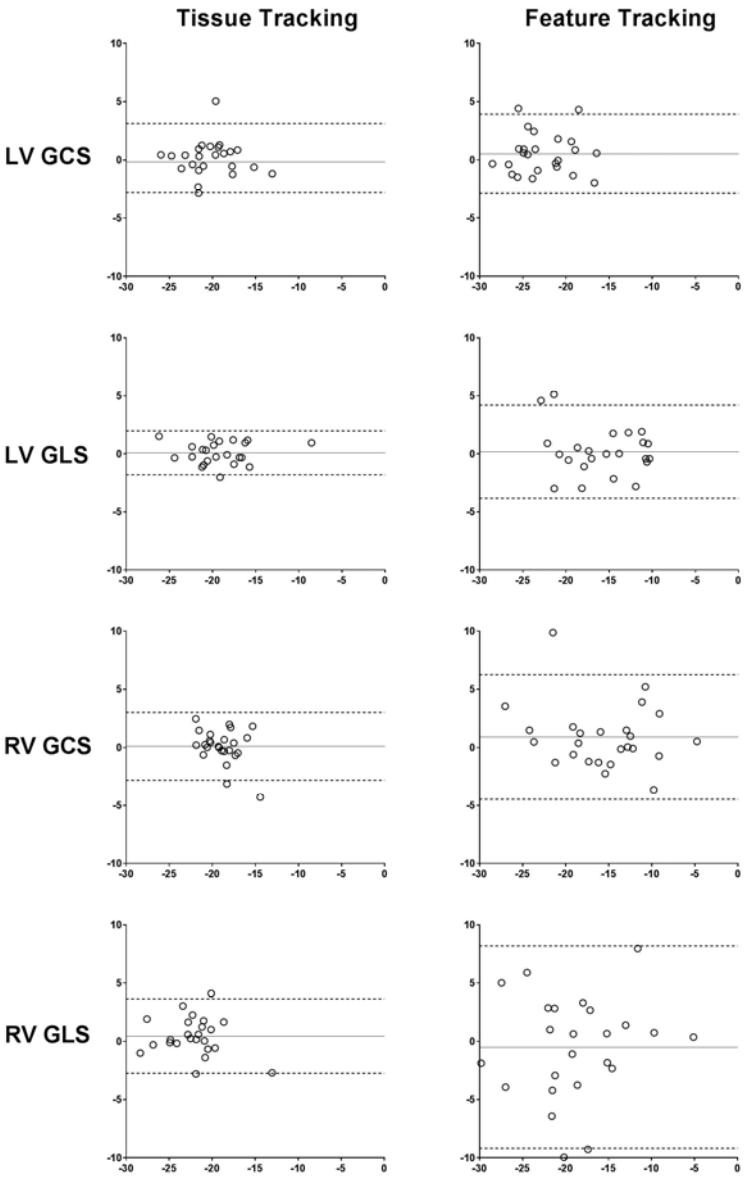

Bland Altman analysis of intraobserver variability for tissue tracking and feature tracking

ID#: 357496

Free-Breathing Retrospectively Cardiac Gated Balanced Steady-State Free Precession Cine Imaging: Evaluation of Clinical Performance in 100 Pediatric Patients

James C. Wilkinson, MD[1] Amol Pednekar, PhD[2], Siddharth Jadhav, MD[2], Prakash Masand, MD[3], Tobias Schlingmann, MD, PhD[4], Pamela Ketwaroo, MD[3], Cory Noel, MD[4]

1. Texas Children's Hospital, Baylor College of Medicine, Houston, TX

2. Texas Children's Hospital, Houston, TX

3. Texas Children's Hospital

4. Texas Children's Hospital / Baylor College of Medicine, TX

Background: Breath-holding requirement may limit acquisition of diagnostic quality cine balanced steady-state free precession (bSSFP) images in sedated pediatric patients. Cardiovascular disease affects the ability to tolerate a thermal challenge, making it prudent to ensure that specific absorbed energy (SAE) does not exceed 1.8 kJ/kg (0.5°C rise in body temperature) [1] in sedated pediatric patients. We evaluated image quality and safety of the respiratory-triggered (RT) bSSFP sequence with prospective arrhythmia rejection and retrospective cardiac gating [2].

Methods: All pediatric CMR studies from September 2016 to March 2017 were reviewed to evaluate clinical performance of RT sequence with respect to breath-held (BH) studies. Two experienced CMR readers reviewed RT cine CMR studies. RT images were graded based on: blood to myocardial contrast, signal uniformity, and delineation of the endocardial contour throughout the cardiac cycle, on the scale of 1 to 5 where 5 corresponds to image quality (IQ) equivalent to best possible with BH sequence [Fig. 1]. Additionally, radio-frequency (RF) power deposition data logged during the 50 consecutive RT-sequences was analyzed.

Results: From 390 pediatric CMR studies, 100 (81 sedated and 19 uncooperative for breath holding) were performed with free-breathing cine imaging [Table. 1]. The imaging parameters for RT cine bSSFP were as follows: TR/TE/flip angle = 2.5-2.7ms/1.25-1.35ms/60°; SENSE factor = 1.3-2; temporal resolution 35-45ms. All 100 patients had diagnostic free-breathing cine CMR. IQ scores ranked as excellent (38), good (54), to moderate (8) [Fig. 2]. Two-sided Wilcoxon signed rank test indicated that IQ scores by two observers ($p = 0.49$) were comparable. The effective SAR was 0.71 ± 0.1W/kg [Fig. 3]. The SAE per slice for RT was 20.1 ± 5.1 J/kg, which is 49.4 ± 5.6% of the alternative (equivalent 4 NSA) sequence. Thus keeping the total SAE for 40 to 50 slices to half below the recommended safe limit of 1.8 kJ/kg. Previous studies have shown no difference in the ventricular volumetric indices estimated with RT and BH techniques [2]. Over that last 3 years, a quarter of our cardiac MRI were conducted exclusively with RT sequence, in a wide range of age and cardiac diseases. Furthermore, our ability to utilize the RT sequence provides an opportunity to obtain high quality CMR data in a historically difficult population.

Conclusion: Respiratory-triggered, retrospectively cardiac–gated bSSFP sequence with prospective arrhythmia rejection can be performed safely with consistent good quality in sedated and uncooperative pediatric CMR studies exclusively.

Ref: 1) Health Phys. 2004, 87:197-216; 2) JCMR 2015, 17:1.

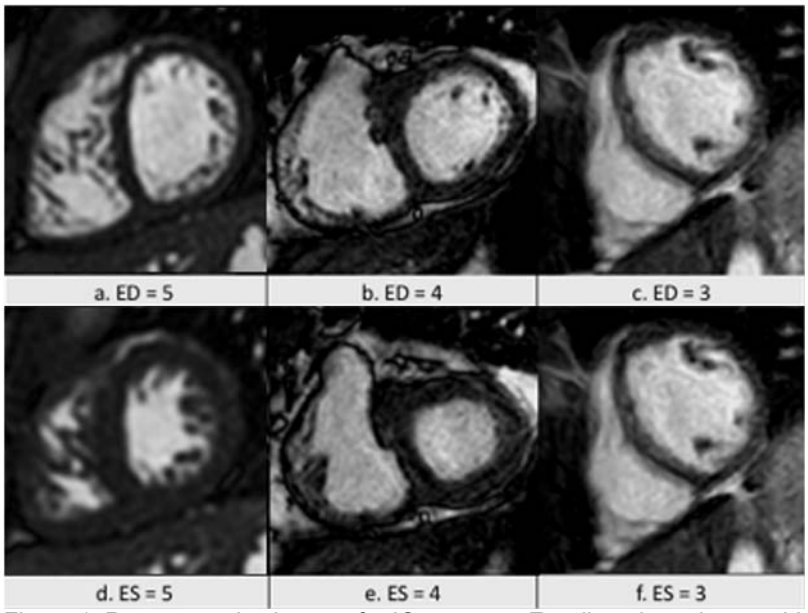

Figure 1. Representative images for IQ scores 5: Excellent; hyperintense blood pool with excellent contrast against myocardium throughout the cardiac cycle, nearly artifact free. 4: Good; blood pool is significantly brighter than myocardium, myocardial signal intensity is fairly uniform throughout the cardiac cycle, with some motion artifact that does not affect overall IQ. 3: Moderate; image is of diagnostic IQ but features significant loss of blood to myocardial contrast or with noticeable variation in myocardial signal throughout cardiac cycle, with noticeable artifact. Less than 3: Poor blood pool to myocardial contrast with borderline to non-diagnostic quality. ED end-diastole; ES end-systole.

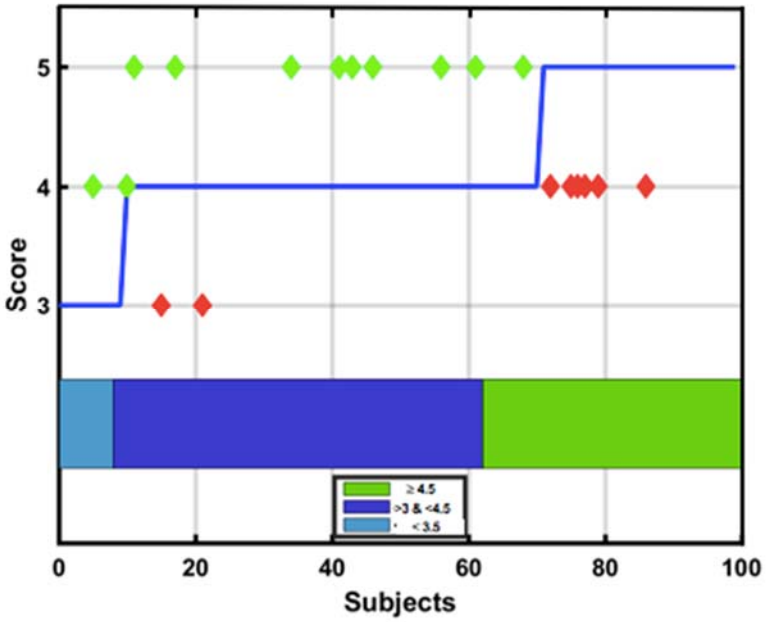

Figure 2. IQ scores and inter-observer variability. Blue line - O1, green diamonds - O2>O1, red diamond - O2<O1. Bar - (O1+O2)/2 categorized to excellent (green), good (purple), and moderate (teal). IQ = Image Quality; O1 = observer 1 IQ score; O2 = observer 2 IQ score.

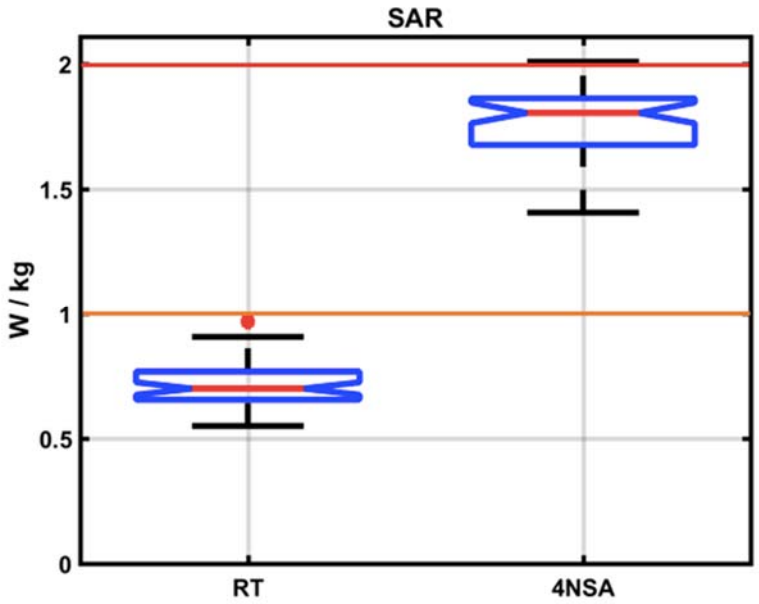

Figure 3. Box-plot for SAR in RT (actual) and 4NSA (calculated) techniques. Red line - 2 W/kg; Orange line: 1 W/kg prudent for pediatric sedated cardiac patients. RT = respiratory triggered; 4NSA = number of signal averages.

Characteristics of the study population

	Total	Sedated	Non-sedated
Number	100	81	19
Age	10.2±8.8	9.1±8.7	15±7.5
Sex (female/male)	59/41	49/32	10/9
Height (cm)	126.5±32.6	120±31.9	154.3±18.4
Weight (kg)	33.2±22.4	28.5±18.8	53±25.9
BSA (m^2)	1.1±0.5	1.0±0.4	1.5±0.4
HR (beats/min)	88.4±19.4	90.9±20.1	77.8±11.7
Acquired disease	18	15	3
Congenital disease	82	66	16

Note.–The data are presented as the mean ± standard deviation or as the number of subjects

BSA body surface area, *HR* heart rate

ID#: 358119

Combined evaluation of aortic pulse wave velocity, epicardial fat volume, left ventricular strain and fibrosis in patients with hypertension and diabetes mellitus

Rami Homsi[1] Michael Meier-Schroers[2], Daniel Kuetting[3], Ulrike Schlesinger-Irsch[2], Darius Dabir[4], Alois Sprinkart[2], Hans Schild[4], Daniel Thomas, MD[4]

1. University Hospital Bonn, Department of Radiology, Bonn, N/A, Germany

2. University Hospital Bonn, Department of Radiology, N/A, Germany

3. University Hospital Bonn, Department of Radiology, Bonn, Nordrhein-Westfalen, Germany

4. University Hospital Bonn, Department of Radiology, Germany

Background: Cardiovascular (CV) disease is the number one cause of death. It is important to early identify individuals with increased risk in order to enable preventive measures and an optimal treatment. This may be achieved by combined quantifications of different parameters such as:

- aortic pulse wave velocity (PWV) which is a measure of aortic stiffness
- epicardial fat volume (EFV), which – when increased – shows unfavorable metabolic and inflammatory activities associated with cardiovascular events such as myocardial infarctions
- left ventricular (LV) fibrosis and strain, sensitive indicators for sub-clinical diseases, such as myocardial ischemia, hypertension, and early heart failure

Normally different methods are needed in order to reach good accuracies. In this context, MRI is not widely used, although it can accurately measure these parameters, without a meaningful harm and within a single examination. With this background, the purpose of this multi-parametric MRI approach in patients with increased CV risk was to assess PWV, EFV, LV fibrosis and strain, and, to relate the results to the presence of hypertension (HTN) and diabetes mellitus (DM).

Methods: 31 hypertensive patients without DM (HTN-PTs) and 12 hypertensive patients with DM (DM-PTs) were examined at 1.5 Tesla. No patient had coronary artery disease and all had a normal LV-ejection fraction (LVEF). Additionally 20 healthy controls were included. PWV was determined at the aortic arch by flow-measurements in the proximal ascending and descending aorta. EFV was determined using a 3D axial ECG- and respiratory navigator gated mDixon-sequence and LV T1 relaxation times (T1) to detect myocardial fibrosis using a MOLLI scheme. ECG-gated SSFP-cine images were used to assess LVEF and to perform systolic circumferential and longitudinal strain analysis (CS, LS).

Results: Age and gender did not differ significantly between the groups. BMI was higher in DM-PTs compared to controls (Figure 1). Results were adjusted for BMI. There were no relevant differences regarding LVEF and end-diastolic volume index (LVEDVi). As expected interventricular septal diameter (IVSD) was higher in hypertensive patients. EFV was lowest in controls, higher in HTN-PTs and highest in DM-PTs. PWV was highest LV strain was lowest in DM-PTs. T1 was higher in DM-PTs and HTN-PTs (Figure 1 and 2).
Figure 3 show an example of the flow measurements to determine PWV (A, B), a reduced CS&LS curves in a hypertensive male (red) compared to a control (blue; C, D) with their T1, wich is higher in the hypertensie male (E) compared to the control (F). Figure 3 E shows a fat image (arrows pointing to the epicardial fat).

Conclusion: A multi-parametric MRI approach to different CV risk and prognostic parameters revealed an increased EFV and aortic stiffness, as well as signs of LV fibrosis and a reduced LV strain despite a normal LVEF. Possible mechanisms may relate to cardiac remodelling, aortic wall stretching and additive effects of DM such as insulin sensitivity disturbances, endothelial dysfunction and an increased inflammatory burden. The increased EFV may also play a role by metabolic & inflammatory mechanisms such as the reduction of anti-inflammatory and flow-regulating adipokines, cardiac steatosis and lipotoxicity. Multi-parameteric MRI approaches can easily be integrated into a routine MRI exam; it may be supportive for a more accurate risk evaluation, help to early identify individuals at risk and enable preventive measures and optimal treatments.

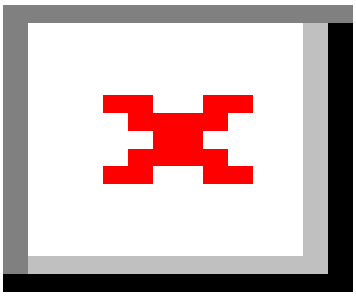

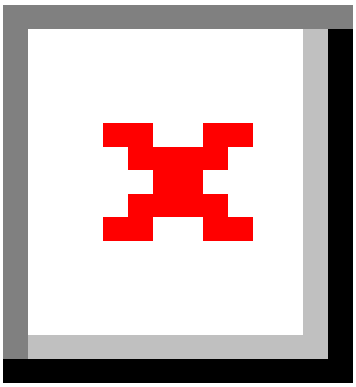

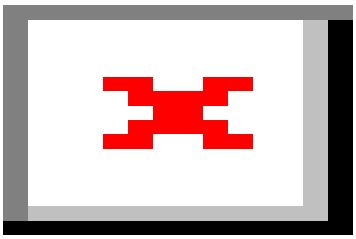

ID#: 353742

Late gadolinium enhancement predicts worse prognosis, adverse remodelling and need for defibrillator implantation in non-ischemic dilated cardiomyopathy

Andrea Barison, MD, PhD[1] Alberto Aimo[2], Alessandro Ortalda[3], Giancarlo Todiere, MD, PhD[4], Chrysanthos Grigoratos[4], Claudio Passino[4], Paolo Camici, FACC FESC[3], Giovanni D. Aquaro[4], Michele Emdin, FESC MHFS[4]

1. Fondazione Toscana Gabriele Monasterio, Pisa (Italy), Pisa, Toscana, Italy

2. Scuola Superiore Sant'Anna, Pisa, Toscana, Italy

3. Vita Salute University and San Raffaele Hospital, Lombardia, Italy

4. Fondazione Toscana Gabriele Monasterio, Pisa (Italy), Toscana, Italy

Background: Reverse remodeling (RR) is the recovery from systolic dysfunction on guideline-recommended treatment. There are currently no established predictors of RR among patients with non-ischemic dilated cardiomyopathy (NIDCM). RR is particularly important in patients with left ventricular ejection fraction (LVEF) ≤35%, who have indication to defibrillator implantation for primary prevention. We sought to investigate whether the presence and extent of late gadolinium enhancement (LGE) at cardiac magnetic resonance (CMR) could predict both a worse prognosis and the lack of RR during follow-up.

Methods: We included NIDCM patients with a left ventricular ejection fraction (LVEF) <45% at baseline CMR, who underwent a second CMR scan within 5 years from the first scan. RR was defined as ≥10% reduction in LV end-diastolic volume index (LVEDVi) and ≥10% LVEF increase. The end-point was a composite of all-cause death, cardiovascular hospitalization, appropriate defibrillator discharge, ventricular assist device implantation or heart transplant. LGE was both visually assessed and quantified as percentage of LV mass (LGE%).

Results: Seventy-one patients were enrolled (age 57±14 years, 43 males, 61%, median LVEF 35%, [interquartile range 27-41%]). LGE was present in 42 patients (59%); at quantitative analysis, median LGE mass was 9 g [5-18], and median LGE% was 7% [3-12%]. Over a median 42-month follow-up [15-73 months], the endpoint occurred in 36 patients (51%). Patients with LGE had a significantly worse prognosis (P=0.043), with best quantitative LGE cut-point ≥7% at ROC analysis (P=0.017). During the interval between the 2 CMR scans (median 28 months [15-44 months]), 22 patients (31%) experienced RR (baseline LVEF 26[18-32]%, follow-up LVEF 54[46-59]%, p<0.01). LGE absence predicted RR irrespectively of baseline LVEDVi, LV end-systolic volume index, and LVEF.
In the subset of 35 patients with baseline LVEF ≤35%, those with either LGE at qualitative analysis or LGE≥7% at quantitative analysis experienced a worse prognosis. Twenty-five (69%) patients crossed the 35% LVEF threshold during follow-up: both LGE absence and quantitative LGE <7% were associated with crossing of the 35% LVEF threshold for defibrillator implantation.

Conclusion: In patients with NIDCM, the absence of LGE at baseline CMR was associated with better prognosis and RR. In patients with baseline LVEF <35%, LGE absence was associated with more frequent crossing of the 35% LVEF threshold for defibrillator implantation.

ID#: 360640

Statistical Shape Modeling of the Left Ventricle in Tetralogy of Fallot Using Cardiac Magnetic Resonance Imaging

Nickolas Forsch, BS[1] Sanjeet R. Hegde, MD, PhD[2], Andrew D. McCulloch, PhD[3], Alistair Young, PhD[4], Jeff Omens, PhD[3], James C. Perry, MD[2], Kathleen Gilbert, BE(hons), PhD[5]

1. UC San Diego, San Diego, CA

2. UC San Diego/Rady Children's Hospital, San Diego, CA

3. UC San Diego, La Jolla, CA

4. University of Auckland, New Zealand, GRAFTON, Auckland, New Zealand

5. University of Auckland, New Zealand, New Zealand

Background: Despite advances in surgical techniques to treat tetralogy of Fallot (TOF), postoperative electromechanical and structural sequelae continue to cause adverse long-term remodeling of the ventricles that is poorly understood. While current methods of image-based patient prognosis can identify TOF patients who are at risk of future complications, they do not adequately differentiate patients or elucidate the underlying mechanisms of remodeling. Better methods of quantifying left ventricular (LV) shape and systolic wall motion have the potential to identify shape biomarkers that predict long-term LV remodeling and elucidate the mechanisms of remodeling. The goal of this study is to find relationships between LV shape and abnormal systolic wall motion in TOF that can help explain mechanisms of adverse remodeling and therefore long-term risk.

Methods: Image-based computational models of three-dimensional (3D) LV geometry were developed using CIM (*Cardiac Image Modeller, v8.1.6, Auckland, New Zealand*) and cardiac magnetic resonance images (cMRI) of 84 patients with TOF. The models were compared to a statistical shape atlas of average LV shape in an asymptomatic control population to derive Z-scores for orthogonal modes of shape and systolic wall motion. Z-scores statistics were calculated for the first eight modes of end-diastolic (ED) shape and the first twelve modes of systolic wall motion. Relationships between ED shape modes and systolic wall motion were found using partial least squares regression analysis.

Results: ED modes revealed a wide distribution of shape and significant differences between age groups for several modes. Systolic wall motion modes 3, 5, and 10 (representing basal and apical longitudinal displacement, as well as lateral free wall radial displacement near the apex) were distinctly abnormal, with mean Z-scores falling outside of the 5^{th} and 95^{th} percentile of the asymptomatic atlas (Figure 1). From multiple regression analysis, the combination of ED modes 2, 3, and 8 (representing sphericity, baseplane orientation, and global wall thickness) significantly correlated with systolic wall motion mode 3, with an adjusted R-squared value of 0.21 after controlling for multiple predictors (p-value < 0.0001). Similarly, the combination of ED modes 1, 2, and 7 (representing size, sphericity, and wall curvature and thickness) significantly correlated with abnormal systolic wall motion mode 10, with an adjusted R-squared value of 0.24 (p-value < 0.0001).

Conclusion: Shape modeling of the LV in TOF revealed distinct modes of systolic wall motion that are abnormal compared to an asymptomatic control population, and correlated with a combination of ED shape modes. This analysis revealed ED shape biomarkers which are potentially important in determining LV function in TOF patients, and ultimately patient outcomes. Further analysis of LV shape and function in TOF using models of biomechanics has the potential to confirm and explain relationships between shape and function that determine long-term LV remodeling.

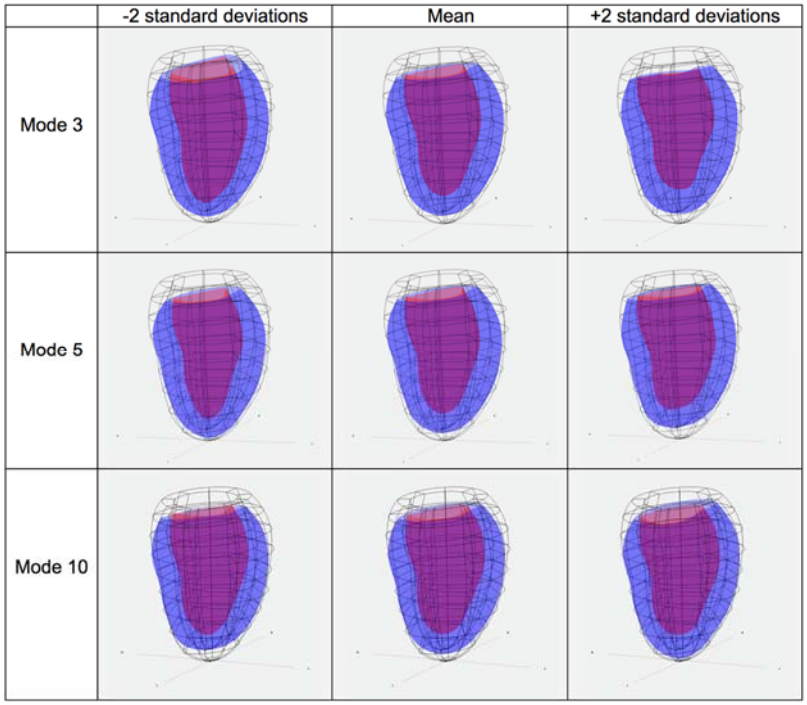

Figure 1: Abnormal modes of systolic wall motion between end-systole and end-diastole. Mean and ±2 standard deviations of the LV atlas for the asymptomatic control population are shown to illustrate the physical variation in the modes. Displacement vectors of wall motion are illustrated as an LV shape that describes the systolic displacement from the mean ED shape (gray wireframe).

ID#: 360719

Machine Learning of 3D Myocardial Deformation from Cine MRI for the Identification of Segmental Viability in Patients with Ischemic Cardiomyopathy

Alessandro Satriano, Ph.D.[2]Matthew Magyar-Ng[1], Yoko Mikami, MD, Ph.D.[3], Aidan Cornhill, BMSc, HBA[3], Jacqueline A. Flewitt, MSc[2], Naeem Merchant, MD[1], Carmen P. Lydell, MD[2], Andrew G. Howarth, MD, Ph.D[3], Nowell M. Fine, MD, M.Sc.[4], James White, MD, FRCP(C)[3]

1. Stephenson Cardiac Imaging Centre, AB, Canada

2. Stephenson Cardiac Imaging Centre, Libin Cardiovascular Institute of Alberta, University of Calgary, Calgary, AB, Canada

3. Stephenson Cardiac Imaging Centre, Libin Cardiovascular Institute of Alberta, University of Calgary, AB, Canada

4. Libin Cardiovascular Institute of Alberta, AB, Canada

Background: Late gadolinium enhancement (LGE) imaging is a reference standard for the identification of myocardial viability following myocardial infarction. With a desire to fully exploit the value of non-contrast imaging techniques, efforts to discriminate viability from deformation analysis (e.g. strain) have been attempted. However, isolated strain measures have shown only modest accuracy in this role. In this study we aimed to evaluate the role of machine learning to classify segmental viability using multiple geometrical (wall thickness) and functional (strain amplitude and time to systolic peak strain) parameters available from contemporary 3D feature-tracking based strain analysis.

Methods: 2D-multiplanar cine and LGE imaging acquired at 3T in 98 patients with ischemic cardiomyopathy was analyzed by segmental analysis to provide 1568 unique myocardial segments. Blinded analysis was performed to determine percent segmental fibrosis (cvi42, Circle Cardiovascular Imaging, Calgary, >5SD threshold) and deformation (GIUSEPPE: validated in-house 3D strain software). The latter provided strain measures for each cardiac phase in conventional (radial, circumferential, and longitudinal) and principal strain (maximum, minimum, and secondary) directions in addition to mean diastolic wall thickness (WT). All segments were classified as viable (<50% LGE) or non-viable (≥50% LGE) with corresponding deformation measures provided to a Feature Correlation Based Filter (FCBF) to identify those with strongest discriminatory power. Three parameters were selected and modelled using a Random Forest algorithm trained to identify segmental viability.

Results: Mean age was 62.2 ± 10.0 years with mean LVEF 40.6 ± 13.4%, and 17 female subjects (17%). A total of 1396 viable (LGE<50%) and 172 non-viable (LGE≥50%) were available. Non-viable segments showed reduced WT ($p<0.005$), reduced strain amplitude for all directions ($p<0.0001$), while time to peak strain was significantly elevated in the radial, longitudinal and minimum principal directions ($p<0.05$). Individually, these measures performed modestly for the classification of segmental viability; the highest AUC was found for circumferential strain (AUC: 0.73). FCBF identified maximum PS amplitude, longitudinal time to peak, and WT as strongest parameters for viability classification (example case in Figure 1). Collectively provided to Random Forest modelling, an AUC of 0.88 (sensitivity 91%, specificity 95%, PPV 59%, NPV 99%) was achieved for classification of segmental viability.

Conclusion: Machine learning based modelling of combined strain analyses improves classification of segmental viability compared to individual strain measures. Following validation in an external cohort, such modelling may expand the clinical value of 3D strain analysis.

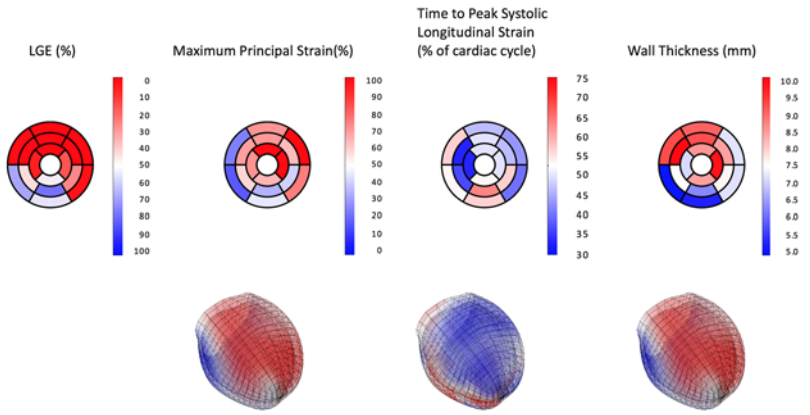

Figure 1: ICM patient with infero-septal LGE. It can be observed that the infer-lateral enhancement corresponds to regional reduced maximum principal strain amplitude, delayed peak-systolic longitudinal contraction, and reduced end-diastolic wall thickness.

ID#: 361082

Regional function after acute myocardial infarction: strain analysis is superior to wall thickening in detecting microvascular injury

Henk Everaars[1]Lourens Robbers[2], Aernout M. Beek, MD, PhD[3], Pierre Croisille[4], Alexander Hirsch, MD, PhD[5], Paul Teunissen, MD, PhD[6], Niels van Royen, MD, PhD[6], Felix Zijlstra[5], Jan Piek[7], Albert C. van Rossum, MD, PhD[8], Robin Nijveldt, MD, PhD[6]

1. VU univeristy medical center, Diemen, Noord-Holland, Netherlands

2. VU university medical center, Noord-Holland, Netherlands

3. VU University Medical Center, Amsterdam, The Netherlands, Noord-Holland, Netherlands

4. Creatis Medical Imaging Research Center, Rhone-Alpes, France

5. Erasmus Medical Center, Netherlands

6. VU University Medical Center, Netherlands

7. Academic Medical Center, Amsterdam, Netherlands

8. VU University Medical Center, Noord-Holland, Netherlands

Background: The presence of MVI after ST-segment elevation myocardial infarction (STEMI) is associated with poor functional recovery and outcome. However, there is limited data on the effect of MVI on regional function, which can be quantified with cardiovascular magnetic resonance imaging (CMR) by analysis of wall thickening or strain. The aim of this study was to compare the diagnostic performance of strain and wall thickening analysis in discriminating between infarcted and non-infarcted myocardium, and in differentiating infarcted myocardium with microvascular injury (MVI) from infarcted myocardium without MVI, in patients with an acute myocardial infarction.

Methods: Seventy-one patients with a successfully treated STEMI underwent CMR imaging at 2-6 days after reperfusion. Imaging protocol included cine imaging, late gadolinium enhancement and myocardial tissue tagging. Regional circumferential and radial strain and strain rates were analyzed in a 16-segment model as well as absolute and relative wall thickening. Strain and wall thickening were stratified according to presence of hyperenhancement and MVI.

Results: Hyperenhancement was detected in 418 (38%) of 1096 segments and was accompanied by MVI in 145 (35%) of hyperenhanced segments. Wall thickening, circumferential and radial strain were all significantly diminished in segments with hyperenhancement and decreased even further if MVI was also present (all $p<0.001$). Peak circumferential strain (CS) surpassed all other strain and wall thickening parameters in its ability to discriminate between hyperenhanced and non-enhanced myocardium (all $p<0.05$). Furthermore, CS was superior to both absolute and relative wall thickening in differentiating infarcted segments with MVI from infarcted segments without MVI ($p=0.02$ and $p=0.001$, respectively).

Conclusion: Strain analysis is superior to wall thickening in differentiating between normal and infarcted myocardium and in discriminating infarcted myocardium with MVI from infarcted myocardium without MVI. Peak circumferential strain is the most accurate marker of regional contractile function.

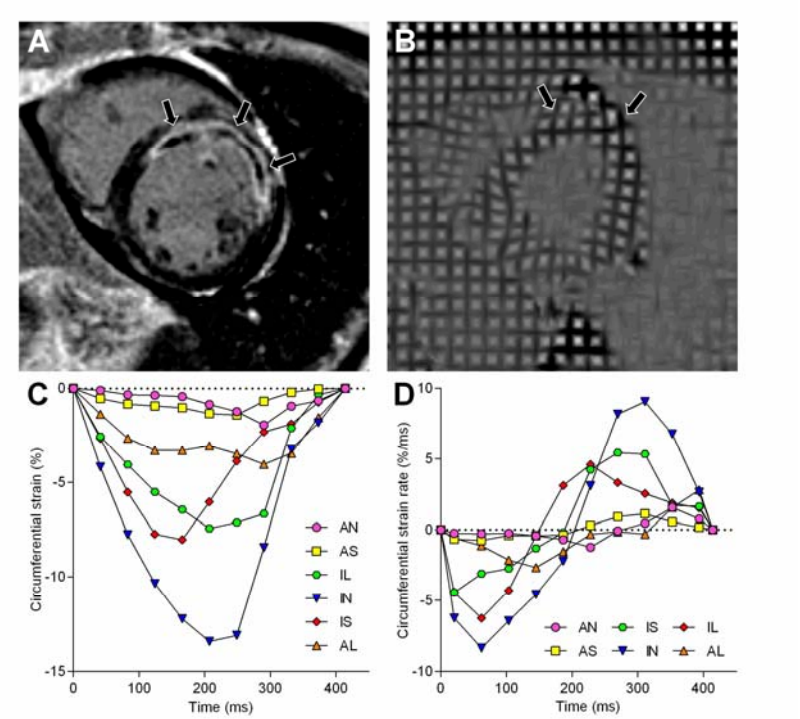

Example of strain and strain rate analysis in a patient after acute anterior myocardial infarction

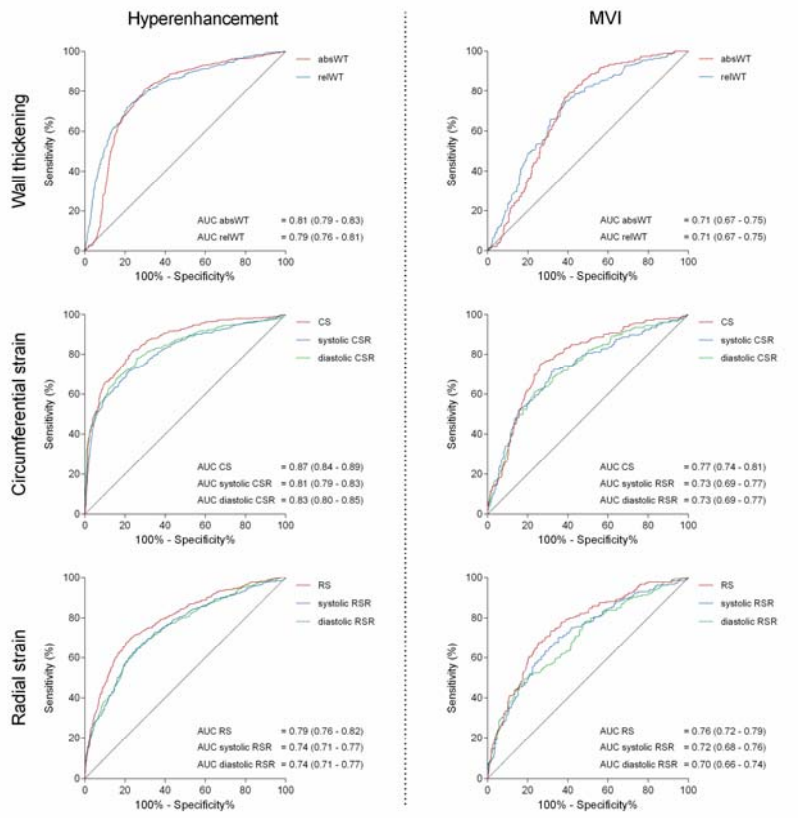

Receiver-operator characteristic curves of wall thickening and strain

Diagnostic performance of strain and wall thickening parameters in detecting hyperenhancement and microvascular injury

ID#: 362265

Longitudinal prospective CMR study in pediatric thalassemia major patients

Alessia Pepe, MD, PhD[1]Maddalena Casale, MD, PhD[2], Aldo Filosa, Napoli[3], Laura Pistoia, MSc[1], Nicolò Schicchi, MD[4], Gennaro Restaino, MD[5], Emanuele Grassedonio, MD[6], Petra Keilberg, RT[7], Massimo Allò, MD[8], Rosamaria Rosso, MD[9], Vincenzo Positano, MSc[1], Antonella Meloni, PhD[1]

1. Fondazione G. Monasterio CNR Regione Toscana, Pisa, Toscana, Italy

2. Azienda Ospedaliera di Rilievo Nazionale, Napoli, Campania, Italy

3. Azienda Ospedaliera di Rilievo Nazionale "A. Cardarelli", Napoli, Campania, Italy

4. Azienda Ospedaliero-Universitaria Ospedali Riuniti "Umberto I-Lancisi-Salesi", Ancona, Marche, Italy

5. Fondazione di Ricerca e Cura, Campobasso, Molise, Italy

6. Policlinico "Paolo Giaccone", Palermo, Sicilia, Italy

7. Fondazione G. Monasterio CNR-Regione Toscana, Pisa, Toscana, Italy

8. Presidio Ospedaliero ASL 5, Crotone, Calabria, Italy

9. spedale “Ferrarotto” - Azienda Ospedaliero-Universitaria Policlinico “Vittorio Emanuele”, Catania, Sicilia, Italy

Background: No data are available in literature on longitudinal prospective study in pediatric patients with thalassemia major (TM) evaluating, on repeated cardiovascular magnetic resonance (CMR) assessments, changes in myocardial iron overload (MIO) and biventricular function, and the development of myocardial fibrosis.

Methods: We considered 68 TM patients enrolled MIOT (Myocardial Iron Overload in Thalassemia) project with less than 18 years at the first CMR scan and who performed a follow-up (FU) study at 18±3 months. Myocardial and hepatic iron burdens were quantified by the T2* technique. Atrial dimensions and biventricular function were quantified by cine images. Late gadolinium enhancement (LGE) images were acquired to detect macroscopic myocardial fibrosis.

Results: At the baseline CMR, 16 (23.5%) patients showed MIO (global heart T2*<20 ms). Figure 1 shows the changes in cardiac iron levels. 25 patients changed the chelation therapy after the baseline CMR. The LV end-diastolic volume index and all RV volumes as well as the LV mass index were significantly lower at the FU MRI. No significant improvement in left or right global systolic function was found (Table 1).

For 40 patients the presence of myocardial fibrosis was investigated at both baseline and FU scans. Six patients (15.0%) had myocardial fibrosis at the baseline CMR and myocardial fibrosis was detected for all of them also at the FU. The extent of myocardial fibrosis was comparable between the two scans (0.77±0.42 % vs 0.79±0.51%; P=0.686). At the FU 4 new occurrences of myocardial fibrosis were detected (two patients without baseline MIO and two with baseline MIO). In patients with baseline MIO no significant correlation was found betweenthe percentage change in cardiac iron and the changes in hepatic iron or the baseline hepatic iron.

Conclusion: In our longitudinal analysis, a high rate of improvement in MIO was observed over a period of 18 months, with normalization of cardiac T2* in 25% of overloaded patients after a tailored chelation therapy. Furthermore, for the first time, myocardial fibrosis was longitudinally studied in a pediatric TM population. Myocardial fibrosis seems to be not progressive at the mid-FU but not reversible over a period of 18 months.

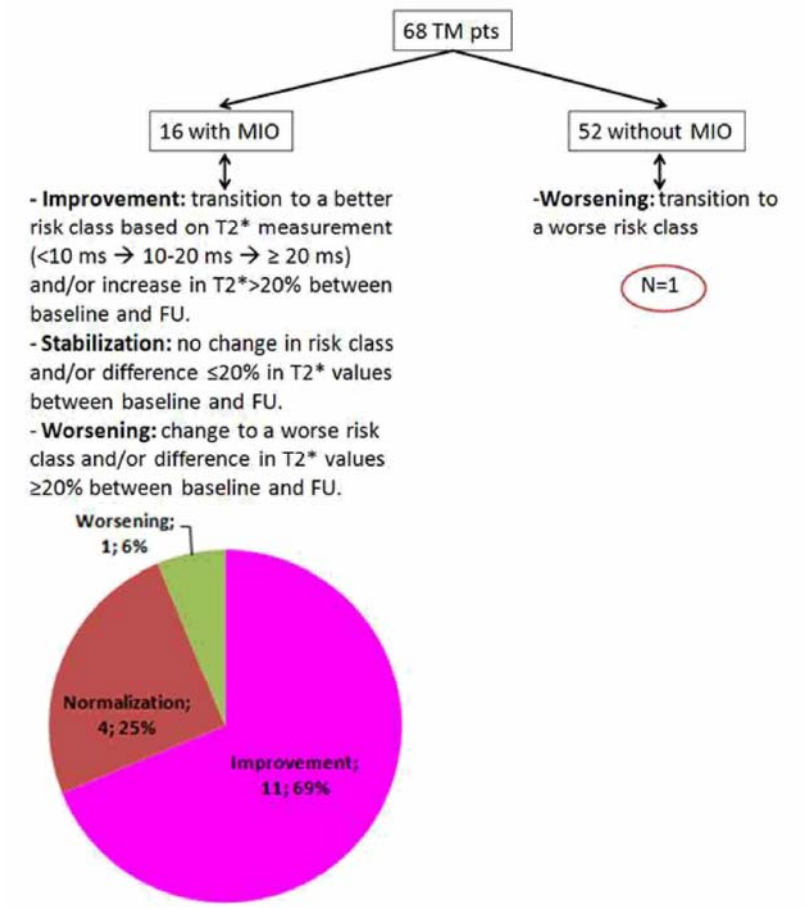

Figure 1

Table 1

Variable	Baseline Value	FU Value	Difference	P-value
Global Heart T2* (ms)	29.72 ± 11.21	31.38 ± 10.32	1.66 ± 6.53	0.031
N. of segments with T2* < 20 ms	4.44 ± 6.06	3.54 ± 5.44	-0.89 ± 3.41	0.046
Mid-septum T2* (ms)	32.49 ± 12.75	34.96 ± 12.97	2.47 ± 9.73	0.052
LV end-diastolic volume index (ml/m2)	93.96 ± 19.26	91.09 ± 21.14	-2.86 ± 19.97	0.027
LV end-systolic volume index (ml/m2)	37.62 ± 10.99	35.65 ± 11.39	-1.97 ± 11.41	0.055
LV stroke volume index (ml/m2)	56.04 ± 11.25	55.38 ± 12.63	-0.66 ± 12.39	0.379
LV mass index (g/m2)	55.14 ± 12.88	60.20 ± 18.49	5.59 ± 19.12	0.012
LV ejection fraction (%)	60.13 ± 6.22	60.93 ± 6.27	0.79 ± 6.83	0.566
RV end-diastolic volume index (ml/m2)	88.97 ± 19.65	82.21 ± 18.32	-6.76 ± 21.15	0.003
RV end-systolic volume index (ml/m2)	33.59 ± 9.89	30.99 ± 11.81	-2.59 ± 13.32	0.014
RV stroke volume index (ml/m2)	55.47 ± 12.59	50.89 ± 10.89	-4.73 ± 13.03	0.003

RV ejection fraction (%)	61.99 ± 6.71	62.51 ± 8.07	0.52 ± 9.05	0.426

ID#: 362315

The strong link between pancreas and heart in thalassemia major.

Alessia Pepe, MD, PhD[1] Laura Pistoia, MSc[1], Massimiliano Missere, MD[2], Antonino Vallone, MD[3], Paolo Preziosi, MD[4], Daniele De Marchi, RT[5], Maria Paola Smacchia, MD[6], Crocetta Argento, MD[7], Antonella Quarta, MD[8], Andrea Olivi, MSc[9], Vincenzo Positano, MSc[1], Antonella Meloni, PhD[1]

1. Fondazione G. Monasterio CNR Regione Toscana, Pisa, Toscana, Italy

2. Fondazione di Ricerca e Cura "Giovanni Paolo II", Campobasso, Molise, Italy

3. Azienda Ospedaliera "Garibaldi" Presidio Ospedaliero Nesima, Catania, Sicilia, Italy

4. Ospedale "Sandro Pertini", Roma, Lazio, Italy

5. Fondazione G. Monasterio CNR Regione Toscana, Toscana, Italy

6. Policlinico Umberto 1, Roma, Lazio, Italy

7. Ospedale “San Giovanni Di Dio”, Agrigento, Sicilia, Italy

8. Ospedale "A.Perrino "Brindisi, Brindisis, Puglia, Italy

9. Fondazione G. Monasterio CNR-Regione Toscana, Pisa, Toscana, Italy

Background: Some preliminary data have postulated a correlation between pancreatic iron overload and heart iron and function in thalassemia major (TM) patients.
In the present study we explored systematically in a multicenter study the link heart-pancreas in a large cohort of TM patients.

Methods: We considered the first 232 TM patients (129 M, mean age 36.95±9.83 years) enrolled in the E-MIOT (Extension-Myocardial Iron Overload in Thalassemia) project.
T2* measurements were performed over pancreatic head, body and tail and global value was the mean. Myocardial iron overload (MIO) was quantified using a T2* segmental approach. Biventricular function parameters were assessed by cine images. Late gadolinium enhancement (LGE) images were acquired to detect myocardial fibrosis.

Results: A significant correlation between pancreatic and cardiac iron was reconfirmed in this more numerous population and a normal pancreas T2* showed negative predictive value of 100% for cardiac iron (Figure 1).
Pancreatic iron was correlated to the LV ejection fraction (EF), but not to the right ventricular (RV) EF.
LGE sequences were acquired in 101 TM patients and 43 (42.57%) of them showed macroscopic myocardial fibrosis. Global pancreas T2* values were significantly lower in patients with fibrosis (6.27±4.12 ms vs 11.15±9.23 ms; P=0.021).
Twenty-two patients showed cardiac complications (11 arrhythmias, 6 heart failure, 2 pulmonary hyperthension, 1 vascular disease, and 2 others) and of them 21 had pancreatic iron. Patients with cardiac complications showed a significant lower global pancreas T2* (7.55±6.11 ms vs 14.31±13.39 ms; P=0.024).

Conclusion: Pancreatic iron is a strong predictor not only for cardiac iron, but also for cardiac complications supporting a more profound link between pancreatic iron and heart disease in TM. More studies are needed to evaluate the prognostic role of pancreatic iron on cardiac complications.

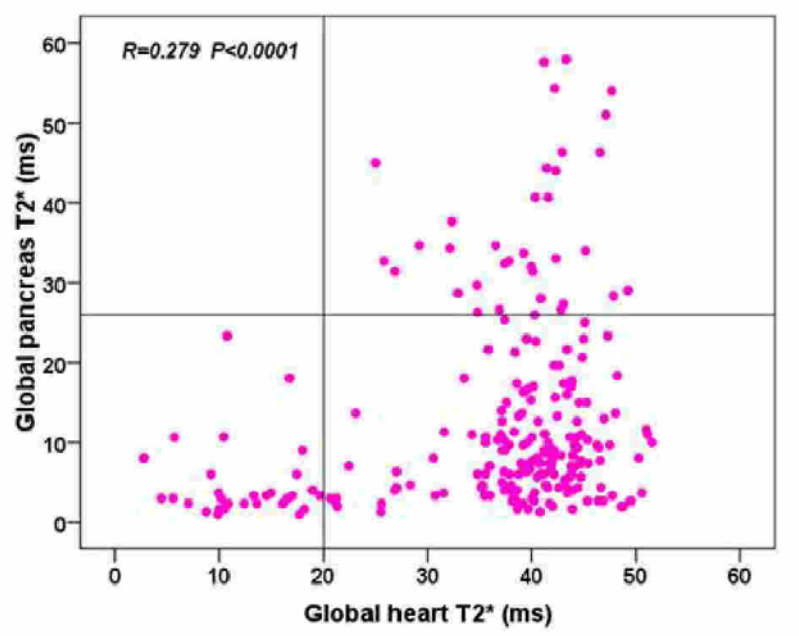
R=0.279 P<0.0001
Global pancreas T2* (ms)
Global heart T2* (ms)
0
10
20
30
40
50
60

Figure 1

ID#: 368637

Prediction of infarct size and adverse cardiac outcomes by tissue tracking-cardiac magnetic resonance imaging in ST-segment elevation myocardial infarction

Yeonyee Elizabeth. Yoon, MD[1] Sang-Eun Lee, MD[2], In-Jeong Cho, MD[2], Hyo Eun Park, MD[3], Jun-Bean Park, MD[3], Wonjae Lee, MD[4], Hong-Mi Choi, MD[4], Goo-Yeong Cho, MD[4], Hyuk-Jae Chang, MD, PhD[2], Eun-Ju Chun, MD[4]

1. Seoul National University Bundang Hospital, Seongma, Republic of Korea

2. Severance Cardiovascular Hospital, Yonsei-Cedar Sinai Integrative Cardiovascular Imaging Research Center, Yeonsei University Health System, Seoul, South Korea, Republic of Korea

3. Seoul National University Hospital, Republic of Korea

4. Seoul National University Bundang Hospital, Republic of Korea

Background: Although there has been increasing interest in the role of myocardial deformation imaging in acute myocardial infarction (MI), most previous studies were performed with speckle tracking echocardiography. In particular, the role of tissue tracking-cardiac magnetic resonance imaging (TT-CMR) in the evaluation of MI patients has never been evaluated. In this study, we investigated whether quantification of global left ventricular (LV) strain by TT-CMR can estimate the infarct size and clinical outcomes in patients with acute MI.

Methods: We retrospectively registered 247 consecutive patients (58±12 years; male, 81%) who underwent concurrent cine and late gadolinium enhanced (LGE) CMR imaging within 1 month after ST-segment elevation MI, and 20 age- and sex-matched controls (58±11 years; male, 80%). TT-CMR analysis was applied to cine images to measure global radial, circumferential, and longitudinal peak strains of LV (GRS, GCS, and GLS, respectively). Adverse cardiac events were defined as cardiac death and hospitalization for heart failure.

Results: During the follow-up (median, 7.8 years), 20 patients (8.1%) experienced adverse events. GRS, GCS, and GLS significantly decreased in MI patients compared to controls (29.5 ± 9.9 vs. 47.4 ± 16.0; p<0.001, -13.1 ± 4.3 vs. -20.2 ± 4.0; p<0.001, -14.0 ± 3.2 vs. -17.4 ± 2.7; p<0.001, respectively) and closely related to LGE extent. (Figure 1) When strain values were evaluated as binary variables divided by their median value, GRS <29.1%, GCS>-13.1%, GLS>-14.1% were the significant predictors for adverse events (HR; 4.391; p=0.008, HR; 4.219; p=0.010, and HR; 9.476; p=0.003, respectively) and were associated with poor event-free survival rates (Figure 2). However, when adjusted to diabetes, LV end-systolic volume index, LV ejection fraction, and LGE extent in the multivariate analysis, only GLS>-14.1% remained as an independent predictor (adjusted HR, 5.709; p =0.003) while GRS<29.1% and GCS >-13.1% were not (adjusted HR, 2.155; p=0.242, and adjusted HR, 2.139; p=0.276, respectively)

Conclusion: Calculations of the GRS, GCS, and GLS by TT-CMR significantly related to the infarct size and composite endpoint of cardiac death and heart failure admission. Especially, our findings suggest that assessment of the GLS provides strong prognostic information in patients with ST-segment elevation MI, even after adjustment for the presence of left ventricular dysfunction and extensive myocardial scar changes.

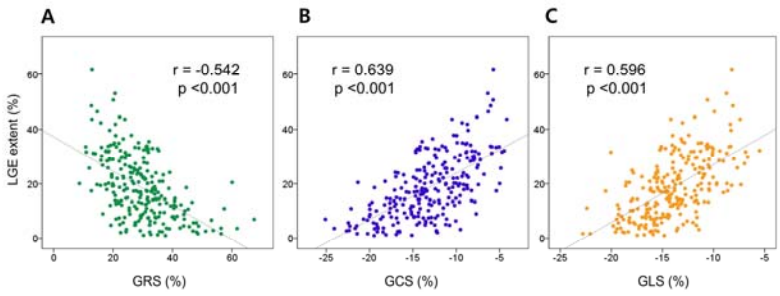

Figure 1. Correlation of the late gadolinium enhancement (LGE) extent and global peak systolic strains (GRS, GCS, and GLS)

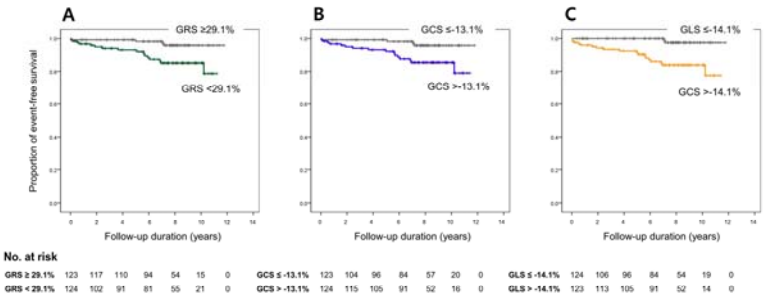

Kaplan-Meier event-free sruvival estimates stratified by GRS, GCS, and GLS

ID#: 368642

Impact of Diffuse Myocardial Fibrosis on Left Ventricular Dysfunction in Patient with Atrial Fibrillation Evaluation with Cardiovascular Magnetic Resonance T1 mapping

Lei Zhao[1] Xiaohai Ma[2]

1. Beijing Anzhen Hospital, Capital Medical University, Beijing, China (People's Republic)

2. Beijing Anzhen Hospital, Capital Medical University, China (People's Republic)

Background: Atrial fibrillation (AF) and heart failure (HF) frequently coexist and both conditions are associated with worse prognosis. The mechanisms linking AF to HF are incompletely understood, but likely include hemodynamic and myocardial factors. Comprehensive cardiovascular magnetic resonance (CMR) can accurately quantify left ventricle (LV) function and myocardial fibrosis. Using CMR T1 mapping, we examined the potential relationship between myocardial fibrosis and LV dysfunction in patients with AF.

Methods: A total of 150 subjects including 50 patients with persistent AF, 50 patients with paroxysmal AF patients, and 50 controls, underwent CMR. Contrast CMR included cine sequences and a histologically validated T1 mapping sequence were performed and analyzed. Left atrial volume (LAV), LV ejection fraction (EF) and circumferential strain indices, LV native T1 time and extracellular volume (ECV) were compared across patient with persistent and paroxysmal AF and controls.

Results: Patients with persistent AF had the worst CMR quantitative parameters (P<0.01). LV native T1 time and ECV correlated with LAV, LV EF and strain indices in paroxysmal and persistent AF patients, respectively (all P<0.05). There were significant differences of LV native T1 time and ECV between AF patients with EF $\geq$50%, EF between 40% and 49%, EF P<0.01). LV native T1 time and ECV had moderate discriminatory ability for identify AF patients from controls; compared within AF patients, LV native T1 time and ECV had moderate to good discriminatory ability for identify AF patients with EF $\geq$50% and identify AF patients with EF <40%.

Conclusion: Diffuse ventricular fibrosis assessed with T1 mapping correlated with declining LV function in patients with AF. CMR assessment of diffuse fibrosis with T1 mapping appears to identify precursors of HF in patients with AF, potentially facilitating future studies focused on HF treatment and prevention in AF.

ID#: 368725

Aortic Remodeling after Anthracycline Therapy

Thiago Ferreira. de Souza, MD, Msc[1] Thiago Quinaglia A. C. Silva, MD, PhD[2], Ravi Shah, MD[3], Tomas G. Neilan, MD, MPH[4], Lício Velloso, MD, PhD[2], Wilson Nadruz, MD, PhD[5], Fabricio P. Brenelli, MD, PhD[5], José Roberto Mattos, MD, PhD[6], Cesar Nomura, MD, PhD[7], Rob J. van der Geest, PhD[8], Michael Jerosch-Herold, PhD[9], OTAVIO R. COELHO-FILHO, MD, PhD, MPH[10]

1. UNICAMP, Campinas, Sao Paulo, Brazil

2. State University of Campinas - UNICAMP, Sao Paulo, Brazil

3. Massachusetts General Hospital, Harvard Medical School, Boston, MA, USA, Newburyport

4. Massachusetts General Hospital, Harvard Medical School, Boston, MA, USA, MA

5. State University of Campinas, Sao Paulo, Brazil

6. State University of Campinas - UNICAMP - UNICAMP, Sao Paulo, Brazil

7. Heart Institute - University of Sao Paulo, Sao Paulo, Brazil

8. Department of Radiology, Leiden University Medical Center, The Netherlands, Leiden, Zuid-Holland, Netherlands

9. Department of Radiology, Brigham & Women`s Hospital & Harvard Medical School, Boston, United States., Boston, MA

10. State University of Campinas - UNICAMP, Campinas, Sao Paulo, Brazil

Background: Anthracycline therapy is commonly associated with adverse effects including irreversible cardiomyopathy, and also vascular remodeling. The nature of vascular remodeling in this setting remains controversial, with some reports demonstrating an increase of pulse wave velocity (PWV), and others a decrease. The goal of this study was to investigate the vascular remodeling using PWV by cardiac magnetic resonance (CMR) imaging in breast cancer patients treated with anthracycline (240 mg/m^2).

Methods: Twenty-seven women with breast cancer (mean-age 51.8±8.9 years, BMI 26.9±3.6 kg/m^2), underwent CMR prior, and up to 3-times after anthracycline, for assessment of left ventricular ejection fraction (LVEF), mass, volumes, maximal left atrial (LA) volume, a marker of diastolic dysfunction, and PWV measured in the aortic arch, using a phase-contrast technique.

Results: At baseline, all subjects had normal LVEF (69.4±3.6%), LV mass-index (51.4±8.0g/m^2), PWV (6.26±2.35m/s) and aortic wall thickness (2.55±0.49mm). At (351-700] days after anthracycline, LVEF and LV mass-index declined significantly to 58±6% and 36±6 g/m^2 respectively (all, $P<0.001$). PWV at baseline was associated with age ($\rho=0.85$; P<1e-4, Figure 1), triglycerides ($\rho=0.60$; P<1e-3), total-cholesterol ($\rho=0.36$; P=0.04), creatinine (P=0.024), serum urea ($\rho=0.48$; P=0.004), and LA-volume index ($\rho=-0.32$, P=0.004). PWV decreased significantly after anthracyclines only after the follow-up periods reached (231,368] and (368,700] days post-anthracycline (P=0.03 and P=0.01, respectively; Figure 2). PWV remained negatively associated with LA volume index at baseline (P=0.029) with simultaneous adjustment by age (P<0.001), but after anthracyclines this association became significantly weaker (P=0.009), suggesting that the change of PWV post-anthracyclines is unrelated to LA indices of diastolic dysfunction (Figure 3). Interestingly, serum triglycerides above its median at baseline identified patients who experienced a significant decline of PWV after anthracyclines (P<0.01) as illustrated in Figure 4.

Conclusion: The decrease of PWV after anthracycline therapy may be associated with lipid disturbances associated with anthracycline therapy. Triglycerides play a prominent role in negative vascular remodeling, and our findings suggest that particularly patients with high triglycerides levels before therapy may undergo a decrease of PWV after anthracyclines, independent of the degree of any pre-existing diastolic dysfunction and age.

Figure 1

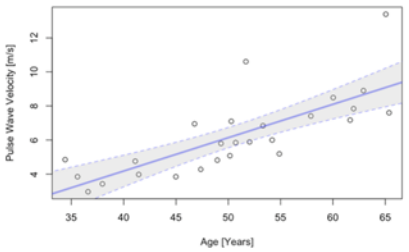

Figure 2

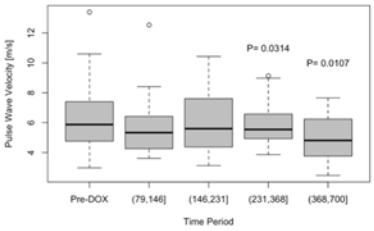

Figure 3

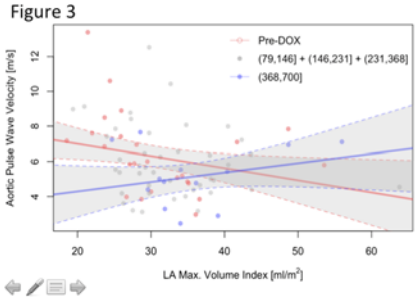

Figure 4

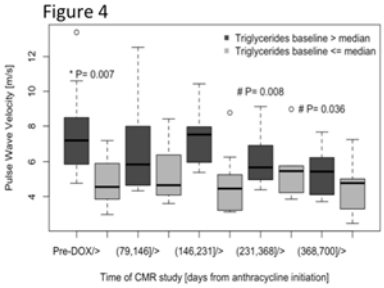

ID#: 368766

Quantifying Inflammation in Atherosclerotic Plaque: a Fluorine-19 MRI Mouse Study at 3T

Roberto Colotti[1] Emeline Darçot[2], Maxime Pellegrin, PhD[2], Anne Wilson, PhD[2], Stefanie Siegert, PhD[2], Jerome Yerly, PhD[3], Matthias Stuber, PhD[3], Ruud B. van Heeswijk, PhD[2]

1. Lausanne University Hospital (CHUV), Lausanne, Vaud, Switzerland

2. Lausanne University Hospital (CHUV), Switzerland

3. Center for Biomedical Imaging (CIBM), Lausanne, Switzerland, Vaud, Switzerland

Background: One of the ultimate goals of fluorine-19 (^{19}F) MRI of perfluorocarbon (PFC) emulsions is direct quantification and monitoring of inflammation in diseases such as atherosclerosis in patients in a clinical setting [1, 2]. In this light, we here aimed to: 1) demonstrate the feasibility of quantitative ^{19}F MRI in small inflammation foci (atherosclerotic plaques) at 3T, and 2) characterize and visualize the PFC-incorporating immune cell populations involved in the inflammation process.

Methods: Apolipoprotein-E-knockout (ApoE$^{-/-}$) mice were fed with a high-fat diet to exacerbate atherosclerosis. Thirteen animals received 2×200µL of perfluoropolyether (PFPE, Celsense) intravenously. All experiments were performed on a 3T clinical system (Siemens Prisma). A ^{19}F/^{1}H volume RF coil and an external reference (concentration C_{PFC}=22mM) were used for absolute quantification. ECG-triggered 2D ^{1}H GRE imaging was used to visualize the anatomy. ^{19}F images were obtained using an optimized 3D TSE pulse sequence [3]. After ^{19}F-^{1}H co-registration, the plaques were manually segmented, and their ^{19}F SNR, signal-volume, SNR-signal-volume product (i.e. the ^{19}F signal-integral), and PFC concentration were quantified. Five additional ApoE$^{-/-}$ mice were injected with fluorescein-isothiocyanate (FITC) PFPE and five control ApoE$^{-/-}$ mice were injected with non-fluorescent-PFPE for post-mortem imaging flow cytometry (ImageStream) [4] to characterize the small leukocyte population sizes.

Results: While their in vivo SNR was low at 5.4±1.8, ^{19}F MR hotspots were detected in the aorta or its branches in all mice (Fig.1). The absolute PFC concentration by MRI was 0.7±0.3mM, the plaque signal-volume 2.1±1.3mm^3 and the ^{19}F signal-integral 12.2±8.7mm^3. Among leukocytes, the PFC-labeled cells were mainly dendritic cells, macrophages and neutrophils at a ratio of 9:1:1. Small PFC spots were observed in macrophages (area=4.6±4.2µm^2, relative brightness=16.4±13.7) and neutrophils (area=3.7±1.8µm^2, relative brightness=16.5±9.8), as opposed to the dendritic cells (area=22.0±18.0µm^2, relative brightness=70.0±54.9, Fig.2). The PFC signal-integral (area*relative brightness) for dendritic cells was ~20× higher than for macrophages and neutrophils.

Conclusion: ^{19}F MR allowed for the noninvasive quantification of PFC and thus inflammation in atherosclerotic plaques in mice at clinical magnetic field strength. Imaging flow cytometry demonstrated that the advanced plaques studied here contained more dendritic cells than macrophages, which agrees well with previous studies [5]. Surprisingly, a significant population of CD45-negative cells (i.e. not leukocytes) took up the PFC nanoparticles - this population might include fibroblasts, epithelial cells or leukocytes that lost their receptors. In conclusion, we have developed a quantitative ^{19}F MRI technique for inflammation studies on a human MRI system, which will aid the translation to the human setting. **References.** [1] Chen et al., Nanomed Nanobiotechnol 2010 [2] van Heeswijk et al., Radiology 2015, [3] Colotti et al., MRM 2017 [4] Basiji et al., J Immunol Methods 2015 [5] Choi et al., Immunity 2011.

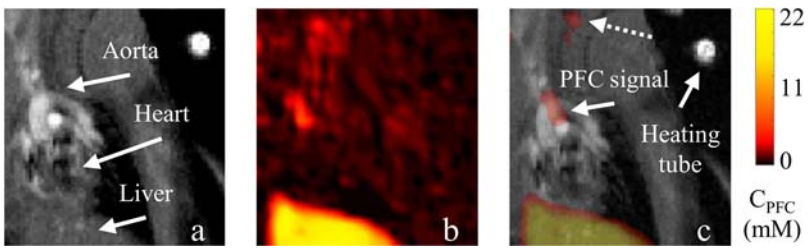

Figure 1. In vivo quantification of PFC in atherosclerotic plaques at 3T. a) In-vivo 1H double oblique MR image

through the liver, the heart and the aorta and b) corresponding 19F MR image. The color bar indicates the PFC concentration CPFC. The 19F MR dataset has been normalized to the known CPFC of the external reference. 19F MRI showed a patchy PFC distribution with hotspots mainly in the aortic arch and its branches (brachiocephalic and left subclavian arteries). c) The 19F/1H fusion MR image shows a plaque in the aortic arch, indicated by the solid arrow. 19F signal was also observed in the subcutaneous fat, where the anesthetic isoflurane accumulates (dotted arrow).

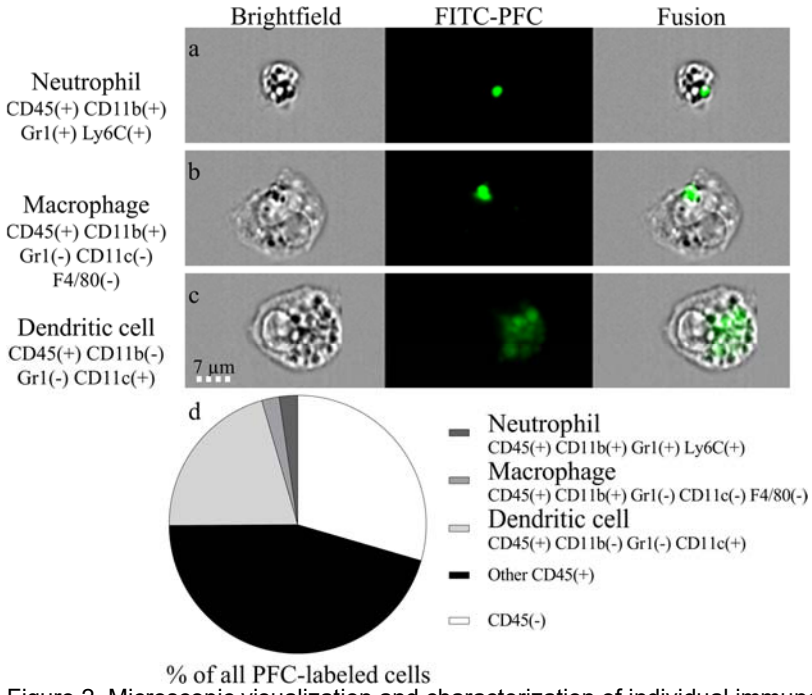

Figure 2. Microscopic visualization and characterization of individual immune cells that took up the PFC nanoparticles. For simplicity, only one anatomical and one fluorescent channel are shown in this image - from left to right: brightfield (gray), FITC-PFC (green) and their fusion. a) An example of a neutrophil, b) macrophage and c) dendritic cell with internalized PFC nanoparticles. d) The dendritic cells constituted a high percentage of the PFC-labeled cells (20.6%), while a similar low percentage of macrophages and neutrophils was measured (~2.3%). 45.4% of the CD45-positive events were not specifically classified, while 29.5% of the PFC-labeled cells were CD45-negative, i.e. not leukocytes.

ID#: 368769

Assessment of focal myocardial scar by native T1 value and extra cellular volume in patient with cardiac sarcoidosis: comparison with late gadolinium enhancement cardiac imaging.

Makito Sato, MD[1] Yoshiaki Ohyama, MD, PhD[2], Masahiko Kurabayashi, MD, PhD[3]

1. Gunma University Hospital, Maebashi City, Gumma, Japan

2. Clinical Investigation and Research Unit, Gunma University Hospital, Japan

3. Gunma University Hospital, Gumma, Japan

Background: Late gadolinium enhancement (LGE) is an essential part of a cardiac MRI examination to evaluate myocardial scar in patients with cardiac sarcoidosis. T1 mapping technique has been developed and established especially for diffuse cardiomyopathies, while there is few study for focal assessment of myocardial injury or fibrosis using T1 map. We examined whether T1 mapping technique can apply for focal myocardial scar quantitatively in patients with cardiac sarcoidosis using 3T MRI imaging.

Methods: We retrospectively examined patients with known or suspected cardiac sarcoidosis who underwent Gd-enhanced cardiac MRI (Skyra 3T, Siemens) for assessment of cardiac involvement from May 2015 to June 2017. Pixel based T1 value was obtained by MyoMaps technique in mid portion of left ventricular short axis before and after contrast enhance. Focal T1 value was measured by using 10mm^2 circular region of interest, which are placed center of each myocardium according to AHA 17-segmentation model (Figure1). Native T1 value and extra cellular volume (ECV) that was calculated from pre and post contrast T1 value and hematocrit were obtained in each patients and segments. Late gadolinium enhancement (LGE) was assessed semi-quantitatively at the same slice of MyoMaps, by grading each segments according to maximum invasion depth of enhancement (group 0: no LGE involvement, group 1: ≤25%, group 2: 26-50%, group 3: 51-75%, group 4: >75%).

Results: After excluding cases with lack of data or severe artifacts, 174 segments in 29 patients (aged 61+/-12 years, 8 men) were eligible for the study. Of 29 patients, 16 patients were LGE positive. In segment analysis, higher focal native T1 value was associated with higher grade of LGE involvements (group 0: n=130, native T1= 1220+/-62, group 1: n=13, 1277+/-63, group 2: n=16, 1298+/-78, group 3: n=9, 1422+/-122, group 4: n=6, 1461+/-152; p trend < 0.001) (Figure2). Greater ECV was also associated with higher grade of LGE (group 0: 27.2+/-3.3 (%), group 1: 27.8+/-2.6, group 2: 33.4+/-10.8, group 3: 49.0+/-14.8, group 4: 53.6+/-19.5; p trend < 0.001) (Figure2). The ROC curve for focal native T1 and focal ECV to detect deep LGE involvement (segments classified as Group 3 or 4) shows their high accuracy to detect myocardial injury (Figure3).

Conclusion: Focal assessment of native T1 and ECV is highly correlated with focal LGE. Native T1 assessment may be an alternative technique for the assessment of left ventricular scar quantification in patients with contraindication of contrasts.

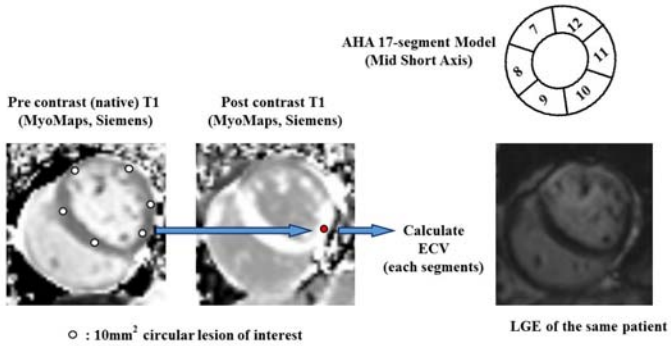

Figure1: Focal native T1 and ECV assessment

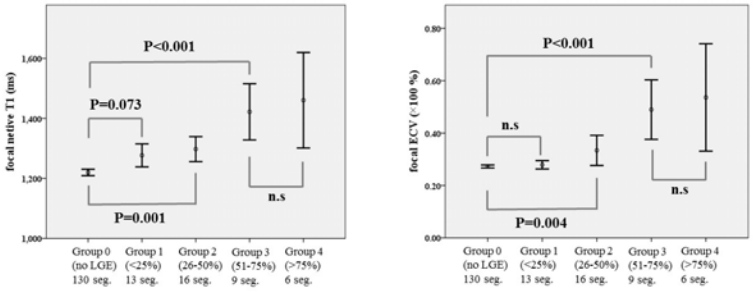

Figure2: LGE grade and native T1 value or ECV in each segment

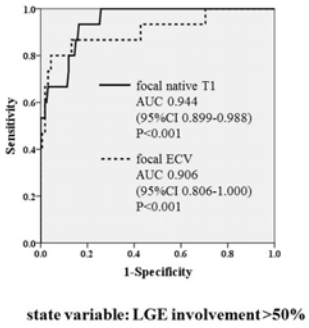

Figure3: ROC curve (per segment analysis)

ID#: 368961

The CMR Impact on Pacemaker/ICD Parameters; an in vivo Reproducibility Study Pre and Post MRI; Cause for Alarm?

Robert W. Biederman, MD, FACC, FAHA[1] Loretta Gevenosky, R.N.[1], Ronald Williams, RT(R)(MR), B.A.[1], Richard Lombardi, RT (mr)(r)[2], Christopher Bonnet, M.D.[1], Moneal Shah, M.D.[3], Mark Doyle, Ph.D.[1]

1. Allegheny General Hospital, Pittsburgh, PA

2. Allegheny General Hospital

3. Allegheny General Hospital, pittsburgh, PA

Background: The evolution of pacemaker/ICD safety in the MRI field has triggered considerable interest in the possibility of more routine use. However, several limitations to widespread adoption of this seemingly implausible concept just a few years ago remain. Chief among them is the unresolved impact of high magnetic field, RF amplitude and oscillatory forces on the electronics with possible high field damage on the capacitor, solenoid and other microcircuitry. However, given recent vender refinements and improved shielding over the last 10 years, we hypothesized that the impact on such circuitry may be far less than expected.

Methods: Systematic interrogation of consecutive pts who underwent clinically indicated MRI were evaluated over 24 months. Routine interrogation was performed within 10 minutes prior to entry into the bore of a dedicated CMR scanner (GE, I.5T, WI). As well, re-interrogation was performed within 10 minutes after departure of the MRI. At time of interrogation pre and post MRI, a separate, repeat interrogation was performed within 5 in of each other such that 2 sets of PM/ICD parameters were obtained (total=4). A cardiologist guided interrogation, configuration and reconfiguration of the pacemaker/ICD';s and was present for entire scan.

Results: No complications to either pt or device occurred during any of 276 MRI';s. Altogether, 161 PM and 115 ICD';s underwent MRI';s (avg 22±13mm). This cohort was comprised of neuro/neurosurgical (70%), orthopedic (11%) and cardiac (19%) cases. There were no differences in any PM/ICD parameter(s) when compared in any order pre to post MRI scan, see Table.

Conclusion: Intrinsic variability and inherent changes triggered by the MRI environment are statistically and clinically negligible thereby removing yet another of the remaining fears and apprehensions for primary pacemaker/ICD failure and destruction as we move towards a more uniform acceptance of this technology for clinically meaningful use and acceptance.

Region	Pacer Variable	Pre	Post	p (Pre-Post)
Atria	Impedance	455±109	453±109	0.35
	Sensing	2.98±1.71	3.19±2.05	0.98
	Threshold (Amplitude)	0.79±0.42	0.81±0.43	0.25
	Threshold (Pulse Width)	0.45±0.11	0.44±0.05	0.11
RV	Impedance	499±117.09	490±117.75	0.04
	Sensing	10.46±14.27	16.67±53.23	0.12
	Threshold (Amplitude)	0.91±0.78	0.87±0.35	0.35
	Threshold (Pulse Width)	0.53±0.71	0.48±0.15	0.26
LV	Impedance	648±190.17	663±185.01	0.13
	Threshold (Amplitude)	1.05±0.54	1.03±0.51	0.17
	Threshold (Pulse Width)	0.59±0.24	0.57±0.24	0.29

ID#: 368973

When Ordered by LVEF, Internal and External Energy Expenditure Exhibit a Strong Periodicity in the Cardiovascular System; a New Paradigm?

Robert W. Biederman, MD, FACC, FAHA[1]Mark Doyle, Ph.D.[1], Geetha Rayarao, M.S.[2], Victor Farah, MD[1]

1. Allegheny General Hospital, Pittsburgh, PA

2. Allegheny General Hospital, PIttsburgh, PA

Background: Recently, we showed that a cardiovascular impedance index (Im) could be derived from cardiovascular magnetic resonance (CMR) imaging measurements of aortic flow. The Im varied in a distinctively periodic manner over multiple patients when arranged by left ventricular (LV) ejection fraction (EF) leading to a distinct pattern of periodic discontinuities. We hypothesize that a relationship exists between internal and external energy expenditure of the left ventricle with respect to the Im positions of discontinuity, as ascertained by CMR.

Methods: Data from male and female subjects (n= 112) who underwent CMR imaging was obtained to calculate internal energy (end-systolic volume x pulse pressure) and external energy (stroke volume x pulse pressure). Both internal and external energy were plotted with respect to EF, and positions of transition of the impedance index were noted on these plots.

Results: The internal energy exhibited a gradual increase with decreasing EF, while the external energy exhibited a gradual decrease with decreasing EF (Figure la and b). In addition to these overall trends, internal and external energy expenditure curves exhibited 4 major peaks of elevated expenditure (—100% change from baseline). The two central peaks occurred at transition positions of the Imi, while the upper and lower major peaks occurred at the mid-point between higher and lower impedance transition points.

Conclusion: The cardiovascular impedance index imposes a unique and unforseen periodicity on the energy expenditure of the heart detectable via CMR corresponding to high intensity peaks at predictable positions with respect to the impedance index. Unexpectedly, physical properties of the heart appear to be governed more by harmonic principles similar to other solid, not classical fluid, mechanical structures or physiology. Herein, on and off-resonance dictates cardiac performance more than classical cardiac physiology. Potentially, subsequent patient outcomes may be similarly governed.

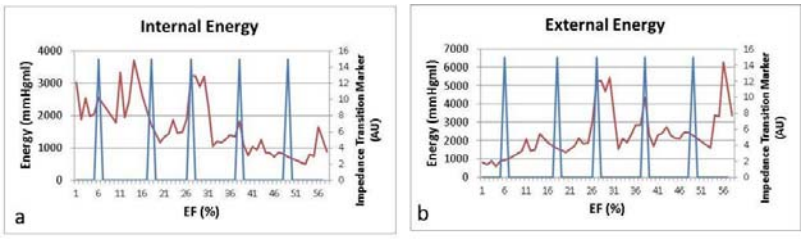

Table 1

ID#: 368979

Metallic Implants in the MRI Environment; Effect on Loops, Stimulators and Retained Pacemaker/ICD Leads

Robert W. Biederman, MD, FACC, FAHA[2]Prabhakaran Gopalakrishnan, M.D.[1], Loretta Gevenosky, R.N.[2], Ronald Williams, RT(R)(MR), B.A.[2], Richard Lombardi, RT (mr)(r)[1], Moneal Shah, M.D.[3], Christopher Bonnet, M.D.[2], Mark Doyle, Ph.D.[2]

1. Allegheny General Hospital

2. Allegheny General Hospital, Pittsburgh, PA

3. Allegheny General Hospital, pittsburgh, PA

Background: Performance of MRI is infrequently conducted on patients with metallic devices/objects within the body. However, recent work has suggested that with an appropriate protocol, pacemakers/ICD';s may in fact be considerably safer than previously considered. However, it is clear that we can extrapolate that notion to other metallic devices and retained leads. In principle, these may have even less ability to be manipulated to 'safe'; or 'safer'; MRI modes. Hypothesis: We propose that MRI in patients with loops, stimulators and retained pacemaker/ICD leads potentially may be safer than previously thought.

Methods: An evaluation of consecutive patients with Loops/Linqs recorders, stimulators and retained pacemaker/ICD leads underwent MR (GE 1.5T Excite,WI) over ~5 years. Great care was taken to maintain acceptable SAR (W/kg) bore and reduce induced electromagnetic RF potentials. Additionally, BP, HR, 02 saturations, as well as, visual monitoring was performed after informed consent with both patient and family members was obtained.

Results: The average MRI was 35±9min for the cohort of 50 patients representing 62 MRI exams. The devices consisted of: 9 Loops/Linqs, 28 neurostimulators (brain and vagal nerve), 2 bladder stimulators, 1 gastric stimulator and 10 retained/fragmented pacemaker/ICD leads. This represents 32 neuro/neurosurgical cases, 13 cardiac and 3 musculoskeletal cases. There was no (0%) immediate (peri-MRI exam) morbidity/mortality. Local follow-up data was available in 79% with a mean of 396±650 days (median 256 days; 5 days-10.9 years) and no (0%) short term (>1 year) device-related complications. Importantly, with careful attention to positioning and scanner sequences, no safety or device issues were encountered in any patient to include those few patients that under went repeat scans (>1 MRI scan in 9 patients).

Conclusion: In this early experience, we show that loop recorders, stimulators and retained pacemaker/ICD leads appear safe when combined with similar considerations for intact PM/ICD';s interrogations even when imaging within the thoracic cavity and heart. To our knowledge, this is the first study to comprehensively evaluate all such non-intact PM/ICD devices, stimulators, recorders and retained fragments and to recognize safety.

ID#: 366897

Integration of 4D-Flow into routine clinical practice of congenital and non-congenital cardiac MRI-18 months experience demonstrating decreased scan times, physician monitoring, and patient breath hold times.

Melany B. Atkins, MD

Fairfax Radiological Consultants, Inova Fairfax Hospital, Arlington, VA

Background: Phase Contrast Imaging is paramount for evaluation of flow dynamics in congenital heart disease as well as valvular disease and is a widely accepted technique in routine clinical practice. Traditional 2D phase contrast imaging is a time-consuming process that requires constant physician monitoring, advanced technologist training, and repetitive scans most commonly requiring patient breath holding. More recent technological advancements in 3D-phase contrast imaging capable of cardiac-phase-resolved whole-volume velocity encoding in three dimensions, referred to as 4D flow, allows for comprehensive flow analysis with ease of acquisition, less physician oversight, and lack of breathholding.

Methods: 237 patients were scanned (189 on a GE 3T Signa Architect system and 48 on a GE 3T 750W) utilizing the 4D-Flow sequence after the administration of intravenous gadolinium or Fereheme. 17 patients received IV Fereheme administered as a 3mg/kg dose diluted as 1 part Fereheme to 4 parts saline via injector at 2cc/sec, among which 1 patient developed diffuse hives after Fereheme injection requiring 50mg IV Benadryl. 215 patients received intravenous Gadovist. 5 patients received dual injection with Gadovist followed by Fereheme. All post-processing (e.g. eddy current phase correction and flow measurements) was performed utilizing Arterys.

Results: Of the 237 patients, the 4D flow sequence failed on 4 patients due to severe cardiac arrhythmia. 4 scans demonstrate aliasing, limiting image processing. The flow analysis successfully processed on the remaining 229 patients. 25 patients had previous cardiac MRI exams utilizing 2D phase contrast. Average total exam time with 4D Flow was 52 minutes. Average total exam time of the prior studies utilizing 2D phase contrast was 71 minutes.

Conclusion: 4D-Flow imaging is an invaluable tool for acquiring flow data, in adult and pediatric congenital heart disease as well as in valvular heart disease, that has been integrated into our routine clinical outpatient practice. We found decreased exam time most notable in our adult and pediatric congenital population and significantly improved flow imaging with reduced failure rate compared to conventional 2D phase contrast. The utilization of Fereheme allows for improved contrast and resolution over Gadovist; however, both agents afford the ability to evaluate flow dynamics and function in the entire volume set. For patients requiring both delayed enhancement imaging and flow, the dual injection protocol is a time effective way to acquire both data sets. The integration of 4D flow with free breathing acquisition has allowed us to image younger patients without anesthesia and reduced the need for physician monitoring.

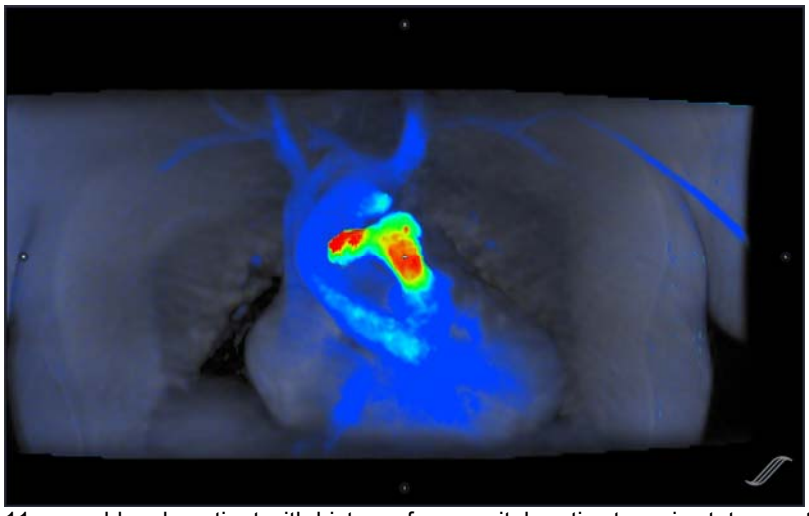

11 year old male patient with history of congenital aortic stenosis status post Ross procedure. 3D image demonstrates mild pulmonic stenosis. The total imaging time utilizing 4D flow was 36 minutes. The prior examination utilizing 2D phase contrast took 81 minutes for a total time savings of 45 minutes.

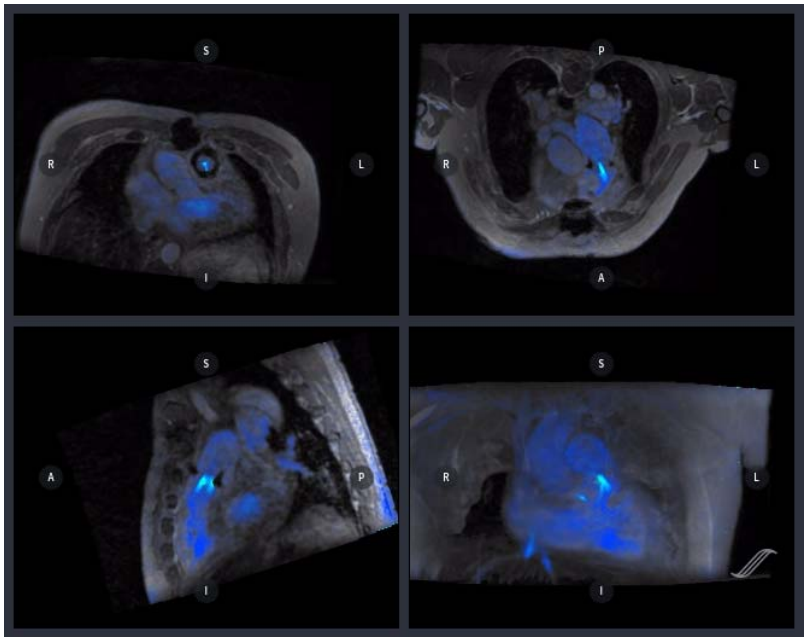

56 year old male with history of Tetrology of Fallot status post repair and pulmonic valve replacement 6 years prior. End-systolic images demonstrate mild pulmonic regurgitation and trivial aortic regurgitation. Scan time for this study was 30 minutes. The prior examination required 58 minutes.

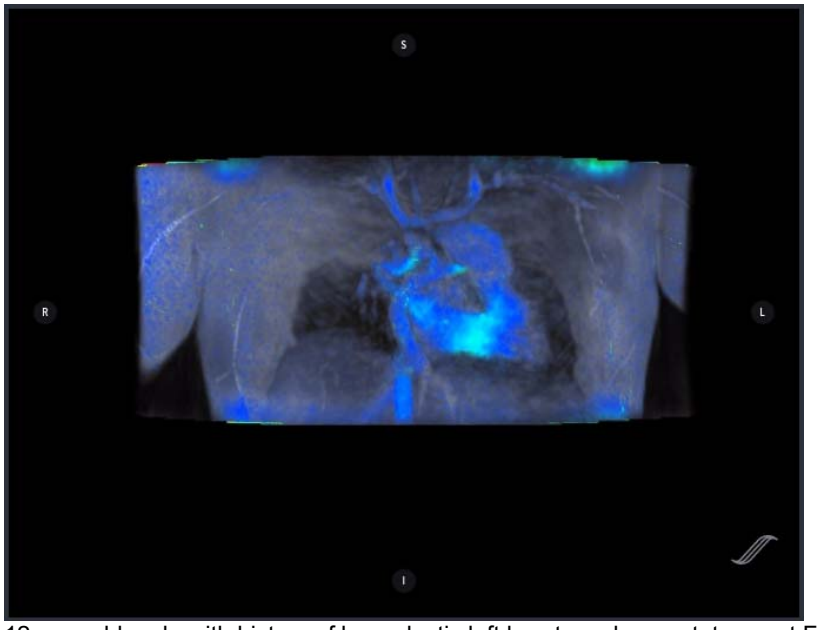

12 year old male with history of hypoplastic left heart syndrome status post Fontan. 3D image demonstrating a patent Fontan. This examination required 51 minutes to complete. The prior examination was completed in 55 minutes with limited phase contrast data due to patient's inability to breath hold and motion.

ID#: 367188

Absence of T1 hyperintensity in the brain of high-risk iron loaded thalassemia patients after multiple high doses of Gadobutrol for cardiac LGE

Alessia Pepe, MD, PhD[1] Antonella Meloni, PhD[1], Domenico Montanaro, MD[2], Daniele De Marchi, RT[3], Petra Keilberg, RT[3], Laura Pistoia, MSc[1], Anna Spasiano, MD[4], Tommaso Casini, MD[5], Caterina Cinzia De Bari, MD[6], Sara De Cori, MD[2], Vincenzo Positano, MSc[1]

1. Fondazione G. Monasterio CNR Regione Toscana, Pisa, Toscana, Italy

2. Fondazione G. Monasterio CNR-Regione Toscana, Pisa, Toscana, Italy

3. Fondazione G. Monasterio CNR Regione Toscana, Toscana, Italy

4. Azienda Ospedaliera di Rilievo Nazionale "A. Cardarelli", Napoli, Campania, Italy

5. Ospedale "Meyer", Firenze, Toscana, Italy

6. Ospedale, Arezzo, Toscana, Italy

Background: Late gadolinium enhancement (LGE) cardiovascular magnetic resonance (CMR) is a unique non-invasive technique validated to detect necrosis/fibrosis. However, many studies have reported an association between increased signal intensities (SI) on unenhanced T1-weighted MR images in different brain regions and the history of repeated intravenous administrations of Gadolinium based contrast agents (GBCA) in patients with normal renal function.
We conducted a prospective study aimed to evaluate signal changes in the dentate nucleus (DN), globus pallidus (GP), pons, and thalamus (normalized to the deep cerebellum white matter) in T1-MRI images after serial injections of Gadobutrol for the LGE-CMR in patients with thalassemia.

Methods: Among the thalassemic patients who underwent a brain MR within a pilot study for iron overload assessment, we selected two groups of patients: 15 patients transfused and chelated with≥4 Gadobutrol administrations at a high dose (0.2 mmol/Kg per scan), 8 thalassemia patients who never received Gadobutrol. Moreover, we included 13 healthy subjects who never received Gadobutrol as control group. All three groups were scanned at 1.5T and 3T.
Iron overload was assessed by the T2* technique.

Results: Signal intensity (SI) ratios at 1.5T in all regions were comparable among the three groups (see Table) and were not correlated with the number of Gadobutol administrations. No correlation was detected between SI ratios and T2* values.
SI ratios at 1.5 T were significantly higher and not correlated with SI ratios at 3T.

Conclusion: It is important to underline that thalassemia patients represent an high-risk population for the GBCA accumulation, due to the fact that, in presence of siderosis, ferric ions can compete with Gadolinium ions for the ligand, destabilizing the gadolinium complex. Nevertheless, our study describes the lack of increased SI after repeated administration of Gadobutrol, a nonionic macrocyclic agent. All our patients were chelated when they received the GBCA. Different studies showed the ability of all three iron chelators to chelate other metals. So, a potential role of chelation therapy may be supposed.
Moreover, it is highlighted that SI ratios in the sampled areas differ between 1.5T and 3T.

Anatomical region	Controls	Thalassemia patients GBCA-naïve	Thalassemia patients with 4≥GBCA adm.	P-value
DN/cerebellum	1.06 ± 0.05	1.03 ± 0.03	1.04 ± 0.04	0.198
GP/cerebellum	1.12 ± 0.04	1.14 ± 0.06	1.14 ± 0.04	0.354
Pons/cerebellum	0.99 ± 0.03	1.02 ± 0.04	1.01 ± 0.04	0.098
Thalamus/cerebellum	1.04 ± 0.07	1.08 ± 0.05	1.09 ± 0.05	0.051

ID#: 367365

Effect of General Anesthesia on Cardiac Magnetic Resonance Derived Cardiac Function in Tetralogy of Fallot.

Steve Muyskens, MD, FACC[1] Tony Roshan, OMS-II[2], Kevin Honan, OMS-II[2], Johnbosco Umejiego, MPH[3]

1. Cook Children's Medical Center, Fort Worth, TX

2. Texas College of Osteopathic Medicine, University of North Texas Health Sciences Center

3. Cook Children's Medical Center

Background: Surgical palliation of tetralogy of Fallot (TOF) results in excellent short-term survival, however, residual defects result in increased long-term mortality. Depressed right ventricular (RV) and left ventricular (LV) ejection fractions (EF) are associated with adverse outcomes. While cardiac magnetic resonance (CMR) imaging is the preferred modality to assess these patients, some may require sedation for successful data acquisition. General anesthesia (GA) has been shown to depress EF and heart rate (HR) in animal models, however, the effect in patients with congenital heart disease has not been well described.

Methods: A retrospective review was conducted of all CMR patients referred with TOF between January 1, 2011, and May 31, 2017. Patients with significant aortic or mitral valve disease, history of cardiomyopathy, undergoing conscious sedation, or receiving inotropic support were excluded. The cohort was separated into GA and non-sedated groups. A standard anesthetic regimen using sevoflurane was used in all patients. Propensity score matching (PSM) was utilized to adjust for selection bias. The kernel matching algorithm was used in matched subjects to calculate the mean differences in LVEF, RVEF, HR, and cardiac index (CI).

Results: A total of 114 patients met criteria, 31 patients were administered GA (mean age 15 years, range 2 - 45, 48% male) while 83 patients received no sedation (mean age 19 years, range 11 - 53, 53% male). The unmatched analysis showed a significant depression in LVEF (49.9 vs 56.8%, $p<0.001$), RVEF (42.1 vs 47.2%, $p<0.001$), and CI (3039 vs 3414 ml/min/m2, $p=0.03$) in the GA group. There was no significant difference in HR (75.9 vs 74.9 bpm, $p=0.86$). Patients were then matched by age, body surface area, QRS duration, and echo derived pulmonary regurgitation, pulmonary stenosis, RV dilation, and LVEF. After PSM adjustment, the GA group had a decrease of 9.7% (47.8 vs 57.5%, $p=0.007$), 8.3% (40.9 vs 49.2%, $p<0.001$) and 1344 ml/min/m2 (2715 vs 4059 ml/min/m2, $p<0.001$) in LVEF, RVEF, and CI respectively. There was a notable trend in HR depression (71.0 vs 81.8 bpm, $p=0.243$) between the groups, but this was not statistically significant.

Conclusion: General anesthesia with sevoflurane results in myocardial depression and significantly depressed CMR derived LVEF, RVEF, and CI. Furthermore, it may be inappropriate to use this data to determining surgical timing for pulmonary valve replacement. Additional studies examining the effect of GA and the use of alternative sedation protocols should be conducted.

ID#: 370108

Left-Ventricular Strain Measured by 2D vs 3D Tissue Tracking Requires Separate Normal Values

Volker Rasche, PhDYangyang Qu, MSc, Jan Paul, PhD, Dominik Buckert, MD, PhD

University Hospital of Ulm, Ulm, Baden-Wurttemberg, Germany

Background: CMR strain analysis by tissue tracking provides additional insight into left-ventricular (LV) mechanical function. Reference values for volunteers without history of cardiovascular disease are required as important step towards broad clinical application.
As different tissue tracking algorithms are available, the dependency of the respective reference values needs to be investigated. In this study, we investigate and compare global and regional strain values obtained from 2D and 3D tissue tracking algorithms.

Methods: 150 adult healthy volunteers were investigated. Global and regional peak strain (radial, circumferential and longitudinal) was derived by post-hoc CMR tissue tracking (cvi42 v5.3.8, Circle, Calgary, Canada) in standard steady-state free precession (SSFP) cine images acquired at 1.5T. Strain was calculated in the 17-segment AHA model applying 2D (short axis stack or long axes separately) and 3D (short axis stack and long axis 2-, 3-, 4-chamber view) tracking. Segments with clearly incorrect results (i.e. negative radial, positive circumferential or longitudinal strain) were excluded on a per-patient basis.
Reproducibility was assessed per segment by analysis of the Intraclass Correlation Coefficient (ICC) based on the re-evaluation of 20 volunteers two month after initial analysis.

Results: Global peak strains (average of 16 segmental peak strains) resulted as 47.6% ± 9.4% vs 48.1% ± 13.5% for radial, -23.6% ± 2.7% vs -17.4% ± 2.6% for circumferential, and -21.2% ± 3.2% vs -16.2% ± 2.3% for longitudinal shortening as obtained by 2D and 3D tracking, respectively. The results were significantly different except for the radial direction.
From a total of 2400 (150 patients * 16 segments) analyzed segments, with 2D/3D tracking 14/4 (radial), 211/2 (circumferential), and 213/8 (longitudinal) segments had to be excluded. In 2D tracking, especially values from basal segments appeared more erroneous. Regional peak strain was significantly different between 2D and 3D tracking for almost all segments across all directions. No systematic tendency of over-/underestimation of strain between the different methods was apparent.
Segmental ICC analysis ranged from 0.83-0.98/0.93-0.99 (radial), 0.76-0.98/0.93-1.00 (circumferential), and 0.62-0.99/0.91-0.99 (longitudinal) for 2D/3D tracking, respectively.

Conclusion: Global and regional strain differed significantly between the 2D and 3D tracking approach, indicating the necessity of algorithm-specific reference values. Considering the higher reproducibility and lower exclusion rates by inclusion of the long axis cine data, 3D tracking appears superior and should be preferred.

Peak radial strain (%)	2D	n_{2D}	3D	n_{3D}	p value: 2D vs 3D
1. Basal anterior	51.1 ± 17.9	150 (100.0%)	59.3 ± 24.7	150 (100.0%)	0.004
2. Basal anteroseptal	27.8 ± 13.2	150 (100.0%)	31.8 ± 15.1	150 (100.0%)	0.019
3. Basal septal	21.3 ± 11.2	145 (96.7%)	27.8 ± 14.0	149 (99.3%)	<0.001
4. Basal inferior	38.4 ± 19.5	142 (94.7%)	51.1 ± 22.8	150 (100.0%)	<0.001
5. Basal posterior	68.1 ± 25.5	149 (99.3%)	76.4 ± 31.3	150 (100.0%)	0.062
6. Basal lateral	75.8 ± 25.6	150 (100.0%)	78.4 ± 31.6	150 (100.0%)	0.573
7. Mid anterior	50.3 ± 15.3	150 (100.0%)	39.8 ± 13.7	150 (100.0%)	<0.001
8. Mid anteroseptal	35.9 ± 10.9	150 (100.0%)	29.9 ± 12.6	150 (100.0%)	<0.001
9. Mid septal	33.6 ± 9.8	150 (100.0%)	26.1 ± 10.3	150 (100.0%)	<0.001
10. Mid inferior	40.0 ± 14.7	150 (100.0%)	31.9 ± 14.0	150 (100.0%)	<0.001
11. Mid posterior	53.0 ± 17.3	150 (100.0%)	38.3 ± 18.1	148 (98.7%)	<0.001
12. Mid lateral	59.5 ± 19.5	150 (100.0%)	43.5 ± 18.7	150 (100.0%)	<0.001
13. Apical anterior	55.5 ± 19.5	150 (100.0%)	68.2 ± 30.3	150 (100.0%)	<0.001
14. Apical septal	48.2 ± 15.5	150 (100.0%)	56.5 ± 23.5	150 (100.0%)	0.002
15. Apical inferior	51.2 ± 18.4	150 (100.0%)	58.6 ± 24.0	149 (99.3%)	0.014
16. Apical lateral	51.1 ± 16.3	150 (100.0%)	52.0 ± 22.8	150 (100.0%)	0.629

Figure 1: Peak radial strain in the AHA 17-segment model as measured by 2D vs 3D tracking, as well as the number n of included datasets per segment.

Peak circumferential strain (%)	2D	n_{2D}	3D	n_{3D}	p value: 2D vs 3D
1. Basal anterior	-27.1 ± 5.2	146 (97.3%)	-19.8 ± 2.9	150 (100.0%)	<0.001
2. Basal anteroseptal	-18.6 ± 5.8	140 (93.3%)	-13.6 ± 3.2	148 (98.7%)	<0.001
3. Basal septal	-15.7 ± 6.3	81 (54.0%)	-14.2 ± 2.9	150 (100.0%)	<0.001
4. Basal inferior	-21.9 ± 6.5	78 (52.0%)	-14.5 ± 3.1	150 (100.0%)	<0.001
5. Basal posterior	-29.0 ± 5.9	122 (81.3%)	-14.9 ± 3.6	150 (100.0%)	<0.001
6. Basal lateral	-30.3 ± 4.6	145 (96.7%)	-18.5 ± 3.3	150 (100.0%)	<0.001
7. Mid anterior	-21.1 ± 4.6	148 (98.7%)	-20.5 ± 3.5	150 (100.0%)	0.158
8. Mid anteroseptal	-19.9 ± 4.5	150 (100.0%)	-15.5 ± 3.4	150 (100.0%)	<0.001
9. Mid septal	-17.5 ± 4.4	149 (99.3%)	-18.6 ± 3.9	150 (100.0%)	0.012
10. Mid inferior	-18.5 ± 5.3	145 (96.7%)	-20.8 ± 3.5	150 (100.0%)	<0.001
11. Mid posterior	-24.8 ± 5.2	147 (98.0%)	-20.9 ± 4.0	150 (100.0%)	<0.001
12. Mid lateral	-24.3 ± 5.5	149 (99.3%)	-20.4 ± 4.1	150 (100.0%)	<0.001
13. Apical anterior	-26.8 ± 3.8	148 (98.7%)	-14.8 ± 3.2	150 (100.0%)	<0.001
14. Apical septal	-24.9 ± 4.9	147 (98.0%)	-13.7 ± 3.4	150 (100.0%)	<0.001
15. Apical inferior	-26.0 ± 4.2	147 (98.0%)	-19.3 ± 3.9	150 (100.0%)	<0.001
16. Apical lateral	-27.1 ± 4.2	147 (98.0%)	-18.8 ± 4.0	150 (100.0%)	<0.001

Figure 2: Peak circumferential strain in the AHA 17-segment model as measured by 2D vs 3D tracking, as well as the number n of included datasets per segment.

Peak longitudinal strain (%)	2D	n_{2D}	3D	n_{3D}	p value: 2D vs 3D
1. Basal anterior	-18.3 ± 6.2	137 (91.3%)	-13.6 ± 4.3	147 (98.0%)	<0.001
2. Basal anteroseptal	-12.5 ± 3.9	114 (76.0%)	-12.4 ± 3.9	150 (100.0%)	0.248
3. Basal septal	-13.3 ± 3.9	131 (87.3%)	-10.6 ± 3.2	149 (99.3%)	<0.001
4. Basal inferior	-19.5 ± 6.1	123 (82.0%)	-9.8 ± 3.9	141 (94.0%)	<0.001
5. Basal posterior	-25.2 ± 6.2	136 (90.7%)	-12.5 ± 3.7	149 (99.3%)	<0.001
6. Basal lateral	-26.3 ± 7.0	144 (96.0%)	-12.7 ± 3.9	148 (98.7%)	<0.001
7. Mid anterior	-26.2 ± 4.7	142 (94.7%)	-20.7 ± 3.4	150 (100.0%)	<0.001
8. Mid anteroseptal	-19.7 ± 3.9	143 (95.3%)	-17.5 ± 3.4	150 (100.0%)	<0.001
9. Mid septal	-20.6 ± 3.5	144 (96.0%)	-17.1 ± 3.5	150 (100.0%)	<0.001
10. Mid inferior	-23.0 ± 5.1	137 (91.3%)	-19.3 ± 3.7	150 (100.0%)	<0.001
11. Mid posterior	-23.3 ± 4.6	140 (93.3%)	-21.0 ± 4.0	150 (100.0%)	<0.001
12. Mid lateral	-26.7 ± 5.1	145 (96.7%)	-20.4 ± 3.9	150 (100.0%)	<0.001
13. Apical anterior	-22.0 ± 7.0	144 (96.0%)	-15.1 ± 3.2	150 (100.0%)	<0.001
14. Apical septal	-21.5 ± 4.0	150 (100.0%)	-16.7 ± 3.8	150 (100.0%)	<0.001
15. Apical inferior	-21.3 ± 6.0	147 (98.0%)	-20.5 ± 5.1	149 (99.3%)	0.188
16. Apical lateral	-19.4 ± 5.7	140 (93.3%)	-18.9 ± 3.6	150 (100.0%)	0.363

Figure 3: Peak longitudinal strain in the AHA 17-segment model as measured by 2D vs 3D tracking, as well as the number n of included datasets per segment.

ID#: 369989

Can Cardiac Magnetic Resonance Feature Tracking Predict Clinical Cardiovascular Events in Asymptomatic Aortic Stenosis Patients with Normal Ejection Fraction?

Moon Young Kim, MD, MSEun-Ah Park, MD, PhD, Whal Lee, MD, PhD, Seung-Pyo Lee, MD, PhD

Seoul National University Hospital, Republic of Korea

Background: Cardiac magnetic resonance (CMR) feature tracking is a fascinating tool which allows the more concise analysis of myocardial strain through myocardial contouring of basic cine images compared to tissue tagging regarded as a gold standard CMR method. Echocardiographic global longitudinal strain emerges as a potentially useful tool in assessing subclinical left ventricular (LV) dysfunction in aortic stenosis (AS). The aims of this study are to determine the most valuable CMR strain parameters for evaluating AS and to assess whether they predict clinical cardiovascular events (CVEs) in asymptomatic AS patients with normal ejection fraction (EF).

Methods:

A prospectively collected cohort of 123 moderate to severe AS patients (60 males, age 68.6±9.20) and 32 control subjects (14 males, age 67.9±4.35) were enrolled. They underwent echocardiography and 3 T CMR imaging. Short axis and 2-, 3-and 4-chamber cine images were analyzed using feature tracking software (Circle, cvi42, Calgary, Canada) to assess LV radial, circumferential and longitudinal strain parameters including peak strain (PS), time to peak of strain (T2PS), PS rates, peak displacement, time to peak of displacement and peak velocities in 2-and 3-dimensional manners (Figures 1-3). After obtaining CMR imaging, CVEs, including cardiac death, heart failure and AS associated symptom development, were followed up for the median 28.0 months. Relative risk (RR) for CVE in asymptomatic AS patients with normal EF were calculated using the Chi-Square tests.

Results:

All PSs were lower and four T2PS parameters were longer in AS patients than in controls ($p<.05$, Table 1). Severe AS patients showed more impaired PS values than moderate AS ($p<.05$, Table 1). Only two-dimensional long-axis (LAX) global radial and longitudinal PSs revealed a significant gradual decrease in the order of control, moderate and severe AS groups ($p<.000$). There were significant linear correlations between global PS parameters and other cardiac functional indices; EF, LV mass index and native T1 value calculated from CMR, and e'; velocity and left atrial diameter obtained by echocardiography ($p<.05$, Table 2). Among 67 asymptomatic AS patients with normal EF, 22 experienced CVEs during the follow-up period. The RRs for CVE were 3.1 ($p=.027$, 95% confidence interval 1.1-8.7) for LAX global radial PS with a cutoff value of 27%, and 2.9 ($p=.026$, 1.1-7.7) for LAX global longitudinal PS with a cutoff of -17.5%.

Conclusion: Two-dimensional LAX global radial and longitudinal PS values can reflect cardiac dysfunction according to the degree of AS and may predict CVE in asymptomatic AS patients with normal EF.

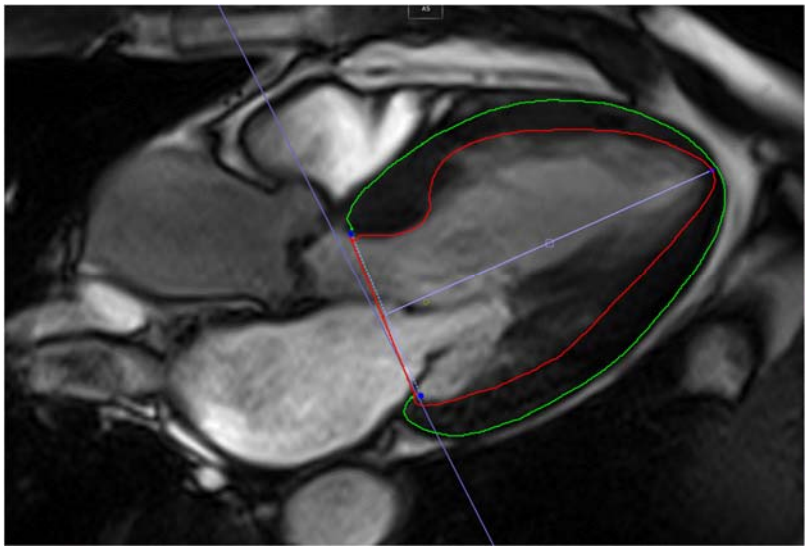

A 72 year-old male with severe AS. Figure 1. The first step for assess myocardial strain; defining the axis of LV and drawing endocardial and epicardial contours.

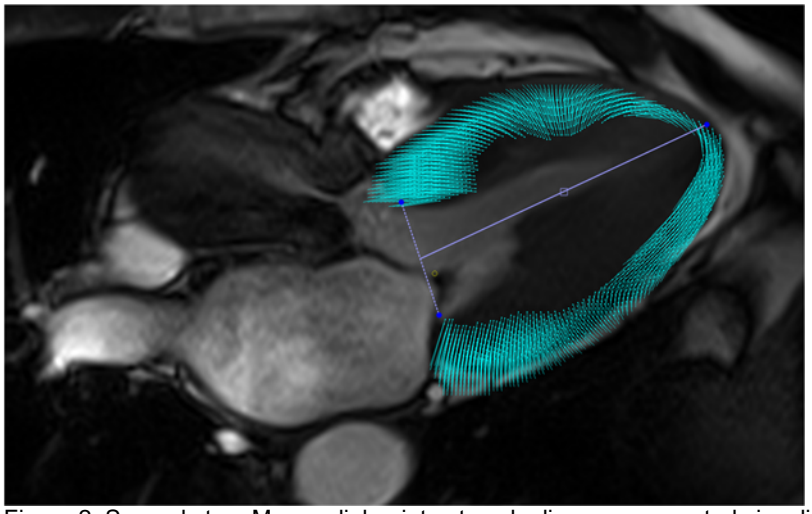

Figure 2. Second step; Myocardial points at each slice are connected visualizing motion lines from end-diastolic to end-systolic phases.

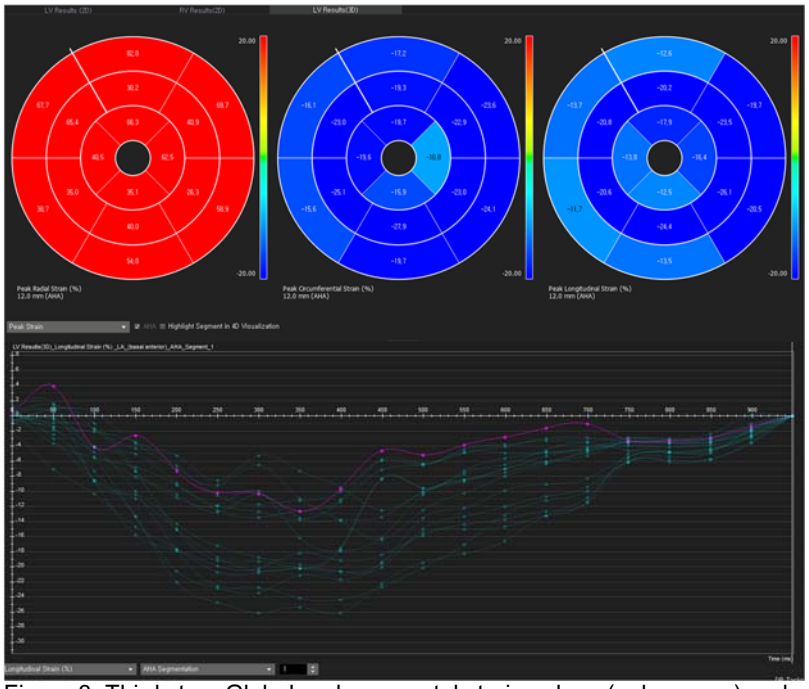

Figure 3. Third step; Global and segmental strain values (polar maps) and phasic graphs are obtained.

Table 1. Differences of feature tracking global parameters between AS and control subjects and between moderate and severe AS subjects.

	AS	Normal	p value	Moderate AS	Severe AS	p value
PEAK STRAIN (%)						
SAX RADIAL	42.55 ± 12.84	47.04 ± 8.57	.023*	45.91 ± 10.87	40.62 ± 13.47	.028*
SAX CIRCUMFERENCIAL	-19.38 ± 4.09	-21.07 ± 2.69	.008*	-20.43 ± 3.38	-18.78 ± 4.33	.031*
LAX RADIAL	26.60 ± 9.58	36.29 ± 7.77	.000*	29.75 ± 7.51	24.79 ± 10.15	.003*
LAX LONGITUDINAL	-14.96 ± 4.04	-18.97 ± 2.33	.000*	-16.47 ± 3.15	-14.09 ± 4.23	.001*
3D RADIAL	42.84 ± 15.04	47.64 ± 10.78	.046*	47.28 ± 13.23	40.27 ± 15.41	.013*
3D CIRCUMFERENCIAL	-18.18 ± 4.06	-20.07 ± 2.13	.001*	-19.34 ± 3.37	-17.51 ± 4.27	.016*
3D LONGITUDINAL	-15.88 ± 3.83	-17.98 ± 2.25	.000*	-16.79 ± 3.51	-15.36 ± 3.91	.045*
TIME to PEAK of STRAIN (ms)						
SAX RADIAL	321.66 ± 41.19	319.83 ± 47.64	.829	325.00 ± 37.16	319.73 ± 43.23	.499
SAX CIRCUMFERENCIAL	326.80 ± 48.45	319.41 ± 42.73	.433	333.45 ± 50.64	322.97 ± 46.71	.252
LAX RADIAL	373.86 ± 60.78	331.79 ± 45.21	.000*	359.05 ± 57.13	382.41 ± 61.18	.040*

LAX LONGITUDINAL	382.51 ± 63.39	328.72 ± 51.38	.000*	372.14 ± 62.75	388.49 ± 62.98	.171
3D RADIAL	330.40 ± 40.19	311.66 ± 34.23	.017*	326.47 ± 36.93	332.68 ± 41.79	.413
3D CIRCUMFERENCIAL	343.20 ± 48.20	315.84 ± 34.65	.000*	336.73 ± 48.29	346.94 ± 47.75	.261
3D LONGITUDINAL	353.29 ± 48.53	342.02 ± 42.79	.237	356.51 ± 50.99	351.43 ± 46.96	.580

SAX: short axis, LAX: long axis, 3D: three dimensional, *: p <.05

Table 2. Linear correlation (Pearson correlation coefficient) between global peak strain parameters and other cardiac functional indices.

	CMR			Echocardiography	
	LV EF	LV MASSi	PreT1 values	e';	LA diameter
***SAX** RADIAL*	.620**	-.456**	-.318**	.233**	-.224*
***SAX** CIRCUMFERENCIAL*	-.648**	.433**	.297**	-.228*	.239**
***LAX** RADIAL*	.604**	-.461**	-.432**	.274**	-.335**
***LAX** LONGITUDINAL*	-.645**	.453**	.451**	-.261**	.354**
***3D** RADIAL*	.650**	-.491**	-.352**	.262**	-.208*
***3D** CIRCUMFERENCIAL*	-.759**	.455**	.391**	-.144	.242**
***3D** LONGITUDINAL*	-.714**	.364**	.422**	-.186*	.282**

EF: ejection fraction, MASSi: myocardial mass index, preT1: precontrast T1 value, *: p <.05, **: p <.001

ID#: 367899

Hemodynamic effects of pharmacological stress with adenosine in patients with left ventricular systolic dysfunction

Gaurav S. Gulsin, MBChB(Hons) MRCP(UK)[1] Ahmed M.S.E.K. Abdelaty, University of Leicester[2], Abhishek Shetye, BSc(Hons) MBChB[3], Jeffrey Khoo, FRCP DPhil[4], Gerald P. McCann, MBChB, MD[5], Jayanth Arnold, BMBCh DPhil[6]

1. The University of Leicester, Nottingham, England, United Kingdom

2. University of Leicester, UK, United Kingdom

3. University of Leicester, United Kingdom

4. University Hospitals of Leicester NHS Trust, Leicester, England, United Kingdom

5. University of Leicester, Leicester, England, United Kingdom

6. Department of Cardiovascular Sciences and NIHR Biomedical Research Centre, Glenfield Hospital, Leicester, England, United Kingdom

Background: Stress cardiovascular magnetic resonance (CMR) perfusion imaging has emerged as a highly sensitive non-invasive investigation for the assessment of myocardial ischemia. However there are scarce data pertaining to the diagnostic accuracy of stress MRI in patients with heart failure. In clinical practice, the most commonly used vasodilator stress agent is adenosine. Conventionally, a heart rate increase >10 beats per minutes (bpm) and/or systolic blood pressure decrease >10mmHg are considered to constitute a satisfactory hemodynamic response to adenosine. In patients with heart failure, this response may be diminished by altered adenosine receptor expression and/or signal transduction. In this study, we sought to evaluate the hemodynamic response to intravenous adenosine in patients with left ventricular (LV) systolic dysfunction (LVSD).

Methods: We retrospectively examined 500 consecutive patients referred for clinical stress CMR between January 2016 and June 2016. Blood pressure and heart rate responses with intravenous adenosine (140µg/kg/min) were compared in patients with normal, mild-moderately impaired and severely impaired LV systolic function (ejection fraction [EF]>55%, 36-55% and <35%, respectively).

Results: At baseline, there was no difference in rate pressure product between the three groups.Following 2 minutes of adenosine infusion (prior to any dose increase), there was a significant difference between the groups in the rate pressure product change, with diminished heart rate (pTable 1). An increase in the dose of adenosine (up to 210 µg/kg/min) was required in more patients with severe LVSD (41%) than those with mild-moderately impaired and normal LV systolic function (24% and 19%, respectively, p Even with increased dose of adenosine in subjects with severe LVSD, the peak hemodynamic response remained blunted (**Table 1**).With multivariate analysis, beta-blocker usage (p=0.033), age (p<0.001) and LV EF (p<0.001) were independent predictors of the heart rate response to adenosine at 2 minutes. Age (p=0.002) and LV EF (p=0.012) were the only predictors of the rate pressure product response to adenosine at 2 minutes.

Conclusion: Patients with reduced LVEF referred for stress perfusion MRI have a blunted hemodynamic response to adenosine. This may limit the diagnostic accuracy of stress perfusion CMR in patients with LV systolic dysfunction and further prospective studies are warranted.

Change in hemodynamic parameters after two minutes' adenosine (140 µg/kg/min) infusion and at peak stress, in patients with severe LV impairment, mild-moderate LV impairment and normal LV function.

	EF≤35%	**EF 36-55%**	**EF>55%**	
	n=251	n=121	n=128	*p*-value
Change in hemodynamic parameters after 2 mins adenosine infusion				
ΔSBP (mmHg)	-2.0±14.2	-5.0±17.7	-7.4±19.9	0.02
ΔDBP (mmHg)	-3.1±9.9	-3.9±15.1	-4.5±9.5	0.46
ΔHR (bpm)	5.6±9.9	12.2±10.6	15.4±10.3	<0.001

ΔRPP	647±1786	1320±1969	1622±2131	<0.001
Peak change in hemodynamic parameters achieved during adenosine infusion				
ΔSBP (mmHg)	-8.4±15.4	-9.6±17.4	-11.4±19.4	0.30
ΔDBP (mmHg)	-6.8±11.1	-6.7±14.4	-6.3±10.4	0.95
ΔHR (bpm)	9.1±11.0	14.0±10.1	17.1±10.4	<0.001
ΔRPP	1116±1874	1628±1915	2108±2365	<0.001

ID#: 367904

Assessment of Pulmonary Artery Mean Pressure with MRI and 4D flow vortex assessment.

Lindsey A. Crowe[1] Gabriel Guglielmi[2], Anne-Lise Hachulla, MD[3], Maurice Beghetti, Pulmonary Hypertension program[4], Frederic Lador[5], Jean-Paul Vallée[5]

1. Geneva University Hospitals, Geneva, Geneve, Switzerland

2. Geneva University Hospitals, Carouge, Geneve, Switzerland

3. Geneva University Hospital, Geneve, Switzerland

4. Pediatric Cardiology Unit, Centre Universitaire Romand de Cardiologie et Chirurgie Cardiaque Pédiatrique, University of Lausanne and Geneva, Switzerland

5. Geneva University Hospitals, Geneve, Switzerland

Background: A robust non-invasive method to estimate increased pulmonary artery mean pressure (mPAP) is needed. Recently, a 2D velocity encoding MRI study has shown that vortex duration in the pulmonary artery (PA) was related to mPAP (Reiter, Radiology, 2015;**275**(1):71). This present study investigated the potential of 4D flow MRI to assess mPAP.

Methods: Eighteen patients with suspected Chronic Thromboembolic Pulmonary Hypertension (CTEPH) were assessed by right heart catheterization (RHC) and cardiac MRI, including a 4D phase contrast flow sequence on a Siemens 3T PRISMA. Streamlines were reconstructed in the pulmonary artery and the duration of the vortical blood flow, defined as closed concentric ring-shaped curves parallel to the pulmonary artery (PA), was measured as a % of the cardiac cycle. The vortex duration was compared to the RHC mPAP, right ventricular volume (RVV), PA diameter and PA distensibility.

Results: CTEPH was confirmed in 11 / 18 patients. The mPAP was 28.7 ± 14.6 mmHg (10-66 mmHg). On the 4D flow data, a vortex was observed in most of the patients, to a greater or lesser extent. A long duration vortex is illustrated in figure 1. Vortex duration measurement was reproducible, with intraobserver ICC = 0.94 and interobserver ICC = 0.88. Vortex duration correlated excellently with mPAP with R^2=0.69, p=0.000018 (figure 2) and outperformed all the other parameters (mPAP correlations with; RVV: R^2=0.13, p=0.14; PA diameter: R^2=0.409, p=0.008; PA distensibility: R^2=0.17, p=0.09). Vortex duration correlations with the other 2D derived MRI parameters were only moderate for PA diameter (RVV: R^2=0.11, p=0.19; PA diameter: R^2=0.47, p=0.003; PA distensibility: R^2=0.14, p=0.13).

Conclusion: The cause of vortex could be explained by two hypotheses: Computational Fluid Dynamics suggests that a change from narrow to wider vessel (PA dilatation) would cause a vortex. This could also explain the moderate correlations of mPAP and vortex duration with PA diameter. Alternatively a pressure increase could cause an outflow obstruction. Three quantified flow directions are needed for vortices. This is not available in clinical 2D breathold flow quantification. 3D volume with '4D Flow'; gives the whole velocity field in one acquisition. Vortex duration derived from 4D flow MRI was the most promising MRI parameter to assess PA pressure and the effect observed by Reiter is confirmed. Further work should include the development of automated method to facilitate the vortex duration measurement.

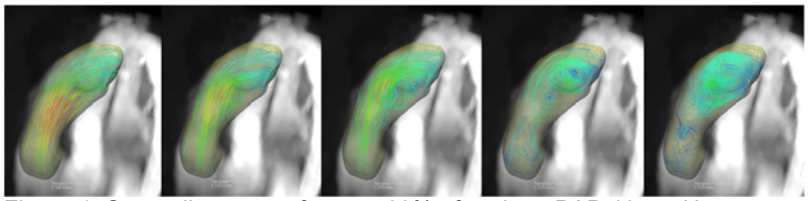

Figure 1. Streamline vortex frames, 60% of cycle, mPAP 46 mmHg.

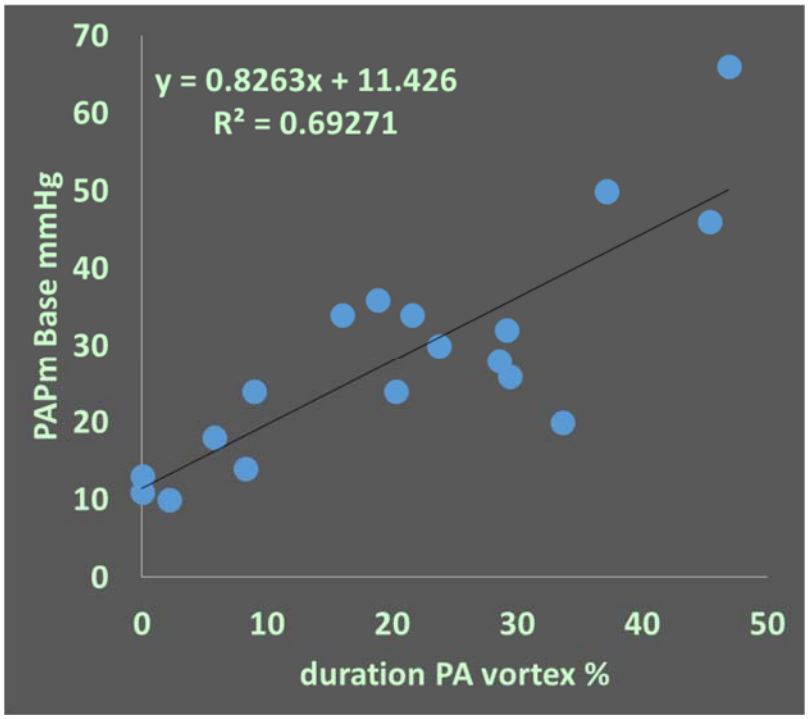

Figure 2. MRI 4D Flow Vortex duration showed excellent correlation with mPAP with R2 = 0.69, p=0.000018, and outperformed all the other parameters.

ID#: 367529

Reduced Myocardial Perfusion Reserve in Systolic Heart Failure is related to NYHA class but not Degree of LV Dysfunction.

Louise AE. Brown, MBChB, BMedSc[1] Sebastian C. Onciul[1], David A. Broadbent, MSc[2], Graham J. Fent, MBChB, BSc[3], Pankaj Garg, MD, PhD[4], James R. Foley, MBChB BSc (Hons)[3], Pei G. Chew, MBChB(Hons) [5], Kristopher D. Knott, MBBS MA[6], Erica Dall'Armellina, Sr., MD, DPhil[7], Hui Xue, PhD[8], John P. Greenwood, PhD[1], Peter P. Swoboda, PhD[3], James C. Moon, MD[9], Peter Kellman, Ph.D.[8], Sven Plein, MD PhD[1]

1. University of Leeds, England, United Kingdom

2. Leeds Teaching Hospitals NHS Trust, England, United Kingdom

3. University of Leeds, Leeds, England, United Kingdom

4. University of Leeds, UK, Leeds, England, United Kingdom

5. University of Leeds, Liverpool, England, United Kingdom

6. University College London, London, England, United Kingdom

7. Leeds Institute of Cardiovascular and Metabolic Medicine, Division of Biomedical Imaging,University of Leeds, United Kingdom

8. National Heart, Lung, and Blood Institute, Bethesda, MD

9. Barts Heart Centre, England, United Kingdom

Background: Left ventricular systolic dysfunction (LVSD) is associated with reduced myocardial perfusion reserve (MPR) even in the absence of proven ischaemic heart disease and patients may have typical angina symptoms, despite the lack of angiographic coronary artery disease. Severity of MPR reduction has been suggested as a prognostic marker in both ischaemic and non-ischaemic cardiomyopathy. We hypothesised that reduction in MPR was associated with worsening symptomatology (represented by NYHA class) and systolic dysfunction (ejection fraction, EF).

Methods: 24 patients referred from cardiology clinics with LVSD of unknown cause underwent adenosine stress perfusion CMR (Siemens 3T). First pass stress and rest myocardial perfusion CMR data were acquired in three short axis slices with 0.05mmol/kg intravenous Gadovist using a recently reported free-breathing motion corrected method with in-line quantification of perfusion maps. For stress, adenosine was administered at 140mcg/kg/min over 5 minutes. Segments showing regional perfusion defects or containing scar were excluded from further quantitative analysis. Myocardial blood flow (MBF) was calculated globally for the remaining left ventricle. MPR was calculated as stress MBF/rest MBF. NYHA class was taken from patient symptoms at the time of referral for CMR. EF was calculated from a short axis cine data set and classified as: normal-mild (≥45%), moderate (35-44%) and severe (≤34%) impairment. ANOVA with post hoc Bonferroni correction was used to compare means of the three groups.

Results: Patients were grouped both by NYHA class and by EF severity, comparisons of these groups are shown in Table 1. No significant difference was seen between groups with respect to age, resting heart rate and resting MBF. MPR was associated with NYHA class (Figure 1). More severe reduction in MPR was associated with a higher NYHA class, there was a significant decrease in MPR between asymptomatic patients and those with exercise limitation (Mean MPR 2.87 ±0.82, 1.75 ±0.41, 1.41 ±0.47 for classes I, II and III respectively, $p < 0.001$). No significant difference was seen between NYHA II and III (1.75 vs 1.41, $p=0.21$). Myocardial perfusion reserve was not correlated with severity of LV dysfunction (Figure 2).

Conclusion:

Reduction in MPR is associated with NYHA class in systolic heart failure, independent of ejection fraction. These findings suggest potential therapeutic targets for symptomatic improvement, including use of vasodilators, even in the absence of coronary disease.

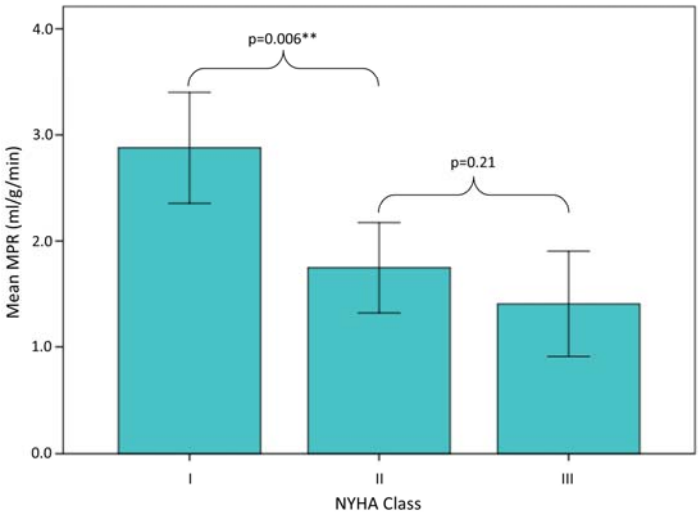

Figure 1 – Mean MPR by NHYA classification. Error bars represent 95% CI of the mean.
** = significant at p<0.01

Figure 1 - MPR and NYHA class

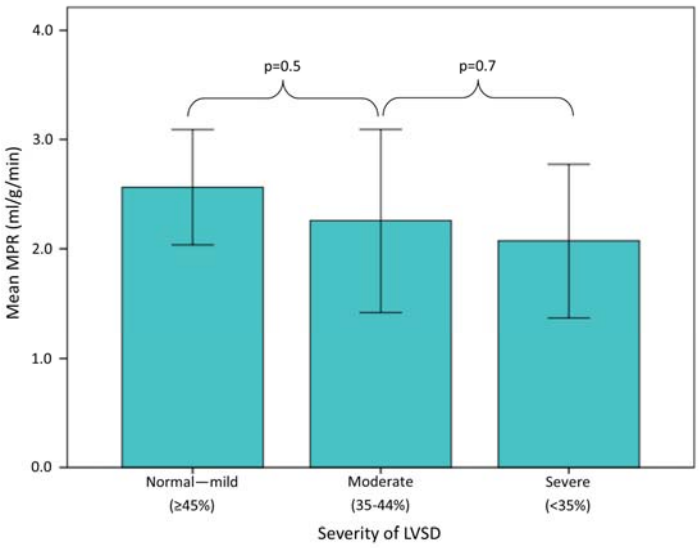

Figure 2 – Mean MPR by severity of LV dysfunction. Error bars represent 95% CI of the mean

Figure 2 - MPR and LVSD severity

Patient Characteristics Between Groups

	NYHA I	NYHA II	NYHA III	p
Age	65.0 ±8.9	66.5 ±14.4	68.2 ±12.2	0.85
EF %	42.3 ±13.8	32.0 ±11.9	26.8 ±5.7	0.04*
Resting HR	69.4 ±11.5	71.0 ±11.1	67.0 ±17.8	0.87

Rest MBF (ml/g/min)	0.83 ±0.45	0.80 ±0.41	0.56 ±0.07	0.373
Stress MBF (ml/g/min)	2.28 ±0.82	1.37 ±0.63	0.80 ±0.41	0.007**
MPR	2.87 ±0.82	1.75 ±0.41	1.41 ±0.47	<0.001**
	Normal-mild EF	Moderate EF	Severe EF	
Age	60.4 ±6.5	72.4 ±5.7	64.9 ±13.1	0.14
Rest HR	71.6 ±6.8	60.0 ±7.2	73.6 ±14.7	0.07
Rest MBF (ml/g/min)	0.89 ±0.60	0.82 ±0.48	0.66 ±0.18	0.498
Stress MBF (ml/g/min)	2.19 ±1.29	1.75 ±1.07	1.44 ±0.94	0.413
MPR	2.56 ±0.42	2.26 ±0.90	2.07 ±1.1	0.629

Table 1 - comparison of patient groups
* significant at p=0.05. ** significant at p=0.01

ID#: 367583

New occurrences of macroscopic myocardial fibrosis in thalassemia at long term by multiple follow-up

Alessia Pepe, MD, PhD[1] Antonella Meloni, PhD[1], Laura Pistoia, MSc[1], Stefania Renne, MD[2], Valentina Vinci, MD[3], Priscilla Fina, MD[4], Nicola Giunta, MD[5], Vincenzo Positano, MSc[1], Angelo Peluso, MD[6], Maria Caterina Putti, MD[7], Antonella Massa, MD[8], Maria Grazia Bisconte, MD[9]

1. Fondazione G. Monasterio CNR Regione Toscana, Pisa, Toscana, Italy

2. Presidio Ospedaliero "Giovanni Paolo II", Lamezia Terme, Calabria, Italy

3. Azienda Ospedaliera "Garibaldi" Presidio Ospedaliero Nesima, Catania, Sicilia, Italy

4. Ospedale "Sandro Pertini", Roma, Lazio, Italy

5. ARNAS Civico Di Cristina-Benfratelli, Palermo, Sicilia, Italy

6. Ospedale "SS. Annunziata" ASL Taranto, Taranto, Puglia, Italy

7. Azienda Ospedaliero-Università di Padova, Padova, Veneto, Italy

8. Ospedale "Giovanni Paolo II", Olbia, Sardegna, Italy

9. Presidio Ospedaliero "Annunziata", Cosenza, Calabria, Italy

Background: To date in thalassemia patients it is recommended to repeat cardiac magnetic resonance (CMR) scans for iron quantification every 1 or 2 years based on the myocardial iron overload (MIO). Also in these patients, late gadolinium enhancement (LGE) *has been demonstrated to be a strong predictor for cardiac events.* However, many studies have shown an association between intravenous gadolinium based contrast agents (GBCA) exposure and neuronal tissue deposition. So, it appears prudent at this time to revisit institutional protocols for GBCA administration, in particular in the follow up (FU) studies.
Thus, we investigated the evolution of myocardial fibrosis in terms of new occurrences over a period of 6 years in thalassemia patients who underwent to multiple FU.

Methods: We considered 52 patients with thalassemia major (28.78±8.59 years; 28 females) consecutively enrolled in the Myocardial Iron Overload in Thalassemia (MIOT) Network who underwent 5 LGE CMRs (baseline + 4 follow-up) using Gadobutrol (0.2 mmoli/kg). The time interval between two subsequent scans was 18±3 months.

Results: At the baseline CMR**,** 44 patients (84.6%) wereLGE□negative.
Eight new occurrences of myocardial fibrosis were detected at the first follow-up (FU). At the second FU, 2 out of the 36 previously LGE-negative patients had myocardial fibrosis. At the third FU, 9 new occurrences of myocardial fibrosis were detected. At the forth FU, 3 patients showed myocardial fibrosis for the first time. The figure shows a simplifying flow-chart.
The 22 patients who developed myocardial fibrosis during the follow-up showed comparable frequency of diabetes and HCV infection and comparable baseline cardiac iron than patients who remained always LGE-negative.

Conclusion: A serial monitoring of thalassemia patients revealed an high number of new occurrences of myocardial fibrosis, suggesting the importance of repeating the LGE CMR over time using 'low risk' macrocyclic agents.

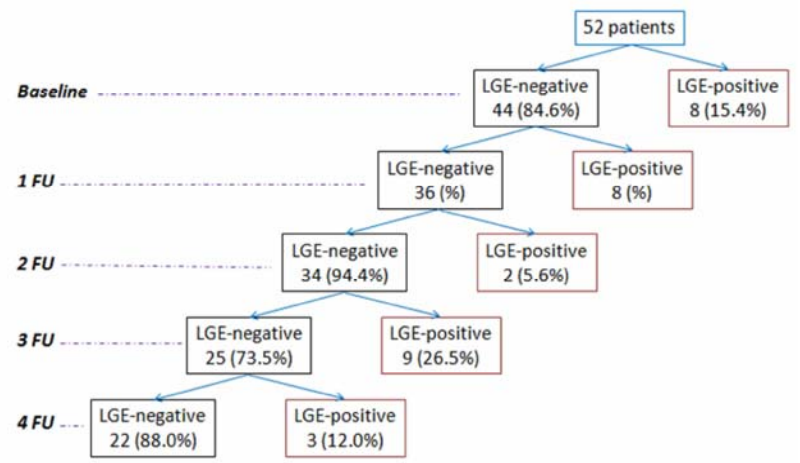
52 patients
Baseline
LGE-negative
44 (84.6%)
LGE-positive
8 (15.4%)
1 FU
LGE-negative
36 (%)
LGE-positive
8 (%)
2 FU
LGE-negative
34 (94.4%)
LGE-positive
2 (5.6%)
3 FU
LGE-negative
25 (73.5%)
LGE-positive
9 (26.5%)
4 FU
LGE-negative
22 (88.0%)
LGE-positive
3 (12.0%)

ID#: 369307

Effects of Blood Pressure on Aortic Morphology and Stiffness in the Adult Population

Kwan Woo Paik[1] Jennifer Bryant, PhD[2], Weng Kit Lye[3], Thu-Thao Le, PhD[2], Boyang Su, PhD[2], Stuart Alexander Cook, Professor[4], Calvin WL. Chin, Assistant Professor[3]

1. Duke NUS Medical School, Singapore, Singapore

2. National Heart Centre Singapore, Singapore

3. Duke-NUS Medical School, Singapore

4. Duke-NUS Medical School, N/A, Singapore

Background: The effects of blood pressure and aortic arch morphology are not well described in the adult population without congenital heart pathologies. We aim to examine determinants associated with aortic morphology (ascending aortic diameter: $Aortic_{Diameter}$ and aortic arch angle: $Arch_{Angle}$) and arterial stiffness (pulse wave velocity: PWV) in an adult population. We hypothesize that blood pressure does not have a strong and independent effect on aortic morphology and arterial stiffness.

Methods: Cardiovascular magnetic resonance (1.5T Aera, Siemens) was performed in 378 adults without congenital heart diseases (hypertension, n= 202; males, n= 221 (58%); age= 52 ± 14 years). All patients did not have cardiovascular diseases such as myocardial infarction, ischemic heart disease, heart failure and stroke. $Aortic_{Diameter}$ was measured in the standard axial dark-blood image at the level of the pulmonary artery bifurcation. We measured $Arch_{angle}$ in the parasagital "candy cane" view (Figure 1) which demonstrated excellent inter-observer reproducibility (1.0 ± 3.0°) in 20 patients. Aortic arch stiffness was measured using the ARTFUN software, as the ratio of aortic arch length to flow transit time. The association of blood pressure on aortic morphology and arterial stiffness was determined using correlation and multivariable linear regression to adjust for potential confounders.

Results: Compared to those without hypertension, hypertensive patients had wider $Arch_{Angle}$ (59.7 ± 10.5° versus 55.1 ± 9.6°; P<0.001), larger $Aortic_{Diameter}$ (31.3 ± 4.0mm versus 27.3 ± 4.0mm; P<0.001) and increased PWV (6.9 ± 2.4m/s versus 5.2 ± 2.1m/s; P<0.001). In the cohort, systolic blood pressure (SBP) correlated modestly with $Aortic_{Diameter}$ (r= 0.29; P<0.0001), Angle (r= 0.17; P<0.001) and PWV (r= 0.40; P<0.0001). Weaker correlations were observed in the hypertensive patients ($Aortic_{Diameter}$: r= 0.09; P= 0.20; $Arch_{Angle}$: r= -0.08; P= 0.28; PWV: r= 0.26; P<0.0001). In multivariable analysis, age was the strongest determinant associated with $Aortic_{Diameter}$ (standardized beta, ß: 0.59; P<0.0001) and PWV (ß: 0.57; P<0.0001), independent of sex, height, weight and SBP. Height (ß: -0.43; P<0.0001) and weight (ß: 0.68; P<0.0001), but not SBP (ß: 0.08; P= 0.10), were the strongest independent determinants associated with $Arch_{Angle}$. Similar results were observed when hypertension status was used instead of SBP.

Conclusion: Compared to blood pressure, age and allometric parameters had stronger and independent effects on aortic morphology and aortic arch stiffness in the adult population.

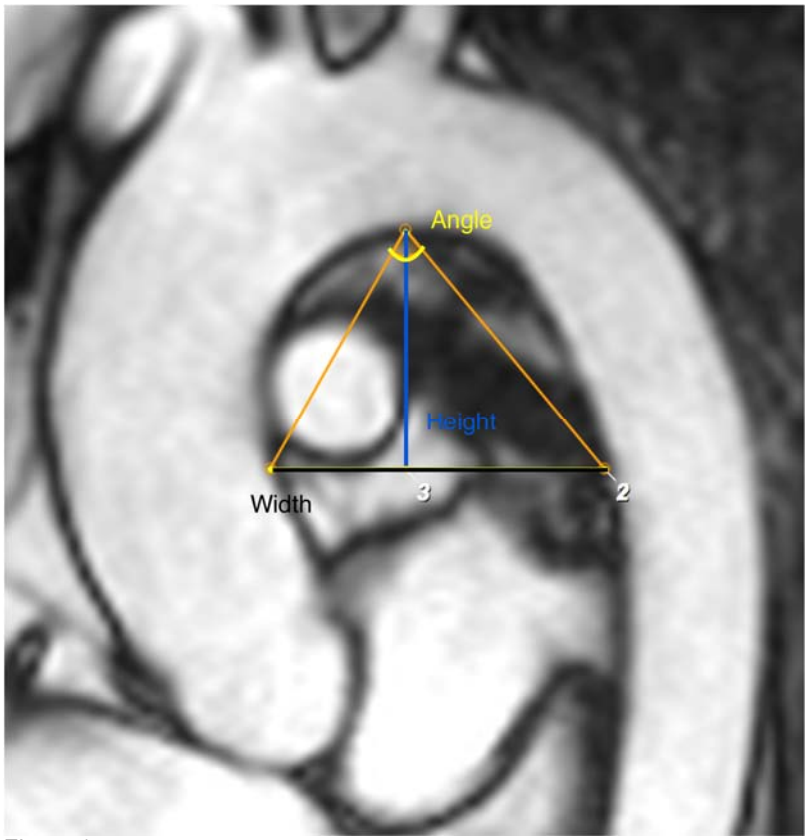

Figure 1

ID#: 369361

Longitudinal, lateral and septal contribution to ventricular stroke volume remains unchanged after long-duration spaceflight

Katarina Steding-Ehrenborg, RPT, PhD[1] Robert Jablonowski, MD, PhD[2], Per M. Arvidsson, MD, PhD[3], Michael W. Bungo, MD, PhD[4], Benjamin D. Levine, MD, PhD[5]

1. Lund University, Department of Clinical Sciences Lund, Clinical Physiology, Skane University Hospital, Lund, Sweden, Lund, Sweden

2. Lund University, Skane Lan, Sweden

3. Lund University, Skane University Hospital, Department of Clinical Sciences Lund, Clinical Physiology, Lund, Sweden, Lund, Skane Lan, Sweden

4. The University of Texas Health Science Center at Houston, USA

5. Institute for Exercise and Environmental Medicine, Texas Health Presbyterian Hospital Dallas, Dallas, Texas, USA and University of Texas Southwestern Medical Center, Dallas, Texas, USA

Background: Long-duration space flight has negative effects on cardiac morphology and function. In-flight echocardiography has revealed decreased global longitudinal strain and increased sphericity of the left ventricle (LV). The aim of this study was to use cardiac magnetic resonance imaging (CMR) to evaluate cardiac pumping mechanics of the left and right ventricle (RV) in astronauts before and after missions to the International Space Station (ISS).

Methods: Thirteen astronauts (four women) underwent CMR before and after missions onboard ISS. Nine (two women) astronauts also underwent a follow-up examination 29±10 days after return to Earth. Ventricular dimensions, atrioventricular plane displacement (AVPD), longitudinal, lateral and septal contribution to stroke volume (SV) of the LV and RV were measured. To account for missing values, mixed-model statistics were used to test for changes between examinations.

Results: For LVAVPD, pre-flight, post-flight and follow-up measures were all 14±2 mm (p=0.95). RVAVPD was 19±4 mm, 19±2 mm and 19±3 mm respectively (p=0.98). Both LV and RV end-diastolic volumes (EDV) and mass were unchanged (LVEDV p=0.76 and LV mass p=0.55, RVEDV p=0.78 and RV mass p=0.25). LV longitudinal contribution to SV did not change (p=1.0). Furthermore, lateral and septal contribution to SV remained stable (p=0.07, p=0.06). Similar results were seen for the RV with no differences for longitudinal, lateral or septal contribution to SV (p=1.0, p=0.48, p=0.54).

Conclusion: Cardiac pumping mechanics measured as longitudinal, lateral and septal contribution to SV did not differ before and after long-duration space flight. Thus, previous changes observed in microgravity using echocardiography did not persist after return to Earth.

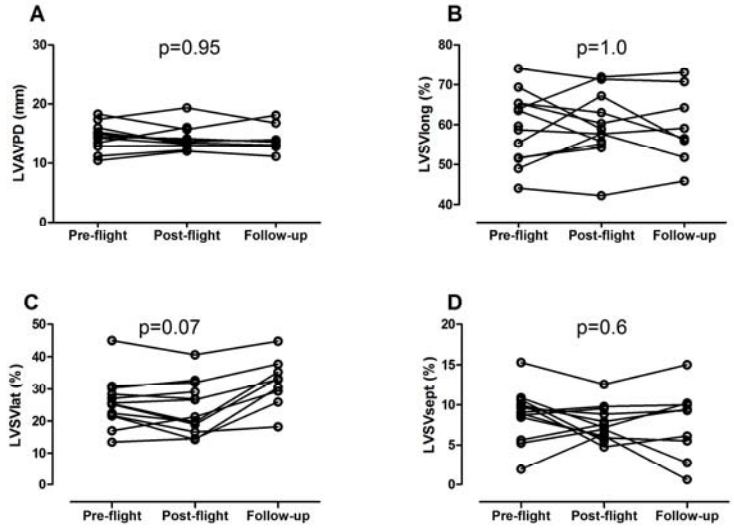

LV atrioventricular plane displacement and contribution of longitudinal, lateral and septal pumping to stroke volume

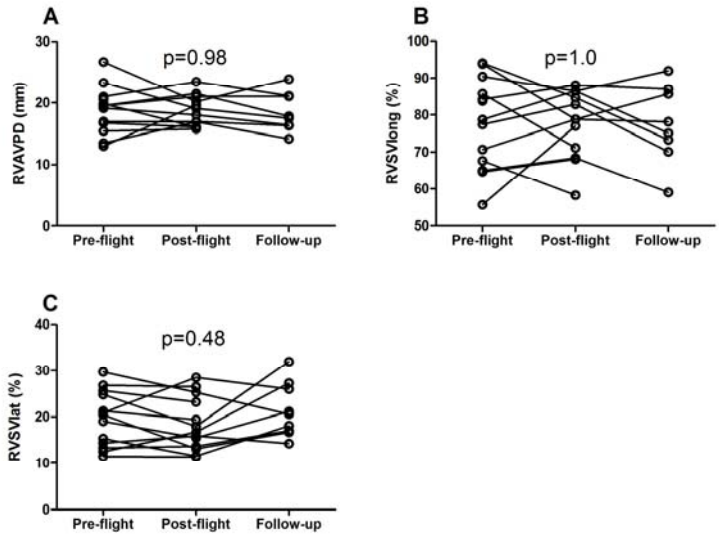

RV atrioventricular plane displacement and contribution of longitudinal and lateral pumping to stroke volume

ID#: 369445

Characterization of Ischemic Cardiomyopathy with Water-Fat Separation via End-to-end Deep Learning

James W. Goldfarb, PhD

St Francis Hospital

Background: Water-fat separation is a post-processing technique typically applied to multiple-echo magnetic resonance (MR) images to identify fat, provide images with fat suppression and quantify the amount and/or type of fat or lipids in specific tissues. This is most commonly accomplished with analytical multi-parameter modeling of the MR signal and individual pixel fitting yielding water and fat images, T2* maps andoff-resonance maps. These images can be used for detection of fatty metaplasia and intramyocardial hemorraghe, Convolutional neural networks (CNNs) offer a completely different post processing workflow via deep machine learning when compared to conventional water-fat separation model-based method. Machine learning is a type of artificial intelligence that provides computers with the ability to learn a task without being explicitly programmed. It focuses on the development of computer programs that can change when exposed to new data. In this work, the task will be MR water-fat separation and the data will be a series of gradient-echo cardiovascular MR studies. In this proof-of-concept study we tested the feasibility of an end-to-end machine learning water-fat separation solution for characterization of ischemic cardiomyopathy.

Methods: Water-fat separation of 1204 gradient-echo acquisitions from 90 imaging sessions (control, acute and chronic myocardial infarction) was performed using a conventional model based method with modeling of R2* and off-resonance and multi-peak fat spectrum. A U-Net convolutional neural network (Figure 1) for calculation of water-only, fat-only, R2* and off-resonance images was trained with 900 gradient-echo bipolar gradient-echo acquisitions and the conventional method';s results using Keras 2.0 and TensorFlow 1.2 (both freely available software). Training on n=900 [training set] (x12 echo-times) complex images (validation on n=100 images [validation set]) with 75 epochs was performed using the Adam optimizer with Nestrov momentum. Training was performed over 75 epochs. Data augmentation was performed by horizontal and vertical mirroring of the images. Water and fat images from the data not used for training (n=304, [test set]) were “predicted” using the trained CNN.

Results: The U-Net CNN was easily trained and provided water-fat separation results visually comparable to conventional methods. Myocardial fat deposition in chronic myocardial infarction and intramyocardial hemorrhage in acute myocardial infarction were well visualized in the DML results (Figure 2). Predicted values for R2*, off-resonance, water and fat signal intensities were all well correlated with conventional model based water fat separation (Figure 3, R^2=0.99, p<0.001). DML images had a 14% higher signal-to-noise ratio (p<0.001) when compared to the conventional method.

Conclusion: The feasibility of water-fat separation using an end-to-end CNN approach was demonstrated. The CNN approach showed visually comparable images with slightly higher signal to noise in typical cardiac image planes. Quantitative image signal intensities, R2* and off-resonance values showed excellent correlation with a conventional analytical model based method. The method worked well in areas with fold-over aliasing artifacts and a bipolar gradient acquisition. CNN based water-fat separation is a promising method capable of learning the water-fat separation problem with corrections for bipolar gradients, a multi-peak model, R2* and off-resonance.

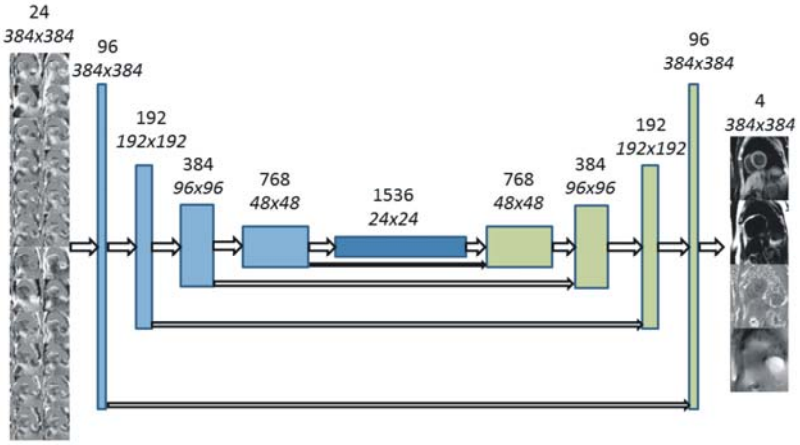

Figure 1: U-Net convolutional neural network used for water-fat separation. The input to the CNN is 24 images (12 echo times, real and imaginary components). The output is four images: water only, fat only, R2* and off-resonance.

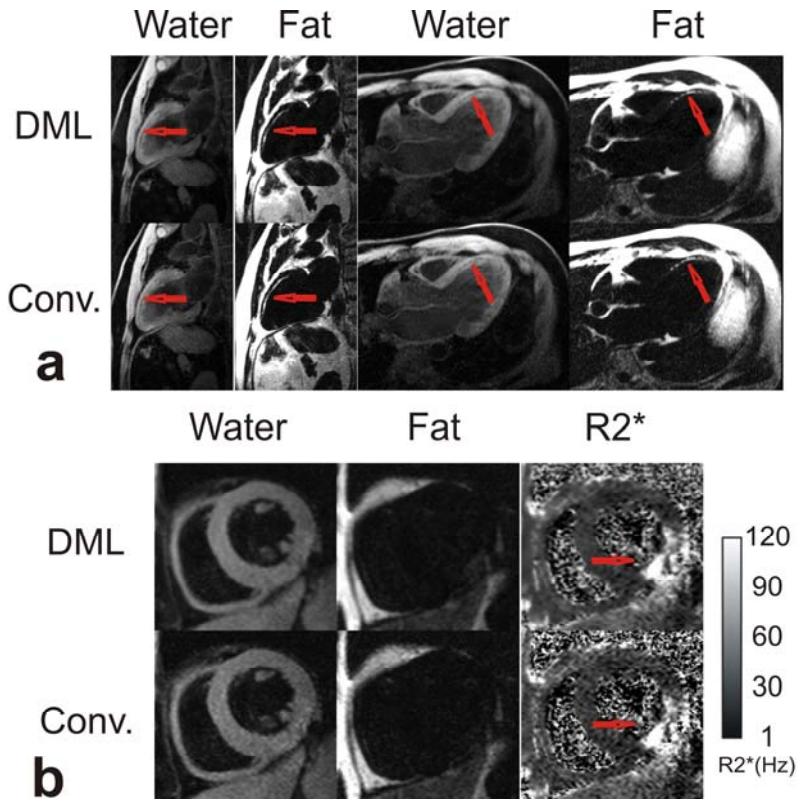

Figure 2: Water-fat separation performed comparatively well in multiple cardiac planes with deep machine learning (DML) when compared to the conventional (Conv.) method. Subjects with chronic (a) and acute (b) myocardial infarctions show fat deposition and intramyocardial hemorrhage (red arrows).

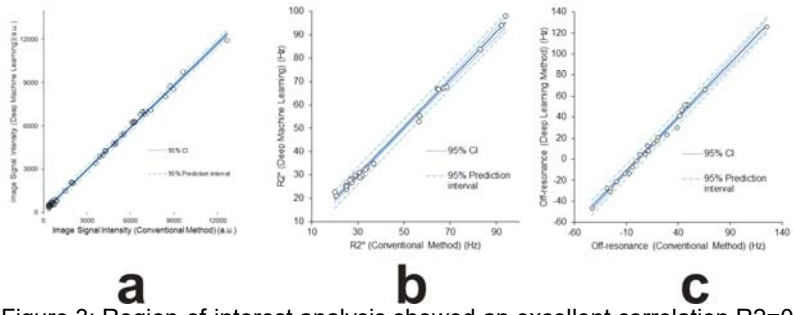

Figure 3: Region-of-interest analysis showed an excellent correlation R2=0.99 between deep machine learning and the conventional method for (a) image signal intensities in water and fat images (b) R2* and (c) off-resonance quantitative values.

ID#: 369465

Quantitative Regional Fibrosis Burden in Duchenne Muscular Dystrophy Patients by Cardiac Magnetic Resonance Imaging

Ramkumar Krishnamurthy, Ph.D., D-ABMP-MRI[1] Sanjay Subramanian, B.S.[2], Houchun Harry Hu, PhD[3], Linda Cripe, MD[4], Rajesh Krishnamurthy, MD[5], Kan Hor, MD[4]

1. Nationwide Children's Hospital, OH

2. University of Michigan

3. Nationwide Children's Hospital, Dublin, OH

4. Nationwide Children's Hospital, Columbus, OH

5. Nationwide Children's Hospital

Background: Cardiac magnetic resonance imaging is used for assessment of ventricular function by ejection fraction (EF) and myocardial fibrosis by late gadolinium enhancement (LGE) for DMD patients. Earlier studies have shown that LGE precedes decline in EF[1-2]. However, there is limited data on quantitative regional fibrosis variability in DMD that might help disease monitoring. In this study, we sought to determine the regional variability between different slice locations, and hypothesize that apical LGE is associated with a later stage of the disease, when EF is abnormal.

Methods: In this retrospective IRB approved study, LGE images of 87 DMD children acquired for clinical indications from November 2015 until June 2017 were analyzed. Using a Matlab program, an observer (SS) drew contours on three short axis slices (basal, mid-level and apical), delineating the endocardium and epicardium, as well as a remote normal region (Figure 1) yielding mean and standard deviation. Area of fibrosis (scar) was defined as regions with signal intensity > 6X standard deviations from the remote normal mean. The scar burden (%) was defined as the ratio of area identified as scar within the slice to total area of the slice. This was calculated globally at the base, mid-ventricular and apical levels, as well as septal and lateral walls, and compared with EF.

Results: The age, ejection fraction and regional scar burden at three short axis levels are shown in table 1 and figure 2. It can be seen that a. There is minimal scar present in the apical slices (8 /34 patients with scar). Patients with scar at apical slice always had scar at basal or mid-ventricular locations. Apical scar occurs at a later age. b. The scar burden is high at the lateral walls when compared to the septal walls (17.1% in lateral vs 0.7 % in septal walls in patients >19 years old) (Figure 2). c. Scar burden increases with age (Figure 2, table 1), while EF decreases with age and increasing scar burden.

Conclusion: Septal involvement occurred in older patients with reduced EF. LGE is more significant at the basal and mid-ventricular level and spares the apical level until older age, when EF is abnormal. Apical LGE only occurs in conjunction with basal and mid-ventricular LGE and never in isolation. Future studies are needed to assess the mechanism of this pattern of LGE.

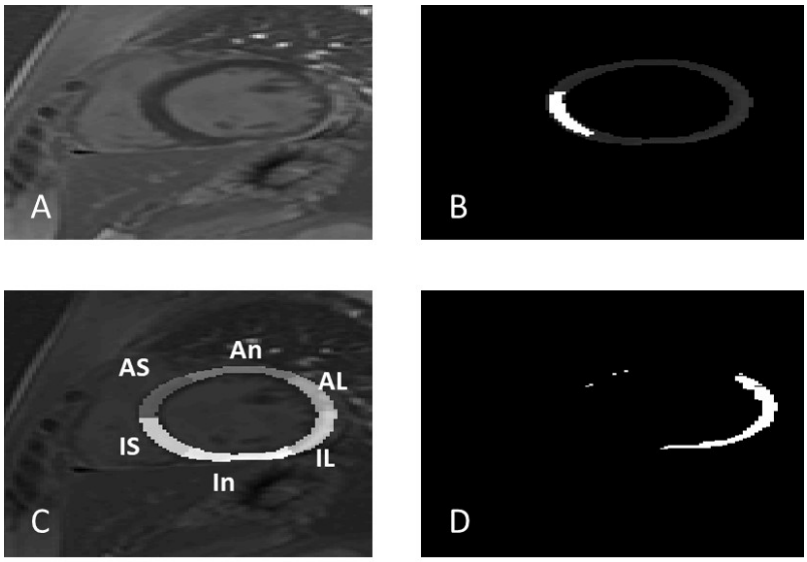

A late gadolinium enhanced (LGE) phase insensitive inversion recovery (PSIR) image obtained at the basal short axis level is shown (A). An observer manually drew contours delineating the endocardium as well as epicardium using a custom written Matlab program. Remote normal ROI was also drawn for each slice (B). The program semi-automatedly identified the six segments across the short axis slice (C), as well as the region of hyper-enhancement within the slice.

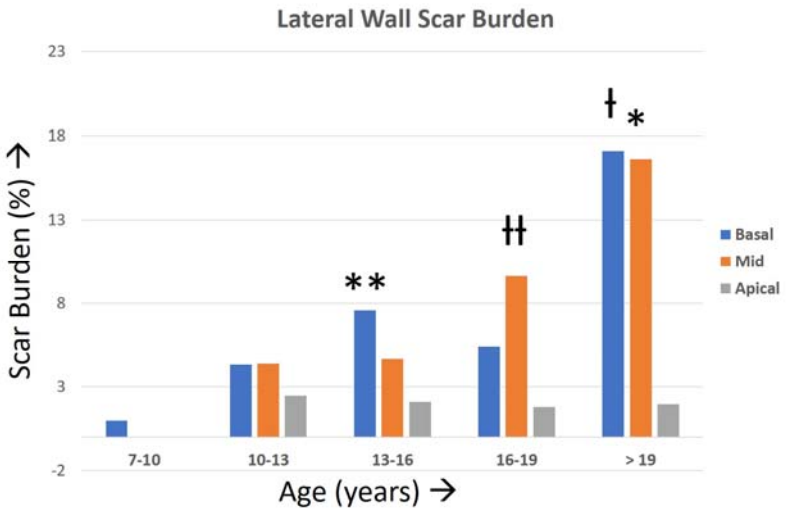

Figure 2: Lateral wall scar burden (%) is listed for different age groups across the three slices. ǂ □p< 0.05 for SB at >19 years vs. all age groups * □ p< 0.05 for SB at >19 years vs. all age groups except 16-19 years ǂ ǂ □p< 0.05 for SB at 16-19 years vs. all age lower groups ** □ p< 0.05 for SB 13-16 years vs. all lower age groups

Age (years)	n	Ejection Fraction (%)	Total # scar	Scar burden (%) across age groups. Expressed as mean ± SD								
				Basal			Mid-Ventricle			Apical		
				# scar	Septal	Lateral	# scar	Septal	Lateral	# scar	Septal	Lateral
7 - 10	18	61.5 ± 3.6	3	2	0 ± 0	0.98 ± 3.6	1	0 ± 0	0 ± 0	0	0 ± 0	0 ± 0
10 - 13	19	60.2 ± 4.5	5	5	0 ± 0	4.3 ± 9.5	4	0 ± 0	4.4 ± 12	1	0 ± 0	2.5 ± 10.7
13 - 16	22	54 ± 11.6	9	9	0 ± 0	7.6 ± 12.6	9	0.1 ± 0.3	4.9 ± 12	2	0.2 ± 0.7	2.1 ± 9.3
16 - 19	16	52 ± 13.6	9	9	0 ± 0	5.4 ± 7.7	8	0.16 ± 0.5	9.6 ± 15.6	3	0 ± 0	1.8 ± 4.9
> 19	12	48 ± 11.1	8	7	0.7 ± 1.8	17.1 ± 17	8	1.0 ± 3.5	16.6 ± 19.3	2	0 ± 0	2 ± 5.3

Table 1: Information related to patients recruited for this study is shown. The patient group is divided into 5 sub groups based on the age. '# scar' denotes the number of patients with scar in that sub group of patients. As expected, the ejection fraction decreased with age, while the scar burden increased with age. More scar is seen in the lateral wall when compared to the septum. From

Table 1: Information related to patients recruited for this study is shown. The patient group is divided into 5 sub

groups based on the age. '# scar' denotes the number of patients with scar in that sub group of patients. As expected, the ejection fraction decreased with age, while the scar burden increased with age. More scar is seen in the lateral wall when compared to the septum.

ID#: 369553

Dynamic Cardiac Off-resonance Mapping for Real-time Spiral De-blurring

Matthew C. Restivo, PhD[1] Adrienne E. Campbell-Washburn, PhD[2]

1. National Heart, Lung, and Blood Institute, National Institutes of Health, Bethesda, MD

2. National Heart, Lung, and Blood Institute, National Institutes of Health, MD

Background: Real-time spiral MRI is appealing for MR guided interventions due to the speed and RF efficiency.[1] Off-resonance distorts spiral MR images resulting in image blurring, which can be corrected if the off-resonance is known.[2] However, it may be difficult to obtain an accurate map during real-time cardiac imaging because cardiac and breathing motion create dynamic spatial off-resonance.

Therefore, we seek a way to measure the variation in off-resonance with physiological motion and assess potential correction strategies.

Methods: A dynamic off-resonance mapping sequence was created by repeatedly acquiring two consecutive images with the acquisition time (TE) of the second image delayed 1 ms relative to the first. The difference in phase between the two images is proportional to the off-resonance.

We examined mapping sequences with 1, 4, 8, and 16 shot variable density spiral interleaves to determine the optimal tradeoff between readout duration and frame rate (fig 1). The sequence was executed using 100 repetitions, covering at least 6 cardiac cycles and 1 respiratory cycle. After mapping, conjugate phase reconstruction using multi-frequency interpolation[2] was used to correct the first map image and assess de-blurring. Images are reconstructed and deblurred using a Gadgetron[3] process running on an inline reconstruction server. This infrastructure enables image deblurring online during real-time MRI.[4]

Results: Shorter readouts lead to less blurring and, generally, more accurate maps; however, at the cost of longer imaging duration (fig 1).

The off-resonance map varies dynamically with cardiac motion, but only a small number of pixels are affected (fig 2). Using a dynamic map that varies with physiological motion improves the correction near fat/muscle boundaries compared to a static map measured at a single time point (white arrows fig 2). Similar results were seen in long axis views as well as in other subjects.

Although breathing motion changes position of the air/tissue interface relative to the FOV (fig 3), this affect is also small and limited. A significant difference in average off-resonance values in the myocardium between inhalation and exhalation was not observed.

Conclusion: Real-time spiral imaging is improved by map based off-resonance correction. Readouts under 8 ms are sufficient for this application. Shorter readouts may be required in the presence of higher off-resonance (i.e. implants). A modest additional improvement at tissue boundaries can be gained by using an off-resonance map from a matching physiological state, at the expense of temporal resolution.

1) Campbell-Washburn,et.al.JCMR.2015;17:114.
2) Man,et.al.MRM1997;37:785–792.
3) Hansen,et.al.MRM2013;69:1768–177.
4) Restivo,et.al.Proc.ISMRM2017:5424

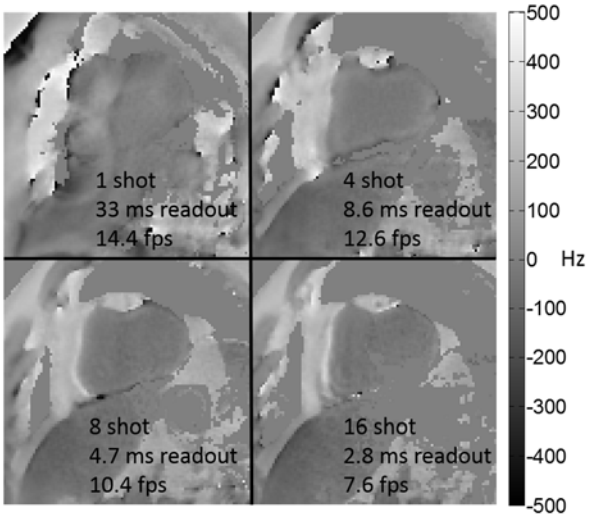

Off-resonance maps in the heart derived from spiral image acquisitions. The fat and myocardium are visible in the 4-shot map. The 8-shot map appears clearer. The 16-shot map has the least blurring, but is also the slowest (132 ms acquisition) and therefore may be corrupted by motion between the two mapping acquisitions.

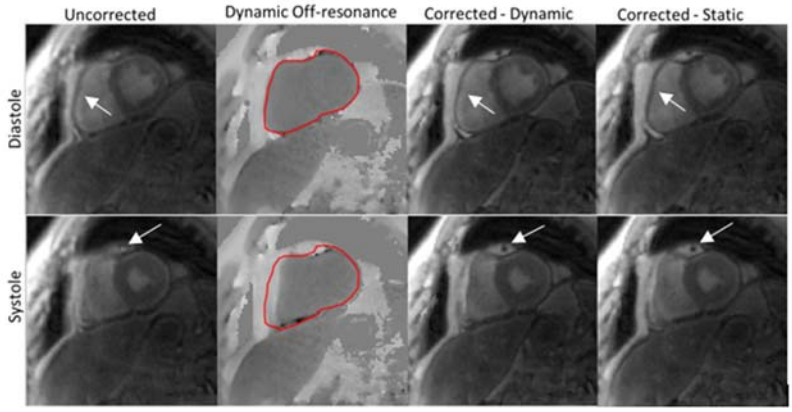

Comparison of off-resonance correction strategies at distinct points in the cardiac cycle. One strategy uses a dynamic off-resonance map acquired for every image and the other uses a single static map acquired at the beginning of the sequence. White arrows point to locations of noticeable blurring and corresponding correction. Red outline in the off-resonance map highlights the shift in position of the fat/myocardium boundaries from diastole to systole. Off-resonance is displayed from -500 to 500 Hz. Static map was acquired near systole.

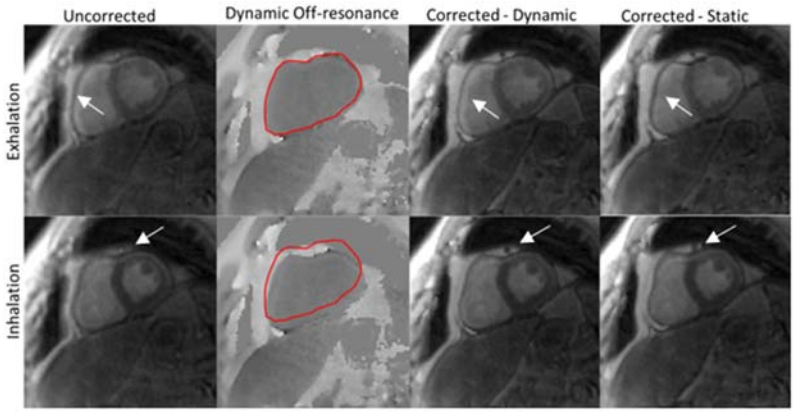

Comparison of off-resonance correction strategies at distinct points in the respiratory cycle. Red outline in the off-resonance map highlights the shift in position of the heart from exhalation to inhalation. Static correction used a map from the opposite respiratory state for maximum inaccuracy.

ID#: 378324

Cardiovascular Magnetic Resonance Predictors of Left Ventricular Remodeling 1 Year After Mitral Valve Repair

Ariane Binoti. Pacheco, MD[1]Ahmad Ali. Abdouni, MD[2], Bernardo B. da Cunha Lopes, MD[3], Carlos M. Brandão, MD, PhD[4], Rosse C. Osorio, MD[5], Pablo Pomerantzeff, MD, PhD[2], Carlos E. Rochitte, MD, PhD[6]

1. Heart Institute - InCor - University of São Paulo Medical School, São Paulo, Brazil, Espirito Santo, Brazil

2. Heart Institute - InCor - University of São Paulo Medical School, São Paulo, Brazil, Brazil

3. Heart Institute - InCor - University of São Paulo Medical School, São Paulo, Brazil, Sao Paulo, Brazil

4. Heart Institute, InCor, University of São Paulo Medical School, São Paulo, Brazil, Sao Paulo, Sao Paulo, Brazil

5. Heart Institute - InCor - University of São Paulo Medical School, São Paulo, Brazil, Salvador, Bahia, Brazil

6. Heart Institute - InCor - University of São Paulo Medical School and Hospital do Coração - Heart Hospital - HCOR, São Paulo, Brazil

Background: Mitral valve repair (MVR) is the treatment of choice for mitral regurgitation of degenerative etiology. Cardiovascular magnetic resonance (CMR) has been able to accurately identify patients that will demonstrate a more favorable reverse left ventricle (LV) remodeling after MVR. However, it is unclear which CMR parameter better predicts LV remodeling. Our objective was to investigate the relationships of pre-operatory CMR parameters with the magnitude of LV reverse remodeling 1 year after MVR.

Methods: From July 2014 to August 2016, 36 patients with severe mitral regurgitation of degenerative etiology and prolapse of the posterior leaflet with clinical indication to undergo MVR were selected. Seven were excluded because mitral valve replacement (3) or not performing baseline CMR exam (4). Twenty-nine patients were included: 17 patients were male (58.6%) and 12 were female (41.4%); mean age was 63.3 years. All patients were submitted to CMR before and one year after the surgery for the evaluation of degree of mitral valve regurgitation, left ventricular volumes, function and mass. The cardiac reverse remodeling was defined as LV end diastolic volume index (EDVi as ml/m2) change, and measured as EDVi at 1-year follow-up minus EDVi at baseline. All measurements were performed using CVi42 software (Circle Cardiovascular Imaging Inc., Calgary, Canada).

Results: The mitral regurgitation was classified as moderate in 8(27.5%) patients and mild in another 3 (10.3%) by CMR. Of the 29 patients who had MVR, 6 did not have the complete baseline and follow-up CMR data (1 died, 2 refused to follow-up CMR, 2 with suboptimal baseline CMR, and 1 with both latter limitations). Regarding functional class (NYHA), one patient was in Class I (3.4%), 5 patients in Class II (17.3%), 19 in Class III (65.5%) and 4 in Class IV (13.8%) in the preoperative period. After surgery, there was a significant improvement in functional class, with 13 patients in Class I (59.1%), 8 in Class II (36.4%) and one patient in Class III (4.5%). There was a mean reduction of EDVi of 25.3± 48.7ml/m2 1 year after MVR for the entire patient group. This EDVi reduction correlated significantly with baseline pre-operatory regurgitant volume(r=-0.83, Figure 1), regurgitant fraction(r=-0.69, Figure 2), EDV index (r=0.52) and LV mass index(r=-0.40). In a multivariate stepwise linear regression, regurgitante volume was the only independent predictor of EDVi change 1 year after MVR.

Conclusion: In patients with mitral regurgitation the baseline regurgitant volumes measured by CMR precisely predict the magnitude of reverse left ventricular remodeling 1 year after mitral valve repair. Our results support the use of CMR parameters, particularly regurgitant volume, on the decision process prior to surgical mitral valve repair.

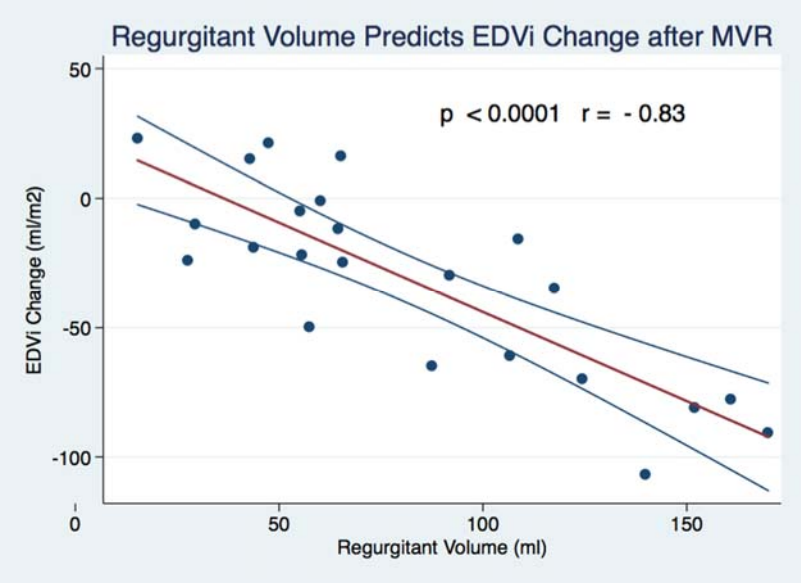

Regurgitant Volume correlation to End Diastolic Volume Index Change After MVR

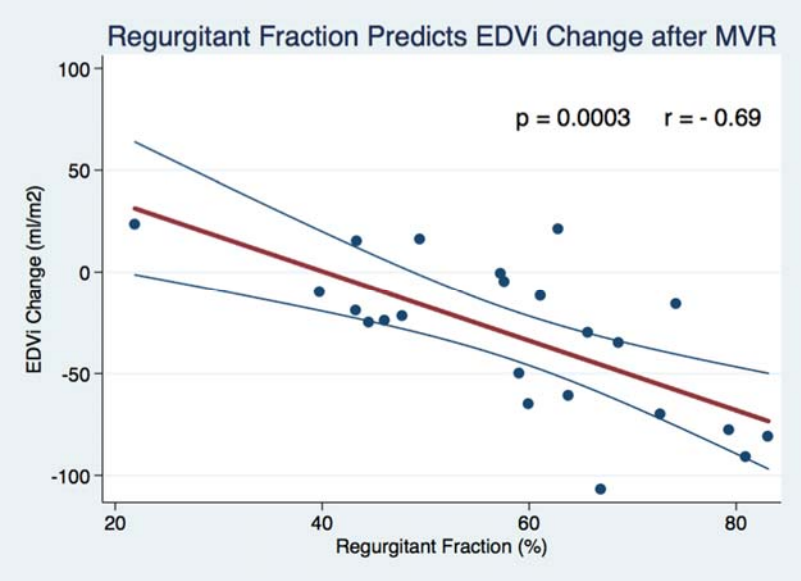

Regurgitant Fraction correlation to End Diastolic Volume Index Change After MVR

ID#: 378306

Does Native Myocardial T1 Relaxation Time and Extracellular Volume Fraction Improve After Autologous Stem Cell Transplantation in Cardiac Amyloidosis: A Case Series.

Luis Eduardo. Enriquez Rodriguez, MD[1] Jeremy R. Stone, MD[2], Victor Mor-Avi, PhD[3], Roberto M. Lang, MD[3], Amit R. Patel, MD[3]

1. Hospital Clinico San Carlos, Madrid, Madrid, Spain

2. University of Chicago Medicine, Chicago, NE

3. University of Chicago, IL

Background: Introduction: Treatment of cardiac AL amyloidosis with chemotherapy followed by autologous stem cell transplantation (ASCT) is associated with improved outcomes. However, currently little is known about the impact of ASCT on advanced cardiac magnetic resonance (CMR) and echocardiography (ECHO) biomarkers of AL cardiac amyloidosis burden such as native myocardial T1 relaxation time (T1), extracellular volume fraction (ECV), and global longitudinal strain (GLS). The aim of this case series is to determine whether ASCT is associated with improved T1, ECV, and GLS in patients with AL cardiac amyloidosis.

Methods: Methods: Four patients with AL cardiac amyloidosis underwent ECHO and CMR (1.5T) including cine-CMR, T1, ECV, and late gadolinium enhancement before and after ASCT. Left ventricular ejection fraction (LVEF), T1, and ECV were calculated from CMR images using commercially available software. GLS was calculated from ECHO images using commercially available software. Measurements from before ASCT were compared to those after ASCT using a 2 tailed t-test. A p-value

Results: Results: Mean age was 64 ± 8 years and 50% of patients were female. The average time between ASCT and CMR was 18 ± 8 months. T1 and ECV decreased significantly following ASCT (T1: 1190 ± 26 ms vs 1126 ± 58ms, p=0.035 and ECV: 41 ± 6% vs 28 ± 10%, p= 0.026). GLS also improved following ASCT (-14 ± 3% to -20 ± 2%, p=0.016). There was a statistically non-significant increased in LVEF after ASCT. See table for details. See figure for example.

Conclusion: Conclusions: T1, ECV, and GLS all improve following ASCT in patients with AL cardiac amyloidosis, suggesting a reduction in amyloid burden. These findings suggest that these advanced CMR and ECHO parameters may be useful imaging-based biomarkers of the burden of AL cardiac amyloidosis.

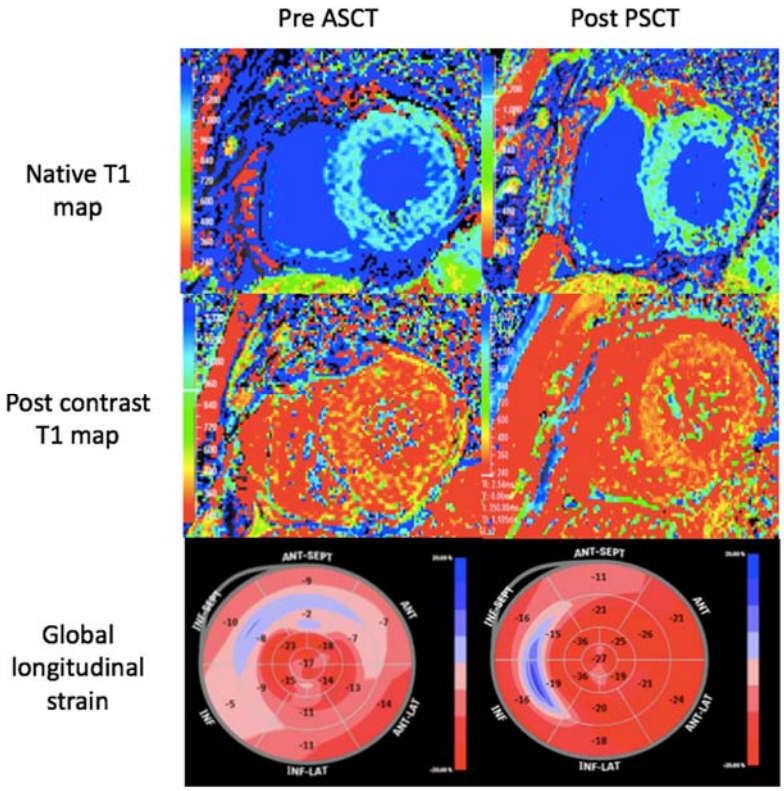

Figure 1. Improvement in native T1 map, post contrast T1 map and LGS after ASCT in patient 4.

Table 1. Demographic, CMR and echocardiographic parameters in patients with AL cardiac amyloid before and after ASCT.

Case	Age (years)	Sex	pre native T1 relaxation time (mseg)	post native T1 relaxation time (mseg)	p	pre ECV	post ECV	p	pre LVEF (%)	post LVEF (%)	p	pre LGS (%)
1	64	M	1210	1147		48	39		44	50		-14
2	54	F	1203	1171		NA	NA		57	58		-19
3	63	M	1195	1148		37	21		55	57		-12
4	73	F	1153	1041		38	23		60	64		-12
Mean	64		1190	1127	0.04	41	28	0.03	54	57	0.06	-14

ID#: 378321

TEMPORAL VARIABILITY of QUANTITATIVE MYOCARDIAL CMR and BLOOD BIOMARKERS IN HEALTHY VOLUNTEERS

Mustafa A. Altaha, MBBS[1]Mark T. Nolan, MBBS[2], Paul M. Yip, PhD, FCACB, DABCC[2], Kim A. Connelly, MD, PhD[3], Maria Michalowska, BSc.[4], Bernd Wintersperger, MD, EBCR, FAHA[5], Paaladinesh Thavendiranathan, MD, MSc[2]

1. University Health Network, University of Toronto, Faculty of Medicine, Institute of Medical Science, Toronto, ON, Canada

2. University Health Network, University of Toronto, Toronto, ON, Canada

3. St. Michaels Hospital and University of Toronto, Toronto, ON, Canada

4. University Health Network, Toronto, ON, Canada

5. University Health Network and University of Toronto, Toronto, ON, Canada

Background: There is a growing interest in using quantitative cardiac-MRI (CMR) tissue-characterization techniques to sequentially follow patients with a goal of detecting pre-clinical myocardial changes. However, there is limited data on the variability of these CMR parameters. In this study, we sought to quantify the expected temporal and observer variability of T2, native-T1, and extra-cellular volume fraction (ECV) measurements and compare to variability in serum biomarkers in healthy volunteers.

Methods: Thirty healthy volunteers (60% female, age: 45.5±13.7 years, range: 23–80 years), with no cardiovascular disease, risk factors, or medications, were prospectively recruited to undergo 3-CMR studies at 1.5T at 3-month intervals (90.4±10.9 days). T2 maps were obtained using a T2-prepared single-shot SSFP technique, and native (5(3)3)- and post-contrast (4(1)3(1)2)-T1 maps were obtained using a MOLLI technique at basal, mid, and apical short-axis locations. Based on native-/post-contrast MOLLI data, ECV values were calculated. LVEF was measured using short-axis SSFP cines. All measurements were performed using commercially-available software (CVI42) by two observers blinded to all clinical and each other';s data. Each volunteer had blood draw within 2 hours of the CMR exam, and high-sensitivity troponin-I (TnI) and B-type natriuretic peptide (BNP) levels were measured. Temporal, inter-observer, and intra-observer variability were calculated as the coefficient of variation (CoV) and as the Standard Error of the Measurement (SEM) using one- and two-way ANOVA.

Results: Mean LVEF at the three time points were: at baseline =59.9±3.8%, at 3-month =59.0±4.7%, and at 6-month =59.5±4.5%. The mean tissue-characterization and biomarkers values were: T2 =51.8ms, native-T1 =1003.6ms, ECV =24.9%, TnI =2.1ng/ml, and BNP =22.5pg/ml (Table-1). Over the 6 months, the whole-myocardial temporal variability was: T2 =1.5ms, native-T1 =12.4ms, ECV =1.4%, TnI =0.4ng/ml, and BNP =9.8pg/ml (Figure-1). Amongst the tissue-characterization techniques, native-T1 had the smallest temporal variability. Between the biomarkers, TnI had lower temporal variability, although slightly larger than that of all tissue-characterisation techniques (Table-1). The inter- and intra-observer variability for CMR measurements were small (Table-1). There were no statistically significant changes in LVEF, T2, native-T1, and ECV measurements over time.

Conclusion: The temporal variability of T2, native-T1, ECV and TnI in healthy volunteers was low, with native-T1 having the lowest temporal variability. The temporal variability of tissue-characterisation techniques was lower than that for blood biomarkers. Whole-myocardial temporal changes in T2>1.8ms, native-T1 values >14.6ms, and ECV>1.7% can be considered to represent changes that extend beyond variability attributable to physiological and technical factors. The inter- and intra-observer reproducibility of these measurements were excellent.

Table-1. Temporal Variability, Repeatability, Reproducibility, and Normal Values for T2, native-T1, ECV, Troponin-I and BNP

Variable	Mean^ (95% CI)	Temporal Variability			Repeatability	Reproducibility
		SEM[&] (95% CI)	P-value[$]	CoV[&] (95% CI)	SEM	SEM
T2 (Whole LV) * (ms)	51.8 (50.5–53.1)	1.5 (1.3–1.8)	0.389	2.7 (2.3–3.2)	0.71	0.84
Native-T1 (Whole LV) * (ms)	1003.6 (995.5–1011.7)	12.4 (10.8–14.6)	0.358	1.1 (0.9–1.3)	7.3	8.5
ECV (Whole LV) * (%)	24.9 (23.9–25.9)	1.4 (1.3–1.7)	0.558	4.8 (3.8–5.8)	0.28	0.44
Troponin-I [@] (ng/ml)	2.1 (1.9–2.3)	0.40 (0.35–0.46)	0.203	5.7 (1.6–9.8)		
BNP [#] (pg/ml)	22.5 (14.3–30.7)	9.8 (8.6–11.5)	0.620	24.3 (18.5–30.2)		

*mean of measurements from 3 slices (base, mid, and apex); ^Mean values from the baseline measurements of the first reader; [@]Troponin-I Values below 2 were given a score of 2; [#] BNP Values below 10 were given a score of 10, [&]Averaged from two readers; [$]Linear mixed model - correlation compound symmetry;

Figure-1. Temporal Changes for T2, native-T1, ECV, Troponin-I and BNP

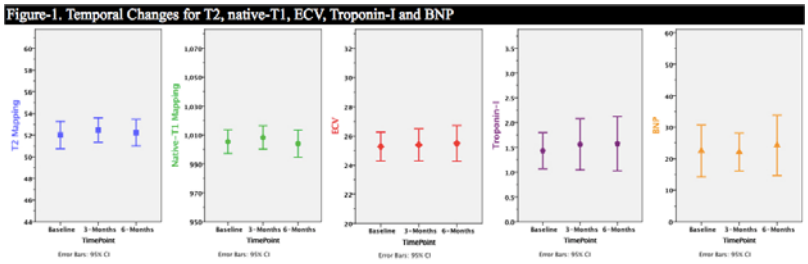

ID#: 378343

Deep Learning Approach for Left Ventricular Endocardium Segmentation in Long-Axis Cardiac MR Imaging

Liang Zhong, PhD[5] Shuang Leng, Ph.D.[1], Xulei Yang, PhD[2], Xiaodan Zhao, PhD[1], Yi Su, PhD[3], Ru San Tan, MBBS, MRCP[4]

1. National Heart Centre Singapore, Singapore

2. Institute of High Performance Computing, Singapore, N/A, Singapore

3. Institute of High Performance Computing, Singapore

4. National Heart Centre Singapore; Duke-NUS Medical School, Singapore, Singapore

5. National Heart Centre Singapore; Duke-NUS Medical School, Singapore

Background: The segmentation of left ventricular (LV) endocardium in long-axis views of cardiac magnetic resonance (CMR) imaging is a prerequisite for downstream assessment of LV structure and function. As manual delineations are tedious and time-consuming, the current study sought to develop a computational method to segment LV endocardium automatically based on deep learning (DL).

Methods: Sixty subjects (30 controls, 30 patients) were used for training and testing the proposed framework, including 4800 images from 40 subjects (20 controls, 20 patients) for training the model and 2400 images from 20 subjects (10 controls, 10 patients) for performance testing, where images were acquired in 4-, 3-, and 2-chamber long-axis views using a 3T Philips MR scanner (Ingenia, Philips Healthcare). The proposed framework (Fig. 1) was based on DL with fully convolutional networks (FCN) architecture[1,2], which includes 8 convolutional layers, 3 max-pooling layers, and 3 up-sampling layers. LV contour tracking analysis was manually conducted by a CMR expert with more than 20-year experience using the QMass software (Medis, Netherlands) and endocardial contours were retrieved as ground truth. The proposed DL method was evaluated using the Dice metric (DM), Pearson';s correlation (R), Bland Altman analysis and intra-class correlation coefficient (ICC).

Results: One example of the segmentation results was shown in Fig. 2 for a 71-year-old female healthy volunteer, where the DM values were 0.95 for 4-chamber view, 0.96 for 3-chamber view, and 0.95 for 2-chamber view. Table 1 presents the evaluation results for all 20 subjects in the testing set in terms of DM values. The overall DM of the output from the proposed model was 0.93 ± 0.04 (range: 0.76 – 0.97) with best results in the 2-chamber view (DM = 0.94 ± 0.02, range: 0.89 – 0.97). The results by comparison with ground truth for LV volumetric measurements were as follows (Table 2): **End-diastolic volume**: R = 0.975, Bias = -1.8 ml, ICC = 0.983; **End-systolic volume**: R = 0.992, Bias = 3.1 ml, ICC = 0.989; **Ejection fraction**: R = 0.971, Bias = -1.1%, ICC = 0.985. The proposed DL-based segmentation process took less than 3 seconds per subject (or < 30 milliseconds per image over 120 images for each subject).

Conclusion: The proposed framework offers a promising means to achieve fully automated segmentation of the LV endocardium in long-axis CMR images using an appropriately trained deep convolutional neural networks. **Reference**

1. Long J, Shelhamer E, Darrell T. Fully convolutional models for semantic segmentation. CVPR 2015.
2. Yang XL, Gobeawan L, Yeo SY, Tang WT, Wu ZZ, Su Y. Automatic segmentation of left ventricular myocardium by deep convolutional and de-convolutional neural networks. CINC Computing in Cardiology 2016.

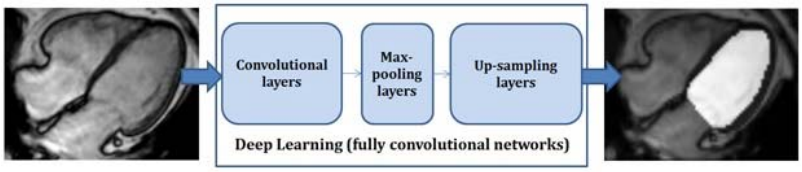

Figure 1. The framework of the proposed method.

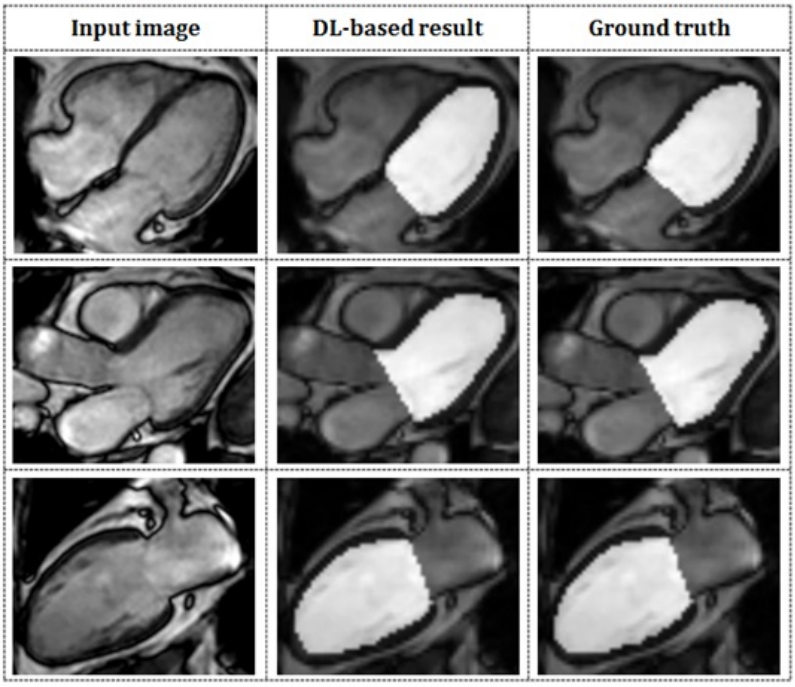

Figure 2. One example of segmentation results for a 71-year-old female healthy volunteer: DM = 0.95 for 4-chamber view (top row), DM = 0.96 for 3-chamber view (middle row), DM = 0.95 for 2-chamber view (bottom row). DL: deep learning; DM: Dice metric.

Table 1: Evaluation results of proposed framework in terms of DM values for all 2400 images from 20 subjects in testing set.

CMR long-axis views	DM
4-chamber	0.92 ± 0.04 (range: 0.76 – 0.96)
3-chamber	0.92 ± 0.05 (range: 0.76 – 0.96)
2-chamber	0.94 ± 0.02 (range: 0.89 – 0.97)
Overall	0.93 ± 0.04 (range: 0.76 – 0.97)
Data expressed as mean ± SD. CMR: cardiac magnetic resonance; DM: Dice metric.	

Table 2: Performance evaluation by correlation, Bland Altman analysis, and ICC between DL-based results and ground truth for EDV, ESV and EF.

Variables	Correlation R	Bias (limits of agreement)	ICC (95% CI)
EDV, ml	0.975	-1.8 (-49.3, 45.6)	0.983 (0.957, 0.993)
ESV, ml	0.992	3.1 (-33.4, 39.7)	0.989 (0.973, 0.996)
EF, %	0.971	-1.1 (-8.7, 6.5)	0.985 (0.961, 0.994)

EDV: end-diastolic volume; ESV: end-systolic volume; EF: ejection fraction; ICC: intra-class correlation; CI: confidence interval.

ID#: 378354

Diffuse myocardial fibrosis in heart failure with preserved and reduced ejection fraction assessed by CMR native T1 and extracellular volume fraction mapping on 3T

Xiaodan Zhao, PhD[1] Shuo Zhang, PhD[2], Xiu Ting Li, PhD[3], Yi Ying Han, BSc[4], David Sim, MBBS, MRCP[1], Fazlur Rehman Jaufeerally, MBChB[5], Arthur Mark Richards, MBChB, MD (Distinction), PhD, DSc, FRACP, FRCP,FAHA, FRSNZ[6], Seet Yoong Loh, MBBS, MRCP, M.Med [7], Dinna K.N. Soon, MBBS, MRCP, FAMS[8], Sheldon S. G. Lee, MBBS[9], Angela S Koh, MBBS, MPH, MMed, MRCP, FESC, FACC[1], Carolyn SP Lam, MBBS, PhD, MRCP, MS, FACC, FAMS, FESC[1], Liang Zhong, PhD[10], Ru San Tan, MBBS, MRCP[11]

1. National Heart Centre Singapore, Singapore

2. Philips Healthcare, Singapore, Singapore

3. Singapore Bioimaging Consortium, Singapore

4. Clinical Imaging Research Centre, Singapore

5. Singapore General Hospital; Duke-NUS Medical School, Singapore

6. National University Hospital, Singapore

7. Tan Tock Seng Hospital, Singapore

8. Khoo Teck Puat Hospital, Singapore

9. Changi General Hospital, Singapore

10. National Heart Centre Singapore; Duke-NUS Medical School, Singapore

11. National Heart Centre Singapore; Duke-NUS Medical School, Singapore, Singapore

Background: Myocardial fibrosis plays an important role in the pathogenesis and prognosis of heart failure (HF). Cardiovascular magnetic resonance (CMR) myocardial T1 and extracellular volume (ECV) fraction mapping techniques can detect and quantify diffuse fibrosis. We aimed to characterize and compare the extent of diffuse myocardial fibrosis in patients with HF with preserved (HFpEF) versus reduced ejection fraction (HFrEF).

Methods: HF patients from 6 centers in the country were prospectively enrolled to undergo CMR on a single 3.0T scanner (Philips, Ingenia) that was used throughout the study. In addition to late gadolinium enhancement (LGE) imaging for detection of focal macrofibrosis, native and post-contrast T1 mapping were performed using standard MOLLI imaging sequences with optimized with a second-based scheme at the mid and basal left ventricular (LV) short-axis (SAX) levels. Typical imaging parameters were: field of view 340 × 290 mm^2, acquired pixel size 1.8 × 1.8 mm^2 interpolated to 1.0 x 1.0 mm^2, slice thickness 8 mm; TR/TE 2.8ms/1.38 ms; flip angle 35°, minimal inversion time 87.7 ms; SENSE imaging factor 2. ECV maps were generated after applying off-line image motion correction and co-registration, as well as same-day hematocrit results. For comparison between HFpEF and HFrEF groups, pre-specified regions of interest (ROIs) for T1 and ECV analyses included (1) the entire myocardium within either the mid or basal SAX slice; (2) focal lesion area corresponding to LGE; remote myocardial tissue without LGE at the (3) LV septum; (4) LV lateral wall; and (5) right ventricular wall. Analysis of variance (ANOVA) was performed; p-value smaller than 0.05 indicated statistically significant difference.

Results: 107 HF patients (mean age 57±11 years; male-female ratio 85:22) were enrolled. 27 were HFpEF (mean age 57 years, mean LVEF 57%); and 80, HFrEF (mean age 58 years, mean LVEF 30%). Of 214 acquired SAX slices, 13 slices failed image quality checks and only 201 SAX slices were analyzed. Within either HFpEF or HFrEF group, the slices were stratified into subgroups with and without focal lesions (i.e. LGE). **Figure 1** demonstrates four typical slice images in each subgroup.Image slices in HFpEF subjects without focal lesion (subgroup 2) had the lowest native T1 and ECV values that were significantly different from the other 3 subgroups (**Table**). T1 and ECV values in the slices generally increased in this order: HFrEF without focal lesion, HFpEF with focal lesion, and HFrEF with focal lesion. In the slices without LGE (subgroups 2 and 4), native T1 and ECV were significantly different for entire SAX, septum, and lateral ROIs (**Figure 2)**. Significant differences were consistently detected at the base and mid anteroseptal (S2 and 8) and inferoseptal (S3 and 9) segments. No significant between-group differences were detected for right ventricular wall segments; as well as all segments for post-contrast T1.

Conclusion: HFrEF carries larger diffuse fibrosis burden than HFpEF; and the presence of LGE not unexpectedly increases quantifiable fibrosis amount in either group. In hearts without focal LGE, quantitation of native T1 and ECV at the base to mid septum reproducibly discriminates between HFpEF and HFrEF, and may be the preferred

ROI for noninvasive detection of diffuse fibrosis, monitoring of progression and response to treatment in HF patients.

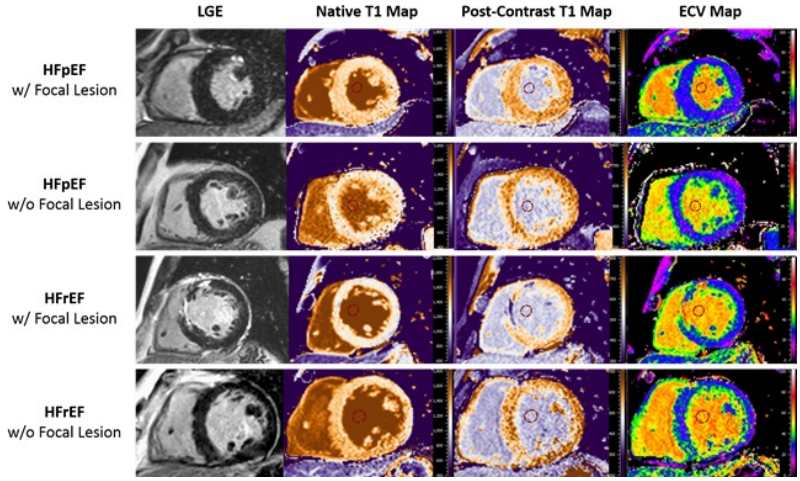

Figure 1. Cardiac magnetic resonance parametric maps of late gadolinium enhancement (LGE), native T1, post-contrast T1 and extracellular volume (ECV) in heart patients from the four subgroups (see text).

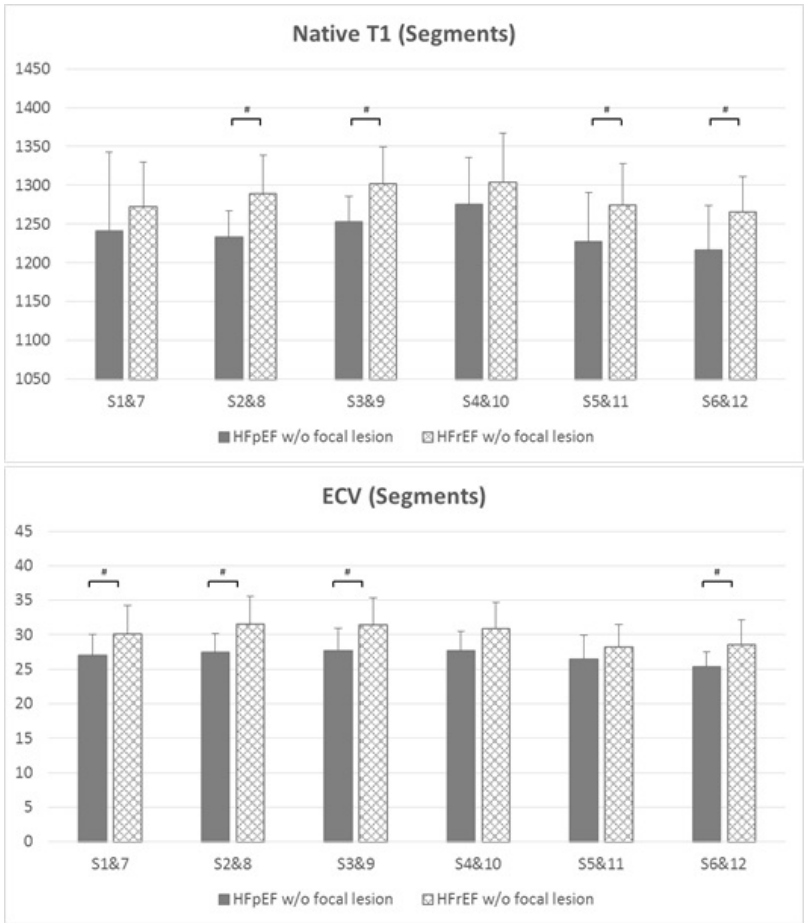

Figure 2. Comparison of segmental native T1 and extracellular volume values in HFpEF versus HFrEF both without focal macrofibrosis lesions (n = 78 slices). [# P < 0.05 between subgroup 2 and 4 (subgroup 2 = HFpEF focal lesion -, 4 = HFrEF focal lesion -). S1&7, S2&8, S3&9, S4&10, S5&11, S6&12 refer to the anterior, anteroseptal, inferoseptal, inferior and inferolateral walls, respectively of the standard American Heart Association 17-segment heart model; mean values of the base and mid left ventricular parameters are indicated.]

Table. Cardiac magnetic resonance findings of myocardial native T1, post-contrast T1 and extracellular volume in the four subgroups of image slices (n = 201 slices) stratified by preserved versus reduced ejection fraction, and presence versus absence of focal late gadolinium enhancement.

	Subgroup 1 HFpEF Focal lesion + (n = 27)	**Subgroup 2 HFpEF Focal lesion -** (n = 26)	**Subgroup 3 HFrEF f Focal lesion +** (n = 96)	**Subgroup 4 HFrEF Focal lesion -** (n = 52)	**ANOVA P value**
Native T1 [ms]					
SAX	1273 ± 51	1239 ± 43#	1284 ± 52#	1284 ± 43#	<0.001
Septum	1262 ± 53*	1221 ± 31*#	1266 ± 46#	1280 ± 45#	<0.001
Lateral	1220 ± 54	1195 ± 48#	1237 ± 52#	1250 ± 51#	<0.001
RV	1316 ± 90	1284 ± 105	1298 ± 81	1292 ± 83	0.561
Post-contrast T1 [ms]					
SAX	583 ± 64	620 ± 49#	583 ± 71#	598 ± 57	0.052
Septum	589 ± 66	623 ± 45	604 ± 71	593 ± 54	0.165
Lateral	606 ± 62	629 ± 54	626 ± 61	614 ± 65	0.353
RV	580 ± 70	604 ± 48	599 ± 67	595 ± 48	0.463
ECV [%]					
SAX	31.8 ± 5.4*	26.8 ± 2.3*#	33.0 ± 5.4#§	30.2 ± 3.1#§	<0.001
Septum	31.0 ± 5.1*	26.3 ± 2.9*#	30.6 ± 4.7#	30.6 ± 3.4#	<0.001
Lateral	28.4 ± 4.6*	25.1 ± 2.3*#	28.1 ± 4.3#	27.9 ± 4.3#	0.010
RV	33.0 ± 5.4	30.0 ± 5.3	31.7 ± 5.7	30.6 ± 4.7	0.157

+ denote present, - denotes absent;

*p<0.05 HFpEF+ and other three groups;#p<0.05 HFpEF+ and HFrEF-;$ p<0.05 HFpEF+ and HFrEF+;§ p<0.05 HFrEF- and HFrEF+

ID#: 378380

Focused, Whole Body Vascular MR Imaging in Less than Five Minutes with Ferumoxytol

Puja Shahrouki, M.D.[1] Kim-Lien Nguyen, M.D.[2], Biraj Bista, M.D.[3], John M. Moriarty, M.D.[4], Stephen T. Kee, M.D.[4], Brian G. DeRubertis, M.D.[4], Sarah N. Khan, M.D.[4], Takegawa Yoshida, M.D.[4], J. Paul Finn, M.D.[4]

1. Department of Radiology, David Geffen School of Medicine at UCLA, Los Angeles, CA

2. Division of Cardiology, David Geffen School of Medicine at UCLA and VA Greater Los Angeles Healthcare System, CA

3. Department of Radiology, David Geffen School of Medicine at UCLA, Santa Monica, CA

4. Department of Radiology, David Geffen School of Medicine at UCLA, CA

Background: Whereas vascular MR imaging has been widely used for more than two decades, the prolific rise of CT angiography (CTA) has underscored the advantages in speed and practicality of modern CTA when compared to contrast enhanced MR angiography (CEMRA). Beyond challenges in workflow, the relatively long magnet time associated with conventional MR techniques serves to discourage patients with even modest levels of claustrophobia. Furthermore, recent controversies surrounding the safety of gadolinium based contrast agents (GBCA) has added further uncertainty in the cost-benefit balance point of conventional CEMRA. We hypothesize that with the use of ferumoxytol (Feraheme, AMAG Pharmaceuticals), comprehensive vascular imaging of the thorax, abdomen and pelvis can be performed in as little as 5 minutes magnet time.

Methods: Eight examinations were carried out in 7 claustrophobic patients (age 11 to 63 years, 4 males) with renal failure (6 dialysis-dependent and 1 with diseased-donor renal transplant). All patients expressed reluctance to undergo the MR examination due to claustrophobia, but agreed to a trial of up to 10 minutes in the scanner bore. Following localizer sequences, breath held, high-resolution 3-D ferumoxytol enhanced MR angiography (FEMRA) was carried out in one (n=1) or two (n=7) overlapping stations on a 3.0T MR system (Magnetom TIM Trio or Magnetom Skyra, Siemens Medical Solutions) or a 1.5T MRI system (Magnetom TIM Avanto, Siemens Medical Solutions). Acquisition time for each station was 16-20 seconds and voxel dimensions were on the order of 1 mm x 1.2 mm x 1.3 mm. Overlapping stations were spliced using vendor software (Image Compose, Siemens). The total scanning time was measured from the beginning of localizer image acquisition to the end of the ultimate FEMRA acquisition. Scanner tuning and coil adjustment routines preceded localizer acquisition. Patient-specific machine shimming was not performed and the default shim settings were employed to minimize adjustment time.

Results: All examinations were completed successfully without adverse events. The average scanning was 6.27 minutes (range 4.16 to 10.10 minutes) and tune up time was less than one minute. All scans were considered of high diagnostic quality and supported full visualization of arterial and venous anatomy from the neck to the thighs.

Conclusion: Comprehensive vascular imaging of the thorax, abdomen and pelvis can be completed in as little as 5 minutes in the scanner bore using focused MR angiographic image acquisition, following infusion of ferumoxytol. The implications for imaging of claustrophobic patients and for vascular MRI workflow and scanner efficiency are profound.

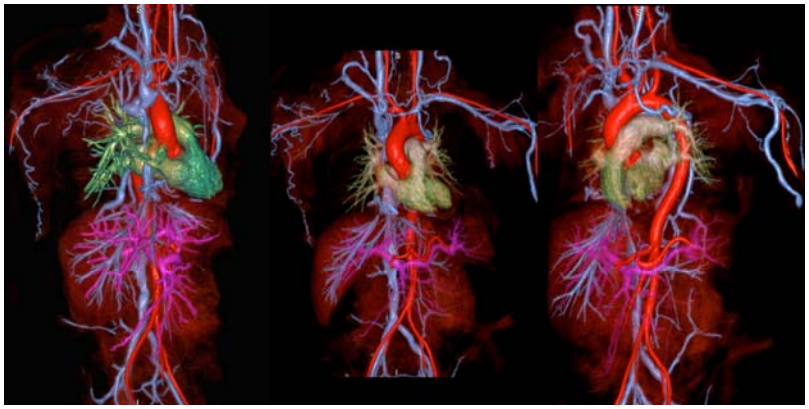

Reconstructed 3-D volume rendered images from 3.0 T FEMRA in a claustrophobic 35 year-old female with a scanning time of 6 minutes and 57 seconds.

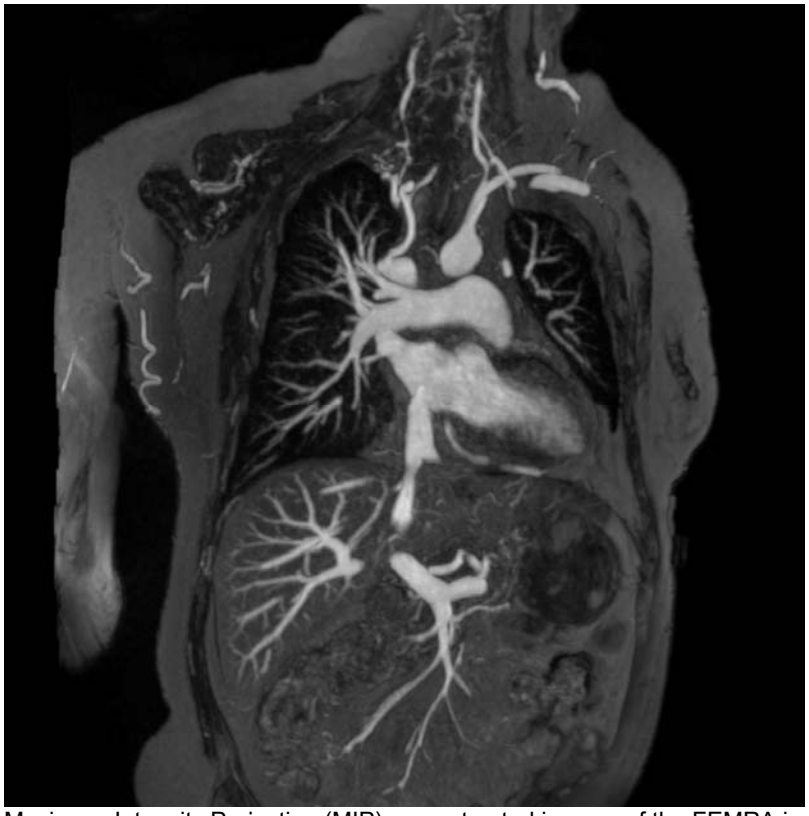

Maximum Intensity Projection (MIP) reconstructed images of the FEMRA in the 35 year-old claustrophobic female.

ID#: 378387

Imaging 4D tricuspid annulus morphology and motion in congenital heart diseases using long-axis CMR imaging

Liang Zhong, PhD[6] Shuang Leng, Ph.D.[1], Watcharee Prasertkulchai, MSc[2], Shuo Zhang, PhD[3], Xiaodan Zhao, PhD[1], Varinsawat Thirawut, MD[2], Sukit Yamwong, MD[4], Ru San Tan, MBBS, MRCP[5], Tarinee Tangcharoen, MD[2]

1. National Heart Centre Singapore, Singapore

2. Ramathibodi Hospital, Bangkok, Thailand

3. Philips Healthcare, Singapore, Singapore

4. Ramathibodi Hospital, Mahidol University, Bangkok, Thailand

5. National Heart Centre Singapore; Duke-NUS Medical School, Singapore, Singapore

6. National Heart Centre Singapore; Duke-NUS Medical School, Singapore

Background: Imaging-based assessment of tricuspid annulus (TA) lags far behind that of the mitral annulus. In this study, we advance the right ventricular (RV) imaging using radially rotational long-axis cardiovascular magnetic resonance (CMR) to quantify 4D dynamics and morphology of the TA

Methods: Study population consisted of 13 patients (38 ± 16 years) with congenital heart disease and 4 normal controls (39 ± 24 years). Cine CMR was performed in the right ventricle in long axis with 18 radially rotational planes and 10° angular equidistance (Fig. 1(A)). By tracking the TA motion trajectory in the spatiotemporal dimension along the annular region for all cardiac phases (Fig. 1(B-C)), four dynamic parameters (Fig. 1(E-F)) were obtained. These include peak systolic velocity (Sm), peak early diastolic velocity (Em), peak late diastolic velocity (Am), and tricuspid annular plane systolic excursion (TAPSE). In addition, the spatiotemporal morphological measurements were derived based on TA reconstruction (Fig. 1D) for all successive frames throughout the cardiac cycle including the 3D area, perimeter, diameter, and height.

Results: Feature tracking analysis was feasible in all subjects. The TA morphological parameters at end-diastole (ED) were not significantly different from those at end-systole (ES). Despite no significant differences in the measurements of TA morphology between patient and normal groups (Table 1), the TA peak velocities Sm, Em, Am and maximal displacement TAPSE in the patient group (8.3 ± 2.0, 7.7 ± 2.6, 9.1 ± 4.0 cm/s, and 15.0 ± 3.4 mm) were significantly smaller than those in the normal group (11.0 ± 1.5, 11.6 ± 3.2, 12.6 ± 1.4 cm/s, and 21.4 ± 3.4 mm, all $P < 0.05$)(Fig. 2).

Conclusion: Feature tracking in radially rotational long-axis cine CMR provided a comprehensive and distinctive profile for 4D TA dynamics and morphology, which may help to further study different cardiac diseases and guide surgical planning including in vivo evaluation of the TA prosthetic ring. Current study also demonstrated impaired tricuspid annular velocities and displacements in clinically diagnosed CHD.

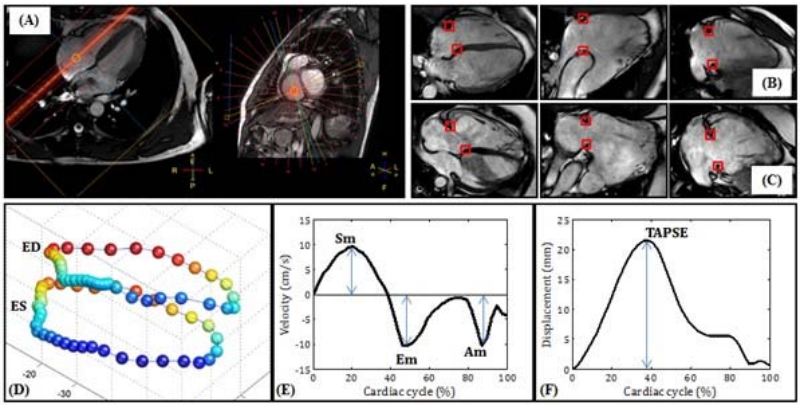

Figure 1. (A) Radially rotational long-axis RV cine CMR in 18 planes. Motion tracking of the TA (red rectangle) in (B) normal and (C) patient (selected planes of 4-chamber, RV inflow/outflow, and RV 2-chamber). (D) Reconstructed TA ring at end-diastole (ED) and end-systole (ES). (E) TA velocity curve. (F) TA displacement curve. Sm: peak systolic velocity; Em: peak early diastolic velocity; Am: peak late diastolic velocity; TAPSE: tricuspid annular plane systolic excursion.

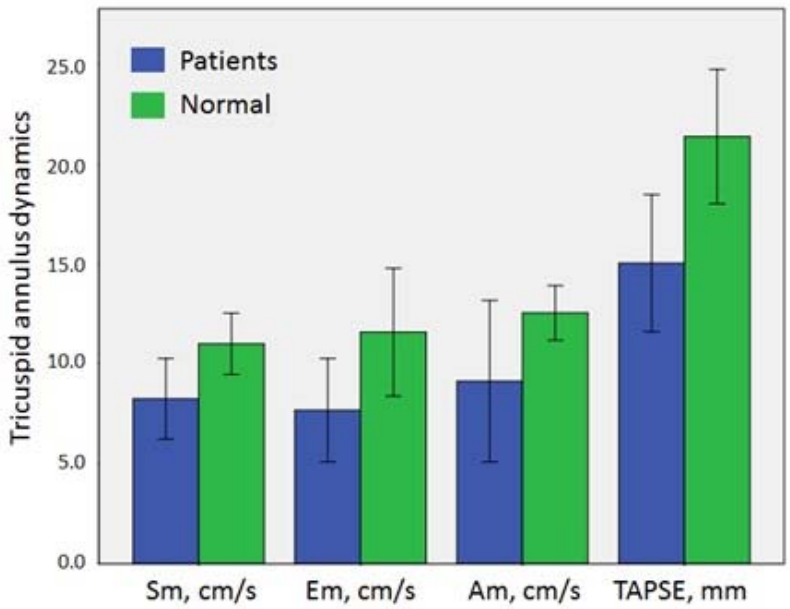

Figure 2. Significantly reduced tricuspid annulus dynamics in patients compared to normal (all P < 0.05).

Table 1. Tricuspid annulus morphology in normal and patient groups.

Parameters		**Normal**	**Patients**	***P* value***
3D Area, cm2	Average	13.6 ± 2.5	11.6 ± 2.6	0.141
	ED	12.5 ± 3.0	11.2 ± 2.6	0.571
	ES	13.2 ± 2.1	11.1 ± 2.6	0.100
Perimeter, mm	Average	136.4 ± 11.1	125.6 ± 13.8	0.089
	ED	129.3 ± 15.6	122.7 ± 13.8	0.428
	ES	135.5 ± 8.6	123.6 ± 14.5	0.113
AS-PL Diameter, mm	Average	39.0 ± 4.3	33.5 ± 5.4	0.113
	ED	39.6 ± 5.8	33.0 ± 5.5	0.056
	ES	37.9 ± 3.9	32.6 ± 5.1	0.113
AL-PS Diameter, mm	Average	39.8 ± 3.9	34.9 ± 4.9	0.070
	ED	36.1 ± 4.0	33.8 ± 5.1	0.308
	ES	38.8 ± 4.0	34.0 ± 4.2	0.070
AS-PL to AL-PS Diameter Ratio	Average	0.98 ± 0.10	0.97 ± 0.19	0.734
	ED	1.09 ± 0.05	0.99 ± 0.22	0.213

	ES	0.98 ± 0.13	0.97 ± 0.16	0.734
Height, mm	Average	7.2 ± 1.1	6.5 ± 3.1	0.428
	ED	6.6 ± 1.6	6.6 ± 2.8	0.610
	ES	7.2 ± 1.4	6.5 ± 3.5	0.428
Data were presented as mean ± SD. AS-PL: anteroseptal to posterolateral; AL-PS: anterolateral to posteroseptal; ED: end diastole; ES: end systole. **P* values obtained using Mann-Whitney U test.				

ID#: 378153

Left ventricular Performance in Takotsubo Syndrome and Aborted Myocardial Infarction: preliminary data of a prospective multicenter CMR study

Nadine Abanador-Kamper[1]Lars Kamper[2], Witali Pomjanski[3], Harald Lapp[4], Haage Patrick[2], Jeanette Schulz-Menger, MD[5], Melchior Seyfarth[1]

1. Department of Cardiology, HELIOS Medical Center Wuppertal, University Hospital Witten/Herdecke, Wuppertal, Germany; Center for Clinical Medicine Witten/Herdecke University Faculty of Health, Wuppertal, Germany, Germany

2. Radiology, HELIOS University Hospital Wuppertal, University Witten/Herdecke, Germany; Center for Clinical Medicine Witten/Herdecke University Faculty of Health, Wuppertal, Germany, Germany

3. Department of Cardiology, HELIOS University Hospital Wuppertal, University Witten/Herdecke, Germany; Center for Clinical Medicine Witten/Herdecke University Faculty of Health, Wuppertal, Germany, Germany

4. HELIOS Klinikum Erfurt, Germany

5. Working Group on Cardiovascular Magnetic Resonance, Experimental and Clinical Research Center a joint cooperation between the Charité Medical Faculty and the Max-Delbrueck Center for Molecular Medicine HELIOS Klinikum Berlin Buch, Germany, Berlin, Germany

Background: Rapid recovery of left ventricular function (LVEF) has been previously described in Takotsubo syndrome (TTS). Temporary course of LVEF recovery in aborted myocardial infarction (aborted MI) has not been reported, so far. Aim of this study was to assess LVEF recovery in both entities as well as myocardial tissue changes.

Methods: Between May 2016 and August 2017 we prospectively included a total of 38 patients with TTS and aborted MI into a multicenter CMR study. Aborted MI was defined as first, reperfused STEMI with a maximum symptom to intervention time of two hours. CMR was performed on a 1.5 T scanner. Initial scan was performed 3 days (interquartile range 2-4) after PCI. Scan protocol included a state of the art cine SSFP to evaluate the LV function. Myocardial injury was assessed by blackblood and fat suppressed T2-weighted sequence (myocardial oedema) and a 2D IR sequence (LGE) for focal fibrosis and microvascular obstruction (MO). Each was quantified using cvi42®. Two follow-up scans were performed after one and three months assessing LVEF and myocardial oedema.

Results: Initial LVEF was decreased in TTS (n=12) and aborted MI (n=26); (50.3±7.9% vs. 57.5±9.6%, P=0.014, Figure 1). LVEF increased similarly during follow-up scans in both groups (65.3±4.5% vs. 61.7±8.6%, *P*=0.089 and 66.1±4.1% vs. 62.5±8.11%, *P*=0.081). T2 size between both groups did not significantly differ throughout all scans (Figure 1). Mean T2 size was initially 29.9±17.4% in TTS and 30.4±21.7% in aborted MI (*P*=0.472) and was resolved in both groups after one month (3.9±5.5% vs. 5.9±6.5%, *P*=0.190). LGE size was significantly larger in aborted MI compared to TTS (8.0±9.5% vs. 0.0±0.0%, *P*=0.010) during the initial scan. MO size was greater in aborted MI compared to TTS (0.0±0.0% vs. 0.2±0.4%, P=0.231; Figure 2).

Conclusion: Our preliminary data show a similar recovery of systolic LV function in aborted MI compared to TTS with a better initial LVEF but larger focal fibrosis in aborted MI.

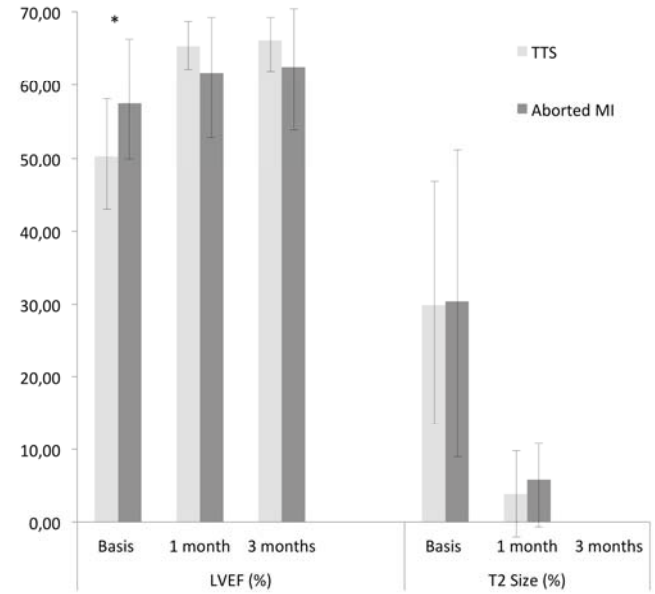

Figure 1 Temporal course of mean LVEF and mean myocardial oedema size between TTS and aborted MI

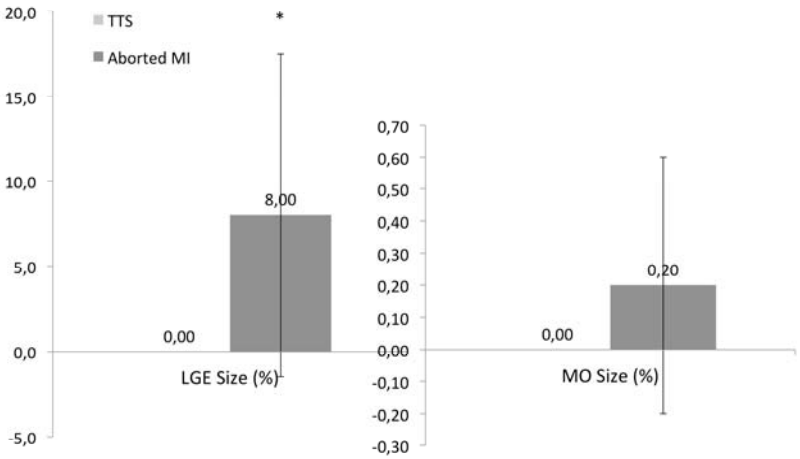

Figure 2 Mean size of LGE and MO in TTS and aborted MI after initial scan

ID#: 378163

T1 mapping for non-invasive quantification of diffuse myocardial fibrosis in children and adolescents with primary inherited cardiomyopathy

Nadya Al-Wakeel - Marquard, M.D.[1] Franziska Degener, M.D.[2], Marcus Kelm, M.D.[2], Boris Schmitt, M.D.[2], Titus Kuehne, PhD M.D.[3], Sabine Klaassen, M.D.[4], Felix Berger, PhD M.D. [5], Daniel Messroghli, M.D.[2]

1. German Heart Center Berlin, Berlin, Berlin, Germany

2. German Heart Center Berlin, Germany

3. Charité -Universitätsmedizin Berlin, Berlin, Germany

4. Experimental and Clinical Research Center, a joint cooperation between the Charité Medical Faculty and the Max-Delbrück-Center for Molecular Medicine, Germany

5. German Heart Center Berlin, Berlin, Germany

Background: In adults with primary inherited cardiomyopathy (CM) increased diffuse myocardial fibrosis (DMF) in association with adverse clinical outcome has been described. However, its relevance in pediatric patients remains relatively unknown. This study aimed to non-invasively evaluate extracellular volume (ECV) reflecting DMF with cardiovascular magnetic resonance (CMR) T1 mapping and to analyze correlations with clinical baseline data, ventricular function, exercise capacity and pro brain natriuretic peptide (proBNP) as a biomarker for heart failure in children and adolescents with primary inherited CM.

Methods: In total, 19 patients (mean age 13.0±3.9 years, 7 female) with CM (dilated CM (DCM), n=4; hypertrophic CM (HCM), n=6; left ventricular non-compaction CM (LVNC), n=7; restrictive CM, n=1; arrhythmogenic right ventricular CM, n=1) and 8 healthy controls (15.3±4.7 years, 5 female) were prospectively enrolled. Standardized CMR imaging at 1.5 Tesla with modified Look-Locker Inversion recovery (MOLLI) T1 mapping, cardiopulmonary exercise testing (CPEX) and blood sampling were performed. Circumferential and septal ECV were calculated in midventricular and basal short axis planes.

Results: Septal ECV in DCM was significantly higher than in HCM (42.7±4.3% vs. 22.9±2.8%, p=0.015) and was significantly elevated compared to controls (26.7±3.6%, p=0.012). In the patient group, circumferential and septal ECV were associated with age at CMR (r=-0.75 and -0.82, p<0.01, respectively) and body surface area (r=-0.76 and -0.80, p<0.01, respectively). Circumferential ECV correlated significantly with LV ejection fraction (EF), maximum oxygen consumption from CPEX and proBNP (r=-1.0, -1.0 and 1.0, p<0.01, respectively) in DCM, and with LV EF and indexed LV end systolic volume in HCM (r=0.90, p=0.037, respectively). In LVNC, septal ECV was related to indexed LV stroke volume (r=0.90, p=0.037).

Conclusion: ECV was significantly associated with younger age and smaller body size in children and adolescents with primary inherited CM. Furthermore, our results indicate an increase of DMF in correlation with markers of heart failure including impaired LV function, reduced exercise capacity and elevated levels of proBNP in pediatric DCM. Further longitudinal studies are necessary to investigate the prognostic significance and utility of non-invasive ECV measurements in guiding therapy in children and adolescents with primary inherited CM.

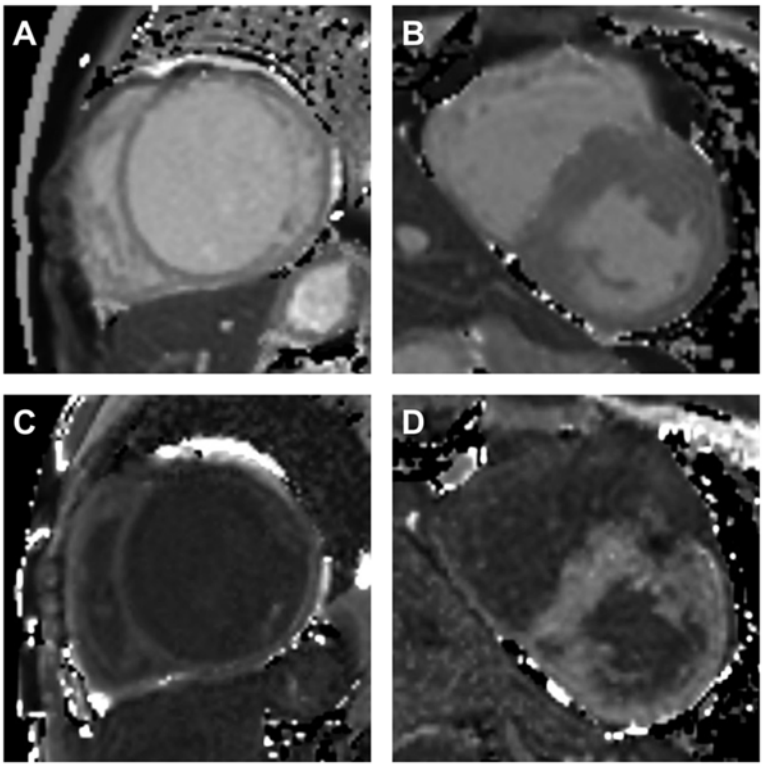

Figure 1. Exemplary native (upper row) and post-contrast (lower row) T1 maps in midventricular short axis plane in pediatric patients with dilated (A + C) and hypertrophic cardiomyopathy (C + D).

ID#: 378173

Extensive analysis of hemodynamics parameters on 4D flow MRI data of patients with bicuspid aortic valve using finite element methods

Julio Sotelo, Sr.[1] Lydia Dux-Santoy[2], Andrea Guala[3], José F. Rodríguez-Palomares, MD, PhD[3], Arturo Evangelista[4], Joaquín Mura[1], Daniel Hurtado[1], Sergio Uribe[1]

1. Pontificia Universidad Católica de Chile, Santiago, Chile

2. Hospital Universitari Vall d´Hebron. Vall d'Hebron Institut de Recerca. Universitat Autònoma de Barcelona, Catalonia, Spain

3. Hospital Universitari Vall d´Hebron. Vall d'Hebron Institut de Recerca. Universitat Autònoma de Barcelona, Barcelona, Catalonia, Spain

4. Hospital Universitari Vall d´Hebron. Vall d'Hebron Institut de Recerca. Universitat Autònoma de Barcelona, Spain

Background: Bicuspid-aortic-valve (BAV) is the most common congenital defect. Recent studies in BAV-patient found that these patients exhibit altered blood flow in the aorta, changing different hemodynamics parameters (HP). Different procedures need to be applied to calculate these HP. The purpose of this work is to propose a single methodology based on finite-element analysis to obtain several 3D quantitative maps of different HP from 4D-flow data set of BAV-patients and healthy volunteers.

Methods: A total of 14 healthy volunteer and 49 BAV-patients were included in the study. The 4D-flow data was acquired at Hospital Universitari Vall d´Hebron in a 1.5T GE-MR Sigma Scanner using the Vastly Undersampled Isotropic Projection Reconstruction technique. The patient demographics, clinical description and MR acquisition parameters are shown in the figure1. The process for creating the tetrahedral mesh is summarized in figure2a. Our work was development using three different software Matlab, Python and Paraview. Sixteen different regions were analyzed for each volunteer and patient, between the level of valsalva and the heart apex figure2b. In all these regions we analyze the mean, maximum and minimum values of HP at peak systole to find differences between volunteers and patients. The normal distribution of each data was studied using the Lilliefors test. Results between patients and volunteers were compared using a t-student test (for normal distribution data) and a wilcoxon test (for non-normal distribution data).

Results: The figure3a shows the list with each HP analyzed in the figure3b. In the figure3b we can see the results of HP with significant differences ($p<0.05$) between volunteers and BAV-patients (yellow box). We have observed that the HP in the regions of the ascending aorta (1 to 4) showed significant differences between volunteers and BAV-patients (RN+RL, RL, RN), compared to other regions. It can also be inferred that the eccentricity of flow was the most differentiating HP between volunteers and BAV-patients, for the entered vessel. Figure3c shows the 3D maps of eccentricity of flow, and the vessel centerline and the main flow centerline used to calculate this HP for one representative volunteer and one BAV-patient (RL).

Conclusion: We present a method that allowed us to obtain several 3D maps of different HP derived from a single 4D-flow data set. The great advantage of the proposed approach is that from a single segmentation of the 4D-flow data we can obtain several quantitative HP in 3D.

Table1: Patient demographics, clinical description and MR parameters used to acquire in-vivo data.

	Volunteers	BAV-Patients
Patient Demographic:		
Gender	9 Male - 5 Female	29 Male - 20 Female
Age (years)	49±17	45±14
Weight (Kg)	79±10	71±12
Height (cm)	169±8	169±10
BSA (m^2)	1.9±0.1	1.8±0.2
Stroke Volume (ml)	87.2±19.3	93.0±27.0
Ejection Fraction (%)	61.1±8.7	59.4±9.0
Phenotype	--	30 RL - 19 RN
Clinical Description: *		
Aortic Regurgitation	--	8(0) - 36(1) - 4(2) - 1(3) [a]
Aortic Stenosis	--	39(0) - 7(1) - 3(2) - 0(3) [a]
Hypertension	--	36(0) - 8(1) - 5(2) [b]
Diabetes	--	48(0) - 0(1) - 1(2) [c]
Dyslipidemia	--	42(0) - 1(1) - 6(2) [d]
MR Parameters:		
FOV (mm)	400x400x400	400x400x400
Voxel size (mm)	2.5x2.5x2.5	2.5x2.5x2.5
Cardiac Phases	39.3±6.8	40.0±7.8
VENC (cm/s)	200	200
Temporal Resolution (ms)	24.9±1.7	27.7±1.4
TE/TR (ms)	1.9-3.7 / 4.2-6.4	
Flip Angle (º)	8º	
HR (bpm)	61.4±10.4	56.6±11.3
Acquisition Time (min)	8-10	

* We show the number of BAV-patients, and the score in parenthesis.
[a] 0 = absent, 1 = mild, 2 = moderate, 3=severe.
[b] 0 = No, 1 = Yes, controlled, 2 = Yes, non-controlled.
[c] 0 = No, 1 = Yes, oral antibiotics, 2 = Yes, insulin.
[d] 0 = No, 1 = Yes, without treatment, 2 = Yes, with treatment.

Figure 1.- Table1: Patient demographics, clinical description and MR parameters used to acquire in-vivo data.

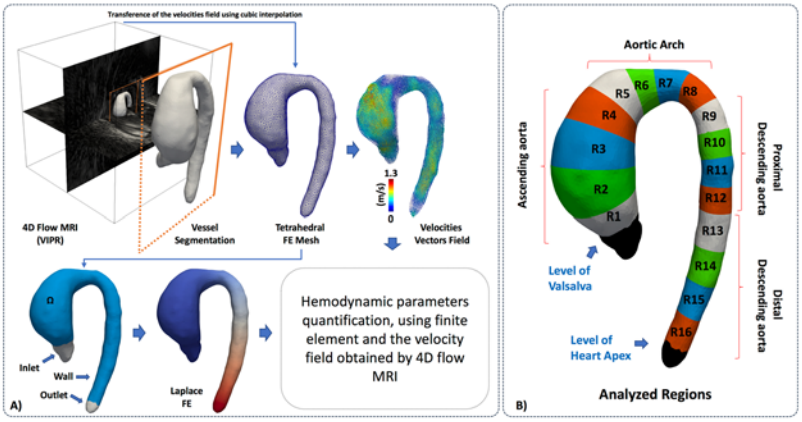

Figure 2.- A) Process for creating the tetrahedral finite element mesh used for the hemodynamic parameters quantification. In B) we show the sixteeen regions used to compare the geometrical parameters between volunteer and BAV-patient.

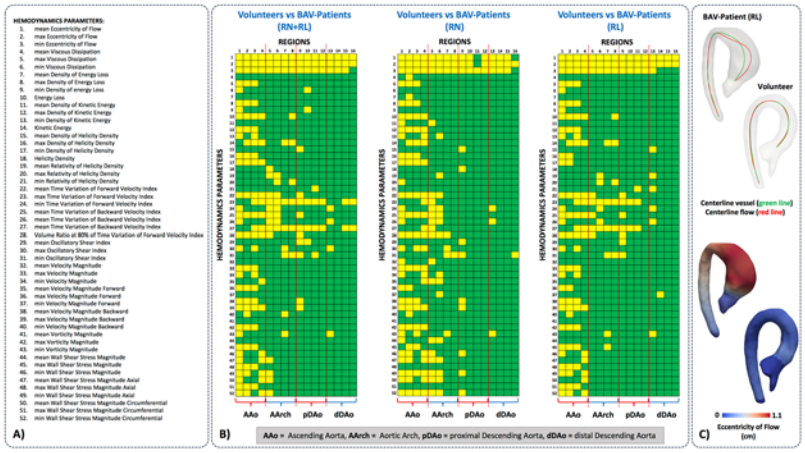

Figure 3.- In A) we shows the list with each HP analyzed in the figure3b. In B) we show the results of hemodynamics parameters with significant differences ($p<0.05$) between volunteers and BAV-patients (yellow box). In C) we shows the 3D maps of eccentricity of flow, and the vessel centerline and the main flow centerline used to calculate this HP for one representative volunteer and one BAV-patient (RL).

ID#: 378180

Impact of Aortic Valve Replacement on flow profiles in the ascending Aorta

Sarah Nordmeyer, MD[1] Marcus Kelm, M.D.[2], Leonid Goubergrits[3], Felix Berger, PhD M.D. [4], Titus Kuehne, PhD M.D.[5]

1. Deutsches Herzzentrum Berlin, Berlin, Berlin, Germany

2. German Heart Center Berlin, Germany

3. Charité - Universitätsmedizin Berlin, Biofluid Mechanics Laboratory, Berlin, Germany

4. German Heart Center Berlin, Berlin, Germany

5. Charité -Universitätsmedizin Berlin, Berlin, Germany

Background: Complex flow profiles in the ascending aorta have been associated with progression in aortic dilation, which affects morbidity and mortality of patients. We aimed to compare blood flow profiles in the ascending aorta in patients before and after aortic valve replacement (AVR) with 4D VEC-MRI. Computational Fluid Dynamics (CFD) virtually assessed the effect of modified surgical technique on flow profiles in the ascending aorta.

Methods: 34 patients underwent 4D VEC-MRI before and after AVR (n=27, biological AVR (BAVR); n=7, mechanical AVR (MAVR)). 7 healthy volunteers served as controls. Assessment of helical, vortical and eccentric flow in the ascending aorta was performed to calculate an “eccentricity score” (ES) and “complex flow score” (CFS). CFD analysis was performed in 4 cases (n=2, BAVR; n=2, MAVR).

Results: Before AVR, all patients showed a higher degree of complex flow profiles than healthy volunteers (ES: 2.5 vs. 1, $p<0.0001$; CFS: 4.7 vs. 1, $p<0.0001$). After BAVR, the degree of complex flow profiles fell only moderately (ES: 2.7 vs. 2.3, $p<0.001$; CFS: 4.7 vs. 4.3, $p<0.0001$) and remained altered compared to healthy volunteers (ES: 2.3 vs. 1, $p<0.0001$; CFS 4.3 vs. 1, $p<0.0001$). After MAVR, the degree of complex flow profiles fell strongly (ES: 2.3 vs. 1, $p=0.02$; CFS: 4.3 vs. 1, $p=0.02$) and did not show a significant difference to healthy volunteers ($p=0.5$ and $p=0.7$, respectively). A subsequent CFD analysis in 4 cases suggested that changes in the rotational position of the MAVR or changes in size and angulation of the BAVR could improve flow profiles.

Conclusion: AVR using biological valves did not restore normal blood flow profiles in the ascending aorta. Mechanical valves, however, showed flow profiles that were more comparable to healthy volunteers. The use of CFD might be helpful to adapt the surgical technique for optimized flow profiles in the ascending aorta.

ID#: 378183

Identifying left atrial enlargement by CMR: comparison between two widely used methods for volumes quantification

Thamara Morais, MD[1]Antonildes Nascimento. Assuncao, Jr., MD[2], Thalita Canevari, MD[3], Andrea Bercht, MD[4], Antonio Paiva, MD[1], Jose Araujo-Filho, MD[1], Roberto N. Dantas, Jr., MD[2], Cesar Nomura, MD, PhD[1], Jose Parga, MD, PhD[1]

1. Heart Institute (InCor), University of Sao Paulo, Brazil

2. Heart Institute (InCor), University of Sao Paulo, Sao Paulo, Sao Paulo, Brazil

3. Heart Institute (InCor), University of Sao Paulo, São paulo, Brazil

4. Heart Institute (InCor), University of Sao Paulo, Sao Paulo, Brazil

Background: Left atrial (LA) enlargement is related to cardiovascular morbidity and mortality. CMR provides high quality images and accurately estimates LA volumes by using equations of 2D based dimensions. We sought to investigate the agreement of LA assessment using the biplane area-length (Bi-ALM) (Pritchett et al, 2003. JACC) and the linear regression equation (LR) (Maceira, 2010. JCMR).

Methods: This study included 10 healthy volunteers and 13 patients with advanced ischemic and non-ischemic cardiomyopathies referred to CMR. Using a standard SSFP sequence, LA quantification was performed using 2 (2ch), 4 (4ch) and 3 chamber (3ch) views as follows: 1) Bi-ALM: 0.85 x Area4ch x Area2ch/ mean of the length in 4ch and 2ch; 2) LR: 3.31 + 1.9*Area3ch + 1.1*Area4ch + 1.1*TransverseDiameter2ch + 0.9*TransverseDiameter4ch − 1.7*AnteroposteriorDiameter3ch. LA enlargement was considered when the indexed LA volume (LAVi) >53ml/m^2 (Maceira, 2010. JCMR).

Results: The two methods strongly correlated (r=0.93, p2). Importantly, when diagnosing LA enlargement, the agreement was especially high with no significant misclassification. Of note, while LR yields higher LAVi than Bi-ALM when the volume is at a normal range, LAVi by Bi-ALM tends to provide higher values when the dilatation is greater. In this scenario, however, this disagreement might not be clinically relevant (Figure).

Conclusion: Biplane area-length and the linear regression equation have excellent concordance in estimating LA volumes as well as in identifying patients with LA enlargement.

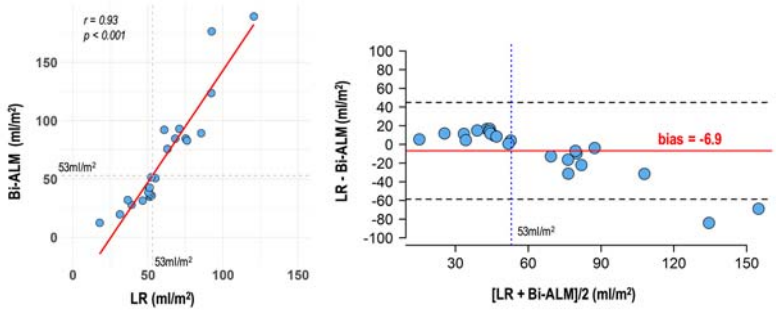

Correlation and agreement between biplane area-length and the linear regression equation in measuring LAVi.

ID#: 378056

Myocardial strain assessed by CRM tissue-tracking in the differential diagnosis of left ventricular hypertrophy.

Ilaria Dentamaro, MD[1] Alejandro Quijada-Fumero, MD[2], Lucia Rodríguez Eyras, MD[3], Nicolas Ezequiel. Villalva, MD[4], Filipa X. Valente, MD[5], Victor Pineda, MD[6], Gisela Teixidó-Turà, MD, PhD[7], Ruben Fernandez-Galera, MD[8], David Garcia-Dorado, MD, PhD[9], Arturo Evangelista[8], Hug Cuellar, MD, PhD[10], José F. Rodríguez-Palomares, MD, PhD[11]

1. Hospital Vall d'Hebron Barcelona, Bari, Puglia, Italy

2. (1) Hospital Vall d'Hebron, Department of Cardiology. VHIR, Universitat Autònoma de Barcelona, Barcelona, Spain., S/C de Tenerife, Canarias, Spain

3. (1) Hospital Vall d'Hebron, Department of Cardiology. VHIR, Universitat Autònoma de Barcelona, Barcelona, Spain., Mar del Plata, Buenos Aires, Argentina

4. (1) Hospital Vall d'Hebron, Department of Cardiology. VHIR, Universitat Autònoma de Barcelona, Barcelona, Spain, BARCELONA, Catalonia, Spain

5. Hospital Universitari Vall d´Hebron. Vall d'Hebron Institut de Recerca. Universitat Autònoma de Barcelona, Barcelona, Spain

6. (2) Hospital Vall d'Hebron, Department of Radiology. VHIR, Universitat Autònoma de Barcelona, Barcelona, Spain., Spain

7. Hospital Vall d'Hebron, Spain

8. Hospital Universitari Vall d´Hebron. Vall d'Hebron Institut de Recerca. Universitat Autònoma de Barcelona, Spain

9. (1) Hospital Vall d'Hebron, Department of Cardiology. VHIR, Universitat Autònoma de Barcelona, Barcelona, Spain., Spain

10. Hospital Universitari Vall d'Hebron, Spain

11. Hospital Universitari Vall d´Hebron. Vall d'Hebron Institut de Recerca. Universitat Autònoma de Barcelona, Barcelona, Catalonia, Spain

Background: Differential diagnosis of left ventricular hypertrophy is crucial since different entities present different management and prognosis. However, this differential diagnosis can be challenging in clinical practice, mainly in when the administration of gadolinium-chelated administration is limited for renal dysfunction. Thus, the aim of our study was to analyze the role of the deformation parameters derived from CMR to characterize patients with cardiac hypertrophy.

Methods: The study included 90 consecutive patients referred to our CMR unit to study left ventricular hypertrophy: 30 with mild left ventricular hypertrophy due to hypertension, 30 with a genetic confirmed hypertrophic cardiomyopathy and 30 with histologic confirmed cardiac amyloidosis. Left ventricular volumes, ejection fraction and myocardial mass were assessed using cine sequences. Tissue-tracking CMR was performed to determine radial, circumferential and longitudinal strain.

Results: Left ventricular hypertrophy was significantly higher in patients with cardiac amyloidosis compared to the rest of the population ($p<0.001$) with no differences in left ventricular volumes. Also, all deformation parameters were significantly more impaired in cardiac amyloidosis ($p<0.001$) (Table 1). Among all different CMR derived variables, longitudinal strain constituted the best parameter to differentiate between hypertensive cardiomyopathy versus hypertrophic/amyloidosis. A cut-off value of longitudinal strain > -15% excluded hypertensive cardiomyopathy with a sensitivity of 82% and specificity 81% (AUC: 0.82, $p<0.001$) (Figure 1).

Conclusion: Deformation parameters (specially global longitudinal strain) constitute excellent alternatives to differentiate between hypertensive cardiomyopathy versus other causes of left ventricular hypertrophy with worse prognosis and should be included in the differential diagnosis flowchart.

	Hypertension	Hypertrophic	Amyloidosis	P-value
Septal thickness (mm)	9 ± 3	12 ± 3	14 ± 2	<0,001
End-diastolic volume (mm)	130 ± 27	125 ± 30	138 ± 36	0,282
End-sistolic volume (mm)	52 ± 11	44 ± 13	67 ± 29	0,124
Ejection Fraction (%)	59 ± 4	64 ± 7	53 ± 11	<0,001
Myocardial mass (gr)	86 ± 22	117 ± 37	148 ± 52	<0,001
Wall motion score index	1 ± 0	1,1 ± 0,4	1,1 ± 0,2	0,002
Global radial strain (%)	51 ± 9	43 ± 9	39 ± 15	<0,001
Global circumferential strain (%)	-23 ± 2	-20 ± 2	-18 ± 5	<0,001
Global longitudinal strain (%)	-18 ± 2	-15 ± 2	-12 ± 4	<0,001

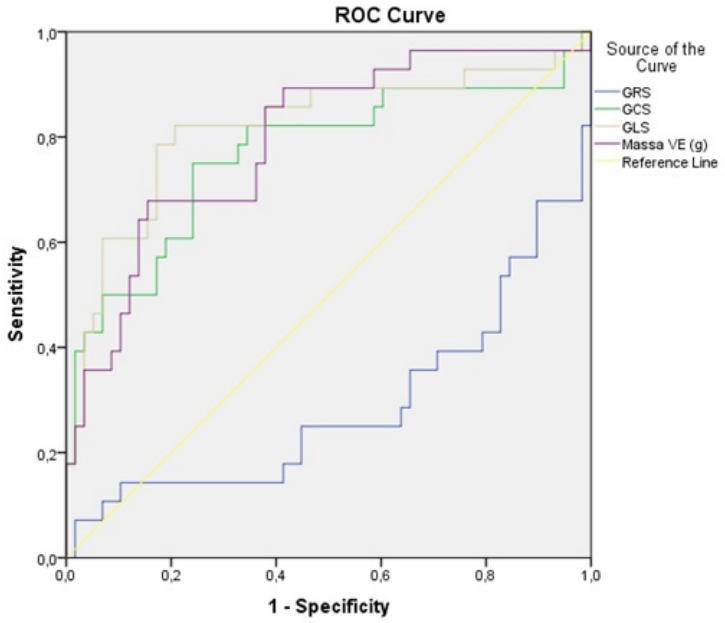

ID#: 378069

Quantification of left ventricle trabeculae in hypertrophied cardiomyopathy, in comparison with healthy subjects

Mathieu Finas, medical doctor[1] Zakarya Bentatou, MS[2], Stanislas Rapacchi, PhD[3], Stéphanie Bricq, PhD[4], Alain Lalande, PhD[5], Frank Kober, PhD[6], Monique Bernard, PhD[7], Alexis Jacquier, MD PhD[8]

1. CHU GRENOBLE ALPES, Saint-égrève, Rhone-Alpes, France

2. Aix Marseille Univ, CNRS, CRMBM, Marseille, France, France

3. Aix-Marseille Université CNRS, Marseille, France

4. Le2i, FRE2005, CNRS, Arts et Métiers, Univ. Bourgogne Franche-Comté, France, Dijon, Bourgogne, France

5. University hospital of Dijon and University of Dijon, Dijon, Bourgogne, France

6. Aix Marseille University CNRS, Marseille, France

7. Aix Marseille University, Marseille, France

8. Aix Marseille Université APHM, France

Background: Hypertrabeculation is the main symptom of left ventricular non-compaction (LVNC) however a trabeculated phenotype can overlap with other cardiomyopathies, such as hypertrophic cardiomyopathy (HCM). We used a semi-automated method to assess global and segmental trabeculated mass (T) across the LV in a cohort of HCM patients, in comparison with healthy subjects.

Methods: Patients with HCM were retrospectively recruited during the year 2015. Healthy volunteers were prospectively recruited to match the patients regarding baseline characteristics. For each subject T, compacted mass (C) and papillary muscles (PM) masses were evaluated with a semi-automated software. The T/C and [PM+T]/C ratios were then computed. A group analysis comparing patients with HCM to controls and a subgroup analysis comparing patients with global LV hypertrophy (“LVH+”, C mass>85g/m²), patients without global hypertrophy (LVH-) and controls were conducted for each parameter. 75 subjects were recruited in each group. We further studied segmental distribution of T/C across the LV to find a correlation between T and C increase.

Results: T/C and [T+PM]/C ratios differed significantly between patients with HCM and controls (13.4±3.1% versus 9.9±2.6%, $p<0.05$ and 17.8±3.2%, versus 13.9±2.9% $p<0.001$). Only T/C ratio differ slightly between LVH+ and LVH- subjects (12.7±2.9%, versus13.9±3.2%, $p=0.04$). However a significant difference was noticed between LVH- patients and controls for the both parameters (14.2±3.3% versus 9.9±2.6, $p<0.001$ and 18.7±2.9 versus 13.9±-2.9, $p<0.001$). Among patients, the most trabeculated segments were 7, 12, 13 and 16 and the most compacted segments were 1, 3 and 9. A positive strong correlation was observed between T and C in segments 11 and 16. No correlation was found between T/C ratio and LV functional parameters.

Conclusion: T/C and [PM+T]/C ratios could provide a diagnostic help in HCM patients without LV hypertrophy. Segmental distribution of T and C seems to correlate in HCM patients.

ID#: 378075

Chagas myocardial fibrosis undistinguishable from myocardial infarction by LGE: Can T1 mapping help?

Thamara Morais, MD[1] Antonildes Nascimento. Assuncao, Jr., MD[2], Rodrigo de Jesus Louzeiro. Melo, MD[1], Fabio Fernandes, MD, PhD[1], Barbara Ianni, MD, PhD[1], Charles Mady, MD, PhD[1], Cesar Nomura, MD, PhD[1], Carlos E. Rochitte, MD, PhD[3]

1. Heart Institute (InCor), University of Sao Paulo, Brazil

2. Heart Institute (InCor), University of Sao Paulo, Sao Paulo, Sao Paulo, Brazil

3. Heart Institute - InCor - University of São Paulo Medical School and Hospital do Coração - Heart Hospital - HCOR, São Paulo, Brazil

Background: Patients with Chagas Heart disease (CD) frequently present late gadolinium enhancement (LGE) classified as an ischemic pattern and that is undistinguishable from myocardial infarction. In fact, those patients frequently present low coronary artery disease (CAD) risk profile and are referred to unnecessarily non-invasive and invasive tests. We aimed to compare tissue composition of infarct-like LGE in CD with true myocardial infarction in coronary heart disease (CHD) patients using T1 mapping pulse sequence.

Methods: Patients with CD (n=6) and CHD, acute (n=7) and chronic settings (n=7), referred to CMR and T1 mapping were included in this analysis. All cases with CD had a LGE pattern classified as an ischemic (subendocardial or transmural) without obstructive coronary artery disease by non-invasive or invasive angiography. T1 mapping was acquired using a modified Look-Locker inversion recovery sequence (MOLLI), with T1 values measured before (native T1) and after 15 minutes of the administration of contrast agent. Extracellular volume was calculated using contemporaneous hematocrit. The regions of interest were drawn on T1 mapping images using matched areas seen on LGE images. LGE images were acquired using 2D IR-prepped GRE with standard parameters. T1 times were measured using CVI42 (Circle Cardiovascular Imaging, Calgary, Canada).

Results: CD patients presented greater ECV values in LGE myocardial areas than patients with CHD, with either chronic or acute myocardial infarction (respectively: 41% versus 36%, p=0.03; 41% versus 35%, p=0.01). There was a trend towards to a higher native T1 among patients with CD when compared with chronic myocardial infarction (Figure 1 and 2).

Conclusion: Extracellular space within Chagas myocardial fibrosis areas were significantly more expanded than in acute and chronic myocardial infarction, paralleling pathological findings of a loose fibrous tissue in Chagas disease. These initial results indicate a potential role of T1 mapping and, particularly extracellular myocardial volume measurements, in differentiating Chagas fibrosis from myocardial infarction.

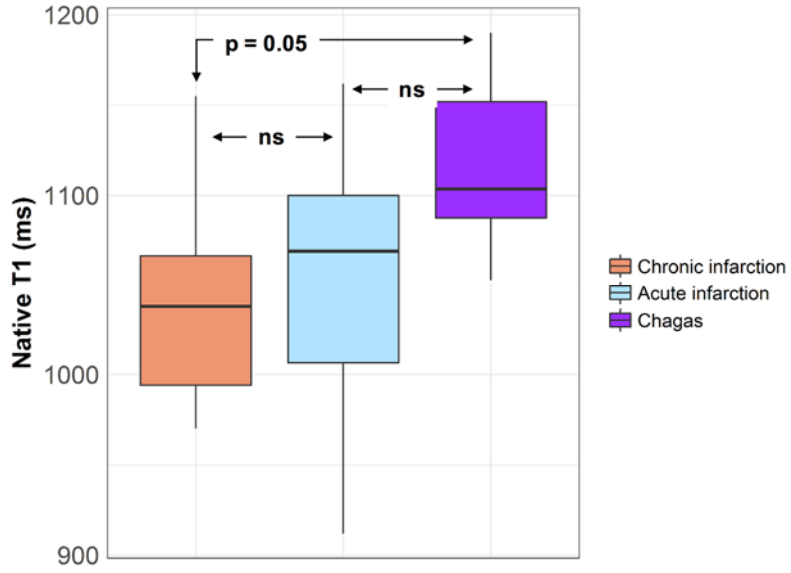

Figure 1. Boxplot showing native T1 differences within LGE regions of patients with Chagas heart disease and ischemic heart disease.

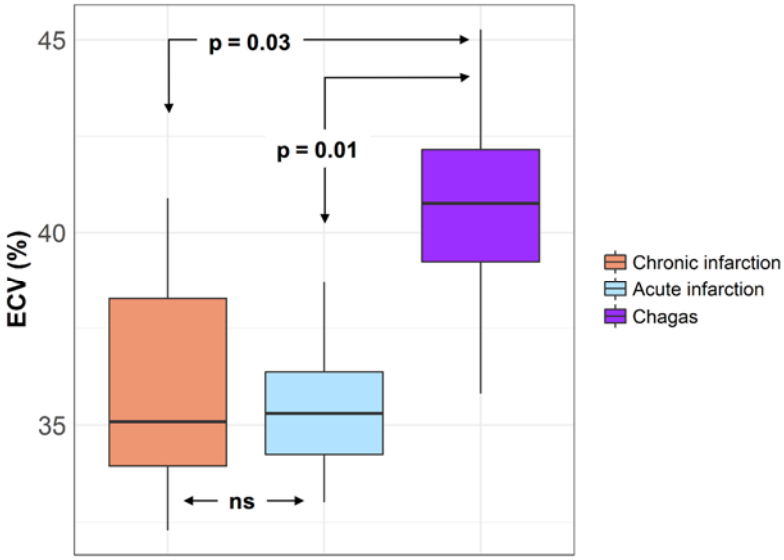

Figure 2. Boxplot showing ECV differences within LGE regions of patients with Chagas heart disease and ischemic heart disease.

ID#: 378133

Semi-automatic geometrical characterization of patients with bicuspid aortic valve using finite element methods

Julio Sotelo, Sr.[1] Lydia Dux-Santoy[2], Andrea Guala[3], José F. Rodríguez-Palomares, MD, PhD[3], Arturo Evangelista[4], Joaquín Mura[1], Daniel Hurtado[1], Sergio Uribe[1]

1. Pontificia Universidad Católica de Chile, Santiago, Chile

2. Hospital Universitari Vall d´Hebron. Vall d'Hebron Institut de Recerca. Universitat Autònoma de Barcelona, Catalonia, Spain

3. Hospital Universitari Vall d´Hebron. Vall d'Hebron Institut de Recerca. Universitat Autònoma de Barcelona, Barcelona, Catalonia, Spain

4. Hospital Universitari Vall d´Hebron. Vall d'Hebron Institut de Recerca. Universitat Autònoma de Barcelona, Spain

Background: The progression of the Bicuspid Aortic Valve (BAV) defect can vary with time, and the typical manifestation related with the function of the aorta are aneurysm, dissection and other complications. Manual methods have been developed to analyze the geometry of great vessels in patients with BAV. In this work, we propose a methodology based on the Laplace formulation using finite elements methods that will allow us to obtain geometrical parameters of the aorta of patients with BAV from the $I^{PC\text{-}MRA}$ image obtained by 4D flow.

Methods: We developed a finite-element based computational framework to obtain the Laplace distribution from the $I^{PC\text{-}MRA}$ image obtained by 4D-flow MR data (figure1a). The algorithm is based in a standard Galerkin FE problem for the Laplace equation. A total of 14 healthy volunteer and 49 BAV-patients (30 with fusion of the right / left coronary cusp (RL) and 19 with right / non-coronary cusp (RN)) were included in the study. The 4D-flow data was acquired at Hospital Universitari Vall d´Hebron in a 1.5T GE-MR Sigma scanner using the VIPR technique. The patient demographic and MR acquisition parameters are shown in the figure2. Sixteen different regions were analyzed between volunteer and BAV-patient figure1b. In each region, each geometrical parameter were analyzed. The normal distribution of the data was studied using the Lilliefors test. Results between patients and volunteers were compared using a t-student test (for normal distribution) and a wilcoxon test (for no normal distribution). We performed the correlation of different hemodynamic parameters with the diameter of the aorta.

Results: In the figure3a we show the results of geometrical parameters with significant differences ($p<0.05$) between volunteers and BAV-patients (yellow box). We have observed that the geometrical parameters in the regions of the ascending aorta and aortic arch (1 to 8) show more significant differences between volunteers and BAV-patients with RL phenotype, in comparison with RN. We observed the most relevant parameter in our analysis is the diameter of the vessel. In figure3b we show different geometric parameters studied, the centerline for one representative volunteer and two BAV-patients with phenotypes (RN and RL). The hemodynamic parameter that showed a stronger correlation with the diameter was the mean eccentricity in the ascending aorta ($R=0.62$ and $y= 1.207x + 0.025$).

Conclusion: We have presented a novel method that allow us the semiautomatic analysis of geometric parameters of the aorta in 3D from the angiographic data obtained by 4D flow. The versatility of the method permit applies it to any type of volumetric segmentation from images of MR or CT.

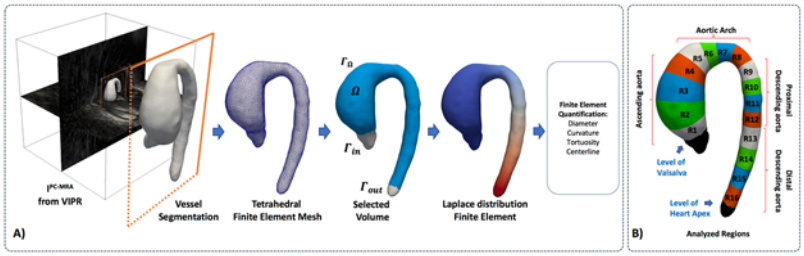

Figure 1.- A) Process for creating the tetrahedral finite element mesh used for the Laplace formulation. In B) we show the sixteeen regions used to compare the geometrical parameters between volunteer and BAV-patient.

Table1: Patient demographics and MR parameters used to acquire in-vivo data.

	Volunteers	BAV-Patients
Patient Demographic:		
Gender	9 Male - 5 Female	29 Male - 20 Female
Age (years)	49±17	45±14
Weight (Kg)	79±10	71±12
Height (cm)	169±8	169±10
BSA (m^2)	1.9±0.1	1.8±0.2
Stroke Volume (ml)	87.2±19.3	93.0±27.0
Ejection Fraction (%)	61.1±8.7	59.4±9.0
Phenotype	--	30 RL - 19 RN
MR Parameters:		
FOV (mm)	400x400x400	400x400x400
Voxel size (mm)	2.5x2.5x2.5	2.5x2.5x2.5
Cardiac Phases	39.3±6.8	40.0±7.8
VENC (cm/s)	200	200
Temporal Resolution (ms)	24.9±1.7	27.7±1.4
TE/TR (ms)	1.9-3.7 / 4.2-6.4	
Flip Angle (º)	8º	
HR (bpm)	61.4±10.4	56.6±11.3
Acquisition Time (min)	8-10	

Figure 2.- Table 1: Patient demographics and MR parameters used to acquire in-vivo data

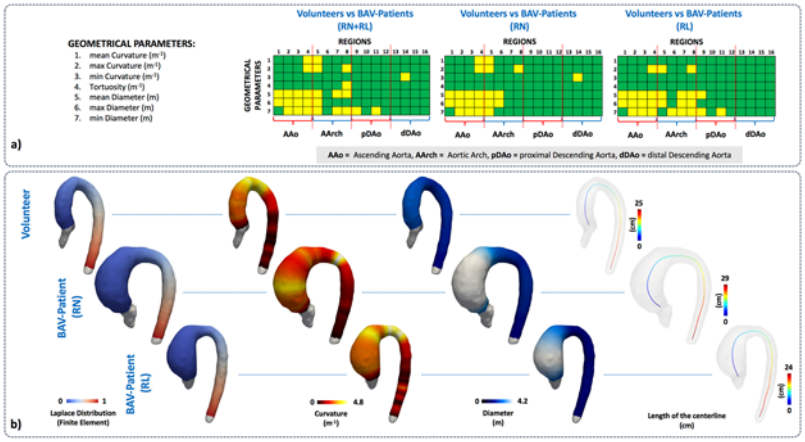

Figure 3.- In A) we show the results of geometrical parameters with significant differences ($p<0.05$) between volunteers and BAV-patients (yellow box). In B) we show different geometric parameters studied, the centerline for one representative volunteer and two BAV-patients with phenotypes (RN and RL).

ID#: 378269

Quantification of Late Gadolinium Enhancement with Contrast-enhanced Cardiovascular MR Imaging for Coronary Artery Chronic Total Occlusion

Yi He[1]Lijun Zhang[2], Xiantao Song[3], Jianan Li[3], Wei Dong[4], Hongzhi Mi[4], Jian Jiao[4], Jing An, M.D.[5], Ruiyu Dou[6]

1. Beijing Anzhen Hospital, Capital Medical University, Beijing China, China (People's Republic)

2. Radiology Department, Beijing Anzhen Hospital, Capital Medical University, Beijing, China (People's Republic)

3. department of cardiology,beijing anzhen hospital, China (People's Republic)

4. department of nuclear medcine, beijing anzhen hospital, China (People's Republic)

5. Siemens Shenzhen Magnetic Resonance Ltd., China (People's Republic)

6. department of radiology,beijing anzhen hospital, China (People's Republic)

Background: To determine the most accurate and reproducible semiautomated grayscale thresholding technique for quantifying late gadolinium enhancement (LGE) with PET as a gold standard in patients with coronary artery chronic total occlusion (CTO).

Methods:

65 patients with known CTO underwent LGE cardiovascular magnetic resonance (CMR) imaging on a 3T scanner (MAGNETOM Verio, Siemens Healthcare, Erlangen, Germany). Positron Emission Tomography (PET[MB1]) was performed within one week. The presence and quantity of LGE were determined with gray-scale thresholds of 2 SDs, 4 SDs, 5 SDs, 6 SDs and 8 SDs above the mean signal intensity for the normal remote myocardium. Receiver operating characteristic curves (ROC) analysis was used for the strongest correlation gray-scale thresholding value with PET as a standard on the segment–based analysis.

Results:

65 patients and 1040 segments were analyzed. Based on SPECT and PET analyses, nonviable myocardium was identified in 29 (45%) patients and 88 (8%) segments. Based on CMR, the mean total enhanced mass was 25 g ± 16.7 at 2 SDs, 15 g ± 14.4 at 4 SDs, 13 g ± 14.0 at 5 SDs, 10 g ± 11.3 at 6 SDs, 7 g ± 9.0 at 8 SDs, above the mean signal intensity for the normal remote myocardium. With the SPECT/PET as the standard, the 5-SD threshold had the strongest correlation ($r = 0.79$, $P < .0001$) compared with other thresholds of 2-SD ($r = 0.43$), 4-SD ($r = 0.76$), 6-SD ($r = 0.78$), and 8-SD ($r = 0.70$). With PET as the standard, the AUC for 5-SD method was 0.99 (95% CI, 0.98–0.99) in segment-based analysis. Sensitivities and specificities were 0.94 and 0.96 for detecting infarction with cutoff value of SIE (the segmental infarct extent) being 41%. The 5-SD threshold quantification showed high inter- and intraobserver agreement (ICC=0.96, $P < .0001$; ICC=0.85, $P < .0001$).

Conclusion:

Semiautomated LGE cardiovascular MR gray-scale thresholding with 5 SDs above the mean signal intensity for the normal remote myocardium yields the strongest correlation of the extent of LGE identified with SPECT/PET and is highly reproducible in patients with CTO. This objective method should be considered for quantifying LGE in patients with CTO.

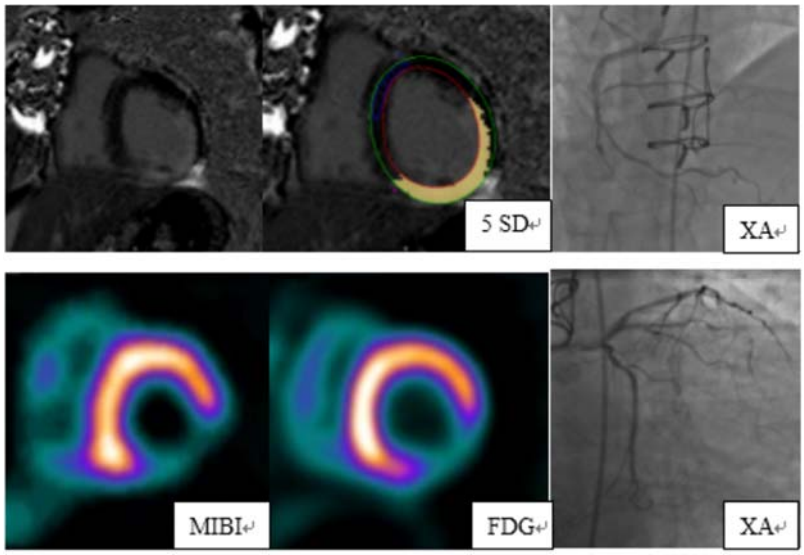

Men, 61-year-old, with right coronary artery chronic total occlusion and coronary artery bypass; Left top two images show LGE imaging before planimetry and thresholding techniques were performed and 5 SDs above mean. Left bottom two images show MIBI and FDG uptake were transmural match defect

ID#: 378287

Right ventricular strain quantification using Cardiac Magnetic Resonance with Multimodality Tissue Tracking in The Multi-Ethnic Study of Atherosclerosis (MESA) Chronic Obstructive Pulmonary Disease (COPD) study.

Michio Ozaki, BS,RT[1] Harisha Garimella[2], Bharath Ambale-Venkatesh, Ph.D[1], Tomoki Fujii, MS, RT[3], Elzbieta Chamera, RDCS[4], Colin O. Wu, PhD[5], Steven Kawut, MD,MS[6], R Graham Barr, MD,PhD[7], Martin R. Prince, MD, PhD[8], David A. Bluemke, MD,PhD[9], Joao A.C. Lima, MD, MBA[4]

1. Johns Hopkins University

2. University of Maryland

3. Showa University, Shinagawa-ku, Tokyo, Japan

4. Johns Hopkins University, Baltimore, MD

5. National Institutes of Health, MD

6. Hospital of the University of Pennsylvania

7. Columbia University Medical Center

8. Cornell University, NY

9. National Institutes of Health Clinical Center

Background: Chronic Obstructive Pulmonary Disease (COPD) is not detected until the later stages when symptoms are predominant. Right ventricular (RV) function is a potentially useful early marker of COPD. The purpose of this study was to assess the reproducibility of RV strain in COPD.

Methods: A total of 40 cases that was stratified, by 20 COPD and 20 Non- COPD participants were randomly selected from the MESA COPD study. We measured RV circumferential strain (EccRV) and RV longitudinal strain (EllRV) by using the pixel based multimodality tissue tracking software (MTT; Toshiba, Japan) on Steady State Free Precession images. EccRV was determined from 3 short-axis cine images. EllRV was determined from 2 long-axis cine images – one perpendicular to the mid-RV and the other perpendicular to the inferior-RV as seen on short-axis images. In order to evaluate RV segmental strain, RV myocardium was divided into 6 equal segments in the long-axis images (segment 1 to 6 were placed in order from apex to base). Similarly, for EccRV, strains were obtained across the base, mid, and apex regions across the anterior, middle, and superior RV segments on short-axis image cine images. Inter-observer reproducibility was determined by comparing analysis by 2 observers, while intra-observer reproducibility was based on two reads by the same reader at least 2 weeks apart. Intra-class correlation coefficient was used for assessment of reproducibility with values representing good-to-excellent (0.8-1.0), fair-to-good (0.6-0.8) and poor (<0.6) reproducibility.

Results: For each parameter, Intra-observer reproducibility was better than Inter-observer reproducibility. Global strain parameters were most reproducible for both Ell_{RV} and Ecc_{RV}. Regional strain (mid- and inferior regions for EllRV; and base, mid, and apical regions for EccRV) reproducibility was similar to global strain reproducibility. In general, segmental strain parameters were less reproducible than regional or global strain parameters. While intra-observer reproducibility was generally acceptable at the segmental level (ICC>0.6), intra-observer reproducibility was generally not.

Conclusion: RV strain quantifications using CMR with MTT had good reproducibility in intra-observer analysis, particularly at the global and regional levels, and was fair at the segmental level. Care should be taken, however, when multiple readers are used for segmental analysis of feature-tracking strain.

Parameters	Regions	Segments	Observer 1		Observer 2	Intra-observer ICC	Inter-observer ICC
			1st Reading	2nd Reading			
Ecc_{RV}	Global		-14.86 ± 4.65	-15.57 ± 4.90	-15.21 ± 3.62	0.89	0.59
Ecc_{RV}	Base	Anterior	-11.46 ± 7.35	-12.99 ± 5.88	-10.74 ± 3.73	0.74	0.19
Ecc_{RV}	Base	Mid	-12.55 ± 5.26	-12.94 ± 5.34	-12.75 ± 4.58	0.64	0.54
Ecc_{RV}	Base	Inferior	-13.10 ± 4.96	-13.86 ± 4.92	-13.02 ± 4.23	0.70	0.49
Ecc_{RV}	Base	Average	-12.07 ± 4.32	-12.90 ± 4.75	-11.96 ± 3.22	0.73	0.44
Ecc_{RV}	Mid	Anterior	-13.64 ± 6.30	-13.61 ± 5.52	-13.68 ± 6.07	0.84	0.62
Ecc_{RV}	Mid	Mid	-14.66 ± 6.73	-16.11 ± 6.18	-15.82 ± 5.89	0.61	0.34
Ecc_{RV}	Mid	Inferior	-15.34 ± 5.82	-16.71 ± 6.11	-14.64 ± 4.26	0.75	0.31
Ecc_{RV}	Mid	Average	-14.32 ± 5.92	-15.15 ± 5.54	-14.55 ± 4.56	0.80	0.53
Ecc_{RV}	Apex	Anterior	-15.84 ± 7.26	-15.09 ± 7.76	-17.37 ± 5.81	0.73	0.25
Ecc_{RV}	Apex	Mid	-18.99 ± 8.53	-19.20 ± 8.57	-18.34 ± 6.02	0.79	0.48
Ecc_{RV}	Apex	Inferior	-18.11 ± 8.14	-19.62 ± 6.85	-20.50 ± 6.29	0.70	0.52
Ecc_{RV}	Apex	Average	-17.51 ± 7.35	-17.61 ± 7.29	-18.18 ± 5.32	0.87	0.52

Intra-observer and inter-observer reproducibility for multimodality tissue tracking strain parameters in MESA COPD by using interclass correlation coefficient (ICC)

Parameters	Regions	Segments	Observer 1		Observer 2	Intra-observer ICC	Inter-observer ICC
			1st Reading	2nd Reading			
Ell_{RV}	Global		-35.08 ± 7.35	-35.27 ± 7.82	-33.77 ± 5.32	0.86	0.52
Ell_{RV}	Mid	Segment1	-33.80 ± 18.07	-34.81 ± 19.22	-33.80 ± 13.20	0.82	0.18
Ell_{RV}	Mid	Segment2	-33.84 ± 16.93	-33.35 ± 17.46	-36.99 ± 13.94	0.85	0.52
Ell_{RV}	Mid	Segment3	-31.21 ± 21.55	-33.47 ± 19.66	-29.26 ± 13.53	0.70	0.49
Ell_{RV}	Mid	Segment4	-36.67 ± 19.84	-35.80 ± 18.87	-31.90 ± 14.75	0.70	0.38
Ell_{RV}	Mid	Segment5	-42.15 ± 19.34	-38.90 ± 22.05	-39.30 ± 15.82	0.65	0.48
Ell_{RV}	Mid	Segment6	-42.36 ± 18.09	-42.36 ± 18.74	-37.61 ± 13.19	0.57	0.12
Ell_{RV}	Mid	Average	-31.60 ± 11.29	-30.91 ± 10.56	-29.79 ± 8.23	0.81	0.53
Ell_{RV}	Inferior	Segment1	-40.04 ± 14.97	-38.22 ± 13.20	-30.35 ± 12.92	0.47	0.44
Ell_{RV}	Inferior	Segment2	-34.43 ± 17.52	-39.17 ± 17.43	-29.33 ± 13.39	0.74	0.25
Ell_{RV}	Inferior	Segment3	-27.56 ± 14.97	-33.54 ± 20.18	-26.59 ± 12.09	0.65	0.41
Ell_{RV}	Inferior	Segment4	-32.15 ± 19.51	-29.36 ± 22.84	-31.17 ± 12.62	0.78	0.54
Ell_{RV}	Inferior	Segment5	-33.93 ± 16.13	-33.57 ± 16.86	-35.88 ± 13.32	0.58	0.39
Ell_{RV}	Inferior	Segment6	-37.03 ± 16.29	-36.04 ± 17.58	-36.70 ± 12.91	0.62	0.61
Ell_{RV}	Inferior	Average	-29.64 ± 10.06	-30.73 ± 11.55	-26.96 ± 7.14	0.88	0.41

Intra-observer and inter-observer reproducibility for multimodality tissue tracking strain parameters in MESA COPD by using interclass correlation coefficient (ICC)

ID#: 378289

Decision Support Software Ensures Appropriate Cost-Effective Use of Cardiac Magnetic Resonance

Christopher J. Francois, MD[1] Mark L. Schiebler, M.D.[2], Richard Bruce, MD[3], Jeffrey P. Kanne, MD[3]

1. University of Wisconsin - Madison, Madison, WI

2. UW Madison School of Medicine and Public Health, Madison, WI

3. University of Wisconsin School of Medicine and Public Health, Madison, WI

Background: The Protecting Access to Medicare Act of 2014 advocates using Appropriate Use Criteria for advanced imaging services, including cardiac magnetic resonance (CMR). Decision support software (DSS) assists ordering providers with determining and documenting appropriateness of CMR for a specific clinical indication. The primary aim of this study was to assess the distribution of appropriate and inappropriate outpatient CMR orders at a tertiary academic referral center. A secondary aim was to determine reasons for "usually not appropriate" or indeterminate orders.

Methods: All outpatient CMR orders requested between 1/1/2018 and 6/30/2018 were reviewed for appropriateness based on data from ACRSelect™ software. Orders were scored green for "appropriate", yellow for "may be appropriate," and red for "usually not appropriate." Orders for which the appropriateness is indeterminate, no score is given. The electronic health record (EHR) was reviewed for each patient for whom CMR orders were yellow, red, or no score to determine if the score should have been reassigned green for appropriate.

Results: In the first six months of 2017, 222 outpatient CMR orders were placed. The distribution of the final decision support scores were 69% green, 3% yellow, 2% red, and 26% no score (Figure 1). After adjudication, all yellow orders were appropriate, 75% of red orders were appropriate, and 86% of no score orders were appropriate. Upon final review, 213/222 (96%) CMR orders were appropriate, 2/222 (1%) CMR orders were usually not appropriate and 7/222 (3%) CMR orders could not be scored. The main reasons for changing the score of a CMR order to appropriate included congenital heart disease, dyspnea suspected to be of cardiac origin, and suspected infiltrative cardiomyopathy (Table 1). The 7/222 orders that were not scored after adjudication were all requested for pre-pulmonary vein isolation in patients with atrial fibrillation, without other criteria for which CMR is considered appropriate.

Conclusion: The majority of CMR orders placed within our system are requested for appropriate indications. After thorough review of the EHR in cases when orders were not considered appropriate by the DSS, the vast majority of these orders were also found to be appropriate. These findings indicate that CMR is being used wisely and suggest that with training, most orders that currently are not initially identified as appropriate could be appropriate with correct identification of the indication for CMR.

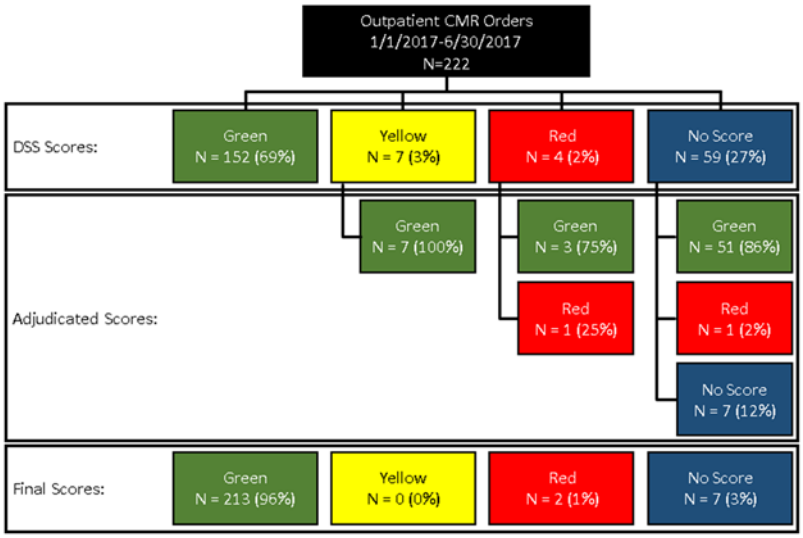

Flowchart outlining the distribution of scores for outpatient CMR orders. The electronic medical record of orders not scored green by DSS were reviewed to determine if patients had signs or symptoms that would indicate that the CMR order would be appropriate.

Summary of changes made to orders considered

Adjudicated Score	N	Reason for Exam(s)
Red	2	Aorta aneurysm (N=1) Aortic dissection (N=1)
Yellow	0	
Green	58	Infiltrative cardiomyopathy (N=15) Dyspnea, cardiac origin (N=14) CHD (N=14) Prior PTCA/CABG (N=7) Cardiomyopathy/HFrEF (N=6) HCM (N=4) ARVC (N=3) Cardiac mass (N=1) Chest pain, high probability CAD (N=1) Valvular heart disease (N=1)
No score	7	Atrial fibrillation

Note: The number of indications found to be appropriate is greater than the number of orders because several patients had more than one appropriate indication for CMR.

ID#: 378219

Focal regions of hypoenhancement visualized by early gadolinium enhancement imaging in patients with hypertrophic cardiomyopathy

Tushar Acharya[1] Sujata M. Shanbhag, MD, MPH[2], Andrew E. Arai, MD[3], W. Patricia Bandettini, MD[4]

1. National Heart, Lung, and Blood Institute, NIH, Bethesda, MD

2. NIH/NHLBI, Bethesda, MD

3. National Heart, Lung and Blood Institute, National Institutes of Health, Bethesda, MD

4. National Heart, Lung and Blood Institute, National Institutes of Health, MD

Background: Resting perfusion defects from micro- and macrovascular obstruction may be seen on early gadolinium enhancement imaging (EGE) in acute myocardial infarction. We report a systematic evaluation of similar findings of focal hypoenhancement in patients with hypertrophic cardiomyopathy (HCM).

Methods: Out of the 280 cases with imaging findings of HCM (between 2011 and 2016), EGE imaging was performed on 226. Cases where HCM was in the differential but not the definite imaging diagnosis (n=35) were excluded. Focal myocardial hypoenhancement on EGE were confirmed by at least two readers and consensus was established on each read. Various imaging parameters were compared between those with and without the hypoenhancement foci using Wilcoxon and chi-square tests for continuous and categorical variables respectively.

Results: Median EGE imaging time was 1 minute after gadolinium contrast administration. Of the 191 cases of HCM, 14 had resting hypoenhancement defects (age range 28-82 years). Patients with defects had greater left ventricular mass (217 g vs 158 g; P=0.015), maximum wall thickness (24 mm vs 19 mm; P<0.001), and end-diastolic volume (187 ml vs 166 ml; P=0.03), and lower ejection fraction (56% vs 64%; P=0.003) compared to those without hypoenhancement defects. Imaging observations like morphological HCM variant, systolic anterior motion of mitral valve, flow acceleration, and cavity obliteration were statistically similar between comparison groups. Among the 14 cases, areas of hypoenhancement on EGE corresponded to dense fibrosis on late gadolinium enhancement imaging. These patients neither had a history of myocardial infarction, nor a recent chest pain syndrome.

Conclusion: Hypoenhancement defects can be seen on EGE in patients with HCM and are more common in those patients with more severe extent of disease. These findings may represent severe resting focal perfusion defects with a mechanism of severe microvascular dysfunction and ischemia. This is the first report to describe this imaging finding outside of myocardial infarction.

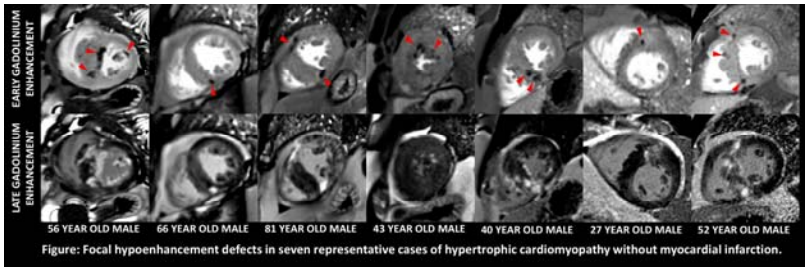

Focal hypoenhancement defects in seven representative cases of hypertrophic cardiomyopathy without myocardial infarction.

ID#: 378225

Comprehensive 3D flow characterization in patients with Dilated Cardiomyopathy (DCM) from 4D flow MRI data using a finite element method and 17-Segment Bullseyes

Pamela Franco[1] Julio Sotelo, Sr.[2], Bram Ruijsink, MD[3], Eric Kerfoot[4], Joaquín Mura[2], Daniel Hurtado[2], Sergio Uribe[2]

1. Pontificia Universidad Católica de Chile, Santiago, Region Metropolitana, Chile

2. Pontificia Universidad Católica de Chile, Santiago, Chile

3. King's College London, London, England, United Kingdom

4. King's College London, United Kingdom

Background: Dilated cardiomyopathy (DCM) is a disease of the heart muscle, that is characterized by the enlargement of the left ventricle and systolic dysfunction. Cardiac MR is the gold standard to measure cardiac function using b-SSFP cine images. Over the last years, 4D flow MRI had offered the opportunity to assess 3D blood flow characteristic. It has mainly been applied in the great vessels to evaluate different cardiovascular conditions, and few research has also been done in the ventricles. The purpose of this work is to use a finite element analysis over 4D flow MRI to perform a comprehensive assessment of different flow parameters in the left ventricle of DCM patients.

Methods: 4D flow MRI data of9 healthy volunteers and 14 patients with DCM were acquired in a clinical MR Scanner of 1.5T (Philips). Data analysis include registration of 4D flow data with cine SSFP data and segmentation of the cine SSFP images. For the LV segmentation, we applied Otsu thresholding and manual correction to generate a LV mask. Subsequently, we generated a tetrahedral mesh using the iso2mesh MATLAB toolbox. Once the mesh was constructed, we computed the velocity vector at each node of the mesh from the 4D flow MRI datasets by using a cubic interpolation. 3D maps of vorticity, helicity density, relative helicity density, viscous dissipation, energy loss and kinetic energy fields were calculated using Python. Finally, LV mesh and results were divided into 17 subvolume segments (AHA) using ParaView. MATLAB was used to perform the different bullseyes of the mean parameters measures, during systole and diastole in each group of subjects. The statistical analysis for comparing quantitative variables between volunteer and patients was performed using a Mann-Whitney U Test.

Results: Figure 1 shows regional partitioning of the LV for one sample patient, including the visualization of some hemodynamic parameters, at diastole. Table 1 summarizes the mean parameters values at systole and diastole for each LV segment. Statistical differences at diastole of vorticity magnitude, helicity density and viscous dissipation was found in at least 3 areas of the LV. Bullseyes of these parameters are shown in figure 2.

Conclusion: We characterized the hemodynamic of the LV of DCM patients using the Bullseyes and a finite-element technique. This approach allows estimating different hemodynamic parameters from 4D flow MRI. The results indicate that some parameters reveal statistical differences between volunteers and patients, particularly during diastole.

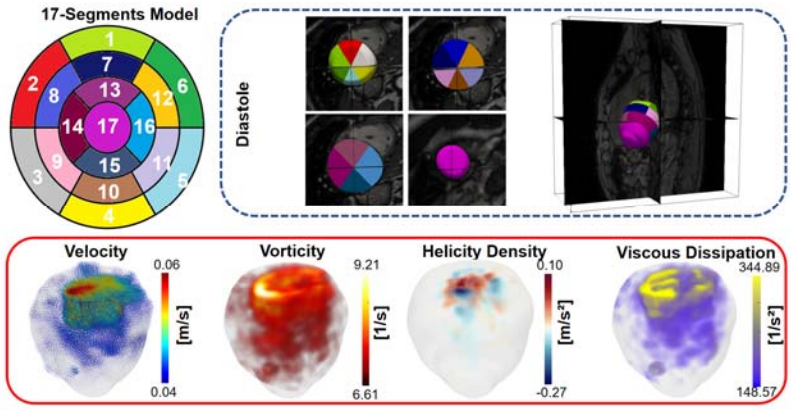

Figure 1: Regional partitioning of the LV for one simple patient, including velocity, vorticity, helicity density and viscous dissipation during diastole. We adjusted the colorbar range for visualization purposes.

		Percent Change [%]			
Mean parameters	**Cardiac Phases**	**Basal**	**Mid-Cavity**	**Apical**	**Apex**
Velocity Magnitude [m/s]	Systole	16.80	10.90	-11.84	-25.02*
	Diastole	10.12	11.47	9.40	9.29*
Vorticity Magnitude [1/s]	Systole	9.93	3.94	-15.04*	-31.86*
	Diastole	9.36	18.19*	18.41*	16.35*
Helicity Density [m/s^2]	Systole	68.96	57.97	21.05	-92.63*
	Diastole	78.64*	146.23*	-11.12	64.29*
Relativity Helicity Density	Systole	-385.57	25.96	-26.14	34.64*
	Diastole	169.92*	-217.27	85.84	51.75*
Viscous Dissipation [1/s^2]	Systole	19.14	10.96	-30.27	17.73*
	Diastole	9.08	28.51*	32.87*	35.71*
Energy Loss [W]	Systole	33.78	17.21	-625.11	68.38*
	Diastole	18.49	52.45*	57.44	81.05*
Kinetic Energy [J]	Systole	17.25	11.49	-11.82	-26.64*
	Diastole	9.43	10.49	8.21	9.70*

Table 1: Mean parameters values in the basal, mid-cavity, apical and apex segments of the LV, during systole and diastole. The percentage change in mean parameters measures between volunteers and patients. Where * is $p<0.05$ considered statistically significant.

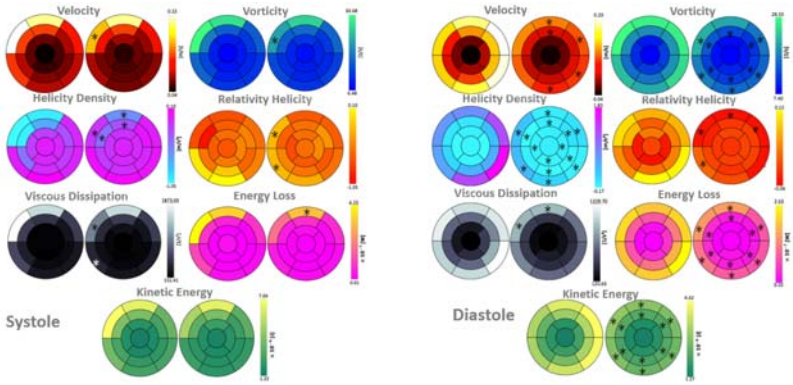

Figure 2:Regional partitioning of the LV for one simple patient, including velocity, vorticity, helicity density and viscous dissipation during diastole. We adjusted the colorbar range for visualization purposes.

ID#: 378238

Reproducibility and Performance of SASHA and MOLLI T1 Mapping in Volunteers at 1.5T and 3T

Kelvin Chow, PhD[1] Jacqueline A. Flewitt, MSc[2], Rosa Sandonato, RN, BScN[3], Carmen P. Lydell, MD[2], James White, MD, FRCP(C)[3], Richard Thompson, PhD[4], Andrew G. Howarth, MD, Ph.D[3]

1. Siemens Medical Solutions, Chicago, IL

2. Stephenson Cardiac Imaging Centre, Libin Cardiovascular Institute of Alberta, University of Calgary, Calgary, AB, Canada

3. Stephenson Cardiac Imaging Centre, Libin Cardiovascular Institute of Alberta, University of Calgary, AB, Canada

4. Department of Biomedical Engineering, University of Alberta, AB, Canada

Background: Expansion of the extracellular volume (ECV) and increased myocardial fibrosis are characteristic features of myocardial remodeling in disease. T_1 mapping has been used to non-invasively assess fibrosis for a wide spectrum of cardiomyopathies, but accurate and reproducible T_1 methods are required for individual diagnoses in clinical practice. SASHA T_1 mapping is accurate and robust to confounders such as B_0 and B_1 field heterogeneity and T_2, but reduced precision compared to MOLLI has limited its appeal. A variable flip angle (VFA) readout has been proposed to increase SNR and reduce image artifacts, but has not been investigated at 3T. The purpose of this study was to characterize the reproducibility and performance of SASHA with VFA and MOLLI T_1 mapping in normal volunteers scanned at 1.5T and 3T.

Methods: Nine healthy volunteers (44±10 years old, 2 female) were imaged on 1.5T MAGNETOM Avanto and 3T MAGNETOM Skyra systems (Siemens Healthcare, Erlangen, Germany) an average of 69±53 days apart. SASHA T_1 mapping was performed using a VFA readout with typical sequence parameters of: 360×270 mm^2 field of view, 256×150 matrix size, and parallel imaging acceleration factor 2. MOLLI had matched acquisition parameters with a 35° flip angle at 1.5T and a 20° flip angle at 3T to reduce sensitivity to B_0 and B_1 heterogeneity. SASHA and MOLLI data were acquired using an investigational prototype sequence on basal and mid-ventricular short-axis slices. Native T_1 data were acquired twice with the subject exiting and re-entering the scanner room and complete re-localization between scans. All T_1 imaging was repeated 22±2 minutes after intravenous administration of 0.15 mmol/kg of gadobutrol (Gadovist, Bayer Inc., Mississauga, Canada). T_1 maps were calculated using a 2-parameter model for SASHA and a Look-Locker corrected 3-parameter model for MOLLI. The left ventricular myocardium and blood pool were manually segmented with care taken to avoid regions with visible artifacts. T_1 values were characterized by the mean and coefficient of variation (CoV), both calculated over all segmented pixels from both slices.

Results: Measured T_1 values were consistent with published literature and are detailed in Table 1. The CoV in native myocardial T_1 at 1.5T was 5.9±0.8% and 5.7±0.9% for SASHA and MOLLI respectively, improving to 4.6±0.9% and 4.9±1.5% respectively at 3T. The smaller reduction in CoV from the higher field strength in MOLLI (14% vs 22% in SASHA) is consistent with the reduced flip angle used in MOLLI at 3T to mitigate dependence on B_0 and B_1 inhomogeneities. CoV was not statistically different between SASHA and MOLLI at either 1.5T or 3T ($p>0.05$). Both SASHA and MOLLI techniques were highly reproducible at both 1.5T and 3T, with a scan-rescan difference in native myocardial T_1 of 0.4±1.0% and 0.3±1.4% for SASHA and MOLLI respectively. ECV was not statistically significantly different between field strengths for both SASHA and MOLLI ($p>0.05$).

Conclusion: Myocardial T_1 values measured using SASHA with a VFA readout and 2-parameter model have comparable precision to MOLLI at both 1.5T and 3T with a 22% increase in precision at 3T compared to 1.5T. Both SASHA and MOLLI have excellent scan-rescan reproducibility with consistent ECV measurements across field strengths. Robustness to confounders and flexibility of enabling free-breathing and 3D acquisitions make SASHA a promising candidate for non-invasive fibrosis imaging.

Performance of SASHA and MOLLI T1 mapping techniques in 9 healthy volunteers

	1.5T	3T

	SASHA	MOLLI	SASHA	MOLLI
Native myocadial T_1 (ms)	1187±27	998±26	1508±43	1259±41
Native blood T_1 (ms)	1690±80	1578±55	2160±121	1768±79
Post-contrast myocardial T_1 (ms)	594±41	510±37	677±54	594±47
Post-contrast blood T_1 (ms)	347±37	347±40	367±41	369±42
Extracellular volume (%)	20.3±1.6	23.5±1.7	19.9±1.5	23.0±1.6
Native myocardial T_1 CoV (%)	5.9±0.8	5.7±0.9	4.6±0.9	4.9±1.5
Native blood T_1 CoV (%)	5.8±1.0	3.0±0.6	5.2±1.3	3.5±1.2
Native myocardial T_1 scan-rescan difference (%)	0.5±1.0	0.4±1.2	0.3±1.0	0.1±1.5

ID#: 378410

T1 and T2 mapping of myocardium in Coronary Artery Bypass Grafting

John-Paul Tantiongco, BSc (Honous) BMBS[1] Robert A. Baker, PhD[2], Joseph Selvanayagam, FRACP, DPhil[3], Craig Bradbrook, MR[4]

1. Flinders University, Bedford Park, South Australia, Australia

2. Flinders Medical Centre and Flinders University, Adelaide, Australia, Bedford Park, South Australia, Australia

3. Flinders University, Adelaide, SA, Australia, Bedford Park, South Australia, Australia

4. Flinders Medical Centre, Adelaide, Australia, Bedford Park, South Australia, Australia

Background: The current gold standard for imaging irreversible myocardial injury is late gadolinium enhancement (LGE) CMR. More recently, T1 and T2 mapping have been shown to be useful in detecting myocardial injury without the need for contrast, however these techniques have not yet been evaluated systematically in a coronary artery bypass grafting (CABG) surgery setting. In a prospective study of CABG patients, we sought to evaluate the utility of T1 and T2 mapping to detect perioperative myocardial injury compared to conventional LGE CMR and biochemical markers.

Methods: 61 patients underwent CABG +/- AVR had CMR approximately 1 week preoperatively and approximately 3 weeks postoperatively. Cardiac troponin T testing (cTnT) was measured at time=0, 6, 12, 24, 48, 72 and 120 hr after cross clamp application. CMR protocol consisted of CINE, T1 mapping (ShMOLLI), T2 mapping (FLASH), T2 STIR and LGE imaging. 6 normal volunteers also underwent the same CMR protocol. Receiver operating characteristics (ROC) area under the curve (AUC) optimal cut off was obtained using Youden';s index. LGE (full width half max) in the postoperative scan with corresponding positive T2 STIR (+5SD relative to skeletal muscle) was considered as new LGE. Perioperative myocardial infarction (PMI) was defined according to the 3rd universal definition of myocardial infarction (Type 5) with troponin >10xULN plus loss of viable myocardium (new LGE).

Results: A new PMI was identified in 23 patients (37.7%). The correlation between cTnT AUC and new LGE was strong (0.82, $p<0.0001$). Using new LGE per segment as the gold standard, ROC AUC for T1 and T2 was 0.66 (95%CI 0.61, 0.72) and 0.66 (95%CI 0.61, 0.72) respectively. Importantly, the postoperative T1 and T2 were significantly higher in new LGE segments compared to those without new LGE (see Figure 1 and 2). Optimal cut off for new LGE, for T1 and T2 in this cohort is 985.6 msec (95%CI 946.8, 1024.4, $p<0.0001$) and 48.0 msec (95%CI 45.0, 51.2, $p<0.0001$) respectively.

Conclusion: This is the first time T1 and T2 have been quantitated in a CABG population. Post-operative T1 and T2 increased significantly in patients with new LGE. However, T1 and T2 values also increased in segments without new LGE, although to a lesser extent. This may signify reversible myocardial injury resulting from cardioplegia and/or ischaemia reperfusion injury. T1 and T2 mapping shows promise in monitoring and assessing myocardial injury in this setting.

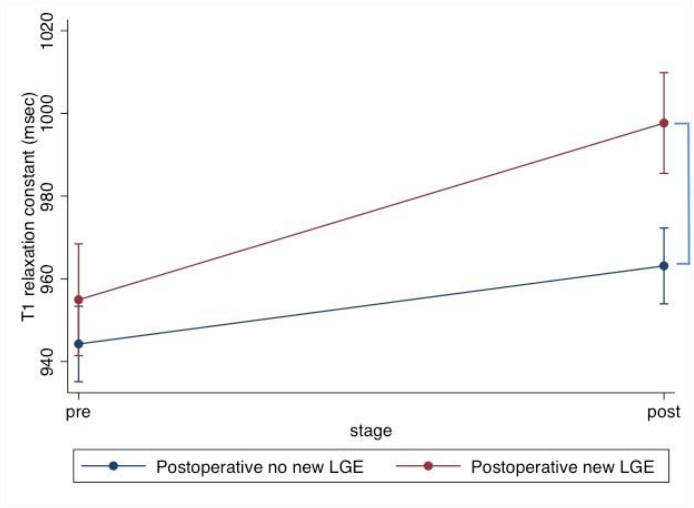

Figure 1 Segmental T1 mapping relaxation constant according to new LGE. (* p<0.0001)

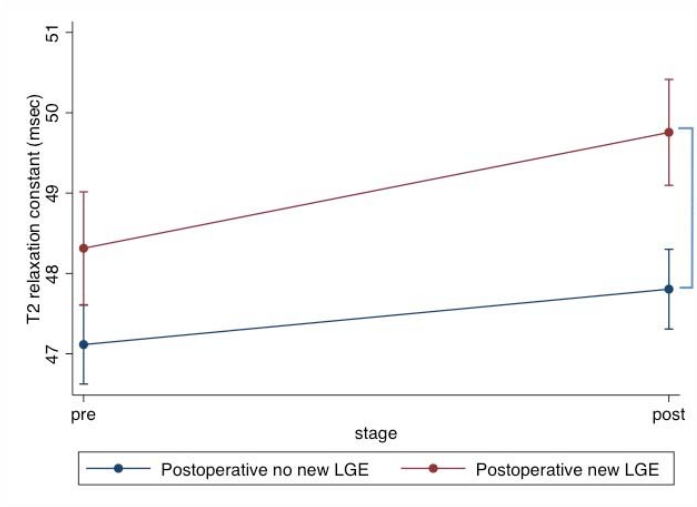

Figure 2 Segmental T2 mapping relaxation constant according to new LGE. (* p<0.03)

ID#: 378413

Improved aortic distensibility after renal sympathetic de-nervation in patients with resistant hypertension. A multi-center CMR study.

Lukas Stoiber, MD[1] Felix Mahfoud, MD[2], Seyedeh Mahsa Zamani[3], Tomas Lapinskas, MD[4], Burkert Pieske, MD[5], Sebastian Kelle, MD[5], Philipp Stawowy, MD[3]

1. German Heart Center Berlin, Germany

2. Saarland University, Homburg, Germany, Germany

3. German Heart Institute Berlin, Berlin, Berlin, Germany

4. Medical Academy, Lithuanian University of Health Sciences, Kaunas, Kauno Apskritis, Lithuania

5. German Heart Center Berlin, Berlin, Berlin, Germany

Background: The blood pressure (BP) lowering efficacy of renal sympathetic denervation (RDN) in patients with resistant hypertension (RH) is mixed. However, determinants of arterial compliance may help to predict response to therapy. Aortic distensibility (AD) can easily be obtained by CMR and represents a well-established parameter of aortic stiffness. This study was aiming to investigate the effects of RDN on central vasculature and to assess whether pre-treatment AD can potentially provide useful information on response to RDN.

Methods: We analyzed data of 65 patients (mean age 64.4 ± 9.6 years) with RH included in a multicenter trial. All participants underwent RDN and a standardized CMR protocol was performed both at baseline and 6-month follow-up. The change in cross sectional aortic area per unit change in BP was used to determine AD.

Results: Maximum aortic areas increased from 604.7 ± 157.7 mm² to 621.1 ± 157.3 mm² (p=0.011). Office BP decreased significantly from 173/92 ± 24/16 mmHg at baseline to 151/85 ± 24/17 mmHg (p-3 $mmHg^{-1}$ to 2.02 ± 0.93 10^{-3} $mmHg^{-1}$ (p<0.001). Increase of AD at follow-up was more pronounced in younger patients (p=0.005) and responders to RDN (p=0.002). Patients with high baseline AD were significantly younger (61.4 ± 10.1 years vs. 67.1 ± 8.4 years, p=0.022). There was no significant correlation of baseline AD to response to RDN.

Conclusion: Aortic distensibility reflects the heterogeneity of aortic stiffness in patients undergoing RDN. We observed significant improvement of AD across all age groups and regardless of the BP change following RDN. Future trials are needed to determine how this will impact the outcome of patients post RDN.

ID#: 378423

Reference values for myocardial T1, T2 and Extracellular Volume Fraction at 3.0 Tesla in the Hamburg City Health Population Study

Jan Schneider, MD[1] Clemens Spink, MD[2], Ersin Cavus, MD[3], Sebastian Bohnen, MD[3], Maxim Avanesov, MD[4], Enver Guner. Tahir, MD[5], Ulf Radunski, MD[6], Gerhard Adam, MD[7], Stefan Blankenberg, MD[8], Gunnar Lund, MD[6], Kai Müllerleile, MD[9]

1. University Heart Center, Germany

2. Department for Diagnostic and Interventional Radiology and Nuclear Medicine University Medical Center Hamburg-Eppendorf, Hamburg, Germany

3. University Heart Center Hamburg, Hamburg, Germany

4. UKE, Hamburg, Germany

5. University Medical Center Hamburg-Eppendorf, Hamburg, Hamburg, Germany

6. University Medical Center Hamburg-Eppendorg, Hamburg, Germany

7. University Medical Center Hamburg-Eppendorf, Hamburg, Germany

8. University Heart Center Hamburg, Germany

9. UKE, Germany

Background: The Hamburg City Health (HCH) study is a single center, prospective, population-based cohort study, which includes a comprehensive cardiovascular magnetic resonance (CMR) protocol. We present reference values for myocardial T1, T2 and extracellular volume fraction (ECV) from a pilot population and the first 1000 participants.

Methods: We excluded 181 subjects with a history of coronary artery disease (CAD) and/or scar on CMR. The final study population consisted of 1103 consecutive individuals, 525 female (48%) with a median age of 65 (range 30 to 80) years. CMR was performed on a 3.0 Tesla scanner (MAGNETOM Skyra, Siemens Healthcare, Erlangen, Germany) including native T1 (5b(3b)3b modified Look-Locker inversion recovery (MOLLI) scheme) as well as T2 mapping (T2 prepared fast-low-angle shot, FLASH sequence) in all subjects. Post-contrast T1 mapping (4b(1b)3b(1b)2b MOLLI scheme) was available for calculation of ECV in a subgroup of 389 unselected subjects. Global myocardial T1, T2 and ECV were defined as the mean values measured with certified post-processing software (cvi42, Circle Cardiovascular imaging, Calgary, Canada) on three representative short-axis slices. Data are presented as median and interquartile range.

Results: Median global myocardial T1, T2 and ECV were 1183 ms (1161 to 1209 ms), 39.3 ms (37.7 to 41.1 ms) and 28.0 % (26.5 to 30.0 %), respectively. Female subjects had significantly higher global myocardial T1 (1195 ms (1173 to 1220 ms) vs. 1174 ms (1149 to 1197 ms); $p<0.0001$), T2 (40.3 ms (38.6 to 41.8 ms) vs. 38.6 ms (37.3 to 40.2 ms); $p<0.0001$) and ECV (29.0 % (27.0 to 31.0 %) vs. 27.0 % (26.0 to 29.0 %); $p<0.0001$) values compared to male subjects. There was a significant inverse correlation of heart rate with global myocardial T2 ($r=-0.48$; $p<0.0001$), but not with T1 ($r=0.05$; $p=0.1036$) or ECV ($r=0.08$; $p=0.1443$), respectively. There were very weak or not-significant correlations of age with global myocardial T1 ($r=-0.02$; $p=0.4784$), T2 ($r=-0.08$; $p=0.0062$) and ECV ($r=-0.04$; $p=0.4072$).

Conclusion: The HCH-study provides robust reference values for myocardial T1, T2 and ECV at 3.0 Tesla using commercially available sequences in a large population. Our findings clarify the need for gender specific normal values for myocardial T1, T2 and ECV. Heart rate had a significant effect on measured myocardial T2, but not on T1 and ECV values in our setting. Interestingly, we did not find a relevant correlation of age with myocardial T1, T2 and ECV in our cohort.

ID#: 378425

Expanding the limits of cardiovascular MR: amyloid detection in the liver and spleen

Michele Boldrini[1] Andrea Baggiano[2], Ana Martinez Naharro, MD[3], Tushar Kotecha, MRCP(UK) MBChB[4], Tamer Rezk, BSc[1], Rohin Francis, MBBS[1], Richa Manwani, MRCP FRCPath[5], Daniel S. Knight[3], Hossam Fayed, MBChB MSc MRCP(UK)[6], Helen J. Lachmann, MD[7], James Moon, MD[8], Peter Kellman, PhD[9], Julian D. Gillmore[10], Philip N. Hawkins[10], Marianna Fontana, MD, PhD[1]

1. UCL Department of CMR, Royal Free Hospital, England, United Kingdom

2. Centro Cardiologico Monzino, Istituto di Ricovero e Cura a Carattere Scientifico, Italy

3. UCL Department of CMR, Royal Free Hospital, London, England, United Kingdom

4. Royal Free London NHS Foundation Trust, London, England, United Kingdom

5. UCL National Amyloidosis Center, Royal Free Hospital, United Kingdom

6. UCL Department of Cardiac MRI, Royal Free Pulmonary Hypertension Service, Pond Street, England, United Kingdom

7. University College London, England, United Kingdom

8. UCL, England, United Kingdom

9. National Heart, Lung, and Blood Institute, National Institutes of Health, Bethesda, MD

10. National Amyloidosis Centre, University College London, England, United Kingdom

Background: Background: Systemic amyloidosis is a disease characterized by amyloid infiltration into different organs and tissues. CMR is the reference standard to assess cardiac amyloid infiltration, that can be visualized with LGE and measured with ECV. The utility of ECV in detecting and quantifying amyloid in other organs has never been investigated. **Aim:** The aim of this study is to assess, in a large prospective cohort of patient suspected systemic amyloidosis, the ability of ECV to detect amyloid infiltration in the liver and spleen. This was done using standard acquisition for cardiac studies, with no extra image acquisition.

Methods: Methods: 732 consecutive patients with suspected systemic amyloidosis were prospectively enrolled into the study between 2015 and 2017. All patients underwent scintigraphy with 123I-labeled serum amyloid P component (SAP scan), the reference standard for assessment of amyloid burden in the spleen and liver: uptake in the spleen and liver was classified into four categories (no amyloid, small, medium, large). All patients underwent a standard cardiac MR protocol including acquisition of three short axis slices with pre and post contrast T1 mapping (by Modified Look-Locker Inversion recovery, MOLLI) and online ECV mapping reconstruction. The liver and spleen ECV was measured on the ECV maps acquired for the left ventricular short axis (Figure 1).

Results: Results: There was a good correlation between ECV and amyloid burden in the liver and spleen as assessed by SAP scintingraphy (Spearman's coefficient of rank correlation: 0.465 (liver), 0.603 (spleen), $p<0.0001$) (Figure 2). The ECV showed a very good diagnostic accuracy to detect amyloid in the liver (AUC 0.870; 95% CI 0.837 to 0.899; sens 78%, spec 81%) and in the spleen (AUC 0.896; 95% CI 0.865 to 0.922; sens 83%, spec 84%) (both $p<0.0001$) (Figure 3).

Conclusion: Conclusions: CMR has a high sensitivity for the detection and quantification of amyloid in the spleen and liver. This does not require any additional image acquisition and can therefore be easily integrated into routine clinical practice. ECV of the liver and spleen could significantly improve the diagnostic pathway for extra-cardiac amyloid but also has the potential to become an important tool to monitor treatment response.

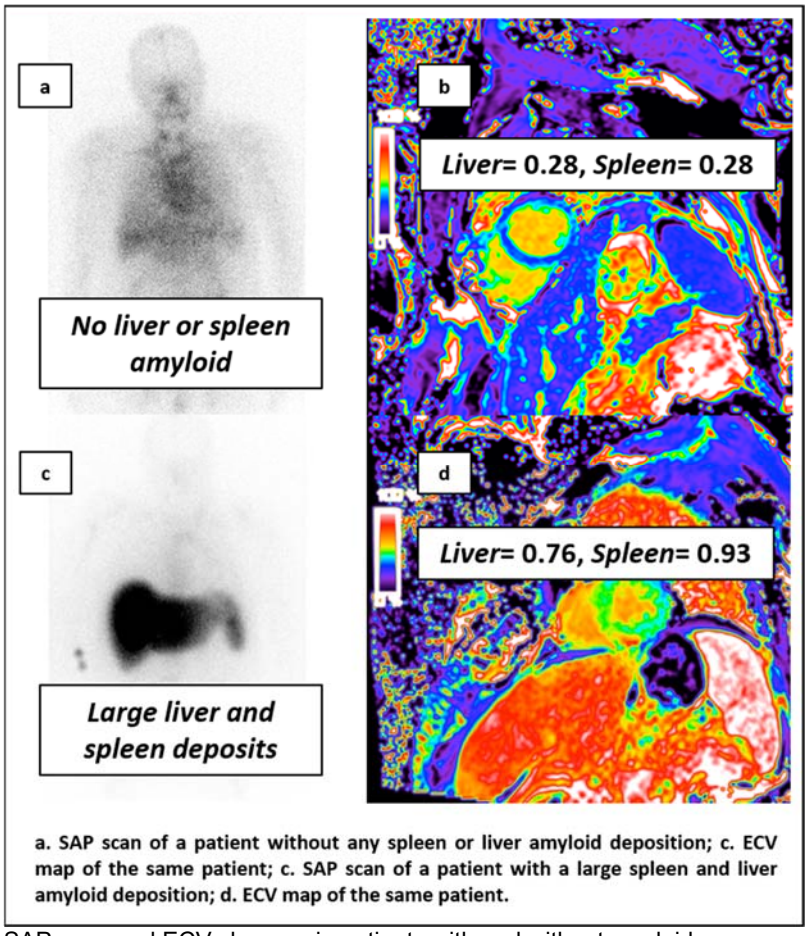

SAP scan and ECV changes in patients with and without amyloid

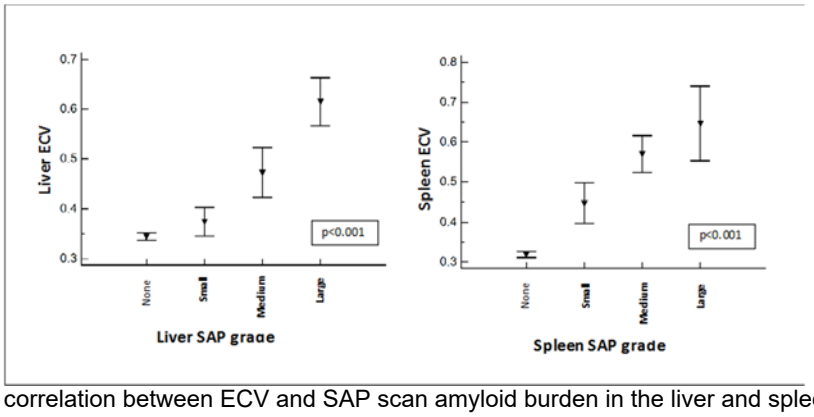

correlation between ECV and SAP scan amyloid burden in the liver and spleen

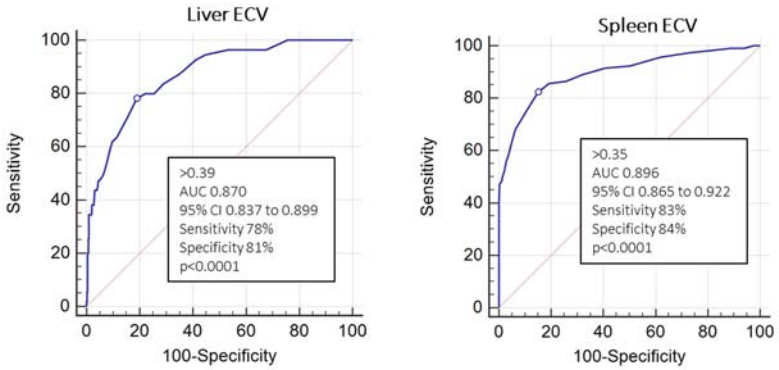

ECV diagnostic accuracy to detect amyloid in the liver and spleen

ID#: 378438

Relation of global and segmental Pulse Wave Velocities of the thoracic aorta with ageing and Left Ventricular remodelling by using 4D flow analysis in healthy volunteers.

Gilles Soulat, MD[1] Umit Gencer, Msc[2], Nadjia Kachenoura, PhD[3], Olivier Villemain, MD[2], Emmanuel Messas, MD, PhD[2], Pierre Boutouyrie, MD, PhD[4], Stéphane Laurent, MD, PhD[2], Elie Mousseaux, MD, PhD[2]

1. European Hospital Georges Pompidou APHP; INSERM U970 PARCC Paris descartes University, Paris, Ile-de-France, France

2. European Hospital Georges Pompidou APHP; INSERM U970 PARCC Paris descartes University, Ile-de-France, France

3. Sorbonne Universités, UPMC Univ Paris 06, INSERM UMRS 1146, CNRS UMR 7371, Laboratoire d'Imagerie Biomédicale, F-75013, Paris, France, Paris, Ile-de-France, France

4. European Hospital Georges Pompidou APHP; INSERM U970 PARCC Paris descartes University, Paris, France

Background: In CMR, thoracic aorta (TA) Pulse Wave Velocity (PWV) is usually estimated after 2D phase contrast (PC) acquisition. Preliminary studies showed that PWV could also be estimated after using 4DflowPC, despite the lower temporal resolution compared to 2DPC. Thanks to the full 4DFlow TA coverage, it is now feasible to estimate PWVs globally along the all TA but also regionally along the ascending and descending TA segments. The Objective of our work was to compare the relationship between 2DPC PWV, global or segmental TA 4DPC PWV and aging, left ventricle (LV) concentric remodelling and thickness in healthy volunteers.

Methods: Acquisitions were performed at 3 Tesla (GEHC, 750w). PWVs were estimated after PC through plane acquisition perpendicular to ascending and descending TA (2DPWV) and after the full coverage of the heart and TA by the 4Dflow volume. TAPWV was estimated after estimating the length and the transit time between upslopes of the valve to diaphragm flow curves while AAPWV was estimated between the valve to isthmus, and DAPWV from aortic isthmus to diaphragmatic aorta.

Results: 57 healthy volunteers (25 male, age 50.9y ±17.3) were included. 2D PWV and TAPWV were strongly correlated with age (r=0.76 and r=0.77 respectively).DAPWV was significantly higher than AAPWV for the 2nd and 3rd quartiles of age. LV thickness and LV Mass/End diastolic volume (EDV) ratio were better related to TAPWV(r=0.35, p<0.01 and r=0.49 p<0.001) than 2D PWV (r= 0.17, p=NS and r=0.36 p<0.01). Furthermore, AAPWV was better related to LV thickness and Mass/EDV (r= 0.43, p<0.01 and r=0.48 p<0.01) than DAPWV (r=0.14 p=NS and r=0.35, p<0.05).

Conclusion: All PWVs were highly correlated with aging, but increase PWV occur earlier along DA than along AA. However, both the global TAPWV and the segmental AAPWV were better related to LV thickness and remodelling than 2D PWV and DAPWV. Further studies are required to validate the interest of segmental TA stiffness in aortic diseases.

ID#: 378444

Relationship between breathing pattern and aortic flow measurement: head-to-head comparison between high temporal resolution free-breathing phase contrast CMR and standard breath-hold phase contrast sequence

Gabriella Vincenti, 1) Division of Cardiology and Center of Cardiac Magnetic Resonance, Cardiovascular Department, University Hospital of Lausanne, CHUV, Switzerland.[1]Anna Giulia Pavon, Division of Cardiology and Center of Cardiac Magnetic Resonance, Cardiovascular Department, University Hospital of Lausanne, CHUV, Switzerland.[2], Pier Giorgio Masci, 1) Division of Cardiology and Center of Cardiac Magnetic Resonance, Cardiovascular Department, University Hospital of Lausanne, CHUV, Switzerland.[3], Pierre Monney, 1) Division of Cardiology and Center of Cardiac Magnetic Resonance, Cardiovascular Department, University Hospital of Lausanne, CHUV, Switzerland.[3], Tobias Rutz, 1) Division of Cardiology and Center of Cardiac Magnetic Resonance, Cardiovascular Department, University Hospital of Lausanne, CHUV, Switzerland.[3], Stamatia Zoi Pagoulatou, Laboratory of Hemodynamics and Cardiovascular Technology, Swiss Federal Institute of Technology, Lausanne, Switzerland[4], Gregoire Berchier, Department of Radiology, University Hospital of Lausanne, CHUV, Switzerland.[5], Juerg Schwitter, 1) Division of Cardiology and Center of Cardiac Magnetic Resonance, Cardiovascular Department, University Hospital of Lausanne, CHUV, Switzerland.[3]

1. 1) Division of Cardiology and Center of Cardiac Magnetic Resonance, Cardiovascular Department, University Hospital of Lausanne, CHUV, Switzerland, Switzerland

2. Division of Cardiology and Center of Cardiac Magnetic Resonance, Cardiovascular Department, University Hospital of Lausanne, CHUV, Switzerland., Switzerland

3. 1) Division of Cardiology and Center of Cardiac Magnetic Resonance, Cardiovascular Department, University Hospital of Lausanne, CHUV, Switzerland., Switzerland

4. Laboratory of Hemodynamics and Cardiovascular Technology, Swiss Federal Institute of Technology, Lausanne, Switzerland, Switzerland

5. Department of Radiology, University Hospital of Lausanne, CHUV, Switzerland., Switzerland

Background: Percutaneous aortic and mitral valve interventions are increasingly performed in routine cardiology. Accordingly, there is a need for precise quantification of valve function. Total systolic aortic flow measured by phase contrast MRI and left ventricular stroke volume (LVSV) allow quantification of mitral insufficiency. To this goal, various aortic flow measurements were evaluated. Purpose: To evaluate the influence of breath-holding during flow measurements by comparing a high temporal resolution free-breathing (Flow-FBhighres) phase-contrast sequence with a standard (Flow-BHstandard) and high-resolution (Flow-BHhighres) breath-hold sequence.

Methods: In 23 patients without relevant valvular disease (3 women, 20 men, 57±16y), a conventional phase-contrast sequence was applied in the proximal ascending aorta during breath-holding (Flow-BHstandard; spatial/temp resolution 1.9x1.9mm2/40.9ms; slice thickness 10mm, segments 4; cardiac phases 20; acquisition duration 17 beats) and a modified high temporal resolution phase-contrast sequence was applied during free breathing (Flow-FBhighres; spatial/temporal resolution 2.1x2.1mm2/9.9ms; segments 1; cardiac phases 60; acquisition duration 262 beats). In a subset of 13 patients, an additional high-resolution breath-hold sequence was applied (Flow-BHhighres; spatial/temporal resolution 3.75x3.75mm2/9.4ms; segments 1; cardiac phases 60; acquisition duration 26 beats) at the same aortic position. In order to verify whether patients performed accidentally a Valsalva-like maneuver during breath-holding, a cine real-time acquisition of a modified LV short-axis view (=single-oblique coronal orientation) was also acquired during breath-holding in these 13 patients and the difference between the LV end-diastolic cavity at the beginning and the end of the breath-hold was measured.

Results: Aortic flow measured by Flow-FBhighres was higher than by Flow-BHstandard (82±15ml vs 69±22ml, $p<0.02$, n=23, see Figure) and tended to be higher vs Flow-BHhighres (75±21ml, $p=0.07$, n=13). In comparison with the LVSV of 82±22ml, Flow-FBhighres was not different ($p=0.95$), while Flow-BHstandard and Flow-BHhighres tended to underestimate flow ($p=0.06$, n=23 and $p=0.34$, n=13, respectively). The acquisition duration for Flow-FBhighres, Flow-BHstandard, and Flow-BHhighres were 234±42s, 15±3s, and 23±4s, respectively. The underestimation of aortic flow by Flow-BHstandard vs Flow-FBhighres (expressed as percentage of Flow-FBhighres) correlated positively with a reduction in LV cavity size during breath-holding (change expressed as percentage of cavity size at the beginning of breath-holding) with $p<0.015$ and $r=0.66$.

Conclusion: Aortic flow may be underestimated when measured with a standard breath-hold phase-contrast pulse sequence and this underestimation may partly be explained by a Valsalva-like maneuver provoked by breath-

holding. A high temporal resolution free-breathing phase-contrast acquisition may avoid this source of error. Further studies are needed to confirm these findings.

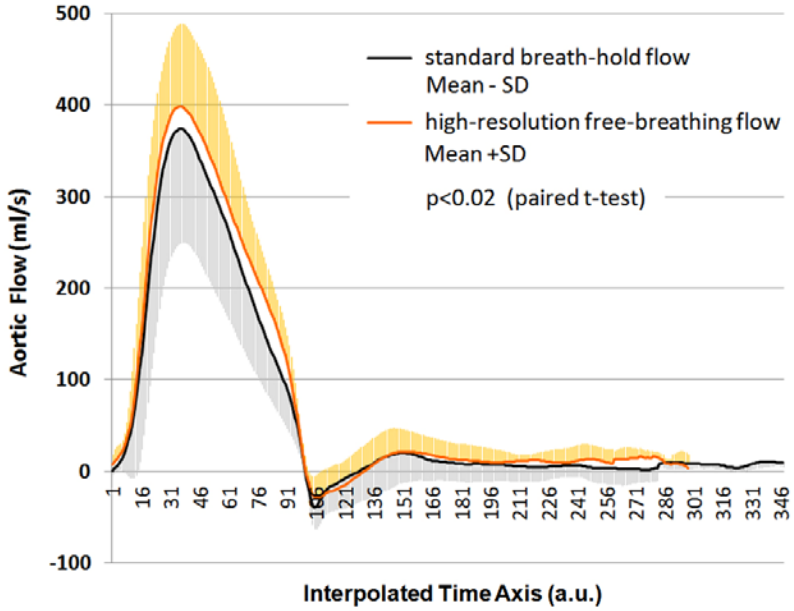

Standard breath-hold vs high resolution free breathing aortic flow measurements (a.u. = arbitrary units)

ID#: 378485

Atrial fibrosis detected using LGE-MRI is a progression phenomenon accelerated by atrial fibrillation: Comparison between patients without and with Atrial fibrillation.

Christian Mahnkopf, MD[1]Marcel Mitlacher[2], Mariella Zuber[3], Mathias Forkmann, MD[3], Johannes Brachmann, MD, PhD[2]

1. Klinikum Coburg, Dept. of Cardiology, Bayern, Germany

2. Klinikum Coburg, Dept. of Cardiology, Coburg, Bayern, Germany

3. Klinikum Coburg, Dept. of Cardiology, Coburg, Germany

Background:

The clinical relevance of left atrial fibrosis in well known. However, the progression of atrial fibrosis (LA-SRM) is still an unknown. In this study we report the progression of atrial fibrosis in patients without history of atrial fibrillation (AF). We also detail the effect of new onset AF on the progression of AF.

Methods:

A total of forty-two patients (27male, 65.9±8.6 years) with stable sinus rhythm and no known history of AF underwent LGE-MRI at two differnt time points to assess for LA-SRM . Each LGE-MRI was segmented by isolating the LA-Wall and quantified for the relative extent of fibrotic remodeling using a semi-automated software (Figure 1).

Results:

Fibrosis was detectable in all patients. The degree of LA-SRM ranged from 4.5% to 28.8%. The average of LA-SRM overall was 12.9±5.9%. All patients underwent 2nd LGE-MRI of the LA after 766±564 days. The degree of change in atrial fibrosis in second MRI ranged from 0.10% to 27.00%. Degree of LA-SRM in the second MRI was significantly higher in all patients compared to first MRI (12.9±5.9% vs. 17.34±6.8%; $p<0.05$). New onset AF was detected in 7 patients (16.6%; 3 male; 68.1 years) during follow up. Comorbidities (hypertension, congestive heart failure, diabetes mellitus, etc.), medication (ACI, ARB, beta-blocker, etc.) age and gender were comparable to patients who showed stable sinus rhythm. Compared to patients with no know AF, patients with new onset AF showed a significant higher degree of LA-SRM in the second MRI (20.5±6.9% vs. 16.7±6.7%; Figure 1).

Conclusion:

Cardiac MRI allows the detection of fibrotic changes in the left atrium. Our preliminary results indicate that atrial fibrosis is a progressive disease. The fact that patients with a new onset AFIB showed a significantly higher degree of LA-SRM suggests that AF itself triggers the progression of LA-SRM.

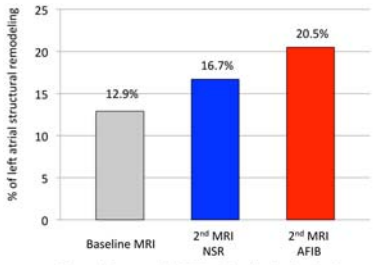

Figure 1: Degree of LA-SRM at Baseline is given in the grey column. Degree of LA-SRM at the second MRI was higher in patients with new onset atrial fibrillation (red column) compared to those patients with stable sinus rhythm (blue column).

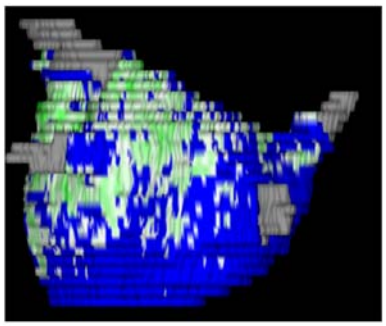

ID#: 378489

T1 mapping for cardiac iron in children

Amna Abdel-Gadir, MBBS.MRCP(UK)[1] Daniel Sado, BM, MRCP[2], Katia Devorha. Menacho, MD[3], Sabrina Nordin, MRCP [4], Louise McGrath, BSc MSc[5], Stefan K. Piechnik, PhD, MScEE[6], Anna Herrey, MD PhD MRCP[7], Charlotte Manisty, MRCP PhD[8], Malcolm J. Walker, MD[9], James C. Moon, MD[7]

1. University College London and Barts Heart Centre, London, England, United Kingdom

2. Kings College Hospital, London, England, United Kingdom

3. Barts Heart Centre, London, England, United Kingdom

4. Barts Heart Centre, United Kingdom

5. University College London, United Kingdom

6. University of Oxford, England, United Kingdom

7. Barts Heart Centre, England, United Kingdom

8. Barts Heart Centre and University College London, United Kingdom

9. University College London, London, United Kingdom

Background: Management of iron overload in paediatric patients has been transformed by the CMR T2* measurement. Clinical guidelines recommending early CMR scanning for iron quantification has led to an increase in number of patients referred at an early age. In adults, T1 mapping appears to detect early cardiac iron in adult patients missed by T2*. We explored T1 mapping for cardiac iron in children.

Methods: A single centre observational study of 21 paediatric patients at risk of cardiac iron overload in a tertiary hospital in London. All patients underwent CMR T2* and native T1 mapping using shortened modified look locker inversion recovery (ShMOLLI) sequences of the midventricular short axis slice at 1.5T (Siemens Avanto).

Results: Mean patient age was 14.0 ± 2.9 year (76% male). Referral diseases were beta-thalassaemia major (n=9), sickle cell anaemia (n=8), and the remainder thalassaemia intermedia, acute lymphoblastic leukaemia, hereditary spherocytosis and congenital sideroblastic anaemia (n=1 each). All patients had normal LV systolic function (LVEF 67 ± 5%). Mean T2* and native T1 values were 33.1 ± 10.8ms and 905 ± 101.4ms, respectively. Across the cohort there is a strong relationship between myocardial T2* and T1 (r^2= 0.73; figure 1). Two (9.5%) patients had low T2* (<20ms). 4 patients (19%) had low T1 values (<898ms) with both the low T2* patients having low T1 (table 1). The low T2* patients were followed up at one year. T2* and T1 both improved with T2* normalising in one but T1 remaining low in both.

Conclusion: Cardiac iron detection by T1 in children is potentially more sensitive than T2*. Further research is required to assess its significance.

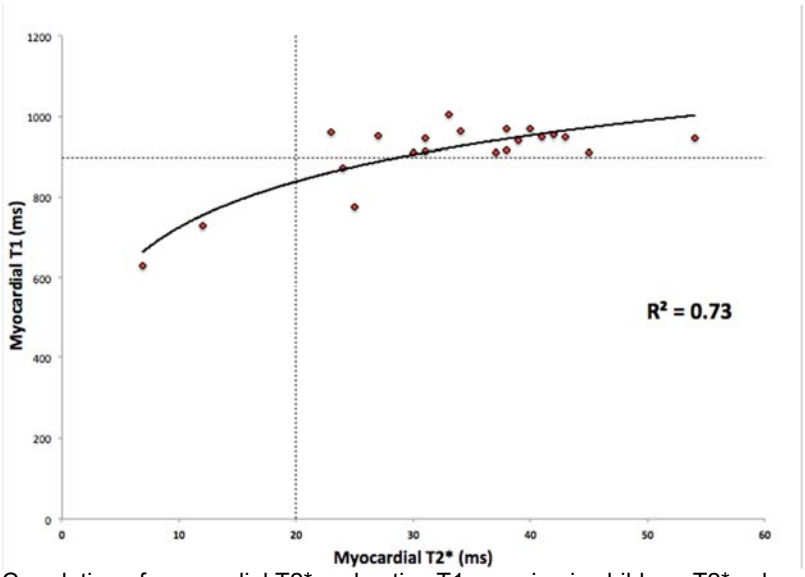

Correlation of myocardial T2* and native T1 mapping in children. T2* values less than 20ms indicate the presence of myocardial iron. 2 patients with normal T2* values have low T1 (<898ms).

Demonstrating the grouping of patients according to T2* and T1 values. 2 patients with low T2* have low T1 and 2 patients with normal T2* have low T1 values.

	T1 (<898ms)	T1 (>898ms)
T2* (<20ms)	2	0
T2* (>20ms)	2	17

ID#: 378453

How assess Early to late peak mitral filling ratio (E/A) obtained after acquisition of a full coverage 4D flow of the heart and great vessels is highly and better related to normal aging than such ratio obtained at echocardiography

Yousef Alattar, -[1]Gilles Soulat, MD[2], Umit Gencer, Msc[1], Nadjia Kachenoura, PhD[3], Olivier Villemain, MD[1], Emmanuel Messas, MD, PhD[1], Elie Mousseaux, MD, PhD[1]

1. European Hospital Georges Pompidou APHP; INSERM U970 PARCC Paris descartes University, Ile-de-France, France

2. European Hospital Georges Pompidou APHP; INSERM U970 PARCC Paris descartes University, Paris, Ile-de-France, France

3. Sorbonne Universités, UPMC Univ Paris 06, INSERM UMRS 1146, CNRS UMR 7371, Laboratoire d'Imagerie Biomédicale, F-75013, Paris, France, Paris, Ile-de-France, France

Background: Doppler echocardiography (US) remains the modality of choice to assess the LV diastolic filling and function by studying trans-mitral blood flow velocities. Early studies with 2D Phase contrast (PC) at CMR have also shown nice results. Quantitative LV filling analysis can now be provided by 4D flow CMR despite the lower temporal resolution. The goal of our study was to compare the results of 4DPC transmitral flow at different levels with 2DPC and US, by studying their correlation with aging in healthy volunteers (HV).

Methods: HV underwent US and CMR (3Tesla GE 750w) the same day. Early (E_{US}) and late (A_{US}) filling peak velocity were recorded using US. In CMR, 2DPC section was placed perpendicular to the trans-mitral flow at the level of the tips of mitral leaflets permitting estimation of the early filling peak flow rate (Ef_{2D}) and velocity (Ev_{2D}) as well as atrial filling peak flow rate and peak velocity (Af_{2D} and Av_{2D}). After 10 minutes acquisition time of a 4D flow volume covering the full heart (Venc:200m/s, fixed 34 ms temporal resolution, 50 phases), transmitral flow rate and velocity were calculated at the level of tip of the mitral leaflet, mitral annulus and also by using a mitral tracking (Ef_{4DTL}, Af_{4DTL}, Ev_{4DTL}, Av_{4DTL}, Ef_{4Dann}, Af_{4Dann}, Ev_{4Dann}, Av_{4Dann}, $Ef_{4Dtrack}$, $Af_{4Dtrack}$, $Ev_{4Dtrack}$, $Av_{4Dtrack}$, respectively).

Results: In 50 HV (mean age 51.4 ±17 years), E and A maximal velocity values estimated by 4DPC were significantly lower than US values (-18.7 $cm.s^{-1}$; -29.9 $cm.s^{-1}$, -23 $cm.s^{-1}$; p4DTL,L Ev_{4Dann}, $Ev_{4Dtrack}$, respectively and -13.8 $cm.s^{-1}$, -18.4 $cm.s^{-1}$, -22.1 $cm.s^{-1}$ for Av_{4DTL} Av_{4Dann}, , $Av_{4Dtrack}$; p<0,0001 respectively) while E/A using velocty was only lower at annulus level (-0.23; p<0.01). But, all E/A ratios derived from flow rate 4DPC estimates were better correlated with E/Av_{US} than E/A ratios derived from velocities. All E/A were highly correlated with age but Ef/Af_{2D} and Ef/Af_{4Dann}(r=-0.84 p<0.0001 and r=-0.82 p<0.0001 respectively) had higher correlation coefficient than E/A_{US} (r= -0.63, p<0.0001).

Conclusion: LV filling and diastolic function parameters such as E/A ratio can be estimated by using a non-dedicated full thoracic heart and great vessel coverage 4DPC with close results compared to TTE and 2PC. Despite significantly lower absolute velocity values in 4DPC compared to US due to the lower temporal resolution, 4DPC Ef/Af ratio at the annulus level was better correlated with normal aging than US.

ID#: 378454

Role of T1 mapping in patients with granulomatous cardiomyopathy

Richa Kothari, DNB, MBBS[1]Karthik Gadabanahalli. Ashok, MBBS, MD[2], Vimal Raj, India[1]

1. Narayana Institute of Cardiac Sciences, India

2. Narayana institute of cardiac sciences, Karnataka, India

Background: Cardiac MR is excellent in assessing patients with granulomatous cardiomyopathy as it can demonstrate both active/inflammatory phase of the disease and chronic phase where scarring andfibrosis are present. Tuberculosis related cardiomyopathy has a high prevalence in India and is often not well diagnosed. CMR is being increasingly used to study these patients and there is significant reliance on delayed enhancement imaging to establish the diagnosis. T1 mapping may have a role in diagnosing granulomatous, in particular tuberculous cardiomyopathy.

Methods: Functional imaging was done using cine steady state free precession (SSFP) sequences in various cardiac planes. The ventricular volumes were calculated with the help of Philips intellispace (ISP) software. Short Tau inversion recovery (STIR) sequences were used to determine edema. Delayed enhancement images were acquired to calculate the amount of fibrosis. All scans were performed on Philips 3T Ingenia systems. Pre and post contrast single slice T1 images were obtained following the shMOLLI protocol. These images were stacked and run through ISP software which creates parametric image maps of the shMOLLI data and then quantified.

Results: Fourteen patients with granulomatous cardiomyopathies were included. Areas of edema and enhancement were evaluated on STIR and delayed gadolinium enhancement sequences. Percentage of fibrosis was determined. Native T1 values and myocardial extracellular volume (ECV) fraction calculated. The average T1 native values were 1368+/-68 with a range from 1262+/-69 to 1519+/-75 msec. The average T1 enhanced values were 686+/-65 with a range from 535+/-44 to 795+/-89 msec. These average values are higher than our cohort of normal volunteer T1 native values of 1250+/-50 msec. Patients with raised T1 native and ECV values had significant LV myocardial late gadolinium enhancement. The patients with relatively normal T1 and ECV values were seen to have predominantly right ventricular or left ventricular apical disease.

Conclusion: Significant incremental information is available by T1 mapping along with delayed gadolinium enhancement imaging in diagnosis of patients with granulomatous cardiomyopathy. Multislice T1 mapping sequence could be advantageous to overcome limited cardiac coverage of conventional single-slice T1 mapping technique and to accurately detect the diffuse myocardial fibrosis in these patients.

ID#: 378456

Left Ventricle Replacement fibrosis detected by Cardiac Magnetic Resonance (CMR) is associated with Major Adverse Cardiovascular Events (MACE) in Systemic Sclerosis Patients

Gilles Soulat, MD[7] Elie Mousseaux, MD, PhD[1], Lucia Agoston-coldea, MD, PhD[2], Zora Marjanovic, MD[3], Rica Stanciu, MD[4], Christophe Deligny, MD, PhD[5], Ludivine Perdrix, MD[6], Arshid Azarine, MD[6], Dominique Farge, MD, PhD[8]

1. European Hospital Georges Pompidou APHP; INSERM U970 PARCC Paris descartes University, Ile-de-France, France

2. Department of Medical Sciences, Iuliu Hatieganu University of Medicine and Pharmacy, Cluj-Napoca, Romania;, Romania

3. tement d'hématologie, Saint-Antoine Hospital Paris, Assistance Publique des Hôpitaux de Paris, Paris, France , France

4. Unité Clinique de Médecine Interne, Maladies Auto-immunes et Pathologie Vasculaire, UF04, Hôpital Saint-Louis, Assistance Publique des Hôpitaux de Paris, Paris Denis Diderot University, France, France

5. Service de Médecine Interne, centre hospitalier universitaire Pierre Zobda Quitman, Fort de France, Martinique, France, France

6. Hôpital Européen Georges Pompidou, Assistance Publique Hôpitaux de Paris, Université Paris Descartes, France, France

7. European Hospital Georges Pompidou APHP; INSERM U970 PARCC Paris descartes University, Paris, Ile-de-France, France

8. Unité Clinique de Médecine Interne, Maladies Auto-immunes et Pathologie Vasculaire, UF04, Hôpital Saint-Louis, Assistance Publique des Hôpitaux de Paris, Paris Denis Diderot University INSERM UMRS 1160, France;, France

Background: Although usually clinically silent, cardiac involvement is the leading cause of death in Systemic Sclerosis (SSc), ahead of pulmonary fibrosis. Despite repeated transthoracic-echocardiography (TTE), heart involvement remains underdiagnosed in SSc. We conducted a prospective single center, longitudinal study to compare the detection of myocardial abnormalities using baseline CMR and TTE in SSc patients and assess whether late gadolinium enhancement (LGE) and cardiac remodeling parameters on CMR are associated with an increased risk of Major Adverse Cardiovascular Events (MACE) during follow-up.

Methods: All consecutive patients referred in our institution for SSc were included in the study between September 2009 and 2013 with complete clinical follow-up including TTE and 1.5 T CMR. To establish presence of CMR remodeling changes, 58 healthy controls were matched for age and gender. Functional indices of both ventricles and atrium, and presence of LGE of right ventricle (RV) and left ventricle (LV) were analyzed. Outcomes during subsequent follow-ups were defined by the occurrence of MACE.

Results: Among the 58SSc patient mean disease duration was 9.3 $\pm$ 8.9 years. When measuring LV function parameters by echocardiography, only lower LV end-systolic diameters (p=0.01) and longer mitral deceleration time (p=0.001) were found in SSc patients, compared to controls. On CMR, 44 SSc patients (75%) had at least one abnormality, namely: either LGE (29.3%), or RV (32.7%) end-systolic dilatation. When patients with LV-LGE were compared to those without LGE in either the LV or RV, the LV end-diastolic (p<0.001), LV end-systolic (p<0.001), RV end-diastolic (p=0.001) and RV end-systolic (p< 0.01) volumes were markedly greater and LVEF was significantly decreased in LGE-positive patients (p<0.001).LV-LGE was not associated with pulmonary arterial systolic pressure (PASP) or E/E' TTE estimates. After a mean follow-up of 19 months (range: 6 to 60), MACE occurred in 11 (19%) patients. Probability of survival was lower in SSc patients with LV-LGE (n=15) compared to those without (n=41) (p=0.02).In a multivariable prediction model adjusted with age and sex, presence of LV-LGE on CMR was associated with decreased survival in SSc patients and was predictor of MACE (OR, 2.43, 95%CI [1.39-15.1]; p=0.015) independent of both E/E' on echocardiography (OR, 1.42 [1.05-1.90]; p=0.020) and LVEF on CMR.

Conclusion: Presence of LV-LGE in SSc patients is an independent risk factor for MACE. CMR is also a sensitive technique to detect impaired remodeling and dysfunction of both LV and RV not related to elevated PASP

ID#: 378460

Potential role for T2 mapping and myocardial strain (DENSE) analysis for surveillance of acute myocarditis

Amrit S. Lota, BMBCh BA[1] Dominique Auger, MD, PhD[2], Andrew D. Scott, PhD[3], Simon J. Newsome, MA MSc[4], Peter D. Gatehouse, PhD[5], Brian Halliday, BSc MBChB[6], Upasana Tayal, BMBCh[7], Rick Wage, DCR (R)[8], James S. Ware, MRCP PhD[9], Raad Hashem Mohiaddin, MD PhD[10], David N. Firmin, PhD[11], Stuart Cook, MRCP PhD[12], John Cleland, MD PhD[13], Dudley J. Pennell, MD[14], Sanjay Prasad, MD[14]

1. CMR Unit Royal Brompton Hospital and National Heart and Lung Institute, Imperial College London, London, England, United Kingdom

2. RBH, England, United Kingdom

3. Royal Brompton Hospital, London, England, United Kingdom

4. London School of Hygiene and Tropical Medicine, England, United Kingdom

5. NIHR Cardiovascular Biomedical Research Unit, Royal Brompton Hospital, London, England, United Kingdom

6. Royal Brompton Hospital and National Heart and Lung Institute, Imperial College London, London, England, United Kingdom

7. Royal Brompton Hospital, England, United Kingdom

8. Royal Brompton Hospital NHS trust, England, United Kingdom

9. Imperial College London, United Kingdom

10. Royal Brompton Hospital and Imperial; College London, London, England, United Kingdom

11. 1. Cardiovascular Magnetic Resonance Unit, Royal Brompton Hospital, Sydney Street, London, SW3 6NP, UK, England, United Kingdom

12. National Heart and Lung Institute, Imperial College London, United Kingdom

13. Imperial College, London, England, United Kingdom

14. Royal Brompton Hospital and Imperial College, London, England, United Kingdom

Background: Acute myocarditis (AM) remains a challenging diagnosis with poorly defined markers of risk and recovery. Ongoing subclinical inflammation is implicated in progression to dilated cardiomyopathy but non-invasive detection is currently limited. T2 mapping by CMR and myocardial strain analysis by echocardiography can detect myocardial oedema and dysfunction associated with myocarditis.[1] We investigated the temporal changes in T2 mapping and strain assessed by CMR displacement encoding with stimulated echoes (DENSE) in AM.

Methods: Nineteen prospective patients (mean age 34±16years, 17 men) with AM defined by clinical presentation and Lake Louise Criteria underwent CMR at baseline (<2 weeks from presentation) and 3 months at 3T (Skyra, Siemens). T2 mapping was performed using T2-prepared balanced steady-state free-precession single-shot images with 4 T2-prep times (0-75ms). TE/TR=1.1/2.5ms, flip-angle=35^{o}, GRAPPA x2, 6/8ths partial Fourier, 1.9x2.2x8mm^3 spatial resolution and 360x285mm^2 field of view (FOV). Reduced FOV cine spiral DENSE was acquired at 3.3x3.3x8.0mm^3 spatial resolution, 224x224x8mm^3 FOV, 30ms temporal resolution and 2-direction encoding at 0.06cycles/mm in mid short-axis and 4 chamber planes.[2] Troponin-I and BNP were measured on the same day in all patients.

T2 was measured in a global region of interest drawn by a single blinded observer in the mid short-axis slice using CMR Tools. Results were compared with T2 values from 9 healthy volunteers (27±6 years, 5 men). Global longitudinal, radial and circumferential strain were obtained from DENSE data.[3] Baseline to follow-up measurements were compared using Wilcoxon matched pairs signed-rank test and correlations between changes in variables using Spearman';s rank correlation coefficient.

Results: In patients with AM, mean global T2 at baseline was 43.5±2.2ms compared to 39.9±1.2ms in healthy volunteers (p<0.001). Mean LVEF was 61±7.6% at baseline and longitudinal, circumferential and radial strain were -14.9±2.0, -17.6±2.5 and 44.3±11.6% respectively. At follow-up (mean 82±18 days), there was a decrease in troponin (p=0.002) and BNP (p=0.013), despite persistent elevation in global T2 (42.6±2.3ms, p=0.53) and persistent impairment in circumferential strain (-17.6±2.1%, p=0.98). Change in circumferential strain showed good correlation with change in LVEF (R=-0.71, p<0.001), change in mean T2 (R=-0.65, p=0.02) and change in T2 standard deviation (R=-0.70, p=0.01).

Conclusion: Despite normalisation of troponin, BNP and LVEF within 3 months of presentation of acute myocarditis, T2 values and circumferential strain remained elevated and impaired, possibly reflecting persistent subclinical disease. This may provide incremental value in the surveillance of AM patients. Variability in T2 values may reflect regional myocardial heterogeneity, hence providing complementary information to absolute T2.[4] Further investigation is required to evaluate the prognostic utility of both techniques on long-term clinical outcomes.

References:
1. Løgstrup EHJ CVI 2016
2. Scott JCMR 2016
3. Gilliam 2016 https://github.com/denseanalysis/denseanalysis
4. Baeßler JCMR 2015

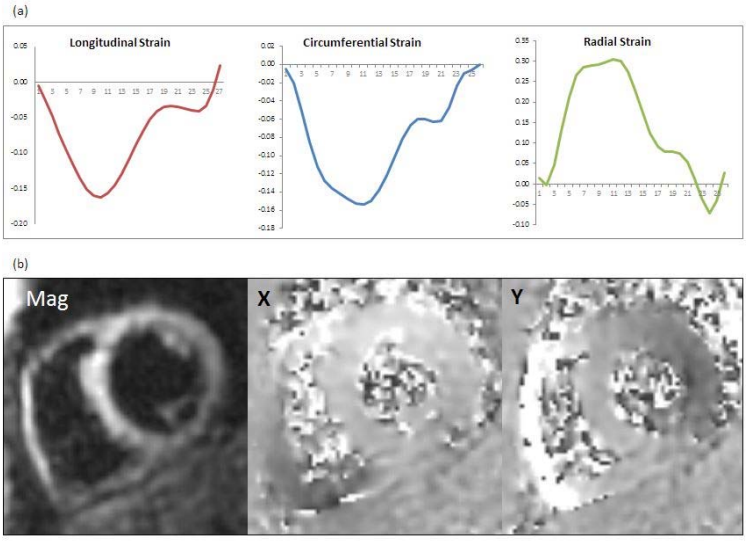

Figure 1. (a). Example of global strain-time curves in a patient with acute myocarditis using CMR displacement encoding with stimulated echoes (DENSE) [y-axis absolute strain, x-axis frame number], (b). Circumferential strain is measured in short-axis DENSE data. Example DENSE magnitude, X-encoded and Y-encoded images are shown here.

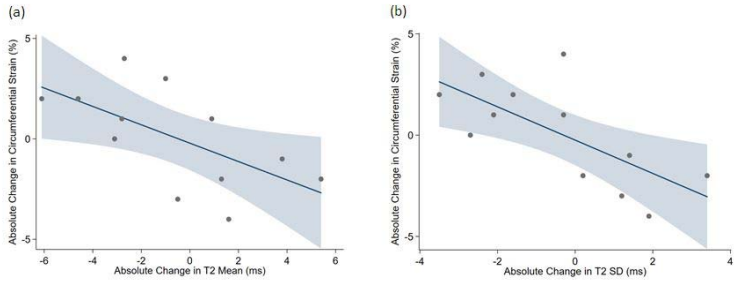

Figure 2. Spearman correlation coefficients between change in baseline and follow-up circumferential strain and (a) mean T2 and (b) standard deviation of T2.

ID#: 378631

Abnormal blood flow dynamics are associated with anatomical torsion of the aortic arch and eccentric geometry of the RV in Patients with Hypoplastic Left Heart Syndrome after three-stage palliation

Dominik D. Gabbert, PhD[1]Patrick Trotz[2], Felix Wadle[2], Hans-Heiner Kramer, MD[2], Arash Kheradvar, PhD, MD[3], Eva Kis, MD[4], Jens Scheewe, MD[2], Carsten Rickers, MD[1]

1. Department of Congenital Heart Disease and Paediatric Cardiology, University Hospital Schleswig-Holstein UKSH, Schleswig-Holstein, Germany

2. University Hospital Schleswig-Holstein, Campus Kiel, Germany

3. Edwards Lifesciences Center for Advanced Cardiovascular Technology, University of California, Irvine, Germany

4. Department of Pediatric Cardiology, UKSH, Christian-Albrechts University Kiel, Germany and Gottsegen György Hungarian Institute of Cardiology, Pediatric Heart Centre, Budapest, Hungary, Germany

Background: The reconstructed aortic arch of patients with Hypoplastic Left Heart Syndrome (HLHS) has an important impact for long-term prognosis. 4D Flow MRI allows determining a variety of novel fluid-dynamic parameters (e.g. helicity, circulation, vorticity in defined volumes of the vessel). Therefore, we thought to test the hypothesis that aortic arch geometry effects blood flow dynamics and may effect right ventricular function in HLHS.

Methods: Twenty-three HLHS patients (median age: 4.5; 2-17 years; all NYHA I) underwent a comprehensive MRI examinations including 4D-flow acquisitions 1.8 (0.4-14.1) years after completion of the Fontan circulation. Volumetric data were used to estimate right ventricular (RV) function. With an in-house analysis software (C++ based), novel parameters of blood flow dynamics were calculated within the cardiac cycle along the entire thoracic aorta from the neo-aortic valve towards diaphragm and were correlated with geometric parameters (such as geometric torsion which describes the twist of a curvature out of the plane) and parameters of the RV.

Results: Peak effective torsion (geometric torsion multiplied with curvature) of the neo-aortic root correlated significantly with peak helicity density of the blood flow (p2 = 0.33, rho=0.59). The peak relative helicity density correlated with the variation (difference between maximum and minimum) of the aortic diameters (p=0.03, adj. R^2=0.18, rho=0.46) as well as with the maximum diameter of the aorta (p=0.04, adj. R^2=0.15, rho=0.44). RV function (EF 57%±10%), volumes and mass did not correlate with any of the flow parameters. The mass-to-volume ratio, a parameter of eccentric geometric remodeling of the RV, correlated inversely with the peak helicity density (p=0.05, adj. R^2=0.14, rho=-0.43).

Conclusion: Our data show that abnormal blood flow patterns in the thoracic aorta in HLHS after three-stage palliation are strongly associated with geometric torsion of the aortic arch, variations of the aortic diameters and eccentric RV geometry. Our findings may trigger modifications of surgical reconstruction to optimize fluid-dynamic conditions in the future.

ID#: 378650

A fully automated myocardium segmentation from 3D Cardiovascular MR images

Kevin Urbain[1]Xi Peng[2], Matthew Bramlet[1], Brent Cross[1], Brad Sutton, PhD[3]

1. JumpTrade Medical Simulation Center

2. University of Illinois at Urbana-Champaign, Urbana, IL

3. University of Illinois at Urbana-Champaign

Background: Myocardium segmentation from cardiovascular MR (CMR) scans is necessary to create patient-specific heart models for presurgical planning in children with complex congenital heart disease (CHD). Manual segmentation is most reliable but labor intensive, and prone to vary among observers. Although significant efforts have been devoted to developing automatic or semi-automatic segmentation methods, it is still a challenge because of the high complexity of patient-specific anatomies and the similar contrast of the surrounding tissues. In this work, we develop a fully automated method for myocardium segmentation from 3D CMR scans.

Methods: The workflow of the proposed fully automated method is illustrated in Fig. 1. The steps are: a) heart cropping. A non-rigid registration method is used to focus the algorithm on the heart volume using a reference cardiac data set with a reference mask for the heart volume. b) Bias field correction. The performance of deep learning based method depends on the complexity of the nonlinear mapping of image features and segmented structure. Bias field correction can be used to reduce the signal intensity variation induced by the MR sequence and coils. c) Myocardium segmentation. After bias field correction, convolutional neural network is exploited to obtain myocardium labels from the images. Specifically, a CNN with contracting path and expansive path using U-net structure are used in this study. 3D Cardiovascular MR datasets were collected using bSSFP sequence (TR 3.93ms, TE 1.65ms, IT 47ms, FA 65 degrees, resolution ~1.1×1.1×2.6mm³) with ECG and respiratory-navigator gating from CHD patientson a 1.5T GE scanner with IRB approval. Image size and resolution varied across subjects. Manual segmentation was conducted on the obtained images (8 for training/ 1 for testing) taking approximately 2 hours per patient. Due to the small number of datasets available for training, value augmentation was used, such as: rotation, shearing, flipping, and elastic transformation. The network was trained on a NVIDIA TITAN Xp graphic processor for 3 days. The entire automated segmentation pipieline takes about 12 minutes on a desktop with an Intel CPU (Xeon E5-2650 v3 @ 2.30GHz).

Results: The cropped heart images with and without bias field correction are shown in Fig. 2, with corresponding myocardium labels shown in Fig. 3. The overall bias field (Fig. 2c) was successfully removed from the raw images, leading to improved differentiation between the myocardium and surround tissues (indicated by red arrows and circles in Fig. 3b). To compare the automated segmentation with manual segmentation, both labels were color coded and overlaid on the magnitude images (Fig. 3d). As can be seen, automated segmentation reached 95% agreement with the manual method.

Conclusion: This work proposes a fully automated segmentation method for whole heart myocardium segmentation. Our preliminary results based on patient datasets demonstrate the feasibility of the proposed method in replacing time-consuming manual segmentation. Future work will include improving the segmentation accuracy by collecting more training datasets and improving the network structure.

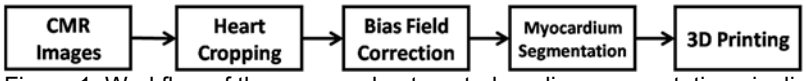

Figure 1. Workflow of the proposed automated cardiac segmentation pipeline.

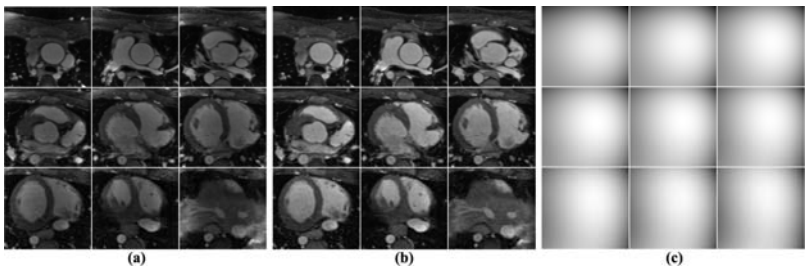

Figure 2. A set of representative slices of the cropped heart images (a) with and (b) without bias field correction. (c) the associated bias field estimated from the MICO method.

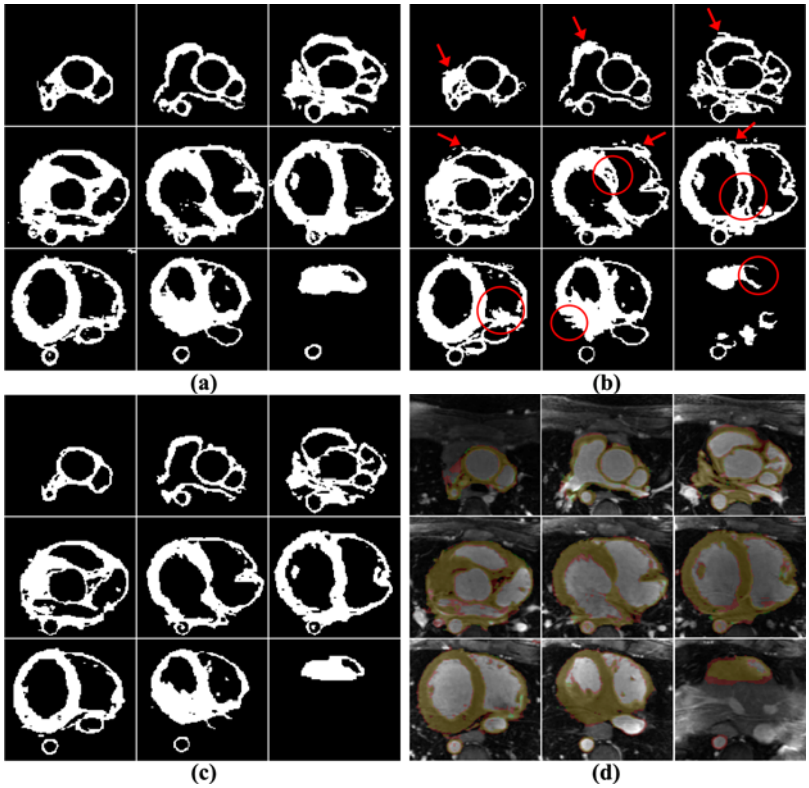

Figure 3. Myocardium labels from (a) automated segmentation with bias field correction, (b) automated segmentation without bias field correction, and (c) manual segmentation. (d) Color coded myocardium labels overlaid on top of the magnitude images. Yellow: agreement between fully automated method and manual segmentation; Red: extra regions captured by the automated method; Green: Regions not captured by the automated method.

ID#: 378662

Should Left Ventricular Global Longitudinal Strain Replace Ejection Fraction as the Preferred Measurement to Quantify Left Ventricular Systolic Function?

Valentina Volpato, MD[1]Roberto M. Lang, MD[1], Amit R. Patel, MD[1], Victor Mor-Avi, PhD[1], John E. Blair, MD[1], Luis Landeras, MD[2], Keigo Kawaji, PhD[3], Neha Goyal, MD[1], Noreen T. Nazir, MD[1], Kohei Matsumoto, MA[3]

1. University of Chicago, IL

2. University of Chicago

3. University of Chicago, Chicago, IL

Background: Cardiac magnetic resonance (CMR) is the reference standard for quantifying left ventricular ejection fraction (LVEF). Recent echocardiographic studies have suggested that because of its higher reproducibility global longitudinal strain (GLS) may be superior to LVEF for quantifying left ventricular systolic function. However, little is known about how these two parameters compare in terms of reproducibility with cardiac MRI. We compared the inter- and intra-observer variability of LVEF measured using cine-CMR against GLS measured using strain-encoded (SENC) CMR.

Methods: CMR imaging was prospectively performed in 15 patients with known or suspected coronary artery disease, including 8 with a prior myocardial infarction. We used a 1.5T scanner (Achieva, Philips) with a 5-channel surface array coil to obtain a stack of left ventricular short-axis cine images using steady-state free precession (TR 2.9 ms, TE 1.5 ms, flip angle 60°, temporal resolution ~40 ms). LVEF was calculated using the standard method of disks (QMass, Medis). In addition, SENC images were obtained (TR=13ms; TE=0.7ms; FA=30; 256x256mm2; slice thickness=10mm; 24ms SENC magnetization prep prior to continuous 40ms -3 spiral interleaves- temporal phase over the R-R interval) during a single heart beat at the basal, mid and apical short axis to measure GLS (Myostrain, Myocardial Solutions). Inter- and intra- observer variability were assessed using intra-class correlation coefficients (ICC) and coefficients of variation (CoV).

Results: LVEF and GLS were successfully measured in all patients. The ICC and CoV values for LVEF and GLS showed that both indices are highly reproducible with similar inter- and intra-observer variability (Table).

Conclusion: Our findings suggest that due to their similar reproducibility, CMR-derived GLS and LVEF provide similar value for the measurement of myocardial systolic function. If confirmed in future studies, the implications of this finding are that GLS may be interchangeable with LVEF in clinical studies.

Reproducibility of Left Ventricular Ejection Fraction and Global Longitudinal Strain

Parameter	Mean ± SD (%)		ICC	CoV
LVEF	52.1 ± 11.6	Inter-observer variability	0.96	2%
		Intra-observer variability	0.99	2%
GLS	-15.9 ± 3.1	Inter-observer variability	0.99	2%
		Intra-observer variability	0.98	3%

LVEF, Left Ventricular Ejection Fraction; GLS, Global Longitudinal Strain;
ICC, intra-class correlation coefficient; CoV, coefficient of variation.

ID#: 378663

Cardiac MR-Derived Global and Regional Myocardial Strain is Similar in Both HIV-positive and HIV-negative Patients with Heart Failure

Bradley D. Allen, MD[1] Amer Ahmed Syed, MD[2], James Carr, MD[3], Matthew Feinstein, MD[2], Jeremy D. Collins, MD[3]

1. Northwestern University Department of Radiology, Chicago, IL

2. Northwestern University

3. Northwestern University, Chicago, IL

Background: Human immunodeficiency virus (HIV) infection appears to be associated with cardiac dysfunction beyond that expected from epicardial coronary artery disease alone. Metabolic dysfunction, virus- and medication-related toxicity, and microvascular dysfunction may all contribute to HIV-associated cardiomyopathy. Previous studies have suggested that myocardial strain is reduced in otherwise healthy HIV+ patients (1) and late gadolinium enhancement (LGE) is increased relative to non HIV patients even when controlling for coronary artery disease in this group.(2) Myocardial strain is a sensitive quantitative marker of cardiac dysfunction that may be useful in evaluating cardiac disease in HIV+ patients. Our aim in the current study was to compare regional and global strain in a well-matched cohort HIV+ and HIV- patients with heart failure.

Methods: Subjects were compiled from an electronic cohort (HIVE-4CVD) which includes HIV+ patients and controls matched for demographics and cardiovascular disease in a 1:2 ratio. The current nested study included 18 HIV+ subjects (48 ± 11 years, 13:5 M:F) and 12 HIV- subjects (48 ± 11 years, 10:2 M:F) who 1)had adjudicated heart failure, and 2) had clinically indicated CMR. Balanced SSFP, ECG-gated cine MRI in short axis was performed at the base, mid, and apex and in the 4-chamber orientation. Ejection fraction and regional (base, mid, apex) and global strain was evaluated from the cine images using dedicated software (cvi42, Circle, Calgary, Canada) (Figure). Peak circumferential (Ecc) and radial (Err) strain and strain at each short axis slice and averaged to obtain global strain, while global longitudinal strain (GLS) and strain rate was measured from the 4-chamber series. Groups were compared using t-test with $\alpha = 0.05$.

Results: The left ventricular ejection fraction was low in both groups, but there was no difference between HIV+ and HIV- groups (37 ± 20% vs. 38 ± 21%, $p = 0.90$). Strain measurements correlated with ejection fraction in both groups (for example, global Err: HIV+, $r=0.75$, HIV-, $r=0.73$). There was no difference in global or regional Ecc or Ecc rate, Err or Err rate, GLS or GLS rate between groups (Table).

Conclusion: No difference in strain was observed in heart failure patients irrespective of HIV status in this well-matched cohort. This finding suggests that the final common pathway of functional deterioration is similar irrespective of myocardial insult. Our study highlights the importance of having a well-matched cohort, in this case heart failure patients, to a limit the likelihood of a false positive HIV effect. Future analyses will compare relative degrees of coronary artery disease and LGE in attempt to better isolate the impact of HIV status in this heart failure group.

1. Holloway CJ, Ntusi N, Suttie J, et al.Comprehensive cardiac magnetic resonance imaging and spectroscopy reveal a high burden of myocardial disease in HIV patients. Circulation. 2013;128(8):814-22.

2. Feinstein MJ, Mitter SS, Yadlapati A, et al.HIV-Related Myocardial Vulnerability to Infarction and Coronary Artery Disease. Journal of the American College of Cardiology. 2016;68(18):2026-7.

			HIV+	HIV-	p-value
Age			48.1 ± 10.5	48.4 ± 11.3	0.94
EF%			36.7 ± 20.2	37.7 ± 20.7	0.90
Peak Strain (%)	Radial	Basal	24.2 ± 13	22 ± 11.2	0.64
		Mid	21.2 ± 17.1	24.7 ± 17.2	0.59
		Apical	28.3 ± 28.7	25.6 ± 21.7	0.81
		Global	19.6 ± 15.7	21.9 ± 12.2	0.66
		Long Axis	16.6 ± 12.9	17.7 ± 9.2	0.79
	Circumferential	Basal	-12.6 ± 6.6	-12.5 ± 4.8	0.97
		Mid	-11.6 ± 9	-14.1 ± 7.9	0.44
		Apical	-12.2 ± 17.7	-12.5 ± 14.2	0.97
		Global	-9.7 ± 9.1	-12.3 ± 5.6	0.39
	Long Axis		-8.9 ± 8.7	-11.3 ± 4.8	0.38
Peak Systolic Rate (1/s)	Radial	Basal	1.5 ± 1.2	1.6 ± 1	0.76
		Mid	1.7 ± 1.2	1.9 ± 1.3	0.74
		Apical	1.3 ± 3	2.2 ± 2.5	0.50
		Global	1.2 ± 1.2	1.8 ± 1	0.19
		Long Axis	1.2 ± 0.7	1.2 ± 0.7	0.89
	Circumferential	Basal	-0.9 ± 1.1	-0.8 ± 0.6	0.71
		Mid	-0.9 ± 0.8	-1.2 ± 0.6	0.36
		Apical	-0.3 ± 2.5	-0.4 ± 1.9	0.92
		Global	-0.6 ± 1	-0.9 ± 0.6	0.36
	Long Axis		-0.8 ± 0.6	-0.8 ± 0.3	0.99

Table: Strain findings in HIV+ and HIV- patients.

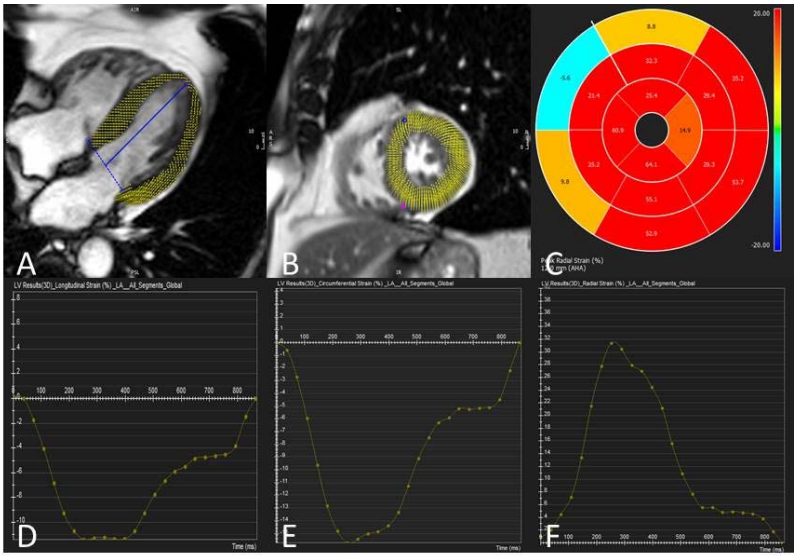

Figure: Example of strain analysis in an HIV+ patient showing longitudinal strain (A) and short axis strain (B) deformation vectors. C :16 segment heat map of radial strain. D-F: Time resolved longitudinal, circumferential, and radial strain.

Figure

ID#: 378582

Impact of angulation on CMR based measurements of descending aortic distensibility. A method agreement study on intra- and inter-observer variability.

Lukas Stoiber, MD[1] Niky Ghorbani[1], Marcus Kelm, M.D.[1], Titus Kuehne, PhD M.D.[2], Tomas Lapinskas, MD[1], Burkert Pieske, MD[3], Sebastian Kelle, MD, PhD[4]

1. German Heart Center Berlin, Germany

2. Charité -Universitätsmedizin Berlin, Berlin, Germany

3. German Heart Center Berlin, Berlin, Berlin, Germany

4. German Heart Center Berlin, Berlin, Germany

Background: Aortic distensibility (AD) represents a well-established parameter of aortic stiffness. However, it remains unclear whether AD can be obtained with high reproducibility in standard CMR images of the descending aorta. We aimed to test intra- and inter-observer agreement of AD measurements based on different angulations of the descending aorta using cardiovascular magnetic resonance (CMR).

Methods: 31 patients underwent advanced CMR imaging using a Philips Ingenia 3.0 Tesla Scanner (Philips Healthcare, Best, The Netherlands). In addition to the standard four chamber cine imaging, we performed an angulation of the descending aorta to obtain strictly transversal and orthogonal cross sectional aortic areas. Qmass software version 8.1 (Medis Suite version 2.1., Medis, the Netherlands) was then used to contour the aortic wall by two experienced Observers. AD was determined as the change in cross sectional aortic area per unit change in BP. All measurements were repeated 3 times and 10 measurements were used to obtain inter-observer variability. To assess intra-observer agreement, the analysis was repeated in ten patients after 4 weeks.

Results: Mean values of Observer 1 were 2.80 ± 1.99 10^{-3} $mmHg^{-1}$ for transversal AD, 3.26 ± 2.27 10^{-3} $mmHg^{-1}$ for 4- chamber AD and 2.49 ±1.96 10^{-3} $mmHg^{-1}$ for strictly orthogonal AD. For Observer 2, respective values were 2.26 ± 2.06 10^{-3} $mmHg^{-1}$, 2.94 ± 2.37 10^{-3} $mmHg^{-1}$ and 2.36 ± 2.06 10^{-3} $mmHg^{-1}$. We found a strong correlation between 4-chamber AD and transversal AD (Observer 1: r^2 = 0.807; Observer 2: r^2 = 0.805) as well as between 4-chamber AD and orthogonal AD (Observer 1: r^2 = 0.845; Observer 2: r^2 = 0.845). Intra-observer agreement was excellent for transversal AD (ICC 0.89; 95% CI: 0.59-0.97), 4-chamber AD (ICC 0.98; 95% CI: 0.91-0.99) and strictly orthogonal AD (ICC 0.87; 95% CI: 0.50-0.97). Inter-observer agreement was also excellent for transversal AD (ICC 0.80; 95% CI: 0.22-0.95), 4-chamber AD (ICC 0.92; 95% CI: 0.70-98) and strictly orthogonal AD (ICC 0.91; 95% CI: 0.62-98). Bland-Altman plots demonstrate intra- and inter-observer reproducibility for AD (Figure 1).

Conclusion: AD measurements using either 4-chamber cine, transversally angled or orthogonally angled imaging of the descending aorta are highly reproducible. This allows an accurate and rapid assessment of arterial compliance and may help to predict changes of the central vasculature.

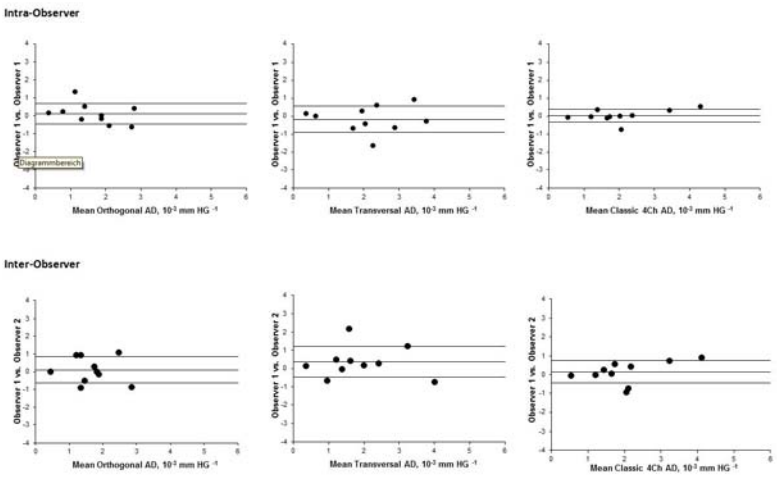

Bland-Altman plots with limits of agreement (1.96 standard deviation) demonstrate the intra-observer and inter-

observer reproducibility for aortic area based aortic distensibility in different CMR planes. The middle-dashed line is the mean of difference of measures. The upper and lower dotted lines are ± 1.96 standard deviation.

ID#: 378591

Clinical Significance of Late Gadolinium Enhancement at Right Ventricular Insertion Point in Non-ischemic Dilated Cardiomyopathy Patients

Jin-Young Kim[1] In-Cheol Kim[2], Hyungseop Kim[1], Sang-Woong Choi[3]

1. Keimyung University Dongsan Medical Center, Republic of Korea

2. Keimyung University Dongsan Medical Center, Daegu, Republic of Korea

3. keimyung university dongsan medical center, DAEGU, Republic of Korea

Background: To investigate the relationship between right ventricle (RV) function and prognosis with late gadolinium enhancement (LGE) at RV insertion point among non-ischemic dilated cardiomyopathy (DCM) patients.

Methods: We retrospectively enrolled 55 DCM patients (40 men, mean age, 58 ± 15 years old) who underwent cardiac magnetic resonance (CMR) to assess myocardial fibrosis. According to the findings of LGE, DCM was classified as follows; No LGE (n=25, 45%), focal LGE detected only in the right ventricle insertion point (RVIP) (n=14, 25%), and LGE detected at the RVIP and mid wall (n=16, 29%). Severe RV dysfunction was defined as RV ejection fraction (EF) less than 30% by CMR. Pulmonary artery systolic pressure (PASP) was compared in patients with echocardiographic measurement at the time of CMR. Follow up echocardiography data after treatment was compared in available patients.

Results: Severe RV dysfunction rate was significantly higher in patients with LGE (RVIP only and RVIP and mid wall) than no LGE (p=0.006). However, there was no significant difference of severe RV dysfunction between LGE at RVIP only and LGE at RVIP and mid wall group (p>0.05). There was a tendency of increased PASP according to the level of LGE (no LGE: 31.3 ± 9.8 mmHg, LGE at RVIP: 39.7 ± 14.4 mmHg, LGE at RVIP and mid wall, 41.3 ± 11.7mmHg, p=0.093). Among the patients who were feasible with the echocardiographic follow up (37 patients, median follow up 343 days, interquartile range 104 to 509 days), left ventricle (LV) EF recovery (defined by LVEF> 45% with absolute increased EF more than 10%) rate was lowest in RVIP with mid-wall type, and highest in no LGE type (no LGE: 66.7%, LGE at RVIP only: 33.3%, LGE at RVIP and mid wall 23.1%, p=0.053). Among the patients who were feasible with the echocardiographic follow up (37 patients, median follow up 343 days, interquartile range 104 to 509 days), left ventricle (LV) EF recovery (defined by LVEF> 45% with absolute increased EF more than 10%) rate was lowest in RVIP with mid-wall type, and highest in no LGE type (no LGE: 66.7%, LGE at RVIP only: 33.3%, LGE at RVIP and mid wall 23.1%, p=0.053).

Conclusion: The LGE at RVIP with or without mid wall involvement was related with severe RV dysfunction and poor outcome in non-ischemic DCM patients.

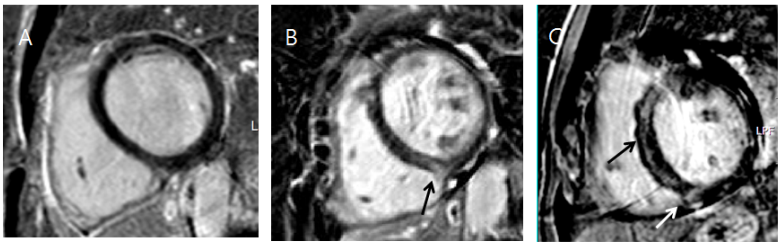

Three different Late Gadolinum Enhancement (LGE) patterns of non-ischemic dilated cardiomyopathy patients in our study. A) No demonstrable LGE at the myocardium. B) Focal LGE at right ventricle insertion point. C) LGE at right ventricle insertion point and mid wall.

ID#: 378596

Late gadolinium enhancement patterns in patients with hypereosinophilia: does CMR help identifying the etiology?

Julien Pagniez, MD[1]Morgan Dubois, MD[2], Guillaume Lefevre, MD, PhD[2], Lorette Averlant, MD[2], Benjamin Longere, MD[1], Valentina Silvestri, MD[1], Jean-Emmanuel Kahn, MD[3], Francois Pontana, MD, PhD[4]

1. Lille University Hospital, Nord-Pas-de-Calais, France

2. Lille University Hospital, France

3. Hopital Foch Paris, France

4. Lille University Hospital, Lille, Nord-Pas-de-Calais, France

Background: The purpose of this study was to assess the prevalence and the patterns of cardiac abnormalities detected by cardiac magnetic resonance (CMR) in patients with hypereosinophilia according to the underlying disease.

Methods: Thirty consecutive patients without history of ischemic cardiopathy (15 males; mean age = 47.7 ± 21) referred for hypereosinophilia were prospectively enrolled. Hypereosinophilia was related to: idiopathic hypereosinophilic syndrome (HES) n=13; eosinophilic granulomatosis with polyangiitis (EGPA) n=6; parasitic infection n=3; hemopathy n=4; and allergy n=4. Cine functional parameters, T1 and T2 values on parametric mapping and late gadolinium enhancement (LGE) were independently assessed by two observers.

Results: Left ventricle (LV) and right ventricle (RV) ejection fractions were altered in 19 patients (63%) and 7 patients (23%) respectively. LV and RV dilatation was observed in 7 patients (23%) and 2 patients (7%) respectively. Increased myocardial T1 and T2 values were found respectively in 10/21 patients (48%) and 4/21 patients (19%). LGE was detected in 13 patients (43%). Among them, 5 patients presented a myocarditis enhancement pattern (HES n=2, EGPA n=2, parasitic infection n=1), 5 patients presented a vasculitis enhancement pattern (EGPA n=3, parasitic infection n=1, hemopathy n=1) and 3 patients presented an endomyocardial fibrosis pattern (HES n=2, EGPA n=1); p = 0.59.

Conclusion: LGE was observed in almost half of the patients with hypereosinophilia with three different patterns (myocarditis, vasculitis and endomyocardial fibrosis), independently of the etiological diagnosis suggesting a non-specific myocardial toxicity of the eosinophils.

ID#: 378513

The influence of abnormal left atrial area on pulmonary haemodynamic assessment by septal curvature: an analysis of 114 patients with same day right heart catheter and CMR studies

Hossam Fayed, MBChB MSc MRCP(UK)[1] Tushar Kotecha, MRCP(UK) MBChB[2], Michele Boldrini[3], Ana Martinez Naharro, MD[4], Adam Mitchell, MBChB[5], Benjamin Schreiber, MD[6], Marianna Fontana, MD, PhD[3], John G. Coghlan, MD, MRCPI, FRCP[7], Vivek Muthurangu, MD[8], Daniel Knight, MD[9]

1. UCL Department of Cardiac MRI, Royal Free Pulmonary Hypertension Service, Pond Street, England, United Kingdom

2. Royal Free London NHS Foundation Trust, London, England, United Kingdom

3. UCL Department of CMR, Royal Free Hospital, England, United Kingdom

4. UCL Department of CMR, Royal Free Hospital, London, England, United Kingdom

5. Royal Free Hospital, United Kingdom

6. Royal Free London, United Kingdom

7. Royal Free Hospital, London, England, United Kingdom

8. Institute of Cardiovascular Science, University College London, England, United Kingdom

9. UCL Department of CMR, Royal Free London Pulmonary Hypertension Service, United Kingdom

Background: Interventricular septal curvature (SC) metrics have been shown to estimate right ventricular (RV) afterload in pulmonary arterial hypertension. However, the influence of raised left atrial pressure on this relationship is an unstudied but important consideration when investigating unselected patients for evidence of raised RV afterload.

Methods: One-hundred and fourteen consecutive patients attended for same day CMR and right heart catheterization (RHC) over an 18-month period at the Royal Free National Pulmonary Hypertension Service (PH). The indications included either diagnosis/exclusion of PH or monitoring of PH on pulmonary vasodilator therapy. SC was measured in short axis cine images at papillary muscle level in the mid-ventricle using an in-house plugin for the OsiriX platform. The relationship between CMR-derived SC and mPAP measured by RHC was studied using linear regression. Patients were classified according to the presence or absence of left atrial dilatation as specified by the upper limit of normal for left atrial area indexed for body-surface area (LAi > or ≤16cm^2/m^2 respectively).

Results: Participants were predominantly female (84%). One-third of patients (n=38) had no PH. The aetiologies for the 76 patients who had PH were as follows: Group 1 (PAH), n=53 (46%); Group 2 (PH due to left heart disease), n=15 (13%); Group 3 (PH secondary to lung disease), n=2 (1.8%); Group 4 (chronic thromboembolic PH), n=6 (5.3%). In the overall cohort of patients, there was a good correlation between SC and mPAP (r=-0.77, p<0.001, figure 1a). This correlation improved when analysing those patients with normal left atrial area (n=91, r=-0.84, p<<0.001, figure 1b). Importantly, the correlation between SC and mPAP was weak in patients with left atrial dilatation (n=23, r=-0.49, p<0.05 figure 1c).

Conclusion: We have demonstrated a good correlation between CMR-derived septal curvature and mPAP at contemporaneous RHC study. Furthermore, this relationship between septal curvature and mPAP is excellent in patients with normal left atrial area but, importantly, is much weaker in patients with left atrial dilatation. This is likely due to the degree of septal curvature being due to the difference between RV end-systolic pressure and left ventricular (LV) early-diastolic pressure. Therefore, septal curvature will be confounded in patients with raised LV diastolic pressure, for which left atrial area is a surrogate marker. In summary, septal curvature and indexed left atrial area are simple but important metrics when investigating patients for evidence of raised RV afterload by CMR. Specifically, septal curvature may not be a clinically reliable surrogate of mPAP in patients with left atrial dilatation.

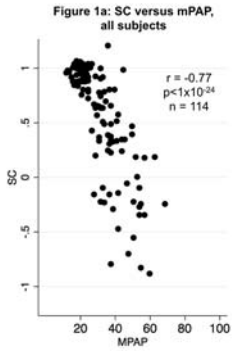
Figure 1a: SC versus mPAP, all subjects
r = -0.77
p<1x10-24
n = 114
SC
MPAP
20 40 60 80 100
-1 -.5 0 .5 1

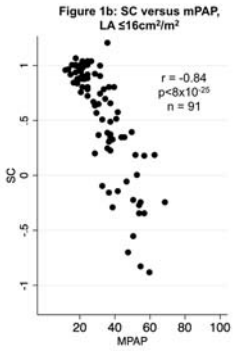
Figure 1b: SC versus mPAP, LA ≤16cm²/m²
r = -0.84
p<8x10-25
n = 91
SC
MPAP
20 40 60 80 100
-1 -.5 0 .5 1

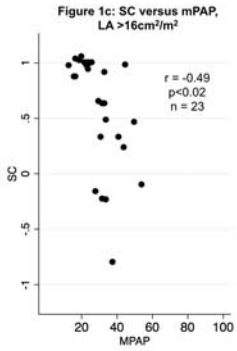
Figure 1c: SC versus mPAP, LA >16cm²/m²
r = -0.49
p<0.02
n = 23
SC
MPAP
20 40 60 80 100
-1 -.5 0 .5 1

ID#: 378517

Impact of Indexation Method and Body Mass Index on Prevalence of High Left Ventricular Mass: The Framingham Heart Study

Michael L. Chuang, MD, ScM[1] Philimon N. Gona, PhD[2], Saadia Qazi, DO, MPH[3], Carol J. Salton, AB[4], Jane J. Lee, PhD[5], Christopher J. O'Donnell, MD, MPH[6], Warren J. Manning, MD[7]

1. Beth Israel Deaconess Medical Center, Newton, MA

2. University of Massachusetts Boston, Framingham, MA

3. Boston VAMC, MA

4. Beth Israel Deaconess Medical Center, MA

5. Boston Children's Hospital

6. Boston VAMC

7. Beth Israel Deaconess Medical Center, Harvard Medical School, Boston, MA

Background: High left ventricular mass (LVM) is associated with excess cardiovascular morbidity and mortality. LVM is often indexed to height (HT) or body surface area (BSA), to account for differences in body size, prior to assessment of whether LVM is high. If LVM increases appropriately with greater body mass index (BMI) then indexation to HT may inappropriately identify obese individuals (defined has having BMI≥30 kg/m^2) as having excess LVM. Conversely, BSA-indexation may underestimate the prevalence of high LVM among the obese. We sought to determine whether indexation to BSA vs. HT affects prevalence of high LVM across BMI strata in a community-dwelling cohort.

Methods: We stratified Framingham Offspring study participants who underwent bSSFP CMR at 1.5T (N=1475, 47% men; aged 65±9y) by sex and BMI category (normal, NL=18.5 to 24.9; overweight, OW=25.0 to 29.9; the obese category was subdivided into OB1=30.0 to 34.9 and OB2≥35 kg/m^2). LVM was measured from contiguous short-axis images, then indexed to HT(m) and to BSA(m^2). For each indexation method we identified participants in the sex-specific top quartile (TQ) of LVM, then tabulated number (and %) of participants with TQ LVM for each BMI category.

Results: The Table shows proportion of participants with TQ LVM by BMI category. Unindexed (raw) or HT-indexed LVM showed a monotonically increasing gradient of TQ LVM with greater BMI category: fewer than 10% of NL participants had TQ LVM; approximately 22% of OW participants were in the TQ; 34% (men) or over 40% (women) OB1 participants were in the TQ, while >50% (men) and >70% (women) of those in OB2 had TQ LVM. In contrast, BSA-indexation gave nearly uniform TQ-LVM status across BMI categories, i.e. the prevalence of TQ LVM/BSA was approximately 25% among NL, OW and both OB strata; if anything, the proportion of TQ LVM may have decreased in the highest OB2 category.

Conclusion: The association of high LVM with BMI varies by indexation method. BSA-indexation yields similar prevalence of TQ LVM across BMI strata, while HT-indexation shows greater prevalence of TQ LVM among the obese, particularly among women. Further (outcomes based) work is needed to identify optimal methods for indexation of LVM.

Distribution of Top-Quartile Left Ventricular Mass by Indexation Method, Sex and BMI Category

BMI Category (kg/m^2)	**NL** (18.5 - 24.9)	**OW** (25.0 - 29.9)	**OB1** (30.0 - 34.9)	**OB2** (≥35.0)
Men, N	126	355	170	43
LVM, raw	11 (8.7%)	81 (22.8%)	59 (34.7%)	23 (53.5%)
LVM/HT	8 (6.3%)	79 (22.3%)	58 (34.1%)	29 (67.4%)
LVM/BSA	32 (25.4%)	90 (25.4%)	42 (24.7%)	10 (23.3%)

Women, N	294	293	126	68
LVM, raw	28 (9.5%)	65 (22.2%)	51 (40.5%)	51 (75.0%)
LVM/HT	23 (7.8%)	66 (22.5%)	54 (42.9%)	52 (76.5%)
LVM/BSA	68 (23.1%)	72 (24.6%)	38 (30.2%)	17 (25.0%)

ID#: 378493

Intraventricular kinetic energy increase exceeds rise in viscous energy loss during stress in Fontan patients: a 4D Flow CMR study

Vivian P. Kamphuis, MD[1]Mohammed Elbaz, PhD[2], Pieter J. van den Boogaard, BSc[3], Lucia J.M. Kroft, MD[4], Albert de Roos, MD, PhD[3], Nico A. Blom, MD, PhD[5], Willem Helbing, MD, PhD[6], Arno A.W. Roest, MD, PhD[7], Jos J.M. Westenberg, PhD[4]

1. Leiden University Medical Center, Netherlands Heart Institute, Den Haag, Zuid-Holland, Netherlands

2. Department of Radiology, Leiden University Medical Center, Leiden, the Netherlands, AB, Canada

3. Department of Radiology, Leiden University Medical Center, Leiden, The Netherlands, Zuid-Holland, Netherlands

4. Department of Radiology, Leiden University Medical Center, Leiden, The Netherlands, Leiden, Zuid-Holland, Netherlands

5. Division of Pediatric Cardiology, Department of Pediatrics, Leiden University Medical Center, Leiden, The Netherlands, Zuid-Holland, Netherlands

6. Department of Pediatrics, division of Pediatric Cardiology, Erasmus Medical Center, Rotterdam, the Netherlands, Zuid-Holland, Netherlands

7. Department of Pediatrics, Leiden University Medical Center, Leiden, The Netherlands, Zuid-Holland, Netherlands

Background: Patients with a Fontan circulation exhibit diminished exercise capacity. Cardiovascular magnetic resonance (CMR) has been used to show an abnormal ventricular stress response in these patients. However, the influence of (pharmacologic) stress on intraventricular energetics by 4D Flow CMR in Fontan patients has not been shown. Therefore, the purpose of this study was to noninvasively assess intraventricular kinetic energy (KE) and viscous energy loss (EL, the KE that is lost due to friction between the blood and surrounding structures) from 4D flow CMR during rest and stress in Fontan patients.

Methods: Seven patients with a Fontan circulation (age 17±4 years) underwent whole-heart 4D Flow CMR at 3T (Ingenia, Philips Healthcare) at rest and with Dobutamine 7.5 µg/kg/min (VENC=150 cm/s, spatial resolution 3×3×3 mm^3, 30 retrospectively reconstructed phases over one cardiac cycle). The systematic ventricle was manually segmented. The amount of intraventricular KE was computed as $½mv^2$, with mass (m) being the voxel volume multiplied by the density of blood (1.025 g/ml) and (v) as the magnitude of the 3-directional velocity. The time-average KE over systole ($KE_{systole}$), diastole ($KE_{diastole}$) and the total cycle (KE_{cycle}) were calculated. Furthermore, EL was computed over systole ($EL_{systole}$), diastole ($EL_{diastole}$) and total cardiac cycle (EL_{cycle}) using the Navier-Stokes energy equations. To assess the amount of viscosity-induced EL relative to the average KE produced, we computed the EL_{index} as: EL_{cycle}/KE_{cycle}. The Wilcoxon signed rank paired test was used to compare rest with stress parameters.

Results: Detailed results are shown in **Table 1** and **Figure 1**. Dobutamine stress resulted in a significant increase in $KE_{systole}$ (1.8 versus 5.2 mJ, P=0.02), $KE_{diastole}$ (1.3 versus 2.5 mJ, P=0.03) and KE_{cycle} (1.7 versus 3.6 mJ, P=0.02). $EL_{systole}$ and EL_{cycle} increased ($EL_{systole}$: 0.3 versus 0.5 mJ, P=0.02; EL_{cycle}: 0.5 versus 0.8 mJ, P=0.02) but $EL_{diastole}$ did not show significant increase. Notably, EL_{index} showed a significant decrease after pharmacologic stress (0.3 versus 0.2, P=0.02).

Conclusion: This is the first study evaluating the 4D Flow CMR based intraventricular energetics at rest and during pharmacological stress. Pharmacologic stress resulted in an increase in intraventricular kinetic energy and viscous energy loss, but the increase in kinetic energy was relatively higher than the rise in viscous energy loss. This may indicate energetic imbalance during stress in Fontan patients'; hemodynamics which could contribute to impaired exercise capacity in these patients.

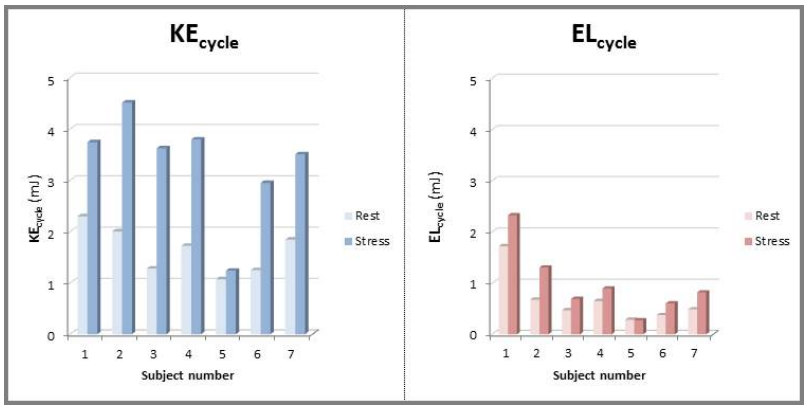

Figure 1 Energetics at rest and stress

Table 1. Quantitative analysis of energetics at rest and stress

Quantitative analysis of energetics at rest and stress					
	Rest	Dobutamine stress	Difference	Difference (%)	*P*-value
	Median [IQR]	Median [IQR]	*Stress-Rest* Median [IQR]	*(Stress-rest)/rest * 100%* Median [IQR]	
HR (bpm)	87 [79-102]	118 [113-119]	31 [18-36]	35 [19-43]	0.02
EDV (mL)	167 [145-181]	167 [131-176]	−5 [-13-7]	−3 [−9-5]	0.50
ESV (mL)	91 [62-98]	72 [58-75]	−19 [-26-13]	−27 [−31-20]	0.40
SV (mL)	70 [62-98]	92 [72-96]	10 [-6-15]	15 [-6-19]	0.13
EF (%)	47.0 [42.0-57.2]	56.1 [55.6-64.7]	10.2 [6.1-11.7]	41 [35-49]	0.03
CO (L/min)	6.5 [5.5-7.7]	10.0 [8.3-11.0]	2.7 [2.3-3.2]	20 [12-27]	0.02
$KE_{systole}$ (mJ)	1.8 [1.2-2.8]	5.2 [3.7-6.0]	2.7 [2.1-3.9]	166 [55-193]	0.02
$KE_{peak\text{-}systole}$ (mJ)	3.4 [2.0-4.9]	9.4 [6.9-10.9]	5.5 [3.3-6.6]	154 [90-232]	0.02
$KE_{diastole}$ (mJ)	1.3 [1.2-1.6]	2.5 [2.0-2.8]	1.1 [0.4-1.4]	95 [25-111]	0.03
$KE_{E\text{-}peak}$ (mJ)	2.0 [1.8-2.4]	3.2 [1.3-3.6]	1.0 [-0.5-1.8]	43 [-30-80]	0.18
$KE_{A\text{-}peak}$ (mJ)	1.9 [1.5-2.5]	3.8 [2.7-4.7]	1.6 [0.3-2.4]	83 [10-127]	0.02
KE_{cycle} (mJ)	1.7 [1.2-2.0]	3.6 [2.9-3.8]	1.7 [1.4-2.3]	120 [63-136]	0.02
$EL_{systole}$ (mJ)	0.3 [0.2-0.4]	0.5 [0.3-0.8]	0.3 [0.1-0.4]	72 [28-98]	0.02
$EL_{peak\text{-}systole}$ (mW)	1.1 [0.8-2.2]	4.4 [2.7-5.6]	2.8 [1.7-4.5]	156 [88-316]	0.02
$EL_{diastole}$ (mJ)	0.3 [0.2-0.4]	0.3 [0.2-0.5]	0.1 [-0.03-0.2]	38 [-21-56]	0.18
$EL_{E\text{-}peak}$ (mW)	1.0 [0.6-1.2]	1.1 [0.7-2.7]	0.4 [-0.3-1.4]	74 [-33-106]	0.24
$EL_{A\text{-}peak}$ (mW)	1.0 [0.7-1.2]	1.8 [0.9-2.3]	0.5 [0.1-1.5]	41 [8-132]	0.02
EL_{cycle} (mJ)	0.5 [0.4-0.7]	0.8 [0.6-1.3]	0.2 [0.2-0.6]	48 [35-67]	0.03

EL_{index}	0.3 [0.3-0.4]	0.2 [0.2-0.3]	-0.1 [-0.1-0.04	-17 [-37-15]	0.02

IQR = interquartile range; HR = heart rate; EDV = end diastolic volume; ESV = end systolic volume; SV = stroke volume; EF = ejection fraction; CO = cardiac output; EL = viscous energy loss; EDV = end diastolic volume; e-peak = peak early diastole; a-peak = peak late diastole

ID#: 378545

Evaluation of Estimation Methods for Missing Premature Ventricular Contractile Beats During Real-Time CMR Slice Acquisition

Saharsh Dass, BS[1] Francisco Contijoch, PhD[2], Zachary Rodgers, MD, PhD[3], Srikant K. Iyer, PhD[4], Walter R. Witschey, PhD[5], Yuchi Han, MD, MMSc[5]

1. University of Pennsylvania, Claymont, DE

2. University of California Los Angeles, CA

3. University of Pennsylvania, PA

4. University of Pennsylvania

5. University of Pennsylvania, Philadelphia, PA

Background: In order to assess the function of premature ventricular contractile beats, we use 2D real time imaging along with ECG synchronization to detect different beat types and a semi-automated segmentation post-processing pipeline for quantification.[1,2,3] However, PVC might not be present at all slice positions during imaging.[1] In this work we investigate the efficiency of four classical empirical, statistical, and fitting methods[4] for estimating missing PVC slice volume data. This simple approach is shown suitable for quantifying PVC global volume.

Methods: We have 10 full data sets including PVC beats in all slices. We tested different methods for estimating left ventricular global volumes and ejection fraction in six hypothetical situations with one and two missing mid-ventricular slices, one missing apical and basal slice, and a three and two slice protocol. We evaluated four techniques using Matlab which included: linear (L) and cubic spline (S) interpolation/extrapolation, 2nd order polynomial fit (P2), and a PVC-Sinus Ratio (R) method. The accuracy of the methods were assessed using mean absolute error (MAE),[4] coefficient of efficiency (R^2),[4] mean absolute percentage error (MAPE), and proportion of estimates less than 10% error (P_{10}).[5] Bland-Altman and correlation analysis were used to display differences between the estimation methods and standard measurements for each parameter and includes the bias and limits of agreement (LOA) of double standard deviation (±2SD).[2,6]

Results: Each of the methods varied in efficiency under different simulations. The results are shown in Table 1 with favorable methods bolded for each simulation and parameter. In all simulations, the EDV and ESV parameters had MAPE ≤ 10.24% and P_{10} ≥ 50%. The SV and EF parameters had a wider range (MAPE ≤ 27.97% and P_{10} ≥ 20%) and were used for comparing suitable methods. Lower MAE and MAPE, and R^2 closer to 1 suggested suitable[4] techniques for each simulation and they were penalized based on P_{10}.[5] These are as follows: 1 mid-vent missing: L & P2 (MAE, MAPE, R^2),
2 mid-vent missing: L & S (MAE, MAPE, R^2),
Apical missing: R (MAE, MAPE, R^2),
Basal missing: R (MAE, MAPE, R^2),
3 slice protocol: P2 & S (MAE, MAPE, R^2), and
2 slice protocol: L (R^2). Estimating the 2 mid-vent missing, apical and basal slices yielded MAPE ranging from 5.08 – 18.09 for SV and EF. However, the L and P2 technique on 2 slice protocol yielded MAPE > 20% and P_{10} ≤ 30% for SV and EF. Figure 1 shows the performance of each technique for subjects 9 and 10, and the challenge in a 2 slice protocol. Bland-Altman plots shows negligible biases of the selected suitable P2 technique for 1 mid-vent missing and a 3 slice protocol (Figure 2).

Conclusion: In this work, simple classical techniques are shown for estimating PVC EDV and ESV slice volume data and the results are comparable to that of complex models used in other contexts[6,7] for reduced slice acquisition. In cases with only 2 slices in the stack, estimating the SV and EF can be compromised.

Simulation	Method	EDV					ESV					SV					EF				
		MAE	R^2	MAPE	$MAPE_{std}$	P_{10}	MAE	R^2	MAPE	$MAPE_{std}$	P_{10}	MAE	R^2	MAPE	$MAPE_{std}$	P_{10}	MAE	R^2	MAPE	$MAPE_{std}$	P_{10}
1 mid-vent missing	L	1.27	1.00	1.39	1.34	100	1.00	1.00	1.44	0.89	100	0.93	0.99	5.52	5.97	80	**0.79**	**0.99**	**4.47**	5.15	80
	S	1.37	1.00	1.48	1.54	100	**0.97**	**1.00**	**1.39**	0.85	100	1.11	0.99	6.75	7.24	80	0.93	0.99	5.37	6.07	80
	P2	**1.10**	**1.00**	**1.21**	1.48	100	1.20	1.00	1.74	1.09	100	**0.82**	**0.99**	**5.12**	6.47	80	0.87	0.99	4.74	5.37	80
	R	1.63	1.00	1.77	1.18	100	1.64	0.99	2.38	1.63	100	1.56	0.97	8.29	7.25	70	1.56	0.97	7.12	7.19	80
2 mid-vent missing	L	**1.70**	**0.99**	**2.17**	2.63	100	1.21	1.00	1.71	1.53	100	**1.47**	**0.98**	**10.56**	12.67	60	1.59	0.97	9.06	11.18	60
	S	1.86	0.99	2.34	2.60	100	**1.15**	**1.00**	**1.65**	1.92	100	1.62	0.97	10.83	12.52	70	**1.78**	**0.97**	**9.45**	10.95	70
	P2	2.27	0.99	2.40	1.59	100	1.80	0.99	2.45	2.31	100	2.05	0.97	12.65	13.64	70	2.07	0.96	10.99	13.63	70
	R	2.65	0.98	2.69	3.18	90	2.12	0.98	2.93	2.68	100	2.03	0.97	12.19	9.10	50	1.94	0.97	11.19	7.47	50
Apical Missing	L	2.81	0.98	3.14	3.08	90	1.45	1.00	2.41	2.08	100	1.92	0.97	13.56	11.73	40	1.74	0.98	11.41	10.30	40
	S	2.95	0.98	3.33	3.95	90	2.14	0.99	3.13	2.49	100	2.22	0.94	15.22	16.76	50	2.05	0.97	13.44	15.37	50
	P2	**1.83**	**0.99**	**1.86**	1.70	100	**1.35**	**1.00**	**2.28**	2.25	100	1.89	0.97	13.60	14.59	60	2.15	0.96	12.24	14.00	60
	R	3.27	0.99	3.58	1.43	100	2.70	0.99	4.10	2.58	100	**0.95**	**0.99**	**5.08**	3.87	80	**0.88**	**0.99**	**4.79**	3.91	80
Basal Missing	L	5.09	0.97	5.34	2.87	100	2.95	0.98	3.74	2.27	100	2.66	0.95	16.35	13.89	40	1.91	0.97	10.86	11.60	70
	S	5.25	0.97	5.64	2.97	100	3.45	0.98	4.37	2.28	100	2.72	0.95	16.91	14.24	40	2.37	0.96	13.14	11.29	60
	P2	4.53	0.97	4.96	2.56	100	**2.46**	**0.99**	**3.51**	2.57	100	2.77	0.95	18.09	16.17	40	2.21	0.96	12.48	14.51	70
	R	**3.15**	**0.98**	**3.42**	2.85	100	2.78	0.98	4.05	3.28	100	**1.88**	**0.98**	**10.39**	7.51	50	**1.69**	**0.98**	**9.23**	7.05	60
3 Slices	L	4.90	0.95	5.18	2.78	100	4.16	0.95	5.85	4.29	90	2.54	0.94	13.26	7.56	40	2.43	0.96	12.47	8.61	60
	S	3.52	0.98	3.77	2.67	100	3.73	0.97	5.29	3.60	90	1.97	0.97	10.68	9.38	60	**2.08**	**0.97**	**10.80**	10.02	60
	P2	**3.17**	**0.98**	**3.48**	2.84	100	**3.64**	**0.97**	**5.22**	3.57	90	**1.71**	**0.98**	**10.21**	10.16	70	2.11	0.97	10.84	10.05	60
2 Slices	L	6.54	0.94	**6.51**	4.15	80	**4.23**	**0.96**	**5.65**	3.56	90	4.76	**0.85**	27.97	21.31	30	**3.94**	**0.90**	**22.54**	17.07	30
	P2	**5.46**	**0.94**	6.64	6.74	70	7.03	0.91	10.24	6.76	50	**4.64**	0.84	**26.83**	25.47	30	5.18	0.82	27.44	25.39	20

Table 1. Selection criteria used for comparing the estimation methods for hemodynamic measurements in all simulations. Mean absolute error (MAE), correlation of efficiency (R2), mean absolute percentage error (MAPE) and standard deviation (MAPEstd), and proportion of percentage error estimates within 10% (P10). Highlighted cells displays lowest MAE and MAPE, and highest R2.

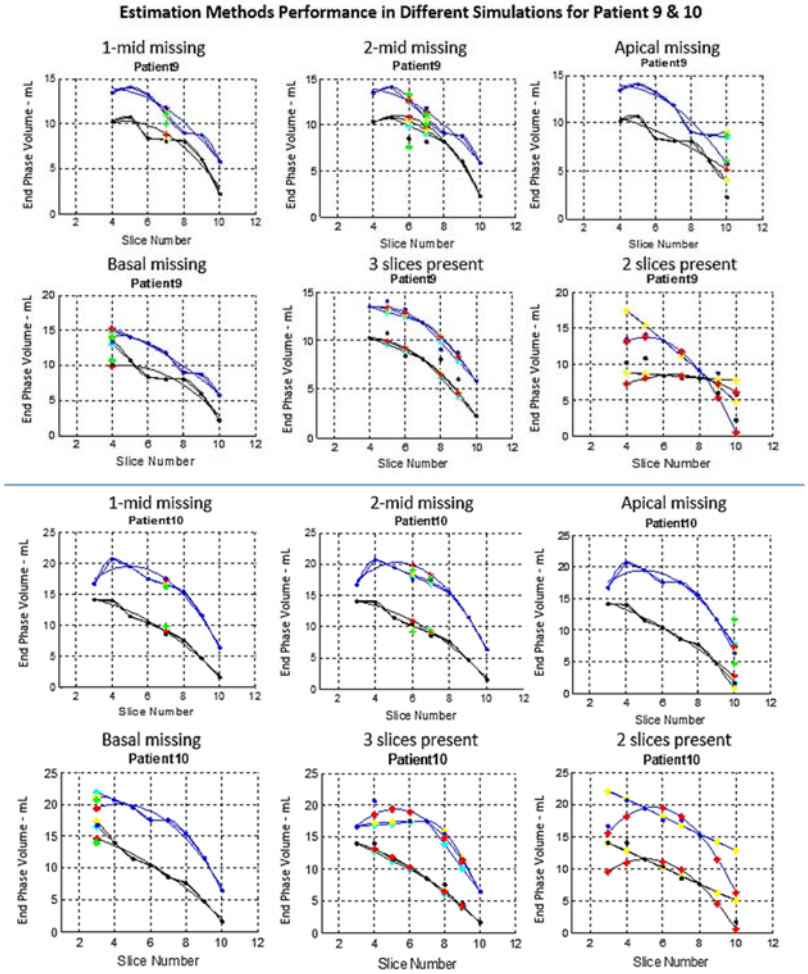

Figure 1. Top panel and bottom panel illustrate the performance of estimation methods for all simulations in patient 9 and 10, respectively. EDV (blue) and ESV (black) slice data were estimated (colored dots)

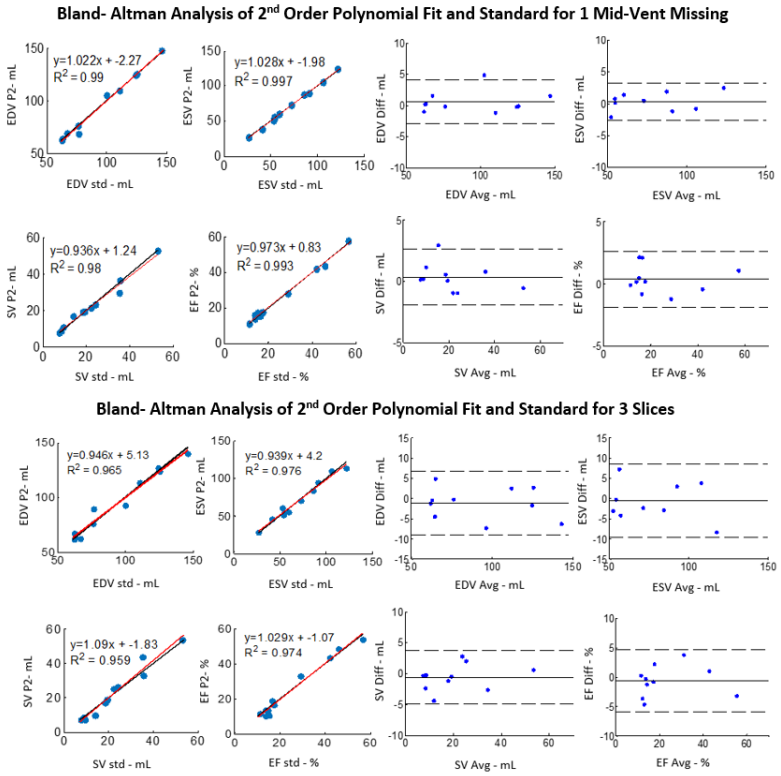

Figure 2. Analysis of selected 2nd order polynomial fit for EDV, ESV, SV and EF in two simulations. Left: correlation analysis shows consistency with estimation. Right: Bland-Altman plots display negligible biases.

ID#: 378559

Remodelling of right ventricular compartments after pulmonary valve replacement or reconstruction in patients with repaired tetralogy of Fallot

Eva Kis, MD[1]Dominik D. Gabbert, PhD[2], Carsten Rickers, MD[2]

1. Department of Pediatric Cardiology, UKSH, Christian-Albrechts University Kiel, Germany and Gottsegen György Hungarian Institute of Cardiology, Pediatric Heart Centre, Budapest, Hungary, Germany

2. Department of Congenital Heart Disease and Paediatric Cardiology, University Hospital Schleswig-Holstein UKSH, Schleswig-Holstein, Germany

Background: Pulmonary valve replacement or reconstruction (PVR) is considered to be an effective therapy to reduce right ventricular (RV) dilatation in patients with tetralogy of Fallot (ToF). However, little is known about the remodelling of RV compartments (right ventricular outflow tract (RVOT) and RV corpus) after PVR. Therefore, our aim was to investigate separately the right ventricular compartments before and after PVR with MRI.

Methods: Twenty five patients with ToF (median age: 17.7; 5.3- 48.2 years) underwent PVR for pulmonary insufficiency and RV dilatation. MRI was performed before (median 0.5 year) and after surgery (median 1.8 years). We used an in-house software for segmental analysis of the RV. The method provides an automatic contour detection algorithm for the determination of the RV blood volume and enables the user to segregate the blood volume of the RVOT and RV corpus based on anatomic landmarks and to generate volume-time-curves over a cardiac cycle. Enddiastolic (EDVi) and endsystolic (ESVi) times were normalized to the patient´s RR times.

Results: After PVR we measured a significant reduction in RV volumes (EDVi: pre: 155.0 ml/m², post: 121.3 ml/m²; p=0.015 and ESVi: pre: 96.5 ml/m², post: 62.2 ml/m²; p=0.001) and a significant increase of RV ejection fraction (pre: 39%, post: 46%; p=0.003).There was a significant reduction in RVOT volumes (EDVi pre: 21.0 ml/m², post: 9.1 ml/m²; p=0.001 and ESVi: pre: 15.0 ml/m², post:11.9 ml/m²; p=0.019). There was also a significant reduction in RV muscular corpus EDVi: pre: 102.2 ml/m², post: 87.3 ml/m²; p=0.015, but not in ESVi: pre: 63.3 ml/m², post: 57.9 ml/m²; p=0.078). From RV time-volume curves we derived delay times in RV EDVi to RVOT EDVi before (0.91- 1.0) and after (0.92-1.0) PVR. RV-RVOT ESVi delay was significantly reduced after PVR (pre: 0.44-0.54; post: 0.44-0.48; p< 0.01). The change in QRS duration was not significantly different (pre PVR: 150 ms; post PVR: 140 ms; p=0.98).

Conclusion: After PVR in ToF patients we have observed significant RV volume reduction and decrease in RV-RVOT ESVi delay. Segmental analysis of the RV compartments showed that the RVOT as well as the RV corpus (not affected by the operation) have improved, indicating the benefical effects of the operation for the entire RV. Separate analysis of RV compartments may clarify the optimal point in time for reoperation.

ID#: 377654

Distribution of left ventricular trabeculation across gender and age in a cohort of 140 healthy Caucasian subjects

Zakarya Bentatou, MS[1]Mathieu Finas, MD[2], Frank Kober, PhD[3], Maxime Guye, MD PhD[4], Stéphanie Bricq, PhD[5], Alain Lalande, PhD[6], Stanislas Rapacchi, PhD[7], Monique Bernard, PhD[8], Alexis Jacquier, MD PhD[9], Jean-Nicolas Dacher, MD, PhD[10]

1. Aix-Marseille Univ, CNRS, CRMBM, Marseille, France, France

2. Département de Radiologie, Aix Marseille Université, Hôpital Universitaire La Timone, Marseille, France, France

3. Aix Marseille University CNRS, Marseille, France

4. Aix Marseille University CNRS, France

5. Le2i, FRE2005, CNRS, Arts et Métiers, Univ. Bourgogne Franche-Comté, France, Dijon, Bourgogne, France

6. University hospital of Dijon and University of Dijon, Dijon, Bourgogne, France

7. Aix-Marseille Université CNRS, Marseille, France

8. Aix Marseille University, Marseille, France

9. Aix Marseille Université APHM, France

10. University Hospital of Rouen, Department of Radiology - Cardiac Imaging Unit, Rouen France, Haute-Normandie, France

Background: The diagnosis of left ventricular non-compaction (LVNC) is usually made using echocardiography and/or cardiac MRI, the latter providing increased resolution and contrast. This uncommon disease characterized by an excess of trabeculations of the left ventricle (LV)(Breckenridge, Cardiology in the Young, 2007) remains poorly documented and challenging to diagnose. Detection using MRI has been recently investigated (Bricq, JMRI, 2016; Captur, Radiology, 2015). LVNC has highly variable clinical manifestations, ranging from no symptoms to arrhythmias and disabling heart failure (Weiford, Circulation, 2004). Therefore, there is a need for reliable quantification of trabeculations in the LV myocardium and its variations in a healthy population. Our purpose was, using cine-MRI, 1) to analyse the distribution of LV compacted (C) and trabeculated (T) myocardium masses across age and gender in a healthy population and to compare them to LV volumes and calculated cardiac function parameters, and 2) to provide reference values of these LV myocardium masses.

Methods: One hundred and forty healthy subjects, were prospectively recruited: 14 men and 14 women for each of the 5 following age groups [20-29], [30-39], [40-49], [50-59] and [60-69]. All volunteers underwent cardiac magnetic resonance imaging at 1.5T with a stack of short-axis cine sequences covering the entire LV. End-diastolic volume (EDV), C and T myocardium masses were quantified using the semiautomatic method proposed by Bricq et al. (Bricq, JMRI, 2016). Ejection fraction (EF) and T/C ratio were computed. A multivariate test was performed to measure the impact of age, gender, EF and EDV on the C, T and T/C ratio.

Results: The mean EF was 63.7±6.3 %, the mean EDV was 75.9±16.2 ml/m2, the mean C mass was 57.2±11.7 g/m2 and the mean T mass was 4.7±2.4 g/m2. The T/C ratio was 8.2±3.9 %. Multivariate ANOVA test showed that the compacted mass was influenced by EDV ($p<0.0001$), EF ($p=0.001$) and gender ($p<0.0001$), and the T mass depended on EDV ($p<0.0001$), gender ($p=0.002$) and age ($p<0.0001$) while the ratio T/C was only impacted by age (significant decrease, $p=0.0003$).

Conclusion: We have proposed reference values for T, C and T/C in a cohort of healthy subjects. While the compacted and trabeculated myocardium masses appear to relate separately to the cardiac function, age and gender, their ratio T/C appears to only decrease with age.

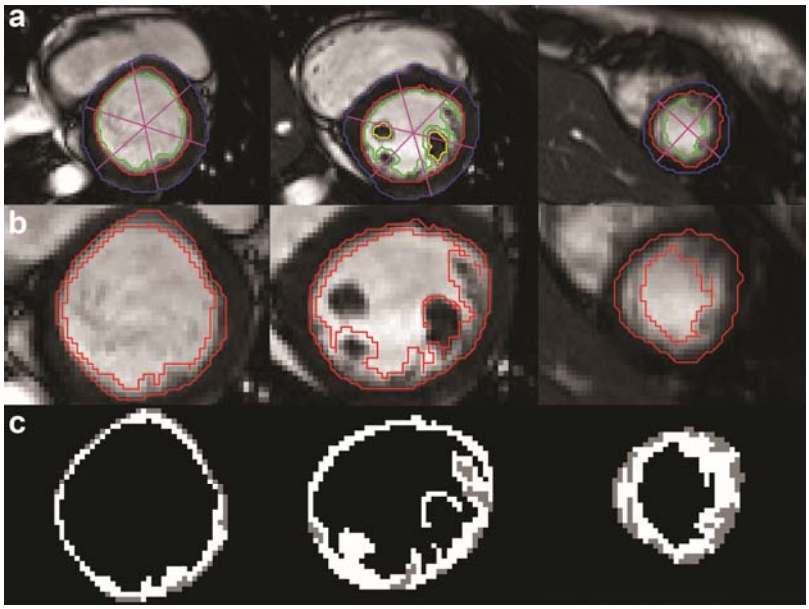

Example of the 16-segment left ventricular segmentation over base (left), median (middle) and apex (right). (A) Epical border in blue (manually drawn), endocardial border in red (manually drawn), trabeculae border in green (automatically segmented), papillary muscles in yellow (included in the compacted mass, semi-automatically segmented) and the 16 segments delineations in magenta. (B) To help the operator refine the segmentation of the trabeculae, the original image is displayed with the endocardial and the trabeculae borders (red line). (C) A semiautomatic thresholding tool helps suppress blood (white pixels) and isolate trabeculae (gray pixels).

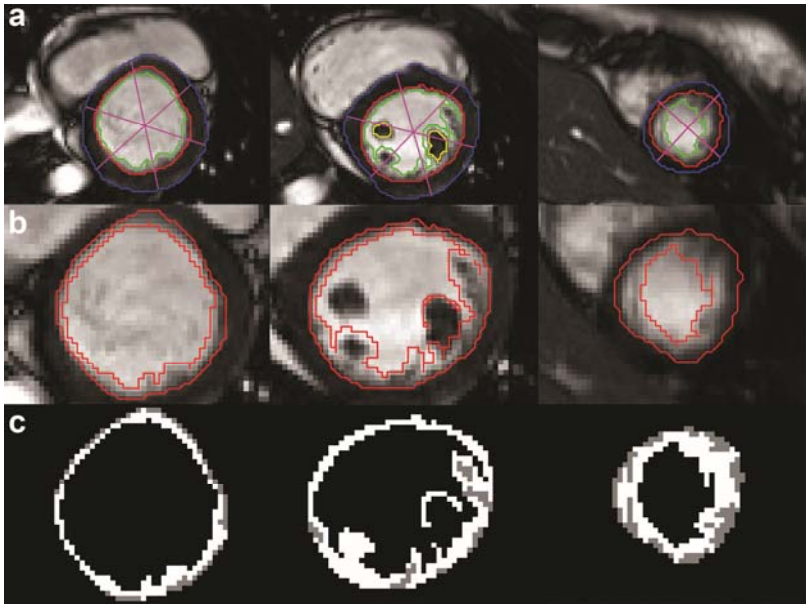

Example of the 16-segment left ventricular segmentation over base (left), median (middle) and apex (right). (A) Epical border in blue (manually drawn), endocardial border in red (manually drawn), trabeculae border in green (automatically segmented), papillary muscles in yellow (included in the compacted mass, semi-automatically segmented) and the 16 segments delineations in magenta. (B) To help the operator refine the segmentation of the trabeculae, the original image is displayed with the endocardial and the trabeculae borders (red line). (C) A semiautomatic thresholding tool helps suppress blood (white pixels) and isolate trabeculae (gray pixels).

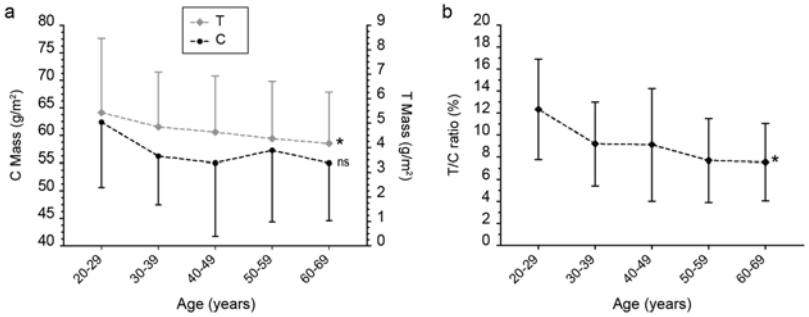

Influence of age on left ventricular masses. (A) Distribution of left ventricular compacted (C) and trabeculated myocardium masses (T), and (B) T/C ratio by age groups. The values are represented as connected means ± standard deviation (SD) for age groups [20-29], [30-39], [40-49], [50-59] and [60-69]. ns, non-significant p value; *, p=0.0003.

ID#: 377659

Patient specific prospective respiratory motion correction for efficient, free-breathing cardiovascular MRI

Michael A. Bush, M.S.[1] Orlando Simonetti, PhD[2], Rizwan Ahmad, PhD[2], Yingmin Liu, Ph.D.[1], Ning Jin, PhD[3]

1. The Ohio State University, Columbus, OH

2. The Ohio State University, OH

3. Siemens Healthineers

Background: CMR techniques are susceptible to respiratory motion induced artifacts that can lead to **poor image quality, repeated scans, and decreased throughput** and thus represent a significant obstacle to clinical utility. Repeated breath-holding is not possible for many patients, and navigator gating typically results in rejection of 60% to 80% of data, **reducing scan efficiency by a factor of 2.5 to 5**[1]. In combination with navigator gating, prospective slice repositioning is often applied that assumes a 0.6 ratio of heart to diaphragm motion in the head-foot direction. This simplistic approach does not account for patient-to-patient variation, inspiratory vs. expiratory differences, or the complete 3D nature of that motion. To address these shortfalls, **we developed a method that uses a patient-specific prospective motion correction model to correct for respiratory motion on-the-fly.**

Methods: Training images consisting of two orthogonal views of the heart are acquired each heartbeat repeatedly over a one minute period, simultaneous with a respiratory navigator signal tracking the diaphragm. Then, the position of the heart is detected in the training images and used to tune patient-specific motion model parameters relating navigator position to heart position in three directions, as shown in **Figure 1**. The patient-specific model is used together with navigator data to determine the position of the heart as it moves with respiration and to prospectively correct slice position on a beat-by-beat basis. The proposed prospective motion correction (**PROCO**) method was tested by acquiring series of single shot images in 5 normal volunteers to compare residual motion following PROCO acquisition with both free-breathing with no-correction (**NOCO**), and traditional navigator gating (**Gated**).

Results: Residual motion estimated using retrospective non-rigid registration showed that**NOCO** had greater residual motion than **PROCO** with p-values of 0.0266 for Vertical and 0.0577 for Horizontal motion. In addition, **PROCO** residual motion is not significantly different from **Gated** with p-values of 0.465 for Vertical and 0.1593 for Horizontal motion, as summarized in **Table 1**. The model was able to track **the bulk motion of the heart throughout the entire respiratory cycle**, illustrating the importance of tracking through-plane motion. In **Figure 2**,papillary muscles show significant in-plane and through-plane motion during NOCO acquisitions, while PROCO tracked the papillary muscles in-plane and through-plane.

Conclusion: PROCO significantly reduces residual motion while maintaining 100% acceptance rate. Several cardiac imaging applications stand to benefit from this technique, including 2D and 3D perfusion, myocardial parameter mapping, and late gadolinium enhancement. 1. Jhooti P, Keegan J, Firmin DN. A fully automatic and highly efficient navigator gating technique for high-resolution free-breathing acquisitions: Continuously adaptive windowing strategy. *Magn Reson Med*. 2010;64(4):1015-1026. doi:10.1002/mrm.22491.

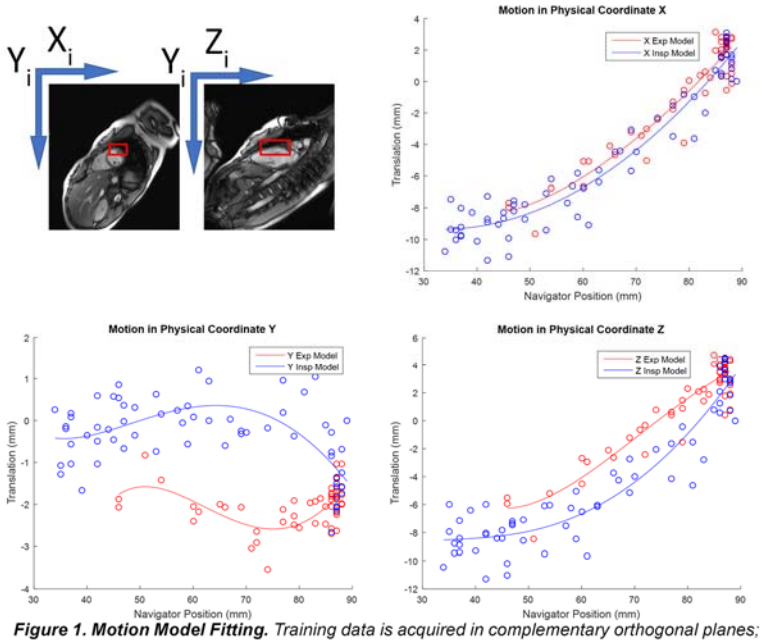

Figure 1. Motion Model Fitting. *Training data is acquired in complementary orthogonal planes; an ROI is placed on relevant anatomical features following image registration* ***(A)****. This allows extraction of three dimensional motion of the heart in the image coordinate system, denoted by the subscript "i". The motion is classified as inspiratory or expiratory, transformed into the MRI physical coordinate system and characterized with polynomial fits.*

Motion Model Fitting

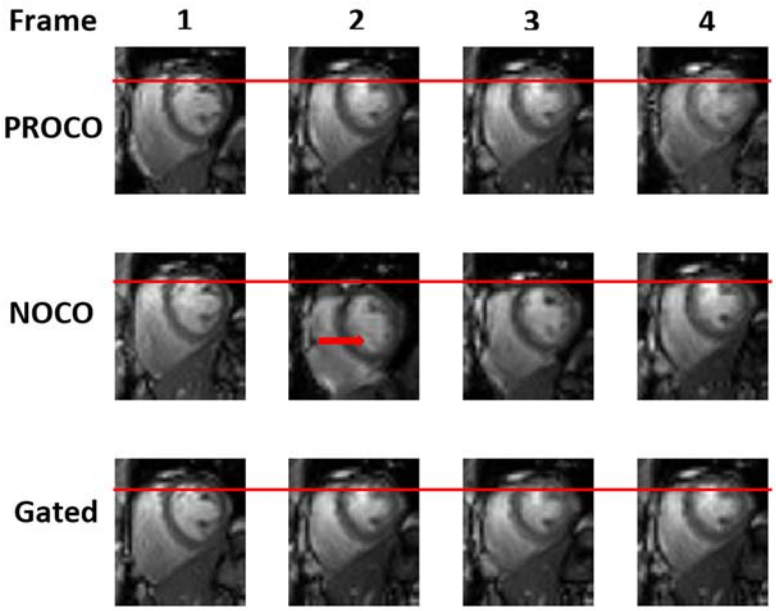

Figure 2. Real-time Testing. *Three scans were run; an initial reference scan with 100% acceptance, free breathing and no correction* ***(NOCO)****; a traditional navigator gated scan with an acceptance window of 4mm* ***(Gated)****, and a scan incorporating the patient-specific 3D prospective motion correction model* ***(PROCO)****. The red lines serve as a baseline position of the papillary muscles, and illustrate changes in position over 4 frames of one complete respiratory cycle. Displacement and loss of the papillary muscles through-plane is shown in the* ***NOCO*** *images, while the motion is absent in both* ***PROCO*** *and* ***Gated*** *images.* ***PROCO*** *was acquired at 100% efficiency, compared to roughly 32% efficiency for* ***Gated****.*

Real-time Testing

Table 1. Summary of residual motion

Direction	**NOCO** *100% AR*	**PROCO** *100% AR*	**Gated** *37.4±0.12% AR*
Vertical	14.39±7.22 mm	3.55±0.75 mm	3.23±1.24 mm
Horizontal	7.07±3.42 mm	3.18±0.5 mm	2.43±0.63 mm

ID#: 377685

Feasibility of Interventional Procedure Planning using Quiescent-Interval Single-Shot (QISS) MRA in Patients with Peripheral Artery Disease

Taylor M. Duguay, BS[1] Thomas M. Todoran, MD[2], Megha Penmetsa, BS[2], Stephen R. Fuller, BS[2], Pal Suranyi, MD, PhD[2], Carlo N. De Cecco, MD, PhD[2], Domenico Mastrodicasa, MD[3], U. Joseph Schoepf, MD[2], Akos Varga-Szemes, MD, PhD[2]

1. Medical University of South Carolina, Charleston, SC

2. Medical University of South Carolina, SC

3. Department of Neuroscience, Imaging and Clinical Sciences, "G. D' Annunzio" University, Chieti, Italy, Abruzzi, Italy

Background: CT angiography (CTA) is considered standard of care in patients with peripheral artery disease (PAD) for interventional procedure planning. However, patients with PAD frequently experience renal insufficiency, which increases the risk associated with contrast administration. Quiescent-interval single-shot (QISS) MRA, a non-contrast technology, has been proven to be highly accurate in detecting significant stenosis in patients with PAD. This study investigated the feasibility of interventional procedure planning using QISS-MRA in PAD patients.

Methods: Twenty-one PAD patients (67±8 years) underwent lower extremity CTA (Siemens Force) and QISS-MRA on a 1.5T system (Siemens Avanto) prior to digital subtraction angiography (DSA) (Siemens Axiom Artis). QISS-MRA was performed covering the abdominal aorta and lower extremities using a prototype sequence (FOV 400×260mm^2, TR/TE 3.5/1.4ms, flip angle 90°, in-plane resolution 1.0×1.0mm^2). Segmental vascular diameter was measured based on an 18-segment model, and compared among QISS-MRA, CTA, and DSA using the Friedman-test. >50% stenosis was considered significant. For each significant stenosis observed on QISS-MRA, the length and diameter of the intravascular stent needed to reinstate flow in the vessel was estimated. The estimated stent size was compared to the actual dimension of the stent implanted during the intervention using Wilcoxon and Bland-Altman tests. Additionally, diagnostic accuracy of QISS-MRA against DSA for detecting PAD was calculated.

Results: After excluding non-diagnostic segments due to inadequate image quality, a total of 346 segments were analyzed with QISS-MRA. Significant stenosis was detected in 82 (23.6%) segments. Vascular diameters showed good agreement among QISS-MRA, CTA, and DSA (overall P>0.05). Based on DSA evaluation, 25 stents were implanted involving 31 segments. Average stent diameter estimated based on QISS-MRA was 8.4±2.8mm, which was in good agreement with the actual diameter of the implanted stent (8.1±3.7mm, P=0.0934; Bland-Altman bias 0.3mm). However, QISS-MRA-based stenosis length measurement underestimated the length of the stent necessary to bridge the stenosis (35.5±11.9mm vs 40.1±13.9mm, P=0.0215, respectively; Bland-Altman bias -4.6mm). The sensitivity and specificity of QISS-MRA in detecting >50% stenosis was 85.1% and 95.9% in this study population.

Conclusion: The prediction of stent diameter required to treat stenosis in patients with PAD was feasible using QISS-MRA. QISS-MRA slightly underestimated the actual stent length, which is most likely attributed to the fact that implanted stents usually extend beyond the proximal and distal ends of a stenosis. Based on these preliminary results, QISS-MRA seems promising for the non-contrast evaluation of vascular anatomy in PAD patients prior to intervention.

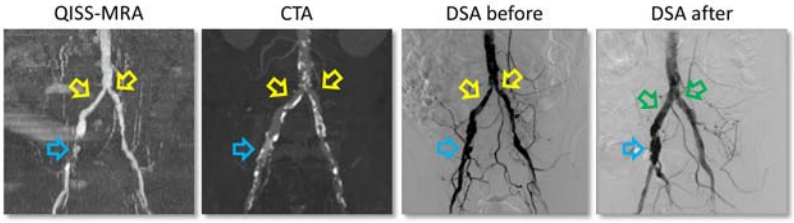

Corresponding QISS-MRA, CTA and DSA images in a 65-year-old man with PAD. Artifact on QISS-MRA (blue arrow) is attributed to previously implanted intra-vascular stent. QISS-MRA shows stenosis of the left and right common iliac arteries (yellow arrows) in agreement with CTA and DSA. Stents were placed to maintain flow following balloon angioplasty (green arrows).

ID#: 377610

Measuring the effects of strain on the diffusion tensor in myocardial tissue: Design and initial testing of a phantom

Andrew D. Scott, PhD[1]Priyanka Sukumaran[2], Pedro F. Ferreira, PhD[3], Jennifer Keegan, PhD,MSc[4], Sonia Nielles-Vallespin, PhD, MSc[5], Dudley J. Pennell, MD[6], David N. Firmin, PhD[7]

1. Royal Brompton Hospital, London, England, United Kingdom

2. Imperial College London, United Kingdom

3. Cardiovascular Magnetic Resonance Unit, Royal Brompton Hospital, Sydney Street, London, SW3 6NP, UK, England, United Kingdom

4. Royal Brompton Hospital , Imperial College, England, United Kingdom

5. NIH, MD

6. Royal Brompton Hospital and Imperial College, London, England, United Kingdom

7. 1. Cardiovascular Magnetic Resonance Unit, Royal Brompton Hospital, Sydney Street, London, SW3 6NP, UK, England, United Kingdom

Background: Microstructural measures obtained by diffusion tensor cardiovascular magnetic resonance (DT-CMR) with stimulated echo acquisition mode (STEAM) are sensitive to myocardial strain during the diffusion time[1]. Models of this effect consider the myocardium as a jelly-like material[2], but recent studies have questioned its applicability in anisotropic materials like myocardium[3,4]. We have recently compared porcine DT-CMR results between in-vivo, in-situ arrested, ex-vivo and histology[5]. However, differences in loading between pre- and post-mortem studies confound comparisons. We design and test a CMR compatible phantom which allows a co-registered comparison of DT-CMR in myocardial tissue with and without cyclical strain.

Methods: A respiratory motion phantom[6] was modified (figure 1) to cyclically compress tissue slabs with variable trajectories and amplitudes and synchronised CMR triggering. The phantom consists of a trolley in the bore, which compresses the tissue, driven by a microprocessor (Taranis, Smartdrive UK) controlled microstepping motor. The metallic motor assembly is separated from the bore via 2.3m plastic rods.
The microprocessor was programmed to produce trapezoidal and sine^2 compression (figure 1), with amplitudes 4-8mm, 1s period. Trapezoidal motion allows imaging while the phantom is stationary while sine^2 is more physiological. The microprocessor provided a trigger signal each period, which was used to trigger the scanner.
A jelly (Rowntrees UK) ~100x100x13mm^3 and a lamb's ventricular septum (butcher';s shop) ~70x50x13mm^3 were imaged. Imaging was performed at 3T (Siemens Skyra) using a flexible surface coil. Monopolar STEAM-EPI DT-CMR was performed in a short-axis-like plane with 6 diffusion directions and b=500smm^{-2}. Compression was transmural and acquisitions were performed in both the relaxed and contracted state while stationary and with one cyclical period during the diffusion time. Cine DENSE[7] was obtained for strain.

Results: Figure 2 shows example DT-CMR parameter maps for the jelly and lamb septum whilst static and moving cyclically while the water molecules diffuse. Figure 3 compares the diffusion tensor in jelly and the sheetlet plane (1st and 2nd eigenvectors) between equivalent static and moving acquisitions. For the lamb septum, the glyphs rotate between the relaxed and contracted states for both the static and dynamic acquisitions.

Conclusion: We have developed a phantom able to simulate myocardial contraction in order to directly assess the contribution of strain on STEAM DT-CMR. Despite the absence of active cardiomyocyte contraction these initial results suggest that the sheetlets rotate when the myocardium is compressed.

References 1.Reese MRM1995.DOI:10.1002/mrm.1910340603
2.Reese JMR-B 1996.DOI:10.1006/jmrb.1996.0139
3.Ferreira JCMR2014.DOI:10.1186/1532-429X-16-S1-P3388
4.Ferreira MRM2017.DOI:10.1002/mrm.26850
5.Nielles-Vallespin JACC2017.DOI:10.1016/j.jacc.2016.11.051
6.Scott JMRI2011.DOI:10.1016/j.mri.2010.11.004
7.Zhong MRM2010.DOI:10.1002/mrm.22503
8.Tseng MRM1999.DOI:10.1002/(SICI)1522-2594(199908)42:23.0.CO;2-F

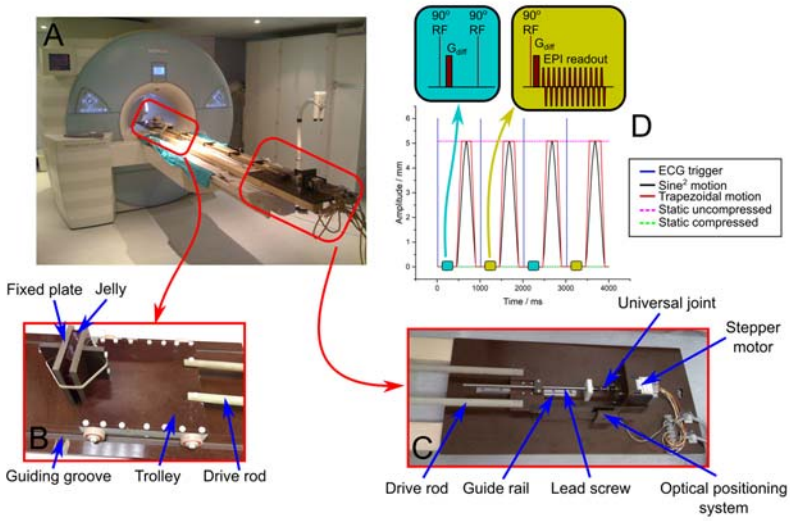

Figure 1: The phantom setup in the scanner (A) and details of both the compressing trolley (B) and the drive apparatus (C). Motion traces the phantom produces with an example of a simplified sequence diagram in the case of imaging in the uncompressed state are shown in D. Gdiff - diffusion encoding gradient.

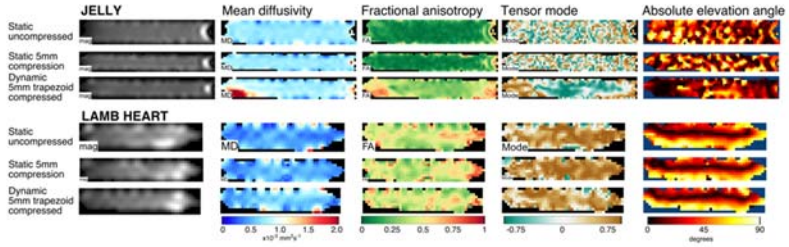

Figure 2: Example DT-CMR parameter maps obtained in the jelly and lamb heart section for both static and dynamic acquisitions, where the heart moves cyclically while the water molecules diffuse. Strain during the mixing time results in an increase in fractional anisotropy and a more coherent (negative) tensor mode. In the lamb heart, the effects of strain on the rotational invariants is subtle. Absolute elevation angle is used due to difficulties in defining the local co-ordinate system for helix angle, but demonstrates the typical transmural change in the orientation of the primary eigenvector expected. Only results from trapezoidal motion have been included here to isolate the effects of strain from those of bulk motion.

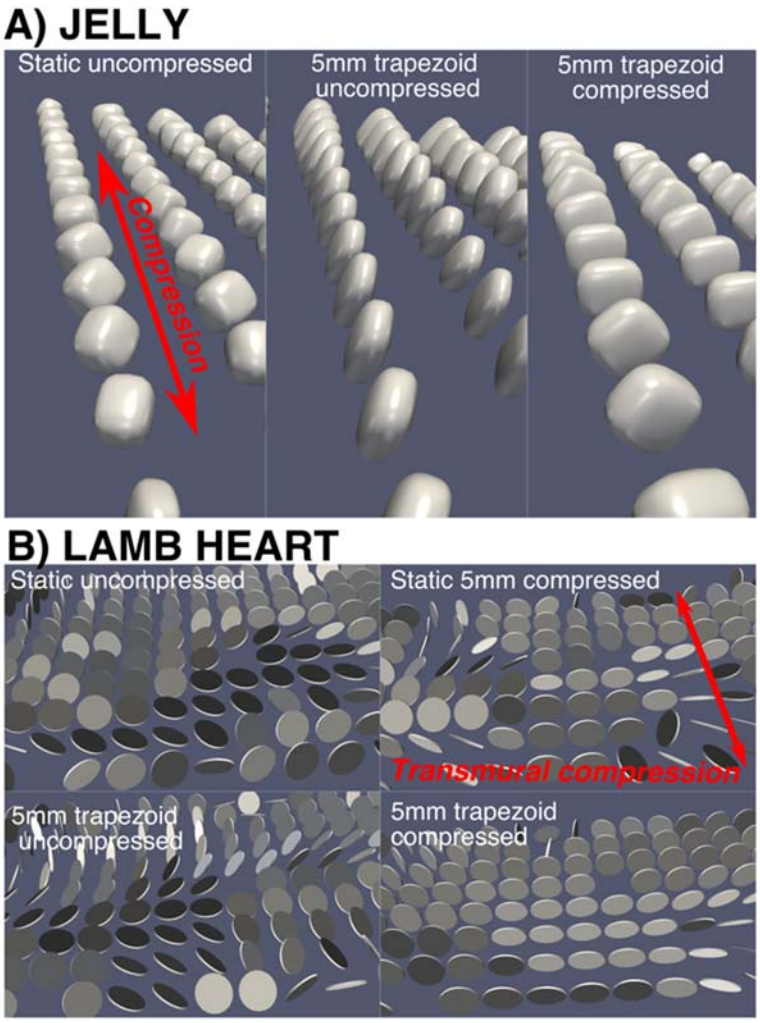

Figure 3: A) The effects of strain on the diffusion tensor obtained in jelly. Diffusion tensors are represented as superquadric glyphs. Without strain the glyphs are close to cuboidal, whereas in the uncompressed dynamic acquisition they are stretched along the direction of compression and in the dynamic compressed acquisition the glyphs are shortened along the direction of motion, in keeping with the results in [8]. B) A comparison of the measured sheetlet plane (first and second eigenvectors lie within the plane of the discs) in equivalent and co-registered static and dynamic acquisitions. While there are some differences in sheetlet orientation between the static and dynamic acquisitions, in both cases they demonstrate results similar to those found in-vivo[3]. The discs tend towards wall perpendicular in the uncompressed state (systolic-like, flat discs) and more wall parallel in the compressed state (diastolic-like, more vertical discs).

ID#: 377619

Simultaneous Multi-Slice (SMS) CINE at 7T with embedded reference dataset

Stanislas Rapacchi, PhD[1] Thomas Troalen, PhD[2], Maxime Guye, MD PhD[3], Monique Bernard, PhD[4], Alexis Jacquier, MD PhD[5], Frank Kober, PhD[6]

1. Aix-Marseille Université CNRS, Marseille, France

2. Siemens Healthineers, France

3. Aix Marseille University CNRS, France

4. Aix Marseille University, Marseille, France

5. Aix Marseille Université APHM, France

6. Aix Marseille University CNRS, Marseille, France

Background: One strong benefit expected from 7 Tesla Cardiac MRI exams is to achieve high resolution imaging, notably high-resolution cardiac dynamic MRI (Cine). However, increasing the resolution of Cine MRI is inherently limited by the duration of a breath-hold. Moreover, 2D Cine MRI resolution is highly anisotropic, with thick slices. Therefore, Cine MRI could benefit from higher SNR at 7T to acquire thinner slices and thus improve longitudinal resolution with short-axis views. Within these considerations, the increased number of slices shifts the problem of limited breath-hold duration to the issue of a repeated number of breath-hold. In this work, we propose to accelerate Cine MRI at 7T using a novel Simultaneous Multi-Slice (SMS) technique(BarthMRM2016).

Methods: Acquisitions were performed on a 7T MRI scanner (Siemens) using a 32Rx/8Tx cardiac coil (MRITOOLS) employed as a single Tx channel with a predefined phase set. Eight healthy volunteers were recruited after written consent was obtained. A 2D FLASH-Cine sequence with retrospective cardiac gating was modified with CAIPIRINHA-SMS excitations(BreuerMRM2006). A Hadamar(SouzaJCAT1988) SMS phase-shift pattern is introduced to allow for slice separation by combining data along the cardiac phase dimension (Figure1). The resulting k-spaces can then serve for calibration of SMS-reconstruction. Cine parameters were SMS3x–GRAPPA2x, 1.8x1.8x4mm^3 reconstructed to 0.9x0.9x4mm^3, 28ms resolution, 15-37deg excitation, ~10s breath-hold/scan. The same acquisitions were performed without SMS acceleration for comparison. Image reconstruction was implemented online using Gadgetron(HansenMRM2013).

Results: Figure 2 shows the results from one volunteer of the 3 slices and the long axis reformat. The 3 slices are well separated and image contrast is sufficient for assessing cardiac function. SNR measurements in the septum showed a significant loss between SMS and regular Cine (5.8±2.2 vs 11.0±3.0, $p<0.01$). Similarly, blood-myocardium CNR was reduced (3.1±1.3 vs 7.1±2.5, $p<0.01$) due to the SAR-limited SMS excitations when compared to single-slice excitations. The resliced Cine in long axis view highlight revealed few SMS slices that had poorer image quality.

Conclusion: Accelerated high resolution Cine using SMS offers multiple perspectives, from simply reducing the examination time to reaching higher resolution to refine imaging of subtle pathologies such as ventricular non-compaction. The novel SMS technique detailed here shows promises for rapid high-resolution Cine which could also benefit clinical field MRI. However, the reduced flip angle imposed by SAR to account for increased power of multi-bands excitations impacts the image noise and contrast.

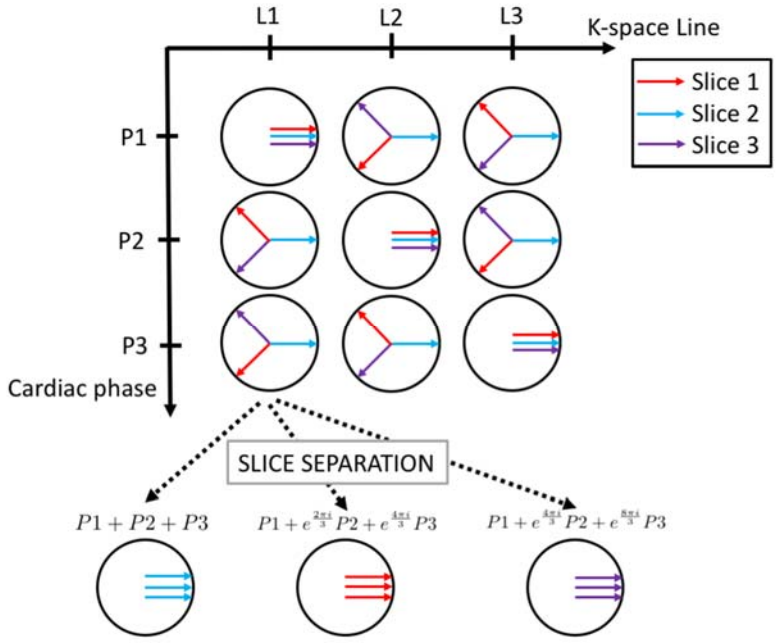

Example of Hadamar radiofrequency CAIPIRINHA phase shifts for different k-space lines and different cardiac phases.

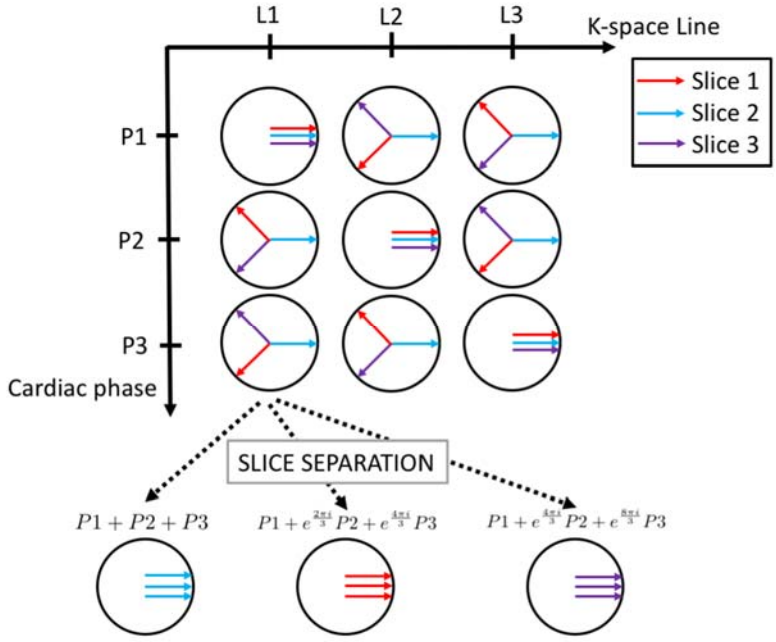

Figure 1: Proposed Hadamar multi-band radiofrequency CAIPIRINHA phase shifts for SMS-3 for different k-space lines and different cardiac phases. The slice separated dataset serves to calibrate SMS reconstruction.

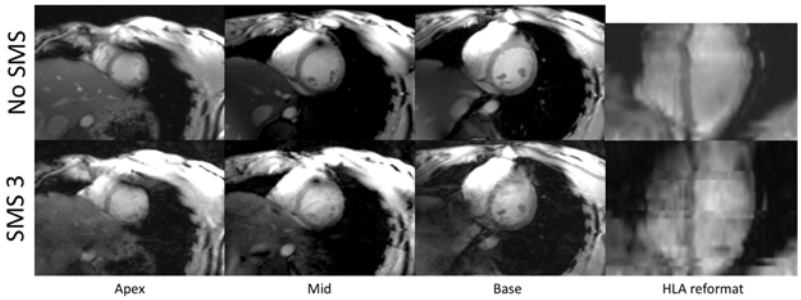

Figure 2: Example of a SMS3-GRAPPA2 FLASH-CINE acquisition in a healthy volunteer. The 3 levels of the left ventricle (apex, mid and base) are covered in a 10s breath-hold.

ID#: 377526

23Na MRI Reveals Altered Levels of Tissue Sodium Concentrations in Obese Teenagers

Marcus Kelm, M.D.[1] Sophie Roth[2], Lajos Marko, M.D.[3], Annika Bickenbach, M.D.[4], Peter Kühnen, M.D.[4], Susanna Wiegand, PhD M.D. [4], Dominik Müller, PhD[3], Sebastian Kelle, MD[5], Peter Linz, Dr. rer. nat.[6], Felix Berger, PhD M.D. [7], Titus Kuehne, PhD M.D.[8]

1. German Heart Center Berlin, Germany

2. Institute for Computational and Imaging Science in Cardiovascular Medicine, Charité - Universitätsmedizin Berlin, Germany, Germany

3. MDC, Germany

4. Charité-Universitätsmedizin Berlin, Germany

5. German Heart Center Berlin, Berlin, Berlin, Germany

6. Institut für Physiologie und Pathophysiologie; Universitätsstrasse 17; 91054 Erlangen, Germany

7. German Heart Center Berlin, Berlin, Germany

8. Charité -Universitätsmedizin Berlin, Berlin, Germany

Background: Early onset obesity is likely to culminate in high incidences of diabetes mellitus 2, hypertension and chronic kidney disease. Hence, the identification of risk factors for secondary complications is of essential clinical interest. In this context the tissue sodium metabolism is only incompletely understood. Due to clinical availability of high-field ^{23}Na Magnetic Resonance Imaging (^{23}Na-MRI) significant associations between Na^+ accumulation and refractory hypertension have been observed in adult populations. In our study, we aimed to investigate to which extent these alterations can already be observed in adolescent patients.

Methods: In 25 teenagers between the age of 13 and 16, 13 overweight and obese patients (BMI 25.9-41.0) as well as 12 controls (BMI 16.77-26.18) underwent ^{23}Na-MRI of the left lower leg on a 3T MRI scanner using a ^{23}Na knee coil to measure Na^+ content in relevant tissue compartments. Four reference standards containing aqueous solutions of 10, 20, 30 and 40 mmol/L NaCl were used to calibrate tissue sodium contents and scanned with the subject's calf. Besides, blood pressure and anthropometrics were measured and participants filled in a questionnaire about salt intake.

Results: The median (interquartile range) Na^+ content of the triceps surae muscle was significantly lower in obese patients compared to healthy controls: 11.6 (0.59) vs. 15.4 (1.96) mmol/L, p+ concentrations of the tibial bone marrow showed no significant difference with 5.2 (5.27) vs. 3.0 (7.37) mmol/L, p=0.142, similar as Na^+ concentrations of subcutaneous fat: 7.42 (3.36) vs. 8.83 (2.39) mmol/L, p=0.211 and skin: 12.99 (1.91) vs. 12.29 (2.44) mmol/L, p=0.328. In the obesity group hypertension was present in 69% of all cases while none of the control group had hypertension (p+ content of the skin in male than in female (13.3 vs 11.5, p=0.011).

Conclusion: Obesity and hypertension were inversely related to muscle Na^+ content. These results are opposing to those from adult populations indicating essential changes in Na^+ metabolism at a later stage of the disease or later in life. Although the diagnostic value of ^{23}Na-MRI for the detection of cardiovascular complications and disease stages still needs further evaluation it can already help to better understand the early impact of obesity and might be helpful in secondary prevention and disease monitoring.

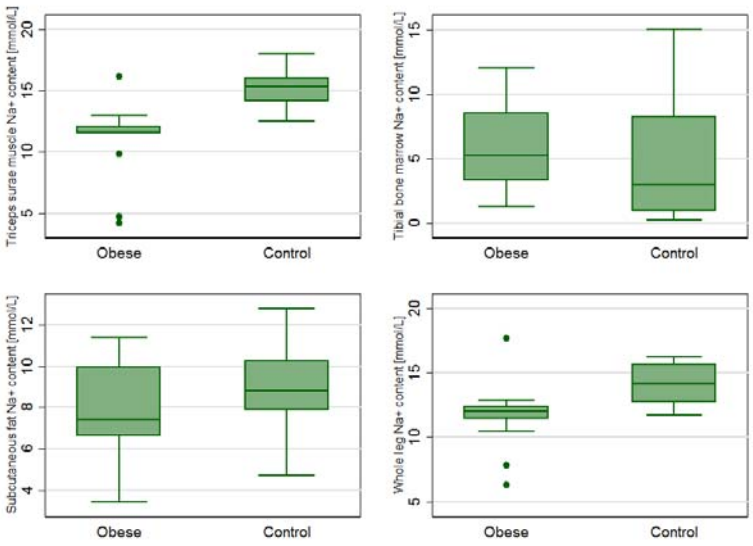

Tissue sodium content in different compartments

ID#: 377530

Intraventricular Vorticity increases during Stress in Fontan patients: Volumetric Analysis by 4D Flow CMR

Vivian P. Kamphuis, MD[1]Mohammed Elbaz, PhD[2], Pieter J. van den Boogaard, BSc[3], Lucia J.M. Kroft, MD[4], Albert de Roos, MD, PhD[3], Nico A. Blom, MD, PhD[5], Willem Helbing, MD, PhD[6], Arno A.W. Roest, MD, PhD[7], Jos J.M. Westenberg, PhD[4]

1. Leiden University Medical Center, Netherlands Heart Institute, Den Haag, Zuid-Holland, Netherlands

2. Department of Radiology, Leiden University Medical Center, Leiden, the Netherlands, AB, Canada

3. Department of Radiology, Leiden University Medical Center, Leiden, The Netherlands, Zuid-Holland, Netherlands

4. Department of Radiology, Leiden University Medical Center, Leiden, The Netherlands, Leiden, Zuid-Holland, Netherlands

5. Division of Pediatric Cardiology, Department of Pediatrics, Leiden University Medical Center, Leiden, The Netherlands, Zuid-Holland, Netherlands

6. Department of Pediatrics, division of Pediatric Cardiology, Erasmus Medical Center, Rotterdam, the Netherlands, Zuid-Holland, Netherlands

7. Department of Pediatrics, Leiden University Medical Center, Leiden, The Netherlands, Zuid-Holland, Netherlands

Background: The magnitude of vortical blood flow density in a ventricle (**Figure 1**), quantitatively expressed in the vorticity (curl of velocity), could be affected by geometrical and hemodynamic factors. These factors also determine ventricular function and therefore, the vorticity could be a useful marker in the assessment of systolic and diastolic ventricular (dys-)function. To our knowledge, it is unknown how intraventricular vorticity changes in relation to ventricular size and shape during (pharmacologic) stress in Fontan patients. Therefore, the purpose of this study was to noninvasively assess intra-ventricular vorticity as well as ventricular size and shape from 4D flow CMR during rest and stress in Fontan patients.

Methods: Seven patients with a Fontan circulation (age 17±4 years) underwent whole-heart 4D Flow CMR at 3T MRI (Philips Healthcare) at rest and with Dobutamine 7.5 µg/kg/min (VENC=150 cm/s, spatial resolution $3\times3\times3mm^3$, 30 retrospectively reconstructed phases over one cardiac cycle). The ventricular volume was segmented and for each acquired time-phase, voxel-wise vorticity magnitude (1/s) was computed over the segmented ventricular volume. Then, for each time-phase, the instantaneous integral vorticity magnitude was computed as the cumulative sum of voxel-wise vorticity and multiplied by voxel volume to give the integral in ml/s. Ventricular vorticity was assessed at peak systole ($vorticity_{peak\text{-}systole}$) and peak diastole ($vorticity_{peak\text{-}diastole}$). In order to study ventricular size and shape, the end diastolic volume (EDV) and stroke volume (SV) were computed as well as a sphericity index (SI), as the short- to long-axis ratio in the cine transversal images. The Wilcoxon signed rank test was used to compare the rest with stress parameters, with $P<0.05$ considered significant.

Results: Detailed results are shown in **Table 1** and **Figure 2**. Between rest and stress, there was no significant difference in EDV (167 mL versus 167 mL, *P*=0.50), ESV (91 mL versus 72 mL, *P*=0.40) or SV (70 mL versus 92 mL, *P*=0.13) and SI (0.8 versus 0.9, *P*=0.74). However, Dobutamine stress resulted in a significant increase in $vorticity_{peak\text{-}systole}$ (5429 versus 6513 ml/s, *P*=0.02) and $vorticity_{peak\text{-}diastole}$ (4692 versus 5881, *P*=0.03).

Conclusion: This is the first study evaluating 4D Flow CMR based intraventricular vorticity at rest and during pharmacological stress in Fontan patients. In this study, despite non-significant differences in ventricular size and shape, pharmacologic stress resulted in a significant increase in intraventricular vorticity during systole and diastole, suggesting this change was hemodynamic-driven.

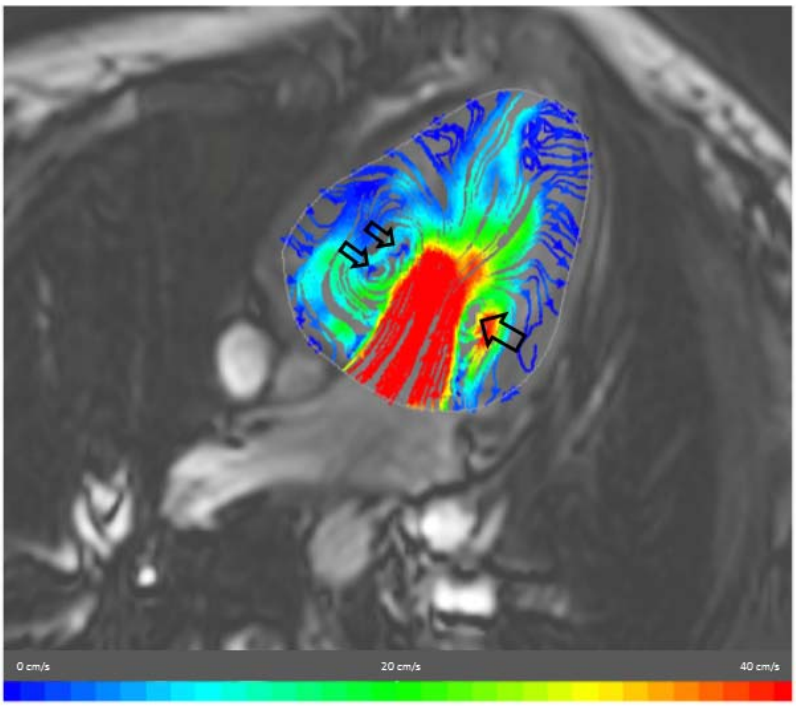

Figure 1. Streamline representation in the 4-chamber view of a Fontan patient with a double inlet left ventricle at peak diastole. Vortex cores are indicated with an arrow.

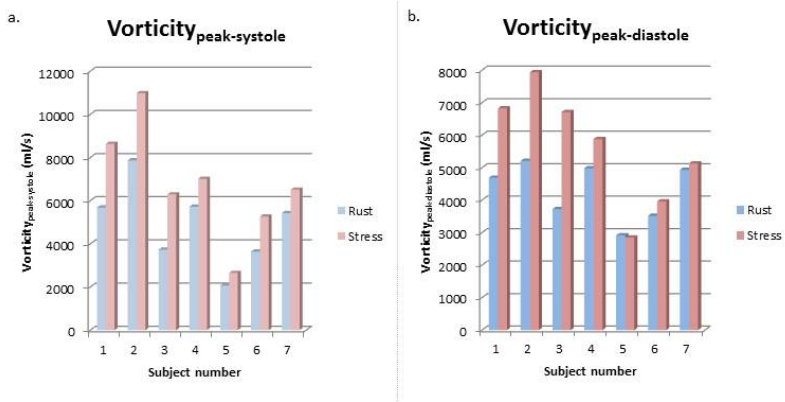

Figure 2. Vorticity at rest and stress

Table 1. Quantitative analysis of vorticity at rest and stress

Quantitative analysis of vorticity at rest and stress					
	Rest	Dobutamine stress	Difference	Difference (%)	P-value
	Median [IQR]	Median [IQR]	Stress-Rest Median [IQR]	(Stress-rest)/Rest*100% Median [IQR]	

HR (bpm)	87 [79-102]	118 [113-119]	31 [18-36]	35 [19-43]	0.02
EDV (mL)	167 [145-181]	167 [131-176]	-5 [-13-7]	-3 [-9-5]	0.50
ESV (mL)	91 [62-98]	72 [58-75]	-19 [-26-13]	-27 [-31-20]	0.40
SV (mL)	70 [62-98]	92 [72-96]	10 [-6-15]	15 [-6-17]	0.13
EF (%)	47 [42-57]	56 [56-65]	10 [6-12]	41 [35-49]	0.03
CO (l/min)	6.5 [5.5-7.7]	10,0 [8.3-11.0]	2.7 [2.3-3.2]	20 [12-27]	0.02
Sphericity index	0.8 [0.7-1.1]	0.9 [0.7-1.3]	-0.1 [-0.2-0.2]	-6.5 [-16.1-15.0]	0.74
$Vorticity_{peak\text{-}systole}$ (ml/s)	5429 [3644-5719]	6513 [5267-8631]	1624 [1084-2947]	39 [23-52]	0.02
$Vorticity_{peak\text{-}diastole}$ (ml/s)	4692 [3518-4984]	5881 [3961-6826]	896 [198-2729]	18 [4-52]	0.03
IQR = interquartile range; HR = heart rate; EDV = end diastolic volume; ESV = end systolic volume; SV = stroke volume; EF = ejection fraction; CO = cardiac output; LV = left ventricle; e-peak = peak early diastole; a-peak = peak late diastole					

ID#: 377546

Diastolic flow in the descending aorta by cardiovascular magnetic resonance imaging for quantification of aortic regurgitation

Andreas Kammerlander, MDFranz Duca, MD, Caroline Zotter-Tufaro, MD, Julia Mascherbauer, MD

Medical University of Vienna, Austria

Background: Echocardiography is the standard method for quantification of aortic regurgitation (AR). However, accurate estimation of AR severity by echo may be challenging due to inherent limitations of applied methods. Cardiovascular magnetic resonance imaging (CMR) has recently been advertised as an accurate method for AR quantification, irrespective of acoustic windows. The present prospective study sought to evaluate the usefulness of CMR for the quantification of AR.

Methods: 228 consecutive patients (33% female, 57±18 years) with varying degrees of AR by echocardiography (90 mild, 57 moderate, and 42 severe, 39 with inconclusive echocardiographic results - “moderate to severe” AR) were invited to undergo CMR within 4 weeks. CMR consisted of standard protocols including phase-contrast velocity-encoded imaging for regurgitant fraction (RegF) at the sinutubular junction and assessment of holodiastolic retrograde flow (HRF) in the descending aorta. Severe AR was defined as the presence of HRF in the descending aorta by CMR.

Results: Left ventricular (LV) end-diastolic volumes (EDV) by CMR significantly increased with increasing AR severity by echo (LVEDV: mild: 151±60ml, moderate: 184±71ml, “moderate to severe”: 210±93ml, severe: 238±68ml; p<0.001). Among the 186 patients with non-severe AR by echo, 10% had HRF by CMR, indicating severe AR. Among the 42 patients with severe AR by echo, 38% did not show HRF by CMR, suggesting overestimation of AR severity in these patients. In patients with inconclusive echo results, 44% had HRF in the descending aorta, indicative for severe AR. Presence of HRF by CMR was associated with significantly higher RegF at the sinutubular junction (9±12% versus 38±18%, p<0.001) and more dilated LVs (165±61ml versus 250±85ml, p<0.001).

Conclusion: Quantification of AR by CMR is feasible and highly reproducible. HRF in the descending aorta by CMR is an easily measurable marker that is very helpful for the distinction between severe and non-severe AR, especially when echocardiographic results are inconclusive.

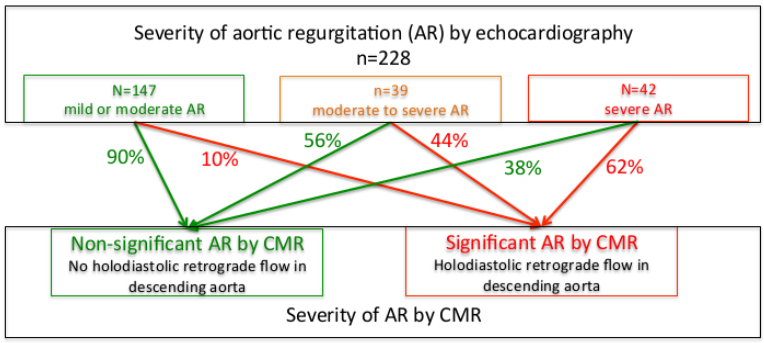

Central illustration

ID#: 377555

Energy Loss and Kinetic Energy of the Left Ventricle in Patients with Paroxysmal Atrial Fibrillation

Julio Garcia, PhD[1] Mohammed S.M. Elbaz, PhD[2], Michael Bristow, MD[3], Carmen P. Lydell, MD[4], Andrew G. Howarth, MD, Ph.D[3], Bobby Heydari, MD, MPH[3], Frank S Prato, PhD[5], Maria Drangova, PhD[6], Rebecca E. Thornhill, PhD[7], Pablo Nery, MD[8], Stephen Wilton, MD[9], Allan Skanes, MD[10], Faramarz F. Samavati, PhD[2], James White, MD, FRCP(C)[3]

1. University of Calgary, Calgary, AB, Canada

2. University of Calgary, AB, Canada

3. Stephenson Cardiac Imaging Centre, Libin Cardiovascular Institute of Alberta, University of Calgary, AB, Canada

4. Stephenson Cardiac Imaging Centre, Libin Cardiovascular Institute of Alberta, University of Calgary, Calgary, AB, Canada

5. Lawson Health Research Institute, ON, Canada

6. Imaging Research Laboratories, Robarts Research Institute, ON, Canada

7. Medical Imaging, The Ottawa Hospital, ON, Canada

8. Electrophysiology, University of Ottawa, ON, Canada

9. Cardiac Sciences, Libin Cardiovascular Institute of Alberta, University of Calgary, AB, Canada

10. Department of Medicine, University of Western Ontario, ON, Canada

Background: Atrial fibrillation (AF) is a common arrhythmia associated with elevated morbidity and mortality from systemic thrombo-embolism. Characterization of left ventricle (LV) hemodynamics may provide valuable detail of LV efficiency to adapt during AF. Besides the routine anatomic measurements, there are few biomarkers of hemodynamics performance. Thus, this study aimed to employ 4D flow MRI to non-invasively quantify volumetric viscous energy loss (EL) and kinetic energy (KE) to assess the LV energetic performance in patients with paroxysmal AF during systole and diastole versus healthy controls (HC).

Methods: 34 subjects (20 with paroxysmal AF, and 14 HC) were enrolled in an IRB-approved study protocol. Patients were required to be in sinus rhythm and not have >mild mitral insufficiency. Imaging was performed using a 3T MRI scanner (Prisma or Skyra, Siemens, Erlangen, Germany) using a standardized protocol inclusive of ECG-gated 4D flow with adaptive navigator respiratory gating with whole heart coverage (Fig. 1A). 4D flow spatial resolution was 1.9-3.5x2.0-3.2x1.8-3.5 mm3, and temporal resolution was 39-47 ms. 4D flow dataset pre-processing included: eddy-current correction, flow aliasing, and calculation of 3D phase contrast angiography (3D PC-MRA). The 3D PC-MRA was used to segment the left sided chambers and proximal aorta, Fig. 1B. The LV was isolated, Fig. 1C, and used to calculate KE ($KE=1/2\times rho\times v^2$, where rho is the blood density = 1.06 g/mL and v the velocity field); and EL ($EL=\mu\sum(DV)$, where the dynamic viscosity was $\mu=0.004$ Pa.s, D was the viscous dissipation on a voxel-by-voxel basis, and V was the voxel volume. Volumetric median and total summation from KE and EL was obtained at peak systole and peak diastole (Fig. 2). All parameters were normalized to volume size.

Results: Age was 52±9 years in AF subjects and 42±12 years in HC (p=0.007). No significant differences were found for KE between both groups (Table 1). At peak diastole, significantly decrease in EL was found in AF patients compared to HC for normalized median EL (HC: 1.8±0.9 mW/m3 vs. AF: 1.2±0.6 mW/m3, p=0.048), and total EL (HC: 13.98±9.27 W/m3 vs. AF: 7.26±2.71 W/m3, p=0.004).

Conclusion: In the studied AF patients, the main hemodynamics alterations in the LV from 4D Flow MRI, expressed in significantly reduced EL, are diastolic while systolic energetics are largely maintained. Such results may indicate that in AF patients, diastolic hemodynamic alterations and potential subsequent impaired diastolic function may precede possible systolic impairment. The reported decline in diastolic EL levels might be a result of impaired preload in these patients. These results could encourage future studies towards investigating the impact of altered LV hemodynamic on diastolic and systolic function in left atrial diseases.

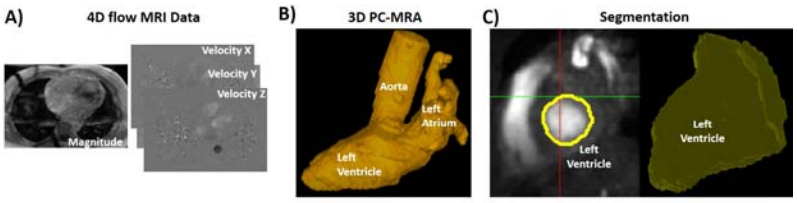

Figure 1. Workflow. Panel A shows an example of 4D flow MRI data which were pre-processed for eddy currents, Maxell terms and aliasing. Panel B shows the segmentation of the left side of the heart including the aorta, left atrium and the left ventricle. Panel C shows the isolation of the left ventricle for energetic measurements.

Figure 1

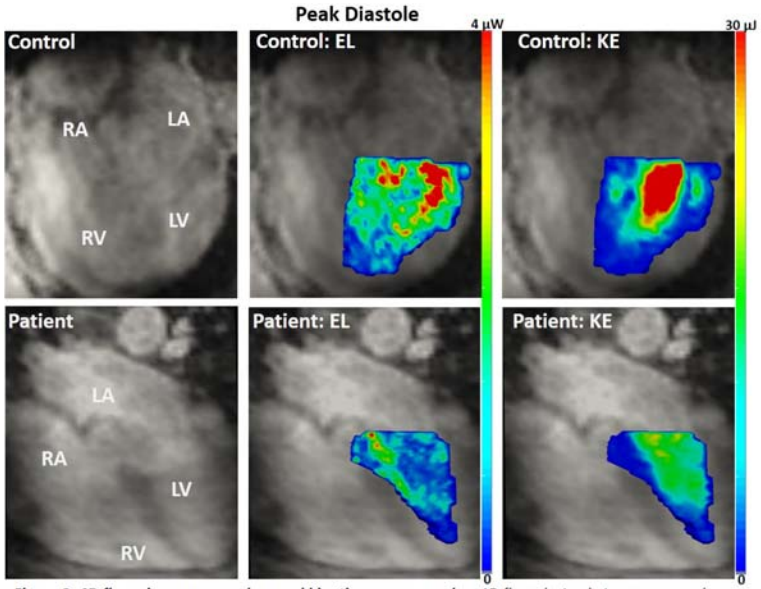

Figure 2. 4D flow viscous energy loss and kinetic energy samples. 4D flow-derived viscous energy loss and kinetic energy maps shown in cross-sectional 4 chambers view in an example control vs AF patient. RA: right atria; RV: right ventricle; LA: left atria; LV: left ventricle; EL: viscous energy loss; KE: kinetic energy.

Figure 2

Table 1. Summary of measurements.

Group	Peak Systole Median Normalized KE (mJ/m3)	Peak Diastole Median Normalized KE (mJ/m3)	Peak Systole Median Normalized EL (mW/m3)	Peak Diastole Median Normalized EL (mW/m3)	Peak Systole Total Normalized KE (mJ/m3)	Peak Diastole Total Normalized KE (mJ/m3)	Peak Systole Total Normalized EL (mW/m3)	Peak Diastole Total Normalized EL (mW/m3)
Control	5.18±5.11	5.54±3.74	1.63±1.04	1.81±0.91	61.25±28.28	50.01±5.11	16.33±9.52	13.98±9.27
Atrial Fibrillation	7.31±10.31	7.17±7.79	1.53±1.66	1.28±0.61	67.87±33.94	39.42±20.70	13.73±8.01	7.26±2.71
P-value	0.485	0.473	0.835	**0.048**	0.554	0.186	0.396	**0.004**

Figure 3

ID#: 377556

Additive Prognostic Value of Left Ventricular Myocardial Deformation in Patients with light chain amyloidosis

Ke Wan, MD[1] Yucheng Chen, MD[2], Jie Wang, BMSci[3], Jiayu Sun, MD[2], Yuchi Han, MD, MMSc[4], Hong Liu[5], Weihao Li, BMSci[6], Xiaoyue Zhou[7]

1. Cardiology Division, West China Hospital, Sichuan University, Guoxue Xiang No. 37, Chengdu, Sichuan Province 610041, China, Sichuan, China (People's Republic)

2. Sichuan University West China Hospital, Sichuan, China (People's Republic)

3. Department of Cardiology, West China Hospital, Sichuan University, ChengDu, Sichuan, China (People's Republic)

4. University of Pennsylvania, Philadelphia, PA

5. Sichuan University West China Hospital, Chengdu, Sichuan, China (People's Republic)

6. Cardiology Division, West China Hospital, Sichuan University, Chengdu, Sichuan, China (People's Republic)

7. Siemens Healthineers Northeast Asia Collaboration, Shanghai, Shanghai, China (People's Republic)

Background:

Cardiac amyloidosis (CA) is the major determinant of outcome in amyloidosis. Late gadolinium enhancement (LGE) and myocardial strain has been proposed as strong prognostic factors in amyloidosis. This study sought to determine whether myocardial deformation can provide additive prognostic information on LGE in patients with light-chain (AL) amyloidosis.

Methods:

We included 83 AL amyloidosis patients underwent cardiovascular magnetic resonance (CMR) in the period January 2012 to December 2015. The extent of LGE (no LGE, subendocardial LGE, and transmural LGE) and left-ventricular (LV) myocardial deformation [global longitudinal strain (GLS), global circumferential strain (GCS) and global radial strain (GRS)] using deformable registration algorithms on cine steady-state free-precession were assessed. Patients were prospectively followed until censuring date on 1 May 2017. The endpoint was all-cause mortality.

Results:

During a median follow-up of 36 months, 53 patients died. LV ejection fraction, GLS, GLS and GRS predicted mortality. The receiver operating characteristic curve revealed global circumferential strain (GCS) had highest prognostic value among LV deformation parameters for predicting 1-year death (area under the curve, 0.904). NYHA class >II [hazard ratio (HR): 2.442, p =0.013] and GCS (hazard ratio: 1.168; p =0.015) were independent predictors for all-cause mortality after adjustment for Mayo clinic stages, left ventriclar mass index and transmural LGE. GCS provided additive value to predict outcome in sub-endocardial LGE group (GCS >-9.1% versus GCS ≤ -9.1% log-rank p< 0.001). In contrast, EF did not provide incremental prognostic value in this subgroup.

Conclusion:

Myocardial deformation derived by CMR provides additive information on LGE pattern of all-cause mortality in patients with AL amyloidosis.

Univariate hazards analysis for overall survival in patients with AL amyloidosis

	Hazard ratio	95 % CI	P Value
Clinic data			
Age(for 1-y increase)	0.996	0.971-1.021	0.724
NYHA functional class ≥II	5.537	3.044-10.070	<0.001

Mayo clinic stage(for I increase)	1.807	1.253-2.604	0.002
Biomakers			
Log NT-pro BNP (pg/ml)	1.768	1.430-2.187	<0.001
Log Troponin-T (ng/L)	2.022	1.555-2.630	<0.001
CMR data			
LVEF(for 1% increase)	0.958	0.940-0.977	<0.001
LVEDV index (ml/m2)	1.003	0.990-1.017	0.657
LVESV index (ml/m2)	1.024	1.008-1.040	0.003
LV mass index (g/m2)	1.013	1.006-1.020	<0.001
Transmural LGE	4.995	2.724-9.157	<0.001
GLS (%)	1.299	1.182-1.427	<0.001
GCS (%)	1.307	1.197 -1.427	<0.001
GRS (%)	0.948	0.927-0.970	<0.001

Multivariate Cox proportional hazard models in patients with AL amyloidosis

Models	**Hazard ratio**	**95 % CI**	**P Value**
Biochemical model			
Log NT-pro BNP (pg/ml)	1.167	0.824-1.652	0.385
Log Troponin-T (ng/L)	1.162	0.786-1.719	0.451
GCS (%)	1.219	1.079-1.377	0.001
CMR Model			
LVEF(for 1% increase)	0.985	0.950-1.022	0.418
LVESV index (ml/m2)	0.983	0.956-1.011	0.223

LVmass index(g/m2)	1.004	0.995-1.014	0.354
Transmural LGE	2.524	1.022-6.236	0.045
GCS (%)	1.191	1.057-1.342	0.004
Comprehensive clinical model			
NYHA functional class >II	2.442	1.208-4.858	0.013
Mayo clinic stages(for I increase)	1.111	0.743-1.661	0.609
LVmass index(g/m2)	1.001	0.992-1.010	0.833
Transmural LGE	1.861	0.812-4.264	0.142
GCS (%)	1.168	1.031-1.323	0.015
Comprehensive clinical model, cardiac involvement (n=65)			
NYHA functional class >II	2.128	1.043-4.343	0.038
Mayo clinic stage(for I increase)	1.074	0.646-1.787	0.783
LVmass index(g/m2)	1.001	0.992-1.010	0.786
Transmural LGE	1.654	0.713-3.838	0.241
GCS (%)	1.183	1.024-1.367	0.023

ID#: 377457

Is there a need for a different clinical management of the bicuspid aortic valve aortopathy? A 4D flow-derived regional biomechanics comparison with tricuspid aortic valve and Marfan subjects

Andrea Guala[1] Lydia Dux-Santoy[2], Aroa Ruiz-Muñoz, MSc[3], GIULIANA MALDONADO, MD[4], Gisela Teixido-Tura, MD, PhD[2], Nicolas Villalva, MD[2], Filipa X. Valente, MD[4], Laura Gutierrez, MD[3], Laura Galian, MD[3], David Garcia-Dorado, MD, PhD[3], Arturo Evangelista[3], José F. Rodríguez-Palomares, MD, PhD[1]

1. Hospital Universitari Vall d´Hebron. Vall d'Hebron Institut de Recerca. Universitat Autònoma de Barcelona, Barcelona, Catalonia, Spain

2. Hospital Universitari Vall d´Hebron. Vall d'Hebron Institut de Recerca. Universitat Autònoma de Barcelona, Catalonia, Spain

3. Hospital Universitari Vall d´Hebron. Vall d'Hebron Institut de Recerca. Universitat Autònoma de Barcelona, Spain

4. Hospital Universitari Vall d´Hebron. Vall d'Hebron Institut de Recerca. Universitat Autònoma de Barcelona, Barcelona, Spain

Background: Bicuspid aortic valve (BAV) is a cardiac congenital disease associated with ascending aorta (AAo) dilation. A diameter threshold is used as prophylactic aortic resection criteria. This threshold is lower in BAV compared to tricuspid aortic valve (TAV) subjects in the presence of concomitant cardiovascular risk factor. This caution derives from a comparison with Marfan syndrome (MFS) patients, but the level of evidence is low.
We aim to investigate whether regional aortic biomechanics (AD and PWV) are intrinsically altered in BAV patients with respect to TAV and MFS individuals. Also, we assessed the best biomechanical marker for clinical follow-up.

Methods: One hundred and thirty-six BAV, 44 Marfan and 54 TAV patients (including 18 with AAo aneurysm) without severe valvular disease were included. The 1.5T CMR protocol comprised a 4D flow MRI study, to assess AAo and descending aorta (DAo) PWV, and two double-oblique 2D bSSFP cine CMR to compute distensibility (AD) in both AAo and DAo.
Three-dimensional geometry of the aorta were reconstructed from 4D flow-derived non-contrast-enhanced angiography, centerline was computed and 100 analysis planes were identified. For each plane average velocity waveform was extracted. The aorta was divided in AAo and DAo. The transit time between velocity waveforms was calculated with the most robust method currently available, which exploit wavelet analysis of the systolic upslope. AAo and DAo 2D CINE PC-MRI were used to compute distensibility.

Results: PWV and AD were similar in BAV and TAV subjects both without (table 1) and with (table 2) AAo dilation if properly adjusted for well-known confounding factors such as age, blood pressure and local diameter. Differently, MFS patients presented lower distensibility and higher PWV in the AAo and DAo.
PWV in BAV patients presented a biphasic trend with respect to the AAo diameter. There was a decrease of its value from 30 until 45 mm. From this point the PWV increased with diameter, showing a markedly increase in aortic stiffness.
In the multivariable analysis based on clinical (age, sex, BSA, BP) and biomechanics variables (AD and PWV), PWV was superior to predict aortic dilation compared to AD.

Conclusion: Aortic biomechanics in BAV patients did not differ from TAV patients when adjusting for age, blood pressure and aortic diameters, but markedly differ from Marfan patients. Thus, it seems that BAV may benefit of a similar clinical approach than TAV patients. PWV should be preferred over AD for the follow-up of BAV patients.

Unadjusted and adjusted analysis of AAo and DAo aortic mechanical parameters in healthy volunteers and non-dilated BAV and MFS patients. PWV [m/s], AD [10-6 cm2/dyne]

				BAV Vs TAV		BAV Vs MFS	
	NON-DILATED TAV	NON-DILATED BAV	NON-DILATED MFS	Unadjusted	Adjusted for age, DBP and AAo diameter	Unadjusted	Adjusted for age and AAo diameter
N	36	30	27	p value	p value	p value	p value
AAo PWV	5.4	4.35	6.81	0.121	0.353	<0.001	0.035

AAo AD	4.2	1.8	2.0	0.001	0.418	0.572	0.015
DAo PWV	7.4	8.2	10.1	0.207	0.157	0.240	0.015
DAo AD	3.1	2.1	2.3	0.001	0.422	0.869	0.041

Table 2: Unadjusted and adjusted analysis of AAo and DAo aortic mechanical parameters in dilated BAV, TAV and MFS patients. PWV [m/s], AD [10-6 cm2/dyne]

				BAV Vs TAV		BAV Vs MFS	
	DILATED TAV	DILATED BAV	DILATED MFS	Unadjusted	Adjusted for age, DBP and AAo diameter	Unadjusted	Adjusted for age, BSA, DBP, SBP and AAo diameter
N	18	106	17	p value	p value	p value	p value
AAo PWV	2.9	3.0	8.6	0.922	0.952	<0.001	0.001
AAo AD	0.9	1.7	1.9	0.016	0.450	0.928	0.032
DAo PWV	11.6	10.9	12.4	0.159	0.710	0.219	<0.001
DAo AD	1.1	1.9	2.2	0.004	0.352	0.620	0.011

ID#: 377194

Progressive myocardial injury in myotonic dystrophy type II (DM2) - CMR-Follow-up study

Edyta Blaszczyk, MD[1]Carolin Lim, PhD Stunden[2], Luisa Schmacht, MD[1], Ulrike Grieben, MD[3], Peter Kellman, PhD[4], Simone Spuler, MD[5], Jeanette Schulz-Menger, MD[1]

1. Working Group on Cardiovascular Magnetic Resonance, Experimental and Clinical Research Center a joint cooperation between the Charité Medical Faculty and the Max-Delbrueck Center for Molecular Medicine HELIOS Klinikum Berlin Buch, Germany, Berlin, Germany

2. Working Group on Cardiovascular Magnetic Resonance, Experimental and Clinical Research Center a joint cooperation between the Charité Medical Faculty and the Max-Delbrueck Center for Molecular Medicine HELIOS Klinikum Berlin Buch, Germany, Germany

3. Muscle Research Unit, Charite Berlin Germany, Berlin, Berlin, Germany

4. National Heart, Lung, and Blood Institute, National Institutes of Health, Bethesda, MD

5. Charité Universitätsmedizin Berlin, Berlin, Germany

Background: Myotonic dystrophy type II (DM2) is a autosomal dominant inherited multisystemic disorder characterized by progressive skeletal muscle weakness, metabolic changes as well as cardiac involvement. Approximately 25% of patients with preserved ejection fraction show fibrosis and/or fat infiltrations in CMR[1]. Arrhythmias are known in DM2 but its relation to myocardial injury as well as evidence for progression of myocardial changes are still unknown. We aimed to investigate a potential progression of cardiac involvement in DM2 using CMR.

Methods: Participants of a former CMR-Study[1] with a genetically confirmed diagnosis of DM2 were prospectively included in a follow up study. Scan protocol was similar. We performed at 1.5T Siemens assessment of left ventricle (LV) function by state of the art SSFP cine-imaging as well as tissue differentiation: T2-mapping (SSFP single-shot images); Fat imaging: multi-echo sequence for fat/water separation[2]; T1-mapping (MOLLI:native T1:5s(3s)3s and postcontrast:4s(1s)3s(1s)2s 15 minutes after injection of gadoteridol (0.2 mmol/kgbw); Late enhancement imaging (LGE) to detect focal myocardial fibrosis. Data were analyzed using cvi42. Arrhythmia and conduction anomaly were analyzed using a 12 lead electrocardiogram (ECG) and 24hour ECG-monitoring (Holter).

Results: CMR was performed in 14 patients (age 54.6±7, 12 females). Due to arrhythmias mapping is only available in 11. Mean follow up time was 3.9 +/- 0.32 years. LV parameters did not change (Table 1). Focal fibrosis as well as focal fat infiltration was detected in two more patients (Figure 1). Native T1 values did not differ (basal: CMR1: 1041±38 vs. CMR2: 1025±41 ms, p=0.11, medial: CMR1: 1025 ± 41 vs. CMR2: 1002 ±30 ms, p=0.16). Interestingly, new arrhythmias as well as new conduction abnormalities were recorded (Table 2). The rhythm and conduction abnormalities were mostly detectable in patients with focal myocardial injury (Figure 2).

Conclusion: CMR is not only able to detect myocardial injury in preserved ejection fraction in DM2, but also the progression of the disease showing new fibrotic lesions as well as fatty lesions. A relation to conduction anomalies as well as other forms of arrhythmias seems to be present.

1. Schmacht L, Traber J, Grieben U, et al. Cardiac Involvement in Myotonic Dystrophy Type 2 Patients With Preserved Ejection Fraction: Detection by Cardiovascular Magnetic Resonance. Circulation Cardiovascular imaging 2016;9.

2. Kellman P, Hernando D, Arai AE. Myocardial Fat Imaging. Current cardiovascular imaging reports 2010;3:83-91.

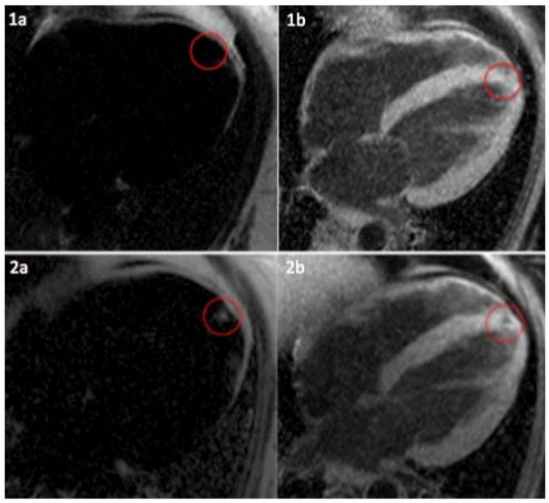

Figure 1. 4-chamber view. Patient with new apical fat infiltration. CMR 1: fat-separated image (1a) and water-separated image (1b) without evidence of fat infiltration. CMR 2: new apical fat infiltration, bright in the fat-separated image (2a) and hypointense (2b) in the water-separated image.

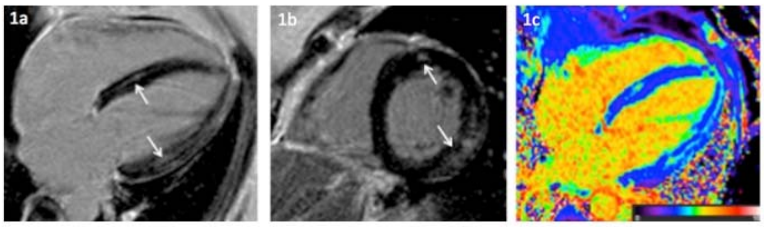

Figure 2. DM2 Patient with fibrosis and conduction abnormalities (Block AV I˚ and left anterior hemiblock). Myocardial fibrosis (arrows) with non-ischemic LGE-pattern in 4-chamber view (1a) and in midventricular short axis (1b). ECV Map with increased global ECV values (34ms) in 4-chamber view (1c).

Table 1. Mean ± SD measured values during the first and the second scan. HR=heart rate; LVEF= left ventricular ejection fraction; LVEDV-I=left ventricular end-diastolic volume index; SV-I=stroke volume index; LA=left atrium; RA=right atrium. * p <0.05

	CMR 1	CMR 2	p value

LVEF [%]	66 ± 5	63 ± 4	0.16
LVEDV-I [ml/m²]	0.71 ± 0.12	0.74 ± 0.16	0.44
SV-I [ml/m²]	0.50 ± 0.07	0.48 ± 0.09	0,14
LA cm^2	23 ± 4	21 ± 6	0.26
RA cm^2	21 ± 3	20 ± 4	0.77
T1 native basal	1041 ± 38	1024 ±46	0.11
T1 native medial	1025 ± 41	1002 ±30	0.16

Table. 2. Recorded arrhythmias during the first and the second exam. Fibrosis and fat deposits recorded during the second scan. SVT: supraventricular tachycardia; AV Block: atrioventricular block; VES: ventricular extrasystoles; LAH: left anterior hemiblock.

	Exam 1	**Exam 2**	**Fibrosis**	**Fat**
SVT	0	4	2	2
AV Block I	3	4		1
AV Block II	0	1		
VES	0	1	1	1
LAH	1	2		1

ID#: 376984

4D flow MRI assessment of the thoracic aorta using variable density k-t acceleration. Feasibility, reproducibility and clinical implication in ascending aneurysm on bicuspid aortic valve.

Kaoru Tanaka, M.D., PhD[1] Pim Pullens, PhD[2], Jan Nijs, M.D.[3], Stéphane Guy. Carlier, M.D., PhD[4], Peng Lai, Ph.D.[5], Ann Shimakawa, PhD[6], Johan De Mey, M.D., PhD[2], Hubert Raeymaekers, PhD[7]

1. Universitair Ziekenhuis Brussel, Brussel, Belgium

2. Universitair Ziekenhuis Brussel, Belgium

3. Universitair Ziekenhuis Brussel, jette, Brussels Hoofdstedelijk Gewest, Belgium

4. UMONS, Mons, Belgium

5. GE Healthcare, Menlo Park, CA

6. GE Health care, CA, CA

7. Universitair Ziekenhuis Brussel, Brussels, Brussels Hoofdstedelijk Gewest, Belgium

Background: We have previously reported our experience of 4D flow MRI from variable density k-t acceleration (VD kat-ARC) in healthy aorta compared to conventional parallel imaging. We sought to evaluate in patients with an ascending aneurysm and bicuspid aortic valve (BAV) VD kat-ARC 4D flow and vascular stiffness and central aortic blood pressure derived from brachial cuff measurements.

Methods: Non-contrast enhanced ECG gated 4D flow was performed in 5 patients with known type I BAV using a 3T GE Discovery 750w and a 32-channel cardiac coil. Imaging parameters were: 380 x 304 mm^2 FOV; 2.1x2.1 mm^2 resolution, 46 sagittal slices, 45-50ms temporal resolution and 8 x acceleration. Scans were repeated twice, except in patient 1. Before and after the MRI, central pulsatile indices and pulse wave velocity (PWV) were measured using a validated brachial cuff-based device (Mobil-O-Graph, IEM, D). Large vessels compliance was computed as 4D flow stroke volume / central pulse pressure (CPP). The CAAS MR 4D flow software (Pie Medical imaging, NL) allowed visualization of streamlines and computation of wall shear stress (WSS), 2D flow, displacement and MRI derived PWV. Agreement between repeated scans was evaluated by Bland-Altman analysis. Flow analysis was done in Matlab R2017a.

Results: All patients were male, 44-58 y-old, normotensive in sinus rhythm. 4D flow scans were successfull in all. The aneurysm types were: 1 aortic root type, 1 tubular type and 3 mixed type. Ascending aorta diameter measured 44-50 mm, sinus of Valsalva 26-47 mm. PWV and CPP measurements were of good quality and comparable before and after MRI scans. 4D flow scan time was 5-6 minutes, depending on the heart rate. All datasets were successfully post processed. Bland-Altman plots of the velocity and flow measurements at the same level of the ascending aorta showed high reproducibility on consecutive scans. Figure 1 shows in grey the average flow curve during a cardiac cycle of our 8 healthy controls (mean, SD) and individual patients'; flow curves, some with aortic regurgitation. Visually assessed streamlines as shown in Figure 2 demonstrated counter clockwise rotational flow characteristic of BAV type I. Table 1 gives 4D flow and pressure derived parameters. The mean PWV from Mobil-O-Graph and MRI was not different (respectively 6.8 and 6.7 m/s, paired t-test NS). The average WSS in normal controls was 1010 MPa. Highest values seen in BAV were locally 3-4 times higher (Table 1 and Figure 3).

Conclusion: We could demonstrate in patients with BAV the feasibility of k-t VD 4D flow in a clinically acceptable time. Repeated flow and velocity measurements had a good agreement. Individual flow curves can show pathologic regurgitation and be combined with pulse pressure measurements to fully characterize aortic biomechanical properties. Further inclusion and validation are ongoing.

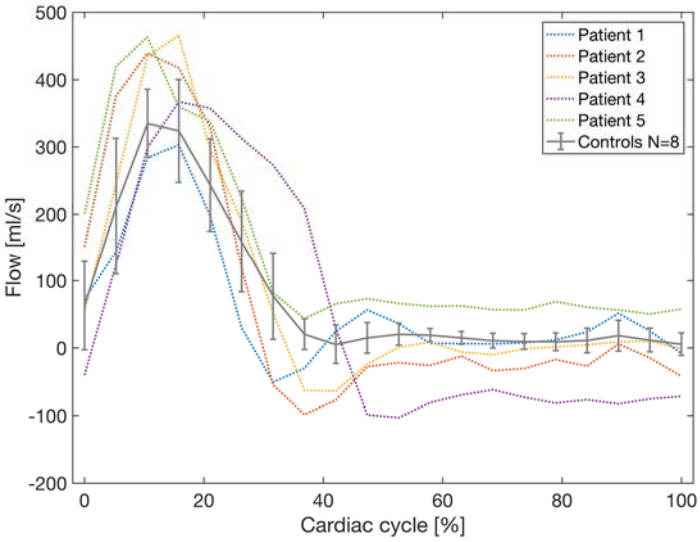

Flow curves during a cardiac cycles

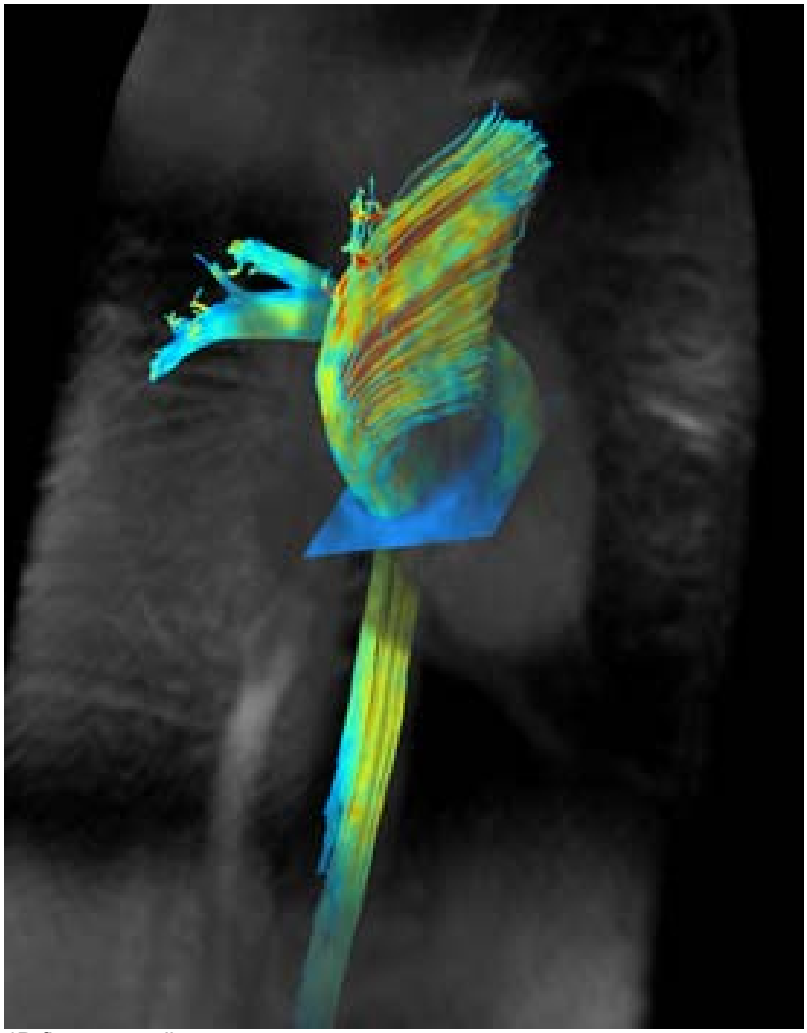

4D flow streamline

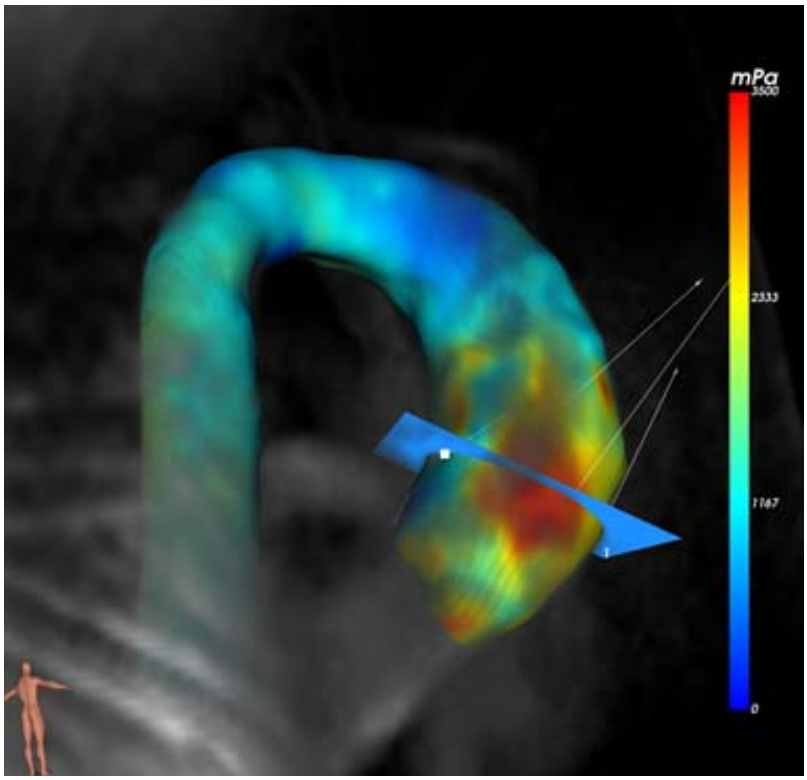

4D flow wall shear stress

4D Flow and Pressure Derived Parameters

Forward Flow Volume from MRI (ml)	84-132
Central Pulse Pressure (mmHg)	35-59
Compliance (ml/mmHg)	1.58-2.88
PWV (m/s)	6.1-7.8
PWV by 4Dflow (m/s)	4.64-10.8
Highest WSS (MPa)	2870-3884
Flow displacement from MRI	9-21

[min-max] values

ID#: 376996

Supine, prone, right and left postures - gravitational effects on human pulmonary vascular physiology studied with MRI

Björn Wieslander, MD PhD[1] Joao Genio Ramos, MD[2], Malin Ax, MD[3], Johan Petersson, MD PhD[3], Martin Ugander, MD, PhD[4]

1. Department of Clinical Physiology, Karolinska Institutet and Karolinska University Hospital, Stockholm, Sweden, Stockholm, Stockholms Lan, Sweden

2. Department of Clinical Physiology, Karolinska Institutet and Karolinska University Hospital, Stockholm, Sweden, Sweden

3. Department of Physiology and Pharmacology, Section of Anesthesiology and Intensive Care Medicine, Karolinska Institutet, and Function Perioperative Medicine and Intensive Care, Karolinska University Hospital, Stockholm, Sweden, Sweden

4. Karolinska Institutet, and Karolinska University Hospital, Stockholm, Sweden, Stockholms Lan, Sweden

Background: During intensive care and/or surgery, body position can be altered to optimize pulmonary ventilation and perfusion. Also, body positioning may serve as a gravitational stress test on the pulmonary vasculature, which could have diagnostic utility. The effect of body position on the distribution of pulmonary blood flow and on pulmonary vascular distensibility measured as the pulmonary blood volume variation (PBVV) has not been systematically characterized in humans. We aimed to characterize the normal physiology of gravitational effects upon the distribution of pulmonary blood flow and unilateral PBVV.

Methods: We performed through-plane phase contrast cardiovascular magnetic resonance imaging (PC-CMR) blood flow measurements at 1.5T (Siemens Aera) in healthy volunteers (n=10, age 27±3 years, 50% male) in supine, prone and both lateral decubitus positions in the pulmonary trunk, both pulmonary arteries, and all four pulmonary veins. By subtracting summed venous flow from arterial flow per time frame, we calculated both right and left PBVV in all positions, expressed as percent of lung blood flow volume per heart cycle.

Results: Supine cardiac index was (mean±SD) 3.3 ± 0.3 L/min/m2 and did not change with body position (Friedman';s p=0.73). In the lateral decubitus position, dependent pulmonary arterial blood flow increased compared to the same lung in the non-dependent position by 70% ± 54% and 74% ± 35% for the right and left lung, respectively ($p<0.01$ for both). Also in the lateral decubitus position, unilateral PBVV was increased in the non-dependent lung compared to the same lung in the dependent position by 119% ± 93% and 152% ± 47% for the right and left lung, respectively ($p<0.01$ for both). Between the supine and prone positions, there was no change in the blood flow distribution to the upper and lower lung lobes, measured as the summed flow through the summed upper and lower pulmonary veins, respectively ($p>0.47$ for both).

Conclusion: Blood flow is increased to the dependent lung in the lateral decubitus position, while PBVV is greatly increased in the non-dependent lung. The supine and prone positions did not affect the relative blood flow to upper and lower lung lobes. These results demonstrate that the gravitational effects of the lateral decubitus position have a pronounced effect on pulmonary blood flow distribution and vascular distension in healthy volunteers. Further studies are justified to determine whether gravitational stress testing through measurement of the unilateral PBVV in the lateral decubitus position has a role in characterizing diseases affecting the pulmonary vasculature.

FIGURE 1

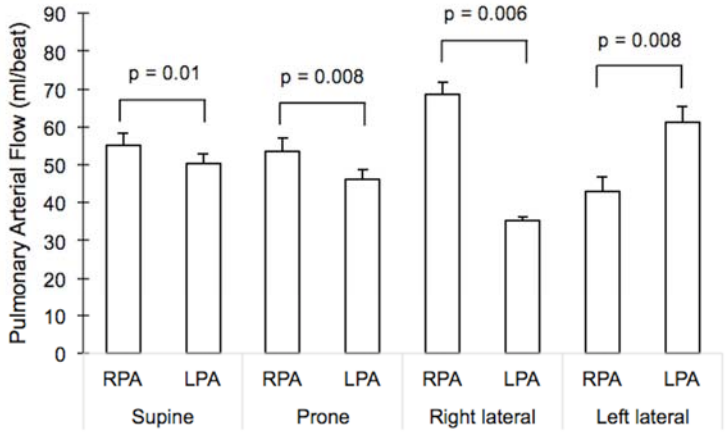

Figure 1 legend: Comparison between the right and left arterial flow volumes in each scanning position. The p-values correspond to the result of a Wilcoxon signed-rank test between the respective sub-samples. RPA: Right pulmonary artery, LPA: left pulmonary artery.

Pulmonary arterial blood flow per side and body position

FIGURE 2

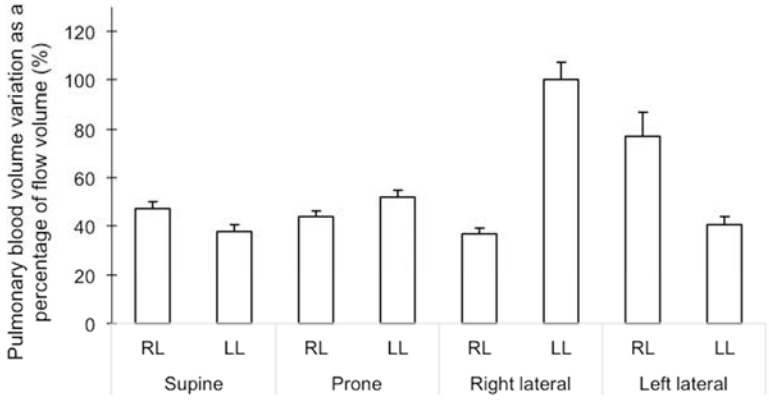

Figure 2 legend: Comparison between the right and left PBVV as a percentage of unilateral arterial flow (stroke volume) in each scanning position. The p-values correspond to the result of a Wilcoxon signed-rank test between the respective sub-samples. RL: right lung, LL: left lung.

Pulmonary blood volume variation per side and body position

ID#: 377249

Is 2-D Echocardiography Adequate for Detection of Pericardial Effusion in Women?

Selena J. Chandler[1] Sreya Brahmandam[2], Daniel R. Morgenstern, MS[3], Ellianna J. Hoff[4], J. Ronald Mikolich, MD[5]

1. Sharon Regional Health System, Willoughby, OH

2. Sharon Regional Health System, OH

3. University of Toledo College of Medicine, PA

4. Sharon Regional Health System

5. Northeast Ohio Medical University (NEOMED), Youngstown, OH

Background: Current criteria for pericarditis include chest pain, pericardial rub on auscultation, ECG changes and pericardial effusion. Friction rubs and ECG changes may be transient and short lived. Often the detection of an effusion is critical to the diagnosis. Cardiac MRI (CMR) is able to detect pericardial effusions, even when small due to superior spatial resolution. This study was designed to evaluate 2-D Echo and CMR detection rates of pericardial effusion when diagnosing pericarditis.

Methods: An institutional cardiac imaging database was queried for patients with chest pain who underwent a cardiac MRI and were found to have pericarditis on LGE imaging. The study cohort was composed of those patients who also had a 2-D echo proximate to the cardiac MRI. The presence or absence of pericardial effusion detected by both modalities was tabulated for each patient and detection rates were computed. Detection rates of effusion were also analyzed separately for males and females.

Results: Of 4,608 database patients, 173 patients were found to have evidence of pericarditis on CMR via LGE imaging; 103 (59.5%) were female, and 70 (40.5%) were male. 75 of the 103 females (70.87%) had pericardial effusion detected by CMR while only 16 (16.5%) females had pericardial effusion detected by 2-D Echo. A total of 59 of 103 females (57.3%) went undetected by 2-D Echo for pericardial effusion, but were detected by CMR. Of the 70 males, 39 (55.7%) had pericardial effusion detected by CMR, while 31 (44.3%) had pericardial effusion detected by 2-D Echo. A total of 8 of 70 (11.4%) males were undetected by 2-D Echo for pericardial effusion, but were detected by CMR. The undetected pericardial effusions missed in both sexes were all classified as small. An example of a small pericardial effusion detected CMR, but not detected by 2-D echo is shown in Figure 1.

Conclusion: These data suggest that pericardial effusions are undetected significantly more often (over twice as often) in women than in men when using 2-D Echo to diagnose pericarditis ($p<0.0001$). In addition, CMR detects pericardial effusions in women significantly (5 times) more often than 2-D Echo ($p<0.0001$). Wider use of Cardiac MRI may be advisable for detecting pericardial effusion when evaluationg patients with chest pain, especially women with symptoms suspicious of pericarditis.

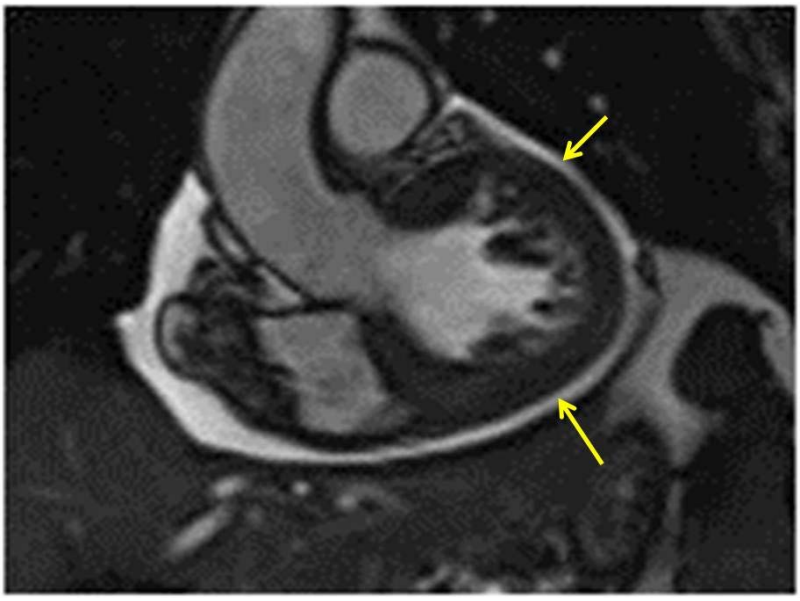

ID#: 377450

T1-Mapping in healthy volunteers - Influence of age and contrast media

Edyta Blaszczyk, MD[1]Serkan Doganguezel, MD[1], Luisa Schmacht, MD[1], Johannes Schueler, MD[1], Florian von Knobelsdorff, MD[2], Jeanette Schulz-Menger, MD[1]

1. Working Group on Cardiovascular Magnetic Resonance, Experimental and Clinical Research Center a joint cooperation between the Charité Medical Faculty and the Max-Delbrueck Center for Molecular Medicine HELIOS Klinikum Berlin Buch, Germany, Berlin, Germany

2. Dept. of Cardiology, Clinic Agatharied, University of Munich, Hausham, Bayern, Germany

Background: Parametric mapping plays an increasing role in myocardial assessment applying CMR. The quantification of diffuse changes remains challenging and different influencing factors such as type of pulse sequence and field strengths have been described.We aimed to assess the impact of type and dosage of contrast media on myocardial extracellular volume (ECV) values and the influence of age on native myocardial T1 values.

Methods: Thirty-five healthy volunteers (16 female) were divided in three age groups (group 1: 18-39 years, group 2: 40-59 years, group 3: 60-80 years) ([1]) for assessing the influence of age on native T1 values. Scans were performed at 1.5T Siemens, Avanto. Assessment of left ventricle (LV) function was performed using steady-state free-precession cine imaging, Parametric T1 mapping was done using Modified Look Locker Inversion Recovery (MOLLI) technique (scheme 5s(3s)3s (native) and 4s(1s)3s(1s)2s (post-contrast) in a mid-ventricular short-axis slice. In 18 volunteers gadoteridol (0.15 mmol / kg body weight) and in 17 volunteers gadobutrol (0.2 mmol / kg body weight) was administered (Table 1). ECV maps were calculated by incorporating the blood T1 and the hematocrit.

Results: Each 210 myocardial segments of native T1 maps, post contrast maps and ECV maps were acquired. 70/630 segments (11%) had to be excluded due to artifacts and incorrect motion correction. There was no significant difference regarding native T1 times between age groups (group 1: 978 ms ± 35ms; group 2: 997 ms ± 33ms, group 3: 972 ms ±21ms, p>0.05). Detailed values for each segment are shown in table 2. In the gadoteridol-group, ECV-values were significantly higher than in the gadobutrol group (26.3 ± 2.2% vs. 23.9 ± 2.9%, p

Conclusion: In healthy volunteers, age did not significantly influence native myocardial T1 values. Type and dosage of contrast media significantly influenced myocardial ECV. The study supports the need for standardized reference values.

1. von Knobelsdorff-Brenkenhoff F, Prothmann M, Dieringer MA, et al. Myocardial T1 and T2 mapping at 3 T: reference values, influencing factors and implications. Journal of cardiovascular magnetic resonance : official journal of the Society for Cardiovascular Magnetic Resonance 2013;15:53.

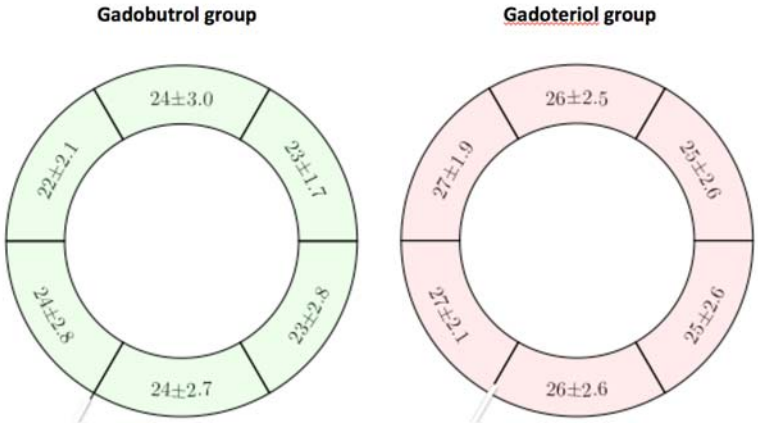

Figure 1. Detailed values of ECV for each contrast media (mid-ventricular slice). Gadoteridol-calculated ECV had significant higher values of the medial slice than gadobutrol-calculated ECV (p<0.01).

Table 1. Patients characteristic in different contrast media groups. BMI = body mass index; HR=heart rate; LVEF= left ventricular ejection fraction; LVEDV-I=left ventricular end-diastolic volume index; SV-I=stroke volume index; LVM-I=left ventricular mass index. SR=sinus rhythm. * p <0.05

	0.15 mmol Gadobutrol/kg	**0.2 mmol Gadoteridol/kg**
Number of patients	18	17
Gender [♂ / ♀]	14/ 4	5 / 12
Age [years]	30 ± 4	54 ± 6*
BMI [kg/m^2]	22.7 ± 2.5	24.4 ± 2.8
HR [min^{-1}]	67 ± 12	75 ± 10
LVEF [%]	61 ± 3	64 ± 5
SV [ml/]	95 ± 14	75 ± 13*

Table 2. Detailed values of native T1 for each age group. There was no significant difference in native T1 times between age groups (p>0.05).

Segment	**Age group 1**	**Age group 2**	**Age group 3**
Anterior	957 ± 47	1004 ± 56	942 ± 27
Anteroseptal	974 ± 42	993 ± 28	961 ± 22
Inferoseptal	989 ± 33	1007 ± 38	1002 ± 44
Inferior	985 ± 35	1010 ± 55	970 ± 48
Inferolateral	975 ± 38	995 ± 41	983 ± 30
Anterolateral	962 ± 32	986 ± 55	959 ± 29

ID#: 377376

Semiautomatic segmentation of the blood pool for real time cines from exercise stress CMR

Boyang Su, PhD[1] Yiu-Cho Chung, PhD[2], Thu-Thao Le, PhD[3], Calvin WL. Chin, Assistant Professor[4], Stuart Cook, PhD[3]

1. National Heart Research Institute Singapore, Singapore

2. Siemens Healthcare Pte. Ltd, Singapore, N/A, Singapore

3. National Heart Centre Singapore, Singapore

4. Duke-NUS Medical School, Singapore

Background: Exercise bike test can detect underlying cardiovascular abnormalities not apparent at rest. In combination with cardiac magnetic resonance (CMR), cardiac volumes at each stage of bike exercise can be assessed with good reproducibility. However, blood pool segmentation of the exercise real-time cine images (ExRT-cine) are challenging compared to breath-hold cine images acquired at rest. ExRT-cines have low spatial resolution, reduced blood-myocardium contrast and respiratory motion which increases with workload. Moreover, manual segmentation for the large number of cines from multi-stage is time consuming. Here, we propose a semiautomatic blood pool segmentation tool that minimizes user intervention, and gives cardiac volumes throughout the cardiac cycle from ExRT-cines.

Methods: MR study: An MR compatible ergometer (Lode BV, Netherlands) was used for the bike exercise test. Real time imaging of the heart was performed at a 1.5T MR clinical scanner (MAGNETOM Aera, Erlangen, Germany). Free-breathing real time cine MRI covering two heart beats was performed at baseline and after each stage of exercise. The scans were performed from apex to base. **Segmentation:** The blood pool of the first frame of the mid-ventricular slice was manually segmented. The radius and centroid of the blood pool contour defined the mask. Subsequent iterative search for blood pool regions in neighboring slices was done using the mask and appropriate constrains (e.g., smoothness and area). In each slice, the search started from the frame with the centroid and propagated towards the rest of the cine (Figure 1). **Evaluation:** The method was applied to five healthy volunteers who underwent bike exercise test. Manual contours at systole and diastole were compared to the contours from semi-automatic segmentation.

Results: Figure 1 showed how manual contours compared to automatic contours in one healthy volunteer (at stage of 100W_1min). The semi-automatic contours and the manual contours matched very well. Figure 2 showed the temporal variation of blood pool areas from several slices and the corresponding cardiac volumes obtained from cine images acquired a. Despite breathing, cardiac volumes in the two consecutive cycles were similar.

Conclusion: The proposed method generates blood pool contours from ExRT-cine images throughout the acquisition periods at various stages of exercise with minimal user intervention. Therefore, the images at all phases could be utilized instead of only end-of-diastole and end-of-systole.

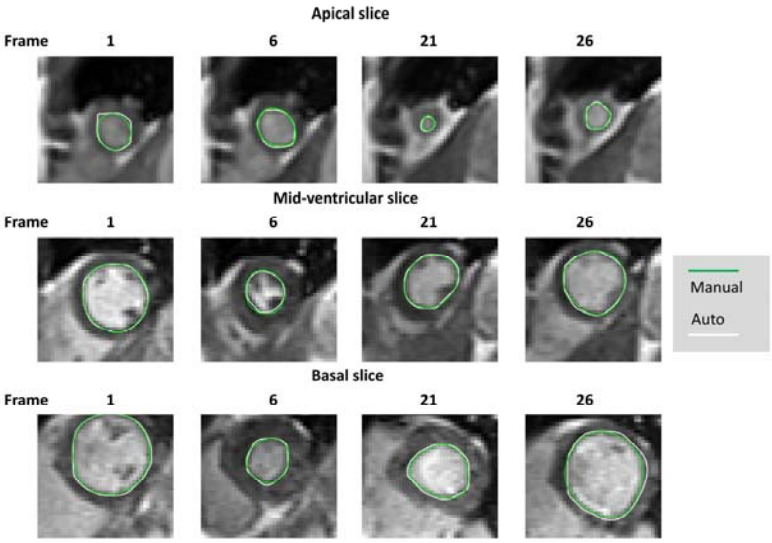

Endocardial contours at apical, middle and basal slices with manual delineation superimposed

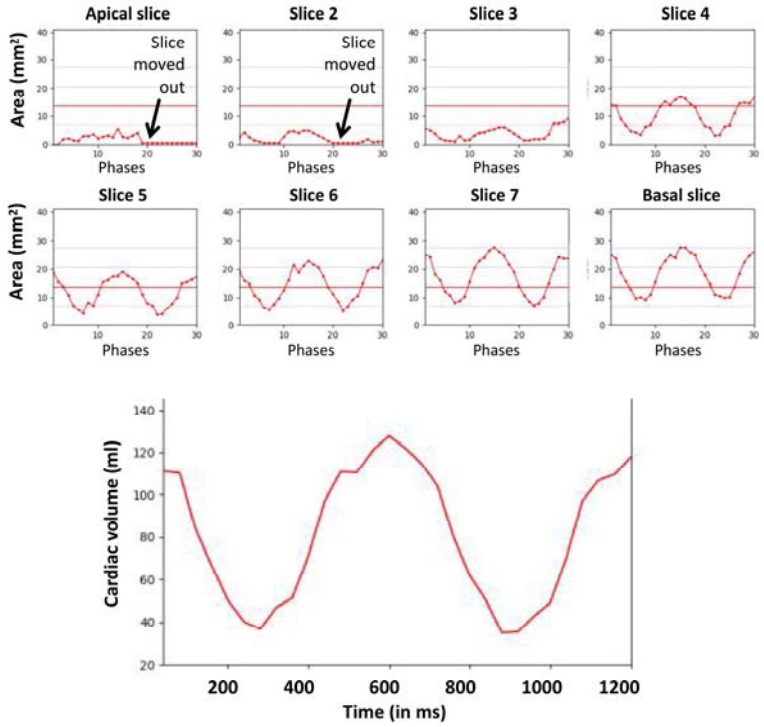

Area plots of endocardium from apex to base at stage of 100W_1min and corresponding cardiac volume

ID#: 377485

Impact of age and dilation on ascending aorta longitudinal and circumferential strain in bicuspid aortic valve patients

Andrea Guala[1]Lydia Dux-Santoy[2], Gisela Teixido-Tura, MD, PhD[2], GIULIANA MALDONADO, MD[3], Nicolas Villalva, MD[2], Filipa X. Valente, MD[3], Laura Gutierrez, MD[4], Laura Galian, MD[4], Teresa Gonzalez-Alujas, MD, PhD[4], Ruben Fernandez-Galera, MD[4], Augusto Sao-Aviles, PhD[4], David Garcia-Dorado, MD, PhD[4], Arturo Evangelista[4], José F. Rodríguez-Palomares, MD, PhD[1]

1. Hospital Universitari Vall d´Hebron. Vall d'Hebron Institut de Recerca. Universitat Autònoma de Barcelona, Barcelona, Catalonia, Spain

2. Hospital Universitari Vall d´Hebron. Vall d'Hebron Institut de Recerca. Universitat Autònoma de Barcelona, Catalonia, Spain

3. Hospital Universitari Vall d´Hebron. Vall d'Hebron Institut de Recerca. Universitat Autònoma de Barcelona, Barcelona, Spain

4. Hospital Universitari Vall d´Hebron. Vall d'Hebron Institut de Recerca. Universitat Autònoma de Barcelona, Spain

Background: Several investigations have related aortic dilation (aneurysm) with biomechanical alteration in bicuspid aortic valve (BAV) patients. Circumferential and longitudinal strain are interrelated, as an increase in strain in one direction is inversely related to the deformation in the other direction. Moreover, longitudinal aortic valve movement have an important, functional role in left ventricle (LV) function. However, any study investigated the impact of ascending aortic longitudinal strain on the resulting cinematic interaction between the LV and the aorta, which has important functional implication in both LV diastolic filling and systolic function. We quantified longitudinal and circumferential ascending aorta (AAo) strain in BAV patients and we characterize how they relates to local dilation and age.

Methods: Seventy BAV patients with no severe valvular disease and 21 matched healthy volunteers were included in the study. CINE MRI images were collected with sagittal, coronal and aortic valve views. Image registration in-house Matlab code were used to track aortic valve movement throughout the cardiac cycle. Longitudinal movement was obtained through projection of the movement in the direction of the centerline at the level of the aortic valve, and mean longitudinal AAo strain was computed dividing longitudinal movement with AAo length. Circumferential strain was quantified with double-oblique 2D CINE MRI in the AAo at the level of the pulmonary artery bifurcation. AAo dilation was defined using a threshold of z-score > 2.

Results: BAV patient has reduced circumferential (p<0,001) and longitudinal (p=0.03) strain when compared to healthy volunteers. Among BAV patient, 73% (52) had dilated AAo. Longitudinal and circumferential strain were not different comparing BAV with and without AAo dilation nor with respect to BAV fusion pattern. Interestingly, age was strongly, negatively related to both AAo circumferential (R=0.44) and longitudinal (R=0.54) strain in the BAV population.

Conclusion: BAV patients have reduced circumferential and longitudinal AAo deformation and ageing negatively impact both strain. The reduction of aortic valve longitudinal systolic movement entails the impairment of functional aorto-ventricular mechanical interaction. Longitudinal studies are needed to investigate whether this information might be used for the evaluation of aorto-ventricular interaction in the clinical management of BAV patients.

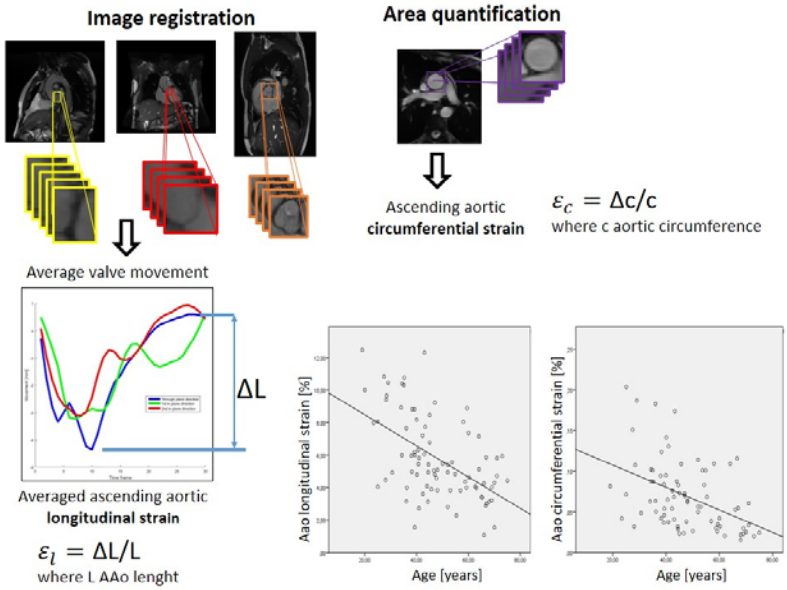

Methods and results

ascending (AAo) circumferential and longitudinal strain in healthy controls and BAV patients. *statistically-significant difference (p<0.05) with respect to controls

	CONTROLS	ALL BAV	NON-DILATED BAV	DILATED BAV
N	21	70	18	52
AAO circunferencial strain	14.7±3	7.6±4.6*	7.9±3.1*	7.4±4.7*
AAo longitudinal strain	8.2±2.7	6.1±2.6*	6.4±2.3*	6.1±2.7*

ID#: 377496

Pre-clinical Changes in Diabetic Cardiomyopathy are Detectable by Cardiovascular Magnetic Resonance Strain Analysis

Alice M. Mezincescu, MRCP[1] Caroline Scally, MBChB, MRCP[2], Amelia Rudd, BSc[2], Hassan Abbas, MBChB, MRCP[1], Trevor Ahearn, PhD[3], Dana Dawson, MD, PhD[2]

1. University of Aberdeen, United Kingdom

2. University of Aberdeen, Aberdeen, Scotland, United Kingdom

3. NHS Grampian, Aberdeen, Scotland, United Kingdom

Background: Diabetic cardiomyopathy (DC) is defined as myocardial dysfunction in patients with diabetes in the absence of hypertension or structural heart disease. Early detection is important in order to prevent progression to heart failure. In this study we hypothesized that cardiac magnetic resonance strain analysis is able to diagnose sub-clinical DC.

Methods: Fifteen *asymptomatic* males with type 2 diabetes (diet-controlled or on metformin alone) with no other previous medical history and 15 healthy male controls underwent cardiac magnetic resonance (CMR) imaging using a 3T Phillips Achiva (Best, the Netherlands) scanner and a cardiac coil. A standard protocol for cine imaging and late gadolinium enhancement (LGE) was used. Left ventricular volumes, mass and ejection fraction were calculated using CMRTools (Cardiovascular Solutions, London, UK). Feature tracking strain analysis was performed using Segment Version: R5859 (Medviso, Lund, Sweden). Longitudinal strain analysis was performed in 2, 3 and 4 long axis cines; radial and circumferential strain in the stack of short axis cines. All data is presented as mean±SD.

Results: Mean age of the diabetic patients was 56±7 years versus 49±17 years in healthy controls, p=0.1. The diabetic group had a higher body mass index (31±4 kg/m^2 for the diabetics vs 27±3 kg/m^2 for healthy controls, p=0.01). The average duration of diabetes was 4±2 years and their HbA1C was 54.9 ±12.6 mmol/mol. There was no difference in LV end-systolic or end-diastolic volumes, mass or calculated EF between diabetic patients and healthy volunteers respectively [55±12 vs 56±23 mls (p=0.9), 132± 23 vs 146±36 mls (p=0.2), 167±30 vs 157±34 g (p=0.4),59±6 versus 63±7 % (p =0.1)]. LGE was unremarkable in all participants. However feature tracking strain analysis demonstrated significant alterations in longitudinal and circumferential strain, as seen in Table 1.

Conclusion: Feature tracking strain analysis identifies pre-clinical changes in cardiac function in otherwise asymptomatic type 2 diabetics and is a promising clinical tool for the detection and monitoring of early stages of diabetes cardiomyopathy.

Feature tracking strain parameters in diabetics versus healthy controls.

Left ventricular strain parameter	Diabetics	Healthy controls	P value
Global longitudinal strain, %	-15±2*	-17±2	**0.005**
Global radial strain, %	26±11	27±12	0.8
Radial strain – basal, %	19±10	23±14	0.3
Radial strain – mid-ventricular, %	33±9	34±13	0.8
Radial strain – apical, %	27±18	25±13	0.7
Global circumferential strain, %	-16±3*	-21±3	**0.0002**
Circumferential strain – basal, %	-15±3*	-19±3	**0.001**
Circumferential strain – mid-ventricular, %	-15±3*	-20±3	**0.0003**
Circumferential strain – apical, %	-18±5*	-24±5	**0.003**

ID#: 377940

Inter-study Reproducibility of Strain Assessed by Displacement Encoding with Stimulated Echoes (DENSE) and Feature-tracking in Patients post-Myocardial Infarction.

Kenneth Mangion, MD MRCP[1] Caroline E Haig, PhD[2], Christie McComb, PhD[3], David Corcoran, MBChB BSc (Hons)[1], Daniel A. Auger, PhD[4], Hany Eteiba, MD[5], Mitchell Lindsay, MD[5], Margaret McEntegart, MBChB PhD[6], Stuart Hood, MD FRCP[7], Mark Petrie, MD[8], Keith G. Oldroyd, MD (Hons); FRCP[5], Stuart Watkins, MD, FRCP[6], Andrew Davie, MB ChB[5], Richard Good, MBChB MD[9], Paul Rocchiccioli, MD, FRCP[10], Aadil Shaukat, MBChB MD[9], Christopher Loughrey, PhD[11], Frederick H. Epstein, PhD[12], Colin Berry, PhD FRCP[1]

1. University of Glasgow, Glasgow, Scotland, United Kingdom

2. Robertson Centre for Biostatistics, Glasgow, Scotland, United Kingdom

3. university of glasgow, United Kingdom

4. University of Virginia Health System, Charlottesville, VA

5. Golden Jubilee National Hospital, Scotland, United Kingdom

6. Golden Jubilee National Hospital, Glasgow, Scotland, United Kingdom

7. NHS Greater Glasgow and Clyde, Scotland, United Kingdom

8. Glasgow University, Scotland, United Kingdom

9. Golden Jubilee National Hospital, United Kingdom

10. West of Scotland Regional Heart & Lung Centre - Golden Jubilee National Hospital, Clydebank, Scotland, United Kingdom

11. University of Glasgow, United Kingdom

12. University of Virginia, VA

Background: Myocardial strain derived from Displacement ENcoding with Stimulated Echoes (DENSE) cardiac magnetic resonance (CMR) provides information on myocardial contraction with high precision and accuracy. Feature-tracking obviates the need for additional breath-held scans for bespoke strain imaging. High inter-study reproducibility is necessary for precision imaging. We aimed to 1. investigate the inter-study reproducibility of DENSE and feature-tracking in patients after ST elevation myocardial infarction (STEMI); 2. estimate what sample size would be required to detect a 5% change in the magnitude of myocardial strain in patients post-STEMI.

Methods: We undertook a prospective, single center cohort study. Participants provided written informed consent (ethics reference 14/WS/0085) and underwent CMR at 1.5 T (MAGNETOM Avanto, Siemens) 6 months post-MI. Patients underwent 2 CMR studies 15 minutes apart. Scan 1 included localizers, mid-LV short axis and horizontal long axis acquisitions with cine imaging and 2D spiral cine-DENSE. Scan 2 included axial stacks of cine (balanced steady-state free precession), 2D spiral cine-DENSE, and delayed-enhancement phase-sensitive inversion-recovery pulse sequences. Feature-tracking and DENSE measures of segmental and global strain parameters were calculated. Left ventricular (LV) circumferential and radial strain were derived from the short axis imaging and LV longitudinal strain was derived from the horizontal long axis views. Inter-study reproducibility and study sample sizes required to demonstrate 5% changes in absolute strain were determined at 90% power, assuming an α error of 0.05.

Results: 36 patients were investigated (mean age: 58 ± 8 years, 81% male, 42% anterior MI, 11% diabetes, 14% current smokers). Global and segmental strain as assessed by DENSE had smaller bias, narrower limits of agreement, and higher intra-class correlation co-efficients and strength of correlation (Table 1). Sample size calculations revealed that smaller sample sizes would be required to detect a 5% change in absolute segmental and global strain with DENSE when compared with feature-tracking (table 2).

Conclusion: 2D spiral cine-DENSE derived strain has higher inter-study reproducibility when compared with feature-tracking. Sample sizes to detect a 5% difference in repeat measurements of strain are smaller with DENSE when compared with feature-tracking. These results have implications for the choice of strain-technique in clinical studies in patients with STEMI.

Test-retest reproducibility assessment.

	Mean bias ± SD	95% Limits of agreement	ICC	Correlation
Circumferential strain- global				
DENSE	0.35 ± 1.52	-2.70, 3.39	0.91	0.84
Feature-tracking	-2.52 ± 4.83	-12.19, 7.16	0.68	0.56
Circumferential strain- segmental				
DENSE	0.84 ± 3.95	-7.06, 8.74	0.88	0.79
Feature-tracking	5.32 ± 9.62	-13.92, 24.57	0.71	0.56
Longitudinal strain- global				
DENSE	0.44 ± 1.72	-2.99, 3.88	0.83	0.72
Feature-tracking	-1.26 ± 4.82	-10.90, 8.37	0.73	0.560
Longitudinal strain- segmental				
DENSE	-0.11 ± 4.50	-9.10, 8.88	0.74	0.59
Feature-tracking	-0.21 ± 15.26	-30.72, 30.31	0.84	0.73
Radial strain- global				
DENSE	0.05 ± 5.21	-10.37, 10.46	0.91	0.84
Feature-tracking	-2.92 ± 12.47	-27.86, 22.01	0.52	0.37
Radial strain- segmental				
DENSE	0.16 ± 7.80	-15.43, 15.76	0.84	0.72
Feature-tracking	-2.12 ± 22.58	-47.27, 43.04	0.66	0.49

DENSE- displacement encoding with stimulated echoes, FT- feature tracking, ICC- intra-class correlation co-efficient.

Sample size estimation for detection of 5% change in global and segmental strain

Sample size estimation, at 90% power

Circumferential strain	
DENSE- global	2
Feature-tracking- global	20
DENSE- segmental	13
Feature-tracking- segmental	78
Longitudinal strain	
DENSE- global	2
Feature-tracking- global	20
DENSE- segmental	17
Feature-tracking- segmental	196
Radial strain	
DENSE- global	23
Feature-tracking- global	131
DENSE- segmental	51
Feature-tracking- segmental	428

ID#: 377944

The Importance of extra Cardiac anatomy when reporting

Luke Dancy, MBBS MRCP[1] Daniel Sado, BM, MRCP[1], Andrew Cox[2]

1. Kings College Hospital, London, England, United Kingdom

2. King's College Hospital, London, United Kingdom

Background: Phaeochromocytoma is a rare neuroendocrine tumour of the adrenal medulla. It can present with a variety of non specific cardiac and non cardiac symptoms, with the diagnosis therefore frequently being delayed.. Although there is no role for cardiovascular magnetic resonance (CMR) in the workup of this disease, as the presentation is so diverse and non specific, it maybe found unexpectedly on anatomical imaging. In the last 18 months there have seen 3 such cases. On each occasion a clearly visible adrenal mass was not identified by the first reporting physician. This highlighted the importance of careful examination of the extra cardiac anatomy when reporting CMR.
We invited 10 Cardiologists who work in CMR at various levels of SCMR accreditation, to report one of these cases to see what proportion would identify the extra cardiac abnormality and in doing so make the correct diagnosis.
The case in question was that of a young female patient presenting with palpitations and presyncope. She had undergone 24 hour EKG monitoring showing intermittent AV dissociation. Transthoracic Echocardiogram was normal and resting EKG unremarkable. Her CMR showed a large mass above the right kidney originating from the adrenal gland. It was heterogeneous in character consistent with the MR appearances of Pheochromocytoma, which was subsequently proven following triple phase CT and plasma / urine metanephrine assessment.

Methods: 10 Cardiologists (9 Specialist Registrars or fellows and 1 Consultant, 8 at SCMR level 2 accreditation and 2 level 3) agreed to take part.
Anonymised DICOMs were provided to each participating Cardiologist to look at on their preferred reporting software. Each were given the case history and informed that transthoracic echocardiography had been reported as normal.
Each was allowed as long as required to report the scan which consisted of localisers, black and white blood HASTE imaging, Long and short axis cines, T1 and T2 mapping, Early Gadolinium images and Late Gadolinium images.
Each participant was asked to commit to a report of the CMR offering where possible an explanation for the patients symptoms.

Results: Of the 10 reports, none detected the adrenal mass.
All 10 identified the cardiac function, structure and tissue characterisation as normal.
None were able to offer Phaeochromocytoma as a differential

Conclusion: Extra Cardiac anatomy presents a significant challenge to Cardiologists when reporting CMR studies. This is particularly the case for assessment of abdominal problems, which are often not well seen on the limited anatomical images we generally acquire. Such problems are rare, but the 100% miss rate in this study (which was clearly biased from the outset to help people find an unusual diagnosis by the mere fact that we were asking people to look at the case) of a large abdominal mass which has potential to confer significant morbidity and mortality risk begs the question of how we can improve training in CMR such that this would be avoided, both to improve patient care and avoid potential litigation problems. We suggest that a small amount of formal training for CMR Cardiologists in chest and upper GI Radiology would be invaluable in this regard.

ID#: 377866

Can Feature Tracking Derived Strain Identify Subclinical Myocardial Involvement in Systemic Iron Overload?

Hari Rajagopal, MBBS[1] Rakesh Donthula, MBBS[2], Shubhika Srivastava, MBBS[3], Gina LaRocca, MD[4], Javier Sanz, MD[5], Santosh Uppu, MD[6]

1. Icahn school of Medicine, Mount Sinai New York

2. Icahn School of Medicine at Mount Sinai (Elmhurst)

3. Icahn School of Medicine, Mount Sinai New York

4. Mount Sinai's Zena and Michael A. Wiener Cardiovascular Institute, NY

5. Mount Sinai's Zena and Michael A. Wiener Cardiovascular Institute

6. Mt Sinai medical center, New York, NY

Background: Myocardial Iron overload (MIO) is directly related to development of heart failure independent of liver iron concentration, MIO cannot be predicted from serum Ferritin or conventional cardiac functional parameters. Cardiac magnetic resonance imaging (CMR) T2* is used to quantify myocardial iron concentration, but controversy exists with heterogenous MIO when cardiac T2* is measured at a single midpapillary ventricular short-axis level. Feature tracking (FT) allows quantitative segmental myocardial strain analysis using traditional cine CMR images. We hypothesized left ventricular (LV) segmental strain would be a more sensitive indicator for early myocardial involvement in patients with systemic iron overload (SIO) even before the development of myocardial T2* abnormalities.

Methods: Patients with SIO and structurally normal hearts who underwent CMR at our institution from 2007-2017 on 1.5 T scanner were studied retrospectively. Consecutive healthy subjects with normal cardiac anatomy, function and no MIO were selected as controls. FT was performed on CMR cine images; longitudinal strain analysis was performed in long axis four (4CLS), three (3CLS) and two chamber (2CLS) views, circumferential strain was calculated at basal (BCS), midventricular (MCS), and apical (ACS) short axis views. Global and segmental strain data was compared to T2* value in liver and myocardium. Sensitivity, specificity, and optimal threshold values of strain were determined by comparison to controls. Descriptive statistics, t-tests, logistic regression analysis, and receiver operator characteristic curves were utilized.

Results: Twenty-one SIO patients and eleven age/sex matched controls were analyzed by FT. There was no evidence of ventricular volume overload in cases. All cases had preserved contractility and yet significantly diminished global longitudinal (GLS), 4CLS, 3CLS, global circumferential (GCS), BCS and ACS strain when compared with controls (Table 1). Multivariate logistic regression analysis identified GLS, 3CLS, GCS and BCS as the most predictive for low hepatic T2* (p= <0.001 for all). GLS and GCS demonstrates good sensitivity and specificity, 3CLS and ACS demonstrates excellent sensitivity for abnormal hepatic T2*. MCS strain remains unaffected and normal in cases (Table 2).

Conclusion: FT derived longitudinal and circumferential strain is sensitive and specific to identify subclinical myocardial systolic dysfunction in patients with SIO irrespective of overt abnormalities in contractility or CMR T2*, and thus might be an useful objective tool in addition to current CMR techniques.

Summary Statistics

	Cases	Control	p-value
N	21	11	
Median age (years, range)	37 (15-70)	39 (18-72)	
Male (%)	6 (29%)	3 (27%)	
BSA (m^2)	1.68 ± 0.2	1.8 ± 0.3	0.18
Hepatic T2* (msec)	4.2 ±2.8	NA	

Myocardial T2* (msec)	31.1±10.1	NA	
Indexed left ventricular (LV) end-diastolic volume (ml/m^2)	73 ± 24	78 ± 25	0.58
LV ejection fraction (%)	62.9 ± 4	62.2 ± 5.6	0.68
Global Longitudinal Strain	-19.9 ± 5.9	-25.2 ± 2.6	< 0.001
4C Longitudinal Strain	-21.5 ± 5.6	-25.2 ± 4	0.05
3C Longitudinal Strain	- 20.1 ± 4.8	-27.8 ± 3.2	<0.001
2C Longitudinal Strain	- 20.1 ± 6.8	-23.4 ± 3.2	0.07
Global Circumferential Strain	-31.5 ± 7.4	-37.1 ± 5.7	0.02
Circumferential Basal Strain	-28.1 ± 5.7	-33.7 ± 6.4	0.02
Circumferential Mid-ventricular Strain	-25.7 ± 6	-27.1 ± 3.2	0.4
Circumferential Apical Strain	-38.7 ± 12.8	-50.5 ± 11.7	0.01

Mean ± standard deviation unless as indicated

Receiver Operating Characteristic Curves for Strain and Hepatic Iron Overload

Strain	Hepatic iron Overload				
	Area Under the Curve	Optimal Threshold Value	Sensitivity (%)	Specificity (%)	p-value
Global Longitudinal Strain	0.75	-22	75	91	<0.01
4C Longitudinal Strain	0.65	-23.5	65	67	0.1
3C Longitudinal Strain	0.88	-24.9	92	67	<0.01
2C Longitudinal Strain	0.76	-18.2	50	91	0.07
Global Circumferential Strain	0.74	-33.6	75	83	<0.01

Circumferential Basal Strain	0.74	-33	70	83	0.01
Circumferential Mid-ventricular Strain	0.58	-24	50	83	0.3
Circumferential Apical Strain	0.72	-50	85	58	0.01

ID#: 377765

Right Ventricular Dysfunction in Left Ventricular Non-Compaction

Rina Verma, MD[1] Shermeen Memon, MD[2], Joshua Newman, MD[2], Alexander Turin, MD[2], Nathan Bibliowicz, DO[2], Mushabbar Syed, MD, FACC[3]

1. Loyola University Medical Center, Glen Ellyn, IL

2. Loyola Medical Center, IL

3. Loyola University Medical Center, IL

Background: Left ventricular noncompaction (LVNC) is a genetic disorder which is increasingly being diagnosed with the more widespread use of cardiac magnetic resonance (CMR) imaging. In the current study, we evaluated the prognostic value of reduced RVEF (right ventricular ejection fraction) in patients with LVNC.

Methods: All CMRs were done at a single tertiary care hospital between 2012 and 2016. We studied 40 patients who met CMR criteria for LVNC (≥ 3 segments of noncompacted to compacted myocardial ratios ≥ 2.3 measured at end-diastole in both 4- and 2-chamber views). Reduction in RVEF was defined as RVEF ≤ 45%. All patients were followed for at least one year for clinical events.

Results: Patients with LVNC and reduced RVEF had significantly lower left ventricular ejection fractions (LVEF), higher left ventricular end-diastolic volume indices (LVEDVi) and had more admissions for heart failure and ICD placement, compared to those with LVNC and normal RVEF (Table 1).

Conclusion: This study demonstrates that reduced RVEF is a negative prognostic marker in patients with LVNC.

Table 1: LNVC with or without reduced RVEF

	Overall 40 (100.0%)	LVNC with reduced RVEF 18 (45.0 %)	LVNC without reduced RVEF 22 (55.0%)	p-value
LV Ejection Fraction, median (IQR)	37.0 (22.5 – 50.0)	22.9 (19.7 – 25.6)	47.4 (41.5 – 55.7)	<.001
LV End Diastolic Volume Index, median (IQR)	123.5 (89.1 - 174.2)	70.3 (130.0 – 202.5)	93.2 (78.2 – 125.2)	<.001
LV End Systolic Volume Index, median (IQR)	75.2 (41.8 – 126.2)	120.2 (85.8 – 151.6)	52.0 (36.5 – 80.8)	<.001
Atrial arrhythmias (atrial fibrillation/atrial flutter), n (%)	10 (25.0)	5 (27.8)	5 (22.7)	,731
Ventricular arrhythmias (ventricular tachycardia/NSVT), n(%)	4 (10.0)	3 (16.7)	1 (4.5)	.204
Thromboembolic Events, n (%)	5 (12.5)	2 (11.1)	3 (13.6)	1.000
Admission for Heart Failure, n (%)	17 (42.5)	14 (77.8)	3 (13.6)	<.001
ICD Placement, n (%)	15 (37.5)	11 (61.1)	4 (18.2)	.005

ID#: 378013

Small pericardial and pleural effusions - always a sign for inflammation? A CMR study in healthy females.

Agnieszka Töpper, MD[1] Yashraj Bhoyroo, MD[2], Stephanie Funk, MD[3], Edyta Blaszczyk, MD[4], Oliver Ehrling[5], Ludger Heisterkamp, MD[6], Elke Nickel[5], Jeanette Schulz-Menger, MD[4]

1. Working Group on Cardiovascular Magnetic Resonance, Experimental and Clinical Research Center a joint cooperation between the Charité Medical Faculty and the Max-Delbrueck Center for Molecular Medicine HELIOS Klinikum Berlin Buch, Department of Cardiology and Nephrology, Berlin, Germany., Berlin, Berlin, Germany

2. Working Group on Cardiovascular Magnetic Resonance, Experimental and Clinical Research Center a joint cooperation between the Charité Medical Faculty and the Max-Delbrueck Center for Molecular Medicine HELIOS Klinikum Berlin Buch, Germany, Germany

3. Working Group on Cardiovascular Magnetic Resonance, Experimental and Clinical Research Center, a joint cooperation between the Charité Medical Faculty and the Max-Delbrueck Center for Molecular Medicine and HELIOS Hospital Berlin Buch, Berlin, Berlin, Germany

4. Working Group on Cardiovascular Magnetic Resonance, Experimental and Clinical Research Center a joint cooperation between the Charité Medical Faculty and the Max-Delbrueck Center for Molecular Medicine HELIOS Klinikum Berlin Buch, Germany, Berlin, Germany

5. Working Group on Cardiovascular Magnetic Resonance, Experimental and Clinical Research Center, a joint cooperation between the Charité Medical Faculty and the Max- Delbrueck Center for Molecular Medicine; and HELIOS Hospital Berlin Buch, Germany

6. Department of Radiology HELIOS Hospital Berlin Buch, Germany, Germany

Background: The appearance of small amount of pericardial and pleural fluid is a frequent finding in routine CMR. It seems to be related to inflammation, but data are conflicting. It is known, that fluid in different parts of the body is related to the menstrual cycle. We aimed to analyse the relation between pericardial (PE) and pleural (PLE) effusion and the menstrual cycle in healthy premenopausal women

Methods: We prospectively screened 147 healthy female. They were scanned twice at predefined time-points during menstrual cycle to cover the period of possible fluid retention. Scan I was performed at day 5 (3-7) and scan II from day 24 to the first day of flow. Follicular stimulating hormone (FSH) as well as inflammatory and cardiac blood markers were quantified. The scan protocol at 3.0T included: full coverage of the thorax using transaxial true fast imaging with steady-state free precession (SSFP, sth. 6/0mm, TE 2.1ms, TR 4.3ms, FA 54°) for assessment of PLE and state of the art cine SSFP (sth. 7/3mm, TE 1.3ms, TE 39ms, FA 45°) for assessment PE and of left ventricular (LV) morphology and function. Differentiation between fat and water was supported by native T1 mapping (MOLLI: 5s(3s)3s; TT385ms, TE1.3ms, TR500ms, incremental TI, FA 35°) positioned similar to cine SSFP. PLE was quantified using signal intensity based algorithm in the transaxial stack. PE was quantified in diastole in short axis stack based on either signal intensity algorithm or by manual contouring.

Results: We could include 35 female, 30 (mean age 31 years, table 1) completed both CMR. FSH at scan I confirmed the premenopausal state. All females had normal LVEF and LVEDV at both time points (table 2) 29 had small amount of PLE and 28 PE at both time points. The amount was not significantly different between both time points. (Table 2) Absolute values did not exceed 34ml and 26ml for pericardial and pleural fluid respectively. There was no correlation to the level of TSH, hsCRP and hsTroponin as well as WBC. NTproBNP-level (did not exceed the normal range) correlated weak to amount of pleural fluid at first scan (Pearsons correlation coefficient .403 p-value .027; 2-sided)

Conclusion: CMR has the unique capability to detect small effusions without any contrast-media application within a fast scan. Small amounts of fluids are also assessable in healthy female independent of the phase of menstrual cycle. Our data suggest that in case of normal LV morphology small amounts of pericardial and pleural effusion are not necessarily indicating an inflammatory stage.

Table1: Basic characteristics of the examined females

PARAMETER	MEAN±SD
Age (years)	31±5.4

Body weight (kilograms)	61.7±6.7
Body height (centimeters	166.63±5.7
Menstrual cycle length (days)	28.47±1.7
Follicle stimulating hormone (U/l)	5.89±2.9
High sensitive CRP (mg/l)	2.16±2.49
High sensitive Troponin (ng/l)	3.77±2.4
White blood cell (Gpt/l)	6.61±1.7
NT-pro-BNP (ng/l)	56.80±22.6

Table 2: Comparisons of the left ventricular function and amounts of pleural and pericardial effusions across menstrual cycle

PARAMETER	Scan I MEAN±SD	Scan II MEAN±SD	p value
LVEDV (ml)	117.03±16.8	117.93±14.7	.637
LVESV (ml)	41.23±13.6	38.70±9.8	.377
LVEF (%)	67.87±4.6	68.40±5.1	.625
PERICARDIAL FLUID (ml)	10.07±6.7	9.10±5.8	.425
PLEURAL FLUID (ml)	9.80±6.1	9.53±5.7	.742

ID#: 377973

Local longitudinal strain from tagged MRI can help distinguish between hypertrophic cardiomyopathy and septal knuckle

Teodora Chitiboi, PhD[1] Lennart Tautz, MS[2], Anja Hennemuth, Dr.[3], Mark Sherrid, MD[4], Leon Axel, PhD, MD[1]

1. NYU School of Medicine, New York, NY

2. Fraunhofer MEVIS, Bremen, Germany

3. Charite - Universitätsmedizin Berlin, Berlin, Germany

4. New York University Langone Medical Center, New York City, NY

Background: Hypertrophic cardiomyopathy (HCM) is commonly associated with asymmetrical increases in myocardial wall thickness, often in the basal part of the septum. While the ejection fraction for HCM patients is typically preserved or increased, there can be locally reduced wall deformation[1]. In contrast, “Septal Knuckle” is a similar-appearing condition, without underlying cardiomyopathy. We hypothesized that tagged MRI can be used for distinguishing between these different conditions.

Methods: We analyzed tagged cines acquired in 25 consecutive patients referred for clinical CMR for HCM (15 with basal or diffuse septal hypertrophy, 3 with apical hypertrophy, 3 who turned out to be normal, and 4 with septal knuckle) and 17 normal volunteers. SPAMM-tagged MRI[2] was acquired (1.5T Aera, Siemens, Erlangen, Germany) in a single three-chamber (3CH) view during one breath hold, with 1.25x1.25x6mm spatial resolution and 30-50ms temporal resolution (depending on breath hold capability). Tagged images were semi-automatically segmented[3] and the myocardium was divided into 7 segments which were tracked over the cardiac cycle (Fig.1.A). The deformation field between each two consecutive temporal frames was computed using a multi-resolution non-rigid registration approach based on local phase[4], which is especially suited for tagged MRI because of its robustness to temporal intensity changes and tag fading. The 2D Green-Lagrange strain tensor was then computed for the myocardium, using the integrated deformation field. The strain tensor was then projected onto a heart-centric frame of reference, using the local normal and tangent to the epicardial wall as axes. The resulting strain tensor consists of tangential (longitudinal stretch) and radial (wall thickening) strain components, as well as the shear.

Results: Fig.2. shows the average tangential strain (± standard deviation) in the basal septal segment of the myocardium over time for the normal volunteers, and the “normal”, HCM and septal knuckle patients. The average longitudinal strain magnitude at end-systole is significantly larger in normal (Fig.1.B) compared to HCM patients (Fig.1.D) $p<0.0001$. Although we currently only have a very small number of patients with septal knuckle (Fig.1.C), the figure suggests that the strain magnitude is slightly reduced compared to normal subjects but much larger compared to HCM patients.

Conclusion: Tagged MRI is simple and fast to acquire, and allows regional deformation quantification; it offers the potential to distinguish between HCM and septal knuckle. Future studies including a larger number of patients with septal knuckle will permit clinical assessment of this.

[1]Circulation 1994;90:854-867 [2]Radiology 1989;171:841–845 [3]SPIE 2016;p.978404 [4]STACOM 2011;pp.78-87

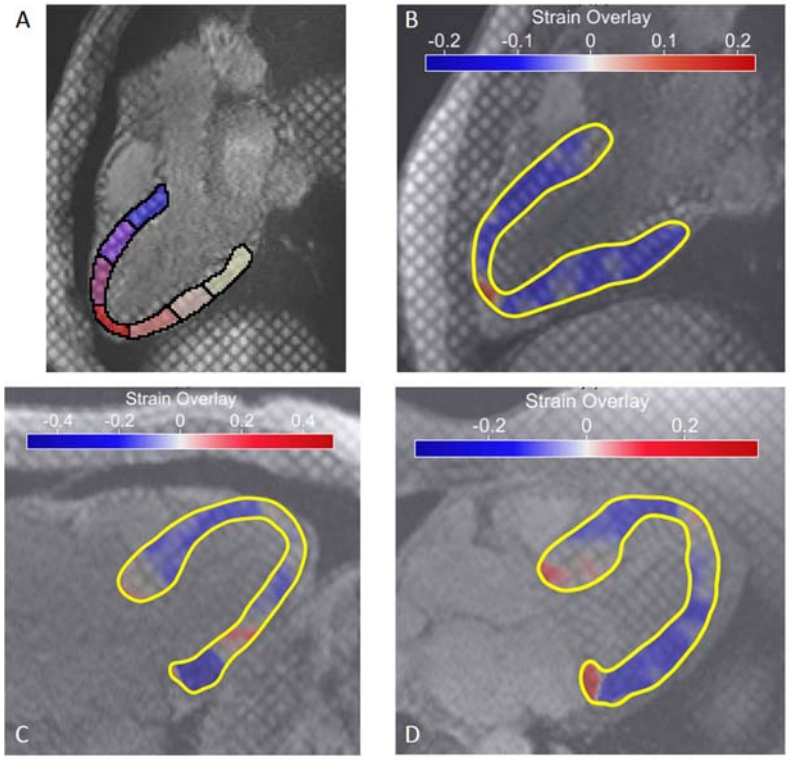

Fig.1. The myocardium in 3CH view divided in 7 segments tracked throughout the cardiac cycle (A); Tangential strain at end-systole for a normal volunteer (B), septal knuckle (C), and HCM (D).

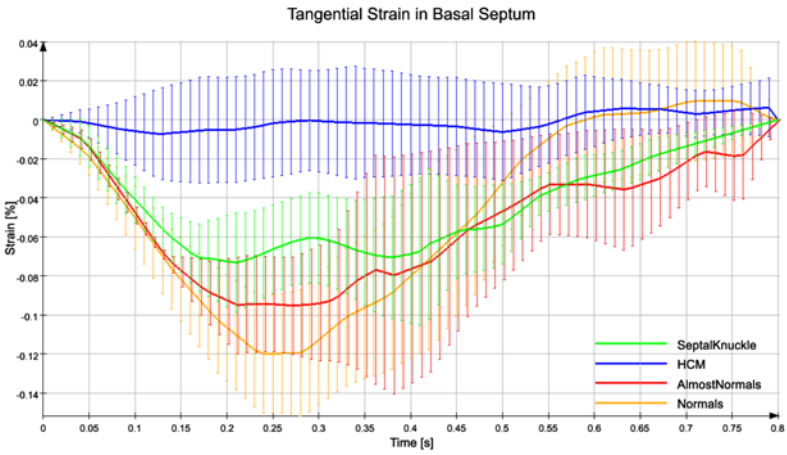

Fig.2. Average tangential strain (± standard deviation) for the basal septum over the cardiac cycle for the normal volunteers and patients, HCM patients and septal knuckle cases.

ID#: 377986

Impact of image motion correction on the evaluation of stress perfusion CMR

Florian von Knobelsdorff, MD[1] Stephanie Reiter, MD[2], Anne Menini, PhD[3], Berthold Höfling, MD[2], Günter Pilz, MD, Professor[2]

1. Dept. of Cardiology, Clinic Agatharied, University of Munich, Hausham, Bayern, Germany

2. Cardiology at Clinic Agatharied, University of Munich, Bayern, Germany

3. General Electric Global Research Center, Bayern, Germany

Background: Image post-processing has been developed to correct for inadequate cardiac and respiratory motion of CMR stress perfusion images. Preliminary results of our group have recently shown in a small cohort that motion correction (MoCo) improves image quality and may facilitate image interpretation. Aim of this continuing study is to analyze the impact of MoCo on the evaluation of stress perfusion CMR in a larger clinical setting.

Methods: Sixty-two patients (mean age 66±10years, 42 males; n=27 without coronary artery stenosis >50%, n=35 with coronary artery stenosis >50%) underwent CMR at 1.5 T (GE Signa HDX 23) including a standard stress-rest-perfusion protocol: three short axes of the left ventricle, spatial resolution 2.0x3.1x8mm^3, adenosine as stressor and 2 x 0.1mmol/kg gadodiamid as contrast agent. Image reconstruction was done both conventionally and with MoCo, which consists in: i) image intensity normalization, ii) group-wise motion extraction with iterative non-rigid registration using a cross-correlation similarity metric, and iii) motion warping of the native images with the combined displacement field. Two SCMR level III readers did the image evaluation by consensus. Each of the 16 AHA segments was evaluated regarding the presence of i) perfusion deficits, ii) dark rim artifacts, iii) uncertain signal loss or iv) normal perfusion patterns. The general image quality (A=non-diagnostic, B=diagnostic, but imperfect, C=good, D=excellent) and the level of diagnostic confidence (A=not confident, B=confident, C=very confident) were assessed once for each dataset.

Results: 53 segments (non-MoCo) and 52 segments (MoCo) were classified as ‘perfusion deficit';. ‘Dark rim artifacts'; were present in 113 (non-MoCo) and 109 (MoCo) segments. Nine vs. 7 segments were classified as ‘uncertain signal loss';. 817 (non-MOCO) and 824 segments (MOCO) were classified as normal. General image quality was rated superior for MoCo compared to non-MoCo, with 92% vs. 63% being ‘good'; or ‘excellent'; (Figure 1). Diagnosis based on MoCo images was rated more often as “very confident” compared to non-MoCo (71% vs. 45%, Figure 2).

Conclusion: While the presence of perfusion deficits, dark rim artifacts, uncertain signal loss and normal perfusion pattern was concordant on non-MoCo and MoCo images, the motion correction of CMR perfusion images clearly improved general image quality and thus increased the readers'; confidence of image evaluation.

Figure 1. General image quality.

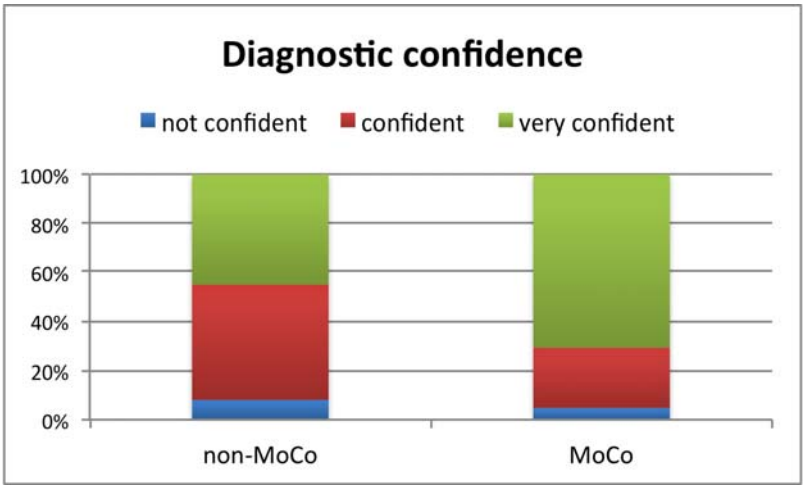

Figure 2. Level of diagnostic confidence.

ID#: 377720

Evaluation of right ventricular cardiac magnetic resonance feature tracking strain analysis in patients with chronic thromboembolic pulmonary hypertension before and after pulmonary endarterectomy

Julia Vietheer, MD[1] Sabine Zitzmann, MD[2], Christoph Liebetrau, MD[1], Till Keller, MD[1], Jan Sebastian Wolter, MD[1], Steffen Kriechbaum, MD[1], Ulrich Fischer-Rasokat, MD[1], Stefan Guth, MD[3], Christoph Wiedenroth, MD[3], Christian W. Hamm, PhD[1], Andreas Rolf, MD[1]

1. Kerckhoff-Heart-Center, Department of Cardiology, Bad Nauheim, Germany, Germany

2. Kerckhoff-Heart-Center, Department of Cardiology, Bad Nauheim, Germany, Frankfurt, Germany

3. Kerckhoff-Heart-Center, Department of Thoracic surgery, Bad Nauheim, Germany, Germany

Background: Increased afterload of the right ventricle (RV) in chronic thromboembolic pulmonary hypertension (CTEPH) causes right heart failure and ultimately death. Beside the volumetric measurement of right ventricular function in cardiac magnetic resonance (CMR) feature tracking (FT) strain analysis is a promising new method of quantifying global and regional myocardial dysfunction. It holds the promise to detect early reduction of RV function, when EF is still normal and is supposed to be a load independent measure of contractility. In this study we investigated strain and strain rate by CMR-FT under different loading conditions at baseline and 12 months after pulmonary endarterectomy (PEA) in patients with CTEPH.

Methods: Steady state free precession (SSFP) cine CMR sequences were analyzed retrospectively using the FT module from cvi42 (circle cardiovascular imaging, Calgary, Canada), yielding six strain parameters (global circumferential strain (GCS), global radial strain (GRS), global longitudinal strain (GLS), global circumferential strain rate (GCSR), global radial strain rate (GRSR), global longitudinal strain rate (GLSR)) in 29 patients with CTEPH before and 12 months after PEA. As surrogate marker for afterload we computed artery elastance (Ea) from volumetry and right heart cath (RHC) as mean pulmonary artery pressure (mPAP) divided by stroke volume and as surrogate marker for contractility we computed end-systolic elastanceSteady (Ees) as mPAP divided by endsystolic volume.

Results: All global RV strain and strain rate parameters showed a significant improvement at 12 month matching the improved right ventricular systolic function measured by CMR volumetry. All strain parameters showed significant correlations with the afterload parameter Ea before and 12 month after PEA but not with contractility parameter Ees.

Conclusion: All strain parameters reflected the improvement of RV global function 12 month after PEA, however strain was not load independent and rather a function of afterload than of contractility.

baseline characteristics

Table 1. baseline characteristics. SD – standard deviation, BNP – brain natriuretic peptid, NYHA – New York Heart Association, SixMWT – six minute walking test, PAMP – pulmonary artery mean pressure, PVR – pulmonary vascular resistance, TAPSE – tricuspid annular plane systolic excursion, EDV – end-diastolic volume, ESV – end-systolic volume, EF – ejection fraction, RV – right ventricle, SAX – short axis, LAX – long axis, GRS(R) – global radial strain (rate), GCS(R) – global circumferential strain (rate), GLS(R) – global longitudinal strain (rate)

Patients characteristics	Observation number	Mean value (SD)
Age (years)	29	55.3(16.7)
Gender (female,n,%)	29	8(27%)
Gender (male,n,%)	29	21(73%)

NT-Pro BNP (pg/ml)	24	1098(947)
NYHA functional class	29	3(0.6)
SixMWT (m)	14	356(103)
Right heart catheterization measures		
PAMP (mmHg)	24	40.7(9.3)
PVR (dsc^{-5})	23	600(277.7)
Echocardiographic measures		
TAPSE (mm)	25	16.3(5.0)
CMR measures of function		
RVEDV index (ml/m²)	29	84(25.9)
RVESV index (ml/m²)	29	58.6(23.1)
RVSV index (ml/m²)	29	25.7(11.3)
RVEF (%)	29	31(12.9)
CMR measures of strain		
RV GRS SAX (%)	29	16.6(7.8)
RV GCS SAX (%)	29	-7.2(7.4)
RV GLS LAX (%)	29	-11.3(9.1)
RV GRSRsyst SAX (1/s)	29	0.76(0.72)
RV GCSRsyst SAX (1/s)	29	-0.41(0.57)
RV GLSRsyst LAX (1/s)	29	-0.91(0.57)

ID#: 377722

4D Flow CMR using semi-automated retrospective valve tracking for assessment of severe mitral regurgitation

Carmen P.S. Blanken, BS[1] Geertruida P. Bijvoet, MD[2], Pim van Ooij, MS, PhD[3], Steven A.J. Chamuleau, MD, PhD[2], Aart J. Nederveen, MS, PhD[3], Stefan M. Boekholdt, MD, PhD[3], Tim Leiner, MD, PhD[4], R. Nils. Planken, MD, PhD[3]

1. Academic Medical Center Amsterdam, Amsterdam, Noord-Holland, Netherlands

2. Utrecht University Medical Center, Netherlands

3. Academic Medical Center Amsterdam, Netherlands

4. Utrecht University Medical Center, Utrecht, Utrecht, Netherlands

Background: Mitral regurgitation (MR) is a common valvular heart defect. Quantification of MR is clinically performed using 2-dimensional (2D) Doppler echocardiography and 2D phase-contrast (PC) MRI. These techniques are limited by geometrical assumptions and operator dependency. Furthermore, quantifying MR severity is challenging due to complex anatomy and cardiac motion. Severe MR often presents with eccentric regurgitation patterns. We aim to evaluate the accuracy of 4D flow cardiac MRI (CMR) using semi-automated retrospective valve tracking for assessment of severe MR.

Methods: 10 patients (80% male, mean age 59 ± 10y) with echocardiographically confirmed asymptomatic severe MR and without other valvular disease underwent CMR including 4D flow at 1.5T. Retrospective tracking of the mitral valve (MV) and aortic valve (AV) annulus was performed using 2D cine bSSFP by dedicated software (CAAS MR 4D Flow 2v0, Pie Medical Imaging, The Netherlands). Time-resolved streamlines were generated for visual verification (Figure 1). 2D PC-MRI of the AV was obtained and short-axis bSSFP planimetric measurements were used to determine left-ventricular (LV) stroke volume.

4D flow-derived LV inflow and outflow were calculated as combinations of MV and AV antegrade and retrograde flows. MR volume was calculated using 4D flow data by assessment of a) regurgitant MV flow and b) LV inflow minus antegrade AV flow. Furthermore, MR volume was derived from 2D CMR data by subtracting antegrade AV flow from LV stroke volume. MR volumes were divided by LV inflow (4D flow) or stroke volume (2D CMR) to obtain MR fractions. Agreements and differences were assessed with Pearson';s correlation and Student';s t test respectively. $P<0.05$ was considered significant.

Results: 4D flow-derived MR fraction by direct quantification of regurgitant MV flow (0.20±0.08) was lower than 2D CMR-derived MR fraction (0.36±0.11) ($p=0.001$). 4D flow-derived MR fraction by indirect quantification based on LV inflow and AV antegrade flow (0.38±0.12) equaled 2D CMR results ($p=0.69$) (Figure 2). 4D flow-derived LV outflow (122±27ml) was lower than LV stroke volume from bSSFP planimetry (152±30ml) ($p=0.03$), whereas LV inflow (152±38ml) showed no difference ($p=0.96$). Antegrade AV flow by 4D flow (90±22ml) corresponded well with 2D-PC measurement (95±19ml) ($p=0.70$).

Conclusion: In patients with severe and complex MR, quantification of MR fraction using 4D flow CMR and semi-automated retrospective valve tracking results in underestimation compared to a 2D CMR-based approach when regurgitation is quantified directly. Indirect 4D flow-derived quantification combining mitral and aortic flow corresponds well with 2D CMR. Future work should aim to overcome the observed underestimation of MR.

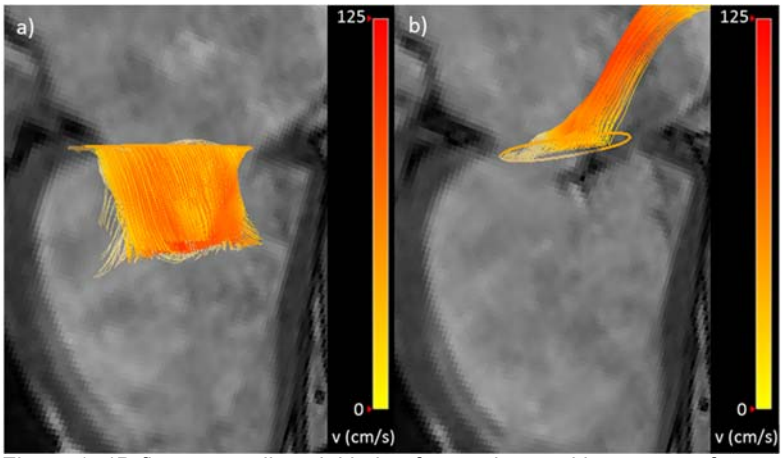

Figure 1. 4D flow streamlines initiating from valve tracking contour for a patient with echocardiographically confirmed severe mitral regurgitation, for a) diastolic inflow and b) systolic regurgitation. Cine bSSFP background shows the left ventricle (bottom) and left atrium (top), separated by the mitral valve.

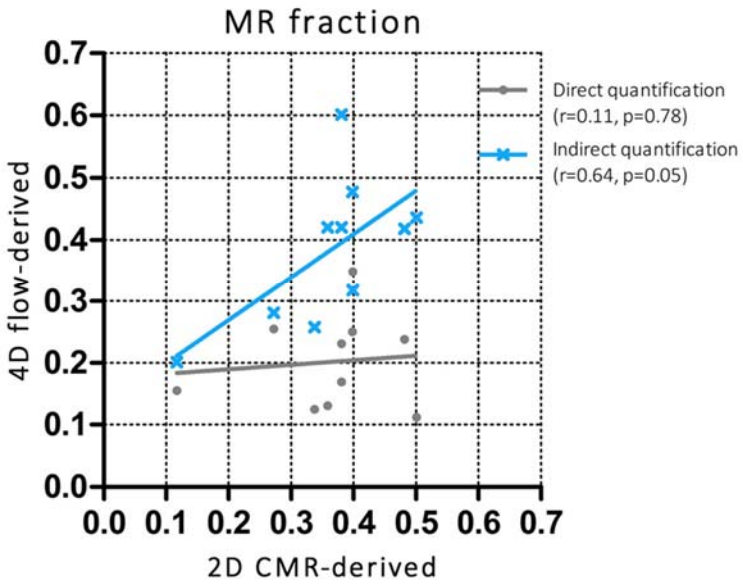

Figure 2. 4D flow-derived MR fraction calculated as a) MV retrograde volume/LV inflow volume (grey) and b) (LV inflow volume - AV antegrade volume)/LV inflow volume (blue), plotted against 2D CMR-derived MR fraction calculated as (LV stroke volume - AV antegrade volume)/LV stroke volume. Corresponding Pearson's correlation coefficients and p-values are shown in the legend.

ID#: 377724

Fluid-dynamic changes in post ischemic dilated cardiomyopathy before and after surgical ventricular restoration: an integrated methodological approach based on CMR 4D flow

Antonia Camporeale, MD[1] Gabriella Di Giovine, MD[2], Silvia Pozzi, M.Sc.[3], Filippo Piatti, M.Sc.[3], Silvia Pica, MD[4], Serenella Castelvecchio, MD[4], Lorenzo Menicanti, MD[4], Andreas Greiser, PhD[5], Emiliano Votta, PhD[3], Alberto Redaelli, PhD[3], Massimo Lombardi, MD[6]

1. IRCCS Policlinico San DOnato, Milano, Italy

2. IRCCS Policlinico San Donato, Milano, Italy

3. Politecnico di Milano, Milan, Italy, Italy

4. IRCCS Policlinico San Donato, Italy

5. Siemens Healthcare GmbH, Erlangen, Germany, Germany

6. IRCCS Policlinico San Donato, Milan, Italy, Lombardia, Italy

Background: To date, the contribution of Cardiac Magnetic Resonance (CMR) in the study of post-ischemic dilated cardiomyopathy (iDCM) consisted of the analysis of LV volume, function and location/extension of ischemic scar. Recently, the use of 4D Flow sequences in the characterization of intraventricular flow patterns allowed to quantify the frictional force on the left ventricular wall (Wall Shear Stress, WSS), and a base-to-apex gradient in WSS has been described in healthy subjects. These aspects related to intra-ventricular fluid-dynamic have never been analysed in iDCM. We aimed to assess through 4D Flow the fluid-dynamic adaptation of iDCM and to characterize changes after surgical ventricular restoration against controls.

Methods: Study population included 20 patients (all males, age=64±11 years) with iDCM and LV dysfunction (EF<35%) and 11 healthy controls (9 males, age=40±15 years). Patients and controls underwent a CMR protocol including Cine images, LGE images and 4D Flow with acquisition volume targeted on LV cavity. 4 patients repeated CMR 6 months after surgical intervention (coronary-artery bypass + surgical ventricular restoration). LGE was quantified as percentage of LV mass. Custom in-house algorithms were used to segment Cine-based 3D masks of the endocardium on which peak diastolic WSS [Piatti et al., 2017] was quantified for LV base, midLV and apex. A base-to-apex gradient (DELTA WSS) was calculated. Nt-proBNP was dosed in patients with iDCM at baseline and at 6 months follow up.

Results: In patients with iDCM, positive correlation between DELTA WSS and LV_EDV ind (R2=0,5, p<0,05) and between DELTA WSS and LV_ESV ind (R2=0,5, p<0,05) were found (Fig.1). This is probably due to the loss of the flow force at apical level following LV dilatation and remodeling. DELTA WSS also showed a negative correlation with LV EF (R2=-0,5, p<0,05) and a positive correlation with LGE extension (R2=0,5, p<0,05). These correlations were not present in healthy controls. At 6 months follow up, a reduction in LV EDV (128 vs 101 ml/m2; p 0,2), ESV (91 vs 63 ml/m2; p 0,1) and NT-proBNP (4497 vs 1237 ng/l; p 0,25) and an increase in LV EF (29 vs 40%; p 0,09) was observed. Moreover, surgical intervention seemed to invert the relationship between DELTA WSS and morpho-functional LV parameters described before surgery.

Conclusion: The integration of fluid-dynamic with Cine- and LGE-derived parameters yielded an innovative characterization of iDCM pathophysiology. The changes in DELTA WSS according to LV volumes and function may be useful in understanding the effect of surgical ventricular restoration on cardiac performance.

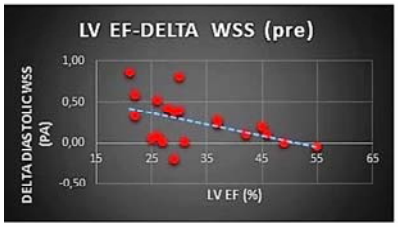
LV EF-DELTA WSS (pre)
DELTA DIASTOLIC WSS (PA)
1,00
0,50
0,00
-0,50
15
25
35
45
55
65
LV EF (%)

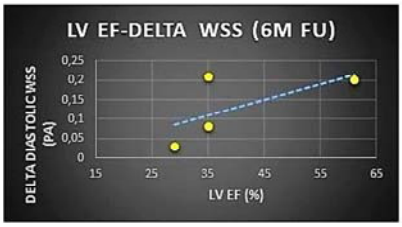
LV EF-DELTA WSS (6M FU)
DELTA DIASTOLIC WSS (PA)
0,25
0,2
0,15
0,1
0,05
0
15
25
35
45
55
65
LV EF (%)

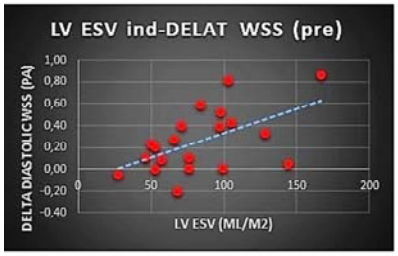
LV ESV ind-DELAT WSS (pre)
DELTA DIASTOLIC WSS (PA)
1,00
0,80
0,60
0,40
0,20
0,00
-0,20
-0,40
0
50
100
150
200
LV ESV (ML/M2)

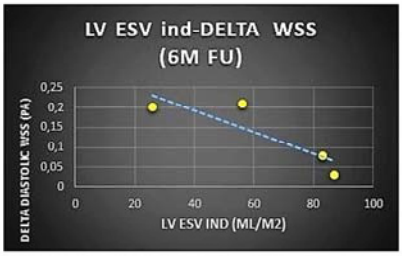
LV ESV ind-DELTA WSS (6M FU)
DELTA DIASTOLIC WSS (PA)
0,25
0,2
0,15
0,1
0,05
0
0
20
40
60
80
100
LV ESV IND (ML/M2)

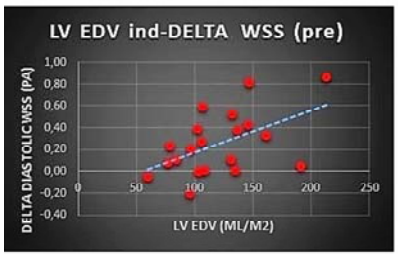
LV EDV ind-DELTA WSS (pre)
DELTA DIASTOLIC WSS (PA)
1,00
0,80
0,60
0,40
0,20
0,00
-0,20
-0,40
0
50
100
150
200
250
LV EDV (ML/M2)

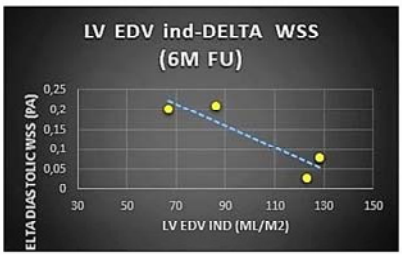
LV EDV ind-DELTA WSS (6M FU)
DELTA DIASTOLIC WSS (PA)
0,25
0,2
0,15
0,1
0,05
0
30
50
70
90
110
130
150
LV EDV IND (ML/M2)

ID#: 377639

Persistent Structural and Functional Left Ventricular Alterations One Year After Takotsubo Cardiomyopathy

Caroline Scally, MBChB, MRCP[1] Amelia Rudd, BSc[1], Alice M. Mezincescu, MRCP[2], Hassan Abbas, MBChB, MRCP[2], Trevor Ahearn, PhD[3], Heather M. Wilson, BSc (Hons) PhD[1], Graham Horgan, MSc PhD [2], Paul Broadhurst, MD[4], Dana Dawson, MD, PhD[1]

1. University of Aberdeen, Aberdeen, Scotland, United Kingdom

2. University of Aberdeen, United Kingdom

3. NHS Grampian, Aberdeen, Scotland, United Kingdom

4. Aberdeen Royal Infirmary, Aberdeen, Scotland, United Kingdom

Background: Takotsubo cardiomyopathy is an acute form of left ventricular systolic (LV) dysfunction precipitated by acute emotional or physical stress. Despite the rapid restoration of the LV ejection fraction within days to weeks after the acute event, we have previously demonstrated incomplete recovery of regional native T1 and extracellular volume (ECV) matrix as well as subtle systolic/diastolic abnormalities at 4 months after the acute event. In the longer term (1 year or more after presentation), these patients remain symptomatic and we have already shown significant myocardial energetic impairment in their hearts. We hypothesize that the LV structural/functional abnormities seen at 4 months fail to normalize during longer-term follow up in keeping with the abnormal myocardial energetics and symptoms.

Methods: Twenty four patients (mean age 65±9 years) with a previous diagnosis of takotsubo and 18 age and co-morbidity matched controls (mean age 61±6 years) were recruited; all were female. Cardiac magnetic resonance (CMR) was performed on a 3T Philips Achieva scanner. T1 mapping was acquired with 3(3)3(3)5 and 5(3)3 schemes for native/post contrast T1. Standard cardiac analysis was performed using CMRTools (Cardiovascular Solutions, London, UK). T1 maps and Feature tracking LV myocardial strain were analysed in Segment (Medviso, Lund, Sweden) in each of the 17 myocardial segments.

Results: Median time to follow-up was 20 months (13-36). The acute takotsubo event was apical in 20 and mid-cavity in 4 patients. As seen form Table 1, there was no difference in the indexed LV volumes, mass or the LV ejection fraction between the two groups. Native T1 values were significantly higher in the takostubo group compared to controls throughout the LV: basal segments (p=0.005), mid-cavity segments (p<0.001) and apical segments (p<0.001). However, there was no significant difference in the ECV between the two groups in any LV region. The takotsubo group showed significantly decreased global longitudinal strain (p=0.04), mean (whole LV) circumferential strain (p=0.005), circumferential strain in the apical segments (p=0.008) and mean (whole LV) radial strain (p=0.03) when compared to the controls.

Conclusion: In patients with prior takotsubo, native myocardial T1 remains significantly elevated at least one year after the acute event, this is accompanied by persistent subtle abnormalities in LV systolic function. These findings likely contribute to the long-term mortality and morbidity in these patients.

Native T1, ECV values and feature tracking strain analysis in takotsubo patients vs controls.

	Takotsubo Patients (n=24)	Controls (n=18)	p value
LVEF (%)	67±8	63±7	0.2
LVEDV i (ml/m2)	71±12	75±10	0.5
LVESV i (ml/m2)	24±8	28±6	0.2
LV Mass i (g/m2)	64±8	62±12	0.6

Native T1 (ms)			
Basal	1262±7*	1223±1	0.005
Mid-cavity	1250±8*	1189±10	<0.001
Apical	1300±19*	1165±19	<0.001
Whole heart	1267± 9*	1196 ±10	<0.001
ECV (%)			
Basal	28± 0.5	28±1.0	0.6
Mid-cavity	26± 0.6	26±1	0.7
Apical	28.±0.1	27± 1	0.9
Whole heart	27 0.1	27 0.1	0.9
Longitudinal strain (%)			
2 chamber	-18.±0.6	-19.7±0.9	0.2
3 chamber	-17.8±0.5	-18.6±0.8	0.5
4 chamber	-17.6±0.5*	-19.8±0.7	0.009
Global	-17.8±0.4*	-19.4±0.7	0.04
Circumferential strain (%)			
Basal	-16.3±0.9	-18.7±0.8	0.06
Mid-cavity	-16.9±0.7	-19±0.9	0.06
Apical	-20.9±1.0*	-27.5±2.1	0.008
Mean LV	-18.0±0.7*	-21±1.0	0.005
Radial strain (%)			
Basal	38.5±2.9	48.2±5.5	0.1
Mid-cavity	42.8±2.7	48.6 ±3.9	0.2
Apical	26.0±4.9	32.5±6.4	0.4
Mean LV	35.7±1.9*	43.1±2.7	0.03

LVEF; Left ventricular ejection fraction, LVEDVi; indexed LV end diastolic volume, LVESVi; indexed LV end-systolic volume; ECV; Extracellular Volume,

*p<0.05, takotsubo patients vs controls.

All data shown as mean ± SEM

ID#: 377516

Parameters of biventricular dyssynchrony in patients with repaired and unrepaired Ebstein's anomaly - assessment by tissue tracking cardiovascular magnetic resonance

Simona Marcora[1]Roland Weber[2], Angela Oxenius[3], Christine Attenhofer Jost[4], Emanuela R. Valsangiacomo Buechel[5]

1. Azienda Ospedaliera Papa Giovanni XXIII , Bergamo, Bergamo, Italy

2. University Children's Hospital Zurich, Zurich, Switzerland

3. University Children's Hospital Zurich, Zurich, Zurich, Switzerland

4. Klinik im Park, Zurich, Switzerland

5. University Childre's Hospital Zurich, ZUrich, Switzerland

Background:

Different factors, such as left ventricular (LV) non-compaction (LVNC) and the atrialized right ventricle (RV) may influence synchrony in patients with Ebstein anomaly (EA). We sought to assess parameters of ventricular synchrony by using feature tracking (FT) CMR and the influence of severity of TV displacement and presence of LVNC.

Methods:

Biventricular function was prospectively assessed by cine CMR using the SSFP sequence in 20 patients with EA. Median age was 44.5 (17-64) years, 9 females. Mean TV displacement 41 ± 36 mm. LVNC was found in 12 patients (60%). Six patients underwent TV repair. Image temporal resolution was < 25 msec. Short-axis (SAX) and long-axis 4 chamber (LAX) images were analyzed by FT (software Qstrain, Medis Version 3.3) to assess global and regional time to peak (TTP) in both ventricles. Wall delay was defined as the TTP difference between the septum and the lateral segments (free wall) on SAX and LAX images.

Results:

LV SAX showed a significant wall delay in the basal (69±84 ms; $p<0.01$) and mid ventricular segments (42±48 ms; $p<0.01$) but not at the apex (-4±57ms; n.s). Mean septal TTP decreased from the basal to the apical segments (370 ± 108 ms vs 334 ± 60 ms (p 0.04) vs 293 ± 69 ms ($p<0.01$) figure 1.Global TTP and free wall TTP did not differ among segments.LV LAX had similar TTP values in the septum and free wall (326 ± 86 ms vs 312 ± 66 ms). RV free wall TTP was significantly delayed compared to the septum (383 ± 114 ms vs 338 ± 123ms; p 0.04; wall delay 75±87ms) and LV free wall (312±67 ms; $p<0.01$). Mean RV EF% was 39±10 and LV EF% 53±10. TV displacement correlated with wall delay in the LV mid-ventricular segments (r 0.57, $p<0.01$), but not in other LV or RV segments. LV EF% correlated with basal LV SAX wall delay (r - 0.53, p 0.014), but not with global or regional TTP. RV EF% correlated weakly only with global RV TTP (r - 0.46, p 0.04). LVNC did not affect synchrony parameters.

Conclusion:

Significant global and segmental differences in TTP are present in both ventricles of EA patients. LV shows intraventricular dyssynchrony in septal basal and mid-ventricular segments that correlates with the severity of TV displacement. In the RV wall delay is greater in the free wall than the septum and the LV free wall, indicating interventricular dyssynchrony.

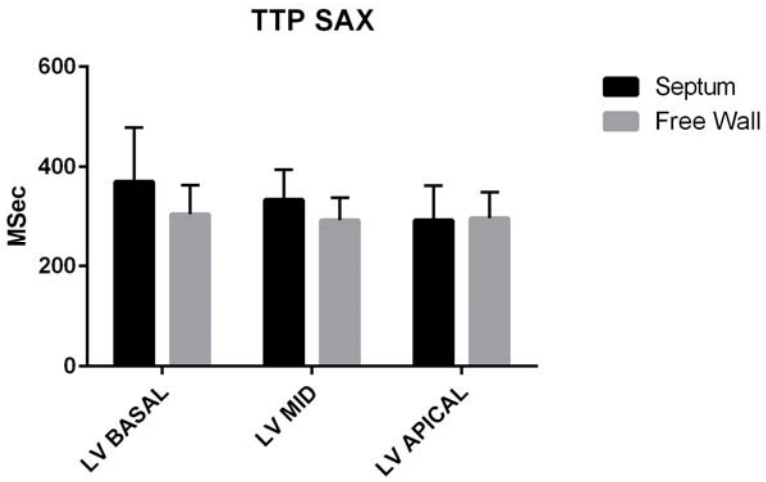
TTP SAX
600
400
200
0
MSec
Septum
Free Wall
LV BASAL
LV MID
LV APICAL

ID#: 377695

Safety of Regadenoson Stress Cardiac Magnetic Resonance Imaging in Heart Transplant Recipients

Felipe Kazmirczak, MD[1] Prabhjot Nijjar, MD[2], Mehmet Akçakaya, Ph.D.[3], Chetan Shenoy, M.D.[4]

1. University of Minnesota

2. University of Minnesota, MN

3. Electrical and Computer Engineering, University of Minnesota; Center for Magnetic Resonance Research, University of Minnesota, Minneapolis, MN

4. Cardiovascular Division, Department of Medicine, University of Minnesota, Minneapolis, MN

Background: Vasodilator stress testing by cardiovascular magnetic resonance imaging (CMR) is a promising non-invasive technique to detect coronary artery vasculopathy (CAV) in heart transplant recipients. However, adenosine is associated with super-sensitivity of the denervated sinus and atrioventricular nodes after heart transplantation, resulting in exaggerated sinus node and atrioventricular node suppression. In non-transplant patients, regadenoson – a newer selective adenosine 2A receptor agonist – has been shown not to be associated with high-degree atrioventricular blocks in contrast to a 4-5% incidence with a 6-minute infusion of adenosine. However, data on the safety of regadenoson after heart transplantation are limited since heart transplant recipients were excluded from pre-approval studies of regadenoson. There are no data on the safety of regadenoson early after transplantation.

Methods: We studied consecutive heart transplant recipients who underwent regadenoson stress CMRs at our institution between April 2012 and June 2017. All recipients received 0.4 mg of regadenoson by rapid intravenous injection, followed immediately by a saline flush and within 1-2 minutes by 0.075 mmol/kg of gadolinium contrast for stress imaging. We assessed for adverse effects.

Results: Sixty-one regadenoson stress CMRs were performed in 44 heart transplant recipients at a median of 2.75 (interquartile range 1.02 - 7.25) years after transplantation. Twenty-six (43%) were performed within two years after heart transplantation. All studies were completed. One had to be temporarily interrupted due to abdominal cramps after regadenoson injection; the patient received a second dose of regadenoson after 20 minutes without any further symptoms. Adverse effects requiring an intervention occurred in two patients (3%); one had chest pain requiring nitroglycerin and one had hypotension requiring intravenous fluids. Minor adverse effects occurred in 21% of the studies, including dyspnea, nausea and headache. There were no occurrences of death, myocardial infarction, ventricular arrhythmias, asystole, sinus pause, high-degree atrioventricular block, or atrial fibrillation. There were no emergency room evaluations or hospitalizations.

Conclusion: We found a low rate of adverse effects requiring an intervention, and importantly, no occurrences of sinus node dysfunction or high-degree atrioventricular block, including in the first two years after heart transplantation. There were no serious adverse events. Unlike adenosine, regadenoson appears to be a safe after heart transplantation. Our findings highlight that regadenoson stress CMR is a safe non-invasive modality for the surveillance of CAV. Further studies are warranted to evaluate the accuracy of regadenoson stress CMR for the detection of CAV.

ID#: 377781

Congenital Aortic Arch Repair in Bicuspid Aortic Valve Results in Altered 4D Flow Characteristics

Lajja Desai, M.D.[1] Haben Berhane, M.A.[2], Nazia Husain, MBBS, MPH[3], Kelly Jarvis, PhD[4], Joshua D. Robinson, MD, FACC[5], Cynthia K. Rigsby, MD, FACR[5], Michael Markl, PhD[6]

1. Northwestern University School of Medicine, Ann and Robert H. Lurie Children's Hospital of Chicago, Chicago, IL

2. Ann & Robert H. Lurie Children's Hospital of Chicago

3. Ann & Robert H. Lurie Children's Hospital of Chicago, IL

4. Northwestern University, IL

5. Ann & Robert H. Lurie Children's Hospital of Chicago, Chicago, IL

6. Northwestern University, Chicago, IL

Background: Bicuspid aortic valve (BAV) affects 1-2% of the population and is associated with aortic flow abnormalities such as abnormal outflow jet patterns and vortex flow implicated in the development of severe aortic complications including aneurysms and dissection. BAV can also accompany congenital abnormalities of the aortic arch such as coarctation, or more severely, interrupted aortic arch (IAA). IAA patients typically undergo neonatal surgical repair; however, the long-term impact of repair on flow characteristics is poorly understood. The aim of this 4D flow MRI study was to investigate changes in aortic hemodynamics in pediatric BAV patients with IAA repair in comparison to BAV alone and healthy controls.

Methods: 4D flow MRI (spatial resolution=2.0-3.4 x 1.6-2.4 x 1.8-2.4 mm^3, temporal resolution=35.7-40.8 ms, venc=120-400 cm/s) of the thoracic aorta was performed in 15 age-matched (p=0.19) subjects: BAV + IAA (n=5, age=21.2 +/- 8.4, 2 female), BAV alone (n=5, age=14.9 +/- 2.9, 2 female), and controls (n=5, age=15.8 +/- 1.7, 2 female). Data analysis included corrections for phase offset errors (eddy currents, Maxwell terms) and velocity aliasing (Matlab, Mathworks, USA) and 3D aorta segmentation using 3D PC-MRA images (Mimics, Materialise, Belgium). Aortic peak systolic velocities in the ascending aorta (AAo), transverse arch, and proximal descending aorta (DAo) were generated from velocity maximum intensity projections (MIPs), and retrograde flow fractions were quantified using analysis planes. Aortic blood flow visualization was performed by velocity color-coded 3D pathlines (EnSight, CEI, Apex, USA). Secondary flow patterns (helices/vortices) were defined as none, mild (>2 360 degree turns).

Results: Comparison of MIPs and 3D blood flow visualization are shown in Figures 1 and 2. T-test analysis between any two groups did not show statistically significant differences in peak systolic velocity and regurgitation at any location; however, when BAV + IAA and BAV alone groups were combined and compared against controls, there was a statistically significant increase in AAo and transverse arch peak systolic velocities (p=0.005, 0.01, Table 1). In addition, patients with IAA repair had pronounced helix flow downstream of the graft (Table 1, Figure 2). In the DAo, helical flow was seen in 4/5 and vortex flow in 1/5 of BAV + IAA patients versus no flow derangement in BAV alone or controls.

Conclusion: In addition to increased AAo and transverse arch systolic flow velocities in BAV patients with or without repaired IAA, IAA repair specifically resulted in DAo flow pattern derangement compared to BAV alone and pediatric controls. Although t-test analysis did not show statistically significant differences between the three groups, this is likely related to the small cohort size of this pilot feasibility study. Future studies are warranted to further investigate the impact of flow changes associated with congenital aortic arch abnormalities in larger cohorts.

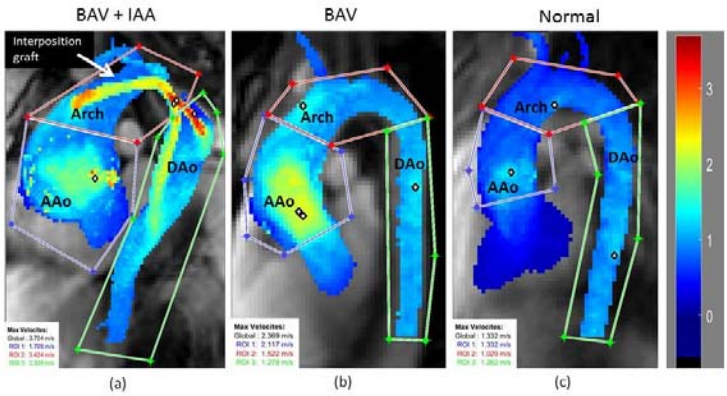

Fig 1. Representative MIPs of aortic peak systolic velocities in the ascending (AAo, ROI 1), transverse arch (ROI 2) and descending aorta (DAo, ROI 3). (a) Female BAV + IAA patient with right and left cusp fusion, 18 years of age at time of scan, status post AAo – DAo interposition Gortex graft repair at < 30 days of age and at 1 year of age, (b) Male BAV patient with right and non cusp fusion, 13 years of age at time of scan, no prior surgeries, (c) Female healthy control without BAV, 14 years of age at time of scan.

Comparison of Aortic Peak Systolic Velocity MIPs Between Groups

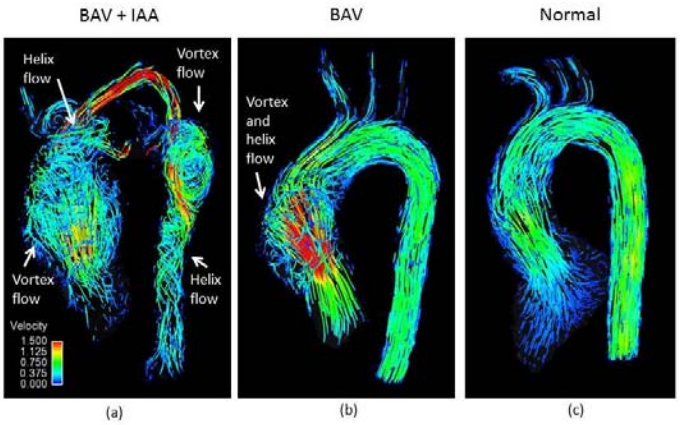

Fig 2. 4D pathline MRI images comparing flow patterns in the BAV + IAA (a), BAV (b) and control patients (c) from Figure 1. Secondary flow patterns (helices/vortices) were graded on a 4 point scale (none, mild, moderate, severe). (a) IAA patient with scan 17 years post repair showing mild helix and severe vortex flow in the AAo and severe helix and vortex flow in the DAo, (b) BAV patient with no prior surgeries showing moderate helix and mild vortex flow in the AAo, and (c) Control patient showing no helix or vortex flow.

Comparison of 4D Flow Pathline MRI Images Between Groups

Comparison of Peak Systolic Velocities, Regurgitation and Flow Grading Between Groups

		Peak Systolic Velocity (m/s)			Regurgitation (%)			Flow Grading			
	Age at Scan	AAo	Transverse Arch	DAo	AAo	Transverse Arch	DAo	AAo - Helix	AAo - Vortex	DAo - Helix	DAo - Vortex

BAV + IAA	19.9	1.9	2.0	1.8	13.7%	8.5%	8.8%	1 (0-2)	1 (0-3)	1 (0-3)	0 (0-3)
BAV Alone	14.9	2.4	1.6	1.5	8.7%	12.5%	9.9%	1 (1-3)	1 (0-1)	0	0
Control	15.8	1.3	1.1	1.3	6.0%	4.2%	3.4%	0	0	0	0

Table 1. Comparison of average peak systolic velocity via MIP ROIs and regurgitation via analysis planes at the AAo, transverse arch and DAo and median flow grading with ranges (none=0, mild=1, moderate=2, severe=3) in the AAo and DAo.

ID#: 377795

Evaluation of aortic stiffness for repaired coarctation of aorta by pulse-wave velocity with MRI

Qiong Yao, ChinaXi-hong Hu, china

Children's Hospital of Fudan University, China (People's Republic)

Background:

Patients with repaired coarctation of aorta (CoA) usually have increased vessel stiffness. The purpose of this study is to evaluate the degree of vascular stiffness in patients with reconstructed CoA and the relation with left ventricular hypertrophy by pulse-wave velocity (PWV) with MRI.

Methods: We retrospectively reviewed cardiac MRI from 22 patients with repaired CoA. PWV was calculated by phase contrast sequence while cardiac function and the thickness of myocardium were evaluated by echocardiography. Another 22 healthy children were included in the control group and there was no difference in age and sex.

Results:

The averaged PWV of research group was significantly higher than the control group (4.42±3.02m/s vs 2.73±0.76m/s, p=0.02). In research group, patients with moderate restenosis had the highest PWV of the three groups. In ROC analysis, the cut-off value was 3.37m/s and the sensitivity and specificity were the highest to distinguish mild from moderate stenosis. Correlations between left ventricular end-diastolic volume, left ventricular end-systolic volume, ejection fraction and myocardium thickness with PWV were not demonstrated.

Conclusion: PWV in repaired group was higher, especially in the moderate restenosis group, implicating more severe vascular remodeling.

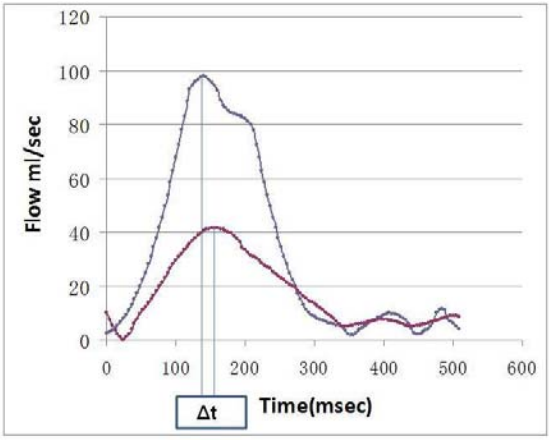

velocity-time flow

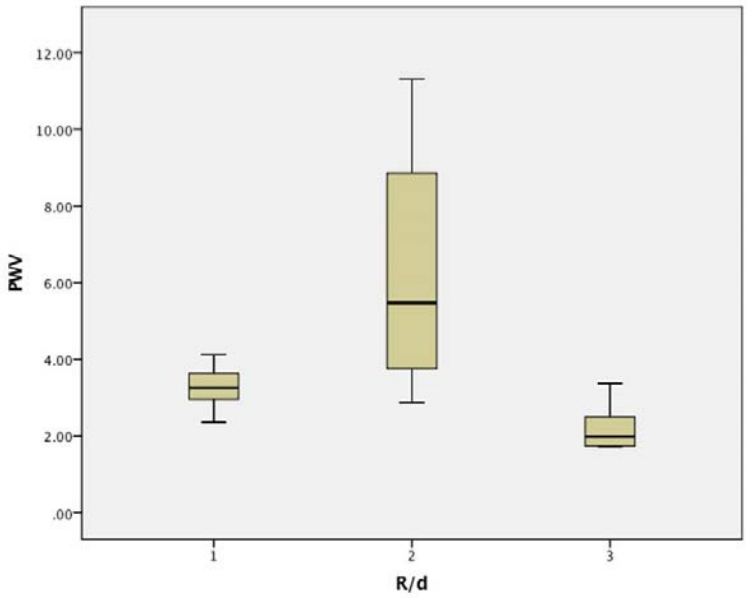

PWV in three groups

PWV between control and surgery group

		PWV	p
control		2.73±0.76	0.02
surgery		4.42±3.02	
	slight	4.10±2.86	0.04
	moderate	6.42±3.26	
	severe	2.27±0.69	

ID#: 377801

The prevalence of myocarditis in Dengue patients: Non-invasive detection of cardiac involvement and evaluation of cardiac function using contrast-enhanced MRI

Mohamad Nazrulhisham Mad Naser, MBBS (UM), MIntMed (UM)[3]Noor Khairiah A. Karim, MBBS (UM), MRad (UM)[1], Yang Faridah Abdul Aziz, MBBS (UM), MRad (UM)[2], Nor Ashikin Md Sari, MBBS (UM), MIntMed (UM)[4], Raja Rizal Azman Raja Aman, MBBS (London), MRad (UM)[2], Sharifah Faridah Syed Omar, MBChB (Manchester), MMed (Internal Medicine) (UM)[4], Ravinderjit Singh Mahinder Singh, MBChB BAO (Ire), MRCP (UK)[5]

1. Regenerative Medicine Cluster, Advanced Medical and Dental Institute, Universiti Sains Malaysia, Malaysia, Bertam, Kepala Batas, Malaysia

2. Department of Biomedical Imaging, Faculty of Medicine, University of Malaya, Malaysia, Kuala Lumpur, Malaysia

3. Department of Cardiology, Hospital Pulau Pinang, Malaysia, Georgetown, Pulau Pinang, Malaysia

4. Department of Medicine, Faculty of Medicine, University of Malaya, Malaysia, Kuala Lumpur, Malaysia

5. Department of Medicine, Faculty of Medicine, University of Malaya, Malaysia; KPJ Klang Specialist Hospital, Malaysia, Selangor, Malaysia

Background: Dengue fever is a major public health problem in Malaysia. Cardiac involvement and dysfunction may influence the outcome of the disease. The purpose of this study was to assess the presence of myocarditis in dengue patients and monitor the outcome by using Cardiac Magnetic Resonance imaging (CMR).

Methods: Sixty consecutive eligible patients with positive dengue IgM antibody (52 patients uncomplicated dengue with presence of warning signs; 8 severe dengue) within the age of 18 to 45 years old were recruited. Those with known co-morbidities, cardiomyopathy, valvular and coronary artery disease (CAD) were excluded. All consented and clinically stable patients underwent baseline CMR within the period of 2 to 4 weeks from day 1 of Febrile Phase. Analysis of the images was performed to detect any cardiac involvement and assess the cardiac function. Myocarditis was diagnosed based on ‘Lake Louis Consensus Criteria';. Similar protocol was applied for follow-up CMR scheduled approximately 8 to 10 weeks later to detect any long-term sequelae. The CMR findings were compared with patients'; long term clinical outcome using New York Heart Association functional classification.

Results: In the baseline scan, the CMR findings were abnormal in 18 patients (30.0%) whereby 16.7% had impaired left ventricular ejection fraction (LVEF), 11.7% had wall motion abnormalities and 8.3% had pericardial effusion. Seven patients (11.7%) had abnormal non-ischaemic fibrosis. The midmyocardial was the most frequent site of late gadolinium enhancement (LGE), with predilection for the anteroseptal wall. None of the cases had positive hyperaemic phase or oedema images. The recruitment period bias may explain these findings. Three of these 7 patients had impaired LVEF and of these, two had associated wall motion abnormalities and one had pericardial effusion. Thirty-two patients came for the follow-up scan and of these, three patients had reduction of LVEF although with no LGE in the baseline scan, which may suggest negative left ventricular (LV) remodelling. On the other hand, four patients showed LVEF improvement. All patients remained subclinical throughout the study period (on 1-year follow up).

Conclusion: In the absence of risk factors for CAD, normal valvular status and normal LV geometry, the presence of abnormal fibrosis (11.7%) and impaired LV function (16.7%) among this study population indicates high likelihood of dengue cardiomyopathic process. Hence, CMR utility should be recommended in dengue patients especially if there is suspicion of dengue-related myocarditis. However, the major drawback of this study is significant dropout (46.7%) among the subjects which limit the outcome.

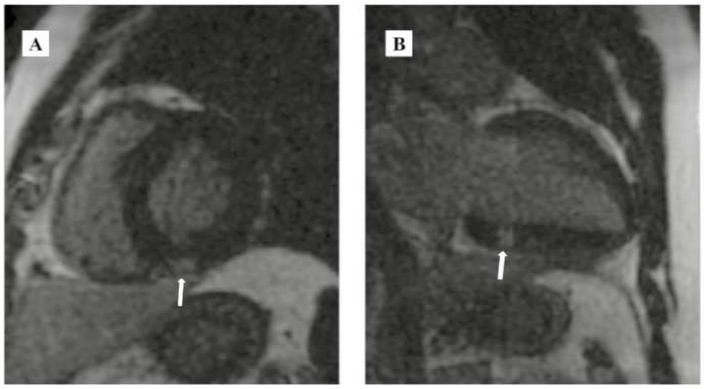

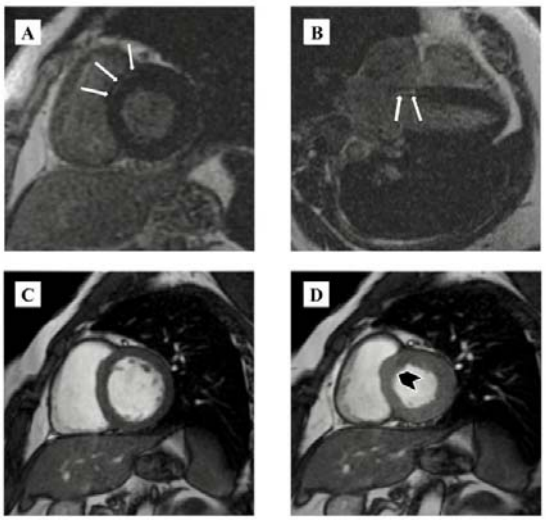

Positive findings (wall motion abnormalities, impaired LVEF, myocardial late gadolinium enhancement and presence of pericardial effusion) on baseline and follow-up CMR scans in study population

Patient no.	Baseline CMR scan (n=60)					
	Wall motion abnormality/ LVEF (%)	T2-weighted with fat suppression signal intensity	T1-weighted early gadolinium enhancement	Late gadolinium enhancement Location/ Segment no. (according to 17-segment model)	Pericardial effusion	Wall motio abnormali LVEF (%

1	N/58%	N	N	N	P	N/62%
2	Global hypokinesia/ 49%	N	N	Subepicardial/ Segment 10	N	
4	N/69%	N	N	N	P	N/63%
7	N/69%	N	N	N	P	N/62%
10	N/71%	N	N	Midmyocardial/ Segment 7	N	
11	N/69%	N	N	Midmyocardial/ Segment 8	P	
14	N/55%	N	N	Midmyocardial/ Segment 7,12	N	
16	Regional hypokinesia/ 55%	N	N	N	N	Regiona hypokines 55%
19	N/59%	N	N	N	P	
24	Global hypokinesia/ 46%	N	N	N	N	N/57%
28	N/60%	N	N	N	N	N/52%
33	N/52%	N	N	N	N	
34	Global hypokinesia/ 47%	N	N	N	N	N/65%
38	N/59%	N	N	N	N	N/51%
39	N/78%	N	N	Midmyocardial/ Segment 9	N	
45	Regional hypokinesia/ 53%	N	N	N	N	N/64%
48	N/61%	N	N	N	N	N/51%
49	N/51%	N	N	N	N	N/64%

53	N/60%	N	N	Midmyocardial/ Segment 8	N	
56	Regional hypokinesia/ 55%	N	N	Subepicardial/ Segment 2	N	
60	Global hypokinesia/ 46%	N	N	N	N	

LVEF, left ventricular ejection fraction; P, positive; N, negative

ID#: 377729

Acute adverse events in cardiac MR imaging with Gadolinium based contrast agents: results from the European Society of Cardiovascular Radiology (ESCR) MRCT registry in 72,839 patients.

Johannes Uhlig, MD MPH[1] Christian Luecke, MD[2], Matthias Grothoff, MD[2], Andreas Schuster, MD PhD MBA FESC[3], Philipp Lurz, MD, PHD[4], Alexis Jacquier, MD PhD[5], Daniel Thomas, MD[6], Joachim Lotz, MD[7], Matthias Gutberlet, MD[8]

1. University Medical Center Göttingen, Institute for Diagnostic and Interventional Radiology, Niedersachsen, Germany

2. Department of Diagnostic and Interventional Radiology, University of Leipzig -Heart Centre, Leipzig, Germany, Germany

3. Department of Cardiology and Pneumology, University Medical Center Göttingen, Germany; Department of Cardiology, Royal North Shore Hospital, Sydney, Australia; The Kolling Institute, Northern Clinical School, University of Sydney, Sydney, Australia, Niedersachsen, Germany

4. University of Leipzig - Heart Centre, Department of Internal Medicine / Cardiology, Sachsen, Germany

5. Aix Marseille Université APHM, France

6. University Hospital Bonn, Department of Radiology, Germany

7. University Medical Center Göttingen, Goettingen, Niedersachsen, Germany

8. University of Leipzig - Heart Centre, Department of Diagnostic and Interventional Radiology, Sachsen, Germany

Background: Gadolinium based contrast agents (GBCA) are generally considered safe in clinical practice. However, there are no studies on GBCA in cardiac MR that adjust for potential confounders such as stress test imaging or main indication.

Methods: GBCA enhanced CMR from the multinational, multicenter European Society of Cardiovascular Radiology MR/CT Registry were included. AAEs were classified according to the American College of Radiology Manual on Contrast Media. Multivariable logistic regression was used to model the likelihood of AAEs in various GBCA, adjusting for pharmacological stressor, main indications, age and sex. Sensitivity analyses were conducted, assessing the influence of GBCA volume and concentration on adverse events. Further sensitivity analyses assessed acute adverse events of severe category.

Results: In the study population of 72,839 GBCA enhanced cardiac MR, a total of 260 acute adverse events were reported (0.36%), with a minority of severe adverse events (n=24, 0.033%). Patients without pharmacological stress imaging had a lower acute adverse event rate (n=120/54,285, 0.22%). In comparison, patients receiving pharmacological stressor imaging were more likely to develop acute adverse events (n=140/18,554, 0.75%). Highest acute adverse event rates were reported for regadenoson (n=34/1,151, 2.95%), and dobutamine (n=7/482, 1.45%), mainly attributable to dyspnea (n=24), but the only 7 (0.041%) severe AAEs occurred in the adenosine group.Compared to the most frequently used Gadobutrol [56%], acute adverse events were more likely for the less frequently used Gadoteridol [4%] (OR=3.16, 95% CI: 2.10-4.74, p<0.001), and less likely for the second frequently used Gadoteracid [20%] (OR=0.64, 95% CI: 0.44-0.93, p=0.018), after multivariable adjustment. In comparison to patients with known coronary artery disease, those with suspected or known cardiomyopathy, myocarditis and imaging indications classified as others were less likely to experience acute adverse events (OR=0.5, p=0.006; OR=0.39, p<0.001; OR=0.5, p=0.005, respectively). There was statistically significant multiplicative interaction between GBCA and pharmacological stressor (p<0.01). For example, comparing adenosine to regadenoson, the acute adverse event rate differed by the factor 9 for Gadobutrol (0.52% versus 4.56%), while rates were comparable for Gadoteracid (0.3% versus 0.47%), independent of the stressor used. However, no significant difference in the frequency of AAEs depending on the molecular structure, ionicity or chelate stability of GBCAs was found.

Conclusion: GBCA enhanced CMR is generally safe with event rates comparable to those of other body regions. The likelihood of acute adverse events increases with stress imaging and depends on the pharmacological stressor, and main indication.

Acute adverse events by stress imaging and pharmacological stressor.

	Molarity [mmol/ml]	Molecular Structure	Ionic/ Non-ionic	Thermodynamic chelate stability	Total No. 72,839	no stress No. 54,285 (74,5%)	stress No. 18,554 (25.5%)	adenos No. 16, (91.2%
All GBCA [% of pts.]					260/72,839 (0.36%)	120/54,29 (0.22%)	140/18,554 (0.75%)	99/16,9 (0.59%)
Gadobutrol (Gadovist®) [56%]	1.0	Cyclic	Non-ionic	21.8	143/40,620 (0.35%)	59/30,366 (0.19%)	84/10,254 (0.82%)	52/9,38 (0.55%)
Gadoteridol (Prohance®) [4%]	0.5	Cyclic	Non-ionic	23.8	29/2,994 (0.97%)	15/2,290 (0.66%)	14/704 (1.99%)	11/669 (1.64%)
Gadoteracid (Dotarem®) [20%]	0.5	Cyclic	Ionic	25.8	35/14,257 (0.25%)	24/10,780 (0.22%)	11/3,477 (0.32%)	9/3,014 (0.30%)
Gadobenate (Multihance®) [10%]	0.5	Linear	Ionic	22.6	27/7,092 (0.38%)	15/4,768 (0.31%)	12/2,324 (0.52%)	11/2,18 (0.50%)
Gadopentetate (Magnevist®) [8%]	0.5	Linear	Ionic	22.1	23/5,624 (0.41%)	6/4,120 (0.15%)	17/1,504 (1.13%)	14/1,3 (1.01%
Gadodiamide (Omniscan®) [3%]	0.5	Linear	Non-ionic	16.9	3/2,252 (0.13%)	1/1,961 (0.05%)	2/291 (0.69%)	2/282 (0.71%)

ID#: 377761

Right Ventricular Myocardium T1 and T2 Mapping in Patients with Repaired Tetralogy of Fallot

Matheus Godoi, MD[1]Dario Firmino, MDI[1], Isaac Torquato, MD[1], Flavio M. Lauand, MD[2], Jamil Calil-Neto, MD[1], Hilka Carvalho, MD[1], Natália Salvatti, MD[1], Tiago Magalhães, MD, PHD[1], Valeria Moreira, MD[1], Adriano C C. Carneiro, MD[3], Carlos E. Rochitte, MD, PhD[4]

1. Hospital do Coração - Heart Hospital - HCOR, São Paulo, Brazil, Brazil

2. Hospital do Coração - Heart Hospital - HCOR, São Paulo, Brazil, São Paulo, Sao Paulo, Brazil

3. Hospital do Coração - Heart Hospital - HCOR, São Paulo, Brazil, Sao Paulo, Sao Paulo, Brazil

4. Heart Institute - InCor - University of São Paulo Medical School and Hospital do Coração - Heart Hospital - HCOR, São Paulo, Brazil

Background: In patients with surgically repaired Tetralogy of Fallot (rTOF), adverse left (LV) and right ventricular (RV) remodeling is associated with functional health status. Focal myocardial fibrosis evaluated by cardiovascular magnetic resonance (CMR) has been shown to correlate to severity of RV overload and severity of clinical presentation. Recent new mapping techniques by CMR have allowed the detection of myocardial T1 and T2 values in LVand also in RV. Despite of the hypothesis that mapping values and ECV could be associated to ventricular remodeling, there is a poverty of data systematically comparing to RV remodeling in rTOF patients. Thus, our objective was to investigate whether right ventricular ECV, native T1 and T2 values are associated to RV remodeling.

Methods: Eleven patients (5 women) with rTOF with mean age of 23.0±13.1 years (12 to 53 years old) underwent cardiac CMR examination at a 1.5T GE scanner (Discovery MR 450w) including T1 (SMART1map, a single point saturation-recovery with true T1 estimation) and T2 mapping (multi-echo fast spin-echo – MFSE) sequences, both acquired during systolic phase to allow thicker and better defined RV walls. T1 map images were also acquired 15 minutes after contrast injection (0.2mMol/Kg of gadolinium based contrast) for ECV measurements. Cine MRI and delayed enhancement using standard SSFP and IR prepped GRE sequences were also acquired. RV dilation was defined as indexed end diastolic volume equal or greater than 100ml/m2.

Results: Patients with and without RV dilatation showed no significant differences in RV or LV ECV values. However, RV myocardium native T1 values were significantly higher in patients with RV dilation compared to those without (1401.7±50.3 vs. 1240.0±37.5ms, p = 0.048, Figure). Within patients without RV dilatation, RV and LV native T1 values were similar, while within patients with RV dilation significantly higher RV than LV native T1 values was observed (1401.7±50.3 vs. 1257.1±38.3ms, p = 0.0002, Figure). Additionally, in a multiple linear regression native LV T1 was an independent predictor of RV dilatation (p=0.047). Left ventricular T2 (57.7±3.6 vs. 51.4±2.8ms, p=ns) and RV T2 values (55.4±2.7 vs. 61.7±3.8ms, p=ns) were similar between patients with and without RV dilatation.

Conclusion: Repaired tetralogy of Fallot patients with right ventricular dilatation have significantly higher native T1 values in the right ventricular myocardium than patients without dilatation. Extracellular volume and T2 values for left and right ventricular myocardium were similar regardless of the right ventricular dilatation. Higher T1 values in dilated right ventricles might be an indication of increased collagen content in this clinical scenario. Further larger studies are warranted.

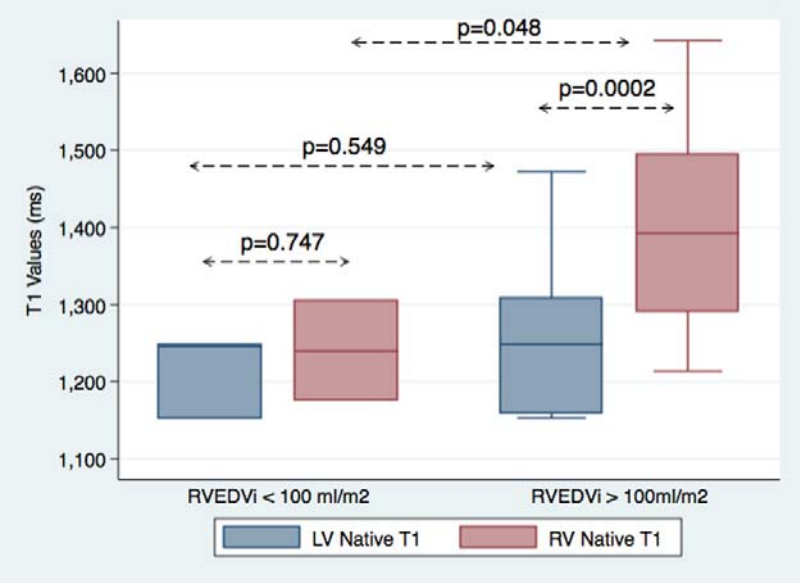

LV and RV Native T1 in Patients With and Without RV Dilatation

ID#: 374801

Frequency and distribution pattern of cardiac involvement in patients with limb-girdle muscular dystrophy (LGMD) - a multi-parametric CMR study

Pauline Schumacher[1], Anca R. Florian[2], Alexandru Patrascu[3], Michael Bietenbeck[4], Udo Sechtem, Prof. Dr.[3], Ali Yilmaz, Prof. Dr.[5]

1. University Hospital Münster, Germany

2. University Hospital Münster, Muenster, Nordrhein-Westfalen, Germany

3. Robert-Bosch Hospital Stuttgart, Baden-Wurttemberg, Germany

4. University Hospital Muenster, Nordrhein-Westfalen, Germany

5. University Hospital Münster, Nordrhein-Westfalen, Germany

Background: Limb-girdle muscular dystrophies (LGMD) are rare neuromuscular disorders that are characterized by muscle weakness and wasting predominantly affecting the extremities (proximal to a greater extent than distal). The LGMD family consists of several autosomal-dominant and -recessive forms, and a distinction between the different types requires protein analysis in skeletal muscle biopsies as well as genetic studies. Major causes of morbidity and mortality are cardiac and/or respiratory failure, however, data on the frequency and pattern of cardiac disease in LGMD are quite limited.

Methods: In a prospective two-center-study, 21 male patients with different forms of genetically-proven LGMD (median age 35yrs; range 15yrs to 73yrs) underwent comprehensive cardiac evaluations including multi-parametric cardiovascular magnetic resonance (CMR) imaging. The CMR study included (amongst others) cine- and late gadolinium enhancement (LGE)-imaging with quantification of myocardial damage.

Results: The study group comprised N=9 patients with LGMD-2I, N=4 with LGMD-2B, N=3 with LGMD-1B, N=3 with LGMD-2A, N=1 with LGMD-2C and N=1 with LGMD-2D. In all study patients (N=21), median left ventricular ejection fraction (LV-EF) was 56% with N=12 (57%) patients showing a reduced LV-EF. Median LV end-diastolic volume (LV-EDV) was 80ml/m² and a dilated LV was observed in N=2 (10%) patients only. Median right ventricular ejection fraction (RV-EF) was 57% with all patients showing a preserved RV-EF. Myocardial damage as assessed by LGE-imaging was detected in N=12 (57%) patients with a median myocardial damage extent of 5% (range 0 to 29%) and a subepicardial distribution pattern in the inferolateral LV wall segments in 7 out of 12 LGE-positive patients and an intramural septal pattern in the remaining 5 out of 12 LGE-positive patients. There were N=3 LGE-positive patients with a preserved LV-EF and N=3 patients showing a reduced LV-EF without the presence of LGE. Taken together, a pathological CMR finding was observed in N=15 (71%) patients with genetically-proven LGMD.

Conclusion: Cardiac involvement is a frequent finding in patients with different forms of LGMD and mostly characterized by either a subepicardial LGE-pattern in the inferolateral wall or an intramural LGE-pattern in the septal wall. The prognostic implications of these findings have to be evaluated in future studies.

ID#: 375550

Pediatric hematopoietic stem cell transplantation (HSCT) late effects on cardiovascular function and myocardial tissue characteristics

Elisabeth H.M. Paiman, MD[1]Marloes Louwerens, MD[2], Dorine Bresters, MD, PhD[3], Jos J.M. Westenberg, PhD[4], Qian Tao, PhD[5], Rob J. van der Geest, PhD[5], Arjan C. Lankester, MD, PhD[6], Arno A.W. Roest, MD, PhD[7], Hildo J. Lamb, MD, PhD[8]

1. Department of Radiology, Leiden University Medical Center, Leiden, The Netherlands, Netherlands

2. Department of Internal Medicine, Leiden University Medical Center, Leiden, The Netherlands, Netherlands

3. Department of Pediatrics, Leiden University Medical Center, Leiden, The Netherlands, Netherlands

4. Department of Radiology, Leiden University Medical Center, Leiden, The Netherlands, Leiden, Zuid-Holland, Netherlands

5. Department of Radiology, Leiden University Medical Center, The Netherlands, Leiden, Zuid-Holland, Netherlands

6. Department of Pediatrics, Leiden University Medical Center, Leiden, Netherlands

7. Department of Pediatrics, Leiden University Medical Center, Leiden, The Netherlands, Zuid-Holland, Netherlands

8. Department of Radiology, Leiden University Medical Center, Leiden, The Netherlands, Zuid-Holland, Netherlands

Background: Pediatric hematopoietic stem cell transplantation (HSCT) recipients are at increased risk of cardiovascular disease later in life. As HSCT long-term survival has significantly improved over the last decades, with a growing number of HSCT indications, greater understanding of the long-term complications is needed. Aim of this study is to assess the subclinical late effects in young adulthood of pediatric HSCT on cardiovascular function and myocardial tissue characteristics.

Methods: A total of 16 patients (age 22.1 ± 1.5 years, men: 11/16), who were treated with HSCT during childhood, and 16 healthy controls (age 22.1 ± 1.8 years, men: 10/16) underwent 3.0T cardiac MRI. Left ventricular ejection fraction (LVEF), global longitudinal and circumferential strain (GLS and GCS), longitudinal and circumferential peak systolic and early peak diastolic strain rate were extracted from bSSFP cine MRI. The ratio of early and late peak filling rate (E/A) and the estimated LV filling pressures (E/Ea) were based on 4D velocity-encoded MRI. LV myocardial tissue characteristics were assessed with proton-magnetic resonance spectroscopy (1H-MRS) and native T1 mapping. Aorta pulse wave velocity was measured using 2D velocity-encoded MRI (see Figure 1).

Results: Ten patients were transplanted for a hematologic malignancy (in preparation for HSCT, 6 received anthracycline therapy); 6 for a non-malignant disorder. Age at time of HSCT was 7.2 ± 5.3 years. MRI was performed 14.8 ± 5.0 years after HSCT. In the patient group compared to the control group, LVEF (54 ± 6% vs. 59 ± 5%, p=0.026) and GLS (-20.7 ± 3.5% vs. -23.3 ± 2.5%, p=0.019), but not GCS, were reduced. LV myocardial tissue characteristics, including myocardial triglyceride content and native T1 relaxation time, diastolic function and aorta stiffness were comparable for patients and controls (see Table 1).

Conclusion: In young adults with a history of childhood HSCT for malignant or non-malignant disease, but without clinical symptoms of cardiovascular disease, LVEF and GLS were reduced, while GCS was preserved, as compared to healthy controls in the same range of age. No differences in LV myocardial tissue characteristics, diastolic function and aorta stiffness were found between post-HSCT patients and healthy controls.

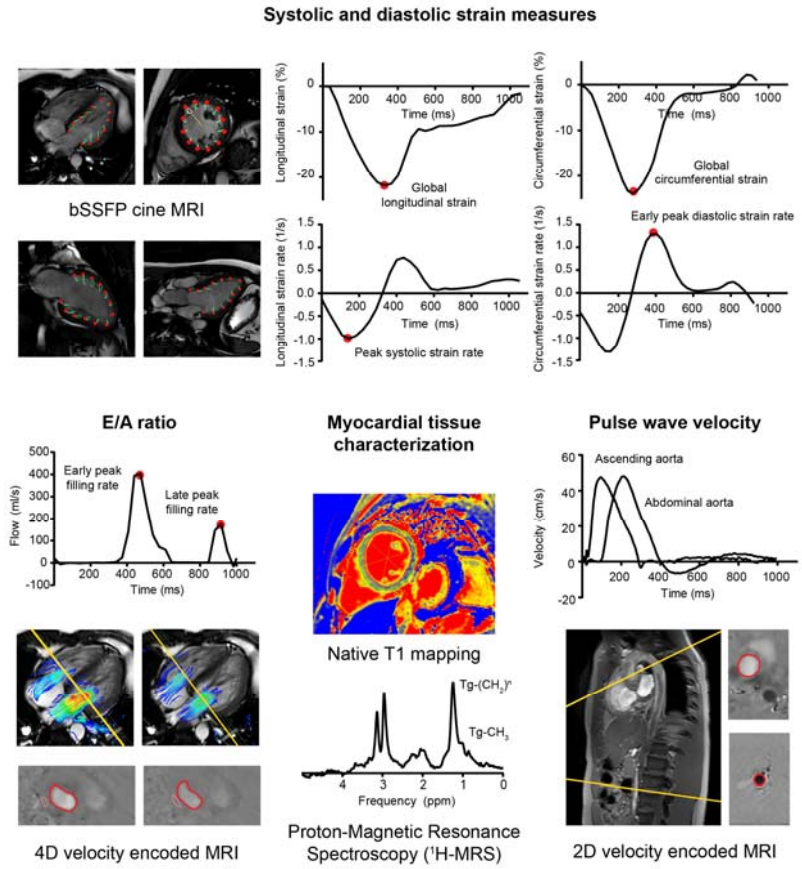

Figure 1. Cardiovascular function and myocardial tissue characteristics were measured using several MRI techniques. Example of a 22-year-old man, who was transplanted for a non-malignant bone marrow failure disorder at the age of 8 years. (upper panel) Longitudinal and circumferential strain curves were extracted from bSSFP 2-, 3- and 4-chamber and mid-ventricular short-axis cine MRI, using feature tracking. (lower panel, left) E/A ratio was based on 4D velocity encoded MRI, with retrospective mitral valve tracking. E/A ratio = early peak filling rate/late peak filling rate. (lower panel, mid) Myocardial tissue characterization comprised native T1 mapping and proton-magnetic resonance spectroscopy (1H-MRS) in the mid-ventricular septum. (lower panel, right) Aorta pulse wave velocity was calculated from through-plane 2D velocity encoded MRI transecting the ascending aorta and abdominal aorta, above the aortic bifurcation (aorta pulse wave velocity = $\Delta x/\Delta t$ (Δx: distance between ascending and abdominal aorta; Δt: transit time of the onset of the systolic velocity wave front).

MRI measures of cardiovascular function and myocardial tissue characteristics.

	Post-HSCT patients (n=16)	Healthy controls (n=16)	P-value
LV systolic function			
LV ejection fraction, %	54 ± 6	59 ± 5	0.026
Global longitudinal strain, %	-20.7 ± 3.5	-23.3 ± 2.5	0.019
Global circumferential strain, %	-23.2 ± 3.6	-24.3 ± 3.5	0.384
Longitudinal peak systolic strain rate, 1/s	-0.95 ± 0.20	-1.07 ± 0.20	0.102
Circumferential peak systolic strain rate, 1/s	-1.21 ± 0.22	-1.33 ± 0.25	0.175

LV diastolic function			
E/A ratio	2.21 ± 0.55	2.23 ± 0.51	0.915
E/Ea ratio	9.19 ± 2.63	7.55 ± 2.44	0.090
Longitudinal early diastolic strain rate, 1/s	1.01 ± 0.26	1.18 ± 0.32	0.105
Circumferential early diastolic strain rate, 1/s	1.28 ± 0.29	1.40 ± 0.34	0.297
LV myocardial tissue characteristics			
Myocardial triglyceride content, %	0.47 ± 0.18	0.50 ± 0.12	0.264
Native T1 relaxation time, ms	1211 ± 36	1229 ± 29	0.125
Aorta stiffness			
Aorta pulse wave velocity, m/s	4.40 ± 0.26	4.31 ± 0.29	0.468

ID#: 375600

Arterial geometry, flow and stiffness indices from thoracic aorta and carotid MRI in elderly hypertensives

Etienne Charpentier[1] David Rosenbaum, MD, PhD[1], Antonio Gallo, MD[2], Thomas Dietenbeck, PhD[2], Kevin Bouaou[2], Alain De Cesare, PhD[2], Xavier Girerd, MD[3], Alban Redheuil, MD, PhD[1], Nadjia Kachenoura, PhD[2]

1. Sorbonne Universités, UPMC Univ Paris 06, INSERM UMRS 1146, CNRS UMR 7371, Laboratoire d'Imagerie Biomédicale, Paris, Ile-de-France, France

2. Sorbonne Universités, UPMC Univ Paris 06, INSERM UMRS 1146, CNRS UMR 7371, Laboratoire d'Imagerie Biomédicale, Ile-de-France, France

3. Groupe hospitalier de la Pitié Salpétrière, APHP, Paris, France, Ile-de-France, France

Background: Vascular aging of the aorta and carotids is a major player in cardiovascular morbidity and overall mortality. Nevertheless, morphological and functional relationships between these two arterial sites remain largely unknown. The aim of our study was to assess during the same MRI examination geometry, flow and stiffness indices of the thoracic aorta and carotids in elderly hypertensive patients.

Methods: Fifty elderly hypertensive patients (mean age: 74±5 years, 68% males) had 3T MRI of the thoracic aorta and carotids as well as blood pressure measurements. Stiffness indices (strain and distensibility), lumen diastolic area and flow parameters in three different arterial sites: ascending aorta (AA), descending aorta (DA) and common carotid artery (CCA) were assessed using automated analysis (Artfun-LIB-UPMC) of SSFP cine and phase contrast images. Strain was calculated as (Systolic–Diastolic)/Diastolic area (%) and used to calculate distensibility as D=strain/PP where PP is the pulse pressure. Flow parameters included net global as well as forward (V_{FF}) and backward flow (V_{BF}) volumes. The backward to forward flow volume ratio (V_{BF}/V_{FF}) was calculated. We measured vessel wall thickness and the wall-to-lumen ratio (WLR) using QMass (MEDIS) on a proton density weighted-dark blood sequence. In this study, CCA measures were defined as the average of the two common carotid arteries.

Results: WLR and local distensibility increased gradually from AA to AD and CCA. Global common carotid net flow represented 24% of AA flow. BF volume decreased gradually from AA to AD and CCA as illustrated by the highest V_{BF}/V_{FF} value in the AA (Table 1). In the three sites, increased V_{BF}/V_{FF} ratio was related to increased vessel lumen area (AA: r^2=0.46, p<0.001; r^2=0.16, p=0.0049; CCA: r^2=0.15, p=0.0248). CCA distensibility was positively associated with AA (r^2=0.21, p=0.0051) and DA (r^2=0.26, p=0.0016) distensibilities. In multivariate analysis, these two associations remained significant independently of age and systolic blood pressure.

Conclusion: In elderly hypertensive patients, ascending aorta distensibility was lower than descending aorta and carotid distensibilities. The degree of CCA stiffness was significantly and positively associated with thoracic aorta stiffness. Flow analysis shows that backward flow exists predominantly in the thoracic aorta, particularly the ascending aorta and to a much lesser extent in carotids and essentially determined by local arterial geometry.

MRI measurements of ascending aorta (AA), descending aorta (DA) and common carotid artery (CCA) geometry, stiffness and flow.

	AA	DA	CCA
Geometry			
Lumen diastolic area, cm^2	9.30±2.18	5.11±1	0.41±0.11
Vessel wall thickness, mm	1.82±0.28	1.96±0.32	1.24±0.14
Wall-to-lumen ratio, %	11.1±2.2	16.1±3.2	40.1±10.4
Arterial stiffness			
Strain, %	5.88±2.57	8±3	20.7±10.3
Distensibility, $kPa^{-1}.10^{-3}$	7.64±3.69	10.4±4.61	26.3±14.4

Flow parameters			
Global flow volume, mL	59.1±15.5	48.5±13.1	6.70±1.81
Backward flow volume, mL	31.8±16.9	6.70±4.22	0.07±0.06
V_{BF} to V_{FF} ratio, %	33.7±10.9	11.9±6.42	1.03±0.78

ID#: 375687

Native T1 measurements from CMR identify severity of myocardial disease over time in patients with Duchenne muscular dystrophy on therapy

Laura Olivieri, M.D.[1] Imani Mojerie, B.S.[2], Karin Hamann, RN[2], Russell Cross, M.D.[3], Heather Gordish, PhD[2], Christopher Spurney, MD[4]

1. Children's National Medical Center, Washington, DC

2. Children's National Medical Center

3. Children's National Medical Center, Washington

4. Children's National Health System, Washington, DC

Background: Duchenne muscular dystrophy (DMD) is an X-linked inherited disorder causing dilated cardiomyopathy with variable onset and progression. Native T1 mapping by cardiac magnetic resonance (CMR) can detect subclinical fibrosis and correlates with extent of disease. It is unknown how fast the rate of change is with medical therapy directed towards DMD cardiomyopathy. We hypothesize that native T1 values will change minimally over time with treatment, thus our aim was to measure native T1 using a Modified Look-Locker (MOLLI) and Saturation Recovery (SASHA) sequences in boys with DMD treated with cardiac medications.

Methods: With IRB approval and informed consent/assent, 16 boys with DMD underwent two CMR exams with standard cine volumetry, late gadolinium enhancement (LGE) and native T1 mapping imaging using MOLLI and SASHA on a 1.5T MR scanner (Figure 1). Native T1 was measured in the septum and lateral wall in the base and mid portions of the heart using the “middle third” technique, and LGE extent and severity were scored 0-6. T1 measurements, ejection fraction (LVEF) and LGE scores were compared between the two time points.

Results: Sixteen DMD subjects (age 15.2±4.2 years; LVEF 56±7% at the first scan) underwent baseline CMR and followup CMR at an average of 14.1±2.8 months. At the time of followup scan, the subjects were 16.4±4.4 years old with LVEF 52±8%. All boys were on therapies directed at heart failure, including lisinopril, perindopril, and aldactone. Native T1 did not significantly change over the follow-up period. Septal T1 values were 1034±19 and 1020±37, (p=0.13) at the baseline and follow-up scans using MOLLI method, and lateral T1 values by MOLLI were 1074±44 and 1061 ± 48 at the baseline and followup exam (p=o.18). Eight boys developed new systolic dysfunction with an LVEF that decreased ≥5% but did not have a significant difference in rate of change in septal T1 values compared the subjects with no decrease in LVEF.

Conclusion: While on cardioprotective therapies, Native T1 levels did not change significantly in DMD subjects over one year. Native T1 mapping is a useful technique for monitoring subclinical myocardial changes and treatment effects over time.

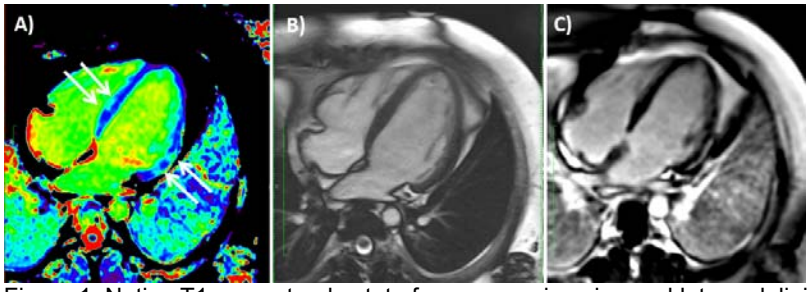

Figure 1. Native T1 map, steady-state free precession cine and late gadolinium enhancement images are depicted for a boy with DMD in panels A, B, and C, respectively. Arrows in panel A indicate irregular distribution of green pixels in the basal lateral wall and mid septum, corresponding to regions of elevated T1, while the myocardium on the LGE image is universally nulled, showing the limitation of LGE to detect diffuse fibrosis

ID#: 375884

Discordance of Aortic Regurgitation grading between Cardiac Magnet Resonance Imaging and Transthoracic Echocardiography.

Ulf Neisius, MD PhDThomas Hauser, MD MPH, Apranta Deka. Patel, MD, Warren J. Manning, MD

Beth Israel Deaconess Medical Center, Harvard Medical School, Boston, MA

Background: Cardiovascular magnetic resonance (CMR) allows direct quantification of aortic regurgitant volume (AR_{Vol}) and regurgitant fraction ($AR_{\%}$) by blood flow assessment in the proximal aorta. Advantages of CMR over transthoracic echocardiography (TTE) for AR assessment are highlighted in contemporary guidelines. We hypothesized that TTE and CMR grading systems are discordant.

Methods: We identified all patients referred for a CMR demonstrating at least moderate aortic regurgitation who also had a TTE within 6 months. Serial CMR scan were available in 13 patients leading to an additional inclusion of less than moderate CMR grades (n=13). CMR grades were calculated based on $AR_{\%}$ cut-off values suggested by ASE/SCMR guidelines ($AR_{\%}$ <30% mild, 30-49% moderate, ≥50% severe) [1] and by Gelfand et al. ($AR_{\%}$ % ≤15% mild, 16-48% moderate, >48% severe) [2]. Both CMR grading systems lack a minimal/trivial grade. TTE aortic regurgitation grades were extracted from reports interpreted by Level 3 trained readers.

Results: 127 studies in 116 patients (57.6±16.1 years, female 22%) were identified (median interval between CMR and TTE 44 days, range 0-182 day). The distribution of TTE and ASE/SCMR or Gelfand AR grades are summarized in the Table. Using the Kruskal-Wallis test, the TTE AR severity increased with volumetric CMR characterization of AR severity for both AR_{Vol} (13 ml [9;16], 18 ml [12;26], 30 ml [22;46], 65 ml [48;203]; P<0.001) and $AR_{\%}$ (18% [17;22], 19% [17;32], 30% [20;38], 48% [37;57]; P<0.001). Using the ASE/SCMR and Gelfand thresholds, CMR and TTE grading correlated mildly with a Spearman';s ρ=0.423 and ρ=0.286 (both, P<0.001), respectively. The agreement between TTE and CMR as assessed by the κ-statistic was low (ASE/SCMR, κ=0.134, CI (0.028, 0.240), P=0.007; Gelfand, κ=0.072, CI (-0.038, 0.182), P=0.107) with similar κ-values for both CMR grading systems.

Conclusion: TTE and CMR grading of aortic regurgitation severity are discordant using thresholds recommended both by the ASE/SCMR or Gelfand. These data highlight the need for CMR specific outcome research, as CMR/TTE grading system are not interchangeable.

1. Zoghbi WA, Adams D, Bonow RO, et al. Recommendations for noninvasive evaluation of native valvular regurgitation: a report from the American Society of Echocardiography developed in collaboration with the Society for Cardiovascular Magnetic Resonance. J Am Soc Echocardiogr. 2017;30:303-371. 2. Gelfand EV, Hughes S, Hauser TH, et al. Severity of mitral and aortic regurgitation as assessed by cardiovascular magnetic resonance: optimizing correlation with doppler echocardiography. J Cardiovasc Magn Resonance. 2006;8:503-507.

Agreement between CMR and TTE in severity of aortic regurgitation

		ASE/SCMR			Gelfand			
	AR Grade	Mild	Moderate	Severe	Mild	Moderate	Severe	n
TTE	None	17	0	0	2	15	0	17
	Mild	23	9	1	3	29	1	33
	Moderate	40	30	7	4	65	8	77
	Severe	2	6	5	0	8	5	13
	n	82	45	13	9	117	14	140

AR, aortic regurgitation; ASE, American Society of Echocardiography; SCMR, Society of Cardiovascular Magnetic Resonance; TTE, transthoracic echocardiography.

ID#: 375972

Active metallic-braided catheters and metallic guidewires equipped with miniature resonant floating RF traps (MBaluns) for heat amelioration: Designs and Validation

Ehud J. Schmidt, PhD[1] Eric Meyer[2], Ronald D. Watkins, CA[3], Hassan Elahi[2], Jeffrey Schweitzer, MS[4], Gregory Olson, BSME[5], Henry Halperin, MD, MA[2]

1. Johns Hopkins University, Towson, MD

2. Johns Hopkins University, Baltimore, MD

3. Stanford University, Redwood City, CA

4. St. Jude Medical, St. Paul, MN

5. Abbott, Plymouth, MN

Background: Conventional cardio-vascular invasive devices (catheters, guidewires) are frequently constructed of metallic tubes/rods or reinforced with metallic braids, since metal has desirable mechanical properties (yield stress, shear modulus), for thin (<3mm) long (>1000mm) structures which are manipulated from their proximal end. MRI-compatible devices contain minimal-length (<wavelength/4) metal, primarily to reduce body-coil-induced radiofrequency (RF) common-mode currents, which may heat surrounding tissues during high specific-absorption-rate (SAR) imaging. Additionally, sensors on the distal catheter (MR-tracking micro-coils, ECG-measuring/impedance-tracking electrodes) have cables running up the catheter shaft, which also receive body-coil induced currents. These cables currently require individual heat-amelioration solutions (transformers, resistors), which take-up space, and may attenuate desired (differential-mode) signals. Diagnostic MRI surface-coil cable-assemblies, which enclose multiple coaxial cables, are overlaid by periodic floating resonant RF traps (Baluns) [1] , attenuating common-mode.
Objective: Develop Miniature Baluns (MBaluns) for metallic-braided catheters or metallic-guidewires, permitting MRI-compatible constructs similar to conventional interventional devices. Test devices electrically and during MRI.

Methods: Novel MBaluns were electro-magnetically simulated, utilizing loosely-wound solenoids surrounding insulated, non-ferrous metallic tubes and braids, encompassing multiple micro-coaxial cables. We constructed; (1) A 1mm outer-diameter (OD) active guidewire (Fig. 1), based on a 0.5mm OD nitinol tube with an MR-Tracking coax passing within. MBalun-design1; 150mm spaced, 50mm-length/MBalun with 150 windings, 0.3mm pitch, 38 gage wire. (2) An 8 Fr irrigated EP catheter (Fig. 2), based on a 1.7mm OD tinned-copper braid, with 4 MR-tracking coaxes passing within. MBalun-design2; 150mm spaced, 15mm-length/MBalun with 50 windings, 0.3mm pitch, 38 gage wire. MBaluns were resonated at 63.8 MHz (1.5T) with miniature capacitors.
Network analyzer tests evaluated; (a) minimal desired (differential-mode) RF signal attenuation. (b) Strong attenuation of induced (common mode) signal on coaxial cables. (c) Strong attenuation of induced signal on metallic braids and tubes. Common-mode signals were induced onto the assemblies using larger transmit-coils. High SAR MRI tests were performed utilizing minimal-TR 90-degree flip-angle Steady-State-Free-Precession and 180-degree single-shot (ETL=256) Fast-Spin-Echo.

Results: Differential-mode signals were not (±0.2dB) attenuated, relative to control catheters without MBaluns. Common-mode signals (Fig. 3), responsible for heating, were attenuated by 15dB/Balun (1) and 8 dB/Balun (2). Common-mode propagation on the metallic-tube (1) or metallic-braid (2) were attenuated by 15dB/MBalun and 9dB/MBalun, respectively. No (±5degrees) flip-angle increase was observed around the shafts of (1) or (2) during MRI imaging (Fig. 4).

Conclusion: Common-mode RF-propagation was efficiently attenuated using MBaluns, allowing construction of MRI-compatible metallic devices (guidewires, catheters). **References**: [1] Seeber, ISMRM 2003 #2477 **Acknowledgements:** R01-HL094610, Abbott

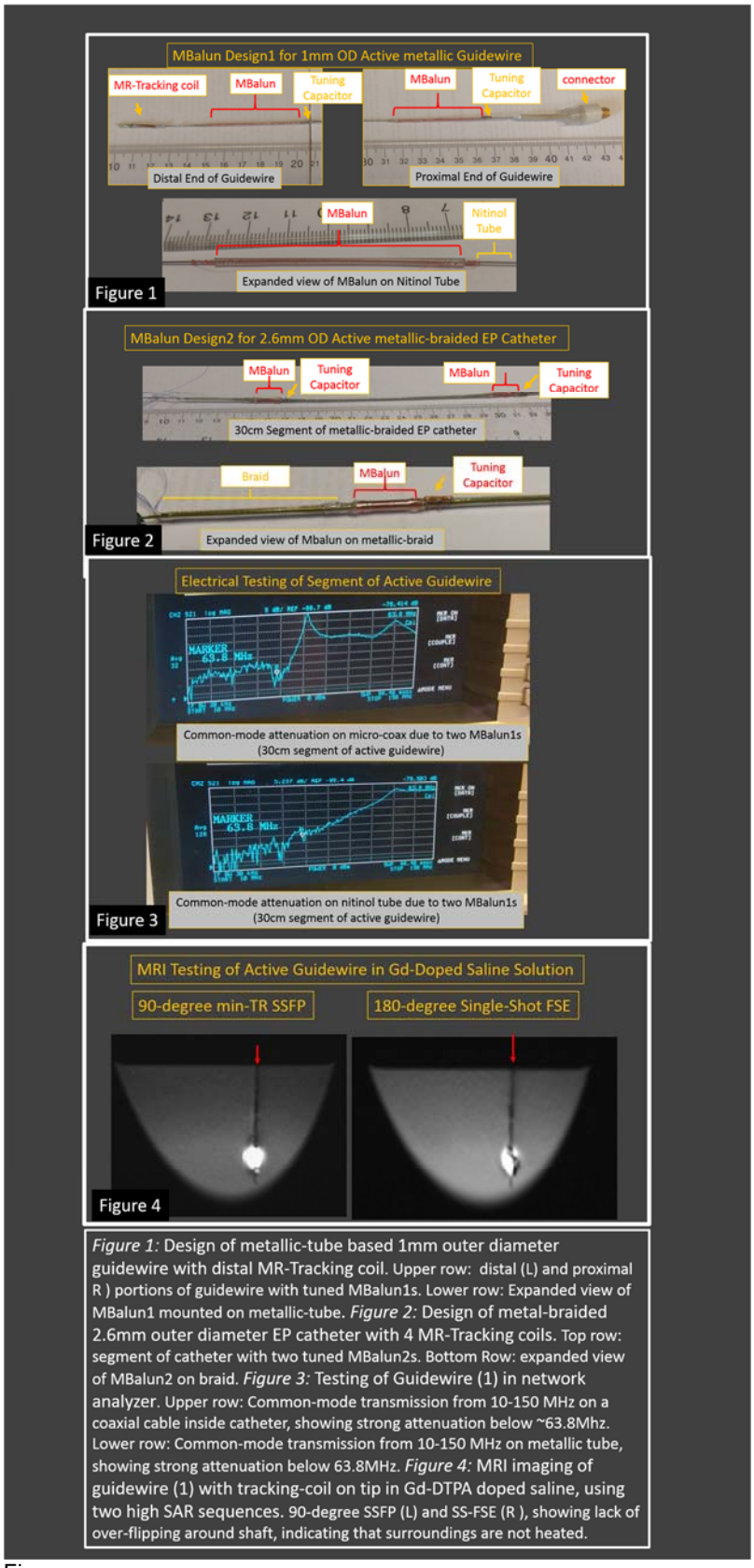

Figure 1: Design of metallic-tube based 1mm outer diameter guidewire with distal MR-Tracking coil. Upper row: distal (L) and proximal R) portions of guidewire with tuned MBalun1s. Lower row: Expanded view of MBalun1 mounted on metallic-tube. *Figure 2:* Design of metal-braided 2.6mm outer diameter EP catheter with 4 MR-Tracking coils. Top row: segment of catheter with two tuned MBalun2s. Bottom Row: expanded view of MBalun2 on braid. *Figure 3:* Testing of Guidewire (1) in network analyzer. Upper row: Common-mode transmission from 10-150 MHz on a coaxial cable inside catheter, showing strong attenuation below ~63.8Mhz. Lower row: Common-mode transmission from 10-150 MHz on metallic tube, showing strong attenuation below 63.8MHz. *Figure 4:* MRI imaging of guidewire (1) with tracking-coil on tip in Gd-DTPA doped saline, using two high SAR sequences. 90-degree SSFP (L) and SS-FSE (R), showing lack of over-flipping around shaft, indicating that surroundings are not heated.

Figure

ID#: 375975

Prevalence and clinical relevance of extra-cardiac findings in CMR imaging

Cesare Mantini[1]Francesco Bianco[1], Domenico Mastrodicasa, MD[2], Valentina Bucciarelli[1], Antonio Raffaele Cotroneo[1], Sabina Gallina[1], Fabrizio Ricci[3], Filippo Cademartiri[4]

1. Department of Neuroscience, Imaging and Clinical Sciences, "G. D' Annunzio" University, Chieti, Italy, Italy

2. Department of Neuroscience, Imaging and Clinical Sciences, "G. D' Annunzio" University, Chieti, Italy, Abruzzi, Italy

3. Department of Neuroscience, Imaging and Clinical Sciences, "G. D' Annunzio" University, Chieti, Italy, Pescara, Italy

4. Cardiovascular Imaging Center, SDN IRCCS, Naples, Italy, Italy

Background: The discovery of extra-cardiac findings (ECF) during cardiovascular magnetic resonance (CMR) is relatively common and might have clinical implications resulting in *de novo* diagnosis, referral for further imaging or early treatment initation. In this study, we sought to estimate the prevalence of ECF detected from clinically indicated CMR scans, and to determine the associated downstream effect on clinical management and resource utilization.

Methods: ECF were retrospectively evaluated in 500 consecutive patients undergoing CMR for different cardiovascular diseases. Two independent radiologists retrospectively reviewed transaxial balanced steady state free precession (bSSFP) multi-slice images acquired with a field of view including thorax and upper abdomen. The ECF were classified as clinically non-significant (benign, not supposed to require further investigations), clinically significant (potentially or absolutely considered to be of clinical significance, mandatory to be reported and monitored), and major (remarkable pathology, mandatory to be reported, further investigated and treated). A 15-month clinical follow-up was obtained from hospital records and referring physicians.

Results: Of 500 patients, 108 patients (21.6% of study population) had a total of 153 ECF, 59 (38.8%) non-significant, 76 (50%) significant and 18 (11.7%) major. The most frequent ECF were pleural effusion (35, 23%), hepatic cysts (27, 17.8%), renal cysts and ascending aorta dilatation (14, 9.2%). Of 94 significant and major ECF, 46 (36 clinically significant and 10 major) were previously unknown and more common in older patients. The 10 newly diagnosed major ECF (2% of study population and 6.5% of all IEFs), including tumors in 5 patients (1% of study population), were confirmed by downstream evaluations and required specific treatment. Patients with major ECF were older than patients without. Significant and major newly diagnosed ECF both required additional diagnostic tests respectively in 44% and 100% of cases.

Conclusion: ECF are increasingly being spotted by radiologists and cardiologists on CMR scans. Significant and major newly diagnosed ECF commonly requires further investigations. The detection of previously unknown major ECF has a strong impact on the course of patients'; clinical history. Knowledge and correct identification of most frequent ECF would allow early diagnosis and faster treatment initiation of unknown extra-cardiac pathologies in patients referred to CMR imaging for other reasons.

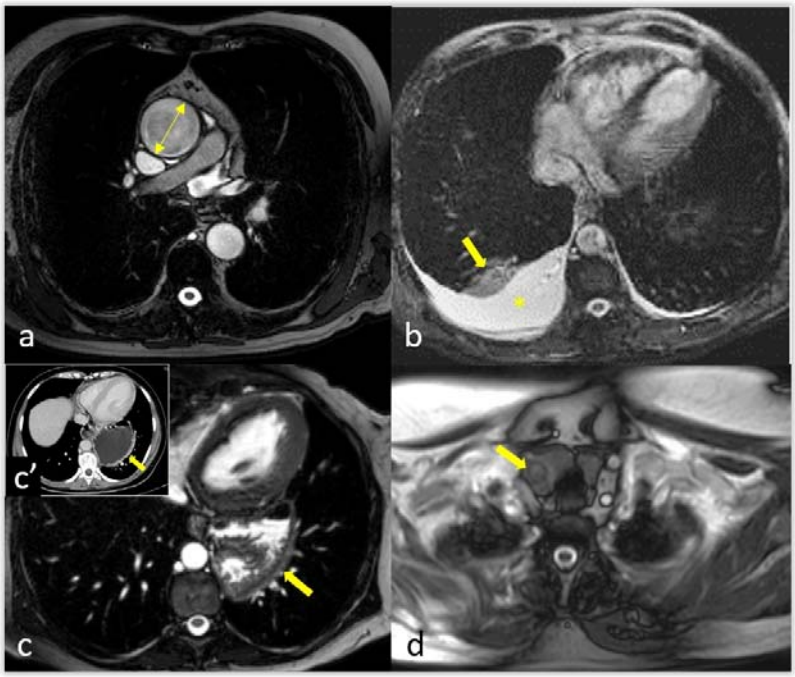
a
b
c'
c
d

ID#: 375745

Feasibility of noncontrast T1 and T2 parametric mapping in assessment of acute ventricular ablation lesions in children

Laura Olivieri, M.D.[1] Elena K. Grant, MBChB[2], Russell Cross, M.D.[3], Jeffrey Moak, MD[2], Charles Berul, MD[2]

1. Children's National Medical Center, Washington, DC

2. Children's National Medical Center

3. Children's National Medical Center, Washington

Background: Catheter ablation to treat ventricular arrhythmias in children is not always 100% effective using current techniques due to inadequate lesion development. Acute post-procedural presence of ablation lesions can be confirmed with contrast-enhanced cardiovascular magnetic resonance (CMR) using late gadolinium enhancement imaging (LGE), but LGE lacks quantitative information regarding extent of the lesion and resulting edema/tissue injury of the lesion. As concerns about exogenous contrast arise, it is important to determine if endogenous contrast mechanisms can be used to identify and describe the ablation lesion. Non-contrast, parametric mapping may further characterize and therefore identify inadequate lesions or gaps to guide further ablation and reduce risk of arrhythmia recurrence.

Methods: This pilot feasibility study assessed feasibility of endogenous contrast parametric mapping in acute post-procedure ablation lesions by MRI. Two children underwent ventricular tachycardia ablation were transferred immediately post-ablation to a 1.5T MRI scanner for imaging following appropriate consent/assent. Noncontrast T1 and T2 mapping were performed, along with standard LGE. T1 mapping was performed using a modified Look-Locker sequence on a 1.5T MR scanner. Immediate and short term arrhythmia recurrences were assessed.

Results: Patients were 17 and 9 years old with structurally normal hearts and normal function who underwent radiofrequency catheter ablation in the septal surface of the right ventricular outflow tract and below the right coronary cusp, respectively, with acute procedural success.). LGE was identified at the reported ablation site in both patients. Figure 1 shows CMR techniques used to visualize these ablation lesions in both patients. Both patients had regions of elevated native T1 (1547±583 and 1300±38) in the endocardium with a deeper and peripheral regions of lower T1 with high variance of signal intensity (872±345, 854±685) compared to remote myocardium (1040±86, 1059±51). T2 was elevated in both patients (132±26, 91±13) compared to remote myocardium (58±11, 51±8). The area of T1 abnormality was lower than area of T2 abnormality in identical slice positions (44 m2 vs 56 mm2, 98 mm2 vs. 151 mm2). Neither patient has experienced recurrence in 3 months of follow-up.

Conclusion: Ventricular ablation lesion visibility by noncontrast MRI in the acute post-procedure setting is feasible. MRI identification with parametric mapping may lend new insight into quantifying lesion adequacy which may provide the unique temporal opportunity for additional ablation therapy to decrease arrhythmia recurrence.

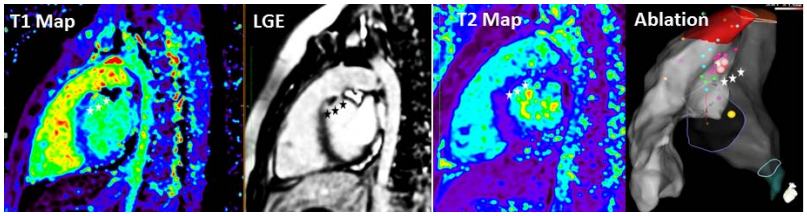

Figure 1. Sagittal view of a ventricular ablation lesion. The first panel shows native (noncontrast) T1 mapping using MOLLI technique where white stars indicate elevated T1 values (green) in the region around the site with a core of low T1 values (purple) and normal myocardium is blue/green; the second panel is an LGE image showing a core of dark tissue surrounded by a halo of bright enhancement as indicated by black stars, with normal myocardium being nulled; the third panel is a T2 map showing a diffuse region of elevated T2 values in the myocardium (blue) as indicated by the white stars whereas remote myocardium is purple. The final panel is the map of the ablation lesion placement in the right ventricular outflow tract, which correlates with the other imaging modalities.

ID#: 375769

Impact of gender and age on CMR parameters in repaired tetralogy of Fallot: insights from a large, prospective, international study of children and adults with chronic pulmonary regurgitation. From the CORRELATE study investigators

Benedetta Leonardi, MD[1] Camilla Calvieri[2], Christopher A. Caldarone, MD[3], Nagib Dahdah, MD[4], Frederic Dallaire, MD[5], Christian Drolet, MD[6], Jasmine Grewal, MD[7], Paul Khairy, MD, PhD[8], Brian McCrindle, MD[9], Najaf Nadeem, MD[10], Ming Yen Ng, BMBS FRCR[11], Edythe Tham, MD[12], Judith Therrien, MD[13], Isabelle Vonder Muhll, MD[14], Andrew Warren, MD[15], Michael Farkouh, MD, MSc[16], Rachel Wald, MD[17]

1. Ospedale Pediatrico Bambino Gesu, Rome, Rome, Lazio, Italy

2. Ospedale Pediatrico Bambino Gesù Roma, Lazio, Italy

3. Hospital for Sick Children, toronto, ON, Canada

4. Centre Hospitalier Universitaire (CHU) Sainte-Justine, Montreal, Quebec, Canada, Canada

5. University of Sherbrooke, Canada

6. CHU de Québec, PQ, Canada

7. St. Paul's Hospital - Providence Health Care, Vancouver, British Columbia, Canada, Vancouver, BC, Canada

8. Montreal Heart Institute, PQ, Canada

9. The Hospital for Sick Children (SickKids), Toronto, Ontario, Canada, Canada

10. Queen Elizabeth II (QEII) Health Sciences Centre - Halifax Infirmary, Halifax, Nova Scotia, Canada, Canada

11. The University of Hong Kong, Hong Kong

12. Stollery Children's Hospital, Edmonton, Alberta, Canada, Canada

13. Sir Mortimer B. Davis Jewish General Hospital, Montreal, Quebec, Canada, Canada

14. University of Alberta, Edmonton, AB, Canada

15. Izaak Walton Killam (IWK) Health Centre, Halifax, Nova Scotia, Canada, Canada

16. University of Toronto, toronto, ON, Canada

17. Division of Cardiology, University of Toronto, ON, Canada

Background: Ventricular volumes and function are important considerations for determining appropriate timing of pulmonary valve replacement (PVR) in the context of chronic pulmonary regurgitation (PR). The impact of gender and age on cardiac magnetic resonance (CMR) measures in patients with repaired tetralogy of Fallot (rTOF) and significant PR remains incompletely understood. Our objective was to explore gender and age-related differences in ventricular volumes, ventricular function, ventricular mass, atrial dimensions and length of dyskinetic right ventricular outflow tract (RVOT) segment in children and adults with rTOF.

Methods: Patients with rTOF and age ≥12 years were prospectively enrolled in Canada, Europe and Asia as part of the CORRELATE study (a comprehensive outcomes registry late after tetralogy of Fallot repair). All patients had moderate or severe PR and a CMR study completed within 18 months of study entry (with steady-state free-precession imaging for assessment of ventricular and atrial dimensions, and phase contrast flow analysis for quantification of PR). All CMR analyses were completed at a centralized facility by a blinded reader. Right ventricle (RV) and left ventricle (LV) volumes/function/mass were indexed to body surface area; atrial area was measured in ventricular systole; length of RVOT dyskinetic segment was recorded in systole and diastole. Patients were classified according to gender and age (<18 and ≥18 years). Statistical analysis included the student's t test and ANOVA for normally distributed variables; non-parametric tests were used for non-normally distributed data. A P value <0.05 was considered statistically significant.

Results: A total of 573 patients were studied (55% male, age 29±14 years at study entry); 25% of the population was <18 years. CMR measurements stratified by age and gender are shown in the Table. There were gender differences in all the parameters measured with the exception of PR. There were statistically significant differences in RV volumes, RV systolic function, biventricular mass, biatrial dimensions and length of dyskinetic RVOT segment in children versus adults; LV volumes were not statistically significant between age groups and LV systolic function showed borderline statistical significance.

Conclusion: With the exception of PR, all of the CMR measurements studied differed according to gender. There are important differences in children as compared with adults in measurements RV volumes, biventricular function, biventricular mass, biatrial dimensions and length of RVOT dyskinetic segment. Further study is required to better understand rate of change over time in CMR measurements and how these findings may contribute to clinical decision making regarding optimal timing of PVR.

Gender and Age Differences in CMR Parameters

	FEMALE ≥18years (N=191)	FEMALE <18years (N=65)	MALE ≥18years (N=238)	MALE <18years (N=79)	GENDER p value	AGE p value
PR_FRACTION	40 ± 14	38 ± 13	39 ± 15	37 ± 12	0.536	0.272
LVEDVi	80 ± 14	84 ± 14	89 ± 20	89 ± 14	<0.001	0.080
LVESVi	34 ± 8	37 ± 8	42 ± 13	39 ± 9	<0.001	0.653
RVEDVi	147 ± 36	141 ± 28	166 ± 45	154 ± 38	<0.001	0.011
RVESVi	80 ± 25	74 ± 21	97 ± 32	83 ± 24	<0.001	<0.001
LV EF (%)	57 ± 6	56 ± 5	53 ± 7	57 ± 7	<0.001	0.049
RV EF (%)	46 ± 6	48 ± 7	42 ± 8	46 ± 6	<0.001	<0.001
LV Mass	73 ± 15	65 ± 13	108 ± 25	79 ± 20	<0.001	<0.001
RV Mass	50 ± 10	47 ± 11	69 ± 16	56 ± 13	<0.001	<0.001
Right Atrial Area	20 ± 6	16 ± 4	24 ± 7	17 ± 4	<0.001	<0.001
Left Atrial Area	17 ± 4	13 ± 3	19 ± 5	14 ± 3	0.002	<0.001
Length of dyskinetic RVOT segment in systole	33 ± 11	25 ± 6	38 ± 13	27 ± 6	0.002	<0.001
Length of dyskinetic RVOT segment in diastole	33 ± 10	25 ± 8	38 ± 13	28 ± 7	0.001	<0.001

EF=ejection fraction; LVEDVi=left ventricular end-diastolic volume; LVESVi=left ventricular end-systolic volume; PR= pulmonary regurgitation; RVEDVi=right ventricular end-diastolic volume; RVESVi=right ventricular end-systolic volume; RVOT=right ventricular outflow tract

ID#: 375787

Early and late peak mitral inflow kinetic energy mapping of the left ventricle is associated with age in the healthy population

Saul Crandon, M.Res.[1] Pankaj Garg, MD, PhD[2], Peter P. Swoboda, PhD[3], James R. Foley, MBChB BSc (Hons)[3], Graham J. Fent, MBChB, BSc[3], Louise AE. Brown, MBChB, BMedSc[4], Pei G. Chew, MBChB(Hons) [5], Sebastian C. Onciul[4], Malenka Bissell, PhD[6], Jos J.M. Westenberg, PhD[7], Rob J. van der Geest, PhD[8], Erica Dall'Armellina, Sr., MD, DPhil[9], John P. Greenwood, PhD[4], Sven Plein, MD PhD[4]

1. University of Leeds, United Kingdom

2. University of Leeds, UK, Leeds, England, United Kingdom

3. University of Leeds, Leeds, England, United Kingdom

4. University of Leeds, England, United Kingdom

5. University of Leeds, Liverpool, England, United Kingdom

6. Leeds Institute of Cardiovascular and Metabolic Medicine, United Kingdom

7. Department of Radiology, Leiden University Medical Center, Leiden, The Netherlands, Leiden, Zuid-Holland, Netherlands

8. Department of Radiology, Leiden University Medical Center, The Netherlands, Leiden, Zuid-Holland, Netherlands

9. Leeds Institute of Cardiovascular and Metabolic Medicine, Division of Biomedical Imaging,University of Leeds, United Kingdom

Background: Diastolic function can be assessed using the peak velocity of early and late mitral filling (peak E- and A-waves respectively). However, even in physiologic aging, peak mitral velocities have been shown to deteriorate. This is due to ventricular stiffening, which can impair diastolic relaxation. It is unknown whether a kinetic energy (KE) assessment of mitral filling offers similar measurements when compared to a traditional transmitral velocity evaluation. The aim of this work was to investigate the association between diastolic velocities and LV flow KE with increasing age.

Methods: A total of 53 healthy volunteers underwent CMR at 1.5T (Ingenia CV, Philips Healthcare, Best, The Netherlands). The CMR protocol included: 2-chamber, 3-chamber, 4-chamber cines and 4D flow CMR with isotropic voxel size ($3\times3\times3mm^3$), parallel imaging (SENSE 2), VENC 150cm/s in all three directions and using echo-planar imaging (EPI) to factor 5 for read-out acceleration. Free breathing was allowed and no respiratory motion correction was used. Peak E- and A-wave velocities were derived by validated retrospective valve tracking methods. Peak E- and A-wave mitral inflow KE parameters were derived by mapping the entire LV KE in diastole and were normalised by end-diastolic volume. Correlation analysis and multiple linear regression with backwards elimination methods were used to assess association.

Results: Age was negatively correlated with peak E-wave velocity ($r= -0.27$, $p=0.05$) and peak E-wave flow KE ($r= -0.54$, $p<0.0001$). Both peak A-wave velocity and peak A-wave flow KE also demonstrated an association to age ($r= 0.40$, $p=0.003$ and $r= 0.58$, $p<0.0001$ respectively). A strong correlation was also seen between the E/A velocity ratio and E/A flow KE ratio ($r= 0.77$, $p<0.0001$), with both being negatively correlated to increasing age ($r= -0.55$, $p<0.0001$ and $r= -0.69$, $p<0.0001$ respectively). A multiple linear regression of all velocity and KE parameters found that peak E-wave flow KE ($\beta= -0.79$, $p<0.00001$) and A-wave flow KE ($\beta= 1.31$, $p<0.00001$) were independently associated with age.

Conclusion: Peak E-wave and A-wave flow KE are more closely associated with age than traditional mitral filling velocities in healthy volunteers. Further research is warranted to investigate whether LV flow KE parameters can offer improved classifications of diastolic function in patient populations.

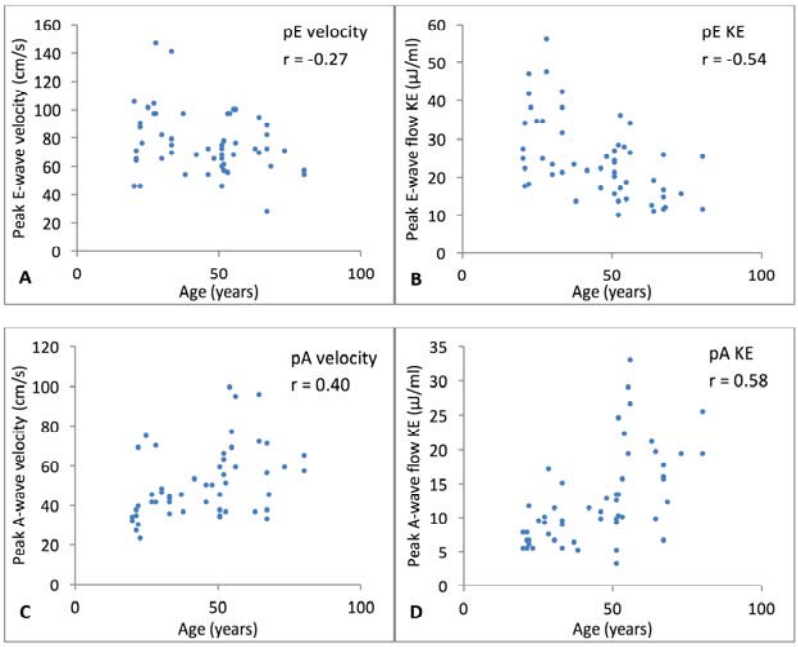

Figure 1. Correlation plots of age against various KE flow parameters. Panel A = age vs peak E-wave velocity, Panel B = age vs peak E-wave KE, Panel C = age vs peak A-wave velocity, Panel D = age vs peak A-wave KE. Peak E and A velocities are given as cm/s, whereas peak E and A flow KE values are given as µJ/mL.

Figure 2. Left ventricular flow kinetic energy (KE) mapping in early diastole in a healthy volunteer in 4-chamber (left-hand panel) and 2-chamber views (right-hand panel).

Table 1. Baseline characteristics of the 53 healthy volunteers.

Characteristic	Mean	SD
Age (yrs)	45	17
Male (n)	N=31	
BSA (m^2)	1.8	0.2
LVEDVi (ml/m^2)	85.9	18.1

LVESVi (ml/m^2)	33.2	10.2
SVi (ml/m^2)	52.7	9.8
EF (%)	61.8	5.2
LVEDMi (g/m^2)	52.2	10.1
LV peak E-wave velocity (cm/s)	76.7	22.0
LV peak A-wave velocity (cm/s)	51.0	17.6
LV peak E-wave KE(μJ/ml)	24.7	10.4
LV peak A-wave KE (μJ/ml)	12.7	6.9
E/A ratio	1.6	0.6
KE E/A ratio	2.6	1.8

ID#: 375795

Evaluation of Myocardial T1 Mapping and Extracellular Volume (ECV) After Pediatric Heart Transplantation

Margaret M. Samyn, MD[1] Adam Gordon, BS[2], Ann Punnoose, MD[3], Ke Yan, PhD[2], Benjamin Goot, MD[4], Joseph Cava, MD PhD[5], Mary Krolikowski, MSN, RN[2], Steve Kindel, MD[6]

1. Medical College of Wisconsin/ Children's Hospital of Wisconsin, Milwaukee, WI

2. Medical College of Wisconsin

3. Children's Hospital of Wisconsin, Milwaukee, WI

4. Medical College of Wisconsin, WI

5. Medical College of Wisconsin/ Children's Hospital of Wisconsin, WI

6. Medical College of Wisconsin/Children's Hospital of Wisconsin, WI

Background: Cardiac allograft health may be affected by donor ischemic time, cell/antibody mediated rejection, coronary allograft vasculopathy, and chronic immunosuppressive therapy. Coronary allograft vasculopathy and episodic rejection result in fibrotic remodeling of the myocardium detectable by cardiac magnetic resonance imaging (CMR), especially by assessing longitudinal relaxation times (T1). Acquisition of native and post contrast T1 allows for calculation of extracellular volume (ECV). These data may serve as biomarkers for allograft health, although few studies have looked at pediatric transplant recipients. This pilot study sought to characterize a pediatric heart transplant population by CMR.

Methods: Eleven pediatric heart transplant patients underwent CMR scans on a Siemens 3 Tesla Skyra® scanner from September 2016 to July 2017 at Children's Hospital of Wisconsin. Standard cardiac cine imaging was performed. T1 basal, mid, apical short axis left ventricular (LV) images were obtained before (native T1) and approximately 15 minutes after the administration of 0.2 mmol/kg gadodiamide (Gd). Cardiac volumetric data, T1 mapping (native and post Gd contrast), late Gd enhancement, and extracellular volume (ECV) were determined using CMR software (CVI42, Circle® Cardiovascular Imaging software). Relationships between CMR data and clinical data (donor ischemic time, number of rejection episodes, time from transplant, New York Heart Association (NYHA) class) were investigated using Pearson's correlation coefficients.

Results: 3 females and 8 males (median age 14.5 years, range 8.9 - 19.3 years) were scanned with median time from transplant (9 years, range 6.2 - 17.8 years). All were NYHA class 1, and none had coronary allograft vasculopathy. T1 and ECV data are given in the table. Median ECV at basal, mid, and apical LV were 28, 28, and 29 % - with some subjects above normal range (25.3 ± 3.5%). A significant negative correlation was seen for time from first rejection and native T1 for the entire LV (r= - 0.88, p=0.047), indicating that more recent rejection corresponded with increased T1. No other correlations were significant, although a few trends were noted.

Conclusion: As the first pilot 3T CMR pediatric heart transplant myocardial characterization study, these data are intriguing and warrant further investigation to understand the utility of T1 mapping and ECV as measures of cardiac allograft health.

T1 and ECV Data for Pediatric Transplant Recipients

	Native T1 median (range) n = 8 (msec)	Post Gd T1 median (range) n = 8 (msec)	ECV median (range) n = 8 (%)
Basal LV Global Intra ventricular septum Free wall	 1235 (1182 - 1322) 1239 (1217 - 1353) 1233 (1150 - 1313)	 517 (419 - 575) 520 (415 - 578) 517 (423 - 579)	 28 (24 - 32)

Mid LV			
Global	1243 (1079 - 1323)	512 (416 - 581)	28 (25 - 33)
Intra ventricular septum	1245 (1086 - 1298)	517 (423 - 583)	
Free wall	1247 (1089 - 1365)	513 (410 - 574)	
Apical LV			
Global	1247 (1101 - 1412)	500 (415 - 573)	29 (25 - 37)
Intra ventricular septum	1252 (1077 - 1390)	500 (413 - 579)	
Free wall	1266 (1116 - 1446)	507 (414 - 572)	

ID#: 375814

Ventricular volume assessment in Adult Congenital Heart Disease using single breath-hold Compressed-Sensing Cardiac Cine MR

Srinivas Ananth Narayan, MRCPCH, MD[1] Phuoc Duong, MD[2], Bram Ruijsink, MD[3], Radhouene Neji, PhD[4], Christoph Forman, PhD[5], Michaela Schmidt[5], Carmel Hayes, Ph.D.[6], Yaso Emmanuel, MRCP[7], Alessandra Frigiola, MRCP[8], Kuberan Pushparajah, MRCPCH, MD[9], Reza Razavi, MD, PhD[3]

1. Kings College London, Harrow, United Kingdom

2. King's College London, United Kingdom

3. King's College London, London, England, United Kingdom

4. Siemens Healthcare, MR Research Collaborations, Siemens Healthcare Limited, United Kingdom

5. SIEMENS HEALTHCARE GmbH, Erlangen, Bayern, Germany

6. Siemens Healthineers, Bayern, Germany

7. Guys and St. Thomas Hospital, United Kingdom

8. Guys and St. Thomas NHS Trust, United Kingdom

9. Kings College London, United Kingdom

Background: Patients with congenital heart disease (CHD) frequently have difficulty with serial breathholds needed for accurate ventricular volume assessment and complying with the long duration needed for cardiac MRI. Accelerated acquisition techniques such as Compressed-Sensing (CS), permitting acquisition of reduced data amount and recovery of the remaining portion of data by well-defined algorithms, has been reported to be useful in non-CHD patients. Once validated, this could reduce scan duration and avoid volumetric error caused by inconsistent breath-holds.
Our prospective study aims to compare ventricular volume measurement in healthy volunteers and patients with CHD using CS single breath-hold multi-slice, real-time cine b-SSFP (balanced steady-state free precession) with the current standard multiple-breath-hold 2D segmented cine b-SSFP (2D-cine) stack (Table 1).

Methods: Healthy volunteers and CHD patients were imaged with 1.5T scanner (MAGNETOM® Aera, Siemens). A prototype CS cine sequence was performed with a single breath-hold (14-24s) immediately after the standard 2D-cine sequence using the same geometry, slice thickness and at least two-thirds the phases of the 2D-cine sequence. Image quality was scored on a five-point Likert scale (Table 2). Ventricular volumes were calculated using manual endocardial contouring (Circle® cmr42®) in visually identified end-systolic and diastolic phases independently by two experienced MR physicians. Use of gadolinium-based contrast, image quality acquisition and reporting time were recorded. Statistical comparisons were made using Intra-class correlation coefficient and Bland-Altman analysis.

Results: 21 patients with CHD and 5 volunteers (15 male, median 71kg (45-130kg), median 24yrs (18-55 yrs.)) were included (Table 3). A gadolinium-based contrast was used in 19% of the cases. Scan time (seconds) was significantly ($p<0.05$) shorter for CS (21±2s) compared to conventional stacks (422±111s). Image quality score was 3.8±0.5 for CS and 4.5±0.5 for 2D-cine ($p<0.05$, Figure 1). Bland-Altman analysis (Figure 2) revealed no significant differences in ventricular volumes obtained by either method (RVEDV $p = 0.09$, RVESV $p=0.14$, LVEDV $p=0.09$, LVESV $p=0.74$). Two-way mixed-effects model of the intra-class correlation coefficient (ICC) demonstrated good-to-excellent inter-observer reliability scores (ICC average measures 0.72 to 0.96). There was no significant difference in reporting time between the 2 sequences; CS (536±171s) vs. 2D-cine (553±131s) ($p= 0.22$).

Conclusion: CS cine sequence allows accurate assessment of ventricular volumes in adult CHD, with reduced scanning time and reliable slice registration within a single breath-hold. This is invaluable for patients with learning difficulties or claustrophobia when a pure volumetric assessment is needed. It could help increase the throughput of patients in a busy clinical environment.

Main Diagnosis	N	Percentage
Volunteers (normal heart)	5	18
Coarctation of Aorta	3	11
Patent foramen ovale	3	11
Aortic stenosis	2	8
Pulmonary atresia, ventricular septal defect (repaired)	2	8
Tetralogy of Fallot	2	8
Patent ductus arteriosus	2	8
Marfan Syndrome	2	8
Ventricular septal defect (repaired)	1	4
Transposition of the great arteries (post arterial switch operation)	1	4
Total anomalous pulmonary venous drainage (repaired)	1	4
Ebstein's anomaly (unrepaired)	1	4
Mitral valve disease	1	4
Total	26	100

Table 3: Diagnosis in patients recruited

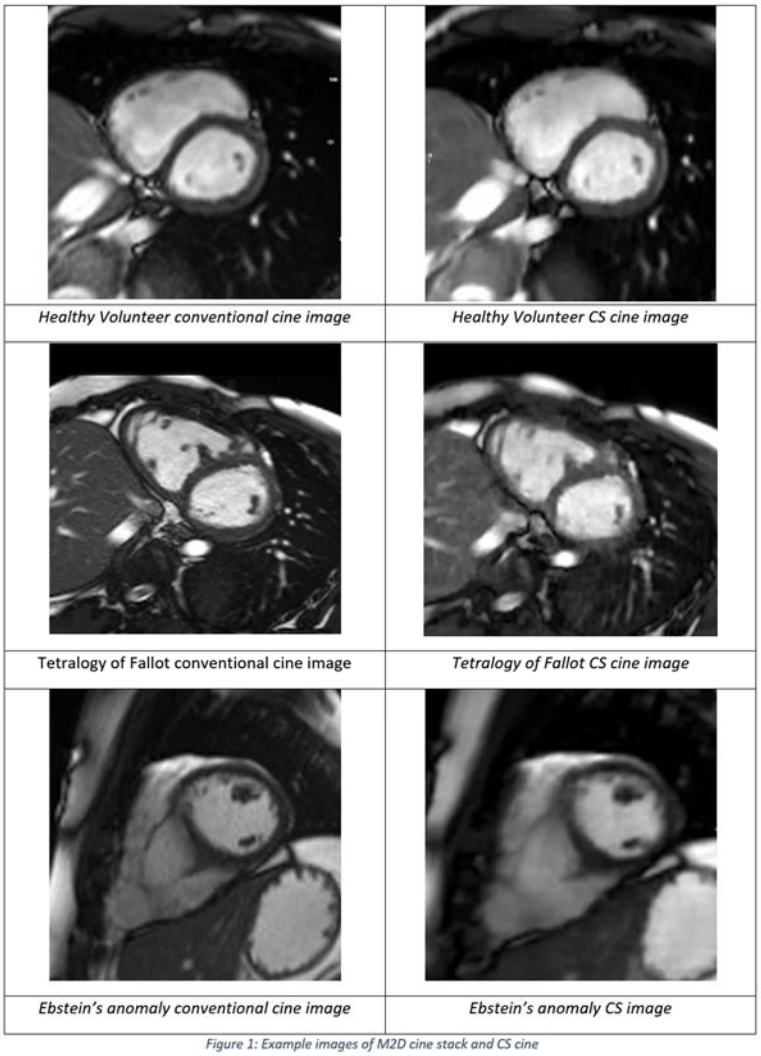

Figure 1: Example images of M2D cine stack and CS cine

Figure 1: Example images of M2D cine stack and CS cine

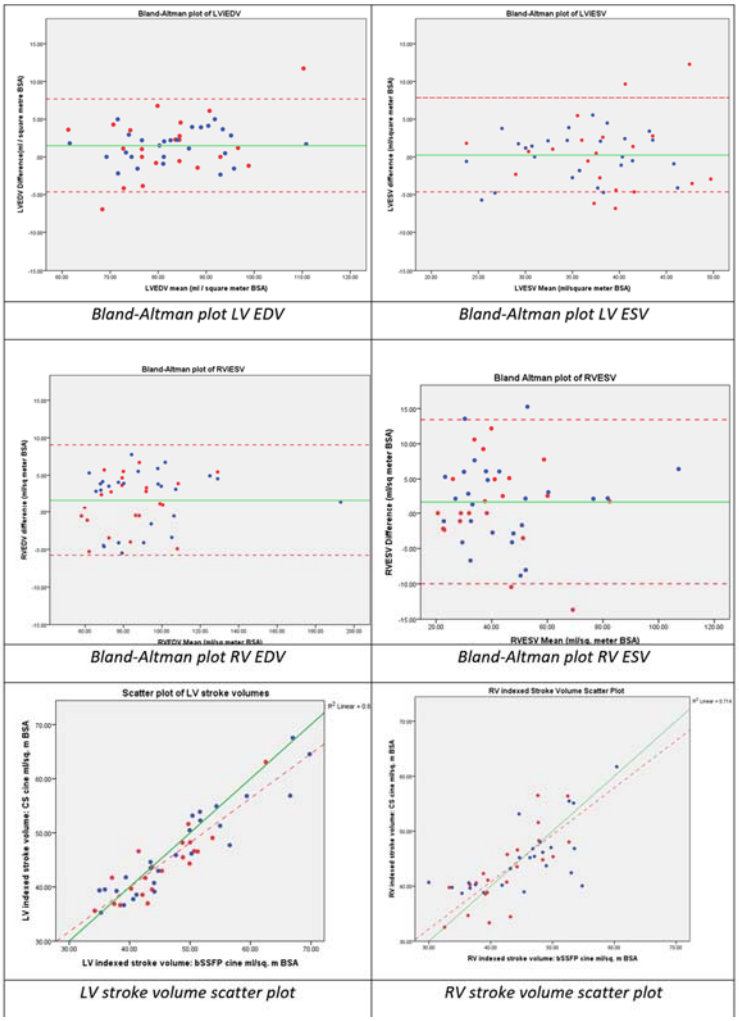

Figure 2: Top four figures show Bland-Altman analysis of ventricular volumes (normalised for body surface area) between two methods (CS compared to conventional cine). The green continuous line is the mean difference (Cine Volume - CS volume) and red hashed lines are 95% confidence limits. The bottom two figures show scatter plot of LV and RV stroke volumes respectively. The green continuous line marker indicates the reference identity line, and the red dotted line is the linear fit line. Note that LV volumes tend to me more accurate (R2= 0.85) than RV (R2 = 0.71). In all figures, red dots indicate physician PD and blue dots physician SAN. [BSA = Body Surface Area, LV = Left Ventricle, RV = Right Ventricle, ESV=End Systolic Volume, EDV=End Diastolic Volume, SV=Stroke Volume (EDV-ESV)

Table 1: Image Protocol Parameters

Parameter	CS breath hold ECG Triggered sequence	M2D Cine stack
Field of view (mm)	320-360	320-360
Recon Matrix	192x105	192x105
Number of 'sections';	10-14	10 – 14
Breathholds (n)	1	4 - 8
Breath hold duration (s)	14 – 24	8 – 14 per segment
Number of profiles per cardiac phase	16 – 24	30

Acquired Voxel	2.7x1.9x10	1.5 x 1.5 x 7 – 10
Recon Voxel	1.9	1.125
Repetition time (ms)	2.6	3 – 4
Echo time (ms)	1.11	1.6 – 2
Flip angle	57	60
Triggering	Retrospective	Prospective
Acceleration factor	10.4	2
Iterations	60	NA

Table 2: Five-point Likert Scale used for qualitative grading of cine images

Score	Description of quality
1	Non-diagnostic with significant artefact affecting volumetric analysis
2	Inferior quality, moderate artefact affecting volumetric analysis
3	Adequate quality, mild artefact affecting volumetric analysis
4	Superior quality, minimal artefact
5	Excellent quality, no artefact

ID#: 375206

Infarct healing during long-term follow-up after ST-elevation myocardial infarction

Hans-Josef Feistritzer, MD[1]Gert Klug, MD[1], Sebastian Reinstadler, MD[1], Martin Reindl[1], Christina Tiller, MD[1], Lukas Müller[1], Agnes Mayr, MD[2], Bernhard Metzler, MD[1]

1. University Clinic of Internal Medicine III, Cardiology and Angiology, Medical University of Innsbruck, Austria

2. University Clinic of Radiology, Medical University of Innsbruck, Austria

Background: Infarct healing is sought to be a dynamic process occurring in the subacute and chronic phase after ST-elevation myocardial infarction (STEMI) and is preferentially investigated by means of cardiac magnetic resonance (CMR) imaging. Previous studies indicate a reduction of infarct size (IS) during the post-infarct period. However, these studies are limited by either a short period of follow-up or small sample sizes. We aimed to investigate the change of IS, assessed by CMR, during a 12 months period of follow-up in a large cohort of STEMI patients all treated by primary percutaneous coronary intervention (PPCI).

Methods: In this prospective observational study, we included 141 consecutive revascularized STEMI patients. CMR scans were performed 2 [2-4] and 367 [365-380] days after infarction to assess infarct characteristics. IS was expressed as percentage of left ventricular myocardial mass. Biomarkers were measured in clinical routine using standard assays.

Results: IS significantly decreased between baseline (17% [8-26%]) and 12 months (9% [3-14%]) ($p < 0.001$). Patients without IS reduction (n = 9, 6%) showed a higher rate of diabetes (n = 3, 33% vs. n = 8, 6%; $p = 0.024$) compared to patients with IS reduction (n = 132, 94%). IS reduction was higher in younger patients and patients without hypertension (both $p = 0.023$). Peak natriuretic peptide levels at baseline were lower in patients showing high IS reduction ($p = 0.034$).

Conclusion: In mechanically reperfused STEMI patients IS decreases during 12 months. Young age, absence of hypertension and low levels of natriuretic peptides are associated with more pronounced IS reduction.

ID#: 375222

Repeatability of myocardial T1 and T2 mapping using MR Fingerprinting and comparison to clinical standards

Shivani Pahwa, MD[1] Jesse I. Hamilton, B.S.[2], Sanjay Sridaran, BS[3], Joseph A. Adedigba[4], Rahul Thomas, MD[5], Gregory O'Connor, BS[6], Ozden Kilinc[2], Nicole Seiberlich, Ph.D.[7], Vikas Gulani, MD, PhD[8], Sanjay Rajagopalan, MD[9], Mark Griswold, Ph.D.[10]

1. University Hospitals Cleveland Medical Center/CWRU

2. Case Western Reserve University, Cleveland Heights, OH

3. Case Western Reserve University School of Medicine, Cleveland Heights, OH

4. Tulane University, New Orleans, LA

5. University Hospitals Cleveland Medical Center, Cleveland, OH

6. CWRU School of Medicine

7. Case Western Reserve University, Clevelad, OH

8. Case Western Reserve University, Cleveland, OH

9. University Hospitals

10. Case Western Reserve University; University Hospitals, OH

Background: Multiple weighted images collected along an inversion recovery or T_2 decay curve are typically required for T_1 or T_2 mapping[1,2]. Traditional cardiac relaxometry techniques are prone to errors due to deviations of the signals collected from the relaxation model, as well as motion and variations in heart rate[1,2]. MR Fingerprinting (MRF) allows simultaneous mapping of multiple tissue properties and includes the timing of cardiac motion into the signal model, yielding relaxometry maps with fewer deleterious effects from motion[3,4]. The hypotheses of this work were that MRF-derived simultaneous measurements of normal myocardial T_1 and T_2 are comparable to clinical standard techniques, and intra- and inter-reader repeatability of these measurements are also similar to clinical standards

Methods: T_1 and T_2 maps were acquired in three short axis slices in 30 healthy volunteers (M:F- 16:14; average heart rate 71 bpm) at 1.5 T (Siemens Aera) using an MRF sequence with ECG triggering in diastole and a breathhold duration of 15 heartbeats (192x192 matrix, 300mm^2, 1.6x1.6x8.0mm^3 spatial resolution, TR 5.1ms, FA 4-25deg) [3]. T_1 maps were also acquired using MOLLI with a 5(3)3 acquisition pattern, and T_2 maps were collected using a T_2 prepared bSSFP sequence with preparation times of 0, 25, and 55ms[4,5]. Repeatability of the methods was tested by acquiring a single mid-ventricular slice at the beginning and the end of the scan in all volunteers. Acceptable image quality couldn';t be obtained with any of the tested sequences to evaluate segment 17.
MRF data were processed in MATLAB to generate T_1 and T_2 maps, and regions of interest (ROI) drawn across standardized myocardial AHA segments. Deming regression analysis was used to compare proportional and systematic errors between the sequences. Same day repeatability repeatabilty, intra- and inter-reader agreement (between two readers) were assessed using intra-class coefficient (ICC).

Results: The average myocardial T_1 relaxation time was 974.2+/-73.1 ms with MRF and 973.2+/- 34.4 ms with MOLLI (Figures 1,2); the average T_2 relaxation time was 41.1+/- 4.2 ms with MRF and 46.5+/-2.6 ms with bSSFP (Figure 1,2). Deming regression analysis revealed no proportional or systematic errors in the acquisition methods at segmental and slice levels. ICC revealed fair to excellent agreement for same day repeated measurements for T_1 and T_2 relaxation times for MRF, MOLLI and bSSFP (Table 1). Good to excellent agreement was obtained for intra-reader repeatability measurements (Table 2a). Fair to excellent agreement was obtained in inter-reader variability except for segment 11, where the agreement was poor (Table 2b).

Conclusion: MRF provides repeatable normative cardiac relaxometry values in normal volunteers. **References:**

1. Hamlin, et al. RadioGraphics 2014; 34:1594-1611
2. Kellman, et al. *Journal of Cardiovascular Magnetic Resonance* 2014;16:2
3. Hamilton, et al. Magnetic Resonance in Medicine. 2016 Apr 1. doi: 10.1002/mrm.26216.

4. Messroghli DR, et al. Magn Reson Med 2004; 52:141–146.
5. Piechnik SK, et al. J Cardiovasc Magn Reson 2010;12:69

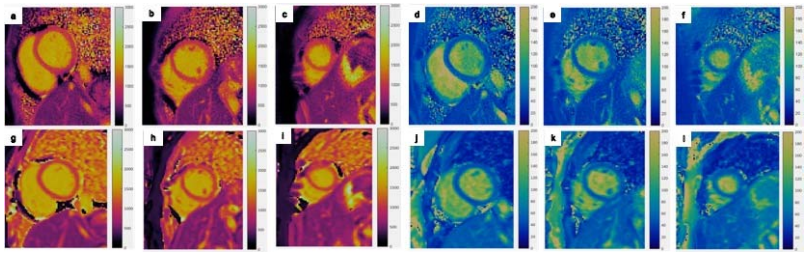

Figure 1: Short axis views through the heart. The top row depicts MRF-derived maps: base (T1-a; T2-d), mid (T1-b; T2-e) and apex (T1-c; T2-f); the bottom row depicts MOLLI (T1) and bSSFP (T2) derived maps- base (T1-g; T2-j), mid (T1-h; T2-k) and apex (T1-i; T2-l).

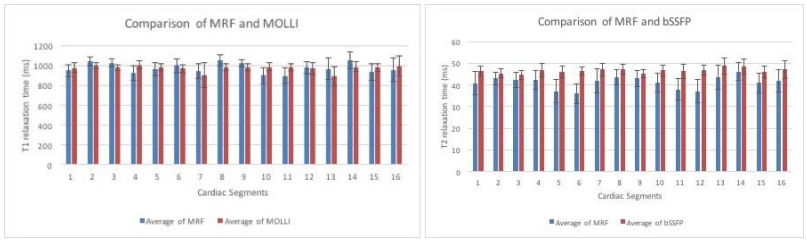

Figure 2. A comparison of myocardial T1 and T2 relaxation time (ms) obtained in normal volunteers in 16 AHA* segments using MRF, MOLLI (T1) and T2-prepared bSSFP (T2). Segment 17 was not evaluated because acceptable quality could not be obtained with any of the tested sequences *AHA = American Heart Association. Error bars represent standard deviation.

Repeatability for MRF, MOLLI and bSSFP tested on mid-ventricular slice acquired twice at the beginning and the end of the scan using intra-class coefficient (ICC)* in 30 volunteer datasets

	MOLLI	MRF T1	bSSFP	MRF T2
Segment 7	0.847	0.933	0.816	0.846
Segment 8	0.646	0.94	0.848	0.865
Segment 9	0.714	0.768	0.745	0.81
Segment 10	0.779	0.64	0.846	0.715
Segment 11	0.818	0.811	0.802	0.85
Segment 12	0.801	0.88	0.836	0.821
Average	0.877	0.911	0.823	0.868

*ICC values <0.40 indicate poor correlation; 0.40-0.59 indicates fair correlation; 0.60-74 indicates good correlation; 0.75-1.00 indicates excellent correlation

-

Intra-reader repeatability (a), and inter-reader repeatability (b) for MRF for two repeated measurements at mid- ventricular slice level in 20 volunteers datasets using intra-class coefficient (ICC)*.

	a) Intra-reader repeatability		b) Inter-reader repeatability	
	MRF T1	**MRF T2**	**MRF T1**	**MRF T2**
Segment 7	0.938	0.94	0.788	0.885
Segment 8	0.96	0.951	0.958	0.806
Segment 9	0.84	0.842	0.724	0.462
Segment 10	0.909	0.923	0.645	0.915
Segment 11	0.777	0.963	0.366	0.918
Segment 12	0.939	0.965	0.826	0.937
Average	0.95	0.951	0.835	0.883

*ICC values < 0.40 indicate poor correlation, 0.40-0.59 indicates fair correlation; 0.60-74 indicates good correlation; 0.75-1.00 indicates excellent correlation.

ID#: 374932

Automatic Image-Based Background Phase Correction in the Presence of Wrap-Around Artifact

Aaron A. Pruitt, B.S.[1] Yingmin Liu, Ph.D.[1], Ning Jin, Ph.D.[2], Orlando Simonetti, PhD[3], Rizwan Ahmad, PhD[3]

1. The Ohio State University, Columbus, OH

2. Siemens Medical Solutions USA, Inc., OH

3. The Ohio State University, OH

Background: Residual background phase (BP) offsets in phase-contrast (PC) MRI can negatively impact flow quantification accuracy in the great vessels of the heart, which may lead to mischaracterization of intracardiac shunts or valvular regurgitation fraction [1]. Commonly utilized polynomial regression of static pixels in the phase image is unreliable in the presence of significant wrap-around artifact [2]. In this work, we present an extension of our recently proposed Outlier Rejection (OR) scheme [3] to identify and exclude wrap-around artifact from the fitting and demonstrate its improvement on flow quantification *in vivo*.

Methods: Nineteen healthy volunteers (age range, 19-44, two females) were scanned on a 3T system (MAGNETOM Trio, Siemens Healthineers). For each volunteer, breath-held 2D PC-MRI datasets from different imaging planes transecting the ascending aorta, the pulmonary arteries, and the descending aorta at the level of the abdomen were acquired using routine clinical parameters. Out of 103 datasets, 29 were collected with and 74 were collected without the wrap-around artifact. As reference, all PC-MRI acquisitions were repeated on a stationary phantom immediately after the volunteer was removed from the magnet. Background phase was corrected with a second order polynomial using weighted least squares (WLS) alone and WLS with the addition of OR. The general procedure for OR is summarized in Figure 1. Flow volume was calculated for each vessel before and after background phase correction and the results were compared to stationary phantom correction.

Results: An example in Figure 2 demonstrates the impact of wrap-around artifact on background phase correction. Here, WLS alone fails to exclude the wrap-around leading to an erroneous background phase correction. Addition of OR successfully excludes the artifact, decreasing flow quantification error by 6.5 % in the ROI. Figure 3 compares measured flow volumes after WLS and WLS+OR correction to the values obtained after stationary phantom correction using Bland-Altman analysis. When wrap-around artifact is not present, WLS and WLS+OR show comparable agreement with the stationary phantom correction, with limits of agreement (LOA) 5.7% and 4.7%, respectively. Both show stronger agreement than no correction (LOA 22%). In the presence of wrap-around artifact, WLS alone performs worse overall (LOA 16%) than no correction (LOA 8.6%); however, addition of outlier rejection outperforms both with LOA of 3.4%. A small bias of 0.65% was detected in this last case (p=0.05).

Conclusion: These preliminary results demonstrate that the performance of polynomial regression degrades in the presence of wrap-around artifact and the proposed outlier rejection scheme is robust to such artifact. Future studies aim to evaluate the clinical impact of WLS+OR in patient populations. **References 1.** Gatehouse et al. JCMR 2010 12:5 **2.** Gatehouse et al. JCMR 2012 14:72 **3.** Pruitt et al. Proc ISMRM 2017 2844.

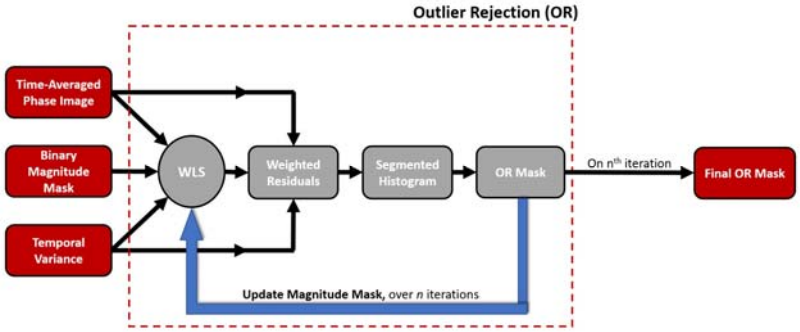

Figure 1. General procedure for Outlier Rejection (OR). The magnitude mask is initialized using only the center 50% of pixels in the phase encoding direction. After a weighted least squares (WLS) fitting with second order polynomial, the histogram of residuals is segmented to identify and exclude pixels (outliers) with high weighted residual. We empirically observed that two iterations of the above procedure were adequate.

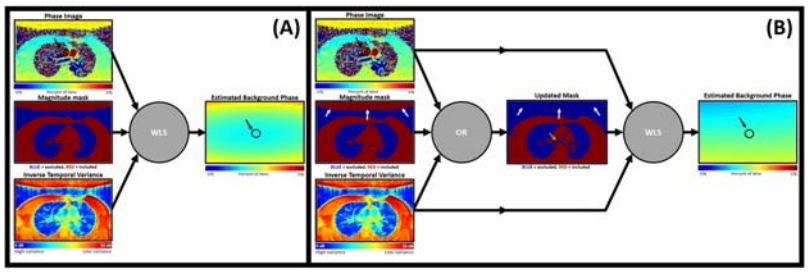

Figure 2. (A) Example of the WLS method in the aorta. Note, how the wrap-around artifact has influenced the correction map. (B) Same example from A using WLS+OR. Here, the wrap-around artifact is almost entirely excluded (white arrows). Regions of steady flow are also excluded using WLS+OR (green arrow). The difference in measured flow volume in the ROI (black arrow) between A and B is 4.52 mL or 6.5%.

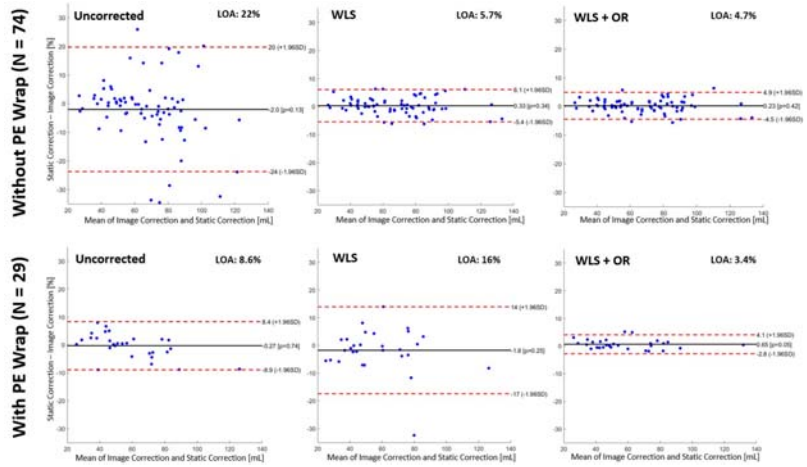

Figure 3. Bland-Altman plots comparing WLS and WLS+OR to stationary phantom correction. WLS and WLS+OR are comparable when wrap-around artifact is not present and are both superior to no correction. When wrap-around artifact is present, WLS alone performs worse than no correction; however, WLS+OR shows a major improvement over both methods.

ID#: 375138

The role of cardiovascular magnetic resonance imaging in prediction of developement of pulmonary hypertension in patients with severe aortic stenosis

Audrone Vaitiekiene, MD[1] Birute Gumauskiene, MD[2], Lina Padervinskiene, MD[2], Antanas Jankauskas, Assoc. prof[2], Dziugas Kreckauskas, MD[3], Gryte Galnaitiene, MD[2], Paulius Simkus, MD[2], Egle Ereminiene, Prof.[2]

1. Lithuanian University of Health sciences, Kauno Rajonas, Kauno Apskritis, Lithuania

2. Lithuanian University of Health Sciences, Lithuania

3. Vilnius University Hospital Santaros Klinikos, Lithuania

Background: Development of pulmonary hypertension (PH) in patients with severe aortic stenosis (AS) is associated with poor outcomes. Therefore, it is important to define the underlying mechanisms of PH. The aim of the study was to determine the clinical value of left ventricle (LV) fibrosis and feature tracking using cardiovascular magnetic resonance (CMR) in patients with isolated severe AS and PH.

Methods: 27 patients with isolated severe AS (aortic valve area (AVA) < 1 cm^2), who underwent Doppler-echocardiography and CMR evaluations before aortic valve replacement were prospectively enrolled. Patients with documented coronary heart disease, chronic obstructive pulmonary disease, atrial fibrillation or mitral regurgitation were excluded from the study. Pulmonary hypertension was estimated using Doppler echocardiography and defined as pulmonary systolic pressure (PSP) ≥ 45 mmHg. CMR protocol included cine imaging in two, three, four chamber and short axis views, phase contrast velocity encoding, late gadolinium enhancement (LGE). Left ventricle end-diastolic and end-systolic volumes (EDV, ESV), LV mass and ejection fraction (EF) were calculated using a semi-automatic Syngovia analysis marking endocardial and epicardial borders. Fibrosis quantification was evaluated calculating fibrosis and LV mass ratio by marking areas of LGE manualy and dividing to LV myocardial mass (Slice thickness in all images was equal). LV feature tracking analysis was performed using Medis program. LV global longitudinal and circumferential strain and strain rate (GLS, CS, GLSR, CSR, respectively) were quantified from standard cine images. Statistical analysis was performed using Microsoft Excel and “SPSS for Windows 23.0”.

Results: Data of 27 patients were analysed. Patients were classified into group A (AVA vs. 103,29±7,64g/ m^2) were not different between groups (p>0,05), as well as LV EF 50,4±5,32% vs. 59,77±2,68% (p>0,05). LV strain and strain rate didn‘t differ between groups (LV GLS(-15,9±3% vs. -17,78±1,26%), LV CS (-30,56±4,76% vs. -35,76±2,17%, p>0,05), GLSR (-0,8±0,2% vs. -0,67±0,35%, p=0,35), CSR (-1,8±0,6% vs. 1,6±0,9%, p=0,64)). LV fibrosis area and myocardial mass ratio were significantly higher in group of patients with AS and PH, compared with AS group without PH (1,94±2,22 mm^2/g vs. 0,68±0,95mm^2/g, p=0,05).

Conclusion: The extent of LV fibrosis, not LV strain and strain rate has impact on developing pulmonary hypertension in patients with isolated severe aortic stenosis.

ID#: 374818

Parameters of biventricular deformation in patients with repaired and unrepaired Ebstein's anomaly - assessment by tissue tracking cardiovascular magnetic resonance

Simona Marcora[1]Roland Weber[2], Angela Oxenius[3], Christine Attenhofer Jost[4], Emanuela R. Valsangiacomo Buechel[5]

1. Azienda Ospedaliera Papa Giovanni XXIII , Bergamo, Bergamo, Italy

2. University Children's Hospital Zurich, Zurich, Switzerland

3. University Children's Hospital Zurich, Zurich, Zurich, Switzerland

4. Klinik im Park, Zurich, Switzerland

5. University Childre's Hospital Zurich, ZUrich, Switzerland

Background: Ebstein's anomaly (EA) of the tricuspid valve (TV) is a complex disease of the right heart. Cardiac output is influenced by right ventricular (RV) function, contraction of the atrialized RV (before and after repair) , left ventricular (LV) function, including non-compaction (LVNC). We sought to assess LV and RV myocardial deformation in unrepaired and repaired EA by using feature tracking (FT) CMR and the influence of other factors on myocardial deformation and global function.

Methods: Biventricular function was prospectively assessed by cine CMR using the SSFP sequence in 20 patients (pts) with EA. Short-axis and long-axis images were analyzed by FT (software Qstrain, Medis Version 3.3) for assessing endocardial circumferential (GCS) and longitudinal strain (GLS) of both ventricles. Image temporal resolution was < 25 msec. Median age was 44.5 (17-64) years, weight 68 (51-108) kg, 9 females. Six pts (30%) had undergone TV repair, LVNC was present in 12 (60%) cases. FT strain results were compared with our own previously published normal values. Correlation with LVNC, degree of TV displacement, ventricular volumes and ejection fraction (EF %) was tested.

Results: Mean RV endiastolic volume (RVEDV) was 137±34 ml/m2; RV endsystolic volume (RVESV) 86±33 ml/m2, RVEF% 39±10. RV dilatation (> 110ml/m2) was present in 18/20 pts, independently from valve repair. Mean LVEDV was 87±26 ml/m2; LVESV 42±16 ml/m2; LVEF% 53±10. LV GCS was normal (-26.3±8% vs -26.1±3.8%). GLS was decreased in the LV and RV compared to normal subjects (LV GLS -16.6±4% vs 21.3±4.8; p<0.01 and RV GLS -12±6% vs 18.9±4.6; p<0.001). RV GLS was more decreased in the RV septum than in the RV free wall (12.2±6% vs 22.8±7.3; p 0.0002). Presence of LVNC, previous TV repair, degree of TV displacement did not influence EF%, nor global strain values of both ventricles (p > 0.05). LV GCS correlated with LV GLS (r 0.749, p<0.001), LVESV and LVEF% (r 0.7128; p<0.001). A weak correlation was also found between LV GCS and RV GLS (r 0.55; p 0.01). LV GLS correlated with LVESV (r-0.52; p 0.01), LVEF% (r 0.7128; p<0.001), RV GLS (r 0.49; p 0.029), but not with RVEF%. RV GLS significantly correlated with RVESV (r -0.5;p 0.02) and RVEF % (r 0.54;p 0.01). LVEF% and RVEF% did not correlate to each other.

Conclusion: Patients with EA have a dilated RV with decreased RV GLS and EF% independently from the severity of TV displacement or TV repair. Deformation of RV septum is more affected than the free wall. LV GCS is normal, but LV GLS is decreased. Presence of LVNC does not affect LVEF% or LV myocardial deformation.

ID#: 374669

Extra-cardiac findings detected by CMR in a Thai population with Thalassaemia major - findings from the TIC-TOC study

Amna Abdel-Gadir, MBBS.MRCP(UK)[1] Yongkasem Vorasettakarnkij, Co-first author[2], Hataichanok Ngamkasem[3], Sabrina Nordin, MRCP [4], Katia Devorha. Menacho, MD[5], Heerajnarain Bulluck, MBBS PhD[6], Emmanuel Ako, MBBS[7], Peter Kellman, Ph.D.[8], Stefan K. Piechnik, PhD, MScEE[9], Juliano L. Fernandes, MD, PhD[10], Charlotte Manisty, MRCP PhD[11], Mark Westwood, MBBS MD FRCP FESC[12], Malcolm J. Walker, MD[13], James C. Moon, MD[14], Monravee Tumkosit, MD[15]

1. University College London and Barts Heart Centre, London, England, United Kingdom

2. Chulalongkorn University and King Chulalongkorn Memorial Hospital, Bangkok, Thailand

3. Phyathai Sriracha Hospital, Sriracha, Chon Buri, Thailand

4. Barts Heart Centre, United Kingdom

5. Barts Heart Centre, London, England, United Kingdom

6. Papworth Hospital NHS Trust, Cambridge, UK, England, United Kingdom

7. Royal Brompton and Harefield NHS Trust, United Kingdom

8. National Heart, Lung, and Blood Institute, Bethesda, MD

9. University of Oxford, England, United Kingdom

10. Jose Michel Kalaf Research Institute, Campinas, Brazil

11. Barts Heart Centre and University College London, United Kingdom

12. Barts, England, United Kingdom

13. University College London, London, United Kingdom

14. Barts Heart Centre, England, United Kingdom

15. Chulalongkorn University and King Chulalongkorn Memorial Hospital, Thailand

Background: CMR is essential for cardiac iron quantification. In the TIC-TOC study, we performed ultrafast CMR in the developing world. We report the extra-cardiac and incidental findings.

Methods: A single center study in a government hospital in Bangkok, Thailand utilizing ultrafast CMR scanning of the heart and liver for iron quantification. Patients were recruited by the Chulalongkorn Thalassemia Support Group, and were receiving regular blood transfusions. Images were analyzed by a certified radiologist and level 3 CMR accredited cardiologist.

Results: 148 patients were recruited (30.8 ± 13 years; 61% female). CMR was performed using a 1.5T scanner (Aera, Siemens). Each scan was typically 9-10 breath-holds – localizers/pilots, dark blood T2* and T1 mapping of the myocardium and liver, SSFP long axis cines (SA stack if these abnormal), and an anatomical HASTE stack. Patients did not receive contrast agents. Mean scan duration was 7.8 ± 2.1 minutes with complete analysis within 1 minute of last image acquisition. Nearly all patients (99%) had liver iron loading (figure 1a). 105(71%) had extra cardiac findings (table 1). 60(57%) had more than one extra cardiac abnormality. Findings were (in descending order) paravertebral extramedullary hematopoiesis (n=61; 40%, figure 1b), splenomegaly (n=34; 23%), hepatomegaly (n=25; 17%), main pulmonary artery dilatation (n=22; 15%, figure 1c), and pericardial effusions (n=14; 10%). Rare but important findings were hepatocellular carcinoma (patient was urgently referred for treatment, but died) and one large atrial septal defect (referred for closure, figure 1d).

Conclusion: Ultrafast CMR in the developing world detects a high prevalence of significant extra-cardiac findings.

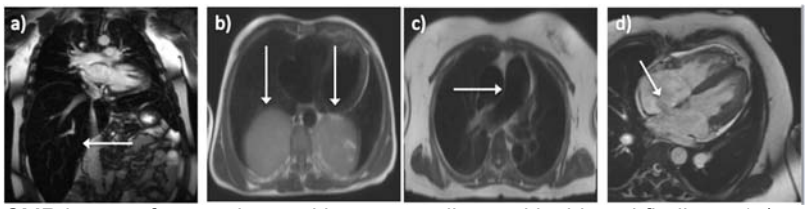

CMR images from patients with extra-cardiac and incidental findings. 1a) a severely iron overloaded liver; 1b) paravertebral extramedullary haematopoiesis; 1c) main pulmonary artery dilatation; 1d) atrial septal defect.

Table 1. Extra cardiac findings in transfusion dependent thalassaemia patients

Findings	**n**	**%**
Extramedullary haematopoiesis • Paravertebral • Rib expansion • Enlarged thymus	 61 6 5	 40 4 3
Hepatomegaly	25	17
Splenomegaly	34	23
MPA dilatation	22	15
Pericardial effusion	14	10
Pleural effusions	2	1.4
Scoliosis	3	2
Splenectomy	7	5
Cysts • Liver • Spleen	 2 1	 1.4 0.7
ASD	1	0.7
Liver mass	1	0.7
Breast prosthesis	1	0.7
Mediastinal lymphadenopathy	1	0.7

ID#: 374544

Impact of a breathing-maneuver stimulus on myocardial oxygenation and left ventricular strain in patients with coronary artery disease

Barbara Spicher[1]Dominik P. Guensch, MD, DESA[2], Kyohei Yamaji, MD[2], Silvia Luescher[3], Yasushi Ueki, MD[2], Bernd Jung, PhD[4], Hendrik von Tengg-Kobligk, MD[5], Stephan Windecker, MD[6], Balthasar Eberle, MD[7], Kady Fischer, PhD[8]

1. Inselspital Bern, Anesthesia, Switzerland, Bern, Switzerland

2. University Hospital Bern, Inselspital, Switzerland

3. University Hospital Bern, Inselspital, Bern, Bern, Switzerland

4. Inselspital Bern, Institute for Diagnostic, Interventional and Pediatric Radiology, Bern, Switzerland

5. Inselspital, Switzerland

6. Department Cardiology, University Hospital Bern, Bern Switzerland, Bern, Bern, Switzerland

7. Department of Anesthesiology, Inselspital / University Hospital Bern, Bern, Bern, Switzerland

8. McGill University Health Center, University Hospital Bern, Montreal, PQ, Canada

Background:

Oxygenation-Sensitive (OS)-CMR can detect myocardial oxygenation changes during a vasoactive stimulus. Recently, we have used voluntary hyperventilation and breath-holding as a replacement to pharmacological vasodilators to detect oxygenation deficits in coronary artery disease (CAD). OS cines provide the advantage that they can also provide information on myocardial contractility from the same image acquisition. The functional significance of these oxygenation changes during this stimulus on contractility has yet to be investigated.

Methods: Nine patients with a diameter stenosis >50% in a coronary artery (assessed by quantitative coronary angiography, QCA) and 6 healthy subjects were studied. OS images were acquired in a 3T scanner with an ECG-triggered cine sequence in a basal and mid-ventricular slice (1 image/4 heartbeats). After acquisition of a baseline cine, the participants were instructed to hyperventilate for 60s (30 breathes/min) and an OS-cine was repeated immediately thereafter in the same slice locations for the duration of the subsequent maximal breath-hold. Peak radial strain was obtained from each cine measurement using feature tracking software, and OS-signal was measured at each end-systolic measurement. The oxygenation was assessed as a %-change in signal. Δ-change in peak radial strain was calculated for the response over hyperventilation, and for the 30s mark of the breath-hold.

Results:

All patients completed the breathing maneuvers including an extended breathhold after hyperventilation (52±28s). In healthy controls, hyperventilation significantly reduced oxygenation, while increasing the peak radial strain (Table). The breath-hold had a reverse effect with increasing oxygenation and strain returning to baseline levels. With apnea, the remote territory in CAD patients had a significant decrease in strain, following the trend of the controls, while the strain response of the myocardium perfused by a stenosed vessel did not return to baseline. This was accompanied by a drop in oxygenation in the same segments.

Specifically with hyperventilation, the ability of tissue to significantly drop oxygenation during hyperventilation signifies a normal vascular reactivity, which is accompanied by an increase in contractility seen in the controls. In the post-stenotic segments, we observed that an abnormal oxygenation response resulted in a more pronounced attenuation in the radial strain response (r=-0.68, p=0.04) after hyperventilation (figure). This correlation was not seen in remote myocardium and healthy controls.

Conclusion: An impaired oxygenation response after a hyperventilation and a short apneic stimulus translated into attenuated strain responses in the post-stenotic tissue of coronary artery disease patients as compared to remote myocardium and healthy volunteers.

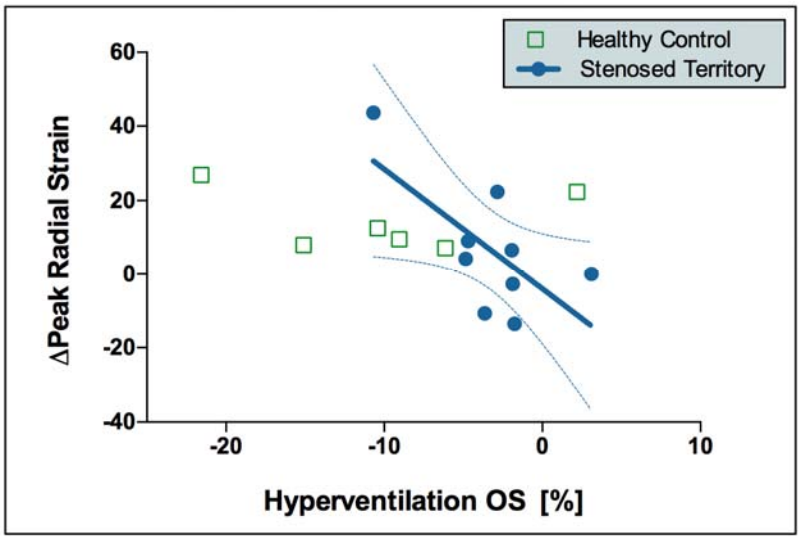

Hyperventilation induces a myocardial oxygenation drop in healthy controls (green), along with an increase in peak radial strain, although these two measurements are not correlated. However for territories subtended to a significant coronary stenosis, the oxygenation response in these territories is abnormal, which is associated with a drop in peak radial strain (r=0.68, p=0.04).

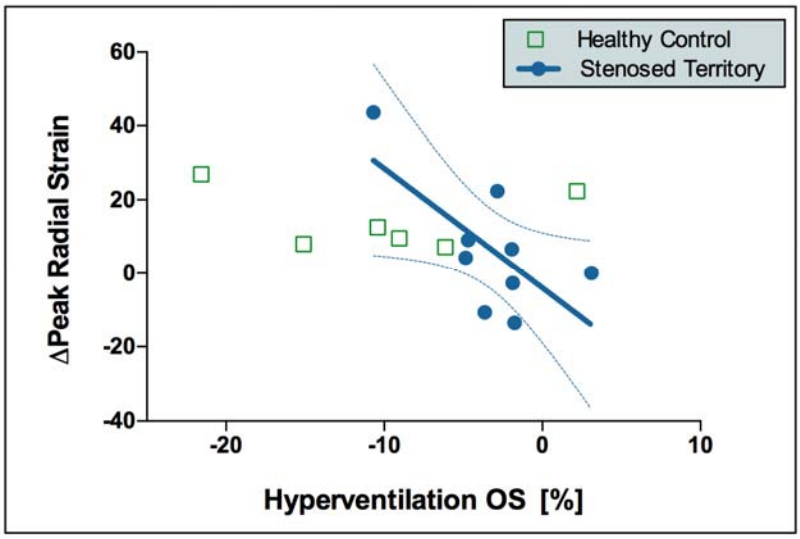

Hyperventilation induces a myocardial oxygenation drop in healthy controls (green), along with an increase in peak radial strain, although these two measurements are not correlated. However for territories subtended to a significant coronary stenosis, the oxygenation response in these territories is abnormal, which is associated with a drop in peak radial strain (r=0.68, p=0.04).

Response of myocardial oxygenation (OS%) and peak radial strain (Δ) to the breathing maneuvers.

	Hyperventilation			Breath-Hold		
	Healthy Control	*Post-Stenotic*	*Remote*	*Healthy Control*	*Post-Stenotic*	*Remote*
OS (%)	-10.0±8.0*	-3.3±3.6	-1.9±5.2	+12.4±7.7*	-1.3±1.7	0.6±7.2
Strain (Δ)	+14.4±8.3*	+6.5±17.6	+5.4±10.6	-14.8±5.9*	-4.4±16.1	-11.1±8.0*

*The myocardial oxygenation response (OS%) and the change in peak radial strain across hyperventilation and subsquent breath-holding (30s) is shown for healthy control subjects, and for CAD patients separated into territories substended to a coronary artery stenosis and remote territory. *p<0.05 for significant change across maneuver.*

ID#: 374638

Papillary muscle mass quantification using cardiovascular magnetic resonance for the diagnosis of pediatric left ventricular non-compaction

Jason N. Johnson, MD MHS[1] Kyle Robillard, BS[2], Anthony Merlocco, MD[3], Jeffrey A. Towbin, MD[4]

1. LeBonheur Children's Hospital, University of Tennessee, Memphis, TN

2. University of Tennessee Health Science Center

3. LeBonheur Children's Hospital, University of Tennessee, TN

4. Le Bonheur Children's Hospital, St. Jude Children's Research Hospital, University of Tennessee Health Science Center, Memphis, TN

Background: Cardiovascular magnetic resonance (CMR) is commonly used to diagnose left ventricular non-compaction (LVNC), but few studies focus on papillary mass as potential diagnostic criteria, especially in children. This study was performed to compare CMR characteristics including papillary mass in children with LVNC with normal controls.

Methods: From July 2013 – March 2017, a retrospective cohort study of 86 children (27 LVNC myopathy, 21 isolated LVNC, and 38 normal controls) was performed. The non-compacted to compacted (NC/C) ratio was measured from multiple CMR views. Left ventricular (LV) volumes, ejection fraction (LVEF), compacted mass (LVCM), non-compacted mass percentage (LVNCM%), and papillary mass indexed (LVPMi), were measured by short axis (Figure 1). LV papillary mass percentage (LVPM%) was calculated as a percentage of the compacted mass, excluding the non-compacted mass. CMR measurements were compared using a non-parametric Kruskal Wallis test. Receiver operating characteristic curve (ROC) analysis was performed.

Results: There was no difference in median age in isolated LVNC compared to controls but LVNC myopathy were older (isolated LVNC 14.7 years (IQR 12.6-16.5) vs control 14.6 (13.3-16.0) p=0.59, vs LVNC myopathy 17.3 (15.5-18) p<0.01). There was no difference in median BSA in isolated LVNC compared to controls or LVNC myopathy (isolated LVNC 1.6 m2 (IQR 1.2-1.8) vs control 1.8 (1.6-1.9) p=0.08, vs LVNC myopathy 1.8 (1.6-1.9) p=0.14). There was no difference in gender in isolated LVNC compared to controls or LVNC myopathy (isolated LVNC male 57% vs control 55% p=0.8, vs LVNC myopathy 67% p=0.2). There was no difference between patients with isolated LVNC and controls in LV end-diastolic volume indexed, left atrial volume indexed, or LVEF (Table 1). The maximum NC/C ratio and LVNCM% were higher while the LVPMi and LVPM% were lower in isolated LVNC compared to controls (Table 1). There was no difference in LVNCM%, LVPMi, or LVPM% between isolated LVNC and LVNC myopathy (Table 1). The ROC analysis (Figure 2) using NC/C ratio >2.3 as the standard diagnostic criteria of LVNC revealed that a LVNCM% above 12% was predictive of LVNC with a specificity of 97% (CI: 85-99) and a sensitivity of 94% (CI: 85-99). A LVPM% lower than 5.6% was predictive of LVNC with a specificity of 92% (CI: 86-98) and a sensitivity of 88% (CI: 82-94).

Conclusion: A papillary mass percentage less than 5.6% is diagnostic for LVNC with high sensitivity and specificity in children. Papillary mass percentage has a similar sensitivity and specificity as the non-compacted mass percentage, and could be used as diagnostic criteria for LVNC in children.

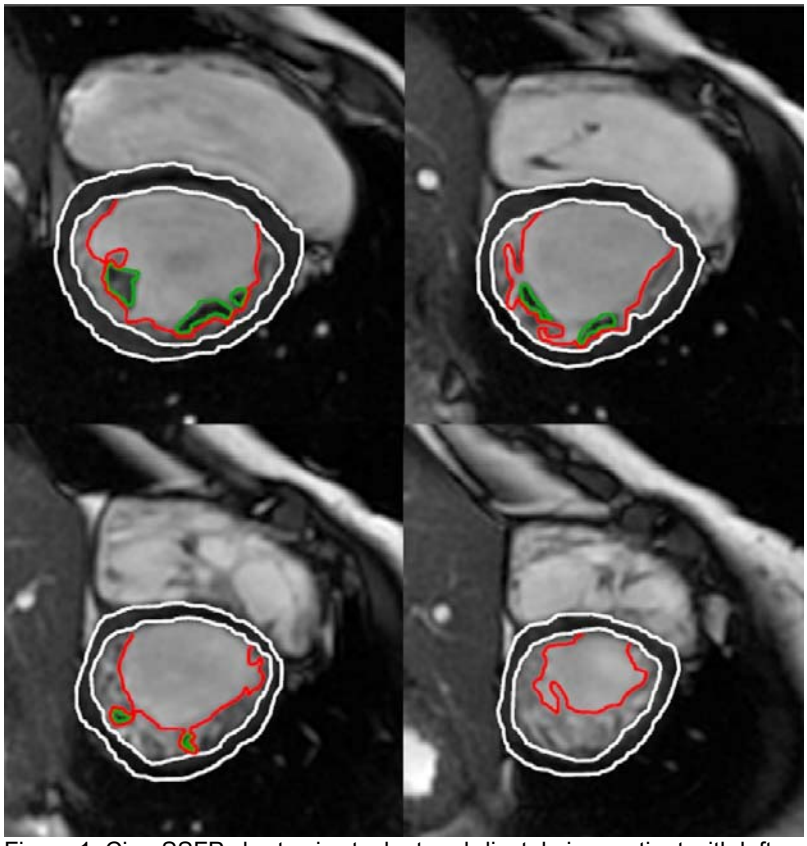

Figure 1. Cine SSFP short axis stack at end-diastole in a patient with left ventricular non-compaction. The white lines define left ventricular compacted mass, red lines define left ventricular non-compacted mass, and green lines define left ventricular papillary mass.

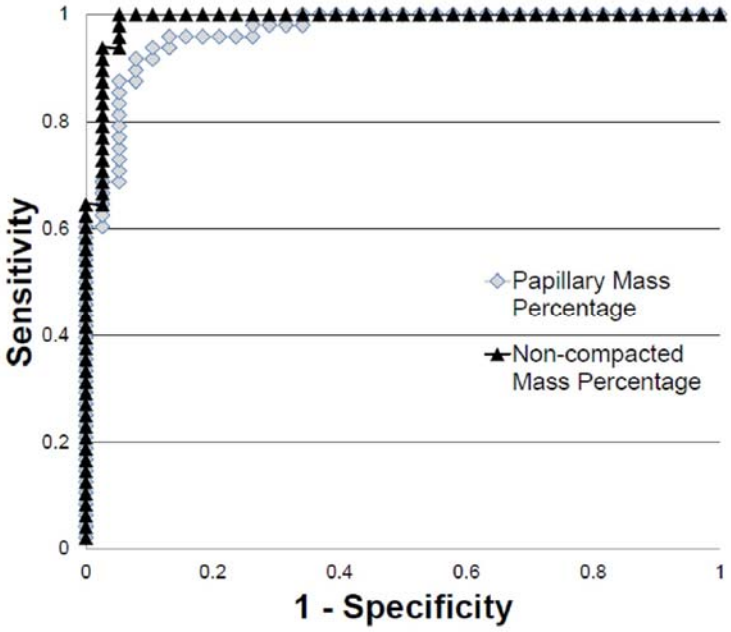

Figure 2. Receiver operating characteristic curves of non-compacted mass percentage and papillary mass percentage to predict left ventricular non-compaction.

Table 1. CMR measurements in children with LVNC and controls

CMR measurements (median, IQR)	Isolated LVNC n=21	LVNC Myopathy n=27	Control n=38
LVEDVi (ml/m^2)	81.9 (71.0-86.7)	92.7 (83.9-104.7) p=0.009	77.3 (67.6-87.9) p=0.192
LVESVi (ml/m^2)	35.7 (31.8-37.4)	46.1 (39.2-60.3) p=0.003	32.9 (27.8-37.6) p=0.209
LVEF (%)	57.2 (55.3-58.8)	50.3 (39.6-55.8) p<0.001	57.7 (54.8-60.7) p=0.757
LAVi (ml/m^2)	26.0 (24.0-29.0)	33.0 (25.0-37.5) p=0.032	27.0 (22.0-29.0) p=0.287
Maximum NC/C ratio	3.3 (2.9-4.1)	3.6 (2.9-4.9) p=0.041	1.1 (0.9-1.5) p<0.001
LVNCM% (%)	17.5 (15.5-21.1)	19.7 (15.5-25.5) p=0.182	5.4 (4.0-6.6) p<0.001
LVPMi (g/m^2)	2.5 (2.1-2.8)	3.0 (2.1-3.3) p=0.158	4.4 (3.9-5.3) p<0.001
LVPM% (%)	4.5 (3.5-5.2)	4.0 (3.6-5.0) p=0.425	7.7 (6.5-9.1) p<0.001

CMR = cardiovascular magnetic resonance; IQR = interquartile range; LVNC = left ventricular non-compaction; LVEDVi = left ventricular end-diastolic volume indexed; LVESVi = left ventricular end-systolic volume indexed; LVEF = left ventricular ejection fraction; LAVi = left atrial volume indexed; NC/C = non-compacted to compacted; LVNCM% = left ventricular non-compacted mass percentage; LVPMi = left ventricular papillary mass indexed; LVPM% = left ventricular papillary mass percentage. Comparisons made to the isolated LVNC group with corresponding p-values.

ID#: 374705

Automatic Ventricular Segmentation Using a Convolutional Neural Network: results from Circle Cardiovascular Imaging on UK Biobank Cardiac MR CINE Images

Alireza Sojoudi, MSc[2] Rotem Golan, MSc[1], Xuexin Gao, PhD[3], Qiao Wei, PhD[4], Philipp Barckow[5], Kenneth Fung, MBBS MRCP[6], Young Jin Kim, MD, PhD[7], Aaron Lee, PhD, MBBS[8], Nay Aung, MD, MRCP[8], Mihir M. Sanghvi, MB BS, BSc[8], Filip Zemrak, MD, PhD, MRCP[9], Jose Miguel Paiva, MSc[8], Elena Lukaschuk, MSc[10], Valentina Carapella, DPhil[11], Stefan K. Piechnik, PhD, MScEE[12], Stefan Neubauer, MD, FRCP[12], Steffen E. Petersen, MD DPhil MPH FRCP[13]

1. Circle Cardiovascular Imaging Inc., AB, Canada

2. Circle Cardiovascular Imaging Inc, Calgary, Canada

3. Circle Cardiovascular Imaging Inc, Panarctic Plaza, Calgary, Canada, AB, Canada

4. Circle Cardiovascular Imaging Inc., Calgary, AB, Canada

5. Circle Cardiovascular Imaging Inc., Berlin, Berlin, Germany

6. William Harvey Research Institute, NIHR Cardiovascular Biomedical Research Unit at Barts, Queen Mary University of London, Charterhouse Square, London, EC1M 6BQ, UK, London, England, United Kingdom

7. Severance Hospital, Yonsei University College of Medicine, Seoul, Republic of Korea

8. William Harvey Research Institute, NIHR Cardiovascular Biomedical Research Unit at Barts, Queen Mary University of London, Charterhouse Square, London, EC1M 6BQ, UK, England, United Kingdom

9. William Harvey Research Institute, London, England, United Kingdom

10. University of Oxford, Oxford, England, United Kingdom

11. University of Oxford, Oxford, United Kingdom, England, United Kingdom

12. University of Oxford, England, United Kingdom

13. Queen Mary University of London, London, England, United Kingdom

Background: Manual left and right ventricular (LV and RV) volumes and function analysis is time consuming and operator dependent. Automated and semi-automated LV analysis tools could be helpful, especially in high volume clinical and research centres. Circle Cardiovascular Imaging develops and markets cardiovascular post-processing software that allows for the evaluation and analysis of MRI and CT images. A Convolutional Neural Network has been trained by Circle researchers to be able to automatically generate contours for left ventricle (endo and epi) and right ventricle (endo). LV and RV volumes and function are then calculated from the contours. The aim of this study is to assess performance of the trained Convolutional Neural Network against manual analysis for LV and RV volumes and function.

Methods: We trained a convolutional neural network using 3929 studies randomly selected out of 4908 studies in UK Biobank data who underwent cardiac magnetic resonance (CMR) imaging at 1.5T (Aera, Siemens) scanners as part of this population cohort study. The remaining 979 studies were used to evaluate the performance of the trained CNN.
Fully automated LV and RV analysis was performed with the trained CNN after acquiring a short axis CINE stack with retrospective balanced steady state free precession sequence. Various clinical operators performed manual LV and RV analysis of the same images on cvi42 software.
We used Pearson';s correlation coefficients and two-way random single measures agreement intraclass correlation coefficients (ICC) to compare LV and RV end-diastolic volume (EDV), end-systolic volume (ESV), stroke volume (SV) and ejection fraction (EF) from manual and trained CNN. The limits of agreement between measurements were also compared using the Bland-Altman plots for visual analysis.

Results: For LV volume and function analysis, there was an excellent agreement between trained CNN results and manual in the directly measured LV volumes – EDV and ESV - (ICC>0.98 and ICC>0.96 respectively): the difference between the trained CNN and manual EDV and ESV was on average less than 1%. Parameters calculated from the measured volumes - SV and EF - had good agreement (ICC>0.95 and 0.86 respectively).
For RV volume and function analysis, there was an excellent agreement between trained CNN results and manual in the directly measured RV volumes – EDV and ESV - (ICC>0.95 and ICC>0.92 respectively): the difference between the trained CNN and manual EDV and ESV was on average 2% and 5% respectively. Parameters calculated from the measured volumes – RV SV and EF - had good agreement (ICC>0.89 and 0.77 respectively).

Conclusion: Trained CNN automated LV analysis tool performs well compared to manual analysis. This proves that machine learning algorithms will play an important role in the future of medical image processing. However, these models need to be tested and possibly modified in clinical settings.

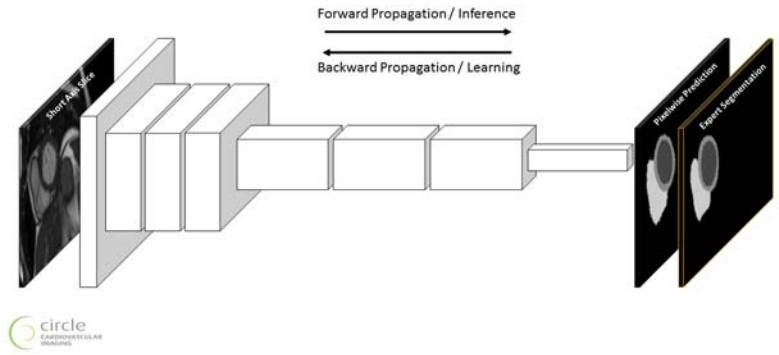

Convolutional Neural Networks for Semantic Segmentation

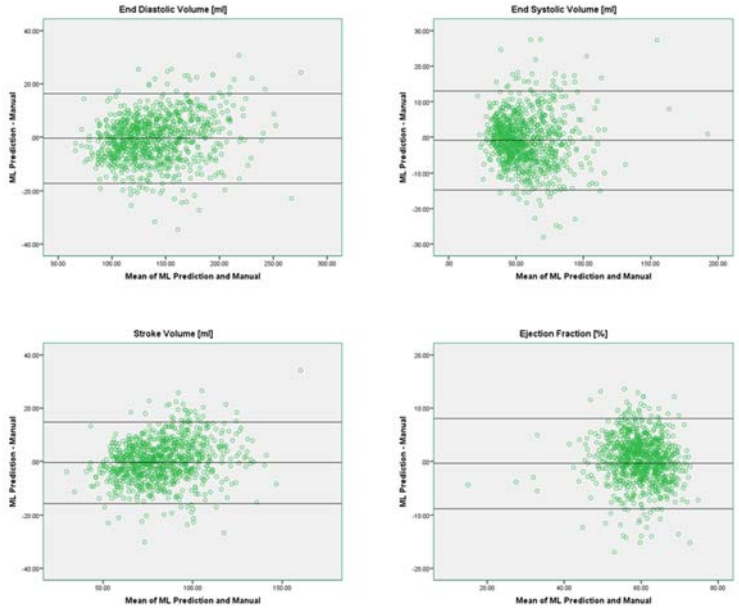

Bland-Altman plots showing differences between trained CNN and manual analysis of LV volumes (EDV, ESV), LV Stroke Volume (SV) and LV Ejection Fraction (EF).

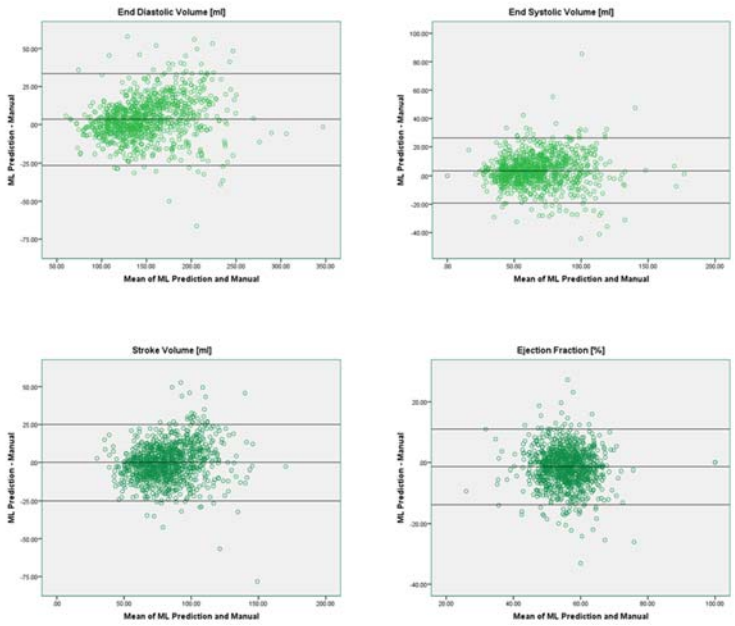

Bland-Altman plots showing differences between trained CNN and manual analysis of RV volumes (EDV, ESV), RV Stroke Volume (SV) and RV Ejection Fraction (EF).

The agreement between manual and fully automated trained CNN for the analysis of left ventricular (LV) volumes and function with Pearson's correlation and intraclass correlation coefficients (ICC).

[n = 979]	CNN	Manual	Mean diff	□2	*p-value*	ICC	95% CI ICC	*p-value*
EDV [ml]	138.90	139.33	-0.42±8.55	0.96	<0.001	0.983	0.981 to 0.985	<0.001
ESV [ml]	56.34	57.24	-0.89±7.08	0.93	<0.001	0.964	0.959 to 0.969	<0.001
SV [ml]	82.55	82.08	-0.46±7.76	0.92	<0.001	0.956	0.950 to 0.961	<0.001
EF [%]	59.82	59.44	-0.37±4.30	0.77	<0.001	0.869	0.850 to 0.885	<0.001

The agreement between manual and fully automated trained CNN for the analysis of right ventricular (RV) volumes and function with Pearson's correlation and intraclass correlation coefficients (ICC).

[n = 979]	CNN	Manual	Mean diff	$\square^2$	*p-value*	ICC	95% CI ICC	*p-value*
EDV [ml]	151.17	147.65	3.51±15.33	0.92	<0.001	0.95	0.94 to 0.96	<0.001
ESV [ml]	68.96	65.43	3.53±11.61	0.87	<0.001	0.92	0.90 to 0.94	<0.001
SV [ml]	82.21	82.22	−0.01±12.78	0.80	<0.001	0.89	0.87 to 0.90	<0.001
EF [%]	54.84	56.34	−1.4±6.32	0.60	<0.001	0.73	0.69 to 0.77	<0.001

ID#: 374743

Abnormal Myocardial Perfusion Reserve in Hypertrophic Cardiomyopathy: Always the same features no matter the phenotype? A Perfusion Mapping Study.

Claudia Camaioni, MD[1]Kristopher D. Knott, MBBS MA[2], Gabriella Captur, MD PhD MRCP MSc[3], Fabrizio Ricci[4], Hui Xue, PhD[5], Redha Boubertakh, PhD[6], Luis Lopes, MD, PhD [7], Saidi A. Mohiddin, FRCP, FESC[8], Steffen E. Petersen, MD DPhil MPH FRCP[9], Charlotte Manisty, MRCP, PHD[10], Sven Plein, MD PhD[11], Peter Kellman, PhD[12], James Moon, MD[13]

1. Barts Heart Center, London, England, United Kingdom

2. University College London, London, England, United Kingdom

3. Barts Heart Centre, London, England, United Kingdom

4. Department of Neuroscience, Imaging and Clinical Sciences, "G. D' Annunzio" University, Chieti, Italy, Pescara, Italy

5. National Heart, Lung, and Blood Institute, Bethesda, MD

6. QMUL, England, United Kingdom

7. Barts Heart Centre; UCL, United Kingdom

8. Barts Heart Centre, England, United Kingdom

9. Queen Mary University of London, London, England, United Kingdom

10. Barts Heart Centre and University College London, England, United Kingdom

11. University of Leeds, England, United Kingdom

12. National Heart, Lung, and Blood Institute, National Institutes of Health, Bethesda, MD

13. UCL, England, United Kingdom

Background: Microvascular ischaemia in hypertrophic cardiomyopathy (HCM) is present in most patients but its place in clinical care and in the pathophysiology of the disease is not well understood. Similarly, the pattern of hypertrophy has not proved easy to understand (asymmetric vs apical vs concentric). We explored the role of ischaemia in HCM using perfusion mapping and compared it to hypertrophy extent, pattern and scar.

Methods: 51 HCM patients with unobstructed coronary arteries and 21 healthy volunteers (HV) underwent free-breathing adenosine stress perfusion CMR using Gadgetron in-line perfusion mapping to deliver pixel-by-pixel myocardial blood flow (MBF, ml/min/g) for three short axis views (± long axis) at stress/rest. Transmural endocardial and epicardial MPR (tm-, endo-, epiMPR) were calculated per segment and correlated with segmental wall thickness (WT) and late gadolinium enhancement (LGE), quantified by the 6 SD method. All analyses were performed on a per-segment basis *(Fig. 1).*

Results: 31 patients with asymmetric hypertrophy (ASH) and 20 patients with apical HCM (aHCM), with similar baseline characteristics, were enrolled (mean age 58 years. men 81%) for a total of 816 segments *(Tab. 1).* 336 segments were analysed from the HV group. Mean tm-MPR in HCM group was 2.32±0.89, in the HV group was 3.7±0.7.
MPR and wall thickness: MPR decreased significantly with increasing tertiles of WT in both HCM subgroups *(Fig. 2)*.
MPR and LGE: MPR fell with increasing tertiles of LGE, but only in the aHCM subgroup.
MPR and LVH pattern: According to an explorative multivariate regression analysis *(Tab. 2)*, WT was the only significant predictor of stress MBF and MPR (tm, endo and epi), while LGE was the only significant predictor of resting MBF.

Conclusion: Perfusion reserve is reduced in HCM. Notably, factors predicting this reduction may be different between morphologic variants of HCM. In this study, perfusion reserve is inversely correlated with hypertrophy magnitude in both ASH and aHCM, but it falls with scar only in aHCM.

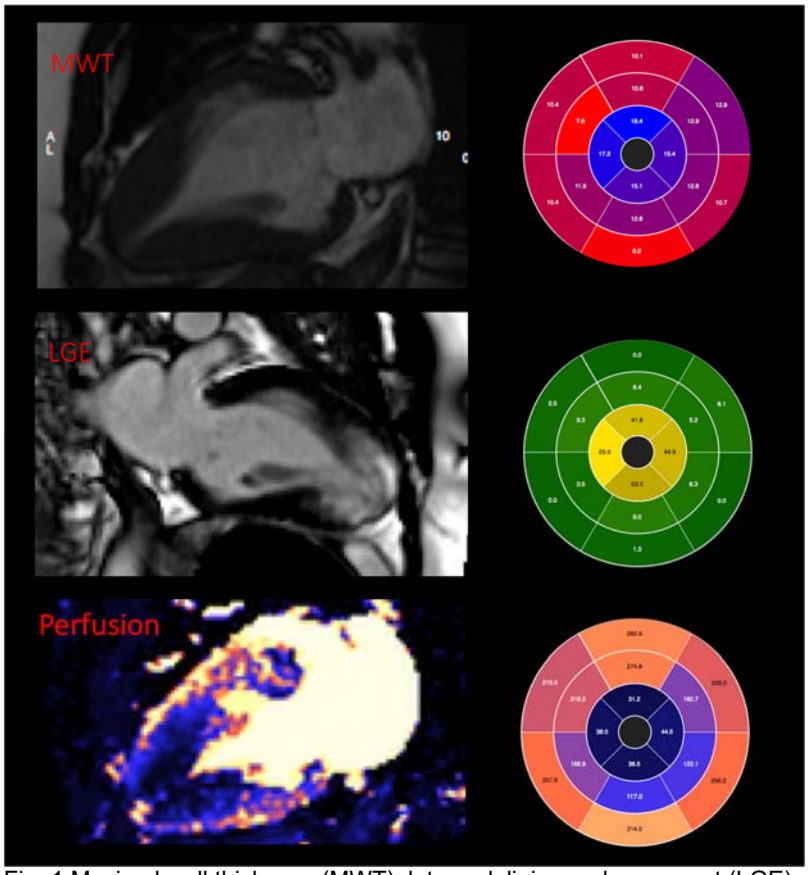

Fig. 1 Maximal wall thickness (MWT). late gadolinium enhancement (LGE) and perfusion mapping 16 segments analysis (CVI42 software).

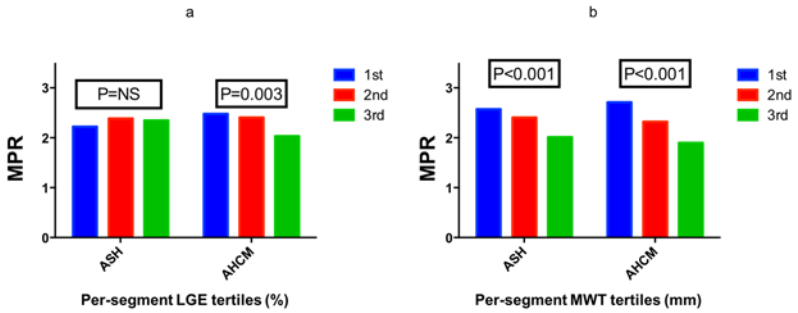

Fig.2: The MPR trend according with the increasing tertiles of LGE (a) and max wall thickness (MWT) (b) in asymmetrical hypertrophic cardiomyopathy (ASH) and apical hypertrophic cardiomyopathy (aHCM).

Tab.1 HCM population baseline characteristics.

	overall	ASH	aHCM	P-value
n	51	30	21 58.8 ± 14.24	---

Age years	57.8 ± 14	57 ± 15	4 (19)	0.666
Female gender	10 (19)	6 (20)	1.9 ± 0.2	0.933
BSA	2 ± 0.2	2 ± 0.2	82.9 ± 19.3	0.225
LV Mass_ind (g/m2)	166.8 ± 58.7	85.5 ± 27	71 ± 13	0.717
LVEDI (ml/m2)	74.4 ± 14.7	76.7 ± 15.5	11.4 ± 1.9	0.174
Average WT mm	11.2 ± 2.3	11.1 ± 2.6	8.6 ± 6.4	0.632
LGE %	8.4 ± 7.3	8.2 ± 7.9	74.4 ± 8	0.855
EF %	72.9 ± 7.6	71.8 ± 7.2	3 (14)	0.233
Diabetes n (%)	9 (17)	6 (20)	7 (33)	0.598
Hypertension n (%)	22 (43)	15 (50)	2.3 ± 0.7	0.237
tmMPR	2.3 ± 0.9	2.3 ± 1	2 ± 0.7	0.91
endoMPR	2 ± 0.8	1.9 ± 0.7	2.5 ± 0.8	0.828
epiMPR	2.5 ± 1	2.6 ± 1.1		0.89

Tab.2 Multivariable Linear Regression continuous and by LGE and MWT tertiles. MPR: myocardial perfusion reserve; LGE: late gadolinium enhancement; MWT: maximal wall thickness; tm: transmural.

816 segments	β	95%CI	P-value
MPR			
LGE	0.003	-0.002. 0.009	0.253
MWT	-0.067	-0.087. -0.046	<0.001*
MPR by LGE and MWT tertiles			
LGE bottom	ref	-	-
LGE 2nd	0.103	-0.077. 0.283	0.262
LGE top	0.156	-0.039. 0.35	0.117
MWT bottom	ref	-	-

MWT second	-0.273	-0.454. -0.092	0.003*
MWT top	-0.701	-0.897. '-0.505	<0.001*
tm stress			
LGE	-0.237	-0.663. 0.188	0.274
MWT	-5.002	-6.556. -3.447	<0.001*
tm stress - by LGE and MWT tertiles			
LGE bottom	ref	-	-
LGE 2nd	18.961	5.349. 32.573	0.006*
LGE top	-0.243	-14.984. 14.497	0.974
MWT bottom	ref	-	-
MWT second	-26.227	-39.913. -12.541	<0.001*
MWT top	-52.125	-66.96. -37.29	<0.001*
tm rest			
LGE	-0.162	-0.278. -0.046	0.006*
MWT	-0.06	-0.483. 0.363	0.78
tm rest - by LGE and MWT tertiles			
LGE bottom	ref	-	-
LGE 2nd	2.683	-1.036. 6.402	0.157
LGE top	-5.708	-9.735. -1.68	0.006*
MWT bottom	ref	-	-
MWT second	-1.724	-5.463. 2.016	0.366
MWT top	0.0651	-4.002. 4.105	0.98

ID#: 376485

Cardiac output assessment during and after pregnancy in women with heart disease as compared with normal controls using cardiovascular magnetic resonance imaging (MoMs Heart Study)

Robin A. Ducas, BSc, MD[1] Brahmdeep Saini[2], Catriona J. Bhagra, MD[3], Kenichiro Yamamura[4], Davide Marini, MD, PhD[5], Mathew Sermer, MD[6], Mike Seed, MBBS[7], Rachel Wald, MD[8]

1. University of Toronto, Toronto, Canada

2. SickKids, Canada

3. Cambridge University and Papworth Hospitals NHS Foundation Trust, United Kingdom

4. University of Toronto, Canada

5. SickKids, ON, Canada

6. Mount Sinai Hospital, Toronto, Canada

7. The Hospital for Sick Children, Toronto, ON, Canada

8. Division of Cardiology, University of Toronto, ON, Canada

Background: Mothers with heart disease are at increased risk of pregnancy-related complications. In women with heart disease, insufficient cardiac output (CO) has been implicated in poor maternal and fetal outcomes. Phase contrast flow analysis using cardiovascular magnetic resonance imaging (CMR) is the reference standard for non-invasive measurement of CO but has not been used to measure flows in pregnant women with cardiac disease. **Hypothesis:** Antepartum assessment of CO will be feasible and will highlight differences in flows in women with heart disease as compared with controls.

Methods: Pregnant women with moderate or severe structural/functional heart disease were matched with healthy controls. Participants were scanned using a 1.5T Siemens scanner during the third trimester of pregnancy (corresponding to peak CO) and six months postpartum (surrogate for baseline). Phase contrast CMR was used to quantify CO (measured by summation of superior vena cava and descending aorta flows, L/min) and cardiac index (CI, L/min/m2). Calculation of CI in pregnancy was achieved using pre-pregnancy body surface area for both groups. Between group findings were compared using the Student';s t-test.

Results: Twelve women with heart disease (mean age 34±4 years) and 12 matched controls (mean age 33±4 years) were studied. Heart disease included left ventricular (LV) systolic dysfunction n=4 (LV ejection fraction [LVEF] 40-50% n=2 and LVEF <40% n=2), systemic right ventricle n=1, ≥moderate/severe aortic regurgitation n=4, ≥moderate mitral regurgitation n=1, severe tricuspid regurgitation n=1, and ≥moderate pulmonic regurgitation n=1. Cardiovascular medications (beta-blockade or diuretics) were used in 10 women with heart disease (83%). Four women (33%) with heart disease experienced a cardiovascular complication in pregnancy (arrhythmia n=2 and heart failure n=2). The CO/CI values are shown (Table 1). There was no difference in antepartum CO/CI in women with heart disease versus controls (p=0.686 for CO and p=0.520 for CI). The magnitude of adaptive change in CO (difference between antepartum and postpartum) was greater in women with heart disease versus controls (p=0.04) although CI did not differ significantly between the groups (p=0.066). There were no fetal or neonatal complications in this study.

Conclusion: Antepartum CMR measurement of CO/CI is feasible in women with cardiac disease. The magnitude of adaptive change in CO during pregnancy is larger in women with heart disease as compared with controls. Further study of a larger population of women with a wider range of cardiac lesions may provide greater insights into hemodynamic adaptations to pregnancy in women with heart disease.

Phase contrast flow assessment of cardiac output during and after pregnancy in women with heart disease as compared with controls.

	Antepartum		Postpartum		Delta antepartum-postpartum	
	CO (+/- SD)	CI (+/- SD)	CO (+/- SD)	CI (+/- SD)	CO (+/- SD)	CI (+/- SD)

Women with heart disease	7.3 (+/- 1.1)	4 (+/-0.6)	4.9 (+/- 1.4)	2.6 (+/- 0.6)	2.4 (+/- 1.2)*	1.4 (+/- 0.8)**
Controls	7.0 (+/- 1.5)	4.2 (+/- 0.8)	5.6 (+/- 1.2)	3.3 (+/- 0.5)	1.4 (+/- 0.9)	0.8 (+/- 0.6)

* p value 0.04 for delta antepartum-postpartum CO in women with heart disease versus controls.

** p value 0.066 for delta antepartum-postpartum CI in women with heart disease versus controls.

CI = cardiac index in liters/minute/meter2; CO = cardiac output in liters/minute; SD = standard deviation

ID#: 376524

Association between Aortic Regurgitation Severity and Post-Valve Replacement Left Ventricular Remodeling: Cardiovascular Magnetic Resonance Imaging vs Transthoracic Echocardiography.

Ulf Neisius, MD PhDThomas Hauser, MD MPH, Apranta Deka. Patel, MD, Warren J. Manning, MD

Beth Israel Deaconess Medical Center, Harvard Medical School, Boston, MA

Background: Isolated aortic regurgitation (AR) leads to LV volume overload and dilatation. Timely aortic valve replacement (AVR) is followed by a decrease in LV cavity size which indirectly reflects on disease severity prior to surgery. We sought to investigate the relationship between preoperative AR severity assessment by cardiovascular magnetic resonance (CMR) or transthoracic echocardiography (TTE) and post-surgical remodeling.

Methods: We retrospectively identified consecutive patients with chronic AR and no significant aortic stenosis (n=18) who underwent CMR and TTE within 1 year of AVR. CMR and TTE scans were interpreted by level 3 trained readers.

Results: A total of 18 patients (age 41 [37;62], 78% male, 33% bicuspid) proceeded to AVR. The median interval between preoperative CMR and TTE was 52 days (range 0 – 364 days). AVR was followed by TTE scans (median 92 days, range 30 – 554 days). The change in TTE (biplane Simpson or Teichholtz formula) LV end-diastolic volume (ΔLVEDV) post-AVR was 67±43 ml. ΔLVEDV correlated with CMR aortic regurgitant volume (AR_{vol}) and regurgitant fraction ($AR_{\%}$) (ΔLVEDV to AR_{vol}, R=0.605, P=0.008; ΔLVEDV to $AR_{\%}$, R=0.589, P=0.010). Using the AR severity system of Gelfand et al. [1] (mild ≤15%, moderate 16-25%, moderate-severe 26-48%, severe >48%), ΔLVEDV was different between patients with moderate-severe (grade 3) and severe AR (grade 4) by CMR (45.3±34.7 ml vs 100.4±24.5 ml, P=0.005) and TTE (70.6±46.0 ml vs 99.5±16.1 ml, P=0.312) (Figure). The correlation of ΔLVEDV with CMR grades (ρ=0.61, P=0.007) was stronger in comparison to TTE (ρ=0.42, P=0.08).

Conclusion: CMR quantification of AR volume relates to post-surgical LV remodeling in isolated AR. The stronger correlation between CMR AR severity (vs TTE) and ΔLVEDV suggests an improvement in predicting remodeling. Such might be relevant in the clinical decision process prior to AVR.

1. Gelfand EV, Hughes S, Hauser TH, Yean SB, Goepfer L, Kissinger KV, Rofsky NM, Manning WJ. Severity of mitral and aortic regurgitation as assessed by cardiovascular magnetic resonance: optimizing correlation with doppler echocardiography. J Cardiovasc Magn Resonance. 2006;8:503-507.

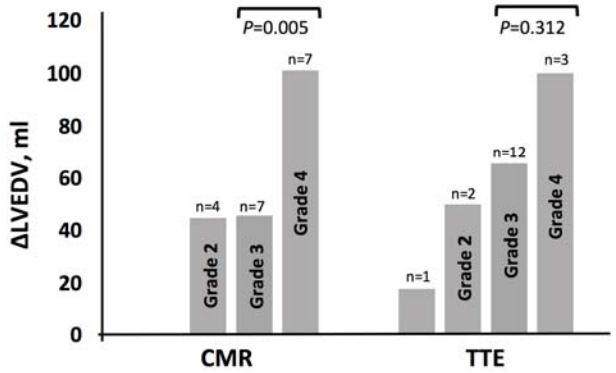

CMR, cardiovascular magnetic resonance; TTE, transthoracic echocardiography; ΔLVEDV, change in left ventricular end-diastolic volume after aortic valve replacement; Grade 1, mild aortic regurgitation; Grade 2, moderate aortic regurgitation; Grade 3, moderate-severe aortic regurgitation; Grade 4, severe aortic regurgitation.

Relation between ΔLVEDV post aortic valve replacement and CMR (light grey) or TTE (dark grey) grading systems.

ID#: 376296

Architecture and pipeline to enable large scale analysis of 4D flow MRI data

Michael B. Scott, MS[1] Ozair Rahman, MD[2], Alex Powell, MS[3], Kathryn Alpert, MS[4], Alexandr Kogan, MS[4], Lei Wang, PhD[3], Jeremy D. Collins, MD[1], James Carr, MD[1], Michael Markl, PhD[1], Alex J. Barker, PHD[1]

1. Northwestern University, Chicago, IL

2. Northwestern University, Feinberg School of Medicine, Chicago, IL

3. Northwestern University Feinberg School of Medicine, Chicago, IL

4. Northwestern University Feinberg School of Medicine

Background: The most common congenital heart disease, bicuspid aortic valve (BAV), affects 1-2% of the population. BAV is associated with aortic flow abnormalities that are implicated in the development of aortopathy, but determination of the hemodynamic contributions to aortopathy in BAV patients is challenging as it requires a complex analysis workflow across large cohorts. Scaling up to thousands of patients or multiple researchers/centers requires automation and standardization of existing workflows to reduce inter-observer errors and allow for adaptable workflows to investigate imaging biomarkers or add subjects. In this pilot study, an aortic 4D flow analysis pipeline was developed that uses remote data archiving and high-performance computing capable of analyzing large cohorts. Here it is used to detect changes in aortic structure and hemodynamics in a cohort of BAV patients.

Methods: To pilot the technique, a small subset of 41 BAV patients (29 male, age 44.7±11.8 years) who underwent baseline and follow-up 4D flow MRI (follow up 2.68±0.66 years) were used in this IRB approved and HIPAA compliant study. Pre-processing included correction for phase offsets (eddy currents, Maxwell terms, velocity aliasing) and 3D segmentation of the thoracic aorta. A remote data archival platform (Fig 1, Northwestern Neuroimaging Data Archive, NUNDA) was used to communicate with a high-performance computing cluster (Northwestern QUEST; scalable to 679 nodes and 16,028 2.5-2.8 GHz cores) executing a custom analysis pipeline. The pipeline included (see Fig 2): 1) automatic detection of the center line and three main branches of the aorta from the segmentation, 2) identification and volume quantification of the ascending aorta (AAo) from the aortic sinus to the takeoff of the innominate artery, 3) placement of 10 equidistant planes along the AAo for calculation of net flow and retrograde fraction, 4) calculation of a velocity maximum intensity projection (MIP) and peak velocity across the aortic valve, 5) archival of computed parameters to the NUNDA database. The results from the unsupervised execution of steps 1-5 for the cohort were compared to manual analysis of the AAo volume and peak transvalvular velocity.

Results: Bland-Altman analysis shows low bias (0.1%) and limits of agreement (7.8%) between the manual and automatic volume measurements (Fig 3). Significant growth was detected using both manual (7.3±10.7 ml, P=0.001) and automated approaches (8.0±14.3 ml, P=0.006), with no significant difference between the methods (p=0.78). No significant difference was seen in peak velocity, from 2.1±0.7 m/s to 2.2±0.9 m/s.

Conclusion: The semi-automated pipeline replicated manual quantification of AAo volume and allowed for hemodynamic quantification; additional parameters such as diameter and wall shear stress can be easily added to the workflow. This is an important step towards running large cohorts of patients with 4D flow MRI in an increasingly automated fashion.

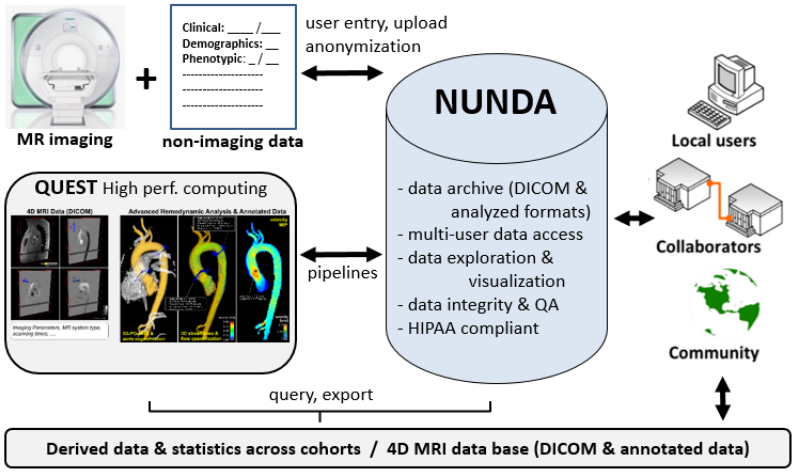

Fig 1: an overview of the NUNDA platform. Imaging, demographic, and pre-processed data can be uploaded to the archive. NUNDA can send data to the Quest High Performance Computing Cluster for a pipeline analysis, then store the outputs of the code for each patient. Raw and processed data can be easily shared between researchers and institutions in a secure manner.

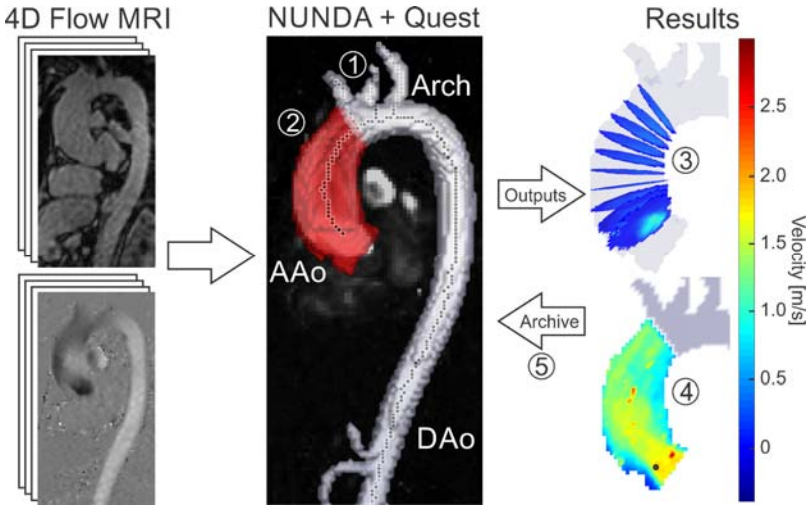

Fig 2: 4D flow MRI data magnitude (top left) and phase (bottom left) images are combined into a phase-contrast MRA that is used to manually segment the aorta (center). These pre-processed inputs are uploaded to NUNDA, where 1) the centerline of the aorta and three main branches is fit, 2) the volume of the ascending aorta is automatically determined, 3) planes are automatically placed for hemodynamic analysis, 4) velocity maximum intensity plot (MIP) is generated. The dark circle in the MIP shows the location of the maximum velocity. Finally, 5) the results are archived in NUNDA.

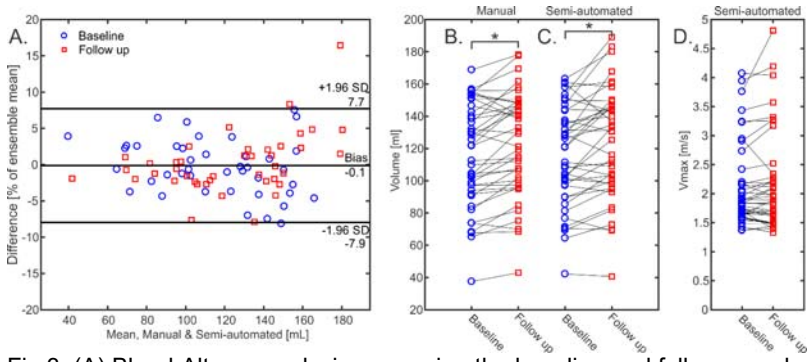

Fig 3: (A) Bland-Altman analysis comparing the baseline and follow up volume measurements between manual and semi-automated methods. The manual measurements are shown in (B); the semi-automated measurements are shown in (C). No significant difference exists between the volumes found using either method (p=0.78), but both methods show significant growth over the follow-up period (p=0.001 manual, p=0.006 automated). (D) Change in maximum velocity in the AAo over the follow up period.

ID#: 376608

Myocardial strain from high-temporal tagging and feature tracking MRI: Relation to myocardial fibrosis in cardiomyopathy

Eri Watanabe, MD, PhD[1]Michinobu Nagao, MD, PhD[1], Kenji Fukushima, MD, PhD[2], Risako Nakao, MD[2], Akiko Sakai, MD, PhD[1], Shuji Sakai, MD, PhD[3], Nobuhisa Hagiwara, MD, PhD[2]

1. Tokyo Women's Medical University, Shinjuku-ku, Tokyo, Japan

2. Tokyo Women's Medical University, Japan

3. Tokyo Women's Medical University, Tokyo, Japan

Background: Feature tracking MRI (FT) has been recently developed as a new technique for quantification of left ventricular (LV) deformation using conventional cine images. In contrast, myocardial strain analysis by tagging-MRI has been considered as the gold standard method for LV deformation. The aim of this study is to compare LV myocardial strain by FT to those derived from tagging-MRI in patients with hypertrophic cardiomyopathy (HCM) and dilated cardiomyopathy (DCM). In addition, we investigate the relationship between late gadolinium enhancement (LGE) and myocardial strains from the two techniques.

Methods:

Data of cardiac MRI with 3-Tesla scanner for 25 patients who consisted of 8 patients with HCM, 10 patients with DCM, and 7 controls was analyzed. For each subject, basal, mid and apical level of LV short-axis cine images with 20 phases per cycle were analyzed using FT. The same level tagging images with 50 phases per cycle and TFEPI glid pulse were analyzed using tagging-MRI. Using 16-segment model, LV peak circumferential strains (Ecc) and peak radial strains (Err) were calculated by the two methods. Ecc and Err were used as strain parameters, and were compared among the three patient groups and between segments with and without LGE.

Results:

Ecc and Err from the two methods were significantly lower for patients with DCM than controls. Ecc from tagging-MRI was significantly lower for patients with HCM than controls (-12.9±1.8% vs. -16.0±1.9%, p=0.007). There was no difference in Ecc and Err from FT and in Err from tagging-MRI between the two groups.

In HCM, Ecc and Err from tagging-MRI were significantly lower for segments with LGE than those without LGE (-14.3±2.8% vs.-10.6±3.0%, p<0.0001, 22.4±9.1% vs. 11.9±5.8%, p<0.0001, respectively). Use of optimal cutoff thresholds of Ecc and Err differentiated segments with LGE from those without LGE, with areas under the curve (AUC) of 0.82 and 0.84. In contrast, there was no difference in Ecc and Err from FT between segments with and without LGE.

In DCM, Ecc from tagging-MRI was significantly lower for segments with LGE than those without LGE (-10.7±4.5% vs.-8.0±3.6%, p=0.0006). Err from the two method was significantly lower for segments with LGE than those without LGE (tagging-MRI: 14.0±7.8% vs. 6.5±3.9%, p<0.0001, FT: 45.9±27.1% vs. 29.1±19.5%, P=0.0006). Use of optimal cutoff thresholds of Err from tagging-MRI and FT differentiated segments with LGE from those without LGE, with AUC of 0.80 and 0.69.

Conclusion:

Tagging-MRI can detect the impairment of myocardial strains caused by fibrosis in cardiomyopathy, in comparison to FT technique.

ID#: 376593

Clinical feasibility of 4D phase-contrast flow CMR imaging in hemodynamic assessment of congenital heart disease patients: A comparison with 2D flow

Liang Zhong, PhD[7] Jun-Mei Zhang, PhD[1], Shuo Zhang, PhD[2], Watcharee Prasertkulchai, MSc[3], Pankaj Garg, MD, PhD[4], Rob J. van der Geest, PhD[5], Xiaodan Zhao, PhD[1], Ju Le Tan, MBBS[1], Ru San Tan, MBBS, MRCP[6], Tarinee Tangcharoen, MD[3]

1. National Heart Centre Singapore, Singapore

2. Philips Healthcare, Singapore, Singapore

3. Ramathibodi Hospital, Bangkok, Thailand

4. University of Leeds, UK, Leeds, England, United Kingdom

5. Department of Radiology, Leiden University Medical Center, The Netherlands, Leiden, Zuid-Holland, Netherlands

6. National Heart Centre Singapore; Duke-NUS Medical School, Singapore, Singapore

7. National Heart Centre Singapore; Duke-NUS Medical School, Singapore

Background: Whole-heart 4D phase-contrast flow (4D flow) cardiovascular magnetic resonance (CMR) imaging provides qualitative and quantitative flow information without breath hold or respiratory gating. Recent technological advances have improved the acquisition speed, rendering its wider clinical adoption imminent. We report our initial experience with 4D flow quantitation in healthy volunteers and patients with congenital heart disease, and compared the results with conventional 2D flow technique.

Methods: Free-breathing whole-heart 4D flow CMR scans were performed on a 1.5T system (Philips, Achieva) without respiratory navigator gating, with velocity encoding in all three orthogonal directions, isotropic spatial resolution of 3 × 3 × 3 mm^3, and temporal resolution of 20 cardiac phases per cardiac cycle. The 3D volume covered the thorax from apex of the heart to the aortic arch. Detailed imaging parameters are summarized in **Table 1**. 4D and 2D flows were measured in the (1) ascending aorta (Ao), distal to coronary artery orifices; (2) mid portion of the pulmonary trunk (PA); (3) right; and (4) left pulmonary arteries at least 4 mm distal to the pulmonary bifurcation. In patients with malformed and/or incompetent aortic or pulmonary valves, regurgitation fractions in the Ao or PA, respectively, were also measured and the results compared between 4D and 2D flow techniques. In addition, intra-cardiac kinetic energy was measured and compared between patients and healthy volunteers. Data analysis was performed with commercial software (MASS, Leiden, the Netherlands). The descriptive results were cross-tabulated.

Results: 4 patients (37 ± 16 years) and 4 healthy volunteers (37 ± 12 years) were enrolled. In the former, distinct abnormal flow features such as cardiac shunt or regurgitation can directly be visualized from 4D flow. **Figure 1** demonstrated three typical flow patterns with selected 4D flow images for patients with atrial septal defect (A), tricuspid regurgitation (B), and turbulence resulted from pulmonary artery banding (C). 4D flow results were generally in good agreement with 2D flow for both velocity and volume, as well as for regurgitant fractions (**Table 2A**). Among patients, calculated kinetic energy in the left ventricle was numerically lower than in healthy controls (**Table 2B**), but the numbers were too small for definitive comparisons. A typical example is illustrated in **Figure 2**, which depicts the kinetic energy for a repaired Tetralogy of Fallot patient with systolic energy loss, compared with a healthy subject.

Conclusion: Free-breathing non-respiratory gated 4D flow CMR facilitates visualization and quantitation of cardiovascular flow with good quality in both healthy and pathological flow conditions, and with reasonable acquisition times. It is feasible to be used in patients with congenital heart disease, who require complex and detailed evaluation of cardiovascular hemodynamics.

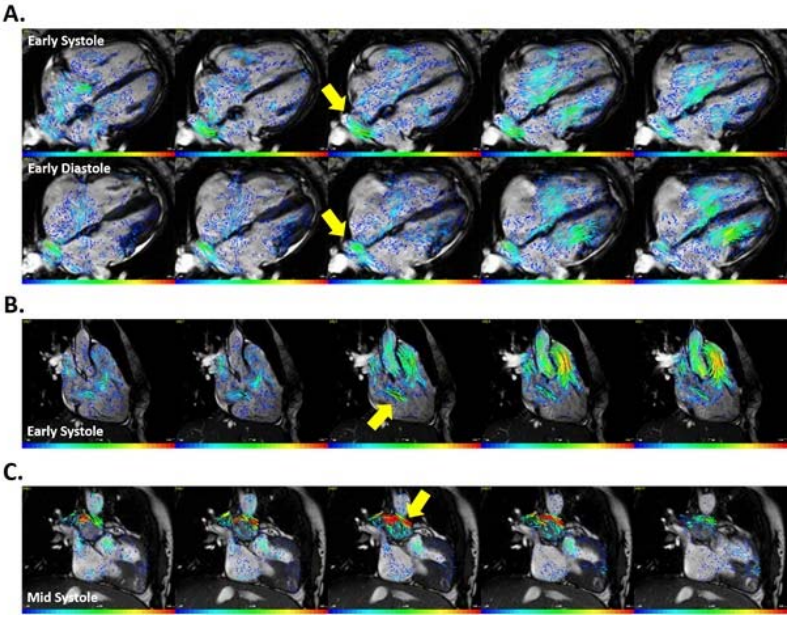

Figure 1. 4D flow visualization in CHD patients. (A) Shunt in atrial septal defect (ASD) during early systole (upper) and diastole (bottom); (B) tricuspid regurgitation; (C) turbulence in pulmonary artery banding (PAB). Flow abnormalities seen with flow vectors were indicated with yellow arrows, respectively

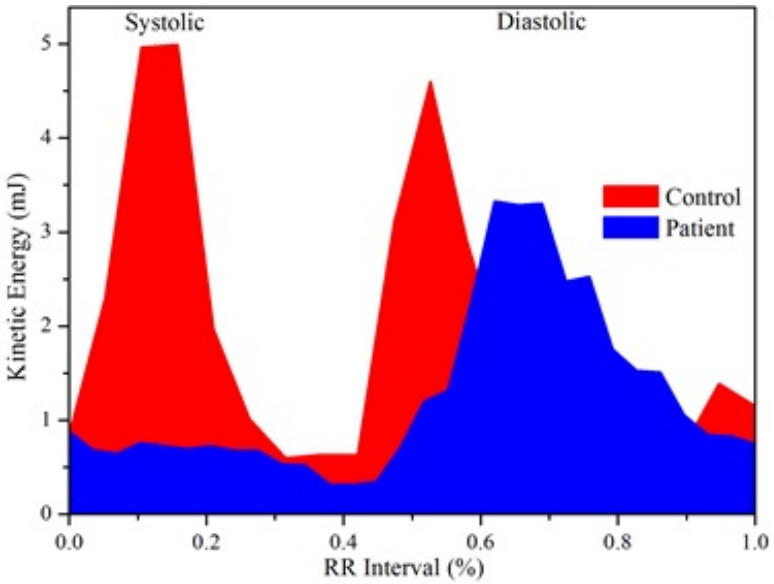

Figure 2. Kinetic energy in the left ventricle derived from 4D flow measurement for a patient with total corrected Tetralogy of Fallot (TOF) and a healthy control

Table 1. 4D and 2D flow CMR imaging parameters

	2D	4D
Field of view (mm^2)	280 × 280	340 × 340
Matrix size	156 × 156	112 × 111

Number of slices	1	67
Acquired voxel size (mm^3)	1.8 × 1.8 × 10	3.0 × 3.0 × 3.0
Reconstructed voxel size (mm^3)	1.3 × 1.3 × 7	1.5 × 1.5 × 1.5
TR / TE (ms)	4.4 / 2.8	3.5 / 2.0
Flip angle (°)	15	10
Cardiac gating	Retrospective	Retrospective
Cardiac phases	40 to 60	20
Sense factor	1.5	2.6 × 1.2
Velocity encoding (cm/s)	150 (max 220)	150 (max 220)
Respiratory motion	free breathing	free breathing
Number of signal averages	3	1
Scan time (min)	1 to 3	5 to 8

Table 2. (A) Percentage difference between 4D and 2D flow CMR measurements on peak velocity, systolic flow and regurgitation fraction (RF) and (B) Comparison of left ventricle (LV) flow kinetic energy between patients and controls from 4D flow analysis.

(A)	AO	PA	RPA	LPA
Peak velocity (cm/s)	9.60%	4.40%	4.50%	3.80%
Systolic flow (ml)	14.90%	12.40%	15.20%	8.30%
Regurgitation fraction (%)	-	9.10%	3.60%	-

(B)						
Flow energy LV (mJ)	Full RR		Systole		Diastole	
	Avg	Max	Avg	Max	Avg	Max
Patients	1.2±0.8	3.4±2.2	1.1±1.2	2.1±2.9	1.2±0.7	2.5±0.9
Controls	1.6±0.7	4.0±1.1	1.8±1.2	2.9±2.1	1.4±0.6	3.9±0.9

ID#: 376598

Diffuse and focal myocardial fibrosis late after Norwood procedure

Naira Mkrtchyan, Dr. Med.[1] Nerejda Shehu, Dr.[2], Heiner Latus, Dr.[3], Heiko Stern, Prof. Dr.[4], Peter Ewert, Prof. Dr.[4], Christian Meierhofer, Dr. Dr.[3], Silke Brodkorb, Dr.[3]

1. Pediatric Cardiology and Congenital Heart Disease, German Heart Center Munich, Munich, Germany

2. Pediatric Cardiology and Congenital Heart Disease, German Heart Center Munich, Muenchen, Bayern, Germany

3. Pediatric Cardiology and Congenital Heart Disease, German Heart Center Munich, Munich, Bayern, Germany

4. Pediatric Cardiology and Congenital Heart Disease, German Heart Center Munich, Bayern, Germany

Background: The modification of placing the shunt from the right ventricle to the pulmonary arteries, also known as Sano procedure, for hypoplastic left heart syndrome (HLHS) has been associated with improved postoperative hemodynamics and outcome but at the cost of a ventriculotomy that may have detrimental long-term sequelae. The conventional modified Blalock-Taussig shunt (MBT) avoids any incision into the ventricle. However, the diastolic run-off of the MBT can cause hemodynamic instability and unpredictable coronary steal phenomenon. This study analyses cardiovascular magnetic resonance (CMR) measurements of myocardial extracellular volume fraction (ECV) and late gadolinium enhancement (LGE) in the systemic right ventricle late after the Norwood procedure (≥9 years). This analysis should determine the frequency, location, and patterns of myocardial fibrosis and evaluate the relationship between diffuse myocardial fibrosis and ventricular performance in patients with Sano procedure or MBT procedure.

Methods: A total of 13 patients with HLHS, all with total cavopulmonary connection (TCPC) were evaluated prospectively by CMR. The entire cohort was divided into 2 groups: 9 patients with Sano Shunt (age median 11 yrs, range 9 to 13 yrs) and 4 patients with MBT (age median 13.5 yrs; range 13 to 14 yrs). The native T1 times (T1) and ECV in the free wall of the right ventricle (RVAW) away from scar, in the interventricular septum (IVS) and in the myocardium bordering the LGE area in patients after Sano shunt were compared with corresponding segments of MBT hearts and correlated with hemodynamic parameters.

Results:

RV ejection fraction and RV size did not differ between groups. LGE was present in 9 (100%) of the Sano shunt patients (at ventriculotomy site) and in 1 (25%) of the MBT patient (one papillary muscle). Median ECV was not significantly different between groups (Tab 1). There was no correlation between ECV and right ventricular volumes or ejection fraction.

Conclusion: In this patient cohort late after completion of TCPC, focal myocardial fibrosis (LGE) was common only at ventriculotomy site and was not associated with adverse ventricular mechanics. Myocardial extracellular volume does not differ depending on the surgical technique (Sano/MBT).

Different levels of calculated ECV fraction in patients with Sano procedure and MBT procedure

ECV [%]	Sano shunt	MBT shunt	p Value
RVAW	24.8 (18-31)	24.0 (20-27)	p=0,94
IVS	25.9 (19-40)	24.0 (20-25)	p=0,50
above scar	28.0 (17-31)	22.3 (22-29)	p=0,26
below scar	22.9 (20-31)	22.0 (19-27)	p=0,71

ID#: 376689

Respiratory Effects on Ventricular Performance using 4D Flow MRI

Alejandro Roldán-Alzate[2]David Rutkowski[1], Christopher J. Francois[2]

1. UW-Madison, WI

2. UW-Madison, Madison, WI

Background: Hemodynamic and energy metrics such as, ventricular flow (Q), kinetic energy (KE), and vorticity, can be used to evaluate cardiac function through the analysis of blood velocity and flow patterns in the heart. The rational for the energy metrics is rooted in the concept of external cardiac work, which is the total work performed on circulating blood from the heart.Such metrics can be quantified with four-dimensional (4D) flow magnetic resonance imaging (MRI). The purpose of this study was to examine the effects of respiratory variations on these metrics, and their relation to cardiac efficiency, through the use of respiratory-gated 4D flow MRI.

Methods: Fifteen healthy volunteers were prospectively recruited according to an IRB-approved and HIPAA-compliant protocol. Subjects were scanned using respiratory- and cardiac-gated 4D Flow MRI. After scanning, data were separated into two sets based on the inspiration and expiration phases of the respiratory cycle. Flow data was analyzed in Matlab (Mathworks, Natick, MA) and Ensight (CEI, Apex, NC) to calculate right ventricle KE (KE_{RV}), left ventricle KE (KE_{LV}), vorticity, and flow through the great vessels (Fig. 1). Cardiac efficiency was assessed based on the Q_{MPA}/KE_{RV} and Q_{AAo}/KE_{LV} ratios. Peak values of measured hemodynamic parameters were compared between respiratory plateaus and correlations between the parameters were examined.

Results: Ventricular efficiency was higher during inspiration than during expiration, due to a combination of higher flow rates and lower kinetic energy (RV: p=0.004; LV: p=0.27) (Fig. 2). Efficiency was also higher in the left ventricles than in the right ventricles of these volunteers. Right ventricular efficiency had a moderate positive correlation (RV: r=0.60,p=0.03) with the magnitude of vorticity, and vorticity values were higher in expiration than in inspiration (LV: p=0.04; RV: p=0.06) (Fig. 3).

Conclusion: The ventricular efficiency parameters indices showed positive correlations with the degree of vorticity in these subjects. This observation agrees with the concept that vortical flow structures work to conserve energy by more efficiently transferring the cardiac work to fluid motion. Furthermore, we observed that LV vorticity was, on average, higher than RV vorticity, which is presumed to support the higher efficiency of the LV. In general, ventricular kinetic energy, cardiac flow magnitude, and ventricular flow structures change with respiration. In conclusion, the effects of respiratory variation should be considered when studying ventricular performance.

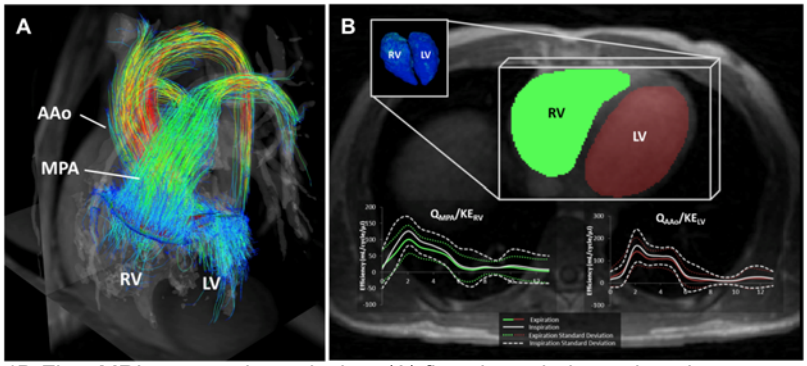

4D Flow MRI was used to calculate (A) flow through the main pulmonary artery (MPA) and ascending aorta (Aao) and (B) kinetic energy in the right (RV) and left (LV) ventricles. Cardiac Efficiency was analyzed through calculation of the great vessel flow (Q) to KE ratio.

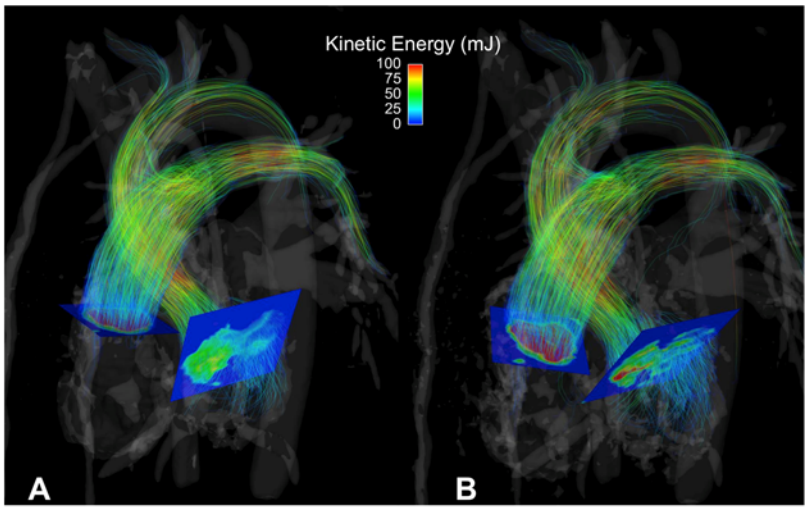

Analysis planes in the center of the RV and LV illustrate the local KE variation during inspiration (A) and expiration (B)

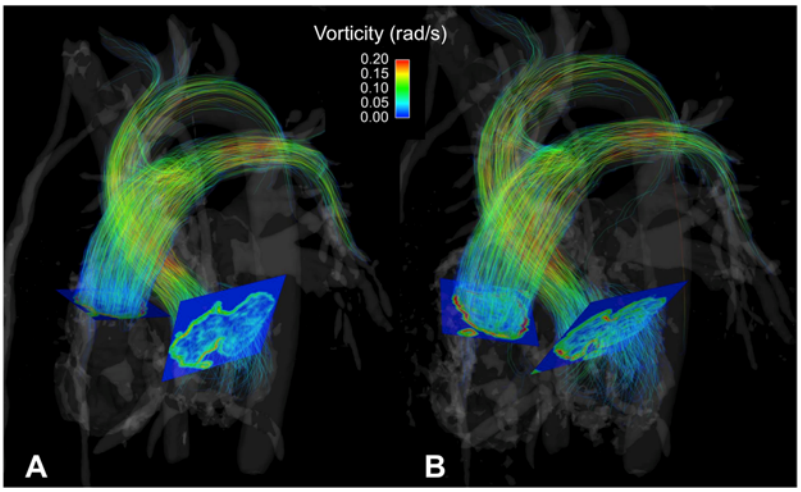

Analysis planes in the center of the RV and LV illustrate the local vorticity variation during inspiration (A) and expiration

ID#: 376713

Focal Scar and Diffuse Myocardial Fibrosis on CMR in Patients with History of Repaired Tetralogy of Fallot

Hubert Cochet[5]Antoine Allain-Nicolai[1], Claudia Camaioni, MD[2], Soumaya Sridi[3], Hubert Nivet[3], Francois Laurent[4], Michel Montaudon[4]

1. CHU Bordeaux, L'Etang-Salé, Reunion

2. Barts Heart Center, London, England, United Kingdom

3. CHU Bordeaux, France

4. Unité d'imagerie cardio-thoracique, CHU Bordeaux, Pessac, Aquitaine, France

5. IHU LIRYC - CHU / Université de Bordeaux, France

Background: Left and right ventricular (LV and RV) remodeling in repaired tetralogy of Fallot (TOF) is poorly understood. We analyzed the correlates of focal scar and diffuse fibrosis in patients with history of TOF repair by using cardiac magnetic resonance (CMR)

Methods: Patients with prior TOF repair underwent CMR including cine imaging to assess ventricular volumes and ejection fraction (EF), T1 mapping to assess LV and RV diffuse fibrosis, and high resolution late gadolinium-enhanced (LGE) imaging to quantify scar size. Structural imaging data were related to clinical characteristics and functional imaging markers. In 40 patients, cine and T1 mapping results were compared to 40 age- and sex-matched controls.

Results: Sixty-four patients with TOF repair were enrolled (age 25±14 years, 19 women), including 18 with prior PV replacement. Compared to controls, TOF patients showed lower LV and RVEF and higher RV volume, RV wall thickness, and native T1 and ECV values on both ventricles. Scar size related to LVEF and RVEF while LV and RV native T1 related to RV dilatation. Patients with history of ventricular arrhythmia showed larger scars and longer native T1. Patients with history of PV replacement showed larger scar on RV outflow tract but LV and RV native T1 were shorter.

Conclusion: Focal scar and biventricular diffuse fibrosis are detected on CMR after TOF repair. Scar size relates to systolic dysfunction, and diffuse fibrosis to RV dilatation. Both may be implicated in ventricular arrhythmias. The finding of shorter T1 after PV replacement suggests that diffuse fibrosis may reverse with therapy.

Characteristics of TOF patients with vs. without history of PV replacement			
Demographics	**History of PVR (N=18)**	**No history of PVR (N=46)**	**P value**
Age (years)	27±13	25±15	0.50
Female gender	5 (28%)	14 (30%)	0.84
Clinical history			
Age at repair (months)	22 [12-38]	17 [9-36]	0.70
History of atrial arrhythmia	2 (11%)	8 (17%)	0.61
History of ventricular arrhythmia	6 (33%)	10 (22%)	0.34
Clinical symptoms			
NYHA functional class	1.5±0.8	1.6±0.6	0.79
Maximum exercise capacity (Watts)	113±34	111±35	0.84
ECG			
QRS duration (ms)	144±28	139±26	0.55
TTE			
PV stenosis	10 (56%)	23 (50%)	0.44
CMR			
Cine MR (N=64)			
LVEDV (mL/m2)	74±15	78±17	0.36
LVEF (%)	56±11	59±9	0.32
RVEDV (mL/m2)	107±26	140±39	**0.002**
RVEF (%)	43±15	51±9	**0.01**
RV wall thickness (mm)	4.0±1.0	3.5±1.0	0.05
Velocity encoded MR (N=64)			
PV regurgitation fraction (%)	0 [0-7.5]	40 [29-48]	**<0.001**
T1 mapping (N=64)			
LV native T1 (ms)	993±49	1022±51	**0.04**
RV native T1 (ms)*	996±46	1053±83	**0.01**
LGE MR (N=40)			
RVOT scar size (cm2)	11 [7-15]	6 [3-9]	**0.02**
Septal scar size (cm2)	5 [4-9]	4 [3-8]	0.72
Other scar on LV or RV	2 (11%)	3 (7%)	0.42
Total scar size (cm2)	16 [13-32]	11 [8-16]	**0.03**
Data are expressed as mean±SD when normaly distibuted, and median [interquartile range Q1-Q3] otherwise. * only available in 17 patients with prior PVR and 41 patients with no prior PVR			

Characteristics of TOF patients with and without PV replacement

Characteristics of TOF patients with vs. without ventricular arrhythmia			
	Ventricular arrhythmia (N=16)	**No ventricular arrhythmia (N=48)**	**P value**
Demographics			
Age (years)	34±14	23±14	**0.005**
Female gender	8 (50%)	11 (23%)	**0.04**
Clinical history			
Age at repair (months)	30 [18-42]	16 [9-36]	0.05
History of PVR	6 (38%)	12 (25%)	0.34
History of atrial arrhythmia	8 (50%)	2 (4%)	**<0.001**
Clinical symptoms			
NYHA functional class	1.8±0.7	1.5±0.6	0.18
Maximum exercise capacity (Watts)	103±29	116±36	0.25
ECG			
QRS duration (ms)	148±34	138±23	0.19
TTE			
PV stenosis	7 (44%)	26 (54%)	0.34
CMR			
Cine MR (N=64)			
LVEDV (mL/m2)	84±21	76±14	0.08
LVEF (%)	52±15	60±6	**0.003**
RVEDV (mL/m2)	141±43	127±37	0.24
RVEF (%)	42±12	51±10	**0.006**
RV wall thickness (mm)	3.6±1.3	3.6±0.9	0.83
Velocity encoded MR (N=64)			
PV regurgitation fraction (%)	28 [0-41]	33 [15-43]	0.47
T1 mapping (N=64)			
LV native T1 (ms)	1044±58	1004±46	**0.006**
RV native T1 (ms)*	1083±83	1025±74	**0.02**
LGE MR (N=40)			
RVOT scar size (cm2)	8 [5-13]	7 [3-9]	0.22
Septal scar size (cm2)	9 [7-12]	3 [2-5]	**<0.001**
Other scar on LV or RV	5 (31%)	0 (0%)	**0.003**
Total scar size (cm2)	20 [16-34]	11 [7-13]	**<0.001**

Data are expressed as mean±SD when normaly distibuted, and median [interquartile range Q1-Q3] otherwise. * only available in 12 patients with ventricular arrhythmia and 46 patients with no ventricular arrhythmia.

Characteristics of TOF patients with and without ventricular arrhythmia

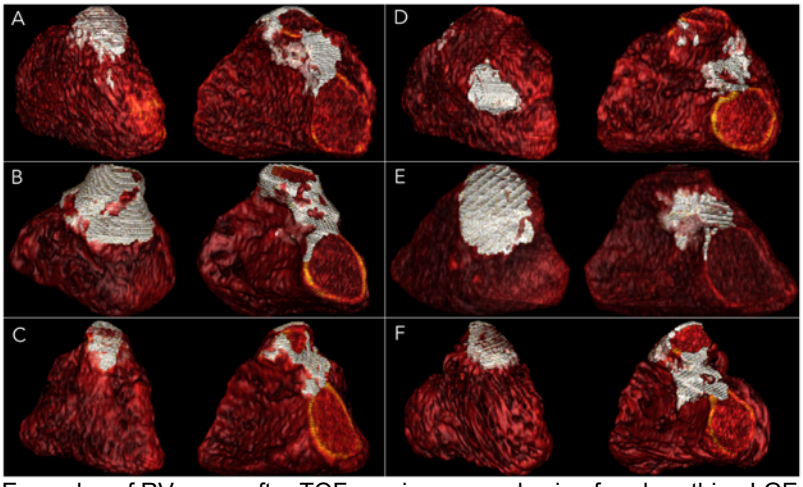

Examples of RV scars after TOF repair assessed using free-breathing LGE-CMR

ID#: 376666

Minimising noise floor effects in spiral diffusion tensor cardiovascular magnetic resonance

Margarita Gorodezky, M. Sc.[1] Andrew D. Scott, PhD[2], Pedro F. Ferreira, PhD[3], Sonia Nielles-Vallespin, PhD, MSc[4], Dudley J. Pennell, MD[5], David N. Firmin, PhD[6]

1. Cardiovascular Magnetic Resonance Unit, Royal Brompton Hospital, England, United Kingdom

2. Royal Brompton Hospital, London, England, United Kingdom

3. Cardiovascular Magnetic Resonance Unit, Royal Brompton Hospital, Sydney Street, London, SW3 6NP, UK, England, United Kingdom

4. NIH, MD

5. Royal Brompton Hospital and Imperial College, London, England, United Kingdom

6. 1. Cardiovascular Magnetic Resonance Unit, Royal Brompton Hospital, Sydney Street, London, SW3 6NP, UK, England, United Kingdom

Background: Diffusion tensor cardiovascular magnetic resonance (DT-CMR) can provide novel information on the myocardial microstructure. In diffusion weighted imaging, diffusivity is measured through signal attenuation where a high diffusivity leads to low signal intensities (SI). However, with large attenuations the SI is artefactually elevated due to the noise floor, which results in errors in DT-CMR parameters including an underestimation of the mean diffusivity (MD)[1]. This work demonstrates a method to reduce noise floor effects in DT-CMR data obtained using a STEAM sequence with a spiral readout[2].

Methods: Short-axis peak-systolic DT-CMR data from 10 healthy volunteers (SIEMENS, 3T-Skyra) obtained using STEAM echo-planar-imaging (EPI) and STEAM spiral, as described by Gorodezky et al.[3]. b=600s/mm^2 / 150s/mm^2 with 8/1 average in 6 diffusion directions were acquired at 2.8x2.8mm^2. For noise floor measurements an agar phantom (40g/l) was also imaged with identical protocols and was repeated with the RF pulses switched off. A product SENSE x2 reconstruction was used for the EPI. The spiral data was reconstructed offline (MATLAB) using both a sum-of-squares (SoS)[4] and a coil sensitivity weighted technique (CSW) (maximal SNR[4]). For CSW coil sensitivity maps were calculated from each of the 2 b≈0s/mm^2 images obtained in each breath-hold and averaged over all breath-holds. The diffusion tensor was calculated with in-house software (MATLAB) and the DT-CMR parameter were compared in the left ventricle (LV), the SNR in septal wall and the standard deviation of the transverse angle (stdTA) was used as quality measurements.

Results: Figure 1 shows example magnitude images and DT-CMR results. The noise floor is clearly suppressed in the magnitude images. The DT-CMR parameters and quality measures are compared in figure 2. Histograms of the noise floor obtained in the phantom are shown in figure 3, demonstrating the effect of applying CSW. Applying CSW restores the MD values obtained with a spiral to similar values to those obtained with an established EPI technique and results in a reduced stdTA.

Conclusion: Despite the higher SNR obtained using SoS reconstruction of spiral data, the noise floor is higher than when using EPI acquisitions with a SENSE reconstruction, which accounts for coil sensitivities. Using coil sensitivity information in reconstructions of spiral DT-CMR data reduces the background noise floor and avoids the underestimation of MD demonstrated with SoS reconstruction of the spiral data. **References:**

1. Jones D.: MRM 2014
2. Gorodezky M: SCMR 2016: R021
3. Gorodezky M: ISMRM 2016: Abstract 3109
4. Roemer P: MRM 1990

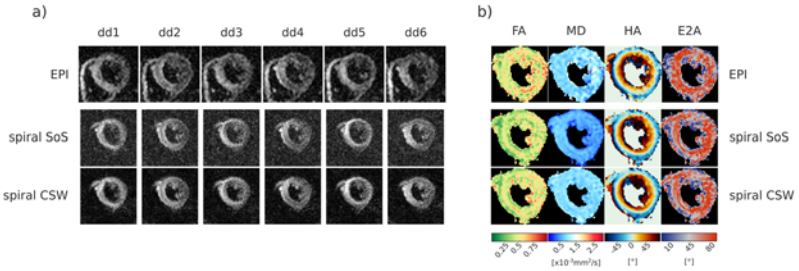

Figure 1: The diffusion weighted images for the STEAM EPI and both reconstructions of the STEAM spiral sequence in all 6 directions for b=600s/mm2 (a). The calculated DT-CMR parameter maps for both sequences and all three reconstructions. The fractional anisotropy (FA), mean diffusivity (MD), helical angle (HA), and secondary eigenvector angulation (E2A) are shown (b).

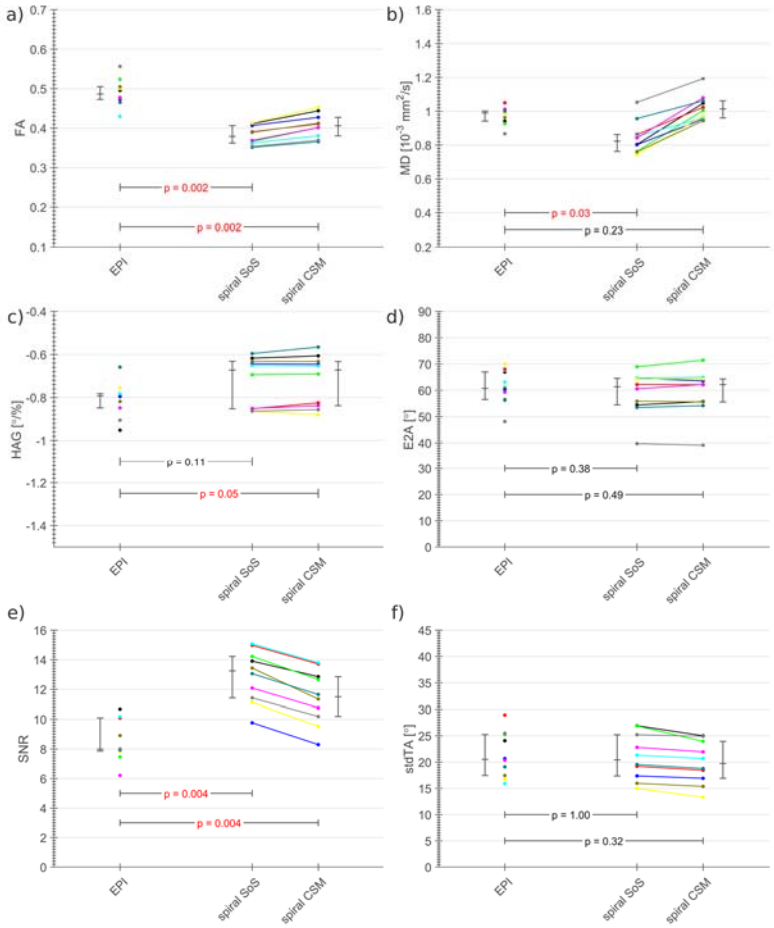

Firgure 2: DT-CMR and quality parameters averaged over the left ventricle are compared between the sequences and the reconstructions. The mean FA (a), MD (b), helical angle gradient (HAG) (c), and median E2A (d) are shown. The SNR (e) was calculated over the septal wall and the standard deviation of the transverse angles (stdTA) over the left ventricle.

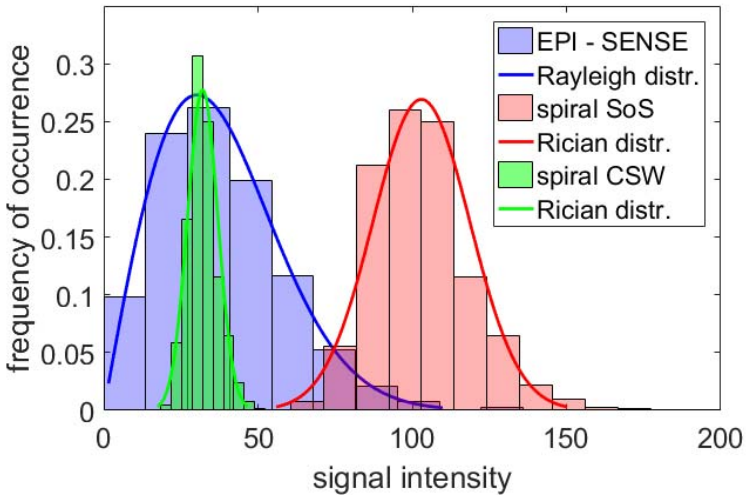

Figure 3: The comparison of the noise distribution in a phantom for the three compared reconstructions with either Rayleigh (EPI) or Rician (spiral SoS and CSW) fits. The noise images were acquired using the sequence employed in vivo with radio frequency pulses of 0°. Noise images were normalized by the mean signal intensity obtained with the radio frequency pulses switched on.

ID#: 376667

The value of shunt size and ventricular volumes at rest and during dobutamine stress in predicting the effect of transcutaneous closure of atrial septal defect

Sigurdur S. Stephensen[1] Ellen Ostenfeld, M.D., Ph.D.[2], Håkan Arheden, MD PhD[3], Marcus Carlsson, MD, PhD[4]

1. Clinical Physiology, Lund University, Lund, Sweden., Iceland

2. Lund University, Dept of Clinical Sciences, Clinical Physiology, Lund, and Skane University Hospital, Lund, Skane Lan, Sweden

3. Lund University, Skåne University Hospital, Department of Clinical Sciences Lund, Clinical Physiology, Lund, Sweden, Lund, Sweden

4. Lund University, Skane University Hospital, Department of Clinical Sciences Lund, Clinical Physiology, Lund, Sweden, Skane Lan, Sweden

Background: Even though many patients with atrial septal defect (ASD) experience improved exercise capacity after ASD closure, this is not true for all patients. The aim of the study was to investigate if pulmonary-to-systemic flow ratio (QP/QS), and right ventricular (RV) function during stress in ASD patients could better predict the outcome of transcutaneous ASD closure, with regards to exercise capacity and to determine the time course of ventricular remodelling after ASD closure.

Methods: Nineteen patients scheduled for ASD closure were included. Seventeen patients underwent CMR at rest and during dobutamine-atropine stress and 16 patients underwent follow up CMR at rest on day 1 and 3 and 12 months after transcutaneous closure of the ASD. Peak oxygen uptake (VO_2) was measured on ergospirometry before and 12 months after ASD closure.

Results: Peak oxygen uptake as percent of predicted value (VO_2 %) increased after ASD closure (P2 did not(P=0.07). Improved VO_2 % was related in a negative manner toQP/QS at rest (P2% was not related to right ventricular size at rest (P=0.16 for RV end-diastolic volume indexed to body surface area (RVEDVI)) or during stress (P=0.96 for RVEDVI). Left ventricular volumes normalized quickly whereas right ventricular remodelling had started on day one after ASD closure and continued for up to 12 months.

Conclusion: Improvement of peak oxygen uptake after ASD closure in adult patients is not straight forward and we found that patients with smaller shunts had a larger improvement in predicted exercise capacity. Quantifications of shunt size or RV function during dobutamine stress did not predict treatment effect. Ventricular remodelling is fast in the left ventricle but is a continuing process over the first year after ASD closure in the right ventricle.

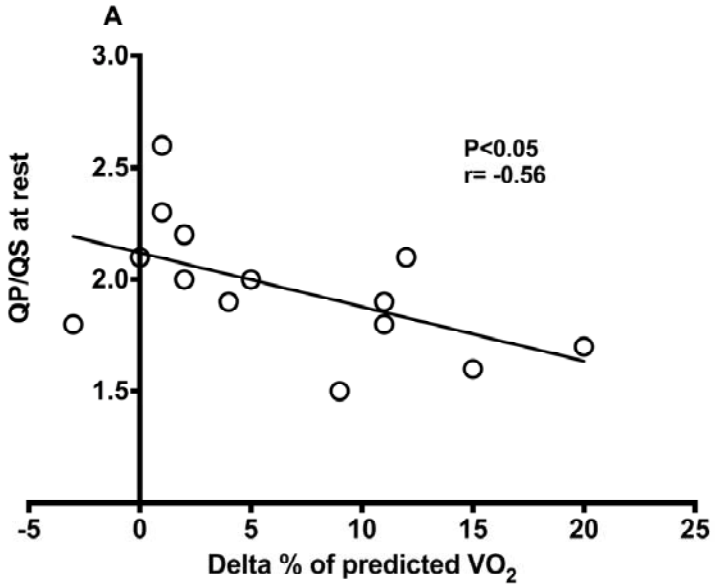

Linear regression analysis between the improvement in VO2 peak presented as percentage of predicted value and pulmonary-to-systemic flow ratio (QP/QS) at rest before ASD closure.

ID#: 376743

Combined T1 mapping and stress perfusion CMR: A promising non-contrast assessment of myocardial perfusion in children.

Lazaro E. Hernandez, MD[1] David A. Parra, M.D.[2], Jianli Niu[1], Jonathan H. Soslow, M.D., M.S.C.I.[3]

1. Joe DiMaggio Children's Hospital, Hollywood, FL

2. Vanderbilt University Medical Center, Division of Pediatric Cardiology, Nashville, TN

3. Vanderbilt University Medical Center, Nashville, TN

Background: Native T1 mapping is sensitive to changes in myocardial water content. Recent work demonstrated the efficacy of myocardial stress/rest T1 mapping for detection of myocardial ischemia in adult patients with coronary artery disease without the need for gadolinium contrast administration. We hypothesized that changes in T1 times after regadenoson administration could detect myocardial perfusion defects in children without the use of gadolinium contrast.

Methods: 14 patients [7 hypertrophic cardiomyopathy; 3 exertional chest pain with abnormal stress test; 3 anomalous origin of the left coronary artery and 1 heart transplant] underwent stress perfusion CMR with regadenoson (1.5 T scanner). T1 maps were performed at stress and rest in the base, mid, and apical short axis slices using a modified Look-Locker inversion recovery (MOLLI) sequence. The percent change in T1 (%ΔT1) defined as [T1stress-T1rest]/T1rest) was calculated for the entire myocardium, each slice, and each segment (using the 16-segment model). Myocardial perfusion reserve index (MPRI) and late gadolinium enhancement (LGE) were also analyzed in each slice and segment. Spearman's correlation, logistic regression and Mann Whitney U were used to examine the ability of %ΔT1 and MPRI to differentiate normal and abnormal myocardial perfusion defined by subjective perfusion analysis and LGE.

Results: The mean age was 16.6 ± 2.0 years. All patients had normal perfusion at rest. Four patients had abnormal perfusion during stress with LGE in the same region. Mean T1 values at rest were 1050 ±50 ms in patients with abnormal perfusion and 976 ± 22 ms in patients with normal perfusion. A mean myocardial %ΔT1 ≥ 2.5 % differentiated between normal and abnormal myocardial perfusion (p=0.007) in 92.8% of the cases (13/14) using the mid-LV slice (Fig.A). Myocardial %ΔT1 analyzed by individual myocardial segment (n=204) distinguished normal (n=165) from abnormal (n=39) myocardial perfusion with an OR=0.027 (95% CI 0.0051 to 0.1474) (Fig.B). Although MPRI was decreased in some of the poorly perfused segments [OR=0.0013 (95% CI 0.0001 to 0.0133)], myocardial %ΔT1 appears to be more sensitive (sensitivity 97.4%/specificity 96.9%) than MPRI (sensitivity of 71.8 %/specificity of 98.8 %) to separate cardiac segments with normal and abnormal perfusion (Fig.C). No significant correlation was found between myocardial %ΔT1 and MPRI (rho=0.29).

Conclusion: Our data suggest that myocardial %ΔT1 is a sensitive method to differentiate between normally and abnormally perfused myocardium and holds promise for detecting myocardial perfusion defects without the need for gadolinium contrast agents.

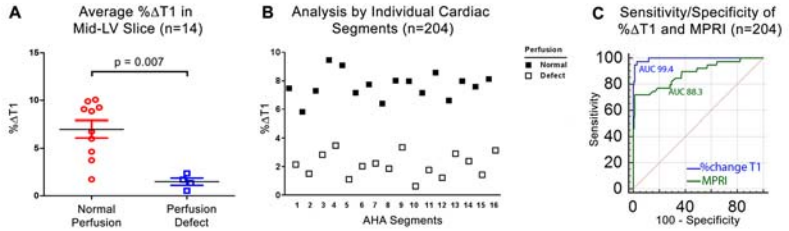

T1% of Change and MPRI to detect abnormal myocardial perfusion.

ID#: 376768

Patients with repaired Tetralogy of Fallot and pulmonary regurgitation have higher hemodynamic forces in the right ventricle compared to controls

Pia Sjöberg, M.D.[1]Einar Heiberg, PhD[2], Ronny Gustafsson, M.D, PhD[3], Shahab Nozohoor, M.D, PhD[3], Johannes Töger, PhD[4], Per M. Arvidsson, MD, PhD[5], Håkan Arheden, MD PhD[6], Marcus Carlsson, MD, PhD[7]

1. Lund University, Skane University Hospital, Department of Clinical Sciences Lund, Clinical Physiology, Lund, Sweden, Sweden

2. Lund University, Skåne University Hospital, Department of Clinical Sciences Lund, Clinical Physiology, Lund, Sweden, Skane Lan, Sweden

3. Lund University, Skane University Hospital, Department of Clinical Sciences Lund, Cardiothoracic Surgery, Lund, Sweden, Sweden

4. Lund University, Skåne University Hospital, Malmö, Sweden

5. Lund University, Skane University Hospital, Department of Clinical Sciences Lund, Clinical Physiology, Lund, Sweden, Lund, Skane Lan, Sweden

6. Lund University, Skåne University Hospital, Department of Clinical Sciences Lund, Clinical Physiology, Lund, Sweden, Lund, Sweden

7. Lund University, Skane University Hospital, Department of Clinical Sciences Lund, Clinical Physiology, Lund, Sweden, Skane Lan, Sweden

Background: Indications for pulmonary valve replacement in patients with repaired Tetralogy of Fallot (rToF) and pulmonary regurgitation (PR) are debated. The status of right ventricular (RV) function is important in this decision but remains elusive. Intracardiac hemodynamic forces have been suggested as marker for ventricular dysfunction and can be quantified by 4D flow cardiac magnetic resonance imaging (CMR). Therefore, the aim of this study was to investigate if the RV hemodynamic forces in patients with rToF differ from controls.

Methods: Patients with rToF, PR>20% and no pulmonary stenosis (n=14, 5 females, median age 24 years, range 18-52 years) underwent CMR including 4D flow, using retrospective ECG triggering, at 1.5 T (Achieva, Philips Healthcare, Best, The Netherlands, or Magnetom Aera, Siemens Healthcare, Erlangen, Germany). Healthy volunteers (n=15, 2 females, median age 28 years, range 23-46 years) were used as controls. Intraventricular pressure gradients were computed using the Navier-Stokes equation with 4D flow data as input. Global hemodynamic force was calculated by integrating the pressure gradients over the RV volume for each point in time. Root mean square (RMS) forces for systole and diastole were computed in three directions, Figure 1.

Results: Figure 2 shows RV hemodynamic forces in all subjects with similar patterns but with greater variation in the patient group. Figure 2 also shows a visualization of the forces in the diaphragm-right ventricular outflow tract direction in a patient with rToF. RMS forces are summarized in Figure 3.

Conclusion: Patients with rToF and PR have higher forces in the RV during diastole compared to healthy controls even when indexing for volume. A possible explanation could be the forces caused by the PR volume, but also increased radial pumping causing higher acceleration of blood flow entering the RV. These results suggest that analysis of hemodynamic forces might provide important information about the ventricular function in patients with rToF and contribute to the understanding of the pathophysiology of the volume-loaded RV. Hemodynamic forces may thus be a new measure to help optimizing the timing for pulmonary valve replacement. Acknowledgments We thank Andreas Greiser, Siemens Healthcare, Erlangen, Germany, for providing the Siemens 4D flow prototype (work-in-progress package WIP785K).

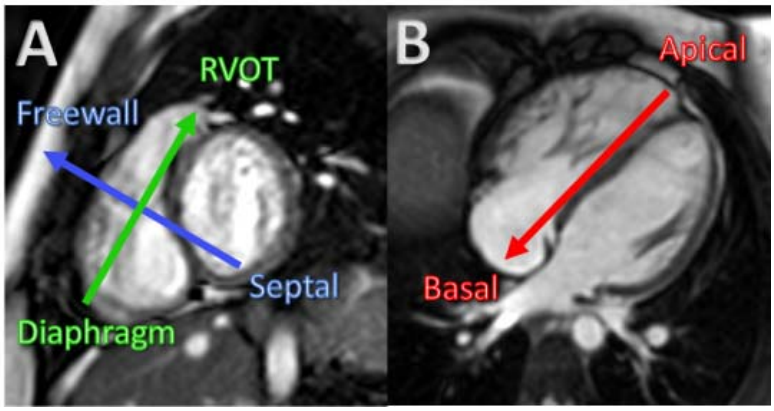

Figure 1. Direction of forces in the right ventricle. A: Septal-freewall and Diaphragm-RVOT (right ventricular outflow tract), B: Apical-basal

Figure 2. Upper panel: Hemodynamic forces in the right ventricle of patients with repaired Tetralogy of Fallot (rToF) and controls. Values are mean ± SD. Lower panel: Visualization of forces in the diaphragm-right ventricular outflow tract direction in a patient with repaired Tetralogy of Fallot and pulmonary regurgitation.

Force direction		Systole			Diastole		
		rToF	Controls	P-value	rToF	Controls	P-value
Septal-freewall	N	0.075 ±0.029	0.058 ±0.019	0.12	0.056 ±0.029	0.042 ±0.012	0.53
	N/I	0.40±0.14	0.40 ± 0.12	0.84	0.27 ± 0.10	0.29 ± 0.13	0.77
Diaphragm-RVOT	N	0.21 ± 0.12	0.17 ±0.059	0.25	0.10 ±0.074	0.040 ±0.015	<0.0001
	N/I	0.93±0.37	1.02 ± 0.29	0.33	0.46 ± 0.25	0.27 ± 0.12	0.015
Apical-basal	N	0.19 ±0.11	0.13 ±0.056	0.051	0.15 ±0.076	0.079 ±0.030	0.0009
	N/I	0.93±0.46	0.79 ± 0.31	0.33	0.71 ± 0.32	0.49 ± 0.14	0.025

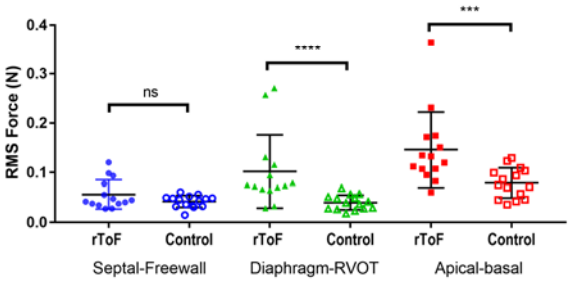

***p<0.001, ****p<0.0001

Figure 3. Upper panel shows RMS force in the right ventricle of patients with repaired Tetralogy of Fallot (rToF) and controls. Lower panel shows diastolic RMS force in the right ventricle of patients with rToF and controls. Bar and whiskers show mean ± SD. RVOT, right ventricular outflow tract.

ID#: 376855

Feasibility Study of a Single Breath-hold, 3D mDIXON Pulse Sequence for Late Gadolinium Enhancement Imaging of Ischaemic Scar

James R. Foley, MBChB BSc (Hons)[1] Graham J. Fent, MBChB, BSc[1], Pankaj Garg, MD, PhD[2], David A. Broadbent, MSc[3], Laura E. Dobson, MD[4], Pei G. Chew, MBChB(Hons) [5], Louise AE. Brown, MBChB, BMedSc[4], Erica Dall'Armellina, Sr., MD, DPhil[6], Peter P. Swoboda, PhD[1], Sven Plein, MD PhD[4], David M. Higgins, PhD[7], John P. Greenwood, PhD[4]

1. University of Leeds, Leeds, England, United Kingdom

2. University of Leeds, UK, Leeds, England, United Kingdom

3. Leeds Teaching Hospitals NHS Trust, England, United Kingdom

4. University of Leeds, England, United Kingdom

5. University of Leeds, Liverpool, England, United Kingdom

6. Leeds Institute of Cardiovascular and Metabolic Medicine, Division of Biomedical Imaging,University of Leeds, United Kingdom

7. Philips, Leeds, England, United Kingdom

Background:

Late gadolinium enhancement (LGE) imaging is well validated for the diagnosis and quantification of myocardial infarction (MI), and the transmural extent of MI identifies likelihood of functional recovery following revascularization. 2D LGE imaging involves multiple breath-holds for the acquisition of each short axis slice to cover the entire left ventricle. 3D LGE methods cover the entire ventricle in a single breath hold; however breath-hold duration is typically long with images susceptible to motion artifacts. We evaluated a rapid 3D mDIXON pulse sequence for image quality and quantitation of MI.

Methods:

92 patients with prior MI underwent an identical 1.5T CMR protocol (Ingenia, Philips Healthcare, Best, The Netherlands). For LGE imaging, an intravenous bolus of 0.15mmol/kg gadobutrol (Gadovist®, Bayer Inc.) was administered. Optimal inversion time to null myocardium was determined by a Look-Locker sequence. 2D and 3D LGE were performed 10 minutes following contrast administration in random order to avoid bias. Imaging parameters included: (i) 2D breath-hold phase sensitive inversion recovery (PSIR) - 12 slices covering the full LV (thickness 10mm, no gap, repetition time 6.1ms/echo time 3.0ms, flip angle 25º); (ii) 3D mDIXON - 24 slices (slice thickness 5mm, repetition time 4.0ms/echo time 1.21ms and 2.5ms, flip angle 15º). Data were analysed using CVI[42] (Circle Cardiovascular Imaging Inc. Calgary, Canada). Image quality was defined on a 4-point scale (4=non-diagnostic, 3=acceptable diagnostic quality 2=good quality, 1=excellent quality). Myocardial transmurality and scar mass was calculated using the full-width half-maximum method.

Results: Image quality was comparable between 3D and 2D LGE (1.4±0.6 vs. 1.3±0.5; P=0.162). 3D LGE was associated with greater scar tissue mass (3D: 18.9±17.5g vs 2D 17.8±16.2g P=0.03), although not statistically significantly different when scar tissue expressed as a %LV mass (3D 13.4±9.9% vs 12.7±9.5% P= 0.07). For 3D vs. 2D scar mass there was strong and significant positive correlation and Bland Altman analysis showed a mean bias of 1.1g (95%CI: -5.7–7.9) (Fig 1). There was excellent agreement (κ=0.870) between 3D and 2D LGE on a segmental level analysis of scar transmurality at a binary threshold of 50% transmural extent (typical clinical threshold for determining viability status). Time taken for 3D image acquisition took just 5% of the time required for 2D images: 3D (15.6±1.4s) compared to 2D (311.6±43.2s) P<0.0001.

Conclusion: Single breath-hold 3D mDIXON LGE imaging allows quantitative assessment of MI and transmurality with comparable image quality in a vastly shorter acquisition time compared to 2D LGE imaging.

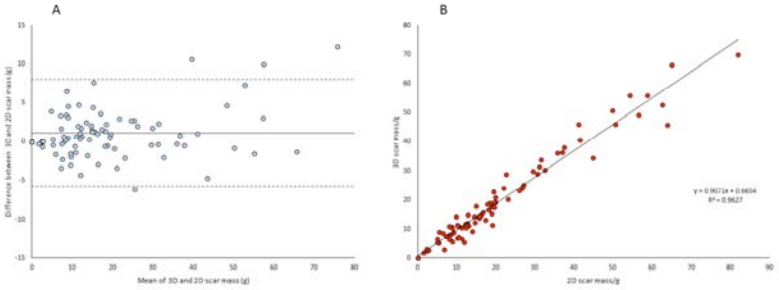
A
B
Mean of 3D and 2D scar mass (g)
2D scar mass/g

ID#: 376885

Contributions of Afterload and Contractility to Adverse Effects of Chemotherapy on Myocardial Function

Nathaniel Reichek, MD FACC[1] Derek Knight[2], Alim Merchant[3], Marie Grgas[4], Haoyi Zheng, MD[5], Bhoomie Mehrotra, MD[3]

1. St. Francis Hospital-The Heart Center and Stony Brook University, Northport, NY

2. St. Francis Hospital, Port Washingotn, NY

3. St. Francis Hospital

4. St. Francis Hospital, Greenvale, NY

5. St Francis Hospital

Background: Afterload excess(AE) and reduced contractility(C) are principal causes of systolic myocardial dysfunction. We';ve previously quantitated AE in nonischemic cardiomyopathy, aortic stenosis and normals(NL) using a simplified afterload index and demonstrated significant inverse relationships to left ventricular ejection fraction(LV EF) and circumferential and longitudinal strains and strain rates in each group. Mirsky's wall stress indices were not as effective. In addition, the relative contributions of AE and reduced C to dysfunction in populations can be determined and contributions in individuals estimated from such data. Since left ventricular ejection fraction(LV EF) impacts chemotherapy management, and anthracycline induced LV mass reduction, a potential contributor to AE, has been reported(Neilan et al, JACC 2012), we examined AE in subjects(S, n= 31) in a CMR cardiotoxicity study and NLs (n=54).

Methods: EF, end-systolic volume(V) and mass(M) were assessed from SSFP short axis cine acquisition stacks on Avanto and Skyra scanners using Medis Mass and cuff systolic pressure(P) was obtained during scans. Afterload was expressed as: PxV over M(PV/M). Alternative more complex wall stress indices were also explored(Mirsky's, Alter's and Arts' stress indices). Contributions of AE and impaired C to EF reduction in the population and estimates of their contributions in individuals were determined by comparing S and NL regressions of PV/M vs EF to total EF reduction. All analyses were blinded.

Results: In S (ages 61.2$\pm$12.7y, 67% female) mean EF was 54.7$\pm$9.6% and PV/M 89.7$\pm$22.2. In NL (age 59.2$\pm$13.5y, 46.2% female,) mean EF was 58.1$\pm$5.1%(p=0.02 vs S) and PV/M 86.4$\pm$20.1 (p=ns). In S, the regression equation for PV/M versus EF was: PV/M=2.4 EF+22.2, r=-0.71 while in NL, PVM=2.75 EF+24.6, r=-0.69, both p<0.0001. Arts'; fiber stress index and Alter';s stress index x P performed comparably but Mirsky';s and Alter';s modified stress indices did not. Overall, afterload excess accounted for 76.2% of EF reduction, impaired contractility 23.8% in the study population, but estimated values in individuals ranged widely(PV/M:31.7%-95.6%) and higher PV/M% was associated with lower EF.

Conclusion: Afterload excess was the principal cause of LV systolic dysfunction in chemotherapy patients, as has previously been described using single beat elastance estimates in systolic heart failure patients (Ky et al, JACC 2013), but relative contributions of AE and contractility varied widely among individuals. Reported anthracycline-related LV mass reductions, which can cause AE, likely play an important role.

ID#: 376892

Left atrial strain assessment in children with repaired tetralogy of Fallot

Richard M. Friesen, MD[1] Brian D. Soriano, MD[2], Mark R. Ferguson, MD[2], Sujatha Buddhe, MD MS[1]

1. Seattle Children's Hospital, Seattle, WA

2. Seattle Children's Hospital, WA

Background: Decreased exercise tolerance, left ventricular dysfunction and atrial arrhythmias have been widely described in patients with repaired tetralogy of Fallot (rTOF). While right atrial (RA) functional properties were previously evaluated, studies evaluating left atrial (LA) strain are limited in rTOF, particularly in children. In adults, LA conduit function in early diastole is a known potential marker of ventricular diastolic dysfunction, which may precede more overt signs of heart failure. Our study aims to evaluate LA strain by cardiac MRI (CMR) as it relates to functional and volumetric indices in children with rTOF.

Methods: This study is a retrospective analysis of rTOF patients who underwent clinically indicated CMR. Clinical, exercise test results and traditional CMR data were collected. LA strain and strain rate were evaluated from SSFP cine images using dedicated CMR-FT software (2D CPA MR, TomTec, Germany) in the four chamber and vertical long axis views. Correlations with clinical, volumetric and functional indices were performed.

Results: Thirty patients with mean age of 13.1yrs (range 7.8-17.8 yrs) were included. Mean LA early negative strain rate (SRe) corresponding to conduit function was -0.70 ± 0.44. Similarly, mean peak positive strain rate (SRs) corresponding to reservoir function was 0.91 ± 0.48 and mean peak late negative strain rate (SRa) corresponding to contractile booster pump function was -0.58 ± 0.48. Of all the indices, LA conduit function, estimated by early negative strain rate (SRe) had better correlation with exercise test based peak oxygen consumption VO2 (-0.67, p = 0.02) and right ventricular ejection fraction (RVEF) (-0.43, p = 0.02). This correlation was better than conduit function assessment by strain (passive strain Ɛe) which was approaching significance (-0.46 and 0.33 respectively; p =0.07). Also, LA global longitudinal strain had a modest correlation with VO2 (r = -0.53, p = 0.03).

Conclusion: Left atrial conduit function and global longitudinal strain in patients with rTOF is associated with decreased RVEF and VO2 max and this assessment is better when using strain rate parameters. Impaired LA conduit function may be an early marker of ventricular diastolic dysfunction in rTOF and may be a surrogate for exercise intolerance and poor outcomes. Further studies are indicated to more thoroughly evaluate LA strain as it pertains to clinical outcomes in these patients.

ID#: 376895

Ferumoxytol-Enhanced Magnetic Resonance Venography in Central Venous Occlusion

Puja Shahrouki, M.D.[1] Biraj Bista, M.D.[2], John M. Moriarty, M.D.[3], Stephen T. Kee, M.D.[3], Brian G. DeRubertis, M.D.[3], Sarah N. Khan, M.D.[3], Takegawa Yoshida, M.D.[3], Kim-Lien Nguyen, M.D.[4], J. Paul Finn, M.D.[3]

1. Department of Radiology, David Geffen School of Medicine at UCLA, Los Angeles, CA

2. Department of Radiology, David Geffen School of Medicine at UCLA, Santa Monica, CA

3. Department of Radiology, David Geffen School of Medicine at UCLA, CA

4. Division of Cardiology, David Geffen School of Medicine at UCLA and VA Greater Los Angeles Healthcare System, CA

Background: As therapy prolongs survival in patients with cancers and organ failure, central venous obstruction is becoming a common and potentially severe clinical complication of venous cannulation. The approach to treatment of venous occlusion is guided largely by anatomic considerations and current approaches to imaging of central veins face many challenges. Ultrasound is of limited value in the chest and conventional CT and MRI techniques are complicated by unpredictable dynamics of venous enhancement with extracellular contrast agents. Furthermore, these agents may be contraindicated in patients with renal failure. We hypothesized that steady state MR imaging with ferumoxytol (Feraheme, AMAG pharmaceuticals), a purely intravascular iron-based contrast agent, would support comprehensive assessment of native and collateralized veins in patients with suspected venous obstruction.

Methods: Forty-four consecutive adult patients with CKD (age 45 ± 17, 26 male) and suspected venous obstruction underwent ferumoxytol-enhanced magnetic resonance venography (FE-MRV) on a 3.0T MRI system (Magnetom TIM Trio, Magnetom Prisma Fit or Magnetom Skyra, Siemens Medical Solutions) or 1.5T MRI system (Magnetom TIM Avanto, Siemens Medical Solutions) between June 2013 to May 2017. All patients underwent continuous monitoring of heart rate, blood pressure and pulse oximetry throughout the examination. Two blinded reviewers independently assessed FE-MRV exams for overall image quality. Twenty-one named vessel segments were scored on a 4-point scale, where scores ≥2 were considered of diagnostic quality. All segments of diagnostic quality within the field of view were analyzed for occlusion. The presence of venous collaterals was scored on a 2-point scale in patients with occlusion (1 = no collaterals; 2 = collaterals present). Disagreements were resolved by consensus of the primary reviewers with a third senior reviewer. Interobserver agreement was determined by using AC1 statistic.

Results: All FE-MRV studies were considered diagnostic, with 100% and 99.5% (888/893) segments being considered of diagnostic quality by the two observers respectively with excellent interobserver agreement (AC1=0.91). The average image quality score for observer 1 and 2 were 3.94 and 3.90 respectively (AC1=0.80). 10.6% (95/888) segments were found to be occluded (ICC=0.93). The interobserver agreement for the presence of collaterals was good (AC1=0.57).

Conclusion: FE-MRV is a powerful, practical and reliable technique for mapping of central thoracic and abdominal veins and can be used to inform image guided therapy. It may set a new standard in venous imaging and may play a pivotal role in patients in whom conventional contrast agents are contraindicated or ineffective.

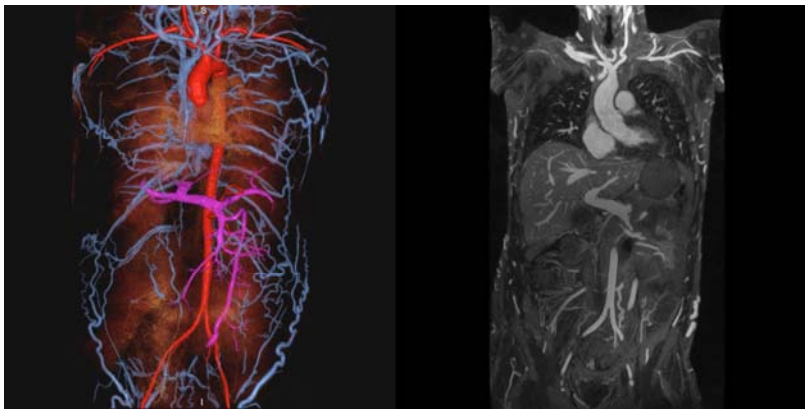

Reconstructed 3-D volume rendered image (left) and FE-MRV (right) of a 33 year-old male with multiple venous occlusions in the neck and pelvic region with extensive collateralization.

ID#: 376896

Differentiation of left ventricular mechanics in high- and low-gradient aortic stenosis by cardiac magnetic resonance (CMR) feature tracking

Sabine Zitzmann, MD[1]Julia Vietheer, MD[2], Anja Dingeldey, MD[2], Christoph Liebetrau, MD[2], Till Keller, MD[2], Jan Sebastian Wolter, MD[2], Steffen Kriechbaum, MD[2], Ulrich Fischer-Rasokat, MD[2], Christian W. Hamm, PhD[2], Andreas Rolf, MD[2]

1. Kerckhoff-Heart-Center, Department of Cardiology, Bad Nauheim, Germany, Frankfurt, Germany

2. Kerckhoff-Heart-Center, Department of Cardiology, Bad Nauheim, Germany, Germany

Background:

Introduction: Three subtypes of severe aortic stenosis (sAS) are distinguished by gradient, ejection fraction and flow state. Paradoxical low-flow, low-gradient (PLFLG) sAS has a poor prognosis despite preserved ejection fraction and is characterized by severe subendocardial fibrosis. Cardiac magnetic resonance (CMR) feature tracking (FT) allows separate analysis of subendocardial function (global longitudinal strain/strain rate [GLS/GLSR]) and subepicardial function (global circumferential strain/strain rate [GCS/GCSR]). Global radial strain/strain rate (GRS/GRSR) accounts for both functional units.

Hypothesis: The goal of this study was to examine whether PLFLG sAS has some unique mechanical properties defined by its strain and strain rate. We speculated that PLFLG sAS differs from the two other subtypes in longitudinal strain and strain rate.

Methods:

Methods: Steady state free precession(SSFP) cine CMR sequences of 88 patients from a previously published cohort were analyzed retrospectively for strain and strain rate using the FT module from cvi42 (circle cardiovascular imaging, Calgary, Canada), yielding six strain parameters. Of the 88 patients, 52 had normal-flow, high-gradient (NFHG) sAS, 18 had paradoxical low-flow, low-gradient (PLFLG) sAS, and 13 had classical low-flow, low-gradient (LFLG) sAS.

Results:

Results: Both PLFLG and NFHG sAS patients had reduced GLS and systolic GLSR with preserved GCS and systolic GCSR, whereas classical LFLG sAS patients had markedly reduced longitudinal and circumferential strain (Table 1). There was no significant difference between PLFLG and NFHG sAS. Instead, we found markedly increased diastolic strain rates in PLFLG sAS patients, a unique feature that was not present in either of the other subtypes and is indicative of severely impaired diastolic function (Table 1).

Conclusion:

Conclusion: As expected all three subtypes of sAS showed impaired strain and strain rates. However PLFLG sAS does not differ from the two other subtypes in longitudinal strain and strain rate. Interestingly CMR FT analysis shows a unique diastolic strain rate pattern in patients with PLFLG sAS.

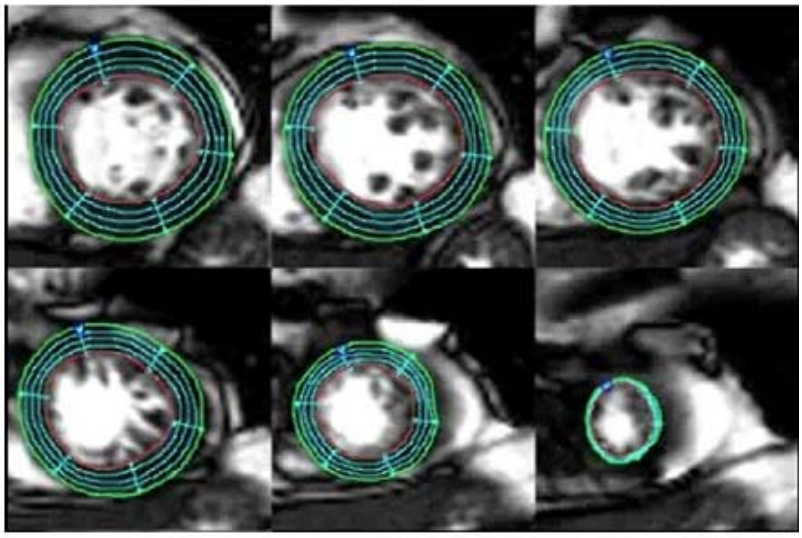

CVI42 feature tracking module (circle cardiovascular imaging, Calgary, Canada). Manual contour definition of endo- and epicardial borders.

CVI42 feature tracking module (circle cardiovascular imaging, Calgary, Canada). Manual contour definition of endo- and epicardial borders.

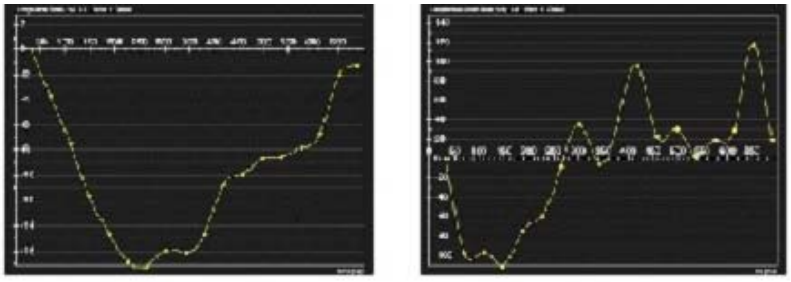

Computation of 2D strain and strain sates

Computation of 2D strain and strain sates

Table 1. Symbols indicate significance on zero point zero one level of post hoc Scheffé test

Results	***LFLG***	***NFHG***	***PLFLG***	***p-value***
Strain %				
GRS	14.8 ± 7.2*§	30.9 ± 12.1*	30.4 ± 15.7§	0.0001
GCS	-9.6 ± 3.9*§	-17.0 ± 4.8*	-16.0 ± 9.5§	0.0002
GLS	-8.5 ± 2.8*§	-14.7 4.9*	-14.0 ± 8.8§	0.001
Syst. Strain Rate 1/s				
GRSR	0.9 ± 0.4*§	2.2 ± 1.1*	1.8 ± 1.1§	0.0002

GCSR	-0.6 ± 0.2*§	-1.0 ± 0.3*	-1.0 ± 0.6§	0.0009
GLSR	-0.4 ± 0.3*§	-0.8 ± 0.3*	-0.9 ± 0.1§	0.0001
Diast. Strain Rate 1/s				
GRSR	-0.8 ± 0.6*§	-1.9 ± 1.0*†	-2.5 ± 1.1§†	0.0001
GCSR	0.6 ± 0.3*§	0.8 ± 0.6*†	1.2 ± 0.4§†	0.003
GLSR	0.4 ± 0.4*§	0.7 ± 0.3*†	0.9 ± 0.4§†	0.0005

ID#: 376909

Pediatric cancer survivors have no MRI evidence of diffuse myocardial fibrosis and demonstrate preserved systolic and diastolic function

Wadi Mawad, MD[1] Luc Mertens, MD, PhD[2], Paul Nathan, MD[2], Joseph Pagano, MD[2], Eugenie Riesenkampff, MD[2], Seema Mital, MD[2], Paul Kantor, MD[3], Mark Greenberg, MD[1], Lars Grosse-Wortmann, MD[2]

1. The Hospital for Sick Children, Toronto, ON, Canada

2. The Hospital for Sick Children, ON, Canada

3. Stollery Children's Hospital, AB, Canada

Background: Anthracycline chemotherapy is frequently used in pediatric cancer treatment, but is known to cause dose-dependent cardiotoxicity, usually detected by systolic dysfunction on echocardiography. Native T1 times (NT1) and extracellular volume fraction (ECV), measured by cardiac magnetic resonance (CMR), have been shown to reflect diffuse myocardial fibrosis in other disease states. Previous studies in pediatric cancer survivors (PCS) found elevated NT1 and ECV on CMR as well as abnormal diastolic function on echocardiography. We aimed to quantify the myocardial fibrosis burden and correlate this with anthracycline dose and with echocardiographic diastolic ventricular function in a cohort of PCS.

Methods: We assessed CMR in a cohort of PCS who had received treatment with anthracyclines. T1 mapping was performed using a modified Look-Locker inversion recovery (MOLLI) technique. Diastolic function was assessed by echocardiographic data within 12 months of CMR. Using unpaired t-test, CMR and echocardiographic parameters were compared to a cohort of normal controls of similar age and gender in a cross-sectional manner.

Results: 41 PCS (mean age 15.3 years) and 42 controls (mean age 14.5 years) were included (Table 1). Mean left ventricular (LV) native T1 values and ECV were not significantly different in PCS compared to controls. Cumulative anthracycline dose did not correlate with ECV or NT1. The PCS group had statistically lower LV ejection fraction (EF), LV mass index (Mi) as well as LV mass/volume ratio compared to controls; however, the average LV EF in PCS was within the normal range. Diastolic function was normal in the PCS cohort. While remaining within normal range, septal E/E'; and average E/E'; were statistically slightly higher in PCS compared to controls. Neither NT1 nor ECV correlated with diastolic function indices or LV EF.

Conclusion: Measures of myocardial mass,markers of diffuse myocardial fibrosis and parameters of diastolic function were normal in this cohort of PCS, suggesting no adverse cardiac tissue remodeling. However, the slight reduction in LV EF and LVMi and the slight increase in septal and average E/E'; found here indicate that lifelong monitoring of cardiac function is likely warranted.

Table 1

	Cancer survivors (n=41)	Controls (n=42)	p
Age (years)	15.3 ± 2.7	14.5 ± 2.3	NS
BSA (m^2)	1.65 ± 0.30	1.72 ± 0.32	NS
Female: Male (%)	46 : 54	43 : 57	NS
Cumulative anthracycline dose (mg/m^2)	197 ± 100		
Time between last anthracyclinedose and CMR (years)	9.0 ± 3.6		
Cardiac MR			

LVEDVi (Z-score)	0.12 ± 1.3	0.37 ± 1.6	NS
LVMi (Z-score)	-1.41 ± 1.7	-0.59 ± 1.9	0.04*
LVEF (%)	55 ± 5	58 ± 5	0.001*
LVEF (Z-score)	-1.5 ± 1.1	-0.75 ± 1.1	0.002*
LVM/Vol (g/mL)	0.55 ± 0.11	0.60 ± 0.10	0.03*
LV T1 (ms)	999 ± 38	991 ± 37	NS
ECV (%)	23 ± 4	23 ± 4	NS
Echocardiography			
	Cancer survivors (n=39)	Controls (n=115)	
Heart rate (BPM)	71 ± 11	68 ± 13	NS
Mitral E velocity (cm/s)	97 ± 16	99 ± 16	NS
Mitral A velocity (cm/s)	43 ± 11	42 ± 11	NS
Mitral E/A	2 ± 1	2 ± 1	NS
Mitral E DT (ms)	174 ± 38	149 ± 18	<0.001*
Mitral A duration (ms)	123 ± 32	118 ± 20	NS
PV S/D	0.73 ± 0.25	0.73 ± 0.23	NS
PVa velocity (cm/s)	13 ± 11	18 ± 10	NS
PVa duration (ms)	74 ± 58	103 ± 24	NS
IVRT (ms)	70 ± 13	75 ± 7	NS
Septal E' (cm/s)	14 ± 2	15 ± 2	0.001*
Lateral E' (cm/s)	18 ± 3	19 ± 2	NS
Septal E/E'	7.0 ± 1.4	6.5 ± 1.2	0.04*
Lateral E/E'	5.8 ± 1.8	5.3 ± 0.9	NS
Average E/E';	6.4 ± 1.4	5.9 ± 0.9	0.02*
LV MPI	0.33 ± 0.05	0.31 ± 0.09	NS

Values are expressed as mean ± SD

*significant p-value as obtained by two-tailed, unpaired t-test

ID#: 377094

Quantitative assessment of left ventricular volumes and function using real-time strain-encoded CMR imaging: method agreement analysis

Tomas Lapinskas, MD[1] Lukas Stoiber, MD[2], Sebastian Kelle, MD, PhD[3], Christian Stehning, PhD[4], Rolf Gebker, MD, PhD[2], Amit R. Patel, MD[5], Keigo Kawaji, PhD[6], Remigijus Zaliunas, MD, PhD[7], Burkert Pieske, MD[2], Sebastian Kelle, MD[2]

1. Medical Academy, Lithuanian University of Health Sciences, Kaunas, Kauno Apskritis, Lithuania

2. German Heart Center Berlin, Berlin, Berlin, Germany

3. German Heart Center Berlin, Berlin, Germany

4. Philips Research Laboratories, Hamburg, Germany

5. University of Chicago, IL

6. University of Chicago, Chicago, IL

7. Lithuanian University of Health Sciences, Kaunas, Kauno Apskritis, Lithuania

Background: Left ventricular (LV) volumes and ejection fraction (EF) are important measures of every cardiac imaging study. Recently introduced real-time strain-encoding (SENC) cardiovascular magnetic resonance (CMR) imaging provides much faster quantitative assessment of these parameters. The main purpose of the study was to assess reliability of measurements derived using new fast real-time SENC technique and compare with conventional cine imaging.

Methods: Twelve healthy volunteers and 23 patients with known or suspected coronary artery disease underwent advanced CMR imaging using a 1.5 T MRI scanner (Ingenia, Philips Healthcare, Best, The Netherlands). SENC images were acquired using newly developed real-time free-breathing technique (Myocardial Solutions, Inc., Morrisville, North Carolina, USA) that takes total acquisition of three heartbeats to acquire three long-axis SENC loops. LV end-diastolic (LVEDV) and end-systolic (LVESV) volumes as well as LVEF and myocardial mass (LVM) were calculated from three long-axis SENC images using dedicated MyoStrain version 4.2. software (Morrisville, NC) (Figure 1) and from a stack of short-axis cine images using Medis Suite version 3.0 (Leiden, The Netherlands). Reliability of the two methods was calculated using Lin';s concordance correlation coefficient (Rc).

Results: SENC imaging and analysis were fast with a 15 second scan time and a 90 second post-processing time for a complete quantitative assessment. Reliability analysis demonstrated excellent concordance in the measurements of LVEDV (Rc = 0.84), LVESV (Rc = 0.95) and LVEF (Rc = 0.83). The measurement of LVM showed substantial concordance (Rc = 0.79) between SENC and conventional cine imaging.

Conclusion: Real-time SENC imaging technique provides fast and accurate quantitative assessment of LV volumes and function. In addition, the same dataset can be used for quantitative myocardial strain analysis.

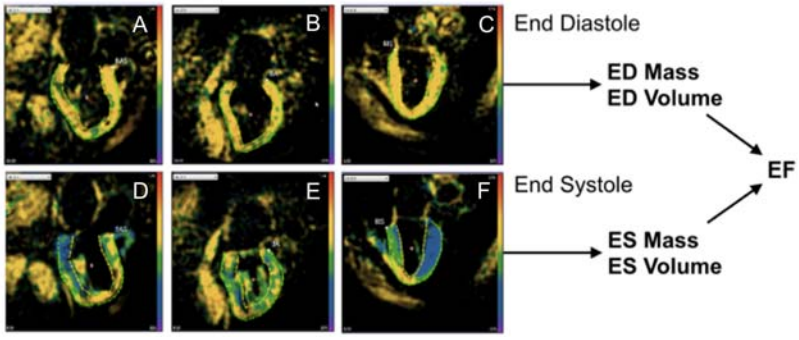

The images of the upper row demonstrate how LVEDV and LV end-diastolic mass are calculated from LV three- (A), two- (B) and four-chamber (C) views. The images of the lower row show how LVESV and LV end-systolic mass are estimated from the corresponding LV planes: three- (D), two- (E) and four-chamber (F) views.

ID#: 377105

Inter- and intraobserver reproducibility of right ventricular cardiac magnetic resonance feature tracking in patients with CTEPH (chronic thromboembolic pulmonary hypertension) after PEA (pulmonary endarterectomie)

Sabine Zitzmann, MD[1] Julia Vietheer, MD[2], Christoph Liebetrau, MD[2], Till Keller, MD[2], Jan Sebastian Wolter, MD[2], Steffen Kriechbaum, MD[2], Ulrich Fischer-Rasokat, MD[2], Stefan Guth, MD[3], Christoph Wiedenroth, MD[3], Christian W. Hamm, PhD[2], Andreas Rolf, MD[2]

1. Kerckhoff-Heart-Center, Department of Cardiology, Bad Nauheim, Germany, Frankfurt, Germany

2. Kerckhoff-Heart-Center, Department of Cardiology, Bad Nauheim, Germany, Germany

3. Kerckhoff-Heart-Center, Department of Thoracic surgery, Bad Nauheim, Germany, Germany

Background:

Introduction: Due to the complex three-dimensional anatomy, measurements of the right ventricle (RV) are challenging. Volumetry in cardiac magnetic resonance (CMR) is currently gold standard in the evaluation of RV ejection fraction (EF). Furthermore strain analysis by CMR feature tracking (FT) is emerging as a quantification technique, which might detect even subtle changes of RV function both as screening and follow up tool. However data on the reproducibility of FT derived measures of RV strain are lacking.

Aim: The aim of this study was to investigate the reproducibility of CMR derived strain and strain rate parameters in a well defined cohort of patients with chronic thromboembolic hypertension (CTEPH) 12 month after pulmonary endarterectomy (PEA).

Methods:

Methods: 85 patients underwent CMR 12 month after PEA. Right heart catheterization measurements were obtained within 24 hours of CMR to characterize the hemodynamic state. Steady state free precession (SSFP) cine CMR sequences were analyzed retrospectively using the FT module from cvi42 (circle cardiovascular imaging, Calgary, Canada), yielding six strain parameters (GCS, GRS, GLS, GCSR, GRSR, GLSR). For intraobserver analysis, two observer analysed CMR images of 30 patients twice. For interobserver analysis, two observers analysed the same datasets once. Intra- and interobserver reproducibility were tested in all patients using intraclass correlation coefficients (ICCs).

Results:

Results: All global RV strain and strain rate parameters showed an excellent intraobserver reproducibility (Table 1). The interobserver reproducibility of CMR derived strain and strain rate parameters was moderate but still significant (Table 1).

Conclusion:

Conclusion: CMR RV-FT using the CVI42 algorithm is highly reproducible in patients with CTEPH. Therefore it seems to be an excellent and comprehensive tool to quantitatively asses RV function and could improve the diagnostic accuracy in the follow-up workflow for patients with CTEPH.

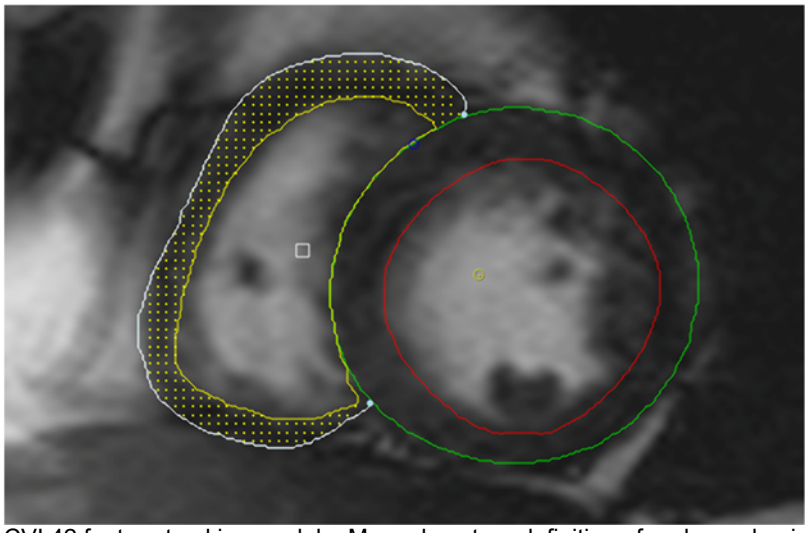

CVI 42 feature tracking module. Manual contour definition of endo- and epicardial borders

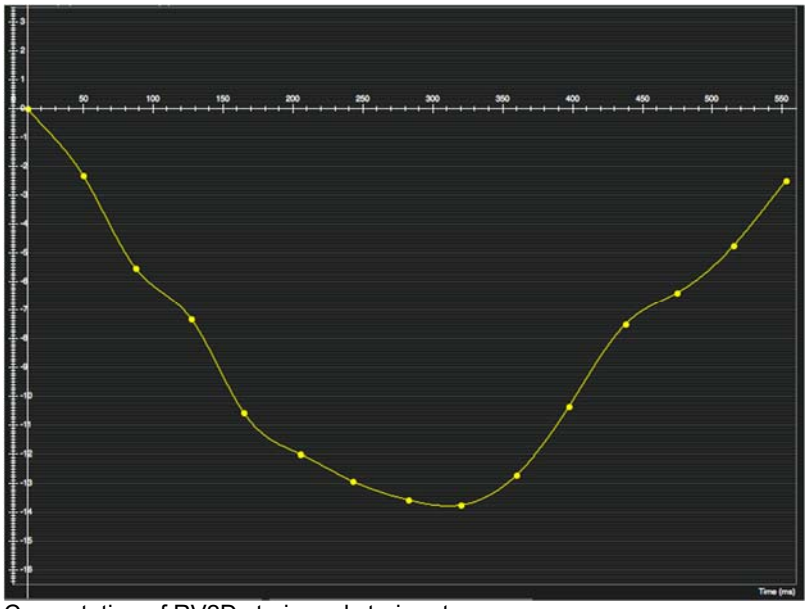

Computation of RV2D strain and strain rates

Table 1. Inter- intraobserver agreement. ICC - intraclass correlation coefficient, SE - standard error, SAX - short axis, LAX - long axis, GRS(R) - global radial strain (rate), GCS(R) - global circumferential strain (rate), GLS(R) - global longitudinal strain (rate)

CMR measures of strain	**ICC**	**SE**
Intra-observer	0.89	0.03
RV GRS SAX (%)	0.96	0.01

RV GCS SAX (%)	0.99	0.002
RV GLS LAX (%)	0.82	0.05
RV GRSRsyst SAX (1/s)	0.95	0.01
RV GCSRsyst SAX (1/s)	0.74	0.07
RV GLSRsyst LAX (1/s)		
Inter-observer	0.50	0.13
RV GRS SAX (%)	0.53	0.13
RV GCS SAX (%)	0.71	0.09
RV GLS LAX (%)	0.50	0.13
RV GRSRsyst SAX (1/s)	0.46	0.14
RV GCSRsyst SAX (1/s)	0.14	0.18
RV GLSRsyst LAX (1/s)		

Table 2. Patients characteristics. SD - standard deviation, BNP - brain natriuretic peptid, NYHA - New York Heart Association, SixMWT - six minute walking test, PAMP - pulmonary artery mean pressure, TAPSE - tricuspid annular plane systolic excursion, EF - ejection fraction, EDV - end-diastolic volume, ESV - end-systolic volume, RV - right ventricle, SAX - short axis, LAX - long axis, Ea - PA endsystolic pressure/volume ratio, Emax - RV endsystolic pressure/volume ratio, GRS(R) - global radial strain (rate), GCS(R) - global circumferential strain (rate), GLS(R) - global longitudinal strain (rate)

Patients characteristics	**Observation number**	**Mean value (SD)**
Age (years)		
Gender (female,n,%)	85	55.9(16.6)
Gender (male,n,%)	85	34(40%)
NT-Pro BNP (pg/ml)	85	51(60%)
NYHA functional class	71	334(646)

SixMWT (m)	85	1.3(0.48)
PAMP (mmHg)	42	471(121)
TAPSE (mm)	84	21.7(7.9)
RVEDVindex (ml/m²)	79	17.3(3.2)
RVESVindex (ml/m²)	85	76.8(22.7)
RVSVindex (ml/m²)	85	46.5(17.5)
RVEF (%)	85	30.4(12.8)
Ea (PAMP/RVSVindex)	85	39.1(10.7)
Emax (PAMP/RVESVindex)	83	0.79(0.39)
Ea/Emax	83	0.56(0.75)
RV GRS SAX (%)	85	1.69(0.69)
RV GCS SAX (%)	85	21.2(8.9)
RV GLS LAX (%)	85	-12.5(7.0)
RV GRSRsyst SAX (1/s)	85	-16.1(10.9)
RV GCSRsyst SAX (1/s)	85	1.12(0.54)
RV GLSRsyst LAX (1/s)	85	-0.69(0.46)
	85	-1.08(0.76)

ID#: 374301

Gender differences in cardiac remodelling in patients with type 2 diabetes

Eylem Levelt, MBBS, DPhil[1] Gaurav S. Gulsin, MBChB(Hons) MRCP(UK)[2], Daniel Swarbrick, MBBS, BMedSci[3], Lavanya Athithan, MBBCh, MRCP[4], Matthew PM. Graham-Brown, MBChB, MRCP[5], Jamal Nasir. Khan, MBChB (Hons), PhD[1], Melanie J. Davies, CBE[3], Kieran Clarke, PhD[6], Stefan Neubauer, MD, FRCP[7], Gerald P. McCann, MBChB, MD[3]

1. University of Leicester, England, United Kingdom

2. The University of Leicester, Nottingham, England, United Kingdom

3. University of Leicester, Leicester, England, United Kingdom

4. University of Leicester, Nottingham, England, United Kingdom

5. University Hospitals Leicester NHS Trust, Leicester, United Kingdom

6. University of Oxford, United Kingdom

7. University of Oxford, England, United Kingdom

Background: Diabetes is a stronger risk factor for cardiovascular disease (CVD) in women than in men. While doubling the risk of CVD in men, this risk is almost tripled for women, highlighting the need to better understand gender-related differences in diabetes-associated CVD. Heart failure (HF) is the primary cause of death in patients with diabetes. Consequently, patients with diabetes have been extensively phenotyped with a nuanced description of cardiac disease burden; adverse features such as LV concentric remodelling and impaired contractile function have been shown. Given the striking gender differences in mortality from CVD, we aimed to determine the effect of gender on the phenotypic expression of diabetic heart disease in young adults with T2D.

Methods: Sixty-two male (mean age 44±8years, BMI 33±5kg/m^2, mean HBA1c 7.8±1.8%), sixty-seven female (44±10years, BMI 35±6kg/m^2, HBA1c 7.6±1.2%) T2D patients on oral glucose lowering treatment; sixteen male (48±17years, BMI 25±3kg/m^2) and fourteen female (50±10years, BMI 25±4kg/m^2) healthy volunteers were recruited. Subjects with diagnosed CVD were excluded. Left ventricular (LV) volumes, mass and function, and left atrial (LA) volumes and function were assessed using CMR imaging. To determine peak systolic global circumferential strain and diastolic strain rate, tissue tracking software was utilised.

Results: CMR findings are detailed in Table 1. Participants in all groups were of similar age, and there were no significant differences in BP, diabetes duration, diabetes treatment or metabolic profile between the two diabetes groups. Concentric remodeling was present in both sexes (P<0.0001). However, the degree of concentric hypertrophy was greater in males (12%, P=0.0015). Biplane LA ejection fraction (EF) was significantly reduced in male diabetics compared to female diabetics (P=0.0380). Similarly, peak systolic circumferential strain (P<0.0001) and diastolic strain rates (P=0.0010) were both significantly reduced in males with T2D compared to females. There were no significant differences in LA EF, and LV strain parameters in female diabetics compared to female controls.

Conclusion: In young adults with T2D, male gender adversely affects the phenotypic expression of diabetic heart disease, with greater LV concentric hypertrophy, worse LV and LA function, compared to female gender. These striking differences in the cardiac phenotype promote awareness of gender-specific risk factors in search of treatment and prevention of diabetes-associated HF. Our results suggest the higher diabetes-associated CVD risk in women may not be related to HF events. Further large-scale studies looking at gender differences in HF-related mortality in T2D are needed.

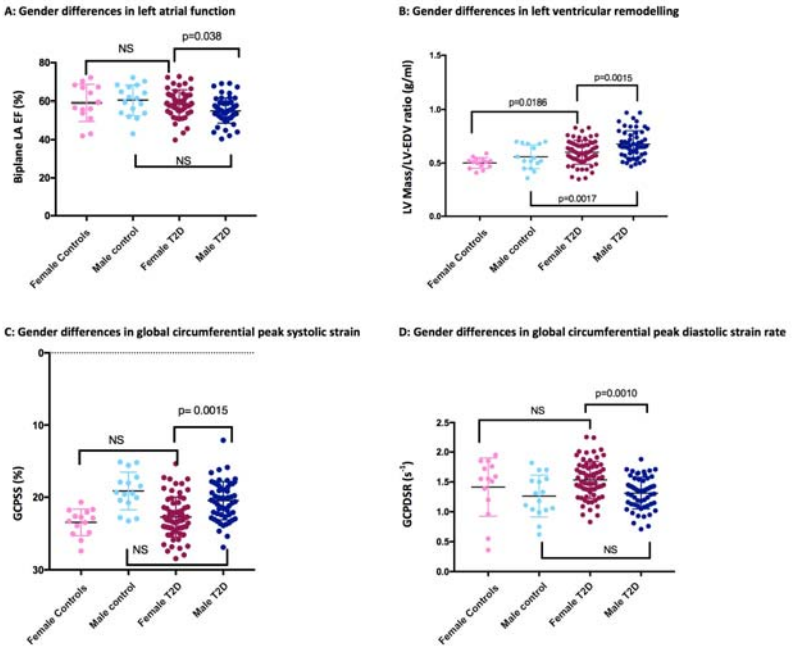

Figure

Table 1: CMR Findings

	Female Controls N=14	Male Controls N=16	Female T2D Patients N=67	Male T2D Patients N=62	P value
LV end-diastolic volume indexed to BSA, ml/m^2	81 ± 13	93 ± 19**	73 ± 12	78 ± 12	<0.0001
LA biplane end-systolic volumes, ml	71 ± 16	63 ± 16	70 ± 19	72 ± 21	0.9383
Biplane LA EF, %	59 ± 10	60 ± 8**	59 ± 7	55 ± 6†	0.0094
LV mass, g	71 ± 12	101 ± 30***	85 ± 20†	114 ± 22	<0.0001
LV mass index, g/m^2	41 ± 6	51 ± 14***	43 ± 7	52 ± 8†	<0.0001
LV mass to LV end-diastolic volume, g/ml	0.50 ± 0.10	0.56 ± 0.11***	0.60 ± 0.11*	0.67±0.13 **,†	<0.0001
Peak systolic circumferential strain, negative (-), %	23.5 ± 1.8	19.1 ± 2.6***	22.7 ± 2.8	20.5 ± 2.6†	<0.0001
Peak circumferential diastolic strain rate, s^{-1}	1.41 ± 0.48	1.26 ± 0.35	1.53 ± 0.31	1.26 ± 0.35†	0.0005

Values are mean ±standard deviations or percentages. T2D indicates type 2 diabetes; CMR, cardiac magnetic resonance; LV, left ventricular.
*P<0.05 female T2D vs female controls, with Bonferroni Correction
†P<0.05 female T2D vs male T2D, with Bonferroni Correction
**P<0.05 male T2D vs male controls, with Bonferroni Correction
***P<0.05 male vs female controls, with Bonferroni Correction

Table

ID#: 374297

The Costly Paradox of CMR. Is it a disruptive Health-Care Technology?

Nelu-Mihai Trofenciuc[1] Adina Pop-Moldovan[2], David Pop[3], Liviu Cirin[4], Mircea Fica Onel[2], Aurora Bordejevic[3], Horia Branea[3], Mirela Cleopatra Tomescu[1]

1. Victor Babes University of Medicine and Pharmacy Timisoara, Timisoara, Timis, Romania

2. Vasile Goldis Western University of Arad, Romania

3. Victor Babes University of Medicine and Pharmacy Timisoara, Romania

4. Victor Babes University of Medicine and Pharmacy Timisoara, Arad, Arad, Romania

Background: The new global medical economy is characterized by increased uncertainty, openness, flexibility, and choices, all of which impact lifestyle, business models, the working environment (for doctors as an example), the educational system, and national security.
"Disruptive Health-Care Technologies" are defined as those that are established in one market, but then penetrate and overwhelm another market. These incursions are accelerated by economic factors, and capitalise on functionality, reliability, and advancements supported by the original medical market.

Methods: We analysed health statistic data, in the period of 2010-2014, from an online Global Health Observatory data repository regarding medical device implementation (MRI with CMR capability) for 178 countries listed in World Health Organisation databank. Inclusion criteria was country with low (Li) or high income (Hi) rate. Exclusion criteria was country with no collected data (or not reported) and country with middle income. As a measurement unit, we used MRI exams per 1 000 population and MRI units per 1 million population.

Results: Out of 178 (100%) countries only 81 (45,76%) meet our inclusion criteria (Hi-Li countries). Out of those 54(66,66%) were Hi and 27(33,34%) Li. There were 5,02 (100%) MRI units for Hi-Li per 1 million population with 2,98 (59,36%) units for Hi and 2,04 (40,64%) for Li. As for MRI exams per 1.000 population there where 15,05 (100%) examination for Hi-Li with a distribution of 8,87(58,93%) for Hi and 6.18(41,07%) for Li countries.

Conclusion: If heavily industrialised countries lead detached as a number of MRI/CMR physical units when it comes to their use for the benefit of patients, the race is quite tight. These conflicting data can be explained by the simple fact that Hi countries have a national health care system based on medical insurance individual ("you pay, you live") while Li countries have a predominantly governmental health system with equal access for all population to all health high-tech facilities and investigations ("we pay, you live"). Responding to time and medical cost pressures, and the desire to do a highly tech care to the patient, will drive the CMR trend away from isolated, complex, academic only large-scale devices from Hi countries toward integrated, modular, and simpler networked technologies ("MIoT -medical *internet of things #MIoT*) with an increased success rate in developing countries.

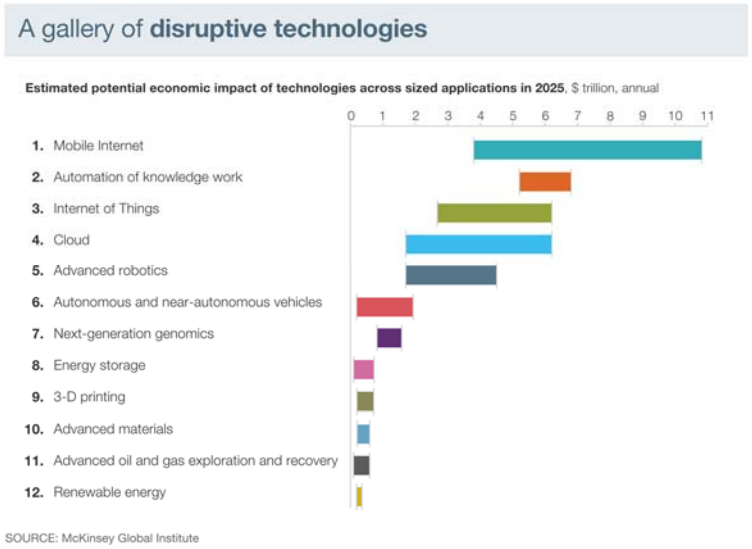

Disruptive technologies

ID#: 374271

Diagnostic Value of Cardiac MR Parameters in Acute Myocarditis: A Meta-Analysis

Sarah L. Blissett, MD MHPE[1] Yehuda Chocron[2], Bojan Kovacina, MD [2], Jonathan Afilalo, MD MSc[3]

1. McGill University, Montreal, PQ, Canada

2. McGill University, Canada

3. Jewish General Hospital, McGill University, Montreal, PQ, Canada

Background: Cardiac magnetic resonance (CMR) is the non-invasive test of choice for the diagnosis of acute myocarditis. While diagnostic criteria were elaborated in 2009, numerous studies have since examined the yield of traditional and novel CMR parameters to achieve greater accuracy. The aim of this meta-analysis was to synthesize these studies and determine the pooled diagnostic value of various CMR parameters for acute myocarditis.

Methods: MEDLINE and EMBASE were systematically searched for original studies that reported CMR parameters in adult patients suspected of acute myocarditis. Abstracts were screened and analyzed by two independent reviewers. Each CMR parameter's binary prevalence, mean value and standard deviation were extracted. Parameters were meta-analyzed using a random-effects model to generate standardized mean differences, defined as the number of standard deviations separating myocarditis patients and controls, with values >0.8 suggesting large differences. Heterogeneity was assessed using the I^2 statistic, with values <50% suggesting low heterogeneity.

Results: After screening 1,414 abstracts, 78 studies were included encompassing 3316 myocarditis patients and 1076 controls. For binary parameters, pooled prevalence was: positive late gadolinium enhancement (LGE) 77% (95% CI 69 to 84, I^2=93%), positive early gadolinium enhancement (EGE) ratio 66% (95% CI 57 to 74, I^2=82%), positive T2 ratio 52% (95% CI 43 to 61, I^2=90%), and pericardial effusion 35% (95% CI 26 to 44, I^2=88%). For continuous parameters, pooled standardized mean differences between myocarditis patients and controls were, in descending order of magnitude: T2 mapping time 2.26 (95% CI 1.50 to 3.02, I^2=83%), extracellular volume ratio 1.64 (95% CI 0.87 to 2.42, I^2=83%), LGE percentage 1.30 (95% CI 0.95 to 1.64, I^2=0%), T1 mapping time 1.18 (95% CI 0.35 to 2.01, I^2=89%), T2 ratio 1.17 (95% CI 0.80 to 1.54, I^2=76%), and EGE ratio 0.93 (95% CI 0.66 to 1.19, I^2=0%). Prolonged T1 mapping time had the highest sensitivity (82%), pericardial effusion had the highest specificity (99%), and the Lake Louise criteria had a pooled sensitivity of 78% and specificity of 74%.

Conclusion: Parametric mapping and pericardial effusion should be integrated in the diagnostic criteria for myocarditis. All CMR parameters analyzed discriminate effectively between myocarditis patients and controls; however, the observed between-study heterogeneity highlights the difficulty in establishing a reference standard for the diagnosis of myocarditis, and the need for future studies to adopt consistent CMR acquisition and measurement protocols.

ID#: 374428

Effect of obesity on native T1 values assessed by T1 mapping in hypertrophic cardiomyopathy

Jie Wang, BMSci[1] Weihao Li, BMSci[2], Jiayu Sun, MD[3], Yuchi Han, MD, MMSc[4], Yucheng Chen, MD[3]

1. Department of Cardiology, West China Hospital, Sichuan University, ChengDu, Sichuan, China (People's Republic)

2. Cardiology Division, West China Hospital, Sichuan University, Chengdu, Sichuan, China (People's Republic)

3. Sichuan University West China Hospital, Sichuan, China (People's Republic)

4. University of Pennsylvania, Philadelphia, PA

Background: Obesity is associated with cardiac steatosis in healthy adults. In addition, obesity are independently associated with increased left ventricle (LV) mass and could induce progression of heart failure symptoms in patients with hypertrophic cardiomyopathy (HCM). However, it is unclear whether increased of LV mass due to obesity will be accompanied by progression of fibrosis. Therefore, we aimed to assess the impact of body mass index (BMI) on myocardial fibrosis assessed by T1 mapping in hypertrophic cardiomyopathy.

Methods: We consecutively recruited 30 obese HCM patients (BMI＞28 kg/㎡) and 30 age- and sex-balanced pre-obese (BMI 24-28kg/㎡) and non-obese (BMI＜24 kg/㎡) HCM patients. We assessed the relationship of BMI to LV mass, native T1, extracellular (ECV) and late gadolinium enhancement (LGE) determined by cardiovascular magnetic resonance (CMR) on a 3T scanner (Siemens Trio, Gemany).

Results: LV mass and native T1 had significant associations with BMI ($p < 0.05$, respectively) in HCM patients. In addition, native T1 decreased with increasing of BMI. The first multivariable model (LV mass, LGE, and ECV) demonstrated that BMI were only associated with LV mass (Beta 0.304, P =0.004) . In a second multivariable model (LV mass, native T1 and LGE) , BMI were associated with both LV mass (Beta 0.309, P =0.003) and native T1 (Beta -0.277, P =0.01) but not LGE.

Conclusion: In HCM patients, obesity is independently associated with increase in LV mass and decrease in native T1 but not association of extracellular fibrosis (ECV and LGE). These new findings suggest obesity may not promote progression of myocardial fibrosis but increase cardiac steatosis in HCM.

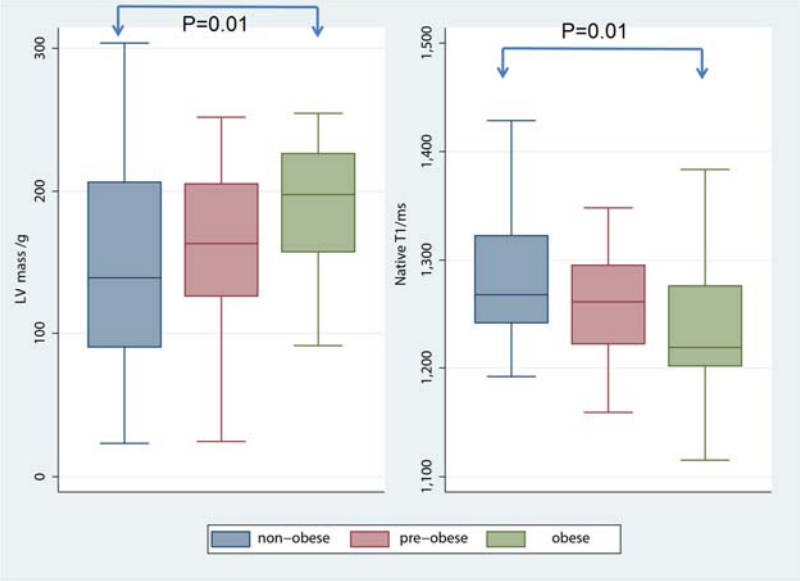

LV mass and native T1 comparisons between different subgroups patients with hypertrophic cardiomyopathy.

Baseline patient characteristics and tissue characteristics.

	Non-obese BMI＜24（n=30）	Pre-Obese BMI 24-28（n=30）	Obese BMI ＞28（n=30）
Age(years)	49.0±14.5	53.6±10.8	50.7±14.9
Male gender, n（%）	18（60%）	18（60%）	18（60%）
Body surface area（㎡）	1.6±0.1*	1.7±0.1*	1.9±0.2
height（cm）	160.6±6.6	162.4±8.8	162.9±10.3
Weight（kg）	56.5±6.7	67.7±6.8	80.9±9.9
Hypertension	9（30%）	8（26.7%）	8（26.7%）
Left ventricle ejection fraction(%)	61.8±12.6	63.2±7.6	66.4±7.1
LVEDVi, mL/㎡	84.0±22.7	77.4±12.0	78.0±17.1
Maximum LV wall thickness (mm)	23.1±4.4	23.0±4.5	22.3±6.0
LVMass, g	143.8±71.0*	156.8±64.3	195.9±70.0
LVMassi, g/㎡	93.2±45.6	91.8±36.9	103.9±34.1
With LV outflow obstruction	14（46.7%）	18（60%）	12（40%）
LGE %（Median, IQR）	5.9（3.2, 10.0）	3.8（0, 9.4）	4.7（0.9, 8.8）
Native-T1	1280.5±66.9*	1257.9±50.8	1241.3±64.1
Extracellular volume（ECV）	31.0±5.6	29.2±5.4	29.4±6.7

*p＜0.05 vs. Obese group；Continuous variables normally distributed are presented as mean±SD, non-normally distributed as median and IQR.

ID#: 374437

Comparison of the tissue characteristics between MYH7 and MYBPC3-caused hypertrophic cardiomyopathy with CMR in Chinese people

Jie Wang, BMSci[1] Jiayu Sun, MD[2], Yang Dong, BMsci[3], Yuchi Han, MD, MMSc[4], Yucheng Chen, MD[2]

1. Department of Cardiology, West China Hospital, Sichuan University, ChengDu, Sichuan, China (People's Republic)

2. Sichuan University West China Hospital, Sichuan, China (People's Republic)

3. Cardiology Department West China Hospital Sichuan University, Sichuan, China (People's Republic)

4. University of Pennsylvania, Philadelphia, PA

Background: Phenotypic differences between hypertrophic cardiomyopathy (HCM) with MYH7 (β-myosin heavy chain) and MYBPC3 (β-myosin-binding protein C) mutations have been inconsistent. In addition, MYH7 mutation could lead to different clinical manifestations and disease progression in different HCM individuals. In this study, we compared the tissue characteristics in HCM patients with the two different genotypes using late gadolinium enhancement(LGE) and T1-mapping with cardiovascular magnetic resonance（CMR）.

Methods: 35 consecutive patients with familial HCM underwent genetic testing by next-generation sequencing (NGS) of a 140 genes on the cardiomyopathies panel. All patients underwent CMR myocardial tissue characterization using conventional CMR fibrosis assessment and T1 mapping by modified look-locker sequence (MOLLI) before and after injection of gadolinium with 3.0 T scanner. The global and segmental myocardial T1 and extracellular volume（ECV）were calculated by dedicated software.

Results: Genetic testing revealed a pathogenic mutation in 33 of 35 patients (94.3%). The most common genes identified were MYH7 (n=19) and MYBPC3 (n=9); 57.6% and 27.3% of genopositive patients, respectively. The tissue characteristics of these 2 groups were similar, including the presence of LGE (79% versus 78%; P=0.94), percent LGE of the total left ventricular mass (%LGE; 19.2±14.2 versus 15.2±10.2; P=0.70), average global and segmental myocardial T1 and ECV (all $P > 0.05$). However, in the MYH7 group, both %LGE and ECV in the global and segmental models showed wider standard deviation reflecting higher variability using coefficient of variation (COV).

Conclusion: Our study showed a lack of group differences in tissue characteristics between MYH7- and MYBPC3-associated HCM when assessed by CMR. However, MYH7 mutation exhibit larger variability at the individual level and segmental level within the individual compared to MYBPC3.

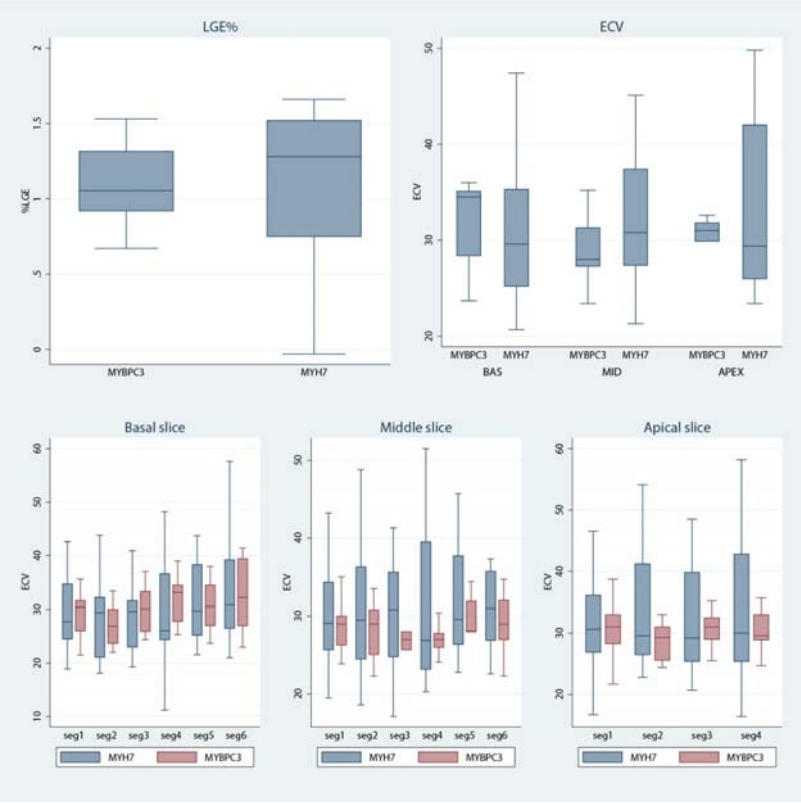

Global and segmental fibrosis characteristics assessed using LGE and T1 mapping on cardiovascular magnetic resonance. Continuous variables normally distributed are presented as mean±SD, non-normally distributed as median and IQR. Extracellular volume(ECV).Basal slice(BAS),Middle slice (MID),Apical slice(APEX);Segment(Seg).

Basaline Characteristics of hypertrophic cardiomyopathy patients.

Variable	MYH7(n=19)	MYBPC3(n=9)	P
Age(years)	43.4±3.9	41.9±5.8	0.83
Male gender, n（%）	12(63.2)	5(55.6)	0.70
LVEF,%	59.7±9.9	65.2±6.9	0.14
LVEDVi, mL/㎡	77.6±23.7	79.2±12.7	0.84
LV maximal wall thickness, mm	21.±1.3	22.0±3.0	0.78
BMI	23.6±2.9	21.3±3.5	0.71
BSA	1.7±0.2	1.6±0.2	0.09
Syncope, n (%)	5(26.3)	1(11.1)	0.36
NSTV on 24 holter monitor, n(%)	2(10.5)	1(11.1)	0.96

Family history of SCD, n(%)	18(94.7)	8(88.9)	0.14
Maximal wall thickness≥30mm, n（%）	2(10.5)	1(11.1)	0.96

Continuous variables normally distributed are presented as mean±SD, non-normally distributed as median and IQR; Body surface area (BSA); Body mass index(BMI);Nonsustained ventricular tachycardia(NSVT); sudden cardiac death(SCD).

ID#: 374439

Global Longitudinal Strain is reduced during maximum myocardial hyperaemia in patients with significant coronary artery disease.

Pankaj Garg, MD, PhD[1] Saul Crandon, M.Res.[2], Peter P. Swoboda, PhD[3], James R. Foley, MBChB BSc (Hons)[3], Graham J. Fent, MBChB, BSc[3], Tarique Musa, MBBS[4], Louise AE. Brown, MBChB, BMedSc[4], Pei G. Chew, MBChB(Hons) [5], Sebastian C. Onciul, MD[2], David Ripley, MBChB[4], Bara Erhayiem, BMBS[4], Laura E. Dobson, MD[4], Adam K. McDiarmid, MD[4], Erica Dall'Armellina, MD, PhD[6], John P. Greenwood, PhD[4], Sven Plein, MD PhD[4]

1. University of Leeds, UK, Leeds, England, United Kingdom

2. University of Leeds, United Kingdom

3. University of Leeds, Leeds, England, United Kingdom

4. University of Leeds, England, United Kingdom

5. University of Leeds, Liverpool, England, United Kingdom

6. Oxford University, England, United Kingdom

Background: Myocardial perfusion imaging during hyperaemic stress is commonly used to detect coronary artery disease (CAD). It remains unclear if patients with perfusion defect on first-pass perfusion imaging during peak myocardial hyperaemia have subtle loss of myocardial function. Therefore, the main aim of this study was to investigate the relationship between peak stress left ventricular global longitudinal strain (GLS), strain rate (GLSR), myocardial early (E';) and late diastolic velocities (A';) with adenosine stress first-pass perfusion cardiovascular magnetic resonance imaging (CMR).

Methods: 44 patients met the inclusion criteria and underwent CMR imaging. The CMR protocol included: rest/stress horizontal long-axis (HLA) cine, rest/stress first pass adenosine perfusion and late gadolinium enhancement imaging. Rest and stress HLA cine CMR images were analysed using feature-tracking software for the assessment of myocardial deformation. The presence of perfusion defects was scored on a binomial scale.

Results: Patient demographics and study results are detailed in Table 1 and Figure 1. In patients with hyperaemia induced perfusion defects, rest GLS (-16.9±3.7 vs -19.6±3.4; P-value=0.02), E'; (-86±22 vs -109±38; P-value=0.02), GLSR (69±31 vs 93±38; P-value=0.01) and stress GLS (-16.5±4 vs -21±3.1; P<0.001) were significantly reduced when compared to patients with no perfusion defects. Stress GLS was the strongest independent predictor of perfusion defects (OR 1.43 95% CI 1.14-1.78, P-value<0.001). A threshold of -19.8% for stress GLS demonstrated 78% sensitivity and 73% specificity for the presence of hyperaemia-induced perfusion defects.

Conclusion: At peak myocardial hyperaemic stress, GLS is reduced in the presence of a perfusion defect in patients with suspected CAD. This reduction is most likely caused by reduced endocardial blood flow at maximal hyperaemia because of transmural redistribution of blood flow in the presence of significant coronary stenosis.

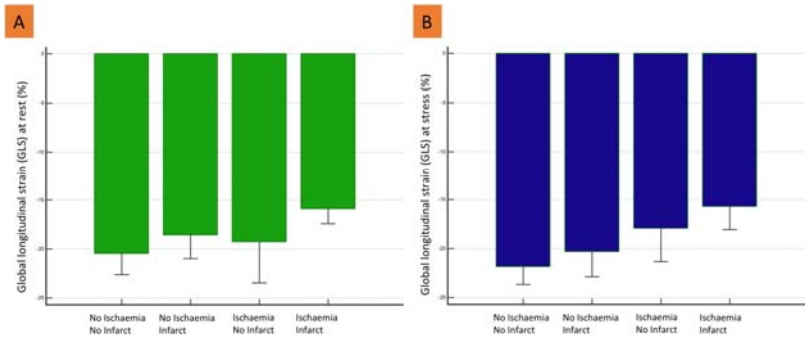

Multiple comparison bars of rest (Panel A: green bars) and stress (Panel B: blue bars) global longitudinal function strain in patients with/without myocardial infarction and perfusion defect (whiskers: standard deviations; SD).

Study demographics and baseline CMR parameters

Characteristics	All patients	Perfusion defect	No perfusion defect	P-value
Demographics	(n=44)	(n=22)	(n=22)	
Age (years)	64±12	64±12	63±13	0.53
Gender (male/female)	31/13	16/6	15-Jul	0.75
Current smoker [no. (%)]	13 (30)	7 (16)	6 (14)	0.75
Hypertension [no. (%)]	13 (30)	7 (16)	6 (14)	0.75
Diabetes Mellitus [no. (%)]	12 (27)	6 (14)	7 (16)	0.45
Dyslipidaemia [no. (%)]	7 (16)	3 (7)	4 (9)	0.69
Baseline CMR parameters				
LV EDV, (ml/m2)	143 ±45	151±46	133±43	0.19
LV ESV, (ml/m2)	55±32	63±39	45±21	0.06
LV SV, (ml/m2)	86±29	87.6±18	84.4±37	0.72
LV EF, (%)	64±13	61±13	67±12	0.07
LV Mass, (grams)	111±35	112±26	109±43	0.76
Rest strain parameters				
GLS (%)	-18±4	-16.9±3.7	-19.6±3.4	0.02
GLSR (s-1)	-98±11	-86±22	-109±38	0.02
E'; (s-1)	80±39	69±31	93±38	0.04
A'; (s-1)	80±29	74.5±25	86.7±33	0.18
Stress strain parameters				
GLS (%)	-19±4	-16.5±4	-21.2±3.1	<0.001
GLSR (s-1)	-104±54	-98±45	-112±60	0.36
E'; (s-1)	97±41	90±50	106±32	0.21
A'; (s-1)	93±50	88±43	113±81	0.2

ID#: 374447

The effect of imaging gradients on estimates of cardiac DTI metrics

Cyril Tous, ME, MR, MB, BE, B.Sc[1] Alistair Young, PhD[2], Beau Pontre, PhD[3]

1. The University of Auckland, Auckland, Auckland, New Zealand

2. University of Auckland, New Zealand, GRAFTON, Auckland, New Zealand

3. The University of Auckland, New Zealand

Background: Diffusion tensor imaging in the heart is used to elucidate the fibre architecture in the myocardial tissue. Most diffusion models consider only a scalar b-value, assuming that the effects of the imaging gradients are negligible and do not contribute to diffusion-dependent signal loss. Ignoring the effects of the additional gradients can lead to significant errors in the estimation of mean diffusivity (MD), and affecting the characterisation of the diffusion tensor and fractional anisotropy (FA). This study compares how the inclusion or exclusion of the imaging gradients affects diffusion metrics that characterise the myocardial fibre orientation.

Methods: We scanned five specimens fixed in formalin for 37-59 years with a diffusion-weighted spin-echo sequence. Imaging parameters were: b=800s/mm2, TR=1s, TE=57ms, slices = 3 (at mid-ventricle), slice thickness = 4mm, matrix=100x100, field of view= 200x200; acquisition voxel = 2x2x4 . We calculated the helix angle (HA), transverse angle (TA) and sheet angle (SA) using either a b-matrix that included the imaging gradients ($bmatrix_{ALL}$) or one that only considered the diffusion-encoding gradients ($bmatrix_{DIFF}$). Akaike';s information criterion (AIC) and root-mean-square (RMS) scores were used to assess the polynomial fit of the measured angles across the myocardial wall.

Results: Using $bmatrix_{ALL}$ in the analysis results in increased helix angles throughout the myocardial wall as compared to $bmatrix_{DIFF}$, with higher extreme values at the epicardium and endocardium (Figure 1a). In addition, the sheet angle is decreased in the septum and increased elsewhere when using $bmatrix_{ALL}$ (Figure 1c).There was a significant difference between the $bmatrix_{ALL}$ and $bmatrix_{DIFF}$ in the AIC of HA ($p<0.002$), TA ($p<0.002$), SA ($p<0.002$) and the RMS of HA ($p<0.01$), TA ($p<0.001$), SA ($p<0.05$). The borderline significance in the SA RMS is likely a result of the uncertainty in accurately differentiating the second and third eigenvectors in regions of interest with low SNR.

Conclusion: The inclusion of the imaging gradients in the b-matrix will result in changes to the degree of diffusion-weighting, related to the orientation of the imaging gradients in relation to the diffusion-encoding gradients. As a result, the calculation of diffusion metrics that characterise the myocardial fibre orientation - such as HA, TA, SA - will depend on whether these gradients are taken into account during analysis. Analysis software that fails to account for the presence of the imaging gradients when defining the b-matrix will have angle calculation errors.

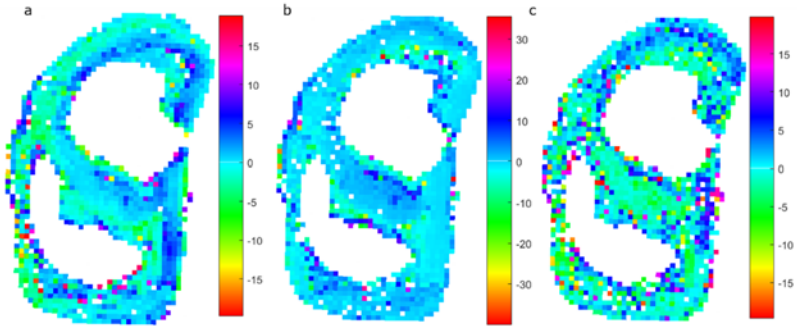

Difference of HA map (a), TA map (b), SA map(c) between bmatrix_ALL and bmatrix_Diff. Each mapping considers two standard deviation of the mean difference. The mean differences are HA_diff=0.57°±9.98°, TA_diff=0.14°±18.48°, SA_diff=0.14°±11.00°.

ID#: 374459

Feasibility and Reproducibility of Automated Mapping of Left Ventricular Kinetic Energy using Four-dimensional Flow Imaging in post MI patients and healthy volunteers.

Pankaj Garg, MD, PhD[1] Saul Crandon, M.Res.[2], Peter P. Swoboda, PhD[3], James R. Foley, MBChB BSc (Hons)[3], Graham J. Fent, MBChB, BSc[3], Louise AE. Brown, MBChB, BMedSc[4], Pei G. Chew, MBChB(Hons) [5], Sebastian C. Onciul, MD[2], Malenka Bissell, Md, DPhil[6], Jos J.M. Westenberg, PhD[7], Rob J. van der Geest, PhD[8], John P. Greenwood, PhD[4], Sven Plein, MD PhD[4], Erica Dall'Armellina, MD, PhD[9]

1. University of Leeds, UK, Leeds, England, United Kingdom

2. University of Leeds, United Kingdom

3. University of Leeds, Leeds, England, United Kingdom

4. University of Leeds, England, United Kingdom

5. University of Leeds, Liverpool, England, United Kingdom

6. Oxford University, United Kingdom

7. Department of Radiology, Leiden University Medical Center, Leiden, The Netherlands, Leiden, Zuid-Holland, Netherlands

8. Department of Radiology, Leiden University Medical Center, The Netherlands, Leiden, Zuid-Holland, Netherlands

9. Oxford University, England, United Kingdom

Background: Doppler echocardiography is the mainstay for the non-invasive assessment of left ventricle (LV) haemodynamics. However, Doppler echocardiography has several limitations relating to 2D-planar assessment, through-plane motion and high intra- and inter-operator variability. Four-dimensional flow (4D flow) cardiovascular magnetic resonance (CMR) imaging allows quantifying different intra-cavity LV flow kinetic energy (KE) components in three dimensions (3D). This can be done using short-axis cine imaging to extrapolate KE information by superimposing the endocardial contours on the acquired 4D flow whole LV data. The reliability of this technique remains unknown for haemodynamic assessment. Therefore, the main aim of this pilot work was to test intra-/inter-observer accuracy, precision and intra-class correlation (ICC) for different LV flow KE components.

Methods: Ten patients with myocardial infarction (MI) and 10 healthy volunteers (HV) underwent CMR on 1.5T Ingenia Philips. CMR protocol included cines and 4D flow. 4D flow was acquired using previously validated EPI accelerated sequence. Automated image registration was performed to correct for any misalignment between the cine and 4Dflow scan. KE parameters were normalized by end-diastolic volume and included the following: averaged LV flow KE, the proportion of in-plane KE and minimal KE of the LV flow. Diastolic KE flow components assessed were averaged diastolic KE, peak E-wave KE, peak A-wave KE and the time difference (TD) of peak early inflow propagation. For systole, averaged systolic KE was computed. For inter-observer tests, two observers contoured the SAX LV cine volumetric stack blinded to each other';s analysis. Automated KE parameters were again generated using the new endocardial contours. For intra-observer tests, LV SAX cines were re-contoured after 3 months. Akin to inter-observer tests, automated KE parameters were generated using the new endocardial contours.

Results: Mean age of HV was not different to MI patients (52±12 versus 59±15, p=0.26). Baseline CMR volumetric results and LV flow KE components are detailed in Table 1. LV flow KE for the complete cardiac cycle was lower in patients with MI (7±3μJ/ml versus 10±4μJ/ml, p=0.03). Similarly, LV systolic KE was lower in MI patients. HV had higher mitral inflow peak E-wave KE versus MI patients (22±9μJ/ml versus 14±7μJ/ml, p=0.04). Intra-/inter-observer results are detailed in Table 2. All LV flow KE components demonstrated high accuracy (bias

Conclusion: Automated LV flow KE assessment is feasible and demonstrates a high degree of repeatability to map the LV flow haemodynamics. In this pilot study, patients with previous MI, appear to have altered LV flow KE components.

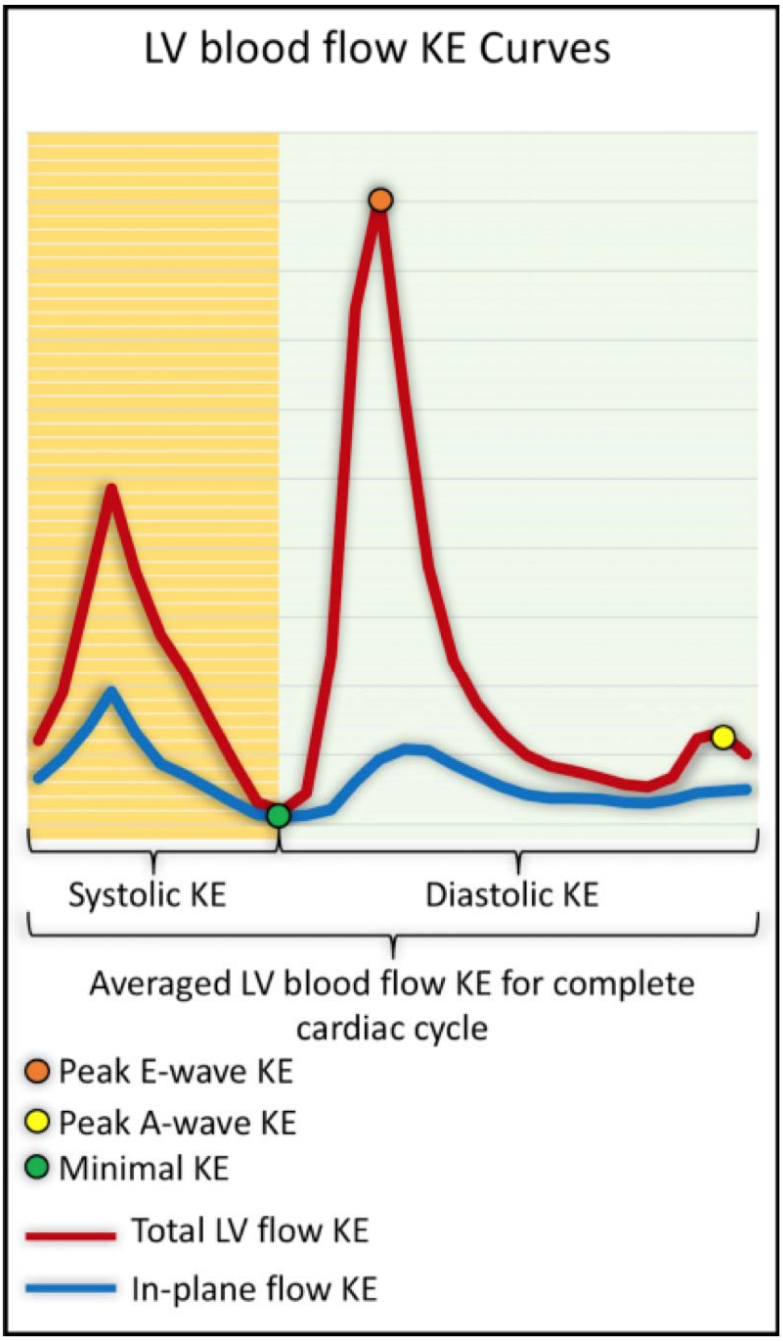

Left ventricular blood flow kinetic energy mapping. The graph describes all the LV flow KE components studied in this pilot work. The in-plane refers to KE in the plane of the short-axis scan.

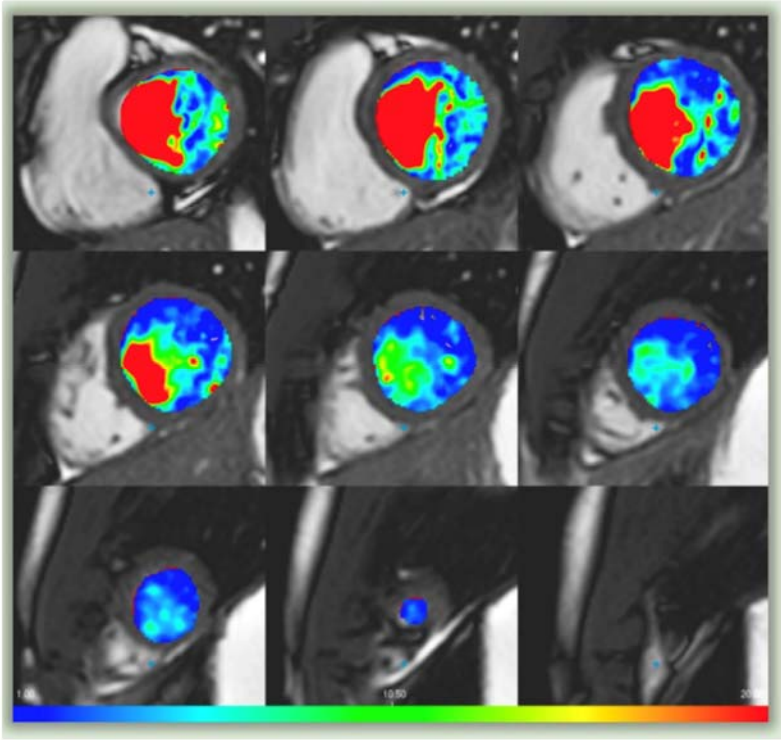

Automated mapping of LV flow KE. This figure demonstrates how the endocardial contours were used to map the KE of LV blood flow. The KE map represented here is during peak systole.

Study demographics and baseline results. *μJ/ml

Subject	**MI patients** (n=10)		**HV** (n=10)		**P-value**
	Mean	SD	Mean	SD	
Age (yrs)	59	15	52	12	0.26
Male (n)	6		5		0.67
Height (cm)	170	11	166	7	0.34
Weight (kg)	79	19	72	11	0.33
BSA (m^2)	1.9	0.3	1.8	0.1	0.28
LVEDV (ml)	148	33	148	35	1.00
LVESV (ml)	74	20	55	12	0.02
SV (ml)	74	16	93	26	0.07
EF (%)	51	7	63	5	0.001
Mass (g)	98	18	88	22	0.30
LV averaged KE*	7	3	10	4	0.03
LV minimal KE*	0.7	0.4	1.2	0.4	0.01
LV systolic KE*	8	3	12	5	0.03
LV diastolic KE*	6	2	10	4	0.05

LV peak E-wave KE*	14	7	22	9	0.04
LV peak A-wave KE*	13	5	16	8	0.33
In-plane proportion of KE (%)	37	20	55	23	0.07

Intra-observer and inter-observer global KE parameters. (Bias, LL, UL are expressed as percentage).

	Intra-observer tests						Inter-observer tests					
	Bias	LL	UL	ICC	95% CI	P	Bias	LL	UL	ICC	95% CI	P
	Global LV kinetic energy parameters											
Averaged LV	1	-8	10	0.998	0.99 to 0.99	0.97	-3	-15	10	0.997	0.99 to 0.99	0.90
Minimal	5	-23	32	0.98	0.94 to 0.99	0.86	-6	-33	21	0.98	0.94 to 0.99	0.79
Systolic	-2	-24	20	0.99	0.96 to 0.99	0.97	-1	-21	18	0.99	0.97 to 0.99	0.92
Diastolic	3	-15	21	0.99	0.97 to 0.99	0.94	-4	-20	12	0.99	0.97 to 0.99	0.91
Peak E-wave	5	-11	20	0.99	0.98 to 0.99	0.84	-4	-18	9	0.99	0.98 to 0.99	0.85
Peak A-wave	3	-12	19	1.00	0.99 to 0.99	0.88	-5	-21	11	0.99	0.98 to 0.99	0.79
In-plane	-1	-14	12	1.00	0.99 to 0.99	0.97	1	-15	16	1.00	0.98 to 0.99	0.97

CI=confidence interval, LV=left ventricle, LL=lower-limit, P=p-value, UL=upper limit, ICC= intra-class correlation coefficient.

ID#: 373545

During vasodilatory stress, which hemodynamic indicator correlates best with myocardial perfusion as measured by first pass contrast enhanced cardiac MRI.

Richard Coulden, MB BS[1] Emer Sonnex, MPhil[2]

1. University of Alberta Hospital, Canada

2. University of Alberta Hospital, Edmonton, AB, Canada

Background: Vasodilatory pharmacological stress is widely used in myocardial stress perfusion imaging but inadequate stress remains a concern. Heart rate and blood pressure changes are currently used as markers of hemodynamic response but are known to be unreliable. We compare biplane LV function assessment during dipyridamole stress and following reversal with aminophylline with semi-quantitative assessment of myocardial perfusion.

Methods: 24 patients undergoing cardiac MRI stress perfusion on clinical grounds were recruited. All had 2 and 4 chamber long axis (LAX) cine SSFP sequences at peak stress following first pass perfusion and following rest perfusion imaging. Dipyridamole (0.56mg/kg) was given over 4 minutes with stress perfusion imaging at 6 minutes. Stress was reversed with IV aminophylline (200mg). Rest perfusion was performed 20 minutes later. Both LAX cine sequences were repeated. Heart rate and BP were monitored with measurements taken to match LAX cine acquisitions at peak stress and 20 mins post aminophylline. 17 patients (71%) had normal LV function and perfusion. In these 17, cardiac output and myocardial signal intensity curves at stress and post-aminophylline 'rest' were derived using standard software (Circle Cardiovascular Imaging, Calgary).

Results: As anticipated, heart rate and rate pressure product correlate with peak myocardial time-signal intensity gradients during first pass perfusion but correlation was relatively poor (R^2 = 0.32 & 0.35 respectively). Cardiac output shows better correlation, particularly when normalized to lean body mass (LBM) (R^2 = 0.70). Using dipyridamole stress, there was no change in BP between stress and 'rest' (p>0.05).

Conclusion: In patients without demonstrable ischemic heart disease, cardiac output normalised to LBM correlates best with semi-quantitative estimates of myocardial perfusion. This is readily assessed during pharmacological stress and is a better indicator of myocardial response to vasodilator stress than standard hemodynamic parameters. It has yet to be shown whether similar correlations apply to other vasodilatory stress agents (eg. adenosine and regadenoson).

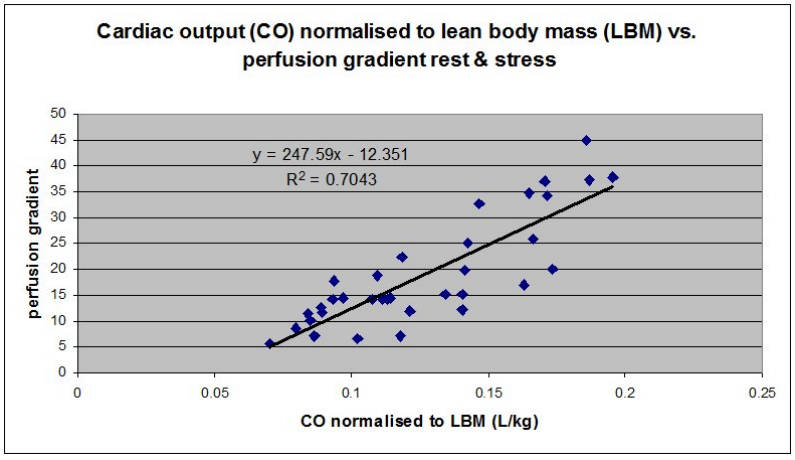

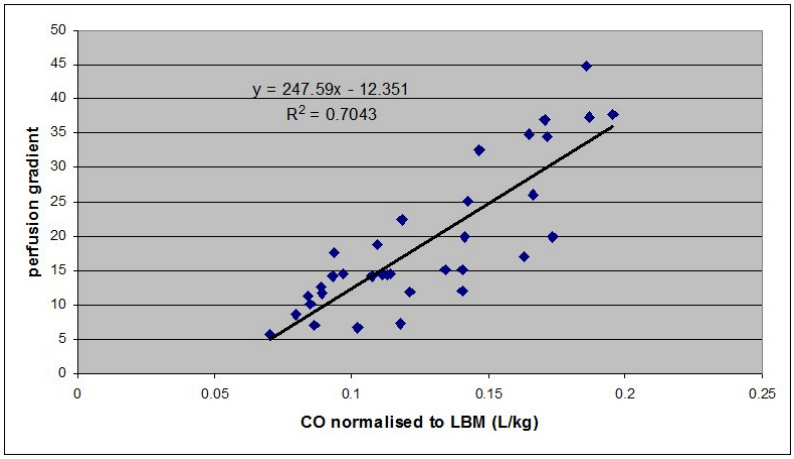

Cardiac output (CO) normalised to lean body mass (LBM) vs perfusion gradient rest & stress

ID#: 373875

Image-based patient-specific simulations of atrial flow can predict regions of blood stasis in sinus rhythm and atrial fibrillation

Desmond Dillon-Murphy, PhD MSc[1] David Nordsletten, PhD[2], Mitchell Brown[3], Henry Chubb, MRCP MRCPCH[4], Mark O'Neill, MD DPhil[5], Oleg Aslanidi, PhD[6], Adelaide de Vecchi, PhD[3]

1. Kings College London, London, England, United Kingdom

2. King's College London, England, United Kingdom

3. King's College London, United Kingdom

4. Kings college London, England, United Kingdom

5. King's College London, London, England, United Kingdom

6. King's College London, London, United Kingdom

Background:

Atrial fibrillation (AF), the most common cardiac arrhythmia, affects over 30 million people worldwide and is associated with increased morbidity, heart failure and stroke. Disorganised atrial activation and contraction in AF affects atrial flow dynamics, reducing cardiac output and increasing the risks of blood stasis and clot formation. In this study, we combine patient MR imaging and CFD simulations of the left atrium (LA) to compare the complex flow dynamics and their changes between patients in sinus rhythm (SR) and AF.

Methods:

Cine MRI data for the LA volume (bSSFP, effective TR 2.7 ms, TE 1.3 ms, 1.25x1.25 mm^2 in-plane, slice thickness 10 mm, 50 phases) and Doppler ultrasound measurements of the mitral valve (MV) flow velocity (FV) were acquired from 2 patients in SR (P01) and AF (P02). Segmentations of the LA were performed on each Cine MRI dataset at a chosen moment of the cardiac cycle (end-systole) to create a patient-specific 3D atrial mesh, with an algorithm based on temporal sparse free-form deformations then used to track the LA wall motion. The respective wall velocity was applied at the LA-blood interface to deform the mesh throughout the cardiac cycle, and patient-specific MV flow waveforms were applied at the MV face. CFD simulations of the patient-specific LA flow were performed using *CHeart* (ALE Navier-Stokes solver).

Results:

Simulations for SR patient showed FVs within a physiological range of 0-2 m/s (average FV over the LA over one cardiac cycle $FV_{LA,mean}$ = 0.16 m/s), with blood forming several high-speed vortices (Fig. 1). Simulations for AF patient showed a smaller number of slower vortices ($FV_{LA,mean}$ = 0.1 m/s). The simulation results are in good agreement with previous patient measurements using 4D flow MRI and PC-MRI – while having an advantage of resolving the flow dynamics in LA regions potentially affected by AF. Thus, the slowest FVs were seen in the LA appendage, with the average FV decreased from 0.05 m/s in SR to 0.04 m/s in AF (Table 1).

Conclusion:

This study describes a novel MRI-based computational workflow for exploring the global dynamics of 3D atrial flow, and provides insights into the flow differences between SR and AF patients – such as reduced FV in specific LA regions, which are linked with the increased risk of clot formation in patients with AF. The workflow can be utilised for improving thromboembolic risk assessment in challenging patient populations with low empirical CHADS2VaSc score.

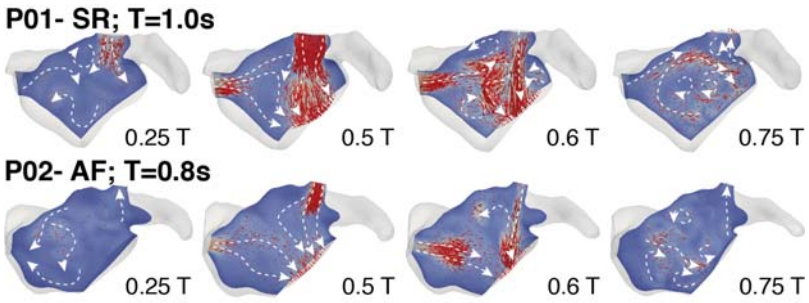

Figure 1. Blood flow in LA of patients in SR and AF. For each patient, snapshots of FV are shown for 4 moments of time through the cardiac cycle with period T. FV magnitude is illustrated in a coronal slice (blue - 0, red - 1 m/s), with red arrows showing the flow directions. Large white arrows indicate vortices and flow patterns characteristic of the atrial flow dynamics.

Table 1. Maximum and average FVs in LA and its appendage (LAA) of patients in SR and AF. FVs are measured over one cardiac cycle and across the entire 3D spatial domain (LA or LAA).

	Sinus rhythm, SR	**Atrial fibrillation, AF**
Maximum LA flow velocity, FV_{max}	1.90 m/s	1.40 m/s
Average LA flow velocity, FV_{mean}	0.16 m/s	0.10 m/s
Maximum LAA flow velocity, $FV_{LAA,\ max}$	0.70 m/s	0.20 m/s
Average LAA flow velocity, $FV_{LAA,\ mean}$	0.05 m/s	0.04 m/s

ID#: 373901

Native T1 measurements in pediatric heart transplant patients correlate with history of prior rejection episodes

Ashish Doshi, MD, PhD[1] Tina Doshi, MD[2], Ileen Cronin, FNP-BC[3], Imani Mojerie, B.S.[4], Adrienne E. Campbell-Washburn, PhD[5], Russell Cross, M.D.[6], Joshua Kanter, MD[3], Sairah Khan, MD[4], Janet Scheel, MD[7], Elena K. Grant, MD[4], Laura Olivieri, M.D.[1]

1. Children's National Medical Center, Washington, DC

2. Johns Hopkins Medical Institutions, Baltimore, MD

3. Children's National Medical Center, DC

4. Children's National Medical Center

5. National Heart, Lung, and Blood Institute, National Institutes of Health, MD

6. Children's National Medical Center, Washington

7. Washington University School of Medicine, St. Louis, MO

Background: Cardiac transplant patients are at risk for cellular rejection, which can cause myocardial injury and tissue fibrosis, limiting the lifespan of the graft. Rejection episodes can be asymptomatic, so patients frequently undergo invasive cardiac catheterizations with endomyocardial biopsies for rejection monitoring. Even with routine surveillance biopsies and anti-rejection therapies, the average graft lifespan is 10.7 years in adults and 16.1 years in children. A noninvasive method for assessing cardiac fibrosis could provide prognostic information on graft health. Native T1 mapping by cardiac magnetic resonance (CMR) correlates with tissue fibrosis in a number of disease states. We hypothesize that history of prior rejection episodes correlates with native T1 levels in transplant patients.

Methods: With IRB approval and consent/assent, 15 heart transplant patients (age 12.8±4.8 years, cardiac index 3.2±0.9 L/min/m^2) underwent non-contrast CMR, MR-guided right heart catheterization, and endomyocardial biopsy in a combined 1.5T scanner/cardiac catheterization suite. CMR included cine volumetry and native T1 mapping using MOLLI. T1 measurements were taken in the base/mid regions of the septum and left ventricular lateral wall using the “middle third” technique, and averaged. Ordered logistic regression analysis was performed with the outcome of number of prior rejection episodes (0, 1, or ≥2) as a function of average T1 level, biopsy grade at the time of CMR (ISHLT grade 0R, 1R, or 2R), and time since transplantation.

Results: Twenty-three studies from fifteen patients were analyzed. T1 levels were 1012±44 (mean±SD) for patients with no prior rejection episodes (n=11), 1028±23 for one prior episode (n=5), and 1089±46 for two or more prior episodes (n=7). Fifteen patients had biopsy grade 0R, four had grade 1R, and four had grade 2R at the time of CMR. Time since transplantation ranged from 41 to 6364 days. Controlling for biopsy grade and time since transplantation, history of rejection significantly correlated with average T1 level ($p<0.05$). The odds ratio for each additional rejection episode was 1.36 (95% CI 1.03-1.8) per 10-unit increase in T1 level.

Conclusion: History of prior rejection correlates with native T1 level, even when controlling for current biopsy result and time since transplantation. Native T1 mapping may have potential as a noninvasive method to evaluate for subclinical fibrosis as a marker of overall graft health.

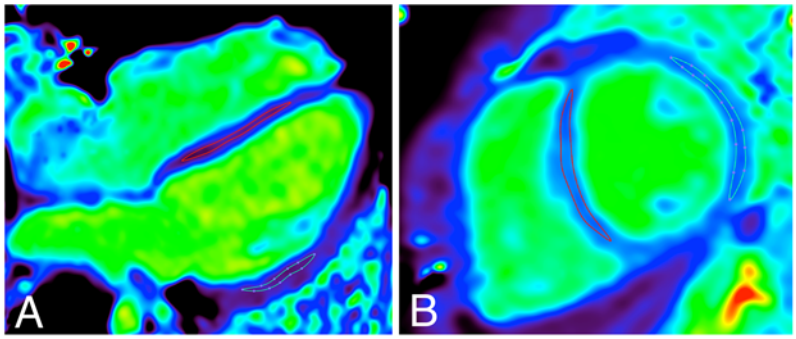

Middle third method for measuring native T1 level in the base and mid regions of the septum and left ventricular lateral wall in the (A) four-chamber view and (B) short-axis view. T1 level was averaged among all four regions.

ID#: 373905

Method for objective automatic assessment of wall motion abnormality from cineMR images

Iulia A. Popescu[1]Christopher Kelly[2], Alessandra Borlotti, PhD[3], Keith M. Channon, MD, FRCP[4], Stefan K. Piechnik, PhD, MScEE[4], Vicente Grau, PhD[5], Erica Dall'Armellina, Sr., MD, DPhil[6]

1. University of Oxford, Centre for Clinical Magnetic Resonance Research, United Kingdom

2. University of Oxford, United Kingdom

3. University of Oxford, Oxford, England, United Kingdom

4. University of Oxford, England, United Kingdom

5. University of Oxford, Oxford, UK, Oxford, England, United Kingdom

6. Leeds Institute of Cardiovascular and Metabolic Medicine, Division of Biomedical Imaging,University of Leeds, United Kingdom

Background:

Assessment of functionally abnormal wall motion is the key diagnostic outcome of contemporary cardiac imaging. We propose a novel objective method for classifying the wall motion using local similarity in strain patterns extracted from cine MR images exclusively.

Methods:

20 (6 female) patient datasets were analysed from the OxAMI (Oxford Acute Myocardial Infarction) clinical study. Images were acquired on a 3.0T Siemens TIM-Trio MRI scanner, in the acute stage of myocardial infarction. The CMR protocol included functional and LGE imaging of matching short axis slices with full left ventricular (LV) coverage. The LV contours were manually drawn using the cmr[42] (Circle Cardiovascular Imaging, Calgary, Alberta, Canada) software. We used a novel clustering method to generate locally similar regions in the left ventricular mask based on radial strain (Err) curves and subsequently group together these regions into three categories: normokinesis, hyperkinesis and hypo/akinesis (Fig. 1). This method uses only cine MRI images to perform the analysis, and LGE images are used to validate the proposed method.

Results: All patients had a positive LGE with a LV% 28±14% with ejection fraction (EF) of 46±8%. The average percentage per patient of myocardium with decreased Err was 84±11% and significantly larger than the LGE extent (p=0.00013). The regions of reduced contractility were co-localized with LGE positive regions (degree of concordance: 87%) (Figure 1). The Err in regions with different degrees of LGE segmental damage fraction are: Err=8±4% in segments with ≤ 50% LGE, Err=6±4% in segments with 51%<Err≤75% and Err=3±3% with LGE>75%.

Conclusion: The proposed method is suitable for segmentation applications where quantification of tissue properties within a ROI is required. Local clustering provides an objective and robust metric for assessing localized changes in the myocardium, overcoming the averaging effects of segmental analysis, as in the case of 16 AHA segments model and hence it could potentially be a more accurate assessment tool for the extent of damage post myocardial infarction, including the extent of area at risk and clinical improvements post treatments.

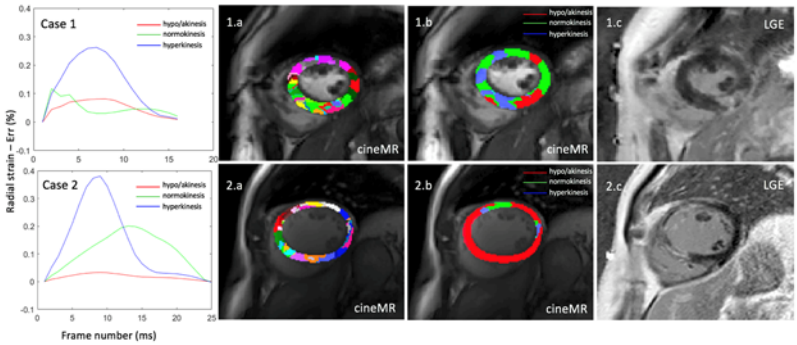

Fig.1: ROI based assessment of wall motion abnormalities using a clustering method: Exemplary cases. From left to right: Panels Case 1. and Case 2. mean radial strain curve per cluster; Panels 1.a and 2.a colour coded map showing regions of myocardium with similar values of Err as assessed from cine images; Panels 1.b and 2.b: colour

coded mask showing the final division of the myocardium in normokinetic (green), hyperkinetic=blue and hypo/akinetic=red regions of interest, based on differences in Err in local regions; Panels 1.c and 2.c corresponding LGE images.

ID#: 373973

Left Ventricle Remodeling in Patients with Bicuspid Aortic Valve

Kenichiro Suwa, MD[1] Amir Ali Rahsepar, MD[2], Ahmadreza Ghasemiesfe, M.D[3], Julia Geiger, MD[4], Ryan Dolan, MD[2], Alex J. Barker, PHD[2], Jeremy D. Collins, MD[5], Michael Markl, PhD[2], James Carr, MD[2]

1. Northwestern University School of Medicine, Hamamatsu University School of Medicine, Evanston, IL

2. Northwestern University, Chicago, IL

3. Yale New Haven Health, Bridgeport Hospital, Milford, CT

4. Imaging Department, Children's University Hospital, Switzerland

5. Northwestern University School of Medicine, Chicago, IL

Background: Bicuspid aortic valve (BAV) is associated with aortic valve stenosis (AS) and regurgitation (AR) and can result in left ventricular (LV) remodeling. However, due to heterogeneous morphological characteristics of the aortic valve, the association between BAV and LV remodeling is unclear. The goal of this study was to assess the impact of BAV, as well as AS and AR, on metrics of LV remodeling measured by electrocardiogram (ECG), transthoracic echocardiography (TTE), and CMR.

Methods: This retrospective study included 156 patients with BAV or trileaflet aortic valve (TAV) who underwent CMR. The BAV cohort was comprised of patients with AS and AR (BAV-ASR: n=11), AS (BAV-AS: n=30), AR (BAV-AR: n=28), or neither AS nor AR (BAV-no AS/AR: n=47). TAV-controls (n=40) demonstrated no AS/AR. AS and AR were defined as moderate or greater in severity. All patients underwent cardiac magnetic resonance (CMR), including cine CMR and T1-mapping, using 1.5 or 3T scanner (Avanto or Skyra, Siemens, Germany). T1-mapping was performed using Modified Look-Locker Inversion recovery (MOLLI) in basal, mid-ventricular, and apical short axis orientation. Regional native T1 and post-Gd-contrast T1 were measured based on the AHA 16-segment model. Global ECV was calculated with patient specific hematocrit and native and post-Gd-contrast T1 values using commercial clinical software (cvi42, v5.3, Circle, Canada). CMR analysis included calculation of measures of global cardiac LV volume, mass, and function (Figure 1). ECG-related parameters, including Sokolow-Lyon product ((SV1 + RV5) × QRS width) and Cornell product ((RaVL + SV3) × QRS width), and TTE-derived E/e' were also measured.

Results: As summarized in Table 1, there were no differences in ECG, TTE and CMR parameters between BAV patients with normal valve function (BAV-no AS/AR) and TAV-controls. However, presence of aortic valve dysfunction resulted in elevated Sokolow-Lyon product for BAV-ASR (P=0.017) and BAV-AR (p=0.001) patients and increased Cornell product (p=0.04) and E/e' (p<0.001) in BAV-AS patients compared to BAV-no AS/AR patients. In addition, LVEDVi and LVMi were elevated in BAV-ASR and BAV-AR patients compared to BAV-no AS/AR (LVEDVi: 101±29 ml/m2 and 112±32 ml/m2 vs. 74±15 ml/m2, p=0.005 and p<0.001, LVMi: 75±7 g/m2 and 64±14 g/m2 vs. 47±9 g/m2, respectively p<0.001). ECV demonstrated no difference between BAV subgroups.

Conclusion: Normal functioning BAV did not result in LV remodeling; however, concomitant AS and/or AR was associated with significant LV remodeling. Additional work is needed to assess ECV by subgroup and severity of aortic valve dysfunction.

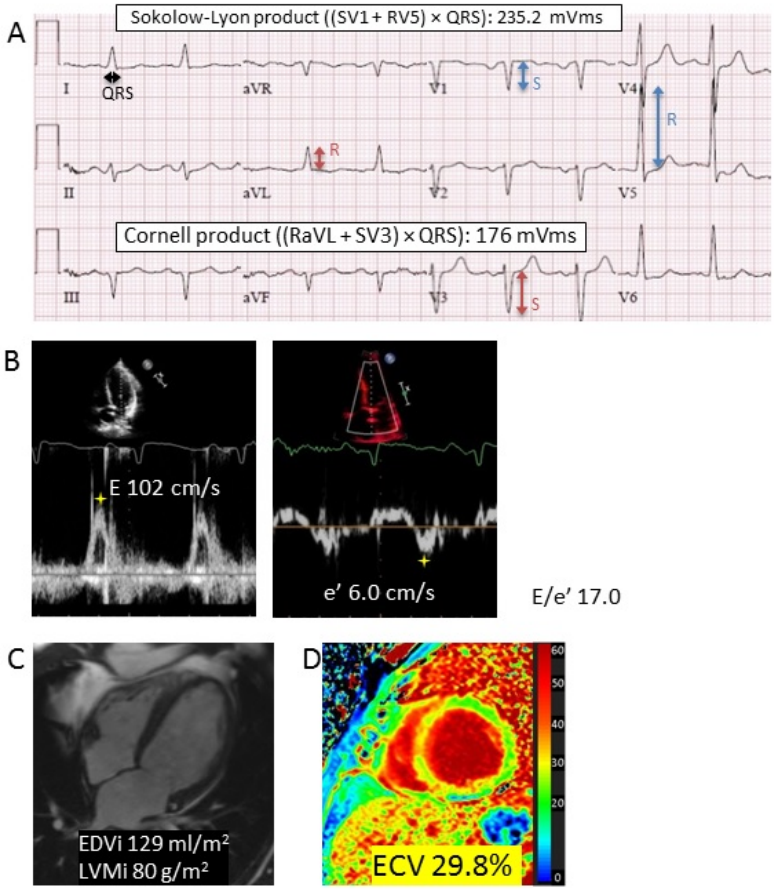

Figure 1. ECG (A), TTE (B), bSSFP image (C) and ECV map (D) by cardiac magnetic resonance in a patient with BAV and AS as well as AR.

ECG, TTE, and CMR characteristics between subgroup in BAV according to AS and/or AR and TAV

	BAV				TAV
	ASR (n=11)	AS (n=30)	AR (n=28)	no AS/AR (n=47)	control (n=40)
ECG					
Sokolow-Lyon product (mVms)	269±80*‡§	186±67	266±129*‡§	183±68	183±70
Cornell product (mVms)	219±84	197±136‡	177±65	133±65	141±82
TTE					
E/e';	12.3±3.8	14.4±5.5†‡§	9.8±3.8	9.9±3.8	10.2±3.7

	BAV				TAV
	ASR (n=11)	AS (n=30)	AR (n=28)	no AS/AR (n=47)	control (n=40)
CMR					
LVEDVi (ml/m^2)	101±29*‡§	70±18	112±32*‡§	74±15	74±12
LVMi (g/m^2)	75±7*‡§	57±15‡	64±14‡§	47±9	50±10
EF (%)	61±12	66±8	62±6	62±6	62±8
ECV (%)	26.2±3.5	25.6±2.6	25.8±3.4	25.2±2.6	24.6±2.3

*: p<0.05 compared to BAV-AS, †: p<0.05 comared to BAV-AR, ‡: p<0.05 compared to BAV-no AS/AR, §: p<0.05 compared to TAV-control.

ID#: 374024

Comparison between 4D and 2D CMR flow in quantitative assessment of pulmonary blood flow in surgically repaired tetralogy of Fallot patients

Mahmoud N. Shaaban, MBBCh, MSc.[1] Dina Haroun, MBBCh,MSc[2], Salem Deraz, MD[3], Abd Elrahman Elafifi, MD[4], Walid Simry, MD, FEBCTS[5], Fatma R. Elkafrawy, MBBCh, MSc.[6], Sameh Khalil, MSc[7], Wesam E. El Mozy, MD, MSc[8], Soha Romeih, MD,PhD, FESC[4]

1. Aswan Heart Center (Magdi Yacoub Foundation) - Cardiology department, Tanta University, Tanta, Al Gharbiyah, Egypt

2. Radiology fellow Aswan Heart Center (Magdi Yacoub Heart Foundation),assistant lecturer Radiology department - Kasr Al Ainy Cairo university., Egypt

3. Menoufia University, Al Minufiyah, Egypt

4. Aswan Heart Centre, Egypt

5. Aswan Heart Center - Magdi Yacoub Foundation, Egypt

6. Radiology fellow at Aswan Heart center (Magdi Yacoub Foundation) -Assistant Lecturer at Radiology Dep., Alexandria university, Aswan, Aswan, Egypt

7. Aswan Heart Center - Magdi Yacoub Foundation, Cairo, Egypt

8. Magdi Yacoub Foundation - Aswan Heart Centre, Aswan, Egypt

Background: Tetralogy of Fallot (TOF) accounts for 10% of all congenital heart defects (CHD). Surgical correction of TOF, usually performed in the first year of life, consists of ventricular septal defect (VSD) closure and reconstruction of the right ventricle outflow tract (RVOT) either by trans-annular patch, right ventricle (RV) to pulmonary artery (PA) conduit or a valve-preserving technique. The most common post-surgical complication is pulmonary insufficiency or stenosis which can lead to RV dysfunction/failure. CMR is the image modality of choice to follow up a repaired TOF. However, the standard 2D CMR flow usually underestimates the pulmonary flow incompetence as well as the pulmonary flow velocity. Recently, 4D CMR flow is introduced for an accurate quantitative flow assessment in patients with complex CHD.

Methods: Twenty-one surgically repaired TOF patients had CMR exam as a part of clinical follow-up on 1.5T scanner(Siemens Magnetom Aera, Siemens Medical Systems, Erlangen, Germany) to assess the RV volumes and systolic function. 2D and 4D CMR flows for pulmonary flow quantification on MPA, LPA and RPA were compared.(Figure 1 & 2)

Results: Patients'; median age was 9 years (range 3–42 years), 52 % were females, median age at total repair was 7.5 years (range 1.5–37 years), 11 patients had RV-PA conduit, 6 Patients had RVOT patch and 4 Patients had transannular patch. The pulmonary regurgitation was quantitatively better assessed by 4D CMR flow (Regurgitation fraction “RF” was 44±7% by 4D flow vs 36±7% by 2D flow), however, it was not statistically significant. By 4D CMR flow, 33% had significant pulmonary regurgitation (RF> 25%), and their RV-EDVI was significantly increased compared to the rest (150 ± 39 ml/m^2 compared to 91 ± 22 ml/m^2). Forward flow volumes were equally measured by 4D and 2D CMR flows of main and central pulmonary arteries. Peak systolic velocities across the main and central pulmonary arteries, were higher by 4D CMR flow (1.8±0.7 m/sec vs 1.4±0.4 m/sec by 2D CMR flow at MPA, 1.7±0.5 m/sec vs 1.3±0.5 m/sec by 2D CMR flow at RPA, 1.7±0.7 m/sec vs 1.1±0.5 m/sec by 2D CMR flow at LPA). (Table)

Conclusion: We reported a comparison between 2D and 4D CMR flow for quantitative assessment of pulmonary blood flow in surgically repaired TOF. 4D CMR flow provides an accurate quantitative assessment of pulmonary regurgitation and a higher peak pulmonary flow velocity. Accurate quantitative pulmonary blood flow assessment would help in the patients'; management.

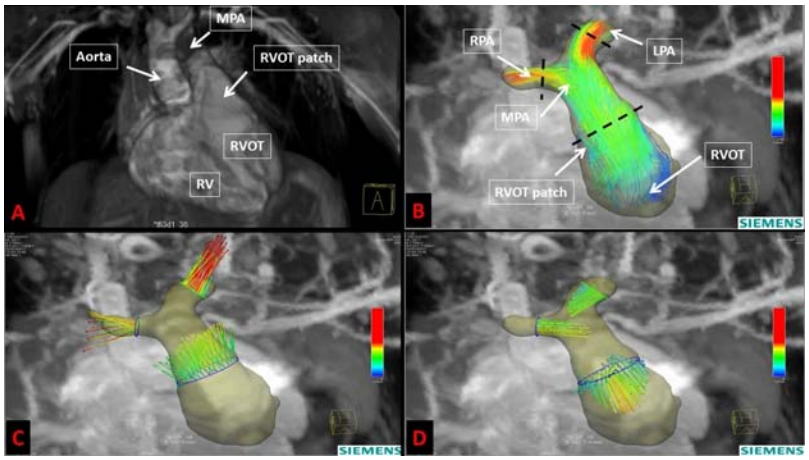

Figure. 1: 4D CMR flow of a surgically repaired TOF patient with RVOT patch. A: 3D whole heart SSFP image in a coronal view showing the RVOT patch and a dilated RV. B: particle tracing color map showing flow in main, left and right pulmonary arteries, flow planes were acquired at demonstrated levels. C-D: Vector velocity maps during systolic phase (C) showing forward flow, and during diastolic phase (D) showing backward flow in main, left and right pulmonary arteries. MPA: main pulmonary artery, RPA: right pulmonary artery, LPA: left pulmonary artery, RVOT: right ventricle outflow tract.

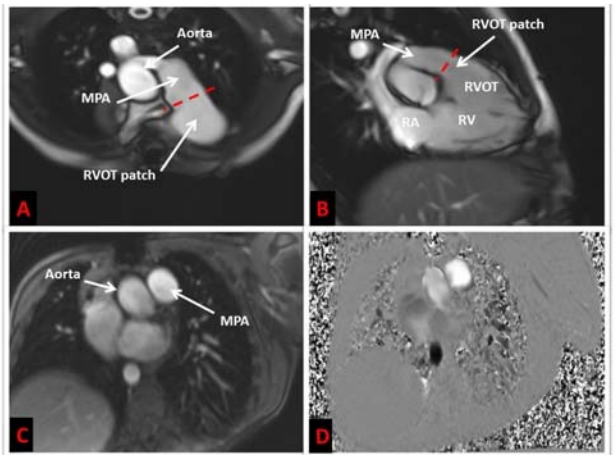

Fig. 2: CMR images of the same patient. A-B: SSFP cine images showing the main pulmonary artery in 2 orthogonal planes, flow was measured at demonstrated levels. C-D: 2D phase contrast through plane flow across the main pulmonary artery, (C) is an anatomy image, (D) is a phase contrast image. MPA: main pulmonary artery, RVOT: right ventricle outflow tract, RV: right ventricle, RA: right atrium.

Table. Peak systolic velocities and forward flow volumes across the main and central pulmonary arteries.

		2D	4D	P value
Peak systolic velocity (m/sec)	MPA	1.4 ± 0.4	1.8 ± 0.7	0.01 *
	RPA	1.3 ± 0.5	1.7 ± 0.5	0.03 *
	LPA	1.1 ± 0.5	1.7 ± 0.7	0.01 *
Forward flow volume (ml)	MPA	52 ± 23	50 ± 22	0.16
	RPA	30 ± 14	28 ± 13	0.66

	LPA	25 ± 14	22 ± 13	0.53

* is considered statistically significant.

MPA: main pulmonary artery, RPA: right pulmonary artery, LPA: left pulmonary artery.

ID#: 374090

Accelerating mutli-slice reduced field of view cardiac T2-ADC mapping with a restore pulse

Kévin Moulin[1] Eric Aliotta, PhD[2], Daniel B. Ennis, PhD[3]

1. Department of Radiological Sciences, University of California, Los Angeles, CA

2. UCLA

3. Department of Radiological Sciences, University of California, Los Angeles, CA, USA., CA

Background: Joint T2 and apparent diffusion coefficient (ADC) mapping is an efficient way to characterize myocardial edema (increased T_2)and the degree of diffuse and focal myocardial fibrosis (increased ADC) [1]. Reduced field-of-view (rFOV) approaches are preferred to improve sequence efficiency and reduce EPI distortion, but current methods are not compatible with interleaved multi-slice acquisitions. The ***objective*** of this study was to design and evaluate a multi-slice rFOV joint T_2+ADC mapping strategy [1] enabled through the use of a 180° RF pulse [2] to "restore" the z-magnetization after readout and improve SNR-efficiency and substantially reduce scan times.

Methods: A navigator based free-breathing cardiac gated spin echo EPI sequence with convex optimized diffusion encoding (CODE, motion compensated with M_1=M_2=0) gradients [3] was modified to support multi-slice rFOV acquisitions through the addition of a 180° restore pulse after the EPI readout [2]. Healthy volunteers (N=6) were imaged on a 3T scanner (Prisma, Siemens). CODE-M_1M_2 diffusion encoding was used to acquire joint T_2+ADC maps at mid-systole (TD=100ms) with 2.3x2.3x5.0mm resolution. Reference (b-value=0) images were obtained at two TEs (TE_1=22ms with two averages, TE_2=59ms with ten averages) and b-value=350s/mm^2 images were obtained at TE=59ms using six diffusion directions and eight averages. All data were acquired under free breathing conditions using navigator based slice following [4] (tracking factor=0.6). Multi-slice rFOV acquisitions with (MS-rFOV+RESTORE) and without (MS-rFOV) the restore pulse were compared to a reference single-slice rFOV (SS-rFOV) acquisition (Table 1). SNR was calculated from the repeated b-value=0 images at TE =59ms. SNR, T_2, and ADC were compared as described in [1] after manual segmentation of the LV and automatic rejection of corrupted signals [5]. SNR-efficiency (SNR/√(Scan time)) was also compared.

Results: Figure 1 shows example DWI, T2, and ADC maps of the same basal slice acquired with MS-rFOV+RESTORE, MS-rFOV, and SS-rFOV. T_2, ADC, and SNR distributions across volunteers are reported in Figure 2. No statistical differences were found for ADC or T2 between MS-rFOV+RESTORE or MS-rFOV and SS-rFOV. Higher SNR was observed for SS-rFOV and MS-rFOV+RESTORE compared to MS-rFOV. Overall the best SNR-efficiency per slice was obtained with MS-rFOV+RESTORE (7.6±1 min$^{-1/2}$) compared to MS-rFOV (6.2±0.6 min$^{-1/2}$) and SS-rFOV (4.2±0.7 min$^{-1/2}$).

Conclusion: The proposed MS-rFOV+RESTORE strategy offers higher SNR-efficiency than traditional SS-rFOV techniques while enabling multi-slice acquisitions and thereby reduced scan times.

[1] Aliotta et al. MRM 2017. [2] Eun-Kee et al MRM 2005. [3] Aliotta et al. MRM. 2016. [4]Moulin et al. MRM 2016. [5] Aliotta et al. SCMR 2015.

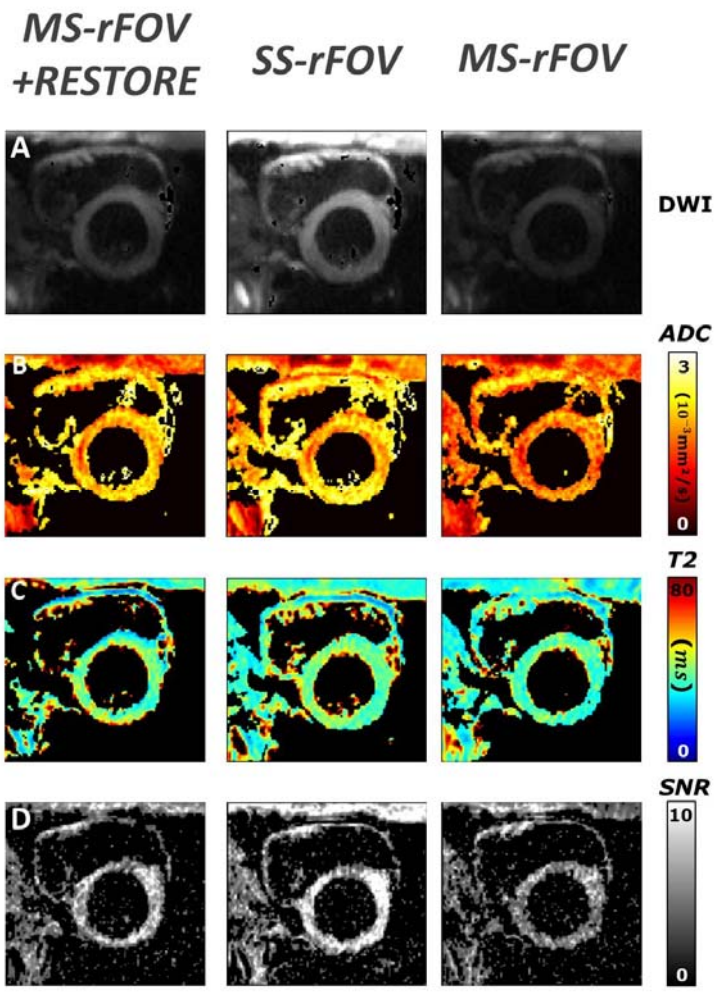

Figure 1: Example of basal DWI images at b-values 350s/mm² A) and corresponding B) ADC maps, C) T2 maps , D) SNR maps for the rFOV+Restore, Reference and rFOV acquisitions.

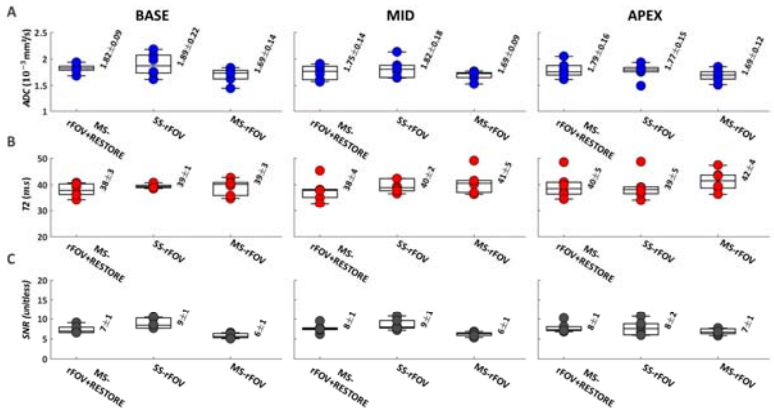

Figure 2: Population distribution and mean ± standard deviation of A) ADC, B) T2 and C) SNR reported from ROI in volunteers (N=6). For each volunteer the same basal, mid and apical slices have been compared in the three acquisitions.

Protocols details

	MS-rFOV+RESTORE	SS-rFOV	MS-rFOV
Number of slices	8	8	3
TR	1 RR	1 RR	4 RR
Total number of images	480	480	180
Scan time per slice	1 min	1 min	4 min
Total scan time	8 min	8 min	12 min

ID#: 374038

Increased Homing of Mast Cells to Sites of Iron-Driven Inflammation Promotes Macrophage Foam Cell Formation and Fatty Degeneration of Hemorrhagic Myocardial Infarction

Ivan Cokic, MD[1]Hsin-Jung Yang, PhD[2], Richard LQ. Tang, MD[3], Joseph Francis, B.V.Sc., Ph.D[4], Rohan Dharmakumar, PhD[5]

1. Cedars-Sinai Medical Center, Los Angeles, CA

2. Cedars-Sinai Medical Center

3. Cedars-Sinai Medical Center, CA

4. Louisian State University, LA

5. Cedars-Sinai Medical, CA

Background: Recently, there has been substantial interest in understanding the role of cardiac mast cells in mediating adverse ventricular remodeling post-MI. Mast cells exert their physiological and pathological effects by secreting cytoplasmic granules containing a variety of mediators (proteoglycans, histamine, proteases (chymase and tryptase), and proinflammatory cytokines). These biologically active mediators are released upon mast cells activation and influence the local tissue microenvironment. Activated mast cells are also known to promote cholesterol uptake/retention by macrophages and their transformation into foam cells. CMR studies over the past two decades have taught us that, in the modern era of mechanical reperfusion, nearly 50% of all MIs are hemorrhagic. Moreover, recent reports indicate that hemorrhagic MIs resolve into chronic iron deposition, which in turn mediates prolonged chemotactic attraction for new monocytes/macrophages. Since iron is a known potent mast cell activator, we hypothesized that mast cells and iron deposits in hemorrhagic MIs act synergistically to promote activation of macrophages and their transformation into foam cells.

Methods: Ten dogs were subjected to 3-hr occlusion of the LAD artery, followed by reperfusion, and underwent T2* and LGE CMR on day 7 post-MI and followed for 6 months. Animals were sacrificed 6 months post-MI at which time the hearts were explanted for histopathological analysis of iron deposits, mast cells, macrophages, phospholipid oxidation products and foam cells.

Results: All dogs exhibited the presence of intramyocardial hemorrhage in subacute MI, as evidenced by T2* CMR (Figure 1A & B). Histopathological studies demonstrated the presence of both iron and fat deposits within all chronic MIs. Moreover, sparse fat deposits (foam cells) within scars were exclusively colocalized with iron deposits (Figure 1C & D), oxidized phospholipid products, foam cells, as well as the activated mast cells and macrophages (Figure 1E-L).

Conclusion: Taken together, our results suggest that increased mast cell homing to sites of iron-driven inflammation promotes macrophage foam cell formation and adverse left ventricular remodeling post-MI.

Figure 1

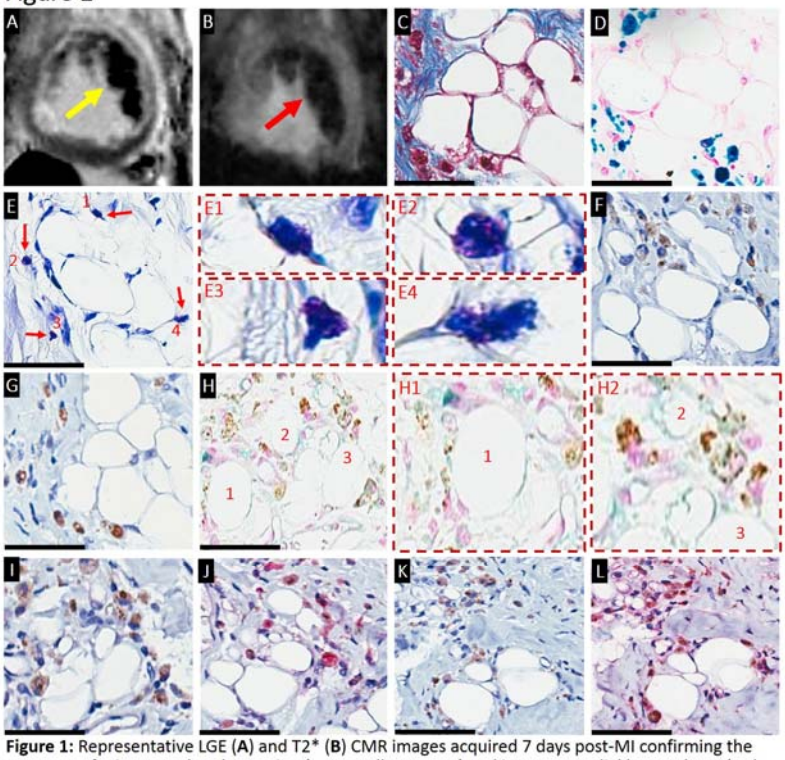

Figure 1: Representative LGE (**A**) and T2* (**B**) CMR images acquired 7 days post-MI confirming the presence of microvascular obstruction (MVO, yellow arrow) and intramyocardial hemorrhage (red arrow), respectively. Corresponding serial histology sections from 6-month-old hemorrhagic MI were stained with elastin-modified Masson's trichrome stain **(C)**, Prussian Blue **(D)**, Toluidine Blue **(E)** as well as the anti-MAC387 **(F)**, anti-E06 **(G)**, anti-CD36 **(H)**, anti-CD163 **(I)**, anti-MMP9 **(J)** , anti-TNF-α **(K)** and anti-IL-1β **(L)** antibodies. Scale bar equals 50 µm.

Summary of key findings presented in Figure 1C-L:

(C) Isolated fat depots were found within old MI scar. **(D)** Persistent iron deposits (blue stain) co-localized with fat depots in the scar tissue. **(E)** Mast cells (arrows) co-localized with fat deposition. Note the individual mast cells in E1-E4. **(F)** New macrophages (MAC387+) were recruited to the iron-laden fat-developing territory (brown staining). **(G)** Increased generation of oxidized phospholipids in the "iron-mast cell-macrophage-fat territory" was demonstrated by intense E06 staining (red staining). **(H)** Fat depots within "iron-mast cell territory" stained positive for CD36 (green) indicating macrophage-derived foam cell formation. Note the individual foam cells in H1-2. **(I)** CD163-positive macrophages (pink staining) co-localized with foam cells indicating iron-induced macrophage-to-foam cell transformation. Positive staining for MMP9 **(J)**, TNF-alpha **(K)** and IL-1 beta **(L)** (all stained red) in the "iron-mast cell-macrophage-fat territory" indicates that hemorrhagic infarcts lead to prolonged mast cell-mediated inflammatory response culminating in fatty degeneration of post-MI scar.

ID#: 373723

Substantial prevalence of a type II left ventricular contraction pattern by feature tracking CMR in patients with non-specific intraventricular conduction delay

Daniel E. Loewenstein[1] Björn Wieslander, MD PhD[2], Karin Johansson[3], Igor Klem, MD[4], Brett D. Atwater, MD[5], Martin Ugander, MD, PhD[6]

1. Karolinska Institutet, Stockholm, Stockholms Lan, Sweden

2. Department of Clinical Physiology, Karolinska Institutet and Karolinska University Hospital, Stockholm, Sweden, Stockholm, Stockholms Lan, Sweden

3. Karolinska Institutet, Sweden

4. Duke University Medical Center, Durham, NC

5. Duke University School of Medicine, NC

6. Karolinska Institutet, and Karolinska University Hospital, Stockholm, Sweden, Stockholms Lan, Sweden

Background: Patients with non-specific intraventricular conduction delay (IVCD) are less likely to respond to cardiac resynchronization therapy (CRT) compared to patients with left bundle branch block (LBBB). A type II contraction pattern in LBBB has been associated with improved CRT response. The aim of this study was to explore the prevalence of a type II left ventricular (LV) contraction pattern in patients with IVCD.

Methods: We retrospectively identified 38 patients with IVCD, defined as QRS duration ≥120ms and absence of fulfilling electrocardiographic morphologic criteria for left or right bundle branch block and available clinically acquired cardiovascular magnetic resonance (CMR) images. CMR feature tracking (Segment, Medviso AB, Lund, Sweden) was used to measure the earliest to latest segment delay (ELSD) in circumferential short-axis strain, a previously validated measure of dyssynchrony in LBBB. Contraction patterns were classified based on the absence (type I) or presence (type II) of a line of block in circumferential short-axis strain.

Results: Among IVCD patients, 21/38 (55%) had a type II contraction pattern and 17/38 (45%) had a type I contraction pattern. In patients with a type II pattern the mid-ventricular inferior segment was the most frequent site of latest mechanical activation (LMA) (8/24, 33% of cases) while, the lateral wall segments (anterolateral and inferolateral) together were the most frequent sites of LMA in patients with a type I pattern (18/26, 69% of cases)

Conclusion: Approximately half of patients with IVCD demonstrate a type II contraction pattern identifiable using CMR feature tracking, which has previously been associated with favorable CRT response in patients with LBBB. The site of LMA in these patients is frequently located elsewhere than the LV lateral wall which is most frequently targeted for LV lead deployment at CRT implantation. Congruence between site of LMA and site of CRT lead deployment has previously been associated with favorable CRT response. These initial findings deserve further study with regards to the ability to predict CRT response in IVCD.

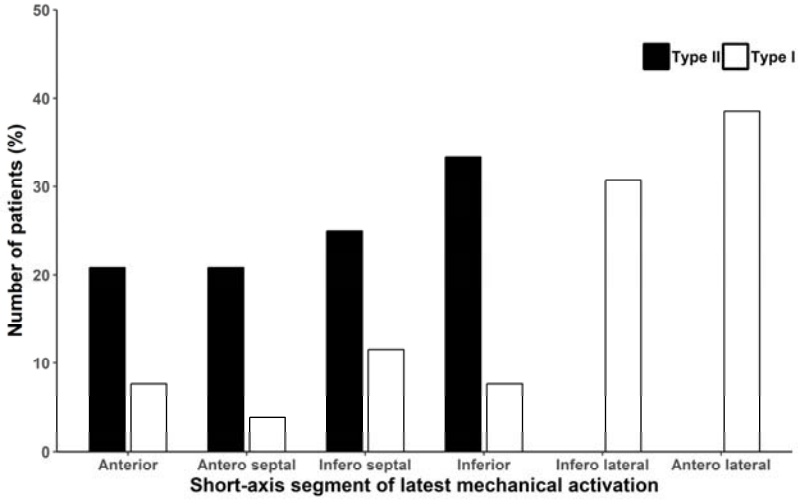

Figure 1. Distribution of site of latest mechanical activation stratified by contraction pattern.

ID#: 373737

Impact of CMR in the diagnosis of acute coronary syndrome with unobstructed coronary arteries

Nadine Abanador-Kamper[1] Lars Kamper[2], Witali Pomjanski[1], Patrick Haage[3], Melchior Seyfarth[1]

1. Department of Cardiology, HELIOS Medical Center Wuppertal, University Hospital Witten/Herdecke, Wuppertal, Germany; Center for Clinical Medicine Witten/Herdecke University Faculty of Health, Wuppertal, Germany, Germany

2. Department of Diagnostic and Interventional Radiology, HELIOS University Hospital Wuppertal, University Witten/Herdecke, Germany, Germany

3. Department of Diagnostic and Interventional Radiology, HELIOS Medical Center Wuppertal, University Hospital Witten/Herdecke, Wuppertal, Germany; Center for Clinical Medicine Witten/Herdecke University Faculty of Health, Wuppertal, Germany., Germany

Background: Finding the underlying diagnosis in patients with acute coronary syndrome (ACS) and unobstructed coronary arteries still remains a diagnostic challenge. We aimed to analyze impact of CMR parameter to distinguish between different diagnoses.

Methods: A total of 213 patients with elevated high-sensitivity troponin but unobstructed coronary arteries that underwent CMR (1.5 T) two days after coronary angiography were enrolled. Left ventricular ejection function (LVEF) was analyzed with SSFP sequences. T2-weighted sequences were used to assess myocardial oedema. LGE was evaluated using a 3D IR sequence. The consensus diagnosis was based on clinical, laboratory and CMR data.

Results: A final diagnosis was detected in 97% of patients. Myocardial infarction with non-obstructed coronary arteries (MINCOA) was diagnosed in 40%, acute myocarditis in 24% and Takotsubo syndrome (TTS) in 33%. Median LVEF was 50% in TTS, 60% in MINOCA and 60% in myocarditis, P=0.001. T2-volume was 13.4%±11.4% in TTS, 4.6%±7.9% in MINOCA and 1.8%±2.7% in myocarditis, P<0.001. After multinominal logistic regression analysis LVEF (OR 0.95; 95% CI 0.92-0.99, P=0.04) and T2-size (OR 1.09; 95% CI 1.04-1.14, P=0.001), age (OR 1.05; 95% CI 1.03-1.08, P<0.001), gender (OR 9.53; 95% CI 3.13-28.95, P<0.001) and current smoking (OR 0.92; 95% CI 0.83-1.03, P=0.03) remained independent predictors for TTS diagnosis compared to MINOCA. Independent predictors for MINOCA diagnosis compared to patients with myocarditis were LGE size (OR 1.29; 95% CI 1.15-1.45, P<0.001), age (OR 1.04; 95% CI 1.02-1.06, P=0.002) and peak value of CK (OR 1.00; 95% CI 1.00-1.00, P=0.04).

Conclusion: CMR parameters as impaired LVEF and increased T2-size combined with age, female gender, lack of current smoking remained independent predictors for the diagnosis of TTS compared to MINOCA. Increased LGE-size, age and peak value of CK were independent predictors for MINOCA compared to myocarditis.

ID#: 373745

Differences in intracellular lifetime of water between patients with and without concentric and eccentric left ventricular hypertrophy cannot be detected in a clinical setting at 1.5T

Magnus Lundin, MD[1] Sara Demirtas[2], Andreas Sigfridsson, PhD[3], Peder Sorensson, MD, PhD[4], Martin Ugander, MD, PhD[5]

1. Karolinska institutet, CMR group, Stockholms Lan, Sweden

2. Karolinska Institutet, Stockholm, Stockholms Lan, Sweden

3. Karolinska Institute, Stockholm, Stockholms Lan, Sweden

4. Karolinska Institutet, Stockholms Lan, Sweden

5. Karolinska Institutet, and Karolinska University Hospital, Stockholm, Sweden, Stockholms Lan, Sweden

Background: Measurement of the myocardial extracellular volume fraction (ECV) assumes a dynamic equilibrium with rapid exchange of an extracellular contrast agent between myocardium and blood. This equilibrium would be manifested by a linear relationship between 1/T1 (R1) of myocardium and R1 of blood. This relationship has been shown to be non-linear for high R1 values in mice, and this has been used to calculate the intracellular lifetime of water (tau) and thereby estimate myocardial cell size. We sought to determine whether it is possible to detect difference in myocardial cell size using tau between patient groups with and without overt left ventricular hypertrophy in a clinical setting.

Methods: Patients referred for cardiovascular magnetic resonance (CMR) evaluation of suspected heart disease were prospectively enrolled. T1-mapping was undertaken at 1.5T (Siemens Aera) using a modified Look-Locker inversion recovery (MOLLI) sequence before and approximately 4, 14 and 25 minutes after an intravenous bolus of a gadolinium-based extracellular contrast agent (gadoteric acid, 0.2 mmol/kg). Patients were categorized according to left ventricular (LV) mass index (LVMi) and thickness to volume-ratio (TVR), defined as mean LV end-diastolic wall thickness divided by LV end-diastolic volume index. Patient groups were defined as normotrophic (normal LVMi, normal TVR), concentric hypertrophy (high LVMi, high TVR), and eccentric hypertrophy (high LVMi, normal TVR). Regions of interest were placed in the LV blood pool and midmurally in the LV myocardium of a midventricular short-axis slice at all time points. Myocardial segments with artefacts or focal lesions were excluded. Tau was calculated using non-linear fitting of the relationship between R1 in the myocardium and blood at different contrast concentrations using published methods, see Figure.

Results: The intracellular lifetime of water (tau) was (median [interquartile range]) 110 [65-163] ms for the normotrophic group (*n*=19), and did not differ for concentric hypertrophy (*n*=23, 66 [9-119] ms, *p*=0.14 vs normal) or eccentric hypertrophy (*n*=19, 93 [5-116] ms, *p*=0.08 vs normal).

Conclusion: It is not possible to detect differences in the intracellular lifetime of water in patients with and without concentric or eccentric left ventricular hypertrophy using MOLLI T1-maps at 1.5T and a double dose bolus of a clinical contrast agent.

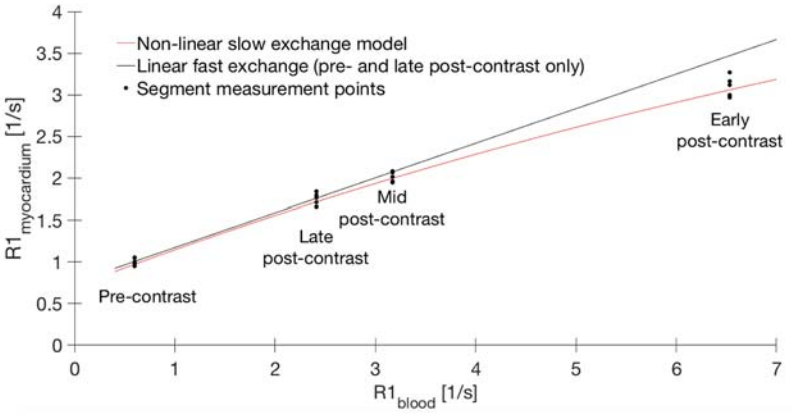

Representative example of non-linear curvefitting from one patient.

Patient data and results.

Patient data and results for the three groups of patients, given as median [inter-quartile range] except for gender. *p*-values calculated using the chi-square test for ratios and the Mann-Whitney U-test for distributions, * denotes statistical significance.

	Normotrophic	Concentric hypertrophy	*p* vs normotrophic	Eccentric hypertrophy	*p* vs normotrophic
Number of patients	19	23		19	
Male sex [%]	74	61	0.38	58	0.31
Age [years]	35 [26–59]	60 [55–66]	0.001 *	67 [54–70]	0.001 *
TVR [-]	76 [70–80]	126 [119–151]	<0.001 *	70 [66–72]	<0.001 *
LVMi [g/m^2]	73 [65–78]	100 [95–119]	<0.001 *	99 [95–114]	0.02 *
Max. R_1 blood [1/s]	5.8 [5.3–7.8]	6.5 [5.7–7.3]	0.47	6.2 [5.7–7.5]	0.45
ECV [%]	27 [25–29]	28 [23–29]	0.96	29 [26–30]	0.04 *
tau [ms]	110 [65–163]	66 [9–119]	0.14	93 [5–116]	0.08

ID#: 373748

Systolic Flow Displacement Correlates with Ascending Aortic Growth in Patients with Isolated Bicuspid Aortic Valve

Nicholas S. Burris, MD[1] Harkamal Singh, BS[2], Jimmy C. Lu, MD[3], Michael D. Hope, M.D.[4], Prachi Agarwal, MD[5]

1. University of Michigan, Ann Arbor, MI

2. University of Michigan

3. University of Michigan, Dexter, MI

4. University of California, San Francisco, CA

5. University of Michigan, MI

Background: Despite the strong association of eccentric blood flow with ascending aortic dilation in cross-sectional studies of bicuspid aortic valve (BAV), little data exists concerning the association of eccentric blood flow with the risk of future aortic growth. Systolic flow displacement is an emerging marker of aortic blood flow eccentricity that is derived from MRI phase-contrast data. Several small studies have shown that systolic flow displacement correlates with ascending aortic growth rate in adult BAV patients with associated congenital heart disease. We hypothesized that MRI-derived systolic flow displacement in the ascending aorta will correlate with growth of the ascending aorta among a population of young patients with isolated BAV.

Methods: We retrospectively identified 25 patients with isolated BAV, baseline cardiac MRI studies that included 2D phase-contrast sequences (2D PC) in tubular ascending aorta, and two or more echocardiograms. Patients with connective tissue disease, interval aortic valve replacement and off-axis/aliased 2D PC data were excluded leaving 17 patients for analysis. Considering that pediatric (<18 y, n=6) and adult (≥18 y, n=11) patients were included, maximal aortic diameters at the tubular segment were transformed into z-scores. Systolic flow displacement was measured using a research version of commercial flow analysis software (Medis, Netherlands).

Results: Among 17 patients [mean age: 20.4 ± 11.0 y (range 9-45), 53% male) the majority had RL fusion pattern (11/17). No patients had history of hypertension or atherosclerosis and the majority had either no/mild aortic stenosis (16/17) or insufficiency (14/17) at baseline. The mean interval between echocardiography studies was 4.9 ± 3.1 years and the mean z-score growth rate was 0.28 ± 11.0 Δz/y (range 0 - 0.89). Flow displacement showed a moderate correlation with aortic stenosis severity at baseline ($r=0.67$, $p<0.01$). There was a moderate correlation between flow displacement and z-score growth rate ($r=0.61$, $p=0.01$), and flow displacement was the only significant predictor of z-score growth after adjusting for age and severity of valve dysfunction by multi-linear regression ($p=0.04$).

Conclusion: Systolic flow displacement correlates with aortic growth rate in a young cohort of patients with isolated BAV and without co-morbid cardiovascular disease, further supporting a flow-mediated mechanism of progressive aortopathy. Future work is needed to validate these findings in larger populations; however, flow displacement can be easily measured from routine 2D PC data and is a promising marker of risk for BAV aortopathy.

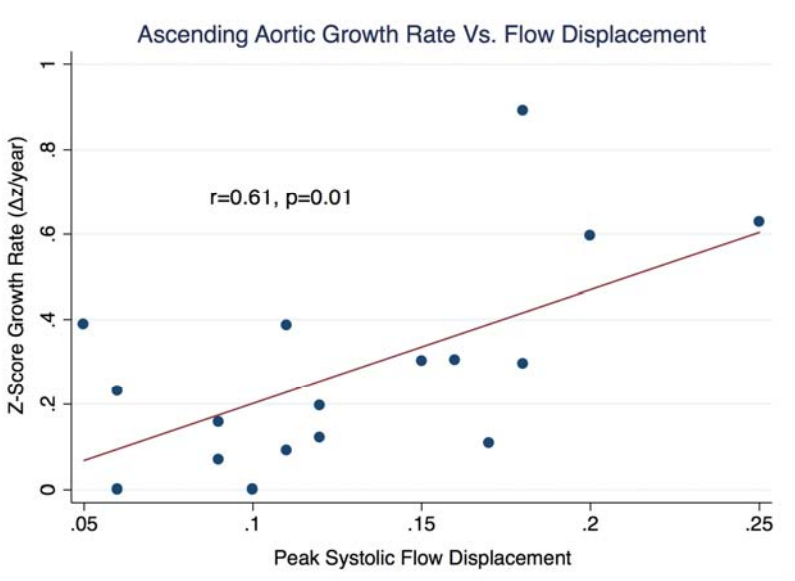
Ascending Aortic Growth Rate Vs. Flow Displacement
r=0.61, p=0.01
Z-Score Growth Rate (Δz/year)
0
.2
.4
.6
.8
1
.05
.1
.15
.2
.25
Peak Systolic Flow Displacement

ID#: 373703

Myocardial triglyceride content and cardiac function in patients with left ventricular hypertrophy: comparison between severe aortic valve stenosis, hypertensive heart disease, and hypertrophic cardiomyopathy

Eiryu Sai, M.D., Ph.D.[1] Kazunori Shimada, M.D.[2], Tatsuro Aikawa, M.D.[2], Takayuki Yokoyama, M.D., Ph.D.[2], Makoto Hiki, M.D., Ph.D.[2], Shohei Ouchi, M.D.[2], Yuko Kawaguchi, M.D.[2], Shinichiro Doi, M.D.[2], Sakiko Miyazaki, M.D., Ph.D., MPH[2], Tetsuro Miyazaki, M.D., Ph.D.[2], Shinichiro Fujimoto, M.D.[2], Shinya Okazaki, M.D.[2], Shigeki Aoki, M.D.[2], Hiroyuki Daida, M.D.[2]

1. Juntendo Tokyo Koto Geriatric Medical Center, Juntendo University Graduate School of Medicine, Tokyo, Japan

2. Juntendo University Graduate School of Medicine, Japan

Background: Pressure overload of heart leads to cardiac hypertrophy and consequent heart failure. Left ventricular (LV) wall stress induced by pressure overload has been reported to cause a switch from fatty acid to glucose in myocardial substrate metabolism, resulting in increased free fatty acid overload in the myocardium. However, the effect of pressure overload on cardiac metabolism in patients with heart diseases, such aortic valve stenosis (AS) and hypertrophic obstructive cardiomyopathy (HOCM), has not yet been fully investigated.

Methods: We performed cardiac magnetic resonance imaging and proton magnetic resonance spectroscopy in 67 patients diagnosed with severe AS (n = 17), hypertensive heart disease (HHD, n = 12), and hypertrophic cardiomyopathy (HCM, n = 38) based on echocardiography, histology, and/or late gadolinium enhancement patterns. We divided patients with HCM into non-obstructive HCM group (n = 26) and HOCM group (n = 12) according to the LV outflow tract gradient. Pressure overload is defined as the presence of AS, HHD, and HOCM. We excluded patients who underwent percutaneous transluminal septal myocardial ablation.

Results: There was a significant difference in the myocardial triglyceride (MTG) content between the AS (2.01% ± 1.63%), HHD (2.48% ± 1.20%), non-obstructive HCM (1.00% ± 0.79%), and HOCM (1.19% ± 0.77%) groups (P_{trend} = 0.003). The levels of MTG content were significantly higher in the AS and HHD groups than in the non-obstructive HCM and the HOCM groups (all $P < 0.05$). There is no significant difference of MTG content between the HOCM and the non-obstructive HCM groups. MTG content was significantly associated with stroke volume ($r = -0.35$, P = 0.004), LV mass ($r = -0.37$, P = 0.003), use of renin–angiotensin inhibitor (β = 0.31, P = 0.01), presence of pressure overload (β = 0.27, P = 0.02), and diagnosis of HCM (β = −0.42, P = 0.0001). In a multivariate analysis, LV mass volume and diagnosis of HCM were independent factors for changes in MTG content.

Conclusion: Although pressure overload due to AS and HHD may increase MTG content, these tendencies were not observed in HOCM. These data suggest that the cardiac triglyceride metabolism in HOCM may be different from that in AS and HHD.

ID#: 373709

Myocardial tissue differentiation in critically ill patients with septic shock - setup and initial results from a proof-of-concept study

Fabian Muehlberg, M.D.[1] Jan Soennichsen, M.D.[2], Edyta Blaszczyk, MD[3], Johannes Kuttner, M.D.[2], Joerg Brederlau, M.D.[2], Jeanette Schulz-Menger, MD[3]

1. Charité University Medicine Berlin & HELIOS Clinic Berlin-Buch, Berlin, Germany

2. HELIOS Clinic Berlin-Buch, Germany

3. Working Group on Cardiovascular Magnetic Resonance, Experimental and Clinical Research Center a joint cooperation between the Charité Medical Faculty and the Max-Delbrueck Center for Molecular Medicine HELIOS Klinikum Berlin Buch, Germany, Berlin, Germany

Background: Patients with severe septic shock have very poor prognosis with mortality rates of up to 60% despite advances in intensive care medicine over the last decades. Sepsis-induced cardiomyopathy plays an important and limiting role in these patients. We wanted to investigate myocardial tissue differentiation in critically ill, sedated and ventilated patients with septic shock using CMR and follow-up echocardiography.

Methods: Patients with septic shock will be recruited in this proof-of-concept study (total n=15). Four patients have completed the study protocol so far. All patients received a CMR scan within 48h after initial catecholamine peak and a transthoracic echocardiography 24 hours prior to CMR. Follow-up echocardiography was done at 48 and 96 hours after CMR scan. Left ventricular ejection fraction (LVEF) was assessed biplanar in both imaging modalities. CMR was performed on 1.5T AvantoFit® (SIEMENS Healthineers®, Erlangen, Germany). An anesthesiologist monitored patients during the entire scan with continuous invasive blood pressure monitoring and realized breathholds during scan through manual ventilation breaks. (Figure 1) CMR protocol included cine-SSFP sequences (LAX/SAX package), midventricular T1 mapping (native T1: 5s(3s)3s and post-contrast: 4s(1s)3s(1s)2s), motion-corrected T2 mapping and late gadolinium enhancement using single-shot a PSIR sequence (7mm slice thickness/0mm gap SAX). All post-processing was done with CVI42® (Circle cardiovascular imaging, Calgary, Canada).

Results: 28 patients with septic shock were screened; four patients could be included so far. Major exclusion criteria were excessive body diameter due to massive fluid administration during septic shock and therapy limitation. All four CMR scans were completed without critical complications. One patient needed to be excluded from analysis due to atrial fibrillation during the scan. All patients showed contracting pattern of typical or inverse Tako-tsubo cardiomyopathy and had impaired left ventricular ejection fraction (figure 2). On 48 and 96 hours follow-up, LVEF improved in all patients (figure 2). Parametric mapping revealed pathologically increased native T1 (1100±38.1ms) and T2 times (63.8±3.4ms) as well as increased ECV (27.2±2.9ms) in all patients (see table 1). No patient had visually detectable LGE lesions.

Conclusion: In this small subset of patients, septic shock leads to tako-tsubo-like cardiomyopathy with severe myocardial edema and inflammation. CMR is safely feasible in critically ill, sedated and ventilated patients using extensive monitoring and experiences staff.

Figure 1. CMR setup for sedated /ventilated patients.
A) Positioning of MR-safe ventilators, monitoring unit and injections pumps
B) During scan an intensive care specialist monitors patient continuously in the scanner room and receives commands for endexspiratory breathhold via headphone.

CMR setup

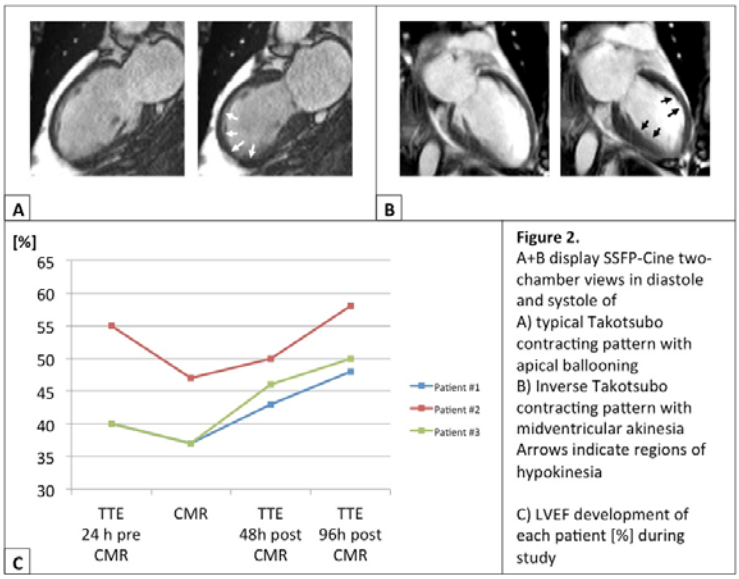

Figure 2.
A+B display SSFP-Cine two-chamber views in diastole and systole of
A) typical Takotsubo contracting pattern with apical ballooning
B) Inverse Takotsubo contracting pattern with midventricular akinesia
Arrows indicate regions of hypokinesia

C) LVEF development of each patient [%] during study

Functional analysis

	#1	#2	#3
Native T1 [ms]	1085 ± 58.4	1124 ± 30.7	1091 ± 25.2
T2 [ms]	64.3 ± 10.8	61.6 ± 5.8	65.4 ± 4.1
Extracellular volume [%]	26.9 ± 3.6	26.3 ± 2.2	28.5 ± 2.8

Table 1. Parametric mapping analysis

Parametric mapping analysis

ID#: 373713

Diagnostic potential of texture analysis applied on cardiac magnetic resonance T1 and T2 mapping in patients with biopsy-proven chronic myocarditis

Philipp Lurz, MD, PHD[1] Bettina Baeßler, M.D.[2], Christian Luecke, MD[3], Karin Klingel, MD[4], Julia Anna. Lurz, MD[5], Karl-Philipp Rommel, MD[6], David Maintz, MD[2], Matthias Gutberlet, MD[7], Holger Thiele, MD[8]

1. University of Leipzig - Heart Centre, Department of Internal Medicine / Cardiology, Sachsen, Germany

2. University Hospital of Cologne, Department of Radiology, Nordrhein-Westfalen, Germany

3. University of Leipzig - Heart Centre, Department of Diagnostic and Interventional Radiology, Niedersachsen, Germany

4. Department of Molecular Pathology, Institute for Pathology and Neuropathology - University Hospital Tuebingen, Baden-Wurttemberg, Germany

5. Heart Center Leipzig, Dept. of Electrophysiology, Leipzig, Sachsen, Germany

6. University Leipzig - Heart Center, Germany

7. University of Leipzig - Heart Center, Sachsen, Germany

8. Heart Center Leipzig - University Hospital, Sachsen, Germany

Background: Texture analysis (TA) comprises a wide range of techniques modeling spatial distributions of pixel grey-levels for recognizing, classifying, and segmenting data based on their underlying texture. Especially in the complex scenario of chronic myocarditis, TA mightimprove the still somehow limited diagnostic performance of conventional imaging and analyses.

Methods: Fourty patients with clinical chronic heart failure (EF<45%; symptom duration > 14 days) and suspicion for underlying chronic myocarditis were prospectively included. Patients underwent biventricular endomyocardial biopsy (EMB), cardiac catheterization and CMR imaging at 1.5T including native T1 and T2-mapping as well as standard Lake Louise criteria (LLC). TA was applied on T1 and T2-maps using a freely available software package by drawing a region of interest encompassing the entire myocardium. Step-wise dimension reduction and texture feature selection was performed for selecting texture features enabling the diagnosis of DCM-like chronic myocarditis, using EMB as the reference standard.

Results: Mean symptom duration was 121±164 days and mean EF was 26±11%. EMB confirmed the presence of myocarditis in 26 patients (EMB+), whereas 14 patients had no signs of inflammation (EMB-). Similar to standard LLC, mean myocardial T1 and T2 demonstrated poor diagnostic performance in receiver operating curve (ROC) analyses (area under the curve [AUC]: 0.52 for LLC, 0.54 for T1 and T2, respectively). The texture features derived from T2 maps, T2 Kurtosis and T2 Run-length Non-uniformity, however, yielded a superior diagnostic performance with an AUC of 0.82 and a sensitivity / specificity of 88 / 77% (Figure).

Conclusion: TA is feasible when being applied on myocardial T1 and T2-maps and delivers interesting novel parameters for the diagnosis of chronic DCM-like myocarditis.

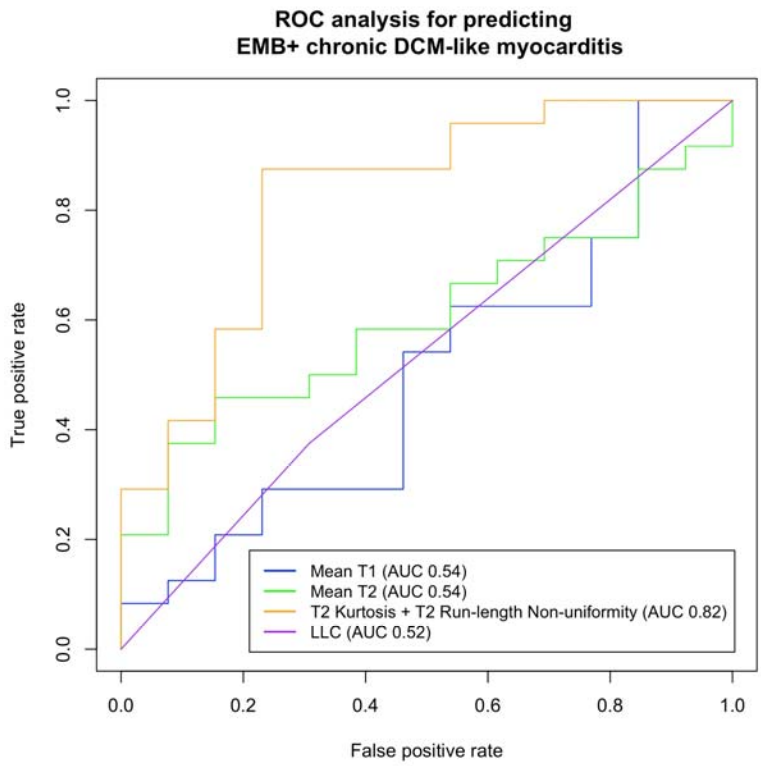

ROC Analysis

ID#: 373716

Impact of global and local left ventricular remodeling in severe ischemic mitral regurgitation

Fausto Pizzino[1]Alessandro Pingitore[2], Giovanni D. Aquaro[3], Anna Terrizzi[4], Stefano Maffei[5], Gianluca Di Bella[6]

1. Fondazione Toscana Gabriele Monasterio and Scuola Superiore Sant'Anna di Pisa, Massa, Toscana, Italy

2. Istituto di Fisiologia Clinica - CNR, Italy

3. Fondazione Toscana Gabriele Monasterio, Pisa (Italy), Toscana, Italy

4. Università di Messina, Messina, Italy, Sicilia, Italy

5. Fondazione Toscana Gabriele Monasterio - Ospedale del Cuore, Toscana, Italy

6. Università degli Studi di Messina, Dipartimento di Medicina Clinica e Sperimentale, Sicilia, Italy

Background: Ischemic mitral regurgitation (IMR) is a common consequence of myocardial infarction (MI) impacting on symptoms and prognosis. IMR is caused by the imbalance between the “closing forces” and the “tethering forces”. These last are a common consequence of left ventricle (LV) dysfunction and remodeling occurring after a MI. Cardiac magnetic resonance (CMR) is the criterion standard method in the evaluation of cardiac function, remodeling and scar burden. Our aim was to provide parameters derived by CMR associated to severe IMR.

Methods: we included patients with old-date MI (>90 days) referring to our Institution from January 2008 to June 2014. Patients with recent myocardial ischemia, prosthetic rings or valves, cardiomyopathies, history of malignancy or chemotherapy treatment were excluded. All patients underwent to CMR with a 1.5 Tesla scanner. Collected parameters were LV ejection fraction (LVEF), LV end-diastolic (LVEDVI) and end-systolic volume indexed (LVESVI), wall motion score indexed (WMSI), global late gadolinium enhancement extension (G-LGE). WM and LGE transmural extension in inferior and inferolateral wall and medial papillary muscle LGE (MPM-LGE) were also evaluated. Echocardiography was performed within 4 days from CMR, a regurgitant orifice area >0.4 cm^2 or a vena contracta >7 mm identified severe IMR.

Results: We enrolled 422 consecutive patients (age 65±13 years), among these, 38 (9%) had severe IMR (severe IMR-group). Severe IMR-group had higher LV volumes and G-LGE and lower LVEF and WMSI. Prevalence of MPM-LGE was also higher in severe IMR-group as well as the presence of dyskinesia in inferolateral wall. LVEF and volumes were interrelated, c-statistics analysis revealed that LVESVI was the best model associated to severe IMR in comparison to LVEDV and LVEF. A best cut-off value of 62 ml/m^2 was identified by ROC curve analysis (AUC 0.755, sensitivity 81.6, specificity 61.2%, P62ml/m^2 (OR 7, 95%-CI 3-16.3, P16% (OR 2.2, 95%-CI 1.1-4.4, P=0.02) were associated with severe IMR. At multivariate analysis only LVEDVI>62ml/m^2 (OR 6.4, CI 2.7-15.4, P<0.001) and dyskinesia in inferolateral wall (OR 4.7, CI 1.2-18.4, P=0.02) were independently associated to severe IMR. Patients with both risk factors had a 28.7-fold and 7.5-fold higher risk to have severe MR in comparison to subject with 0 and 1 risk factor respectively (P=0.001 and P<0.001).

Conclusion: Patients with previous MI presenting with increased LVEDVI and with dyskinetic inferolateral wall have higher risk to have severe IMR.

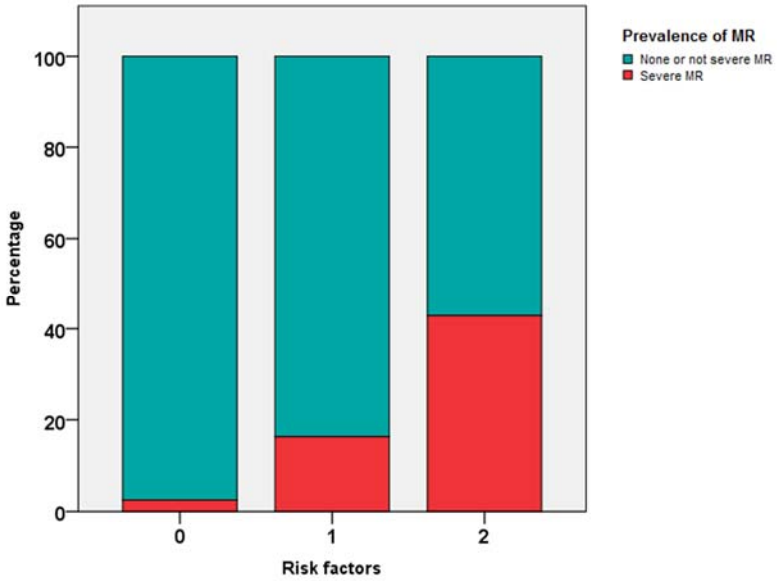

Prevalence of severe mitral regurgitation in patients presenting 0,1 or 2 risk factors (end diastolic volume > 62 ml/m2 and dyskinesia in inferolateral wall)

ID#: 373719

Simulating diffusion tensor cardiovascular magnetic resonance using a histology-based virtual microstructure

Jan N. Rose, MSc[1] Sonia Nielles-Vallespin, PhD, MSc[2], Pedro F. Ferreira, PhD[3], David N. Firmin, PhD[4], Andrew D. Scott, PhD[5], Denis J. Doorly, PhD[6]

1. Imperial College London, London, England, United Kingdom

2. NIH, MD

3. Cardiovascular Magnetic Resonance Unit, Royal Brompton Hospital, Sydney Street, London, SW3 6NP, UK, England, United Kingdom

4. 1. Cardiovascular Magnetic Resonance Unit, Royal Brompton Hospital, Sydney Street, London, SW3 6NP, UK, England, United Kingdom

5. Royal Brompton Hospital, London, England, United Kingdom

6. Imperial College London, London, United Kingdom

Background: Diffusion tensor cardiovascular magnetic resonance (DT-CMR) is unique in that it enables an inference of the underlying tissue microstructure. Recent work[1,2] has demonstrated abnormalities in DT-CMR parameters for hypertrophic and dilated cardiomyopathy patients. However, the exact relationship between measured DT-CMR signal and underlying pathology is not well understood. Numerical simulations are a promising approach to synthesise the DT-CMR data of a known microstructure, thus allowing for the *in silico* investigation of physiological changes such as myocyte hypertrophy or disarray.

Methods: An efficient algorithm was developed to perform Monte Carlo random walk simulations for arbitrary cell geometries. A realistic membrane transit model[3] was implemented that can accommodate variable intra and extra-cellular diffusivities (D_i, D_e).
The virtual microstructure was based on pig histology using 10μm radial-longitudinal sections of a mid-myocardial transmural block[2]. Myocyte cross-sections were manually segmented (figure 1) and repeated to fill a voxel, applying a 10deg/mm transmural rotation. A second substrate was created by artificially thickening the myocytes to account for tissue shrinkage during fixation and match *in vivo* estimates of extra-cellular volume fraction (ECV=21%).
We studied the effect of membrane permeability, varied from P=0 (impermeable) to 100μm/s (erythrocytes[4]), with D_i=1.5mm^2/ms and D_e=3.0mm^2/ms. Another study varied the intra-cellular diffusivity, D_i=0.5–3.0mm^2/ms with fixed D_e=3.0mm^2/ms and realistic[4] permeability of P=25μm/s.
Three pulse sequences were simulated: Stejskal–Tanner pulse gradient spin-echo (PGSE)[5], second-order motion-compensated spin echo (M012-SE)[6], and monopolar stimulated echo acquisition mode (STEAM)[7]. A 2.8x2.8x8.0mm^3 voxel was seeded with 10^4 particles. The b-value was set to 450s/mm^2 in 6 encoding directions.

Results: Figure 2A shows the effect of varying permeability. For all values tested, the DT-CMR results vary very little from the impermeable case. This agrees with others[3,8,9] who studied PGSE-like sequences, but did not investigate the long diffusion times used with STEAM.
Figure 2B shows a strong dependence of the DT-CMR parameters on intra-cellular diffusivity, which is partly a reflection of the small ECV.

Conclusion: We have demonstrated the feasibility of performing Monte Carlo random walk simulations of DT-CMR with realistic imaging voxel size for a range of typical *in vivo* DT-CMR pulse sequences (covering both short and long mixing times).
The observation that DT-CMR results are unaffected by permeability is interesting and prompts further investigation, including high b-value simulations and particle concentration tracking.

References

1. Ferreira JCMR 2014 16(1):87
2. Nielles-Vallespin JACC 2017 69(6):661
3. Fieremans NBM 2010 23(7):711
4. Ogura JJPhysiol 2002 52(4):333

5. Stejskal JCP 1965 42(1):288
6. Welsh TMI 2015 34(9):1843
7. Reese MRM 1995 34(6):786
8. Bates TMI 2017 36(6):1316
9. Hall TMI 2009 28(9):1354

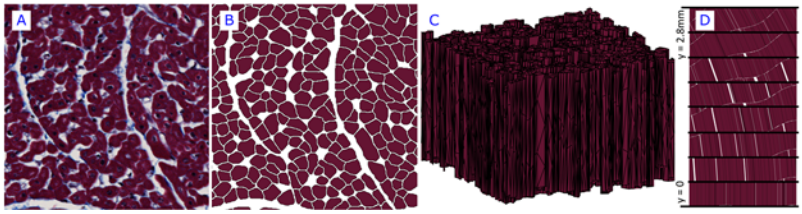

Part of the Masson trichrome-stained pig heart histology (A) and corresponding segmentation (B), which was used to generate 3D myocytes (C). The full segmented tissue block (~400x500μm2) was replicated along all three directions and rotated 10deg/mm every instance in the transmural direction (D) to fill the entire DT-CMR voxel.

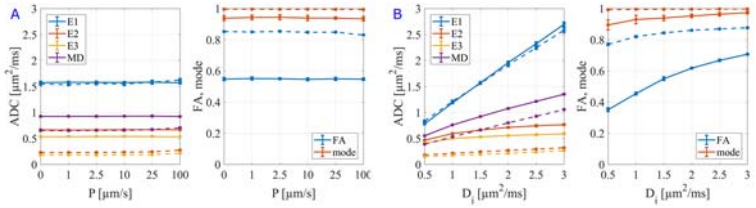

Results for PGSE (-) vs STEAM (--) shown as mean ± 1σ. (A) Increasing the intra-cellular diffusivity Di towards extra-cellular diffusivity (De=3.0μm2/ms) increases the diffusion tensor eigenvalues (E1—E3) and mean apparent diffusivity (MD), but also fractional anisotropy (FA). (B) Varying the permeability P has no obvious effect.

ID#: 373643

Inability of Iron-Loaded Macrophages to Switch from Glycolytic to Oxidative Phenotype Promotes Foam Cell Formation and Fat Deposition in Hemorrhagic MI: Early Findings from a PET/MRI Study with Histological Validation

Ivan Cokic, MD[1] Jane Sykes, BS[2], John Butler, BSc MRT(MR)[3], Michael S Kovacs, PhD[4], Hsin-Jung Yang, PhD[5], Damini Dey, PhD[6], Frank S. Prato, PhD[7], Rohan Dharmakumar, PhD[8]

1. Cedars-Sinai Medical Center, Los Angeles, CA

2. Lawson Health Research Institute, ON, Canada

3. Lawson Health Research Institute, London, ON, Canada

4. Lawson Health Research Institute, Canada

5. Cedars-Sinai Medical Center

6. Cedars Sinai Medical Center, CA

7. Lawson Health Research Institute, University of Western Ontario, ON, Canada

8. Cedars-Sinai Medical, CA

Background: While pro-inflammatory (M1) macrophages are highly dependent on glucose as an energy substrate, anti-inflammatory (M2) macrophages are preferentially fueled by fatty acid (FA) β-oxidation. Failure to switch from M1 to M2 macrophage phenotype can lead to prolonged inflammatory response accompanied by increased glucose transporter 1 (GLUT1)-mediated glucose metabolism, decreased FA beta oxidation, increased intracellular lipid accumulation, and macrophage-to-foam cell transformation. Recent studies in the field of venous leg ulcers have shown that chronic iron-overloading of macrophages can prevent the physiologic switch from glycolytic M1 to oxidative M2 phenotype. A growing body of evidence now shows that iron-laden scar tissue of hemorrhagic myocardial infarction (HMI) is preferentially populated by M1-polarized macrophages. We investigated the metabolic profile of HMI in both acute and chronic settings using ^{18}F-fluorodeoxyglucose (^{18}FDG)-PET/MRI. We hypothesized that the inability of iron-loaded macrophages to switch from glycolytic to oxidative phenotype underlies fatty degeneration of HMI via macrophage lipid accumulation and their transformation into foam cells.

Methods: Canines (n=3) were subjected to 3-hour occlusion of the LAD artery, followed by reperfusion. All dogs underwent in-vivo T2*, LGE and ^{18}FDG-PET/MRI acquired at baseline, week 1, and week 10 post-MI in a hybrid clinical PET/MR scanner. To suppress myocardial uptake of ^{18}FDG, animals were fasted, infused with 20% fat emulsion (I.V.) and treated with 2000 units of heparin. Two hours after the lipid infusion, ^{18}FDG-PET images were acquired simultaneously with T2* and LGE images (in that order). The same imaging protocol was repeated for post-mortem in-situ imaging at week 12 post-MI after which explanted hearts underwent histopathological evaluation. Long-axis LGE and T2*-weighted MR images were independently fused with ^{18}FDG-PET images and target-to-background ratios (TBRs) in MI regions positive and negative for T2* losses were computed and averaged.

Results: HMIs exhibited a glycolytic phenotype throughout the chronic phase of MI as evidenced by increased ^{18}FDG metabolism on weeks 1, 10, and 12 post-MI (Figure 1). TBRs were greater than 2.0 in all regions of MI at week 1, but by weeks 10 and 12 only iron-rich regions showed TBR>2 (Table 1). Retention of the glycolytic phenotype in macrophages undergoing foam cell transformation was confirmed by intense immunoreactivity for GLUT1 (Figure 2).

Conclusion: These findings underscore a key role for iron in macrophage-to-foam cell transformation in HMI. We conclude that ^{18}FDG-PET/CMR has the capacity to evolve as a non-invasive imaging modality for identifying subjects at risk for fatty degeneration of infarcted myocardium.

Figure 1

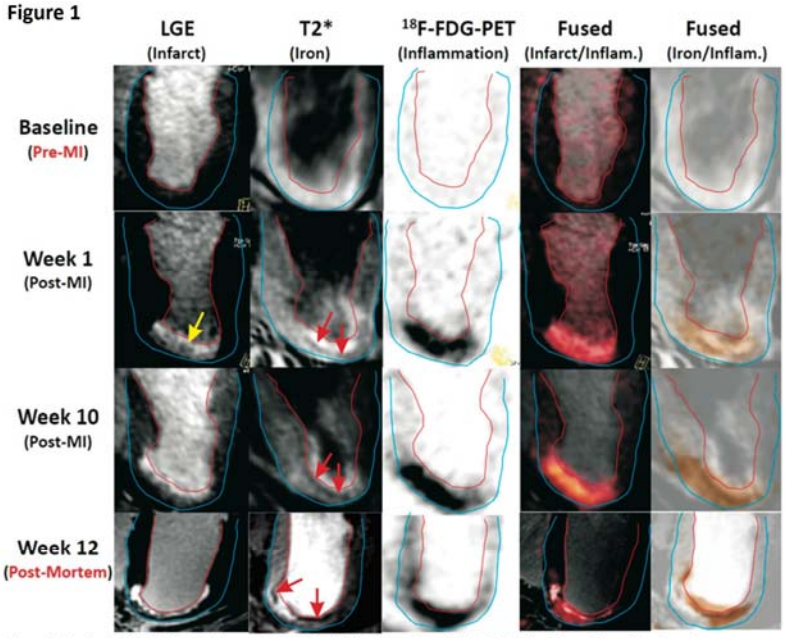

Figure 1. Cardiac PET/MR-Based Evidence of Failed Switching From Glycolytic to Oxidative Macrophage Phenotype in Hemorrhagic MI. Representative serial long-axis PET (^{18}FDG) and MRI (T2* and LGE) images from a dog with hemorrhagic MI. Baseline PET/CMR showed no MI, T2* losses, or 18-fluorodeoxyglucose (^{18}FDG) signals. In contrast, ^{18}FDG-positive signals persisted in the infarcted iron-laden myocardium throughout the chronic phase of MI. Arrows show microvascular obstruction (week 1, yellow arrow) and hemorrhage/iron (red arrows).

Table 1

Time after MI	Mean T2* (MI/Iron+)	Mean T2* (MI/Iron-)	Mean TBR (MI/Iron+)	Mean TBR (MI/Iron-)
Week 1	13 ± 3 ms	40 ± 3 ms	2.7 ± 0.4	2.8 ± 0.4
Week 10	11 ± 2 ms	37 ± 4 ms	2.8 ± 0.5	1.2 ± 0.1
Week 12 (post mortem)	11 ± 2 ms	37 ± 2 ms	2.6 ± 0.5	1.1 ± 0.1

Table 1: Relationship between T2* and ^{18}FDG target-to-background ratios (TBRs) in acute and chronic MIs with history of reperfusion hemorrhage. "Iron+" and "Iron-" denotes with and without iron.

Figure 2

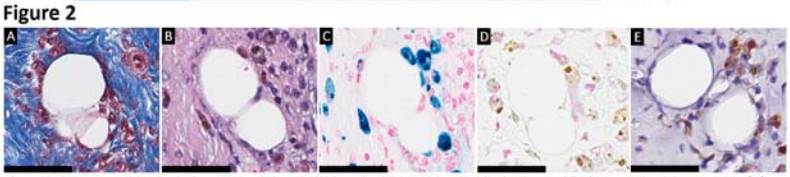

Figure 2. Contiguous histological sections of chronic (12-week-old) MI stained with elastin-modified Masson's trichrome stain **(A)**, H&E stain **(B)**, Prussian Blue stain **(C)**, anti-CD36 (foam cell marker; green staining) antibody **(D),** and anti-GLUT1 (red staining) **(E)** antibody. Scale bar equals 50 μm.

ID#: 373559

Left ventricular function and left atrial size: insights from parametric CMR

Robert D. Adam, MBBS, BSc (Hons)[1] Bashir Alaour, MD[2], Eleanor Jones[2], David Gant[2], Jane Long[3], Charles Peebles, MBBS, FRCR[3], James Shambrook, BM, FRCR[3], Stephen Harden, MBBS, FRCR[3], Ausami Abbas, MBBS, FRCR[3], Andrew Flett, MBBS, MD(Res)[2]

1. University Hospital Southampton, Winchester, United Kingdom

2. University Hospital Southampton, United Kingdom

3. University Hospital Southampton, England, United Kingdom

Background: T1 mapping is a rapidly evolving field and is emerging as a novel quantitative tissue characterisation technique with potential applications in fibrosis, oedema, fat, iron and other patho-physiology. Its significance is not yet fully explored but has the potential to add insights into disease processes and aid in refining diagnosis.

Methods:

401 consecutive consenting patients referred for CMR between December 2014 and August 2017 were scanned on a 1.5T Magnetom Avanto (Siemens Healthcare, Erlangen) using a MOLLI (WIP#448, 5:3:3 acquisition scheme). In each case, separate ROI';s were placed in the mid septal wall and the left ventricular cavity to derive a myocardial and blood pool pre and post contrast T1 time. The HCT was estimated from the pre contrast blood T1 and extracellular volume (ECV) calculated using conventional methods. Patients were grouped according to LVEF; ≤40% (low EF) or ≥41% (preserved EF) and further sub divided into normal or dilated indexed left atrial area (LAAi) according to recognised gender specific reference ranges. LV volumes and mass were also acquired. Comparison was performed using single tailed unpaired t-test.

Results: Baseline characteristics and results are given in **table 1**. The groups were well matched for gender, incidence of diabetes and hypertension. As expected, in both group';s patients with a dilated LA were more likely to have atrial fibrillation. ECV was significantly higher in the low EF group compared to the preserved EF group (mean =0.30±0.09 vs. 0.25±0.04, respectively, psee figure 1).

Conclusion: We have shown that markers of diffuse fibrosis are significantly elevated in patients with low EF vs preserved EF. These markers of fibrosis appear to play a significant role in left atrial dilatation in patients with preserved EF. In patients with low EF, diffuse fibrosis has no significant role in left atrial dilatation, rather that this is determined by other factors including atrial fibrillation and LV adverse remodelling.

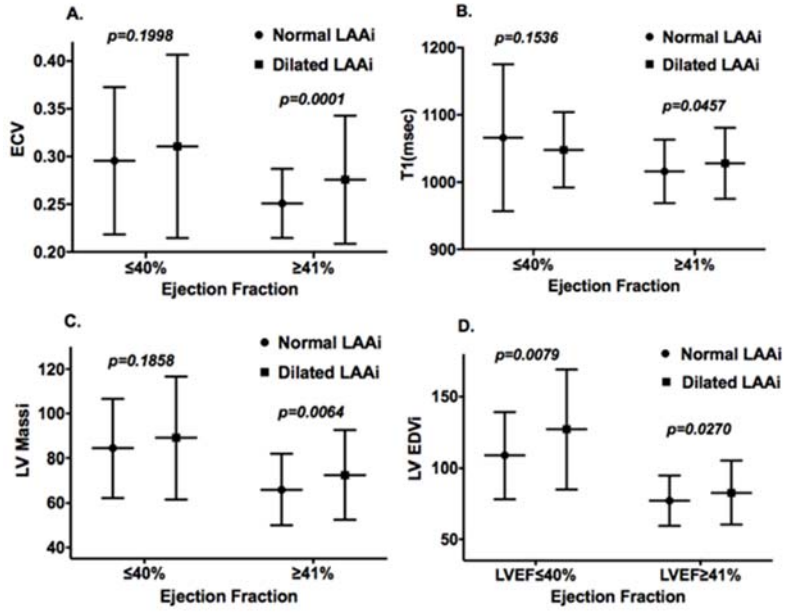

Figure 1. Left atrial area vs. Ejection fraction.

Variable	LVEF≤40%			LVEF≥41%		
	Normal LAAi	Dilated LAA	P Value	Normal LAAi	Dilated LAAi	P Value
Number	48	48	-	258	47	-
Female	14 (27%)	12 (25%)	0.64	85 (33%)	15 (32%)	0.89
Hypertension	22 (46%)	23 (48%)	0.83	106 (41%)	28 (60%)	0.19
Diabetic	16 (33%)	7 (15%)	0.31	44 (17%)	5 (11%)	0.27
AF/Flutter	7 (15%)	29 (60%)	<0.001*	10 (4%)	12 (26%)	<0.001*
Age Mean (SD)	64.46 (12.7)	67.13 (12.4)	0.151	58.66 (16)	67.35 (14)	<0.001*
LVEF Mean (SD)	30.86 (6.2)	28.05 (7.6)	0.025*	58.64 (8.2)	58.04 (11.2)	0.334
LV Massi Mean (SD)	84.43 (22.2)	89.01 (27.5)	0.186	65.96 (15.9)	72.55 (20.1)	0.006*
LV EDVi Mean (SD)	108.7(30.5)	127.1(42.1)	0.008*	77.2 (17.7)	82.86 (22.3)	0.027*
T1(msec) Mean (SD)	1066 (109.3)	1048 (56.0)	0.154	1016 (47.2)	1029 (52.9)	0.046*
ECV Mean (SD)	0.30(0.08)	0.31 (0.10)	0.200	0.25(0.04)	0.28(0.07)	<0.001*

Table 1. *Statistically significant

ID#: 373570

Native T1 Values Can Identify Pediatric Patients with Myocarditis

Rohan Kumthekar, M.D.[1]Imani Mojerie, B.S.[2], Russell Cross, M.D.[3], Laura Olivieri, M.D.[4]

1. Children's National Health System, Washington, DC

2. Children's National Medical Center

3. Children's National Medical Center, Washington

4. Children's National Health System

Background: Late gadolinium enhancement (LGE) on cardiac magnetic resonance (CMR) imaging is a sensitive marker of myocarditis in children, but can be falsely negative in early or diffuse disease where myocardial changes cannot be detected qualitatively. Non-contrast native T1 mapping is a CMR method used to quantify T1 changes indicating myocardial fibrosis in adult inflammatory conditions, but is relatively untested in children with smaller hearts and higher heart rates. We hypothesize native T1 values will detect changes in pediatric patients with myocarditis compared to those with normal hearts.

Methods: With IRB approval, ten pediatric patients with myocarditis (average age 9.7 years) and ten normal pediatric subjects with normal function and chamber size and no LGE (average age 10.4 years) were included in the study. Patients were confirmed to have myocarditis by chest pain, increased troponin or dysfunction, and positive LGE findings. All subjects underwent CMR with LGE imaging and native T1 mapping using Modified Look-Locker (MOLLI) and Saturation Recovery Single Shot Acquisition (SASHA) techniques. Regions of interest (ROI) were drawn in the lateral and septal walls of both four-chamber and short-axis slices to generate average T1 values. Medians and IQRs were calculated and compared using Mann-Whitney U tests. Multiple group comparisons were done using Kruskal-Wallis tests, and then Mann-Whitney U tests with Bonferroni correction.

Results: Pediatric myocarditis patients had significantly higher native T1 values versus controls with both T1 mapping methods. The median native T1 using MOLLI was 1123 (IQR 1030-1213) and 1009 (IQR 987.0-1031) for myocarditis and controls, respectively ($p < 0.0001$). Using SASHA, median native T1 was 1227 (IQR 1187-1341) and 1194 (IQR 1164-1215) for myocarditis and controls, respectively ($p = 0.0057$). There were no significant regional differences in T1 values amongst myocarditis patients despite regional variation of LGE. Median native T1 values using MOLLI were higher amongst the five myocarditis patients with left ventricular ejection fraction (LVEF) 55% (1183 (IQR 1119-1321) vs. 1053 (IQR 994.1-1123), respectively ($p = 0.0004$)).

Conclusion: Native T1 values are significantly different in pediatric patients with myocarditis vs. patients with normal hearts, regardless of technique. T1 values using MOLLI were significantly higher in patients with myocarditis and low EF than in patients with myocarditis and normal EF.

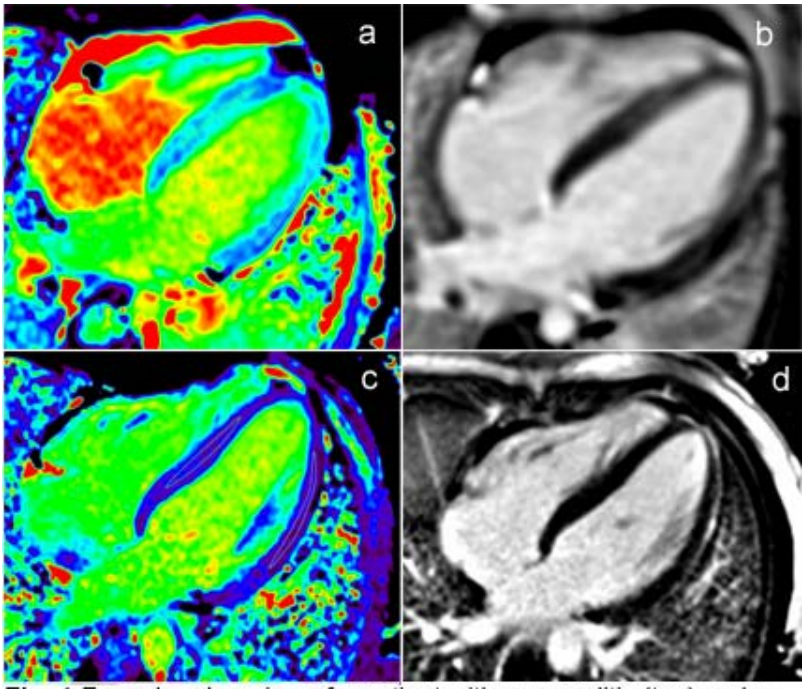

Fig. 1 Four chamber view of a patient with myocarditis (top) and a patient with a normal heart (bottom) depicting a stark difference in T1 maps (a, c) relative to a subtle difference between late gadolinium enhancement images (b, d).

Figure 1

ID#: 373572

Unexpected extracardiac and non-ischaemic cardiac findings in a large cohort of patients undergoing stress perfusion cardiac magnetic resonance.

Chrysanthos Grigoratos, MD[1] Ignazio Alessio Gueli, MD[2], Antonella Meloni, PhD[3], Andrea Barison, MD, PhD[4], Giancarlo Todiere, MD, PhD[5], Alessia Pepe, MD, PhD[3], Giovanni D. Aquaro[5]

1. Institute of Life Sciences, Scuola Superiore Sant'Anna, Pisa, Italy, Italy

2. Cardio-Thoracic Department, Cisanello Hospital, Pisa, Italy

3. Fondazione G. Monasterio CNR Regione Toscana, Pisa, Toscana, Italy

4. Fondazione Toscana Gabriele Monasterio, Pisa (Italy), Pisa, Toscana, Italy

5. Fondazione Toscana Gabriele Monasterio, Pisa (Italy), Toscana, Italy

Background: Baseline cardiac magnetic resonance (CMR) ability to detect unexpected cardiac findings as well as extracardiac findings (EF) has already been demonstrated. Stress-CMR has proven to be a valuable asset in non-invasive ischaemia assessment but its potentiality to uncover unexpected non-ischaemic cardiac findings (NICF) has been scarcely investigated.

Methods: We retrospectively analyzed all stress perfusion CMRs performed in our center from 2007 to 2017. Images were reviewed randomly from five different experienced cardiologists in order to detect EF, as well as previously unknown NICF. EF were divided in accordance with previous studies either as minor (MiEF) or major (MaEF).

Results: A total of 370 stress perfusion CMRs (262 male patients, mean age 61 years ± 13) were analyzed. Stress perfusion agent used was either adenosine (89 exams, 24% of tests) or dipyridamole (281 exams, 76%). A total of 66 EF were observed (17.8%), with the majority of them being considered of minor importance (42 MiEF, 63.6%). MiEF found were: pleural effusion (2), simple renal (23) and small and/or isolated hepatic (7) cysts, vertebral (4) and hepatic (1) hemangiomas, scoliosis (1), gallblader stones (3), and elevated hemidiaphragm (1). The 24 MaEF observed were:pulmonary nodule/mass (5), splenic mass (2), multiple hepatic cysts (7), complex renal cysts (5), dilated aorta (3) or dilated pulmonary artery (1), and aberrant right subclavian artery (1) and left vena cava superior persistent (1). The total number of NICF was 75 (20%). More than half patients (39, 52%) presented areas of non-ischaemic fibrosis. Moreover, 10 patients (3.7%) showed right ventricular (RV) regional wall motion abnormalities with or without evidence of associated RV fatty infiltration, 11 patients findings in keeping with hypertrophic cardiomyopathy, 2 with cardiac amyloidosis, 6 cases of small intraventricular thrombus, 3 cases of bicuspid aorta, and 5 cases of coronary abnormalities (1 coronary bridge, 3 abnormal coronary origin and one coronary malformation).

Conclusion: Stress perfusion CMR allows the diagnosis of an important number of EF (17.8%) and unexpected NICF (20%), with potential therapeutic implications and/or changes in patients'; prognosis.

ID#: 373583

Prevalence of aneurysm of the ascending aorta in hypertensive patients

Jordan T. Long[1] Brandon M. Mikolich, MD[2], J. Ronald Mikolich, MD[3]

1. Sharon Regional Health System, Boardman, OH

2. Sharon Regional Health System, PA

3. Northeast Ohio Medical University (NEOMED), Youngstown, OH

Background: Hypertension (HTN) is a known risk for development of aneurysm of the ascending aorta (AAscAo), which is among the top 10 cardiovascular (CV) disorders resulting in claim payment in malpractice actions in the United States. Of those claims, AAscAo has the highest per claim payment ($417 K). For these reasons, early diagnosis and follow-up of AAscAo is important from both clinical and medico-legal perspectives. This study was designed to evaluate the prevalence of AAscAo in hypertensive patients using CMR.

Methods: An institutional cardiac imaging database was queried for all patients with a diagnosis of HTN. The study cohort was composed of patients with HTN who had a diameter of the ascending aorta > 3.5 cm, measured perpendicular to flow on CMR. The prevalence of AAscAo was then computed for the study cohort.

Results: Of the 3,543 patients in the database, 2,283 with a diagnosis of hypertension were identified. Of the patients with HTN, 999 had AAscAo based on an ascending aorta diameter > 3.5 cm, measured perpendicular to flow on CMR. The prevalence of AAscAo in hypertensive patients using this retrospective approach is 43.76%. The aneurysm size distribution is shown in Table 1.

Conclusion: The prevalence of AAscAo in hypertensive patients occurs at a higher rate than expected. The majority of aneurysms are in the range of 3.51 to 4.10 cm, allowing ample time for follow-up and potential intervention. Given this high prevalence, an imaging modality capable of visualizing the thoracic aorta seems preferable. However, the ACC/AHA guidelines for Hypertension list 2-D echo as a Class II indication for hypertensive patients when heart failure or structural disease is suspected. Unfortunately, 2-D echo has a limited 90-degree field of view of the heart, often limiting visualization of the ascending aorta, potentially resulting in a lower detection rate of AAscAo. However, cardiac MRI is not similarly limited, given its full field view capability, suggesting that CMR may be the preferred imaging modality for hypertensive patients.

AAscAo (cm)	3.51 - 3.80	3.81 - 4.10	4.11 - 4.40	4.41 - 4.70	> 4.70
%	32.93	31.93	19.92	9.51	5.71

ID#: 373461

Prevalence and clinical relevance of incidental extra-cardiac findings in the Hamburg City Health Study - a prospective single-center population study of German middle-aged and old population compared with published pooled data

Maxim Avanesov, MD[1] Jan Schneider, MD[2], Clemens Spink, MD[3], Sebastian Bohnen, MD[4], Ersin Cavus, MD[4], Enver Guner. Tahir, MD[5], Ulf Radunski, MD[6], Kai Müllerleile, MD[7], Stefan Blankenberg, MD[8], Gerhard Adam, MD[9], Gunnar Lund, MD[9]

1. UKE, Hamburg, Germany

2. University Heart Center, Germany

3. Department for Diagnostic and Interventional Radiology and Nuclear Medicine University Medical Center Hamburg-Eppendorf, Hamburg, Germany

4. University Heart Center Hamburg, Hamburg, Germany

5. University Medical Center Hamburg-Eppendorf, Hamburg, Hamburg, Germany

6. University Medical Center Hamburg-Eppendorg, Hamburg, Germany

7. UKE, Germany

8. University Heart Center Hamburg, Germany

9. University Medical Center Hamburg-Eppendorf, Hamburg, Germany

Background: Incidental extra-cardiac findings (IEF) are increasingly found on CMR scans with large heterogeneity of the reported prevalence of 8 to 81%. Moreover, the prevalence varies largely among studies with cardiologists or radiologists as observers, which represents a potential selection bias. We aimed to characterize IEF in a large German single-center cohort study by combined radiological and cardiological consensus evaluation and to compare the results with available pooled data of 7062 patients.

Methods: 1102 individuals between 45-74 years (mean age 66±8 years, 57% male) were prospectively studied by CMR at 3.0 Tesla (MAGNETOM™ Skyra, Siemens Healthcare, Erlangen, Germany). Two observers (cardiologist and radiologist) evaluated the amount, origin and clinical relevance of IEF by consensus on Localizers and T2 HASTE sequences in coronal, axial, and parasagittal orientation. In 548 individuals (50%) an additional volumetric interpolated breath-hold examination (VIBE) sequence was performed in coronal and axial orientation after i.v. application of 0.15 mmol/kg gadoterate meglumine (Dotarem®, Guerbet, Aulnay, France). All IEF were categorized as relevant or irrelevant for additional diagnosis or therapy. Relevant IEF were defined as findings needing additional diagnostic examination or findings of an unclear origin. Irrelevant IEF consisted of benign findings without need for further investigation. Comparison of proportions of our data with pooled data was performed by a chi-square test. Comparison of means of two independent proportions was done by t-test. Statistical significance was defined as $p<0.05$.

Results: 893 individuals (81%) of our study group showed 2338 IEF on CMR compared with 2751 IEF in the pooled data ($p<0.001$). Significantly more individuals in our group had clinically relevant IEF compared with the pooled dataset (15% (n=166) vs. 12% (n=847), $p<0.05$). Irrelevant IEF were found more often in our group (66%, n=727) vs. pooled data (17%, n=1625), $p<0.001$). However, our group was significantly older compared with the pooled data group (66±8 years vs. 57±16 years, $p<0.001$). The majority of individuals with relevant IEF (89%, 147/166) were older than 55 years.

Conclusion: IEF are very common in middle-aged and old population with 81% prevalence, which is at the upper range of the reported prevalence. Both relevant and irrelevant findings were significantly more often observed than previously reported. The majority of our study group with clinically relevant IEF was older than 55 years, indicating a progression of the amount and relevance of IEF with increased age.

Table 1: Prevalence of incidental extra-cardiac findings (IEF) depending on different age groups and sex

	Incidental extra-cardiac findings (IEF)		
Demographics	*Individuals with relevant IEF*	*Individuals with Irrelevant IEF*	*Total number of individuals with IEF*

Age (y)			
45-55 (n=213)	19 (2)	125 (11)	144 (13)
56-65 (n=336)	57 (5)	207 (19)	264 (24)
66-75* (n=510)	82 (7)	368 (33	450 (41)
>75* (n=41)	8 (1)	27 (2)	35 (3)
Total	166 (15)	727 (66)	893 (81)
Sex			
Men (n=627)	87 (8)	430 (39)	517 (58)
Women (n=475)	79 (7)	297 (27)	376 (42)

*Data are numbers of individuals (%). *Individuals were 74 years old at time of inclusion into the study*

ID#: 373330

Relation of low-density lipoprotein cholesterol with microvascular injury and clinical outcome in revascularized ST-elevation myocardial infarction

Martin Reindl[1] Sebastian Reinstadler, MD[1], Hans-Josef Feistritzer, MD[1], Agnes Mayr, MD[2], Gert Klug, MD[1], Bernhard Metzler, MD[1]

1. University Clinic of Internal Medicine III, Cardiology and Angiology, Medical University of Innsbruck, Austria

2. University Clinic of Radiology, Medical University of Innsbruck, Austria

Background: Microvascular injury (MVI) after primary percutaneous coronary intervention (PPCI) for ST-elevation myocardial infarction (STEMI) is a major determinant of adverse clinical outcome. Experimental data indicate an impact of hypercholesterolemia on MVI, however, there is a lack of clinical studies confirming this relation. We aimed to investigate the association of cholesterol concentrations on admission with MVI visualized by cardiac magnetic resonance (CMR) imaging and clinical outcome in STEMI patients treated by PPCI.

Methods: In this prospective observational study, we included 235 consecutive revascularized STEMI patients. Cholesterol (total cholesterol, low-density lipoprotein (LDL) and high-density lipoprotein (HDL) cholesterol) and triglyceride concentrations were determined at presentation. CMR scans were performed 2 [2-4] days after infarction to assess infarct characteristics including MVI. Clinical endpoint was the occurrence of major adverse cardiac events (MACE) comprising all-cause mortality, non-fatal reinfarction and new congestive heart failure.

Results: Patients with MVI (n=129, 55%) showed higher levels of total cholesterol (204[172-226] vs. 185[168-212] mg/dl;p=0.01) and LDL cholesterol (142[113-166] vs. 118[103-149] mg/dl;p=0.001), whereas HDL cholesterol and triglycerides did not differ significantly. In multivariable analysis including all significant clinical and CMR determinants of MVI, LDL concentration emerged as independent predictor of MVI (odds ratio 1.02 (95%CI:1.01-1.02);p=0.002). Furthermore, increased LDL cholesterol (>150mg/dl) significantly predicted the occurrence of MACE (hazard ratio 3.09 (95%CI:1.22-7.87);p=0.01).

Conclusion: In STEMI patients undergoing PPCI, baseline LDL cholesterol concentrations were independently associated with MVI, revealing a clinically relevant link between LDL metabolism and MVI in acute STEMI.

ID#: 373345

Cardiac Magnetic Resonance T2 Mapping in the Surveillance of Acute Allograft Rejection in Pediatric Cardiac Transplant Patients

Neeta J. Sethi, MD[1]Russell R. Cross, MD[2], Ileen F. Cronin, ARNP[3], Elena K. Grant, MD[4], Joshua Kanter, MD[4], Janet Scheel, MD[5], Sairah Khan, MD[2], Adrienne E. Campbell-Washburn, PhD[6], Laura Olivieri, M.D.[7]

1. Children's National Health System, Washington, DC

2. Children's National Medical Center, Washington, DC

3. Children's National Medical Center, DC

4. Children's National Medical Center

5. University of Washington in St Louis

6. National Heart, Lung, and Blood Institute, National Institutes of Health, MD

7. Children's National Health System

Background: Monitoring for acute allograft rejection is fundamental to care after cardiac transplantation. Endomyocardial biopsy (EMB) is the current gold standard test for screening. However, this invasive procedure is limited by potential significant complications and its high false negative rate with blinded sampling. The use of cardiac magnetic resonance (CMR) T2 mapping has been described in adult transplant patients as a predictor of biopsy-proven rejection, but this has not been extensively studied in pediatric patients. Thus, our aim was to evaluate T2 mapping in its ability to detect biopsy-proven allograft rejection in pediatric cardiac transplant patients.

Methods: With IRB approval and informed consent/assent, 9 pediatric transplant patients underwent 12 comprehensive CMR and interventional cardiac catheterization on a 1.5T scanner, co-located with an interventional catheterization suite. All were asymptomatic outpatients presenting for routine surveillance; one patient had a repeat study a month later to reassess rejection. T2 mapping and volumetry were obtained, followed by transfer to the catheterization laboratory for RV EMB. Regions of interest were hand-drawn by a blinded reviewer using the middle-third technique in the left ventricular septum and lateral wall from a short axis and four-chamber slice (Figure 1). Right and left ventricular ejection fractions (RVEF, LVEF), cardiac index (CI), T2 mean and standard deviation, and biopsy results were compared with one-way ANOVA analyses.

Results: Five of the nine patients were male, with average age of 11.4 years. Cardiac allograft age ranged from 0.6- 17 years, average 7.5 years. Average RVEF 54%, LVEF 57%, and CI 3.3L/min/m^2. Acute cellular rejection was present in 4/12 EMBs; 2-stage 1R, 2-stage 2R. Three of those four with rejection were from the same patient. There was a significant trend between increasing T2 value and higher grades of rejection (Figure 1), with a statistically significant difference in the mean T2 values of those with grade 0 vs 2R (53.1ms vs 61.3ms respectively, p value <0.05), consistent with adult transplant literature where > 60ms increases risk of rejection. All patients with T2 measurements > 57ms had biopsy-proven rejection except one patient with an average T2 value of 57.7ms had biventricular systolic dysfunction (RVEF 42%, LVEF 48%) with a grade 0 biopsy, raising the possibility of a false negative biopsy result.

Conclusion: CMR with quantitative T2 mapping may offer a novel, non-invasive method for screening pediatric cardiac transplant patients for acute allograft rejection. More data is needed to understand the relationship between T2 and rejection.

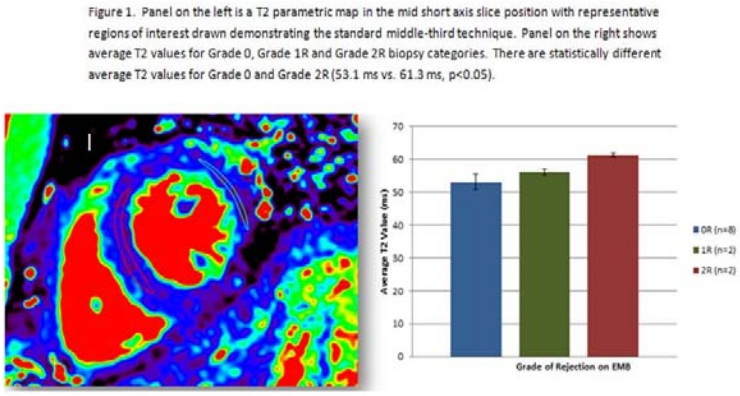

Figure 1. Panel on the left is a T2 parametric map in the mid short axis slice position with representative regions of interest drawn demonstrating the standard middle-third technique. Panel on the right shows average T2 values for Grade 0, Grade 1R and Grade 2R biopsy categories. There are statistically different average T2 values for Grade 0 and Grade 2R (53.1 ms vs. 61.3 ms, $p<0.05$).

ID#: 373395

Impact of atrial fibrillation during ST-elevation myocardial infarction on infarct characteristics and prognosis

Sebastian Reinstadler, MD[1] Thomas Stiermaier, MD[2], Charlotte Eitel, MD[3], Georg Fuernau, MD[3], Mohammed Saad, MD[3], Janine Pöss, MD[3], Suzanne de Waha, MD[3], Steffen Desch, MD[4], Bernhard Metzler, MD[1], Holger Thiele, MD[5], Ingo Eitel, MD[3]

1. University Clinic of Internal Medicine III, Cardiology and Angiology, Medical University of Innsbruck, Austria

2. University Heart Center Lübeck, Lübeck, Schleswig-Holstein, Germany

3. University Heart Center Lübeck, Germany

4. University Leipzig - Heart Center, Germany

5. University Heart Center Luebeck, Sachsen, Germany

Background: AF is frequently observed in patients with ST-elevation myocardial infarction (STEMI) and associated with worse clinical outcome. However, the mechanisms for this increased risk are not fully understood. The purpose of this study was to investigate the relationship of the presence of atrial fibrillation (AF) to cardiac magnetic resonance (CMR) derived myocardial salvage and damage as well as clinical outcomes.

Methods: This multicenter CMR study enrolled 786 STEMI patients. CMR parameters (infarct size, myocardial salvage index, microvascular obstruction and myocardial function) were assessed 3 (interquartile range [IQR] 2-4) days post-STEMI and compared between patients with or without AF during hospitalization. Major adverse cardiac events (MACE) were assessed as a composite of all-cause death, re-infarction and new congestive heart failure at 12 months.

Results: AF was documented in 48 (6.1%) patients. There was no significant difference in infarct size (18[IQR9-29] vs. 17[IQR 9-25]% of left ventricular mass (%LV),p=0.34), myocardial salvage index (51[IQR 34-69] vs. 51[IQR 33-69],p=0.83), or microvascular obstruction (0.6[IQR 0-2.0] vs. 0.0[IQR 0-1.8]%LV,p=0.34) between groups. Patients with AF had significantly lower left ventricular (47[IQR 34-54] vs. 51[IQR 44-58]%,p=0.003) and left atrial (42[IQR 17-57] vs. 53[IQR 45-59]%,p<0.001) ejection fraction. AF was associated with MACE, even when adjusting for clinical risk factors (odds ratio=2.48[95% confidence interval:1.22-5.03],p=0.012) or CMR prognosis markers (odds ratio=3.77[95% confidence interval:1.83-7.79],p=0.001).

Conclusion: This CMR study found no major differences in myocardial salvage, infarct size or microvascular damage in STEMI patients with or without AF. AF was, however, associated with cardiac dysfunction and independently related to MACE.

ID#: 373398

Accelerated Cardiac Diffusion Tensor Imaging Using Joint Low-Rank and Sparsity Constraints

Sen Ma, MSChristopher Nguyen, PhD, Anthony G. Christodoulou, PhD, Debiao Li, PhD

Cedars-Sinai Medical Center, Los Angeles, CA

Background: Cardiac diffusion tensor imaging (CDTI) shows promise for revealing the myofiber organization non-invasively [1]. However, CDTI is challenging due to long scan times (>10min) resulting from the need for multiple diffusion directions and signal averages, limiting its clinical feasibility [2]. This work accelerates CDTI using an imaging framework jointly combining a phase-corrected low-rank (LR) model and compressed sensing (CS), reducing scan time while preserving the image features used to assess heart failure.

Methods: Diffusion-weighted images (DWI) exhibit LR structure due to the correlated diffusion behaviors along different directions, especially when a phase correction is performed to compensate for the eddy current-induced phase inconsistency [3]. The LR constraint can be explicitly expressed using a partially separable model [4]. Additionally, DWIs possess transform sparsity which can be integrated with the LR constraint to achieve higher acceleration [5]. Data were collected on a 3T Siemens Biograph mMR scanner from n=6 explanted human heart failure cadavers using a DW spin echo sequence. 12 diffusion directions were acquired at b-value of 1000s/mm^2. Retrospective undersampling was performed where the non-diffusion k-space were fully sampled and the diffusion k-space were sampled with Gaussian density. The phase map was estimated from a simple sparse reconstruction (CS Only) [6]. The proposed method (LR/CS) was compared to methods using no phase correction (No PC) [7], low-resolution phase correction (Low-Res PC) [3], and CS Only, all of which have been reported to accelerate DTI.

Results: Fig. 1 shows the reconstructed DWIs, helix angle (HA) maps, and helix angle transmuralities (HAT) at 2x acceleration using the proposed method, No PC and Low-Res PC. The proposed method yielded least normalized error (4.5%) and restores the transmural change of HA with the best accuracy (HAT: -1.02°/%TD). Fig. 2 shows the reconstructed HA maps and statistical analysis on HAT using the proposed method and CS Only. The proposed method improved the reconstruction, showed no significant difference in HAT up to 6x acceleration, and yielded significantly lower bias at 6x and 8x. Fig. 3 shows the same analysis for mean diffusivity (MD). The proposed method preserved more accurate MD features, showed higher tolerance for acceleration (16x) and significantly lower bias above 12x.

Conclusion: We have presented an acceleration method for ex vivo cardiac diffusion tensor imaging by incorporating a phase-corrected low-rank (LR) model and compressed sensing (CS). The proposed method improved measurement quality compared to previously published LR and/or CS methods, showing great promise for reducing scan time (currently 6x). Further validation needs to be conducted in vivo.

References:

[1] Tseng *JMRI* 2003
[2] Mekkaoui *NMR Biomed* 2017
[3] Gao *MRM* 2014
[4] Liang *IEEE ISBI* 2007
[5] Zhao *IEEE TMI* 2012
[6] Wu *MRM* 2014
[7] Huang *Techno Health Care* 2016

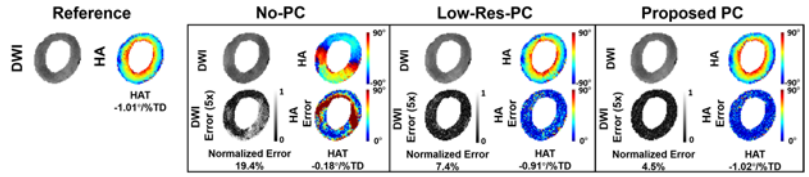

Fig. 1 Comparison between no phase correction (No-PC), low-resolution phase correction (Low-Res-PC), and the proposed method at 2x acceleration. DWI, HA and HAT are evaluated.

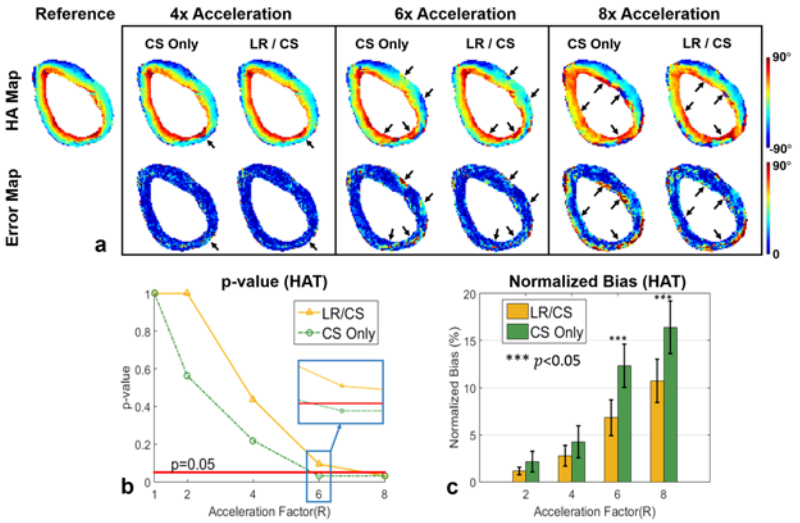

Fig. 2 (a) Reference and reconstructed HA maps using CS Only and LR/CS at 4x, 6x, and 8x acceleration. Black arrows point at the regions where differentiable between the two methods. (b) p-value between reference and reconstructed HAT using CS Only and LR/CS at 2x, 4x, 6x, and 8x acceleration. The significance level (p=0.05) is labeled in red. (c) Normalized bias between reference and reconstructed HAT using CS Only and LR/CS.

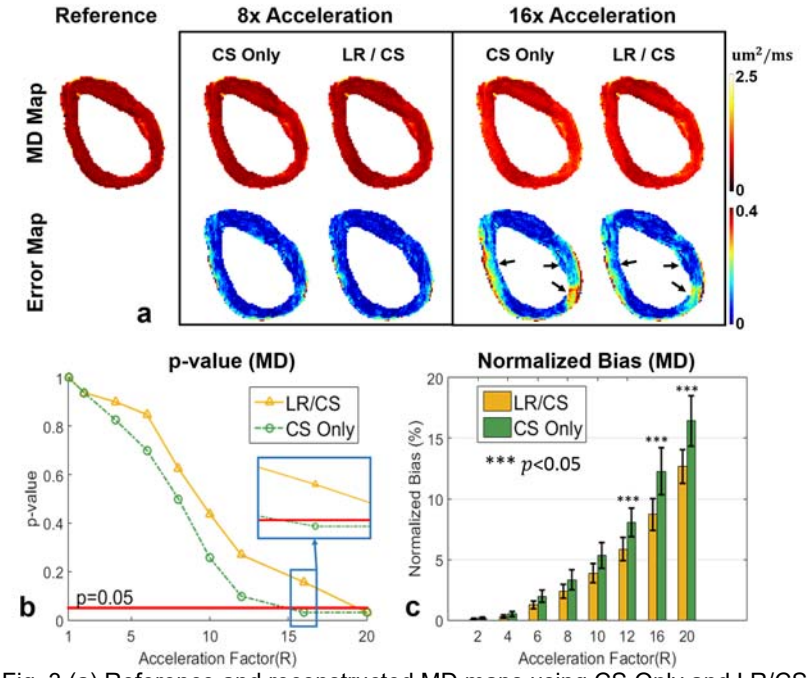

Fig. 3 (a) Reference and reconstructed MD maps using CS Only and LR/CS at 8x and 16x acceleration. Black arrows point at the regions where differentiable between the two methods. (b) p-value between reference and reconstructed MD values using CS Only and LR/CS at 2x, 4x, 6x, 8x, 10x, 12x, 16x and 20x acceleration. The significance level (p=0.05) is labeled in red. (c) Normalized bias between reference and reconstructed MD values using CS Only and LR/CS.

ID#: 373417

Artefacts in 1.5 Tesla and 3 Tesla cardiac magnetic resonance imaging in patients with leadless cardiac pacemakers

Daniel Kiblboeck[1]Christian Reiter[2], Juergen Kammler[2], Pierre Schmit[2], Thomas Lambert[2], Joerg Kellermair[2], Hermann Blessberger[2], Stefan Schwarz[2], Thomas Lukas[2], Franz Fellner[2], Alexander Kypta[2], Clemens Steinwender[2]

1. Kepler University Hospital Linz, Austria, Linz, Oberosterreich, Austria

2. Kepler University Hospital Linz, Austria, Austria

Background: There is only limited data on patients with leadless cardiac pacemakers (LCP) undergoing magnetic resonance imaging (MRI). The aim of this prospective, single-center study was to evaluate artefacts on cardiac magnetic resonance (CMR) images in patients with LCPs.

Methods: Fifteen patients with Micra^{TM} LCPs, which were implanted at least six weeks prior to CMR scan, were enrolled and randomized in a 1:1 ratio to either 1.5 Tesla or 3 Tesla CMR imaging. Artefacts were categorized into grade 1 (excellent image quality), grade 2 (good), grade 3 (poor) and grade 4 (non-diagnostic) for each myocardial segment. One patient was excluded because of an incomplete CMR investigation due to claustrophobia.

Results: LCPs caused an arc-shaped artefact (1.14 ± 0.23cm^2) at the apex of the right ventricle (RV). Out of 224 analyzed myocardial segments of the left ventricle (LV) 158 (70.5%) were affected by grade 1, 27 (12.1%) by grade 2, 17 (7.6%) by grade 3 and 22 (9.8%) by grade 4 artefacts. The artefact burden ratio per patient of affected myocardial segments by grade 3 and 4 artefacts was significantly higher in the 3 Tesla group compared to the 1.5 Tesla group (3.7 ± 1.6 vs 1.9 ± 1.4 myocardial segments, p = 0.03). A high artefact burden was particularly observed in the mid anteroseptal, inferoseptal and apical septal myocardial segments of the LV and in the mid and apical segments of the RV. Quantification of LV function and assessment of valves was feasible in all patients. We did not observe any clinical or device-related adverse events.

Conclusion: CMR imaging in patients with LCPs is safe and feasible with excellent to good image quality in the majority of myocardial segments of the LV. The artefact burden is comparable small allowing an accurate evaluation of LV function, cardiac structures and valves. Artefacts on CMR images may be reduced by the use of 1.5 Tesla MRI scanners.

ID#: 373297

Focal myocardial fibrosis in high endurance exercise ahtletes

Blanca Domenech, MD[1]María Sanz-de la Garza, MD PhD[2], Diego Navarrete[2], Rosario J. Perea Palazón, MD PhD[3], Felip Burgos, RN, PhD[2], Adelina Doltra, MD, PhD[4], Karina Durán, MD[2], Susanna Prat, MD, PhD[2], Marta Sitges, MD, PhD[5]

1. Hospital Josep Trueta, Spain

2. Hospital Clinic, Spain

3. Hospital Clínic. Universitat de Barcelona, Barcelona, Catalonia, Spain

4. Hospital Clínic de Barcelona, Barcelona, Spain

5. Hospital Clínic de Barcelona, Spain

Background: Myocardial fibrosis is frequently seen in the late stages of various cardiac diseases and it is well known to be a predictive factor for adverse cardiac outcome, such as sudden cardiac death. Nevertheless, as focal fibrosis in the right ventricle (RV) insertion point has also been identified in general population, its meaning and its clinical impact is currently uncertain. Besides, recent studies suggest that focal fibrosis is even more common in endurance athletes. Thus, our aim was to assess the presence of focal fibrosis and its relationship with cardiac remodelling/adaptation, among a group of highly–trained resistance athletes.

Methods: Highly trained endurance athletes (>12 hours training/week during the last 5 years) underwent a resting cardiac magnetic resonance (CMR) to assess biventricular dimensions and function, pulmonary artery distensibility and the estimated pulmonary vascular resistance. The presence of myocardial fibrosis was detected by late gadolinium enhancement (LGE).

Results: Eighty-five athletes were consecutively recruited: 36 years (31-40), 38 women (44,7%). Among them, 25 (29 %) showed LGE confined to the interventricular septum, commonly where the RV attaches the septum (Figure 1). Other specific LGE patterns, such as subendocardial, myocarditic or hypertrophic, were not identified in our population. All athletes showed larger right atrial area, RV end-diastolic volume, and RV stroke volumes (RV-EDV (ml/m2): 105±16 and RV-SV: 57±9.5). Normal systolic function was found. There were no differences in RV volume, pulmonary artery distensibility or estimated pulmonary resistances among athletes with positive vs negative LGE.

Conclusion: The presence of focal fibrosis in our group of highly-trained endurance athletes was higher than the reported in the literature among the general population with exclusive focal LGE confined to the RV insertion point. This was observed together with harmonic right ventricular dilatation and increased right atrial cavity size. These findings suggest that this pattern of LGE might be another feature of the athlete';s heart with a potentially benign prognostic significance.

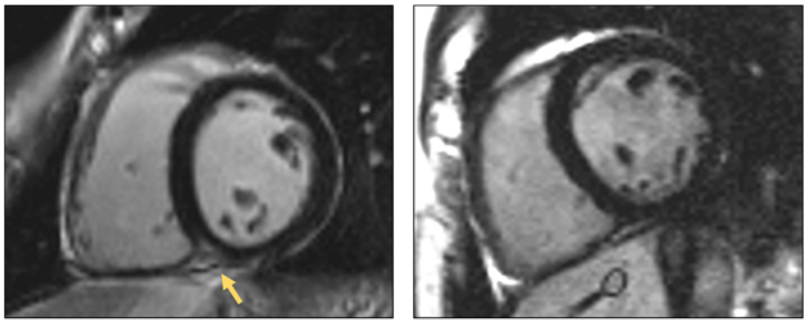

Figure 1. Late gadolinium enhancement (LGE) in two athletes. Left image shows a focal LGE confined where the RV joints the septum (indicated with an arrow), compared to right image that shows an athlete with a normal study.

Figure 1. Late gadolinium enhancement (LGE) in two athletes. Left image shows a focal LGE confined where the RV joints the septum (indicated with an arrow), compared to right image that shows an athlete with a normal study.

ID#: 373245

Spin-Spin Dephasing on Cine-CMR for Assessment of Blood Pool Stasis - A Novel Physiologic Marker for Post-Myocardial Infarction Left Ventricular Thrombus

Neil Mehta, MD[1] Saadat Khan, MD[2], Jiwon Kim, MD[3], Meridith P. Pollie, BS[1], Javid Alakbarli, MD[1], Alexi Geevarghese, BA[4], Martin A. Janich, PhD[5], Maggie Fung, MA[6], John Heitner, MD[7], Oliver Wieben, PhD[8], Jonathan W. Weinsaft, MD[9]

1. Weill Cornell Medical College

2. Weill Cornell Medical College, Brooklyn, NY

3. Weill Cornell Medical College, New York, NY

4. Weill Cornell Medical College, NY

5. GE Healthcare, Germany

6. GE Global Research

7. New York Methodist Hospital, NY

8. University of Wisconsin-Madison, Madison, WI

9. Weill Cornell Medical Center, NY

Background: Left ventricular thrombus (LVT) is a serious consequence of myocardial infarction (MI); non-contrast imaging (via cine-CMR or echocardiography) is limited for detection and prediction of LVT. Spin-spin dephasing on steady-state free precession (SSFP) cine-CMR increases with blood stasis but has yet to be tested as a marker of left ventricular (LV) dysfunction or actual LVT.

Methods: The population comprised consecutive ST-segment elevation MI patients prospectively imaged via a standardized CMR (1.5T) protocol. Delayed-enhancement (DE)-inversion recovery CMR was the reference for LVT, which was defined via established criteria based on avascular (non-enhancing) tissue properties. SSFP cine-CMR (typical TR 3.5msec, TE 1.1msec, flip angle 60^{o}) was read blinded for LVT, and quantified for LV function, morphology, and dephasing: Regional LV function (stroke volume, ejection fraction, peak ejection rate) was quantified via automated segmentation of short axis images using standardized landmarks in the LV base (LV-BA), mid (LV-MID), and apex (LV-APX). Spin-spin dephasing was quantified via signal intensity in matched long axis locations using ROIs ($0.5cm^2$) in the LV blood pool (excluding trabeculae or tissue prominences suspicious for LVT). Cine (SSFP) and DE-CMR were analyzed independently.

Results: 215 patients underwent CMR 4.0±1.1 weeks post-MI (LAD 56%, LCX 9%, RCA 35%); 8% (n=18) had LVT (17/18 LAD) on DE-CMR, among whom cine-CMR detected LVT in 72% (via blinded analysis). Patients with LVT on DE-CMR had increased SSFP dephasing in the LV-APX ($p<0.001$) and LV-MID ($p=0.041$; Figure [mean±SE]), corresponding to decreased LV stroke volume (LV-APX: 2.5±0.9 vs 3.5±1.3; $p=0.002$| LV-MID: 4.9±1.5 vs 5.7±1.2; $p=0.006$), EF (LV-APX: 36.4±15.6 vs 61.4±20.7, $p<0.001$| LV-MID: 43.4±14.3 vs 57.4±13.6, $p<0.001$) and peak ejection rate (LV-APX: 10.4±6.3 vs 16.4±8.2, $p=0.003$| LV-MID: 23.9±10.1 vs. 27.0±7.9, $p=0.12$) in each respective region. LV-BA dephasing differences between patients with and without LVT were of lesser magnitude ($p=0.054$; Figure), paralleling non-significant differences in basal stroke volume (6.9±1.0 vs 6.3±1.4, $p=0.09$), EF (50.6±6.4 vs 51.5±10.2, $p=0.71$), and peak ejection rate (31.4±11.5 vs 27.9±15.7, $p=0.36$). In multivariate analysis, LVT was independently associated with both LV aneurysm (HR 37.4; $p<0.001$) and LV-APX dephasing (HR 1.1 per 10 units SI; $p=0.009$). Among patients with LVT, those in the largest tertile of LVT size had greater SSFP dephasing in LV-BA, LV-MID, and LV-APX (all $p\leq0.01$) than patients with smaller LVT.

Conclusion: Spin-spin dephasing on SSFP cine-CMR is a novel marker of blood pool stasis that parallels contractile dysfunction. SSFP dephasing magnitude is associated with presence and size of LVT.

Figure

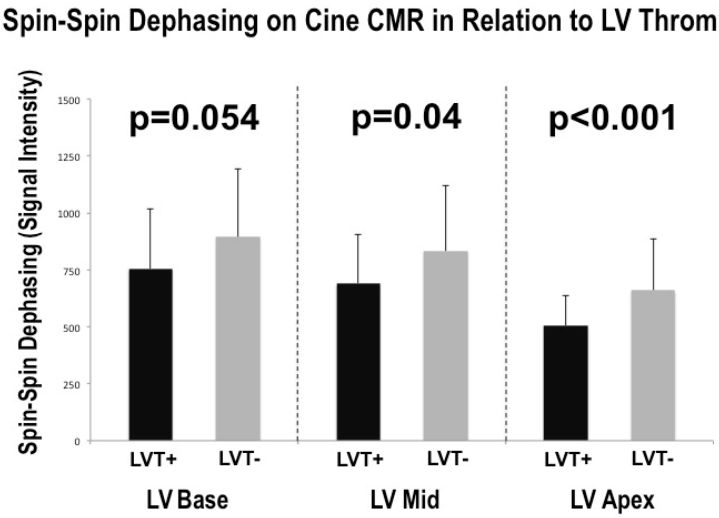

Cine-CMR (SSFP) derived blood pool signal intensity among patients with (black) and without (grey) LV thrombus on DE-CMR (data reported as mean±standard error). Note decreased SSFP blood pool signal intensity in the mid (p=0.04) and apical LV (p<0.001) among patients with LV thrombus as defined independently by DE-CMR.

ID#: 373208

Left Ventricle Segmentation via Deep Learning Networks: Superfast and Accurate Analysis of Cine MRI

Qian Tao, PhD[3] Wenjun Yan[1], Xinyi Li[2], Zeju Li[2], Yuanyuan Wang, Ph.D.[2], Rob J. van der Geest, PhD[3]

1. Fudan University, Shanghai, Shanghai, China (People's Republic)

2. Fudan University, Shanghai, China (People's Republic)

3. Department of Radiology, Leiden University Medical Center, The Netherlands, Leiden, Zuid-Holland, Netherlands

Background: Cine MR is commonly used for assessment of left ventricular (LV) function. Given the high number of images in one acquisition, it typically requires substantial manual input to analyze the Cine data, which is tedious and subjective. We aim to develop and validate a Deep Learning based approach to realize fast and accurate analysis of Cine MR for clinical use.

Methods: A total of 142 post-infarction subjects were included, who underwent an MR examination (Philips 1.5T Intera) including multi-slice short-axis Cine. The endocardial and epicardial contours of the LV were manually or semi-automatically traced using the MASS software (research version 2017, Leiden University Medical Center) by experienced clinical observers. The manual tracing focused on the end-diastolic and end-systolic phase, and in a majority of cases, intermediate phases were automatically detected and manually adjusted, if needed. We divided the cohort into a training set of 100 subjects (22,965 annotated images) and a testing set of 42 subjects (9,106 annotated images). The state-of-art U-shape convolutional neural network (CNN), called UNET architecture, was adopted to learn the segmentation of the LV myocardium from the training set. The resulting UNET was applied to the independent testing set to automatically identify the blood pool and myocardium region. The evaluation was performed on those slices where the manual annotation was present. Using the manual contour as gold standard, the average perpendicular distance (APD) on both endocardial and epicardial side were evaluated. In addition, clinical parameters including LV ejection fraction (LVEF) and LV mass were further evaluated on the 42 testing subjects.

Results: For all 9,106 images, compared to manual contour tracing, the APD of the contour obtained from UNET was 0.72 ± 0.61 pixel (IQR 0.51 - 0.82) for the endocardial boundary and 0.70 ± 0.28 pixel (IQR 0.51 - 0.83) for the epicardial boundary. For the 42 testing subjects, the estimated cardiac parameters from UNET was not significantly different from those derived from manual annotation, with LVEF 30.0 ± 9.9% vs 28.8 ± 10.4 (p=0.3), LV mass 126.6 ± 34.2 ml vs. 128.4 ± 37.2 ml (p=0.4). The execution time per image was 0.01 second on average using graphics processing unit (GPU) acceleration, and 0.36 second without GPU.

Conclusion: We demonstrated that the UNET architecture can achieve superfast segmentation of short-axis Cine MR, with good agreement to manual contour tracing, without any user-interaction. Future work is warranted to further increase the robustness of the method, as well as its compatibility to MR data from different vendors and obtained with varying scan protocols.

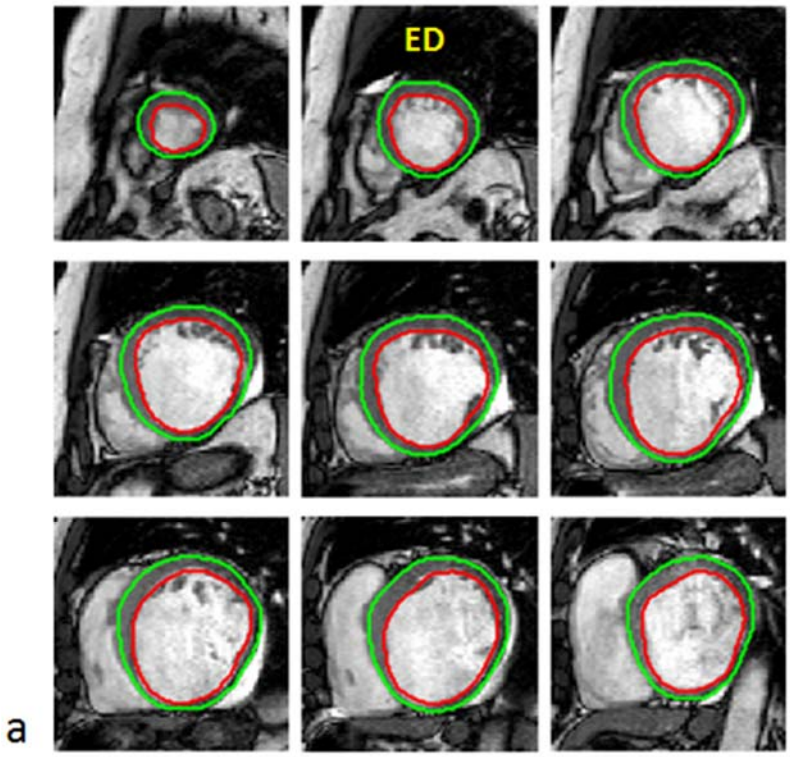

a

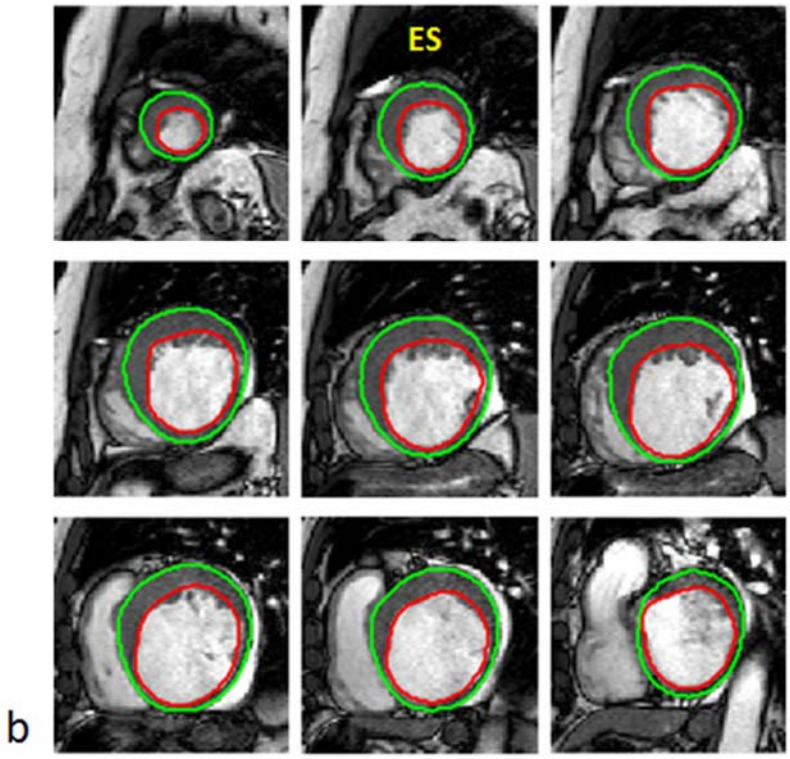

b

LV segmentation of a short-axis stack in a testing subject. a. The LV contour in the end-diastolic phase. b. The LV contour from the end-systolic phase. The estimated LVEF is 19.8%, compared to 19.2% from manual contour tracing.

Comparison of clinical parameters measured from cine MR, by manual and automatic segmentation. The p value of paired T-test is also reported.

	EDV (ml)	ESV (ml)	LVEF (%)	LV mass (ml)
Manual	238.0 ± 97.4	177.2 ± 102.7	30.0 ± 9.9	126.6 ± 34.2
Deep-learning	234.6 ± 92.7 (p=0.1)	174.8 ± 97.7 (p=0.3)	28.8 ± 10.4 (p=0.1)	128.4 ± 37.2 (p=0.4)

ID#: 378465

Females have higher myocardial blood flow, myocardial blood volume and myocardial extracellular volume compared to males - both at rest and during adenosine stress cardiovascular magnetic resonance

Jannike Nickander, MD[1]Raquel Themudo, MD, PhD[2], Andreas Sigfridsson, PhD[3], Hui Xue, PhD[4], Peter Kellman, PhD[5], Martin Ugander, MD, PhD[6]

1. Karolinska Institutet, Stockholm, Stockholms Lan, Sweden

2. Karolinska Institutet, Stockholms Lan, Sweden

3. Karolinska Institute, Stockholm, Stockholms Lan, Sweden

4. National Heart, Lung, and Blood Institute, Bethesda, MD

5. National Heart, Lung, and Blood Institute, National Institutes of Health, Bethesda, MD

6. Karolinska Institutet, and Karolinska University Hospital, Stockholm, Sweden, Stockholms Lan, Sweden

Background: Women have a worse outcome after a clinically suspected acute coronary syndrome compared to men. Multiple factors underlie this difference in outcome. However, knowledge on sex differences in myocardial blood flow and blood volume in healthy individuals is scarce. Therefore, the aim of this study was to investigate sex differences in myocardial perfusion and myocardial blood volume in healthy individuals at rest and during adenosine stress cardiovascular magnetic resonance imaging (CMR).

Methods: Healthy volunteers (n=41, mean±SD age 26±5 years, 51% female) underwent CMR at 1.5T (Siemens Aera). Quantitative myocardial blood flow (MBF) [ml/min/g] and myocardial blood volume (MBV) [%] maps were computed by Gadgetron inline perfusion mapping software using first pass perfusion imaging during adenosine stress (140 microg/kg/min infusion) and at rest following an intravenous contrast bolus (0.05 mmol/kg, gadobutrol). A native midventricular short axis T1 map (MOLLI) was acquired before and during adenosine stress. The same midventricular short axis T1 map (MOLLI) was also acquired after administration of contrast (0.2 mmol/kg, gadobutrol), at rest and during adenosine stress. This rendered both rest and stress extracellular volume fraction (ECV) maps.

Results: Compared to males, females had higher rest and stress values for MBF (rest 0.94±0.21 vs 0.79±0.16 ml/min/g, p=0.02; stress 3.80±0.55 vs 3.02±0.69 ml/min/g, p<0.001), Figure 1, MBV (rest 9.2±0.6 vs 8.6±0.8%, p<0.01; stress 12.5±1.0 vs 11.5±0.9%, p<0.01), Figure 2, and ECV (rest 29±2 vs 25±3%, p<0.01; stress 33±2 vs 29±3%, p<0.01), Figure 3. MBV and ECV were correlated (R^2 = 0.35, p<0.001), and there was no difference in the rest-to-stress increase in MBV compared to the rest-to-stress incrase in ECV (3.7±2.6 vs 3.1±1.2 %-points, p=0.28).

Conclusion: MBF, MBV and ECV are higher in female healthy volunteers compared to males, both at rest and during adenosine stress. ECV measures at rest and stress provide independent validation of the accuracy of stress-induced changes in MBV. Increased MBV contributes to the higher ECV found in females compared to males. Taken together, these findings provide mechanistic insight into sex differences in myocardial physiology.

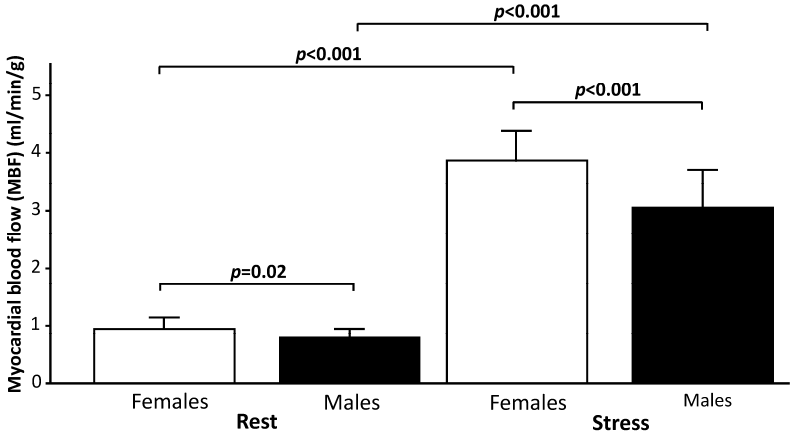

Differences in myocardial blood flow between males and females at rest and during adenosine stress

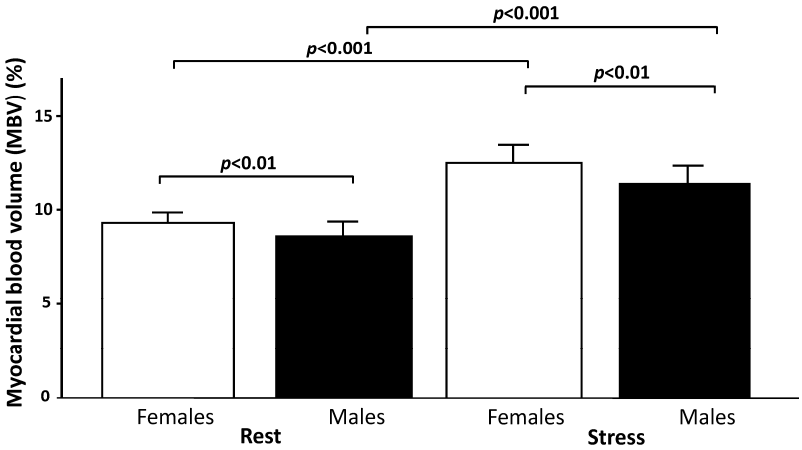

Differences in myocardial blood volume between males and females at rest and during adenosine stress

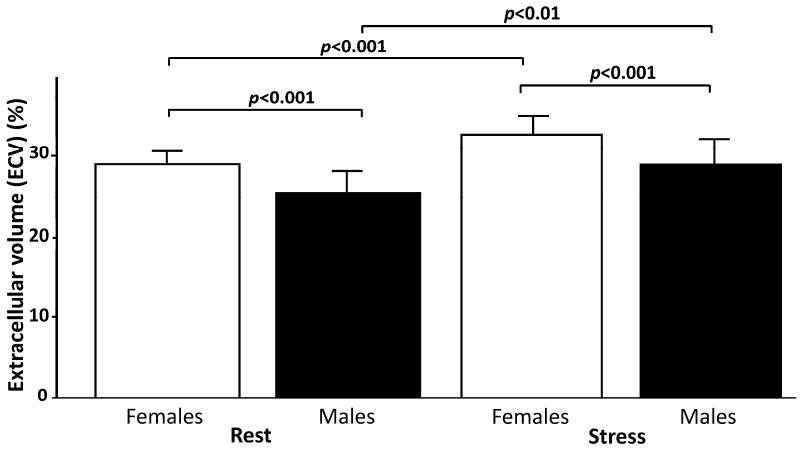

Differences in extracellular volume between males and females at rest and during adenosine stress

ID#: 378769

Utility of three-dimensional whole heart imaging (3D-WHI) in the detection of acute myocarditis in paediatric patients

Davide Curione, MD[1]Paolo Ciliberti, MD[2], Teresa Pia Santangelo, MD[2], Enrica Rossi, MD[3], Aurelio Secinaro, MD[2]

1. Bambino Gesù Children's Hospital and Research Institute, Rome, Italy, Roma, Lazio, Italy

2. Bambino Gesù Children's Hospital and Research Institute, Rome. Italy, Lazio, Italy

3. Bambino Gesù Children's Hospital and Research Institute, Rome, Italy, Italy

Background: The aim of our study was to assess the utility of three-dimensional whole heart imaging (3D-WHI), a T2/T1 weighted-sequence routinely used in paediatric and congenital heart disease (CHD) patients as it provides high signal-to-noise ratio and isotropic voxel resolution images with respiratory navigator gating (free-breathing) and ECG triggering, in the diagnosis of acute myocarditis.

Methods: 27 paediatric patients (age range 5-20 years, mean 11 years) undergoing cardiovascular magnetic resonance (CMR) for suspected acute myocarditis were retrospectively analysed. Black-blood STIR, early and delayed enhancement sequences were obtained in all patients and the presence of at least 2 of the 3 “Lake Louise criteria” was used to confirm or rule out the diagnosis. 3D-WHI, acquired after contrast administration, was subsequently evaluated for concordant myocardial tissue abnormalities, comparing the findings with the “Lake Louise Criteria” in order to assess 3D-WHI diagnostic accuracy.

Results: In our study 3DWHI showed a sensitivity of 93%, a specificity of 75%, a positive predictive value (PPV) of 82% and a negative predictive value (NPV) of 90%. The overall diagnostic accuracy was 85%. In detail, in three cases where black-blood STIR, early and/or delayed enhancement images were ambiguous or artefacted, myocardial tissue abnormalities on 3D-WHI helped to suggest the diagnosis of acute myocarditis and to define the extact extent of the disease.

Conclusion: 3D-WHI might play a role in the diagnosis of acute myocarditis in paediatric patients, particularly when the “Lake Louise criteria” are uncertain. This might be especially true when artefacts related to reduced patient compliance are present, given 3D-WHI is a sequence with high spatial resolution and signal-to-noise ratio that requires only minimal patient cooperation.

ID#: 378811

Long-term prognosis of acute myocarditis with chest pain: incidence and characteristics of recurrences

Esther Perez David, MD, PhD[1] Elena Montalvo, MD[2], Rosa Colina, MD[3], Raquel Prieto-Arevalo, MD, PhD[3], Ana Gonzalez-Mansilla, MD, PhD[3], Raquel Yotti, MD, PhD[3], Teresa Mombiela, MD, PhD[3], Adolfo Villa, MD, PhD[4], Javier Bermejo Thomas, MD, PhD[3], Francisco Fernandez-Aviles, MD, PhD[3]

1. Hospital Gregorio Maranon, Majadahonda, Madrid, Spain

2. Hospital del Sureste, Spain

3. Hospital Gregorio Maranon, Madrid, Spain

4. Hospital Gregorio Maranon,, Madrid, Spain

Background: The purpose of our study was to evaluate long-term prognosis of patients admitted to our institution with chest pain, normal coronary angiogram and myocarditis as final diagnosis, and to analyse whether clinical and cardiovascular magnetic resonance (CMR) parameters obtained in the acute setting could be useful to predict recurrences.

Methods: Consecutive patients (p) admitted to our institution between 2004 and 2015 for troponin-positive chest pain and normal coronary arteries or non-flow-limiting CAD in coronary angiography, with final diagnosis of myocarditis based on CMR (Lake Louise criteria) were analysed. All CRM studies were performed with Philips Intera and Achieva 1.5T scanner. Clinical data including age, sex, characteristics of chest pain, examination findings, troponin levels, ECG recordings, transthoracic echocardiography, and coronary angiogram were reviewed. Prospective follow-up of clinical events (death or new episode of myocarditis) was performed, by means of review of medical records or telephonic interview.

Results: 93 p were included. Mean age was 37± 13 years and 80 (86%) were male. Median follow-up was 47 months (range: 10-152 months). No fatal cardiovascular events were recorded. A p died 50 months after acute myocarditis due to lung cancer. 12 p (12.9%) had myocarditis recurrence during follow-up (recurrence incidence: 11,2 cases/100 patient-year). 3 p were readmitted < 1 month after initial discharge following reduction of treatment. Acute myocarditis recurred late after onset (>1 year after initial episode) in the rest of the cases. All cases had chest pain, without heart failure. No significant differences in clinical variables parameters were observed between patients with and without myocarditis recurrence. No differences existed regarding CMR parameters, including LVEF, location or extension of late enhancement. A description of both groups can be seen in table 1.

Conclusion: Long-term prognosis of acute myocarditis with chest pain is good. However, Incidence of recurrences is not negligible (13%) and may occur late after onset of the initial episode. In our series, clinical and CMR parameters from acute phase were not useful to predict recurrences.

Basal characteristics of patients with and without recurrence of myocarditis.

	RECURRENCE (N=12)	**NO RECURRENCE (N=81)**	p
Age	32±10	37±13	0.2
Male sex	12 (100%)	66(68%)	0.2
Infectious disease	52 (66%)	7 (58%)	0.3
LVEDV	166+/-29	180+/-25	0.2
LVESV	71+/-19	80+/-17	0.1
LVEF	0,57 +/-0.06	0,51 +/-0.17	0.1

ID#: 378686

The length of posterior mitral valve leaflet distinguish hypertrophic cardiomyopathy from Fabry disease

Diego Perez de Arenaza, MD[1], Ezequiel Espinosa, MD[1]Santiago del Castillo, MD[2], Laura Dragonetti, MD[3], Mariano Falconi, MD[4], Juan Benger[1], Marcelo Andres. Pietrani, MD[5], Cesar Belziti, MD[1]

1. Hospital Italiano de Buenos Aires, Argentina

2. Hospital Italiano de Buenos Aires, Turdera, Buenos Aires, Argentina

3. Hospital Aleman de Buenos Aires, Argentina

4. Hospital Italiano de Buenos Aires, Ciudad Autonoma de Buenos Aires, Argentina

5. Hospital Italiano de Buenos Aires, CABA, Buenos Aires, Argentina

Background: In hypertrophic cardiomyopathy (HCM) mitral valve leaflets are elongated. Fabry disease (FD) is a storage disease mimicking HCM but with specific therapy so distinguishing it is important. Hypothesis: The aim of this study was to assess if the length of mitral valve leaflets is useful to distinguish sarcomeric HCM from FD, using cardiovascular magnetic resonance (CMR).

Methods: Methods: We included 14 patients with molecular diagnosis of FD and 14 patients matched by gender with sarcomeric HCM and negative Fabry All patients had a maximal left ventricular (LV) wall thickness ≥15mm. The length of anterior and posterior mitral leaflets were assessed by CMR (figure 1).

Results: HCM and FD patients had a similar age and gender (through matching), but also LV ejection fraction, mass and wall thickness. Patients with HCM had smaller end systolic volumes, larger left atrium volumes, longer posterior mitral leaflet (14.7mm±2.5 vs. 10.2±1.4, p<0.001) (e.g. figure 2) and have greater rate of rest LV outflow tract obstruction (57.1 vs. 7.1%, p=0.005) compared with patients with FD. In a logistic regression analysis, posterior mitral leaflets length was the only variable retained as an independent predictor of diagnosis of HCM (OR 4.10 95% CI 1.20 to 14.0, p=0.024). The area of the receiving operating curve (ROC) relating PML length with HCM diagnosis was 0.93 (95% CI: 0.82–1.00), and the highest likelihood ratio corresponded to a posterior mitral valve length of 12.5mm, with sensitivity of 85.7% and specificity of 92.8% (figure 3).

Conclusion: The length of the mitral valve leaflets may help to distinguish HCM from FD.

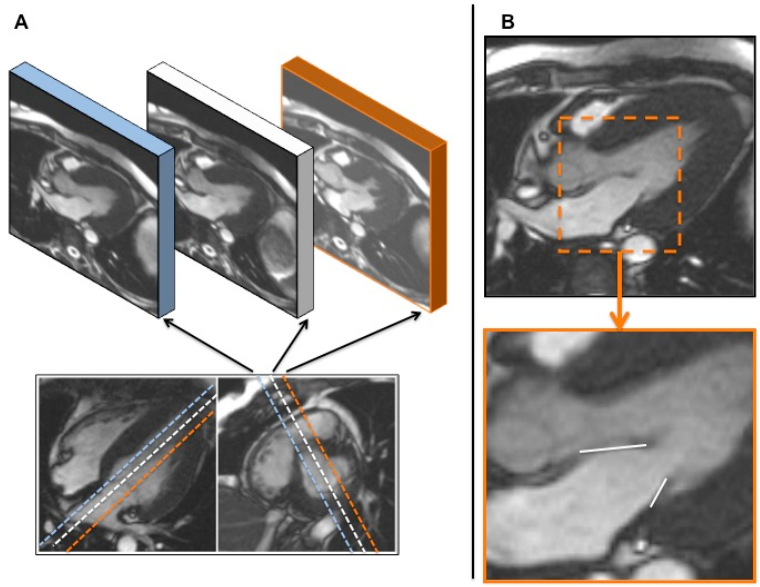

Figure 1, Three cine images on 3-chamber view were obtained with a thickness of 8mm and a gap 20%. B. The 3-chamber view which most clearly displayed the mitral valve length was selected for leaflet analysis.

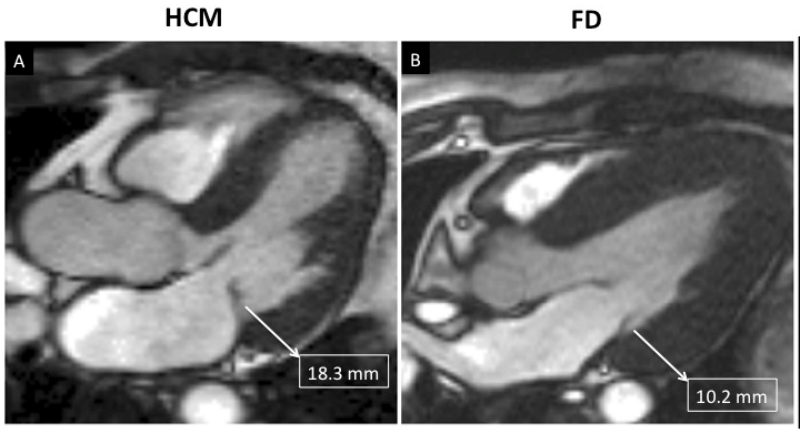

Figure 2. Measurement of posterior mitral leaflets in three chamber long axis cine. A. Male patient with hypertrophic cardiomyopaty (HCM) with asymmetrical septal left ventricular hypertrophy, increased left ventricular mass (214g, 113g/m2) and elongated posterior mitral leaflet of 18.3mm. B. Male patient with Anderson-Fabry disease (FD) with symmetrical left ventricular hypertrophy, increased left ventricular mass (296g, 161g/m2) and relatively short posterior mitral leaflet of 10.2mm.

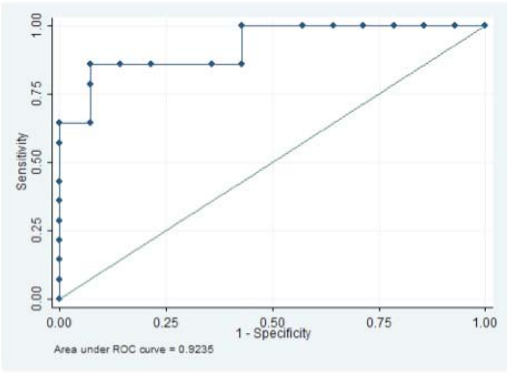

Figure 3. Area of the receiving operator curve (ROC) relating length of posterior mitral leaflet with diagnosis of HCM

ID#: 378699

Importance of LV filling pressure parameters on atrial remodeling: a pilot study

Dana C. Peters, PhD[7]Ricardo Gonzales[1], Chenxi Hu, PhD[2], Felicia Seemann, MS[3], Karl Grunseich, M.D.[2], Michael Quail, MD[4], Lauren A. Baldassarre, MD[2], Albert J. Sinusas, MD[5], Judith L. Meadows, MD[6], Hamid R. Mojibian, MD[6]

1. Universidad de Ingenieria y Tecnologia, Lima, Peru

2. Yale University, CT

3. Skane University Hospital, Department of Clinical Physiology, Lund University, and Department of Biomedical Engineering, Lund University, Sweden

4. King's College London, United Kingdom

5. Yale University, New Haven, CT

6. Yale School of Medicine, CT

7. Yale University

Background: Left atrial (LA) remodeling—which is associated with development of atrial fibrillation (AF), and recurrent AF after therapy-- can be characterized by changes in volume, atrial ejection fractions (EF), strain and increased atrial fibrosis. Many factors may influence LA remodeling. We sought to investigate the role of left ventricular (LV) filling pressures, as estimated using a cardiac magnetic resonance (CMR) derived measure of transthoracic echocardiographic (TTE) parameters e';, E and A on LA remodeling (1,2).

Methods: Forty two patients without AF were imaged on a Siemens 1.5T for diverse indications in an IRB approved study. LA fibrosis was quantified by 3D late gadolinium enhancement (LGE) as % fibrosis of the atrial myocardium. Phasic LV volumes were measured on short-axis cine imaging to generate LV volume vs. time curves. The derivative yielded CMR-derived E and A (Figure 1A-B). Long axis cine were used to measure LA volume using the biplane method at begin and end atrial systole, and pre-atrial kick phases. Additionally, they were used to measure CMR-derived e';, as recently validated against TTE (3,4). All volumes and mass were indexed to BSA.

Results: E/A agreed strongly with recent (<3 months, N=13) TTE measures of E/A (Table 1, Figure 1C-D). e'; septal strongly correlated with passive LA EF and age (Figure 2), as did E/A, but neither were correlated with LV EF (Figure 2B), LV EDVi or LV mass index (Table 1). Lower e'; septal correlated with increased minimum LA volume. e'; septal showed a significant decrease with extent of atrial fibrosis in tertiles (Figure 2D).

Conclusion:

We previously demonstrated that CMR-derived e'; is well correlated with its TTE counterpart (3,4). Here we show an E/A correlation with TTE which is reasonable, but may be limited by insufficient temporal resolution of CMR cine. E/A and e'; are metrics of LV diastolic dysfunction and increased LV filling pressure, not commonly evaluated by CMR. In our study, they were strongly associated with parameters of LA remodeling—including fibrosis--but not with LV remodeling. While it is known from TTE that e'; is highly correlated with LA strain, the very excellent correlation between LA EF and e'; is not well recognized.
References: 1) Westenberg et al., Current cardiovascular imaging reports 2011. 2) Kawaji K et al. Circ Cardiovascular Imaging 2009. 3) Gonzales R et al. SCMR 2018 (submitted). 4) Seemann F et al., BMC Med Imaging 2017.

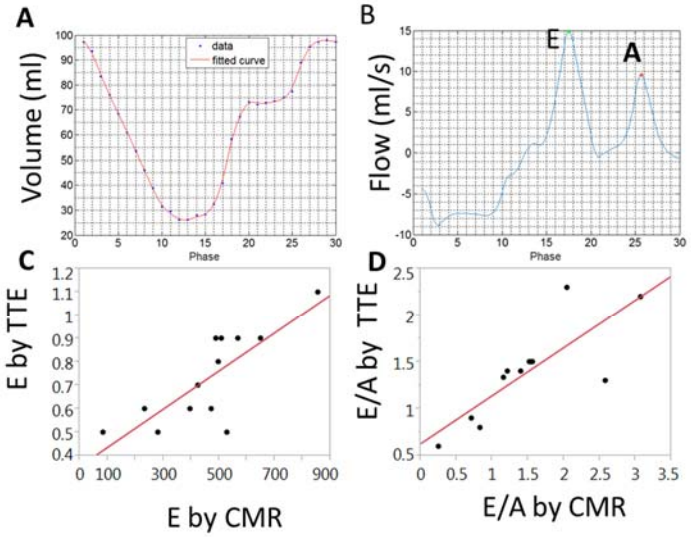

Figure 1: A) Exemplary LV volume vs. time curve obtained from the volumetric cine data in one patient. B) The derivative yields the flow, showing early (E) and late filling (A). C) Comparison of recent TTE measurement of E with E by CMR shows a strong correlation (R^2=0.62, p=0.001). D) E/A by TTE correlates well with E/A by CMR (R^2=0.53, p=0.005).

Figure 1

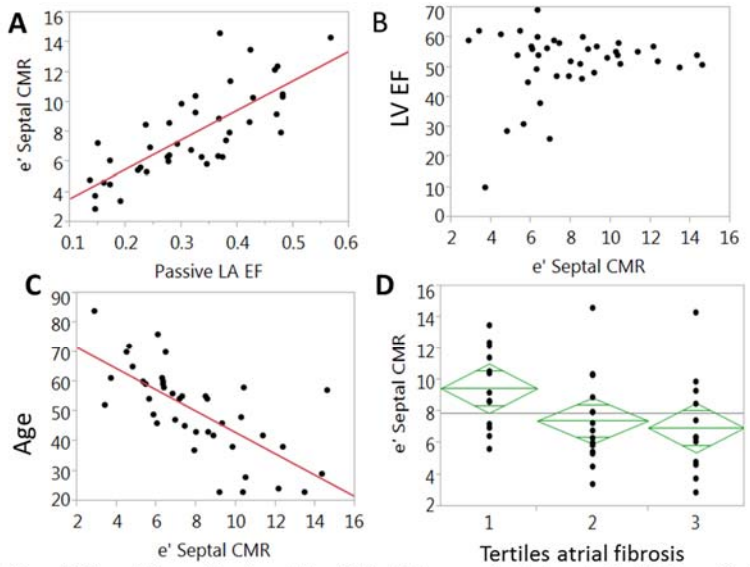

Figure 2: Correlations with e' septal by CMR. A) In our cohort, e' septal by CMR was highly correlated with passive LA EF (R^2=0.59, p<0.001). B) LVEF did not correlate with e' septal, possibly because of the presence of patients with low e' and preserved EF. C) Age correlated very strongly (R^2=0.49) to e' septal. D) e' was lower in patients with greater atrial fibrosis.

Figure 2

vs. CMR septal e'			vs. CMR E/A		
	R^2	p		R^2	p
TTE E/A	--	--		0.53	0.005
LA Parameters					
LA min vol (ml/m^2)	0.14	0.015		0.008	NS
LA max vol(ml/m^2)	0.003	NS		0.02	0.34
Passive LA EF (%)	0.59	<0.001		0.34	<0.001
Active LA EF (%)	0.08	0.08		0.007	NS
Overall LA EF (%)	0.46	<0.001		0.17	0.007
Tertiles LGE (%)	--	0.03		--	0.20
LV Parameters					
LV EF (%)	0.03	0.29		0.0	NS
LV EDVI (ml/m^2)	0.03	0.25		0.07	0.10
LV mass index (kg/m^2)	0.0	NS		0.0	NS
CMR septal e' (cm/s)	--	--		0.46	<0.001
Age (years)	0.49	<0.001		0.51	<0.001

Table 1

ID#: 378719

Visualization of 4D MRI vascular flow patterns in pediatric pulmonary arterial hypertension

Anar K. Shah, DO[1] Michal Schäfer, MSc[2], Lorna Browne, MD[3], Dunbar Ivy, MD[4], Vitaly Kheyfets, PhD[5], Uyen Truong, MD[3]

1. Children's Hospital Colorado, Denver, CO

2. University of Colorado Denver, Franktown, CO

3. Children's Hospital Colorado, CO

4. Children's Hospital Colorado

5. University of Colorado Denver

Background: Pulmonary arterial hypertension (PAH) is a multifactorial disease with the etiology and survival in the pediatric PAH population being distinctly different compared to the adult population. PAH pathology consists of progressively rising pulmonary vascular resistance, elevated mean pulmonary arterial pressure, and stiffening of the arterial walls. These vascular parameters are usually measured by invasive right heart catheterization – the gold standard for establishing disease severity. 4D MRI allows for noninvasive evaluation of vascular velocity in a spatiotemporal manner. Flow patterns in pediatric PAH are complex and not well defined, but may give insight into disease pathophysiology. The aim of this study was to demonstrate the potential application of 4D MRI flow patterns in the pulmonary vasculature of pediatric PAH patients as a marker of the disease.

Methods: Four patients with PAH (14.5 ± 2.5 years, PVR 7.9 ± 2.4 Wood units/m^2, mean PA pressure 42.3 ± 16.7 mmHg) and four healthy control patients (12.8 ± 3.5 years) underwent whole heart 4D MRI assessment on a 3T Philips MRI system (Ingenia, Philips Medical Systems) using a retrospective vector cardiogram controlled cardiac-gated gradient echo sequence with free breathing, velocity encoding of 120 cm/s in all three directions, spatial resolution of 2.0 x 2.0 x 2.5 mm, TR 42 msec, and 14 heart phases reconstructed over one cardiac cycle. Velocity data was processed in ParaView (Kitware, Clifton, NY) for visualization with streamlines seeded along the right ventricular outflow tract and proximal branch pulmonary arteries.

Results: Streamline visualization in the four pediatric PAH patients revealed flow patterns in the main and right pulmonary arteries that greatly differed from the normotensive control patients. Example velocity streamlines generated are shown in Figure 1 for a single control patient and PAH patient, and were representative of the findings in all patients in each group. In the PAH patients, a vortex of blood flow was seen in the main pulmonary artery with the rotation direction antegrade anteriorly and retrograde posteriorly. Additionally, there was helical flow into the right pulmonary artery. Neither finding was observed in the control patients. These findings are consistent with altered 4D flow patterns seen in adult pulmonary hypertensive patients.

Conclusion: 4D MRI with streamline visualization is feasible in the pediatric population. Flow patterns differ significantly from healthy control patients. Vortex formation in the main pulmonary artery with helical flow into the right pulmonary artery is present in pediatric patients. Clinically, patients with PAH are known to have dilation of their pulmonary vasculature with abnormal wall stiffness. The altered flow pattern may reflect an inefficient pulmonary circulation that furthers disease progression. Further quantitative evaluation is underway, and comparison of flow patterns to vascular markers by catheterization is in progress.

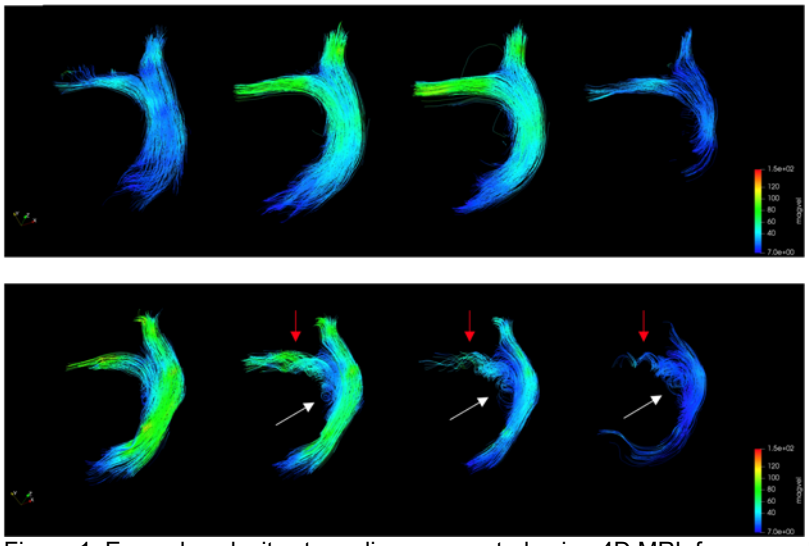

Figure 1: Example velocity streamlines generated using 4D MRI, for a sample normotensive (top panel) and PH patient (bottom panel), at 4 points in the cardiac cycle: early systole, mid-systole, late systole, and early diastole. The white arrows highlight the location of vortex formation, and the red arrows demonstrate helical flow in the right pulmonary artery.

ID#: 378752

Cardiac and Respiratory Self-Gated Motion-Corrected Free-breathing Spiral Cine Imaging

Ruixi Zhou, MS[1] Yang Yang, PhD[2], Matthew J. Van Houten, MS[1], Christopher M. Kramer, MD[3], Michael Salerno, MD, PhD[2]

1. University of Virginia, Charlottesville, VA

2. University of Virginia, VA

3. University of Virginia Health System, Charlottesville, VA

Background: In current clinical practice, breath-held ECG-gated Cartesian cine images are typically acquired to assess cardiac function. This approach is inefficient as it requires 10-12 breath-holds to cover the left ventricle, and it is susceptible to respiratory-motion artifacts and ECG gating artifacts, particularly at 3T. Thus, there is a growing interest in self-gated free-breathing approaches. We developed a continuous-acquisition respiratory and cardiac self-gated cine sequence for free-breathing cardiac function acquisition, and developed a motion-compensated reconstruction strategy.

Methods: 13 volunteers were imaged on a 3T scanner (Prisma, Siemens Healthineers). Gradient echo cine data were acquired continuously for 20 seconds per slice using a pulse sequence consisting of a single spiral trajectory rotated by the golden angle. Sequence parameters included: TR 7.8ms, TE 1ms, slice thickness 8mm, resolution 1.5x1.5mm. Self-gating respiratory and cardiac signals were determined by gridding an 8x8 central region of k-space for each spiral arm for all coils, followed by low-pass temporal filtering, principal component analysis, and band-pass filtering of the derived temporal-basis functions (Figure 1). For each heartbeat, a static image was reconstructed using all spiral arms following each self-gating trigger. These images were rigidly-registered to derive the respiratory motion. The cardiac self-gating signal was used to retrospectively bin the data across the cardiac cycle. Cine images were reconstructed using motion-corrected compressed sensing with spatial total variance as the sparse term, with a reconstructed temporal resolution of 40ms. Images were graded on a 5 point scale (1-worst, 5-best) by an experienced cardiologist. Cine Images covering the whole heart were acquired in two subjects. The accuracy of self-gating as compared to the acquired ECG signal was assessed using Bland-Altman analysis.

Results: Figure 1 shows the cardiac and respiratory self-gating pipeline. The derived respiratory component is consistent with the respiratory signal derived from rigid registration, and the cardiac cycle lengths matched those of the ECG. Figures 2 and 3 show images at diastole and systole covering the whole heart in 1 subject. The average image quality score was 4.0±0.8. There was good agreement between the self-gating and ECG signal, with a mean bias of 0.57 ms.

Conclusion: Our self-gated free-breathing spiral cardiac cine imaging strategy acquires high quality cine images with temporal and spatial resolution typical for breath-held cine imaging without the need for ECG gating or breath-holding. This strategy could provide a simpler, more efficient protocol for clinical CMR imaging particularly for patients who may have difficulty holding their breath.

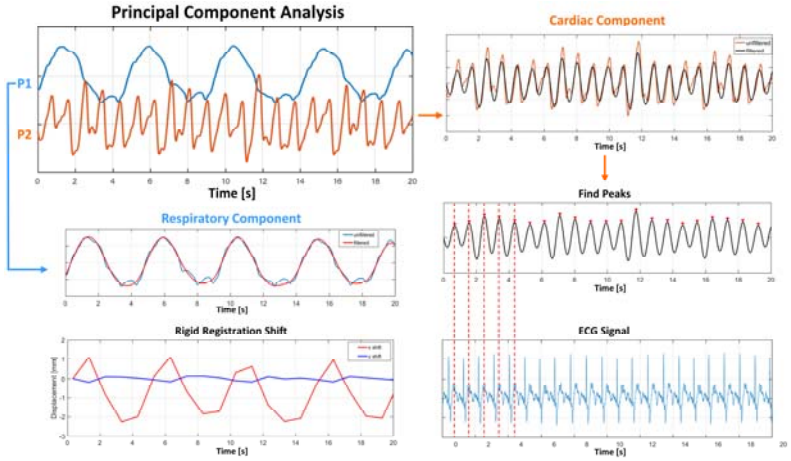

Figure 1: Pipeline for extracting the cardiac and respiratory components for self-gating. A central k-space region is gridded, and after low-pass temporal filtering, PCA is performed. The first principal component (blue) shows the respiratory component, whereas the second principal component (orange) shows the cardiac component. After

band-pass filtering, the respiratory and cardiac self-gating signals are derived. The derived respiratory component is consistent with the respiratory signal derived from rigid registration, and the cardiac cycle lengths matched those of the ECG signal.

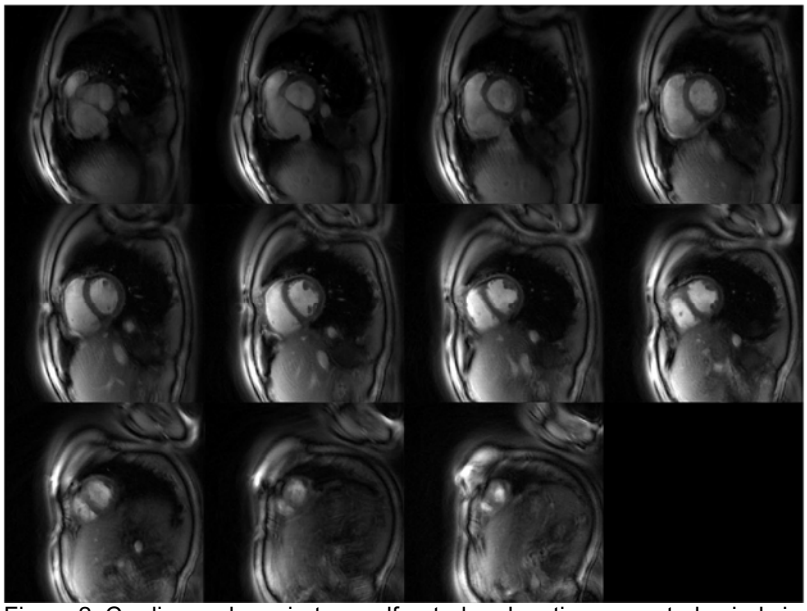

Figure 2: Cardiac and respiratory self-gated and motion-corrected spiral cine end diastolic images covering the whole heart from one subject.

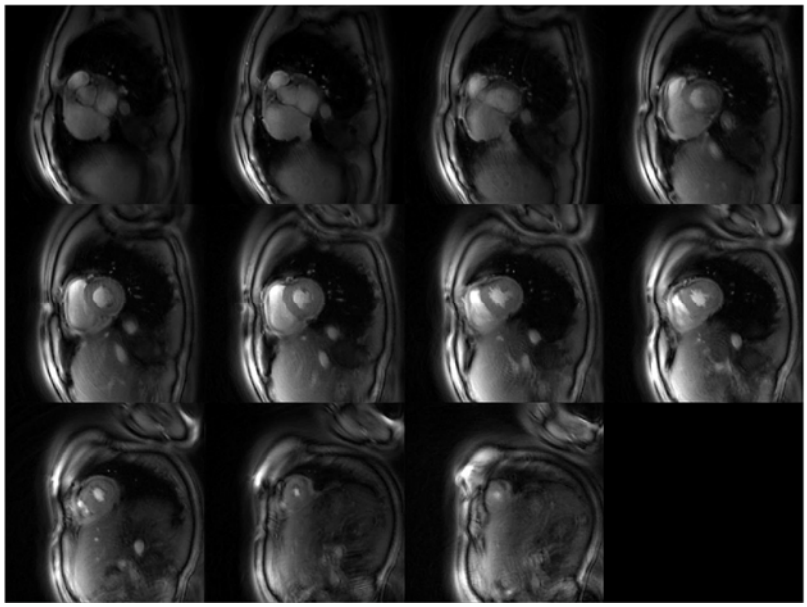

Figure 3: Cardiac and respiratory self-gated and motion-corrected spiral cine end systolic images covering the whole heart from one subject.

ID#: 378838

Prevalence of extracardiac findings on adenosine stress perfusion CMR in patients with preserved ejection fraction

Sohail Iqbal, MBBS[1] Pamela Brown, MBBS[2], Matthias Schmitt, MD, PhD[3], Gaetano Nucifora, MD, PhD[4]

1. University Hospital South Manchester, Manchester, United Kingdom

2. University Hospital South Manchester, Whitby, England, United Kingdom

3. University Hospital South Manchester, United Kingdom

4. University Hospital of South Manchester, United Kingdom

Background: Adenosine Stress Perfusion CMR plays an important role in the diagnostic work-up and risk stratification of patients with suspected or known coronary artery disease (CAD) and consequently is increasingly used in routine clinical practice. Relevant non-cardiac diseases may be incidentally found on CMR images, occasionally explaining patients'; clinical symptoms. While the reported prevalence of extra-cardiac findings in CMR imaging is about 17% [1], the prevalence in the cohort of patients referred to adenosine stress perfusion CMR may be higher, as several of the cardiovascular risk factors for atherosclerosis are also risk factors for malignancy. The aim of this study was therefore to investigate the prevalence of extracardiac findings in patients with preserved LVEF referred to adenosine stress perfusion CMR imaging.

Methods: A total of 775 consecutive patients (mean age of 63±13 years, 1.85:1 male: female) referred to adenosine stress CMR were included. The study population was then divided in three groups, according to their age (young age: 19 to 39 years, n = 58 patients; middle age: 40 to 64 years, n = 406 patients; old age: 65 to 89 years, n = 311 patients) and the prevalence of extra-cardiac findings assessed.

Results: Overall, 183 (23.6%) extracardiac findings were observed in 164 (21%) patients. As shown in Figure 1, the prevalence of extracardiac findings was significantly higher in old age group (n = 94, 30%) in comparison to the young patients (n = 7, 12%) and middle-age patients (n = 63, 16%). Furthermore, 12 patients (4%) in the old age group had more than one findings compared to 4 patients (1%) in middle age group. Similarly, clinically significant findings were higher in the old age group (6 patients, 2%) including three lung cancer patients (Figure 2); one of these patients had advanced disease and expired two months after initial diagnosis.

Conclusion: The overall prevalence of extra-cardiac findings in patients referred to adenosine stress perfusion CMR is similar to that previously described in patients referred to CMR imaging. Older patients have higher prevalence of extra-cardiac findings with increasing chance of clinically significant disease compared to young and middle age groups, with potentially significant impact on management and additional work-up.

Reference: Dunet V, Schwitter J, Meuli R, et al. Incidental extracardiac findings on cardiac MR: Systematic review and meta-analysis. J Magn Reson Imaging. 2016; 43:929-39. doi: 10.1002/jmri.25053. Epub 2015 Sep 23.

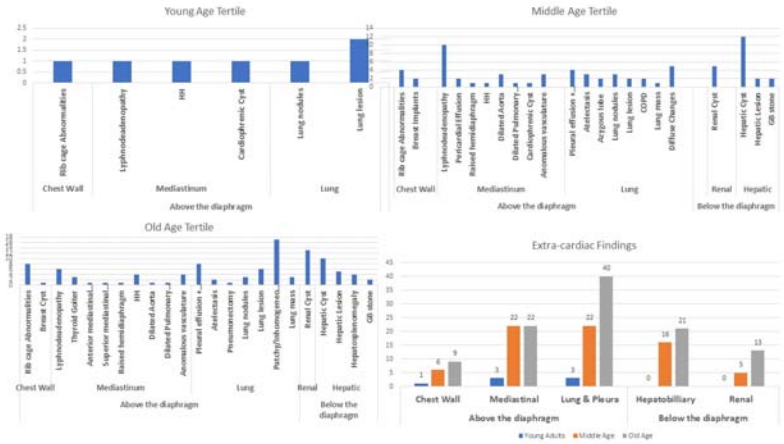

Figure 1 depicting extracardiac findings in 3 age groups

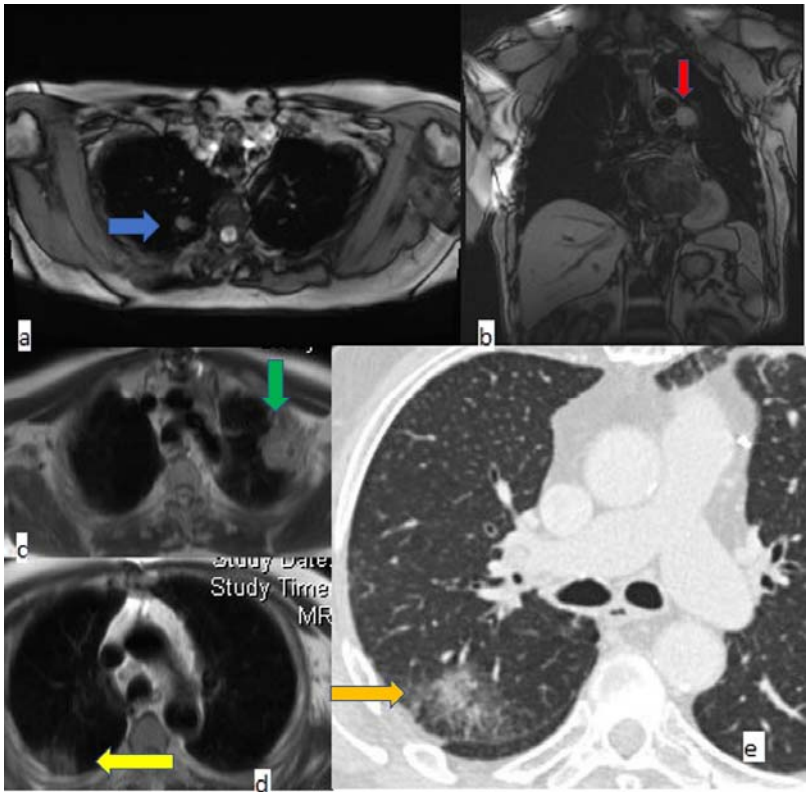

Figure 2a, RUL lung mass; 2b, mediastinal cystic lesion; 2c, advanced LUL lung mass; 2d, RLL infiltrative mass lesion; 2e, Follow up CT of RLL infiltrative mass lesion

ID#: 378880

Rest Perfusion Characteristics in Patients with Chronic Hemorrhagic Myocardial Infarctions: Early Findings

Eric Johnson[1] Andreas Kumar, MD, MSc[2], Rohan Dharmakumar, PhD[3]

1. Cedars-Sinai Medical Center and UCLA, Beverly Hills, CA

2. Northern Ontario School of Medicine, Sudbury, ON, Canada

3. Cedars-Sinai Medical, CA

Background: Pathological accumulation of erythrocyte-derived iron is known to scavenge nitric oxide, causing endothelial dysfunction and reduced microcirculatory blood flow. Given that hemorrhagic myocardial infarctions (hMI) are associated with iron accumulation within infarct territories, we hypothesized that the resting blood flow in the chronic phase of hMI territories would be lower than in non-hMI territories. We studied this in a small cohort of ST-elevation myocardial infarction (STEMI) patients treated with percutaneous coronary intervention (PCI) and serially followed with CMR.

Methods: STEMI patients (n=10) treated with PCI were recruited for the initial CMR (3-5 days post-PCI) and were followed with CMR at 6 months PCI (n=8; 2 dropped off). Following localizers, T2*-weighted, contrast-enhanced rest perfusion and LGE images were acquired in short-axis orientation on a clinical 1.5T system. Rest perfusion scans were acquired over 3 slices (basal, mid-ventricular and apical) that were matched to T2* and LGE scans. Based on acute MI T2*, patients were identified to have had hMI or non-hMI. All image analysis was performed in CVI42. Rest-perfusion images obtained at 6 months were analyzed by first segmenting the LGE images for infarct regions using the mean+5SD criterion. The infarct contour was copied and propagated across the time-resolved perfusion images, adjusting for respiratory motion. A remote region, identified on the LGE was also propagated in a similar fashion. For each subject, *Relative Perfusion Index* was calculated as *Perfusion Index* of infarct zone / *Perfusion Index* of remote zone, where *Perfusion Index* is the upslope of signal intensity of the myocardium normalized by the upslope of the signal intensity of the blood pool. Student';s t-test was used to determine if the mean *Relative Perfusion Index* of hMI and non-hMI patients were different. Statistical significance was set at $p<0.05$.

Results: Perfusion defects and T2* losses were visible in chronic MI regions in patients with hMIs, but not in patients with non-hMIs. Representative findings supporting this are shown in Fig. 1. Mean Relative Perfusion Index of hMIs were significantly lower than non-hMI (0.72±0.14 vs. 0.92±0.20, p=0.03; Fig.2).

Conclusion: This is the first evidence demonstrating that the rest perfusion in the chronic phase of hMI is lower than non-hMI. While our early findings support the notion that resting perfusion is reduced in chronic hMIs, additional studies are needed to establish the mechanism underlying the rest perfusion defects in chronic hMIs. If confirmed, hemorrhage-mediated hypoperfusion could evolve as a pathological contributor to adverse remodeling observed in hMIs.

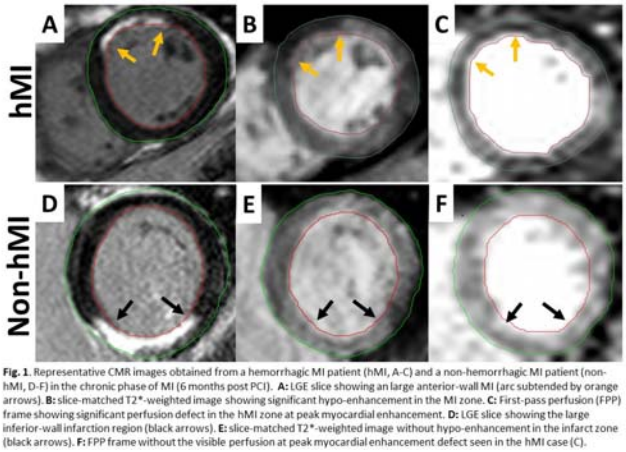

Fig. 1. Representative CMR images obtained from a hemorrhagic MI patient (hMI, A-C) and a non-hemorrhagic MI patient (non-hMI, D-F) in the chronic phase of MI (6 months post PCI). **A:** LGE slice showing an large anterior-wall MI (arc subtended by orange arrows). **B:** slice-matched T2*-weighted image showing significant hypo-enhancement in the MI zone. **C:** First-pass perfusion (FPP) frame showing significant perfusion defect in the hMI zone at peak myocardial enhancement. **D:** LGE slice showing the large inferior-wall infarction region (black arrows). **E:** slice-matched T2*-weighted image without hypo-enhancement in the infarct zone (black arrows). **F:** FPP frame without the visible perfusion at peak myocardial enhancement defect seen in the hMI case (C).

Fig. 1. Representative CMR images obtained from a hemorrhagic MI patient (hMI, A-C) and a non-hemorrhagic MI patient (non-hMI, D-F) in the chronic phase of MI (6 months post PCI). A: LGE slice showing an large anterior-wall MI (arc subtended by orange arrows). B: slice-matched T2*-weighted image showing significant hypo-enhancement in the MI zone. C: First-pass perfusion (FPP) frame showing significant perfusion defect in the hMI zone at peak

myocardial enhancement. D: LGE slice showing the large inferior-wall infarction region (black arrows). E: slice-matched T2*-weighted image without hypo-enhancement in the infarct zone (black arrows). F: FPP frame without the visible perfusion at peak myocardial enhancement defect seen in the hMI case (C).

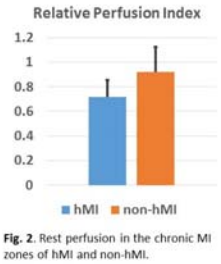

Fig. 2. Rest perfusion in the chronic MI zones of hMI and non-hMI.

Fig. 2. Rest perfusion in the chronic MI zones of hMI and non-hMI.

ID#: 378889

Clinical and morpho-functional evaluation of young athletes with exercise-induced ventricular arrhythmias: a study performed by cardiac magnetic resonance

Alberto Cipriani, MD[1]Patrizio Sarto, MD[2], Martino Donini, MD[1], Matteo Cesarotto, MD[1], Manuel De Lazzari, MD, PhD[1], Laura Merlo, MD[2], Cinzia Pegoraro, MD[2], Ilaria Rigato, MD, PhD[1], Benedetta Giorgi, MD[1], Domenico Corrado, MD, PhD[1], Sabino Iliceto, MD, PhD[1], Barbara Bauce, MD, PhD[1], Martina Perazzolo Marra, MD, PhD[1]

1. Department of Cardiac, Thoracic and Vascular Sciences, University of Padova, Italy, Italy

2. Department of Prevention, UOC Sport Medicine, Azienda ULSS 9 Treviso, Italy, Italy

Background: Exercise-induced ventricular arrhythmias (EIVA) are associated with higher long-term mortality in asymptomatic middle-aged individuals. Nonetheless, clinical substrates accounting for this increased risk are unknown. The detection of EIVA in young athletes raised the issue if they represent a benign condition or on the contrary should be considered a marker for an undiagnosed cardiac disease. Contrast–enhanced cardiac magnetic resonance (CE-CMR) provides a non-invasively myocardial tissue characterization and with the addition of feature tracking (FT) integrated software enables the assessment of left ventricular (LV) strain, which constitutes a sensitive marker for contractile dysfunction. The aim of the present study was to characterize the clinical and imaging profile of a cohort of young athletes showing EIVA and to determine
the possible morphological substrate of EIVA in this specific population. Moreover, to compare the CE-CMR features of EIVA athletes with those of athletes presenting ventricular arrhythmias (VA) that disappear during exercise. Finally, to investigate through a CMR-FT analysis whether young athletes with EIVA present early abnormalities of LV systolic function.

Methods: Clinical, electrocardiographic, 24-Holter electrocardiographic (ECG) monitoring and CE-CMR findings of 34 athletes (74% male, age: 15-50 years) with EIVA (group A) were compared to those of 24 athletes (75% male, age: 15-50 years) presenting VA that disappear during exercise (group B).

Results: Athletes of group A were older compared to those of group B (25 years vs 17 years, p=0.02) and were characterised by more complex VA (couplets and non-sustained ventricular tachycardia) compared to group B (25 vs 11, p=0.03; 14 vs 2, p=0.006). Analysis of VA morphology showed that the two groups differed in terms of site of VA origin, as athletes of group A presented more frequently a right bundle branch block-superior axis morphology (p=0.02), whereas in subjects of group B the left bundle branch block-inferior axis morphology was more common (p=0.001). At CE-CMR no differences between the two groups regarding LV and right ventricle dimensions, stroke volumes and systolic function were found. On post-contrast sequences, late gadolinium enhancement (LGE) was identified in 22/34 (62%) athletes of group A compared to 4/24 (17%) athletes of group B (p<0.001). LGE was localized in the left ventricle and junctional sites more often in athletes with EIVA (p=0.001, p=0.03) and presented a non-ischemic pattern in 21/34 (62%) athletes of group A, consisting in stria (38%) or spot (24%). CMR-FT analysis did not report significant differences in global peak radial, circumferential and longitudinal strain measurements between the groups.

Conclusion: Non-ischemic myocardial fibrosis is a common CE-CMR finding in young athletes with EIVA, even if the causative role of this morphological substrate in their origin needs to be researched. Nonetheless, detection of EIVA during screening for competitive sports activity should always suggest to perform a CE-CMR evaluation for a detailed morphological and tissue characterization.

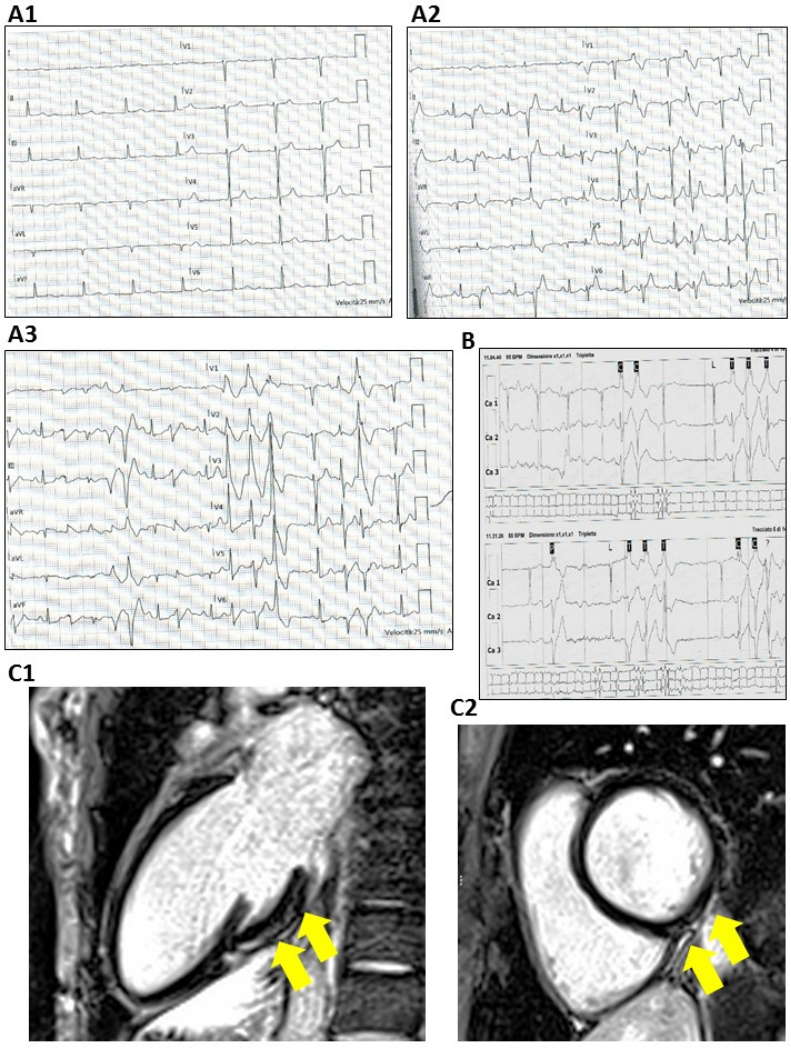

41-year old woman. Panel A1-A2-A3 show the development of exercise-induced ventricular arrhythmias at exercise stress test. Arrhythmias have right bundle branch block-superior axis morphology. Panel B. On 24h ECG monitoring, couplet and non-sustained ventricular tachycardia were recorded. Panel C1-C2. Contrast-enhanced cardiac magnetic resonance revealed intramural late gadolinium enhancement stria on inferobasal wall of left ventricle.

ID#: 378890

Left ventricle wall motion disorders in myocardial infarction depicted by compressed sensing real-time cine imaging.

Benjamin Longere, MD[1]Marc-Henry Chavent, MD[2], Michaela Schmidt[3], Christoph Forman, MS[3], Valentina Silvestri, MD[1], Julien Pagniez, MD[1], Francois Pontana, MD, PhD[4]

1. Lille University Hospital, Nord-Pas-de-Calais, France

2. Lille University Hospital, France

3. SIEMENS HEALTHCARE GmbH, Erlangen, Bayern, Germany

4. Lille University Hospital, Lille, Nord-Pas-de-Calais, France

Background: Cardiac magnetic resonance (CMR) provides an accurate evaluation of wall motion disorders that occur after myocardial infraction (MI), usually using steady-state free precession (SSFP) cine sequences. On the other hand, compressed sensing (CS) imaging dramatically drops scan time. We compared the accuracy of a prototype CS real-time cine sequence (Sparse 2D, Siemens Healthineers) to the reference SSFP cine sequence for the depiction of wall motion disorders.

Methods: We prospectively included 100 consecutive adult patients (77 males, 23 females; mean age = 63.12 ±11.3 y/o) referred for either initial work-up or follow-up of MI by CMR. The same CMR protocol was performed for every patient: (a) the reference segmented multi-breath-hold SSFP cine sequence including one short-axis stack and both vertical and horizontal long-axis slices (Group 1) and (b) the CS real-time single-breath-hold evaluated sequence (Group 2) providing the same slice number, position and thickness. Additional short-axis, 2-chambers and 4 chamber delayed gadolinium-enhanced stacks were achieved to assess MI. Wall motion disorders were independently and blindly sought in both groups by two radiologists, referring to the American Heart Association left ventricle segmentation. Statistical difference was evaluated by paired Wilcoxon signed-rank test and differential diagnosis performance was appreciated by ROC curve analysis.

Results: For every patient in both groups at least one segment suffered from wall motion abnormalities. The 1700 segments read in Group 1, were rated as normokinetic (n = 360; 21.2%), hypokinetic (n= 783; 46.1%), akinetic (n= 526; 30.9%) or dyskinetic (n= 31; 1.8%). No significant difference was assessed regarding wall motion disorder depiction in Group 2 compared to Group 1 (p = 1.0). The CS prototype sequence sensitivity and specificity were 99.63% (95%CI [99.1-99.9]) and 99.72% (95%CI [98.5-100]), respectively. Area under the curve was 0.997 (95%CI [0.993-0.999]; p < 0.0001).

Conclusion: The single-breath-hold compressed sensing real-time cine sequence is reliable to assess wall motion abnormalities in the context of myocardial infarction. Since patients suffering from MI may present shortness of breath or arrhythmia due to myocardial fibrosis, the use of CS cine imaging can significantly reduce scan time without compromising detection accuracy of LV-wall motion disorders.

ID#: 378894

Automatic Artifacts Detection as Operative Scan-aided Tool in an Autonomous MRI Environment

Wenwen Jiang[1]Okai Addy, Ph.D.[2], William Overall, Ph.D.[3], Juan Santos, Ph.D.[3], Bob Hu, MD[3]

1. Heartvista, Inc, Los Altos, CA

2. HeartVista, Inc, Los Altos, CA

3. HeartVista, CA

Background:

Artifacts in magnetic resonance imaging may reduce the quality of examinations or may be confused with pathology. Image artifacts may not be recognized by operators and lead to suboptimal physician interpretations. Ideally, any suboptimal images should be identified and reacquired with optimal imaging parameters while the patient is still on the table. We propose an intelligent scan control framework that detects image artifacts during the scan and self-corrects imaging parameters or triggers a rescan in an autonomous MRI environment.

Methods:

Imaging acquisition was performed on a 1.5 T GE Signa TwinSpeed scanner with an 8-channel cardiac coil using the HeartVista autonomous MRI environment (HeartVista, Inc. Los Altos, CA). Data was acquired with a multi-slice Double Inversion Fast Spin Echo sequence with the field of view ranging from 32×32 to 48x48 cm^2, 256 x 96 to 168 matrix size, TE/TR/TI = 20-120 us/31.6 ms/758 us and echo train length = 24. SPIRiT parallel reconstruction [1] was performed. 500 cardiac patient studies using this protocol (5962 images) were randomly divided into a training set of 5762 images and a test set of 200 images. An experienced operator manually labeled images into two categories: with motion artifacts or without motion artifacts. A modified Inception [2] convolutional neural network was used with TensorFlow [3] on a system equipped with a GeForce GTX Titan X GPU.

The resulting predictive models were integrated into the HeartVista scan-control platform system to provide prospective scan guidance during automated scanning.

Results:

The inception model resulted in an overall accuracy = 85%, sensitivity = 86% and specificity = 84.5%. Figure 1 shows randomly selected examples of the confusion matrix. We have integrated the prediction model into the autonomous MRI environment, shown in Figure 2, to trigger rescan operation. If the prediction indicates the current slice has artifacts, then the system prompts the operator to reacquire the scan.

Conclusion:

A scan-aided artifact detection mechanism has been presented using deep learning, and was integrated into the HeartVista autonomous MRI system. It is able to provide effective scan suggestions for technicians.

The proposed method illustrates the efficacy of automatically detecting one type of artifacts. However, it can be easily extendable to other kinds of artifacts. We are currently training a deep learning model that can recognize different artifacts and their source, e.g. flow artifacts, off-resonance artifacts, etc. and provide corresponding operative scan suggestions or even self-tune the scan protocols to optimize the image quality based on the detected image artifact sources.

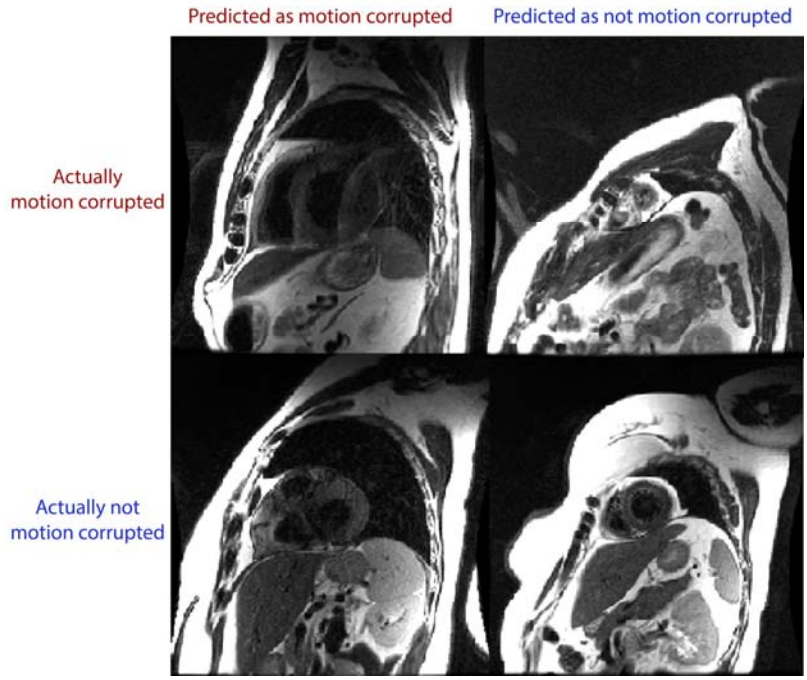

Examples of Confusion Matrix for Motion Artifact Detection

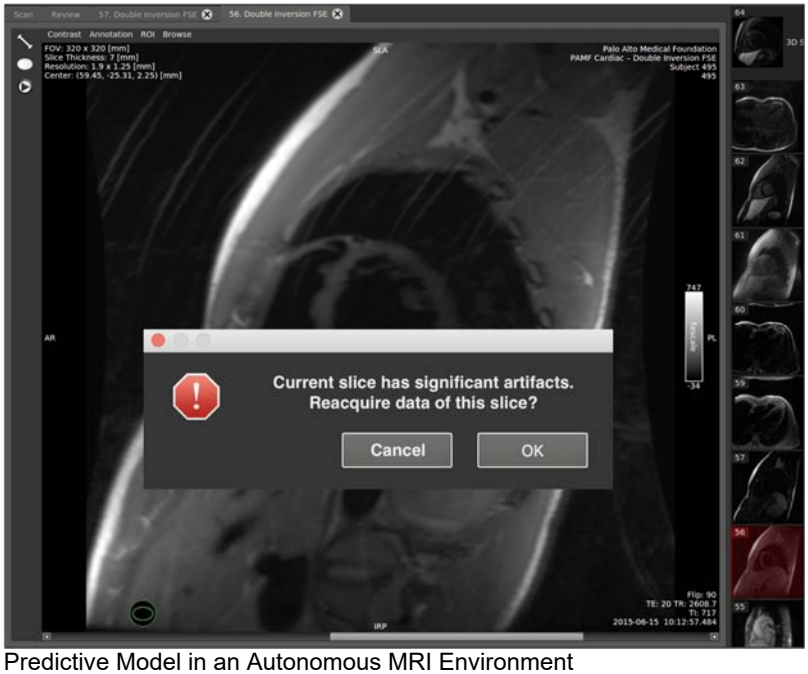

Predictive Model in an Autonomous MRI Environment

ID#: 378896

Single Breath Hold 4D Flow Acquisition of the Aortic Valve

Adam V. RIch, Ph.D.[1] Yingmin Liu, Ph.D.[2], Ning Jin, Ph.D.[3], Lee Potter, PhD[4], Orlando Simonetti, PhD[4], Rizwan Ahmad, PhD[4]

1. The Ohio State University

2. The Ohio State University, Columbus, OH

3. Siemens Medical Solutions USA, Inc., OH

4. The Ohio State University, OH

Background: Standard phase-contrast MRI (PC-MRI) with through-plane velocity encoding is routinely used to quantify flow in the great vessels. For patients with aortic valve stenosis (AVS), this technique, however, tends to underestimate the peak velocity due to misalignment of the imaging plane and aortic jet. As demonstrated in Figure 1, 4D flow imaging eliminates image plane alignment and location issues at the cost of increased scan time. In this work, we demonstrate the feasibility of single breath-hold 4D flow imaging using our recently proposed acceleration technique called ReVEAL [1].

Methods: Data from five healthy volunteers and five patients with aortic valve stenosis were collected on a 1.5T scanner (Avanto, Siemens Healthineers) using 18-channel coil array. Imaging was performed over a 48 mm thick slab that covered the aortic valve and was approximately normal to the dominant blood flow direction. Two 4D flow datasets were acquired per subject: a free-breathing reference scan using respiratory navigator at an acceleration factor of R = 3 and a single breath-hold acquisition using VISTA sampling [2] with acceleration rate R = 21–27. The datasets were collected using prospectively triggered segmented acquisition with referenced four-point encoding. In-slab resolution was 3 mm or better, through-slab resolution was 6 mm, and temporal resolution was 35-38 ms. Other scan parameters were as follows: TE 2.4ms, TR 4.7ms, VENC 130-500 cm/s, and flip angle 10°. The free-breathing datasets were reconstructed using GRAPPA and the breath-held datasets were reconstructed using ReVEAL.

Results: In Figure 2, Bland-Altman analyses are presented for peak velocity for healthy volunteers and AVS patients. For both healthy subjects and patients, the discrepancy between GRAPPA and ReVEAL was less than 20% of the peak velocity values reported by GRAPPA. Representative magnitude and velocity maps are shown in Figure 3, with GRAPPA exhibiting more noise than ReVEAL. Similar BA analyses were also performed for stoke volume (not shown) in healthy volunteers with mean difference of 0.1 ml and 95% confidence interval of ±10 ml.

Conclusion: These preliminary results suggest that clinically relevant hemodynamic parameters in the vicinity of the aortic valve can be adequately quantified within a single breath-hold using ReVEAL. In contrast, rate-3 GRAPPA acquisition took, on average, more than 10 minutes. Future studies will combine ReVEAL with respiratory navigator-based free-breathing acquisition and evaluate the clinical impact of this technique in a larger cohort of patients. [1] Rich et al., Magn Reson Med. doi: 10.1002/mrm.25904, [2] Ahmad et al., Magn Reson Med. doi: 10.1002/mrm.25507

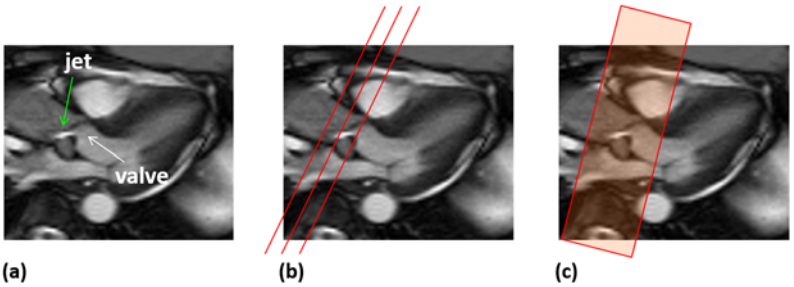

Figure 1 Aortic valve imaging. (a) An example showing skewed aortic jet. (b) Depiction of 2D PC-MRI where multiple imaging planes are sequentially acquired to capture the peak velocity. Even with this multi-plane acquisition, a misalignment between the jet and the imaging plane can lead to velocity underestimation. (c) Volumetric coverage and multi-directional encoding employed in 4D flow imaging avoids the underestimation associated with planar imaging.

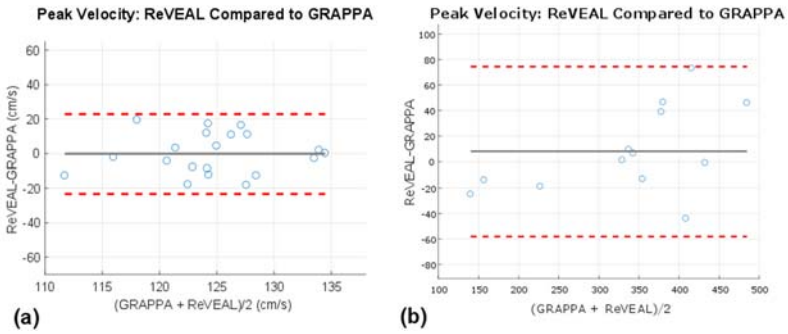

Figure 2 Bland Altman analyses for peak velocity for ReVEAL compared to GRAPPA. (a) Bland Altman for healthy volunteers. (b) Bland Altman for AVS patients. For each subject, the quantification was performed at multiple locations downstream of the aortic valve.

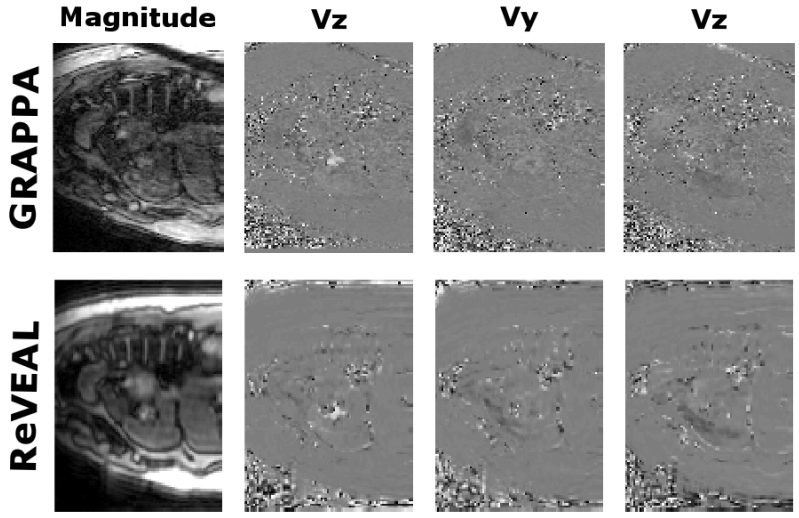

Figure 3 An example of GRAPPA and ReVEAL reconstructions for a patient with AVS

ID#: 378940

Myocardial Characterization and Strain as a Diagnostic Tool in Pediatric Patients Receiving Anthracycline Chemotherapy

Cory V. Noel, M.D.[1] Amol Pednekar, PhD[2], Prakash Masand, MD[3], James Wilkinson, M.D.[4], Nino Rainusso, M.D., PhD[4]

1. Texas Children's Hospital - Baylor College of Medicine, Houston, TX

2. Texas Children's Hospital, Houston, TX

3. Texas Children's Hospital

4. Texas Children's Hospital - Baylor College of Medicine

Background: Cancer therapy-related cardiac dysfunction (CTRCD) is a growing clinical issue observed in survivors of pediatric cancer. The usual surveillance method for CTRCD is by transthoracic echocardiography, but early alterations in imaging biomarkers remain poorly explored. MRI can quantify cellular changes and the ramifications regarding mechanical properties of the myocardium along with the assessment of global ventricular function which may have utility in earlier detection of CTRCD. T2 mapping correlates with myocardial edema, an early feature of cardiotoxicity. The purpose of our ongoing study is to examine the effectiveness of CMR myocardial tissue characterization by T2 mapping, along with myocardial longitudinal strain for early detection of CTRCD in a pediatric clinical model.

Methods: Ten pediatric patients, (aged 10-16 years), with a new diagnosis of solid bone tumor receiving anthracycline-based chemotherapy (AC) were prospectively recruited. All patients received dexrazoxane at a dose of 10 times AC dosage. The patients underwent a CMR at baseline prior to AC, and a subsequent CMR within 24 to 72 hours of reaching 150 mg/m^2 or 225 mg/m^2 depending on clinical condition. Acquisition Protocol: All scans performed in a 1.5T clinical MRI scanner (Philips Ingenia). The right and left ventricular ejection fractions (RVEF, LVEF) were quantified from bSSFP cine sequence obtained in the short axis. T_2 mapping and strain (Fast-Strain Encoded for longitudinal strain $\varepsilon_{L)}$ imaging was performed in 3 short-axis slices; basal, mid-ventricular, and apical. Data Analysis: The T_2 was measured manually (cvi^{42}, Calgary, CA) and global T_2 was calculated as a mean of anterior, lateral, inferior and septal ROIs. The global myocardial ε_L was calculated (myocardial solutions, Morrisville, NC). Paired t-test and box plot analysis was performed on the pre and post treatment data.

Results: The data acquisition and parametric measurements were successful in all study participants. There was significant decrease in global T_2, global $\varepsilon_{L,}$ LVEF, and RVEF between the baseline and within 72hrs post-AC CMR (Table 1). The mean drop in both LVEF and RVEF was more than 5%. T_2 elongated by more than 14% and ε_L strain worsened by an average of 1.6% (a change of 9%). Figure 1 depicts Box and Whisker plots for all parameters.

Conclusion: MR-based myocardial tissue characterization with T_2 along with myocardial strain, may be useful diagnostic tools in pediatric patients in the earlier detection of CTRCD receiving AC. Larger clinical trials are needed to determine the value of these CMR techniques for the prediction of global dysfunction in this pediatric population.

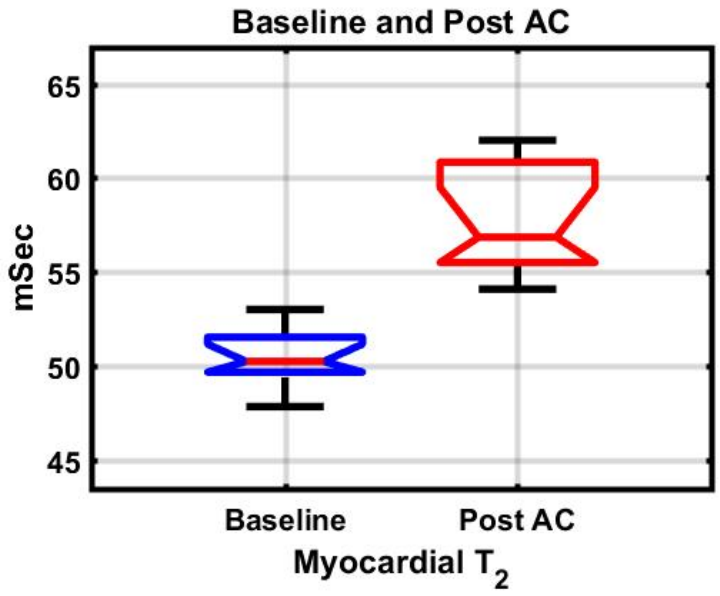

Global myocardial T2 at Baseline and Post AC

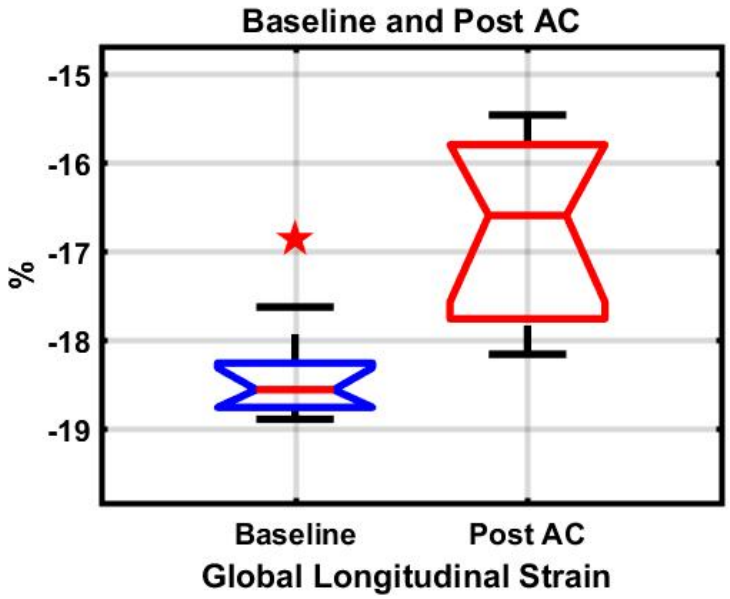

Global longitudinal strain (εL) at Baseline and Post AC

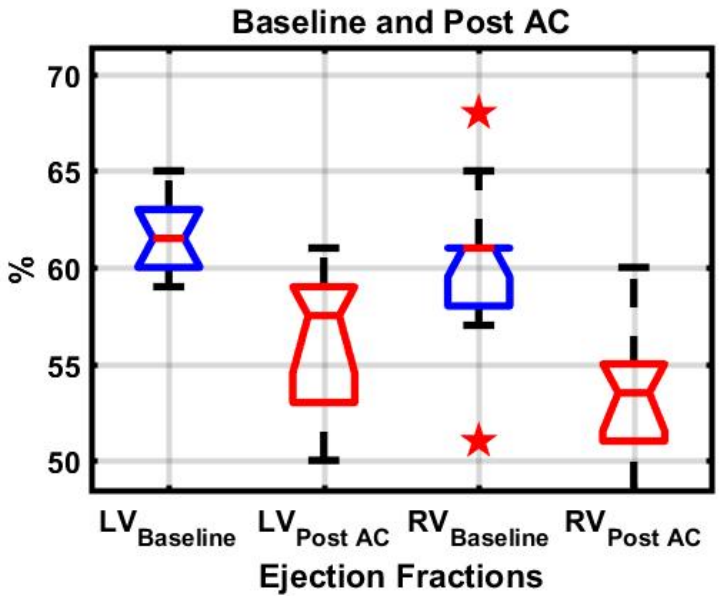

Global ventricular ejection fractions at Baseline and Post AC

Cardiac MR derived myocardial tissue characterization (T2), strain (εL), and ventricular ejection fractions at baseline and within 72hrs after receiving anthracycline-based chemotherapy. Post AC = within 72hrs after receiving anthracycline-based chemotherapy

	Global T_2 (mSec)	Global ε_L (%)	LVEF (%)	RVEF (%)
Baseline	50.4 ± 1.62	-18.35 ± 0.63	61.8 ± 2.2	60.2 ± 4.57
Post AC	57.6 ± 2.8	-16.72 ± 1.02	56.2 ± 3.71	53.4 ± 4.09
p value	0.000007	0.00017	0.00097	0.0023
Mean Diff.	-7.21	-1.62	5.6	6.8
Confidence Interval	-8.98 to -5.44	-2.22 to -1.03	2.96 to 8.2	3.14 to 10.46

AC - Anthracycline Chemotherapy; LVEF - Left ventricular ejection fraction; RVEF - Right ventricular ejection fraction

ID#: 378850

Compressed Sensing real-time Cine Imaging in patients with cardiac arrhythmia: Does it help to reduce mis-triggering artifacts?

Francois Pontana, MD, PhD[1] Alexandre Bridoux, MD[2], Paul-Edouard Allard, MD[2], Michaela Schmidt[3], Christoph Forman, MS[3], Julien Pagniez, MD[4], Valentina Silvestri, MD[4], Benjamin Longere, MD[4]

1. Lille University Hospital, Lille, Nord-Pas-de-Calais, France

2. Lille University Hospital, France

3. SIEMENS HEALTHCARE GmbH, Erlangen, Bayern, Germany

4. Lille University Hospital, Nord-Pas-de-Calais, France

Background: The purpose of this study was to evaluate the impact of a Compressed Sensing (CS) real-time prototype cine sequence (Sparse 2D cine, Siemens Healthineers) on mis-triggering artifacts and image quality in patients with arrhythmia, in comparison with the reference cine-imaging technique.

Methods: 71 consecutive adult patients (41 males; mean age = 59 ±20.6 years) referred for cardiac magnetic resonance (CMR) examination with concomitant irregular heart rate (defined by R-R interval variation > 10%) during scanning, were prospectively enrolled. For each patient, two series of cine images were systematically acquired: (a) a standard segmented multi-breath-hold steady-state free precession (bSSFP) sequence including a short-axis stack, one four-chamber slice, one two-chamber slice (Group 1) and (b) an additional real-time CS single-breath-hold prototype sequence (Group 2) providing the same slice number, position and thickness as the reference technique. Two observers independently assessed mis-triggering artifacts, objective and subjective image quality for both acquisition techniques.

Results: The mean heart rate variation was 38.3% ±22.7 (range: 11-121). A total of 599 cine slices were evaluated in each Group (mean number of slices per patient = 8.4 ±1.9). The number of slices with mis-triggering artifacts per patient was higher in Group 1 than in Group 2 (85.9% ±22 vs 3.2% ±0.8, $p<0.0001$). The European CMR registry standardized artifacts score was lower in Group 2 than in Group 1 (1.55 ±1.45 vs 2.87 ±0.53 respectively, $p<0.0001$). Subjective image quality score was improved in Group 2 compared to Group 1 (2.56 ±0.73 vs 1.92 ±0.77 respectively, $p<0.0001$).

Conclusion: Compressed Sensing real-time cine imaging drastically reduces mis-triggering artifacts and improves image quality of CMR cine acquisition in patients with arrhythmia.

ID#: 378946

T1/T2 mapping for diagnosis of myocarditis in pediatric patients

Matthew Cornicelli, MD[1] Cynthia K. Rigsby, MD, FACR[1], Elfriede Pahl, MD, FACC[2], Joshua D. Robinson, MD, FACC[1]

1. Ann & Robert H. Lurie Children's Hospital of Chicago, Chicago, IL

2. Ann & Robert H Lurie Children's Hospital of Chicago

Background: Myocarditis is an important cause of heart failure, dilated cardiomyopathy and sudden death in children. Accurate diagnosis is challenging due to the heterogeneity of disease presentation and limitations of available testing. CMR is increasingly used for diagnosis in pediatric patients but techniques remain variable across centers and findings are largely qualitative, with significant interobserver variability. Newer quantitative CMR techniques, such as T1 and T2 mapping (T1M/T2M) with calculation of extra-cellular volume (ECV), have improved diagnostic performance in adults compared to standard "Lake Louise" criteria (LLC), however, limited data exist in pediatrics. This study aimed to determine if T1, T2 and ECV values are abnormal in pediatric patients with myocarditis as compared to a healthy control population.

Methods: We performed a retrospective case controlled study of patients <21 years old with a clinical diagnosis of acute myocarditis (n=23) who underwent CMR at our institution between 2014 and 2017, and compared them to healthy patients (n=39) with structurally normal hearts. T1M and T2M were added to a standard CMR protocol including T2-weighted, early and late gadolinium enhancement imaging. T1, T2 and ECV values were determined using a 16-segment model (Figure 1). An independent t-test was performed to compare our primary endpoints of mean global T1, ECV, and T2 values between study patients and controls.

Results: For the 23 patients meeting our inclusion criteria, all were hospitalized and underwent CMR at mean 4.5 (range 1-26) days after diagnosis. Additional characteristics of myocarditis and controls are presented in Table 1. For our primary outcomes, patients with acute myocarditis had significantly higher mean global T1 (1097.9 ± 77.0 vs 989.6 ± 34.3 ms), ECV (29.8 ± 5.1 vs 23.3 ± 2.4%) and T2 (52.8 ± 4.6 vs 46.7 ± 2.6 ms) values compared to controls (all p-values <0.001, Table 1). Only 57% of patients had the presence of 2 out of 3 CMR characteristics described by LLC.

Conclusion: In pediatric patients with acute myocarditis, mean global T1, ECV, and T2 values are elevated compared to healthy controls. Mapping techniques can reduce the uncertainty in interpreting relative signal intensities on conventional imaging. Establishing cut points for diagnostic accuracy is limited by lack of a reference gold standard but study in larger patient cohorts and combination of T1M/T2M with other CMR findings may improve diagnostic performance.

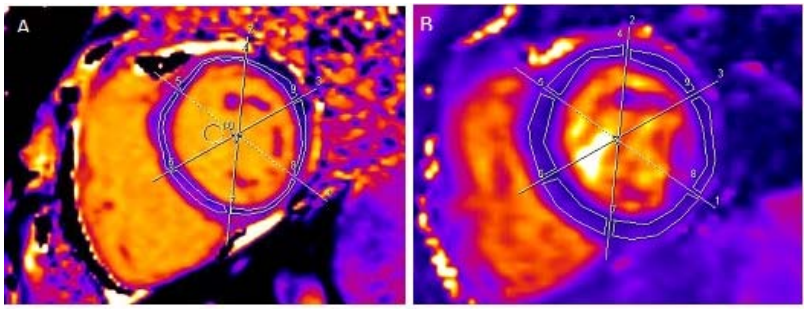

Figure 1 demonstrates: (a) T1 pre-contrast mapping of the basal slice in a patient with acute myocarditis. ROIs are drawn according to the AHA 16 segment model, with an elevated mean global T1 value of 1176 ± 46 ms. Increased signal intensity is noted in the basal lateral wall. (b) T2 mapping of the basal slice in the same patient revealed elevated mean global T2 value of 56 ± 3 ms. The maximum segmental value in the anterolateral segment was 60ms.

Figure 1

	Control (n=39)	Acute Myocarditis (n=23)	p-value
Patient Demographics			

Age at CMR (years)	16.1 ± 2.4	14.0 ± 4.0	0.02
Gender (% male)	69%	61%	0.50
ICU admission	-	13 (57%)	-
Required Inotropes	-	13 (57%)	-
Treated with IVIG	-	12 (52%)	-
Presence of Arrhythmias	-	4 (17%)	-
Elevated Troponin	-	22 (96%)	-
Ventricular Function			
LV Ejection Fraction by Echo (%)	62 ± 5	51 ± 17	0.003
LV Ejection Fraction <45% by Echo	0	9 (39%)	
LV Ejection Fraction by MRI	57 ± 5	52 ± 11	0.01
LV Ejection Fraction <45% by MRI	0	5 (22%)	
LV End Diastolic Volume Indexed (ml/m^2)	92 ± 16	92 ± 23	0.89
Standard MRI Findings			
Abnormal Early Gadolinium Enhancement	-	3 (13%)	-
Abnormal Late Gadolinium Enhancement	-	20 (86%)	-
Abnormal T2-Weighted Imaging	-	13 (57%)	-
Abnormal by Lake Louise Criteria	-	13 (57%)	-
Myocardial Mapping			
Native (Pre-Contrast) Global T1 (ms)	989.6 ± 34.3	1097.9 ± 16.1	<0.0001
ECV (%)	23.3 ± 2.4	29.8 ± 5.1	<0.0001
Global T2 (ms)	46.7 ± 2.6	52.8 ± 4.6	<0.0001
Segmental max T2 (ms)	52.4 ± 4.2	61.2 ± 7.0	<0.0001

ID#: 378984

Numerical Simulation of Pulmonary Hypertension: Effect of 2D Flow and 4D Flow MRI-Based Inlet Boundary Conditions

Christopher J. Francois, MD[4] Sylvana García-Rodríguez[1], James A. Leschke, DO[2], Alejandro Roldán-Alzate[3]

1. University of Wisconsin-Madison, Madison, WI

2. Aurora St. Luke's, New Berlin, WI

3. UW-Madison, Madison, WI

4. University of Wisconsin - Madison, Madison, WI

Background: Computational fluid dynamics (CFD)1 and 4D flow MRI2-4 have been independently used to study pulmonary hypertension (PH) hemodynamics. CFD analyses typically approximate in vivo flow using parabolic velocity or plug flow profiles for inlet boundary conditions. The purpose of this study was to measure effects of 4D flow MRI-derived velocity on PH CFD models.

Methods: After IACUC approval, six adult female beagles were anesthetized. Right heart catheterization (RHC) and cardiac magnetic resonance (CMR) measurements were performed before and after acute PH induction by injection of embolizing micro-beads (150-500 μm) into the right atrium and ventricle. Pulmonary capillary wedge pressure (PCWP) was measured. 4D Flow MRI was performed following administration of 0.1 mmol/kg of gadobenate dimeglumine. Data was reconstructed to 20 time frames for post-processing using retrospective ECG gating and a temporal filter for view sharing. The main and proximal pulmonary arteries were segmented from the 4D flow MRI angiographic images. Surfaces were smoothed and inlet and outlet planes were defined. Volumes were discretized with tetrahedral elements. 4D flow MRI velocity data was analyzed to calculate volumetric flow rate for each time step. CFD was performed using blood fluid properties (density 1050 kg/m3; viscosity 0.0035 Pa*s). No-slip boundary conditions were defined at rigid walls. Two inlet conditions were compared: 1) 2D Flow: time-varying velocity normal to the inlet, using 4D flow MRI-average flow divided by inlet area, and 2) 4D Flow: three-directional inlet velocity from 4D flow MRI, varying in time. Outlets were assigned the PCWP from RHC. The impact of the two inlet conditions on peak systolic CFD calculations of flow distribution to the left (LPA) and right (RPA) pulmonary arteries, peak velocity, pressure gradient, peak WSS, and time-averaged WSS (TAWSS) were assessed.

Results: Table 1 summarizes the results. Mean differences in systolic and diastolic parameters were small, but the range of differences was broad (Figs. 1-2). In general, mean velocity, WSS and TAWSS tended to decrease post-PH by an average of 28.5%, 31.3% and 27.5%, respectively, the last two especially at proximal main vessels. 4D Flow inlets showed slightly higher PH effect.

Conclusion: MRI flow-based inlet conditions for simulations of pulmonary artery hemodynamics were developed. Although mean differences in parameters between 2D and 4D flow MRI inlet conditions were small, regional values showed much greater variation. Given the large ranges of differences locally, it is critical to consider CFD inlet boundary condition definition when modeling proximal pulmonary circulation.

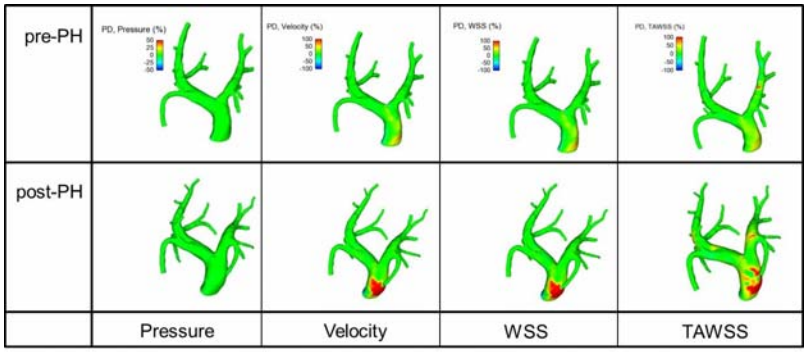

Percent difference distributions comparing CFD hemodynamic parameters as a result of 2D Flow and 4D Flow inlet conditions. Representative case, Dog 2.

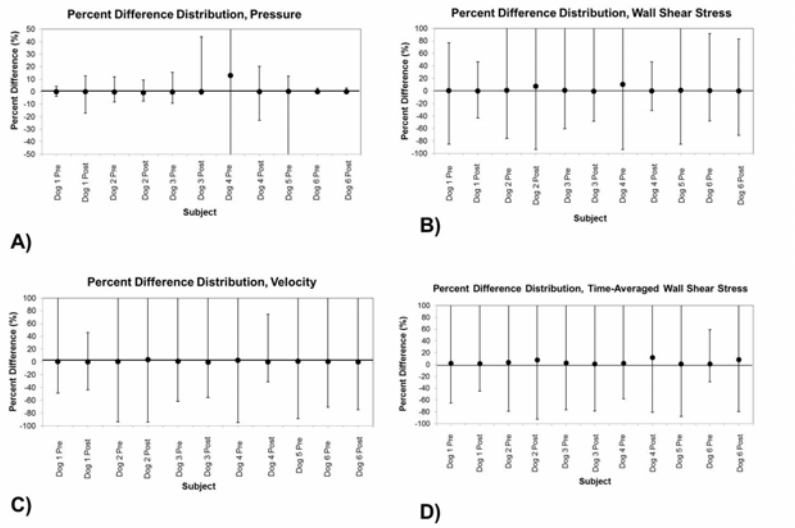

Graphs depicting the mean and range of percent difference comparing 2D Flow and 4D Flow-based CFD inlets. Results correspond to A) pressure gradient, B) velocity, C) WSS at peak systole and D) TAWSS.

Volumetric mean of percent difference (%), comparing various CFD hemodynamic parameters resulting from 2D Flow and 4D Flow inlets before and after PH induction.

Dog	Pre/post	Pressure			Velocity			WSS			TAWSS	
		Min	Max	Mean	Min	Max	Mean	Min	Max	Mean	Min	Max
1	Pre	-3.55	4.33	-0.080	-48.6	105	0.70	-85.0	77.0	0.68	-65.0	345
	Post	-17.2	12.7	0.11	-43.6	46.2	0.39	-43.6	46.2	0.22	-45.0	248
2	Pre	-8.20	11.9	-0.26	-93.7	238	0.88	-75.7	100	1.18	-79.1	390
	Post	-7.40	9.40	-0.71	-94.4	1830	3.68	-93.8	2170	7.32	-92.3	1170
3	Pre	-9.33	15.5	-0.15	-61.9	196	1.08	-60.3	123	1.03	-76.5	151
	Post	-2.10	44.0	-0.061	-55.7	139	-0.14	-48.5	112	-0.28	-78.4	171
4	Pre	-100	2590	12.3	-94.7	1190	2.80	-93.5	1240	10.5	-58.1	236
	Post	-23.0	20.2	0.10	-31.4	74.6	0.20	-31.3	46.4	0.11	-80.7	996

5	Pre	-88.0	12.2	0.17	-88.8	1000	0.91	-84.9	567	1.01	-88.0	250
6	Pre	-1.62	2.59	0.001	-71.0	131	0.48	-47.7	91.8	0.76	-29.0	59.1
	Post	-1.63	3.03	0.03	-74.7	103	0.16	-71.0	82.9	-0.027	-79.7	834
Average		-23.8	248	1.10	-68.9	460	1.01	-66.8	424	2.05	-70.2	441

ID#: 379036

Left ventricular cardiac magnetic resonance parameters of elite, young and masters athletes with quantitative analysis of papillary muscle and trabecular mass

Ibolya Csecs[1] Csilla Czimbalmos[2], Ferenc Suhai[2], Zsofia Dohy[2], Vencel Juhasz[2], Tamas Simor[3], Attila Toth[4], Bela Merkely[2], Hajnalka Vago[2]

1. Semmelweis University Heart and Vascular Center, Tet, Hungary

2. Semmelweis University Heart and Vascular Center, Hungary

3. University of Pecs, Hungary

4. Semmelweis University, Heart and Vascular Center, Hungary

Background:

Cardiac magnetic resonance (CMR) imaging is the gold standard method of evaluation left ventricular volumes, ejection fraction and mass. Using semi-automatic threshold-based (TB) quantification software, quantitative measurement of papillary muscles and trabeculation (TPM) is available based on the different signal intensity of chamber blood and myocardium.

Our goal was to evaluate left ventricular CMR parameters for athletes focusing on age and gender differences and to study how quantitative analysis of left ventricular trabeculation and papillary muscles (TPM) alter normal LV values.

Methods:

CMR examination was performed on 159 elite (121 male, mean age 25±7 y) and 68 age and gender matched sedentary controls (41 m, mean age 27±6 y). 27 masters (43.5±5.8 y) and 52 young (15.9±4.7 y) male athletes were also enrolled. Left ventricular ejection fraction, end-diastolic (LVEDVi), end-systolic, stroke volumes and mass (LVMi) were determined. Using TB analysis (Medis 7.6 QMass software Leiden, The Netherland) TPM, TPMi (TPM/BSA) and TPM% (TPM/EDM*100) were calculated.

Results: Comparing athletes and sedentary controls left ventricular volume indices and mass index were higher in athletes both with and without quantifying TPM ($p<0.001$). TPM index was higher in athletes (male 20.8±4.3 g/m2 vs 18.3±3.1 g/m2, female 16.9±3.5 g/m2 vs 13.6±4.1 g/m2), however control group had higher TPM% (male 20.9±2.5 % vs 19.2±3.9 %, female 22.2±5.8 % vs 19.7±4 %), suggesting a more pronounced hypertrophy of the compact myocardium in athlete';s heart. Comparing male elite, young and masters athletes, LVEDVi (121.3±15.1 vs 112.8±17.0 vs 106.4±18.0) and LVMi (87.0±13.1 vs 79.0±19.8 vs 72.3±18.0) were the highest in elite group ($p<0.001$). Masters athletes had the lowest TPMi among athletes, while their TPM% was significantly higher compared to elite and young athletes ($p<0.001$), which suggests a less intense cardiac adaptation.

Conclusion: Quantitative analysis of myocardial trabeculation could fundamentally alter normal left ventricular parameters in athlete population. Measuring trabecular mass could help us to better know the cardiac adaptation in athletes, and new CMR parameters could help to differentiate between physiological and pathological conditions.

ID#: 379111

Simultaneous multi-slice bSSFP CMR: Is it feasible?

Vanessa Landes, MS[1] Terence R. Jao, PhD[2], Krishna S. Nayak, PhD[1]

1. University of Southern California, Los Angeles, CA

2. University of Southern California, CA

Background: Simultaneous multislice (SMS) imaging combines parallel imaging with multi-band RF pulses and 3D Fourier encoding to significantly reduce scan times. SMS with bSSFP CMR faces unique challenges. bSSFP requires high flip angles (~30-50°) and short RF durations (usually <0.7ms) to avoid off-resonance banding artifact. This is demanding on the RF transmit subsystem. In addition, cardiac coils are sensitive to a large abdominal volume making spurious slice excitation a potential source of artifact. Here, we examine the feasibility of multi-band excitation with adequate spacing to cover 16 of 17 LV myocardial segments (1).

Methods: Several multi-band pulses were designed and tested using the Shinnar Le-Roux algorithm (2) with TBW 2/4, 3-4 slices, duration 0.5-0.96 ms, and with/without optimized phase schedules (3). The pulse with the best tradeoff between minimal spurious slice excitation and shortest duration is proposed to simultaneously acquire 3 short-axis views: 0.648 ms, 30° FA, 3-band, TBW=2, 0.7 cm thickness, and slice centers at z=-2,0,2 cm. Experiments were performed using an 8-channel cardiac coil on a 3T HD23 GE scanner. Phantom experiments A uniform tube phantom filled with water (3 feet long, 5 cm diameter) was used to measure the excitation profile of the 3-band pulse (20 cm FOV, 500x96 matrix) as 10 averaged center phase encode (PE) lines. A fully sampled 3-band dataset was acquired with steady-state bSSFP imaging and encoding at z=-10:2:10 cm using blipped gradients (4). The center PE of reconstructed data at each z-location was plotted to visualize signal contribution from different slices. In-vivo experiments 3 short-axis slices with encoded signal at z=-10:2:10 were acquired with both steady-state and transient bSSFP imaging in a healthy volunteer (M,23) with institutional approval.

Results: Z-profile shows max side-lobe excitation of <2.4% in Figure 1. Imperfections in reconstructed images are predominantly from main 3-band signal leaking into the wrong reconstructed slice in Figure 2. In-vivo results are seen with 11 encoded slices in Figure 3.

Conclusion: SMS excitation is compatible with bSSFP CMR in humans and provides <2.4% signal in the stop-band region. Future work will test this pulse with SMS acquisition for various applications inlcuding cardiac ASL (5). VERSE algorithm or other techniques can be explored to reduce pulse duration and banding artifact (6). **Funding:** NIH R01-HL130494 **References:** (1) Cerqueira MD: AHA. 2002. (2) Pauly J: IEEE. 1991. (3) Wong E: ISMRM. 2012. (4) Setsompop K: MRM. 2012. (5) Kober F: JCMR. 2016. (6) Conolly S: JMRI. 1988.

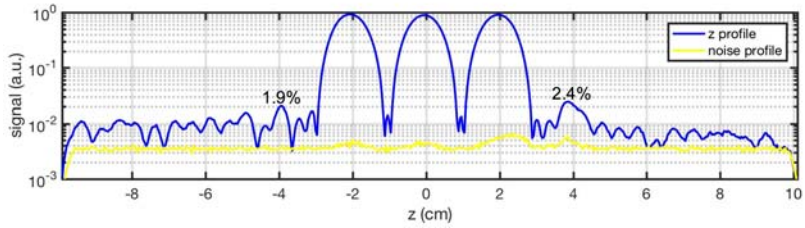

Figure 1: The z-profile of the RF pulse is determined by the average of 10 phase encodes in the acquired image. The noise profile is determined by the average of 10 phase encodes outside the excited region. The signal in the z-profile is consistently higher than the noise profile. Signal of side-lobes at z=±4 is 2.4% and 1.9%, respectively, indicating minimal spurious slice excitation.

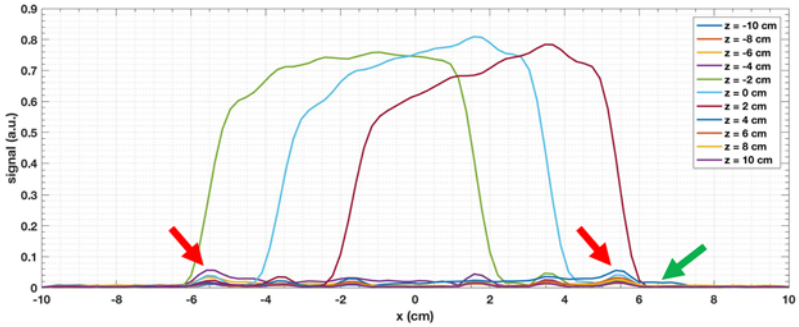

Figure 2: Middle phase encode of reconstructed fully-sampled data with the proposed 3-band pulse in a uniform cylinder phantom, tilted on an angle with the scanner to accentuate differences between excited slices. Slices are encoded at z = -10:2:10 about the SMS pulse with slice centers z=-2,0,2. Imperfections in slice separation at the edge of other excited slices is due to through-slice phase accrual of blipped-CAIPI acquisitions (red arrows). This can be reduced by increasing spacing between slices or by acquiring thinner slices. Slices with z > 7 contain <2% max excited signal, indicating minimal excitation of spurious side slices (green arrow).

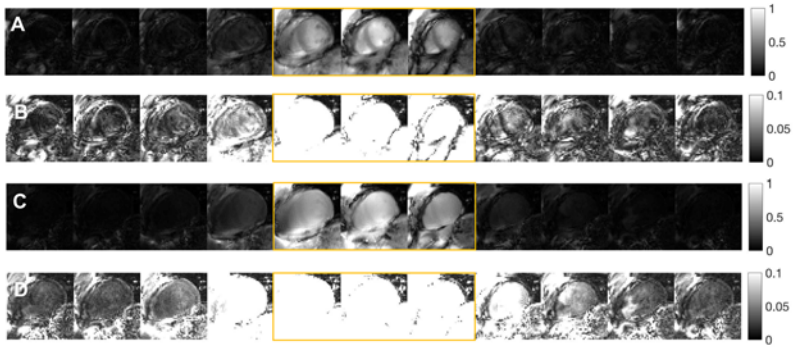

Figure 3: Reconstructed fully-sampled data of 3 short-axis views in the heart using the proposed 3-band pulse with 11 encoded slices using blipped gradients with steady-state bSSFP (A, B) and transient bSSFP after 19 catalyzation steps (C, D). Images are shown with scaling from 0-100% (A,C) and 0-10% (B,D) max signal intensity in the blood pool. Desired slices are boxed (orange). Residue is a superposition of the three imaging slices.

ID#: 379169

Association of Left Ventricular Remodeling and Systolic Function with Native T1 Mapping

Connie W. Tsao, MD, MPH[1] Ulf Neisius, MD PhD[2], Lana Myerson, BS[3], Shiro Nakamori, MD, PhD[4], Warren J. Manning, MD[2]

1. Beth Israel Deaconess Medical Center, Boston, MA

2. Beth Israel Deaconess Medical Center, Harvard Medical School, Boston, MA

3. Beth Israel Deaconess Medical Center

4. Beth Israel Deaconess Medical Center, MA

Background: Adverse left ventricular (LV) remodeling and systolic function are associated with adverse cardiovascular events. Characterizing myocardial tissue with native T1 mapping is of interest to understand pathologic changes that occur with adverse remodeling and decline in systolic function.

Methods: We prospectively studied 28 subjects (71% men, 63±7 years) with (n=13, 46%) and without (n=15, 54%) heart failure (HF) at rest using a 1.5T (Philips Achieva, Best, NL) CMR system. Cine bSSFP acquisitions were obtained in the short-axis orientation (repetition time / echo time [TR/TE] = 3.3/1.6 msec; flip angle = 60°; field of view [FOV] = 320 × 320 mm^2; acquisition matrix = 188 × 188; slice thickness = 8 mm; gap = 2 mm). LV mass, volumes, stroke volume, and ejection fraction were quantified by semi-automated tracing of end-diastolic and end-systolic contours of the LV endocardium (Extended MR WorkSpace, v. 2.3.6.3, Philips). Native T1 mapping was acquired using the slice-interleaved technique (STONE sequence [Weingartner et al, MRM 2014]) (diastolic acquisition, 5 slices, TR/TE = 2.8/1.4 msec, flip angle = 70°, FOV = 360 × 350 mm^2, voxel size = 2.1 × 2.1 mm^2, slice thickness = 8 mm, turbo field echo factor = 86, parallel imaging SENSE factor = 2). Native T1 maps were generated after motion correction. Native T1 mapping measures were independently analyzed by a reviewer blinded to LV measures (MatLab, MathWorks, Natick, MA). The Pearson correlation of LV remodeling measures and T1 were evaluated (SPSS, IBM, NY).

Results: Native T1 was greater in the individuals with as compared to those without HF (1111±59 vs.1077±33, p=0.03). Native T1 was associated with LV end-diastolic (r=0.40, p=0.037) and end-systolic volume (r=0.44, p=0.021), and negatively associated with ejection fraction (r=-0.46, p=0.015). There was a trend toward correlation of native T1 with LV mass/end-diastolic volume, a measure of concentricity (r=0.43, p=0.08).

Conclusion: Measures of LV remodeling and systolic function are related to native T1. Further analyses may determine directionality of the associations and association with cardiovascular outcomes.

ID#: 379182

Association of Baseline Demographics with T1, T2 and ECV Values in Healthy Volunteers

Mark T. Nolan, MBBS[1]Mustafa A. Altaha, MBBS[2], Maria Michalowska, BSc.[3], Bernd J. Wintersperger, MD, FAHA[4], Paaladinesh Thavendiranathan, MD, MSc[1]

1. University Health Network, University of Toronto, Toronto, ON, Canada

2. University Health Network, University of Toronto, Faculty of Medicine, Institute of Medical Science, Toronto, ON, Canada

3. University Health Network, Toronto, ON, Canada

4. Department of Medical Imaging, University of Toronto, Toronto, ON, Canada

Background: Cardiac Relaxometry provides quantifiable cardiovascular MRI (CMR) imaging biomarkers (T1, T2,ECV) which may allow for identification of diffuse fibrosis and/or edema in early pathological states, and therefore provide treatment management and prognostic information. Prior to clinical use of imaging biomarkers at individual patient level, its important to understand their variability based on basic patient demographics. Our objective was to identify and quantify any significant association between age/gender/BMI with T1/T2/ECV measurements in cohort of healthy volunteers.

Methods: 32 healthy volunteers (inclusion criteria: age >18, no significant medical history, no regular medications) were prospectively recruited (age 45.1 ± 13.5 years, range 23 – 80, 57.6% female, BMI 25.2 ±4.4 kg/m^2) to undergo CMR examinations at 1.5T. T2 maps obtained using a T2-prepared single-shot SSFP technique, and native (5(3)3)- and post-contrast (4(1)3(1)2)-T1 maps were obtained using MOLLI technique at basal, mid and apical short-axis locations. Based on native-/post-contrast MOLLI data, ECV values were calculated. All measurements were performed using commercially available software (CVI42). Each volunteer had blood drawn within 2 hours of CMR exam to measure hematocrit.. Student';s t-test used to compare means. Pearson';s coefficient used to assess correlation. Multivariable linear regression models used to assess association independence.

Results: Mean values for T1, T2 and ECV were 1003.3 ± 21.1 msec, 52.0 ± 3.6 msec and 24.9 ± 2.6%. No significant correlation seen between age and T1 (r=-0.01, p=0.96), T2 (r=0.31, p=0.08) or ECV (r=-0.09, p=0.63). Males had lower values compared with females for T1 (999.3 ± 20.2 vs. 1010.2 ± 19.3, p=0.026) and ECV (23.1 ± 1.7 vs. 26.2 ± 2.4, p=0.0002) with no significant difference for T2. Volunteers with BMI>25 kg/m^2 had lower ECV values compared with volunteers with BMI>25 kg/m^2 (24.0 ± 2.4 vs. 25.9 ± 2.6, p=0.038), but there was no difference between T1 and T2. Multivariate linear regression confirmed independent effect of gender on T1 (β =-18.5, p=0.02, multiple R^2 0.25) and independent effects of gender (β -3.47, p=0.0004, multiple R^2 0.09) and BMI (β -0.19, p=0.03, multiple R^2 0.03). No significant association with hematocrit with T1 or T2, and no independent demographic effects on T2.

Conclusion: Gender and BMI are independently associated with ECV values. Apart from a small significant effect of gender on T1, there was no other significant association between baseline demographics and T1/T2 values. When ECV measurements are used clinically for detecting pathology, patients BMI and gender should be considered.

Table 1: Association of Baseline Demographics with CMR Imaging Biomarkers

Correlation (Pearson's)

	Age		Gender		BMI	
	β	p	β	p	β	p
T1	-0.01	0.96	-0.4	**0.02**	-0.26	0.14
T2	0.31	.08	-0.30	0.10	-0.16	0.38
ECV	-0.09	0.63	-0.58	**0.0004**	-0.30	0.09

Mean ± SD

	Age<60 years	Age>60 years	p	Male	Female	p	BMI<25 kg/m²	BMI>25 mg/m²	p
T1 (msec)	1002.3 ± 20.9	1008.5 ± 24.0	0.61	999.3 ± 20.2	1010.2 ±19.3	**0.026**	1010.3 ± 20.4	997.12 ± 20.4	0.08
T2 (msec)	51.9 ± 3.6	53.0 ± 3.5	0.52	50.7 ± 3.5	52.9 ± 3.4	0.1	52.1 ±4.2	51.93 ± 3.1	0.91
ECV (%)	25.0 ± 2.5	24.3 ± 3.6	0.69	23.1 ± 1.7	26.2 ±2.4	**0.0002**	25.9 ± 2.6	24.01 ± 2.4	**0.038**

Table

ID#: 379188

Effects of the High Flow Arterio-venous Fistula on Right Ventricular Contractility in Hemodialysis Patients

Sheena C. Bhagirath[1] Pranav Bhagirath[2]

1. OLVG Teaching Hospital, Amsterdam, Noord-Holland, Netherlands

2. OLVG Teaching Hospital, VU Medical Center, Netherlands

Background: The presence of an arterio-venous fistula (AVF) in hemodialysis patients is a source of constant volume overload. The inability of the right ventricle (RV) to adapt to these conditions leaves it more susceptible to dysfunction as compared to the left ventricle (LV). Early recognition of RV failure in this population, especially in relation to the AVF flow, could contribute towards improved and personalized therapeutic strategies. In this study we utilize tissue-tracking cardiac magnetic resonance to describe the relation between AVF flow and RV contractility. It is hypothesized that the RV contractility will be decreased in patients with a high flow AVF due to volume overload related RV dysfunction.

Methods: Hemodialysis patients (n=7) and age-matched controls (n=5) underwent CMR. Acquisitions were obtained prior to and after dialysis to distinguish between the effects of AVF flow and volume status (fluid overload). The patients were divided in Group 1 (low flow, 1000ml/min) based on the AVF flow measured using ultrasonography. Global longitudinal (GLS), global circumferential (GCS) and global radial strain (GRS) of the RV were calculated with the tissue-tracking module of Circle Cardiovascular Imaging using short- and long-axis cine images.

Results: The contractility parameters between the groups were similar prior to dialysis. After dialysis, there were no significant changes observed between Group 1 (n=4) and the control group (n=5). In comparison to the control group, patients in group 2 (n=3) had a significantly lower GLS (-16.5±3.0% vs. -28.1±4.4%, P<0.05) and GRS (31.0±8.5% vs. 71.7±23.7%, P<0.05) after the dialysis session. No significant change was observed for the GCS between the control group and group 2 (-3.6±10.6% vs. -15.6±3.5%, P=0.06).

Conclusion: These findings suggest that patients with high AVF flow have significantly lower contractile parameters and thereby have at an increased risk for developing right ventricular dysfunction. Tissue-tracking analysis offers the possibility to detect subtle early changes in right ventricular contractility and could have significant therapeutic consequences in this patient group.

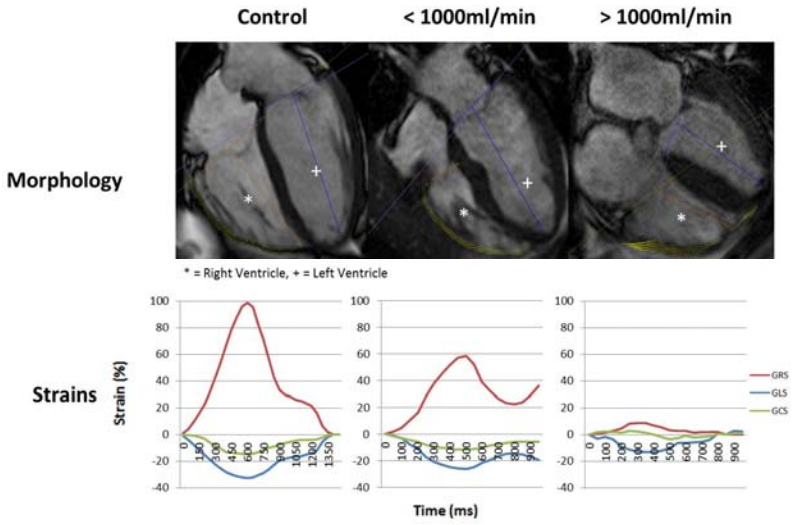

ID#: 379197

Left anterior fascicular block is associated with increased left ventricular scar burden and reduced left ventricular ejection fraction but not with mortality

Johan von Schéele[1] Brett D. Atwater, MD[2], Igor Klem, MD[3], Björn Wieslander, MD PhD[4], Martin Ugander, MD, PhD[5]

1. Karolinska Institutet, and Karolinska University Hospital, Stockholm, Sweden, Sweden

2. Duke University School of Medicine, NC

3. Duke University Medical Center, Durham, NC

4. Department of Clinical Physiology, Karolinska Institutet and Karolinska University Hospital, Stockholm, Sweden, Stockholm, Stockholms Lan, Sweden

5. Karolinska Institutet, and Karolinska University Hospital, Stockholm, Sweden, Stockholms Lan, Sweden

Background: Left anterior fascicular block (LAFB) is a conduction abnormality that has recently been associated with increased mortality. The cause of LAFB remains unknown. The aims of this study were to investigate whether LAFB by 12-lead electrocardiography (ECG) was associated with left ventricular (LV) scar burden, reduced LV ejection fraction (EF) and impaired survival.

Methods: Patients were included if they underwent ECG ≤180 days prior to cardiovascular magnetic resonance imaging (CMR). LAFB (n=55) and normal conduction controls (n=1881) were compared with regards to LV scar burden by CMR late gadolinium enhancement, EF, a dysfunction index, and survival. The dysfunction index has been previously described and was calculated as the difference between maximum possible EF in relation to scar size, and the measured EF. LAFB was defined by 12-lead ECG as a frontal plane QRS axis between -45 to -90 degrees in the absence of hypertrophy, and with QRS duration less than 120 ms.

Results: Compared to controls, patients with LAFB had an increased amount of LV scar (median [interquartile range], 0.7 [0.0-8.5] vs 0.0 [0.0-0.7] %LV mass, p<0.001) and reduced EF (56 [45-60] vs 60 [55-64] %, p=0.005), but no difference in dysfunction index (21 [14-23] vs 21 [16-26] % points of EF, p=0.26). LAFB was associated with increased amount of LV scar (5% increments, odds ratio [95% confidence interval] 1.29 [1.15-1.44], p<0.001), reduced EF (5% decrements, 1.12 [1.03-1.23], p=0.009). Compared to controls, LAFB was associated with a higher prevalence of any scar (58% vs 28%, p<0.001), and specifically more non-ischemic scar (24% vs 10%, p=0.001) but not more ischemic scar (29% vs 19%, p=0.07). No association was found between LAFB and survival (p=0.44).

Conclusion: LAFB is associated with increased LV scar burden and reduced EF, but these differences were not of a large enough magnitude to affect survival. No difference in dysfunction index was found, and this implies that when decreased EF is found in LAFB, the reduction in EF is caused by either scar or other causes, to the same extent as in normal conduction, in patients who have undergone CMR for any reason.

ID#: 379207

Left Atrial Longitudinal Strain by CMR Feature Tracking in ST Elevation Myocardial Infarction

Ariane Binoti. Pacheco, MD[3]Bernardo da Cunha Lopes, MD[1], Rosse C. Osorio, MD[2], Wilson Mathias, MD, PhD[4], Carlos E. Rochitte, MD, PhD[5]

1. Heart Institute - InCor - University of São Paulo Medical School, São Paulo, Brazil, Brazil

2. Heart Institute - InCor - University of São Paulo Medical School, São Paulo, Brazil, Salvador, Bahia, Brazil

3. Heart Institute - InCor - University of São Paulo Medical School, São Paulo, Brazil, Espirito Santo, Brazil

4. Heart Institute - InCor - University of São Paulo Medical School, São Paulo, Brazil, Sao Paulo, Sao Paulo, Brazil

5. University of São Paulo Medical School, Sao Paulo, Brazil

Background: Left atrial (LA) function and diastolic volume are predictors of cardiovascular events. The quantification of left atrial deformation by CMR feature tracking (CMR-FT) is scarcely studied, especially in acute scenarios as ST elevation myocardial infarction (STEMI), where LA volume is usually not modified. We sought to explore the feasibility and relationship of the left atrial (LA) total longitudinal strain (sum of passive and active strain, TLS) obtained by CMR-FT with LV functional and tissue characterization data.

Methods: Forty-three patients at 3-5 days after STEMI and 12 healthy volunteers underwent CMR with cine SSFP sequence with a temporal resolution of at least 50ms in a 1.5T scanner (Achieva, Philips). Left atrial TLS were retrospectively analyzed using a dedicated CMR-FT software (CVi42 version 5.6.3, Circle Cardiovascular Imaging, Calgary, Canada). Two and four-chamber cine views were analyzed by two independent observers. The mean LA TLS were measured and the following analyses were performed: interobserver reproducibility, comparison between groups and correlation with LVEF and MI size. Two STEMI sub-groups based on median TLS value (15%) were defined for additional comparisons.

Results: Left atrial TLS measured by CMR-FT were feasible in all patients and healthy volunteers. Interobserver reproducibility was good as demonstrated by Figure 1 (mean difference = - 0.61, CI -0.15 to 1.38). Left atrial TLS was significantly lower in patients with STEMI compared to healthy controls (16.8±3.12 and 24.2±3.2, $p < 0.001$, Figure 2), and shown a moderate positive correlation with LVEF ($r = 0.44$, $p = 0.03$), and moderate to weak negative correlation with MI size as total mass and %LV ($r = - 0.37$ and $r = - 0.33$, $p < 0,05$). In contrast, LA volume index has shown no significant correlation with LVEF and MI size. STEMI patients with TLS ≥ 15% showed significantly higher LV ejection fraction and salvaged myocardium, and smaller infarct size and area at risk (as % of LV mass, Figure 3).

Conclusion: Left atrial strain was feasible, reproducible and significantly lower in STEMI patients compared to normal healthy volunteers. Within STEMI subgroup lower left atrial total longitudinal strain was associated with worse STEMI CMR left ventricle functional and tissue characterization data.

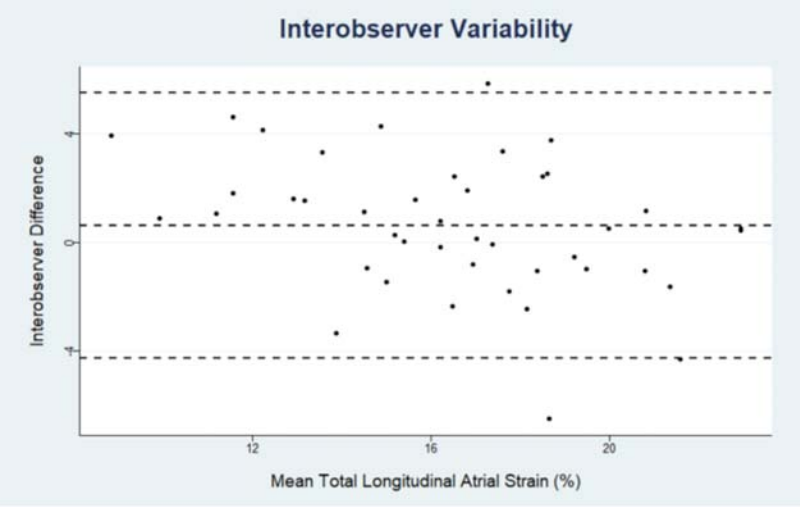

Interobserver Variability

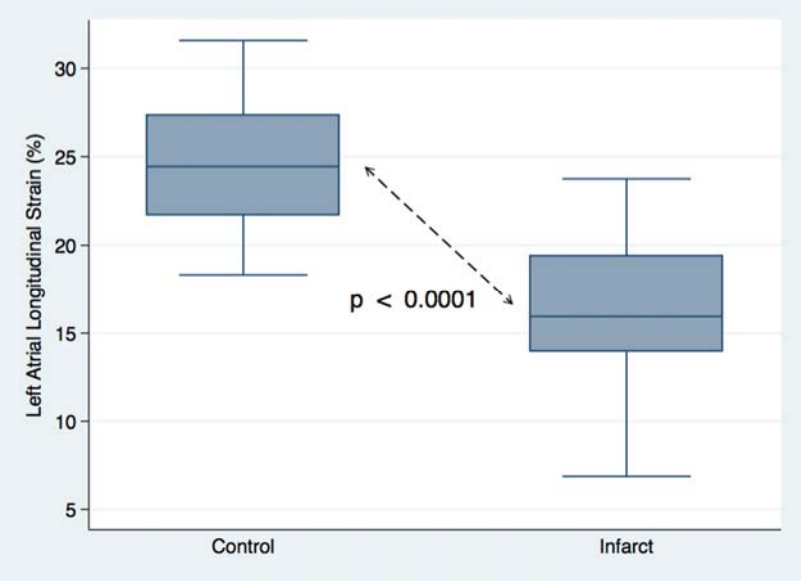

Left Atrial Total Longitudinal Strain - Infarct versus Controls

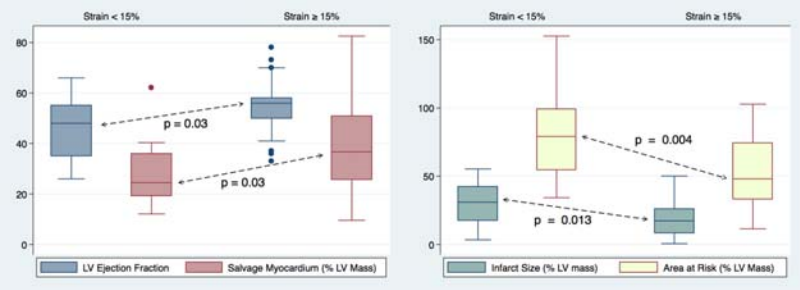

Left Atrial Total Longitudinal Strain in STEMI Subgroups - Left Ventricle Ejection Fraction, Salvaged Myocardium, Infarct Size and Area at Risk Comparisons

ID#: 379219

Characterization of Cardiac Function and Rotational Mechanics in Boys with Duchenne's Muscular Dystrophy

Patrick Magrath, MS [1]Nancy Halnon, MD[2], Pierangelo Renella, MD[3], Daniel B. Ennis, PhD[4]

1. University of California, Los Angeles, Los Angles, CA

2. University of California, Los Angeles, Los angeles, CA

3. UCLA and CHOC Children's Hospital, CA

4. Department of Radiological Sciences, University of California, Los Angeles, CA, USA., CA

Background: Duchenne';s Muscular Dystrophy (DMD) is a fatal genetic disorder affecting 1 in 3000 boys. DMD has a severe impact on heart health, prompting recent clinical trials to include cardiac MRI biomarkers as end-points. Previous reports have indicated that boys with DMD have reduced peak systolic midwall circumferential strain (E_{cc}) {Hor *et al*. Pediatr Cardiol 2015} and LV twist {Reyhan *et al*., MRM 2016} compared to normal controls. Our ***objective*** was to further characterize both peak systolic midwall LV E_{cc} and LV twist in a cohort of boys with DMD compared with healthy volunteers.

Methods: *Study population*: In this IRB-approved and HIPAA-compliant prospective study, boys with DMD (N=17, age=15±5 years) and healthy volunteers (N=7, age=21±5 years) underwent a cardiac MRI examination after obtaining informed consent. *MRI Protocol:* Subjects were imaged at either 1.5T or 3T (Siemens Avanto/Skyra) using: 2D CINE images (1.4x1.4x6mm, TE/T_{Res}=1.2/45.1 ms) and basal, mid, and apical LV short-axis tagged images (1.4x 1.4x8mm, TE/T_{Res}=2.12/24-48 ms, 11-31 phases, tag spacing = 8mm). *Data Processing and Statistical Analysis:* LV Ejection Fraction (EF) was quantified from cine images (Qmass, Medis and Argus, Siemens). Global LV midwall peak systolic E_{cc} and peak LV twist were estimated from tagged MR images (Diagnosoft, Myocardial Solutions). Normally distributed data were compared with a two-tailed t-test. Non-parametric data were compared with a Kruskal-Wallice test. A Holm-Sidak post hoc correction accounted for multiple comparisons. Effect size (Cohen';s *d*) was computed to determine the non-overlap of statistically significant results.

Results: Table 1 and Figure 1 summarize LV ejection fraction, global E_{cc}, and LV twist in boys with DMD and normal volunteers. There was no significant difference in EF between groups (63.0±8.7% vs. 63.7± 2.9%, p = N.S.). A significant reduction in LV twist (9.3°±4.7° vs. 13.7°±3.1°, p< 0.02) was observed in boys with DMD compared to volunteers. Global peak systolic E_{cc} (-16.0±6.7% vs. -18.8±3.4%, p=0.035) was decreased, but not significant after post-hoc correction. The effect size for E_{cc} and LV twist were 0.5 and 1.1, which corresponds to a 33% and a 59% non-overlap of patient and volunteer data respectively. Figure 2 shows a plot of EF vs. E_{cc} and EF vs. LV twist

Conclusion: These results suggest that LV twist measured by MR tagging may be an earlier and more sensitive indicator of changes in cardiac function than EF in boys with DMD. Peak systolic E_{cc} was also decreased, but not significantly. LV twist has a larger effect size and consequently may be a more sensitive measure of early dysfunction. These results corroborate the strain reports of Hor *et al*. and twist results of Rehyan *et al*. The normal volunteers were not precisely age-matched, but peak systolic E_{cc} is known to decrease with age whereas twist remains relative constant until middle age {Reyhan *et al*., JCMR 2013}.

Acknowledgements: This work was supported by NIH NHLBI R01 HL131975.

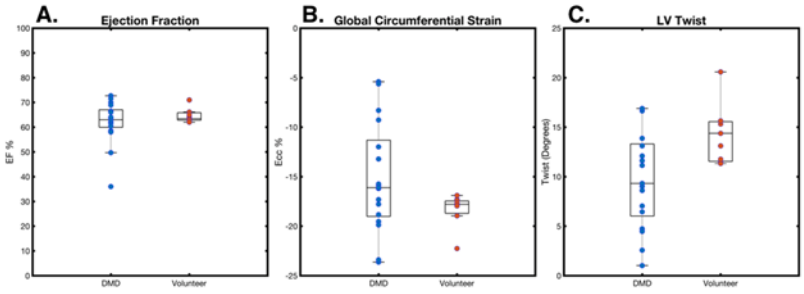

Figure 1. (A) Ejection Fraction, (B) Peak Systolic Ecc, and (C) LV Twist for boys with DMD and Normal Volunteers.

There is no significant difference between patients and volunteers for EF. There is a significant difference in peak LV twist. Ecc is borderline after post-hoc correction. Peak global Ecc and LV twist may be a effective indicators of early cardiac involvement prior to changes in EF.

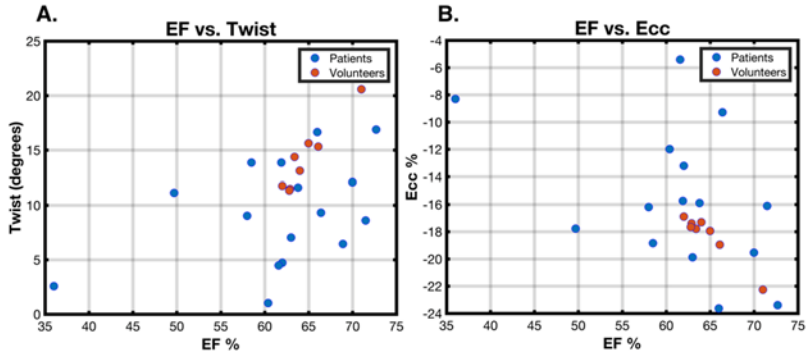

Figure 2. (A) Peak LV twist plotted as a function of ejection fraction (EF) and (B) peak global Ecc plotted as a function of EF for volunteers (red) and boys with DMD (blue). All volunteers had normal twist, EF, and Ecc. Notably, many patients with DMD presented with normal EF, but a pronounced decrease in LV twist and Ecc. `This suggests that for patients with normal EF and reduced twist or Ecc, these measures may be early indicators of involvement

Table 1. Rotational Mechanics

Table 1. Rotational Mechanics	DMD Patients	Normal Volunteers
Global Ecc (%)	-16.0 ± 6.7	-18.8 ± 3.4
Twist (degrees)	9.3 ± 4.7*	13.7 ± 3.1*
LV Ejection Fraction (%)	63.0 ± 8.7	63.7 ± 2.9

Rotational Mechanics and circumferential strain in N = 17 boys with DMD and N = 7 Normal Volunteers shown as median ± standard deviation). * denotes a statistically significant difference at a confidence level of level of p<.05 and post hoc correction.

ID#: 379220

Impact of Arterio-venous Fistula Flow on Ventricular Contractility in Hemodialysis Patients - a Cardiac Magnetic Resonance Study

Sheena C. Bhagirath[1] Pranav Bhagirath[2]

1. OLVG Teaching Hospital, Amsterdam, Noord-Holland, Netherlands

2. OLVG Teaching Hospital, VU Medical Center, Netherlands

Background: The arterio-venous fistula (AVF) in hemodialysis patients often leads to a substantial increase in cardiac output. The resulting high-output state can have detrimental effects in the long term. In this study the relation between AVF flow and ventricular contractility parameters was investigated using cardiac magnetic resonance imaging (CMR).

Methods: CMR was performed in 7 hemodialysis patients and 5 age-matched controls. CMR acquisitions were obtained prior to and after dialysis to differentiate between the effects of AVF flow and volume status (fluid overload). AVF flow, measured using ultrasonography, was used to subdivide the patients in Group 1 (low flow, 1000ml/min). Short- and long-axis cine images were used for calculating global longitudinal strain (GLS), global circumferential strain (GCS) and global radial strain (GRS) with the tissue-tracking module of Circle Cardiovascular Imaging.

Results: There were no significant differences in the contractility parameters between the three groups prior to dialysis. Following dialysis, no significant changes in contractility were observed between Group 1 (n=4) and the control group (n=5). In comparison to the control group, patients in group 2 (n=3) had a significantly lower GLS (-14.2±2.3% vs. -20.4±3.3%, P<0.05), GCS (-13.5±1.6% vs. -22.3±2.1%, P<0.05) and GRS (23.3±4.7% vs. 45.0±8.4%, P<0.05) after the dialysis session.

Conclusion: These findings suggest that patients with high AVF flow are at an increased risk for developing ventricular dysfunction. Tissue-tracking analysis can be used to detect subtle early changes in contractility and could improve the diagnosis and prognosis of this patient group.

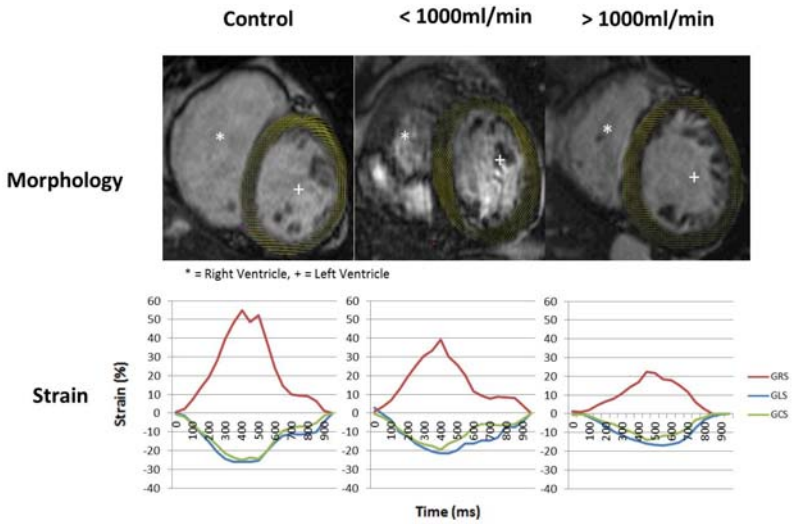

ID#: 379252

MRI findings in patients underwent different types of Total Cavo Pulmonary Connection.

Paolo Ciliberti, MD[1]Valentina Valenti, MD[2], Paolo Ciancarella, MD[3], Carmela Napolitano, MD[1], Giuseppe Muscogiuri, MD[2], Teresa Pia Santangelo, MD[1], Enrica Rossi, MD[4], Davide Curione, MD[5], Adriano Carotti, MD[2], Aurelio Secinaro, MD[1]

1. Bambino Gesù Children's Hospital and Research Institute, Rome. Italy, Lazio, Italy

2. Bambino Gesù Children's Hospital and Research Institute, Rome. Italy, Italy

3. bambino Gesù Children's Hospital and Research Institute, Rome. Italy, Italy

4. Bambino Gesù Children's Hospital and Research Institute, Rome, Italy, Italy

5. Bambino Gesù Children's Hospital and Research Institute, Rome, Italy, Roma, Lazio, Italy

Background: Cardiac Magnetic Resonance (CMR) is nowadays the "gold standard" diagnostic technique for patients underwent Total Cavo Pulmonary Connection (TCPC) completion. Little is known about long term MRI findings after different types of Fontan palliations.

Methods: We retrospectively reviewed CMR performed between 2008 and 2017 in patients underwent TCPC completion in a single center. All the studies comprehended ventricular function assessment and a complete set of cardiac flow allowing calculation of cardiac index and effective cardiac index (measured from the sum of SVC and IVC net flow). Atrio ventricle valve regurgitation was calculated by a combined analysis of volumes and cardiac flows. Medical, surgical and clinical data were collected from hospital records.

Results: One hundred eighteen (118) patients were included. Mean age at MRI was 19.8 ± 6.7 years, mean age at TCPC was 5.4 ± 4.7 years and mean time from TCPC completion was 14.3 ± 6.7 years. Extracardiac tunnel was the most common type of palliation (105 pts; 89%) followed by the Classic Fontan (8 pts; 7%) and intracardiac lateral tunnel (5 pts; 5%). 72 patients (61%) had a left main ventricle, 30 patients (25%) had a right main ventricle, and 16 patients (14%) presented a complex biventricular arrangement. Mean end diastolic indexed volume was 96.9 ± 27.4 ml, mean ventricle ejection fraction was 49.6 ± 21.3%. The cardiac index calculated by the net ascending aorta antegrade flow was 3 ± 0.7 L/min/m2, whilst the effective cardiac index measured by the SVC and IVC net flow was 2.5 V 0.6 L/min/m2. A significant AV valve regurgitation (RF > 20%) was present in 9 patients (7%). Comparing the three subgroups of different type of palliation there were no differences in term of EF ($p = 0.75$), of patients presenting EF < 45% ($p = 0.63$), and of presence of at least moderate AV valve regurgitation ($p=0.88$). Percentage of systemic to pulmonary collateral was also comparable among the different subgroups ($p = 0.2$), as well as the RPA/LPA net antegrade flow ($p= 0.8$), suggesting no significant differences in term of pulmonary arteries flow distribution. No differences were found in term of MACE (death, heart transplant, and listing for heart transplant due to failing). Despite the comparable findings a significant difference was found in term of cardiac index measured by the ascending net flow ($p < 0.001$) between the Extracardiac conduit and the Classic Fontan subgroups. No significant differences were found for CI among the other subgroups. A similar trend almost reaching the statistical significance ($p = 0.06$) was also found in term of effective cardiac index .

Conclusion: Despite comparable value of ventricle function, AV valve regurgitation and percentage of systemic to pulmonary collaterals, cardiac index measured by CMR is higher in patients with Extracardiac Tunnel Fontan compared to the ones underwent Classic Fontan. This finding suggests a better efficiency of the Fontan system in this subgroup, and confirms that cardiac output in Fontan patients is not only related to ventricle function but is dependent on the combination of many different factors.

ID#: 379257

Accuracy in Evaluating Cardiac Geometry, Function and Ventricular Strain in Children with Chronic Heart Failure from the MD-Pedigree study: Echocardiography versus Cardiac MRI

Aurelio Secinaro, MD[1]Agnese Ricotta, MD[2], Lilia Oreto, MD[2], Giuseppe Muscogiuri, MD[2], Paolo Ciliberti, MD[1], Gabriele Rinelli, MD[2], Marcello Chinali, MD[2]

1. Bambino Gesù Children's Hospital and Research Institute, Rome. Italy, Lazio, Italy

2. Bambino Gesù Children's Hospital and Research Institute, Rome. Italy, Italy

Background: Echocardiography is the exam of choice for routine repeated evaluation of heart failure children, however its accuracy has been questioned as compared to CMR, which represents the gold standard for evaluating cardiac geometry. Few data are currently available on the accuracy of echocardiographic parameters as compared to cardiac MRI in chronic HF pediatric population.

Methods: Data from 34 children with chronic HF and dilated cardiomyopathy (age 9 ± 6 years; range 0-18; 40% girls) enrolled in the MD-Paedigree Study cardiomyopathy protocol were evaluated. All patients were in stable chronic HF. Both echocardiographic examination and CMR were performed in all patients. Data reported include: left ventricular volumes from both biplane 2D and 3D data, Ejection fraction, LV mass, left atrial volume, mitral regurgitation and left ventricular global longitudinal strain. Comparison between measurements was performed by Pearson correlation and analysis of interclass correlation coefficient (ICC) with Blant-Altman plots.

Results: Echocardiography showed good accuracy for all measurements of LV diastolic volume as compared to MRI (2D-Apical 4ch= ICC 0.91, 2D-Apical 2ch= ICC 0.86, 3D-Full volume= ICC 0.90) with best correlation found for composite apical Biplane LV volume (BP LV diastolic volume = ICC 0.92) with deviation from MRI due to a general underestimation (mean difference -12%). Similar results were also observed for LV systolic volume (BP LV diastolic volume = ICC 0.91), again due to systemic underestimation from echocardiography (mean difference -13%). Accordingly, despite systematic underestimation of both systolic and diastolic LV volumes, measurement of biplane ejection fraction, showed excellent accuracy as compared to cardiac MRI (ICC= 0.95, mean difference -0.4%). A good correlation was also observed for echocardiographic left ventricular mass LV mass (ICC 0.89) , while low correlation could be observed for atrial volume measured by biplane method (ICC 0.68), longitudinal global LV strain (ICC 0.71, mean difference – 14%) and degree of mitral valve regurgitation (ICC 0.53), all due to underestimation at echocardiography. Of note however, in Cox regression model only echocardiographic global longitudinal strain (Hazard Ratio=0.8; p=0.04), but not MRI global longitudinal strain (p=0.26), was informative of incident cardiovascular events, possibly owing to the lower temporal resolution of cardiac MRI as compared to echocardiography. This was also suggested by the significant correlation between differences among methods in global strain and heart rate (R^2: -0.24; p=0.014), as also displayed in panel D.

Conclusion: In our population of pediatric patients with chronic HF-dilated cardiomyopathy echocardiography shows systematic underestimation in the evaluation of cardiac volumes and of mitral regurgitation as compared to CMR. On the other hand, echocardiography shows higher prognostic value in the analysis of cardiac mechanics, as compared to CMR, as the latter seems to be significantly affected by high heart rate.

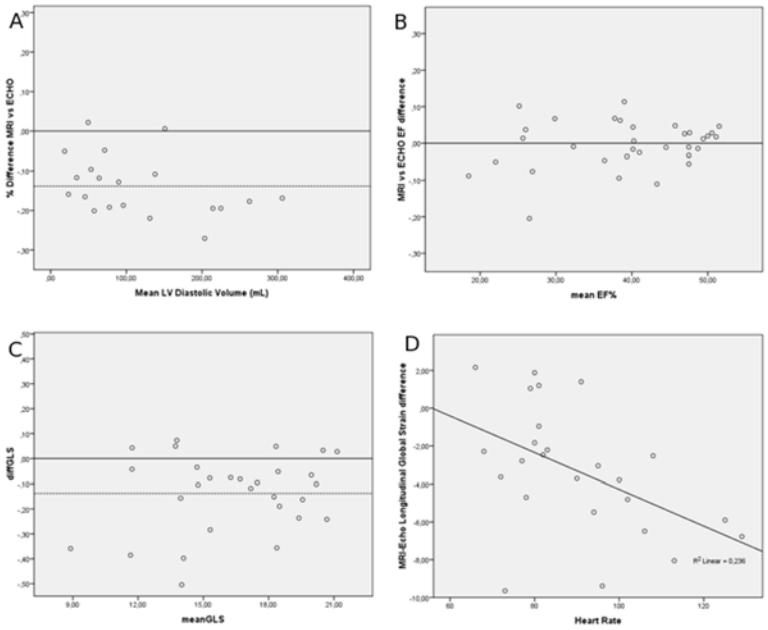

Head-to-head comparison of cardiac MRI and echocardiography for: LV diastolic volume (panel A), LV ejection fraction (panel B), and LV global longitudinal strain (panel C). Impact of heart rate on differences among MRI and echocardiographic longitudinal strain (panel D).

ID#: 379346

CMR-Feature Tracking by Magnetic Resonance Imaging Post Cancer Therapy in Survivors of Hodgkin's Lymphoma

Elizabeth Hillier, B.Sc., PhD Student[1] Negar Mousavi[2], Selwynne M. Hawkins[1]

1. McGill University, Montreal, PQ, Canada

2. McGill University, PQ, Canada

Background: Radiation and chemotherapy remain effective treatments for many different types of cancers. However, the clinical benefit of these therapies is counterbalanced by an increased risk of cardiovascular disease. Strain imaging by echocardiography has been used to monitor subclinical left ventricular dysfunction with the use of Global Longitudinal Strain (GLS) values as a surrogate marker. However, Feature-Tracking with Cardiac Magnetic Resonance Imaging (CMR-FT) offers more potential to detect sub-clinical left ventricular dysfunction. CMR-FT allows endo- and epi-cardial contouring to gain measurements from the entire myocardium as opposed to just regions of interest as in echocardiography. In this pilot study, the novel FT-CMR technique was used to assess left ventricular strain parameters of patients treated with and without chemo- and radiotherapy for Hodgkin';s lymphoma, to determine if there was long-lasting, sub-clinical left ventricular dysfunction post treatment.

Methods: This study performed CMR scans on 13 patients treated with chemotherapy and radiation therapy (CT+RT), six patients with only chemotherapy (CT), and four patients treated only with radiation therapy (RT). CMR-FT values were obtained from SAX SSFP cine images using cvi^{42} tissue tracking (Circle Cardiovascular Imaging). Global peak circumferential strain (E_{cc}), global peak longitudinal strain (E_{ll}), and segmental circumferential strain values were obtained. All values obtained from the patients enrolled in this study are compared to previously published CMR-FT normal values. All data is presented as mean±SD, and segementation values are based on the American Heart Association (AHA) method.

Results: The CT group mean values are: age=29.83±5.3, sex=4M & 2F, and time (in months) since treatment ended (TSTE)=66.67±44.58. RT group values are: age=46.75±4.7, sex= 3F & 1M, and TSTE=262.5±60.1. CT+RT group values are: age=37.77±10.8, sex= 9F & 1M, and TSTE=79.69±90.51. CMR-FT analysis showed no significant E_{cc} difference between CT (-17.12±3.0), RT (-19.62±3.5), or CT+RT (-19.27) and the normal E_{cc} value. All AHA segments are significantly different than normal values in the RT group, $p<0.01$. All segments are significantly different than normal values in the CT group except for segments 11 ($p=0.6808$) and 12 ($p=0.1975$), and all are significant in the CT+RT group except for segments 8 ($p=0.0511$), 9 ($p=0.1232$), 11 ($p=0.0738$), and 12 ($p=0.1392$).

Conclusion: CMR-FT analysis suggests the presence of significant left ventricular strain abnormalities in all treatment groups, including those only treated with radiation therapy. The long mean time from the end of treatment for radiation therapy may indicate that this form of treatment may have long-term sub-clinical effects on left ventricular function. This further reinforces the need for the development of more sensitive ways to diagnose and monitor left ventricular function in cancer survivors.

E_{CC}	RT+CHEMO			CHEMO only			RT only		
Subject	Mean	P (2-tailed)	Sig (p<0.05)	Mean	P (2-tailed)	Sig (p<0.05)	Mean	P (2-tailed)	Sig (p<0.05)
1	-22.04 ± 3.4	< 0.0001	*	-19.15 ± 2.1	0.0041	*	-19.92 ± 2.5	0.0007	*
2	-18.33 ± 4.1	< 0.0001	*	-14.84 ± 2.2	0.0010	*	-17.24 ± 1.6	< 0.0001	*
3	-15.99 ± 3.3	< 0.0001	*	-15.52 ± 2.9	0.0013	*	-14.11 ± 2.3	< 0.0001	*
4	-15.74 ± 2.8	< 0.0001	*	-16.86 ± 4.2	0.0059	*	-14.42 ± 2.1	< 0.0001	*
5	-18.29 ± 4.3	< 0.0001	*	-18.56 ± 4.1	0.0167	*	-17.2 ± 2.9	0.0002	*
6	-21.3 ± 3.7	0.0005	*	-20.76 ± 3.0	0.0351	*	-18.39 ± 4.0	0.0050	*
7	-22.32 ± 4.6	0.0004	*	-19.44 ± 1.7	0.0018	*	-19.42 ± 2.9	0.0006	*
8	-19.8 ± 5.9	0.0113	*	-19.34 ± 3.4	0.0511		-18 ± 3.1	0.0030	*
9	-21.42 ± 4.5	0.0244	*	-21.21 ± 3.2	0.1232		-17.59±4.7	0.0145	*
10	-22.69 ± 3.9	< 0.0001	*	-23.58	0.0007	*	-20.84±6.1	0.0224	*
11	-25.46 ± 4.6	0.6808		-21.97 ± 3.0	0.0738		-20.85 ± 4.8	0.0470	*
12	-24.26 ± 4.1	0.1975		-22.68 ± 3.1	0.1392		-18.26±5.6	0.021	*
13	-18.61 ± 4.4	< 0.0001	*	-14.56 ± 2.2	0.0021	*	-15.89 ± 3.6	0.0012	*
14	-19 ± 5.3	< 0.0001	*	-15.59 ± 2.8	0.0018	*	-15.63 ± 4.4	0.0014	*
15	-19.56 ± 4.3	< 0.0001	*	-18.3 ± 1.6	0.0004	*	-18.7 ± 5.1	0.0004	*
16	-19.64 ± 5.0	< 0.0001	*	-18.35 ± 2.1	0.0023	*	-18.23 ± 3.0	0.0004	*

Segmental circumferential strain in all three treatment groups compared to normal values

ID#: 379141

How cardiac magnetic resonance imaging could help the differential diagnosis in MINOCA? - Single center data of a 5-year period

Hajnalka Vágó[1] Ibolya Csecs[2], Csilla Czimbalmos[3], Ferenc Imre. Suhai, MD[4], Ibolya Csecs, MD[5], Liliana Szabo[3], Andrea Szucs[3], Anna Kiss[3], Tamas Simor[6], Attila Toth[7], Bela Merkely[3]

1. Heart and Vascular Center of Semmelweis University, Hungary

2. Semmelweis University Heart and Vascular Center, Tet, Hungary

3. Semmelweis University Heart and Vascular Center, Hungary

4. Semmelweis University, Budapest, Pest, Hungary

5. Heart and Vascular Center of Semmelweis University, Budapest, Pest, Hungary

6. University of Pecs, Hungary

7. Semmelweis University, Heart and Vascular Center, Hungary

Background:

The results of routinely used diagnostic methods in MINOCA patients are not conclusive in many cases. The aim of our study was to establish the diagnostic role of cardiac magnetic resonance (CMR) imaging and to determine the CMR characteristics of patients with clinical signs of STEMI but normal coronary angiography.

Methods:

In our study 195 consecutive patients (140 male; 38±16 y) with positive troponin levels, persistent chest pain and localized ST-elevation underwent CMR examination following coronary angiography in the first 1-7 days. Follow-up CMR scan was performed after 3-6 months in a subgroup of 75 patients with myocarditis, adverse cardiac event (hospitalization due to heart failure or arrhythmia, cardiac death) was recorded.
We prepared cine movie in long and short-axis planes, T2-weighted spectral inversion recovery, and delayed contrast enhancement images. Left ventricular end-diastolic and end-systolic volumes, ejection fraction (EF), mass (LVM) were evaluated and myocardial necrosis/scar was quantified. We analysed laboratory parameters (high sensitive troponin-T, creatin-kinase MB, C-reactive protein) and determined cardiovascular risk factors.

Results:

CMR proved myocarditis in 125 pts (106 male), myocardial infarction (MI) in 30 cases (17 male), Tako-Tsubo cardiomyopathy (CMP) in 16 women, myocardial contusion in one case and in 23 pts (16 male) there was no CMR abnormality. In 35% of the cases (N=69) CMR findings modified the original diagnosis. Hypertension was a less frequent cardiovascular risk factor in pts with myocarditis.
EF was lower in Tako-Tsubo CMP (42.1±9.6 vs MI:56.3±6.8; vs myocarditis:55.2±8.2; $p<0.001$), but there was no difference between myocarditis and MI. The extent of necrosis was larger in myocarditis than in MI (20.7±15.1g vs 14.2±11.3g; $p<0.01$). There was a significant positive correlation between the extent of necrosis and laboratory parameters, and a negative correlation between the extent of necrosis and EF, and between the hsTnT and EF both in myocarditis and MI ($p<0.05$).
Comparing acute and follow-up CMR parameters EF increased (54.7±8.3 vs 60.2±5.0%), the scar persisted in 75%, but shrank (20.2±13.3 vs 6.6±7.1g) and the LVM decreased (128.0±28.4 vs 112.7±23.6g) ($p<0.001$). Patients who had scar on the follow-up CMR had a lower EF and larger necrosis in the acute phase (53.2±8.2 vs 59.7±6.6%) compared to patients without scar on the follow-up CMR. During follow-up (mean:1409±716 days) no adverse cardiac event occurred.

Conclusion: CMR has proved to play an essential role in refining the diagnosis and in providing precise morphological and functional information for MINOCA pts. However, in myocarditis mimicking STEMI the scar remains in 75% of the cases, the clinical and CMR follow-up proved good prognosis.

ID#: 379149

Velocity sensitivity of inner-volume cardiac echo planar imaging

Ahsan Javed, MSKrishna S. Nayak, PhD

University of Southern California, Los Angeles, CA

Background: Inner volume echo planar imaging (IV-EPI) has recently been shown to be feasible and useful for cardiac diffusion tensor imaging (DTI) (1) and cardiac arterial spin labelling (ASL) (2). One previous study demonstrated the sensitivity of IV-EPI to velocity-selective saturation effects caused by the crusher gradients around the 180º refocusing-pulse (see Fig. 1). In this study, we characterize the effect of velocity-cutoff (V_{cut}) on myocardial signal both in systolic and diastolic IV-EPI images.

Methods: One subject was scanned on a GE 3T scanner using single-shot partial-Fourier IV-EPI, sequence shown in Fig 1. Eleven images were acquired at each V_{cut} for a total of 121 images at 11 equally spaced from 5cm/s to 30cm/s during systole and diastole. V_{cut} was calculated using the equation : $V_{cut}=\gamma AT$, γ where is the gyromagnetic-ratio, A is the area of each crusher gradient in Fig. 1, and T is the separation between them (3). The partial-Fourier data was reconstructed using GE-Orchestra homodyne reconstruction and converted to SNR units (4). Images for each V_{cut} were aligned using advanced normalization tools (ANTs) (5) and then averaged before manual-segmentation. The myocardium was divided into 6-segments and the data for each segment was fitted to the model $S=M_o sinc(v_z/V_{cut})$, M_o is the scaling term in SNR units and v_z is the longitudinal-velocity in cm/s.

Results: Results are shown in Fig. 2 and 3. The longitudinal-velocity of the myocardium was estimated to be 0cm/s during diastole and 1.84 - 4.0cm/s during systole. The velocity was higher in the lateral-wall than the septal-wall, consistent with literature (6,7). However, the residue for the fitting was particularly high for myocardium in diastole, suggesting inaccuracy of the model or by an inadequate range of V_{cut} unable to capture velocity saturation effects in myocardium during diastole.

Conclusion: This study suggests that to avoid myocardial velocity saturation effects in IV-EPI, it is appropriate to use a Vcut>>5cm/s at mid-diastole or Vcut>>20cm/s at end-systole. This study will have to be repeated in several subject to be more conclusive. This study demonstrates the ability to experimentally characterize velocity saturation effects of IV-EPI using a simple model originally derived for blood-flow in blood-vessels. This data may also inform the development of better models for myocardial longitudinal-velocity distribution.

Funding:

NIH R01-HL130494 **References**
1. Lau-AZ(MRM-2015).
2. Javed-A(ISMRM-2017).
3. Wong-EC(MRM-2006).
4. Kellman-P(MRM-2005).
5. Avants B(Insight-2009).
6. Greaves-K(HLC-2004).
7. Codreanu-I(JCMR-2010).

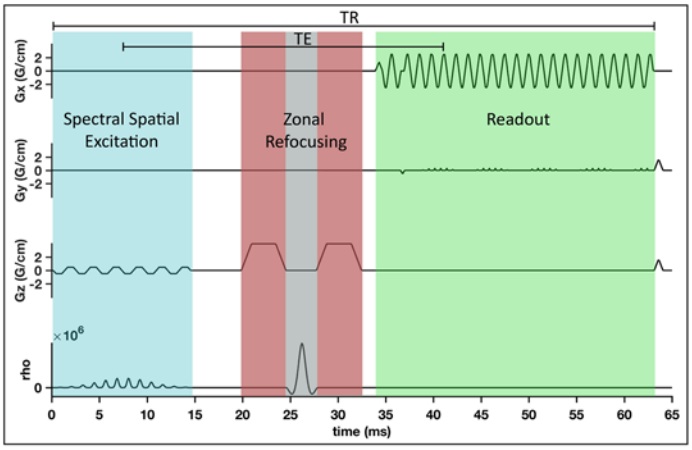

Figure 1: EPI image acquisition, which is comprised of a (blue) 90º spectral-spatial excitation pulse, (gray) 180º spin echo pulse that is spatially selective in the y direction, (red) z crusher gradients that suppress signal from outside the inner volume and suppress flowing blood above a cut off velocity Vcut, and a (green) single-shot partial Fourier EPI readout. The imaging parameters were TE = 32.9 ms , matrix size: 128 x 64, partial k-space ratio: 5/8, FOV 28x14 cm. TE was kept constant at 32.9 ms for all Vcut.

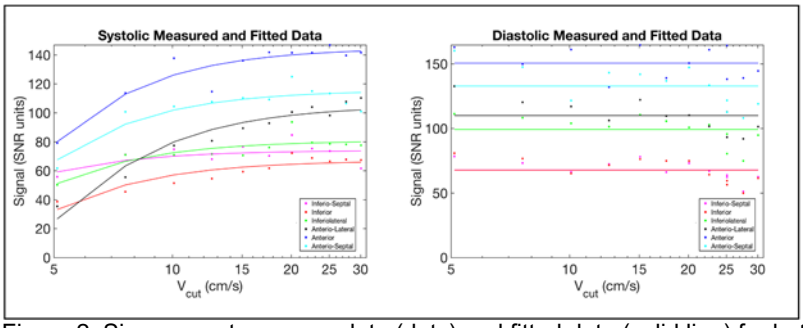

Figure 2: Six segment measure data (dots) and fitted data (solid line) for both systole (left) and diastole (right). Increasing velocity cutoff increased the signal in systole. However, the signal during diastole remained relatively constant with change in velocity cutoff. The model fitting error is larger in diastole than in systole.

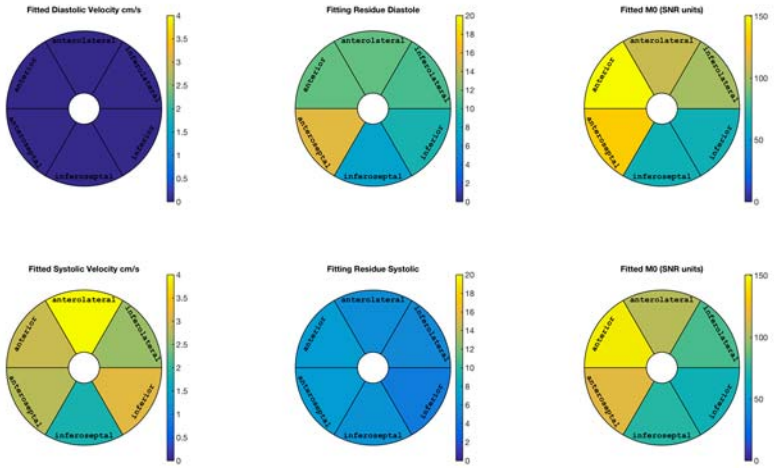

Figure 3: Bullseye plots showing estimated velocities, residue of fit and M0 of myocardium. The RMSE residue shows the accuracy of the fit. Mo includes proton density, coil sensitivity, T2* weighting, and B1+ inhomogeneity.The velocity during diastole is estimated to be 0 cm/s with a large fitting residue. The velocity during systole is estimated to be > 0cm/s however it varies from 1.84 cm/s - 4.0 cm/s through out the myocardium. In

general the residue is low and about the same through out the myocardium and myocardial velocity is higher in the lateral wall compared to the septal wall. The M0 is smoothly varying throughout the myocardium.

ID#: 379379

Genotype-Phenotype correlation in ARVC - a CMR study

Silvia Castelletti, MD[1] Rachel Bastiaenen, PhD[2], Caroline Coats, PhD[3], Antonis Pantazis, MD[4], James C. Moon, MD[5]

1. Istituto Auxologico Italiano, N/A, Italy

2. Guy's and St Thomas NHS Foundation Trust, London, England, United Kingdom

3. UCLH, Scotland, United Kingdom

4. Royal Brompton Hospital, England, United Kingdom

5. Barts Heart Centre, England, United Kingdom

Background: Arrhythmogenic Right Ventricular Cardiomyopathy (ARVC) is a rare inherited cardiac disease characterized histologically by fibro-fatty replacement and clinically by arrhythmias, heart failure and sudden cardiac death. Although initially though RV only, LV and biventricular involvement is increasingly recognized. Mutations in five desmosomal genes account for 30-60% of cases particularly plakophilin-2 (PKP2) and desmoplakin (DSP). Predominant LV involvement is typically observed in disease due to DSP mutations but appears rare in PKP2 mutations carriers. The capability of modern cardiovascular magnetic resonance (CMR) sequences to image fibrosis has led to better recognition of LV involvement. We compared CMR tissue characterization findings in a (single/multi centre) cohort of patients with ARVC due to PKP2 and DSP mutations.

Methods: A prospective tertiary centre study of 30 unrelated probands with either pathogenic PKP2 (n=16) or DSP gene mutation (n=14) and fulfilled ARVC modified 2010 task force criteria (TFC). CMR was performed according to a standard ARVC protocol including dedicated RV views and 3rd generation MOCO late gadolinium enhancement on a 1.5-T Magnet (Avanto Siemens Medical Solution).

Results: In the DSP group compared to PKP2 group, left ventricular ejection fraction (LVEF) was lower (59±8% vs 67±7%; p=0.007) and LV volumes were greater (LV end diastolic volume 82±8mL/m^2 vs 69±11mL/m^2, p=0.001). Fatty infiltration was only detected in 3 patients – these were all in the DSP group (n=3, 21%) and the abnormal fat signal was observed in the LV. The pattern of late enhancement was strikingly different between the groups: LV late gadolinium enhancement (LGE) was more prevalent in the DSP group (54% vs 13%, p=0.03) but RV LGE was higher in PKP2 patients (50% vs 38%, p=0.6).

Conclusion: ARVC has a gene specific phenotype for both structural and tissue abnormalities with the RV affected in PKP2 and LV in DSP.

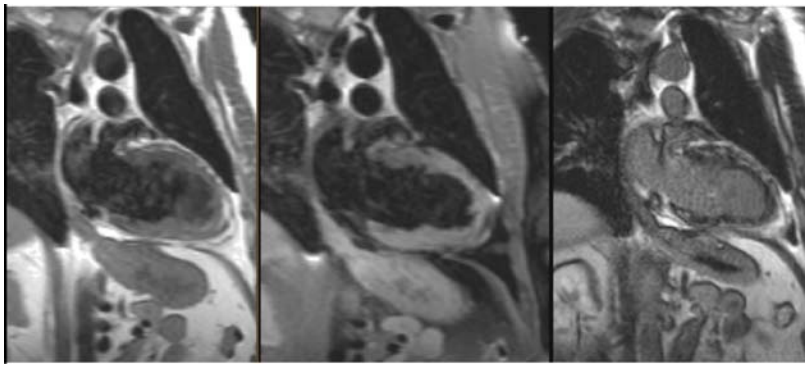

DSP patient

ID#: 379353

Association of myocardial deformation by tissue tracking CMR with fibrosis in patients with Fabry disease

Rui Placido, MD[1]Ana G. Almeida[2], Patricio Aguiar[1], Gustavo Lima da Silva[1], Tatiana Guimaraes[2], Claudio David[2], Fausto J. Pinto[1]

1. Santa Maria University Hospital, Cardiology Department, Lisbon Academic Medical Center, CCUL, Lisbon, Portugal, Lisboa, Portugal

2. Santa Maria University Hospital, Cardiology Department, Lisbon Academic Medical Center, CCUL, Lisbon, Portugal, Lisbon, Lisboa, Portugal

Background: Myocardial fibrosis is a common trait in Fabry cardiomyopathy and is associated with disease progression and prognosis. This study aimed to assess the myocardial deformation in patients with Fabry disease (FD) in order to evaluate the role of tissue tracking CMR as a method for the non-invasive determination of myocardial fibrosis.

Methods: We included 45 patients with Fabry disease (35.8 ± 11.9 year-old; 24 males), all in sinus rhythm and without contraindications to CMR. LV volumes, ejection fraction were assessed by cine CMR. Myocardial fibrosis was evaluated by late gadolinium enhancement (LGE) from a stack of short-axis planes and the percentage of LGE areas of LV mass was quantified. Regional myocardial deformation was assessed by tissue tracking CMR (cvi42, Calgary) from cine CMR images obtained in long and short-axis planes, in order to measure the global longitudinal, radial and circumferential systolic strain.

Results: In twenty-two patients (49%) LGE was found, located predominantly at the basal lateral and posterior segments, with a mean volume of 1.8±1.1% of total LV mass. Patients with LGE had a lower global systolic longitudinal strain than those without (-15.8±3.0% versus -19.2±2.1%, respectively; p2.5% was associated with lower longitudinal strain values in comparison with segments with <2.5%; (-8.9 ± 5.9% vs -11.9±6.5%) There was no difference between these 2 groups regarding the LV volumes, ejection fraction, radial or circumferential strain. ROC analysis revealed that the global longitudinal systolic strain of basal postero-lateral segments was the most powerful predictor to distinguish between patients with and without LGE (sensitivity 89%; specificity 91%, AUC=0.812; p<0.01).

Conclusion: LGE was associated with lower longitudinal strain in the LV segments with fibrosis in patients with Fabry disease, as assessed by tissue tracking LGE, which may represent a surrogate marker of fibrosis.

ID#: 379364

Utilization of Superparamagnetic Iron Oxide Contrast Agents for the Determination of Myocardial Adipose Inflammation Using T2 Star as a Marker for Coronary Artery Disease in HIV Positive Patients

Korey M. Haddox, D.O.[1] Saagar Sanghvi, M.D.[2], Jonathan Forquer, D.O.[2], Carl F. Fichtenbaum, M.D.[3], Robert O'Donnell, M.D., M.S.[1], David M. Harris, MD[4]

1. University of Cincinnati Medical Center, Cincinnati, OH

2. University of Cincinnati Medical Center, OH

3. University of Cincinnati Medical Center

4. University of Cincinnati, Cincinnati, OH

Background: Coronary artery disease (CAD) is a common cause of morbidity and mortality in individuals infected with HIV. The pathogenesis of CAD involves a host of inflammatory and immunologic processes, and inflammation in adipose tissue may be associated with the progression of atherosclerotic disease, especially in HIV-infected patients. Cardiac MRI (cMRI) allows for the detection of monocyte activity, using superparamagnetic iron oxide contrast agents (SPIO). SPIOs are phagocytosed by monocytes which migrate to areas of inflammation. Tissue T2 star changes signify the presence of monocyte/macrophages, indicating inflammation. Here, we evaluate the ability of cMRI to measure inflammation in pericardial adipose tissue as a potential surrogate marker for CAD risk.

Methods: Patients with or without HIV and/or CAD were identified by the Infectious Disease Center and the cardiac catheterization laboratory. Each participant had an initial contrasted cMRI for evaluation of baseline characteristics including structure, function, edema, and scar. Feraheme 5 mg/kg IV was administered after the initial cMRI to a maximum dose of 510 mg and a repeat cMRI was obtained 48-72 hours later. T2 star values were measured for the myocardium, liver, and pericardial fat by a blinded physician both before and after the administration of IV iron (Image 1).

Results: Three patients with HIV and CAD, four with HIV and no CAD, and four with CAD without HIV were enrolled. There were 8 males and 3 females ranging in age from 44 to 69 years (average 59 years). The T2 star values obtained for the myocardium, pericardial fat, and liver after the administration of Feraheme were consistently less than those obtained prior to administration (p = 0.015, 0.035, 6.97x10-8 respectively). The average decrease in T2 star was 8.06 (SD 12. 5 ms) for pericardial fat, 13.0 (SD 16.4 ms) for myocardium, and 19.4 (SD 4.7 ms) for liver. The greatest decrease in T2 star values for pericardial fat were seen in the cohort with both HIV and CAD (Table 1) with an average decline of 14.8 ms (SD 20.6 ms). However, this decrease was not statistically significant when compared to the cohort with HIV without CAD (p 0.31) which had an average decrease of 6.5 ms (SD 7.0) or to the cohort with CAD without HIV (p = 0.28) which had an average decrease of 4.6 ms (SD 4.0).

Conclusion: Inflammation of pericardial adipose tissue can be reliably quantified on cMRI with the use of SPIOs. This pilot study shows the feasibility of quantifying inflammation in pericardial fat in HIV positive patients and SPIOs may represent a novel technique for evaluating CAD risk in this population.

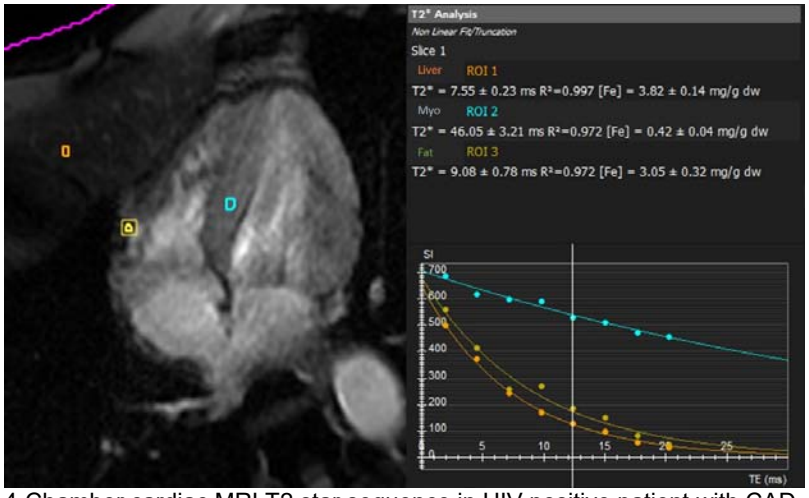

4-Chamber cardiac MRI T2 star sequence in HIV positive patient with CAD

Average decline in T2 star values following the administration of IV iron oxide contrast agent

COHORT	MYOCARDIUM	LIVER	PERICARDIAL FAT
HIV+/CAD+	2.1 ms (SD 6.0)	21.1 ms (SD 7.1)	14.8 ms (SD 20.6)
HIV+/CAD-	13.6 ms (SD 7.9)	19.1 ms (SD 4.3)	6.5 ms (SD 7.0)
HIV-/CAD+	20.7 ms (SD 22.3)	18.3 ms (SD 1.2)	4.6 ms (SD 4.0)

ID#: 379399

Extracellular Volume Imaging, Aortic Distensibility and CMR-Feature Tracking by Magnetic Resonance Imaging Post Mediastinal Radiotherapy in Survivors of Hodgkin's Lymphoma

Ying Jia Gong[1] Elizabeth Hillier, B.Sc., PhD Student[2], Edward Hulten[3], Kelly Davison[4], Tiago Teixeira[5], Marcio Bittencourt[6], Chantal Séguin[4], Silke Friedrich[4], Matthias Friedrich[4], Christine Lambert[7], Tarek Hijal[7], Carolyn Freeman[7], Negar Mousavi[7]

1. McGill University, Lachine, Canada

2. McGill University, Montreal, PQ, Canada

3. Walter Reed National Military Medical Centre

4. McGill University, Canada

5. Centro Hospitalar entre Douro e Vouga, Portugal

6. University of São Paulo, Brazil

7. McGill University, PQ, Canada

Background: Radiotherapy (RT) for Hodgkin';s lymphoma often involves incidental exposure of the cardiovascular system to ionizing radiation causing myocardial fibrosis and increased vascular stiffness. Novel quantitative imaging of extracellular volume fraction (ECV), aortic distensibility, and CMR-Feature Tracking (CMR-FT) may be able to detect subclinical cardiovascular injury such as diffuse myocardial fibrosis and adverse vascular remodeling. We aimed to determine whether the myocardial extracellular volume was increased or the aortic distensibility was decreased in patients treated with mediastinal radiation therapy. Additionally, CMR-FT analysis was utilized to assess if global peak systolic strain values were reduced when compared to previously-published normal values.

Methods: This was a prospective pilot study. Cardiac magnetic resonance imaging was performed in 14 lymphoma patients who received mediastinal radiotherapy and 4 lymphoma patients who did not, with T1 mapping before and after injection of gadolinium contrast. CMR-FT analysis was performed to obtain global peak longitudinal (E_{ll}) and peak circumferential (E_{cc}) strain values.

Results: The radiation-treated cohort consisted of 4 males and 10 females with a median age of 42.5 years (range 21-58), presenting at a median of 124 months after radiotherapy with a mean left ventricular ejection fraction of 62±7%. The indexed LV mass was 57±7 g/m^2, native T1 for myocardium was 1272±44 msec, and the ECV was 28.0±5.0%. The distensibility of the ascending aorta was 17.2±9.8mmHg$^{-1}\cdot10^{-3}$ and that of the descending aorta was 16.8±9.4mmHg$^{-1}\cdot10^{-3}$. The control group consisted of 4 males with a median age of 26.5 years (range 25-37), and mean left ventricular ejection fraction of 56.5±3%. The index LV mass was 67±10 g/m^2, native T1 for myocardium was 1232±71 msec, and the ECV was 28.3±5.6%. The distensibility of the ascending aorta was 21.8±5.6mmHg$^{-1}\cdot10^{-3}$ and that of the descending aorta was 17.0±0.7mmHg$^{-1}\cdot10^{-3}$. The tracked E_{ll} values were significant for both the radiation-treated cohort (-16.07±1.997; p-16.81±2.292, pE_{cc} values were significant.

Conclusion: In this pilot study, mediastinal radiotherapy was not associated with an increase in ECV values or aortic distensibility. However, CMR-FT suggests there may be long-term underlying subclinical functional impairments of the left ventricle. Further research and larger-scale studies are still needed to validate these findings and to evaluate the effect of new advanced radiation techniques on the cardiovascular system.

ID#: 379400

3D dark-blood interleaved with gray-blood (DIG) vessel wall imaging of the aortic arch

Zhaoyang Fan, PhD[1] Qi Yang, MD PhD[2], Guoxi Xie, PhD[3], Xiaoming Bi, PhD[4], Debiao Li, PhD[5]

1. Cedars-Sinai Medical Center, CA

2. Cedars-Sinai Medical Center, China (People's Republic)

3. School of Basic Science, Guangzhou Medical University, Guangzhou, China; Shenzhen Institutes of Advanced Technology, Chinese Academy of Sciences, China (People's Republic)

4. Siemens Healthineers, Los Angeles, CA, United States, CA

5. Cedars-Sinai Medical Center, Los Angeles, CA

Background: Atherosclerotic disease of the aortic arch has been considered a potential cause of cryptogenic stroke. Vessel wall MR can directly probe atherosclerotic lesions to provide comprehensive assessment of plaque burden and instability. However, its clinical adoption for aortic arch imaging is hindered by long imaging time associated with the needs for 3D and multi-contrast imaging. In this work, we proposed a motion-compensated, time-efficient 3D dark-blood interleaved with gray-blood (DIG) vessel wall MR technique that is potentially useful for detecting intraplaque hemorrhage and calcification as well as measuring plaque burden.

Methods: The DIG technique acquires dark-blood and gray-blood data in consecutive heartbeats. At the beginning (i.e. R wave) of the first heartbeat, the blood in the left ventricle is inverted with a localized inversion preparation. During the subsequent approach to the nulling point, the blood spins are distributed in the ascending aorta (AAo), aortic arch (AAr), and proximal descending aorta (DAo). Dark blood images are then acquired at the aortic arch quiescent phase (typically 150 – 250 ms). Gray-blood images are acquired at the same phase during the second heartbeat. To improve navigator efficiency, two independent respiratory navigators are used for the interleaved acquisition. Five healthy volunteers (1 F, aged 24-61 y) were scanned on a 3T system (MAGNETOM Verio, Siemens) equipped with a 32-channel cardiac coil. Major imaging parameters were: FLASH readout, candy-cane orientation, FOV 216×152×54 mm^3, isotropic spatial resolution 1.23mm, flip angle 10^o, parallel imaging GRAPPA 2, 33 segments/heartbeat, navigator acceptance window ±5 mm. The contrast-to-noise ratio (CNR) between the vessel wall and lumen was measured for AAo, AAr, and DAo, respectively. Visual comparison between DIG images and 2D T1-weighted TSE images at two selected locations were performed.

Results: Spatially co-registered dual-contrast images were acquired with DIG imaging with 4:36 to 6:38 min. As shown in Figure 1, on dark-blood images, blood signals were adequately suppressed in AAo, AAr, and proximal DAo, resulting wall-lumen CNR of 55.2±1.2, 53.7±0.6, 47.9±3.0, respectively; neutral contrast between the vessel wall and lumen was obtained on gray-blood images with slightly higher signal intensity in the vessel wall (CNR = 5.8±1.5, 3,8±3.1, 2.8±4.1 for the three locations). Reformatted aortic wall cross-sections from 3D DIG imaging were visually comparable to that from 2D TSE in terms of wall delineation quality (Figure 2).

Conclusion: 3D DIG vessel wall imaging provides high-quality dual-contrast images for the aortic arch. Evaluation of its utility to assess plaque burden and high-risk plaque composition is underway.

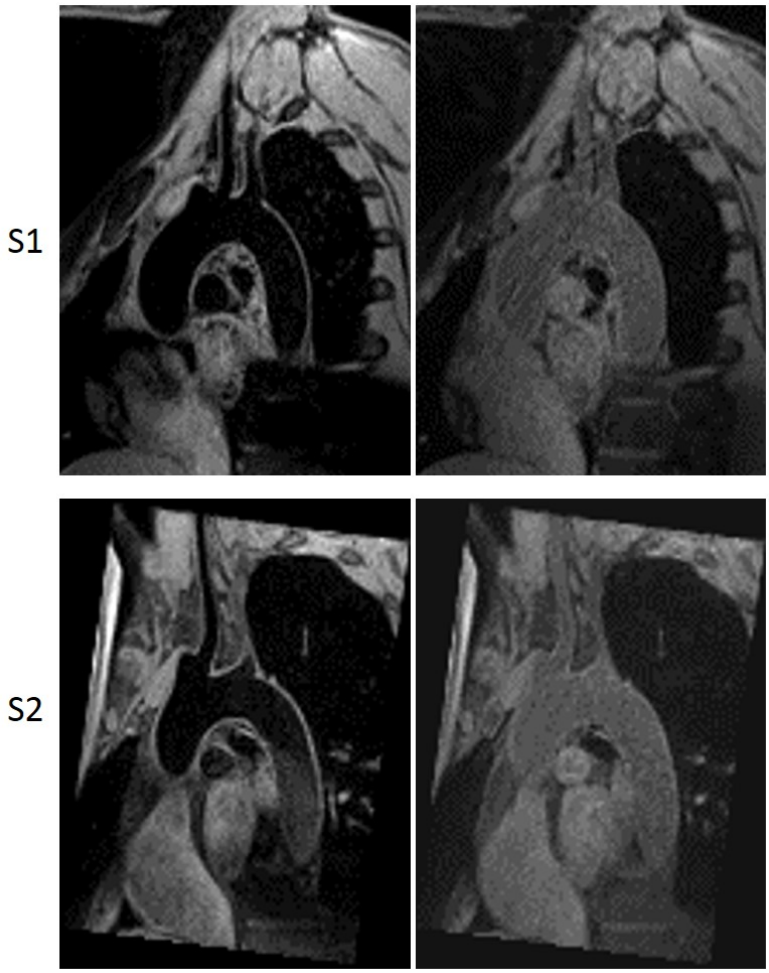

Figure 1. Two representative DIG imaging cases. 3D dark-blood and gray-blood images are inherently co-registered and can be reformatted into cross-sectional view to better visualize the vessel wall.

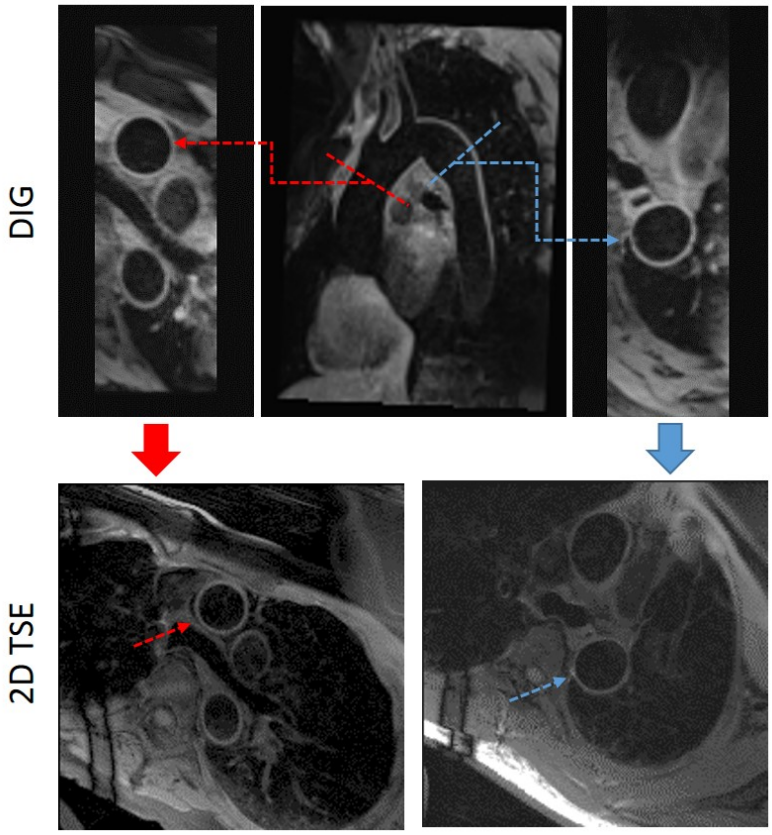

Figure 2. Visually comparable quality of vessel delineation from 3D DIG and 2D TSE.

ID#: 379420

Effects of Vitamin D on Cardiac structure and Function in patients with Chronic Kidney Disease: Insights in myocardial deformation using magnetic resonance-feature tracking technique

Emmanuel Androulakis[1], Debasish Banerjee, MD[2]Nihil Chitalia[2], David Goldsmith[3], Nick Bunce[4], Konstantinos Bratis[5]

1. St George's University Hospital, London, United Kingdom

2. Cardiology Clinical Academic Group and ^Renal Unit, St Georges University Hospital NHS Foundation Trust, United Kingdom

3. Renal Unit, Guys Hospital, United Kingdom

4. St. George's Hospital, United Kingdom

5. St George's NHS Trust, London, England, United Kingdom

Background: Vitamin D is associated with decreased cardiovascular-related morbidity and mortality, possibly by modifying cardiac structure and function, yet firm evidence for either remains lacking. We aimed to determine the effects of vitamin D supplementation on left ventricular structure and function as well as on myocardial deformation indices assessed, for the time to the best of our knowledge, by cardiac magnetic resonance feature tracking (CMR-FT) in patients with chronic kidney disease.

Methods: This a subgroup analysis of a double blind, randomized, placebo-controlled trial, on stable non-diabetic chronic kidney disease stage 3b and 4 without significant comorbidity or no prior cardiac disease. Patients were randomized to receive 600,000 units of cholecalciferol (Group 1, n=28) or matched placebo (Group 2, n=28) by directly observed therapy over 6 visits between week 4 and 42. All patients underwent a cardiac MRI study in a 3T scanner with acquisition of SSFP cines at baseline and 52 weeks follow-up. The primary endpoint was left ventricular (LV) volume, function and mass index (LVMI) change between baseline and 6 months. Secondary endpoints included changes in 2-dimension peak systolic LV myocardial longitudinal, radial and circumferential strain and strain rates examined in 11 patients form Group 1, 11 patients form Group 2, compared with 10 healthy controls (Group 3) with the use of CMR feature tracking (CMR-FT).

Results: All 3 groups were matched regarding basic demographics and cardiovascular risks factors. Routine indices of LV systolic function were normal in both groups (Group 1; LVEF: 61.1±5.9, LV mass: 96.7±27.8 g, LV end diastolic volume 156.4±37.6 ml/Group 2; LVEF: 63.7±5.9, LV mass: 104.8±32.2, LV end diastolic volume 149.8±30.9ml). Left ventricular volumes, ejection fraction and LVMI values did not differ either between groups 1 and 2 either at baseline or post vitamin D supplementation (p=NS for all). With regards to CMR-FT analysis, comparisons were made between normal controls and (i) Group 1, (ii) Group 2. Peak systolic LV myocardial longitudinal, radial and circumferential strain and strain rates did not change significantly following vitamin D supplementation or placebo (p=NS for all).

Conclusion: In this study, 6 months therapy with vitamin D supplementation did not alter LV volumes, systolic function and LVMI as well as global strain and strain rates values derived by CMR-FT.

ID#: 379438

Utilization of compressed sensing image acceleration in pediatric cardiac magnetic resonance imaging

Timothy Slesnick[1] Sassan Hashemi, MD[2], Gary McNeal, M.S.[3], Christoph Forman, PhD[4], Denver Sallee III[1], W. James Parks[1]

1. Emory University School of Medicine, Children's Healthcare of Atlanta

2. Children's Healthcare of Atlanta, Atlanta, GA

3. Siemens Healthineers, Granbury, TX

4. SIEMENS HEALTHCARE GmbH, Erlangen, Bayern, Germany

Background: Image acceleration techniques are used in cardiac magnetic resonance (CMR) to improve acquisition times, increase temporal resolution, and allow parameter manipulation to improve spatial resolution. Applications of compressed sensing (CS) techniques have limited experience in pediatric patients.

Methods: Patients were prospectively enrolled and underwent 2D cine SSFP imaging with CS using prototype sequences. The sequences utilize sparse, incoherent sampling and non-linear iterative reconstruction, with the most recent version performing regularization in all dimensions (readout, phase encoding, and time dimensions) during reconstruction. Several variants were tested, including single shot (real-time) and multi heartbeat acquisitions. Prospective gating was used, with number of acquired phases determined primarily by the sequence variant and heart rate.

Results: Forty patients were enrolled; median age was 16 years (8-20 years), with a variety of cardiac diagnoses, with bicuspid aortic valve (n=10) and repaired tetralogy of Fallot (n=6) most common. The real-time variant (TE 1.18, TR 2.8, base resolution 208 yielding spatial resolution of 1.7x1.7 mm) produced good image quality, but temporal resolution was limited (typically 14-20 phases reconstructed) (Figure 1a). Importantly, an entire stack of short axis images can be acquired in a single breath hold, convenient for rapid imaging and for exercise CMR imaging. A 4 heartbeat variant using a coherent mSENSE sampling pattern (TPAT) with non-linear iterative reconstruction (similar TE, TR, base and resultant spatial resolution) yielded improved signal to noise and temporal resolution (typically 25-40 phases), while still allowing acquisition of multiple slices per breath hold (3 breath holds performed to obtain a short axis stack) (Figure 1b). A 12 heartbeat variant allowed increase in the base resolution to acquire non-interpolated, 1x1 mm pixels with excellent signal and contrast to noise and markedly increased temporal resolution (50+ phases). This required single slice breath holds, similar to traditional imaging, but produced superior image quality (Figure 1c).

Conclusion: Compressed sensing can be successfully applied to pediatric patients with congenital heart disease, even with increased resting heart rates. Real-time CS imaging offers the most rapid acquisition, but had limited temporal resolution. Multi-heart beat imaging produced superior spatial and temporal resolution with excellent signal and contrast to noise compared to traditional cine SSFP imaging. Hybrid variants, with coherent sampling but non-linear iterative reconstruction, offer spatial and temporal resolution similar to traditional cine SSFP images while allowing multiple slice per breath hold acquisition.

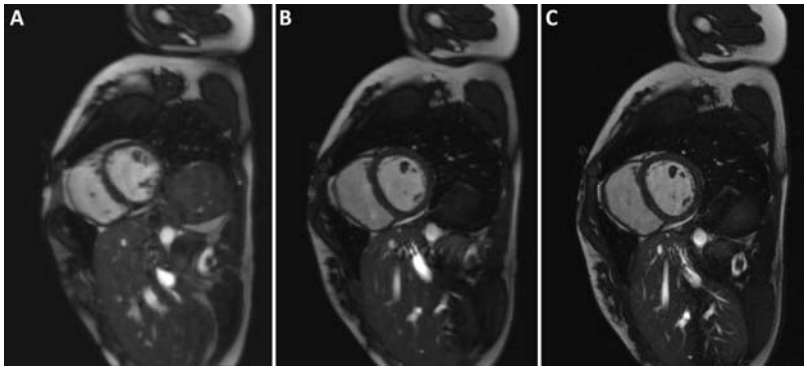

Figure 1: Compressed sensing short axis images, including real-time (a), 4 heartbeat (b), and 12 heartbeat (c) variants.

ID#: 379441

Usefulness of early assessment of Takotsubo cardiomyopathy patients with cardiac magnetic resonance imaging

Emmanuel AndroulakisSitara Khan, Michael Papadakis

St Georges University Hospital NHS Foundation Trust, United Kingdom

Background: There is a growing body of evidence suggesting thatcardiac magnetic resonance imaging (MRI) adds further value in the management of patients with Takotsubo cardiomyopathy, by assessing left ventricular function and tissue characterisation. There is only few data derived from small scale studies with MRI performed after the initial acute presentation, but it is unclear whether there is an optimal timeframe for detecting abnormalities.

Methods: A retrospective analysis was performed of 31 patients who were diagnosed with Takotsubo cardiomyopathy based on clinical presentation, echocardiographic features, and the absence of obstructive coronary artery disease on coronary angiography. All patients underwent a cardiac MRI study in a 3T scanner with acquisition of SSFP cines, STIR and late gadolinium enhancement (LGE) sequences. Studies were analysed to assess for any differences that existed between patients studied early (Group 1, within 30 days of presentation, n=15), and those studied late (Group 2, after 30 days of presentation, n=16).

Results: The two groups were similar with regards to age and other classical risk factors for cardiovascular disease (p=NS for all). The mean time from presentation to MRI was 6.1±2.3 days in Group 1, and 111±14 days in Group 2. A wall motion abnormality was detected in 11/15 (73%) in Group 1 vs 2/16 (13%) in Group 2 (Odds ratio [OR]=5.87, 95% Confidence Interval (CI): 1.11 to 30.96, p=0.042). Moreover, the LV ejection fraction was significantly lower in Group 1 compared to Group 2 (46.8±4.0% vs. 61.1±3.7%, p=0.013). LGE was detected in 5/15 (33%) in the early group vs 2/16 (13%) in the late group though the difference did not reach statistical significance (p=0.41), potentially due to small size effect. Of note, there were no significant differences between groups in troponin or BNP levels (p=0.70, p=0.49 respectively).

Conclusion: This study demonstrated that early assessment of Takotsubo cardiomyopathy patients (within 30 days) with cardiac MRI provides much more valuable information in regards to wall motion abnormality, left ventricular systolic impairment and potentially LGE imaging compared to the late assessment. This may have significant implications on current clinical practice, signifying the best time frame within which cardiac MRI should be performed in this vulnerable population.

ID#: 379451

MR imaging for aortic annular sizing

James Carr, MD[3]Pascale Aouad, MD[1], Ali Serhal, MD[2], Michael Markl, PhD[3], Jeremy D. Collins, MD[4], Julie Blaisdell[3], Kelly Jarvis, PhD[5], Louise Collins, M.Eng[1], Marcos P. Ferreira Botelho, MD[6], Marcos Botelho, MD[2]

1. Northwestern Memorial Hospital

2. NorthShore University HealthSystem, IL

3. Northwestern University, Chicago, IL

4. Northwestern University School of Medicine, Chicago, IL

5. Northwestern University, IL

6. The University of Texas Health Science Center at Houston, Houston, TX

Background: Aortic annulus sizing is crucial in pre-procedural planning for transcatheter aortic valve replacement (TAVR). ECG-gated CT angiography (CTA) was traditionally used to evaluate the annulus size and to assess the vascular access. However, CTA requires the administration of iodinated contrast media which can be contraindicated in patients with impaired renal function or with history of severe allergic reaction. In the last few years, some authors reported promising results for alternative imaging with non-contrast MRI. The main limitation of these sequences is the long scanning time. The purpose of this study was to evaluate a new 3D cine MRI technique (3D k-t SSFP) and to compare its accuracy in annulus measurement to other MR sequences and to the CTA.

Methods: 6 volunteers and 7 TAVR candidates were prospectively enrolled. The volunteers underwent only an MRI exam while the TAVR candidates underwent an MRI and the gold standard CTA. The non-contrast MR sequences obtained to compare for annular sizing are: 3D cine, Nav 3D SSFP and the 3D bSSFP k-t1 which is a novel sequence derived from 4D flow using only magnitude images. Annular area was obtained on each of these sequences at mid diastole and at the systolic phase with the corresponding maximal annular area. Quiescent interval slice selective (QISS) non-contrast MRA was additionally acquired in the 7 patients to evaluate for coronary artery heights and vascular access.

Results: There was an excellent correlation of the aortic annular area measured on 3D bSSFP k-t1 by comparison to the 3D cine (r=0.95), Nav 3D SSFP (r=0.92) and CTA (r=0.99) with no statistically significant difference (p value of 0.8, 0.9 and 0.4 respectively). As assessed by Bland-Altman analysis, there was no significant systemic difference between annular area measurements on 3D bSSFP k-t1 and 3D cine, Nav 3D SSFP and CTA with a mean difference of 0.27%, 0.18% and 0.0048% respectively.

Conclusion: The novel studied MR technique 3D bSSFP k-t1 demonstrated excellent correlation with CTA and with other MR sequences. This technique has a great potential as an alternative for assessment of annular sizing in patients undergoing pre-TAVR evaluation.

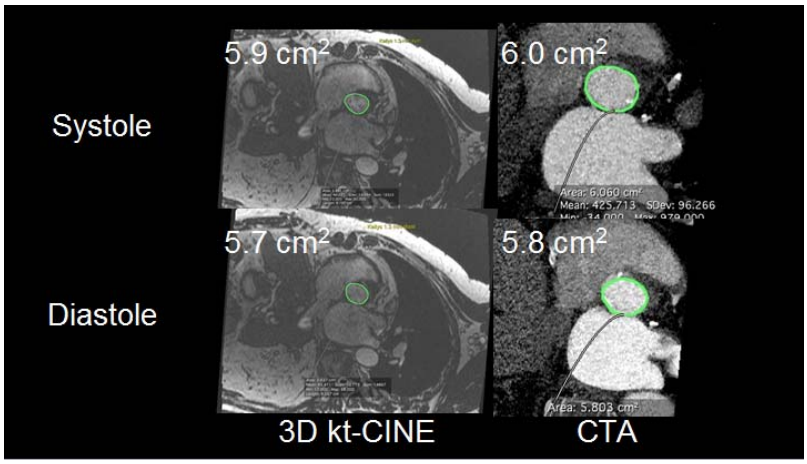

annular area measurement on systole and diastole 3D bSSFP k-t1 vs. CTA

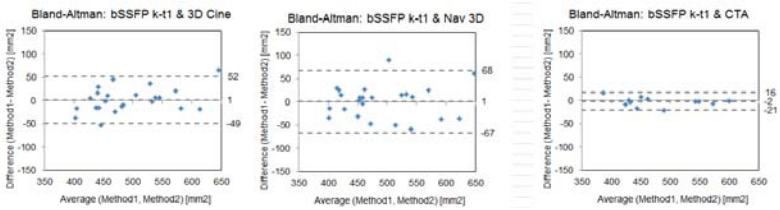

Bland-Altman plots comparing annular area measurements between 3D bSSFP k-t1 and each of 3D cine, Nav 3D SSFP and CTA

ID#: 379457

Myocardial Extracellular Volume Expansion and Cardiomyocyte Hypertrophy Measured by CMR Correlate With Friedreich's Ataxia Ranking Score in Patients Without Heart Failure.

Karen Girotto, MD[1], OTAVIO R. COELHO-FILHO, MD, PhD, MPH[3]Thiago Quinaglia A. C. Silva, MD, PhD[1], Michael Jerosch-Herold, PhD[2], Marcondes França, MD, PhD[1]

1. State University of Campinas - UNICAMP, Sao Paulo, Brazil

2. Harvard Medical School, Boston, MA

3. State University of Campinas - UNICAMP, Campinas, Sao Paulo, Brazil

Background: Heart Failure (HF) is the most common cause of death in Friedreich';s ataxia (FRDA), a mitochondrial disease caused by homozygous GAA expansions in the FXN gene, and characterized by neurodegeneration, and hypertrophic cardiomyopathy. The cardiac phenotype in FRDA is highly variable, and frequently the first overt manifestation is cardiomyopathy with HF. Myocardial interstitial fibrosis is a hallmark of FRDA';s cardiomyopathy with potential prognostic implications in the transition to HF. Myocardial tissue characterization by cardiac magnetic resonance (CMR) can provide phenotyping at the tissue level to describe LV remodeling in FRDA';s cardiomyopathy, and in the CMR tissue phenotype holds promise as surrogate endpoint to investigate therapies with anti remodeling properties.

Methods: Twenty-seven FRDA';s patients (mean age 26.6±9.3years, 15 female) without HF, and with genetic diagnosis and GAA repeat length quantification, underwent CMR, including assessment of myocardial extracellular volume fraction (ECV), and intracellular lifetime of water (τ_{ic}), a measure of cardiomyocyte hypertrophy. Friedreich';s ataxia neurological ranking score (FARS.3) designed to measure disease severity in FRDA, was determined in all patients. 15 healthy volunteers (mean age 34.9±8.5, 4 female) underwent CMR for comparison. Look-Locker gradient-echo imaging for T1 quantification before and after contrast was combined with a 2-site model for transcytolemmal water exchange to estimate ECV and τ_{ic}. Cine CMR and LGE imaging were also performed in matching locations.

Results: FRDA patients had normal LVEF with significant increased LV mass-index (LVMASSi) compared to healthy controls (LVEF: 67%±11 vs. 63.9±9, P=NS; LVMASSi 62.7±23 vs. 45.1±7 g/m^2, p<0.001) were notably higher in FRDA patients (ECV: 0.36 ± 0.05 vs. 0.25±0.01, p<0.0001; τ_{ic}: 0.13±0.07 vs. 0.06±0.02, p=0.001). ECV demonstrated a negative association with LVEDV-index (r=-0.6, p<0.001). τ_{ic} was negatively associated with the FARS3 ranking (r=-0.55, P=0.02), and FARS3 was positively associated with time since diagnosis/onset (r=-0.7, p<0.001, Figure-1), suggesting that the progression of FRDA in the heart may result in regression of cardiomyocyte hypertrophy. Cardiomyocyte mass-index [(1−ECV)xLVmass/BSA)] correlated inversely with age at the time of MRI (r=-0.43, P=0.03), indicating that with advancing age FRDA patients develop some degree of LV atrophy, and that hypertrophy may transition into an LV "burn-out" phase. Compared to ECV, LVEDVi and LVEF, τ_{ic} was the only imaging parameter capable to efficiently identify patients with FARS3 < median (Figure 2) (p<0.05 only for τ_{ic}).

Conclusion: LV mass index, ECV and intracellular lifetime of water were notably elevated in FRDA patients, consistent with a cardiac hypertrophy phenotype in FRDA. The negative association of τ_{ic} with FARS3 scale, and the increase of FARS3 with duration since initial diagnosis suggest that regression of cardiomyocyte hypertrophy may be a useful cardiac biomarker to follow cardiomyopathy progression in FRDA.

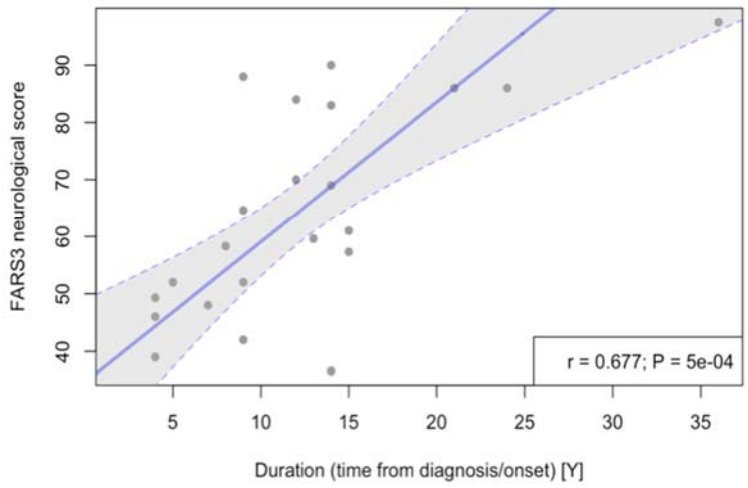

FIGURE-1

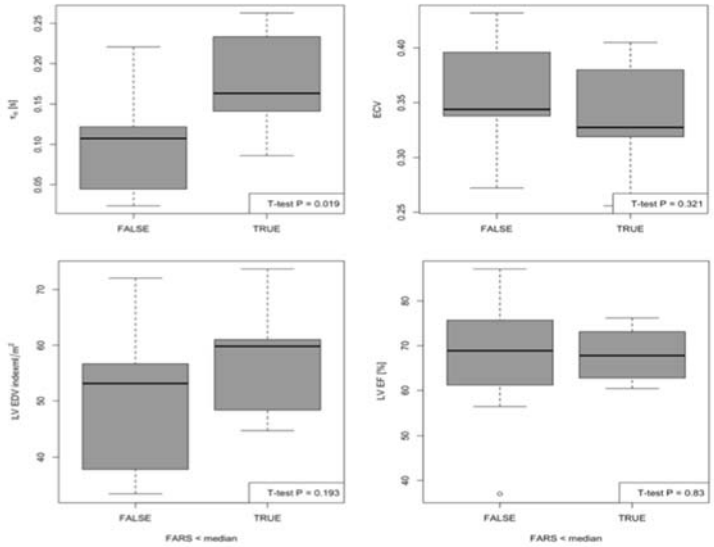

FIGURE-2

ID#: 379506

Myocardial Strain Before and After Percutaneous Mitral Commisurotomy for Severe Mitral Stenosis

Raouf Mahmoud. AbdelRaouf[2] Ahmad E.Mostafa[1], Ahmed Fathy. F. Tamara, MD Cardiology[3], Haitham Badran, MD,PhD[1], Sameh S.Raafat, Immediate and short-term effect of balloon mitral valvuloplasty on global and regional biventricular function: a two-dimensional strain echocardiographic study[1], Diaa Kamal[4], Ahmed A.Tharwat[1], Ahmed S.Ibrahim[1], Sarah Moharem-Elgamal, MD[5]

1. Ain shams university hospital, Egypt

2. Dar Al Fouad hospital, 6th october city, Egypt, Cairo, Al Qahirah, Egypt

3. Ain Shams Faculty Of Medicine, Egypt

4. Ain Shams University, Cairo, Egypt

5. Bristol Heart Institute, Bristol NIHR Biomedical Research Centre (Cardiovascular Section), University of Bristol, United Kingdom

Background: Severe rheumatic mitral stenosis(MS) can alter the hemodynamic load and left ventricular(LV) function,despite the presence of normal ejection fraction(EF)**.**Little is known about the effect of MS on the LV and after the relief of this obstruction.In our study,we aimed to assess the impact of percutaneous mitral commisurotomy(PMC) on LV global and regional function using cardiac magnetic resonance imaging(CMR).

Methods: Twenty patients(median age 36 years, 12 women and 8 men) with clinically significant MS(mitral valve area <1.5cm^2) were recruited. Trans-thoracic echocardiography(TTE) was performed to assess the suitability of patients to undergo PMC and to assess the adequacy of the intervention afterwards.All patients scheduled to undergo PMC underwent CMR 1 week prior to and 2 months after the procedure. Cine and myocardial tagging images were analyzed using dedicated post-processing software(Myocardial Solutions,Inc.,North Carolina,USA) to assess the LV EF, LV end diastolic volume(LVEDV), LV end systolic volume(LVESV),LV global circumferential strain(GCS), LV regional circumferential strain (RCS) of the 16 LV segments,and circumferential uniformity ratio estimate(CURE) to identify LV mechanical synchronization.Continuous numerical values were expressed as mean ± SD. Numerical and continuous data obtained by CMR were compared by the paired t-Test.

Results: Enrolled patients showed a significant improvement of LV EF post PMC (62.8±10.05% vs 60.15±9.96%, P<0.0142).There was a similar improvement of GCS post PMC (-15.5±2.46 vs -12.63±2.67, P>0.0001).Upon evaluation of RCS, all 16 LV segments demonstrated improvement post procedure, however, statistically significant values were only noted in basal infero-lateral (-15.32±3.75 vs -11.96±7.95,P<0.0488)and apical inferior segments (-13.54±3.35 vs -11.71±3.82, P<0.0379).Moreover, CURE index showed a significant increase in post PMC comparing to pre PMC(0.91±0.03 vs 0.83±0.04, P<0.0001)denoting improved LV mechanical synchronization.

Conclusion: The assessment of PMC patients by CMR may provide us with an additional insight on the functional impact of MS on the LV and its improvement post PMC.

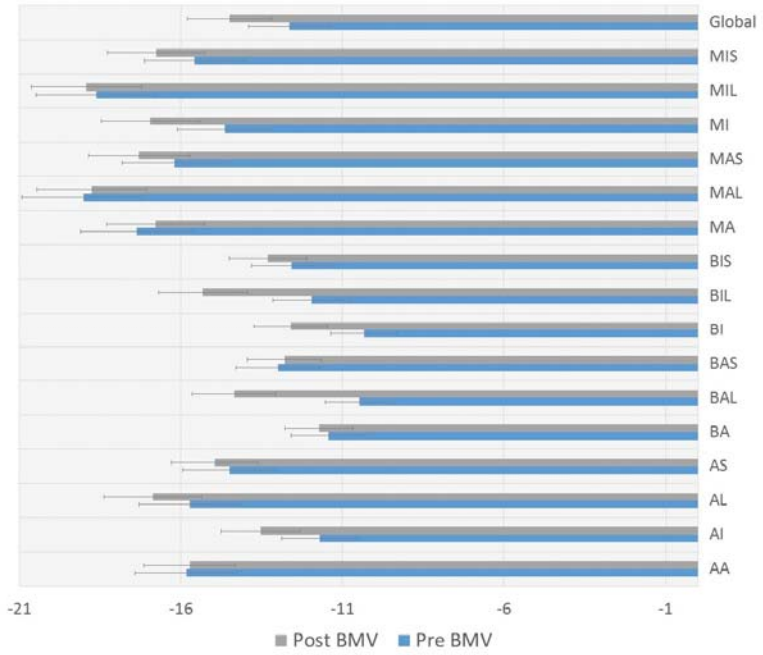

Regional Circumferential Strain of The 16 Left Ventricular Segments Before and After Percutaneous Mitral Commisurotomy.

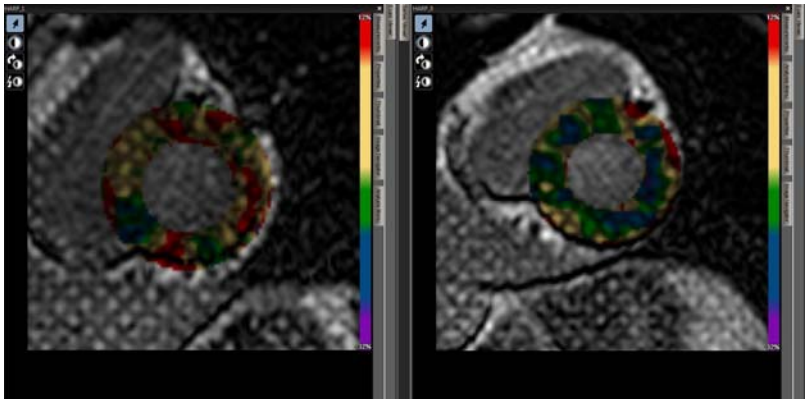

Color Coding Map for Regional Circumferential Strain at mid-cavity segment. Left panel: pre PMC, Right panel: after PMC.

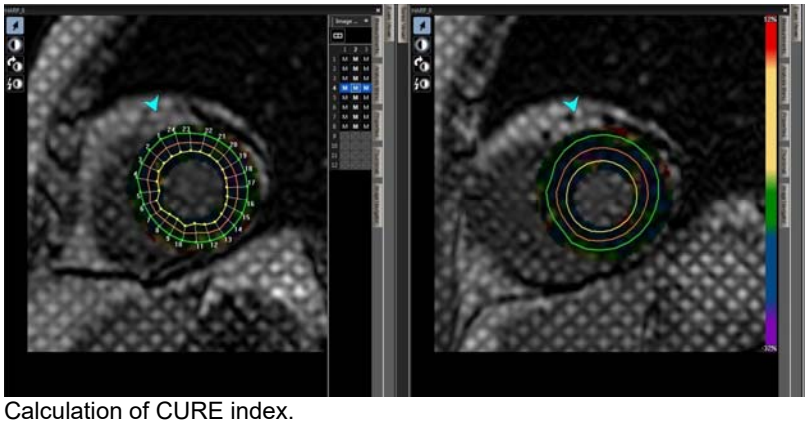

Calculation of CURE index.

ID#: 379523

Role of global circumferential strain in patients with myocarditis and normal ejection fraction assessed by CMR

Bostjan Berlot, MD[1]Slavica Ponorac, MD[2], Matjaž Baraga, MD[2]

1. University Medical Centre Ljubljana, Nova Gorica, Slovenia

2. University Medical Centre Ljubljana, Slovenia

Background: Background: Impairment of left ventricular (LV) deformation in patients with acute myocarditis is an independent predictor of cardiovascular outcomes despite normal LV ejection fraction (EF). Cardiovascular magnetic resonance myocardial feature tracking (CMR-FT) can provide quantitative measurements of myocardial deformation. The aim of our study was to assess changes in myocardial circumferential strain in patients who had LV EF above 50% at admission and did not experience major adverse cardiac event during follow up.

Methods: We retrospectively analyzed CMR studies of 34 patients with acute myocarditis. CMR-FT was applied on standard short axis view of vector-ECG gated CMR cine SSFP sequences. Global myocardial circumferential strain (GCS) value was measured at the baseline and at 6 months follow up. CMR-FT analyses was performed on commercially available software (Medis QStrain RE 2.0, Leiden, The Netherlands). Paired t-test was used to compare interval parameters.

Results: Mean age of patients was 28 ± 9 years and 82% were male. The average duration of follow-up was approximately 7.4 ± 4.2 months. There was a significant difference between the baseline and follow up in EF (57.8 ± 5.5 vs. 60.2 ± 6.0, $p<0.001$), LV mass/BSA (57.3 ± 10.9 vs. 54.4 ± 9.4, $p=0.001$), EDV/BSA (77.8 ± 12.7 vs. 80.0 ± 13.4, $p<0.001$) and ESV/BSA (33 ± 7.2 vs 32.1 ± 7.2, $p<0.001$). GCS showed borderline significant interval with clear trend of reduction between baseline and follow up (-22.7 ± -4.6 vs. -23.2 ± -3.6, $p=0.07$).

Conclusion: GCS showed trend of reduction during the follow up in myocarditis patients with normal ejection fraction and could be used as an additional parameter to predict change in cardiac function. Further studies assessing mechanical deformation in myocarditis are required to assess potential for improving outcome prediction in myocarditis.

ID#: 379541

Improved CMR protocol for semi-quantitative assessment of myocardial stress perfusion in children

Shivani G. Patel, MBBS[1] Cynthia K. Rigsby, MD, FACR[2], Joshua D. Robinson, MD, FACC[2]

1. Ann and Robert H Lurie Children's Hospital of Chicago, Chicago, IL

2. Ann & Robert H. Lurie Children's Hospital of Chicago, Chicago, IL

Background: In children, stress perfusion CMR is useful in a broad array of disease processes but presents many technical challenges. Adenosine is the most common stress agent but requires continuous infusion through a separate IV. After achieving vasodilation, faster heart rates and inadequate breath-holding complicate image acquisition. Regadenoson is a newer vasodilator with selective cardiac A2A adenosine receptor activity which produces fewer side effects and allows for bolus dosing, precluding a second IV. Implementation of motion corrected (MOCO) sequences can allow for better image quality and more quantitative analysis but have not been described in children. Our study aim was to further assess the safety and efficacy of an improved stress perfusion protocol using regadenoson and MOCO for improved image quality and semi-quantitative analysis.

Methods: We conducted a retrospective study of all patients who underwent stress perfusion MRI (Fig. 1) at our center from 2014-2017. Regadenoson dose was 0.4 mg for patients >40 kg and 6-10 mcg/kg for smaller patients. Stress response data and presence of major adverse events such as arrhythmia, hypotension, AV block or bronchoconstriction, need for termination of exam and other side effects were documented. Each exam was reviewed in consensus by 2 experienced CV imagers to assess image quality (5 point scale), perfusion deficits, wall motion abnormality and late gadolinium enhancement. A splenic hypoperfusion score (3 point scale) was assigned as a marker of adequacy of vasodilation. Semi-quantitative analysis was performed (Medis 3.0) to obtain time signal intensity curves for 6 segments in every apical, mid and basal slice. The relative upslope of myocardial signal intensity compared to blood pool was calculated for each segment at rest and stress. Myocardial perfusion reserve index (MPRI) was calculated as the ratio of the stress and rest relative upslopes.

Results: Table 1 shows patient demographics and hemodynamic response to regadenoson. All patients completed stress perfusion imaing; 1 patient had inadequate image quality for semi-quantitative analysis. Splenic hypoperfusion score was higher in the rest vs stress images (1.83 vs 1.13, $p<0.005$) and there was no difference between patients who had standard vs weight based dosing ($p=1$). Image quality of MOCO images was significantly better than conventional perfusion images (4.63 vs 4.01 at rest, $p<0.005$; 4.41 vs 3.84 at stress, $p< 0.005$). Reversible perfusion deficits were seen in 6/38 patients, LGE in 3/38 patients and wall motion abnormality in 1/38 patients. Semi-quantitative analysis showed lower global mean MPRI in the 6 patients with reversible perfusion deficits (1.13 vs 0.83, $p=0.005$).

Conclusion: Regadenoson is a safe and effective vasodilator for pediatric myocardial stress perfusion MRI. MOCO sequences provide better image quality for qualitative analysis of perfusion deficits and allow semi-quantiative assessment of myocardial perfusion.

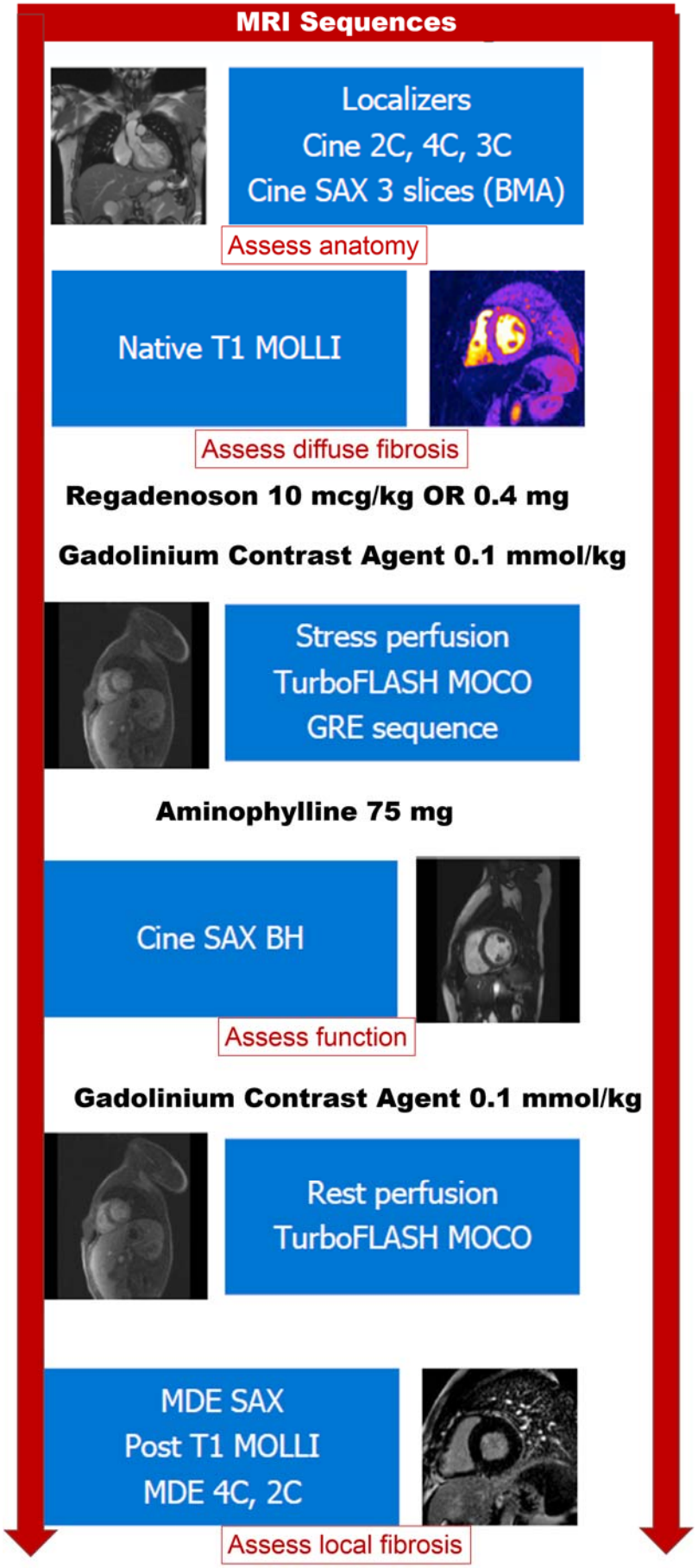
MRI Sequences
Localizers
Cine 2C, 4C, 3C
Cine SAX 3 slices (BMA)
Assess anatomy
Native T1 MOLLI
Assess diffuse fibrosis
Regadenoson 10 mcg/kg OR 0.4 mg
Gadolinium Contrast Agent 0.1 mmol/kg
Stress perfusion
TurboFLASH MOCO
GRE sequence
Aminophylline 75 mg
Cine SAX BH
Assess function
Gadolinium Contrast Agent 0.1 mmol/kg
Rest perfusion
TurboFLASH MOCO
MDE SAX
Post T1 MOLLI
MDE 4C, 2C
Assess local fibrosis

Stress Perfusion MRI protocol

Patient demographics and hemodynamic response to regadenoson

	N=38
Age	Median 15 years (range 5 to 20 years)
Weight	Median weight 61 kg (range 28 to 99 kg)
Height	Median height 163 cm (range 142 to 192 cm)
BSA	1.67 m^2 (range 1.05 to 2.3 m^2)
Gender	Males 23 (60%), Females 15 (40%)
Most common indications	Orthotopic heart transplant (n=12) Kawasaki disease (n=11) Coronary artery revision (n=9)
Baseline heart rate	84 ± 18 beats/min (range 56 to 132 beats/min
Peak heart rate	123 ± 20 beats/min (range 86 to 172 beats/min) *Significant rise in heart rate ($p < 0.005$)
Rise in heart rate	56±37%
Time between regadenoson and aminophylline	3.6 ± 1.3 minutes (range 2 to 9 minutes)
Major adverse events	None
Transient side effects	12/30 patients Nausea/gastrointestinal discomfort (n=4) Limb tingling (n=4) Chest pain (n=3) Headache (n=3)

ID#: 379545

Characterizing Left Ventricular Displacements During Active Diastolic Filling with CINE DENSE

Patrick Magrath, MS [1]Luigi E. Perotti, PhD[2], Ilya Verzhbinsky[3], Daniel B. Ennis, PhD[4], Michael Loecher, PhD[5]

1. University of California, Los Angeles, Los Angles, CA

2. UCLA, Los Angeles, CA

3. University of California, Los Angeles

4. Department of Radiological Sciences, University of California, Los Angeles, CA, USA., CA

5. University of California Los Angeles

Background: Heart Failure with Preserved Ejection fraction (HFpEF) accounts for 50% of all heart disease in the United States {Udelson et al., Circulation 2016}. Understanding the mechanics of active left ventricular (LV) filling as a consequence of atrial systole is a target for gaining mechanistic insight into HFpEF {Shah *et al.,* 2016}. Quantitative LV imaging during atrial systole is challenging due to: 1) the brevity of the event (30-90ms); 2) the relatively small displacements; and 3) tag fading at the end of the QRS.
Displacement Encoding with Stimulated Echoes (DENSE) is a robust technique for quantifying LV kinematics during systole {Kim *et al*., Radiology, 2002}. DENSE is typically triggered at the QRS pulse and is sensitized to capture systolic displacements without multiple phase wraps by utilizing encoding strengths (k_e) of 0.04-0.08 cycles/mm.
O*bjectives*: 1) To adapt the DENSE acquisition strategy to reliably measure LV filling displacements during atrial systole; and 2) To characterize the LV filling displacements to enable optimizing the cine DENSE acquisition for sensitively capturing the LV response to atrial systole.

Methods: *Animal Study:* Healthy female Yorkshire pigs (N=8) were scanned (IACUC approved) at 3T (Siemens Prisma). A long-axis 2D CINE image (T_{Res}=10ms) was used identify atrial systole (first time point in diastasis after which the mitral valve fluttered). A stack of x-, y- and z-displacement encoded 2D DENSE slices were acquired using a pulse-ox trigger delay of ~50ms prior to the beginning of atrial systole. DENSE parameters: nav. gated, bal. 4-point encoding, 3-point phase cycling, 2.5x2.5x8mm, 15 ms (view shared) temp res., 10 spiral interleaves, 2800-3400 points/spiral, 3 averages, k_e=0.14 cycles/mm, 2.5-4min/slice. *Human Study:* Healthy volunteers (N=4) were enrolled with consent and scanned at 3T (Siemens Prisma) in a single slice with identical imaging parameters. *Data Processing:* DENSE images were processed in Matlab {Spottiswoode *et al.*, IEEE, 2007} to yield x- ,y- , and z-displacements.

Results: *Animal Study:* Figure 1: x- ,y- ,z- and total displacements in all slices captured during LV filling throughout atrial systole. Peak total LV displacements in all slices with respect to diastasis were 0.59±0.16mm. *Human Study:* Figure 2: peak x- ,y- ,z- and total displacements in the LV during atrial systole in a mid-ventricular slice. Peak total LV displacements were 0.42±0.14mm. *Optimal encoding strength:* Optimal experimental design would capture the maximum displacements during atrial systole without phase wrapping by selecting the correct k_e [cycles/mm]. In volunteers, 99.7% (3 standard deviations) of all peak displacements fell within [-0.1 to 0.8] mm suggesting an optimal encoding strength of ~0.8mm of displacement without phase wrapping. This accords with k_e=1.11 cycles/mm for three-point + null encoding or k_e=0.49 cycles/mm for balanced 4-point encoding, which has greater phase sensitivity by a factor of {Zhong *et al.*, MRM, 2007}.

Conclusion: With an appropriate pulse-ox trigger delay & encoding strength, imaging LV filling during atrial systole is possible with DENSE. A k_e~0.5 cycles/mm can LV filling during atrial systole. This is higher than the k_e of 0.04-0.08 cycles/mm used during systolic DENSE imaging. Increased encoding strengths are limited by intravoxel dephasing {Aletras *et al.*, MRM, 2004}. Intravoxel dephasing, not encoding strength, is the limiting factor for imaging LV motion during atrial systole.

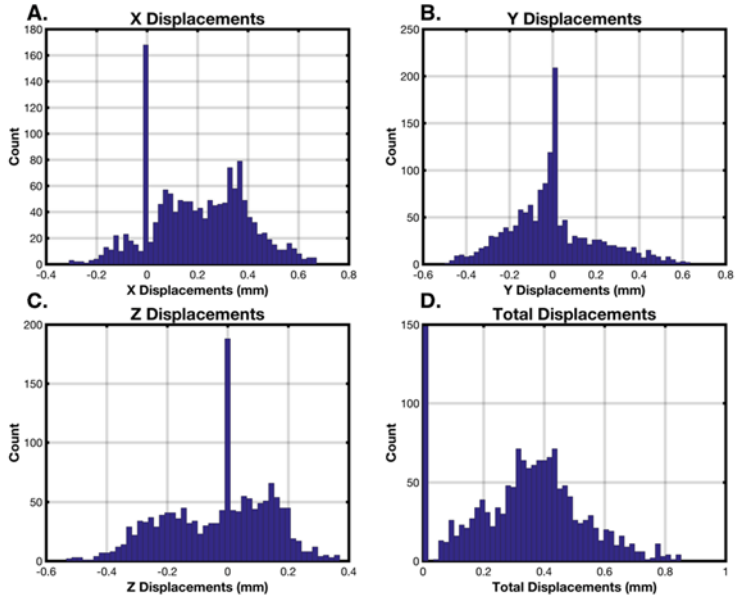

Figure 1: A. X displacement B. Y displacement C. Z displacement and D. Total displacement across all slices during LV filling throughout the atrial kick in N=8 healthy Yorkshire pigs.

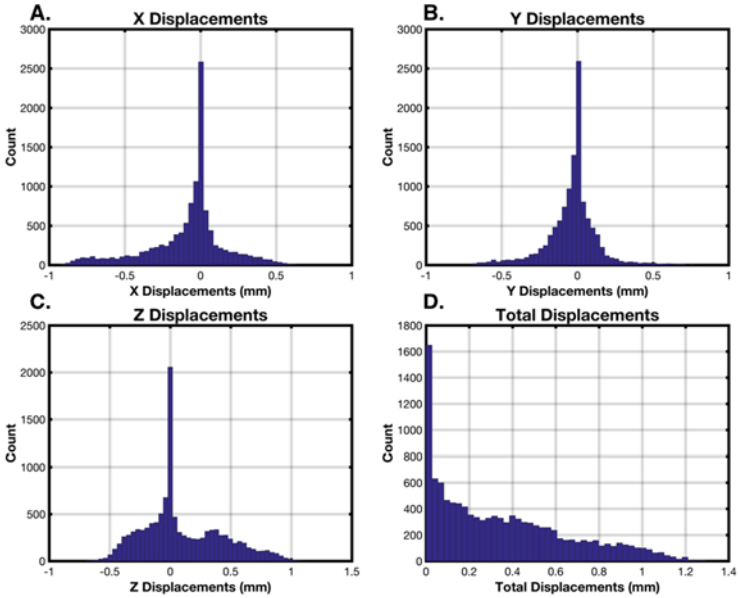

A. X displacement B. Y displacement C. Z displacement and D. Total displacement across in a mid-ventricular short axis DENSE slice during LV filling throughout the atrial kick in N=4 healthy volunteers.

ID#: 379560

Personal Profiling using Genotyping and Metabolomics Markedly Accentuates Therapeutic Response of Omega-3 Fatty Acid on Post-AMI Remodeling - The OMEGA-REMODEL Randomized Multicenter Trial

Raymond Y. Kwong, MD, MPH[1] Bobby Heydari, MD, MPH[2], Kana Fujikura, MD, PhD[3], Kyoichi Kaneko, MD, PhD[4], Shuaib Abdullah, MD[5]

1. Brigham and Womens Hospital, Boston, MA

2. Stephenson Cardiac Imaging Centre, Libin Cardiovascular Institute of Alberta, University of Calgary, AB, Canada

3. Brigham and Women's Hospital, Boston, MA

4. Brigham and Women's Hospital and Showa University, Brookline, MA

5. University of Texas-Southwestern Medical Center

Background: Personal profiling may substantially overcome the challenges in therapeutic drug discovery. Adverse cardiac remodeling is the key mechanism that leads to post-AMI heart failure, which has remained the most significant cause of morbidity and mortality despite of the advance in primary coronary interventions. In the OMEGA-REMODEL trial, we observed a significant yet modest improvement of cardiac remodeling from high dose (4g/d) omega-3 fatty acid (O3-FA) during the initial 6 months of AMI. We hypothesized that personal profiling using a wide array of clinical characteristics, baseline cardiac structures, genomics and metobolomics will result in strengthening of O3-FA';s benefits on cardiac remodeling.

Methods: The OMEGA-REMODEL trial enrolled 384 AMI pts from 3 centers and randomized pts 1:1 to 4g/d of O3-FA or placebo for 6 months. CMR was performed at baseline and at 6 months of study treatment. Improvement in cardiac remodeling was defined by both reduction of LVESV and non-infarct fibrosis. Overall, O3-FA resulted in reduction of LVESV compared to placebo (-5 vs -0.9 ml, $p<0.001$). Effect modification of this therapeutic response were screened in 142 common remodeling risk markers from categories of patient demographics (N=43), angiographic features (N=8), fatty-acid related genotypes (N=3), cardiac structures (N=15), metabolomics of inflammation (21), insulin resistance (N=9), lipidomics (31), and dietary habits in fish (N=12). Effect modification was assessed using a 3-way interaction term added to the model with reduction of LVESV as the dependent variable and drug assignment, treatment visit, and the effect modifier of interests included as main independent variables. Benjamin-Hochberg procedure corrected for multiple testing.

Results: Consistent with known genetic polymorphism of fatty acid desaturase (RS-1535) metabolism, pts with G-G allele experienced improved remodeling due to O3-FA compared to non-GG pts (Fig 1). Evidence of marked systemic inflammation on AMI admission (Fig 2) accentuated beneficial cardiac remodeling from O3-FA. In contrary, presence of high insulin resistance by all markers (only 3 shown in Fig 3, top panel) attenuated, whereas presence of protection against insulin resistance accentuated (Fig 3, bottom panel), improvement in cardiac remodeling from O3-FA. In patients treated with O3-FA, personal profiling using genetic polymorphism, admission white cell count, and markers of insulin resistance resulted in a 28-fold enhanced reduction of LVESV during the first 6 months post AMI (11 vs. 0.4 ml reduction, $p<0.0001$).

Conclusion: Personal profiling using pt genotype and relevant metabolomics may markedly enhance therapeutic benefits of anti-inflammatory remodeling benefits of O3-FA after an AMI.

FADS genotype polymorphism likelihood of LVESV improvement in the first 6 months of AMI

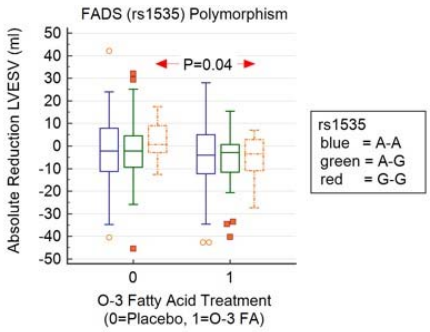

Fig 1

High WBC and Neutrophil Counts at Index AMI Arrival Accentuates Remodeling Benefits from O3-FA

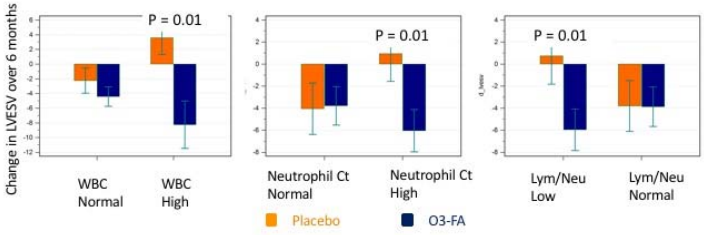

Fig 2

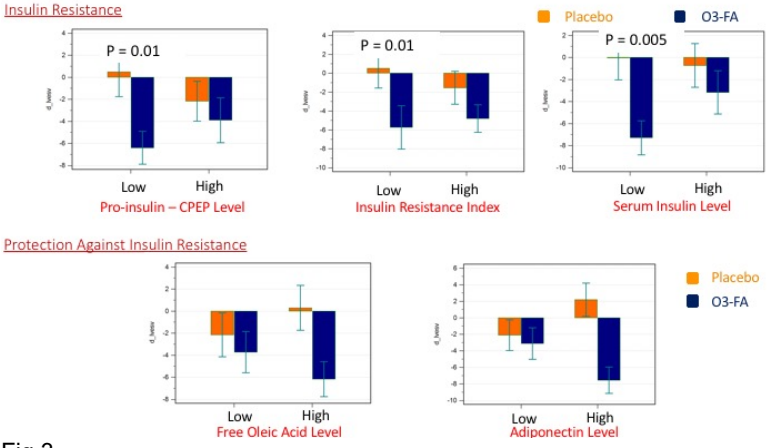

Fig 3

ID#: 379484

Comprehensive structure and function assessment by CMR in pediatric heart transplant patients.

Nazia Husain, MBBS, MPH[1] Shivani G. Patel, MBBS[2], Arleen Li, BS[3], Haben Berhane, M.A.[4], Cynthia K. Rigsby, MD, FACR[5], Joshua D. Robinson, MD, FACC[5]

1. Ann & Robert H. Lurie Children's Hospital of Chicago, IL

2. Ann and Robert H Lurie Children's Hospital of Chicago, Chicago, IL

3. Ann & Robert H Lurie Children's Hospital of Chicago, IL

4. Ann & Robert H. Lurie Children's Hospital of Chicago

5. Ann & Robert H. Lurie Children's Hospital of Chicago, Chicago, IL

Background: Heart transplant recipients (HTX) present a unique set of anatomic and pathophysiologic considerations; requiring frequent monitoring for development of life-threatening complications such as rejection and cardiac allograft vasculopathy (CAV). Comprehensive CMR evaluation has an increasing role in management of adult HTX but data in children are limited. Specifically, the feasibility of stress perfusion CMR for evaluation of perfusion abnormalities has not been systematically evaluated. The aim of this study was to describe our center's experience with multi-parametric CMR assessment in pediatric heart transplant patients.

Methods: We performed retrospective chart review of 17 pediatric HTX who underwent comprehensive CMR evaluation with stress perfusion imaging. 16/17 underwent cardiac catheterization within 1 month. Protocol included standard cine imaging, T1/T2 mapping, delayed enhancement, myocardial perfusion at rest and stress (using regadenoson). T1, T2, ECV values were calculated (using a 16 segment model); deformation variables (global longitudinal and circumferential strain; GLS and GCS) were obtained using Tomtec (feature tracking software) and semi-quantitative stress perfusion was analyzed using Medis Suite 3.0 (QMASS, Netherlands). Previously described perfusion variables (relative upslope and myocardial perfusion reserve index; MPRI) were calculated. HTX patients were compared with historical controls (n=15) who had CMRs with rest perfusion performed for various indications.

Results: HTX and controls had no significant demographic differences (Table 1). HTX were 10.4 +/- 4.9 years post-transplant. Five had clinically unimportant rejection (Grade 1R/1A) and 1 had antibody-mediated rejection on recent endomyocardial biopsy; 3 had CAV on coronary angiography. Compared to controls (Table 2), HTX had significantly smaller end-diastolic ventricular volumes (LVEDV p=0.03; RVEDV p=0.01); lower GCS (p=0.02) and higher mean pre-contrast T1 (p=0.02). Increasing T2 values were strongly associated with worsening GCS (R2=0.7, p=<0.01). Of the 3 HTX suspected to have CAV, qualitative assessment showed a perfusion deficit in only one patient and one could not tolerate stress perfusion. Semi-quantitative perfusion analysis in HTX showed a mean MPRI of 0.78 +/- 0.21 (median 0.8; range 0.46 to 1.36).

Conclusion: In this small pediatric HTX cohort with a low incidence of rejection or vasculopathy, we showed that comprehensive CMR assessment demonstrates significant structure-function relationships between T2 values and GCS. Stress perfusion with semi-quantitative analysis is feasible but further studies in higher risk patients are needed to elicit its relationship with CAV. Larger patient cohorts and longitudinal follow-up may determine clinical significance of these findings.

Demographics

	HTX cases (n=17)	Controls (n=15)	p-value
Sex (M:F)	(8:9)	(5:10)	0.44
Age at CMR (years)	15.8 +/- 2.8	16.7 +/- 1.9	0.11
Age at Transplant	10.4 +/- 4.9		
Height (cms)	163.7 +/- 11.2	170.1+/-10.2	0.10
Weight (kgs)	61.5 +/- 16.5	61.5 +/- 13.3	0.99

BSA (m2)	1.66 +/- 0.2	1.68 +/- 0.2	0.79

CMR structure and function variables

	HTX		Controls		p-value
	mean	stdev	mean	stdev	
LVEDV (ml)	133.29	40.02	152.93	35.57	NS
LVEDV indexed to BSA (ml/m2)	78.88	13.72	89.33	11.92	0.03
LVESV (ml)	57.71	26.68	64.67	14.25	NS
LVESV indexed to BSA (ml/m2)	34.94	13.61	37.93	5.3	NS
LV Cardiac Output indexed to BSA (ml/m2/min)	4.5	0.78	3.78	0.7	0.01
LV ejection fraction (%)	58.35	7.04	57.67	3.39	NS
LV mass	81.82	22.75	79.33	27.95	NS
LV mass indexed to BSA (ml/m2)	48.71	8.15	45.73	11.82	NS
RVEDV (ml)	129.35	37.91	153.2	37.3	NS
RVEDV indexed to BSA (ml/m2)	76.94	12.74	89.2	11.48	0.01
RVESV (ml)	57.29	26.19	67.93	16.48	NS
RVESV indexed to BSA (ml/m2)	32.88	10.1	39.53	5.49	0.03
RV Cardiac output indexed to BSA (ml/m2/min)	4.4	0.68	7.79	16.12	NS
RV Ejection Fraction (%)	58.12	7.38	51.73	14	NS
GLS (%)	-20.79	5.43	-23.21	2.8	0.13
GCS (%)	-24.46	8.33	-29.75	3.15	0.02
Pre-T1 (msec)	1062.12	47.76	1015.70	30.91	0.02
ECV (%)	25.31	7.75	26.41	1.90	NS
T2 (msec)	49.56	4.42	51.00	1.00	NS

ID#: 379489

T1 mapping abnormalities in patients with aortic stenosis. Relationship with clinical features and myocardial deformation assessed by tissue tracking

Ana G. Almeida, MD, PhD[1] Rui Placido, MD[2], Gustavo Lima Silva, MD[3], Ana Francisco, MD[3], Claudio David, MD[3], Luis Rosário, MD, PhD[4], Pedro Carrilho-Ferreira, MD[4], Fausto Pinto, MD, PhD[3]

1. University Hospital Santa Maria, Lisbon, Portugal, Lisbon, Portugal

2. Santa Maria University Hospital, Cardiology Department, Lisbon Academic Medical Center, CCUL, Lisbon, Portugal, Lisboa, Portugal

3. Cardiology - University Hospital Santa Maria, Lisbon, Lisboa, Portugal

4. University Hospital Santa Maria, Lisbon, Portugal, Portugal

Background: In patients with aortic stenosis, myocardial fibrosis underlines the progression to LV dysfunction, which impacts prognosis and clinical decision. Diffuse fibrosis may be assessed currently by CMR using T1 mapping, •Additionally, deformation abnormalities of left ventricle (LV) myocardium may precede changes in LV ejection fraction and potentially influence the prognosis.•We aimed to assess the presence and amount of diffuse fibrosis in patients with severe aortic stenosis by native CMR T1 mapping and to evaluate its association with strain changes by CMR feature tracking and the clinical features and biomarkers

Methods: We included 54 consecutive patients (63+/-5 year-old, 63% male) with severe aortic stenosis as assessed by echocardiography according to EACVI and ASE guidelines •Patients with atrial fibrillation, coronary artery disease or associated cardiomyopathy, EF<50%, general contra-indications to CMR were excluded.
All patients underwent: a) Clinical: NYHA class, angina, syncope; b) NTproBNP values c) CMR – 3T system (Philips Achieva) –SSFP cine in short-axis and long-axis for volumes and function; Native T1 mapping by MOLLI sequence, in a mid-short-axis plane; Peak global longitudinal strain, using tissue tracking (cvi42, Circle, Calgary); LGE, representing replacement fibrosis
A control group of 27 normal individuals was included for comparison.

Results: In compatison with the control group, patients with aortic stenosis had a larger LV end-diastolic volume (p=0.001), a larger LV mass (p=0.001), a larger left atrial volume (p=0.002), higher T1 values (1256±38 versus 1125±18 ms, p=0.004) and lower global longitudinal strain (-18.4 versus -21.2%, p=0.003). No LGE was present in any of the groups.
In the aortic stenosis patients, T1 values correlated significantly with the peak global longitudinal strain by tissue tracking (r=0.61, p =0.001), with the indexed left atrial volume (r=0.41, p=0.02) and with the NTproBNP values (r=0,81, p=0,002).No relationship was found with the aortic valve area, the LV volume, ejection fraction or mass.
In comparison with asymptomatic patients, the ones in class ii/III or with angina showed higher native T1 values (1312±31 versus 1216±45, p=0,001) and a lower global longitudinal strain (-17.1±1,2 versus -19.5±3.1, p=0.01).

Conclusion: Both Native T1 and longitudinal strain values in patients with severe aortic stenosis were higher than in controls suggesting the presence of myocardial fibrosis. Furtermore, In symptomatic patients, these parameters were significantly different from the ones in asymptomatic patients.
CMR T1 mapping and strain provide tools for the possibility of early detection of myocardial disease, and participate in the decision on timing to operate on and influence the post-operative recovery and outcomes.

ID#: 379591

Mind the Gap: Insights into Recurrent Atrial Fibrillation Post Cryoablation with Novel Cylindrical Navigator and 3-Tesla Imaging

Ibrahim M. Saeed, MD[2]Joseph S. Soltys, Ph.D[1], Sanjaya Gupta, MD[2], Martin A. Janich, PhD[3]

1. Cardiovascular Imaging Technologies, Kansas City, MO

2. Saint Luke's Mid-America Heart Institute, Kansas City, MO

3. GE Healthcare, Germany

Background: Pulmonary vein isolation (PVI) with cryoablation is a procedure to treat patients with atrial fibrillation (AF) that is 85% successful at restoring normal rhythm. For the 15% with recurrent AF post ablation, optimal treatment is often unclear. CMR with late gadolinium enhancement (LGE) has demonstrated the ability to visualize post-ablation scarring. However results linking the continuity of these left atrial LGE scars with recurrence of AF have been inconclusive and mostly focused on continuity of radiofrequency ablation lesions. Previously we have reported on the importance of parameters for visualization of LA-LGE post cryoablation. In this work we demonstrate advantages of a 3-Tesla platform to identify why AF recurs even when a cryoablation scars appears continuous.

Methods: After obtaining IRB-approved consent, all patients were imaged post-cryoablation using 3D, IR-prepped, cardiac/respiratory navigated FGRE sequence acquired axially (temporal resolution ≤15% RR-interval.) Images on 1.5-T (Signa HDxt, or Optima 450w, General Electric) were performed with 0.15 mmol/kg injection of gadobenate-dimeglumine, standard 90-180 navigator pulse, and voxel size 1.6 x 1.6 x 2.6 mm. On 3-T (Discovery 750, GE), images had similar orientation but lower dose of gadobenate (0.1 mmol/kg), but with a cylindrical navigator, fat-sat preparation, voxel size of 1.2 x 1.2 x 2.0 mm. Follow up data regarding recurrence of AF was available for 3-T. Contrast between blood pool and LGE were calculated from ROIs on multi-planar reformatted slices of each PV antrum demonstrating the most continuous lesion (Osirix, Pixmeo, CH).

Results: On 1.5-T, 122/132 PVs were imaged (33 pts (11F, 64±10y) and 39/40 PVs on 3-T (5 pts (2F, 62±8y). A two-sided students T-test (assumed unequal variance) indicated significant increase in contrast between observed LGE and blood pool in each PV (p=0.04) at higher field strength despite lower contrast dosage. At 3-T, average LGE was 12.7%±5.6% brighter than blood pool, vs 7.9%±10.7% on 1.5-T. In the 3-T cohort, recurrent AF was observed in pts with an area of apparent “no reflow” within the PV antrum (Figure).

Conclusion: LGE is seen in PVI lesions from cryoablation on both 1.5 and 3.0 Tesla field strengths, with increased confidence in obtaining quality images. The cylindrical navigator on 3-T allows for smaller voxel, decreased gadolinium dosage, and improved contrast-to-noise that is clinically significant in this limited data set. This limited 3-T data also suggests potential mechanisms for recurrent AF, warranting further studies. This study was supported in part by the American College of Cardiology-Missouri Chapter and GE.

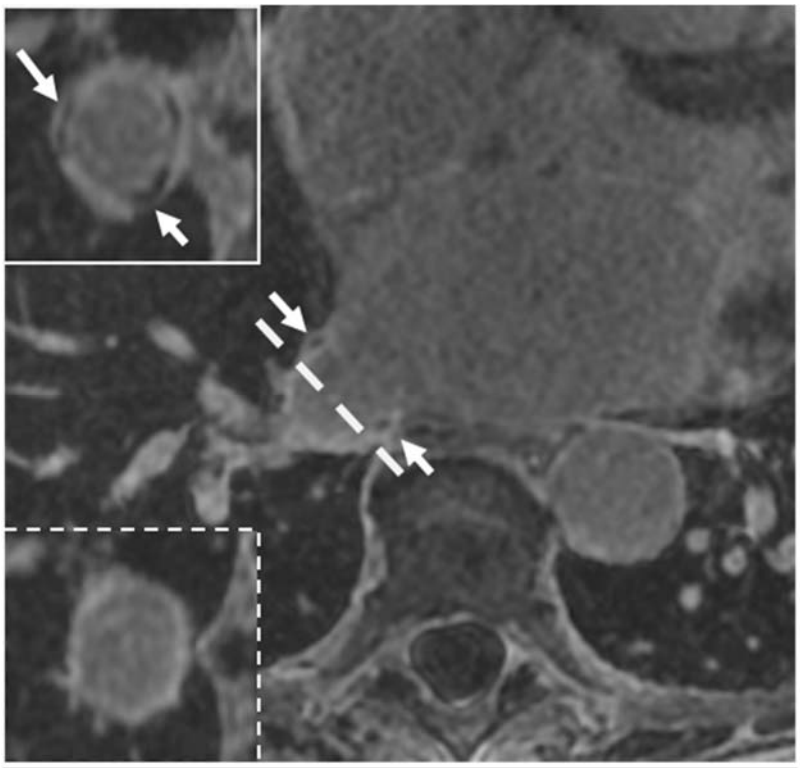

Figure: Axial view of left atrial cryoablation PVI attempts imaged at 3T. An arrow of "no reflow" was noted (arrows on multi-planar reformat in upper inset) in 2 of 5 patients, despite an apparently continuous LGE ring just distal (dashed line in lower inset). Both patients with "no reflow" phenomenon had recurrent AF.

3T LA LGE

ID#: 379592

Management of unbalanced pulmonary blood flow in univentricular patients: surgical intervention by intra-pulmonary septation and evaluation by CMR and catheterization

Keisuke Sato, MD

Shizuoka Children's Hospital, Department of Cardiology, Shizuoka City, Shizuoka, Japan

Background: Unbalanced pulmonary blood flow is believed to cause evil situations against univentricular patients in their way to Fontan circulation. For those patients, IPAS (making a septum in pulmonary artery and modified Blalock-Taussig shunt to hypoplastic pulmonary artery) is performed to apply high blood pressure to high pulmonary vascular resistance. But the indication for removal of IPAS has been vague. The aim of this study is to investigate whether pulmonary vascular resistance calculated by CMR and catheterization provides indication for removal of IPAS.

Methods: 5 univentricular patients with unbalanced pulmonary blood flow who underwent IPAS and CMR/Catheterization study were eligible for this retrospective study. All CMR examination was performed with MAGNETOM Symphony 1.5T (Siemens). Pulmonary blood flow analysis was performed with phase contrast images at pulmonary arteries and pulmonary veins.

Results: The diagnosis of five patients was hypoplastic left heart syndrome for 2 patients, single ventricle for 2 patients and Ebstein';s anomaly for 1 patient. One patient (Ebstein';s anomaly) was after total cavopulmonary connection (TCPC) and the other 4 patients were after bidirectional Glenn procedure (BDG). The age at IPAS was 3.5±1.5 years old. In four BDG patients, the ratio of pulmonary arterial blood flow, pulmonary venous blood flow and pulmonary vascular resistance improved successfully. Before IPAS, the ratio of pulmonary arterial blood flow, pulmonary venous blood flow and pulmonary vascular resistance were 0.19±0.14, 0.57±0.22, 2.62±0.52 respectively. After IPAS, the ratio of pulmonary arterial blood flow, pulmonary venous blood flow and pulmonary vascular resistance were 0.67±0.23, 0.89±0.20, 1.74±0.37 respectively. Three of the four BDG patients removed IPAS and one of them is waiting for removal of IPAS. In one TCPC patient, the ratio of pulmonary arterial blood flow, pulmonary venous blood flow and pulmonary vascular resistance was not improved.

Conclusion: Pulmonary vascular resistance calculated by CMR and catheterization provides indication for removal of IPAS.

ID#: 379611

Resolution of Late Gadolinium Enhancement in a Series of Pediatric Patients with Clinical Myocarditis

Marc V. Lee, MD[1] Jason N. Johnson, MD MHS[2], Jeffrey A. Towbin, MD[3]

1. University of Tennessee Health Science Center, Memphis, TN

2. LeBonheur Children's Hospital, University of Tennessee, Memphis, TN

3. Le Bonheur Children's Hospital, St. Jude Children's Research Hospital, University of Tennessee Health Science Center, Memphis, TN

Background: Pediatric patients with acute myocarditis may present with nonspecific signs and symptoms including chest pain and troponin elevation. Cardiac magnetic resonance imaging (CMR) can show areas of myocardial necrosis or fibrosis by late gadolinium enhancement (LGE) in a significant portion of these patients. The evolution or progression of LGE in clinically resolved myocarditis in children is not well studied.

Methods: This was a retrospective case series at a tertiary care children';s hospital of 10 patients with clinical diagnosis of myocarditis based on history and laboratory data with LGE positive CMR who underwent repeat CMR for reevaluation following convalescence from hospitalization for myocarditis. The presence of LGE, interval LGE changes, left ventricle (LV) volumes, LV mass, and left atrial volumes were recorded.

Results: 7 patients with LGE positive CMR (85% male, median age 15, interquartile range 8-17) underwent repeat studies to reevaluate LGE burden. Median time to follow-up CMR was 11months (IQR 3.5-15). 4 patients (57%) demonstrated either interval complete resolution of LGE (Table). During the median follow-up period of 25 months (IQR 23-26), no adverse clinical events of mortality, significant arrhythmia, or cardiac transplantation were reported.

Conclusion: CMR is useful in surveillance for changes in LGE burden in pediatric patients with history of myocarditis who have clinical resolution of illness. Clinical outcome in a small series of patients with LGE positive myocarditis appears favorable following hospital discharge.

Characteristics of Myocarditis Patients with LGE (+) CMR

Patient	Presenting Symptom	Peak Troponin	Initial LGE Distribution	Initial LVEF	Time to Follow-up CMR	Follow-up LGE Distribution	Follow-up LVEF
1	Chest pain, myalgias, fever, vomiting and diarrhea	9.3	Basal inferior, inferolateral	34%	11	No change	54%
2	Chest pain, fever, headache	5.2	Basal inferolateral	55%	15	**No LGE**	54%
3	Chest pain, dyspnea, nasal congestion, headache	1.9	Basal inferior	54%	11	**No LGE**	54%

4	Chest pain, upper respiratory infection, abdominal pain	5.0	Basal inferolateral	61%	3.5	No change	63%
5	Chest pain, arrhythmia, fever, fatigue	1.35	Basical to apical lateral	59%	16	No change	56%
6	Chest pain, presyncope, malaise, upper respiratory infection	13.9	Mid-inferolateral	67%	15	**No LGE**	65%
7	Chest pain, dyspnea, cough, fatigue	14.7	Basal inferolateral	67%	2	**No LGE**	63%

ID#: 379613

A bump in the road - what is this arch?

Nilanjana Misra, MBBS, FAAP

Cohen Children's Medical Center of NY, New Hyde Park, NY

Description of Clinical Presentation: 4 year old boy recently emigrated from Bangladesh who was referred to Cardiology for a murmur heard on routine evaluation. He was completely asymptomatic from the cardiac standpoint denying any chest pain, breathing difficulties, stridor, feeding problems, palpitations or syncope. He was 89th percentile by weight and 99th percentile by height. He was fully saturated on room air, with no discrepancy in blood pressure in 4 extremities. Examination revealed a well appearing child with no dysmorphic features and no respiratory distress. Cardiac examination was significant for a grade III/VI harsh systolic ejection murmur along the left upper sternal border and equal pulses bilaterally with no radio femoral delay.

Diagnostic Techniques and Their Most Important Findings: Transthoracic echocardiogram showed normal segmental anatomy. There was a thickened, doming pulmonary valve with mild to moderate stenosis (PSIG of 39 mm Hg). Tricommissural aortic valve, mildly dilated aortic root with no evidence of stenosis or regurgitation. There was a patent arch. Head and neck vessels were visualized on another plane but origins from the arch were not adequately visualized. Likely left arch. Turbulent flow with peak gradient of 100mmHg was at the level of the right brachiocephalic artery. Normal biventricular systolic function.

Cardiac MRI was recommended and showed the following:

- Normal segmental anatomy
- Dephasing jet artifact across the pulmonary valve suggestive of stenosis
- Good sized main pulmonary artery with continuous branch arteries
- Tricommissural aortic valve. No evidence of aortic regurgitation on cine imaging and PC flows
- Ascending aorta terminated abruptly with some distance between ascending aorta and distal transverse arch
- Transverse arch was short, giving off the left common carotid and left subclavian arteries along the inner curvature
- Right brachiocephalic artery was stenotic (almost string like) and appeared to come off close to the left common carotid artery from the transverse arch
- Right subclavian artery and right common carotid artery were good size
- Ascending aorta communicates to a vascular structure that connects to the transverse descending aorta. This vessel was widely patent and had a course to the left of the trachea and inferior to the short transverse arch
- Normal biventricular morphology and ejection fractions

In summary, the ascending aorta is interrupted at the level of origins of the right brachiocephalic trunk and left common carotid - like a Type C interruption. There is a persistent fifth arch that courses inferior to the short transverse arch (the fourth arch). The ascending aorta communicates with the distal transverse arch/descending aorta via the persistent fifth arch which is widely patent. There is mild change in caliber of the vessels but no discrete stenosis. The origin of the right brachiocephalic artery is stenotic. Given the size of the right subclavian and common carotid arteries, it is likely that it is being perfused retrograde from the Circle of Willis.

Learning Points from this Case: Based on these findings and the fact that the patient is clinically asymptomatic, no interventions were recommended. Parents were counselled about routine surveillance and to notify cardiology about syncopal episodes given concern for possible subclavian/carotid steal. Review of literture shows presence of Type A Interruption of 4th arch with persistent 5th arch but none similar to our case. This case highlights the importance of CMR in defining the vascular anatomy in patients where structures are not adequately visualized on echocardiogram.

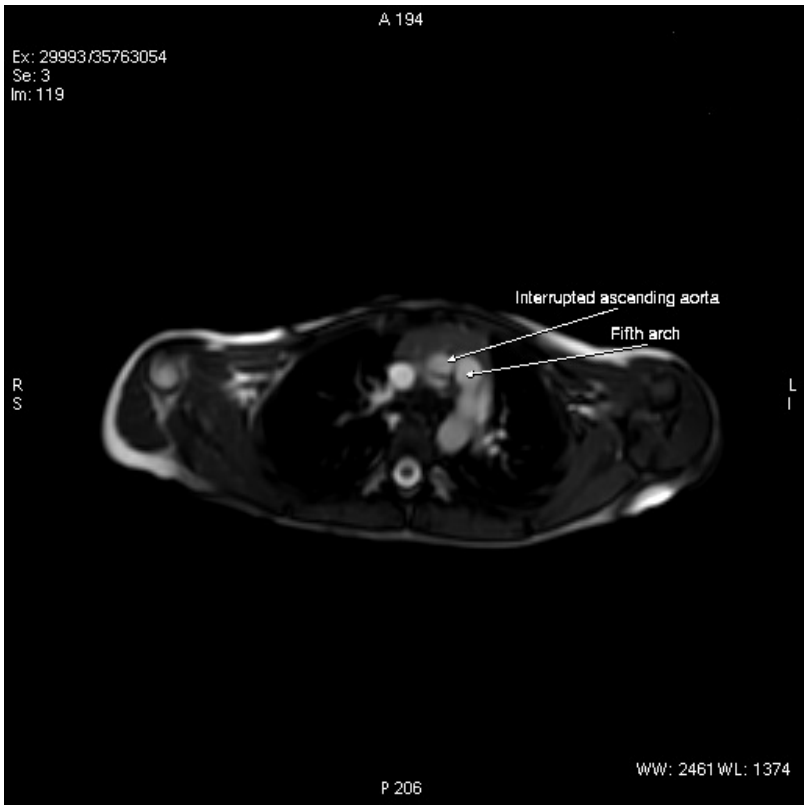

Axial SSFP showing an arch to left of trachea and another vessel in cross section just along its side.

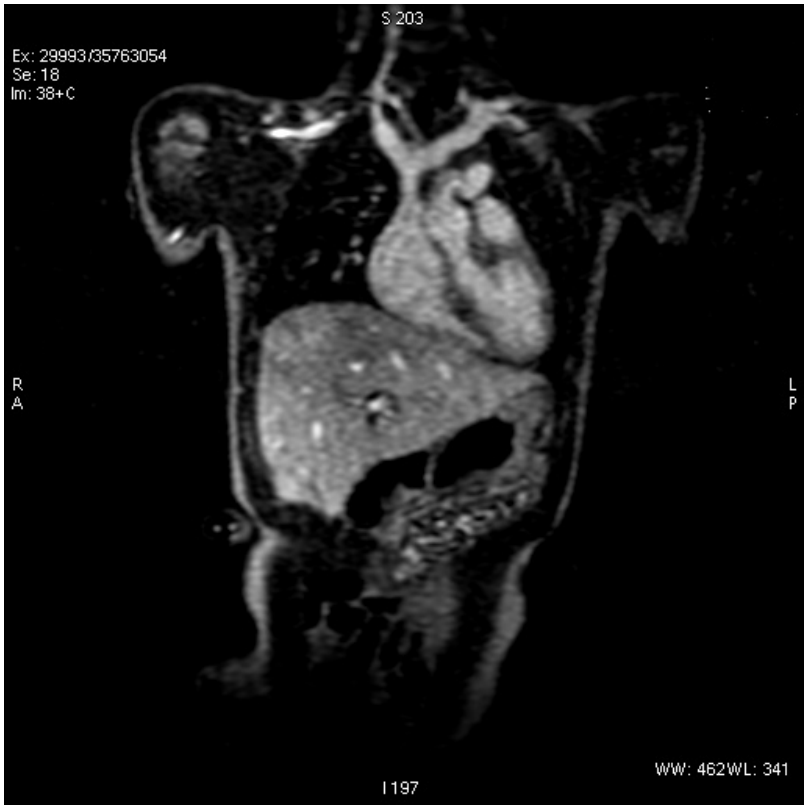

MRA in coronal plane showing a ? tortuous arch

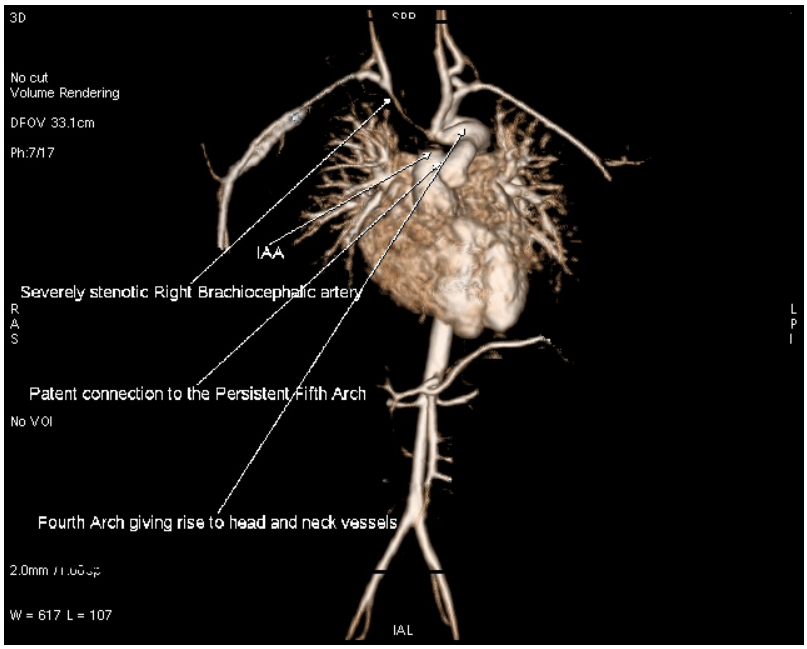

3D reformat of the arch showing the interruption and the persistent fifth arch

ID#: 379479

Recurrent chest pain following surgical repair of cor triatriatum in a young teenager

Rukmini R. Komarlu, MD

Cleveland Clinic Children's Hospital, Beachwood, OH

Description of Clinical Presentation: An obese 14 year old female presented with recurrent history of several weeks of severe chest pain (worse on laying flat, relieved slightly with leaning forward), shortness of breath with back pain. Her past medical history was significant for repair of cor triatriatum and atrial septal defect at an outside institution, 10 months prior to presentation. She had developed post pericardiotomy syndrome soon after the surgery and had undergone multiple hospitalizations for suspected pericarditis, 2, 4 and 10 months following surgery with therapy with ibuprofen and aspirin, with resolution of symptoms following the first 2 hospitalizations. She had been followed for pericardial effusion. However recently her chest pain had become unresponsive to standard therapy with anti-inflammatory medications during this admission. An echocardiogram revealed small circumferential pericardial effusion with normal biventricular systolic function and no residual atrial shunt; but imaging was difficult due to limited acoustic windows.

Diagnostic Techniques and Their Most Important Findings: Cardiac MRI was performed for assessment of pericardial constriction. This revealed small pericardial effusion. There was diffuse thickening of the pericardium. There was circumferential increased pericardial signal intensity on T2 STIR imaging suggesting pericardial edema. There was significant circumferential pericardial delayed enhancement noted. There was diastolic septal bounce, conical deformity of the ventricles with respirophasic septal shift. These findings were consistent with constrictive pericarditis. There was normal biventricular systolic function and normal valvar function. Triple therapy was instituted with steroids, colchicine and ibuprofen. A repeat cardiac MRI done 5 months later revealed significant improvement with mild thickening of the pericardium and patchy minimal increased pericardial signal intensity on T2 STIR imaging as well as mild circumferential pericardial enhancement.

Learning Points from this Case: Cardiac MRI was crucial in establishing the diagnosis of constrictive pericarditis in this patient with history of recurrent episodes of pericarditis, following surgery. This enabled institution of appropriate therapy with improvement in symptoms and markers of inflammation. Pericarditis should remain in the differential diagnosis of chest pain especially in the post-surgical patient.

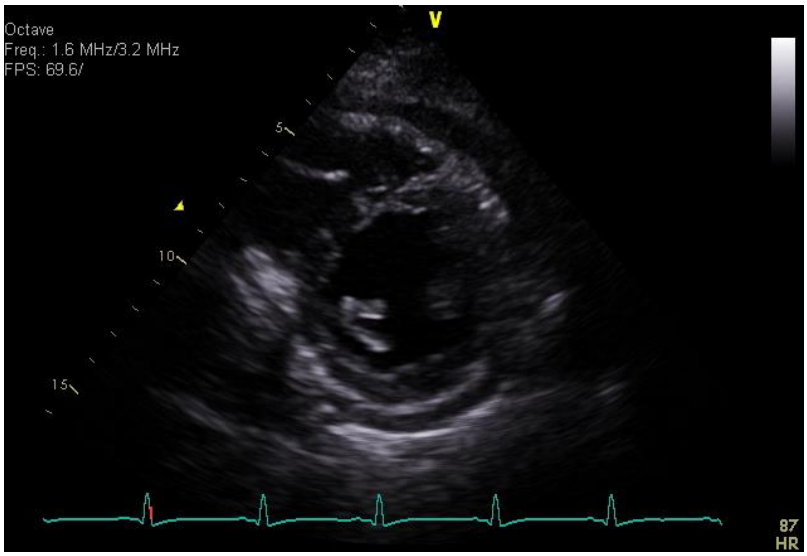

Echocardiogram showing small circumferential pericardial effusion

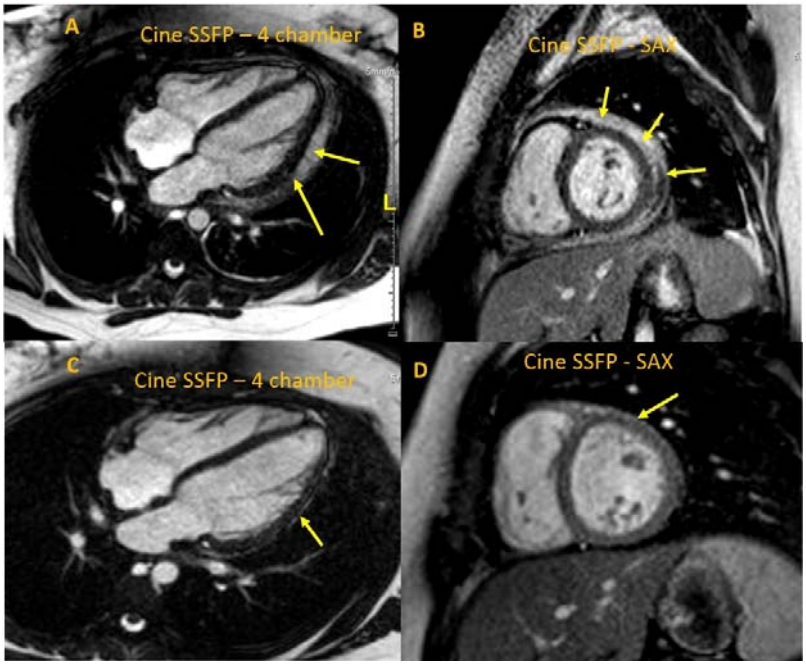

Cine SSFP imaging: Arrows reveal thickened pericardium in A-B; C-D reveals absence of thickened pericardium following therapy

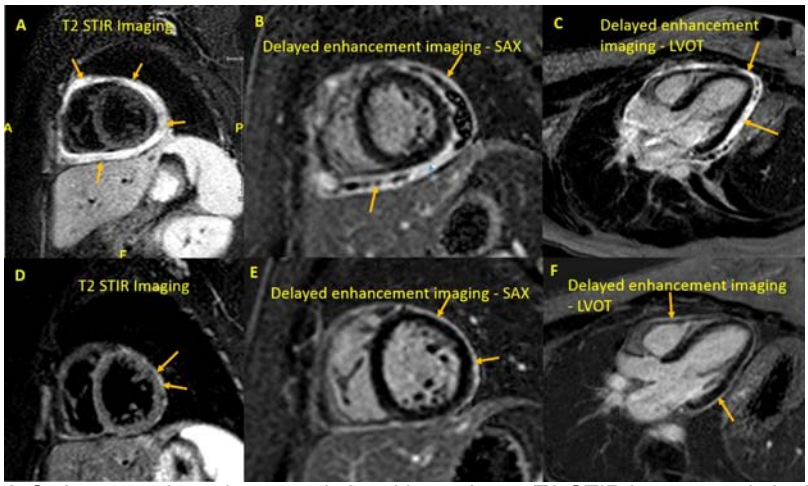

A-C: Arrows point to increased signal intensity on T2 STIR images and significant pericardial enhancement; Images D-F show improvement following therapy

ID#: 379596

Imaging of acute myocarditis in patient with systemic lupus erythematosus

Andreja Cercek Cerne, MD, PhD

University Medical Centre Ljubljana, Slovenia

Description of Clinical Presentation: Myocarditis is a rare manifestation of systemic lupus erythematosus (SLE). Here we present a multimodality imaging approach in this potentially life threatening cardiovascular complications.

Diagnostic Techniques and Their Most Important Findings: A 26-year-old female patient with SLE was admitted to our hospital due to myocarditis mimicking acute coronary syndrome. At presentation she had increased troponin I level (TnI 37 mcg/L) and ischemic changes in the ECG. Coronary angiography excluded obstructive coronary artery disease. Echocardiography revealed low mildly impaired left ventricular ejection fraction (LVEF) 50%, thickened LV walls (1.2 cm) and reduced global longitudinal strain (GLS) (-13%) (Figure 1). Cardiac magnetic resonance imaging (CMR) showed areas of late gadolinium enhancement (LGE) in basal lateral and anterior LV walls. The diagnosis was confirmed with endomyocardial biopsy; fine granular immune complexes and complement deposition in the walls of myocardial blood vessels and perivascular tissue were detected by immunofluorescence microscopy; PCR for viral nucleic was negative (Figure 2). At first, the patient was treated with high-dose of steroids on a top her immunosuppressive medications. This treatment resulted in transient relief of symptoms and troponin I level normalization. However, tapering of steroids resulted in relapse of myocarditis after 30 days of initial event. CMR showed additional areas of subepicardial LGE. Again, the patient received elevated dose of steroids and in addition the immunosupressive therapy was modified to include biological therapy. At 6 months follow-up the patient was asymptomatic and LVEF (58%), LV wall thickness (0.9 cm) as well as GLS (-20%) were normal (Figure 1). In addition, CMR showed significant reduction of LGE. At 3 years follow-up, she remained asymptomatic, with normal LV systolic in diastolic function.

Learning Points from this Case: CMR may help in diagnosing and treatment follow-up of patients with acute SLE myocarditis. With immunosuppressive medications and cardiovascular support, the long-term outcome is usually favourable.

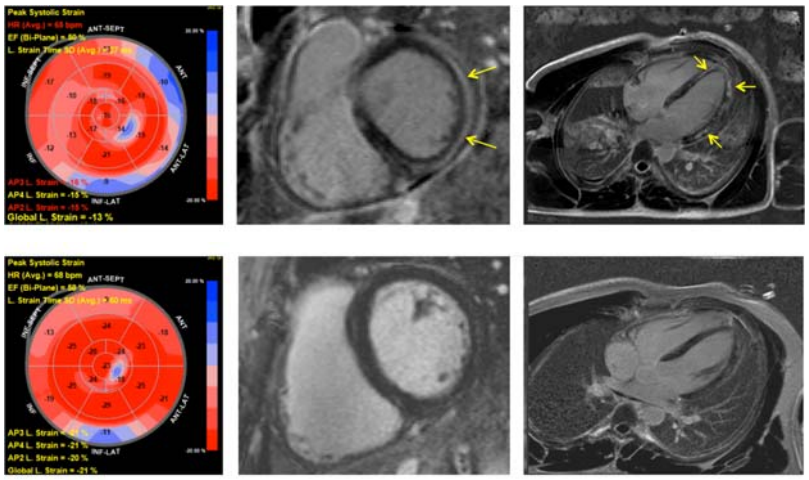

Fgure 1. Magnetic resonance imaging (MRI) and ultrasonographic 2D speckle tracking imaging of patient with SLE myocarditis at presentation and at 6 months follow-up.

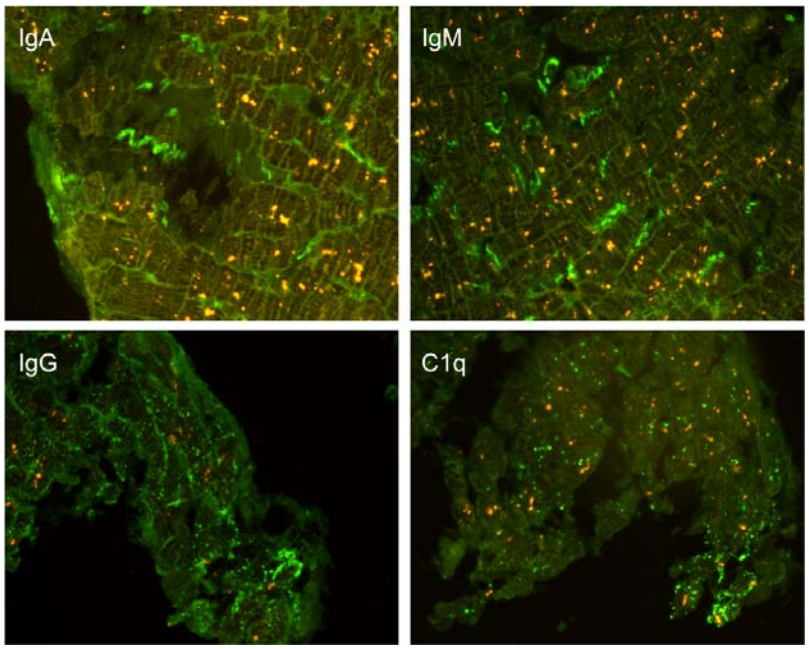

Figure 2. Endomyocardial biopsy-imunohistochemistry

ID#: 379492

A Clinical Situation Where Cardiac MRI Made a Difference

Abdalla Elagha, Cairo university

cairo university, Zamalek, Al Qahirah, Egypt

Description of Clinical Presentation: A 45-year old previously healthy male, presented with a three-month history of atypical chest pain followed by progressive shortness of breath on exertion. ECG revealed inverted abnormal T-wave in inferior and anterior precordial leads. Echocardiography demonstrated normal left ventricular function, and marked hypertrophy of the left ventricular apex. Apical hypertrophic cardiomyopathy was given as preliminary diagnosis, and medical treatment including B-blockers was prescribed, which does not improve patient's symptoms.

Diagnostic Techniques and Their Most Important Findings: Cardiac MRI was requested for further investigations. Unexpectedly, the CMR study showed completely different picture. The left ventricular apical cavity is completely obliterated by a large mass (5 x 2.5 cm) obliterating the left ventricular apex and adjacent apical regions. It has a low signal in T1W & T2W images. By applying fat saturation sequence, the signal of this mass did not decrease in intensity, which means it is not a fatty mass. On First-Pass perfusion study, the left ventricular mass did not show any uptake of the contrast. On Delayed Hyperenhancement technique, This mass did not enhance, which means (with other supporting evidences form other sequences) it is a large thrombus, and not an apical HCM. However, this was not the only clue given by DHE images; It demonstrates areas of increased signal in several myocardial segments, all affection was limited only to the endocardial surface. Endocardial fibrosis was depicted at the apex, apical & mid anterior segments, apical, mid, & basal inferior segments ,apical lateral & septal segments. The endocardial fibrosis was extending into a small area of right ventricular apex. All CMR findings denoted a process of "Endomyocardial fibrosis." Moreover, CMR study showed a large circumferential pericardial effusion, significant mitral regurgitation, nevertheless, the left ventricular systolic function was preserved. All these finding followed by laboratory findings (esinophilia on CBC) confirmed the diagnosis of Loffler's endocarditis.

Learning Points from this Case: In general, This syndrome results in an obliterative, restrictive cardiomyopathy thought to result from toxic damage from the intracytoplasmic granular content of activated eosinophils. It occurs in temperate climates and is associated with a hypereosinophilic syndrome. Patients have endocardial thickening and obliteration of the cardiac apex. It is usually an aggressive disease, however, corticosteroids and cytotoxic drugs in the early phase of disease may improve symptoms and survival. In this educational case, cardiac MRI made a substantial role in clinical management, primarily by changing diagnosis from apical HCM to Loffler's disease.

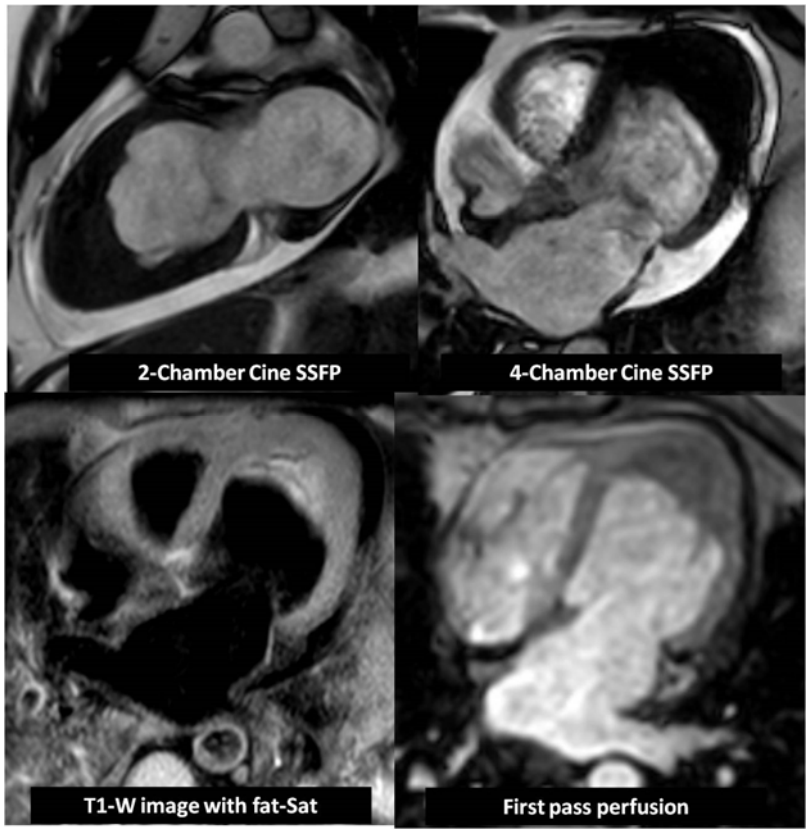

On SSFP pulse sequence, the left ventricular apical cavity is completely obliterated by a large mass (5 x 2.5 cm) obliterating the left ventricular apex and adjacent apical regions, that appears in two-chamber view (A) and four-chamber view (B). By applying fat-saturation pulse sequence, the signal of the apical mass did not decrease in intensity, which means it is not a fatty mass (C) . On First-Pass perfusion study, the left ventricular mass did not show any uptake of the contrast. (D)

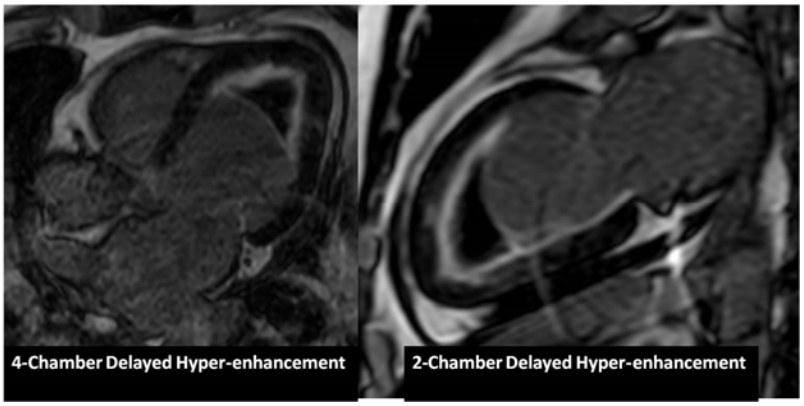

On Delayed Hyperenhancement technique, in four-chamber view (A) and two-chamber view (B), the apical mass did not enhance, which means it is a thrombus. Moreover, It demonstrates areas of increased signal in several myocardial segments, all affection was limited only to the endocardial surface. Endocardial fibrosis was depicted at the apex, apical & mid anterior segments, apical, mid, & basal inferior segments ,apical lateral & septal segments. The endocardial fibrosis was extending into a small area of right ventricular apex.

ID#: 379576

Left Ventricular Aneurysm After Blunt Force Trauma in a Pediatric Patient

Michael Brock, MD[1]Jennifer G. Co-Vu, MD[2], John-Anthony Coppola, MD[2], Frank Y. Han, MD[3], Arun Chandran, MD[4], Renata Shih, MD[1]

1. University of Florida Congenital Heart Center, FL

2. University of Florida, Gainesville, FL

3. University of Florida Congenital Heart Center, Gainesville, FL

4. University of Florida, FL

Description of Clinical Presentation:

A 9 year old male was admitted to the Pediatric Intensive Care Unit (PICU) after a motor vehicular accident where he was ran over by a trailer. He fell from the truck and sustained injury after the trailer rolled over his chest. After admission to the PICU he had several nonsustained runs of ventricular tachycardia (VT). Echocardiographic findings showed a large left ventricular (LV) aneurysm of the inferoseptal wall and a muscular ventricular septal defect (VSD). To better delineate the extent of the aneurysm, CMR was done with findings detailed below.

Diagnostic Techniques and Their Most Important Findings: CMR was done on a Siemens Avanto scanner (Erlangen, Germany) at 1.5 T. Cine SSFP which showed a mid inferior and inferoseptal LV aneurysm as well as a muscular VSD. On delayed enhancement imaging, there is full-thickness hyperenhancement of the region of the aneurysm. He had an exploratory median sternotomy which revealed an anterior right ventricular contusion and a mildly contused area on the back of the LV, with no free rupture or area of what surgeons thought was a pseudoaneursym. Surgeons decided that no surgical intervention was needed at the time. About a month later, he returned with palpitations and tachycardia. Because of concern for enlargement of the aneurysm, a repeat CMR was done. With Cine SSFP, a much larger LV aneurysm was demonstrated at the mid inferior and inferoseptal region. On delayed enhancement imaging, there was again, delayed enhancement demonstrated throughout the wall of the aneurysm.

Learning Points from this Case:

Left ventricular aneurysms are quite rare, especially in the pediatric population. CMR is essential in defining the size and extent of the aneurysm. It is also central in the surgical decision making process. In review of the literature, there are a few case reports of post-traumatic cardiac aneurysms of which include true and pseudoaneurysms. This is the second case in the literature that demonstrates CMR findings of a traumatic LV aneurysm, and the first case that demonstrates such a large aneurysm in the realm of pediatrics – where the patient also survived the initial trauma. Surgical isolation of the LV aneurysm was subsequently performed and the patient is currently being followed closely as an outpatient.

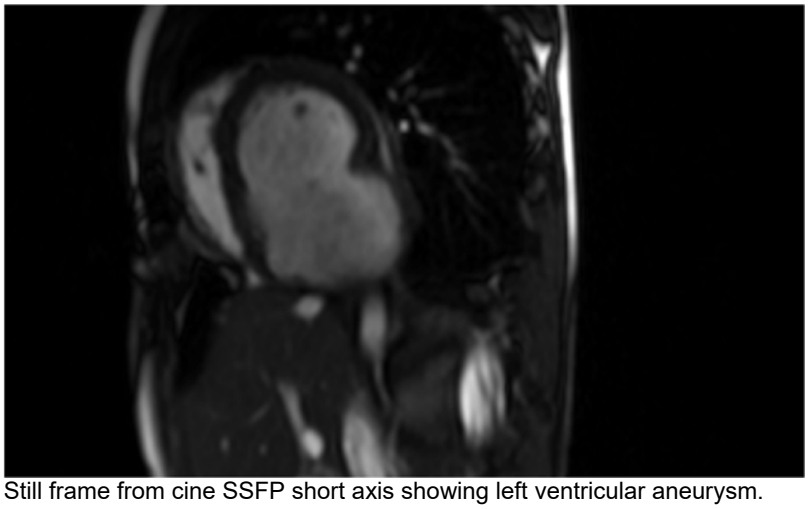

Still frame from cine SSFP short axis showing left ventricular aneurysm.

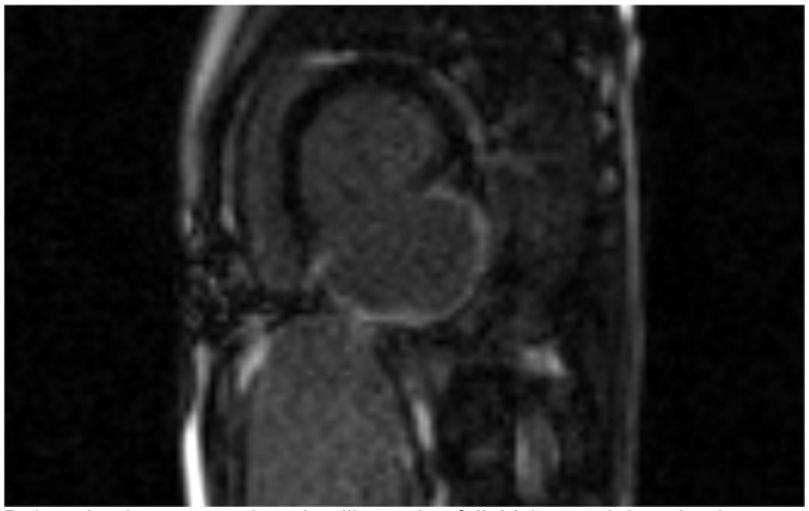

Delayed enhancement imaging illustrating full thickness delayed enhancement of the aneurysmal wall and normal enhancement of the remainder of the LV wall.

ID#: 379375

A rare case of giant submitral left ventricular diverticulum

Rui Placido, MD[1] Ana G. Almeida[1], Tatiana Guimaraes[2], Susana Goncalves[1], Paula Campos[3], Fausto J. Pinto[1]

1. Santa Maria University Hospital, Cardiology Department, Lisbon Academic Medical Center, CCUL, Lisbon, Portugal, Lisboa, Portugal

2. Santa Maria University Hospital, Cardiology Department, Lisbon Academic Medical Center, CCUL, Lisbon, Portugal, Lisbon, Lisboa, Portugal

3. Santa Maria University Hospital, Radiology Department, Lisboa, Portugal

Description of Clinical Presentation: A 36-year-old Guinean woman was referred to our centre for a closer examination of systolic murmur. She had no cardiovascular complaints.

Diagnostic Techniques and Their Most Important Findings: Echocardiographic examinations depicted a large sacular structure at the left ventricular posterior wall in the submitral region. There was paradoxical contraction with no evidence of thrombus at its distal end. The outpouching structure was connected to the left ventricle (LV) through a large neck. In diastole, blood flowed from the LV into the cavity, and in systole blood flowed from the cavity into the LV. These findings indicate that this cavity itself contracts. No other cardiac abnormalities were found. To better delineate the whole shape of the cavity and its relation with the LV chambrer, a computed tomographic (CT) scan was requested. It allowed precise measurement of the outpouching structure (9x7 cm), delineation of its morphology and excluded coronary artery disease. To confirm whether the wall of the cavity consists of muscle, cardiac magnetic resonance (CMR) was performed. We could clearly confirm that the wall of the cavity consisted of muscle with no fibrosis. A diagnosis of congenital large submitral left ventricular diverticulum was made. The patient refused surgery and is followed at our cardiology clinic.

Learning Points from this Case: Left ventricular (LV) diverticulum is a rare condition and it is important to differentiate it from pseudoaneurysm. The increasing use of noninvasive imaging modalities can help to demonstrate different types of ventricular outpouching structures. While definite diagnoses need to be made by histopathologic evaluation, a review of the literature showed that there are different clinical and radiologic criteria for distinguishing these lesions. CMR with its advanced sequences can adequately characterize these outpouchings, allowing to better understand their natural history and to guide proper management decisions with accurate diagnosis.

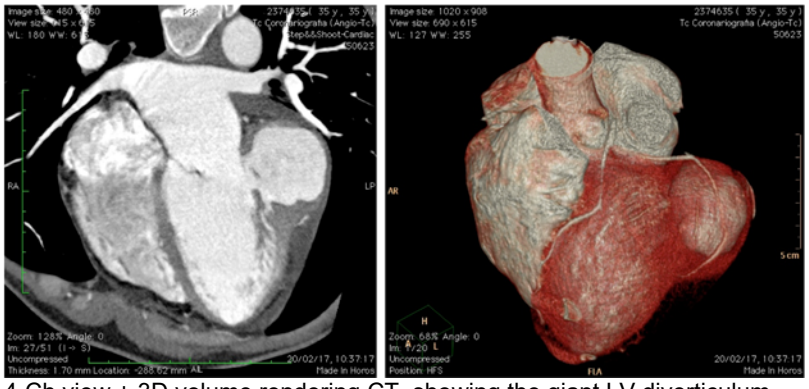

4-Ch view + 3D volume rendering CT, showing the giant LV diverticulum

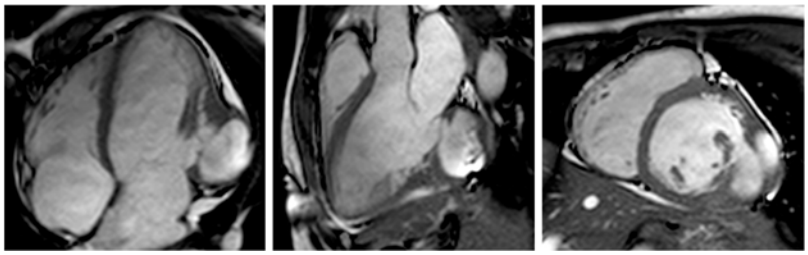

4-Ch, 3-Ch, SA view, depicting the giant LV diverticulum

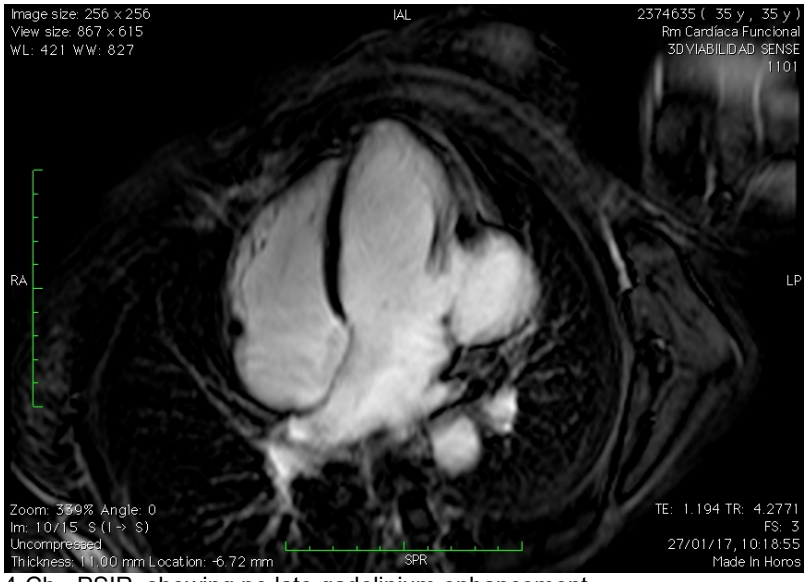

4-Ch - PSIR, showing no late gadolinium enhancement

ID#: 379385

3D “modeling” and “printing” based on MR and CT data in neonate with complex twisted heart: new frontier for clinical decision and optimal surgical approach

Aurelio Secinaro, MD[1]Giuseppe Muscogiuri, MD[2], Adriano Carotti, MD[2], Paolo Ciliberti, MD[1]

1. Bambino Gesù Children's Hospital and Research Institute, Rome. Italy, Lazio, Italy

2. Bambino Gesù Children's Hospital and Research Institute, Rome. Italy, Italy

Description of Clinical Presentation: A newborn male (2.7 Kg) with diagnosis of Goldenhar syndrome, right lung hypoplasia, right sided heart, twisted supero-inferior ventricles with hypoplastic LV, aortic coarctation and large ventricular septal defect underwent computed tomography angiography (CTA) and cardiovascular magnetic resonance (CMR) in order to better define cardiovascular anatomy and hemodynamic consequence related to the complex malformation.

Diagnostic Techniques and Their Most Important Findings: CTA was acquired using post-iodinate contrast ECG-gated high-pitch acquisition modality (Somatom Definition Flash, Siemens). CMR sequences were focused on the evaluation of anatomical morphology, flows and function. In particular, CMR anatomy was assessed using a 3D T1 turbo spin echo with respiratory triggering. Both CTA and CMR volumetric sequence were acquired in systolic phase avoiding the artefact due to ventricular tachycardia.
Data achieved from CTA and CMR were combined using a post-processing software (MIMICS, Materialise) in order to evaluate and isolate cardiac chambers, myocardium, great vessels and proximal coronary arteries.
The left ventricle volumes (indexed LVEDV 21 ml/m2) and aortic forward flow (>1 l/min/m2) were considered adequate to support biventricular circulation with no evidence of endomyocardial fibroelastosis at late gadolinium enhancement imaging.
Stereolithography (STL) file was obtained from 3D data from CTA and CMR. Hollow model was printed out with TuskT (rigid and trasparent) material and divided in three pieces in order to optimize intracardiac views and better define relationship between structures.
VSD septal defect, its margin and its relationship with surrounding structures such as outflow tracts, RV free wall and branching right coronary artery course were identified and three-dimensionally displayed.
Surgical LV to aorta connectibility and VSD closure were considered feasible and biventricular repair was successfully performed.

Learning Points from this Case: Modern advanced integrated imaging approach supported by new 3D technologies provides additional insight into complex congenital heart disease in neonates, as in twisted or criss-cross heart. 3D printed models can reduce uncertainties as regards to the patient';s specific anatomy and effectively help in the clinical decision□making.

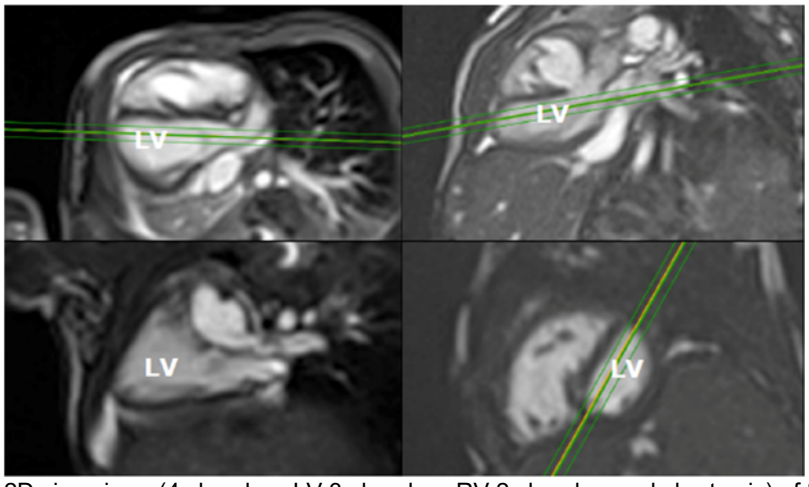

2D cine views (4 chamber, LV 3 chamber, RV 2 chamber and short axis) of the right sided complex twisted heart

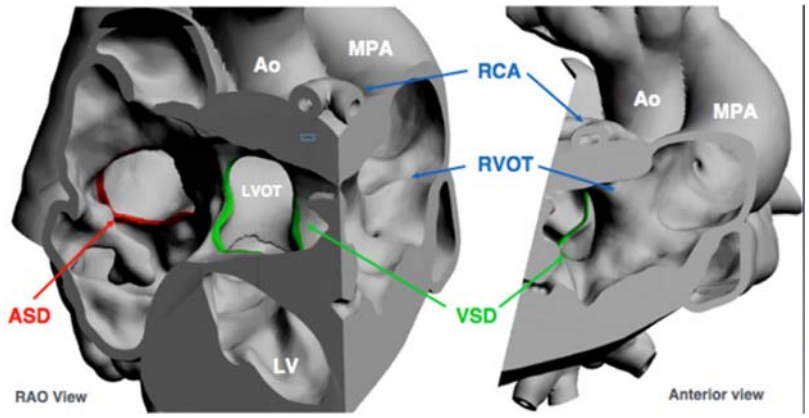

3D "segmented" heart with a "hollow" reconstruction that includes views of heart chambers, defects and coronaries.

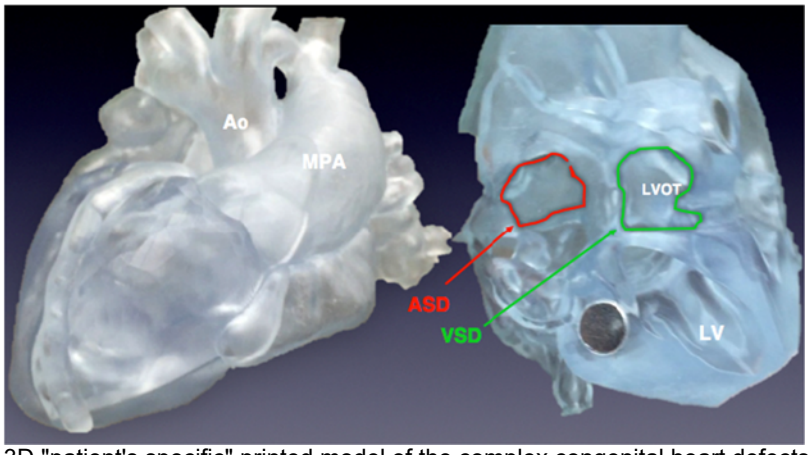

3D "patient's specific" printed model of the complex congenital heart defects with direct visualisation of anatomy, proportions and anatomical relationship of structures potentially involved in the surgical procedure

ID#: 379161

An unexplained arrhythmias: the fine line between cardiac sarcoidosis and arrhytmogenic cardiomyopathy.

Martina Previato, MD[1]Alice Niero, MD[2], Stefania Rizzo, MD, PhD[3], Manuel De Lazzari, MD, PhD[4], Alberto Cipriani, MD[4], Pietro Zucchetta, MD[5], Sabino Iliceto, MD, PhD[4], Carmelo Lacognata, MD[6], Giuseppe Tarantini, MD, PhD[7], Franco Bui, MD[5], Cristina Basso, MD, PhD[3], Martina Perazzolo Marra, MD, PhD[4]

1. Depatment of Cardiac, Thoracic and Vascular Sciences. University of Padua. Italy., Italy

2. Depatment of Cardiac, Thoracic and Vascular Sciences. University of Padua. Italy, Italy

3. Depatment of Cardiac, Thoracic and Vascular Sciences. University of Padua., Italy

4. Department of Cardiac, Thoracic and Vascular Sciences, University of Padova, Italy, Italy

5. Nuclear Medicine Unit, Department of Medicine, DIMED, University Hospital of Padua, Padua, Italy, Italy

6. Radiology, Azienda Ospedaliera Padova, Italy, Italy

7. Department of Cardiac, Thoracic and Vascular sciences, University of Padua, Italy

Description of Clinical Presentation: For an episode of palpitations, a previously healthy 46-year-old caucasian man underwent a 24-h ECG monitoring that showed 1618 ventricular premature beats, more than 500 runs of non-sustained ventricular tachycardia (NSVT) and some episodes of sustained ventricular tachycardia that resolved spontaneously. Echocardiography revealed regional thickening of the septum, hypokinesis of the basal segment of the septum and inferior wall and mildly reduced left ventricle ejection fraction (49%). Chest x-ray was normal. A myocardial SPECT scan showed fixed perfusion defects in the inferior and septal segments but coronary arteries were normal at coronary angiography. A first Cardiac magnetic resonance (CMR) confirmed regional hypertrophy and hypokinesis of the inferior and infero-septal basal wall and revealed multiple areas of intense LGE with non-ischemic pattern. The patient was then referred to our centre for the execution of an endomyocardial biopsy (EMB) with the suspicion of myocarditis or hypertrophic/infiltrative cardiomyopathy. Endomyocardial biopsy was inconclusive (probably due to sampling error). Screening for inherited metabolic diseases and anti-heart antibodies and laboratory investigations for sarcoidosis were negative. Thoracic HRCT showed subcentimeter mediastinal adenopathy and mild thickening of the peribronchovascular interstitium.

Diagnostic Techniques and Their Most Important Findings: The coexistence of ventricular tachycardia, segmental LV dysfunction and the distribution and intensity/of intense of LGE fostered the suspicion of cardiac sarcoidosis (CS). We decided to perform a hybrid simultaneous positron emission tomography/magnetic resonance imaging (FDG-PET/3TMRI; *Siemens Healthcare, Erlangen, Germany*) study; in preparation for the scan, the patient was asked to follow a low-carbohydrate and high-proteic diet and fast for at least 12 hours prior to the study, to suppress the high physiological uptake of 18F-FDG naturally present in the myocardium. Image acquisition was initiated 60 minutes after FDG administration; MR images were used for anatomical localization and MR-based attenuation correction was performed. The scan showed good concordance of myocardial LGE distribution and regions of increased FDG myocardial uptake (Figure 1); maximum intensity projection PET images also revealed FDG uptake on bilateral hilar, mediastinal and abdominal lymphnodes. The presence of FDG avid lymphadenopathy and the evidence of active myocardial inflammation (increased myocardial FDG uptake) within an area of “scar” (LGE) were indicative of active sarcoidosis. Biopsy of one of the lymphnodes later revealed granulomas consistent with sarcoidosis (Fig.1c). The final diagnosis of active sarcoidosis with predominant cardiac involvement was made and corticosteroid therapy was initiated.

Learning Points from this Case: Prompt diagnosis of CS is therefore of utmost importance but it is still a difficult challenge: with the advent of hybrid PET/MR systems, we have now the opportunity to combine detailed morphological assessment with functional imaging: the pattern of injury can be co-localised with disease activity to further improve diagnostic accuracy. The same scan also provides insight into the stage of activity of the disease, allowing classification of patients into distinct groups (active-inflammatory phase or chronic phase) that informs prognosis and indication for therapy.

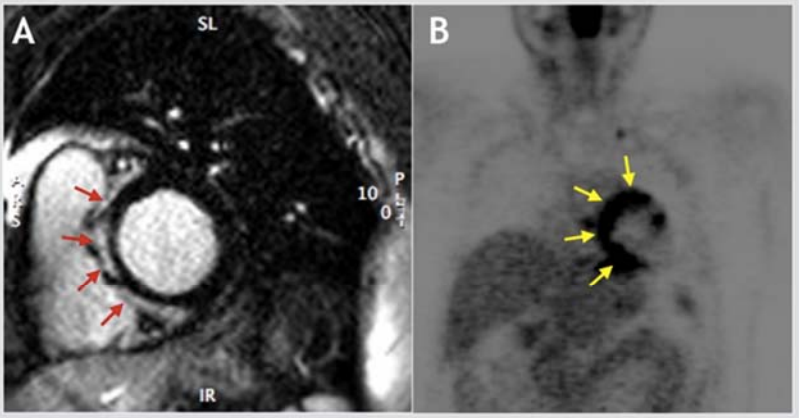

Figure 1. CMR short-axis view; late gadolinium enhanced images (*Panel A*). LGE was observed as a midmyocardial stria of intense hyperenhancement with variable extension to the epicardium and the right endocardium in the basal segments of the septum and as an epicardial stria in the basal and medial anterior segments (*red arrows*).
Maximum intensity projection image of ^{18}F-fluorodeoxyglucose (FDG) PET (*Panel B*). FDG strong uptake was detected in the myocardium (*yellow arrows*), in the basal anterior, septal and inferior walls of the left ventricle.

Image 1

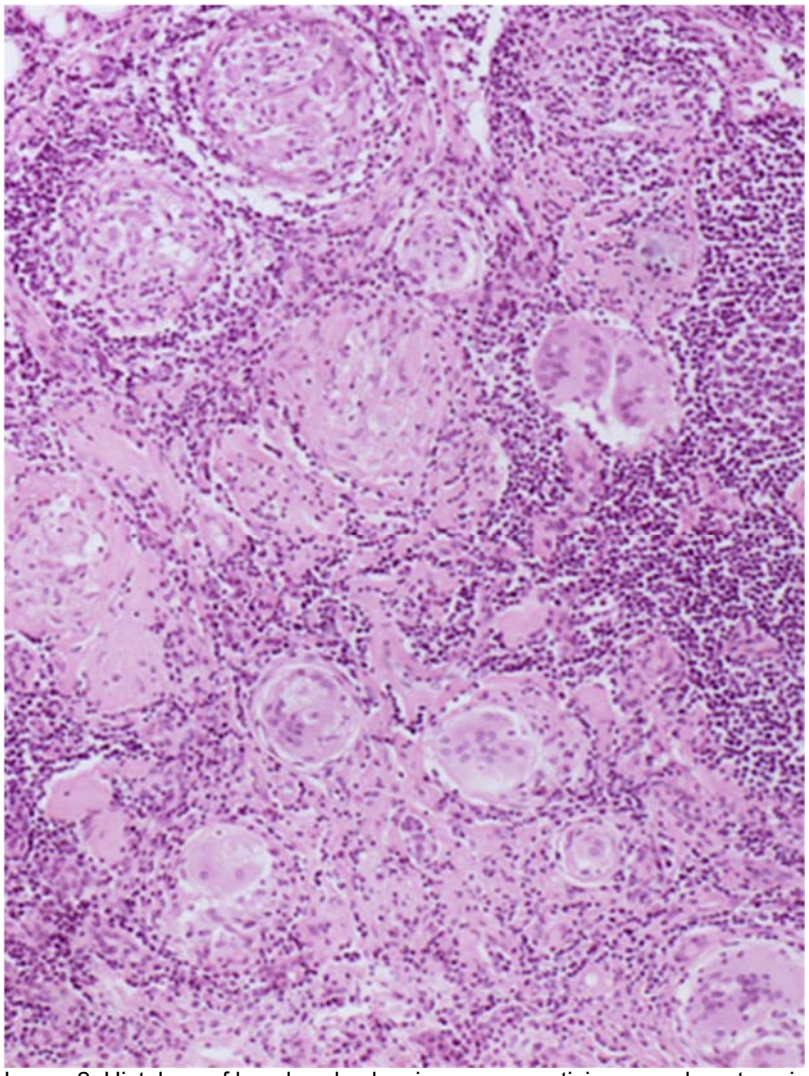

Image 2. Histology of lymphnode showing non necrotizing granulomatous inflammation with giant cells

ID#: 379019

Approaching to the Etiology of a Right Ventricle Mass with Cardiac Magnetic Resonance

Katia Devorha. Menacho, MD[1] Sabrina Nordin, MRCP[2], Sara Elizabeth. Ramírez Flores[3], Camilla Torlasco, MD[4], Amna Abdel-Gadir, MBBS.MRCP(UK)[5], James Moon, MD[6]

1. Barts Heart Centre, London, England, United Kingdom

2. Barts Heart Centre, United Kingdom

3. HOSPITAL FAP / CLÍNICA INTERNACIONAL, Lima, Lima, Peru

4. University of Milan-Bicocca. IRCCS Istituto Auxologico Italiano, Milan, Italy, Milan, Lombardia, Italy

5. University College London and Barts Heart Centre, London, England, United Kingdom

6. UCL, England, United Kingdom

Description of Clinical Presentation:

A 69 year-old asymptomatic man with elevated liver enzymes underwent liver investigation. A Transjugular liver biopsy incidentally detected significant tricuspid regurgitation triggering cardiology review.

Diagnostic Techniques and Their Most Important Findings:

Electrocardiogram showed first-degree heart block and right bundle branch block.

Echocardiogram had poor windows but suggested an RV filling defect. There was moderate to severe TR. CMR was requested.

CMR revealed a large RV mass 6x6x5cm filling half of the RV, without RVOT obstruction, tethering and distorting the tricuspid valve (TV) resulting in severe TR. **Figure 1 a-c**. The RV was dilated, half of the RV myocardium was unaffected and trying to function normally. Septum flattening suggesting RV volume loading from TR. **Figure 1d**.

The mass looked encapsulated, with a heterogeneous texture with T1 and T2 weighted imaging **(Figure 2 a-c)** and mapping **(Figure 3 a, b)** excluding fat and fluid (cyst).

Rest perfusion imaging showed the mass to be vascular **(Figure 4a-c)**. Late gadolinium enhancement showed a heterogeneous appearance with probable partial fibrotic capsule. **Figure 4d**.

The CMR interpretation was of a vascular partial encapsulated tumour, probably cardiac haemangioma. However, malignancy could not be completely ruled out (Angiosarcoma vs metastasis) so surgery is scheduled.

Patient underwent cardiac surgery. Tumour was excised intact. Successful post-operative recovery, currently patient is clinically stable. Pathology specimen was confirmed to be a cardiac cavernous hemangioma. Tumour was surrounded by fibrous tissue. The results of histology will be available for presentation.

Learning Points from this Case: - Cardiac hemangioma is a rare benign primary cardiac tumour. Most of these tumours are asymptomatic, and frequently discovered by accident. However. Hemangiomas have the potential to cause significant morbidity and mortality secondary to its spatial relation to adjacent structures and size of tumour. Particularly, for this patient, its relation with the RV and the tricuspid valve caused severe TR and increase RV pressure. - CMR helps plan surgery, can add value to mass characterisation, excluding cysts, thrombus and fat, but on many occasions a tissue diagnosis is still needed. - The most important characteristics of cardiac cavernous hemangioma by CMR is a capsulated mass, iso-intense on T1, hyper-intense on T2, and gradual centripetal contrast enhancement capture.

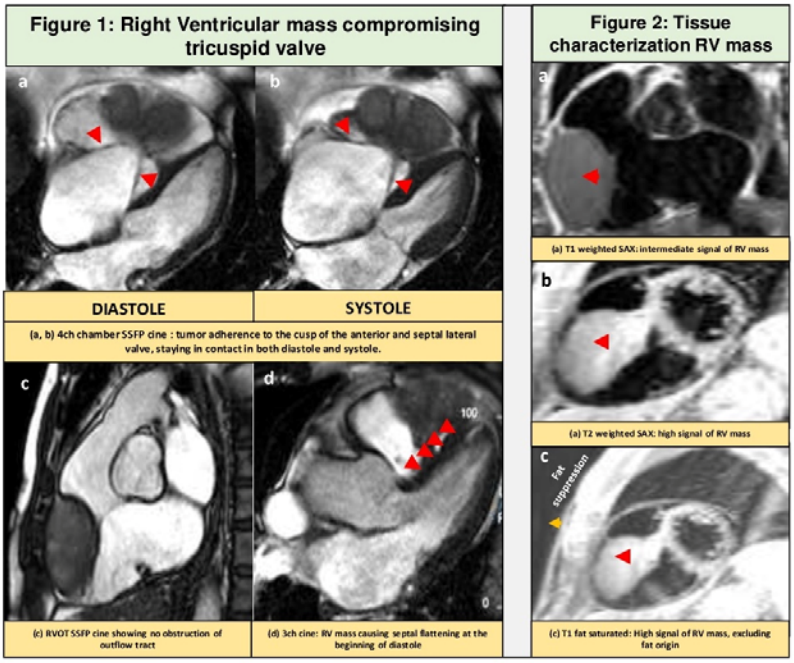

Right Ventricle Cardiac Mass Characteristics

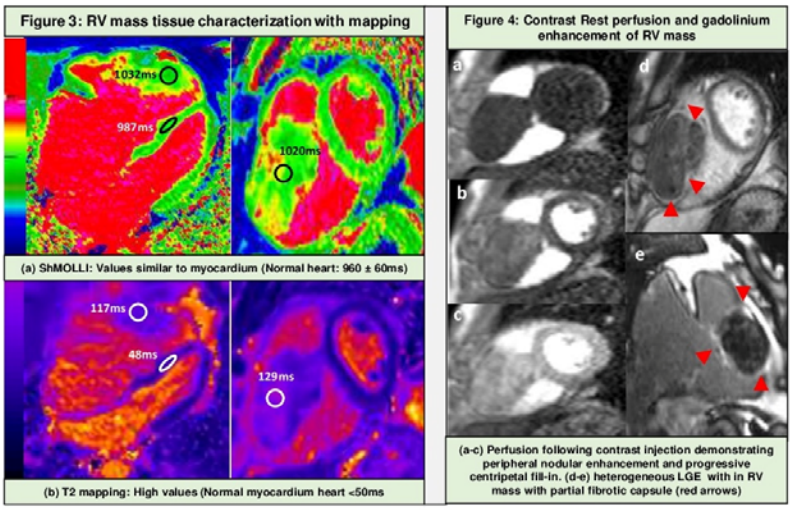

Right Ventricle Mass: CMR Mapping, Perfusion and Gadolinium Assessment

ID#: 378844

CMR relaxometry in Freidreich ataxia

Elena Giulia Milano, MD[1]Estefania De Garate, MD[2], Tobias A. Fuchs, MD, FESC, FSCCT[3], Iwan Harries, MD[2], Sarah Moharem-Elgamal, MD[3], Anna Baritussio, MD[2], Chiara Bucciarelli-Ducci, MD, PhD[2]

1. Bristol Heart Institute, Italy

2. Bristol Heart Institute, Bristol NIHR Biomedical Research Centre (Cardiovascular Section), University of Bristol, Bristol, England, United Kingdom

3. Bristol Heart Institute, Bristol NIHR Biomedical Research Centre (Cardiovascular Section), University of Bristol, United Kingdom

Description of Clinical Presentation: A 25-year old male recently diagnosed with Friedreich's ataxia (FRDA) underwent a cardiology evaluation with electrocardiogram (ECG) and transthoracic echocardiography. He complained of shortness of breath on exertion. On physical examination, he presented high blood pressure and a loud systolic murmur. ECG showed sinus rhythm with voltage criteria for left ventricular hypertrophy (LVH), T wave changes in the inferolateral leads; echocardiography showed biventricular hypertrophy with preserved systolic function and mild intracavity gradient in the left ventricle, unremarkable mitral and aortic valve. He was then referred to our cardiac magnetic resonance (CMR) Unit for further assessment.

Diagnostic Techniques and Their Most Important Findings: CMR was performed using a 1.5 Tesla scanner. Imaging protocol included cine images (Figure 1a), native and post contrast T1 mapping (shMOLLI, Figure 1b), early and late gadolinium enhancement (LGE) images (Figure 1c, d). There was an asymmetric LVH, with markedly increased septal wall thickness. Native T1 values were mildly reduced in the septum (909 ms) and low normal in the lateral walls (942ms) (normal range 953 ± 23 ms at 1.5 Tesla). Post contrast T1 values were diffusely reduced. On late images, there is a patchy diffuse LGE in the lateral walls (Figure 1c and d, yellow arrows).

Learning Points from this Case: FRDA is an inheritable mitochondrial disorder due to the mutation of frataxine. Although the underlying pathophysiology of the disease is not completely clear, it is commonly accepted that frataxine is involved in mitochondrial iron metabolism. Cardiomyopathy represents a significant cause of morbidity and mortality in patients affected by FRDA, in particular they usually present with LVH. Raman et al measured normal myocardial T2* values in a population of FRDA patients, suggesting it was not possible to detect iron aggregates using this technique (1). Myocardial T1 mapping has been proposed as a method of detection of mild iron overload. In this case, the reduced native T1 values may be explained with a mild cardiac iron accumulation. Reduced native T1 values are also observed in lipid accumulation (AFD), but in a patient with an already confirmed diagnosis of FRDA, the coexistence of these rare conditions is unlikely. T1 mapping could be a useful tool to detect early myocardial changes in patients with FRDA and should be routinely acquired in these patients. Further studies are necessary to confirm these findings. 1. Subha V. Raman, Kavita Phatak, et al. Impaired myocardial perfusion reserve and fibrosis in Friedreich ataxia: a mitochondrial cardiomyopathy with metabolic syndrome Eur Heart J. 2011 Mar; 32(5): 561-567.

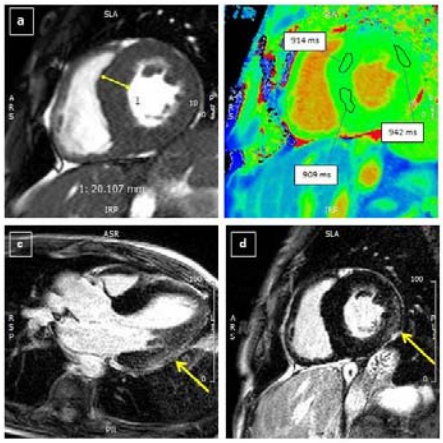

Figure 1 a) Basal short axis cine showing septal hypertrophy; b) Native T1 mapping values in basal short axis; c) basal short axis showing LGE in the lateral wall (yellow arrow); d) 3-chamber showing LGE in the lateral wall (yellow arrow).

ID#: 378787

Cardiac sarcoidosis with features mimicking hypertrophic obstructive cardiomyopathy

Stacey Elangovan, MD[1] Harold Litt, MD-PhD[2]

1. Hospital of the University of Pennsylvania, Philadelphia, PA

2. Perelman School of Medicine of the University of Pennsylvania, Philadelphia, PA

Description of Clinical Presentation: A 51 year old man with a clinical diagnosis of pulmonary sarcoidosis presented for evaluation for myocardial sarcoidosis with cardiac MRI and PET/CT following two syncopal events, the first of which occurred ten years prior to the second. Prior workup included echocardiograms performed after both episodes, which were normal, and an EKG performed after the second episode that demonstrated Mobitz Type I second degree AV block and bradycardia.

Diagnostic Techniques and Their Most Important Findings: MRI of the heart was performed on a 1.5 tesla unit. Function was assessed with cine imaging in short axis slices covering the ventricles and in 4-chamber, 2-chamber, and LVOT orientations. Native T1 mapping was performed in short axis slice, and late gadolinium enhancement (LGE) images were obtained after intravenous administration of 29 mL of Gadoterate meglumine.

Cardiac PET/CT was also performed the same day following overnight fasting and a diet consisting of low carbohydrates and high fat content during the previous meal. Images were obtained from the lower neck to the upper abdomen 50 minutes after injection of 5.898 mCi F-18 FDG. Low-dose unenhanced CT images were obtained concurrently for anatomic correlation and attenuation correlation.

MRI demonstrated basal anteroseptal wall thickening to 22 mm with regional hypokinesis in the area of thickening, patchy increased T2 signal throughout the myocardium, left ventricular outflow tract flow acceleration, very mild systolic anterior motion of the mitral valve, and intense multifocal LGE, including nodular enhancement in the papillary muscles and right ventricle. Mediastinal and hilar lymphadenopathy was also present.

PET/CT demonstrated intense patchy focal FDG uptake throughout the myocardium of the left ventricle as well as in the base of the left ventricle. Abnormal FDG uptake was also identified in thoracic lymph nodes, and low-dose CT images demonstrated irregular thickening with ground glass opacity in a perilymphatic distribution.

Learning Points from this Case: This case demonstrates overlapping features of cardiac sarcoidosis with those seen in hypertrophic cardiomyopathy (HCM), including basal anteroseptal wall thickening, left ventricular outflow tract flow acceleration, systolic anterior motion of the mitral valve, abnormal T2 signal, and patchy LGE of the myocardium. However, the features that help to distinguish cardiac sarcoidosis, as seen in this case, from HCM include the intensity and multifocality of the LGE and the presence of mediastinal and hilar lymphadenopathy. The diagnosis of sarcoidosis is supported by the PET/CT findings also suggestive of myocardial, pulmonary, and mediastinal sarcoidosis.

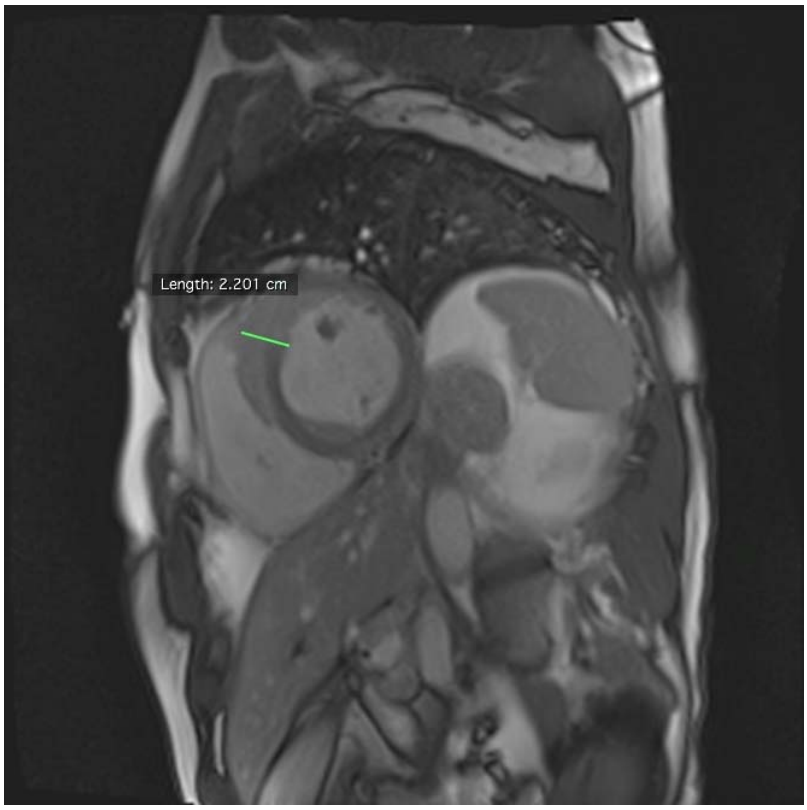

Short-axis image demonstrating basal anteroseptal hypertrophy to 22 mm in diastole. The native T1 is 1100 ms in the thickened area and 965 ms in the normal thickness inferior wall.

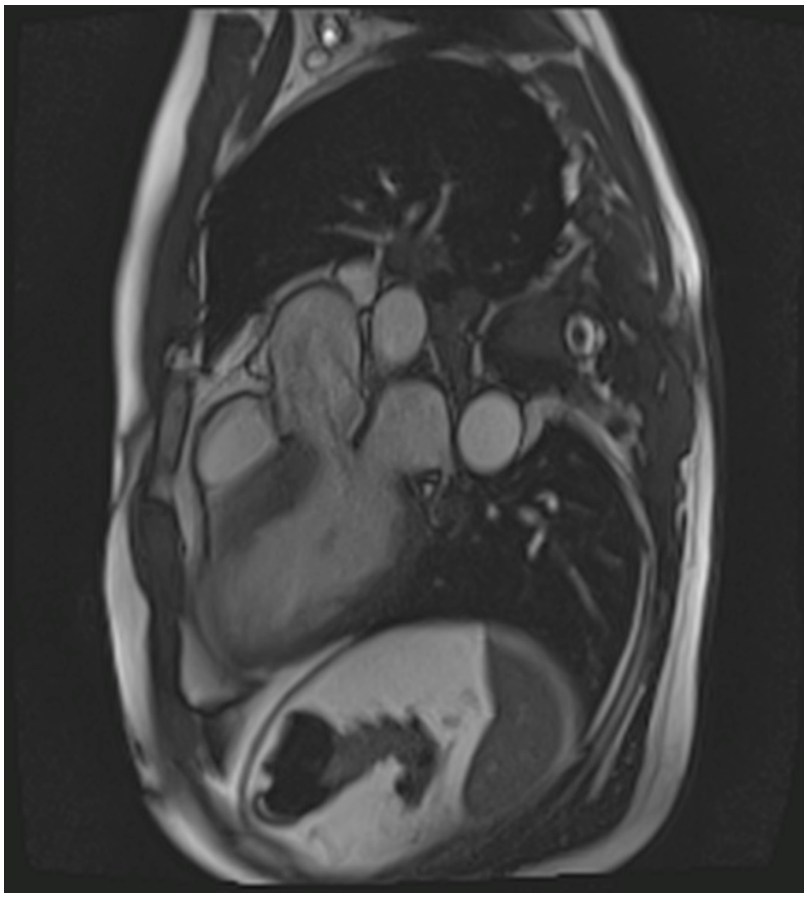

Left ventricular outflow tract image showing jet indicating flow acceleration

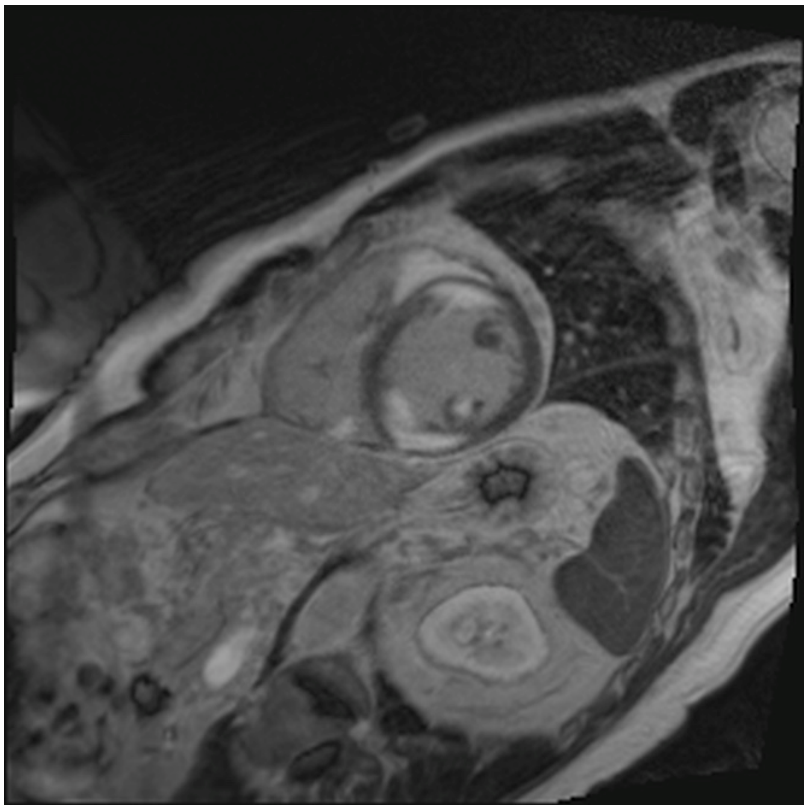

Short axis late gadolinium enhancement image demonstrating intense multifocal nodular enhancement, including right ventricular and papillary muscle enancement

ID#: 373108

Thrombosed Saphenous Vein Graft Aneurysm Mistaken for a Right Atrial Mass

Roshin C. Mathew, MD[1] Adrián I. Löffler, MD[2], Ara Maranian, MD[3], Christopher M. Kramer, MD[2], Michael Salerno, MD, PhD[4]

1. University of Virginia Health System, VA

2. University of Virginia Health System, Charlottesville, VA

3. Novant Health Prince William Cardiology

4. University of Virginia, VA

Description of Clinical Presentation:

A 78 y/o male with history of abdominal aortic aneurysm (AAA) s/p endovascular repair (2016), CAD s/p 5-vessel coronary artery bypass grafting (CABG) (1996) complained of persistent dyspnea and fatigue since his AAA repair. Initially, symptoms were thought to be attributed to post-operative deconditioning; however, due to extensive cardiac history, it was decided to pursue a workup with an echocardiogram and a regadenoson nuclear single-photon emission computed tomography (SPECT) stress test. Stress testing showed no abnormalities. Echocardiogram revealed normal left ventricular function of with an EF of 60-65% and a right atrial mass measuring 3.2cmx2.9cm that was thought to be thrombus (Figure1). Patient was started on anticoagulation, and referred for CMR to further characterize the right atrial mass.

Diagnostic Techniques and Their Most Important Findings:

A CMR was performed on a General Electric 1.5 Tesla Signa with the following sequences: Axial Haste, dark-blood T1/T2 weighted imaging, FIESTA short and long axis cine images, and multi-contrast delayed enhancement (MDE). A circular mass-like structure measuring (3.4x3.2cm) is located along the infero-lateral wall of the right atrium near the IVC junction (Figure 2A). The mass is hypo-intense on T2 weighted imaging and is isointense on T1 imaging, and does not demonstrate LGE, suggesting thrombus. Careful inspection of the mass demonstrated a small lumen extending from a vein-graft proximally and exiting into the posterior descending artery (rPDA) (Figure 2B). Taken together these findings were consistent with a large thrombosed SVG to the rPDA compressing the right atrium.

Learning Points from this Case:

Anticoagulation was discontinued, and patient underwent coronary and graft angiography with subsequent percutaneous intervention to the SVG with three covered stents (Figure 3). Since the procedure, patient has felt improved.

Large aorta-coronary saphenous vein graft aneurysms are a rare, late complication of CABG. A thrombosed SVG could easily be mistaken for a right atrial mass. The presence of a lumen and the continuity with the SVG provided the key information differentiating this pathology from a right atrial mass. This case and two others in the literature demonstrated that CMR is capable of identifying and characterizing the aneurysm for either monitoring or possible intervention[1,2]. There are no current guidelines for treatment and are currently addressed on a case by case basis, depending on the severity or complications related to the aneurysm.

[1] Lupetin AR, et al. Cardiovasc Intervent Radiol. 1995 Sep-Oct;18(5):330-2
[2] Yatskar L, et al. Echocardiography. 2005 Mar;22(3):263-5

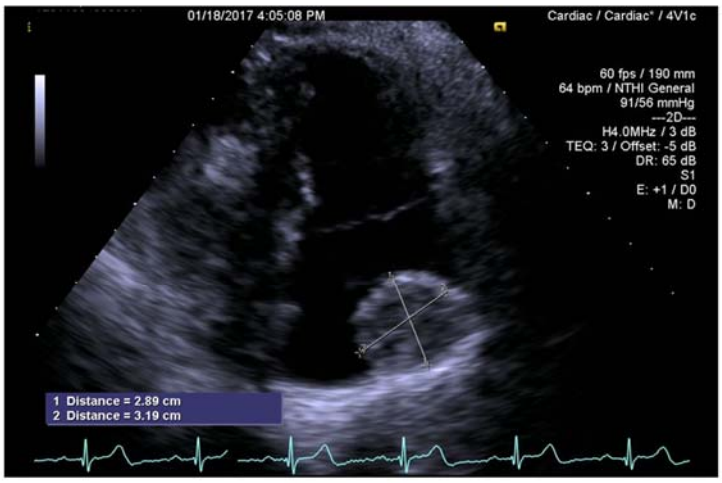

Figure 1: Right ventricular inflow echocardiographic view showing a large right atrial mass

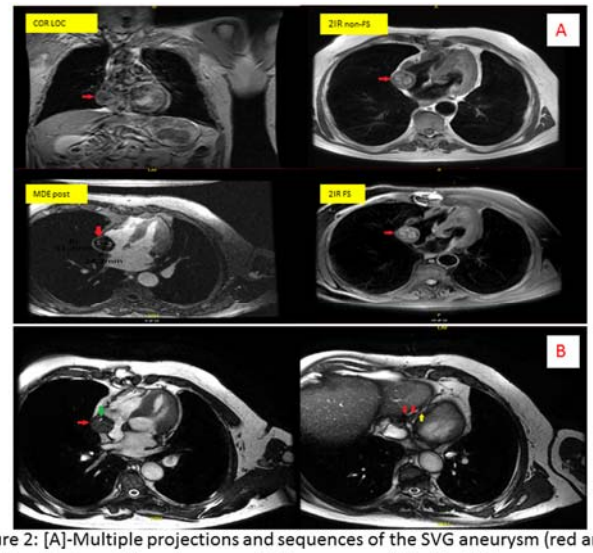

Figure 2: [A]-Multiple projections and sequences of the SVG aneurysm (red arrow). [B]-Visualization of the entrance point (green arrow) into the SVG aneurysm and the attachment to the rPDA (yellow arrow).

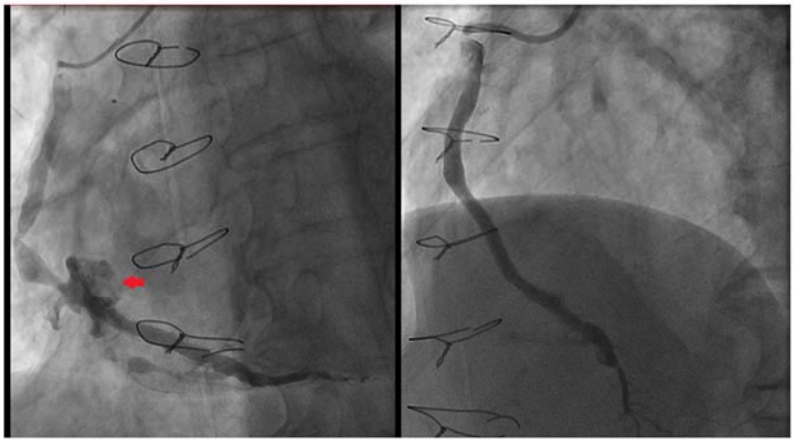

Figure 3: [Left]-Angiographic visualization of the SVG graft aneurysm (red arrow). Note the ectatic segments of the SVG and a stenosis proximal to the aneurysm. [Right]-Angiography performed after percutaneous intervention with covered stents in the SVG.

ID#: 374213

Intracardiac bronchogenic cyst

Yoo Jin Lee, M.D.[1]Klaus Hagspiel, MD[2], Michael Salerno, MD, PhD[2], Patrick T. Norton, MD[2]

1. University of Virginia Medical center

2. University of Virginia, VA

Description of Clinical Presentation: A 59 year old man with hypertension and hyperlipidemia presented after an intra-atrial mass was discovered on an abdominal CT performed for gross hematuria. On further questioning, the patient reported intermittent palpitations for the past 4 years which subsided with short breath holds. Echocardiogram and cardiac MRI was ordered for further characterization of the mass.

Diagnostic Techniques and Their Most Important Findings: On the original abdominal CT, a well-defined mass measuring 3 cm x 2.7 cm was located in the right atrium adjacent to the interatrial septum (Fig. 1). The density of the mass measured 15 HU on CT, suggesting a fluid filled structure. Further characterization with MRI was performed using SSFP cine (Fig. 2A, 2B), dark blood T2-weighted STIR (2C), gradient echo cine (2D), and late gadolinium enhancement (LGE) phase sensitive inversion recovery (2E). Multi-planar SSFP imaging revealed a cystic-appearing mass arising from the interatrial septum immediately inferior to the noncoronary aortic cusp. The mass contained a high water content based on STIR imaging and was hypointense relative to myocardium on gradient echo cine. The mass was without enhancement and markedly hypointense on phase reconstructed LGE images. Echocardiogram demonstrated an anechoic lesion deforming the atrial septum (Fig.3). The constellation of finding were consistent with a simple cyst. The gradient echo cine signal characteristic were slightly confounding, as a myxoma could have a similar appearance. Despite this, the finding on CT, T2-weighted and LGE MRI sequences, and echocardiogram all point to the diagnosis of an intracardic cyst. When imaging cardiac masses, multi-planar imaging is used to determine the overall size and anatomical relationship to surrounding structures. SSFP cine imaging can be used to visualize motion of the mass as well as obstruction to blood flow. First pass perfusion, immediate post-contrast imaging, and LGE imaging can provide information about the presence and dynamics of contrast enhancement. PSIR phase reconstructed images provide an additional benefit of detecting fluid-filled lesions, which have signal characteristics similar to pericardial fluid, as was seen in this case. This patient was observed and has not developed significant symptom. To date, the lesion has been stable for three year as determined by annual transthoracic echocardiography.

Learning Points from this Case: 1. Although rare, a mainly cystic mass such as intracardiac bronchogenic cyst may be found within the cardiac chambers to be confused with atrial myxoma due to the similar location and morphology when further characterization of the mass is not provided. 2. The differential diagnosis for an intracardiac cystic mass includes bronchogenic cysts, post-traumatic cysts, hydatid cysts, blood cysts, teratomas, and cavernous lymphangioendotheliomas. 3. Although the treatment for intracardiac bronchogenic cysts are not in consensus, they are preferably resected for the following reasons: to address symptoms of obstruction or arrhythmia; to exclude other malignancy even when asymptomatic; due to possibility of further growth and rare malignant transformation of this benign lesion. 4. As most reported cases were resected, this case with documented 3 years' stability free of growth and symptom is notable.

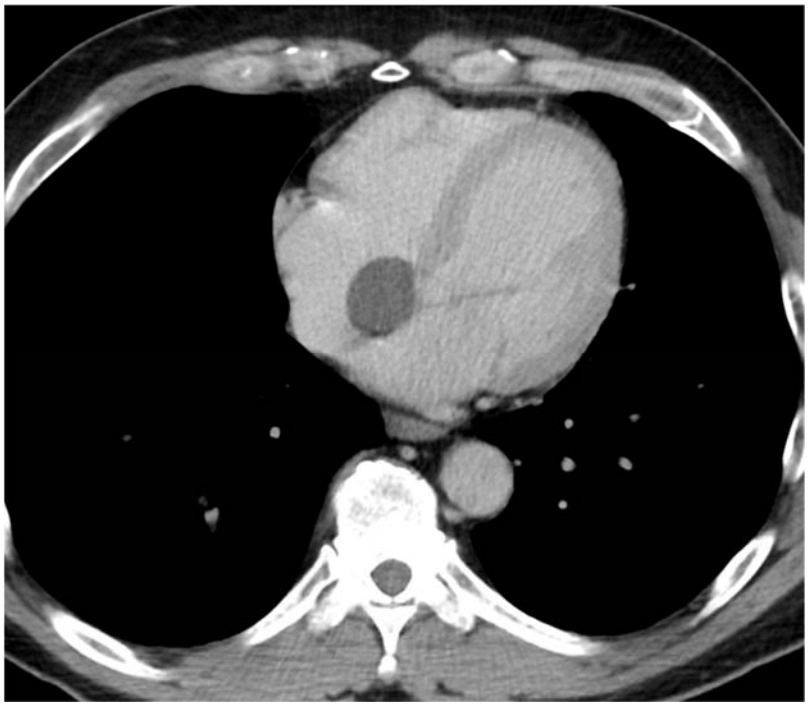

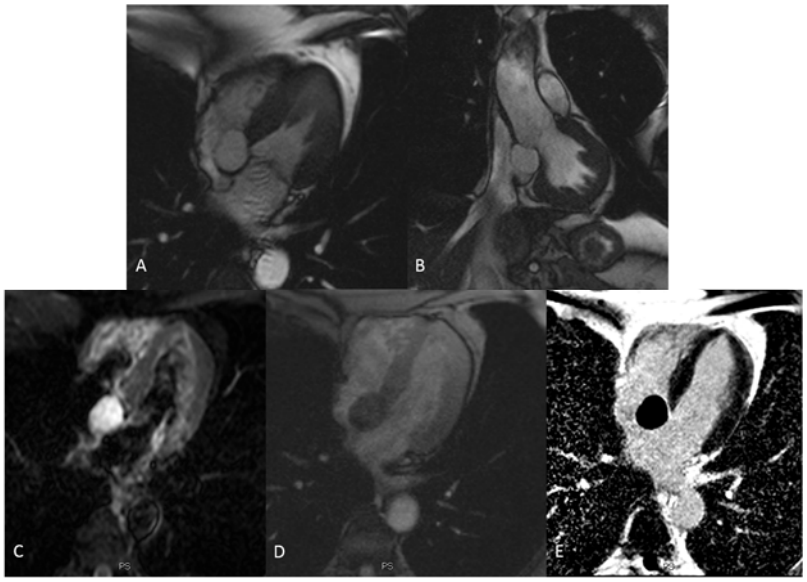
A
B
C
D
E

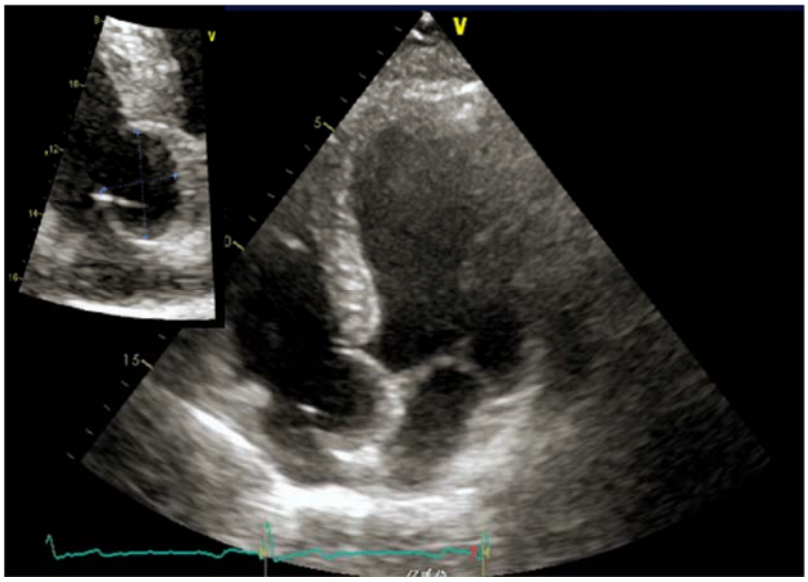

ID#: 374234

Large Left Atrial Appendage Aneurysm: Imaging Identification of a Rare Anomaly

Noelle C. Garster, MD, MS[1] Andrew E. Kott, M.D.[1], Russell C. Dabrowski, MD[1], Dhiraj Baruah, MBBS, MD[2], Jason C. Rubenstein, MD[1]

1. Medical College of Wisconsin, Milwaukee, WI

2. Medical College of Wisconsin, brookfield, WI

Description of Clinical Presentation: A 58 year-old female with history of anxiety and tobacco use presented for routine physical examination after several years without healthcare contact. She reported symptoms of atypical chest pain, dyspnea on exertion and intermittent palpitations. Family history was significant for bicuspid aortic valve in multiple family members. Initial evaluation included 48 hour ambulatory Holter monitoring which was negative for atrial fibrillation and demonstrated only one brief episode of atrial tachycardia. Transthoracic echocardiogram was completed, demonstrating normal biventricular size and function and no significant valvular disease. However, an unusually large, presumed vascular structure was seen and noted to be externally compressing the lateral wall of the left ventricle. This prompted further imaging including cardiac MRI.

Diagnostic Techniques and Their Most Important Findings: The primary finding on cardiac MRI was identification of an aneurysmal left atrial appendage measuring 5.2 x 3.9 cm. No clot or shunt was noted. Three-dimensional MR angiography of the left atrium revealed otherwise normal left atrial and pulmonary venous anatomy. The patient was started on anticoagulation for primary prevention of a cardiac thromboembolism and referred to cardiothoracic surgery. Full surgical excision of the aneurysmal left atrial appendage via median sternotomy is currently planned.

Learning Points from this Case: Left atrial appendage aneurysm is a rare anomaly, with fewer than 150 cases reported in the medical literature. It is characterized by localized outpouching or diffuse enlargement of the left atrial appendage and is often identified in the second to fourth decades of life. Palpitations and dyspnea are the most commonly reported symptoms. It is important to recognize, as it is associated with cardiovascular morbidity and mortality by predisposing to atrial tachyarrhythmia and thromboembolic events including stroke. Surgical resection is the standard of care, and prompt surgical consultation is advised for patients with this finding on cardiac imaging. Cardiac MRI can provide clarification if left atrial appendage aneurysm is suspected on echocardiography and can serve an important role in surgical planning. This rare anomaly should be kept in mind as we encounter lesions adjacent to the left heart border on cardiac imaging studies.

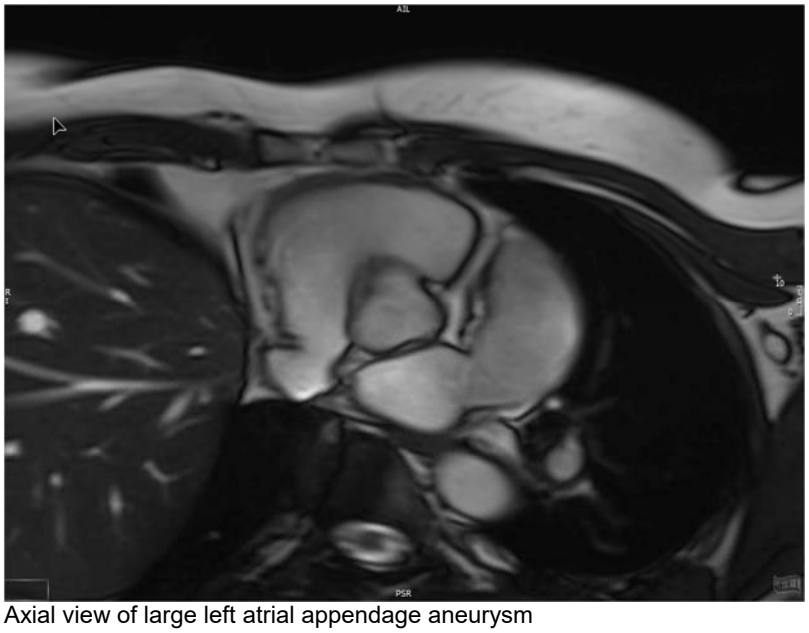

Axial view of large left atrial appendage aneurysm

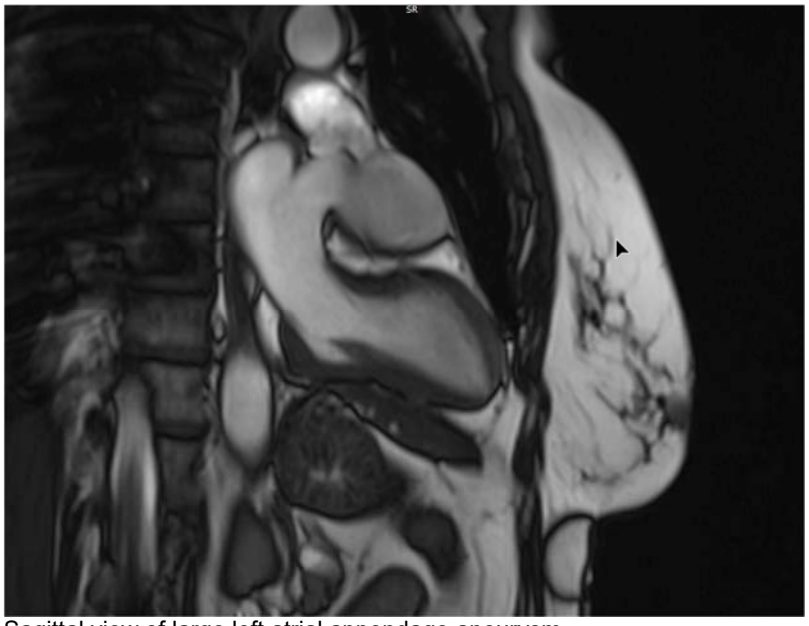

Sagittal view of large left atrial appendage aneurysm

ID#: 374291

Giant cell myocarditis: Cardiac MR findings and pathology correlation on endomyocardial biopsy and explanted heart.

Mohamed A. M. Abdelrazek[1] Eric Charles Belanger, MD, FRCPC[2], Joao R. Inacio, MD, radiologist[2], Giselle Revah, MD, FRCPC[3], Carole Dennie[2], Elena Pena, MD[2]

1. Ottawa University, Ottawa, ON, Canada

2. University of Ottawa, ON, Canada

3. University of Ottawa, Ottawa, ON, Canada

Description of Clinical Presentation: A 30-year-old female, presented to the Emergency Department (ED) with acute shortness of breath, chest pain, ankle swelling and generalized weakness. She had a prior history of ulcerative colitis but was otherwise healthy. There was no family history of cardiac disease. Laboratory tests, including TnI and serology for HIV, hepatitis and CMV were negative. There was a positive IgG test for EBV in keeping with past infection. Antinuclear antibodies (ANA) were also positive (1:80).

Diagnostic Techniques and Their Most Important Findings: ECG demonstrated sinus tachycardia. Echocardiography revealed significant global left ventricular (LV) hypokinesis and the LV ejection fraction (EF) was estimated at 24%. The right ventricular (RV) systolic function was also moderately reduced. Coronary angiography was normal. Cardiac magnetic resonance (CMR) was subsequently performed confirming biventricular systolic dysfunction (LVEF= 19% and RVEF= 22%) with global biventricular hypokinesis and preserved ventricular volumes. There was diffuse late-gadolinium enhancement (LGE) involving the sub epicardial and subendocardial layers of the LV and the RV side of the septum and RV free wall. Two small intracavitary LV apical thrombi were seen. SAO T2-SPAIR images showed no increase in signal to suggest acute inflammation. There were pericardial and bilateral pleural effusions. RV endomyocardial biopsy was performed which demonstrated giant cell myocarditis. The patient underwent orthotopic cardiac transplantation and pathological examination of the explanted heart confirmed areas of active and healing myocarditis containing multiple groups of giant cells. There was extensive biventricular scarring involving the LV to a greater extent than the RV, in a pattern that mirrored the distribution of LGE on MR.

Learning Points from this Case: Giant cell myocarditis is very rare type of myocarditis, characterized by development of acute heart failure. The pattern of MR late gadolinium enhancement is nonspecific and commonly involves multiple layers of the myocardium. The appearance on MR overlaps with other types of cardiomyopathy such as sarcoidosis, ARVC and viral myocarditis. The diagnosis is usually obtained from endomyocardial biopsy. CMR may help direct endomyocardial biopsy as well as monitor ventricular function.

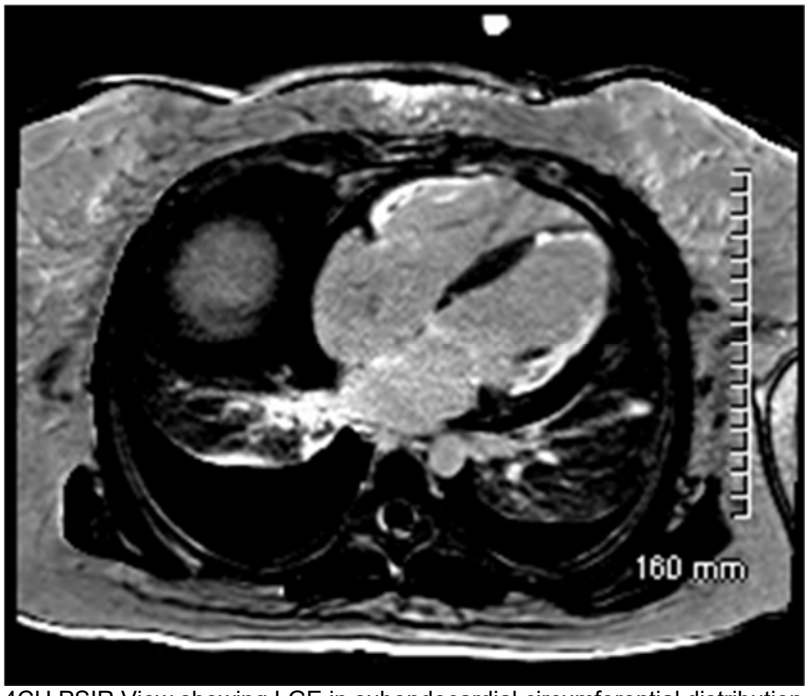

4CH PSIR View showing LGE in subendocardial circumferential distribution in both ventricles. Note is made of pleural and pericardial effsuions

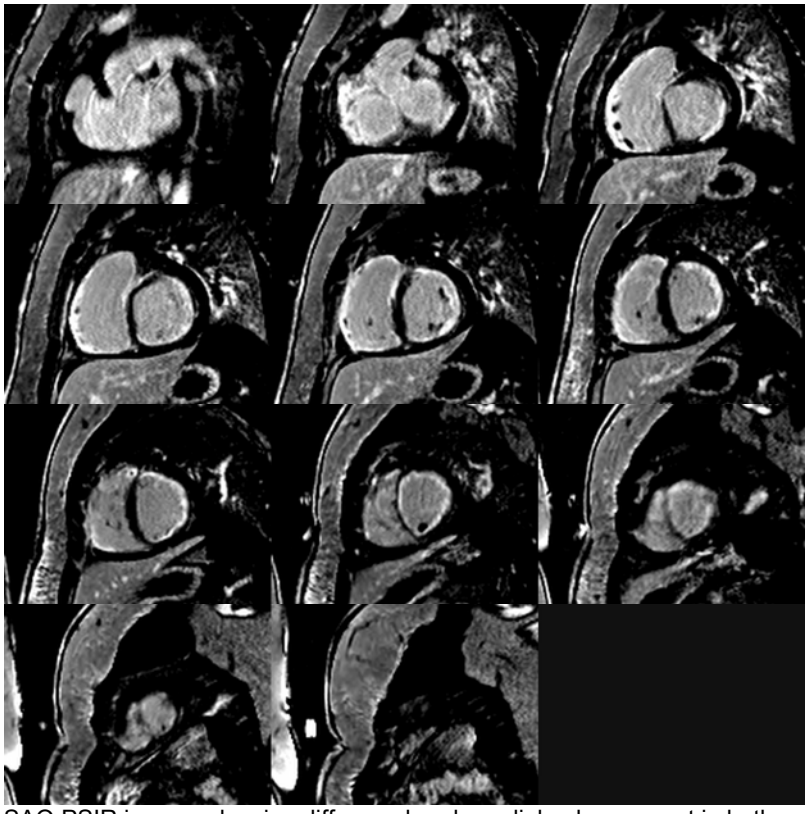

SAO PSIR images showing diffuse subendocardial enhancement in both ventricles. There is LV thrombus.

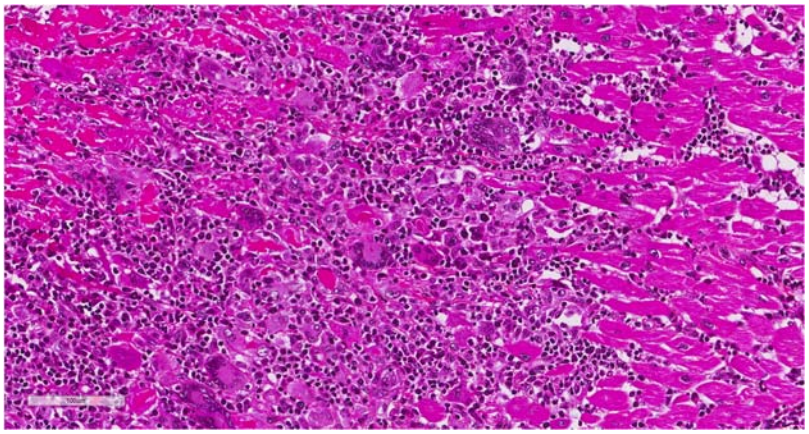

Microscopic picture from the explanted heart showing active inflammation

ID#: 374396

Is it an aneurysm or a pseudoaneurysm? Does CMR has any special clue to tell us?

Lilia M. Sierra-Galan, MD, MCvT[5]Armando I. Fajardo-Juarez, MD[1], Baldemar E. Castro-Montes, MD, MSc[2], Angel L. Alberto-Delgado, MD[3], Dipan J. Shah, MD[4]

1. American British Cowdray Medical Center, Distrito Federal, Mexico

2. H+ Hospital, Queretaro, Queretaro de Arteaga, Mexico

3. Central Military Hospital, Mexico, City, Distrito Federal, Mexico

4. Houston Methodist DeBakey Heart & Vascular Center

5. American British Cowdray Medical Center, CDMX, Distrito Federal, Mexico

Description of Clinical Presentation: A 61-year-old man with family history of early onset ischemic heart disease (IHD) who present for effort dyspnea. His is a current smoker and has dyslipidemia. He played basketball routinely 3 times a week and in the last 4 weeks he started to experience effort dyspnea during games. His physical examination showed no precordial myocardial impulse, audible fourth heart sound and the rest of his examination unremarkable. His ECG reveals, inferior myocardial necrosis with ischemic changes. He was admitted to the hospital for IHD workup. Troponin-I was normal and his Echo showed mildly enlarged left ventricle (LV), moderate LV dysfunction with regional wall motion abnormalities (RWM) of inferolateral (IL) akinesia and the loss of wall integrity in basal IL segment highly suggestive of ventricular pseudoaneurysm (VP). He was sent to a CMR evaluation, which confirmed the moderate to severe LV dysfunction with RWM abnormalities in the basal IL segments and mild LV dilatation; findings consistent with old IL myocardial necrosis with no residual myocardial ischemia (MI) and a VP contained by the pericardium and a thrombus. Mild pericardial effusion was noted. He was sent to the Cath lab in preparation for surgery and multivessel disease was found. The surgery consisted of successful off-pumb bypass grafting with LIMA to LAD, venous grafts to a ramus and to PDA and in the plication of a LV aneurysm. He was discharged from the hospital 5 days after procedure in excellent conditions, in functional class I NHYA and in the following 5 months he remains free of events.

Diagnostic Techniques and Their Most Important Findings: Routine laboratory tests showed normal troponin-I and elevated cholesterol levels, the rest were unremarkable. ECG showed an old inferior myocardial necrosis with ischemic T waves in inferior and in V5-V6 leads, and low QRS complex voltage in V5-V6 leads. Chest-X-ray was unremarkable. Echo showed moderate LV dysfunction, LVEF of 40%, LV mildly dilated and with RWM abnormalities due to IL akinesia and an image suggestive of loss of wall integrity in the basal IL segment suggestive of VP, no thrombus was noted. CMR showed mild LV dilatation with moderate to severe LV dysfunction, LVEF 36% and RWM abnormalities due to akinesia of basal and mid inferior and of basal IL segments, dyskinesia of mid IL segment which also had aneurysmal morphology and hypokinesia of the apical inferior segment. LGE with ischemic pattern, subendocardial (50-75% of wall thickness (WT)) in basal inferior, transmural in basal IL, subendocardial (>75% of WT) in mid inferior, subendocardial (50-75% of WT), in the mid IL, transmural in the most proximal portion of the apical inferior segments, and in the IL papillary muscle. No MI and mild pericardial effusion were noted. Findings were compatible with an old myocardial infarction, no residual ischemia and a VP in the basal-mid IL segments contained by the surrounding pericardium and a laminar thrombus in the territory of a large RCA. Invasive coronary angiography (ICA) showed a severely diseased RCA with retrograde filling from left coronary system, moderate stenosis of LAD and severe stenosis of a ramus.

Learning Points from this Case: Cardiac VP are very rare and a challenging diagnosis where CMR has an important role due to its high spatial resolution and unique property of tissue characterization. This diagnosis is a surgical emergency due to its high risk of rupture and systemic thromboembolism. It is important to consider the possibility of mechanical complications in the myocardial infarction setting and to remember that CMR play an important role.

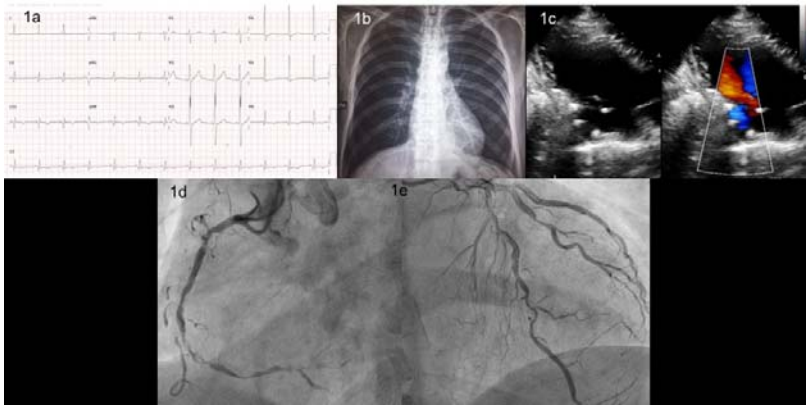

1a. ECG showing an old inferior myocardial necrosis with ischemic T waves in inferior and in V5-V6 leads, and low QRS complex voltage in V5-V6 leads. 1b. Normal chest x-ray. 1c. Echo showing mildly dilated LV and an image suggestive of loss of wall integrity (color Doppler) in the basal inferolateral segment suggestive of ventricular aneurysm. 1d-e. Invasive coronary angiography showing significant multivessel disease.

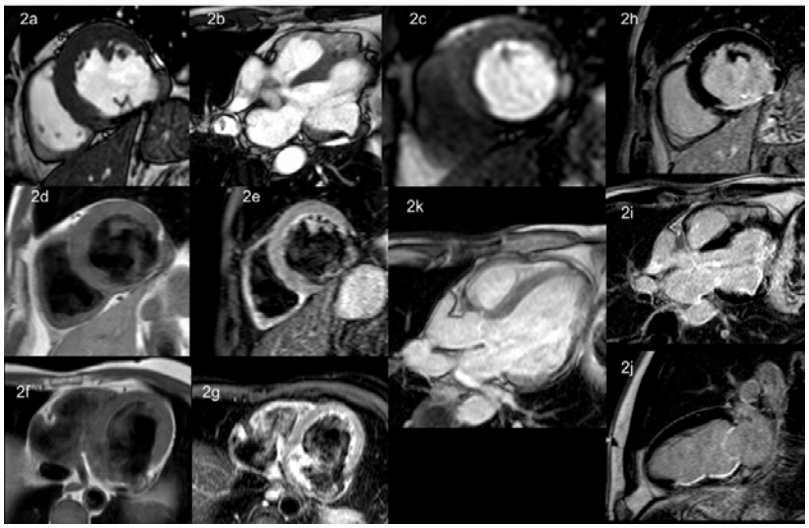

2a-b. SSFP in basal short-axis (2a) and 3-chambers long axis (2b) views showing the aneurysmal basal inferolateral segment. 2c. First pass perfusion in basal short-axis view showing pass of contrast to the aneurysmal cavity. 2d-g. T1-W (2d and 2f), T2-W STIR (2e and 2g) short axis and 4-chambers views, showing the apparent loss of wall integrity of basal inferolateral segment. 2h-j. LGE images, 2h short-axis view showing the old-myocardial necrosis, an apparent loss of segmental integrity and an image suggestive of thrombus. 2i 3 and 2j 2-chambers long axes views showing the old myocardial infarction and the aneurysmal appearance of basal inferolateral segment (2i). 2k. Long-TI LGE image in 3-chambers view showing the hipointense area corresponding to the thrombus.

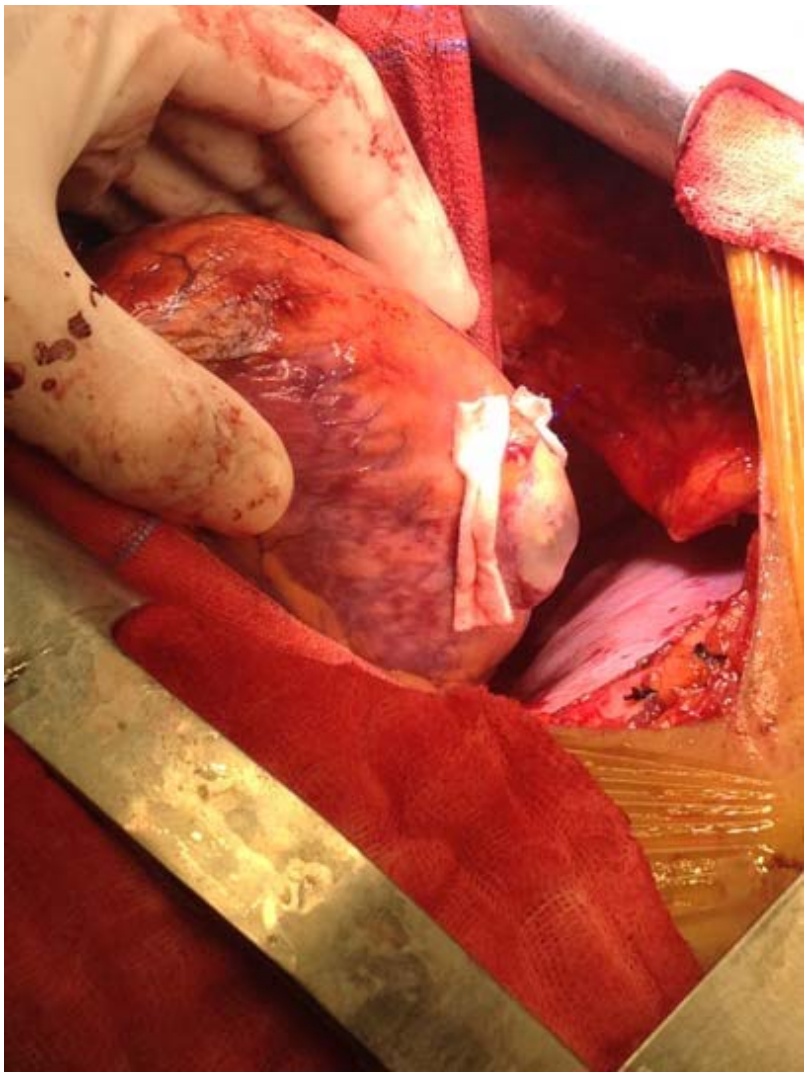

Off-pump CABG surgery showing the plication of a LV aneurysm.

ID#: 376600

All left ventricular hypertrophies are not created equal: a case of left ventricular metastasis from breast cancer.

Alessandra Scatteia, MD[1]Pasquale PG. Guarini, MD[2], Carmine Emanuele. Pascale, RT[3], Santo Dellegrottaglie, MD, PHD[4]

1. Division of Cardiology, Ospedale Medico-Chirurgico Accreditato Villa dei Fiori, Acerra, Naples, Italy, Naples, Campania, Italy

2. Division of Cardiology, Ospedale Medico-Chirurgico Accreditato Villa dei Fiori, Acerra, Naples, Italy, Italia, Campania, Italy

3. Division of Cardiology, Ospedale Medico-Chirurgico Accreditato Villa dei Fiori, Acerra, Naples, Italy, Campania, Italy

4. Division of Cardiology, Ospedale Medico-Chirurgico Accreditato Villa dei Fiori, Acerra, Naples, Italy; The Zena and Michael A. Wiener Cardiovascular Institute and Marie-Josee and Henry R. Kravis Center for Cardiovascular Health, Mount Sinai School of, Campania, Italy

Description of Clinical Presentation: A 55-year old woman was referred to our echocardiography laboratory following a recent diagnosis of breast cancer. Her personal history was positive for frequent ventricular ectopic heartbeats since the age of 40, when no secondary cause for the ectopics was identified. The family history was negative for cardiac disease as well as for sudden cardiac death. At the time of presentation, she was asymptomatic and was not on regular medications. ECG showed voltage criteria for left ventricular (LV) hypertrophy with T wave inversions in the lateral leads, which had not been described in previous ECGs.

Diagnostic Techniques and Their Most Important Findings: Transthoracic echocardiography (TTE) showed apical LV hypertrophy, mainly involving the apical anterior and antero-lateral walls, with preserved ejection fraction (EF). TTE raised the suspect of hypertrophic cardiomyopathy and she was referred for a cardiovascular magnetic resonance (CMR) examination to clarify the diagnosis. Cine SSFP images showed a normal functioning LV, with no regional wall motion abnormalities. However, a roughly oval area of severely increased wall thickness (max. = 26 mm) was noted in the apical antero-lateral LV wall (Figure 1-A). Within the area of LV hypertrophy there appeared to be a mass, irregular in shape and margins with heterogeneous signal intensity, extending to the postero-medial papillary muscle. This mass had heterogeneous but mainly high signal intensity in STIR T2-weighted images (Figure 1-B) and isointense signal in FSE T1-weighted images (Figure 1-C). First-pass rest-perfusion and late gadolinium enhancement (LGE) images demonstrated delayed perfusion and extensive enhancement of the mass (Figure 1-D). Based on those findings, a suspect of cardiac metastasis from breast cancer was made and the patient was then referred to the Oncological Department for further examination and treatment.

Learning Points from this Case: Cardiac metastases are rare, yet more common than primary heart tumours. They are generally associated with poor prognosis as they usually present in very subtle ways causing a delay in clinical diagnosis. In fact, the exact incidence of cardiac metastases for the most common cancers is still unknown. About two-third of all cardiac metastases involve the pericardium and only one-third the epicardium or the myocardium, where they usually form small, multiple lesions. Rarely, a single large mass is observed and can be easily misdiagnosed as an area of LV hypertrophy. This case highlights the role played by CMR in recognizing secondary cardiac lesions, with the potential to improve the characterization of patients with metastatic cancer.

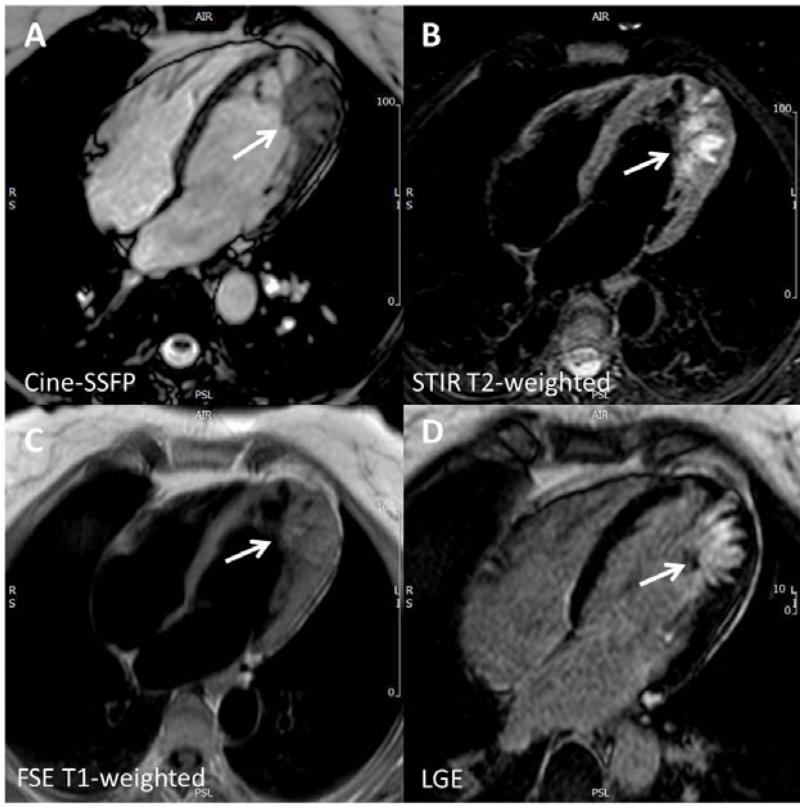

Cine SSFP, STIR t2-weighted, FSE T1-weighted and LGE images showing tissue characterization of the mass

ID#: 376574

Acute Right Ventricular Myocardial Infarction Mimicking Anterior Myocardial Infarction characterized by CMR: expected the unexpected

Anna Giulia Pavon, Cardio-Thoracic Vascular Department, San Raffaele Hospital, Milan, Italy[1]Pierre Monney, 1) Division of Cardiology and Center of Cardiac Magnetic Resonance, Cardiovascular Department, University Hospital of Lausanne, CHUV, Switzerland.[2], Gabriella Vincenti, 1) Division of Cardiology and Center of Cardiac Magnetic Resonance, Cardiovascular Department, University Hospital of Lausanne, CHUV, Switzerland.[3], Tobias Rutz, 1) Division of Cardiology and Center of Cardiac Magnetic Resonance, Cardiovascular Department, University Hospital of Lausanne, CHUV, Switzerland.[2], Juerg Schwitter, 1) Division of Cardiology and Center of Cardiac Magnetic Resonance, Cardiovascular Department, University Hospital of Lausanne, CHUV, Switzerland.[2], Pier Giorgio Masci, 1) Division of Cardiology and Center of Cardiac Magnetic Resonance, Cardiovascular Department, University Hospital of Lausanne, CHUV, Switzerland.[2]

1. Cardiac MR Center-Cardiologiy Unit-University Hospital-CHUV-Lausanne, Switzerland, Lombardia, Italy

2. 1) Division of Cardiology and Center of Cardiac Magnetic Resonance, Cardiovascular Department, University Hospital of Lausanne, CHUV, Switzerland., Switzerland

3. 1) Division of Cardiology and Center of Cardiac Magnetic Resonance, Cardiovascular Department, University Hospital of Lausanne, CHUV, Switzerland, Switzerland

Description of Clinical Presentation: Background: anterior ST segment elevation (STE) is a hallmark of anterior left ventricular (LV) myocardial infarction (MI) as a consequence of abrupt occlusion of left anterior descending (LAD) coronary artery. Herein, we present an unusual case of an isolated right ventricular (RV) MI showing pronounced anterior STE.

Diagnostic Techniques and Their Most Important Findings: A 56-year-old man was admitted to our Institution because of long-lasting typical chest pain. He had unremarkable past medical history, and he was not under medication. At hospital admission ECG showed anterior STE in the precordial antero-septal leads (Figure 1 Panel A) without mirroring ST depression in the opposing leads. Invasive coronary angiography disclosed severe stenosis of LAD and proximally occluded right coronary artery (RCA) with good collateral circulation from left system for the interventricular posterior branch (Rentrop grade 3; Panel B, C and D). Remarkably, no branches for the right ventricle (RV) were visualized from either RCA or collateral circulation. In view of ECG findings, the operator treated LAD stenosis and judged RCA disease as a chronic total occlusion. The patient underwent CMR 6 days after the acute event. Cine imaging by steady-state free-precession sequence showed akinetic RV inferior and lateral free-walls resulting in reduced global systolic function (ejection-fraction of 43%). The left ventricle (LV) had normal regional systolic function except for slight hypokinesia of the inferior septum whereas global systolic function was normal (ejection-fraction 60%). T2-mapping technique showed myocardial edema confined to the inferior septum and extensive edema of the RV free-wall (Panel E) Fifteen minutes after bolus administration of 0.2 mmol/kg of Gadobutrol (Gadovist, Bayer-Germany), post-contrast 2D segmented T1-weighted gradient-echo phase-sensitive inversion-recovery sequence showed extensive RV late gadolinium enhancement (LGE) with extensive microvascular obstruction (Figure1 Panel E). Tiny subendocardial LGE was observed the mid inferior septum (Figure 1, Panel F).

Learning Points from this Case: Anterior STE in precordial leads without reciprocal changes on 12-lead ECG should evocate isolated acute RV infarction. This rare condition is caused by atherothrombotic complication of marginal branches nourishing the RV free-wall as a result of the abrupt occlusion of either non-dominant RCA or dominant RCA / left circumflex but with well developed collaterals for the interventricular posterior branch.

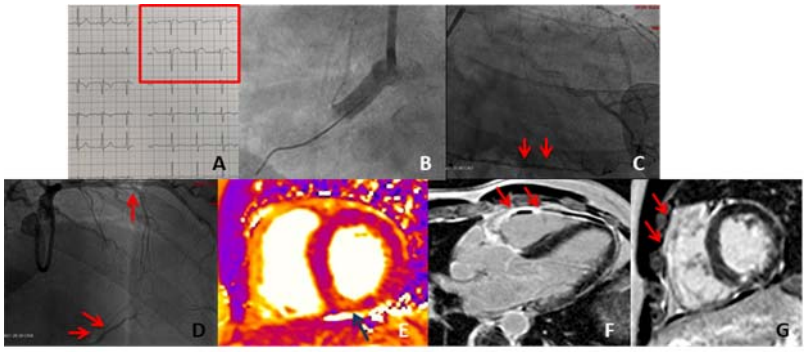
A
B
C
D
E
F
G

ID#: 376577

A Cardiac Mass Missed on CT and Echocardiography: The Added Value of CMR

Akhil Narang, MD[1]Neha Goyal, MD[2], Samir Undevia, MD[3], Tae Song, MD[3], Jeanne DeCara, MD[3], Karima Addetia, MD[3]

1. University of Chicago, Chicago, IL

2. University of Chicago, IL

3. University of Chicago

Description of Clinical Presentation: A previously healthy 50 year-old female presented to the emergency room with progressive shortness of breath. Computed tomography (CT) was negative for a pulmonary embolism but was notable for a large pericardial effusion (Figure A) that was confirmed on transthoracic echocardiogram (TTE, Figure B). Due to concern for tamponade, she underwent large-volume pericardiocentesis with pericardial drain placement. Follow-up TTE suggested a persistent large residual pericardial effusion. She was then referred for a surgical pericardial window during which a large mass, adherent to the epicardium and pericardium, was noted. Pericardial window was aborted and biopsy revealed synovial sarcoma. She was then referred to our institution for further management. A cardiac MRI (CMR) was obtained to further characterize the mass.

Diagnostic Techniques and Their Most Important Findings: CMR was used to evaluate the signal properties and morphology of the mass. Steady-state free precession cine sequences revealed a normal LV ejection fraction (62%). An extra-cardiac mass measuring 8x4 cm was noted adjacent to the posterior and lateral walls of the LV and LA (Figure C1 and C2). First pass perfusion imaging revealed contrast uptake suggesting vascularity of the mass (Figure D) and T2-weighted imaging demonstrated hyperenhancement of the mass suggesting inflamed/edematous tissue (Figure E). The patient was then referred for surgical resection of the mass (Figure F). One month after hospital discharge, the patient developed lower extremity edema and ascites. A repeat TTE did not demonstrate underlying etiology. A repeat CMR was obtained which showed complete resection of the mass but a thickened pericardial sac with hyperenhancement on T2-weighted imaging (Figure G). Tagged sequences revealed tethering of the pericardium suggestive of pericarditis with signs of constrictive physiology. The patient was managed medically with diuretics and her symptoms improved.

Learning Points from this Case: Multiparametric CMR imaging allows for integration of multiple parameters to delineate the etiology of cardiac masses and evaluate complications after their resection. In this case, both CT and TTE identified a pericardial effusion but were unable to delineate the pericardial mass that was seen on CMR. First-pass perfusion demonstrated contrast uptake within the mass suggesting vascularity and excluded hematoma or cyst. Hyperintense T2-weighted signal within the mass suggested the presence of edema due to active inflammation from a tumor. After resection, pericarditis with signs of pericardial constriction was diagnosed with repeat CMR showing an inflamed pericardium with tethered motion. CMR is a robust tool that allows for more accurate tissue characterization over CT and TTE.

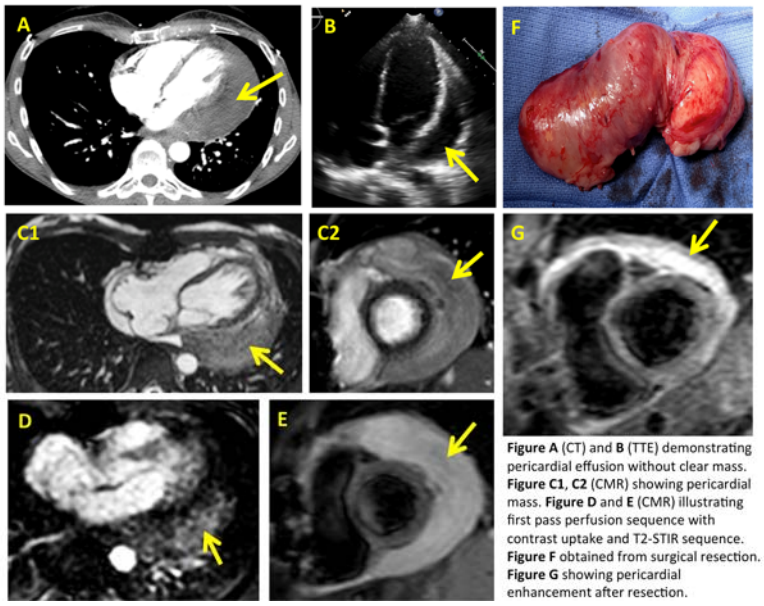

Figure A (CT) and **B** (TTE) demonstrating pericardial effusion without clear mass. **Figure C1**, **C2** (CMR) showing pericardial mass. **Figure D** and **E** (CMR) illustrating first pass perfusion sequence with contrast uptake and T2-STIR sequence. **Figure F** obtained from surgical resection. **Figure G** showing pericardial enhancement after resection.

ID#: 376582

Out of Hospital Cardiac arrest in a 14-year-old soccer player: don't forget the coronaries!

Alessandra Scatteia, MD[1] Giuseppe Limongelli, MD, PhD[2], Pasquale PG. Guarini, MD[3], Carmine Emanuele. Pascale, RT[4], Paolo Calabrò, MD, PHD[5], Santo Dellegrottaglie, MD, PHD[6]

1. Division of Cardiology, Ospedale Medico-Chirurgico Accreditato Villa dei Fiori, Acerra, Naples, Italy, Naples, Campania, Italy

2. Department of Cardiothoracic Sciences, Luigi Vanvitelli-Campania University - Monaldi Hospital, AORN Colli, Naples, Italy, Campania, Italy

3. Division of Cardiology, Ospedale Medico-Chirurgico Accreditato Villa dei Fiori, Acerra, Naples, Italy, Italia, Campania, Italy

4. Division of Cardiology, Ospedale Medico-Chirurgico Accreditato Villa dei Fiori, Acerra, Naples, Italy, Campania, Italy

5. Department of Cardiothoracic Sciences, Luigi Vanvitelli-Campania University - Monaldi Hospital, AORN Colli, Naples, Italy;, Campania, Italy

6. Division of Cardiology, Ospedale Medico-Chirurgico Accreditato Villa dei Fiori, Acerra, Naples, Italy; The Zena and Michael A. Wiener Cardiovascular Institute and Marie-Josee and Henry R. Kravis Center for Cardiovascular Health, Mount Sinai School of, Campania, Italy

Description of Clinical Presentation: A 14-year-old boy was admitted to our Emergency Department following a resuscitated cardiac arrest secondary to ventricular fibrillation which occurred while he was playing soccer. He had been regularly practicing soccer for 7 years, with periodic screening visit for sport eligibility, and never complained of any significant symptom. The family history was negative for cardiac diseases as well as for sudden cardiac death (SCD). At the admission he had no signs of infection and a mild troponin rise was recorded.

Diagnostic Techniques and Their Most Important Findings: ECG and transthoracic echocardiography suggested left ventricular hypertrophy (LVH) and raised the suspect of hypertrophic cardiomyopathy, with possible indication to ICD implantation. To clarify the diagnosis and to assess the presence and extent of myocardial fibrosis, he was referred for a cardiovascular magnetic resonance (CMR) study. Cine SSFP images showed mild symmetric LVH (maximal wall thickness = 10,4 mm), with no regional wall motion abnormalities and preserved left ventricular ejection fraction. Right ventricular dimensions and function were normal. STIR T2-weighted images showed a subendocardial area of high signal intensity involving the basal-to-mid infero-lateral wall as well as the anterolateral papillary muscle (Figure 1-A arrowheads), where a limited area of enhancement was also noted on LGE images (Figure 1-B arrowhead). A coronary magnetic resonance angiography was thus performed (navigator-gated T2-prep whole-heart technique), which highlighted an anomalous origin of the left coronary artery (LCA) form the right coronary sinus (Figure 1-C) with a slit-like orifice and interarterial ("malignant") course (Figure 1-D). The right coronary artery (RCA) had normal origin and course. The patient was then referred to the cardio-thoracic department for surgical correction.

Learning Points from this Case: In Italy the incidence of cardiomyopathies-related SCD in young athletes declined since the introduction of a cardiovascular screening program including ECG. Instead, 9-33% of sudden cardiac deaths in youngsters are attributable to coronary artery anomalies (CAA). In the present case, CMR had a pivotal role in reaching the diagnosis, firstly identifying an "ischemic-like" lesion and then spotting the anomalous origin of the LCA with the associated interarterial course. In young subjects experiencing aborted SCD, CAA should always be kept into consideration and CMR considered as fundamental part of the evaluation process, as it combines the possibility for tissue characterization with the assessment of coronary artery origin and course.

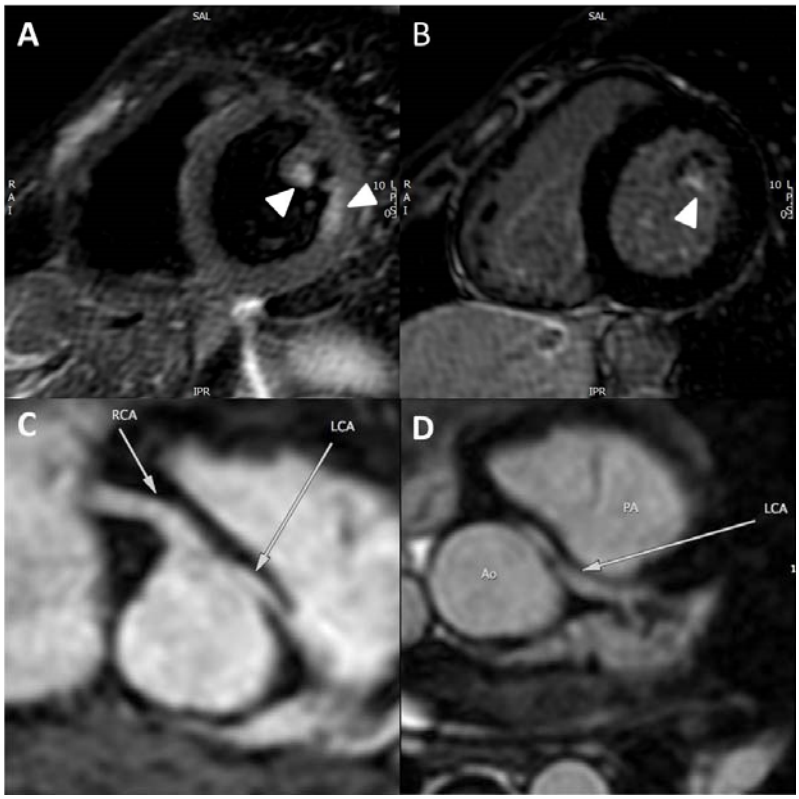

Oedema and ischemic enhancement caused by the abnormal left coronary artery

ID#: 375555

Comprehensive cardiovascular magnetic resonance for isolated cardiac cyst

Anna Giulia Pavon, Cardio-Thoracic Vascular Department, San Raffaele Hospital, Milan, Italy[1] Pierre Monney, 1) Division of Cardiology and Center of Cardiac Magnetic Resonance, Cardiovascular Department, University Hospital of Lausanne, CHUV, Switzerland.[2], Gabriella Vincenti, 1) Division of Cardiology and Center of Cardiac Magnetic Resonance, Cardiovascular Department, University Hospital of Lausanne, CHUV, Switzerland.[3], Tobias Rutz, 1) Division of Cardiology and Center of Cardiac Magnetic Resonance, Cardiovascular Department, University Hospital of Lausanne, CHUV, Switzerland.[2], Pier Giorgio Masci, 1) Division of Cardiology and Center of Cardiac Magnetic Resonance, Cardiovascular Department, University Hospital of Lausanne, CHUV, Switzerland.[2], Juerg Schwitter, 1) Division of Cardiology and Center of Cardiac Magnetic Resonance, Cardiovascular Department, University Hospital of Lausanne, CHUV, Switzerland.[2]

1. Cardiac MR Center-Cardiologiy Unit-University Hospital-CHUV-Lausanne, Switzerland, Lombardia, Italy

2. 1) Division of Cardiology and Center of Cardiac Magnetic Resonance, Cardiovascular Department, University Hospital of Lausanne, CHUV, Switzerland., Switzerland

3. 1) Division of Cardiology and Center of Cardiac Magnetic Resonance, Cardiovascular Department, University Hospital of Lausanne, CHUV, Switzerland, Switzerland

Description of Clinical Presentation: Hydatid disease is mostly caused by the Echinococcus granulosus and it is a rare parasitic disease, which mainly involves liver and lung. Cardiac involvement is rare, and it occurs usually in the context of multiorgan involvement. The diagnosis remains challenging particularly when the disease is confined to the heart and the serology is negative. Herein, we present a case of a suspected isolated hydatid cardiac disease in a young African man studied by comprehensive cardiovascular magnetic resonance (CMR).

Diagnostic Techniques and Their Most Important Findings: A 35-year old man was referred to CMR due to an incidental finding of an aspecific lesion in the left ventricular (LV) lateral wall visualized at abdominal CT scan performed for aspecific abdominal pain, fever and weight loss. At CT the lesion was hypodense (4 Hounsfield unit) suggesting fluid content (panel A) The patient underwent CMR (1.5 T Siemens Aera, Erlangen, Germany) and breath-hold cine steady-state free precession (SSFP) imaging revealed a lesion of 10x12x20 mm embedded in the LV lateral wall (panel B). The lesion was highly hyperintense on SSFP and T2-weighted short-TI (STIR) imaging (Panel C and D), showing well defined boundaries without invading the adjacent myocardium. On native T1- and T2-mapping (panel D and E, respectively) the mass had 3660ms and 300ms relaxtion times, respectively, (for comparison, blood pool had native T1 and T2 values of 1634ms and 167ms, respectively). T2 was slightly elevated at the surface of the mass indicating mild peri-lesional edema. At first-pass perfusion imaging during bolus injection of 0.1 mmol/kg of gadolinium-based contrast-agent (Gadobutrol, Gadovist, Bayer Healthcare, Germany), the lesion was not perfused (panel F) and on post-contrast imaging mild late gadolinium enhancement (LGE) was detected at the surface of the mass (panel G). The patient underwent total-body 18-FDG PET-CT scan confirming a mild inflammation around the cardiac lesion, and the exam excluded other organ involvement (panel H). After interdisciplinary discussion, considering the high false-negative rate by blood testing described in literature, especially in patients with small and extraepatic hydatid cysts, the diagnosis of an isolated hydatic intra-myocardial cyst was retained. Accordingly, antihelminthic treatment was started, and clinical and imaging follow-up will be performed after at least 6 months of treatment.

Learning Points from this Case: An isolated hydatid intra-myocardial cyst is an extremely rare condition; in our case CMR had a matchless value in pursuing the most probable diagnosis with a major impact on patient's management.

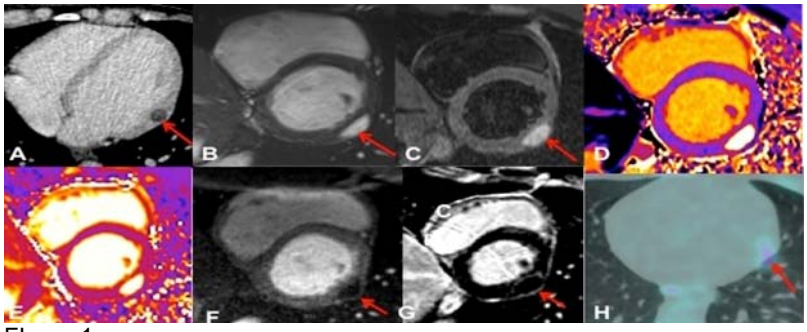

FIgure 1

ID#: 377930

Right ventricular outflow tract obstruction in the setting of hypertrophic cardiomyopathy

Bharath Sathya, MD[1] Andrew E. Arai, MD[2], W. Patricia Bandettini, MD[3]

1. National Institutes of Health/NHLBI, Bethesda, MD

2. National Heart, Lung and Blood Institute, National Institutes of Health, Bethesda, MD

3. National Heart, Lung and Blood Institute, National Institutes of Health, MD

Description of Clinical Presentation: A 42-year-old Vietnamese female presented for evaluation of a cardiac murmur with CMR after a technically challenging transthoracic echocardiogram, perhaps related to her breast implants. She had been experiencing occasional lightheadedness and palpitations associated with activity. She has a non-significant family history. Her physical examination was notable for a 3/6 systolic murmur at the left upper sternal border and 2/6 systolic murmur at the left lower sternal border which both did not significantly change with hand grip.

Diagnostic Techniques and Their Most Important Findings: On cine CMR, there was severe asymmetric septal hypertrophy extending from the basal left ventricle to the apex. The maximal septal thickness was 31 mm and was in the anteroseptum adjacent to the right ventricular outflow tract (RVOT). Myocardial T1 was prolonged within the hypertrophied septal wall. There was also myocardial fibrosis in this area on late gadolinium enhancement imaging. On velocity encoded phase contrast imaging, there was flow acceleration in the right ventricular outflow tract occurring in systole adjacent to the area of maximal septal hypertrophy. The maximum velocity measured was 2.7 m/s in the RVOT at rest. The flow acceleration appeared to be caused by the interventricular septal hypertrophy. There was minimal flow acceleration in the left ventricular outflow tract and no associated systolic anterior motion of the mitral valve. These findings are most consistent with a diagnosis of hypertrophic cardiomyopathy with associated right outflow tract obstruction. Based on her risk profile, the patient was offered an implantable defibrillator but declined for cosmetic reasons.

Learning Points from this Case: 1. This case demonstrates a rare finding of dynamic, hemodynamically significant right ventricular outflow tract (RVOT) obstruction secondary to protrusion of the hypertrophied interventricular septal wall into the RVOT. Prior literature has only described the finding of a fixed right ventricular outflow obstruction secondary to right ventricular hypertrophy usually at the crista supraventricularis (Malik R et al. Echocardiography 2014).
2. The preferred modality of treatment for this patient is not well defined. There have been reported reductions in resting gradients with medication. Surgical myomectomy with resection of the right ventricular muscular tissue has also been described in the setting of more prominent right ventricular outflow tract hypertrophy.
3. Cardiac MRI was useful in identifying high risk features in this patient including the 31 mm septal thickness and involvement of 18% of the myocardium on late gadolinium enhancement.

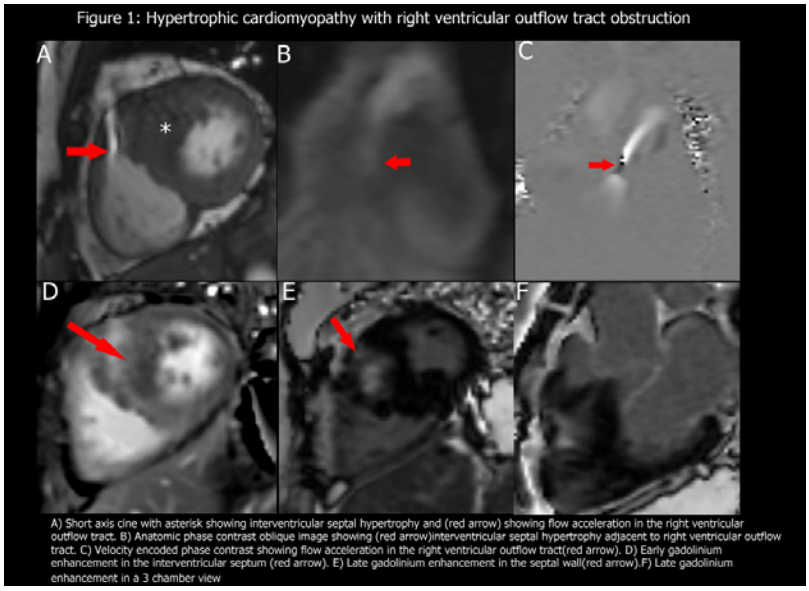

ID#: 378012

Regadenoson myocardial stress perfusion CMR in a 2-month-old with transposition of the great arteries status post arterial switch with left coronary obstruction

James C. Wilkinson, MD[1] Amol Pednekar, PhD[2], Cory Noel, MD[3]

1. Texas Children's Hospital, Baylor College of Medicine, Houston, TX

2. Texas Children's Hospital, Houston, TX

3. Texas Children's Hospital / Baylor College of Medicine, TX

Description of Clinical Presentation: We present a patient with transposition of the great arteries (TGA) who underwent arterial switch operation (ASO) at 5 days of life at an outside institution. Pre-operatively, the right coronary artery (RCA) originated to the right side of the posterior commissure with an intramural course. The post-operative echocardiogram demonstrated normal biventricular function. At 2 months of age he was noted to have severe left ventricular dysfunction (left ventricle ejection fraction (LVEF) of 42%), normal right ventricular function, moderate mitral valve regurgitation and echogenic papillary muscles. He underwent cardiac catheterization which demonstrated absence of prograde flow and LCA occlusion. The patient was transferred to our institution on a continuous infusion of milrinone.

Diagnostic Techniques and Their Most Important Findings: We performed a myocardial stress perfusion cardiac magnetic resonance (CMR) using regadenoson, a direct A2A agonist, to induce coronary hyperemia. The patient was sedated with propofol. Regadenoson was administered at a weight-based dose of 8 mcg/kg (adult dose 0.4 mg), without complication. Following the regadenoson administration, perfusion analysis was performed utilizing first-pass of 0.1 mmol/kg of gadolinium. The LVEF at rest was 48%. The heart rate (HR) at rest was 115 beats per minute (bpm) with a peak HR of 145 bpm during stress. The systolic blood pressure was 90 and 84 mmHg, diastolic pressure was 54 and 48 mmHg at rest and stress states respectively. A small resting perfusion defect was detected in the antero-lateral wall at the basilar level. Perfusion analysis during stress demonstrated a large sub and mid-myocardial perfusion defect which encompassed the majority of the interventricular septum, in addition to the anterior and lateral wall, consistent with LCA distribution. There was enhancement of the antero-lateral papillary muscles as well as a small portion of the subendocardial region of the antero-lateral ventricular wall, at rest and stress states. Ultimately, attempts to recanalize the LCA were unsuccessful and the patient was managed medically.

Learning Points from this Case: We were able to safely and accurately perform a myocardial stress perfusion CMR, using weight-based dosing of regadenoson (8 mcg/kg), in a 2-month-old with TGA, status post ASO with LCA obstruction. To our knowledge, this is the youngest patient to undergo such a procedure involving pharmacologic stress CMR. We believe there is potential in using myocardial stress perfusion CMR, in conjunction with late gadolinium enhancement, and wall motion analysis to safely detect, analyze, and guide treatment in coronary artery disease and ischemia in infants and young children.

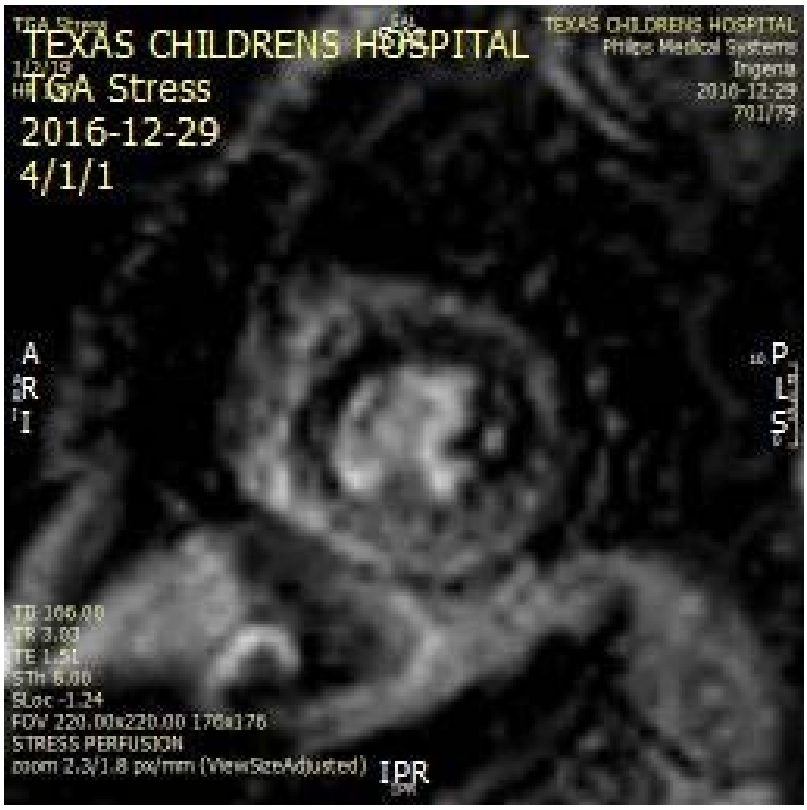

Figure 1. Dynamic T1-Weighted Spoiled Gradient Echo first-pass perfusion sequence at the mid-ventricular level demonstrating inducible perfusion defect of anterior septum, anterior and lateral left ventricular wall.

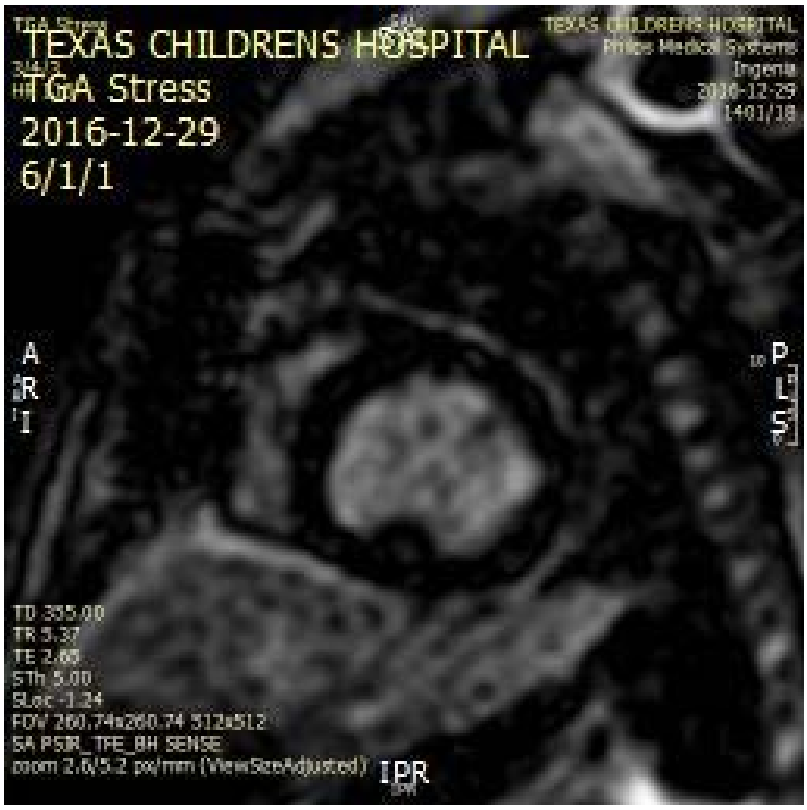

Figure 2. Phase-sensitive inversion recovery sequence at corresponding ventricular level demonstrating area of enhancement of antero-lateral mitral valve papillary muscle and antero-lateral ventricular wall.

ID#: 377250

When the heart knows first: high grade neuroendocrine carcinoma of the heart.

Jitka Starekova, MD[1] Theresa Wisst, MD[2], Felix Kreidel, MD[2], Tobias Spangenberg, MD[3], Dietmar Kivelitz, Priv.-Doz., MD[4]

1. University Medical Center Hamburg-Eppendorf (UKE), Hamburg, Germany

2. Asklepios Klinik St.Georg, Hamburg, Germany

3. Asklepios Klinik St.Gerog, Hamburg, Germany

4. Asklepios Klinik St.Georg, Hamburg, Hamburg, Germany

Description of Clinical Presentation: A previously healthy 50-year-old man presented to the emergency department with progressive chest pain during deep inspiration for the last 2 days. The ECG showed indistinct abnormalities (T negativation, ST depression of inferior left ventricle wall). An acute myocardial infarction was ruled out. The D-dimer test was positive.
The following examinations revealed tumorous masses of the left (LV) and right ventricle (RV) as well as involvement of the right coronary aortic cusp. The histopathology revealed a high grade small cell neuroendocrine carcinoma (NEC). The primary tumour remains unknown and no other metastases were detected. No symptoms of carcinoid syndrome were present.

Diagnostic Techniques and Their Most Important Findings: A CT angiogram was negative for pulmonary embolism or lung malignancy, however the scan revealed a large homogeneous intramural mass of the inferolateral wall of the LV with an intracavitary component and involvement of the pericardial space. Furthermore, moderate haemorrhagic pericardial effusion was present.
Cardiac MRI (CMR) showed additionally a smaller similar mass in the RV free wall and on the right coronary cusp of the aortic valve which was missed in previously performed transthoracic echocardiography (TTE) and CT. Global cardiac function was normal. Complementary dermatologic evaluation, abdominal CT, brain MRI and Scintigraphy excluded any other suspect malignant lesions. Pericardiocentesis and cardiac biopsy was performed. Histologic examination revealed a high grade small cell neuroendocrine carcinoma.

Learning Points from this Case: Cardiac tumours can be either primary or metastatic. Primary cardiac tumours are very uncommon (various postmortem studies show an incidence of 0.001% to 0.28%). Cardiac metastases are much more common, ranging from 2.3% to 18% in literature. Most such primary tumours are melanomas, sarcomas, lung, breast and hematologic malignancies.
Neuroendocrine carcinomas of the heart are extremely rare and usually metastatic (incidence 1-4%). They appear to be more common in males with average age at diagnosis of 58 years. Majority metastasize from gastrointestinal tract or bronchopulmonary system, however in individual cases the primary tumour remains unknown. They are commonly associated with carcinoid syndrome and their occurrence in the absence of liver involvement is exceedingly rare.
There are no specific clinical symptoms in patients with cardiac metastases, however they usually present with dyspnoea, arrhythmias or accentuation of carcinoid syndrome.
In general survival rates in patients with distant metastases of high grade NEC are about 4 %.
As a single method; MRI is superior to echocardiography in the detection and quantification of cardiac metastases, as the smaller lesion can be missed in the echocardiography.
Treatment is usually palliative chemotherapy, because patients rarely have solitary disease that is amenable to resection. In symptomatic patients, medical treatment should be considered (e.g. ß-blockers, Somatostatin analogues, Interferon-α).
The follow-up intervals depend on individual clinical situation. The imaging follow-up schedule ranges in progressive disease from every 3 to 6 months.

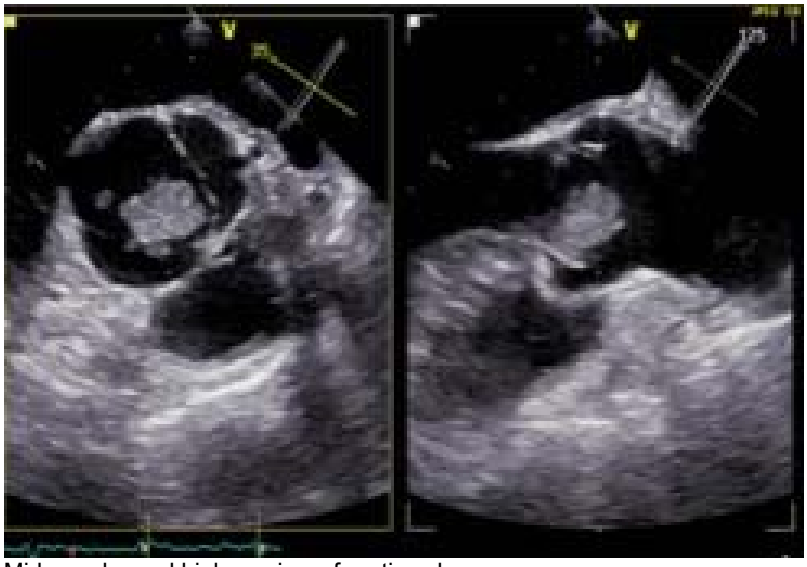

Mid-esophageal biplane view of aortic valve

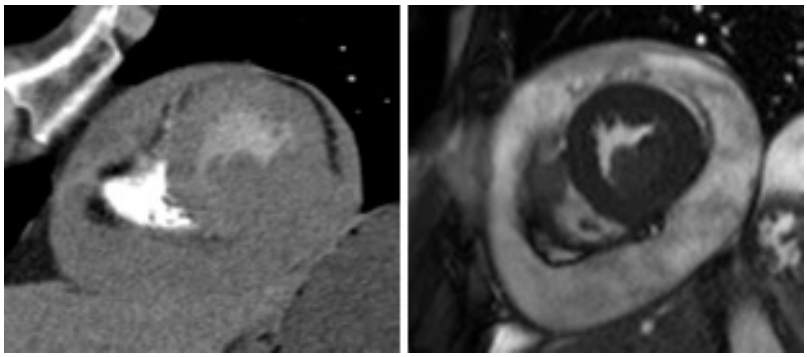

Short-axis CT and CMR

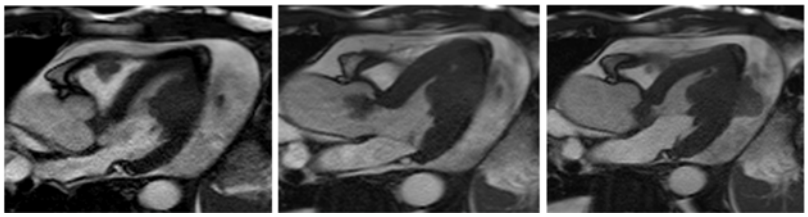

Long-axis (3-chamber view) CMR

ID#: 377368

Serial CMR Follow Up of Left Ventricular Pseudoaneurysm and Aneurysm In a Child With May-Thurner Syndrome.

Ronak Naik, MD, FACC[1] Abdul H. Khan, MD[2], Jason N. Johnson, MD MHS[3]

1. University of Tennessee Health Science Center, Memphis, TN

2. Lebonheur Children's Hospital, Memphis, Tennessee, Cordova

3. LeBonheur Children's Hospital, University of Tennessee Health Sciences Center, Memphis, TN

Description of Clinical Presentation: A 4 year old child presented with abdominal pain and high fever for two days with limping, hallucinations, and pustular rash. Hypoxia and hypotension developed requiring mechanical ventilation and ionotropic support. Laboratory findings were significant for pancytopenia, elevated CRP, and blood culture positive for methicillin susceptible staphylococcus aureus. CT abdomen showed multiple septic emboli in the lungs and thrombosis of left common and external iliac veins along with narrowing of left common iliac vein as it passed underneath the right common iliac artery – characterized as May-Thurner Syndrome. He developed bilateral micro hemorrhagic septic emboli to the brain, bones, and a mobile vegetation in the right ventricular outflow tract on echocardiogram. During hospital course lowest LV ejection fraction of 45-50% noted for which he was started on atenolol and enalapril. No coagulation disorder, immunological disorder or rheumatological disorders were found.

Diagnostic Techniques and Their Most Important Findings: Transthoracic echocardiogram one month after hospital discharged showed akinesia of the inferior and inferolateral wall segments concerning for possible aneurysm so a CMR was obtained. Contrast-enhanced CMR with sedation showed a normal left atrial volume (17ml/m2) and left ventricular chamber size (LVEDVI 74ml/m2). A pseudoaneurysm of the mid inferior wall (opening 5 mm, and 7x9x10 mm in size) and an aneurysm of the mid inferolateral wall (opening 2 mm, and 7x10x15 mm in size) of the left ventricle noted(Figure 1). Gadolinium contrast is seen entering the cavity of the pseudoaneurysm and aneurysm on perfusion sequences (Figure 2). There was normal global left ventricular systolic function (LVEF 66%) with dyskinesia of the mid inferior wall and hypokinesia of the mid inferolateral wall in the area of pseudoaneurysm and aneurysm respectively. Subendocardial late gadolinium enhancement (LGE) of the inferior and lateral apical wall, mid inferolateral wall, and basal to mid anterolateral wall, and transmural LGE of the mid inferior wall (correlating to the area of pseudoaneurysm)(Figure 3). No evidence of thrombus in the aneurysm or pseudoaneurysm. A repeat contrast-enhanced CMR was performed 6 months later showed no significant change in LV systolic function, pseudoaneurysm or aneurysm size, or LGE pattern. He is currently being managed conservatively on atenolol, aspirin, and valsartan. Lovenox was changed to Coumadin with goal INR of 2-3. He is currently active, ambulatory and without any cardiac symptoms.

Learning Points from this Case: Ventricular pseudoaneurysm and aneurysms are very rare in pediatric population. This is the first case describing both in pediatric patient. May-Thurner syndrome predisposes to deep vein thrombosis, and with superimposed bacteremia, septic emboli can seed multiple organ systems leading to infarcts, a process that has not been described before in May-Thurner sydrome. Cardiac MRI provided superior visualization to help differentiate between pseudoaneurysm and aneurysms, determine embolic etiology, and provided serial information on changes in aneurysmal size and viability pattern.

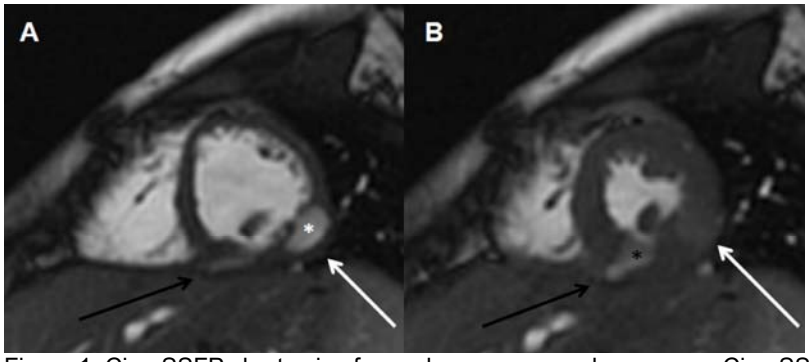

Figure 1. Cine SSFP short axis of pseudoaneurysm and aneurysm. Cine SSFP short axis at end-diastole (A) and end-systole (B) with the pseudoaneurysm (black arrows and asterix) in the inferior wall and the aneurysm (white arrows and asterix) in the inferolateral wall.

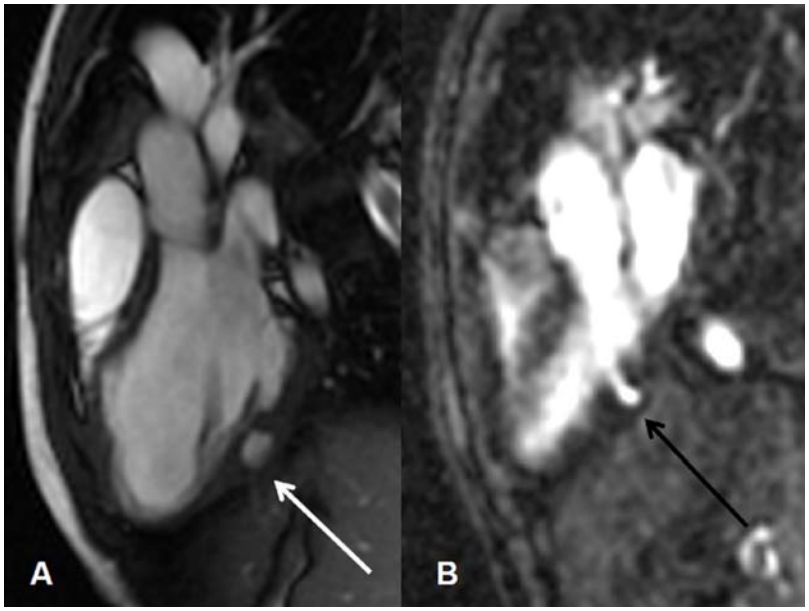

Figure 2. Cine SSFP and perfusion left ventricular outflow tract of the aneurysm. Cine SSFP left ventricular outflow tract (A) of the aneurysm (white arrow) and perfusion sequence (B) with gadolinium contrast in the aneurysm (black arrow).

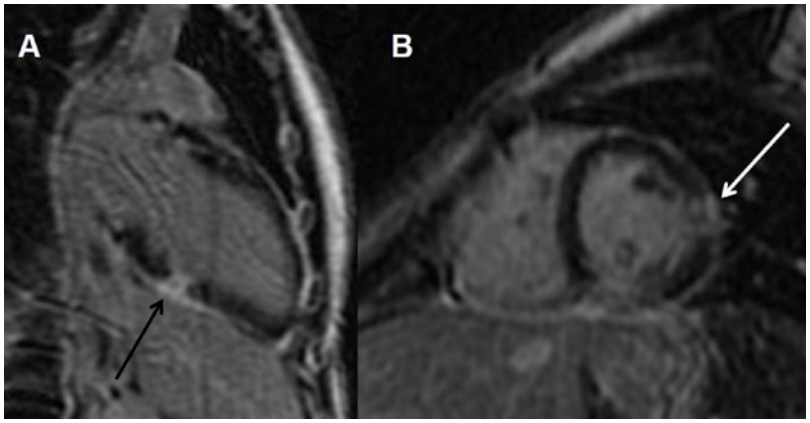

Figure 3. Two chamber left ventricle and short axis delayed enhancement. Two chamber left ventricle (A) with transmural late gadolinium enhancement (LGE) of the mid inferior wall (black arrow). Mid short axis (B) with sub-endocardial LGE of the anterolateral wall (white arrow).

ID#: 377693

Myocardial Edema as a Novel Biomarker of Risk in Familial Dilated Cardiomyopathy

Mohamed Elamin, M.D.[1] Andrea Cardona, MD[2], Subha Raman, MD, MSEE[3], Karolina Zareba, MD[4]

1. The Ohio State University, Hilliard, OH

2. The Ohio State University Wexner Medical Center, Columbus, OH

3. The Ohio State University, Columbus, OH

4. The Ohio State University Wexner Medical Center, OH

Description of Clinical Presentation: Early diagnosis and prognosis assignment in individuals at risk of familial dilated cardiomyopathy can be challenging. We present two cases of geno-positive, asymptomatic siblings referred for screening cardiac magnetic resonance (CMR) carrying a known dilated cardiomyopathy (DCM)-causing gene mutation who demonstrated strikingly similar myocardial edema by CMR T2 mapping.

Diagnostic Techniques and Their Most Important Findings: Two asymptomatic Caucasian male siblings (ages 39 and 36 years) with known family history of DCM, whose mother suffered sudden cardiac death, presented for genetic screening. They were both found to carry RBM20 gene. Both siblings had normal physical exam findings, ECGs and echocardiograms. CMR was done to assess for early myocardial changes. Both brothers exhibited increased left ventricular (LV) sphericity (Figure 1) with strikingly elevated myocardial T2 values in multiple LV segments (Figures 2). The older brother had top normal LV size (LV end-diastolic volume index 98 ml/m^2) and mild global systolic dysfunction, (LV ejection fraction 49%). Myocardial T2 elevation was found predominantly in the anterior and inferolateral walls (> 75 msec, normal <59 mesc); Figure 2 a and b. Late gadolinium imaging (LGE) demonstrated patchy mid-myocardial fibrosis in the septal and inferolateral walls (Figure 3). The younger brother had mild LV dilatation (LV end diastolic volume index = 115 ml/m^2) and preserved systolic function (LV ejection fraction 57%) with no myocardial scar or infiltrate by LGE. However, myocardial T2 elevation was present in the mid-inferolateral wall (>70 msec, Figure 2 c and d).

Learning Points from this Case: Early identification of structural and functional changes in geno-positive individuals at risk of familial DCM is challenging but very important to guide initiation of appropriate cardioprotective therapy. CMR can uniquely and non-invasively identify early myocardial tissue alterations that precede clinically-apparent disease. T2 mapping has been shown to identify early inflammatory changes in acute myocarditis and cardiac sarcoidosis before irreversible myocardial fibrosis ensues. However, the role of T2 mapping in asymptomatic subjects with DCM is not established. In these two asymptomatic individuals with RBM20 mutation associated with familial DCM, only one exhibited abnormal LGE findings. However, T2 values were significantly elevated in both. RBM20 gene encodes for a nuclear protein which regulates alternative splicing of expressed genes that have a key role in cardiac function. There are no reports describing T2 signal abnormalities in early familial DCM. Understandably, an association between specific genes, in this case RBM20, and cardiac tissue characterization is lacking. Myocardial characterization with T2 mapping could be used as a novel marker to identify a potentially treatable early phenotype of genetic DCM, improve risk stratification, and monitor response to therapy.

We present a novel observation between genetic DCM and T2 signal abnormalities. Further investigation of the relationship between T2 mapping in the context of familial DCM will help elucidate its role in early detection and management.

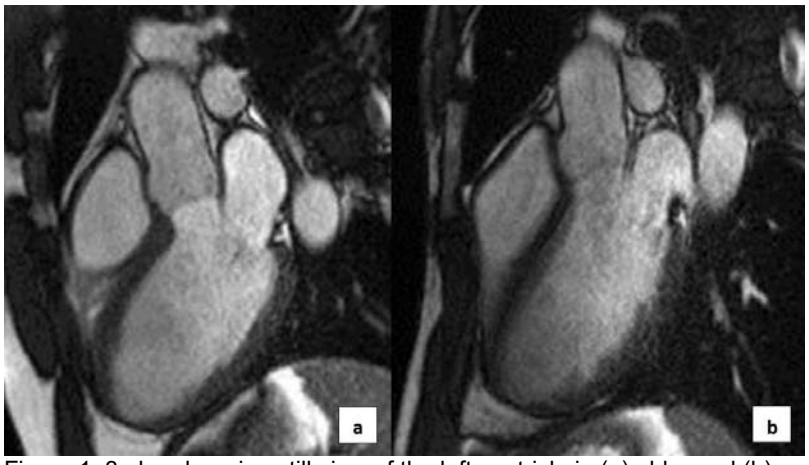

Figure 1. 3-chamber cine still view of the left ventricle in (a) older and (b) younger sibling demonstrating the similarly globular (spherical) shape hearts in both patients.

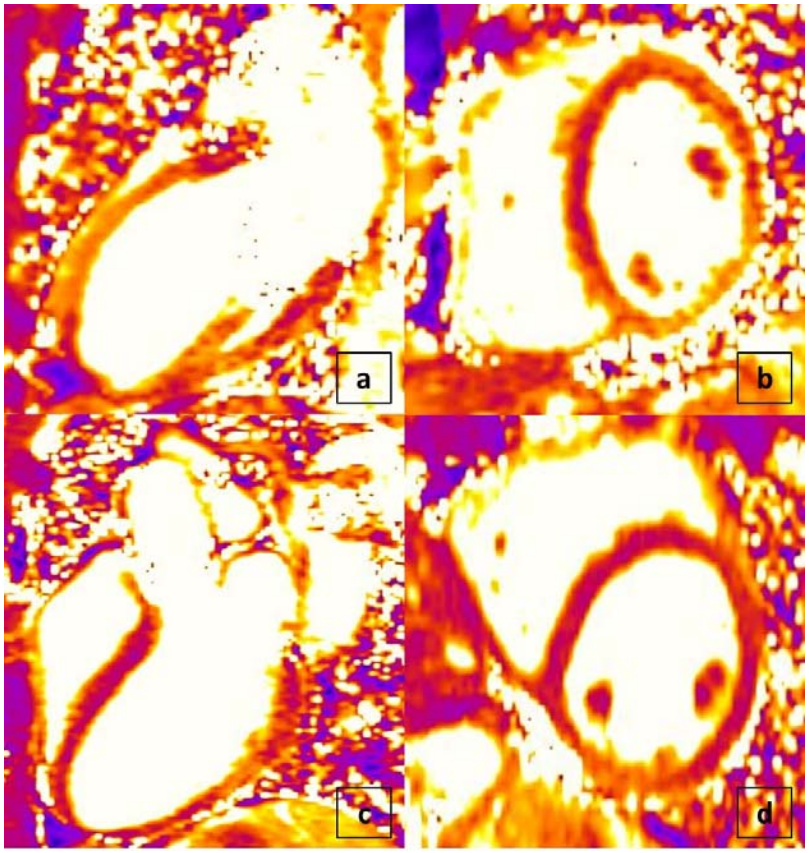

Figure 2. T2 mapping of the left ventricle in 2-chamber (a) and mid short axis (b) views demonstrating elevated T2 values (> 75 ms) predominantly in the anterior and inferolateral walls in a 39 year old male carrier of RBM20 mutation. T2 mapping of the left ventricle in 3-chamber (c) and mid short axis (d) views demonstrating elevated T2 values (>70 ms) in the mid-inferolateral wall in a 36 year old male carrier of RBM20 mutation.

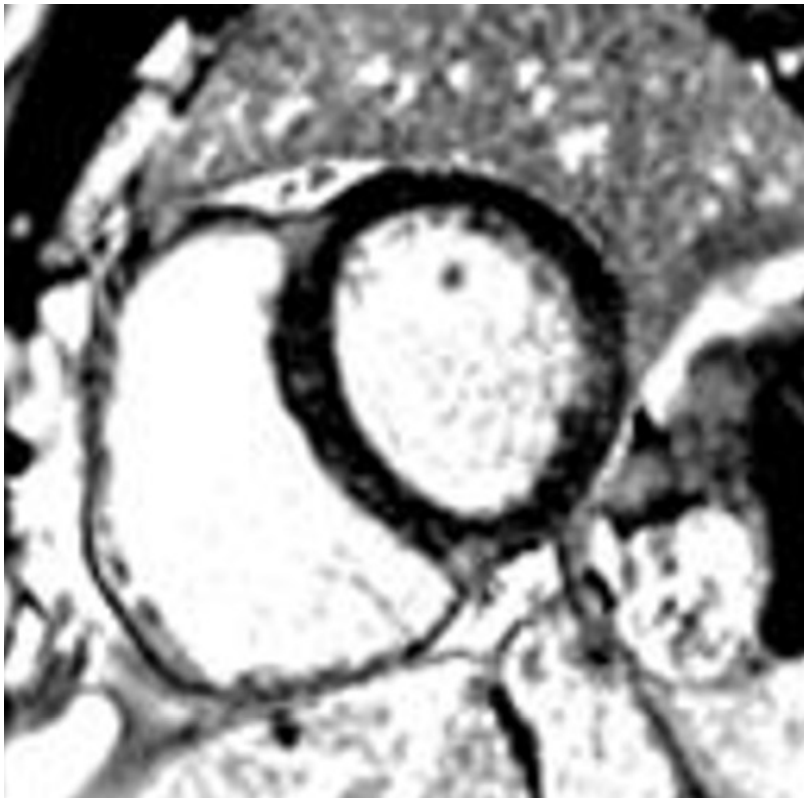

Figure 3. Late gadolinium enhancement imaging of the mid short axis view demonstrating patchy mid-myocardial fibrosis in the septal and inferolateral walls in a 39 year old male carrier of RBM20 mutation.

ID#: 378494

Growing from within: dyspnea due to progressive stenosis of multiple heart vessels

Filipa X. Valente, MD[1]Laura Gutierrez, MD[2], Ignacio Ferreira, MD, PhD[3], Victor Pineda, MD, PhD[3], Nazarena Pizzi, MD[3], Albert Roque, MD[3], Hug Cuellar, MD, PhD[3], David Garcia-Dorado, MD, PhD[4], Arturo Evangelista, MD, PhD[5], José F. Rodríguez-Palomares, MD, PhD[6]

1. Hospital Universitari Vall d´Hebron. Vall d'Hebron Institut de Recerca. Universitat Autònoma de Barcelona, Barcelona, Spain

2. Hospital Universitari Vall d´Hebron. Vall d'Hebron Institut de Recerca. Universitat Autònoma de Barcelona, Spain

3. Hospital Universitari Vall d'Hebron, Spain

4. (1) Hospital Vall d'Hebron, Department of Cardiology. VHIR, Universitat Autònoma de Barcelona, Barcelona, Spain., Spain

5. Hospital Vall d'Hebron, Spain

6. Hospital Universitari Vall d´Hebron. Vall d'Hebron Institut de Recerca. Universitat Autònoma de Barcelona, Barcelona, Catalonia, Spain

Description of Clinical Presentation: A 42-year-old woman was evaluated in the outpatient clinic complaining of exertional dyspnea over the previous two months. She also referred occasional precordial chest pain at rest of 5-10 minutes duration. She had a history of arterial hypertension, obesity and was a former smoker. A transthoracic echocardiogram showed a dilated right ventricle and a D-shaped left ventricle suggestive of elevated right systolic pressure, dilation of the right atrium, severe estimated systolic pulmonary arterial pressure (62 mmHg), absence of atrial septal defects or inferior vena cava dilation, and moderate pericardial effusion. Chest CT showed no signs of pulmonary embolism. Ventilation/perfusion scintigraphy was normal as was the 6-min walking test. She was referred for a CMR for further study.

Diagnostic Techniques and Their Most Important Findings: CMR showed a large irregular mediastinal mass (53x28x49 mm) occupying the anterior interventricular sulcus, infiltrating the basal anterior and antero-septal wall of the left ventricle as well as the pulmonary artery. The mass caused severe reduction of the pulmonary lumen (> 90% stenosis) and involved circumferentially the aortic root and ascending aorta as well as the coronary arteries (Figure 1). The right ventricle was hypertrophic, dilated and presented mild systolic dysfunction. These findings were considered suggestive of a lymphoproliferative disorder and, less likely, an undifferentiated sarcoma. Cardiac CT showed similar findings as well as diffuse and severe stenosis of the left main and proximal-mid anterior descending and circumflex arteries (Figure 2). Whole-body PET/CT showed an extensive hypermetabolic activity, with no extra-cardiac foci. Guided by these findings, echocardiography was repeated and showed the mass occupying the pulmonary artery and causing severe stenosis (transpulmonary velocity > 4.5 m/s, Figure 3).

Learning Points from this Case: Percutaneous biopsy of the mass provided insufficient material for diagnosis; therefore, surgical biopsy was performed through a median thoracic sternotomy and multiple samples were sent for pathologic study. As the results were awaited, the patient complained of precordial chest pain, and ST-segment changes were observed on the ECG; she had a sudden cardiac arrest and advanced life support was started. She was transferred to the cath lab where an intra-aortic balloon was implanted and left main stem occlusion was visualized. Percutaneous coronary interventions were performed; however, the patient did not recover spontaneous cardiac activity. The final pathology diagnosis was of IgG4 vasculitis. IgG4-related disease is an immune-mediated fibroinflammatory condition that can affect multiple organs and lead to tumefactive tissue-destructive lesions. It is a rare and generally treatable disease. The most common vascular manifestation is aortitis with aneurysm formation. In this case, we illustrate a very unusual presentation of the disease which delayed the correct diagnosis and corresponding treatment.

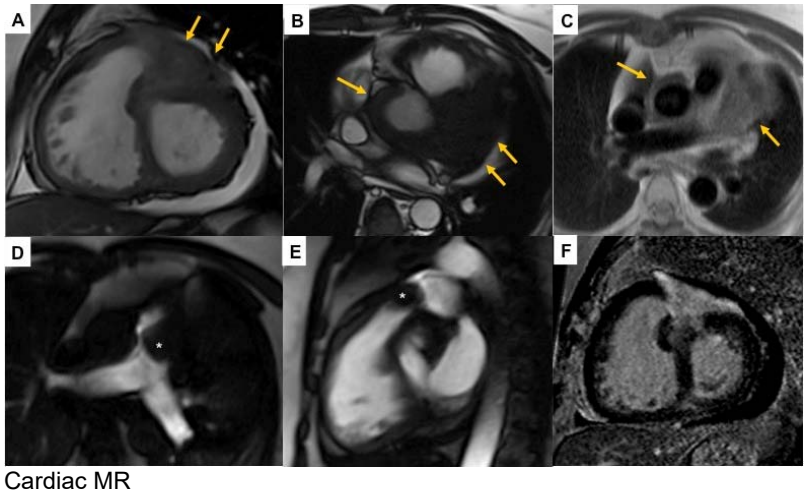

Cardiac MR

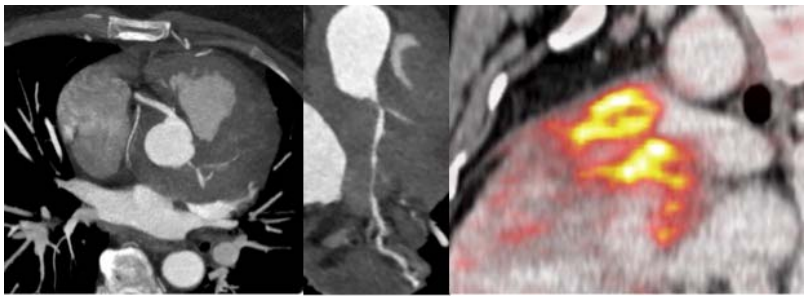
Cardiac PET/CT

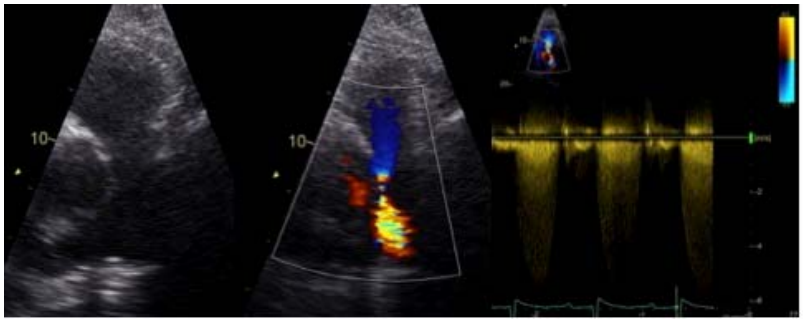

Transthoracic echocardiogram

ID#: 378365

Optimizing 3D whole heart imaging in complex congenital heart disease: ferumoxytol and respiratory suspension

Wilson King, MD[1] Douglas A. Hokeness, RT[2], Chetana Reddy, MD[3], Nadeem Parkar, MD[3]

1. Saint Louis University, Des Peres

2. SSM Cardinal Glennon Hospital, Okawville, IL

3. Saint Louis University

Description of Clinical Presentation:

A 4-year-old girl presented to cardiology clinic with a diagnosis of dextrocardia, double outlet right ventricle with an inlet VSD with normally related great arteries, and previously underwent a pulmonary artery band and Glenn shunt. She became progressively cyanotic saturating 75%. Echocardiography suggested the left ventricle was possibly large enough for biventricular repair. Cardiac MRI was performed to determine whether the patient could undergo a biventricular conversion with a Rastelli operation, or required single ventricle completion with a Fontan.

Diagnostic Techniques and Their Most Important Findings:

Ferumoxytol (3 mg/kg dose, 8 mg/mL concentration) was given as a slow infusion over 15 minutes in a supervised holding area. The patient was brought to the 1.5 T GE Signa MRI suite where she was intubated, ventilated, and paralyzed by cardiac anesthesia.

After the localizers, a cine IR sequence was performed to determine the optimal inversion time to null the myocardium. A 3D whole heart sequence with end-diastolic ECG-gating and respiratory navigator was performed using an ultrafast gradient echo (FGRE) readout with an inversion recovery (IR) time of 170 ms (Flip angle: 15 degrees, TR 3.3 ms, TE 1.5 ms). Although the overall image quality was acceptable, visible respiratory navigator bands crossed areas of interest. The 3D whole heart IR-FGRE sequence was repeated without the respiratory navigator. Instead, anesthesia provided five 30 second breath-holds during which images were acquired. Image quality was significantly improved without navigator band artifact.

Excellent contrast between the myocardium and blood pool was obtained, delineating the superior-inferior relationship of the normal-sized right ventricle and hypoplastic left ventricle, as well as the inlet ventricular septal defect and common atrium. Decompressing veins from the Glenn shunt were clearly seen. Smaller structures such as coronary arteries, semilunar valves, and the lumen across the tightened pulmonary artery band were easily resolved.

Use of an exclusive intravascular contrast agent in conjunction with a 3D whole heart sequence utilizing anesthesia-assisted breath-holds allows acquisition of high quality images in a short period of time. This technique can be used for 3D modeling, 3D printing, and advanced surgical planning.

Learning Points from this Case:

1. Ferumoxytol, an exclusive intravascular contrast agent, is extremely useful for obtaining high quality intracardiac and extracardiac vascular imaging for congenital heart disease.

2. Contrast-enhanced 3D whole heart imaging can be performed with improved image quality and decreased scanning time by utilizing anesthesia-assisted breath-holds instead of respiratory navigators.

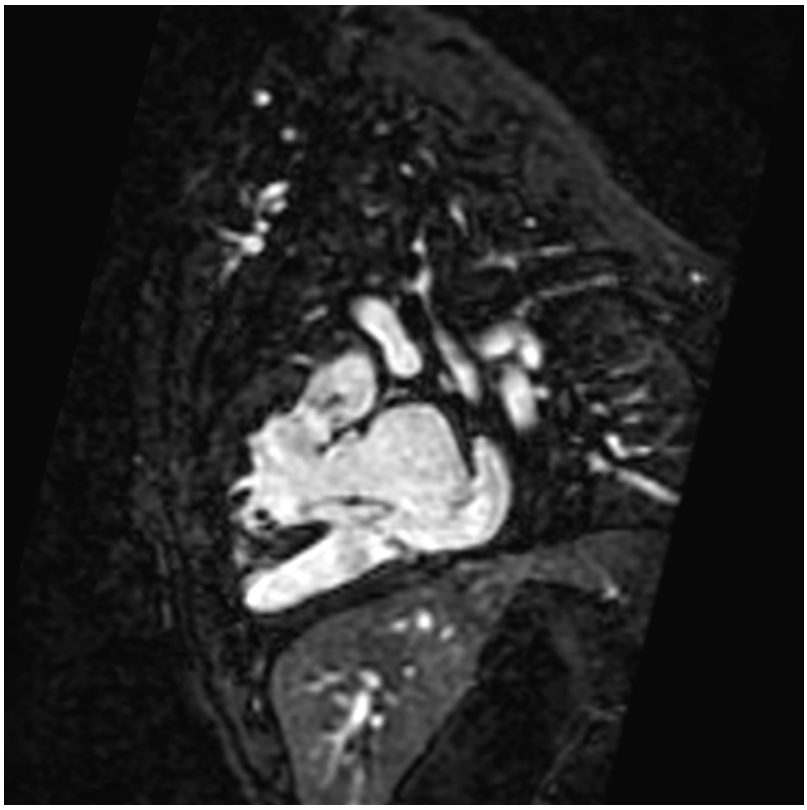

3D Whole Heart coronal oblique reformat demonstrating inferior left ventricle, superior right ventricle, and aortic valve

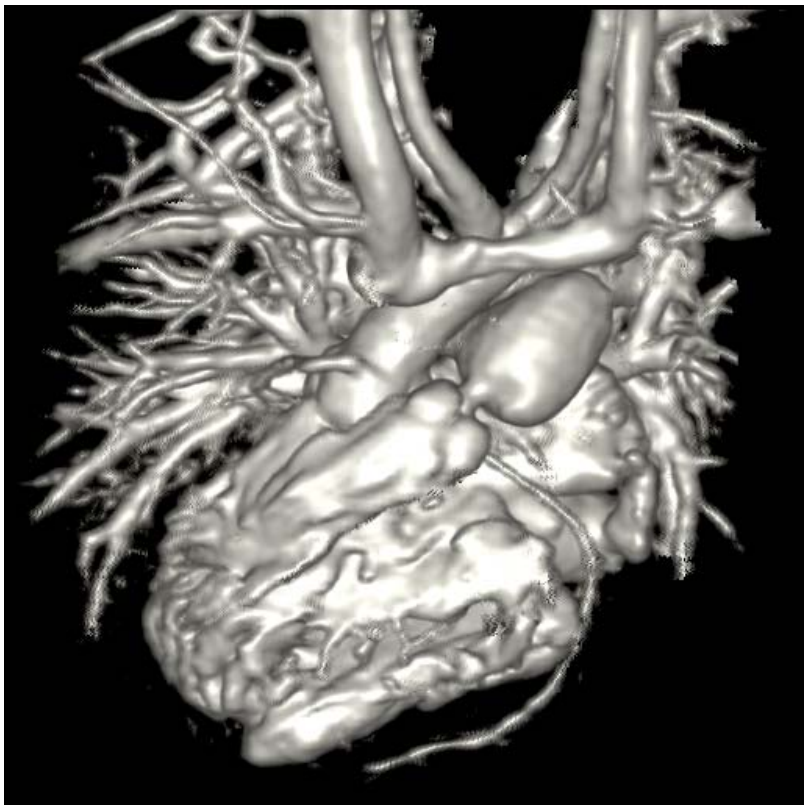

Anterior 3D reconstruction demonstrating posterior aorta and anterior banded main pulmonary artery both originating from the superiorly oriented right ventricle. Note left and right coronary arteries

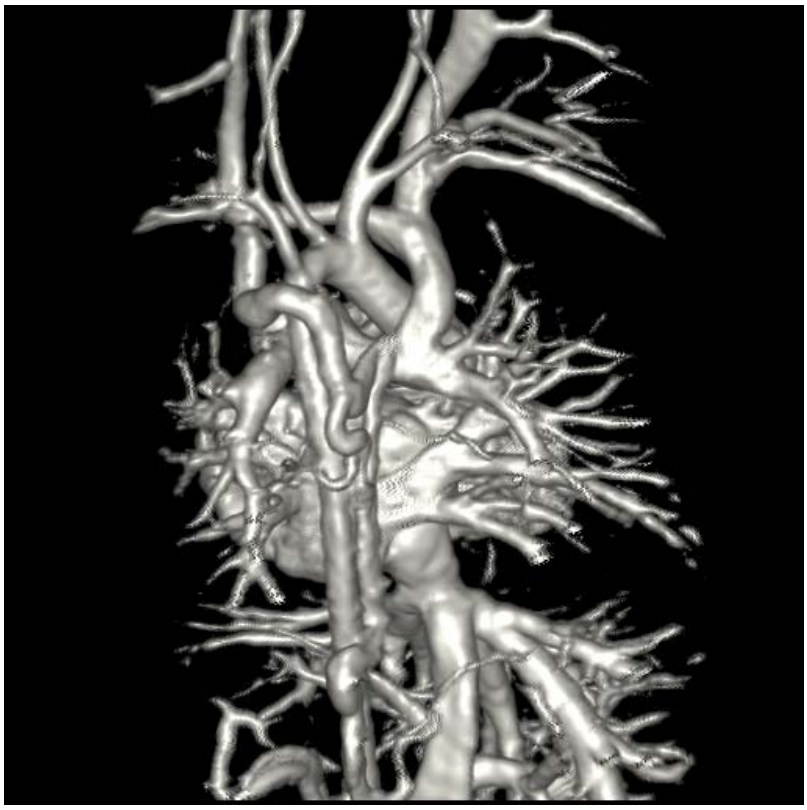

Posterior 3D reconstruction demonstrating Glenn shunt and decompressing veins. Note opacification of all extracardiac vascular structures

ID#: 367521

Advances in prediction of interventional outcome in univentricular hearts

Petter Frieberg, MD, MSc[1] Petru Liuba, MD, PhD[2], Marcus Carlsson, MD, PhD[3]

1. Lund University, Department of Clinical Sciences Lund, Clinical Physiology, Skane University Hospital, Lund, Sweden, Lund, Sweden

2. Lund University, Department of Clinical Sciences Lund, Pediatric Heart Center, Skane University Hospital, Lund, Sweden, Lund, Sweden

3. Lund University, Skane University Hospital, Department of Clinical Sciences Lund, Clinical Physiology, Lund, Sweden, Skane Lan, Sweden

Description of Clinical Presentation: We present two related cases in children with Fontan circulation where CMR acquisition of anatomy and flow was used in support of Computational Fluid Dynamic (CFD) simulations to predict an unfavorable outcome of an invasive Y-graft intervention and to evaluate a new endovascular device. The first case is a female 15 year old patient with univentricular heart and heterotaxy including bilateral superior vena cava (SVC) and absence of the hepatic segment of the inferior vena cava (IVC) with azygos continuation (Figure 1A). This patient had earlier Kawashima procedure followed by surgical implantation of an 18 mm Gore-Tex conduit between the hepatic veins and the left part of the central pulmonary artery (PA). Due to competitive flow, severe hypoplasia of the central PA developed, leading to hepatic flow circulation almost entirely to the left lung. Due to the lack of the hepatic flow to the right lung, widespread arterio-venous malformations in this lung developed subsequently with secondary symptomatic cyanosis. The patient`s hepatic conduit was surgically replaced with a bifurcated Y-graft with the intent to distribute hepatic blood equally to both lungs.

Diagnostic Techniques and Their Most Important Findings: CFD simulation predicted that there would be no flow in the right branch of the Y-graft (Figure 1B), which was later confirmed by post-op 4D CMR (Figure 1C). Consecutive follow-up CMR measurements over three years showed a continuous shift in Fontan inflows resulting in a small but increasing fraction of blood flowing in the right Y-graft branch (Figure 2). The most important findings are that acute post-op hemodynamics could be accurately predicted with CFD simulation based on pre-op CMR information, but changes probably due to circulatory adaptation affect the medium term redistribution of flows. The second case is a female 13 year old patient with univentricular heart with anatomy similar to the first case, and no hepatic blood flow to the contralateral lung (Figure 3A). Using CFD simulations and experiences from the previous patient, a Y-graft implantation was ruled out at the surgical meeting. We hypothesized that if the hypoplastic PA could be stent-dilated and hemiazygos flow could be reduced with an endovascular device (Figure 3B), some hepatic blood could reach the LPA. In close partnership with Occlutech (Occlutech GMBH, Jena, Germany), a prototype flow reducer for endovascular implantation was developed. Ethical approval was obtained for animal trials with device implantation in IVC and flow measurements in CMR. Two weeks post-implantation, a hemodynamic shift was seen from IVC toward SVC. In the patient CFD- and one-dimensional model, negligible acute changes were seen in the Fontan flows following device implantation. However, after approximating the redistribution seen in animal trials to the patient CFD model, 20-25% of the hepatic flow is predicted to pass through the dilated PA (Figure 3C). The most important findings are that CFD simulations can be used to design new treatment options and test them in silico before animal trials in Fontan patients.

Learning Points from this Case: We have learned that patient-specific CFD flow simulations can be very useful to predict acute post-interventional hemodynamic changes and to evaluate interventional options. Longer term flow distribution is harder to predict, making consecutive post-interventional CMR examinations invaluable. Results from complementary animal trials in combination with CFD can be translated to the patient scenario to try to estimate longer term flow redistribution.

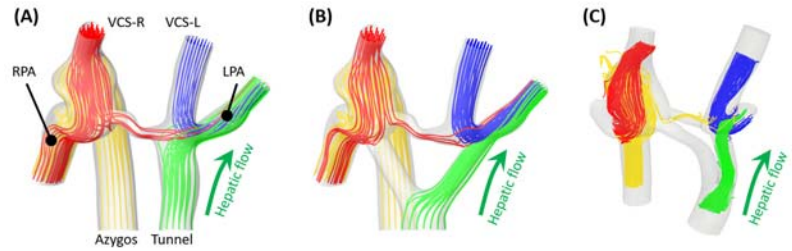

Figure 1: First case, pre-op Fontan flows with no hepatic flow to RPA (A). A computer simulation predicted that

there would be no flow in the right branch of a surgically implemented Y-graft (B), which was later confirmed by a post-op 4D CMR (C).

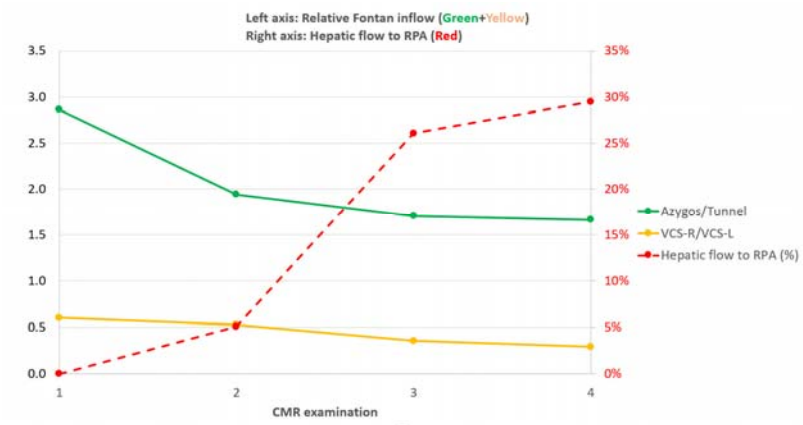

Figure 2: Consecutive post-op CMR flow measurements showed an unexpected increase of hepatic flow through the Y-graft to the RPA from 0% to 30% (Red). Inferior right-sided Fontan inflows have decreased significantly relative to inferior left-sided inflows (Green). A slight decrease is also seen in superior right-sided inflows relative to superior left-sided inflows (Yellow).

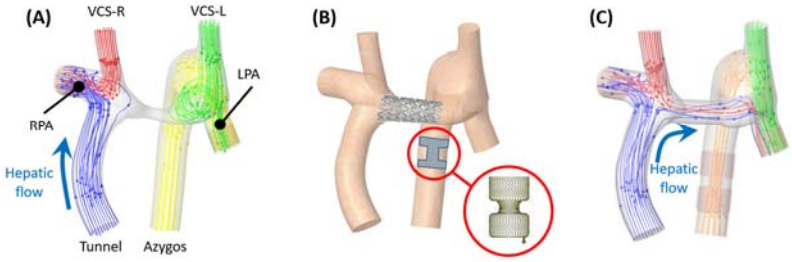

Figure 3: Second case, pre-op Fontan flows with no hepatic flow to LPA (A). The central PA is proposed to be dilated and an endovascular flow reducer to be implanted in the hemiazygos (B). Computer simulation based on flow redistribution seen in animal trials predict that hepatic blood then could reach the LPA (C).

ID#: 367179

Pixel-wise Quantitative Stress Perfusion Imaging of Coronary Microvascular Dysfunction

David Corcoran, MBChB BSc (Hons)[1] Vanessa Orchard[2], Tom Ford, MBChB (Hons), FRACP[3], Li-Yueh Hsu, D.Sc.[4], Andrew E. Arai, MD[5], Colin Berry, PhD FRCP[1]

1. University of Glasgow, Glasgow, Scotland, United Kingdom

2. Golden Jubilee National Hospital, United Kingdom

3. University of Glasgow, United Kingdom

4. National Heart, Lung and Blood Institute, National Institutes of Health

5. National Heart, Lung and Blood Institute, National Institutes of Health, Bethesda, MD

Description of Clinical Presentation: A 49-year-old female patient gave a 5-year history of typical Canadian Cardiovascular Society class 2 anginal symptoms. The patient had no traditional risk factors for obstructive epicardial coronary artery disease. At exercise electocardiography testing, the patient performed 12 minutes of a full Bruce protocol, developing 1mm down-sloping infero-lateral ST-segment depression from stage 3. At initial presentation 5 years previously, she had undergone invasive coronary angiography which demonstrated unobstructed epicardial coronary arteries. Given her ongoing symptoms despite 3 anti-anginal agents, the patient was referred to our institution for coronary physiology testing to investigate for coronary microvascular dysfunction as the cause of her angina.

Diagnostic Techniques and Their Most Important Findings: Invasive diagnostic coronary angiography again demonstrated smooth unobstructed epicardial coronary arteries (Figure 1). We proceeded to invasive coronary physiology testing of the left anterior descending artery (Figure 2). Coronary microvascular resistance was borderline elevated (Index of microcirculatory resistance = 25), and coronary epicardial and microvascular vasodilatory function was impaired (coronary flow reserve = 1.7). Invasive coronary endothelial function testing with acetylcholine was normal (Figure 2). These metrics are consistent with coronary microvascular dysfunction. The patient subsequently underwent adenosine stress perfusion CMR at 1.5T. SSFP cine imaging confirmed a structurally normal heart with preserved left ventricular function (LVEDVi = 85ml, LVESVi = 31ml, LVEF = 63%). There was no myocardial fibrosis on late gadolinium enhancement imaging. Dual-sequence SSFP perfusion imaging was performed following intravenous adenosine stress (140 µg/kg/min for 3 minutes) and again at rest 15 minutes later. Myocardial blood flow (MBF) was quantified on a pixel-by-pixel basis from the perfusion images using a modified Fermi-constrained deconvolution algorithm. Qualitatively, there was an inducible circumferential subendocardial perfusion defect, most marked in the basal myocardial segments (Figure 3). The global stress MBF was reduced (1.9 ml/g/min), and the global myocardial perfusion reserve (MPR = stress MBF/rest MBF) was reduced at 1.7, consistent with the invasively measured CFR.

Learning Points from this Case: This case demonstrates the clinical utility of pixel-wise quantitative stress perfusion CMR in patients with angina, non-invasive evidence of ischaemia, and angiographically unobstructed epicardial coronary arteries. This clinical entity is termed ischaemia and no obstructive coronary artery disease (INOCA), and is recognised as a condition of unmet clinical need. Stress perfusion CMR in these patients complements invasive tests of coronary microvascular function, by confirming the non-invasive evidence of inducible myocardial ischaemia, and allowing accurate quantification of ischaemic burden. In future, this technique may be used to track treatment response to novel therapeutics for patients with coronary microvascular dysfunction.

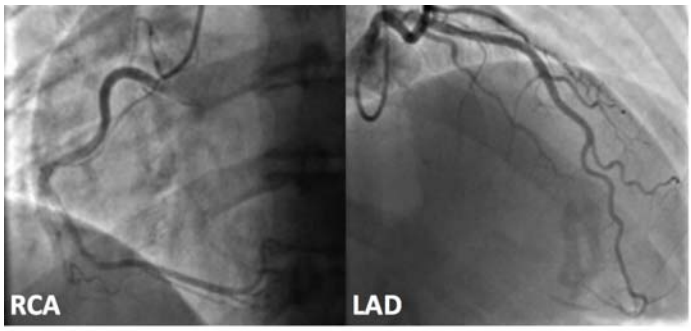
RCA
LAD

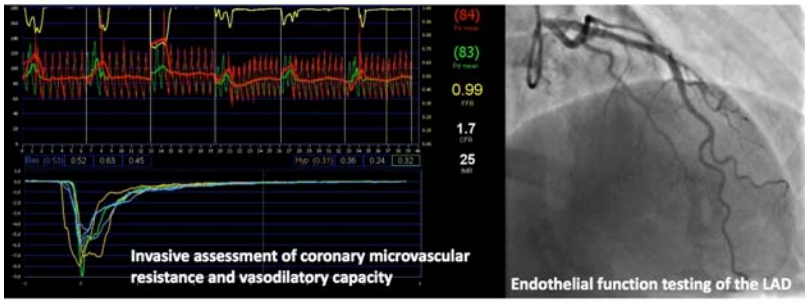
(84)
(83)
0.99
1.7
25
Invasive assessment of coronary microvascular resistance and vasodilatory capacity
Endothelial function testing of the LAD

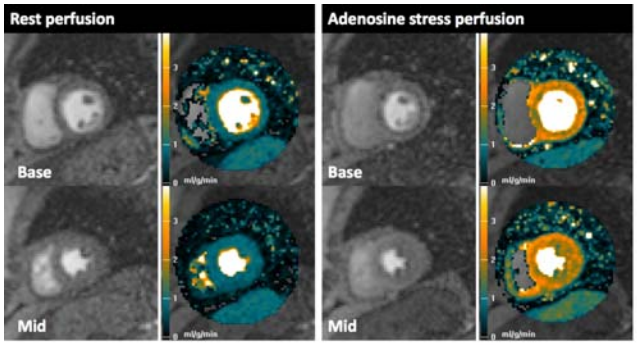
Rest perfusion
Adenosine stress perfusion
Base
Base
Mid
Mid

ID#: 357136

Resting perfusion defect in a case of acute fulminent myocarditis

Yue-Hin Loke, MD[1] John Berger, III, M.D.[2], Laura Olivieri, M.D.[3]

1. Children's National Health System, Washington Dc, DC

2. Children's National Medical Center

3. Children's National Medical Center, Washington, DC

Description of Clinical Presentation: Patient is a previously healthy 13-year-old year old female who presented with acute onset of fevers and chest pain, hemodynamically stable. Her EKG demonstrated ST segment elevation in the lateral leads, with elevated troponin (29ng/mL), and echocardiogram findings of mildly decreased systolic function (left ventricular ejection fraction = 50%) with apical hypokinesis. She was admitted to the hospital for continued observation and workup.

Diagnostic Techniques and Their Most Important Findings: 24 hours into admission, cardiovascular magnetic resonance (CMR) was performed with Siemens 1.5T scanner to obtain volumetry, T2-weighted imaging, myocardial perfusion, early gadolinium enhancement (EGE) and late gadolinium enhancement (LGE). Gadolinium-based contrast was administered at 0.15 mmol/kg via peripheral IV for enhancement imaging.

Cine steady-state free procession (SSFP) images demonstrated mildly depressed left ventricular function, with akinesis in the apical lateral wall. T2-weighted imaging demonstrated left ventricular myocardial edema in the long and short axis at the apex of both ventricles. A moderate-sized subendocardial resting perfusion defect was visible (Figure 1) in the akinetic apical lateral wall qualitatively and using the quantitative perfusion map. In this same territory, there was mild subendocardial EGE and a region of subendocardial LGE. Additional regions of patchy, atypical LGE were seen in the basal to mid inferoseptum as well.

In light of the atypical finding of a subendocardial perfusion defect, the patient underwent cardiac catheterization for endomyocardial biopsy and coronary angiography. Selective angiography of both coronary arteries demonstrated normal coronary artery patterns with good visualization of the coronary tree and no filling defects. Biopsies demonstrated significant lymphocytic and histiocytic inflammation with muscle damage, consistent with acute myocarditis.

Over the next day, the patient experienced rapidly progressive cardiac dysfunction and ventricular arrhythmia, requiring extracorporeal mechanical oxygenation support for four days. She experienced frequent arrhythmias including polymorphic ventricular tachycardia and complete heart block. Her clinical status improved over two weeks, and by discharge her systolic function had normalized on echocardiogram and she had no ventricular ectopy. A repeat CMR was undertaken for prognostication purposes which demonstrated resolution of the T2-weighted abnormalities and resting perfusion defect (Figure 2). There was a decrease in the LGE territory with resolution of the septal LGE, and persistence of the subendocardial LGE and regional wall motion abnormality previously seen at the apex.

Learning Points from this Case: This case demonstrates a rare incident of how the hallmark features of myocarditis on MRI (myocardial edema, hyperemia and myocyte fibrosis) were seen with a classic subendocardial infarction and resting perfusion defect, which are very atypical in myocarditis. The subendocardial resting perfusion defect and LGE, raised concerns for possible focal coronary artery disease despite the heterogenous and subepicardial involvement seen in the rest of the heart. Her cardiac catheterization demonstrated a clean coronary tree, and ultimately, the patient';s clinical course was consistent with acute fulminant myocarditis with complete recovery. Infarct-like patterns on LGE imaging in clinical myocarditis have been reported in adults in the past, but are very rare in the pediatric population.

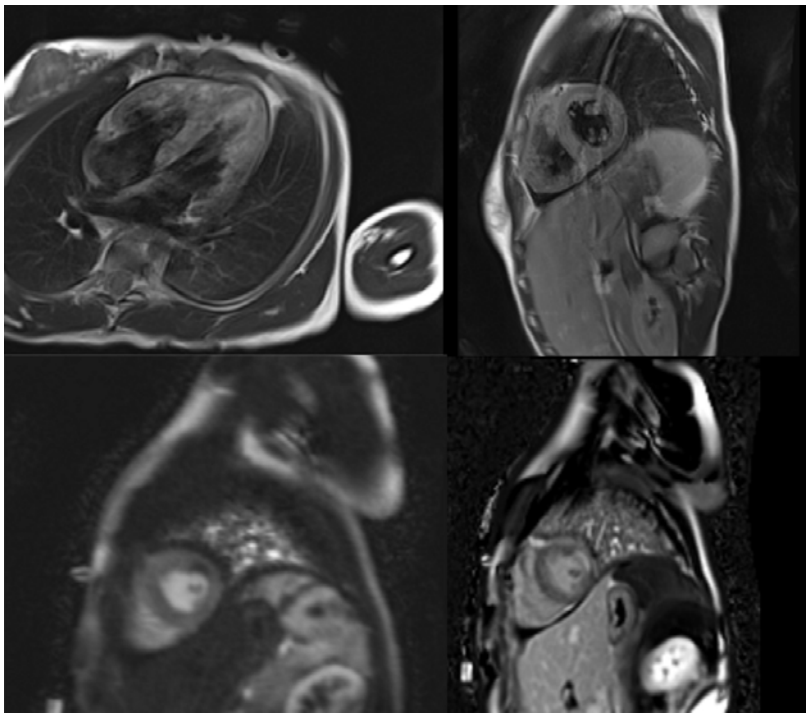

Figure 1. Initial MRI scan on presentation.

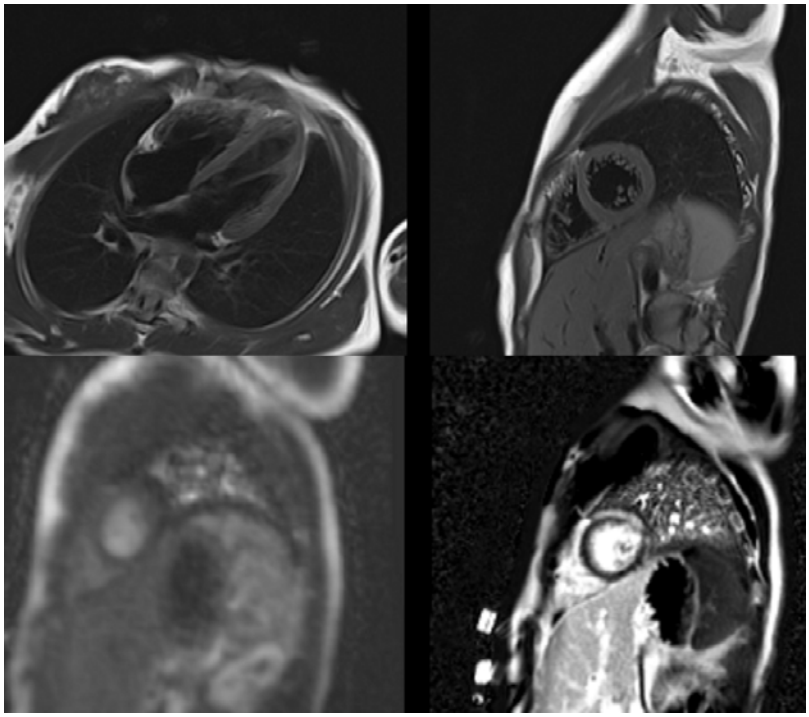

FIgure 2. Follow-up MRI scan two months later.

ID#: 363919

Chronic Intramyocardial Hemorrhage Detected by T1 and T2 star Mapping after Reperfusion of ST-Segment-Elevation Myocardial Infarction: A Case Report

Yohei Yamauchi[1] Yumiko Kanzaki[2], Kenichiro Yamamura[2], Masako Yuki[2], Masaaki Hoshiga[2]

1. Osaka Medical college, Takatsuki, Osaka, Japan

2. Osaka medical college, Japan

Description of Clinical Presentation: A 63-year-old male was admitted to our institute for 3 hours of prolonged chest pain. The electrocardiogram showed ST-segment elevation in leads I, aVL, and V1–V6, with reciprocal ST-segment depression in leads III and aVF (Figure 1). Furthermore, transthoracic echocardiography revealed severe hypokinesis in the anterior wall of the left ventricle and a left ventricular ejection fraction of 40%. Emergency coronary angiography demonstrated that the proximal portion of the left anterior descending coronary artery had an acute thrombus with delayed antegrade coronary artery flow [Thrombolysis in Myocardial Infarction (TIMI) grade 1]. After a successful primary percutaneous coronary intervention with a drug-eluting stent (duration of ischemia < 4 hours), TIMI grade 2 flow was achieved. The peak creatine kinase concentration was 9224 U/L with creatine kinase-MB fraction of 561 U/L at 4 hours after coronary reperfusion. He remained symptom-free for 4 months under medical treatment after acute myocardial infarction, and underwent cardiovascular magnetic resonance (CMR) for myocardial tissue characterization.

Diagnostic Techniques and Their Most Important Findings: CMR was performed on a 3-Tesla scanner (Ingenia; Philips Medical Systems, Best, the Netherlands) using a 32-channel phased-array cardiac coil. A late gadolinium enhancement (LGE) image revealed *a* transmural area of hyperenhancement (white arrow) in mid-anterior wall and anterior-septum (Figure 2A). T2 star mapping revealed a hypointense region (black arrow) in the midcardium of the anterior-septal wall, suggesting intramyocardial hemorrhage (IMH) (Figure 2B, 2C). Native T1 mapping clearly detected a low T1 value corresponding to the area of IMH on T2 star map (Figure 2D).

Learning Points from this Case: IMH detected by the combination LGE and T2 star imaging reflects severe reperfusion injury in ST segment elevation myocardial infarction (STEMI) and is associated with a larger myocardial infarction size, adverse left ventricular remodeling, and worse clinical outcomes. Native T1 mapping, in this case, could detect IMH after reperfusion for STEMI. Notably, native T1 mapping without an intravenous contrast agent might have the potential of detecting IMH, even in the chronic phase.

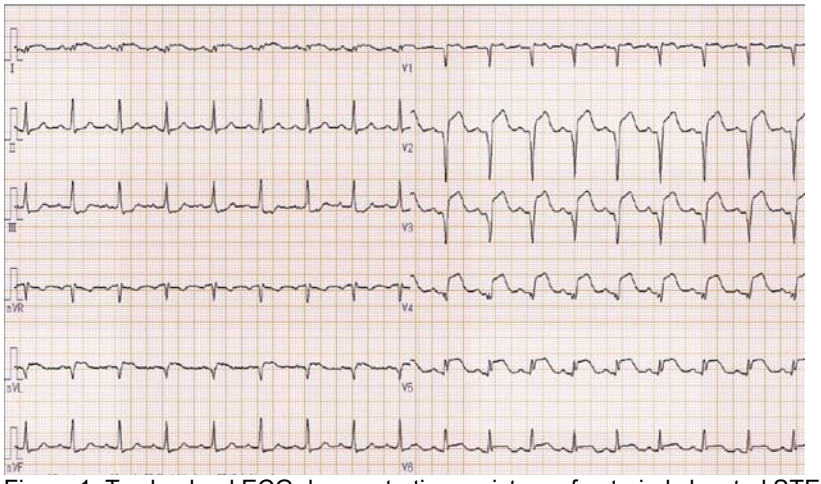

Figure 1. Twelve-lead ECG demonstrating a picture of anteriorly located STEMI.

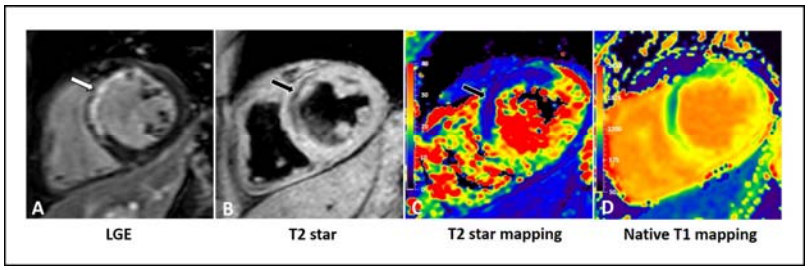

Figure 2. Middle left ventricular short axis of the patient with LGE, T2 star, and T1 mapping images.

ID#: 365476

Utilization of 4D Flow for evaluation of adult congenital heart disease: a case of congenital pulmonary atresia status post repair

Melany B. Atkins, MD

Fairfax Radiological Consultants, Inova Fairfax Hospital, Arlington, VA

Description of Clinical Presentation: 28 year old female patient with history of congenital pulmonary atresia and neonatal hypoplastic right ventricle status post balloon atrial septectomy, balloon pulmonary valvotomy and BT shunt placement. This was followed by BT shunt takedown, atrial septal patch, and surgical pulmonary valvotomy with excellent results. A recent echocardiogram demonstrated mild right ventricular dilatation, tricuspid regurgitation and pulmonic regurgitation. The patient was sent for cardiac MRI to evaluation ventricular volumes, pulmonary regurgitant fraction, tricuspid regurgitant fraction, central pulmonary artery evaluation, and evaluation of scar.

Diagnostic Techniques and Their Most Important Findings: 3T MRI on a GE Signa Architect Magnet was performed utilizing multiplanar Fiesta Imaging, 4D Flow, post-contrast dynamic MRA, and phase sensitive MDE. A dual injection of 20ccs gadobutrol and 5.5ccs (3mg/kg) of Ferumoxytol was utilized. Scan time 41 minutes. Post-processing performed via Arterys. 4D flow produces both magnitude and phase images reconstructable in any 3D plane in a scan time in this patient of 9 minutes 53 seconds. The utilization of a blood pool agent allows for improved contrast and resolution which affords for better myocardial contouring for functional analysis from the 4D Flow sequence. The function was calculated utilizing both traditional short axis fiesta images and the 4D flow sequence demonstrating no significant difference in volume or functional measurements. Pulmonary regurgitant fraction and tricuspid regurgitant fraction were also calculated via 4D Flow.

The images demonstrate mild right ventricular dilatation with an end diastolic volume index of 111 ml/m2. The pulmonary regurgitant fraction was calculated to 22%. The tricuspid regurgitant fraction was calculated to 22% utilizing the valve tracking feature on Arterys. There is no residual pulmonic stenosis or branch pulmonary artery stenosis.

Learning Points from this Case: Utilizing 4D Flow for acquisition of all flow data allows for decreased scan time, requires less physician supervision, requires no breath holding, and allows for accurate flow analysis. In addition, given the whole heart coverage, flow can be measured at any data point in the coverage window after the fact. Although function was calculated utilizing both 4D flow and traditional short axis fiesta images, additional scan time could be saved by only acquiring function via the 4D Flow sequence.

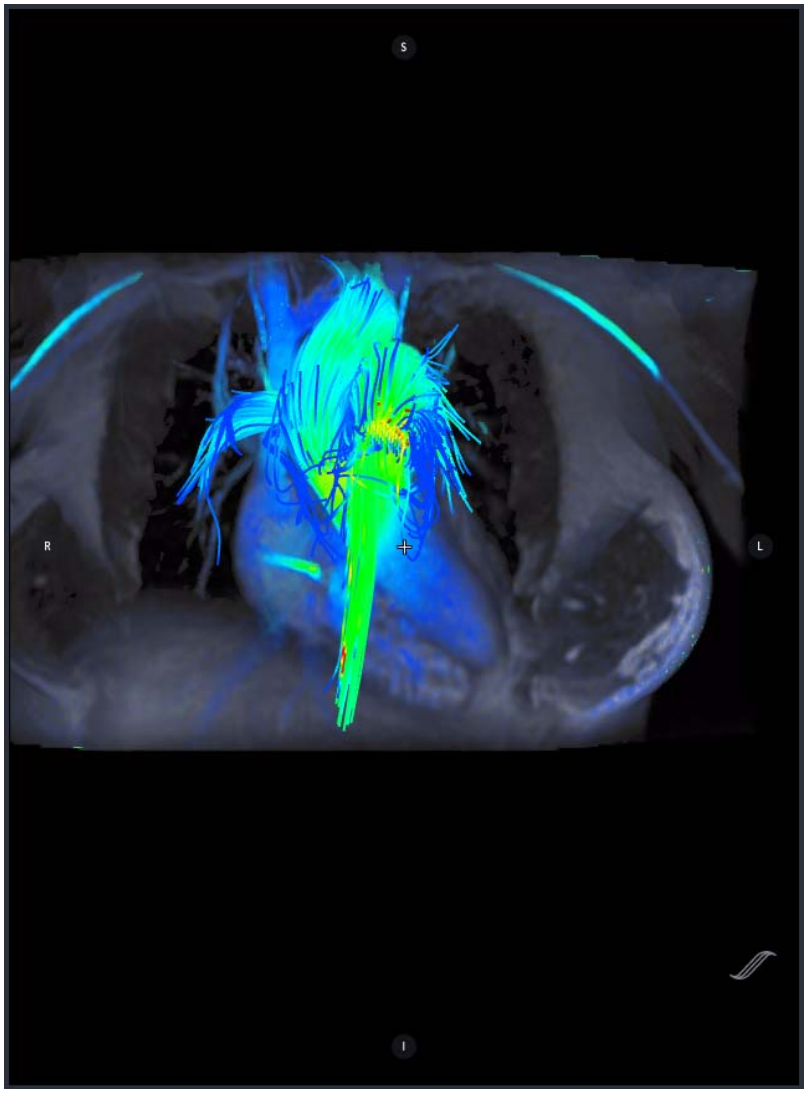

4D flow 3D images demonstrating mild right ventricular dilatation and tricuspid regurgitation.

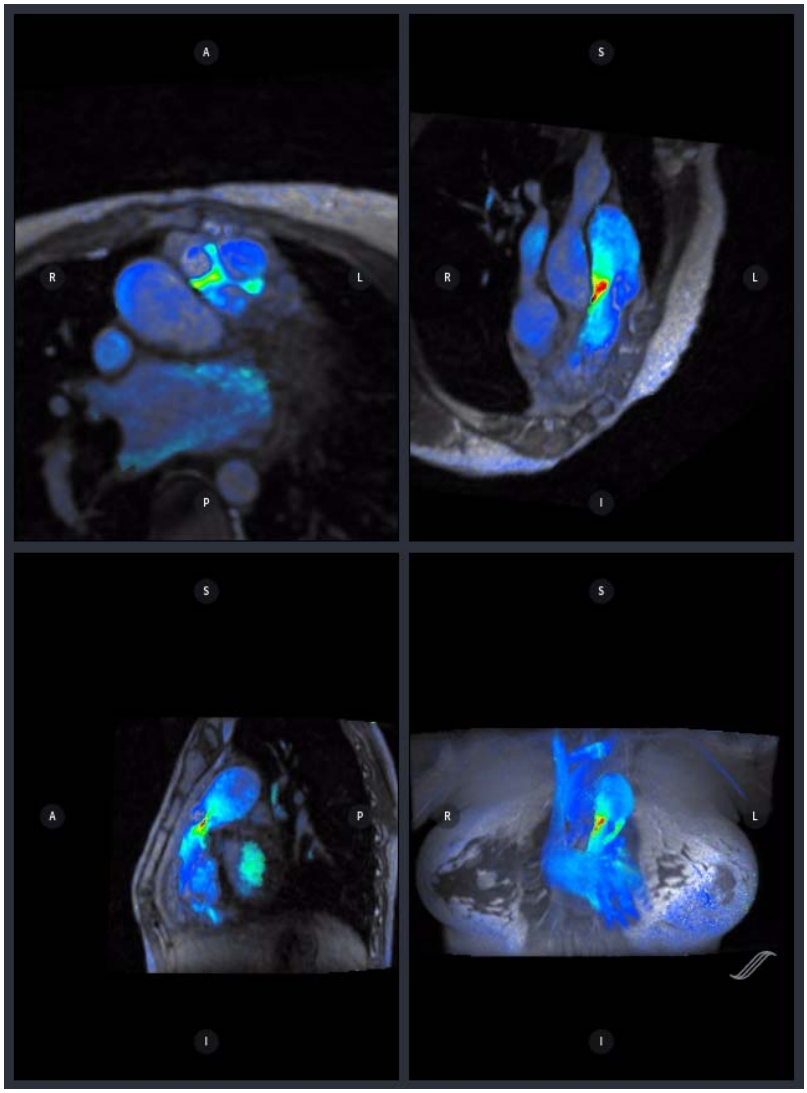

3D and oblique 4D flow images demonstrate pulmonic regurgitation with a regurgitant fraction of 22%. No significant residual pulmonic stenosis.

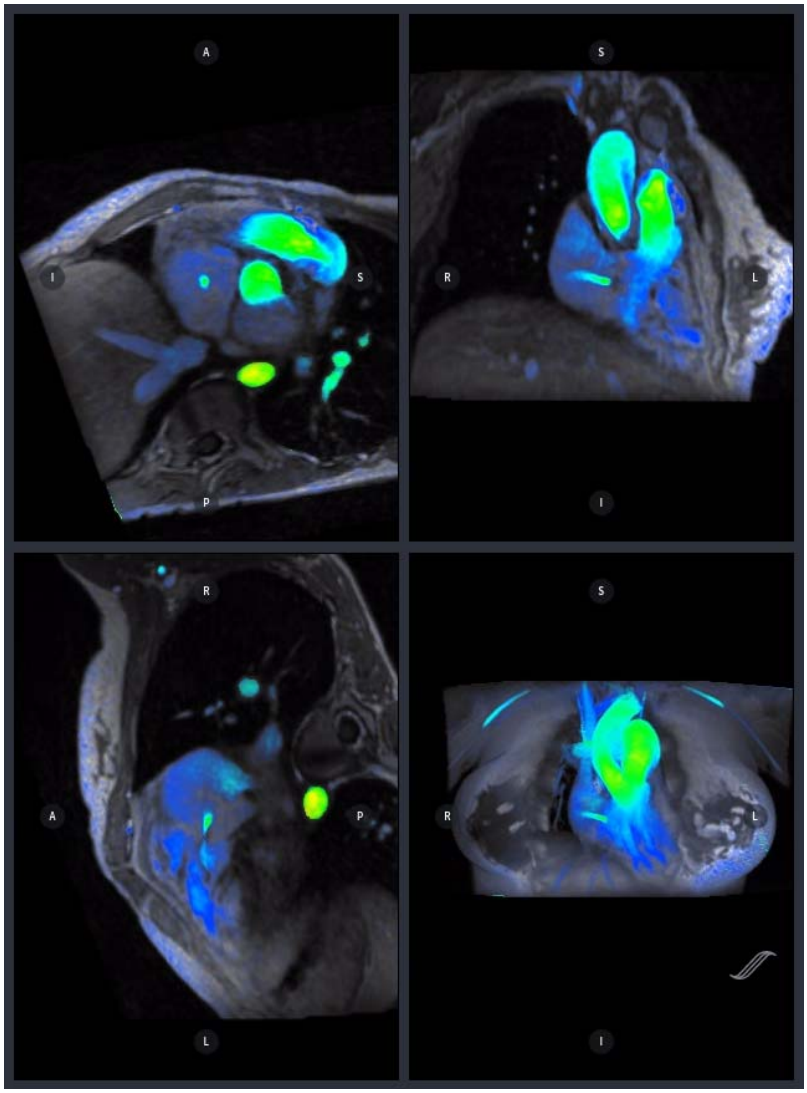

3D and oblique 4D flow images demonstrating tricuspid regurgitation with a regurgitant fraction of 22%.

ID#: 371267

Primary pericardial hydatidosis (Echinococcoccosis): a great mimicker.

Manphool Singhal[1]Paramjeet Singh[2], Subhash Varma[3], Sanjay Jain, MD DM[4], Sachin Mahajan[4]

1. Post Graduate Institute of Medical Education and Research, Chandigarh. India. 160012, Chandigarh, Chandigarh, India

2. Post Graduate Institute of Medical Education and Research, Chandigarh. India. 160012, India

3. Post Graduate Institute of Medical Education and Research. Chandigarh. India. 160012, Chandigarh, Chandigarh, India

4. Post Graduate Institute of Medical Education and Research. Chandigarh. India. 160012, India

Description of Clinical Presentation: 37 year female presented with complaints of dull aching chest pain shortness of breath and low grade fever for 4 weeks. Cardiovascular and respiratory system examination were normal. Electrocardiographic (ECG), cardiac enzymes, hemogram and blood cultures were unremarkable.

Diagnostic Techniques and Their Most Important Findings: Posterior-anterior chest radiograph showed cardiomegaly, convex aorto-pulmonary window with a peripherally calcified mass like lesion. 2D- transthoracic echocardiogram revealed a cyst like lesion adjacent to the left ventricle, but it could not assess further due to calcifications. A differential diagnosis of a teratoma, peripherally calcified loculated pericardial effusion (tubercular), calcified pulmonary artery or left ventricle aneurysm was considered. CT demonstrated a well marginated, thick peripherally calcified cystic lesion adjacent to free wall of left ventricle. MRI characterized the lesion with typical internal membranes and T2 hypointense wall that did not show contrast enhancement confirming diagnosis of pericardial hydatid cyst with impending rupture. Positive hydatid serology (1:1600) further substantiated the diagnosis. Ultrasound abdomen did not reveal any other cyst confirming it to be an isolated pericardial hydatid cyst. The cyst was excised and histopathology confirmed the radiological diagnosis.

Learning Points from this Case:

1. Isolated pericardial hydatidosis is an extremely rare disease and can have vivid clinical presentation.
2. It a great mimicker of cardiac mass and calcified aneurysms.
3. Cardiac MR is diagnostic with characteristic findings of a cystic lesion with internal membranes, T2 hypointense wall that does not enhance on post contrast imaging.

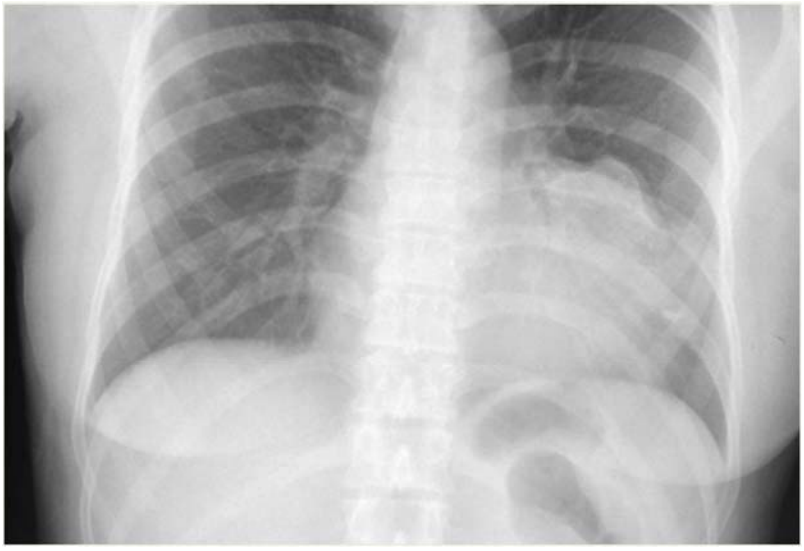

Figure 1:- Posterio-anterior chest radiograph shows cardiomegaly, convex aorto-pulmonary window with a peripherally calcified mass like lesion silhouetting left cardiac border.

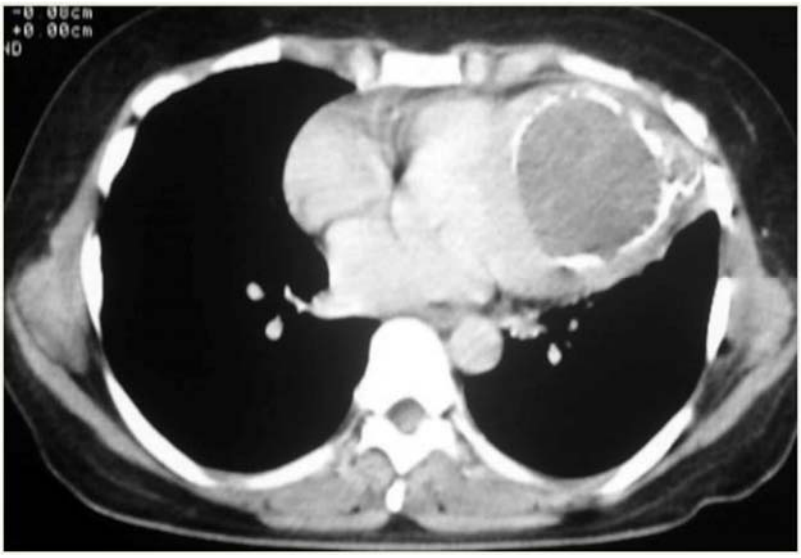

Figure 2:- Axial contrast enhanced computed tomography (CT) image shows a well marginated, peripherally calcified cystic lesion adjacent to free wall of left ventricle.

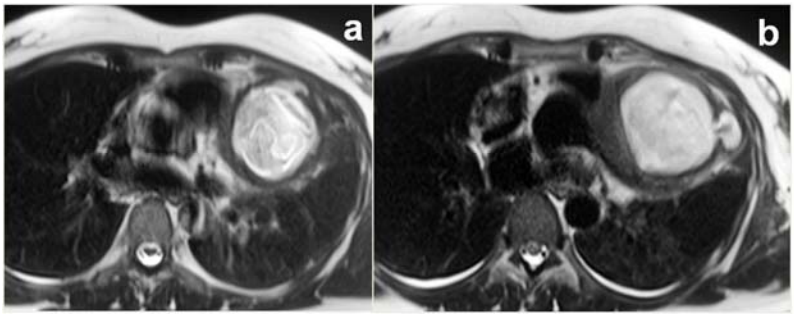

Figure 3:-Black blood T2-HASTE axial cardiac MRI images show a cystic lesion with typical internal membranes (a) T2 hypointense wall (a &b). Note protrusion of internal contents through pericyst on lateral aspect (b) suggesting impending rupture.

ID#: 371041

Unusual Cause of Chest Pain

Tatiana Stipalova, 1st Department of Internal Medicine/Cardioangiology, St. Anne´s Faculty Hospital and Masaryk University, Brno, Czech Republic[1]Roman Panovsky, International Clinical Research Center, 1st Department of Internal Medicine/Cardioangiology[2], Michal Rezek, 1st Department of Internal Medicine/Cardioangiology, St. Anne´s Faculty Hospital and Masaryk University, Brno, Czech Republic[3], Vera Feitova, International Clinical Research Center, Department of Medical Imaging[2]

1. International Clinical Research Center, St. Anne´s Faculty Hospital, Brno, Czech Republic, Bilovice Ned Svitavou, Czech Republic

2. St. Anne´s Faculty Hospital, Brno, Czech Republic, Czech Republic

3. 1st Department of Internal Medicine/Cardioangiology, St. Anne´s Faculty Hospital and Masaryk University, Brno, Czech Republic, Brno, Czech Republic

Description of Clinical Presentation: A 58-year-old woman presents to cardiology department with a week of chest pain in the left precordium without any radiation. She denies dyspnoea, nausea, vomiting, fevers or chills. Her medical history includes total thyroidectomy due to struma nodosa and parathyroid adenoma extirpation both 9 years ago with benign histology findings. Currently her medication includes levothyroxine and for last 2 days cefuroxime for an acute bronchitis. Physical examination revealed normal vital signs. Electrocardiogram shows sinus rhythm with heart rate 80 beats per minute, incomplete right bundle branch block and inverted T waves in precordial leads. Laboratory findings showed elevated high sensitive troponin T 101 ng/l (cut off 14 ng/l)

Diagnostic Techniques and Their Most Important Findings: A coronary angiogram demonstrated no significant stenosis of coronary arteries. An echo revealed a suspicious mass in the apex of right ventricle and interventricular septum. The patient underwent cardiac magnetic resonance where 2 pathologic masses were described, first in the apex of right ventricle spreading to the apical part of interventricular septum and surrounding pericardium, the second mostly in the pericardium next to the basis of right vetricle and right atrium. This highly suspected tumorous masses couldn';t be surgically removed. Endomyocardial biopsy confirmed the diagnosis of diffuse large B-cell lymphoma and the patient was immediately transferred to the hemato-oncology department to start the combination of chemotherapy. Follow up echo 2 months later showed significant reduction of the mass, patient is clinically stable, scheduled for further evaluation.

Learning Points from this Case: The importance of advanced cardiac imaging for clarification of unusual cause of chest pain with elevated cardiac markers and normal coronary angiogram.

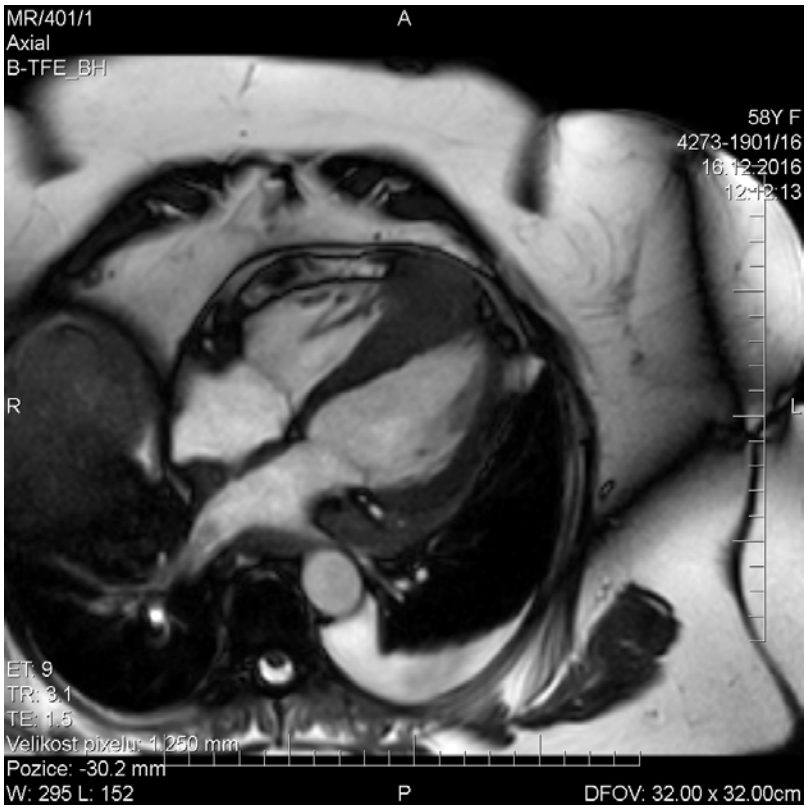

Infiltrative mass in balanced turbo field-echo sequence

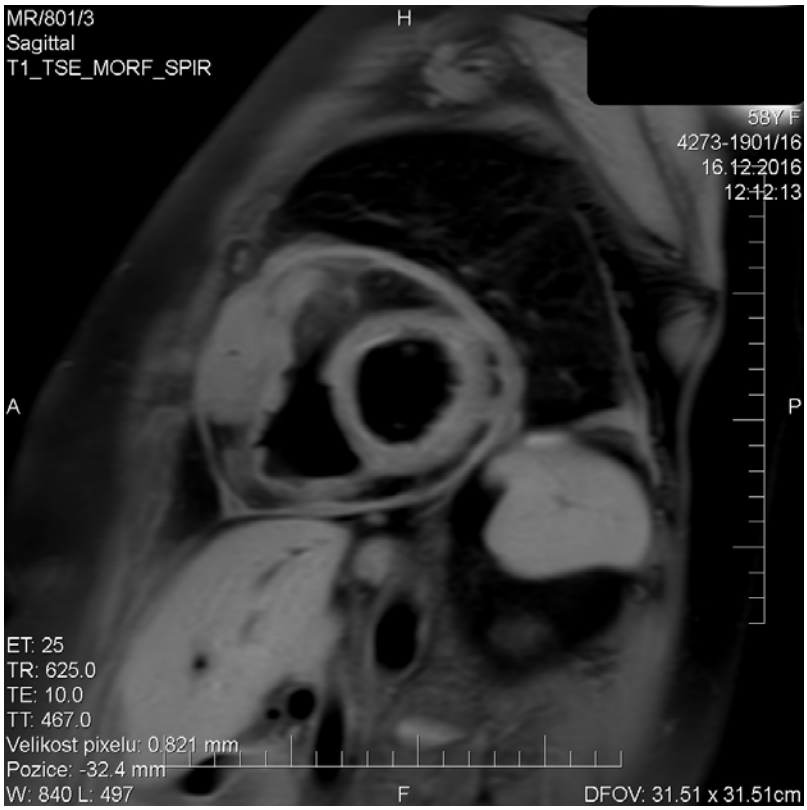

Tumorous mass affecting free wall of the right ventricle in T1 sequence

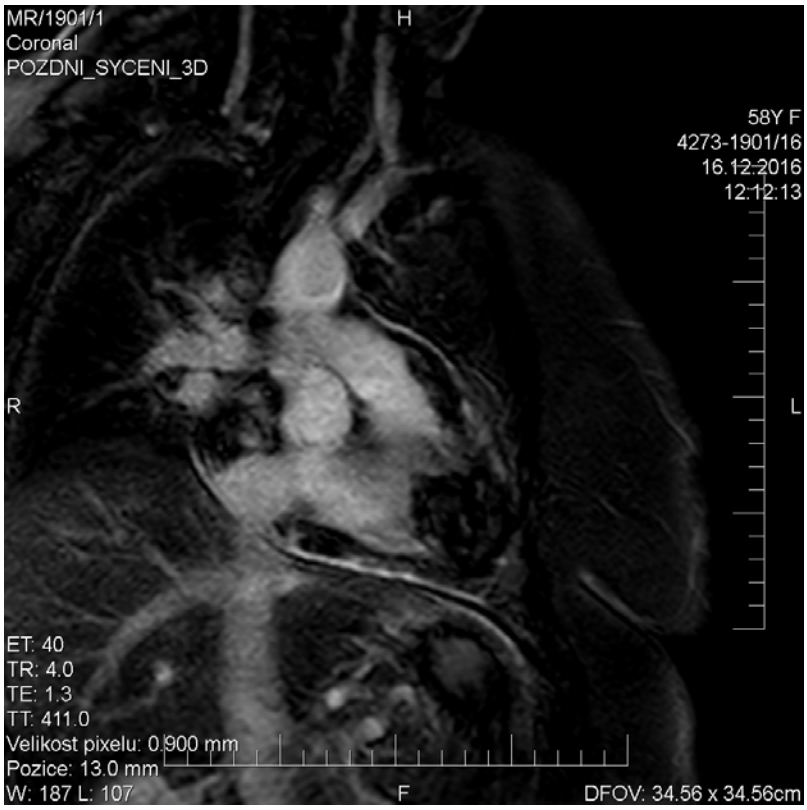

Absence of gadolinium deposition in the tumorous mass in LGE sequence

ID#: 370892

Tuberculous Pericarditis. From overt pathology to healing. Insights from CMR

Enric Cascos-Garcia[1]Albert Teis[2], Francisco Gual-Capllonch[3], Gladys Junca[4], Angel Caballero[3], Antoni Bayes-Genis, Department of Medicine, Universitat Autònoma de Barcelona, Barcelona[3]

1. Hospital Universitari Germans Trias i Pujol. Badelona. Barcelona, Barcelona, Spain

2. Hospital Universitari Germans Trias. Badalona. Bacelona. Spain., Badalona, Spain

3. Hospital Universitari Germans Trias i Pujol, Spain

4. Hospital Universitari Germans Trias i Pujol. Badelona. Barcelona, Spain

Description of Clinical Presentation: A 35 years-old african man with history of not treated malaria arrived to emergency department due to abdominal pain, fever and constitutional syndrome. Physical examination revealed signs of right heart failure. Chest X-Ray showed increase of cardiac silhouette. Completed blood tests were performed, being HCV, HBV, HIV, CMV, Parvovirus, Toxoplasma and Syphilis all negative. Autoimmunity test were also negative. Mantoux test was positive, but sputum culture was negative. Chest-TC exam showed thoracic adenopathies and high densitiy pericardial effusion. Biopsy of the adenopathies was performed, but histology was non-diagnostic. A transthoracic echocardiogram showed pericardial space fullfilled by high density material and signs of constriction. All this prompted a cardiac MR study (see below). CMR findings suggested a pericardial inflammatory process. Pericardial biopsy was performed through minithoracotomy. Anatomopathologycal histology was compatible with tuberculosis infection. Tuberculostatic treatment was started and right heart failure signs resolved few months after. Follow-up CMR was performed; all pathologic finding resolved (see below).

Diagnostic Techniques and Their Most Important Findings: A complete CMR study was performed. Breath hold and free breathing SSFP-cine images were performed at standanrd 2ch, 3ch, 4ch and short axis projections. Peridardium space was fully infiltrated by an homogeneous mass (fig 1A). Mid-ventricular septal bounce and superior and inferior vena cava dilatation were detected. Mid lateral left-ventricular wall motion was partialy restricted due to infiltration. The mass was highly hyperintense on T2-weighted images (Fig 1B) and slightly hyperintense on T1-weighted images (fig 1C). It was not perfused, but presented severe heterogeneous enhancement 10 minutes after injection of gadolinium-derived contrast agent (Gd). Moreover, mid lateral left ventricular subepicardial enhencement was detected (fig 1D).
Follow-up study after treatment showed complete resolution of the pericardial infiltration, with no pericardial thickening and no signs of constriction (Fig 2A, 2B). Only mild enhancement of the pericardium was detected 10 minuts after Gd injection (fig 2C).

Learning Points from this Case: Tuberculosis is a known cause of constrictive pericarditis. However, if treated at a very early stage of the disease, constriction physiology could not be present or even disappear. The present case is demonstrative of the MRI appearance of acute pericardial tuberculosis and its evolution after correct treatment.

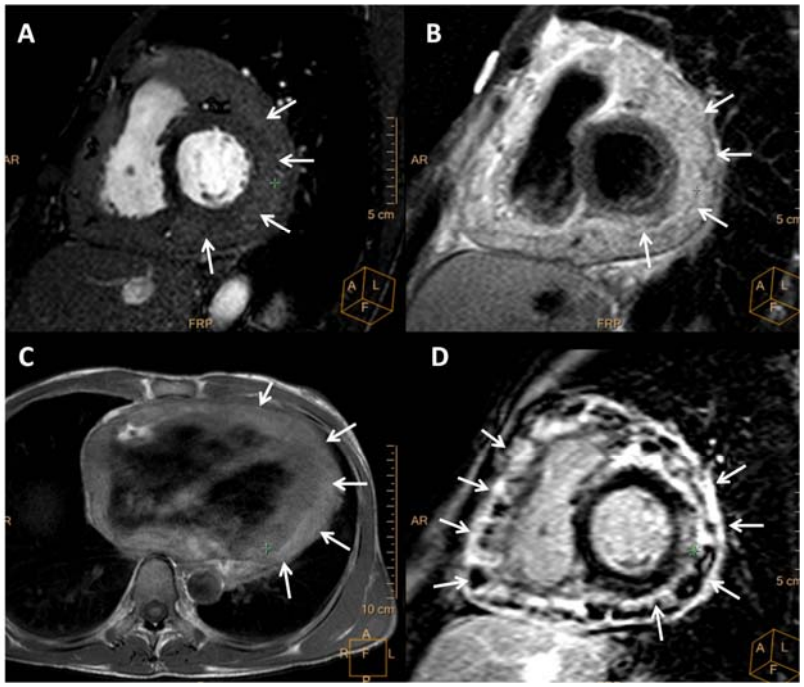

Basal CMR

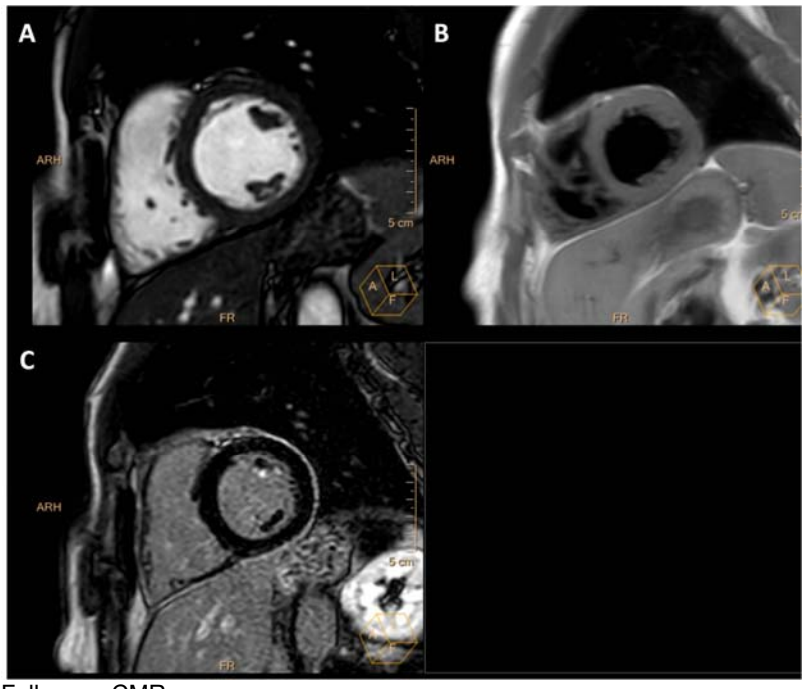

Follow-up CMR

ID#: 371568

Could CMR guide the surgical plan in patients with transposition of the great arteries?

Mahmoud N. Shaaban, MBBCh, MSc.[1] Sameh Khalil, MSc[2], Fatma R. Elkafrawy, MBBCh, MSc.[3], Dina Haroun, MBBCh,MSc[4], Ahmed M. Ismail[5], Hatem Hosny[6], Wesam E. El Mozy, MD, MSc[7], Soha Romeih, MD,PhD, FESC[8]

1. Aswan Heart Center (Magdi Yacoub Foundation) - Cardiology department, Tanta University, Tanta, Al Gharbiyah, Egypt

2. Aswan Heart Center - Magdi Yacoub Foundation, Cairo, Egypt

3. Radiology fellow at Aswan Heart center (Magdi Yacoub Foundation) -Assistant Lecturer at Radiology Dep., Alexandria university, Aswan, Aswan, Egypt

4. Radiology fellow Aswan Heart Center (Magdi Yacoub Heart Foundation),assistant lecturer Radiology department - Kasr Al Ainy Cairo university., Egypt

5. Aswan Heart Center - Magdi Yacoub Foundation, Egypt

6. Aswan Heart Centre, Aswan, Egypt

7. Magdi Yacoub Foundation - Aswan Heart Centre, Aswan, Egypt

8. Aswan Heart Centre, Egypt

Description of Clinical Presentation: Transposition of great arteries (TGA) with ventricular septal defect (VSD) and left ventricle outflow tract obstruction (LVOTO) can present challenge for accurate delineation of morphology and, subsequently, the management. An 8-year-old boy, known since early childhood to have cyanotic heart disease. He was asymptomatic apart from mild cyanosis with exertion. The patient presented by progressive dyspnea and worsening cyanosis (with oxygen saturation at rest of 70%). Echocardiography showed TGA, VSD and LVOTO caused by a subpulmonic muscular ring creating a peak systolic gradient of 60 mmHg.(Figure 1) Multiple questions were raised to decide the possible management strategy including, whether LV was still conditioned, LVOTO could be relieved, pulmonary valve (PV) morphology and function, and the hemodynamic significance of the VSD. CMR examination was performed on 1.5T scanner (Siemens Magnetom Aera, Siemens Medical Systems, Erlangen, Germany) to assess the LV volumes, mass and function, in addition to quantitative shunt calculation, and assessment of LVOTO level.

Diagnostic Techniques and Their Most Important Findings: CMR showed mildly dilated systemic right ventricle (RV) “EDVI 109 ml/m^2” with slightly impaired systolic function. LV was significantly dilated ‘EDVI 262ml/m^2'; with preserved systolic function, and mass “127 g/m^2”.(Table1) A muscular subpulmonic ring was very adherent to PV creating a significant LVOTO with maximum velocity >3 m/sec. PV was a tri-leaflet valve with limited mobility of the anterior cusp seemed likely to be degenerated by the turbulent flow. In addition, there was moderate pulmonary incompetence (RF 24%) with no stenosis.(Figure 2) A significant left to right shunt across the VSD was calculated, where pulmonary flow was 94ml, while aortic flow was 32ml. QP/QS was 2.9 on room air that increased to 3.6 by 100% oxygen, denoting reactive pulmonary vascular bed.(Table 2) Based on CMR data, LV was still conditioned and volume overloaded. LVOTO was believed to be resectable, and PV would still function as an adequate neo-aortic valve after possible repair. Heart team decision was to proceed for an arterial switch operation. The child had a successful arterial switch with VSD closure, resection of the LVOTO, and neo-aortic valve repair. Post-operative Echo showed good LV systolic function, mild neo-aortic valve incompetence and no residual VSD. He had a smooth post-operative course.

Learning Points from this Case: CMR, being a comprehensive noninvasive imaging modality can provide enormous anatomical data as well as quantitative functional analysis. This can play an important role in understanding the hemodynamics of complex CHD and therefore guide patient management.

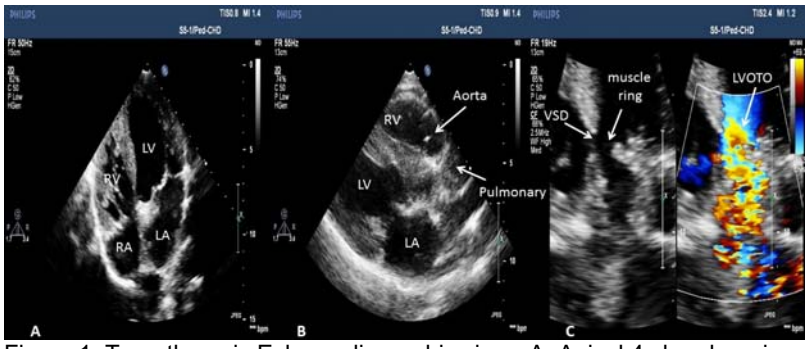

Figure 1. Transthoracic Echocardiographic views A. Apical 4 chamber view showing AV concordance. B. Parasternal long axis view showing VA discordance with the aortic valve arising anteriorly from the right ventricle and the pulmonary valve arising posteriorly from the left ventricle. Subpulmonic muscular ring is noted. C. Apical 5 chamber view showing conoventricular VSD and pulmonary valve arising from the left ventricle. The subpulmonic muscular ring closely related to pulmonary vale with turbulent flow across. RV: right ventricle, RA: right atrium, LV: left ventricle, LA: left atrium, VSD: ventricular septum defect, LVOTO: left ventricle outflow tract obstruction.

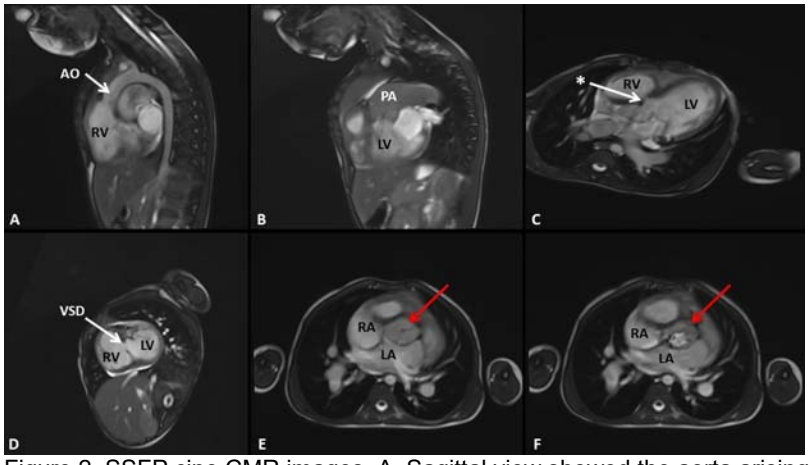

Figure 2. SSFP cine CMR images. A. Sagittal view showed the aorta arising anteriorly from the right ventricle. B. Sagittal view showed markedly dilated main pulmonary artery arising posteriorly from the left ventricle. C. 3 chamber view showed subpulmonic muscular ring causing LVOTO (Asterisk sign). D. Short axis view showing conoventricular VSD. E-F short axis views at the level of pulmonary valve in diastole (E) showed trileaflet pulmonary valve and in systole (F) showed limited mobility of the anterior pulmonary cusp (red arrows). AO: aorta, RV: right ventricle, PA: pulmonary artery, LV: left ventricle, VSD: ventricular septal defect, RA: right atrium, LA: left atrium.

Table 1. Bi-ventricular volumes and function.

	EF (%)	EDV (ml)	ESV (ml)	SV (ml)	EDVI (ml/m^2)	ESVI (ml/m^2)	SVI (ml/m^2)
RV "Systemic ventricle"	44	89	50	39	109	61	48
LV "Subpulmonic ventricle"	62	214	82	133	262	100	163

RV: right ventricle, LV: left ventricle, EF: ejection fraction, EDV: end diastolic volume, ESV: end systolic volume, SV: stroke volume, EDVI: end diastolic volume index, ESVI: end systolic volume index, SVI: stroke volume index.

Table 2. Quantitative flow analysis of the aorta and pulmonary artery measured by phase contrast flow on room air and 100 % oxygen.

Room air				
	Net flow (ml)	Forward flow (ml)	Backward flow (ml)	Regurgitant fraction (%)
MPA	94	124	30	24
Aorta	32	32	0	0
QP/QS = 2.9				
100 % Oxygen				
	Net flow (ml)	Forward flow (ml)	Backward flow (ml)	Regurgitant fraction (%)
MPA	126	134	8	6
Aorta	35	35	0	0
QP/QS = 3.6				

MPA: main pulmonary artery.

ID#: 371603

The classic cardiac involvment in Erdheim-Chester disease

Klaus Schumacher[1] Elker P. F. Abreu[2], Lilian Sande[3], Eduardo Miquelino. Oliveira, Jr.[4], Alexandre P. Borges[5], Thiago Quinaglia A. C. Silva, MD, PhD[6], Otávio Coelho-Filho, MD, PhD[6]

1. State University of Campinas - UNICAMP, Brazil

2. State University of Campinas - UNICAMP, Campinas, Sao Paulo, Brazil

3. State University of Campinas, Brazil

4. Radiology Department of Medical Center, Sao Paulo, Brazil

5. Radiology Department of Medical Center, Brazil

6. State University of Campinas - UNICAMP, Sao Paulo, Brazil

Description of Clinical Presentation: A previously healthy 68-year-old man presented to emergency department with diffuse abdominal pain. Physical examination was normal and an initial abdominal ultrasound showed symmetrical infiltration of the perirenal fat and fascia taking the appearance of ‘hairy kidneys';. Subsequent abdominal computed tomography (CT) scan confirmed the perirenal infiltration and also demonstrated infiltration within the retroperitoneal space. A CT guided biopsy of the retroperitoneal space was positive for xanthomatous infiltration, characterized by foamy histiocytes, giant and chronic inflammatory cells, consistent with Erdheim-Chester Disease. Abdominal CT scan also suggested cardiac involvement with a large pericardial effusion and possible infiltration in the atrium walls. Further investigation with cardiac magnetic resonance (CMR) showed typical cardiac involvement (infiltration with hypointense tissue within the atrioventricular groove, right atrium walls and periaortic space).

Diagnostic Techniques and Their Most Important Findings: Our patient underwent multimodality investigation of a rare systemic inflammatory disease including abdominal ultrasound and CT, CMR, brain MRI and CT guided biopsy. Erdhein-Chester Disease was confirmed by retroperitoneal biopsy of the infiltrated tissue. We summarized the most important findings on each method: 1) abdominal ultrasound demonstrated symmetrical infiltration of the perirenal fat and fascia taking the appearance of ‘hairy kidneys';, 2) abdominal CT with iodinated contrast evidenced extensive soft density tissue within the descending aorta (perivascular) and perirenal space, signs of mesenteric paniculitis and a large pericardial effusion, 3) brain MRI was positive for retro-orbital lesions and extra-axials lesions around the magnum foramina and finally 4) CMR demonstrated typical cardiac involvement, with hypointense tissue infiltration within the atrioventricular groove, right atrium walls and periaortic space (Figures 1 and 2) (Movie 1). Characteristically, the cardiac infiltration appeared as a hypointense tissue in cine SSFP images and isointense in both black blood T1 and T2 weighted images. Finally, infiltrated tissue had diffuse delayed enhancement on LGE-imaging.

Learning Points from this Case: - Erdheim-Chester disease (ECD) is a rare form of non-Langerhans cell histiocytosis. Most patients with ECD will have bone pain, explicated by bone lesions that usually are symmetric and affect diaphysis and metaphysis of long bones; the majority will also have commitment of other organs (central nervous system, skin, eyes, retroperitoneal, pulmonary, cardiac and others).
- The cardiac lesions are the third most common extra-skeletal finding.
- CMR allows a comprehensive characterization of localization, extension and nature of the lesions, as well as the definition of the fibrous nature of tissue.
- Pericardial effusion is a very common feature that goes along with the cardiac infiltration (more than 80% of cases).

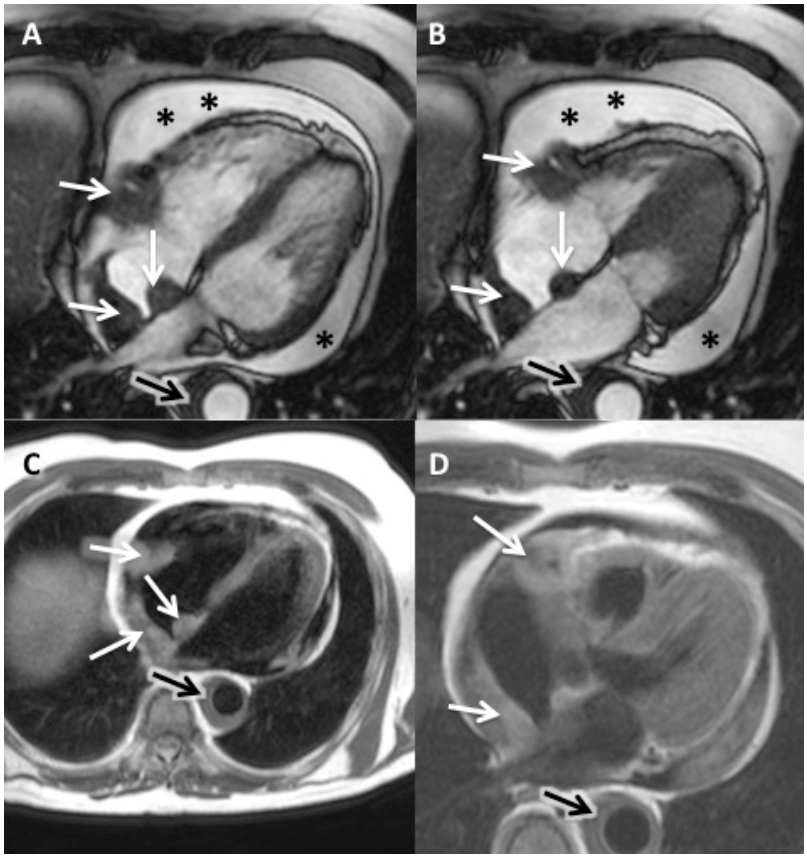

A and B: 4 chamber SSFF cine images in diastole (A) and systole (B) demonstrating normal biventricular function with infiltration of hypointense tissue within the right atrioventricular groove surrounding the right coronary artery and the right atrium walls (septal and upper walls) (with arrows). The 4 chamber cine images (A and B) also demonstrated a large pericardial effusion without signs of tamponade (*). C and D: In T2-weighted (C) and T1-weighted (D) axial black-blood images, the tissue infiltration appeared predominately as isointense to the myocardium. Black arrows also showed that infiltration extended to peri-advential region of the descending aorta.

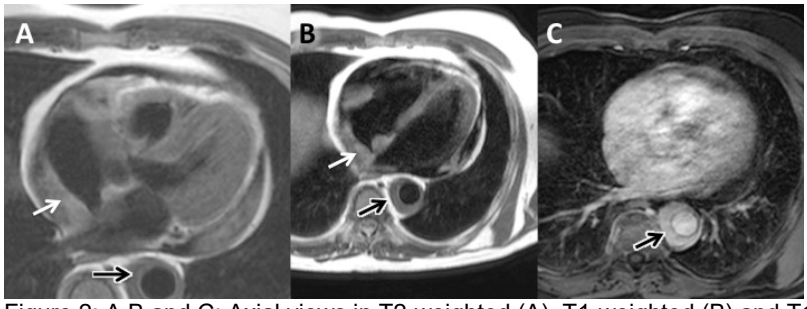

Figure 2: A,B and C: Axial views in T2-weighted (A), T1-weighted (B) and T1-weighted after contrast (C) demonstrating the infiltration within the atrium walls and the descending aorta.

ID#: 371512

Cardiac Amyloidosis with Normal Transthoracic Echo

Adrián I. Löffler, MD[1]Roshin C. Mathew, MD[2], Patrick T. Norton, MD[3], Christopher M. Kramer, MD[1], Michael Salerno, MD, PhD[3]

1. University of Virginia Health System, Charlottesville, VA

2. University of Virginia Health System, VA

3. University of Virginia, VA

Description of Clinical Presentation: A 58-year-old female with a history of tobacco abuse presented to the emergency department with complaints of progressive dyspnea on exertion, orthopnea, paroxysmal nocturnal dyspnea, and lower extremity edema. Labs were notable for a troponin I of 0.07 ng/mL, serum albumin of 1.0 g/dL, and serum creatinine of 0.9 mg/dL. Electrocardiogram showed sinus tachycardia with low voltage in some but not all of the precordial and limb leads. Transthoracic echocardiogram demonstrated hyperdynamic left ventricular (LV) ejection fraction (EF 65-70%), normal atrial size, and normal septal end diastole diameter, measuring 10mm. Diastolic function parameters were normal: mitral valve septal e'; velocity 11 cm/s, mitral valve lateral e'; velocity 12 cm/s, Average E/E'; 8.95. Speckle-tracking echocardiography demonstrated normal segmental and global longitudinal strain (Figure 1). CMR was performed to evaluate for cardiac amyloid given concerns for nephrotic syndrome and symptoms consistent with heart failure. Significant findings included increased native myocardial T1 values, elevated extracellular volume (ECV), atrial wall thickening and enhancement, and difficultly nulling the myocardium following contrast administration, all supportive of cardiac amyloidosis. Urine and serum protein electrophoresis revealed a spike in IgA lambda monoclonal protein. 24-hour urine protein study demonstrated 12 grams of protein consistent with nephrotic syndrome. Renal biopsy demonstrated lamba-restricted amyloidosis consistent with AL-type Amyloid. Bone marrow biopsy contained 66% plasma cells with atypical features and lamba restriction. She was subsequently started on bortezomib, cyclophosphamide, and dexamethasone.

Diagnostic Techniques and Their Most Important Findings: CMR was performed on a Siemens 1.5 T Aera scanner. Steady state free precession cine images (2A and 2E), native and post-contrast T1 mapping (2B, 2F and 2C, 2G), and delayed contrast-enhanced phase sensitive inversion recovery images were obtained (2D and 2H). Left atrial and right atrial sizes were normal, LV mass index was normal (37.37 g/m^2) and systolic function was hyperdynamic with EF calculated at 74%. Small bilateral pleural effusions and a small pericardial effusion were present. There was atrial wall thickening and enhancement (2E and 2H). There was markedly increased native T1 globally (1140-1170 ms). ECV calculated to be 0.49 consistent with marked expansion of the extracellular volume. Following contrast administration, there was difficulty nulling of the myocardium due to increased blood gadolinium clearance in amyloid patients.

Learning Points from this Case: In this patient with normal wall thickness and strain by echocardiography, the advanced tissue characterization provided with CMR was able to suggest the diagnosis of cardiac amyloidosis. CMR tools such as native T1 mapping, ECV assessment, and LGE can provide important clues when morphological and functional features do not suggest amyloid cardiomyopathy. Amyloid cardiomyopathy has been shown to be an underappreciated cause of HFpEF, particularly where traditional findings on echocardiogram are not seen. This is especially true in AL amyloid which has been shown to have much smaller LV mass compared to the ATTR group.

References: 1) Maceira AM, et al. Cardiovascular Magnetic Resonance in Cardiac Amyloidosis. Circulation. 2005;111:186–193. 2) Dungu JN, et al. CMR-Based Differentiation of AL and ATTR Cardiac Amyloidosis. JACC Cardiovasc Imaging. 2014. 2:133-42.

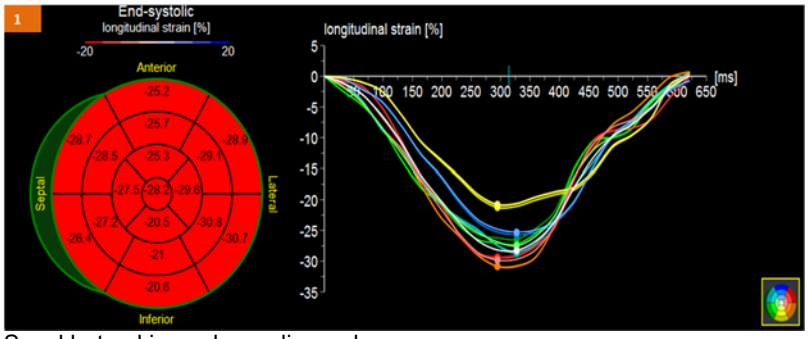

Speckle-tracking echocardiography

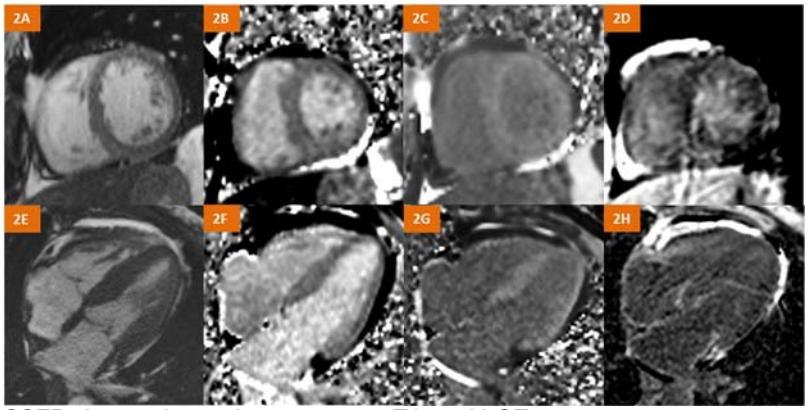

SSFP cine, native and post-contrast T1, and LGE.

ID#: 371471

The use of CMR in diagnosing and quantifying an unusual extracardiac shunt

Luca Conti, MD [1]Kentaro Yamagata[2], Alexander Borg, MD, FESC[3]

1. Mater Dei Hospital, San Gwann, Malta

2. Mater Dei Hospital, Malta

3. Mater Dei Hospital, N/A, Malta

Description of Clinical Presentation: A previously healthy 33-year old female consulted a respiratory physician in view of a 1-month history of dry cough. A trial of inhaled corticosteroids initially helped, but her symptoms later recurred. She was noted to have a high pitch continuous murmur, grade 3/6, parasternally at the right second intercostals.

Diagnostic Techniques and Their Most Important Findings: An asymmetrical right-sided upper mediastinal mass was noted on a CXR. This lesion was characterised further using a contrast CT. This showed a pulmonary lesion involving the right anterior upper and middle lobe measuring 4x6x14cm in size and widespread lymphadenopathy (Figure 1). TTE was performed to identify the underlying cause of the continuous murmur. Left ventricular dimensions were within normal limits, showing good global and regional left ventricular systolic function. The inter-atrial septum was intact, with no evidence of intracardiac shunts. No valvular pathologies were noted. A CMR was performed to further characterize the lesion. The lesion was noted to have a dense vascular supply on first-pass perfusion CMR (Figure 2). Phase-contrast MRI allowed the comparative quantification of cardiac blood flow in the pulmonary circulation with that in the systemic circulation. Forward flow volume across the aortic valve was 77mls and that across the pulmonary valve was 60mls, resulting in a Qp/Qs ratio of 0.79. In the absence of any obvious intracardiac shunt, this was suggestive of a communication, probably within the mass, between the pulmonary and systemic circulation (Figure 3). Interestingly, on perfusion imaging, the mass filled mostly during the pulmonary phase, implying that most of the supply was from the pulmonary artery. This is in keeping with the Qp/Qs ratio <1 indicating right-to-left shunting. The histological features and immunoprofile of the lesion biopsied were suspicious for Nodular Sclerosing Hodgkin';s Lymphoma.

Learning Points from this Case: CMR provides useful data for the assessment of tumour vascularity and is the non-invasive modality of choice for calculating the shunt ratio. Determination of the Qp/Qs ratio by phase-contrast CMR is reliable and safe compared to invasive oximetry. A Qp/Qs ratio of >1 implies a left-to-right shunt, and if <1 a right-to-left shunt is present. This provides clinically useful information in assessing the degree of ventricular volume overload in the presence of shunts between the pulmonary and systemic circulation. We present a case illustrating how CMR led to a diagnosis of extracardiac shunting within a vascular lung mass, which was also the cause of a prominent murmur.

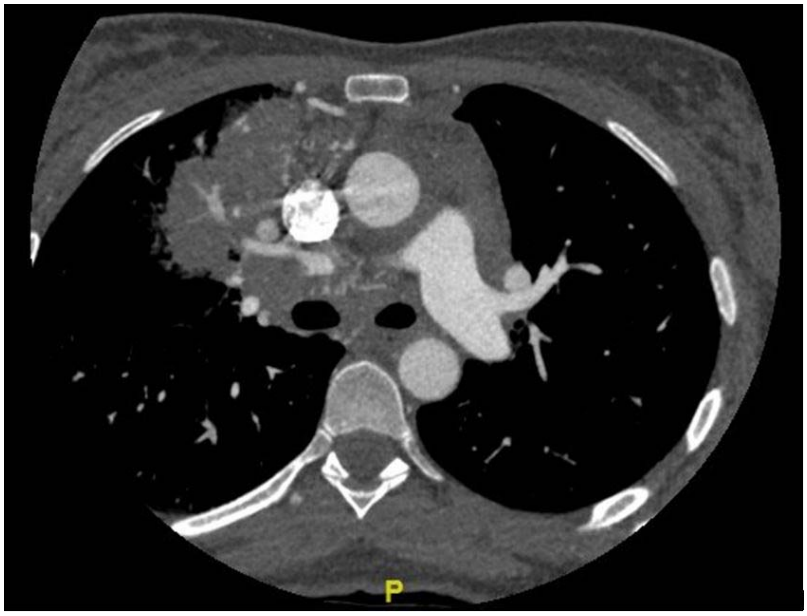

An ECG-gated CT angiogram showing a large pulmonary mass within the anterior mediastinum surrounding but not obstructing the superior vena cava. Caudally, it extends anterior to right atrium and ventricle, and posterior to right lung hilum. In posterior mediastinum, it also extends posterior to left atrium. At its most caudal extent, it stops just short of the right cardiophrenic recess. The right upper lobe pulmonary artery runs through the mass.

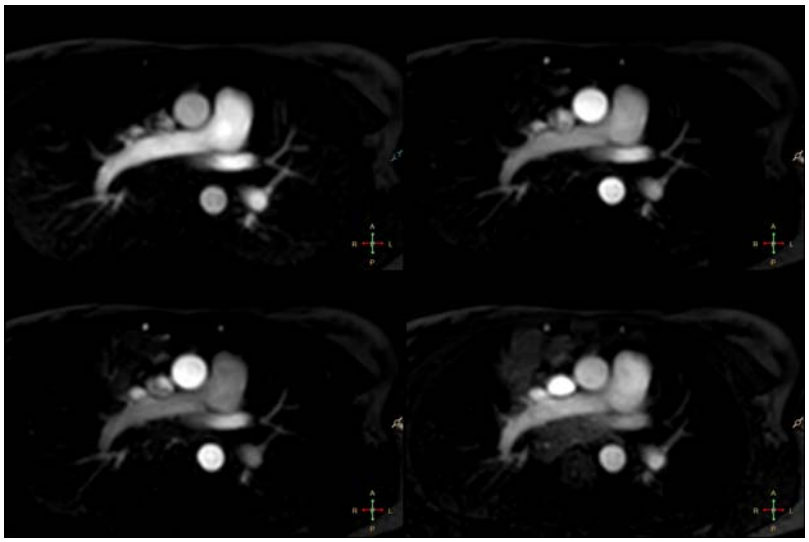

On CMR perfusion imaging, the mass fills avidly, implying that it is a highly vascular lesion. Interestingly, it fills mostly during the pulmonary phase, implying that most of the supply is from the pulmonary artery (i-iv).

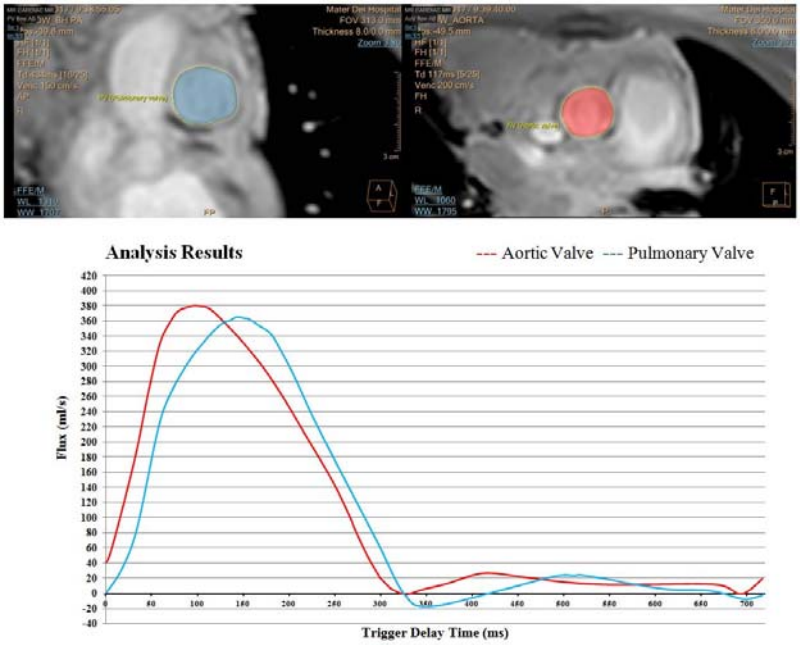

Images demonstrating MR quantification of the Qp/Qs ratio. Top left phase contrast CMR image showing a blue-shade circle indicating the plane through which pulmonary velocity was measured. Top right phase contrast CMR image showing a red-shade circle indicating the plane through which aortic velocity was measured. The above plot demonstrates the volumes passing through the pulmonary and aortic planes during multiple points of the cardiac cycle. The volume is plotted versus time, and the areas under the curves are calculated. The area under the pulmonary curve was calculated to be 60.4mls/beat and under the systemic curve was 76.9mls/beat. A Qp/Qs ratio of 0.79 was obtained.

ID#: 371931

Primary cardiac lymphoma. A CMR clue to recognize it.

Bianca V. Granados-Pinedo, MD[1] Angel L. Alberto-Delgado, MD[2], Julio C. Sauza-Sosa, MD[3], Jorge Marcuschamer-Miller, MD[1], Fernanda Ortiz-Haro y Nassar, MD[1], Teresa C. Cuesta-Mejias, MD[4], Lilia M. Sierra-Galan, MD, MCvT[5]

1. American British Cowdray Medical Center, Mexico

2. Central Military Hospital, Mexico, City, Distrito Federal, Mexico

3. American British Cowdray Medical Center, Mexico, Distrito Federal, Mexico

4. American British Cowdray Medical Center, Distrito Federal, Mexico

5. American British Cowdray Medical Center, CDMX, Distrito Federal, Mexico

Description of Clinical Presentation: A 58-year-old male presented with intermittent oppressive epigastric and precordial pain, fever, chills, night sweats and persisting unintended weight loss for two months. He has long-term systemic hypertension and previous myocardial infarction back in 2010 treated with PCI and stenting, he stopped medical treatment by his own decision and lost for follow-up for more than 10 years. On his physical examination, he had a systolic aortic murmur and the rest was unremarkable. His attending was concern about myocardial ischemia and associated infection, so he ordered a CCTA to evaluate newly developed significant CAD and stent patency, which showed significant coronary lesions and an extra cardiac mass; and an Echo also found an anterior mediastinal mass; to better characterization of the mass, a CMR was done that showed myocardial ischemia and an epicardial large irregular mass comprised within the pericardium that causes imprisonment of RCA. The mass was highly suspicious of primary cardiac lymphoma (PCL) and a CT-guided pericardial biopsy was taken that confirmed the diagnosis of diffuse large B-cell type PCL provided by CMR. Angioplasty and stenting of significant coronary artery lesions were performed and a permanent pacemaker installed due to high grade A-V block in preparation for chemotherapy cycles with rituximab, cyclophosphamide, doxorubicin hydrochloride, vincristine sulfate and prednisone. Patient is asymptomatic at 12-months follow-up and his PET-CT scan showed complete remission of lymphoma.

Diagnostic Techniques and Their Most Important Findings: Routine laboratory tests revealed increased levels of LDH, the rest was unremarkable. His chest X-ray showed cardiomegaly and no abnormal masses. CCTA showed significant lesions in mid LAD and ramus, with intermedia lesions in proximal LAD and LCx; global pericardial thickening of 11 mm and epicardial mass next to right side of the heart with apparent malignant characteristics and mildly dilated ascending aorta. Echo revealed an anterior mediastinal mass. CMR showed right ventricular dysfunction, myocardial ischemia and LGE with ischemic pattern in LAD territory; partial pericardial thickening, maximum thickness of 7 mm with mild pericardial effusion and no signs of constriction. An epicardial large irregular mass comprised within the pericardium that causes imprisonment of RCA, involves RA wall and caused mild external constriction of RV outflow tract; additional nodules, two extracardiac smaller attached to right-sided pericardium, one in the LV outflow tract, one attached to one right papillary muscle, within the inferior LV myocardium and in the interatrial septum. Tissue characterization demonstrated a heterogeneous and isointense/hipointense aspect in T1-W, hiperintense in T2-W and T2-W STIR and patchy heterogeneous enhanced in T1-W post-Gd sequences; with low and delayed first-pass perfusion enhanced suggestive of low-vascularity; and heterogeneous LGE with complete signal null with PSIR protocol; highly suggestive of a malignant type. A PCL was proposed as first differential diagnosis. A PET-CT scan confirmed a malignant mass in the mediastinum.

Learning Points from this Case: PCL is extremely rare, about 1.3% of all primary cardiac tumors, and there are no unified criteria for diagnosis, which is particularly difficult due to its nonspecific clinical manifestations. CMR is the best choice based on its tissue characterization ability and high spatial resolution to provide special clues for the diagnosis.

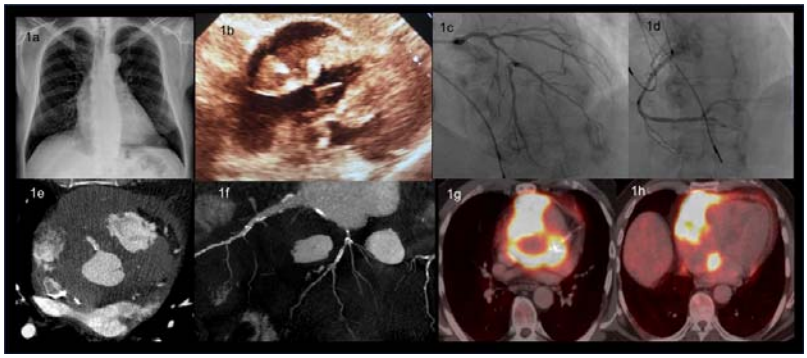

1a. Chest X-ray showing cardiomegaly and no masses. 1b. Echo showing free RV thickened and invade by a mass. 1c-d. ICA with significant lesions in LAD and ramus (1c) and normal RCA (1d). 1e. CCTA showing in an axial view a large extra cardiac mass with RCA imprisonment and in 2D MIP the coronary arteries lesions (1f). 1g-h. PET/CT showing the highly radiotracer pickup mass.

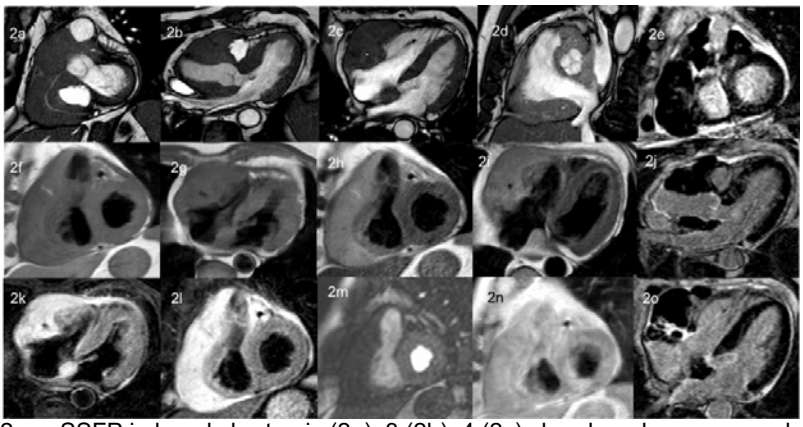

2a-c. SSFP in basal short-axis (2a), 3 (2b), 4 (2c) chambers long axes and aortic valve (2d) views showing the mass surrounding the right sided heart and the RCA imprisonment. 2f-g. T1-W, 2h-i. T2-W, 2k-2l. T2-W STIR and 2n. T1-W post-Gd short and 4-chambers views, respectively; showing the different signal intensity of the mass in comparison the myocardium. 2m. First pass perfusion basal image showing the low and delayed contrast enhanced. 2e, 2j and 2o. LGE images in basal short axis (2e), 3 (2j) and 4-chambers (2o) long axes views showing the nulling of the mass.

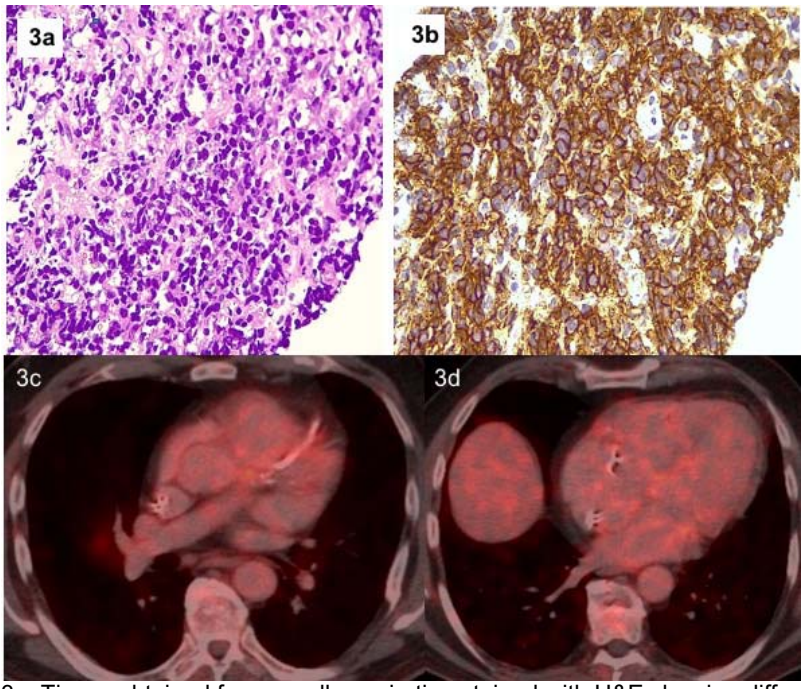

3a. Tissue obtained from needle aspiration stained with H&E showing diffuse infiltrate of mononuclear cells 3b. CD20 positive for malignant cells lymphoma type. PET/CT showing the absence of highly radiotracer pickup mass.

ID#: 371889

Comprehensive coronary artery aneurysm assessment by CMR

Martin MairFabian Gisler, Claudia C. Deluigi, Thierry Carrel, Lorenz Raber, Andreas Wahl, Kerstin Wustmann

University Hospital Bern, Bern, Switzerland

Description of Clinical Presentation: A 77yo male with a history of arteria lusoria aneurysm treated 12 years ago using a hybrid surgical/interventional technique (carotid-subclavian artery bypass and TEVAR into the distal aortic arch). In 2017, a non-ECG-triggered angio-CT showed a large (>3cm) and partially thrombosed aneurysm of the proximal right coronary artery (RCA). Retrospective review of previous CT-scans confirmed its presence at least since 2012. The last coronary angiography from 2005 showed no aneurysm. Patient`s symptoms were unspecific with only mild exercise-induced shortness of breath. CMR was requested to evaluate the size of the aneurysm, the amount of thrombotic material and myocardial ischemia and late gadolinium enhancement (LGE).

Diagnostic Techniques and Their Most Important Findings: By cine-SSFP and ECG-triggered 3D-SSFP, a large aneurysm (32x35x39mm) of the proximal segment of the RCA was confirmed. The entrance of the proximal RCA into the aneurysmatic sack was not clearly visualized, suggesting either a stenosis or kinking of the RCA. Half of the volume of the aneurysm was filled with thrombotic material. Left and right ventricular function were normal. Adenosine-stress-perfusion revealed a transmural perfusion deficit of the inferior and inferolateral segments (basal to apical). Resting-perfusion showed a slightly delayed arrival of contrast medium in these segments. These findings were consistent with prognostically relevant inferior and inferolateral ischemia. Also there was evidence of bloodpooling in the RCA aneurysm leading to a delayed contrast arrival at rest. Only circumscribed subendocardial LGE of the basal inferolateral segment was detected. Due to the presence of relevant ischemia and evidence of possible thromboembolism, the case was discussed with our cardiac surgeons. Coronary angiography confirmed a subtotal RCA stenosis at the level of the entrance of the RCA into the aneurysm, while the left coronary system showed only mild coronary sclerosis. Surgical repair consisted in opening of the aneurysm and closure of the stenosed RCA at the entrance into the aneurysm with reconstruction using a short saphenous vein segment. Postoperative course was uneventful.

Learning Points from this Case: Coronary aneurysms are rare. Approximately 50% of cases are due to atherosclerosis. Other etiologies include congenital, inflammatory (Takayasu arteritis, Kawasaki disease, rheumatoid arthritis, polyarteriitis nodosa), connective tissue disease, mycotic aneurysms or complications of percutaneous coronary interventions. Atherosclerosis and post-stenotic aneurysm formation is the suggested cause in this case. CMR is useful to assess the size of the aneurysm, to estimate the amount of thrombotic material and to assess the prognostic impact with regard to myocardial ischemia and LGE. Comparison of stress- and resting-perfusion CMR helped to assess myocardial ischemia as well as blood pooling in the aneurysm.

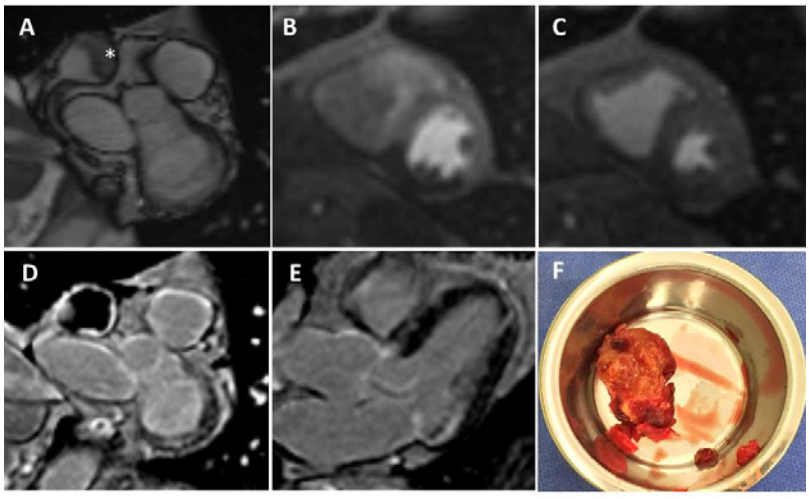

A) cine still frame, *RCA aneurysm; B) adenosine-stress-perfusion; C) resting-perfusion; D) post contrast with thrombus in the aneurysm; E) LGE inferolateral basal; F) resected aneurysm.

ID#: 371737

Complex pericardial cyst and congestive hepatopathy: The role of cardiac MRI with pathologic validation

Vinh Q. Nguyen, MD[1] Virginia K. Workman, MD[2], Kristin Stendahl, MD[2], Jeffrey Sklar, MD, PhD[2], Lawrence Young, MD[2], Hamid R. Mojibian, MD[3], Judith L. Meadows, MD[3], Steffen Huber, MD[3], Isabel Oliva, MD[4], Anna Bader, MD[2], Jonathan Killam, MD[2], Imran Hafeez, MD[2], Mariana L. Henry, BS[2], Lauren A. Baldassarre, MD[5]

1. Yale School of Medicine, New Haven, CT

2. Yale School of Medicine

3. Yale School of Medicine, CT

4. Yale School of Medicine, MADISON, CT

5. Yale University, CT

Description of Clinical Presentation: A 53-year-old man with undifferentiated liver disease was referred for liver transplant evaluation due to persistent ascites despite placement of a peritoneal cavity to superior vena cava shunt. A pre-transplant chest x-ray showed extensive pericardial calcification and cardiovascular magnetic resonance (CMR) imaging was obtained. A large pericardial mass and a right atrial thrombus were discovered. The patient was hospitalized and his clinical course was notable for bacterial peritonitis with secondary dissemination via his peritoneovenous shunt. He eventually died from septic shock with multi-organ failure. An autopsy was performed.

Diagnostic Techniques and Their Most Important Findings: CMR imaging was performed on a Siemens 1.5T scanner. Cine images acquired using steady state free precession sequences revealed LVEF 52%, RVEF 41%, and interventricular septal bounce. A large mass (13 x 7.5 cm) was seen compressing the right atrium and right ventricle (Image 1). T1-weighted and T2-weighted images with fat saturation were obtained. The mass had a heterogeneous composition and did not demonstrate contrast enhancement on first-pass rest perfusion nor late gadolinium enhancement (LGE) imaging. Long inversion time LGE images (600 ms) demonstrated a large thrombus in the right atrium associated with the shunt tip.

Autopsy revealed a 14 cm pericardial cystic mass containing old blood products and mural calcification. The epicardium was covered in fibrous tissue, indicating chronic pericarditis, supportive of myocardial constriction. The cystic lesion was adherent to but did not invade the myocardium (Image 2). On H&E stain, there were clusters of neutrophils, suggesting an infectious component (Image 3).

Learning Points from this Case: The majority of pericardial cysts are asymptomatic. However, this large space-occupying cyst compromised cardiac function and was complicated by chronic inflammation and fibrosis, leading to constrictive pericarditis and congestive hepatopathy. Chylous ascites found in this patient was likely due to central venous hypertension that impaired lymphatic drainage and augmented hepatic lymph production. In this case, the CMR identified the previously unknown pericardial cyst, and the findings of mass effect and ventricular interdependence supported a diagnosis of constrictive pericarditis. First-pass perfusion and nonenhancement on long inversion time LGE differentiated the mass as a cyst over a tumor and thrombus.

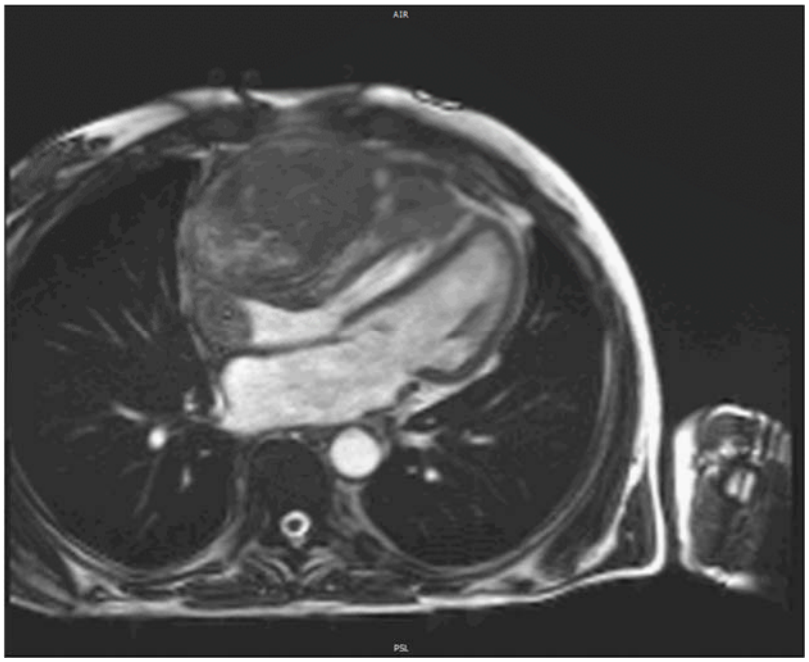

Four-chamber steady state free precession imaging revealed a large heterogeneous pericardial cyst occupying a large part of the mediastinum with compressive effects on the right atrium and right ventricle. Also note presence of right atrial thrombus.

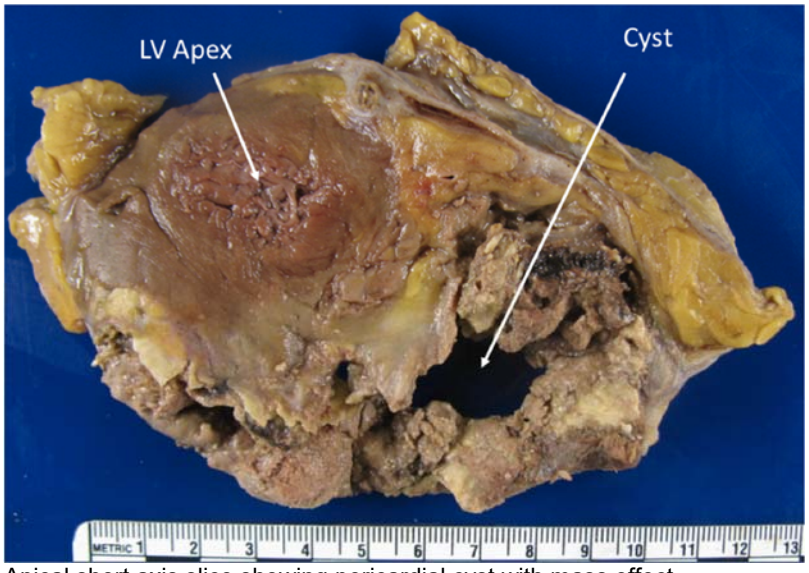

Apical short axis slice showing pericardial cyst with mass effect.

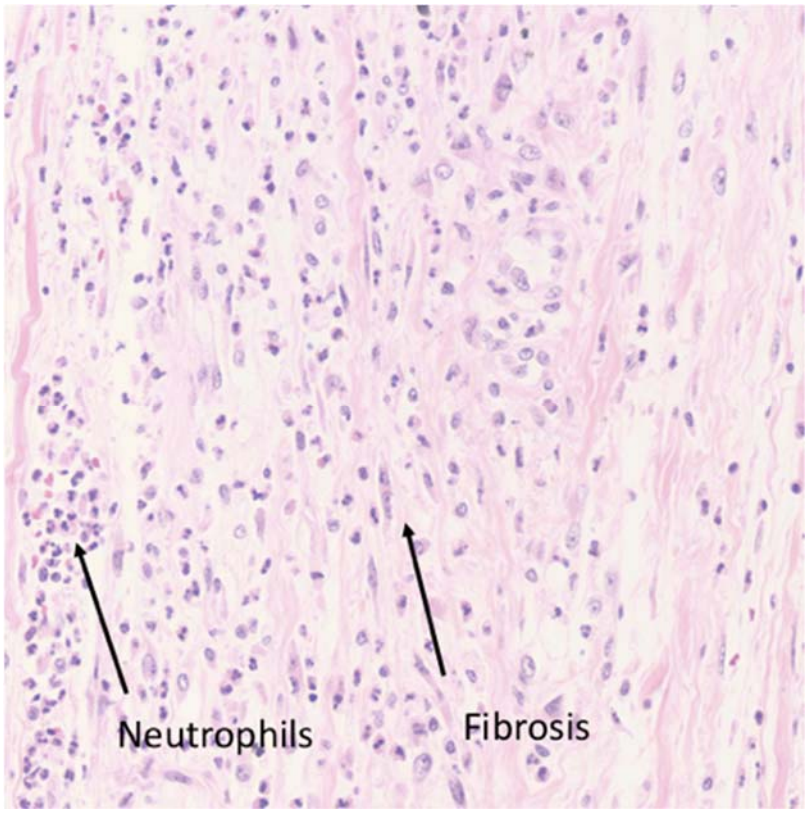

H&E stain of the cyst wall showing neutrophil infiltration with areas of fibrosis.

ID#: 372468

T1 mapping detect distal bed matrix changes in coronary artery lesions' configuration changes in developing ischemia, a case report

Ahmed Kharabish, MSc, PhD[1] Zahra A. Zadeh, MD[2], Mathias Langer[3], Tobias Krauß, MD[4]

1. Bad Krozingen Heart Center, Freiburg University, Germany, Germany

2. Freiburg University Hospital, Freiburg, Baden-Wurttemberg, Germany

3. Univ. Hospital, Germany

4. Freiburg University Hospital, Germany

Description of Clinical Presentation:

Configuration changes of coronary artery lesions take place and lead to cardiac events. Through new cardiac magnetic resonance imaging (CMRI) techniques; namely the T1 mapping, may provide an early tool in detecting any accompanying undergoing matrix changes before ischemia develops.

Diagnostic Techniques and Their Most Important Findings:

A patient presented with recently developed atypical chest pain, was sent to CMRI to assess ischemia. A previous CT coronary & catheter (Figure 1) showed mild atherosclerotic changes of the left anterior descending artery (LAD). The patient was scanned using protocol of adenosine stress MRI; cine images, dynamic gadolinium enhanced images under Adenosine stress and without adenosine as well as late gadolinium enhancement (LGE). In addition; three cuts SAX T1 mapping sequence were performed pre and post contrast in basal, mid and apical levels. Extracellular volume (ECV) was measured in all scanned segments. ECV above 30% was considered expanded.
No myocardial segments showed ischemic defect by adenosine. No scarring was detected in LGE (Figure 2). The test was considered negative for ischemia (Figure 2). However, mid ventricular segments of the anterior and antero-septal walls showed evidence of ECV expansion (Figure 2). It was accidently discovered that the patient had a new CT angiography, two days before the recent CMRI. Images of new CT showed a stenosis of >50% in segment 6 of the left anterior descending coronary which coincides with areas of ECV expansion. The lesion in the recent CT was mixed and of a higher grade when compared to the previous invasive angiography. A one year interval was between the new CT and the previous coronary CT and catheter.

Learning Points from this Case:

Configuration changes in coronary artery lesions may take place. These changes may lead to cardiac events, such as STEMI or Non- STEMI infarctions. Moreover, those configuration changes may lead to micro-embolization, which in turn may lead to subtle matrix changes. A phenomenon; to be studied if proved, that may predict ischemic events, where CMRI would provide a modality for assessment.

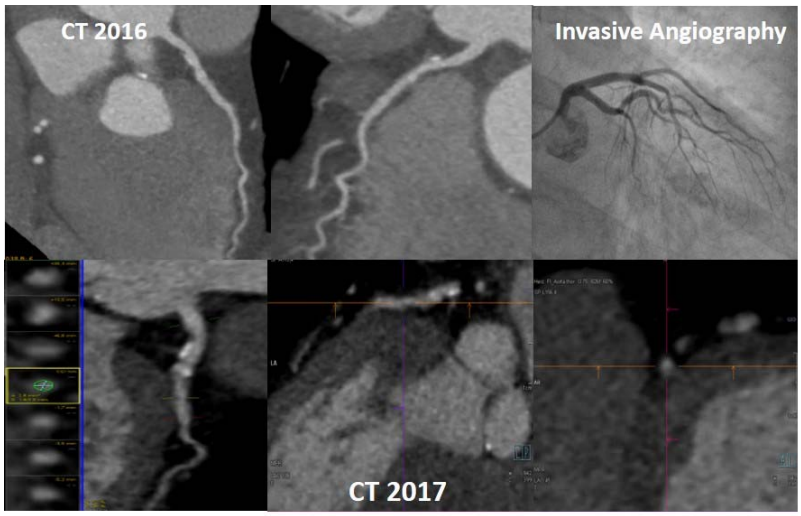

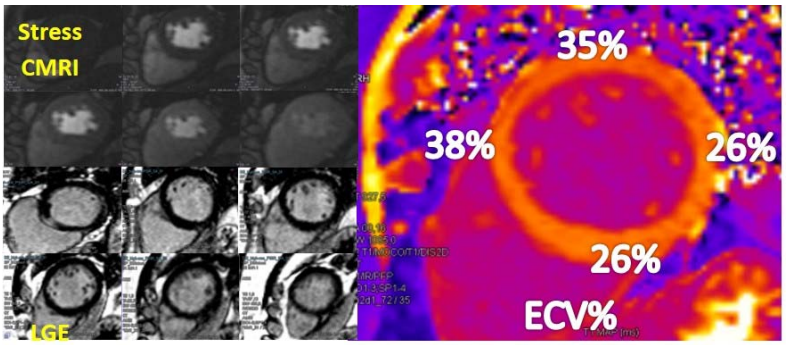
Stress
CMRI
LGE
35%
38%
26%
26%
ECV%

ID#: 372434

The dissociation between pathological progression and clinical stability: A Case Report of Hypertrophic Cardiomyopathy

David Wen[1], Betty Raman, MBBS, FRACP[2]Rina Ariga, MBBS, MRCP[3], Stefan Neubauer, MD, FRCP[3], Masliza Mahmod, MBChB, DPhil[3]

1. University of Oxford, United Kingdom

2. University of Oxford, Division of Cardiovascular Medicine, Oxfordshire, England, United Kingdom

3. University of Oxford, England, United Kingdom

Description of Clinical Presentation: Hypertrophic cardiomyopathy (HCM) is an evolutive disease with few studies mapping the natural course of pathological abnormalities. We present a case of HCM phenotyped on serial cardiac magnetic resonance (CMR) imaging to highlight the dissociation between phenotype and clinical symptoms in HCM, and the challenges presented for clinical management. A patient was referred at the age of 19 years for the management of HCM detected incidentally on echocardiogram. He was asymptomatic with no family history of sudden cardiac death (SCD), and no history of hypertension, aortic valve disease, syncope, abnormal blood pressure response on exercise testing or ventricular tachycardia on 24-hour ECG monitoring.

Diagnostic Techniques and Their Most Important Findings: Initial echocardiogram revealed moderate hypertrophy (1.6cm) and normal LVEF (61%) with no outflow tract obstruction. Cine and late gadolinium enhancement (LGE) imaging on CMR revealed a maximum thickness of 1.8cm with small areas of patchy LGE in hypertrophied segments (Fig 1). LV strain assessed on CMR feature tracking was normal (Table 1). Risk of SCD on European Society of Cardiology (ESC) risk calculator was 2.16% resulting in conservative management.

At 4 year follow up, although remaining asymptomatic, he was noted to have a significant increase in left ventricular hypertrophy to 2.6cm on CMR with increased areas of LGE compared to the previous scan whilst LV strain worsened marginally (Table 1). His SCD risk on ESC risk score remained low at 2.92%. He was commenced on a beta blocker. Genetic testing revealed a TRP-792 frame shift mutation in the myosin binding protein C (MYBPC3) gene (C2373dupG).

At 6 year follow up, a further increase in wall thickness on CMR to 3.2cm was observed. He remained asymptomatic during this period. There were widespread areas of LGE throughout the myocardium noted along with further impairment in LV strain compared to the initial scan (Table 1). Despite these differences in subtle markers of contractility, LVEF did not vary significantly over 6 years. ESC risk stratification this time was 2.75%. Due to the low risk and absence of any LVOT obstruction, the decision to implant a primary prevention ICD was deferred.

Learning Points from this Case: The present case describes the natural history of pathological abnormalities in a young adult with HCM despite a benign asymptomatic clinical course suggesting that pathological progression can occur silently. Conventional SCD risk stratification does not account for progression rate of wall thickness or fibrosis and further studies examining the prognostic value of rate of pathological progression in HCM are required.

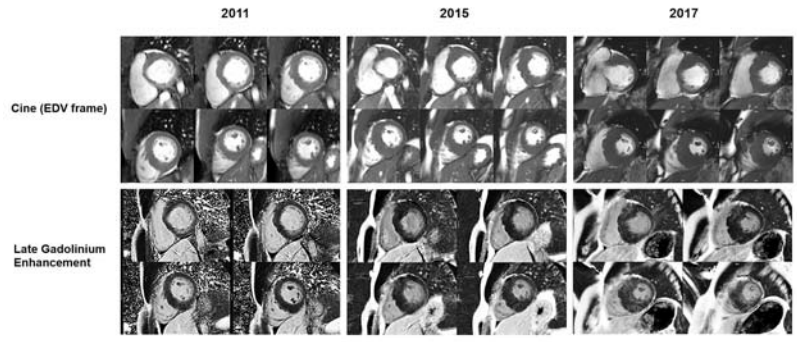

Cine and LGE reveal progression of left ventricular wall thickness and fibrosis over 6 years.

Table 1: CMR indices on serial imaging.

	2011	2015	2017
LV EDV (ml)	167	156	154
LV ESV (ml)	67	58	48
LV stroke volume (ml)	100	98	106
LV EF (%)	60	63	69
LV mass (g)	126	155	203
LV mass index (g/m^2)	74	82	108
LV wall thickness (cm)	1.8	2.6	3.2
LA EDV (ml)	24	44	60
LA ESV (ml)	70	92	114
LA EF (%)	66	52	47
LA AP diameter (mm)	31	37	38
Total enhanced mass (g)	2	4	12
Relative enhanced mass (%)	1.59	2.58	5.91
Global radial strain (%)	44.32	43.53	39.85
Global circumferential strain (%)	-22.23	-19.61	-16.83
Global longitudinal strain (%)	29.27	26.91	19.71
ESC Risk Score for SCD at 5 years (%)	2.16	2.92	2.75

LV Left ventricular; LA Left atrial; EDV End diastolic volume; ESV End systolic volume; EF Ejection fraction; AP Antero-posterior; ESC European society of cardiology; SCD sudden cardiac death

ID#: 372862

A 20 year-old female with chest pain, pericardial effusion and pericardial mass.

Arlene Sirajuddin, MD[1] Raffit Hassan, MD[2], Markku M. Miettinen, MD[3], Christine Alewine, MD, PhD[4], Anish Thomas, MBBS, MD[2], Emerson Padiernos, ANP-BC, CRNP[2], R. Taylor Ripley, MD[2], Andrew E. Arai, MD[5]

1. National Institutes of Health, Bethesda, MD

2. Thoracic and GI Oncology Branch, NIH/CCR/NCI, MD

3. Laboratory of Pathology, NIH/NCI, MD

4. Laboratory of Molecular Biology, NIH/CCR/NCI, Bethesda, MD

5. National Heart, Lung and Blood Institute, National Institutes of Health, Bethesda, MD

Description of Clinical Presentation: The patient is a 20 year-old female former smoker who has a past history of working with mosaics. She presented with of a 2-month history of worsening chest pain which eventually prompted a trip to the emergency room. At the emergency room, a chest radiograph revealed an enlarged cardiac silhouette and a CT pulmonary angiogram showed a moderate to large complex pericardial effusion. Subsequent cardiac MRI showed a large pericardial effusion, thickening of the pericardium, but also a mass within the pericardial space. PET imaging demonstrated hypermetabolism of the pericardial mass and mediastinal lymph nodes. CT guided needle biopsy of the mass revealed an epithelioid malignant mesothelioma arising from the pericardium. The patient underwent surgical resection via median sternotomy followed by adjuvant chemotherapy with six cycles of Cisplatin and Pemetrexed. Final pathology of the mass showed a 5.6 cm mass involving the pericardium composed of solid sheets of epithelioid eosinophilic cells with focal tubulopapillary differentiation and showing lymphovascular invasion. The tumor cells were positive for calretinin, keratins5/6, mesothelin, and WT-1, and negative for BER-EP4, supporting the diagnosis of malignant mesothelioma.

Diagnostic Techniques and Their Most Important Findings: Cardiac MRI definitely documented the intrapericardial mass and showed all of the findings of pericardial mesotheliomia: mass within the pericardial space that enhanced relatively homogeneously on first pass perfusion and heterogeneously on late gadolinium enhancement, complex pericardial effusion containing septations, and thickening of the parietal pericardium. CT angiogram showed a large complex effusion, however did not definitely diagnose the presence of the mass which lead to the cardiac MRI. However, CT was ultimately able to guide the biopsy that lead to definitive diagnosis. PET/CT images showed hypermetabolic activity of the pericardial mass as well as the pericardium, highly suggestive of malignancy.

Learning Points from this Case: 1. Pericardial masses are extremely uncommon. Pericardial thickening and effusion associated with this mass increase likelihood of malignancy. Pericardial mesothelioma is the most common of the malignant pericardial masses. Lymphoma, metastatic disease, and various sarcomas are in the differential diagnosis. 2. Mesothelioma can arise from mesothelial cells in four different locations in the body: pericardium, pleura, peritoneum, and tunica vaginalis testis (in males). Pericardial mesothelioma makes up less than 1% of all mesotheliomas and can invade adjacent myocardium, pleura, or lung and can also metastasize to lymph nodes. 3. Symptoms of pericardial malignancy are nonspecific, and imaging with cardiac magnetic resonance imaging is key to making an accurate diagnosis.

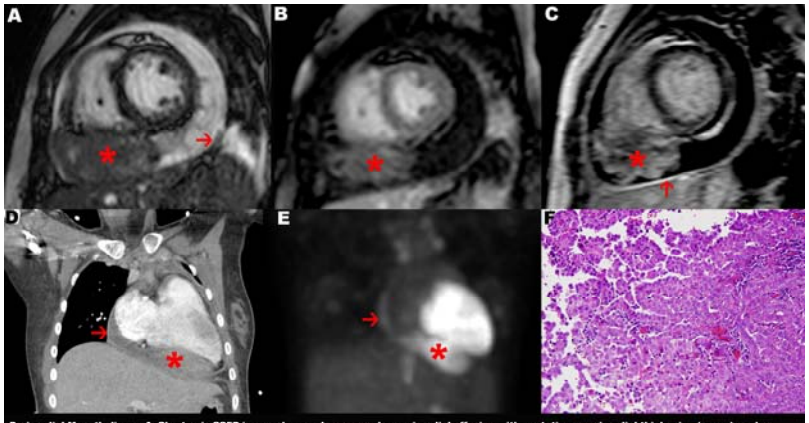

Pericardial Mesothelioma. A: Short axis SSFP image shows a large complex pericardial effusion with septations, pericardial thickening (arrow), and a mass in the pericardial space (*). B: First pass perfusion imaging shows relatively homogenous perfusion of the mass (*). C: Late gadolinium enhancement imaging shows heterogenous enhancement of the mass (*) and some pericardial enhancement (arrow). D: Coronal CT image of the chest shows a large pericardial effusion with heterogenous density within it (*) and pericardial thickening (arrow). E: Coronal PET image shows hypermetabolic activity of the mass withinthe pericardial space (*) as well as hypermetabolism of the pericardium (arrow). Mediastinal lymph nodes also show hypermetabolic activity. F: Photomicrograph shows tumor composed of sheets of malignant epithelioid cells showing focal tubulopapillary differentiation (Original magnification, x200, Hematoxylin and eosin stain).

ID#: 372947

Unknown systemic lupus erythematosus initially suspected by CMR.

Lilia M. Sierra-Galan, MD, MCvT[4]Angel L. Alberto-Delgado, MD[1], Maria-Elena Soto, MD, PhD[2], Ingrid E. Flandes--Aguilar, MD[3]

1. Central Military Hospital, Mexico, City, Distrito Federal, Mexico

2. American British Cowdray Medical Center, Mexico City, Distrito Federal, Mexico

3. American British Cowdray Medical Center, Distrito Federal, Mexico

4. American British Cowdray Medical Center, CDMX, Distrito Federal, Mexico

Description of Clinical Presentation: A 47-year-old woman with no previous relevant medical history presented to the ER 8 months before with the first episode of atypical chest pain consistent with osteochondritis; the second episode occurred 4 months before by presenting to the ER with typical chest pain, elevated troponin-I and STEMI due to proximal LAD occlusion by coronary thrombus treated with PCI, thrombus aspiration and stenting. At her third episode, she presented at ER with typical chest pain, on her physical examination she had elevated jugular venous pressure, no precordial myocardial impulse and distant heart sounds were found; the rest was unremarkable. A type III B acute coronary syndrome (ACS) was diagnosed, invasive evaluation showed normal coronary arteries, patent LAD stent, and a LV pseudoaneurysm. An Echo showed a LV pseudoaneurysm and she was schedule to surgery to treat the pseudoaneurysm. To proper planning the surgical procedure CMR was done that showed thrombosed LV aneurysm and raised the suspicion of autoimmune underlying etiology instead of ischemic origin. Surgery was successfully performed and CMR findings were confirmed. Laboratory specific test confirmed the diagnosis of Systemic Lupus Erythematosus (SLE). She was discharged 5 days after surgery, asymptomatic and in functional class I NYHA with medical treatment for SLE, she remains asymptomatic and free of new episodes for the last 14 months.

Diagnostic Techniques and Their Most Important Findings: At the first episode, routine laboratory test and ECG were normal. At the second episode, elevated troponin-I and ST elevation MI were found. At the third episode, routine laboratory tests showed normal troponin-I, ECG showed old anterior myocardial necrosis and unspecific ST-T changes in anterior and lateral walls. Chest-X-ray showed significant increase in heart silhouette mainly prominent in left contour of the heart. Invasive angiography showed normal coronary arteries with patent stent in proximal LAD and the ventriculography showed a large LV aneurysm of the anterior wall. An Echo showed regional wall motion abnormalities (RWMA) and an image that was diagnosed as pseudoaneurysm. CMR showed LV dysfunction, RWMA and late gadolinium enhancement (LGE) consistent with previous myocardial infarction (MI), a thrombosed large left ventricular aneurysm of anterior wall, mild pericardial thickening with LGE and large pericardial effusion. Tissue characterization of the thrombus showed that had two different components, an old and a recent one, corresponding to two separate events. Biopsy tissue confirmed CMR findings of old MI, LV aneurysm of anterior wall with two different type of thrombus, a chronic and an acute one. Immunofluorescence analysis of pericardial fluid was positive for anti-nuclear antibodies with homogeneous pattern; and from peripheral blood, positive for anti-nuclear antibodies with fine-speckled pattern; consistent with SLE.

Learning Points from this Case: Twenty percent of ACS in youth are related to non-atherosclerotic factors such as coronary abnormalities, connective tissue disorders and autoimmune diseases, from these, SLE and anti-phospholipid syndrome (APS) can cause MI; SLE is the most frequent. It is always important to consider prothrombotic states such as SLE and APS in ER in young adults with ACS. CMR has a key role in this clinical scenario due to its ability to delineate all components of the disease, to differentiate between pseudo-aneurysm and aneurysm, to characterized the associated thrombus, the inflammation of the pericardium and to orient the possible etiology.

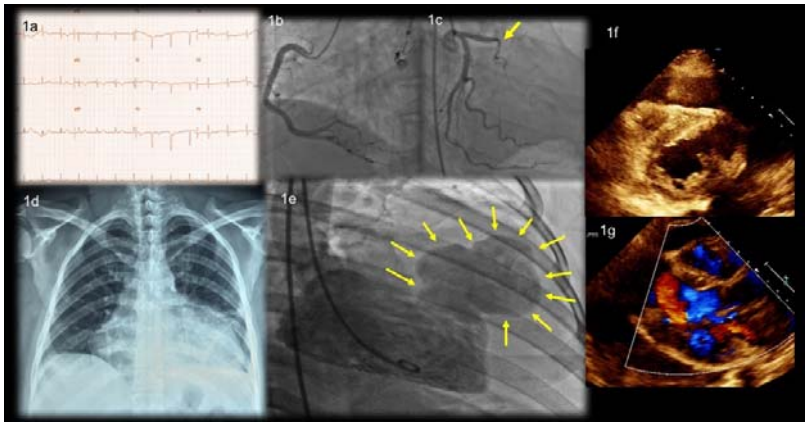

1a. ECG showing old anterior myocardial necrosis and unspecific ST-T changes in anterior and lateral walls. 1b-c. Invasive coronary angiography of second episode. 1b. Normal RCA. 1c. LAD proximally occluded. 1d-g. Third episode. 1d. Chest x-ray showing significant cardiomegaly mainly prominent in left contour of the heart. 1e. Invasive ventriculography showing large LV aneurysm of the anterior wall. 1f-g. Echo showing an image diagnosed as pseudoaneurysm in the anterior mid-apical segments with communication to LV cavity with color Doppler (1g).

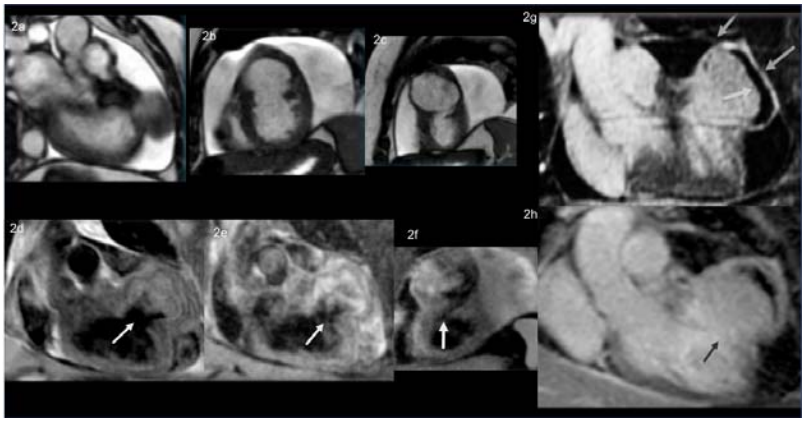

2a-c. SSFP. 2a. 3-chambers long axis view, 2b-c. Apical short-axis views showing the anterior aneurysm and the large pericardial effusion. 2d. T1-W and 2e. T2-W STIR 3-chambers long-axes and 2f. T2-W apical short-axis views showing the different signal intensity of the thrombus and its components. 2g. LGE sequence in 3-chambers view projection showing the aneurysmal wall of the infarcted anterior segment with the lined thrombus confirmed by 2h. LGE with very long TI showing its hipointense signal.

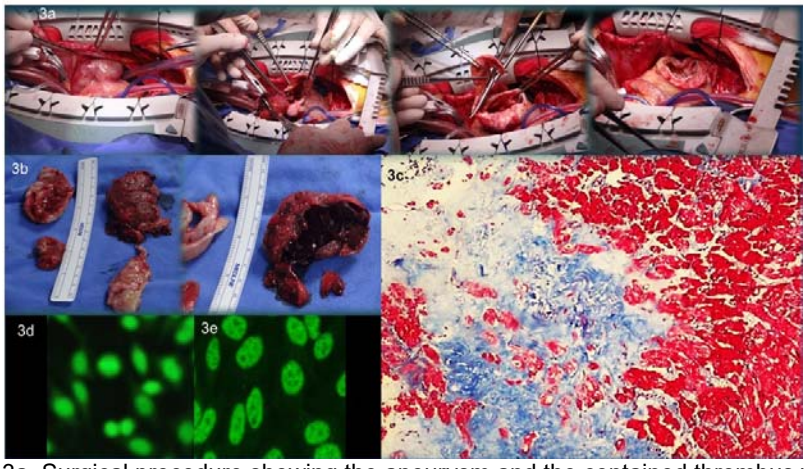

3a. Surgical procedure showing the aneurysm and the contained thrombus with its two components. 3b. Macroscopic views of the surgical pieces that shows the LV that constituted the aneurysm and the two-different age

of the thrombus and its histological aspect (3c). 3d. Positive anti-nuclear antibodies from the pericardial fluid with homogeneous pattern and 3e. from the peripheral blood with fine speckled pattern.

ID#: 372678

Improving recognition of intra-myocardial fat by CMR

Ana Martinez Naharro, MD[1] Tushar Kotecha, MRCP(UK) MBChB[2], Rohin Francis, MBBS[3], Daniel S. Knight[1], Philip N. Hawkins[4], Peter Kellman, PhD[5], Marianna Fontana, MD, PhD[3]

1. UCL Department of CMR, Royal Free Hospital, London, England, United Kingdom

2. Royal Free London NHS Foundation Trust, London, England, United Kingdom

3. UCL Department of CMR, Royal Free Hospital, England, United Kingdom

4. National Amyloidosis Centre, University College London, England, United Kingdom

5. National Heart, Lung, and Blood Institute, National Institutes of Health, Bethesda, MD

Description of Clinical Presentation: A 51 year-old gentleman with no relevant past medical history presented with one week of pre-syncopal episodes culminating in an episode of collapse. Admission resting ECGs revealed sinus rhythm with paroxysmal episodes of ventricular tachycardia. Transthoracic echocardiography examination was performed suggesting moderate biventricular dysfunction. To further investigate the cause of the non-sustained ventricular tachycardia and to exclude any possible structural heart disease, a cardiac magnetic resonance (CMR) was performed.

Diagnostic Techniques and Their Most Important Findings: Cine SSFP imaging showed mild biventricular dilatation, mild biventricular systolic impairment with no regional wall motion abnormalities, and, interestingly, revealed multiple regions of low signal from basal to distal septum. The CMR protocol, which included native T1 mapping, T2*, late gadolinium enhancement images (LGE), and fat/water separated sequences, provided clear identification of multiple areas of fatty infiltration from basal to distal interventricular septum of the LV. All the sequences were concordant with low T1 values on native T1 mapping matched by evidence of fat on fat/water sequence and late gadolinium enhancement (LGE) on the delayed enhancement images.

Learning Points from this Case: Among the various CMR techniques employed, only fat/water separated sequences confirmed definitive evidence of fatty infiltration. LGE image sequences are not sufficient to definitively demonstrate fatty infiltration. Furthermore, gadolinium injection inherently changes the tissue T1 and T2 parameters, further reducing the ability to identify relatively small regions of fatty infiltration. Sequences other than the fat/water separated sequences are in agreement with this finding; however, the abnormal intraventricular signal could be due to other changes in the tissue.

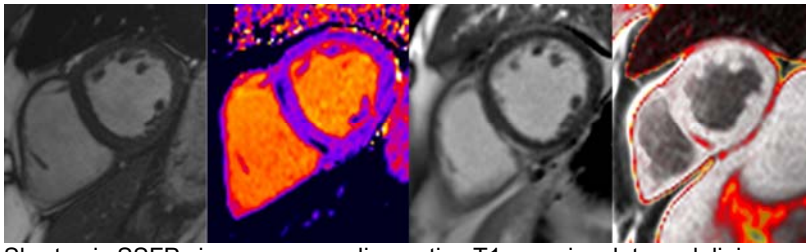

Short axis SSFP cine, corresponding native T1 mapping, late gadolinium enhancement and fused fat/water separated sequence confirming intramyocardial fat

ID#: 372609

Athlete's Heart or Hypertrophic Cardiomyopathy?

Dina Radenkovic, BSc; MBBS Candidate [1] Gabriella Captur, MD PhD MRCP MSc[2], Luis Lopes, MD, PhD [3], James Moon, MD[4], Perry Elliot, MBBS; MD; FRCP; FESC; FACC[5]

1. Barts Heart Centre & UCL Medical School, London, UK, London, England, United Kingdom

2. Barts Heart Centre, London, England, United Kingdom

3. Barts Heart Centre; UCL, United Kingdom

4. UCL, England, United Kingdom

5. University College London, United Kingdom

Description of Clinical Presentation: A 33-year-old weightlifter presented to cardiology clinic five years ago with palpitations but no syncope. Physical examination was normal. He had a family history of sudden cardiac death (SCD) - father and grandfather at 24 and 50 years respectively, both with no known prior cardiac disease. Differential diagnoses at the time included hereditary channelopathy or familial cardiomyopathy.

Diagnostic Techniques and Their Most Important Findings: At presentation ECG suggested left ventricular hypertrophy (LVH) by voltage criteria with high take-off ST segments anteriorly and T wave inversion laterally. Holter monitoring showed rare ventricular ectopy. Echocardiography showed mild concentric LVH with preserved ejection fraction (69%). Cardiovascular magnetic resonance (CMR) showed a maximal wall thickness of 13mm in the septum and no scar. Prior to CMR, he had reduced weightlifting to three sessions per week and denied anabolic steroid use. At this stage, the diagnosis of athlete';s heart remained plausible. Over the next five years he underwent a series of tests including ajmaline provocation, exercise stress test, and repeated Holter monitoring that were unremarkable. In 2017 he became symptomatic of chest pain, palpitations and pre-syncope. Echocardiography and CMR were repeated. The echocardiogram reported mild LVH with maximal wall thickness of 14mm at the mid-infero septum, but CMR one month later revealed a maximal wall thickness of 17mm anteroseptally, and in an asymmetric HCM distribution. Side-by-side comparison of the two CMR studies 5 years apart showed definite progression of the LVH (**Fig 1**). There was also new patchy late gadolinium enhancement in the mid to apical antero-septum (**Fig 2**) with a matching increase in the native myocardial T1 signal by MOLLI (**Fig 3**). 24-Hour Holter monitoring at this time picked up an 11-beat salvo of regular wide complex tachycardia representing either nonsustained ventricular tachycardia (NSVT) or aberrancy.

Learning Points from this Case: If NSVT is confirmed, this young man';s 5-year SCD risk [1] could be as high as 6.1% - enough to alter his management from watchful wait and annual cardiology follow up, to consideration of an implantable-cardioverter defibrillator. He has now been commenced on a beta-blocker. This case illustrates the utility of CMR in the noninvasive assessment and longitudinal follow-up of patients with a family history of SCD and suspected HCM. Here CMR permitted earlier HCM diagnosis and risk stratification with practical clinical implications in terms of drug therapy and potential future device implantation.

1. doi:10.1093/eurheartj/ehu284

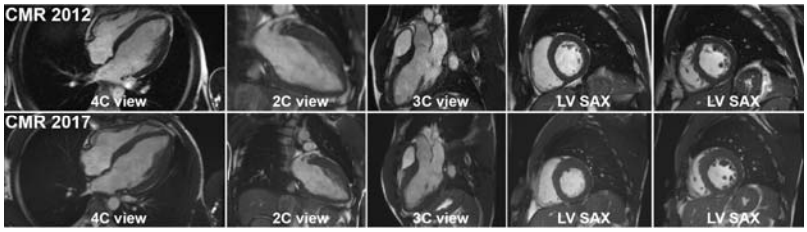

Two CMR studies 5 years apart demonstrating definite progression of left ventricular hypertrophy.

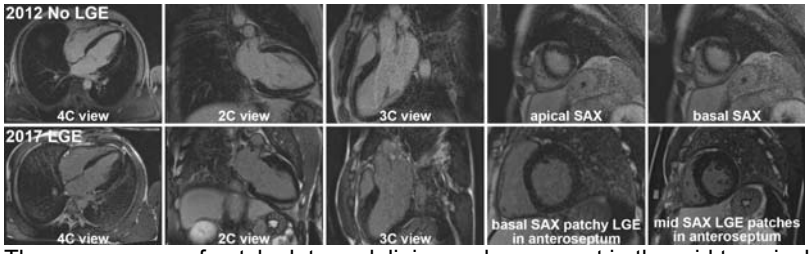

The appearance of patchy late gadolinium enhancement in the mid to apical antero-septum was noted in the CMR performed in 2017 but was not present in 2012.

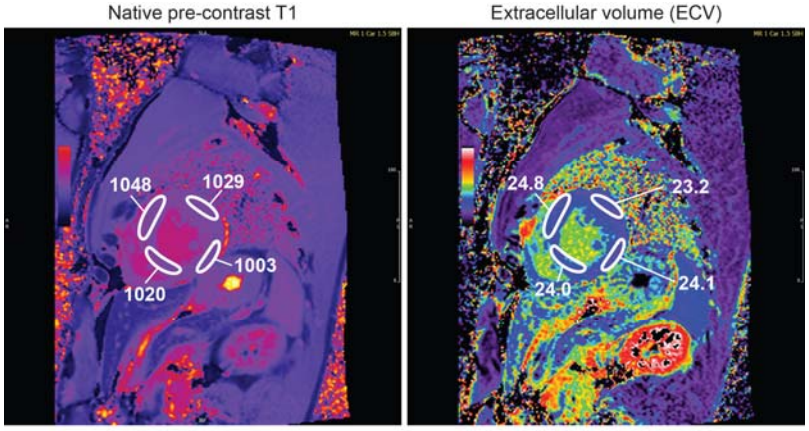

The changes were supported by the increase in the native myocardial T1 signal by MOLLI (Modified Look-Locker Inversion Recovery).

ID#: 372662

Syncope on exertion in a young male

Julia W. Erath, M. D. [1] Valentina O. Puntmann, MD, PhD [2], Emmanouil Chavakis, M. D. [3], Achim Grünewaldt, M. D. [4], Christian Hügel, M. D. [5], Tommaso D'Angelo, MD [6], Eike Nagel, MD, PhD [7], Stefan Hohnloser, M. D. [8]

1. University Hospital Frankfurt, Goethe University, Cardiology/Clinical Electrophysiology, Frankfurt, Germany

2. Universitaetsklinikum Frankfurt, Frankfurt Am Main, Germany

3. University Hospital Frankfurt, Goethe University, Division of Cardiology, Germany

4. University Hospital Frankfurt, Goethe University, Frankfurt, Hessen, Germany

5. University Hospital Frankfurt, Goethe University, Germany

6. University of Messina, Messina, Sicilia, Italy

7. University Hospital Frankfurt; Institute for Experimental and Translational Cardiovascular Imaging; DZHK Centre for Cardiovascular Imaging, Frankfurt, Germany

8. University Hospital Frankfurt, Goethe University, Cardiology/Clinical Electrophysiology, Germany

Description of Clinical Presentation: We report the case of a 34-year-old male patient presenting with a history of recurrent syncope on exertion. At rest, the 12-lead ECG showed first-degree AV block with undisturbed intraventricular conduction (fig. 1A). On exercise treadmill testing (fig.1 B), second-degree AV-block with two-to-one AV-conduction was observed with increasing workload at 100W suggesting infra-hissian block (fig. 1 C). Long-term ECG monitoring one day later demonstrated intermittent third-degree AV-block (fig. 1D). Echocardiography showed mildly impaired RV and LV function. Cardiac magnetic resonance (CMR) with late gadolinium enhancement (LGE) revealed moderately reduced left ventricular (LV) global systolic function (LVEF 45%) with sharply demarcated intramyocardial enhancement within the mid-anterior septal segment, corresponding with the region of the bundle of His (fig. 2A).

Diagnostic Techniques and Their Most Important Findings: Native T1 and T2 mapping values were elevated, consistent with the presence of myocardial inflammation. Together with bihilar lymphadenopathy on CMR, the findings were highly suggestive of cardiac involvement in systemic sarcoidosis. Subsequent bronchioalveolar lavage revealed with an increased CD4/CD8 lymphocytes ratio lung and paratracheal lymphnode biopsy provided the histological proof of non-caseating granuloma.

Learning Points from this Case: Although cardiac sarcoidosis is a rare disease, young people with a history of syncope and complete heart block should be actively screened to initiate early treatment. Cardiac MRI seems to be a suitable, non-invasive diagnostic tool to monitor myocardial involvement.

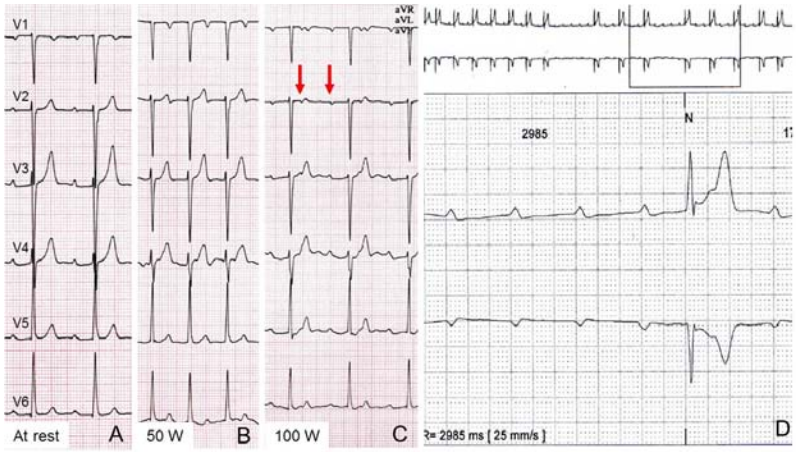

ECG at 25mm/s paper speed at rest (panel A), at exercise 50 W (panel B), at exercise 100 W (panel C) and during Holter monitoring (panel D).

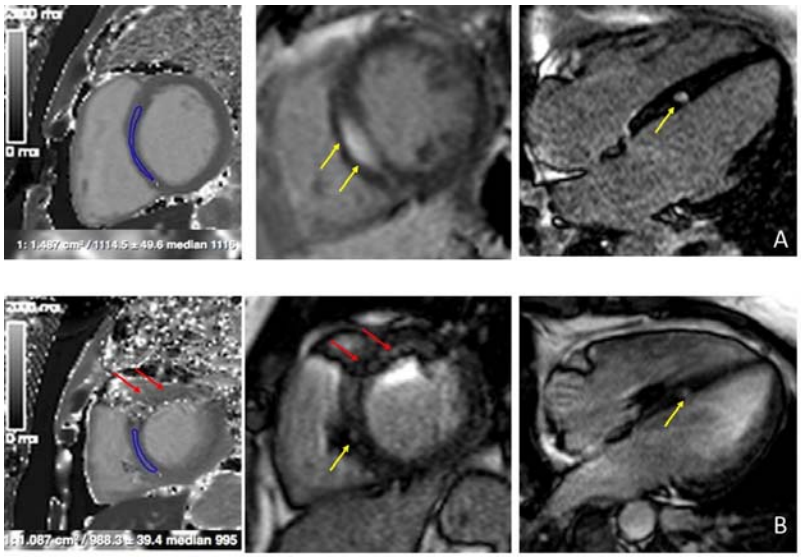

Cardiac MRI on initial presentation (panel A) and during follow-up (panel B).

ID#: 372337

In patients with vanishing white matter disease, could cardiac MRI reveal a concealed pathology?

Dina Haroun, MBBCh,MSc[1]Sameh Khalil, MSc[2], Fatma R. Elkafrawy, MBBCh, MSc[3], Mahmoud N. Shaaban, MBBCh, MSc.[4], Reda Sallam, BSc[5], Soha Romeih, MD,PhD, FESC[6], Wesam E. El Mozy, MD, MSc[7]

1. Radiology fellow Aswan Heart Center (Magdi Yacoub Heart Foundation),assistant lecturer Radiology department - Kasr Al Ainy Cairo university., Egypt

2. Aswan Heart Center - Magdi Yacoub Foundation, Cairo, Egypt

3. Aswan Heart Center - Magdi Yacoub Foundation,assistant lecturer Alexandria university, Egypt

4. Aswan Heart Center (Magdi Yacoub Foundation) - Cardiology department, Tanta University, Tanta, Al Gharbiyah, Egypt

5. Aswan Heart Center - Magdi Yacoub Foundation, Al Jizah, Egypt

6. Aswan Heart Centre, Egypt

7. Magdi Yacoub Foundation - Aswan Heart Centre, Aswan, Egypt

Description of Clinical Presentation: A 25-year-old male patient,mentally retarded,presented by recurrent attacks of loss of conscious and convulsions. ECG showed frequent PVCs. Echocardiography revealed dilated ventricles with impaired left ventricle systolic function; EF was 40%. Excess right ventricular apical trabeculations with poor systolic function.The cause of loss of conscious was not clear whether it is due to cardiac or the neurological state. Therefore, cardiac and brain MRI were performed on a 1.5 T scanner (Siemens Magnetom Aera, Siemens Medical Systems, Erlangen, Germany) to assess bi-ventricular systolic function and myocardial tissue characterization as well as the brain integrity.

Diagnostic Techniques and Their Most Important Findings: Cardiac MRI showed normal LV volumes with impaired systolic function, and global hypokinesia. No LV myocardial fibrosis. RV was dilated (EDVI 121 ml/m^2,ESVI 99 ml/m^2) with poor systolic function, EF was 19%. (Table1) Dyskinesia RV free wall at apical level. Transmural myocardial fibrosis of the RV free wall,(Figure 1) with no myocardial fatty infiltration.
Brain MRI showed bilateral symmetrical affection of the diffuse deep cerebral white matter, centrum semiovale, subcortical U-fibres, corticospinal tract and tiny cerebellar foci eliciting bright signal in T2 weight images and FLAIR and low signal intensity in T1 weighted images, sparing the basal ganglia.(Figure 2)
CMR findings fit with the diagnosis of arrhythmogenic right ventricular cardiomyopathy (ARVC) according to the task force criteria (Rastegar et al.,2014). Brain MRI showed a vanishing white matter disease (VMWD). Therefore, RV could be the origin of the arrhythmia causing loss of conscious and VMWD explained his mental status and the convulsions.
Based on MRI findings, cardiac team discussed with the family the probability of intracardiac defibrillator implantation as secondary prevention.
Combination between VWMD and dilated cardiomyopathy have been frequently reported.However, combination between VWMD and ARVC is uncommon, this combination had been once reported by (Hata Y1 et al.,2014) Interestingly that even in this case, the diagnosis of ARVC was discovered only by post mortem histopathology and not during the clinical assessment which would confirm our concern that this combination might be underestimated rather than uncommon.

Learning Points from this Case: In patients with VWMD, the underlying risk of sudden cardiac death due ARVC could be masked with the general neurological state. Raising the awareness of this possible association and considering cardiac MRI as a part routine investigation in this peculiar group of patients might reveal more cases. The association between Tuberous sclerosis and cardiac rhabdomyoma may be a good example to be followed.

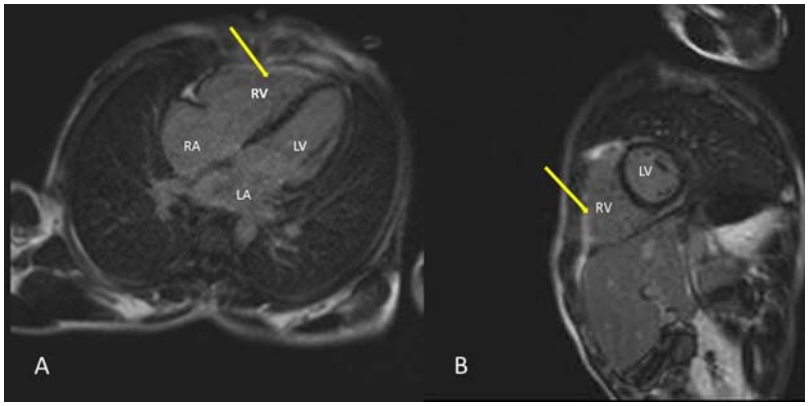

Figure 1: cardiac MRI (A) four chamber view inversion recovery (IR) after 10 minutes of gadolinium injection showed transmural fibrosis of right ventricular free wall (arrow) (B) short axis view IR 10 minutes after LGE apical level showing the transmural fibrosis. RV: right ventricle, LGE: late gadolinium LV: left ventricle, RA: right atrium, LA: left atrium

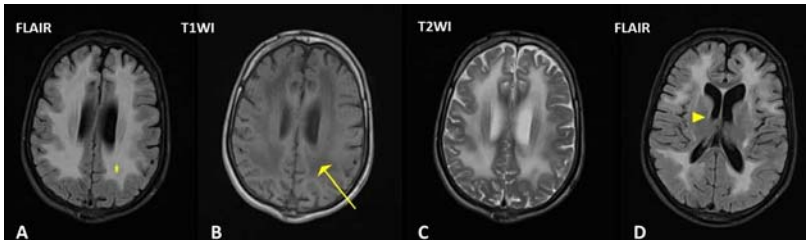

Figure 2: MRI brain axial cuts: (A): FLAIR (fluid attenuated inversion recovery) images showing diffuse bilateral symmetrical deep white matter (asterisk), subcortical U fibers and corticospinal tract sparing the basal ganglia (arrow head) (D); eliciting bright signal in T2WI (T2 weighted images) as well (C) and low signal intensity in T1WI (arrow)(B)

Table 1: Showing Right Ventricular , Left Ventricular functions and volumes :

Ventricle /volume	*EF (%)*	*EDV (ml)*	*ESV(ml)*	*SV(ml)*	*EDVI (ml/m2)*	*ESVI (ml/m2)*	*SVI (ml/m2)*
RV	19	160	130	30	121	99	23
LV	38	87	54	33	66	41	25

RV:right ventricle ,LV:left ventricle ,EF:ejection fraction,EDV:end diastolic volume,ESV:end systolic volume,SV:stroke volume,EDVI:end diastolic volume indexed,ESVI:end systolic volume indexed,SVI:stroke volume indexed.

ID#: 370854

Obstructive cardiac tumor with a capsule: fibroma or rhabdomyoma?

Barbara Burkhardt, M.D.[1] Srikant Das, M.D.[2], Matthew Lemler, M.D.[3], Tarique Hussain, MD, PhD[4]

1. Dept. of Pediatrics, UT Southwestern Medical Center, Dallas, TX

2. University of Arkansas for Medical Sciences, AR

3. University of Texas Southwestern Medical Center, Dallas, TX

4. Dept. of Pediatrics, UT Southwestern Medical Center, TX

Description of Clinical Presentation: A term newborn presented with a loud murmur, and echocardiography showed a 30x18mm interventricular septum (IVS) tumor causing severe left ventricular outflow tract obstruction (LVOTO; Doppler gradient up to 140 mmHg), which required prostaglandin infusion to maintain ductal patency for systemic perfusion. At 1 day of age, cardiac magnetic resonance (CMR) imaging was performed. Based on a hyperintense periphery on LGE, the tumor was thought to be a fibroma, too large for complete resection. The patient was transferred for heart transplant evaluation secondary to concerns that partial resection would leave him at risk for malignant arrhythmias.

Diagnostic Techniques and Their Most Important Findings: A large, single IVS tumor causing LVOTO was confirmed by CMR. On balanced turbo field echo (BTFE), it was mildly hyperintense, especially in the periphery. T1-weighted images showed the tumor as mildly hyperintense. On T2-weighted images, the tumor was clearly hyperintense, but with lower central signal on fat saturated T2. The tumor did not take up contrast during gadolinium perfusion. On late gadolinium imaging (LGE), the tumor appeared very hypointense, but with a thin hyperintense “capsule”, thus giving it the appearance of a fibroma. However, this can also be seen in rhabdomyomas. After review of echocardiography and CMR, the patient went for partial, transaortic tumor resection, and histology confirmed a rhabdomyoma with endocardial fibrosis and scattered dystrophic calcification. Later, a dual chamber pacemaker was implanted due to symptomatic 2:1 atrio-ventricular block.

Learning Points from this Case: The most common cardiac tumors in children are rhabdomyomas and fibromas, and both are commonly located in the ventricular myocardium. Rhabdomyomas have a high chance of spontaneous regression, even if only partially resected. Fibromas are hyperintense on LGE and may have a dark core. Rhabdomyomas are typically hypointense on LGE, but can also present with a fibrotic capsule, thereby mimicking fibromas. Cardiac rhabdomyomas are multiple in more than half of patients, fibromas are often single lesions. Calcifications are more common with fibromas. Both can cause arrhythmias. They look similar on BTFE, T1- and T2-weighted images and don';t take up contrast during gadolinium perfusion. With a finding of a single, “encapsulated” tumor, which is typical of a fibroma, one must be careful not to exclude the differential diagnosis of rhabdomyoma. Septal cardiac tumor resection carries a risk of atrio-ventricular block.

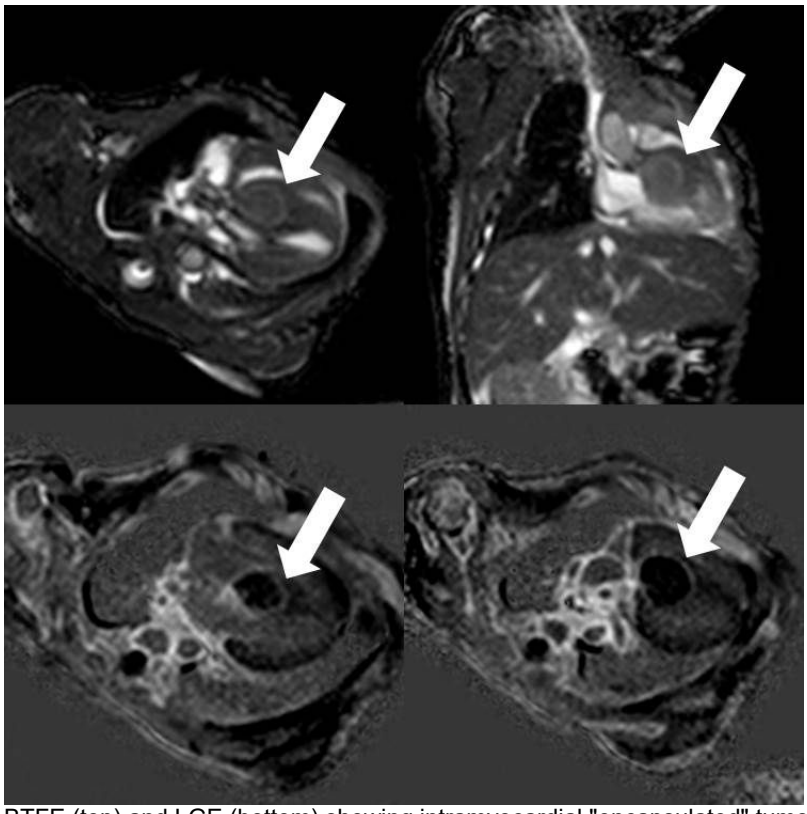

BTFE (top) and LGE (bottom) showing intramyocardial "encapsulated" tumor (arrows) causing LVOT obstruction

ID#: 371332

An interesting case of Myocarditis

Luke Dancy, MBBS MRCP[1] Kevin O'Gallagher, MBBS, MRCP[2], Daniel Sado, BM, MRCP[1]

1. Kings College Hospital, London, England, United Kingdom

2. King's College NHS Foundation Trust, London, UK, United Kingdom

Description of Clinical Presentation: 25 year old male presented acutely with chest pain, dizziness,headache and palpitations. His EKG was unremarkable, but his troponin was mildly elevated. Examination was unremarkable aside from a single significantly elevated blood pressure had been recorded in the emergency department. A CMR was performed with to look for the presumptive diagnosis of myocarditis.

Diagnostic Techniques and Their Most Important Findings: The overall LV function was normal, but with focal wall motion abnormality in the mid anterior wall. The native T1 and T2 were elvated in the basal to mid septum and anterior walls. There was no late enhancement. These findings are consistent with a mild myocarditis.. However, on localaiser and axial anatomical images a large mass was seen just superior to the right kidney in the localiser images. The mass was extremely heterogenous with large fluid filled areas. Triple phase CT and blood and urine metaneprines conformed the diagnosis of phaeochromocytoma which was subsequently removed following pharmacotherapy.

Learning Points from this Case: 1. Myocardtitis has been described in phaeochromocytoma as a presenting symptom
2. The heterogenous nature of the mass on CMR makes it easy to confuse with bowel
3. Attention to the extracardiac anatomy in CMR not only reduces the risk of other pathology being missed but can also assist in the cardiac diagnosis.

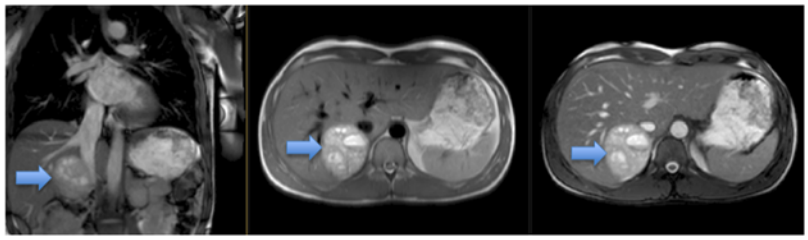

Stills of phaeochromocytoma

ID#: 370955

Asymmetrical thickening of the left ventricular wall

Wooi Kok Lim, MD(USM), MRCPCH(UK)[1] Nor Hanim Mohd Amin, MD(UKM) , MMED(Mal)[2], Martin Ngie Liong Wong, MBBS(Malaya), MRCP(UK)[3]

1. SARAWAK HEART CENTRE , KOTA SAMARAHAN, SARAWAK, MALAYSIA, Kota Samarahan, Sarawak, Malaysia

2. SARAWAK HEART CENTRE , KOTA SAMARAHAN, SARAWAK, MALAYSIA, KOTA SAMARAHAN, Sarawak, Malaysia

3. Sarawak Heart Centre, Kota Samarahan, Sarawak, Malaysia, KOTA SAMARAHAN, Sarawak, Malaysia

Description of Clinical Presentation: A toddler first presented at 6 months of age to the emergency department for fast breathing. She was noted to be having an ventricular tachycardia and was successfully cardioverted medically. A cardiac ultrasound performed, showed she had a thickened left ventricular free wall but there was no significant clear cut mass. The left ventricle free wall did not cause any left ventricular outflow tract obstruction. There was no clear demarcation of the mass and normal ventricular myocardium. She represented many times again to the emergency for breakthrough recalcitrant ventricular tachycardia , and was each time successfully cardioverted. A vast spectrum of anti-arrhythmic agents were used to control her symptoms and presentation. She is currently stable on anti-arrhythmic agents. An elective cardiac magnetic resonance imaging was performed to ascertain the nature of the myocardial mass and the assess the feasibility of tumour resection if there was a clear plain of separation between the normal myocardium and abnormal left ventricular mass.

Diagnostic Techniques and Their Most Important Findings: Electrocardiography-gated, breath-hold cine steady state free precession (SSFP) for axial stacks, left ventricular 4 chambers, 3 chambers, 2 chambers, short axis stacks, and right ventricular 2 chambers and right ventricular outflow track (RVOT) . Electrocardiography-gated, breath-hold cine first pass perfusion sequence. Electrocardiography-gated, breath-hold cine phase contrast flow measurement for Aorta, Pulmonary Artery, 4D Trak Gadolinium bolus with Look-Locker sequence and phase-sensitive inversion recovery PSIR and late gadolinium enhancement (LGE) study. Pre Gadolinium (T1w TSE), Post Gadolinium (T2w TSE, T1w TSE).
Large homogenous left ventricular mass, arising from left ventricular free wall from the apex and extends superiorly towards the mitral valve into the left atrium with a mild left lower pulmonary vein flow obstruction. The mass measures 8.8cm x 3.6 cm x 5.6 cm . Calculated mass volume is 115.3cm^3 . The overall left ventricular myocardial mass 156.1g/m^2 , is significantly contributed by the tumour mass . No clear line of demarcation between the normal myocardium and the tumour mass. The left ventricular ejection fraction is preserved at 54.3%. There is no left ventricular outflow obstruction. Solid homogenous intramyocardial mass in the left ventricular free wall, with CMR features consistent with a cardiac fibroma.

Learning Points from this Case: Cardiac tumour remains a difficult condition to treat. This is more evident in this case when there is no clear demarcation of the tumour and the normal myocardium. The tumour has become a significant part of the left ventricle and contibutes to the cardiac function. It has caused many hospital admissions with recalcitrant ventricular tachycardias and required multiple anti- arrhythmic. As there is no clear separation of normal myocardium and tumour, surgical intervention is impossible. Unlike malignant tumors, fibromas are "benign" and not sensitive to chemotheraphy, thus ruling out use of chemotheraphy. Though benign in nature, the size of the "benign" mass , located at the lateral left ventricular wall , makes up over half of the left ventricular myocardial mass. Should we hold on to our Hippocrates oath "*primum non nocere***",** which means *first , do no harm* , or attempt some intervention to reduce the intramyocardial tumour mass?Will any sort of intervention cause more harm or will the watchful eye cause more harm to not intervening?

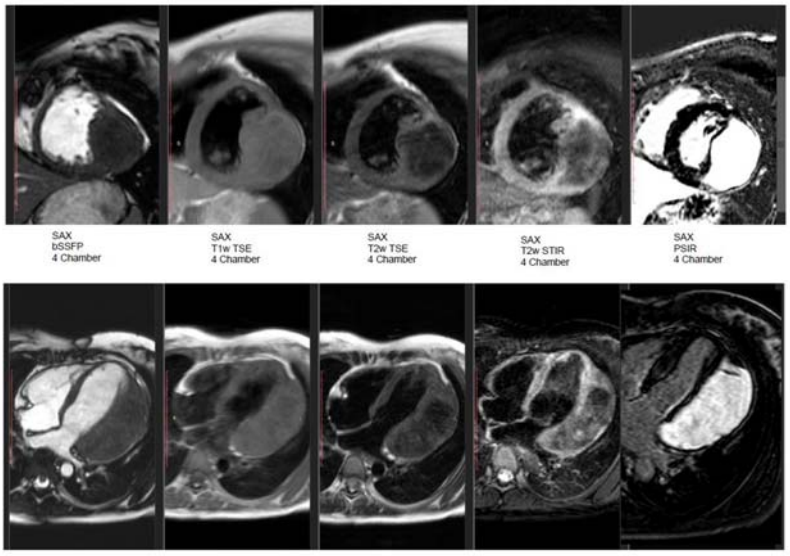

Left ventricular tumor characteristics with different sequences

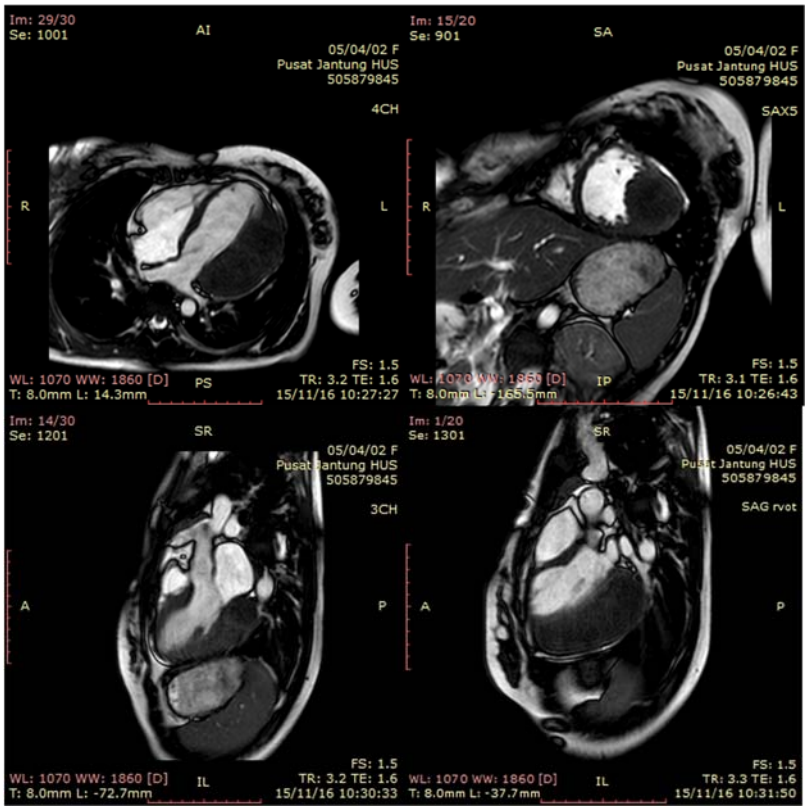

bSSFP images of left ventricular tumor

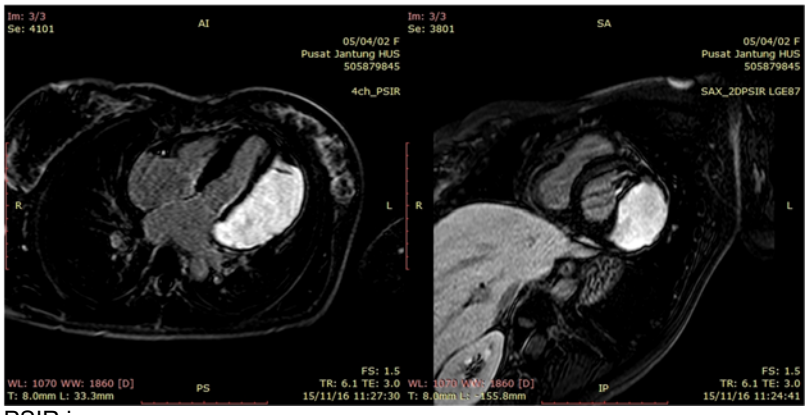

PSIR images

Characteristics of left ventricular tumor

Sequences	**Characteristics**	
bSSFP	Isointense to myocardium	
	T1w TSE	**T2w TSE**
Pre contrast	isointense	hypointense
STIR	-	hypointense
Post contrast	hyperintesnse	
PSIR / LGE	hyperintense	

Characteristics of left ventricular tumor

ID#: 366886

Unusual 'tumor' of the mitral valve presenting with multiple territory cardio-embolic brain infarction

Joseph Lembo, DO[1] Thuy Nguyen, MD[2], Michael O'Loughlin, MD[3]

1. Hartford Hospital, Orange, CT

2. University Hospitals Cleveland Medical Center, Shaker Heights, OH

3. Jefferson Radiology, West Hartford, CT

Description of Clinical Presentation: A 54 year old female with a history of hypertension presented with acute onset memory loss. Head CT demonstrated multiple infarcts involving the bilateral supratentorial white matter, basal ganglia, and cerebellum. A cardio-embolic source was presumed and transthoracic/transesophageal echocardiograms were performed. This demonstrated a circular mass-like lesion in the region of the posterior mitral leaflet and annulus. Cardiac MRI confirmed this finding noting unusual features, possibly representing an abnormally located myxoma. The patient was subsequently referred to surgery. No intra-atrial tumor was noted surgically. The posterior mitral leaflet where it abutted the annulus was diffusely thickened and calcified. When excised, cloudy tan colored fluid was expressed. Following drainage, a residual pocket in the posterior mitral leaflet and annulus was present. The patient underwent a prosthetic mitral valve replacement. Her OR pathology was positive for caseous calcifications only without evidence of tumor cells or infection, consistent with a so-called "toothpaste" tumor. Her recovery was uneventful.

Diagnostic Techniques and Their Most Important Findings: Transthoracic/Transesophageal echocardiograms demonstrated a well-circumscribed, non-mobile, centrally hypoechoic mass associated with the posterior mitral annulus. Mild mitral regurgitation was seen. Cardiac MRI was performed to further characterize, demonstrating an irregularly shaped 2.4 cm mass abutting the inferior left atrial wall and posterior mitral leaflet. This mass was slightly brighter than myocardium on both T1 and T2-weighted images. There was no significant central enhancement with very mild surrounding peripheral enhancement. Operative pathology was consistent with degenerative change, calcification, and chronic inflammation. There was no evidence of infection or extensive replacement by myxoid material.

Learning Points from this Case: Mitral annular calcification (MAC) is a common entity frequently involving the posterior annulus and occasionally the mitral valve apparatus. Caseous calcification is a rare variant that can be seen as a large mass with central echolucency. Echocardiographic prevalence of this caseous variant has been estimated at 0.6% in patients with known MAC and 0.06% of all patients. The internal aspect of the mass becomes a liquefied suspension of calcium, cholesterol, and fatty acids taking a toothpaste-like consistency. This consistency has led to the entity being referred to as a "toothpaste" tumor or caseoma. Caseomas are generally considered benign; however, they have been mistaken for abscesses or cardiac tumors, only truly identified after surgical resection. There is an association between MAC with cardiac conduction abnormalities, higher burden of coronary artery disease, and stroke. However, the caseous nature of these calcifications has not been shown to alter these risks.

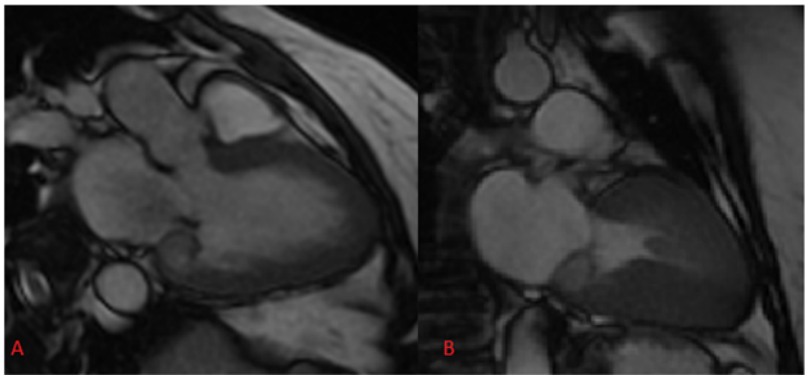

3-Chamber (A) and 2-Chamber (B) FIESTA imaging demonstrates a 2.4 x 1.5 cm mass within the posterior leaflet of the mitral valve. An associated mitral regurgitant jet is seen in the right atrium on the 3-Chamber view.

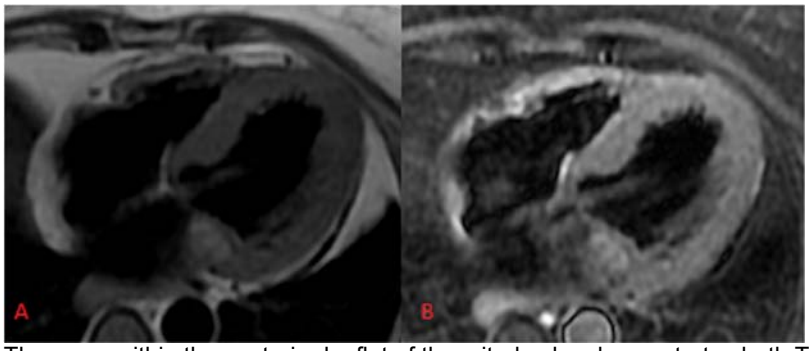

The mass within the posterior leaflet of the mitral valve demonstrates both T1 and T2 central hyperintensity on the Double IR (A) and Triple IR (B) sequences respectively.

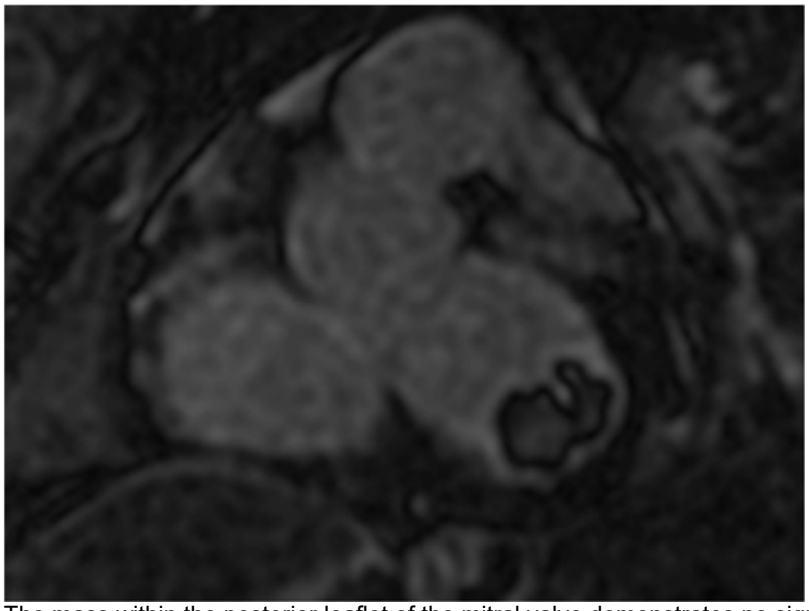

The mass within the posterior leaflet of the mitral valve demonstrates no significant central enhancement with very mild surrounding peripheral enhancement.

ID#: 360125

Incidental dramatic finding with cardiac MRI viability testing: Left Ventricular Free Wall Rupture Missed by Echocardiography

Niels Menck[1] Guido Boerrigter[2], Stefan Loeser[2], Kathrin Schindler[2], Harald Lapp[2]

1. HELIOS Klinikum Erfurt, Erfurt, Thuringen, Germany

2. HELIOS Klinikum Erfurt, Germany

Description of Clinical Presentation: A 57 year old male was referred to our hospital due to 12 hours of persistent angina (NSTEMI). He had pulmonary oedema and a severely reduced left ventricular ejection fraction (LVEF) as assessed by echocardiography done in the emergency room. He immediately underwent transradial angiography, which showed extensive 3-vessel coronary artery disease. The RCA und the mid-LAD were totally occluded (chronic). A thrombotic occlusion of the LCX was responsible for the infarction and the acute cardiac decompensation. Successful percutaneous coronary angioplasty and implantation of a drug eluting stent were performed. After the intervention the patient improved slowly with the support of dobutamine and non-invasive ventilation. Five days post-admission, sudden deterioration occurred. Echocardiography showed pericardial tamponade, which could be drained by percutaneous pericardiocentesis (550 ml haemorrhagic effusion). This was at the time - erroneously- attributed to Dressler syndrome following the subacute myocardial infarction. A successful CTO-recanalization of the mid-LAD was performed 12 days later. The patient was discharged with a readmission planned three months later to address the RCA CTO. Given that the RCA was small and that the LVEF remained reduced, it was decided to first determine the myocardial viability of the inferior wall by cardiac MRI.

Diagnostic Techniques and Their Most Important Findings: A Siemens Aera 1.5T scanner was used for the imaging. The SSFP cine sequences (Figures 1 and 2) showed the known severely reduced LVEF, extensive scarring of the lateral and inferior wall, and an ongoing pericardial effusion with a covered rupture of the free lateral left ventricular wall (long arrows) that was not detected by the other imaging modalities. The late gadolinium enhancement (LGE) sequences (Figure 3) confirmed the extensive left ventricular scar (short arrows) laterally and inferiorly (with microvascular obstruction) and hyperenhancement of the pericardium (long arrows). This was in keeping with the detected covered rupture, which was responsible for the pericardial tamponade 5 days after the initial presentation. The pericardial inflammation saved the patient's life by containing the bleeding and sealing the rupture (pseudoaneurysm). The patient was immediately referred to cardiac surgery.

Learning Points from this Case: Pericardial tamponade is a known, severe complication after myocardial infarction. Sometimes echocardiography provides only a limited view of the lateral wall. This case demonstrates that multiple imaging techniques, including cardiac MRI, should be used to rule out left ventricular free wall rupture in the setting of haemorrhagic pericardial effusion following a myocardial infarction.

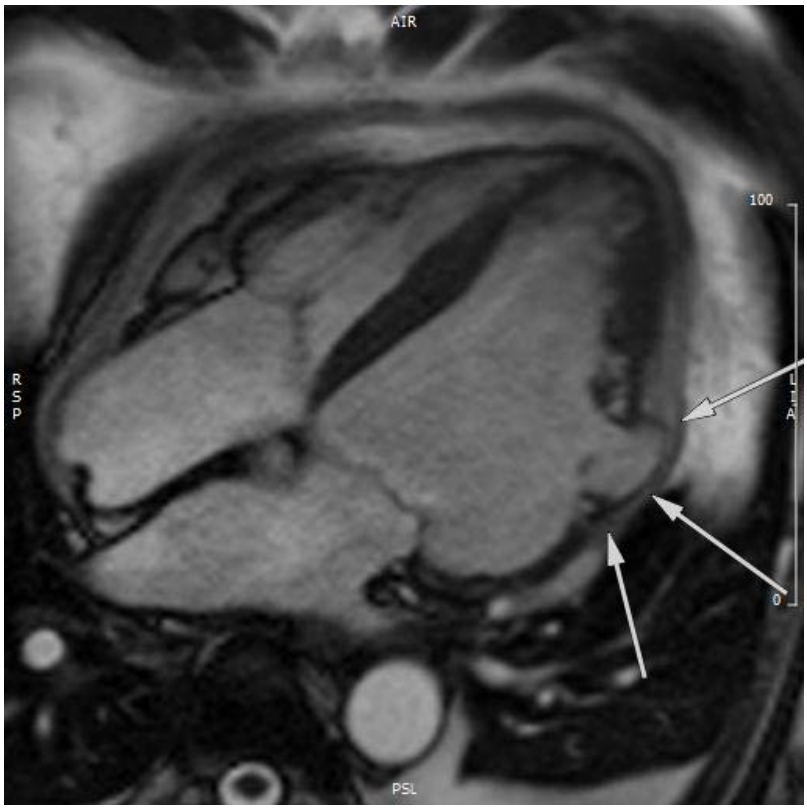

Figure 1: SSFP cine (4 chamber view): covered rupture of the free lateral left ventricular wall (long arrows).

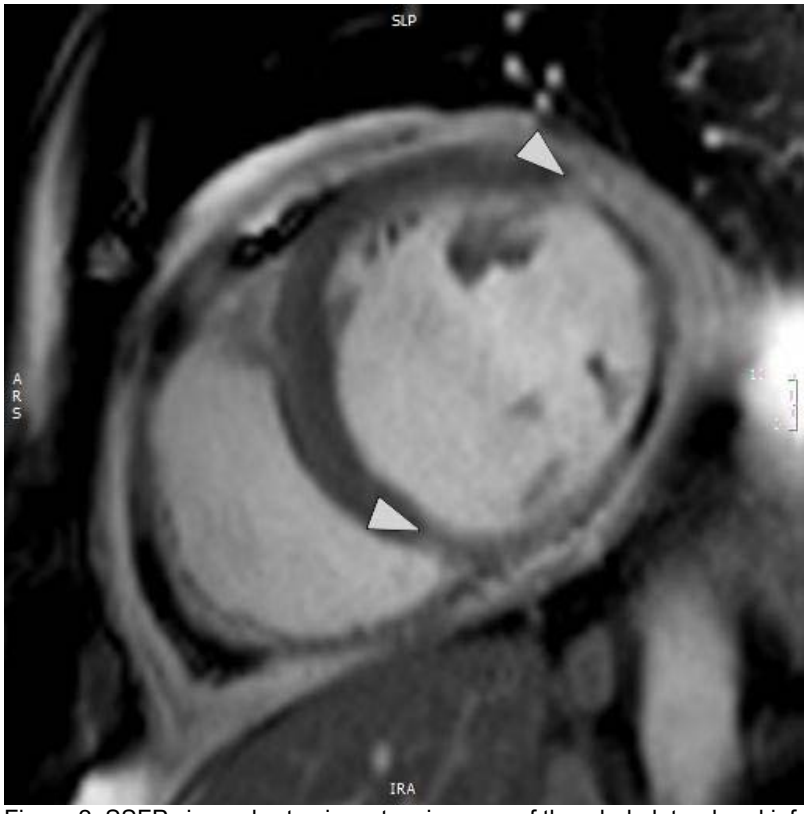

Figure 2: SSFP cine - short axis: extensive scar of the whole lateral and inferior wall.

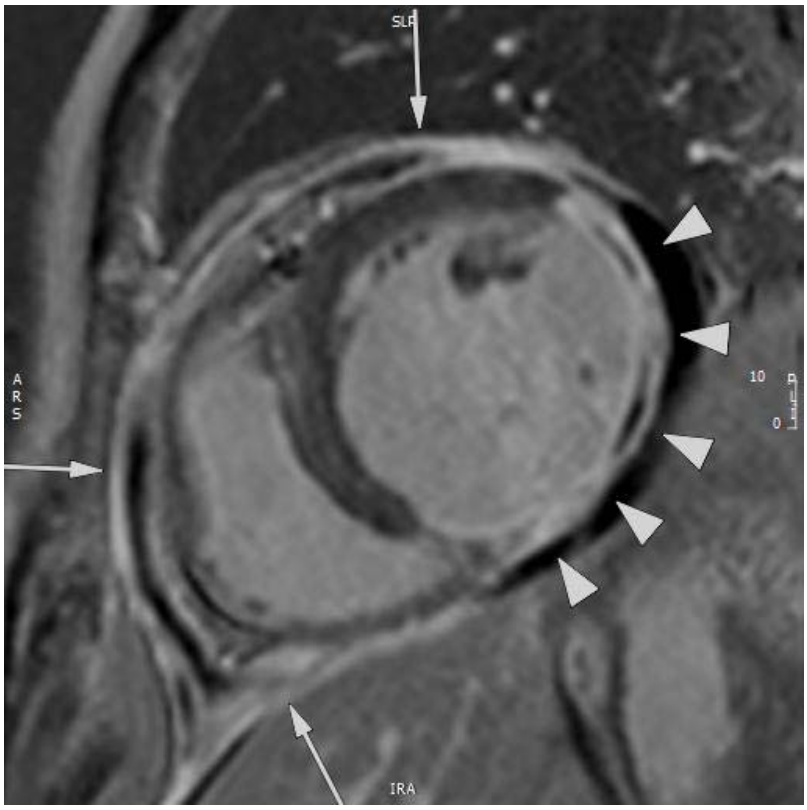

Figure 3: Late gadolinium enhancement (LGE) sequences - short axis: extensive left ventricular scar (short arrows) lateral and inferior (with microvascular obstruction) and a hyperenhancement of the pericardium (long arrows)

ID#: 367206

Fulminant myocarditis with checkpoint inhibitor immunotherapy: Late gadolinium enhancement on cardiovascular magnetic resonance with pathological correlation

Vinh Q. Nguyen, MD[1]Douglas Rottmann, MD[2], Cesia Gallegos, MD[2], Ahmad Charifa, MD[2], Ryan T. Sowell, PhD[3], Brian West, MD[2], Hamid R. Mojibian, MD[4], Harriet M. Kluger, MD[2], Forrester Lee, MD[2], Ralph J. Riello, PharmD[2], Judith L. Meadows, MD[4], Isabel Oliva, MD[5], Steffen Huber, MD[4], Anna Bader, MD[2], Jonathan Killam, MD[2], Imran Hafeez, MD[2], Guoping Cai, MD[2], Mariana L. Henry, BS[2], Lauren A. Baldassarre, MD[6]

1. Yale School of Medicine, New Haven, CT

2. Yale School of Medicine

3. Yale University School of Medicine, New Haven, CT

4. Yale School of Medicine, CT

5. Yale School of Medicine, MADISON, CT

6. Yale University, CT

Description of Clinical Presentation: A 47-year-old woman with metastatic melanoma on nivolumab (anti-PD1 monoclonal antibody) presented with dyspnea and tachycardia. A transthoracic echocardiogram revealed a left ventricular ejection fraction (LVEF) of 26%. Soon after, the patient was hospitalized with acute decompensated heart failure. Cardiovascular magnetic resonance (CMR) imaging revealed a non-ischemic pattern of delayed enhancement, most consistent with a myocarditis. Her clinical course was complicated by cardiogenic shock refractory to inotropic support and immunosuppressive therapy. The patient was eventually made comfort care and died in the hospital. An autopsy was performed and tissue samples were obtained from areas of myocardium with and without late gadolinium enhancement (LGE).

Diagnostic Techniques and Their Most Important Findings: CMR imaging was performed on a Siemens 1.5T scanner. Cine images acquired using steady state free precession sequences revealed four-chamber dilation with severe biventricular failure (LVEF 16%; RVEF 12%). T2-weighted imaging was nondiagnostic due to respiratory motion artifact. LGE-CMR demonstrated mid-wall and epicardial LGE of the basal to mid inferior and inferolateral segments, with a focal area of increased intensity at the inferior RV insertion site (Image 1), involving 15% of the total LV myocardium upon quantitative analysis.

On microscopy, H&E stains showed evidence of significant lymphocytic myocarditis in the regions with LGE (Image 2) but to a lesser degree in the regions without LGE. The infiltrate was composed of almost exclusively T-cells, with an admixture of CD4+ (helper) and CD8+ (cytotoxic) T-cells. Trichrome stain showed moderate fibrosis in the areas of LGE. PD-L1 stain showed focal membrane positivity in the areas of LGE (Image 3).

Learning Points from this Case: Current therapy for metastatic melanoma includes immune checkpoint inhibition, including anti-PD1 therapy. Left ventricular dysfunction and fatal myocarditis are uncommon but possible side effects. Early detection of cardiac toxicity is of significant importance to guide intervention, including immunosuppression and heart failure therapy. This is a unique case demonstrating direct histological correlation of T-lymphocytic infiltration and fibrosis in areas of LGE on CMR, suggesting an acute on subacute/chronic process. Additionally, there was evidence of an inflammatory process, albeit to a lesser degree, in areas without LGE. CMR with more sensitive techniques for detection of inflammation and left ventricular dysfunction may be of incremental value in these patients.

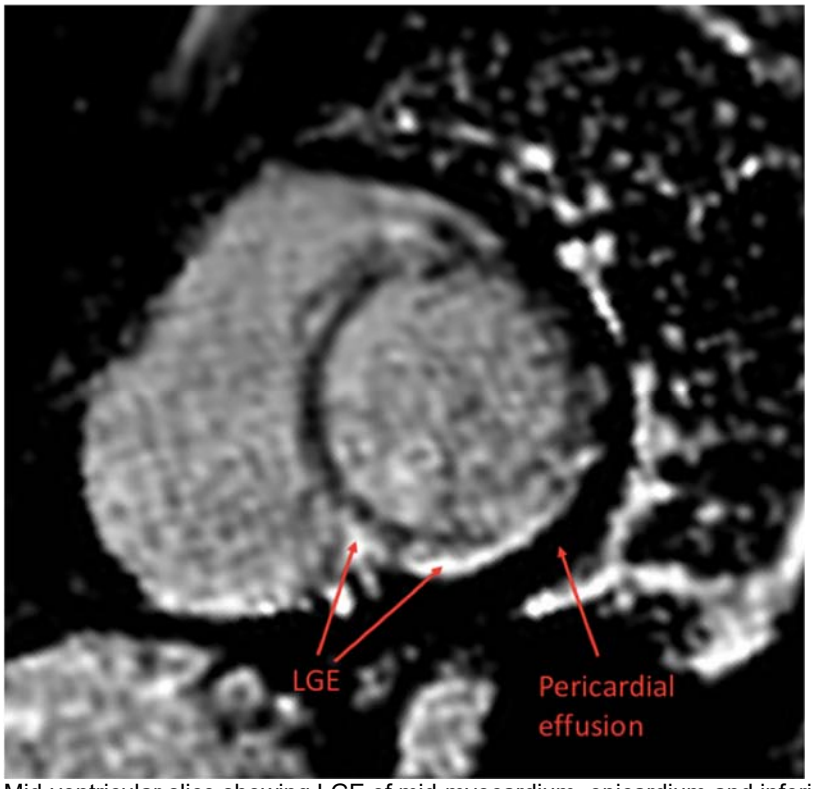

Mid-ventricular slice showing LGE of mid-myocardium, epicardium and inferior RV insertion site.

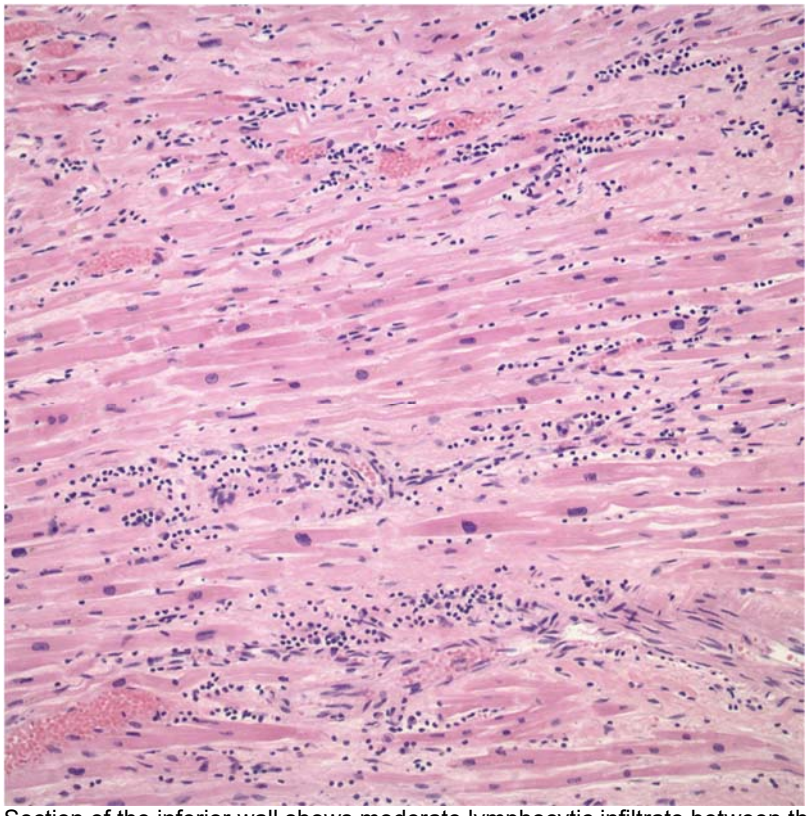
Section of the inferior wall shows moderate lymphocytic infiltrate between the myocytes and myocyte dropout, indicative of a lymphocytic myocarditis. (Hematoxylin & Eosin, 200x).

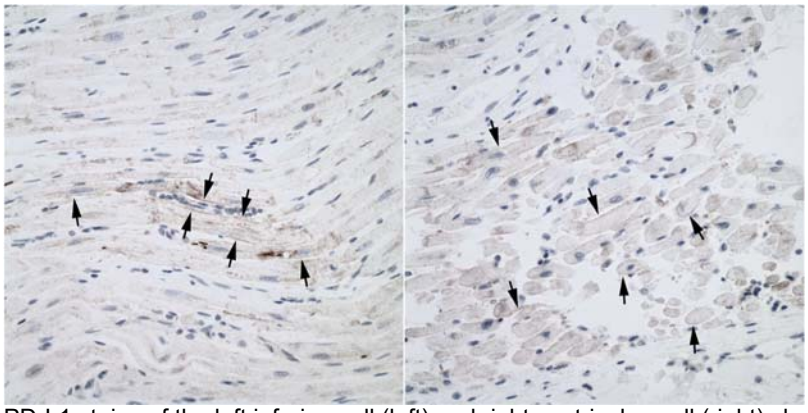

PD-L1 stains of the left inferior wall (left) and right ventricular wall (right) show focal positivity (just over 10% overall). Positive cells have a linear membranous staining pattern (arrows). (PD-L1 22C3 stain, 400x)

ID#: 378297

Intracardiac Cyst: A Mistaken Identity

Iva Golemi, MD[1] Eileen Gajo, BS, MD[2], Amit Pursnani, MD[3]

1. University of Chicago (Northshore), Evansotn, IL

2. University of Chicago (NorthShore), Evanston Hospital

3. NorthShore University HealthSystem, IL

Description of Clinical Presentation: A 48-year-old South American immigrant male presented to our hospital for evaluation of chest pain. The patient complained of non-radiating chest heaviness with outdoor work that resolved with rest and shortness of breath with exertion. Additionally, he described sharp chest pain that occurred multiple times daily, lasting only seconds. He disclosed that several months prior, he was hospitalized at an outside institution for nephrolithiasis and a computed tomography (CT) scan revealed an incidental cyst in his heart.

Diagnostic Techniques and Their Most Important Findings: An initial echocardiogram was unrevealing, but cardiac CT angiography revealed a low-attenuation intra-myocardial mass measuring 1.7x1.5 cm in the apical lateral wall of the left ventricle (A). Further characterization with cardiac MRI showed a well-circumscribed mass of similar measurements that showed lack of enhancement on first pass perfusion (B), and that was SSFP-hyperintense (C). These findings were consistent with an encapsulated cyst. Given the patient';s geographic origin, parasitic testing was done, which was positive for Echinococcus. With a working diagnosis of hydatid cyst, the patient was started on Albendazole. Due to persistent angina, he ultimately underwent surgical extirpation with cautious excision given the possible antigenic nature of the cyst contents. Surprisingly, histological examination revealed myocardium with a unilocular benign cyst lined by a flat single cell layer; no parasites were identified. Final diagnosis of a congenital mesothelial cyst was made. The patient recovered well post-operatively and had resolution of chest pain.

Learning Points from this Case: The true incidence of intramyocardial cysts is unknown, though most case reports are due to echinococcal cysts. Geographical background is always an important component when forming a differential diagnosis; however, congenital anomalies should also be considered in patients with progressive, persistent angina. While most are asymptomatic and can be followed with extended surveillance, they do have the potential to grow and cause compression on the adjacent myocardium and/or vessels, which can subsequently cause chest pain. Advanced imaging with CT and cardiac MRI are helpful in delineating the anatomy of a cyst. They can provide tissue characterization and aid in assessing the potential impact on neighboring structures, including coronary branch vessels, which can possibly lead to more rapid referral to a cardiothoracic surgeon. Thus, congenital cyst identification can be a crucial one and should always be kept within the differential.

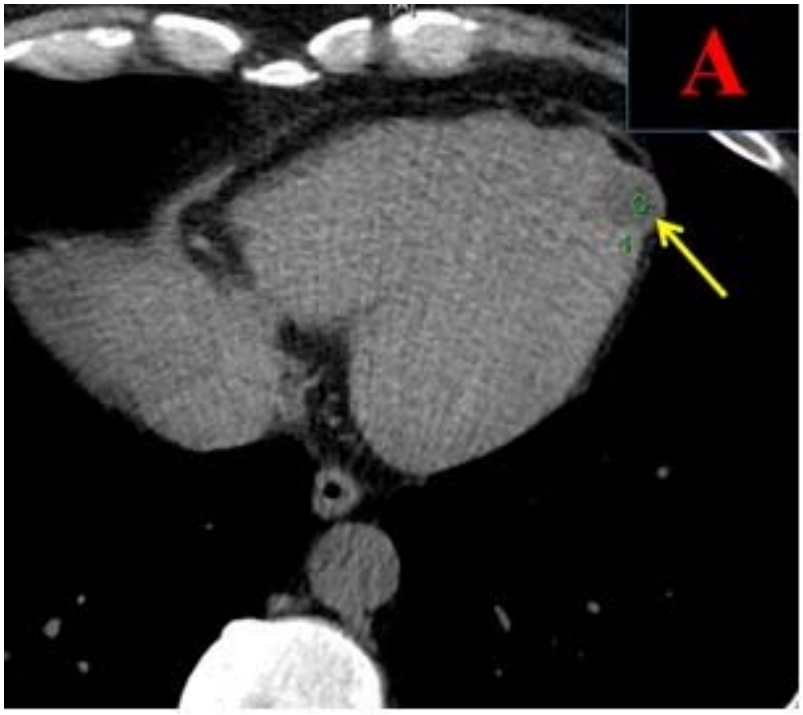

Computed tomography (CT) in the axial plane showing an intramyocardial mass (yellow arrow) measuring 1.7x1.5 cm in the apical lateral wall of the left ventricle.

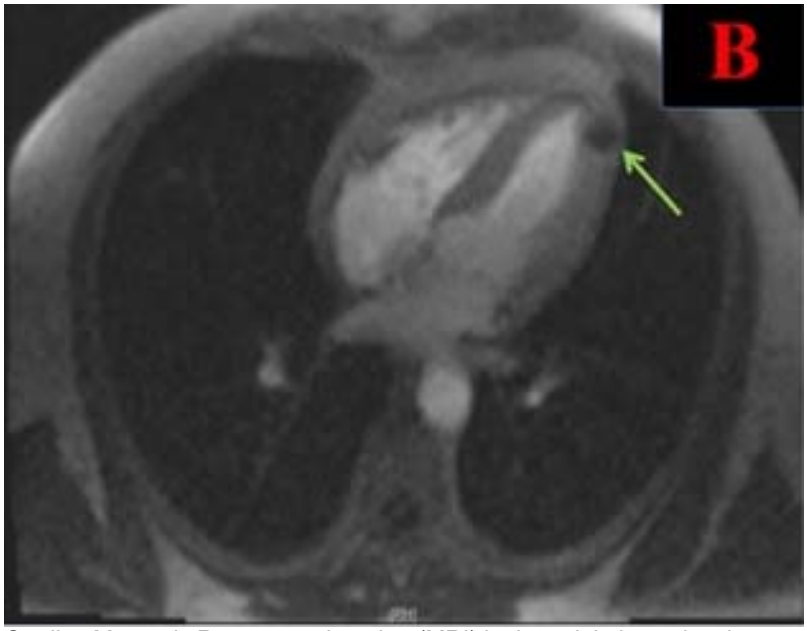

Cardiac Magnetic Resonance Imaging (MRI) in the axial plane showing a well-circumscribed mass (green arrow) measuring 1.7x1.4 cm in the apical wall of the left ventricle with lack of enhancement on first pass perfusion.

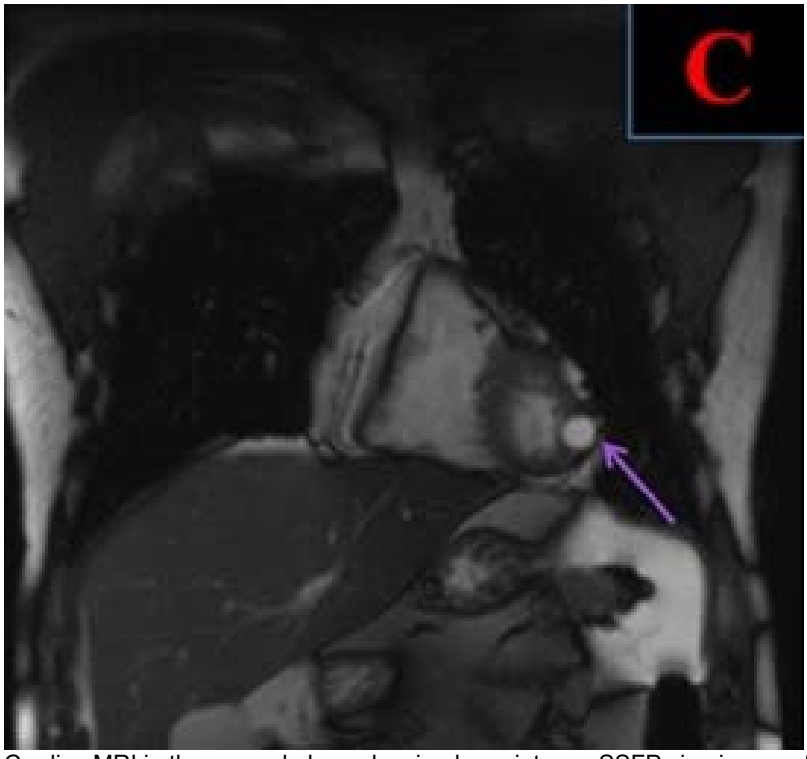

Cardiac MRI in the coronal plane showing hyperintense SSFP cine image of an intramyocardial mass (purple arrow). The mass demonstrated high T2 signal and low intensity signal on T1-weighted images.

ID#: 378491

CMR sees everything - the joy of interventional cardiologists

Tobias A. Fuchs, MD, FESC, FSCCT[1]Elena G. Milano, MD[1], Estefania De Garate, MD[2], Sarah Moharem-Elgamal, MD[1], Konstantina Mitrousi, MD[1], Iwan Harries, MD[2], Amardeep Ghosh Dastidar, MBBS(Hons), MRCP[2], Anna Baritussio, MD[2], Chiara Bucciarelli-Ducci, MD, PhD[2]

1. Bristol Heart Institute, Bristol NIHR Biomedical Research Centre (Cardiovascular Section), University of Bristol, United Kingdom

2. Bristol Heart Institute, Bristol NIHR Biomedical Research Centre (Cardiovascular Section), University of Bristol, Bristol, England, United Kingdom

Description of Clinical Presentation: A 62-year old patient presented with an inferoposterior STEMI.

Diagnostic Techniques and Their Most Important Findings: Invasive coronary angiography revealed a dominant proximally blocked right coronary artery. The patient received primary percutaneous intervention and DES stenting of the right coronary artery. Additionally the left anterior descending artery was found to be moderately to severely diseased. Echocardiography revealed a moderate to severe left ventricular systolic impairment (left ventricular ejection fraction of 36%) and a normally sized right ventricle with impaired radial function. Ten weeks after acute presentation, the patient was referred to undergo a stress CMR in order to investigate the presence of inducible myocardial ischemia and viability in the territory of the left anterior descending artery. Adenosine stress perfusion CMR was performed on a 1.5 Tesla scanner. The SSFP cine images revealed a mildly reduced left ventricular ejection fraction (LVEF 52%) with severe hypokinesia in the proximal to distal right coronary artery territory. There was a billowing of the mitral valve without significant mitral regurgitation. The systolic function of the right ventricle was normal (RVEF 53%) but there was a focal area of marked hypokinesia of the mid portion of the right ventricular free wall. Despite adequate response to adenosine there was no inducible myocardial ischemia. On late gadolinium enhanced images there was a large transmural myocardial infarction of the inferior wall from base to apex corresponding to the proximal to distal RCA territory with a core of microvascular obstruction and a partial infarction of the posterior papillary muscle. Interestingly, additional focal infarction of the right ventricular free wall was found (Figure 1). Overall, there is was no inducible myocardial ischemia but the presence of microvascular obstruction suggested that the RCA infarction war relatively recent . Subsequent review of the coronary angiography demonstrated RV side branch occlusion consistent with the incidental RV infarction (Figure 2).

Learning Points from this Case: CMR is a highly accurate diagnostic tool to assess right ventricular infarction. Despite the thin right ventricular wall, even a small area of late gadolinium enhancement can be detected. Stenting can lead to occlusion of overstented side branches and subsequently to myocardial infarction. Microvascular obstruction can be detected after myocardial infarction and is a poor prognostic indicator.

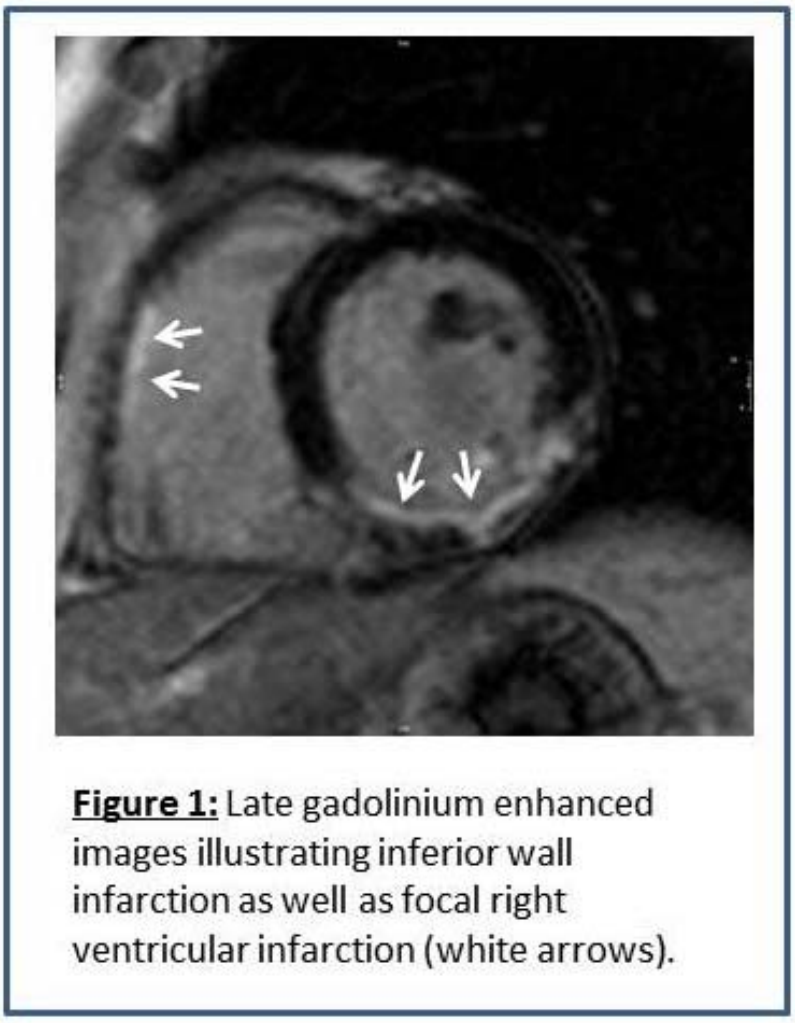

Figure 1: Late gadolinium enhanced images illustrating inferior wall infarction as well as focal right ventricular infarction (white arrows).

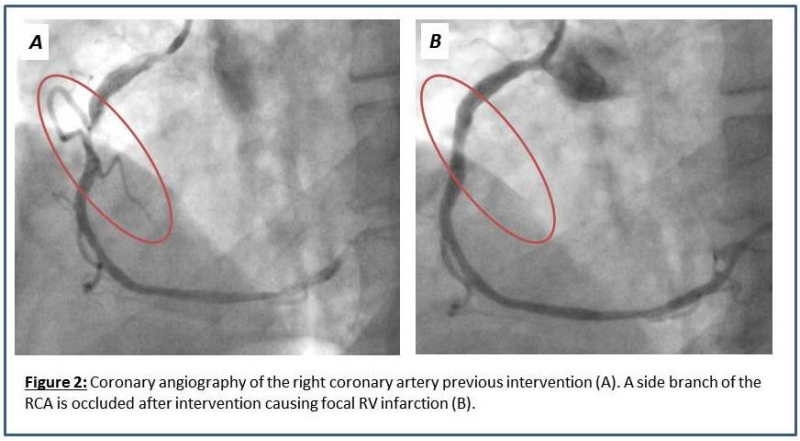

Figure 2: Coronary angiography of the right coronary artery previous intervention (A). A side branch of the RCA is occluded after intervention causing focal RV infarction (B).

ID#: 377963

Risk of Embolization of Left Atrial Myxoma associated with Carney's Complex

Bharath Sathya, MD[1] Andrew E. Arai, MD[2], W. Patricia Bandettini, MD[3], Phillip Corcoran, MD[4], Markku M. Miettinen, MD[5], Constantine Stratakis, MD[6]

1. National Institutes of Health/NHLBI, Bethesda, MD

2. National Heart, Lung and Blood Institute, National Institutes of Health, Bethesda, MD

3. National Heart, Lung and Blood Institute, National Institutes of Health, MD

4. 2. Suburban Hospital, MD

5. Laboratory of Pathology, NIH/NCI, MD

6. National Institutes of Health

Description of Clinical Presentation: A 44-year-old Caucasian female with a past medical history of Carney';s complex (CNC) and cardiac myxoma presented for specialized care of her rare condition. Her past medical history was significant for a cardiac myxoma that had embolized and was resected in 2010. She presented with hemiplegia initially in 2010 and was eventually diagnosed with a cerebrovascular accident secondary to an embolized myxoma. Her physical examination was significant for a right facial droop.

Diagnostic Techniques and Their Most Important Findings: A transthoracic echocardiogram detected a 45 mm x 24 mm mass adherent to the left side of the inter-atrial septum. The mass prolapsed through the mitral valve in diastole with a 5 mmHg trans-mitral gradient. A CMR was recommended to further evaluate the mass. Cine MRI documented a 48 x 20 mm mass that moved partially through the mitral valve in diastole. There was no hemodynamically significant obstruction to flow as the smallest mitral valve orifice measured on phase contrast imaging was approximately 3.86 sq cm. The mass had prolonged T1 and T2 relaxation times but the core of the mass had lower T2 than the periphery. On perfusion imaging, there was minimal uptake of contrast. On late gadolinium enhancement imaging, there was minimal enhancement within the mass. No additional masses were detected. The findings were consistent with a large atrial myxoma. The patient was sent for surgical resection, where a 42 mm x 38 mm x 36 mm mass was excised from the left side of the inter-atrial septum.

Learning Points from this Case: 1. The recurrence of this mass in the same location in the absence of symptoms illustrates the importance of surveillance imaging post resection particularly in CNC patients.
2. Cardiac myxomas are the second most common finding in CNC. It has been described that 57% of patients with CNC have died from cardiac related effects including obstruction, embolic events, or cardiac surgery related complications. Myxomas in CNC develop in the second and third decade of life, and recur more frequently after resection than spontaneous myxomas.
3. This mass was resected due to concerns for embolic potential given the patient';s prior history. The pathological characteristics of the mass (presence of micropapillary elements) are associated with risk of embolization.
4. CMR is warranted in patients with CNC with plans for resection of a myxoma as some patients have more than one tumor, sometimes in different cardiac chambers.
5. Velocity encoded phase contrast imaging can evaluate for a hemodynamically significant obstruction of the mitral valve and residual orifice area.

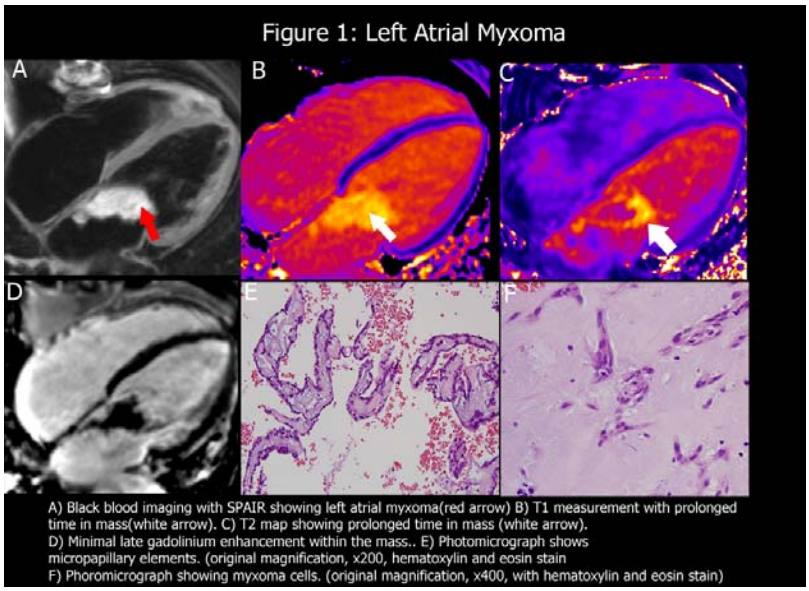
Figure 1: Left Atrial Myxoma
A
B
C
D
E
F
A) Black blood imaging with SPAIR showing left atrial myxoma(red arrow) B) T1 measurement with prolonged time in mass(white arrow). C) T2 map showing prolonged time in mass (white arrow).
D) Minimal late gadolinium enhancement within the mass.. E) Photomicrograph shows micropapillary elements. (original magnification, x200, hematoxylin and eosin stain
F) Phoromicrograph showing myxoma cells. (original magnification, x400, with hematoxylin and eosin stain)

ID#: 377874

Biventricular dysfunction in neuronal ceroid lipofuscinosis: dual pathology or a unifying aetiology?

Lydia Bos[1] Rocio Eiros[2], Rhodri Davies, MRCP, PHD[3], Joao Augusto, MD[4], Ana Gomes[5], Mark Westwood, MBBS MD FRCP FESC[6], Thomas Treibel, PhD[7], James C. Moon, MD[7]

1. Hospital de la Santa Creu i Sant Pau, Spain

2. Barts Heart Centre, London, United Kingdom, Spain

3. Barts Heart Centre, London, United Kingdom, CARDIFF, Wales, United Kingdom

4. Barts Heart Centre, Lisbon, Portugal

5. Barts Heart Centre, Portugal

6. Barts, England, United Kingdom

7. Barts Heart Centre, England, United Kingdom

Description of Clinical Presentation: A 29-year-old African male without cardiovascular risk factors presented in his early 20s with cerebral ataxia, von Willebrand disease and retinitis pigmentosa and was eventually diagnosed with Neuronal Ceroid Lipofuscinosis (NCL). During follow-up, he developed heart failure with biventricular impairment by echocardiography, and subsequently started on betablockers and ACE inhibitors. He was referred for CMR for further myocardial characterisation.

Diagnostic Techniques and Their Most Important Findings: CMR was performed at 1,5T. Extracardiac imaging showed decompensation with a small pericardial effusion, bilateral pleural effusions and ascites. The left ventricle (LV) was non-dilated with severely impaired function (EF = 18%) with some regionality – there was akinesia of the basal-to-mid inferior and inferolateral wall and hypokinesis elsewhere. The right ventricle (RV) had normal cavity size but severe systolic dysfunction. Early gadolinium enhancement showed a small apical LV thrombus (figure 1). There was extensive, bright, clearly defined non-infarct pattern of late gadolinium enhancement in mid wall of LV and RV, particularly in the areas of akinesis (figure 2).

Learning Points from this Case: Neuronal ceroid lipofuscinosis is a rare genetic degenerative disorder that causes excess accumulation of lipopigments in bodily tissues. Cardiac involvement has been described mainly as repolarization disturbances, sinus node dysfunction and ventricular hypertrophy. The pattern of late gadolinium enhancement here is unusual – whilst this may be dual pathology from an unusual myocarditis or dilated cardiomyopathy, we suspect this is the first description of cardiac disease in NCL.

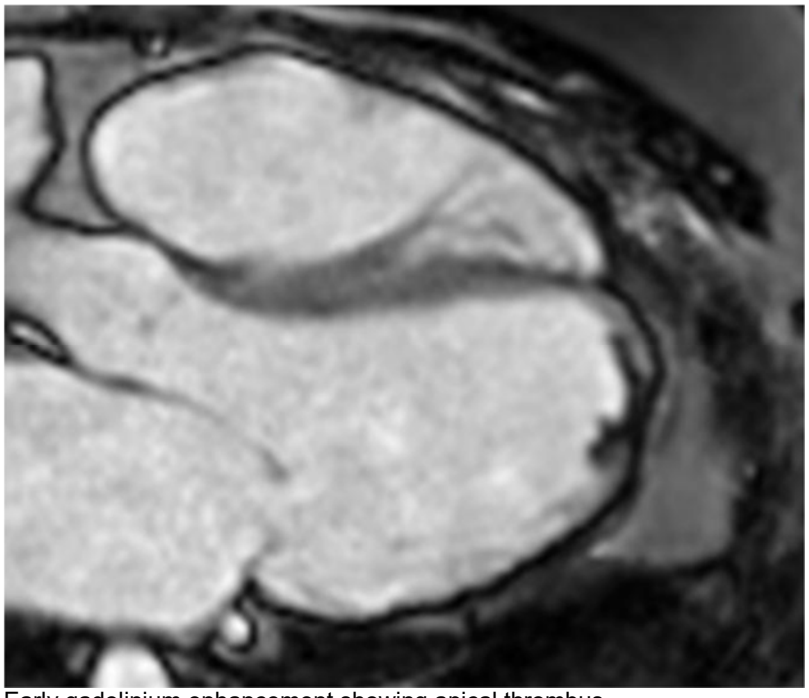

Early gadolinium enhancement showing apical thrombus

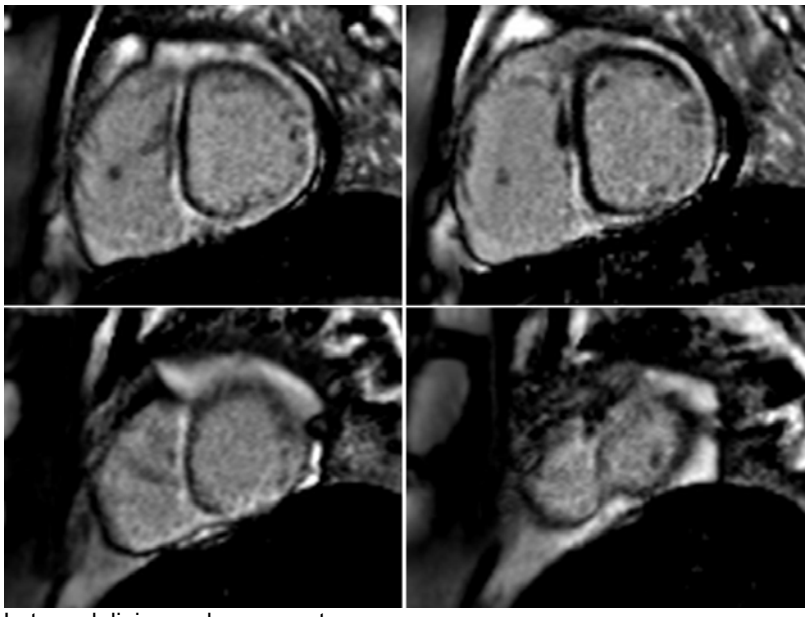

Late gadolinium enhancement

ID#: 374747

Post-MI pericarditis or Dressler syndrome post-open heart surgery? Key role of CMR in the differential diagnosis.

Lilia M. Sierra-Galan, MD, MCvT[1] Angel L. Alberto-Delgado, MD[2], Alejandro Rey-Rodriguez, MD[3], Ingrid E. Flandes-Aguilar, MD[4], Julio Lopez-Cuellar, MD[3], Marco A. Reza-Orozco, MD[5]

1. American British Cowdray Medical Center, CDMX, Distrito Federal, Mexico

2. Central Military Hospital, Mexico, City, Distrito Federal, Mexico

3. American British Cowdray Medical Center, Mexico, Distrito Federal, Mexico

4. American British Cowdray Medical Center, Distrito Federal, Mexico

5. American British Cowdray Medical Center, Mexico

Description of Clinical Presentation: A 50-year-old male patient presented with long-term atypical angina. He had long-term untreated dyslipidemia with 5 consecutive check-up';s positive treadmill stress test but negative SPECT scans. His physical examination was normal and the ECG showed diffuse repolarization abnormality. A CCTA depicted significant lesions in left main coronary artery (LMCA), in proximal LAD and LCx. Invasive coronary angiography (ICA) was schedule but the patient had acute chest pain and presented earlier for an urgent ICA that confirmed CCTA findings. Coronary artery bypass grafting with LIMA to LAD and venous graft to OM-1 was successfully performed and he was discharged from the hospital 5 days later in good condition. Three days later he started with severe chest pain, fatigue, low-grade fever, dyspnea and pleuritic pain; he had pericardial rub and bilateral pleural effusion (PE), he was started on non-steroidal anti-inflammatory (NSAA) drugs and diuretics with incomplete response. An Echo found mildly significant pericardial effusion. The NSAA treatment was reinforced and he remained stable, but his clinical condition (CC) deteriorates 2-weeks later and the drainage of 550 mL of hemorrhagic fluid from PE was performed; with immediate but transient improvement of his CC. The CMR done 3 weeks after surgery due to worsening of symptoms showed a recent small myocardial infarction (MI) in the OM territory, mild pericardial effusion, moderate left PE and thickened, markedly inflamed pericardium with constrictive physiology. A Dressler syndrome (DS) was diagnosed and he was changed into higher doses of NSAA and colchicine with excellent response. His medical treatment started the reduction after 8 months with no further need of invasive procedures. He is completely asymptomatic and free of new events after 10 months of follow-up.

Diagnostic Techniques and Their Most Important Findings: Routine pre-op laboratory tests showed only high cholesterol levels. Pre-op ECG showed diffuse repolarization abnormality. CCTA showed high-grade stenosis in distal LMCA, in proximal LAD and LCx. ICA confirmed CCTA findings. Two-weeks post-op HSCRP was elevated. Post-op echo showed normal LV function with moderate pericardial effusion with inspiratory reduction of transvalvular flows. Chest X-ray showed minimum left PE. First CMR was negative for myocardial ischemia and showed mild LV dysfunction, a small recent MI in the OM territory, mild pericardial effusion, moderate left PE and pericardium globally, mildly thickened and markedly inflamed with constrictive physiology. CMR one week after showed improvement of LV function and non-global, less thickened pericardium with no pericardial effusion but still highly inflamed. CMR four months after showed the old MI, further improvement of LV global function, no pericardial or PE, pericardium slightly inflamed with normal thickness. CMR 8 months later showed minimally inflamed pericardium. Last HSCRP was normal.

Learning Points from this Case: DS is a secondary pericarditis that can occur after MI or open heart surgery and it is immune-mediated, but its incidence has been declining in recent years. CMR has several clues to make the differential diagnosis and to guide proper treatment, such as clearly visualization of the global aspect of pericardial involvement by LGE that strongly suggest the inflammatory component of the disease, which can reinforce the use of full anti-inflammatory medical treatment and to avoid unnecessary invasive procedures or radiation exposure.

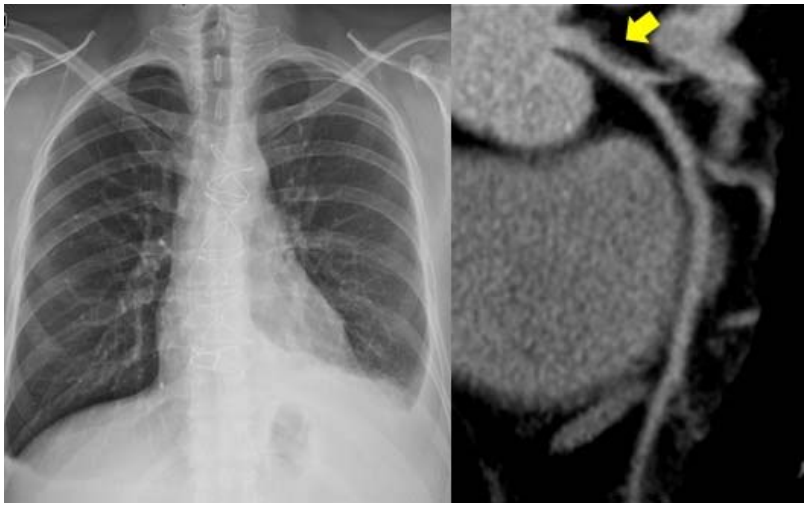

Left side: Chest x-ray showing minimum left pleural effusion. Right side: CCTA showing significant non-calcified plaque in mid-distal left main coronary artery (arrow).

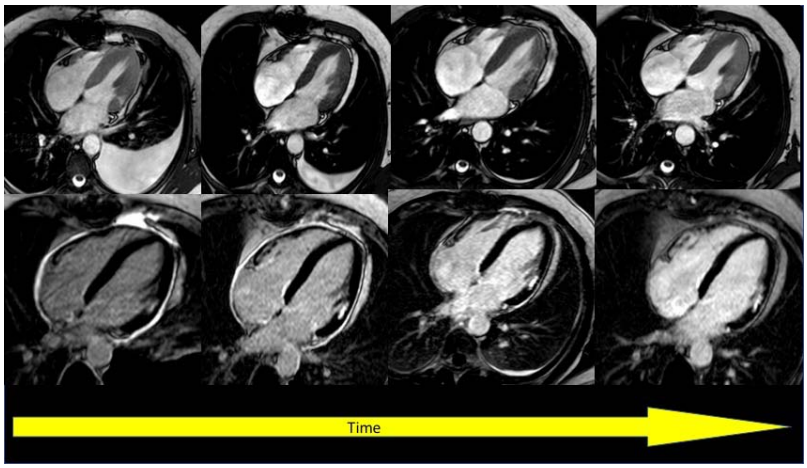

Superior panel. SSFP sequence in 4-chambers long axis views showing the time line from the surgery and the following 8 months; where pleural effusion clearly diminished until disappeared and the pericardial effusion initially increased to became the resolution process until a trivial remaining effusion. Inferior panel. LGE sequence in 4-chambers long axis views showing the time line from the surgery and the following 8 months; where the myocardial infarction stablished and the pericardium was initially thickened and strongly enhanced compatible with inflammation that slowly became not enhanced in almost of normal thickness.

ID#: 374091

Spontaneous coronary artery dissection and Takotsubo cardiomyopathy: MRI demonstration of the underlying mechanism

Antonella Cecchetto[1]Emiliano Dalla Chiara[2], Stefano Bonapace[1], Carmelo Cicciò[1], Clementina Dugo[2], Enrico Barbieri[1]

1. Ospedale Sacro Cuore Don Calabria - Negrar Verona, Italy

2. Sacro Cuore Don Calabria Hospital, Negrar, Verona, Italy

Description of Clinical Presentation: A female of 53 years old, with a history of arterial hypertension, came to the Emergency Room for chest pain from 30 minutes, radiating to the left arm and arising after a familiar fight.

Diagnostic Techniques and Their Most Important Findings: ECG documented anterior ST segment elevation (Fig. 1A) and transthoracic echocardiogram showed apex akinesia. The patient underwent to urgent coronary angiography, that showed spontaneous dissection of distal left anterior descending (LAD) coronary artery (Fig. 1D e 1 E). Apex akinesia with basal segments hyperkinesia was visible, like Takotsubo cardiomyopathy (TTC), at ventriculography (Fig. 1C). There was a rise in Troponin I (2,15 ug/L) to laboratory tests and later ECG documented anterior T waves inversion (Fig. 1B). For a better definition of the left ventricular dysfunction mechanism, the patient underwent to cardiac MRI. We saw apical hypokinesis on cine sequences (Fig. 1F, 1G, 1H), apical oedema on STIR sequences (Fig. 1I, 1L) and no late enhancement after gadolinium injection (Fig. 1M, 1N, 1O).

Learning Points from this Case: Spontaneous coronary artery dissection (SCAD) and TTC can both cause myocardial infarction with subsequent normalization of wall motion abnormality. About this, SCAD can result in prolonged ischemia in the territory of the dissected artery, which can cause myocardial stunning. SCAD and TTC share clinical similarities: predilection for younger women, association with precipitating stressors, ischemic electrocardiographic abnormalities, biomarker positivity and wall motion abnormalities that subsequently normalize. A potential difference between the two conditions is that the wall motion abnormality resulting from SCAD corresponds to the affected artery and may not have the classic apical ballooning appearance of TTC if the distal LAD artery is unaffected. In this case, SCAD of LAD resulted in apex akinesia, because LAD artery was very large and wrapped around the LV apex and supplied the inferior wall. We have a demonstration that SCAD had similar MRI presentation to TTC, because prolonged ischemia causes apical oedema, without late enhancement, a demonstration of myocardial stunning. In conclusion the presence of normal coronary arteries with wall motion abnormalities may prompt an operator to diagnose TTC; however, the angiographer should scrutinize the coronary angiogram to rule out SCAD.

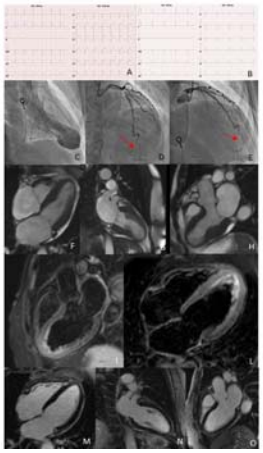

ID#: 378949

Reversible cardiomyopathy in a patient with juvenile hemochromatosis after iron-chelating agents for the treatment of iron overload.

Lorena Squassante. Capeline[1] Cibele Gontijo[2], Davi Zagonel[2], José Eduardo Barbosa[3], Carlos Gonçalves de. Paula Junior[3], Marly Uellendahl, MD, PhD[2], Roberto Cury, MD, Phd[3]

1. University of São Paulo, São Paulo, Sao Paulo, Brazil

2. DASA São Paulo , Universidade Federal de São Paulo - Unifesp, Brazil

3. DASA São Paulo, Brazil

Description of Clinical Presentation:

A 44-year-old Brazilian woman who had diagnosed juvenile hemochromatosis (HAMP mutation on 5';-UTR region) that developed symptoms of congestive heart failure 1 week ago. She had had fatigue at medium exertion, dyspnea and nocturnal paroxysmal dyspnea. She hadn´t had edema, urinary changes or fever. At physical examination, she was good general condition, stained, hydrated, afebrile, acyanotic. Normal heart sounds, without murmurs. Blood pressure 120x60 mmHg and cardiac frequency 90 bpm. Audible vesicular murmur without adventitious noise. Flabby abdomen, without visceromegaly. No edema or signs of clogging.

Diagnostic Techniques and Their Most Important Findings: She was found to have dilated cardiomyopathy in the cardiac magnetic resonance (CMR) with left ventricular ejection fraction (LVEF) of 42%. Her laboratory tests were: hemoglobin (Hb) 11.7 g/dL, transferrin saturation (TS) 100%, serum ferritin (SF) 7,350 ng/mL and CMR using T2* evaluation showed liver iron concentration (LIC) of 40.75mg Fe/g dry (NV<2.0 mg/g) and myocardium iron concentration (MIC) of 2.5mg/g (NV<1.1 mg/g). Five years after treatment with iron-chelants, CMR showed a dramatic improvement of her cardiac function with LVEF of 63% and no detection of iron in myocardium (MIC of 0.69 ng/mL).

Learning Points from this Case: Juvenile hemochromatosis is a rare form of iron overload that frequently causes cardiomyopathy. The mechanism by which disordered iron metabolism induces heart failure is not entirely understood, but myocardial dysfunction appears to be intimately related to the deposition of iron in myocytes. Cardiac function characteristically worsens or improves in proportion to the degree of iron accumulation in cardiac myocytes.
This case indicates that the cardiac function in juvenile hemochromatosis could be reversed once iron overload from treatment with iron-chelating agents.

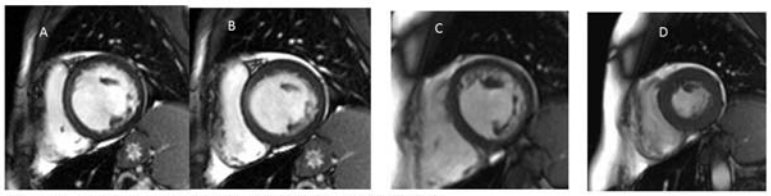

Figure 1: Left ventricular function 2013 (A;B) and 2017 (C;D).

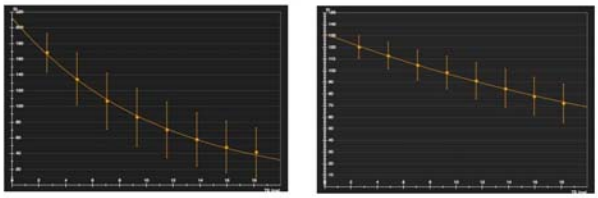
Figure 2: Graphic show iron overload in 2013 on the left and 2017 on the right.

Left ventricular function before and after treatment.

ID#: 378762

CMR diagnosis of microvascular dysfunction? It's all in the map

Tushar Kotecha, MRCP(UK) MBChB[1] Ana Martinez Naharro, MD[2], Rohin Francis, MBBS[3], Hossam Fayed, MBChB MSc MRCP(UK)[4], Michele Boldrini[3], Daniel S. Knight[2], Peter Kellman, PhD[5], Marianna Fontana, MD, PhD[3]

1. Royal Free London NHS Foundation Trust, London, England, United Kingdom

2. UCL Department of CMR, Royal Free Hospital, London, England, United Kingdom

3. UCL Department of CMR, Royal Free Hospital, England, United Kingdom

4. UCL Department of Cardiac MRI, Royal Free Pulmonary Hypertension Service, Pond Street, England, United Kingdom

5. National Heart, Lung, and Blood Institute, National Institutes of Health, Bethesda, MD

Description of Clinical Presentation: Patients with symptoms of angina are commonly referred for stress perfusion CMR and/or coronary angiography for assessment of ischaemia and evaluation of coronary anatomy. The detection of microvascular dysfunction is often a diagnosis of exclusion following the demonstration of unobstructed coronary arteries, although invasive physiological assessment may help.

Diagnostic Techniques and Their Most Important Findings: Here we present the case of a 79-year old lady with hypertension and hyperlipidaemia who reported a 2-year history of classic exertional angina. She underwent stress perfusion CMR at 1.5T which included a new motion corrected myocardial perfusion method with automated in-line perfusion mapping allowing for pixel-wise quantification of myocardial blood flow (MBF). Visual analysis of traditional saturation recovery perfusion images failed to show a perfusion defect, however myocardial perfusion maps showed globally reduced subendocardial perfusion (Figure). She went on to have coronary angiography that showed unobstructed coronary arteries and invasive coronary physiology assessment confirmed the presence of microvascular dysfunction with elevated index of microcirculatory resistance, IMR (LAD 45, Circumflex 24, RCA 58, normal range <20). She was treated with anti-anginal therapy resulting in improvement in symptoms. In contrast, a 58-year old male with hypertension reporting a 3-month history of atypical chest pain underwent coronary angiography showing normal coronaries and normal IMR (LAD 11 and Circumflex 13). Stress perfusion CMR with the same sequences showed normal myocardial blood flow (Figure).

Learning Points from this Case: Here we use myocardial perfusion mapping to detect microvascular dysfunction, confirmed with invasive physiological assessment. Microvascular dysfunction is important to diagnose correctly as the management is with anti-anginal therapy rather than reassurance and other investigations. Myocardial perfusion mapping may be able to differentiate microvascular dysfunction from normal, but larger scale studies are required to confirm this hypothesis.

Figure 1: Myocardial perfusion maps (stress and rest) and coronary angiograms of a patient with microvascular dysfunction confirmed by invasive coronary physiology and a patient with unobstructed coronaries with no evidence of microvascular dysfunction

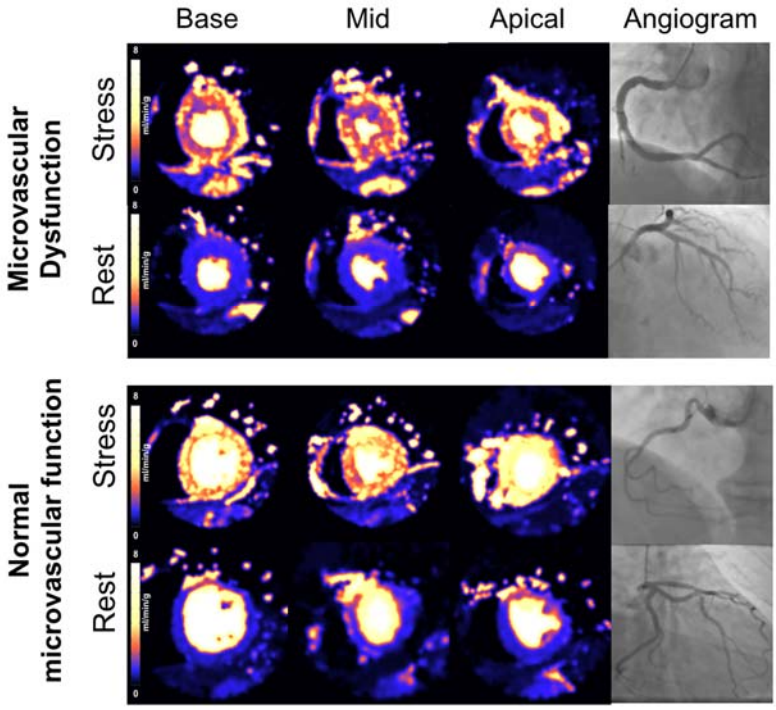

Figures 1 and 2

ID#: 378812

The other toxic face of cocaine

Estefania De Garate, MD[1]Iwan Harries, MD[1], Sarah Moharem-Elgamal, MD[2], Anna Baritussio, MD[1], Tobias A. Fuchs, MD, FESC, FSCCT[2], Elena G. Milano, MD[2], Konstantina Mitrousi, MD[2], Chris Lawton, PGC, BSC[3], Chiara Bucciarelli-Ducci, MD, PhD[1]

1. Bristol Heart Institute, Bristol NIHR Biomedical Research Centre (Cardiovascular Section), University of Bristol, Bristol, England, United Kingdom

2. Bristol Heart Institute, Bristol NIHR Biomedical Research Centre (Cardiovascular Section), University of Bristol, United Kingdom

3. Bristol Heart Institute, Bristol, England, United Kingdom

Description of Clinical Presentation: A 39-year-old male presented with chest pain and troponin rise. He also had a history ongoing cocaine use and smoking habit. Electrocardiogram showed a fixed 1mm ST elevation of the inferolateral leads. His LVEF was normal, but a discoordinate septum was observed on echocardiogram. Angiogram was unremarkable. He was then referred to have Cardiac MRI (CMR) to rule out the presence of myocardial scarring

Diagnostic Techniques and Their Most Important Findings: CMR images were acquired with a 1.5 T scanner, 48 hours after onset of symptoms. Imaging protocol included axial and coronal localizer images, short axis and long axis SSFP cine images; T2-weighted STIR oedema sequences, as well as late gadolinium enhancement (LGE) images. In addition, native and post contrast T1 mapping (MOLLI) and T2 mapping images were acquired for further tissue characterization. CMR findings showed significant patchy epicardial/mid-wall myocardial oedema in the lateral wall from base to apex on T2-STIR; and this finding was confirmed with high T2 mapping values on these areas. LGE images showed patchy myocardial fibrosis in the lateral segments, typically non-ischaemic, in keeping with myocarditis. The T1 mapping values on this area were increased, confirming diffuse fibrosis of these segments. There were no wall motion abnormalities on the cine images. Based on the findings, the final CMR diagnosis of acute myocarditis was established.

Learning Points from this Case: (Toxic) Myocarditis is not amongst the most common cardiac complications of cocaine use; however, it has been described in histology studies of up to 20% of autopsies of patients with detectable cocaine levels, and the use of CMR for assessment of acute chest pain post-cocaine has been described by other groups. This case shows how CMR provides valuable tissue characterization for identifying the cause of acute cocaine-related chest pain.

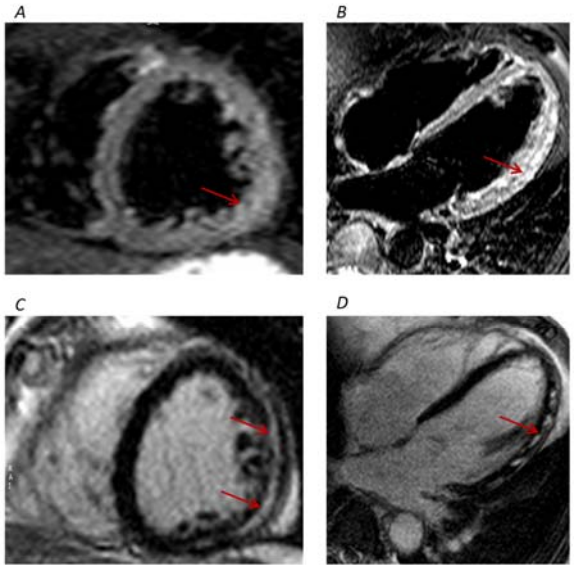

Figure 1. (A & B) short axis and four chamber STIR images showing oedema in the lateral wall. (C & D) late gadolinium images showing epicardial/mid-wall fibrosis in the lateral wall

Figure 1: (A & B) short axis and four chamber STIR images showing oedema in the lateral wall. (C & D) late gadolinium images showing epicardial/mid-wall fibrosis in the lateral wall

ID#: 379203

First Case of Quantitative Perfusion Mapping in Fabry Cardiomyopathy

Rebecca Hughes, MBBS MRCP[1] Kristopher D. Knott, MBBS MA[2], Hui Xue, PhD[3], Peter Kellman, PhD[4], Sabrina Nordin, MRCP[5], James Moon, MD[6]

1. Barts Heart Centre, London, United Kingdom

2. University College London, London, England, United Kingdom

3. National Heart, Lung, and Blood Institute, Bethesda, MD

4. National Heart, Lung, and Blood Institute, National Institutes of Health, Bethesda, MD

5. Barts Heart Centre, United Kingdom

6. UCL, England, United Kingdom

Description of Clinical Presentation: Fabry Disase (FD) is a rare lysosomal storage disorder caused by X-linked mutations in the alpha-galactosidase gene leading to progressive left ventricular hypertrophy, arrhythmia and heart failure. T1 is low due to sphingolipid accumulation except in areas of scar due to pseudonormalisation of T1. Recently, FD has been shown to be an inflammatory cardiomyopathy, with chronically raised troponins associated with high T2 in areas of scar in the absence of thinning. Myocardial infarction is uncommon in FD, however, involvement of the coronary microcirculation can also occur in FD, which may lead to angina symptoms. FD patients can present with ischaemic changes (in both left ventricular hypertrophy (LVH)-positive and LVH-negative patients) but there has been little or no research into myocardial perfusion in FD. We present a case of a 62 year-old male patient with known FD and ischaemic-looking electrocardiogram (ECG) who consented to a perfusion scan.

Diagnostic Techniques and Their Most Important Findings: Cardiac magnetic resonance (CMR) was performed with adenosine stress perfusion and automated inline perfusion mapping. T1, T2 and synthetic ECV maps were also acquired. Adenosine was infused for 4 minutes at 140mcg/kg/min with a good symptomatic and heart rate response. 3 short axis and a 3 chamber slice was acquired at stress and rest. The perfusion maps were analysed and the myocardial blood flow (MBF) at stress and rest calculated. This demonstrated low global MBF at stress (1.1ml/g/min) with the poorest perfusion in the hypertrophied septum (0.72ml/g/min). We have shown stress MBF in healthy volunteers to be around 2-4ml/g/min. Septal T1 was low and there was high T2 in the areas of scar.

Learning Points from this Case: This is the first case of quantitative perfusion using CMR in FD. We have demonstrated globally poor perfusion but with the lowest flow in the areas of greatest glycosphingolipid deposition. We will take this forward with further research investigating the relationship between perfusion, storage and inflammation in FD.

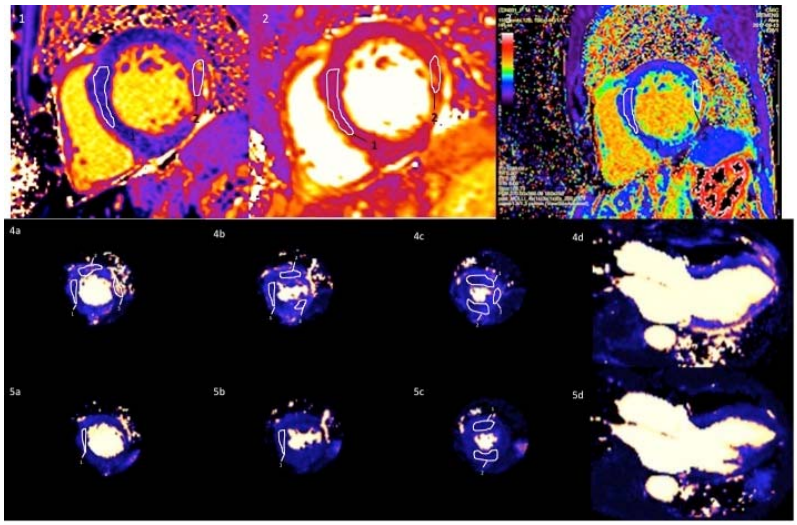

Figure legend 1. T1 imaging at basal level; T1 848ms in area 1 (septum) and 1284ms in area 2 (lateral wall). Normal range T1 1020+/-60ms. Figure legend 2. T2 imaging at basal level; T2 43ms in area 1 and 57ms in area 2. Normal range T2 <50ms. Figure legend 3. ECV imaging at basal level; 59% in area 1, 24% in area 2. Figure legend 4. Adenosine perfusion mapping performed at stress. Basal level (a) demonstrates myocardial blood flow (in ml/g/min) as 0.72 in area 1, 1.15 in area 2 and 1.34 in area 3. Mid ventricular level (b): 0.72 in area 1, 1.00 in area 2, 1.14 in area 3. Figure legend 5. Adenosine perfusion mapping performed at rest. Basal level (a) demonstrates myocardial blood flow (in ml/g/min) as 0.65 in area 1. Mid ventricular level (b): 0.60 in area 1.

ID#: 379284

The "Disappearing" Paraganglioma…..Now you see it, now you don't

Faraz Kureshi, MD, MSc[1] Andrew E. Arai, MD[2], W. Patricia Bandettini, MD[3], Sujata M. Shanbhag, MD, MPH[4], Marcus Y. Chen, MD[2]

1. National Institutes of Health

2. National Heart, Lung and Blood Institute, National Institutes of Health, Bethesda, MD

3. National Heart, Lung and Blood Institute, National Institutes of Health, MD

4. NIH/NHLBI, Bethesda, MD

Description of Clinical Presentation: A 33 year old female with a past medical history notable for a SDHD mutation and metastatic paragangliomas status post removal of several tumors (2005) presented for routine surveillience imaging of a known prior cardiac mass after being lost to follow-up for 10 years. In particular, a cardiac MR (CMR) from 2007 demonstrated a 11 mm nodule in the right side of atrioventricular groove adjacent to the tricuspid annulus and near the diaphragm. On steady state free precession imaging, the signal intesnity of this nodule was between that of myocardium and fat. Although the nodule did not enhance with gadolinium imaging, it was felt to be a paraganglioma. The remainder of her CMR was unremarkable. A CMR was obtained to re-evaluate this mass and screen for other metastatsis. The patient had remained asymptomatic since her prior resections in 2005 and plasma and urinary catecholamine and metanephrine testing were within normal limits.

Diagnostic Techniques and Their Most Important Findings: A CMR was obtained at 3T and included cardiac localization imaging, steady-state free prescession cine and contrast enhanced gadolinium enhancement imaging (8 mm slice thickness without skip) in multiple planes which did not reveal the previously described nodule. Subsequently, a cardiac CT was obtained for further clarification that revealed a 6 x 7 x 11 mm (maximal dimension) discrete contrast enhancing mass outside of the RV free wall, within the pericardium of the basal portion of the right atrial-ventricular groove, adjacent to the mid-distal RCA without impingement of the vessel lumen .

Learning Points from this Case:

- Paragangliomas are extra-adrenal tumors arising from the sympathetic paraganglia.
- The tumor may be catecholamine-secreting and can metastasize.
- Cardiac paragangliomas are particularly rare with only a few hundred cases reported in literature.
- This case highlights the importance of optimizing CMR imaging techniques (slice thickness, skip, imaging planes, etc) when evaluating known/suspected small cardiac masses. This remains particularly important in areas with significant through plane motion (i.e. near the atrial-ventricular groove) to minimize partial volume averaging effects.

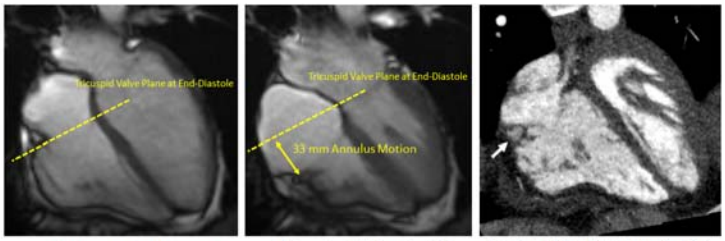

4-Chamber End-Diastole CMR | 4-Chamber End-Systole CMR | Low 4-Chamber Diastole Cardiac CTA Mass (arrow) within right AV groove

Disappearing ganglioma

ID#: 379350

An ill defined right atrial abnormality on echocardiogram in a patient with Erdheim-Chester disease

Faraz Kureshi, MD, MSc[1] Andrew E. Arai, MD[2], Diana Melo, MD[1], Sujata M. Shanbhag, MD, MPH[3], Jeannie Yu, MD[1], W. Patricia Bandettini, MD[4], Marcus Y. Chen, MD[2]

1. National Institutes of Health

2. National Heart, Lung and Blood Institute, National Institutes of Health, Bethesda, MD

3. NIH/NHLBI, Bethesda, MD

4. National Heart, Lung and Blood Institute, National Institutes of Health, MD

Description of Clinical Presentation: A 46 year old male with a history of Erdheim-Chester disease without any cardiac symptoms was evaluated at our institution with a baseline screening trans-throacic echocardiogram for cardiac involvement. An indeterminate hazy echodense area measuring 2.5 X 3 cm was noted in the right atrium near the free wall side of the annulus. The patient was then referred for a cardiac MR (CMR) for further evaluation.

Diagnostic Techniques and Their Most Important Findings: A CMR was obtained at 1.5T and included cardiac localization imaging, steady-state free precession cine. T2-weighted, fat/water separation imaging and contrast enhanced late gadolinium enhancement imaging). There was a large (35 X 18mm) heterogenous mass extending from the base of the right atrioventricular groove along the inferior border of the right heart, encasing the right coronary artery, and continuing along the heart border to the level of the ascending aorta and the right pulmonary artery, and extension to the right atrial appendage. Tissue characterization of the mass suggested that it was water based on fat-water separation imaging with an intermediate signal intensity on T2-weighted steady-state free precession imaging. Enhancement of the mass on first-pass perfusion and delayed gadolinium imaging was noted. A subsequent coronary CT angiogram did not reveal any right coronary artery infiltration or obstruction.

Learning Points from this Case:

- Erdheim Chester disease is rare non-Langerhans histiocytosis, characterized by xanthomatous tissue infiltration with foamy histiocytes.
- Infiltrative lesions may be skeletal or extra-skeletal.
- In our single center cohort of 58 patients with biopsy proven Erdheim-Chester disease, cardiac involvement is realtively common (40%) with the most common site being the right atrioventricular sulcus, followed by right atrium and aorta.
- Baseline screening for infiltrative cardiac lesions secondary to Erdheim-Chester disease should be systematically performed with cardiac MR or cardiac CT as lesions may be missed on echocardiography.

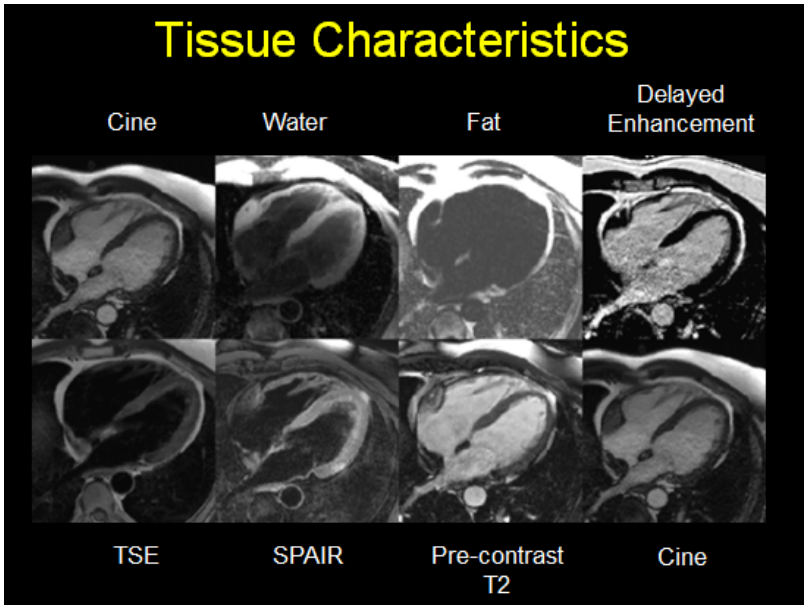

ECD infiltrative lesion

ID#: 379430

Right ventricular sarcoidosis, mimic for arrhythmogenic right ventricular cardiomyopathy

Nicholas Tadeo, MD[1]Nasir Sulemanjee, MD[2], Rahul N. Sawlani, MD[2], Erik Skulborstad

1. Aurora Health Care - Saint Luke's Medical Center, Oak Creek, WI

2. Aurora Health Care - Saint Luke's Medical Center

Description of Clinical Presentation: Case 1
A 62 year-old male presented with ventricular tachycardia. Subsequent evaluation included an electrocardiogram (ECG) demonstrating pathognomonic epsilon waves and a cardiac magnetic resonance study (CMR), interpreted as meeting major criteria for ARVC.

Case 2
A 28 year-old male presented with ventricular tachycardia arrest requiring cardioversion. Initial ECG revealed subtle epsilon waves raising concern for ARVC and an echocardiogram demonstrated asymmetric septal basal hypertrophy as well as RV dysfunction

Diagnostic Techniques and Their Most Important Findings:

Case 1
In the following two years, subsequent pre-transplant evaluation included an ECG which demonstrated RBBB without T wave inversion, an echocardiogram and right heart catheterization revealing significant right heart dysfunction and dilatation.

However, a retrospective re-interpretation of the outside CMR revealed findings consistent with sarcoidosis, including regional areas of irregular RV hypertrophy with associated edema on T2 black-blood imaging. Contrast had not been administered for the exam.

Further evaluation with a chest CT and myocardial inflammation positron emission tomography (PET) revealed PET-positive adenopathy as well as biventricular tracer uptake. Endobronchial ultrasound guided biopsy (EBUS) of a mediastinal lymph node confirmed scant ill-defined granulomas consistent with clinical history of sarcoidosis. Currently the patient is receiving steroid therapy and will be re-assessed for cardiac transplant based upon response.

Case 2
Subsequent CMR demonstrated findings compatible with RV predominant cardiac sarcoidosis, including irregular RV hypertrophy with intense delayed enhancement, edema on black-blood imaging and T2 mapping, and mediastinal lymphadenopathy. An EBUS biopsy of a mediastinal lymph node was consistent with the diagnosis. The patient had an automatic implantable cardiac defibrillator (AICD) placed and is currently receiving steroid therapy.

Learning Points from this Case: ARVC remains a challenging diagnosis, with presenting features and diagnostic criteria that significantly overlap with RV-predominant sarcoidosis. In addition, the latter diagnosis carries a potentially more favorable prognosis and different treatment strategy, and therefore must be considered in the differential diagnosis. Most importantly, these cases highlight that appropriate use of and expertise in CMR are critical to achieving the correct diagnosis.

ID#: 379121

A case of noonan's syndrome: hypertrophic cardiomyopathy in adulthood

Rola Khedraki, MD[1]Marta Alhama-Belotto, MD[2], George Wesbey, MD[3], Jorge Gonzalez, MD[4]

1. Scripps Clinic

2. Scripps Clinic, San Diego, CA

3. Scripps Clinic, CA

4. Scripps Clinic, La Jolla, CA

Description of Clinical Presentation: The patient is a 28 year-old male with history of Noonan syndrome who was found to have hypertrophic cardiomyopathy (HCM) on workup of his intermittent palpitations and atypical chest pain on outpatient echocardiogram. He had a history of multiple cardiac congenital anomalies including ASD and VSD (both repaired), RVOT obstruction and pulmonary stenosis. He also had evidence of apical and asymmetric left ventricular hypertrophy. He did not have any functional limitations and his physical exam was only remarkable for a crescendo-decrescendo systolic ejection murmur at the left and right upper sternal borders.

Diagnostic Techniques and Their Most Important Findings: The patient underwent CMR evaluation with conventional cine images, volumetric phase-contrast 4D flow MRI and delayed enhancement imaging. 4D flow images identified an unroofed coronary sinus with a non-significant left to right shunt (Qp:Qs of 1.3) (Fig. 1). Cine images of the RVOT showed mild pulmonary artery dilatation. Phase contrast through the pulmonic valve calculated mild pulmonic stenosis with a pressure gradient of 19 mmHg. CMR images of the left ventricle show severe asymmetrical hypertrophy of the LV with apical thickening (Fig. 2 & 5). Delayed imaging showed areas of late gadolinium enhancement (LGE) at the level of the apical segments that represented <15% of the total myocardium (Fig. 3 & 4). No LVOT obstruction was identified (Fig. 6).

Learning Points from this Case: Noonan syndrome is an autosomal dominant disorder with an incidence of 1:1000 to 1:2500 live births. There are four main genetic mutations that have been associated with this syndrome with the most common being a mutation in the PTPN11 gene on chromosome 12q24. The syndrome is characterized by minor facial dysmorphism, webbed neck, short stature, and cardiac disease. The most common cardiac manifestations are pulmonary stenosis and HCM. Noonan syndrome HCM can be seen alongside congenital cardiac defects that are not typically seen in classic HCM cases. Despite the similarities in myofiber disarray in Noonan syndrome-HCM and nonsyndromic HCM, their genetic etiologies and prognosis differ with poorer outcomes seen in Noonan syndrome-HCM. Possibly as a result of the associated congenital structural abnormalities in this syndrome. Importantly, in a retrospective study by Colquitt et al. who examined the progression of cardiac disease in patients with Noonan-HCM, it was uncommon for HCM to phenotypically express itself beyond early childhood. Therefore, this case is not only uncommon because of the syndromic association of Noonan and HCM but also because the patient's HCM was discovered later in life. Also, it highlights the important role of CMR and 4D flow in patients with congenital heart disease since patient was never diagnosed with an unroofed coronary sinus ASD prior to the utilization of this modality.

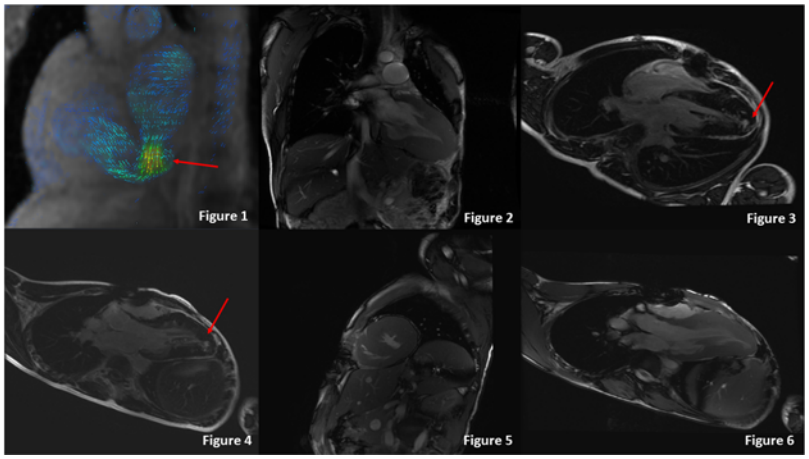

ID#: 378823

Anterior STEMI - A lucky escape

Tushar Kotecha, MRCP(UK) MBChB[1] Rohin Francis, MBBS[2], Ana Martinez Naharro, MD[3], Hossam Fayed, MBChB MSc MRCP(UK)[4], Michele Boldrini[2], Daniel S. Knight[3], Peter Kellman, PhD[5], Marianna Fontana, MD, PhD[2]

1. Royal Free London NHS Foundation Trust, London, England, United Kingdom

2. UCL Department of CMR, Royal Free Hospital, England, United Kingdom

3. UCL Department of CMR, Royal Free Hospital, London, England, United Kingdom

4. UCL Department of Cardiac MRI, Royal Free Pulmonary Hypertension Service, Pond Street, England, United Kingdom

5. National Heart, Lung, and Blood Institute, National Institutes of Health, Bethesda, MD

Description of Clinical Presentation: This 62-year old male was admitted with a 4-day history of cardiac chest pain. He had no significant past medical history. ECG at presentation showed anterior ST elevation with Q waves. In view of ongoing chest pain, he was taken directly for coronary angiography, which showed an occluded left anterior descending artery. This was treated with primary angioplasty that was complicated by angiographic no reflow. Post-procedure, he received a 12-hour infusion of glycoprotein IIb/IIIa inhibitor and was commenced on dual anti-platelet therapy with aspirin and ticagrelor. Two days later, transthoracic echo suggested left ventricular (LV) apical thrombus and he was referred for cardiovascular magnetic resonance (CMR) to assess further.

Diagnostic Techniques and Their Most Important Findings: CMR performed on day four post-presentation (Figure 1) showed heterogeneous signal from the pericardial space adjacent to the apical infarct suggestive of a self-contained myocardial rupture with associated pericardial haematoma. On early gadolinium imaging, there was extensive microvascular obstruction (MVO) affecting the mid-anterior wall, all apical segments and the apical cap, and an apical thrombus (Figure 1). On late gadolinium imaging, there was transmural late gadolinium enhancement affecting the same segments. This presented a treatment dilemma regarding anti-platelets and anticoagulation given the contained myocardial rupture, apical thrombus and recent angioplasty. He was treated with ongoing dual anti-platelets but no anticoagulation and made an uneventful clinical recovery. He underwent repeat CMR at 6 months that showed complete resolution of the rupture and no remaining thrombus.

Learning Points from this Case: Late-presenting myocardial infarction is often associated with angiographic no reflow and the formation of LV thrombus, which is usually managed with aggressive anticoagulation. However, extensive infarction also carries risk of spontaneous myocardial rupture, which is usually fatal. In this case, early CMR allowed for diagnosis of the rupture before commencement of anticoagulation for the apical thrombus, which could have led to further haemorrhage into the pericardium.

Figure 1: CMR scans performed four days post-presentation and at 6 months.
SSFP cine images at end-diastole showing self-contained myocardial rupture (white arrows), which has resolved at follow up
Early gadolinium (EGE) imaging showing extensive microvascular obstruction and apical thrombus (black arrows) at 4 days, which resolved at follow up

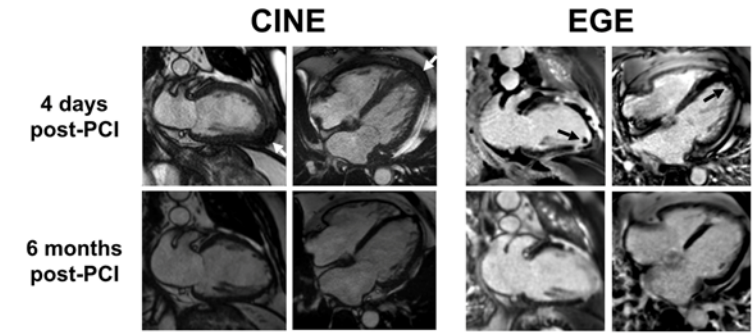

Figure 1

ID#: 379433

Gluten free diet to prevent myocardial infarction ? How cardiac MRI solved the enigma

Soufiani Aida[1]Ougnou Hind[2], Fagouri Rim[2], TAZI Mezalek Zoubida[2]

1. Ibn Sina Hospital, Rabat, Rabat-Sale-Zemmour-Zaer, Morocco

2. Ibn Sina hospital, Morocco

Description of Clinical Presentation: A 28-year-old woman with no cardiovascular risk factors (CVRF) presented with lipothymia. She has a history of spontaneous abortion and of abdominal discomfort. The physical examination was normal excepting a 18 kg / m2 BMI. The electrocardiogram revealed Q waves in V4-V5-V6 leads (Fig.1) that did not exist on a previous EKG (Fig.2).

Diagnostic Techniques and Their Most Important Findings: The echocardiography showed a mild global hypokinesia and the ejection fraction was estimated at 54%. The cardiac MRI diagnosed a lateral infarction (Fig. 3) with a transmural late gadolinum enhacement distribution. Coronary angiography was normal. Blood tests revealed protein C and S deficiency. A malabsorption syndrome was suspected. Tissue transglutaminase antibodies were positive and a duodenal biopsy confirmed the diagnosis of a celiac disease. An anticoagulation and a gluten-free diet were started, the patient is presently stable with a one-year follow-up.

Learning Points from this Case: Prevalence of infarction with normal coronary artery (INCA) is around 4%. Cardiac MRI provides diagnosis through its tissue characterization and can eliminates myocarditis or takotsubo syndrome. A coronary spasm (15.5%), thrombophilia (14%) or emboli should be investigated. Recent studies suggest that INCA has a better prognosis than patient group with coronary stenosis > 50%. Secondary prevention must take into account the etiological assessement.
Hypercoagulability during celiac disease is explained by thrombocytosis, hyperhomocysteinaemia and deficiency in coagulation inhibitors, favored by the malabsorption of vitamin K (as for our patient).
This case highlight the role of MRI in case of infarction with normal coronary artery, and the importance of etiological assessement especially in a young patient without cardiovascular risk factor.

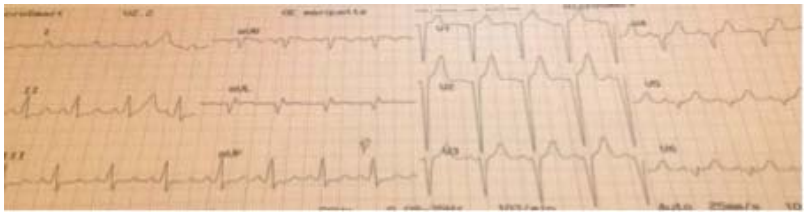

Fig. 1 : Admission electrocardiogram: Q waves in V4-V6 leads.

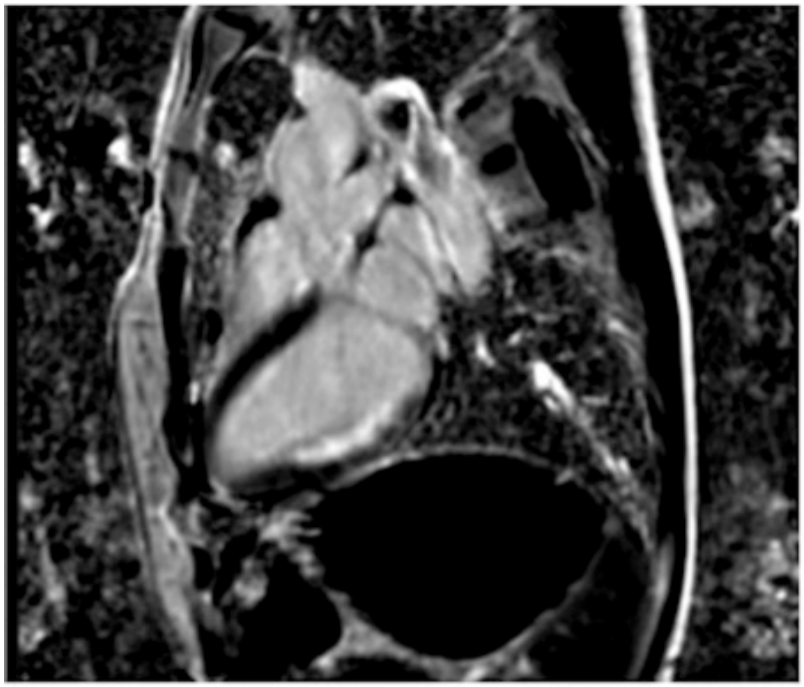

Fig. 2: Cardiac MRI, late gadolinium enhancement (LGE) sequence, left ventricle long axis view showing almost transmural LGE at the medial and apical segments of the infero-lateral wall.

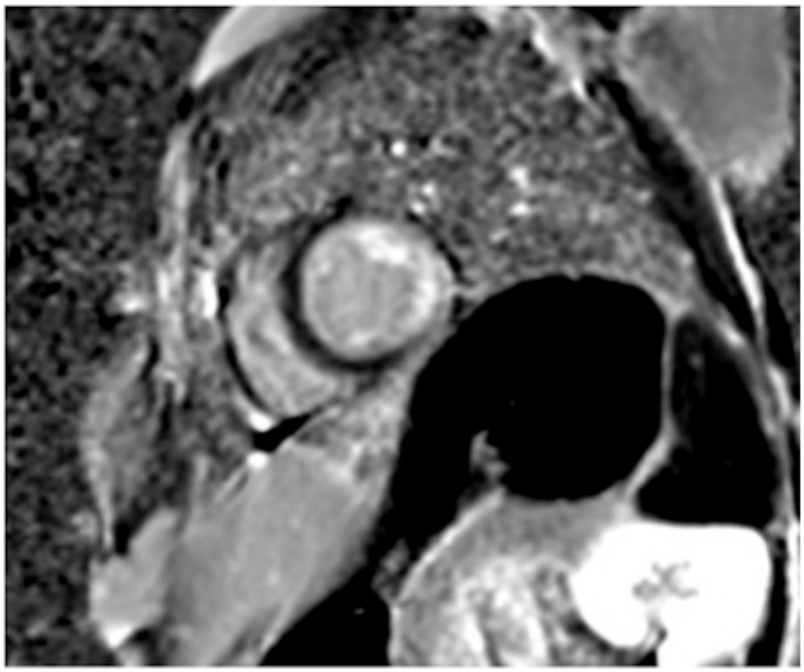

Fig. 3 : Cardiac MRI, late gadolinium enhancement (LGE) sequence, left ventricle short axis view showing almost transmural LGE at the medial and apical segments of the infero-lateral wall.

ID#: 379476

A Rare Etiology Of Mitral Regurgitation Revealed By CMR

Abdalla Elagha, Cairo university

cairo university, Zamalek, Al Qahirah, Egypt

Description of Clinical Presentation: A 37 year-old asymptomatic athletic healthy male, was found to have an apical pan-systolic murmur during routine checkup. Transthoracic echocardiography revealed severe mitral valve regurgitation (MR) in a nearly "normal-appearance" mitral valve apparatus.

Diagnostic Techniques and Their Most Important Findings: To solve this dilemma, cardiac MRI (CMR) was requested, which revealed an abnormal communicating orifice located between A1& A2 scallops of anterior mitral leaflet **(Figure1:A- C)**. The communicating orifice measured about 9 mm at its maximal diameter(area =0.4cm^2) **(Figure1:D)**. Actually, severe MR was caused by unexpected perforation, reaching posterior wall of left atrium. Noticeably, blood escaped through this orifice in early diastole, even before opening of the normal orifice of mitral valve. The anterior mitral leaflet appeared elongated. Mitral valve prolapse was also noticed, together with dilated mitral valve annulus. Left ventricular end-diastolic and left atrial dimensions were markedly increased. Despite presence of severe mitral regurgitation,however, left ventricular systolic function(EF= 62%) was preserved. The patient was advised to have a surgical mitral valve repair. At surgery, perforation was confirmed and sealed by both sutures and a patch closure. At two-month follow-up visit, left ventricular dimensions returned back to normal and MR disappeared.

Learning Points from this Case: Mitral leaflet perforation is a rare cause of mitral regurgitation, usually occurs following infective endocarditis, which is not the etiology here. Although the patient is tall(195cm),however, there was no confirmatory (clinical or laboratory) evidence of "Marfan syndrome" or other connective tissue disease. Cardiac MRI is a powerful imaging tool that can reveal fine structural details with excellent resolution, in comparison to echocardiography.

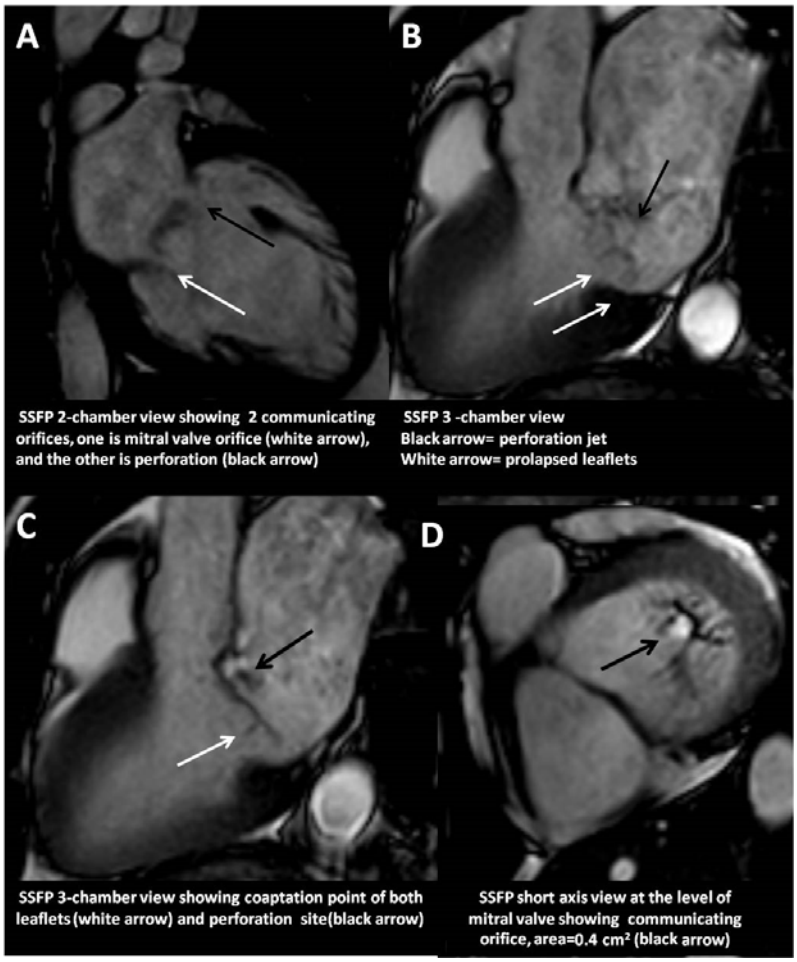

severe MR was caused by unexpected perforation, reaching posterior wall of left atrium.

ID#: 374238

Right Superior Vena Cava Drainage into the Left Atrium Diagnosed in the Peripartum Period

Magdalena Janus, PhD, MD[1]Justyna Rajewska-Tabor, PhD, MD[2], Andrzej Siniawski, PhD, MD[3], Agnieszka Graczyk-Szuster, MD[3], Szymon Rozmiarek, MPhys[2], Jolanta Miszczak-Śmiałek, MD[4], Malgorzata B. Pyda, Prof., PhD, MD[1]

1. 1st Department of Cardiology, Poznan University of Medical Sciences, Poznań, Poland

2. 1st Department of Cardiology, Poznan University of Medical Sciences, Wielkopolskie, Poland

3. 1st Department of Cardiology, Poznan University of Medical Sciences, Poland

4. Provincial Hospital in Poznan, Poland

Description of Clinical Presentation: Isolated right superior vena cava drainage into the left atrium is an extremely rare cardiac anomaly. We present the case of a woman who suffered cerebral air embolism in the peripartum period associated with isolated drainage of the right SVC into the LA. In June 2017, a 38-year-old woman after the birth of her third child, a 38-year-old woman developed abrupt neurological symptoms following the injection in the CVC central vena in a sitting position. Based on CT she was diagnosed with cerebral air embolism. ECG and transthoracic echocardiography revealed nothing pathologyunusual. During hospitalization chest CT was also performed because of persistent hypoxia with saturation at 87%. A suspicion of congenital heart disease with abnormal drainingage of the right superior vena cava into the left atrium was raised.

Diagnostic Techniques and Their Most Important Findings: The patient She was referred to our center for further diagnosis, where the . We performed cardiac magnetic resonance with angio MR sequences that confirmed the preliminary diagnosis of an isolated anomalous connection of the right SVC to the LA. Steady-state, free-precession, paracoronal magnetic resonance image showed the superior vena cava emptying into the left atrium (FIG. 1A). The inferior vena cava empties/emptied??? separately to the right atrium. AngioMR performed with contrast medium administration intravenously through a peripheral venous catheter in the right upper extremity showed contrast media medium in the superior vena cava, left heart and aorta without opacification of the right heart or the pulmonary vasculature (FIG 1B). The second AngioMR performed with contrast medium administration intravenously through a peripheral venous catheter in the left lower extremity showed contrast media in the inferior vena cava, right heart and pulmonary vasculature (FIG 1C), and revealed no other systemic to pulmonary shunts or other cardiac abnormalities. Although this anomaly and its potential complications were thoroughly explained to the patient, she refused surgical correction. One of her children was diagnosed with Tetralogy of Fallot disease and is currently under examination.

Learning Points from this Case: Isolated right superior vena cava drainage into the left atrium is an extremely rare cardiac anomaly. Echocardiography is not a sufficient diagnostic method in this case. CMR provides vital information about anomalies and co-morbidity inthis case.

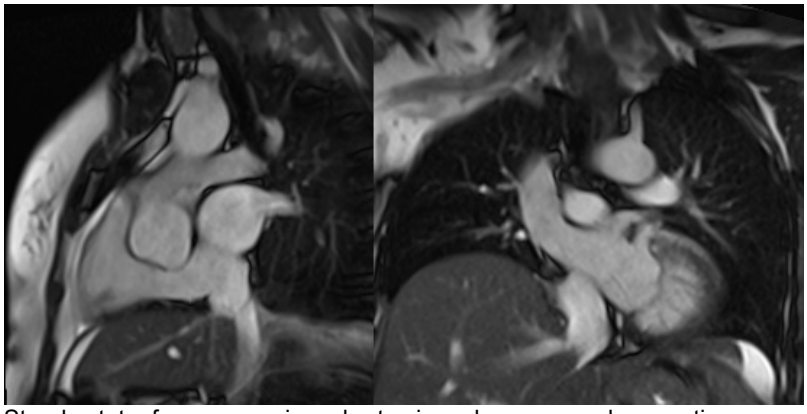

Steady-state, free-precession, short axis and paracoronal magnetic resonance image showed the superior vena cava emptying into the left atrium

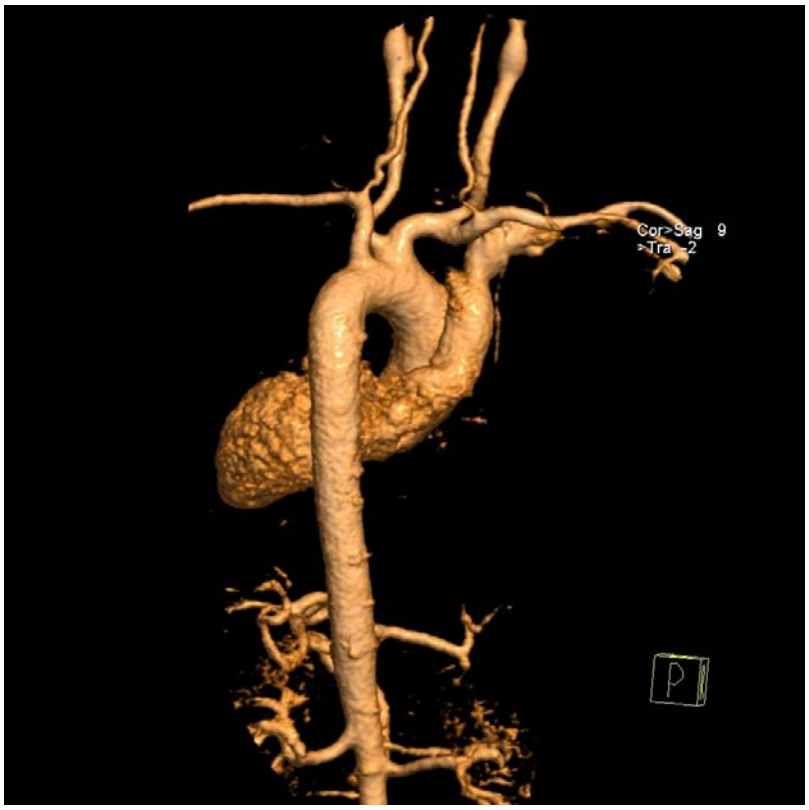

AngioMR 3D reconstruction:contrast material in the superior vena cava, left heart and aorta without opacification of the right heart or the pulmonary vasculature

AngioMR 3D reconstruction: contrast material in the inferior vena cava, right heart and pulmonary circulation

ID#: 373553

A nice case (of a wrong diagnosis) of hypertrophic cardiomyopathy.

Chrysanthos Grigoratos, MD[1] Giancarlo Todiere, MD, PhD[2], Andrea Barison, MD, PhD[3], Giovanni D. Aquaro[2]

1. Institute of Life Sciences, Scuola Superiore Sant'Anna, Pisa, Italy, Italy

2. Fondazione Toscana Gabriele Monasterio, Pisa (Italy), Toscana, Italy

3. Fondazione Toscana Gabriele Monasterio, Pisa (Italy), Pisa, Toscana, Italy

Description of Clinical Presentation: A 65 years-old female asymptomatic patient during a routine visit was found with precordial T wave inversion on electrocardiogram. Echocardiography showed left ventricular (LV) apical hypertrophy and was therefore scheduled for cardiac magnetic resonance (CMR) with an apical hypertrophic cardiomyopathy (HCM) query.

Diagnostic Techniques and Their Most Important Findings: CMR confirmed hypertrophy in the apical segments (Panel A) and a significant relative hypertrophy with apical (13 mm) to basal (8 mm) segment ratio of 1.6 and diffuse myocardial oedema in T2-weighted sequences in the hypertrophic segments (Panel B). LV indexed mass was above normal limits whereas global and regional wall motion was normal, as well as biventricular volumes. Myocardial fibrosis assessed by means of late gadolinium enhancement (LGE) was absent (Panel C). Findings were in keeping with an initial form of apical HCM. Given however the presence of extensive acute myocardial damage, a follow-up scan was arranged after 8 months to assess oedema and fibrosis evolution. Rather unexpectedly following scan did not confirm previous findings. Apical hypertrophy disappeared (Panel D), as well as myocardial oedema (Panel E). Myocardium showed no areas of fibrosis (Panel F). Second CMR was deemed normal and previous findings re-interpreted as secondary to acute inflammatory process causing myocardial oedema and pseudohypertrophy.

Learning Points from this Case: In the light of all above information, first CMR findings were either due to myocarditis with a rather atypical presentation given the absence of symptoms, signs of infection and LGE in CMR or stress cardiomyopathy once again with atypical presentation since no regional wall motion abnormalities were seen and patient has had no chest pain over the past months. A phone call to patient';s GP revealed how she decided to have a medical visit because of the sudden death of a dear friend of her some weeks before the first CMR. A Tako-tsubo cardiomyopathy, with a silent presentation, mimicking an apical HCM was clearly the case

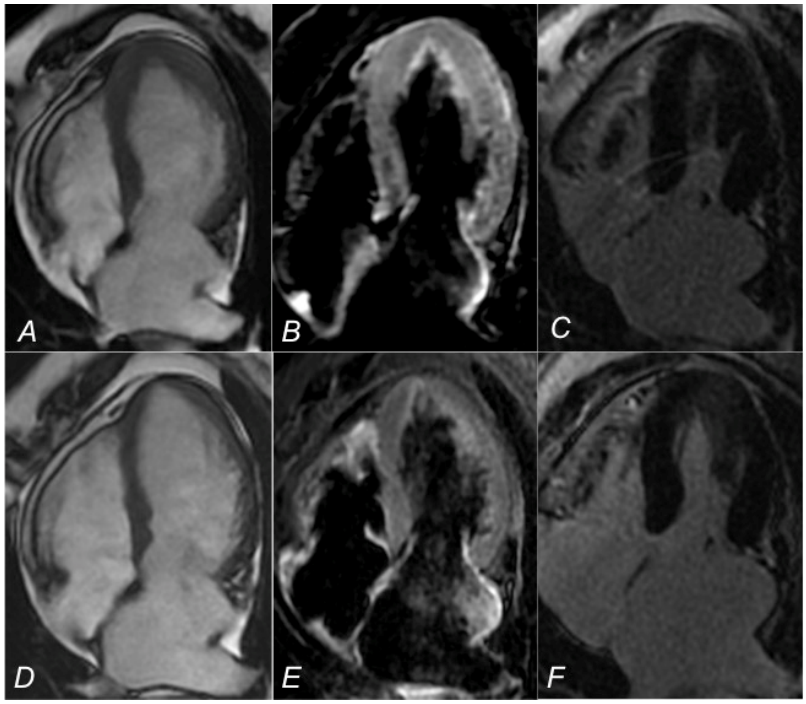

ID#: 375588

An Unusual Case of Tethered Right Coronary Cusp

Ranjini Srinivasan, National Institute of Health[1] Sujata M. Shanbhag, MD, MPH[2], Marcus Y. Chen, MD[3]

1. National Institute of Health

2. NIH/NHLBI, Bethesda, MD

3. National Heart, Lung and Blood Institute, National Institutes of Health, Bethesda, MD

Description of Clinical Presentation: A 39 year old woman presented to a cardiologist with a history of long-standing chest pain and dyspnea on exertion. She diagnosed as a child with a “congenital heart abnormality,” however she did not recall the details. She underwent a stress echocardiogram, which was showed ST segment and T wave abnormalities and she was referred for a coronary angiogram. On coronary angiography, the left coronary system was normal, however, the right coronary artery could not be cannulated, nor did the right coronary artery fill by aortic angiography. She was referred for cardiac MRI (CMR) for further evaluation.

Diagnostic Techniques and Their Most Important Findings: A cardiac MRI cine sequences in the 3-chamber show the right coronary cusp (RCC) tethered to the sinotubular junction (STJ) resulting in obstruction of the right coronary sinus. Phase-contrast and cine imaging of the aortic valve demonstrate that tenting of the RCC led to moderate aortic insufficiency. Black blood imaging of the aortic valve showed stagnant blood within the right coronary sinus. A regadenoson stress perfusion was performed demonstrates near-circumferential perfusion defects. However, cine images illustrate normal biventricular systolic function. No myocardial infarction or scar was detected by late gadolinium enhancement imaging. Under further assessment by coronary CTA, the RCC tip was once again seen tethered to the sintotubular junction wall, obstructing flow into the right coronary artery. On the arterial phase of contrast administration, there was poor opacification of the right sinus of Valsalva. On delayed imaging, the right coronary artery and the right coronary sinus appears to fill retrograde from the left coronary system. The patient almost immediately underwent a mechanical aortic valve replacement after the CMR and CTA. She is currently doing well without symptoms.

Learning Points from this Case: • Occlusion of the coronary os by a tethered aortic valve leaflet is rare but has been reported in the literature. Some patients may present early in life with ventricular dysfunction or sudden death, but patients who develop collaterals may present later in life with symptom of chest pain, dyspnea or syncope. • Stress perfusion testing can determine the extent of perfusion defects due to the coronary obstruction, even in the absence of compromised ventricular function. • Not only can CMR imaging and CT angiography diagnose this condition without the use of invasive techniques, but they can also further delineate anatomic details, assesses ischemic burden, and assess myocardial scar.

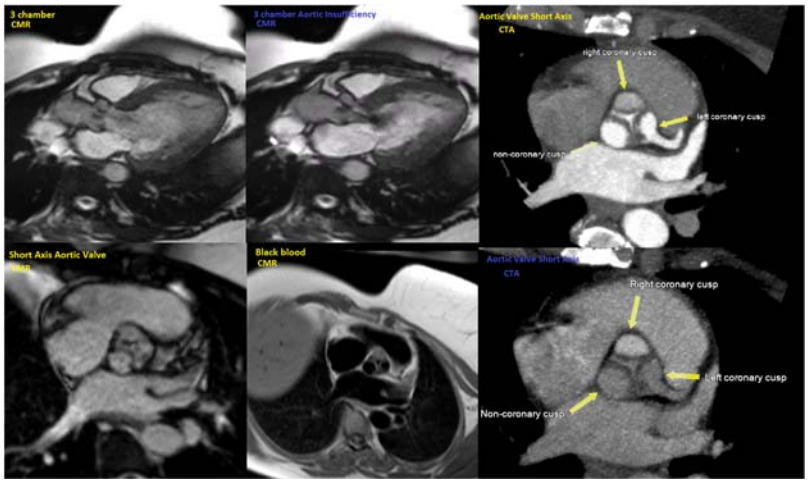

CMR images show tethering of the right coronary cusp to the sinotubular junction, with moderate aortic insufficiency, and stagnant blood flow in the right coronary sinus. The right coronary artery fills on late gadolinium enhancement imaging. CTA images show normal filling of the left and non-coronary cusp and delayed filling of the right coronary cusp.

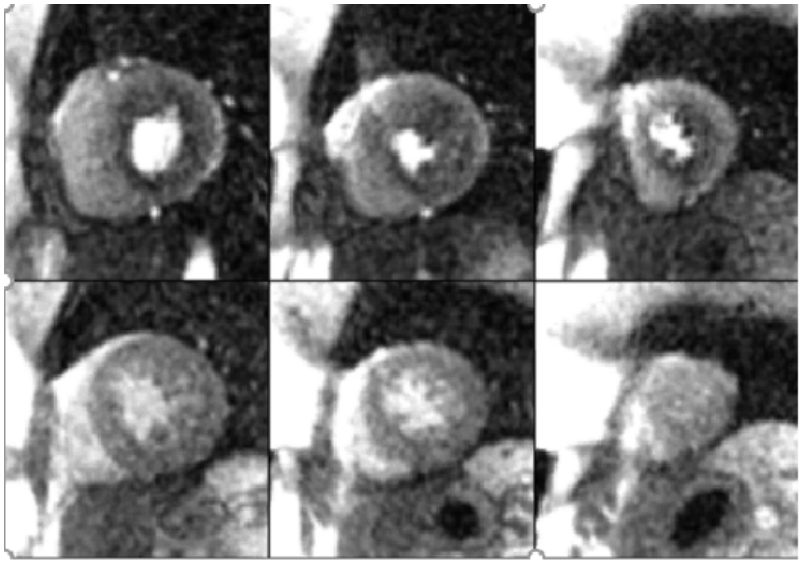

Near-circumferential perfusion defects with regadenason stress perfusion

ID#: 375593

Long term complications of the Takeuchi repair for Anomalous Left Coronary Artery off the Pulmonary Artery (ALCAPA)

Ranjini Srinivasan, National Institute of Health[1]Marcus Y. Chen, MD[2], Andrew E. Arai, MD[2]

1. National Institute of Health

2. National Heart, Lung and Blood Institute, National Institutes of Health, Bethesda, MD

Description of Clinical Presentation: A 19 year old woman with anomalous left coronary artery off the pulmonary artery (ALCAPA) presented after a myocardial infarction. She underwent a Takeuchi repair, which involves creation of an aortopulmonary window and an intrapulmonary tunnel to baffle the aorta to the ostium of the anomalous coronary. After the infarct she developed left ventricular dysfunction. The intrapulmonary baffle led to main pulmonary artery (MPA) stenosis which required pulmonary artery patch plasty at the age of 30. By 39 years old, she had severe pulmonary insufficiency and right ventricular dilation by echocardiography and was referred for cardiac magnetic resonance imaging (CMR).

Diagnostic Techniques and Their Most Important Findings: The patient underwent yearly CMR. Sequences performed included steady state free procession in multiple planes, velocity encoded phase-contrast imaging and late gadolinium enhancement (LGE). The initial studies showed free pulmonary insufficiency with elevated right ventricular volumes (indexed end diastolic volume (EDVi) of 105 ml/m2). LGE showed myocardial infarction with focal wall motion abnormalities, as well as akinesis and thinning of the mid and apical anterior walls and apex. Eventually, EDVi increased to 140 ml/m2 and she developed atrial fibrillation, which was the deciding factor in surgery. She underwent an open pulmonary valve replacement with a bioprosthetic valve at the age of 49. A Melody valve was not an option due to the close proximity of the left main coronary artery to the baffle. Subsequent CMR showed improved right ventricular size (EDVi 85 ml/2) with minimal regurgitation through the bioprosthetic valve. She also underwent cardiac computed tomography (CTA) which showed ectasia of the left main coronary artery. At the age of 51, she passed away from a cerebral vascular event.

Learning Points from this Case: • The Takeuchi procedure is no longer as routine for ALCAPA repair as direct reimplantion of the anomalous coronary ostia, but patients who have undergone this procedure are at risk of long-term complications. These include MPA stenosis in the region of the intrapulmonary baffle, baffle leak, diminished left ventricular systolic function and mitral regurgitation.
• Timing of pulmonary valve replacement is based on multiple factors, most importantly RV EDVi (recent studies suggest >150 ml/m2), RV and LV ejection fraction, presence of RVOT aneurysm or tachyarrhythmia. This patient did not meet RV volume criteria but development of arrhythmia prompted surgical repair.
• CMR plays a key role in evaluation of the relationship between the coronary arteries and the pulmonary artery and in this case, guided the decision for type of intervention.

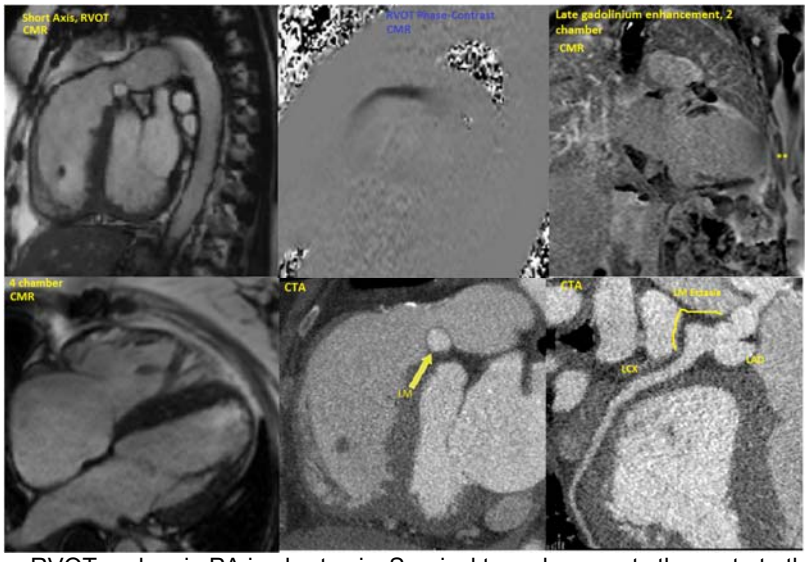

a. RVOT and main PA in short axis: Surgical tunnel connects the aorta to the left main coronary artery in the posterior aspect of the reconstructed main pulmonary artery. b. RVOT velocity encoded phase contrast: Diastolic

frame with severe pulmonary insufficiency c. LGE 2-Chamber view: Transmural MI of most of the anterior wall and part of the apex. d. 4-chamber view: Severe dilation of the right ventricle e. CTA RVOT: Relationship of the coronary baffle to the RVOT and MPA f. CTA Left Coronary: Takeuchi baffle with ectasia of the left main, circumflex, and origin of the LAD.

ID#: 377607

When big is bigger - a multimodality imaging case.

Camilla Torlasco, MD[1]Miriam Revera, MD, PhD[2], Silvia Castelletti, MD[3], Simonetta Blengino, MD[3], Franco Cernigliaro, MD[3], Gianfranco Parati, MD, PhD[3]

1. University of Milan-Bicocca. IRCCS Istituto Auxologico Italiano, Milan, Italy, Milan, Lombardia, Italy

2. IRCCS Istituto Auxologico Italiano, Milan, Italy, Lombardia, Italy

3. IRCCS Istituto Auxologico Italiano, Milan, Italy, Italy

Description of Clinical Presentation: This is the case of a 78year-old woman with past medical history of silent anterior myocardial infarction treated with medical therapy. Functional Class NYHA III. Admitted for pulmonary oedema not responsive to medical therapy, echocardiogram showed severely reduced left ventricle (LV) systolic function, mid akinesia and apical aneurysm. Coronary angiogram showed chronically occluded proximal left anterior descending(LAD) artery and a bare metal stent was implanted. After 5-days, she was asymptomatic at rest but with persistently low blood pressure and high heart rate, and a routine echocardiogram was suspicious for ventricular septal defect(VSD). A haemodynamic study excluded that complication, so the patient was referred for cardiac magnetic resonance (CMR) to investigate cardiac structure and function and explain the echo findings.

Diagnostic Techniques and Their Most Important Findings: Haemodynamic study: right atrial, right ventricle and mixed venous SO2 saturation: 63%, 62% and 61% respectively. Rest echocardiogram showed moderate LV dilatation (LV end diastolic diameter:49mm, LV end diastolic volume [EDV]:163ml, indexed [EDVi]:95ml), akinesia of mid-ventricular segments and aneurysm of the LV apex, reduced LV systolic function (ejection fraction [EF]:30%). A small eccentric jet, apparently originating from the posterior IV septum and directed toward the LV cavity was observed, compatible with a VSD but without clear shunt. Fig 1. CMR (1.5T) confirmed LV septum integrity, but showed severely dilated LV (LVEDV:419ml, LVEDVi:242ml, LVESV:342ml, LVESVi:197ml). RV size and function were normal (REDV:80ml, RVESV:46ml). The mid-ventricular walls were hypokinetic with normal thickness. An extensive apical aneurism, involving all the distal LV segments, was noted. LVEF: 19%. Transmural LGE, matching the extension of the aneurysm, was present. Fig 2.

Learning Points from this Case: 1) LV aneurysm is a frequent occurrence after anterior, non-revascularised MI. It carries unfavourable prognosis owed to ventricular arrhythmias, thrombi and ruptures, and should always be looked for.
2) A combined multimodality imaging approach helps in complex conditions. Echocardiogram and CMR are particularly fit for this purpose as they provide high availability, cost effectiveness and possibility to use in an emergency setting, versus infinite planarity and gold standard assessment of function, mass and volumes and tissue characterisation.

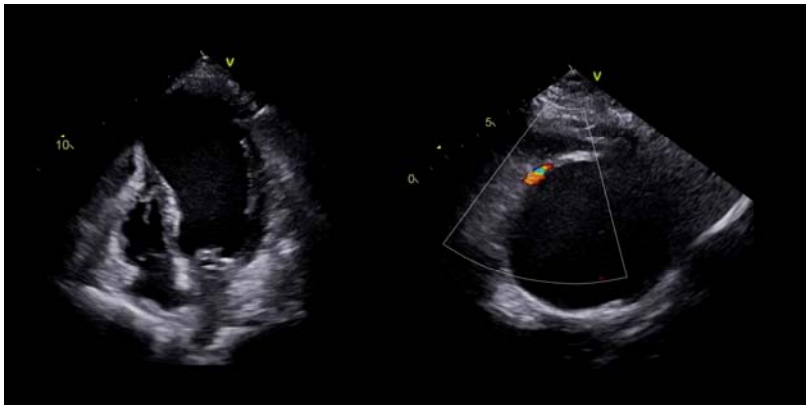

Fig 1: on the left, 4chamber view. On the right, cross section of the aneurysm with a jet suspicious for VSD.

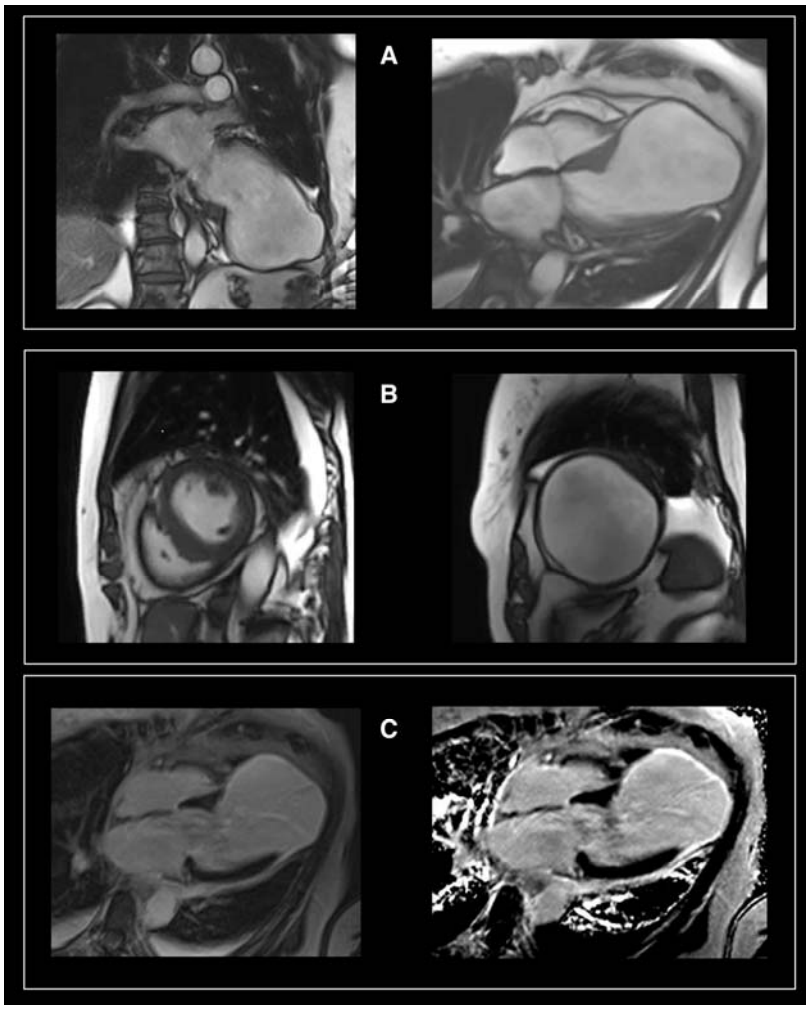

Fig 2: PanelA: cine 4ch, 2ch. The aneurysm involves the distal and apical segments, but basal and mid ventricular are spared. PanelB: basal SAX, distal (aneurysm) SAX. PanelC: transmural LGE, matching the aneurysm. Other segments are spared.

ID#: 377505

The vanishing coronary artery syndrome

Mihiri C. Wettasinghe, MBBS, MD (Radiology)[1] Sara Elfawal, MBCHB, MD [2], Praveen PG Rao, MRCP, FRCR[3], Aparna Deshpande, MRCP FRCR[3]

1. University Hospitals of Leicester NHS Trust, Leicester, England, United Kingdom

2. Department of Radiology - University of Alexandria, Egypt

3. University Hospitals of Leicester, United Kingdom

Description of Clinical Presentation: We present an interesting case of a young female who developed Left Main Stem (LMS), occlusion following mediastinal radiotherapy (RT) with curative intent for invasive thymoma within a short latent period. A 49 year old female with no cardiac risk factors presented with gradual onset of typical exertional angina. She had thymectomy for invasive thymoma one year prior to presentation followed by mediastinal RT to ensure complete marginal clearance. Her exertional chest pain started a few months after completion of RT course. Basic investigations including full blood count, renal function, bone profile, cardiac enzymes, ECG and echocardiography were normal. Exercise tolerance test was equivocal. She was referred for non-invasive CT coronary angiogram (CTCA).

Diagnostic Techniques and Their Most Important Findings: There were no coronary artery calcific plaques. CTCA demonstrated normal non-obstructive dominant Right Coronary Artery (RCA). The LMS, Left Anterior Descending (LAD) and Circumflex (Cx) were not opacified in the arterial phase. As there was “ghosting” of the LAD/Cx, a very delayed 9-minute scan without further contrast injection showed opacification of the LAD and small Cx, indicating backfilling from collaterals. Although she had no coronary angiograms prior to the RT, the staging pre-surgical CT thorax convincingly demonstrated opacified LMS and LAD. Subsequent Invasive Coronary Angiogram (ICA) failed to cannulate/opacify the LMS and its branches.Dominantnormal RCA supplying collaterals to the left-sided circulation was demonstrated. Cardiac Magnetic Resonance (CMR) stress perfusion study showed circumferential almost transmural inducible ischaemia in the LAD and Cx territories. There was no evidence of myocardial infarction or infiltrative cardiomyopathy. The left ventricular function was normal.

Learning Points from this Case: In the several cases reported in the literature, coronary/cardiac complications following mediastinal RT developed after a latent period of 3-30 years. To our best knowledge, this is the first case reporting the development of significant coronary artery disease (CAD) within one year of RT. A combination onset of typical angina symptoms in low-risk patients and multi-modality imaging including cardiac CT and CMR helped in identifying the coronary artery occlusion and myocardial ischemia. Our hypothesis is that she developed RT induced coronary artery occlusive disease as the pre-surgical CT convincingly demonstrated a normal proximal LAD. Although this is a rare case, we hope to raise awareness among oncologists and cardiologists.

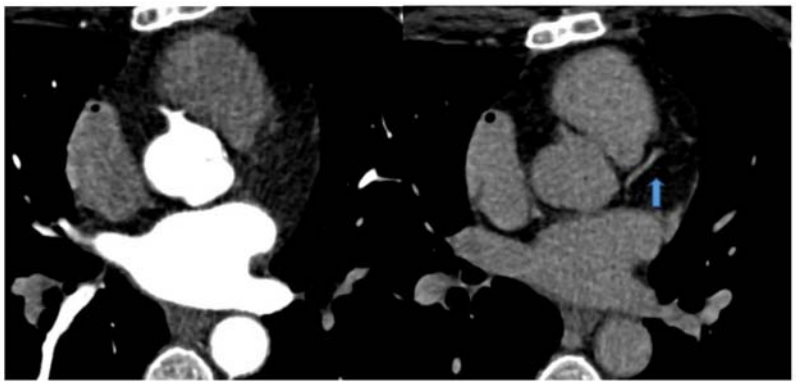

Figure 1a

Figure 1b

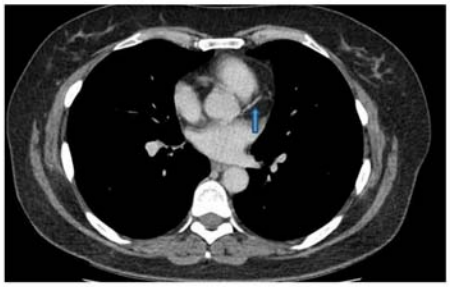

Figure 1c

Figure 1a and 1b - Delayed filling of the LAD (blue arrow in figure 1b), which was not seen in the initial angiogram (Figure 1a). Figure 1c demonstrates the LAD in the pre-surgical staging scan done one year back (blue arrow)

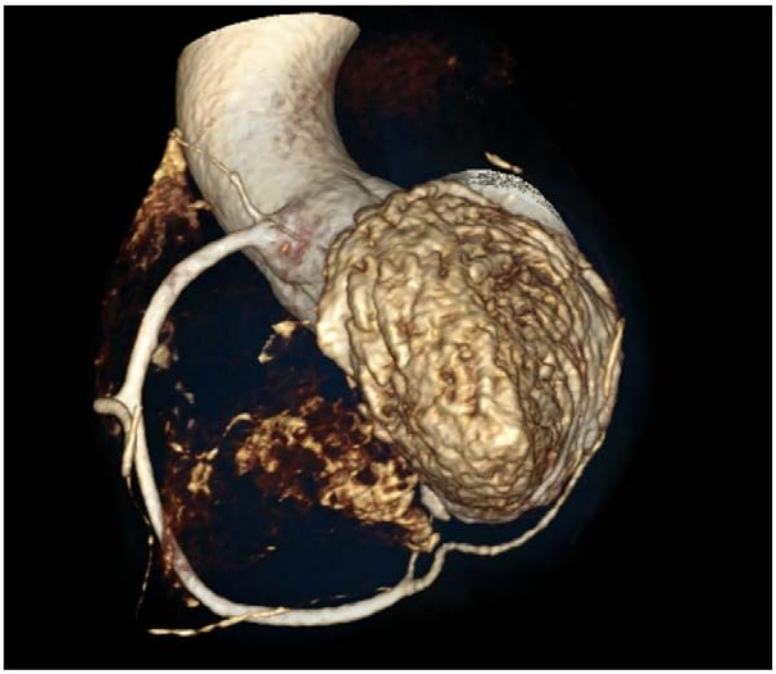

Figure 2a

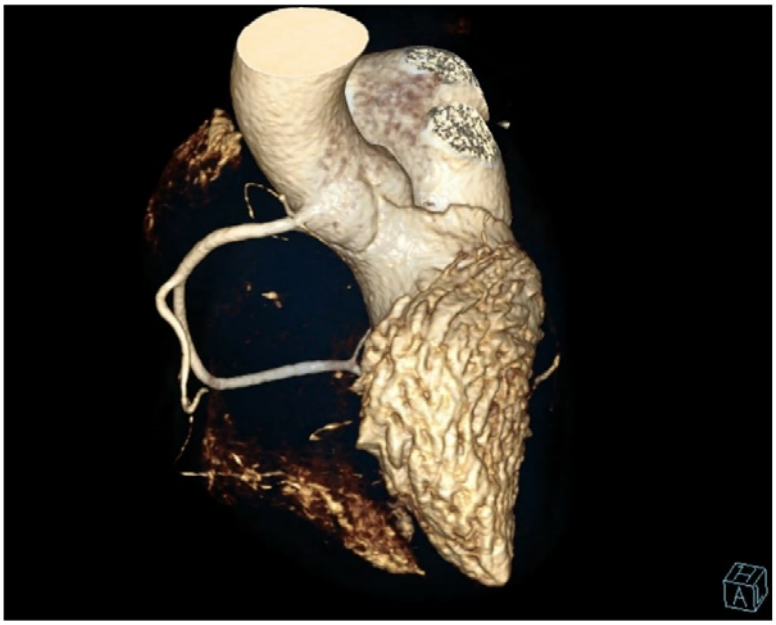

Figure 2b

Figure 2a and figure 2b: : 3D coronary CT angiogram images showing RCA with collaterals extending to the left coronary arterial territory

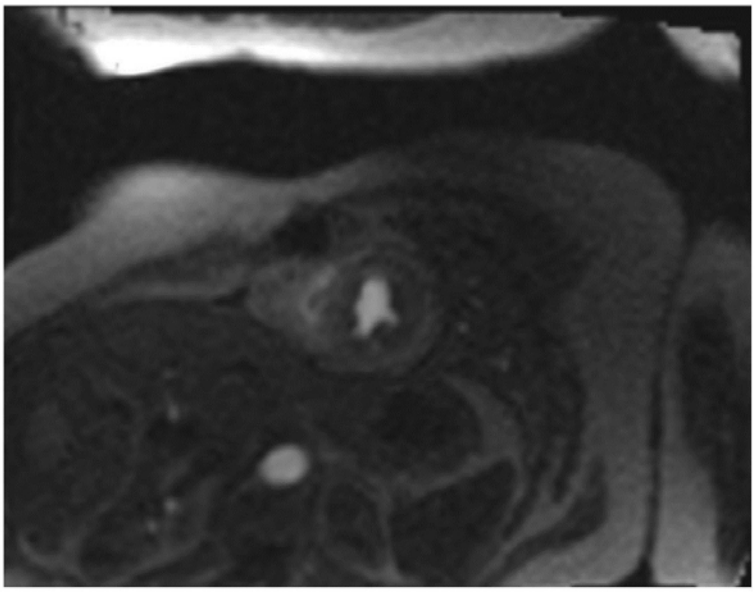

Figure 3a

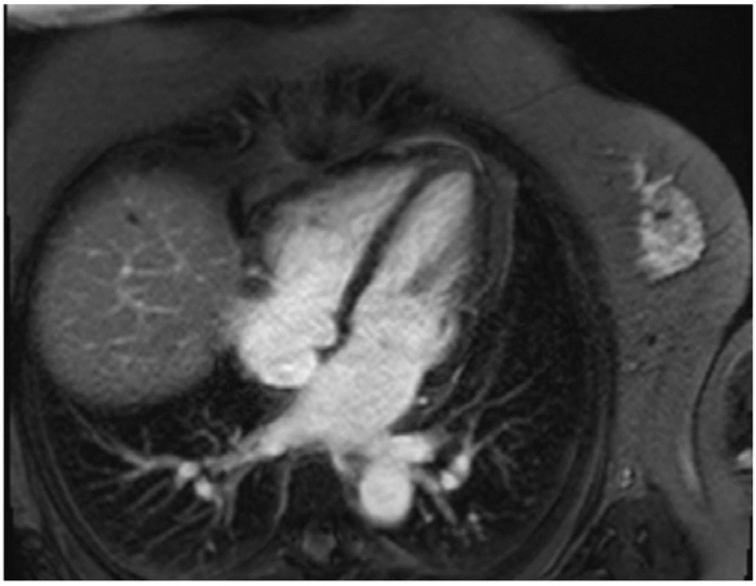

Figure 3b

CMR stress perfusion images showing significant almost circumferential transmural inducible ischaemia (Figure 3a) and No late gadolinium enhancement in delayed CMR (Figure 3b)

ID#: 378520

Revealing the Unexpected: Cardiac Magnetic Resonance in the Diagnosis of Sinus of Valsalva Aneurysm

Katia Devorha. Menacho, MD[1] Sabrina Nordin, MRCP[2], Amna Abdel-Gadir, MBBS.MRCP(UK)[3], Camilla Torlasco, MD[4], Sara Elizabeth. Ramírez Flores[5], James Moon, MD[6], Daniela A. Salazar[7], Jorge Luis. Alave[8]

1. Barts Heart Centre, London, England, United Kingdom

2. Barts Heart Centre, United Kingdom

3. University College London and Barts Heart Centre, London, England, United Kingdom

4. University of Milan-Bicocca. IRCCS Istituto Auxologico Italiano, Milan, Italy, Milan, Lombardia, Italy

5. HOSPITAL FAP / CLÍNICA INTERNACIONAL, Lima, Lima, Peru

6. UCL, England, United Kingdom

7. Universidad Peruana Cayetano Heredia, Lima, Lima, Peru

8. Asociación Civil Impacta Salud y Educación, Peru

Description of Clinical Presentation:

A 34 year-old lady with 6 months of breathlessness and palpitations on exertion. Past history of type 1 Diabetes Mellitus, cardiac surgery at the age of 3 in Germany for an unknown indication and, at 23, an ST elevation inferior infarct treated with 2 stents to the RCA. Currently on no regular medication.

Diagnostic Techniques and Their Most Important Findings:

Echocardiography showed normal LV dimensions, preserved function. CMR was requested to assess previous infarction and rule out new inducible ischaemia.

First localizer sequences highlighted a significant abnormality of the RCA ostium and the aortic root. ***Figure 1a, b.*** Coronal/ Right ventricle outflow tract RVOT **(Figure 2a)** and Aortic Valve cine SSFP **(Figure 2b)** showed a 2cm right coronary Sinus of Valsalva aneurysm protruding into the right ventricle, causing RVOT obstruction in systole and mild PR. The right coronary artery (white arrows) arises from the apex of the aneurysmal sinus. Late gadolinium enhancement was negative for thrombus in the aneurysmal segment **(Figure 3a)**. Small old infarction in the basal inferior wall **(Figure 3b).** No evidence of abnormalities in the rest of the aorta, **Figure 4.**

Conclusion: A Sinus of Valsalva Aneurysm (SVA) arising from the right coronary cusp was diagnosed by CMR. Echo confirmed no shunt/rupture and CT showed two patents stents inserted at proximal and distal segments of RCA with no apparent stenosis. After considering the scenario, symptoms and RVOT obstruction in a young patient from the aneurysm, surgical repair is planned.

Learning Points from this Case:

- SVA is a rare condition of thinning of the wall of the aortic sinus, enlarging with time and typically remaining undetected until complications appear, as here.

- CMR revealed it and provided a valuable functional information, studying left ventricular hemodynamic pattern and aorto-cardiac shunt.

- A previous infarct at the age of 23, with no other cardio metabolic factor risk factor, even with T1DM, raises the possibility of an additional pathophysiologic mechanism in this case, not purely explained by atherosclerosis, such as thrombus embolization from the aneurysm. It remains uncertain why it hasn';t been discovered at that time. SVA should be considered as differential diagnosis on a young individual without major cardiovascular risk factors who has sudden acute MI.

- Echocardiogram plays a key role in the diagnosis of right SVA. Although highly diagnostic, it is operator dependant, and SVA can be missed. This diagnosis remained unnoticed until CMR exam.

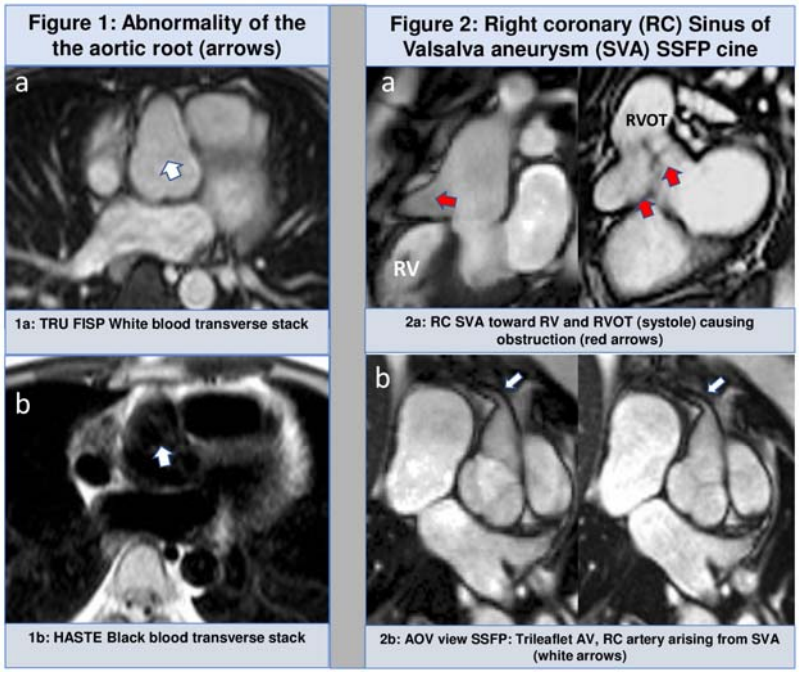

Figure 1 and 2: Abnormality of the RCA ostium and the aortic root.

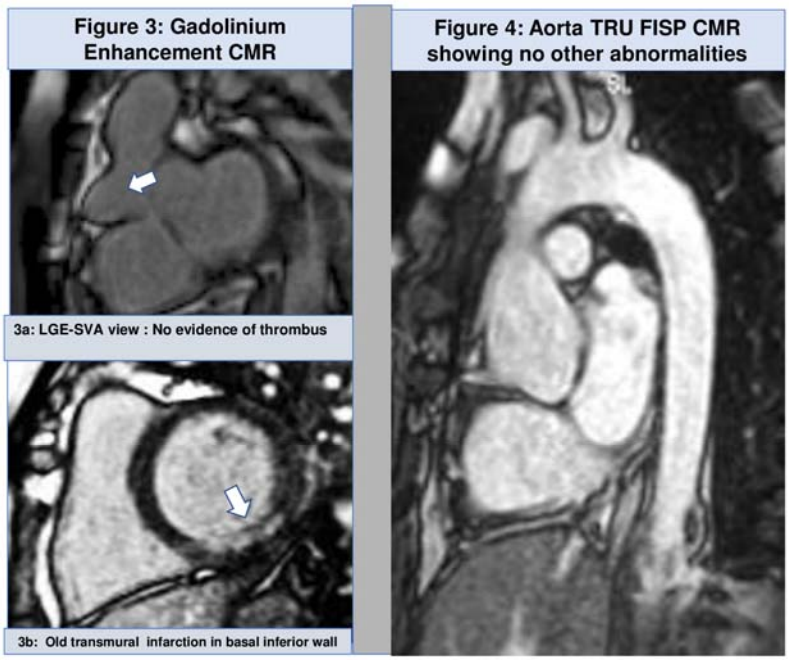

Figure 3 and 4: Late Gadolinium Enhancement and Aorta Assessment

ID#: 378333

Subvalvular left ventricular outflow tract aneurysm in the setting of remote bicuspid aortic valve endocarditis

Thuy Nguyen, MD[1] Joseph Lembo, DO[2], Michael O'Loughlin, MD[3]

1. University Hospitals Cleveland Medical Center, Shaker Heights, OH

2. Hartford Hospital, Orange, CT

3. Jefferson Radiology, West Hartford, CT

Description of Clinical Presentation: A 58 year old female presented to her cardiologist with intermittent palpitations. Past medical history was notable for infectious endocarditis involving her bicuspid aortic valve 30 years prior. Electrocardiogram showed occasional benign premature ventricular contractions. She underwent a transthoracic echocardiogram which demonstrated a small pericardial effusion, a mildly insufficient bicuspid aortic valve, and an apparent pulsatile structure near the posterior sinus of Valsalva. Further evaluation with cardiac MRI demonstrated a 4.3 cm aneurysmal out-pouching extending from the left ventricular outflow tract into the left atrium. At surgery, the orifice of the aneurysm measured 1.8 x 1.0 cm in size with a thick fibrous margin amenable to patch repair. Followup evaluation demonstrated significant decrease in size of the aneurysm without persistent internal flow. Mild aortic insufficiency persisted.

Diagnostic Techniques and Their Most Important Findings: Pre-surgical transthoracic/transesophageal echocardiograms demonstrated a small pericardial effusion, a bicuspid aortic valve with fusion of the right and left posterior cusps, mild aortic insufficiency, and a pulsatile mass near the posterior sinus of Valsalva. Pre-surgical cardiac MRI demonstrated similar findings, adding information regarding the pulsatile mass which appeared as an out-pouching from the subvalvular left ventricular outflow tract consistent with a subannular ventricular aneurysm. The aneurysm bulged posteriorly and inferiorly with respect to the left main coronary artery causing distortion of left atrium. No significant turbulent flow in the left atrium was demonstrated. Post-surgical cardiac MRI and transthoracic echocardiogram demonstrated a significant decrease in size of aneurysm although mild aortic insufficiency persisted.

Learning Points from this Case: Aneurysmal out-pouching of the left ventricular outflow tract (LVOT) is a rare clinical entity with nonspecific clinical presentation. These tend to be pseudoaneurysms rather than true aneurysms, contained only by a thickened epicardial or pericardial wall. They most commonly occur through the mitral-aortic intervalvular fibrosa, a point of weakness that is fibrous, avascular, and prone to infection/trauma. LVOT pseudoaneurysms have been documented in a variety of settings including prior cardiac surgery, prosthetic aortic valve replacement, infective endocarditis, chest trauma, myocardial infarction, and congenital heart disease. Symptoms are usually vague secondary to mass effect on surrounding structures (LVOT itself, coronary arteries, pulmonary artery, left atrium, or left main bronchus). However, rupture of the pseudoaneurysm can be fatal. Both transthoracic and transesophageal echocardiograms can aid in detection and anatomic delineation but cross-sectional imaging may ultimately be needed to establish the actual origin. Localization and description of the neck is especially important for surgical planning.

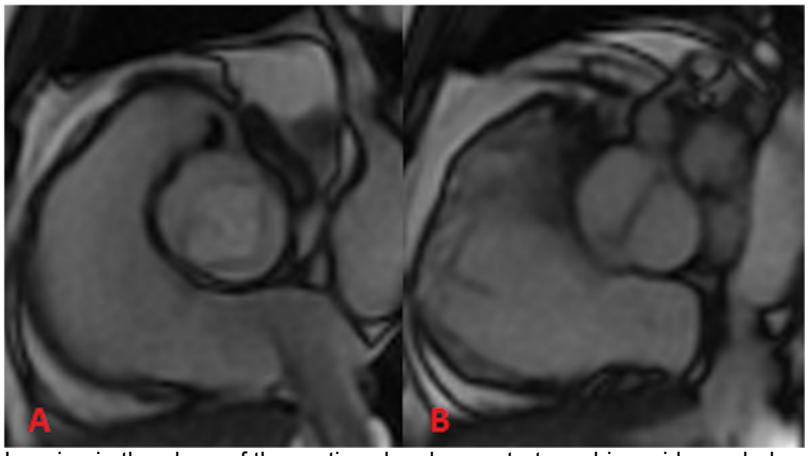

Imaging in the plane of the aortic valve demonstrates a bicuspid morphology; Open (A) and Closed (B).

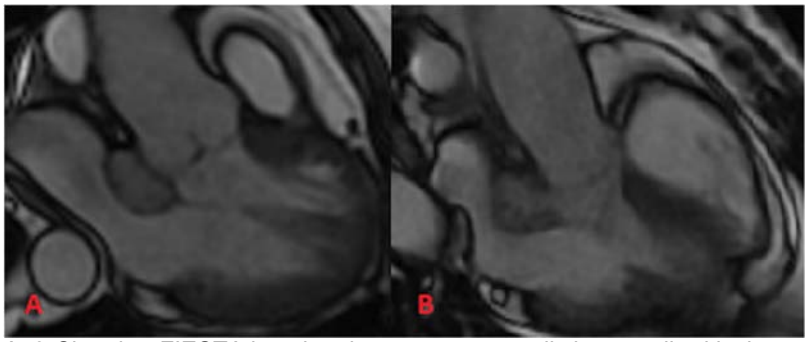

A. 3-Chamber FIESTA imaging demonstrates a well circumscribed lesion posterior to the aortic valve that deforms the left atrium. B. Slightly off axis imaging demonstrates that this lesion directly communicates with the left ventricular outflow tract.

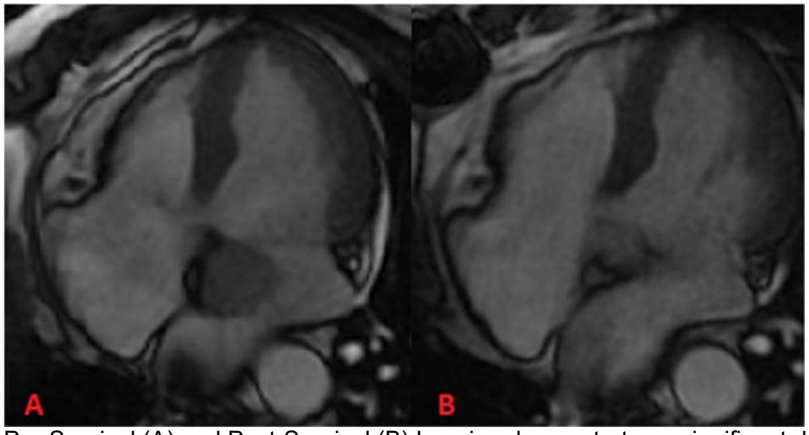

Pre-Surgical (A) and Post-Surgical (B) Imaging demonstrates a significant decrease in size of the LVOT aneurysm and less deformity of the left atrial chamber.

ID#: 378393

Ferumoxytol-Enhanced MR Venography in End-Stage Renal Disease

Puja Shahrouki, M.D.[1] Adam Plotnik, M.D.[2], Justin P. McWilliams, M.D.[2], J. Paul Finn, M.D.[2]

1. Department of Radiology, David Geffen School of Medicine at UCLA, Los Angeles, CA

2. Department of Radiology, David Geffen School of Medicine at UCLA, CA

Description of Clinical Presentation: A 19 year-old male with a complicated history of oxalosis and end-stage renal disease (ESRD; creatinine 6.0 mg/dL, eGFR 12 mL/min/1.73 m^2) with bilateral nephrectomies on hemodialysis, was suspected to have thrombus at the catheter tip on echocardiography. Further imaging was required to evaluate the thrombotic burden, but magnetic resonance angiography with gadolinium-based contrast agents was contraindicated because of concerns about nephrogenic systemic fibrosis.

Diagnostic Techniques and Their Most Important Findings: High-resolution magnetic resonance venography (MRV) was carried out on a Siemens Magnetom Prisma Fitscanner (Malvern, PA) at 3.0 T following intravenous infusion of the renal-safe ultrasmall, superparamagnetic iron oxide (USPIO) particle, ferumoxytol in a dose of 3.5 mg/kg. Ferumoxytol enhanced-MRV (FE-MRV) confirmed the presence of catheter-associated thrombus and excluded additional thrombus in the entire thoracoabdominal vasculature. Following continued uncomplicated anticoagulation, interventional radiology successfully performed Permacatheter replacement 16 days later without complications. Within 24 hours, the patient';s post-procedural renal function improved to creatinine 4.6 mg/dL and eGFR 16 mL/min/1.73 m^2. The patient subsequently had 4 additional FE-MRVs over the course of 16 months for a range of different angiographic indications without any adverse events (Figure 1-3). As noted in Figure 3, right renal transplantation was carried out in the interim. Of the five FE-MRVs, no additional imaging was required prior to clinical intervention or decision making. Of note, laboratories reflecting iron metabolism and storage were monitored throughout the course of the 16 months and no significant change was noted.

Learning Points from this Case: FE-MRV has significant clinical impact in patients with ESRD by giving clinicians confident diagnostic assessment with minimal need for additional imaging. Repeated FE-MRV was performed safely without affecting renal function or significant change in iron storage or metabolism.

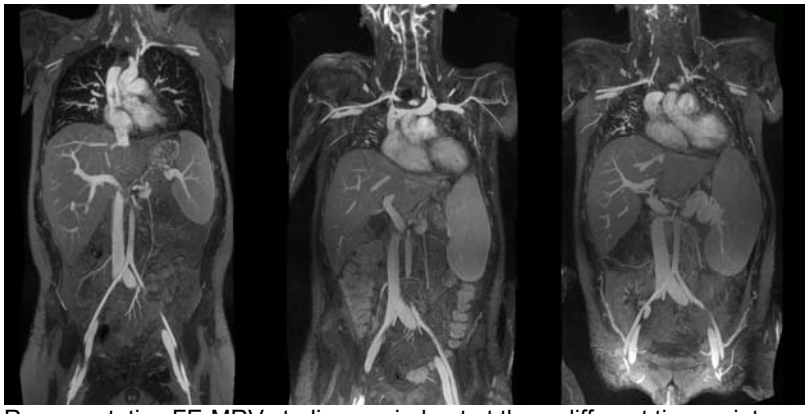

Representative FE-MRV studies carried out at three different time points over a 16-month period.

ID#: 378261

An incidental finding in a young female following a motor vehicle collision status post hysterectomy two weeks prior

Rydhwana Hossain, MD[1] Adam Herder, MD[2], Charles White, MD[2]

1. University of Maryland, Burtonsville, MD

2. University of Maryland

Description of Clinical Presentation: A 36-year-old female originally from Cameroon with past medical history of uterine fibroids status post hysterectomy 2 weeks prior, presented to the emergency department with pain after being involved in a motor vehicle collision several days earlier. She was found to be in hypertensive urgency with blood pressure of 250/120. Routine chest radiograph demonstrated a 1.2 cm right lung nodule prompting further evaluation with chest CT. Contrast enhanced chest CT demonstrated two right lung nodules in addition to a large intracardiac right ventricular (RV) mass (Figure 1). The patient was admitted to the cardiac surgery unit and underwent preoperative cardiac MRI and left heart catheterization.

Diagnostic Techniques and Their Most Important Findings: CMR with multiplanar CINE SSFP, T1 TSE (Dark Blood), first pass and delayed-contrast imaging were performed. CMR demonstrated an oblong soft tissue mass measuring 4.9cm within the right ventricular outflow tract (Figure 2). This mass abutted the pulmonary valve and appeared to be in close contact with the right ventricular papillary muscle. The mass was isointense to myocardium on T2 weighted sequences and demonstrated heterogeneous enhancement on post contrast imaging. The left ventricular systolic function was preserved. A cardiac catheterization revealed moderate proximal to mid LAD atherosclerotic disease. Given the presence of a partially obstructing RVOT mass with pulmonary nodules, the patient was taken to cardiac surgery. A midline sternotomy was performed and a RV intracardiac mass was identified encircling the tip of a papillary muscle supporting chordae tendinae of the anterior leaflet of the tricuspid valve. The lesion was smoothly marginated with benign non-hemorrhagic appearance(Figure 3). The lesion was excised and histology demonstrated a whorled fascicular pattern of bland spindle cells and cigar shaped nuclei; very few mitosis or atypia. Immunohistochemistry stains for smooth muscle actin, desmin, and estrogen and progesterone receptors were positive, indicating a smooth muscle tumor of uterine origin consistent with a benign metastasizing leiomyoma (BML).

Learning Points from this Case: First case described by Steiner in 1939, BML is a rare disorder affecting women with history of uterine leiomyoma with metastasis to extrauterine sites. The lungs are most common site of metastasis, with other rare various locations such as the heart. To our knowledge only 5 case reports have been published on BML with cardiac metastasis. CMR can provide useful additional information to assist the diagnosis, characterize the lesion, and aid in management of cardiac masses; although large obstructing intracardiac masses like our case require resection for accurate diagnosis and prevention of complications.

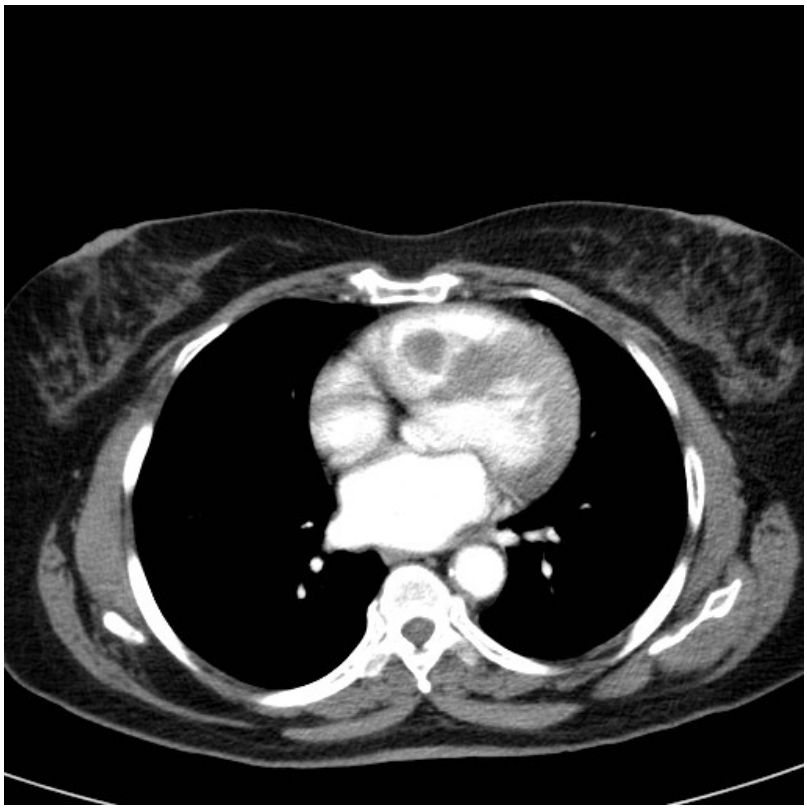

Figure 1, chest CT

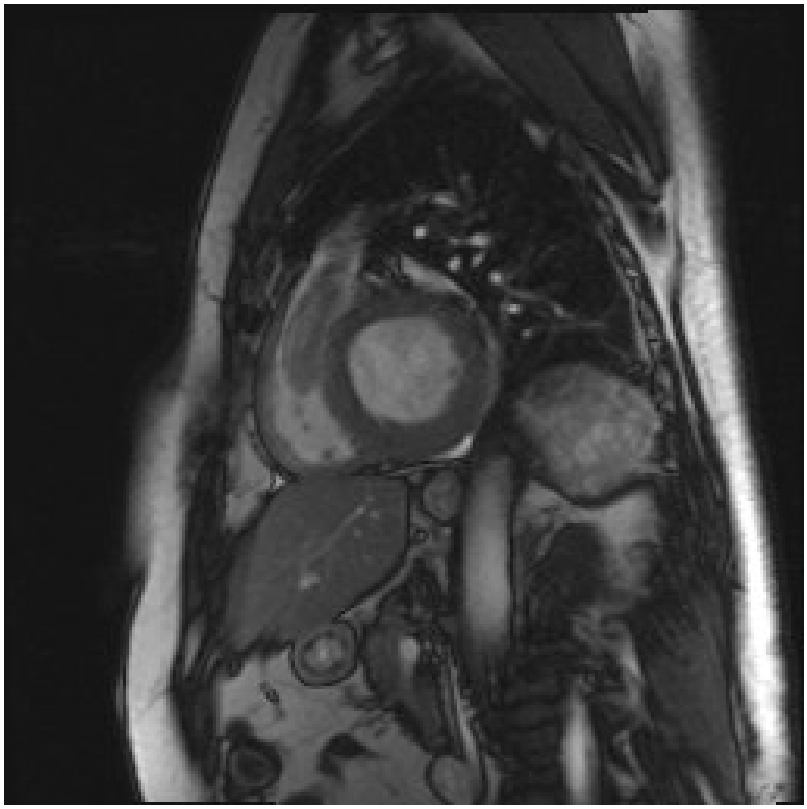

Figure 2, Sax SSFP right ventricular mass

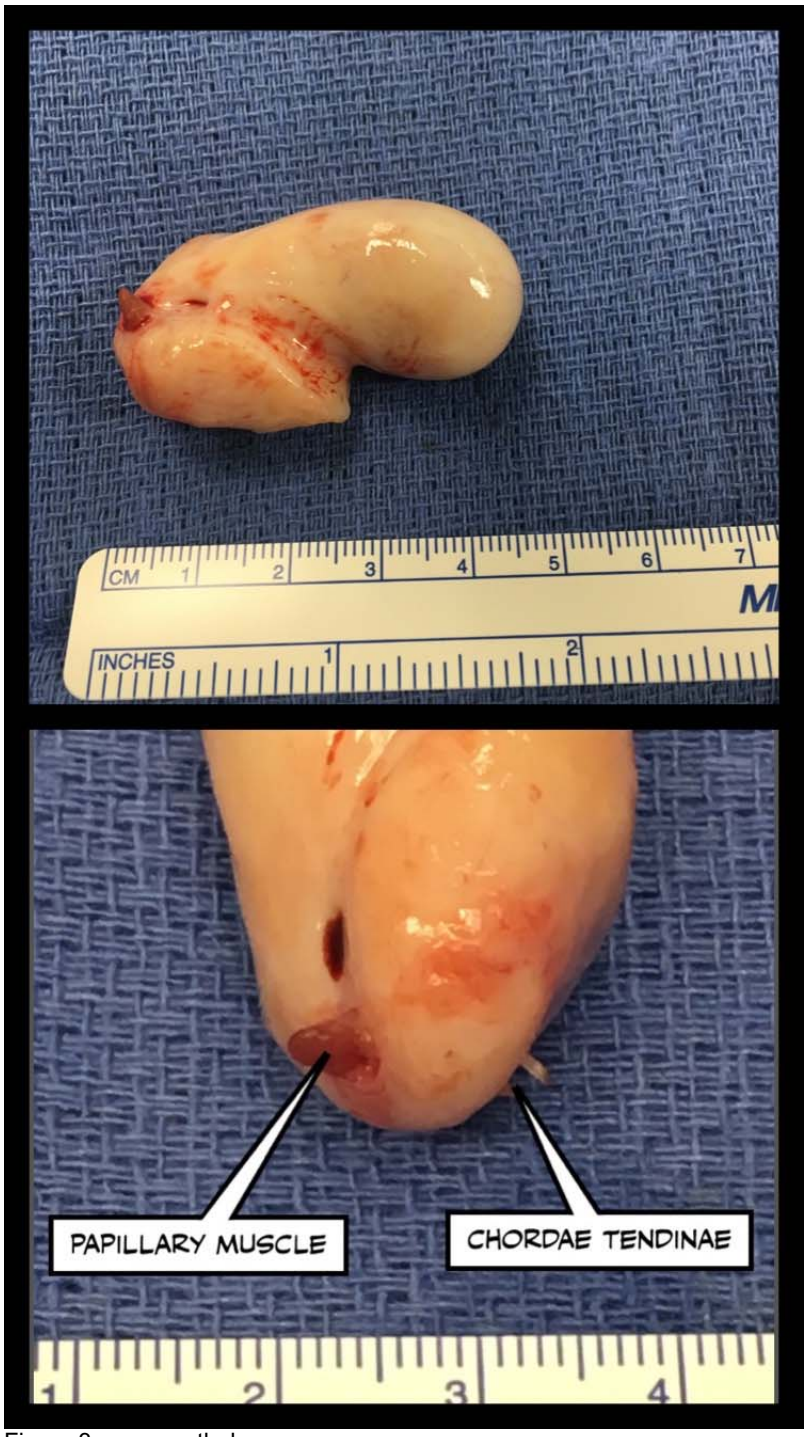

Figure 3, gross pathology

ID#: 367211

An unusual case of asymmetrical 'Left Ventricular Hypertrophy'

Emma Burnhope, BM, MRCP[1] Adriana Villa, MD[2], Amedeo Chiribiri, MD PhD[3], Reza Razavi, MD, PhD[3], Tevfik F. Ismail, PhD MRCP[4]

1. King's College, London, London, England, United Kingdom

2. St. Thomas' Hospital, London; King's College London, London, England, United Kingdom

3. King's College London, London, England, United Kingdom

4. King's College London; Guy's and St Thomas' Hospitals NHS Foundation Trust, London, England, United Kingdom

Description of Clinical Presentation: A 30-year-old man was incidentally noted to have a murmur on clinical examination. He denied any cardiovascular symptoms and had no other relevant past medical or surgical history, and in particular, no history of epilepsy. He took no regular medications. There was no relevant family history of cardiac or any other disease, however, he mentioned having been told about a murmur since childhood. Clinical examination was unremarkable other than for a grade 2/6 ejection systolic murmur heard at the left sternal edge. There were no stigmata of a neurocutaneous syndrome. His 12-lead ECG met voltage criteria for left ventricular hypertrophy with associated repolarisation changes. He was referred for further investigation to exclude hypertrophic cardiomyopathy. A transthoracic echocardiogram (TTE), unexpectedly revealed a large mass in the interventricular septum measuring approximately 60x30mm. Systolic function was normal as was valve morphology and function. There was no significant LV intracavity gradient or outflow tract gradient at rest or on Valsalva.

Diagnostic Techniques and Their Most Important Findings: He subsequently underwent Cardiovascular Magnetic Resonance (CMR) at 1.5T for further assessment and tissue characterisation. This confirmed a non-dilated LV with good systolic function. The septal mass was solitary with relatively homogenous signal characteristics and measured 49x66mm (Image 1). The mass was isointense on T1-weighted spin echo sequences but hyperintense on T2-weighted imaging with no signal drop on spectral pre-saturation of fat signal (Image 2). There was minimal contrast enhancement following first-pass perfusion imaging and on late gadolinium imaging (Image 3). The MRI characteristics were most in-keeping with a rhabdomyoma. The main differential is a cardiac fibroma, but the latter tends to be hypointense on T2-weighted sequences, and to exhibit marked contrast hyperenhancement on late enhancement imaging. Interval scans over 5 years have shown no significant change in lesion size or signal characteristics supporting the diagnosis of a benign cardiac tumour.

Learning Points from this Case: CMR continues to play a vital role in the assessment of suspected cardiac or pericardial masses. In comparison to TTE, it affords better quantification of mass size, location and relationships to surrounding structures. It can more readily identify local invasion or extra-cardiac spread. Its superior tissue contrast and tissue characterisation properties facilitate differential diagnosis. Rhabdomyomas are benign tumours of striated muscle and can occur in the heart or may be extra-cardiac, often presenting as head and neck tumours. There is a known association with tuberous sclerosis. Anatomically, they are classically intramyocardial with a preponderance for either the left or right ventricle and frequently occur in multiples. While rhabdomyomas are the most common cause of benign paediatric cardiac tumour, they are uncommonly seen in adulthood with <100 reports of extra cardiac rhabdomyoma and even fewer cardiac presentations. The natural history in children is of partial or complete tumour regression, although this does not appear to apply to our particular example. In asymptomatic patients, no treatment is usually indicated due to this typical regression, however, if there is left ventricular outflow tract obstruction or arrhythmia, surgical excision offers curative treatment and an excellent prognosis.

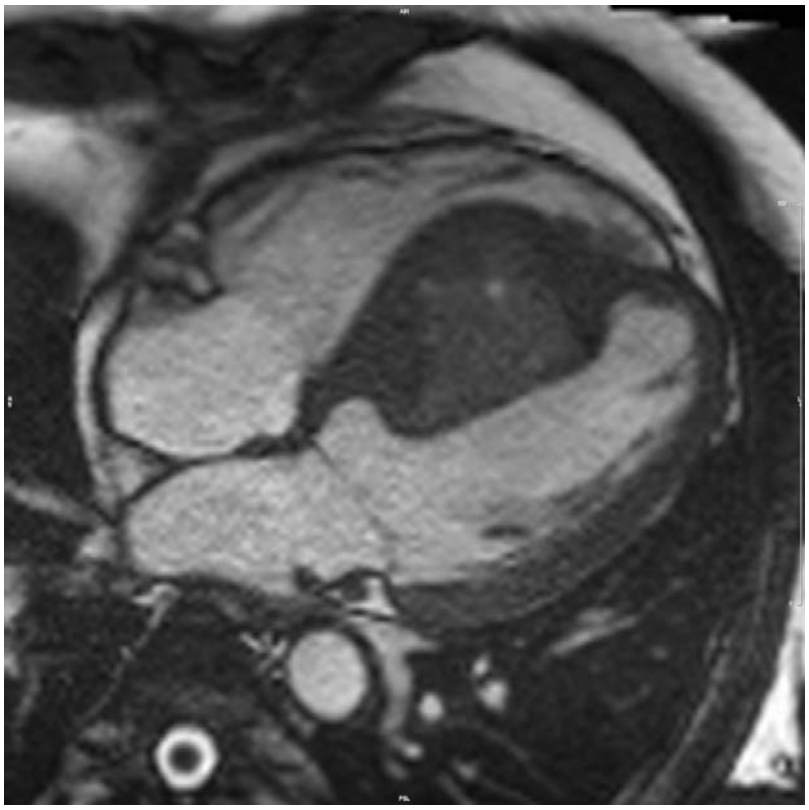

Four Chamber SSFP-cine sequence demonstrating the mass in the interventricular septum.

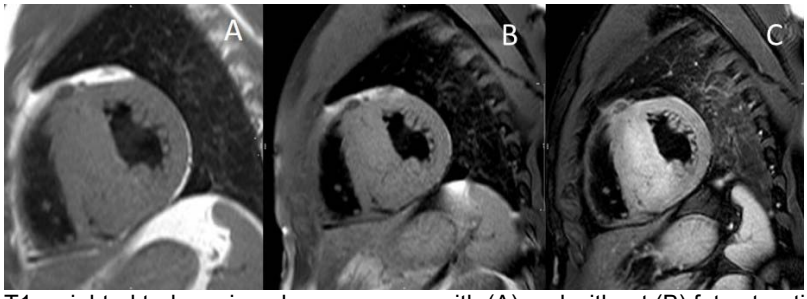

T1-weighted turbo spin-echo sequences with (A) and without (B) fat saturation and T2-weighted spin echo sequences with fat saturation (C).

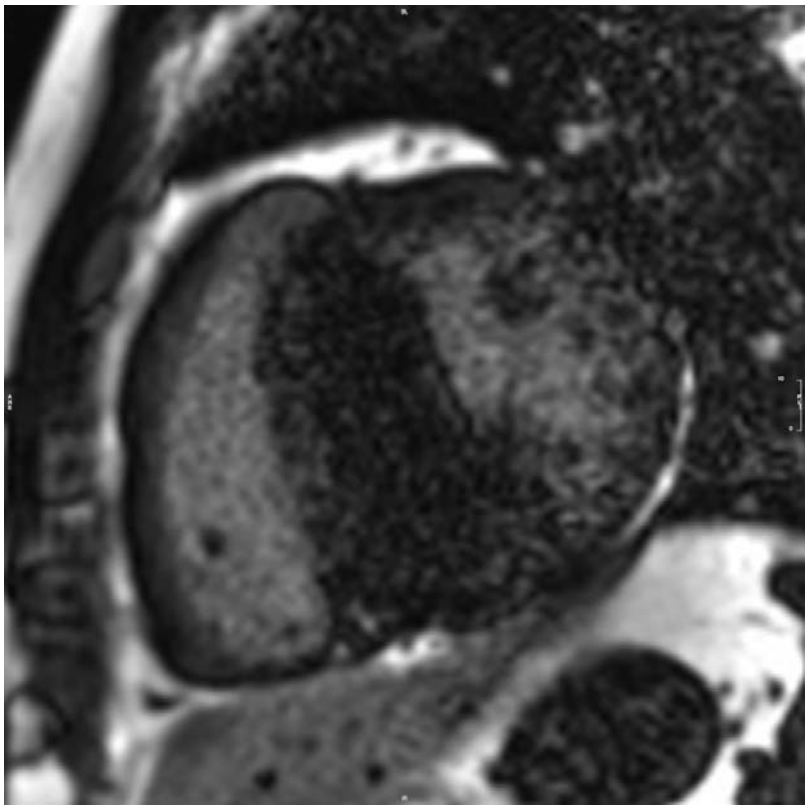

Late gadolinium enhancement

ID#: 367651

Small & highly mobile cardiac masses: how to image?

Riad Abou Zahr, MD[1] Naseem Uddin, MD [2], Kavita Sharma, MD [2], Tarique Hussain, MD, PhD[3]

1. University of Texas Southwestern Medical Center UTSW, Dallas, TX

2. University of Texas Southwestern Medical Center

3. Dept. of Pediatrics, UT Southwestern Medical Center, TX

Description of Clinical Presentation: An 11 year old female with no significant past medical history presented with Sydenham chorea. During work up for acute rheumatic fever, echocardiography demonstrated only an incidental mass on the mitral valve. An electrocardiogram was unremarkable. CMR was performed & findings were suggestive of fibroelastoma (Image 1) which was surgically resected with no complications. Pathologic examination revealed benign fibromyxoid growth with endothelial proliferation not consistent with a papillary fibroelastoma or a cardiac myxoma (Images 2 & 3).

Diagnostic Techniques and Their Most Important Findings: The patient was pre-medicated with Metoprolol 25 mg. Heart rate during scan was 66-68 beats/min. Sequences included:
2D cine balanced steady state free precession (bSSFP) in 2, 3, and 4 chambers and short axis across the mitral valve plane views
T1 double inversion recovery (DIR) Turbo Spine Echo (TSE) across the mass with and without fat saturation (FS)
T2 weighted DIR TSE with FS
First pass perfusion with injection of Gadobutrol
Phase-sensitive inversion recovery (PSIR) in a short axis slice across the mass for late gadolinium enhancement
3D IR bSSFP whole heart sequence with continuous Gadobutrol infusion and image based navigation

Findings: A homogeneous 5.6 mm x 5 mm x 4.9 mm T1 and T2 isointense mass with a smooth surface,attached between the middle and the posterior segment of the posterior mitral valve leaflet that moved with the valve. The mass did not show contrast uptake nor delayed gadolinium enhancement. It was most consistent with a fibroelastoma. Differential diagnoses include thrombus and endocarditis lesion

Learning Points from this Case: CMR finding was a small isointense (T1 & T2), non-perfused, homogeneous mass attached to the posterior mitral valve leaflet, most likely a papillary fibroelastoma.
Imaging small and highly mobile cardiac masses in children can be challenging. Cine bSSFP sequences can be used to locate the mass, both in position and time. The plane where the mass is best seen should be recorded and ideally positioned in free-breathing. If breath-holding is used, consistent breath-holding in end expiration should be used across all sequences. Timing of the still period of the mass in this plane can be achieved using high-temporal resolution cine imaging (60 to 80 phases).
For all sequences, the trigger delay (Td) and acquisition window should be manually adjusted to this ‘still'; period. This includes Td for DIR images (which are often set at default values). This also includes perfusion images and late enhancement.
For high heart rates, it is important to increase TR times for TSE imaging appropriately (e.g standard T2 weighting is achieved with TR of 1500-2000 ms and so in children, it may be necessary to switch the default (every second heart-beat) to every third or even every fourth.
Using consistent rest periods and respiratory compensation, it is possible to image small & highly mobile masses with full tissue characterization.

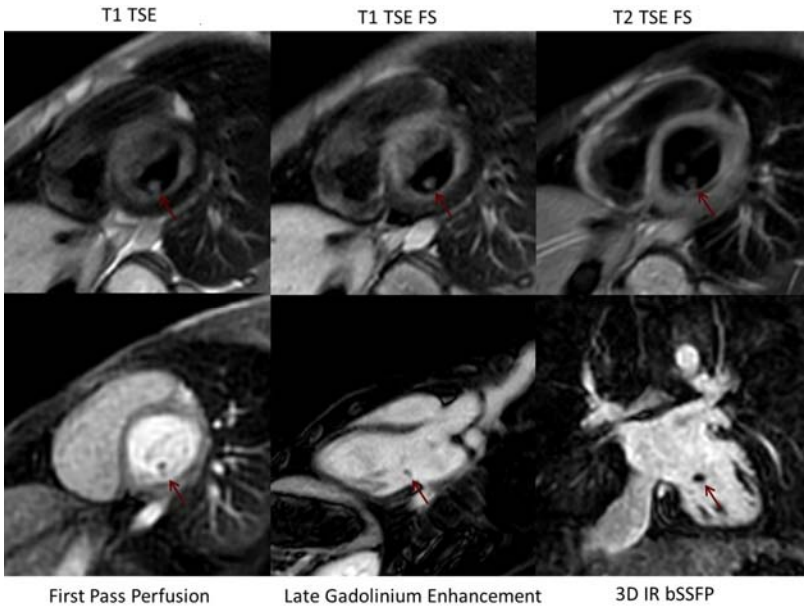

Tumor characterization

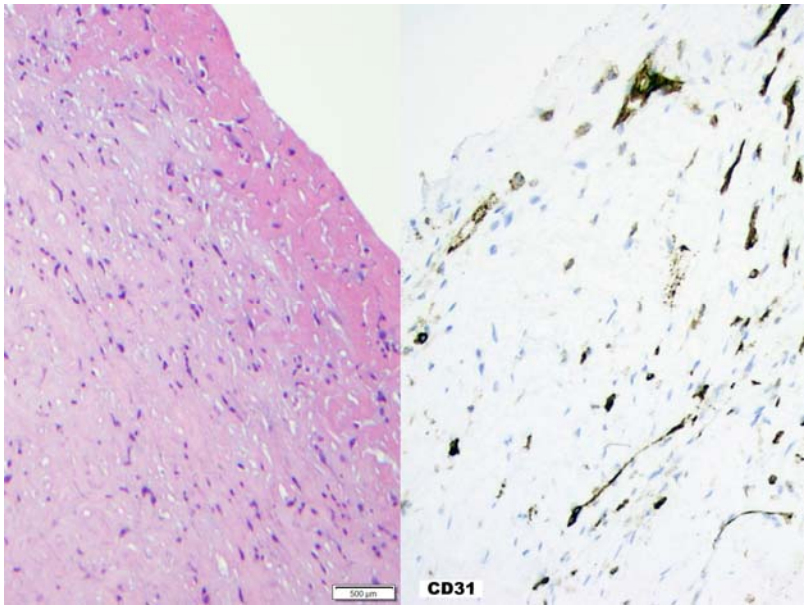

Benign fibromyxoid growth with endothelial proliferation

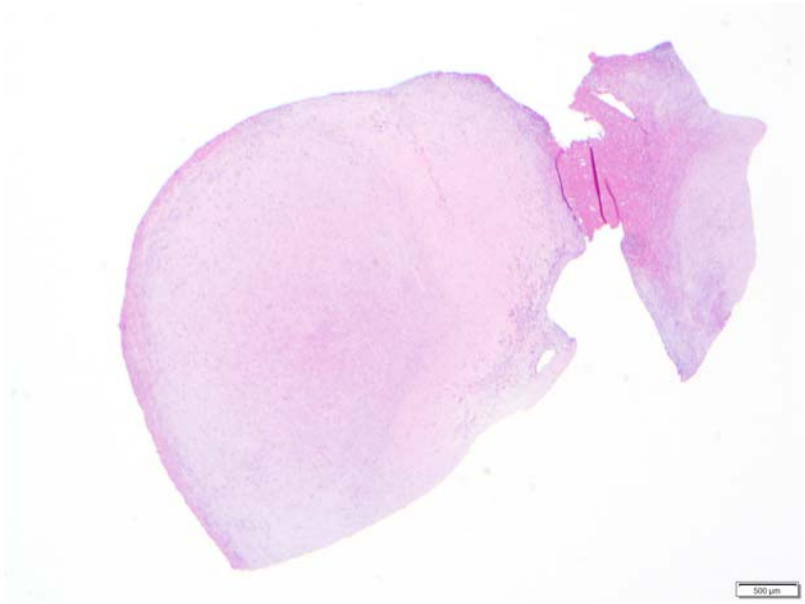

Whole lesion

ID#: 370463

Three-Dimensional printed cardiac model in assisting surgical planning in Heterotaxy patient with complex systemic and pulmonary venous drainage

Arpit Agarwal, MD[1] Dilachew Adebo, MD, FAAP, FACC[2]

1. University of Texas Medical School at Houston, Houston, TX

2. University of Texas Medical School at Houston

Description of Clinical Presentation: A four-year-old female child born with a diagnosis of heterotaxy syndrome consisting of abdominal situs inversus, interrupted inferior vena cava with azygous continuation to superior vena cava (SVC), atrial situs ambiguous, atrioventricular (AV) discordance, balanced AV canal defect, L-looped ventricles and ventriculo-arterial concordance. She had been doing well and remained relatively asymptomatic from a cardiac standpoint. Pre-surgery cardiac catheterization revealed pulmonary vascular resistance of 0.83 wood units m^2 and Qp:Qs of 2.3:1. To further delineate the complex pulmonary and systemic venous connections cardiac magnetic resonance imaging was performed which revealed right sided atrium receiving all four pulmonary veins and the superior vena cava along with right hepatic veins. The left sided atrium was severe hypoplastic and received only left hepatic veins. Three dimensional cardiac model was printed to determine feasibility of biventricular repair. A complete biventricular repair of her defect was done by performing a Mustard like procedure to baffle the systemic and pulmonary veins along with repair of her atrioventricular septal defect. The surgical outcome was good and patient was discharged home five days after the procedure. To our knowledge, this is the first case demonstrating the role of 3D modelling in surgical planning of heterotaxy patient with complex systemic and pulmonary venous connection and atrioventricular septal defect.

Diagnostic Techniques and Their Most Important Findings: The findings of cardiac magnetic resonance imaging and three-dimensional (3D) printed cardiac model demonstrated that all four-pulmonary veins, superior vena cave and right hepatic veins draining into the right sided atrium. The 3D printed cardiac model also revealed the relative position of ostium of these vessels in the right sided atrial cavity. The openings of all four pulmonary veins were posterior to the opening of superior vena cava and the right hepatic veins (Figure 1). The left sided atrium was severely hypoplastic and received only left hepatic veins (Figure 2).There was interrupted inferior vena cava with azygous continuation to superior vena cava and atrioventricular septal defect (Figure 3). Based on these findings the patient underwent complete repair of AV canal defect and atrial switch procedure (Mustard-like operation). With the help of a single bovine pericardial patch the AV defect was repaired. The superior end of the patch was fashioned to direct the SVC and hepatic venous flow towards the left sided morphologic right ventricle. The use of three-dimensional printed cardiac model was of paramount importance in pre-planning of this complex cardiac surgery. We report this interesting case of complex systemic and pulmonary venous drainage who underwent successful biventricular repair with help of cardiac magnetic resonance imaging and three dimensional printed cardiac model.

Learning Points from this Case: The cardiac magnetic resonance imaging and three dimensional printed cardiac model can be a useful tool in understanding complex systemic and pulmonary venous drainage which is frequently encountered in patients with heterotaxy syndrome. The use of three-dimensional printed cardiac model is of paramount importance in pre-planning of such complex cardiac surgery for better surgical outcome.

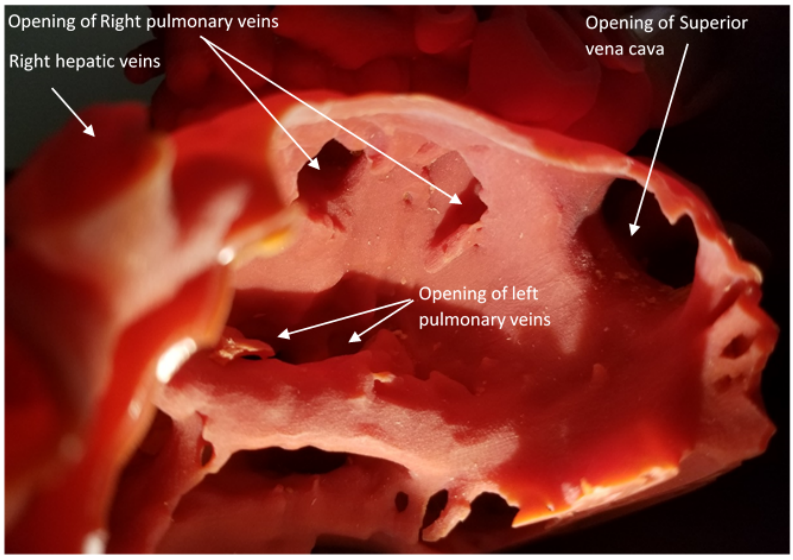

Figure 1

Right Sided Atrium

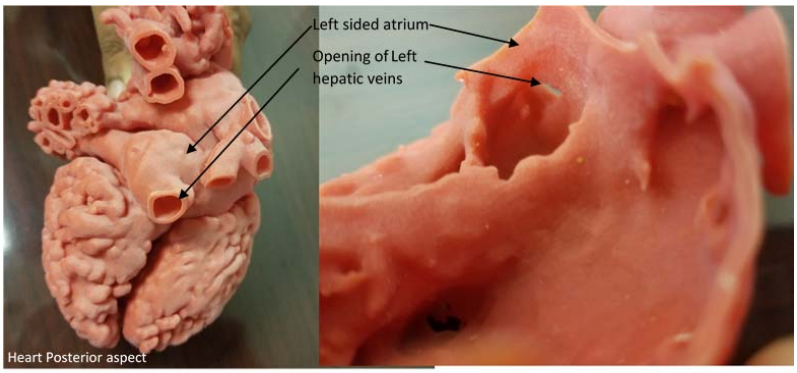

Figure 2

Left Sided Atrium

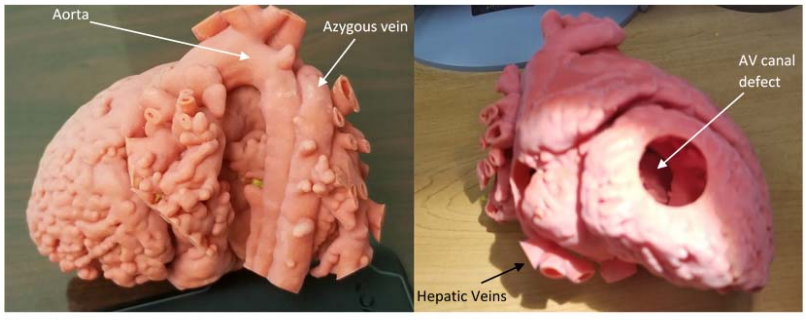

Figure 1

Heterotaxy Syndrome with Atrioventricular Canal Defect

ID#: 371215

A strange worm in the right heart...

José Miguel. Correia, Hospital Cuf Viseu

Centro Hospitalar de Tondela Viseu EPE, Portugal

Description of Clinical Presentation:

A 38 years old female patient, with an history of asthma, was referred to the emergency department because of chest pain and an abnormal ambulatory transthoracic echocardiogram (TTE), describing an important mobile mass in the right atrium. The physical exam didn';t show significant findings. The EKG and initial blood work was normal.

She was admitted in the cardiology ward for further study. The differential diagnosis included a local thrombus, a right atrial myxoma / other less common primary cardiac tumor, or possibly a tumor infiltrating the vena cava from a nearby organ.

Diagnostic Techniques and Their Most Important Findings:

To delineate this cardiac mass, initially a transesophageal echocardiogram (TEE) was performed, showing a "worm-like", very elongated, filiform mass, of significant dimensions (fig.1), that seemed to emerge from the inferior vena cava, without any attachment to other cardiac structures, occupying the right atria and prolapsing to the right ventricle during diastole. Those findings didn't seem compatible with a myxoma, and the location and shape were atypical for a thrombus.

For better study, a cardiovascular magnetic resonance (CMR) was requested, showing the already described filiform mass, now clearly seen to be implanted in the inferior vena cava (fig.2A), near the junction with the right atrium, without any evidence of venous invasion from nearby structures (fig.2C). This lesion didn't have any signs of vascularity in the perfusion sequences (fig.2B) and no evidence of enhancement in early or delayed enhancement sequences (fig. 3).

The CMR findings were compatible with a thrombus.

Due to the significant dimensions and important embolic risk, the case was discussed with the cardiothoracic surgical team, and a decision was made to remove the mass.

While waiting for surgery, the patient suffered a massive pulmonary embolism. She was submitted to thrombolysis with good clinical response and quick recovery. A follow-up TTE failed to show any significant mass on the right atrium. A control CMR study confirmed the absence of the previous described mass in the right heart. The clinical evolution and exam findings corroborated the initial CMR diagnosis.

This way, obviously, surgery was no longer needed, and she was discharged on oral anticoagulation. Subsequent ambulatory study confirmed the presence of a prothrombotic state, with the diagnosis of antiphospholipid syndrome being made.

Learning Points from this Case: In conclusion, this unusual case illustrates the importance of CMR in studying the nature of cardiac masses.

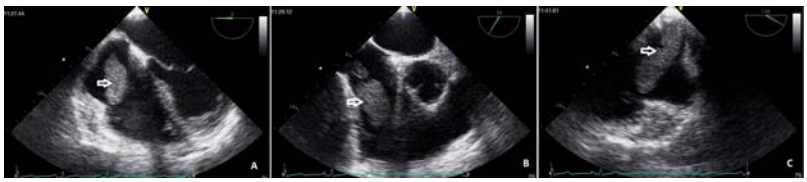

TEE images in different planes

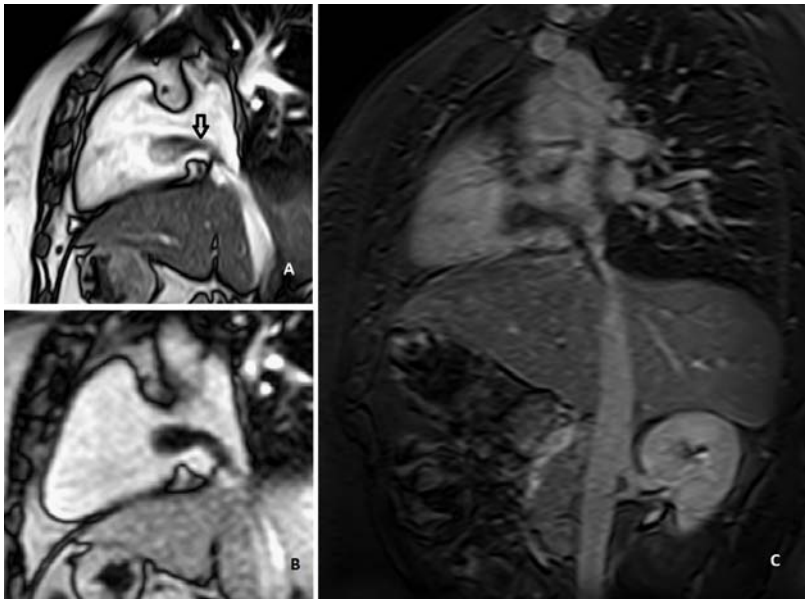

CMR images (A - cine (SSFP); B - Perfusion sequence; C - MR angiography, venous phase)

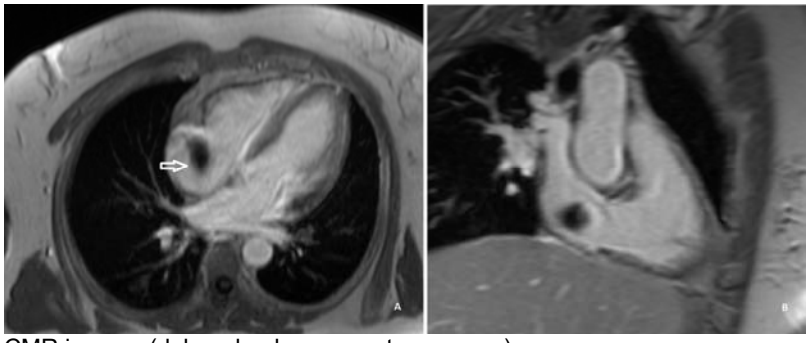
CMR images (delayed enhancement sequence)

ID#: 372491

CMR and CT/PET Correlation in a Case of Metastatic Pancreatic Plasmacytoma

Roshin C. Mathew, MD[1] Adrián I. Löffler, MD[2], Robert Burress, MD[3], Michael Salerno, MD, PhD[4], Christopher M. Kramer, MD[2]

1. University of Virginia Health System, VA

2. University of Virginia Health System, Charlottesville, VA

3. University of Virginia Health System

4. University of Virginia, VA

Description of Clinical Presentation: A 68 y/o female with recently diagnosed pancreatic plasmacytoma s/p biliary stent for extrinsic common bile duct (CBD) compression presented to the hospital for re-obstruction of CBD on 7/25/17 with significantly elevated hepatobiliary enzymes. The patient underwent succesful repeat biliary stent placement. With stabilization and improvement in symptoms, the patient underwent whole body PET/CT to evaluate for progression of disease and staging.

Diagnostic Techniques and Their Most Important Findings: Whole Body PET/CT was performed using a a Siemens Biograph40 CT scanner to obtain 4mm axial slices from head to foot. Images were reconstructed in axial, sagittal, and coronal projections along with attenuated and non-attenuated PET images. Whole body PET/CT revealed significant FDG uptake of an infiltrative mass of the pancreatic tail. In addition, patient was found to have increased FDG uptake in local lymph nodes. Noted in the images were ill-defined lesions demonstrating FDG uptake within the suprahepatic inferior vena cava (IVC) and right atrium that could be thrombus versus metastasis(Figure 1). CMR was performed on a Siemens AERA 1.5 Tesla CMR scanner to obtain the following sequences: Axial HASTE and steady state free procession images, multiplanar steady state free procession cine images in both the axial and short axis orientations, T1 and T2 weighted images with and without fat saturation, first pass contrast enhanced perfusion images, and delayed contrast-enhanced phase sensitive inversion recovered images. CMR showed two masses (Figure 2), one at the junction of the IVC and right atrium (11x14mm) and another as part of the interatrial septum (12x8mm). Both masses demonstrated similar first pass enhancement to normal myocardium. In addition, there was no pre- or post-contrast T1 or T2 mapping abnormalities, no late gadolinium enhancement, and no loss of signal from fat saturation(Figure 3). The masses demonstrated myocardial tagging properties similar to the myocardium.

Learning Points from this Case: Due to the increased FDG uptake in a metabolically active acute thrombus, it can be difficult to differentiate thrombus from other metabolically active tissue using PET/CT[1]. CMR can help rule out thrombus as in this case. In all sequences that were applied, the cardiac masses behaved morphologically like normal myocardium and not like thrombus(Figure 3). Utilizing the results of both imaging modalities, the cardiac masses are metastatic pancreatic plasmacytoma lesions. In this case, therapeutic anticoagulation was never started and inpatient chest radiation and chemotherapy was initiated.

[1] Rondina MT, et al. (18)F-FDG PET in the evaluation of acuity of deep vein thrombosis. Clin Nucl Med. 2012 Dec;37(12):1139-45

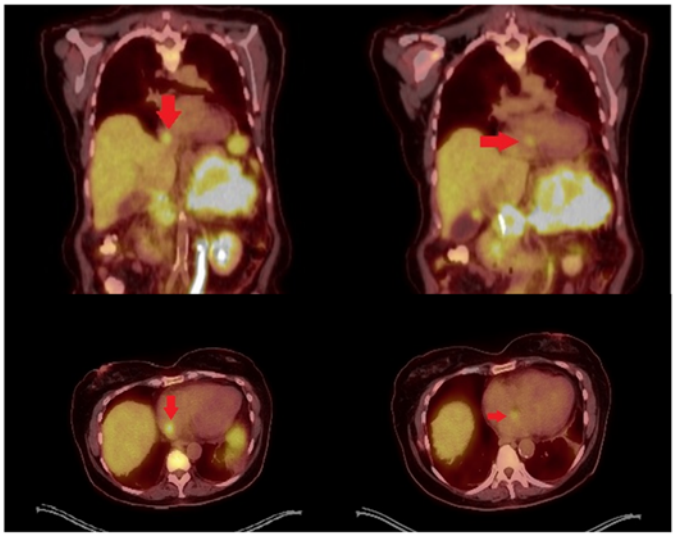

Figure 1: Axial and coronal PET/CT images shows increased FDG uptake in the area of the inferior vena cave and right atrium (left) and the intra-atrial septum (right)

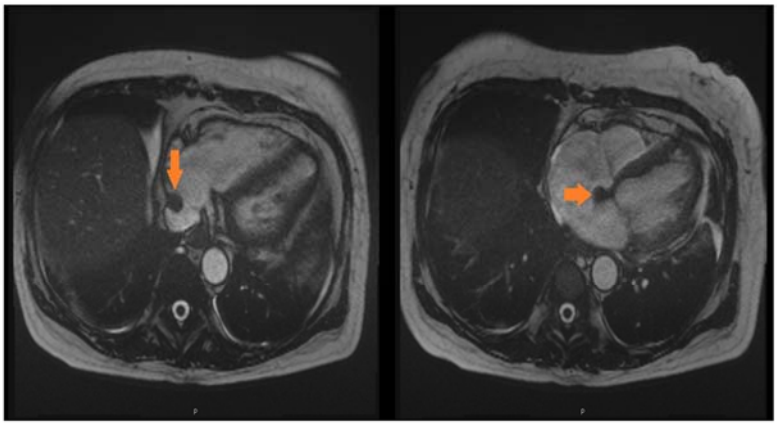

Figure 2: Pre-contrast axial images showing a masses (arrows) in the area of the inferior vena cava and right atrium (left) and intra-atrial septum (right) correlating to PET/CT images seen in Figure 1

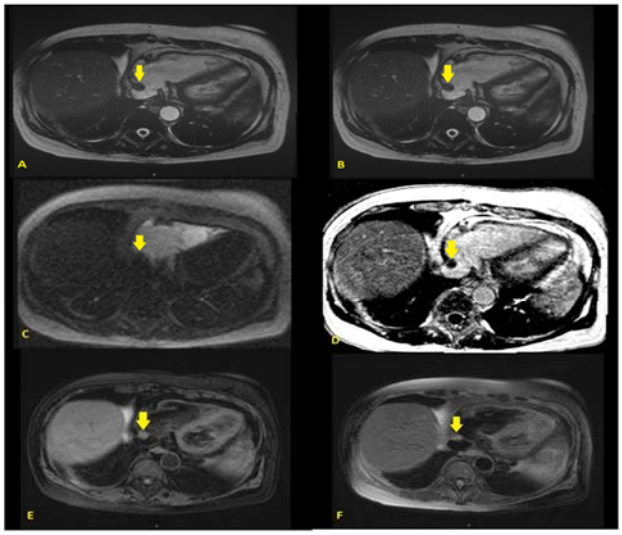

Figure 3: Images of the right atrial/inferior vena cava mass (arrow) using various sequences: (A) pre-contrast, (B) post-contrast, (C) first-pass perfusion, (D) late gadolinium enhancement, (E) T1 fat sat, and (F) T2 Fat Sat.

ID#: 371755

Sever pulmonary stent stenosis after failed Ross procedure

Gladys Juncà[1] Albert Teis[2], Jorge López Ayerbe[3], Francisco Gual-Capllonch[4], Antoni Bayes-Genis, Department of Medicine, Universitat Autònoma de Barcelona, Barcelona[4]

1. Hospital Universitari Germans Trias i Pujol. Badelona. Barcelona, Spain

2. Hospital Universitari Germans Trias. Badalona. Bacelona. Spain., Badalona, Spain

3. Hospital Universitari Germans Trias i Pujol. Badalona., Spain

4. Hospital Universitari Germans Trias i Pujol, Spain

Description of Clinical Presentation: A 52-years smoker caucasian male with medical history of hypertension and dyslipidemia was affected of anuloaortic ectasia with severely dilated ascending aorta and severe aortic regurgitation. Surgery was performed, repairing the aortic root using David's technique plus ascending proximal aorta replacement with Dacron graft. In 2005, sever aortic regurgitation with LV disfunction was detected, and he submitted to a Ross procedure. During follow-up, sever stenosis of the pulmonary homograft was observed and a percutaneous stent in the pulmonary homograft was implanted. Few years years later, severe stenosis of the pulmonary stent and RV dilatation and dysfunction was detected on a rutinary transthoracic echocardiogram. This prompted a cardiovascular MR exam.

Diagnostic Techniques and Their Most Important Findings: A complete CMR examination was perfomed. Breath-hold SSFP-cine images at standard 2CH, 3CH, 4CH and short axis projections were performed. Moreover, additional oblique cines of the right ventricular and right ventricular outflow tract (RVOT) were performed. Moderate RV dilatation and disfunction was detected (fig.1a-d). With standard SSFP-cine images (figure 1C-D), pulmonary stent stenosis was suspected but not well defined, so we performed additional gradient-echo cine sequences at RVOT level, for better definition of the stent architecture and the severity and level of the stenosis (fig 2a-d). Those confirmed the stenosis of all the stent being more severe at the proximal edge. Additional right ventricular and pulmonary artery 3D-angiography (fig 3) confirmed the critical stent stenosis with a minimal intraluminal area of 0.33cm2. Currently, the patient is awaiting for final clinical decision. .

Learning Points from this Case: This is a complex clinical case with multiple severe complications of previous surgical / percutaneous procedures. Moreover, it might serve to remember two main points: First, metallic artifacts are less prone to appear when using gradient-echo sequences, which allow for better stent / prosthesis valoration. Second, 3D-angyography can be useful for future surgery/percutaneous procedures planification.

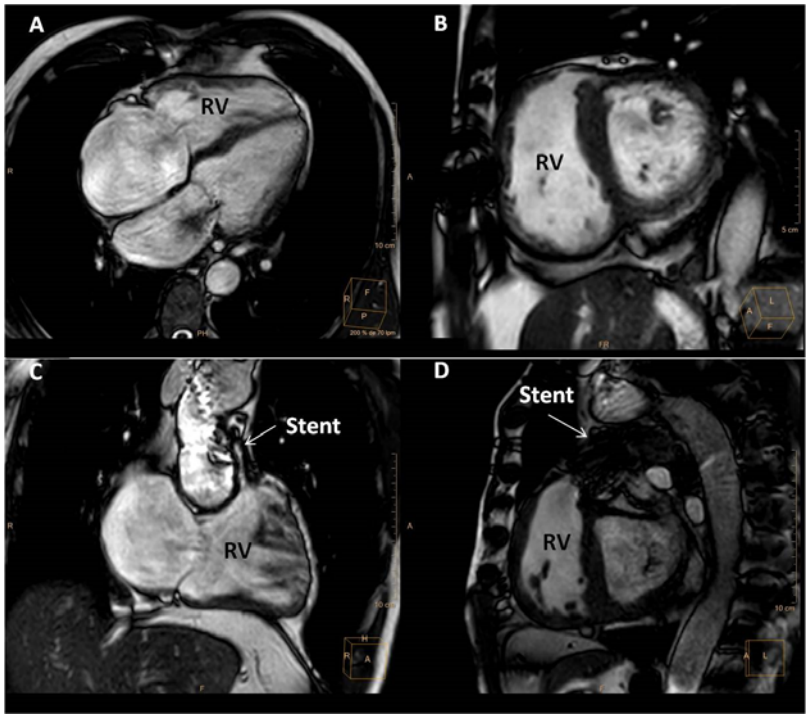

Figure 1

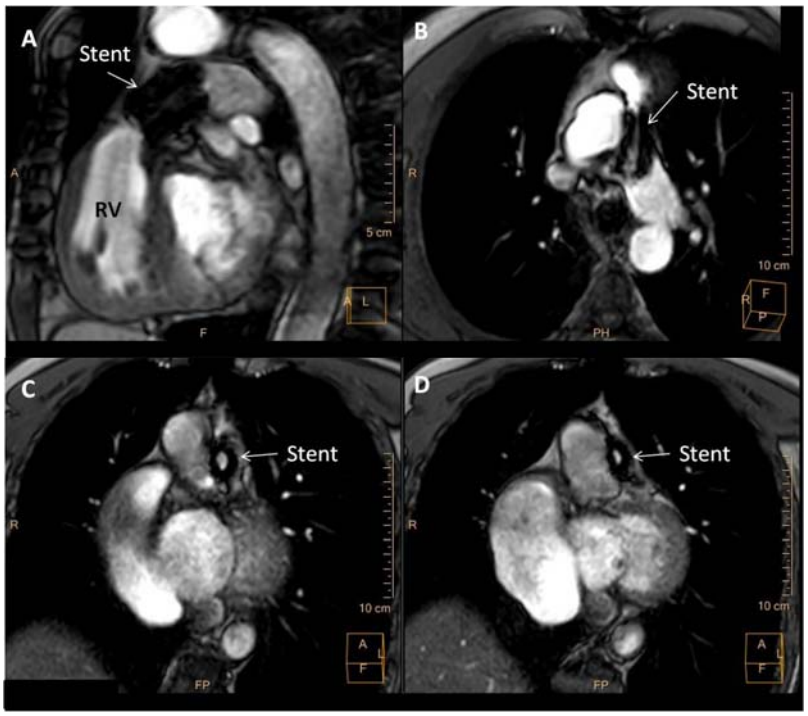

Figure 2

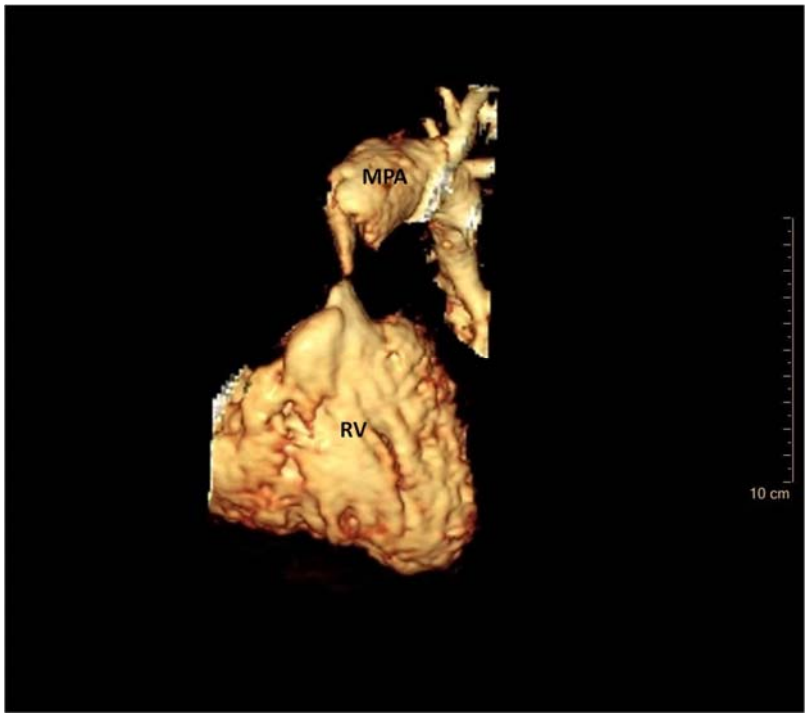

Figure 3

ID#: 371796

A case of Peripartum Cardiomyopathy and Autosomal Dominant Polycystic Kidney Disease

Lucia Occhi, MD[1] Giuseppina Quattrocchi, MD[2], Paola Sormani, MD[3], Angela Milazzo, MD[2], Cristina Giannattasio, MD[4], Patrizia Pedrotti, MD[5]

1. ASST Grande Ospedale Metropolitano Niguarda, Lombardia, Italy

2. Department of Cardiology and Cardiac Surgery ASST Grande Ospedale Metropolitano Niguarda Milano, Italy, Lombardia, Italy

3. ASST GRANDE OSPEDALE METROPOLITANO NIGUARDA, MILANO, Lecco, Lombardia, Italy

4. Department of Cardiology and Cardiac Surgery, ASST Grande Ospedale Metropolitano Niguarda, Milano, Italy, Milano, Lombardia, Italy

5. Department of Cardiology and Cardiac Surgery ASST Grande Ospedale Metropolitano Niguarda, Milano, Italy, Milano, Lombardia, Italy

Description of Clinical Presentation: A 39-year-old woman with Autosomal Dominant Polycystic Kidney Disease (ADPKD) was referred for dyspnea on exertion, peripheral edema and ascites about 2 months after caesarean labor. Pregnancy was complicated by gestational hypertension. Immediate post-partum was unremarkable. A previous echocardiogram was normal.
Laboratory tests showed elevated NTproBNP and Troponin T levels (HSTnT). EKG showed sinus rhythm, left anterior hemiblock and inversion of T waves from V1 to V5.
The patient underwent paracentesis and diuretic therapy.

Diagnostic Techniques and Their Most Important Findings: Echocardiography documented severe bi-ventricular dysfunction, mild mitral insufficiency and an intra-ventricular mobile thrombus.
Coronary artery catheterization showed normal epicardial vessels.
Cardiac Magnetic Resonance (CMR) revealed ventricular chambers of normal size, with severe bi-ventricular dysfunction (LVEF 26%, RVEF 27%), no areas of edema and no late gadolinium enhancement. CMR confirmed the presence of mobile left ventricular (LV) apical thrombus (23 x 10 mm – figure 1). Besides, both pericardial and pleural effusions were present and numerous renal and liver cysts were identified.
Warfarin and recommended therapy for heart failure (HF) with beta-blockers, ACE-inhibitors and mineralocorticoid receptor antagonists was started. Bromocriptine was given in order to block prolactin production.
At discharge systolic LVEF had improved at 42%. CMR follow-up scan 4 months later showed further improvement of biventricular function and resolution of LV thrombus (figure 2). The ample field of view of CMR allowed the detection of severe enlargement of hepatic and renal cysts, with invasion of the thoracic cavity and important supra-elevation of right diaphragm (figure 3). The cysts caused mechanical impairment of ventricular filling, which might become a predominant feature in case of further progression of cystic disease.

Learning Points from this Case: Considering all clinical and instrumental data available, we concluded for the diagnosis of Peripartum Cardiomyopathy (PPCM) which is an idiopathic cardiomyopathy characterized by development of HF toward the end of pregnancy or in the months following delivery, in absence of another identifiable cause for HF.
Besides, pregnancy after the age of 30 years and the presence of history of preeclampsia, eclampsia, or postpartum hypertension are considered risk factors for the development of PPCM. Diagnosis was supported also by the presence of LV thrombus: patients with PPCM are at high risk for thrombus formation due to both the hypercoagulable state of pregnancy and stasis of blood due to LV dysfunction.
To the best of our knowledge, no cases of PPCM associated with ADPKD are described in literature.
CMR allows a comprehensive assessment of heart morphology and function, besides revealing its relation and reciprocal interaction with surrounding organs.

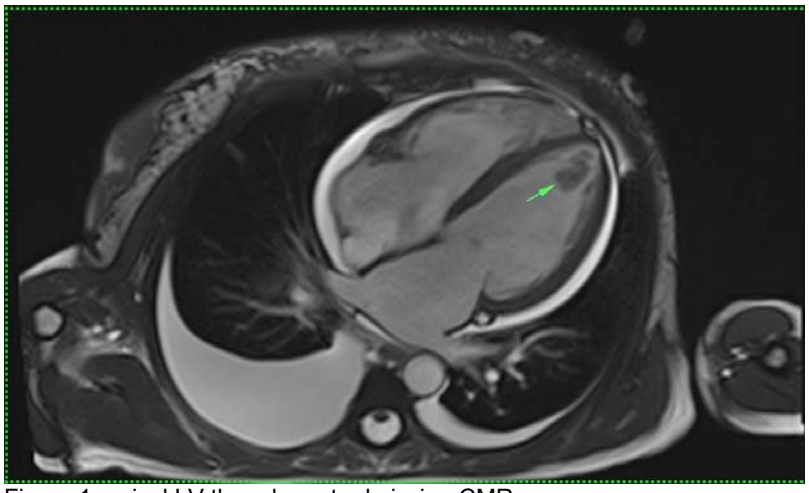

Figure 1: apical LV thrombus at admission CMR

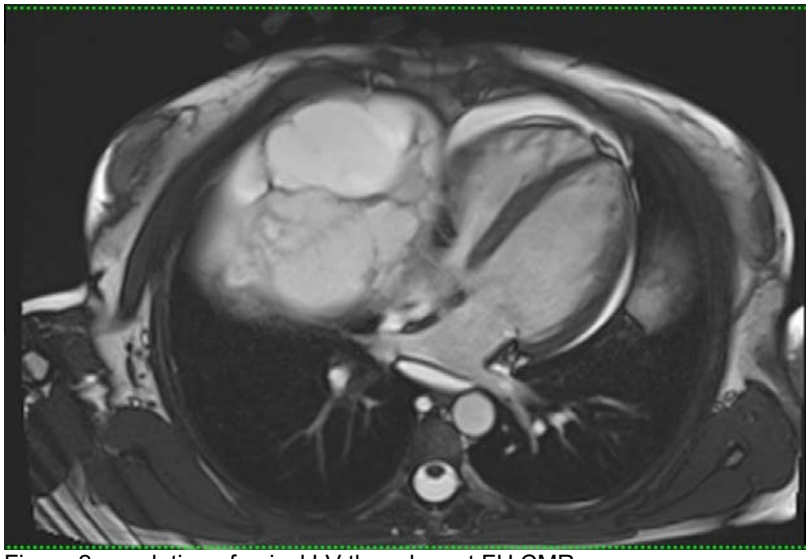

Figure 2: resolution of apical LV thrombus at FU CMR

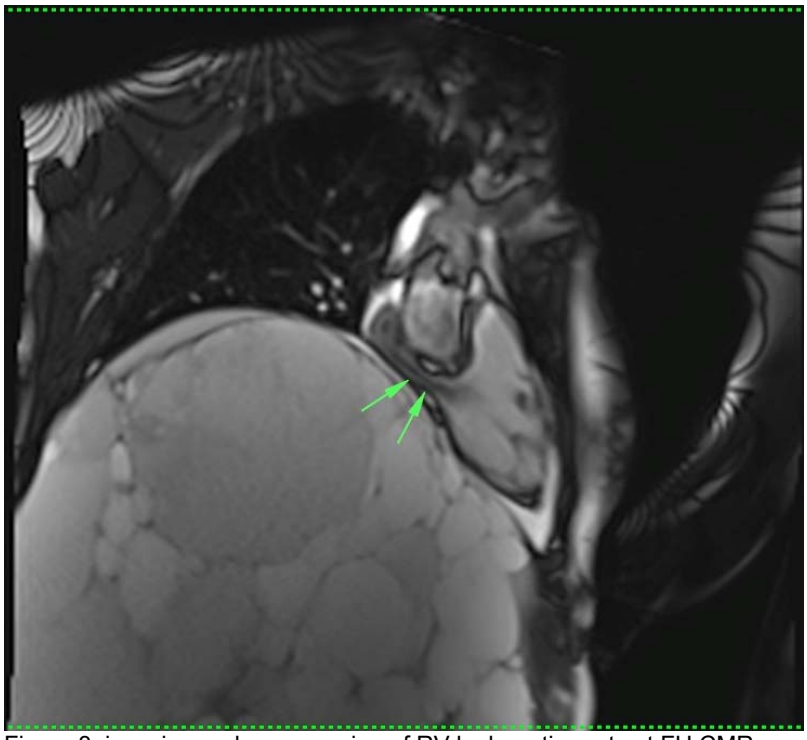

Figure 3: invasion and compression of RV by hepatic cysts at FU CMR

ID#: 371736

Delayed chemotherapy induced cardiomyopathy

JAE SUP JUN[1] Jung Im Jung, M.D., Ph. D.[2], Kyongmin Sarah. Beck[3]

1. Department of Radiology, The Catholic University of Korea, Seoul St. Mary's Hospital, Seoul, Republic of Korea

2. Department of Radiology, Seoul St. Mary's Hospital, College of Medicine, The Catholic University of Korea, N/A, Republic of Korea

3. Seoul St. Mary's Hospital, College of Medicine, The Catholic University of Korea, Republic of Korea

Description of Clinical Presentation: A 44-year-old man with past medical history for Hodgkin';s lymphoma with treatment-related secondary AML presented to our outpatient clinic with dyspnea. His Hodgkin';s lymphoma was initially diagnosed in 2011 and treated with Adriamycin, Bleomycin, Vinblastine, and Dacarbazine (ABVD). His disease remained in remission until April 2015. At that time, therapy-related secondary AML was developed. He received induction chemotherapy using Idarubicin and Cytarabine in May 2015, and then underwent consolidation chemotherapy using Mitoxantrone and Cytarabine in July 2015. During this period, he took transthoracic echocardiography. The patient';s echocardiogram showed mildly reduced left ventricular ejection fraction (LVEF) of 45%. A repeat echocardiogram 4 month later revealed an improved LVEF to 52%. He finally received hematopoietic stem cell transplantation. He achieved complete remission. Two years later, the patient presented with aggravated dyspnea. On chest radiograph, cardiomegaly was noted. Transthoracic echocardiography revealed severely reduced LVEF (25%) with diffuse global hypokinesis of LV wall. Cardiac magnetic resonance (CMR) imaging was performed.

Diagnostic Techniques and Their Most Important Findings: CMR images revealed relatively proportional increase of four chamber size with marked wall thinning of LV. The LVEF was 22%, the left ventricular end diastolic diameter was 6 cm in mid ventricular level, the LV interventricular septum was 8 mm thick, and its mass was 113 g. On cine CMR, global hypokinesis with decreased LV contractile function was noted. On T1 and T2 mapping, T2 relaxation time was 42 ms (apex), 41 ms (mid), and 43 ms (base) (cut-off value in our hospital; 40.5 ± 2.6ms), and native T1 was 1506 ms (apex), 1477 ms (mid), and 1251 ms (base) (cut- off value; 1278 ± 30ms). ECV value was 43.3% (apex), 38.8% (mid), 27.7% (base) (cut- off value; 27.4 ± 2.4%). Native T1 value and ECV were increased in our patient compared with control. Delayed enhancement CMR showed no LGE. Follow up echocardiography performed 1 month later showed no remarkable interval change.

Learning Points from this Case: The present case shows a clinical course of delayed chemotherapy induced cardiomyopathy. Anthracyclines are frequently used in treatment of lymphoma and acute myeloid leukemia as in our patient. The purpose of imaging in patients receiving an cardiotoxic agent is to detect a subclinical decline in left ventricular function. When such a decline is found, the chemotherapy regimens are adjusted to limit cardiotoxic side effect. T1 mapping offers a new approach to evaluate diffuse myocardial fibrosis in patient with dilated cardiomyopathy, which is strongly correlated with diastolic dysfunction. In previous reports, some authors found that native T1 values were longer in dilated cardiomyopathy compared with controls, while post-contrast T1 times were lower and ECV was higher, and suggested that T1 values was the predictor of cardiomyopathy. CMR may be useful for early diagnosis of chemotherapy induced cardiomyopathy.

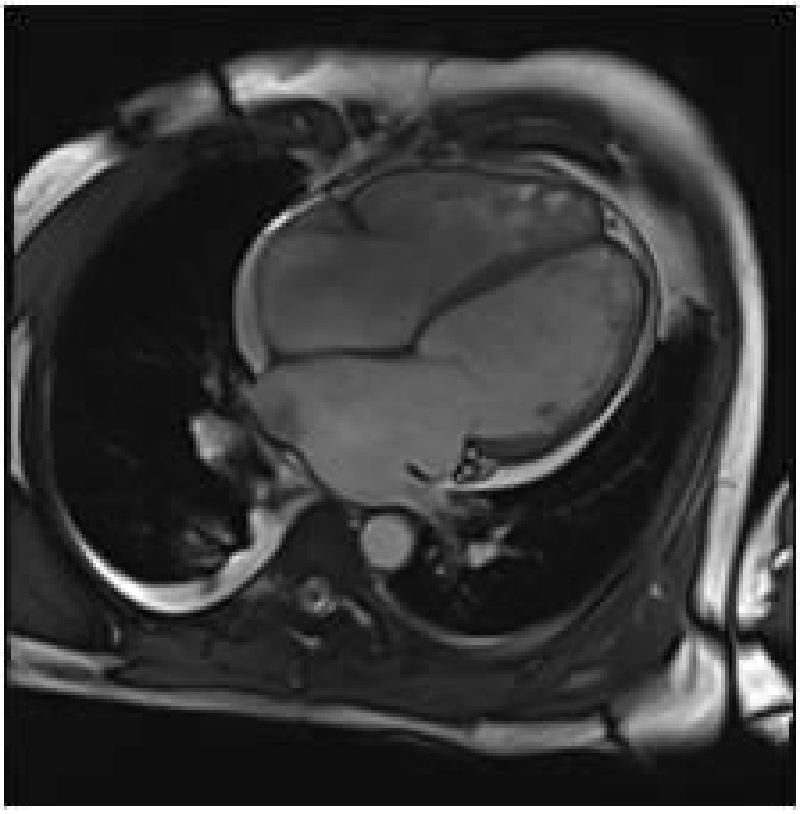

Image 1-2. Cine CMR in the four chamber and the short axis view illustrating proportional increase of four chamber size with marked wall thinning of LV. The left ventricular end diastolic diameter was 6 cm in mid ventricular level. The LV interventricular septum was 8 mm thick.

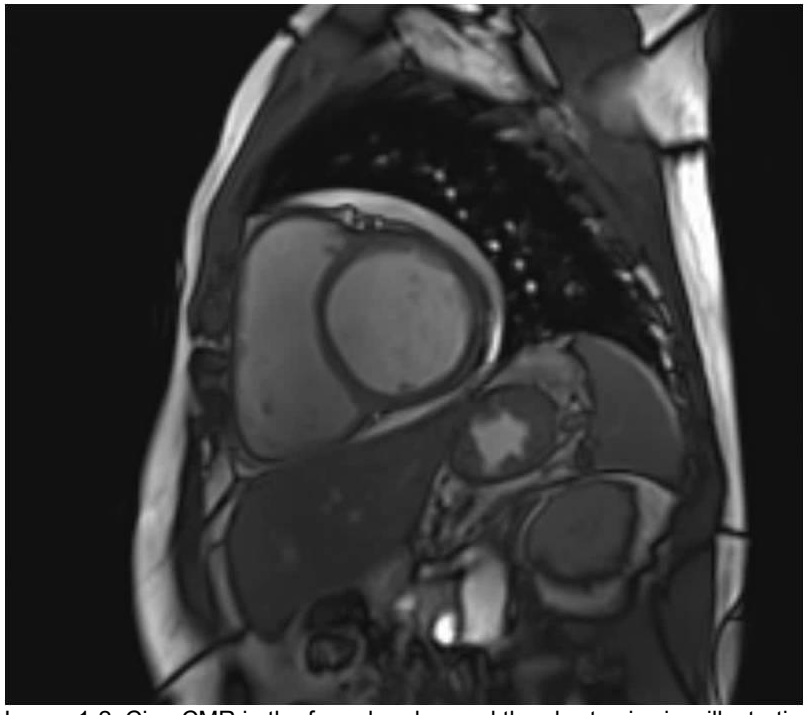

Image 1-2. Cine CMR in the four chamber and the short axis view illustrating proportional increase of four chamber size with marked wall thinning of LV. The left ventricular end diastolic diameter was 6 cm in mid ventricular level. The LV interventricular septum was 8 mm thick.

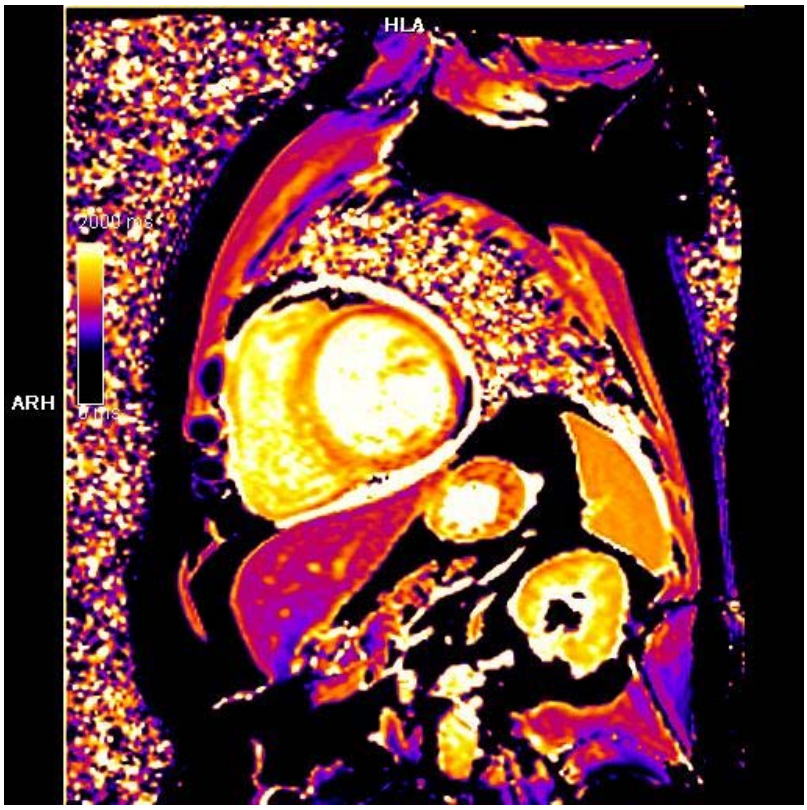

Image 3. T1 mapping images.

ID#: 372574

A case of Fabry's disease misdiagnosed at its onset

Rosario J. Perea Palazón, MD PhD[1] Adelina Doltra, MD, PhD[2], Jose T. Ortiz-Pérez, MD PhD[2], Carlos Brenes, MD[3], Susanna Prat-González, MD PhD[2]

1. Hospital Clínic. Universitat de Barcelona, Barcelona, Catalonia, Spain

2. Hospital Clínic. Universitat de Barcelona, Catalonia, Spain

3. Hospital Clinic. Universitat de Barcelona, Catalonia, Spain

Description of Clinical Presentation: This 54-year-woman presented with a long-standing history of intermittent neurologic symptoms. At the age of 26 she debuted with left hemiparesis and right optic neuritis with partial loss of visual acuity. Clinical and radiological features initially suggested a diagnosis of multiple sclerosis. An ophthalmological check at age 45 detected cornea verticillata and dilating conjunctive vessels, being diagnosed of Fabry';s disease. Aged 46, there was a new episode of optic neuritis. The patient explains repetitive syncopes in adolescence. On physical examination she had inframammary telangiectasias.

Diagnostic Techniques and Their Most Important Findings: FD is an X-linked lysosomal storage disorder, which is caused by deficiency of α-galactosidase A. Glycosphingolipids accumulate in a variety of tissues, so that neurologic, renal, dermatologic, cardiac, ophthalmologic and gastro-intestinal manifestations of the disease are recognized.
Cornea verticillata is characteristic in FD, but not patognomonic.
Brain magnetic resonance depicted confluent periventricular and deep white matter hyperintensities in T2/FLAIR sequence, in relation to chronic ischemic microangiopathy, common findings in this entity.
Cardiac involvement in FD includes ventricular hypertrophy, arrhythmias, chronic heart failure and small vessel disease. 24 hours Holtter demonstrated ventricular extrasystoles and atrial tachycardia. Echocardiogram revealed severe concentric left ventricular (LV) hypertrophy (16 mm), a hallmark of the disease, and grade I diastolic dysfunction. CMR confirmed concentric LV hypertrophy with normal ejection fraction. LGE sequence detected a characteristic intramyocardial pattern, involving the basal and mid-ventricular lateral wall. This is a typical finding that can differentiate FD from other causes of hypertrophy. Native T1-mapping showed a reduced T1 value in the septum (910 ms, N: 1030±25 ms) that narrows the diagnosis, as only lipids and iron can reduce the T1 in the myocardium.
Blood test revealed a glomerular filtration rate of 87ml/min (normal>90) and proteinuria (850mg/24h, normal<150). Proteinuria often present in men is less consistent in women, as well as the eventual development of renal failure.
Alpha-galactosidase A gene sequencing identified a heterozygous positive mutation p.W162G/c.484T>G. This is the most reliable test for confirming the diagnosis.
Early treatment with enzyme replacement therapy is key for prevention and improvement in major affected organs.

Learning Points from this Case:

- FD is a disorder with multiorgan involvement. The initial symptoms sometimes are non-specific, and the disease can be misdiagnosed.
- FD implies severe cardiovascular complications that can be prevented with early enzyme replacement therapy.
- Unexplained LV hypertrophy should be investigated with CMR and typical LGE patterns should be considered in order to rule out FD cardiomyopathy.
- CMR T1-mapping may detect early cardiac involvement in FD.

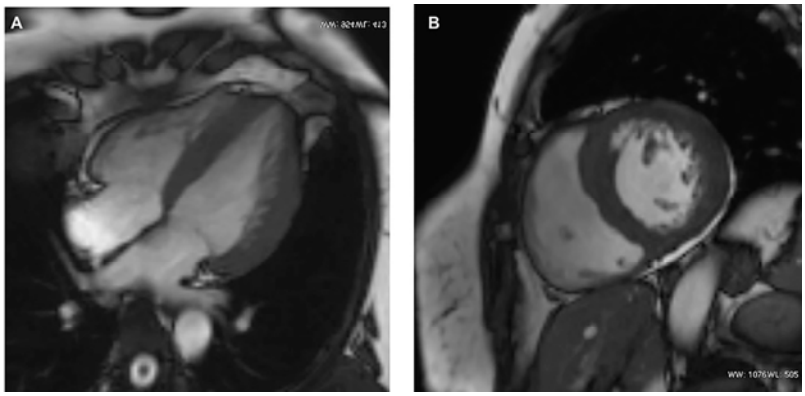

Four-chamber view cine image (A) and short axis (B). A concentric hypertrophy with a basal antero-septal thickness of 16 mm is observed.

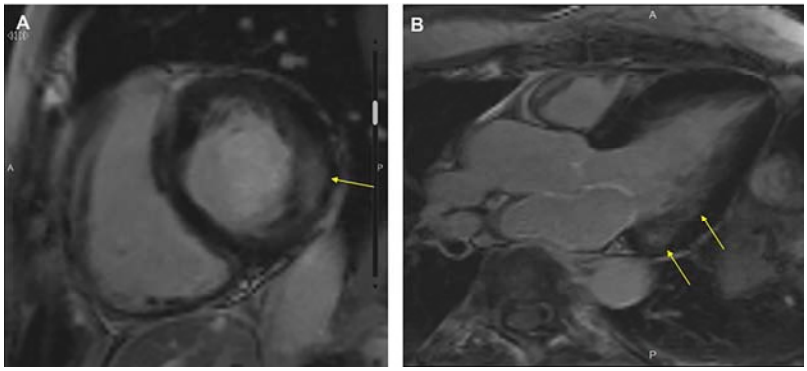

LGE images are shown in short axis (A) and in three-chamber view (B). Late gadolinium enhancement was detected in the basal and mid-ventricular lateral wall with the typical intra-myocardial pattern.

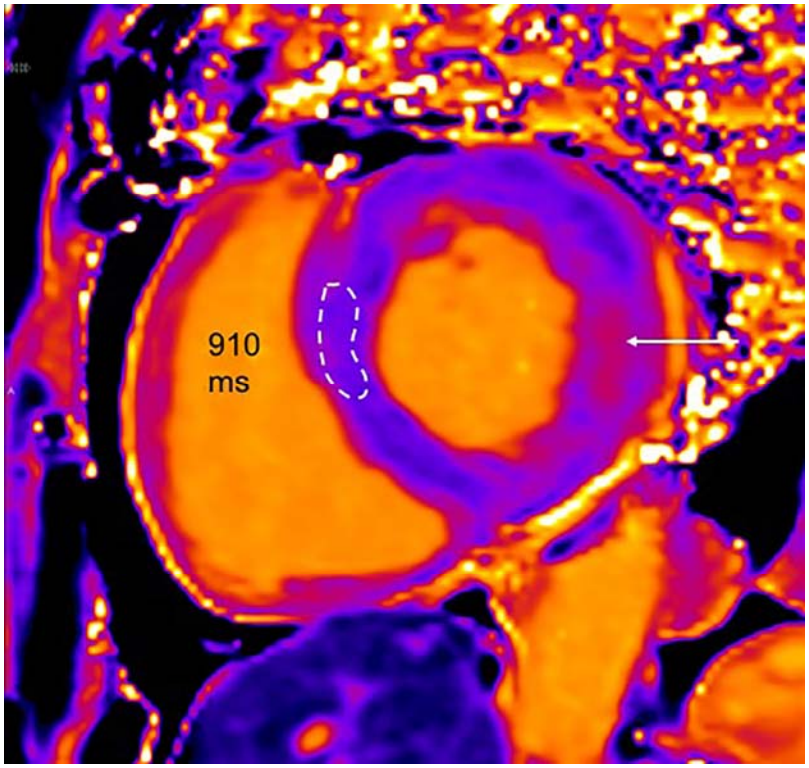

A non-contrast basal short axis T1 map performed with a 3T scanner (Magnetom Trio-Tim, Siemens, Erlangen, Germany) and with a MOLLI sequence (Modified Look-Locker inversion recovery) demonstrates a decreased mean septal T1 value (910 ms) and an increase T1 in the infero-lateral wall (red color, 1231 ms), correlating with the area of late gadolinium enhancement (arrow).

ID#: 372886

Fatal outcome after myocardial infarction and pulmonary damage due to CS gas intoxication

Saoussen AntitIskander Slama, Sarra Chenik, Ilhem Boussabeh, Lilia Zakhama, Soraya Benyoussef

Department of Cardiology, Interior Security Forces Hospital, La Marsa, Tunisia, Tunisia

Description of Clinical Presentation: We report a case of a young healthy man aged of 24 years, who had myocardial infarction in anterior leads and pulmonary edema after exposure to tear gas. Echocardiography ruled out severe hypokinesis of the mid-to-apical segments of the infero-septal and the antero-lateral walls, with altered left ventricular ejection fraction (32%) and apical thrombus. Coronarography revealed a tight thrombosis of the left anterior descending artery (Figure 1). Cardiac magnetic resonance (CMR) confirmed the diagnosis of myocardial infarction with an intra-ventricular thrombus (Figure 2). Hence, he was putted under curative doses of heparin associated with dual anti- platelet aggregation. Pulmonary CT-scan noted diffused alveolo interstitial oedema witch is tightly correlated to acute smoke inhalation. The evolution was initially favorable but then the patient developed cardiopulmonary failure and he was admitted several times for congestive heart failure and pulmonary abscess. Cardiopulmonary transplantation was indicated. He was dead 20 months after intoxication.

Diagnostic Techniques and Their Most Important Findings: Echocardiography ruled out severe hypokinesis of the mid-to-apical segments of the infero-septal and the antero-lateral walls, with altered left ventricular ejection fraction (32%) and apical thrombus. Coronarography revealed a tight thrombosis of the left anterior descending artery (Figure 1). Cardiac magnetic resonance (CMR) confirmed the diagnosis of myocardial infarction with an intra-ventricular thrombus (Figure 2).

Learning Points from this Case: Cardio-pulmonary damage due to tear gaz is extremely rare but exists and can causes fatal outcome. Our observation suggests that CS gas is not as safe as it seems. By encouraging follow-up collection data after every case of exposure and deeply exploring its real toxicity on innocent people, further complications could be detected to make the authorities aware of its potential danger in order to limit its use and avoid undesirable disabilities.

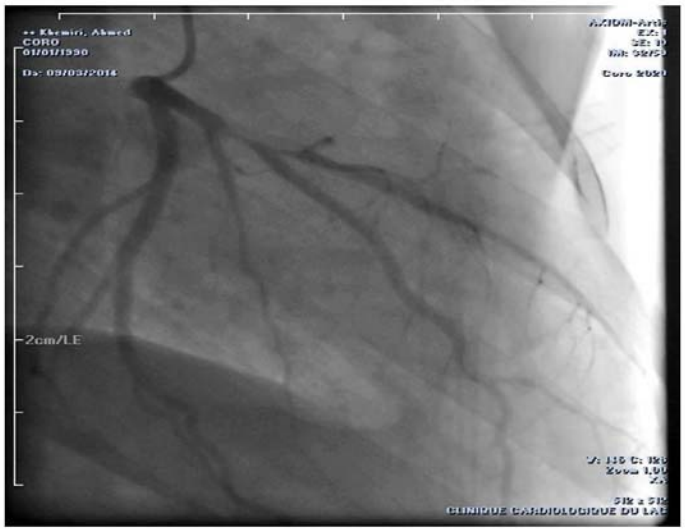

Figure 1. Coronarography: Left descending artery thrombosis

Figure 1. Coronarography: Left descending artery thrombosis

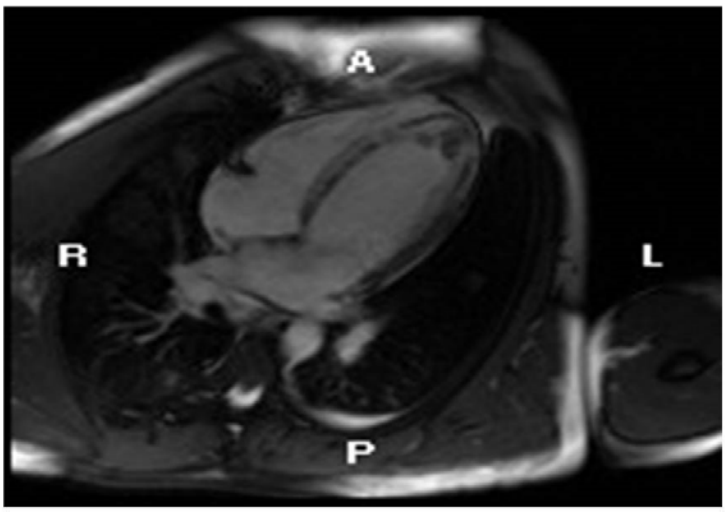

Figure 2. CMR: Subendocardial late enhancement and apical thrombus

Figure 2. CMR: Subendocardial late enhancement and apical thrombus

ID#: 372737

Left Atrial Appendage Mass - Thrombus or Myxoma?

Robert W. Biederman, MD, FACC, FAHA[2]Richard Lombardi, RT (mr)(r)[1]

1. Allegheny General Hospital

2. Allegheny General Hospital, Pittsburgh, PA

Background: History: 67year old male with a history of hypertension presented with dyspnea, cough and wheezing, worse at night.

Technique: SSFP 2, 3, 4 chambers and para-axial views, T1 and T2 for morphology, LGE and LGE with long TI.

Methods: Case description: This patient was referred to CMRI after having a TEE which showed a large mass in the left atrium (LA) and left atrial appendage (LAA) consistent with a myxoma. CMRI showed normal sized LA and a large mass rising out of the LAA into the LA. This homogenous mass was long, mobile, and tubular with dimensions 5.2 x 2.3 cm. It was seen to move in and out prolapsing the mitral valve causing moderate stenosis during the diastolic phase (Figure 1 &2).

Results: The mass was isointense on T1 and hyperintense on T2 suggestive of a myxoma (Figure 2). However, the early gadolinium enhancement gave an impression of a thrombus (Figure 4), but LGE was consistent with neoplasm with an overlying thrombus (Figure 5). The patient underwent surgery with excision of mass and LAA. The histopathology confirmed neoplastic process and the final report came back as myxofibrosarcoma.

Conclusion: Myxofibrosarcoma is a rare primary malignant neoplasm of the heart and often it is difficult to differentiate from myxoma (1). Since this is a very rare finding, the patient will be worked up for metastasis. Treatment of these tumors is surgical excision followed by radiation and/or chemotherapy. This, to our knowledge, is the first myxofibrosarcoma ever diagnosed not only within the LAA but by CMR.

References:

1. Iglesia D, Refoyo E, Ruiz-Cantador J et al. Left atrial myxofibrosarcoma: Diagnostic approach through imaging techniques. J. of Cardiology cases. 2013:2:e91-92.

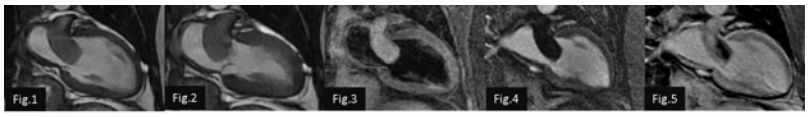

ID#: 372980

The thinking technologist's guide to investigating ventricular tachycardia

Bao Ru Leong, BSc[1] Yun Yun Go, MBBS[2], Hak Chiaw Tang, MBBS[2], Alicia Ting Er, BSc[2], Elizabeth Goh, BSc[3], Anton Lin, BSc[3], Sakinah Hanafi, BSc[3]

1. National Heart Centre Singapore, Singapore, Singapore

2. National Heart Centre Singapore, Singapore

3. National Heart Centre Singapore, N/A, Singapore

Background: A 61-year-old lady with no significant past history of note except hypertension, of which she is on diet control, presented to the emergency department for heartburn and nausea. The electrocardiogram showed right ventricular outflow tract (RVOT) pattern polymorphic ventricular tachycardia. She received cardioversion for a total of 6 times and reverted to sinus rhythm while on intravenous amiodarone infusion. Echocardiogram showed a normal left ventricular ejection fraction, normal left and right ventricular sizes, and no significant valvular problems.

Methods: Cardiac magnetic resonance (CMR) imaging was done to rule out arrhythmogenic right ventricular cardiomyopathy (ARVC), in view of the RVOT morphology of ventricular tachycardia.

Results: No CMR evidence of ARVC was found. In particular, the right ventricle was normal in size and function. However, there was a discrete mid inferoseptal subendocardial lesion on late gadolinium enhancement. Figure 1 and 2 demonstrate the lesion in the delayed enhancement short axis and 4 chamber view. **Learning Points** CMR scan protocols are often decided according to the referral diagnosis. However, protocol modification may be required after initial scan images are obtained. Technologists performing scans need to be aware to manipulate scan sequences accordingly, in consultation with a qualified CMR doctor. Using the above case of tachycardia as an example, the following flow diagram is proposed for technologists to consider during a cardiac MRI examination.

Conclusion: While the presented case is unresolved, we learnt that CMR technologists play a vital role in contributing towards patient management. Technologists need to be vigilant to ensure all necessary scan images are acquired for accurate and timely diagnosis.

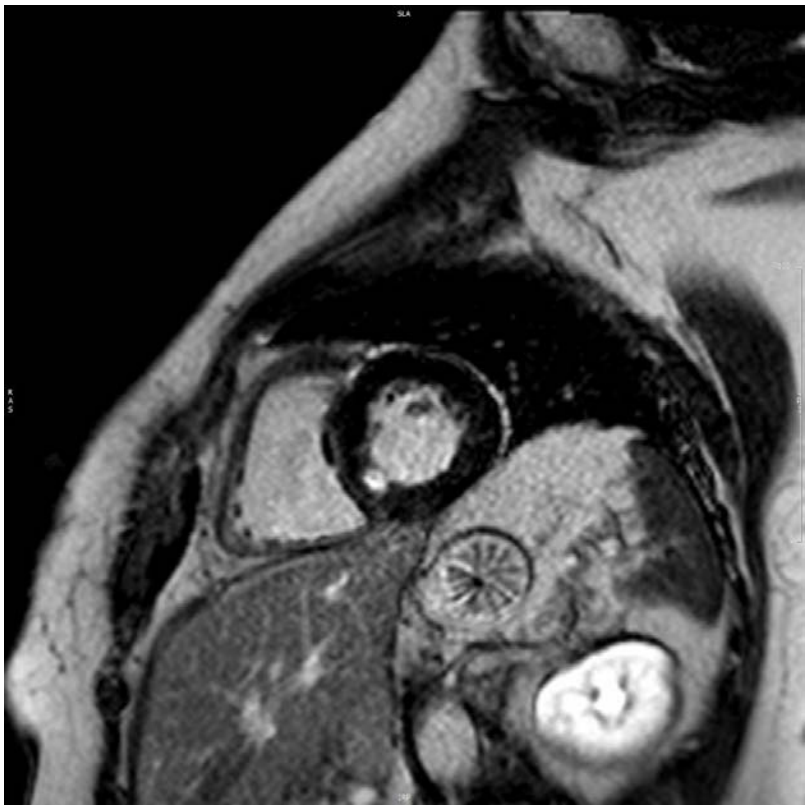

Mid inferoseptal subendocardial lesion demonstrated in short axis view, late gadolinium enhancement sequence

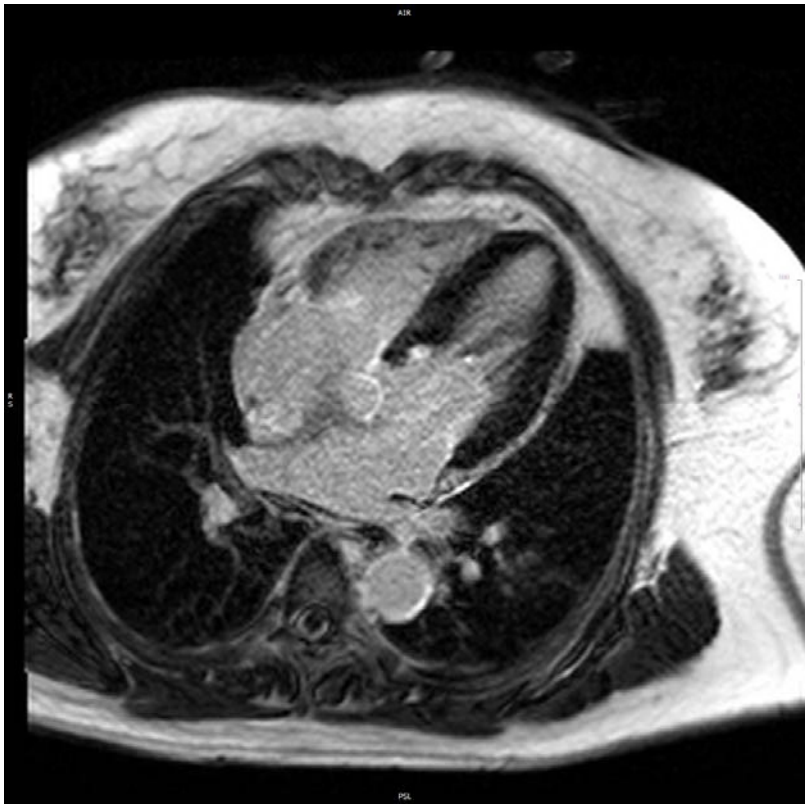

Mid inferoseptal subendocardial lesion demonstrated in 4 chamber view, late gadolinium enhancement sequence

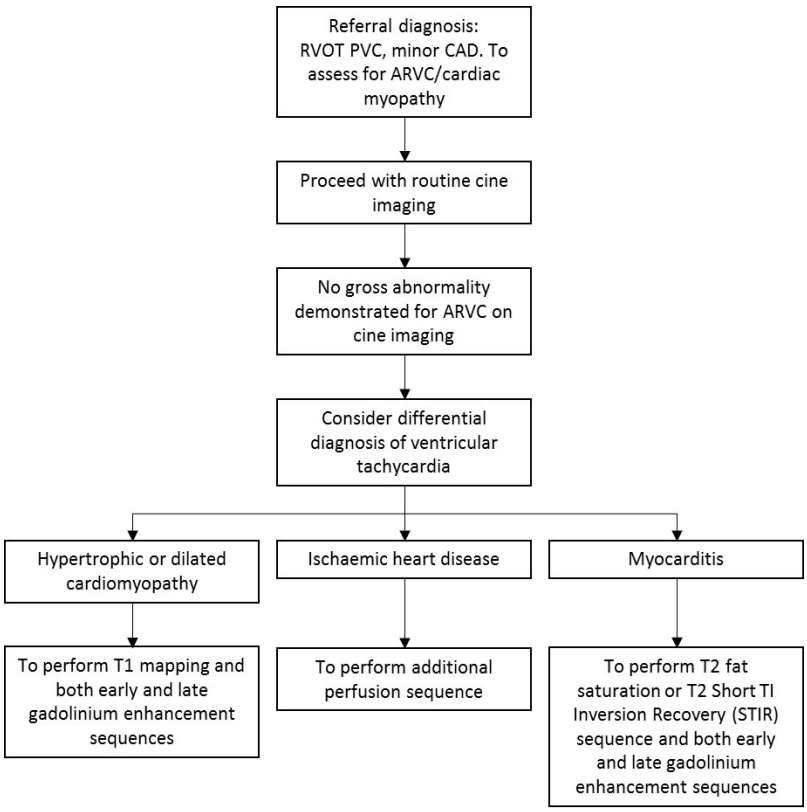

RVOT: right ventricular outflow tract; PVC: polymorphic ventricular complex; CAD: coronary artery disease; ARVC: arrhythmogenic right ventricular cardiomyopathy

Proposed considerations for technologists during CMR acquisition

ID#: 371317

CMR in Children under General Anaesthesia: A Single Institutional Experience

Rick Wage, DCR (R)[1] Inga Voges, MD[2], Mary Lane, MD[3], Sonya Babu-Narayan, PhD[3]

1. Royal Brompton Hospital NHS trust, England, United Kingdom

2. CMR Unit, Royal Brompton Hospital, Lonon, United Kingdom

3. Royal Brompton Hospital NHS trust, United Kingdom

Background: Cardiovascular Magnetic Resonance (CMR) imaging has become routine for paediatric patients as it is frequently advantageous compared with other imaging modalities. However, CMR is time-consuming and requires patient cooperation. Therefore, in small or uncooperative children general anaesthesia (GA) is often required. We describe our experience with a paediatric GA CMR service.

Methods: This is a retrospective analysis of our first paediatric GA scans. All patients referred for GA CMR were discussed for appropriateness in a multidisciplinary meeting before being listed. Prior to each GA a suitable scan protocol and strategy were agreed, creatinine assessed and preceding chest x-ray reviewed. All scans were performed with a 3T scanner (MAGNETOM Skyra, Siemens Healthcare) according to local safety protocols. Anaesthesia was delivered using Datex Ohmeda Aestiva MRI and 3T MR conditional monitoring systems and equipment. Dedicated paediatric resuscitation and difficult intubation trolleys were available. The service was delivered by congenital heart disease cardiologists, paediatric cardiac anaesthetists and a CMR radiographer. The team undergoes regular MRI environment resuscitation simulation training.

Results: Forty-three children with congenital or acquired cardiovascular disease (age 4.6±3.3 years, 3.7 months – 13.6 years, weight 16.5+/-6.6 kg, 20 male) underwent GA 3T MRI. Of these, 37 patients underwent GA CMR (scan duration 51.3±15.2 minutes); 2 out of these 37 patients had a brain MRI under the same GA. Six patients underwent only a brain/neck/vascular MRI (scan time 18.2±6.6 minutes) without cardiac assessment under general radiology co-supervision. The CMR protocol included gadolinium-based contrast application in 32 patients for time-resolved angiography (30/37), myocardial perfusion (2/37) and late gadolinium enhancement (LGE) imaging (25/37). Creatinine was within the normal range in all patients (31.1±11.3 µmol/l). Typical scan parameters were: cine CMR-TR/TE 54.2/1.6 ms, averages 1, slice thickness 5 mm, flip angle 53 deg, phases 25; angiography- FOV 370x370 mm, voxel size 1.4x1.4x1.5 mm, TR/TE 2.58/0.95 ms; LGE- FOV 185x62x270 mm, TR/TE 627/1.7 ms, averages 1, slice thickness 5 mm, flip angle 20 deg. All scans were completed without complications. All scans were diagnostic and contributed to clinical decision-making as intended; in one case, additional unexpected findings led to urgent successful treatment. Example images are shown below: A) cine image of a fibroma (arrow), B) 3D reconstruction of pulmonary arteries, C) endocardial LGE (arrows) in Williams syndrome with coronary artery stenosis.

Conclusion: CMR under GA in paediatric patients benefits from a multidisciplinary approach to implement and deliver a safe and effective service.

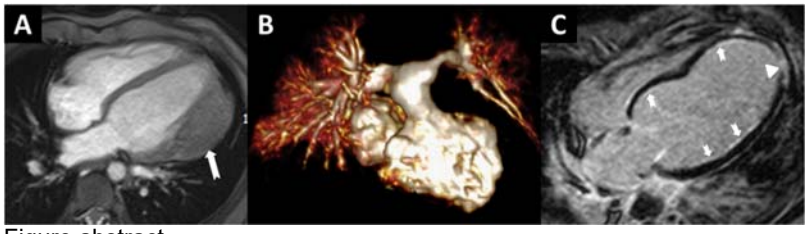

Figure abstract

ID#: 378526

Live detection of left atrial appendage thrombi in cardiac amyloidosis: an emerging clinical problem

Sarah Anderson[1]Donatella Lorusso[1], Michele Boldrini[2], Ana Naharro[1], Tushar Kotecha[1], Hossam Fayed, MBChB MSc MRCP(UK)[3], Julian D. Gillmore[4], Daniel S. Knight[5], Philip N. Hawkins[4], Marianna Fontana, MD, PhD[2]

1. UCL Department of Cardiac MRI, United Kingdom

2. UCL Department of CMR, Royal Free Hospital, England, United Kingdom

3. UCL Department of Cardiac MRI, Royal Free Pulmonary Hypertension Service, Pond Street, England, United Kingdom

4. National Amyloidosis Centre, University College London, England, United Kingdom

5. UCL Department of CMR, Royal Free Hospital, London, England, United Kingdom

Background: Cardiac amyloidosis is a disease characterized by progressive accumulation of amyloid protein in the myocardial interstitium, causing a restrictive cardiomyopathy with significant systolic and diastolic impairment of both right and left ventricle. Recent studies have shown a significant reduction of atrial function directly related to cardiac amyloid infiltration. This has implications in terms of the fluid haemodynamics of both the left atrium and left atrial appendage (LAA), leading to a possible increase in the risk of thrombus formation.

Methods: 106 consecutive patients with cardiac amyloidosis were prospectively enrolled in the study between the 1st of June and the 31st of August 2017. All patients underwent a standard cardiac magnetic resonance protocol including volume, early and late gadolinium images. Early gadolinium images of the LAA where acquired using a 5mm contiguous stack. The images were reviewed by the radiographer after image acquisition and blinded reviewed by two imaging cardiologists.

Results: 106 were enrolled in the study, 49 with transthyretin cardiac amyloidosis (ATTR) and 55 with light chain amyloidosis (AL) cardiac amyloidosis. The prevalence of thrombi was 6.5% in the overall population, 3.7% in ATTR, 2.8% in AL. Of the patients with thrombi, 4 patients were in atrial fibrillation, 3 in sinus rhythm. The prevalence of thrombi in patients with ATTR and atrial fibrillation was 31%. The diagnostic accuracy of the radiographer using the described image acquisition protocol was comparable to the blinded review of the two imaging cardiologists.

Conclusion: LAA thrombi is highly prevalent in patients with cardiac amyloidosis, especially ATTR. Early gadolinium images of the LAA should be included in the routine clinical scan protocol of patients with suspected cardiac amyloidosis. This allows easy live detection of thrombi by technicians performing the scans. This approach could have immediate implications for patient';s management.

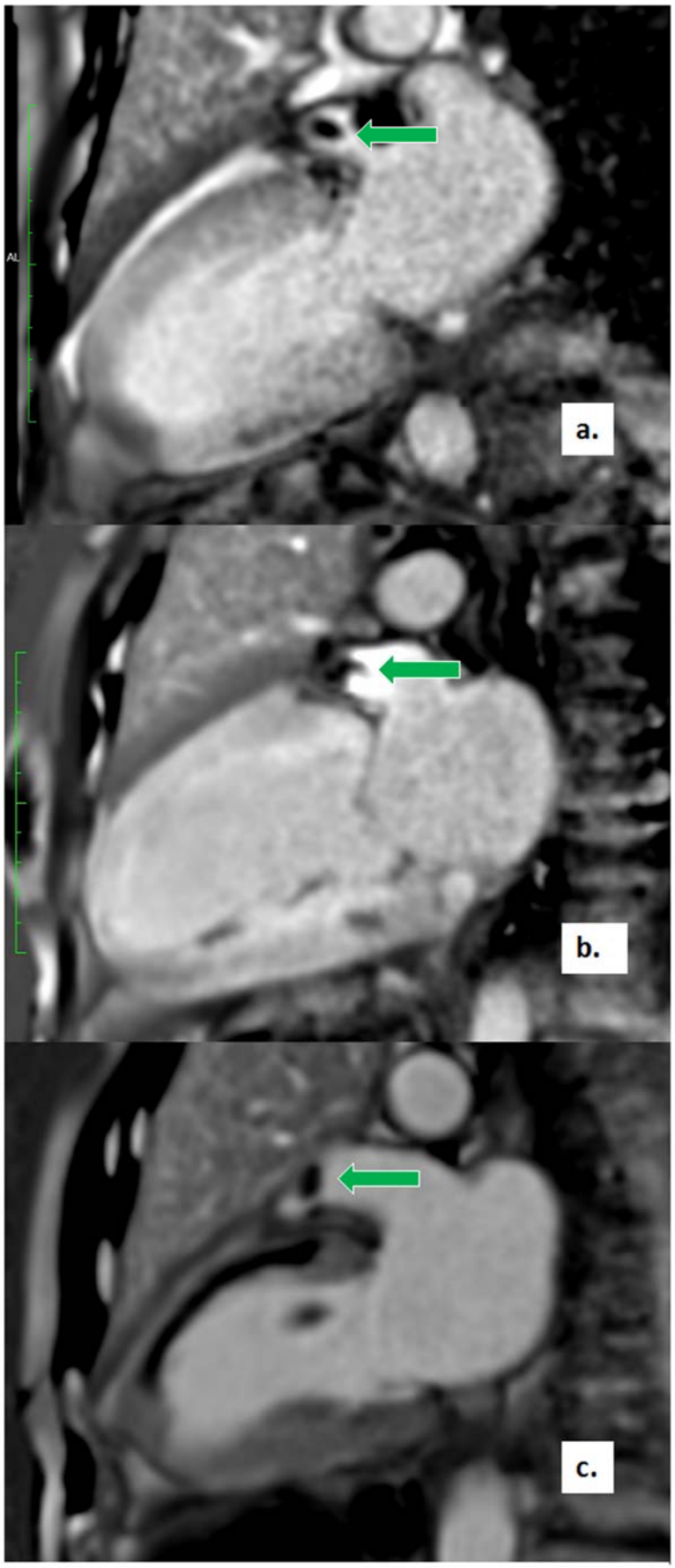

Early gadolinium images demonstrating appendage thrombi: **a.** ATTR patient in sinus rhythm; **b.** AL patient in sinus rhythm; **c.** ATTR

ID#: 378463

Arrhythmia:- Image quality and new techniques

Joana Leal, BSc[1] Michaela M. Hell[2], Fiona Mcmillan[3], Jane M. Francis[4]

1. Oxford Centre for Magnetic Resonance Research, Oxford, England, United Kingdom

2. Department of Cardiology, Faculty of Medicine, Friedrich-Alexander University Erlangen-Nürnberg, Germany, Germany

3. University of Oxford, United Kingdom

4. University of Oxford, OX39DU, England, United Kingdom

Background: Arrhythmia refers to any change in the normal sequence of electrical impulses in the heart. This condition affects over 2 million people in the UK and presents a challenge when performing CMR. The most common types include atrial fibrillation and ectopy. Different CMR techniques have been established to optimise analysis of cardiac function and decrease image artefact in arrhythmic patients. Optimising ECG gating from retrospective to prospective provides a first line solution but different techniques are also available within the Siemens® system. We aim to compare four different sequences and show the advantages and disadvantages of each technique.

Methods: We present an overview of different techniques available at our institution in order to optimise image quality in arrhythmia. In a patient with atrial fibrillation, one long axis cine was acquired using retrospective gating, prospective triggering ssfp (steady state free precession) cine, 2 shot free breathing sequences and real time. Image quality in these four sequences was visually assessed for artefact, miss-triggering and cardiac motion.

Results: When comparing the four sequences, retrospectively gated images showed severe cardiac motion artefacts resulting in markedly reduced image quality. Prospective triggering showed superior image quality compared to retrospective gating, but with the disadvantage of excluding the end diastolic phases. Real time (RT) as a free breathing technique co-related with ECG can be used for the correct process for cardiac function. The image quality is robust and by acquiring at least 3 full cardiac cycles enables a more accurate result. This method produces a large volume of data, needing a high computational demand for acquiring and a dedicated software for processing. The 2 shot free breathing sequence uses retrospective gating and can be adapted from the basic ssfp cine sequence. Image quality is equivalent to standard RT and offers the potential of acquiring the whole volumetric analysis in under minute. Since it is a retrospective technique, it needs at least two regulars RR intervals in order to be acquired without an artefact.

Conclusion: Standard CMR sequences are prone to arrhythmia-induced artefacts resulting in reduced image quality and less accurate results. We reviewed the current developments in CMR to demonstrate the methods available on how to deal with these arrhythmias on an individual patient basis.

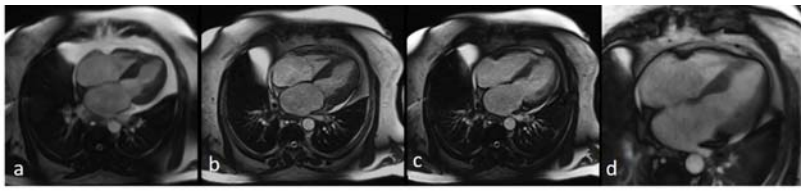

Fig.1 - The images above represent the cine images acquired on a patient in atrial fibrillation using four different sequences as per (a) 2 shot free breathing cine, (b) ssfp cine prospectively triggered, (c) ssfp cine retrospectively gated and (d) Real Time cine.

ID#: 369635

Alcohol Induced Tako-Tsubo Cardiomyopathy (TCM)

Chris Lawton, PGC, BSC[1] Anna Baritussio, MD[2], Chiara Bucciarelli-Ducci, MD, PhD[2]

1. Bristol Heart Institute, Bristol, England, United Kingdom

2. Bristol Heart Institute, Bristol NIHR Biomedical Research Centre (Cardiovascular Section), University of Bristol, Bristol, England, United Kingdom

Background: A 48 year old woman was referred to our CMR Unit after an alcohol withdrawal seizure. Her alcohol intake was ~ 40 units per day. Lateral T wave changes and a slightly raised troponin level were reported. An echo showed moderate systolic dysfunction.

Methods: A Cardiomyopathy protocol was performed which included the following sequences prescribed in long and shorts axis positions; Cine SSFP, T2 mapping, STIR, T1 mapping(MOLLI) (pre and post contrast). Early and Late Gadolinium Imaging

Results: mild hypokinesia of the mid-cavity to apical segments. Normal indexed volumes, EF 59%. Apical LVH (max 10 mm septal apex vs 8 mm lateral apex, normal range <6 mm). Diffuse myocardial oedema of the mid-cavity to apical segments. No myocardial scar or fibrosis. These findings are in keeping with Tako-Tsubo cardiomyopathy (TCM) ,which was most likely precipitated by alcohol withdrawal.

Conclusion: Very few cases are reported of Tako-Tsubo cardiomyopathy after alcohol withdrawal. Sympathetic hyperactivity, increased cathecolamine levels and increased beta-adrenergic activity are all effects of alcohol withdrawal which are known causes of TCM (1,2). A small number of cases of TCM following seizures have been reported, and it is still unknown if they are clinical diverse to non-seizure activated TCM (3).

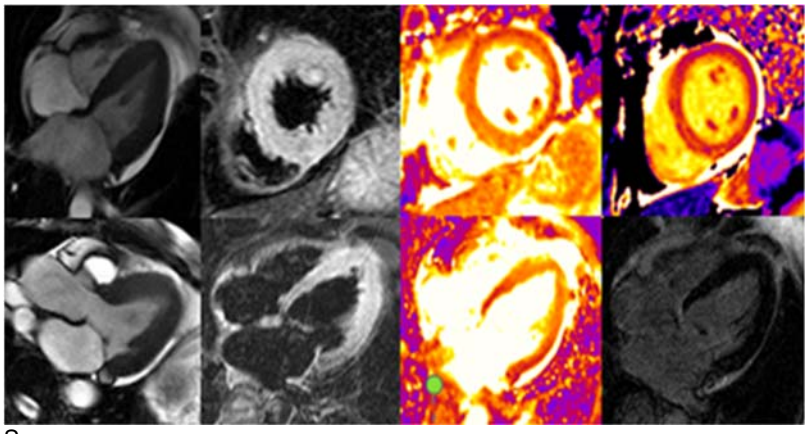

Sequences

ID#: 372736

Where Are You Going to Slice It? Our Look at Aortic Regurgitation

Ronald Williams, RT(R)(MR), B.A.[1] Mark Doyle, Ph.D.[1], Richard Lombardi, RT (mr)(r)[2], Moneal Shah, M.D.[3], Loretta Gevenosky, R.N.[1], Robert W. Biederman, MD, FACC, FAHA[1]

1. Allegheny General Hospital, Pittsburgh, PA

2. Allegheny General Hospital

3. Allegheny General Hospital, pittsburgh, PA

Background: Aortic regurgitation (AR) is the result of an incompetence or aortic valvular irregularity (leaflets, annulus, etc.) allowing blood to flow into the left ventricle during diastole. Valvular abnormalities can be congenital (bicuspid aortic valve) or acquired causes such as rheumatic fever, degenerative aortic valve (AV), post-surgical, uncontrolled hypertension (HTN), dilated aorta unrelated to AV disorders, and inflammatory processes. Long periods of AR, due to the stress imposed on the left ventricle, may lead to left ventricular hypertrophy (LVH), left heart failure, and even death if not treated. AR routinely is evaluated with echocardiography. Cardiac MRI (CMRI), has become the gold standard to evaluate valvular disorders with the ability to image valvular structures, regurgitant flow, anatomical variants. This leads to the question: Where do you slice it/position your location to evaluate AR flow? Above the AV in the ascending aorta (~1 cm above the Sino tubular junction (STJ)), at the STJ, through the sinus of Valsalva, or below the AV in the left ventricular outflow (LVOT)? See (Fig.1) **Hypothesis:** We hypothesize that the optimal location for a phase velocity evaluation of AR is above the AV in the ascending aorta.

Methods: Using Medis Suite, The Leiden, Netherlands, version 2.1.12.0, contours were completed for the LV function, the aortic phase velocity mapping (PVM) on the aorta above and below images. (Fig 2.) The stroke volumes obtained from the LV function (Mass Program), and the Flow programs were tabulated and compared as follows: Aortic PVM Above (APA) to LV Stroke Volume (LVSV); Aortic PVM Below (APB) to LVSV; Regurgitant Volume (RF) Above to RF Below. (See Fig. 3)

Results: We evaluated 10 patients (females 4, average age: 62.25 ±12.9; male 6, average age: 50.83±21.89 yrs.) with visible AR on the 3 chambers and/ or coronal SSFP images. Comparison was made using the stroke volumes as stated above. We found correlation between the RF for Above and below with an r=0.88. However, correlation of the Forward Flow for APA correlates more strongly with the LVSV (r=0.6) than did the flow in the APB (r=0.01)

Conclusion: Though the comparison used low population, we feel that the APA location is more accurate in the evaluate of RF in patients exhibiting AR. Further investigation using this premise would provide a better understanding of the AR in patients, in the future and is likely concordant with the consensus albeit more recent discussions suggest otherwise.

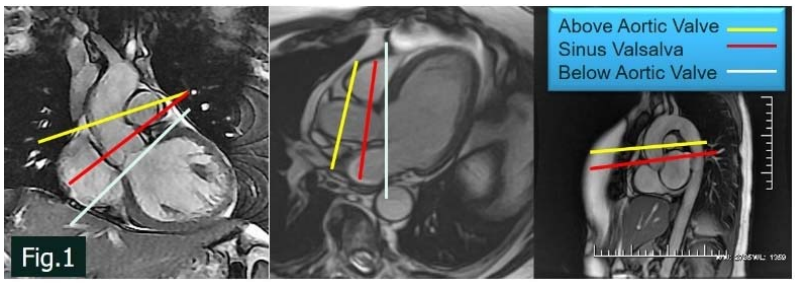

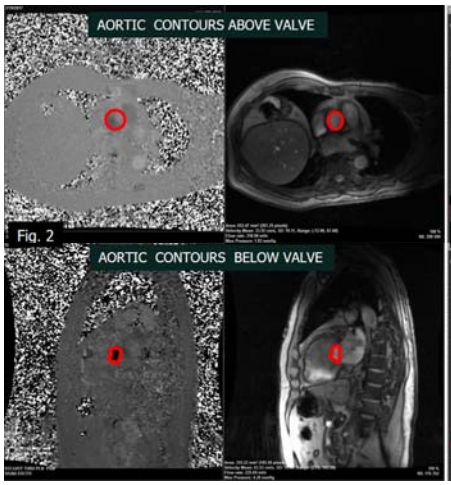
AORTIC CONTOURS ABOVE VALVE
Fig. 2
AORTIC CONTOURS BELOW VALVE

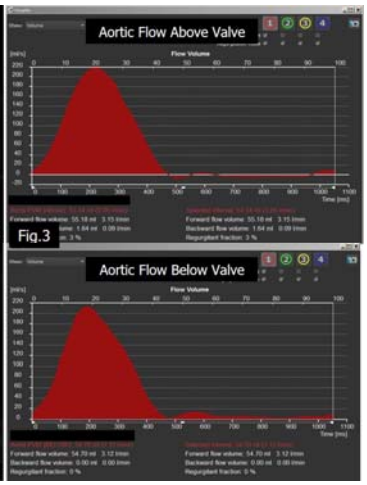
Aortic Flow Above Valve
Fig.3
Aortic Flow Below Valve

ID#: 378770

Effects of non pacer ICD metallic implants in the CMR environment

Robert W. Biederman, MD, FACC, FAHA[1] Loretta Gevenosky, R.N.[1], Prabhakaran Gopalakrishnan, M.D.[2], Ronald Williams, RT(R)(MR), B.A.[1], Richard Lombardi, RT (mr)(r)[2], Moneal Shah, M.D.[3], Christopher Bonnet, M.D.[1], Mark Doyle, Ph.D.[1]

1. Allegheny General Hospital, Pittsburgh, PA

2. Allegheny General Hospital

3. Allegheny General Hospital, pittsburgh, PA

Background: Performance of MRI is infrequently conducted on patients with metallic devices/objects within the body. However, recent work has suggested that with an appropriate protocol, pacemakers/ICD';s may in fact be considerably safer than previously considered. However, it is clear that we can extrapolate that notion to other metallic devices and retained leads. In principle, these may have even less ability to be manipulated to 'safe'; or 'safer'; MRI modes. Hypothesis: We propose that MRI in patients with loops, stimulators and retained pacemaker/ICD leads potentially may be safer than previously thought.

Methods: An evaluation of consecutive patients with Loops/Linqs recorders, stimulators and retained pacemaker/ICD leads underwent MR (GE 1.5T Excite,WI) over ~5 years. Great care was taken to maintain acceptable SAR (W/kg) bore and reduce induced electromagnetic RF potentials. Additionally, BP, HR, 02 saturations, as well as, visual monitoring was performed after informed consent with both patient and family members was obtained.

Results: The average MRI was 35±9min for the cohort of 50 patients representing 62 MRI exams. The devices consisted of: 9 Loops/Linqs, 28 neurostimulators (brain and vagal nerve), 2 bladder stimulators, 1 gastric stimulator and 10 retained/fragmented pacemaker/ICD leads. This represents 32 neuro/neurosurgical cases, 13 cardiac and 3 musculoskeletal cases. There was no (0%) immediate (peri-MRI exam) morbidity/mortality. Local follow-up data was available in 79% with a mean of 396±650 days (median 256 days; 5 days-10.9 years) and no (0%) short term (>1 year) device-related complications. Importantly, with careful attention to positioning and scanner sequences, no safety or device issues were encountered in any patient to include those few patients that under went repeat scans (>1 MRI scan in 9 patients).

Conclusion: In this early experience, we show that loop recorders, stimulators and retained pacemaker/ICD leads appear safe when combined with similar considerations for intact PM/ICD';s interrogations even when imaging within the thoracic cavity and heart. To our knowledge, this is the first study to comprehensively evaluate all such non-intact PM/ICD devices, stimulators, recorders and retained fragments and to recognize safety.

ID#: 378861

Preliminary Comparison between Intravoxel Incoherent Motion (IVIM) imaging with Quantitative Myocardial First Pass Perfusion (FPP) and Extracellular Volume (ECV) Mapping

Christopher Nguyen, PhD[1] Anthony G. Christodoulou, PhD[1], Nan Zhang, MD[2], Sen Ma, MS[1], Zixin Deng, MS[3], Zhanming Fan, MD PhD[4], Debiao Li, PhD[1]

1. Cedars-Sinai Medical Center, Los Angeles, CA

2. Beijing Anzhen Hospital, Capital Medical University, China (People's Republic)

3. Cedars-Sinai Medical Center, CA

4. Beijing Anzhen Hospital, Capital Medical University, Beijing, China (People's Republic)

Background: Contrast-based cardiac magnetic resonance (CMR) including myocardial first pass perfusion (FPP) and extracellular volume (ECV) mapping have demonstrated enormous clinical value in identifying myocardial ischemia[1] and scar[2]. However in renal insufficient patients, conventional Gd-based contrast agents are contraindicative. Therefore, alternative contrast-free CMR techniques are desired. We propose and test the feasibility of the application of a free breathing second order motion compensated spin echo (M2) intravoxel incoherent motion (IVIM) [3,4] CMR, in which a single IVIM scan will yield parameters reflective of myocardial micro-circulation (pseudo perfusion coefficient, D*, and vascular fraction, f) and myocardial tissue microstructure (apparent diffusion coefficient, D) yielding possible surrogates to both quantitative FPP and ECV.

Methods: Healthy normal volunteers (N = 8) were recruited and consented to scan on a 3T clinical system (Verio, Siemens Healthcare) with the following protocol: localizers, CINE, M2 IVIM (reduced FOV EPI, TR = 4s, TE = 79ms, 3 orthogonal directions, b = 10, 20, 30, 40, 50, 70, 100, 150, 200, 250, 300, 350 s/mm^2), Native T1 for ECV (MOLLI [2],), repeated M2 IVIM, FPP (Dual bolus FLASH [5], dilute = 1/10, 0.05 mmol/kg Gd), and Post-contrast T1 for ECV (MOLLI, 0.15 dose for total of 0.2 mmol/kg Gd). M2 IVIM was collected in a free breathing mode and retrospectively motion corrected using an affine transformation and mutual information cost function. Non-linear least squares fit (Levenberg-Marquardt algorithm) was used to fit the IVIM data assuming the following bi-exponential model: $S(t) = So\ e^{-b(fD^*+(1-f)D)}$. Myocardial blood flow (MBF) was calculated from the conventional dual bolus FPP scan using the fully quantitative Fermi model described in Hsu, et al [5]. Conventional ECV maps were created using the native and post-contrast T1 maps and hematocrit [5]. Intra-scan reproducibility of free breathing second order motion compensated (M2) was tested with Bland-Altman plots and intra-class correlation (ICC). An unstable angina patient with invasive angiography showing 70% stenosis at LAD was recruited to test the feasibility of performing free breathing M2 IVIM in a clinical setting.

Results: In healthy normal volunteers, IVIM demonstrated robust image quality without any bulk motion-induced signal loss and substantial intra-scan reproducibility for f (ICC: 0.7) and D (ICC: 0.8) (Fig. 1). D* was highly variable and prone to noise with poor reproducibility (Fig. 1B). For microcirculation, f calculated from IVIM significantly (p2 = 0.86) with MBF calculated from FPP (Fig. 2A). For tissue microstructure, D calculated from IVIM significantly (p2 = 0.83) with ECV (Fig. 2B). For the unstable angina patient, f revealed a deficit in the microcirculation in the LAD territory which was confirmed with invasive x-ray angiography (Fig. 3).

Conclusion: Free breathing M2 IVIM demonstrated high intra-scan reproducibility. Furthermore at rest, a single IVIM scan yielded parameters (f and D) that highly correlated with both quantitative FPP and ECV, respectively, in a group of healthy volunteers. M2 IVIM showed microcirculation deficit in a region corresponding to invasive angiography in an unstable angina patient. Future studies will need be performed in large cohort of patients and under stress conditions to fully realize IVIM';s clinical potential.

[1] Schwitter EHJ 2011, [2] Kellman JCMR 2012, [3] LeBihan, Rad 1988, [4] Callot, MRM 2003, [5] Hsu JMRI 2006.

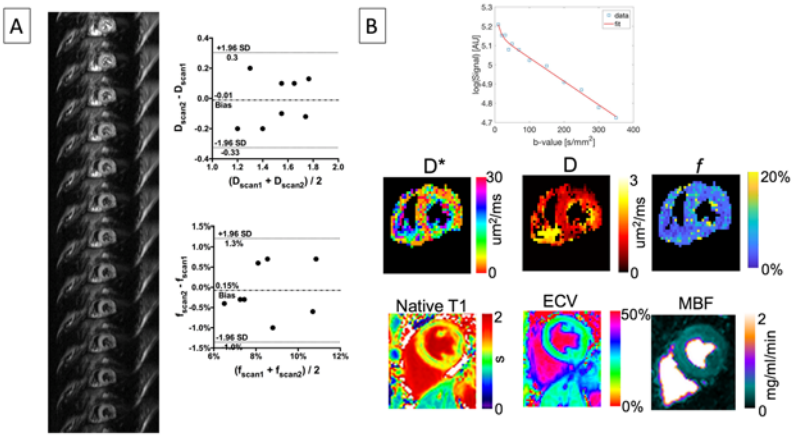

(A) Raw diffusion weighted images and reproducibility Bland Altman plots. (B) Representative f, D*, and D maps with log(signal) vs b-value plot demonstrating goodness of fit. Representative Native T1, ECV, and MBF maps are also shown.

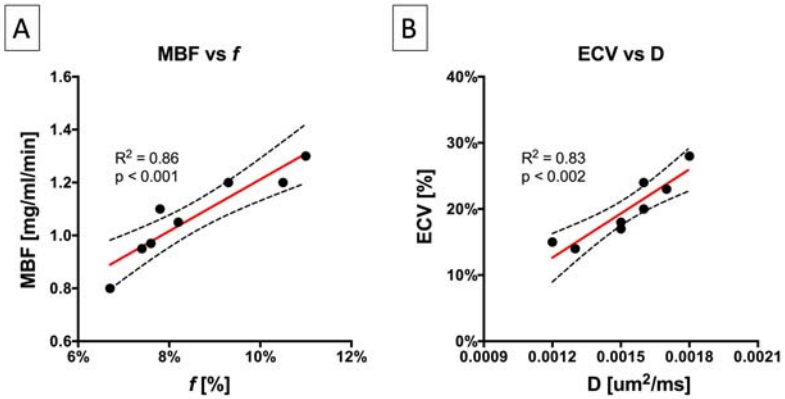

Scatter plots between (A) f vs MBF and (B) ADC vs ECV in normals showing significant correlation.

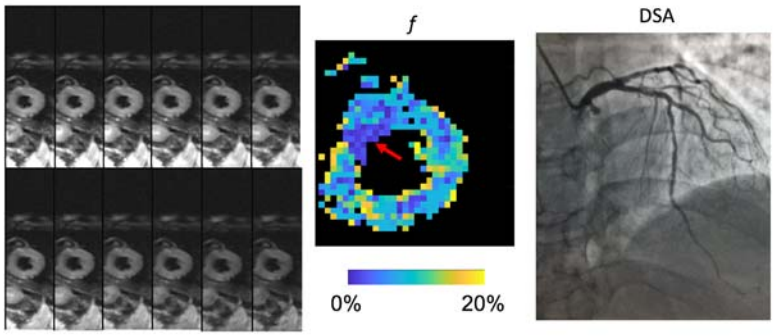

IVIM identifies low microcirculation (red) in endocardial anteroseptal region in unstable angina patient with confirmed 70% stenosis in LAD from DCA.

ID#: 372722

Ultra-high spatial resolution spiral myocardial perfusion imaging with whole heart coverage at 3T

Yang Yang, PhD[1]Matthew J. Van Houten, MS[2], Christopher M. Kramer, MD[3], Michael Salerno, MD, PhD[1]

1. University of Virginia, VA

2. University of Virginia, Charlottesville, VA

3. University of Virginia Health System, Charlottesville, VA

Background: Contrast-enhanced first-pass myocardial perfusion is a valuable noninvasive technique to evaluate patients with known or suspected coronary artery disease (CAD). Canine studies have shown that the endocardium is more sensitive to reduced perfusion, resulting in transmural variations of the severity of ischemia. Conventional CMR perfusion techniques have either limited spatial-temporal resolution, or lack the whole heart coverage needed to fully assess regional differences in perfusion between the endocardium and epicardium. We previously demonstrated high quality perfusion imaging at 1.5T with spiral trajectories, outer-volume suppression (OVS), and simultaneous multi-slice (SMS) imaging, achieving 2 mm spatial resolution with whole heart coverage. The goal of this study was to further develop this spiral pulse sequence to achieve even higher spatial resolution of 1.25 mm at 3T.

Methods: Two different pulse sequences were evaluated in this study including a) an interleaved acquisition of two slices per saturation recovery (SR) block, and b) SMS with a multiband factor of 2 per SR. An optimized 5 hard-pulse SR was used to reduce SAR in 3T. Both sequences utilized an OVS module containing a BIR-4 tip-down pulse, a 2D spiral tip-back pulse, and a spoiler to crush residual signal. The sequence schematic is shown in Figure 1 and detailed parameters are listed in Table 1. Resting first-pass perfusion was performed using both sequences with a 0.075 mmol/kg Gd-DTPA bolus, separated by 20 min contrast washout time, in 9 healthy subjects on a 3T Prisma Siemens scanner. The images were reconstructed by L1-SPIRiT or SMS-L1-SPIRiT using finite temporal difference as the sparsity transform. Image quality of both sequences were graded on a 5-point scale (5 excellent, 1 poor) by an experienced cardiologist.

Results: Figure 2 shows an example of 6 slice perfusion images with 1.25 mm resolution of the OVS + interleaved sequence. Figure 3 shows another example of high spatial resolution perfusion images using an OVS + SMS sequence. Both sequences produced high quality perfusion images. The average image scores of the interleaved and SMS sequences were 3.3±0.5 and 2.9±0.3 respectively (p=0.01). There was some signal dropout in the inferior wall due to off-resonance effects, which could be mitigated by further shortening the spiral readout durations.

Conclusion: We successfully demonstrated the application of an ultra-high resolution spiral perfusion sequence using OVS and SMS techniques. High resolution, whole heart perfusion could be used to quantify regional differences in perfusion of the subendo and subepi myocardium. Further validation will be required in patients undergoing adenosine stress CMR.

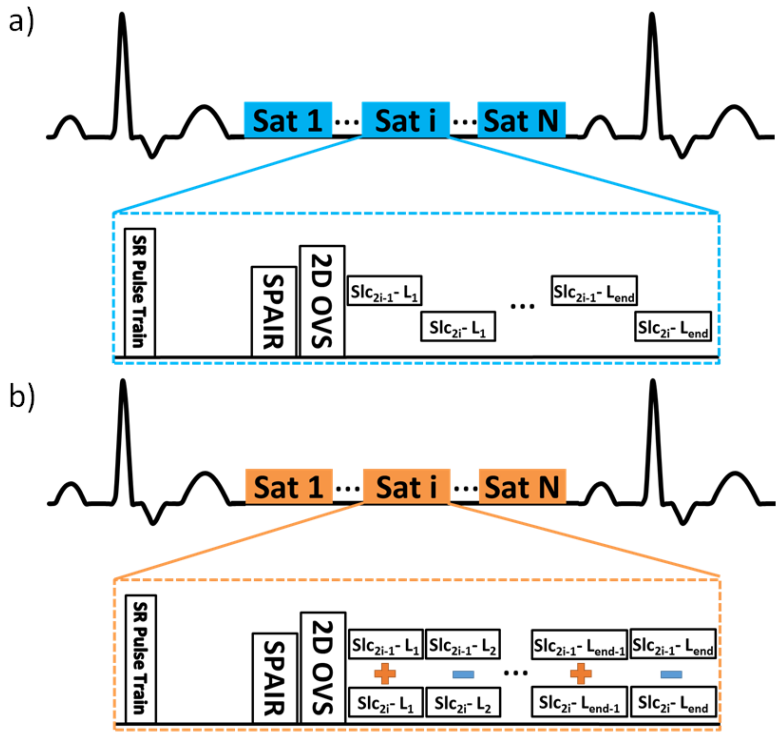

Figure 1. Pulse sequence schematics of (a) OVS with interleaved acquisition and (b) OVS with SMS techniques.

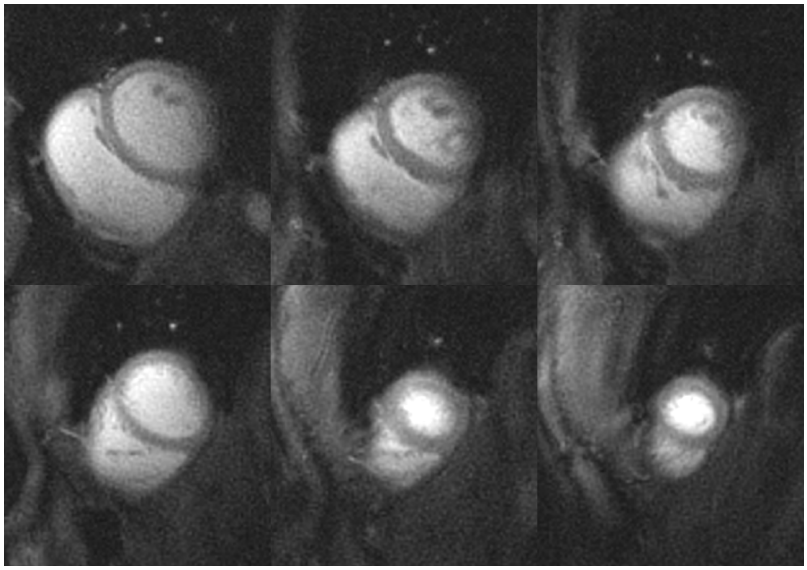

Figure 2. Spiral perfusion images acquired with 1.25mm spatial resolution using the OVS and interleaved acquisition fashion pulse sequence.

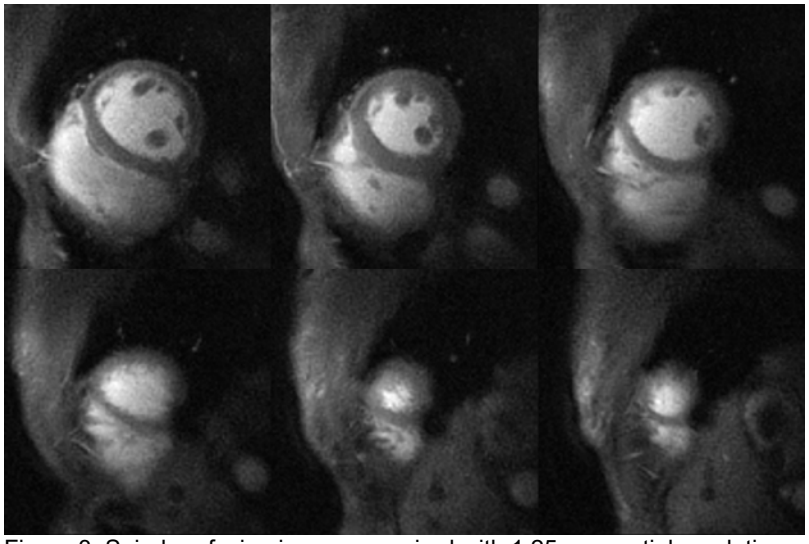

Figure 3. Spiral perfusion images acquired with 1.25mm spatial resolution using the OVS and SMS techniques pulse sequence.

Table 1. Pulse sequence parameters

	Sequence 1 (OVS + interleaved)	Sequence 2 (OVS + SMS)
FOV (mm)	170	170
Spatial resolution (mm)	1.25	1.25
Spiral interleaves	4	8
Spiral readout per interleave (ms)	5	5
# of slices acquired per SR	2	2
Starting density (Nyquist)	1	2
Ending density (Nyquist)	0.16 (6 fold)	0.33 (3 fold)
Temporal resolution (ms)	54.6	62.4
Inversion time (ms)	120	120
Flip angle (degree)	26	18
# of Slices	6-8	6-8

ID#: 373043

Quantification of Native T1 Rest/Stress Reactivity without T1 Mapping: Towards a Noncontrast Surrogate Marker of Myocardial Blood Volume Reserve Using a Novel Gradient-Echo Hybrid 2D/3D Acquisition Scheme

Behzad Sharif, PhD[1] Zulma Sandoval, Ph.D.[1], C. Noel Bairey Merz, MD[2]

1. Cedars-Sinai Medical Center, Los Angeles, Los Angeles, CA

2. Cedars Sinai Medical Center, Los Angeles, CA

Background: Native T1 is sensitive to the water content in all myocardial compartments. In the context of stable ischemic disease, intramyocardial blood volume (MBV) is the main contributor to the myocardial water content. Recently, Liu et al. [1] have shown that, in patients with stress-induced ischemia, *rest/stress native T1 reactivity* measured using shortened MOLLI (shMOLLI) can detect the myocardial territory affected by significant epicardial stenosis. The underlying mechanism is that native T1 reactivity acts as a surrogate marker of MBV reserve, which is significantly reduced in the myocardium distal to the stenosis due to microcirculatory autoregulation [2]. It is known, however, that shMOLLI native T1 values are confounded by magnetization transfer (MT) effects. Consequently, MT also confounds the T1 reactivity derived from shMOLLI. Specifically, in patients who have *diffuse fibrosis concomitant with ischemia*, this confounding effect is likely going to be complex and difficult to account for. We developed a new approach for native T1 reactivity mapping that is free of MT effects and hypothesized that it can accurately quantify T1 reactivity in controlled preclinical rest/stress studies.

Methods: Five Yorkshire farm pigs (30-46 kg) were studied at rest and during intravenous adenosine infusion (rate: 280 µg/kg/min) using a novel T1-weighted pulse sequence *designed to eliminate* the T1-modulating effects of through-plane motion and in-flow. As shown in Fig. 1, the proposed method employs an RF-spoiled gradient-echo steady-state sequence with a fixed flip angle (FA) and TR but 2 distinct RF excitation profiles. Following an initialization phase, the sequence switches to 2D excitation at the R-wave to acquire the selected slice and then switches again to 3D nonselective excitation to drive the out-of-slice spins back to steady state. For the proposed method, native T1 reactivity is computed from the rest/stress myocardial signal intensity (SI) values according to: $(SI_{rest} - SI_{stress}) \div SI_{stress}$. Based on simulations described in Fig. 2, the following parameters were used at 3T: FA=13º, TR/TE = 4.4/1.7 ms, in-plane resolution: 1.4x1.4 mm.

Results: The optimized gradient-echo sequence (no magnetization prep. and low FA) is almost entirely free of MT effects (phantom results not shown). Figure 3 shows representative images and summarizes the septal T1 reactivity results for shMOLLI and the proposed method. Native T1 reactivity estimated using the proposed method closely matched shMOLLI (Fig. 3 caption). The relatively blunted T1 reactivity compared to [1] may be due to a lower level of MBV increase during adenosine stress in anesthetized pigs. This is consistent with other pig studies showing minimal MBV increase in response to adenosine [3]. The mean T2 reactivity in our study was 9.8% ± 3.6%, consistent with prior 3T BOLD studies [4].

Conclusion: We have developed a new approach for quantification of native T1 reactivity that is inherently free of the confounding effects of MT. Our preclinical results demonstrate the feasibility and accuracy of the proposed method based on comparison to shMOLLI in controlled studies of anesthetized pigs. The key advantage of the proposed approach is its potential for achieving a higher level of accuracy as *a non-contrast surrogate for MBV reserve* in presence of myocardial fibrosis, a common finding in patients with suspected ischemia.

References:

[1] Liu et al. JACC Img 2016
[2] Nagel et al. JACC Img 2016
[3] Foltz et al. Circ 2002
[4] Arnold et al. JACC 2012

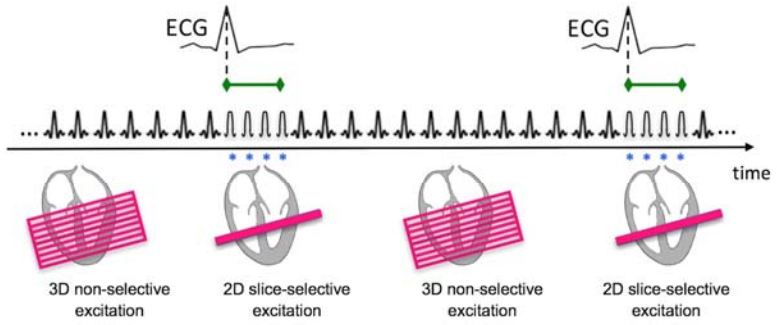

Fig 1. Simplified schematic of the data acquisition scheme for the proposed approach with hybrid 2D/3D continuous excitation to eliminate through-plane motion effects. The proposed method employs an RF-spoiled gradient-echo steady-state sequence (no magnetization prep.) with a fixed flip angle and TR but two different RF excitation profiles. The sequence starts but playing ≈2 seconds of 3D nonselective RF pulses (TR = 4.4 ms) to drive the magnetization to steady state. Following this phase, with the arrival of an R-wave trigger, the sequence switches to slice-selective excitation (marked by blue asterisks) for a brief period (88 ms) to acquire readouts of the 2D slice and then switches again to 3D nonselective excitation to drive the out-of-slice spins back to steady state.

Figure 1.

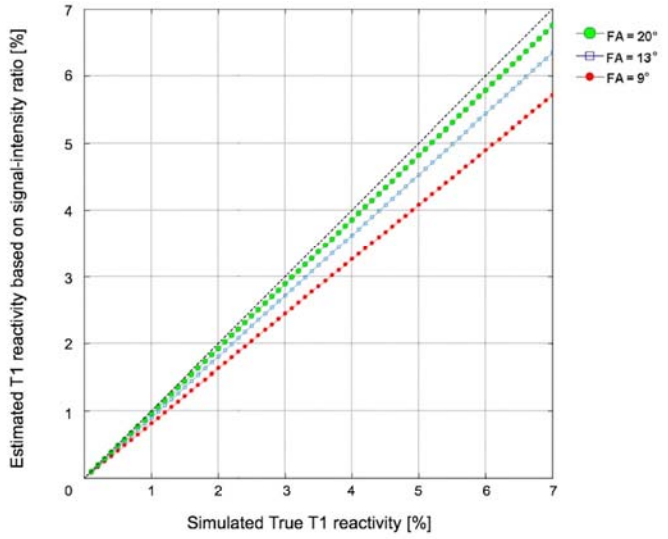

Fig 2. Bloch equation simulations for selection of the optimal pulse sequence parameters at 3T. Several variations of the acquisition scheme (Fig. 1 with TR = 4.4 ms) were simulated using Bloch equations and the estimated T1 reactivity was computed as the inverse ratio of the T1-weighted signal intensities. In the example plots shown here, the ideal scenario is represented by the diagonal dashed line that corresponds to zero underestimation. A high flip angle (FA = 20°) would result in a near-ideal accuracy in the physiologic range of 0% - 7%; however, this comes at the price of poor signal-to-noise ratio (SNR). All animal imaging data were acquired using FA=13°, which achieves sufficient SNR and a relative estimation error of < 10% (i.e., maximum of ≈0.5% underestimation of native T1 reactivity).

Figure 2.

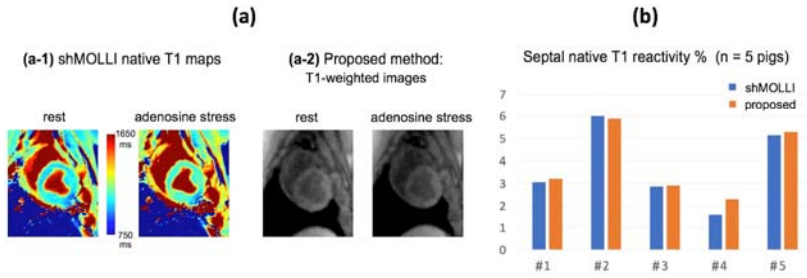

Fig 3. (a): Representative results for rest and adenosine-stress studies: **(a-1)** T1 maps using shMOLLI and **(a-2)** T1-weighted signal intensities using the proposed method. **(b): Estimated septal native T1 reactivity** for the 5 studied pigs using shMOLLI (difference between stress and rest T1, expressed as a percentage of rest T1) and the proposed method (computed based on the rest/stress difference between T1-weighted myocardial signal intensities as described in Methods). The mean shMOLLI rest and stress native T1 values were 1125 ± 31 ms and 1166 ± 21 ms, respectively ($p < 0.01$). The mean native T1 reactivity estimated using shMOLLI and the proposed method were 3.7% ± 1.6% and 3.9% ± 1.4%, respectively ($p = 0.25$).

Figure 3.

ID#: 373102

Splenic T2-Mapping: a Novel Method for the Assessment of Splenic Blood Flow during Adenosine Stress

Tommaso D'Angelo, MD[1] Elen Elen, MD, FIHA[2], Silvio Mazziotti, MD[3], Alfredo Blandino, Md[4], Faraz Pathan, MBBS, FRACP[5], Julian L. Wichmann, MD[6], Christophe Arendt, MD[7], Md. Ibnul Mia[8], Lea Winau, Bsc[9], Melanie Le[10], Valentina O. Puntmann, MD, PhD[11], Eike Nagel, MD, PhD[12]

1. University of Messina, Messina, Sicilia, Italy

2. National Cardiovascular Center Harapan Kita, Jakarta-Indonesia; Institute for Experimental and Translational Cardiovascular Imaging, University Hospital Frankfurt-Germany, Tangerang, Banten, Indonesia

3. University of Messina, Italy

4. Università di messina, Italy

5. Goethe Institute for Experimental and Translational Cardiovascular Imaging, Sydney, New South Wales, Australia

6. University Hospital Frankfurt, Frankfurt, Hessen, Germany

7. Goethe-University Frankfurt, Department of Diagnostic and Interventional Radiology, Frankfurt Am Main, Hessen, Germany

8. Goethe University Hospital Frankfurt, Institute for Experimental and Translational Cardiovascular Imaging, Germany

9. Goethe University Hospital Frankfurt, Hessen, Germany

10. Institute for Experimental and Translational Cardiovascular Imaging, University Hospital Frankfurt, Hessen, Germany

11. Universitaetsklinikum Frankfurt, Frankfurt Am Main, Germany

12. University Hospital Frankfurt; Institute for Experimental and Translational Cardiovascular Imaging; DZHK Centre for Cardiovascular Imaging, Frankfurt, Germany

Background: Inadequate adenosine stress may occur in a relevant proportion of patients undergoing myocardial first-pass perfusion cardiac magnetic resonance (perfusion-CMR). This may lead to false-negative results and suboptimal clinical management. “Splenic switch-off” has recently been proposed as a surrogate sign to determine the effect of adenosine. However, since this sign can only be assessed after contrast-injection, novel methods are emerging to detect reduction of splenic blood volume during adenosine stress and prior to contrast administration. T2-values correlate well with water content within a tissue. We sought to determine the feasibility of using splenic native-T2 as a marker to assess adenosine-stress effect.

Methods: In fifty-three consecutive patients with indications for perfusion-CMR splenic T1- and T2-values were assessed at 3T (n=39) and 1.5T (n=14), respectively using MOLLI and GraSE sequences, performed at rest and during adenosine stress (140µg/kg/min, 4 min) along one mid-ventricular short-axis slice. Changes of T1- (ΔT1) and T2-values (ΔT2) were calculated and expressed as percentages. Perfusion-CMR was performed after intravenous injection of gadobutrol (0.1mmol/kg body-weight). Images were analyzed with the use of a semiautomatic software (Medis, Leiden, The Netherlands) to obtain splenic and myocardial enhancement-ratios. Spleen-to-myocardium perfusion ratio (s/mΔSI) was calculated to quantify splenic blood-flow during perfusion-CMR. The presence of a visual “splenic switch-off” was assessed in consensus by two readers and used as reference standard. Statistical analysis included correlations and receiver operating characteristic (ROC) curves, which were used to assess the accuracy of s/mΔSI, ΔT1 and ΔT2 in predicting the splenic switch-off sign.

Results: All patients were included in the analysis (27 males, mean age 57.2±11.8). The mean splenic native T1- and T2-values were respectively 1254.7±97.9(ms) and 59.3±12(ms) at 3T, and 1147.1±77.2(ms) and 79.0±11.1(ms) at 1.5T, versus stress T1- and T2-values of 1196.5±87.7(ms) and 53.1±11.3(ms) at 3T, and 1099.6±82.3(ms) and 72.6±11.2(ms) at 1.5T (all p<0.001).
s/mΔSI showed a correlation with ΔT2 and ΔT1 respectively of 0.702 and 0.479 (all p<0.001). ΔT2 showed the best accuracy for predicting “switch-off” sign (AUC=0.988), followed by s/mΔSI (AUC=0.964) and ΔT1 (AUC=0.910) (all p<0.001) (Fig.1). The largest difference in terms of accuracy was seen between ΔT2 and ΔT1 (0.0752; p=0.076). Cut-off values were 8.22% for ΔT2 (sensitivity: 94%; specificity 95%) and 3.73% for ΔT1 (sensitivity: 82%; specificity: 84%).

Conclusion: Use of splenic ΔT2 may predict an effective adenosine response prior to fist-pass perfusion-CMR. Eventually, this may allow for preventive dose adaption to minimize false-negative results.

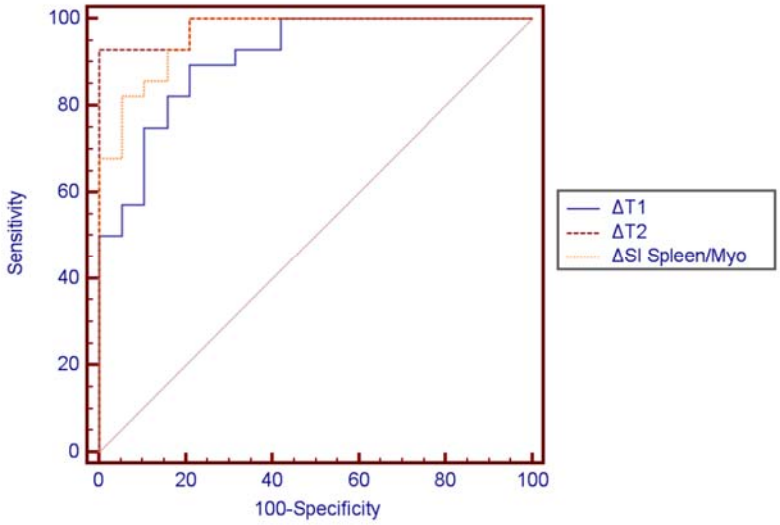

Fig.1

ID#: 372466

Simultaneous Multi Slice (SMS) SSFP first pass myocardial perfusion at 1.5 Tesla.

Muhummad Sohaib Nazir, MBBS MRCP[1] Radhouene Neji, PhD[2], Peter Speier[3], Daniel Stäb, Dr.[4], Michaela Schmidt[5], Christoph Forman, PhD[5], Caroline M. Van De Heyning, MD PhD[6], Reza Razavi, MD, PhD[7], Sven Plein, MD PhD[8], Tevfik F. Ismail, PhD MRCP[9], Amedeo Chiribiri, MD PhD[7], Sébastien Roujol, PhD[7]

1. King's College London, United Kingdom

2. Siemens Healthcare Limited, Frimley, England, United Kingdom

3. Siemens Healthcare GmbH, Germany

4. The University of Queensland, Brisbane St Lucia, Queensland, Australia

5. SIEMENS HEALTHCARE GmbH, Erlangen, Bayern, Germany

6. St. Thomas' Hospital, London; King's College London ; Antwerp University Hospital, Edegem, Belgium

7. King's College London, London, England, United Kingdom

8. University of Leeds, England, United Kingdom

9. King's College London; Guy's and St Thomas' Hospitals NHS Foundation Trust, London, England, United Kingdom

Background: In routine clinical practice, conventional first-pass contrast-enhanced cardiovascular magnetic resonance (CMR) perfusion imaging has limited spatial coverage, usually 3 slices. CMR perfusion with higher spatial coverage may allow detection of perfusion defects that may be missed in a standard 3-slice approach. Simultaneous multi-slice (SMS) imaging is an acceleration technique which enables simultaneous acquisition of multiple slices with minimal signal-to-noise (SNR) penalty and shows potential to increase spatial coverage of CMR perfusion[1]. Robustness of SMS-bSSFP against B_0 inhomogeneities can be ensured by adding Gradient Controlled Local Larmor Adjustment (GC-LOLA)[2]. We sought to evaluate the feasibility of CMR rest perfusion using an SMS GC-LOLA bSSFP prototype sequence and compare to a standard bSSFP sequence.

Methods: Eight patients with no history of myocardial infarction or cardiovascular risk factors and low pre-test probability of ischaemic heart disease were recruited and imaged at 1.5T (MAGNETOM Aera, Siemens Healthcare GmbH, Erlangen, Germany). Two rest contrast perfusion protocols using standard bSSFP imaging (3 slices) and SMS GC-LOLA bSSFP imaging (6 slices) were performed in a random order in each patient using 0.075mmol/kg of Gadovist (Bayer, Berlin, Germany). The two protocols were separated by a minimum time interval of 15 minutes to allow for contrast washout and the imaging parameters were kept constant between both sequences (TR/TE/α: 2.9ms/1.24ms/50° [SMS], TR/TE/α: 2.5ms/1.04ms/50° [standard], voxel size: 1.9x1.9mm^2, slice thickness: 10mm, FOV: 332x332mm^2, TI 120ms [SMS] 105ms [standard], bandwidth 1093Hz). Subjective assessment of image quality (3=excellent, 2=artefact present but diagnostic, 1=non-diagnostic), degree of respiratory artefact (3=none, 2=artefact present but diagnostic, 1=non-diagnostic) and circumferential percentage of dark rim artefact was performed by two experts blinded to the clinical details.

Results: The SMS 6-slice and standard 3-slice sequences produced diagnostic image quality in 7 cases and one case was deemed to have non-diagnostic image quality in both sequences. The standard approach had better image quality (p=0.02) compared to SMS. There was no difference in degree of respiratory artefact (p=0.65) or degree of dark rim artefact (p = 0.81).

Conclusion: We demonstrated the feasibility of first-pass perfusion imaging using SMS GC-LOLA bSSFP. Image quality was diagnostic and comparable to standard bSSFP acquisition but with a two-fold increase in spatial coverage. However, the subjective image quality was superior using a standard approach. Future evaluation in patients with suspected coronary artery disease will determine the clinical utility of this technique.

[1] Staeb, JMRI, 2013:39(6) 1575–1587 [2] Speier, SCMR, 2016, P301

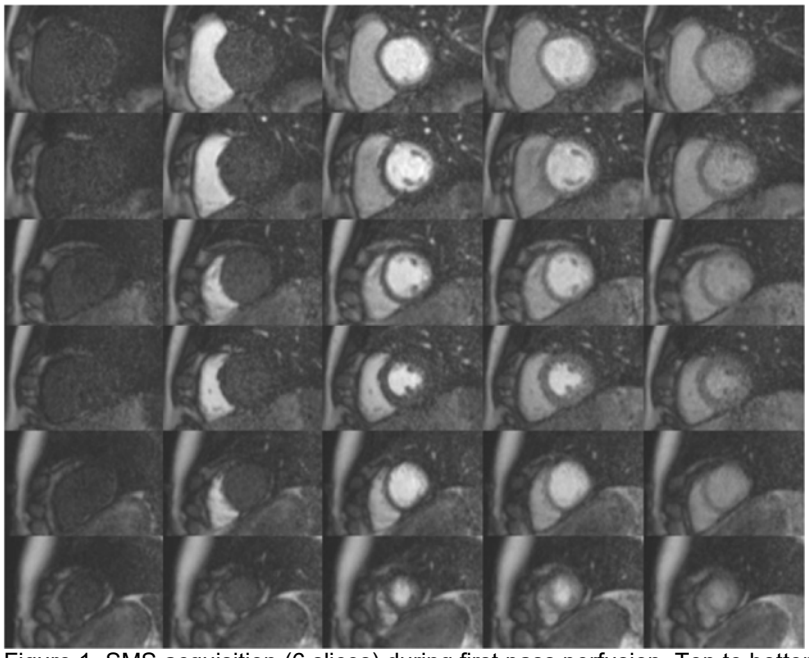

Figure 1. SMS acquisition (6 slices) during first pass perfusion. Top to bottom: base to apex. Left to right: baseline, peak contrast right ventricle, peak contrast left ventricle, peak contrast myocardium and washout.

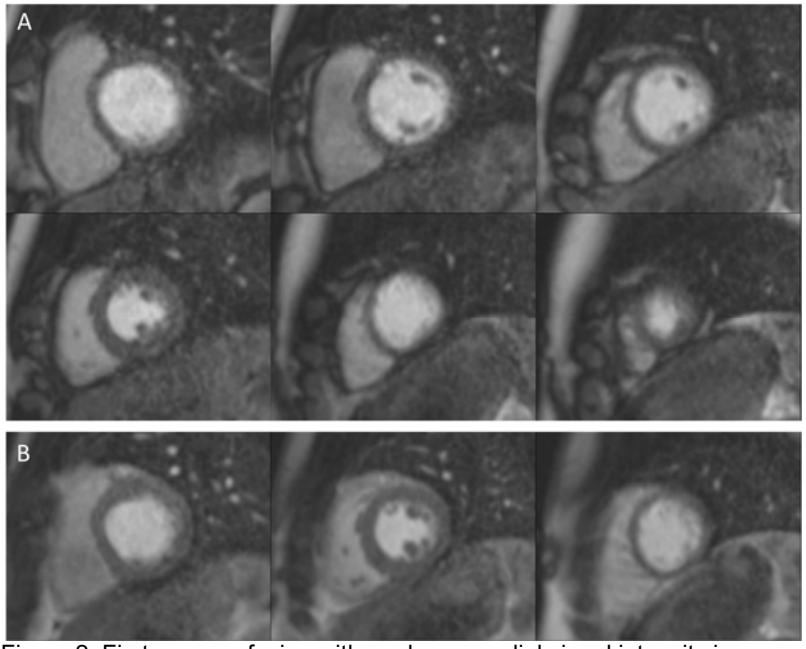

Figure 2. First pass perfusion with peak myocardial signal intensity in one patient using SMS 6-slice bSSFP with spatial coverage from base to apex of the left ventricle (a) and a standard 3-slice bSSFP acquisition (b). Both perfusion images were deemed to be of diagnostic value.

ID#: 366569

Pattern of ischemic injury is modulated by coronary architecture: A quantitative CMR study

Nilesh R. Ghugre, PhD[3] Jennifer Barry, VT, RLAT[1], Xiuling Qi, PhD[1], Graham Wright, PhD[2]

1. Sunnybrook Research Institute, Canada

2. Sunnybrook Research Institute, University of Toronto, ON, Canada

3. Sunnybrook Research Institute, University of Toronto, Toronto, ON, Canada

Background: The severity and pattern of myocardial infarction (MI) is dependent on the coronary architecture and the duration of the ischemia. Porcine models of MI are popular due to their similarity in heart size and coronary anatomy to humans. Recent work in Yorkshire pigs demonstrates that duration of occlusion can produce different patterns of infarction i.e. transmural, heterogeneous or with microvascular obstruction (MVO). The presence and absence of hemorrhage and resolution of edema is also governed by the severity of the initial ischemic injury. Yucatan mini pigs have a slower growth rate and are ideal for chronic studies. Our objective was to compare the coronary structure and the subsequent injury patterns in these two breeds of pigs using quantitative CMR.

Methods: The study involved a) Yorkshire pigs (N=4) with a 90 min occlusion just beyond 2nd diagonal branch of the left anterior descending artery (LAD), followed by reperfusion [3] and b) Yucatan Mini pigs (N=3) with Y1: 90 min occlusion just beyond 2nd diagonal branch of LAD similar to the Yorkshire arm; Y2: 90 min occlusion at 1st diagonal branch of LAD; and Y3: 180 min occlusion at 1st diagonal branch of LAD. Coronary anatomy was studied by X-ray fluoroscopy and CMR studies were conducted on a 3T whole-body system at baseline (healthy) and day 2-3 post-MI. A comprehensive CMR exam was performed in all animals. T2 mapping was performed using a T2-prepared spiral sequence. Hemorrhage was assessed from T2* maps obtained using a multi-echo gradient-echo acquisition. Infarcted and remote myocardial segments were evaluated based on LGE images. Cardiac function was evaluated using cine SSFP and infarct and MVO size by late gadolinium enhancement (LGE).

Results: Ejection fraction (EF) and infarct size and MVO size in Yorkshire and Yucatan minipigs (Y1-Y3) are presented in Table 1. In the Yorkshires, EF was markedly decreased ($p<0.003$) at day 2-3 post-MI in association with the presence of transmural infarction with MVO and hemorrhage. The Yucatan';s Y1 and Y2 with 90 min occlusions demonstrated heterogeneous infarction with no MVO or hemorrhage. With a 180 min occlusion, Y3 presented with transmural infarction with MVO and hemorrhage and substantial EF reduction similar to the Yorkshires. Representative X-ray angiograms and LGE images are shown in Fig. 1. On X-ray angiograms, we noted that Yucatans had a long and extensive left marginal branch (M1) from left circumflex artery (LCX), overlapping with the mid-LAD territory, possibly offering protective collateralization.

Conclusion: Coronary circulation in Yucatan Mini pigs was found to be more extensive than that in Yorkshires and this dictated the infarct size and presence of MVO and hemorrhage. Thus, level and duration of coronary occlusion can produce different ischemic injury patterns depending on the extent of perfusion tree and collateral network. Understanding coronary architecture is important in determining infarct patterns in animals and creating more reproducible injury patterns, which is critical when evaluating novel therapeutics for MI.

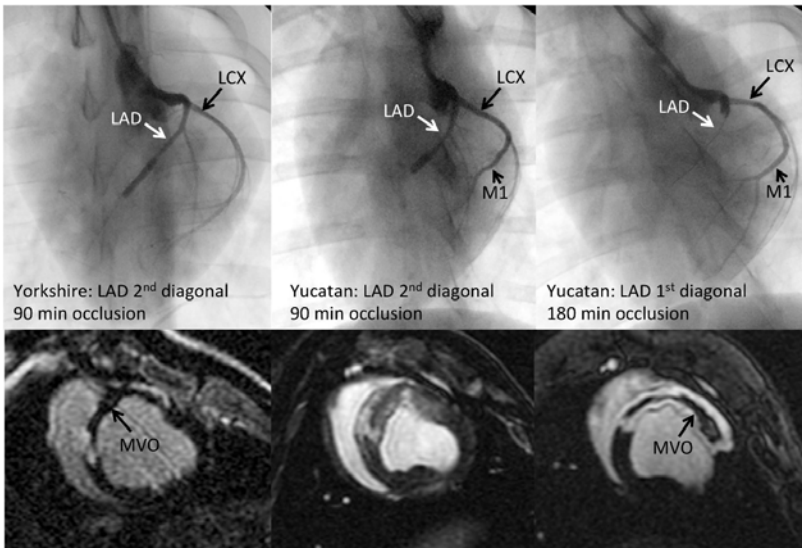

Figure 1: X-ray angiograms and corresponding LGE images at day 2-3 post-MI

Table 1: Cardiac Function and MI and MVO Size

Pig groups – Occlusion level/duration	EF (%)	MI (%)	MVO (%)
	Baseline/Day 2-3	Day 2-3	Day 2-3
Yorkshire: DB2/90 min	45.6±7.7 / 35.8±5.2	17.7±5.0	6.6±3.4
Yucatan (Y1): DB2/90 min	42.8 / 40.2	4.6	No MVO
Yucatan (Y2): DB1/90 min	51.7 / 44.1	19.8	No MVO
Yucatan (Y3): DB1/180 min	55.9 / 29.8	43.9	10.7

DB: Diagonal Branch, EF: Ejection Fraction, MI: Myocardial Infarction, MVO: Microvascular Obstruction

ID#: 366003

Steady-State Pulsed Arterial Spin Labeling Is Faster and Provides Lower Variability for Quantification of Myocardial Perfusion Reserve in Mice Compared to Flow Alternating Inversion Recovery Look-Locker ASL

Sophia X. Cui, B.S.[1] Frederick H. Epstein, PhD[2]

1. University of Virginia, Charlottesville, VA

2. UVA Health System, Charlottesville, VA

Background: Flow Alternating Inversion Recovery Look-Locker (FAIR-LL) arterial spin labeling (ASL) is a well-established method for quantifying myocardial perfusion in mice. Recently, steady-state pulsed ASL (spASL) was introduced as a potentially better method with regard to speed and variability [1]. The original spASL sequence included recovery delay periods such that the method captured the steady-state signal as well as the transition to the steady state. We implemented a modified spASL sequence without the delay periods to further reduce the scan time, as capturing the transition to steady state is not necessary for quantifying perfusion. The modified spASL method was compared to FAIR-LL ASL for quantifying myocardial perfusion reserve in mice.

Methods: Steady-state pulsed ASL without delay periods (Figure 1) was implemented on a 7T Clinscan system (Bruker, Ettlingen, Germany). Acquisitions utilized ECG R-wave detection without gaps to ensure maintenance of the steady state. Five mice underwent perfusion MRI at rest and stress (regadenoson 0.1 μg/g body weight) using a 30-mm diameter birdcage RF coil. Two perfusion quantification methods were performed in each mouse, namely, FAIR-LL ASL and spASL. All scans shared the following parameters: FOV = 38 x 38 mm^2 and voxel size = 0.3 x 0.3 x 1 mm^3. As shown in Figure 1, spASL used an arterial blood tagging scheme consisting of a regional inversion pulse over the left atria and aorta. The corresponding control images used an inversion pulse applied symmetrically below the imaging slice. Parameters for spASL included: TR = 8 ms, TE = 2 ms, flip angle = 7°, averages = 8, and scan time = 5 minutes. Myocardial blood flow (MBF) was quantified as previously described [1]. FAIR-LL ASL was performed with cardio-respiratory gating, fuzzy clustering and a spiral readout, as previously described [2]. Imaging parameter for FAIR-LL ASL included: TR = 7 s, TE = 0.67 ms, flip angle = 3°, averages = 3, number of spiral interleaves = 84, and interleaves per heartbeat = 3. The acquisition was rate-2 accelerated, providing a scan time of 15 minutes. MBF was quantified using the T1-shift method.

Results: Example FAIR-LL ASL and spASL images of the mouse heart are shown in Figure 2. MBF and myocardial perfusion reserve (MPR) for each individual animal are provided in Table 1. Mean rest and stress MBF were 6.1±1.0 and 13.0±0.8 for FAIR-LL ASL, respectively, and were 4.9±0.2 and 10.2±0.5 for spASL, respectively. The t-test shows no significant difference between the rest perfusion measured by the two methods, but there was a significant difference for stress perfusion, $P < 0.05$. MPR was 2.3±0.3 using FAIR-LL, and 2.1±0.1 using spASL, as shown in Figure 3. The t-test showed no significant difference in MPR measure by the two methods. The F test showed a significantly lower variance in MPR measured by spASL.

Conclusion: In one-third of the scan time, spASL without delay periods provided less variability in quantifying MPR in mice compared to FAIR-LL ASL, while maintaining the same spatial resolution. Steady-state pulsed ASL may outperform FAIR-LL ASL for quantitative myocardial perfusion MRI in mice. **References** [1] Troalen et al. MRM, 2013. **70**(5): p. 1389-1398. [2] Vandsburger et al. MRM 2010. **63**(3): p. 648-57.

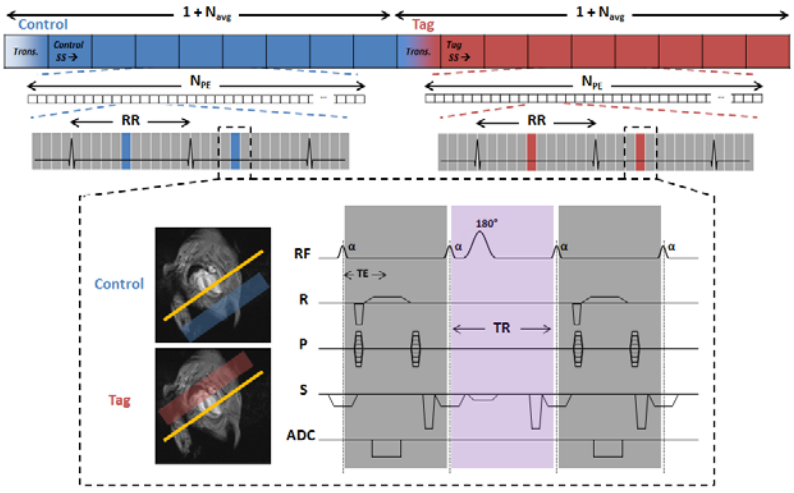

Figure 1. Schematic description of the spASL pulse sequence without delay periods. Two contrasts (control and tag) are collected during each acquisition. For each contrast, the transition to steady state occurs during the first measurement and is not used in image reconstruction. The arterial tagging scheme labels blood by placing an inversion pulse over the atria and aorta, and the control uses an inversion pulse symmetric to the imaging slice.

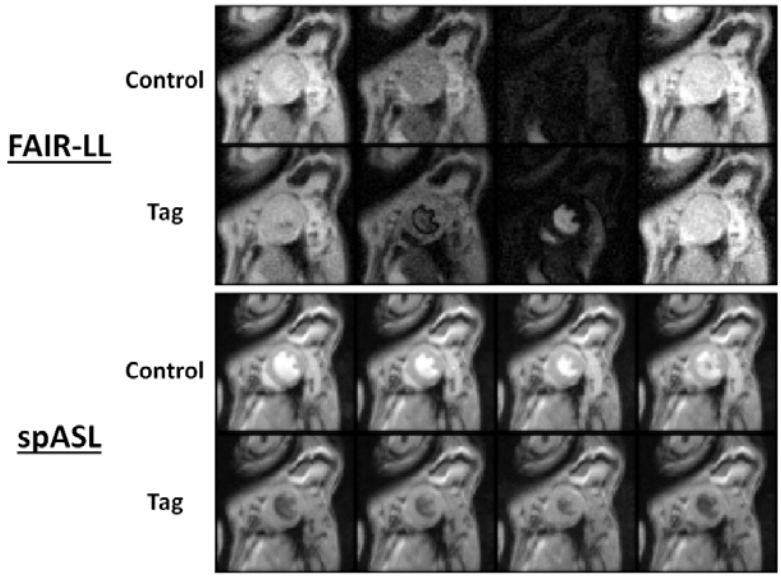

Figure 2. Example FAIR-LL ASL and spASL images of the mouse heart. For FAIR-LL ASL, images are shown at selected inversion times, and for spASL, images are shown at selected cardiac phases.

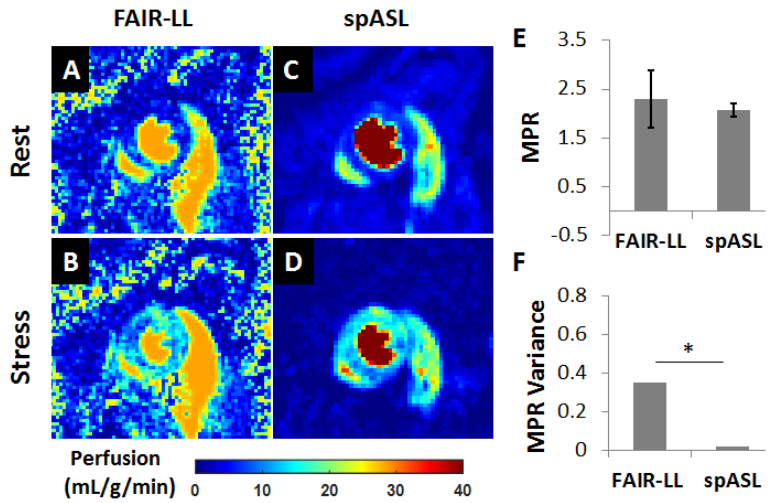

Figure 3. Example perfusion maps at rest (A,C) and stress (B, D) calculated using FAIR-LL ASL (A,B) and spASL (C,D). Mean MPR was similar for FAIR-LL ASL and spASL (E). A significantly lower variance in MPR was measured by spASL compared to FAIR-LL ASL (F).

Table 1. Perfusion and MPR data from 5 mice measured using FAIR-LL ASL and spASL.

Mouse	Weight (g)	Perfusion (ml/g/min)				MPR	
		FAIR-LL		spASL		FAIR-LL	spASL
		Rest	Stress	Rest	Stress		
1	28.5	9.1	16.1	4.5	9.3	1.8	2.1
2	28.5	4.2	12.1	4.7	9.9	2.9	2.1
3	26.8	4.2	11.9	4.8	9.1	2.9	1.9
4	28.5	8.0	13.2	4.9	10.9	1.7	2.2
5	33.5	5.0	11.5	5.7	11.7	2.3	2.1
Mean ± SD	29.1 ± 2.5	6.1 ± 2.3	13.0 ± 1.9	4.9 ± 0.4	10.2 ± 1.1 *	2.3 ± 0.6	2.1 ± 0.1 #

*$P < 0.05$ between stress perfusion measure by FAIR-LL and spASL. # $P < 0.05$ between the variance of MPR measured by FAIR-LL and spASL.

ID#: 370533

Simultaneous quantitative myocardial perfusion with hybrid PET-MRI imaging in a 3D printed phantom using gadolinium contrast and 13-N Ammonia

Muhummad Sohaib Nazir, MBBS MRCP[1] Sarah-May Gould, MPhys MSci[2], Xenios Milidonis, MSc, PhD[2], Sami Jeljeli, PG Dip MMR[3], Radhouene Neji, PhD[4], Tevfik F. Ismail, PhD MRCP[5], Reza Razavi, MD, PhD[6], Paul Marsden[1], Sven Plein, MD PhD[7], Amedeo Chiribiri, MD PhD[6]

1. King's College London, United Kingdom

2. King's College London, London, United Kingdom

3. Kings College London., England, United Kingdom

4. Siemens Healthcare Limited, Frimley, England, United Kingdom

5. King's College London; Guy's and St Thomas' Hospitals NHS Foundation Trust, London, England, United Kingdom

6. King's College London, London, England, United Kingdom

7. University of Leeds, England, United Kingdom

Background: Hybrid PET-MRI imaging allows simultaneous PET and CMR acquisition for cross-validation of techniques. A 3D-printed cardiac phantom that simulates myocardial blood flow (MBF) allows preclinical evaluation of methodology and quantification algorithms in a controlled environment without respiratory or motion artefact. PET is the in-vivo reference standard for MBF quantification and 13-N ammonia is the most widely used PET tracer. We sought to demonstrate the feasibility of simultaneous acquisition of 13-N ammonia PET and dynamic contrast-enhanced CMR and determine the correlation and degree of agreement between the two modalities in a perfusion phantom with known ground truth perfusion rates of the phantom.

Methods: MBF was simulated at five different perfusion rates (1-5 mL/kg/min) in the phantom at fixed cardiac output and heart rate 60 beats/min. 200MBq of 13-N ammonia was administered to the perfusion phantom simultaneously with 0.0075mmol/kg followed by 0.075mmol/kg gadolinium contrast using a dual-bolus technique. Images were acquired using a 3T hybrid PET-MRI scanner (Biograph mMR, Siemens Healthcare, Erlangen, Germany). 3D-PET data were acquired in list mode for 7 minutes following tracer injection and reconstructed into 60 x 3 second bins followed by 8 x 15 second bins. MR-based attenuation correction was carried out using a 3D VIBE Dixon sequence. PET dynamic data were modelled using a single compartment model after ordered subset expectation maximisation (OSEM) reconstruction. For dynamic contrast-enhanced CMR, a FLASH sequence was used and MBF quantified with a Fermi function-constrained deconvolution of the arterial input function and myocardial tissue impulse response. Measurements were performed twice to assess reproducibility.

Results: PET and CMR MBF were highly reproducible with intraclass coefficients 0.97 and 0.96 respectively. There was a very strong correlation (R^2 = 0.91) between phantom and CMR MBF. There was a very strong correlation (R^2 = 0.99) between phantom and PET MBF. PET and CMR MBF estimates had a very strong correlation (R^2 = 0.96). Compared to phantom perfusion MBF, CMR underestimated MBF with a bias of -0.71 ± 0.33 ml/g/min (figure 1), whilst PET overestimated MBF with a bias of +0.71 ± 0.56 ml/g/min. CMR underestimated MBF compared to PET with a bias of -1.42 ± 0.66 ml/kg/min.

Conclusion: A strong correlation was demonstrated between PET, CMR and phantom MBF. However, CMR MBF quantified with Fermi deconvolution underestimated phantom MBF whilst PET overestimated phantom MBF. The perfusion phantom has utility in multimodal imaging to cross validate different perfusion quantification approaches against a true gold-standard prior to in-vivo application.

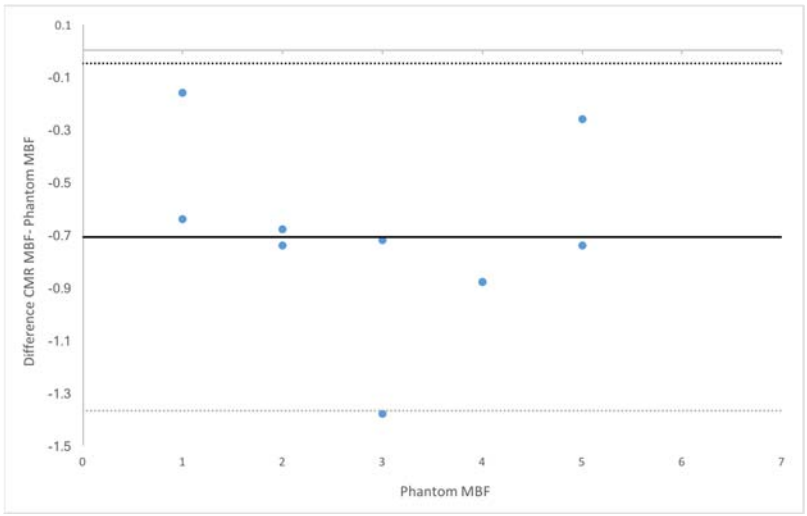

Figure 1. Bland Altman plot demonstrating agreement between CMR and Phantom MBF. Mean difference (solid line) and 95% limits of agreement (dotted line) displayed.

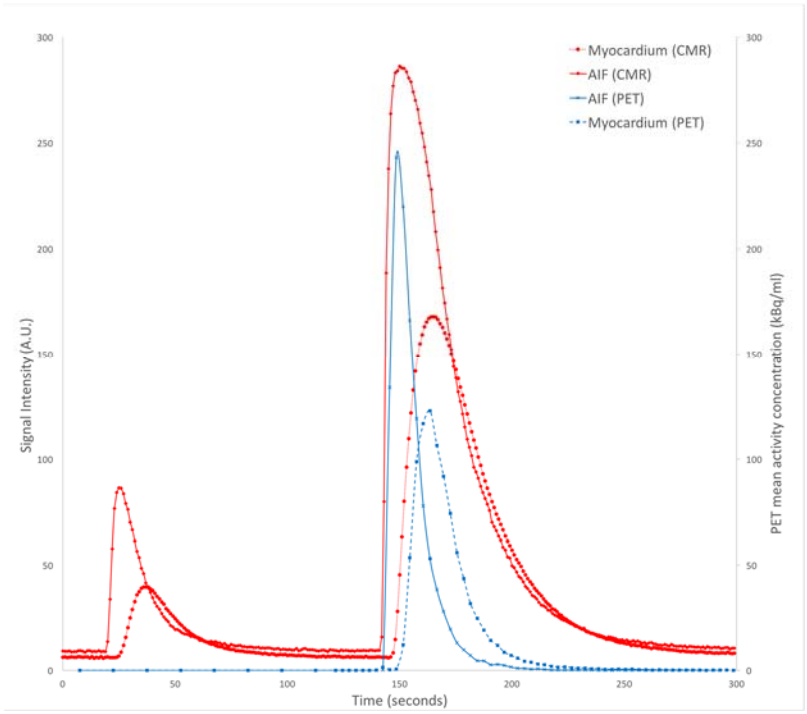

Figure 2. Arterial input function and myocardial response of the perfusion phantom with CMR signal intensity and PET mean activity concentration at a phantom perfusion rate of 5ml/g/min.

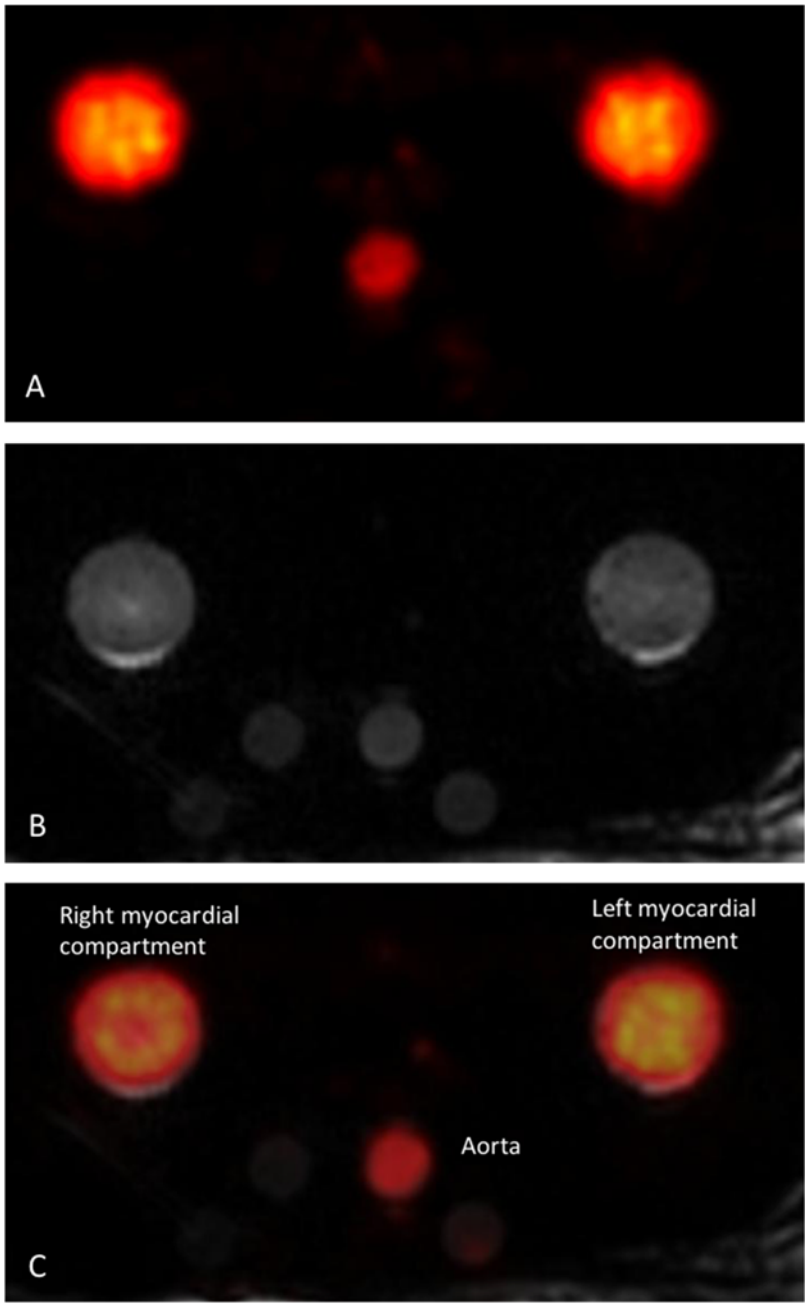

Figure 3. Cross section acquisition of the perfusion phantom during first pass perfusion of 13-N ammonia and gadolinium contrast. (A) PET only, (B) CMR only and (C) hybrid PET-MR imaging.

ID#: 378492

Quantitative perfusion in patients at high risk of coronary artery disease

Kristopher D. Knott, MBBS MA[1] Claudia Camaioni, MD[2], Lizette Cash[3], Anish Bhuva, MRCP, MBBS[4], Louise AE. Brown, MBChB, BMedSc[5], Hui Xue, PhD[6], Charlotte Manisty, MRCP PhD[7], Christos Bourantas[8], Sven Plein, MD PhD[5], Peter Kellman, PhD[9], James C. Moon, MD[10]

1. University College London, London, England, United Kingdom

2. Barts Heart Center, London, England, United Kingdom

3. Barts Heart centre, United Kingdom

4. University College London, and Barts Heart Centre, United Kingdom

5. University of Leeds, England, United Kingdom

6. National Heart, Lung, and Blood Institute, Bethesda, MD

7. Barts Heart Centre and University College London, United Kingdom

8. Barts Health NHS, UCL, United Kingdom

9. National Heart, Lung, and Blood Institute, National Institutes of Health, Bethesda, MD

10. Barts Heart Centre, England, United Kingdom

Background: Gadgetron inline perfusion mapping has been developed to automatically generate myocardial flow maps on the scanner, but needs to proceed through a number of validation steps before it can be used clinically and as a research surrogate endpoint. Perfusion mapping provides myocardial blood flow (MBF) at rest and stress (in ml/g/min), and the ratio, myocardial perfusion reserve (MPR). One of the early validation steps is to assess MBF and MPR in health and in chest pain patients, downstream of a stenosis and in remote myocardium.

Methods: Over the last 4 months, we prospectively recruited a healthy volunteer cohort (n=22) and 22 patients at high risk of coronary artery disease, scheduled for invasive coronary angiogram. Patients with previous CABG or contraindications to perfusion CMR were excluded. Perfusion mapping was acquired in 3 short axis slices during free-breathing adenosine stress and rest scans. MBF was calculated for each myocardial segment from the generated perfusion maps (figure 1). Regions of interest were drawn in in visually ischaemic and remote myocardium in all three slices. MBF values were obtained from all ischaemic / remote myocardial segments.

Results: The patients were older than the healthy volunteers (57 vs 35 years) and had more cardiovascular risk factors. By visual analysis, 13 patients (59%) were found to have stress perfusion defects. On quantitative perfusion mapping, rest MBF was the same in healthy volunteers and in ischaemic and remote regions in patients (volunteers vs remote vs ischaemic: 0.86, 0.79, 0.63ml/g/min, p=NS). Stress MBF in volunteers was 3.07ml/g/min (range 1.86 to 4.28) and was lower in the remote areas of patients (2.33ml/g/min), unpaired t-test p=0.0042 and ischaemic areas (0.81ml/g/min) p<0.0001. 16 patients (73%) had significant CAD by invasive angiography (visually scored). On a per patient basis, perfusion mapping had no false positives, and detected perfusion abnormalities in all of the 16 patients. In 3 however, there was no perfusion defect on the raw perfusion images but visually scored to have significant stenosis on coronary angiography.

Conclusion: Inline quantitative perfusion mapping allows for an objective, non-invasive assessment of coronary artery disease. Initial results demonstrate high specificity for significant coronary artery stenosis. Additionally, CAD patients have reduced remote stress MBF which, requires more exploration.

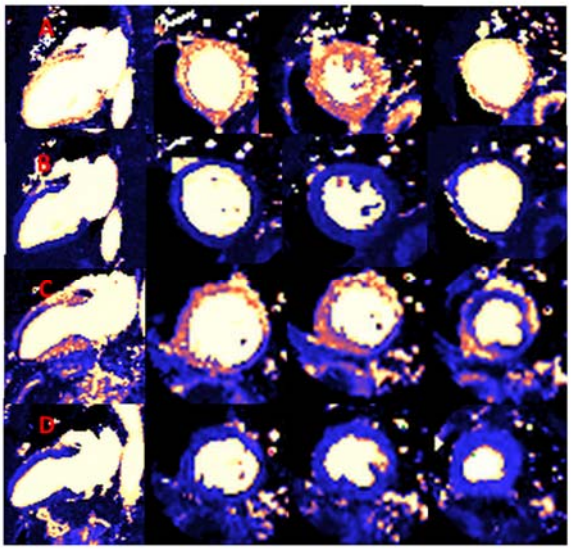

Figure 1. Perfusion maps from a healthy volunteer (A&B) and a CAD patient (C&D) at stress (A&C) and rest (B&D). The perfusion defects are easily visualised. Invasive coronary angiography confirmed significant stenoses of the left anterior descending and circumflex arteries.

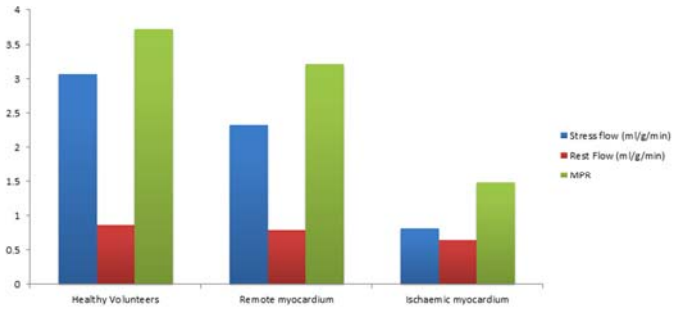

Figure 2. Myocardial blood flow and myocardial perfusion reserve for healthy volunteers and patients at high risk for CAD in ischaemic and remote territories.

ID#: 373671

Magnifying Myocardial BOLD Sensitivity Through Time-Resolved Imaging of Regadenoson Phamacokinetics

Hsin-Jung Yang[1]Damini Dey, PhD[2], Behzad Sharif, PhD[3], Jane Sykes, BS[4], John Butler, BSc MRT(MR)[5], Ivan Cokic, MD[6], Piotr Slomka, PhD[2], Frank S. Prato, PhD[7], Rohan Dharmakumar, PhD[8]

1. Cedars Sinai Medical Center, Los Angeles

2. Cedars Sinai Medical Center, CA

3. Cedars-Sinai Medical Center, Los Angeles, Los Angeles, CA

4. Lawson Health Research Institute, ON, Canada

5. Lawson Health Research Institute, London, ON, Canada

6. Cedars-Sinai Medical Center, Los Angeles, CA

7. Lawson Health Research Institute, University of Western Ontario, ON, Canada

8. Cedars-Sinai Medical, CA

Background: Cardiac stress testing with BOLD CMR has seen major technical advances in the past two decades. Yet, the reliability of BOLD CMR remains a major weakness for its widespread clinical use. A key unresolved obstacle with BOLD CMR is limited sensitivity, which is compounded by the presence of challenging imaging conditions during peak vasodilation, resulting in poor reliability. We hypothesized that if we repeatedly acquired BOLD images following regadenoson injection (a long-acting (tens of minutes) coronary vasodilator) and modeled the signal response to reflect the known pharmacokinetics of regadenoson, the reliability of BOLD CMR can be significantly improved. We tested our hypothesis in a clinically relevant animal model and validated our findings with simultaneously acquired ^{13}N-NH_3 PET perfusion images.

Methods: Intact (n=7) and infarcted (n=2) dogs were studied in a clinical PET/MR system. 2D BOLD (T_2 maps) and ^{13}N-NH_3 PET images were acquired pre- and post-regadenoson administration (p.r.a). Studies were terminated with LGE to identify the infarcted myocardium. T_2 maps p.r.a were repeatedly acquired over 30 mins and were registered to T_2 maps at rest. These time-dependent T_2 maps were then used to model the pharmacokinetics of regadenoson as a mono-exponential process ($T_2(t)=T_{2o}+\Delta T_{2max}\exp(-t/\tau)$). Maximum myocardial BOLD response from regadenoson pharmacokinetics modeling (RPM) was estimated and compared to the conventional BOLD approach(Con) , which relies on a single time-point peak-vasodilation typically estimated at 2 min p.r.a. BOLD CNR between remote and affected zones (CNR= ($\mu MBR_{Remote}-\mu MBR_{Affected}$)/$\delta MBR_{Remote}$, where μ and δ are the mean and standard deviation) were estimated for Myocardial BOLD Response (MBR) based on RPM (MBR_{RPM}) and conventional approach (MBR_{con}) and compared. MBRs were validated against PET (MPR, Myocardial Perfusion Reserve).

Results: In intact dogs, myocardial T_2 dynamics followed the mono-exponential process of RPM (R=0.92 ±0.06). Parameters estimated from RPM (T_{2o}:44.2±6.7ms; ΔT_{2max}:14.7±5.8ms; τ:35.5±26.8min) were in agreement with previous reports. Both MBRs (MBR_{RPM}=27±16% and MBR_{con}=12±6%) were consistent with PET (MPR=3.0±0.6). MBR_{RPM} and MBR_{Con} were highly correlated(R=0.93; $MBR_{RPM}=2.83*MBR_{con}-0.27$), indicating that MBR_{RPM} was ~2.8-fold higher than the MBR_{Con}. In infarcted dogs, significantly higher MBRs in the remote and lower MBRs in the affected regions were observed with both methods (Remote: MBR_{RPM}=27±6%, MBR_{Con}=15±5%; Affected: MBR_{RPM}=1±10%, MBR_{con}=5±7%; both $p<0.05$) and were in agreement with PET (MPR_{remote}=3.7±0.6; $MPR_{affected}$=1.9±0.7;). Mean CNR based on RPM were nearly 2-fold larger than the conventional approach (CNR_{RPM}=3.7±0.6; CNR_{con}=1.9±0.7).

Conclusion: Our findings support the hypothesis that repeatedly acquired BOLD CMR, modeled to reflect the pharmacokinetics of regadenoson, may be used to significantly improve the current limits of BOLD sensitivity.

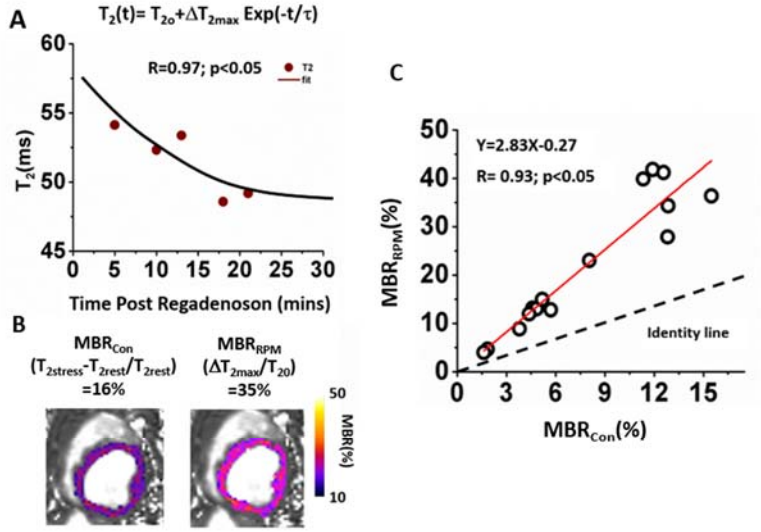

Fig. 1 *Pharmacokinetic Modeling of Regadenoson Leads to Marked Improvement in BOLD Sensitivity in Intact Dogs*: (**A**) shows a representative time-resolved T_2 relaxation estimates and least-squares fitting following regadenoson injection; (**B**) shows the corresponding multi-fold increase in MBR from the RPM compared to conventional MBR estimation; and (**C**) shows the linear regression between RPM-based and conventional estimates of MBR. Note the slope of the regression curve is significantly larger than 1 highlighting the amplification in BOLD signal response uncovered by the RPM that is likely masked by unreliable signal estimates from conventional estimates.

Fig. 1 Pharmacokinetic Modeling of Regadenoson Leads to Marked Improvement in BOLD Sensitivity in Intact Dogs

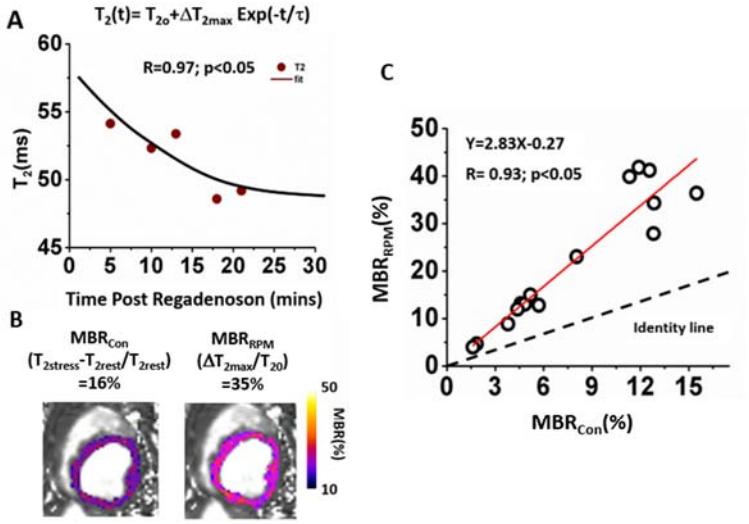

Fig. 1 *Pharmacokinetic Modeling of Regadenoson Leads to Marked Improvement in BOLD Sensitivity in Intact Dogs*: (**A**) shows a representative time-resolved T_2 relaxation estimates and least-squares fitting following regadenoson injection; (**B**) shows the corresponding multi-fold increase in MBR from the RPM compared to conventional MBR estimation; and (**C**) shows the linear regression between RPM-based and conventional estimates of MBR. Note the slope of the regression curve is significantly larger than 1 highlighting the amplification in BOLD signal response uncovered by the RPM that is likely masked by unreliable signal estimates from conventional estimates.

Fig. 1 Pharmacokinetic Modeling of Regadenoson Leads to Marked Improvement in BOLD Sensitivity in Intact Dogs

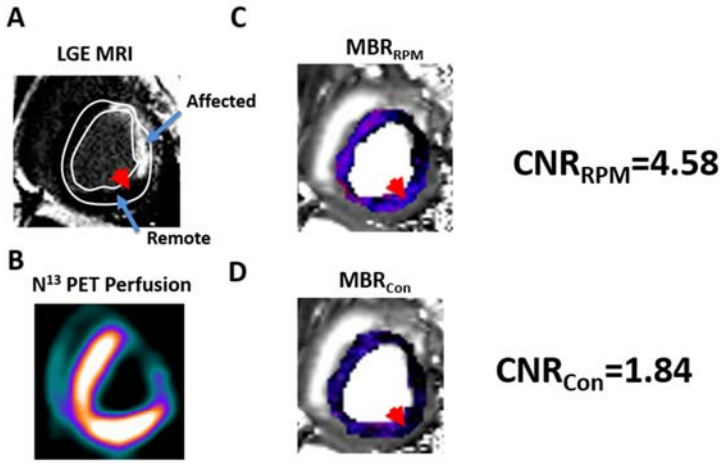

Fig. 2 *Time-Resolved Capture of Regadenoson Pharmacokinetics for Increasing the Detection Sensitivity of Perfusion Defect Territories with BOLD CMR*: (**A**) shows a representative LGE image with an anterior wall chronic infarction; (**B**) shows a significantly reduced perfusion on ^{13}N-NH_3 PET p.r.a in the infarct territory; (**C**) shows the MBR map based on RPM; and (**D**) shows the MBR estimated using the conventional approach based on BOLD signal responses at baseline and 2 minutes p.r.a. Note the improved BOLD CMR delineation of the perfusion defect territory in (**C**) compared to (**D**). The red arrows identify a healthy (remote) region that is hypointense in the conventional MBR and is recovered by MBR_{CRM} from the increased CNR.

Fig. 2 Time-Resolved Capture of Regadenoson Pharmacokinetics for Increasing the Detection Sensitivity of Perfusion Defect Territories with BOLD CMR

ID#: 373693

Cardiac fMRI - A new approach for identifying myocardial oxygenation changes in the heart with unprecedented confidence

Hsin-Jung Yang[1] Ilkay Oksuz, M.sc.[2], Olivia Sobczyk[3], Damini Dey, PhD[4], Jane Sykes, BS[5], John Butler, BSc MRT(MR)[6], Xiaoming Bi, PhD[7], Ivan Cokic, MD[8], Michael S Kovacs, PhD[9], Debiao Li, PhD[8], Piotr Slomka, PhD[4], Joseph Fisher, M.D.[3], Sotirios Tsaftaris[10], Rohan Dharmakumar, PhD[11]

1. Cedars Sinai Medical Center, Los Angeles

2. IMT Institute for Advanced Studies Lucca, Lucca, Toscana, Italy

3. University of Toronto, ON, Canada

4. Cedars Sinai Medical Center, CA

5. Lawson Health Research Institute, ON, Canada

6. Lawson Health Research Institute, London, ON, Canada

7. Siemens Healthcare, CA

8. Cedars-Sinai Medical Center, Los Angeles, CA

9. Lawson Health Research Institute, Canada

10. School of Engineering, University of Edinburgh, Scotland, United Kingdom

11. Cedars-Sinai Medical, CA

Background: BOLD CMR has evolved into a promising method for detecting ischemic heart disease without contrast agents, but its reliability remains poor. In this study, we propose a novel strategy to overcome this barrier through: (i) a fast, free breathing, confounder-corrected, 3D T2 mapping at 3T that is performed with whole-heart coverage, which permits rapid modulation of breathing gases; (ii) repeat stimulation of heart with prospective control of arterial CO_2 ($PaCO_2$); and (iii) a statistical image analysis framework. Using a large animal model we demonstrate that our approach could provide unprecedented amplification in sensitivity and specificity, thus providing an opportunity to markedly improve the reliability of BOLD CMR.

Methods: Canines with (n=5) and without (n=5) LAD stenosis were studied in a clinical PET/MR system. A fast, confounder-corrected, free-breathing 3D T2 mapping sequence was prescribed during rest, under adenosine and under four repeat modulations of $PaCO_2$ (refer to Figs.1A-B). Segmental myocardial T2 values acquired under normocapnia ($PaCO_2$(-)) and hypercapnia ($PaCO_2$(+)) were compared using t-statistics to test the null hypothesis using all the segments available after each stimulation block (hypercapnia and normocapnia pair):

H_0 [Null: *BOLD response present*]: T2 during $PaCO_2$(-) = T2 during $PaCO_2$(+)

H_1 [Alternate: *BOLD response absent*]: T2 during $PaCO_2$(-) ≠ T2 during $PaCO_2$(+) Maps of segmental t-scores determined from increasing number of blocks were constructed as shown in Fig. 1C.

Results: Representative results from animals with and without LAD stenosis are presented in Fig. 2. Panels A and B show a representative t-score and confidence of response (CoR, 1-p values) maps, along with PET validation in a healthy animal. Panels C and D show the aggregate response across all segments. Note that with increasing number of $PaCO_2$ blocks both the t-scores and CoRs increased; and that with 4 blocks, all segments reached CoRs >0.95. Panels E, F, G, and H show the same for an animal with LAD stenosis. While remote segments behaved similar to response observed with healthy animals, the affected segments showed no increase in t-scores or CoRs, which was consistent with PET MPR. These findings were consistent across all animals.

Conclusion: Repeat coronary stimulations with precisely targeted arterial CO_2 can be used to significantly increase the confidence in detecting myocardial BOLD response. These early findings show a means for overcoming the reliability limitations currently associated with BOLD CMR.

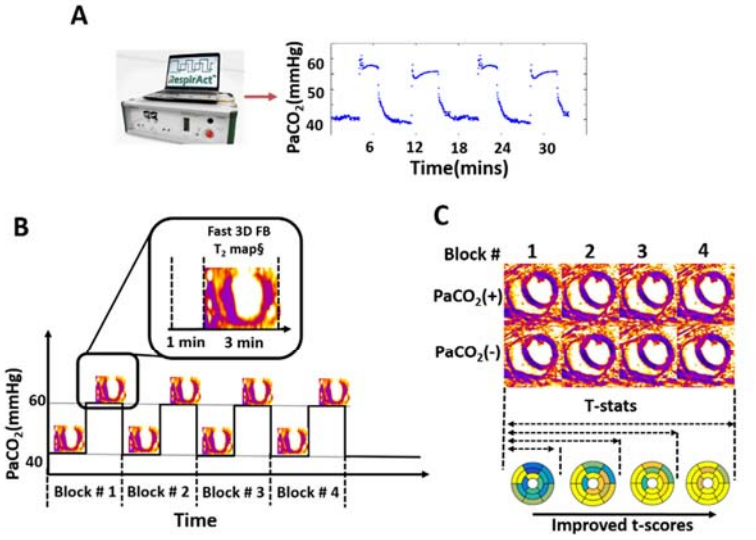

Figure 1. *Image Acquisition Protocol and Framework of Statistical Analysis*. **Panel A** shows the repeat stimulation with a prospective $PaCO_2$ modulation system as previously described. **Panel B** shows image acquisition protocol. Fast 3D, free-breathing, T2 maps were prescribed under normocapnic (-) and hypercapnic (+) states and repeated for 4 times (each representing 1 block). T2 maps acquired from each block were analyzed with t-statistics in **Panel C**. T-scores and CoRs were derived using paired segmental T2 values from repeat blocks. Higher t-scores were observed with integration of repeatedly measured data.

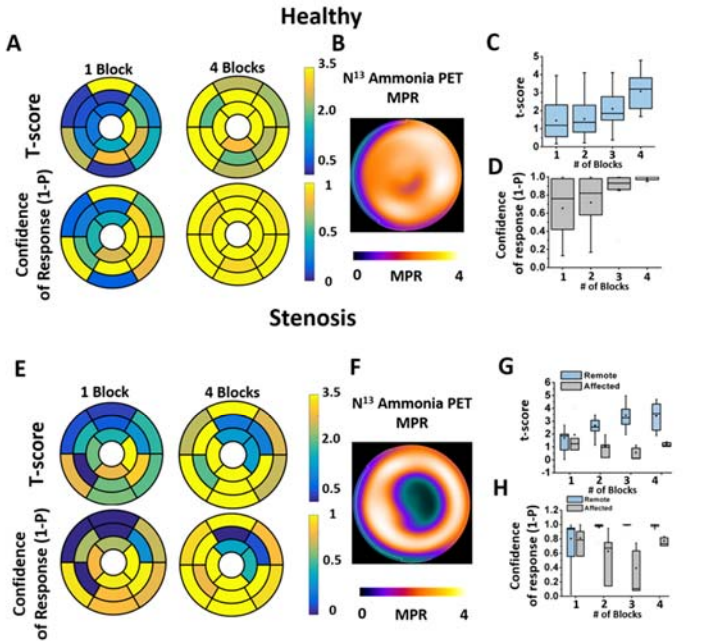

Figure 2. *T-score and CoR from BOLD MRI and PET MPR in Dogs with and without (healthy) Coronary Stenosis*. **Panels A** and **E** show representative segmental t-score and CoR derived from blocks 1 and 4 from a healthy dog and a dog with LAD stenosis are shown, respectively. **Panels B** and **F** show corresponding PET MPR images. The maps from 4 blocks and MPR were highly concordant. Segments with impaired MPR showed significantly lower CoR from 4 blocks. **Panels C, D, G** and **H** show boxplots of t-scores and CoR derived from 1-4 blocks.

Figure 1. Image Acquisition Protocol and Framework of Statistical Analysis.

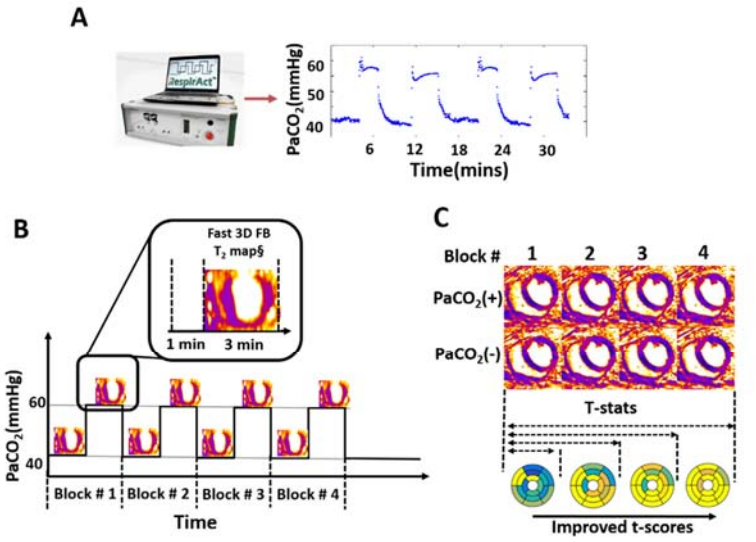

Figure 1. *Image Acquisition Protocol and Framework of Statistical Analysis*. **Panel A** shows the repeat stimulation with a prospective $PaCO_2$ modulation system as previously described. **Panel B** shows image acquisition protocol. Fast 3D, free-breathing, T2 maps were prescribed under normocapnic (-) and hypercapnic (+) states and repeated for 4 times (each representing 1 block). T2 maps acquired from each block were analyzed with t-statistics in **Panel C**. T-scores and CoRs were derived using paired segmental T2 values from repeat blocks. Higher t-scores were observed with integration of repeatedly measured data.

Figure 2. T-score and CoR from BOLD MRI and PET MPR in Dogs with and without (healthy) Coronary Stenosis.

ID#: 375386

Coronary Endothelial Function Testing using Continuous Cardiac ASL-CMR

Ahsan Javed, MS[1] Hung P. Do, PhD[1], Andrew J. Yoon, MD[1], Krishna S. Nayak, PhD[1], Parveen Garg, Md mph[2]

1. University of Southern California, Los Angeles, CA

2. USC Keck School of Medicine

Background: Coronary magnetic resonance angiography has recently been used to assess coronary endothelial dysfunction (CED) (1), but is limited by the need for high spatial resolution, sensitivity to cardio-respiratory motion, and the ability to image only proximal coronary arterial segments. In this study we demonstrate the feasibility of cardiac arterial spin labeling (ASL) to assess CED by measuring myocardial blood flow (MBF) (2) as a surrogate for coronary blood flow.

Methods: *Acquisition:* Thirty-two patients were enrolled: 10 patients with coronary artery disease (CAD) (> 50% stenosis in at least one major coronary branch as determined by coronary angiography); 12 high-risk patients (with at least two risk factors for cardio-vascular disease and no clinical cardio-vascular disease); and 10 healthy controls. In this study, double-gated cardiac ASL (3) at 3 Tesla was used to continuously measure MBF in a mid-short axis slice using the protocol shown in Figure 1. Stress was induced with sustained isometric handgrip exercise, an endothelial dependent stressor (4), at 30% of each subject';s maximum voluntary contraction. *Data Analysis:* Semi-automated segmentation was used to generate masks for all images (5). The myocardium was divided into six segments and MBF was calculated after a spatial-temporal averaging (6). Rest MBF and stress MBF was calculated from 8 min (~18 pairs) of rest data and 3.5 min of stress data (~6-8 pairs) as shown in Figure 1. MBF reserve was calculated as stress MBF– rest MBF. Temporal SNR (TSNR) was calculated as MBF divided by the estimated standard deviation of MBF (7). Subjects with global rest TSNR < 3, or global stress TSNR < 1 were rejected from data analysis. A student';s t-test was performed to determine statistical significance.

Results: Five healthy, three high-risk, and four CAD patients were excluded due to either the inability to complete the protocol or a low TSNR. Table 1 shows the results and patient demographics. Figure 2 contains the group analysis. There were statistically significant differences in MBF reserve between healthy vs. CAD patients and healthy vs. high-risk subjects with $p<0.01$ and $p<0.05$, respectively.

Conclusion: This study demonstrates the feasibility of using cardiac ASL for non-invasive assessment of CED. Future studies will involve larger patient cohort for more conclusive statistical testing. References

1. Hays AG:JACC. 2010.
2. Kober F:MRM. 2016.
3. Do HP:MRM. 2016.
4. Hays AG:AJPHeart. 2015.
5. Javed A:JCMR. 2015.
6. Jao T:ISMRM. 2012.
7. Zun Z:MRM. 2009.

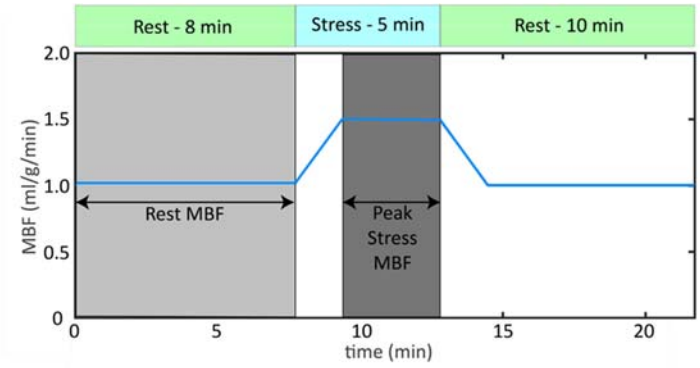

Figure 1:The scan protocol and the ideal expected curve are shown assuming a 50% increase in MBF during peak stress. In this study, cardiac ASL was performed continuously for approximately 23 minutes: 8 min rest, 5 min handgrip stress, and 10 min rest. Data acquired during period marked rest MBF and peak stress MBF was used to calculate rest and peak stress MBF, respectively. The first 1.5 min of data during stress was not used in the calculation of peak stress MBF.

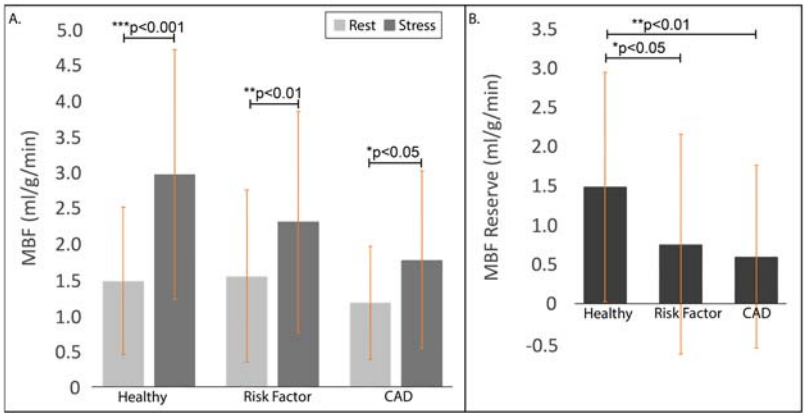

Figure 2: A) Comparison of rest and stress MBF in healthy, high-risk, and CAD groups. The difference between rest and stress MBF was statistically significant in all three groups with ***p<0.001 (healthy), ** p<0.01 (high-risk), and * p<0.05 (CAD). The post-stress resting MBF (not shown) was statistically not different from pre-stress resting MBF in all three patient populations(p>0.41). B) Comparison of MBF reserve in healthy, high-risk, and CAD groups. The difference of MBF reserve between healthy vs. CAD and healthy vs. high-risk was statistically significant with p<0.01 and p<0.05, respectively.

Patient Population	*Demographic*	*Rest MBF*	*Stress MBF*	*MBF Reserve*
Healthy (5 subjects, N=30 segments)	4M/1F , Age: 24-27	1.48±1.03	2.97±1.75	1.49±1.46
High-Risk (9 subject, N=54 segments)	4M/5F , Age: 51-76	1.55±1.20	2.30±1.54	0.76±1.40
CAD (6 subjects, N=36 segments)	4M/2F , Age: 40-75	1.18±0.79	1.78±1.24	0.60±1.16

Table 1: Demographic and measured MBF and MBF reserve from cardiac ASL. Values are reported as mean ± standard deviation and are shown only for patients whose data was used. Age is give as min-max.

ID#: 378327

Myocardial infarction with normal coronary arteries by coronary angiography and the relevance of cardiac magnetic resonance for its diagnostic classification.

Guadalupe M. Pérez Quintana, MD[1] Beatriz E. Domínguez Mendez, MD[2], Héctor González Pacheco, MD[3], David F. Cuevas Cueto, MD[4], Gabriela Melendez Ramírez, Ph.D[5], Roberto Cano Zárate, MD[6], Aloha Meave González, MD[7]

1. Instituto Nacional de Cardiología Ignacio Chávez, Oaxaca, Oaxaca, Mexico

2. Instituto Nacional de Cardiología "Ignacio Chávez", Ciudad De México, Distrito Federal, Mexico

3. National Institute of Cardiology, Distrito Federal, Mexico

4. Instituto Nacional de Cardiología Ignacio Chavez, Zapopan, Jalisco, Mexico

5. Instituto Nacional de Cardiología Ignacio Chavez, Distrito Federal, Mexico

6. Instituto Nacional de Cardiología, Mexico

7. Instituto Nacional de Cardiología Ignacio Chavez, Mexico

Background: Myocardial infarction with coronary arteries without significant obstruction (MINOCA) is identified by the detection of "elevation and / or fall" of troponin associated with at least one of the following: symptoms of myocardial ischemia, electrocardiographic changes indicative of new ischemia, evidence of new viable myocardial loss or new regional abnormality of wall motion, and identification of intracoronary thrombus by angiography or autopsy. It may be considered a work diagnosis that requires routine evaluation to address the underlying causes. This may include CMR imaging, provocative spasm testing, and evaluation of thrombophilia. Adequate diagnostic algorithms should be available in these cases.

Methods: Objectives: To describe the importance of the correlation of imaging methods in the MINOCA for the diagnostic classification. **Hypothesis:** Cardiac Magnetic Resonance allows the non-invasive cardiac and diagnostic classification of the MINOCA. **Material and methods:** We identified all patients admitted to the emergency department of our institute from January 2016 to March 2017 with chest pain and who underwent coronary angiography with a report of normal coronary arteries and underwent magnetic resonance imaging cardiac.

Results: A total of 12 patients were admitted to the emergency room with chest pain and to whom coronary angiography was negative for coronary artery injury and CMRI was also requested. Of the 100% of patients with the characteristics already described, two groups were obtained: 1) Patients with confirmed cardiac magnetic resonance imaging (IMR) accounted for 41% (of all patients), with the following diagnoses: Acute myocardial infarction representing 80% and myocarditis 20% in this group. 2) Patients with a reclassification of their diagnosis of admission to diagnosis obtained by cardiac magnetic resonance, representing 58.3% of the total patients, where the following diagnoses were: myocarditis representing 41%, myopericarditis with 8.3%, and dilated myocardiopathy with 8.3% in this group of patients.

Conclusion: Cardiac magnetic resonance imaging is a useful noninvasive diagnostic method to establish the definitive diagnosis of patients with myocardial infarction with coronary arteries without lesion (MINOCA), in which the potential causes are multiple, therefore adequate evaluation is necessary to optimize therapeutics and improve life prognosis.

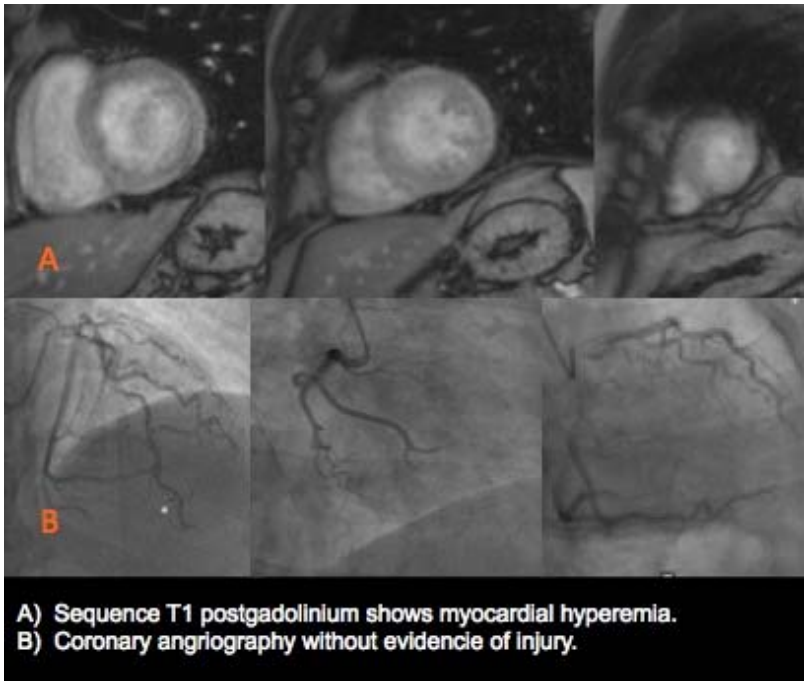

Cardiac Acute Myocarditis whit Resonance with diagnosis of Myocarditis and Coronary angiography

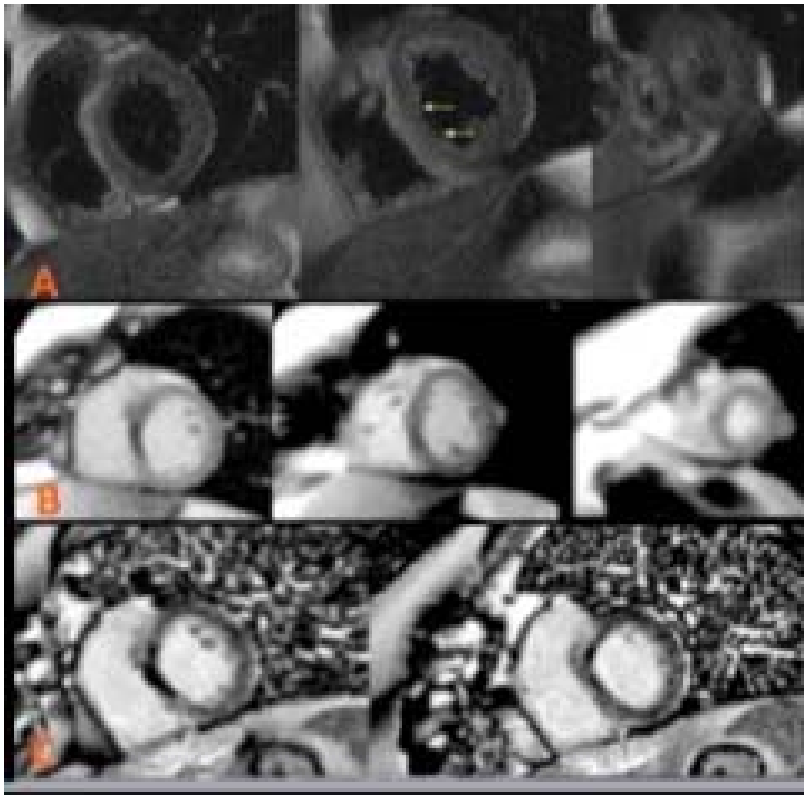

A) Sequence T2 W: Edema inferoseptal.
B) First-pass sequence: with hypointense zone by infarction in third basal anteroseptal and third third inferoseptal.
C) Transmural late reinforcement in basal third with microvascular obstruction in anteroseptal segments with inferoseptal extension, middle subendocardial third and septal apical third.

Acute myocardial infarction of the septal transmural myocardium in basal and middle thirds, with zones of microvascular obstruction.

ID#: 377972

Optimal Flip Angle for Steady Pulsed Arterial Spin Labeled CMR

Hung P. Do, PhD[1] Terence R. Jao, PhD[2], Venkat Ramanan, MSc[3], Graham Wright, PhD[4], Nilesh R. Ghugre, PhD[5], Krishna S. Nayak, PhD[1]

1. University of Southern California, Los Angeles, CA

2. University of Southern California, CA

3. Sunnybrook Research Institute, Toronto, ON, Canada

4. Sunnybrook Research Institute, University of Toronto, ON, Canada

5. Sunnybrook Research Institute, University of Toronto, Toronto, ON, Canada

Background:

Steady-pulsed arterial spin labeling (SPASL) [1–3] is a highly-efficient labeling technique for ASL-CMR [4]. Previous studies used transient balanced steady state free precession (bSSFP) acquisition with a 50º prescribed flip angle, which is known to provide high signal-to-noise ratio (SNR) efficiency [5]. This study aims to identify the optimal flip angle by systematically measuring the influence of flip angle on temporal SNR (TSNR), an indirect measure of the sensitivity of SPASL-CMR to myocardial blood flow (MBF) [6].

Methods:

Data collection:
CMR experiments were performed at 3T on a healthy pig using a single mid short-axis slice, with all imaging in stable mid-diastole (timing identified from a CINE). The CMR protocol consisted of acquiring 32 baseline images in a 32 heartbeat breathhold with different prescribed flip angles (50º, 40º, 30º, 25º, 20º, 15º, 10º, and 5º). B1+ mapping [7] was performed in order to determine the actual flip angles experienced by each myocardial segment.

Data analysis:
Left-ventricular myocardium was manually segmented; regional analysis followed the standard 6-segment model. Measured signal intensity, SNR [8], and TSNR [9] as functions of actual flip angle were assessed, and compared with predictions by Bloch simulation.

Results:

Relative B1+ (shown in Figure 1) varied by 48% across LV myocardium [10]. The measured signal as a function of flip angle follows the same trend as simulations, with <39% discrepancy (shown in Figure 2). The discrepancy may be due to imprecise estimation of equilibrium magnetization. Figure 3 shows calculated TSNR from 6-AHA segments. Spatially varying coil sensitivity is responsible for some of the variation in SNR and TSNR. TSNR was maximum at approximately 25º.

Conclusion:

The preliminary results indicate that a flip angle of 25º instead of 50º will provide superior TSNR for SPASL-CMR. Use of a lower flip angle with preserved TSNR may improve ASL signal strength since there would be reduced saturation effect on inflowing blood perfusion. To better inform SPASL-CMR acquisitions, this study and analysis will need to be repeated in multiple animals, and be repeated for control and labeled images (the current study only included baseline images).

Funding
NIH R01-HL130494

References
1. Capron T: MRM 2013;70:1399–408.
2. Capron T: MRM 2015;74:990–8.
3. Xu J: MRM 2016;75:238–48.
4. Kober F: JCMR 2016;18:22.
5. Smith T: MRM 2010;63:537–42.
6. Zun Z: MRM 2009;62:975–83.
7. Chung S: MRM 2010;64:439–46.

8. Kellman P: MRM 2005;54:1439–47.
9. Triantafyllou C: Neuroimage 2011;55:597–606.
10. Sung K: JMRI 2008;27:643–8.

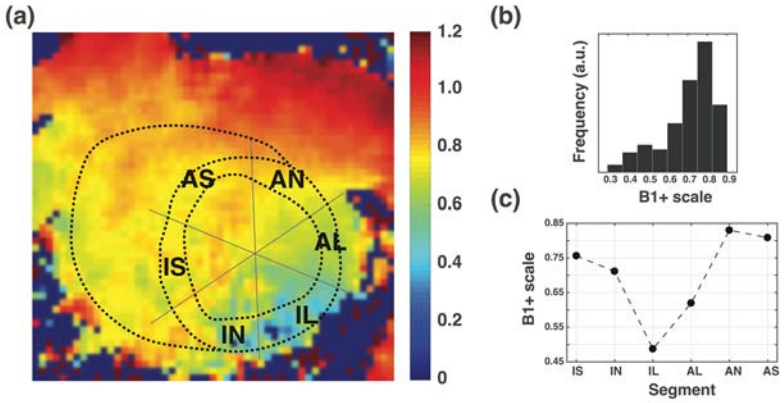

Figure 1: (a) B1+ scale map, (b) histogram of B1+ scale within LV myocardium, and (c) average B1+ scale of each segment. (IS: inferoseptal; IN: inferior; IL: inferolateral; AL: anterolateral; AN: anterior; AS: anteroseptal)

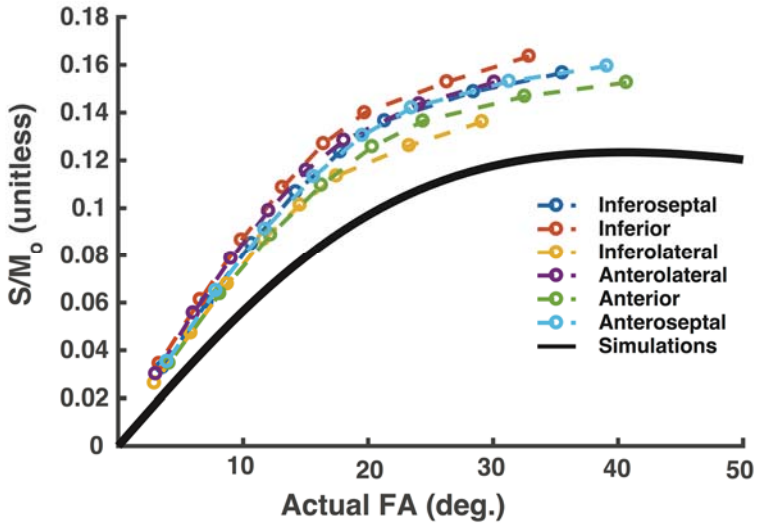

Figure 2: Normalized signal intensity (S/Mo) as a function of actual flip angle, measured from (color) 6 LV myocardial segments, and (black solid) generated using Bloch simulation. Note that SNR is proportional to normalized signal intensity because thermal noise in this acquisition is i.i.d.

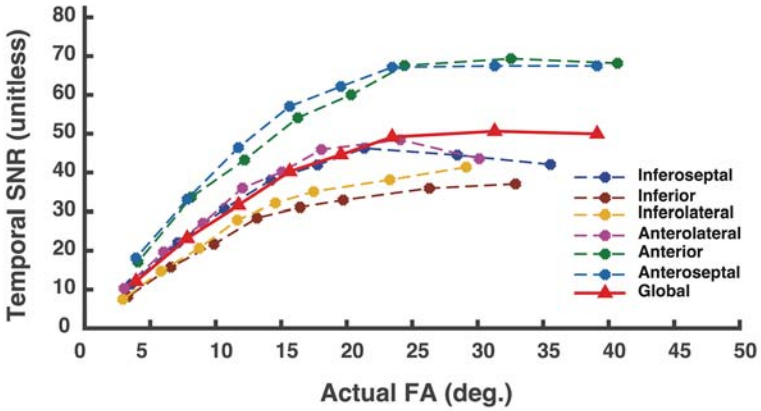

Figure 3: Temporal SNR as a function of actual flip angle from 6 LV myocardial segments. Spatially varying coil sensitivity is partially responsible for the variation. Maximum TSNR was achieved at approximately 25º.

ID#: 369182

Robust motion correction of myocardial perfusion MRI data

Cian Scannell, BSc, MRes[1] Amedeo Chiribiri, MD PhD[2]

1. King's College London, London, United Kingdom

2. King's College London, London, England, United Kingdom

Background: Myocardial perfusion imaging using CMR allows quantitative values relating to myocardial blood flow to be obtained. This analysis requires extraction of time-intensity curves from the data. However, these curves are sensitive to motion, in particular respiratory motion, which hampers the accuracy of the analysis and is viewed as a major bottleneck in the clinical translation of the technique. Many methods have been proposed to account for this motion but thus far none of these have achieved widespread acceptance. We propose a general framework that is robust to the wide variations seen in clinical data and allows accurate analysis of the curves.

Methods: Image registration algorithms are applied in two stages in order to retrospectively align frames from image series that exhibit respiratory motion. In the first stage, the local signal enhancement, which is caused by the passage of the contrast agent, is separated from the baseline images using robust principal component analysis. Non-rigid group-wise registration is performed on a coarse grid in order to eradicate the bulk motion. Hence, in the second stage, the majority of the motion has been accounted for and fine-tuning is performed. The remaining motion appears noise-like and therefore appears in the later components of a PCA decomposition. This allows construction of a completely motion-free synthetic image series using only the early principal components. Frames are then matched to the synthetic series on a fine grid to eradicate motion.

Results: The method is tested using two open source datasets (Wollny et al. (2014) and Pontre et al. (2016)), which contain 80 individual image series. In the first of these datasets, automatically extracted time-intensity curves are compared to the ground-truth (manually obtained) curves before and after applying this method. The mean normalised mean square error improves from 0.76 (0.8) to 0.50 (0.62) and the mean Pearson correlation coefficient improves from 0.77 (0.25) to 0.89 (0.17). In the second dataset, it is shown that there is no statistical difference between pharmacokinetic model parameters computed automatically after this motion correction scheme and the ground-truth values which are obtained through manual motion correction.

Conclusion: The method presented performs at least as well as those described in the literature. The advantage of this method, however, lies in its robustness; satisfactory motion correction is achieved for all frames in a completely automated and unsupervised manner. Further work will be required to validate its performance in a clinical setting.

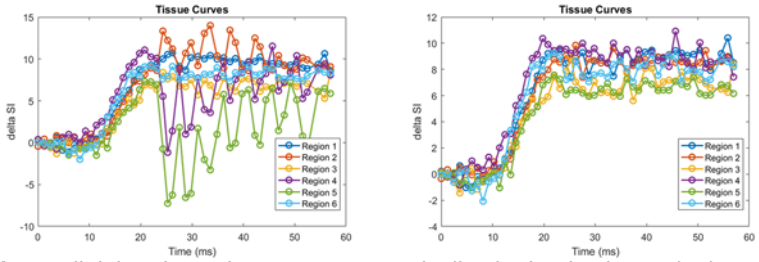

Myocardial time-intensity curves automatically obtained using a single segmentation as a mask for all frames, before (left) and after (right) application of the proposed motion correction scheme

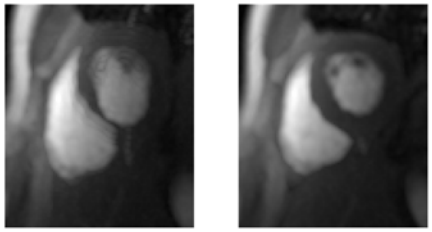

Maximum intensity projections before (left) and after (right) motion correction. These are commonly used for segmenting the myocardium and it is clear to see the effect of the motion on these images.

ID#: 372392

CMR Strain Analysis during Breathing Maneuvers for the Detection of Single Vessel Coronary Artery Disease

Mohamad Rabbani, B.Sc., MDCM Candidate[1] Elizabeth Hillier, B.Sc., PhD Student[1], Kady Fischer, PhD[2], Matthias G. Friedrich, MD[3]

1. McGill University, Montreal, PQ, Canada

2. McGill University Health Center, University Hospital Bern, Montreal, PQ, Canada

3. McGill University Health Centre, PQ, Canada

Background: In patients with suspected coronary artery disease (CAD), testing for inducible myocardial ischemia for identifying severe coronary artery stenosis typically requires the infusion of an inotropic agent such as dobutamine or a vasodilator such as adenosine. This adds cost and the necessity to have a physician present. Furthermore, side effects are frequent. Voluntary breathing maneuvers have been introduced as a method for inducing coronary vasomotion, yet their ability to induce functional abnormalities in unknown. Myocardial strain has become a diagnostic target for CMR and can be used to uncover very mild functional abnormalities. We aimed to evaluate whether myocardial strain is altered in territories of stenotic coronary arteries and whether breathing maneuvers modify this.

Methods: We studied 21 healthy volunteers (11 males, mean age 40 ± 15) and 8 patients with single-vessel CAD (8 male, mean age 60 ± 8) . CMR strain imaging was performed in regular cine images (SSFP, basal and mid ventricular short axis, repeated every 4s) in a 3T MRI scanner. The images were acquired before and during a voluntary breathing maneuver, that consisted of a 60s period of hyperventilation followed by a period of a maximal voluntary breath-hold. We measured segmental (AHA segment classification) left ventricular systolic circumferential strain (E_{cc}) and strain rate (SR). Clinical coronary angiography reports served as the reference standard to define territories subtended by coronary arteries with at least 70% narrowing in the absence of other significant stenosis. The remaining territories were considered remote. Global measurements from the healthy volunteers served as control values.

Results:

E_{cc} showed a significant difference between coronary territories of healthy volunteers and territories subtended by a stenotic coronary artery at time points of 30s into the breath-hold (healthy: -22.1 ± 1.9%, stenotic: -17.5 ± 3.2%, p= 0.003). In patients with CAD, there was a significant difference in E_{cc} between stenotic and remote territories at all time-points: pre-hyperventilation, post-hyperventilation, and 30s into breath-hold. For strain rate, only at time 30s into breath-hold there is a significant different between normal, stenotic and remote territories. ROC analysis at 30s into breath hold revealed that an E_{cc} cut-off value of -20.4% differentiates stenotic from remote territories with a sensitivity of 88% and specificity of 75%, with an area under the curve of 0.82.

Conclusion: In patients with coronary artery disease, CMR strain analysis in combination with a simple breathing maneuver may be useful to identify coronary artery disease and the presence of significant coronary artery stenosis.

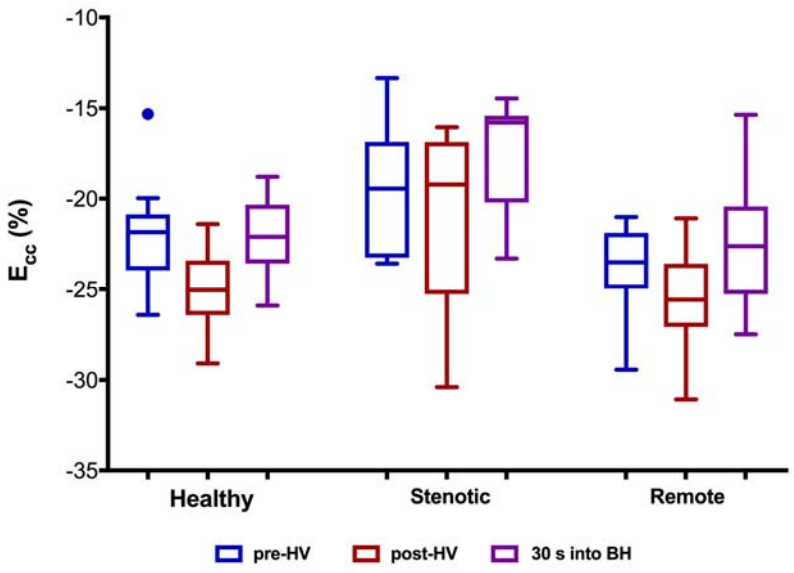

Circumferential Strain (Ecc) differences between healthy, stenotic and remote territories at Pre-hyperventilation, Post-hyperventilation, and 30s into BH (breath-hold)

Changes in Circumferential Strain and Strain Rate during Breathing Maneuvers

	Healthy		Patients				P-value	
			Stenotic Territory		Remote Territory			
	Mean	SD	Mean	SD	Mean	SD	Healthy vs. Stenotic Territory	Stenotic vs. Remote Territory
Circumferential Strain (%)								
Pre-HV	-22.1	2.3	-19.5	3.6	-23.8	2.7	0.051	0.027
Post-HV	-25.0	2.0	-20.9	5.1	-25.5	3.0	0.025	0.046
30s into BH	-22.1	1.9	-17.5	3.2	-22.5	3.7	0.003	0.036
Strain Rate (s^{-1})								
Pre-HV	-1.6	0.3	-1.8	0.7	-2.0	0.3	0.495	0.046
Post-HV	-1.9	0.6	-2.1	0.5	-2.3	0.3	0.379	0.345
30s into BH	-1.5	0.3	-1.0	0.7	-1.9	0.3	0.017	0.002

Results were considered statistically significant if the P-value was <0.05.

Abbreviations:
Pre-HV: Pre-Hyperventilation
Post-HV: Post-Hyperventilation
BH: Breath hold

ID#: 372260

Development of a stress-only perfusion gradient marker for detection of coronary microvascular dysfunction in women with no obstructive CAD: a new quantitative approach validated by invasively measured coronary reactivity

Zulma Sandoval, Ph.D.[1]Ahmed Albadri, MD[1], Janet Wei, MD[1], Louise E J. Thomson, MBChB[2], Babak Azarbal, MD[2], Bruce Samuels, MD[3], Daniel Berman, MD[2], C. Noel Bairey Merz, MD[4], Behzad Sharif, PhD[1]

1. Cedars-Sinai Medical Center, Los Angeles, Los Angeles, CA

2. Cedars-Sinai Medical Center, Los Angeles, CA

3. Cedars-Sinai Medical Center, CA

4. Cedars Sinai Medical Center, Los Angeles, CA

Background: Nearly half of women with symptoms of ischemia and no obstructive coronary artery disease (INOCA) have coronary microvascular dysfunction (CMD) [1]. Invasive assessment of coronary microvascular function using intracoronary adenosine is a predictor of major adverse outcomes in INOCA patients [2]. In the context of obstructive coronary artery disease (CAD), stress-induced myocardial perfusion gradients have been shown to detect the severity of ischemia without the need for a rest exam [3,4]. However, no “stress-only” noninvasive surrogate of coronary reactivity has been established/validated to date. We hypothesized that an optimally-designed marker of stress-induced myocardial blood flow (MBF) gradients will be strongly associated with invasively-measured microvascular reactivity in INOCA patients.

Methods: Twenty women with INOCA based on prior invasive quantitative coronary angiography (obstructive CAD defined as ≥50% stenosis in ≥1 epicardial artery) underwent invasive coronary reactivity testing [2] and adenosine-stress CMR. Microvascular reactivity to vasodilator stress was assessed invasively by measuring the coronary flow reserve (CFR) in response to intracoronary adenosine (100 µg bolus). High-resolution stress/rest CMR perfusion data was acquired in 3 contiguous slices centered at the midventricular position (in-plane resolution: 1.7x1.7 mm) using a dual-bolus protocol. In addition to quantification of transmural myocardial perfusion reserve (MPR), the thickest slice was selected and analyzed for subendocardial/subepicardial stress MBF quantification. Several variations of a marker for *global stress-induced MBF gradients*, including the one used by Mordini et al. [4], were tested against the invasive CFR data using Pearson correlation.

Results: Figure 1 shows representative stress perfusion results and demonstrates the ability to sufficiently delineate “endo/epi” sub-segments (mean transmural width = 7.7 mm). As described in Fig. 2, the optimized definition of global “endo/epi” stress-MBF ratio (last row) achieves a significant correlation vs. invasive CFR ($r = 0.83$, $p < 0.0001$). Figures 3(a) and 3(b) summarize the correlation analyses of the proposed stress-only perfusion gradient marker and the transmural MPR, respectively, vs. invasive CFR (the gold-standard index of microvascular reactivity). Both correlations were statistically significant; however, MPR showed a weaker correlation vs. invasive CFR ($r = 0.45$) compared with the proposed stress-only marker ($r = 0.83$; $p < 0.005$ for difference).

Conclusion: These initial results show, for the first time, that an optimized marker of global stress-induced perfusion gradients can serve as a noninvasive surrogate for detection of abnormal microvascular reactivity to adenosine, which is a hallmark of CMD and an established prognostic marker in women with INOCA. Compared to markers of perfusion reserve that require a comprehensive stress/rest perfusion exam, the proposed stress-only perfusion gradient marker is robust to the confounding effects of the rest-perfusion exam and may represent a novel target for therapeutic strategies involving this cohort. Furthermore, a stress-only CMR perfusion exam will only require half of the amount of gadolinium contrast agent needed to perform a combined stress/rest exam.

References:

[1] Bairey Merz et al. Circ 2017
[2] Pepine et al. JACC 2010
[3] Chiribiri et al. JACC Img 2013
[4] Mordini et al. JACC Img 2014.

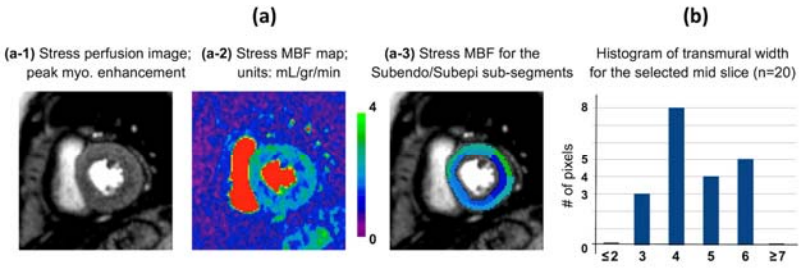

Fig 1. (a): Representative results in a patient with symptoms of ischemia and no obstructive CAD (INOCA) who underwent invasive coronary reactivity testing (the gold-standard test [1,2] for determination of CMD) and stress/rest perfusion CMR. **(a-1):** Stress perfusion image at peak myocardial enhancement phase (1.7x1.7 mm^2 in-plane resolution) after motion compensation and proton-density correction; **(a-2,a-3):** Quantified pixel-wise (a-2) and segmental (a-3) stress MBF maps, demonstrating *global stress-induced perfusion gradients*. Segment division to subendocardial ("endo") and subepicardial ("epi") regions was performed semi-automatically. The stress-induced gradient (mean endo-MBF divided by mean epi-MBF) for this case was 0.80 and the invasive CFR was 1.63, which is considered an abnormal level of coronary reactivity [2]. **(b): Histogram of the transmural segment width** for the thickest mid slice (true pixel units) for the 20 stress scans. For each case, the thickest slice was selected for endo/epi stress MBF quantification (average width = 7.7 mm ≈ 4-5 pixels).

Figure 1.

Definition of Stress-induced MBF Gradient	Pearson corr. (r)	p value
$min\left(\frac{endo_1}{epi_1}, \frac{endo_2}{epi_2}, \cdots, \frac{endo_6}{epi_6}\right)$	0.36	0.124
$\frac{min(endo_1, endo_2, \cdots, endo_6)}{median(epi_1, epi_2, \cdots, epi_6)}$	0.57	< 0.01
$median\left(\frac{endo_1}{epi_1}, \frac{endo_2}{epi_2}, \cdots, \frac{endo_6}{epi_6}\right)$	0.75	< 0.001
$mean\left(\frac{endo_1}{epi_1}, \frac{endo_2}{epi_2}, \cdots, \frac{endo_6}{epi_6}\right)$	0.79	< 0.0001
$\frac{mean(endo_1, endo_2, \cdots, endo_6)}{mean(epi_1, epi_2, \cdots, epi_6)}$	**0.83**	**< 0.0001**

Fig 2. Derivation of the optimal marker of global stress-induced MBF gradients for detection of CMD in the absence of obstructive CAD: Pearson correlation (2 tailed) for 5 different definitions of global stress-induced MBF gradients vs. invasive CFR (index for abnormal microvascular reactivity in INOCA patients). In each row, "endo" and "epi" represent subendocardial and subepicardial stress MBF values, respectively, corresponding to the myocardial segment indicated in the subscript index (total of 6 segments for the thickest slice among the 3 acquired contiguous mid slices). All correlations except for the 1st row were significant. The 2nd row corresponds to the stress MBF marker used by Mordini et al. [4] for detection of obstructive CAD. The bottom two rows provide the strongest correlation vs. the invasive measure. *The last row was selected as the "optimized" marker.*

Figure 2.

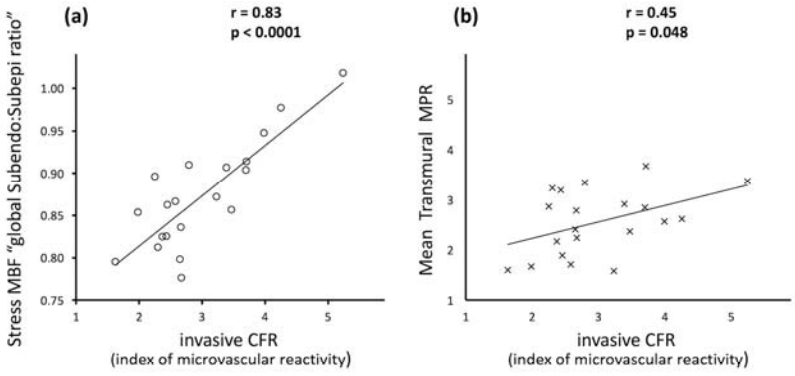

Fig 3. (a): The optimized marker of stress-induced MBF gradient (defined in the last row of Fig. 2) is plotted against CFR (index of microvascular reactivity) measured invasively in response to intracoronary adenosine (n = 20). The significant correlation indicates the potential for noninvasive detection of abnormal coronary reactivity in INOCA patients with suspected CMD based on the optimized marker for stress-induced MBF gradients. **(b):** Mean transmural myocardial perfusion reserve (stress-to-rest MBF ratio averaged over all segments) plotted against invasive CFR. Although the correlation is still significant ($p < 0.05$), the correlation is weaker compared with the stress-only marker in panel (a), which is likely due to the confounding effect of variations in resting flow on perfusion reserve (inconsistent "resting state" during the invasive test vs. the CMR exam). The proposed imaging marker in (a) does not use the resting MBF data and therefore eliminates this confounder.

Figure 3.

ID#: 378974

The Global Myocardial Oxygenation Response to Breathing Maneuvers is Reduced in a Non-Selective Cohort of Patients with Coronary Artery Disease

Giulia Vinco, MD[1] Elizabeth Hillier, B.Sc., PhD Student[2], Michele Pighi, MD[3], Giovanni Benfari, MD[4], Emile Mehanna, MD[5], Matthias G. Friedrich, MD[6]

1. McGill University Health Centre, University of Verona, PQ, Canada

2. McGill University, Montreal, PQ, Canada

3. McGill University Health Centre, Italy

4. University of Verona, Italy

5. McGill University Health Centre

6. McGill University Health Centre, PQ, Canada

Background: Oxygenation-sensitive cardiovascular magnetic resonance (OS-CMR) detects myocardial oxygenation changes by associated changes of signal intensity (SI). The use of a maximal voluntary breath-hold following 1 min of hyperventilation (HVBH) has been shown as an effective vasodilatory stimulus, inducing an increase of myocardial oxygenation in healthy subjects. We aim to analyze the myocardial oxygenation response to breathing maneuvers in patients with angiographic evidence of coronary artery disease (CAD), to assess the ability of this technique to detect significant coronary lesions.

Methods: Subjects with angiographic evidence of significant coronary artery disease (as defined by at least one coronary lesion with a 50% lumen reduction by quantitative coronary angiography) were recruited. Healthy volunteers, without evidence of cardiac/respiratory disease, constituted the control group. All participants underwent a CMR exam in a 3T Siemens scanner. A baseline standard oxygenation-sensitive bSSFP cine was acquired in two short-axis slices (mid-basal and mid-apical). The subjects then performed a combined breathing maneuver by hyperventilating for 60s with a rate of 30 breaths/min paced by a metronome, followed by a maximal voluntary breath-hold at end-expiration (HVBH). During the breath-hold, OS-CMR images were continuously acquired using the OS sequence. SI changes were measured at the end-systolic phase of each cardiac cycle.

Results: Among all participants (n=66), six subjects (3 healthy volunteers and 3 CAD patients) experienced lightheadedness and one CAD patient experienced chest discomfort during the breathing maneuvers. In all cases, adverse effects were reversible within 60 seconds and disappeared with normal breathing. There was no significant difference in the breath-hold duration between healthy and CAD subjects (66. 1 ± 23.5 sec and 64. 5 ± 25.5 sec). Two subjects performed the breathing maneuvers incorrectly, therefore had to be excluded from the analysis. CAD patients had a significantly lower SI response (ΔSI[%]) than healthy volunteers at 30 sec into the breath-hold (+3.6±4.1% vs. +8.3±6.8%, $p<0.05$).

Conclusion: Our data suggest that breathing maneuvers are safe and feasible. Subjects with angiographic evidence of coronary artery disease have a global decrease of the myocardial oxygenation response to a breath-hold stimulus when compared to healthy subjects. OS-CMR with breathing maneuvers is a promising needle-free tool to assess vascular function in the setting of coronary artery disease.

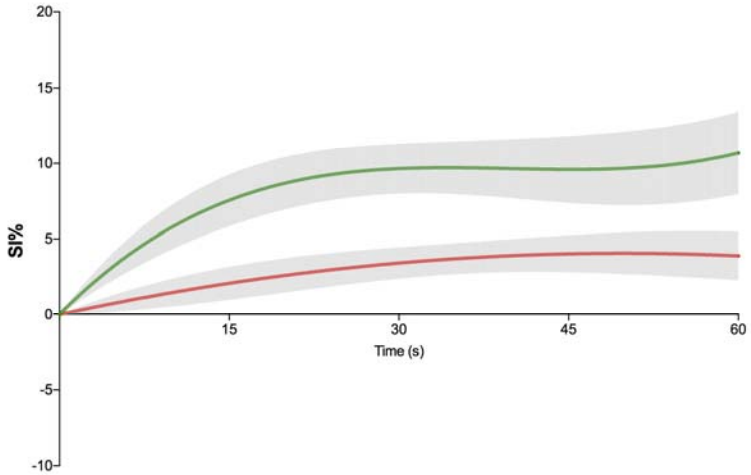

Myocardial oxygenation response curve during the breath-hold in healthy volunteers (green) and CAD patients (red).

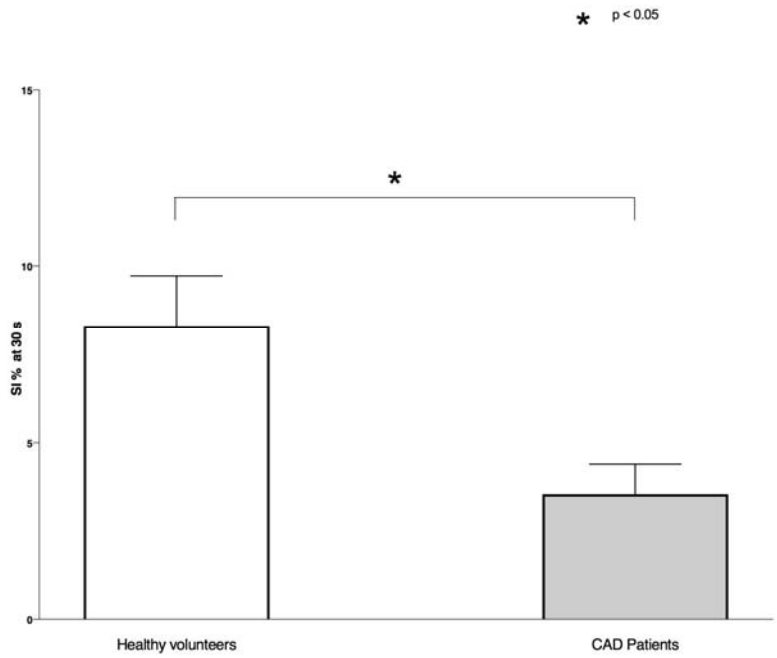

Global myocardial OS-SI % change at 30 s in healthy volunteers and CAD patients